JMIR Medical Informatics

Impact Factor (2023): 3.1
Volume 14 (2026) ISSN 2291-9694 Editor in Chief: Christian Lovis, MD, MPH, FACMI

Contents

Reviews

Digital Public Reporting Systems for Evaluating Health Care Quality: Systematic Review (e80435)
Lanmei Du, Reima Suomi, Elorm Damalie. . . . 8

Machine Learning for Predicting Venous Thromboembolism After Joint Arthroplasty: Systematic Review of Clinical Applicability and Model Performance (e79886)
Junwei Ma, Huifeng Tang, Yunshan Zhang, Xuemei Yi, Tangsheng Zhong, Xinyun Li, Gang Wang. . . . 23

Using Health Information Systems to Support Behavioral Interventions in Local Contexts: Scoping Review (e77296)
Xi Yang, Martin Dijst, Joost Daams, Marc Suhrcke, Haoran Yang, Ronald Cornet. . . . 37

Core Elements, Development, and Implementation Strategies of the Nursing Minimum Data Set: Scoping Review (e84281)
Pascal Müller, Annabell Gangnus, Katrin Gayen, Uta Kirchner-Heklau, Patrick Jahn, Sebastian Hofstetter. . . . 65

Technological Strategies for the Patient Experience in Emergency Departments: Scoping Review (e79782)
Andrés Santafé, Juan Aranda, Wilmer Beltrán, William Guerrero, Maryory Guevara Lozano, Ingrid Bustos. . . . 75

Large Language Model–Based Virtual Patient Systems for History-Taking in Medical Education: Comprehensive Systematic Review (e79039)
Dongliang Li, Syaheerah Lebai Lutfi. . . . 90

Causal Discovery in Observational Medical Research: Scoping Review (e82499)
Zuting Liu, Tian Luo, Hailin Ma, Jiali Mo, Xia Yang, Zhenglong Huang, Jingkun Li, Jie Kuang. . . . 110

Viewpoints

Developing Clinical Decision (Support) Systems Combining the Scientific and Regulatory Perspective: European Insights on Challenges, Requirements, and Practical Guidance (e72809)
Sanne Vrijlandt, Sanne Janssen, Annemarie van Rossum, Niek Achten, Rianne Oostenbrink. . . . 129

Dynamic Personalized Optimization: An AI Functionality Framework for Digital Therapeutics (e75256)
Dohyoung Rim. . . . 138

XSL•FO
RenderX

Ethical Imperatives for Retrieval-Augmented Generation in Clinical Nursing: Viewpoint on Responsible AI Use (e79922)
Xinyi Tu, Chenghao Shi, Peilin Qian, Lizhu Wang. . . . 162

Improving Clinical Decision-Making in Treating Airway Diseases With an Expert System Built Upon the Free AI Tool Google NotebookLM (e78567)
Cheng-Hao Hsu, Ching-Li Hsu, Chih-Hsiang Tsou, Kuo-Fang Hsu, Hung-Yu Yang. . . . 170

Original Papers

Telepathology Development and Stakeholder Perspectives in China: Cross-Sectional Survey (e83514)
Linlin Wang, Fangfang Cui, Xianying He. . . . 144

Experiences With Integrating Medical Terminologies Into User Interfaces for a Decision Support System for Primary Care: Conceptual and Development Study (e74934)
Michaela Neff, Jannik Schaaf, Najia Ahmadi, Michele Zoch, Dania Schütze, Holger Storf. . . . 185

Developing a Suicide Risk Prediction Algorithm Using Electronic Health Record Data in Mental Health Care: Real-World Case Study (e74240)
Linda Hummel, Karin Lorenz-Artz, Joyce Bierbooms, Inge Bongers. . . . 202

Rectal Cancer Radiotherapy Response Prediction: Retrospective Study of Development of a Deep Learning–Based Radiomics Model (e77313)
Yiqun Li, Hengchang Liu, Qiang Wei, Zhenqi Wang, Zhen Hu. . . . 227

Comprehensive Pediatric Health Risk Stratification Using an AI-Driven Framework in Children Aged 2 to 8 Years: Design and Validation Study (e80163)
Jundan Chen, Zhihe Mao. . . . 248

Scalable and Privacy-Conscious End-to-End Processing of Large-Scale Clinical Data for Precision Medicine: Empirical Evaluation Study (e83487)
Jungwoo Lee, Sangwon Hwang, Kyu Lee. . . . 266

Trust in AI-Supported Screening in General Practice Among Urban and Rural Citizens: Cross-Sectional Study (e69777)
Larisa Wewetzer, Katja Goetz, Soenke Freischmidt, Jost Steinhauser. . . . 280

Current Status, Challenges, and Opportunities Associated With Implementing Clinical Data Interchange Standards Consortium Standards in Japanese Academic Medical Centers: Cross-Sectional Survey (e83774)
Kaori Nagai, Noriko Ito, Yuya Ikeda, Toshiki Saito. . . . 291

Iterative Large Language Model–Guided Sampling and Expert-Annotated Benchmark Corpus for Harmful Suicide Content Detection: Development and Validation Study (e73725)
Kyumin Park, Myung Baik, YeongJun Hwang, Yen Shin, HoJae Lee, Ruda Lee, Sang Lee, Je Sun, Ah Lee, Si Yoon, Dong-ho Lee, Jihyung Moon, JinYeong Bak, Kyunghyun Cho, Jong-Woo Paik, Sungjoon Park. . . . 305

Development and Evaluation of SNOMED CT Automated Mapping Tool: Advancing Terminology Standardization and Semantic Interoperability (e82670)
Youngsun Park, Hannah Kang, Jiwon Kim, Soo-Yong Shin, Dosang Cho, Sang Rhee, Hong Park, Kyung-Jae Lee, Sungchul Bae. . . . 329

XSL•FO
RenderX

Design Principles for Interactive Dashboards in Drug Safety Surveillance: Design Science Research (e75936)
Malwina Kotowicz, Mexhid Ferati, Soumitra Chowdhury, Cláudio Martins Pires. 345

Mild Cognitive Impairment Detection System Based on Unstructured Spontaneous Speech: Longitudinal Dual-Modal Framework (e80883)
Yu-Shan Liao, Thiri Wai, Ting-Yun Liao, Ho-Ling Chang, Yu-Ling Chang, Li-Chen Fu. 378

Enhancing Anesthetic Depth Assessment via Unsupervised Machine Learning in Processed Electroencephalography Analysis: Novel Methodological Study (e77830)
Po-Yu Huang, Wei-Lun Hong, Hui-Zen Hee, Wen-Kuei Chang, Ching-Hung Lee, Chien-Kun Ting. 402

Machine Learning Prediction of Progression to Dialysis in Patients With Polycystic Kidney Disease: Population-Based Retrospective Cohort Study (e80343)
Cheng-Hao Chang, Mingchih Chen, Ming-Hsien Tsai, Yen-Chun Huang, Hung-Hsiang Liou, Ben-Chang Shia, Chingying Liang, Yu-Wei Fang.
4 1 4

Exploring Factors Associated With the Stalled Implementation of a Ground-Up Electronic Health Record System in South Africa: Qualitative Insights From the E-Tick Case Study Using the Consolidated Framework for Implementation Research (CFIR) (e73831)
Campion Zharima, Frances Griffiths, Jane Goudge. 435

Development of Quality Indicators for the Correct Use of Electronic Medical Records in Primary Care: Modified Delphi Study (e80057)
Rico Paridaens, Steve Van den Bulck, Michel De Jonghe, Benjamin Fauquert, Liesbeth Meel, Willem Raat, Bert Vaes. 451

Multi-Institutional Drug Use Patterns in Hospitalized Older Patients: Retrospective Cross-Sectional Study (e78353)
Chung Lee, Grace Kim, Suhyun Kim, Jee Hong, Won Hwang, Jong-Yeup Kim, Kye Lee, Kwangsoo Kim, Mingyu Kang, Ju Kim, Suehyun Lee.
4 6 2

Harmonizing Logical Observation Identifiers Names and Codes (LOINC) Codes and Units in Real-World Oncology Data: Method Development and Evaluation (e81254)
Parvati Naliyatthaliyazchayil, Travis Stenerson. 482

Complete Blood Count–Derived Inflammation Indices to Predict 3-Year All-Cause Mortality in Patients With Diabetes and Acute Myocardial Infarction in Critical Care: Retrospective Cohort Study With Single-Center External Validation (e83328)
Tong Zhou, Kun Yang, Ying Yang, Song-Mei Liu. 496

Neutrophil Percentage–to-Albumin Ratio as a Novel Prognostic Biomarker in Adult Diffuse Gliomas: Retrospective Study Integrating 3 Machine Learning Models and Cox Regression (e79945)
Congcong Zhu, Jiyang An, Lili Zhou. 512

CT Radiomics–Based Machine Learning Model for Predicting Capsular and Neural Invasion in Thyroid Carcinoma: Diagnostic Accuracy Study (e77349)
Fang-fang Cong, Ke Tian, Qian Gao, Fulin Wang, Peng Sun, Nan Xu. 536

Effects of Image Degradation on Deep Neural Network Classification of Scaphoid Fracture Radiographs: Comparison Study of Different Noise Types (e65596)
Chihung Lin, Alfred Yoon, Chien-Wei Wang, Tung Chao, Kevin Chung, Chang-Fu Kuo. 557

Exploring Self-Management–Based Mobile Health User Typologies and Associations Between User Types and Satisfaction With Key Mobile Health Functions: Comparative Study of Various Fitness and Weight Management App User Types (e64860)
Tong Wang, Yiwen Fan, Zheng Li, Xiaoyi Jiao, Qichuan Fang, Junhao Ma, Jianbo Lei. 577

XSL•FO
RenderX

Balancing Privacy and Utility in Child and Adolescent Mental Health Services Research: Retrospective Cohort Study on Synthetic Data Generation (e71819)
Mounir Haizoune, Bennett Leventhal, Dipendra Pant, Øystein Nytrø, Kaban Koochakpour, Roman Koposov, Lars Øhlckers, Norbert Skokauskas. . . . 597

Developing a Thai User Interface Terminology for Systematized Nomenclature of Medicine Clinical Terms Implementation in Primary Care: Cross-Sectional Content Coverage Analysis (e80039)
Nat Tangchitnob, Wanchana Ponthongmak, Boonchai Kijsanayotin, Oraluck Pattanaprateep, Sithakom Phusanti, Pongsakorn Atiksawedparit, Kamonporn Suwanthaweemeesuk, Jirayus Siangfu, Gareth McKay, John Attia, Ammarin Thakkinstian. . . . 614

Large Language Models for Psychiatric Diagnosis Based on Multicenter Real-World Clinical Records: Comparative Study (e77699)
Maoqian Sun, Jia Yu, Zhuhong Long, Yun Yang, Tao Xiao, Jiaquan Liang, Jun Feng, Huaili Deng, Guoping Huang. . . . 627

Identifying and Analyzing Bot-Generated Responses in Online Health Care Surveys: Methodological Study (e73622)
Emily Hamovitch, Kaileah McKellar, Walter Wodchis. . . . 641

Chatbot Outreach in Value-Based Preventive Care: Retrospective Analysis (e81370)
Jincy Chacko, Yuane Jia, Kimon Stathakos, Kathleen Mazza, Doran Kim, Michael Diefenbach, Lorena Carlo. . . . 655

Development of a Practical Nomogram for Depression Risk Stratification in Older Adults With Hypertension and Diabetes: Retrospective Analysis of Data From the China Health and Retirement Longitudinal Study (e81529)
Ting Peng, Ying Zhang, Rujia Miao, Jiangang Wang. . . . 671

Two-Minute Deep Learning–Powered Brain Quantitative Mapping: Accelerating Clinical Imaging With Synthetic Magnetic Resonance Imaging (e79389)
Yawen Liu, Hongxia Yin, Zuofeng Zheng, Wenjuan Liu, Tingting Zhang, Linkun Cai, Haijun Niu, Han Lv, Zhenghan Yang, Zhenchang Wang, Pengling Ren. . . . 683

Nomograms Based on X-Ray Radiomics for Predicting Pain Progression in Knee Osteoarthritis Using Data From the Foundation for the National Institutes of Health: Development and Validation Study (e78338)
Yingwei Sun, Jing Liu, Chunbo Deng, Chengbao Peng, Shinong Pan, Xueyong Liu. . . . 699

Linking Electronic Health Records for Multiple Sclerosis Research: Comparative Study of Deterministic, Probabilistic, and Machine Learning Linkage Methods (e79869)
Ohoud Almadani, Yasser Albogami, Adel Alrwisan. . . . 712

Knowledge-Guided Explainable Recommendation Tool for Cancer Risk Prediction Models Using Retrieval-Augmented Large Language Models: Development and Validation Study (e78519)
Shumin Ren, Xin Zheng, Jing Zhao, Jiale Du, Yuxin Zhang, Cheng Bi, Jie Song, Jinyi Zhang, Hongmei Lang, Fan Zhang, Bairong Shen. . . . 721

Impact of Age on Hospital Outcomes Following Minimally Invasive Posterior Lumbar Interbody Fusion: Retrospective Analysis of the Nationwide Inpatient Sample Database from 2016 to 2020 (e76424)
Yu-Jun Lin, Fu-Yuan Shih, Jin-Fu Huang, Chun-Wei Ting, Yu-Chin Tsai, Lin Chang, Yu-Hua Huang, Ming-Jung Chuang. . . . 737

Machine Learning–Based Risk Prediction for Coronary Heart Disease Complicated by Hyperhomocysteinemia: Retrospective Study (e80809)
Ming-Yuan Du, Meng-Ke Lyu, Hai-long Liu, Yi-zhuo Li, Hai-feng Yan, Xiao-hui Li. . . . 748

Bridging Population Patterns and Individual Prediction: Framework for Prospective Multimorbidity Study (e84261)
Qianyao Zhang, Runtong Zhang, Weiguang Ma, Butian Zhao, Xiaomin Zhu. . . . 762

XSL•FO
RenderX

Enhanced Prediction of Atrial Fibrillation in Patients With Ischemic Stroke Through Electronic Medical Records and Text Mining: Algorithm Development and Validation (e78117)
Yu-Wei Chen, Sheng-Feng Sung, Ya-Han Hu, Yu-Hsuan Yang. 795

Research on the Prediction of Coal Workers' Pneumoconiosis Based on Easily Detectable Clinical Data: Machine Learning Model Development and Validation Study (e80156)
Haiquan Li, Jiaqi Jia, Xu Shi, Yudie Dong, Songquan Wang, Yuming Cui, Wenlu Hang, Dekun Zhang. 812

Assessing the Impact of Sociodemographic Factors on Artificial Intelligence Models in Predicting Dementia: Retrospective Cohort Study (e80405)
Xingyi Liu, Muskan Garg, Maria Vassilaki, Jennifer St Sauver, Ronald Petersen, Momin Malik, Chung Wi, Young Juhn, Sunghwan Sohn. . . . 8 2 7

Screening for Clinically Significant Nephrolithiasis Based on Simple Health Checkup Clinical and Urine Parameters in General Populations: Multicenter Machine Learning Study (e80764)
Hao-Wei Chen, Pei-Siou Wei, Yu-Chen Chen, Jeng-Yih Wu, Chia-I Lin, Yii-Her Chou, Yung-Shun Juan, Wen-Jeng Wu, Chung-Yao Kao, Jung-Ting Lee. 845

Prediction of First and Multiple Antiretroviral Therapy Interruptions in People Living With HIV: Comparative Survival Analysis Using Cox and Explainable Machine Learning Models (e78964)
Donald Salami, Emily Koech, Janet Turan, Kristen Stafford, Lilly Nyagah, Stephen Ohakanu, Anthony Ngugi, Manhattan Charurat. 863

Prospective Diagnostic Accuracy and Technical Feasibility of Artificial Intelligence-Assisted Rib Fracture Detection on Chest Radiographs: Observational Study (e77965)
Shu-Tien Huang, Liong-Rung Liu, Ming-Feng Tsai, Ming-Yuan Huang, Hung-Wen Chiu. 883

Machine Learning Prediction of Pharmacogenetic Testing Uptake Among Opioid-Prescribed Patients Using Electronic Health Records: Retrospective Cohort Study (e81048)
Mohammad Yaseliani, Je-Won Hong, Jiang Bian, Larisa Cavallari, Julio Duarte, Danielle Nelson, Wei-Hsuan Lo-Ciganic, Khoa Nguyen, Md Hasan. 899

Development of Venous Thromboembolism Risk Prediction Models Based on Whole Blood Gene Expression Profiling Using 20 Machine Learning Algorithms: Comprehensive Analysis Study (e75565)
Yedong Huang, Xiaoyun Chen, Guannan Bai, Yajun Zhao, Dapeng Kuang, Lin Zhang, Wei Lu. 914

Automated Classification of Lymphoma Subtypes From Histopathological Images Using a U-Net Deep Learning Model: Comparative Evaluation Study (e72679)
Jin Zhao, Xiaolian Wen, Li Ma, Liping Su. 925

Deep Learning for Dynamic Prognostic Prediction in Minimally Invasive Surgery for Intracerebral Hemorrhage: Model Development and Validation Study (e86327)
Jingxuan Wang, Jian Shi, Qing Ye, Danyang Chen, Yuhao Sun, Chao Pan, Yingxin Tang, Ping Zhang, Zhouping Tang. 938

Ranking-Aware Multiple Instance Learning for Histopathology Slide Classification: Development and Validation Study (e84417)
Ho Kim, Gisu Hwang, Won Jeong, Young Ko. 953

Early Prediction of Delirium in Postcardiac Surgery Patients: Machine Learning Model Development and External Validation (e73283)
Huixiu Hu, Yuxiang Wang, Houfeng Li, Qinglai Zang, Jing Huang, Ying Zhang, Jinjing Wu, Long Liu, Zhen Xing, Yaohua Yu. 967

Ensemble Machine Learning Models for Predicting Patients With High Usage: Model Validation and Economic Impact Analysis (e77202)
Joshua Tan, Le Quan, Hao Tan, Su-Yen Goh, Julian Thumboo, Marianne Au, Yong Bee, Jen Tan. 982

XSL•FO
RenderX

Enhanced Magnetic Resonance Imaging–Based Knee Cartilage Segmentation Using a Swin-UNet Conditional Generative Adversarial Network: Development and Validation Study (e86155)
Jun Park, Ji-Hoon Nam, Shakhboz Abdigapporov, Jong-Keun Kim, Yong-Gon Koh, Byung Cho, Hyuck Kwon, Kwan Park, Kyoung-Tak Kang. . 9 9 5

Leveraging Naturalistic Driving Digital Biomarkers for Early Mild Cognitive Impairment Detection: Deep Learning Strategies (e83622)
Firas Al-Hindawi, Teresa Wu, Yutong Wen, Peter Serhan, Erica Forzani, Francis Tsow, Yonas Geda. 1009

Patient Experiences With Outpatient Pharmacy Services in Hospitals Using Automated Pharmacy Systems: Cross-Sectional Study (e80963)
Ali Buabbas, Fatemah Alsaleh, Mariam Alsanafi, Maryam Safar, Ahmad Al-Sultan, Talal Zaman. 1034

Identification and Localization of Breast Tumor Components via a Convolutional Neural Network Based on High-Frequency Ultrasound Combined With Histopathologic Registration: Prospective Study (e81181)
Jia-Qian Yao, Wen-Wen Zhou, Zhi-Fei Chai, Fei Ren, Tong-Yi Huang, Tian-Tian Zhen, Hui-Juan Shi, Xiao-Yan Xie, Ze Zhao, Ming Xu. 1060

Prompting and Fine-Tuning Large Language Models for Parkinson Disease Diagnosis: Comparative Evaluation Study Using the PPMI Structured Dataset (e77561)
Hyun-Ji Shin, Young Jeong, Sungmin Jun, Do-Young Kang. 1072

Applicability of Existing Gender Scores for German Clinical Research Data: Scoping Review and Data Mapping (e74162)
Lea Schindler, Hilke Beelich, Elpiniki Katsari, Daniele Liprandi, Sylvia Stracke, Dagmar Waltemath. 1093

Approval of AI-Based Medical Devices in China From 2020 to 2025: Retrospective Analysis (e85538)
Lingli Zhang, Jianzhou Yan. 1119

Tailoring Discharge Summaries to Health Care Providers' Needs (Part 1 of the Framework and Implementation of AI Tools Project): User-Centered Design Approach (e80613)
Mieke Deschepper, Helga Rogge, Mathias Syx, Kirsten Colpaert. 1132

Evaluating GPT-4 Responses on Scars or Keloids for Patient Education: Large Language Model Evaluation Study (e78838)
Mingjun Rao, Tang Xiujun, Wang Haoyu. 1144

Large Language Models in Patient Health Communication for Atherosclerotic Cardiovascular Disease: Pilot Cross-Sectional Comparative Analysis (e81422)
Pengfei Li, Yinfei Xu, Xiang Liu, Zhean Shen, Yi Wang, Xinyi Lv, Ziyi Lu, Hui Wu, Jiaqi Zhuang, Yan Chen. 1153

Multi-Evidence Clinical Reasoning With Retrieval-Augmented Generation for Emergency Triage: Retrospective Evaluation Study (e82026)
Hang Wong, Tsz Wong. 1168

Machine Learning Algorithms to Predict Venous Thromboembolism in Patients With Sepsis in the Intensive Care Unit: Multicenter Retrospective Study (e80969)
Yan Zhang, Xia Ren, Luojie Liu, Junjie Zha, Yijie Gu, Hongwei Ye. 1187

Evaluation of Large Language Models for Radiologists' Support in Multidisciplinary Breast Cancer Teams: Comparative Study (e68182)
Hong Jiang, Chun Yang, Wenbin Zhou, Cheng-liang Yin, Shan Zhou, Rui He, Guanghui Ran, Wujie Wang, Meixian Wu, Juan Yu. 1208

XSL•FO
RenderX

Artificial Intelligence Models for Predicting Triage in Emergency Departments: Seven-Month Retrospective Comparative Study of Natural Language Processing, Large Language Model, and Joint Embedding Predictive Architectures (e83318)
Edouard Lansiaux, Ramy Azzouz, Emmanuel Chazard, Amélie Vromant, Eric Wiel. . . . 1224

Application of a Large Visual Language Model on Tongue Image Description Generation and Physical Constitution Reasoning in Traditional Chinese Medicine (TongueVLM): Model Development and Validation Study (e87237)
Chengdong Peng, Jun Gao, Nuo Yang, Yong Wang, Renming Chen, Changwu Dong. . . . 1245

Large Language Model–Enabled Editing of Patient Audio Interviews From "This Is My Story" Conversations: Comparative Study (e80205)
Bikram Bains, Sampath Rapuri, Edgar Robitaille, Jonathan Wang, Arnav Khera, Catalina Gomez, Eduardo Reyes, Cole Perry, Jason Wilson, Elizabeth Tracey. . . . 1258

Implementation Report

Scaling Wireless Continuous Vital Sign Monitoring Across an 8-Hospital Health System: Digital Health Implementation Report (e78216)
Ngoc-Anh Nguyen, Grace Lee, Brendan Holderread, Terrie Holman, Sarah Pletcher, Roberta Schwartz. . . . 216

Letter to the Editor

Enhancing Predictive Accuracy of Mood Symptoms Using Wearable Devices and Machine Learning in Bipolar Disorder (e92172)
P Nair, Priyanka D'Souza. . . . 1030

Corrigenda and Addendas

Correction: Comprehensive Pediatric Health Risk Stratification Using an AI-Driven Framework in Children Aged 2 to 8 Years: Design and Validation Study (e92491)
Jundan Chen, Zhihe Mao. . . . 1032

Correction: Exploring the Potential of Claude 3 Opus in Renal Pathological Diagnosis: Performance Evaluation (e88845)
JMIR Editorial Office. . . . 1033

Editorial

AI Scribes: Are We Measuring What Matters? (e89337)
Enrico Coiera, David Fraile-Navarro. . . . 1057

Research Letter

AI-Enabled Customer Relationship Management Platforms for Patient Services in Health Care, Early Lessons From Governance, and Program-Level Outcomes (e83564)
Anup Gupta. . . . 1115

XSL•FO
RenderX

Digital Public Reporting Systems for Evaluating Health Care Quality: Systematic Review

Lanmei Du, MSc; Reima Suomi, PhD; Elorm Damalie, MSc

Department of Management and Entrepreneurship, Turku School of Economics, University of Turku, Rehtorinpellonkatu 3, Turku, Finland

Corresponding Author:
Lanmei Du, MSc
Department of Management and Entrepreneurship, Turku School of Economics, University of Turku, Rehtorinpellonkatu 3, Turku, Finland

Abstract

Background: Health care public reporting (PR) refers to making information about the quality and performance of health care providers available to the public. The primary targeted use of PR is the selection of a health care provider. Previous studies suggest that PR has improved health care quality; however, the overall adoption rate of PR systems remains low. Misalignment between PR information and users' actual needs can explain this gap.

Objective: This study conducts a systematic literature review of PR systems in health care, aiming to explore how data encoding and presentation influence user utilization, with particular attention to the impact of data inconsistencies and inaccuracies on actual use.

Methods: A literature search was conducted on 5 electronic databases (Web of Science, CINAHL, Embase, PsycINFO, and PubMed), focusing on studies providing information in health care from an individual perspective. Subsequently, the quality of the included studies was assessed using the Mixed Methods Appraisal Tool (McGill University). Finally, a total of 25 empirical studies were included in this study.

Results: Among the 25 studies, 40% (10/25) investigated website presentation formats, 20% (5/25) explored dashboard-based data presentation formats in PR systems, 48% (12/25) examined data quality, and 20% (5/25) addressed user heterogeneity. Quantitative methods were used in 80% (20/25) of studies, while qualitative and mixed method designs accounted for 16% (4/25) and 4% (1/25), respectively. Findings suggest that standardized website and dashboard guidelines improve data reliability and user comprehension and that user heterogeneity mediates the effects of structural and process indicators on outcomes. Data collection was completed in February 2025, and the study was projected to be fully completed by September 2025.

Conclusions: This study provides an integrated structure-process-outcome–based framework for PR in health care. By presenting data through dashboards, inconsistencies and inaccuracies in data across different web pages can be mitigated, thereby decreasing conflicting information and improving comprehension in PR systems. Based on the literature findings and identified knowledge gaps, this study also proposes future research directions for online PR.

(JMIR Med Inform 2026;14:e80435) doi:10.2196/80435

KEYWORDS

digital health; public reporting systems; data and information process; health literacy; quality indicators

Introduction

Background

Digital health refers to the development and use of digital technologies to enhance health-related knowledge and practices [1]. It is not only a technological concept but also profoundly shapes how people access health information. For instance, a 2023 report by Digitalis Medical indicates that 7% of all daily Google searches are health-related, equating to approximately 70,000 health care searches every minute [2].

The core function of public reporting (PR) systems is to assist individuals in selecting health care providers and services [3]. Improving the use of the PR system requires understanding how data are encoded and decoded in digital health. This understanding is crucial for individuals who use the PR system to proactively manage their health and engage in recommended behaviors [4].

Previous studies have shown that inconsistencies or errors in PR data can affect trust and reduce users' confidence in the reporting system [5]. Such inconsistencies not only challenge data reliability but also influence how users understand PR information. However, empirical research on these data inconsistencies remains fragmented. For example, some studies suggest that information presentation affects users' actual use of PR systems [6,7]. Moreover, these studies largely remain focused on information presentation formats, while research on

XSL•FO
RenderX

data heterogeneity within systems remains limited, underscoring the complexity of PR data usage.

Patient activation measure (PAM) refers to an individual's knowledge, skills, and confidence essential for managing their own health and health care [8,9]. Although patients show strong interest in accessing PR information to make informed health care decisions, the overall adoption of the PR system remains low, largely due to information presentations that do not match patients' comprehension levels [10-12]. Therefore, exploring data generated in real-world physician-patient co-management contexts may help alleviate data communication challenges and support informed decision-making [13,14].

To address this gap, this study conducts a systematic literature review to provide an overview of current research on PR in digital health information systems. To achieve this objective, we address the following research questions: (1) How do system-level structural indicators influence process indicators, and subsequently influence outcome indicators? and (2) How do decoding errors in PR systems and user-system interactions influence users' information use?

Accordingly, we systematically identified and reviewed 25 empirical studies on information presentation in PR in health care contexts. Drawing upon the structure-process-outcome (SPO) theoretical framework, we categorized and synthesized the structural indicators (website guidelines and dashboard guidelines), process indicators (data quality guidelines and data process criteria), and outcome indicators (user satisfaction and surgical mortality). Meanwhile, we position user heterogeneity as a mediating variable that links process indicators to outcome indicators. Specifically, variations in contextual and individual-level factors (age, gender, political affiliation, employment status, income, and area of residence) can influence the interactions of users' engagement with information.

The remainder of this paper is structured as follows: the "Methods" section describes the methodology for planning and conducting the literature review, focusing on recent research; the "Results" section presents the findings in response to the 2 research questions; and the "Discussion" section discusses the progress and identifies challenges in current literature, concluding with recommendations for future research. Checklist 1 presents the PRISMA-P (Preferred Reporting Items for Systematic Review and Meta-Analysis Protocols) 2020 checklist which outlines recommended items to address in a systematic review protocol. Multimedia Appendix 1 contains the search strategies used in each database. Multimedia Appendix 2 shows the Mixed Methods Appraisal Tool (MMAT; McGill University) quality assessment report. Multimedia Appendix 3 contains the key characteristics of the included studies. Multimedia Appendix 4 includes additional details of the included studies.

Theoretical Background

Overview

The presentation of information in public reports significantly influences user engagement with these systems [15]. To gain an understanding of individual users' attitudes toward the PR system and how this forms health information adoption behavior, it is necessary to explore the information presented in the PR systems. While information is composed of data, the way data is structured determines how information is understood [16]. Based on this premise, this study assesses whether existing PR data align with users' informational needs and examines how such alignment influences users' adoption of PR systems.

PR and Quality Indicators

PR in health care refers to the disclosure of performance-related information about providers, organizations, or systems to the general public. Such information is typically nonanonymous, identifying specific professionals or institutions, thereby enabling direct comparison and accountability [17,18]. By disclosing the performance data, individuals (patients and nonpatients) can choose higher-performing providers and make health plan decisions [17,19].

The assessment of PR systems, rather than direct health care delivery, has increasingly drawn academic attention. Donabedian [20] addresses this issue by conceptualizing health care quality through the SPO framework. In health care, structure indicators refer to the system's resources and organizational arrangements, and process indicators include all service delivery activities such as diagnosis, treatment, nursing, and patient education. Finally, outcome indicators reflect the resulting health effects, including patient health improvements, satisfaction, and mortality rates. By applying the SPO framework in this manner, we shift the focus from assessing health care delivery quality to evaluating how PR system structures and processes influence user outcomes.

In recent times, we have also seen that PR in health care is demanded from the perspective of environmental, social, and governance (ESG) reporting, which involves public disclosure of an organization's performance and its impacts on environmental, social, and governance factors [21]. Currently, PR seems to be moving toward health care processes beyond basic clinical activity, such as PR on clinical trials [22]. In the era of the current artificial intelligence revolution, the impact of artificial intelligence on PR is, of course, an important topic [23,24].

Although defining and measuring quality in health care remains challenging, extensive evidence supports the essential role of the SPO framework in measuring health care quality [20,25]. Within the structural dimension, PR systems are an important component [25]. The health care system is depicted through structural indicators, which in turn influence process indicators, ultimately affecting outcome indicators [20]. PR has to inform its users of all these health care components. Previous research on process indicators in PR primarily focused on operational standardization, consistency, and service standard implementation [15,26]. However, few studies have examined the structural dimension from an individual-system interaction perspective.

At the process level, patient-physician collaboration (PPC) generates substantial user data [27]. During interactions between health care organizations and users, systems serve as supporting tools that can enhance treatment efficiency. The data generated in this process holds significant value for collection and use

XSL•FO
RenderX

[28]. The fine details of PPC, however, remain a difficult item to document in PR.

Existing research has paid insufficient attention to patient-generated data from the PPC process, particularly in the digital era, where the processes of data collection, organization, and use remain inadequate compared to the opportunities that digital data processing could offer. Such gaps may lead to unintended consequences, including users' mistrust of PR systems.

Finally, outcome indicators include subjective or functional metrics, such as in our sample, patient satisfaction and mortality rate [29,30]. Online PR websites enable individuals to interact directly with information, whereas individuals often rely on their own knowledge to evaluate content [17]. In contrast, in offline settings, user interaction is typically mediated by health care institutions, resulting in a more indirect experience [31].

Previous research indicates that attitudes formed through direct experience are more effective in predicting behavior than those formed through indirect experience [32]. However, studies examining interactions between individuals and system information in online environments in a PR context remain relatively limited. Taken together, these gaps highlight the need for a framework that integrates system information processing into the SPO dimensions of PR.

Sociotechnical Theory

According to Bostrom and Heinen [33], sociotechnical theory suggests that information systems should be designed so that the individual and technology operate as an integrated whole. In other words, the design of information systems should not only focus on data collection, processing, and transmission; the interaction between humans and information should also be emphasized. Within the context of PR, this principle is embodied through the interaction between PPC, user heterogeneity, and system-level demand for data reliability and standardization.

The operational goal of any PR system is to serve as a channel through which health care organizations and governments convey PR information to the public. This process enables individuals to filter health care information via the selection pathway and make health care choices suited to their needs [12]. PR information selection is both receptive and selective, and at the system stage, it primarily involves information processing.

In the context of PR, effective information processing is critical because it shapes how users understand and use performance data to make informed decisions. The information processing in PR systems involves a series of systematic steps that transform raw health data into actionable information for diverse stakeholders such as policymakers, providers, and the public [34]. On the PR website, data are symbols that represent the properties of objects and events [35].

Information consists of processed data, with the processing directed at increasing its usefulness [16]. System information processing involves integrating data from multiple sources into a central database, which is then retrieved and displayed on websites [36]. Regarding quality indicators, many individuals still experience significant analytical challenges, particularly when information is not clearly presented [37]. Thus, it is necessary for the PR system to reduce information asymmetries and empower patients, families, and payers to select high-quality providers [38].

These studies provide insights into the interaction between PR information and individuals, particularly regarding how end users use PR information. Previous research has primarily focused on issues of data inconsistency and low accuracy in PR [39]. However, previous studies have provided insufficient investigation into how data inconsistency issues can be effectively addressed within the field of information systems. Specifically, it is equally important to consider the objective quality of the data, incorporating data guidelines to address data inconsistency.

These findings underscore the critical role of data quality in shaping the adoption of PR systems. However, extant research demonstrates several notable limitations. First, the analytical depth remains constrained. Most studies focus primarily on information presentation as the primary mode of data delivery; however, they often overlook how data processing within systems fundamentally influences website presentation and user interpretation.

Second, investigations in the PR domain have predominantly adopted an awareness-to-behavior framework, emphasizing the role of awareness in guiding user actions [17]. Nevertheless, the complex interrelations between data quality and adoption remain underexplored, resulting in substantive gaps between PR systems and users' actual attitudes. Consequently, there is a pressing need to examine online PR systems through a lens that integrates the system and individuals.

Methods

Overview

A systematic literature review requires clearly defined research questions, a transparent search process, data extraction, and data presentation [17,40]. Typical reviews cover a span of approximately 10 years. In this study, the time frame was set from 2016 to 2025. The rationale for selecting studies after 2015 is that, from this year onward, PR increasingly transitioned to internet-based platforms. The system reached its peak in July 2015, but then declined rapidly and has remained at a relatively low level since [41]. Additionally, the Hospital Consumer Assessment of Healthcare Providers and Systems star ratings system was launched, enhancing patients' visual understanding of hospital quality information [42].

We used the guidelines of Okoli and Schabram [43] and the framework proposed by Webster and Watson [44] to conduct our literature review. This review adopts a structured approach to the literature. As shown in Figure 1, the complete selection and synthesis process is summarized in the PRISMA (Preferred Reporting Items for Systematic Reviews and Meta-Analyses) flow diagram.

XSL•FO
RenderX

Figure 1. PRISMA (Preferred Reporting Items for Systematic Reviews and Meta-Analyses) flow diagram of the selection process for public reporting systems retrieved from 5 databases between 2016 and 2025. EC: exclusion criteria; IC: inclusion criteria.

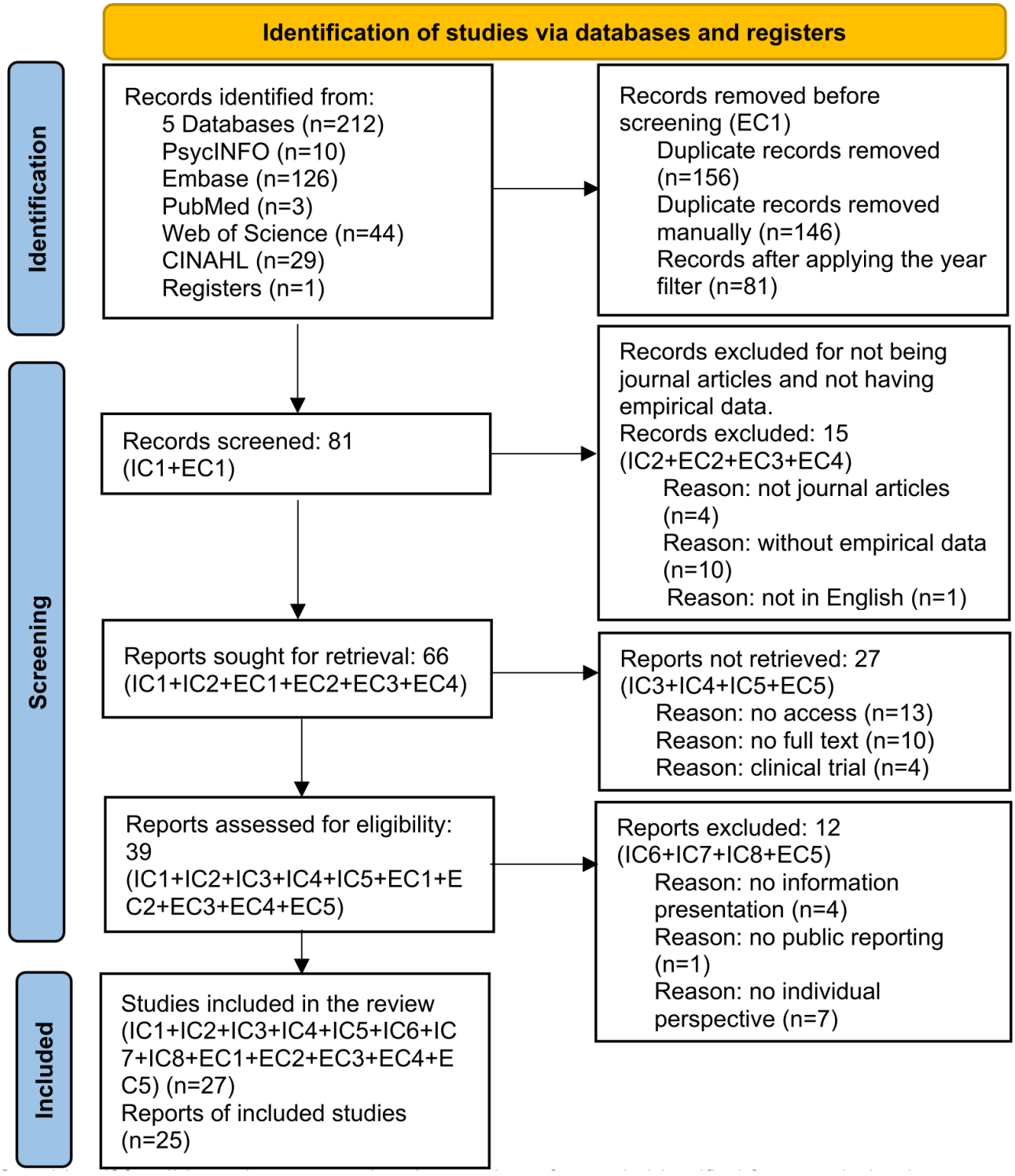

First, when designing the search strategy, efforts were made to capture all studies that met the inclusion criteria [45]. This research aims to explore the presentation of information in PR systems. Therefore, the search term was set to information; meanwhile, the research mainly focuses on PR, and the keyword includes "PR." The search term is provided in Multimedia Appendix 1, and the search date was September 14, 2025.

Second, PR has evolved as an interdisciplinary field, drawing from health policy and behavioral science. Conducting a review can be helpful to fill in the gap of data inconsistency and identify future directions from the information system perspective [46]. Access to these databases was obtained via Volter (Library of the University of Turku), ensuring that the user was logged in to minimize the number of ignored studies due to access issues. The data sources were chosen from Web of Science (multidisciplinary and broad literature search), CINAHL (health and public health information systems), Embase (health and public health information systems), PsycINFO (cognitive science, decision-making, and behavioral economics), and PubMed (biomedicine literature database).

XSL•FO
RenderX

Third, using tools to assess the risk of bias in studies is an important step described in systematic review protocols, as judgments made during this process may influence the analysis and interpretation of the review results [45]. Meanwhile, applying objective and reproducible methods helps ensure the appropriateness and fairness of the study findings [43]. The quality assessment protocol covers study methodology, level of structuring, study outcomes, and research topics. After the deduplication of studies (n=146) in EndNote (Clarivate) combined with manual checking, 81 studies were included in the final scoring pool.

Among the included studies, the methodologies involved both qualitative and quantitative approaches. The scoring table referenced from Hong et al [47] is provided in Multimedia Appendix 2.

Screening Process of the Systematic Review

In the screening process, 81 studies were initially included in the research pool. Review or descriptive studies that were not journal publications and did not contain empirical data were excluded. A total of 66 articles were retrieved, and full-text searches were conducted for these studies. During the full-text review, studies without accessible full text and clinical trial papers were excluded. Ultimately, 39 studies were included in the quality assessment.

Some of these studies examined PR systems from an organizational perspective. This study, however, focuses primarily on the individual perspective, specifically the alignment between individual users and the information presented in the PR system. Studies that explored system processes at the organizational level, which do not directly reflect the information presentation encountered by individual users, were excluded. Additionally, since this study focuses on PR systems in the health care domain, studies from non–health care fields were also excluded.

In Figure 1, abbreviated labels are used to represent inclusion criteria (IC) and exclusion criteria (EC).

The selection was conducted independently and double-checked manually. For clarity, the IC correspond to the following criteria: IC1 indicates studies published between 2016 and 2025, IC2 indicates empirical studies, IC3 indicates studies with open access, IC4 indicates studies with full text availability, IC5 indicates studies published after peer review, IC6 indicates studies focused on information presentation, IC7 indicates studies focused on the individual level, and IC8 indicates studies conducted in health care contexts. The EC corresponds to the following criteria: EC1 indicates studies published outside the 2016 to 2025 timeframe, EC2 indicates nonjournal studies, EC3 indicates nonempirical studies, EC4 indicates studies not published in English, and EC5 indicates clinical trials and other studies not focused on PR systems or individual-level information use.

After the initial full‐text screening, 27 studies were eligible for quality appraisal. The methodological quality of the included studies was assessed using the MMAT (2018 version) [47], a validated instrument specifically developed for appraising empirical studies in mixed-study systematic reviews. The MMAT evaluates 5 categories of study designs—qualitative research, randomized controlled trials, nonrandomized quantitative studies, quantitative descriptive studies, and mixed methods studies—each using 5 methodological criteria.

Following MMAT guidance, studies can be classified as low (1‐2 criteria met), moderate (3 criteria met), or high quality (4‐5 criteria met). All assessments were performed independently by the first and third authors, and discrepancies were resolved through discussion. Two studies with MMAT scores of 1/5 and 2/5 were excluded from the analysis, resulting in a final set of 25 studies for article synthesis.

Literature Synthesis

Thematic and Narrative Synthesis

We conducted a thematic synthesis of the included studies to extract key findings, which were then grouped into distinct themes [45]. Within each theme, dimensional indicators were identified and presented using an integration framework to address the first research question. This approach enables the qualitative integration of evidence across studies, highlighting patterns in structure indicators, process indicators, and outcome indicators.

Given the fragmented and broad scope of research in the field of PR, a narrative synthesis approach was adopted [48]. To enhance the transparency and rigor of the synthesis, descriptive statistics were also used to summarize the number of studies within each category and their methodological characteristics.

Regarding the research questions, the theme under the SPO framework is reported quantitatively, whereas subthemes (eg, website, dashboard, and data) are explored using a narrative approach. During synthesis, studies were grouped based on the specific dimensions of the SPO framework and their relevance to the research questions. Furthermore, a subset of studies investigated how structural indicators and process indicators influence the outcome indicators. Examining findings on the same aspects allows them to extend one another, which can be viewed as a form of confirmation [48].

SPO Framework–Based Results Mapping

Each subtheme in the “Results” section corresponds to a specific type of data extracted from the literature: (1) structure (website and dashboard): indicators describing the system design, presentation, and functionality were collected and summarized; (2) process (data quality and data process): studies reporting on data accuracy, completeness, accessibility, and workflow processes were analyzed; (3) outcome (patient satisfaction and surgical mortality): measures were extracted from studies evaluating the effect of PR systems on users’ decision-making, satisfaction, and clinical outcomes; and (4) user heterogeneity: information on demographic characteristics, health literacy, and contextual factors influencing user interaction with PR systems was also extracted and synthesized.

Quality Assurance and Integration

First, we conducted an initial synthesis using thematic analysis, presenting the study results in Multimedia Appendices 3 and 4. Subsequently, 1 author summarized and categorized the included

XSL•FO
RenderX

studies within an integrative framework. Based on this synthesis, an integrative framework was developed to organize the identified themes, which are further elaborated in the "Results" section.

Results

Overview

Among the 25 studies included in this review, 40% (10/25) explored PR from the perspective of information presentation formats, while 20% (5/25) of the studies focused on the dashboard in online PR. Additionally, 48% (12/25) of the studies examined PR systems from the perspective of data presentation, and 20% (5/25) addressed user heterogeneity. Finally, 12% (3/25) of the studies investigated PR from the perspective of patient satisfaction and surgical mortality.

Meanwhile, 80% (20/25) adopted quantitative methods, 16% (4/25) used qualitative designs, and 4% (1/25) used a mixed methods approach. Regarding data sources, 60% (15/25) collected secondary data (eg, web content analyses), while 40% focused on primary data through surveys, interviews, or focus groups. Data collection was conducted between February 2025 and September 2025.

Structure

Website

Among the included studies, 40% (10/25) of the studies examined PR from the perspective of information presentation formats on websites. For instance, studies found that the format of information presentation on PR websites can significantly influence public understanding and trust, policymaking, and pandemic response [49].

Specifically, the findings show that standardized data guidelines help improve the quality of PR websites, including accuracy, completeness, technical elements, design and aesthetics, readability, usability, and accessibility [50]. For example, challenges in information presentation may also result from mismatches between recommended reading levels for patient education materials (typically up to sixth grade) and the actual readability of websites, which seldom meet the needs of most patients [50]. Such mismatches create a gap between the health information users need and what is actually provided. Appropriate readability facilitates comprehension, enabling better disease management and adoption of healthy lifestyles [51].

Moreover, in terms of presentation formats, we found that online ratings may serve as a valuable source of information for both consumers and policymakers [52]. It is worth noting that storytelling techniques that convey narrative trends on dashboards can help users better understand the information presented in PR [53]. Additionally, supplementing this with characteristics of professional care institutions, which are often under-represented, can enhance the comprehensiveness of PR information [54].

Furthermore, the widespread use of aggregated ratings, such as star systems, may further strengthen consumer responses [55]. Interestingly, research has shown that "breadcrumb navigation" (forward-backward topic navigation) helps maintain the continuity of information, enabling users to quickly review previously read content and efficiently locate needed information [50]. Meanwhile, studies indicate that participants accessing "drill-down scores" tend to engage more deeply with the provided data (manifested as increased interactions on the website), but their impact on physician selection is lower than that of participants accessing "roll-up scores" [56].

Additionally, studies have found that over 90% of websites do not include accessibility features for individuals with disabilities, such as hearing, cognitive, neurological, motor, language, or visual impairments [51,57,58]. Therefore, considering accessibility benefits not only for disabled users but also the general population (eg, those using mobile devices, with slow internet, or limited bandwidth), it provides equal access to information for elderly individuals or residents in remote areas [51,57,58].

Dashboard

In our sample, a lot of discussion revolved around dashboards. We see them as a subcategory of web-based information, offering more dynamic and versatile analysis possibilities than static websites.

Overall, 20% (5/25) of studies examined the presentation of information on dashboards. Relevant and high-quality data are crucial for constructing dashboards, and research indicates that data sources are key factors in dashboard development [59,60]. Dashboards are especially useful in presenting epidemic and pandemic trends, such as those of COVID-19 [61], but can also be used in classical resource selection performed by PR users.

In terms of content presentation, dashboards should serve as tools that clearly link current trends with past policy decisions and individual behaviors, thereby enhancing the use of indicators [61]. However, evidence suggests that known and validated presentation techniques were overall underused, especially explanatory narratives [61]. To enhance usability, effective dashboards include: (1) understanding the audience and their information needs; (2) managing the type, quantity, and flow of displayed information; (3) clearly reporting data sources and methods; (4) linking time trends with policy decisions; (5) providing "close-to-home" data; (6) segmenting populations into relevant subgroups; and (7) using storytelling and visual cues [61].

Among these studies, the predominant approach involved data provision (specificity of geographic breakdowns, range of indicators reported, and explanations of data sources or calculations) and advancements enabled by the technologies employed (customization of time trends and interactive or visual chart elements) [53]. Meanwhile, studies also note that the clarity of data sources and methods has improved in dashboard development [53]. Teams differ in how they explore and define the purposes of dashboards. Some view dashboards as tools for presenting raw data to the public, while others attempt to provide explanations through narrative or visualization [59].

Moreover, 8% (2/25) of studies viewed the purpose of dashboards as solely presenting data (raw numbers) for the

XSL•FO
RenderX

public to interpret independently, whereas others sought to provide explanations through narrative or visual methods [53]. Additionally, incorporating storytelling elements and visual cues within dashboards has been shown to enhance users' ability to process information effectively [53]. For example, the development of dashboards that allow users to create profiles and receive personalized scores enables consumers to "see themselves in the data" [62].

Process

Data Quality

Overall, 48% (12/25) of studies examined PR from the perspective of website data. Notably, 32% (8/25) of studies indicated that standardized data guidelines help improve the quality of PR websites [15,45-47,58,59]. Additionally, some research described implementing check types within a data quality framework covering conformance, completeness, and plausibility, including both verification and validation [63].

Data Process

In the context of PPC, the generation of data encompasses multiple sources and activities. By using the data quality framework, data were collected across 4 domains, multiple measures, and time periods to examine access and equity; efficiency and sustainability; quality, safety, and patient orientation; and employee engagement [60].

Among these studies, 28% (7/25) investigated chart information on PR websites. The use of publicly reported data by consumers, policymakers, and researchers has grown substantially [64]. Most websites use charts, graphical elements, and quantitative descriptions as tools to convey differences between hospitals [65]. In addition, some research suggests adding charts to improve navigation [15]. For example, appropriate disease-related images and illustrations help patients better understand the information [50].

Meanwhile, the trend toward simplified composite rating systems may be reasonable to improve consumer responses to PR [55]. Previous research identified seven key elements that enhance user understanding [7]. The elements include unmarked bar charts, bar charts with simple symbols, bar charts with traffic light indicators, bar charts with thumbs-up symbols, provider rankings based on performance, clearly indicating whether higher values represent better performance, and implying quality levels through performance ranges without explicitly marking scale directions [7].

Furthermore, the transparent communication of standardized databases provides a crucial supplement to the missing components commonly observed in observational research [63]. This transparency can enhance the effectiveness of PR tools, as consumers may question the reliability of the quality information provided and consequently avoid using report cards [66].

Within the PPC process, presenting data in a structured format on dashboards can facilitate clear communication between health care providers and patients [67]. Meanwhile, PR websites can also serve as supplementary materials recommended by physicians, thereby reducing the need for face-to-face education and consultation [50].

Moderating Variable

User Heterogeneity

Overall, 20% (5/25) of the studies examined user heterogeneity, suggesting that themes such as simplicity, trust, collaboration, software and data integration, and adaptability have facilitated the development of PR systems [67]. However, the use of identical data across different websites may result in confusion or even contradictions regarding the same provider [15].

Moreover, research has highlighted that improvements in data timeliness, the level of detail available, and the categorization of comparable population groups can enhance the quality and effectiveness of PR [60]. For instance, individuals with higher health literacy tend to spend more time reviewing PR information than those with lower health literacy [68].

Individual Characteristics and Contextual Factors

Similarly, individual characteristics and contextual factors, such as age, political orientation, employment status, income level, and residential area, significantly influence users' adoption of PR information [38]. Younger adults are generally more likely than older adults to trust information from all sources [38]. In addition, political orientation, employment status, income level, and residential location are correlated with trust in medical quality information from companies, government agencies, or family and social network sources [38]. Collectively, these findings indicate that both individual characteristics and contextual factors are critical determinants of the perception of PR information.

Outcome

Patient Satisfaction

Overall, although patients generally prefer to obtain health information from medical professionals, the media remains an important source of information [69]. Within the PPC process, patient satisfaction primarily depends on the quality of care and service delivery. Specifically, patient satisfaction appears to depend largely on postoperative pain levels and access to timely appointments [70].

Surgical Mortality

In addition, studies have pointed out that the variables influencing patient risk levels in surgical mortality include demographic factors such as age, weight, and prematurity, surgical factors such as the type of procedure, as well as disease-related factors [71].

A Framework to Understand the PR Quality Indicators in Health Care

The framework used in this study is based on the Donabedian quality model [20]. As shown in Figure 2, the system constitutes a key component of structural indicators [20]. User heterogeneity functions as a mediating mechanism linking the structural indicators and process indicators to outcome indicators. Specifically, the structural indicators and process indicators features of PR systems jointly shape users' perception of the information [38].

XSL•FO
RenderX

Figure 2. Integrative structure-process-outcome (SPO) framework for public reporting systems in health care.

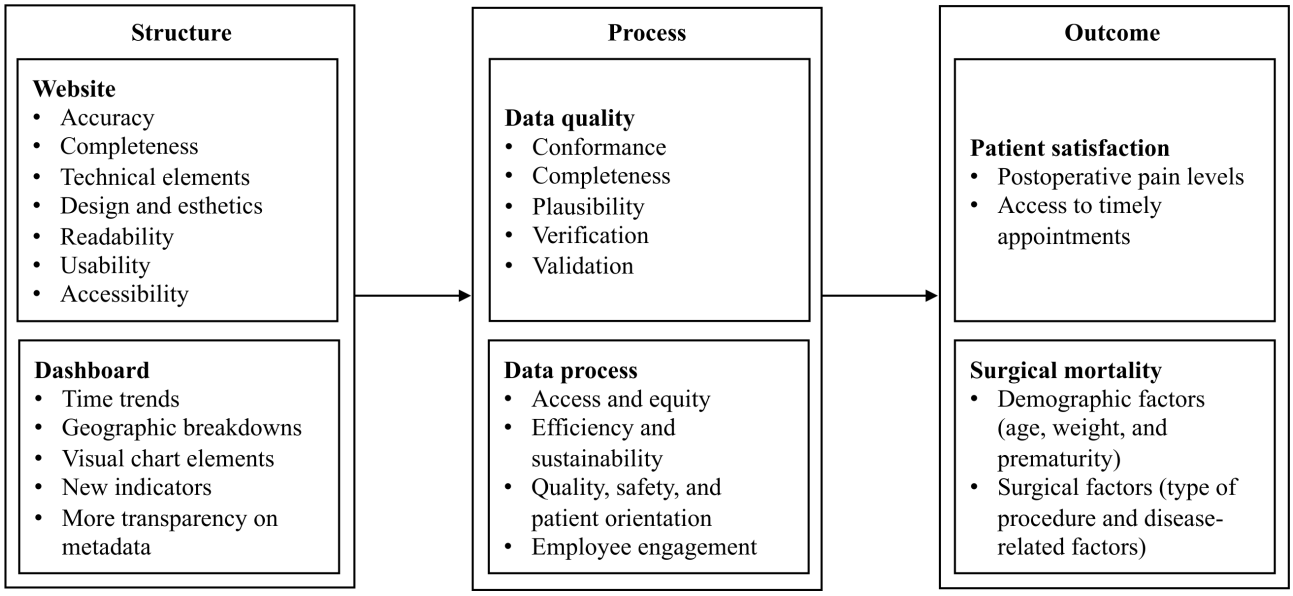

The presentation format of PR websites refers to the channel through which users directly interact with the displayed content of the PR systems. Adherence to the website quality dimension and the dashboard quality dimension in the presentation format facilitates users' understanding of the system in a structured context.

Previous studies have indicated that data inconsistencies negatively affect the actual use of the system, thereby influencing users' adoption of the system [72]. The reviewed study indicates that the dashboards present data that have been processed and integrated within the underlying data architecture, resulting in higher accuracy and consistency. This, in turn, helps users use information that is more reliable and precise.

While structural indicators define the foundational quality of PR websites, process indicators determine how these systems function and generate reliable data. In terms of process indicators, data quality encompasses conformance, completeness, plausibility, verification, and validity. Data processes include accessibility and equity, efficiency and sustainability, quality, safety, patient-centered orientation, as well as employee engagement.

Building on the research gap regarding data inconsistency in existing PR, this study examines the dimensional indicators of data generated within process metrics. Standardizing data generated through PPC processes facilitates process-level data handling, thereby supporting the further use of the data. This aligns with prior findings from reviewed studies indicating that standardized data guidelines help users make better-informed health decisions [51].

User heterogeneity consists of individual characteristics and contextual design features [37]. Prior research suggests that dashboard design often fails to account for distinct user groups, leading to limited engagement [59]. Integrating contextual factors, health literacy levels, and individual characteristics into the design of PR systems allows for a more targeted presentation of information, thereby enhancing user comprehension and decision-making [37,59,68].

Previous research has shown that demographic variations influence information perception [73]. In line with this evidence, the reviewed studies identify multiple factors associated with users' interactions with PR systems, including age, gender, political orientation, employment status, and region of residence. Beyond demographic variations, health literacy and contextual design features jointly shape how users interpret and use PR data [37].

The reviewed studies have demonstrated that audiovisual and narrative information can positively influence satisfaction measures; contextual features such as storytelling techniques, interactivity, and visual chart elements enhance user understanding [37]. Health literacy plays a critical role in users' ability to interpret PR data. The reviewed studies found that individuals with higher health literacy are better able to comprehend PR information, which may explain their longer visual attention to such content [68]. This suggests that health literacy influences both the depth and quality of patient engagement in PPC processes. To address this, design features such as explanatory narratives [59], temporal trends and interactive functions [57], and appropriate visual chart elements can assist users with varying levels of health literacy in better understanding PR information [68].

This study further notes that within PR, patient satisfaction is primarily affected by postoperative pain levels (higher pain correlates with lower satisfaction) and access to timely appointments [70], consistent with previous findings linking health status to user satisfaction. Meanwhile, demographic factors (age, weight, and prematurity) and surgical factors (type of procedure and disease-related factors) influence surgical mortality [71].

By mapping the reviewed studies to the SPO framework, we illustrate that system data are no longer confined solely to structural indicators; they also play a role in process and outcome indicators. Accordingly, this study identifies website guidelines and dashboard guidelines under structural indicators, data quality and data processes under process indicators, and patient satisfaction and surgical mortality under outcome

XSL•FO
RenderX

indicators. Furthermore, the underlying database sources are displayed within dashboards, helping to address inconsistencies between databases across different systems.

Discussion

Principal Findings

Health technology assessment ensures that medical innovations genuinely improve patient outcomes rather than merely increasing the burden [74]. In this literature review, we synthesized the findings of 25 empirical studies by categorizing them under structural indicators, process indicators, and outcome indicators [20]. Our main findings indicate that structural indicators (website and dashboard guidelines) and process indicators (data quality and data processes) jointly influence user outcomes, such as satisfaction and surgical mortality, with user heterogeneity mediating these effects.

This study adopts a dual perspective of the individual and the system in selection pathways to systematically examine the mechanisms through which information presentation and user interaction operate within PR systems [19]. Existing literature indicates that the presentation of information within information systems not only supports patients in selecting health care providers and using report cards [68] but also influences the quality of user decision-making [55]. Consistent with prior research, the mode of information presentation, the level of aggregation, and report personalization significantly affect the extent of user engagement in decision-making [7,62]. However, this study finds that the operability and data-display characteristics of dashboards play a unique role in supporting individualized decisions [53,61] and that the supplementation of online information can enhance users' understanding of the data [51]. Additionally, the personal and contextual characteristics of health care information sources affect users' adoption in PR systems [37].

Regarding consistency, most studies emphasize the importance of PR dashboards for user decision-making [67], while user health literacy and individual characteristics modulate actual information use [68]. This study further highlights that the standardized design of data and websites can enhance decision-making effectiveness [60]. Unified dashboard guidelines, along with aggregation and search functionalities, can reduce information conflicts and increase user comprehension and trust [59,68].

In terms of heterogeneity, studies have examined the impact of different information types (eg, online reviews, report cards, and dashboards during the pandemic) and diverse user groups (classified by age and health status) on decision-making [54]. Specifically, users differ in their focus on data operability versus information sources [37,61]. Common challenges in PR include missing information, delayed updates, complex formats, lack of standardization, and limited accessibility for users with low health literacy [51,68].

Regarding the user selection pathway, the system is considered a critical avenue for decision-making. Dashboards can mitigate existing issues in PR, such as missing data, delayed updates, and information confusion. As Donabedian [20] noted, while quality indicators are difficult to measure, their establishment contributes to improving actual health care quality. Standardized data guidelines and structured information presentation can support more effective decisions within structural and process indicators, while reducing information asymmetry and enhancing the quality of health services [55].

In summary, by referencing different PR scenarios and information types, this study proposes practical system optimization recommendations and categorizes differences among user groups as user-consciousness heterogeneity, which serves as a moderating variable. It emphasizes the role of standardized guidelines in facilitating the flow of information.

Future Research Agenda

Overview

In the era of digital health, the adoption of PR has evolved. From the perspective of availability, it is possible to examine the innovativeness of technologies in shaping users' perceptions of what they can accomplish [75]. Information systems, as a critical component of structural indicators [20], also play a significant role in enhancing patient awareness [15]. Based on the classification of diverse user groups and the multiple roles involved in the PPC process, incorporating dashboards and other visualization tools into system design can facilitate the adoption of PR information.

Based on the analysis of the studies included in this review, the public's understanding and use of PR remain at a preliminary stage across different population groups [76,77]. To advance the practical use of PR information, future studies should adopt diverse methodological and theoretical approaches to explore how enhancing awareness can foster trust between health care organizations and various demographic groups. Research on this topic should be further expanded along four key dimensions: conceptual understanding, thematic exploration, methodological innovation, and technological development.

Conceptual Agenda

User attitudes are fundamental determinants of behavioral intentions and actual behaviors [17]. Underlying these attitudes are user cognitions, particularly awareness and understanding, which align with levels 1 and 2 of the PAM. While existing research highlights the role of health literacy in PR and its connection to PAM, little attention has been paid to its functional and interactive dimensions [78].

Although system design and information presentation can foster awareness and literacy, the conceptual link between the two remains underexplored. From a systems perspective, perception marks the initial awareness stage; subsequent information processing drives decision-making and system adoption. Information framing, as shown in media studies, shapes comprehension and interpretation [79]. Empirical evidence shows that most patients remain at level 1 of PAM [10]. Enhancing health literacy may help users progress from basic awareness to initial engagement.

XSL•FO
RenderX

Thematic Agenda

This study notes that participants with more severe health conditions tend to seek care more frequently than healthier individuals, making the process of choosing a physician particularly important for them. Notably, significant differences in decision quality are observed among these participants [56]. Previous research on the design of PR websites has largely focused on conditions such as hypertension, diabetes, and infectious diseases [15]. The future PR system should pay greater attention to the needs of patients with complex conditions, such as those with multiple comorbidities.

Moreover, this study points out that contextual factors, health literacy, and individual characteristics affect an individual's adoption. Future research should explore how individuals' emotional states and literacy capacities interact with and interpret PR information. For instance, Shaller [80] proposed a context-based consumer choice framework that emphasizes the integration of users' decision contexts, emotional states, and literacy capacities.

Methodological Agenda

Primary data collection was primarily used in surveys, experiments, and semistructured interviews, whereas qualitative approaches, such as interviews, focus groups, and thematic content analysis, remained less common. Mixed method studies were rare, typically combining expert evaluation with descriptive and thematic analyses.

Methodologically combining natural language processing, causal inference, and experimental designs could advance the understanding of how system-level indicators interact with user heterogeneity, health literacy, and decision-making behaviors in the PR system.

Technological Agenda

In health care organizations, the PPC extends beyond physicians and patients to include family members, friends, caregivers, and other stakeholders. Future system designs that integrate and accommodate these multiple roles could enhance communication between actual users and the system.

Previous studies have indicated that patients with poorer health conditions exhibit more pronounced differences in decision-making [56]. Population segmentation can be categorized into low-health-demand, multiple comorbidities, medically complex, and frail groups [77]. Future research could explore the heterogeneity of responses across these groups in relation to information presentation. For example, web design could incorporate switchable versions to accommodate the health information needs of patients with different health conditions.

Limitations

First, this study retrieved literature through keyword searches within selected databases. This approach may have limited the scope of study selection and potentially excluded relevant studies from other databases.

Second, this study explored PR systems from the perspective of individuals in health care. Even though employees act as individual users of the PR system, broadening the search term to include employees of health care organizations in their dual roles can bring new insights. It can be helpful to explore the interaction between employees in the organization and individuals within the sociotechnical theory. Additionally, given that qualitative research methods are interpretive, potential subjective biases may exist when evaluating study findings.

Conclusions

This study provides the following contributions to the existing literature. First, we synthesized within the SPO framework. By systematically analyzing current research on the use of PR information presentation, this study provides an overview of the website and dashboard dimensions in the structure indicators, data quality and data process in the process indicators, and patient satisfaction and surgical mortality in the outcome indicators. Moreover, this study contributes to the literature by identifying contextual factors, such as health literacy, individual characteristics, political affiliation, employment status, income, and area of residence that influence users' perceptions.

Second, this study builds a connection between data appearing during PPC and the PR systems in the structure quality dimension. Finally, this research outlines future research directions from conceptual, methodological, thematic, and information system perspectives. These insights provide valuable guidance for advancing research in this field, bridging existing gaps, and improving the overall quality of academic inquiry.

Acknowledgments

The authors thank Professor Hongxiu Li for her guidance in conceptualizing the study and providing comments on the manuscript. We also acknowledge the librarians at the University of Turku for their assistance with refining the search strategies. Finally, the authors are grateful to the anonymous reviewers for their comments on the conceptual framing and comments regarding the search strategy.

Funding

LD was financially supported by the Chinese Scholarship Council (grant 202306770017). The funder had no role in the study design, data collection, analysis, interpretation, or manuscript writing.

XSL•FO
RenderX

Data Availability

All extracted data, coding notes, and synthesis outputs generated in this study are publicly available in the Open Science Framework repository at [81]. This includes structured data files (ciw/ris/nbib). Access is unrestricted. Researchers can download and use these materials for noncommercial purposes. During the preparation of this manuscript, generative artificial intelligence (AI; ChatGPT) was used solely for translation and language polishing purposes. All outputs generated by the AI were carefully reviewed and verified by the authors to ensure accuracy and appropriateness. The AI was not involved in study design, data collection, analysis, interpretation, or in writing the scientific content of the manuscript.

Authors' Contributions

Conceptualization: LD, RS
Data curation: LD
Formal analysis: LD, ED
Investigation: LD, ED
Methodology: LD
Resources: RS
Supervision: RS
Validation: LD, ED
Visualization: LD
Writing–original draft: LD
Writing–review & editing: LD, ED

Conflicts of Interest

None declared.

Multimedia Appendix 1
Search strategies in each database.
[DOCX File, 17 KB - medinform_v14i1e80435_app1.docx]

Multimedia Appendix 2
Mixed Methods Appraisal Tool (MMAT) quality assessment report.
[DOCX File, 54 KB - medinform_v14i1e80435_app2.docx]

Multimedia Appendix 3
Key characteristics of the included studies.
[DOCX File, 50 KB - medinform_v14i1e80435_app3.docx]

Multimedia Appendix 4
Details of the included studies.
[DOCX File, 40 KB - medinform_v14i1e80435_app4.docx]

Checklist 1
PRISMA-P checklist.
[DOCX File, 27 KB - medinform_v14i1e80435_app5.docx]

References

1. Evans L, Evans J, Pagliari C, Källander K. Scoping review: exploring the equity impact of current digital health design practices. Oxf Open Digit Health 2023 Jan 1;1(8):qad006. [doi: 10.1093/oodh/oqad006]
2. All the healthcare marketing statistics to pay close attention to in 2023. Digitalis Medical. 2021. URL: https://digitalismedical.com/blog/healthcare-marketing-statistics/ [accessed 2026-03-13]
3. Salampessy BH, Portrait FRM, van der Hijden E, Klink A, Koolman X. On the correlation between outcome indicators and the structure and process indicators used to proxy them in public health care reporting. Eur J Health Econ 2021 Nov;22(8):1239-1251. [doi: 10.1007/s10198-021-01333-w] [Medline: 34191196]
4. Greene J, Hibbard JH. Why does patient activation matter? An examination of the relationships between patient activation and health-related outcomes. J Gen Intern Med 2012 May;27(5):520-526. [doi: 10.1007/s11606-011-1931-2] [Medline: 22127797]

XSL•FO
RenderX

5. Knopik C. Evaluating data integrity and reporting challenges in public health: lessons from COVID-19 data collection in Washington state. : Science, Public Health Policy and the Law; 2024 URL: https://publichealthpolicyjournal.com/wp-content/uploads/2024/10/Knopik_SciencePublicHealthPolicyAndTheLaw_v5.2019-2024.Oct_2024.pdf [accessed 2026-02-27]
6. Kurtzman ET, Greene J. Effective presentation of health care performance information for consumer decision making: a systematic review. Patient Educ Couns 2016 Jan;99(1):36-43. [doi: 10.1016/j.pec.2015.07.030] [Medline: 26277826]
7. Sander U, Emmert M, Dickel J, Meszmer N, Kolb B. Information presentation features and comprehensibility of hospital report cards: design analysis and online survey among users. J Med Internet Res 2015 Mar 16;17(3):e68. [doi: 10.2196/jmir.3414] [Medline: 25782186]
8. Alemu W, Girma E, Mulugeta T. Patient awareness and role in attaining healthcare quality: a qualitative, exploratory study. Int J Afr Nurs Sci 2021;14:100278. [doi: 10.1016/j.ijans.2021.100278]
9. Janamian T, Greco M, Cosgriff D, Baker L, Dawda P. Activating people to partner in health and self-care: use of the patient activation measure. Med J Aust 2022 Jun 6;216 Suppl 10(Suppl 10):S5-S8. [doi: 10.5694/mja2.51535] [Medline: 35665937]
10. Chen M, Zhang X, Liu C, Chen H, Wang D, Liu C. Effects of public reporting of prescription indicators on patient choices: evidence from propensity scores matching. Front Pharmacol 2023 Oct 9;14:1110653. [doi: 10.3389/fphar.2023.1110653]
11. Chimonas S, Fortier E, Li DG, Lipitz-Snyderman A. Facts and fears in public reporting: patients' information needs and priorities when selecting a hospital for cancer care. Med Decis Making 2019 Aug;39(6):632-641. [doi: 10.1177/0272989X19855050] [Medline: 31226909]
12. Cacace M, Geraedt M. Public reporting as a quality strategy. Eur J Public Health 2017 Nov 1;27(suppl_3):ckx187-ckx751. [doi: 10.1093/eurpub/ckx187.751]
13. Schlesinger M, Grob R, Shaller D. Using patient‐reported information to improve clinical practice. Health Serv Res 2015 Dec;50(Suppl 2):2116-2154. [doi: 10.1111/1475-6773.12420] [Medline: 26573890]
14. Greene SM, Tuzzio L, Cherkin D. A framework for making patient-centered care front and center. Perm J 2012 Sep;16(3):49-53. [doi: 10.7812/TPP/12-025]
15. Sapin M, Ehlig D, Geissler A, Vogel J. Public reporting in five health care areas: a comparative content analysis across nine countries. Health Policy 2025 Feb;152:105222. [doi: 10.1016/j.healthpol.2024.105222] [Medline: 39700634]
16. Ackoff R. Ackoff's Best: His Classic Writings on Management: Wiley; 1999.
17. Cacace M, Geraedts M, Berger E. Public reporting as a quality strategy. In: Reinhard B, Niek K, Dimitra P, Wilm Q, editors. Improving Healthcare Quality in Europe: Characteristics, Effectiveness and Implementation of Different Strategies: WHO Regional Office for Europe (with OECD); 2019:331-355.
18. Totten AM, Wagner J, Tiwari A, O'Haire C, Griffin J, Walker M. Closing the quality gap: revisiting the state of the science (vol. 5: public reporting as a quality improvement strategy). Evid Rep Technol Assess (Full Rep) 2012 Jul(208.5):1-645. [Medline: 24422977]
19. Berwick DM, James B, Coye MJ. Connections between quality measurement and improvement. Med Care 2003 Jan;41(1 Suppl):I30-I38. [doi: 10.1097/00005650-200301001-00004] [Medline: 12544814]
20. Donabedian A. Evaluating the quality of medical care. Milbank Mem Fund Q 1966 Jul;44(3):166-206. [Medline: 5338568]
21. Pratici L, Salvatore FP, Fanelli S, Zangrandi A, Milone M. Using ESG paradigm as a basis for social reporting in nonprofit organizations: evidence from cases in healthcare. Manag Decis 2025 Feb 13;63(2):586-609. [doi: 10.1108/MD-10-2023-2012]
22. Chan AW, Karam G, Pymento J, et al. Reporting summary results in clinical trial registries: updated guidance from WHO. Lancet Glob Health 2025 Apr;13(4):e759-e768. [doi: 10.1016/S2214-109X(24)00514-X] [Medline: 40155113]
23. Agha RA, Mathew G, Rashid R, et al. Revised Strengthening the Reporting of Cohort, Cross-Sectional and Case-Control Studies in Surgery (STROCSS) guideline: an update for the age of artificial intelligence. Prem J Sci 2025. [doi: 10.70389/PJS.100081]
24. Non LR, Marra AR, Ince D. Rise of the machines - artificial intelligence in healthcare epidemiology. Curr Infect Dis Rep 2025 Dec;27(1):4. [doi: 10.1007/s11908-024-00854-8]
25. Donabedian A. The quality of care. How can it be assessed? JAMA 1988;260(12):1743-1748. [doi: 10.1001/jama.260.12.1743] [Medline: 3045356]
26. Quality improvement and monitoring at your fingertips. Agency for Healthcare Research and Quality. 2016. URL: https://qualityindicators.ahrq.gov/ [accessed 2026-03-05]
27. Staehelin D, Dolata M, Stöckli L, Schwabe G. How patient-generated data enhance patient-provider communication in chronic care: field study in design science research. JMIR Med Inform 2024 Sep 10;12(1):e57406. [doi: 10.2196/57406] [Medline: 39255481]
28. Fiske A, Degelsegger-Márquez A, Marsteurer B, Prainsack B. Value-creation in the health data domain: a typology of what health data help us do. Biosocieties 2022 Apr 12:1-25. [doi: 10.1057/s41292-022-00276-6] [Medline: 35432575]
29. Tang Y, Liu C, Zhang X. Performance associated effect variations of public reporting in promoting antibiotic prescribing practice: a cluster randomized-controlled trial in primary healthcare settings. Prim Health Care Res Dev 2017 Sep;18(5):482-491. [doi: 10.1017/S1463423617000329] [Medline: 28606190]
30. Yang L, Liu C, Wang L, Yin X, Zhang X. Public reporting improves antibiotic prescribing for upper respiratory tract infections in primary care: a matched-pair cluster-randomized trial in China. Health Res Policy Syst 2014 Oct 10;12:61. [doi: 10.1186/1478-4505-12-61] [Medline: 25304996]

XSL•FO
RenderX

31. Kwame A, Petrucka PM. A literature-based study of patient-centered care and communication in nurse-patient interactions: barriers, facilitators, and the way forward. BMC Nurs 2021 Sep 3;20(1):158. [doi: 10.1186/s12912-021-00684-2] [Medline: 34479560]
32. Fazio RH, Zanna MP. Direct experience and attitude-behavior consistency. Adv Exp Soc Psychol 1981;14:161-202. [doi: 10.1016/S0065-2601(08)60372-X]
33. Bostrom RP, Heinen JS. MIS problems and failures: a socio-technical perspective. MIS Q 1977 Sep 1;1(3):17-32. [doi: 10.2307/248710]
34. Prang KH, Maritz R, Sabanovic H, Dunt D, Kelaher M. Mechanisms and impact of public reporting on physicians and hospitals' performance: a systematic review (2000-2020). PLoS ONE 2021;16(2):e0247297. [doi: 10.1371/journal.pone.0247297] [Medline: 33626055]
35. Miller GA. The magical number seven plus or minus two: some limits on our capacity for processing information. Psychol Rev 1956 Mar;63(2):81-97. [Medline: 13310704]
36. Sivarajkumar S, Mohammad HA, Oniani D, et al. Clinical information retrieval: a literature review. J Healthc Inform Res 2024 Jun;8(2):313-352. [doi: 10.1007/s41666-024-00159-4] [Medline: 38681755]
37. Moore AR, Hudson C, Amey F, Chumbler N. Trusting sources of information on quality of physician care. Inquiry 2020;57:46958020952912. [doi: 10.1177/0046958020952912] [Medline: 32830580]
38. Pross C, Averdunk LH, Stjepanovic J, Busse R, Geissler A. Health care public reporting utilization - user clusters, web trails, and usage barriers on Germany's public reporting portal Weisse-Liste.de. BMC Med Inform Decis Mak 2017 Apr 21;17(1):48. [doi: 10.1186/s12911-017-0440-6] [Medline: 28431546]
39. Zhang Y, Callaghan-Koru JA, Koru G. The challenges and opportunities of continuous data quality improvement for healthcare administration data. JAMIA Open 2024 Oct;7(3):ooae058. [doi: 10.1093/jamiaopen/ooae058] [Medline: 39091510]
40. Kitchenham B, Pearl Brereton O, Budgen D, Turner M, Bailey J, Linkman S. Systematic literature reviews in software engineering—a systematic literature review. Inf Softw Technol 2009 Jan;51(1):7-15. [doi: 10.1016/j.infsof.2008.09.009]
41. Li J. Public reporting and consumer demand in the home health sector. Med Care Res Rev 2024 Apr;81(2):122-132. [doi: 10.1177/10775587231221852] [Medline: 38235538]
42. Beckett MK, Quigley DD, Cohea CW, et al. Trends in HCAHPS survey scores, 2008–2019: a quality improvement perspective. Med Care 2024 Jun 1;62(6):416-422. [doi: 10.1097/MLR.0000000000002001] [Medline: 38728680]
43. Okoli C, Schabram K. A guide to conducting a systematic literature review of information systems research. SSRN Electron J 2010. [doi: 10.2139/ssrn.1954824]
44. Webster J, Watson RT. Analyzing the past to prepare for the future: writing a literature review. MIS Q 2002 Jun 1;26(2):xiii-xxiii. [doi: 10.2307/4132319]
45. Higgins JPT, Thomas J, Chandler J, et al, editors. Cochrane Handbook for Systematic Reviews of Interventions: Wiley; 2019. URL: https://onlinelibrary.wiley.com/doi/book/10.1002/9781119536604 [accessed 2026-02-27] [doi: 10.1002/9781119536604]
46. Jasperson J(, Carte TA, Saunders CS, et al. Review: power and information technology research: a metatriangulation review. MIS Q 2002 Dec 1;26(4):397-459. [doi: 10.2307/4132315]
47. Hong QN, Fàbregues S, Bartlett G, et al. The Mixed Methods Appraisal Tool (MMAT) version 2018 for information professionals and researchers. Educ Inf 2018 Nov 1;34(4):285-291. [doi: 10.3233/EFI-180221]
48. Sandelowski M, Voils CI, Barroso J. Defining and designing mixed research synthesis studies. Res Sch 2006;13(1):29. [Medline: 20098638]
49. Hennessee I, Clennon JA, Waller LA, Kitron U, Bryan JM. Considerations for improving reporting and analysis of date-based COVID-19 surveillance data by public health agencies. Am J Public Health 2021 Dec;111(12):2127-2132. [doi: 10.2105/AJPH.2021.306520] [Medline: 34878867]
50. Siddhanamatha HR, Heung E, de los Angeles Lopez-Olivo M, et al. Quality assessment of websites providing educational content for patients with rheumatoid arthritis. Semin Arthritis Rheum 2017 Jun;46(6):715-723. [doi: 10.1016/j.semarthrit.2017.01.006] [Medline: 28258768]
51. Lopez-Olivo MA, des Bordes JKA, Syed MN, et al. Quality appraisal of educational websites about osteoporosis and bone health. Arch Osteoporos 2021 Feb 10;16(1):28. [doi: 10.1007/s11657-021-00877-x] [Medline: 33566216]
52. Temkin-Greener H, Mao Y, McGarry B. Online customer reviews of assisted living communities: association with community, county, and state factors. J Am Med Dir Assoc 2023 Jun;24(6):841-845.e3. [doi: 10.1016/j.jamda.2023.02.007] [Medline: 36934775]
53. Barbazza E, Ivanković D, Wang S, et al. Exploring changes to the actionability of COVID-19 dashboards over the course of 2020 in the Canadian context: descriptive assessment and expert appraisal study. J Med Internet Res 2021 Aug 6;23(8):e30200. [doi: 10.2196/30200] [Medline: 34280120]
54. Ryskina KL, Andy AU, Manges KA, Foley KA, Werner RM, Merchant RM. Association of online consumer reviews of skilled nursing facilities with patient rehospitalization rates. JAMA Netw Open 2020 May 1;3(5):e204682. [doi: 10.1001/jamanetworkopen.2020.4682] [Medline: 32407501]
55. Perraillon MC, Konetzka RT, He D, Werner RM. Consumer response to composite ratings of nursing home quality. Am J Health Econ 2019;5(2):165-190. [doi: 10.1162/ajhe_a_00115] [Medline: 31579236]

XSL•FO
RenderX

56. Cerully JL, Parker AM, Rybowski L, et al. Improving patients' choice of clinician by including roll-up measures in public healthcare quality reports: an online experiment. J Gen Intern Med 2019 Feb;34(2):243-249. [doi: 10.1007/s11606-018-4725-y] [Medline: 30446909]
57. Reid RO, Deb P, Howell BL, Conway PH, Shrank WH. The roles of cost and quality information in Medicare Advantage plan enrollment decisions: an observational study. J Gen Intern Med 2016 Feb;31(2):234-241. [doi: 10.1007/s11606-015-3467-3] [Medline: 26282952]
58. Emmert M, Wiener M. What factors determine the intention to use hospital report cards? The perspectives of users and non-users. Patient Educ Couns 2017 Jul;100(7):1394-1401. [doi: 10.1016/j.pec.2017.01.021] [Medline: 28189471]
59. Barbazza E, Ivanković D, Davtyan K, et al. The experiences of 33 national COVID-19 dashboard teams during the first year of the pandemic in the World Health Organization European Region: a qualitative study. Digit Health 2022;8:20552076221121154. [doi: 10.1177/20552076221121154] [Medline: 36060614]
60. Lloyd S, Cliff C, FitzGerald G, Collie J. Can publicly reported data be used to understand performance in an Australian rural hospital? Health Inf Manag 2021;50(1-2):35-46. [doi: 10.1177/1833358320948559] [Medline: 32935590]
61. Ivanković D, Barbazza E, Bos V, et al. Features constituting actionable COVID-19 dashboards: descriptive assessment and expert appraisal of 158 public web-based COVID-19 dashboards. J Med Internet Res 2021 Feb 24;23(2):e25682. [doi: 10.2196/25682] [Medline: 33577467]
62. Smith MA, Bednarz L, Nordby PA, et al. Increasing consumer engagement by tailoring a public reporting website on the quality of diabetes care: a qualitative study. J Med Internet Res 2016 Dec 21;18(12):e332. [doi: 10.2196/jmir.6555] [Medline: 28003173]
63. Blacketer C, Defalco FJ, Ryan PB, Rijnbeek PR. Increasing trust in real-world evidence through evaluation of observational data quality. J Am Med Inform Assoc 2021 Sep 18;28(10):2251-2257. [doi: 10.1093/jamia/ocab132] [Medline: 34313749]
64. Hsu SH, Hung P, Wang SY. Factors associated with hospices' nonparticipation in medicare's hospice compare public reporting program. Med Care 2019 Jan;57(1):28-35. [doi: 10.1097/MLR.0000000000001016] [Medline: 30489545]
65. Downing NS, Cloninger A, Venkatesh AK, et al. Describing the performance of U.S. hospitals by applying big data analytics. PLoS One 2017;12(6):e0179603. [doi: 10.1371/journal.pone.0179603] [Medline: 28662045]
66. Kast K, Otten SM, Konopik J, Maier CB. Web-based public reporting as a decision-making tool for consumers of long-term care in the United States and the United Kingdom: systematic analysis of report cards. JMIR Form Res 2023 Dec 14;7:e44382. [doi: 10.2196/44382] [Medline: 38096004]
67. Gephart SM, Tolentino DA, Quinn MC, Wyles C. Neonatal intensive care workflow analysis informing NEC-Zero clinical decision support design. Comput Inform Nurs 2023 Feb 1;41(2):94-101. [doi: 10.1097/CIN.0000000000000929] [Medline: 35470306]
68. Yılmaz NG, Timmermans DR, Van Weert JC, Damman OC. Breast cancer patients' visual attention to information in hospital report cards: an eye-tracking study on differences between younger and older female patients. Health Informatics J 2023;29(1):14604582231155279. [doi: 10.1177/14604582231155279] [Medline: 36840473]
69. Walsh-Childers K, Braddock J, Rabaza C, Schwitzer G. One step forward, one step back: changes in news coverage of medical interventions. Health Commun 2018 Feb;33(2):174-187. [doi: 10.1080/10410236.2016.1250706] [Medline: 27983868]
70. Shah NS, Umeda Y, Newyear B, et al. Patients with higher postoperative pain after ambulatory shoulder surgery reported lower satisfaction: a prospective observational study. AME Surg J 2022 Dec 1;2:32-32. [doi: 10.21037/asj-22-11]
71. Jacobs JP. The society of thoracic surgeons congenital heart surgery database public reporting initiative. Semin Thorac Cardiovasc Surg Pediatr Card Surg Annu 2017 Jan;20:43-48. [doi: 10.1053/j.pcsu.2016.09.008] [Medline: 28007064]
72. Rambur B, Vallett C, Cohen JA, Tarule JM. Metric-driven harm: an exploration of unintended consequences of performance measurement. Appl Nurs Res 2013 Nov;26(4):269-272. [doi: 10.1016/j.apnr.2013.09.001] [Medline: 24206760]
73. Wong YK, Low KL, Pooke TG. Factors associated with dimensions of patients' trust in chiropractic doctors in the international medical university healthcare chiropractic center: an exploratory study. J Chiropr Med 2022 Jun;21(2):83-96. [doi: 10.1016/j.jcm.2022.02.003] [Medline: 35774631]
74. Facey K, Henshall C, Sampietro-Colom L, Thomas S. Improving the effectiveness and efficiency of evidence production for health technology assessment. Int J Technol Assess Health Care 2015 Jan;31(4):201-206. [doi: 10.1017/S0266462315000355] [Medline: 26646858]
75. Zheng H, Xia W, Ma J. Affordance types and their determinants in patient mobile health portals use: an empirical investigation. J Med Internet Res 2025 Aug 27;27(2025):e74351. [doi: 10.2196/74351] [Medline: 40865120]
76. Kumpunen S, Trigg LJ, Rodrigues R. Public reporting in health and long-term care to facilitate provider choice. : World Health Organization; 2014 URL: https://iris.who.int/server/api/core/bitstreams/ca6534be-7003-4d72-892a-45023ddbbf01/content [accessed 2026-02-27]
77. Langton JM, Wong ST, Burge F, et al. Population segments as a tool for health care performance reporting: an exploratory study in the Canadian province of British Columbia. BMC Fam Pract 2020 May 31;21(1):98. [doi: 10.1186/s12875-020-01141-w] [Medline: 32475339]
78. Nutbeam D. Health literacy as a public health goal: a challenge for contemporary health education and communication strategies into the 21st century. Health Promot Int 2000 Sep 1;15(3):259-267. [doi: 10.1093/heapro/15.3.259]

XSL•FO
RenderX

79. de Vreese CH, Boomgaarden HG, Semetko HA. (In)direct framing effects: the effects of news media framing on public support for Turkish membership in the European Union. Communic Res 2011 Apr;38(2):179-205. [doi: 10.1177/0093650210384934]
80. Shaller D, Kanouse DE, Schlesinger M. Context-based strategies for engaging consumers with public reports about health care providers. Med Care Res Rev 2014 Oct;71(5 Suppl):17S-37S. [doi: 10.1177/1077558713493118] [Medline: 23819945]
81. Understanding user behavior toward public reporting in digital health: a systematic review. OSF. URL: https://osf.io/62bdk/overview [accessed 2026-03-13]

Abbreviations

EC: exclusion criteria
ESG: environmental, social, and governance
IC: inclusion criteria
MMAT: Mixed Methods Appraisal Tool
PAM: patient activation measure
PPC: patient-physician collaboration
PR: public reporting
PRISMA: Preferred Reporting Items for Systematic Reviews and Meta-Analyses
PRISMA-P: Preferred Reporting Items for Systematic Review and Meta-Analyses Protocols
SPO: structure-process-outcome

Edited by A Benis; submitted 10.Jul.2025; peer-reviewed by H Maheshwari, Y Oyende, Z Guo; revised version received 09.Feb.2026; accepted 17.Feb.2026; published 18.Mar.2026.

Please cite as:
Du L, Suomi R, Damalie E
Digital Public Reporting Systems for Evaluating Health Care Quality: Systematic Review
JMIR Med Inform 2026;14:e80435
URL: https://medinform.jmir.org/2026/1/e80435
doi:10.2196/80435

© Lanmei Du, Reima Suomi, Elorm Damalie. Originally published in JMIR Medical Informatics (https://medinform.jmir.org), 18.Mar.2026. This is an open-access article distributed under the terms of the Creative Commons Attribution License (https://creativecommons.org/licenses/by/4.0/), which permits unrestricted use, distribution, and reproduction in any medium, provided the original work, first published in JMIR Medical Informatics, is properly cited. The complete bibliographic information, a link to the original publication on https://medinform.jmir.org/, as well as this copyright and license information must be included.

XSL•FO
RenderX

Machine Learning for Predicting Venous Thromboembolism After Joint Arthroplasty: Systematic Review of Clinical Applicability and Model Performance

Junwei Ma[1], BSc; Huifeng Tang[2], MSN; Yunshan Zhang[2], BSc; Xuemei Yi[2], BSc; Tangsheng Zhong[3], DN; Xinyun Li[1], BSc; Gang Wang[2], MSN

[1]School of Nursing, Jilin University, Changchun, China

[2]The Second Operation Room, First Hospital of Jilin University, No. 71 Xinmin Street, Chaoyang District, Changchun, China

[3]Nursing Department, First Hospital of Jilin University, Changchun, China

Corresponding Author:
Gang Wang, MSN
The Second Operation Room, First Hospital of Jilin University, No. 71 Xinmin Street, Chaoyang District, Changchun, China

Abstract

Background: There is increasing research on machine learning in predicting venous thromboembolism after joint arthroplasty, but the quality and clinical applicability of these models remain uncertain.

Objective: This systematic review aims to evaluate the predictive performance and methodological quality of machine learning models for venous thromboembolism risk after joint replacement surgery.

Methods: Web of Science, Embase, Scopus, CNKI, Wanfang, Vipro, and PubMed were searched until December 15, 2024. The risk of bias and applicability were evaluated using the PROBAST (Prediction Model Risk of Bias Assessment Tool) checklist. A qualitative comprehensive analysis was conducted to extract and describe the data related to the model's characteristics and performance.

Results: This review encompassed 34 prediction models from 9 studies. The most frequently used machine learning models were extreme gradient boosting and logistic regression. The results showed that all studies had significant heterogeneity and high risk of bias. Although some models reported nearly flawless area under the curve (>0.9), they lacked external validation and may have overfitted. The models tested on large external datasets demonstrated more conservative performance.

Conclusions: The predictive performance of machine learning models varied greatly. Although the reported area under the curve values indicated that some models have good discriminative ability, this performance varied greatly and was inconsistent among the included studies. These models have a high risk of bias, and it is necessary to take this into account when they are used in clinical practice. Future studies should adopt a prospective study design, ensure appropriate data handling, and use external validation to improve model robustness and applicability.

Trial Registration: PROSPERO CRD42024625842; https://www.crd.york.ac.uk/PROSPERO/view/CRD42024625842

(JMIR Med Inform 2026;14:e79886) doi:10.2196/79886

KEYWORDS

joint arthroplasty; venous thromboembolism; machine learning; meta-analysis; systematic review

Introduction

Joint replacement surgery is one of the main treatment methods for severe joint injuries, which can alleviate patients' pain and improve joint function [1,2]. In recent years, due to the aging population and the advancement of medical technology, more and more patients have undergone joint replacement surgery. But surgical complications are a big risk that can change how well joint replacement surgery works. Venous thromboembolism (VTE), including deep vein thrombosis (DVT) and pulmonary embolism (PE), is a serious postoperative complication that significantly affects the prognosis of patients [3,4].

Studies have shown that for patients who did not receive preventive medication before undergoing major orthopedic surgeries, such as total hip arthroplasty (THA) or total knee arthroplasty (TKA), the incidence of postoperative VTE can be as high as 26.6% to 60.8% [5]. Asymptomatic VTE may not present any obvious clinical symptoms but can be detected through ultrasound examination or other diagnostic techniques. Some patients with VTE may experience discomfort and swelling in the affected limb, and their functional condition may be poor, which may even affect their postoperative recovery [6,7]. Furthermore, PE also has a significant impact on patients'

XSL•FO
RenderX

lives and prognosis. Studies have shown that up to 34% of postoperative deaths may be caused by PE [8,9].

Being able to accurately identify which patients are at high risk of VTE is of great significance for the prognosis of these patients. Accurate predictions can maximize the effectiveness of anticoagulant drugs and reduce side effects, such as bleeding [10,11]. Through the analysis of vast volumes of high-dimensional data, machine learning (ML) may uncover hidden patterns and intricate nonlinear relationships, aiding illness early warning [12,13]. In recent studies, ML models have been developed to predict the incidence of postoperative VTE. The most commonly used algorithms include extreme gradient boosting (XGB), random forest (RF), and support vector machine (SVM) [14]. In the prediction of VTE, ML technology exhibits many advantages. For instance, compared to traditional approaches, it can provide superior predictions by combining several types of information, such as imaging data, biomarkers, and clinical data [15,16]. Although these studies provide new methods for the field, there are some uncertainties in the consistency and reliability of the results in the existing literature owing to the single data source, small sample size, and the model's limited capacity for generalization. In addition, there are justified concerns about bias, explainability, and applicability [17]. Therefore, this study aimed to assess the effectiveness and methodological quality of ML models in predicting VTE following joint replacement through a systematic review in order to provide evidence-based support for their clinical application, identify current research gaps, and offer guidance for future high-quality studies.

Methods

Registration of the Study

This study adheres to PRISMA (Preferred Reporting Items for Systematic Reviews and Meta-Analyses; Checklist 1) guidelines for conducting systematic reviews [18]. The study protocol was registered on PROSPERO (International Prospective Register of Systematic Reviews; registration number: CRD42024625842).

Data Sources and Search Strategy

A comprehensive search was conducted in both Chinese and English databases, including Web of Science, Embase, Scopus, CNKI, Wanfang, Vipro, and PubMed, from the time of their formation until December 15, 2024. The following search terms were applied: "joint arthroplasty," "venous thromboembolism," "machine learning," "risk prediction," "prediction models," and their synonyms and variant terms. A manual search of reference lists containing studies to find related publications was conducted. For detailed search strategies, see Multimedia Appendix 1, which includes keyword combinations and database settings.

Inclusion or Exclusion Criteria

The following were the inclusion criteria: (1) studies on patients after joint replacement; (2) observational studies, case-control studies, cohort studies, and randomized controlled trials; (3) postoperative VTE risk was predicted using an ML model; (4) studies that provide performance evaluation metrics (eg, accuracy, sensitivity, specificity, area under the curve [AUC]) for the model and give clear statistical analysis results; and (5) studies published in English or Chinese.

The following were the exclusion criteria: (1) review articles, case reports, opinion pieces, commentaries, conference abstracts, and other nonoriginal research; (2) studies that do not mention particular kinds of ML models or algorithms; (3) animal experiments, simulation studies, and other nonclinical research; and (4) studies for which the entire text was not retrievable.

Study Selection and Data Synthesis

The retrieved results were imported into EndNote 21, and duplicates were eliminated. Two researchers trained in systematic evaluation techniques independently conducted the study selection process based on preestablished eligibility criteria. First, the titles and abstracts of the literature were screened, and the studies failing to meet the eligibility criteria were initially excluded. Second, it was filtered through full-text reading, and if 2 researchers disagreed, a third researcher stepped in to reach an agreement.

The data extraction process was also performed independently by 2 researchers following CHARMS (Critical Appraisal and Data Extraction for Systematic Reviews of Prediction) guidelines [19], and a third researcher settled any discrepancies. There are 2 groups into which the data taken from the chosen studies are separated: (1) basic information: author, year of publication, country, study design, participants, data source, clinical outcome, and sample size and (2) model information: missing data handling, candidate predictors, screening variable methods, prediction timepoint, prediction horizon, model development, internal verification, external verification, model performance, number of variates, calibration, and method of visualization.

Risk of Bias Assessment

The included studies' applicability and bias risk were evaluated using the PROBAST (Prediction Model Risk of Bias Assessment Tool) tool. The assessment has 20 questions, including 4 basic areas: participants, predictors, outcomes, and analysis. There are answers to the questions in each domain: "yes/probably" (low risk of bias), "no/probably not" (high risk of bias), and "no information" (unclear). A domain was deemed to have a high risk of bias if its answer contained "no/probably not." If every question had a "yes/probably yes" response, the domain was deemed to have a low risk of bias. When there is "no information," it is deemed to be highly biased if it cannot be explained by the original or additional material. If each domain was considered low risk, then the total bias risk was considered low. Furthermore, the total risk of bias was deemed high if any domains were deemed to be at high risk.

The bias risk in each model is assessed independently by 2 researchers, and if there are differences, they will be discussed to reach an agreement. Due to the majority of research using various models or having several outcomes, the bias risk is evaluated independently for each model and outcome. Finally, since there are no differences in the risk of bias between models in a single study, each study only shows the result once.

XSL•FO
RenderX

Results

Results of Literature Screening

The study selection process is detailed in the PRISMA flow diagram (Figure 1). A total of 4344 records were initially identified from 6 electronic databases (PubMed, n=2001; Embase, n=661; Web of Science, n=1415; Wanfang, n=112; CNKI, n=73; and Wipro, n=82). After removing 1466 duplicates, 2878 unique records remained for screening. During the title and abstract screening phase, 2863 records were excluded because they were either unrelated to the topic (n=2,641) or were nonoriginal research, such as reviews and newspaper articles. This left 15 reports to be sought for full-text retrieval. The subsequent critical appraisal excluded 6 studies based on predefined criteria: 3 did not use an ML approach, 2 had incomplete outcome data, and 1 did not involve a model development process. Ultimately, 9 studies met the full inclusion criteria and were included in this systematic review.

Figure 1. Literature screening process. CNKI: China National Knowledge Infrastructure.

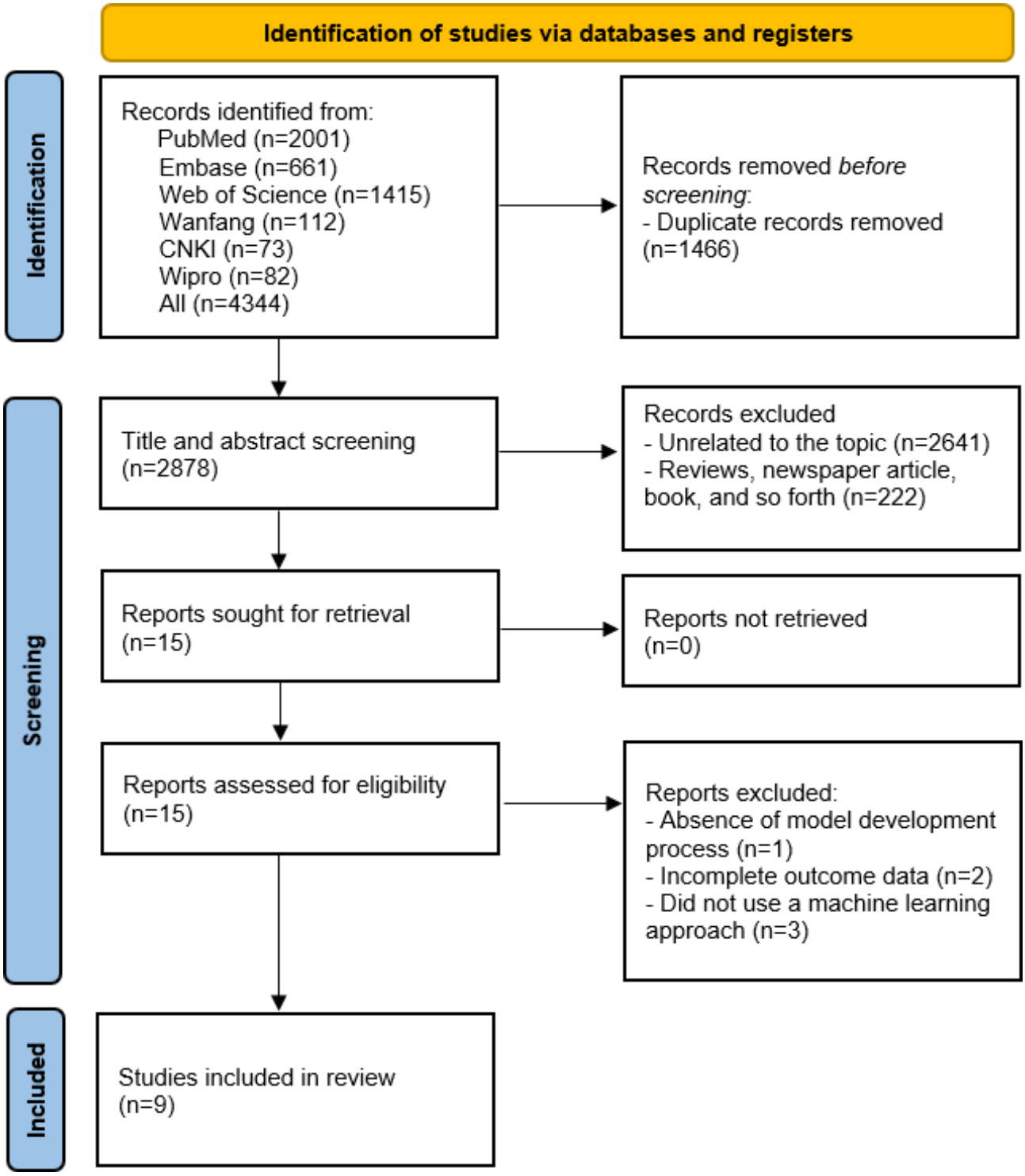

XSL•FO
RenderX

General Study Characteristics

Table 1 shows the basic characteristics of the 9 studies. These studies were published from 2018 to 2024 and included 1 prospective study [3] and 8 retrospective studies [20-27]. Among them, 4 studies [3,20,21,25] were conducted in China; 3 studies [22-24] were from the United States; 1 was conducted in the Netherlands; and 1 transnational study used data from the Netherlands, the United Kingdom, and Denmark. In terms of study population, 2 studies [3,20] focused on patients with THA, 1 study [21] targeted patients with TKA, and the remaining studies [22-27] focused on both THA and TKA. In terms of clinical outcomes, 2 studies [20,21] concentrated solely on DVT, while the remaining 7 studies [3,22-27] evaluated both DVT and PE. In addition, the studies' sample sizes ranged from 60 to 3,92,661. Cases of VTE ranged from 24 to 4042, with an incidence of 0.9% to 40%.

Table . Basic characteristics of the included studies.

Author (year)	Country	Research type	Data source	Participants	Clinical outcome	Cases/sample size
Ding et al (2023) [3]	China	Prospective study	Shanghai Changzheng Hospital	THA[a]	VTE[b]	76/1481
Chen and Jiang (2022) [21]	China	Retrospective study	Clinical database of a hospital in Chongqing	TKA[c]	DVT[d]	24/60
Harris et al (2019) [22]	United States	Retrospective study	VASQIP data, VA Corporate Data Warehouse	TKA, THA	VTE	566/70,569
Rasouli Dezfouli et al (2022) [23]	United States	Retrospective study	The Cerner Health Facts data warehouse	TKA, THA	VTE	4042/392,661
Shohat et al (2023) [24]	United States	Retrospective study	Rothman Orthopedic Institute at Thomas Jefferson University	TKA, THA	DVT, PE[e]	308/35,963
Wang et al (2023) [25]	China	Retrospective study	A health system	TKA, THA	VTE	1161/6897
Xu et al (2024) [20]	China	Retrospective study	A hospital in Wenzhou, China	THA	DVT	92/333
Sweerts et al (2022) [26]	Netherlands	Retrospective study	Multiple databases from the Dutch	TKA, THA	VTE	26/3776
Nemeth et al (2024) [27]	Netherlands, Denmark, England	Retrospective study	Multiple databases from the United Kingdom, the Netherlands, and Denmark	TKA, THA	VTE	897/64,032

[a]THA: total hip arthroplasty.

[b]VTE: venous thromboembolism.

[c]TKA: total knee arthroplasty.

[d]DVT: deep vein thrombosis.

[e]PE: pulmonary embolism.

Characteristics and Performance of ML Models

Table 2 provides a detailed summary of the methodological design and data characteristics of the included studies. Table 3 presents a summary of the performance of the model development, validation, and inclusion of the studies. Among the 9 studies included, 5 studies [3,20,23-25] evaluated multiple ML algorithms, and 4 studies [21,22,26,27] used a single algorithm. Across these studies, 15 kinds of ML algorithms were used to develop 34 predictive models, and each study developed 1-5 models. Logistic regression (LR) and XGB were the most common algorithms, appearing in 5 studies (5/9, 56%) each. This is followed by RF (3/9, 33%) [23-25] and SVM (3/9, 33%) [20,24,25]. In particular, the XGB model showed strong performance in predicting DVT and PE, with an AUC range of 0.71 - 0.982. Figure 2 details the frequency of the model used.

XSL•FO
RenderX

Table . Summary of methodological design and data characteristics of the included studies.

Author (year)	Missing data handling	Candidate predictors	Screening variable methods	Prediction timepoint	Prediction horizon	Number of variates
Singh et al (2019) [1]	Data were excluded, or mean imputation, or mode imputation	67	LASSO[a] regression	Preoperative	During postoperative hospitalization	27
Yau et al (2022) [2]	NR[b]	NR	Single-factor analysis	Postoperative	Within 3-5 days after surgery	8
Ding et al (2023) [3]	Treats missing data as a separate category	NR	NR	Preoperative	Within 30 days after surgery	22
Simon et al (2023) [4]	NR	NR	Genetic algorithm	Preoperative	Within 30 days after surgery	25
Lee et al (2013) [5]	NR	56	Univariate analysis	Postoperative	Within 90 days after surgery	27
Malcolm et al (2020) [6]	NR	66	NR	Preoperative	Within 5 weeks after surgery	66
Lewis et al (2019) [7]	missForest	26	Recursive feature elimination	Postoperative	During postoperative hospitalization	10
Meng et al (2021) [8]	Multiple imputation	5	Literature, clinical reasoning, eyeballing	Preoperative	Within 1 year after surgery	5
Runner et al (2021) [9]	No missing data	39	LR[c]	Preoperative	Within 90 days after surgery	12

[a]LASSO: least absolute shrinkage and selection operator regression.

[b]NR: not reported.

[c]LR: logistic regression.

XSL•FO
RenderX

Table . Summary of model development, validation, and performance of included studies.

Author (year)	Model development	Internal verification	External verification	AUC[a] (95% CI)	Calibration	Method of visualization
Singh et al (2019) [1]	MLP[b], XGB[c], AdaBoost[d], GBC[e], KNN[f], LR[g]	10-fold cross-validation, random split validation	None	0.955 (0.917 - 0.993); 0.982 (0.954 - 1.000); 0.980 (0.944 - 1.000); 0.978 (0.953 - 1.000); 0.837 (0.743 - 0.931); 0.944 (0.878 - 1.000)	NR[h]	ROC[i] curve, DCA[j] curve, Shapley additive explanations, nomogram
Yau et al (2022) [2]	XGB	Random split validation	None	0.832 (0.748 - 0.916)	NR	ROC curve
Ding et al (2023) [3]	LASSO[k]	Internal cross-validation	Yes	0.613 (0.608 - 0.617)	Calibration plot	Calibration curve
Simon et al (2023) [4]	RF[l], GBT[m], TE[n], FCDNN[o]	Random split validation	None	0.698; 0.638; 0.635; 0.780	NR	ROC curve
Lee et al (2013) [5]	XGB, RF, LASSO, SVM[p]	Random split validation, repeated cross-validation	None	DVT[q]: 0.759 (0.667 - 0.881); 0.71; 0.68; 0.64; PE: 0.774 (0.683 - 0.835); 0.8; 0.8; 0.67	Calibration plot	ROC curve, PR[r] curve, calibration curve
Malcolm et al (2020) [6]	XGB, RF, SVM, BPNN[s], LR, EM[t]	5-fold cross-validation, GridSearchCV	None	0.914 (0.894 - 0.935); 0.907 (0.883 - 0.931); 0.903 (0.874 - 0.930); 0.910 (0.8949 - 0.926); 0.885 (0.868 - 0.902); 0.921 (0.896 - 0.936)	NR	ROC curve
Lewis et al (2019) [7]	XGB, KNN, SVM, NB[u], MLP[v], LR	Random split validation, 10-fold cross-validation	None	0.800 (0.674 - 0.927); 0.755 (0.634 - 0.874); 0.753 (0.627 - 0.878); 0.681 (0.571 - 0.788); 0.739 (0.611 - 0.846); 0.579 (0.450 - 0.696)	Brier score	Shapley additive explanations, feature importance
Meng et al (2021) [8]	Multiple imputation	LR	None	0.663 (0.627 - 0.699)	Hosmer-Lemeshow, calibration plot, Brier score	ROC curve, calibration curve
Runner et al (2021) [9]	No missing data	LR	Yes	0.65 (0.63 - 0.67) external validation: 0.64 (0.61 - 0.67)	Calibration plot	Calibration curve

[a]AUC: area under the curve.

[b]MLP: multilayer perceptron.

[c]XGB: extreme gradient boosting.

[d]AdaBoost: adaptive boosting.

[e]GBC: gradient boosting classifier.

[f]KNN: k-nearest neighbors.

[g]LR: logistic regression.

[h]NR: not reported.

[i]ROC: receiver operating characteristic.

[j]DCA: decision curve analysis.

XSL•FO
RenderX

[k]LASSO: least absolute shrinkage and selection operator regression.

[l]RF: random forest.

[m]GBT: gradient boosting tree.

[n]TE: tree-based ensemble methods.

[o]FCDNN: fully connected deep neural network.

[p]SVM: support vector machines.

[q]DVT: deep vein thrombosis.

[r]PR: precision-recall.

[s]BPNN: back propagation neural network.

[t]EM: ensemble method.

[u]NB: naive Bayes.

[v]MLP: multilayer perceptron.

Figure 2. Frequency of machine learning models. adaBoost: adaptive boosting; BPNN: back propagation neural network; EM: ensemble method; FCDNN: fully connected deep neural network; GBT: gradient boosting tree; GBC: gradient boosting classifier; KNN: k-nearest neighbors; LASSO: least absolute shrinkage and selection operator regression; LR: logistic regression; MLP: multilayer perceptron; NB: naive Bayes; RF: random forest; SVM: support vector machine; TE: tree-based ensemble methods; XGB: extreme gradient boosting.

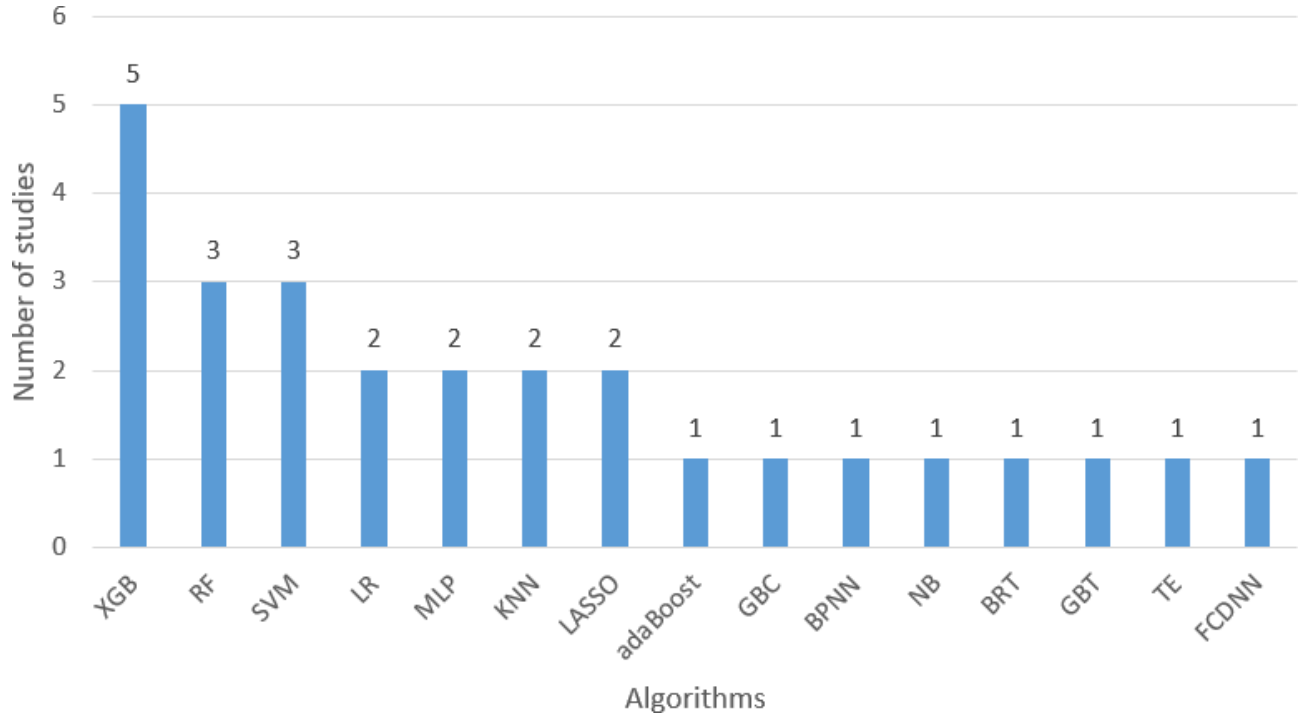

The included studies used a variety of metrics to evaluate ML models, of which AUC was the most common (8/9, 89%). The predicted AUC range for DVT and PE was 0.579 - 0.982. One study did not report AUC but reported C-statistic [22]. XGB, popularized by Chen and Guestrin [28] in 2016, is a widely adopted ML algorithm on the basis of gradient boosting [29,30]. The included XGB studies [3,20,21,24,25] reported AUC ranging from 0.71 to 0.982, demonstrating strong model performance. LR estimates the association of one or more independent variables with binary dependent variables [31,32]. The included LR studies [3,20,25-27] reported AUC ranging from 0.579 to 0.944. RF is a widely used ML algorithm that helps mitigate overfitting and improves the model's stability and accuracy by aggregating the outcomes from various decision trees [33]. It functions as a modeling algorithm as well as a variable selection technique. Three studies [23-25] used RF, with reported AUC ranging from 0.698 to 0.907. In addition, calibration plots were provided in 3 studies [22,24,27]; Brier scores were provided in 1 study [20]; and 1 study [26] also provided Hosmer-Lemeshow, calibration plot, and Brier score. The other 4 studies did not include data on calibration performance. Additional reported metrics encompass accuracy, sensitivity, and specificity.

These 9 studies differ in terms of the optimal timing for risk assessment. Six studies have created preoperative prediction models [3,22,23,25-27] to identify high-risk individuals before surgery. The last 3 studies focused on postoperative prediction, assessing immediate risks using postoperative data [20,21,24]. Additionally, there is diversity in the risk assessment's predictive horizon. Its duration ranges from a brief period following the procedure, such as "within 3 - 5 days after surgery" or "during the postoperative hospital stay" [3,20], to a lengthy risk assessment that might continue for up to a year following the procedure [26]. Common time horizons include 30 days [22,23] and 90 days [24,27].

From a low of 5 [26] to a high of 66 [25], the number of predictor variables that ultimately made it into the model varied

XSL•FO
RenderX

widely. The descriptive analysis of the predictive factors used in each study (as shown in Figure 3) shows that a constant core set of variables is regularly utilized, despite the wide variations in the number of predictive factors used in each investigation. These variables can be broadly classified into four categories: (1) demographic and biological characteristics of the patients (such as age, gender, BMI); (2) major comorbidities (such as hypertension, diabetes, coronary heart disease, and malignant tumors); (3) specific VTE risk histories (such as previous VTE); and (4) key laboratory indicators (such as D-dimer).

Figure 3. Frequency of the predictors. APTT: activated partial thrombin time; ASA: American Society of Anesthesiologists; VTE: venous thromboembolism.

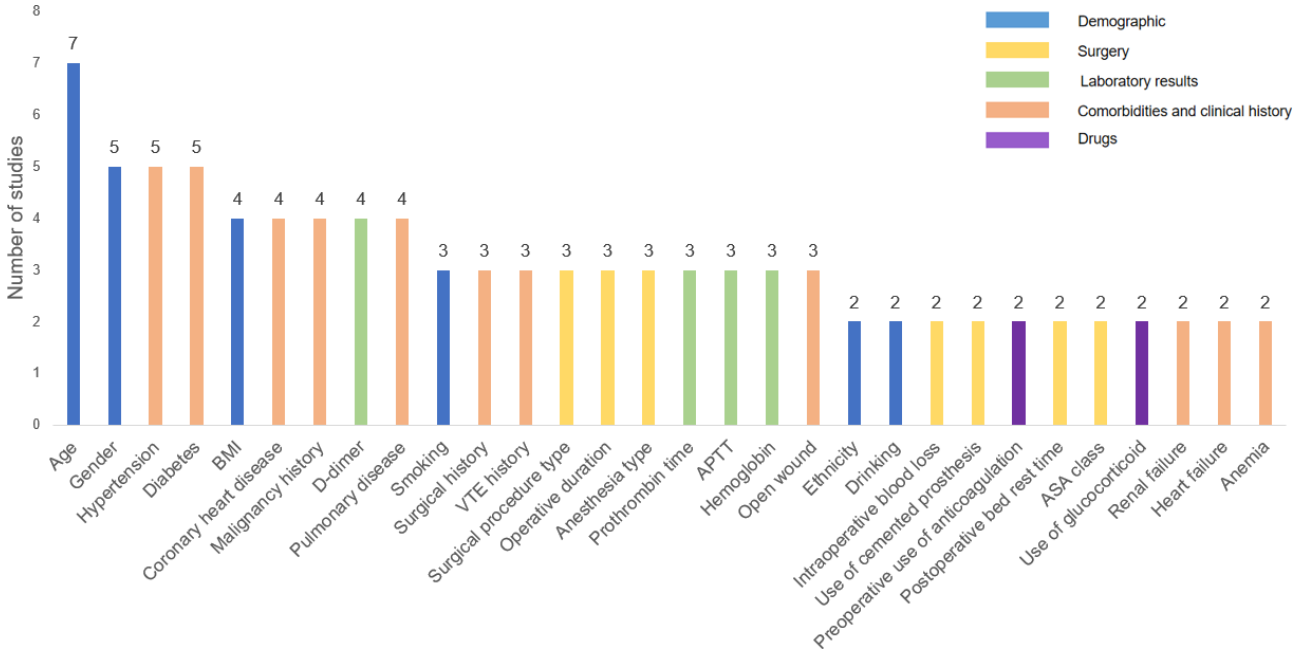

Model Validation

All of the models in the included studies underwent internal validation; however, only 2 studies [22,27] used external validation and reported the AUC value of external validation. The main methods used for internal validation were k-fold cross-validation and random-split validation. External validation plays a key role in confirming whether a model can maintain good performance in different populations and clinical settings. The absence of external validation will limit the generalization and clinical application of these models.

Assessing Risk of Bias

According to the PROBAST evaluation, all models had a high risk of bias (Table 4). The assessment results showed that the main sources of bias were concentrated in the “participants” and “analysis” domains. In the participants domain, 8 studies had a high risk of bias, mainly because these studies relied on retrospective data. In the analysis domain, all models had a high risk of bias. The PROBAST assessment pointed out several specific methodological issues: 4 studies [21,23-25] did not perform model calibration, 4 studies [3,21,23,25] did not report the handling of missing data, and 2 studies [21,23] were insufficient in measures to prevent model overfitting. In contrast, the outcome domain was rated as having a low bias risk level in all studies. In terms of applicability assessment, only 1 study [25] had poor applicability because the model was overly complex and required 66 predictor variables.

XSL•FO
RenderX

Table . Prediction Model Risk of Bias Assessment Tool (PROBAST) results of the included studies.

Author (year)	Risk of bias				Applicability			Overall	
	Participants	Predictors	Outcome	Analysis	Participants	Predictors	Outcome	Risk of bias	Applicability
Ding et al (2023) [3]	+[a]	+	+	–[b]	+	+	+	–	+
Chen et al (2023) [21]	–	+	+	–	+	+	+	–	+
Harris et al (2019) [22]	–	+	+	–	+	+	+	–	+
Rasouli et al (2022) [23]	–	+	+	–	+	+	+	–	+
Shohat et al (2022) [24]	–	+	+	–	+	+	+	–	+
Wang et al (2023) [25]	–	–	+	–	+	–	+	–	–
Xu et al (2024) [20]	–	+	+	–	+	+	+	–	+
Sweerts et al (2022) [26]	–	+	+	–	+	+	+	–	+
Nemeth et al (2024) [27]	–	+	+	+	+	+	+	–	+

[a]Low risk of bias.

[b]High risk of bias.

Discussion

Principal Findings

VTE is a common and serious postoperative complication that is preventable [10]. Risk assessment and management-based strategies can help prevent or reduce the occurrence of VTE [34]. Therefore, selecting an appropriate predictive model for VTE is crucial. This systematic review examined the methodological quality and clinical applicability of ML methods in predicting VTE after joint replacement surgery. Among the reviewed studies, 15 ML algorithms were utilized to construct 34 predictive models. XGB and LR were the most used model types, followed by RF and SVM. The AUC values of the models ranged from 0.579 to 0.982, indicating that the discrimination ability of the models varied greatly, and some of the models showed excellent performance. Two research [1,6] reports demonstrated extremely high discrimination ability, with their AUC values exceeding 0.9. Such high performance often raises concerns about overfitting, where the model learns specific statistical noise specific to the training data rather than the generalizable underlying biological signals, leading to an optimistically biased performance estimate. Moreover, these models have not yet undergone external validation. This deficiency is a major limitation. In the clinical environment of joint replacement, there may be significant differences among patients, and surgical techniques as well as VTE prevention protocols may also vary among different medical institutions. Models trained based on data from a single hospital are likely to learn the specific treatment patterns of that hospital rather than a universally applicable VTE prediction signature. This may lead to unreliable prediction results when the model is applied to different patient groups. The risk of overfitting and the lack of reliable external validation seriously undermine the clinical value of these highly performing models. These models can only be considered for practical application after undergoing extensive external validation.

Another finding is that the XGB model demonstrates superior predictive performance compared to other models. For instance, 2 studies [3,20] compared the XGB and SVM models with the LR models, and the results showed that the XGB and SVM models outperformed the LR model. This supremacy is probably due to the smart way the algorithm was made. First, XGB has strong built-in features (such as regularization) that keep the model from overfitting when working with small datasets, making it stable even when the data are noisy. Second, XGB is very good at identifying the most important risk factors on its own. It can also capture complicated nonlinear interaction relationships, which typical linear models cannot do. Furthermore, the fact that XGB functions so effectively most likely indicates that the research team spent a great deal of time and energy optimizing the hyperparameters and determining the ideal configurations for their particular dataset. However, research has indicated that LR models may be more successful and easier to apply in some situations, whereas XGB and SVM models may not necessarily perform better. LR's fundamental structure makes it simple to comprehend and analyze. Additionally, it produces dependable findings and has strong convergence, particularly when used for small datasets [35]. The Caprini score is a clinically prevalent instrument utilized to evaluate VTE risk by analyzing many clinical risk factors, including age, surgical history, malignancy, and obesity [36]. One study [25] compared the Caprini Score to ML models and showed that the ML models were better at predicting VTE risk. Although the predictive performance of most models ranged

XSL•FO
RenderX

from moderate to good, the risk of bias in all studies restricted the applicability of these models in clinical practice.

Related Work

The PROBAST assessment results indicate that all the models have a high risk of bias, suggesting that their predictive performance in practical applications may be lower than the reported levels. This widespread bias is mainly due to the flaws in the research design and the statistical analysis methods adopted by the models. In terms of the research design, most studies rely on retrospective data, which increases the risk of selecting an unrepresentative patient population, thereby weakening the generalization ability of the models beyond the original dataset. Additionally, there are numerous flaws in the analysis aspects of the model construction and testing processes. The main issues are that some studies did not check the calibration process. This makes it impossible for us to determine whether the "30% risk of venous thrombosis" predicted by the model truly means a 30% probability in reality, thus preventing its use in clinical decision-making. Some studies also failed to provide enough protections against the "overfitting" problem, in which the model just remembered the noise in the training data instead of identifying the true risk patterns, while others did not provide solutions for handling missing patient data. These analytical flaws make these models likely to perform poorly when applied to new patients. Furthermore, the actual usability is also an issue. One model used an excessive 66 predictive variables, making it overly complex and unsuitable for clinical use. To raise the accuracy and clinical application of predictive models, future studies should apply more rigorous methodological methods. Moreover, the significant bias risk indicates inconsistency in the development and validation of current models, which could influence their widespread application. Future studies should give priority to enhancements in a number of important domains, including the research design (ie, cohort or case-control study design), the number of events, the method for predictor selection, the processing of complicated data, and the processes of model calibration and fitting.

One serious and widespread flaw in these studies is the absence of model calibration reports. Although most of the included studies reported high discrimination metrics such as AUC, the discrimination does not guarantee that the predicted probabilities are accurate. Calibration addresses a more fundamental clinical question: Does the predicted "30% risk of venous thrombosis" really mean that there will be a 30% incidence rate among a group of similar patients? Inaccurate calibration might have very harmful consequences. For example, a model that consistently overestimates risks may incorrectly identify patients with low risks as having high risks [37]. This may lead to the improper use of potent anticoagulant drugs, thereby exposing patients to a serious risk of bleeding, a risk that could have been avoided. However, if the model underestimates the risks, it may prevent doctors from taking necessary preventive measures to ensure the safety of patients with high risk. This could lead to potentially fatal thrombosis incidents [38]. Consequently, owing to the absence of calibration data, most of these models are unreliable for informing individual patient decisions, irrespective of their quoted AUC values. Future research must prioritize calibration as the principal measure of model performance. We strongly urge that studies include both visual calibration plots and quantitative indicators (such as the Brier Score) at the same time to make sure their predictions are accurate in the actual world. Additionally, most of the included studies did not provide reports on the sensitivity and specificity of their models. This affects the overall assessment of model performance, as the reported AUC values may not fully reflect its clinical applicability. Future research should follow standardized reporting guidelines to evaluate its model performance.

External validation is critical to confirm the generalizability of the model's performance and its applicability to different populations [39,40]. However, all the studies used internal validation methods, such as K-fold cross-validation or random split validation, and only 2 studies conducted external validation. Most of these models lack external validation, further increasing the challenge of clinical implementation. In such a sensitive sector as health care, where predictive models are finally meant to be employed in real-world situations, these ML models may not accurately reflect their applicability and dependability without outside validation [41]. Future studies should incorporate external validation where possible, such as in different hospitals or using publicly accessible databases, to optimize the model generalization through data synthesis and larger datasets [42]. Additionally, we advise temporal validation to assess the model's resilience at different points in time.

The ML model's predictive variables found in this study have a number of important effects on clinical practice. First, the predictive factors frequently used in these models play a very important role in current clinical practice and future research. For instance, D-dimer is a well-known clinically validated biomarker for VTE. Studies have shown that it is highly sensitive in predicting the risk of VTE. Prothrombin time, activated partial thromboplastin time, and international normalized ratio are a few other markers that may assist physicians better understand the risk of blood clots and quickly identify and treat patients with high risk [43]. Another established risk factor for VTE is age. Research has indicated that the risk of VTE rises with age. People over the age of 60 years account for around 70% of occurrences of VTE [44]. Considering age while evaluating patients before surgery may enhance outcomes and diminish complication rates. Common chronic disorders, such as diabetes and hypertension, were also among recurring factors. Research has shown that these disorders can raise VTE incidence. A personalized anticoagulant treatment strategy might help those with past histories of these disorders lower their VTE risk even more [45]. Second, the results of the 9 studies on the predictors can guide the development of future predictive models and contribute to later studies on related risk elements. For instance, 1 study [20] included bone cement prosthesis as a predictor in the model, although further study is required to confirm its association with VTE. However, variance in the choosing and reporting of predictors in these studies may affect the comparability and practical utility of the models in different clinical settings.

Limitations

To our knowledge, this is the first study to evaluate ML in predicting VTE in patients undergoing joint replacement

XSL•FO
RenderX

surgery. Nevertheless, the study had certain limitations. First, most of the included studies have been conducted in China and the United States. This geographical concentration restricts the general applicability of the model to different areas. Second, numerous studies focused solely on developing predictive models without considering external validation or practical application of the model. The absence of external validation may affect the credibility of our pooled estimates. Third, since the traditional methods used to assess publication bias (such as funnel plots and Egger or Begg tests) are not applicable to AUC data, no quantitative assessment of publication bias was conducted for the included studies. However, the risk of publication bias remains: “positive” studies (eg, high AUC values) are more likely to be published than “negative” or inconclusive ones. Therefore, the studies included in this review may overestimate the true performance of these models. Finally, the included studies exhibited a high risk of bias and insufficient transparency. These methodological shortcomings could affect the accuracy of model predictions, therefore reducing the dependability and application of the conclusions.

Conclusions

The study identified 9 studies with a total of 34 ML models for predicting VTE after joint replacement. Most studies have modest to good discriminative ability from their AUC values. However, among these 9 studies, only 2 of them underwent effective external validation. The widespread neglect of external validation has left the generalization capabilities of these models, which performed well on the original dataset, completely unknown. In addition, these studies also show a high risk of bias and significant heterogeneity. Most of the studies had significant methodological shortcomings, including a lack of rigorous study design and absence of calibration measurements. These deficiencies will affect the reliability of the model in clinical applications and reduce the promotion value of the model. To improve the prediction capabilities of ML models, future research must closely follow the PROBAST criteria, which place a strong emphasis on meticulous study design and quality control. External validation is also necessary to improve the generalization and applicability of ML models in clinical settings.

Funding

This work was supported by the Jilin Provincial Department of Science and Technology (grant number 20210203091SF).

Data Availability

The datasets used and/or analyzed during this study are available from the corresponding author upon reasonable request.

Authors' Contributions

Conceptualization: JM
Data curation: HT, YZ
Formal analysis: HT, JM, XY
Funding acquisition: GW
Investigation: GW
Methodology: GW, JM, XY
Project administration: GW
Resources: HT
Software: HT
Supervision: GW
Validation: TZ, XY, YZ
Visualization: JM, XL
Writing – original draft: JM
Writing – review & editing: XY, YZ

Conflicts of Interest

None declared.

Multimedia Appendix 1
Details of the search strategy.
[DOCX File, 24 KB - medinform_v14i1e79886_app1.docx]

Checklist 1
PRISMA checklist.
[PDF File, 206 KB - medinform_v14i1e79886_app2.pdf]

References

XSL•FO
RenderX

1. Singh JA, Yu S, Chen L, Cleveland JD. Rates of total joint replacement in the United States: future projections to 2020-2040 using the national inpatient sample. J Rheumatol 2019 Sep;46(9):1134-1140. [doi: 10.3899/jrheum.170990] [Medline: 30988126]
2. Yau LK, Henry FU, Man Hong C, et al. Swelling assessment after total knee arthroplasty. J Orthop Surg (Hong Kong) 2022;30(3):10225536221127668. [doi: 10.1177/10225536221127668] [Medline: 36122907]
3. Ding R, Ding Y, Zheng D, et al. Machine learning-based screening of risk factors and prediction of deep vein thrombosis and pulmonary embolism after hip arthroplasty. Clin Appl Thromb Hemost 2023;29:10760296231186145. [doi: 10.1177/10760296231186145] [Medline: 37394825]
4. Simon SJ, Patell R, Zwicker JI, Kazi DS, Hollenbeck BL. Venous thromboembolism in total hip and total knee arthroplasty. JAMA Netw Open 2023 Dec 1;6(12):e2345883. [doi: 10.1001/jamanetworkopen.2023.45883] [Medline: 38039005]
5. Lee WS, Kim KI, Lee HJ, Kyung HS, Seo SS. The incidence of pulmonary embolism and deep vein thrombosis after knee arthroplasty in Asians remains low: a meta-analysis. Clin Orthop Relat Res 2013 May;471(5):1523-1532. [doi: 10.1007/s11999-012-2758-9] [Medline: 23264001]
6. Malcolm TL, Knezevic NN, Zouki CC, Tharian AR. Pulmonary complications after hip and knee arthroplasty in the United States, 2004-2014. Anesth Analg 2020 Apr;130(4):917-924. [doi: 10.1213/ANE.0000000000004265] [Medline: 31206434]
7. Lewis S, Glen J, Dawoud D, et al. Venous thromboembolism prophylaxis strategies for people undergoing elective total knee replacement: a systematic review and network meta-analysis. Lancet Haematol 2019 Oct;6(10):e530-e539. [doi: 10.1016/S2352-3026(19)30155-3] [Medline: 31444124]
8. Meng H, Zhu Y, Zhang J, et al. Incidence and risk factor for preoperative deep vein thrombosis (DVT) in isolated calcaneal fracture, a prospective cohort study. Foot Ankle Surg 2021 Jul;27(5):510-514. [doi: 10.1016/j.fas.2020.06.007] [Medline: 32595018]
9. Runner RP, Shau DN, Staley CA, Roberson JR. Utilization patterns, efficacy, and complications of venous thromboembolism prophylaxis strategies in revision hip and knee arthroplasty as reported by American Board of Orthopaedic Surgery Part II candidates. J Arthroplasty 2021 Jul;36(7):2364-2370. [doi: 10.1016/j.arth.2021.01.072] [Medline: 33674164]
10. Chong J, Curtain C, Gad F, et al. Development and implementation of venous thromboembolism stewardship across a hospital network. Int J Med Inform 2021 Nov;155:104575. [doi: 10.1016/j.ijmedinf.2021.104575] [Medline: 34560489]
11. Agarwal AR, Das A, Harris A, Campbell JC, Golladay GJ, Thakkar SC. Trends of venous thromboembolism after total hip arthroplasty in the United States: analysis from 2011 to 2019. J Am Acad Orthop Surg 2023 Apr 1;31(7):e376-e384. [doi: 10.5435/JAAOS-D-22-00708] [Medline: 36727960]
12. Wei C, Wang J, Yu P, et al. Comparison of different machine learning classification models for predicting deep vein thrombosis in lower extremity fractures. Sci Rep 2024 Mar 22;14(1):6901. [doi: 10.1038/s41598-024-57711-w] [Medline: 38519523]
13. Khera R, Haimovich J, Hurley NC, et al. Use of machine learning models to predict death after acute myocardial infarction. JAMA Cardiol 2021 Jun 1;6(6):633-641. [doi: 10.1001/jamacardio.2021.0122] [Medline: 33688915]
14. Ryan L, Mataraso S, Siefkas A, et al. A machine learning approach to predict deep venous thrombosis among hospitalized patients. Clin Appl Thromb Hemost 2021;27:1076029621991185. [doi: 10.1177/1076029621991185] [Medline: 33625875]
15. Guan C, Ma F, Chang S, Zhang J. Interpretable machine learning models for predicting venous thromboembolism in the intensive care unit: an analysis based on data from 207 centers. Crit Care 2023 Oct 24;27(1):406. [doi: 10.1186/s13054-023-04683-4] [Medline: 37875995]
16. Hou T, Qiao W, Song S, et al. The use of machine learning techniques to predict deep vein thrombosis in rehabilitation inpatients. Clin Appl Thromb Hemost 2023;29:10760296231179438. [doi: 10.1177/10760296231179438] [Medline: 37365805]
17. Arina P, Kaczorek MR, Hofmaenner DA, et al. Prediction of complications and prognostication in perioperative medicine: a systematic review and PROBAST assessment of machine learning tools. Anesthesiology 2024 Jan 1;140(1):85-101. [doi: 10.1097/ALN.0000000000004764] [Medline: 37944114]
18. Salameh JP, Bossuyt PM, McGrath TA, et al. Preferred reporting items for systematic review and meta-analysis of diagnostic test accuracy studies (PRISMA-DTA): explanation, elaboration, and checklist. BMJ 2020 Aug 14;370:m2632. [doi: 10.1136/bmj.m2632] [Medline: 32816740]
19. Moons KGM, de Groot JAH, Bouwmeester W, et al. Critical appraisal and data extraction for systematic reviews of prediction modelling studies: the CHARMS checklist. PLoS Med 2014 Oct;11(10):e1001744. [doi: 10.1371/journal.pmed.1001744] [Medline: 25314315]
20. Xu Q, Yu B, Zhou P, Dai S, Dong X. Construction of interpretable prediction model for lower limb deep vein thrombosis in patients undergoing total hip arthroplasty based on machine learning and SHAP. Chin J Hosp Stat 2024;31(1) [FREE Full text]
21. Chen Y, Jiang Y. Construction of prediction model of deep vein thrombosis risk after total knee arthroplasty based on XGBoost algorithm. Comput Math Methods Med 2022 Jan 25;2022:3452348. [doi: 10.1155/2022/3452348] [Medline: 35116072]

XSL•FO
RenderX

22. Harris AHS, Kuo AC, Weng Y, Trickey AW, Bowe T, Giori NJ. Can machine learning methods produce accurate and easy-to-use prediction models of 30-day complications and mortality after knee or hip arthroplasty? Clin Orthop Relat Res 2019 Feb;477(2):452-460. [doi: 10.1097/CORR.0000000000000601] [Medline: 30624314]
23. Rasouli Dezfouli E, Delen D, Zhao H, Davazdahemami B. A machine learning framework for assessing the risk of venous thromboembolism in patients undergoing hip or knee replacement. J Healthc Inform Res 2022;6(4):423-441. [doi: 10.1007/s41666-022-00121-2] [Medline: 36744082]
24. Shohat N, Ludwick L, Sherman MB, Fillingham Y, Parvizi J. Using machine learning to predict venous thromboembolism and major bleeding events following total joint arthroplasty. Sci Rep 2023 Feb 7;13(1):2197. [doi: 10.1038/s41598-022-26032-1] [Medline: 36750656]
25. Wang X, Xi H, Geng X, et al. Artificial intelligence-based prediction of lower extremity deep vein thrombosis risk after knee/hip arthroplasty. Clin Appl Thromb Hemost 2023;29:10760296221139263. [doi: 10.1177/10760296221139263] [Medline: 36596268]
26. Sweerts L, Hoogeboom TJ, van Wessel T, van der Wees PJ, van de Groes SAW. Development of prediction models for complications after primary total hip and knee arthroplasty: a single-centre retrospective cohort study in the Netherlands. BMJ Open 2022 Aug 24;12(8):e062065. [doi: 10.1136/bmjopen-2022-062065] [Medline: 36002218]
27. Nemeth B, Smeets M, Pedersen AB, et al. Development and validation of a clinical prediction model for 90-day venous thromboembolism risk following total hip and total knee arthroplasty: a multinational study. J Thromb Haemost 2024 Jan;22(1):238-248. [doi: 10.1016/j.jtha.2023.09.033] [Medline: 38030547]
28. Chen TQ, Guestrin C. XGBoost: a scalable tree boosting system. Presented at: 22nd ACM SIGKDD International Conference on Knowledge Discovery and Data Mining (KDD); Aug 13-17, 2016. [doi: 10.1145/2939672.2939785]
29. Liang D, Wang L, Liu S, et al. Global incidence of diarrheal diseases—an update using an interpretable predictive model based on XGBoost and SHAP: a systematic analysis. Nutrients 2024 Sep 23;16(18):3217. [doi: 10.3390/nu16183217] [Medline: 39339819]
30. Davagdorj K, Pham VH, Theera-Umpon N, Ryu KH. XGBoost-based framework for smoking-induced noncommunicable disease prediction. Int J Environ Res Public Health 2020 Sep 7;17(18):6513. [doi: 10.3390/ijerph17186513] [Medline: 32906777]
31. Tolles J, Meurer WJ. Logistic regression: relating patient characteristics to outcomes. JAMA 2016 Aug 2;316(5):533-534. [doi: 10.1001/jama.2016.7653] [Medline: 27483067]
32. Moore A, Bell M. XGBoost, a novel explainable AI technique, in the prediction of myocardial infarction: a UK Biobank cohort study. Clin Med Insights Cardiol 2022;16:11795468221133611. [doi: 10.1177/11795468221133611] [Medline: 36386405]
33. Strobl C, Malley J, Tutz G. An introduction to recursive partitioning: rationale, application, and characteristics of classification and regression trees, bagging, and random forests. Psychol Methods 2009 Dec;14(4):323-348. [doi: 10.1037/a0016973] [Medline: 19968396]
34. Raskob GE, Angchaisuksiri P, Blanco AN, et al. Thrombosis: a major contributor to global disease burden. Semin Thromb Hemost 2014 Oct;40(7):724-735. [doi: 10.1055/s-0034-1390325] [Medline: 25302681]
35. Chen X, He L, Shi K, Wu Y, Lin S, Fang Y. Interpretable machine learning for fall prediction among older adults in China. Am J Prev Med 2023 Oct;65(4):579-586. [doi: 10.1016/j.amepre.2023.04.006] [Medline: 37087076]
36. Caprini JA. Thrombosis risk assessment as a guide to quality patient care. Dis Mon 2005;51(2-3):70-78. [doi: 10.1016/j.disamonth.2005.02.003] [Medline: 15900257]
37. Ghadri JR, Cammann VL, Jurisic S, et al. A novel clinical score (InterTAK Diagnostic Score) to differentiate takotsubo syndrome from acute coronary syndrome: results from the International Takotsubo Registry. Eur J Heart Fail 2017 Aug;19(8):1036-1042. [doi: 10.1002/ejhf.683] [Medline: 27928880]
38. Zaka A, Mutahar D, Gorcilov J, et al. Machine learning approaches for risk prediction after percutaneous coronary intervention: a systematic review and meta-analysis. Eur Heart J Digit Health 2024 Oct;6(1):23-44. [doi: 10.1093/ehjdh/ztae074] [Medline: 39846069]
39. Looi JL, Chan C, Pemberton J, et al. External validation of a clinical score to differentiate takotsubo syndrome from non-ST-elevation myocardial infarction in women. Heart Lung Circ 2023 Jun;32(6):696-701. [doi: 10.1016/j.hlc.2023.04.002] [Medline: 37121882]
40. Riley RD, Ensor J, Snell KIE, et al. External validation of clinical prediction models using big datasets from e-health records or IPD meta-analysis: opportunities and challenges. BMJ 2016 Jun 22;353:i3140. [doi: 10.1136/bmj.i3140] [Medline: 27334381]
41. Zobeiri A, Rezaee A, Hajati F, Argha A, Alinejad-Rokny H. Post-cardiac arrest outcome prediction using machine learning: a systematic review and meta-analysis. Int J Med Inform 2025 Jan;193:105659. [doi: 10.1016/j.ijmedinf.2024.105659] [Medline: 39481177]
42. Mao A, Su J, Ren M, Chen S, Zhang H. Risk prediction models for falls in hospitalized older patients: a systematic review and meta-analysis. BMC Geriatr 2025 Jan 14;25(1):29. [doi: 10.1186/s12877-025-05688-0] [Medline: 39810076]
43. Alhabibi AM, Eldewi DM, Wahab MAA, Farouk N, El-Hagrasy HA, Saleh OI. Platelet-derived growth factor-beta as a new marker of deep venous thrombosis. J Res Med Sci 2019;24:48. [doi: 10.4103/jrms.JRMS_965_18] [Medline: 31160915]

XSL•FO
RenderX

44. Wang H, Rosendaal FR, Cushman M, van Hylckama Vlieg A. Procoagulant factor levels and risk of venous thrombosis in the elderly. J Thromb Haemost 2021 Jan;19(1):186-193. [doi: 10.1111/jth.15127] [Medline: 33090602]
45. Anghele AD, Marina V, Dragomir L, Moscu CA, Anghele M, Anghel C. Predicting deep venous thrombosis using artificial intelligence: a clinical data approach. Bioengineering (Basel) 2024 Oct 25;11(11):1067. [doi: 10.3390/bioengineering11111067] [Medline: 39593727]

Abbreviations

AUC: area under the curve
CHARMS: Critical Appraisal and Data Extraction for Systematic Reviews of Prediction
DVT: deep vein thrombosis
LR: logistic regression
ML: machine learning
PE: pulmonary embolism
PRISMA: Preferred Reporting Items for Systematic Reviews and Meta-Analyses
PROBAST: Prediction Model Risk of Bias Assessment Tool
PROSPERO: International Prospective Register of Systematic Reviews
RF: random forest
SVM: support vector machine
THA: total hip arthroplasty
TKA: total knee arthroplasty
VTE: venous thromboembolism
XGB: extreme gradient boosting

Edited by A Benis; submitted 30.Jun.2025; peer-reviewed by S Mohanadas, T Shi; revised version received 18.Nov.2025; accepted 29.Dec.2025; published 12.Feb.2026.

Please cite as:
Ma J, Tang H, Zhang Y, Yi X, Zhong T, Li X, Wang G
Machine Learning for Predicting Venous Thromboembolism After Joint Arthroplasty: Systematic Review of Clinical Applicability and Model Performance
JMIR Med Inform 2026;14:e79886
URL: https://medinform.jmir.org/2026/1/e79886
doi:10.2196/79886

© Junwei Ma, Huifeng Tang, Yunshan Zhang, Xuemei Yi, Tangsheng Zhong, Xinyun Li, Gang Wang. Originally published in JMIR Medical Informatics (https://medinform.jmir.org), 12.Feb.2026. This is an open-access article distributed under the terms of the Creative Commons Attribution License (https://creativecommons.org/licenses/by/4.0/), which permits unrestricted use, distribution, and reproduction in any medium, provided the original work, first published in JMIR Medical Informatics, is properly cited. The complete bibliographic information, a link to the original publication on https://medinform.jmir.org/, as well as this copyright and license information must be included.

XSL•FO
RenderX

Using Health Information Systems to Support Behavioral Interventions in Local Contexts: Scoping Review

Xi Yang[1,2], MArch; Martin Dijst[2,3], Prof Dr; Joost G Daams[4], MA; Marc Suhrcke[5,6], Prof Dr; Haoran Yang[7,8], Prof Dr; Ronald Cornet[1], Prof Dr

[1]Department of Medical Informatics, Amsterdam Public Health Research Institute, Amsterdam UMC, University of Amsterdam, Meibergdreef 15, Amsterdam, The Netherlands

[2]Department of Urban Development and Mobility, Luxembourg Institute of Socio-Economic Research, Esch-sur-Alzette, Luxembourg

[3]University of Luxembourg, Esch-sur-Alzette, Luxembourg

[4]Medical Library, Research Support, Amsterdam UMC, University of Amsterdam, Amsterdam, The Netherlands

[5]Department of Living Conditions, Luxembourg Institute of Socio-Economic Research, Esch-sur-Alzette, Luxembourg

[6]Centre for Health Economics, University of York, York, United Kingdom

[7]School of Geographic Sciences, East China Normal University, Shanghai, China

[8]Liwa Institute of Skin Health, East China Normal University, Shanghai, China

Corresponding Author:
Ronald Cornet, Prof Dr
Department of Medical Informatics, Amsterdam Public Health Research Institute, Amsterdam UMC, University of Amsterdam, Meibergdreef 15, Amsterdam, The Netherlands

Abstract

Background: Individual-level behavioral interventions are designed to improve health behaviors and manage noncommunicable diseases. Neighborhood geo-referenced contexts (NGRCs) significantly impact the success of these interventions. Integrating NGRC data into health information systems (HISs), including electronic medical records (EMRs), electronic health records (EHRs), and personal health records (PHRs), can enhance personalized NGRC-focused behavioral interventions and improve health outcomes. Despite the potential benefits, there is a notable gap in the literature about NGRC-focused behavioral interventions using HISs.

Objective: This scoping review aims to review the current status and stakeholder insights of NGRC-focused behavioral interventions using HISs.

Methods: Two reviewers examined publications indexed by MEDLINE (Ovid) and Scopus. Publications reporting on NGRC-focused behavioral interventions using HISs were included. We extracted data on study characteristics, population attributes, diseases, health setting characteristics, HISs, NGRCs, behavioral interventions, outcomes, and conclusions, with suggestions for future research.

Results: The literature search identified 24 studies for inclusion. Of these, EHRs or EMRs were mostly used in 20 studies, with limited focus on PHRs. HISs were not used in the entire process of NGRC-focused behavioral interventions in 23 studies. Behavioral interventions in 21 studies focused exclusively on social needs interventions, with comparatively limited attention given to lifestyle change interventions. NGRCs mainly focused on built environments (n=24), with less attention to natural (n=1) and social (n=4) environments. The spatiotemporal characteristics of NGRCs were described in limited detail. “Destination accessibility” was the main focus within built environments. Other characteristics (“density,” “design,” “diversity,” and “distance”) were less studied. Stakeholders’ perspectives highlighted the value, convenience, patient autonomy, and privacy of integrating content (NGRCs) and/or technology (HISs) into behavioral interventions, despite the persistence of certain social concerns. We summarized 15 recommendations in terms of NGRC-focused behavioral interventions using HISs.

Conclusions: PHRs have the potential to actively integrate more diverse, dynamic, and/or high-resolution NGRCs. Additionally, PHRs can participate in the entire process of NGRC-focused behavioral interventions, particularly in outpatient lifestyle change interventions. Health care providers can support these interventions to help achieve public health goals and advance health equity.

(JMIR Med Inform 2026;14:e77296) doi:10.2196/77296

KEYWORDS

health information system; behavioral intervention; environments; geo-referenced contexts; neighborhood geo-referenced contexts

XSL•FO
RenderX

Introduction

Behavioral interventions are strategies and techniques to influence health-related behaviors at the personal, community, and public policy levels [1]. They may encourage individuals to quit smoking or to exercise regularly. At the community level, behavioral interventions aim to change behaviors by modifying the environments that support them [1]. For example, enhancing existing sidewalks with improved lighting, repainting bike lane markings, and adding benches can create a more enjoyable experience that encourages walking and cycling. At the public policy level, the government or private groups can share health information to encourage behavioral change [1]. The absence of individual-level behavioral interventions poses a significant challenge in managing noncommunicable diseases (NCDs), which account for 70% of global deaths annually [2], as effective interventions for NCDs require long-term engagement and multiple follow-ups to detect relapses or late effects as soon as possible [3].

Neighborhood geo-referenced contexts (NGRCs) have been identified as barriers or facilitators to the acceptance of, participation in, and adherence to individual-level behavioral interventions [4]. NGRCs refer to the physical and social environments of a location or locations along one's daily activities, and they influence people's health-related behaviors [5-8]. NGRCs are a spatial manifestation of the social determinants of health (SDoH), which refer to the conditions in which people are born, grow, live, work, and age, as well as the broader systems and forces that shape these daily life conditions [9]. Beyond the social and natural environments in NGRCs, the built environment is characterized using the 5D framework, which includes *density*, *diversity*, *design*, *distance*, and *destination accessibility*. The failure to address NGRCs is evident from the focus on limited prevention programs or resources in health care settings aimed at addressing individual attitudes and behaviors, along with the limited resources for preventive care [10]. NGRC-focused behavioral interventions allow health care providers to tailor interventions to specific contexts, offering a more personalized approach. These interventions can be categorized into social needs interventions (eg, arranging transportation) and individual lifestyle change interventions (eg, walking in a nearby park). To achieve NGRC-focused behavioral interventions, studying the interaction between NGRCs and modifiable health-related behaviors is essential [11-13].

Health information system (HIS) data have been used to investigate the relationships between NGRCs and health behaviors among health providers, HIS vendors, payers, and researchers [14-24]. A HIS is a system for collecting and processing data, information, and knowledge in health care settings [25]. The category includes (1) provider-centric electronic medical record (EMR) systems used within a single health care setting, (2) electronic health record (EHR) systems spanning multiple settings, and (3) patient-centric personal health record (PHR) systems. Among PHRs, standalone PHRs are not integrated with EMRs or EHRs, whereas tethered and interconnected PHRs are linked to EMRs or EHRs [25-27]. These systems enable various stakeholders, such as health providers, patients, and caregivers, to access and process multimodal data, such as diagnoses, medication use, treatments, NGRCs, and behavioral information.

At the individual level, HISs can enhance NGRC-focused behavioral intervention via comprehensive NGRC data capture and effective intervention prescription, monitoring, and assessment [3]. HISs can help collect NGRC data during routine clinical care, supplemented by patient-reported information, or through linkage with publicly available external data sources like geographic information systems. At the community and policy levels, HISs can support cost-effective, large-volume, and time-efficient assessments of large-scale public health efforts, such as environmental interventions to support behavioral changes, compared with traditional surveys [28].

Although integrating NGRCs with HISs is not new [29], many reviews on the functionalities and features of EHRs, EMRs, and PHRs lack clarity regarding NGRCs [30-44]. Additionally, several systematic reviews have investigated the linkage between NGRC data and clinical data sources (eg, EHRs) for population health research, but they lack specifics regarding behavioral interventions [45,46]. Recent systematic reviews on SDoH screening, linkage, extraction, analysis, and interventions within HISs, especially EHRs, similarly show limited attention to NGRCs and/or intervention-based approaches [47-50]. Given the increasing interest and existing research gap in using HISs to prepare, prescribe, monitor, and assess NGRC-focused behavioral interventions, we conducted, to our knowledge, the first scoping review of the literature in this field to distinguish it from broader SDoH-focused reviews and those lacking an intervention-based approach [46,50]. This review excluded standalone PHRs, as they are independent of provider-centric EHRs or EMRs.

This scoping review aimed to answer the following questions:

1. To what extent and what types of HISs have been used in NGRC data capture, intervention prescriptions, monitoring, and assessments of NGRC-focused behavioral interventions, and across the 4 stages?
2. What types, spatiotemporal characteristics, and databases of NGRCs have been utilized in each type of behavioral intervention supported by HISs?
3. What are stakeholders' insights regarding the use of HISs and/or NGRCs in behavioral interventions?
4. What are the gaps in research on the use of NGRCs and HISs in behavioral interventions?

Methods

Checklist

The analysis adhered to the PRISMA-ScR (Preferred Reporting Items for Systematic Reviews and Meta-Analyses extension for Scoping Reviews) checklist (Checklist 1) [51].

Search for Relevant Research

An information specialist from the Amsterdam Medical Center library (JGD) was consulted to help define key concepts and establish the evaluation framework, which included selecting the appropriate databases, relevant keywords, and MeSH terms.

XSL•FO
RenderX

MEDLINE (Ovid) and Scopus were searched from inception on April 29, 2024, to include studies up to the search date.

The search strategy could be conceptually summarized as follows: ([GRCs] AND (([neighborhoods] AND ([chronic care model] OR ([HISs] AND [health behaviors]))) OR ([community health facilities] AND [health behaviors]))), involving the following four elements related to our research questions: (1) HISs, (2) geo-referenced contexts (GRCs), (3) neighborhoods, and (4) health behaviors. Detailed information regarding the search terms in Scopus is shown in Textbox 1. The inclusion and exclusion criteria are presented in Textbox 2. For search terms in MEDLINE, refer to Table S2 in Multimedia Appendix 1.

Textbox 1. Search terms in Scopus.

[GRCs] AND (([neighborhoods] AND ([chronic care model] OR ([HISs] AND [health behaviors]))) OR ([community health facilities] AND [health behaviors]))

(((TITLE-ABS-KEY((("electronic health" or personal or digital or medical or patient or participant) W/1 record) OR (("electronic health" or personal or digital or medical or patient or participant or subject or adult) W/2 data) OR ehr or referral OR ((screen or screening) W/4 ("social determinant" or "social need" or sdoh))) OR ABS("clinical data" or "clinical information" or "clinical record")) AND TITLE-ABS-KEY(((socio or socioeconomic or social or psychosocial) W/0 (risk or stress or vulnerable or vulnerability or disadvantage or status)) or (((socio or socioeconomic or social or psychosocial) W/1 (need or environment)) or "health need") or ((socio or socioeconomic or social or psychosocial) W/2 (determinant or exposure or factor or problem)) or sdoh or hrsn or health equity or patient contextual or "life circumstance" or (socioeconomic W/0 (factor or deprivation or status)) or (socio W/1 (factor or deprivation or status)) or (community and (prevalence or risk)) or (community W/1 (type or context or factor or health*)) or (environment* PRE/0 (factor or design)) or ((community or environment*) W/2 exposure)) AND (TITLE-ABS-KEY(("residence characteristic" or "place of birth" or "birth place" or domicile or "health service area" or "catchment area" or neighbourhood or housing or census or urban or rural or county or counties or household) OR geocode or geocoding or "geo-code" or "geo-coding" OR (geograph W/2 (code or coding or data or divers or distribute or distribution or disparity or inequity or information or measure or measurement or record or residence)) OR ((patient W/0 context) or (contextual W/1 data)) OR ((demograhic W/2 (data or information or record)) or census) OR ((area or community) W/2 (factor or resource or research or impact or level or link or linked or linking or linkage)) OR (social W/2 information)) or ABS((demograhic W/3 factor) OR ((regional or region) W/9 patient) OR ((personal or individual) W/1 (sdoh or "social determinant")) OR "family centered" OR (social W/2 (risk or problem or factor)) OR geography or geographies)) OR (TITLE-ABS-KEY(((socio or socioeconomic or social or psychosocial) W/0 (risk or stress or vulnerable or vulnerability or disadvantage or status)) or (((socio or socioeconomic or social or psychosocial) W/1 (need or environment)) or "health need") or ((socio or socioeconomic or social or psychosocial) W/2 (determinant or exposure or factor or problem)) or sdoh or hrsn or health equity or patient contextual or "life circumstance" or (socioeconomic W/0 (factor or deprivation or status)) or (socio W/1 (factor or deprivation or status)) or (community and (prevalence or risk)) or (community W/1 (type or context or factor or health*)) or (environment* PRE/0 (factor or design)) or ((community or environment*) W/2 exposure)) AND TITLE-ABS-KEY((community W/1 (register or registry or data or record or program or provider)) or "community health center" or "community mental health center"))) AND (TITLE-ABS-KEY(((health or unhealth) PRE/1 behavior) or ((healthy or unhealthy) PRE/1 behavior) or smoking or tobacco or diet or food or nutrition or lifestyle or alcohol or "physical activit" or sedentary or (("social determinant" or SDOH) W/0 (screen or screening))))) OR ((TITLE-ABS-KEY ("chronic care model")) AND (TITLE-ABS-KEY (("residence characteristic" OR "place of birth" OR "birth place" OR domicile OR "health service area" OR "catchment area" OR neighbourhood OR housing OR census OR urban OR rural OR county OR counties OR household) OR geocode OR geocoding OR "geo-code" OR "geo-coding" OR (geograph W/2 (code OR coding OR data OR divers OR distribute OR distribution OR disparity OR inequity OR information OR measure OR measurement OR record OR residence)) OR ((patient W/0 context) OR (contextual W/1 data)) OR ((demograhic W/2 (data OR information OR record)) OR census) OR ((area OR community) W/2 (factor OR resource OR research OR impact OR level OR link OR linked OR linking OR linkage)) OR (social W/2 information)) OR ABS ((demograhic W/3 factor) OR ((regional OR region) W/9 patient) OR ((personal OR individual) W/1 (sdoh OR "social determinant")) OR "family centered" OR (social W/2 (risk OR problem OR factor)) OR geography OR geographies)) AND (TITLE-ABS-KEY (((socio OR socioeconomic OR social OR psychosocial) W/0 (risk OR stress OR vulnerable OR vulnerability OR disadvantage OR status)) OR (((socio OR socioeconomic OR social OR psychosocial) W/1 (need OR environment)) OR "health need") OR ((socio OR socioeconomic OR social OR psychosocial) W/2 (determinant OR exposure OR factor OR problem)) OR sdoh OR hrsn OR health AND equity OR patient AND contextual OR "life circumstance" OR (socioeconomic W/0 (factor OR deprivation OR status)) OR (socio W/1 (factor OR deprivation OR status)) OR (community AND (prevalence OR risk)) OR (community W/1 (type OR context OR factor OR health*)) OR (environment* PRE/0 (factor OR design)) OR ((community OR environment*) W/2 exposure))))

XSL•FO
RenderX

Textbox 2. Inclusion and exclusion criteria.

Inclusion criteria

- Study type: Original empirical research studies.
- Health information systems (HISs) and behavioral interventions: Used HISs to prepare, prescribe, monitor, and/or assess behavioral interventions.
- Neighborhood geo-referenced contexts (NGRCs): Used one or more NGRC attributes about the outside world to assist and/or adjust behavioral interventions.
- NGRCs and behavioral interventions: Studies in which NGRC and intervention data pertain to concurrent or longitudinal periods. Studies in which NGRC attributes and intervention attributes use either objective or subjective measurements.

Exclusion criteria

- Study type: Study protocols without substantive findings and studies without results (eg, experimental descriptions and commentaries).
- HISs: Studies for which it cannot be confirmed whether the records are part of an HIS due to an unspecified format (electronic or paper), or it is not explicitly stated whether these data are connected to HISs. Studies on standalone personal health records managed solely by patients and/or caregivers without the integration of data in medical settings (eg, hospitals). Studies using an HIS that was not focused on interventions but was used as a database to identify participants for empirical studies.
- NGRCs: Studies focusing only on broad geographic categories (eg, county, city, region, nation, and urban/rural), using sensors without specific attributes, NGRCs about health services, or economic factors (eg, transportation reimbursement). Studies for which it cannot be determined whether NGRCs were involved due to a lack of specific details on social determinants of health screening tools and interventions.

Results

Search Term Coverage and Rationale

GRCs include (1) built environments from the 5D dimensions (density, diversity, design, distance, and destination accessibility); (2) natural environments; and (3) social environments, which encompass neighborhood socioeconomic status and neighborhood social relationships. Neighborhoods include (1) static administrative areas, (2) various delineations surrounding each participant's address, (3) perceived neighborhoods, and (4) geographic areas encompassing all locations visited by an individual in their daily activities. For the definitions and examples of NGRCs and neighborhoods, see Table S1 in Multimedia Appendix 1 [1,9,26,52-76]. We used 3 different search strategies because some concepts can be merged and replaced by related ones. For example, HISs and health behaviors are 2 critical elements of the chronic care model, which is a valuable framework for patient empowerment, supporting self-management and enhancing health outcomes [53-56]. Consequently, substituting HISs and health behaviors with search terms pertinent to the chronic care model while connecting them with GRCs and neighborhoods constituted the second part of the search strategy. Additionally, community health facility workers may use HISs to address neighborhood-related issues. Therefore, replacing HISs and neighborhoods with search terms relevant to community health facilities (eg, community health centers and community data) while linking these terms with GRCs and health behaviors formed the third part of our search strategy.

Eligibility Criteria

All original peer-reviewed scientific studies in English indexed up to April 29, 2024, were included, while non–peer-reviewed studies and gray literature were excluded. Textbox 2 outlines the inclusion and exclusion criteria.

Selection Process

First, we screened titles and abstracts and excluded studies according to the inclusion and exclusion criteria. When uncertainty arose, studies were retained for the full-text screening stage. Second, XY and MD independently conducted a full-text review and extracted the relevant NGRCs, HISs, and behavioral interventions from the potentially included papers. Any disagreements were first addressed by referring to a predefined inclusion/exclusion checklist. If consensus was not reached using the checklist, the reviewers discussed each case, and, if necessary, a third reviewer (RC) made the final decision. Although interrater reliability was not calculated, this structured approach ensured consistent and transparent decision-making.

Data Extraction

We extracted data from the included studies using a 7-item table. These seven items included: (1) study attributes; (2) population attributes, diseases, and health setting characteristics; (3) HISs; (4) NGRCs; (5) behavioral interventions; (6) results; and (7) conclusions and future studies. Table S3 in Multimedia Appendix 1 provides further details.

Figure 1 presents the PRISMA flowchart, which includes the identification, screening, and selection process. A total of 24 peer-reviewed studies were finally included.

XSL•FO
RenderX

Figure 1. PRISMA (Preferred Reporting Items for Systematic reviews and Meta-Analyses) flowchart. HIS: health information system; NGRC: neighborhood geo-referenced context.

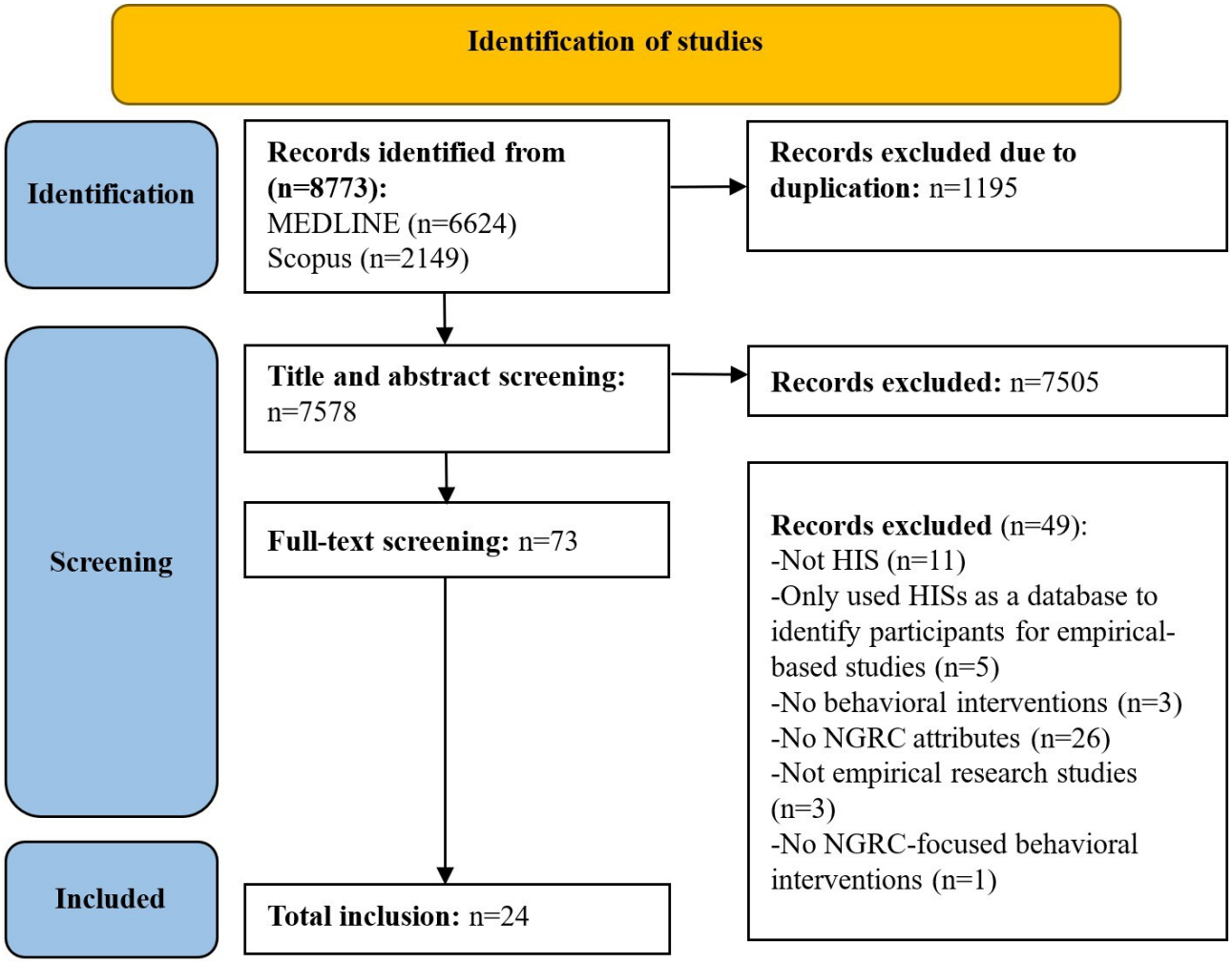

Study Characteristics

We reviewed the descriptive characteristics of all 24 included papers. Basic characteristics of the studies are presented in Table S4 in Multimedia Appendix 1, including information on (1) the type, number, gender, age distributions, and language of participants, and (2) the study type and year of publication. The characteristics with appropriate properties for summarization include (1) the type, NCD, and health and computer literacy of participants, and (2) health settings. All studies were conducted in the United States. Details are provided in Table S5 in Multimedia Appendix 1.

We divided the studies by participant type as follows: 2 studies [29,77] focused solely on providers, 4 studies concentrated on caregivers [78-81], 13 studies examined patients only [10,82-93], and 5 studies involved both health providers and patients [93-97]. Among patients, most studies focused on adults.

Summarization of the Results

Overview

In this section, we aim to summarize the findings from the 24 included articles to address the first 3 research questions. Each of these themes is explored in detail in the subsections that follow.

Question 1: Question Regarding HISs

We summarized whether HISs were used and the types of HISs used. Table 1 presents HIS usage across all stages, while Table S5 in Multimedia Appendix 1 lists the types of HISs. Table S4 in Multimedia Appendix 1 provides the specific names of the HISs.

Table 2 details the stage 1 NGRC data capture, including the settings (eg, health care settings, such as hospitals, and non–health care settings, such as homes), those collecting data (eg, patients, providers, and systems), and those documenting it (systems or providers).

XSL•FO
RenderX

Table . The role of HISs[a] in the entire process of NGRC[b]-focused behavioral interventions, including situations and actors.

Group and study	NGRC data capture (n=18)	Prescription (n=13)				Monitoring (n=2)	Assessment (n=11)
		Digital prescriptions (n=6)		Prescriptions by HPs[c] and documented in HISs (n=7)			
		Tools	Interventions	Types of HPs	Interventions		
Social needs interventions							
Buitron de la Vega et al [82]	HISs[d]	EHR[d,e]	Referral guides[d]	—[f]	—	—	—
Cordova-Ramos et al [78]	HISs[d]	—	—	Nurses[d]	—	—	—
Fortin et al [79]	HISs[d]	—	—	Social workers[d]	EHR-based resource maps[d]	—	—
Lynch et al [94]	HISs[d]	—	—	—	—	Manual documentation[d]	—
Palakshappa et al [95]	HISs[d]	A tablet-based patient portal[d]	CRLs[g] and TIAtHPs[d,h]	—	—	—	—
Percac-Lima et al [85]	HISs[d]	—	—	—	—	—	The percentage of CRC[i] screening[d]
Russell et al [84]	HISs[d]	—	HISs[d]	Nurses[d]	—	—	—
Wallace et al [86]	—	—	—	—	—	—	HCUD[d,j]
Wright et al [96]	HISs[d]	—	HISs[d]	Social workers[d]	—	—	—
Wu et al [97]	HISs[d]	—	—	—	—	—	HCUD and medication adherence[d]
Roth et al [88]	—	—	—	—	—	—	HCUD, HbA_{1c} levels, and blood pressure[d]
Tanumihardjo et al [87]	HISs[d]	—	—	—	—	—	HbA_{1c}, LDL[k], and blood pressure[d]
Holt et al [29]	HISs[d]	Web-based PatientWisdom patient portal[d]	Resource linkages and TIAtHPs[d]	—	—	—	—
Bechtel et al [89]	—	—	—	—	—	—	HCUD[d]
Taber et al [90]	HISs[d]	—	—	—	—	—	—
Stark et al [80]	HISs[d]	Healthy Planet app[d]	CRLs[d]	—	—	—	—
Gupta et al [91]	HISs[d]	NowPow embedded in EMR[d,l]	Resource linkages[d]	—	—	Automatic documentation[d]	HCUD[d]
Britto et al [92]	HISs[d]	—	—	Researchers[d]	HISs[d]	—	The percentage of patients with well-controlled asthma[d]

XSL•FO
RenderX

Group and study	NGRC data capture (n=18)	Prescription (n=13)				Monitoring (n=2)	Assessment (n=11)
		Digital prescriptions (n=6)		Prescriptions by HPs[c] and documented in HISs (n=7)			
		Tools	Interventions	Types of HPs	Interventions		
Glasser et al [81]		EHR-integrated CommunityRx[d]	Resource linkages[d]	—	HISs[d]	—	—
Loo et al [93]	HISs[d]	—	—	EDCS[d,m]	HISs[d]	—	—
Percac-Lima et al [98]	HISs[d]	—	—	Navigators[d]	HISs[d]	—	HCUD[d]
Lifestyle change interventions							
Jilcott et al [10]	—	—	—	—	—	—	HCUD, blood lipids, glucose, pressure, BMI, and body composition[d]
Johnston et al [83]	—	—	—	—	—	—	HCUD[d]
The entire care process							
Kane et al [77]	HISs[d]	—	—	—	—	—	—

[a]HIS: health information system.

[b]NGRC: neighborhood geo-referenced context.

[c]HP: health provider.

[d]HISs have functioned in this category.

[e]EHR: electronic health record.

[f]Not applicable.

[g]CRL: community resource list.

[h]TIAtHP: timely intervention alert to health provider.

[i]CRC: colorectal cancer.

[j]HCUD: health care utilization data.

[k]LDL: low-density lipoprotein.

[l]EMR: emergency medical record.

[m]EDCS: emergency department clinical staff.

XSL•FO
RenderX

Table . The role of HISs[a] in NGRC[b] data capture.

Group and study	NGRC preparation (n=18)								
	H/NH[c]	NGRC data collection (n=18)						NGRC data documentation (n=18)	
		Patient-administered electronic collection (n=5)		Patient-administered paper-based collection (HPs[d] to assist if needed) (n=2)	HP-administered collection (n=10)		System-administered collection (n=1)	System (n=5)	HPs (n=13)
		Tools	Types of HPs		V/E[e]	Types of HPs			
Social needs interventions									
Buitron de la Vega et al [82]	H	—[f]	—	Medical assistants[g]	—	—	—	—	Medical assistants[g]
Cordova-Ramos et al [78]	H	—	—	—	V[g]	Nurses[g]	—	—	Nurses[g]
Fortin et al [79]	H	REDCap[g]	—	—	—	—	—	—	CTAs[g,h]
Lynch et al [94]	H	—	—	—	E[g]	Medical assistants[g]	—	—	Medical assistants[g]
Palakshappa et al [95]	H	Tablet-based patient portal[g]	—	—	—	—	—	HISs[g]	—
Percac-Lima et al [85]	H	—	—	—	V[g]	Navigators[g]	—	HISs[g]	Navigators[g]
Russell et al [84]	H	eScreening platform[g]	CTAs[g]	—	—	—	—	—	—
Wright et al [96]	H	—	—	Nurses[g]	—	—	—	—	Nurses[g]
Wu et al [97]	H	—	—	—	V[g]	Pharmacists[g]	—	—	Pharmacists[g]
Tanumihardjo et al [87]	H	—	—	—	V[g]	CHWs[g,i]	—	—	CHWs[g]
Holt et al [29]	NH	Web-based PatientWisdom patient portal[g]	—	—	—	—	—	HISs[g]	—
Taber et al [90]	H	—	—	—	V[g]	Pharmacists, nurses, social workers, and CHWs[g]	—	—	Pharmacists, nurses, social workers, and CHWs[g]
Stark et al [80]	NH	Healthy Planet app[g]	—	—	—	—	—	HISs[g]	—
Gupta et al [91]	H	—	—	—	E[g]	Without specificity[g]	—	—	Without specificity[g]
Britto et al [92]	H	—	—	—	V[g]	Researchers[g]	—	—	Researchers[g]

XSL•FO
RenderX

Group and study	NGRC preparation (n=18)								
	H/NH[c]	NGRC data collection (n=18)						NGRC data documentation (n=18)	
		Patient-administered electronic collection (n=5)		Patient-administered paper-based collection (HPs[d] to assist if needed) (n=2)	HP-administered collection (n=10)		System-administered collection (n=1)	System (n=5)	HPs (n=13)
		Tools	Types of HPs		V/E[e]	Types of HPs			
Loo et al [93]	H	—	—	—	V[g]	Nurses and clinicians[g]	—	—	Nurses[g]
Percac-Lima et al [85]	H	—	—	—	V[g]	Navigators[g]	—	—	Navigators[g]
Entire care process									
Kane et al [77]	H	—	—	—	—	—	Publicly available datasets[g]	HISs[g]	—

[a]HIS: health information system.

[b]NGRC: neighborhood geo-referenced context.

[c]H/NH: physical health settings (H), and non–health care settings (NH).

[d]HP: health provider.

[e]V/E: verbal surveys embedded in electronic health records (EHRs) or electronic medical records (EMRs) (E), or surveys not embedded in EHRs or EMRs (V).

[f]Not applicable.

[g]HISs have functioned in this category.

[h]CTA: care team assistant.

[i]CHW: community health worker.

Question 2: Question Regarding NGRCs

We summarized the reviewed studies in terms of behavioral intervention types as follows: (1) social needs interventions, (2) lifestyle change interventions, and (3) whole care without specifying the behavioral intervention type. This categorization agrees with the information in Table S1 in Multimedia Appendix 1. Table 3 summarizes the types and spatiotemporal characteristics of NGRC attributes.

XSL•FO
RenderX

Table . The types and spatiotemporal characteristics of NGRCs[a] related to social needs interventions, lifestyle interventions, and the entire care process.

Group and NGRC	B/N/S[b]	Neighborhood type (address)	Data source[c]	SDoH[d] screening	Ob/Su[e]	I/O[f]	Li/So/E[g]	Reference
Social needs interventions (n=21)								
Transportation barriers (inpatient)	B	PNs[h]	Sc	Yes	Su	I	So	[78,82,84,92,94,96,98]
Transportation barriers (outpatient)	B	PNs	Sc	Yes	Su	O	So	[29,80,81,93,97]
Neighborhood safety (individuals' fears and feelings of insecurity in their environment)	S	PNs	Sc	Yes	Su	I	So	[90]
Lifestyle interventions (n=2)								
Design: sidewalk/bike lane shortage	B	PNs (RDs[i])	—[j]	Yes	Su	I	So	[10]
Density: intensive fast foods, insufficient healthy food options (eg, food stores, restaurants, farmer's markets, and fruit stands), and healthy breakfast access	B	PNs (RDs)	—	Yes	Su	I	So	[10]
Density: recreational facility scarcity for walking (eg, parks, gyms, and tracks), affordable exercise facilities, and suitable physical activity programs	B	PNs (RDs)	—	Yes	Su	I	So	[10]
Traffic	B	PNs (RDs)	—	Yes	Su	I	So	[10]
Design: lack of streetlights	B	PNs (RDs)	—	Yes	Su	I	So	[10]
Distance to a high-risk location, such as a bar or supplier the individual used to frequent	B	Daily routes	L	No	Ob	O	Li	[83]

XSL•FO
RenderX

Group and NGRC	B/N/S[b]	Neighborhood type (address)	Data source[c]	SDoH[d] screening	Ob/Su[e]	I/O[f]	Li/So/E[g]	Reference
Living in an environment where alcohol use is prevalent or normalized	S	PNs (RDs)	Sc	No	Su	O	Li	[83]
Community crime	S	PNs (RDs)	Sc	No	Su	I	So	[10]
Verbal abuse from people on the street and speeding drivers	S	PNs (RDs)	Sc	No	Su	I	So	[10]
Air pollution from cars or factories	N	PNs (RDs)	Sc	No	Su	I	So	[10]
The entire care process (n=1)								
Food desert status (yes/no) and low food access census tract (yes/no)	B	Census tracts (RDs)	P	No	Ob	I	E	[77]
Location type (urban/rural)	B	Census tracts (RDs)	P	No	Ob	I	E	[77]
Total population, low-income population, children aged 0-17 years, seniors aged 65 years or older, and housing units lacking vehicle access among populations with limited access, defined by how far the closest supermarket is (0.5, 1, 10, and 20 miles away)	S	Census tracts (RDs)	P	No	Ob	I	E	[77]

XSL•FO
RenderX

Group and NGRC	B/N/S[b]	Neighborhood type (address)	Data source[c]	SDoH[d] screening	Ob/Su[e]	I/O[f]	Li/So/E[g]	Reference
Community-level socioeconomic and demographic data, including age, race, ethnicity, nationality distribution, median age, median family and household income, education level distribution, median home value and gross rent, renter-occupied household distribution, total population, total housing units, and low-income census tract (yes/no)	S	Census tracts (RDs)	P	No	Ob	I	E	[77]

[a]NGRC: neighborhood geo-referenced context.

[b]B/N/S: built environment (B), natural environment (N), or social environment (S).

[c]Source: NGRC screening (Sc), location-aware devices (L), or public datasets (P).

[d]SDoH: social determinants of health.

[e]Ob/Su: objective (Ob) or subjective (Su).

[f]I/O: inpatient (I) or outpatient (O).

[g]Li/So/E: lifestyle change interventions (Li), social needs interventions (So), or entire care process (E).

[h]PN: perceived neighborhood.

[i]RD: residential address.

[j]Not available.

We specified substructures for the categorization of social needs interventions, lifestyle change interventions, and whole care. Social needs interventions used actively collected, subjective, and static measures of perceived neighborhood social and built environments. Lifestyle change interventions included (1) actively collected, subjective, and static measures of perceived neighborhood social, natural, and built environments at residential addresses, and (2) passively collected, objective, real-time, and location-based distances to high-risk areas (eg, bars). Whole care included passively collected, objective, and static social and built environment indicators derived from the census tract of residential addresses.

In social needs interventions, actively collected, subjective, and static measures of perceived transportation barriers and neighborhood safety were the only 2 assessed NGRCs (21/24, 88%). These were assessed using electronic or paper-based surveys [29,78-82,84-98]. The focus on transportation barriers (21/24, 88%) may reflect their relative ease of mitigation through interventions (eg, door-to-door transportation to medical appointments [8,92]). These interventions were shaped by specific health service settings and available community resources. Similarly, transportation barriers were assessed using a variety of question formats, time frames, destination types, and SDoH screening tools. Despite these efforts, detailed information, such as transport mode, distance, travel time, and the locations of perceived neighborhoods, was generally rarely collected. Additional details are presented in Table 4.

XSL•FO
RenderX

Table . Additional details regarding transportation barriers.

Questions about NGRCs[a]	Timespan	Survey frequency	SDoH[b] screening tools	Reference
Transportation barriers to attending medical appointments (eg, CRC[c] screening) or obtaining medications (n=10)				
Do you have trouble getting transportation to medical appointments?	—[d]	—	Tool for Health and Resilience In Vulnerable Environments Social Determinants of Health (THRIVE)	[82,93]
Do you have trouble with transportation to or from NICUs[e]? For example, paying for parking or getting a ride to the hospital.	—	—	Tool for Health and Resilience In Vulnerable Environments Social Determinants of Health (THRIVE)	[78]
Query regarding transportation barriers to CRC screening	—	—	—	[85]
Query regarding transportation barriers to CT[f] screening tests (eg, lung cancer and chest)	—	—	—	[98]
Query regarding transportation to appointments	—	—	—	[92]
Have you missed any medical appointments because of difficulties with transportation?	Past 6 and 12 months	Annually	Health Risk Assessment (HRA)	[87]
Have you ever not seen a doctor because you did not have a way to get to the clinic or hospital?	Past 12 months	—	HealthLeads	[86]
Has a lack of transportation kept you from medical appointments or from getting medications? (query 1)	Past 12 months	—	Intensifying Community Referrals for Health (SINCERE)	[80]
Has a lack of transportation kept you from medical appointments or from getting medications? (query 2)	Past 3 months	—	Monteliore's 10-question SDoH survey	[91]
Transportation barriers to attending medical appointments, meetings, or work, or getting things needed for daily living (n=9)				
Has a lack of transportation kept you from medical appointments, meetings, or work, or from getting things needed for daily living? (query 1)	Past 12 months	—	Health-Related Social Needs (HRSN)	[79,95]
Has a lack of transportation kept you from medical appointments, meetings, or work, or from getting things needed for daily living? (query 2)	Past 12 months	—	Protocol for Responding to and Assessing Patients' Assets, Risks, and Experiences (PRAPARE)	[87]
Has a lack of transportation kept you from medical appointments, meetings, or work, or from getting things needed for daily living? (query 3)	—	—	Protocol for Responding to and Assessing Patients' Assets, Risks, and Experiences (PRAPARE)	[88,94]
Has a lack of transportation kept you from medical appointments, meetings, or work, or from getting things needed for daily living? (query 4)	—	—	Assessing Circumstances and Offering Resources for Needs	[84]
Has a lack of transportation kept you from work, attending medical appointments including dialysis treatments, or getting things you need for your daily living?	—	Monthly [96]; — [89]	The Core 5 Determinants of Health Screening Tool	[89,96]
Query regarding challenges in finding affordable, reliable, or handicap-accessible transportation to obtain resources such as medical care, food, or medications	—	—	—	[90]
Transportation barriers without specifying which destinations were affected (n=3)				
Query regarding transport	—	—	—	[29,81]

XSL•FO
RenderX

Questions about NGRCs[a]	Timespan	Survey frequency	SDoH[b] screening tools	Reference
By the way, we have this new resource team that can help with things not related to health care, like food, housing, and transportation. Is this something you want to talk about?	—	Weekly	—	[97]

[a]NGRC: neighborhood geo-referenced context.

[b]SDoH: social determinants of health.

[c]CRC: colorectal cancer.

[d]Information not available.

[e]NICU: neonatal intensive care unit.

[f]CT: computed tomography.

Lifestyle change interventions assessed actively collected, subjective, and static measures of social, natural, and built environments at participants' perceived residential neighborhoods. These were assessed with "neighborhood assessment" during follow-up visits [10]. These assessments showed the multifaceted interplay between NGRCs and lifestyle behaviors. The environmental barriers to healthy eating and physical activity included air quality, food environment density, physical activity facility density, streetlight design, and neighborhood safety (Table 3). The absence of subsequent similar studies highlights the practical challenges of consistently partnering with community groups and agencies to address environmental barriers to lifestyle change.

In addition, passively collected, objective, real-time, and location-based distances to high-risk areas (eg, bars) were assessed using GPS data from the A-CHESS (Addiction Comprehensive Health Enhancement Support System) app [83] (Figure 2). Unlike approaches that depend on community-level resources of residential addresses, A-CHESS optimizes users' daily routes. This suggests that leveraging existing environments along these routes—not just around residential areas—can be practical without requiring extensive organizational collaboration. A-CHESS also supports weekly surveys to actively assess participants' perceived alcohol use in their residential neighborhoods [83]. While transportation barriers are relatively stable, neighborhood social cultures, such as drinking behaviors, fluctuate rapidly, requiring active and higher-resolution data collection to capture their health effects.

In whole care, passively collected, objective, and static social and built environment indicators based on the census tract level of the residential address were displayed in the Envirome Web Service [77]. Integrated with the Cerner Millennium EHR, this service displays socioeconomic data, food desert status, and contextual information at the census tract level using public datasets (eg, the US Department of Agriculture and the 2010 Decennial Census). Compared with A-CHESS, the Envirome Web Service offers broader, population-level coverage of social and built environment factors through passive data collection but lacks dynamic, route-specific, or nonresidential contextual information.

XSL•FO
RenderX

Figure 2. The A-CHESS (Addiction Comprehensive Health Enhancement Support System) app [83] supports recovery from alcohol use disorder by providing 24/7 smartphone access to services such as cognitive-behavioral therapy, addiction-related resources, and alcohol-free events. The left panel displays a list of identified high-risk locations, the middle panel summarizes risky situations based on weekly surveys, and the right panel shows the app's homepage. Using GPS, A-CHESS monitors when users approach predesignated high-risk locations, such as bars, and sends an alert asking whether they intend to be there. No alert is issued if the user is not near a high-risk location. The screenshots were captured from the app link [99].

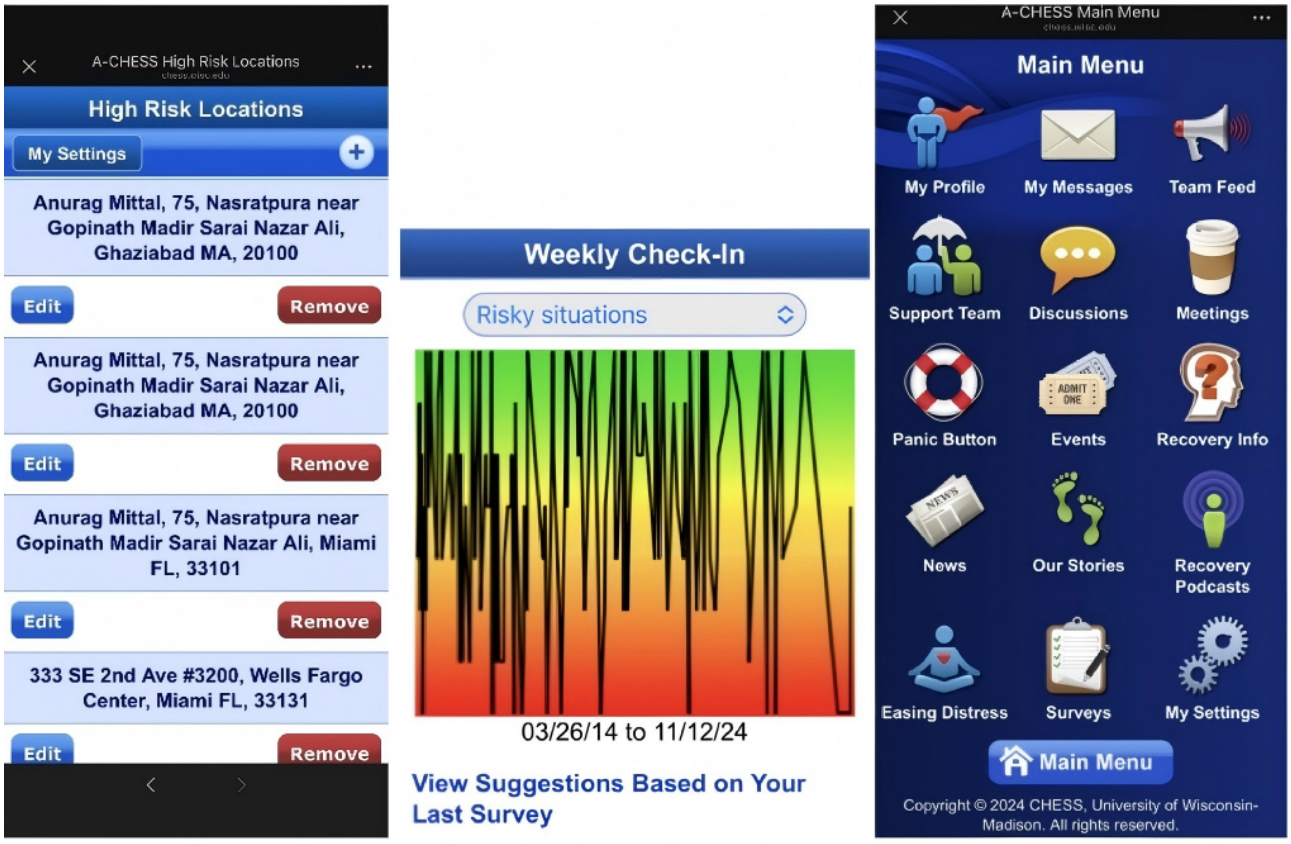

Question 3: Question Regarding Stakeholders' Insights

We summarized stakeholders' insights on the use of NGRCs and/or HISs in social needs interventions and whole care from 10 included studies. The details are shown in Table S6 in Multimedia Appendix 1.

Seven studies mentioned attitudes toward NGRC integration. Six out of the seven studies on social needs interventions found that patients, caregivers, and providers valued addressing transportation barriers for comfort and convenience [84,93,96,97]. However, challenges remain in addressing patients' concerns about potential discrimination, such as reduced courtesy or respect, as well as providers' discomfort with stigmatizing questions [81,86,93,96,97]. At the core, the challenge lies in balancing actionable social needs interventions and sensitive care. The last study [77] examined providers' views on NGRC data needs, clinical usefulness, and data visualizations in whole care. Providers emphasized the need for clear definitions and simple visualizations to make complex data more actionable in practice [77].

Nine studies examined HIS integrations from 3 aspects: value and convenience, patient autonomy, and privacy. The efficiency and convenience of electronic NGRC capture tools were recognized by providers, patients, and caregivers, particularly when patients completed them before visits [29,77,86,95-97]. However, providers also expressed concerns about increased workload, time constraints, unfitness to the workflow, and the possibility of raising unmet patient expectations [29,86,94-96]. These concerns underscore the need to integrate NGRC-focused behavioral interventions seamlessly into clinical workflows to avoid a higher administrative burden. Patient autonomy and engagement were enhanced [77,86,95-97]. Improved autonomy can support person-centered and team-based care. However, the absence of data on patients' digital literacy could lead to misinterpretation of patients' attitudes (eg, acceptability, adoption, and usage of HISs), especially for those with low literacy levels, as higher digital literacy can alleviate social concerns [29,84]. Privacy was improved by reducing patients' feelings of judgment and promoting greater honesty in disclosure [84,86,95]. Improved privacy suggests that well-designed digital systems can mitigate stigma associated with sensitive NGRCs.

Discussion

Principal Findings and Recommendations

In this scoping review, we reviewed the current state of NGRC-focused behavioral interventions using HISs in order to propose recommendations for future studies. We included 24 studies, and nearly half of the studies (11/24, 46%) were conducted in 2023 or later (Table S4 in Multimedia Appendix 1). Due to unstructured reporting in many of the included studies, reliably extracting data was difficult. We organized our findings and recommendations according to the 4 research questions.

XSL•FO
RenderX

Question 1: Question Regarding HISs

The predominant reliance on provider-centric EHRs/EMRs and the limited and inconsistently described use of HISs across the entire NGRC-focused behavioral intervention cycle significantly constrain the integration of NGRCs into behavioral interventions. Apart from the unspecified type of HIS in 1 study [10], most included studies relied on provider-centric EHRs/EMRs (20/24, 83%), with limited use of more patient-empowered PHRs. Only 3 studies used tethered PHRs, and none utilized interconnected PHRs (Table S5 in Multimedia Appendix 1). The reliance on provider-centric EHRs/EMRs may lead to difficulties in monitoring and assessment. Therefore, most studies (23/24, 96%) did not apply HISs in the entire process (NGRC data capture, intervention prescription, monitoring, and assessment). HISs were mainly used for (1) NGRC data capture (18/24, 75%), with limited patient-led (5/24, 21%) or system-led (1/24, 4%) cases; (2) intervention prescriptions (13/24, 54%); and (3) assessments (11/24, 46%) focusing on health care utilization, with minimal use in monitoring (2/24, 8%). Limited monitoring and a narrow focus on health care utilization data for assessments leave the sustainability of behavior change largely unaddressed. Given its critical role in improving long-term health outcomes, future research should aim to establish integrated frameworks that embed tethered or interconnected PHRs consistently across the 4 phases. Furthermore, the lack of details on HIS functionalities limits the ability to synthesize evidence and derive practical design recommendations for future interventions. Future studies should provide sufficient details to ensure reproducibility.

Although HISs have been used frequently in NGRC data capture, the dominance of active collection (eg, patient-administered or provider-administered surveys; 22/24, 92%) and the underuse of passive collection (eg, linkage with public datasets; 1/24, 4%) and GPS data (1/24, 4%) have left existing data underutilized, and active collection may cause user information to be unclear. On one hand, the majority of studies (17/24, 71%) relied on manual NGRC collection and documentation into EHRs/EMRs by stakeholders (Table S6 in Multimedia Appendix 1). Active data collection likely contributes to negative provider attitudes due to increased workload and limited consultation time. This potentially hinders the integration of NGRCs into routine care. Self-completed assessments using tethered or interconnected PHRs may address providers' concerns, and both patients and providers hold positive attitudes toward them (Table S6 in Multimedia Appendix 1). However, tethered or interconnected PHRs were underutilized in the included studies. The gap between positive stakeholder attitudes and practice suggests missed opportunities to reduce provider burden and engage patients more actively in their care using PHRs. On the other hand, although the A-CHESS app achieved passive data collection, it relied solely on HISs as assessment tools and had limited provider access to behavioral data, which constrained the understanding of how HISs and providers influence behavior change and its sustainability. Similarly, the Envirome Web Service [77] passively collected NGRC data via public dataset linkages. However, the lack of detailed descriptions of the use of HISs in subsequent steps (eg, monitoring and assessment) further limited insights into their role in supporting sustained behavior change.

The complexity of provider types and roles in the entire process of NGRC-focused behavioral interventions (Table 1) further complicates implementation in clinical settings. Future studies should clearly define the responsibilities of every provider to enhance coordination across care teams, thereby improving intervention fidelity and consistency.

In summary, implementing tethered or interconnected PHRs throughout the intervention process, particularly in outpatient settings, is recommended (Figure 3). Connection with EHRs/EMRs can also achieve provider support. By ensuring privacy, security, and controlled access, PHRs can enhance user acceptance and usage [100]. Secure data exchange among patient apps, public datasets, sensors, and EMRs/EHRs can enable tailored interventions, timely issue detection, improved communication, greater engagement and adherence, better care coordination, higher satisfaction, and reduced treatment burden [86,101]. We have summarized 3 recommendations in Textbox 3.

XSL•FO
RenderX

Figure 3. Tethered and interconnected advantages of PHRs in NGRC-focused behavioral interventions. The image has been modified [3]. EHR: electronic health record; EMR: electronic medical record; NGRC: neighborhood geo-referenced context; PHR: personal health record.

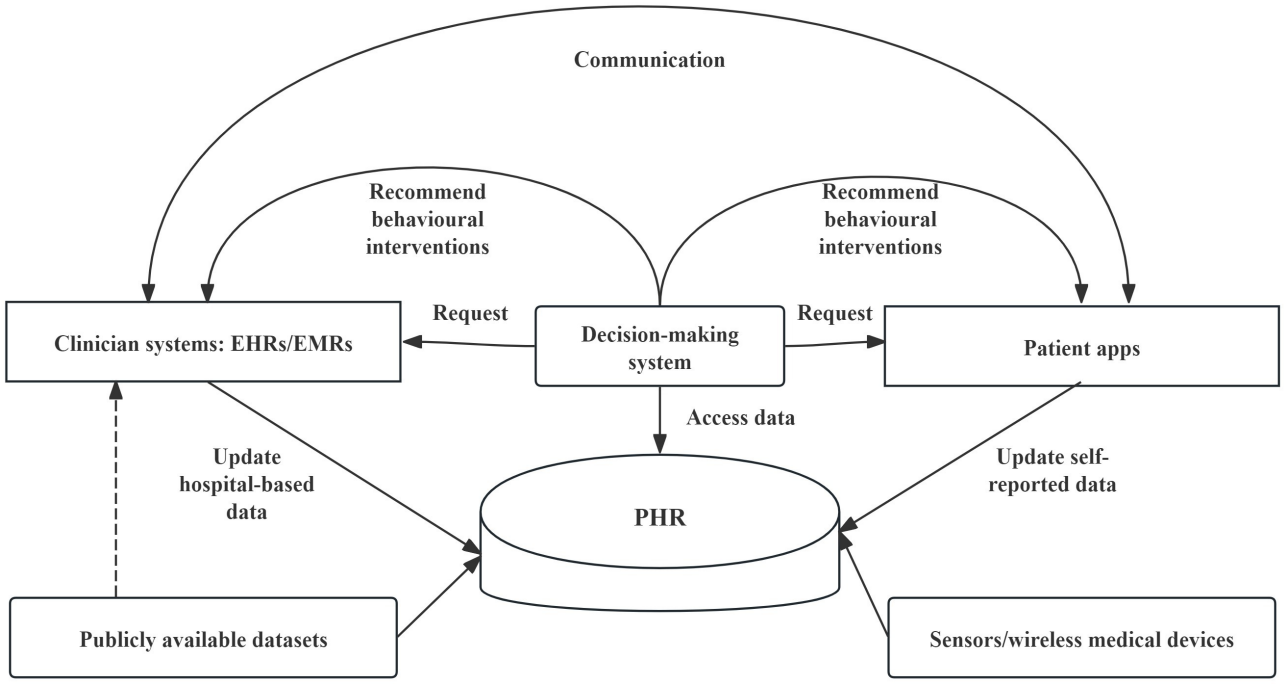

XSL•FO
RenderX

Textbox 3. Recommendations.

Recommendations regarding the types and roles of health information systems (HISs) in the entire process of neighborhood geo-referenced context (NGRC)–focused behavioral interventions

1. Consider tethered or interconnected personal health records (PHRs), especially in outpatient settings, in the entire process of NGRC-focused behavioral interventions.
    - Use tethered or interconnected PHRs to actively or passively collect multiple NGRCs and generate a more comprehensive view of patients' NGRCs [84]. PHRs can passively obtain location-related NGRCs through connections with electronic health records (EHRs)/electronic medical records (EMRs), public datasets (eg, government data and cohorts), sensors, and wireless medical devices. The locations can include not only the residential address but also regularly visited places or GPS-derived data. On the other hand, PHRs can also embed patient- or caregiver-completed surveys to actively collect perceived NGRCs. Determining the optimal timing and frequency of data capture is essential to balance user burden and data quality [82,84,102,103].
    - Clinical decision support systems (CDSSs) can use NGRC data from PHRs to personalize behavioral interventions, delivering recommendations to patients via apps and to providers via EHRs/EMRs. For instance, real-time CDSS alerts sent at optimal intervals can support providers in adjusting NGRC-focused interventions.
    - Consider integrating PHRs with other portable devices (eg, patient apps, sensors, and wireless medical devices) to allow real-time monitoring through surveys, GPS, and sensors.
    - Integrating PHRs with EHRs/EMRs and other portable devices can provide sufficient long-term follow-up data. CDSSs can then use these data to assess and adapt NGRC-focused behavioral interventions [46,85,104], allowing the evaluation of the sustainability of outcomes and the identification of interventions that produce lasting effects.
2. Incorporate the support of health care providers throughout NGRC-focused behavioral interventions. This support can be provided through (1) providers' guidance on CDSS recommendations and (2) direct patient-provider communication.
    - Explore the roles of various health care providers in the entire process of NGRC-focused behavioral interventions.
3. Balance active and passive NGRC data collection to achieve higher acceptability, feasibility, and effectiveness of NGRC-focused behavioral interventions [24,84,86].

Recommendations regarding the types, spatiotemporal characteristics, and datasets of NGRCs in each type of behavioral intervention

1. Accommodate NGRC-focused social needs interventions with lifestyle change interventions.
2. Include a broader range of NGRCs with detailed spatiotemporal information for different behavioral interventions.
    - Expand the focus beyond influential built environments to also include key natural and social environments for specific behaviors.
    - Incorporate a comprehensive 5D (density, diversity, design, distance, and destination accessibility) framework of built environments.
    - Optimize NGRC spatiotemporal resolution using an evolutionary approach. Apply high-resolution or real-time data when available for precise interventions; otherwise, use static or coarse data (eg, administrative datasets) to capture neighborhood influences. Combining dynamic and static NGRCs can mitigate challenges such as the modifiable areal unit problem, the uncertain geographic context problem, and neighborhood effect averaging.
    - Prioritize key subjective and objective NGRCs for specific behaviors (eg, cycling and walking) and standardize their definitions, spatiotemporal attributes, and measurements through multidisciplinary collaboration. Such efforts should leverage and expand existing terminologies (eg, "community details" in Systematized Nomenclature of Medicine—Clinical Terms [SNOMED CT] and Logical Observation Identifiers Names and Codes [LOINC]) and ontologies (Social Determinants of Health Ontology [SOHO] [105] and social determinants of health ontology [SDoHO] [106]) [24].
    - Assess the availability of influential objective NGRCs in existing datasets and explore opportunities to collect missing objective and subjective data through passive methods (eg, sensors). When certain NGRCs cannot be captured passively, develop self-administered questionnaires to obtain the remaining information. Finally, evaluate the quality, usability, and improvement potential of patient-completed data.
3. Address both technical and social considerations (eg, ethical issues) in NGRC data collection [92].

Recommendations regarding stakeholders' insights on the use of HISs and/or NGRCs in behavioral interventions

1. Assess stakeholder acceptance, attitude, and preferred interactive features for various NGRC-focused behavioral interventions using HISs, particularly those targeting lifestyle changes. For example, evaluate patients' willingness and desired features in PHR-based self-management tools, and design EHR/EMR features that fit providers' workflows to mitigate concerns like time constraints and workload.
2. Develop and iteratively test efficient, user-friendly data visualization tools for stakeholders [33,107-111].
3. Explore stakeholders' perspectives on integrating diverse and/or real-time NGRCs into behavioral interventions, extending beyond transportation barriers to broader applications. Future research should identify which NGRCs stakeholders consider most actionable and relevant for specific interventions, and determine effective, nonstigmatizing data collection methods. For example, assess patient willingness to share GPS data when they can control access to their information.
4. Consider stakeholders' computer and health literacy when evaluating their attitudes toward NGRC-focused behavioral interventions using HISs.

XSL•FO
RenderX

5. Iteratively build support systems, responding to negative feedback by aligning patient expectations and addressing stakeholders' social concerns.

Recommendations regarding research designs

1. Adopt standardized and detailed descriptions of NGRCs [24], HIS functionalities, intervention designs, and relevant disease contexts—ideally guided by common metadata standards or consensus-based frameworks—to enhance transparency, comparability, and collaboration across studies.
2. Evaluate the feasibility, acceptability, adoption, sustainability, effectiveness, cost-effectiveness, ethics issues, and mechanisms of change of NGRC-focused behavioral interventions using HISs, with detailed descriptions of research design for reproduction, testing, and comparison. For example, in research design, the only difference between the intervention and control groups should be whether the intervention is NGRC-focused, in order to isolate the effect of NGRCs.
3. Initiate comparative studies examining how different NGRCs and HIS functionalities influence specific intervention effectiveness, which would further inform the design of evidence-based interventions.

Generalizability

1. Explore the unique challenges and context-specific solutions relevant to countries outside the United States.

Question 2: Question Regarding NGRCs

The dominance of structured, measurable social needs interventions in the involved studies likely reflects that health care prioritizes short-term outcomes. In contrast, long-term lifestyle change interventions are overlooked. This may be due to operational challenges, including reimbursement constraints, lower adherence, long-term evaluation, etc [112-115]. However, lifestyle change interventions are crucial for preventing NCDs. To raise attention on lifestyle change interventions, incorporating NGRCs is beneficial for improving adherence and effectiveness. Future studies should focus on leveraging NGRC data to design and evaluate personalized, NGRC-focused lifestyle interventions aiming at advancing patient-centered and preventive care.

Current research has largely overlooked NGRCs beyond transportation barriers within the "destination accessibility" dimension of built environments. Neglecting other 4D elements, as well as social (eg, community crime, neighborhood safety, and socioeconomic data; included in 4 studies) and natural environments (specifically air pollution; included in 1 study), may limit our understanding of how specific NGRCs can inform behavioral interventions. Within the built environment domain, the exploration of "density," "distance," and "design" in the "5D" framework was limited, and "diversity" was not addressed. Future studies should systematically explore other less-studied NGRCs, such as social, natural, and other built NGRCs, to inform more holistic solutions of behavioral interventions using HISs.

Insufficient attention to objective, dynamic, and/or high-resolution NGRCs has left several key methodological challenges largely unaddressed. These include the modifiable areal unit problem, uncertain geographic context problem, neighborhood effect averaging problem, and problem of temporal variations in NGRCs (Figure 4) [60,116-120]. One likely reason is that 22 studies (92%) relied on actively collected, subjective, and static NGRC data, which require substantial participant effort and are therefore difficult to scale for capturing dynamic and/or high-resolution NGRCs. Passive data collection methods (eg, GPS tracking and linkage with public datasets) could help overcome these limitations by enabling more dynamic and/or high-resolution NGRC measurement. However, passive approaches alone cannot capture all real-time and/or high-resolution NGRCs, particularly those related to individual perceptions. Therefore, active data collection remains essential for assessing perceived NGRCs. While some studies have focused exclusively on perceived measures, others have underscored the added value of combining subjective and objective NGRCs to more comprehensively understand their associations with behavioral outcomes [121-124]. When collecting perceived dynamic and/or high-resolution NGRCs, issues, such as user vagueness and the quality of self-reported data, must be carefully considered. Future work should prioritize developing optimized and balanced approaches that integrate active and passive data collection, thereby leveraging dynamic and/or high-resolution NGRC measures to advance behavioral intervention research.

XSL•FO
RenderX

Figure 4. The top-left figure displays the modifiable areal unit problem. The mean value does not change with aggregation, but the variance declines [118,119]. The top-right figure presents how the neighborhood effect averaging problem operates in individual air pollution exposures [116,120]. The bottom figure shows the uncertain geographic context problem, which arises because of the spatial uncertainty in the actual areas that exert contextual influences on the individuals being studied, and the temporal uncertainty in the timing and duration in which individuals experienced these contextual influences [60,117].

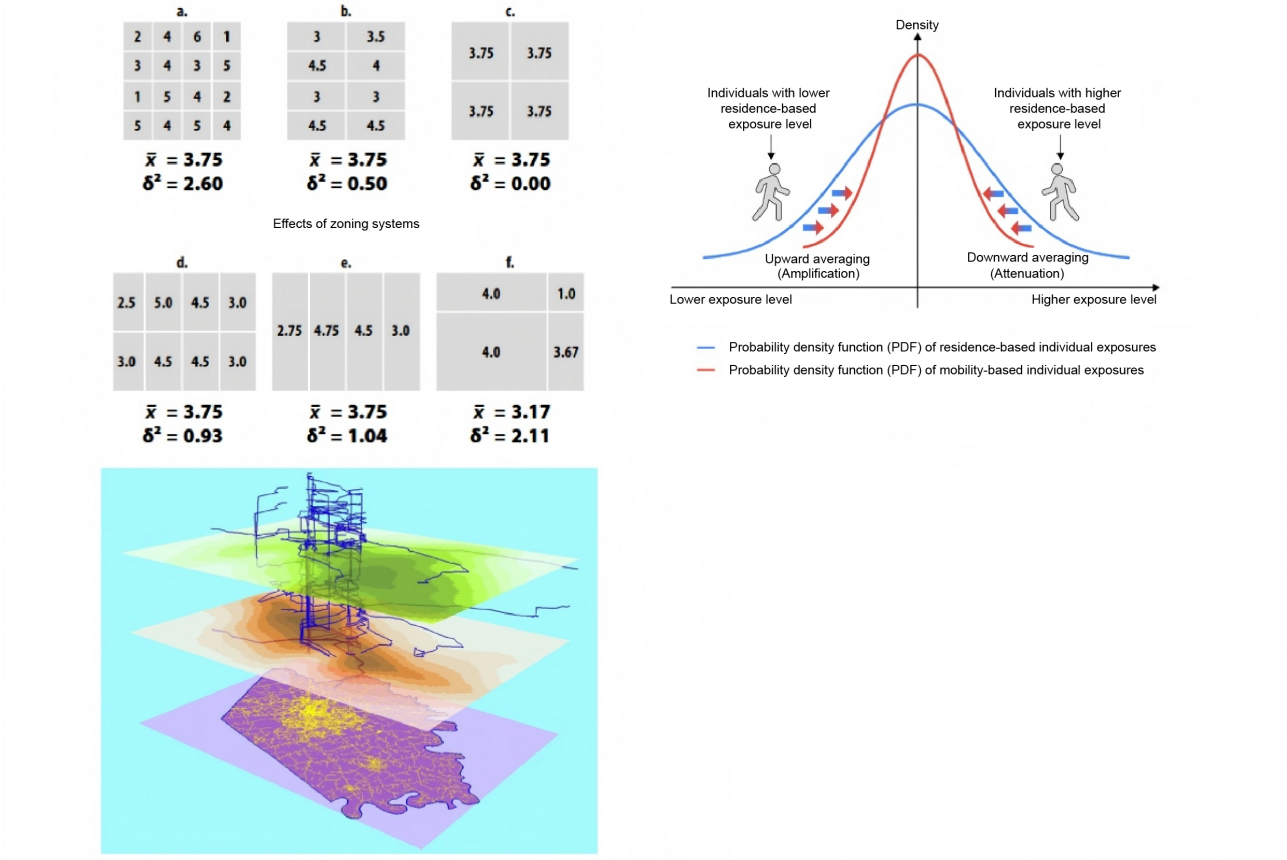

Furthermore, all involved studies illustrated the ongoing challenges of balancing granularity and comprehensiveness in assessing NGRCs. On the one hand, actively collected, subjective NGRC measures provide individualized insights but are limited in granularity and comprehensiveness. On the other hand, passively collected, objective indicators offer broad coverage but often lack individual insights and granularity, potentially due to existing dataset constraints. This trade-off underscores the need for integrated approaches that combine active and passive data to capture the complex, dynamic interplay between NGRCs and health behaviors.

To improve the granularity and comprehensiveness of NGRCs in various behavioral interventions, especially lifestyle change interventions, HISs—preferably tethered or interconnected PHRs in outpatient settings—should be considered. We have summarized 3 recommendations in Textbox 3.

Question 3: Question Regarding Stakeholders' Insights

Improved perceived value, convenience, patient autonomy, and privacy were consistently reported as outcomes of integrating technological (HISs) and content (NGRCs) innovations into behavioral interventions in all 10 included studies. On the other hand, social concerns persisted, including provider workload and the potential for discrimination. These benefits and concerns could be influenced by participants' computer literacy, which was rarely reported in the studies. Given this gap, future research should explore how to balance technological and content innovations with unresolved social concerns, accounting for variations in computer literacy.

The NGRC information needs of providers, the clinical usefulness of NGRC data, and the usefulness of NGRC-related data visualizations are not yet well supported by existing evidence. Future studies should investigate which NGRCs should be presented in HISs, how they should be used in practice, and which interactive features best support their use.

Stakeholders' insights into the integration of NGRCs and/or HISs into lifestyle interventions were not explored in the included studies. This highlights a critical gap in both technological and content innovations, as well as in addressing social concerns and in the integration of HISs and NGRCs into lifestyle change interventions.

We have summarized 5 recommendations focusing on enhancing NGRC and/or HIS integrations in behavioral interventions in Textbox 3.

Question 4: Question Regarding Research Design

We found limited coverage and inconsistent health outcomes of NGRC-focused behavioral interventions using HISs. Health outcomes focused mainly on health care utilization (eg, emergency visits), with limited coverage of clinical indicators, including medication adherence [97], asthma control [92], cancer screening [98], and blood pressure [87]. This limited coverage of clinical health outcomes limits the understanding of long-term

XSL•FO
RenderX

behavior change and highlights the need for more comprehensive assessments. Moreover, the inconsistent health care utilization outcomes [88,91] may be caused by the inconsistent and/or insufficient reporting of 5 aspects. These aspects include (1) NGRC attributes (eg, definitions and spatiotemporal characteristics), (2) HIS types and functionalities, (3) assessment methods (eg, clinical metrics [eg, HbA_{1c}] and health care utilization), (4) stakeholders (eg, only HISs or various health providers), and (5) targeted diseases. Such heterogeneity causes low interstudy comparability and reproducibility. It also limits the ability to determine which behavioral interventions, leveraging specific NGRCs via particular HIS functions, are most effective, thereby complicating the translation of findings into evidence-based practice.

No studies have addressed key issues such as cost-effectiveness and ethical considerations. Future research should examine these critical factors to ensure successful implementation.

To develop evidence, we have summarized 3 recommendations in Textbox 3.

Generalizability of the Results

Our objective was to synthesize global literature on NGRC-focused behavioral interventions supported by HISs. However, we were unable to identify published, peer-reviewed studies conducted outside of the United States. Initiatives, such as the European Health Data Space (EHDS) [125] and China's Healthy China Initiative [126], reflect growing efforts to integrate SDoH, including NGRCs, into HISs. On one hand, contextual differences do not preclude transferability. The contextual differences include cultural norms, socioeconomic conditions, and geographic contexts. With appropriate localization and system-level adaptation, the core principles identified in United States–based studies can be effectively applied in diverse settings. However, the limited diversity of study settings may obscure unique challenges and solutions relevant to low-resource or non-Western countries. Addressing these gaps is essential, and future research should ensure that context-specific NGRC-focused behavioral interventions using HISs are inclusive, adaptable, and globally relevant (Table 3). On the other hand, technological and political differences across the world do not influence the generalizability of our study. These differences include (1) HIS infrastructure, architecture, and integration capabilities, and (2) data standards, privacy regulations (eg, the European General Data Protection Regulation [127]), and governance policies. The commonalities of these differences help support the generalizability of the findings [128].

Strengths and Limitations

Our review has 4 key strengths. First, this article reviews the current state of NGRC-focused behavioral interventions using HISs. This provides a comprehensive analysis from 3 perspectives: technology, NGRC content, and stakeholders' insights. Second, we searched a wide range of databases, leading to publications from diverse disciplines, including medical journals, environmental journals, and computer science conferences. Third, we consulted a library information specialist to develop the search strategy, ensuring its comprehensiveness and accuracy, which thus enhanced the research's quality and credibility. Finally, to provide readers with sufficient context and allow them to assess the reliability of the evidence, we extracted and reported descriptive information, including study type, publication year, and sample size (Table S4 in Multimedia Appendix 1). We did not conduct a critical appraisal of the included studies, as it is not mandatory in scoping reviews. According to the Joanna Briggs Institute (JBI) methodology for scoping reviews [129], a critical appraisal is generally unnecessary unless it is directly relevant to the review objectives. Additionally, most quality assessment tools, including the Mixed Methods Appraisal Tool (MMAT) [130], primarily evaluate study design, data collection, and methodological rigor. Therefore, applying such tools would not provide meaningful information for our objectives (eg, HIS functionalities and NGRC indicators).

Our study also has several limitations that should be considered. First, NGRCs are ambiguous, suggesting that they are open to multiple interpretations or are vague. For example, in various studies, neighborhood safety may refer to different things, but there are no clear details of this concept in the studies. However, resolving this ambiguity is challenging because of the lack of standardized definitions and the context-dependent characteristics of NGRCs. Therefore, future studies should adopt detailed and consistent definitions of NGRCs, ideally guided by standardized terminologies or ontologies. These terminologies or ontologies can leverage and expand existing terminologies (eg, "community details" in Systematized Nomenclature of Medicine—Clinical Terms [SNOMED CT] and Logical Observation Identifiers Names and Codes [LOINC]) and SDoH ontologies [24].

Possible Mechanisms and Implications for Clinicians or Policymakers

HISs are often seen as passive recorders of health data. However, tethered or interconnected PHRs can actively participate in the entire process of NGRC-focused behavioral interventions, especially in outpatient lifestyle change interventions, with the relatively limited help of health care providers. For example, platforms like the iManageCancer platform for cancer patients and the iManageMyHealth app for their physicians provide personalized content from reliable public resources on cancer. However, these platforms do not currently consider NGRC factors and focus on behavioral interventions [3]. This underscores the importance for providers and policymakers to utilize tethered or interconnected PHRs to collect comprehensive, dynamic, and static NGRCs; deliver timely behavioral interventions in outpatient settings; monitor behaviors and the health status; and assess interventions. By doing so, they can achieve public health goals and promote health equity.

Conclusion

In this study, we found that most NGRC-focused behavioral interventions utilized transportation barriers to support social needs interventions. Meanwhile, HISs were involved only in specific aspects of the NGRC-focused behavioral intervention process. To achieve comprehensive dynamic and/or

XSL•FO
RenderX

high-resolution NGRC considerations and the full integration of HISs throughout the behavioral intervention process, given the limited and heterogeneous evidence, further research is needed to determine how tethered or interconnected PHRs can effectively support NGRC-focused interventions, especially lifestyle change interventions. During implementation, it is essential to address social concerns alongside technological (eg, HIS integration) and content innovations (eg, NGRC integration). We compiled a list of 15 recommendations for future research. These recommendations are likely to accelerate the integration of tethered or interconnected PHRs in NGRC-focused behavioral interventions.

Acknowledgments

Generative artificial intelligence (AI) tools were used for writing assistance. Generative AI tools (eg, ChatGPT) were used for language editing and minor improvements in phrasing after the original writing was completed. We would like to thank Valerie Moran from Luxembourg Institute of Socio-Economic Research (LISER) for shaping the thematic focus and structure of this scoping review.

Funding

The study was funded by the China Scholarship Council (CSC) (file number: 202208140027).

Authors' Contributions

XY, MD, and RC are the guarantors of the integrity of the entire study. All authors contributed to the study's conceptualization and design. JGD performed the literature search. XY, MD, and RC contributed to study selection and interpretation. XY wrote the manuscript. MD, RC, HY, MS, and JGD reviewed and edited the manuscript. All authors read and approved the manuscript.

Conflicts of Interest

None declared.

Multimedia Appendix 1
Additional information to support the scoping review.
[DOCX File, 62 KB - medinform_v14i1e77296_app1.docx]

Checklist 1
PRISMA-ScR checklist
[PDF File, 151 KB - medinform_v14i1e77296_app2.pdf]

References

1. Anderson NB, Bulatao RA, Cohen B, National Research Council (US) Panel on Race, Ethnicity,and Health in Later Life. Critical Perspectives on Racial and Ethnic Differences in Health in Late Life: National Academies Press (US); 2004. [doi: 10.17226/11086] [Medline: 20669464]
2. Lunde P, Nilsson BB, Bergland A, Kværner KJ, Bye A. The effectiveness of smartphone apps for lifestyle improvement in noncommunicable diseases: systematic review and meta-analyses. J Med Internet Res 2018 May 4;20(5):e162. [doi: 10.2196/jmir.9751] [Medline: 29728346]
3. Schera F, Schäfer M, Bucur A, et al. iManageMyHealth and iSupportMyPatients: mobile decision support and health management apps for cancer patients and their doctors. Ecancermedicalscience 2018;12:848. [doi: 10.3332/ecancer.2018.848] [Medline: 30079110]
4. Burgess E, Hassmén P, Pumpa KL. Determinants of adherence to lifestyle intervention in adults with obesity: a systematic review. Clin Obes 2017 Jun;7(3):123-135. [doi: 10.1111/cob.12183] [Medline: 28296261]
5. Cummings KM, Fong GT, Borland R. Environmental influences on tobacco use: evidence from societal and community influences on tobacco use and dependence. Annu Rev Clin Psychol 2009;5:433-458. [doi: 10.1146/annurev.clinpsy.032408.153607] [Medline: 19327036]
6. Basta LA, Richmond TS, Wiebe DJ. Neighborhoods, daily activities, and measuring health risks experienced in urban environments. Soc Sci Med 2010 Dec;71(11):1943-1950. [doi: 10.1016/j.socscimed.2010.09.008]
7. Kepper MM, Myers CA, Denstel KD, Hunter RF, Guan W, Broyles ST. The neighborhood social environment and physical activity: a systematic scoping review. Int J Behav Nutr Phys Act 2019 Dec 9;16(1):124. [doi: 10.1186/s12966-019-0873-7] [Medline: 31815626]
8. Popkin B, Duffey K, Gordonlarsen P. Environmental influences on food choice, physical activity and energy balance. Physiol Behav 2005 Dec 15;86(5):603-613. [doi: 10.1016/j.physbeh.2005.08.051]

XSL•FO
RenderX

9. Healthy People 2030 - social determinants of health. Department of Health and Human Services, Office of Disease Prevention and Health Promotion. URL: https://odphp.health.gov/healthypeople/priority-areas/social-determinants-health [accessed 2025-10-15]
10. Jilcott SB, Keyserling TC, Samuel-Hodge CD, et al. Linking clinical care to community resources for cardiovascular disease prevention: the North Carolina Enhanced WISEWOMAN project. J Womens Health (Larchmt) 2006 Jun;15(5):569-583. [doi: 10.1089/jwh.2006.15.569] [Medline: 16796484]
11. Christian BJ. Translational research - the intersection between sociocultural and environmental factors and the health of children and families. J Pediatr Nurs 2017;37:127-131. [doi: 10.1016/j.pedn.2017.09.013] [Medline: 28988617]
12. Diez Roux AV, Mair C. Neighborhoods and health. Ann N Y Acad Sci 2010 Feb;1186(1):125-145. [doi: 10.1111/j.1749-6632.2009.05333.x] [Medline: 20201871]
13. Samuels-Kalow ME, Camargo CA. The use of geographic data to improve asthma care delivery and population health. Clin Chest Med 2019 Mar;40(1):209-225. [doi: 10.1016/j.ccm.2018.10.012] [Medline: 30691713]
14. Alharthy A, Hosler AS, Leckman-Westin E, Kammer JR. Association between tobacco retailer density and smoking among adults with diabetes and serious mental illness in New York state. Prev Chronic Dis 2022 Jan 6;19:E01. [doi: 10.5888/pcd19.210270] [Medline: 34990338]
15. Cottrell EK, Hendricks M, Dambrun K, et al. Comparison of community-level and patient-level social risk data in a network of community health centers. JAMA Netw Open 2020 Oct 1;3(10):e2016852. [doi: 10.1001/jamanetworkopen.2020.16852] [Medline: 33119102]
16. Edmonds AT, Rhew IC, Jones-Smith J, et al. Neighborhood disadvantage, patterns of unhealthy alcohol use, and differential associations by gender, race/ethnicity, and rurality: a study of Veterans Health Administration patients. J Stud Alcohol Drugs 2022 Nov;83(6):867-878. [doi: 10.15288/jsad.21-00110] [Medline: 36484584]
17. García R, Muñoz MA, Navas E, Vinyoles E, Verdú-Rotellar JM, Del Val JL. Variability in cardiovascular risk factor control in patients with heart failure according to gender and socioeconomic status. J Womens Health (Larchmt) 2022 May;31(5):690-697. [doi: 10.1089/jwh.2021.0404] [Medline: 35041531]
18. Howell NA, Tu JV, Moineddin R, Chu A, Booth GL. Association between neighborhood walkability and predicted 10-year cardiovascular disease risk: the CANHEART (Cardiovascular Health in Ambulatory Care Research Team) cohort. J Am Heart Assoc 2019 Nov 5;8(21):e013146. [doi: 10.1161/JAHA.119.013146] [Medline: 31665997]
19. Kurani SS, Lampman MA, Funni SA, et al. Association between area-level socioeconomic deprivation and diabetes care quality in US primary care practices. JAMA Netw Open 2021 Dec 1;4(12):e2138438. [doi: 10.1001/jamanetworkopen.2021.38438] [Medline: 34964856]
20. Mathur R, Schofield P, Smith D, Gilkes A, White P, Hull S. Is individual smoking behaviour influenced by area-level ethnic density? A cross-sectional electronic health database study of inner south-east London. ERJ Open Res 2017 Jan;3(1):00130-2016. [doi: 10.1183/23120541.00130-2016] [Medline: 28435842]
21. Miranda O, Fan P, Qi X, et al. DeepBiomarker2: prediction of alcohol and substance use disorder risk in post-traumatic stress disorder patients using electronic medical records and multiple social determinants of health. J Pers Med 2024 Jan 14;14(1):94. [doi: 10.3390/jpm14010094] [Medline: 38248795]
22. Rodriguez-Mireles S, Lopez-Valcarcel BG, Galdos-Arias P, Perez-Diaz E, Serra-Majem L. Socioeconomic disparities in diet and physical activity in children: evidence from well-child visit electronic health records in the Canary Islands, Spain. J Epidemiol Community Health 2024 May 9;78(6):354-359. [doi: 10.1136/jech-2023-220335] [Medline: 38458631]
23. To D, Joyce C, Kulshrestha S, et al. The addition of United States census-tract data does not improve the prediction of substance misuse. AMIA Annu Symp Proc 2021;2021:1149-1158. [Medline: 35308901]
24. DesRoches CM, Wachenheim D, Harcourt K, Garcia A, Shah R. Collecting, documenting, and using social determinants of health data: patient and clinician views. : OpenNotes; 2025 URL: https://www.opennotes.org/wp-content/uploads/2025/02/ASTP_OpenNotes_SDOH-FinalReport_508.pdf [accessed 2026-02-06]
25. Haux R. Health information systems - past, present, future. Int J Med Inform 2006;75(3-4):268-281. [doi: 10.1016/j.ijmedinf.2005.08.002] [Medline: 16169771]
26. Kim JW, Ryu B, Cho S, et al. Impact of personal health records and wearables on health outcomes and patient response: three-arm randomized controlled trial. JMIR Mhealth Uhealth 2019 Jan 4;7(1):e12070. [doi: 10.2196/12070] [Medline: 30609978]
27. Tang PC, Ash JS, Bates DW, Overhage JM, Sands DZ. Personal health records: definitions, benefits, and strategies for overcoming barriers to adoption. J Am Med Inform Assoc 2006;13(2):121-126. [doi: 10.1197/jamia.M2025] [Medline: 16357345]
28. Cottrell EK, O'Malley JP, Dambrun K, et al. The impact of social and clinical complexity on diabetes control measures. J Am Board Fam Med 2020;33(4):600-610. [doi: 10.3122/jabfm.2020.04.190367] [Medline: 32675271]
29. Holt JM, Cusatis R, Asan O, et al. Incorporating patient-generated contextual data into care: clinician perspectives using the consolidated framework for implementation science. Healthcare (Basel) 2020 Mar;8(1):100369. [doi: 10.1016/j.hjdsi.2019.100369]

XSL•FO
RenderX

30. Abd-Alrazaq AA, Bewick BM, Farragher T, Gardner P. Factors that affect the use of electronic personal health records among patients: a systematic review. Int J Med Inform 2019 Jun;126:164-175. [doi: 10.1016/j.ijmedinf.2019.03.014] [Medline: 31029258]
31. Andrikopoulou E, Scott P, Herrera H, Good A. What are the important design features of personal health records to improve medication adherence for patients with long-term conditions? A systematic literature review. BMJ Open 2019 Sep 26;9(9):e028628. [doi: 10.1136/bmjopen-2018-028628] [Medline: 31558449]
32. Aslani N, Ahmadi M, Samadbeik M. A systematic review of the attributes of electronic personal health records for patients with multiple sclerosis. Health Technol 2020 May;10(3):587-599. [doi: 10.1007/s12553-019-00387-4]
33. Azizi A, Aboutorabi R, Mazloum-Khorasani Z, Hoseini B, Tara M. Diabetic personal health record: a systematic review article. Iran J Public Health 2016 Nov;45(11):1388-1398. [Medline: 28032056]
34. Chiesa V, Chiarenza A, Mosca D, Rechel B. Health records for migrants and refugees: a systematic review. Health Policy 2019 Sep;123(9):888-900. [doi: 10.1016/j.healthpol.2019.07.018] [Medline: 31439455]
35. Crameri KA, Maher L, Van Dam P, Prior S. Personal electronic healthcare records: what influences consumers to engage with their clinical data online? A literature review. HIM J 2022 Jan;51(1):3-12. [doi: 10.1177/1833358319895369]
36. Eastway J, Lizarondo L. Experiences of adult patients with chronic non-communicable disease using electronic personal health records for self-management: a qualitative systematic review protocol. JBI Database System Rev Implement Rep 2019 Nov;17(11):2334-2342. [doi: 10.11124/JBISRIR-2017-003941] [Medline: 31232888]
37. Fernández-Alemán JL, Seva-Llor CL, Toval A, Ouhbi S, Fernández-Luque L. Free web-based personal health records: an analysis of functionality. J Med Syst 2013 Dec;37(6):9990. [doi: 10.1007/s10916-013-9990-z] [Medline: 24221916]
38. Genitsaridi I, Kondylakis H, Koumakis L, Marias K, Tsiknakis M. Evaluation of personal health record systems through the lenses of EC research projects. Comput Biol Med 2015 Apr;59:175-185. [doi: 10.1016/j.compbiomed.2013.11.004] [Medline: 24315661]
39. Harahap NC, Handayani PW, Hidayanto AN. Functionalities and issues in the implementation of personal health records: systematic review. J Med Internet Res 2021 Jul 21;23(7):e26236. [doi: 10.2196/26236] [Medline: 34287210]
40. Jabour A, Jones JF. Facilitators and barriers to patients' engagements with personal health records: systematic review. In: Stephanidis C, Antona M, editors. Universal Access in Human-Computer Interaction Applications and Services for Quality of Life UAHCI 2013 Lecture Notes in Computer Science: Springer; 2013, Vol. 8011:472-481. [doi: 10.1007/978-3-642-39194-1_55]
41. Kharbouch M, Idri A, Fernandez-Aleman JL, Redman L, Toval A, Stelate Y. Reviewing the features and functionalities of contraception mPHRs. Health Policy Technol 2022 Sep;11(3):100633. [doi: 10.1016/j.hlpt.2022.100633]
42. Kneale L, Demiris G. Lack of diversity in personal health record evaluations with older adult participants: a systematic review of literature. J Innov Health Inform 2017 Jan 15;23(4):881. [doi: 10.14236/jhi.v23i4.881] [Medline: 28346131]
43. Thompson MJ, Reilly JD, Valdez RS. Work system barriers to patient, provider, and caregiver use of personal health records: a systematic review. Appl Ergon 2016 May;54:218-242. [doi: 10.1016/j.apergo.2015.10.010] [Medline: 26851482]
44. Zhao JY, Song B, Anand E, et al. Barriers, facilitators, and solutions to optimal patient portal and personal health record use: a systematic review of the literature. AMIA Annu Symp Proc 2017;2017:1913-1922. [Medline: 29854263]
45. Golembiewski E, Allen KS, Blackmon AM, Hinrichs RJ, Vest JR. Combining nonclinical determinants of health and clinical data for research and evaluation: rapid review. JMIR Public Health Surveill 2019 Oct 7;5(4):e12846. [doi: 10.2196/12846] [Medline: 31593550]
46. Schinasi LH, Auchincloss AH, Forrest CB, Diez Roux AV. Using electronic health record data for environmental and place based population health research: a systematic review. Ann Epidemiol 2018 Jul;28(7):493-502. [doi: 10.1016/j.annepidem.2018.03.008] [Medline: 29628285]
47. Chishtie JA, Tea J, Ester M, et al. Integration of screening and referral tools for social determinants of health and modifiable lifestyle factors in the Epic electronic health record system: scoping review. J Med Internet Res 2025 Sep 15;27:e73615. [doi: 10.2196/73615] [Medline: 40953441]
48. Arroyave Caicedo NM, Parry E, Arslan N, Park S. Integration of social determinants of health information within the primary care electronic health record: a systematic review of patient perspectives and experiences. BJGP Open 2024 Apr;8(1):BJGPO.2023.0155. [doi: 10.3399/BJGPO.2023.0155] [Medline: 37673433]
49. Chen M, Tan X, Padman R. Social determinants of health in electronic health records and their impact on analysis and risk prediction: a systematic review. J Am Med Inform Assoc 2020 Nov 1;27(11):1764-1773. [doi: 10.1093/jamia/ocaa143] [Medline: 33202021]
50. Li C, Mowery DL, Ma X, et al. Realizing the potential of social determinants data in EHR systems: a scoping review of approaches for screening, linkage, extraction, analysis, and interventions. J Clin Trans Sci 2024;8(1). [doi: 10.1017/cts.2024.571]
51. Tricco AC, Lillie E, Zarin W, et al. PRISMA extension for scoping reviews (PRISMA-ScR): checklist and explanation. Ann Intern Med 2018 Oct 2;169(7):467-473. [doi: 10.7326/M18-0850] [Medline: 30178033]
52. Health informatics — electronic health record — definition, scope and context. : ISO (the International Organization for Standardization); 2005 ISO/TR 20514:2005(en) URL: https://www.iso.org/obp/ui/en/#iso:std:iso:tr:20514:ed-1:v1:en [accessed 2026-02-06]

XSL•FO
RenderX

53. Coleman K, Austin BT, Brach C, Wagner EH. Evidence on the chronic care model in the new millennium. Health Aff (Millwood) 2009;28(1):75-85. [doi: 10.1377/hlthaff.28.1.75] [Medline: 19124857]
54. Siminerio LM, Piatt GA, Emerson S, et al. Deploying the chronic care model to implement and sustain diabetes self-management training programs. Diabetes Educ 2006;32(2):253-260. [doi: 10.1177/0145721706287156] [Medline: 16554429]
55. Siminerio LM, Piatt G, Zgibor JC. Implementing the chronic care model for improvements in diabetes care and education in a rural primary care practice. Diabetes Educ 2005;31(2):225-234. [doi: 10.1177/0145721705275325] [Medline: 15797851]
56. Stellefson M, Dipnarine K, Stopka C. The chronic care model and diabetes management in US primary care settings: a systematic review. Prev Chronic Dis 2013;10:E26. [doi: 10.5888/pcd10.120180] [Medline: 23428085]
57. Boonstra A, Broekhuis M. Barriers to the acceptance of electronic medical records by physicians from systematic review to taxonomy and interventions. BMC Health Serv Res 2010 Aug 6;10(1):231. [doi: 10.1186/1472-6963-10-231] [Medline: 20691097]
58. Tang PC, Lee TH. Your doctor's office or the internet? Two paths to personal health records. N Engl J Med 2009 Mar 26;360(13):1276-1278. [doi: 10.1056/NEJMp0810264] [Medline: 19321866]
59. Stimson RJ, Golledge RG. Spatial Behavior: A Geographic Perspective: Guilford Press; 1996.
60. Kwan MP. The uncertain geographic context problem. Annals of the Association of American Geographers 2012 Sep;102(5):958-968. [doi: 10.1080/00045608.2012.687349]
61. Rodríguez DA, Evenson KR, Diez Roux AV, Brines SJ. Land use, residential density, and walking. Am J Prev Med 2009 Nov;37(5):397-404. [doi: 10.1016/j.amepre.2009.07.008]
62. Giles-Corti B, Donovan RJ. Socioeconomic status differences in recreational physical activity levels and real and perceived access to a supportive physical environment. Prev Med 2002 Dec;35(6):601-611. [doi: 10.1006/pmed.2002.1115] [Medline: 12460528]
63. Giles-Corti B, Donovan RJ. Relative influences of individual, social environmental, and physical environmental correlates of walking. Am J Public Health 2003 Sep;93(9):1583-1589. [doi: 10.2105/ajph.93.9.1583] [Medline: 12948984]
64. Crawford D, Cleland V, Timperio A, et al. The longitudinal influence of home and neighbourhood environments on children's body mass index and physical activity over 5 years: the CLAN study. Int J Obes 2010 Jul;34(7):1177-1187. [doi: 10.1038/ijo.2010.57]
65. Zhang R, Wulff H, Duan Y, Wagner P. Associations between the physical environment and park-based physical activity: a systematic review. J Sport Health Sci 2019 Sep;8(5):412-421. [doi: 10.1016/j.jshs.2018.11.002] [Medline: 31534816]
66. Luik AI, Zuurbier LA, Hofman A, Van Someren EJW, Tiemeier H. Stability and fragmentation of the activity rhythm across the sleep-wake cycle: the importance of age, lifestyle, and mental health. Chronobiol Int 2013 Dec;30(10):1223-1230. [doi: 10.3109/07420528.2013.813528] [Medline: 23971909]
67. Feinglass J, Lee J, Semanik P, Song J, Dunlop D, Chang R. The effects of daily weather on accelerometer-measured physical activity. J Phys Act Health 2011 Sep;8(7):934-943. [doi: 10.1123/jpah.8.7.934] [Medline: 21885884]
68. Ferguson T, Curtis R, Fraysse F, et al. Weather associations with physical activity, sedentary behaviour and sleep patterns of Australian adults: a longitudinal study with implications for climate change. Int J Behav Nutr Phys Act 2023 Mar 14;20(1):30. [doi: 10.1186/s12966-023-01414-4] [Medline: 36918954]
69. Hu X, Knibbs LD, Zhou Y, Ou Y, Dong GH, Dong H. The role of lifestyle in the association between long-term ambient air pollution exposure and cardiovascular disease: a national cohort study in China. BMC Med 2024 Mar 5;22(1):93. [doi: 10.1186/s12916-024-03316-z] [Medline: 38439026]
70. Strak M, Janssen N, Beelen R, et al. Associations between lifestyle and air pollution exposure: potential for confounding in large administrative data cohorts. Environ Res 2017 Jul;156:364-373. [doi: 10.1016/j.envres.2017.03.050] [Medline: 28395240]
71. Michie S, van Stralen MM, West R. The behaviour change wheel: a new method for characterising and designing behaviour change interventions. Implement Sci 2011 Apr 23;6(1):42. [doi: 10.1186/1748-5908-6-42] [Medline: 21513547]
72. Nair BR, Browne W. Chronic disease management: seizing the moment in medical education. Pharm Med 2008 Nov;22(6):351-354. [doi: 10.1007/BF03256731]
73. Irizarry T, DeVito Dabbs A, Curran CR. Patient portals and patient engagement: a state of the science review. J Med Internet Res 2015 Jun 23;17(6):e148. [doi: 10.2196/jmir.4255] [Medline: 26104044]
74. Kamiński M, Kręgielska-Narożna M, Bogdański P. Seasonal variation in lifestyle behavior in Poland: Google searches and market sales analysis. BMC Public Health 2021 Aug 6;21(1):1516. [doi: 10.1186/s12889-021-11543-9] [Medline: 34362345]
75. Wagner EH, Austin BT, Davis C, Hindmarsh M, Schaefer J, Bonomi A. Improving chronic illness care: translating evidence into action. Health Aff (Millwood) 2001;20(6):64-78. [doi: 10.1377/hlthaff.20.6.64] [Medline: 11816692]
76. Venerandi A, Mellen H, Romice O, Porta S. Walkability indices—the state of the art and future directions: a systematic review. Sustainability 2024 Aug 6;16(16):6730. [doi: 10.3390/su16166730]
77. Kane NJ, Wang X, Gerkovich MM, et al. The Envirome Web Service: patient context at the point of care. J Biomed Inform 2021 Jul;119:103817. [doi: 10.1016/j.jbi.2021.103817] [Medline: 34020026]

XSL•FO
RenderX

78. Cordova-Ramos EG, Jain C, Torrice V, et al. Implementing social risk screening and referral to resources in the NICU. Pediatrics 2023 Apr 1;151(4):e2022058975. [doi: 10.1542/peds.2022-058975] [Medline: 36919445]
79. Fortin K, Vasan A, Wilson-Hall CL, Brooks E, Rubin D, Scribano PV. Using quality improvement and technology to improve social supports for hospitalized children. Hosp Pediatr 2021 Oct;11(10):1120-1129. [doi: 10.1542/hpeds.2020-005800] [Medline: 34475224]
80. Stark K, Mathur M, Fok C, et al. Evaluation of a clinic-based, electronic social determinants of health screening and intervention in primary care pediatrics. Acad Pediatr 2024 Mar;24(2):302-308. [doi: 10.1016/j.acap.2023.12.010] [Medline: 38160752]
81. Glasser NJ, Lindau ST, Wroblewski K, et al. Effect of a social care intervention on health care experiences of caregivers of hospitalized children: a randomized clinical trial. JAMA Pediatr 2023 Dec 1;177(12):1266-1275. [doi: 10.1001/jamapediatrics.2023.4596] [Medline: 37902777]
82. Buitron de la Vega P, Losi S, Sprague Martinez L, et al. Implementing an EHR-based screening and referral system to address social determinants of health in primary care. Med Care 2019 Jun;57 Suppl 6 Suppl 2(Suppl 2):S133-S139. [doi: 10.1097/MLR.0000000000001029] [Medline: 31095052]
83. Johnston DC, Mathews WD, Maus A, Gustafson DH. Using smartphones to improve treatment retention among impoverished substance-using appalachian women: a naturalistic study. Subst Abuse 2019;13:1178221819861377. [doi: 10.1177/1178221819861377] [Medline: 31312084]
84. Russell LE, Cohen AJ, Chrzas S, et al. Implementing a social needs screening and referral program among veterans: Assessing Circumstances & Offering Resources for Needs (ACORN). J Gen Intern Med 2023 Oct;38(13):2906-2913. [doi: 10.1007/s11606-023-08181-9] [Medline: 37165261]
85. Percac-Lima S, Grant RW, Green AR, et al. A culturally tailored navigator program for colorectal cancer screening in a community health center: a randomized, controlled trial. J Gen Intern Med 2009 Feb;24(2):211-217. [doi: 10.1007/s11606-008-0864-x] [Medline: 19067085]
86. Wallace AS, Luther B, Guo JW, Wang CY, Sisler S, Wong B. Implementing a social determinants screening and referral infrastructure during routine emergency department visits, Utah, 2017-2018. Prev Chronic Dis 2020 Jun 18;17:E45. [doi: 10.5888/pcd17.190339] [Medline: 32553071]
87. Tanumihardjo JP, Kuther S, Wan W, et al. New frontiers in diabetes care: quality improvement study of a population health team in rural critical access hospitals. J Gen Intern Med 2023 Mar;38(Suppl 1):56-64. [doi: 10.1007/s11606-022-07928-0] [Medline: 36864269]
88. Roth SE, Gronowski B, Jones KG, et al. Evaluation of an integrated intervention to address clinical care and social needs among patients with type 2 diabetes. J Gen Intern Med 2023 Mar;38(Suppl 1):38-44. [doi: 10.1007/s11606-022-07920-8] [Medline: 36864267]
89. Bechtel N, Jones A, Kue J, Ford JL. Evaluation of the core 5 social determinants of health screening tool. Public Health Nurs 2022 Mar;39(2):438-445. [doi: 10.1111/phn.12983] [Medline: 34628675]
90. Taber KA, Williams JN, Huang W, et al. Use of an integrated care management program to uncover and address social determinants of health for individuals with lupus. ACR Open Rheumatol 2021 May;3(5):305-311. [doi: 10.1002/acr2.11236] [Medline: 33779065]
91. Gupta D, Self S, Thomas D, Supra J, Rudisill C. Understanding the role of a technology and EMR-based social determinants of health screening tool and community-based resource connections in health care resource utilization. Med Care 2023 Jul 1;61(7):423-430. [doi: 10.1097/MLR.0000000000001800] [Medline: 36729786]
92. Britto MT, Vockell ALB, Munafo JK, et al. Improving outcomes for underserved adolescents with asthma. Pediatrics 2014 Feb;133(2):e418-e427. [doi: 10.1542/peds.2013-0684] [Medline: 24470645]
93. Loo S, Anderson E, Lin JG, et al. Evaluating a social risk screening and referral program in an urban safety-net hospital emergency department. J Am Coll Emerg Physicians Open 2023 Feb;4(1):e12883. [doi: 10.1002/emp2.12883] [Medline: 36704207]
94. Lynch S, Street NW, Sharpe L, Kellish A. Social determinants of health screening: primary care PRAPARE tool implementation. J Nurse Pract 2024 Apr;20(4):104955. [doi: 10.1016/j.nurpra.2024.104955]
95. Palakshappa D, Benefield AJ, Furgurson KF, et al. Feasibility of mobile technology to identify and address patients' unmet social needs in a primary care clinic. Popul Health Manag 2021 Jun;24(3):385-392. [doi: 10.1089/pop.2020.0059] [Medline: 32924796]
96. Wright QC, Wiencek CA, Williams IC. Utilizing a tailored approach to standardized screening of health-related social needs. J Nurs Care Qual 2024;39(2):114-120. [doi: 10.1097/NCQ.0000000000000745] [Medline: 37729002]
97. Wu L, Chang C, Lo K, et al. Telephone-based social health screening by pharmacists in the nonadherent Medicare population. J Manag Care Spec Pharm 2023 Nov;29(11):1184-1192. [doi: 10.18553/jmcp.2023.29.11.1184] [Medline: 37889865]
98. Percac-Lima S, Ashburner JM, Rigotti NA, et al. Patient navigation for lung cancer screening among current smokers in community health centers a randomized controlled trial. Cancer Med 2018 Mar;7(3):894-902. [doi: 10.1002/cam4.1297] [Medline: 29464877]
99. University of Wisconsin–Madison - Center for Health Enhancement Systems Studies. URL: https://center.chess.wisc.edu/ [accessed 2025-04-12]

XSL•FO
RenderX

100. Hosseini A, Emami H, Sadat Y, Paydar S. Integrated personal health record (PHR) security: requirements and mechanisms. BMC Med Inform Decis Mak 2023 Jul 10;23(1):116. [doi: 10.1186/s12911-023-02225-0] [Medline: 37430242]
101. Dao KP, De Cocker K, Tong HL, Kocaballi AB, Chow C, Laranjo L. Smartphone-delivered ecological momentary interventions based on ecological momentary assessments to promote health behaviors: systematic review and adapted checklist for reporting ecological momentary assessment and intervention studies. JMIR Mhealth Uhealth 2021 Nov 19;9(11):e22890. [doi: 10.2196/22890] [Medline: 34806995]
102. Fukuoka Y, Gay C, Haskell W, Arai S, Vittinghoff E. Identifying factors associated with dropout during prerandomization run-in period from an mHealth physical activity education study: the mPED trial. JMIR Mhealth Uhealth 2015 Apr 13;3(2):e34. [doi: 10.2196/mhealth.3928] [Medline: 25872754]
103. Owen JE, Jaworski BK, Kuhn E, Makin-Byrd KN, Ramsey KM, Hoffman JE. mHealth in the wild: using novel data to examine the reach, use, and impact of PTSD coach. JMIR Ment Health 2015;2(1):e7. [doi: 10.2196/mental.3935] [Medline: 26543913]
104. Oikonomidi T, Ravaud P, LeBeau J, Tran VT. A systematic scoping review of just-in-time, adaptive interventions finds limited automation and incomplete reporting. J Clin Epidemiol 2023 Feb;154:108-116. [doi: 10.1016/j.jclinepi.2022.12.006] [Medline: 36521653]
105. Kollapally NM, Chen Y, Xu J, Geller J. An ontology for the social determinants of health domain. Presented at: 2022 IEEE International Conference on Bioinformatics and Biomedicine (BIBM); Dec 6-8, 2022. [doi: 10.1109/BIBM55620.2022.9995544]
106. Dang Y, Li F, Hu X, et al. Systematic design and data-driven evaluation of social determinants of health ontology (SDoHO). J Am Med Inform Assoc 2023 Aug 18;30(9):1465-1473. [doi: 10.1093/jamia/ocad096] [Medline: 37301740]
107. Brennan PF, Downs S, Casper G. Project HealthDesign: rethinking the power and potential of personal health records. J Biomed Inform 2010 Oct;43(5 Suppl):S3-S5. [doi: 10.1016/j.jbi.2010.09.001] [Medline: 20937482]
108. Thomas Craig KJ, Fusco N, Gunnarsdottir T, Chamberland L, Snowdon JL, Kassler WJ. Leveraging data and digital health technologies to assess and impact social determinants of health (SDoH): a state-of-the-art literature review. Online J Public Health Inform 2021;13(3):E14. [doi: 10.5210/ojphi.v13i3.11081] [Medline: 35082976]
109. Estiri H, Patel CJ, Murphy SN. Informatics can help providers incorporate context into care. JAMIA Open 2018 Jul;1(1):3-6. [doi: 10.1093/jamiaopen/ooy025] [Medline: 31984312]
110. United States, National Committee on Vital and Health Statistics. Information for health; a strategy for building the national health information infrastructure. : United States Department of Health and Human Services; 2001 URL: https://stacks.cdc.gov/view/cdc/26030 [accessed 2026-02-06]
111. Wetta RE, Severin RD, Gruhler H. An evidence-based strategy to achieve equivalency and interoperability for social-behavioral determinants of health assessment, storage, exchange, and use. Health Informatics J 2020 Jun;26(2):1477-1488. [doi: 10.1177/1460458219882265] [Medline: 31659920]
112. Deslippe AL, Soanes A, Bouchaud CC, et al. Barriers and facilitators to diet, physical activity and lifestyle behavior intervention adherence: a qualitative systematic review of the literature. Int J Behav Nutr Phys Act 2023 Feb 14;20(1):14. [doi: 10.1186/s12966-023-01424-2] [Medline: 36782207]
113. Burgess E, Hassmén P, Welvaert M, Pumpa KL. Behavioural treatment strategies improve adherence to lifestyle intervention programmes in adults with obesity: a systematic review and meta-analysis. Clin Obes 2017 Apr;7(2):105-114. [doi: 10.1111/cob.12180] [Medline: 28199047]
114. Freeman KJ, Grega ML, Friedman SM, et al. Lifestyle medicine reimbursement: a proposal for policy priorities informed by a cross-sectional survey of lifestyle medicine practitioners. Int J Environ Res Public Health 2021 Nov 5;18(21):11632. [doi: 10.3390/ijerph182111632] [Medline: 34770148]
115. Middleton KR, Anton SD, Perri MG. Long-term adherence to health behavior change. Am J Lifestyle Med 2013;7(6):395-404. [doi: 10.1177/1559827613488867] [Medline: 27547170]
116. Kim J, Kwan MP. Assessment of sociodemographic disparities in environmental exposure might be erroneous due to neighborhood effect averaging: implications for environmental inequality research. Environ Res 2021 Apr;195:110519. [doi: 10.1016/j.envres.2020.110519] [Medline: 33253702]
117. Kwan MP. How GIS can help address the uncertain geographic context problem in social science research. Ann GIS 2012 Dec;18(4):245-255. [doi: 10.1080/19475683.2012.727867]
118. Dark SJ, Bram D. The modifiable areal unit problem (MAUP) in physical geography. Progress in Physical Geography: Earth and Environment 2007 Oct;31(5):471-479. [doi: 10.1177/0309133307083294]
119. Andresen MA. Modifiable areal unit problem. In: Barnes JC, Forde DR, editors. The Encyclopedia of Research Methods in Criminology and Criminal Justice: John Wiley & Sons, Inc; 2021:854-855. [doi: 10.1002/9781119111931.ch164]
120. Kwan MP. The neighborhood effect averaging problem (NEAP): an elusive confounder of the neighborhood effect. Int J Environ Res Public Health 2018 Aug 27;15(9):1841. [doi: 10.3390/ijerph15091841] [Medline: 30150510]
121. Hinckson E, Cerin E, Mavoa S, et al. Associations of the perceived and objective neighborhood environment with physical activity and sedentary time in New Zealand adolescents. Int J Behav Nutr Phys Act 2017 Oct 25;14(1):145. [doi: 10.1186/s12966-017-0597-5] [Medline: 29065897]

XSL•FO
RenderX

122. Nyunt MSZ, Shuvo FK, Eng JY, et al. Objective and subjective measures of neighborhood environment (NE): relationships with transportation physical activity among older persons. Int J Behav Nutr Phys Act 2015 Sep 15;12(1):108. [doi: 10.1186/s12966-015-0276-3] [Medline: 26373320]
123. Jáuregui A, Salvo D, Lamadrid-Figueroa H, Hernández B, Rivera-Dommarco JA, Pratt M. Perceived and objective measures of neighborhood environment for physical activity among Mexican adults, 2011. Prev Chronic Dis 2016 Jun 9;13:E76. [doi: 10.5888/pcd13.160009] [Medline: 27281391]
124. Zhao L, Shen Z, Zhang Y, Sheng F. Study on the impact of the objective characteristics and subjective perception of the built environment on residents' physical activities in Fuzhou, China. Sustainability 2019 Dec 31;12(1):329. [doi: 10.3390/su12010329]
125. Regulation - EU - 2025/327 - EN - EUR-lex. European Union EUR-Lex. URL: https://eur-lex.europa.eu/eli/reg/2025/327/oj/eng [accessed 2025-11-28]
126. 中共中央 国务院印发《"健康中国2030"规划纲要》[Article in Chinese]. The State Council of the People's Republic of China. URL: https://www.gov.cn/zhengce/2016-10/25/content_5124174.htm [accessed 2025-11-28]
127. Regulation - 2016/679 - EN - gdpr - EUR-Lex. European Union EUR-Lex. URL: http://data.europa.eu/eli/reg/2016/679/oj [accessed 2025-11-24]
128. Sittig DF, Wright A, Coiera E, et al. Current challenges in health information technology-related patient safety. Health Informatics J 2020 Mar;26(1):181-189. [doi: 10.1177/1460458218814893] [Medline: 30537881]
129. Critical appraisal tools: JBI's critical appraisal tools assist in assessing the trustworthiness, relevance and results of published papers. JBI (Joanna Briggs Institute). URL: https://jbi.global/critical-appraisal-tools?utm_source=chatgpt.com [accessed 2025-10-17]
130. Hong QN, Fàbregues S, Bartlett G, et al. The Mixed Methods Appraisal Tool (MMAT) version 2018 for information professionals and researchers. EFI 2018 Dec 18;34(4):285-291. [doi: 10.3233/EFI-180221]

Abbreviations

A-CHESS: Addiction Comprehensive Health Enhancement Support System
EHR: electronic health record
EMR: electronic medical record
GRC: geo-referenced context
HIS: health information system
NCD: noncommunicable disease
NGRC: neighborhood geo-referenced context
PHR: personal health record
SDoH: social determinants of health

Edited by A Benis; submitted 11.May.2025; peer-reviewed by A Yan, A Azizi; accepted 29.Dec.2025; published 25.Feb.2026.

Please cite as:
Yang X, Dijst M, Daams JG, Suhrcke M, Yang H, Cornet R
Using Health Information Systems to Support Behavioral Interventions in Local Contexts: Scoping Review
JMIR Med Inform 2026;14:e77296
URL: https://medinform.jmir.org/2026/1/e77296
doi:10.2196/77296

© Xi Yang, Martin Dijst, Joost G Daams, Marc Suhrcke, Haoran Yang, Ronald Cornet. Originally published in JMIR Medical Informatics (https://medinform.jmir.org), 25.Feb.2026. This is an open-access article distributed under the terms of the Creative Commons Attribution License (https://creativecommons.org/licenses/by/4.0/), which permits unrestricted use, distribution, and reproduction in any medium, provided the original work, first published in JMIR Medical Informatics, is properly cited. The complete bibliographic information, a link to the original publication on https://medinform.jmir.org/, as well as this copyright and license information must be included.

XSL•FO
RenderX

Core Elements, Development, and Implementation Strategies of the Nursing Minimum Data Set: Scoping Review

Pascal Müller[1], MSc; Annabell Gangnus[1], Dr Rer Med; Katrin Gayen[1], Dip; Uta Kirchner-Heklau[1], MSc; Patrick Jahn[1], Prof Dr; Sebastian Hofstetter[1,2], PhD

[1]Health Service Research Working Group, Acute Care, Department of Internal Medicine, Faculty of Medicine, University Medicine Halle (Saale), Martin-Luther-University Halle-Wittenberg, Magdeburger Straße 12, Halle (Saale), Germany

[2]Dorothea-Erxleben-Learning-Centre, Faculty of Medicine, University Medicine Halle (Saale), Martin-Luther-University Halle-Wittenberg, Halle (Saale), Germany

Corresponding Author:
Pascal Müller, MSc
Health Service Research Working Group, Acute Care, Department of Internal Medicine, Faculty of Medicine, University Medicine Halle (Saale), Martin-Luther-University Halle-Wittenberg, Magdeburger Straße 12, Halle (Saale), Germany

Abstract

Background: Nursing care systems face significant challenges due to demographic changes, a workforce shortage, and rising demand for care services. Digital assistive technologies offer potential to address these challenges, but systematic and standardized nursing data are essential to evaluate both innovations and broader care processes. The Nursing Minimum Data Set (NMDS) provides a foundational framework for capturing structured information on nursing care, yet there is no international consensus on its core content, development, and practical use.

Objective: This scoping review aims to map current international literature regarding (1) the core content elements of NMDS, (2) methodological approaches used in NMDS development, and (3) implementation and use of NMDS in different nursing settings.

Methods: Following the JBI (Joanna Briggs Institute) methodology and Arksey and O'Malley framework, a systematic search was conducted on July 2, 2025, in the MEDLINE (via PubMed) and CINAHL (via EBSCO) databases using the term "nursing minimum data set." Inclusion was restricted to studies in English or German focusing on the content, development, or implementation of the NMDS. The research team reviewed studies in an independent and double-blinded fashion for eligibility based on predefined criteria, with discrepancies resolved by consensus. Eligible studies were narratively summarized, with extraction structured into categories based on the review's research questions.

Results: From 1908 initially identified articles, 26 (1.4%) studies met the inclusion criteria. Considerable heterogeneity was found in the structure and scope of the NMDS, with datasets comprising 16 to 145 items. Despite variation, 4 central domains consistently emerged: patient demographics, medical care information, nursing care elements, and institutional or organizational data. NMDS development typically followed a participatory, multistage approach involving literature analysis, stakeholder consensus building, and validation through pretesting and real-world application. Implementation and use of the NMDS serve multiple functions, including documenting nursing care processes, supporting workload measurement and resource planning, quality assurance, benchmarking, and demonstrating nursing's contribution to patient outcomes. However, successful implementation depends on technical, legal, organizational, and educational strategies. Core challenges include a lack of standardized terminology, inconsistent legal frameworks, and varying levels of staff training and acceptance.

Conclusions: The NMDS provides a robust basis for standardized nursing documentation, quality assurance, and health system planning, but international variability and ongoing challenges in harmonization, integration, and acceptability persist. Advancing the NMDS requires collaborative efforts for interoperability, investment in digital infrastructure, and targeted education. Further research should focus on comparative effectiveness, cross-context validation, and strategies to reduce documentation burden while maximizing data utility.

(JMIR Med Inform 2026;14:e84281) doi:10.2196/84281

KEYWORDS

Nursing Minimum Data Set; standardized nursing data; nursing informatics; nursing documentation; core nursing data elements; health information systems; digital health

XSL•FO
RenderX

Introduction

The nursing care system in Germany is confronted with significant challenges, including demographic shifts, a shortage of nursing personnel, and increasing demand for care services [1]. From 2014 to 2021, expenditures on long-term care insurance increased more than 2-fold, rising from €25.5 billion (US $30 billion) to €53.9 billion (US $63.4 billion) [2]. To ensure the sustainability of care provision, there is a need for innovative digital solutions. Digital assistive technologies have been shown to have considerable potential in promoting participation and autonomy, as well as reducing care dependency [3]. However, research focusing on the etiology and progression of care needs, as well as the ramifications of digital innovations, has been disproportionately underrepresented to date [4].

Robust and standardized nursing data are essential to evaluate these innovations and their impact on care. The Nursing Minimum Data Set (NMDS) is defined as "a minimum set of items of information with uniform definitions and categories concerning the specific dimension of nursing which meets the information needs of multiple data users in the health care system" [5]. The NMDS provides a structured basis for capturing nursing care across populations, settings, and regions. It facilitates the monitoring of trends in care delivery and resource use, serves as a foundational element for research by establishing connections with broader health information systems, and contributes to the formulation of health policy, thereby ensuring the visibility of nursing contributions in health care planning and decision-making [6]. With a focus on influencing factors and opportunities to prevent or reduce care dependency, the NMDS can also serve as a framework for assessing the impact of digital innovations.

Despite its potential, there is a lack of clarity regarding which elements should be included in a core nursing dataset, how such elements are developed, and what barriers or success factors influence its implementation in practice. The objective of this scoping review is to map the current state of the literature by addressing the following research questions:

1. Which content elements comprise a nursing minimum dataset?
2. Which methodological approaches have been used in its development?
3. What is the implementation and use of such a dataset in different nursing settings?

Methods

This scoping review was conducted in accordance with the JBI (Joanna Briggs Institute) methodology [7] and guided by the framework of Arksey and O'Malley [8], which structures the process into the following phases: identifying relevant studies, study selection, data presentation, and synthesis of results. To enhance rigor and transparency, the reporting process adhered to the PRISMA-ScR checklist (Preferred Reporting Items for Systematic Reviews and Meta-Analyses extension for Scoping Reviews; Checklist 1) [9].

Search Strategy

A systematic search was conducted on July 2, 2025, in the MEDLINE (via PubMed) and CINAHL (via EBSCO) databases using the search term "nursing minimum data set," applied identically in both databases. "Nursing minimum data set" is an internationally established and unambiguous term for the concept of interest. Preliminary searches using broader terms such as "nursing data" or "nursing data set" yielded numerous irrelevant results, mostly referring to general medical datasets including nursing-related variables but not specifically designed for nursing care. Searches in other databases (eg, Google Scholar and Europe PMC) produced even more irrelevant hits.

Using the precise term "nursing minimum data set" maximized specificity and relevance. PubMed's Automatic Term Mapping further captured synonyms and MeSH (Medical Subject Headings) terms. This focused approach aligns with Freguia et al [10] but extends their work by also analyzing the development and implementation of the NMDS. The MEDLINE and CINAHL databases were selected due to their comprehensive coverage of peer-reviewed nursing and health services research. No date restrictions were applied, and reference lists of the included articles were manually screened to minimize the risk of missing eligible studies.

The detailed inclusion and exclusion criteria are enumerated in Textbox 1. Exclusion criteria were based on our aim to map the conceptual, methodological, and implementation aspects of the NMDS rather than secondary applications or specialized derivatives. Studies focusing solely on specific clinical conditions, measurement tools, isolated settings (eg, palliative care), or context (eg, quality management) were excluded. Publications on other datasets (eg, the Minimum Data Set Resident Assessment Instrument [11]) or nursing classifications were also excluded. Language was restricted to English and German to ensure reliable screening and data extraction. Although this may introduce language bias, the majority of conceptual NMDS literature is published in these languages.

XSL•FO
RenderX

Textbox 1. Inclusion and exclusion criteria.

Inclusion criteria

- Primary and secondary studies with abstracts available
- Language: German or English
- Description of content, development, implementation, and use in practical applications of the Nursing Minimum Data Set

Exclusion criteria

- Secondary analyses of the Nursing Minimum Data Set
- Reference to interventions, specific clinical pictures, or medications
- Reference to quality management, personnel indicators, or specific settings
- Comparison of measurement instruments
- In cases of duplicate publication, only the most comprehensive or earliest version was included to avoid double-counting

Study Selection and Data Extraction

The study selection followed the JBI methodology for transparency and reproducibility. Duplicate removal and screening were conducted using Rayyan (Rayyan Systems, Inc) [12], a web-based collaborative platform enabling independent and blinded review. Duplicates were first removed automatically using the software's matching algorithms based on title, author, DOI, journal, and year and then manually checked to resolve partial matches or inconsistent metadata.

Titles and abstracts of remaining records were independently screened by 2 reviewers (PM and AG) using Rayyan's blinded mode. Records identified as potentially eligible by at least 1 reviewer proceeded to full-text review. Discrepancies were resolved through discussion, with a third reviewer (KG) consulted if consensus could not be reached. The process was independent of study design and focused on studies addressing the conceptualization, development, or implementation of the NMDS. The number of records at each stage is presented in the PRISMA (Preferred Reporting Items for Systematic Reviews and Meta-Analyses) flow diagram. Reference lists of the included studies were manually screened to identify further eligible studies.

To systematically extract and present relevant information, included studies were narratively summarized in a data-charting form. The studies were categorized and analyzed according to the following classifications: "overview" (eg, definition and elements); "development" (eg, methods and processes); and "implementation" (eg, evaluation, availability, reliability, and validity). The primary categories were derived deductively from the review questions. Subcategories were subject to refinement and expansion in an iterative manner as novel themes and patterns emerged from the included studies. This framework enabled the synthesis of structured and flexible approaches, capturing the breadth of the research field.

Results

Study Selection

The database search conducted in July 2025 yielded 1908 results (PubMed: n=1820, 95.4%; CINAHL: n=88, 4.6%). After removing duplicates, 1869 (N=1908, 98%) records remained for title and abstract screening. Of these, 1823 (N=1869, 98%) were excluded due to unavailability of full texts or because they focused on data infrastructure, storage, or evaluation frameworks unrelated to NMDS content, development, or implementation. A total of 36 (N=1869, 2%) articles underwent double-blind full-text review. After applying all eligibility criteria, 23 (N=1869, 1.2%) articles were included. Screening reference lists added 3 more studies, resulting in a total of 26 included studies. No conflicts occurred among independent reviewers. The selection process is presented in the PRISMA flowchart [13] (Figure 1). A comprehensive list of the included studies and the data extraction table are provided in Multimedia Appendix 1 [6,10,14-37].

XSL•FO
RenderX

Figure 1. PRISMA (Preferred Reporting Items for Systematic Reviews and Meta-Analyses) flowchart illustrating the study selection process.

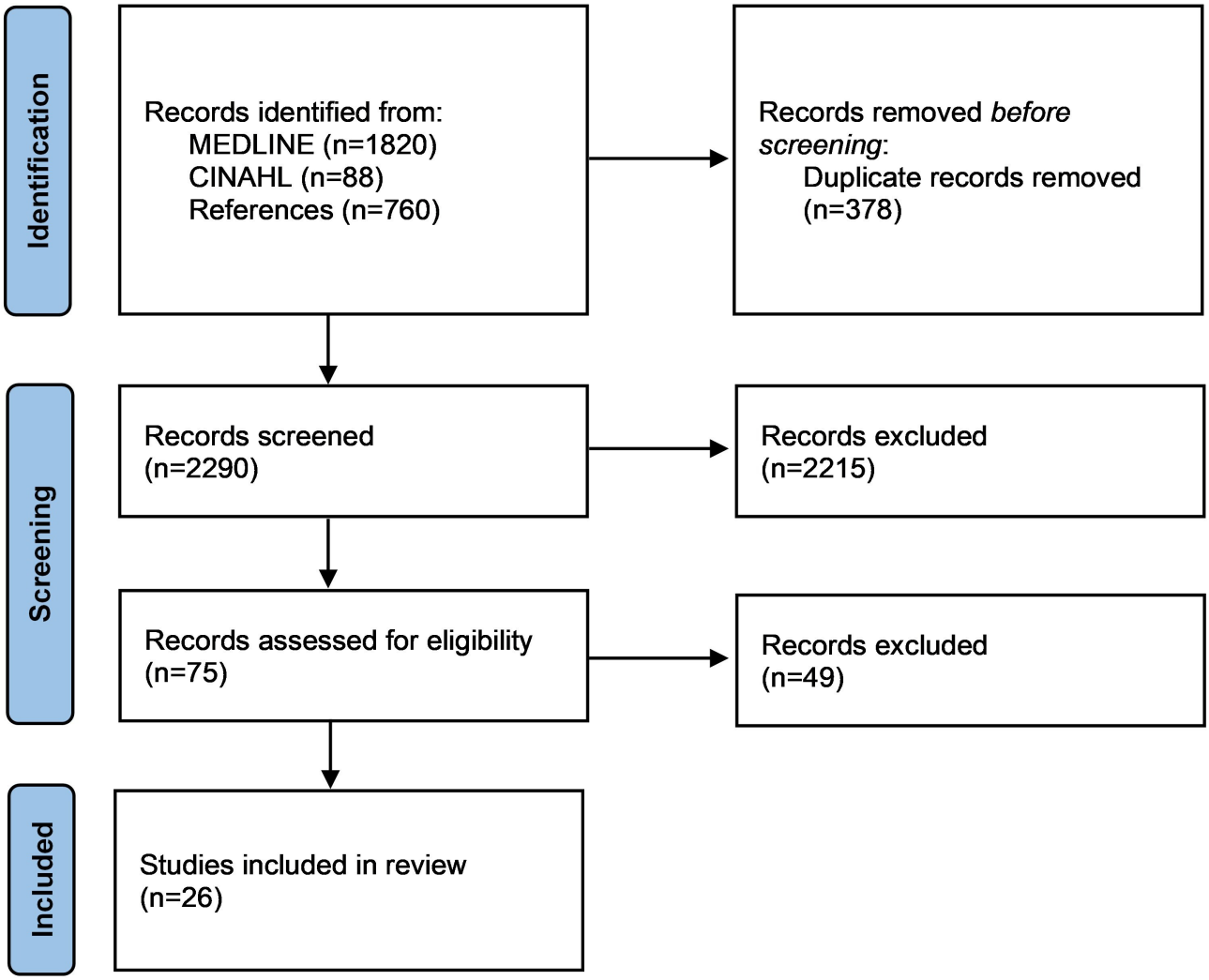

Main Characteristics of the Included Studies

The 26 studies originated from 9 countries. Most were from the Netherlands (n=6, 23.1%), the United States (n=4, 15.4%), Austria (n=4, 15.4%), Belgium (n=4, 15.4%), and Ireland (n=3, 11.5%). Additional studies were conducted in Finland (n=2, 7.7%), and 1 (3.8%) each from Italy, Germany, and Thailand. The majority of reported NMDS initiatives have their origins in the United States [10,16,19,25,29], Belgium [10,19,25,29,32-34,36], Canada [10,19,25,29], Thailand [10,25,27,29,37], Switzerland [25,29], and the Netherlands [18,20-23,25,29]. Additional origins including Ireland [14,26,29], Germany [17,29], Finland [24,25,29,35], Australia [19,25,29], Sweden [25], Brazil [25], Japan [25], Austria [28,30,31], and Scotland [19] were mentioned in several studies, which also referenced a European [10,19,25] and an international NMDS [19,25]. Most of the studies focused on universal nursing settings. However, there have also been investigations of specific settings such as hospitals, long-term care facilities, nursing homes, home health care agencies, and public health contexts.

The articles encompassed a period from 1988 to 2022. The predominant language of publication was English (n=24, 92.3%), with 2 (7.7%) articles published in German. The study designs exhibited heterogeneity, encompassing theoretical papers (n=9, 34.6%), mixed methods studies (n=7, 26.9%), quantitative studies (n=9, 34.6%), and a single qualitative study. The predominant focus was the development of the NMDS [14,17,21,27,28,30,33-36], followed by evaluation [16,20,22,31] and implementation [24,26,32]. A subset of these studies was also partially cited in the included systematic review [29] and umbrella review [10].

Data Elements

The datasets have been designed to capture comprehensive and comparable information on nursing practice, patient status, and care context. This facilitates the monitoring, evaluation, and enhancement of nursing care delivery at both the individual and system levels. A review of the existing literature revealed a considerable variation in the number of elements comprising an NMDS, ranging from 16 to 145 items per dataset. Despite this variation, 4 key categories consistently emerged: patient demographics, medical care information, core nursing care elements, and institutional or organizational data (Textbox 2).

The patient's demographic information is typically documented on an initial admission to the health care facility and subsequently serves as a foundational reference point for the patient's characteristics. The medical care items in question prioritize crucial medical information. While certain elements are documented on a single occasion during the patient's hospital

XSL•FO
RenderX

stay, details concerning medical procedures and medications are frequently recorded throughout the patient's stay. Core nursing care elements are typically collected continuously throughout the duration of hospitalization. The exception to this is nursing outcomes, which are generally assessed at discharge. Risk assessments and nursing diagnoses, on the other hand, are updated as the patient's status changes. Institutional or organizational data link patient- and care-level information with structural and organizational attributes, thereby supporting contextual analysis of care processes.

Textbox 2. The datasets are designed to capture information on nursing practice, patient status, and care context.

Patient demographics (3-8 items)

- Personal identification (pseudonymized)
- Date of birth and age
- Gender
- Race and ethnicity
- Place of residence
- Address and phone number

Medical care information (4-7 items)

- *International Classification of Diseases* codes
- Medical history (patient and family)
- Drug allergies or other allergies
- Procedures
- Laboratory tests
- Medication
- Dead or alive codes and resuscitation status
- Admission or encounter date
- Discharge information (date and summary)
- Length and progression of stay
- Health status (stability, severity, complications, and critical events)

Nursing care elements

- Nursing diagnosis (17-48 items)
- Nursing interventions (8-170 items)
- Nursing outcome (4-40 items)
- Intensity of nursing care (3-4 items)
- Nursing process (10 items)
- Client status (activities of daily living)
- Discharge plan
- Care planning (goals of the shift and goals of nursing care)
- Medical instruments' use before discharge

Institutional or organizational data

- Health care setting (4-5 items): type of institution, main point of service, type of nursing delivery system, and other disposition point
- Resource allocation (4 items): number and qualification of available nurses, number of nursing hours available, number of beds, and nurse-to-patient ratios
- Institutional or provider identifiers: service or agency number, health record number, nurse identifier, and physician identifier
- Expected payer of the bills or health insurance

XSL•FO
RenderX

NMDS Development

The development of the NMDS generally follows a three-stage process: (1) selection and definition of relevant data elements based on literature analysis, document analysis, and interdisciplinary consensus; (2) validation and consensus building through expert rounds, pretesting, and reliability assessments; and (3) application and testing the feasibility in real-world settings.

Selection and Definition of Data Elements

Potential items were chosen for clinical relevance and feasibility through literature reviews, analysis of clinical records (n=15-45 per study), and collaborative expert panels or Delphi processes. Participants included field nurses, nurse managers, nursing scientists, informatics specialists, and policy representatives (n=22-287 per study). Semistructured interviews and questionnaires were central, supported by focus groups and multiple rounds of expert panels (up to 11 with n=5-88 participants). The goal was to ensure that the items reflected actual practice, captured the diversity of nursing activities, and could be coded in a feasible manner. Critical decisions included choosing terminology and coding schemes, unit of data collection (eg, patient day or episode of care), and timing of data entry.

Refinement and Validation

The refinement of items and structures was achieved through consensus-building methods, such as repeated Delphi rounds and focus groups, along with pretests and reliability assessments, including Cohen κ and intraclass correlation coefficient. These methods often incorporated interdisciplinary and practice-based feedback, facilitating the continuous improvement and refinement of the research instruments. In the preliminary phase, the expert participants engaged in deliberations concerning the relevance, frequency, and practical feasibility of each item. In addition, they addressed the conceptualization, frequency, and relevance of the items, along with the data that were routinely collected. Lists of nursing diagnoses, interventions, and outcomes were developed and discussed for clarity and practicality. Subsequent rounds entailed the refinement and evaluation of the wording and definitions for their usefulness and feasibility, as well as the systematic testing of the definitions and coding rules. The resulting data collection instruments provided multiple response options for each item, thereby generating a broad range of analyzable variables. Each data element was carefully defined and accompanied by specific operational instructions, including scoring schemes that frequently used 5-point Likert scales to evaluate interventions and diagnoses.

The documentation of nursing care is typically implemented through the use of standardized classification systems. However, a universal system has yet to be established across all NMDS implementations. Instead, a variety of established frameworks are used, including the International Classification of Nursing Practice [38], the North American Nursing Diagnosis Association-I classification [39], the Omaha System [40], and the Home Health Care Classification [41], among others. The NMDS has been designed to either specify a preferred system or permit cross-mapping between local and international standards. The ability to exchange data and information seamlessly across different systems and between different countries is paramount for the comparability of data at both the national and international levels.

Reliability and validity testing constituted a fundamental component of the second stage. Pretests were conducted using samples ranging from 4 to 214 participants, often comparing the extracted information from patient records (n=20 to nearly n=300,000) by pairs of raters (research staff and clinical nurses). The coding agreement was subsequently quantified. The validity of the content was determined through its alignment with existing literature and user evaluations.

Feasibility Testing and Application

The final development stage focused on evaluating the usability and practical implementation of the NMDS. This included structured pilot applications in real nursing settings, such as hospitals, nursing homes, ambulatory care, and home health agencies. Typically, a longitudinal design with repeated measurements over a defined observation period (eg, 7 d or 1 admission episode) was selected. Consequently, the NMDS demonstrated its efficacy in the domains of care process description, workload measurement, resource planning support, benchmarking, and quality improvement across diverse nursing settings.

One such function is to systematically describe the diversity of nursing care and patient populations through frequency analyses of nursing diagnoses, interventions, and outcomes. The application of advanced analytical approaches, such as relative to an identified distribution analysis, has been demonstrated to facilitate the illustration of variations in nursing practice and complexity across a variety of settings, age groups, and medical diagnoses. In addition, the NMDS is instrumental in evaluating the intensity of nursing care. By establishing a correlation between the implementation of each nursing intervention and the temporal and experiential parameters of the nursing personnel involved, health care institutions can facilitate a quantitative assessment of the workload associated with each patient or unit of care. Classification systems such as the nursing diagnosis index or patient dependency models (eg, the San Joaquin classification) are used to establish a correlation between patient needs and staffing requirements, thereby facilitating evidence-based staffing decisions and resource allocation.

A further central benefit of the NMDS is its ability to demonstrate nursing's contribution to patient outcomes. For instance, path analysis can be used to examine the relationship between nursing interventions and patient progress, as illustrated by improvements in functional indices (eg, the Barthel index) during hospitalization. In the context of quality management and patient safety, outcome indicators facilitate the identification of care problems and the evaluation of improvement strategies through the integration of validated assessment instruments. The longitudinal use of these tools adds further value by enabling the tracking of care trends and patient outcomes over extended periods. These analyses are valuable for clinical managers and policymakers in the context of epidemiological

XSL•FO
RenderX

analysis, benchmarking institutions, highlighting areas of best practice, and supporting the dissemination of evidence-based interventions. This facilitates the formulation of strategic decisions regarding care processes and resource distribution.

A comprehensive implementation strategy must encompass not only technical solutions, such as increasing automation and electronic data collection, but also legal, organizational, and educational strategies. For instance, the implementation of the NMDS in specific contexts was terminated due to the absence of a legal foundation or inadequate institutional endorsement. The quality and utility of collected data are contingent on nurses' familiarity with the NMDS content and vocabulary. Educational initiatives are required to enhance nurses' comprehension of the significance of structured data collection and its pertinence for clinical decision-making, quality assurance, and the development of interoperable hospital information systems. To reduce the workload associated with NMDS documentation, it may be necessary to minimize the scope of collected variables, with a push toward electronic and automated data collection.

Discussion

Principal Findings

This scoping review offers a comprehensive mapping of the extant literature on the NMDS with regard to content elements, methodological development processes, and implementation and use across nursing settings. Synthesizing evidence from diverse international contexts and research designs, this review addresses the critical knowledge gaps identified in the introduction and provides an informed basis for further research and policy development in the field of standardized nursing data.

A salient finding of this review is the substantial heterogeneity observed in the structure and length of reported NMDSs, which vary from 16 to 145 items. Nevertheless, 4 core domains consistently emerged: patient demographics, medical care information, nursing care elements, and institutional or organizational data. This convergence on key domains, despite variation in the level of detail and specific items, underscores both the complexity of capturing nursing care and the international consensus on the essential pillars of nursing-relevant information. The comprehensive integration of nursing diagnoses, interventions, and outcomes signifies a worldwide transition toward outcome-oriented, evidence-based nursing practice. However, the absence of a universally adopted classification system for these categories—variously using systems such as the North American Nursing Diagnosis Association-I classification, the International Classification of Nursing Practice, or local taxonomies—continues to challenge the comparability of nursing data both within and across countries. This diversity underscores the necessity for enhanced harmonization to facilitate broader benchmarking, interoperability, and secondary data use.

The development of the NMDS is characterized by rigorous, iterative, and participatory processes. Most of the studies used a 3-stage approach: first, systematic identification and selection of content elements (frequently drawing from the literature, expert consultations, and clinical record analyses); second, consensus building and validation (frequently relying on Delphi processes, focus groups, and pretesting); and third, pilot implementation in real-world settings. The consistent engagement of field nurses, managers, scientific experts, and policy stakeholders supports both the clinical relevance and the practical feasibility of the resulting datasets. However, methodological diversity—particularly in the degree of stakeholder inclusion, the criteria for item selection, and the approach to validation—limits the extent to which the results can be compared and generalized. A fundamental finding is that consensus and interdisciplinary involvement significantly enhance acceptance and operationalization. However, disparities in contextual adaptation and infrastructure availability necessitate context-sensitive approaches, superseding the notion of a universally optimal solution.

The review demonstrates a wide range of applications of the NMDS, encompassing care process documentation, workload measurement, resource planning, quality assurance, benchmarking, and outcome evaluation. Analytical techniques such as frequency analysis, relative to an identified distribution analysis, and path analysis facilitate the sophisticated use of NMDS data. This includes the identification of care trends and variations, the mapping of nursing workload, and the demonstration of the impact of nursing care on patient outcomes. NMDS data have demonstrated their relevance for supporting clinical management, health policy, and epidemiological surveillance in multiple health care systems.

However, the implementation of NMDS is not without challenges. Achieving success in this endeavor necessitates the implementation of a multifaceted approach, encompassing not only technical solutions such as electronic and automated data collection but also legal, organizational, and particularly educational strategies. In certain settings, the discontinuation of NMDS initiatives was attributed to a lack of legal foundation, inadequate institutional support, or suboptimal integration into health information systems. The collection of consistent and high-quality data is contingent upon nurses' familiarity with the terminology and documentation standards. Consequently, training and change management are imperative. Furthermore, the balancing of data comprehensiveness with feasibility, as well as the minimization of documentation burden, emerges as a recurring theme in the pursuit of long-term sustainability.

Strengths and Limitations

A central strength of this review is its comprehensive and systematic approach, which adheres to established methodological frameworks (JBI and PRISMA-ScR) and uses a transparent, replicable search and data extraction process. The program's emphasis on international literature and a diverse array of study types contributes to the generalizability and relevance of the findings. The use of independent, blinded screening and iterative data charting enhances the rigor and credibility of the synthesis.

Several limitations of this review should be acknowledged. First, only 2 databases and a single search term were used. Preliminary scoping checks indicated that broader terms or additional databases yielded mostly irrelevant results, suggesting

XSL•FO
RenderX

a low likelihood of missing studies specifically addressing the NMDS. As NMDS initiatives are sometimes embedded in national health IT programs, relevant reports may appear in gray literature or regional journals not indexed in the MEDLINE or CINAHL databases. Nevertheless, the potential remains that studies using alternative terminology or published outside the MEDLINE and CINAHL databases were not captured. This structural publication bias should be considered when interpreting the findings. Second, the exclusion criteria may limit the mapping breadth by underrepresenting NMDS adaptations in non–English-speaking and non–German-speaking countries or highly specialized settings. This potential exclusion could introduce publication bias and limit the capture of ongoing or context-specific innovations. Third, as is typical for scoping reviews, no formal quality appraisal of included studies was conducted, which may have affected the weight assigned to individual findings. Fourth, the heterogeneity of study designs, settings, and health care systems complicates a direct comparison and synthesis of findings. To conclude, while this review identifies fundamental content and process elements, as well as prevalent barriers and success factors, it does not provide a meta-analytic estimate of the impact of the NMDS on patient or system outcomes.

Conclusions

This scoping review highlights the heterogeneity and evolving consensus on the structure, development, and implementation of the NMDS. Despite international variations, 4 core domains consistently emerged: patient demographics, medical care information, nursing care elements, and institutional or organizational data. The NMDS can enhance the visibility, quality, and effectiveness of nursing care across health care systems, provided that challenges related to standardization, interoperability, and acceptance are addressed.

To translate these findings into practice, policymakers and health care managers should prioritize the standardization of nursing documentation through appropriate legal frameworks, investment in digital infrastructure, and targeted educational initiatives for nursing staff. Practical steps include establishing interoperable digital nursing records; providing structured training on NMDS use; and implementing pilot programs to assess the feasibility, usability, and data utility. Researchers are encouraged to evaluate the NMDS across diverse settings, conduct comparative effectiveness studies, and explore strategies to reduce documentation burden while maximizing actionable insights for care management, resource planning, and policy decisions. Overall, the review underscores that advancing the NMDS requires interdisciplinary collaboration, context-sensitive implementation, and ongoing evaluation to ensure that standardized nursing data meaningfully inform clinical practice and health system planning.

Funding

This research was funded by the Federal Ministry of Research, Technology, and Space (grant 01ZZ2401A). The study has been funded for a 5-year period, starting in November 2024. The study was funded for €4,559,301.88 (US $5,369,253.83). The funder had no involvement in the study design, data collection, analysis, interpretation, or the writing of the manuscript. The authors acknowledge the financial support of the Open Access Publication Fund of the Martin-Luther University Halle-Wittenberg.

Data Availability

The datasets generated or analyzed during this study are available from the corresponding author on reasonable request.

Conflicts of Interest

None declared.

Multimedia Appendix 1
Data extraction sheet.
[XLSX File, 82 KB - medinform_v14i1e84281_app1.xlsx]

Checklist 1
PRISMA-ScR checklist.
[PDF File, 119 KB - medinform_v14i1e84281_app2.pdf]

References

1. Behrendt S, Tsiasioti C, Schwinger A. Pflegeprävalenzen und inanspruchnahme in der räumlichen verortung. In: Schwinger A, Kuhlmey A, Greß S, Klauber J, Jacobs K, Behrendt S, editors. Pflege-Report 2024: Springer; 2024:3-25. [doi: 10.1007/978-3-662-70189-8_1]
2. Rothgang H, Müller R. Wirkungen der Pflegereformen und Zukunftstrends: Barmer; 2021.
3. Assistive technology. World Health Organization. 2024. URL: https://www.who.int/news-room/fact-sheets/detail/assistive-technology [accessed 2025-08-08]

XSL•FO
RenderX

4. Blüher S, Stein T, Schilling R, Grittner U, Kuhlmey A. Vermeidung von pflegebedürftigkeit – herausforderungen für forschung und praxis. In: Jacobs K, Kuhlmey A, Greß S, Klauber J, Schwinger A, editors. Pflege-Report 2021: Springer; 2021:91-102. [doi: 10.1007/978-3-662-63107-2_6]
5. Werley HH, Lang NM. Identification of the Nursing Minimum Data Set: Springer; 1988.
6. Werley HH, Devine EC, Zorn CR, Ryan P, Westra BL. The Nursing Minimum Data Set: abstraction tool for standardized, comparable, essential data. Am J Public Health 1991 Apr;81(4):421-426. [doi: 10.2105/ajph.81.4.421] [Medline: 2003618]
7. von Elm E, Schreiber G, Haupt CC. Methodische anleitung für scoping reviews (JBI-methodologie). Z Evid Fortbild Qual Gesundhwes 2019 Jun;143:1-7. [doi: 10.1016/j.zefq.2019.05.004] [Medline: 31296451]
8. Arksey H, O'Malley L. Scoping studies: towards a methodological framework. Int J Soc Res Methodol 2005 Feb;8(1):19-32. [doi: 10.1080/1364557032000119616]
9. Tricco AC, Lillie E, Zarin W, et al. PRISMA extension for scoping reviews (PRISMA-ScR): checklist and explanation. Ann Intern Med 2018 Oct 2;169(7):467-473. [doi: 10.7326/M18-0850] [Medline: 30178033]
10. Freguia F, Danielis M, Moreale R, Palese A. Nursing minimum data sets: findings from an umbrella review. Health Informatics J 2022;28(2):14604582221099826. [doi: 10.1177/14604582221099826] [Medline: 35634983]
11. Long-term care facility resident assessment instrument 3.0 user's manual. Centers for Medicare & Medicaid Services. 2025. URL: https://www.cms.gov/files/document/draftmds-30-rai-manual-v1201october2025-1.pdf [accessed 2025-08-25]
12. Hirt J, Nordhausen T. Digitale anwendungen für die studienauswahl im rahmen von systematischen evidenzsynthesen. Pflege 2019 Oct;32(5):277-278. [doi: 10.1024/1012-5302/a000690] [Medline: 31538877]
13. Moher D, Liberati A, Tetzlaff J, Altman DG, PRISMA Group. Preferred reporting items for systematic reviews and meta-analyses: the PRISMA statement. PLoS Med 2009 Jul 21;6(7):e1000097. [doi: 10.1371/journal.pmed.1000097] [Medline: 19621072]
14. Butler M, Treacy M, Scott A, et al. Towards a nursing minimum data set for Ireland: making Irish nursing visible. J Adv Nurs 2006 Aug;55(3):364-375. [doi: 10.1111/j.1365-2648.2006.03909.x] [Medline: 16866831]
15. Coenen A, Schoneman D. The nursing minimum data set: use in the quality process. J Nurs Care Qual 1995 Oct;10(1):9-15. [doi: 10.1097/00001786-199510010-00004] [Medline: 7579551]
16. Devine EC, Werley HH. Test of the nursing minimum data set: availability of data and reliability. Res Nurs Health 1988 Apr;11(2):97-104. [doi: 10.1002/nur.4770110205] [Medline: 3363179]
17. Eberl I, Bartholomeyczik S. The Belgian Nursing Minimum Data Set II (B-NMDS II) and its transfer to German hospitals: results of the first investigation phase, the translation and adaption process of the instrument. Pflege 2010 Oct;23(5):309-319. [doi: 10.1024/1012-5302/a000064] [Medline: 20886449]
18. Goossen WT. Exploiting the Nursing Minimum Data Set for the Netherlands. Stud Health Technol Inform 2001;84(Pt 2):1334-1338. [Medline: 11604944]
19. Goossen WT, Epping PJ, Feuth T, Dassen TW, Hasman A, van den Heuvel WJ. A comparison of nursing minimal data sets. J Am Med Inform Assoc 1998;5(2):152-163. [doi: 10.1136/jamia.1998.0050152] [Medline: 9524348]
20. Goossen WT, Epping PJ, Feuth T, van den Heuvel WJ, Hasman A, Dassen TW. Using the Nursing Minimum Data Set for the Netherlands (NMDSN) to illustrate differences in patient populations and variations in nursing activities. Int J Nurs Stud 2001 Jun;38(3):243-257. [doi: 10.1016/s0020-7489(00)00075-4] [Medline: 11245862]
21. Goossen WT, Epping PJ, Van den Heuvel WJ, Feuth T, Frederiks CM, Hasman A. Development of the Nursing Minimum Data Set for the Netherlands (NMDSN): identification of categories and items. J Adv Nurs 2000 Mar;31(3):536-547. [doi: 10.1046/j.1365-2648.2000.01308.x] [Medline: 10718872]
22. Goossen W, Dassen T, Dijkstra A, Hasman A, Tiesinga L, van den Heuvel W. Validity and reliability of the Nursing Minimum Data Set for the Netherlands (NMDSN). Scand J Caring Sci 2003 Mar;17(1):19-29. [doi: 10.1046/j.1471-6712.2003.00112.x] [Medline: 12581291]
23. Goossen WTF. Statistical analysis of the Nursing Minimum Data Set for The Netherlands. Int J Med Inform 2002 Dec 18;68(1-3):205-218. [doi: 10.1016/s1386-5056(02)00077-1] [Medline: 12467803]
24. Kaakinen P, Torppa K. Implementation of a structured nursing documentation in a special care unit. Stud Health Technol Inform 2009;146:367-369. [Medline: 19592867]
25. Mac Neela P, Scott PA, Treacy MP, Hyde A. Nursing minimum data sets: a conceptual analysis and review. Nurs Inq 2006 Mar;13(1):44-51. [doi: 10.1111/j.1440-1800.2006.00300.x] [Medline: 16494666]
26. Morris R, Matthews A, Scott AP. Validity, reliability and utility of the Irish Nursing Minimum Data Set for General Nursing in investigating the effectiveness of nursing interventions in a general nursing setting: a repeated measures design. Int J Nurs Stud 2014 Apr;51(4):562-571. [doi: 10.1016/j.ijnurstu.2013.07.011] [Medline: 23992666]
27. Phuphaibul R. Nursing data set development in Thailand. Stud Health Technol Inform 2006;122:991. [Medline: 17102504]
28. Ranegger R, Hackl WO, Ammenwerth E. A proposal for an Austrian Nursing Minimum Data Set (NMDS): a Delphi study. Appl Clin Inform 2014;5(2):538-547. [doi: 10.4338/ACI-2014-04-RA-0027] [Medline: 25024767]
29. Ranegger R, Ammenwerth E. Nursing Minimum Data Sets (NMDS) - a literature review relating to objective and data elements. Pflege 2014 Dec;27(6):405-425. [doi: 10.1024/1012-5302/a000393] [Medline: 25416487]
30. Ranegger R, Hackl WO, Ammenwerth E. Development of the Austrian Nursing Minimum Data Set (NMDS-AT): the third Delphi round, a quantitative online survey. Stud Health Technol Inform 2015;212:73-80. [Medline: 26063260]

XSL•FO
RenderX

31. Ranegger R, Hackl WO, Ammenwerth E. Implementation of the Austrian Nursing Minimum Data Set (NMDS-AT): a feasibility study. BMC Med Inform Decis Mak 2015 Sep 17;15:75. [doi: 10.1186/s12911-015-0198-7] [Medline: 26384111]
32. Sermeus W, Delesie L, Van den Heede K, Diya L, Lesaffre E. Measuring the intensity of nursing care: making use of the Belgian Nursing Minimum Data Set. Int J Nurs Stud 2008 Jul;45(7):1011-1021. [doi: 10.1016/j.ijnurstu.2007.05.006] [Medline: 17588580]
33. Sermeus W, Van den Heede K, Michiels D, et al. A nation-wide project for the revision of the Belgian Nursing Minimum Dataset: from concept to implementation. Stud Health Technol Inform 2004;110:21-26. [Medline: 15853247]
34. Sermeus W, van den Heede K, Michiels D, et al. Revising the Belgian Nursing Minimum Dataset: from concept to implementation. Int J Med Inform 2005 Dec;74(11-12):946-951. [doi: 10.1016/j.ijmedinf.2005.07.005] [Medline: 16153887]
35. Turtiainen AM, Kinnunen J, Sermeus W, Nyberg T. The cross-cultural adaptation of the Belgium Nursing Minimum Data Set to Finnish nursing. J Nurs Manag 2000 Sep;8(5):281-290. [doi: 10.1046/j.1365-2834.2000.00194.x]
36. Van den Heede K, Michiels D, Thonon O, Sermeus W. Using nursing interventions classification as a framework to revise the Belgian nursing minimum data set. Int J Nurs Terminol Classif 2009;20(3):122-131. [doi: 10.1111/j.1744-618X.2009.01124.x] [Medline: 19659842]
37. Volrathongchai K, Delaney CW, Phuphaibul R. Nursing Minimum Data Set development and implementation in Thailand. J Adv Nurs 2003 Sep;43(6):588-594. [doi: 10.1046/j.1365-2648.2003.02757.x] [Medline: 12950564]
38. Hinz M, Dörre F, König P. In: Tackenberg P, editor. ICNP: Internationale Klassifikation für die Pflegepraxis: Huber; 2003.
39. Herdman TH, Kamitsuru S, Lopes C. NANDA-I-Pflegediagnosen: Definitionen und Klassifikation 2024-2026: Thieme RECOM; 2025.
40. Martin KS, Norris J. The Omaha System: a model for describing practice. Holist Nurs Pract 1996 Oct;11(1):75-83. [doi: 10.1097/00004650-199610000-00011] [Medline: 8945176]
41. Saba VK. Nursing classifications: Home Health Care Classification System (HHCC): an overview. Online J Issues Nurs 2002;7(3):9. [Medline: 12410634]

Abbreviations

JBI: Joanna Briggs Institute
MeSH: Medical Subject Headings
NMDS: Nursing Minimum Data Set
PRISMA: Preferred Reporting Items for Systematic Reviews and Meta-Analyses
PRISMA-ScR: Preferred Reporting Items for Systematic Reviews and Meta-Analyses extension for Scoping Reviews

Edited by A Benis; submitted 17.Sep.2025; peer-reviewed by AG Kirkova-Bogdanova, MA Zoubi; revised version received 17.Nov.2025; accepted 01.Jan.2026; published 27.Feb.2026.

Please cite as:
Müller P, Gangnus A, Gayen K, Kirchner-Heklau U, Jahn P, Hofstetter S
Core Elements, Development, and Implementation Strategies of the Nursing Minimum Data Set: Scoping Review
JMIR Med Inform 2026;14:e84281
URL: https://medinform.jmir.org/2026/1/e84281
doi:10.2196/84281

© Pascal Müller, Annabell Gangnus, Katrin Gayen, Uta Kirchner-Heklau, Patrick Jahn, Sebastian Hofstetter. Originally published in JMIR Medical Informatics (https://medinform.jmir.org), 27.Feb.2026. This is an open-access article distributed under the terms of the Creative Commons Attribution License (https://creativecommons.org/licenses/by/4.0/), which permits unrestricted use, distribution, and reproduction in any medium, provided the original work, first published in JMIR Medical Informatics, is properly cited. The complete bibliographic information, a link to the original publication on https://medinform.jmir.org/, as well as this copyright and license information must be included.

XSL•FO
RenderX

Technological Strategies for the Patient Experience in Emergency Departments: Scoping Review

Andrés Santiago Santafé[1]; Juan Manuel Aranda[1], PhD; Wilmer Jair Beltrán[1]; William Javier Guerrero[1], PhD; Maryory Guevara Lozano[2], MSc; Ingrid Xiomara Bustos[3], RN

[1]Faculty of Engineering, Universidad de La Sabana, Campus del Puente del Común, Km 7 Autopista Norte de Bogotá, Chía, Cundinamarca, Colombia

[2]Faculty of Nursing and Rehabilitation, Universidad de La Sabana, Chía, Cundinamarca, Colombia

[3]Clínica Universidad de La Sabana, Chía, Cundinamarca, Colombia

Corresponding Author:
Juan Manuel Aranda, PhD
Faculty of Engineering, Universidad de La Sabana, Campus del Puente del Común, Km 7 Autopista Norte de Bogotá, Chía, Cundinamarca, Colombia

Abstract

Background: Technology has improved patient care in hospitals, enhancing the overall patient experience. However, digitalization raises questions on effectively integrating technological strategies to ensure assertive communication of information during emergency department (ED) journeys. Keeping patients well-informed boosts their service perception and satisfaction, a factor often neglected by institutions in EDs.

Objective: This paper analyzes relevant studies on technological strategies designed for EDs aimed at improving patient experience, focusing on communication and information access. We analyze the technologies, outcomes, impacts, and challenges of the strategies.

Methods: A scoping review was conducted using the PRISMA-ScR (Preferred Reporting Items for Systematic Reviews and Meta-Analyses Extension for Scoping Reviews) guidelines and CADIMA tool. Searches were performed in Scopus, PubMed, IEEE Xplore, and CINAHL databases. Articles published from January 2018 to December 2024 were included. Quality appraisal was performed using the Crowe Critical Appraisal Tool version 1.4. Three reviewers independently examined the title and abstract for eligibility based on the inclusion and exclusion criteria.

Results: Sixteen eligible studies were included. Four technological strategy categories were identified: artificial intelligence−based, simulation-based, infrastructure and hardware technologies, and interfaces and information systems. Mobile and web applications were the main technologies adopted in the studies.

Conclusions: Technological strategies hold significant potential to enhance patient experiences in EDs by providing real-time updates on medical status and care progress. However, their effectiveness depends on usability, literacy, and system design. Existing literature highlights the impact and challenges of deploying and using these strategies in EDs. However, no studies have systematically evaluated long-term outcomes or cost-effectiveness across diverse ED settings.

(JMIR Med Inform 2026;14:e79782) doi:10.2196/79782

KEYWORDS

scoping review; PRISMA-ScR framework; emergency department; patient journey; communication technology; patient experience

Introduction

The emergency department (ED) constitutes the gateway to health care for many people, being the place where treatment begins for a wide spectrum of diseases, some of which are life-threatening and require immediate attention [1]. The typical patient journey in the ED involves triage classification, medical evaluation, necessary examinations, medications, or procedures, reevaluation, and finally discharge or observation [2]. However, challenges such as overcrowding, uncomfortable facilities, and poor communication continue to hinder timely and efficient ED patient care, negatively impacting both patient experience and institutional performance [3]. In fact, effective and assertive communication of information about the ED patient journey has been found to be associated with patient satisfaction; thus, studies indicated that the lack of information on the progress and delays has a greater effect on patient satisfaction than perceived waiting times while visiting the ED [4]. In addition, it leads to feelings of powerlessness for patients and their family members [5]. Patients who feel well informed tend to have a better perception of the service [6], leading to higher satisfaction with the care and reduced anxiety [7], which in turn contributes to greater institutional efficiency [8].

XSL•FO
RenderX

With recent technological innovations, the potential to address communication challenges in EDs has increased significantly. Technologies that enhance communication and improve information accessibility have shown promise in improving the patient experience in the ED [9]. However, due to the rapid pace of technological advancement and the growing use of digital solutions in health care, there is an urgent need to review existing evidence to guide future implementation efforts.

This scoping review aims to analyze relevant studies and describe the evidence on technological strategies implemented in EDs worldwide that enhance patients' experiences during their journey in the ED. A technological strategy refers to the approach and implementation of technologies and supporting infrastructure within ED workflows to improve patient experience throughout their journey. Regarding the ED patient experience, the review focuses on two dimensions: communication and access to information. Communication refers to the exchange of timely, accurate, and comprehensible information between health care providers and patients or family members regarding medical status and progress updates during the ED visit. Access to information refers to patients' ability to obtain and understand relevant details about their journey in the ED. The following research questions (RQ) were addressed:

- What technological strategies exist to improve patient experience in EDs, considering dimensions such as communication and information accessibility?
- What infrastructure and technologies support technological strategies?

The scoping review offers a comprehensive and interdisciplinary perspective, integrating insights from clinical, technological, and human-centered design domains. The primary innovation of this study lies in its integrative and multidimensional approach to evaluating technological interventions in EDs, specifically through the lens of patient communication and information accessibility—dimensions often underrepresented in prior reviews. Unlike earlier works that focus predominantly on clinical outcomes or operational efficiency, this review foregrounds the patient experience and satisfaction as central evaluative criteria. It also identifies a critical knowledge gap: the lack of standardized frameworks for evaluating the long-term effectiveness, cost-efficiency, and scalability of these technologies across diverse health care settings. Additionally, the review highlights the insufficient attention given to the adaptability of these tools for vulnerable populations, such as those with low digital literacy or disabilities, and the need for participatory design approaches to ensure equitable and sustainable implementation.

Methods

Databases and Search Keywords

To analyze the current and future landscape of technological strategies in EDs, a scoping review was conducted following the PRISMA-ScR (Preferred Reporting Items for Systematic Reviews and Meta-Analyses Extension for Scoping Reviews) guidelines [10]. Studies were retrieved from Scopus, PubMed, IEEE Xplore, and CINAHL in January 2025. The inclusion of CINAHL and PubMed ensures coverage of nursing and clinical perspectives that are highly relevant to patient care and workflow improvements, complementing the technical focus of IEEE Xplore and the multidisciplinary scope of Scopus. The keywords used in the search queries included technology, strategy, ED, communication, and access to information. The complete search strategy was as follows: ("Technolog*") AND ("Strateg*" OR "Approach*" OR "Solution*" OR "Framework*" OR "System*" OR "Model*") AND ("Emergency Department*" OR "Emergency Service, Hospital" OR "Emergency Room*" OR "Emergency Medical Service*") AND ("Communication" OR "Access to Information"). The final database search queries for the period January 2018 to December 2024 are summarized in Multimedia Appendix 1.

Inclusion and Exclusion Criteria

To ensure the quality of the articles, only those that met the inclusion and exclusion criteria presented in Textbox 1 were considered in the review process. These criteria were chosen to focus on studies that specifically examine technological strategies designed for EDs and their impact on patient experience, particularly in the dimensions of communication and information accessibility. Three reviewers independently applied the criteria to refine the list of eligible articles. In cases of uncertainty, the decision was made collectively after discussion.

XSL•FO
RenderX

Textbox 1. Inclusion and exclusion criteria.

Inclusion criteria

- Documents published between 2018 and 2024 (including both years)
- Documents published in peer-reviewed journals or conference proceedings
- Full-text articles available in English
- The research setting is at least a hospital or an emergency department (ED), regardless of the age or sex of the patients who have used the ED
- Technological strategies specifically designed for EDs aimed at improving the patient's experience during their ED journey, focusing on communication and access to information
- Studies reporting on at least one patient-centered outcome (satisfaction, experience, or well-being)

Exclusion criteria

- Technological strategies outside the health care sector or those presented as telemedicine, remote medicine, or prehospital solutions
- Patients who have not used hospital or ED services
- Articles that do not present a descriptive evaluation, case study, or empirical evidence regarding the design, implementation, or impact of technological interventions on patient experiences in EDs
- Protocol-only studies or incomplete data reports

Study Selection

A 3-step filtering process was implemented to refine the selection of studies relevant to our RQ:

- In the first filter, *identification*, duplicates were removed. This process ensured the uniqueness of each record for accuracy and to avoid redundancy.
- The second filter involved *screening* by title and abstract, which significantly narrowed down the selection, based on our inclusion and exclusion criteria. This step focuses on identifying papers that are most relevant to ED's technological advancements.
- The third filter involved a full-text review to assess the *eligibility* of studies that addressed our RQ, culminating in the final selection of studies included in the review.

CADIMA was used for both the first and second filtering stages. CADIMA is an open-access online tool developed by the Julius Kühn-Institut during the EU-funded Global Response Against Child Exploitation project to support the conduct of systematic reviews [11].

Data Charting

The data charting process for the studies included in this review was structured into three rigorous rounds to explore the categories of technological strategies in EDs comprehensively. In the first round, we extracted fundamental attributes from each study, such as the authors, publication year, journal, and keywords. This process allowed us to understand the distribution of research over time and identify key categories within the field. A standardized data charting form was jointly developed in Microsoft Excel by three reviewers and piloted on a subset of studies to ensure consistency and clarity before full data extraction.

In the second round, we delved deeper into technological strategies applied in the studies. The charting form included variables such as the affected dimension (communication or access to information), technology and infrastructure used, impact on patient experience, measurement tools for usability or satisfaction, preferred information by patients, implementation details (approach, settings, challenges), and implementation outcomes.

Finally, in the third round, each paper was independently reviewed by three reviewers to ensure consistency and reduce bias in the analytical process. Any discrepancies were discussed and resolved by consensus. The charting process was iterative, and adjustments were made to the Excel form when new variables or categories emerged.

Quality Appraisal

Each selected paper underwent a quality appraisal conducted independently by two reviewers using the Crowe Critical Appraisal Tool version 1.4 (CCAT) [12]. This step was undertaken to assess the methodological rigor and credibility of the included evidence, supporting a more reliable interpretation of the findings in relation to our research questions. The CCAT is a widely used instrument recognized for its high reliability in evaluating research papers [13]. This instrument is organized into 8 categories comprising 22 items. Each category is scored on a 6-point scale ranging from 0 (lowest) to 5 (highest). The overall score is calculated as a percentage, and we arbitrarily considered acceptable a score above 60%. Prior to the appraisal, both reviewers were familiarized with the CCAT manual to ensure consistent interpretation of criteria. In cases of discrepancies between the reviewers' assessments, consensus was reached through discussion of the arguments and evidence.

Synthesis of Results

We grouped the studies by technological strategy category and summarized their associated challenges, as well as related patient experience outcomes and impacts. The strategy categories were defined using a content-based grouping approach: we reviewed all included studies, examined the technologies and their stated purposes, and clustered similar technologies based on their primary function and orientation toward improving ED patient

XSL•FO
RenderX

experience. The synthesis mapped the relationship between each strategy and its impact on communication and access to information, highlighting key outcomes, impacts, and challenges. Technologies and IT infrastructures were tabulated by strategy category, while patients' preferred information and satisfaction improvements were synthesized narratively.

Results

Flow Diagram and Number of Studies

The scoping review process is detailed in the flow diagram shown in Figure 1, presenting the stepwise filtering and the number of studies included at each step. In the *identification* step, 976 papers were identified and selected. Papers were imported into the CADIMA, where duplicates were removed, resulting in 923 papers. These papers were *screened*, applying the defined inclusion and exclusion criteria, where 21 papers were classified as eligible. Finally, after *full-text* reading, 16 papers were selected for further analysis; 5 articles did not contribute to the RQ.

Figure 1. Flow diagram of the scoping review process. RQ: research question.

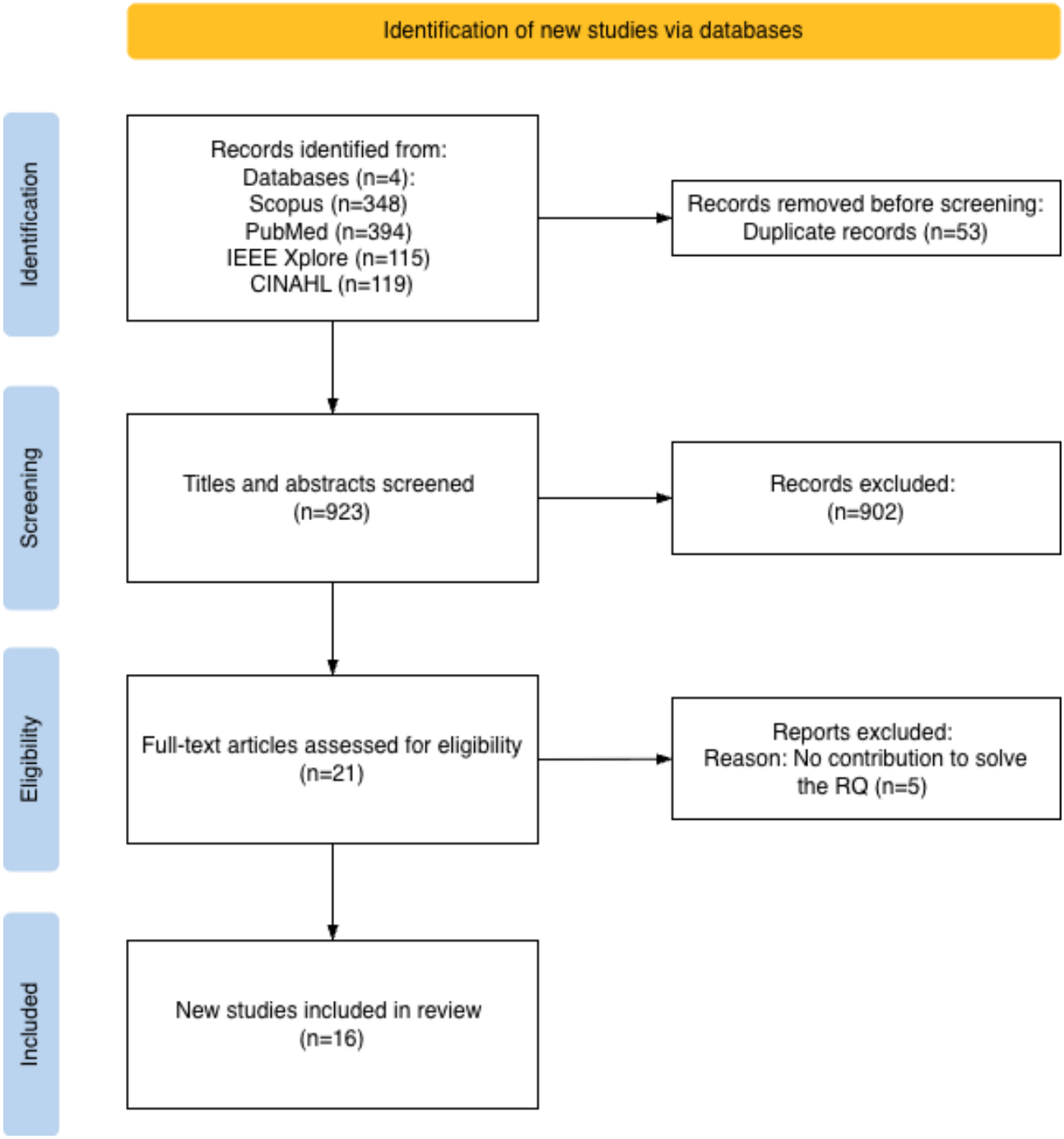

XSL•FO
RenderX

General Description and Characteristics of Studies

The set of 16 studies, published between 2018 and 2024 in journals such as *Journal of Medical Internet Research* and *Applied Clinical Informatics*, examines a range of technological strategies designed to improve patient experience in EDs. These studies address key aspects, including the design and implementation of solutions, the technological and infrastructural components that support them, patients' preferences for information delivery, system usability, and the assessment of their impact on patient satisfaction and overall experience. Methodologically, the articles include qualitative evaluations, observational pilot studies, and mixed methods research, reflecting a diversity of approaches (see Multimedia Appendix 2).

The reviewed literature reveals an interdisciplinary orientation, with collaborations among computer scientists, clinicians, designers, and data analysts. Notably, studies originate from diverse regions, including the United States [14-19], the United Kingdom [20], Italy [21], Israel [22,23], Denmark [5], Australia [24], Thailand [25], Malaysia [26], South Korea [27], and Greece [28]. Finally, the quality appraisal of the 16 studies revealed that 87.5% (n=14) were of high quality and 12.5% (n=2) of medium quality (see Multimedia Appendix 2).

Key Findings on Technological Strategies

Technological Strategies

Based on revised studies and following the process described in the Synthesis of Results subsection, we categorized the technological strategies that help to enhance patient journey experiences in EDs into four primary categories, as outlined below.

1. Interfaces and information systems: This category encompasses tools and information systems designed to provide access to comprehensive patient medical information and ED stage updates, enhancing patients' understanding of their journeys through the ED and facilitating communication with medical staff.
2. Infrastructure and hardware technologies: This category includes strategies focused on the underlying IT infrastructure necessary for ED operations. It encompasses advanced computing systems, integration devices, and hardware that are critical for patient care and tracking.
3. Artificial intelligence (AI)–based strategy: This category includes strategies that utilize machine learning (ML) and deep learning models for predictive analytics and pattern recognition in EDs.
4. Simulation-based strategy: This category encompasses simulation strategies, which are essential for evaluating the performance of health care operations, analyzing patient flow, and modeling complex interactions within ED settings.

Figure 2 illustrates the distribution of these strategy categories by dimension within the reviewed literature. Interfaces and information systems strategies were the most frequently cited, appearing in 14 studies, followed by infrastructure and hardware technologies and AI-based strategies, each appearing in 3 studies, and the simulation-based category, appearing in 2 studies. All categories addressed both dimensions, except the simulation-based category. These findings indicate a clear preference for integrated solutions and reveal a gap in studies dedicated exclusively to communication strategies.

XSL•FO
RenderX

Figure 2. Distribution of articles by technological strategy category and dimension focus.

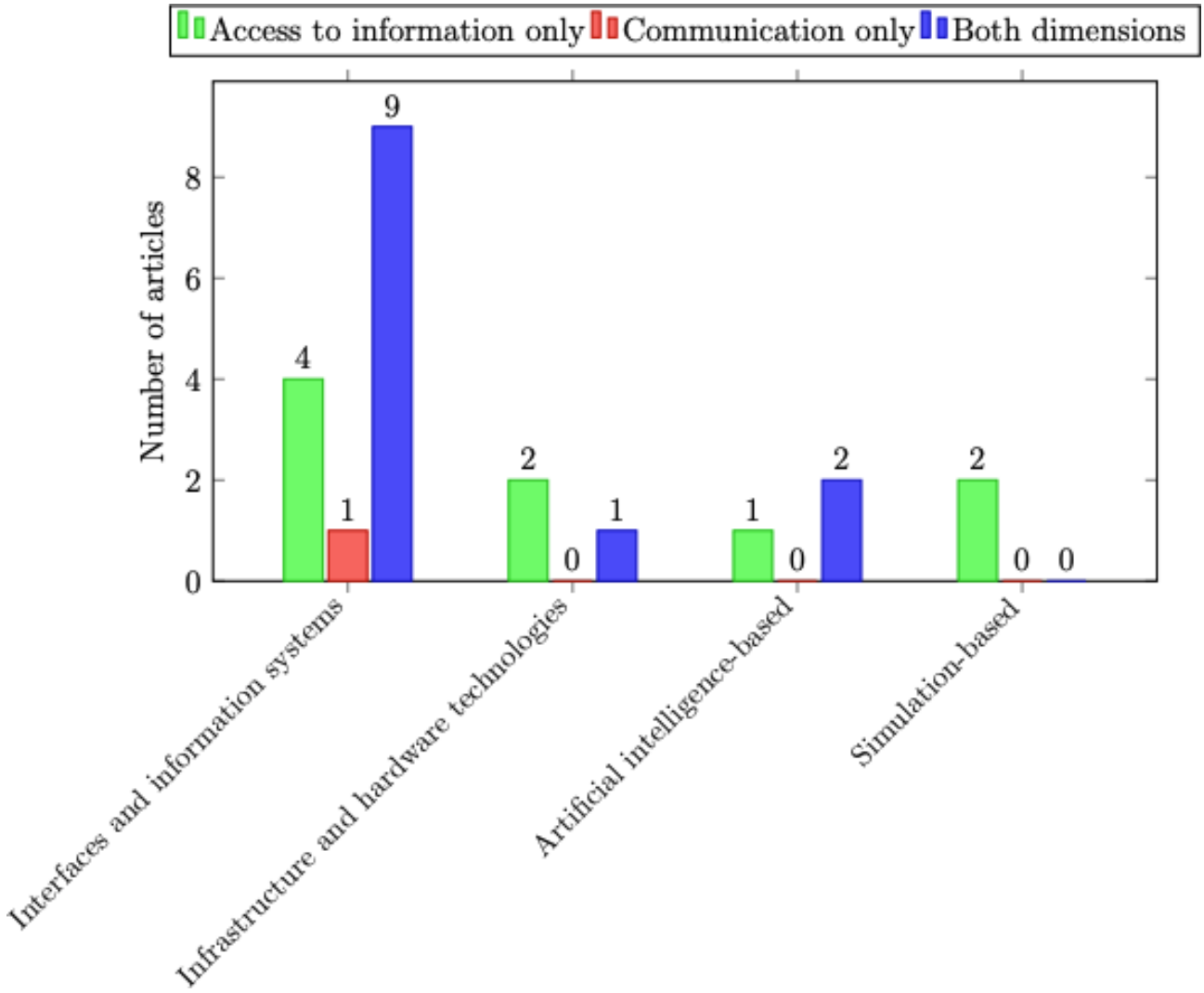

Table 1 provides a comprehensive overview of the key technological strategies implemented in EDs to enhance patient experience. For each strategy, the table details the specific dimension(s) addressed (communication and access to information), the implementation approach used and the target population (patients, family members, or health care staff), the measurement methods used to assess outcomes, the observed outcomes and their impact on patient experience and satisfaction, and the implementation challenges encountered. The results reveal a strong emphasis on systems that integrate both communication and access to information, particularly through interfaces and information systems such as digital whiteboards [16], clinical logic platforms [5], and discharge tools [17,24]. These solutions consistently aim to enhance patient and family engagement, improve satisfaction, and streamline information flow during care transitions [22].

XSL•FO
RenderX

Table . Key technological strategies for patient experience in EDs.

References	Dimension	Strategy category	Description	Measurement methods	Outcomes and impact	Challenges
Westphal et al [22]	Comm[a] and ATI[b]	AI, Int & IS[c]	• MyED: Web application providing real-time information about ED[d] journeys, procedures and expected waiting times • Target population: patients, family	Deployment survey, interviews, usage analytics	Improved patient understanding of the ED journey; positive reactions to comprehensive health information; enhanced transparency	Delays in synchronizing data from hospital databases; limited engagement period due to short ED visits
Marshall et al [16]	Comm	Int & IS	• Digital whiteboards: E-paper displays showing real-time orienting and clinical information in ED rooms • Target population: patients, Family	Satisfaction survey (Likert), custom quantitative perception survey	96% of patients preferred rooms with whiteboards; higher overall ED satisfaction; more likely to recommend hospital to family/friends	Not integrated with EHR[e]; updates not truly real-time; potential privacy concerns
Østervang et al [5]	Comm and ATI	Int & IS	• Cetrea Clinical Logistics for patients: hospital information system displaying time estimates, staff names, and educational videos • Target population: patients, family	SUS[f] surveys (Likert), qualitative semistructured interviews	Increased sense of control reduced uncertainty; improved communication with health care professionals; positive impact on family members; usability rated close to excellent (83.6 SUS)	Difficult for older patients; privacy concerns; IT support dependency; content limitations
Steel et al [17]	ATI	Int & IS	• MyEDCare: Mobile app for discharge instructions and information comprehension • Target population: patients	ED Consumer Assessment of Health Care Providers and Systems patient satisfaction scores, usage analytics	Reduced 72-hour, 9-day, and 30-day unscheduled return ED visits; positive impact on patients' perceptions of ED nursing; improved patient safety	Patient difficulties understanding complex information; technical issues; software bugs
Doyle et al [24]	Comm and ATI	Int & IS	• PETS[g]/REDCap[h] digital discharge system: discharge system: digital tools for pediatric patient registry and discharge information. • Target population: patients, family	SUS scores (Likert), confidence surveys, semistructured interviews	Parents felt more confident with digital discharge information; preferred digital engagement for clinical research; high usability ratings (94 SUS)	Parent concerns about understanding instructions; technical issues

XSL•FO
RenderX

References	Dimension	Strategy category	Description	Measurement methods	Outcomes and impact	Challenges
Jaafar et al [26]	Comm and ATI	I&H[i]	• Patient Tracking System (TrackMe): Mobile app with wireless wristbands for real-time updates on patient location • Target population: staff, family	Satisfaction surveys (Likert)	Enhanced family engagement; decreased anxiety through real-time updates about patient status and location; high user satisfaction (mean >4.0)	Resistance to adoption among staff; training needs; connectivity and infrastructure requirements

[a]Comm: communication.

[b]ATI: access to information.

[c]Int & IS: interfaces and information systems.

[d]ED: emergency department.

[e]EHR: electronic health record.

[f]SUS: System Usability Scale.

[g]PETS: Parent Engagement Through Technology Solutions.

[h]REDCap: Research Electronic Data Capture.

[i]I&H: infrastructure and hardware.

Common measurement methods include satisfaction surveys, usability scales, and structured interviews, reflecting a focus on patient-centered evaluation (see the *Measuring Usability, Patient Experience, and Satisfaction Improvement* subsection for more information). Reported outcomes and impact generally include improved understanding of care processes [22], reduced anxiety [5,26], and better communication with health care professionals [5], although challenges persist, such as technical limitations [17], integration with existing systems [16], and resistance to adoption [26]. Notably, infrastructure-based tools such as patient tracking systems [26] complement these efforts by supporting real-time updates, but they face barriers related to cost and implementation complexity. Overall, the evidence suggests a trend toward multidimensional strategies that prioritize transparency and communication while highlighting gaps in scalability and interoperability. In addition, the literature provides limited discussion on how these strategies can adapt to dynamic changes in ED protocols [22], ensure equity among diverse patient populations—including individuals with disabilities or lower digital literacy [5,18,24]—and effectively support digitally underserved or vulnerable groups [16,17].

Technologies and IT Infrastructures

Table 2 provides an overview of the main technologies and IT infrastructures used in ED settings, grouped by strategy category.

XSL•FO
RenderX

Table . Overview of technologies and IT infrastructures used in EDs, grouped by strategy category.

Strategy category and technology/infrastructure	Description and outcome	References
Interfaces and information systems		
Mobile app	Provides a patient-friendly health information and communication interface through a smartphone app, designed to deliver real-time and comprehensive medical data—such as health status, triage classification, vital signs, discharge instructions, and location within the ED[a] journey—while also enabling communication with patients' next of kin and supporting guidance for effective illness management, thereby improving health care services and enhancing patient satisfaction.	[17,20,26-28]
Web dashboard	Delivers a user-friendly, graphical web interface that provides real-time updates on patients' medical status—including triage classification, clinical conditions, and vital signs—along with their ED treatment progression, open clinical note access, care pathways, and discharge instructions. This interface enhances transparency and patient engagement during the ED stay.	[5,14,18,19,22-25,28]
Digital whiteboard	Provides an electronic paper interface via a digital whiteboard that communicates relevant real-time clinical information to ED patients, including status updates, orientation details, care team assignments, safety alerts, patient orders, and disposition information. This interface enhances patient understanding of their journey through the ED.	[16]
Patient-centered information system	Provides an information system accessible across various devices and interfaces (web and desktop applications), designed to deliver real-time updates and detailed information—including procedures, treatments, associated waiting times, nurse and physician responsible for care, and current and upcoming stages—directly to patients and their family members. This enhances patients' understanding of their individual journeys through the ED and supports informed decision-making and communication.	[5,22]
Infrastructure and hardware technologies		
Internet of Medical Things	Includes IoT[b] devices (eg, wearables) for real-time monitoring of ED patients, providing vital insights into their health status, vital signs, patient stratification for special services, and physical location within the ED. This information supports clinical decision-making and enhances communication by delivering timely and essential updates to both medical staff and patients' families about the health care process.	[26-28]
Computing infrastructure	Covers advanced computing infrastructures, such as cloud computing, that support real-time data storage, processing, and analysis in EDs.	[26,28]
Artificial intelligence–based		
ML[c] algorithms	Encompasses ML algorithms like random forest for predictive analytics in EDs, providing insights into patient treatment, stratification, and predicting waiting times based on workload and patient characteristics.	[14,15,22]
Simulation-based		

XSL•FO
RenderX

Strategy category and technology/infrastructure	Description and outcome	References
Discrete-event simulation	Provides a simulation-based model in R to estimate individual treatment times from aggregated ED data, aiming to assess delays, improve waiting time estimates, and enhance understanding of patient flow.	[21]
Petri net model	Comprises a simulation-based model in Python using Colored Petri Nets to model and analyze ED processes and workflows, supporting improvements in patient flow across treatment paths and enhancing decision-making efficiency.	[15]

[a]ED: emergency department.

[b]IoT: Internet of Things.

[c]ML: machine learning.

Interfaces and information systems emerge as the most significant strategy category for directly improving patient experience through enhanced communication and transparency (14 studies). Within this category, *mobile* and *web dashboard applications* are the most widely adopted technologies (5 and 9 studies, respectively). For example, the Parent Engagement Through Technology Solutions (PETS) [24] and MyEDCare [17] mobile apps support patients and caregivers during discharge by improving comprehension and reinforcing key information about the ED journey. Complementing these mobile tools, the MyED system [22] and the Cetrea Clinical Logistics (CCL) dashboard for patients [5] were designed as web dashboard applications to enhance patients' understanding of their care trajectory by displaying completed, ongoing, and anticipated procedures, as well as identifying the clinicians responsible for their care. Additionally, digital whiteboards, leveraging E-paper technology, deliver real-time notifications on delays and post-discharge instructions, functioning as integral components of the IT infrastructure [16].

Building on these interface-focused solutions, *infrastructure and hardware technologies* provide the foundation for real-time monitoring and data exchange. This category integrates *Internet of Medical Things* (*IoMT*) components with robust *computing infrastructure*. IoMT technologies enable real-time sensing and location tracking through dedicated hardware: beacon devices worn as patient bracelets and beacon readers (gateways) enable continuous wireless monitoring of patient location and status [26]; wearable biosensors capture physiological signals such as heart rate and oxygen saturation, supported by real-time location devices, Wi-Fi hotspots, and Bluetooth-to–Wi-Fi gateways for data transmission [28]; and near-field communication (NFC) tags paired with mobile electronic medical record (EMR) devices (eg, smartphones) allow location-based access to patient information [27]. Computing infrastructure complements these technologies by offering backend systems for secure data storage, processing, and decision support, including cloud-based databases and local servers operating within private networks [26,28]. Examples of strategies include TrackMe [26], which combines beacon-enabled bracelets with a mobile app and a 3-tier architecture for real-time updates; the NFC-integrated Mobile EMR System [27], which accelerates access to patient records; and IntelTriage [28], which uses wearable biosensors and LAN-based communication to monitor vital signs and geo-location, supported by a decision-support subsystem for dynamic prioritization.

Building on these physical infrastructures, *AI-based* strategies leverage computational techniques to enhance decision-making and operational efficiency. Predictive models such as *machine learning algorithms* [14,15] and random forest [22] approaches analyze EMR data—including length of stay, procedures, and clinical notes—to generate actionable insights. For example, the AI-enabled non-English language preference prioritization strategy [14] computes complexity scores for patients with a non-English language preference, while the AI/ML model presented in Gehlot et al [15] provides deeper insights into treatment details and patient experiences, thereby supporting more accurate patient routing based on acuity. Similarly, the MyED strategy [22] combines random forest models with operations research techniques, such as process discovery and queue mining, to predict waiting times for specific procedures and deliver real-time updates to patients through a responsive mobile interface.

Finally, *simulation-based* approaches complement predictive analytics by modeling complex ED workflows to optimize patient flow. Techniques such as *discrete-event simulation* and *Petri Net models* are used to estimate waiting times, identify bottlenecks, and validate algorithms for time-to-treatment predictions. These models support more reliable and equitable resource allocation. Reported strategies use these models to simulate care pathways and assess workflow constraints, enabling validation of predictive algorithms for waiting time and treatment prioritization [21]. A notable example is presented in Gehlot et al [15], where a Colored Petri Net–based simulation is integrated with Python-based AI/ML components to evaluate and refine triage processes, aiming to improve clinical outcomes and enhance patient experience.

Further details on usability, patient experience, and satisfaction impacts are provided in Table 1 and discussed in the subsection *Measuring Usability, Patient Experience, and Satisfaction Improvement*.

Patient's Preferred Information

The selected studies displayed a wide variety of topics that patients preferred on their journey through the ED. Specifically, patients preferred detailed information on their medical status

XSL•FO
RenderX

and progress updates [18,26], including triage status [15,28], treatment, and discharge instructions [17,19,24]. Additionally, patients valued comprehensive medical information related to their vital signs [18,25,28], laboratory results [27] and medical orders [16,18], nursing care plans [15,25,28], and the nurse and physician responsible for care [5,16]. Patients also appreciated personalized medical information and updates on procedures, associated waiting times [5,21], as well as current and upcoming stages of their ED stay [16,22]. They also favored precise tracking of their location in the ED [26,27], safety, and disposition information [16]. These preferences highlight a significant trend toward personalized health care information, underscoring the need for technological strategies to focus on delivering precise, individualized health data and highlighting the importance of accuracy and clarity in the patient communication tools of the ED.

Measuring Usability, Patient Experience, and Satisfaction Improvement

Usability evaluations are essential in health care technology to identify design flaws early and prevent ineffective implementations [24]. Among reviewed studies, the System Usability Scale (SUS) was the most frequently used instrument [5,18,24,27]. SUS is a 10-item Likert questionnaire that generates a score from 0 to 100, interpreted using a grading scheme (eg, >90: “A” [excellent]; <60: “F” [poor]). To illustrate, the PETS mobile discharge tool scored 94/100 (A grade—Excellent), indicating superior design and strong patient acceptance [24]. Similarly, the CCL patient information system achieved near-excellent usability with a mean SUS score of 83.6/100 (B+ grade—Acceptable) [5]. In contrast, NFC-integrated mobile EMR and REDCap eConsent interfaces scored 71.9/100 and 78/100 (B grade—acceptable), reflecting moderate usability and less direct impact on patient experience [24,27]. The electronic health record display for ED patient health status and care plan progress received a mean SUS score of 69.6 out of 100 (C grade—marginally acceptable) [18], suggesting limited effectiveness in improving patient experience.

While SUS provides a standardized measure, complementary approaches are often necessary to capture user perceptions more comprehensively. Likert-scale satisfaction surveys (typically 5- or 10-point) are commonly used to assess design quality, content relevance, and overall user-friendliness [16,25,26]. For example, the web application for emergency trauma patients, using a 10-point Likert scale, reported a mean usability score of 4.09 (SD 0.74) [25]. Similarly, the TrackMe patient-tracking system, using a 5-point Likert scale, reported a mean usability score of 4.0 (SD 1.2) and a mean satisfaction score of 4.4 (SD 1.0), indicating a generally positive user experience during ED waiting periods [26]. These findings reinforce that usability and satisfaction are interrelated but distinct constructs, underscoring the need for multidimensional assessment.

Patient experience and satisfaction are closely linked to usability, which strongly influences technology acceptance in clinical settings. In ED environments, these areas are typically assessed using mixed methods that combine SUS scores, Likert-scale measures, and validated instruments such as Hospital Consumer Assessment of Health Care Providers and Systems (CAHPS) and ED-CAHPS [16,17], complemented by semistructured interviews for contextual insights into patient perceptions [5,22,24]. For example, semistructured interviews in the MyED study showed that patients who used the solution demonstrated significantly better understanding of their ED journey compared with nonusers ($F_{8,299}$=2.519; P=.01) [22]. Using satisfaction surveys, the digital whiteboards intervention improved patient-reported communication about delays (1.96 vs 2.48; P=.03) and clarity of post-discharge instructions (2.41 vs 2.83; P=.02), and users were more likely to recommend the facility (9.66 vs 9.22; P=.05) [16]. Operational benefits were also reported in the MyEDCare study: patients receiving digital discharge instructions had significantly fewer unscheduled ED returns at 72 hours and 30 days compared with those receiving standard paper-based discharge (P=.003 and P<.001) and higher ED-CAHPS scores in nursing communication domains (eg, “Nurses explain in a way you understand”: 86.5 vs 81.9; P=.03) [17].

Collectively, these findings underscore that usability is not merely a design metric but a critical driver of patient experience, satisfaction, and even clinical outcomes in ED technology implementations. In addition, the evidence shows that *Interfaces and Information Systems*—particularly *mobile and web applications*—provide the greatest added value for improving patient experience, primarily by enhancing communication, transparency, and comprehension.

Discussion

Principal Findings

The integration of advanced digital technologies in EDs represents a rapidly evolving but still unstructured field. Among the 16 studies included in this review, 9 reported interventions that achieved measurable improvements in communication, patient satisfaction, or reductions in service fragmentation [5,16-18,22,24-27]. Despite the promising results (see subsection *Measuring Usability, Patient Experience, and Satisfaction Improvement*), the absence of standardized frameworks, definitions, and evaluation models limits comparability and scalability across settings [29]. Developing a shared conceptual and operational framework is essential to ensure consistency in research and guide technology implementation within ED systems.

Patient-facing technologies such as mobile apps, real-time dashboards, and web-based platforms have enabled patients to access individualized health information, often in real time, enhancing their sense of involvement in emergency care [22]. Some tools demonstrated significant benefits—for example, MyEDCare improved patient comprehension and experience (86.5 vs 81.9; P=.03) [17], and digital whiteboards reduced perceived uncertainty (2.41 vs 2.83; P=.02) [16]. However, implementation challenges were common. The MyED system faced difficulties synchronizing live data from hospital databases, and short ED visits limited patient engagement [22]. Usability issues were also reported among older adults, who requested simplified functions [5]. These findings underscore the need for participatory design approaches that incorporate patient perspectives prior to implementation [30]. Ultimately,

XSL•FO
RenderX

usability remains a critical determinant of successful adoption and effective use [31].

Technological impact extends beyond patient interaction to clinical workflows. Real-time data systems and mobile-based discharge tools require adjustments in routines, new training protocols, and additional coordination. While these tools can enhance communication and data accuracy, they often introduce extra responsibilities, increasing cognitive and operational burden on health care professionals [24]. This tension—between intended benefits such as efficiency and the reality of added workload—has been documented in multiple studies [32,33]. Understanding nursing staff perceptions and acceptance is therefore essential for successful adoption [34]. Policymakers and ED managers must consider these trade-offs when planning technological strategies to avoid overburdening staff while pursuing efficiency goals [16].

Additionally, the integration of wearable devices (eg, TrackMe, IntelTriage) and patient-facing platforms (eg, CCL, MyED) is reshaping care dynamics by fostering patient autonomy [5] and involvement in decision-making [20,23]. Although these innovations hold promise for improved outcomes and satisfaction [16,17,23], they raise concerns regarding workflow implications (eg, TrackMe increased nurses' workload [26]; fears of delays with MyED [22]), digital literacy barriers (eg, limited access to Open Notes among non-English speakers [23]; usability issues for older users of CCL [5]), and communication norms (eg, risks of patients viewing information before staff [22]; potential reduction in nurse/physician time) [5]). These factors must be addressed to ensure equitable and safe implementation.

Finally, the economic cost required for the investment, implementation, and maintenance of advanced technologies in EDs must be carefully considered. These expenses may include infrastructure upgrades, software development, technical support, and training for health care personnel [19]. Given the potential financial implications, future studies should explore the cost-benefit relationship of these technological strategies, assessing their feasibility, sustainability, and overall value in diverse health care settings [17].

Strengths and Limitations

A key strength of this study is its multidimensional approach, which provides a holistic view by examining various facets of ED care, including communication and information accessibility. This comprehensive perspective was achieved by focusing on emerging technologies, such as AI and IoT, which represent the forefront of operational efficiency and diagnostic accuracy in EDs. The recent literature (2018 - 2024) grounds the study's findings in current technological trends, ensuring relevance. However, limitations include a focus on English articles, which may have excluded relevant studies in other languages, potentially restricting generalization. Furthermore, since many technologies analyzed are relatively new (eg, IoMT, AI), few studies directly address their long-term impacts. Variability in environments where these technologies are implemented can also affect reproducibility, especially in resource-limited settings. The recent temporal range may not capture emerging trends or long-term effects, highlighting the need for ongoing research to understand their sustained impact.

Conclusions

This scoping review synthesized current technological strategies designed to enhance patient experiences in EDs, primarily through improved communication and access to information. The limited number of studies identified (n=16, published between 2018 and 2024) underscores the nascent and fragmented nature of this research area. Existing evidence suggests that patient-facing tools—such as mobile apps, real-time dashboards, and web-based platforms—can improve information transparency and engagement, while clinical workflow solutions, including digital whiteboards and mobile discharge systems, support communication accuracy and care coordination. Emerging innovations like IoT-wearable monitoring devices further demonstrate potential for promoting patient autonomy and continuous observation. However, these benefits are tempered by persistent implementation challenges. Usability barriers among older adults, technical integration issues, and increased workload for health care professionals remain significant obstacles. Equity concerns related to digital literacy and language accessibility further complicate adoption, raising questions about inclusiveness and fairness in technology-driven care. Importantly, none of the reviewed studies conducted systematic evaluations of long-term outcomes or cost-effectiveness across diverse ED contexts, limiting the evidence base for sustainable integration. Future research should move beyond descriptive assessments toward rigorous, standardized evaluation frameworks that capture clinical, economic, and experiential outcomes. Participatory and inclusive design approaches are essential to address usability and equity gaps, while comprehensive cost-effectiveness analyses will inform scalability and resource allocation. Advancing this agenda is critical to ensure that technological innovations in EDs are not only effective but also equitable, sustainable, and adaptable across varied health care settings.

Acknowledgments

The authors would like to acknowledge all the institutions that supported this work: Clínica Universidad de La Sabana, CAPSAB–Control y Automatización de Procesos Universidad de La Sabana and Sistemas Logísticos–Facultad de Ingeniería, and Cuidado de Enfermería Unisabana-Facultad de Enfermería y Rehabilitación, Universidad de La Sabana (project ING-299-2022). The authors also thank Rosario Lozano and Santiago Lozano for their valuable assistance during the screening and data extraction processes. During the preparation of this work, the authors used ChatGPT (OpenAI 2025) and Copilot (Microsoft 2025) to improve the readability of the paper. After using this tool/service, the authors reviewed and edited the content as needed and take full responsibility for the content of the publication.

XSL•FO
RenderX

Funding

This research is supported by Universidad de La Sabana, grant agreement ING-299-2022—"Estrategias Tecnológicas Para Aumentar La Eficiencia En La Ruta De Atención Del Usuario En Servicios De Urgencias De La Clínica Universidad De La Sabana, 2023-2024"—call for the promotion of the academic career and categorization of researchers–2022.

Data Availability

All data generated or analyzed during this study are included in this manuscript and multimedia appendices.

Authors' Contributions

Writing – original draft: ASS, JMA
Methodology: ASS, JMA, WJB, WJG, MGL, IXB
Conceptualization: ASS, JMA, WJB, WJG, MGL, IXB
Investigation: ASS, JMA, WJB
Visualization: ASS, JMA, MGL, IXB
Data curation: ASS, JMA
Writing – review & editing: JMA, WJB, WJG
Funding acquisition: JMA, WJG

Conflicts of Interest

None declared.

Multimedia Appendix 1
Database search queries and results.
[DOCX File, 15 KB - medinform_v14i1e79782_app1.docx]

Multimedia Appendix 2
Crowe Critical Appraisal results.
[XLSX File, 15 KB - medinform_v14i1e79782_app2.xlsx]

Checklist 1
PRISMA-ScR checklist.
[DOCX File, 110 KB - medinform_v14i1e79782_app3.docx]

References

1. Tsai WC, Liu CF, Lin HJ, et al. Design and implementation of a comprehensive AI dashboard for real-time prediction of adverse prognosis of ED patients. Healthcare (Basel) 2022 Aug 9;10(8):1498. [doi: 10.3390/healthcare10081498] [Medline: 36011155]
2. Mora-Meza D, Espejo-Díaz JA, Guerrero WJ. A simulation approach to analyze the operational response plans in an emergency department under the COVID-19 pandemic. In: Montoya-Torres JR, Guerrero WJ, Cortés-Murcia DL, editors. Operations Research and Analytics in Latin America: Proceedings of ASOCIO/IISE Region 16 Joint Conference 2022: Springer; 2023:149-158. [doi: 10.1007/978-3-031-28870-8_12]
3. Sonis JD, Aaronson EL, Lee RY, Philpotts LL, White BA. Emergency department patient experience: a systematic review of the literature. J Patient Exp 2018 Jun;5(2):101-106. [doi: 10.1177/2374373517731359] [Medline: 29978025]
4. Yoo J, Soh JY, Lee WH, Chang DK, Lee SU, Cha WC. Experience of emergency department patients with using the Talking Pole device: prospective interventional descriptive study. JMIR mHealth uHealth 2018 Nov 22;6(11):e191. [doi: 10.2196/mhealth.9676] [Medline: 30467105]
5. Østervang C, Jensen CM, Coyne E, Dieperink KB, Lassen A. Usability and evaluation of a health information system in the emergency department: mixed methods study. JMIR Hum Factors 2024 Feb 21;11:e48445. [doi: 10.2196/48445] [Medline: 38381502]
6. Sonis JD, Rogg J, Yun B, Raja AS, White BA. Improving the patient experience: ten high-yield interventions. : American Academy of Emergency Medicine News; 2016 URL: https://apps.aaem.org/UserFiles/file/MarApr16CommonSense_OMC.pdf [accessed 2025-06-26]
7. Bissonette S, Chartrand J, Bailey L, Lalonde M, Tyerman J. Interventions to improve nurse-family communication in the emergency department: a scoping review. J Clin Nurs 2024 Jul;33(7):2525-2543. [doi: 10.1111/jocn.17068] [Medline: 38476035]
8. Sangal RB, Orloski CJ, Shofer FS, Mills AM. Improving emergency department patient experience through implementation of an informational pamphlet. J Patient Exp 2020 Apr;7(2):225-231. [doi: 10.1177/2374373519826246] [Medline: 32851144]

XSL•FO
RenderX

9. Goldfine CE, Knapp A, Goodman GR, et al. Media and technology usage and attitudes in emergency department patients. Front Digit Health 2022;4:894683. [doi: 10.3389/fdgth.2022.894683] [Medline: 36386045]
10. Tricco AC, Lillie E, Zarin W, et al. PRISMA extension for scoping reviews (PRISMA-ScR): checklist and explanation. Ann Intern Med 2018 Oct 2;169(7):467-473. [doi: 10.7326/M18-0850] [Medline: 30178033]
11. Kohl C, McIntosh EJ, Unger S, et al. Online tools supporting the conduct and reporting of systematic reviews and systematic maps: a case study on CADIMA and review of existing tools. Environ Evid 2018 Dec;7(1):8. [doi: 10.1186/s13750-018-0115-5]
12. Crowe M. Crowe Critical Appraisal Tool (CCAT) user guide. : Conchra; 2013 Nov 19 URL: https://conchra.com.au/wp-content/uploads/2015/12/CCAT-user-guide-v1.4.pdf [accessed 2025-11-21]
13. Crowe M, Sheppard L, Campbell A. Comparison of the effects of using the Crowe Critical Appraisal Tool versus informal appraisal in assessing health research: a randomised trial. Int J Evid Based Healthc 2011 Dec;9(4):444-449. [doi: 10.1111/j.1744-1609.2011.00237.x] [Medline: 22093394]
14. Strechen I, Wilson P, Eltalhi T, et al. Harnessing health information technology to promote equitable care for patients with limited English proficiency and complex care needs. Trials 2024 Jul 4;25(1):450. [doi: 10.1186/s13063-024-08254-y] [Medline: 38961501]
15. Gehlot V, Rokowski P, Sloane EB, Wickramasinghe N. Taxonomy, tools, and a framework for combining simulation models with AI/ML models. Presented at: 2022 Annual Modeling and Simulation Conference (ANNSIM); Jul 18-20, 2022. [doi: 10.23919/ANNSIM55834.2022.9859494]
16. Marshall ADA, Hasdianda MA, Miyawaki S, et al. A pilot of digital whiteboards for improving patient satisfaction in the emergency department: nonrandomized controlled trial. JMIR Form Res 2023 Mar 21;7:e44725. [doi: 10.2196/44725] [Medline: 36943360]
17. Steel PAD, Bodnar D, Bonito M, et al. MyEDCare: Evaluation of a smartphone-based emergency department discharge process. Appl Clin Inform 2021 Mar;12(2):362-371. [doi: 10.1055/s-0041-1729165] [Medline: 33910262]
18. Wang X, Kim TC, Hegde S, et al. Design and evaluation of an integrated, patient-focused electronic health record display for emergency medicine. Appl Clin Inform 2019 Aug;10(4):693-706. [doi: 10.1055/s-0039-1695800] [Medline: 31533171]
19. Gesell SB, Golden SL, Limkakeng AT Jr, et al. Implementation of the HEART pathway: using the consolidated framework for implementation research. Crit Pathw Cardiol 2018 Dec;17(4):191-200. [doi: 10.1097/HPC.0000000000000154] [Medline: 30418249]
20. Rathbone AL, Neill S, Prime S, Thomas N, Everett K. Supporting parents with acutely ill children: environment scan and user evaluation of mobile applications (the SuPa kids project). Int J Med Inform 2024 Sep;189:105504. [doi: 10.1016/j.ijmedinf.2024.105504] [Medline: 38833841]
21. Lusa L, Bukovšek D. Providing patients visiting emergency departments with useful information using public real time data: a case study based on Italian data. J Eval Clin Pract 2019 Jun;25(3):404-411. [doi: 10.1111/jep.13059] [Medline: 30407698]
22. Westphal M, Yom-Tov GB, Parush A, et al. A patient-centered information system (MyED) for emergency care journeys: design, development, and initial adoption. JMIR Form Res 2020 Feb 25;4(2):e16410. [doi: 10.2196/16410] [Medline: 32130144]
23. Sangal RB, Powers E, Rothenberg C, et al. Disparities in accessing and reading open notes in the emergency department upon implementation of the 21st Century CURES Act. Ann Emerg Med 2021 Nov;78(5):593-598. [doi: 10.1016/j.annemergmed.2021.06.014] [Medline: 34353651]
24. Doyle S, Pavlos R, Carlson SJ, et al. Efficacy of digital health tools for a pediatric patient registry: semistructured interviews and interface usability testing with parents and clinicians. JMIR Form Res 2022 Jan 17;6(1):e29889. [doi: 10.2196/29889] [Medline: 35037889]
25. Pearkao C, Potisopha W, Wonggom P, Jumpamool A, Apiratwarakul K, Lenghong K. Outcomes of emergency trauma patients after the implementation of web application operating systems. Asian Nurs Res (Korean Soc Nurs Sci) 2023 Aug;17(3):174-179. [doi: 10.1016/j.anr.2023.06.003] [Medline: 37355036]
26. Jaafar R, Lam MC, Abdullah MN, et al. Enhancing healthcare service delivery via patient tracking system using mobile apps technology: a case study. J Eng Sci Technol 2022;17(5):3526-3538 [FREE Full text]
27. Jung KY, Kim T, Jung J, et al. The effectiveness of near-field communication integrated with a mobile electronic medical record system: emergency department simulation study. JMIR mhealth uHealth 2018 Sep 21;6(9):e11187. [doi: 10.2196/11187] [Medline: 30249577]
28. Mavropodi R, Zouka M, Bamidis P, et al. The architecture of an intelligent incident response system in health environments. Presented at: 2019 4th South-East Europe Design Automation, Computer Engineering, Computer Networks and Social Media Conference (SEEDA-CECNSM); Sep 20-22, 2019. [doi: 10.1109/SEEDA-CECNSM.2019.8908329]
29. Hampiholi N. Elevating emergency healthcare - technological advancements and challenges in smart ambulance systems and advanced monitoring and diagnostic tools. Int J Comput Trends Technol 2024;72(1):1-7. [doi: 10.14445/22312803/IJCTT-V72I1P101]

XSL•FO
RenderX

30. Østervang C, Lassen A, Schmidt T, Coyne E, Dieperink KB, Jensen CM. Development of a health information system to promote emergency care pathways: a participatory design study. Digit Health 2022;8:20552076221145856. [doi: 10.1177/20552076221145856] [Medline: 36601282]
31. Rochat J, Ehrler F, Siebert JN, Ricci A, Garretas Ruiz V, Lovis C. Usability testing of a patient-centered mobile health app for supporting and guiding the pediatric emergency department patient journey: mixed methods study. JMIR Pediatr Parent 2022 Mar 15;5(1):e25540. [doi: 10.2196/25540] [Medline: 35289754]
32. Alowad A, Samaranayake P, Ahsan K, Alidrisi H, Karim A. Enhancing patient flow in emergency department (ED) using lean strategies–an integrated voice of customer and voice of process perspective. Bus Process Manag J 2021 Jan 25;27(1):75-105. [doi: 10.1108/BPMJ-11-2019-0457]
33. Al Harbi S, Aljohani B, Elmasry L, et al. Streamlining patient flow and enhancing operational efficiency through case management implementation. BMJ Open Qual 2024 Feb 28;13(1):e002484. [doi: 10.1136/bmjoq-2023-002484] [Medline: 38423585]
34. Aranda JM, Moreno-Fergusson ME, Guerrero WJ, et al. Technology acceptance and use among nursing staff in Latin American hospitals: a mixed methods study. Int J Nurs Stud Adv 2025;8:100290. [doi: 10.1016/j.ijnsa.2024.100290] [Medline: 39872435]

Abbreviations

AI: artificial intelligence
CAHPS: Consumer Assessment of Health Care Providers and Systems
CCAT: Crowe Critical Appraisal Tool
CCL: Cetrea Clinical Logistics
ED: emergency department
EMR: electronic medical record
IoMT: Internet of Medical Things
ML: machine learning
NFC: near-field communication
PETS: Parent Engagement through Technology Solutions
PRISMA-ScR: Preferred Reporting Items for Systematic Reviews and Meta-Analyses Extension for Scoping Reviews
RQ: research question
SUS: System Usability Scale

Edited by A Benis; submitted 27.Jun.2025; peer-reviewed by E Bai, R Clay-williams; revised version received 27.Nov.2025; accepted 01.Jan.2026; published 09.Mar.2026.

Please cite as:
Santafé AS, Aranda JM, Beltrán WJ, Guerrero WJ, Guevara Lozano M, Bustos IX
Technological Strategies for the Patient Experience in Emergency Departments: Scoping Review
JMIR Med Inform 2026;14:e79782
URL: https://medinform.jmir.org/2026/1/e79782
doi:10.2196/79782

© Andrés Santiago Santafé, Juan Manuel Aranda, Wilmer Jair Beltrán, William Javier Guerrero, Maryory Guevara Lozano, Ingrid Xiomara Bustos. Originally published in JMIR Medical Informatics (https://medinform.jmir.org), 9.Mar.2026. This is an open-access article distributed under the terms of the Creative Commons Attribution License (https://creativecommons.org/licenses/by/4.0/), which permits unrestricted use, distribution, and reproduction in any medium, provided the original work, first published in JMIR Medical Informatics, is properly cited. The complete bibliographic information, a link to the original publication on https://medinform.jmir.org/, as well as this copyright and license information must be included.

XSL•FO
RenderX

Review

Large Language Model–Based Virtual Patient Systems for History-Taking in Medical Education: Comprehensive Systematic Review

Dongliang Li[1], MSc; Syaheerah Lebai Lutfi[2], PhD

[1]Artificial Intelligence & Software Engineering, School of Computer Sciences, Universiti Sains Malaysia, Penang, Malaysia

[2]Medical Informatics Department, College of Medicine and Health Sciences, Sultan Qaboos University, Al Seeb, Oman

Corresponding Author:
Syaheerah Lebai Lutfi, PhD
Medical Informatics Department
College of Medicine and Health Sciences
Sultan Qaboos University
PO Box 35
Al Khoudh
Al Seeb, 123
Oman
Phone: 60 134526001
Email: s.lutfi@squ.edu.om

Abstract

Background: Large language models (LLMs), such as GPT-3.5 and GPT-4 (OpenAI), have been transforming virtual patient systems in medical education by providing scalable and cost-effective alternatives to standardized patients. However, systematic evaluations of their performance, particularly for multimorbidity scenarios involving multiple coexisting diseases, are still limited.

Objective: This systematic review aimed to evaluate LLM-based virtual patient systems for medical history-taking, addressing four research questions: (1) simulated patient types and disease scope, (2) performance-enhancing techniques, (3) experimental designs and evaluation metrics, and (4) dataset characteristics and availability.

Methods: Following PRISMA (Preferred Reporting Items for Systematic Reviews and Meta-Analyses) 2020, 9 databases were searched (January 1, 2020, to August 18, 2025). Nontransformer LLMs and non–history-taking tasks were excluded. Multidimensional quality and bias assessments were conducted.

Results: A total of 39 studies were included, screened by one computer science researcher under supervision. LLM-based virtual patient systems mainly simulated internal medicine and mental health disorders, with many addressing distinct single disease types but few covering multimorbidity or rare conditions. Techniques like role-based prompts, few-shot learning, multiagent frameworks, knowledge graph (KG) integration (top-k accuracy 16.02%), and fine-tuning enhanced dialogue and diagnostic accuracy. Multimodal inputs (eg, speech and imaging) improved immersion and realism. Evaluations, typically involving 10-50 students and 3-10 experts, demonstrated strong performance (top-k accuracy: 0.45-0.98, hallucination rate: 0.31%–5%, System Usability Scale [SUS] ≥80). However, small samples, inconsistent metrics, and limited controls restricted generalizability. Common datasets such as MIMIC-III (Medical Information Mart for Intensive Care-III) exhibited intensive care unit (ICU) bias and lacked diversity, affecting reproducibility and external validity.

Conclusions: Included studies showed moderate risk of bias, inconsistent metrics, small cohorts, and limited dataset transparency. LLM-based virtual patient systems excel in simulating multiple disease types but lack multimorbidity patient representation. KGs improve top-k accuracy and support structured disease representation and reasoning. Future research should prioritize hybrid KG-chain-of-thought architectures integrated with open-source KGs (eg, UMLS [Unified Medical Language System] and SNOMED-CT [Systematized Nomenclature of Medicine - Clinical Terms]), parameter-efficient fine-tuning, dialogue compression, multimodal LLMs, standardized metrics, larger cohorts, and open-access multimodal datasets to further enhance realism, diagnostic accuracy, fairness, and educational utility.

(JMIR Med Inform 2026;14:e79039) doi:10.2196/79039

XSL•FO
RenderX

KEYWORDS

large language model; virtual patient; medical education; history-taking; simulated patients

Introduction

Since 2020, large language models (LLMs) such as GPT-3.5 (OpenAI) [1] and GPT-4 (OpenAI) [2] have significantly enhanced virtual patient systems in medical education. Unlike traditional methods relying on resource-intensive standardized patients or high-fidelity simulators [3], LLMs provide scalable, low-risk, and cost-effective solutions by simulating realistic patient interactions across a wide range of clinical scenarios, including internal medicine, mental health disorders, and surgical and orthopedic cases [4]. This capability addresses key challenges in medical education, such as limited exposure to diverse clinical cases and the high costs of traditional simulation approaches.

Early virtual patient systems, often based on models like BERT (Bidirectional Encoder Representations from Transformers), struggled to generate natural dialogues and adapt to complex clinical scenarios, limiting their effectiveness in medical training [5,6]. In contrast, modern LLMs, leveraging prompt-based techniques for role and scenario customization, demonstrate improved contextual understanding, enabling clinically relevant responses. However, these systems still face challenges with hallucination, defined as the generation of factually incorrect or contextually irrelevant content, which may compromise the accuracy of medical history-taking in virtual patient simulations [7,8].

To ensure effective clinical training, continuous improvement and validation of LLMs are essential to mitigate hallucination rate and ensure the reliability of generated information [7]. Recent studies have incorporated techniques such as Supervised Fine-Tuning (SFT) [9] and Retrieval-Augmented Generation (RAG) [10] to enhance contextual adaptability and diagnostic accuracy, as measured by metrics like top-k accuracy and GTPA@k. However, the specific disease types simulated by LLMs, such as such as neurological and rheumatological or rare multiple disease types and potential gaps in simulation capabilities remain underexplored partly due to variations in experimental design and datasets.

Despite progress, systematic comparative evaluations of these techniques in virtual patient systems are lacking. Existing literature reviews often broadly discuss LLMs in medical education without focusing on virtual patient history-taking, limiting insights into domain-specific challenges [11]. Thus, a systematic literature review is critical to consolidate fragmented research, identify challenges, and guide future work.

Previous systematic reviews have explored LLMs in medical education but lack specificity. For instance, Lucas et al [11] reviewed LLMs' implications for teaching effectiveness, ethics, and reliability but did not focus on virtual patient history-taking. García-Torres et al [12] used a hybrid human-LLM methodology to evaluate virtual patients' impact on clinical reasoning but provided limited technical details on prompt design, knowledge graph (KG) integration, or fine-tuning. Similarly, Fatima et al [13] conducted a cross-disciplinary review of ChatGPT in research, clinical practice, education, and patient interaction but did not systematically analyze virtual patient history-taking. Recent empirical studies on LLM-powered virtual patients with automated feedback have prioritized educational outcomes over methodological comparisons [8].

In contrast, this review specifically examines LLM-based virtual patient systems for clinical history-taking. It systematically analyzes prompt engineering, external knowledge integration, model fine-tuning, and evaluation strategies, synthesizing their implications for medical education and effective clinical training. By adopting this methodological focus, this work addresses gaps in prior reviews, which were either too broad or lacked technical depth.

Given this research gap, a systematic literature review is essential to consolidate fragmented research and guide future studies. This paper addresses four core research questions (RQs), as outlined in Figure 1:

- RQ1: what types of patients, conditions, or diseases, such as internal medicine or rare and multiple disease types, are simulated in LLM-based virtual patient systems?
- RQ2: what techniques do LLMs use to enhance medical history-taking capabilities in clinical interviews?
- RQ3: how are experimental designs structured to evaluate LLM-based virtual patient systems, and what evaluation metrics, such as top-k accuracy or System Usability Scale (SUS), are used?
- RQ4: what public datasets are available, and what are their characteristics for training, simulating, and evaluating medical history–taking in virtual patient systems?

XSL•FO
RenderX

Figure 1. Overview of 4 research questions on large language model–based virtual patient systems, covering simulation types, enhancement techniques, evaluation strategies, and datasets.

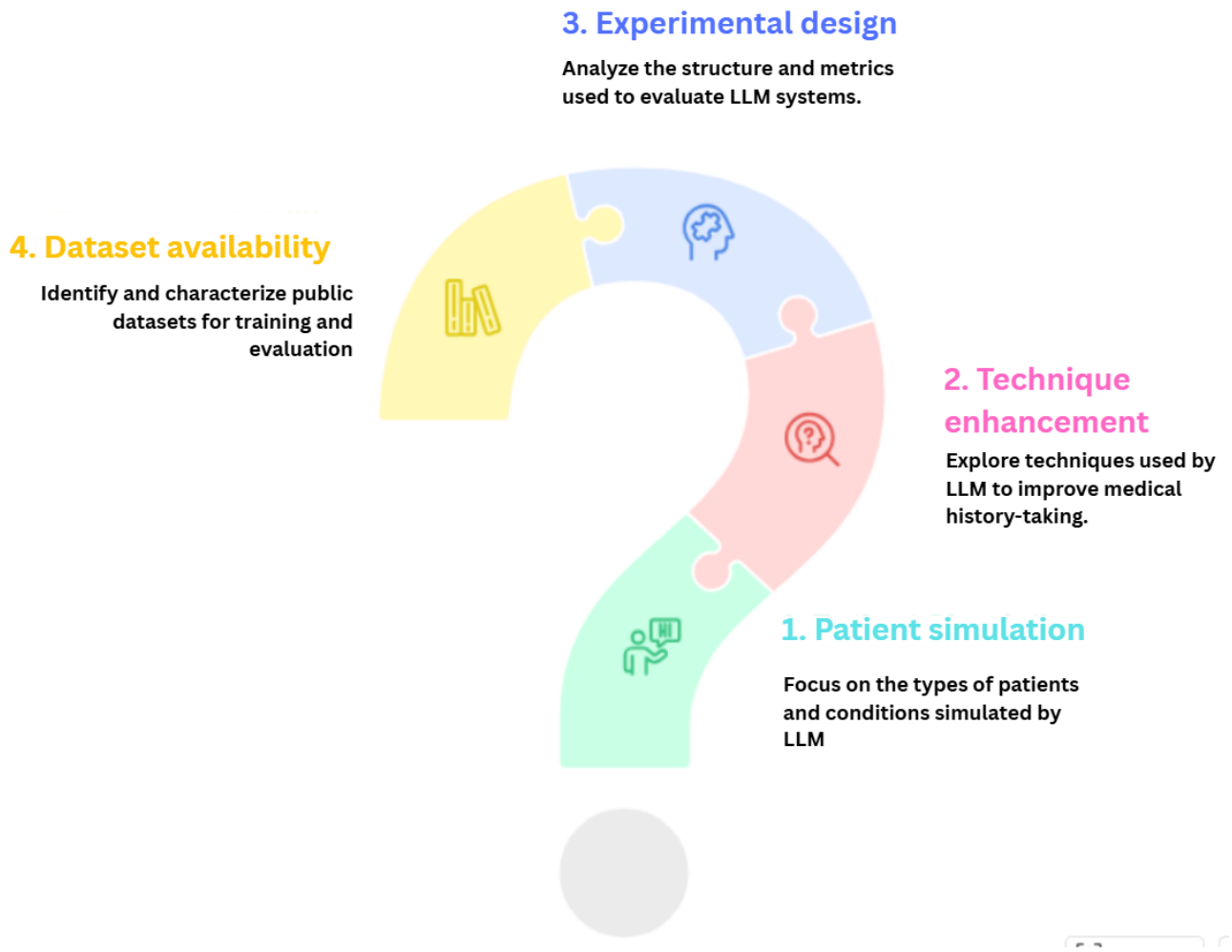

This systematic literature review addresses these questions to guide researchers in understanding the potential, limitations, and ethical challenges of LLMs in virtual patient systems. It is critical for advancing effective clinical training tools in medical education. The paper is structured as follows, the first section introduces the background of virtual patient systems and LLM applications; the second section describes the literature search methodology and evaluation criteria; the third section presents results, analyzing effectiveness and challenges; the fourth section discusses findings in the context of existing literature; and the fifth section concludes with key findings and recommendations for future research.

Methods

Overview

This study conducted a systematic literature review adhering to PRISMA (Preferred Reporting Items for Systematic Reviews and Meta-Analyses) 2020 guidelines. The research topic and target population were clearly defined, a comprehensive search strategy was formulated, and key search terms were identified. Search results were exported as CSV files via Mendeley (Mendeley Ltd) and Zotero (Corporation for Digital Scholarship) and manually screened. Abstracts were initially evaluated, followed by a comprehensive full-text assessment to confirm relevance and quality.

Eligibility Criteria

Population

The population includes medical students and physicians engaged in medical history–taking. Artificial intelligence (AI)–based virtual patients refer to LLM-based systems simulating patients for training in history-taking. Only transformer-based LLMs (eg, GPT series) are included, excluding older models like BERT (Google AI) or pre-Transformer architectures. Studies focusing on anesthesia, emergency procedures, or intraoperative scenarios are excluded, as these are nontraditional history-taking contexts. Preoperative history-taking for surgical and orthopedic patients is included. This ensures a focus on transformer-based LLMs for history-taking, emphasizing educational and clinical skill development while excluding irrelevant clinical settings. Only studies where LLMs serve as virtual patients for active history-taking and patient communication are included, excluding those focused solely on medical interviews without history-taking.

XSL•FO
RenderX

Intervention

The intervention involves transformer-based LLM technologies applied to medical history-taking, including prompt design, model fine-tuning, KG integration, and other LLM-related techniques. These aim to enhance diagnostic accuracy, interaction quality, and overall performance in virtual patient systems.

Outcomes

Outcomes include performance metrics such as top-k accuracy (eg, top-1 accuracy), empathy scores, readability, system stability (eg, response consistency), user experience (eg, SUS, Chatbot Usability Questionnaire [CUQ]), and other relevant indicators, such as κ (Cohen κ) and *P* value. These metrics evaluate the effectiveness of transformer-based LLM virtual patient systems in medical history–taking.

Inclusion and Exclusion Criteria

Inclusion and exclusion criteria were established to ensure relevance and quality, as shown in Textbox 1. Inclusion criteria prioritize studies with technical depth, validated outcomes, recent publication, and a focus on Transformer-based LLM virtual patients for history-taking, excluding nontransformer models.

Textbox 1. Inclusion and exclusion criteria for transformer-based large language model (LLM) virtual patient studies.

Inclusion criteria:

- IC1: the study population included medical students or physicians involved in medical history–taking or communication training.
- IC2: the intervention involved Transformer-based LLMs (eg, GPT series) used as virtual patients for history-taking or communication training in traditional consultation settings.
- IC3: the study was published between January 1, 2020, and August 18, 2025, including peer-reviewed articles and preprints.
- IC4: the study reported measurable outcomes related to diagnostic performance, communication effectiveness, empathy, readability, or user experience.
- IC5: preoperative history-taking scenarios (eg, surgical or orthopedic patients) were included if they involved conventional patient–clinician consultation processes.

Exclusion Criteria:

- EC1: based on earlier or nongenerative transformer models (eg, BERT [Bidirectional Encoder Representations from Transformers] and GPT-2) rather than modern LLMs.
- EC2: focused solely on medical interviews without explicit medical history–taking.
- EC3: published before January 2020.
- EC4: duplicate titles or redundant publications.
- EC5: review or commentary papers.
- EC6: non-English language studies.
- EC7: focused on anesthesia, emergency procedures, or intraoperative contexts (except preoperative consultations).

Information Sources

A systematic literature search was conducted across 9 authoritative databases PubMed, Scopus, Web of Science, IEEE Xplore, ACM Digital Library, SpringerLink, ERIC, arXiv, and ACL Anthology, covering studies published between January 2020 and August 18, 2025, in medicine, AI, education, and virtual technologies. A secondary search used a snowballing strategy, identifying additional sources from 15 initial articles and relevant publications, including theses from ProQuest. Including peer-reviewed articles and grey literature (eg, preprints from arXiv and theses) ensured comprehensive coverage of the rapidly evolving fields of AI and medical education.

Search Strategy

Two search strategies were used for this systematic review. The first query combined virtual patient terms (eg, virtual patient, simulated patient, AI patient, conversational patient, chatbot patient, intelligent virtual agent, and dialogue agent) with LLM-related keywords (eg, LLM, ChatGPT, GPT-4, GPT, transformer model, generative AI, AI-powered tutor, and natural language generation) and was applied to structured databases including PubMed, Scopus, Web of Science, IEEE Xplore, and ACM Digital Library. The second, simplified query included only virtual patient terms and was applied to broader repositories, namely SpringerLink, ERIC, arXiv, and ACL Anthology, to ensure comprehensive coverage, as strict LLM keywords reduced results in these databases (see Multimedia Appendix 1 for more details).

Selection Process and Data Collection

The literature screening and data collection process followed PRISMA 2020 guidelines [14] (checklist provided in Multimedia Appendix 2). Titles and abstracts were manually screened for relevance to LLM-based virtual patient history-taking, with GPT-3.5 Turbo used for auxiliary verification. Full-text evaluations were conducted for studies meeting preliminary inclusion criteria. A multidimensional quality assessment form recorded key study characteristics and outcomes, as detailed in Multimedia Appendices 3 and 4. The ChatPDF tool was used to cross-check content, and final inclusion decisions were made with the supervising researcher's input.

XSL•FO
RenderX

Quality and Risk of Bias Assessment

A reviewer with a computer science background, under the supervision of an experienced research advisor, conducted the quality assessment. A customized multidimensional assessment framework was developed to evaluate the technical quality of the included studies, as described in Multimedia Appendices 3 and 4. Conventional appraisal tools such as the Joanna Briggs Institute Critical Appraisal Checklist (2020) were adapted because they were not fully suitable for LLM-based virtual patient research. The framework incorporated 6 evaluation dimensions methodology clarity, dataset transparency, completeness of system evaluation, innovation or integration level, reproducibility and openness, and the presence of control or baseline comparisons. Each dimension was rated on a 3-point scale ranging from 0 to 2, with 2 indicating the highest quality. The total score for each study, therefore, ranged from 0 to 12. Based on the overall score, studies were categorized into 3 quality levels, high (9-12 points), medium (5-8 points), and low (0-4 points). This classification ensured a consistent and transparent interpretation of the technical quality across studies. The assessment emphasized methodological rigor, technical implementation, system architecture, model training strategies, multimodal integration, and evaluation methods to identify potential sources of bias.

Risk of bias was also assessed across 5 domains—selection or reporting bias, implementation bias, evaluation bias, data bias, and reporting completeness bias—to capture variations in study design, data transparency, technical implementation, and reporting quality. This combined approach ensured a systematic evaluation of both methodological soundness and potential bias in LLM-based virtual patient studies.

Based on the aforementioned screening and evaluation methods, the research results will be presented in detail in the next section.

Results

Overview

This section reports the results of literature selection, study characteristics, and findings related to the 4 RQs, avoiding interpretive discussion.

Study Selection Results

During identification (see Figure 2 for the 2020 flow diagram for systematic reviews, including database and register searches), 848 records were retrieved from 10 databases. During abstract screening, 672 records were excluded, and after removing 46 duplicates, 130 unique full-text articles were assessed. Of these, 66 were excluded for reasons including lack of extractable data (n=3), duplicate content (n=6), non-LLM models (n=13), focus not on LLM applications (n=5), nonroutine clinical settings (n=2), no history-taking focus (n=36), or nonrelevance to LLM technologies (n=1), leaving 64 eligible articles. During multidimensional evaluation, 20 studies were excluded for limited relevance, 11 for insufficient technical detail, and 4 for other reasons, yielding 29 articles from database searches. An additional 12 articles were identified through snowballing, of which 2 were excluded as irrelevant, resulting in 10 included snowballed studies. The final synthesis comprised a total of 39 studies [8,10,15-51] (6 high-quality, 33 moderate-quality) (see Multimedia Appendix 5).

Figure 2. PRISMA flow diagram.

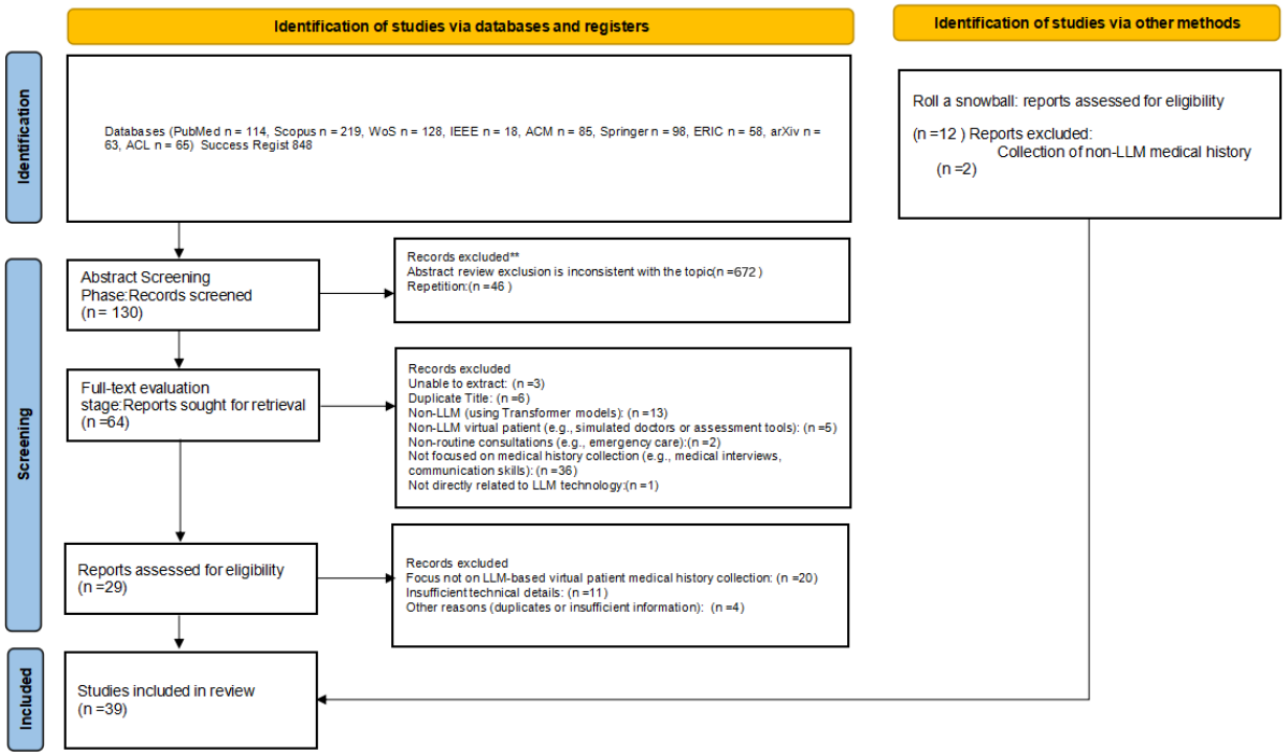

XSL•FO
RenderX

Quality and Risk of Bias Assessment Results

Most studies achieved the highest rating (2 points) for methodological clarity, indicating well-defined research procedures and consistent experimental designs. Scores for dataset transparency and system evaluation completeness varied considerably, with approximately 45%-55% of studies receiving moderate ratings (1 point) due to insufficient details regarding data sources or evaluation frameworks. Innovation and integration levels were generally high, with about 80% of studies receiving high ratings (2 points), reflecting notable progress in multimodal integration and technological creativity. Reproducibility and openness received moderate ratings (1 point) in approximately 60% of studies, as some provided replication details whereas others lacked information on model configurations or training strategies. Control or baseline comparison obtained the lowest scores (0-1 point), with only 25%-30% of studies incorporating explicit comparative or controlled analyses. Overall, 6/39 (15%) studies were rated as "high quality," and 33/39 (85%) as "moderate quality," suggesting strong methodological design and innovation but highlighting the need for improved dataset transparency, evaluation completeness, and reproducibility (see Multimedia Appendix 5 for details).

Risk of bias was assessed across five domains—selection and reporting bias, implementation bias, evaluation bias, data bias, and reporting completeness bias—as illustrated in Figure 3.

Figure 3. Overview of risk of bias distribution across studies.

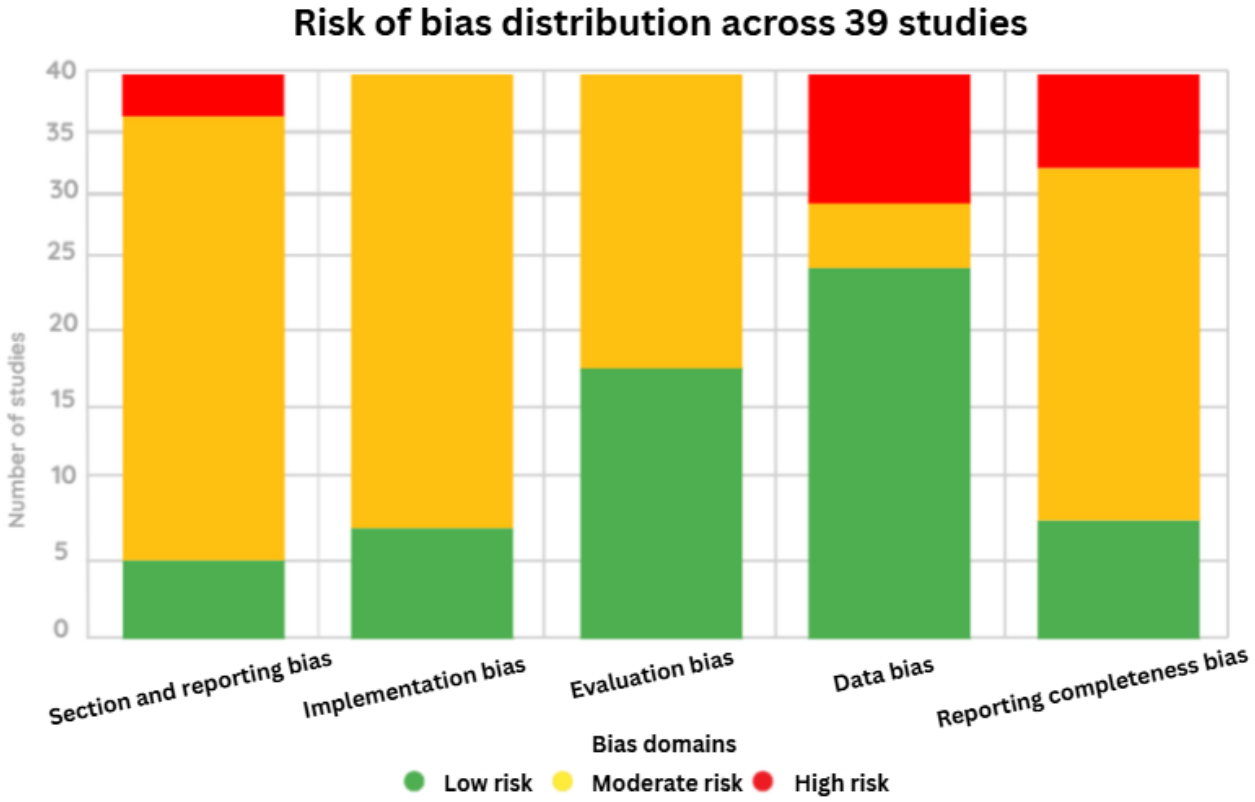

Selection and reporting bias was evident in disease coverage. Approximately 95% (37/39) of studies simulated specific disease types (eg, internal medicine or mental health disorders), but only 50% (20/39) addressed multiple disease stages, thereby limiting generalizability to multimorbidity contexts.

Implementation bias was observed in the limited reporting of model development details. While 80% (31/39) of studies described model types, only 35% (14/39) provided information on training procedures, fine-tuning processes, prompt engineering, reinforcement learning with human feedback (RLHF), domain-specific adaptation, or multimodal integration. This resulted in high technical heterogeneity.

Evaluation bias was reflected in the uneven assessment of educational and user experience outcomes. Approximately 70% (27/39) of studies evaluated educational outcomes, and 65% (25/39) assessed user experience using instruments such as the SUS or the Chatbot Usability Questionnaire (CUQ). However, only 30% (12/39) of studies conducted comparative or controlled evaluations, which limited the interpretability of effectiveness findings.

Data bias stemmed from moderate dataset transparency. Fewer than half of the studies (18/39, 45%) explicitly identified data sources or quality control procedures, constraining reproducibility.

Reporting completeness bias was identified in the limited documentation of personalization mechanisms and quality control for generated outputs, reported in only 25%-30% (10-12/39) of studies, suggesting incomplete methodological reporting.

In summary, this multidimensional quality and bias assessment systematically examined the technical features, methodological design, and potential biases of LLM-based virtual patient research. The findings highlight the need to improve dataset

XSL•FO
RenderX

transparency, enhance the comprehensiveness of system evaluation, and include controlled comparative studies to strengthen reproducibility and scientific validity. Details of the screening results and full bias assessment are provided in Multimedia Appendix 6.

Finding for RQ1: What Types of Patients Are Simulated in LLM-Based Virtual Patient Systems?

This section presents a descriptive statistical analysis and classification of patient types simulated by LLMs in virtual patient history-taking systems, based on a systematic literature review. The classification uses disease categories from Table 1, grouping similar disease types (eg, internal medicine and mental health disorders). For each category, the number of studies, specific simulation scenarios, disease complexity (eg, low: single symptom; medium: multisystem involvement; high: rare or complex interactions), number of simulated cases (if specified), and disease stage (eg, acute and chronic) are summarized.

Table 1. Classification of patient types simulated in virtual patient systems.

Disease category	Simulation scenarios	Complexity	Number of cases	Stage	References
Internal medicine	Chest/abdominal pain, diabetes, COPD[a], COVID-19, hypertension, multisymptom	Medium-high	3-500+	Acute-chronic	12 studies [15,20-30]
Mental health disorders	Depression, PTSD[b], ADHD[c], TRD[d], CBT[e] models	High	1-106	Acute-chronic	8 studies [18,31-35,37]
Surgical/orthopedic	Plastic surgery, hand surgery, joint pain	Medium	3-10	Acute–chronic	4 studies [16,20,24,38]
Neurological/rheumatological	Stroke, meningitis, concussion, polymyositis, brain hemorrhage	High	1-4	Acute	6 studies [20,21,36,39-41]
Ophthalmological	Eye conditions, pain with redness/photophobia	Medium	1-24	Acute	3 studies [17,20,42]
Dermatological	Ear cyst, telogen effluvium, skin conditions	Medium	1-394	Acute-chronic	4 studies [19,25,43,44]
Rare/multiple disease types[f]	Rare diseases, unspecified conditions, broad patient scenarios	High	8-5230	Diverse	10 studies [8,10,25,45-51]

[a]COPD: chronic obstructive pulmonary disease.

[b]PTSD: posttraumatic stress disorder.

[c]ADHD: attention deficit hyperactivity disorder.

[d]TRD: treatment-resistant depression.

[e]CBT: cognitive behavioral therapy.

[f]Only [25] involves rare disease simulation, using the RareBench dataset with 421 rare disease cases. Other references in the "rare/multiple disease types" category focus on multiple disease types or unspecified/broad patient scenarios.

Summary of Research Focus and Coverage

A systematic descriptive analysis of the literature indicates that research primarily focuses on internal medicine, particularly gastrointestinal (eg, abdominal pain, heartburn, hematemesis [20-23,27,28]), respiratory (eg, cough, chronic obstructive pulmonary disease, COVID [20,21,23,29,30]), cardiovascular (eg, chest pain, hypertension [20-22,30]), metabolic and endocrine (eg, diabetes [10,23,24]), and fatigue-related conditions (eg, chronic fatigue [15,26]). These conditions are well-suited for effective clinical training, with LLMs effectively simulating both acute and chronic management scenarios, though vague symptoms like fatigue remain underexplored.

Mental health disorders are a significant focus, including depression and related disorders (eg, suicidal ideation and treatment-resistant depression) [15,32-35], posttraumatic stress disorder (posttraumatic stress disorder; eg, combat trauma) [18,31], attention-deficit/hyperactivity disorder [31], and other mental health conditions (eg, cognitive impairment, cognitive behavioral therapy [CBT] models) [32,37]. These simulations emphasize emotional and psychological complexity, suitable for empathy and CBT training, though behavioral disorders like attention-deficit/hyperactivity disorder are less explored.

Rare and multiple disease types are well represented, focusing on heterogeneous case collections and electronic health record (EHR)–driven simulations [8,46-51], as well as rare disease modeling (eg, 421 rare diseases [10,25,45]). These studies highlight the scalability and diversity of LLMs in simulating complex and varied clinical conditions.

Less studied areas include neurological and rheumatological diseases (eg, stroke, meningitis, and polymyositis [20,21,36,39-41]), dermatological diseases (eg, ear cyst, telogen effluvium, and skin conditions [19,25,43,44]), surgical and orthopedic diseases (eg, joint pain, plastic surgery, and hand surgery [16,20,24,38]), and ophthalmological diseases (eg, eye pain, photophobia, and multiple eye conditions [17,20,42]). These areas, due to specialized or visual simulation requirements, have received less attention, revealing significant research gaps.

XSL•FO
RenderX

Overall, research focuses on internal medicine and mental health disorders due to their prevalence and clinical relevance. Rare and multiple disease types demonstrate LLMs' scalability and generalization potential. In contrast, specialized domains such as surgical and orthopedic, neurological and rheumatological, dermatological, and ophthalmological diseases remain underexplored, presenting opportunities for further innovation in simulation-based medical education.

Finding for RQ2: What Techniques do LLMs Use to Enhance Medical History–Taking Capabilities in Clinical Interviews?

To address RQ2, LLMs use advanced techniques to enable realistic, dynamic, and accurate virtual patient simulations for medical history-taking, providing medical students and professionals with effective clinical training platforms that closely resemble real-world scenarios. The following sections categorize core LLM technologies for history-taking into prompt engineering, KGs and structured data, model fine-tuning and training, and speech interaction, as summarized in Table 2.

Table 2. Technical metrics, evaluation scores, and key strengths and limitations of LLM virtual patient techniques.

Category and technique (source)[a]	Top-k accuracy (%)	Hallucination rate (%)	IRR[b] (%)	AS[c] (%)	Strengths	Limitations
Prompt design						
Role-based prompts [10,23]	81.4	4.97	2.08	28	Realistic role-play; multiagent;	Long prompts inconsistent; complex cases limited
Few-shot [25]	Not used: 25%, used: 52%				Simple, effective;	Limited depth
Multiagent prompt frameworks [21,24]	—[d]	—	—	—	Consistent dialogue	Higher computation
KG[e]						
Entity-relation triples [17]	—	—	—	—	Structured triples	Small-scale realism
Entity layering [10]	97.42	—	—	—	High diagnostic accuracy and interpretability	Limited semantic layers
KG+history and few-shot [10]	97.85	—	—	—	Role continuity	Context overflow
KG+multiagent prompts [10]	97.85	—	—	—	Modular roles	High cost
Fine-tuning						
SFT[f] [17]	—	(Before fine-tuning 3.71%, after fine-tuning 0.31%)	4.79	87.00	Reduces hallucination rate; better reasoning	Limited turn validation
LoRA[g] [17]	—	—	—	—	Efficient tuning	Limited scalability evidence
Speech interaction						
TTS[h] [28,51]	—	—	—	—	Realistic voice; multimodal input	Recognition errors possible

[a]All techniques listed are LLM-based Transformer architectures.

[b]IRR: information-related response rate.

[c]AS: Anthropomorphism Score.

[d]Not available.

[e]KG: knowledge graph.

[f]SFT: supervised fine-tuning.

[g]LoRA: low-rank adaptation.

[h]TTS: text-to-speech.

Prompt Design for Realistic Patient Simulation

1. Role-based prompt design: detailed prompts embed patient demographics, personality traits (eg, Big Five), and clinical symptoms to simulate authentic patient behavior. For instance, Borg et al [41] developed virtual patient cases with approximately 2000 tokens per prompt, including detailed medical histories and contextual information, occupying a significant portion of the LLM's 4096-token context window. Implementations include structured prompts with role context, medical history, and behavioral constraints [16-20,22,24-29,31,33-41,43-46,51]. For

XSL•FO
RenderX

example, Bodonhelyi et al [37] used Satir model roles (eg, "accuser"') to achieve up to 95% dialogue consistency. This ensures consistent role-playing but requires instructor oversight to maintain medical accuracy [36].

2. Few-shot and dialogue history–based prompting: prompts incorporate dialogue history and few-shot examples to maintain conversational coherence and mimic gradual information disclosure. MEDDxAgent uses structured examples to guide diagnostic reasoning, improving top-k accuracy from 25% to 52% in complex cases [25]. Limitations include token constraints, which may restrict handling of intricate scenarios.
3. Multiagent prompt frameworks: multiple agents (eg, patient agent, doctor agent, and behavior controller) collaborate to generate realistic and personalized clinical dialogues, reducing reliance on single prompts and minimizing hallucination rate. For example, EvoPatient, developed by Du et al [18], uses a patient–doctor dual-agent system for natural dialogue via unsupervised learning. LLM-based generative agents integrate memory flows, retrievers, and cognitive mechanisms to enhance dialogue realism and training effectiveness [24]. Additionally, AI self-play agents such as AMIE simulate diagnostic conversations through internal and external self-play loops, applying multirole strategies within a single model to improve diversity and dialogue adaptation [21].

Knowledge Graphs and Structured Data

1. Dynamic KG retrieval: MedDiT uses KG agents to retrieve relevant subgraphs via SPARQL queries, linearizing them into natural language prompts to reduce token load and context loss, achieving significant token reduction [47].
2. Hierarchical KG modeling: AI Patient integrates layered KG with a Reasoning RAG multiagent framework, boosting accuracy from 68.94% to 94.15%. For the difficult "family and social history" category, accuracy improved from 13.33% to 85.56%, showing the value of structured KG reasoning. Compared to role-based prompts, the KG-based method performs better in multiclass tasks. With entity layering [10], accuracy rose by 16.02% (81.4% to 97.42%) in challenging categories such as allergy and social history.

Model Fine-Tuning and Training

1. Instruction fine-tuning and self-play: AMIE uses real and simulated medical dialogues with self-play loops (inner and outer) to optimize diagnostic performance, outperforming primary care physicians (PCPs) [19,45].
2. SFT and LoRA (Low-Rank Adaptation): Liu et al [17] fine-tuned Qwen2.5-72B-Instruct on MedDialog, reducing the hallucination rate from 3.71% to 0.31% [17]. At the same time, in terms of information-related response rate and Anthropomorphism Score (AS).
3. Chain-of-thought (CoT) and RLAIF+MoM: CureFun uses CoT and RAG, while Kumar et al's [26] RLAIF+MoM framework structures ambiguous symptoms, achieving up to 95% output clarity [23].

Speech Interaction

1. TTS and STT integration: Takata et al [28] use Google application programming interface (API) and Unity for synchronized speech [51] and emotional facial expressions, outperforming traditional platforms in interaction realism. Thesen et al [51] leverage Whisper-3 for immersive speech processing, achieving high student satisfaction.
2. Multimodal enhancements: AMIE integrates image uploads (eg, skin photos) to support history-taking, outperforming PCPs in diagnostic accuracy [19]. Ryu et al [35] enhances realism with patient image uploads.

In conclusion, LLM technologies achieve consistent and realistic virtual patient dialogues through multilevel prompt design, few-shot examples, and multiagent mechanisms. The use of KGs and structured data enhances information retrieval and medical history modeling, improving classification and recognition accuracy. Model fine-tuning techniques (SFT, LoRA, self-play, CoT, RLAIF+MoM) effectively reduce hallucination rate, optimize reasoning, and enhance diagnostic performance. Furthermore, speech interaction and multimodal integration improve interaction immersion and provide diagnostic support.

Findings for RQ3: How Are Experimental Designs Structured to Evaluate LLM-Based Virtual Patient Systems, and What Evaluation Metrics Are Used?

To address RQ3, this review synthesized 32 studies listed in Table 3 to examine the experimental design, evaluation methods, and metrics of LLM-based virtual patient systems, focusing on medical education, high diagnostic accuracy, and effective clinical training. Of the 39 identified studies (see Multimedia Appendix 5), 7 were excluded due to the absence of formal evaluations (eg, Takata et al [28] described planned behavioral experiments without data collection; Rodrigo et al [46] outlined testing plans but reported no results; Geer [31] focused on design without providing quantitative outcomes; Li et al [47] emphasized system architecture but lacked performance metrics; Staples et al [34] relied solely on qualitative feedback; Kumar et al [26] discussed workflow but lacked quantified results; Lee et al [15] provided expert Likert scores without statistical analysis). Due to high heterogeneity in evaluation metrics (eg, top-k accuracy, hallucination rate, CUQ, inconsistent scales and dimensions, lack of statistical information such as SDs or confidence intervals in many studies, and large variations in sample sizes that could bias pooled analyses), a meta-analysis was not performed. Instead, a structured narrative synthesis was adopted, supplemented with tabular summaries in Tables 2 and 3, which present the technical approaches and corresponding evaluation metrics.

XSL•FO
RenderX

Table 3. Merged quantitative and qualitative evaluation details for virtual patient systems.

Authors	Participants (N)	Identity	Comparisons	Analysis method	Results	Evaluation type
Du et al [18]	None	AI[a]	Evolved vs Nonevolved	Stats[b]	Relevance 0.7589; Faithfulness 0.8786	Q[c]
Holderried et al [8]	106	Med students	GPT-4 vs Human	κ [d]	Top-k accuracy >99%;κ=0.832	Q
Tu et al [21]	20	PCPs[e]	AMIE vs PCPs	Stats	AMIE better on 28/32 expert metrics	Q
Yamamoto et al [20]	145	Med students	AI vs Traditional	t and MWU[f]; Likert[g]	OSCE: 28.1 vs 27.1 (P^h=.01)	M[i]
Cook et al [50]	3	Physicians	GPT-4.0 vs 3.5	1–6 scale, multivar.	GPT-4.0 higher authenticity, feedback	Q
Haider et al [16]	None	AI	GPT-4o vs Claude vs Gemini	Stats	Nonsignificant differences; high baseline	Q
Brugge et al [39]	21	Med students	Feedback vs Control	Wilcoxon, ICC[j]=0.924	CRI-HTI: 3.60 vs 3.02 (P^k≈.05)	Q
Holderried et al [22]	28	Med students	None	Stats; Spearman	Script Q 60.3%; Answers 94.4%	Q
Leypold et al [38]	3	Hand surgeons	None	Likert (1–5)	Mean=4.6 (Understand 5.0; History 4.2)	Q
Borg et al [40]	15	Med students	Robot vs VP	*t* test; Thematic	Authenticity 4.5 vs 3.9 (P^l=.04)	M
Radel et al [36]	40	Med students	Feedback vs None	*t* test; Likert	Improved scores with feedback (P^m<.05)	M
Luo et al [42]	184	Med students	LLMDP vs Traditional	*t* test; Pearson	78.13 vs 67.08 (P^n<.001)	M
Thesen et al [51]	94	Med students	None	Likert; *t* test	Comfort 61% to 76% (P^o<.001)	M
Laverde et al [24]	86	Med students	Agent vs Others	CUQ[p]	CUQ: 86.25/100	Q
Benfatah et al [29]	12	Nursing students	None	Pearson; Likert	Total score 19.42; Clarity r=0.701	M
Geer [31]	None	AI	None	Descr[q]	High similarity; no quant data	QL[r]
Borg et al [41]	15	Med students	Robot vs VIC	Wilcoxon; Text	Authenticity 4.47 vs 3.93 (P^s≈.03)	M
Ng et al [49]	100	Med students	Hybrid vs Baselines	Acc[t]; failure and confusion	Top-k accuracy 98.7%; failure 2.0%	Q
Wang et al [32]	N/S	Experts	Expert vs GPT-4	Stats; Subjective	Experts rated higher, GPT-4 underestimated	QL
Zheng et al [48]	N/S	Experts	None	Weighted F_1-score; Fuzzy labels	High professionalism and ethics	M
Rose et al [25]	None	AI	GPT-4o vs Llama3.1	Stats	GTPA@1 0.96; RareBench 0.45	Q
Liu et al [17]	None	AI	Proposed vs Baselines	Stats	Hallucination Rate 0.31%; Anthropomorphism 0.87	Q
Chen et al [33]	25	Patients and Psychiatrists	Prompt D1–D4	Stats	Fluency 3.28; Empathy 3.43; Dx 55.56%	Q
Liao et al [43]	N/S	Students, laypeople	GPT-4 vs others	Stats	Dx 53.33%; Coverage rate:15.36%-33.89%%	Q
Johri et al [44]	None	AI	GPT-4 vs 3.5	Stats	MCQ 0.919; FRQ 0.684	Q

XSL•FO
RenderX

Authors	Participants (N)	Identity	Comparisons	Analysis method	Results	Evaluation type
Bodonhelyi et al [37]	N/S	Psych experts	Accuser vs Rationalizer	Likert; Emotion; Stats	Realism 3.8 vs 3.7	M
Rashidian et al [30]	2	Clinicians	AI vs Doctors	κ; Likert	Symptom top-k accuracy 97.7%; κ=0.74	M
Tu et al [45]	20	PCPs	AMIE vs PCPs	Stats	AMIE better on 28/32 expert metrics	Q
Saab et al [19]	43	Patients, specialists	AMIE vs PCPs	Stats; *P* values	*Top*-1 accuracy: 0.65 vs 0.53 (P^{u}<.001)	Q
Li et al [23]	8	Med experts	Auto vs Manual	Spearman; Pearson	ρ=0.81; *r*=0.85 (P^{v}<.05)	Q

[a]AI: artificial intelligence.

[b]Stats: statistical analysis.

[c]Q: Quantitative.

[d]κ: Cohen κ.

[e]PCP: primary care physician.

[f]t and MWU: *t* test/Mann-Whitney *U* test.

[g]Likert: Likert scale.

[h]*P*: Objective Structured Clinical Examination performance comparison between AI-trained and traditionally trained students showed a difference of 28.1 vs 27.1, respectively (Mann–Whitney *U* test, *P*=.01).

[i]M: Mixed.

[j]ICC: intraclass correlation coefficient.

[k]*P*: Feedback group scored 3.60 on CRI-HTI vs 3.02 in control group (ANOVA, ICC=0.924, *P*=.049).

[l]*P*: Robot vs virtual patient authenticity ratings were 4.5 vs 3.9 (*t* test; *P*=.04).

[m]*P*: Students receiving feedback showed higher Likert-scale scores compared to control (*t* test; *P*=.04).

[n]*P*: LLMDP-trained students scored 78.13 (SD 8.35) on history acquisition; traditional group scored 67.08 (SD 7.21), with a mean difference of 11.05 points (*P*<.001).

[o]*P*: Comfort scores improved from 61% to 76% after intervention (*t* test; *P*<.001).

[p]CUQ: Chatbot Usability Questionnaire.

[q]Descr: Descriptive.

[r]QL: Qualitative.

[s]*P*: Robot vs VIC comparison yielded authenticity ratings of 4.47 vs 3.93 (Wilcoxon test; *P*=.035).

[t]Acc: Accuracy.

[u]*P*: Original article did not provide comparative statistical values such as means or test statistics, only reported model accuracy with significance levels.

[v]*P*: Among the 8 evaluated cases, exact *P* values for comparisons 1 and 2 were *P*<.001 and *P*=.04, respectively; the remaining 6 ranged from *P*=.003 to *P*=.011. As per reporting guidelines, *P*=.000 was converted to *P*<.001.

Commonalities and Specificities in Experimental Design

Commonalities

Most studies involved medical or health professional students, typically 10-50 participants, with some including residents or practicing physicians as evaluators (usually 3-5 experts) [10,19,36]. A few studies used AI agents for large-scale automated testing [18,25]. Tasks primarily covered core clinical competencies, including history-taking accuracy [10,36], diagnostic reasoning [45], role-playing [37], and multiturn dialogues [41].

Evaluation paradigms were categorized into 3 types quantitative (18 studies) using randomized controlled trials (RCTs) or comparative experiments with statistical tests (eg, ANOVA, *t* tests, and correlation) [39,45]; qualitative (1 study) using expert interviews, thematic analysis, or questionnaires [32]; and mixed (13 studies) integrating objective metrics (eg, top-k accuracy, and F_1-score) with subjective scales (eg, Likert, CUQ) [36,40]. Comparative baselines included model comparisons (GPT-4 and 4o, Claude, and Gemini) [16], AI versus human physicians [19,45], with or without feedback or platform comparisons [40,41], and variations in prompt strategies, multimodality, or RAG and KG [49]. Most studies applied blinding and reported rater consistency (eg, κ) [8,39]. Details of each study's evaluation type are provided in Table 3 (Evaluation type column).

Specificities

Some studies implemented AI self-play for scalability [18], or AI doctor-AI patient automated evaluation [16]. Social robot-LLM hybrids were used to enhance realism [40,41]. Comparative baselines varied, including direct AI versus human physician comparisons [19,45], modular and hybrid architecture comparisons (eg, RASA or KG or LLM) [49], and multimodel comparisons (GPT-4.5 and 4o, Claude 3.7, and Gemini 2.5)

XSL•FO
RenderX

showing nonsignificant differences, indicating a high performance baseline [16].

Evaluation Metrics: Commonalities and Specificities

Evaluation metrics in LLM-based virtual patient systems generally fall into 5 categories: clinical accuracy and knowledge, communication and interaction quality, robustness and stability, training efficacy and feedback quality, and system performance. Clinical accuracy and knowledge were assessed using metrics such as top-k accuracy [19], GTPA@k [25], information coverage [43], hallucination rate [17,19], and fidelity and relevance [18], evaluating diagnostic and information-gathering capabilities. Communication and interaction quality were measured through readability (Flesch and Flesch–Kincaid) [10], CUQ [22], and Anthropomorphism Score [17,37], reflecting language clarity and interaction naturalness. Robustness and stability were evaluated via paraphrase robustness [10], leak resistance [18], and rater consistency metrics, including κ [8] and intraclass correlation coefficient (ICC) [39]. Training efficacy and feedback quality focused on learning outcomes and user experience, assessed through Objective Structured Clinical Examination (OSCE) score improvements [39], and usability scales (such as CUQ). System performance metrics, including latency, failure rate [49], and confusion or clarification rates [49], captured efficiency and reliability. Specificities included unique metrics such as span-level F_1-score [10] for knowledge extraction, cosine similarity-based fidelity and relevance [18], weighted F_1-score or fuzzy labels for professionalism and ethics [39], and system-level confusion, clarification, or failure rates. Automated evaluation metrics such as GTPA@k [25] provided standardized measures for diagnosis, while expert ratings revealed realism biases, including underestimation by GPT-4. Usability was further examined through instruments such as the CUQ (score of 77/100), 7-dimensional Likert scales combined with ANOVA for accuracy, realism, and empathy, and system latency and confusion reporting (0.5%). These metrics collectively enable comprehensive assessment of both the technical performance and experiential quality of LLM-based virtual patient systems. The calculation formula for the indicators is detailed in Multimedia Appendix 7.

Evaluation Results

The synthesis of evaluation results from the 32 included studies indicates that LLM-based virtual patient systems demonstrate high diagnostic accuracy across key metrics. Quantitative results showed top-k accuracy ranging from 0.45 to 0.98 (based on 34 models and 300 patient cases); Saab et al [19] reported that AMIE achieved a Top-1 Accuracy of 0.65, compared to 0.53 for PCPs, with $P<.001$. Information coverage averaged 33.89% to 94.4% (eg, Liao et al [43] reported 33.89%, based on 150 cases; Holderried et al [22] reported 94.4%, based on 502 questions explicitly covered in case scripts, with a total of 826 answers), while hallucination rate remained low, ranging from 0.31% to 5% (eg, Liu et al [17] conducted experiments with up to 5 dialogue rounds, achieving a hallucination rate of 0.31%).

In terms of communication quality, CUQ scores ranging from 77 to 86.25 (eg, Laverde et al [24] reported 86.25). Training effectiveness was evident in OSCE performance (eg, Yamamoto et al [20] reported posttraining 28.1 vs pretraining 27.1, $P=.01$; Luo et al [42] reported that medical students trained using the LLM-based digital patient system (LLMDP) achieved a medical history acquisition score of 78.13 (SD 8.35), while the control group trained with traditional real patients scored 67.08 (SD 7.21). The difference between groups was 11.05 points, with $P<.001$, indicating a highly statistically significant difference). Robustness metrics such as κ ranged from 0.74 to 0.832 (eg, Holderried et al [8] reported 0.832; Rashidian et al [30] reported 0.74).

Mixed methods studies reported improvements in authenticity (eg, Borg et al [40] reported postuse 4.5 vs preuse 3.9; $P=.04$) and comfort (Thesen et al [51] reported that among 69 participants, average preuse comfort was 61%, increasing to 76% postuse, indicating higher student-reported comfort after training; $P<.001$). Automated baseline systems, such as EvoPatient, achieved a relevance of 0.7589 and a faithfulness of 0.8786 (Du et al [18]), while multimodel comparisons showed no significant differences among top LLMs (Haider et al [16]).

These results highlight the effectiveness of LLM-based systems in simulating realistic interactions, although specific metrics—such as the low failure rate of 2.0% reported by Ng et al [49] (based on 200 dialogue trials) and the high ICC of 0.924 reported by Brugge et al [39]—indicate that further standardization is needed.

The reviewed studies exhibit consistent commonalities in participant composition, task objectives, and evaluation paradigms, typically involving small to medium student samples and multisource evaluations with experts and AI, focusing on history-taking and diagnostic reasoning. Specificities are evident in comparative settings (AI vs humans, multimodel comparisons) and statistical methods such as bootstrap, false discovery rate (FDR), and ICC. Across studies, 5 key evaluation aspects were assessed using objective metrics. Clinical accuracy and knowledge were measured using top-k accuracy [19,21], GTPA@k [25], information coverage [22,43], and span-level F_1-score [18], capturing high diagnostic accuracy and knowledge acquisition. Authenticity was evaluated using hallucination rate [17] and fidelity metrics [18]. Interaction experience was assessed via CUQ [24] and Anthropomorphism Score [17], reflecting communication quality and user perception. Robustness and consistency were quantified using κ [30] and ICC [39]. System performance was captured through latency, failure rate, and confusion rate [21,49]. These categories collectively enable a comprehensive assessment of both technical and experiential quality, highlighting the systems' effectiveness while indicating areas for further standardization and evaluation refinement.

Finding for RQ4: What Public Datasets Are Available, and What Are Their Characteristics for Training, Simulating, and Evaluating Medical History-Taking in Virtual Patient Systems?

A variety of datasets support the development and evaluation of virtual patient systems, ranging from real-world EHRs to structured synthetic clinical scenarios. Table 4 summarizes key datasets used in recent studies, which are either publicly

XSL•FO
RenderX

available or accessible through formal application processes. These datasets provide diverse clinical data resources for effective clinical training and evaluation.

MIMIC-III (Medical Information Mart for Intensive Care-III) is a comprehensive publicly available medical dataset, containing detailed EHR data from over 40,000 intensive care unit (ICU) patients [10]. It covers multiple disease types, including internal medicine and neurological and rheumatological conditions, serving as a critical resource for virtual patient system development. However, its ICU-focused nature, primarily reflecting acute or severe diseases, limits its applicability to noncritical care scenarios, such as outpatient consultations, mental health disorders, or chronic disease management [10].

DDxPlus provides clinical dialogue data for respiratory diseases [25], suitable for training virtual patient systems in specific domains within internal medicine. The iCraft-MD dataset focuses on dermatological cases [25], and RareBench contains region-specific subsets of rare and multiple disease types [25]. While valuable for specialized applications, their scope is limited for building generalized, multitask virtual patient systems.

The medical-NLP corpus provides a broad range of clinical dialogues and records [18], while CCKS 2019 offers a Chinese medical KG dataset, enabling multilingual history-taking simulations [17,56]. The Open-i dataset includes multimodal chest X-ray images and textual descriptions, supporting dynamic image generation alongside history-taking [47]. MedQA provides multiple-choice and long-form medical question-answering data, useful for fine-tuning LLMs for diagnostic dialogues [45]. These datasets enhance multimodal and question-answering capabilities, though their coverage is narrower than MIMIC-III.

In summary, current datasets primarily focus on critical care or specific medical domains, with limited publicly available, diverse resources. These datasets have limitations in generalizability, multitask applicability, and multilingual support for virtual patient systems. Combining MIMIC-III (broad coverage) [10], DDxPlus and iCraft-MD (specialized domains) [25], and CCKS 2019 (multilingual support) [17,56] provides partial coverage. However, further development of diverse, emotionally annotated, and non-English datasets is needed to enhance system generalizability and conversational fidelity.

Table 4. Datasets used in virtual patient systems.

Dataset Name	Index	Description	Access requirements
MIMIC-III[a]	[10]	EHR[b] database from Beth Israel Deaconess Medical Center, over 40,000 ICU[c] patients (2001-2012), including vital signs, medications, laboratory results, diagnostic codes.	Access via PhysioNet; requires CITI training and DUA [52].
DDxPlus	[25]	Synthetic dataset for respiratory diseases, with clinical dialogues and diagnoses.	CC-BY[d]; publicly available, allows commercial use with attribution [53].
iCraft-MD	[25]	Synthetic dermatology dataset from public medical question banks and expert cases.	MIT License; publicly available [54].
RareBench	[25]	Rare disease dataset with regional subsets (Europe, Canada, and China).	Apache-2.0; publicly available [55].
medical-nlp	[18]	Medical NLP[e] corpus with clinical dialogues and records.	GNU General Public License v3.0; publicly available on GitHub [18].
CCKS 2019	[17]	Chinese medical knowledge graph dataset with entity recognition, relation extraction, QA[f] tasks.	Research use only; cite source [56].
Open-i	[47]	Multimodal dataset with 3314 chest x-ray images and textual descriptions.	Open Data Commons Open Database License; publicly available via NIH Open-i project [57].
MedQA	[45]	Multiple-choice and long-form medical QA dataset for diagnostics.	Publicly available via GitHub [45].

[a]MIMIC-III: Medical Information Mart for Intensive Care-III.

[b]EHR: electronic health record.

[c]ICU: intensive care unit.

[d]CC-BY: Creative Commons Attribution.

[e]NLP: natural language processing.

[f]QA: question-answering.

Discussion

Principal Findings

Current LLM-based virtual patient systems exhibit significant limitations in disease coverage, complex case simulation, multimorbidity representation, specialty applicability, multimodal capabilities, and standardization of evaluation metrics, indicating a need for systematic optimization to enhance clinical fidelity, educational adaptability, and interaction quality.

XSL•FO
RenderX

Limitations and Future Directions in Virtual Patient Type Simulation Research

The systematic review reveals several limitations in current virtual patient systems regarding disease coverage, case complexity modeling, and support across medical specialties [20,32]. First, research is heavily concentrated on internal medicine (eg, gastrointestinal, respiratory, and metabolic disorders) and mental health disorders, accounting for over half of the studies [15,32]. This focus reflects the strengths of LLMs in language-driven tasks and the availability of relevant data, but it highlights significant gaps in surgical and orthopedic, ophthalmological, and dermatological domains. Scenarios requiring procedural operations, image recognition, or multimodal interactions are underrepresented, with current systems lacking effective modeling mechanisms [16,43]. This finding aligns with RQ1, indicating that most simulations focus on specific disease categories, leaving certain specialty areas insufficiently covered.

Although some studies involve multiple disease types, current virtual patient systems mainly use single-disease trajectories, with each virtual patient representing only one disease [21,25]. multimorbidity simulations—patients with 2 or more coexisting chronic or acute diseases—are limited. Clinical multimorbidity requires complex decisions, including drug interactions, overlapping symptoms, and conflicting management priorities. Dataset analysis for RQ4 shows most datasets focus on a single primary disease, lacking comprehensive multimorbidity cases. Without simulating this complexity, virtual patient systems have limited use in advanced medical education and clinical reasoning. Future research should emphasize role construction and dialogue design for multimorbidity scenarios to support integrated management across multiple diseases.

Furthermore, current systems exhibit instability in simulating vague or atypical symptoms (eg, chronic fatigue, low mood, attention deficits), demonstrating weak extraction of unstructured chief complaints and incoherent reasoning processes, which limits support for comprehensive clinical assessments [10,31]. Incorporating KGs and CoT reasoning mechanisms may improve knowledge organization and causal chain construction, enhancing models' reasoning and response capabilities in complex clinical scenarios [58,59]. Open-source KGs, such as UMLS (Unified Medical Language System) [60], SNOMED-CT (Systematized Nomenclature of Medicine - Clinical Terms) [61] can be integrated to provide structured, high-coverage medical knowledge. Leveraging these KGs allows LLMs to reference verified entities and relationships during dialogue generation, reducing hallucinations and enhancing reasoning in multimorbidity or complex symptom scenarios.

Additionally, coverage of specialty domains remains limited, particularly in surgical and orthopedic, ophthalmological, and dermatological contexts requiring procedural or visual recognition skills. These fields show constraints in case complexity, multimodal interaction support, and procedural training, limiting educational adaptability and clinical fidelity [43]. This observation is consistent with findings from RQ1 and RQ4, indicating that certain specialty cases and complex patient scenarios remain underrepresented.

In summary, current virtual patient systems require systematic optimization in disease coverage balance, case complexity, multimorbidity simulation, specialty applicability, multimodal capabilities, and interaction depth. These improvements are expected to enhance clinical fidelity, educational adaptability, and natural human-computer interaction, providing a foundation for advancing intelligent medical education and clinical decision support systems.

Technical Challenges and Solutions of LLM-Based Virtual Patient Simulation

In virtual patient simulation, prompts guide LLMs to generate dialogues conforming to specific role characteristics. However, overly long prompts lead to information loss, affecting dialogue quality and coherence. Specifically, GPT-style models based on autoregressive decoder architectures process prompts sequentially from left to right, prioritizing information at the beginning (primacy effect) and end (recency effect), while middle information may be ignored or inadequately processed, impacting content completeness and accuracy [62]. Additionally, few-shot learning maintains role settings using limited historical dialogues, but balancing information completeness and avoiding overload in multiturn complex dialogues remains challenging. To address this, core information should be prioritized at the prompt's beginning and end, with emotional content placed in the middle to ensure accurate and consistent information transmission.

Compared to single-prompt methods, multiagent frameworks decompose dialogue generation into modular components, with agents handling specific functions such as patient history or simulated emotions, or leveraging adversarial training to enhance dialogue quality [18,21,24]. However, multiagent systems increase computational costs, as each agent independently calls APIs, leading to higher financial burdens. Additionally, fine-tuning using older APIs may cause "memory loss," affecting dialogue context continuity. Dialogue saving and restoration mechanisms are necessary to ensure information consistency. To reduce costs and improve efficiency, dialogue compression and summarization mechanisms can simplify context input, and noncritical tasks can be assigned to lower-cost APIs to balance performance and expense.

Research on fine-tuning GPT-style models and integrating KGs remains limited. Liu et al [17] proposed a SFT strategy using synthetic medical records and manually annotated dialogues, significantly enhancing the realism and anthropomorphism of patient history collection dialogues on the Qwen-72B model (Alibaba Cloud), reducing Hallucination Rate from 3.71% to 0.31%. However, their training process did not explicitly embed disease names into the Transformer model, limiting specific disease knowledge mastery. Prior studies indicate that incorporating disease names as labels or input features improves semantic understanding and generalization, particularly for simulating patient histories for specific diseases [58,59]. Combining CoT methods with fine-tuning to guide step-by-step reasoning for complex medical knowledge is underexplored and presents a potential direction for medical dialogue systems.

KGs systematically represent structured medical knowledge, but there is a lack of studies comparing disease embeddings

XSL•FO
RenderX

trained by LLMs with KG embeddings to evaluate differences in knowledge representation and reasoning capabilities. KGs' clear entity and relation structures complement LLMs' limitations in sparse knowledge or verification, while LLM-trained embeddings as a baseline reveal constraints in semantic understanding and improvements from KG enhancement. Future research should establish a unified evaluation framework integrating supervised fine-tuning, LoRA, and CoT reasoning to explore the complementary roles of KG and LLM embeddings, advancing medical dialogue models in logical reasoning and knowledge accuracy.

Evaluation Design Suggestions and Summary of Metrics

Evaluation methods and metrics in LLM-based virtual patient systems are diverse, reflecting the multidimensional nature of performance and educational outcomes. However, the lack of standardized frameworks hinders cross-study comparison and generalizability. Diagnostic accuracy is often measured by top-k accuracy (eg, 65% [19]) and GTPA@k [25], though these coarse metrics may not capture system capabilities. Information Coverage and Hallucination Rate assess retrieval fidelity but usually rely on manual verification. Interaction quality metrics—such as semantic similarity (0.7589 [18]) and user scores (eg, CUQ=77 [22])—highlight interactivity but are limited by subjectivity and small samples. External studies also report high usability, such as SUS=88.1[31], a 10-item scale measuring ease of use, confidence, and learnability, reinforcing the systems' educational value despite inconsistent evaluation standards.

Moreover, system performance assessment remains insufficient. Some studies report response delays affecting conversation naturalness, but lack quantitative measures or systematic evaluations. The absence of standardized key performance indicators exacerbates framework fragmentation, hindering effective implementation and broader application in medical education and effective clinical training [41].

To address fragmented metrics, a unified and scientifically grounded evaluation framework is necessary. Key performance indicators with recommended thresholds are proposed to guide system design and assessment:

- Top-1 accuracy (≥0.80): AMIE achieved a top-1 accuracy of 0.65, outperforming primary care physicians (0.53) [19], while *GTPA*@1 reached 0.96 [25]. A threshold of 0.80 ensures reliable diagnostic performance.
- Hallucination rate (≤0.05): GPT-4o demonstrated a Hallucination Rate of 0.31% [17], with rates below 5% reported in [19], supporting medical safety standards.
- Information coverage (≥0.50): coverage of critical history items was 33.89% [43], indicating room for improvement. A 50% threshold ensures adequate information capture.
- Empathy and Anthropomorphism Score (≥0.75, standardized 0-1 scale): GPT-4o scored 0.87 [17], and [37] reported approximately 0.76, indicating desired human-like interaction and empathy.
- Usability (SUS≥80, CUQ≥75): SUS of 88.1 [59] and CUQ of 77 [22] meet standards for satisfactory usability.
- Robustness (leak resistance≥0.90): a value of 0.9412 was reported in [18], indicating compliance with privacy and ethical requirements.
- Rater consistency (κ and ICC≥0.80): high interrater reliability was observed, with ICC=0.924 [39] and κ=0.832 [8].

Challenges of Data Diversity: Limitations in Corpus Coverage and Adaptability

Existing datasets for training and evaluating LLM-based virtual patient systems are diverse, encompassing real-world EHRs, synthetic clinical scenarios, and multimodal or multilingual resources [10,17,18,25,45,47,56]. Table 4 summarizes key datasets, which are either publicly available or accessible through formal application processes. Analysis reveals several limitations impacting system development.

Mainstream datasets like MIMIC-III primarily reflect intensive care scenarios, containing records from ICU patients with acute or critical conditions, often within internal medicine or neurological and rheumatological categories [10]. This bias limits generalizability to nonacute settings, such as outpatient consultations, mental health disorders, or chronic disease management. Specialized datasets, including DDxPlus (internal medicine), iCraft-MD (dermatological), and RareBench (rare and multiple disease types), provide tailored resources [25]. While valuable for specific domains, their narrow coverage limits suitability for general-purpose or multitask system training.

Linguistic and cultural diversity is limited, as most corpora are English-based and originate from Western health care systems [17,18,45,47,56]. The lack of datasets in other languages, such as Chinese [17,56], and integration with local KGs or region-specific disease contexts constrains performance in multilingual and cross-cultural environments. Modality limitations are evident; most datasets provide textual information and lack multimodal inputs like images, speech, or physiological signals [47], restricting interaction realism and diagnostic reasoning.

Data accessibility and format heterogeneity affect usability. Access requirements, annotation styles, field definitions, and dialogue formats vary [10,17,18,25,45,47,56], hindering integration and comprehensive training. Standardization of data formats and unified interfaces is necessary to reduce development costs and support broader adoption. Additionally, task alignment poses challenges, as datasets like MedQA [45] are structured for multiple-choice or question-answering tasks, requiring extensive adaptation for dialogue generation.

Combining broadly covering datasets like MIMIC-III [10] with domain-specific (DDxPlus, iCraft-MD, RareBench) [25] and multilingual or multimodal datasets (CCKS 2019 [17,56], Open-i [47], medical-nlp [18], MedQA [45]) can partially address gaps. However, developing diverse, emotionally annotated, non-English, and multimodal datasets is essential to enhance generalizability, robustness, and interaction fidelity.

XSL•FO
RenderX

Conclusion

This systematic review, conducted per PRISMA 2020 guidelines, evaluated studies (January 2020-August 18, 2025) on LLM-based virtual patient systems for medical history collection, sourced from 9 databases PubMed, Scopus, Web of Science, IEEE Xplore, ACM Digital Library, Springer, ERIC, arXiv, and ACL Anthology. Following rigorous screening, deduplication, and quality appraisal, 6 high-quality and 33 moderate-quality studies were included, addressing 4 research questions, simulated patient types, performance-enhancing technologies, experimental designs, and evaluation metrics.

Key findings include (1) systems primarily simulate internal medicine and mental health disorders (acute and chronic), with limited coverage of rare and multiple disease types, multimorbidity, and specialties like surgical and orthopedic, neurological and rheumatological, dermatological, and ophthalmological, restricting applicability in complex clinical reasoning and education [15,16,32,43]. (2) Technologies such as role-based prompts, few-shot learning, multiagent frameworks, KGs, and fine-tuning (eg, SFT, LoRA, CoT, RLAIF+MoM) enhance dialogue coherence, retrieval accuracy (+16.02% with KGs) [10], and high diagnostic accuracy, while multimodal integration (eg, speech) improves immersion [18,25]. (3) Evaluations involved medical students and practitioners, using mixed methods (top-k accuracy, F_1-score, SUS, CUQ, and expert ratings) with comparisons across AI models, physicians, or prompt variations; small sample sizes (10-50 students and 3-10 experts) and inconsistent metrics limit generalizability [19,40]. (4) Systems demonstrated high diagnostic accuracy: top-k accuracy 0.45-0.98, information coverage 33.89%-94.4%, Hallucination Rate 0.31%-5%, and high usability (SUS≥80), often outperforming junior physicians [18,43]. Dataset limitations (eg, MIMIC-III ICU bias, restricted access, low multilingual and multimodal diversity) hinder cross-study comparability [10,17,25].

The key discussion points are summarized: (1) Disease coverage is imbalanced, favoring internal medicine and mental health disorders over surgical and orthopedic, dermatological, ophthalmological, and multimorbidity scenarios, limiting effective clinical training [16,43]. Future systems should prioritize multimorbidity and diverse patient populations (cultural and linguistic) to enhance realism [17,56]. (2) Prompt design endures information loss in long prompts; placing critical information at prompt ends and using dialogue compression or multiagent frameworks can mitigate this [18,60]. KG-LLM integration and fine-tuning improve performance, with potential for further gains via hybrid KG-CoT approaches [58,59]. (3) Fragmented evaluation frameworks, inconsistent metrics, and small participant pools reduce reliability. A standardized framework with thresholds (eg, top-1 accuracy≥0.80, hallucination rate≤0.05, SUS≥80, CUQ≥75,κ and ICC≥0.80) and larger samples (50-100 students, 5-10 experts) is needed [19,39]. (4) Dataset biases (eg, ICU focus), format heterogeneity, and privacy restrictions limit inclusivity. Open-access, ethically compliant, multimodal, and multilingual datasets are essential for equitable systems [10,45,47].

Future research should focus on large-scale longitudinal studies, standardized evaluation metrics, diverse open-access datasets (eg, UMLS [60] and SNOMED-CT [61]), and advanced integration of KGs, multimodal training, and optimized prompts to enhance the realism, high diagnostic accuracy, and fairness of LLM-based virtual patient systems in medical education [17,18,59].

Acknowledgments

We thank Sultan Qaboos University for partially funding this project. The corresponding author is also affiliated with Universiti Sains Malaysia (USM). Additional supporting materials related to this work are provided in Multimedia Appendix 8.

Funding

The authors thank Sultan Qaboos University (Oman) for the funding of this paper.

Conflicts of Interest

None declared.

Multimedia Appendix 1
Database Search Strategies.
[DOCX File , 13 KB - medinform_v14i1e79039_app1.docx]

Multimedia Appendix 2
PRISMA Checklist.
[DOCX File , 26 KB - medinform_v14i1e79039_app2.docx]

Multimedia Appendix 3
Joanna-Briggs Institute Quality Assessment Questionnaire.
[DOCX File , 13 KB - medinform_v14i1e79039_app3.docx]

XSL•FO
RenderX

Multimedia Appendix 4
Multidimensional assessment table.
[DOCX File , 15 KB - medinform_v14i1e79039_app4.docx]

Multimedia Appendix 5
Quality Assessment Result.
[DOCX File , 27 KB - medinform_v14i1e79039_app5.docx]

Multimedia Appendix 6
Risk of Bias Assessment for 39 Included Studies.
[DOCX File , 26 KB - medinform_v14i1e79039_app6.docx]

Multimedia Appendix 7
Calculation Formulas for Evaluation Metrics.
[DOCX File , 23 KB - medinform_v14i1e79039_app7.docx]

Multimedia Appendix 8
Other file screening process, source files, etc.
[ZIP File (Zip Archive), 1137 KB - medinform_v14i1e79039_app8.zip]

References

1. Brown TB, Mann B, Ryder N, Subbiah M, Kaplan J, Dhariwal P, et al. Language models are few-shot learners. 2020 Presented at: NIPS'20: Proceedings of the 34th International Conference on Neural Information Processing Systems; 2020 December 06; Red Hook, NY, United States p. 1877-1901.
2. OpenAI, Achiam J, Adler S, Agarwal S, Ahmad L, Akkaya I, et al. GPT-4 technical report. ArXiv. Preprint posted online on March 4, 2024.
3. Lim AS, Lee SWH. Is technology enhanced learning cost-effective to improve skills?: the Monash objective structured clinical examination virtual experience. Simul Healthc 2022;17(2):131-135. [doi: 10.1097/SIH.0000000000000526] [Medline: 33273417]
4. Cook DA. Creating virtual patients using large language models: scalable, global, and low cost. Med Teach 2025;47(1):40-42. [doi: 10.1080/0142159X.2024.2376879] [Medline: 38992981]
5. Song W, Hou X, Li S, Chen C, Gao D, Wang X, et al. An intelligent virtual standard patient for medical students training based on oral knowledge graph. IEEE Trans Multimedia 2023;25:6132-6145. [doi: 10.1109/tmm.2022.3205456]
6. Babu A, Boddu SB. BERT-based medical chatbot: enhancing healthcare communication through natural language understanding. Explor Res Clin Soc Pharm 2024;13:100419 [FREE Full text] [doi: 10.1016/j.rcsop.2024.100419] [Medline: 38495953]
7. Chow JCL, Wong V, Li K. Generative pre-trained transformer-empowered healthcare conversations: current trends, challenges, and future directions in large language model-enabled medical chatbots. BioMedInformatics 2024;4(1):837-852. [doi: 10.3390/biomedinformatics4010047]
8. Holderried F, Stegemann-Philipps C, Herrmann-Werner A, Festl-Wietek T, Holderried M, Eickhoff C, et al. A language model-powered simulated patient with automated feedback for history taking: prospective study. JMIR Med Educ 2024;10:e59213 [FREE Full text] [doi: 10.2196/59213] [Medline: 39150749]
9. Yi Y, Kim KJ. The feasibility of using generative artificial intelligence for history taking in virtual patients. BMC Res Notes 2025;18(1):80 [FREE Full text] [doi: 10.1186/s13104-025-07157-8] [Medline: 39994780]
10. Yu H, Zhou J, Li L, Chen S, Gallifant J, Shi A, et al. AIPatient: simulating patients with EHRs and LLM powered agentic workflow. ArXiv. Preprint posted online on July 29, 2025. [doi: 10.48550/arXiv.2409.18924]
11. Lucas HC, Upperman JS, Robinson JR. A systematic review of large language models and their implications in medical education. Med Educ 2024;58(11):1276-1285. [doi: 10.1111/medu.15402] [Medline: 38639098]
12. García-Torres D, Vicente Ripoll MA, Fernández Peris C, Mira Solves JJ. Enhancing clinical reasoning with virtual patients: a hybrid systematic review combining human reviewers and ChatGPT. Healthcare (Basel) 2024;12(22):2241 [FREE Full text] [doi: 10.3390/healthcare12222241] [Medline: 39595439]
13. Fatima A, Shafique M, Alam K, Fadlalla Ahmed TK, Mustafa M. ChatGPT in medicine: a cross-disciplinary systematic review of ChatGPT's (artificial intelligence) role in research, clinical practice, education, and patient interaction. Medicine (Baltimore) 2024;103(32):e39250 [FREE Full text] [doi: 10.1097/MD.0000000000039250] [Medline: 39121303]
14. Page MJ, McKenzie JE, Bossuyt PM, Boutron I, Hoffmann TC, Mulrow CD, et al. The PRISMA 2020 statement: an updated guideline for reporting systematic reviews. Syst Rev 2021;10(1):89 [FREE Full text] [doi: 10.1186/s13643-021-01626-4] [Medline: 33781348]

XSL•FO
RenderX

15. Lee WY, Han SY, Kim JH, Lee BW, Han Y, Lee S. Gen-SynDi: leveraging knowledge-guided generative AI for dual education of syndrome differentiation and disease diagnosis. Applied Sciences 2025;15(9):4862. [doi: 10.3390/app15094862]
16. Haider SA, Prabha S, Gomez-Cabello CA, Borna S, Genovese A, Trabilsy M, et al. Synthetic patient-physician conversations simulated by large language models: a multi-dimensional evaluation. Sensors (Basel) 2025;25(14):4305 [FREE Full text] [doi: 10.3390/s25144305] [Medline: 40732431]
17. Liu Z, Tu Q, Ye W, Xiao Y, Zhang Z, Cui H. Exploring the inquiry-diagnosis relationship with advanced patient simulators. ArXiv. Preprint posted online on March 11, 2025.
18. Du Z, Zheng L, Hu R, Xu Y, Li X, Sun Y, et al. Llms can simulate standardized patients via agent coevolution. ArXiv. Preprint posted online on June 7, 2025.
19. Saab K, Freyberg J, Park C, Strother T, Cheng Y, Weng WH, et al. Advancing conversational diagnostic AI with multimodal reasoning. ArXiv. Preprint posted online on May 6, 2025. [doi: 10.48550/arXiv.2505.04653]
20. Yamamoto A, Koda M, Ogawa H, Miyoshi T, Maeda Y, Otsuka F, et al. Enhancing medical interview skills through AI-simulated patient interactions: nonrandomized controlled trial. JMIR Med Educ 2024;10:e58753 [FREE Full text] [doi: 10.2196/58753] [Medline: 39312284]
21. Tu T, Schaekermann M, Palepu A, Saab K, Freyberg J, Tanno R, et al. Towards conversational diagnostic artificial intelligence. Nature 2025;642(8067):442-450. [doi: 10.1038/s41586-025-08866-7] [Medline: 40205050]
22. Holderried F, Stegemann-Philipps C, Herschbach L, Moldt J, Nevins A, Griewatz J, et al. A Generative Pretrained Transformer (GPT)-powered chatbot as a simulated patient to practice history taking: prospective, mixed methods study. JMIR Med Educ 2024;10:e53961 [FREE Full text] [doi: 10.2196/53961] [Medline: 38227363]
23. Li Y, Zeng C, Zhong J, Zhang R, Zhang M, Zou L. Leveraging large language model as simulated patients for clinical education. ArXiv. Preprint posted online on April 25, 2024.
24. Laverde N, Grévisse C, Jaramillo S, Manrique R. Integrating large language model-based agents into a virtual patient chatbot for clinical anamnesis training. Comput Struct Biotechnol J 2025;27:2481-2491. [doi: 10.1016/j.csbj.2025.05.025] [Medline: 40547455]
25. Rose D, Hung C, Lepri M, Alqassem I, Gashteovski K, Lawrence C. Meddxagent: a unified modular agent framework for explainable automatic differential diagnosis. ArXiv. Preprint posted online on February 26, 2025. [doi: 10.48550/arXiv.2502.19175]
26. Kumar R, Gattani D, Singh K. Enhancing medical history collection using llms. 2024 Presented at: ACSW '24: Proceedings of the 2024 Australasian Computer Science Week; 2024 May 13; NSW, Sydney, Australia p. 140-143.
27. Choi D, Jung Y, Kim J, Oh N, Oh H, Lee S, et al. LLM-Based clinical history taking system: a persona-driven approach. Stud Health Technol Inform 2025;329:1866-1867. [doi: 10.3233/SHTI251254] [Medline: 40776271]
28. Takata T, Yamada R, René A. Development of a virtual patient model for Kampo medical interview: new approach for enhancing empathy and understanding of Kampo medicine pathological concepts. 2024 Presented at: 2024 Joint 13th International Conference on Soft Computing and Intelligent Systems and 25th International Symposium on Advanced Intelligent Systems (SCIS&ISIS); 2024 November 01; Himeji, Japan p. 1-5.
29. Benfatah M, Marfak A, Saad E, Hilali A, Nejjari C, Youlyouz-Marfak I. Assessing the efficacy of ChatGPT as a virtual patient in nursing simulation training: a study on nursing students' experience. Teach Learn Nurs 2024;19(3):e486-e493. [doi: 10.1016/j.teln.2024.02.005]
30. Rashidian S, Li N, Amar J, Lee J, Pugh S, Yang E, et al. AI agents for conversational patient triage: preliminary simulation-based evaluation with real-world EHR data. ArXiv. Preprint posted online on June 4, 2025.
31. Kenny PG, Parsons TD. Virtual standardized llm-ai patients for clinical practice. Annual Review of Cybertherapy And Telemedicine 2024;22:177-182.
32. Wang R, Milani S, Chiu J, Zhi J, Eack S, Labrum T, et al. PATIENT-Ψ: using large language models to simulate patients for training mental health professionals. ArXiv. Preprint posted online on October 3, 2024.
33. Chen S, Wu M, Zhu K, Lan K, Zhang Z, Cui L. LLM-empowered chatbots for psychiatrist and patient simulation: application and evaluation. ArXiv. Preprint posted online on May 23, 2023. [doi: 10.48550/arXiv.2305.13614]
34. Staples P, Clarke P, Leininger C, Principato C, Shafiei M, Goodwin G. Building virtual patients for training mental health professionals. PsyArXiv 2025.
35. Ryu JW, Kwon CY, Park JS, Lim SR, Jeon HL, Kim HJ. Development and application of a chatgpt-based simulation training platform for korean medicine. Journal of Oriental Neuropsychiatry 2024;35(4):413-427.
36. Rädel-Ablass K, Schliz K, Schlick C, Meindl B, Pahr-Hosbach S, Schwendemann H, et al. Teaching opportunities for anamnesis interviews through AI based teaching role plays: a survey with online learning students from health study programs. BMC Med Educ 2025;25(1):259 [FREE Full text] [doi: 10.1186/s12909-025-06756-0] [Medline: 39966894]
37. Bodonhelyi A, Stegemann-Philipps C, Sonanini A, Herschbach L, Szép M, Herrmann-Werner A. Modeling challenging patient interactions: LLMs for medical communication training. Preprint posted online on April 8, 2025. [doi: 10.48550/arXiv.2503.22250]
38. Leypold T, Schäfer B, Boos AM, Beier JP. Artificial intelligence-powered hand surgery consultation: GPT-4 as an assistant in a hand surgery outpatient clinic. J Hand Surg Am 2024;49(11):1078-1088 [FREE Full text] [doi: 10.1016/j.jhsa.2024.06.002] [Medline: 39066762]

XSL•FO
RenderX

39. Brügge E, Ricchizzi S, Arenbeck M, Keller MN, Schur L, Stummer W, et al. Large language models improve clinical decision making of medical students through patient simulation and structured feedback: a randomized controlled trial. BMC Med Educ 2024;24(1):1391 [FREE Full text] [doi: 10.1186/s12909-024-06399-7] [Medline: 39609823]
40. Borg A, Georg C, Jobs B, Huss V, Waldenlind K, Ruiz M, et al. Virtual patient simulations using social robotics combined with large language models for clinical reasoning training in medical education: mixed methods study. J Med Internet Res 2025;27:e63312 [FREE Full text] [doi: 10.2196/63312] [Medline: 40053778]
41. Borg A, Parodis I, Skantze G. Creating virtual patients using robots and large language models: a preliminary study with medical students. 2024 Presented at: HRI '24: Companion of the 2024 ACM/IEEE International Conference on Human-Robot Interaction; 2024 March 11 - 15; Boulder CO USA p. 273-277. [doi: 10.1145/3610978.3640592]
42. Luo M, Bi S, Pang J, Liu L, Tsui C, Lai Y, et al. A large language model digital patient system enhances ophthalmology history taking skills. NPJ Digit Med 2025;8(1):502 [FREE Full text] [doi: 10.1038/s41746-025-01841-6] [Medline: 40760042]
43. Liao Y, Meng Y, Wang Y, Liu H, Wang Y, Wang Y. Automatic interactive evaluation for large language models with state aware patient simulator. ArXiv. Preprint posted online on July 21, 2024. [doi: 10.2139/ssrn.4890649]
44. Johri S, Jeong J, Tran BA, et al. CRAFT-MD: A conversational evaluation framework for comprehensive assessment of clinical LLMs. 2024 Presented at: AAAI 2024 Spring Symposium on Clinical Foundation Models; March 25-27, 2024; Stanford University, Stanford, California.
45. Tu T, Azizi S, Driess D, Schaekermann M, Amin M, Chang P, et al. Towards generalist biomedical AI. NEJM AI 2024;642(3):442-450. [doi: 10.1056/aioa2300138]
46. Rodrigo MMT, Castaneda S, Hernandez RB, Alaan JAMV, Caoile PSP, Chidrome KD. Project caladrius: The design of a virtual patient for philippine medical education. 2025 Presented at: 7th International Conference, AIS 2025, Held as Part of the 27th HCI International Conference, HCII; 2025 June 22–27; Gothenburg, Sweden p. 232-244. [doi: 10.1007/978-3-031-92970-0_17]
47. Li Y, Zeng C, Zhang J, Zhou J, Zou L. Meddit: A knowledge-controlled diffusion transformer framework for dynamic medical image generation in virtual simulated patient. ArXiv. Preprint posted online on August 22, 2024. [doi: 10.24963/ijcai.2024/1267]
48. Zheng W, Turner L, Kropczynski J, Ozer M, Nguyen T, Halse S. Llm-as-a-fuzzy-judge: Fine-tuning large language models as a clinical evaluation judge with fuzzy logic. ArXiv. Preprint posted online on June 12, 2025. [doi: 10.48550/arXiv.2506.11221]
49. Ng HW, Koh A, Foong A, Ong J. Real-time hybrid language model for virtual patient conversations. 2023 Presented at: International Conference on Artificial Intelligence in Education; 2023 3 July; Tokyo, Japan p. 780-785. [doi: 10.1007/978-3-031-36272-9_71]
50. Cook DA, Overgaard J, Pankratz VS, Del Fiol G, Aakre CA. Virtual patients using large language models: scalable, contextualized simulation of clinician-patient dialogue with feedback. J Med Internet Res 2025;27:e68486 [FREE Full text] [doi: 10.2196/68486] [Medline: 39854611]
51. Thesen T, O'Brien WN, Stone S, Pinto-Powell R. Generative AI as the first patient: practice, feedback, and confidence. Med Sci Educ 2025:1-6. [doi: 10.1007/s40670-025-02473-x]
52. Johnson AEW, Pollard TJ, Shen L, Lehman LH, Feng M, Ghassemi M, et al. MIMIC-III, a freely accessible critical care database. Sci Data 2016;3:160035 [FREE Full text] [doi: 10.1038/sdata.2016.35] [Medline: 27219127]
53. Fansi TA, Goel R, Wen Z, Martel J, Ghosn J. DDXPlus: a new dataset for automatic medical diagnosis. ArXiv. Preprint posted online on October 13, 2022.
54. Li J, Lai Y, Li W, Ren J, Zhang M, Kang X. Agent hospital: a simulacrum of hospital with evolvable medical agents. ArXiv. Preprint posted online on January 17, 2025. [doi: 10.48550/arXiv.2405.02957]
55. Chen X, Mao X, Guo Q, Wang L, Zhang S, Chen T. RareBench: can LLMs serve as rare diseases specialists? 2024 Presented at: KDD '24: The 30th ACM SIGKDD Conference on Knowledge Discovery and Data Mining; 2024 August 25 - 29; Barcelona Spain p. 4850-4861. [doi: 10.1145/3637528.3671576]
56. Han X, Wang Z, Zhang J, Wen Q, Li W, Tang B. Overview of the CCKS 2019 knowledge graph evaluation trackntity, relation, event and QA. ArXiv. Preprint posted online on March 9, 2020. [doi: 10.48550/arXiv.2003.03875]
57. Demner-Fushman D, Kohli M, Rosenman M, Shooshan S, Rodriguez L, Antani S, et al. Preparing a collection of radiology examinations for distribution and retrieval. J Am Med Inform Assoc 2016;23(2):304-310 [FREE Full text] [doi: 10.1093/jamia/ocv080] [Medline: 26133894]
58. Huang K, Altosaar J, Ranganath R. Clinicalbert: modeling clinical notes and predicting hospital readmission. ArXiv. Preprint posted online on November 29, 2020. [doi: 10.5860/choice.189890]
59. Steenstra I, Nouraei F, Bickmore T. Scaffolding empathy: training counselors with simulated patients and utterance-level performance visualizations. 2025 Presented at: CHI '25: Proceedings of the 2025 CHI Conference on Human Factors in Computing Systems; 2025 1 May; Yokohama Japan p. 1-22. [doi: 10.1145/3706598.3714014]
60. Bodenreider O. The unified medical language system (UMLS): integrating biomedical terminology. Nucleic Acids Res 2004;32(Database issue):D267-D270 [FREE Full text] [doi: 10.1093/nar/gkh061] [Medline: 14681409]

XSL•FO
RenderX

61. Fung KW, Hole WT, Nelson SJ, Srinivasan S, Powell T, Roth L. Integrating SNOMED CT into the UMLS: an exploration of different views of synonymy and quality of editing. J Am Med Inform Assoc 2005;12(4):486-494 [FREE Full text] [doi: 10.1197/jamia.M1767] [Medline: 15802483]
62. Liu N, Lin K, Hewitt J, Paranjape A, Bevilacqua M, Petroni F. Lost in the middle: how language models use long contexts. ArXiv. Preprint posted online on November 20, 2023. [doi: 10.1162/tacl_a_00638]

Abbreviations

AI: artificial intelligence
API: application programming interface
AS: Anthropomorphism Score
BERT: Bidirectional Encoder Representations from Transformers
CoT: chain-of-thought
CUQ: Chatbot Usability Questionnaire
EHR: electronic health record
FDR: false discovery rate
ICC: intraclass correlation coefficient
ICU: intensive care unit
KG: knowledge graph
LLM: large language model
LLMDP: LLM-based digital patient system
LoRA: Low-Rank Adaptation
MIMIC-III: Medical Information Mart for Intensive Care-III
OSCE: Objective Structured Clinical Examination
PCP: primary care physician
PRISMA: Preferred Reporting Items for Systematic Reviews and Meta-Analyses
RAG: retrieval-augmented generation
RCT: randomized controlled trial
RLHF: reinforcement learning with human feedback
RQ: research question
SFT: supervised fine-tuning
SNOMED-CT: Systematized Nomenclature of Medicine - Clinical Terms
SUS: System Usability Scale
UMLS: Unified Medical Language System

Edited by A Benis; submitted 14.Jun.2025; peer-reviewed by W Wang, E Chang; comments to author 11.Aug.2025; accepted 23.Oct.2025; published 02.Jan.2026.

Please cite as:
Li D, Lebai Lutfi S
Large Language Model–Based Virtual Patient Systems for History-Taking in Medical Education: Comprehensive Systematic Review
JMIR Med Inform 2026;14:e79039
URL: https://medinform.jmir.org/2026/1/e79039
doi:10.2196/79039
PMID:

©Dongliang Li, Syaheerah Lebai Lutfi. Originally published in JMIR Medical Informatics (https://medinform.jmir.org), 02.Jan.2026. This is an open-access article distributed under the terms of the Creative Commons Attribution License (https://creativecommons.org/licenses/by/4.0/), which permits unrestricted use, distribution, and reproduction in any medium, provided the original work, first published in JMIR Medical Informatics, is properly cited. The complete bibliographic information, a link to the original publication on https://medinform.jmir.org/, as well as this copyright and license information must be included.

XSL•FO
RenderX

Review

Causal Discovery in Observational Medical Research: Scoping Review

Zuting Liu[1,2], MPH; Tian Luo[1,2], MS; Hailin Ma[1,2], MBBS; Jiali Mo[1,2], MPH; Xia Yang[1,2], MS; Zhenglong Huang[1,2], MPH; Jingkun Li[3*], PhD; Jie Kuang[1,2*], PhD

[1]Department of Epidemiology, School of Public Health, Jiangxi Medical College, Nanchang University, Nanchang, China

[2]Jiangxi Provincial Key Laboratory of Disease Prevention and Public Health, Nanchang University, Nanchang, China

[3]Department of Biostatistics, School of Public Health, Harbin Medical University, Harbin, China

[*]these authors contributed equally

Corresponding Author:
Jie Kuang, PhD
Department of Epidemiology
School of Public Health, Jiangxi Medical College
Nanchang University
No. 1299 Xuefu Avenue
Nanchang, 330019
China
Phone: 86 15807008572
Email: kuangjie@ncu.edu.cn

Abstract

Background: Observational data are fundamental to medical research but present formidable challenges for causal inference. Machine learning–based causal discovery algorithms have emerged as a promising solution to identify causal structures directly from such data. However, the current literature is skewed toward theoretical and methodological innovations, with a critical gap in systematic assessments of performance in medical research settings and a lack of practical guidance for clinicians and researchers on selecting and applying these algorithms in specific medical contexts.

Objective: This study aimed to systematically map and synthesize the application of causal discovery methods in observational medical research, detailing the methodologies used, their application domains, the robustness of the findings, and the practical challenges encountered.

Methods: Following the PRISMA-ScR (Preferred Reporting Items for Systematic Reviews and Meta-Analyses Extension for Scoping Reviews) guidelines, we conducted a systematic search of Scopus, Web of Science, PubMed, MEDLINE, Embase, and CINAHL from inception to May 2025. We included studies that applied any causal discovery algorithms within a medical research context, encompassing both analyses of real-world observational data and method-validation studies using synthetic or benchmark datasets with a clear medical focus. Purely methodological papers and studies based solely on experimental data were excluded. Data were extracted and synthesized using a descriptive analysis focused on study characteristics, algorithm types, application domains, reported numerical results, and implementation challenges.

Results: Out of 2296 identified publications, 72 (3.1%) met the inclusion criteria. Our synthesis revealed three key themes. The first theme was methodological landscape, where constraint-based algorithms were the most prevalent (38/72, 52.8%), with the fast causal inference (10/72, 13.9%) and Peter-Clark algorithms (9/72, 12.5%) being most common. Score-based (19/72, 26.4%) and hybrid (14/72, 19.4%) methods also represented significant and growing segments (methods were not mutually exclusive). The second theme was application domains and findings, where the majority of studies (54/72, 75%) were in clinical research, with a strong focus on mental health (19/72, 26.4%; eg, identifying symptom networks in schizophrenia and posttraumatic stress disorder) and chronic diseases (19/72, 26.4%; eg, elucidating progression pathways in Alzheimer and diabetes). Etiological research was the primary objective (28/72, 38.9%). Public health applications (18/72, 25%) frequently assessed the causal impacts of behavioral interventions. The third theme was implementation challenges and innovations, where common challenges included pervasive unmeasured confounding, limited sample sizes (noted in more than 20% of studies), and reliance on unvalidated causal assumptions. Emerging innovations focused on longitudinal data frameworks and the integration of multimodal data sources to strengthen causal claims.

XSL•FO
RenderX

Conclusions: This review underscores the growing application of causal discovery algorithms in medical research while also highlighting challenges such as the lack of standardized validation frameworks and persistent confounding. Future efforts must focus on developing evaluation standards and fostering interdisciplinary collaboration to translate these powerful computational techniques into reliable tools for medical research and practice.

(JMIR Med Inform 2026;14:e82499) doi:10.2196/82499

KEYWORDS

causal discovery; medical research; observational data; algorithm; scoping review

Introduction

The advent of big data has driven significant advances in machine learning (ML), yet current methodologies often focus on identifying correlations rather than uncovering underlying causal relationships [1]. This limitation is particularly critical in medicine, where understanding causality is essential for effective clinical decision-making. Contemporary causal research addresses 2 interrelated challenges: causal discovery (identifying causal structures and directions between variables) and causal inference (quantifying effects within predefined causal frameworks) [2-5]. Causal discovery is concerned with deducing the causal structure and directionality among variables from data, with the primary objective of elucidating direct and indirect causal pathways by constructing causal graphs. Typically, it relies on statistical principles such as conditional independence tests to discern potential causal structures from correlational patterns. In contrast, causal inference focuses on quantifying the magnitude of the effect of specific interventions on an outcome variable, presuming a known or assumed causal structure. Therefore, inferring causal relationships, that is, causal discovery, from observational medical data is critical for advancing precision and personalized medicine. A central class of computational methods developed for causal discovery, such as the Peter-Clark (PC) algorithm and fast causal inference (FCI), aims to learn a causal graph that represents the underlying data-generating mechanism. The growing scale and accessibility of diverse medical data resources, encompassing real-world records, such as surgical, therapeutic, and diagnostic information, as well as genetic, lifestyle, and environmental data, have become invaluable for such research [6]. However, these data are often affected by confounding, selection bias, and missing data, posing substantial challenges to deriving reliable causal conclusions. Although randomized controlled trials (RCTs) remain the gold standard for medical decision-making [7], the limits of RCTs and the growing abundance of observational data underscore an urgent need for more robust causal discovery methodologies.

Observational datasets, particularly those derived from real-world settings, offer significant advantages for medical research, including large sample sizes, accessibility, and the ability to reflect real-world clinical scenarios. Previous studies have demonstrated their potential to elucidate disease etiology [8-10], optimize treatment strategies [11,12], and refine prognostic models [13,14]. However, the specific application of causal discovery methods to harness these datasets remains particularly challenging and fragmented. Key barriers include unmeasured confounding, complex data structures, and a lack of consensus on methodological best practices. As a result, there is an insufficient synthesis of how these methods can be robustly applied, validated, and translated into clinical insights. This scoping review aims to fill this gap by systematically analyzing causal discovery methods applied to observational medical studies. Specifically, we critically assess: (1) The evolving methodological landscape and algorithm suitability across clinical contexts; (2) High-impact application domains and translational outcomes; (3) Persistent implementation challenges, such as unmeasured confounding and sample limitations. By mapping these dimensions, we provide a foundation for advancing causal discovery in digital health and precision medicine.

Methods

Study Design

This scoping review adhered to Arksey and O'Malley's framework for scoping review [15] and the PRISMA-ScR (Preferred Reporting Items for Systematic Reviews and Meta-Analyses extension for Scoping Reviews) guidelines [16] (Multimedia Appendix 1). Our primary research question was: "What are the methodologies, clinical applications, and implementation challenges of causal discovery in observational medical research?" The aim was to synthesize evidence to guide future methodological development and clinical translation. Given the rapidly evolving nature of this field, no temporal restrictions were applied.

Search Strategy

To comprehensively review studies of causal discovery algorithms in medical research and its subtypes, 2 researchers (XY and ZH) performed a systematic literature search of Scopus, Web of Science, PubMed, MEDLINE, Embase, and CINAHL in May 2025 and was restricted to studies published in English, using the following search strategies: "causal discovery/causal structure discovery/causal structure learning/causal graph discovery/learning causal models." The search was focused on biomedical databases (PubMed, Embase, etc) as this review aims to map applications in medical research. While computer science–focused databases, such as IEEE Xplore or ACM Digital Library, include methodological developments, they primarily emphasize algorithmic innovation; seminal methodological papers with medical applications are typically also indexed within the selected biomedical sources. The search strategy was designed in consultation with an information specialist. The entire search strategy for the 6 databases is displayed in Multimedia Appendix 2.

XSL•FO
RenderX

Eligibility Criteria

Two researchers (HM and JM) independently screened studies based on predefined inclusion and exclusion criteria by examining their titles, abstracts, and full texts. Studies met the following inclusion criteria: (1) application focus: empirical implementation of causal discovery algorithms in medical or health contexts. (2) Data and methodology: the study applied a causal discovery approach within the observational research paradigm. This included analyses of real-world observational medical data as well as method-validation studies that used synthetic or benchmark datasets to address a medical research question or simulate a medical data environment. (3) Output: the study generated an explicit causal graph or causal structure. (4) Language: English-language publications. The exclusion criteria were: (1) The study purely focused on methodological or theoretical papers without medical applications. (2) Experimental (RCT) or basic science studies. (3) Duplicate publications, brief abstracts, or conference summaries lacking full methodological and results sections. (4) Studies where causal discovery was not the primary methodology. Discrepancies in study eligibility were resolved through consensus between 2 independent reviewers (JK and JL).

Data Extraction and Synthesis

Screening was performed using Rayyan [17], with dual-reviewer verification at all stages. A standardized electronic form was used to extract the following data items: (1) study characteristics: year of publication, country or region of corresponding author affiliation, study design, and sample size; (2) causal discovery methods: specific algorithms, methodological category, and the primary software or package used for implementation; (3) data properties: data type, dimensionality, and temporal features; (4) application domain and specific clinical or public health objectives; and (5) validation approaches and key reported limitations.

Data synthesis was conducted in 2 complementary ways to align with the scoping review's descriptive aims. First, a descriptive quantitative analysis summarized structured characteristics (eg, causal discovery algorithms, software tools, and application domains) using frequencies and percentages. Second, for textual data on reported methodological considerations and challenges, an inductive content summary was performed. Two reviewers (ZL and TL) independently identified recurrent issues and patterns, which were then discussed, consolidated, and organized into overarching descriptive themes (eg, methodological landscape and challenges). This process ensured the results reflected both the quantitative distribution and qualitative substance of the included literature. While this scoping review did not undertake a formal critical appraisal of individual studies using standardized quality assessment or risk-of-bias tools, we systematically extracted study-reported methodological limitations and implementation challenges as a prespecified data item during full-text screening. These author-reported limitations were subsequently subjected to inductive qualitative synthesis, alongside other extracted textual data, to identify recurrent patterns and to develop the descriptive themes presented in the "Challenges" section. This approach was intended to map commonly reported methodological issues in the literature rather than to appraise or grade the quality of individual studies.

Results

Article Selection

After the removal of duplicates, 2296 unique records were identified for screening. Of these, 72 studies [8-14,18-82] (3.1%) met the inclusion criteria and were included in the final synthesis (Figure 1). After eliminating 2548 duplicates (52.6%), title or abstract screening excluded 1909 records (39.4%). A full-text review of 387 articles led to the exclusion of 315 (81.4%) due to reasons such as a methodological focus (201/315, 63.8%), duplicate publications or abstracts (50/315, 15.9%), and basic research or experimental designs (64/315, 20.3%).

XSL•FO
RenderX

Figure 1. PRISMA-ScR (Preferred Reporting Items for Systematic Reviews and Meta-Analyses Extension for Scoping Reviews) flowchart for the study selection process. RCT: randomized controlled trial.

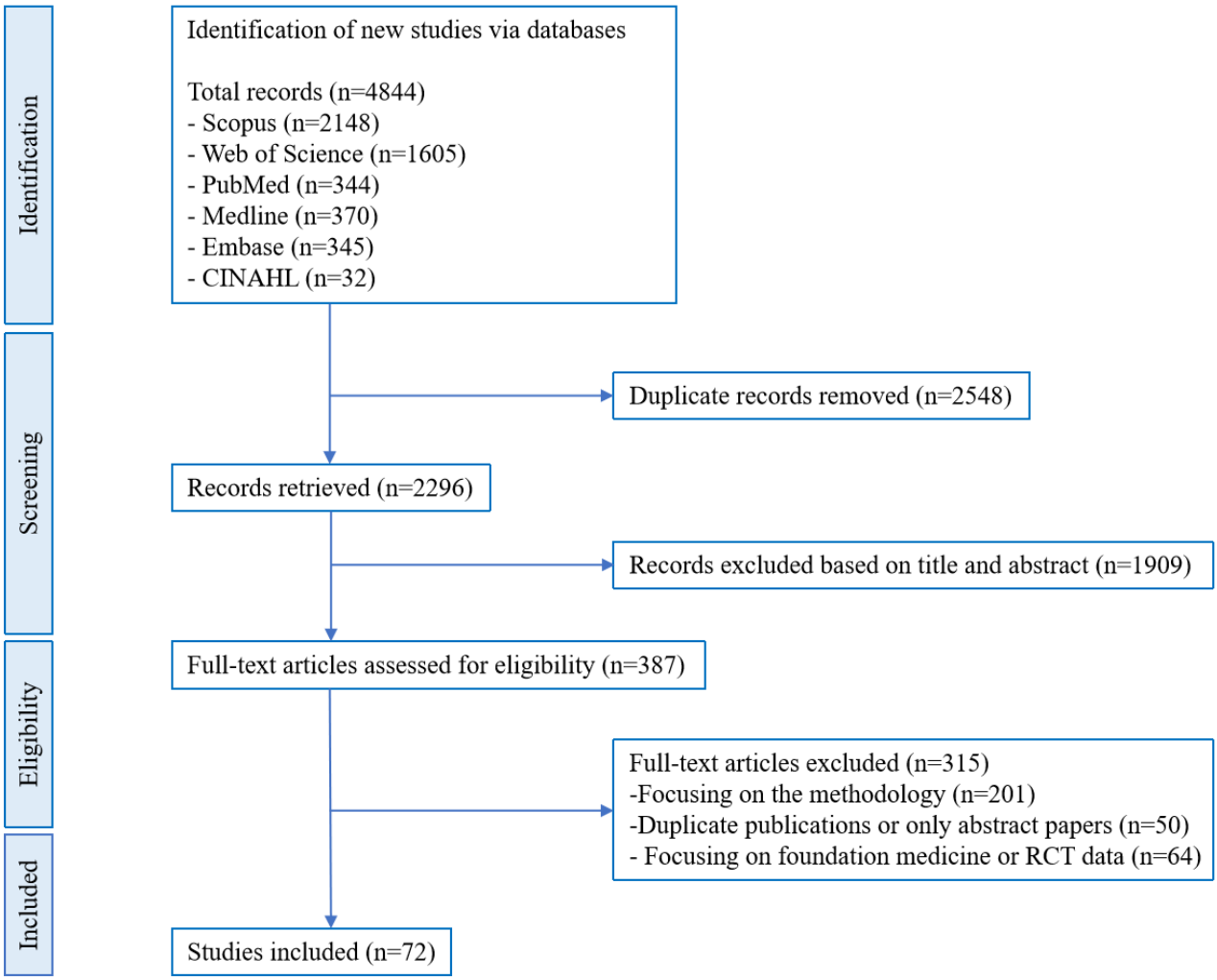

Characteristics of the Articles

The characteristics of the included studies (N=72) [8-14,18-82] are summarized in Table 1, covering publication year, country or region, and document type. The number of annual publications progressively increased from 2017 to 2025, with the years 2023-2025 accounting for the majority (46/72, 63.9%). Publications peaked in 2023 and 2024. The majority of studies were peer-reviewed journal articles (64/72, 88.9%), with the remaining studies being conference proceedings. The studies originated from 18 distinct countries or regions, with the United States contributing the largest proportion (25/72, 34.7%), followed by China (8/72, 11.1%), the Netherlands (6/72, 8.3%), and Japan (4/72, 5.6%), accounting for a combined total of 59.7% of publications. Three primary themes emerged from the analysis: (1) methodological landscape, that is, dominant causal discovery approaches and typologies in medical research; (2) application domains, that is, multidimensional implementation scenarios across observational studies; and (3) challenges, that is, methodological limitations and barriers to clinical translation.

XSL•FO
RenderX

Table 1. Characteristics of the studies used in the review, including the year, type, and country of publication (N=72).

Features	Studies, n (%)	References
Year of publication		
2025	14 (19.4)	[8-10,13,18-26,82]
2024	16 (22.2)	[11,14,27-40]
2023	16 (22.2)	[41-56]
2022	8 (11.1)	[57-64]
2021	5 (6.9)	[12,65-68]
2020	7 (9.7)	[69-75]
2019	2 (2.8)	[76,77]
2018	1 (1.4)	[78]
2017	3 (4.2)	[79-81]
Type of publication		
Journal article	64 (88.9)	[8-14,18-31,33,34,37,38,41-48,50,51,53-63,65-82]
Conference article	8 (11.1)	[32,35,36,39,40,49,52,64]
Country of publication		
United States	25 (34.7)	[18,20,22,23,26,28,36,38,43,46,47,51,56-58,60,61,63,65-67,70,73,74,79]
China	8 (11.1)	[19,29,33,42,52,69,77,78]
Netherlands	6 (8.3)	[9,27,59,71,80,81]
Japan	4 (5.6)	[39,40,49,75]
Other countries	29 (40.3)	[8,10-14,21,24,25,30-32,34,35,37,41,44,45,48,50,53-55,62,64,68,72,76,82]

Themes

Theme 1: Methodological Landscape

Causal discovery methodologies are broadly divided into several major categories: constraint-based, score-based, continuous optimization, functional causal models, and hybrid methods. It should be noted that these categories are not mutually exclusive; a single study could use methods from more than one category. Thus, the percentages reported below are calculated based on the total number of included studies (N=72) [8-14,18-82] and may sum to more than 100%. Among the 72 studies analyzed, constraint-based methods constituted the predominant approach (38/72, 52.8%) [8-10,12,14,18,24,25,27,29-32,34-38,43,45,48,52,53,55,57-59,63,64,68,70,71,73,74,77,79-81], followed by score-based (19/72, 26.4%) [8,11,18-20,23,24,26,28,32,33,35,39,42,61,67,73,74,82], hybrid (14/72, 19.4%) [8,13,22,23,33,41,46,47,51,56,60,63,65,69], continuous optimization (9/72, 12.5%) [29,33,36,40,44,49,50,54,62], and functional causal models (5/72, 6.9%) [21,32,66,75,78]. At the algorithmic level, FCI (10/72, 13.9%) [10,18,29,34,38,43,58,63,73,74] and PC (9/72, 12.5%) [12,18,25,27,29,35,36,53,70] algorithms were the most implemented constraint-based methods, whereas greedy fast causal inference (GFCI) (10/72, 13.9%) [13,22,23,41,46,47,51,60,63,65] and Non-combinatorial Optimization via Trace Exponential and Augmented Lagrangian for Structure learning (6/72, 8.3%) [36,40,49,50,54,62] demonstrated notable dominance within the hybrid and continuous optimization categories, respectively. Additionally, time-series causal discovery (eg, Peter-Clark momentary conditional independence) was actively explored in 11 studies [32,44,48,55,64,66,68,72,76,77,82]. These findings highlight a clear trajectory toward the adoption of more integrated, scalable, and nonparametric causal discovery frameworks. The reviewed studies used methodologies from 2 distinct conceptual frameworks. The majority used structural causal discovery algorithms (eg, PC, FCI, and NOTEARS) to learn causal graphs or networks. An analysis of implementation tools revealed the software landscape for causal discovery (Table 2). Of the 72 included studies, 45 (62.5%) [8-10,12,13,18-22,24,26-28,30,32,36-39,41,43,44,46-48,50,51,54,55,57,60-63,65,68-71,74,75,77,79] explicitly specified the software or package used. Among these, R was the most prevalent environment, used in 22 studies [8-10,12,18,20,22,24,26-28,30,37,38,48,55,57,60,61,68,74,82] (22/45, 48.9% of reporting studies, or 22/72, 30.6% of all studies), with the *pcalg* package being the most frequently cited. The standalone Tetrad suite was used in 10 studies [13,18,41,43,46,47,51,63,65,74] (10/45, 22.2% of reporting studies, or 10/72, 13.9% overall). Out of 45 studies, Python and MATLAB were implemented in 7 [9,21,32,36,50,54,62] (15.5%) and 8 [32,44,69-71,75,77,79] (17.7%) of the software-reporting studies, respectively. A notable finding regarding transparency was that 27 studies [11,14,23,25,29,31,33-35,40,42,45,49,52,53,56,58,59,64,66,67,72,73,76,78,80,81] (37.5% of the total) did not report any software details, posing a significant barrier to reproducibility. For details, refer to Table 2.

XSL•FO
RenderX

Table 2. Characteristics of the studies used in the review, including author, causal discovery method, method type, software, disease or area, and type of data.

Authors	Causal discovery method	Method type	Software	Disease or area	Type of data	Validation methods
Gururaghavendran and Murray [18]	PC[a], FCI[b], FGES[c], GRaSP[d]	Constraint-based; Score-based	R (*pcalg*), Tetrad	Cardiovascular mortality	Cohort	Internal stability assessment; Expert review
Petrungaro et al [8]	PC-stable[e], Inter-IAMB[f], HC[g], Tabu[h], MMHC[i], H2PC[j]	Constraint-based; Score-based; Hybrid	R (*bnlearn*)	Sepsis	Cross-sectional	None reported
Li et al [19]	GES[k]	Score-based	Python (DoWhy, Causal Discovery Toolbox)	Alzheimer disease	Cohort	None reported
Korvink et al [20]	GES	Score-based	R (*pcalg*, *dagitty*)	Public health	Cross-sectional	None reported
Penson et al [9]	BCCD[l]	Constraint-based	R (*lavaan*, *RU-causal*)	Chronic fatigue	Cross-sectional	None reported
Noh et al [21]	LiNGAM[m]	Functional-based	Python (DoWhy)	Diabetes	Cross-sectional	Statistical verification
Tseng et al [22]	GFCI[n]	Hybrid	R (*lavaan*)	Autism	Cohort	None reported
Yu et al [10]	FCI and MGM[o]	Constraint-based	R (*rCausalMGM*)	Dementia	Cohort	None reported
Bronstein et al [23]	GFCI, GraSP, GraSP-FCI[p]	Score-based; Hybrid	Not specified	Clinical high risk for psychosis	Cohort	Internal stability assessment
Giuliani et al [13]	GFCI	Hybrid	Tetrad	Schizophrenia	Cross-sectional	None reported
Colineaux et al [24]	Hill climbing, Inter-IAMB, ARACNE[q]	Constraint-based; Score-based	R (*bnlearn*)	Health care use	Cohort	Expert review
Ribeiro-Dantas et al [14]	iMIIC[r]	Constraint-based	Not specified	Breast cancer	Cohort	Expert review; Internal stability analysis
Verveen et al [27]	PC	Constraint-based	R (*pcalg*)	COVID-19	Cohort	None reported
Ren et al [28]	GGES[s]	Score-based	R (*pcalg*)	Esophageal cancer	Cohort	None reported
Guo et al [29]	PC, FCI, and GAE[t]	Constraint-based; Continuous optimization-based	Not specified	Nonsuicidal self-injury	Cross-sectional	None reported
Foraita et al [30]	Modified PC[u]	Constraint-based	R (*pcalg*, *tPC*, *micd*)	Childhood obesity	Cohort	None reported
Ribeiro et al [31]	AnchorFCI[v]	Constraint-based	Not specified	Cardiometabolic diseases	Cross-sectional	Internal stability analysis
Sabzevar et al [32]	RDCM[w], MVGC[x], PCMCI[y], Var-LINGAM[z]	Constraint-based; Score-based; Functional-based	MATLAB, Python	Schizophrenia	Cross-sectional (fMRI time series)	None reported
Zhang et al [33]	MMHC, H2PC, CBAMN[aa]	Score-based; Continuous optimization-based; Hybrid	Not specified	Acute kidney injury	Cohort	Internal stability analysis; Statistical verification; Independent dataset validation
Bernasconi et al [11]	SEM[ab]	Score-based	Not specified	Breast cancer	Cohort	Expert review
Fay et al [25]	PC	Constraint-based	Not specified	Aortic Morphology	Cross-sectional	None reported

XSL•FO
RenderX

Authors	Causal discovery method	Method type	Software	Disease or area	Type of data	Validation methods
Gąsior et al [41]	GFCI	Hybrid	Tetrad	Congenital heart disease	Cross-sectional	None reported
Gao et al [42]	RL[ac]-based causal discovery (IIE[ad] strength)	Score-based	Not specified	Type 2 diabetes	Cross-sectional	None reported
Lee et al [43]	FCI	Constraint-based	Tetrad	Cardiac surgery (CABG[ae] and AVR[af])	Cohort	None reported
Miley et al [51]	GFCI	Hybrid	Tetrad	Schizophrenia	Cohort	Independent dataset validation
Thomas et al [44]	DYNOTEARS[ag]	Continuous optimization-based	MATLAB	Sleep disorders	Cross-sectional	None reported
Vowels et al [45]	SAM[ah]	Constraint-based	Not specified	Mental health (depression and anxiety)	Cross-sectional and cohort	None reported
Bao et al [57]	Modified PC, MMPC, IAMB[ai], GS[aj]	Constraint-based	R (*bnlearn*)	HIV	Cross-sectional	Statistical verification; Internal stability assessment
Singh et al [58]	FCI	Constraint-based	Not specified	In-hospital mortality	Cross-sectional	None reported
Pierce et al [46]	GFCI	Hybrid	Tetrad	PTSD[ak]	Longitudinal time-series	None reported
Langwerden et al [59]	BCCD	Constraint-based	Not specified	Mental disorders	Cross-sectional	None reported
Bronstein et al [60]	GFCI	Hybrid	R (*rcausal*)	Eating disorders	Cross-sectional	None reported
Ganopoulou et al [12]	PC	Constraint-based	R (*MXM*)	Coronary chronic total occlusions	Cross-sectional	None reported
Rawls et al [65]	GFCI	Hybrid	Tetrad	Alcohol use disorder	Cross-sectional	None reported
Li et al [66]	ANM[al]	Functional-based	Not specified	COVID-19	Longitudinal time-series and cross-sectional	None reported
Wang et al [69]	PKCL[am]	Hybrid	MATLAB	T2DM[an] and osteoporosis	Cross-sectional	Expert review
Saxe et al [70]	GLL-PC[ao] and TPC[ap]	Constraint-based	MATLAB	PTSD	Cohort	None reported
Lee et al [47]	GFCI	Hybrid	Tetrad	Nursing home hospitalization	Cohort	Expert review
Andersen et al [48]	TPC	Constraint-based	R (*causalDisco*)	Mental health (stress and depression)	Cross-sectional and cohort	Independent dataset validation
Shen et al [67]	FGES, Modified FGES (temporal constraints)	Score-based	Not specified	T2DM	Cohort	Independent dataset validation
Petersen et al [68]	TPC	Constraint-based	R (*causalDisco*)	Depression	Cohort	Internal stability assessment
Schoenmacker et al [71]	BCCD	Constraint-based	MATLAB	ADHD[aq]	Cohort	None reported
Ahangaran et al [72]	PCDSD[ar]	Probabilistic graphical model	Not specified	Amyotrophic lateral sclerosis	Longitudinal time-series	None reported
Wang et al [73]	FCI[b] and LSTM[as]	Constraint-based; Score-based	Not specified	Knee osteoarthritis	Cohort	None reported
Chen et al [78]	McDSL[at]	Functional-based	Not specified	Acute kidney injury	Cohort	None reported

XSL•FO
RenderX

Authors	Causal discovery method	Method type	Software	Disease or area	Type of data	Validation methods
Galatzer-Levy et al [79]	SVM[au], LGMM[av], and HITON-PC[aw]	Constraint-based	MATLAB	PTSD	Cohort	None reported
Sokolova et al [80]	BCCD	Constraint-based	Not specified	ADHD and ASD[ax]	Cross-sectional	None reported
van Dijk et al [81]	BCCD	Constraint-based	Not specified	The Wechsler Adult Intelligence Scale-IV	Cross-sectional	None reported
Li et al [49]	NOTEARS[ay]	Continuous optimization-based	Not specified	General health status	Longitudinal time-series	None reported
Shen et al [74]	FCI, FGES, and SEM	Constraint-based; Score-based	Tetrad, R (*lavaan*)	Alzheimer disease	Cohort	Expert review
Mouches et al [62]	NOTEARS	Continuous optimization-based	Python (CausalNex)	Brain aging and CVD[az]	Cross-sectional	None reported
Shen et al [61]	FGES	Score-based	R (*rcausal*)	White matter hyperintensities	Cohort	None reported
Zhang et al [63]	FCI and GFCI	Constraint-based; Hybrid	Tetrad	COVID-19-associated AKI[ba]	Longitudinal time-series	None reported
Park et al [50]	NOTEARS	Continuous optimization-based	Python (CausalNex)	Quality of life and mental health	Cross-sectional	None reported
Fu et al [26]	GES	Score-based	R (package unspecified)	Progressive supranuclear palsy	Cohort	None reported
Nogueira et al [64]	ItsPC[bb]	Constraint-based	Not specified	ICU[bc] survival analysis	Cohort	None reported
Li et al [34]	FCI and PPCIT[bd]	Constraint-based	Not specified	Hospital-acquired pressure injury and spinal cord injury	Cohort	Statistical verification
Kazemi et al [35]	PC, GES, and GIES[be]	Constraint-based; Score-based	Not specified	Maternal quality of life (obesity and stress-related)	Cohort	Statistical verification
Naik et al [36]	NOTEARS and PC	Constraint-based; Continuous optimization-based	Python (CausalNex, gcastle, pgmpy)	Non–small cell lung cancer	Cross-sectional	None reported
Ribeiro Santiago et al [82]	Bayesian Structure Learning (partition MCMC[bf])	Score-based	R (*BiDAG*, *blavaan*)	Adolescent emotional disorders (depression or anxiety)	Cohort	Expert review
McCormick et al [37]	GGM[bg], PC-stable, and SEM	Constraint-based	R (*bnlearn*, *lavaan*, *EGAnet*)	Oral health	Cross-sectional	None reported
Zeng et al [38]	FCI	Constraint-based	R (*rCausalMGM*)	Childhood Sjögren's	Cohort	None reported
Li et al [52]	PC	Constraint-based	Not specified	Primary liver cancer	Cohort	None reported
Nagaraj et al [53]	PC	Constraint-based	Not specified	Stress-related disorders	Longitudinal time-series	None reported
Vigneshwaran et al [54]	NOTEARS	Continuous optimization-based	Python (CausalNex)	Brain aging and gray matter atrophy	Cross-sectional	None reported
Petersen et al [55]	TPC	Constraint-based	R (*causalDisco*)	CVD and depression	Cohort	Expert review
Zhang et al [40]	NOTEARS	Continuous optimization-based	Not specified	Psychological stress and obesity-related risks	Longitudinal time-series	Expert review
Tosaki et al [39]	Causal Bayesian network	Score-based	INGOR	Atherosclerosis, hypertension, diabetes, dyslipidemia, osteopenia, chronic kidney disease, COPD[bh], and obesity	Cohort	None reported

XSL•FO
RenderX

Authors	Causal discovery method	Method type	Software	Disease or area	Type of data	Validation methods
Fung et al [56]	Causal Bayesian network	Hybrid	Not specified	COVID-19	Cross-sectional	Statistical verification
Ahangaran et al [76]	PCDSD	Probabilistic graphical model	Not specified	Amyotrophic lateral sclerosis	Longitudinal time-series	None reported
Yang et al [77]	CD-SF[bi] and CD-SU-SF[bj]	Constraint-based	MATLAB	Lung cancer	Cross-sectional	None reported

XSL•FO
RenderX

Authors	Causal discovery method	Method type	Software	Disease or area	Type of data	Validation methods
Itahashi et al [75]	LiNGAM[bk]	Functional-based	MATLAB	Adolescent mental issues	Cohort	None reported

[a]PC: Peter-Clark algorithm.
[b]FCI: fast causal inference.
[c]FGES: fast greedy equivalence search.
[d]GRaSP: greedy relaxation of the sparsest permutation.
[e]PC-stable: Peter-Clark stable.
[f]Inter-IAMB: interleaved incremental association Markov blanket.
[g]HC: hill climbing.
[h]Tabu: tabu search.
[i]MMHC: max-min hill climbing.
[j]H2PC: hybrid of HPC and PC.
[k]GES: greedy equivalence search.
[l]BCCD: Bayesian Constraint-based Causal Discovery.
[m]LiNGAM: linear non-Gaussian acyclic model.
[n]GFCI: greedy fast causal inference.
[o]MGM: mixed graphical model.
[p]GraSP-FCI: greedy relaxation of the sparsest permutation fast causal inference.
[q]ARACNE: algorithm for the reconstruction of accurate cellular networks.
[r]iMIIC: interpretable multivariate information-based inductive causation.
[s]GGES: greedy generalized equivalence search.
[t]GAE: graph autoencoder.
[u]Modified PC: modified Peter-Clark algorithm.
[v]AnchorFCI: anchor fast causal inference.
[w]RDCM: regression dynamic causal modeling.
[x]MVGC: multivariate Granger causality.
[y]PCMCI: Peter-Clark momentary conditional independence.
[z]VarLINGAM: vector autoregressive linear non-Gaussian acyclic model.
[aa]CBAMN: cycle-breaking algorithm based on modified NOTEARS.
[ab]SEM: structural expectation-maximization.
[ac]RL: reinforcement learning.
[ad]IIE: inverse information entropy strength.
[ae]CABG: isolated coronary artery bypass grafting.
[af]AVR: isolated aortic valve replacement.
[ag]DYNOTEARS: dynamic noncombinatorial optimization via trace exponential and augmented lagrangian for structure learning.
[ah]SAM: structural agnostic modeling.
[ai]IAMB: incremental association Markov blanket.
[aj]GS: grow-shrink.
[ak]PTSD: posttraumatic stress disorder.
[al]ANM: additive noise model.
[am]PKCL: prior-knowledge-driven local causal structure learning.
[an]T2DM: type 2 diabetes mellitus.
[ao]GLL-PC: global-local learning Peter-Clark algorithm.
[ap]TPC: temporal Peter-Clark algorithm.
[aq]ADHD: attention-deficit/hyperactivity disorder.
[ar]PCDSD: probabilistic causal discovery in sequential datasets.
[as]LSTM: long short-term memory.
[at]McDSL: multiple-cause discovery combined with structure learning.
[au]SVM: support vector machine.
[av]LGMM: latent growth mixture modeling.
[aw]HITON-PC: HITON-PC algorithm.
[ax]ASD: autism spectrum disorder.

XSL•FO
RenderX

[ay]NOTEARS: noncombinatorial optimization via trace exponential and augmented Lagrangian for structure learning.

[az]CVD: cardiovascular disease.

[ba]AKD: acute kidney injury.

[bb]ItsPC: irregular time-series PC.

[bc]ICU: intensive care unit.

[bd]PPCIT: predictive permutation conditional independence tests.

[be]GIES: greedy interventional equivalence search.

[bf]MCMC: Markov chain Monte Carlo.

[bg]GGM: Gaussian graphical model.

[bh]COPD: chronic obstructive pulmonary disease.

[bi]CD-SF: causal discovery based on the streaming feature.

[bj]CD-SU-SF: causal discovery with symmetrical uncertainty based on the streaming feature.

[bk]LiNGAM: linear non-Gaussian acyclic model.

Theme 2: Application Domains

Examination of the 72 studies [8-14,18-82] indicated that causal discovery applications were dominated by clinical research (54/72, 75%), with public health comprising the remainder (18/72, 25%). Etiological investigation emerged as the predominant focus within clinical research, followed by predictive modeling, highlighting the method's central role in elucidating disease mechanisms and enabling clinical prognosis. This application profile demonstrated the adaptability of causal discovery methodologies across the spectrum from individual-level clinical research to population health studies.

Causal Discovery Methodological Approaches to Disease Categories

Among the 54 clinical studies [8-14,18,19,21-23,25-29,31-34,36,38,39,42-46,51-54,58-61,63-65,67,69-81], mental health represented the most extensively examined area (19/72, 26.4%) [13,22,23,27,29,32,45,46,51,53,59,60,65,70,71,75,79-81], with significant attention to schizophrenia (3/72, 4.2%) [13,32,51], posttraumatic stress disorder (3/72, 4.2%) [46,70,79], autism spectrum disorder (2/72, 2.8%) [22,80], and attention-deficit/hyperactivity disorder (2/72, 2.8%) [71,80]. Chronic disease investigations equally comprised 26.4% (19/72) of studies [9-12,14,19,21,26,28,31,36,38,42,52,69,72-74,76], spanning neurodegenerative diseases [10,19,26,72-74,76] (particularly Alzheimer disease [10,19,26,74] and amyotrophic lateral sclerosis [72,76]), malignancies [11,14,28,36,52], diabetes [21,42], and other chronic conditions [9,12,31,38,69]. Additional clinical applications included acute illnesses [8,33,78], pharmacological research [18,63], and other various specialized clinical scenarios [25,34,39,43,44,54,58,61,64,67,77], collectively demonstrating the extensive penetration of causal discovery methodologies in clinical research. For details, refer to Table 2.

Research Focus and Clinical Applications

The 54 clinical studies [8-14,18,19,21-23,25-29,31-34,36,38,39,42-46,51-54,58-61,63-65,67,69-81] showed a distinct concentration in research aims. Etiological exploration represented the predominant focus (28/72, 38.9%) [8-10,18,22,23,25,27,29,31,39,42-46,51,54,60,61,63,65,69-71,74,75,80], establishing causal discovery as a core methodology for investigating disease mechanisms. Predictive modeling constituted the second major application area (13/72, 18.1%) [19,21,26,33,34,58,64,72,73,76-79], while prognostic evaluation [13,14,28,52] and disease diagnosis [32,36,38,53] each accounted for 4 studies respectively. Collectively, these 4 domains accounted for 49 investigations (49/72, 68.1%), underscoring the method's primary use in addressing fundamental clinical questions from causation to outcome assessment.

For example, in a study by Zhang et al [63], causal discovery methods were applied to construct causal networks of COVID-related acute kidney injury using longitudinal electronic health record (EHR) data. Specifically, the FCI and GFCI algorithms were used to automatically identify the development of COVID-19–related acute kidney injury with minimal prior assumptions about pathway connectivity. The results provided a more refined understanding of how remdesivir and other risk factors contribute to acute kidney injury, identifying critical time points for potential intervention and offering valuable insights for clinical decision-making [63]. Similarly, Sokolova et al [80] demonstrated the application of the Bayesian constraint-based causal discovery algorithm to cross-sectional phenotypic data, which revealed directional relationships between attention-deficit/hyperactivity disorder and autism spectrum disorder symptom domains that traditional correlational methods failed to elucidate, generating novel hypotheses regarding the etiological mechanisms underlying their comorbidity [80].

However, the limited applications in clinical decision support development (1/72, 1.4%) [67] and measurement scale implementation (2/72, 2.8%) [59,81] suggested that the translation of causal discovery into practical clinical tools remained underdeveloped, highlighting substantial potential for future research and implementation in real-world health care settings.

Public Health Research Applications

Public health domains were addressed in 25% (18/72) of studies [20,24,30,35,37,40,41,47-50,55-57,62,66,68,82], demonstrating the expanding relevance of causal discovery beyond clinical settings. Health behavior interventions constituted the largest subgroup (8/72, 11.1%) [30,35,37,40,41,49,56,62], primarily focusing on lifestyle quantification and health promotion. Disease management decision-making and health care optimization strategies were examined in 9.7% (7/72) of studies [20,24,47,50,66,68,82], encompassing social determinants of

XSL•FO
RenderX

health, health care use patterns, and nursing home hospitalization reduction. The remaining studies addressed infectious disease transmission research [57,66] and life-course epidemiology [55]. These applications collectively demonstrated the methodological versatility of causal discovery in tackling population-level health challenges and informing public health policy.

Theme 3: Challenges

Common Observational Study Challenges

Medical observational studies using causal discovery methods consistently faced several fundamental limitations. Unmeasured confounding represented the most prevalent challenge (32/72, 44.4%) [11,12,18,20,21,25-27,29,37,38,41,43,44,52-57,59,62,63,65,66,70,71,73,75,82-84], potentially introducing spurious discoveries and biased effect estimates. Sample size limitations were reported in 29.2% (21/72) of studies [9,10,23,24,27,30,31,35,38,40,41,49,55,61,63,69,71,73,78,81,85], restricting statistical power and generalizability. Data quality issues emerged across multiple investigations, including substantial missing data and discretization-induced biases [10,12,30,33,47,49,54,77]. The absence of longitudinal designs in several studies further hindered the verification of temporal directionality in causal relationships [10,13,19,29,54,74,86].

Causal Discovery-Specific Methodological Issues

The application of causal discovery algorithms revealed distinct methodological challenges. Unvalidated algorithmic assumptions were identified in 18.1% (13/72) of studies [8,9,37,43,44,48,52,57,61,71,82,87,88], compromising validity when core assumptions such as causal sufficiency and the Markov property were violated. Limited cross-disease validation [21] and insufficient external validation [59] constrained the broader applicability of findings. Additionally, overreliance on prior knowledge introduced subjectivity into the discovery process, potentially influencing causal structure learning and interpretation [24,36,74,89,90].

Proposed Methodological Improvements

To address these challenges, future research should focus on the following. First, developing confounder-robust algorithms, as demonstrated by AnchorFCI in cardiometabolic disease research [31], and integrating domain knowledge in neurodegenerative studies [10]. Second, advancing longitudinal causal discovery frameworks for irregularly sampled temporal data in EHRs, as seen in nephrotoxicity and intensive care unit studies [63,64]. Third, enabling multimodal data integration strategies, such as coupling neuroimaging with EHRs or synthesizing wearable data with clinical assessments to explore lifestyle diseases [40,49,61]. Finally, incorporating artificial intelligence (AI) architectures like large language models, deep learning, and reinforcement learning to enhance clinical interpretability and model transferability across institutions [21,25,36,42,58,67].

Discussion

Principal Findings

This scoping review represents the first systematic mapping of causal discovery algorithms in observational medical research. It synthesizes key methodological, translational, and implementation gaps across clinical and public health domains. Despite the field's nascent stage, research momentum has accelerated markedly, reflecting growing translational potential. The scarcity of qualifying studies (72 of 2296 screened) underscores both the emergent nature of these methods and the novelty of this review. Our integration of fragmented evidence establishes a foundational framework for interdisciplinary refinement, advancing beyond traditional observational research limitations and supporting the causal discovery's role in medical settings.

Translational Gaps in Application Domains

Clinical research concentrates on etiological exploration, leveraging causal graphs to deconstruct complex diseases (eg, mental health and chronic conditions). However, a severe imbalance exists between mechanism discovery and clinical decision support development (1/72, 1.4%), revealing a critical mechanism-application dissociation. This translational gap primarily stems from 4 interconnected barriers: most methods remain at the proof-of-concept stage without large-scale clinical validation, creating a fundamental trust deficit; existing tools lack seamless integration with clinical workflows and EHR systems; real-world data quality issues and computational demands hinder practical implementation; and crucially, statistically robust findings often fail to translate into clinically actionable recommendations that clinicians can readily understand and apply at the point of care. Public health applications focus on behavior interventions (eg, lifestyle-outcome linkages) and system optimization (eg, health care use patterns), but face domain-specific confounders (eg, policy shifts). Cross-domain translation requires context-adapted methodological frameworks.

Methodological Challenges to Practical Translation

Causal discovery in observational medical research remains dominated by constraint-based (eg, PC and FCI) and score-based methods (eg, GES and FGES), valued for their reliability in exploratory analysis and high-dimensional data, as well as their inherent interpretability; their graphical outputs and testable assumptions align well with clinical reasoning. However, their limitations in identifying causal directions, handling unmeasured confounding, and computational efficiency have spurred new approaches: continuous optimization (eg, NOTEARS) enhances scalability, although often at the cost of transparency; hybrid methods (eg, GFCI) improve robustness; functional models (eg, LiNGAM) enable direction identification; and time-series approaches (eg, PCMCI) capture dynamic causality. This interpretability-scalability trade-off critically guides model selection in clinical settings, where trust and actionable insight depend on understandable outputs. This evolution marks a transition toward more robust, scalable, and temporally-aware causal inference.

XSL•FO
RenderX

Unmeasured confounding remains fundamental, distorting effect estimates and causal structures. Partial ancestral graph algorithms (eg, FCI and RFCI [91]) and negative control designs [92] offer partial solutions but lack universal robustness. Small-sample limitations undermine statistical power and generalizability, particularly in rare diseases or early-phase studies. Transfer learning [93], multimodal data fusion (eg, Cov-Pneum dataset [94]), and cross-disease validation mitigate data scarcity [95], while embedding expert knowledge (eg, in Bayesian networks) reduces model uncertainty. Beyond these challenges, translating causal discovery into practice requires concerted action on 2 fronts: establishing benchmark datasets and implementing a rigorous, explainable, multitiered validation framework. We strongly recommend the curation of medical benchmark datasets derived from gold-standard sources, such as large-scale RCTs or well-validated longitudinal cohorts, to provide a critical foundation for fairly evaluating and comparing algorithms. For instance, the study by Gururaghavendran and Murray [18] used a zero placebo effect as the benchmark to compare multiple causal discovery algorithms, demonstrating that guidance from expert insight and prior knowledge significantly enhances their performance.

Explainable artificial intelligence techniques hold significant potential for improving the causal discovery process. Hasan and Gani [96] introduced a knowledge-guided causal AI system that integrates domain-specific prior knowledge as structural constraints with observational data to refine causal graph discovery. The results show that this approach also lowers computational demands while improving reliability [96]. One study introduced a new causal discovery approach, called REX, leveraging ML models coupled with interpretability techniques, showing REX's effectiveness and robustness in accurately recovering true causal structures, along with its applicability to real-world problems [97]. In addition, moving beyond theoretical sensitivity analyses, a robust validation strategy must integrate internal validation (eg, using bootstrap to assess graph stability), external validation on independent datasets, and most importantly, rigorous evaluation of biological and clinical plausibility against established knowledge or new experimental findings. This comprehensive approach is essential for bridging the current trust gap and generating clinically actionable insights.

Future Directions

To propel the field beyond current methodological constraints and accelerate clinical translation, the following strategic advancements warrant prioritized investigation:

1. Advancing temporal causal inference: integrate time-series data (eg, EHRs) with target trial emulation frameworks to resolve temporal ambiguity, mitigate time-varying confounding, and strengthen causal directionality inference [98].
2. Enabling multimodal data integration: leverage causal ML methodologies to unify heterogeneous data sources (eg, EHRs, genomics, and behavioral data), thereby facilitating robust estimation of individualized treatment effects and bridging critical evidence gaps [10,36,99].
3. Developing AI-enhanced causal discovery: synthesize deep learning (for high-dimensional feature extraction), reinforcement learning (for adaptive decision-making), and causal representation learning to enhance the accuracy, scalability, and interpretability of causal inference in complex biomedical systems [21,25,42,100].
4. Accelerating clinical translation: it is imperative to establish reproducible benchmarking frameworks and standardized reporting guidelines. We encourage journals to adopt policies that actively promote code and data availability, thereby enhancing transparency and reproducibility. The integration of sensitivity analyses into routine methodological reporting should be considered essential for evaluating the robustness of inferred causal relationships. Furthermore, the development of cross-institutional validation protocols and standardized tools that facilitate the incorporation of clinical domain knowledge into causal discovery pipelines will be critical for fostering broader clinical adoption.
5. Enhancing interpretability: improving the interpretability of causal discovery outputs and building clinical trust requires heightened methodological transparency and consistent reporting standards. The field should move toward developing domain-specific reporting guidelines for causal discovery in medicine, which would detail the algorithms used, parameter settings, and evaluation metrics. Systematically embedding interpretability-focused techniques, such as feature importance analysis or causal pathway explanation, can help bridge inferred causal structures with established clinical evidence.

Ultimately, the real-world impact of causal discovery hinges on its ability to deliver comprehensible and actionable insights that resonate with clinical researchers and practitioners. However, whether causal discovery can genuinely drive scientific progress, generate novel insights, and inform scholarly discourse in fields can ultimately be determined only through its repeated application in practice, coupled with rigorous and transparent reporting of the results [101].

Strengths and Limitations

This review provides a timely, comprehensive synthesis of causal discovery algorithms across diverse medical domains. Nevertheless, limitations exist: First, restricting the search to English-language publications may have excluded valuable non-English evidence. Second, our review reveals a pronounced geographic concentration of research, with the majority of studies originating from the United States and China. This likely reflects disparities in access to large-scale digital health infrastructure, advanced computational resources, and targeted research funding. Consequently, the current evidence base and its associated methodological trends may not be fully representative of global research activity or directly generalizable to health care settings in other regions. Third, the search was conducted within biomedical databases and relied on a core set of terms centered on "causal discovery." While this approach efficiently captured studies self-identifying with this paradigm, it is possible that some relevant applications published under different terminology (eg, "Bayesian network structure learning") in computational science venues were not retrieved. Finally, while we mapped application breadth, a formal assessment of reporting quality or bias risk was not

XSL•FO
RenderX

conducted; future work should implement standardized appraisal tools to systematically evaluate methodological rigor.

Conclusions

Causal discovery is emerging as a pivotal approach in medical observational research, offering transformative potential for etiological exploration and clinical decision-making. However, critical barriers impede clinical translation, notably the absence of standardized validation frameworks and persistent confounding. Future progress necessitates rigorous evaluation standards and AI-causal methodology integration to enable robust, generalizable real-world decision support.

Acknowledgments

In accordance with journal policy, we confirm that no generative artificial intelligence tools were used in the writing of this manuscript or in the generation of its scientific content. Artificial intelligence–assisted tools were used solely for minor language polishing and proofreading. All conceptualization, analysis, intellectual interpretation, and authorship of the final manuscript are solely attributable to the human authors.

Data Availability

All data generated or analyzed during this study are included in this published article and Multimedia Appendices 1-2.

Funding

This study was supported by the National Natural Science Foundation of China (grant numbers 82360667 and 82160645), the Natural Science Foundation of Jiangxi Province (grant number 20212BAB206091), and the National Undergraduate Training Program for Innovation and Entrepreneurship (grant number 202510403077).

Authors' Contributions

JK and JL were involved in the concept and design of the review. ZL, TL, HM, JM, XY, and ZH made major contributions to literature search, data collection, data analysis, and data interpretation. ZL and JK wrote and edited the manuscript. All authors read and approved the final manuscript.

JK and JL are co-corresponding authors of this paper. JL can be reached at ljk545464@163.com.

Conflicts of Interest

None declared.

Multimedia Appendix 1
PRISMA-ScR checklist.
[DOCX File , 72 KB - medinform_v14i1e82499_app1.docx]

Multimedia Appendix 2
Queries used for the database search.
[DOCX File , 19 KB - medinform_v14i1e82499_app2.docx]

References

1. Hernán MA. The c-word: scientific euphemisms do not improve causal inference from observational data. Am J Public Health 2018;108(5):616-619. [doi: 10.2105/AJPH.2018.304337] [Medline: 29565659]
2. Nogueira AR, Pugnana A, Ruggieri S, Pedreschi D, Gama J. Methods and tools for causal discovery and causal inference. WIREs Data Min Knowl Discov 2022;12(2):e1449. [doi: 10.1002/widm.1449]
3. Spirtes P, Zhang K. Causal discovery and inference: concepts and recent methodological advances. Appl Inform (Berl) 2016;3:3 [FREE Full text] [doi: 10.1186/s40535-016-0018-x] [Medline: 27195202]
4. Peters J, Janzing D, Schölkopf B. Elements of Causal Inference: Foundations and Learning Algorithms. In: Computer Reviews. Cambridge: The MIT Press; 2017.
5. Spirtes P, Glymour C, Scheines R. Causation, Prediction, and Search. Cambridge, MA: MIT Press; 2000.
6. Kaufman H, Rappoport N, Gilad A, Linial M. Advancing causal inference in medicine using biobank data. J Biomed Inform 2025;171:104903. [doi: 10.1016/j.jbi.2025.104903] [Medline: 40953713]
7. Bothwell LE, Greene JA, Podolsky SH, Jones DS. Assessing the gold standard--lessons from the history of RCTs. N Engl J Med 2016;374(22):2175-2181. [doi: 10.1056/NEJMms1604593] [Medline: 27248626]
8. Petrungaro B, Kitson NK, Constantinou AC. Investigating potential causes of sepsis with bayesian network structure learning. Appl Intell 2025;55(7):17. [doi: 10.1007/s10489-025-06405-5]

XSL•FO
RenderX

9. Penson A, Bucur IG, Walraven I, Grootenhuis MA, Maurice-Stam H, van der Heiden-van der Loo M, et al. Structural equation modeling to explore putative causal factors for chronic fatigue in childhood cancer survivors: a DCCSS LATER study. J Cancer Surviv 2025. [doi: 10.1007/s11764-024-01738-5] [Medline: 40019719]
10. Yu X, Lophatananon A, Holmes V, Muir KR, Guo H. Investigating causal networks of dementia using causal discovery and natural language processing models. NPJ Dement 2025;1(1):4. [doi: 10.1038/s44400-025-00006-2] [Medline: 40351535]
11. Bernasconi A, Zanga A, Lucas PJF, Scutari M, Trama A, Stella F. A causal network model to estimate the cardiotoxic effect of oncological treatments in young breast cancer survivors. Prog Artif Intell 2024. [doi: 10.1007/s13748-024-00348-7]
12. Ganopoulou M, Kangelidis I, Sianos G, Angelis L. Causal models for the result of percutaneous coronary intervention in coronary chronic total occlusions. Applied Sciences 2021;11(19):9258. [doi: 10.3390/app11199258]
13. Giuliani L, Sanmarchi F, Mucci A, Rucci P, Caporusso E, Bucci P, et al. Investigating the causal pathways among psychopathological variables, cognitive impairment, and real-life functioning in people with schizophrenia. Schizophrenia (Heidelb) 2025;11(1):1 [FREE Full text] [doi: 10.1038/s41537-024-00545-2] [Medline: 39753575]
14. Ribeiro-Dantas MDC, Li H, Cabeli V, Dupuis L, Simon F, Hettal L, et al. Learning interpretable causal networks from very large datasets, application to 400,000 medical records of breast cancer patients. iScience 2024;27(5):109736 [FREE Full text] [doi: 10.1016/j.isci.2024.109736] [Medline: 38711452]
15. Arksey H, O'Malley L. Scoping studies: towards a methodological framework. Int J Soc Res Methodol 2005;8(1):19-32. [doi: 10.1080/1364557032000119616]
16. Tricco AC, Lillie E, Zarin W, O'Brien KK, Colquhoun H, Levac D, et al. PRISMA extension for scoping reviews (PRISMA-ScR): checklist and explanation. Ann Intern Med 2018;169(7):467-473 [FREE Full text] [doi: 10.7326/M18-0850] [Medline: 30178033]
17. Ouzzani M, Hammady H, Fedorowicz Z, Elmagarmid A. Rayyan-a web and mobile app for systematic reviews. Syst Rev 2016;5(1):210 [FREE Full text] [doi: 10.1186/s13643-016-0384-4] [Medline: 27919275]
18. Gururaghavendran R, Murray EJ. Can algorithms replace expert knowledge for causal inference? A case study on novice use of causal discovery. Am J Epidemiol 2025;194(5):1399-1409. [doi: 10.1093/aje/kwae338] [Medline: 39218433]
19. Li C, Wang S, Xia Y, Shi F, Tang L, Yang Q, et al. Risk factors and predictive models in the progression from MCI to alzheimer's disease. Neuroscience 2025;565:312-319. [doi: 10.1016/j.neuroscience.2024.11.056] [Medline: 39645072]
20. Korvink M, Biondolillo M, Van Dijk JW, Banerjee A, Simenz C, Nelson D. Detection of potential causal pathways among social determinants of health: a data-informed framework. Soc Sci Med 2025;373:118025. [doi: 10.1016/j.socscimed.2025.118025] [Medline: 40164049]
21. Noh MJ, Kim YS. Diabetes prediction through linkage of causal discovery and inference model with machine learning models. Biomedicines 2025;13(1):124 [FREE Full text] [doi: 10.3390/biomedicines13010124] [Medline: 39857708]
22. Tseng A, Francis SM, Rawls E, Conelea C, Grissom NM, Kummerfeld E, et al. Integrating causal discovery and clinically-relevant insights to explore directional relationships between autistic features, sex at birth, and cognitive abilities. Psychol Med 2025;55:e89. [doi: 10.1017/S0033291725000571] [Medline: 40098476]
23. Bronstein MV, Kummerfeld E, Bearden CE, Cornblatt BA, Walker EF, Woods SW, et al. Delineating empirically plausible causal pathways to suicidality among people at clinical high risk for psychosis. J Psychopathol Clin Sci 2025;134(3):239-250. [doi: 10.1037/abn0000969] [Medline: 39913476]
24. Colineaux H, Lepage B, Chauvin P, Dimeglio C, Delpierre C, Lefèvre T. Contribution of structure learning algorithms in social epidemiology: application to real-world data. Int J Environ Res Public Health 2025;22(3):348 [FREE Full text] [doi: 10.3390/ijerph22030348] [Medline: 40238329]
25. Fay L, Hepp T, Winkelmann MT, Peters A, Heier M, Niendorf T, et al. Determinants of ascending aortic morphology: cross-sectional deep learning-based analysis on 25 073 non-contrast-enhanced NAKO MRI studies. Eur Heart J Cardiovasc Imaging 2025;26(5):895-907. [doi: 10.1093/ehjci/jeaf081] [Medline: 40052574]
26. Fu M, Sankararaman S, Vossel KA, Chang TS. Identifying common disease trajectories of progressive supranuclear palsy with electronic health records. Mov Disord Clin Pract 2025;12(10):1528-1538. [doi: 10.1002/mdc3.70119] [Medline: 40344390]
27. Verveen A, Nugroho FA, Bucur IG, Wynberg E, van Willigen HDG, Davidovich U, et al. Long-term sequelae of SARS-CoV-2 two years following infection: exploring the interplay of biological, psychological, and social factors. Psychol Med 2024;54(15):1-11. [doi: 10.1017/S0033291724002721] [Medline: 39618323]
28. Ren S, Beeche CA, Iyer K, Shi Z, Auster Q, Hawkins JM, et al. Graphical modeling of causal factors associated with the postoperative survival of esophageal cancer subjects. Med Phys 2024;51(3):1997-2006. [doi: 10.1002/mp.16656] [Medline: 37523254]
29. Guo X, Wang L, Li Z, Feng Z, Lu L, Jiang L, et al. Factors and pathways of non-suicidal self-injury in children: insights from computational causal analysis. Front Public Health 2024;12:1305746 [FREE Full text] [doi: 10.3389/fpubh.2024.1305746] [Medline: 38532971]
30. Foraita R, Witte J, Börnhorst C, Gwozdz W, Pala V, Lissner L, et al. A longitudinal causal graph analysis investigating modifiable risk factors and obesity in a European cohort of children and adolescents. Sci Rep 2024;14(1):6822 [FREE Full text] [doi: 10.1038/s41598-024-56721-y] [Medline: 38514750]

XSL•FO
RenderX

31. Ribeiro AH, Crnkovic M, Pereira JL, Fisberg RM, Sarti FM, Rogero MM, et al. AnchorFCI: harnessing genetic anchors for enhanced causal discovery of cardiometabolic disease pathways. Front Genet 2024;15:1436947 [FREE Full text] [doi: 10.3389/fgene.2024.1436947] [Medline: 39717478]
32. Sabzevar S, Masoudnia S, Araabi BN, Nazemzadeh M, Tavakoli H. Enhanced diagnosis of schizophrenia using integrated node embedding and causal discovery on imbalanced fMRI data. 2024 Presented at: Proceedings of the 10th International Conference on Signal Processing and Intelligent Systems (ICSPIS) 2024; December 25-26, 2024; Shahrood, Iran p. 234-239. [doi: 10.1109/icspis65223.2024.10931071]
33. Zhang M, Zhang X, Dai M, Wu L, Liu K, Wang H, et al. Development and validation of a multi-causal investigation and discovery framework for knowledge harmonization (MINDMerge): A case study with acute kidney injury risk factor discovery using electronic medical records. Int J Med Inform 2024;191:105588. [doi: 10.1016/j.ijmedinf.2024.105588] [Medline: 39128399]
34. Li Y, Scheel-Sailer A, Riener R, Paez-Granados D. Mixed-variable graphical modeling framework towards risk prediction of hospital-acquired pressure injury in spinal cord injury individuals. Sci Rep 2024;14(1):25067 [FREE Full text] [doi: 10.1038/s41598-024-75691-9] [Medline: 39443567]
35. Kazemi K, Ryhta I, Azimi I, Niela-Vilen H, Axelin A, Rahmani AM, et al. Impact of physical activity on quality of life during pregnancy: a causal ML approach. Annu Int Conf IEEE Eng Med Biol Soc 2024;2024:1-6. [doi: 10.1109/EMBC53108.2024.10782584] [Medline: 40040140]
36. Naik N, Khandelwal A, Joshi M, Atre M, Wright H, Kannan K. Applying large language models for causal structure learning in non small cell lung cancer. 2024 Presented at: Proceedings of the IEEE 12th International Conference on Healthcare Informatics (ICHI); June 3-6, 2024; Orlando, FL p. 688-693. [doi: 10.1109/ichi61247.2024.00110]
37. McCormick KM, Ribeiro Santiago PH, Jamieson L. The impact of COVID-19 on the oral health self-care practices of Australian adults. J Public Health (Berl.) 2024 Jun 05;34(3):525-534. [doi: 10.1007/s10389-024-02287-y]
38. Zeng W, Thatayatikom A, Winn N, Lovelace TC, Bhattacharyya I, Schrepfer T, et al. The Florida scoring system for stratifying children with suspected Sjögren's disease: a cross-sectional machine learning study. Lancet Rheumatol 2024;6(5):e279-e290. [doi: 10.1016/S2665-9913(24)00059-6] [Medline: 38658114]
39. Tosaki T, Uchino E, Harada Y, Sakuragi M, Koyanagi Y, Okajima S. Subgrouping causal networks of disease onset in large-scale health and medical data using supercomputer Fugaku. 2024 Presented at: Proceedings of the IEEE International Conference on Bioinformatics and Biomedicine (BIBM); December 3-6, 2024; Lisbon, Portugal p. 4384-4391. [doi: 10.1109/bibm62325.2024.10822105]
40. Zhang J, Cong R, Deng O, Li Y, Lam K, Jin Q. Analyzing lifestyle and behavior with causal discovery in health data from wearable devices and self-assessments. 2024 Presented at: Proceedings of the IEEE International Conference on E-Health Networking, Application and Services, HealthCom 2024; November 18-20, 2024; Nara. [doi: 10.1109/healthcom60970.2024.10880758]
41. Gąsior JS, Młyńczak M, Williams CA, Popłonyk A, Kowalska D, Giezek P, et al. The discovery of a data-driven causal diagram of sport participation in children and adolescents with heart disease: a pilot study. Front Cardiovasc Med 2023;10:1247122 [FREE Full text] [doi: 10.3389/fcvm.2023.1247122] [Medline: 38075979]
42. Gao XE, Hu JG, Chen B, Wang YM, Zhou SB. Causal discovery approach with reinforcement learning for risk factors of type II diabetes mellitus. BMC Bioinformatics 2023;24(1):296 [FREE Full text] [doi: 10.1186/s12859-023-05405-x] [Medline: 37480046]
43. Lee JJR, Srinivasan R, Ong CS, Alejo D, Schena S, Shpitser I, et al. Causal determinants of postoperative length of stay in cardiac surgery using causal graphical learning. J Thorac Cardiovasc Surg 2023;166(5):e446-e462 [FREE Full text] [doi: 10.1016/j.jtcvs.2022.08.012] [Medline: 36154975]
44. Thomas A, Niranjan M, Legg J. Causal analysis of physiological sleep data using granger causality and score-based structure learning. Sensors (Basel) 2023;23(23):9455 [FREE Full text] [doi: 10.3390/s23239455] [Medline: 38067827]
45. Vowels LM, Vowels MJ, Carnelley KB, Millings A, Gibson-Miller J. Toward a causal link between attachment styles and mental health during the COVID-19 pandemic. Br J Clin Psychol 2023;62(3):605-620 [FREE Full text] [doi: 10.1111/bjc.12428] [Medline: 37300241]
46. Pierce B, Kirsh T, Ferguson AR, Neylan TC, Ma S, Kummerfeld E, et al. Causal discovery replicates symptomatic and functional interrelations of posttraumatic stress across five patient populations. Front Psychiatry 2022;13:1018111 [FREE Full text] [doi: 10.3389/fpsyt.2022.1018111] [Medline: 36793783]
47. Lee K, Kummerfeld E, Robinson E, Anderson L, Rantz M. Data-driven analytics to discover APRN's impact on nursing home hospitalization: causal discovery analysis. J Am Med Dir Assoc 2023;24(11):1746-1754. [doi: 10.1016/j.jamda.2023.05.003] [Medline: 37302798]
48. Andersen TO, Sejling C, Jensen AK, Drews HJ, Ritz B, Varga TV, et al. Nighttime smartphone use, sleep quality, and mental health: investigating a complex relationship. Sleep 2023;46(12):zsad256. [doi: 10.1093/sleep/zsad256] [Medline: 37758231]
49. Li YX, Deng O, Ogihara A, Nishimura S, Jin Q. Causal discovery of health features from wearable device and traditional Chinese medicine diagnosis data. 2023 Presented at: Proceedings of the 25th International Conference on Human-Computer Interaction, HCI International 2023; July 23, 2023; Copenhagen, Denmark p. 556-569. [doi: 10.1007/978-3-031-48041-6_37]

XSL•FO
RenderX

50. Park CH, Kwon J, Lee JT, Ahn S. Impact of criterion versus norm-referenced assessment on the quality of life in Korean medical students. J Korean Med Sci 2023;38(17):e133 [FREE Full text] [doi: 10.3346/jkms.2023.38.e133] [Medline: 37128877]
51. Miley K, Meyer-Kalos P, Ma S, Bond DJ, Kummerfeld E, Vinogradov S. Causal pathways to social and occupational functioning in the first episode of schizophrenia: uncovering unmet treatment needs. Psychol Med 2023;53(5):2041-2049 [FREE Full text] [doi: 10.1017/S0033291721003780] [Medline: 37310333]
52. Li X, Qian XL, Liang LT, Kong LJ, Dong QL, Chen JJ. Causally-aware intraoperative imputation for overall survival time prediction. 2023 Presented at: Proceedings of the IEEE/CVF Conference on Computer Vision and Pattern Recognition (CVPR); June 17-24, 2023; Vancouver, BC p. 15681-15690. [doi: 10.1109/cvpr52729.2023.01505]
53. Nagaraj S, Goodday S, Hartvigsen T, Boch A, Garg K, Gowda S, et al. Dissecting the heterogeneity of "in the wild" stress from multimodal sensor data. NPJ Digit Med 2023 Dec 20;6(1):237. [doi: 10.1038/s41746-023-00975-9] [Medline: 38123810]
54. Vigneshwaran V, Wilms M, Forkert ND. The causal link between cardiometabolic risk factors and gray matter atrophy: an exploratory study. Heliyon 2023;9(11):e21567 [FREE Full text] [doi: 10.1016/j.heliyon.2023.e21567] [Medline: 38027770]
55. Petersen AH, Ekstrøm CT, Spirtes P, Osler M. Constructing causal life-course models: comparative study of data-driven and theory-driven approaches. Am J Epidemiol 2023;192(11):1917-1927 [FREE Full text] [doi: 10.1093/aje/kwad144] [Medline: 37344193]
56. Fung H, Sgaier SK, Huang VS. Discovery of interconnected causal drivers of COVID-19 vaccination intentions in the US using a causal Bayesian network. Sci Rep 2023 May 16;13(1):6988. [doi: 10.1038/s41598-023-33745-4] [Medline: 37193707]
57. Bao L, Li C, Li R, Yang S. Causal structural learning on MPHIA individual dataset. J Am Stat Assoc 2022;117(540):1642-1655 [FREE Full text] [doi: 10.1080/01621459.2022.2077209] [Medline: 36620488]
58. Singh H, Mhasawade V, Chunara R. Generalizability challenges of mortality risk prediction models: a retrospective analysis on a multi-center database. PLOS Digit Health 2022;1(4):e0000023 [FREE Full text] [doi: 10.1371/journal.pdig.0000023] [Medline: 36812510]
59. Langwerden RJ, Van der Heijden PT, Claassen T, Derksen JJL, Egger JIM. The structure of dimensions of psychopathology in normative and clinical samples: applying causal discovery to MMPI-2-RF scales to investigate clustering of psychopathology spectra and -factors. Front Psychiatry 2022;13:1026900 [FREE Full text] [doi: 10.3389/fpsyt.2022.1026900] [Medline: 36440421]
60. Bronstein MV, Everaert J, Kummerfeld E, Haynos AF, Vinogradov S. Biased and inflexible interpretations of ambiguous social situations: associations with eating disorder symptoms and socioemotional functioning. Int J Eat Disord 2022;55(4):518-529 [FREE Full text] [doi: 10.1002/eat.23688] [Medline: 35132668]
61. Shen X, Raghavan S, Przybelski SA, Lesnick TG, Ma S, Reid RI, et al. Causal structure discovery identifies risk factors and early brain markers related to evolution of white matter hyperintensities. Neuroimage Clin 2022;35:103077 [FREE Full text] [doi: 10.1016/j.nicl.2022.103077] [Medline: 35696810]
62. Mouches P, Wilms M, Bannister JJ, Aulakh A, Langner S, Forkert ND. An exploratory causal analysis of the relationships between the brain age gap and cardiovascular risk factors. Front Aging Neurosci 2022;14:941864 [FREE Full text] [doi: 10.3389/fnagi.2022.941864] [Medline: 36072481]
63. Zhang J, Kummerfield E, Hultman G, Drawz PE, Adam TJ, Simon G, et al. Application of causal discovery algorithms in studying the nephrotoxicity of remdesivir using longitudinal data from the EHR. AMIA Annu Symp Proc 2022;2022:1227-1236 [FREE Full text] [Medline: 37128413]
64. Nogueira AR, Ferreira CA, Gama J. Temporal nodes causal discovery for in intensive care unit survival analysis. 2022 Presented at: Proceedings of the EPIA Conference on Artificial Intelligence; August 31, 2022; Lisbon, Portugal p. 587-598. [doi: 10.1007/978-3-031-16474-3_48]
65. Rawls E, Kummerfeld E, Zilverstand A. An integrated multimodal model of alcohol use disorder generated by data-driven causal discovery analysis. Commun Biol 2021;4(1):435 [FREE Full text] [doi: 10.1038/s42003-021-01955-z] [Medline: 33790384]
66. Li Z, Xu T, Zhang K, Deng HW, Boerwinkle E, Xiong M. Causal analysis of health interventions and environments for influencing the spread of COVID-19 in the United States of America. Front Appl Math Stat 2021;6:611805. [doi: 10.3389/fams.2020.611805]
67. Shen X, Ma S, Vemuri P, Castro MR, Caraballo PJ, Simon GJ. A novel method for causal structure discovery from EHR data and its application to type-2 diabetes mellitus. Sci Rep 2021;11(1):21025 [FREE Full text] [doi: 10.1038/s41598-021-99990-7] [Medline: 34697394]
68. Petersen AH, Osler M, Ekstrøm CT. Data-driven model building for life-course epidemiology. Am J Epidemiol 2021;190(9):1898-1907. [doi: 10.1093/aje/kwab087] [Medline: 33778840]
69. Wang W, Hu G, Yuan B, Ye S, Chen C, Cui Y, et al. Prior-knowledge-driven local causal structure learning and its application on causal discovery between type 2 diabetes and bone mineral density. IEEE Access 2020;8:108798-108810. [doi: 10.1109/access.2020.2994936]

XSL•FO
RenderX

70. Saxe GN, Ma S, Morales LJ, Galatzer-Levy IR, Aliferis C, Marmar CR. Computational causal discovery for post-traumatic stress in police officers. Transl Psychiatry 2020;10(1):233 [FREE Full text] [doi: 10.1038/s41398-020-00910-6] [Medline: 32778671]
71. Schoenmacker GH, Groenman AP, Sokolova E, Oosterlaan J, Rommelse N, Roeyers H, et al. Role of conduct problems in the relation between attention-deficit hyperactivity disorder, substance use, and gaming. Eur Neuropsychopharmacol 2020;30:102-113. [doi: 10.1016/j.euroneuro.2018.06.003] [Medline: 30292416]
72. Ahangaran M, Jahed-Motlagh MR, Minaei-Bidgoli B. A novel method for predicting the progression rate of ALS disease based on automatic generation of probabilistic causal chains. Artif Intell Med 2020;107:101879. [doi: 10.1016/j.artmed.2020.101879] [Medline: 32828438]
73. Wang Y, You L, Chyr J, Lan L, Zhao W, Zhou Y, et al. Causal discovery in radiographic markers of knee osteoarthritis and prediction for knee osteoarthritis severity with attention-long short-term memory. Front Public Health 2020;8:604654 [FREE Full text] [doi: 10.3389/fpubh.2020.604654] [Medline: 33409263]
74. Shen X, Ma S, Vemuri P, Simon G, Alzheimer's Disease Neuroimaging Initiative. Challenges and opportunities with causal discovery algorithms: application to Alzheimer's pathophysiology. Sci Rep 2020;10(1):2975 [FREE Full text] [doi: 10.1038/s41598-020-59669-x] [Medline: 32076020]
75. Itahashi T, Okada N, Ando S, Yamasaki S, Koshiyama D, Morita K, et al. Functional connectomes linking child-parent relationships with psychological problems in adolescence. Neuroimage 2020;219:117013 [FREE Full text] [doi: 10.1016/j.neuroimage.2020.117013] [Medline: 32504815]
76. Ahangaran M, Jahed-Motlagh MR, Minaei-Bidgoli B. Causal discovery from sequential data in ALS disease based on entropy criteria. J Biomed Inform 2019;89:41-55 [FREE Full text] [doi: 10.1016/j.jbi.2018.10.004] [Medline: 30339928]
77. Yang J, Li N, Fang S, Yu K, Chen Y. Semantic features prediction for pulmonary nodule diagnosis based on online streaming feature selection. IEEE Access 2019;7:61121-61135. [doi: 10.1109/access.2019.2903682]
78. Chen W, Hu Y, Zhang X, Wu L, Liu K, He J, et al. Causal risk factor discovery for severe acute kidney injury using electronic health records. BMC Med Inform Decis Mak 2018;18(Suppl 1):13 [FREE Full text] [doi: 10.1186/s12911-018-0597-7] [Medline: 29589567]
79. Galatzer-Levy IR, Ma S, Statnikov A, Yehuda R, Shalev AY. Utilization of machine learning for prediction of post-traumatic stress: a re-examination of cortisol in the prediction and pathways to non-remitting PTSD. Transl Psychiatry 2017;7(3):e0 [FREE Full text] [doi: 10.1038/tp.2017.38] [Medline: 28323285]
80. Sokolova E, Oerlemans AM, Rommelse NN, Groot P, Hartman CA, Glennon JC, et al. A causal and mediation analysis of the comorbidity between attention deficit hyperactivity disorder (ADHD) and autism spectrum disorder (ASD). J Autism Dev Disord 2017;47(6):1595-1604 [FREE Full text] [doi: 10.1007/s10803-017-3083-7] [Medline: 28255761]
81. van Dijk MJAM, Claassen T, Suwartono C, van der Veld WM, van der Heijden PT, Hendriks MPH. Evaluating WAIS-IV structure through a different psychometric lens: structural causal model discovery as an alternative to confirmatory factor analysis. Clin Neuropsychol 2017;31(6-7):1141-1154. [doi: 10.1080/13854046.2017.1352029] [Medline: 28726544]
82. Ribeiro Santiago PH, Smithers L, Townsend M, Quintero A, Sawyer A, Soares G, et al. The longitudinal network of peer problems and emotional symptoms among Australian adolescents: Bayesian structure learning of directed acyclic graphs. Dev Psychol 2025;61(8):1479-1494. [doi: 10.1037/dev0001915] [Medline: 39869684]
83. Cheek C, Zheng H, Hallstrom BR, Hughes RE. Application of a causal discovery algorithm to the analysis of arthroplasty registry data. Biomed Eng Comput Biol 2018;9:1179597218756896 [FREE Full text] [doi: 10.1177/1179597218756896] [Medline: 29511363]
84. Bilgel F, Karahasan BC. Understanding covid-19 mobility through human capital: a unified causal framework. Comput Econ 2023:1-41 [FREE Full text] [doi: 10.1007/s10614-023-10359-6] [Medline: 36844967]
85. Młyńczak M, Krysztofiak H. Discovery of causal paths in cardiorespiratory parameters: a time-independent approach in elite athletes. Front Physiol 2018;9:1455 [FREE Full text] [doi: 10.3389/fphys.2018.01455] [Medline: 30425645]
86. Constantinou A, Kitson NK, Liu Y, Chobtham K, Amirkhizi AH, Nanavati PA, et al. Open problems in causal structure learning: a case study of COVID-19 in the UK. Expert Syst Appl 2023;234:121069. [doi: 10.1016/j.eswa.2023.121069]
87. Huie JR, Vashisht R, Galivanche A, Hadjadj C, Morshed S, Butte AJ, et al. Toward a causal model of chronic back pain: challenges and opportunities. Front Comput Neurosci 2022;16:1017412 [FREE Full text] [doi: 10.3389/fncom.2022.1017412] [Medline: 36714527]
88. Anderson LM, Lim KO, Kummerfeld E, Crosby RD, Crow SJ, Engel SG, et al. Causal discovery analysis: a promising tool in advancing precision medicine for eating disorders. Int J Eat Disord 2023;56(11):2012-2021. [doi: 10.1002/eat.24040] [Medline: 37548100]
89. Tao Z, Chi M, Chen L, Ban T, Tu Q, Gao F, et al. Clinical causal analysis via iterative active structure learning. Memetic Comp 2025;17(1):13. [doi: 10.1007/s12293-025-00439-5]
90. Jin W, Ni Y, Spence AB, Rubin LH, Xu Y. Directed cyclic graphs for simultaneous discovery of time-lagged and instantaneous causality from longitudinal data using instrumental variables. J Mach Learn Res 2025;26:22. [Medline: 41394884]
91. Colombo D, Maathuis MH, Kalisch M, Richardson TS. Learning high-dimensional directed acyclic graphs with latent and selection variables. Ann Statist 2012;40(1):294-321. [doi: 10.1214/11-aos940]

XSL•FO
RenderX

92. Lipsitch M, Tchetgen Tchetgen E, Cohen T. Negative controls: a tool for detecting confounding and bias in observational studies. Epidemiology 2010;21(3):383-388 [FREE Full text] [doi: 10.1097/EDE.0b013e3181d61eeb] [Medline: 20335814]
93. Taghados Z, Azimifar Z, Monsefi M, Jahromi MA. CausalCervixNet: convolutional neural networks with causal insight (CICNN) in cervical cancer cell classification-leveraging deep learning models for enhanced diagnostic accuracy. BMC Cancer 2025;25(1):607 [FREE Full text] [doi: 10.1186/s12885-025-13926-2] [Medline: 40181353]
94. Agarwal S, Arya KV, Meena YK. MultiFusionNet: multilayer multimodal fusion of deep neural networks for chest X-ray image classification. Soft Comput 2024;28(19):11535-11551. [doi: 10.1007/s00500-024-09901-x]
95. Tang X, Guo R, Mo Z, Fu W, Qian X. Causality-driven candidate identification for reliable DNA methylation biomarker discovery. Nat Commun 2025;16(1):680 [FREE Full text] [doi: 10.1038/s41467-025-56054-y] [Medline: 39814752]
96. Hasan U, Gani M. A knowledge-guided framework to enhance causal reasoning and human-AI collaboration. : IEEE; 2025 Presented at: Proceedings of the IEEE International Conference on Pervasive Computing and Communications Workshops and other Affiliated Events (PerCom Workshops); March 7-21, 2025; Washington DC, DC, USA. [doi: 10.1109/percomworkshops65533.2025.00041]
97. Renero J, Maestre R, Ochoa I. ReX: causal discovery based on machine learning and explainability techniques. Pattern Recognition 2026;172:112491. [doi: 10.1016/j.patcog.2025.112491]
98. Hernán MA, Robins JM. Using big data to emulate a target trial when a randomized trial is not available. Am J Epidemiol 2016;183(8):758-764 [FREE Full text] [doi: 10.1093/aje/kwv254] [Medline: 26994063]
99. Weberpals J, Feuerriegel S, van der Schaar M, Kehl KL. Opportunities for causal machine learning in precision oncology. NEJM AI 2025;2(8):AIp2500277. [doi: 10.1056/aip2500277]
100. Jiao L, Wang Y, Liu X, Li L, Liu F, Ma W, et al. Causal inference meets deep learning: a comprehensive survey. Research (Wash D C) 2024;7:0467 [FREE Full text] [doi: 10.34133/research.0467] [Medline: 39257419]
101. Petersen AH, Ekstrøm CT, Spirtes P, Osler M. Causal discovery and epidemiology: a potential for synergy. Am J Epidemiol 2024;193(10):1341-1342. [doi: 10.1093/aje/kwae101] [Medline: 38825335]

Abbreviations

AI: artificial intelligence
EHR: electronic health record
FCI: fast causal inference
GFCI: greedy fast causal inference
ML: machine learning
PC: Peter-Clark algorithm
PRISMA-ScR: Preferred Reporting Items for Systematic Reviews and Meta-Analyses extension for Scoping Reviews
RCT: randomized controlled trial

Edited by A Coristine; submitted 15.Aug.2025; peer-reviewed by JMI Arockiasamy, C Ma; comments to author 26.Oct.2025; revised version received 16.Feb.2026; accepted 19.Feb.2026; published 13.Mar.2026.

Please cite as:
Liu Z, Luo T, Ma H, Mo J, Yang X, Huang Z, Li J, Kuang J
Causal Discovery in Observational Medical Research: Scoping Review
JMIR Med Inform 2026;14:e82499
URL: https://medinform.jmir.org/2026/1/e82499
doi:10.2196/82499
PMID:

©Zuting Liu, Tian Luo, Hailin Ma, Jiali Mo, Xia Yang, Zhenglong Huang, Jingkun Li, Jie Kuang. Originally published in JMIR Medical Informatics (https://medinform.jmir.org), 13.Mar.2026. This is an open-access article distributed under the terms of the Creative Commons Attribution License (https://creativecommons.org/licenses/by/4.0/), which permits unrestricted use, distribution, and reproduction in any medium, provided the original work, first published in JMIR Medical Informatics, is properly cited. The complete bibliographic information, a link to the original publication on https://medinform.jmir.org/, as well as this copyright and license information must be included.

XSL•FO
RenderX

Developing Clinical Decision (Support) Systems Combining the Scientific and Regulatory Perspective: European Insights on Challenges, Requirements, and Practical Guidance

Sanne E W Vrijlandt[1], MD; Sanne W C M Janssen[2], MD; Annemarie M C van Rossum[2], Prof Dr; Niek B Achten[3], PhD; Rianne Oostenbrink[1], PhD

[1]Department of Pediatrics, Division of General Pediatrics, Erasmus MC-Sophia Children's Hospital, University Medical Center, Dr. Molewaterplein 40, Rotterdam, The Netherlands

[2]Department of Pediatrics, Division of Pediatric Infectious Diseases and Immunology, Erasmus MC-Sophia Children's Hospital, University Medical Center, Rotterdam, The Netherlands

[3]Department of Pediatrics, Erasmus MC-Sophia Children's Hospital, University Medical Center, Rotterdam, The Netherlands

Corresponding Author:
Rianne Oostenbrink, PhD
Department of Pediatrics, Division of General Pediatrics, Erasmus MC-Sophia Children's Hospital, University Medical Center, Dr. Molewaterplein 40, Rotterdam, The Netherlands

Abstract

Clinical decision-making is a critical process where physicians balance risks and benefits. Clinical Decision Support Systems (CDSSs) are increasingly used to help in this process. The regulatory landscape for CDSSs is evolving significantly, with the new European Medical Device Regulation (MDR) now requiring, CE certification for certain CDSSs. This shift poses challenges for health care providers to develop CDSSs in an effective and useful manner while adhering to regulations. This viewpoint comments on diverse challenges and provides solutions to develop a reliable, well integrated and practical tool for clinical use. Using three tools (the Early Onset Sepsis Calculator, Feverkidstool, and Neonatal Procalcitonin Intervention Study algorithm) as examples, we explore the development of CDSSs across four core characteristics: scientific basis, technical aspects, safety, and sustainability. These characteristics recur across the main development processes; scientific development, regulatory assessment, and implementation in routine practice. Successful integration of CDSSs into clinical practice requires a comprehensive understanding of the interconnections between these processes. For example, decisions on algorithm validation and platform selection in the scientific process influence choices for technical safety during the regulatory process. Developers should consider both regulation requirements and clinical needs, to create CDSSs that are not only compliant but also adaptable to the rapidly changing healthcare landscape. We outline a developer's checklist, for practical guidance, but also appeal for structural support, including national protocols and dedicated hospital roles, to help developers implement CDSSs successfully.

(JMIR Med Inform 2026;14:e72809) doi:10.2196/72809

KEYWORDS

clinical decision support systems; regulatory requirements; pediatrics; infection diseases; diagnostic reasoning

Juggling Risks and Benefits Using Tools—A Doctor's Evolving Job

Clinical decision-making involves a delicate balancing act between risks and benefits. It requires the synthesis of a physician's clinical intuition with objective variables. For instance, deciding whether to start or stop antibiotic treatment in children at risk for severe bacterial infections illustrates this process. Distinguishing between early-stage bacterial illness and viral or physiological causes in neonates and febrile children is particularly challenging, and wrong decisions can have fatal consequences. To aid in making accurate decisions, clinicians may use clinical decision support systems (CDSSs). As these tools become more integral to clinical practice, the regulatory framework governing them is evolving, with significant implications for their development and implementation.

Until 2017, European regulations allowed CDSSs to be used without Conformité Européenne (CE) certification under the Medical Device Directive. However, the introduction of the Medical Device Regulation (MDR) (Textbox 1) expanded the definition of medical devices to include CDSSs [1]. The MDR's implementation has made CE certification more stringent, linking it directly to a CDSS's risk classification (Figure 1) [2]. For instance, any CDSS classified from Class II onwards now requires approval from a notified body. Proper classification is the responsibility of the developer. And using only CE-certified CDSSs is the responsibility of the user. Currently, a transition period allows for the legal use of both CE-certified and noncertified CDSSs until 2028. After this period, hospitals and

XSL•FO
RenderX

healthcare professionals will bear the responsibility for verifying the certification status of CDSSs used in practice. To aid this verification process, certified devices will be listed in the European Database on Medical Devices (EUDAMED), creating a centralized repository for medical devices used within the European Union.

Textbox 1. Highlights from the Medical Device Regulation (MDR) regulatory process

Key changes introduced by the MDR for Clinical Decision Support Systems (CDSSs):

- Risk classification: To ensure safe usage, a 4-scale classification system was added to address appropriate safety measures according to their risk. Additionally, Rule 11 of the MDR regulation states that "software intended tools to provide information which is used to take decisions with diagnosis or therapeutic purposes is classified as class IIa". As a result, CDSSs are at least classified as class IIa.
- Notified bodies: With more devices falling into higher risk classifications, including CDSSs, more devices need to be revised by notified bodies. Also, stricter requirements account for the approval of the impartial notified bodies.
- Post marketing surveillance: It is mandatory for manufacturers to actively monitor and report on the performance and safety of a device (article 10). This obligation also requires data collection post-implementation ensuring ongoing effectiveness and safety of CDSSs.
- Transparency: The MDR mandates the registration of CDSSs in the European Database on Medical Devices (EUDAMED). This is mandatory to improve insight in which tools are CE-certified by different stakeholders (regulatory authorities, manufacturers, and practitioners).

Figure 1. Medical software device classification.

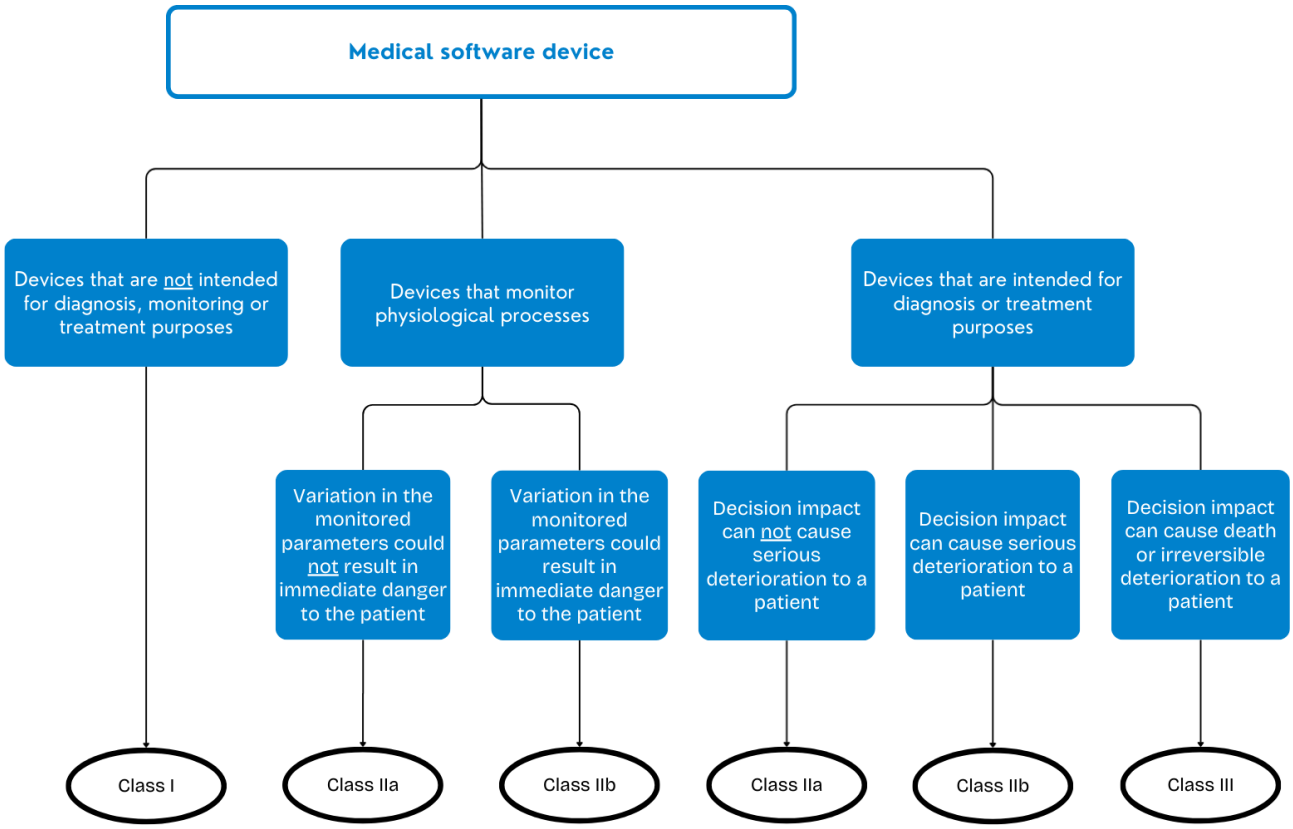

Successful adoption of CDSSs in routine practice depends on overcoming regulatory and (scientific) developmental hurdles [3]. This viewpoint addresses these obstacles and identifies key improvements needed in the development of CDSSs. While the focus is on the European regulatory environment as regulatory pathways differ across regions, for example, in the United States, where the Food and Drug Administration regulates similar tools under a different framework, some principals may be relevant internationally. Our aim is to support clinical researchers and developers who are at the early stages of CDSS development by providing early insight into the scientific and regulatory considerations that will shape the trajectory of their tool development. This viewpoint synthesizes existing requirements and real-world experiences to clarify key obstacles and areas where alignment is needed. By understanding these challenges early, developers may better anticipate what is required to progress toward successful evaluation and clinical implementation.

Learning From the Past: Exploring CDSSs With Diverse Characteristics

In this viewpoint we explore three CDSSs designed to assist in the diagnosis and management of pediatric bacterial infections: the Early Onset Sepsis (EOS) Calculator [4], the Feverkidstool (FKT) [5], and the Neonatal Procalcitonin Intervention Study (NeoPInS) algorithm [6]. We described variability in the development and functionality of the CDSSs using previously

XSL•FO
RenderX

defined characteristics, including the scientific foundation, the technical design, safety considerations, and sustainability (Table 1) [7].

XSL•FO
RenderX

Table . Key characteristics of three pediatric clinical decision support systems.

Characteristics of CDSS	Feverkidstool	EOS[a] calculator	NeoPInS[b]	Regulated by the MDR[c] [1]
Usage	Helps pediatric ED[d] physicians assess the risk of serious bacterial infection and bacterial pneumonia in febrile children (>1 mo and <18 y) presenting to the emergency department	Helps doctors and nurses estimate the risk of early-onset neonatal sepsis to guide antibiotic use and clinical management in newborns born at ≥34 weeks	Helps doctors guide the management of suspected early onset neonatal sepsis by supporting decisions on safely discontinuing g antibiotics in neonates born at ≥34 weeks of gestational age	
Scientific basis				
Scientific evidence (highest support)	Stepped-wedge cluster-randomized controlled trial	Meta-analysis and parallel cluster randomized trial	Individually randomized controlled trial	No
Current evidence/validation	(international) external validation	(international) external validation	(international) external validation	No
Reproducibility	In the application a link to the algorithm is provided	In the application a link to the algorithm is provided	No direct link to the algorithm is provided	No
Technical aspect				
CDSS[e] requirement for algorithm	Tool is required for algorithm	Tool is required for algorithm	A flowchart with reference values is sufficient	No
Platform	Web-based application; accessible through smartphone, tablet, and computer, and integration in the EHR[f]	Webbased application accessible through smart-phone, tablet, and computer, open-source Shiny application, and integration in the EHR	A smart-phone application Print out the flowchart and use it on paper	Yes
Safety				
Accuracy and reliability	Technical assessment	Technical assessment	Superior and noninferior intervention study	Yes
CE-certification	In 2024 under the Medical Device Regulation as a class IIa product	The application in 2021 under the MDD as a class Ia product. The original web-application is not CE-certified[g] by itself but covered by the EHR certification	In 2021 under the Medical Device Directive as a class Ia product	Yes
CDSS's final outcome	Risk score with advice	Risk score and prescriptive guidance	Prescriptive guidance	No
Privacy	Data is stored anonymously according to the in ISO13485 and NEN7510-1 mentioned manners	Usage is anonymous, and data is not stored (apart from general storage by using a webpage). If embedded in the EHR, privacy is guaranteed by hospital security systems	Data within the software is stored by the application supplier according to the applicable laws and regulations	Yes
Sustainability				
Funding sources for development and implementation	National funding supported by ZonMW[h] for development and implementation	Private funding by Kaiser Permanente for development and implementation. EHR implementation is provided by EHR manufacturers.	Private funding by The Thrasher Foundation, The NutsOhra Foundation and the Sophia Foundation for Scientific research for development and implementation	No
Safety monitored during usage	Clinical evaluation report and a post marketing surveillance plan	Clinical evaluation RCT[i]	Clinical evaluation RCT and superior and noninferior intervention study	Yes

[a]EOS: early onset sepsis.

[b] NeoPInS: Neonatal Procalcitonin Intervention Study.

XSL•FO
RenderX

[c]MDR: Medical Device Regulation.
[d]ED: emergency department.
[e]CDSS: clinical decision support system.
[f]EHR: electronic health record.
[g]CE: Conformité Européenne.
[h]ZonMW: the Dutch National Health Council.
[i]RCT: randomized controlled trial.

Scientific Basis

Across the three CDSSs we examined, the scientific basis emerged as a central yet variably addressed component. The tools differed in the type and strength of evidence underpinning their recommendations. The EOS Calculator mainly draws from meta-analyses of observational studies [8] with a later parallel cluster-randomized trial [9], while NeoPInS and the FKT are based on an individually randomized and stepped-wedge cluster-randomized controlled trials, respectively [6,10].

All three tools included in our analysis underwent international external validation; however, validation strategies can vary considerably, and some CDSSs rely solely on internal validation [3]. Despite the centrality of the scientific foundation, the MDR does not specify requirements for the level of evidence, leaving developers to navigate this crucial aspect independently. Both clinicians and developers should be aware that the MDR procedure does not confirm a tool's scientific validity.

Transparency also varied across tools. All three publicly display their algorithms in their initial publications [4-6], and both the EOS Calculator and FKT additionally provide algorithm access via their websites, with the EOS Calculator even providing the full algorithm directly on their website. As reproducibility of a CDSS is closely linked to algorithm transparency, this variability may have implications for independent evaluation nevertheless; transparency is not regulated by the MDR.

Finally, the scope plays a significant role in the MDR classification process, as the intended use directly affects the tool's risk classification (Figure 1). While CDSSs often focus on diagnostic support, as the EOS Calculator, FKT and NeoPINS, their scope can extend beyond diagnosis as they may offer insights into prognosis, treatment, or risk assessment.

Overall, the scientific basis, while not comprehensively covered by MDR regulations, remains critical in CDSS development. Particularly, external validity remains a key consideration, requiring careful attention during development to ensure broad adoption [11]. Moreover, the strength of the scientific foundation and the chosen validation approach influence the market scan and validation processes in the regulatory process.

Technical Aspects

In our three example tools, we observed substantial variation in how the tools were technically designed and implemented. Platforms ranged from protocol- or paper-based formats to web-based applications, mobile apps, and full integration into electronic health record (EHR) systems. The EOS Calculator and FKT both rely on more complex algorithms, requiring digital platforms, whereas NeoPInS could also be delivered in a protocol or on-paper format. Ultimately, all three tools were developed into applications to support broader clinical use. These differences illustrate how algorithm complexity and intended use shape the technical form a CDSS can realistically take.

Protocol or on-paper tools, such as NeoPInS can be embedded within clinical protocols, offering continuous access at low cost. However, they face challenges in scalability and ease of use, as manual calculations are often required. The responsibility for updates and modifications lies with individual hospitals or local departments. Importantly, on-paper tools are not directly subject to the MDR certification requirements as their use does not necessitate an additional CE-mark.

Web-based applications, such as the EOS Calculator and FKT benefit from global accessibility and ease of integration in EHRs with hyperlinks. However, reliance on web-based platforms introduces vulnerabilities like downtime and security concerns. The MDR places the certification responsibility on developers, necessitating a representative for CDSSs used within the EU but developed elsewhere [1]. The complexity increases when web-based tools developed outside the EU, such as the EOS Calculator web-based version, are accessed from inside the EU.

Mobile apps like the NeoPInS (deprecated) and EOS Calculator app (currently for research purpose in the Netherlands), offer tailored user experience on devices like smartphones or tablets. Although apps provide tailored interactions, they are costly to develop and maintain, requiring agreements on intellectual property and updates.

EHR system integration, as seen with the EOS Calculator and FKT, offers user-friendliness by aligning with existing healthcare infrastructure. While cost-effective, integration across diverse EHR systems can be complex due to the lack of a universal standard. Maintenance typically falls under the purview of EHR providers, but algorithm updates may require prior agreements as they are not automatically managed by the provider.

Taken together, our comparison shows that technical design decisions, shaped by algorithm complexity, workflow integration needs, and resource constraints, directly influence reproducibility, long-term sustainability, and regulatory obligations. Because these factors determine whether a CDSS can be reliably adopted, maintained, and scaled, they must be considered early in the development process rather than treated as secondary concerns.

Safety

Our comparison shows that safety considerations are shaped not only by the underlying data flows but also by how directive

XSL•FO
RenderX

a CDSS‘s recommendation is. Although both the FKT and EOS Calculator generate risk scores, the EOS Calculator offers more prescriptive guidance compared to the FKT. The NeoPInS, without a risk score, also provides prescriptive recommendations. These functional differences influence potential clinical risk. However, although the MDR considers intended scope for classification, it does not account for recommendation type.

Compliance with privacy regulations is mandatory, as CDSSs often handle sensitive patient data. Adherence to the MDR ensures comprehensive coverage of data privacy requirements. Privacy responsibilities also differ by platform: for the EOS Calculator and FKT embedded within an EHR, hospital security systems guarantee privacy compliance, whereas for the web applications of the three tools, the developer ensures it.

Beyond privacy, safety also depends on accuracy and reliability; this involves the technical correctness of a tool’s output and its scientific validity. A reliable CDSS consistently produces accurate results, as demonstrated by the validation in our examples. Risk assessment and mitigation strategies address potential issues such as misdiagnosis or cybersecurity threats. Developers can implement security measures like dual authentication to safeguard CDSSs against cyber threats. However, user account requirements and time-consuming login processes, as seen with the NeoPInS and FKT applications, may hinder adoption and have even led to discontinuation of the NeoPInS app.

Overall, safety is paramount for CDSSs, ensuring that these tools benefit patients without causing harm. Safety is not a single requirement but an interplay of privacy protection, accuracy, reliability, and risk mitigation, all of which require continuous monitoring throughout a CDSS’s lifecycle.

Sustainability

The sustainability of a CDSS relies on its integration into daily practice, maintenance costs, and available funding. Funding sources vary, ranging from private investors to governmental organizations and research institutions. The funding party’s priorities can influence platform choice, impacting long-term sustainability. In CDSS development, project-based funding is common, posing challenges for continued financial support once projects conclude.

Integration into the EHR, as seen for both the FKT and EOS calculator, can enhance sustainability by facilitating routine use and reducing the need for parallel systems. At the same time, embedding a CDSS within an EHR may introduce challenges related to ownership and governance, as responsibility for the tool, its maintenance, and updates can become less transparent once it is no longer managed as a standalone application. These issues are particularly relevant in the context of MDR requirements, for example post-market surveillance, which mandates ongoing monitoring and data collection after implementation. For EHR-integrated CDSSs, it may be unclear whether such responsibilities lie with the original developer, the EHR vendor, or the health care organization, potentially complicating compliance and long-term accountability.

Leveraging the Process of Developing Scientifically Valid, Regulatory Proven, and Sustainable CDSSs for Clinical Practice

From the above, we argue that the developmental processes involved integrating CDSSs into clinical practice should not be portrayed as three consecutive phases but are dynamic and interconnected in practice (Figure 2). Also, these processes are crucial in determining how effectively a CDSS can be integrated into clinical practice, ensuring that it is both reliable and useful for healthcare professionals. This requires developers to navigate them with a strategic approach. Understanding the interplay between these processes is crucial for creating CDSSs that are scientifically sound, regulatory-compliant, practically effective, and ultimately sustainable. While the MDR addresses certain aspects of these processes (eg, internal validity, market scan and justification and post marketing surveillance) it does not comprehensively regulate every characteristic (Table 1), leaving gaps that require careful consideration by developers and clinicians. To translate the lessons learned from the three CDSSs into actionable guidance, we therefore synthesized our observations into a developer’s checklist (Textbox 2), which highlights key considerations across scientific development, technical design, safety, and sustainability.

XSL•FO
RenderX

Figure 2. Processes in the clinical decision support system development. CDSS: clinical decision support system; EHR: electronic health record. *Aspects part of the Medical Device Regulation are marked with an asterisk.

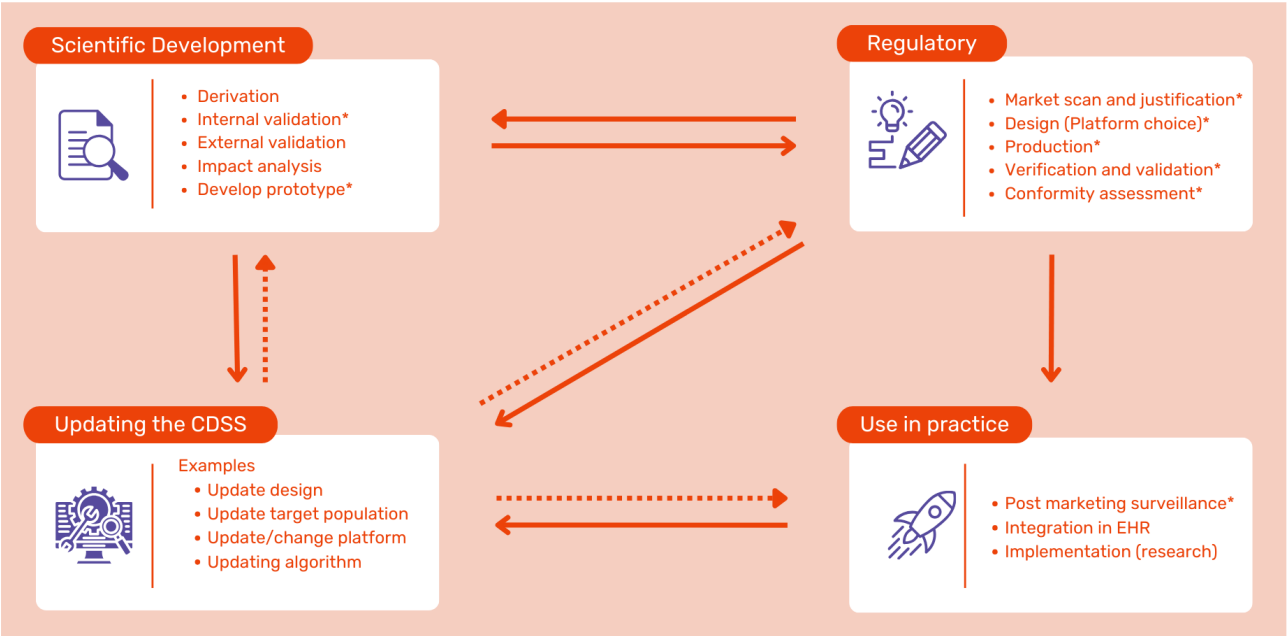

Textbox 2. Developer's checklist for a Clinical Decision Support System (CDSS).

1. Select the technical platform early and ensure it aligns with all integration and implementation requirements.
2. Engage and communicate with end-users early and throughout the development and design of the CDSS to ensure clinical workflow fits.
3. Ensure the tool's guidance matches user expectations (e.g. if it provides advice rather than full decision-making, clarify this to avoid overreliance).
4. Plan for both internal validation and external real-world testing.
5. Integrate privacy and security requirements from the earliest stage to avoid delays later.
6. Realistically estimate Conformité Européenne certification workload, expertise, and timelines.
7. Define clear ownership and a sustainable long-term maintenance plan.
8. Prepare fallback strategies to manage tool downtime safely.
9. Keep access simple (e.g. avoid unnecessary login steps).
10. Ensure full integration with existing hospital and electronic health record systems.

A critical, yet often overlooked, aspect of CDSS development is the early involvement of end-users in the scientific development process, as this can improve both tool design, effectiveness, and facilitate smoother transitions to later stages. Early strategic choices, such as selecting an appropriate technical platform, also have important downstream consequences for validity assessment and future usability. For example, although the EOS Calculator was initially developed as a web-based tool to maximize accessibility, this choice later complicated retrospective validation due to the need for manual data handling.

Validation should therefore be planned as a comprehensive, iterative process, combining internal testing with external, real-world evaluation, while accounting for the workload, expertise, and timelines required for CE certification. Beyond validation, long-term success depends on clear ownership, sustainable maintenance strategies, and predefined fallback procedures to ensure patient safety during tool downtime. Practical design considerations, such as minimizing burdensome login procedures and enabling seamless integration with existing hospital and EHR systems, further support adoption and routine use. Addressing these elements across scientific development, regulatory assessment, and clinical implementation processes enhances not only the reliability of a CDSS but also its lasting impact in clinical practice. Although all three CDSSs underwent these three key processes, their approaches differed (Table 1). As illustrated by the publication dates of manuscripts on development, the processes were timed sequentially from which important lessons were learned regarding the need for earlier and more continuous alignment.

A limitation of this viewpoint is that it focuses primarily on European MDR regulations nevertheless, similar challenges have been observed in other regions of the world. Also, currently novel AI techniques, performing the functions of CDSSs, such as dynamic risk prediction and providing targeted clinical advice, are often not yet recognized as CDSSs by clinicians. As a result, these tools are used without formal consideration of

XSL•FO
RenderX

their regulatory status, posing challenges to the current MDR regulation.

This viewpoint highlights that the complexity of CDSS development currently places a disproportionate burden on individual developers. While foresight and adaptability remain essential, developers cannot be expected to navigate scientific validation, regulatory compliance, and practical implementation alone. To support clinical scientists, our developer's checklist (Textbox 2) provides concrete guidance for successful CDSS development. Beyond these practical recommendations, structural changes are needed at the system level, for example, the creation of national protocols, standardized regulatory guidance, and dedicated support structures within hospitals. The MDR provides an important safety framework, but realizing the full potential of CDSSs requires both practical guidance for developers and systemic changes to ensure that these tools can be safely, efficiently, and effectively implemented to support clinicians and improve patient outcomes.

Acknowledgments

The manuscript text was refined with the assistance of the generative AI tool ChatGPT, version GPT-5 (OpenAI). All revisions were critically reviewed, edited, and approved by the authors.

Funding

The development of the Feverkidstool was supported by funding from the Dutch National Health Council (ZonMW), grant 170992503. Further validation of the tool was also funded by the Dutch National Health Council (ZonMW), grant 836041001. The implementation of the tool and SV were also supported by the Dutch National Health Council (ZonMW), grant 10390162210012. The Neonatal Procalcitonin Intervention Study trial received financial support from the Trasher Foundation, the NutsOhra Foundation, grant 1101-059, and the Sophia Foundation for Scientific Research, grant 681. Additionally, Thermo Fisher provided procalcitonin kits and an unrestricted grant to facilitate the organization of four investigator meetings in 2008, 2009, 2013, and 2015. SJ is supported by the Sophia Foundation for Scientific Research and Tergooi.

Data Availability

Data sharing is not applicable to this article as no datasets were generated or analyzed during this study.

Authors' Contributions

Conceptualization: NA, RO
Supervision: AW, NA, RO
Visualization: SV
Writing – Original Draft: SV, SJ
Writing – Review & Editing: SV, SJ, AW, NA, RO

Conflicts of Interest

None declared.

References

1. Regulation (EU) 2017/745 of the european parliament and of the council of 5 april 2017 on medical devices, amending directive 2001/83/EC, regulation (EC) no 178/2002 and regulation (EC) no 1223/2009 and repealing council directives 90/385/EEC and 93/42/EEC. EUR-Lex (European Union). URL: https://eur-lex.europa.eu/eli/reg/2017/745/oj [accessed 2024-11-24]
2. Keutzer L, Simonsson US. Medical device apps: an introduction to regulatory affairs for developers. JMIR Mhealth Uhealth 2020 Jun 26;8(6):e17567. [doi: 10.2196/17567] [Medline: 32589154]
3. Cowley LE, Farewell DM, Maguire S, Kemp AM. Methodological standards for the development and evaluation of clinical prediction rules: a review of the literature. Diagn Progn Res 2019;3:16. [doi: 10.1186/s41512-019-0060-y] [Medline: 31463368]
4. Puopolo KM, Draper D, Wi S, et al. Estimating the probability of neonatal early-onset infection on the basis of maternal risk factors. Pediatrics 2011 Nov;128(5):e1155-e1163. [doi: 10.1542/peds.2010-3464] [Medline: 22025590]
5. Nijman RG, Vergouwe Y, Thompson M, et al. Clinical prediction model to aid emergency doctors managing febrile children at risk of serious bacterial infections: diagnostic study. BMJ 2013 Apr 2;346:f1706. [doi: 10.1136/bmj.f1706] [Medline: 23550046]
6. Stocker M, van Herk W, El Helou S, et al. Procalcitonin-guided decision making for duration of antibiotic therapy in neonates with suspected early-onset sepsis: a multicentre, randomised controlled trial (NeoPIns). Lancet 2017 Aug 26;390(10097):871-881. [doi: 10.1016/S0140-6736(17)31444-7] [Medline: 28711318]
7. Hak F, Guimarães T, Santos M. Towards effective clinical decision support systems: a systematic review. PLoS One 2022;17(8):e0272846. [doi: 10.1371/journal.pone.0272846] [Medline: 35969526]

XSL•FO
RenderX

8. Achten NB, Klingenberg C, Benitz WE, et al. Association of use of the neonatal early-onset sepsis calculator with reduction in antibiotic therapy and safety: a systematic review and meta-analysis. JAMA Pediatr 2019 Nov 1;173(11):1032-1040. [doi: 10.1001/jamapediatrics.2019.2825] [Medline: 31479103]
9. van der Weijden BM, Janssen SWCM, van der Weide MC, et al. Safety and effectiveness of the early-onset sepsis calculator to reduce antibiotic exposure in at-risk newborns: a cluster-randomised controlled trial. EClinicalMedicine 2025 Sep;87:103419. [doi: 10.1016/j.eclinm.2025.103419] [Medline: 40831464]
10. van de Maat JS, Peeters D, Nieboer D, et al. Evaluation of a clinical decision rule to guide antibiotic prescription in children with suspected lower respiratory tract infection in The Netherlands: a stepped-wedge cluster randomised trial. PLoS Med 2020 Jan;17(1):e1003034. [doi: 10.1371/journal.pmed.1003034] [Medline: 32004317]
11. Abell B, Naicker S, Rodwell D, et al. Identifying barriers and facilitators to successful implementation of computerized clinical decision support systems in hospitals: a NASSS framework-informed scoping review. Implement Sci 2023 Jul 26;18(1):32. [doi: 10.1186/s13012-023-01287-y] [Medline: 37495997]

Abbreviations

CDSSs: clinical decision support systems
CE: Conformité Européenne
EHR: electronic health records
EOS: Early Onset Sepsis
EUDAMED: European Database on Medical Devices
FKT: Feverkidstool
JMIR: Journal of Medical Internet Research
MDR: Medical Device Regulation
NeoPInS: Neonatal Procalcitonin Intervention Study

Edited by A Coristine; submitted 20.Feb.2025; peer-reviewed by C Duesing, G Su, SS Goswami; revised version received 29.Dec.2025; accepted 09.Jan.2026; published 09.Mar.2026.

Please cite as:
Vrijlandt SEW, Janssen SWCM, van Rossum AMC, Achten NB, Oostenbrink R
Developing Clinical Decision (Support) Systems Combining the Scientific and Regulatory Perspective: European Insights on Challenges, Requirements, and Practical Guidance
JMIR Med Inform 2026;14:e72809
URL: https://medinform.jmir.org/2026/1/e72809
doi:10.2196/72809

© Sanne E W Vrijlandt, Sanne W C M Janssen, Annemarie M C van Rossum, Niek B Achten, Rianne Oostenbrink. Originally published in JMIR Medical Informatics (https://medinform.jmir.org), 9.Mar.2026. This is an open-access article distributed under the terms of the Creative Commons Attribution License (https://creativecommons.org/licenses/by/4.0/), which permits unrestricted use, distribution, and reproduction in any medium, provided the original work, first published in JMIR Medical Informatics, is properly cited. The complete bibliographic information, a link to the original publication on https://medinform.jmir.org/, as well as this copyright and license information must be included.

XSL•FO
RenderX

Dynamic Personalized Optimization: An AI Functionality Framework for Digital Therapeutics

Dohyoung Rim, PhD

Rowan Corporation, 18F Yonsei Severance Bld, 10, Tongil-ro, Jung-gu, Seoul, Republic of Korea

Corresponding Author:
Dohyoung Rim, PhD
Rowan Corporation, 18F Yonsei Severance Bld, 10, Tongil-ro, Jung-gu, Seoul, Republic of Korea

Abstract

Dynamic Personalized Optimization (DPO) is introduced as a conceptual framework that defines core artificial intelligence (AI) functions required to deliver real-time, personalized, and optimized treatment in digital therapeutics (DTx). DPO continuously refines therapeutic strategies by integrating patient data, treatment content, usage feedback, and status measurements to provide real-time, personalized treatment. Using predictive AI models, DPO adapts treatment approaches based on patient responses, thereby improving therapeutic effectiveness. Furthermore, this paper explores the potential role of large language models (LLMs) in supporting DPO by processing diverse and complex data formats. By addressing current limitations in real-time personalization within DTx, DPO establishes a structured, AI-driven approach to delivering tailored digital interventions. This framework ultimately aims to enhance treatment efficacy and improve patient engagement.

(JMIR Med Inform 2026;14:e75256) doi:10.2196/75256

KEYWORDS

dynamic personalized optimization; digital therapeutics; AI functionality framework; personalized treatment; large language models

Introduction

Digital Therapeutics (DTx) are software-based interventions designed to prevent, manage, or treat medical conditions and provide direct therapeutic benefits through digital technology [1]. Such digital interventions are particularly important for neurological disorders, which require complex, personalized approaches [2]. Neurological disorders such as tinnitus, depression, and mild cognitive impairment require individualized care that DTx can offer [3,4], but the full potential of DTx is realized only with artificial intelligence (AI) integration [5].

These DTx solutions can continuously monitor patients, deliver real-time feedback, and dynamically adjust treatments to improve outcomes [6]. AI plays a crucial role in DTx by analyzing large-scale patient data to enable real-time personalization and improved treatment outcomes [3,7,8].

This study introduces a functional framework for AI in DTx, which supports real-time personalization through dynamic adaptation. Existing DTx lack a formal framework for real-time personalization. Prior work has identified persistent challenges in dynamic personalization [8,9], including the need for more adaptable models and limitations of static content in DTx. This paper addresses this gap by introducing a new framework called Dynamic Personalized Optimization (DPO).

DPO Framework

Definition and Characteristics of DPO

DPO is a conceptual framework that delineates the core AI functions necessary for DTx to achieve dynamic personalization and optimal therapy. It integrates and analyzes patient data to refine treatment strategies in real time. DPO tailors treatment plans by incorporating patient data and responses to offer individualized therapeutic approaches. A predictive AI model anticipates the patient's future status and optimizes treatment accordingly. DPO dynamically optimizes personalized therapy by integrating clinical data, feedback, and treatment content.

Building on just-in-time adaptive interventions [10], DPO formalizes relevant data types and introduces adaptive treatment content optimization through AI-based prediction of patient feedback or status. While traditional just-in-time adaptive interventions primarily focus on determining the timing of interventions, DPO differentiates itself by continuously optimizing treatment content through AI-based prediction of patient feedback, thereby extending the concept from temporal adaptation to content-level personalization.

Necessity of DPO in DTx

Neurological and other complex disorders require personalized, responsive treatment. DPO is essential to achieving this in DTx, as it continuously tailors therapy based on patient-specific data in real time.

XSL•FO
RenderX

The Four Data Types of DPO

DPO uses four types of data to tailor therapy. User data (U) include information about the patient, such as demographics, medical history, and lifestyle. Status measurement (M) data refer to objective health metrics, including symptom severity and test results. Treatment content data (C) encompass information related to the therapy itself, such as descriptions, types, and formats. Finally, feedback data (F) consist of feedback received after therapy, such as treatment game scores or the patient's reported feelings. AI in DTx uses these 4 types of data to create personalized treatment plans. Figure 1 illustrates how these 4 data types are sequentially processed throughout the therapeutic process.

Figure 1. The treatment process begins with a sequence of 4 data types: initial user data (U), initial patient status (Mi), and a repeated cycle of treatment content (C) and feedback (F), which leads to updated status measurements (M). This treatment-feedback sequence and patient status update continues throughout the treatment period.

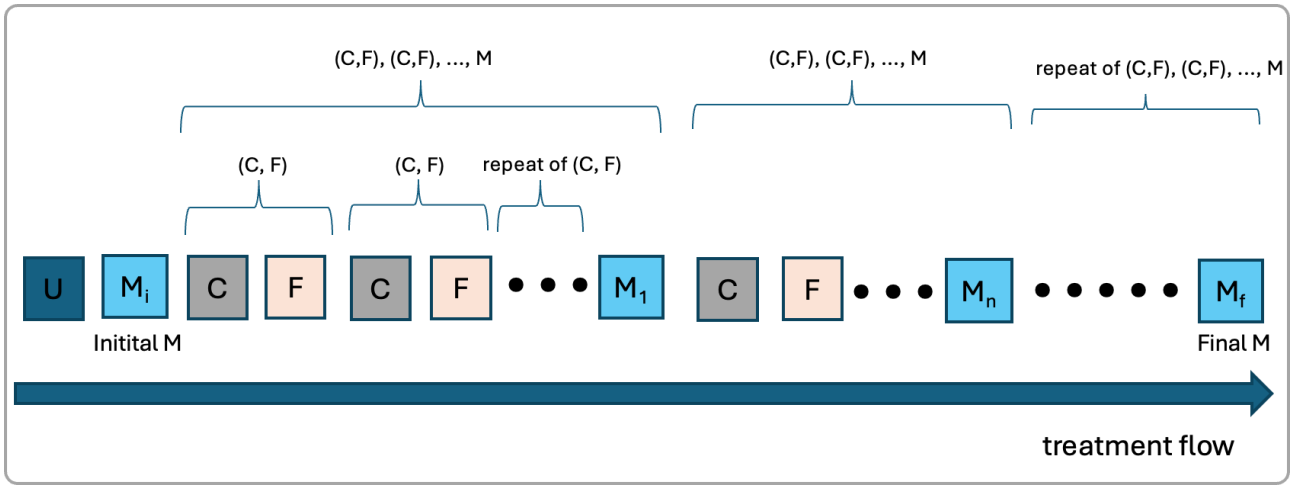

Adaptive Treatment Content Optimization

Within the DPO framework, AI is expected to continuously select the treatment content (C) that yields the greatest improvement in a patient's final status (M_f) relative to the initial status (M_i). However, identifying the "best" content in advance for AI model training is nearly impossible because it varies by individual and context and cannot be known until tried.

Predicting F

As Figure 2 illustrates, instead of directly predicting the optimal content C, this approach focuses on predicting F for a given C. In a DTx environment, real-world data collection yields sequential data (U, M, C, and F) throughout the treatment. An AI model can be trained on these historical data sequences to predict subsequent F. Although F does not directly represent treatment efficacy, it informs future treatment decisions. This approach assumes that feedback (F) is a valid proxy for treatment efficacy. Prior research shows a strong correlation between user engagement in digital interventions and improved treatment outcomes [11], though engagement alone may not fully capture clinical efficacy. Nonetheless, leveraging this correlation, the model can predict F for candidate treatment contents and select the optimal one (C_o) with the highest predicted F.

XSL•FO
RenderX

Figure 2. One optimization approach involves predicting the expected feedback (F) for each candidate content. The optimal content (C_o) is selected based on the highest predicted F. An artificial intelligence (AI) model is trained on historical data sequences to predict F for a given candidate C.

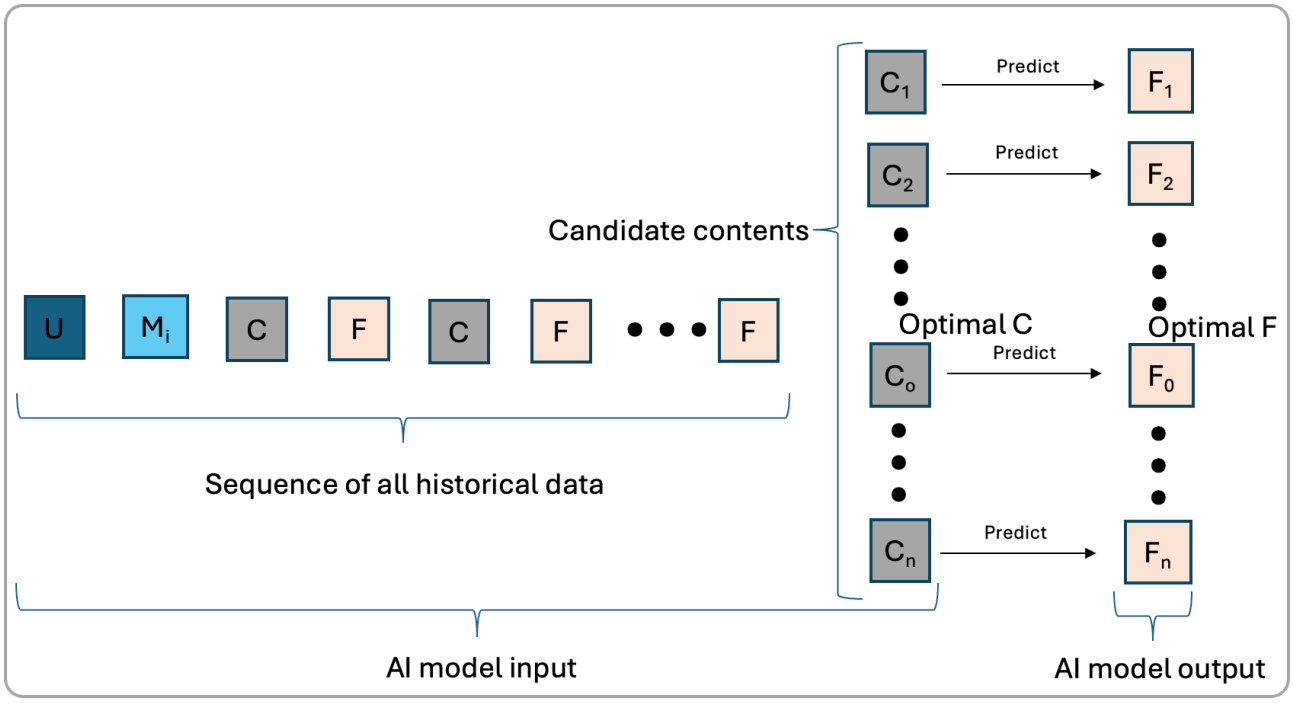

Predicting M

Figure 3 illustrates another approach: predicting the patient's M_f. In this approach, an AI model is trained with prior data sequences as input and M_f as the output. If the model learns this relationship accurately, it can predict M_f for a given input sequence and a candidate C. By predicting M for all candidate C options, the model can select the C_o that most effectively improves M.

Together, these approaches eliminate the need to explicitly label C as the correct answer. Instead, AI predicts F or M_f to dynamically determine the optimal C, ensuring that patients engage with the most effective therapeutic content. However, implementing these AI-driven strategies in practice requires managing complex and heterogeneous DTx data, which poses significant challenges.

Figure 3. An alternative approach involves predicting the final patient status (M_f) for each candidate content. The artificial intelligence (AI) model takes historical data and candidate C as input and predicts the resulting status (M_f). The optimal content (C_o) is selected to maximize improvement in M_f relative to the initial status.

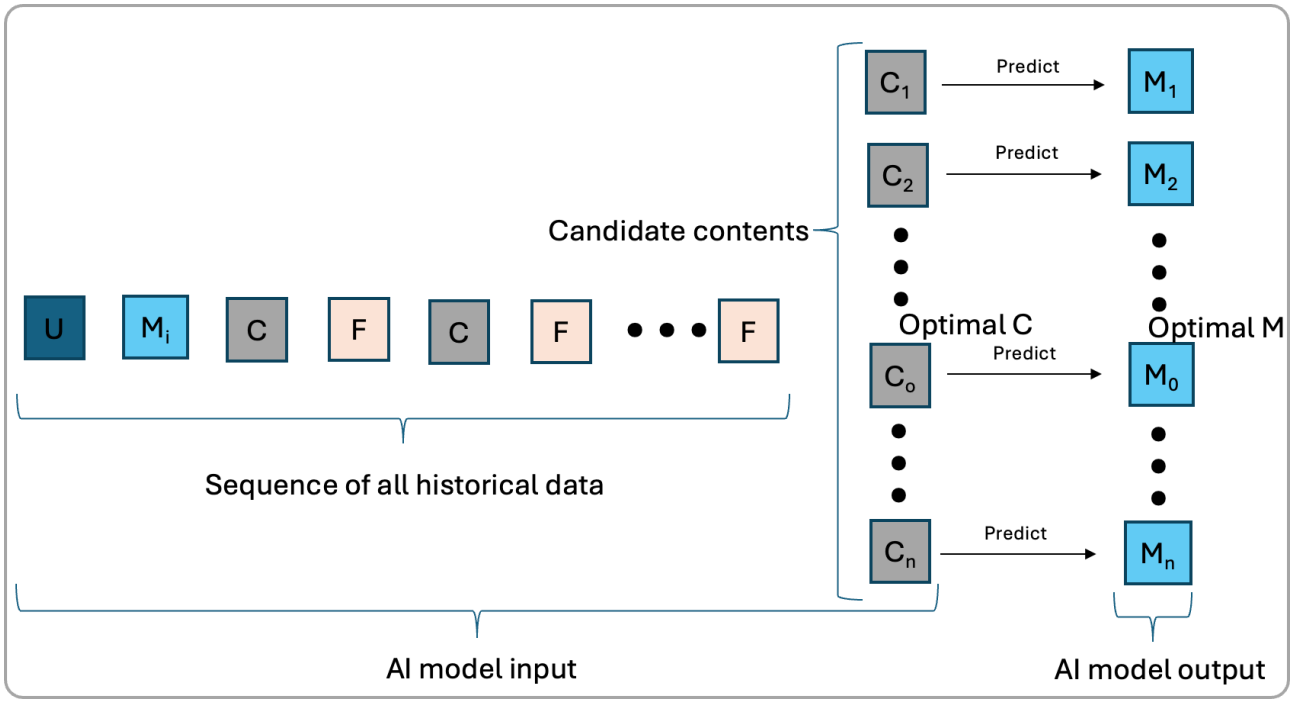

XSL•FO
RenderX

In a cognitive intervention context for mild cognitive impairment (MCI) [12], DPO operates as follows. The system first collects U such as demographic and behavioral information including age, education level, daily activity, and sleep patterns. It also gathers initial measurement data (M_i), such as the Mini-Mental State Examination score [13] representing the patient's baseline cognitive state. Based on these inputs and the history of previously delivered C—for example, cognitive games that train memory, attention, or problem-solving skills—and corresponding F, such as game scores reflecting engagement and task performance, the AI model predicts either the expected F or the postsession M for each candidate content option. The predicted value then guides the system in selecting the next C_o for the patient's subsequent training session. This process of providing C and receiving F repeats over time, allowing the system to refine personalized cognitive training. Through this iterative mechanism, DPO continuously optimizes therapeutic content to enhance cognitive function and engagement in patients with MCI.

Challenges of Data in DTx and LLM Strategy

Overview

DTx data appear in diverse forms—text (eg, clinical notes), numeric measurements, images, and video—varying widely in length and quality. This heterogeneity hinders uniform processing of data by AI. Addressing this issue requires careful data preprocessing, stringent quality control, and AI models capable of integrating disparate data types.

LLMs have significant potential to overcome data processing challenges in DTx [14]. The following strategies describe how LLMs can support DPO.

Integrated Processing of Various Data Formats

LLMs can process diverse data formats (including text, numerical data, and images) thereby enabling comprehensive analysis to improve treatment outcomes [15]. They analyze unstructured text, such as medical records and patient feedback, to extract key details and interpret numerical data like vital signs and laboratory results. Additionally, LLMs use embedding techniques to represent each data modality as a numeric vector, enabling integrated analysis across different data types. This approach allows processing of disparate data types within the same mathematical space.

Processing Variable Data Sizes

LLMs can handle data inputs of widely varying lengths [16,17]—from brief notes and detailed medical records to extensive patient histories and multisource health logs. They can also process time-series data to identify patterns and trends in symptom logs and vital signs. This capability enables real-time monitoring and more adaptive care.

Discussion

The DPO framework proposed in this study has been designed as a structural model applicable to a range of DTx scenarios, offering a systematic functional definition of AI capabilities required for the personalization and adaptive coordination of digital therapeutic content. In DPO, LLMs are not used to generate new therapeutic content but rather serve as analytical tools to integrate and interpret multimodal data for personalized optimization. This paper presents a conceptual design framework and does not include empirical validation for 2 primary reasons. First, DPO is formulated as a high-level functional abstraction rather than a model-specific architecture, and its applicability may be realized through various algorithmic implementations. Therefore, the focus of this work is on the completeness and coherence of the framework design rather than the comparative performance of specific models. Second, the DPO framework is currently undergoing pilot-level integration in several ongoing DTx development pipelines within an industry setting, and early experimental outcomes related to these efforts are planned to be reported in a separate study. Future work will empirically evaluate the implementation and performance of each functional component of the DPO framework—prediction, personalization, and optimization—within actual digital therapeutic contexts using real user data. Additional studies will also explore the generalizability and scalability of DPO across diverse clinical domains, including MCI, depression, and tinnitus, to further establish the framework's practical utility and robustness.

Conclusion

The proposed DPO framework offers a structured approach to operationalizing AI in DTx, with the potential to improve both engagement and therapeutic efficacy. Integrating LLMs into DPO could greatly enhance personalized care delivery and improve health care outcomes. At the same time, ensuring data privacy, security, and safety in digital therapeutics remains essential. Moreover, the responsible use of AI-based DTx requires addressing ethical issues such as transparency, fairness, cybersecurity, and data protection, which must be implemented with accountability [18]. Recent studies on responsible AI deployment further emphasize the importance of governance, transparency, and privacy as key foundations for ethical implementation in health care [19,20]. AI must generate transparent recommendations while ensuring clinical validation and ethical oversight. Overcoming these challenges could enable a new level of personalized treatment and substantially improve patient outcomes. Leveraging advanced AI models for DPO may facilitate the integration of heterogeneous patient data in ways previously unattainable, essentially serving as a "brain" for DTx that learns and adapts to each patient. Going forward, the practical implementation and clinical validation of DPO (potentially with LLMs) are crucial next steps. These efforts must be accompanied by careful attention to ethical and regulatory considerations. If DPO can maintain patient engagement by tailoring content to what is therapeutically optimal for each individual, the therapeutic efficacy of DTx could be substantially enhanced. Such personalized adaptation prevents patient dropout or disengagement caused by monotonous or ineffective content [1], thereby further improving outcomes.

XSL•FO
RenderX

Funding

The author declares no financial support was received for this work.

Authors' Contributions

DR confirms being solely responsible for all aspects of this work, including conceptualizing and designing the study, conducting the analysis, and drafting and revising the entire manuscript.

Conflicts of Interest

None declared.

References

1. Digital therapeutics definition and core principles. : Digital Therapeutics Alliance; 2019.
2. Griñán-Ferré C, Bellver-Sanchis A, Guerrero A, Pallàs M. Advancing personalized medicine in neurodegenerative diseases: The role of epigenetics and pharmacoepigenomics in pharmacotherapy. Pharmacol Res 2024 Jul;205:107247. [doi: 10.1016/j.phrs.2024.107247] [Medline: 38834164]
3. Choi H, Shin J, Kim JH, et al. Digital therapeutics for patients with mild cognitive impairment: Design of a mobile health program. Electronics (Basel) 2024;13(19):3892. [doi: 10.3390/electronics13193892]
4. Armeni P, Polat I, De Rossi LM, Diaferia L, Meregalli S, Gatti A. Exploring the potential of digital therapeutics: An assessment of progress and promise. Digit Health 2024;10:20552076241277441. [doi: 10.1177/20552076241277441] [Medline: 39291152]
5. Darcy A, Beaudette A, Chiauzzi E, et al. Anatomy of a Woebot® (WB001): agent guided CBT for women with postpartum depression. Expert Rev Med Devices 2022 Apr;19(4):287-301. [doi: 10.1080/17434440.2022.2075726] [Medline: 35748029]
6. Palanica A, Docktor MJ, Lieberman M, Fossat Y. The need for artificial intelligence in digital therapeutics. Digit Biomark 2020;4(1):21-25. [doi: 10.1159/000506861] [Medline: 32399513]
7. Smith ME, Sharma D, Rivero-Arias O, et al. Digital thErapy For Improved tiNnitus carE Study (DEFINE): Protocol for a randomised controlled trial. PLoS ONE 2024;19(1):e0292562. [doi: 10.1371/journal.pone.0292562] [Medline: 38180996]
8. Niazi SK. The coming of age of AI/ML in drug discovery, development, clinical testing, and manufacturing: The FDA perspectives. Drug Des Devel Ther 2023;17:2691-2725. [doi: 10.2147/DDDT.S424991] [Medline: 37701048]
9. Hu P, Hu L, Wang F, Mei J. Editorial: Computing and artificial intelligence in digital therapeutics. Front Med 2024;10:1330686. [doi: 10.3389/fmed.2023.1330686]
10. Patel M, Butte A. Challenges in digital therapeutics: Personalization and evidence generation. Journal of Digital Health 2020;5(2):98-105. [doi: 10.1093/ehjdh/ztaa008] [Medline: 37056293]
11. Nahum-Shani I, Smith SN, Spring BJ, et al. Just-in-time adaptive interventions (JITAIs) in mobile health: Key components and design principles for ongoing health behavior support. Ann Behav Med 2018 May 18;52(6):446-462. [doi: 10.1007/s12160-016-9830-8] [Medline: 27663578]
12. Petersen RC, Smith GE, Waring SC, Ivnik RJ, Tangalos EG, Kokmen E. Mild cognitive impairment: clinical characterization and outcome. Arch Neurol 1999 Mar;56(3):303-308. [doi: 10.1001/archneur.56.3.303] [Medline: 10190820]
13. Folstein MF, Folstein SE, McHugh PR. “Mini-mental state”. A practical method for grading the cognitive state of patients for the clinician. J Psychiatr Res 1975 Nov;12(3):189-198. [doi: 10.1016/0022-3956(75)90026-6] [Medline: 1202204]
14. Gan DZQ, McGillivray L, Han J, Christensen H, Torok M. Effect of engagement with digital interventions on mental health outcomes: A systematic review and meta-analysis. Front Digit Health 2021;3:764079. [doi: 10.3389/fdgth.2021.764079] [Medline: 34806079]
15. Zhang K, Meng X, Yan X, et al. Revolutionizing health care: The transformative impact of large language models in medicine. J Med Internet Res 2025 Jan 7;27(1):e59069. [doi: 10.2196/59069] [Medline: 39773666]
16. Belyaeva A, Cosentino J, Hormozdiari F, et al. Multimodal LLMs for health grounded in individual-specific data. Presented at: First International Workshop on Machine Learning for Multimodal Healthcare Data; Jul 29, 2023. [doi: 10.1007/978-3-031-47679-2_7]
17. Gpt-4 technical report. : OpenAI; 2023. [doi: 10.48550/arXiv.2303.08774]
18. Mennella C, Maniscalco U, De Pietro G, Esposito M. Ethical and regulatory challenges of AI technologies in healthcare: A narrative review. Heliyon 2024 Feb 29;10(4):e26297. [doi: 10.1016/j.heliyon.2024.e26297] [Medline: 38384518]
19. Radanliev P, Santos O, Brandon-Jones A, Joinson A. Ethics and responsible AI deployment. Front Artif Intell 2024;7:1377011. [doi: 10.3389/frai.2024.1377011] [Medline: 38601110]
20. Radanliev P. AI Ethics: Integrating transparency, fairness, and privacy in AI development. Appl Artif Intell 2025 Dec 31;39(1). [doi: 10.1080/08839514.2025.2463722]

XSL•FO
RenderX

Abbreviations

AI: artificial intelligence
C: treatment content data
C_o: optimal content
DPO: Dynamic Personalized Optimization
DTx: digital therapeutics
F: feedback data
LLM: large language model
M: status measurement data
MCI: mild cognitive impairment
M_f: final status
M_i: initial status
U: user data

Edited by A Benis; submitted 31.Mar.2025; peer-reviewed by B Tasci, P Radanliev, S Aammou; revised version received 18.Oct.2025; accepted 17.Dec.2025; published 18.Mar.2026.

Please cite as:
Rim D
Dynamic Personalized Optimization: An AI Functionality Framework for Digital Therapeutics
JMIR Med Inform 2026;14:e75256
URL: https://medinform.jmir.org/2026/1/e75256
doi:10.2196/75256

© Dohyoung Rim. Originally published in JMIR Medical Informatics (https://medinform.jmir.org), 18.Mar.2026. This is an open-access article distributed under the terms of the Creative Commons Attribution License (https://creativecommons.org/licenses/by/4.0/), which permits unrestricted use, distribution, and reproduction in any medium, provided the original work, first published in JMIR Medical Informatics, is properly cited. The complete bibliographic information, a link to the original publication on https://medinform.jmir.org/, as well as this copyright and license information must be included.

XSL•FO
RenderX

Telepathology Development and Stakeholder Perspectives in China: Cross-Sectional Survey

Linlin Wang[1*], MM; Fangfang Cui[1*], MM; Xianying He[1,2], MM

[1]National Engineering Laboratory for Internet Medical Systems and Applications, The First Affiliated Hospital of Zhengzhou University, 1 Jianshe Road, Zhengzhou, Henan, China

[2]Shanghai Artificial Intelligence Laboratory, Shanghai, China

[*]these authors contributed equally

Corresponding Author:
Xianying He, MM
National Engineering Laboratory for Internet Medical Systems and Applications, The First Affiliated Hospital of Zhengzhou University, 1 Jianshe Road, Zhengzhou, Henan, China

Abstract

Background: Telepathology is widely recognized for improving diagnostic access in remote areas and is strongly promoted in China to address the shortage of pathologists. However, a comprehensive national assessment of its implementation and multistakeholder perspectives remains lacking.

Objective: This study aims to conduct a comprehensive analysis of the infrastructure, practical application, and user experience of telepathology in China from 2018 to 2023 and to identify the key factors affecting its adoption and satisfaction levels.

Methods: A repeated cross-sectional survey was administered to hospitals across China (2018-2023), alongside a parallel survey of telepathology users (2023). Data were analyzed from hospitals (sample sizes ranging from 464 to 188 across years), pathologists (n=262), and patients (n=141). Regression analysis was applied to investigate factors associated with professional satisfaction and willingness to adopt the technology.

Results: The proportion of hospitals with telepathology software grew at an annual average rate of 7.60%, increasing from 29.5% (137/464) in 2018 to 42.6% (80/188) in 2023. The median number of telepathology cases per hospital increased from 51 to 200, with the fastest growth observed in the eastern region. Among pathologists, 61.1% (160/262) used telepathology weekly, 61.5% (161/262) spent 11 to 20 or 21 to 30 minutes. Pathologists reported a 95.8% (251/262) satisfaction rate, and 95% (249/262) were willing to continue participation. Convenience of system operation and service processes were associated with enhanced satisfaction and sustained engagement willingness (P<.05). Among patients, 92.2% (130/141) received diagnostic results within 24 hours, with 100% (141/141) satisfaction, and 99.3% (140/141) were willing to recommend telepathology.

Conclusions: Telepathology in China grew significantly from 2018 to 2023, with high satisfaction among both pathologists and patients. For sustained development, a multilevel approach is essential: improving system usability, implementing supportive policies (eg, funding and insurance coverage), and conducting targeted promotion of its proven benefits. This integrated strategy is key to making telepathology a sustainable solution for equitable diagnostic access nationwide.

(JMIR Med Inform 2026;14:e83514) doi:10.2196/83514

KEYWORDS

telepathology; digital slide scanners; software; service; usage; satisfaction; perceptions

Introduction

Pathological diagnosis is the gold standard for disease diagnosis, particularly for cancer. However, China's primary medical institutions face a significant shortage of pathologists, especially experienced ones. According to the 2019 China Pathology Quality Report [1], there are only 0.55 pathologists per 100 hospital beds, and 46.3% of secondary hospitals have just 1 pathologist, which is far below the demand for timely and high-quality pathology services. Data from the Pathology Quality Control Center of China [2] reveal that 82% of senior pathologists are concentrated in tertiary hospitals, leaving many primary hospitals without senior-title pathologists. In central and western regions, such as Tibet, Xinjiang, Qinghai, and Guizhou, more than 20% of institutions have no more than 1 pathologist, highlighting a significant imbalance in pathology resource distribution across China.

Telepathology, first proposed in 1987 [3], addresses resource shortages by enabling the transmission of static images, dynamic videos, and whole-slide images (WSIs). As defined in the Basic Functions Specification of Telemedicine Information System (WS/T529-2016), telepathology involves the submission of

XSL•FO
RenderX

diagnostic requests and patient data by an inviting party to an invited expert, who then provides diagnostic opinions and reports. Central to this practice is WSI technology, which converts pathological slides into high-resolution, zoomable digital images and supports the diagnosis of all pathology-dependent diseases, including tumor classification and grading, as well as the identification of specific pathogens or special inflammatory lesions. Its diagnostic reliability is supported by multiple guidelines and studies. The College of American Pathologists (CAP) released relevant validation guidelines in 2013 and 2021 [4,5], and the Royal College of Pathologists issued "Best Practice Recommendations for Implementing Digital Pathology" [6]. Studies by Montgomery et al [7] and Shinohara et al [8] confirmed the high diagnostic accuracy and effectiveness of WSIs in remote diagnosis. Furthermore, Girolami et al's [9] meta-analysis validated the diagnostic concordance between WSIs and light microscopy, reinforcing its role in delivering high-quality diagnostic services to resource-limited regions. At the regulatory and application levels, pathological diagnosis based on WSIs has been approved by the Food and Drug Administrations of the United States, the European Union, and Japan [10-12]. Since the US Food and Drug Administration first authorized a WSI system for primary diagnosis in 2017, multiple integrated digital pathology platforms, combining scanning, storage, viewing, and analysis functions, have received 510(k) clearance [13]. As of December 31, 2025, China's National Medical Products Administration (NMPA) had also approved 71 digital pathology–related medical devices [14]. In practice, WSI-based telepathology has been widely adopted in numerous countries and regions, including Europe [15], Nigeria [16], India [17], Tanzania [18], and Canada [19].

In China, developing a WSI-based telepathology system is a core strategy to address the deficiencies in grassroots pathology services [20]. Preliminary studies have demonstrated the effectiveness of the national cloud-based telepathology platform [21] and its potential to optimize resource allocation [22]. However, the existing literature lacks a comprehensive, long-term, and systematic evaluation of the overall development of telepathology in China. Key questions remain unanswered: What are the national trends and regional disparities in its adoption? As primary users, what are the adoption behaviors, perceptions, and influencing factors among pathologists? Moreover, what are patients' experiences and satisfaction levels with telepathology services? The absence of such critical information limits a thorough understanding of current implementation barriers and hinders targeted interventions.

To address these gaps, this study utilizes nationwide survey data from 2018 to 2023 with the following objectives: (1) to delineate the developmental trends and spatial distribution characteristics of telepathology in China over the past 6 years; (2) to analyze, from the perspective of pathologists, their usage behaviors, attitudes, and key influencing factors; and (3) to conduct the first systematic assessment of patient satisfaction with telepathology services. By integrating multidimensional evidence, including macro-level trends, insights from pathologists, and patient experiences, this study aims to provide an empirical foundation and decision-making support for optimizing China's telepathology infrastructure and promoting the equitable distribution of high-quality pathology resources.

Methods

Study Setting

To understand the current status of and identify obstacles to telemedicine services (telemedicine service items include teleconsultation, telepathology, teleradiology, telemonitoring, tele-outpatient services, etc), the Telemedicine Informationization Professional Committee of China (TIPC) and the National Telemedicine Center of China (NTCC) have conducted web-based surveys on telemedicine since 2018.

Survey on the Development of Telemedicine in Hospitals

This survey targeted hospitals approved by Chinese health administrative departments. The questionnaire was developed by experts with more than 5 years of telemedicine experience and refined annually based on prior findings. Following the initial design, 10 to 18 hospitals were selected for pilot testing, and feedback was incorporated to finalize the questionnaire.

Survey on the Usage and Perceptions of Telemedicine

A survey was conducted among doctors and patients participating in telemedicine services. The questionnaires were designed through needs analysis, a review of telemedicine practices, and relevant literature. After drafting, a pilot test was administered at the Henan Provincial Telemedicine Center and selected subcenters. The instruments were further optimized based on pilot feedback to form the final versions.

Implementation of the Survey

The electronic open survey was an online questionnaire on NTCC's website [23]. The survey announcement was formally issued by TIPC via an official red-headed document. Each annual theme had its own webpage, with up to 42 mandatory questions (the exact number depended on the respondent's answers) across 18 to 25 pages in Chinese. Completion required approximately 8 to 12 minutes based on pilot testing. The surveys were open from July to September 2018, October to November 2019, September to October 2020, and September to October 2023. To ensure data quality, duplicate submission prevention was implemented through IP address verification, response-time logic control, and cross-validation with official hospital records. Response metrics for each questionnaire type were as follows:

- The hospital questionnaire recorded 896 views with a 63.3% (567/896) participation rate and an 81.8% (464/567) completion rate in 2018
- The corresponding figures for 2019, 2020, and 2023 were 482 views (60.8% participation, 82.6% completion), 401 views (61.1% participation, 83.3% completion), and 364 views (63.2% participation, 81.7% completion).
- The doctor questionnaire received 3269 views, achieving a 53.1% (1736/3269) participation rate and a 77.9% (1353/1736) completion rate, including 262 pathologists among the completers.

XSL•FO
RenderX

- The patient questionnaire garnered 3528 views, with a 42.6% (1502/3528) participation rate and a 59.3% (891/1502) completion rate, of whom 141 patients had used telepathology services.

Data Cleaning and Valid Questionnaire

After the collection deadline, data were exported to Excel for cleaning. Hospital questionnaires from identical or conflicting IP addresses that could not be verified against official hospital records (eg, outpatient visits, bed counts) were excluded. Additionally, hospital questionnaires completed in less than 2 minutes and multiple doctor or patient questionnaires submitted from the same IP address within a 3-minute interval were omitted. Valid hospital questionnaires totaled 464 in 2018, 242 in 2019, 204 in 2020, and 188 in 2023.

Study Design

To explore the current status of telepathology development and application in Chinese hospitals, this study used data from TIPC and NTCC. Surveys were conducted in 2018, 2019, 2020, and 2023 across eastern, central, and western China. Due to the COVID-19 pandemic, restrictions on personnel movement during the outbreak disrupted normal work routines and medical services, resulting in the cancellation of surveys that were planned for 2021 and 2022. The eastern, central, and western regions are classified according to standards set by the National Bureau of Statistics of China (Multimedia Appendix 1). The survey coverage area is presented in Multimedia Appendix 2. Pearson chi-square test indicated no significant difference in provincial distribution among these regions across the 4 years (P=.90). Telepathology-related data were selected to assess construction progress and development trends. Based on 2023 survey responses from pathologists and patients who participated in telepathology services, application effectiveness was further analyzed.

This study was reported in accordance with the CHERRIES (Checklist for Reporting Results of Internet E-Surveys) guidelines (Checklist 1) [24]. The hospital questionnaire included 11 repeated survey questions on telepathology, comprising 9 single-choice questions and 2 fill-in questions. Among them, 6 questions related to telepathology infrastructure and service volume, and 5 questions related to telepathology operations and billing. The questionnaire was completed by telemedicine organizers at each hospital. The doctor questionnaire consisted of 24 questions, including basic information (7 questions), telepathology service usage and experience (9 questions), evaluation and attitudes (6 questions), and open-ended questions regarding problems and expectations (2 questions). The patient questionnaire consisted of 19 questions, including basic information (7 questions), usage (7 questions), and evaluation and attitudes (5 questions) (Multimedia Appendix 3).

Data Analysis

Data cleaning was performed to avoid logical problems and ensure data quality. Descriptive statistics were used to analyze the data. Median values and IQR are reported for quantitative data, and percentages are reported for qualitative data. Chi-square tests and Fisher exact probability tests were used to assess differences. Variables selected through univariate analysis were further analyzed using multivariate ordinal logistic regression to identify factors influencing satisfaction and usage intention [25]. All statistical analyses were conducted using SPSS (version 20.0; IBM Corp). All tests were 2-tailed, and P<.05 was considered statistically significant. Chinese maps were generated using ArcMap (version 10.8.1; Esri Corp) and R language (version 4.4.1; R Foundation for Statistical Computing).

Ethical Considerations

This study was approved by the institutional review board at the First Affiliated Hospital of Zhengzhou University (protocol 2021-KS-HNSR181). Ethics approval was obtained with the stipulation that collected data must not expose respondents' identities and only aggregated information would be addressed in the research paper. Informed consent was obtained from all participants. The survey was conducted without compensation. The questionnaire was anonymous, and the data file was stored on the NTCC intranet server. Only research team members who signed confidentiality agreements were permitted to access the data.

Results

The Construction of Telepathology

Digital slide scanners, software, and networks were investigated, as shown in Figure 1. The configuration status of digital slide scanners was not investigated in 2018. In 2019, 2020, and 2023, the number of hospitals equipped with scanners were 85 of 242 (35.1%), 76 of 204 (37.3%), and 68 of 188 (36.2%), respectively, with an annual average growth rate of 0.75%. From 2018 to 2023, the percentages of hospitals deploying telepathology software were 29.5% (137/464), 35.1% (85/242), 43.1% (88/204), and 42.6% (80/188), respectively, with an annual average growth rate of 7.6%. The telepathology service network comprises private networks and the internet. In 2018, 2019, 2020, and 2023, there were 137 (137/464, 29.5%), 100 (100/242, 41.3%), 96 (96/204, 47.1%), and 89 (89/188, 47.3%) hospitals connected to the telepathology service network, respectively. Private networks were consistently more utilized than the internet, with annual ratios of 68.6% (94/137) vs 31.4% (43/137), 74% (74/100) vs 26% (26/100), 67% (64/96) vs 33% (32/96), and 93% (83/89) vs 7% (6/89).

XSL•FO
RenderX

Figure 1. In 2018 - 2020 and 2023, the construction of telepathology infrastructure.

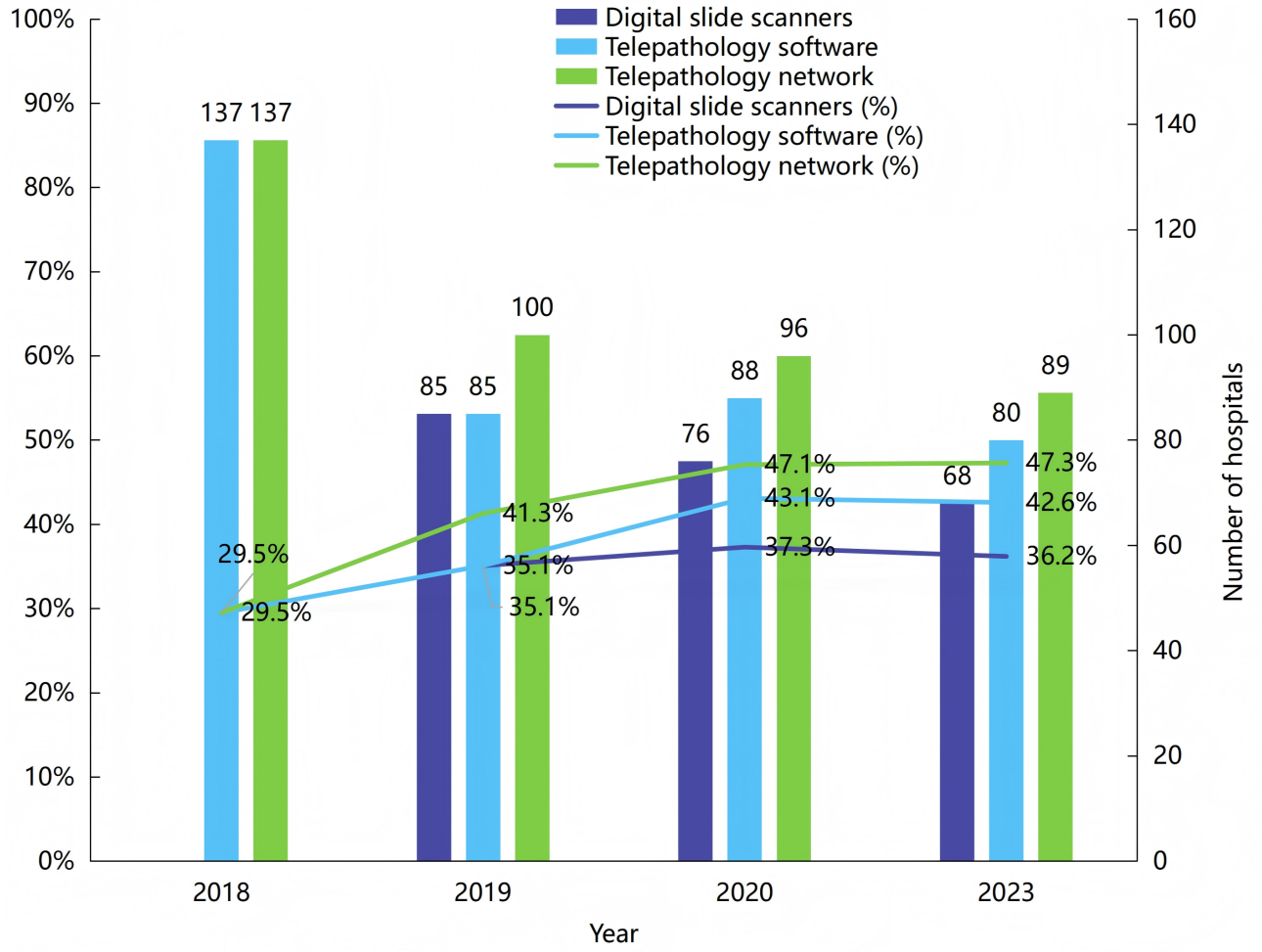

The Current Status of Telepathology Services

In 2018, 2019, 2020, and 2023, the proportions of hospitals providing telepathology services were 23.3% (108/464), 28.9% (70/242), 33.3% (68/204), and 31.4% (59/188), respectively, with an annual average growth rate of 6.1%. Among hospitals with established telepathology systems, the proportions providing telepathology services were 78.8% (108/137) in 2018, 82.3% (70/85) in 2019, 77.3% (68/88) in 2020, and 73.8% (59/80) in 2023. The median numbers of telepathology cases for these years were 51 (IQR 10 - 200), 95 (IQR 18.25 - 228.5), 100 (IQR 27.5 - 223.75), and 200 (IQR 93 - 331.5), respectively. A statistically significant increase was observed from 2018 to 2023, with an annual average growth rate of 31.4%. Table 1 details the regional and hospital-level distribution. From 2018 to 2020, the Central region led in telepathology services; however, by 2023, the Eastern region took over. Significant differences were observed in telepathology services between the Central and Western regions across the years, with annual average growth rates of 17.7% and 27.2%, respectively. Tertiary hospitals consistently reported higher median telepathology case volumes than secondary hospitals, with a statistically significant annual average growth rate of 26.2%.

XSL•FO
RenderX

Table . Distribution of telepathology services in different regions and different levels of hospitals.

Characteristics	Telepathology service volume per year, median (IQR)				*H*	*P* value
	2018	2019	2020	2023		
District						
East	36.5 (10-105)	80 (27.75-215)	31 (11.25-120.75)	359 (164.75-676.25)	4.55	.21
Center	93 (30-226)	141 (60-287)	148 (47-258)	210 (112.5-331.5)	10.11	.02
West	24 (2-180)	13 (2-123.5)	124 (60-776)	80 (36.75-146.75)	11.32	.01
Hospital grade						
Third-level	64 (5-292.25)	124 (60.5-245)	120 (25-274.5)	205 (109.75-420.25)	14.15	<.001
Second-level	50 (14.5-165)	55 (6.5-213)	80 (30-157)	100 (32.5-218)	2.15	.54
Total	51 (10-200)	95 (18.25-228.5)	100 (27.5-223.75)	200 (93-331.5)	17.61	.001

The Operation and Charging Situation of Telemedicine in Hospitals That Carry Out Telepathology Services

Among the hospitals providing telepathology services in 2018, 2019, 2020, and 2023, the percentages with established telemedicine departments were 69.4% (75/108), 77.1% (54/70), 76.5% (52/68), and 72.9% (43/59), respectively. The median numbers of telemedicine staff allocated were 3 (IQR 2 - 5) in 2018 and 2019, 4.5 (IQR 2 - 7) in 2020, and 5 (IQR 2.5 - 7) in 2023. Telemedicine operation modes included hospital self-operation, third-party operation, and mixed operation. Surveys over the 4 years showed that hospital self-operation was the primary mode, accounting for 67.59%, 50%, 67.65%, and 72.88%, respectively (Table S1 in Multimedia Appendix 4).

In 2018, 2019, 2020, and 2023, among hospitals providing telepathology services, the percentages of free services were 30.6% (33/108), 30% (21/70), 35.3% (24/68), and 57.6% (34/59), respectively. For charged services reimbursed by medical insurance, the percentages were 15.7% (17/108), 28.6% (20/70), 22.1% (15/68), and 22% (13/59), respectively (Figure 2). Fee standards were based on 3 factors: administrative department guidelines, hospital-specific standards, and telemedical service provider criteria (Table S1 in Multimedia Appendix 4).

XSL•FO
RenderX

Figure 2. Proportions of hospitals providing telepathology services (free, charged and insured, charged but uninsured) in 2018 - 2020 and 2023

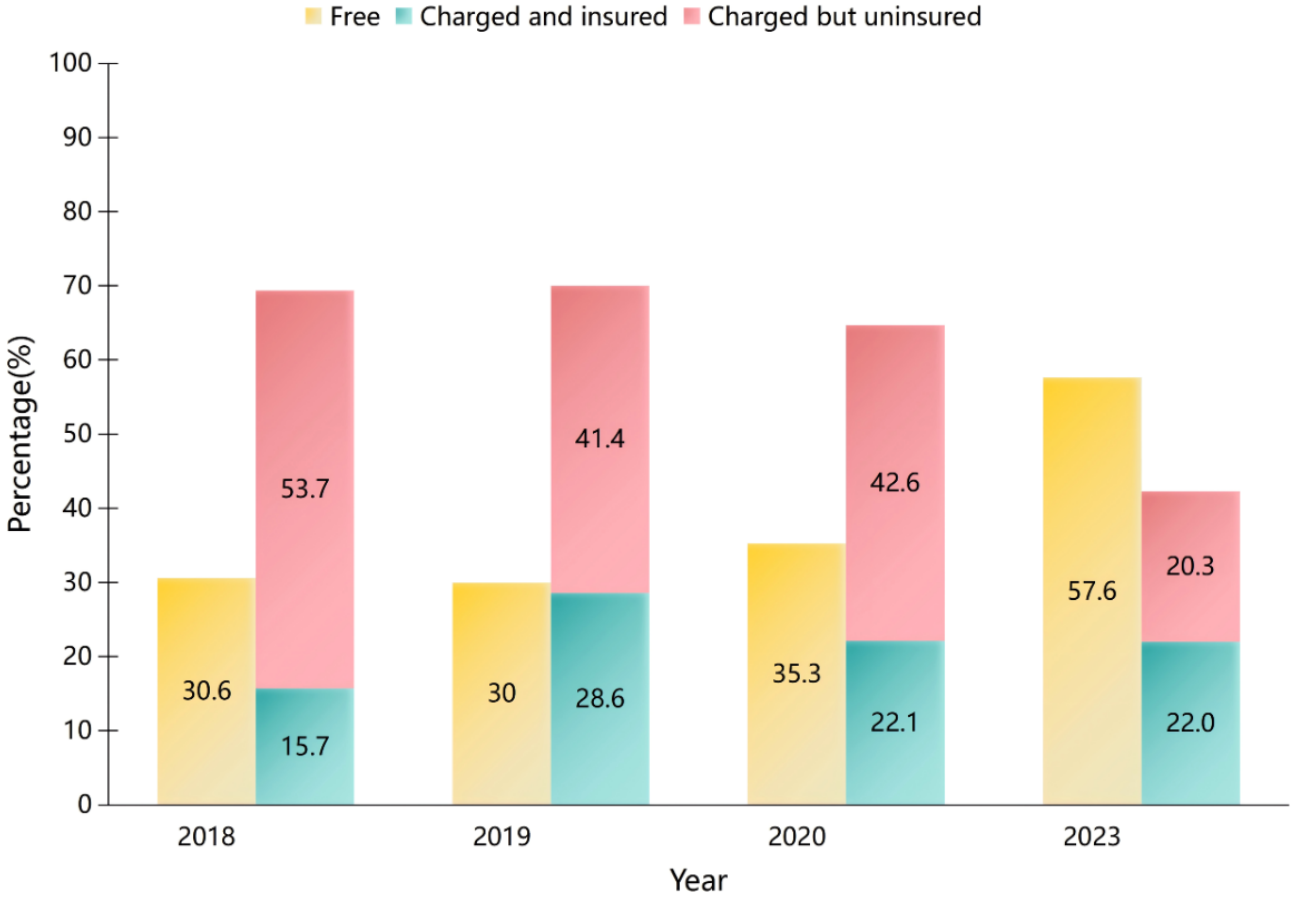

Usage of Telepathology Among Pathologists

A total of 262 valid questionnaires were collected from pathologists, as shown in Table 2. The distribution of these pathologists by region was 69 from the eastern, 61 from the central, and 132 from the western regions. There were 129 (49.2%) males and 133 (50.8%) females with a mean age of 35.3 (SD 9.1, range 20-73) years. The dominant frequency was once a week, accounting for 61.1% (n=160). Combined, those who serviced once a week or 2 to 3 times a week made up 84.4% (n=221) of the total, whereas those servicing 4 to 5 times a week or more accounted for 15.6% (n=41). The average time spent on telepathology services was mainly 11 to 20 minutes (n=78, 29.8%) and 21 to 30 minutes (n=83, 31.7%).

XSL•FO
RenderX

Table . Demographic characteristics and telepathology usage among pathologists.

Characteristics	Participants, n (%)
District	
East	69 (26.3)
Center	61 (23.3)
West	132 (50.4)
Gender	
Male	129 (49.2)
Female	133 (50.8)
Age, y	
<30	76 (35.1)
30-39	106 (39.6)
40-49	60 (20.1)
≥50	20 (5.2)
Education	
Doctoral degree	13 (4.9)
Master's degree	35 (13.3)
Bachelor's degree	149 (56.8)
College diploma and below	65 (24.8)
Professional title	
Senior	23 (8.7)
Deputy senior	30 (11.4)
Intermediate	71 (27)
Primary and below	138 (52.6)
Frequency of telepathology use, time/wk	
1	160 (61.1)
2-3	61 (23.3)
4-5	23 (8.8)
6-7	3 (1.1)
≥8	15 (5.7)
Average duration of telepathology, min	
≤10	44 (16.8)
11-20	78 (29.8)
21-30	83 (31.7)
31-60	42 (16)
>60	15 (5.7)

Pathologists' Evaluation and Satisfaction With Telepathology

As shown in Table 3, 92.7% (n=243) of pathologists considered the system easy to operate, and the service process was convenient. Additionally, 95.5% (n=250) believed that telepathology could reduce patient burdens. The overall satisfaction rate with telepathology services was 95.8% (n=251), and 95% (n=249) of pathologists were willing to continue participation.

XSL•FO
RenderX

Table . The evaluation and satisfaction of telepathology.

Characteristics	Participants, n (%)
Convenience of system operation	
Very convenient	168 (64.1)
Convenient	75 (28.6)
Neutral	8 (3.1)
Inconvenient	9 (3.4)
Very inconvenient	2 (0.8)
Convenience of service process	
Very convenient	149 (56.9)
Convenient	94 (35.9)
Neutral	8 (3.1)
Inconvenient	10 (3.8)
Very inconvenient	1 (0.4)
The role of telepathology in reducing the medical burden of patients	
Very helpful	166 (63.4)
Helpful	84 (32.1)
Neutral	5 (1.9)
Unhelpful	4 (1.5)
Very unhelpful	3 (1.1)
Using intention of telepathology	
Very willing	153 (58.4)
Willing	96 (36.6)
Neutral	10 (3.8)
Unwilling	2 (0.8)
Very unwilling	1 (0.4)
Overall satisfaction	
Very satisfied	147 (56.1)
Satisfied	104 (39.7)
Neutral	6 (2.3)
Dissatisfied	4 (1.5)
Very dissatisfied	1 (0.4)

Factors Influencing Pathologists' Satisfaction and Use Intention of Telepathology

According to the univariate analyses shown in Tables 2 and 3, 6 variables were associated with overall satisfaction (P<.25), and 5 variables were associated with use intention (P<.25) (Table 4). Multivariate ordinal logistic regression analysis revealed that 3 variables were included in the models for pathologists' overall satisfaction and use intention, respectively. Both models met the proportional odds (parallel lines) assumption, with test results showing P=.83 for the satisfaction model and P=.44 for the usage intention model. Convenience of system operation and service processes significantly improved both overall satisfaction and willingness to use telepathology. Compared with an average service duration of ≤10 minutes per session, longer service times were associated with improved willingness to continue using the service. In addition, a moderate frequency of participation enhanced pathologists' overall satisfaction.

XSL•FO
RenderX

Table . Ordinal logistic regression results of the influencing factors of the attitude toward telepathology among pathologists.

Variables	Overall satisfaction		Using intention	
	OR[a] (95% CI)	*P* value	OR (95% CI)	*P* value
Threshold (ref=very satisfied/very willing)				
Very dissatisfied/very unwilling	—[b]	<.001	—	<.001
Dissatisfied/unwilling	—	<.001	—	<.001
Neutral	—	<.001	—	<.001
Satisfied/willing	—	.13	—	.19
Education (ref=doctoral degree)				
College diploma and below	2.53 (0.52-12.39)	.25	1.92 (0.41-8.91)	.41
Bachelor's degree	1.26 (0.30-5.30)	.76	0.87 (0.21-3.53)	.85
Master's degree	0.50 (0.11-2.28)	.37	0.36 (0.08-1.57)	.17
Professional title (ref=senior)				
Primary and below	1.26 (0.40-3.99)	.70	0.54 (0.17-1.70)	.29
Intermediate	1.48 (0.46-3.81)	.51	1 (0.31-3.23)	>.99
Deputy senior	0.89 (0.25-3.21)	.86	0.67 (0.19-2.39)	.54
Frequency of telepathology use (ref=≥8 time/wk)			—	—
1 time/week	0.26(0.06-1.13)	.07		
2-3 times/week	0.21 (0.04-0.96)	.045		
4-5 times/week	0.36 (0.06-1.98)	.24		
6-7 times/week	0.15 (0.01-2.56)	.19		
Average duration of telepathology (ref=≤10 min)				
≥61 min	4.03 (0.93-17.51)	.06	6.68 (1.48-30.23)	.01
31-60 min	1.98 (0.74-5.34)	.18	1.92 (0.75-4.94)	.18
21-30 min	1.76 (0.75-4.12)	.19	2.49 (1.09-5.67)	.03
11-20 min	1.78 (0.75-4.21)	.19	2.30 (1.01-5.26)	.049
Convenience of system operation (ref=Very convenient)				
Very inconvenient	6.21 (0.23-169.52)	.28	2.76 (0.12-64.33)	.53
Inconvenient	0.76 (0.08-7.50)	.81	0.70 (0.08-5.82)	.74
Neutral	0.06 (0.01-0.50)	.01	0.02 (0.00-0.18)	<.001
Convenient	0.44 (0.20-0.94)	.03	0.49 (0.23-1.04)	.06
Convenience of service process (ref=Very convenient)				
Very inconvenient	0.05 (0.00-7.92)	.25	0.08 (0.00-9.46)	.30
Inconvenient	0.07 (0.01-0.54)	.01	0.20 (0.03-1.32)	.09
Neutral	0.08 (0.01-0.70)	.02	0.25 (0.04-1.77)	.17
Convenient	0.22 (0.10-0.46)	<.001	0.29 (0.14-0.59)	.001

[a]OR: odds ratio.

[b]Not applicable.

Patients' Perceptions of Telepathology Service Quality

A total of 141 patients who had used telepathology services participated in the survey, as shown in Table 5. The distribution across eastern, central, and western provinces was 31.9% (n=45), 32.6% (n=46), and 35.5% (n=50), respectively. There were 64 males and 77 females, with a male-to-female ratio of 0.83:1. Ages ranged from 19 to 72 years, with a mean age of 33.5 (SD 10.5) years. Most patients held a bachelor's degree (n=59, 41.8%), followed by an associate degree (n=50, 35.5%). Urban residents accounted for 61% (n=86) of patients. Employee medical insurance was the most common type of coverage

XSL•FO
RenderX

(n=81, 57.5%), followed by the New Rural Cooperative Medical Insurance (n=38, 27%). Notably, 76.6% (n=108) of patients reported an average annual family income below 30,000 yuan (US $4335), which is lower than the national per capita disposable income of 39,218 yuan (US $5667) reported in the 2024 China Statistical Yearbook.

Table . Characteristics of the patients participating in telepathology.

Characteristics	Participants, n (%)
District	
East	45 (31.9)
Center	46 (32.6)
West	50 (35.5)
Age (y)	
<30	61 (43.3)
30-39	46 (32.6)
40-49	23 (16.3)
≥50	11 (7.8)
Gender	
Male	64 (45.4)
Female	77 (54.6)
Education	
Doctoral degree	2 (1.4)
Master's degree	6 (4.3)
Bachelor's degree	59 (41.8)
Associate degree	50 (35.5)
High school and below	21 (14.9)
Other	3 (2.1)
Average annual family income (¥)[a]	
<5000	42 (29.8)
5000-9999	26 (18.4)
10,000-14,999	17 (12.1)
15,000-19,999	7 (5)
20,000-24,999	9 (6.4)
25,000-29,999	7 (5)
30,000-49,999	8 (5.7)
≥50,000	25 (17.7)
Location	
Urban	86 (61)
Rural	55 (39)
Insurance	
Employee medical insurance	81 (57.5)
Medical insurance for urban residents	16 (11.4)
New rural cooperative medical insurance	38 (27)
Business insurance	2 (1.4)
No medical insurance	1 (0.7)
Other	3 (2.1)

[a]Exchange rate at the time of the study: US $1=¥6.92.

XSL•FO
RenderX

A total of 99.3% (140/141) of patients reported that the doctor thoroughly explained telepathology, and 96.5% (136/141) had signed the informed consent form, as shown in Table 6. All patients received diagnostic opinions from senior experts. Within 24 hours, 92.2% (130/141) received results; within 48 hours, 98.6% (139/141) received results. Only 1 patient (1/141, 0.7%) received results within 72 hours. Overall, 98.6% (139/141) of patients were satisfied with the waiting time. All 141 patients found telepathology convenient and beneficial for their condition. Regarding service cost, 63.1% (89/141) were charged, with 52 of 89 (58.4%) considering the charges very reasonable, 36 of 89 (40.5%) reasonable, and only 1 of 89 (1.1%) unreasonable.

XSL•FO
RenderX

Table . Telepathology service quality and patient satisfaction (N=141).

Characteristics	Participants, n (%)
Did doctor introduce telepathology in detail?	
Very detailed	97 (68.8)
Detailed	43 (30.5)
Not detailed	1 (0.7)
Did you sign the informed consent form?	
Yes	136 (96.5)
No	5 (3.5)
Convenience of telepathology service	
Very convenient	96 (68.1)
Convenient	45 (31.9)
Inconvenient	0 (0)
Have you received the expert diagnostic opinion?	
Yes	141 (100)
No	0 (0)
Waiting time (h)	
≤12	101 (71.6)
12.1-24	29 (20.6)
24.1-48	9 (6.4)
48.1-72	1 (0.7)
>72	1 (0.7)
Are you satisfied with the waiting time?	
Very satisfied	88 (62.4)
Satisfied	51 (36.2)
Dissatisfied	2 (1.4)
Is telepathology helpful for diseases?	
Very helpful	100 (70.9)
Helpful	41 (29.1)
Unhelpful	0 (0)
Is there a fee for this service?	
Yes	89 (63.1)
No	52 (36.9)
Is the fee reasonable? (n=89)	
Very reasonable	52 (58.4)
Reasonable	36 (40.5)
Unreasonable	1 (1.1)
Has medical expenses been saved?	
Yes	134 (95)
No	7 (5)
Willingness to recommend to others?	
Very willing	93 (66)
Willing	47 (33.3)
Unwilling	0 (0)

XSL•FO
RenderX

Characteristics	Participants, n (%)
Very unwilling	1 (0.7)
Overall satisfaction	
Very satisfied	91 (64.5)
Satisfied	50 (35.5)
Dissatisfied	0 (0)

Patient Satisfaction With Telepathology Services

The overall satisfaction rate was 100% (141/141), with 64.5% (91/141) reporting being “very satisfied”. Among patients, 95% (134/141) believed that telepathology could save medical expenses, and 99.3% (140/141) were willing to recommend it to others. The main reasons for recommendation included convenience (91/140, 65%), access to quality medical services (22/140, 15.7%), cost saving (11/140, 7.9%), time saving (6/140, 4.3%), and necessity (1/140, 0.7%).

Discussion

Principal Results

Diagnosis consistency between WSI and light microscopy has been confirmed, and telepathology is increasingly adopted worldwide [26]. It is widely used for remote primary diagnosis, second-opinion consultations, quality assurance, education, and research [27]. In China, the government has actively promoted telepathology to address the shortage of pathologists in primary health care institutions. However, although most medical institutions in China have implemented telemedicine systems, the utilization rate has remained below 20%, as highlighted at the 2019 subforum of the Global Health Forum of Boao Forum for Asia: Innovation for Health—The Future of Internet Medicine [28]. The actual use of telepathology in Chinese hospitals remains systematically understudied. Although annual surveys by TIPC and NTCC provide cross-sectional snapshots of telemedicine development, they are largely descriptive and lack dedicated analysis of telepathology or longitudinal assessment. To address this gap, this study provides the first systematic examination of telepathology development in China through long-term trend analysis, regional comparisons, and dual perspectives from both clinicians and patients. Based on these findings, targeted recommendations are proposed to inform policy-making and support the sustainable advancement of telepathology in China.

Regarding telepathology infrastructure construction, the highest proportion is networks, while the lowest is digital slide scanners. This is because invited experts only need to provide diagnostic suggestions based on WSI uploaded by the inviting institutions, eliminating the need for slide scanners. From 2018 to 2023, the number of telepathology service cases in China grew steadily, with the median per hospital increasing from 51 to 200 cases, reflecting an average annual growth rate of 31.4%. However, surveys revealed that the proportion of hospitals with established telepathology systems exceeded the proportion of those actually providing services each year. The ratio of service implementation to system construction ranged from 73.8% (59/80) to 82.3% (70/85), a trend consistent with the reported service utilization rates of 72.3% (60/83) to 89.1% (74/83) in the China CNCTPS telepathology platform report [21]. Hitchcock [29] pointed out that the limited implementation of telepathology in developing countries primarily stems from a lack of standardized equipment, inconsistent image formats, and insufficient training for pathologists. Practices in Nigeria [16] further highlighted the significant time cost associated with image scanning and uploading (5 - 10 min per slide for scanning and 10 - 30 min for uploading to the cloud), which has become a critical bottleneck affecting service efficiency. Research by Indian scholars [17] also indicated that challenges such as the large file sizes of WSI, insufficient transmission speeds, and the need for security protection of patient data and images during internet transmission are key factors limiting the application of telepathology. In response to these challenges, various technical approaches have been proposed in the academic community. Emerging technologies such as IoT [30], blockchain-based digital identity authentication [31], and aspect-oriented programming [32] have been proven effective in reducing data transmission latency, enhancing medical information security, and improving system interoperability. These technologies offer feasible solutions for addressing the challenges of cross-institutional secure retrieval of large WSI files. Therefore, promoting the integrated application of these technologies in telepathology holds significant potential for increasing service utilization rates in the future. Moreover, policy and standardization improvements are crucial. Health authorities should promote WSI standardization, clarify cross-institutional licensing rules, and include telepathology in insurance reimbursement.

From a regional distribution perspective, the development of telepathology varies across different areas. Similarly, a national survey in Ireland [33] indicated that the advancement of telemedicine differs significantly across regions, with multiple regional networks established in the east, while development in the west predominantly consisted of isolated links. Our study reveals that the eastern region experienced the fastest growth, with an average annual growth rate of 58%, likely attributable to its more abundant medical resources, stronger economic foundation, and the advantages of policy piloting and early implementation. From 2018 to 2020, the central region reported the highest median number of telepathology diagnostic cases, which may be associated with its lower urbanization rate and relatively scarce rural healthcare resources. According to the China Statistical Yearbook, the urbanization rate in the eastern region was 68.5%, compared with 56.8% in the central region and 54.1% in the western region. Additionally, data from the China Health Statistical Yearbook indicate that from 2018 to

XSL•FO
RenderX

2020, the central region consistently had the lowest number of health technicians per thousand rural population. These factors likely contributed to a higher demand in the central region. To address regional disparities in China's telepathology services, a systematic policy intervention is essential. This includes: (1) Investment: establishing a dedicated fund for central/western regions and integrating telepathology into medical insurance; (2) Operations: implementing unified technical standards and regional diagnostic centers with performance incentives; (3) Capacity: training local pathology technicians and physicians.

The dominant frequency of telepathology usage among pathologists in China was once a week, accounting for 61.1% (160/262). In contrast, a national survey in the United Kingdom revealed that telepathology was rarely used on a weekly or monthly basis [34]. Meanwhile, surveys in South Africa showed that 11% (8/71) used telepathology weekly [35], and a study in Switzerland reported a 31% (42/134) weekly usage rate for telepathology [36]. The average time spent on telepathology services is mainly 11 to 20 and 21 to 30 minutes (161/262, 61.5%), which aligns with the reported average duration of telemedicine services in China [37]. In contrast, a study from the United Kingdom reported that the time taken for telepathology diagnosis averaged 3.9 minutes [38]. Pathologists' acceptance of telepathology demonstrates a strong global consensus. In our study, 95.8% (251/262) of participating pathologists reported overall satisfaction, with 95% (249/262) willing to continue its use. This aligns with international findings: a Saudi Arabian study noted only 1.6% (1/64) had no intention to use telepathology [39]; a UK study involving 18 pathologists found 88.89% (16/18) were likely to continue digital reporting [40]; and a Japanese study showed 70% (16/23) were interested in the system for consultations [41]. Notably, our survey revealed a higher rate of strong intention to use (153/262, 58.4%) compared to the Saudi study (23/64, 35.9%) [39]. This trend extends beyond pathology, as evidenced by a global survey of urologists from 58 countries, where 80.9% (197/244) intended to continue using telemedicine in clinical practice [42]. When analyzing the influencing factors of satisfaction and using intention among pathologists, this study demonstrated that the convenience of system operations and service process had a significant positive impact on pathologists' satisfaction and willingness to use telepathology. Additionally, longer service durations were also associated with positive impact, consistent with prior research on telemedicine services [37]. However, no significant associations were found between pathologists' satisfaction or willingness to use telepathology and factors such as gender, age, education level, or professional title. This is consistent with the findings from a survey of 64 pathologists in Saudi Arabia [39]. The manual navigation tools required for digital slides and the single-layer 2D nature of WSIs demand careful scrutiny by pathologists to ensure diagnostic accuracy. Shorter duration of telepathology may compromise diagnostic precision. Conversely, an intuitive system interface and streamlined service workflow facilitate smoother telepathology diagnosis, thereby enhancing pathologists' engagement and platform retention. The research suggests that improving pathologists' engagement in telepathology depends on optimizing both system design and workflow. To achieve this, medical institutions should: (1) enhance system usability and streamline the consultation process; and (2) reasonably schedule telepathology sessions based on workload and diagnostic quality requirements.

While research on telemedicine from an end-user perspective is extensive, studies focusing on telepathology user attitudes remain limited. This may be because telepathology often does not require direct patient involvement. Nevertheless, we surveyed 141 telepathology patients to assess their experiences and satisfaction. Among them, 92.2% (130/141) and 98.6% (139/141) received diagnostic results within 24 and 48 hours, respectively, surpassing the rates from our previous analysis of Henan Province's telepathology network (64%, 14,835/23,167 and 82.9%, 19,201/23,167) [21] and exceeding those reported by the Québec Telepathology Network in Canada [43]. All patients expressed satisfaction, aligning with the high patient satisfaction reported in other telemedicine surveys in Canada (248/272, 91%) [44], Norway [45], Argentina (116/116, 100%) [46], and Africa [47]. Higher than the survey in India, which indicated that 78% (39/50) of patients with cancer expressed interest in future telemedicine opportunities [48], 99.3% (140/141) were willing to recommend telepathology to others, citing high-quality service, time savings, and cost savings as key reasons. Based on the findings of this study and international comparative data, telepathology services have demonstrated clear and significant advantages in diagnostic turnaround time and patient satisfaction. Therefore, it is recommended that in future public education and service promotion, the core messages of "high quality (expert diagnosis), high efficiency (rapid response), convenience (localized diagnosis and treatment)" and "high satisfaction (patient endorsement)" be precisely communicated. This approach aims to enhance patient awareness and trust, thereby encouraging patients to more proactively choose telepathology services when faced with diagnostic options.

Limitations

This study analyzes the construction and application of telepathology in China from 2018 to 2023 through a nationwide survey, focusing on digital slide scanners, telepathology software, and network connectivity. It also evaluates the progress of telepathology services across hospitals of varying levels and regions. As the first detailed nationwide report on telepathology in China, this study uniquely examines perspectives from both pathologists and patients, covering usage, satisfaction, and influencing factors analysis. The findings provide a comprehensive understanding of telepathology in China and offer actionable recommendations for its enhanced application.

Although our findings offer valuable insights into telepathology in China, this study has several limitations. The sample was based on voluntary participation rather than a longitudinal cohort follow-up, and the significant shift in policy focus toward internet hospitals may have reduced engagement with this telemedicine-specific survey, contributing to the annual decline in sample size. The survey was conducted through TIPC, the national academic organization for telemedicine, and administered via the NTCC website, with participating hospitals spanning most regions. However, the online nature of the survey

XSL•FO
RenderX

may have introduced selection bias. The survey spanned from 2018 to 2023, a period marked by significant advancements in telemedicine and a shift toward internet-based healthcare, driven by national policies. Policy shifts and potential survey fatigue contributed to a decline in valid responses each year. Additionally, the surveys for 2021 and 2022 were disrupted due to the pandemic. Despite these limitations, the survey encompassed a sufficient number of medical institutions across China, and data analysis revealed a clear growth trend in telepathology development. Therefore, while these limitations exist, their impact on the study's conclusions is likely minimal. Besides, in-depth interviews with surveyed pathologists and patients are still lacking to fully understand the barriers of telepathology, so as to put forward more reasonable suggestions.

Given that this study is based on a comprehensive national survey in which the items related to telepathology were relatively general, future research will involve the design and implementation of a specialized telepathology survey. This survey will categorize questions according to service types—such as routine histopathological diagnosis and intraoperative frozen section consultation—to obtain more granular and in-depth data. This approach aims to comprehensively and thoroughly reveal the actual clinical application landscape and differentiated needs of telepathology. Additionally, we will further explore the perspectives of pathologists and patients towards telepathology through semi-structured interviews, which can help to devise corresponding strategies for the better development of telepathology in China.

Conclusion

This study provides the first systematic examination of telepathology development in China through long-term trend analysis, regional comparisons, and dual perspectives of both clinicians and patients. The findings indicate significant growth in the construction and application of telepathology in China from 2018 to 2023, with high levels of acceptance from both pathologists and patients. Factors such as the convenience of system operation, smoothness of service processes, frequency of use, and average duration per session were significantly associated with pathologists' satisfaction and willingness to use telepathology. To enhance the adoption rate of telepathology services, targeted recommendations are proposed around a synergistic "technology-institution-promotion" framework: at the technological level, integrating cloud computing and artificial intelligence to improve system usability; at the institutional level, establishing dedicated funds for central and western regions, promoting the inclusion of telepathology in medical insurance reimbursement, and refining cross-institutional licensing and performance incentive policies; at the promotional level, accurately communicating its core values of "high quality, high efficiency, convenience, and high satisfaction" to the public to encourage proactive patient choice. Through multidimensional systemic interventions, the technological advantages of telepathology can be translated into sustainable primary healthcare service capabilities.

Funding

This research was supported by grants from the National Key R&D Program of China (2022ZD0160705), the Science and Technology Research Program in Henan province (242102311012, 242102311021), the Basic Research and Appled Basic Research Program in Zhengzhou City (Grant No. 2024ZZJCYJ017), the Key Research of Higher Education in Henan province (23A330007), and the Joint Co-construction Program of Medical Science and Technology of Henan province (LHGJ20210313).

Data Availability

The datasets generated during this study are available upon individual request from the corresponding author.

Conflicts of Interest

None declared.

Multimedia Appendix 1
Map of China Showing the Division of Eastern, Central, and Western Regions.
[PNG File, 23 KB - medinform_v14i1e83514_app1.png]

Multimedia Appendix 2
Distribution of the survey coverage areas in China from 2018 to 2023.
[PNG File, 2983 KB - medinform_v14i1e83514_app2.png]

Multimedia Appendix 3
Survey on the development of telemedicine in Chinese hospitals.
[DOCX File, 42 KB - medinform_v14i1e83514_app3.docx]

Multimedia Appendix 4
Table S1. The operation and charging situation of telemedicine in hospitals that carry out telepathology services.

XSL•FO
RenderX

[DOCX File, 14 KB - medinform_v14i1e83514_app4.docx]

Checklist 1
CHERRIES checklist.
[DOCX File, 18 KB - medinform_v14i1e83514_app5.docx]

References

1. Lu ZH, Chen J. National pathology quality report in 2019 [Article in Chinese]. Zhonghua Bing Li Xue Za Zhi 2020 Jul 8;49(7):667-669. [doi: 10.3760/cma.j.cn112151-20200331-00273] [Medline: 32610375]
2. Yefan Y, Shafei W, Yuan L, et al. Survey report on personnel, equipment, and workload in Chinese pathology departments, 2019-2020 [Article in Chinese]. Chin J Pathol 2023;52(9):985-988. [doi: 10.3760/cma.j.cn112151-20230314-00192]
3. Weinstein RS, Bloom KJ, Rozek LS. Telepathology and the networking of pathology diagnostic services. Arch Pathol Lab Med 1987 Jul;111(7):646-652. [Medline: 3606341]
4. Pantanowitz L, Sinard JH, Henricks WH, et al. Validating whole slide imaging for diagnostic purposes in pathology: guideline from the College of American Pathologists Pathology and Laboratory Quality Center. Arch Pathol Lab Med 2013 Dec;137(12):1710-1722. [doi: 10.5858/arpa.2013-0093-CP] [Medline: 23634907]
5. Evans AJ, Brown RW, Bui MM, et al. Validating whole slide imaging systems for diagnostic purposes in pathology. Arch Pathol Lab Med 2022 Apr 1;146(4):440-450. [doi: 10.5858/arpa.2020-0723-CP] [Medline: 34003251]
6. Cross S, Furness P, Igali L, Snead D, Treanor D. Best practice recommendations for implementing digital pathology. : The Royal College of Pathologists; 2018 Jan URL: https://www.rcpath.org/static/f465d1b3-797b-4297-b7fedc00b4d77e51/Best-practice-recommendations-for-implementing-digital-pathology.pdf [accessed 2025-11-25]
7. Montgomery ND, Liomba NG, Kampani C, et al. Accurate real-time diagnosis of lymphoproliferative disorders in Malawi through clinicopathologic teleconferences: a model for pathology services in sub-Saharan Africa. Am J Clin Pathol 2016 Oct;146(4):423-430. [doi: 10.1093/ajcp/aqw118] [Medline: 27594430]
8. Shinohara S, Bychkov A, Munkhdelger J, et al. Substantial improvement of histopathological diagnosis by whole-slide image-based remote consultation. Virchows Arch 2022 Aug;481(2):295-305. [doi: 10.1007/s00428-022-03327-2] [Medline: 35672584]
9. Girolami I, Pantanowitz L, Marletta S, et al. Diagnostic concordance between whole slide imaging and conventional light microscopy in cytopathology: a systematic review. Cancer Cytopathol 2020 Jan;128(1):17-28. [doi: 10.1002/cncy.22195] [Medline: 31600035]
10. García-Rojo M. International clinical guidelines for the adoption of digital pathology: a review of technical aspects. Pathobiology 2016;83(2-3):99-109. [doi: 10.1159/000441192] [Medline: 27100834]
11. Hanna MG, Pantanowitz L, Evans AJ. Overview of contemporary guidelines in digital pathology: what is available in 2015 and what still needs to be addressed? J Clin Pathol 2015 Jul;68(7):499-505. [doi: 10.1136/jclinpath-2015-202914] [Medline: 25979986]
12. Hanna MG, Reuter VE, Samboy J, et al. Implementation of digital pathology offers clinical and operational increase in efficiency and cost savings. Arch Pathol Lab Med 2019 Dec;143(12):1545-1555. [doi: 10.5858/arpa.2018-0514-OA] [Medline: 31173528]
13. 510(k) clearances. US Food and Drug Administration (FDA). URL: https://www.fda.gov/medical-devices/device-approvals-and-clearances/510k-clearances [accessed 2026-01-04]
14. Digital pathology-related medical device [Article in Chinese]. National Medical Products Administration. URL: https://www.nmpa.gov.cn/datasearch/search-result.html [accessed 2026-01-04]
15. Kayser K. Telepathology in Europe. Anal Cell Pathol 2000;21(3-4):95-96. [doi: 10.1155/2000/757486] [Medline: 11339573]
16. Silas OA, Abdulkareem F, Novo JE, et al. Telepathology in Nigeria for global health collaboration. Ann Glob Health 2022;88(1):81. [doi: 10.5334/aogh.3673] [Medline: 36196362]
17. Feroz A, Mohammed Feroz TP, Bastian TS, Selvamani M. Telepathology: an update on applications, latest advances, and current status in Indian scenario. J Cancer Res Ther 2020;16(4):703-707. [doi: 10.4103/jcrt.JCRT_477_17] [Medline: 32930106]
18. Mremi A, Bentzer NK, Mchome B, et al. The role of telepathology in diagnosis of pre-malignant and malignant cervical lesions: implementation at a tertiary hospital in Northern Tanzania. PLoS ONE 2022;17(4):e0266649. [doi: 10.1371/journal.pone.0266649] [Medline: 35421156]
19. Pare G, Meyer J, Trudel MC, Tetu B. Impacts of a large decentralized telepathology network in Canada. Telemed J E Health 2016 Mar;22(3):246-250. [doi: 10.1089/tmj.2015.0083] [Medline: 26252758]
20. Tong S, Lili N, Zhouping T, Yanyan C. Construction of a remote pathology consultation service platform based on internet hospitals [Article in Chinese]. Chin J Hosp Admin 2024;40(3):236-240. [doi: 10.3760/cma.j.cn111325-20230815-00078]
21. He X, Wang L, Wang L, et al. Effectiveness of a cloud-based telepathology system in China: large-sample observational study. J Med Internet Res 2021 Jul 29;23(7):e23799. [doi: 10.2196/23799] [Medline: 34326037]

XSL•FO
RenderX

22. Chen J, Jiao Y, Lu C, Zhou J, Zhang Z, Zhou C. A nationwide telepathology consultation and quality control program in China: implementation and result analysis. Diagn Pathol 2014;9 Suppl 1(Suppl 1):S2. [doi: 10.1186/1746-1596-9-S1-S2] [Medline: 25565398]
23. NTCC. URL: https://www.ntcc.org.cn [accessed 2026-02-26]
24. Eysenbach G. Improving the quality of web surveys: the Checklist for Reporting Results of Internet E-Surveys (CHERRIES). J Med Internet Res 2004 Sep 29;6(3):e34. [doi: 10.2196/jmir.6.3.e34] [Medline: 15471760]
25. Wang P, Hong J, Tang ZQ, et al. The acceptance of traditional Chinese medicine among patients with Parkinson's disease: a hospital survey. J Integr Med 2024 Mar;22(2):180-187. [doi: 10.1016/j.joim.2024.03.005] [Medline: 38519276]
26. Tsuchihashi Y. Expanding application of digital pathology in Japan--from education, telepathology to autodiagnosis. Diagn Pathol 2011 Mar 30;6 Suppl 1(Suppl 1):S19. [doi: 10.1186/1746-1596-6-S1-S19] [Medline: 21489189]
27. Farahani N, Pantanowitz L. Overview of telepathology. Clin Lab Med 2016 Mar;36(1):101-112. [doi: 10.1016/j.cll.2015.09.010] [Medline: 26851668]
28. Xiaohui W. The utilization rate of telemedicine is less than 20%. Related prices and medical insurance policies will be introduced before September. URL: https://www.chinatimes.net.cn/article/87356.html [accessed 2024-06-02]
29. Hitchcock CL. The future of telepathology for the developing world. Arch Pathol Lab Med 2011 Feb;135(2):211-214. [doi: 10.5858/135.2.211] [Medline: 21284440]
30. Harasees A, Al-Ahmad B, Alsobeh A, Abuhussein A. A secure IoT framework for remote health monitoring using fog computing. Presented at: 2024 International Conference on Intelligent Computing, Communication, Networking and Services (ICCNS); Sep 24-27, 2024; Dubrovnik, Croatia p. 17-24. [doi: 10.1109/ICCNS62192.2024.10776425]
31. Hasan FA, Ashqar HI, AlSobeh A, Darwish O. Blockchain-based national digital identity framework – case of Palestine. Presented at: 2024 International Conference on Intelligent Computing, Communication, Networking and Services (ICCNS); Sep 24-27, 2024; Dubrovnik, Croatia p. 76-83. [doi: 10.1109/ICCNS62192.2024.10776538]
32. AlSobeh AMR, Hammad R, Tamimi AKA. A modular cloud-based ontology framework for context-aware EHR services. Int J Comput Appl Technol 2019;60(4):339-350. [doi: 10.1504/IJCAT.2019.101181]
33. Maher L, Craig A, Menezes G. A national survey of telemedicine in the Republic of Ireland. J Telemed Telecare 2007;13(7):348-351. [doi: 10.1258/135763307782215361] [Medline: 17958936]
34. Dennis T, Start RD, Cross SS. The use of digital imaging, video conferencing, and telepathology in histopathology: a national survey. J Clin Pathol 2005 Mar;58(3):254-258. [doi: 10.1136/jcp.2004.022012] [Medline: 15735155]
35. Eloff E, Schoeman R. Digital pathology in South Africa: a survey and cross-sectional analysis of the current level of use and comparison with the international community. Int J Telemed Appl 2025;2025:7990652. [doi: 10.1155/ijta/7990652] [Medline: 40917478]
36. Unternaehrer J, Grobholz R, Janowczyk A, Zlobec I, Swiss Digital Pathology Consortium (SDiPath). Current opinion, status and future development of digital pathology in Switzerland. J Clin Pathol 2020 Jun;73(6):341-346. [doi: 10.1136/jclinpath-2019-206155] [Medline: 31857377]
37. Ma Q, Sun D, Tan Z, et al. Usage and perceptions of telemedicine among health care professionals in China. Int J Med Inform 2022 Oct;166:104856. [doi: 10.1016/j.ijmedinf.2022.104856] [Medline: 36037593]
38. Leong FJ, Graham AK, Schwarzmann P, McGee JO. Clinical trial of telepathology as an alternative modality in breast histopathology quality assurance. Telemed J E Health 2000;6(4):373-377. [doi: 10.1089/15305620050503834] [Medline: 11242544]
39. Alawashiz R, AlDossary SA. Pathologists' acceptance of telepathology in the Ministry of National Guard Health Affairs Hospitals in Saudi Arabia: a survey study. Digit Health 2023;9:20552076231163672. [doi: 10.1177/20552076231163672] [Medline: 36937697]
40. Browning L, Fryer E, Roskell D, et al. Role of digital pathology in diagnostic histopathology in the response to COVID-19: results from a survey of experience in a UK tertiary referral hospital. J Clin Pathol 2021 Feb;74(2):129-132. [doi: 10.1136/jclinpath-2020-206786] [Medline: 32616541]
41. Nakayama I, Matsumura T, Kamataki A, et al. Development of a teledermatopathology consultation system using virtual slides. Diagn Pathol 2012 Dec 13;7:177. [doi: 10.1186/1746-1596-7-177] [Medline: 23237667]
42. Dubin JM, Wyant WA, Balaji NC, et al. Telemedicine usage among urologists during the COVID-19 pandemic: cross-sectional study. J Med Internet Res 2020 Nov 5;22(11):e21875. [doi: 10.2196/21875] [Medline: 33031047]
43. Perron E, Louahlia S, Nadeau L, et al. Telepathology for intraoperative consultations and expert opinions: the experience of the Eastern Québec Telepathology Network. Arch Pathol Lab Med 2014 Sep;138(9):1223-1228. [doi: 10.5858/arpa.2013-0466-OA] [Medline: 25171705]
44. Strasser L, Hayawi L, Webster RJ, Venkateswaran S, Muir K. Telemedicine in pediatric neurology: a survey of patient and provider experience. J Child Neurol 2025 Feb;40(2):99-115. [doi: 10.1177/08830738241287243] [Medline: 39539164]
45. Moseng D. Teledermatology--experiences from Northern Norway [Article in Norwegian]. Tidsskr Nor Laegeforen 2000 Jun 20;120(16):1893-1895. [Medline: 10925620]
46. Fortini S, Espeche A, Caraballo R. Telemedicine and epilepsy: a patient satisfaction survey of a pediatric remote care program. Epilepsy Res 2020 Sep;165:106370. [doi: 10.1016/j.eplepsyres.2020.106370] [Medline: 32516743]

XSL•FO
RenderX

47. Kurji K, Kiage D, Rudnisky CJ, Damji KF. Improving diabetic retinopathy screening in Africa: patient satisfaction with teleophthalmology versus ophthalmologist-based screening. Middle East Afr J Ophthalmol 2013;20(1):56-60. [doi: 10.4103/0974-9233.106388] [Medline: 23580853]
48. Sharma SK, Kumar M, Datla PKV, et al. Assessment of IPD patients' knowledge and attitudes toward telemedicine at tertiary care hospital of Metro City. J Pharm Bioallied Sci 2025 Sep;17(Suppl 3):S2376-S2380. [doi: 10.4103/jpbs.jpbs_1471_24] [Medline: 41164588]

Abbreviations

CHERRIES: Checklist for Reporting Results of Internet E-Surveys
NTCC: National Telemedicine Center of China
TIPC: Telemedicine Informationization Professional Committee of China
WSI: whole-slide image

Edited by A Rosania; submitted 04.Sep.2025; peer-reviewed by A AlSobeh, C Ling, W Zhang; accepted 01.Feb.2026; published 16.Mar.2026.

Please cite as:
Wang L, Cui F, He X
Telepathology Development and Stakeholder Perspectives in China: Cross-Sectional Survey
JMIR Med Inform 2026;14:e83514
URL: https://medinform.jmir.org/2026/1/e83514
doi:10.2196/83514

© Linlin Wang, Fangfang Cui, Xianying He. Originally published in JMIR Medical Informatics (https://medinform.jmir.org), 16.Mar.2026. This is an open-access article distributed under the terms of the Creative Commons Attribution License (https://creativecommons.org/licenses/by/4.0/), which permits unrestricted use, distribution, and reproduction in any medium, provided the original work, first published in JMIR Medical Informatics, is properly cited. The complete bibliographic information, a link to the original publication on https://medinform.jmir.org/, as well as this copyright and license information must be included.

XSL•FO
RenderX

Ethical Imperatives for Retrieval-Augmented Generation in Clinical Nursing: Viewpoint on Responsible AI Use

Xinyi Tu[1,2*], BSN; Chenghao Shi[1*], MN; Peilin Qian[3], BSN; Lizhu Wang[1], MPH

[1]Department of Nursing, The Second Affiliated Hospital of Zhejiang University School of Medicine, No. 88 Jiefang Road, Shangcheng District, Hangzhou, Zhejiang, China

[2]School of Medicine, Zhejiang University, Hangzhou, Zhejiang, China

[3]School of Nursing, Chinese Academy of Medical Sciences & Peking Union Medical College, Beijing, Beijing, China

[*]these authors contributed equally

Corresponding Author:
Lizhu Wang, MPH
Department of Nursing, The Second Affiliated Hospital of Zhejiang University School of Medicine, No. 88 Jiefang Road, Shangcheng District, Hangzhou, Zhejiang, China

Abstract

Retrieval-augmented generation (RAG) systems have emerged as a powerful technique to enhance the capabilities of large language models by enabling them to access external, up-to-date knowledge in real time, and RAG systems are being increasingly adopted by researchers in the medical field. In this viewpoint article, we explore the ethical imperatives for implementing RAG systems in clinical nursing environments, with particular attention to how these technologies affect patient care quality and safety. The purpose of this paper is to examine the ethical risks introduced by RAG-enhanced large language models in clinical nursing and to propose strategic guidelines for their responsible implementation. Key considerations include ensuring accuracy, fairness, transparency, and accountability, as well as maintaining essential human oversight, as discussed through a structured analysis. We argue that robust data governance, explainable artificial intelligence (AI) techniques, and continuous monitoring are critical components of a responsible RAG implementation strategy. Ultimately, realizing the benefits of RAG while mitigating ethical concerns requires sustained collaboration among health care professionals, AI developers, and policymakers, fostering a future where AI supports patient safety, reduces disparities, and improves the quality of nursing care.

(JMIR Med Inform 2026;14:e79922) doi:10.2196/79922

KEYWORDS

large language models; clinical decision-making; ethics; fairness; transparency

Introduction

Advances in artificial intelligence (AI) are rapidly transforming the health care field, with large language models (LLMs) playing a pivotal role in revolutionizing nursing practice [1,2]. These models enhance human capabilities by learning patterns from large amounts of text data and generating contextually relevant information, offering benefits such as improved decision support, streamlined care planning, and personalized patient education [3]. LLMs can assist nurses by providing comprehensive insights and generating evidence-based recommendations. However, their integration into clinical workflows faces significant challenges [4], partly because LLMs do not operate like traditional rule-based programs. Instead, they generate responses based on statistical patterns learned from large text corpora, rather than performing logical reasoning or interpreting meaning as humans do.

While this generative capability allows LLMs to produce contextually relevant and fluent text, it also gives rise to several critical limitations in specialized clinical applications. These include biases inherited from training data and the "black-box" nature of their decision-making processes, which make it difficult to understand how outputs are produced. Such issues lead to concerns about trust and transparency, ultimately undermining the reliability of model-generated recommendations in high-stakes health care environments [5,6].

To address these shortcomings, the retrieval-augmented generation (RAG) system has emerged as an enhancement to LLMs. By combining external knowledge retrieval with the language patterns an LLM has learned during training, RAG can provide more accurate, up-to-date, and context-sensitive information [7]. In this paper, the term "RAG system" refers to the practical implementation of the RAG approach, in which an LLM retrieves external information from databases or documents and integrates it with the patterns learned during training to generate context-aware responses. While this approach aims to overcome the static nature of traditional LLMs, it introduces new ethical risks, particularly related to the quality and reliability of external data sources, the complexity of information traceability, and privacy concerns [4].

XSL•FO
RenderX

This article examines the ethical challenges introduced by RAG-optimized LLMs in clinical nursing and proposes strategies for responsible implementation. We focus on three core ethical imperatives: ensuring accuracy, fairness, and bias mitigation; promoting transparency, explainability, and trust; and maintaining responsibility, accountability, and oversight. By addressing these challenges proactively, we can harness the benefits of RAG to enhance nursing practice while safeguarding patient well-being.

The Promise and Peril of RAG in Nursing

Overview

RAG offers significant opportunities to enhance clinical nursing practice by providing more accurate, up-to-date, and context-specific information. By combining the language-pattern learning capability of LLMs with external knowledge retrieval, RAG can address some of the limitations of traditional LLMs [8]. However, alongside its potential benefits, RAG also introduces unique risks that need to be carefully considered, particularly in the context of clinical nursing.

The Promise of RAG in Nursing

The primary advantage of RAG lies in its ability to enhance decision support by integrating real-time, relevant knowledge from external sources. In high-pressure environments, such as hospitals, where quick decision-making is critical, RAG can significantly improve the accuracy of clinical recommendations by ensuring they are based on the latest research and guidelines [7,9]. By enabling real-time access to updated information, RAG helps reduce errors that may arise from outdated or incomplete data [9].

Additionally, RAG systems build on what the LLM has learned from language data to provide personalized and context-specific recommendations by incorporating patient-specific data, such as medical history, treatment plans, and current health status. This ability to tailor recommendations to the individual needs of patients ensures that health care providers can deliver more accurate and effective care [10]. In settings with limited resources, RAG can provide vital support for nurses by offering evidence-based recommendations that might otherwise be difficult to access due to time constraints or a lack of available resources [9].

The Peril of RAG in Nursing

Overview of Risks

Despite its advantages, the use of RAG systems in nursing also introduces a range of ethical challenges and risks. Many of these challenges stem from the limitations of the underlying LLMs on which RAG is built—including issues such as bias, opacity, and a lack of accountability. At the same time, RAG introduces additional, system-specific risks because it retrieves and integrates external information dynamically at query time. These additional risks center on data quality, source reliability, semantic coherence, and information provenance and must be carefully addressed in clinical applications.

Common Risks of LLMs

Many of the risks associated with RAG are rooted in the inherent challenges of LLMs, which include the following:

- Bias and fairness: LLMs may perpetuate biases that are present in their training data, such as racial, gender, or cultural biases [11]. Since RAG systems rely on external sources, they can also inherit and even amplify these biases if the external data sources are not sufficiently diverse or representative [4]. This is particularly concerning in nursing, where such biases can lead to unequal treatment and care disparities, potentially exacerbating health inequalities [12].
- Transparency and explainability: The “black-box” nature of LLMs remains a significant issue, making it difficult for clinicians to understand how the model produces its responses [13,14]. While RAG can improve transparency by citing the sources of external information, the process may still be opaque. This lack of explainability can undermine trust in the system, especially when nurses are unable to interpret the reasoning behind a recommendation [5,15].
- Accountability: Another concern is who should bear responsibility when a RAG system provides a recommendation that leads to an error or harm. It may be unclear who is responsible—whether it is the developers of the model, the clinical staff who implemented it, or the health care institution as a whole. This ambiguity complicates accountability and the governance of AI-driven health care systems [16].

Risks Specific to RAG

While many of the risks in RAG are shared with LLMs, there are several risks that are unique to RAG systems due to their reliance on outside information sources.

- Information provenance and quality: RAG systems pull data from many different websites, databases, and documents. Some of these sources may not undergo rigorous peer review, and there may be discrepancies in the information retrieved [17,18]. When the information used by RAG is incomplete or unreliable, the guidance it gives can also be misleading. It can also be difficult to check exactly where the information came from, which makes it harder for nurses to judge whether a recommendation can be trusted [19].
- Semantic integration and coherence: When a RAG system combines information drawn from many sources, the final advice may sound uneven or use different styles of wording. For a nurse using it, this means different parts of the output may suggest slightly different approaches, which can create confusion or reduce confidence in applying the recommendation [20]. Merging text generated from different materials may result in conflicting or incompatible pieces of information, which can cause confusion or misinterpretation [21]. This issue is particularly problematic in clinical contexts, where accuracy and consistency are essential for patient safety [22].
- Privacy and security risks: To offer personalized advice, RAG systems may need access to sensitive patient data, such as medical histories, to provide personalized

XSL•FO
RenderX

recommendations [18,23]. If the system's security is weak, or if it does not meet privacy standards like HIPAA (Health Insurance Portability and Accountability Act) or GDPR (General Data Protection Regulation), confidential information could be exposed. Such data breaches could harm both patients and the health care institution [5].

- Shifting trust foundations: Traditional LLMs depend only on the language relationships learned during training, but RAG depends on both internal and external sources. This means that the reliability of RAG depends not only on the model itself but also on the trustworthiness of the outside information it uses [24,25]. If that outside data is wrong or biased, the recommendations produced by the RAG system may be wrong too, reducing nurses' confidence in using the system [18,19,26].

An example is as follows: A nurse used a RAG-based tool to check evidence for pressure injury prevention. The system retrieved the 2014 second edition of the international pressure ulcer guideline, which recommended turning the patient every 2 hours on standard foam surfaces. However, the upcoming 2025 fourth edition emphasizes individualized repositioning schedules, the use of alternating-pressure mattresses, and closer monitoring for deep tissue injury in high-risk or obese patients. Because the RAG system relied on outdated data, the nurse followed the older 2-hour rule and missed early signs of a deep tissue injury. This case shows how outdated retrieval sources can lead to substandard care and highlights the need for RAG systems to verify and update their evidence sources regularly.

Focused Ethical Challenges

Overview

The introduction of RAG systems into clinical nursing presents several ethical challenges that need to be carefully considered. These challenges are not only rooted in the inherent limitations of how LLMs learn from data but also amplified by the integration of external knowledge sources [18,27]. In this section, we focus on three core ethical challenges: accuracy, bias, and fairness; transparency, explainability, and trust; and responsibility, accountability, and human oversight. These challenges must be addressed to ensure that RAG-enhanced LLMs support ethically evidence-based decisions in nursing practice [28].

Accuracy, Bias, and Fairness

One key ethical concern when using RAG systems is maintaining the accuracy of the information they generate, especially for clinical decisions [3,19]. The accuracy of RAG depends directly on how reliable and up-to-date the outside sources are [9]. If the outside sources are outdated, incomplete, or inaccurate, the systems' recommendations may mislead nurses and lead to unsafe decisions that could harm patients [18,19]. Therefore, RAG systems should only use checked and high-quality data that fits the medical context [18].

Additionally, bias remains a significant challenge. RAG systems can carry bias from both the training data used to develop the LLMs and the outside sources it pulls information from [26,29]. These biases can manifest in various forms, such as racial, gender, or socioeconomic biases, and can show up as racial, gender, or economic differences and may cause unfair care for some patients [30,31]. In clinical settings, where health gaps already exist, AI-related bias can make these gaps worse. For example, if RAG systems draw information from databases that underrepresent minority populations, the resulting recommendations may be less accurate or effective for these groups [32].

To reduce these risks, we need continued work to make AI systems fair [16,18]. This means checking that outside sources cover different patient groups and reviewing the system's outputs regularly for bias. Furthermore, health care institutions and developers should also focus on including a wide range of patients in AI training data and retrieval sources to avoid making health gaps worse [33,34].

Transparency, Explainability, and Trust

Another significant ethical challenge is transparency and explainability. While RAG systems can increase transparency by showing the sources of information, the process by which these models generate their responses is still not very clear [18,35]. Because their internal workings are complex and often hidden, it can be hard for clinicians to see how external data and built-in knowledge come together to form a recommendation [36]. This lack of clarity can reduce trust in the system, since clinicians might hesitate to use a tool whose reasoning process cannot be easily interpreted [15,37,38].

Explainability is particularly important in clinical settings, where nurses and health care professionals need to understand the basis for AI-generated suggestions in order to trust them and incorporate them into their decision-making process [15,39,40]. It is essential for RAG systems to explain their answers in a way that is easy for health care professionals to understand. For example, providing confidence scores or source citations can help clinicians evaluate the reliability of the information and determine whether it fits the patient's situation [38,41].

Enhancing transparency and explainability will not only help build trust in AI systems but also foster responsible and ethical AI adoption in clinical practice. As RAG systems become more integrated into health care systems, transparency will be key to ensuring that their use aligns with professional standards and ethical guidelines [6].

Responsibility, Accountability, and Human Oversight

Responsibility and accountability are key ethical concerns in the context of AI-driven decision-making. One of the main challenges in using RAG systems is that responsibility can become blurred when many parties—such as AI developers, health care providers, and institutions—take part in the same process [42]. If an error occurs because of a recommendation from a RAG system, it may be unclear who should bear responsibility for it. This uncertainty can make legal and ethical management of such situations more difficult [43,44].

To address this issue, it is important to have clear guidelines that define the roles and duties of everyone involved in the AI decision-making process [45]. Health care institutions must ensure that there are well-defined accountability structures in

XSL•FO
RenderX

place to determine who is responsible when AI systems make errors [6]. Furthermore, RAG systems should be designed with human supervision in mind. While they can enhance decision support, they should never replace human judgment. Nurses and clinicians must be able to step in or question the AI-generated recommendations if they believe the advice is not in the patients' best interest [46,47].

Keeping humans actively in each stage of the process, which is often called "human-in-the-loop" oversight, is crucial to maintaining ethical standards in AI-assisted clinical care [48,49]. This approach ensures that clinical decisions are ultimately guided by human expertise, with AI acting only as a support tool. To support this approach, ongoing training for health care professionals on the use of AI systems, along with mechanisms for reporting and addressing errors, will help uphold ethical standards and ensure that the use of RAG systems benefits patients while minimizing risks.

Addressing these ethical concerns requires not only awareness but also systematic strategies to guide responsible use of RAG systems in nursing practice.

Strategies for Responsible RAG Implementation

Overview

Building on the ethical challenges discussed in the *Focused Ethical Challenges* section, it is essential to implement strategies that ensure the responsible and effective use of RAG systems in clinical nursing. While RAG systems offer significant advantages, such as real-time decision support and personalized care recommendations, they also introduce unique risks. To maximize the benefits of RAG and minimize its ethical concerns, we propose several key strategies for responsible implementation. These strategies are designed as direct responses to the ethical challenges identified in the *Focused Ethical Challenges* section, translating theoretical imperatives into actionable guidance for nursing practice.

Data Governance and Bias Mitigation

Building on the discussion of bias and fairness in *Accuracy, Bias, and Fairness*, effective data governance provides the foundation for responsible RAG implementation. Because RAG systems rely on external knowledge sources, ensuring the integrity and representativeness of these data is essential. Biases in the external data used for retrieval can have a significant impact on the outputs generated by the system, potentially leading to unfair or discriminatory outcomes [12,50,51].

To mitigate these risks, bias detection and correction mechanisms must be implemented at multiple stages of the RAG system's development and deployment. Specifically, RAG systems should incorporate bias auditing practices to identify potential biases in the external datasets used for retrieval. This includes regular audits of the data sources to ensure they are inclusive and reflect a broad range of patient demographics and clinical scenarios [12,50]. Additionally, techniques such as fairness-aware machine learning and adversarial debiasing can be employed to reduce the impact of bias in the model's generated recommendations. By continuously monitoring and correcting for bias, health care organizations can help ensure that RAG systems provide fair and equitable information support for all patients [43].

Explainable AI and Transparent Decision-Making

Building on the transparency challenges identified earlier, explainable AI techniques should be integrated into RAG systems to enhance transparency and help nurses and clinicians trust the information these systems produce. By improving the explainability of RAG systems, health care professionals can better assess the basis of AI-generated suggestions and integrate them into their decision-making processes [5].

One effective way to enhance transparency is by incorporating confidence scores and contextual explanations. Confidence scores provide an indication of how certain the system is about a given output, giving clinicians a clearer understanding of the model's reliability [52]. Contextual explanations, on the other hand, help clarify the basis for a given response by linking it to relevant patient data or clinical guidelines. For instance, a RAG system might explain that a particular medication recommendation is based on the patient's medical history, current health status, and recent clinical studies [18]. This additional layer of information will not only improve trust in the system but also empower nurses to make informed decisions based on AI recommendations [47].

Operationalizing Human Oversight and Collaborative Intelligence

Extending the discussion of accountability from the *Responsibility, Accountability, and Human Oversight* section, it is crucial to emphasize the role of human-in-the-loop oversight. RAG systems should not replace human judgment but rather augment it. Nurses, doctors, and other health care professionals should remain central to the decision-making process, with RAG systems serving as assistive tools to support clinical judgment rather than a substitute for clinical expertise [9,19,26].

To ensure the effectiveness of human-AI collaboration, health care organizations should establish clear guidelines for collaborative intelligence. This includes defining roles and responsibilities for both human and AI components of the decision-making process. Nurses and clinicians should be trained to understand the strengths and limitations of RAG systems and to intervene when they believe the AI-generated recommendation is not appropriate for the patient's context [6,37,53]. In addition, RAG systems should be designed to provide options for clinicians to modify or override system-generated outputs when necessary, allowing for greater flexibility and ensuring that human expertise is always part of the decision-making process [19,54,55].

Continuous Monitoring and Evaluation

To ensure the ongoing effectiveness and ethical integrity of RAG systems, continuous monitoring and evaluation are essential. After RAG systems are deployed in clinical practice, they must be regularly assessed for both technical accuracy and ethical impact. This process should include performance audits,

XSL•FO
RenderX

where the system's outputs and their clinical relevance are evaluated against real-world data. Continuous monitoring should also include version control and scheduled updates of external data sources to prevent outdated or inconsistent information from influencing clinical recommendations [56].

Moreover, it is equally important to assess the ethical implications of RAG systems over time. This involves gathering feedback from health care professionals who use the system, as well as patients who are impacted by the decisions. Implementing a structured feedback mechanism is critical to identify potential ethical risks such as new biases, privacy concerns, or trust issues that may arise after the model has been in use for some time [6,57]. By continuously monitoring the performance and ethical consequences of RAG systems, health care organizations can make necessary adjustments to ensure that these systems remain aligned with ethical standards and improve patient care without causing harm.

Conclusion

RAG systems have the potential to significantly enhance nursing practice by providing accurate, context-aware, and timely information support for clinical decisions. By integrating external knowledge sources into clinical reasoning, RAG can improve patient outcomes, particularly in high-pressure environments where rapid, evidence-based decisions are crucial. However, as with any emerging technology, the deployment of RAG systems in clinical settings must be approached with caution, taking into account both the opportunities and the ethical risks they introduce.

The ethical challenges associated with RAG, including issues of accuracy, fairness, transparency, explainability, accountability, and human oversight, must be proactively addressed to ensure that these systems are used responsibly. By implementing robust data governance, ensuring the explainability of AI recommendations, maintaining human-in-the-loop oversight, and continuously monitoring the model's performance and ethical impact, health care organizations can harness the benefits of RAG while minimizing the potential risks.

Ultimately, responsible RAG implementation will require collaboration between health care professionals, AI developers, and policymakers. By prioritizing ethical considerations in the deployment of RAG systems, we can ensure that they support patient safety, reduce health care disparities, and contribute to the overall improvement of nursing practice. Through careful, responsible integration, RAG systems have the potential to transform the future of clinical decision-making and enhance the quality of care delivered to patients worldwide.

Acknowledgments

This paper was language-polished using the generative artificial intelligence (AI) tool ChatGPT by OpenAI. The authors carefully reviewed and revised all AI-generated suggestions to ensure accuracy, clarity, and academic integrity. The authors take full responsibility for the content.

Funding

The authors declare that no financial support was received for the research, authorship, and/or publication of this article.

Authors' Contributions

XT conceived the topic, outlined the article, and contributed to the manuscript's drafting and writing. CS refined the outline and contributed to the manuscript writing. PQ contributed to the manuscript writing. LW provided revisions and guidance as corresponding author and supervisor. All authors contributed to the study's preparation and approved the final version of the manuscript.

Conflicts of Interest

None declared.

References

1. Goktas P, Grzybowski A. Shaping the future of healthcare: ethical clinical challenges and pathways to trustworthy AI. J Clin Med 2025 Feb 27;14(5):1605. [doi: 10.3390/jcm14051605] [Medline: 40095575]
2. Kung TH, Cheatham M, Medenilla A, et al. Performance of ChatGPT on USMLE: potential for AI-assisted medical education using large language models. PLOS Digit Health 2023 Feb;2(2):e0000198. [doi: 10.1371/journal.pdig.0000198] [Medline: 36812645]
3. Nashwan AJ, Abujaber AA. Harnessing large language models in nursing care planning: opportunities, challenges, and ethical considerations. Cureus 2023 Jun;15(6):e40542. [doi: 10.7759/cureus.40542] [Medline: 37465807]
4. Yang X, Chen A, PourNejatian N, et al. A large language model for electronic health records. NPJ Digit Med 2022 Dec 26;5(1):194. [doi: 10.1038/s41746-022-00742-2] [Medline: 36572766]
5. Bhagat SV, Kanyal D. Navigating the future: the transformative impact of artificial intelligence on hospital management - a comprehensive review. Cureus 2024 Feb;16(2):e54518. [doi: 10.7759/cureus.54518] [Medline: 38516434]

XSL•FO
RenderX

6. Markus AF, Kors JA, Rijnbeek PR. The role of explainability in creating trustworthy artificial intelligence for health care: a comprehensive survey of the terminology, design choices, and evaluation strategies. J Biomed Inform 2021 Jan;113:103655. [doi: 10.1016/j.jbi.2020.103655] [Medline: 33309898]
7. Gao Y, Xiong Y, Gao X, et al. Retrieval-augmented generation for large language models: a survey. arXiv. Preprint posted online on Dec 18, 2023. [doi: 10.48550/arXiv.2312.10997]
8. Verma S. Contextual compression in retrieval-augmented generation for large language models: a survey. arXiv. Preprint posted online on Sep 20, 2024. [doi: 10.48550/arXiv.2409.13385]
9. Miao J, Thongprayoon C, Suppadungsuk S, Garcia Valencia OA, Cheungpasitporn W. Integrating retrieval-augmented generation with large language models in nephrology: advancing practical applications. Medicina (Kaunas) 2024 Mar 8;60(3):445. [doi: 10.3390/medicina60030445] [Medline: 38541171]
10. Ceriello A, Gallo M, Candido R, et al. Personalized therapy algorithms for type 2 diabetes: a phenotype-based approach. Pharmgenomics Pers Med 2014;7:129-136. [doi: 10.2147/PGPM.S50288] [Medline: 24971031]
11. Jiao J, Afroogh S, Xu Y, Phillips C. Navigating LLM ethics: advancements, challenges, and future directions. AI Ethics 2025 Dec;5(6):5795-5819. [doi: 10.1007/s43681-025-00814-5]
12. Arora A, Alderman JE, Palmer J, et al. The value of standards for health datasets in artificial intelligence-based applications. Nat Med 2023 Nov;29(11):2929-2938. [doi: 10.1038/s41591-023-02608-w] [Medline: 37884627]
13. Riedemann L, Labonne M, Gilbert S. The path forward for large language models in medicine is open. NPJ Digit Med 2024 Nov 27;7(1):339. [doi: 10.1038/s41746-024-01344-w] [Medline: 39604549]
14. Yoon CH, Torrance R, Scheinerman N. Machine learning in medicine: should the pursuit of enhanced interpretability be abandoned? J Med Ethics 2022 Sep;48(9):581-585. [doi: 10.1136/medethics-2020-107102] [Medline: 34006600]
15. Marey A, Arjmand P, Alerab ADS, et al. Explainability, transparency and black box challenges of AI in radiology: impact on patient care in cardiovascular radiology. Egypt J Radiol Nucl Med 2024;55(1). [doi: 10.1186/s43055-024-01356-2]
16. Pham T. Ethical and legal considerations in healthcare AI: innovation and policy for safe and fair use. R Soc Open Sci 2025 May;12(5):241873. [doi: 10.1098/rsos.241873] [Medline: 40370601]
17. Wang F, Wan X, Sun R, Chen J, Arik SO. Astute RAG: overcoming imperfect retrieval augmentation and knowledge conflicts for large language models. Presented at: Proceedings of the 63rd Annual Meeting of the Association for Computational Linguistics (Volume 1: Long Papers); Jul 27 to Aug 1, 2025. [doi: 10.18653/v1/2025.acl-long.1476]
18. Yang R, Ning Y, Keppo E, et al. Retrieval-augmented generation for generative artificial intelligence in health care. Npj Health Syst 2025;2(1). [doi: 10.1038/s44401-024-00004-1]
19. Ke YH, Jin L, Elangovan K, et al. Retrieval augmented generation for 10 large language models and its generalizability in assessing medical fitness. NPJ Digit Med 2025 Apr 5;8(1):187. [doi: 10.1038/s41746-025-01519-z] [Medline: 40185842]
20. Wang J, Fan X, Shen X, Gao Y. Understanding the dark side of online reviews on consumers' purchase intentions in E-commerce: evidence from a consumer experiment in China. Front Psychol 2021;12. [doi: 10.3389/fpsyg.2021.741065]
21. Picard M, Scott-Boyer MP, Bodein A, Périn O, Droit A. Integration strategies of multi-omics data for machine learning analysis. Comput Struct Biotechnol J 2021;19:3735-3746. [doi: 10.1016/j.csbj.2021.06.030] [Medline: 34285775]
22. Gomersall T, Astell A, Nygård L, Sixsmith A, Mihailidis A, Hwang A. Living with ambiguity: a metasynthesis of qualitative research on mild cognitive impairment. Gerontologist 2015 Oct;55(5):892-912. [doi: 10.1093/geront/gnv067] [Medline: 26315317]
23. Smith E, Eloff JHP. A prototype for assessing information technology risks in health care. Computers & Security 2002 Jun;21(3):266-284. [doi: 10.1016/S0167-4048(02)00313-9]
24. Ayyamperumal SG, Ge L. Current state of LLM risks and AI guardrails. arXiv. Preprint posted online on Jun 16, 2024. [doi: 10.48550/arXiv.2406.12934]
25. Xu H, Wang S, Li N, et al. Large language models for cyber security: a systematic literature review. ACM Trans Softw Eng Methodol 2025. [doi: 10.1145/3769676]
26. Gargari OK, Habibi G. Enhancing medical AI with retrieval-augmented generation: a mini narrative review. Digit Health 2025;11:20552076251337177. [doi: 10.1177/20552076251337177] [Medline: 40343063]
27. Lysandrou G, Owen RE, Mursec K, Le Brun G, Fairley EA. Comparative analysis of drug-GPT and ChatGPT LLMs for healthcare insights: evaluating accuracy and relevance in patient and HCP contexts. arXiv. Preprint posted online on Jul 24, 2023. [doi: 10.48550/arXiv.2307.16850]
28. Nashwan AJ, Cabrega JA, Othman MI, et al. The evolving role of nursing informatics in the era of artificial intelligence. Int Nurs Rev 2025 Mar;72(1):e13084. [doi: 10.1111/inr.13084] [Medline: 39794874]
29. Zeng S, Zhang J, He P, et al. The good and the bad: exploring privacy issues in retrieval-augmented generation (RAG). Presented at: Findings of the Association for Computational Linguistics: ACL 2024; Aug 11-16, 2024. [doi: 10.18653/v1/2024.findings-acl.267]
30. Gupta O, Marrone S, Gargiulo F, Jaiswal R, Marassi L. Understanding social biases in large language models. AI 2025;6(5):106. [doi: 10.3390/ai6050106]
31. Pasupuleti MK. Bias and fairness in large language models: evaluation and mitigation techniques. IJAIRI 2025 May;05(5):442-451. [doi: 10.62311/nesx/rphcr6]

XSL•FO
RenderX

32. Khan B, Fatima H, Qureshi A, et al. Drawbacks of artificial intelligence and their potential solutions in the healthcare sector. Biomed Mater Devices 2023 Feb 8;1(2):1-8. [doi: 10.1007/s44174-023-00063-2] [Medline: 36785697]
33. Lasker A. Exploring ethical considerations in generative AI. IJAR 2024;12(4):531-535. [doi: 10.21474/IJAR01/18578]
34. Sagona M, Dai T, Macis M, Darden M. Trust in AI-assisted health systems and AI's trust in humans. Npj Health Syst 2025;2(1). [doi: 10.1038/s44401-025-00016-5]
35. Weiner EB, Dankwa-Mullan I, Nelson WA, Hassanpour S. Ethical challenges and evolving strategies in the integration of artificial intelligence into clinical practice. PLoS Digit Health 2025 Apr;4(4):e0000810. [doi: 10.1371/journal.pdig.0000810] [Medline: 40198594]
36. Choudhury A, Chaudhry Z. Large language models and user trust: consequence of self-referential learning loop and the deskilling of health care professionals. J Med Internet Res 2024 Apr 25;26:e56764. [doi: 10.2196/56764] [Medline: 38662419]
37. Abgrall G, Holder AL, Chelly Dagdia Z, Zeitouni K, Monnet X. Should AI models be explainable to clinicians? Crit Care 2024 Sep 12;28(1):301. [doi: 10.1186/s13054-024-05005-y] [Medline: 39267172]
38. Sivaraman V, Bukowski LA, Levin J, Kahn JM, Perer A. Ignore, trust, or negotiate: understanding clinician acceptance of AI-based treatment recommendations in health care. Presented at: Proceedings of the 2023 CHI Conference on Human Factors in Computing Systems (CHI '23); Apr 23-28, 2023. [doi: 10.1145/3544548.3581075]
39. Nasarian E, Alizadehsani R, Acharya UR, Tsui KL. Designing interpretable ML system to enhance trust in healthcare: a systematic review to proposed responsible clinician-AI-collaboration framework. Information Fusion 2024 Aug;108:102412. [doi: 10.1016/j.inffus.2024.102412]
40. Sadeghi Z, Alizadehsani R, Cifci MA, et al. A review of explainable artificial intelligence in healthcare. Comput Electr Eng 2024 Aug;118:109370. [doi: 10.1016/j.compeleceng.2024.109370]
41. Benrimoh D, Kleinerman A, Furukawa TA, et al. Towards outcome-driven patient subgroups: a machine learning analysis across six depression treatment studies. Am J Geriatr Psychiatry 2024 Mar;32(3):280-292. [doi: 10.1016/j.jagp.2023.09.009] [Medline: 37839909]
42. Abràmoff MD, Tarver ME, Loyo-Berrios N, et al. Considerations for addressing bias in artificial intelligence for health equity. NPJ Digit Med 2023 Sep 12;6(1):170. [doi: 10.1038/s41746-023-00913-9] [Medline: 37700029]
43. Elendu C, Amaechi DC, Elendu TC, et al. Ethical implications of AI and robotics in healthcare: a review. Medicine (Baltimore) 2023 Dec 15;102(50):e36671. [doi: 10.1097/MD.0000000000036671] [Medline: 38115340]
44. Ferlito B, Segers S, De Proost M, Mertes H. Responsibility gap(s) due to the introduction of AI in healthcare: an Ubuntu-inspired approach. Sci Eng Ethics 2024 Aug 1;30(4):34. [doi: 10.1007/s11948-024-00501-4] [Medline: 39090479]
45. Schiff D, Rakova B, Ayesh A, Fanti A, Lennon M. Principles to practices for responsible AI: closing the gap. arXiv. Preprint posted online on Jun 8, 2020. [doi: 10.48550/arXiv.2006.04707]
46. Habli I, Lawton T, Porter Z. Artificial intelligence in health care: accountability and safety. Bull World Health Organ 2020 Apr 1;98(4):251-256. [doi: 10.2471/BLT.19.237487] [Medline: 32284648]
47. Rony MKK, Parvin MR, Ferdousi S. Advancing nursing practice with artificial intelligence: enhancing preparedness for the future. Nurs Open 2024 Jan;11(1). [doi: 10.1002/nop2.2070] [Medline: 38268252]
48. Harrer S. Attention is not all you need: the complicated case of ethically using large language models in healthcare and medicine. EBioMedicine 2023 Apr;90:104512. [doi: 10.1016/j.ebiom.2023.104512] [Medline: 36924620]
49. Zhang J, Zhang ZM. Ethics and governance of trustworthy medical artificial intelligence. BMC Med Inform Decis Mak 2023 Jan 13;23(1):7. [doi: 10.1186/s12911-023-02103-9] [Medline: 36639799]
50. Nazer LH, Zatarah R, Waldrip S, et al. Bias in artificial intelligence algorithms and recommendations for mitigation. PLoS Digit Health 2023 Jun;2(6):e0000278. [doi: 10.1371/journal.pdig.0000278] [Medline: 37347721]
51. Price WN, Cohen IG. Privacy in the age of medical big data. Nat Med 2019 Jan;25(1):37-43. [doi: 10.1038/s41591-018-0272-7] [Medline: 30617331]
52. Futia G, Vetrò A. On the integration of knowledge graphs into deep learning models for a more comprehensible AI—three challenges for future research. Information 2020;11(2):122. [doi: 10.3390/info11020122]
53. Lawton T, Morgan P, Porter Z, et al. Clinicians risk becoming "liability sinks" for artificial intelligence. Future Healthc J 2024 Mar;11(1):100007. [doi: 10.1016/j.fhj.2024.100007] [Medline: 38646041]
54. Bunnell DJ, Bondy MJ, Fromtling LM, Ludeman E, Gourab K. Bridging AI and healthcare: a scoping review of retrieval-augmented generation—ethics, bias, transparency, improvements, and applications. medRxiv. Preprint posted online on Apr 1, 2025. [doi: 10.1101/2025.04.01.25325033]
55. Zhao X, Liu S, Yang SY, Miao C. MedRAG: enhancing retrieval-augmented generation with knowledge graph-elicited reasoning for healthcare copilot. Presented at: Proceedings of the ACM Web Conference 2025 (WWW '25); Apr 28 to May 2, 2025. [doi: 10.1145/3696410.3714782]
56. Feng J, Phillips RV, Malenica I, et al. Clinical artificial intelligence quality improvement: towards continual monitoring and updating of AI algorithms in healthcare. NPJ Digit Med 2022 May 31;5(1):66. [doi: 10.1038/s41746-022-00611-y] [Medline: 35641814]
57. Pandi-Perumal SR, Akhter S, Zizi F, et al. Project stakeholder management in the clinical research environment: how to do it right. Front Psychiatry 2015;6:71. [doi: 10.3389/fpsyt.2015.00071] [Medline: 26042053]

XSL•FO
RenderX

Abbreviations

AI: artificial intelligence
GDPR: General Data Protection Regulation
HIPAA: Health Insurance Portability and Accountability Act
LLM: large language model
RAG: retrieval-augmented generation

Edited by A Benis; submitted 01.Jul.2025; peer-reviewed by D Paradice, J Shi, S Mohanadas; revised version received 26.Oct.2025; accepted 30.Nov.2025; published 09.Jan.2026.

Please cite as:
Tu X, Shi C, Qian P, Wang L
Ethical Imperatives for Retrieval-Augmented Generation in Clinical Nursing: Viewpoint on Responsible AI Use
JMIR Med Inform 2026;14:e79922
URL: https://medinform.jmir.org/2026/1/e79922
doi:10.2196/79922

© Xinyi Tu, Chenghao Shi, Peilin Qian, Lizhu Wang. Originally published in JMIR Medical Informatics (https://medinform.jmir.org), 9.Jan.2026. This is an open-access article distributed under the terms of the Creative Commons Attribution License (https://creativecommons.org/licenses/by/4.0/), which permits unrestricted use, distribution, and reproduction in any medium, provided the original work, first published in JMIR Medical Informatics, is properly cited. The complete bibliographic information, a link to the original publication on https://medinform.jmir.org/, as well as this copyright and license information must be included.

XSL•FO
RenderX

Viewpoint

Improving Clinical Decision-Making in Treating Airway Diseases With an Expert System Built Upon the Free AI Tool Google NotebookLM

Cheng-Hao Hsu[1], MD; Ching-Li Hsu[2], MD; Chih-Hsiang Tsou[3,4], MD, PhD; Kuo-Fang Hsu[2], MD, PhD; Hung-Yu Yang[1,5,6], MD, PhD

[1]Department of Medicine, College of Medicine, Taipei Medical University, Taipei, Taiwan
[2]Miaoli General Hospital, Ministry of Health and Welfare of Taiwan, Miaoli City, Taiwan
[3]Department of Pulmonology, Jen-Ai Branch, Taipei City Hospital, Taipei, Taiwan
[4]School of Medicine, College of Medicine, National Yang Ming Chiao Tung University, Taipei, Taiwan
[5]Department of Cardiology, Wan Fang Hospital, Taipei Medical University, Taipei, Taiwan
[6]Biomedical Data Center, Wan Fang Hospital, Taipei Medical University, Taipei, Taiwan

Corresponding Author:
Hung-Yu Yang, MD, PhD
Department of Cardiology
Wan Fang Hospital
Taipei Medical University
No.111, Sec. 3, Xinglong Rd.,
Wenshan Dist.,
Taipei
Taiwan
Phone: 886 2 29307930 ext 2818
Email: jaero@tmu.edu.tw

Abstract

We used the free artificial intelligence (AI) tool Google NotebookLM, powered by the large language model Gemini 2.0, to construct a medical decision-making aid for diagnosing and managing airway diseases and subsequently evaluated its functionality and performance in a clinical workflow. After feeding this tool with relevant published clinical guidelines for these diseases, we evaluated the feasibility of the system regarding its behavior, ability, and potential, and we created simulated cases and used the system to solve associated medical problems. The test and simulation questions were designed by a pulmonologist, and the appropriateness (focusing on accuracy and completeness) of AI responses was judged by 3 pulmonologists independently. The system was then deployed in an emergency department setting, where it was tested by medical staff (n=20) to assess how it affected the process of clinical consultation. Test opinions were collected through a questionnaire. Most (56/84, 67%) of the specialists' ratings regarding AI responses were above average. The interrater reliability was moderate for accuracy (intraclass correlation coefficient=0.612; *P*<.001) and good on completeness (intraclass correlation coefficient=0.773; *P*<.001). When deployed in an emergency department (ED) setting, this system could respond with reasonable answers, enhance the literacy of personnel about these diseases. The potential to save the time spent in consultation did not reach statistical significance (Kolmogorov-Smirnov [K-S] D=0.223, *P*=.24) across all participants, but it indicated a favorable outcome when we analyzed only physicians' responses. We concluded that this system is customizable, cost efficient, and accessible to clinicians and allied health care professionals without any computer coding experience in treating airway diseases. It provides convincing guideline-based recommendations, increases the staff's medical literacy, and potentially saves physicians' time spent on consultation. This system warrants further evaluation in other medical disciplines and health care environments.

(JMIR Med Inform 2026;14:e78567) doi:10.2196/78567

KEYWORDS

airway disease; artificial intelligence; AI; artificial intelligence tool; AI tool; emergency department; medical decision-making; NotebookLM; pulmonology

XSL•FO
RenderX

Introduction

Expert Systems and the Decision-Making Aids

An expert system is a knowledge management tool that integrates domain-specific information with an inference engine to facilitate decision-making. When consulted, it delivers timely and relevant solutions to a problem. This concept originated in the 1950s, with medical diagnostic reasoning being among its earliest applications [1,2]. Gradually, expert systems became popular in the 1970s and 1980s [3]. With the advent of the digital era, the concept of expert systems was revisited by the medical community. For instance, oncology, given its rapid evolution and growth in knowledge over the past 2 decades, has required consultation systems to aid patient management.

Knowledge Management and the Large Language Model

Large language models (LLMs) represent a branch of machine learning that has been under development for several years. Their impact became widely recognized on November 30, 2022, when OpenAI released ChatGPT, a free web-based service [4,5]. This milestone illustrated the potential of LLMs to advance toward general purpose artificial intelligence (AI) by enabling natural language–based dialogue. The continuously expanding medical knowledge has traditionally been managed through structured data storage, indexing, and query mechanisms [6] or probabilistic inference algorithms [7]. However, these conventional clinical decision support systems struggle to incorporate new information and adapt to complex clinical contexts [8]. Unlike these approaches, LLM-driven systems enable interaction in natural language, offering a more user-friendly and adaptable knowledge management tool. Such systems can be easily deployed across health care teams, including physicians and allied health care professionals. In this study, we devised a model to understand how this new LLM-based methodology could affect medical decision-making and routine clinical workflow. The process of our project and our key findings were described as follows.

Decision-Making Aid Construction and Assessment

Constructing an Expert System With a Free AI Tool Based on LLM

The free AI tool Google NotebookLM, powered by the LLM Gemini 2.0 [9], provides a platform for knowledge integration through 3 components: a source input pane, a query pane, and a note-taking pane, which function collaboratively (Figure 1). We used this platform to develop a medical decision support system for airway diseases. Relevant published clinical guidelines were uploaded into the source input pane, including the GINA (Global Initiative for Asthma) guideline [10] and the GOLD (Global Initiative for Chronic Obstructive Lung Disease) guideline [11] (version 2021-2025). Additional standard documents from the Taiwan Society of Pulmonary and Critical Care Medicine [12], such as the Taiwan asthma guidelines and the pulmonary rehabilitation guidelines, were also incorporated. The responses of the system to queries were then recorded.

Figure 1. The Google NotebookLM interface.

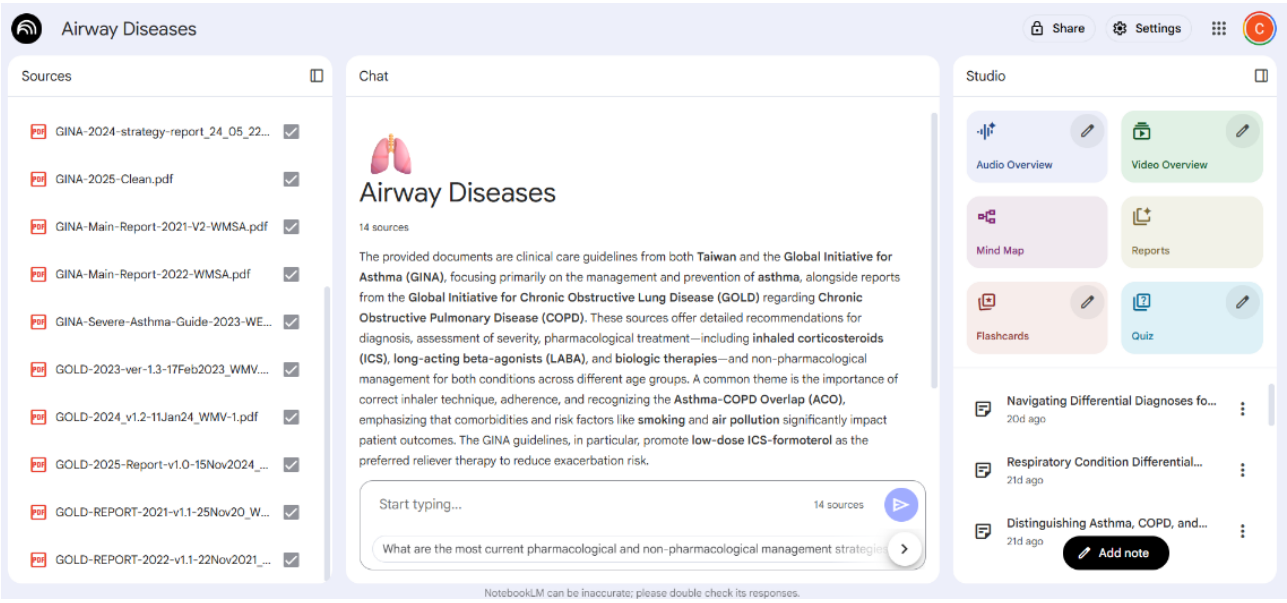

Feasibility Evaluated by Pulmonologists

Query questions were selected to match the essential requirements of eligible AI tools, such as reproducibility, the ability to develop a treatment plan, and the capacity to handle speculative ideas. They were designed by a pulmonologist with expertise in airway diseases and familiarity with these guidelines, and the appropriateness (focusing on accuracy and completeness) of AI responses was judged (Likert scale 1-5) by 3 pulmonologists independently. Airway diseases were selected as the pilot scenario to evaluate the feasibility of our system because standardized clinical guidelines are widely accepted, and they involve fewer complex and controversial data points than other conditions, such as oncological diseases.

Implementation in the Clinical Workflow

The system was introduced to physicians and allied health care professionals in the emergency department (ED), where patients

XSL•FO
RenderX

with airway diseases commonly present for treatment. Feedback was collected through a questionnaire, and the responses were analyzed to assess the system's effectiveness within the clinical workflow.

The ED setting was chosen because clinicians frequently encounter diverse conditions and require rapid access to specialist knowledge. In this context, an expert system capable of answering clinical queries has the potential to reduce the time burden on patients, frontline clinicians, and the specialists consulted.

The complete workflow of the project is summarized in Figure 2.

Figure 2. Flowchart illustrating the process of constructing our artificial intelligence (AI)–based consultation tool for medical decision-making.

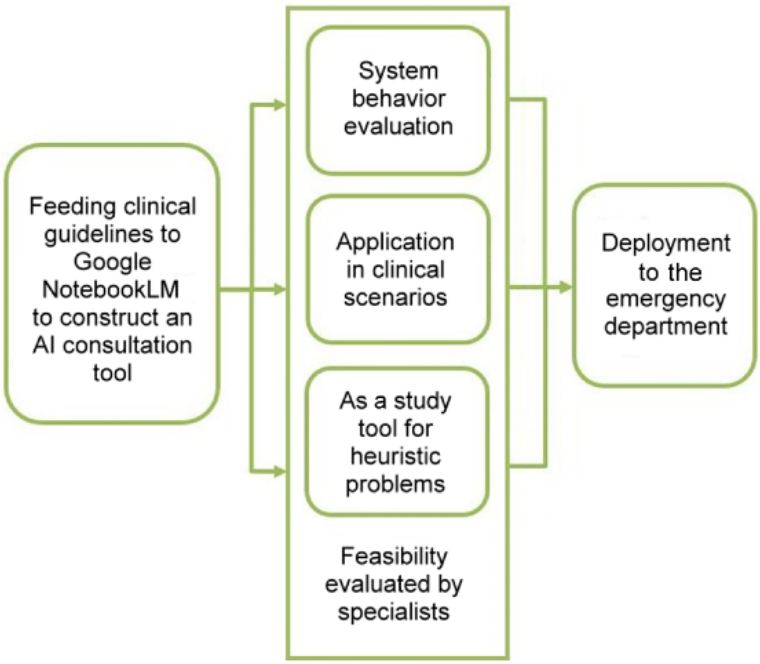

AI Responses to Queries

System Behavior Evaluation

Test 1: Reproducibility

The system consistently generated accurate summaries and responses, each supported by appropriate and reliable references. When prompted to regenerate output from the same sources, this system produced slightly varied responses that retained identical meaning, resembling the variability typically observed in an AI chatbot interaction.

Test 2: Knowledge Consolidation

The asthma and chronic obstructive pulmonary disease (COPD) guidelines contained respective lists of differential diagnoses. When instructed to generate a consolidated table of differential diagnoses for airway diseases, including their distinguishing features and relevant diagnostic tests, the system successfully produced one, as shown in Table 1.

XSL•FO
RenderX

Table 1. Summary of the differential diagnoses for asthma, chronic obstructive pulmonary disease (COPD), and related conditions, including distinguishing symptoms, clinical features, and tests. Full version available in Multimedia Appendix 1.

Condition	Primary differential for	Differentiating symptoms and features	Differentiating tests and findings
Inducible laryngeal obstruction or vocal cord dysfunction	Both asthma and COPD	Dyspnea and inspiratory wheezing (stridor), sometimes with cough and general wheeze	Functional laryngoscopy visualizing vocal cord movement; full flow-volume curve assessing upper airway obstruction
Obesity	Both asthma and COPD	Respiratory symptoms, such as dyspnea and wheeze, that can mimic asthma or COPD, often related to deconditioning or mechanical restriction	Objective measurement of variable expiratory airflow limitation to confirm asthma in obese patients
Tracheobronchomalacia	Both asthma and COPD	Wheeze	Bronchoscopy; high-resolution chest computed tomography scan
Lung cancer	Both asthma and COPD (more common in COPD)	Breathlessness, significant weight loss, hemoptysis, night sweats, and fever	Chest radiograph or computed tomography scan; reduced diffusing capacity for carbon monoxide may be present
Alpha-1 antitrypsin deficiency	Both asthma and COPD (more commonly associated with COPD)	Shortness of breath, with a family history of early-onset emphysema	Blood test confirming alpha-1 antitrypsin deficiency
Tuberculosis	Both asthma and COPD (especially in low- and middle-income countries)	Chronic cough, hemoptysis, dyspnea and/or fatigue, fever, night sweats, anorexia, and weight loss	Sputum induction (to confirm inflammatory phenotype); high-resolution computed tomography of the chest

Test 3: Temporal Order Recognition

The system demonstrated the ability to recognize temporal updates. For instance, it correctly identified that the “ABCD assessment tool” for COPD was replaced by the “ABE assessment scheme” in the 2023 update of the GOLD COPD guideline [11]. When asked to provide treatment recommendations, the system appropriately referred to the most recent guideline version while disregarding outdated ones, as shown in Textbox 1.

Textbox 1. The chronic obstructive pulmonary disease (COPD) grouping follows the most recent version of the clinical guidelines. For full details, refer to Multimedia Appendix 2.

Question

A COPD patient with mMRC=2 and CAT=11, and a history of hospitalization once in the past 1 year. What is his/her treatment suggestion?

Answer

...

3. GOLD Group Classification:

Combining a high symptom burden (mMRC=2, CAT=11) with a high exacerbation risk (one hospitalization), this patient is classified as GOLD Group E [GOLD 2023, p. 40, Figure 2.4; GOLD 2024, p. 29, Figure 2.5; GOLD 2025, p. 38, Figure 2.5]. This classification guides therapeutic recommendations [GOLD 2023, p. 40; GOLD 2024, p. 29; GOLD 2025, p. 38]...

Test 4: Memory Flush

When the COPD guidelines from 2023 onward were deselected from the source input panel, the system could still respond to questions about “ABE assessment” using information retained from previous dialogues, provided those dialogues had not been deleted using the Refresh button (Textbox 2). Interestingly, if the dialogues were deleted and no clues regarding the 2023 update were supplied, the system concluded that “ABE” might be a typographic error for “ABCD” (Textbox 3) or “creatively“ suggested that “B” referred to blood eosinophil count (Textbox 4). This indicates that the AI tool retains dialogue content until it is deliberately erased using the Refresh button.

XSL•FO
RenderX

Textbox 2. The system could respond using information from prior dialogues until those dialogues were removed using the Refresh button.

Question

What is the ABE assessment tool?

Answer

The provided 2021 and 2022 reports do not contain information about merging groups C and D into a single "E" group, nor do they refer to an "ABE" assessment tool. This suggests that the change to the ABE classification, if it occurred, was introduced in a subsequent GOLD report (e.g., the GOLD 2023 report as mentioned in our previous conversation).

Textbox 3. A system response after a memory flush.

Question

Explain the ABE assessment tool for COPD.

Answer

The sources provided do not contain information on an "ABE assessment tool" for COPD. However, they extensively describe the "ABCD" assessment tool used in the Global Initiative for Chronic Obstructive Lung Disease (GOLD) guidelines for COPD management. It is possible that "ABE" in your query was a typographical error for "ABCD" or refers to a concept not detailed in these documents.

Textbox 4. A creative response after a memory flush.

Question

Explain the ABE assessment tool for COPD.

Answer

While the provided sources do not explicitly define or refer to an "ABE assessment tool" as a named entity for evaluating COPD, they do describe a framework for the initiation of pharmacological management that relies on assessing factors commonly associated with "A" (Symptoms), "B" (Blood Eosinophil Count), and "E" (Exacerbation Risk).

Test 5: Handling Multiple Languages

Leveraging Google's multilingual capability, the system could accept a query in Chinese and respond in either English or Chinese. When asked to compare the 2022 Taiwan adult asthma clinical care guidelines, written entirely in Chinese, with the GINA guideline, the system managed to perform the task without difficulty. Language switching did not appear to affect system performance.

Application in Clinical Scenarios

Scenario 1: Requesting Patient Management Suggestions Based on a Simulated Medical Record

As illustrated in Textbox 5, the system generated guideline-based recommendations that were clinically useful.

Textbox 5. Helpful recommendations generated by the system, supported by guideline-based reasoning. For a complete explanation, refer to Multimedia Appendix 3.

Question

I have a patient diagnosed of COPD adequately maintained with Pulmicort, 2 puffs bid. However, he suffered from more and more dyspnea while walking. What is the management suggestion?

Answer

Based on the information in the sources, here are some management suggestions for your patient with COPD who is experiencing increasing dyspnea on walking despite being maintained on Pulmicort (an inhaled corticosteroid - ICS):

1. Consider adding a long-acting bronchodilator...
2. Consider a combination inhaler containing ICS and LABA...
3. Optimize inhaled therapy. Ensure that the patient...
4. Consider pulmonary rehabilitation...
5. Reassess lung function and consider other diagnoses...
6. Review for modifiable risk factors...
7. Consider stepping up ICS dose (with caution)...
8. Assess for features of asthma-COPD overlap (ACO)...
9. Follow-up and reassess...

XSL•FO
RenderX

Scenario 2: Logical Question

The system addressed a logical question regarding the unavailability of pulmonary function testing by providing a structured, entry-by-entry response. It explained the implications separately for COPD and asthma, as shown in Textbox 6.

Textbox 6. The system presented a comparative response for chronic obstructive pulmonary disease (COPD) and asthma. For the complete answer, refer to Multimedia Appendix 4.

Question

Is pulmonary function test necessary for diagnosis? What if there is no pulmonary function test accessible?

Answer

Here's how pulmonary function tests relate to diagnosing airway diseases, and what to do if these tests aren't accessible:

- COPD Diagnosis: Spirometry is essential to confirm a COPD diagnosis...
- Asthma Diagnosis: Asthma diagnosis relies on a combination of characteristic symptom patterns and evidence of variable expiratory airflow limitation...
- Role of Lung Function Testing: Lung function testing is essential to confirm...
- Spirometry: Forced spirometry is the most reproducible and objective measurement of airflow obstruction. It measures...
- When Spirometry Isn't Available for Asthma Diagnosis:
  - Peak expiratory flow (PEF) can be used, although it is less reliable...
  - Assess the patient for a characteristic pattern of respiratory symptoms.
  - Consider a therapeutic trial with SABA and low-dose ICS...
  - Confirm variable expiratory airflow limitation by PEF. A ≥20% improvement in PEF...
  - Improvement in symptoms and PEF after a 4-week therapeutic trial...
- When Spirometry Isn't Available for COPD Diagnosis: When routine spirometry is not available, home measurement of peak expiratory flow (PEF) combined with validated patient questionnaires could be used to support or refute a possible diagnosis of COPD...

Scenario 3: Personalized Rehabilitation Planning

The system generated a tailored rehabilitation plan and schedule that took into account an advanced age condition, as shown in Textbox 7.

XSL•FO
RenderX

Textbox 7. The system produced a detailed, individualized rehabilitation plan for an extremely older adult patient with chronic obstructive pulmonary disease (COPD) and ischemic heart disease. The complete plan is available in Multimedia Appendix 5.

Question

I have a female patient, age 95, with COPD and ischemic heart disease. Please make a rehabilitation plan and schedule for her.

Answer

For your 95-year-old female patient with COPD and ischemic heart disease, a highly individualized, comprehensive, and carefully supervised rehabilitation plan is crucial, taking into accounts her advanced age and multiple comorbidities. This plan draws primarily from the Taiwan Pulmonary Rehabilitation Practical Guideline and the Global Initiative for Chronic Obstructive Lung Disease (GOLD) reports.

I. Overall Approach and Guiding Principles

1. Personalized and Integrated Care:...
2. Specialist Supervision:...
3. Holistic Goals:...

II. Initial Comprehensive Assessment

- Patient Goals and Preferences:...
- Medical History and Physical Examination:...

...

III. Rehabilitation Setting and Schedule

1. Setting: For a 95-year-old patient with significant comorbidities, a supervised setting is highly recommended, such as...
2. Duration: Optimal benefits from pulmonary rehabilitation programs are typically achieved within 6 to 8 weeks...
3. Frequency: Supervised exercise training at least twice weekly is recommended.

IV. Components of the Rehabilitation Plan

1. Exercise Training:...
2. Education and Self-Management:...

...

V. Follow-up and Monitoring

- Regular Review:...
- Response Assessment:...

...

Scenario 4: Vague Question

In this case, the system transformed the ambiguous concept of “prospect” into practical categories of “future challenges” and “research directions.” This approach provided a meaningful response, as illustrated in Textbox 8.

XSL•FO
RenderX

Textbox 8. The system interpreted the vague query as a request for practical insights. The complete answer is provided in Multimedia Appendix 6.

Question

What is the future prospect of airway diseases and their treatment?

Answer

The sources discuss future challenges and research directions for airway diseases such as asthma and Chronic Obstructive Pulmonary Disease (COPD).

Asthma:

- Despite improvements in asthma care and effective medications, many patients worldwide do not benefit from these advances due to inadequate medical facilities and financial resources.
- Future research should focus on clinical and physiological characteristics, biomarkers, outcomes, and underlying mechanisms in patients with respiratory symptoms or chronic airflow limitation...

COPD:

- More research is needed to guide better recognition and safe, effective treatment of COPD.
- There's a need to study clinical and physiological characteristics, biomarkers, outcomes and underlying mechanisms in broad populations of patients with respiratory symptoms or with chronic airflow limitation.
- Future studies should focus on defining phenotypes and mechanisms to ensure the safety of pharmacological treatments...

Scenario 5: Out-of-Scope Questions

The system appropriately declined to answer questions that were beyond the scope of the available sources. It did not fabricate factitious responses, unlike many chatbots.

As a Study Tool for Heuristic Problems

Problem 1: Version Comparison and Trend Analysis

When asked to compare guideline versions across publication years, the system clearly outlined the differences between them. Additionally, when requested to analyze trends in pharmacological use for airway diseases over the past 5 years, it generated a comprehensive summary, as shown in Textbox 9.

XSL•FO
RenderX

Textbox 9. The system analyzed the trend in pharmacological use for airway diseases across the years. A complete list is available in Multimedia Appendix 7.

Question

Find the trend in pharmacological use for COPD and asthma in the past 5 years.

Answer

In the past five years, pharmacological treatment for both Chronic Obstructive Pulmonary Disease (COPD) and asthma has seen a clear trend towards more individualized, exacerbation-focused, and strategically combined therapies, with a strong emphasis on proper inhaler use and minimizing oral corticosteroid exposure.

Overarching Trends for Both COPD and Asthma (Past 5 Years)

1. Individualized and Patient-Centered Care:...
2. Focus on Exacerbation Reduction:...
3. Emphasis on Inhaler Technique and Adherence:...
4. Minimizing Oral Corticosteroid (OCS) Use:...

Trends in COPD Pharmacological Treatment (Past 5 Years): The GOLD reports (2021, 2022, 2023, 2024, 2025) and the 2023 Taiwan COPD Clinical Care Guidelines emphasize these trends:

1. Long-Acting Bronchodilators (LABA and/or LAMA) as First-Line:...
2. Strategic Use of Inhaled Corticosteroids (ICS):...
3. Increasing Role of Triple Therapy (LABA+LAMA+ICS):...

...

Trends in Asthma Pharmacological Treatment (Past 5 Years): GINA reports (2021, 2022, 2023, 2024, 2025) and the 2022 Taiwan Adult Asthma Clinical Care Guidelines highlight significant shifts:

1. Shift Away from SABA Monotherapy:...
2. Introduction of Two Treatment Tracks (GINA):...
3. ICS as the Cornerstone of Controller Therapy:...

...

Problem 2: Further Reading Suggestions

When asked to recommend additional readings on intractable asthma, the system searched both the source text and the reference lists it contained. However, it did not suggest any external articles or books. Notably, the system interpreted the term “intractable asthma” as both “severe asthma” and “difficult-to-treat asthma” to ensure comprehensive coverage, as shown in Textbox 10.

XSL•FO
RenderX

Textbox 10. Suggested further reading items provided by the system. For the complete list, refer to Multimedia Appendix 8.

Question

Can you suggest any further readings about the treatment for intractable asthma?

Answer

For further readings about the treatment of intractable asthma, which is often referred to in the sources as severe asthma or difficult-to-treat asthma, you may find the following publications insightful. These sources provide detailed information on diagnosis, management, and treatment options for patients whose asthma remains uncontrolled despite standard therapies:

Comprehensive Guidelines and Reviews:

- Global Strategy for Asthma Management and Prevention (GINA): The GINA reports are frequently referenced for their comprehensive guidance on asthma management. Specifically, the sections within these reports on "Difficult-to-treat and severe asthma" provide a roadmap for assessment and management. You can refer to the detailed sections in the provided GINA reports, such as:
    - GINA-2023-Report:...
    - GINA-2024-strategy-report:...
    - GINA-2025-Clean:...

...Pharmacological Interventions:

- Biologic Therapies:
    - EAACI Biologicals Guidelines-Recommendations for severe asthma: Agache I et al. offer guidelines and recommendations for biologics in severe asthma.
    - Tezepelumab:...

...

- Add-on treatments (nonbiologic):
    - Tiotropium:...
    - Azithromycin:...
    - Oral Corticosteroids (OCS):...

Diagnostic and Management Strategies:

- Sputum-guided treatment...
- Bronchial Thermoplasty:...
- Importance of Adherence and Inhaler Technique:...

These readings should provide a comprehensive overview of the current understanding and treatment approaches for intractable asthma.

Problem 3: Speculative Question

We designed a question regarding the interchangeability of questionnaires used for evaluating COPD and asthma. Our system provided a reasonable response, as shown in Textbox 11.

Textbox 11. The system addressed this speculative question and provided a supporting rationale.

Question

Can we evaluate asthmatic patients with questionnaires designed for COPD? Can we evaluate COPD patients with questionnaires designed for asthma?

Answer

Asthma and COPD can be difficult to distinguish, especially in older patients and smokers, and these conditions may overlap. Some patients are assigned both diagnoses. While some questionnaires might capture general respiratory symptoms that could be present in both asthma and COPD, it is best to use disease-specific questionnaires to ensure the most appropriate and accurate assessment. There is no evidence that asthma questionnaires can be used for COPD patients, and vice versa.

Problem 4: Diagnostic Skill Training Tool

We instructed the system to generate a simulated case with symptoms and pulmonary function values to test our diagnostic skills. During this exercise, we compared our reasoning and diagnosis with the system's answer to strengthen diagnostic ability, as shown in Textbox 12.

XSL•FO
RenderX

Textbox 12. The system generated a simulated case to facilitate diagnostic training. For the answer, diagnostic rationale, and treatment recommendation, refer to Multimedia Appendix 9.

Question

Please make a case with symptoms and pulmonary function values to test our diagnostic skills.

Answer

Simulated Patient: Mr David Lee

Patient Background: Mr David Lee is a 58-year-old male with a 25 pack-year smoking history, though he states he is currently trying to quit. He reports a chronic cough with some mucus production for the past 8 years. He also experiences intermittent shortness of breath on exertion, particularly when climbing stairs. Lately, he's noticed that his breathing feels tighter in the mornings, and he occasionally hears a whistling sound (wheeze) when breathing out, especially after exposure to cold air. These wheezing episodes are variable in intensity, and he notes that his symptoms sometimes improve with a relative's "asthma inhaler" (a short-acting beta2-agonist, SABA).

Symptoms:

- Chronic cough with mucus production (8 years duration).
- Intermittent dyspnea on exertion (eg, climbing stairs).
- Morning chest tightness.
- Occasional expiratory wheezing, variable in intensity, exacerbated by cold air.
- Reports temporary improvement with SABA.
- Significant smoking history (25 pack-years).

Pulmonary Function Values:

- Pre-Bronchodilator Spirometry:
  - Forced Expiratory Volume in 1 second (FEV1): 60% of predicted
  - Forced Vital Capacity: 80% of predicted
  - FEV1/Forced Vital Capacity Ratio: 65% (indicating airflow limitation)
- Post-Bronchodilator Spirometry (after administering 400 mcg of salbutamol, a SABA):...

Diagnosis, Reasons, and Treatment Suggestion for Mr David Lee

...

Pulmonologists' Judgment on AI Responses to Queries

Most of the 3 pulmonologists' ratings (56/84, 67%) regarding AI responses were above average (Likert scale 4-5), and only 5% (4/84) were below average (Likert scale 1-2). The interrater reliability was moderate for accuracy (intraclass correlation coefficient=0.612; P<.001) and good for completeness (intraclass correlation coefficient=0.773; P<.001) based on a 2-way random-effects model with absolute agreement and single measures options [13]. We also noted that AI responses received more (187/333, 56%) credits from the raters for query questions that required more intelligence (adaptation, deduction, analysis, and planning) to answer, such as scenarios 1 to 3 and problems 1 to 4, than for the other questions. This finding further supports the feasibility of our system.

Responses From the Field Tests in the ED

We collected responses from 20 participants, including 3 physicians, 3 nurse practitioners, 11 ED nurses, and 3 respiratory therapists. Among them, 80% (16/20) expressed interest in the system (Kolmogorov-Smirnov [K-S] D=0.362; P=.008; indicating a deviation from normality). All these participants had prior experience consulting a chatbot. In total, 60% (12/20) of the participants were aware of and ever disturbed by the issue of AI hallucination (K-S D=0.238; P=.18; indicating a normal distribution). All participants in this group thought that guideline-based reasoning provided by the system was essential in clinical practice.

In total, 55% (11/20) of the participants believed that the system could reduce specialty consultation time (K-S D=0.223; P=.24; indicating a normal distribution). Importantly, all participants indicated that the system could enhance their knowledge and diagnostic ability in airway diseases or increase their confidence in explaining conditions to patients.

Discussion

Statistical Findings

Previous studies on LLM-based medical decision support have reported various outcomes [14,15]. These discrepancies may reflect differences in participants' expertise, the difficulty of test questions, and the dimensions measured in study designs. In our evaluation of consultation time, the K-S test indicated a normal distribution of responses. When analyzing only physicians' responses, we observed a trend toward favorable

XSL•FO
RenderX

outcomes, although this did not reach statistical significance (P=.24) across all participants. Thus, the system shows potential for reducing physicians' consultation time, but larger and more comprehensive studies are required to confirm its effectiveness.

What We Expect of a Medical AI Consultation Tool

AI Hallucination and AI Ethics in Medicine

Since the widespread adoption of LLM-based chatbots, users have become increasingly concerned about AI hallucination, that is, plausible but unfounded responses generated without a factual basis. Such errors are unacceptable in medical practice. Amiot and Potier [16] recently emphasized that hallucination is particularly difficult to detect in a health care context. Fortunately, the design of the Google NotebookLM platform mitigates this risk by providing answers supported by explicit references to authoritative sources. With such verifiable citations, concerns about errors, biases, ethics, and safety from autonomous AI actions are substantially reduced.

Beyond a Decision-Making Aid

The project aims to provide a clinical decision-making aid for the diagnosis and management of airway diseases and to assess how this AI tool affected medical staff in the ED during the consultation process. As Wang et al [17] noted, an AI system could uncover subtle relationships in medical data that may elude both traditional decision support tools and human experts. During system development, pulmonologists found that the tool not only consolidated their expertise but also offered novel insights and opportunities to explore speculative ideas, as described in test problems 1 and 3. For medical trainees, the system functions as an effective educational tool, providing not only suggestions but also the underlying reasons.

Limitations Inherent to LLMs

Scope of External Knowledge Considered

NotebookLM generates content strictly from user-provided sources. Because general "common sense" information is often absent from "specialized" clinical guidelines, excluding external knowledge can considerably limit the scope of the system's responses. Moreover, the extent to which external information is incorporated into outputs is undisclosed and therefore unpredictable.

Inability to Pose Differentiating Questions

LLM-based systems generate responses in the form of summaries or abstracts but do not query users. However, accurate clinical decision-making often requires additional patient-specific data obtained through differentiating questions. For example, clarifying whether a patient is a smoker or a nonsmoker or identifying ethnic background (Asian or White) may guide diagnostic pathways. If the system could formulate such discriminative questions and allow users to provide input—ideally guided by Bayesian theorem [18]—its clinical utility would be markedly enhanced. We did not observe this feature in the current implementation.

Future Directions

Once the pilot project is fully operational, the expert system can be refined along several pathways. First, the system should adapt its responses to the user's professional role. For example, when handling a consultation request, it should provide only essential surgical information to an internist while delivering more comprehensive surgical details to a surgeon.

Second, although our study focused on airway diseases and the system demonstrated generally positive performance, its generalizability to other specialties remains uncertain. Disciplines such as oncology, where problems are more complex and controversies are common, may present challenges. Further research is required to determine whether the model can provide reliable and clinically meaningful output in these domains.

Finally, because decision-making, studying, and education are central components of our medical practice routines, integrating such a system into the existing health care information systems presents a logical next step. We expect that this integration could streamline clinical workflows and improve automation across multiple aspects of care delivery.

Conclusions

Our findings suggest that this approach is highly customizable, cost efficient, and accessible to clinicians and allied health care professionals without any computer coding experience in managing airway diseases. It provides convincing guideline-based recommendations, increases the staff's medical literacy, and potentially saves physicians' time spent on consultation. As AI tools gain widespread adoption, we believe that, if validated across additional medical specialties, this methodology could establish a new paradigm in clinical practice. While acknowledging the potential of AI, we emphasize the continued need for human judgment and oversight in evaluating and applying AI-generated recommendations.

Acknowledgments

The authors would like to thank their colleagues Dr Jer-Hwa Chang, Dr Ming-Cheng Wang, Dr Chien-Yeh Chin, Dr Chung-Hui Tang, Dr Tung-Wu Lin, Yung-Chieh Chiu, Feng-Ling Huang, Yu-Ting Su, Tsai-Chi Chen, Yuan-Hsiang Hsieh, Chi-Wen Feng, Syuan-Wen Lai, Yu-Hsiu Liu, Yi-Chen Chiang, Bing-Hua Wu, Ju-Chuan Hsu, Yu-Ping Lin, Cheng-Yang Tu, Pei-Yi Kuo, Chi-Hsin Chang-Chien, Li-Chun Chang, and Pei-Chen Hsieh for their valuable opinions during the evaluation process. We would like to extend our special thanks to Google for providing its free AI tool, NotebookLM [9], which served as the platform for our discussions.

XSL•FO
RenderX

Funding

No external financial support or grants were received from any public, commercial, or not-for-profit entities for the research, authorship, or publication of this article.

Conflicts of Interest

None declared.

Multimedia Appendix 1
Unabridged version of Table 1.
[DOCX File , 24 KB - medinform_v14i1e78567_app1.docx]

Multimedia Appendix 2
Unabridged version of Textbox 1.
[DOCX File , 20 KB - medinform_v14i1e78567_app2.docx]

Multimedia Appendix 3
Unabridged version of Textbox 5.
[DOCX File , 20 KB - medinform_v14i1e78567_app3.docx]

Multimedia Appendix 4
Unabridged version of Textbox 6.
[DOCX File , 19 KB - medinform_v14i1e78567_app4.docx]

Multimedia Appendix 5
Unabridged version of Textbox 7.
[DOCX File , 21 KB - medinform_v14i1e78567_app5.docx]

Multimedia Appendix 6
Unabridged version of Textbox 8.
[DOCX File , 19 KB - medinform_v14i1e78567_app6.docx]

Multimedia Appendix 7
Unabridged version of Textbox 9.
[DOCX File , 21 KB - medinform_v14i1e78567_app7.docx]

Multimedia Appendix 8
Unabridged version of Textbox 10.
[DOCX File , 26 KB - medinform_v14i1e78567_app8.docx]

Multimedia Appendix 9
Unabridged version of Textbox 12.
[DOCX File , 21 KB - medinform_v14i1e78567_app9.docx]

References

1. Ledley RS, Lusted LB. Reasoning foundations of medical diagnosis: symbolic logic, probability, and value theory aid our understanding of how physicians reason. Science 1959 Jul 03;130(3366):9-21. [doi: 10.1126/science.130.3366.9] [Medline: 13668531]
2. Weiss SM, Kulikowski CA, Amarel S, Safir A. A model-based method for computer-aided medical decision-making. Artif Intell 1978 Aug;11(1-2):145-172. [doi: 10.1016/0004-3702(78)90015-2]
3. Leondes CT. Expert Systems: The Technology of Knowledge Management and Decision Making for the 21st Century. New York, NY: Elsevier Science; 2002:1-22.
4. Hu K. ChatGPT sets record for fastest-growing user base - analyst note. Reuters. 2023 Feb 1. URL: https://www.reuters.com/technology/chatgpt-sets-record-fastest-growing-user-base-analyst-note-2023-02-01/ [accessed 2025-05-29]
5. OpenAI. GPT-4 technical report. arXiv. Preprint posted online on March 15, 2023 2023:1-100 [FREE Full text] [doi: 10.48550/arXiv.2303.08774]

XSL•FO
RenderX

6. Salton G. Developments in automatic text retrieval. Science 1991 Aug 30;253(5023):974-980. [doi: 10.1126/science.253.5023.974] [Medline: 17775340]
7. Waxman HS, Worley WE. Computer-assisted adult medical diagnosis: subject review and evaluation of a new microcomputer-based system. Medicine (Baltimore) 1990 May;69(3):125-136. [Medline: 2189054]
8. Bai E, Zhang Z, Xu Y, Luo X, Adelgais K. Enhancing prehospital decision-making: exploring user needs and design considerations for clinical decision support systems. BMC Med Inform Decis Mak 2025 Jan 17;25(1):31 [FREE Full text] [doi: 10.1186/s12911-024-02844-1] [Medline: 39825293]
9. Google NotebookLM. URL: http://notebooklm.google [accessed 2025-05-29]
10. The GINA Asthma Guideline: The Global Strategy for Asthma Management and Prevention. Global Initiative for Asthma (GINA). URL: https://ginasthma.org [accessed 2025-05-29]
11. The GOLD COPD guideline: Global Strategy for the Diagnosis, Management, and Prevention of Chronic Obstructive Pulmonary Disease. Global Initiative for Chronic Obstructive Lung Disease. URL: https://goldcopd.org [accessed 2025-05-29]
12. Home page. The Taiwan Society of Pulmonology and Critical Care Medicine. URL: http://en.tspccm.org.tw/ [accessed 2025-05-29]
13. Koo TK, Li MY. A guideline of selecting and reporting intraclass correlation coefficients for reliability research. J Chiropr Med 2016 Jun;15(2):155-163 [FREE Full text] [doi: 10.1016/j.jcm.2016.02.012] [Medline: 27330520]
14. McDuff D, Schaekermann M, Tu T, Palepu A, Wang A, Garrison J, et al. Towards accurate differential diagnosis with large language models. Nature 2025 Jun;642(8067):451-457 [FREE Full text] [doi: 10.1038/s41586-025-08869-4] [Medline: 40205049]
15. Goh E, Gallo R, Hom J, Strong E, Weng Y, Kerman H, et al. Large language model influence on diagnostic reasoning: a randomized clinical trial. JAMA Netw Open 2024 Oct 01;7(10):e2440969 [FREE Full text] [doi: 10.1001/jamanetworkopen.2024.40969] [Medline: 39466245]
16. Amiot F, Potier B. Artificial intelligence (AI) and emergency medicine: balancing opportunities and challenges. JMIR Med Inform 2025 Aug 13;13:e70903 [FREE Full text] [doi: 10.2196/70903] [Medline: 40802997]
17. Wang D, Wang L, Zhang Z, Wang D, Zhu H, Gao Y, et al. "Brilliant AI doctor" in rural clinics: challenges in AI-powered clinical decision support system deployment. In: Proceedings of the 2021 CHI Conference on Human Factors in Computing Systems. 2021 Presented at: CHI '21; May 8-13, 2021; Yokohama, Japan p. 1-18 URL: https://dl.acm.org/doi/10.1145/3411764.3445432 [doi: 10.1145/3411764.3445432]
18. Hatton GE, Pedroza C, Kao LS. Bayesian statistics for surgical decision making. Surg Infect (Larchmt) 2021 Aug;22(6):620-625 [FREE Full text] [doi: 10.1089/sur.2020.391] [Medline: 33395554]

Abbreviations

AI: artificial intelligence
COPD: chronic obstructive pulmonary disease
ED: emergency department
GINA: Global Initiative for Asthma
GOLD: Global Initiative for Chronic Obstructive Lung Disease
K-S: Kolmogorov-Smirnov
LLM: large language model

Edited by C Perrin; submitted 24.Jun.2025; peer-reviewed by S Habib, VV Khanna, KH Lin; comments to author 28.Jul.2025; accepted 03.Jan.2026; published 29.Jan.2026.

Please cite as:
Hsu CH, Hsu CL, Tsou CH, Hsu KF, Yang HY
Improving Clinical Decision-Making in Treating Airway Diseases With an Expert System Built Upon the Free AI Tool Google NotebookLM
JMIR Med Inform 2026;14:e78567
URL: https://medinform.jmir.org/2026/1/e78567
doi:10.2196/78567
PMID:41483468

©Cheng-Hao Hsu, Ching-Li Hsu, Chih-Hsiang Tsou, Kuo-Fang Hsu, Hung-Yu Yang. Originally published in JMIR Medical Informatics (https://medinform.jmir.org), 29.Jan.2026. This is an open-access article distributed under the terms of the Creative Commons Attribution License (https://creativecommons.org/licenses/by/4.0/), which permits unrestricted use, distribution, and reproduction in any medium, provided the original work, first published in JMIR Medical Informatics, is properly cited. The

XSL•FO
RenderX

complete bibliographic information, a link to the original publication on https://medinform.jmir.org/, as well as this copyright and license information must be included.

XSL•FO
RenderX

Original Paper

Experiences With Integrating Medical Terminologies Into User Interfaces for a Decision Support System for Primary Care: Conceptual and Development Study

Michaela Christina Neff[1], MSc; Jannik Schaaf[1], Prof Dr; Najia Ahmadi[2], MSc; Michele Zoch[2], Dipl-Wi-Inf; Dania Schütze[3], Dr rer med; Holger Storf[1], Prof Dr

[1]Institute of Medical Informatics, University Medicine, Goethe University Frankfurt, Frankfurt, Germany

[2]Institute for Medical Informatics and Biometry, Carl Gustav Carus Faculty of Medicine, Technical University of Dresden, Dresden, Germany

[3]Institute of General Practice, Goethe University Frankfurt, Frankfurt, Germany

Corresponding Author:
Michaela Christina Neff, MSc
Institute of Medical Informatics
University Medicine
Goethe University Frankfurt
Theodor-Stern Kai 7
Frankfurt, 60590
Germany
Phone: 49 69630184439
Email: neff@med.uni-frankfurt.de

Abstract

Background: Clinical decision support systems (CDSSs) have shown promise in improving diagnosis in primary care, particularly for chronic diseases. The SATURN (Smart Physician Portal for Patients With Unclear Disease) project developed a CDSS prototype for primary care in Germany that uses artificial intelligence to reduce diagnostic uncertainty in unclear and rare diseases. It generates recommendations based on clinical data from university hospitals stored in a standardized common data model. However, integrating primary care data in Germany remains challenging due to the use of country-specific vocabularies and heterogeneous data structures. Therefore, integration of medical concepts into general practitioners' user interfaces (UIs) and improved workflow design is needed.

Objective: This study investigates how the UI of a CDSS for primary care should be designed to facilitate the user-friendly entry of medical concepts.

Methods: A structured, iterative user-centered design process of five steps was applied: (1) conceptualization, including analysis of requirements and objectives, (2) implementation of the CDSS UI, (3) analysis of user and expert feedback, (4) workshop with experts in the primary care electronic health record system, and (5) development of an extended concept for the system UI.

Results: This study identified requirements and options for supporting data entry in the UI of a CDSS for primary care, thus providing a framework for future implementation and prototype development. Usability testing revealed the need to refine input support, particularly the language used to make the system easy for general practitioners to use. Further effort is required to map this. In addition, we have identified a system interface to electronic patient records in primary care as essential for the system.

Conclusions: This paper demonstrates how standardized medical terminologies can be integrated into a CDSS UI for primary care. The user-centered design approach has been effective in developing CDSS UIs that align with clinicians' workflows and provide a user-friendly experience. Although the current technical infrastructure presents significant challenges when connecting to primary care electronic health record systems, collaborating with experts enabled us to identify potential interface solutions. Overall, the results indicate a need for optimized physician language input support and interoperability, including standardized data entry, automated tools, and artificial intelligence–based approaches to enhance data quality and usability.

(JMIR Med Inform 2026;14:e74934) doi:10.2196/74934

KEYWORDS

user computer interfaces; primary care; clinical decision support; controlled vocabulary

XSL•FO
RenderX

Introduction

Background and Significance

The use of clinical decision support systems (CDSSs) has been demonstrated to enhance diagnostic accuracy in primary care settings [1,2]. However, the prevailing focus at present is on chronic diseases [1]. In primary care, general practitioners (GPs) play a unique role in the diagnostic and referral processes. They often deal with nonspecific symptoms that may indicate a wide range of potential diagnoses, leading to diagnostic uncertainty. It is therefore essential to provide GPs with adequate support to ensure patient care [3-5]. Although the potential of CDSSs to achieve significant improvements in outcomes has been demonstrated, wide variations remain in the types and methods of CDSS implementation as well as the resulting effectiveness. Further research is required to determine effective implementation strategies for the usage of CDSS in various settings [6].

The SATURN (Smart Physician Portal for Patients With Unclear Disease) project has developed a prototype of a CDSS to address unclear diagnoses in primary care in Germany [7,8]. The development was conducted through an iterative, user-centered development process (UCD) [8]. The CDSS generates recommendations for GPs using 3 artificial intelligence (AI) modules based on clinical data (a machine learning algorithm and a case-based reasoning algorithm) and expert knowledge (a rule-based system). Clinical databases (rather than primary care databases) were used to establish connections between GPs and the knowledge data held by the university medicine. The diagnostic recommendations derived from clinical data are based on comparisons with existing cases [7,8]. Specifically, the data for these existing cases were extracted from the electronic health record (EHR) data of the University Hospitals in Frankfurt and Dresden via Data Integration Centers (DICs). The DIC is a central institution responsible for making medical data from hospital patient care accessible for medical research and clinical exchange in a structured, standardized, and pseudonymized form [9]. The CDSS database has been designed in such a way that EHR data from the 2 hospitals are merged into 1 OMOP database and can be used for the AI modules. Only data, not AI logic, is stored in the database. The AI modules are designed as separate modules.

The OMOP Common Data Model (CDM) is an open-access standardized data model [10] that can be used to ensure interoperability. The OMOP CDM harmonizes medical databases through a uniform structure and standardized terminologies such as SNOMED CT (Systematized Nomenclature of Medicine Clinical Terms) and RxNorm (normalized names for clinical drugs) [10-12]. New EHR patient cases from primary care for which a diagnosis recommendation is to be made will also be stored in this database, along with corresponding flags (flag: without diagnosis). In addition, solved patient cases are stored (flag: with final diagnosis). As the CDSS uses OMOP and is used in primary care, the data entered by primary care GPs must be compatible with the OMOP vocabulary standards. However, the use of standardized vocabulary remains a challenge, particularly in Germany's primary care sector, where the predominant classification of diseases is *ICD-10-GM* (*International Statistical Classification of Diseases and Related Health Problems, Tenth Revision, German Modification*). *ICD-10-GM* is complemented by OPS (Operation and Procedure Codes; German: "Operationen- und Prozedurenschlüssel") for procedural coding procedures [13], along with "Einheitlicher Bewertungsmaßstab" as the basis for billing GPs and contract psychotherapists [14]. Heterogeneous data structures in different countries and country-specific vocabularies (such as *ICD-10-GM*) pose significant challenges for exchanging data and comparing results. To our knowledge, there has been no full systematic integration of primary care data into the OMOP CDM, to date, in Germany. The standardization of data could facilitate the development of common tools. Initial international approaches have shown potential but are limited in their scope [15,16]. Henke et al [17,18] investigated the merging and collaboration of primary care and clinical data in Germany. These studies linked data from the DICs of the Medical Informatics Initiative with routine health insurance data and aimed to increase the coverage of the German vocabulary in the OMOP CDM. Another study examined the cross-sector linkage of primary care data and identified challenges, including system interfaces and data extraction processes [19]. Such projects show the need for using CDMs, such as the OMOP CDM and standardized vocabularies, to harmonize cross-sector data. To integrate medical concepts into GP user interfaces (UIs), the UI must be designed to support and streamline existing workflows [20]. Medical concepts are coded according to standards for terminology, listed in terminology management or the OMOP vocabularies.

Objectives

The objective of this study is to explore how the UI of a CDSS for primary care should be designed to allow the entry of medical concepts in a user-friendly way. To our knowledge, it has not yet been investigated how a CDSS UI for primary care can be comprehensively mapped to enable the standardized data collection and integration of data in Germany. This study outlines the requirements and the available options for CDSS UI for primary care, providing both a technical overview and a conceptual framework to support future CDSS implementations. The CDSS UI implementation focuses on medical vocabularies and the input into the CDSS. Other components of the CDSS, and the iterative conception and development, are covered in previous publications [8,21,22].

Methods

Study Design

As in the whole SATURN project, an iterative UCD was used [23]. In this paper, we focus on data entry into the CDSS (Figure 1). The requirement analysis and underlying data model [24], the ongoing evaluation, as well as other parts of the CDSS, are described in previous publications [8,21,22,25]. The UCD, from the perspective of data input, began with a conceptual design stage. During this stage, the GPs' requirements and necessary medical concepts were analyzed. These concepts were then coded into vocabularies and mapped to the UI design (step: conception). The UI then underwent iterative development in

XSL•FO
RenderX

dialogue with the GPs (step: prototypes), followed by the collection of feedback from users and experts to evaluate its usability and to identify potential improvements (step: system evaluation feedback). EHR experts discussed the automation of medical concept entry (step: workshop with EHR experts). All participant groups were selected using a purposeful sampling approach. Finally (step: extended concept), a draft for the final design concept was created.

Figure 1. Methodological steps of this study for the development process of the CDSS data entry UI. CDSS: clinical decision support system; EHR: electronic health record; UI: user interface.

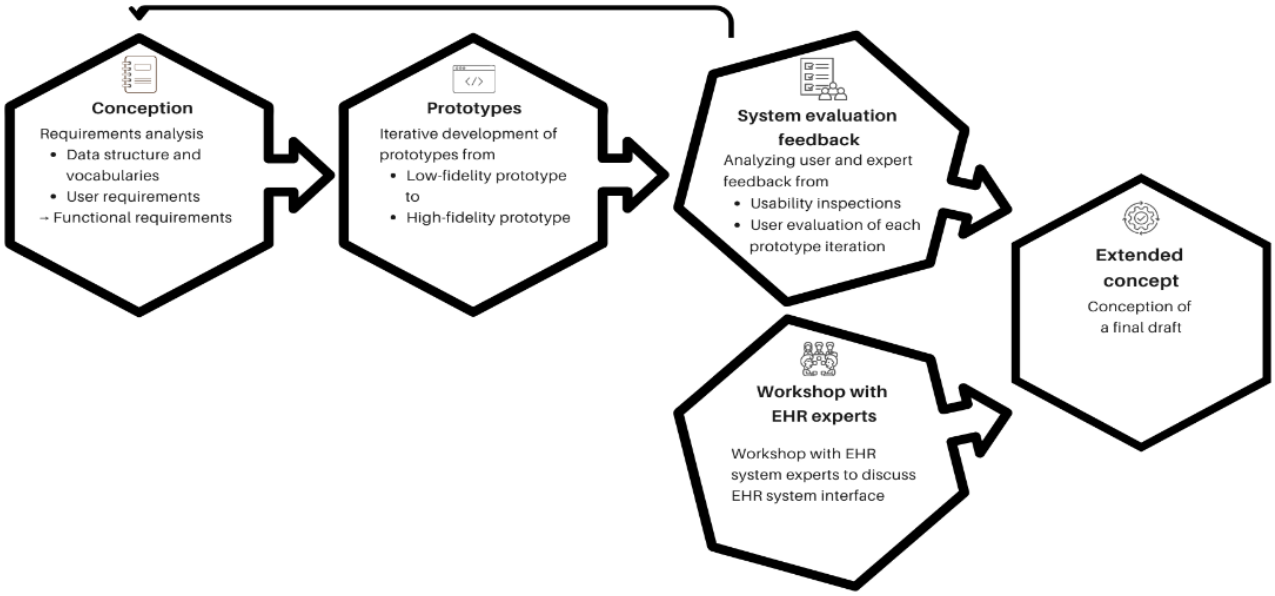

Ethical Considerations

For the conception and development of this study, the SATURN project was previously approved by the Ethics Committee of Goethe University's Medical Faculty (case 2022-1088). The user evaluation was also approved, with the Ethics Committee waiving the need for a separate ethics vote on the inquiry of GPs (case 2022-629). All participants received written information on the study and provided a signed informed consent. All data were pseudonymized before analysis. Participants received €150 (average currency exchange rate in August 2023: US $1=€0.92) for taking part in the usability test.

Participants in the usability inspections and the EHR expert workshop were either project participants or had previously submitted a letter of intent to support the project. All data were pseudonymized before analysis, with only sample data being used for case studies. Participants received no compensation for their participation in the usability inspections.

Conception

In order to facilitate data entry into the CDSS, it is necessary to consider the structure and usage of the vocabularies, as well as the requirements of the end users [21]. The appropriate fields and variables must be defined with the vocabularies for the UI. The data model was defined in a previous study [24] and specifies the following vocabularies, shown in Table 1 [26-37].

All vocabularies shown in Table 1 are fully available in the German language, except for SNOMED CT and Human Phenotype Ontology (HPO). The data to be captured from the requirements and the data model, including its vocabularies, needed to be mapped to the UI and the fields of the UI. To accomplish this, UI data categories were created: basic patient data (patient ID, gender, date of birth, and postcode), diagnosis, symptoms, medication, vital and laboratory values, and procedures. The representation in the UI was described as a UI component with an input format. Where possible, mapping to an OMOP standard concept, such as SNOMED CT and RxNorm, was also ensured and documented. Data in the OMOP CDM are expressed as concepts, which represent the semantic meanings of each data element. A standard concept represents a normative expression of a clinical entity. The others were labelled as nonstandard or source concepts and mapped to the standard concepts [38]. In order to consider the user requirements and data input structure, these were translated into functional requirements. The user requirements collected [21] were analyzed for this purpose and transformed into functional requirements with specific, testable functions that the system should fulfil. Subsequently, use cases and functional requirements were formulated in the following template: [actor] must/should/will [conditions, time aspect] [object] [process description] or something more general [target system] + [priority] + [functionality] + [conditions] [39]. Thus, an example of a functional requirement could be "the system must enable the data to be exported in a usable format." MCN, a medical informatician, carried out the conceptualization step in consultation with the other authors.

XSL•FO
RenderX

Table 1. Selected vocabularies according to the data model for the CDSS[a].

Vocabulary	Description	Availability of the German translation	Progress or version of the German translation in August 2024
ICD-10-GM [b]	Official classification for the encoding of diagnoses in inpatient and outpatient medical care in Germany [26]	Available	*ICD-10-GM* version 2024
HPO[c]	Standardized vocabulary of phenotypic abnormalities encountered in human disease [27]	Translation is not fully available in the German language	The HPO browser allows the display of some German HPO terms or synonyms [28,29], and a study on the translation of HPO terms was conducted as part of the project [30]
LOINC[d]	Database and universal standard for identifying medical laboratory observations [31]	Available	LOINC version 2.76
ATC/DDD[e]	Official classification for pharmacologically active substances. Active substances are divided into different groups according to the organ or organ system on which they act and according to their anatomical, therapeutic, and chemical properties. [32,33]	Available	ATC/DDD version 2024
OPS[f]	Official German classification for the encoding of operations, procedures, and general medical measures [34]	Available	OPS version 2024
SNOMED CT[g]	Systematized Nomenclature of Medicine Clinical Terms [35]	Translation is not fully available in the German language	The German translation group has been actively working on this since 2020 and translated the first national edition with SNOMED CT content into German at the end of 2023 [35-37]

[a]CDSS: clinical decision support system.

[b]ICD-10-GM: International Statistical Classification of Diseases and Related Health Problems, Tenth Revision, German Modification.

[c]HPO: Human Phenotype Ontology.

[d]LOINC: Logical Observation Identifiers Names and Codes Names and Codes.

[e]ATC/DDD: Anatomical Therapeutic Chemical Classification With Defined Daily Doses.

[f]OPS: Operation and Procedure Codes (German: “Operationen- und Prozedurenschlüssel”).

[g]SNOMED CT: Systematized Nomenclature of Medicine Clinical Terms.

Prototypes

The functional requirements defined in the concept were developed and implemented by MCN iteratively (described in more detail in Neff et al [8]) while feedback from users and experts was collected through user evaluations [40,41] and usability inspections [8] (described in section “system evaluation feedback”).

The following intermediate (results) were created in the iterations: (1) low-fidelity prototype (CDSS version 0) [22], (2) first high-fidelity prototype (CDSS version 1) [8], and (3) final high-fidelity prototype (CDSS version 2).

The UI and the vocabulary used were implemented in German wherever possible to suit the German-speaking target. SNOMED CT was used in English due to its limited availability, and HPO was used in an initial partial translation by Noll et al [30]. To ensure good usability, design principles and usability guidelines [42-44] were followed, in addition to the points mentioned above, including principles of dialogue design in accordance with ISO (International Organization for Standardization) 9241 and other ISO standards [43,45,46].

System Evaluation Feedback

The usability of the data entry process was assessed after each developed prototype. Initially, CDSS version 0 was discussed in 2 online user evaluation workshops involving 5 GPs, using a videoconferencing tool. This workshop was conducted and moderated by MCN with support from researchers from the Institute of General Practice (Frankfurt), and key statements were derived [22]. The findings were then documented as user requirements, and new functional requirements were derived where necessary. Usability expert inspections (method: heuristic walkthrough) were carried out in-person by 5 usability experts from the project team to accompany the further development of CDSS versions 1 and 2 (4 inspections conducted and analyzed by MCN: CDSS version 1: 3, CDSS version 2: 1) [8]. Finally, 2 usability evaluations were conducted for CDSS version 1 and version 2. Five GPs who participated in the version 0 evaluation took part in the version 1 evaluation, and 10 GPs (5 of whom were newly recruited) took part in the version 2 evaluation. The evaluations used the thinking-aloud test method, a postsession interview, and the system usability scale. The tests were conducted online by researchers from the Institute of General Practice (Frankfurt) with support from MCN [40].

The tasks that the users were asked to perform in the user evaluation and expert inspections were based on the task model derived from the requirements analysis: perform data entry, review and discuss AI results, plan further diagnosis, refer to specialists, and close the case [21]. The feedback from the expert inspections was categorized as bugs, features, improvements, ideas, or usability heuristics and linked to the individual steps of the task model [8]. When analyzing the feedback from the user evaluations, the usability problems identified in the usability tests were categorized as layout, content, navigation,

XSL•FO
RenderX

comprehensibility, and usability, and also assigned to the steps of the task model [40]. This study focuses on analyzing and interpreting the evaluation results, particularly those concerning the task of "performing data entry." The results of this task were analyzed to inform further development. The analysis of feedback represents an important conceptual intermediate step. Moreover, together with considerations regarding the connection to the primary care EHR system (see Workshop With EHR System Experts), it forms the basis for the final data entry concept within the CDSS.

Workshop With EHR System Experts

As the interface to the primary care EHR system was identified as a key requirement in the analysis and subsequent evaluation iterations, a research workshop was conducted. This workshop was held in a hybrid format, combining in-person participation with remote connections via videoconference [47]. Research workshops focus on analyzing specific cases and collecting reliable and valid data on a participant's future, including organizational change and design. These workshops yield theoretical concepts, methods, and applications that contribute to the discipline. The method involves presenting topics, conducting experiments, and then discussing the findings [48]. The central theme of the workshop was as follows: What should an interface between an EHR system and a decision support system for primary care look like? What is the current state of the art, and what is the vision for the future? The workshop focused on the technical possibilities and challenges of an interface between the CDSS and the EHR system in primary care. The participants were experts in this field, and no GPs were included. However, these experts served as representatives, as it is very difficult to cover the entire spectrum of the system landscape in Germany.

In more detail, the workshop was conducted with (1) project representatives of the SATURN project; (2) representatives from three different companies in the field of EHR systems for primary care, who are considered experts in EHR systems in this study; and (3) two moderators (with medical and medical informatics backgrounds) and one SATURN team member who took notes.

The discussion was supported by a structured discussion guide (Multimedia Appendix 1). This guide addressed the organizational, syntactic, semantic, and structural interface levels of a software. Furthermore, the UI data categories for the decision support system (see description of data categories in the chapter "conception") with related vocabularies were discussed. During the discussion, an initial architectural design was collaboratively sketched on a virtual whiteboard to support the discussion. The workshop analysis was carried out by analyzing the notes and assigning the relevant aspects to the questions in the discussion guide.

Extended Concept

After evaluating the CDSS version 2 prototype, a proposal for an extended concept for future CDSS projects in primary care with the focus on data entry was formulated by MCN in exchange with other authors. This concept considers all the results and describes a design framework that includes UI components, data flows, and system integration.

Results

Overview

The conception and development of the UI for a CDSS—in particular, the process of entering data into the CDSS—led to the development of 3 CDSS prototypes (CDSS versions 0, 1, and 2). CDSS version 2 was developed as a high-fidelity prototype connected to AI modules. Evaluation by users and experts revealed several issues regarding user-friendliness, particularly when entering medications and laboratory values. These issues led to recommendations to improve the search function for symptoms and laboratory values, and to integrate medications from the electronic prescription list. Further improvements to data entry could be achieved by integrating the primary care EHR system. EHR system experts considered middleware to be necessary for this, due to the current data exchange format (data exchange family xDT, which is not transferable via the web). In addition, the low level of standardization for important parameters—such as symptoms, which are currently entered as free text—was identified as a challenge. However, current position papers and technical possibilities may simplify this in the future.

Conception

The results of the conceptualization are presented in 2 tables: Table 2 presents the functional requirements for UI data entry, and Table 3 shows the mapping of the data elements to the UI components and standardization.

Table 3 shows the mapping of the data to be recorded to the UI fields and, if available, the mapping to the standardized international vocabulary of the OMOP database. This is based on the previously defined data model of relevant data entities and vocabularies. The column "mapping to OMOP" represents the mapping to an OMOP standard concept.

Nonstandard vocabularies were mapped in OMOP to SNOMED CT and RxNorm, with the source vocabularies being used in the UI for input. The project aimed to remove free text and to minimize the use of fields not mapped to OMOP.

A few fields were identified as relevant through the requirements analysis, but no direct mapping to OMOP could be established. Symptoms were saved using the HPO vocabulary, which at the time of the project was not supported by OMOP and was not yet available in German. In SATURN, a semiautomatic partial translation was performed for the project using natural language processing [30]. Integration of HPO as vocabulary in OMOP did not take place. HPO and SNOMED CT did not yet have an official mapping at that time—storage therefore took place in the observation table.

XSL•FO
RenderX

Table 2. Functional requirements for UI[a] data entry.

Number	Functional requirement
1	The system must offer the entry of all parameters for diagnoses, procedures, laboratory values, medications, and other clinical entities (in German).
2	The system must contain patient information such as administrative sex and age.
3	The system must generate a unique patient ID for each patient.
4	The system must offer data field-supported input help.
5	The system must ensure the integration of established medical standardized vocabularies used in the data set.
6	The system must allow exclusion diagnoses to be entered in the form (eg, using *ICD*[b] codes).
7	The system must allow time-based documentation during entry.
8	The system must offer the basic functions of a patient file (create, edit, open, or save).
9	The system must enable the continuous processing of a case and the ability to re-request diagnostic suggestions after a change.
10	The system should offer the transfer of a patient ID from the primary care EHR[c] system to the SATURN[d] patient file.
11	The system should offer a parameter query and input support based on previous entries.
12	The system must guarantee the optional input of all data fields.

[a]UI: user interface.

[b]ICD: International Statistical Classification of Diseases and Related Health Problems.

[c]EHR: electronic health record.

[d]SATURN: Smart Physician Portal for Patients With Unclear Disease.

XSL•FO
RenderX

Table 3. Mapping of the data basis to the user interface (with German vocabulary).

UI[a] data category	Mapping to OMOP	Description	UI component	Input format	Additional variables
Patient ID	Person ID	Unique ID of a patient	Auto-generated	Number	—[b]
EHR[c] system patient ID	Person source value	External unique ID of a patient	Text field	Characters or numbers	—
Gender	SNOMED CT[d]	Administrative gender	Radio button	Selection (female, male, unknown, and other)	—
Date of birth	Date of birth	Patient's date of birth	Date picker	Datetime (UTC[e])	—
Postal code	Location ID	Postal code	Text field	Number (5 digits)	—
Diagnosis	SNOMED CT	Diagnosis code, name, and date	Text field with search and date picker	*ICD-10*[f] code	Date of diagnosis
Symptoms	No mapping to SNOMED CT	Symptoms and date	Text field with search and date picker	HPO[g] code	Date of symptom onset
Medication	RxNorm	Drug name, and start or end date	Text field with search and date picker	ATC[h] code	Dose, unit, and days of administration
Vital signs and laboratory values	SNOMED CT	Parameter name, date, and reference range	Text field with search and date picker	LOINC[i] code	Reference range (only laboratory values) and measurement unit
Procedures	SNOMED CT	Procedure name and date	Text field with search and date picker	OPS[j] code	Procedure type

[a]UI: user interface.

[b]Not available.

[c]EHR: electronic health record.

[d]SNOMED CT: Systematized Nomenclature of Medicine Clinical Terms.

[e]UTC: Universal Time Coordinated.

[f]ICD-10: International Statistical Classification of Diseases and Related Health Problems, Tenth Revision.

[g]HPO: Human Phenotype Ontology.

[h]ATC: Anatomical Therapeutic Chemical Classification.

[i]LOINC: Logical Observation Identifiers Names and Codes.

[j]OPS: Operation and Procedure Codes (German: "Operationen- und Prozedurenschlüssel").

Prototypes

The requirements and the associated vocabularies were implemented step by step. The CDSS version 0 was designed as a low-fidelity prototype in the form of mock-ups [22]. This was followed by the development of the following 2 high-fidelity prototypes: (1) CDSS version 1: JavaScript frameworks nuxt.js 2 (Vuetify), and the UI component framework Vuetify 2 were used with initial sample data (without an active interface to AI modules, as yet, and with integrated vocabularies) [8]. (2) CDSS version 2: React.js (Meta Platforms, Inc) and Mantine were used due to the expiring support of nuxt.js 2. The prototype includes all feasible requirements and has a connection to the AI modules.

Figure 2 shows the first step of the data entry in the final high-fidelity prototype.

CDSS version 0 mock-ups, as well as screenshots of the 2 high-fidelity prototypes, CDSS versions 1 and 2, can be found in Multimedia Appendix 2. At the request of user feedback on this prototype, a step-by-step navigation was incorporated below (see also Neff et al [8] for a more detailed description of prototype version 1).

Figure 3 shows an example of how the integration of vocabularies appears using *ICD-10-GM*: users can search for *ICD-10-GM* terms using the code (eg, E05.0) or the disease name (eg, in the German language "Hyperthyreose mit diffuser Struma").

XSL•FO
RenderX

Figure 2. Zoomed-in section of the input template of the CDSS version 2. CDSS: clinical decision support system.

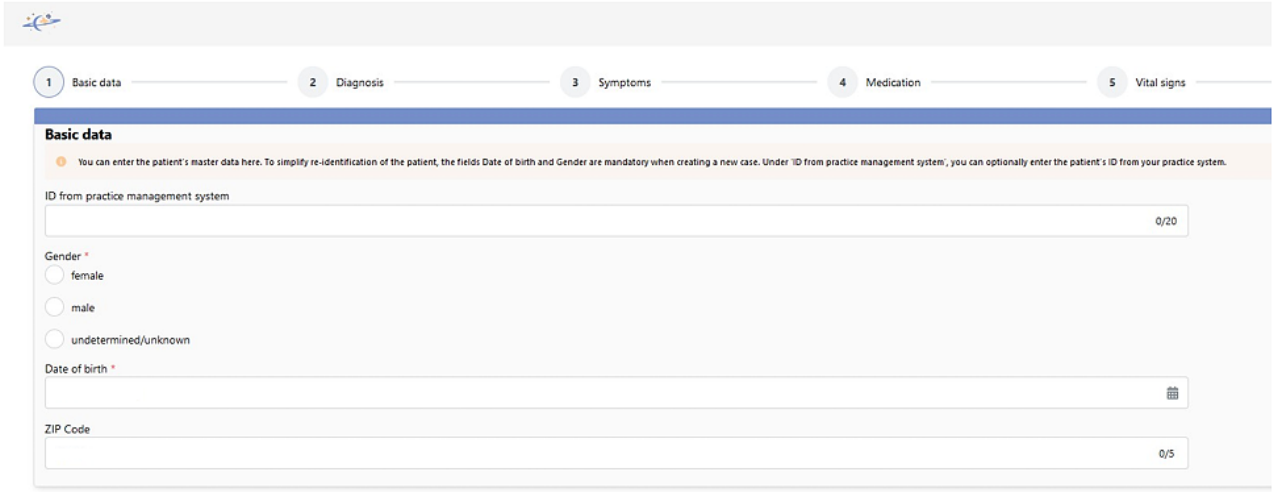

Figure 3. Screenshot of the diagnosis search (CDSS version 2). CDSS: clinical decision support system.

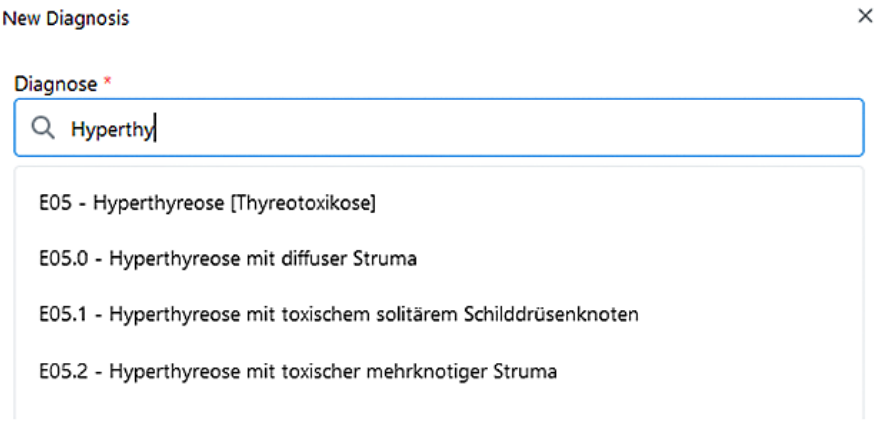

System Evaluation Feedback

During the development of CDSS version 1, expert feedback revealed issues, particularly with search field entry options and inconsistencies between system functions and real clinical practice, for example, the handling of "diagnostic certainty." Feedback also emphasized the importance of automatic saving and clear error messages. Errors were found when entering medications and laboratory values. Some terminology was not displayed in the German language; thus, it is imperative that vocabularies be available in the German language [8]. Detailed information can be found in the publication by Neff et al [8].

In addition to expert feedback from the inspections, further issues were derived from the user evaluations. Feedback on data entry was collated into categories (layout, content, navigation, comprehensibility, and ease of use). The results of the CDSS version 1 usability test (Figure 4) indicated several usability issues. Participants had difficulties entering unlisted symptoms, medications, and tests, and retrieving laboratory values using common abbreviations. Medication data was the biggest problem area. The wide range of laboratory units also caused confusion; thus, specifications for values such as the heart rate were proposed. Some important GPs' diagnostic criteria were absent, with participants proposing their inclusion within the system or the creation of additional free entry fields. The additional fields were proposed to encompass physical examination findings, symptom duration, diagnoses, and family history. GPs also proposed issues for the CDSS version 2 (Figure 4), including automated display of reference range and integration of an updated medication database. GPs were unfamiliar with LOINC (Logical Observation Identifiers Names and Codes) terms, and so better input support was recommended. Participants also recommended focusing on frequency, time, dosage, and extending the search function. This would allow GPs to enter both generic and brand names, as data entry for laboratory values, medications, and diagnoses was considered time-consuming. The information text to each input step was unclear and not sufficiently relevant, and the distinction between some parameter names was not apparent. The GPs also noted several limitations; these included the inability to enter lowercase letters for laboratory reference values and the failure of the symptom search function to recognize certain synonyms.

XSL•FO
RenderX

Figure 4. Summarized results of first and second user evaluations (feedback of the first high-fidelity prototype: version 1, and of the final high-fidelity prototype: version 2). CDSS: clinical decision support system; HPO: Human Phenotype Ontology; LOINC: Logical Observation Identifiers Names and Codes; PMS: patient management system.

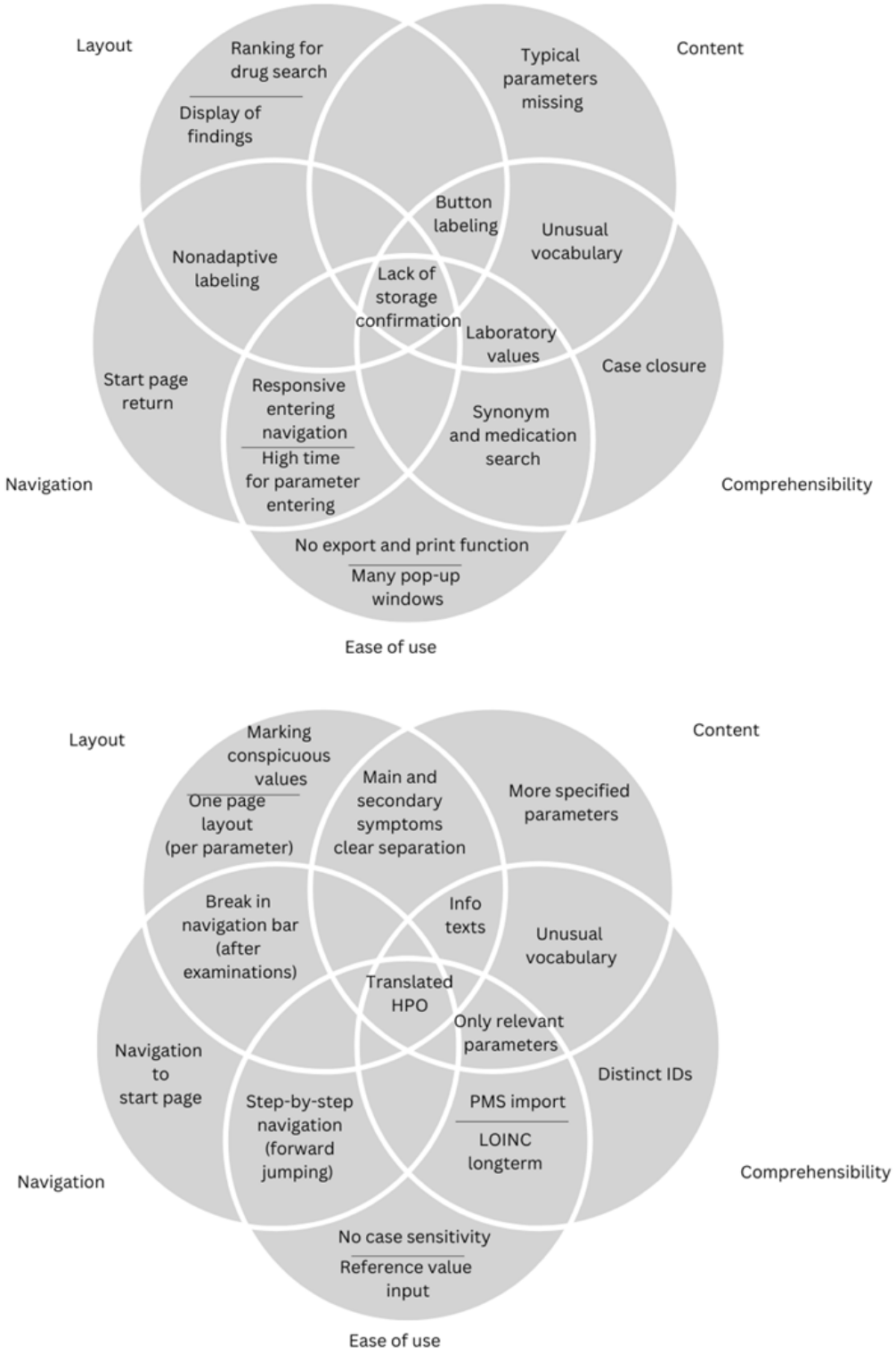

Workshop With EHR System Experts

The workshop was attended by a total of 12 participants (7 women and 5 men): (1) four project representatives (experts with backgrounds in medicine, medical informatics, medical technology, or public health) from the SATURN project; (2) five representatives from three different companies in the field of EHR systems for primary care (experts for EHR systems); (3) the workshop confirmed that currently, the most widely used data transmission standard (syntactically) in primary care in Germany is still the xDT data standard family [49]. These include, in particular: Behandlungsdaten-Transfer (further development completed in 2019) for the transfer of treatment data [50], and Labordaten-Transfer for laboratory values [51].

XSL•FO
RenderX

Both standards are defined by the KBV (Kassenärztliche Bundesvereinigung; umbrella organization of the Associations of Statutory Health Insurance Physicians in Germany) [52]. The data transfer (structural) is currently realized via xDT interfaces and is not transferable via the web. A 2022 position paper ([53]) indicated movement toward FHIR (Fast Healthcare Interoperability Resources from HL7 [Health Level Seven]) and thus web transfer. However, the workshop participants have indicated that not all the necessary FHIR profiles have yet been specified. The JSON format was considered a favorable option for the future, with or without a combination with FHIR. Initial data, such as the MIO "Medizinische Informationsobjekte," representing the new KBV data exchange standard [54], are already available in JSON. Table 4 summarizes the terminology and data structure (semantics) for the participants' description of the status quo for the specific CDSS for the primary care use case. All primary care EHR systems are required to provide an electronic physician letter, as part of the telematics infrastructure (TI) in Germany [55].

Participants concluded based on the status quo that middleware is currently indispensable in Germany for integrating EHR systems with CDSS in primary care due to limited data structures and limited data transfer options. Middleware is required to map data to standard medical terminologies used in the CDSS. Ideally, an interface for diagnoses (billing diagnoses in *ICD-10-GM*), laboratory values, and the electronic physician letter should be available via the EHR system. The CDSS should ensure the addressability of the interface and the import of medications from the electronic medication plan. The electronic physician's letter can be used to extract symptoms and examinations. If the electronic physician letter cannot be sent through the EHR system, a new interface is needed. In the future, other medical devices and wearables will connect to the CDSS via middleware. The workshop participants also provided the following feedback on the potential for future developments: data processing with AI is already partially integrated into the EHR systems in primary care. TI measures have also been implemented and are mandatory for manufacturers in Germany.

These include, besides the physician's electronic letters, electronic medication plans and electronic prescriptions, which are set to increase. Connecting the EHR system to other systems, such as the CDSS, is considered feasible and can be implemented depending on the availability and format of data, using REST (Representational State Transfer), a software architecture paradigm.

Table 4. Semantic description of status quo: terminologies and structured data in primary care EHR[a].

Data category	Status quo (data structure)
Basic patient data	Patient data, such as date of birth and postcode, are considered primitive data types and, therefore, are easy to structure and transfer via an interface.
Diagnosis	Diagnoses are structured as billing and permanent diagnoses, with some stored as "suspected diagnoses" and localizations. Transferring the *ICD-10-GM*[b] codes is, according to the current state of the art, challenging.
Symptoms	Symptoms are typically documented as free text, using, for example, nonstandardized categories in chronological index cards.
Medication	Medications are ideally coded using national medication plans (ATC[c] codes or PZN[d]); EHR systems must implement the standardized national medication plan, which has been mandatory since 2016 [56].
Laboratory and vital signs	Laboratory values comply with the LDT[e] 3 standard, although many laboratories continue to use unstructured data that are not LOINC[f] compliant [52,57]. The KBV[g] is developing an MIO[h] for laboratory values [54]. Vital signs can be recorded as either discrete or continuous measurements for billing purposes.
Procedures	Procedure codes (eg, OPS[i]) are structured in hospital outpatient departments but are rarely used in primary care EHR systems; outpatient procedures are often documented as service code justifications for billing purposes.

[a]EHR: electronic health record.

[b]*ICD-10-GM*: *International Statistical Classification of Diseases and Related Health Problems, Tenth Revision, German Modification*.

[c]ATC: Anatomical Therapeutic Chemical Classification.

[d]PZN: Pharmazentralnummer.

[e]LDT: Labordaten-Transfer.

[f]LOINC: Logical Observation Identifiers Names and Codes.

[g]KBV: Kassenärztliche Bundesvereinigung.

[h]MIO: Medizinische Informationsobjekte.

[i]OPS: Operation and Procedure Codes (German: "Operationen- und Prozedurenschlüssel").

Extended Concept

Overview

The concept is described in the form of a design framework with UI components, data flows, and system integration.

UI Components

The required ontologies will continue to be entered as standardized vocabulary, but will be supported by various factors. These include error-tolerant searching that ignores misspellings and similar spellings, and the use of common

XSL•FO
RenderX

abbreviations [58-60]. These approaches are visualized in Figure 5.

Figure 5. UI component optimizations. LOINC: Logical Observation Identifiers Names and Codes; UI: user interface.

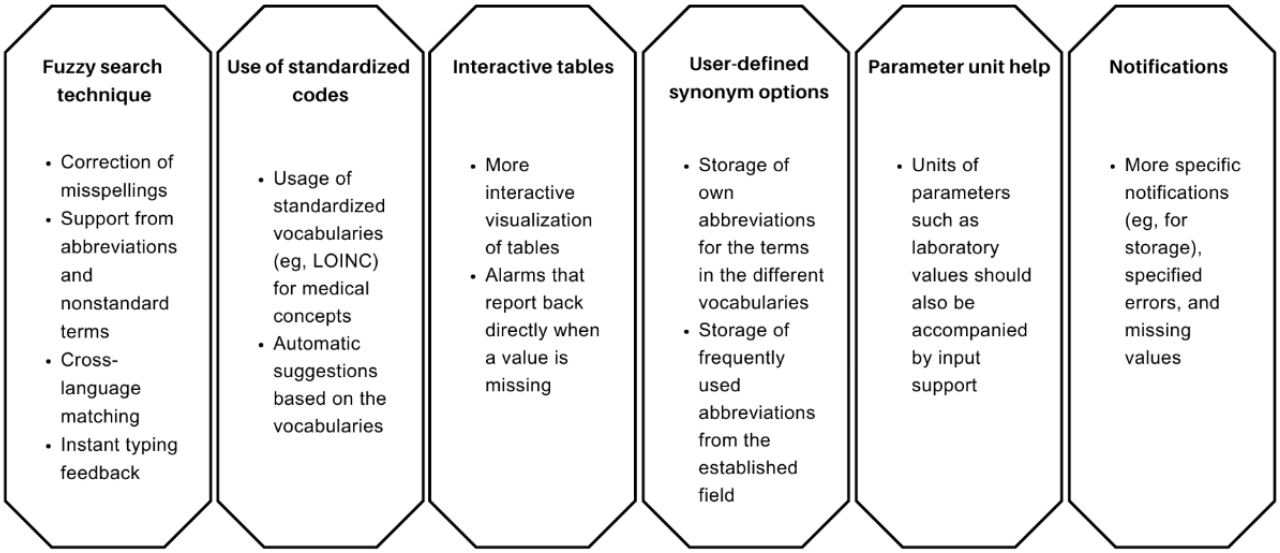

Data Flows

The input of patient data should be possible both via the UI and via an interface to the primary care EHR system or TI applications. Supporting middleware can help with this, especially for laboratory values and medications. The data flow then goes from the UI to the backend for storage, which is connected to the stored database. A data flow from the database via the backend to the UI occurs only when displaying and correcting previously saved cases or when retrieving the vocabularies for input support.

System Integration

System integration is provided by a REST interface from the UI to the backend and REST interfaces to the AI modules.

Discussion

Discussion of Methods

The objective of this study was to investigate how the UI of a CDSS designed for primary care can effectively support GPs in the user-friendly input of standardized vocabulary codes from medical terminologies. It focuses on the CDSS UI, as well as the usability and clarity of medical terminology input.

Methods from software development and UCD were used as part of the iterative process. The UCD design process has been proven to have positive effects in several studies [61-64]. Clinical decision support is generally viewed favorably, providing higher benefits when it improves performance [63]. The current study addresses the integration of the CDSS into the physicians' workflow, an aspect shown in the literature to be essential for CDSS acceptance and usage [65]. To simplify the input of medical terms into the UI for GPs, the UI must be designed to be supportive and user-friendly [20]. One key aspect, therefore, is the reduction of cognitive load. This is described by Miller et al [65] as an important principle for CDSS design: focusing on the input of standardized medical terminology codes can help to reduce the cognitive load on physicians.

The research conducted in this project and other studies has mainly focused on UCD, requirements analysis, and evaluation of CDSS [8,21,63,66]. The formulation of functional requirements and task model methods has proven effective [39,67]. Building on these results, the current study mapped relevant data elements to the UI and collaborated with primary care EHR system experts to develop an extended concept. Zerlik et al [68] took a similar approach in their initial steps, following a UCD process that included requirements definition and iterative development across 3 iterations. We complemented usability expert testing and workshops with feedback from EHR system experts. This approach enabled us to identify potential interfaces to other systems, consistent with recommendations that include different perspectives in the design process [64].

Discussion of the Results

This study identifies requirements and options for entry support in the UI of a primary care CDSS and provides a conceptual framework to support future CDSS implementations. The feedback from the usability test indicates that optimized input support in the language of GPs will be necessary in the future, as will additional mapping work. It is imperative to avoid unfamiliar terms and minimize input restrictions. Ideally, the system would integrate directly with the primary care EHR system in use. The workshop with primary care EHR system experts resulted in initial solution approaches for system interfaces. However, it also highlighted challenges related to limited interoperability, including a simple nonweb-transferable data exchange format and a lack of standardization for important parameters. We propose various optimizations for the UI in our concept for a future CDSS UI. There are several options to better support standardized data entry. Standardizing data entry and using automated tools can significantly improve data quality by minimizing the need for queries and simplifying data collection. Automated features, such as auto-complete, can improve accuracy by relying on predictive modeling. Integration with generative AI can further improve data accuracy and usability. Nevertheless, further research is needed to optimize

XSL•FO
RenderX

the role of standardized data in clinical decision-making and in the research context [69]. AI (eg, machine learning) and natural language processing methods already exist for data integration and mapping, data extraction, and clinical coding.

Models for clinical data extraction, phenotyping, and LOINC mapping also exist [70-74]. A mandatory opt out system for the electronic patient records (ePA) planned for 2025 in Germany, focusing on secure storage and pseudonymized data usage, may facilitate implementing an interface to the ePA data [75,76]. The Unified Medical Language System metathesaurus is another option, already being partially in use, that supports terminology mapping and standardization and enables better interoperability and information retrieval [77]. When searching the medical literature, it is often easier to use the language you are most familiar with. Using one's native language can facilitate the identification of certain concepts that are difficult to translate into English [60]. There is still a need for improvement in this area, particularly regarding the German-language description of symptoms. Further development of standards and translations, as well as data transfer formats such as FHIR for connecting primary care EHR to CDSS, may simplify integration in the future. When implementing in practice, it is important to incorporate the system into the daily workflow and connect it to the practice's own EHR system.

Limitations

This study focused on integrating medical terminologies into the UI, representing 1 task within the task model. The methodological framework was designed to address this objective. However, the steps are transferable to other tasks within the task model. This requires selecting the requirements and involving additional experts (such as EHR system experts) relevant to the task. Further studies in real-world clinical settings, using the implemented system over an extended period, are necessary to develop the CDSS. For the specific task of entering medical terminology into the CDSS, fuzzy search can provide excellent support; however, there are also challenges in the form of high computational effort, false positive results, and balanced precision in different languages [58]. For the integration into practice, the current infrastructure and networking in Germany make it difficult to interface with the primary care EHR system. The slow uptake of ePA in Germany, with only ≈1% penetration by 2023 compared to a target of 80% by 2025, is hampering automation. Barriers to adoption include legal ambiguities, conflicts between stakeholders, and insufficient communication [75,76].

Thanks to their modular structure, the practices will not require significant resources. However, the task here is to ensure secure implementation, including hosting of the AI modules and secure data transfer.

Conclusion

In conclusion, the process of UCD has been shown to be effective in the development of the UI of CDSS, particularly regarding the integration into physicians' workflow and creation of a user-friendly interface. Iterative development with experts identified potential interfaces for other systems. The results indicated a need for optimized entry support in the physician's language and revealed challenges concerning interoperability. Suggestions for improvements include standard data entry, automated tools, and AI to enhance data quality and usability. However, the current infrastructure poses significant challenges for interfacing with primary care EHR systems in Germany. Further studies are required to address these issues.

Acknowledgments

We would like to thank the participants of the workshop with electronic health record system experts and the participants in the expert and user evaluations.

Funding

SATURN is funded by the German Federal Ministry of Health as part of the research focus "Digital Innovation," Module 3: "Smart Algorithms and Expert Systems" (funding code: 2520DAT02B, 2520DAT02C, 2520DAT02D).

Authors' Contributions

Conceptualization: MCN
Data curation: MCN
Formal analysis: MCN
Funding acquisition: JS, HS
Investigation: MCN, JS, DS, NA, MZ
Methodology: MCN, JS, DS, NA, MZ
Resources: MCN
Supervision: JS, HS
Validation: MCN, JS, DS, NA, MZ, HS
Visualization: MCN
Writing – original draft: MCN
Writing – review & editing: MCN, JS, DS, NA, MZ, HS

XSL•FO
RenderX

Conflicts of Interest

None declared.

Multimedia Appendix 1
Discussion guide of EHR expert workshop. EHR: electronic health record.
[DOCX File , 19 KB - medinform_v14i1e74934_app1.docx]

Multimedia Appendix 2
Screenshots of the CDSS user interface (prototypes: CDSS versions 0, 1, and 2). CDSS: clinical decision support systems.
[DOCX File , 718 KB - medinform_v14i1e74934_app2.docx]

References

1. Harada T, Miyagami T, Kunitomo K, Shimizu T. Clinical decision support systems for diagnosis in primary care: a scoping review. Int J Environ Res Public Health 2021 Aug 10;18(16):8435 [FREE Full text] [doi: 10.3390/ijerph18168435] [Medline: 34444182]
2. Sutton RT, Pincock D, Baumgart DC, Sadowski DC, Fedorak RN, Kroeker KI. An overview of clinical decision support systems: benefits, risks, and strategies for success. NPJ Digit Med 2020 Feb 06;3:17 [FREE Full text] [doi: 10.1038/s41746-020-0221-y] [Medline: 32047862]
3. Wübken M, Oswald J, Schneider A. [Dealing with diagnostic uncertainty in general practice]. Z Evid Fortbild Qual Gesundhwes 2013;107(9-10):632-637. [doi: 10.1016/j.zefq.2013.10.017] [Medline: 24315334]
4. Singh H, Schiff GD, Graber ML, Onakpoya I, Thompson MJ. The global burden of diagnostic errors in primary care. BMJ Qual Saf 2017 Jun;26(6):484-494 [FREE Full text] [doi: 10.1136/bmjqs-2016-005401] [Medline: 27530239]
5. Kostopoulou O, Delaney BC, Munro CW. Diagnostic difficulty and error in primary care--a systematic review. Fam Pract 2008 Dec;25(6):400-413. [doi: 10.1093/fampra/cmn071] [Medline: 18842618]
6. Bryan C, Boren SA. The use and effectiveness of electronic clinical decision support tools in the ambulatory/primary care setting: a systematic review of the literature. Inform Prim Care 2008;16(2):79-91 [FREE Full text] [doi: 10.14236/jhi.v16i2.679] [Medline: 18713524]
7. Smartes Arztportal für Patienten mit unklarer Erkrankung (SATURN). Bundesministerium für Gesundheit. 2024. URL: https://www.bundesgesundheitsministerium.de/ministerium/ressortforschung/handlungsfelder/forschungsschwerpunkte/digitale-innovation/modul-3-smarte-algorithmen-und-expertensysteme/saturn.html [accessed 2026-02-17]
8. Neff MC, Schütze D, Holtz S, Köhler SM, Vasseur J, Ahmadi N, et al. Development and expert inspections of the user interface for a primary care decision support system. Int J Med Inform 2024 Dec;192:105651 [FREE Full text] [doi: 10.1016/j.ijmedinf.2024.105651] [Medline: 39413613]
9. Semler SC, Wissing F, Heyder R. German medical informatics initiative. Methods Inf Med 2018 Jul;57(S 01):e50-e56 [FREE Full text] [doi: 10.3414/ME18-03-0003] [Medline: 30016818]
10. OMOP Common Data Model. OHDSI CDM Working Group. URL: https://ohdsi.github.io/CommonDataModel/ [accessed 2026-02-17]
11. Overhage JM, Ryan PB, Reich CG, Hartzema AG, Stang PE. Validation of a common data model for active safety surveillance research. J Am Med Inform Assoc 2012;19(1):54-60 [FREE Full text] [doi: 10.1136/amiajnl-2011-000376] [Medline: 22037893]
12. Reich C, Ostropolets A, Ryan P, Rijnbeek P, Schuemie M, Davydov A, et al. OHDSI Standardized Vocabularies-a large-scale centralized reference ontology for international data harmonization. J Am Med Inform Assoc 2024 Feb 16;31(3):583-590 [FREE Full text] [doi: 10.1093/jamia/ocad247] [Medline: 38175665]
13. ICD-10-GM 2024: BfArM veröffentlicht endgültige Fassung. BfArM. 2025. URL: https://www.bfarm.de/DE/Kodiersysteme/News/ICD-10-GM_2024_BfArM_veroeffentlicht_endgueltige_Fassung.html [accessed 2026-02-17]
14. Einheitlicher Bewertungsmaßstab. Kassenärztliche Bundesvereinigung KdöR. 2025. URL: https://www.kbv.de/html/ebm.php [accessed 2026-02-17]
15. Fruchart M, Quindroit P, Jacquemont C, Beuscart JB, Calafiore M, Lamer A. Transforming primary care data into the observational medical outcomes partnership common data model: development and usability study. JMIR Med Inform 2024 Aug 13;12:e49542 [FREE Full text] [doi: 10.2196/49542] [Medline: 39140273]
16. Ward R, Hallinan CM, Ormiston-Smith D, Chidgey C, Boyle D. The OMOP common data model in Australian primary care data: building a quality research ready harmonised dataset. PLoS One 2024;19(4):e0301557 [FREE Full text] [doi: 10.1371/journal.pone.0301557] [Medline: 38635655]
17. Henke E, Zoch M, Peng Y, Reinecke I, Sedlmayr M, Bathelt F. Conceptual design of a generic data harmonization process for OMOP common data model. BMC Med Inform Decis Mak 2024 Feb 26;24(1):58 [FREE Full text] [doi: 10.1186/s12911-024-02458-7] [Medline: 38408983]

XSL•FO
RenderX

18. Henke E, Zoch M, Kallfelz M, Ruhnke T, Leutner LA, Spoden M, et al. Assessing the use of German claims data vocabularies for research in the observational medical outcomes partnership common data model: development and evaluation study. JMIR Med Inform 2023 Nov 07;11:e47959 [FREE Full text] [doi: 10.2196/47959] [Medline: 37942786]
19. Moser K, Mikolajczyk R, Bauer A, Tiller D, Christoph J, Purschke O, et al. [BeoNet-Halle-development of a multifunctional database for the automated extraction of healthcare data from general practitioner and specialist practices]. Bundesgesundheitsblatt Gesundheitsforschung Gesundheitsschutz 2023 May;66(5):569-577 [FREE Full text] [doi: 10.1007/s00103-023-03691-7] [Medline: 37079066]
20. Meunier PY, Raynaud C, Guimaraes E, Gueyffier F, Letrilliart L. Barriers and facilitators to the use of clinical decision support systems in primary care: a mixed-methods systematic review. Ann Fam Med 2023;21(1):57-69 [FREE Full text] [doi: 10.1370/afm.2908] [Medline: 36690490]
21. Schütze D, Holtz S, Neff MC, Köhler SM, Schaaf J, Frischen LS, et al. Requirements analysis for an AI-based clinical decision support system for general practitioners: a user-centered design process. BMC Med Inform Decis Mak 2023 Jul 31;23(1):144 [FREE Full text] [doi: 10.1186/s12911-023-02245-w] [Medline: 37525175]
22. Neff MC, Schaaf J, Noll R, Holtz S, Schütze D, Köhler SM, et al. Initial user-centred design of an AI-based clinical decision support system for primary care. Stud Health Technol Inform 2024 Jan 25;310:1051-1055. [doi: 10.3233/SHTI231125] [Medline: 38269975]
23. Jokela T, Iivari N, Matero J, Karukka M. The standard of user-centered design and the standard definition of usability: analyzing ISO 13407 against ISO 9241-11. : Association for Computing Machinery; 2003 Presented at: CLIHC03: Latin American Conference on Human-Computer Interaction; August 17-20, 2003; Rio de Janeiro Brazil p. 53-60. [doi: 10.1145/944519.944525]
24. Ahmadi N, Zoch M, Guengoeze O, Facchinello C, Mondorf A, Stratmann K, et al. How to customize common data models for rare diseases: an OMOP-based implementation and lessons learned. Orphanet J Rare Dis 2024 Aug 14;19(1):298 [FREE Full text] [doi: 10.1186/s13023-024-03312-9] [Medline: 39143600]
25. Neff MC, Schaaf J, Schütze D, Storf H. Development of a patient dashboard in a clinical decision support system for primary care. Stud Health Technol Inform 2025 Apr 24;324:170-175. [doi: 10.3233/SHTI250181] [Medline: 40270405]
26. ICD-10-GM. URL: https://www.bfarm.de/EN/Code-systems/Classifications/ICD/ICD-10-GM/_node.html [accessed 2026-02-17]
27. Human Phenotype Ontology. URL: https://hpo.jax.org/ [accessed 2026-02-17]
28. Gargano MA, Matentzoglu N, Coleman B, Addo-Lartey EB, Anagnostopoulos AV, Anderton J, et al. The Human Phenotype Ontology in 2024: phenotypes around the world. Nucleic Acids Res 2024 Jan 05;52(D1):D1333-D1346 [FREE Full text] [doi: 10.1093/nar/gkad1005] [Medline: 37953324]
29. Translations and Mapping. Human Phenotype Ontology. URL: https://hpo.jax.org/data/translations [accessed 2026-02-17]
30. Noll R, Berger A, Facchinello C, Güngöze O, von Wagner M, Hoehl S, et al. Translation of ontological concepts from English into German using commercial translation software and expert evaluation. Stud Health Technol Inform 2024 Jan 25;310:89-93. [doi: 10.3233/SHTI230933] [Medline: 38269771]
31. The international standard for identifying health measurements, observations, and documents. LOINC. URL: https://loinc.org/ [accessed 2026-02-17]
32. Anatomical Therapeutic Chemical (ATC) classification. World Health Organization (WHO). 2024. URL: https://www.who.int/tools/atc-ddd-toolkit/atc-classification [accessed 2026-02-17]
33. ATC-Classification. BfArM. 2025. URL: https://www.bfarm.de/EN/Code-systems/Classifications/ATC/_node.html [accessed 2026-02-17]
34. Operationen- und Prozedurenschlüssel (OPS). BfArM. URL: https://www.bfarm.de/DE/Kodiersysteme/Klassifikationen/OPS-ICHI/OPS/_node.html [accessed 2026-02-17]
35. Germany's BfArM joins SNOMED international for nationwide use of SNOMED CT. SNOMED International. 2021. URL: https://www.snomed.org/news/germany%E2%80%99s-bfarm-joins-snomed-international-for-nationwide-use-of-snomed-ct [accessed 2026-02-17]
36. SNOMED CT. BfArM. 2024. URL: https://www.bfarm.de/DE/Aktuelles/Blog/_docs/2024-03-05-snomed.html [accessed 2026-02-17]
37. Deutsche Übersetzungen von SNOMED CT-Konzepten. BfArM. URL: https://www.bfarm.de/DE/Kodiersysteme/Terminologien/SNOMED-CT/Uebersetzung/_node.html [accessed 2026-02-17]
38. Chapter 5 standardized vocabularies. The Book of OHDSI. URL: https://ohdsi.github.io/TheBookOfOhdsi/StandardizedVocabularies.html [accessed 2026-02-17]
39. Tremp H. Funktionale Anforderungen spezifizieren. In: Tremp H, editor. Agile objektorientierte Anforderungsanalyse Planen - Ermitteln - Analysieren - Modellieren - Dokumentieren - Prüfen Wiesbaden. Heidelberg: Springer Vieweg; 2022:119-143.
40. Köhler SM, Holtz S, Neff MC, Schaaf J, von Wagner M, Müller BS, et al. Evaluating the prototype of a clinical decision support system in primary care: qualitative study. JMIR Form Res 2025 Aug 20;9:e69875 [FREE Full text] [doi: 10.2196/69875] [Medline: 40835411]

XSL•FO
RenderX

41. Köhler SM, Holtz S, Neff M, Schaaf J, Wagner M, Müller BS, et al. Evaluation digitaler Interventionen - Erfahrungen mit Remote-Usability-Test mittels Think-Aloud-Technik. In: 23 Deutscher Kongress für Versorgungsforschung (DKVF) 2024. Düsseldorf: German Medical Science GMS Publishing House; 2024 Sep 10 Presented at: 23. Deutscher Kongress für Versorgungsforschung (DKVF); September 25-27, 2024; Potsdam. [doi: 10.3205/24DKVF415]
42. Geis T, Gerloff N, Lampert-Staimann M, Polkehn K, Reisemann M. Curriculum: Certified Professional for Usability and User Experience. User Requirements Engineering (CPUX-UR). URL: https://www.uxqb.org/ux-training-and-certification/cpux-ur/ [accessed 2026-02-17]
43. DIN. Ergonomics of human-system interaction - Part 11: Usability: Definitions and concepts (ISO 9241-11:2018); German version EN ISO 9241-11:2018. Germany: Beuth Verlag GmbH; 2018:46.
44. Baxter K, Courage C, Caine K. Understanding Your Users: A Practical Guide to User Research Methods. Amsterdam, Netherlands: Morgan Kaufmann; 2015.
45. ISO 9241-210:2019 ergonomics of human-system interaction - part 210: human-centred design for interactive systems. International Organization for Standardization. 2019. URL: https://www.iso.org/standard/77520.html [accessed 2026-02-17]
46. ISO 9241-110:2006 ergonomics of human-system interaction - part 110: dialogue principles. International Organization for Standardization. 2006. URL: https://www.iso.org/standard/38009.html [accessed 2026-02-17]
47. Ellis R, Goodacre T, Mortensen N, Oeppen RS, Brennan PA. Application of human factors at hybrid meetings: facilitating productivity and inclusivity. Br J Oral Maxillofac Surg 2022 Jul;60(6):740-745 [FREE Full text] [doi: 10.1016/j.bjoms.2021.12.055] [Medline: 35300882]
48. Ørngreen R, Levinsen K. Workshops as a research methodology. Electron J e-Learn 2017;15:70-81 [FREE Full text]
49. QMS-Standards in der Arztpraxis. Qualitätsring Medizinische Software. URL: https://www.qms-standards.de/standards/ [accessed 2026-02-17]
50. BDT-Schnittstelle. Qualitätsring Medizinische Software. URL: https://www.qms-standards.de/standards/schnittstellen-archiv/bdt-schnittstelle/ [accessed 2026-02-17]
51. LDT-Schnittstelle. Qualitätsring Medizinische Software. URL: https://www.qms-standards.de/standards/schnittstellen-archiv/ldt-schnittstelle/ [accessed 2026-02-17]
52. Bohrer KJ. Nationale ambulante standards. In: Müller-Mielitz S, Lux T, editors. E-Health-Ökonomie. Wiesbaden: Springer Gabler, Wiesbaden; 2017:647-667.
53. DGIV. 2022. URL: https://dgiv.org/wp-content/uploads/2022/08/DGV-Positionspapier-Digitalisierung.pdf [accessed 2026-02-17]
54. Medizinische Informationsobjekte. Kassenärztlichen Bundesvereinigung. URL: https://mio.kbv.de/site/mio#tab-Rund+um+die+MIOs [accessed 2026-02-17]
55. eArztbrief. Kassenärztliche Bundesvereinigung. 2024. URL: https://www.kbv.de/html/earztbrief.php [accessed 2026-02-17]
56. Anwendungen in der TI- Elektronischer medikationsplan (eMP). Kassenärztliche Bundesvereinigung. URL: https://www.kbv.de/praxis/verordnungen/arzneimittel/medikationsplan [accessed 2024-12-13]
57. Labordatenkommunikation. Kassenärztliche Bundesvereinigung. URL: https://update.kbv.de/ita-update/Labor/Labordatenkommunikation/ [accessed 2026-02-17]
58. Griffon N, Schuers M, Dhombres F, Merabti T, Kerdelhué G, Rollin L, et al. Searching for rare diseases in PubMed: a blind comparison of Orphanet expert query and query based on terminological knowledge. BMC Med Inform Decis Mak 2016 Aug 02;16:101 [FREE Full text] [doi: 10.1186/s12911-016-0333-0] [Medline: 27484923]
59. Wang J, Cetindil I, Ji S, Li C, Xie X, Li G, et al. Interactive and fuzzy search: a dynamic way to explore MEDLINE. Bioinformatics 2010 Sep 15;26(18):2321-2327. [doi: 10.1093/bioinformatics/btq414] [Medline: 20624778]
60. Liu F, Ackerman M, Fontelo P. BabelMeSH: development of a cross-language tool for MEDLINE/PubMed. AMIA Annu Symp Proc 2006;2006:1012 [FREE Full text] [Medline: 17238631]
61. Luna D, Quispe M, Gonzalez Z, Alemrares A, Risk M, Garcia Aurelio M, et al. User-centered design to develop clinical applications. Literature review. Stud Health Technol Inform 2015;216:967. [Medline: 26262269]
62. LeRouge C, Wickramasinghe N. A review of user-centered design for diabetes-related consumer health informatics technologies. J Diabetes Sci Technol 2013 Jul 01;7(4):1039-1056 [FREE Full text] [doi: 10.1177/193229681300700429] [Medline: 23911188]
63. Brunner J, Chuang E, Goldzweig C, Cain CL, Sugar C, Yano EM. User-centered design to improve clinical decision support in primary care. Int J Med Inform 2017 Aug;104:56-64 [FREE Full text] [doi: 10.1016/j.ijmedinf.2017.05.004] [Medline: 28599817]
64. Davies I. Designing user interface requirement patterns for a genomically enabled clinical decision support system using frailty assessment as a prototypical example. 2020. URL: https://open.library.ubc.ca/soa/cIRcle/collections/ubctheses/24/items/1.0392430 [accessed 2026-02-11]
65. Miller K, Mosby D, Capan M, Kowalski R, Ratwani R, Noaiseh Y, et al. Interface, information, interaction: a narrative review of design and functional requirements for clinical decision support. J Am Med Inform Assoc 2018 May 01;25(5):585-592 [FREE Full text] [doi: 10.1093/jamia/ocx118] [Medline: 29126196]
66. Schütze D, Holtz S, Neff MC, Köhler S, Schaaf J, Frischen LS, et al. User-Centered-Design als partizipative Methode in der Versorgungsforschung – Beispiel SATURN-Projekt. Düsseldorf: German Medical Science GMS Publishing House;

XSL•FO
RenderX

2023 Oct 02 Presented at: 22. Deutscher Kongress für Versorgungsforschung (DKVF) 2023; October 04-06, 2023; Berlin. [doi: 10.3205/23DKVF095]
67. Geis T, Polkehn K. Praxiswissen User Requirements: Nutzungsqualität Systematisch, Nachhaltig und Agil in die Produktentwicklung Integrieren: Aus- und Weiterbildung zum UXQB Certified Professional for Usability and User Experience - Advanced Level “User Requirements Engineering” (CPUX-UR). Heidelberg: dpunkt.verlag; Jul 30, 2018.
68. Zerlik M, Jung IC, Sehr T, Hennings F, Kamann C, Brandt MD, et al. A pragmatic methodical framework for the user-centred development of an electronic process support for the sleep laboratory patients' management. Digit Health 2022;8:20552076221134437 [FREE Full text] [doi: 10.1177/20552076221134437] [Medline: 36325436]
69. Madandola OO, Bjarnadottir RI, Yao Y, Ansell M, Dos Santos F, Cho H, et al. The relationship between electronic health records user interface features and data quality of patient clinical information: an integrative review. J Am Med Inform Assoc 2023 Dec 22;31(1):240-255. [doi: 10.1093/jamia/ocad188] [Medline: 37740937]
70. Scheurwegs E, Luyckx K, Luyten L, Daelemans W, Van den Bulcke T. Data integration of structured and unstructured sources for assigning clinical codes to patient stays. J Am Med Inform Assoc 2016 Apr;23(e1):e11-e19 [FREE Full text] [doi: 10.1093/jamia/ocv115] [Medline: 26316458]
71. Isaradech N, Khumrin P. Auto-mapping clinical documents to ICD-10 using SNOMED-CT. AMIA Jt Summits Transl Sci Proc 2021;2021:296-304 [FREE Full text] [Medline: 34457144]
72. Dai HJ, Wang CK, Chen CC, Liou CS, Lu AT, Lai CH, et al. Evaluating a natural language processing-driven, AI-assisted international classification of diseases, 10th revision, clinical modification, coding system for diagnosis related groups in a real hospital environment: algorithm development and validation study. J Med Internet Res 2024 Sep 20;26:e58278 [FREE Full text] [doi: 10.2196/58278] [Medline: 39302714]
73. Badalotti D, Agrawal A, Pensato U, Angelotti G, Marcheselli S. Development of a Natural Language Processing (NLP) model to automatically extract clinical data from electronic health records: results from an Italian comprehensive stroke center. Int J Med Inform 2024 Dec;192:105626 [FREE Full text] [doi: 10.1016/j.ijmedinf.2024.105626] [Medline: 39321491]
74. Sharma H, Mao C, Zhang Y, Vatani H, Yao L, Zhong Y, et al. Developing a portable natural language processing based phenotyping system. BMC Med Inform Decis Mak 2019 Apr 04;19(Suppl 3):78 [FREE Full text] [doi: 10.1186/s12911-019-0786-z] [Medline: 30943974]
75. Rau E, Tischendorf T, Mitzscherlich B. Implementation of the electronic health record in the German healthcare system: an assessment of the current status and future development perspectives considering the potentials of health data utilisation by representatives of different stakeholder groups. Front Health Serv 2024;4:1370759 [FREE Full text] [doi: 10.3389/frhs.2024.1370759] [Medline: 38800500]
76. ePA für alle. gematik. 2024. URL: https://www.gematik.de/anwendungen/epa/epa-fuer-alle [accessed 2026-02-11]
77. Amos L, Anderson D, Brody S, Ripple A, Humphreys BL. UMLS users and uses: a current overview. J Am Med Inform Assoc 2020 Jul 19;27(10):1606-1611 [FREE Full text] [doi: 10.1093/jamia/ocaa084] [Medline: 32683453]

Abbreviations

AI: artificial intelligence
CDM: Common Data Model
CDSS: clinical decision support systems
DIC: Data Integration Centre
EHR: electronic health record
ePA: electronic patient record
FHIR: Fast Healthcare Interoperability Resources
GP: general practitioner
HL7: Health Level Seven
HPO: Human Phenotype Ontology
ICD-10-GM: International Statistical Classification of Diseases and Related Health Problems, Tenth Revision, German Modification
ISO: International Organization for Standardization
KBV: Kassenärztliche Bundesvereinigung
LOINC: Logical Observation Identifiers Names and Codes
OPS: Operation and Procedure Codes (German: “Operationen- und Prozedurenschlüssel”)
REST: Representational State Transfer
SATURN: Smart Physician Portal for Patients With Unclear Disease
SNOMED CT: Systematized Nomenclature of Medicine Clinical Terms
TI: telematics infrastructure
UCD: user-centered development process
UI: user interface

XSL•FO
RenderX

Edited by A Benis; submitted 25.Mar.2025; peer-reviewed by J Walsh, N Blase, H Min; comments to author 05.Oct.2025; accepted 29.Dec.2025; published 20.Feb.2026.

Please cite as:
Neff MC, Schaaf J, Ahmadi N, Zoch M, Schütze D, Storf H
Experiences With Integrating Medical Terminologies Into User Interfaces for a Decision Support System for Primary Care: Conceptual and Development Study
JMIR Med Inform 2026;14:e74934
URL: https://medinform.jmir.org/2026/1/e74934
doi:10.2196/74934
PMID:

©Michaela Christina Neff, Jannik Schaaf, Najia Ahmadi, Michele Zoch, Dania Schütze, Holger Storf. Originally published in JMIR Medical Informatics (https://medinform.jmir.org), 20.Feb.2026. This is an open-access article distributed under the terms of the Creative Commons Attribution License (https://creativecommons.org/licenses/by/4.0/), which permits unrestricted use, distribution, and reproduction in any medium, provided the original work, first published in JMIR Medical Informatics, is properly cited. The complete bibliographic information, a link to the original publication on https://medinform.jmir.org/, as well as this copyright and license information must be included.

XSL•FO
RenderX

Developing a Suicide Risk Prediction Algorithm Using Electronic Health Record Data in Mental Health Care: Real-World Case Study

Linda Hummel[1,2], MSc; Karin C A G Lorenz-Artz[1,2], PhD; Joyce J P A Bierbooms[1], PhD; Inge M B Bongers[1], PhD

[1]Tranzo Scientific Center for Care and Wellbeing, Tilburg School of Social and Behavioral Sciences, Tilburg University, Prof. Cobbenhagenlaan 125, Reitse Poort, Room RP 204, Tilburg, The Netherlands

[2]GGzE Mental Health Care Institute, Eindhoven, The Netherlands

Corresponding Author:
Linda Hummel, MSc
Tranzo Scientific Center for Care and Wellbeing, Tilburg School of Social and Behavioral Sciences, Tilburg University, Prof. Cobbenhagenlaan 125, Reitse Poort, Room RP 204, Tilburg, The Netherlands

Abstract

Background: Artificial intelligence (AI) offers potential solutions to address the challenges faced by a strained mental health care system, such as increasing demand for care, staff shortages, and pressured accessibility. While developing AI-based tools for clinical practice is technically feasible and has the potential to produce real-world impact, only a few are actually implemented into clinical practice. Implementation starts at the algorithm development phase, as this phase bridges theoretical innovation and practical application. The design and the way the AI tool is developed may either facilitate or hinder later implementation and use.

Objective: This study aims to examine the development process of a suicide risk prediction algorithm using real-world electronic health record (EHR) data through a qualitative case study approach for clinical use in mental health care. It explores which challenges the development team encountered in creating the algorithm and how they addressed these challenges. This study identifies key considerations for the integration of technical and clinical perspectives in algorithms, facilitating the evolution of mental health organizations toward data-driven practice. The studied algorithm remains exploratory and has not yet been implemented in clinical practice.

Methods: An exploratory, multimethod qualitative case study was conducted, using a hybrid approach with both inductive and deductive analysis. Data were collected through desk research, reflective team meetings, and iterative feedback sessions with the development team. Thematic analysis was used to identify development challenges and the team's responses. Based on these findings, key considerations for future algorithm development were derived.

Results: Key challenges included defining, operationalizing, and measuring suicide incidents within EHRs due to issues such as missing data, underreporting, and differences between data sources. Predicting factors were identified by consulting clinical experts; however, psychosocial variables had to be constructed as they could not directly be extracted from EHR data. Risk of bias occurred when traditional suicide prevention questionnaires, unequally distributed across patients, were used as input. Analyzing unstructured data by natural language processing was challenging due to data noise, but ultimately enabled successful sentiment analysis, which provided dynamic, clinically relevant information for the algorithm. A complex model enhanced predictive accuracy but posed challenges regarding understandability, which was highly valued by clinicians.

Conclusions: To advance mental health care as a data-driven field, several critical considerations must be addressed: ensuring robust data governance and quality, fostering cultural shifts in data documentation practices, establishing mechanisms for continuous monitoring of AI tool usage, mitigating risks of bias, balancing predictive performance with explainability, and maintaining a clinician "in-the-loop" approach. Future research should prioritize sociotechnical aspects related to the development, implementation, and daily use of AI in mental health care practice.

(JMIR Med Inform 2026;14:e74240) doi:10.2196/74240

KEYWORDS

implementation science; artificial intelligence; prediction algorithms; electronic health records; mental mealth services; suicide prevention

XSL•FO
RenderX

Introduction

Advances in artificial intelligence (AI; see Textbox 1 for a glossary of key terms) may provide promising opportunities for many actual and future challenges that mental health care faces [1], such as increasing demand for care and staff shortages that affect the quality of care and accessibility of mental health care. AI may enhance multiple domains, such as triage and screening, diagnostics, clinical decision-making, care delivery, chronic care management, self-care, and prevention of (psychiatric) symptoms [2].

Textbox 1. Glossary.

Artificial intelligence refers to a computerized system (hardware or software) that is able to perform tasks or reasoning processes that we usually associate with intelligence in a human being [3,4].

Machine learning is part of artificial intelligence. It is able to build algorithms that can detect patterns in large training datasets to explain variation in data or predict outcomes (predictive algorithms) [3,5-7].

Predictive analytics aims to build models which allow for individual (ie, single subject) predictions, thereby moving from the description of patients (hindsight) and the investigation of statistical group differences or associations (insight) toward models capable of predicting current or future characteristics for individual patients (foresight), thus allowing for a direct assessment of a model's clinical use [8].

Natural language processing refers to ML techniques capable of parsing unstructured texts, such as free written texts or spoken language [9]. Natural language processing enables the use of unstructured data that is otherwise largely inaccessible, such as the dynamic fluctuations of symptoms (eg, by analyzing clinical notes) and can identify social and behavioral factors, which are not commonly registered in EHR [10].

Predictive algorithms are a promising subfield of AI, in which machine learning (ML) models generate predictions on an individual patient level to support decision-making in the diagnosis, prognosis, and treatment of patients [5,8,11]. Predictive algorithms have been shown to be more successful than traditional statistical models, as they provide a new way to gain knowledge from a data set. For example, in the field of predicting suicide risk at the individual level, predictive algorithms can yield more accurate predictions [12-15] than traditional statistical models, which predict only slightly better than chance and whose predictive ability has not improved over time, even after 50 years of research [16]. Not all ML models for suicide risk are adequate, although, as performance can vary depending on various factors, such as data quality, nature of the features used as input, preprocessing steps, and the used techniques [12]. In other mental health care domains, ML models are also able to perform better than traditional models, such as the prediction of psychosis, treatment response [17], or opioid use disorder [18].

Algorithms designed for clinical care often use patient data collected during regular clinical care in the organization's electronic health record (EHR). Combining the expanding possibilities of AI with EHR data fuels the transformation into a data-driven mental health care, as the EHR contains rich, real-world, and real-time data. Reusing EHR data to develop algorithms that support clinical practice on an everyday basis opens many possibilities. However, it may be challenging, as these data are usually noisy, heterogeneous, dynamic, and contain both structured and unstructured data (eg, text) and require careful preprocessing [19]. Developing [20] and implementing AI-based algorithms using real-world EHR data has been proven to be feasible and can have a significant clinical impact [21-23]. However, the studies of algorithms that are actually implemented and used in mental health clinical practice are still scarce [24]. Also, there is a gap between the creation of scientifically sound algorithms and their meaningful application in real-world settings, a challenge often referred to as the "AI chasm" [25].

For mental health care to benefit from AI opportunities and the wealth of EHR data, developing algorithms based on real-world EHR patient data intended for clinical use is a crucial first step toward successful implementation and use. The development phase bridges theoretical innovation and practical application. Therefore, the development phase is not only a preparatory step but an integral part of implementation, as the design and development of the AI tool may either facilitate or hinder later implementation and use (eg, through alignment with organizational workflows and engendering trust) [26].

To enable the successful development, implementation, and actual use of AI and ML in mental health clinical practice, implementation science provides a valuable framework [3], as it studies the contextual factors that enable the process of embedding and integrating new practices into actual care [27,28]. Also, it fosters greater attention for the sociotechnical aspects of technology, focusing not only on the development of technological improvements but also the social changes required for their successful implementation and use [17,29-33]. Multiple barriers and facilitators have been identified in the literature, highlighting aspects of AI technology itself (eg, accuracy, transparency, and generalizability); organizational factors (eg, integration with workflows); governance, ethical, and legal issues; perception of staff and patients; or the implementation process (eg, engagement, user-centered design) [34,35]. However, these barriers and facilitators have, for a large part, been identified not primarily on implementation data but rather based on hypothetical implementation, white papers, and thought articles [34,35]. Therefore, more empirical studies are required to fill this knowledge gap [6,17].

To better understand how this development phase unfolds within the specific context of mental health care, we conducted a case study. This study explores the challenges encountered by a development team in creating a suicide risk prediction algorithm using real-world EHR data for clinical application in close collaboration with clinicians, as well as the team's responses to these issues. Ultimately, we aim to identify key considerations relevant to bridging technical and clinical needs in algorithm

XSL•FO
RenderX

development, offering insights for mental health professionals and organizations seeking to move toward data-driven care.

Methods

Research Design

This study is a detailed case study aimed to explore the challenges involved in the development of a suicide risk prediction algorithm using real-world EHR data in mental health care. Using an exploratory, multimethod approach with both inductive and deductive analysis suited to this emerging field, as the study seeks to identify key development considerations applicable to broader contexts [36].

Case Description

Setting and Background

Suicide prevention in the Netherlands is organized through a national policy agenda focused on public awareness, early detection, and professional care. The national helpline 113 Suicide Prevention is available 24/7 by phone or chat. This organization also provides public campaigns and training for professionals and citizens. The National Suicide Prevention Agenda, developed by the Ministry of Health, Welfare and Sport together with 113 and other partners, offers a framework for collaboration between health care, education, municipalities, and the media. Locally, Municipal Health Services, youth health care, schools, and social services work on prevention and early risk identification. In mental health care, suicide prevention is part of standard practice, including staff training and procedures following a suicide incident. The Health and Youth Care Inspectorate monitors suicide prevention and reporting, while knowledge institutes, such as Trimbos, support professionals through guidelines and research.

GGz Eindhoven and the Kempen (Geestelijke Gezondheidszorg Eindhoven en de Kempen [GGzE]) is a mental health institution in southern Netherlands, providing specialized care to around 17,000 patients annually. At GGzE, a protocol is in place in accordance with the national multidisciplinary guideline [37]. All health care professionals are required to complete suicide prevention training courses. Suicide risk assessments are conducted at the start of each treatment trajectory and at other critical moments, for example, during a crisis; at the beginning, end, and after hospitalization; or prior to the extension of patient privileges during admission. A standardized suicide assessment tool, the Suicide Prevention Questionnaire (SPQ), is embedded within the EHR and should be administered at these key points, at least once or twice per year.

To enhance suicide prevention, GGzE explored the feasibility of developing a predictive algorithm using EHR data to support clinicians in identifying suicide risk in individual patients. Key objectives included establishing a reliable measure of suicide incidents, identifying predictive factors, and creating an algorithm with an accuracy target of 70% - 90% [38]. The development team, consisting of 2 data scientists with support from data science, governance, law, and clinical suicide experts (multiple psychologists and psychiatrists), operated under a structured project organization with a steering committee and project group. Both the steering committee and the project group comprised health care professionals as well as staff members with legal, organizational, and other forms of specialized expertise.

The project was embedded in the organization-wide Suicide Prevention Program, which provided consultation and training, developed organizational guidelines and protocols, organized evaluation of suicide incidents and subsequent quality enhancement of clinical practice, ensured evidence-based treatment options regarding suicidality, and developed a reflective learning culture regarding suicidality within the organization. The organization was part of the Suicide Prevention Action Network (Supranet GGZ), in which mental health institutions work together to make the quality of care for suicidal patients transparent, to learn what can be improved, and to improve care where necessary. Within this network, data on suicide incidents were structurally collected and shared, including core indicators on suicide risk.

The Suicide Prediction Algorithm: Description and Performance

The development team designed the algorithm for hospitalized patients with severe mental illness, using the Cross-Industry Standard Process for Data Mining (CRISP-DM) framework [39], a standard method in data mining and ML, to predict suicide risk within 1 month. Data for the algorithm was taken from the EHR and included data from 5044 patients (December 31, 2015, to August 31, 2021) included demographics (eg, age and sex), administrative details (eg, financing type), treatment history (eg, hospitalization count), psychiatric factors (eg, primary diagnosis), current treatment details (eg, duration and intensity), and social factors (eg, social contacts). Consultations with clinicians, interviews, and a literature search resulted in a list of possible predictors of suicide incidents that were derived from the EHR.

The team applied natural language processing (NLP) to clinicians' daily reports, identifying unreported suicide incidents and capturing patient sentiment as an additional predictor, using topic modeling (BERTopic) [40]. Ensemble learning (extreme gradient boosting) [41] strengthened the model. The development team deemed the algorithm successful based on Hicks et al criteria [38]. The team acknowledged that the performance indicator outcomes were exploratory, as the algorithm would be retrained prior to implementation in a pilot phase and subsequently retrained annually in accordance with quality standards.

The predictive algorithm for suicide incidents will be gradually tested in a small-scale pilot project conducted in close collaboration with health care professionals. The algorithm will be implemented solely as an add-on to existing suicide prevention policies. Health care professionals will remain fully responsible for clinical assessment and decision-making. The pilot project will be evaluated at multiple stages throughout its implementation.

Sampling and Participants

The study's participants included 2 core data science professionals who led the development of the suicide risk

XSL•FO
RenderX

prediction algorithm, supported by internal and external experts. The team worked closely with clinicians (multiple psychologists, psychiatrists, and the Medical Director's office) and experts in data science, law, and data governance, as well as with external data science collaborators from other mental health care institutions. The participants were selected by expert sampling, in which participants are included who have demonstrable experience and expertise regarding the study's aim and objective [42,43]. These participants offered crucial insights into the challenges and considerations of algorithm development. The team worked closely with clinicians (eg, psychologists, psychiatrists, and the medical director) and experts in data science, law, and data governance, as well as with external data science collaborators from other mental health care institutions.

Data Collection and Data Analysis

Data for our study on the development process were collected through desk research, reflective meetings, and iterative feedback sessions with the development team. The study proceeded in three phases: (1) desk research and meetings with the development team to draw up a detailed process description, (2) identification of challenges and responses by thematic analysis, and (3) formulation of key considerations.

The detailed process description formed the basis for thematic analysis, which was conducted following the Braun and Clarke approach [44]. An exploratory, multimethod design combining inductive and deductive analysis was used to identify challenges during the algorithm development process. Deductive analysis was guided by the innovation domain of the Consolidated Framework for Implementation Research (CFIR) [28,45] and concepts from AI-related literature.

Data on process steps, challenges, and responses were analyzed and organized in a chart by 1 researcher (LH). Data was discussed by all 4 researchers to derive the main challenges and describe the team's responses. Communicative validation was achieved through discussions with the development team. Triangulation across data sources strengthened the credibility and transferability of findings. Data collection and analysis were iterative and integrated throughout all phases.

Ethical Considerations

Ethical approval was obtained from the Ethical Review Board of Tilburg University (reference TSB_RP1038). Participants received no financial compensation and provided written informed consent prior to participation. All procedures adhered to principles of privacy and confidentiality: no identifying information was collected or published, and any nonessential identifying details were omitted. No images or supplementary materials contain identifiable participant features.

Results

Overview

The encountered challenges and the team's responses are described below, related to the construction of the suicide incidents (dependent variable) and possible predictors (independent variables), and the building of the model. At the start, the concept of the suicide incidents and the predictors had to be defined, operationalized, and measured. Several challenges were encountered during this phase: data was hard to find, data sources yielded different results, and underreporting was suspected. Regarding predicting factors, psychosocial predictors were not available and had to be estimated. To calculate the algorithm, the team used complex models that improved predictive performance but reduced understandability for clinicians.

Regular consultations between the project team and clinical experts during the development process were important to gain an accurate and profound understanding of the phenomena of suicide incidents and their predictive factors.

The Results section will focus on the development team's challenges and their responses to them. In the Discussion section, the results will be contextualized within the literature to formulate key considerations for algorithm development in mental health care.

Defining, Operationalizing, and Measuring Suicide Incidents

Different Data Sources Provide Different Outcomes

The data science team collaborated with health care professionals to define suicide incidents as the dependent variable. Within the organization, a suicide incident was defined as either a fatal suicide or a nonfatal attempt with a certain intention to die. This also covered self-harming or risky behavior that involved a risk of death or failure to avoid such risk. Severe suicide incidents were those that were fatal or caused, or could cause, severe or permanent physical injury [source: GGzE Protocol Reporting suicides and suicide attempts; consulted 2025-09-19]. Clinicians had to distinguish these from self-harm driven by other motives, such as reducing emotional pain.

Organizational protocols prescribed the registration of every suicide incident in a digital registration system. The Medical Director's office kept its own registration. The 2 data sources within the organization yielded different outputs on the total number of suicide incidents:

> *In the Client Details source there is a variable called Suicide Attempt. In addition, a variable called Suicide Incident has been created based on the incident data. […] there are more numbers […] for Suicide Incident than for Suicide Attempt." [Report of the development team and external partners on characteristics of the suicide incident risk algorithm, p. 10].*

The medical director's office clarified to the data science team that they reviewed the registered suicide incidents in the reporting system and recorded only those suicide incidents classified as severe. The team chose to include all suicide incidents, providing more data to train the algorithm and enabling the prediction of both severe and less severe cases. Clinical experts reflected on the overall numbers and considered them to be low, suggesting underregistration, particularly of less severe cases, possibly due to noncompliance with protocols or sensitivities around suicide. Moreover, ambiguity about the intention behind the behavior in less severe cases may have

XSL•FO
RenderX

played a role. For example, behavior without serious injury or risk of injury that primarily served a communicative function.

Using Unstructured Data to Improve Detection of Suicide Incidents Is Challenging

To detect underreported suicide incidents, the development team added text mining using NLP of clinicians' unstructured daily reports. However, the method produced significant data noise, identifying many reports related to suicidality but failing to pinpoint actual suicide incidents. Text analysis was hindered by clinicians' writing habits, such as negation terms ("not feeling suicidal"), the use of synonyms (eg, "jumping off a bridge"), and the use of standard templates (eg, "has the patient expressed suicidality today?").

Manual labeling of cases was tried, but appeared to be very time-consuming and unfeasible as a permanent solution, especially as the algorithm had to be retrained every 6 months due to quality requirements:

> *We still need to be 100% sure that there is/isn't a suicide incident in the daily report data. Possible solution: Read the data yourself and assess whether there is/isn't a suicide incident (label data). Disadvantages: […] Takes a lot of time (for a small dataset it took 3 days)*

The development team responded to these challenges by making efforts to enhance data quality. The organization was in the process of transitioning to another provider of an EHR system. The team recommended including a check mark for suicide incidents [source: Presentation Suicide Predictive Model_2nd iteration, p. 36] within this new system and advocated this solution in the new EHR project team, underlining the importance of these interventions to transform into a data-driven health care organization. Also, a new executive board took the lead of the organization and, consequently, a new multiyear strategy was developed, in which "working data-driven to enhance decision support" was one of the main ambitions [source: GGzE, multiyear strategy 2024 - 2028; consulted 2025-09-19]. This prompted management to take a more active role in ensuring data quality, such as completing suicide-related information. Also, the organization implemented an alternative instrument for the SPQ. This way, the organization aimed to improve data quality. The algorithm would be retrained when the new EHR system was implemented.

However, the team still had to deal with the fact that possible underregistration of suicide incidents, especially less severe cases, was an issue. From a data science perspective, they could interpret this as missing data, which threatened data quality. From a clinical perspective, the possibility that mild incidents were not always reported was a reflection of the ambiguity of the interpretation of a suicide incident: did the patient actually aim to end their life, or should the behavior be interpreted more as self-harming behavior with the intent to decrease pain or to communicate distress?

Defining, Operationalizing, and Measuring Potential Predicting Factors

The development team compiled a list of potential predicting factors by performing a literature review, reviewing factors from well-known suicide risk assessment methods, and interviewing clinicians to leverage their expertise and to involve and engage clinicians in the development process. The list of predictors then had to be defined, operationalized, and measured. Reflective meetings with the development team revealed several challenges they faced, which are described below.

The EHR Lacks Psychosocial Factors: Construction of Predictors is Necessary

Some predicting factors, like previous suicide attempts or substance dependence, could be directly derived from the EHR. Other predicting factors were psychosocial and could not be directly obtained from the EHR, thus requiring the construction of an estimator.

For example, information on the number of contacts of a patient, as registered in the EHR, along with a selection of characterization of these relationships (eg, spouse, sibling, child, and neighbor) was used to construct the factor "social network." Also, the factor "quality of the therapeutic relationship" was operationalized as the number of primary [1] practitioners during hospitalization. Although it was recognized that these operationalizations did not necessarily reflect the actual factors, in the absence of a better alternative, it was decided to operationalize and measure these concepts in this way.

Data Availability Differs Between Subgroups: Risk of Bias

Clinicians considered the SPQ, available in the EHR, the most promising source of predictors. Although protocols required annual administration for all patients, the data science team found a recent SPQ in only 21.95% of cases. Clinicians confirmed that SPQ variables were highly explanatory but acknowledged their limited availability. They suspected that SPQs were often completed only when suicide risk was already suspected, creating bias and overrepresenting high-risk patients. To include all patients, the data science team had to derive estimators from other EHR data. Additional disparities emerged: SPQs were missing more often for youth (0 - 17 y) than for older patients, despite comparable incident rates. These findings were shared with the Child & Youth Department to improve data quality. Ethnicity was also explored as a predictor but was excluded due to frequent missing values.

Overall, the results exposed a gap between organizational protocols (eg, annual SPQ administration, registration of ethnicity) and actual practice. They also revealed different perspectives: clinicians valued SPQ data but were less familiar with data science principles, such as representativeness and external validity, while data scientists emphasized these risks. Close collaboration was deemed essential to identify predictors and minimize bias.

To address these challenges, the development team worked with the Suicide Prevention Program and a national suicide prevention organization to design a digital toolkit as a

XSL•FO
RenderX

replacement for the SPQ. This decision support tool aimed to make risk assessment more user-friendly, link assessments to targeted treatment advice based on the national guideline, and reduce clinician workload through robotic process automation that transferred data directly to the EHR.

Sentiment Analysis to Construct a Time- and Context-Sensitive Predictor

As the literature review and interviews with clinicians emphasized the role of time- and context-related factors in suicide risk (eg, relationship breakup and intoxication), the development team explored ways to integrate these into the model. Since collecting daily data directly from patients was impractical due to severe psychiatric conditions and low cooperation, daily reports by clinicians about patients were identified as the best alternative. These allowed real-time data to strengthen predictive accuracy.

Although detecting suicide incidents in daily reports was challenging, sentiment analysis proved feasible. Patients with suicide incidents showed lower sentiment in the daily notes by clinicians, especially in the most recent entries, compared to those without incidents (internal document: PowerPoint Suicide Predictive Model_2nd iteration, p. 29).

When the development team presented the results to the medical director's office, new applications were discussed. The algorithm was initially designed as an add-on to existing protocols, such as administering an SPQ annually. Given the time-intensive nature of the SPQ, 1 proposal was to let the algorithm preselect high-risk patients for SPQ administration. This would save time by limiting assessments to flagged patients.

Clinical experts, including the medical director, rejected this option, noting that the algorithm was still in development and should not replace established tools. They did, however, acknowledge that SPQs were not consistently administered in practice. As an alternative, they proposed using sentiment analysis as an alert system: if emotional decline was detected and no recent SPQ was available, clinicians would be prompted to administer one. This approach was accepted, as it integrated the algorithm while reinforcing compliance with existing suicide prevention protocols.

Building the Algorithm: High-Performance Model Appears Hard to Understand by Clinicians

After identifying dependent and independent variables, the development team built the algorithm using ensemble learning, which combines weaker models into a stronger one. This approach delivered high predictive power, meeting the project's feasibility goal, but the model was too complex to interpret directly.

The data science team shared the results with clinicians and the steering group, including the model's performance metrics (eg, accuracy, precision, and recall), acknowledging that the results were exploratory as the model would later be retrained. Clinicians appreciated the potential value of the algorithm but emphasized that understanding why suicide risk was elevated was essential for fostering trust, ensuring accountability, and supporting treatment planning. They highlighted that a well-performing algorithm alone would not be sufficient to generate meaningful benefits in clinical practice. The data science team, therefore, identified explainability as a core requirement. They aimed to develop case-level reports that not only flagged risk but also explained the reasons behind it: "Not only: alarm! But also: alarm, for this reason" [Reflective meeting, 2023-11-07].

To address this challenge, a team member engaged in additional training in explainable AI, noting the scarcity of knowledge within mental health care. Additionally, the data science team planned to organize several collaborative sessions with clinicians to cocreate an explainability dashboard that contextualizes the algorithm's outputs. Also, collaborative sessions were planned to facilitate the integration of the algorithm into existing workflows and jointly reflect on the tasks, roles, and responsibilities of each stakeholder in its use.

Discussion

Principal Findings

This study provided a detailed case study of the development of a suicide risk prediction algorithm using real-world EHR data. Its unique contribution lies in demonstrating how algorithm development is carried out within the clinical practice of mental health care, where technical innovation must be aligned with clinical needs, professional values, and organizational structures. By describing the challenges of a development team and their responses to them, this study offers an in-depth description of the development of a predictive algorithm, in which the development process is seen as a first step in the implementation process.

This paper highlights the sociotechnical and organizational aspects of algorithm development, showing how collaboration, joint efforts to enhance data quality, and clinician engagement are essential prerequisites for algorithm development.

Reflection on the Principal Results

Addressing Data Quality Challenges in the EHR

High data quality is essential for AI in mental health care, yet EHR data are often low in quality, incomplete, "soft," and indirect [46,47]. Also, handling unstructured EHR data requires unique approaches [48,49].

Regarding data quality, EHR data quality in mental health is typically problematic. In the current case, suicide incident data were hard to construct and possibly underreported, although this could also be a reflection of real-world clinical assessment issues. Low data quality is noted in the literature, where suicide incidents are frequently underdocumented [50] due to clinicians' workload [7,46] and departmental workflow inconsistencies [51]. Addressing this, data quality issues span all 5 dimensions identified by Weiskopf and Weng [52]: completeness, correctness, concordance, plausibility, and currency. Organizations are faced with challenges on data quality according to each of these dimensions.

Mental health data often rely on "soft" psychological constructs (eg, social support), which are harder to quantify than "hard"

XSL•FO
RenderX

somatic measures (eg, heart rate) [47]. This raises risks for construct validity [53]. Moreover, much of the data reflects professionals' perceptions rather than patients' own, which may diverge significantly [54-57]. Future approaches using direct patient data (eg, real-time sampling and devices) could help improve accuracy [13].

Analysis of unstructured data, like staff notes, showed high noise, with frequent mentions of suicidality but few actual incidents, a challenge also noted in other mental health domains [13,58]. Variations in writing style and negations further complicate analysis [59-61]. Still, NLP offers potential to capture real-time risk fluctuations and enhance predictive accuracy [62-65].

While low data quality in mental health is a barrier for AI, algorithm development may also support quality improvement. In the current case, feedback on data inconsistencies spurred organizational motivation to enhance quality and adapt the EHR system.

Mitigating Risk of Bias to Ensure Performance for Subgroups

When algorithms are trained on data of low quality, risk of bias (RoB) occurs, in which the algorithm may not perform as well for each subgroup, and human biases are repeated and even amplified. When predictors are constructed from EHR data as data are not readily available, selection bias may occur. Algorithms require balanced representation across subgroups, though, to perform effectively. In this case, using SPQ items as predictors risked overrepresenting high-risk patients and weakening performance for others. While EHR data enables inclusion of all hospitalized patients, including minority groups often underrepresented in research [66], bias remains a major concern. As social factors are often key predictors in mental health care [15,67], social data is often missing due to true absence or nonrandom issues, such as patient refusal, confidentiality concerns, or language barriers, and excluding such cases may worsen bias [15,67]. Selection bias also threatens performance when samples do not reflect the broader population [10,68,69]. Bias is therefore considered an additional dimension of data quality, alongside the 5 identified by Weiskopf and Weng [52,70].

By building algorithms from reused EHR data, human biases in the data may be reinforced. The development team acknowledged this risk but considered the potential benefits sufficient to proceed, provided mitigating measures were applied. Since algorithms are trained on subjective EHR data, cognitive biases, such as stereotypes or in-group favoritism [71-73], may become embedded and systematically applied [66,68,69]. In practice, if an algorithm's outcome aligns with a clinician's initial diagnosis, confirmation bias may lead the clinician to ignore contradictory information. If the outcomes differ, precautionary bias might cause them to trust the algorithm over their own judgment [73]. Automation bias could also emerge, where clinicians rely more on the tool than on other information, potentially diminishing their skills [7]. The question remains what mitigating measures are adequate to prevent systematically disadvantaging subgroups. At the same time, algorithms may also reduce bias by integrating fragmented information across professionals and systematically processing both subjective and objective data [74]. Determining under which conditions algorithms amplify or mitigate bias remains an open question for future research.

Actionability, Trust, Accountability, and Communication in Complex Models

Predictive power and understandability have to be balanced in algorithm development. In our study, data scientists prioritized predictive performance, applying a complex model to enhance accuracy, while clinicians emphasized the need for understandability. This reflects the broader trade-off between complex "black box" models, which yield higher predictive power but limited explainability, and simpler "glass box" models, which are more interpretable but often less accurate [75-77]. Initially, the team focused on feasibility, whether an algorithm with sufficient predictive performance could be built from organizational data, rather than on clinical applicability. Clinician feedback prompted the inclusion of explainability as a key objective, as it enhances the actionability of the outcomes, that is, whether clinicians can use the information to identify actions to change the outcome predicted by the algorithm [78]. In suicide prevention, detecting elevated risk is insufficient; clinicians must also understand which factors contributed most, which are modifiable, and which interventions are likely to reduce risk [79,80]. Explainability is crucial for building trust [81-83], and providing an appropriate level of transparency (not too little and not too much) is necessary in designing for trust [84]. Clinicians should be well informed about the actual capabilities of the algorithm, as responsible use of AI systems also depends on the level of correspondence between a user's trust and the technology's capabilities, known as calibration [83]. Explainability may also enhance patient communication and support shared decision-making [76,79,85]. Also, mental health institutions are accountable for care quality, effectiveness, and safety. In our study, clinicians feared that using complex, nonexplainable models would undermine accountability, as evidence-based protocols are easier to justify than black-box algorithms. Given the high-stakes nature of suicide care, caution is warranted when applying complex models [80].

Whether performance or explainability should be prioritized in mental health care remains unresolved, and future research should examine context-specific trade-offs as well as post hoc strategies to enhance explainability [77,86]. Future research should explore what information should be communicated to clinicians and how it should be presented. Moreover, fostering mutual trust and collaboration between clinicians and data scientists throughout the algorithm development process is essential. Technical performance alone does not guarantee clinical usefulness. Instead, cocreation of both the algorithm and its user interface, combined with joint efforts to integrate it into everyday practice, is crucial for enabling clinicians to trust and meaningfully use the algorithm's outcomes.

Below, we present Table 1 summarizing the challenges encountered during the development phase, the corresponding responses by the team and organization, and the broader considerations derived from these experiences.

XSL•FO
RenderX

Table . Challenges, responses, and considerations during algorithm development in mental health care.

The development phase	Challenges	Responses	Considerations
Defining, operationalizing, and measuring suicide incidents	• Inconsistent detection of suicide incidents across data sources.	• Enhanced suicide incident data by integrating clinician insights. • Broadened incident inclusion. • Tested NLP[a] approaches. • Improved EHR[b] registration.	• Ensure sufficient data availability for the predicted outcome. • Consult clinicians to improve data interpretation. • Consider clinical explanations for data quality issues. • Provide user-friendly EHR options for registering suicide incidents.
Defining, operationalizing, and measuring potential predicting factors	• Limited and uneven availability of psychosocial and contextual predictors constrains robust and unbiased model development.	• Developed high-availability estimators. • Addressed data gaps with clinicians. • Implemented a guideline-aligned assessment tool to simultaneously enhance data registration and support clinical decision-making. • Developed a sentiment analysis for contextual risk signals.	• Ensure predictor validity by prioritizing high-availability EHR data. • Address subgroup gaps through data governance. • Supplement psychosocial information via clinicians or patients. • Develop user-friendly assessment tools that integrate required data registration with clinical decision-making support.
Building the algorithm	• Complex models improve prediction but are difficult for clinicians to interpret.	• Established explainability as a core requirement. • Planned cocreation of an explainability dashboard with clinicians before the pilot.	• Balance predictive performance and explainability through close collaboration between data scientists and clinicians.
Toward an implementation pilot	• Effective use requires full integration into clinical workflows and sufficient clinician experience. • Algorithm use may introduce cognitive and decision biases.	• Planned joint data scientist–clinician sessions to integrate the algorithm into workflows and clarify roles. • Positioned the algorithm as an add-on to suicide prevention care, with clinicians' judgment remaining central.	• Organize data scientist–clinician sessions to support workflow integration and clarify roles. • Clearly communicate the algorithm's role and its support function for clinical decision-making. • Calibrate clinicians' expectations to the algorithm's actual capabilities and limitations.

[a]NLP: natural language processing.

[b]EHR: electronic health record.

Limitations

This study provided a detailed case study of the development of a suicide risk prediction algorithm using real-world EHR data, highlighting the tension between technical requirements and clinical needs. Using a qualitative, real-world approach, the study captured contextualized knowledge from the development team, who collaborated closely with clinicians. While generalizability is limited by the single-case design, triangulation and detailed process descriptions support transferability. A key limitation is that clinicians' perspectives were obtained indirectly via the development team rather than through direct engagement, although this was partly mitigated by desk research and targeted questions to include broader stakeholder views.

Conclusions and Future Research

Conclusions

Based on the findings of our case study, we highlight the following 5 main recommendations for mental health organizations that aim to evolve into data-driven practice.

1. Data governance and quality: high-performing algorithms require robust data governance and timely, deliberate data preparation to ensure data quality.
2. Cultural change in data entry: a cultural shift is needed to regard and manage data as a strategic asset for algorithm development.
3. Bias awareness and monitoring: organizations must remain sensitive to potential bias in both data and use, requiring careful data handling and regular evaluation of real-world application.

XSL•FO
RenderX

4. Balancing performance and transparency: predictive performance using complex models must be balanced with clinicians' needs for transparency and explainability to ensure actionability, trust, communication, and accountability.
5. Clinician-in-the-loop: it is essential to define the knowledge, skills, and workflows that enable clinicians to use algorithms responsibly while maintaining final clinical judgment.

For mental health organizations aspiring to evolve toward data-driven care, early preparation is essential. First, building predictive algorithms requires sufficient and well-structured data, which demands timely and deliberate data collection. Reliance on existing organizational protocols alone is insufficient; explicit attention must be given to how relevant variables are defined, recorded, and embedded in the EHR system. A cultural transformation is also critical. Second, data should not be viewed merely as an administrative or accountability tool but as a strategic resource for predictive modeling. However, this is not always aligned with clinical practice and may require a change in working processes for clinicians. This transition requires awareness and commitment from clinicians, whose engagement from the earliest stages of algorithm development is crucial. Collaboration between data scientists and clinicians must begin in an early stage of the development process: data scientists contribute technical and data-analytical expertise, while clinicians bring contextual understanding, interpret data inconsistencies, identify meaningful predictors, and help foster a data-driven culture. Organizations must also recognize potential biases within their data and proactively assess how information from subgroups is collected and represented. Third, ongoing attention to bias is crucial, as it may stem not only from data or model design but also from real-world use. Regular evaluation of both performance and application is essential to ensure quality and responsibility in practice. Decisions regarding model design should balance predictive accuracy with interpretability. Fourth, explainable AI techniques may help translate complex model outputs into clinically meaningful insights, allowing clinicians to understand and act upon algorithmic predictions. Clinicians require not only accurate models but also transparency to understand the reasons for the outcome to ensure actionability, trust, and clinician-patient communication. Institutions should further consider how accountability for algorithm use is shared between individual practitioners and the organization. Finally, advancing toward data-driven mental health care requires investment in clinicians' education and professional development regarding AI. Defining the knowledge, skills, and workflows that enable responsible algorithm use, while maintaining clinical judgment as the ultimate decision point, will be key to realizing the added value of predictive technologies in practice.

Future Research

Future research should further explore how robust data governance structures can be established to ensure data quality and readiness for algorithm development. This includes examining how AI techniques may contribute to improving data quality through automation, standardization, and enhanced data validation. Moreover, studies should investigate how cultural change can be fostered to promote viewing data as a strategic resource rather than an administrative by-product, and how such shifts can be maintained throughout the organization.

Attention to bias should extend beyond data collection and model design to the actual use of algorithms. Future studies are needed to determine under which conditions algorithms amplify or mitigate bias, and how systematic monitoring of real-world application can safeguard fairness and responsible use.

The ongoing tension between predictive performance and explainability also warrants investigation. Research should identify context-specific trade-offs between complex, high-performing models and simpler, more transparent approaches and explore how explainability dashboards can enhance actionability, trust, accountability, and clinician–patient communication.

Finally, future research should examine what knowledge, skills, and workflows clinicians need to engage responsibly with predictive algorithms while maintaining final clinical judgment. Integrating sociotechnical considerations throughout algorithm development will be key to ensuring that AI tools are both effective and ethically grounded in clinical practice.

While much focus has been placed on the technical aspects of ML in mental health care, sociotechnical factors related to successful algorithm development, implementation, and use have been largely overlooked [6,13,15,17,24,25,30,33,87]. More research is needed to explore these issues in real-world settings to ensure responsible and sustainable innovation.

Acknowledgments

All authors contributed to study design and manuscript revision. LH collected and analyzed the data and drafted the initial manuscript, after which all authors contributed to multiple revisions. We thank the GGzE development team for their cooperation.

Data Availability

The datasets generated or analyzed during this study are not publicly available due to the inability to fully anonymize the raw data but are available from the corresponding author on reasonable request.

Conflicts of Interest

None declared.

XSL•FO
RenderX

References

1. WRR [Netherlands Scientific Council for Government Policy]. Sustainable healthcare, a matter of choice. People, resources and public support. : The Hague: Netherlands Scientific Council for Government Policy; 2021 URL: https://english.wrr.nl/publications/reports/2022/05/03/sustainable-healthcare-a-matter-of-choice.-people-resources-and-public-support [accessed 2025-12-05]
2. Transforming healthcare with AI: the impact on the workforce and organisations. : EIT Health and McKinsey & Company; 2020 URL: https://www.mckinsey.com/industries/healthcare/our-insights/transforming-healthcare-with-ai#/ [accessed 2025-12-05]
3. Nilsen P, Svedberg P, Nygren J, Frideros M, Johansson J, Schueller S. Accelerating the impact of artificial intelligence in mental healthcare through implementation science. Implement Res Pract 2022;3:26334895221112033. [doi: 10.1177/26334895221112033] [Medline: 37091110]
4. AI HLEG. A definition of AI: main capabilities and disciplines. : European Union; 2019 URL: https://ec.europa.eu/futurium/en/system/files/ged/ai_hleg_definition_of_ai_18_december_1.pdf [accessed 2025-12-18]
5. Graham S, Depp C, Lee EE, et al. Artificial intelligence for mental health and mental illnesses: an overview. Curr Psychiatry Rep 2019 Nov 7;21(11):31701320. [doi: 10.1007/s11920-019-1094-0] [Medline: 31701320]
6. Koutsouleris N, Hauser TU, Skvortsova V, De Choudhury M. From promise to practice: towards the realisation of AI-informed mental health care. Lancet Digit Health 2022 Nov;4(11):e829-e840. [doi: 10.1016/S2589-7500(22)00153-4] [Medline: 36229346]
7. Monteith S, Glenn T, Geddes J, Whybrow PC, Achtyes E, Bauer M. Expectations for artificial intelligence (AI) in psychiatry. Curr Psychiatry Rep 2022 Nov;24(11):709-721. [doi: 10.1007/s11920-022-01378-5] [Medline: 36214931]
8. Hahn T, Nierenberg AA, Whitfield-Gabrieli S. Predictive analytics in mental health: applications, guidelines, challenges and perspectives. Mol Psychiatry 2017 Jan;22(1):37-43. [doi: 10.1038/mp.2016.201] [Medline: 27843153]
9. Khurana D, Koli A, Khatter K, Singh S. Natural language processing: state of the art, current trends and challenges. Multimed Tools Appl 2023;82(3):3713-3744. [doi: 10.1007/s11042-022-13428-4] [Medline: 35855771]
10. Goodday SM, Kormilitzin A, Vaci N, et al. Maximizing the use of social and behavioural information from secondary care mental health electronic health records. J Biomed Inform 2020 Jul;107:103429. [doi: 10.1016/j.jbi.2020.103429] [Medline: 32387393]
11. Dwyer DB, Falkai P, Koutsouleris N. Machine learning approaches for clinical psychology and psychiatry. Annu Rev Clin Psychol 2018 May 7;14(91–118):91-118. [doi: 10.1146/annurev-clinpsy-032816-045037] [Medline: 29401044]
12. Ehtemam H, Sadeghi Esfahlani S, Sanaei A, et al. Role of machine learning algorithms in suicide risk prediction: a systematic review-meta analysis of clinical studies. BMC Med Inform Decis Mak 2024 May 27;24(1):138. [doi: 10.1186/s12911-024-02524-0] [Medline: 38802823]
13. Kirtley OJ, van Mens K, Hoogendoorn M, Kapur N, de Beurs D. Translating promise into practice: a review of machine learning in suicide research and prevention. Lancet Psychiatry 2022 Mar;9(3):243-252. [doi: 10.1016/S2215-0366(21)00254-6] [Medline: 35183281]
14. Kusuma K, Larsen M, Quiroz JC, et al. The performance of machine learning models in predicting suicidal ideation, attempts, and deaths: a meta-analysis and systematic review. J Psychiatr Res 2022 Nov;155:579-588. [doi: 10.1016/j.jpsychires.2022.09.050] [Medline: 36206602]
15. Nordin N, Zainol Z, Mohd Noor MH, Chan LF. Suicidal behaviour prediction models using machine learning techniques: a systematic review. Artif Intell Med 2022 Oct;132:102395. [doi: 10.1016/j.artmed.2022.102395] [Medline: 36207078]
16. Franklin JC, Ribeiro JD, Fox KR, et al. Risk factors for suicidal thoughts and behaviors: a meta-analysis of 50 years of research. Psychol Bull 2017 Feb;143(2):187-232. [doi: 10.1037/bul0000084] [Medline: 27841450]
17. Salazar de Pablo G, Studerus E, Vaquerizo-Serrano J, et al. Implementing precision psychiatry: a systematic review of individualized prediction models for clinical practice. Schizophr Bull 2021 Mar 16;47(2):284-297. [doi: 10.1093/schbul/sbaa120] [Medline: 32914178]
18. Fouladvand S, Talbert J, Dwoskin LP, et al. A comparative effectiveness study on opioid use disorder prediction using artificial intelligence and existing risk models. IEEE J Biomed Health Inform 2023 Jul;27(7):3589-3598. [doi: 10.1109/JBHI.2023.3265920] [Medline: 37037255]
19. Liu F, Panagiotakos D. Real-world data: a brief review of the methods, applications, challenges and opportunities. BMC Med Res Methodol 2022 Nov 5;22(1):287. [doi: 10.1186/s12874-022-01768-6] [Medline: 36335315]
20. Kessler RC, Hwang I, Hoffmire CA, et al. Developing a practical suicide risk prediction model for targeting high‐risk patients in the Veterans Health Administration. Int J Methods Psych Res 2017 Sep;26(3). [doi: 10.1002/mpr.1575]
21. Delgadillo J, Ali S, Fleck K, et al. Stratified care vs stepped care for depression: a cluster randomized clinical trial. JAMA Psychiatry 2022 Feb 1;79(2):101-108. [doi: 10.1001/jamapsychiatry.2021.3539] [Medline: 34878526]
22. Garriga R, Mas J, Abraha S, et al. Machine learning model to predict mental health crises from electronic health records. Nat Med 2022 Jun;28(6):1240-1248. [doi: 10.1038/s41591-022-01811-5] [Medline: 35577964]
23. McCarthy JF, Cooper SA, Dent KR, et al. Evaluation of the recovery engagement and coordination for health-veterans enhanced treatment suicide risk modeling clinical program in the Veterans Health Administration. JAMA Netw Open 2021 Oct 1;4(10):e2129900. [doi: 10.1001/jamanetworkopen.2021.29900] [Medline: 34661661]

XSL•FO
RenderX

24. DECIDE-AI Steering Group. DECIDE-AI: new reporting guidelines to bridge the development-to-implementation gap in clinical artificial intelligence. Nat Med 2021 Feb;27(2):186-187. [doi: 10.1038/s41591-021-01229-5] [Medline: 33526932]
25. Keane PA, Topol EJ. With an eye to AI and autonomous diagnosis. NPJ Digit Med 2018;1(40):40. [doi: 10.1038/s41746-018-0048-y] [Medline: 31304321]
26. Golden G, Popescu C, Israel S, et al. Applying artificial intelligence to clinical decision support in mental health: what have we learned? Health Policy Technol 2024 Jun;13(2):100844. [doi: 10.1016/j.hlpt.2024.100844]
27. Proctor EK, Landsverk J, Aarons G, Chambers D, Glisson C, Mittman B. Implementation research in mental health services: an emerging science with conceptual, methodological, and training challenges. Adm Policy Ment Health 2009 Jan;36(1):24-34. [doi: 10.1007/s10488-008-0197-4] [Medline: 19104929]
28. Damschroder LJ, Reardon CM, Widerquist MAO, Lowery J. The updated consolidated framework for implementation research based on user feedback. Implementation Sci 2022 Oct 29;17(1). [doi: 10.1186/s13012-022-01245-0] [Medline: 36309746]
29. Wieringa M. What to account for when accounting for algorithms. Presented at: FAT* '20: Proceedings of the 2020 Conference on Fairness, Accountability, and Transparency; Jan 27-30, 2020; Barcelona Spain p. 1-18. [doi: 10.1145/3351095.3372833]
30. Wiens J, Saria S, Sendak M, et al. Do no harm: a roadmap for responsible machine learning for health care. Nat Med 2019 Sep;25(9):1337-1340. [doi: 10.1038/s41591-019-0548-6] [Medline: 31427808]
31. Group T, Vasey B, Clifton DA. DECIDE-AI: new reporting guidelines to bridge the development-to-implementation gap in clinical artificial intelligence. Nat Med 2021 Feb;27(2):186-187. [doi: 10.1038/s41591-021-01229-5] [Medline: 33526932]
32. Sujan M, Furniss D, Grundy K, et al. Human factors challenges for the safe use of artificial intelligence in patient care. BMJ Health Care Inform 2019 Nov;26(1):31780459. [doi: 10.1136/bmjhci-2019-100081] [Medline: 31780459]
33. O'Dell B, Stevens K, Tomlinson A, Singh I, Cipriani A. Building trust in artificial intelligence and new technologies in mental health. Evid Based Ment Health 2022 May;25(2):45-46. [doi: 10.1136/ebmental-2022-300489] [Medline: 35444002]
34. Baldwin H, Loebel-Davidsohn L, Oliver D, et al. Real-world implementation of precision psychiatry: a systematic review of barriers and facilitators. Brain Sci 2022 Jul 16;12(7):35884740. [doi: 10.3390/brainsci12070934] [Medline: 35884740]
35. Hassan M, Kushniruk A, Borycki E. Barriers to and facilitators of artificial intelligence adoption in health care: scoping review. JMIR Hum Factors 2024 Aug 29;11:e48633. [doi: 10.2196/48633] [Medline: 39207831]
36. Fereday J, Muir-Cochrane E. Demonstrating rigor using thematic analysis: a hybrid approach of inductive and deductive coding and theme development. Int J Qual Methods 2006 Mar;5(1):80-92. [doi: 10.1177/160940690600500107]
37. Kerkhof AM, Verwey B, Hummelen JW, et al. Multidisciplinaire Richtlijn Diagnostiek En Behandeling van Suïcidaal Gedrag [Multidisciplinary Guideline on the Assessment and Treatment of Suicidal Behaviour] [Book in Dutch]: Trimbos Institute; 2012. URL: https://psychiatrieweb.nl/pw.spoed/files/docs/suicidaal%20gedrag/richtlijn/120801_MDR_DBSG.pdf [accessed 2025-12-05]
38. Hicks SA, Strümke I, Thambawita V, et al. On evaluation metrics for medical applications of artificial intelligence. Sci Rep 2022 Apr 8;12(1):5979. [doi: 10.1038/s41598-022-09954-8] [Medline: 35395867]
39. Wirth R, Hipp J. CRISP-DM: towards a standard process model for data mining. 2000 Presented at: Proceedings of the 4th International Conference on the Practical Applications of Knowledge Discovery and Data Mining; Apr 18-20, 2000 URL: https://www.semanticscholar.org/paper/CRISP-DM%3A-Towards-a-Standard-Process-Model-for-Data-Wirth-Hipp/48b9293cfd4297f855867ca278f7069abc6a9c24#extracted [accessed 2025-12-05]
40. Grootendorst M. BERTopic: neural topic modeling with a class-based TF-IDF procedure. arXiv. Preprint posted online on Mar 11, 2022. [doi: 10.48550/arXiv.2203.05794]
41. Chen T, Guestrin C. XGBoost: a scalable tree boosting system. Presented at: KDD '16: Proceedings of the 22nd ACM SIGKDD International Conference on Knowledge Discovery and Data Mining; Aug 13-17, 2016; San Francisco, California, USA p. 785-794. [doi: 10.1145/2939672.2939785]
42. Etikan I, Musa SA, Alkassim RS. Comparison of convenience sampling and purposive sampling. AJTAS 2016;5(1):1. [doi: 10.11648/j.ajtas.20160501.11]
43. Singh K. Quantitative Social Research Methods: Sage Publications; 2007. [doi: 10.4135/9789351507741]
44. Braun V, Clarke V. Using thematic analysis in psychology. Qual Res Psychol 2006 Jan;3(2):77-101. [doi: 10.1191/1478088706qp063oa]
45. Damschroder LJ, Aron DC, Keith RE, Kirsh SR, Alexander JA, Lowery JC. Fostering implementation of health services research findings into practice: a consolidated framework for advancing implementation science. Implementation Sci 2009 Dec;4(1):50. [doi: 10.1186/1748-5908-4-50] [Medline: 19664226]
46. Hersh WR, Weiner MG, Embi PJ, et al. Caveats for the use of operational electronic health record data in comparative effectiveness research. Med Care 2013 Aug;51(8 Suppl 3):S30-S37. [doi: 10.1097/MLR.0b013e31829b1dbd] [Medline: 23774517]
47. Wickramarathne TL, Premaratne K, Murthi MN, Scheutz M, Kubler S, Pravia M. Belief theoretic methods for soft and hard data fusion. Presented at: ICASSP 2011 - 2011 IEEE International Conference on Acoustics, Speech and Signal Processing; May 22-27, 2011. [doi: 10.1109/ICASSP.2011.5946964]

XSL•FO
RenderX

48. Sedlakova J, Daniore P, Horn Wintsch A, et al. Challenges and best practices for digital unstructured data enrichment in health research: a systematic narrative review. PLOS Digit Health 2023 Oct;2(10):e0000347. [doi: 10.1371/journal.pdig.0000347] [Medline: 37819910]
49. Tayefi M, Ngo P, Chomutare T, et al. Challenges and opportunities beyond structured data in analysis of electronic health records. WIREs Computational Stats 2021 Nov;13(6). [doi: 10.1002/wics.1549]
50. Anderson HD, Pace WD, Brandt E, et al. Monitoring suicidal patients in primary care using electronic health records. J Am Board Fam Med 2015;28(1):65-71. [doi: 10.3122/jabfm.2015.01.140181] [Medline: 25567824]
51. Parsons A, McCullough C, Wang J, Shih S. Validity of electronic health record-derived quality measurement for performance monitoring. J Am Med Inform Assoc 2012;19(4):604-609. [doi: 10.1136/amiajnl-2011-000557] [Medline: 22249967]
52. Weiskopf NG, Weng C. Methods and dimensions of electronic health record data quality assessment: enabling reuse for clinical research. J Am Med Inform Assoc 2013 Jan 1;20(1):144-151. [doi: 10.1136/amiajnl-2011-000681] [Medline: 22733976]
53. De Choudhury M, Kiciman E. Integrating artificial and human intelligence in complex, sensitive problem domains: experiences from mental health. AI Mag 2018 Sep;39(3):69-80. [doi: 10.1609/aimag.v39i3.2815]
54. Baune BT, Christensen MC. Differences in perceptions of major depressive disorder symptoms and treatment priorities between patients and health care providers across the acute, post-acute, and remission phases of depression. Front Psychiatry 2019;10(335):335. [doi: 10.3389/fpsyt.2019.00335] [Medline: 31178765]
55. Ilkiw-Lavalle O, Grenyer BFS. Differences between patient and staff perceptions of aggression in mental health units. Psychiatr Serv 2003 Mar;54(3):389-393. [doi: 10.1176/appi.ps.54.3.389] [Medline: 12610249]
56. Rossberg JI, Friis S. Patients' and staff's perceptions of the psychiatric ward environment. Psychiatr Serv 2004 Jul;55(7):798-803. [doi: 10.1176/appi.ps.55.7.798] [Medline: 15232020]
57. Van Der Merwe M, Muir-Cochrane E, Jones J, Tziggili M, Bowers L. Improving seclusion practice: implications of a review of staff and patient views. J Psychiatr Ment Health Nurs 2013 Apr;20(3):203-215. [doi: 10.1111/j.1365-2850.2012.01903.x] [Medline: 22805615]
58. Hazewinkel MC, de Winter RFP, van Est RW, et al. Text analysis of electronic medical records to predict seclusion in psychiatric wards: proof of concept. Front Psychiatry 2019;10(188):188. [doi: 10.3389/fpsyt.2019.00188] [Medline: 31031650]
59. Velupillai S, Hadlaczky G, Baca-Garcia E, et al. Risk assessment tools and data-driven approaches for predicting and preventing suicidal behavior. Front Psychiatry 2019;10(36):36. [doi: 10.3389/fpsyt.2019.00036] [Medline: 30814958]
60. Zhang D, Yin C, Zeng J, Yuan X, Zhang P. Combining structured and unstructured data for predictive models: a deep learning approach. BMC Med Inform Decis Mak 2020 Oct 29;20(1):280. [doi: 10.1186/s12911-020-01297-6] [Medline: 33121479]
61. Boggs JM, Kafka JM. A critical review of text mining applications for suicide research. Curr Epidemiol Rep 2022;9(3):126-134. [doi: 10.1007/s40471-022-00293-w] [Medline: 35911089]
62. Boudreaux ED, Rundensteiner E, Liu F, et al. Applying machine learning approaches to suicide prediction using healthcare data: overview and future directions. Front Psychiatry 2021;12:707916. [doi: 10.3389/fpsyt.2021.707916] [Medline: 34413800]
63. Fernandes AC, Dutta R, Velupillai S, Sanyal J, Stewart R, Chandran D. Identifying suicide ideation and suicidal attempts in a psychiatric clinical research database using natural language processing. Sci Rep 2018 May 9;8(1):7426. [doi: 10.1038/s41598-018-25773-2] [Medline: 29743531]
64. Levis M, Levy J, Dent KR, et al. Leveraging natural language processing to improve electronic health record suicide risk prediction for veterans health administration users. J Clin Psychiatry 2023 Jun 19;84(4):22m14568. [doi: 10.4088/JCP.22m14568] [Medline: 37341477]
65. Cusick M, Adekkanattu P, Campion TR Jr, et al. Using weak supervision and deep learning to classify clinical notes for identification of current suicidal ideation. J Psychiatr Res 2021 Apr;136(95–102):95-102. [doi: 10.1016/j.jpsychires.2021.01.052] [Medline: 33581461]
66. Geneviève LD, Martani A, Shaw D, Elger BS, Wangmo T. Structural racism in precision medicine: leaving no one behind. BMC Med Ethics 2020 Feb 19;21(1):17. [doi: 10.1186/s12910-020-0457-8] [Medline: 32075640]
67. Cook LA, Sachs J, Weiskopf NG. The quality of social determinants data in the electronic health record: a systematic review. J Am Med Inform Assoc 2021 Dec 28;29(1):187-196. [doi: 10.1093/jamia/ocab199] [Medline: 34664641]
68. Timmons AC, Duong JB, Simo Fiallo N, et al. A call to action on assessing and mitigating bias in artificial intelligence applications for mental health. Perspect Psychol Sci 2023 Sep;18(5):1062-1096. [doi: 10.1177/17456916221134490] [Medline: 36490369]
69. Suresh H, Guttag J. A framework for understanding sources of harm throughout the machine learning life cycle. Presented at: EAAMO '21: Proceedings of the 1st ACM Conference on Equity and Access in Algorithms, Mechanisms, and Optimization; Oct 5-9, 2021; New York, United States p. 1-9. [doi: 10.1145/3465416.3483305]
70. Lewis AE, Weiskopf N, Abrams ZB, et al. Electronic health record data quality assessment and tools: a systematic review. J Am Med Inform Assoc 2023 Sep 25;30(10):1730-1740. [doi: 10.1093/jamia/ocad120] [Medline: 37390812]

XSL•FO
RenderX

71. Akata Z, Balliet D, de Rijke M, et al. A Research Agenda for Hybrid Intelligence: Augmenting Human Intellect With Collaborative, Adaptive, Responsible, and Explainable Artificial Intelligence. Computer (Long Beach Calif) 2020;53(8):18-28. [doi: 10.1109/MC.2020.2996587]
72. Mouchabac S, Conejero I, Lakhlifi C, et al. Improving clinical decision-making in psychiatry: implementation of digital phenotyping could mitigate the influence of patient's and practitioner's individual cognitive biases. Dialogues Clin Neurosci 2021;23(1):52-61. [doi: 10.1080/19585969.2022.2042165] [Medline: 35860175]
73. Choudhury A, Chaudhry Z. Large language models and user trust: consequence of self-referential learning loop and the deskilling of health care professionals. J Med Internet Res 2024 Apr 25;26:e56764. [doi: 10.2196/56764] [Medline: 38662419]
74. Vitacca M, Giardini A, Gazzi L, Vitacca M. Hidden biases in clinical decision-making: potential solutions, challenges, and perspectives. Monaldi Arch Chest Dis 2022 Sep 7;93(2):36069639. [doi: 10.4081/monaldi.2022.2339] [Medline: 36069639]
75. Hulsen T. Explainable artificial intelligence (XAI): concepts and challenges in healthcare. AI 2023;4(3):652-666. [doi: 10.3390/ai4030034]
76. Amann J, Blasimme A, Vayena E, Frey D, Madai VI, Precise4Q consortium. Explainability for artificial intelligence in healthcare: a multidisciplinary perspective. BMC Med Inform Decis Mak 2020 Nov 30;20(1):310. [doi: 10.1186/s12911-020-01332-6] [Medline: 33256715]
77. Bodria F, Giannotti F, Guidotti R, Naretto F, Pedreschi D, Rinzivillo S. Benchmarking and survey of explanation methods for black box models. Data Min Knowl Disc 2023 Sep;37(5):1719-1778. [doi: 10.1007/s10618-023-00933-9]
78. Singh R, Miller T, Sonenberg L, Velloso E, Vetere F, Howe P, et al. An actionability assessment tool for explainable AI. arXiv. Preprint posted online on Jun 19, 2024. [doi: 10.48550/arXiv.2407.09516]
79. Menger VJ, Spruit MR, Scheepers FE. Kennisontwikkeling in de klinische psychiatrie: leren van elektronische patiëntendossiers [Article in Dutch]. Tijdschr Psychiatr 2021;63(4):294-300 [FREE Full text]
80. Vale D, El-Sharif A, Ali M. Explainable artificial intelligence (XAI) post-hoc explainability methods: risks and limitations in non-discrimination law. AI Ethics 2022 Nov;2(4):815-826. [doi: 10.1007/s43681-022-00142-y]
81. Reddy S, Shaikh S. The long road ahead: navigating obstacles and building bridges for clinical integration of artificial intelligence technologies. J Med Artif Intell 2025;8:7-7. [doi: 10.21037/jmai-24-148]
82. Kaplan AD, Kessler TT, Brill JC, Hancock PA. Trust in artificial intelligence: meta-analytic findings. Hum Factors 2023 Mar;65(2):337-359. [doi: 10.1177/00187208211013988] [Medline: 34048287]
83. Glikson E, Woolley AW. Human trust in artificial intelligence: review of empirical research. Ann R Coll Physicians Surg Can 2020 Jul;14(2):627-660. [doi: 10.5465/annals.2018.0057]
84. Kizilcec RF. How much information?: Effects of transparency on trust in an algorithmic interface. Presented at: CHI '16: Proceedings of the 2016 CHI Conference on Human Factors in Computing Systems; May 7-12, 2016; San Jose, California, USA p. 2390-2395. [doi: 10.1145/2858036.2858402]
85. Luk JW, Pruitt LD, Smolenski DJ, Tucker J, Workman DE, Belsher BE. From everyday life predictions to suicide prevention: clinical and ethical considerations in suicide predictive analytic tools. J Clin Psychol 2022 Feb;78(2):137-148. [doi: 10.1002/jclp.23202] [Medline: 34195998]
86. van der Veer SN, Riste L, Cheraghi-Sohi S, et al. Trading off accuracy and explainability in AI decision-making: findings from 2 citizens' juries. J Am Med Inform Assoc 2021 Sep 18;28(10):2128-2138. [doi: 10.1093/jamia/ocab127] [Medline: 34333646]
87. Barredo Arrieta A, Díaz-Rodríguez N, Del Ser J, et al. Explainable artificial intelligence (XAI): concepts, taxonomies, opportunities and challenges toward responsible AI. Information Fusion 2020 Jun;58:82-115. [doi: 10.1016/j.inffus.2019.12.012]

Abbreviations

AI: artificial intelligence
CFIR: Consolidated Framework for Implementation Research
CRISP-DM: Cross-Industry Standard Process for Data Mining
EHR: electronic health record
GGzE: Geestelijke Gezondheidszorg Eindhoven en de Kempen
ML: machine learning
NLP: natural language processing
RoB: risk of bias
SPQ: Suicide Prevention Questionnaire

XSL•FO
RenderX

Edited by C Perrin; submitted 20.Mar.2025; peer-reviewed by HH Yeh, R Jacobucci; revised version received 18.Nov.2025; accepted 18.Nov.2025; published 14.Jan.2026.

Please cite as:
Hummel L, Lorenz-Artz KCAG, Bierbooms JJPA, Bongers IMB
Developing a Suicide Risk Prediction Algorithm Using Electronic Health Record Data in Mental Health Care: Real-World Case Study
JMIR Med Inform 2026;14:e74240
URL: https://medinform.jmir.org/2026/1/e74240
doi:10.2196/74240

© Linda Hummel, Karin C A G Lorenz-Artz, Joyce J P A Bierbooms, Inge M B Bongers. Originally published in JMIR Medical Informatics (https://medinform.jmir.org), 14.Jan.2026. This is an open-access article distributed under the terms of the Creative Commons Attribution License (https://creativecommons.org/licenses/by/4.0/), which permits unrestricted use, distribution, and reproduction in any medium, provided the original work, first published in JMIR Medical Informatics, is properly cited. The complete bibliographic information, a link to the original publication on https://medinform.jmir.org/, as well as this copyright and license information must be included.

XSL•FO
RenderX

Implementation Report

Scaling Wireless Continuous Vital Sign Monitoring Across an 8-Hospital Health System: Digital Health Implementation Report

Ngoc-Anh Nguyen[1,2,3], MD; Grace Lee[1,2], BA; Brendan Holderread[1,2], MD; Terrie Holman[1], BS; Sarah Pletcher[1,2,4], MD, MHCDS; Roberta Schwartz[1,2], PhD

[1]Center for Connected Care, Innovation & Implementation - Research, Houston Methodist, Houston, TX, United States

[2]Houston Methodist Research Institute, Houston Methodist, Houston, TX, United States

[3]Department of Medicine, Houston Methodist, Houston, TX, United States

[4]Department of Surgery, Houston Methodist, Houston, TX, United States

Corresponding Author:
Ngoc-Anh Nguyen, MD
Center for Connected Care, Innovation & Implementation - Research
Houston Methodist
6560 Fannin Street
Scurlock Tower STB2-133
Houston, TX, 77030
United States
Phone: 1 7132996839
Fax: 1 7137931851
Email: nanguyen@houstonmethodist.org

Abstract

Background: Frequent vital sign (VS) monitoring is central to inpatient safety but is traditionally performed manually every 4 hours, a century-old practice that can miss early clinical deterioration, disrupt patient sleep, and impose a heavy documentation burden on nursing staff. Continuous VS monitoring (CVSM) using wearable remote patient monitoring devices enables near real-time, high-frequency VS measurement while reducing manual workload and preserving patient rest.

Objective: This implementation report describes the large-scale implementation of CVSM across an 8-hospital health system. The initiative aimed to (1) enhance earlier detection of patient health deterioration through continuous, algorithm-driven monitoring; (2) improve nursing workflow efficiency by reducing reliance on manual VS checks; and (3) minimize nighttime disruptions to support patient rest and recovery.

Methods: The program was designed for system-wide scalability and executed from 2022 to 2024 using a 4-phase framework: strategic program design, program planning, go-live preparation, and implementation and optimization. A Food and Drug Administration–cleared wearable device (BioButton) continuously measured heart rate, respiratory rate, and skin temperature, with data integrated into Epic and monitored 24×7 through a centralized virtual operations center. Rollout followed a staggered playbook across approximately 2700 adult non–intensive care unit beds and was supported by leadership engagement, supply chain readiness, staff training, and phased superuser-led adoption.

Implementation (Results): All 8 hospitals achieved full deployment between April 2023 and February 2024, with more than 95% device use rates and 100% nursing staff training completion. A standardized escalation workflow filtered approximately 50% of the alerts at the virtual operations center review stage, substantially reducing frontline alert burden. Operational refinements included revised heart rate and respiratory rate alert thresholds and the removal of temperature as a single alert trigger. Several units extended overnight manual VS intervals from every 4 hours to every 6 to 8 hours, with staff estimating approximately 4 hours saved per nursing shift. Patient care assistants redirected time toward patient mobility and personal care needs, while staff reported growing confidence in device performance over time.

Conclusions: This initiative represents the first system-wide deployment of CVSM across a diverse, multihospital health system. Success was enabled by early strategic alignment, phased rollout, robust IT and monitoring infrastructure, and iterative optimization. The program demonstrates the feasibility of embedding CVSM into routine inpatient care to improve efficiency and patient experience. Transferable strategies, including phased rollouts, centralized monitoring, and structured change management, may

XSL•FO
RenderX

inform other health systems pursuing digital VS redesign. Future work should rigorously evaluate impacts on patient outcomes, cost-effectiveness, and applicability to postacute and ambulatory care settings.

(JMIR Med Inform 2026;14:e78216) doi:10.2196/78216

KEYWORDS

continuous vital sign monitoring; remote patient monitoring; wearable devices; hospital workflow redesign; patient safety; digital health implementation; implementation science

Introduction

Context

This implementation occurred within Houston Methodist (HM), an 8-hospital health system in Texas encompassing the HM Hospital (a quaternary care academic flagship), 6 community hospitals, and 1 long-term acute care (LTAC) facility serving the greater Houston area, together serving a diverse adult population of more than 140,000 annual admissions and 2 million outpatient visits [1].

During the COVID-19 pandemic, HM established a centralized virtual operations center (VOC) and virtual intensive care unit (VICU) providing 24×7 monitoring for approximately 370 intensive care unit (ICU) beds. This infrastructure created favorable conditions for remote patient monitoring (RPM) and ultimately informed the development of the system-wide continuous vital sign (VS) monitoring (CVSM) program. This CVSM program differs from traditional RPM in its continuous, hospital-based, and fully integrated design, with data integrated into the electronic medical record and supported by 24×7 centralized oversight rather than periodic outpatient review.

In 2022, the health system launched a redesign of inpatient VS practices, with this report detailing the program's scale-up and deployment, which were designed from the outset for system-wide implementation.

Problem Statement

Frequent monitoring of VSs—heart rate (HR), respiratory rate (RR), temperature, blood pressure, and oxygen saturation (SpO_2)—is a cornerstone of inpatient safety [2]. On general hospital floors, VSs are routinely collected manually every 4 hours, reflecting a century-old practice that does not account for patient acuity [3,4]. This approach risks missed deterioration between checks, places substantial time demands on nursing staff, and disrupts patients' sleep, with physiological consequences [5-14]. Deteriorating VSs are well-established predictors of ICU transfer and in-hospital mortality, and CVSM, enabled by wearable RPM devices, now allows for unobtrusive, high-frequency VS measurement [7,11,12]. This work directly addresses health system challenges of limited access to timely clinical data and variable adherence to evidence-based monitoring practices, both of which undermine patient safety and workflow efficiency. However, evidence on broad, system-wide implementation across diverse hospital settings remains limited.

Similar Interventions

Previous CVSM implementations have typically been limited to ICUs, single hospitals, or narrow patient groups, demonstrating feasibility but limiting generalizability [15-17]. Our initiative differs by extending CVSM across all adult non-ICU inpatients in an 8-hospital system, integrated with Epic and supported by centralized monitoring. This report describes the implementation and scale-up process.

This report follows JMIR's implementation reporting guidelines for digital health implementation [18] to ensure transparency in describing the implementation context and processes.

Methods

Aim and Objective

The aim of this initiative was to redesign inpatient VS measurement practices to enhance patient safety, patient experience, and staff efficiency through the implementation of CVSM. Specific objectives were to enable early detection of deterioration, reduce nighttime disruptions to promote patient rest and recovery, and improve workflow by decreasing reliance on manual VS checks. Implementation outcomes included system-wide rollout to all eligible beds, 100% nursing staff training completion, optimal device use, and reductions in manual VS collection, with qualitative observations of staff and patient acceptance. Operational metrics (scale-up timeline, device use, alert filtering, and training completion) were directly measured, whereas workflow impacts and staff acceptance were reflected in qualitative, staff-reported estimates.

Implementation Strategy

The implementation strategy was designed for system-wide scalability and organized into 4 phases, with the observed timeline shown in Figure 1.

XSL•FO
RenderX

Figure 1. Four-phase implementation framework and observed timeline for scaling continuous vital sign monitoring across (CVSM) Houston Methodist's 8-hospital health system. EMR: electronic medical record.

Phase 1: Strategic Program Design (1-2 Years Before Implementation)

The health system defined an enterprise-wide vision for CVSM as part of a broader effort to modernize VS monitoring. Strategic goals emphasized embedding continuous monitoring into routine inpatient care, strengthening patient safety through earlier detection of deterioration, and redesigning workflows to mitigate the impact of nursing staff shortages.

A multidisciplinary team of key stakeholders, including clinical, operational, IT, supply chain, and innovation leaders, was engaged early and consistently to ensure clinical and organizational alignment. The team identified use cases and target populations, prioritizing continuous monitoring of all hospitalized, non-ICU patients to address the safety gap created by every-4-hour manual VS checks. Patient eligibility was intentionally broad; CVSM was applied to general adult medical-surgical inpatients, excluding only ICU patients, with no additional eligibility restrictions.

Implementation sites included the academic flagship, 6 community hospitals, and 1 LTAC facility, with monitoring supported by bedside nurses, unit superusers, and the centralized VOC. The multidisciplinary team guided planning and iteratively refined a scalable model for system-wide deployment, supported by superusers at the unit level and centralized monitoring through the VOC.

Phase 2: Program Planning (1Year Before Implementation)

After defining the overall CVSM strategy, the health system conducted market research to evaluate vendor partners and established planning priorities in workflow redesign, Epic integration, staff training, and IT infrastructure, with a standardized playbook to guide hospital rollouts. Vendor selection considered Food and Drug Administration (FDA) clearance, performance, usability, multiparameter monitoring, battery life, patient comfort, Epic integration, and scalability.

A wearable patch device (BioButton; BioIntelliSense) was selected as the FDA-cleared option that best met these criteria. The adhesive patch is worn on the chest with a battery life lasting 7 to 16 days. It continuously collects HR, RR, and skin temperature (additional parameters are listed in Multimedia Appendix 1) [6,17]. Device selection prioritized accurate RR measurement, given its established predictive value for deterioration [14,19]. Although a BioButton device does not measure SpO_2 or blood pressure, these parameters were acceptable through existing bedside monitoring. Continuous SpO_2 monitoring typically requires a tethered probe that disrupts rest and increases alarm burden [20], whereas the BioButton device allows unobtrusive, trended monitoring aligned with program goals to reduce patient disruptions.

From the outset, the program was designed for system-wide scale, leveraging existing institutional resources and establishing a centralized monitoring team at the main academic hospital. Pilot sites included 2 internal medicine units, 1 neurosurgery unit, and 1 neurology unit selected for innovation experience and staff receptiveness. Program management included site-level and system-level leads, who shared responsibilities with the vendor for workflow design, data integration, training, and support **(**roles are detailed in Multimedia Appendix 2).

Participating entities included HM, a quaternary academic health system whose mission emphasizes patient-centered, digitally enabled care, which led workflows, monitoring staff, and supply chain integration, and BioIntelliSense, which provided devices, hubs, dashboard tools, and technical support. The VOC delivered continuous monitoring, with bedside nurses serving as superusers. Intellectual property for the BioButton device remains with BioIntelliSense, while workflows, data integration, and the operational model belong to HM.

XSL•FO
RenderX

The business case projected nursing and patient care assistant (PCA) time savings from extended overnight VS intervals, supporting adoption and sustainability. Internal funding was secured as part of routine service redesign, with no direct costs to patients. Budget categories included devices, hubs, Epic integration, staff training, supply chain processes, and change management. BioButton devices were supplied through a per-bed subscription model, and approximately 2711 BioHub Wi-Fi gateways were installed across all patient rooms. The largest investments were technology procurement and integration, with ongoing costs for training and supply chain support.

Phase 3: Go-Live Preparation (3-6 Months Before Going Live)

Building on program planning, readiness efforts focused on 5 domains: room and BioHub setup, device and supply chain readiness, Epic and IT validation, unit training plans, and kickoff planning. Activities occurred at both system and unit levels (details are provided in Multimedia Appendix 3). Integration with Epic and the monitoring dashboard followed standard institutional IT and security protocols. IT preparations included configuring BioHub connectivity, enabling secure transmission of physiological data, and validating data flow into Epic flowsheets and early warning score logic. A summary of this pathway is shown in Figure 2.

Device and environmental preparations included stocking BioButton devices, labeling return bins, and completing room readiness surveys. Initial stock levels were based on recent admission volumes, with automated reordering through the supply chain. Workflows were established for device return and sanitation.

Kickoff planning finalized rollout sequencing and support allocation. The central monitoring team staffing within the VOC was expanded by reallocating staff after reducing telemetry use. VOC staff completed vendor-led training and competency demonstrations in alert interpretation, escalation protocols, and workflow integration.

Phase 4: Implementation and Optimization

Implementation emphasized 5 core activities: playbook rollout, staff training, go-live support, protocol refinement, and iterative feedback and optimization. Each unit followed an 8-week rollout guided by the playbook, with superuser and vendor support during the go-live phase.

Training followed a train-the-trainer model, with unit leaders and superusers trained first, followed by cascading training to frontline staff. All bedside nurses completed a mandatory learning management system module (100% completion system wide), which covered device application, alert interpretation, escalation protocols, and workflow integration. Adoption was reinforced through superuser rounding, vendor staff presence, and structured communication plans. Training activities were designed to build knowledge, confidence, and consistency among staff and are consistent with approaches described in the implementation science literature [21-23].

Go-live execution proceeded in staggered groups of 4 to 8 units, allowing overlap between training and operational transitions. Kickoff meetings, leadership communication plans, and coordinated supply chain activation supported each launch.

Protocol refinement was embedded throughout the rollout. Initial thresholds and workflows were iteratively adjusted based on frontline experience. VOC champions and superusers reinforced troubleshooting and informed subsequent launches. Sustainability was achieved by embedding CVSM into standard operations, including VOC monitoring workflows, Epic documentation, supply chain logistics, and updated learning management system training modules. Continued superuser engagement and institutional commitment to operational funding reinforced adoption. Full institutionalization of CVSM into existing structures ensured long-term ownership and positioned the program as a core element of HM's broader digital care transformation strategy.

Figure 2. Data flow from the BioButton device through BioHub, BioCloud, and BioDashboard to Epic. AI: artificial intelligence.

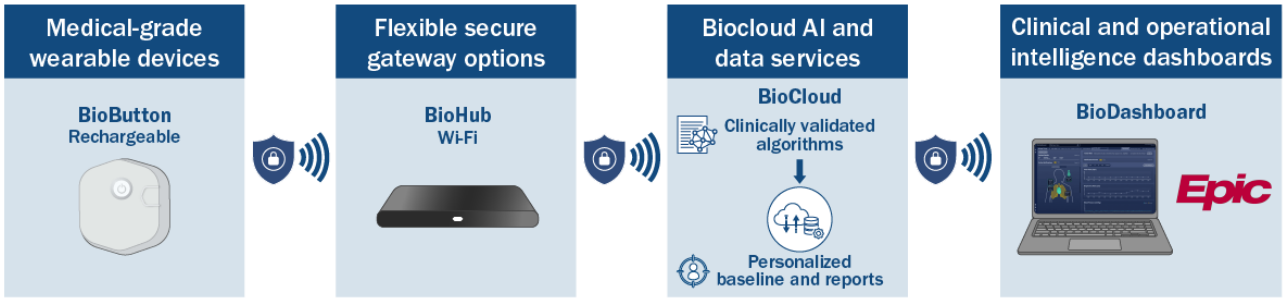

Ethical Considerations

The Institutional Review Board of Houston Methodist Research Institute reviewed this initiative and deemed it *not human research*, as it represented a service redesign implemented as part of standard care.

Implementation (Results)

Coverage

Between April 2023 and February 2024, the program expanded from pilot units to enterprise-wide coverage across all 8 hospitals, encompassing the full adult, non-ICU inpatient population (approximately 2700 beds across the academic flagship, 6 community hospitals, and 1 LTAC facility).

XSL•FO
RenderX

Rollout Approach and Timeline

The enterprise rollout followed a phased road map. Pilot implementation began on 4 units at the main hospital (2 internal medicine units, 1 neurosurgery unit, and 1 neurology unit). Four months later, deployment scaled through staggered 8-week waves of 4 to 8 units, with 3-week offsets to permit overlap between staff training and transitions, allowing the incorporation of iterative learning. This cadence enabled continuous optimization while maintaining operational continuity.

Monitoring and Escalation Workflow

Five months after the pilot launch, HM introduced a standardized escalation protocol embedded in centralized monitoring workflows. When BioButton device–triggered alerts appeared on the VOC dashboard, a VOC technician performed a first-line review to add clinical content and either dismissed nonactionable events or escalated alerts to a VICU nurse. Approximately half of the alerts were dismissed at the VOC step, reducing alert burden for frontline staff. Illustrative case examples are provided in Multimedia Appendix 4.

The VICU nurse notified the bedside nurse or activated the clinical emergency response team when intervention was indicated. This tiered model concentrated clinical escalation on higher-value alerts. Data on clinical emergency response team activations during the study period have been reported previously in a related outcomes study [24].

Outcomes and Post–Go-Live Protocol Refinement

Primary outcomes included system-wide scale-up, reliable Epic integration, and sustained monitoring. Device use exceeded 95%, training completion reached 100%, and approximately 50% of alerts were resolved at VOC review. Secondary outcomes included improved alert specificity, fewer patient refusals, increased staff acceptance, and operational efficiencies (nursing and PCA time savings). Alert thresholds were systematically reviewed with virtual medicine leadership in collaboration with frontline nursing staff, superusers, and the vendor. Baseline thresholds (HR 50-115 beats per minute, RR 11-28 breaths per minute, and skin temperature >36 °C) were operationalized with alerts stratified as single alerts (1 abnormal VS), double alerts (2 abnormalities, typically HR and RR), or triple alerts (3 abnormalities: HR, RR, and skin temperature). Three protocol changes improved the system-wide specificity.

Skin temperature was removed as an isolated escalation criterion and retained only for triple alerts. The RR lower limit was reduced from 11 to 8 breaths per minute to reduce clinically insignificant overnight alerts. The upper HR limit was increased from 115 to 120 beats per minute to reduce nonactionable alerts reported by community hospitals and the LTAC facility. Other parameters (eg, body position and activity) contributed to *low motion* alerts but were not primary triggers.

Collectively, these adjustments improved the balance between sensitivity and specificity, as reflected by observed reductions in nonactionable alerts and staff-reported decreases in false positives during enterprise rollout. The final escalation workflow and logic are depicted in Figures 3 and 4, with detailed initial and revised threshold values in Multimedia Appendix 5.

XSL•FO
RenderX

Figure 3. Escalation workflow for the BioButton device alerts with virtual operations center triage and bedside escalation. Bedside teams are responsible for all button management activities (ie, placement or removal, low battery, and no data). Patient data (from the BioIntelliSense button) will be transmitted into the Epic vital signs flowsheet, and BioDashboard can take up to 20 minutes to fully synchronize. APP: advanced practice provider; CERT: clinical emergency response team; RN: registered nurse; RR: respiratory rate.

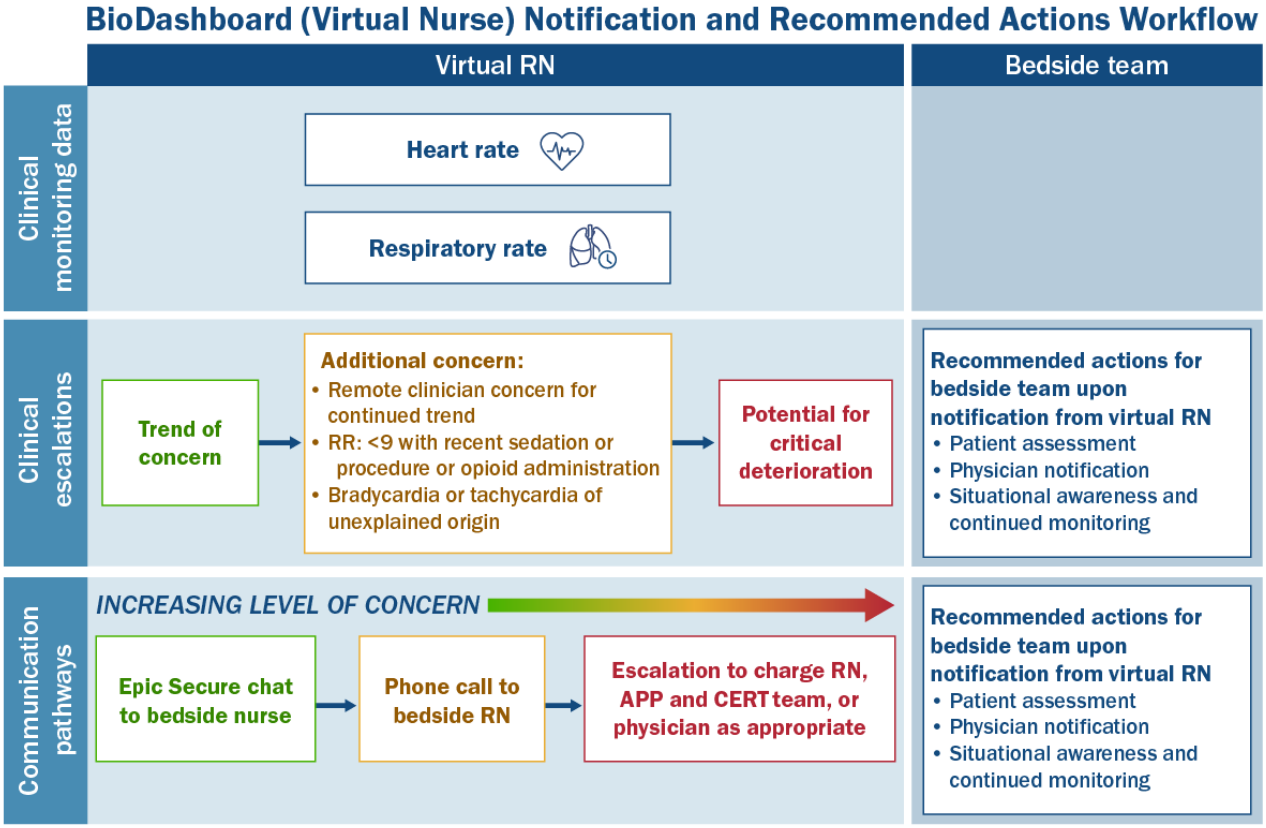

Figure 4. Escalation protocol for respiratory rate (RR) and heart rate (HR) alerts with system-wide thresholds. Final threshold for HR (50-120 bpm) and RR (8-27 bpm). Skin temperature has been removed from the escalation criteria. BDB: BioDashboard.

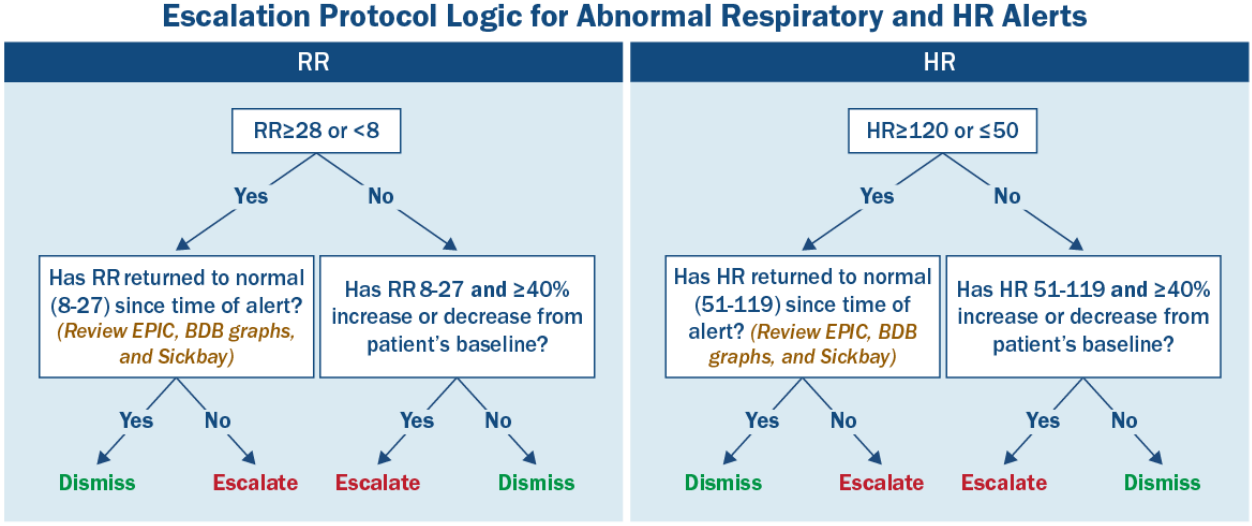

Lessons Learned and Implementation Challenges

Technical and workflow challenges identified during the pilot informed the enterprise rollout. Barcode scanning difficulties (eg, poor label contrast) occasionally impeded device-to-patient matching; staff used device packaging barcodes and Workstations on Wheels carts as interim work-arounds, and the vendor subsequently improved barcode resolution. Rare *double HR* artifacts (concurrent S1 and S2 detections) produced nonactionable alerts and were resolved via algorithm updates.

Variation in device application sometimes caused skin irritation, which was addressed via staff reeducation and the use of adhesive remover spray. Early staff skepticism about using median CVSM values for documentation declined as experience accumulated, and staff perceived CVSM values to be accurate and consistent with routine bedside measurements; patient

XSL•FO
RenderX

refusals decreased with standardized education. These mitigations and training reinforcements were propagated system wide during enterprise rollout.

As noted previously, unintended consequences, including minor skin irritation, initial device hesitancy, and early false positives, were observed and addressed through staff education, supplies, and vendor refinements; no significant harms were reported.

Discussion

Principal Findings

To our knowledge, this initiative represents the first large-scale deployment of wearable CVSM across a diverse, multihospital health system as part of a system-wide redesign initiative [17]. Our goal was to modernize inpatient VS practices by introducing continuous monitoring to support earlier detection, improve outcomes, and enhance both patient and clinician experience. Several units extended overnight VS intervals from every 4 hours to 6 to 8 hours, saving approximately 4 hours per nursing shift and allowing PCAs to focus on patient mobility and personal needs. Together with early clinical benefits, these efficiencies strengthened adoption and staff buy-in.

Weller et al [17] evaluated the same FDA-cleared device in 11,977 patients across urban and rural hospitals, with initial ICU use before expansion to non-ICU settings. They reported low RR alarms most frequently, while in our implementation, elevated RR emerged as the most common alert, underscoring RR's role as a sensitive marker of cardiopulmonary function. This difference likely reflects patient mix, as sedation in ICU patients tends to lower RRs, while elevated RRs in ward patients more often indicate deterioration.

A key distinction of this program was its breadth and scope. Unlike previous efforts limited to ICUs, daytime hours, or narrow diagnostic groups, this program encompassed all adult non-ICU inpatients, deployed continuously (24×7) across the flagship academic hospital, 6 community hospitals, and 1 LTAC facility. This design addressed gaps in every 4-hour VS collection, enabled earlier detection across diverse patient populations, and supported workflow redesign amid nursing staff shortages.

Device selection prioritized accurate RR measurement, given its strong predictive value. Although the BioButton devices do not measure blood pressure or SpO_2, they remained available through existing bedside monitoring. Continuous SpO_2 monitoring was avoided to minimize alarm burden. The device offered unobtrusive, trended monitoring without disturbing patients' rest while capturing key physiological parameters for early detection. The final escalation protocol's emphasis on HR and RR reflected clinical prioritization and not device limitation. Although formal satisfaction and quality metrics are forthcoming, early stakeholder feedback suggests that reduced overnight disruptions improved sleep quality, potentially enhancing patient satisfaction and reducing overnight nursing workload. Prospective studies are needed to evaluate long-term effects on clinical outcomes, alert trends, workflow efficiency, and satisfaction, including patient-reported outcomes.

Limitations

This report has several limitations. No formal satisfaction survey was conducted, and estimates of time savings were based on staff feedback. BioButton device–derived VSs were not independently validated, as accuracy testing of the FDA-cleared device was beyond the scope of this work. The escalation protocol was intentionally delayed in pilot units; therefore, early data reflect monitoring without active escalation, with finalized protocols introduced later and applied retrospectively. Although guided by an internal business case projecting nursing and PCA time savings, no formal health technology assessment was conducted.

Generalizability may be limited by HM's centralized monitoring model; other health systems may face different challenges. Observed alert trends may also differ across settings, as illustrated by differences between ICU-focused studies and our broad non-ICU deployment. Outcome measures, such as clinical impact, workflow efficiency, and adoption, were not prospectively defined, constraining evaluation but informing priorities for future analyses.

Several transferable lessons emerged: (1) structured change management with engagement, champions, and feedback loops supported adoption; (2) phased rollout with iterative refinements reduced risk and enabled optimization; (3) centralized monitoring enabled 24×7 oversight, while hospitals without such infrastructure could adapt using telemetry staff, rapid response teams, or external partners; and (4) alignment of CVSM with institutional priorities secured leadership support and momentum. Table 1 summarizes key lessons and success factors to guide future implementers in scaling similar initiatives.

XSL•FO
RenderX

Table 1. Key lessons and success factors from system-wide CVSMa implementation.

Domain	Challenges encountered	Lessons learned and success factors
Leadership and Governance	Balancing innovation with standardization across 8 hospitals	Early executive sponsorship and system-wide alignment maintained focus, accountability, and resource continuity.
Implementation Approach	Scaling across multiple hospitals while managing operational risk	Staggered enterprise rollout using an 8-week implementation playbook enabled iterative refinement and risk mitigation before full scale-up.
Workflow Integration	Incorporating CVSM data into existing Epic processes	Integration into Epic flowsheets and early warning scores streamlined workflow and improved adoption.
Technology and Infrastructure	Interoperability issues and alert fatigue	Centralized monitoring filtered ~50% of alerts before bedside escalation; iterative threshold refinements improved specificity and reduced alert fatigue.
Training and Adoption	Staff skepticism and learning curve	Superuser model, LMS[b] training, and vendor support during go-live built confidence and sustained engagement.
Change Management	Variation in readiness and engagement across sites	Phased rollout enabled iterative optimization and local adaptation while maintaining operational continuity.
Data Governance	Managing HIPAA[c] compliance and device data retention	Preimplementation IT security review ensured compliance with institutional privacy and security standards.
Sustainability	Maintaining engagement and support after implementation	Integration into standard operations, funding streams, and training infrastructure supported long-term sustainability.
Cultural Readiness	Early staff skepticism about device accuracy and value	Confidence increased with experience and demonstrated accuracy, reinforcing trust and normalization of continuous monitoring.

[a]CVSM: continuous vital sign monitoring.

[b]LMS: learning management system.

[c]HIPAA: Health Insurance Portability and Accountability Act.

Conclusions and Future Implications

This initiative demonstrates the feasibility and operational value of scaling CVSM across a large, diverse health system. Embedding continuous monitoring into standard workflows can improve patient safety, enhance staff efficiency, and build infrastructure for digitally enabled care models.

Future work should rigorously assess clinical outcomes, economic impact, and patient-reported measures while exploring application in postacute and ambulatory settings. Although growing evidence supports continuous monitoring, prospective randomized trials are still needed to confirm clinical and economic benefits. As health systems address workforce shortages and rising patient acuity, wearable monitoring technologies, such as CVSM, could serve as core infrastructure for safer, more efficient, and patient-centered care.

Acknowledgments

The authors thank BioIntelliSense Inc, Houston Methodist (HM) Center for Health Data Science and Analytics, Ms Ellie Kalatzi, HM Department of Strategic Innovation, HM Department of Virtual Operations, HM Department of IT and Informatics, HM supply chain, HM nursing leadership, and HM nursing education for their invaluable contributions to the successful implementation of this quality improvement initiative. The authors also thank Ms Sarah Sossong for her significant contributions to manuscript development, including content drafting and revision, integration of reviewer feedback, and overall editorial guidance.

Funding

No external financial support or grants were received from any public, commercial, or not-for-profit entities for the research, authorship, or publication of this paper.

Data Availability

The datasets generated or analyzed during this study are not publicly available due to institutional privacy policies.

Authors' Contributions

Investigation: NAN, GL, and BH
Program conceptualization and design: SP and RS

XSL•FO
RenderX

Project management: TH
Overall responsibility: SP and NAN
Writing—original draft: GL, NAN, and BH

Conflicts of Interest

None declared.

Multimedia Appendix 1
Physiological parameters measured by the BioButton device, measurement methods, and clinical use cases.
[DOCX File , 15 KB - medinform_v14i1e78216_app1.docx]

Multimedia Appendix 2
Roles and responsibilities of vendor and health system stakeholders in the multidisciplinary implementation team for continuous vital sign monitoring.
[DOCX File , 22 KB - medinform_v14i1e78216_app2.docx]

Multimedia Appendix 3
System-level and unit-level readiness activities by operational domain for continuous vital sign monitoring implementation.
[DOCX File , 23 KB - medinform_v14i1e78216_app3.docx]

Multimedia Appendix 4
Illustrative case examples of early detection and intervention.
[DOCX File , 16 KB - medinform_v14i1e78216_app4.docx]

Multimedia Appendix 5
Initial and revised alarm thresholds with rationale for revisions.
[DOCX File , 14 KB - medinform_v14i1e78216_app5.docx]

Multimedia Appendix 6
iCHECK-DH: Guidelines and Checklist for the Reporting on Digital Health Implementations.
[PDF File (Adobe PDF File), 286 KB - medinform_v14i1e78216_app6.pdf]

References

1. Facts and statistics. Houston Methodist. URL: https://www.houstonmethodist.org/newsroom/facts-statistics/ [accessed 2026-01-07]
2. Lockwood C, Conroy-Hiller T, Page T. Vital signs. JBI Libr Syst Rev 2004;2(6):1-38. [doi: 10.11124/01938924-200402060-00001] [Medline: 27820007]
3. Yoder JC, Yuen TC, Churpek MM, Arora VM, Edelson DP. A prospective study of nighttime vital sign monitoring frequency and risk of clinical deterioration. JAMA Intern Med 2013 Sep 09;173(16):1554-1555 [FREE Full text] [doi: 10.1001/jamainternmed.2013.7791] [Medline: 23817602]
4. Orlov NM, Arora VM. Things we do for no reason™: routine overnight vital sign checks. J Hosp Med 2020 May;15(5):272-274 [FREE Full text] [doi: 10.12788/jhm.3442] [Medline: 32379025]
5. Mann DL. Q4 vital signs: can machine learning protect patients from the machinery of modern medicine? JACC Basic Transl Sci 2019 Jun;4(3):468-469 [FREE Full text] [doi: 10.1016/j.jacbts.2019.05.002] [Medline: 31312769]
6. Weenk M, Bredie SJ, Koeneman M, Hesselink G, van Goor H, van de Belt TH. Continuous monitoring of vital signs in the general ward using wearable devices: randomized controlled trial. J Med Internet Res 2020 Jun 10;22(6):e15471 [FREE Full text] [doi: 10.2196/15471] [Medline: 32519972]
7. Ludikhuize J, Smorenburg SM, de Rooij SE, de Jonge E. Identification of deteriorating patients on general wards; measurement of vital parameters and potential effectiveness of the Modified Early Warning Score. J Crit Care 2012 Aug;27(4):424.e7-424.13. [doi: 10.1016/j.jcrc.2012.01.003] [Medline: 22341727]
8. Al-Moteri M, Plummer V, Cooper S, Symmons M. Clinical deterioration of ward patients in the presence of antecedents: a systematic review and narrative synthesis. Aust Crit Care 2019 Sep;32(5):411-420. [doi: 10.1016/j.aucc.2018.06.004] [Medline: 30025983]
9. Schein RM, Hazday N, Pena M, Ruben BH, Sprung CL. Clinical antecedents to in-hospital cardiopulmonary arrest. Chest 1990 Dec;98(6):1388-1392. [doi: 10.1378/chest.98.6.1388] [Medline: 2245680]
10. Churpek MM, Yuen TC, Edelson DP. Risk stratification of hospitalized patients on the wards. Chest 2013 Jun;143(6):1758-1765 [FREE Full text] [doi: 10.1378/chest.12-1605] [Medline: 23732586]

XSL•FO
RenderX

11. Barfod C, Lauritzen MM, Danker JK, Sölétormos G, Forberg JL, Berlac PA, et al. Abnormal vital signs are strong predictors for intensive care unit admission and in-hospital mortality in adults triaged in the emergency department - a prospective cohort study. Scand J Trauma Resusc Emerg Med 2012 Apr 10;20:28 [FREE Full text] [doi: 10.1186/1757-7241-20-28] [Medline: 22490208]
12. Schmid A, Hoffman L, Happ MB, Wolf GA, DeVita M. Failure to rescue: a literature review. J Nurs Adm 2007 Apr;37(4):188-198. [doi: 10.1097/01.NNA.0000266838.23814.65] [Medline: 17415106]
13. Mok WQ, Wang W, Liaw SY. Vital signs monitoring to detect patient deterioration: an integrative literature review. Int J Nurs Pract 2015 May;21 Suppl 2:91-98. [doi: 10.1111/ijn.12329] [Medline: 26125576]
14. Churpek MM, Adhikari R, Edelson DP. The value of vital sign trends for detecting clinical deterioration on the wards. Resuscitation 2016 May;102:1-5 [FREE Full text] [doi: 10.1016/j.resuscitation.2016.02.005] [Medline: 26898412]
15. Dhala A, Fusaro MV, Uddin F, Tuazon D, Klahn S, Schwartz R, et al. Integrating a virtual ICU with cardiac and cardiovascular ICUs: managing the needs of a complex and high-acuity specialty ICU cohort. Methodist Debakey Cardiovasc J 2023 Aug 01;19(4):4-16 [FREE Full text] [doi: 10.14797/mdcvj.1247] [Medline: 37547898]
16. Dhala A, Sasangohar F, Kash B, Ahmadi N, Masud F. Rapid implementation and innovative applications of a virtual intensive care unit during the COVID-19 pandemic: case study. J Med Internet Res 2020 Sep 03;22(9):e20143 [FREE Full text] [doi: 10.2196/20143] [Medline: 32795997]
17. Weller GB, Mault J, Ventura ME, Adams J, Campbell FJ, Tremper KK. A retrospective observational study of continuous wireless vital sign monitoring via a medical grade wearable device on hospitalized floor patients. J Clin Med 2024 Aug 13;13(16):4747 [FREE Full text] [doi: 10.3390/jcm13164747] [Medline: 39200889]
18. Perrin Franck C, Babington-Ashaye A, Dietrich D, Bediang G, Veltsos P, Gupta PP, et al. iCHECK-DH: guidelines and checklist for the reporting on digital health implementations. J Med Internet Res 2023 May 10;25:e46694 [FREE Full text] [doi: 10.2196/46694] [Medline: 37163336]
19. Cretikos MA, Bellomo R, Hillman K, Chen J, Finfer S, Flabouris A. Respiratory rate: the neglected vital sign. Med J Aust 2008 Jun 02;188(11):657-659. [doi: 10.5694/j.1326-5377.2008.tb01825.x] [Medline: 18513176]
20. Rasooly IR, Makeneni S, Khan AN, Luo B, Muthu N, Bonafide CP. The alarm burden of excess continuous pulse oximetry monitoring among patients with bronchiolitis. J Hosp Med 2021 Dec;16(12):727-729 [FREE Full text] [doi: 10.12788/jhm.3731] [Medline: 34798003]
21. Powell BJ, Waltz TJ, Chinman MJ, Damschroder LJ, Smith JL, Matthieu MM, et al. A refined compilation of implementation strategies: results from the Expert Recommendations for Implementing Change (ERIC) project. Implement Sci 2015 Feb 12;10:21 [FREE Full text] [doi: 10.1186/s13012-015-0209-1] [Medline: 25889199]
22. Damschroder LJ, Aron DC, Keith RE, Kirsh SR, Alexander JA, Lowery JC. Fostering implementation of health services research findings into practice: a consolidated framework for advancing implementation science. Implement Sci 2009 Aug 07;4:50 [FREE Full text] [doi: 10.1186/1748-5908-4-50] [Medline: 19664226]
23. Proctor E, Silmere H, Raghavan R, Hovmand P, Aarons G, Bunger A, et al. Outcomes for implementation research: conceptual distinctions, measurement challenges, and research agenda. Adm Policy Ment Health 2011 Mar 19;38(2):65-76 [FREE Full text] [doi: 10.1007/s10488-010-0319-7] [Medline: 20957426]
24. Narcisse V, Ishaq F, Gomez M, Homer S, Griffin L, Pletcher S, et al. Implementation of remote patient monitoring and earlier CERT activation: effects on ICU transfer and mortality. J Clin Med 2025 Oct 21;14(20):7434 [FREE Full text] [doi: 10.3390/jcm14207434] [Medline: 41156302]

Abbreviations

CVSM: continuous vital sign monitoring
FDA: Food and Drug Administration
HM: Houston Methodist
HR: heart rate
ICU: intensive care unit
LTAC: long-term acute care
PCA: patient care assistant
RPM: remote patient monitoring
RR: respiratory rate
SpO2: oxygen saturation
VICU: virtual intensive care unit
VOC: virtual operations center
VS: vital sign

XSL•FO
RenderX

Edited by C Perrin; submitted 29.May.2025; peer-reviewed by P Helmer, M Haveman; comments to author 19.Aug.2025; revised version received 04.Dec.2025; accepted 03.Jan.2026; published 26.Jan.2026.

Please cite as:
Nguyen NA, Lee G, Holderread B, Holman T, Pletcher S, Schwartz R
Scaling Wireless Continuous Vital Sign Monitoring Across an 8-Hospital Health System: Digital Health Implementation Report
JMIR Med Inform 2026;14:e78216
URL: https://medinform.jmir.org/2026/1/e78216
doi:10.2196/78216
PMID:41482965

©Ngoc-Anh Nguyen, Grace Lee, Brendan Holderread, Terrie Holman, Sarah Pletcher, Roberta Schwartz. Originally published in JMIR Medical Informatics (https://medinform.jmir.org), 26.Jan.2026. This is an open-access article distributed under the terms of the Creative Commons Attribution License (https://creativecommons.org/licenses/by/4.0/), which permits unrestricted use, distribution, and reproduction in any medium, provided the original work, first published in JMIR Medical Informatics, is properly cited. The complete bibliographic information, a link to the original publication on https://medinform.jmir.org/, as well as this copyright and license information must be included.

XSL•FO
RenderX

Rectal Cancer Radiotherapy Response Prediction: Retrospective Study of Development of a Deep Learning–Based Radiomics Model

Yiqun Li[1*], MS; Hengchang Liu[2*], PhD; Qiang Wei[1], MS; Zhenqi Wang[1], MS; Zhen Hu[1], MS

[1]Department of Colorectal and Anal Surgery, Shanxi Provincial People's Hospital, No. 29 Shuangtasi Street, Taiyuan, China

[2]Department of Colorectal Surgery, National Cancer Center/National Clinical Research Center of Cancer/Cancer Hospital, Chinese Academy of Medical Sciences and Peking Union Medical College, Beijing, China

[*]these authors contributed equally

Corresponding Author:
Zhen Hu, MS
Department of Colorectal and Anal Surgery, Shanxi Provincial People's Hospital, No. 29 Shuangtasi Street, Taiyuan, China

Abstract

Background: Radiotherapy (RT) is a cornerstone of multimodal treatment for rectal cancer (RC); yet, substantial interindividual variability in treatment response persists. Deep learning (DL)–based radiomics offers potential for pre-RT response prediction to support personalized decision-making. **Objective:** This study aimed to develop and compare multiple DL radiomics models for predicting RT response in RC, with emphasis on the performance and clinical utility of Transformer architectures. **Methods:** In this single-center retrospective study, 2000 pathologically confirmed patients with RC who received standard RT were included. Pretreatment computed tomographic and dynamic contrast-enhanced magnetic resonance images and clinical variables were collected. Treatment response was categorized according to RECIST (Response Evaluation Criteria in Solid Tumors) version 1.1 as good (complete or partial response) or poor (stable or progressive disease). The primary analysis used magnetic resonance imaging (MRI)–only input; computed tomography (CT) was used for registration and quality control and evaluated in a late-fusion CT + MRI sensitivity analysis. Data were randomly split into training, validation, and test sets (8:1:1), with 5-fold cross-validation within the training set. Test set tumor masks were manually delineated, whereas a U-Net assisted segmentation was performed only within training to prevent data leakage. Convolutional neural network, graph convolutional network, and Transformer classifiers were compared. Class imbalance (approximately 65% vs 35%) was addressed using class weighting. Performance was evaluated using area under the receiver operating characteristic curve (AUROC) and accuracy with 95% CIs obtained by bootstrapping. AUROC differences were assessed using the DeLong test. Clinical usefulness was evaluated using decision curve analysis. Segmentation performance was quantified by Dice coefficient and intersection over union. Model interpretability was assessed using Gradient-Weighted Class Activation Mapping. **Results:** In the MRI-only primary analysis, the Transformer achieved the best performance on the independent test set, with accuracy of 87.0% (95% CI 84.2%-89.5%) and AUROC of 0.921 (95% CI 0.901-0.945), significantly outperforming the convolutional neural network (AUROC 0.881; *P*=.02) and graph convolutional network (AUROC 0.894; *P*=.041). Sensitivity and specificity were 89.2% and 82.9%, respectively. Decision curve analysis demonstrated higher net benefit across threshold probabilities of 0.3-0.7. U-Net segmentation achieved a mean Dice coefficient of 0.892 and intersection over union of 0.814. In sensitivity analysis, CT + MRI late fusion yielded a comparable AUROC to MRI only (0.926 vs 0.921; *P*=.36), with modest incremental net benefit at higher thresholds. **Conclusions:** In this large pre-RT imaging cohort, an MRI-driven Transformer-based DL radiomics model outperformed conventional architectures in predicting RT response in RC and demonstrated superior clinical net benefit. Late fusion of CT and MRI did not significantly improve overall discrimination but may provide incremental benefit in specific decision contexts. Multicenter external validation is warranted.

(JMIR Med Inform 2026;14:e77313) doi:10.2196/77313

KEYWORDS

deep learning; radiomics; rectal cancer; radiotherapy; Transformer model

Introduction

Rectal cancer (RC) remains one of the leading causes of cancer-related incidence and mortality worldwide, with a particularly notable rise among middle-aged and older adult populations. Radiotherapy (RT) is a cornerstone of RC management; however, its therapeutic efficacy varies substantially among patients [1]. Current clinical indicators and conventional imaging approaches show limited ability to accurately predict individual responses to RT [2], often failing

XSL•FO
RenderX

to identify patients who are truly radiosensitive [3,4]. This variability poses a significant challenge in optimizing treatment strategies [2]. Consequently, there is a pressing need for robust predictive tools to guide personalized treatment and improve clinical outcomes.

The advent of radiomics has introduced the ability to extract high-dimensional quantitative features from medical images, uncovering latent biological information and offering novel insights into tumor behavior and treatment response. Unlike traditional imaging techniques, radiomics enables noninvasive prediction of therapeutic efficacy using imaging-derived biomarkers [5,6]. Nevertheless, conventional machine learning models often struggle to manage the complexity of radiomics data, particularly their high dimensionality and inherent nonlinearity [7,8]. This has led to a growing interest in the application of advanced deep learning (DL) algorithms, which offer superior capacity for feature representation and pattern recognition, to enhance the predictive power of radiomics analyses [9].

DL, particularly convolutional neural networks (CNNs), has achieved substantial advances in medical image analysis in recent years [10,11]. These models can automatically extract hierarchical features from imaging data and effectively recognize and classify complex patterns [12]. Compared with traditional approaches, DL offers notable advantages in handling high-dimensional data and performing intricate pattern recognition, making it especially well suited for analyzing radiomics data [13,14]. However, most existing studies have applied single DL algorithms in isolation, with few providing a systematic comparison of multiple models, particularly in the context of predicting RT response in patients with RC [15].

In recent years, the application of artificial intelligence (AI) in RT, cancer diagnosis, and clinical decision support has shifted from research exploration toward clinical deployment. Within the RT workflow, AI has been increasingly implemented in key steps such as organ autosegmentation, target delineation, (semi-)automated treatment planning, dose optimization, and image registration, yielding measurable time savings and improved plan consistency [16]. In the domain of cancer diagnosis, the integration of DL and radiomics has achieved substantial progress in RC lesion segmentation and feature quantification on magnetic resonance imaging (MRI). Such models can automatically localize tumor regions and characterize morphological and textural features of lesions, thereby facilitating earlier and more consistent assessment and diagnosis; this has been substantiated by both systematic reviews of RC lesion segmentation and specific studies on post–neoadjuvant chemoradiotherapy (nCRT) T2-weighted (T2W) MRI segmentation [17]. Moreover, AI models that integrate multimodal data have demonstrated practical value for personalized treatment strategies and risk prediction in clinical decision-making. For RC, a multicenter study showed that late-fusion models combining multiparametric MRI–derived DL or radiomics features with clinical variables outperformed unimodal approaches in predicting early recurrence risk and provided greater clinical net benefit as assessed by decision curve analysis (DCA) [18]. Against this background, this study integrates DL with radiomics to construct a predictive model aimed at accurately assessing the RT response in RC patients, thereby providing intelligent support for treatment optimization.

We systematically compared multiple state-of-the-art DL architectures, including CNNs, graph convolutional networks (GCNs), and Transformer models, for their ability to analyze and process radiomics imaging data in patients with RC. The Transformer architecture, in particular, exhibited superior capability in modeling complex image features through its self-attention mechanism, allowing it to effectively identify key regions relevant to RT response. By comparing these models in terms of feature extraction and predictive performance, this study investigated the potential of the Transformer model in predicting RT response in RC and evaluated its feasibility for clinical application. Unlike traditional applications of AI in tumor detection or initial diagnosis, this study focused on patients with pathologically confirmed RC. Our objective was to predict their responsiveness to RT based on pretreatment imaging, thereby enabling individualized treatment planning and minimizing unnecessary exposure to RT-related risks.

The key innovation of this study lay in the systematic application and comparison of multiple DL algorithms to enhance the accuracy of RT response prediction, with a particular emphasis on exploring the strengths of the Transformer model. By combining DL techniques with radiomics, we aimed to advance current predictive methodologies and develop a more precise model for RT response assessment. This work provides clinicians with a robust, data-driven tool to support personalized therapeutic strategies, ultimately contributing to the broader goal of precision medicine in oncology.

Methods

Ethical Considerations

This study was conducted in strict accordance with ethical standards. The use of imaging and clinical data was approved by the Medical Ethics Committee of Shanxi Provincial People's Hospital. As this was a retrospective analysis, all data were obtained from routine clinical records and were fully deidentified prior to analysis. The ethics committee confirmed that additional informed consent was not required. All data were anonymized before processing, and no identifiable patient images or information was included in the manuscript or supplementary materials. Data were stored on encrypted servers with access restricted to authorized investigators. Since this study did not involve prospective data collection or patient intervention, no monetary or nonmonetary compensation was provided to participants. For any future studies involving identifiable images, written informed consent will be obtained, and the relevant materials will be submitted with the manuscript.

Data Collection

This retrospective study included 2000 patients with RC who were treated at Shanxi Provincial People's Hospital between January 2015 and December 2023. All patients underwent standard RT and had complete paired pretreatment computed tomography (CT) and MRI data, along with follow-up assessments of RT response.

XSL•FO
RenderX

Inclusion criteria were (1) pathologically confirmed RC, (2) receipt of standard RT, (3) availability of complete pretreatment CT and dynamic contrast–enhanced MRI (DCE-MRI) data, and (4) documented RT outcomes with follow-up records. Exclusion criteria were (1) incomplete or poor-quality imaging data, (2) missing essential clinical information or outcome labels, (3) coexisting malignancies or severe systemic diseases, and (4) patients who did not receive standard RT protocols. Treatment regimens followed the Chinese Society of Clinical Oncology guidelines for RC and primarily consisted of long-course RT (50.4 Gy in 28 fractions). Some patients also received concurrent chemotherapy and subsequent surgical intervention, depending on clinical conditions.

To ensure transparency in patient selection, a CONSORT (Consolidated Standards of Reporting Trials)-style flowchart is provided in Figure S1 in Multimedia Appendix 1, detailing the inclusion process, exclusion criteria, final sample size, and classification of patients into RT-sensitive and RT-insensitive groups.

All imaging data were acquired from routine clinical scanning systems at a single institution (Shanxi Provincial People's Hospital), encompassing MRI and CT examinations performed across different years. Detailed information regarding scanner models and acquisition parameters is provided in Table S1 in Multimedia Appendix 2.

Data Preprocessing

Following data collection, the imaging data were preprocessed to ensure quality and consistency. The preprocessing steps included denoising, cropping, normalization, and resolution adjustment. All images were normalized to a range between 0 and 1 and resized to a resolution of 512×512 pixels. To enhance the model's generalization ability, data augmentation techniques such as rotation, flipping, and scaling were applied to generate more diverse training samples and effectively expand the dataset. In addition, clinical data were standardized to harmonize feature values with different units and ranges, ensuring compatibility with model input requirements. The complete data collection and preprocessing workflow is illustrated in Figure S1 in Multimedia Appendix 3.

To prevent data leakage, the statistical parameters required for image normalization (mean and SD) were computed exclusively from the training set and kept fixed for both the validation and test sets. The test set was not involved in estimating normalization parameters at any stage, thereby ensuring independence and rigor in both preprocessing and model evaluation.

All DL models used in this study were trained and inferred on 2D slices; thus, the input features were derived solely from spatial texture information within single images, without relying on voxel-level 3D volume information. During preprocessing, we did not perform volumetric resampling along the *z*-axis to reconcile slice thickness differences (3 mm vs 4 mm), in order to avoid interpolation-induced artifacts that could distort 2D texture features. Because model training and prediction were conducted at the single-slice level, and all patients' images were acquired using consistent scanning sequences and acquisition protocols, variations in slice thickness were expected to have limited impact on grayscale distribution or spatial structure of the input features. Nevertheless, we discuss the potential biases associated with differing slice thicknesses in the "Limitations" section, and we plan to explore full 3D volume resampling and the integration of 3D models in future work to further improve model robustness in cross-device settings.

Data Annotation and Quality Control

To ensure high-quality data for model training, strict annotation and quality control procedures were applied to all imaging data and RT response labels. For the imaging side, radiologists manually delineated tumor regions, with particular attention paid to tumor boundaries and clinically relevant areas. Semiautomated annotation tools were used to assist in the delineation process. All annotations were independently reviewed by 2 associate chief radiologists (ZW and ZH), each with more than 10 years of experience. All delineation results were further validated through random sampling to ensure the consistency and accuracy of boundary recognition.

RT response labels were assigned based on posttreatment MRI evaluations and classified according to the RECIST (Response Evaluation Criteria in Solid Tumors) version 1.1. Patients who achieved a complete response (CR) or a partial response (PR) were categorized as the "good response (GR) group," while those with stable disease or progressive disease were categorized as the "poor response group." All imaging evaluations were performed in a blinded manner, with evaluators unaware of treatment plans and clinical outcomes. Two independent reviewers (ZW and ZH) assessed the follow-up MRIs, and interobserver agreement was assessed using the Cohen κ coefficient, which reached 0.83, indicating good consistency. Final response classifications were determined through consensus and used as ground-truth labels for supervised model training.

In particular, all tumor masks in the test set were manually annotated by experts without reference to any DL model outputs, thereby avoiding error propagation and ensuring the independence and rigor of model evaluation. The U-Net model was used exclusively on the training set to generate tumor masks as auxiliary inputs for the classification models. Its outputs were not used in any segmentation or feature extraction tasks for the test set, minimizing the risk of information leakage.

DL Model Construction and Training

For the patient-level response prediction task, the model first performs independent inference on each 2D slice, producing a probability score indicating the likelihood of belonging to the "GR" category. Subsequently, the predicted probabilities of all slices from the same patient are averaged arithmetically to obtain an aggregated patient-level probability, and a threshold of 0.5 is applied to generate the final patient-level classification label. This aggregation strategy helps smooth slice-to-slice fluctuations caused by differences in imaging position, preventing any single atypical slice from disproportionately influencing the overall judgment. As a result, the stability and robustness of patient-level predictions are enhanced. This study used multiple DL algorithms to process radiomics imaging data and predict

XSL•FO
RenderX

patient responses to RT (Figure S1 in Multimedia Appendix 4). The models compared included CNNs, GCNs, and Transformer models. All models were trained and tested on the same dataset to ensure comparability.

The Transformer model served as the primary focus due to its self-attention mechanism, which enabled the capture of complex global features and provided unique advantages in tumor region recognition. In this model, input images were divided into 16×16 patches and processed with 8 multihead attention heads and 12 Transformer encoder layers. Standard sinusoidal positional encoding was incorporated to preserve spatial structure information. The model was trained using the Adam optimizer, with an initial learning rate of 1e-4 and a cosine annealing strategy for dynamic learning rate adjustment. Training was conducted over 100 epochs, with early stopping applied if validation loss did not decrease for 10 consecutive epochs.

As the comparative baseline, the CNN used a residual networks (ResNet-34) architecture, consisting of 34 residual convolutional layers organized into 4 residual stages with channel dimensions of 64, 128, 256, and 512, respectively. Feature extraction was performed on 2D patches of the input images. The output of the final global average pooling layer was fed into a 2-layer fully connected classification head (hidden layer size=256, activation function=ReLU) to generate predictions of RT response.

The GCN module adopted a 3-layer GCNConv structure, where nodes represented embedded features of image patches or regions of interest (ROIs). The adjacency matrix was constructed based on spatial proximity using a k-nearest neighbors approach (k=8). Each layer used a ReLU activation function, and dropout (P=.30) was applied between layers to mitigate overfitting. The aggregated node features after global pooling were passed to a classification layer. All models were trained under identical conditions, using the same loss function (weighted cross-entropy), optimizer (Adam, learning rate=1×10^{-4}), and training strategy (cosine annealing schedule with early stopping) to ensure a fair performance comparison. Hyperparameter tuning and L2 regularization were applied throughout training to reduce overfitting risks. The final model was independently evaluated on the test set and compared against other networks, with particular emphasis on its performance in feature extraction and classification accuracy.

Given the class imbalance in RT response labels (approximately 65% of patients in the GR group and 35% in the poor response group), a class weighting strategy was introduced during training. Specifically, inverse-frequency weights based on sample distribution were applied in the loss function to enhance the model's sensitivity to the minority class (poor response patients). This approach effectively mitigated the prediction bias caused by unequal class distribution and yielded higher sensitivity and overall stability in the validation set.

In the final implementation of this study, the Transformer architecture was used solely as an image-level classifier. The network consisted of multiple encoder layers and a classification head, without any decoder branch or explicit segmentation output (eg, a "Seg Head"). The tumor segmentation task was performed entirely by an independent U-Net model, and the 2 models operated independently throughout the training and evaluation processes.

Dataset Splitting and Cross-Validation

To evaluate the generalization ability of the models, the dataset was divided into training, validation, and test sets in a ratio of 8:1:1. Random sampling was used to ensure the representativeness of each subset. The 8:1:1 split was chosen based on the sufficiently large sample size (2000 patients), which supported the high-dimensional feature extraction needs of DL models. A larger training set enabled the model to better learn complex nonlinear patterns, while 200 patients each were retained for independent validation and testing. To further improve model stability and generalizability, 5-fold cross-validation was applied during training, with k set to 5. Stratified sampling was used to preserve consistent class distributions across all folds. All models were trained and evaluated on the same data splits, and the average performance metrics across the 5 folds were reported as the final results. This approach ensured robust evaluation, minimized bias, and enhanced the reproducibility of model performance across different subsets.

To evaluate model generalizability, the dataset was divided into training, validation, and testing subsets in an 8:1:1 ratio. All partitions were performed at the patient level, ensuring that all images, slices, and augmented samples from the same patient were assigned exclusively to a single subset to prevent information leakage. Stratified random sampling was applied to maintain consistent class distribution across subsets. To further enhance model robustness and generalization performance, 5-fold cross-validation (k=5) was conducted within the training cohort, also based on patient-level partitioning. This approach ensured the independence of the validation data and the reproducibility of the experimental results.

To avoid data leakage, data augmentation in this study was applied exclusively to the training set, while no augmentation was performed on the validation or test sets. All augmented samples were strictly linked to their original patients and existed only within the training subset, ensuring that none entered the independent test set. Consequently, each test-set patient corresponded to exactly 1 nonaugmented imaging input during inference, which explains why the total count in the confusion matrix matches the original number of patients (n=200).

Model Evaluation and Performance Analysis

Model performance was evaluated using multiple classification metrics, including accuracy, sensitivity, specificity, receiver operating characteristic (ROC) curves, area under the curve (AUC) values, and confusion matrices, to comprehensively assess the predictive accuracy of RT response in RC. Ninety-five percent CIs were calculated for all metrics to strengthen the robustness and interpretability of results.

To statistically compare model performances and verify the relative advantage of the Transformer model, pairwise bootstrap resampling (10,000 iterations) and DeLong's test were performed for AUC comparisons, with P values reported. ROC curves and their confidence intervals were used to visually and

XSL•FO
RenderX

quantitatively compare the classification performance of different models.

Calibration was evaluated on the independent test set by plotting a calibration curve (reliability diagram) using 10 equal-frequency bins (deciles). For each bin, we reported the mean predicted probability and the observed event rate. Overall calibration was quantified with the Brier score (the mean squared error between predicted probabilities and true labels). All calibration analyses were performed once on the test set without any retraining or post hoc recalibration to avoid information leakage. To ensure fairness, the bin boundaries and the evaluation pipeline were kept identical across input settings (MRI-only vs CT + MRI).

During evaluation, particular emphasis was given to evaluating the Transformer model's performance under varying segmentation input conditions. Its prediction results were further analyzed through Gradient-Weighted Class Activation Mapping (Grad-CAM) visualization to interpret attention regions and their clinical relevance. Tumor segmentation performance using the U-Net model was evaluated on the independent test set, with the Dice Similarity Coefficient (DSC) and the Intersection over Union (IoU) used as primary metrics. Manually delineated tumor regions, confirmed by 2 experienced radiologists, served as the gold standard. Failure cases were manually analyzed to identify potential factors contributing to segmentation inaccuracies, such as blurred tumor boundaries, low tissue contrast, or irregular tumor morphology. Detailed segmentation outcomes are shown in the "Results" section, and representative case images are provided in multimedia appendices.

Image Data Analysis Method

The image data analysis pipeline in this study consisted of 2 independent stages: tumor segmentation and image-level classification. First, a U-Net segmentation network was used to delineate tumor regions on the raw MRI or CT images, generating binary masks (Figure S1 in Multimedia Appendix 5). This segmentation model served solely to provide ROIs and did not participate in subsequent classification learning. Next, image patches or ROI features extracted from the masked tumor regions were fed into 3 types of classification models, CNNs, GCNs, and a Transformer classifier (Figure S1 in Multimedia Appendix 6), to predict patients' RT response.

It is important to emphasize that the Transformer model used in this study was a pure classification architecture composed only of an encoder and a multilayer perceptron classification head. It did not include any decoder structure, upsampling pathway, or segmentation outputs. Accordingly, it was entirely independent of the U-Net segmentation model used to generate masks; the 2 models shared no parameters and had no information exchange during training or inference. The GCN was used to model spatial relationships within the tumor region, further enhancing classification performance. The overall model evaluation and performance analysis workflow is shown in Figure S1 in Multimedia Appendix 7.

Input Modalities and Multimodal Fusion Strategy

In the primary analysis, the classifier used MRI-only inputs—pre-RT DCE-MRI and T2W sequences—and extracted features or patches or embeddings strictly within expert-annotated tumor masks, thereby minimizing bias from cross-modal acquisition heterogeneity and registration error. CT was used solely for quality control and, when necessary, rigid registration and was not provided to the classifier. Per reviewer request, we additionally implemented late fusion of CT + MRI under the same data split, loss function, class weighting, and hyperparameter settings as the primary analysis. Specifically, patient-level representations were extracted from CT and MRI with identical backbone encoders; after feature alignment and normalization, the representations were concatenated immediately before the classification head and trained or evaluated jointly (all other procedures unchanged). To ensure a fair comparison, the independent test set was kept fixed (n=200; good responders, n=130 and poor responders, n=70); only the input modality configuration was varied.

Statistical Analysis

This study applied various DL techniques to analyze radiomics imaging data from patients with RC. Initially, CNNs were used to extract features from the image data, capturing fine-grained details of tumor tissues. During image segmentation, deep segmentation networks such as U-Net and Mask R-CNN were used to identify and annotate tumor regions, ensuring accurate localization of key lesions. The self-attention mechanism of the Transformer model was used to manage complex spatial relationships, thereby improving the model's pattern recognition capabilities. GCNs were also applied to extract global and local spatial features from the images, effectively modeling both tumor and peritumoral tissue characteristics. By integrating multiple DL models, the study aimed to achieve accurate predictions of RT response and support personalized treatment recommendations.

During model evaluation, various statistical methods were used to comprehensively assess predictive performance. Metrics, including sensitivity, specificity, precision, and recall, were calculated to evaluate classification outcomes across different categories. Confusion matrices were plotted to visualize model performance in distinguishing between positive and negative RT responses. To assess predictive ability across varying thresholds, ROC curves and AUC values were generated for each model. These statistical analyses facilitated a detailed comparison of the strengths and limitations of each DL approach in predicting RT response in patients with RC.

Results

Dataset Sample Distribution Balance and Generalization Ability

In this study, radiomic imaging data from 2000 patients with RC were collected and randomly divided into training (1600 cases), validation (200 cases), and test (200 cases) sets using an 8:1:1 ratio. Approximately 65% (1300/2000) of patients exhibited a favorable response to RT and were classified as the "sensitive" group, while the remaining 35% (700/2000) were categorized as "nonsensitive." As shown in Table 1, we further compared baseline demographic and clinical characteristics—including age, sex, T stage, N stage, tumor

XSL•FO
RenderX

location, and carcinoembryonic antigen levels—between the training and test sets. None of the variables showed statistically significant differences (P>.05). These results indicate that the random partitioning of the dataset was unbiased and that the training and test sets were highly comparable. This balanced distribution provides a reliable foundation for model training and independent validation, thereby enhancing the generalizability and robustness of the proposed approach.

Table . Baseline demographic and clinical characteristics of patients in the training and testing cohorts[a].

Variable	Training cohort (N=1600)	Testing cohort (N=200)	*P* value
Age (years), mean (SD)	58.7 (10.9)	59.1 (11.2)	.62
Sex, n (%)			.53
Male	980 (61.3)	118 (59.0)	
Female	620 (38.7)	82 (41.0)	
T stage, n (%)			.78
T2	430 (26.9)	50 (25.0)	
T3	930 (58.1)	120 (60.0)	
T4	240 (15.0)	30 (15.0)	
N stage, n (%)			.67
N0	610 (38.1)	80 (40.0)	
N1	710 (44.4)	86 (43.0)	
N2	280 (17.5)	34 (17.0)	
Tumor location, n (%)			.79
Upper rectum	310 (19.4)	36 (18.0)	
Midrectum	860 (53.8)	112 (56.0)	
Lower rectum	430 (26.9)	52 (26.0)	
CEA[b] level (ng/mL), median (IQR)	3.6 (2.1-6.8)	3.8 (2.2-7.0)	.73
Response category, n (%)			>.99
Good response	1040 (65.0)	130 (65.0)	
Poor response	560 (35.0)	70 (35.0)	

[a]This table shows the baseline differences between the training and test sets in demographic characteristics (age and sex), tumor clinical staging (T stage and N stage), tumor location, and CEA level. Statistical comparisons were performed using independent-samples *t* tests, chi-square tests, or Mann-Whitney *U* tests, as appropriate. All *P* values were greater than .05, indicating no significant differences between the training and test sets. This demonstrates that the random allocation process was unbiased and that the cohorts were well matched and comparable.

[b]CEA: carcinoembryonic antigen.

High Accuracy of U-Net Model in Tumor Region Segmentation

In this study, a U-Net segmentation network was applied to automatically segment tumor regions in the imaging data of patients with RC. The results demonstrated excellent performance of the model in tumor recognition and segmentation tasks. On the independent test set, the U-Net model achieved a mean DSC of 0.892 (95% CI 0.881 - 0.904) and a mean IoU of 0.814 (95% CI 0.800 - 0.829), indicating high segmentation consistency and robustness. The model precisely delineated tumor boundaries and clearly separated tumor regions from surrounding structures. The original image is shown in Figure 1A, and the corresponding segmentation mask generated by the U-Net model is shown in Figure 1B.

XSL•FO
RenderX

Figure 1. Tumor region segmentation results. (**A**) Original image. The white arrow indicates the rectal tumor lesion. (**B**) Model segmentation result image (tumor region highlighted).

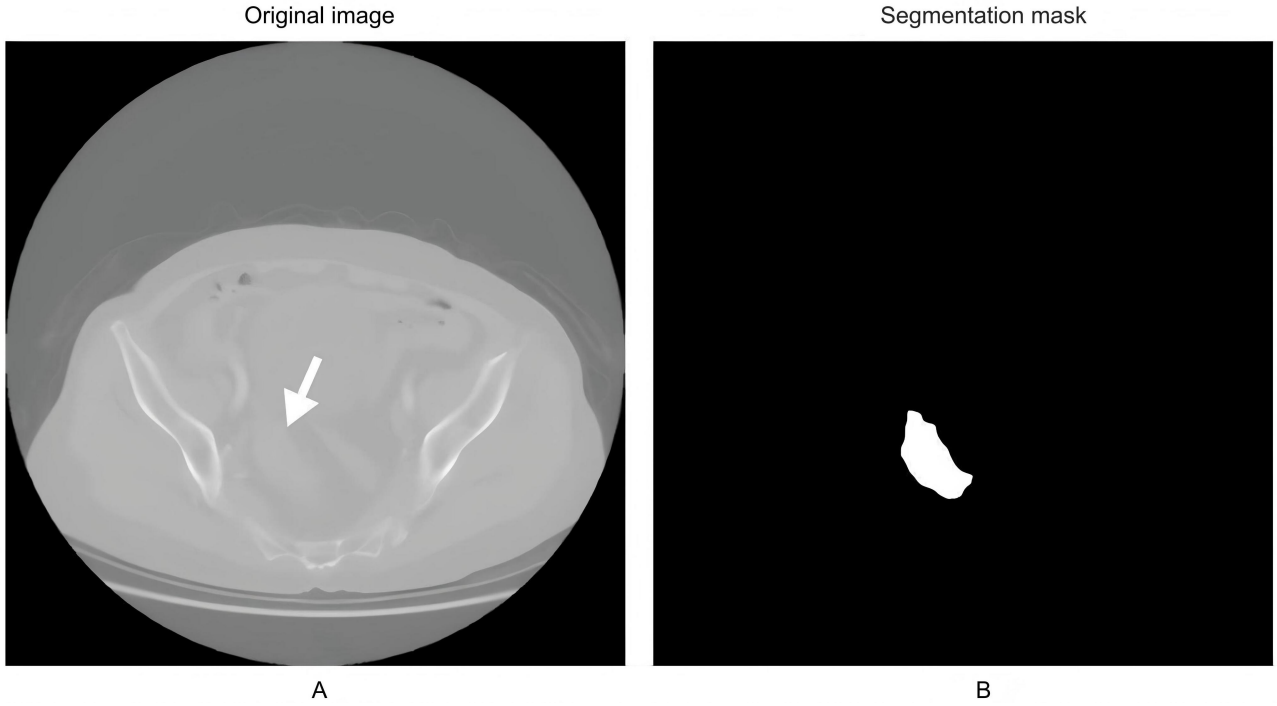

When compared with manually annotated gold-standard segmentations by expert radiologists, the model showed a high degree of agreement in both boundary definition and tumor morphology. Notably, the U-Net model maintained strong performance even when segmenting tumors with irregular shapes or blurred margins. However, a small number of inaccurate segmentations were observed, primarily in cases characterized by indistinct tumor margins, low contrast with adjacent tissues, or atypical tumor morphology. These challenging cases provide directions for future model optimization.

Outstanding Performance of the Transformer Model in Predicting RT Response

This study compared the performance of several DL models in predicting the RT response in patients with RC. The results showed that the Transformer model achieved the highest overall performance, with an accuracy of 87%. As illustrated in Figure 2A, the Transformer leveraged its self-attention mechanism to effectively process complex patterns and fine-grained features within the radiomics imaging data, offering a distinct advantage in capturing global contextual information. In comparison, the CNN (Figure 2D) and GCN (Figure 2E) models achieved accuracies of 82% and 84%, respectively, both lower than that of the Transformer model. Analysis of ROC curves (Figures 2A-2E) further highlighted the Transformer model's superior discriminative ability, as reflected by its AUC value of 0.921 (95% CI 0.901 - 0.945), which exceeded that of the CNN (Figure 2D) and GCN (Figure 2E).

XSL•FO
RenderX

Figure 2. ROC curve comparison of different models. (A) Transformer, (B) U-Net, (C) ResNet, (D) CNN, and (E) GCN. AUC: area under the curve; CNN: convolutional neural network; GCN: graph convolutional network; ROC: receiver operating characteristic.

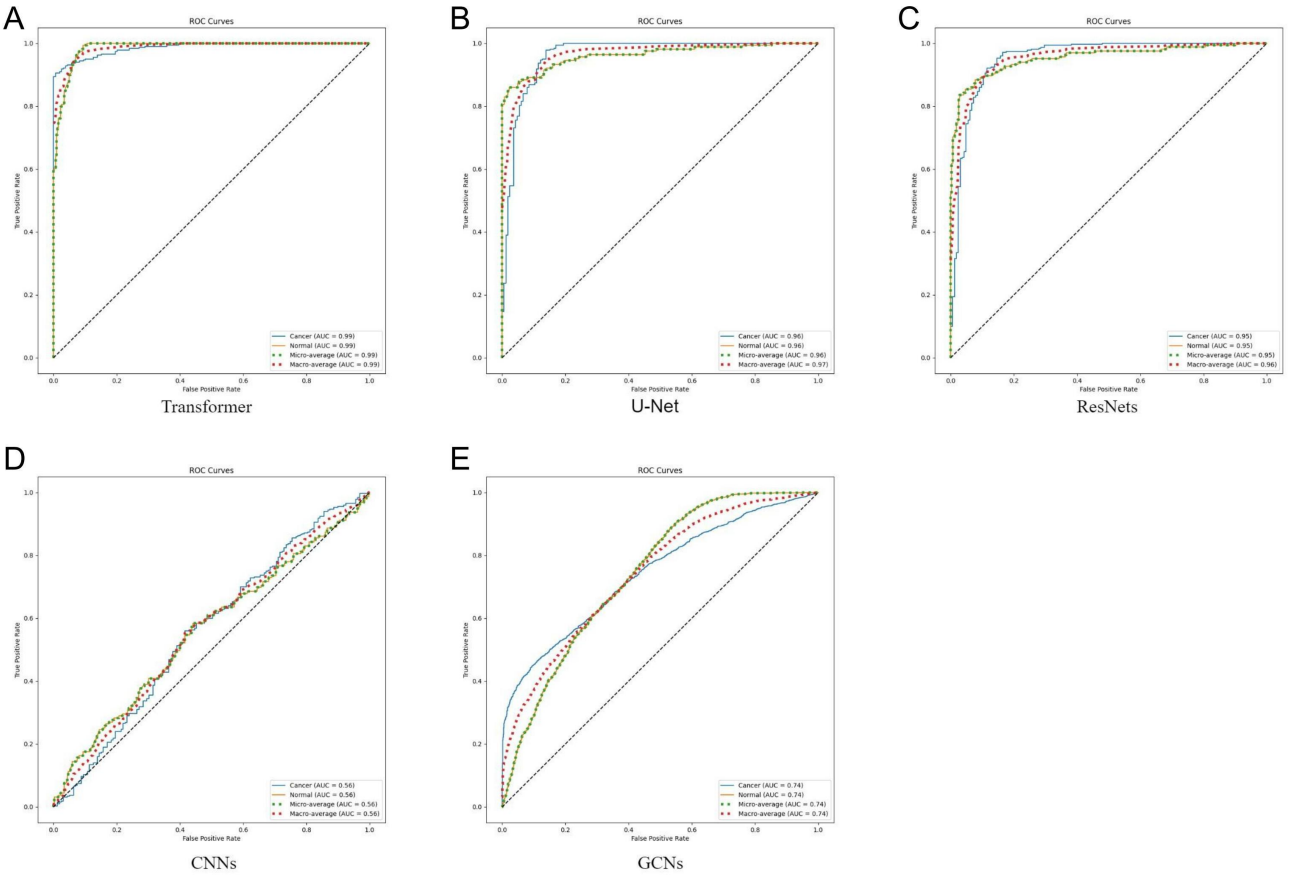

To enhance the robustness of the results, 95% CIs were calculated for all classification metrics across the models (Table 2). On the independent test set, the Transformer model achieved an accuracy of 87.0% (95% CI 84.2% - 89.5%), sensitivity of 89.2% (95% CI 85.3% - 92.4%), specificity of 82.9% (95% CI 79.2% - 88.1%), and an AUC of 0.921 (95% CI 0.901 - 0.945). In contrast, the CNN model reached an AUC of 0.881 (95% CI 0.854 - 0.906), while the GCN model achieved an AUC of 0.894 (95% CI 0.869 - 0.918).

Table . Performance comparison of deep learning models in predicting radiotherapy response[a].

Model	Accuracy	Sensitivity	Specificity	AUC[b]	*P* value vs Transformer
Transformer	87.0% (84.2%-89.5%)	89.2% (85.3%-92.4%)	82.9% (79.2%-88.1%)	0.921% (0.901%-0.945%)	—[c]
CNN[d]	82.0% (78.9%-85.0%)	83.7% (79.4%-87.6%)	80.2% (75.0%-84.6%)	0.881% (0.854%-0.906%)	.02
GCN[e]	84.0% (80.4%-87.2%)	85.9% (81.7%-89.7%)	82.1% (77.0%-86.4%)	0.894% (0.869%-0.918%)	.041

[a]This table compares the performance of 3 deep learning models (transformer, CNN, and GCN) in predicting radiotherapy response in rectal cancer using an independent test set. All metrics are reported as mean values with 95% CI. The primary evaluation metrics include accuracy, sensitivity, specificity, and the area under the curve (AUC). Differences in AUC were assessed using the DeLong test. The results demonstrate that the Transformer model outperformed both CNN and GCN models across all evaluation metrics, with the differences in AUC reaching statistical significance (P<.05).

[b]AUC: area under the curve.

[c]Not available.

[d]CNN: convolutional neural network.

[e]GCN: graph convolutional network.

To evaluate the statistical significance of AUC differences between the Transformer and other models, pairwise bootstrap resampling (10,000 iterations) and DeLong's test were conducted. The results showed that the Transformer model significantly outperformed both the CNN model (P=.02) and the GCN model (P=.041) in terms of AUC. These findings indicated that the Transformer model provided a statistically significant advantage in identifying imaging features associated with RT response.

XSL•FO
RenderX

Confusion Matrix Reveals the Classification Capability of the Transformer Model

To further assess classification performance, a confusion matrix was constructed to evaluate the Transformer model's predictive ability. As shown in Table 3, among the 200 patients in the test set, the model correctly identified 89% of RT-sensitive patients. The false-positive rate, representing RT-insensitive patients incorrectly classified as sensitive, was only 8%. These results further validated the model's effectiveness across both classes, particularly in correctly identifying RT-insensitive patients. The Transformer model significantly reduced misclassification errors, a critical factor in clinical decision-making. Accurate identification of RT-insensitive patients was essential for enabling timely adjustments to treatment plans, avoiding ineffective RT, and ultimately improving patient prognosis and survival outcomes. On the independent test set, the Transformer's calibration curve closely followed the ideal 45° line, with only mild overconfidence observed in the high–predicted-probability region. The corresponding Brier scores were identical for both input settings: MRI-only, 0.145; and CT + MRI (late fusion), 0.145. Overall calibration was therefore comparable between modalities. Taken together with the AUCs (0.921 vs 0.927) and the DCA results, adding CT did not yield a meaningful improvement in global performance, but it produced a slight and consistent gain in net benefit within higher decision-threshold ranges (Figure 3 and Table 4).

Table . Confusion matrix results for the Transformer model[a].

Category	Sensitive class (good response to radiotherapy)	Insensitive class (poor response to radiotherapy)
Predicted as sensitive class	116 (true positive)	12 (false positive)
Predicted as insensitive class	14 (false negative)	58 (true negative)

[a]This table shows the confusion matrix of the Transformer model on the independent test set (magnetic resonance imaging–only, n=200). True positives represent the number of patients correctly predicted as radiotherapy-sensitive (116 cases); false positives represent the number of patients incorrectly predicted as sensitive but actually nonsensitive (12 cases); false negatives represent the number of patients incorrectly predicted as nonsensitive but actually sensitive (14 cases); and true negatives represent the number of patients correctly predicted as radiotherapy nonsensitive (58 cases). Based on this matrix, the calculated performance metrics were as follows: accuracy=87.0%, sensitivity=89.2%, and specificity=82.9%.

XSL•FO
RenderX

Figure 3. Calibration of the Transformer classifier on the independent test set. Reliability curves of the Transformer classifier on the independent test set (n=200) using 10 equal-frequency bins. The dashed line indicates perfect calibration. Curves are shown for both MRI-only and CT + MRI input settings, with the corresponding AUC and Brier score reported within parentheses. AUC: area under the curve; CT: computed tomography; MRI: magnetic resonance imaging.

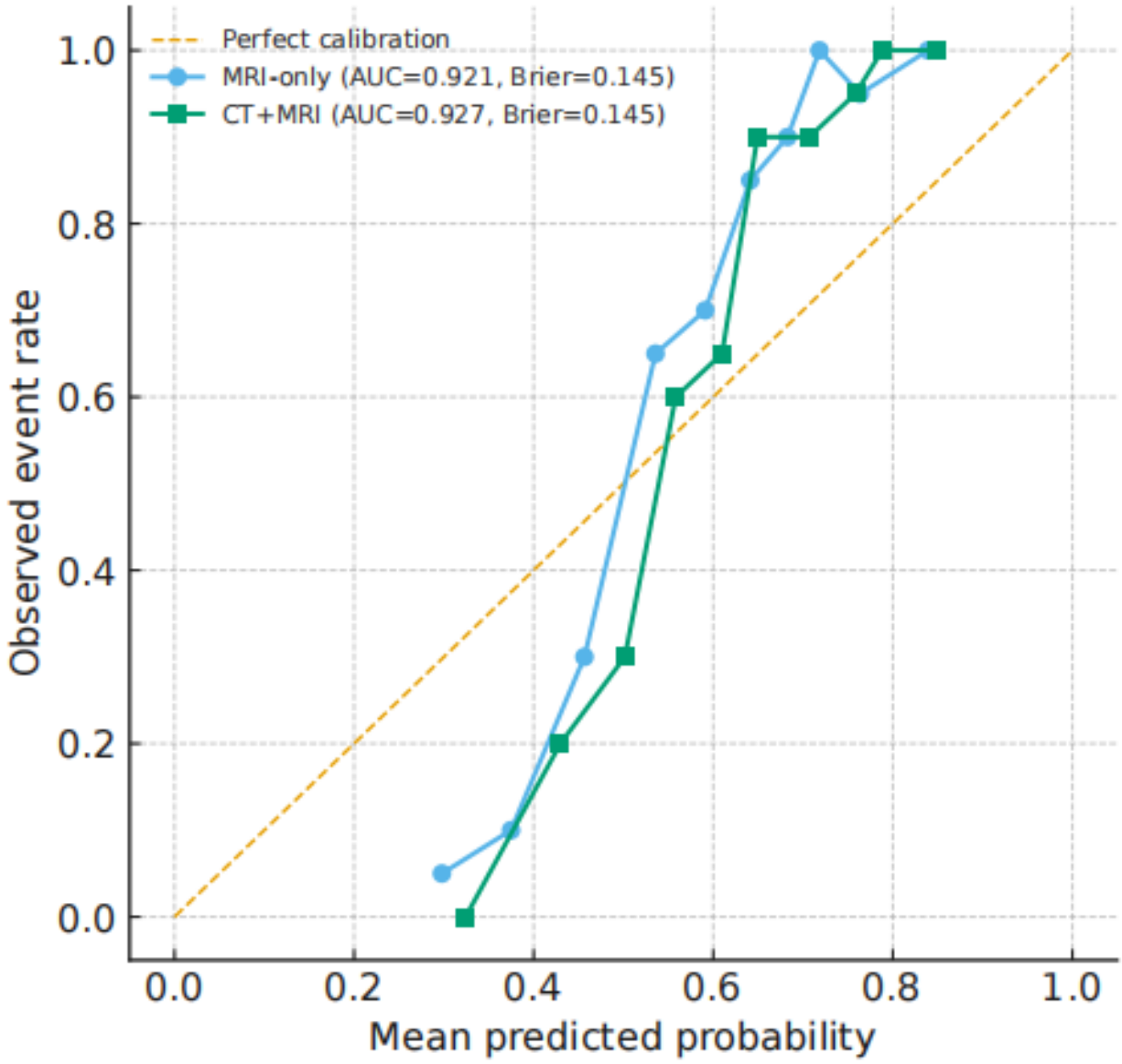

XSL•FO
RenderX

Table . Calibration results of the Transformer model under MRI[a]-only and CT[b] + MRI settings[c].

Setting	Bin	Count	pred_mean	obs_rate	pred_min	pred_max
MRI-only	1	20	0.297790855	0.05	0.182508038	0.338796612
MRI-only	2	20	0.374815574	0.1	0.350143687	0.407613655
MRI-only	3	20	0.456552744	0.3	0.411604379	0.488843116
MRI-only	4	20	0.535671487	0.65	0.489127784	0.56889754
MRI-only	5	20	0.591075985	0.7	0.573348236	0.619675996
MRI-only	6	20	0.641167999	0.85	0.620093517	0.662707158
MRI-only	7	20	0.682686695	0.9	0.663585095	0.697369603
MRI-only	8	20	0.718369677	1	0.697816083	0.742269577
MRI-only	9	20	0.763478434	0.95	0.742374832	0.788465779
MRI-only	10	20	0.839248874	1	0.789370839	0.919921412
CT + MRI	1	20	0.324232379	0	0.240873315	0.387211357
CT + MRI	2	20	0.429795288	0.2	0.389460186	0.473106637
CT + MRI	3	20	0.501537256	0.3	0.473698194	0.538277464
CT + MRI	4	20	0.558194525	0.6	0.538663984	0.585177755
CT + MRI	5	20	0.609770763	0.65	0.586338258	0.625575137
CT + MRI	6	20	0.649248771	0.9	0.626019055	0.677019798
CT + MRI	7	20	0.707037992	0.9	0.683165825	0.735004007
CT + MRI	8	20	0.758477804	0.95	0.737737455	0.775617046
CT + MRI	9	20	0.788180535	1	0.7760233	0.80785209
CT + MRI	10	20	0.847920043	1	0.808998069	0.928076363

[a]MRI: magnetic resonance imaging.

[b]CT: computed tomography.

[c]This table shows the calibration binning results of the transformer model on the independent test set under 2 input settings: MRI-only and CT + MRI. The predicted probabilities (pred_mean) were divided into 10 equal-frequency bins (bin), each containing 20 samples. Obs_rate represents the observed positive rate (proportion of radiotherapy-sensitive patients), while pred_min and pred_max indicate the minimum and maximum predicted probabilities within each bin, respectively. The results show that both input settings exhibit calibration trends close to the ideal diagonal, indicating good agreement between predicted probabilities and observed rates. Notably, the CT + MRI setting demonstrated a slight improvement in net benefit within the higher threshold range.

Grad-CAM Visualization to Validate the Accuracy of Feature Extraction

The effectiveness of the Transformer model was reflected not only in its overall predictive performance but also in the depth and precision of its feature extraction. Grad-CAM was used to visualize the model's feature extraction process. The results revealed that the model primarily focused on tumor boundaries and high-density regions within the tumor. As shown in Figures 4A and 4B, the model was particularly adept at capturing complex structures in heterogeneous tumor areas and using them to predict RT response. The visualization results further demonstrated that the model effectively filtered out irrelevant background information and concentrated on diagnostically significant regions. This selective focus enhanced both the classification accuracy and the clinical interpretability of the model. The ability to highlight meaningful anatomical and pathological features supported the Transformer model as a reliable diagnostic aid for clinicians in treatment planning and response prediction.

XSL•FO
RenderX

Figure 4. Gradient-Weighted Class Activation Mapping (Grad-CAM) visualization of feature extraction in the Transformer model. (A) Original image. (B) Grad-CAM visualization image: displays the areas where the model focuses, particularly on tumor edges and high-density regions. Red areas represent the regions of high attention by the model. CAM: Class Activation Mapping.

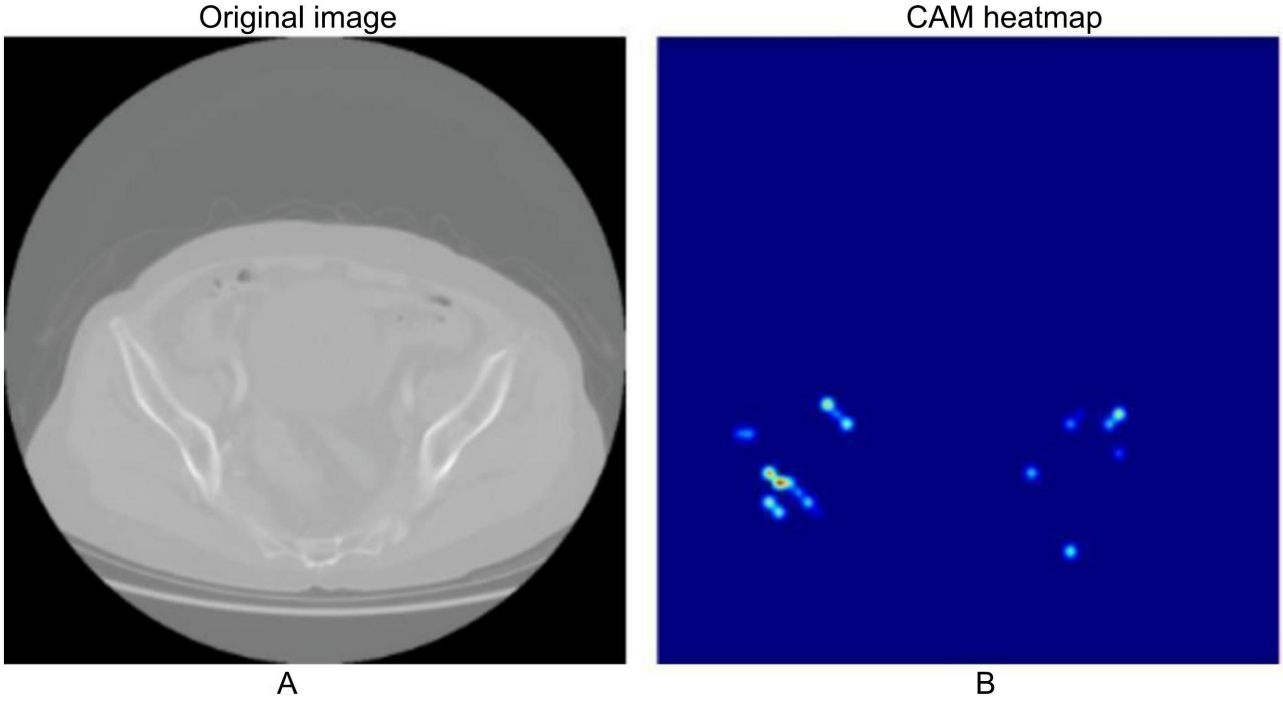

Hyperparameter Optimization and Model Iteration Analysis

During model training and optimization, adjustments to hyperparameters such as learning rate, batch size, and regularization substantially improved the performance of the Transformer model. After 50 training epochs, the validation loss steadily decreased to 0.01, indicating good model convergence and stable training dynamics. As training progressed, the loss curves of the training and validation sets gradually converged, with no apparent signs of overfitting, further confirming the critical role of hyperparameter optimization in enhancing model performance (see Figure 5A for training loss and Figure 5B for validation loss). The model maintained consistently low validation loss and favorable convergence characteristics, establishing a solid foundation for subsequent testing and external validation.

Figure 5. Changes in loss and accuracy for training and validation sets. (A) Loss curve: the loss values for both the training and validation sets decrease gradually over 50 epochs. (B) The validation loss curve (Val loss) indicates that the model stabilized during the later training phase without signs of overfitting.

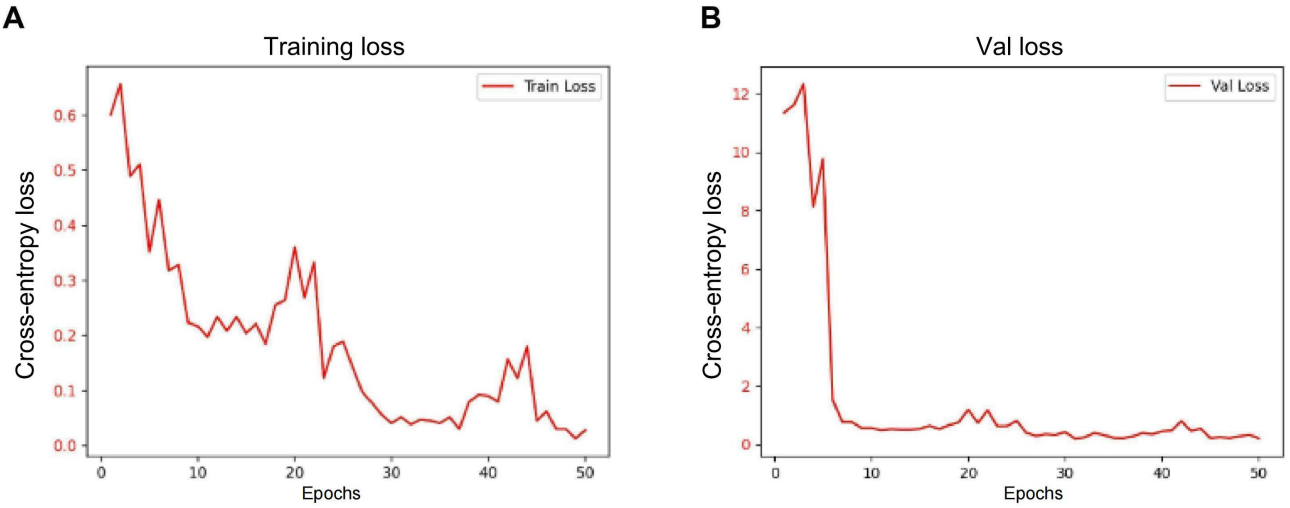

Clinical Benefit Analysis Based on DCA

To further evaluate the potential clinical use of the DL models in RT decision-making, DCA was performed to compare the net benefit of the Transformer, CNN, and GCN models across different probability thresholds (Figure 6). The results showed that across most threshold ranges—particularly between 0.3 and 0.7—the Transformer model achieved a higher net benefit than both the “treat all” and “treat none” strategies, as well as outperforming the CNN and GCN models. This suggests that the Transformer model provides greater decision support capacity in clinical practice.

XSL•FO
RenderX

Figure 6. Decision curve analysis. The figure shows the comparison of net benefit across different probability thresholds for the Transformer, CNN, and GCN models. The dashed lines represent the "treat all" and "treat none" strategies, respectively. The Transformer model demonstrated higher net benefits within the primary clinical decision-making range of 0.3 - 0.7, highlighting its clinical use in predicting radiotherapy sensitivity. CNN: convolutional neural network; GCN: graph convolutional network.

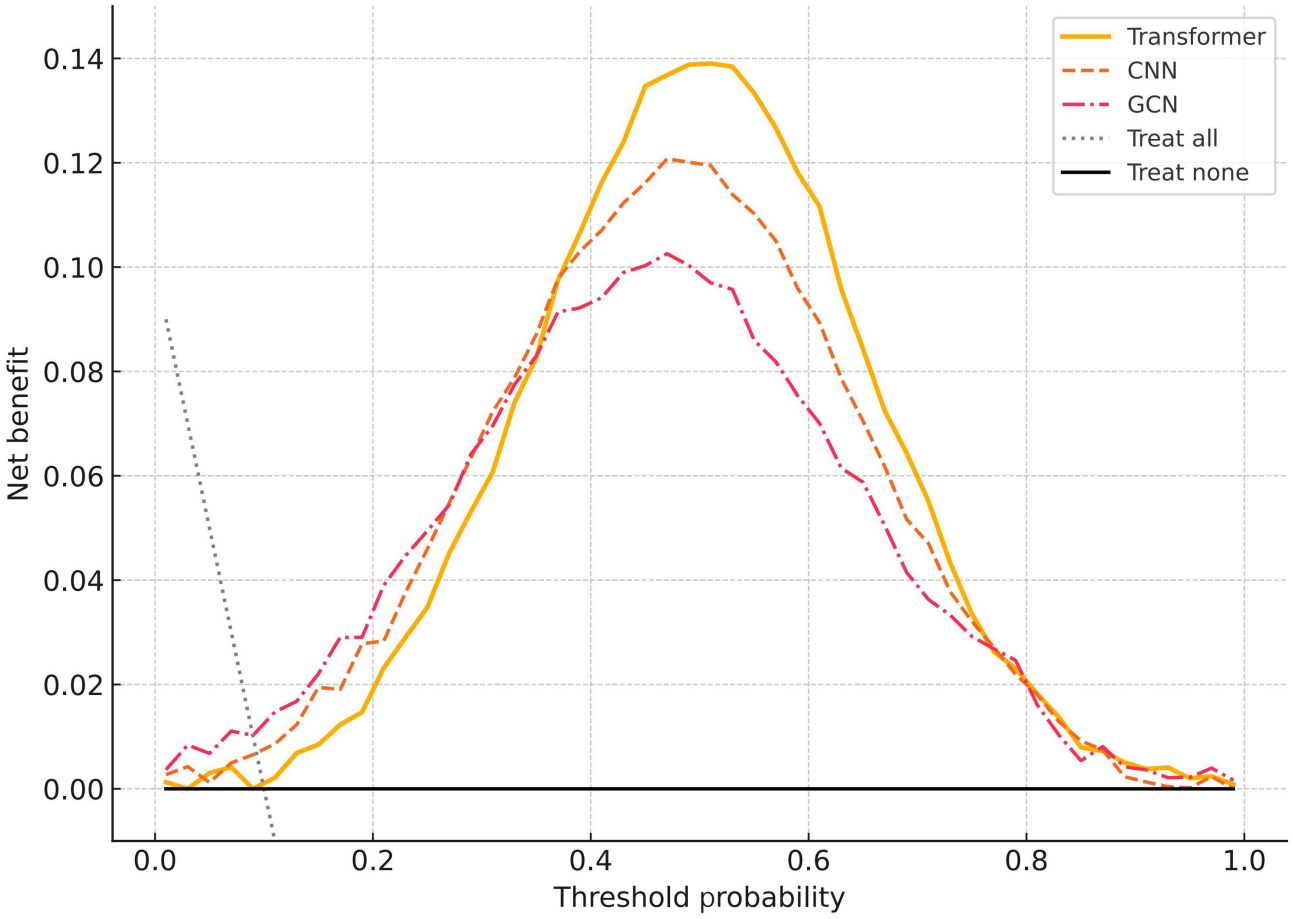

For example, when predicting RT-sensitive patients, the Transformer model maintained a high true-positive rate while significantly reducing the likelihood of unnecessary RT and associated side effects. These findings highlight the model's potential as a valuable tool for individualized RT decision-making.

Sensitivity Analysis of Imaging Input Settings (MRI-Only Versus CT + MRI)

To quantify the incremental value of CT, we compared MRI-only with late-fusion CT + MRI under identical training or validation procedures (same splits, loss, class weighting, and hyperparameters). Using the Transformer as an exemplar, overall discrimination on the independent test set was similar between modalities: Transformer (MRI-only): accuracy 87.0%, AUC 0.921 (95% CI 0.901 - 0.945), sensitivity 89.2% (true positive 116/130), specificity 82.9% (true negative 58/70), Brier score 0.145, and area under the precision–recall curve 0.900; Transformer (CT + MRI): accuracy 87.5%, AUC 0.926 (95% CI 0.905 - 0.948), sensitivity 90.0% (true positive 117/130), specificity 82.9% (true negative 58/70), Brier score 0.142, and area under the precision–recall curve 0.905.

DeLong's test indicated no significant difference in AUC between the 2 settings (P=.36). In DCA, CT + MRI yielded a slight and consistent gain in net benefit at higher threshold probabilities (>0.6), whereas curves largely overlapped within the primary clinical range (0.3 - 0.7). Overall, given a unified MRI acquisition protocol in this single-center cohort, MRI-only achieved robust performance; adding CT did not confer a statistically significant global improvement but may offer marginal clinical value at specific, higher decision thresholds. For completeness, test-set AUCs (95% CI) across all 3 architectures (CNN, GCN, and Transformer) under both input settings are summarized in Table 5, and full classification metrics for the Transformer are provided in Table 6.

XSL•FO
RenderX

Table . Comparison of the Transformer model performance under different input settings[a].

Input setting	Accuracy	AUC	95% CI (AUC[b])	Sensitivity	Specificity	Brier	AUCPR[c]	DeLong test *P* value
MRI[d]-only	87.00%	0.921	0.901 - 0.945	89.2% (116/130)	82.9% (58/70)	0.145	0.9	—[e]
CT + MRI (late fusion)	87.50%	0.926	0.905 - 0.948	90.0% (117/130)	82.9% (58/70)	0.142	0.905	.36

[a]This table compares the predictive performance of the Transformer model under 2 input settings: magnetic resonance imaging (MRI)–only and CT + MRI (late fusion). The main evaluation metrics include accuracy, area under the curve (AUC) with its 95% CI, sensitivity, specificity, Brier score, area under the precision–recall curve (AUCPR), and the DeLong test *P* value for AUC comparison. The results indicate that the overall discriminative performance of the 2 input settings was comparable (AUC difference, *P*=.36). The CT + MRI configuration showed slightly better Brier score and AUCPR at higher threshold ranges, suggesting a minor net benefit under certain clinical decision thresholds.

[b]AUC: area under the curve.

[c]AUCPR: area under the precision–recall curve.

[d]MRI: magnetic resonance imaging.

[e]Not available.

Table . Comparison of AUC[a] values across architectures under MRI[b]-only and CT[c] + MRI settings[d].

Architecture	MRI-only AUC (95% CI)	CT + MRI AUC (95% CI)	DeLong test *P* value
CNN[e]	0.881 (0.854 - 0.906)	0.888 (0.861 - 0.912)	.22
GCN[f]	0.894 (0.869 - 0.918)	0.899 (0.873 - 0.922)	.29
Transformer	0.921 (0.901 - 0.945)	0.926 (0.905 - 0.948)	.36

[a]AUC: area under the curve.

[b]MRI: magnetic resonance imaging.

[c]CT: computed tomography.

[d]This table compares the area under the curve (AUC) performance and corresponding 95% CI of 3 deep learning models—CNN, GCN, and Transformer—under 2 input conditions: MRI-only and CT + MRI. Differences in AUC were evaluated using the DeLong test. The results show that all 3 models exhibited slight improvements in AUC under the CT + MRI condition; however, none of the differences reached statistical significance (*P*>.05). Among the 3, the Transformer model achieved the highest AUC in both settings (MRI-only: 0.921; CT + MRI: 0.926).

[e]CNN: convolutional neural network.

[f]GCN: graph convolutional network.

Computational Efficiency and Inference Time Analysis

To quantitatively evaluate the computational overhead and deployment feasibility of different models in clinical scenarios, we further compared CNNs, GCNs, and Transformer-based models in terms of parameter count, theoretical computational complexity (Floating-Point Operations [FLOPs]), and inference time on an independent test set. Inference-time evaluation was conducted under a fixed hardware configuration (GPU: NVIDIA RTX 3090, 24 GB memory), using FP32 precision, with synchronized timing performed after model warm-up. The timing scope included model forward inference and patient-level probability aggregation (ie, arithmetic averaging of predicted probabilities across all 2D slices belonging to the same patient), while offline image preprocessing and data-loading overheads were excluded.

As summarized in Table 7, the Transformer model exhibits a larger parameter size (86.4 M) and higher FLOPs (17.8 G) than the CNN (ResNet-34) and GCN architectures, reflecting its increased model complexity. Nevertheless, on the test set, the Transformer model achieves an average per-slice inference time of 3.8 milliseconds. At the patient level (median number of slices: 20, IQR 16 - 24), the overall inference time is 78 (IQR 63-95) milliseconds per patient, which remains well within the acceptable range for real-time clinical decision support. By comparison, the patient-level inference times of the CNN and GCN models are 42 milliseconds and 55 milliseconds, respectively.

XSL•FO
RenderX

Table . Computational efficiency and inference latency of the evaluated models[a].

Model	Parameters, millions	FLOPs[b], billions	Inference time per slice (ms), mean (SD)	Average slices per patient, median (IQR)	Inference time per patient (ms)
CNN[c] (ResNet-34)	21.8	3.6	2.1 (0.3)	20 (16-24)	42 (34 - 50)
GCN[d]	28.5	5.2	2.7 (0.4)	20 (16-24)	55 (44 - 66)
Transformer	86.4	17.8	3.8 (0.5)	20 (16-24)	78 (63 - 95)

[a]Parameter counts and FLOPs were calculated based on a single region of interest input. Inference time was measured on an independent test set (n=200) and includes model forward inference as well as patient-level prediction probability aggregation, while offline image preprocessing and data-loading overheads were excluded. All results were obtained under identical hardware and software environments.

[b]FLOPs: Floating-Point Operations.

[c]CNN: convolutional neural network.

[d]GCN: graph convolutional network.

These results indicate that although the Transformer architecture incurs a higher computational cost than conventional convolutional models, its inference latency remains low. Moreover, when weighed against its substantial advantages in predictive performance and clinical net benefit, the increased computational overhead is acceptable for practical clinical applications.

Discussion

Principal Findings

In this study, a DL-based radiomics model was developed to predict RT response in patients with RC. A systematic comparison of multiple models, including CNNs, GCNs, and Transformers, revealed that the Transformer architecture demonstrated the best overall performance. By leveraging its self-attention mechanism, the Transformer effectively captured complex imaging features within key tumor regions, achieving an accuracy of 87% and an AUC of 0.921 on the test set. In addition to its predictive accuracy, the Transformer model demonstrated strong interpretability, as confirmed by Grad-CAM visualization, which highlighted its focus on clinically relevant tumor regions. These findings underscore the model's potential as a reliable and interpretable tool for supporting individualized RT planning in clinical settings.

During training, 5-fold cross-validation (k=5) was adopted based on the following considerations. First, it balanced statistical stability and sample efficiency. In this cohort (n=2000; class ratio ≈65%/35%), k=5 ensured approximately 200 validation cases per fold, providing sufficient positive and negative samples to stably estimate AUC, calibration, and DCA metrics. Larger k would yield smaller validation subsets, increasing variability in calibration and DCA estimates, whereas smaller k would raise estimation bias and reduce the resolution of hyperparameter selection. Second, it accounted for computational cost and practical reproducibility: compared with 10-fold cross-validation, 5 folds substantially reduced training time and resource requirements, making replication in a clinical research setting more feasible. To assess robustness, we conducted sensitivity analyses using k=3 and k=10 and repeated 5-fold cross-validation with different random seeds under the same patient-level stratification. Across all settings, the relative ranking of the Transformer and baseline models remained consistent, fold-to-fold AUC variability was comparable with the main analysis, and no systematic instability or overfitting was observed. Compared with 5 folds, 10 folds primarily increased training time and triggered more frequent early stopping without materially affecting final test performance. Three-folds showed slightly greater variance in validation metrics and reduced hyperparameter discriminability. In summary, k=5 provided an optimal balance among performance stability, computational feasibility, and methodological rigor. To avoid information leakage, cross-validation was performed exclusively within the training set using stratified, patient-level splits; all images, slices, and augmented samples from the same patient were confined to a single fold. The independent test set was reserved for a one-time final evaluation only.

Comparison With Prior Work

RT remains a cornerstone in RC treatment; however, predicting individual response to RT continues to be a major clinical challenge due to significant patient heterogeneity [19]. Radiomics, an emerging technology capable of extracting high-dimensional features from medical images, has opened new avenues for predicting treatment response [20]. However, traditional machine learning approaches have shown limited effectiveness in modeling the high-dimensional, heterogeneous nature of radiomics data [21]. The advent of DL, particularly CNNs, has markedly improved pattern recognition capabilities in this domain [7,9,22]. Unlike prior studies that applied single-model approaches, our work systematically compared 3 advanced DL architectures and identified the Transformer as the most effective model for complex image-based RT response prediction [23].

Several recent studies have attempted to integrate DL into tumor-imaging analysis and RT response prediction. For instance, Xu et al [24] applied CNNs for breast region segmentation using DCE-MRI in breast cancer, demonstrating strong performance in local feature extraction. However, their approach was limited to 2D analysis and failed to account for the complexity of 3D imaging data [24]. Similarly, Mzoughi et al [25] proposed a multiscale 3D CNN for glioma classification based on MRI, achieving approximately 85% accuracy, but still faced limitations in feature representation and generalizability.

XSL•FO
RenderX

Previous studies have systematically evaluated MRI-based radiomics and DL approaches for predicting response to nCRT in RC. A multicenter study published in *Radiology* demonstrated that MRI radiomics models could predict pathological complete response (pCR) with relatively high accuracy [26]. DL models based on post-nCRT T2W MRI also achieved discriminative performance for pCR or GR that was comparable to, or even surpassed, expert radiologist assessment [27]. Beyond single time point models, delta radiomics—which captures changes in features before and after treatment—showed superior performance in predicting nCRT response [28]. In terms of risk stratification and clinical translation, late-fusion multimodal models that integrated multiparametric MRI–derived DL or radiomics features with clinical variables outperformed unimodal models and provided greater clinical net benefit on DCA [18]. Furthermore, several systematic reviews and meta-analyses confirmed the robustness of imaging AI for predicting pCR, reporting pooled AUCs of approximately 0.90 - 0.91; models based on DL or clinical fusion generally outperformed conventional radiomics approaches [29]. These findings are consistent with the results of this study and support our design rationale of introducing more advanced architectures (eg, Transformers) and evaluating clinical use using tools such as DCA.

In contrast, our Transformer-based model achieved an accuracy of 87% and an AUC of 0.921, outperforming the CNN-based approaches in both precision and discriminative capacity. The multihead self-attention mechanism of the Transformer effectively captured global dependencies within tumor regions, demonstrating enhanced robustness and generalizability, especially in cases with complex morphology or blurred tumor boundaries. Compared with previously reported models, our approach offered distinct advantages in architectural innovation, predictive performance, and clinical interpretability, positioning it as a more reliable framework for RT response prediction.

Additionally, the U-Net model also demonstrated satisfactory performance in tumor segmentation, achieving a mean DSC of 0.892 and an IoU of 0.814 on the independent test set, indicating strong consistency with expert annotations. These results underscore the crucial role of accurate segmentation in radiomics workflows, as it ensures high-quality inputs for downstream feature extraction and classification, even in tumors with irregular edges.

Furthermore, Grad-CAM visualization revealed that the Transformer model concentrated on tumor edges and regions of heterogeneous density, areas known to correlate with RT sensitivity [20,21]. This interpretability enhanced the interpretability and clinical credibility of the model.

Limitations

Despite the promising results, this study had several limitations. First, the dataset was derived from a single center, with limited diversity in race, age, and pathological subtypes, which may have constrained the model's generalizability [20]. Although data augmentation and k-fold cross-validation were applied to mitigate this limitation, future studies should incorporate multicenter datasets to assess the model's robustness across broader populations. Second, the imaging data primarily consisted of DCE-MRI, without the integration of additional clinical variables such as genomic data, pathological classification, or treatment history. This single-modality approach may have limited the comprehensiveness of the predictive model [7]. Incorporating multimodal data in future models could improve both predictive accuracy and biological interpretability. Third, although Grad-CAM was used to enhance model interpretability, it functioned as a post hoc visualization method and did not directly reveal the underlying causal mechanisms driving model predictions. Future research that integrates molecular biomarkers and longitudinal follow-up data may help elucidate the biological basis of model outputs and strengthen their interpretability. Fourth, model performance evaluation was conducted on a single-center dataset and validated only on an internal holdout test set comprising 10% of the cohort. External multicenter validation was not performed. Although cross-validation and regularization techniques were used to reduce overfitting, radiomics models are known to be sensitive to cross-center variations—such as differences in imaging parameters, scanner models, and acquisition protocols—which may lead to substantial domain shift in real-world applications. Future studies should incorporate external datasets from multiple institutions to systematically assess robustness, generalizability, and clinical applicability. Fifth, expert-annotated tumor masks were used in the test set to avoid data leakage; however, this evaluation setup represents an "idealized" condition that does not fully reflect real-world clinical workflows. In practice, errors from automatic segmentation networks may propagate to the Transformer classifier, potentially leading to lower end-to-end performance than the manually masked results reported here. Future work will include validation of a fully automated pipeline and quantitative assessment of how segmentation inaccuracies affect downstream prediction tasks. Sixth, MRI slice thickness varied between 3 mm and 4 mm across patients. Although this study adopted a 2D slice–level modeling strategy, in which the inputs primarily rely on in-plane texture and morphological information, and volumetric resampling along the *z*-axis was intentionally avoided to prevent interpolation-induced artifacts, we acknowledge that differences in slice thickness and spatial resolution may still affect the statistical distributions of intensity and texture features, thereby constituting a potential confounding factor in radiomics-based analyses. We performed patient-level splitting for training, validation, and testing and used data augmentation and cross-validation to mitigate instability arising from acquisition-related heterogeneity; however, such effects cannot be completely eliminated. Future work will further explore standardized resampling strategies or explicit modeling of resolution differences (eg, stratification or covariate adjustment) and will incorporate 3D models and multicenter external validation to systematically evaluate the impact of slice thickness and scanner or protocol variability on model generalizability. Seventh, this study combined CR and PR patients into a single "GR" category to improve class balance, a strategy commonly used in statistical modeling. However, this grouping does not optimally reflect clinical practice: "watch-and-wait" strategies are typically suitable only for patients achieving clinical CR or pCR, whereas PR patients still require further treatment. While the binary classification

XSL•FO
RenderX

framework in this study aimed primarily to demonstrate the DL model's ability to predict overall RT response, future research should investigate multiclass models to enhance clinical interpretability and applicability. Eighth, although the Transformer model demonstrated superior predictive performance compared with CNN and GCN models, this improvement comes at the cost of increased computational burden. Transformers generally require larger parameter counts and higher floating-point computation, with the self-attention mechanism imposing substantial overhead when processing high-resolution image patches. To address this concern, we have supplemented the revised manuscript with a detailed comparison of model parameter counts, FLOPs, and patient-level inference time, thereby quantitatively assessing the computational efficiency of different architectures. The results demonstrate that despite its higher computational cost relative to ResNet-34 and the GCN model, the Transformer maintains a patient-level inference time within the acceptable range for real-time clinical decision support, indicating its practical feasibility for deployment under the current experimental settings. Nevertheless, in larger-scale datasets or resource-constrained clinical environments, model complexity and deployment cost may still pose limiting factors. Future work will therefore explore model compression strategies, such as knowledge distillation, structural pruning, and parameter sharing, to further reduce inference latency and computational resource consumption while preserving predictive performance, thereby enhancing the applicability of the model in real-world clinical workflows.

Future Directions

Future research should aim to extend the application of the Transformer-based radiomics model beyond RC, exploring its transferability and adaptability to other solid tumors such as cervical, lung, and esophageal cancers, in order to evaluate cross-cancer generalizability [15,30]. Another promising avenue involves integrating radiomics with additional data modalities, including genomic, transcriptomic, immunomic, and digital pathology features, to develop comprehensive multimodal fusion models. Such models have the potential to enhance predictive accuracy and provide deeper insights into the biological mechanisms underlying treatment response [21]. Furthermore, the development of lightweight and resource-efficient model versions suitable for deployment on edge devices will be critical for facilitating real-world clinical translation, enabling the routine use of DL-based radiomics models at the point of care to support individualized treatment planning and decision-making.

Conclusions

This study successfully constructed a Transformer-based DL radiomics model for predicting RT sensitivity in patients with RC. The results demonstrate that when using pre-RT MRI features as the primary input, the proposed model achieves superior performance in terms of predictive accuracy, interpretability, and model stability, thereby providing a feasible tool for pretreatment risk stratification and personalized RT decision-making. Supplementary analyses indicate that the multimodal integration of CT and MRI does not yield a statistically significant improvement in overall discriminative performance; however, it may offer a modest and consistent clinical net benefit at specific decision thresholds. Further validation using multicenter datasets is warranted, and future studies should more clearly delineate the potential value of multimodal information across different clinical application scenarios.

Funding

No external financial support or grants were received from any public, commercial, or not-for-profit entities for the research, authorship, or publication of this article.

Disclaimer

No generative AI tools were used in the preparation, writing, analysis, or submission of this manuscript.

Data Availability

To enhance the reproducibility of this study, the complete implementation code, including scripts for data preprocessing, feature extraction, model training, and inference, will be made publicly available on GitHub upon publication. All data processing workflows have been automated and standardized to ensure that external users can replicate the model training process under identical data conditions. Considering patient privacy and institutional policy restrictions, the trained model weight files will be provided only upon reasonable academic request and limited strictly to noncommercial research purposes.

Authors' Contributions

YL and HL contributed equally to this work. YL, HL, and QW designed the study and performed data analysis. ZW and ZH were responsible for data collection and curation. YL developed the deep learning models and conducted experiments. ZH supervised the project and provided critical revisions. All authors contributed to the manuscript writing and approved the final version.

Conflicts of Interest

None declared.

Multimedia Appendix 1

XSL•FO
RenderX

Patient inclusion flowchart for rectal cancer. The flowchart illustrates the inclusion and exclusion process. A total of 2450 patients were screened; 200 were excluded for missing imaging data, 120 for poor image quality, 80 for lack of radiotherapy outcome labels, and 50 for not receiving standard radiotherapy. Ultimately, 2000 patients were included for model analysis, with 1300 classified as radiotherapy-sensitive and 700 as radiotherapy-insensitive based on follow-up evaluations.
[PDF File, 345 KB - medinform_v14i1e77313_app1.pdf]

Multimedia Appendix 2
Scanner models and acquisition parameters used in the study.
[DOCX File, 12 KB - medinform_v14i1e77313_app2.docx]

Multimedia Appendix 3
Data collection and preprocessing flowchart. These figures illustrate the entire process from data collection, data anonymization, formatting, normalization, and data augmentation to the final dataset preparation. They depict data preprocessing steps such as denoising, cropping, normalization, and resolution adjustment.
[PDF File, 62 KB - medinform_v14i1e77313_app3.pdf]

Multimedia Appendix 4
Workflow of deep learning model training and validation. This figure illustrates the overall framework of the deep learning analysis pipeline used in this study, including data preprocessing, tumor region segmentation, feature extraction, model training with cross-validation, and performance evaluation. First, preradiotherapy images were cleaned, normalized, and augmented to generate standardized inputs. Subsequently, a U-Net model was used for automatic tumor segmentation, and the resulting masks were used to extract tumor region features from the magnetic resonance images. The Transformer model then performed classification training based on patch embeddings, leveraging multihead self-attention to capture global feature patterns. Five-fold cross-validation was adopted during training to enhance model robustness and generalizability. Finally, performance metrics, including accuracy, sensitivity, specificity, and area under the curve, were computed. This workflow provides a comprehensive overview of the deep learning analysis pathway from raw imaging data to model prediction.
[PNG File, 59 KB - medinform_v14i1e77313_app4.png]

Multimedia Appendix 5
U-shaped convolutional neural network (U-Net) model tumor segmentation process diagram. This diagram illustrates how the U-Net segmentation model extracts features layer by layer through convolution operations, ultimately segmenting the tumor region. It includes the original image input, convolution process, feature extraction, and segmentation results.
[PNG File, 70 KB - medinform_v14i1e77313_app5.png]

Multimedia Appendix 6
Schematic architecture of the transformer classification model. This figure illustrates the overall workflow of the Transformer-based classification model used to predict radiotherapy response in rectal cancer. First, pretreatment magnetic resonance images are processed using tumor-region masks (masked region of interest). The masked images are then divided into fixed-size 16×16 patches, which are linearly projected to obtain patch embeddings. The model consists of 12 Transformer encoder layers, where multihead self-attention mechanisms capture global contextual features. During classification, a dedicated classification token is passed through a multilayer perceptron (MLP head) to produce the final prediction of radiotherapy response (sensitive vs nonsensitive). This architecture operates exclusively at the image level and does not include any segmentation decoder, remaining fully independent from the U-Net segmentation model used elsewhere in the study.
[PNG File, 33 KB - medinform_v14i1e77313_app6.png]

Multimedia Appendix 7
Model evaluation and performance analysis flowchart. This figure illustrates the entire model evaluation process, including the calculation of accuracy, sensitivity, specificity, receiver operating characteristic curve, and area under the curve values, and how these metrics are used to assess the model's classification ability.
[PNG File, 36 KB - medinform_v14i1e77313_app7.png]

References

1. Barbieri P, Posa A, Lancellotta V, et al. Electrochemotherapy in the locoregional treatment of metastatic colorectal liver metastases: a systematic review. Curr Oncol 2024 Nov 20;31(11):7403-7413. [doi: 10.3390/curroncol31110546] [Medline: 39590176]
2. Ocanto A, Teja M, Amorelli F, et al. Landscape of biomarkers and pathologic response in rectal cancer: where we stand? Cancers (Basel) 2024 Dec 2;16(23):4047. [doi: 10.3390/cancers16234047] [Medline: 39682232]

XSL•FO
RenderX

3. Wojakowska A, Marczak L, Zeman M, et al. Proteomic and metabolomic signatures of rectal tumor discriminate patients with different responses to preoperative radiotherapy. Front Oncol 2024;14:1323961. [doi: 10.3389/fonc.2024.1323961] [Medline: 38410100]
4. Ellakwa DES, Mushtaq N, Khan S, et al. Molecular functions of microRNAs in colorectal cancer: recent roles in proliferation, angiogenesis, apoptosis, and chemoresistance. Naunyn-Schmiedeberg's Arch Pharmacol 2024 Aug;397(8):5617-5630. [doi: 10.1007/s00210-024-03076-w]
5. Mendes B, Domingues I, Santos J. Radiomic pipelines for prostate cancer in external beam radiation therapy: a review of methods and future directions. J Clin Med 2024 Jul 3;13(13):3907. [doi: 10.3390/jcm13133907] [Medline: 38999473]
6. Astaraki M, Häger W, Lazzeroni M, Toma-Dasu I. Radiomics and deep learning models for glioblastoma treatment outcome prediction based on tumor invasion modeling. Phys Med 2025 Jan;129:104881. [doi: 10.1016/j.ejmp.2024.104881] [Medline: 39724784]
7. Deasy JO. Data science opportunities to improve radiotherapy planning and clinical decision making. Semin Radiat Oncol 2024 Oct;34(4):379-394. [doi: 10.1016/j.semradonc.2024.07.012] [Medline: 39271273]
8. Wu M, Yan C, Sen G. Computer-aided diagnosis of hepatic cystic echinococcosis based on deep transfer learning features from ultrasound images. Sci Rep 2025;15(1). [doi: 10.1038/s41598-024-85004-9]
9. Zhang H, Dohopolski M, Stojadinovic S, et al. Multiomics-based outcome prediction in personalized ultra-fractionated stereotactic adaptive radiotherapy (PULSAR). Cancers (Basel) 2024 Oct 9;16(19):3425. [doi: 10.3390/cancers16193425] [Medline: 39410044]
10. Toba S, Mitani Y, Yodoya N, et al. Prediction of pulmonary to systemic flow ratio in patients with congenital heart disease using deep learning-based analysis of chest radiographs. JAMA Cardiol 2020 Apr 1;5(4):449-457. [doi: 10.1001/jamacardio.2019.5620] [Medline: 31968049]
11. Ran J, Li D. A faster privacy-preserving medical image diagnosis scheme with machine learning. J Digit Imaging Inform Med 2025;38(5):2716-2728. [doi: 10.1007/s10278-024-01384-4]
12. Alazwari S, Alsamri J, Alamgeer M, Alotaibi SS, Obayya M, Salama AS. Automated gall bladder cancer detection using artificial gorilla troops optimizer with transfer learning on ultrasound images. Sci Rep 2024 Sep 19;14(1):21845. [doi: 10.1038/s41598-024-72880-4] [Medline: 39300284]
13. Thompson HM, Kim JK, Jimenez-Rodriguez RM, Garcia-Aguilar J, Veeraraghavan H. Deep learning-based model for identifying tumors in endoscopic images from patients with locally advanced rectal cancer treated with total neoadjuvant therapy. Dis Colon Rectum 2023;66(3):383-391. [doi: 10.1097/DCR.0000000000002295]
14. Wichtmann BD, Albert S, Zhao W, et al. Are we there yet? The value of deep learning in a multicenter setting for response prediction of locally advanced rectal cancer to neoadjuvant chemoradiotherapy. Diagnostics (Basel) 2022 Jun 30;12(7):1601. [doi: 10.3390/diagnostics12071601] [Medline: 35885506]
15. Fu J, Zhong X, Li N, et al. Deep learning-based radiomic features for improving neoadjuvant chemoradiation response prediction in locally advanced rectal cancer. Phys Med Biol 2020 Apr 2;65(7):075001. [doi: 10.1088/1361-6560/ab7970] [Medline: 32092710]
16. Kawamura M, Kamomae T, Yanagawa M, et al. Revolutionizing radiation therapy: the role of AI in clinical practice. J Radiat Res 2024 Jan 19;65(1):1-9. [doi: 10.1093/jrr/rrad090]
17. Yang M, Yang M, Yang L, et al. Deep learning for MRI lesion segmentation in rectal cancer. Front Med 2024;11. [doi: 10.3389/fmed.2024.1394262]
18. Li Z, Qin Y, Liao X, et al. Comparison of clinical, radiomics, deep learning, and fusion models for predicting early recurrence in locally advanced rectal cancer based on multiparametric MRI: a multicenter study. Eur J Radiol 2025 Aug;189:112173. [doi: 10.1016/j.ejrad.2025.112173] [Medline: 40403678]
19. Kaval G, Dagoglu Kartal MG, Azamat S, et al. Evaluating complete response prediction rates in locally advanced rectal cancer with different radiomics segmentation approaches. Pathol Oncol Res 2024;30:1611744. [doi: 10.3389/pore.2024.1611744] [Medline: 38694706]
20. Nardone V, Reginelli A, Rubini D, et al. Delta radiomics: an updated systematic review. Radiol Med 2024 Aug;129(8):1197-1214. [doi: 10.1007/s11547-024-01853-4] [Medline: 39017760]
21. Kwiatkowska-Miernik A, Wasilewski PG, Mruk B, Sklinda K, Bujko M, Walecki J. Estimating progression-free survival in patients with primary high-grade glioma using machine learning. J Clin Med 2024 Oct 16;13(20):6172. [doi: 10.3390/jcm13206172] [Medline: 39458122]
22. Ramireddy JK, Sathya A, Sasidharan BK, et al. Can pretreatment MRI and planning CT radiomics improve prediction of complete pathological response in locally advanced rectal cancer following neoadjuvant treatment? J Gastrointest Canc 2024 Sep;55(3):1199-1211. [doi: 10.1007/s12029-024-01073-z]
23. Zhu Y, Liu T, Chen J, Wen L, Zhang J, Zheng D. Prediction of therapeutic response to transarterial chemoembolization plus systemic therapy regimen in hepatocellular carcinoma using pretreatment contrast-enhanced MRI based habitat analysis and Crossformer model. Abdom Radiol 2024;50(6):2464-2475. [doi: 10.1007/s00261-024-04709-7]
24. Xu X, Fu L, Chen Y, et al. Breast region segmentation being convolutional neural network in dynamic contrast enhanced MRI. Annu Int Conf IEEE Eng Med Biol Soc 2018 Jul;2018:750-753. [doi: 10.1109/EMBC.2018.8512422] [Medline: 30440504]

XSL•FO
RenderX

25. Mzoughi H, Njeh I, Wali A, et al. Deep multi-scale 3D convolutional neural network (CNN) for MRI gliomas brain tumor classification. J Digit Imaging 2020 Aug;33(4):903-915. [doi: 10.1007/s10278-020-00347-9] [Medline: 32440926]
26. Shin J, Seo N, Baek SE, et al. MRI radiomics model predicts pathologic complete response of rectal cancer following chemoradiotherapy. Radiology 2022 May;303(2):351-358. [doi: 10.1148/radiol.211986] [Medline: 35133200]
27. Jang BS, Lim YJ, Song C, et al. Image-based deep learning model for predicting pathological response in rectal cancer using post-chemoradiotherapy magnetic resonance imaging. Radiother Oncol 2021 Aug;161:183-190. [doi: 10.1016/j.radonc.2021.06.019] [Medline: 34139211]
28. Wang L, Wu X, Tian R, et al. MRI-based pre-Radiomics and delta-Radiomics models accurately predict the post-treatment response of rectal adenocarcinoma to neoadjuvant chemoradiotherapy. Front Oncol 2023;13. [doi: 10.3389/fonc.2023.1133008]
29. Jia LL, Zheng QY, Tian JH, et al. Artificial intelligence with magnetic resonance imaging for prediction of pathological complete response to neoadjuvant chemoradiotherapy in rectal cancer: a systematic review and meta-analysis. Front Oncol 2022;12:1026216. [doi: 10.3389/fonc.2022.1026216] [Medline: 36313696]
30. Abbaspour S, Abdollahi H, Arabalibeik H, et al. Endorectal ultrasound radiomics in locally advanced rectal cancer patients: despeckling and radiotherapy response prediction using machine learning. Abdom Radiol 2022;47(11):3645-3659. [doi: 10.1007/s00261-022-03625-y]

Abbreviation

AI: artificial intelligence
AUC: area under the curve
CNN: convolutional neural network
CONSORT: Consolidated Standards of Reporting Trials
CR: complete response
CT: computed tomography
DCA: decision curve analysis
DCE-MRI: dynamic contrast–enhanced magnetic resonance imaging
DL: deep learning
DSC: Dice Similarity Coefficient
FLOP: Floating-Point Operation
GCN: graph convolutional network
GR: good response
Grad-CAM: Gradient-Weighted Class Activation Mapping
IoU: Intersection over Union
MRI: magnetic resonance imaging
nCRT: neoadjuvant chemoradiotherapy
pCR: pathological complete response
PR: partial response
RC: rectal cancer
RECIST: Response Evaluation Criteria in Solid Tumors
ResNets: residual networks
ROC: receiver operating characteristic
ROI: region of interest
RT: radiotherapy
T2W: T2-weighted
U-Net: U-shaped convolutional neural network

Edited by A Coristine; submitted 11.May.2025; peer-reviewed by JCL Chow, P Sharma; revised version received 08.Jan.2026; accepted 12.Jan.2026; published 17.Mar.2026.

Please cite as:
Li Y, Liu H, Wei Q, Wang Z, Hu Z
Rectal Cancer Radiotherapy Response Prediction: Retrospective Study of Development of a Deep Learning–Based Radiomics Model
JMIR Med Inform 2026;14:e77313
URL: https://medinform.jmir.org/2026/1/e77313
doi:10.2196/77313

XSL•FO
RenderX

© Yiqun Li, Hengchang Liu, Qiang Wei, Zhenqi Wang, Zhen Hu. Originally published in JMIR Medical Informatics (https://medinform.jmir.org), 17.Mar.2026. This is an open-access article distributed under the terms of the Creative Commons Attribution License (https://creativecommons.org/licenses/by/4.0/), which permits unrestricted use, distribution, and reproduction in any medium, provided the original work, first published in JMIR Medical Informatics, is properly cited. The complete bibliographic information, a link to the original publication on https://medinform.jmir.org/, as well as this copyright and license information must be included.

XSL•FO
RenderX

Comprehensive Pediatric Health Risk Stratification Using an AI-Driven Framework in Children Aged 2 to 8 Years: Design and Validation Study

Jundan Chen*, PhD; Zhihe Mao*, BA

School of Physical Education, Hunan University of Arts and Science, 3150 Dongting Road, Changde, Hunan, China

*all authors contributed equally

Corresponding Author:
Zhihe Mao, BA
School of Physical Education, Hunan University of Arts and Science, 3150 Dongting Road, Changde, Hunan, China

Related Article:

This is a corrected version. See correction statement: https://medinform.jmir.org/2026/1/e92491

Abstract

Background: Early life health risks can shape long-term morbidity trajectories, yet prevailing pediatric risk assessment paradigms are often fragmented and insufficiently capable of integrating heterogeneous data streams into actionable, individualized profiles.

Objective: This study aimed to design, implement, and validate an artificial intelligence–driven framework that fuses multimodal pediatric data and leverages advanced natural language processing and ensemble learning to improve early, accurate stratification of key pediatric health risks.

Methods: A retrospective dataset of over 40,000 pediatric participants aged 2 - 8 years was used to train and evaluate the framework. Data were split into training, validation, and test sets (70%, 15%, and 15%, respectively) with a temporally mindful partitioning strategy to approximate prospective evaluation. Baseline comparators included traditional statistical and machine learning models, and the statistical significance of area under the receiver operating characteristic curve (AUC-ROC) differences was assessed using the DeLong test.

Results: The proposed Bidirectional Encoder Representations From Transformers–based model achieved an AUC-ROC of 0.85 (95% CI 0.82 - 0.88), sensitivity of 0.78, specificity of 0.80, and F_1-score of 0.75 on the test set, outperforming multiple baseline models. In an additional manual comparison evaluation, automated and expert assessments aligned with 78% accuracy (78/100), and most discrepancies arose in “equivalent” cases.

Conclusions: This study provides a validated, artificial intelligence–driven, multimodal pediatric health risk stratification framework that translates heterogeneous child health data into clinically actionable risk profiles, demonstrating strong discriminative performance and meaningful agreement with expert assessment. The framework supports proactive, individualized pediatric care and offers a scalable foundation for further validation across broader populations and longitudinal follow-up.

(JMIR Med Inform 2026;14:e80163) doi:10.2196/80163

KEYWORDS

pediatric health; artificial intelligence; AI; risk stratification; ensemble learning; framework design; multisource data fusion; predictive modeling

Introduction

The assessment and early identification of health risks in children represent a critical area of research with profound implications for individual lifelong well-being and public health strategies. Establishing healthy developmental trajectories during childhood is fundamental, as health conditions and risk exposures in early life can significantly influence adult health outcomes and susceptibility to chronic diseases [1,2]. Traditional pediatric health surveillance often relies on periodic checkups, which may not fully capture the dynamic and multifaceted nature of health risks influenced by a complex interplay of genetic, environmental, and lifestyle factors [3,4]. Therefore, developing advanced, data-driven methodologies, such as those explored in recent research on artificial intelligence (AI) and machine learning (ML) for tasks like toxicity prediction and broader research applications, to proactively identify and stratify these risks is of paramount importance. Such systems, potentially incorporating guardian-interactive elements, can empower health

XSL•FO
RenderX

care providers and families with actionable insights for timely preventive interventions, ultimately contributing to a healthier future generation and optimizing health care resource allocation [5]. Global health initiatives increasingly emphasize the importance of leveraging innovative technologies, including advanced AI models, such as large language models adapted for specific domains [6], to enhance child health and well-being. The potential for deep learning to enhance diagnostic and prognostic capabilities in areas like child psychiatry further underscores this trend [7].

The rapid popularization of internet-based medical services, including telehealth, mobile health (mHealth) apps, and online consultation platforms, has significantly reshaped health care delivery and accessibility worldwide [8]. This digital transformation has not only provided patients and caregivers with more convenient access to medical advice and health information but also led to the generation of vast amounts of digital health data [9,10]. While much of the initial adoption has been observed in adult care, the principles of leveraging digital platforms for health monitoring, data collection, and remote consultation, often supported by automated systems for tasks like information synthesis [11], are increasingly recognized as valuable in pediatric care. The experience gained from the broader implementation of digital health solutions, including aspects of data security, interoperability, and user engagement, offers important lessons for developing effective and safe digital health tools specifically for children [12,13]. The expanding digital health infrastructure provides a rich ecosystem for collecting diverse health-related data that, if properly managed and ethically used with robust frameworks, can be invaluable for comprehensive risk assessment in pediatric populations [14,15]. Task-oriented dialogue systems, for instance, show potential for structured data gathering in such contexts. Despite progress in pediatric health surveillance, significant clinical voids persist, particularly in the settings of primary care and population health screening. Current risk assessment paradigms are often fragmented, struggling to effectively integrate heterogeneous data streams, such as structured electronic health record (EHR) data, unstructured clinical notes, parental reports, and real-time wearable sensor data, into a single, cohesive risk profile. This leads to a reactive, rather than proactive, approach to care, where risks are often identified only after they have manifested. This research addresses this gap by proposing a framework designed for the following specific end users: (1) pediatricians in primary care, who can use the system for point-of-care decision support; (2) public health officials, who can leverage population-level risk distributions for resource allocation and strategic planning; and (3) clinical care coordinators, who can manage and monitor high-risk pediatric cohorts more effectively.

The increasing availability of EHR data, administrative data, patient-generated health data, and other health-related information sources has fueled the application of health care big data analytics to improve service quality, operational efficiency, and patient outcomes [16-18]. Effective utilization of these data, supported by primers on data handling and the underlying principles of models like Bidirectional Encoder Representations From Transformers (BERT), can support evidence-based clinical decision-making, enhance population health management, facilitate epidemiological surveillance, and enable the development of personalized health care interventions [19]. To enhance clinical utility and facilitate shared decision-making, it is imperative that the reasons behind a child's risk stratification are transparent and interpretable. Shapley additive explanations (SHAP) are used due to their strong theoretical guarantee of consistency and local accuracy, which can provide a unified and reliable framework for model interpretation [20]. For a given prediction, SHAP assigns an importance value (SHAP value) to each input feature, and it is crucial for unlocking its full potential in transforming health care delivery, research, and policy.

AI algorithms can analyze complex, multidimensional datasets to identify subtle patterns, predict the likelihood of various health conditions, and stratify risk earlier and more accurately than traditional statistical methods [20,21]. Researchers have explored various AI-driven systems for health applications. For example, some systems focus on the early detection of developmental disorders using behavioral or imaging data, while others aim to predict adverse outcomes in neonatal intensive care units or identify children at risk for conditions like asthma, obesity, and mental health issues, sometimes using specific BERT-based approaches for analyzing medical records or predicting conditions like Alzheimer disease (AD-BERT), which, while not pediatric, demonstrates domain-specific adaptation [22]. Common approaches in developing such systems involve the curation of large, representative datasets; rigorous data preprocessing and feature engineering; the application of appropriate ML algorithms; and robust model validation using independent test sets and ideally prospective clinical evaluation [23]. For instance, deep learning models have shown promise in analyzing medical images for pediatric conditions, while ensemble methods and sophisticated scoring mechanisms like BERTScore for evaluating text generation quality [24] (analogous to assessing the quality of AI-generated health summaries) are often used to improve the robustness and accuracy of predictive models based on structured EHR data or textual information [25]. The primary contribution of our framework lies in its advanced natural language processing (NLP) capabilities, which distinguish it from prior AI systems in pediatric care that have largely relied on traditional NLP techniques. Methodologies, such as keyword matching, bag-of-words, and term frequency-inverse document frequency models, while useful, are fundamentally limited in their ability to interpret the complex and nuanced narratives found in clinical texts.

Therefore, this study aimed to design, implement, and validate a comprehensive, AI-driven framework for pediatric health risk stratification. We hypothesize that by integrating multimodal data, including EHRs, parental questionnaires, and wearable sensor data, and leveraging advanced NLP and ensemble learning models, our system can identify and stratify key pediatric health risks (eg, obesity and developmental delay) with greater accuracy and at an earlier stage than traditional assessment methods, thereby providing robust support for clinical decision-making and pre-emptive intervention. A

XSL•FO
RenderX

comparison of pediatric risk stratification frameworks is provided in Table 1.

Table . Comparison of the selection of pediatric risk stratification frameworks.

Study	Key method	Data modalities used	Clinical deployment status
Smith et al [26]	Logistic regression	EHR[a] (structured only)	Retrospective validation
Chen et al [27]	Random forest	EHR and parental surveys	Prototype on retrospective data
Our study	Fine-tuned BERT[b] + ensemble	EHR, surveys, and wearables	Prototype on retrospective data
Lee et al [28]	CNN[c] on images	Medical imaging	Conceptual framework

[a]EHR: electronic health record.

[b]BERT: Bidirectional Encoder Representations From Transformers.

[c]CNN: convolutional neural network.

Methods

Pediatric Health Risk Stratification Framework and Data Foundation

This section addresses the critical, complex, and multifaceted aspects of multimodal data acquisition, encompassing the collection of diverse data types from various sources and the requisite, often intricate, data preparation processes. These preparation stages, including but not limited to data cleaning, normalization, transformation, and feature engineering, are indispensable for effectively fueling the advanced AI models that form the analytical core of this research, ensuring they operate on high-quality, meaningful inputs to generate reliable and actionable insights [29,30]. The overarching goal is to establish robust data and conceptual groundwork upon which sophisticated risk prediction and stratification can be built, ultimately aiming to transform pediatric health care through proactive and personalized interventions. Conceptually, the framework aims to map a complex set of input variables Xdata (representing multimodal pediatric data) through a series of transformations and AI modeling of fAI to an interpretable risk stratification outcome Yrisk :

(1)Yrisk=fAI(Preprocessing(Xdata))

This high-level representation underscores the journey from raw data to actionable risk assessment.

Conceptual Framework for Pediatric Risk Stratification

The creation of a robust pediatric health risk stratification system requires a meticulously defined conceptual framework that delineates the core components, their interactions, and the overall data flow. As depicted in Figure 1, the proposed AI-driven framework is architected to be modular, scalable, and adaptable to diverse pediatric health contexts. Its primary objective is to convert raw, multisource pediatric data into actionable risk profiles, thereby facilitating proactive and personalized health care interventions.

Commencing with *multimodal data input*, the framework assimilates a wide array of data sources pertinent to child health. Subsequently, the *data preprocessing and harmonization* layer comes into play. Given the heterogeneity and potential quality issues inherent in real-world pediatric data, such as missing values, inconsistencies, and varying formats from different sources, this layer uses data cleaning, normalization, transformation, and integration techniques to create a unified and analysis-ready dataset.

Next is the *feature engineering and selection* module, which is dedicated to extracting meaningful features from the preprocessed data that are highly indicative of pediatric health risks. This process may involve creating composite variables, transforming existing features, or applying dimensionality reduction techniques to optimize the input for AI models. Domain knowledge from pediatric medicine is crucial in guiding this process to ensure clinical relevance.

At the core of the framework lies the *AI-powered risk modeling and stratification engine*. This engine uses advanced ML algorithms, with a particular focus on ensemble learning techniques, as discussed in the Introduction, to construct predictive models for various pediatric health risks. Trained on historical data, these models learn complex patterns and relationships between input features and health outcomes or risk states. The output of this engine is not merely a binary prediction but a nuanced risk stratification, which may encompass risk scores, probability estimates, or the identification of distinct risk phenotypes. The determination of weights for each data modality is a critical aspect of our ensemble model. Rather than assigning predetermined, fixed weights, our *stacking* framework uses a data-driven approach.

The final layers of the framework are devoted to *risk profile generation and visualization* and *clinical decision support and intervention pathways*. The generated risk profiles are designed to be interpretable by health care professionals and understandable by caregivers, often incorporating visual aids and clear explanations. This output is intended to seamlessly integrate with clinical workflows, offering evidence-based insights to support shared decision-making regarding preventive strategies, further assessments, or targeted interventions. *Continuous monitoring* and *model updating* are also integral to the framework, ensuring that the AI models maintain their accuracy and relevance as new information emerges and clinical knowledge evolves [31].

XSL•FO
RenderX

Figure 1. Conceptual diagram of the AI-driven pediatric health risk stratification framework. The image visually represents the modules and their interconnections. AI: artificial intelligence.

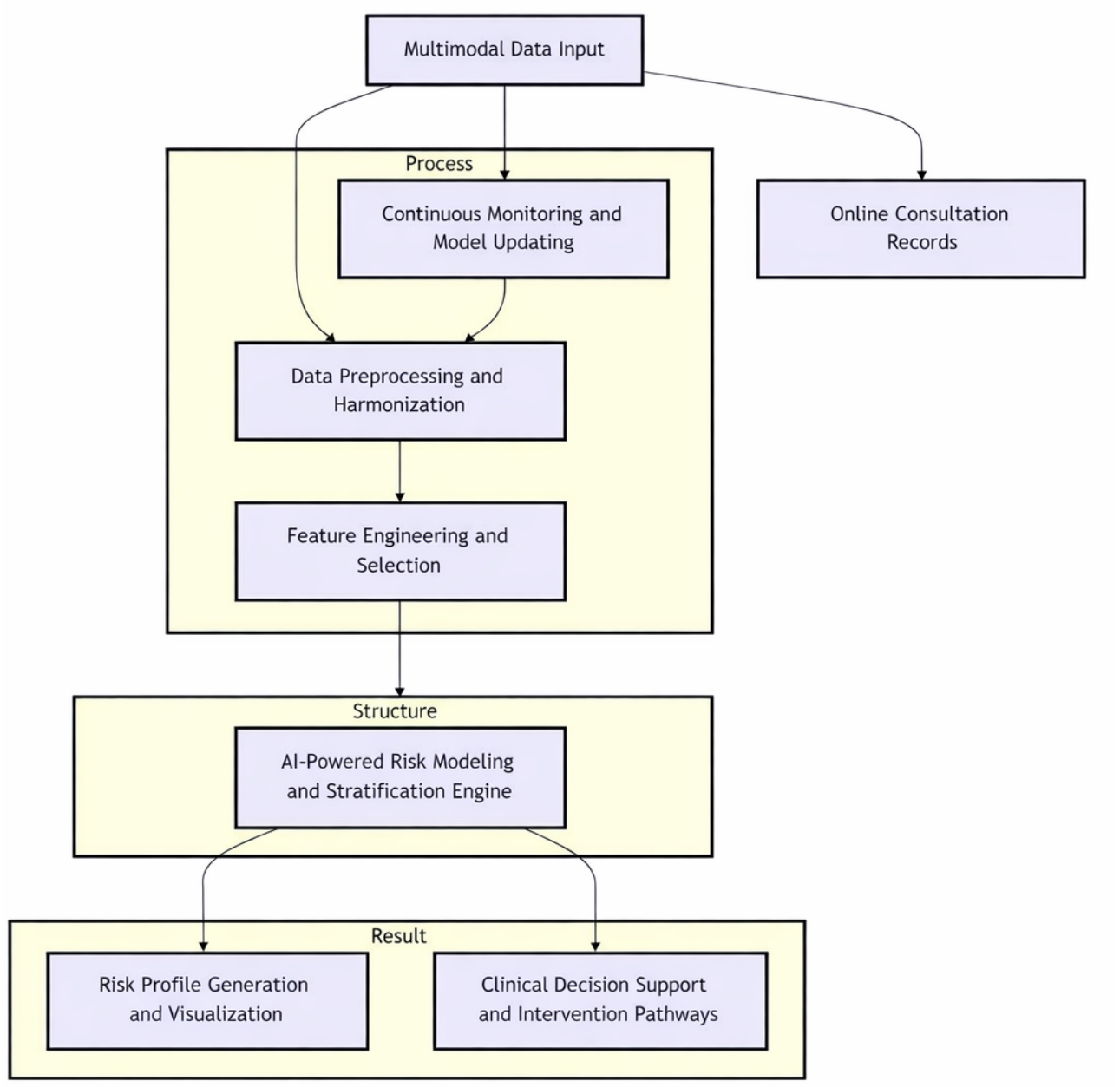

Identification of Key Pediatric Health Domains and Risk Factors

The primary pediatric health domains identified for this framework, as detailed in Table 2, cover a broad spectrum of child well-being. *Patient safety* focuses on risks, such as adverse drug events and medical errors, typically informed by EHR data and incident reports. *Continuous health monitoring* is crucial, tracking growth parameters and developmental milestones using EHR data and wearable sensor inputs. For children with ongoing conditions, *chronic disease management* addresses factors like glycemic control or asthma exacerbation frequency, primarily using EHR data and home monitoring device information. *Mental health* is a significant domain, evaluating behavioral indicators and emotional well-being via parental, teacher, and direct child assessments. Furthermore, *preventive care* adherence is monitored through risk factors, such as vaccination status and well-child visit compliance, drawing from EHR data and parental questionnaires [32]. The interconnected domains of *nutrition* and *growth* consider risks associated with nutritional intake and growth percentiles, also informed by EHR and parental questionnaire data. Lastly, *physical activity* levels and sedentary behavior duration, identified as critical risk factors, are assessed using wearable sensor data and parental questionnaires.

For each identified health domain, a set of specific, measurable risk factors and associated potential data sources is cataloged. This systematic identification ensures that the subsequent data acquisition and AI modeling efforts are focused and aligned with the goal of comprehensive risk assessment. The dynamic nature of these risk factors across different developmental stages (infancy, early childhood, middle childhood, and adolescence)

XSL•FO
RenderX

is also a key consideration in the framework's design and application.

Table . Key pediatric health domains, associated risk factors, and potential data sources.

Key pediatric health domains	Associated risk factors	Potential data sources
Patient safety	Adverse drug events and medical errors	EHR[a] data and incident reports
Health monitoring	Growth parameters and developmental milestones	EHR data and wearable sensor data
Chronic disease management	Glycemic control and asthma exacerbation frequency	EHR data and home monitoring devices
Acute illness severity	Fever severity and respiratory distress indicators	EHR data and parental questionnaire responses
Mental health	Behavioral indicators and emotional well-being	Parental and teacher assessments, and direct child assessments
Preventive care	Vaccination status and well-child visit adherence	EHR data and parental questionnaire responses
Nutrition and growth	Nutritional intake and growth percentiles	EHR data and parental questionnaire responses
Physical activity	Activity levels and sedentary behavior duration	Wearable sensor data and parental questionnaire responses

[a]EHR: electronic health record.

Multimodal Data Acquisition and Preparation

The effectiveness of the AI-driven risk stratification framework is fundamentally dependent on the availability of comprehensive, high-quality, multimodal data that accurately reflect the various factors influencing child health. This section details the strategies for acquiring and preparing such data for input into the framework, emphasizing the critical importance of ethical considerations, including informed consent, data privacy, and security, in full compliance with relevant regulations, such as the General Data Protection Regulation (GDPR) and Health Insurance Portability and Accountability Act (HIPAA), adapted for pediatric populations.

The data sources for this framework are inherently multimodal, encompassing a variety of information types. EHRs serve as a primary source, offering longitudinal clinical data that include diagnoses (ICD codes), procedures, medications, laboratory results, growth chart data, and clinical notes. Access to both structured and unstructured EHR data is essential. *Parental and child questionnaires or surveys* are used to capture information often not systematically recorded in EHRs, such as detailed family history, socioeconomic status, lifestyle factors (diet, physical activity, and sleep), environmental exposures, and patient-reported outcomes or symptoms. *Wearable sensors and mHealth data* provide opportunities for continuous, real-world monitoring of physiological parameters (eg, heart rate, activity levels, and sleep patterns) and behavioral data. *School health records* can contribute information on immunizations, health screenings conducted at school, and potentially attendance or behavioral notes relevant to health [33]. *Public health and environmental databases* can offer community-level data on factors like air quality, neighborhood socioeconomic indicators, and access to health care or recreational facilities. *Genomic data*, when applicable and ethically sourced, can provide valuable genetic risk scores or specific genetic markers associated with pediatric conditions.

The data preparation pipeline, illustrated in Figure 2, involves several key steps to transform raw, multimodal data into an analysis-ready dataset. Initially, data from disparate sources must undergo integration and harmonization. This process includes mapping data elements to common terminologies, resolving inconsistencies, and creating a unified data schema. Data cleaning is then performed to address missing values, correct errors, and remove outliers. Data transformation may be necessary to convert raw data into formats suitable for analysis, such as calculating age-specific *z* scores for growth parameters or deriving summary statistics from time-series sensor data. For instance, if xraw is a raw measurement and μage,sex and σage,sex are the age- and sex-specific mean and SD, respectively, from a reference population, the *z* score can be calculated as follows:

$$z = x_{raw} - \mu_{age,sex} \sigma_{age,sex}$$

This normalization is crucial for enabling comparisons of measurements across different age groups and sexes. Finally, data anonymization or pseudonymization is rigorously applied to protect patient privacy before the data are used for model development. The resulting dataset provides the foundation for the feature engineering and AI modeling stages described in the subsequent part.(2)

XSL•FO
RenderX

Figure 2. Multimodal data acquisition and preparation pipeline.

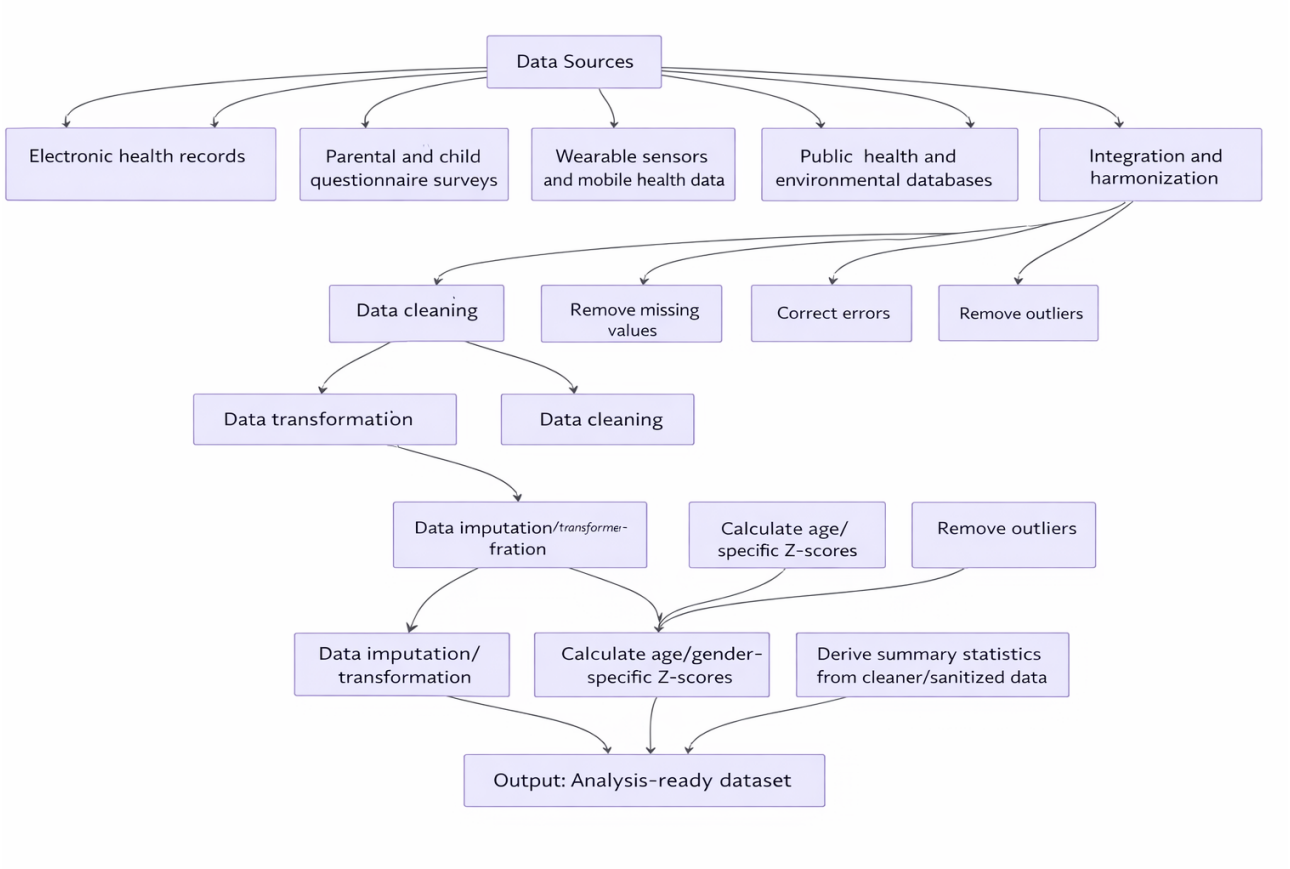

Data Preprocessing and Feature Engineering

The integrity and utility of input data are paramount to the performance and clinical relevance of any AI model, particularly in the pediatric domain, where data can be sparse, longitudinal, and highly variable due to growth and development. Pediatric health data, often derived from multiple heterogeneous sources, such as EHRs, parental questionnaires, school health notes, and wearable sensors, typically present unique challenges, including systematically missing values (eg, developmental assessments not performed at certain ages), measurement noise (eg, variability in home-based measurements), and the presence of irrelevant or redundant information that can obscure true risk signals. Therefore, rigorous data preprocessing and thoughtful, domain-informed feature engineering are indispensable steps to prepare a high-quality dataset for subsequent AI modeling.

The initial phase of preprocessing involves comprehensive data cleaning. Missing data represent a pervasive issue in longitudinal pediatric health care datasets. For instance, growth parameters or developmental screening results might be missing for specific well-child visits. While simple imputation techniques like mean, median, and mode imputation can be applied for variables with a low percentage of missingness and random patterns, they often fail to capture the underlying data structure in pediatric cohorts. More sophisticated methods are typically required, such as k-nearest neighbors imputation, which identifies the k most similar pediatric cases (based on a suite of other observed features) and imputes the missing value for a feature Xj using a weighted average or majority vote from the neighbors [34]. Alternatively, model-based imputation, using algorithms like multivariate imputation by chained equations (MICE), can be used. MICE iteratively models each variable with missing values as a function of other variables in the dataset, cycling through variables until convergence is achieved. For a set of variables X1,…,Xp, MICE specifies a conditional model PXj ∣ X-j,φj for each Xj and iteratively samples from these conditional distributions.

Outlier detection and appropriate treatment are also critical in pediatric data, where extreme values might represent genuine clinical concern or measurement error. Statistical methods, such as the *z* score and IQR, are used. For a data point xi in a feature distribution, its *z* score is calculated as zi=(xi−μ)/σ, where μ is the mean and σ is the SD. Data points with |zi|>θoutlier may be flagged. The IQR method defines outliers as points falling below Q1-1.5×IQR or above Q3+1.5×IQR, where Q1 and Q3 are the first and third quartiles, respectively, and IQR=Q3-Q1. Decisions on handling outliers (removal, transformation, or winsorization) are made cautiously, considering the potential clinical significance of extreme values in child health.

Feature engineering in the pediatric context is a highly domain-driven process focused on creating new, informative features from raw data to capture developmental trajectories, critical exposure periods, and clinically relevant interactions. This enhances model performance and interpretability. In child health, this includes deriving age- and sex-adjusted *z* scores for growth parameters, such as height, weight, BMI, and head circumference, based on standardized pediatric growth charts like World Health Organization (WHO) and Centers for Disease Control and Prevention (CDC) growth standards. It also involves

XSL•FO
RenderX

creating features like developmental velocity, calculated as ΔD/Δt=Dt2-Dt1/t2-t1, reflecting the rate of change in developmental milestone scores between assessments. Additionally, it covers quantifying cumulative exposure to risk factors, such as days with poor air quality and screen time during early childhood, generating features for adherence to pediatric guidelines like vaccination completeness and well-child visit schedules, and creating interaction terms reflecting synergistic effects in child health, such as genetic predispositions interacting with environmental exposures.

To reduce dimensionality, mitigate the risk of overfitting (especially with potentially limited sample sizes in specific pediatric subpopulations), and improve model training efficiency and interpretability, various feature selection techniques are used. These are broadly categorized into filter methods, wrapper methods, and embedded methods. Filter methods evaluate features independently of the AI model, using statistical measures relevant to pediatric outcomes, such as the chi-square test for assessing associations between categorical risk factors (eg, maternal smoking during pregnancy) and a binary child health outcome, and the ANOVA *F* value for assessing the relationship between numerical predictors (eg, birth weight) and different risk groups. Wrapper methods, such as recursive feature elimination, use the performance of a specific AI model to iteratively build and evaluate models with different subsets of features. Embedded methods perform feature selection as an integral part of the model training process. For instance, tree-based algorithms like random forest and gradient boosting inherently provide feature importance scores based on how much each feature contributes to reducing impurity or error across the ensemble of trees. Regularization techniques, such as L1 regularization (Lasso), are particularly useful. The Lasso objective function for a linear model predicting a child's health outcome y based on features X and coefficients β is as follows:

$$(3) LLasso=\sum i=1n\ (yi-\beta 0-\sum j=1p\ xij\beta j)2+\lambda \sum j=1p\ |\beta j|$$

where λ is the regularization parameter that controls the penalty on the sum of absolute values of the coefficients, effectively shrinking less important feature coefficients to zero. The selection of λ is typically done via cross-validation.

To provide an overview of the preprocessing pipeline and feature engineering strategies across different data modalities, the key steps are summarized in Table 3.

Table . Summary of pediatric data preprocessing steps and feature engineering strategies.

Data type	Preprocessing methods	Feature engineering	Examples
Growth indicators	Missing data imputation (KNN[a] and MICE[b])	*z* score calculation and velocity features	Age- and sex-adjusted *z* scores
Early exposure	Outlier detection (*z* score and IQR)	Cumulative exposure and interaction terms	Poor air quality days and screen time
Questionnaires	Data cleaning and encoding	One-hot encoding and label encoding	Vaccination scores and visit adherence
School records	Data integration	Feature extraction	Immunization records and attendance
Wearables	Noise reduction and smoothing	Activity patterns and sleep metrics	Activity levels and sleep duration
Genomics	Data anonymization	Genetic risk scoring	Genetic predispositions

[a]KNN: k-nearest neighbors.

[b]MICE: multivariate imputation by chained equations.

Risk Stratification Algorithm

The process of risk stratification involves translating the continuous risk probabilities or composite risk scores generated by AI models into distinct, actionable risk categories that are meaningful in a clinical context. This is achieved by defining specific thresholds that convert model outputs into discrete risk strata. The thresholds are determined through a combination of clinical expertise, statistical methods, and decision theory principles, ensuring they are both clinically relevant and statistically valid. P(Risk / Xchild) represents the feature vector for a specific child. For a 4-tier stratification system, the risk categories can be defined as follows:

- Low risk: P(Risk /Xchild)<θ1
- Moderate risk: θ≤P(Risk / Xchild)<θ2
- High risk: θ2≤P(Risk / Xchild)<θ3
- Very high risk: P(Risk / Xchild)≥θ3

The selection of the thresholds θ1,θ2,θ3 is guided by clinical expertise, statistical methods, and decision theory. Pediatric specialists define thresholds based on established clinical guidelines, acceptable risk levels for specific age groups, and the availability and efficacy of preventive interventions. Statistical methods, such as using percentiles of the predicted risk distribution in a well-characterized pediatric reference population, can also be used. For example, thresholds might be set to correspond to the 50th, 80th, and 95th percentiles of this distribution. Decision theory principles can further refine threshold optimization by considering a utility function that balances the costs and benefits associated with true positives, false positives, true negatives, and false negatives. This might involve analyzing metrics like Youden J statistic (J=sensitivity+specificity−1) or finding points on the precision-recall curve that correspond to desired tradeoffs for pediatric screening or intervention programs.

XSL•FO
RenderX

When the system is designed to predict multiple distinct health risks for a child, such as the risk of obesity, developmental delay, or asthma exacerbation, the framework requires a mechanism to present these risks in a consolidated and understandable manner. This can be achieved by either displaying the stratified risk level for each condition independently or by developing a composite pediatric health vulnerability index (CPHVI). The CPHVI is calculated by assigning weights wi to each risk score *S*(Ri) based on factors, such as the clinical severity of risk Ri, its impact on long-term child development, its prevalence in the target pediatric population, and its responsiveness to an intervention. To translate the CPHVI into clinical practice, we propose a tiered intervention model based on predefined, clinically meaningful thresholds developed in collaboration with pediatric experts. For example, a CPHVI score exceeding a "high risk" threshold could automatically trigger an alert in the EHR system for the primary care physician, along with a recommendation for a direct referral to a relevant specialist. The formula for the CPHVI is as follows:

$$(4)\text{SCPHVI}=\sum i=1\text{N wi}\cdot\text{S(Ri)}\sum i=1\text{N wi}$$

The determination of the weights wi is a complex task, often requiring expert consensus or data-driven approaches. Another advanced approach involves using unsupervised learning techniques, such as clustering algorithms, applied to the vector of predicted individual risk probabilities for each child. This can help identify common co-occurring risk patterns or distinct pediatric subphenotypes that share similar multirisk profiles, guiding more tailored multifaceted interventions.

To enhance clinical utility and facilitate shared decision-making with families, the reasons behind a child's stratification into a particular risk category must be as transparent and interpretable as possible. Techniques, such as SHAP and Local Interpretable Model-Agnostic Explanations (LIME), are used. For a given prediction f(Xchild), SHAP assigns an importance value (SHAP value, φj) to each input feature j, representing its marginal contribution to pushing the prediction away from a baseline. The sum of SHAP values for all features plus the baseline prediction equals the model's output for that child:

$$(5)\text{fXchild} =\varphi 0+\sum j=1\text{M }\varphi j$$

This allows clinicians to understand which specific factors (eg, low birth weight, specific dietary patterns, and lack of physical activity) are most influential in determining a child's assessed risk level, thereby guiding targeted advice and interventions.

BERT-Based Knowledge Extraction and NLP Modeling

BERT-based NLP is used to extract informative representations from unstructured pediatric clinical text (eg, consultation records, clinical notes, and parental narratives), which are subsequently used as input features for pediatric health risk stratification models.

Pediatric medical journals serve as a vital source of pediatric disease knowledge, encompassing a wealth of information on pediatric diseases, including clinical symptoms, diagnostic methods, treatment approaches, and prognoses. These journals are written by pediatric experts and researchers and are based on extensive clinical practice and scientific research. They contain detailed case studies, research findings, and expert opinions, providing a solid foundation for the extraction and application of pediatric disease knowledge. The knowledge derived from these journals can help health care professionals better understand the characteristics and progression of pediatric diseases, thereby improving the quality of pediatric health care services [14].

The pediatric disease knowledge base is a structured repository that integrates information from pediatric medical journals and other authoritative sources. It includes various aspects of pediatric diseases, such as disease names, symptoms, signs, laboratory test results, imaging findings, treatment methods, and prognoses. This knowledge base is designed to provide comprehensive and accurate information on pediatric diseases, supporting clinical decision-making and research. By organizing and structuring the information from pediatric medical journals, the pediatric disease knowledge base enables efficient retrieval and utilization of pediatric disease knowledge, facilitating the application of this knowledge in clinical practice and research.

The process begins with the ingestion of pediatric medical journal data into our system. These textual data, rich in pediatric disease knowledge, undergo meticulous preprocessing to align with BERT's input requirements. The text is tokenized into a sequence of tokens [T1,T2,…,Tn], where each Ti represents a word or subword unit. Additionally, the pediatric disease knowledge base is incorporated to enhance the model's understanding of pediatric medical concepts. BERT's architecture consists of multiple transformer encoder layers, each equipped with self-attention mechanisms. The input tokens, enriched with special markers like [CLS] and [SEP], pass through these layers, generating a matrix of contextualized embeddings z={z1,z2,…,zn}. These embeddings capture intricate semantic relationships and contextual information within the text, forming the basis for subsequent knowledge extraction tasks.

To identify key pediatric disease entities and their relationships within the text, named entity recognition and relation extraction techniques are applied to the BERT-generated embeddings. For named entity recognition, a linear layer combined with a conditional random field is used. The conditional random field loss function is defined as follows:

$$(6)\text{LNER}=-1\text{N}\sum i=1\text{NlogP(yi} \mid \text{Xi)}$$

where N is the number of samples and Pyi ∣ Xi is the probability of the true label sequence yi given the input sequence Xi. For relation extraction between entities, a classifier is trained using a cross-entropy loss function as follows:

$$(7)\text{LRE}=-\sum i=1\text{M }\sum j=1\text{C yi,jlogy}\hat{}\text{i,j}$$

where M represents the number of entity pairs, C is the number of relation types, and yi,j and y^i,j are the true and predicted probabilities for relation *j* between the entity pair *i*, respectively. The extracted entities and relationships are then integrated into the pediatric disease knowledge base. This knowledge base, enriched with entities and relationships from pediatric medical literature, serves to enhance a medical chatbot's responses. When users input symptoms, the chatbot leverages this

XSL•FO
RenderX

knowledge base to generate accurate and contextually relevant diagnostic suggestions and risk assessments.

Figure 3 illustrates a comprehensive workflow where BERT's robust language understanding capabilities are harnessed to extract valuable pediatric disease knowledge from medical texts. This knowledge is subsequently used to empower a medical chatbot, enabling it to deliver precise and informative responses to user inquiries regarding pediatric symptoms. The integration of BERT with pediatric medical journals and a pediatric disease knowledge base provides a powerful tool for advancing pediatric health care through improved diagnostic accuracy and personalized treatment recommendations.

Our knowledge extraction module is built upon BioBERT, a pretrained language model optimized for the biomedical domain. We chose BioBERT as our base model due to its demonstrated strong performance on various biomedical text mining tasks. For fine-tuning, we used a domain-specific corpus comprising over 50,000 articles from leading pediatric medical journals and over 100,000 deidentified clinical notes. The model was fine-tuned for 5 epochs with a learning rate of $2e^{-5}$. The performance of our fine-tuned model on key NLP tasks was rigorously evaluated on a manually annotated test set of 500 clinical notes, which were dual-annotated by pediatric domain experts to ensure quality.

Figure 3. BERT-driven pediatric disease knowledge extraction and medical dialogue response framework. T denotes the input token sequence obtained after tokenization of the pediatric clinical text, E represents the contextualized embedding vectors produced by the BERT encoder, and Trm refers to the Transformer encoder layers of the BERT model. BERT: Bidirectional Encoder Representations From Transformers.

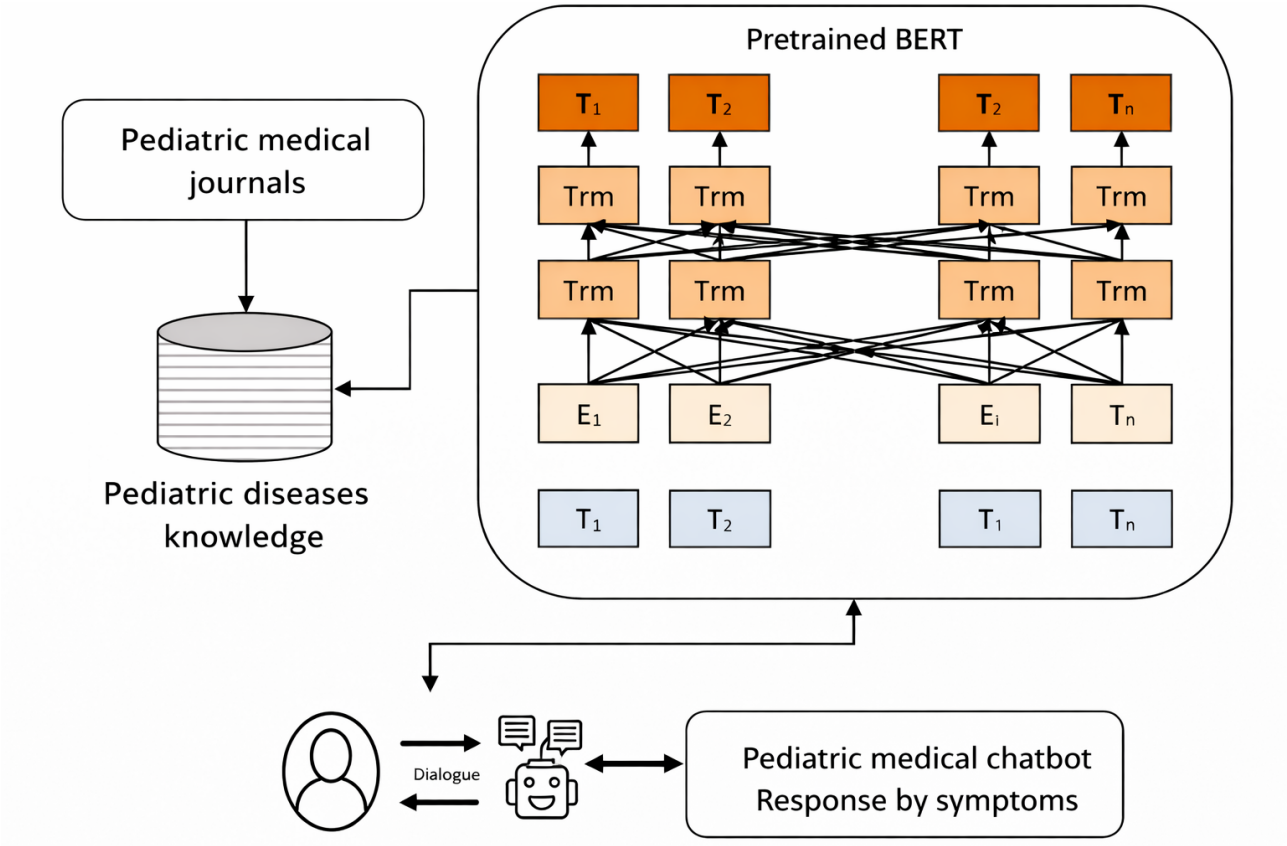

System Architecture Design

The successful deployment, scalability, and usability of the AI-driven pediatric health risk stratification framework critically depend on a meticulously planned and well-engineered system architecture. This architecture must robustly support efficient multimodal data processing pipelines; reliable and timely execution of complex AI models; secure and compliant management of sensitive pediatric health data; and an intuitive, actionable interface for diverse end users, including pediatricians, specialist clinicians, public health officials, researchers, and potentially, with appropriate safeguards, parents or caregivers. A multitier, service-oriented architecture is proposed to ensure modularity, maintainability, and scalability. This typically comprises the following tiers:

1. Data tier: This foundational tier is responsible for the persistent storage and comprehensive management of all relevant pediatric health data. This includes raw input data from diverse sources (EHRs, wearables, and questionnaires), preprocessed and feature-engineered datasets, trained AI models (including their versions and metadata), generated risk profiles for individual children, and audit logs. This tier would likely involve a hybrid database strategy, combining relational databases (MySQL) for structured metadata, patient demographics, and well-defined clinical entities, with potentially NoSQL databases for handling large volumes of heterogeneous, unstructured, or streaming data (like continuous sensor readings). Robust data governance, backup, and recovery mechanisms are integral.
2. Application logic tier (backend services): This is the computational core of the system, housing the data

XSL•FO
RenderX

preprocessing pipelines, sophisticated feature engineering modules, the AI model inference engine, and the risk stratification algorithms. It handles all computational tasks, business logic for risk assessment, and interactions with the data tier. This tier would be developed using scalable and efficient programming languages and appropriate backend frameworks. It may be implemented as a set of microservices to enhance scalability and independent deployability of different functionalities.

3. Presentation tier (frontend interfaces): This tier provides the user interface and user experience for interacting with the system. This could manifest as a secure web-based application accessible via standard browsers, designed with responsive layouts for use on various devices. For specific user groups like parents or children (with age-appropriate design), a dedicated mobile app might be considered. The frontend allows authorized users to view individualized pediatric risk stratification results, explore interactive visualizations of risk factors and trends, access evidence-based decision support information or guideline recommendations, and potentially (for clinicians) trigger further diagnostic or intervention pathways.

Key functional system modules are designed to support the end-to-end pediatric risk stratification process (Figure 4).

1. Pediatric data ingestion and management module: It securely handles the import of data from diverse, often disparate, pediatric health information systems and sources. It performs initial data validation and schema mapping and manages data storage, versioning, and provenance tracking, which are crucial for longitudinal pediatric studies.
2. Preprocessing and pediatric feature engineering module: It implements complex algorithms described in the preceding section, tailored for pediatric data. This module needs to be highly configurable and extensible to accommodate new data types, evolving pediatric clinical knowledge, or updated feature definitions.
3. AI model execution and management engine: It loads versioned, trained AI models and performs inference on new or updated pediatric patient data to generate risk predictions. This engine must be optimized for performance and scalability, especially if real-time or near real-time risk assessment is required for acute pediatric conditions. It also manages the model lifecycle, including retraining triggers and performance monitoring.
4. Pediatric risk stratification and profiling module: It implements the sophisticated algorithms from the preceding section to convert raw model outputs into clinically interpretable risk strata and comprehensive, multidimensional pediatric risk profiles, potentially including age-adjusted interpretations.
5. Reporting, visualization, and alerting module: It generates customized reports, interactive dashboards (eg, showing population-level pediatric risk distributions and trends over time for specific age cohorts), and dynamic visualizations (eg, individual child risk timelines and feature importance charts for specific predictions). It may also include an alerting mechanism for clinicians when a child's risk profile crosses critical, predefined thresholds.
6. User authentication, authorization, and audit module: It ensures secure, role-based access to the system and its sensitive pediatric data, adhering strictly to privacy regulations (eg, HIPAA, GDPR, and Children's Online Privacy Protection Act [COPPA]). Comprehensive audit trails of data access and system actions are maintained.
7. Interoperability layer (application programming interfaces [APIs]): It provides well-defined APIs, possibly using standards like Fast Healthcare Interoperability Resources, to allow secure data exchange and interaction with other clinical systems (eg, pediatric EHRs, laboratory information systems, and clinical decision support tools embedded in existing workflows).

The data flow within the system begins with secure data ingestion from multiple sources into the *data tier*. The *application logic tier* then orchestrates the preprocessing and feature engineering pipelines. The processed features are subsequently fed into the *AI model execution engine* for risk prediction. These predictions are passed to the *risk stratification and profiling module*, and the final, interpretable pediatric risk profiles are stored and made available for secure access and visualization through the *presentation tier* or via the *API layer*. The technology stack will be carefully chosen based on criteria, such as scalability for large pediatric populations, real-time performance requirements, security mandates for child data, ease of development and maintenance, and compatibility with existing health care IT infrastructure. This might include Python with libraries like Pandas, NumPy, Scikit-learn, TensorFlow/Keras, and PyTorch for AI or ML development; web frameworks, such as Django/Flask (Python), Spring Boot (Java), and Node.js, for the backend services; modern JavaScript frameworks like React, Angular, and Vue.js for building responsive and interactive frontend interfaces; and a combination of SQL and NoSQL databases as described for the *data tier*. Containerization technologies like Docker and orchestration tools like Kubernetes may be used for deployment and scaling.

XSL•FO
RenderX

Figure 4. Multitier system architecture diagram for pediatric risk stratification. AI: artificial intelligence.

XSL•FO
RenderX

Prototype System Implementation

The pediatric health risk stratification prototype system integrates multisource data input with advanced AI models to deliver a comprehensive risk assessment platform. As illustrated in Figure 5, the system collects diverse data types, including patient demographics, clinical records, and parent-reported outcomes, which serve as the foundation for subsequent analysis and risk assessment. This integration ensures a holistic view of pediatric health, enabling more accurate and nuanced risk predictions.

At the core of the system is a pretrained BERT model, specifically fine-tuned to handle pediatric health terminology and context. The model processes input text data through multiple Transformer modules, which encode the text to capture complex linguistic patterns and semantic relationships. Feature extraction layers then distil these encoded representations into risk-relevant features. These features are passed to risk assessment components where the actual risk stratification takes place, transforming raw data into actionable insights regarding children's health risks.

The system's implementation leverages a robust technology stack to ensure efficiency, scalability, and user-friendliness. The backend, developed using Python and its rich library ecosystem, handles data processing and model execution. It uses microservices, potentially orchestrated by lightweight frameworks like Flask, to manage distinct functionalities such as data ingestion, preprocessing, and model inference. Data storage follows a hybrid approach, combining PostgreSQL for structured data with MongoDB for unstructured or semistructured content. The frontend, built with modern JavaScript frameworks, offers tailored interfaces for different users, including physicians and parents. It includes features like risk profile visualizations and population-level risk trend dashboards. Docker is used for containerization to ensure smooth deployment and scalability of the application components.

To illustrate the practical utility of the framework, consider a hypothetical clinical scenario. Dr Smith, a pediatrician, begins her day by logging into the system's dashboard. The system flags one of her patients, a 5-year-old child, for a significant increase in the composite risk score for developing obesity. Dr Smith clicks on the patient's profile and is presented with an interactive, multimodal dashboard. An explainable AI feature, using SHAP values, highlights the primary contributing factors: a recent decrease in physical activity levels captured by wearable data and parent-reported dietary logs indicating high consumption of processed foods. Based on these insights, the system provides Dr Smith with evidence-based, actionable recommendations, including a referral to a pediatric nutritionist and a set of tailored educational materials for the parents. This scenario demonstrates how the framework can transform raw data into clinically actionable insights to facilitate timely and personalized preventive care.

XSL•FO
RenderX

Figure 5. Structure of the pediatric health risk stratification prototype system. T denotes the input token sequence obtained after tokenization of the pediatric clinical text, E represents the contextualized embedding vectors produced by the BERT encoder, and Trm refers to the Transformer encoder layers of the BERT model. BERT: Bidirectional Encoder Representations From Transformers; EHR: electronic health record.

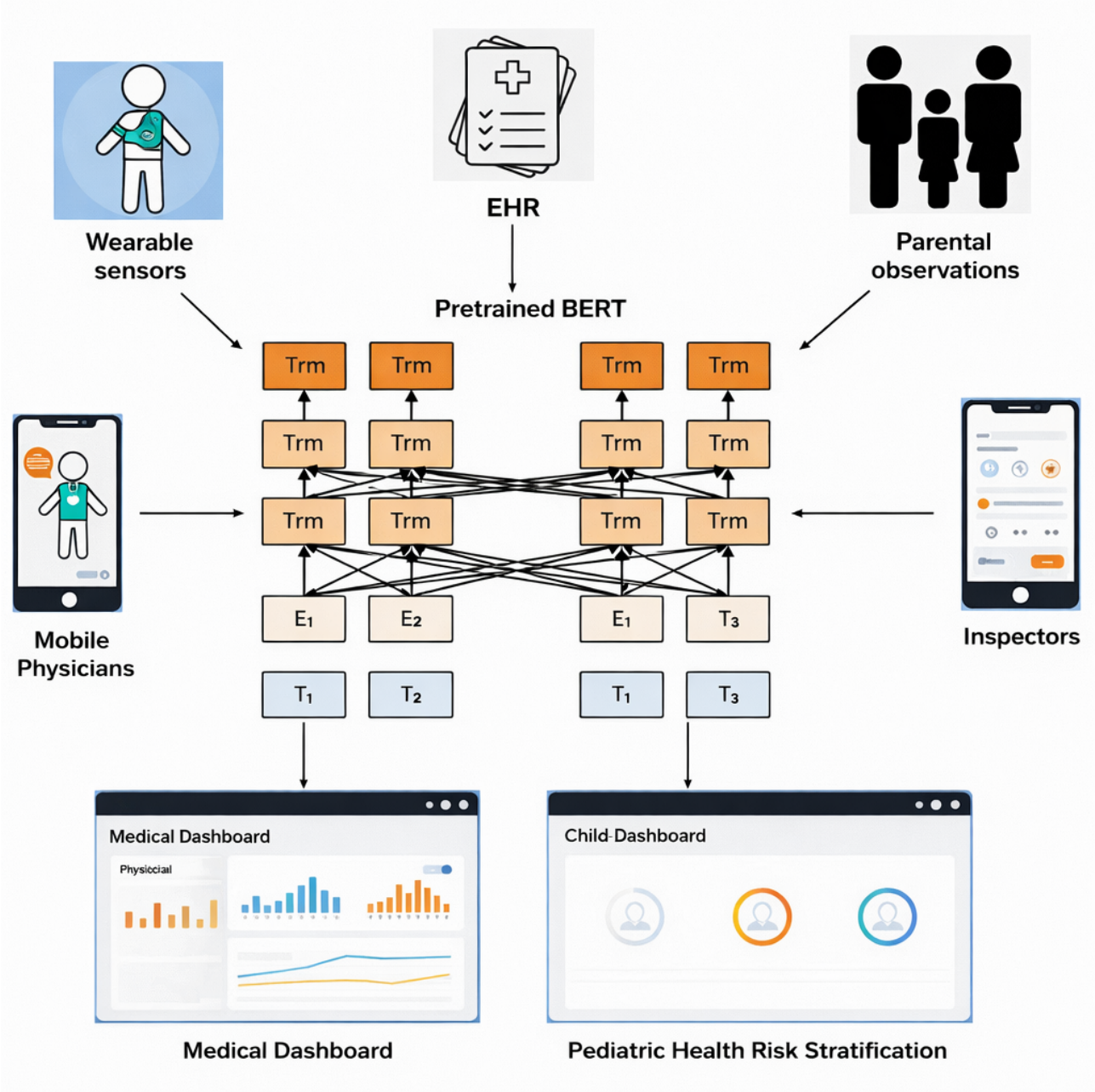

Experimental Setup

The primary dataset used for training and validating the AI models included data from over 40,000 pediatric participants, with an age range of 2 to 8 years at the time of data collection or follow-up. The dataset was partitioned into 3 mutually exclusive sets: a training set (70% of the data), a validation set (15%), and an independent holdout test set (15%). To ensure temporal validity if longitudinal data were used, the split was performed such that data from earlier time periods were used for training and validation, while data from later periods were reserved for testing, mimicking a prospective evaluation.

To benchmark the performance of the proposed AI-driven framework, a selection of robust baseline models was implemented and rigorously evaluated on an identical dataset and predictive task. These comparators included established traditional statistical models frequently used in pediatric risk prediction, specifically logistic regression for binary risk outcomes, where the probability of risk $P(Y=1 \mid X)$ is modeled as $P(Y=1 \mid X)=(1+e^{-(\beta 0+\sum i=1p \beta iXi)})-1$, and Cox proportional hazards models in scenarios where time-to-event data for risk onset were available. Furthermore, simpler yet effective ML algorithms, namely support vector machine (SVM), configured with various kernels (linear and radial basis function), and standard single decision trees, were also incorporated as baselines. In instances where existing, validated pediatric risk scores or established rule-based systems were pertinent to the specific health outcomes under investigation and applicable to the dataset, these were also included in the comparative analysis to provide a comprehensive performance context. To rigorously

XSL•FO
RenderX

assess the statistical significance of our model's superior performance, we used the DeLong test to compare the area under the receiver operating characteristic curve (AUC-ROC) of our proposed model with that of each baseline model.

Ethical Considerations

This study involved research with human participants. The study protocol was reviewed and approved by the Institutional Review Board and Research Ethics Committee of Hunan University of Arts and Science (HUAS-20250504). All procedures were performed in accordance with the ethical standards of the responsible institutional committee and with the principles of the Declaration of Helsinki. Informed consent was obtained from all participants prior to their inclusion in the study. Participants were fully informed about the purpose of the study, the procedures involved, and their right to withdraw at any time without penalty. The privacy and confidentiality of all participants were strictly maintained throughout the study. All data were anonymized prior to analysis, and no personally identifiable information was collected, stored, or reported. No financial or material compensation was provided to participants for their participation in this study.

Results

This section reports the empirical performance of the proposed AI-driven pediatric health risk stratification framework evaluated on the independent test set, in comparison with multiple baseline models.

Table 4 summarizes the predictive performance of the proposed model and baseline methods across targeted pediatric health risks. The proposed model achieved an AUC-ROC of 0.85 (95% CI 0.82 - 0.88), an area under the precision-recall curve of 0.70 (95% CI 0.65 - 0.75), a sensitivity of 0.78, a specificity of 0.80, and an F_1-score of 0.75. In comparison, logistic regression, SVM, random forest, gradient boosting, and a conventional deep learning model yielded lower AUC-ROC and F_1-score values.

Table . Key performance metrics of the proposed artificial intelligence model and baseline models for targeted pediatric risks in the test set.

Model name	AUC-ROC[a], value (95% CI)	AUC-PR[b], value (95% CI)	Sensitivity	Specificity	F_1-score	Brier score
Proposed BERT[c] model	0.85 (0.82 - 0.88)	0.70 (0.65 - 0.75)	0.78	0.80	0.75	0.15
Logistic regression	0.72 (0.68 - 0.76)	0.60 (0.55 - 0.65)	0.65	0.70	0.62	0.20
SVM[d]	0.75 (0.71 - 0.79)	0.65 (0.60 - 0.70)	0.70	0.72	0.66	0.18
Random forest	0.78 (0.74 - 0.82)	0.67 (0.62 - 0.72)	0.72	0.75	0.69	0.17
Gradient boosting	0.80 (0.77 - 0.83)	0.69 (0.64 - 0.74)	0.75	0.76	0.72	0.16
Deep learning	0.83 (0.80 - 0.86)	0.72 (0.67 - 0.77)	0.76	0.79	0.74	0.14

[a]AUC-ROC: area under the receiver operating characteristic curve.

[b]AUC-PR: area under the precision-recall curve.

[c]BERT: Bidirectional Encoder Representations From Transformers.

[d]SVM: support vector machine.

The DeLong test demonstrated that the AUC-ROC of the proposed model was significantly higher than that of each baseline model (all $P<.05$). Paired t tests on F_1-scores similarly indicated statistically significant improvements in predictive accuracy for the proposed model relative to all comparators.

To further assess alignment with expert judgment, a manual comparison evaluation was conducted using 100 randomly selected pairs of online consultation cases. Automated predictions and expert assessments were concordant in 78 cases, corresponding to an agreement rate of 78%.

A confusion matrix (Figure 6) shows that most discrepancies occurred in cases manually labeled as "equivalent," whereas predictions for clearly differentiated cases exhibited higher agreement with expert assessments. Misclassifications were predominantly observed within the equivalent category, while the majority of nonequivalent cases were correctly identified.

XSL•FO
RenderX

Figure 6. Artificial intelligence prediction confusion matrix.

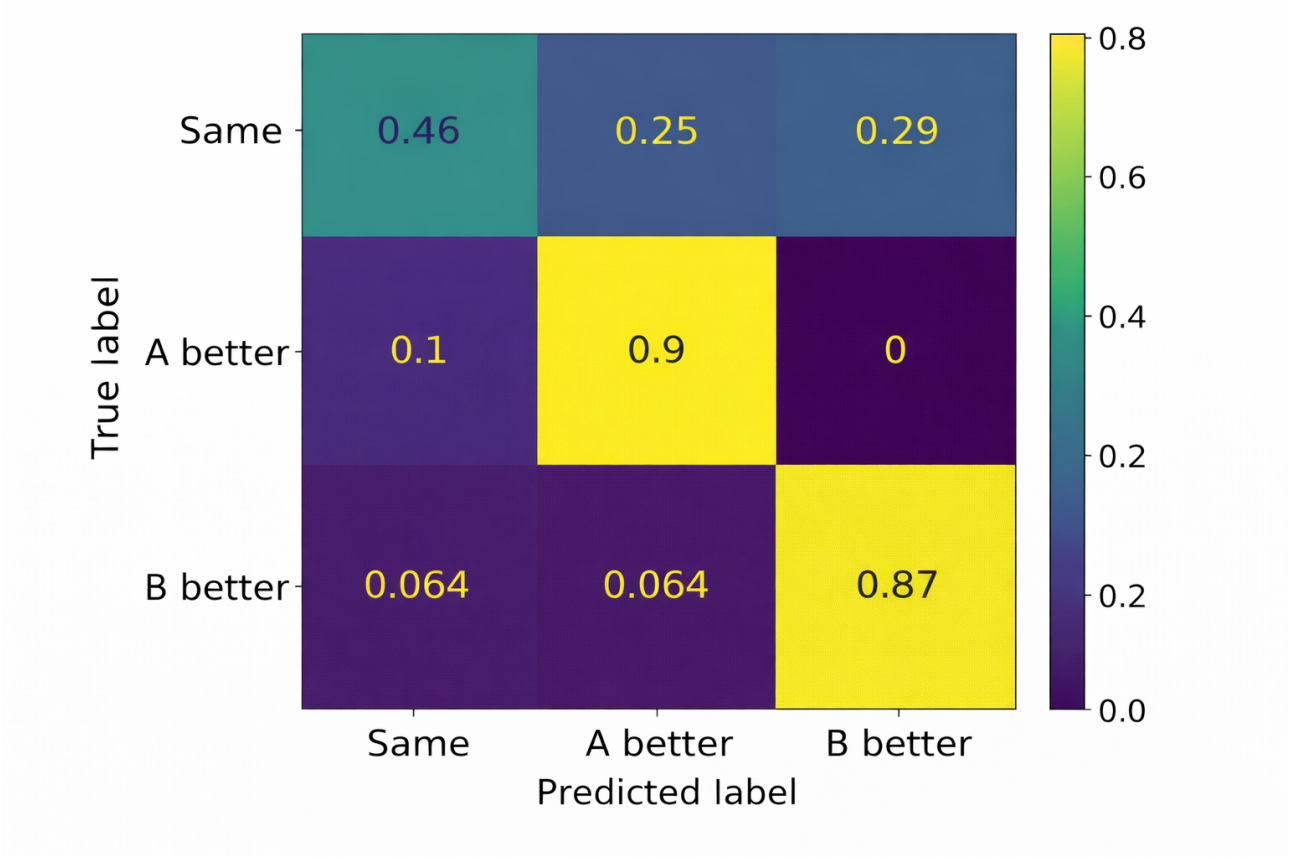

Model performance was further examined across predefined pediatric subgroups, including age categories, sex, and socioeconomic status (Table 5). Comparable AUC-ROC and F_1-score values were observed across all subgroups. For age-based stratification, the AUC-ROC values were 0.84 for children younger than 2 years, 0.85 for those aged 2 - 5 years, and 0.86 for those older than 5 years. Similar performance consistency was observed across sex and socioeconomic strata.

Table . Model performance across different pediatric subgroups for early childhood obesity.

Group	AUC-ROC[a], value (95% CI)	F_1-score
Age		
<2 years	0.84 (0.80 - 0.88)	0.74
2 - 5 years	0.85 (0.82 - 0.89)	0.75
>5 years	0.86 (0.83 - 0.89)	0.76
Sex		
Male	0.85 (0.82 - 0.88)	0.75
Female	0.84 (0.81 - 0.87)	0.74
Status		
Low SES[b]	0.83 (0.79 - 0.87)	0.73
Medium SES	0.85 (0.82 - 0.88)	0.75
High SES	0.86 (0.83 - 0.89)	0.76

[a]AUC-ROC: area under the receiver operating characteristic curve.

[b]SES: socioeconomic status.

XSL•FO
RenderX

Discussion

Conclusions

This study successfully designed and validated a novel AI-driven framework for comprehensive pediatric health risk stratification. The primary findings were threefold. First, the framework demonstrates the capability to effectively integrate heterogeneous, multimodal data sources to create a holistic view of a child's health status. Second, our proposed predictive model, which combines a fine-tuned BERT architecture with an ensemble learning strategy, significantly outperformed established baseline models, such as logistic regression and SVM, in predicting key health risks, achieving an AUC-ROC of 0.85 for early childhood obesity. Third, the prototype system's risk assessments showed substantial agreement with manual expert evaluations (78% accuracy), confirming its potential clinical utility and feasibility. The successful implementation of the prototype system, featuring intuitive dashboards for both clinicians and parents, further illustrates the practical applicability of this approach in facilitating early and personalized interventions, thereby contributing a novel and robust technological foundation for proactive pediatric health care.

Limitations and Future Work

While the presented framework shows considerable promise, certain limitations and avenues for future research warrant discussion. The current validation, though rigorous, was based on a specific dataset of over 40,000 pediatric participants aged 2 - 8 years. Broader validation across more diverse pediatric populations and longitudinal follow-up are essential to ascertain long-term predictive accuracy and generalizability. One limitation of our study is the observed slight dip in model performance for the subgroup of children aged 3 - 5 years, which we attribute to the relative scarcity of rich, unstructured text data for this age cohort. To mitigate this issue in future work, we plan to incorporate alternative text sources. A promising approach, as suggested, is the inclusion of open-ended responses from parental questionnaires. These narratives, which capture detailed parental concerns and observations, can be processed by our fine-tuned BERT model to generate rich semantic features, thereby enriching the feature set for younger children and addressing the data sparsity issue. A crucial direction for future work is the implementation of advanced bias mitigation techniques. We plan to further explore methods, such as adversarial debiasing, which involves training the model to make predictions that are invariant to sensitive attributes, thereby proactively enhancing the fairness and equity of our risk stratification framework.

Funding

The research project was supported by the Education Department of Hunan Province: Multidimensional Risk Assessment and Sports-Health Integrated Intervention Model Development for Postural Health in Children in Northwestern Hunan (project number: 24B0629), and the Aid Program for Science and Technology Innovative Research Team in Higher Educational Institutions of Hunan Province.

Conflicts of Interest

None declared.

References

1. Sales WB, Maranhão EF, Ramalho CST, Macêdo S, Souza GF, Maciel Á. Early life circumstances and their impact on health in adulthood and later life: a systematic review. BMC Geriatr 2024 Nov 28;24(1):978. [doi: 10.1186/s12877-024-05571-4] [Medline: 39609801]
2. Wadsworth ME, Kuh DJ. Childhood influences on adult health: a review of recent work from the British 1946 national birth cohort study, the MRC National Survey of Health and Development. Paediatr Perinat Epidemiol 1997 Jan;11(1):2-20. [doi: 10.1046/j.1365-3016.1997.d01-7.x] [Medline: 9018723]
3. Braveman P, Barclay C. Health disparities beginning in childhood: a life-course perspective. Pediatrics 2009 Nov;124 Suppl 3:S163-S175. [doi: 10.1542/peds.2009-1100D] [Medline: 19861467]
4. Noteboom A, Have MT, de Graaf R, Beekman ATF, Penninx B, Lamers F. The long-lasting impact of childhood trauma on adult chronic physical disorders. J Psychiatr Res 2021 Apr;136:87-94. [doi: 10.1016/j.jpsychires.2021.01.031] [Medline: 33581460]
5. Eadie P, Levickis P, McKean C, et al. Developing preschool language surveillance models - cumulative and clustering patterns of early life factors in the early language in Victoria study cohort. Front Pediatr 2022;10:826817. [doi: 10.3389/fped.2022.826817] [Medline: 35186809]
6. Olsen J, Pedersen LH. Reproductive health indicators and fetal medicine - many things will change. Scand J Work Environ Health 2016 Jun 1;42(6):561-562. [doi: 10.5271/sjweh.3596] [Medline: 27685865]
7. Young C, Grobelna A. Flash Glucose Monitoring Systems in Pediatric Populations With Diabetes: Canadian Agency for Drugs and Technologies in Health; 2021. URL: https://www.ncbi.nlm.nih.gov/books/NBK572013/ [accessed 2026-01-02]
8. Garbarino S, Bragazzi NL. Revolutionizing sleep health: the emergence and impact of personalized sleep medicine. J Pers Med 2024 Jun 4;14(6):598. [doi: 10.3390/jpm14060598] [Medline: 38929819]

XSL•FO
RenderX

9. Stidley CA, Shah VO, Narva AS, et al. A population-based, cross-sectional survey of the Zuni Pueblo: a collaborative approach to an epidemic of kidney disease. Am J Kidney Dis 2002 Feb;39(2):358-368. [doi: 10.1053/ajkd.2002.30557] [Medline: 11840378]
10. Vittoria Togo M, Mastrolorito F, Orfino A, et al. Where developmental toxicity meets explainable artificial intelligence: state-of-the-art and perspectives. Expert Opin Drug Metab Toxicol 2024 Jul 2;20(7):561-577. [doi: 10.1080/17425255.2023.2298827]
11. He O, Chen D, Li Y. A deep-learning approach to predict reproductive toxicity of chemicals using communicative message passing neural network. Front Toxicol 2025;7:1640612. [doi: 10.3389/ftox.2025.1640612] [Medline: 40765625]
12. Sambanis A, Osiecki K, Cailas M, Quinsey L, Jacobs DE. Using artificial intelligence to identify sources and pathways of lead exposure in children. J Public Health Manag Pract 2023;29(5):E208-E213. [doi: 10.1097/PHH.0000000000001759] [Medline: 37129378]
13. Huang YD, Zeng SL, Lin J, et al. Parents' understanding and attitudes toward the application of AI in pediatric healthcare: a cross-sectional survey study. Front Public Health 2025;13:1654482. [doi: 10.3389/fpubh.2025.1654482] [Medline: 40910043]
14. Sezgin E, Jackson DI, Kocaballi AB, et al. Can large language models aid caregivers of pediatric cancer patients in information seeking? A cross-sectional investigation. Cancer Med 2025 Jan;14(1):e70554. [doi: 10.1002/cam4.70554] [Medline: 39776222]
15. Shah U, Khan N, Alzubaidi M, Agus M, Househ M. ArtInsight: a multimodal AI framework for interpreting children's drawings and enhancing emotional understanding. Stud Health Technol Inform 2025 May 15;327(5):808-812. [doi: 10.3233/SHTI250471] [Medline: 40380579]
16. Till AC, Briganti G. Outcomes in machine learning models for child psychiatry: a systematic review of the literature. Psychiatr Danub 2025 Sep;37(Suppl 1):79-84. [Medline: 40982877]
17. Vandewouw MM, Syed B, Barnett N, et al. Using deep learning to predict internalizing problems from brain structure in youth. Transl Psychiatry 2025 Aug 29;15(1):326. [doi: 10.1038/s41398-025-03565-3] [Medline: 40883286]
18. Till AC, Briganti G. AI in child psychiatry: exploring future tools for the detection and management of mental disorders in children and adolescents. Psychiatr Danub 2023 Oct;35(Suppl 2):20-25. [Medline: 37800200]
19. Li Z, Lu F, Wu J, et al. Usability and effectiveness of eHealth and mHealth interventions that support self-management and health care transition in adolescents and young adults with chronic disease: systematic review. J Med Internet Res 2024 Nov 26;26:e56556. [doi: 10.2196/56556] [Medline: 39589770]
20. Zhao H, Zhang Z, Tang J. Enhancing rural healthcare through internet-based remote collaborative outpatient services: a comprehensive evaluation in Changzhi, Shanxi Province. Medicine (Baltimore) 2024;103(36):e39614. [doi: 10.1097/MD.0000000000039614]
21. Liu F, Song T, Yu P, et al. Efficacy of an mHealth app to support patients' self-management of hypertension: randomized controlled trial. J Med Internet Res 2023 Dec 19;25:e43809. [doi: 10.2196/43809] [Medline: 38113071]
22. Hussain SA, Sezgin E, Krivchenia K, Luna J, Rust S, Huang Y. A natural language processing pipeline to synthesize patient-generated notes toward improving remote care and chronic disease management: a cystic fibrosis case study. JAMIA Open 2021 Jul;4(3):ooab084. [doi: 10.1093/jamiaopen/ooab084] [Medline: 34604710]
23. Zayas-Cabán T, Haque SN, Kemper N. Identifying opportunities for workflow automation in health care: lessons learned from other industries. Appl Clin Inform 2021 May;12(3):686-697. [doi: 10.1055/s-0041-1731744] [Medline: 34320683]
24. Šuster S, Baldwin T, Lau JH, et al. Automating quality assessment of medical evidence in systematic reviews: model development and validation study. J Med Internet Res 2023 Mar 13;25:e35568. [doi: 10.2196/35568] [Medline: 36722350]
25. Abbasi M, Khera S, Dabravolskaj J, Aissiou A, Abbasi-Dezfouly R. Family physicians' feedback on the feature design of a digital health platform to streamline the care of older adults. Geriatrics (Basel) 2024 Nov 28;9(6):154. [doi: 10.3390/geriatrics9060154] [Medline: 39727813]
26. Smith J, Cheater F, Bekker H. Parents' experiences of living with a child with a long-term condition: a rapid structured review of the literature. Health Expect 2015 Aug;18(4):452-474. [doi: 10.1111/hex.12040] [Medline: 23311692]
27. Chen J, Lim CP, Tan KH, Govindan K, Kumar A. Artificial intelligence-based human-centric decision support framework: an application to predictive maintenance in asset management under pandemic environments. Ann Oper Res 2025 Jul;350(2):493-516. [doi: 10.1007/s10479-021-04373-w]
28. Lee JG, Jun S, Cho YW, et al. Deep learning in medical imaging: general overview. Korean J Radiol 2017;18(4):570-584. [doi: 10.3348/kjr.2017.18.4.570] [Medline: 28670152]
29. Kalla M, Bradford A, Schadewaldt V, et al. Co-designing a user-centered digital health tool for supportive care needs of patients with brain tumors and their caregivers: interview analysis. JMIR Cancer 2025 May 23;11:e53690. [doi: 10.2196/53690] [Medline: 40408266]
30. Kowalkowski M, Eaton T, Reeves KW, et al. Incorporating patient, caregiver, and provider perspectives in the co-design of an app to guide hospital at home admission decisions: a qualitative analysis. JAMIA Open 2024 Oct;7(3):ooae079. [doi: 10.1093/jamiaopen/ooae079] [Medline: 39156047]

XSL•FO
RenderX

31. Ibrahim ST, Patel J, Katapally TR. Digital citizen science for ethical monitoring of youth physical activity frequency: comparing mobile ecological prospective assessments and retrospective recall. PLOS Digit Health 2025 May;4(5):e0000840. [doi: 10.1371/journal.pdig.0000840] [Medline: 40315264]
32. Sumiya M, Nishimura T, Aizaki K, et al. Addressing the ethical, legal, and social issues of healthtech in education: insights from Japan. JMIR Form Res 2025 Jul 18;9:e72781. [doi: 10.2196/72781] [Medline: 40680270]
33. Pavarini G, Yosifova A, Wang K, et al. Data sharing in the age of predictive psychiatry: an adolescent perspective. Evid Based Ment Health 2022 May;25(2):69-76. [doi: 10.1136/ebmental-2021-300329] [Medline: 35346984]
34. Li E, Lounsbury O, Clarke J, Ashrafian H, Darzi A, Neves AL. Patient and caregiver perceptions of electronic health records interoperability in the NHS and its impact on care quality: a focus group study. BMC Med Inform Decis Mak 2024 Dec 3;24(1):370. [doi: 10.1186/s12911-024-02789-5] [Medline: 39627780]

Abbreviations

AI: artificial intelligence
API: application programming interface
AUC-ROC: area under the receiver operating characteristic curve
BERT: Bidirectional Encoder Representations From Transformers
CPHVI: composite pediatric health vulnerability index
EHR: electronic health record
GDPR: General Data Protection Regulation
HIPAA: Health Insurance Portability and Accountability Act
MICE: multivariate imputation by chained equations
ML: machine learning
NLP: natural language processing
SHAP: Shapley additive explanations
SVM: support vector machine

Edited by A Benis; submitted 05.Jul.2025; peer-reviewed by B Zhang, K Li, MBR Mahmoud; revised version received 18.Oct.2025; accepted 23.Oct.2025; published 26.Jan.2026.

Please cite as:
Chen J, Mao Z
Comprehensive Pediatric Health Risk Stratification Using an AI-Driven Framework in Children Aged 2 to 8 Years: Design and Validation Study
JMIR Med Inform 2026;14:e80163
URL: https://medinform.jmir.org/2026/1/e80163
doi:10.2196/80163

© Zhihe Mao, Jundan Chen. Originally published in JMIR Medical Informatics (https://medinform.jmir.org), 26.Jan.2026. This is an open-access article distributed under the terms of the Creative Commons Attribution License (https://creativecommons.org/licenses/by/4.0/), which permits unrestricted use, distribution, and reproduction in any medium, provided the original work, first published in JMIR Medical Informatics, is properly cited. The complete bibliographic information, a link to the original publication on https://medinform.jmir.org/, as well as this copyright and license information must be included.

XSL•FO
RenderX

Original Paper

Scalable and Privacy-Conscious End-to-End Processing of Large-Scale Clinical Data for Precision Medicine: Empirical Evaluation Study

Jungwoo Lee[1], PhD; Sangwon Hwang[2], PhD; Kyu Hee Lee[2], PhD

[1]Artificial Intelligence Big Data Medical Center, Yonsei University Wonju College of Medicine, Wonju, Republic of Korea

[2]Department of Precision Medicine, Yonsei University Wonju College of Medicine, Wonju, Republic of Korea

Corresponding Author:
Kyu Hee Lee, PhD
Department of Precision Medicine
Yonsei University Wonju College of Medicine
20 Ilsan-ro, Wonju-si, Gangwon-do
Wonju, 26417
Republic of Korea
Phone: 82 82 741 0466
Email: powerpc@yonsei.ac.kr

Abstract

Background: In large-scale clinical data analysis, CSV and traditional relational database management system–based approaches are widely used but impose substantial storage and processing constraints that delay research preparation and hinder multicenter collaboration. Although column-oriented storage formats such as Apache Parquet have gained attention in data science, systematic end-to-end evaluations in clinical environments remain limited, particularly regarding efficiency and scalability.

Objective: This study aimed to empirically evaluate whether a Parquet-based end-to-end pipeline could improve computational efficiency and scalability in large-scale clinical data analysis while preserving predictive performance and protecting privacy.

Methods: Electronic health record data comprising 13.76 million rows from a large academic medical center in Korea were analyzed using Parquet, CSV, PostgreSQL, and DuckDB environments. Standardized SQL workloads and multilabel classification models—implemented using graphics processing unit–accelerated Extreme Gradient Boosting and classifier chain (CC) ensembles to address class imbalance—were applied to evaluate storage efficiency, time to analysis, and predictive performance. Statistical equivalence testing with prespecified clinical margins and bootstrap resampling ensured rigorous comparison, while privacy risks were assessed through advanced membership inference attacks (MIA), including shadow MIA and likelihood ratio attacks.

Results: Compared with CSV, Parquet demonstrated enhanced computational efficiency by lowering disk access from 940.2 to 44.2 seconds (95.3% reduction). End-to-end processing latency was substantially reduced across feature transformation (15.0 vs 9.3 s) and model training (8.1 vs 6.7 s). To address complex clinical correlations, we implemented CC and one-vs-rest architectures, which effectively captured interdependencies between disease labels. Classification performance remained statistically equivalent across area under the receiver operating characteristic curve, area under the precision-recall curve, accuracy, and F_1-score, with all differences falling within prespecified clinical equivalence margins (P<.001). Notably, the CC ensemble demonstrated high technical rigor, minimizing Hamming loss (2.2×10^{-4}) and ensuring robustness even in imbalanced cohorts. MIA performed at chance level (area under the curve=0.500), suggesting no measurable increase in privacy risk.

Conclusions: By significantly mitigating data processing bottlenecks, a Parquet-based pipeline enabled high-throughput, large-scale clinical evidence generation without compromising model integrity or patient privacy. This framework provides a scalable and robust infrastructure for precision medicine, facilitating agile multicenter collaborations and real-world data analysis in resource-constrained clinical environments.

(JMIR Med Inform 2026;14:e83487) doi:10.2196/83487

KEYWORDS

electronic health records; medical informatics; predictive performance; data privacy; precision medicine

XSL•FO
RenderX

Introduction

Clinical data, including diagnostic reports, prescriptions, laboratory results, and imaging data, hold substantial potential for precision medicine, predictive modeling, and collaborative research. The volume of electronic health records (EHRs) generated in clinical practice has grown exponentially with the expansion of digital health systems [1-4]. However, as datasets expand, bottlenecks, such as storage overhead, transmission delays, and slow query execution, become increasingly common. These challenges cannot be resolved simply by expanding storage capacity; instead, they necessitate more efficient frameworks for data storage and processing.

In medical informatics, data are most commonly stored in row-oriented formats, such as CSV files, spreadsheets, and relational databases. Although valued for their simplicity and interoperability, these approaches exhibit clear limitations in storage efficiency and analytic scalability. CSV files are uncompressed and large in size, restricting input and output throughput, while relational databases often underperform in column-level operations. In contrast, column-oriented formats offer high compression and selective input and output, making them well suited for high-volume and cloud-based environments. Among these, Apache Parquet is widely used as a standard solution owing to its scalability and interoperability [5,6]. However, few studies have systematically evaluated its end-to-end performance in clinical pipelines that incorporate deidentification procedures.

A further challenge in clinical data use is balancing privacy protection with data utility. Deidentification is mandatory in multicenter research and machine learning, but it may affect statistical distributions or compromise predictive performance. Understanding how storage architectures interact with deidentification to influence analytic outcomes is therefore of both academic and practical importance [7-13].

Unlike prior studies that focused solely on benchmarking computational efficiency, this work integrates privacy risk assessment and formal equivalence testing into a real-world end-to-end pipeline, thereby providing a clinically meaningful evaluation of Parquet as a foundation for precision medicine and collaborative research. Against this background, this study developed a scalable Parquet-based pipeline for high-volume clinical data and empirically assessed its storage efficiency, computational throughput, and preservation of predictive performance. This study also sought to establish a reliable infrastructure that enables cohort construction, secure data sharing, and clinical decision support in multicenter and precision medicine research [14-23].

Methods

Ethical Considerations

This retrospective observational study was conducted using real-world EHR data. The study protocol was approved by the institutional review board of Wonju Severance Christian Hospital (CR325065). The requirement for informed consent was waived by the institutional review board due to the retrospective nature of the study and the use of deidentified data. All data processing was performed within an independent honest broker system, and investigators had access only to deidentified data. No compensation was provided to the participants as there was no direct contact or intervention involved. The entire process complied with the Personal Information Protection Act of Korea, the Health Insurance Portability and Accountability Act Safe Harbor standard, and the General Data Protection Regulation [24-28].

Integrated End-to-End Clinical Data Processing Workflow

We developed an integrated pipeline connecting 5 core stages: raw EHR ingestion, privacy-preserving preprocessing (ISO 8601 and *k*-anonymity), scalable infrastructure using Apache Parquet, multilabel modeling via graphics processing unit (GPU)–accelerated Extreme Gradient Boosting (XGBoost), and rigorous statistical and privacy audits (Figure 1). To optimize analytic performance, we adopted a column-oriented storage format (Apache Parquet) over the traditional row-oriented structure (eg, CSV) [6]. For comparative evaluation, the same dataset was also maintained in CSV format. While row-oriented structures excel in transactional tasks, columnar storage significantly reduces input and output overhead and enhances compression efficiency for complex analytic queries. This architectural choice is specifically tailored for the high dimensionality and sparse distribution of clinical datasets, ensuring both system scalability and robust privacy protection across the entire workflow.

XSL•FO
RenderX

Figure 1. Integrated workflow for scalable and privacy-preserving clinical data processing. AUROC: area under the receiver operating characteristic curve; AUPRC: area under the precision-recall curve; CC: classifier chains; EHR: electronic health record; GDPR: General Data Protection Regulation; GPU: graphics processing unit; HIPAA: Health Insurance Portability and Accountability Act; ICD-10: International Classification of Diseases, Tenth Revision; KCD: Korean Classification of Diseases, Eighth Revision; LiRA: Likelihood Ratio Attack; MIA: membership inference attack; OvR: one-vs-rest; PIPA: Personal Information Protection Act; TOST: two 1-sided tests; XGBoost: extreme gradient boosting.

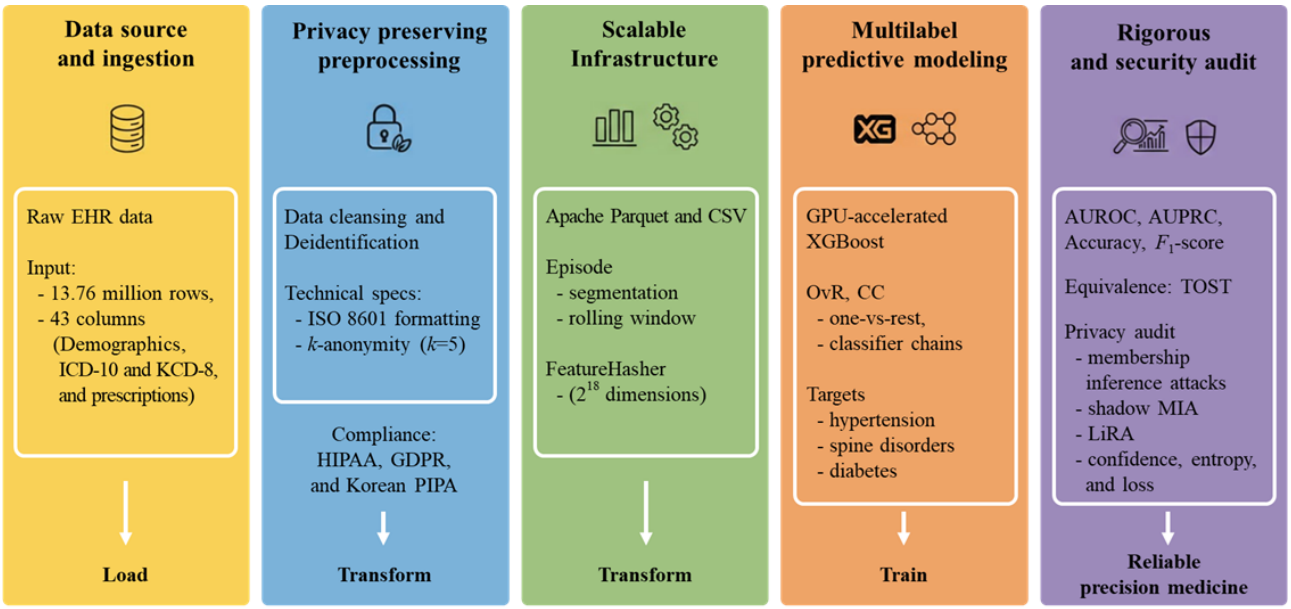

Data Preparation and Transformation

The dataset included patient demographics, diagnostic codes based on the International Classification of Diseases, Tenth Revision (ICD-10) [29-35] and the Korean Classification of Diseases, Eighth Revision (KCD-8), visit type, and prescription records. In total, the dataset comprised approximately 13.76 million rows (43 columns, approximately 3.2 GB), as detailed in Multimedia Appendix 1. After replacing patient identifiers with randomly generated surrogate IDs, quasi-identifiers were generalized to satisfy *k*-anonymity (*k*=5). Data cleansing further ensured quality control by standardizing date fields into the ISO-compliant format (YYYY-MM-DD).

Clinical Data Processing Pipeline

Clinical data processing followed a stepwise pipeline designed to reflect clinical context. In preprocessing, we standardized date formats, removed records with missing sex, and normalized sex codes (eg, “men” to M and “women” to F). Duplicate entries were resolved by retaining only the most recent record for identical combinations of patient, date, and diagnosis code. Visits were segmented into episodes by department changes or temporal gaps, and each episode was assigned an episode identifier. Episode-level summaries included episode duration, event count, and primary diagnosis status. To capture temporal continuity, a 90-day rolling window was applied to compute diagnosis counts and code diversity per patient. Monthly aggregates were then derived, including patient counts, code diversity, and primary diagnosis counts, with patient-month statistics summarized using quantiles (eg, p50 and p90). The diagnostic records for the targeted conditions—including I10.9, E10-E14, and M48.06—were identified and extracted to construct the final summary tables, which were then stored in both CSV and Parquet formats for comparative analysis. The stepwise process is illustrated in Figure 2.

XSL•FO
RenderX

Figure 2. Stepwise scenario of the clinical data processing pipeline.

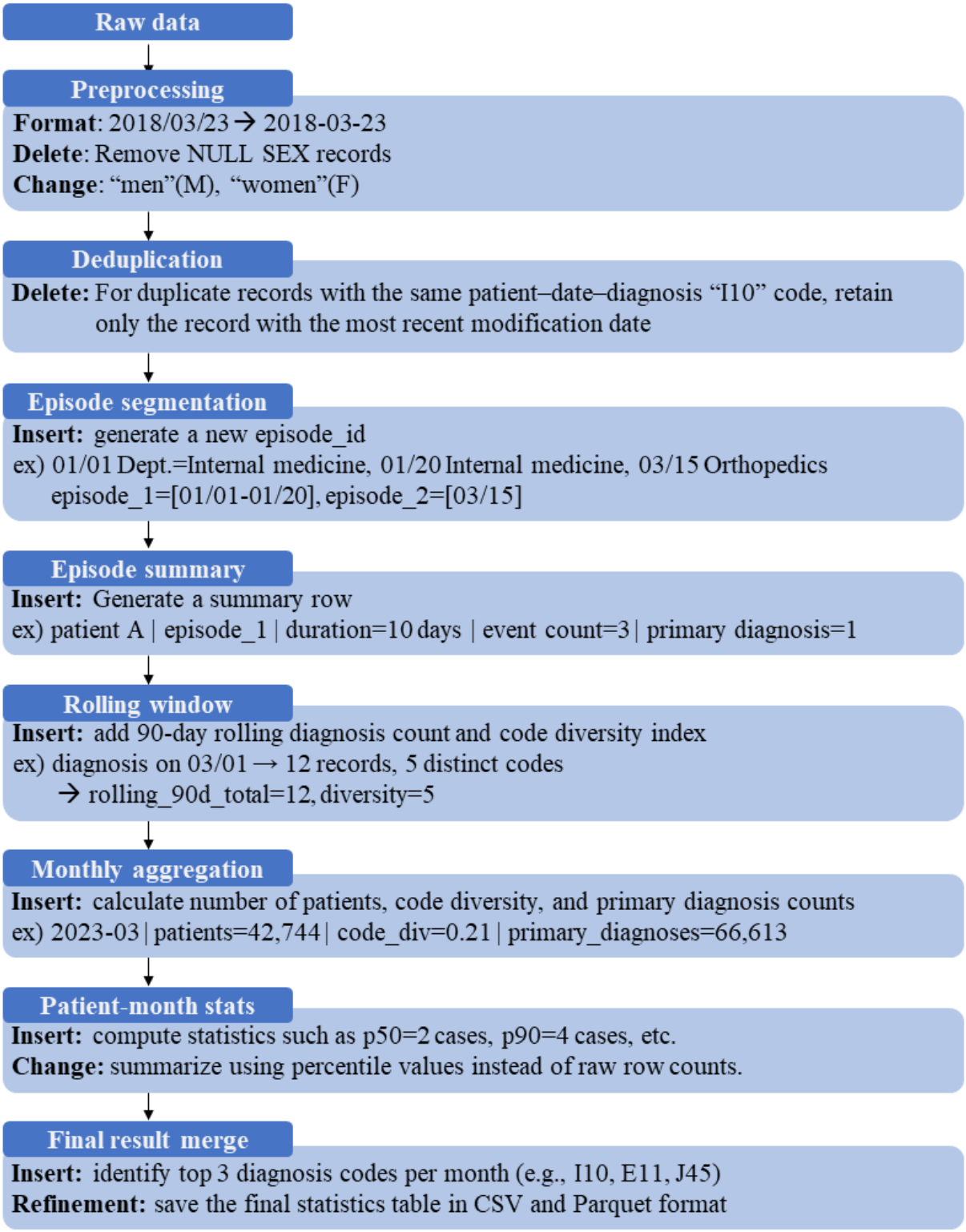

Database Workload Benchmarking

To evaluate the efficiency of storage formats, scenario-based workloads were executed in DuckDB (DuckDB Labs) [36] and PostgreSQL (PostgreSQL Global Development Group) [37] environments. Synthetic example data are provided in Multimedia Appendix 2. Identical datasets were loaded into Parquet-based DuckDB and row-store PostgreSQL, and complex SQL queries—adapted from TPC-DS patterns [38,39] (eg, window functions, multidimensional aggregation, and ROLLUP)—were applied to compare performance. Resource use was further examined by varying chunk sizes (10,000-50,000 records) with detailed results in Multimedia Appendix 3.

Predictive Modeling and Multilabel Strategy

Predictive modeling assessed the impact of storage formats on classification performance for hypertension (I10.9), spinal disorders (M48.06), and diabetes (E10-E14). Patient-level

XSL•FO
RenderX

diagnostic histories were transformed into 2^{18} dimensional sparse vectors (approximately 262,000 features) via FeatureHasher (scikit-learn; Python Software Foundation) [40-42]. The dataset was randomly partitioned into training (65%), validation (15%), and test (20%) subsets with a fixed seed of 42. Classification models were implemented using GPU-accelerated XGBoost with positive class weighting to address imbalance [43-45]. Hyperparameter details are provided in Multimedia Appendix 4.

For multilabel classification, we applied one-vs-rest (OvR) [46] and classifier chains (CC) [47]. To mitigate label-order dependence and evaluate interlabel dependencies, we constructed ensembles of 5 strategically ordered chains encompassing a prevalence gradient—from high-prevalence anchors (hypertension and diabetes) to the sparse target, spinal stenosis (M48.06, 0.50%; Multimedia Appendix 5). Prioritizing M48.06, a domain-independent and sparse condition, served to demonstrate model robustness even without the clustering benefits of related disease families (eg, I-series codes). To ensure the rigorous prevention of label leakage and validate the integrity of the performance gains, all defining ICD-10 codes were strictly excluded from the feature space. This setup ensured that the model's predictive capability relied solely on statistical associations across hundreds of thousands of nondiagnostic features. Model performance was evaluated using area under the receiver operating characteristic curve (AUROC), area under the precision-recall curve (AUPRC), accuracy, and F_1-score, calculated for each label as well as macroaverages and microaverages.

Statistical Evaluation and Privacy Assessment

Model performance was evaluated using AUROC, AUPRC, accuracy, and F_1-score. To assess model reliability, calibration was further evaluated using the Brier score and expected calibration error (ECE), with detailed results provided in Multimedia Appendix 6. CSV and Parquet results were compared using paired runs with shared identifiers. Normality was assessed via the Shapiro-Wilk test, followed by paired 2-tailed *t* tests or Wilcoxon signed-rank tests with Bonferroni correction (P<.05) [48-50].

Equivalence was assessed via two 1-sided tests (TOST) [51] and 95% bootstrap CIs. Equivalence margins (δ) were prespecified at 0.02 for AUROC or AUPRC and 0.01 for accuracy or F_1-score. These thresholds were selected to be narrower than the 0.05 margin commonly used in clinical equivalence trials [52] and are more conservative than performance variances typically observed in the external validation of clinical artificial intelligence (AI) systems [53]. Such strict margins were intended to constrain observed differences to ranges generally regarded as clinically negligible, particularly for high-performing models operating within an elevated accuracy range (0.98-1.00).

To mitigate stochastic variation, a fixed random seed was applied across all experiments, ensuring that observed differences reflected data handling effects rather than algorithmic randomness. Privacy was further audited using membership inference attacks (MIA)—including confidence, entropy, loss-based (Yeom), shadow, and Likelihood Ratio Attack (LiRA) strategies—under patient-level stratified splits (train: 240,596; test: 240,597) to verify model robustness.

Experimental Setup and Reproducibility

All experiments were conducted on a Linux Ubuntu 22.04 server with a 24-core central processing unit (CPU), 128-GB memory, and an NVIDIA RTX 5090 GPU (CUDA 12.2, cuDNN 8.9, driver 550.54). Data processing used Python (version 3.10; Python Software Foundation) with Pandas 1.5.3, PyArrow 12.0.1, scikit-learn 1.3.2, and XGBoost 2.0.3 (GPU-hist). Multiprocessing was implemented using the standard Python multiprocessing module.

As specified in the modeling strategy, XGBoost was configured with a learning rate of 0.08, maximum depth of 6, and 1000 estimators. To handle class imbalance, task-specific *scale_pos_weight* and an ensemble of 5 CCs were used. All random operations used a fixed seed of 42 for reproducibility. For robust performance evaluation, we conducted 20 independent experimental runs and used 5000-iteration bootstrap resampling to compute 95% CIs. Detailed hyperparameters and the statistical framework for equivalence testing are provided in Multimedia Appendix 4.

Results

Storage and Pipeline Efficiency

Conversion to Parquet substantially improved storage efficiency, reducing file size by nearly 6.9-fold relative to CSV. As summarized in Table 1, Parquet also consistently outperformed CSV across the end-to-end pipeline. File loading (input and output) time decreased by more than 95%, and both feature transformation (FeatureHasher) and model training (XGBoost) were faster under Parquet. Although peak CPU memory was about 1.3 GB higher, GPU memory consumption decreased by 326 MB, resulting in stable overall resource use. Resource consumption remained stable at 9 to 10 GB across chunk sizes, reflecting consistent scalability, with efficiency varying by chunk size. The values in Table 1 represent peak use in end-to-end runs, with minor variations arising from measurement conditions, whereas CPU, memory, and disk input and output patterns remained consistent across chunk sizes (Multimedia Appendix 3).

XSL•FO
RenderX

Table 1. System performance comparison between CSV and Parquet formats.

Metric	CSV, mean (SD)	Parquet, mean (SD)	Difference[a] (95% CI)
Time (s)			
Input and output duration	940.2 (53.3)	44.2 (1.6)	−896.0 (−930.0 to −860.0)
Feature transformation	15.0 (0.9)	9.3 (0.7)	−5.7 (−7.0 to −4.5)
Model training	8.1 (1.2)	6.7 (0.9)	−1.4 (−2.5 to −0.3)
Resource use			
Memory maximum (GB)	21.2 (0.8)	22.5 (0.6)	1.3 (0.1 to 2.0)
GPU[b] memory maximum (MB)	4873.0 (582.6)	4547.0 (596.9)	−326.0 (−450.0 to −200.0)

[a]Calculated as the Parquet mean minus CSV mean.

[b]GPU: graphics processing unit.

Classification Performance and Calibration

Single-label results are presented in Table 2. All 3 tasks achieved AUROC values above 0.920, with AUPRC ranging from 0.488 to 0.580. Hypertension (I10.9) yielded the highest F_1-score (0.599), followed by spinal disorders (M48.06, 0.536) and diabetes (E10-E14, 0.521). Macroaveraged performance reached an AUROC of 0.920, an AUPRC of 0.545, an accuracy of 0.934, and an F_1-score of 0.552. Calibration analyses [54,55], reported in Multimedia Appendix 6, demonstrated excellent reliability for hypertension (Brier score 2.1×10^{-5}; ECE 6.0×10^{-6}), while spinal disorders (ECE=0.016) and diabetes (ECE=0.018) showed mild miscalibration but remained within recommended thresholds (ECE<0.020).

Table 2. Per-label classification performance using extreme gradient boosting.

Labels	AUROC[a]	AUPRC[b]	Accuracy	F_1-score
Hypertension	0.920	0.580	0.906	0.599
Spine disorder	0.941	0.488	0.982	0.536
Diabetes[c]	0.899	0.567	0.915	0.521
Macroaverage	0.920	0.545	0.934	0.552

[a]AUROC: area under the receiver operating characteristic curve.

[b]AUPRC: area under the precision-recall curve.

[c]Diabetes mellitus (International Classification of Diseases, Tenth Revision codes: E10-E14).

Table 2 evaluates label-specific discrimination under substantial class imbalance, whereas Table 3 summarizes overall multilabel prediction performance using microaveraged aggregation across all label–instance pairs. Specifically, Table 2 focuses on the predictive performance of individual sparse labels, while Table 3 reflects aggregated performance across all prediction events. Multilabel results in Table 3 confirmed high-performance consistency for both OvR and CC, with AUROC >0.999 and AUPRC >0.998. Subset accuracy was identical (0.999), but CC showed slight improvements in Hamming loss and Jaccard index [56], suggesting modest benefits from capturing label dependencies. A numerical gap was observed between per-label AUPRC (approximately 0.5; Table 2) and multilabel AUPRC (near 1.0; Table 3). This reflects the technical difference in aggregation: multilabel metrics were calculated using microaveraging to evaluate the overall model efficacy.

XSL•FO
RenderX

Table 3. Multilabel classification performance.

Models	AUROC[a]	AUPRC[b]	Hamming loss	Subset accuracy	Jaccard index
One-vs-rest					
Microaverage	0.999	0.998	2.4×10^{-4}	0.999	0.997
Macroaverage	0.999	0.998	—[c]	—	—
Classifier chains					
Microaverage	0.999	0.998	2.2×10^{-4}	0.999	0.997
Macroaverage	0.999	0.998	—	—	—

[a]AUROC: area under the receiver operating characteristic curve.

[b]AUPRC: area under the precision-recall curve.

[c]Not applicable.

Although discrimination remained high across all tasks, calibration analyses revealed modest overconfidence for diabetes and spinal disorder models. These deviations, while within accepted thresholds, emphasize the importance of calibration-aware adjustments when deploying predictive models in clinical workflows.

Database Benchmarking

As summarized in Table 4, DuckDB executed analytic workloads with an approximately 28-fold reduction in wall-clock time compared with PostgreSQL, which required 2546.4 seconds. DuckDB also exhibited higher CPU use (72.1% vs 39.6%), while memory consumption was comparable across systems.

Table 4. Performance comparison of DuckDB and PostgreSQL in scenario-based SQL workloads.

Metrics	DuckDB[a]	PostgreSQL[b]
Wall-clock time (s)	90.2	2546.4
CPU[c] use (%)	72.1	39.6
Memory use (GB)	13.7	14.8
Read throughput (MB/s)	554.7	365.2
Write throughput (MB/s)	1116.0	998.0

[a]DuckDB: column-oriented database optimized for analytical workloads.

[b]PostgreSQL: row-oriented relational database primarily designed for transactional workloads, with support for analytical queries.

[c]CPU: central processing unit.

Equivalence Analysis

Paired experiments (20 runs per condition) were conducted using shared run identifiers, with median and IQR values provided in Table S1 in Multimedia Appendix 7. Several metrics converged across all repetitions, producing zero IQR values and demonstrating high algorithmic stability. Overall, both formats achieved robust numerical consistency across all experimental iterations; for instance, mean AUROC was 1.000 for CSV and 0.984 for Parquet ($\Delta=-0.015$). While other metrics (AUPRC, accuracy, and F_1-score) were slightly higher under the CSV format, paired *t* tests and Wilcoxon signed-rank tests confirmed statistical significance after Bonferroni correction ($P<.001$; Table S2 in Multimedia Appendix 7). However, these numerical variations remained minimal.

Notably, all observed differences fell within the prespecified equivalence margins ($\delta=0.02$ for AUROC and AUPRC and $\delta=0.01$ for accuracy and F_1-score). TOST confirmed statistical equivalence ($P<.05$) across all evaluated metrics, and bootstrap 95% CIs for AUROC Δ (−0.016 to −0.015) further reflected near-zero variability consistent with asymptotic performance stability (Table S3 in Multimedia Appendix 7).

Privacy Assessment

The MIA evaluations, performed based on established methodologies [57-59] and summarized in Table 5, produced area under the curve (AUC) values of 0.501, 0.502, and 0.499 for confidence, entropy, and loss-based strategies, respectively. The maximum advantage did not exceed 0.007, and the gain over random guessing was ≤0.003. Attack performance was indistinguishable from random guessing, indicating no additional privacy risk. Additional shadow and LiRA [60,61] results are available in Multimedia Appendix 8, corroborating these findings.

XSL•FO
RenderX

Table 5. Membership inference attack results across different attack strategies.

Attack strategy	Attack AUC[a] (95% CI)	Advantage	Best accuracy	Gain vs baseline
Confidence	0.501 (0.501-0.503)	0.006	0.503	0.003
Entropy	0.502 (0.502-0.503)	0.007	0.503	0.003
Loss (Yeom)	0.499 (0.498-0.499)	0.002	0.500	0.001

[a]AUC: area under the curve.

Discussion

Principal Findings

This study successfully implemented an integrated end-to-end pipeline (Figure 1) that ensures a seamless transition from raw EHR data ingestion to predictive modeling. By leveraging Apache Parquet, the framework effectively addressed storage and processing bottlenecks—specifically, input and output latency—inherent in traditional row-oriented workflows, substantially enhancing data throughput and accelerating the analytic preparatory phase while maintaining high predictive fidelity. Furthermore, our findings indicate that the minor performance discrepancies between formats are attributable to systematic data handling effects under a strictly controlled environment. Beyond these computational efficiencies, privacy evaluations demonstrated that the optimized workflow maintains rigorous data protection standards, providing a secure foundation for multicenter research operations without introducing additional vulnerabilities.

Although paired statistical tests yielded highly significant *P* values ($P<.001$), this result reflects the sensitivity of paired testing under large-scale data and repeated bootstrap evaluation rather than clinically meaningful divergence. From an equivalence perspective, all performance differences remained well within the prespecified margins, confirming that the Parquet-based pipeline achieves practical performance equivalence to the traditional CSV workflow.

The substantial improvement in multilabel AUPRC compared with per-label performance highlights the system-level predictive advantage gained by explicitly modeling interlabel dependencies. While individual disease prediction remains challenging under substantial class imbalance, the multilabel formulation enables the model to capture clinically meaningful comorbidity structures, thereby reframing the observed performance gap as a reflection of holistic predictive efficacy rather than a metric artifact. This gap was also driven by the extreme class imbalance inherent in clinical datasets (eg, 0.50% prevalence for spinal disorders), where high AUROCs can coexist with lower F_1-scores. By integrating these dependencies within the CC architecture, the model leveraged frequent clinical co-occurrence patterns—such as hypertension and diabetes—to stabilize predictions for sparse conditions, including spinal stenosis. Importantly, the consistent performance observed despite the strict exclusion of all defining ICD-10 codes provided strong evidence against label leakage and underscored the model's reliance on nondiagnostic clinical associations.

Clinical Implications and Research Operations

The clinical implications were considerable. By substantially shortening preparatory phases and enabling analyses to be completed within hours rather than days, Parquet-based pipelines allowed investigators to progress more rapidly from raw data to actionable evidence. Such improvements not only accelerated study initiation but also facilitated the integration of predictive models into research and clinical workflows. In multicenter settings, scalability supported the efficient integration of heterogeneous patient populations without excessive computational cost, thereby enhancing reproducibility and advancing precision medicine initiatives. These efficiencies were directly relevant to clinical workflows and regulatory-grade analyses. They enabled interim analyses and timely regulatory submissions, supporting more responsive and efficient research operations.

Privacy and Security Safeguards

Privacy evaluation reinforced the suitability of this approach. Deidentification procedures satisfied k-anonymity, and MIA yielded chance-level performance. The chance-level performance of multiple MIA methods confirmed that computational gains do not compromise patient confidentiality, a prerequisite for secure collaboration across institutions. Patient-level stratification and consistent pipeline design acted as effective safeguards. While residual risks remain inherent to secondary data use, our findings suggested that Parquet does not introduce additional vulnerabilities. For collaborative research networks—where privacy assurances are essential for sharing—these results provide practical reassurance.

Interpretation of Predictive Performance and Label Dependencies

Classification analyses revealed stable performance for common conditions such as hypertension, whereas imbalanced disorders such as diabetes and spinal disease yielded lower scores. This pattern highlights the need to account for dataset structure and interlabel dependencies when interpreting predictive outputs. The elevated AUROC values likely reflect the combination of high-prevalence conditions and extensive diagnostic feature sets. Consistent with the modeling strategy, defining codes were excluded from the feature space; however, correlated diagnostic features may still have influenced performance estimates.

While performance convergence at elevated levels constrained the sensitivity to subtle comparative differences, it underscored the robustness and reproducibility of the pipeline, supporting its suitability for large-scale clinical research, where stability and reliability are critical. Predictive reliability was not compromised by storage structure, supporting Parquet as a

XSL•FO
RenderX

dependable option for secondary use of EHR data in diverse research settings.

Model Reliability and Calibration

Calibration analyses further showed that hypertension models were well aligned with observed risks, whereas diabetes and spinal disorder tasks exhibited modest miscalibration. These results underscore that even high-performing classifiers may generate overconfident probability estimates, a limitation directly relevant to clinical decision support. Future studies should evaluate calibration-aware techniques, such as temperature scaling or isotonic regression, to improve the reliability of probability estimates (Multimedia Appendix 6).

Beyond technical validation, the findings demonstrated practical value for clinical research operations. Large-scale trials and observational studies often face delays in cohort assembly and iterative validation; Parquet-based pipelines shorten these steps, enabling more adaptive study designs. In multicenter collaborations, they promote secure and efficient data exchange, reducing delays that commonly impede cooperative studies.

Limitations

Several limitations should be acknowledged. First, the datasets analyzed were derived from specific institutional cohorts, which may constrain generalizability to other health care systems. Second, the elevated performance baseline of the predictive models limited the sensitivity to subtle differences between CSV and Parquet formats. Third, while MIA offered a widely accepted proxy for privacy risk, broader adversarial evaluations were not included. Fourth, the evaluation was primarily conducted in on-premise settings, so the scalability of findings in distributed or cloud-based environments remains to be established. Finally, despite the clear efficiency advantages of Parquet, its adoption may introduce a technical learning curve for clinical researchers who are less familiar with column-oriented storage formats or big-data frameworks. Transitioning from traditional row-oriented workflows to optimized columnar architectures requires initial investments in technical training and infrastructure adjustment. However, these upfront efforts are likely to be offset by the long-term gains in scalability and processing speed demonstrated in our results, ultimately supporting more efficient and reproducible clinical evidence generation.

Future Work

Future research should extend the evaluation of Parquet-based pipelines to distributed and cloud-based environments, focusing on both scalability and cost-effectiveness. In addition, validation across hybrid and federated architectures will be important to confirm applicability in multicenter collaborations where data cannot be centralized. Beyond structured EHR data, future studies should also investigate applications to unstructured modalities, such as clinical narratives, imaging metadata, and time-series signals. Such efforts would test the versatility of Parquet-based pipelines in supporting multimodal learning and integrative analyses. Privacy assessments should likewise be expanded to encompass attribute inference, linkage, and other adversarial scenarios, ideally within federated or privacy-preserving analytic frameworks. Moreover, interoperability across international coding standards should be validated using external multicenter datasets to ensure global applicability. Pursuing these directions will enhance the technical robustness of Parquet-based infrastructures while reinforcing their clinical relevance, ultimately enabling secure collaboration and more efficient integration of evidence into patient care.

Conclusions

This study demonstrated that Parquet-based end-to-end processing effectively alleviated the storage and computational bottlenecks inherent in traditional row-oriented and relational database workflows while maintaining predictive fidelity and privacy safeguards. By improving computational efficiency and enabling the rapid preparation of analysis-ready cohorts, Parquet reduces the resources required for large-scale clinical data handling. These efficiencies translate into tangible research benefits, enabling earlier study initiation and more adaptive study designs across diverse clinical research settings.

The integration of efficiency with privacy safeguards further ensures that accelerated workflows remain suitable for secure data sharing across institutions. In parallel, these capabilities support regulatory-grade analyses and health technology assessments, where timely and reproducible evidence is critical. For clinicians and researchers, the central implication is that Parquet-based pipelines reduce the manual effort and computational overhead required to transform raw EHR data into analysis-ready cohorts. This capability not only strengthens multicenter collaboration but also facilitates the timely translation of evidence into clinical decision support.

Ultimately, by aligning computational efficiency with privacy-conscious infrastructure, Parquet-based pipelines reinforce the evidence base that informs clinical decision-making, positioning this approach as a robust foundation for sustainable precision medicine.

Acknowledgments

This work was supported by the National Research Foundation of Korea (NRF) grant funded by the Korea government (grant RS-2025-24683718). This research was supported by the Ministry of Trade, Industry and Energy, Republic of Korea, under the project titled “Research and Development on AI Standardization in the Healthcare Industry Based on Human Big Data and Artificial Intelligence” (grant RS-2025-13882968), funded through the Korea Evaluation Institute of Industrial Technology. This research was supported by a grant from the medical data-driven hospital support project through the Korea Health Information Service, funded by the Ministry of Health and Welfare, Republic of Korea. This research was supported by the Regional Innovation

XSL•FO
RenderX

System and Education program through the Gangwon Regional Innovation System and Education Center, funded by the Ministry of Education and the Gangwon State, Republic of Korea (grant 2025-RISE-10-006).

Funding

This study was funded by the following grants: (1) the National Research Foundation of Korea (NRF) grant funded by the Korea government (grant RS-2025-24683718); (2) a grant from the medical data-driven hospital support project through the Korea Health Information Service, funded by the Ministry of Health and Welfare, Republic of Korea; and (3) the Regional Innovation System and Education program through the Gangwon Regional Innovation System and Education Center, funded by the Ministry of Education and the Gangwon State, Republic of Korea (grant 2025-RISE-10-006). The funders had no involvement in the study design, data collection, analysis, interpretation, or the writing of the manuscript.

Data Availability

The datasets generated or analyzed during this study are available from the corresponding author on reasonable request.

Authors' Contributions

Conceptualization: KHL
Data curation: JL
Formal analysis: JL, KHL
Methodology: SH
Project administration: KHL
Resources: JL
Writing – original draft: JL, SH
Writing – review and editing: KHL

Conflicts of Interest

None declared.

Multimedia Appendix 1
Column definitions for the structured clinical data table.
[XLSX File (Microsoft Excel File), 10 KB - medinform_v14i1e83487_app1.xlsx]

Multimedia Appendix 2
Synthetic example data used for scenario-based workload evaluation.
[XLSX File (Microsoft Excel File), 24 KB - medinform_v14i1e83487_app2.xlsx]

Multimedia Appendix 3
Resource use profiles during Parquet-based data processing across different chunk sizes.
[DOCX File , 252 KB - medinform_v14i1e83487_app3.docx]

Multimedia Appendix 4
Hyperparameter configurations and the formal statistical framework for equivalence testing.
[DOCX File , 16 KB - medinform_v14i1e83487_app4.docx]

Multimedia Appendix 5
Detailed demographic characteristics and visit statistics of the study cohort.
[PNG File , 235 KB - medinform_v14i1e83487_app5.png]

Multimedia Appendix 6
Calibration metrics (Brier score and expected calibration error [ECE] and ECE) for each binary classification task.
[DOCX File , 14 KB - medinform_v14i1e83487_app6.docx]

Multimedia Appendix 7
Integrated statistical performance and equivalence analysis.
[DOCX File , 18 KB - medinform_v14i1e83487_app7.docx]

XSL•FO
RenderX

Multimedia Appendix 8
Membership inference results with shadow and Likelihood Ratio Attack attackers.
[DOCX File , 15 KB - medinform_v14i1e83487_app8.docx]

References

1. Jensen PB, Jensen LJ, Brunak S. Mining electronic health records: towards better research applications and clinical care. Nat Rev Genet 2012 May 02;13(6):395-405. [doi: 10.1038/nrg3208] [Medline: 22549152]
2. Weiskopf NG, Weng C. Methods and dimensions of electronic health record data quality assessment: enabling reuse for clinical research. J Am Med Inform Assoc 2013 Jan 01;20(1):144-151 [FREE Full text] [doi: 10.1136/amiajnl-2011-000681] [Medline: 22733976]
3. Hripcsak G, Albers DJ. Next-generation phenotyping of electronic health records. J Am Med Inform Assoc 2013 Jan 01;20(1):117-121 [FREE Full text] [doi: 10.1136/amiajnl-2012-001145] [Medline: 22955496]
4. Birkhead GS, Klompas M, Shah NR. Uses of electronic health records for public health surveillance to advance public health. Annu Rev Public Health 2015 Mar 18;36:345-359. [doi: 10.1146/annurev-publhealth-031914-122747] [Medline: 25581157]
5. Vohra D. Apache Parquet. In: Practical Hadoop Ecosystem: A Definitive Guide to Hadoop-Related Frameworks and Tools. Berkeley, CA: Apress; 2016:325-335.
6. Apache parquet documentation. Apache Software Foundation. URL: https://parquet.apache.org/ [accessed 2025-06-01]
7. Meystre SM, Friedlin FJ, South BR, Shen S, Samore MH. Automatic de-identification of textual documents in the electronic health record: a review of recent research. BMC Med Res Methodol 2010 Aug 02;10(1):70 [FREE Full text] [doi: 10.1186/1471-2288-10-70] [Medline: 20678228]
8. Negash B, Katz A, Neilson CJ, Moni M, Nesca M, Singer A, et al. De-identification of free text data containing personal health information: a scoping review of reviews. Int J Popul Data Sci 2023 Dec 12;8(1):2153 [FREE Full text] [doi: 10.23889/ijpds.v8i1.2153] [Medline: 38414537]
9. Kushida CA, Nichols DA, Jadrnicek R, Miller R, Walsh JK, Griffin K. Strategies for de-identification and anonymization of electronic health record data for use in multicenter research studies. Med Care 2012 Jul;50 Suppl(Suppl):S82-101 [FREE Full text] [doi: 10.1097/MLR.0b013e3182585355] [Medline: 22692265]
10. El-Hayek C, Barzegar S, Faux N, Doyle K, Pillai P, Mutch SJ, et al. An evaluation of existing text de-identification tools for use with patient progress notes from Australian general practice. Int J Med Inform 2023 May;173:105021. [doi: 10.1016/j.ijmedinf.2023.105021] [Medline: 36870249]
11. Liu J, Gupta S, Chen A, Wang CK, Mishra P, Dai HJ, et al. OpenDeID pipeline for unstructured electronic health record text notes based on rules and transformers: deidentification algorithm development and validation study. J Med Internet Res 2023 Dec 06;25:e48145 [FREE Full text] [doi: 10.2196/48145] [Medline: 38055317]
12. Jabet A, Bérot V, Chiarabini T, Dellière S, Bosshard PP, Siguier M, et al. Trichophyton mentagrophytes ITS genotype VII infections among men who have sex with men in France: an ongoing phenomenon. J Eur Acad Dermatol Venereol 2025 Feb;39(2):407-415. [doi: 10.1111/jdv.20439] [Medline: 39587983]
13. Crane HM, Nance RM, Ruderman SA, Drumright LN, Mixson LS, Heckbert SR, et al. Smoking and type 1 versus type 2 myocardial infarction among people with HIV in the United States: results from the center for AIDS research network integrated clinical systems cohort. J Assoc Nurses AIDS Care 2024 Sep 6;35(6):507-518. [doi: 10.1097/JNC.0000000000000492] [Medline: 39241219]
14. Solomon J, Dauber-Decker K, Richardson S, Levy S, Khan S, Coleman B, et al. Integrating clinical decision support into electronic health record systems using a novel platform (EvidencePoint): developmental study. JMIR Form Res 2023 Oct 19;7:e44065 [FREE Full text] [doi: 10.2196/44065] [Medline: 37856193]
15. Trinkley KE, Kroehl ME, Kahn MG, Allen LA, Bennett TD, Hale G, et al. Applying clinical decision support design best practices with the practical robust implementation and sustainability model versus reliance on commercially available clinical decision support tools: randomized controlled trial. JMIR Med Inform 2021 Mar 22;9(3):e24359 [FREE Full text] [doi: 10.2196/24359] [Medline: 33749610]
16. Yoo J, Lee J, Rhee PL, Chang DK, Kang M, Choi JS, et al. Alert override patterns with a medication clinical decision support system in an academic emergency department: retrospective descriptive study. JMIR Med Inform 2020 Nov 04;8(11):e23351 [FREE Full text] [doi: 10.2196/23351] [Medline: 33146626]
17. Jing X, Min H, Gong Y, Biondich P, Robinson D, Law T, et al. Ontologies applied in clinical decision support system rules: systematic review. JMIR Med Inform 2023 Jan 19;11:e43053 [FREE Full text] [doi: 10.2196/43053] [Medline: 36534739]
18. Sommers SW, Tolle HJ, Trinkley KE, Johnston CG, Dietsche CL, Eldred SV, et al. Clinical decision support to increase emergency department Naloxone Coprescribing: implementation report. JMIR Med Inform 2024 Nov 06;12:e58276 [FREE Full text] [doi: 10.2196/58276] [Medline: 39504560]
19. Barton HJ, Maru A, Leaf MA, Hekman DJ, Wiegmann DA, Shah MN, et al. Academic detailing as a health information technology implementation method: supporting the design and implementation of an emergency department-based clinical decision support tool to prevent future falls. JMIR Hum Factors 2024 Apr 18;11:e52592 [FREE Full text] [doi: 10.2196/52592] [Medline: 38635318]

XSL•FO
RenderX

20. Dong J, Jin Z, Li C, Yang J, Jiang Y, Li Z, et al. Machine learning models with prognostic implications for predicting gastrointestinal bleeding after coronary artery bypass grafting and guiding personalized medicine: multicenter cohort study. J Med Internet Res 2025 Mar 06;27:e68509 [FREE Full text] [doi: 10.2196/68509] [Medline: 40053791]
21. Jung C, Mamandipoor B, Fjølner J, Bruno RR, Wernly B, Artigas A, et al. Disease-course adapting machine learning prognostication models in elderly patients critically ill with COVID-19: multicenter cohort study with external validation. JMIR Med Inform 2022 Mar 31;10(3):e32949 [FREE Full text] [doi: 10.2196/32949] [Medline: 35099394]
22. Alvarez-Romero C, Martinez-Garcia A, Ternero Vega J, Díaz-Jiménez P, Jiménez-Juan C, Nieto-Martín MD, et al. Predicting 30-day readmission risk for patients with chronic obstructive pulmonary disease through a federated machine learning architecture on Findable, Accessible, Interoperable, and Reusable (FAIR) data: development and validation study. JMIR Med Inform 2022 Jun 02;10(6):e35307 [FREE Full text] [doi: 10.2196/35307] [Medline: 35653170]
23. Blasi L, Bordonaro R, Serretta V, Piazza D, Firenze A, Gebbia V. Virtual clinical and precision medicine tumor boards-cloud-based platform-mediated implementation of multidisciplinary reviews among oncology centers in the COVID-19 era: protocol for an observational study. JMIR Res Protoc 2021 Sep 10;10(9):e26220 [FREE Full text] [doi: 10.2196/26220] [Medline: 34387553]
24. Ahmed A, Shahzad A, Naseem A, Ali S, Ahmad I. Evaluating the effectiveness of data governance frameworks in ensuring security and privacy of healthcare data: a quantitative analysis of ISO standards, GDPR, and HIPAA in blockchain technology. PLoS One 2025 May 23;20(5):e0324285 [FREE Full text] [doi: 10.1371/journal.pone.0324285] [Medline: 40408373]
25. Bradford L, Aboy M, Liddell K. International transfers of health data between the EU and USA: a sector-specific approach for the USA to ensure an 'adequate' level of protection. J Law Biosci 2020;7(1):lsaa055 [FREE Full text] [doi: 10.1093/jlb/lsaa055] [Medline: 34221424]
26. Gomase VS, Ghatule AP, Sharma R, Sardana S. Cybersecurity and compliance in clinical trials: the role of artificial intelligence in secure healthcare management. Rev Recent Clin Trials 2025 Apr 25;20(4):332-351. [doi: 10.2174/0115748871366467250413070850] [Medline: 40277117]
27. Scheibner J, Raisaro JL, Troncoso-Pastoriza JR, Ienca M, Fellay J, Vayena E, et al. Revolutionizing medical data sharing using advanced privacy-enhancing technologies: technical, legal, and ethical synthesis. J Med Internet Res 2021 Feb 25;23(2):e25120 [FREE Full text] [doi: 10.2196/25120] [Medline: 33629963]
28. Broen K, Trangucci R, Zelner J. Measuring the impact of spatial perturbations on the relationship between data privacy and validity of descriptive statistics. Int J Health Geogr 2021 Jan 07;20(1):3 [FREE Full text] [doi: 10.1186/s12942-020-00256-8] [Medline: 33413390]
29. Chen PF, Wang SM, Liao WC, Kuo LC, Chen KC, Lin YC, et al. Automatic ICD-10 coding and training system: deep neural network based on supervised learning. JMIR Med Inform 2021 Aug 31;9(8):e23230 [FREE Full text] [doi: 10.2196/23230] [Medline: 34463639]
30. Chen PF, Chen KC, Liao WC, Lai F, He TL, Lin SC, et al. Automatic international classification of diseases coding system: deep contextualized language model with rule-based approaches. JMIR Med Inform 2022 Jun 29;10(6):e37557 [FREE Full text] [doi: 10.2196/37557] [Medline: 35767353]
31. Chen PF, He TL, Lin SC, Chu YC, Kuo CT, Lai F, et al. Training a deep contextualized language model for international classification of diseases, 10th revision classification via federated learning: model development and validation study. JMIR Med Inform 2022 Nov 10;10(11):e41342 [FREE Full text] [doi: 10.2196/41342] [Medline: 36355417]
32. Wu P, Gifford A, Meng X, Li X, Campbell H, Varley T, et al. Mapping ICD-10 and ICD-10-CM codes to phecodes: workflow development and initial evaluation. JMIR Med Inform 2019 Nov 29;7(4):e14325 [FREE Full text] [doi: 10.2196/14325] [Medline: 31553307]
33. Falissard L, Morgand C, Ghosn W, Imbaud C, Bounebache K, Rey G. Neural translation and automated recognition of ICD-10 medical entities from natural language: model development and performance assessment. JMIR Med Inform 2022 Apr 11;10(4):e26353 [FREE Full text] [doi: 10.2196/26353] [Medline: 35404262]
34. Ghasemi P, Lee J. Unsupervised feature selection to identify important ICD-10 and ATC codes for machine learning on a cohort of patients with coronary heart disease: retrospective study. JMIR Med Inform 2024 Jul 26;12:e52896 [FREE Full text] [doi: 10.2196/52896] [Medline: 39087585]
35. Dai HJ, Wang CK, Chen CC, Liou CS, Lu AT, Lai CH, et al. Evaluating a natural language processing-driven, AI-assisted international classification of diseases, 10th revision, clinical modification, coding system for diagnosis related groups in a real hospital environment: algorithm development and validation study. J Med Internet Res 2024 Sep 20;26:e58278 [FREE Full text] [doi: 10.2196/58278] [Medline: 39302714]
36. DuckDB documentation. DuckDB Foundation. URL: https://duckdb.org/ [accessed 2025-05-25]
37. PostgreSQL documentation. PostgreSQL Global Development Group. URL: https://www.postgresql.org/docs/ [accessed 2025-06-10]
38. Tardío R, Maté A, Trujillo J. Beyond TPC-DS, a benchmark for Big Data OLAP systems (BDOLAP-Bench). Futur Gener Comp Syst 2022 Jul;132:136-151. [doi: 10.1016/j.future.2022.02.015]
39. Ding B, Chaudhuri S, Gehrke J, Narasayya V. DSB: a decision support benchmark for workload-driven and traditional database systems. Proc VLDB Endow 2021 Oct 28;14(13):3376-3388. [doi: 10.14778/3484224.3484234]

XSL•FO
RenderX

40. Pedragosa M, Riera G, Casella V, Esteve-Codina A, Steuerman Y, Seth C, et al. Linking cell dynamics with gene coexpression networks to characterize key events in chronic virus infections. Front Immunol 2019 May 3;10:1002 [FREE Full text] [doi: 10.3389/fimmu.2019.01002] [Medline: 31130969]
41. Pang Y, Zhang X, Gao R, Xu L, Shen M, Shi H, et al. Efficacy of web-based self-management interventions for depressive symptoms: a meta-analysis of randomized controlled trials. BMC Psychiatry 2021 Aug 11;21(1):398 [FREE Full text] [doi: 10.1186/s12888-021-03396-8] [Medline: 34380440]
42. Bugiardini R, Cenko E. Sex differences in myocardial infarction deaths. Lancet 2020 Jul 11;396(10244):72-73. [doi: 10.1016/S0140-6736(20)31049-7] [Medline: 32445694]
43. Kaul V, Gross S, Corbett FS, Malik Z, Smith M, Tofani C, et al. Clinical utility of wide-area transepithelial sampling with three-dimensional computer-assisted analysis (WATS3D) in identifying Barrett's esophagus and associated neoplasia. Dis Esophagus 2020 Dec 07;33(12):32607543. [doi: 10.1093/dote/doaa069] [Medline: 32607543]
44. Rajkomar A, Oren E, Chen K, Dai AM, Hajaj N, Hardt M, et al. Scalable and accurate deep learning with electronic health records. NPJ Digit Med 2018 May 8;1(1):18 [FREE Full text] [doi: 10.1038/s41746-018-0029-1] [Medline: 31304302]
45. Wu J, Roy J, Stewart WF. Prediction modeling using EHR data: challenges, strategies, and a comparison of machine learning approaches. Med Care 2010 Jun;48(6 Suppl):S106-S113. [doi: 10.1097/MLR.0b013e3181de9e17] [Medline: 20473190]
46. Rifkin R, Klautau A. In defense of one-vs-all classification. J Mach Learn Res 2004;5:41. [doi: 10.5555/1005332.1005336]
47. Read J, Pfahringer B, Holmes G, Frank E. Classifier chains for multi-label classification. Mach Learn 2011 Jun 30;85(3):333-359. [doi: 10.1007/S10994-011-5256-5]
48. Dunn OJ. Multiple comparisons among Means. J Am Stat Assoc 1961 Mar;56(293):52-64. [doi: 10.1080/01621459.1961.10482090]
49. Bland JM, Altman DG. Multiple significance tests: the Bonferroni method. BMJ 1995 Jan 21;310(6973):170 [FREE Full text] [doi: 10.1136/bmj.310.6973.170] [Medline: 7833759]
50. Choi JE, Kang HW, Hong YM, Sohn S. C-reactive protein and N-terminal pro-brain natriuretic peptide discrepancy: a differentiation of adenoviral pharyngoconjunctival fever from Kawasaki disease. Korean J Pediatr 2018 Jan;61(1):12-16 [FREE Full text] [doi: 10.3345/kjp.2018.61.1.12] [Medline: 29441107]
51. Schuirmann DJ. A comparison of the two one-sided tests procedure and the power approach for assessing the equivalence of average bioavailability. J Pharmacokinet Biopharm 1987 Dec 1;15(6):657-680. [doi: 10.1007/BF01068419] [Medline: 3450848]
52. Walker E, Nowacki AS. Understanding equivalence and noninferiority testing. J Gen Intern Med 2011 Feb 21;26(2):192-196 [FREE Full text] [doi: 10.1007/s11606-010-1513-8] [Medline: 20857339]
53. Rockenschaub P, Akay EM, Carlisle BG, Hilbert A, Wendland J, Meyer-Eschenbach F, et al. External validation of AI-based scoring systems in the ICU: a systematic review and meta-analysis. BMC Med Inform Decis Mak 2025 Jan 06;25(1):5 [FREE Full text] [doi: 10.1186/s12911-024-02830-7] [Medline: 39762808]
54. Glenn WB. Verification of forecasts expressed in terms of probability. Mon Weather Rev 1950 Jan;78(1):1-3. [doi: 10.1175/1520-0493(1950)078<0001:vofeit>2.0.co;2]
55. Dawood T, Chen C, Sidhu BS, Ruijsink B, Gould J, Porter B, et al. Uncertainty aware training to improve deep learning model calibration for classification of cardiac MR images. Med Image Anal 2023 Aug;88:102861 [FREE Full text] [doi: 10.1016/j.media.2023.102861] [Medline: 37327613]
56. Eelbode T, Bertels J, Berman M, Vandermeulen D, Maes F, Bisschops R, et al. Optimization for medical image segmentation: theory and practice when evaluating with dice score or Jaccard index. IEEE Trans Med Imaging 2020 Nov;39(11):3679-3690. [doi: 10.1109/tmi.2020.3002417]
57. Zhang Z, Yan C, Malin BA. Membership inference attacks against synthetic health data. J Biomed Inform 2022 Jan;125:103977 [FREE Full text] [doi: 10.1016/j.jbi.2021.103977] [Medline: 34920126]
58. Cobilean V, Mavikumbure HS, Drake D, Stuart M, Manic M. Investigating membership inference attacks against CNN models for BCI systems. IEEE J Biomed Health Inform 2025 Nov;29(11):8164-8174. [doi: 10.1109/jbhi.2025.3593443]
59. Chen J, Wang WH, Shi X. Differential privacy protection against membership inference attack on machine learning for genomic data. Pac Symp Biocomput 2021;26:26-37 [FREE Full text] [Medline: 33691001]
60. Bohrson CL, Barton AR, Lodato MA, Rodin RE, Luquette LJ, Viswanadham VV, et al. Linked-read analysis identifies mutations in single-cell DNA-sequencing data. Nat Genet 2019 Apr 18;51(4):749-754 [FREE Full text] [doi: 10.1038/s41588-019-0366-2] [Medline: 30886424]
61. Luquette LJ, Miller MB, Zhou Z, Bohrson CL, Zhao Y, Jin H, et al. Single-cell genome sequencing of human neurons identifies somatic point mutation and indel enrichment in regulatory elements. Nat Genet 2022 Oct 26;54(10):1564-1571 [FREE Full text] [doi: 10.1038/s41588-022-01180-2] [Medline: 36163278]

Abbreviations

AI: artificial intelligence
AUC: area under the curve
AUPRC: area under the precision-recall curve

XSL•FO
RenderX

AUROC: area under the receiver operating characteristic curve
CC: classifier chains
CPU: central processing unit
ECE: expected calibration error
EHR: electronic health record
GPU: graphics processing unit
ICD-10: International Classification of Diseases, Tenth Revision
KCD-8: Korean Classification of Diseases, Eighth Revision
LiRA: Likelihood Ratio Attack
MIA: membership inference attack
OvR: one-vs-rest
TOST: two 1-sided tests
XGBoost: extreme gradient boosting

Edited by A Benis; submitted 03.Sep.2025; peer-reviewed by A Kalluchi, Y He; comments to author 19.Jan.2026; accepted 05.Feb.2026; published 04.Mar.2026.

Please cite as:
Lee J, Hwang S, Lee KH
Scalable and Privacy-Conscious End-to-End Processing of Large-Scale Clinical Data for Precision Medicine: Empirical Evaluation Study
JMIR Med Inform 2026;14:e83487
URL: https://medinform.jmir.org/2026/1/e83487
doi:10.2196/83487
PMID:

©Jungwoo Lee, Sangwon Hwang, Kyu Hee Lee. Originally published in JMIR Medical Informatics (https://medinform.jmir.org), 04.Mar.2026. This is an open-access article distributed under the terms of the Creative Commons Attribution License (https://creativecommons.org/licenses/by/4.0/), which permits unrestricted use, distribution, and reproduction in any medium, provided the original work, first published in JMIR Medical Informatics, is properly cited. The complete bibliographic information, a link to the original publication on https://medinform.jmir.org/, as well as this copyright and license information must be included.

XSL•FO
RenderX

Trust in AI-Supported Screening in General Practice Among Urban and Rural Citizens: Cross-Sectional Study

Larisa Wewetzer, Dr Rer Hum Biol; Katja Goetz, Prof Dr Phil, Dipl-Soz; Soenke Freischmidt, Dr Med; Jost Steinhauser, Prof. Dr Med

Institute of Family Medicine, University Medical Center Schleswig-Holstein, Ratzeburger Allee 160, Luebeck, Germany

Corresponding Author:
Larisa Wewetzer, Dr Rer Hum Biol
Institute of Family Medicine, University Medical Center Schleswig-Holstein, Ratzeburger Allee 160, Luebeck, Germany

Abstract

Background: The early detection of diseases is one of the tasks of general practice. Artificial intelligence (AI)–based technologies could be useful for identifying diseases at an early stage in general practices. As approximately 90% of the population regularly consults a general practitioner during one year, this could increase the percentage of citizens who take part in meaningful screening measures.

Objective: This study aimed to evaluate the level of trust among citizens in rural and urban areas in AI-supported early detection measures in general practice.

Methods: This cross-sectional study was conducted in the federal state of Schleswig-Holstein, Germany, from November 2023 to December 2023, on the topic of early detection measures with AI in general practice care, among other things. For this purpose, 5000 adult residents of rural areas (Ostholstein, Pinneberg, and Nordfriesland) and urban areas (the city of Kiel) were invited to take part in the survey. Data analysis was carried out using descriptive statistics, subgroup analysis, and linear and stepwise regression analysis to identify the factors that influenced trust in AI-based diagnoses.

Results: Most respondents (787/1790, 44.0%) considered the introduction of an AI-based screening measure to be a sign of modern medicine. Moreover, 21.7% (n=388) of respondents feared that the introduction of such services could lead to a deterioration in the physician-patient relationship. The role of AI in future care was rated as very important by 35.4% (n=634) of respondents. The stepwise regression analysis showed that a positive attitude toward AI in medicine was the strongest predictor (ß=0.420) of trust in AI-based diagnoses. In contrast, trust in physician diagnoses was associated with lower age (ß=–0.111) and shorter waiting times for test results (ß=0.077).

Conclusions: Trust in general practitioner–based diagnoses was approximately 6 times greater than trust in AI applications. Despite concerns about their impact on the physician-patient relationship, approximately one-third of participants believed that the role of AI in health care will grow.

(JMIR Med Inform 2026;14:e69777) doi:10.2196/69777

KEYWORDS

artificial intelligence; AI; citizens; cross-sectional study; diabetic retinopathy; general practice; trust

Introduction

The basic care of all patients in emergency, acute, and long-term care, as well as in prevention and rehabilitation, constitutes a central responsibility of general medicine [1]. Therefore, the early detection of diseases represents an important aspect of secondary prevention in a general practitioner (GP) practice. Appropriate measures can be initiated through early detection, which can considerably improve the course of an individual illness. GPs are often the first to diagnose diseases such as diabetes, hypertension, and cardiovascular diseases [2].

More than 90% of the population regularly consults their GP per year [1], which offers a significant opportunity to increase the proportion of citizens who take part in appropriate screening measures.

Screening for eye diseases is a promising extension of these early detection measures. Diabetic retinopathy (DR), in particular, can lead to severe visual impairment or even blindness if it is not detected and treated early. The number of people in Germany who become blind as a result of DR is approximately 15,000 per year [3]. DR is therefore the second most common cause of blindness [4]. According to a European study, 48% of patients with diabetes do not undergo the recommended screening examination [5].

The current diagnosis of these diseases requires a referral to an ophthalmologist, which can lead to long waiting times, especially in rural areas with limited access to specialists [6].

XSL•FO
RenderX

In this context, artificial intelligence (AI)–supported technologies could play an important role by complementing and extending traditional screening approaches. For example, in general practice, these technologies may include AI-assisted analysis of skin lesions for cancer screening or algorithms that identify abnormal heart rhythms in long-term electrocardiograms. In this study, we focused on DR as an illustrative example.

AI-assisted diagnostic tools could be used to analyze retinal images without requiring the presence of an eye specialist [7,8]. At the same time, recent studies indicate good diagnostic performance of deep learning algorithms. For example, in a study conducted in 2019, the detection of DR was analyzed on 25,326 retinal images of diabetes patients from Thailand. The algorithm showed a sensitivity of 97%, higher than the 74% observed for human experts, and a specificity of 96%, compared with 98% of specialists [9].

The implementation of AI-supported technologies could enable screening for DR directly in the GP practice as part of disease management programs. In this way, suspicious findings could be detected early, and patients could be referred to ophthalmologists accordingly.

It is still unknown whether trust in AI-supported technologies for early disease detection varies across population groups. However, significant variations in attitudes toward eHealth were observed between urban and rural respondents, highlighting a potential disparity in the future implementation of these technologies in general practice across demographic areas [10,11]. Therefore, the aim of the study was to evaluate the level of trust citizens in rural and urban areas have in AI-supported early detection measures in general practice.

Methods

This cross-sectional study was conducted in accordance with the STROBE (Strengthening the Reporting of Observational Studies in Epidemiology) guidelines [12].

Study Design and Participants

A cross-sectional study on early detection measures using AI in GP care was conducted in the federal state of Schleswig-Holstein, Germany, from November 2023 to December 2023. To this end, 5000 adult citizens from Schleswig-Holstein were invited to take part in the survey. The citizens were randomly selected from the databases of the local registration office.

Following the first invitation, 2 reminders to participate in the study were sent out at 3-week intervals. A stamped and preaddressed return envelope was included in all mailings to facilitate participation. A short version of the questionnaire was enclosed with the third reminder letter. This approach, which is consistent with the Tailored Design Method in survey research, was chosen to maximize the response rate and reduce the participation barrier for citizens who had not yet responded, by minimizing the time required.

Data Collection and Questionnaire

Data were collected using a self-constructed questionnaire in paper form. The development of the questionnaire was rigorously based on the findings of a qualitative study that served as a formal pilot phase and informed the generation of items [13]. This preceding qualitative study explored the determinants of AI implementation for DR screening in primary care. In addition, a subset of items—especially those assessing trust in AI vs physician diagnosis and general attitudes toward AI—was pilot-tested in a small qualitative pretest with GPs (1 female GP and 3 male GPs) to ensure clarity and face validity.

To account for different levels of respondent burden, 2 versions of the questionnaire were used:

- The long version consisted of 35 items, covering all conceptual domains in depth (telemedicine use, attitudes toward AI, perceived impact of AI-supported screening, importance ratings for screening attributes, expectations about examination duration, trust in diagnoses, and sociodemographic variables).
- The short version was reduced to 5 core study-related items, capturing only the core constructs (general attitude toward telemedicine, general attitude toward AI in medicine, trust in AI diagnosis, trust in physician diagnosis, age, gender, and region).

The use of long and short questionnaire versions was chosen because shorter instruments in postal surveys can increase response rates and reduce dropout, especially when sent as reminders [14].

The long questionnaire consisted of five sections:

1. Telemedicine experience and attitudes
2. Attitudes toward AI in health care
3. Perceived impact of AI-based screening in general practice
4. Importance of specific aspects of AI-assisted eye disease screening
5. Trust in AI-based diagnosis vs diagnosis by physicians

The participants' general attitude toward AI applications in general practice was assessed using a 6-point Likert scale ranging from "very positive" to "very negative." In addition, questions were asked about the expected future role of AI in their own health care and the potential impact of integrating AI into general practice.

Participants were asked to rate from a list of options what impact the use of AI-based screening measures would have on their everyday life and care, such as improving or worsening patient care and physician-patient relationships. In addition, specific aspects were asked about the importance of performing AI-based screening tests. The importance of these aspects was rated on a 6-point scale, ranging from "very important" to "very unimportant." Finally, respondents were asked about their trust in diagnoses made by AI compared with diagnoses made by GPs.

The questionnaire also included sociodemographic parameters such as age, gender, and regional origin. Sociodemographic information (age, gender, and regional origin) was collected at the end of the instrument. Regional origin was dichotomized

XSL•FO
RenderX

into rural (Ostholstein, Pinneberg, and Nordfriesland) and urban (Kiel).

Statistical Data Analysis

The analyses were carried out using the SPSS software (version 29.0; IBM Corp). The sociodemographic characteristics of the sample (full and short versions of the questionnaire) were analyzed descriptively. Variables with continuous values were summarized using mean values and SDs. Variables with categorical values were represented by absolute (n) and relative (%) frequencies. The regional origin was dichotomized: the regions Ostholstein, Pinneberg, and Nordfriesland were assigned to the rural area, and the Kiel region to the urban area.

The sociodemographic characteristics of the sample (full and short versions of the questionnaire) were analyzed descriptively. Variables with continuous values were summarized using mean values and SDs. Variables with categorical values were represented by absolute (n) and relative (%) frequencies. The regional origin was dichotomized: the regions Ostholstein, Pinneberg, and Nordfriesland were assigned to the rural area, and the Kiel region to the urban area.

The nonparametric Mann-Whitney *U* test was used to compare the full and short versions of the questionnaire regarding the general preferences of telemedicine and AI. Furthermore, a subgroup analysis was performed by using the nonparametric Mann-Whitney *U* test to assess whether the regional origin (0=rural region and 1=urban region) differed concerning the preferences for telemedicine and AI.

Moreover, linear correlations between trust in diagnosis with AI and trust in diagnosis through physicians, the sociodemographic variables, and various influencing factors were calculated using Spearman correlation coefficient. Testing for connections using a correlation is a common procedure to reduce the number of variables for subsequent model calculations. In a further step, significant correlations identified in this way were taken into account in the linear regression models.

Afterward, 2 stepwise regression analyses were performed to evaluate which factors were strongly associated with the outcome variables. Trust in diagnosis with AI and trust in diagnosis through physicians were the outcome variables, while other aspects, such as preferences for telemedicine and AI, attitudes to early detection measures, and some characteristics of participants (such as gender, age, regional origin), were considered potential predictors and handled as covariates. Additionally, the possibility for multicollinearity was considered in both models. The variance inflation factor (VIF) and the tolerance value were reported for the final step of the regression models. Values for VIF should not exceed 5.0, and tolerance values should not be lower than 0.25 [15]. Statistical significance was set at $P<.05$.

Ethical Considerations

The ethics application for conducting the study was approved by the ethics committee of the University of Lübeck in March 2023 (2023-258_1). All participants provided informed consent prior to participation and were informed that their participation was voluntary and that they could withdraw from the study at any time without consequences. The study involved only the analysis of data collected within the scope of the approved protocol; no additional data were evaluated beyond those covered by the original ethical approval. All data were anonymized prior to analysis, and no personally identifiable information was accessible to the researchers. Appropriate technical and organizational measures were implemented to ensure data protection and confidentiality in accordance with applicable data protection regulations. No incentives were offered for participation.

Results

Description of the Sample

Of the 5000 citizens contacted, 1790 (35.8%) took part in the survey, corresponding to a response rate of almost 36%. Of the participants, 785 (43.9%) were male and 972 (54.3%) were female. A total of 10 participants (0.6%) identified themselves as diverse, while 23 (1.3%) did not specify their gender. Of these participants, 352 (19.7%) chose the short version of the questionnaire. Of these, 160 (44.1%) were male, 189 (52.1%) were female, 3 (0.8%) were diverse, and 7 (1.9%) had missing data for this variable. The average age of all participants was 56 years (range 18-96 years).

Of the 1790 participants, 764 (42.7%) lived in the city and 979 (54.7%) lived in a rural area. Most participants lived in Kiel (764/1790, 42.7%), followed by 520 (29.1%) in Ostholstein, 335 (18.7%) in Pinneberg, and 124 (6.9%) in Nordfriesland districts. Table 1 provides further details on the comparison between the long version and the short version of the questionnaire.

XSL•FO
RenderX

Table . Sociodemographic characteristics of participants (n=1790).

Characteristics[a]	Long version questionnaire (n=1427)	Short version questionnaire (n=363)	*P* value
Gender, n (%)			.64
Female	783 (54.9)	189 (52.1)	
Male	625 (43.8)	160 (44.1)	
Diverse	7 (0.5)	3 (0.8)	
Age (y), mean (SD; range)	55.8 (16.8; 18 - 96)	57 (16.4; 18 - 91)	.11
Regional origin, n (%)			.09
Kiel (urban)	606 (42.5)	158 (43.5)	
Ostholstein (rural)	406 (28.5)	114 (31.4)	
Pinneberg (rural)	275 (19.3)	60 (16.5)	
Nordfriesland (rural)	109 (7.6)	15 (4.1)	
Assessment of local medical care[b], mean (SD)	2.97 (1.43)	2.93 (1.32)	.88

[a]The n values vary due to missing data.

[b]Ranging from 1 (very good) to 6 (very bad).

General Attitude, Future Role of AI, and Trust in Diagnosis Through AI and Physicians

A descriptive analysis of general preferences regarding telemedicine and AI in health care was carried out (Table 2). The variables analyzed included general attitudes toward telemedicine and AI, as well as specific aspects such as trust in diagnoses by AI and the future role of AI in one's own health care.

Table . General preferences for telemedicine and artificial intelligence (AI)—descriptive analysis.

Variables	Long version, mean (SD)	Short version, mean (SD)	*P* value
General attitude to the topic of telemedicine[a]	3.44 (1.50)	3.58 (1.37)	.06
General attitude to applications of AI in medicine[a]	3.35 (1.49)	3.47 (1.47)	.19
Future role of AI for own health care	2.91 (1.48)	—[b]	—
Trust in diagnosis through AI[c]	3.53 (1.43)	—	—
Trust in diagnosis through physician[c]	1.96 (0.82)	—	—

[a]Ranging from 1 (very positive) to 6 (very negative).

[b]Not available.

[c]Ranging from 1 (very small) to 6 (very big). These items were not asked in the short version.

For the general attitude toward applications of AI in medicine, a mean value of 3.35 (SD 1.49) was observed for the long version of the questionnaire, and a mean value of 3.47 (SD 1.47) was observed for the short version.

The assessment of the future role of AI in personal health care had a mean value of 2.91 (SD 1.48). The SD of 1.48 suggests a wide distribution of responses. It was rated important by 35.4% (n=634) of respondents.

Trust in diagnoses by AI is rated with a mean value of 3.53 (SD 1.43). In comparison, trust in diagnoses by physicians had a mean value of 1.96 (SD 0.82).

Subgroup Analysis Concerning Regional Origin and General Preferences to Telemedicine and AI

Participants from urban regions were more positive toward telemedicine ($mean_{urban}$ 3.26, SD 1.5; $mean_{rural}$ 3.56, SD 1.5; $P<.001$) and toward applications of AI in medicine ($mean_{urban}$ 3.11, SD 1.4; $mean_{rural}$ 3.52, SD 1.5; $P<.001$) than participants from rural regions. Moreover, for respondents from urban regions, AI was perceived to play a bigger future role for own health care ($mean_{urban}$ 2.65, SD 1.4; $mean_{rural}$ 3.09, SD 1.5; $P<.001$), and they reported greater trust in diagnoses made by AI ($mean_{urban}$ 3.38, SD 1.4; $mean_{rural}$ 3.63, SD 1.5; $P<.001$) than participants from rural regions. No significant difference was

XSL•FO
RenderX

observed for trust in diagnosis through physicians ($mean_{urban}$ 1.99, SD 0.80; $mean_{rural}$ 1.93, SD 0.81; *P*=.14).

Relevance of AI-Based Screening Measures in the GP Practice

Participants were asked to rate the use of AI-based screening measures in GP practices (Figure 1). Respondents had the opportunity to select several statements that applied.

Figure 1. Response rates for the long version vs short version of the questionnaire.

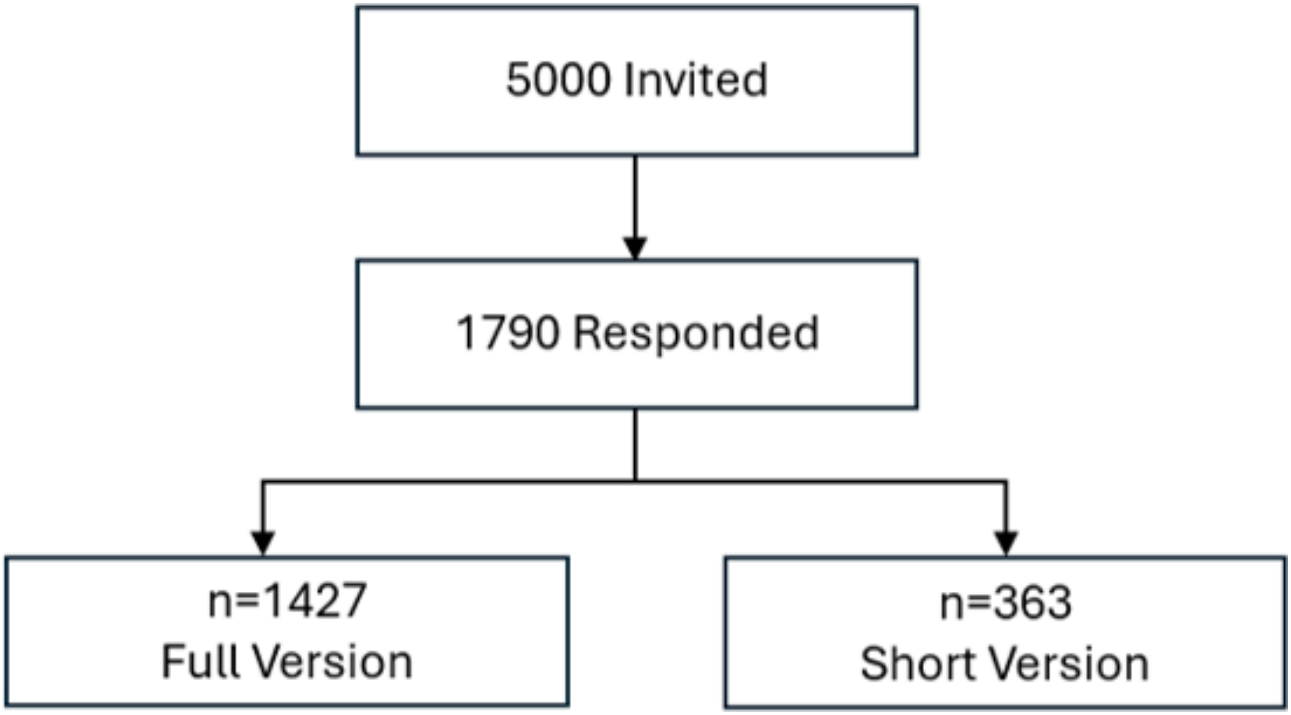

The analysis of the survey results showed a differentiated perception of the AI-based screening measures, which reflected both potential benefits and concerns among the citizens surveyed.

Out of the 1790 respondents, the most frequently mentioned statement was “signs of modern medicine,” selected by 787 (44.0%) participants. The statement “improved patient care” was selected by 618 participants (34.5%), followed by “easing everyday life” with 445 (24.9%) responses. In contrast, 388 (21.7%) participants stated that they would expect a “worsened doctor-patient relationship,” and 270 (15.1%) respondents described the measure as “intensifying uncertainty.”

The statements “improved doctor-patient relationship” (n=167, 9.3%), “signs of unnecessary technologization” (n=162, 9.1%), “deterioration in patient care” (155, 8.7%), and “difficulty in everyday life” (n=37, 2.1%) were selected less frequently (Multimedia Appendix 1).

Aspects of the Implementation of Screening Examinations for Eye Diseases Using AI in GP Practices

In the data received from the long version of the questionnaire, the most important factors from the citizens’ perspective were trust in the GP (mean 1.78, SD 1.24) and the reliability of the examination (mean 1.43, SD 1.01), followed by data security (mean 2.19, SD 1.52).

With regard to organizational factors, the accessibility of the practice (mean 2.14, SD 1.31) and the waiting time for an ophthalmologist appointment (mean 2.13, SD 1.26) were also rated as relevant. The protection against additional examination costs (eg, Individual Health Services; mean 2.30, SD 1.42) was rated as moderately important.

Factors considered less important from the citizens’ perspectives included not having their pupils dilated (mean 3.24, SD 1.65), the duration of the examination (mean 2.93, SD 1.45), and the distance to the nearest ophthalmologist (mean 2.50, SD 1.39).

The results showed that trust in the GP conducting the examination, the reliability of the examination, and data security were the most important aspects considered by the participants when implementing such technologies in GP practices (Table 3).

XSL•FO
RenderX

Table . Evaluation of the aspects of artificial intelligence–supported screening for eye diseases in general practitioner practices.

Variables[a]	Factors, mean (SD; 95% CI)
Trust in general practitioner	1.78 (1.24; 1.71 - 1.86)
Duration of the examination	2.93 (1.45; 2.84 - 3.02)
Waiting time until the test results are available	2.44 (1.29; 2.37 - 2.52)
Data security	2.19 (1.52; 2.10 - 2.29)
Reliability of the examination	1.43 (1.01; 1.37 - 1.49)
Not having the pupils dilated	3.24 (1.65; 3.14 - 3.35)
Accessibility of the practice	2.14 (1.31; 2.06 - 2.22)
Distance to the nearest ophthalmologist	2.50 (1.39; 2.41 - 2.58)
Waiting time for an eye specialist appointment	2.13 (1.26; 2.05 - 2.21)
Waiting time in an ophthalmologist's practice	2.49 (1.31; 2.41 - 2.57)
Protection against additional examination costs	2.30 (1.42; 2.22 - 2.39)
Performance of the examination by medical assistants	2.12 (1.30; 2.04 - 2.20)

[a]Scale from 1=very important to 6=very unimportant.

Factors Associated With Trust in Diagnosis With AI

The stepwise regression analysis is presented in Table 4 and reports only coefficients with statistical significance at the $P<.05$ level. A 9-step model was fitted and explained more than 60% ($R^2=0.602$) of the variance in the dependent variable, "trust in diagnosis through AI." In the first step of the stepwise regression analysis, the variable "general attitude to applications of AI in medicine" showed the highest explained variance ($R^2=0.509$). A higher positive level of attitude toward applications of AI in medicine was strongly associated with higher level of trust in diagnosis through AI. Individual characteristics were not included in the regression model, as $P>.05$. Collinearity statistics ranged between 2.112 (VIF value) and 0.473 (tolerance value) for "general attitude to applications of AI in medicine" and 1.140 (VIF value) and 0.877 (tolerance value) for "improved patient-physician relationship."

Table . Associations of individual characteristics, general preferences for telemedicine and artificial intelligence (AI), and attitudes toward early detection measures in general practitioner care with general trust in AI (results of stepwise linear regression analysis).

Variables[a]	β	*P* value
General attitude to applications of AI in medicine	0.420	<.001
Intensifying uncertainty	0.136	<.001
Future role of AI for own health care	0.164	<.001
Signs of unnecessary technologization	0.120	<.001
Improved physician-patient relationship	−0.063	.003
Providing security	−0.091	<.001
Duration of the examination	0.063	.004
Worsened physician-patient relationship	0.066	.004
Reliability of the examination	0.053	.02

[a]Last step was reported.

Factors Associated With Trust in Diagnosis Through Physicians

The stepwise regression analysis is presented in Table 5 and reports only coefficients with statistically significances at the $P<.05$ level. A 5-step model was fitted and explained more than 4.8% ($R^2\approx.048$) of the variance in the dependent variable, "trust in diagnosis through physicians." For example, a higher positive level of trust in diagnosis through physicians was strongly associated with lower age and greater importance attributed to the waiting time until the test results were available. Collinearity statistics ranged between 1.308 (VIF value) and 0.765 (tolerance value) for "distance to the nearest ophthalmologist" and 1.007 (VIF value) and 0.993 (tolerance value) for "providing security."

XSL•FO
RenderX

Table . Associations of individual characteristics, general preferences for telemedicine and artificial intelligence, and attitudes toward early detection measures in general practice care on general trust in diagnosis through physicians (results of stepwise linear regression analysis).

Variables	β	*P* value
Age of the participants	−0.111	<.001
Waiting time until the test results are available	0.077	.03
Providing security	0.093	.003
Local general medical care	0.089	.005
Distance to the nearest ophthalmologist	0.090	.01

[a]Last step was reported.

Discussion

This study examines citizens' attitudes toward the use of AI in general practice, particularly in the context of early detection measures. The study showed that the introduction of AI-supported technologies is met with mixed reactions.

Differences Between Rural and Urban Areas

Significant differences emerged between urban and rural participants. People from urban areas were significantly more positive about the use of AI in medicine than those from rural areas.

Differences in access to medical services between urban and rural areas are deeply rooted and reflect a complex mix of infrastructural, socioeconomic, and cultural factors [16,17]. While urban areas often provide a wide range of medical services and specialists, some rural areas experience a shortage of physicians, greater distances to health facilities, and limited access to specialized treatment [17].

The introduction of AI and telemedicine is often promoted as a solution to these inequalities by extending access to care. However, emerging research suggests that these technologies are not always met with acceptance [10,11]. The reasons for this are varied and include technological barriers, a lack of trust in digital diagnostic methods, and a preference for in-person physician-patient interactions [12,18,19].

To ensure equal access to care, a deeper understanding of the specific needs and concerns of the rural population is needed. This means not only providing technology but also taking into account the cultural and psychological aspects that influence attitudes toward technology.

Dynamics of Trust in General Practice Care and Technology

This study pointed to a trust deficit in AI-supported technologies. Trust plays an essential role both in interpersonal interactions and in the use of technology. The patient-physician relationship is built on trust, particularly in the physician's commitment to voluntary responsibility and compassionate judgment [20]. This dimension of trust is crucial, as patients in vulnerable health situations depend heavily on the expertise and care of their treating physicians.

This trust is primarily shaped by the quality of the physician-patient relationship, in particular effective communication, interpersonal care, and the physician's knowledge of the patient's individual needs. The study emphasized that these factors play an important role in strengthening patient trust, while other aspects, such as the duration of registration at a practice or the frequency of visits, had less influence on trust [21].

Interpersonal interaction and trust in the treating physician are essential for patient satisfaction and adherence to treatment [20]. Research also highlighted that perceived empathy and individualized care are particularly important to patients, reinforcing the importance of these qualities in maintaining trust in medical professionals [21].

Central to this trust is the concept of continuity of care, particularly relational continuity, in which patients consistently see the same physician over time.

The association between continuity of primary care and patient mortality has been described by categorizing continuity into 3 types: relational continuity, informational continuity, and management continuity. A review of 13 quantitative studies found that greater continuity of care is significantly associated with lower all-cause mortality, particularly among older patients and those with chronic conditions. This protective effect was explained by improved physician knowledge, increased patient confidence, and better adherence to medical advice [22].

Therefore, in an increasingly digitalized world, it is essential that new digital health applications are designed from a patient-centered perspective.

Trust in technologies is predominantly based on functional aspects, such as reliability, security, and predictability [23]. From the perspective of the citizens in our study, the reliability of the examination was the most important factor.

Trust in technology is a construct that is strengthened by a combination of experiences with the technology, trust in users, and trust in regulators. Each of these components plays a critical role in maintaining and fostering trust over time. Past experiences, especially the reliability of the technology, had a significant impact on user trust [24]. In addition, trust is strengthened by the integrity and competence of those who use the technology, especially in the medical field [25], as well as by trust in regulatory authorities responsible for the safety and effectiveness of the technology [26].

The ways in which AI technologies work are currently incomprehensible to the public. This technological opacity requires a certain degree of explainability and interpretability

XSL•FO
RenderX

[27]. This lack of transparency means that damage caused by interaction with an AI system cannot be easily proven or clearly attributed [28]. This poses a major challenge and underlines the urgency of developing mechanisms that clearly regulate responsibility and liability in connection with AI decisions.

AI is often seen as a potential solution to current challenges in the health care system, such as relieving the burden on physicians and promoting a person-centered physician-patient relationship [29,30]. In a systematic analysis of 45 studies, the impact of AI on the person-centered physician-patient relationship was investigated. The researchers identified various ways in which the use of AI tools could promote person-centered care. One of these ways was the use of AI tools in a supportive role [31].

The rising interest in AI for medical applications should not overshadow the need for proper scientific review and evaluation. It is crucial that the medical field maintains its high standards of evidence and ethical responsibility to ensure both the credibility and effectiveness of patient care in an increasingly digital world.

While a large body of research demonstrates the benefits of primary care, there is comparatively less evidence for the use of AI technologies in health care. This discrepancy has substantial implications for evidence-based medicine, where clinical decisions should be based on solid scientific research [32].

A lack of uniform evaluation protocols introduces several challenges, such as doubts concerning the long-term effectiveness, safety of patients, security of data, and ethical dilemmas. To integrate telemedicine and AI into health care systems responsibly and effectively, we need flexible and comprehensive evaluation methods that conform to clinical objectives and regulatory guidelines [33].

The literature highlights that the factors influencing health are complex and influenced by a variety of factors [34,35]. Future studies should continue to explore how aspects beyond technology influence health to ensure that the design of new health systems considers a balanced integration of digital and human resources.

Future Role of AI in Medical Care

While concerns remain about the integration of AI in health care, a significant proportion of participants believed that AI-based early detection measures in general practice could enhance patient care. The application of patient-specific medical data combined with AI assistance systems has the potential to improve treatment outcomes by facilitating prevention, early diagnosis, and individualized therapies. Such advancements could lead to the identification of new medical correlations and innovative approaches to prevention [36].

However, despite these potential benefits, significant challenges and concerns remain. The use of AI necessitates access to substantial amounts of sensitive medical data, raising concerns about data privacy and security. Robust security protocols are essential to safeguard patient privacy and prevent data misuse [37].

The development and integration of AI in health care also bring significant ethical considerations, particularly around accountability for poor decisions or unexpected outcomes. Establishing clear guidelines and defining responsibilities are essential to address these ethical concerns and build trust with patients [38].

In this context, the European Union's "AI Act" represents a critical step toward creating uniform regulations for AI use within the European Union to ensure safety and trustworthiness. This regulation uses a risk-based approach, categorizing AI applications into different risk levels, with high-risk applications, such as those often found in the medical field, subjected to strict requirements. These requirements include transparency, security, and the avoidance of discrimination, all aimed at ensuring that AI systems in the health care sector adhere to high-quality standards and guarantee patient safety [39].

Strengths and Limitations

With a response rate of approximately 36%, the study provides a robust insight into the attitudes and opinions of the population of Schleswig-Holstein on the use of AI in GP practices.

The study was limited to Schleswig-Holstein, which could limit the generalizability of the results to the whole of Germany. Furthermore, the sample could be biased by self-selection of participants who may have had a greater interest in or familiarity with digital technologies. Future studies should therefore aim for a broader geographical spread to improve the representativeness and applicability of the results to the entire German population.

Conclusions

These findings suggest that despite the growing importance of AI in some areas of health care, the traditional physician-patient relationship is seen as absolutely essential. This emphasizes the enduring value of the human elements in health care—personal interaction, empathy, and understanding—features that AI cannot replicate.

Nevertheless, the introduction of AI is still recognized as a sign of modern medicine. People in urban areas are somewhat more open to AI technologies in health care. The integration of AI into health care raises crucial considerations regarding the principles of evidence-based medicine. Balancing technological innovation with the fundamentals of patient-centered care will be crucial in navigating the future landscape of health care.

Funding

This work was supported by grants from the Joachim Herz Foundation as part of the PASBADIA (smartphone-based point-of-care diagnostics) Project.

XSL•FO
RenderX

Authors' Contributions

LW and JS initiated and designed the study. LW and SF coordinated the study. KG carried out data analysis. LW wrote the first draft of the manuscript. All authors (LW, KG, SF, and JS) read earlier versions of the manuscript, provided critical comments, and approved the final manuscript.

Conflicts of Interest

None declared.

Multimedia Appendix 1
Evaluation of an artificial intelligence–based screening measure in general practice.
[DOCX File, 16 KB - medinform_v14i1e69777_app1.docx]

References

1. Fachdefinition allgemeinmedizin [Web page in German]. Deutsche Gesellschaft für Allgemeinmedizin und Familienmedizin. 2024. URL: https://www.degam.de/fachdefinition [accessed 2025-05-25]
2. Prävention: Früherkennungsuntersuchungen und Impfungen [Web page in German]. Kassenärztliche Bundesvereinigung. 2024. URL: https://www.kbv.de/praxis/patientenversorgung/praevention [accessed 2025-05-25]
3. Hörle S, Grüner F, Kroll P. Epidemiologie diabetischer Erblindungen - eine Übersicht [Article in German]. Klin Monatsbl Augenheilkd 2002 Nov;219(11):777-784. [doi: 10.1055/s-2002-36318]
4. Cavan D, Makaroff L, da Rocha Fernandes J, et al. The Diabetic Retinopathy Barometer Study: global perspectives on access to and experiences of diabetic retinopathy screening and treatment. Diabetes Res Clin Pract 2017 Jul;129:16-24. [doi: 10.1016/j.diabres.2017.03.023] [Medline: 28499163]
5. Diabetic retinopathy barometer report. International Diabetes Federation Europe. 2017. URL: https://drbarometer.com/wp-content/uploads/2022/08/drbarometer_global_report-1.pdf [accessed 2025-05-25]
6. Krogh M, Germund Nielsen M, Byskov Petersen G, et al. Patient acceptance of AI-assisted diabetic retinopathy screening in primary care: findings from a questionnaire-based feasibility study. Front Med 2025 Sep 10;12:1610114. [doi: 10.3389/fmed.2025.1610114]
7. Abràmoff MD, Lavin PT, Birch M, Shah N, Folk JC. Pivotal trial of an autonomous AI-based diagnostic system for detection of diabetic retinopathy in primary care offices. NPJ Digit Med 2018;1(1):39. [doi: 10.1038/s41746-018-0040-6] [Medline: 31304320]
8. Ting DS, Cheung CY, Lim G, et al. Development and validation of a deep learning system for diabetic retinopathy and related eye diseases using retinal images from multiethnic populations with diabetes. JAMA 2017 Dec 12;318(22):2211-2223. [doi: 10.1001/jama.2017.18152] [Medline: 29234807]
9. Ruamviboonsuk P, Krause J, Chotcomwongse P, et al. Erratum: author correction: deep learning versus human graders for classifying diabetic retinopathy severity in a nationwide screening program. NPJ Digit Med 2019;2:68. [doi: 10.1038/s41746-019-0146-5] [Medline: 31341955]
10. von Solodkoff M, Strumann C, Steinhäuser J. Akzeptanz von Versorgungsangeboten zur ausschließlichen Fernbehandlung am Beispiel des telemedizinischen Modellprojekts „docdirekt“: ein mixed-methods design [Article in German]. Gesundheitswesen 2021 Mar;83(3):186-194. [doi: 10.1055/a-1173-9903]
11. Strumann C, Steinhäuser J. Evaluation of a direct-to-patient telehealth service in Germany (Docdirekt) based on routine data. Dtsch Arztebl Int 2021 Dec 17;118(50):872-873. [doi: 10.3238/arztebl.m2021.0378] [Medline: 35300786]
12. Vandenbroucke JP, von Elm E, Altman DG, et al. Strengthening the Reporting of Observational Studies in Epidemiology (STROBE): explanation and elaboration. Int J Surg 2014 Dec;12(12):1500-1524. [doi: 10.1016/j.ijsu.2014.07.014] [Medline: 25046751]
13. Held LA, Wewetzer L, Steinhäuser J. Determinants of the implementation of an artificial intelligence-supported device for the screening of diabetic retinopathy in primary care - a qualitative study. Health Informatics J 2022;28(3):14604582221112816. [doi: 10.1177/14604582221112816] [Medline: 35921547]
14. Edwards P, Roberts I, Clarke M, et al. Increasing response rates to postal questionnaires: systematic review. BMJ 2002 May 18;324(7347):1183. [doi: 10.1136/bmj.324.7347.1183] [Medline: 12016181]
15. Field A. Discovering Statistics Using IBM SPSS Statistics: Sage Publications; 2011.
16. Hartley D. Rural health disparities, population health, and rural culture. Am J Public Health 2004 Oct;94(10):1675-1678. [doi: 10.2105/ajph.94.10.1675] [Medline: 15451729]
17. Loftus J, Allen EM, Call KT, Everson-Rose SA. Rural-urban differences in access to preventive health care among publicly insured Minnesotans. J Rural Health 2018 Feb;34 Suppl 1(Suppl 1):s48-s55. [doi: 10.1111/jrh.12235] [Medline: 28295584]
18. Haggstrom DA, Lee JL, Dickinson SL, et al. Rural and urban differences in the adoption of new health information and medical technologies. J Rural Health 2019 Mar;35(2):144-154. [doi: 10.1111/jrh.12358] [Medline: 30830983]

XSL•FO
RenderX

19. LeBlanc M, Petrie S, Paskaran S, Carson DB, Peters PA. Patient and provider perspectives on eHealth interventions in Canada and Australia: a scoping review. Rural Remote Health 2020 Sep;20(3):5754. [doi: 10.22605/RRH5754] [Medline: 32949485]
20. DeCamp M, Tilburt JC. Why we cannot trust artificial intelligence in medicine. Lancet Digit Health 2019 Dec;1(8):e390. [doi: 10.1016/S2589-7500(19)30197-9] [Medline: 33323220]
21. Tarrant C, Stokes T, Baker R. Factors associated with patients' trust in their general practitioner: a cross-sectional survey. Br J Gen Pract 2003 Oct;53(495):798-800. [Medline: 14601357]
22. Baker R, Freeman GK, Haggerty JL, Bankart MJ, Nockels KH. Primary medical care continuity and patient mortality: a systematic review. Br J Gen Pract 2020 Sep;70(698):e600-e611. [doi: 10.3399/bjgp20X712289] [Medline: 32784220]
23. Lankton N, McKnight DH, Tripp J, Marshall University, Michigan State University, Baylor University. Technology, humanness, and trust: rethinking trust in technology. JAIS 2015;16(10):880-918. [doi: 10.17705/1jais.00411]
24. Hafizoğlu FM, Sen S. Understanding the influences of past experience on trust in human-agent teamwork. ACM Trans Internet Technol 2019 Nov 30;19(4):1-22. [doi: 10.1145/3324300]
25. Wewetzer L, Held LA, Goetz K, Steinhäuser J. Determinants of the implementation of artificial intelligence-based screening for diabetic retinopathy-a cross-sectional study with general practitioners in Germany. Digit Health 2023;9:20552076231176644. [doi: 10.1177/20552076231176644] [Medline: 37274367]
26. Li X, Hess TJ, Valacich JS. Why do we trust new technology? A study of initial trust formation with organizational information systems. The Journal of Strategic Information Systems 2008 Mar;17(1):39-71. [doi: 10.1016/j.jsis.2008.01.001]
27. Herzog C. Technological opacity of machine learning in healthcare. Presented at: 2nd Weizenbaum Conference: Challenges of Digital Inequality; May 16-17, 2019 URL: https://www.ssoar.info/ssoar/bitstream/handle/document/62580/ssoar-2019-herzog-Technological_Opacity_of_Machine_Learning.pdf;jsessionid=2A48C886E963221F3FD376851A02F14A?sequence=1 [accessed 2025-05-25]
28. Beck S, Faber M, Gerndt S. Rechtliche Aspekte des Einsatzes von KI und Robotik in Medizin und Pflege [Article in German]. Ethik Med 2023 Jun;35(2):247-263. [doi: 10.1007/s00481-023-00763-9]
29. Aminololama-Shakeri S, López JE. The doctor-patient relationship with artificial intelligence. AJR Am J Roentgenol 2019 Feb;212(2):308-310. [doi: 10.2214/AJR.18.20509] [Medline: 30540210]
30. Printz C. Artificial intelligence platform for oncology could assist in treatment decisions. Cancer 2017 May 15;123(6):905-905. [doi: 10.1002/cncr.30655] [Medline: 28263386]
31. Sauerbrei A, Kerasidou A, Lucivero F, Hallowell N. The impact of artificial intelligence on the person-centred, doctor-patient relationship: some problems and solutions. BMC Med Inform Decis Mak 2023 Apr 20;23(1):73. [doi: 10.1186/s12911-023-02162-y] [Medline: 37081503]
32. Evidence summary: the benefits of relational continuity. Alberta Medical Association. 2017. URL: https://www.albertadoctors.org/resource-centre/relational-continuity-resources/evidence-summary-the-benefits-of-relational-continuity/ [accessed 2025-05-25]
33. Burrell DN. Dynamic evaluation approaches to telehealth technologies and artificial intelligence (AI) telemedicine applications in healthcare and biotechnology organizations. Merits 2023;3(4):700-721. [doi: 10.3390/merits3040042]
34. Stronks K, Kunst AE. The complex interrelationship between ethnic and socio-economic inequalities in health. J Public Health (Oxf) 2009 Sep;31(3):324-325. [doi: 10.1093/pubmed/fdp070] [Medline: 19589801]
35. Deutekom M, Vansenne F, McCaffery K, Essink-Bot ML, Stronks K, Bossuyt PMM. The effects of screening on health behaviour: a summary of the results of randomized controlled trials. J Public Health (Oxf) 2011 Mar;33(1):71-79. [doi: 10.1093/pubmed/fdq050] [Medline: 20667898]
36. Budde K, Dasch T, Kirchner E, et al. Künstliche Intelligenz: Patienten im Fokus [Article in German]. Dtsch Arztebl 2020;117(49):A-2407 [FREE Full text]
37. Jiang F, Jiang Y, Zhi H, et al. Artificial intelligence in healthcare: past, present and future. Stroke Vasc Neurol 2017 Dec;2(4):230-243. [doi: 10.1136/svn-2017-000101] [Medline: 29507784]
38. Parikh RB, Obermeyer Z, Navathe AS. Regulation of predictive analytics in medicine. Science 2019 Feb 22;363(6429):810-812. [doi: 10.1126/science.aaw0029] [Medline: 30792287]
39. On artificial intelligence - a European approach to excellence and trust. European Commission. 2020. URL: https://commission.europa.eu/system/files/2020-02/commission-white-paper-artificial-intelligence-feb2020_en.pdf [accessed 2025-05-25]

Abbreviations

AI: artificial intelligence
DR: diabetic retinopathy
GP: general practitioner
STROBE: Strengthening the Reporting of Observational Studies in Epidemiology
VIF: variance inflation factor

XSL•FO
RenderX

Edited by A Benis; submitted 08.Dec.2024; peer-reviewed by A Wahbeh, L Buhr, M Bleckwenn; revised version received 15.Dec.2025; accepted 17.Dec.2025; published 12.Feb.2026.

Please cite as:
Wewetzer L, Goetz K, Freischmidt S, Steinhauser J
Trust in AI-Supported Screening in General Practice Among Urban and Rural Citizens: Cross-Sectional Study
JMIR Med Inform 2026;14:e69777
URL: https://medinform.jmir.org/2026/1/e69777
doi:10.2196/69777

© Larisa Wewetzer, Katja Goetz, Soenke Freischmidt, Jost Steinhauser. Originally published in JMIR Medical Informatics (https://medinform.jmir.org), 12.Feb.2026. This is an open-access article distributed under the terms of the Creative Commons Attribution License (https://creativecommons.org/licenses/by/4.0/), which permits unrestricted use, distribution, and reproduction in any medium, provided the original work, first published in JMIR Medical Informatics, is properly cited. The complete bibliographic information, a link to the original publication on https://medinform.jmir.org/, as well as this copyright and license information must be included.

XSL•FO
RenderX

Current Status, Challenges, and Opportunities Associated With Implementing Clinical Data Interchange Standards Consortium Standards in Japanese Academic Medical Centers: Cross-Sectional Survey

Kaori Nagai[1], MSN; Noriko Ito[1], MEng; Yuya Ikeda[2], BEng; Toshiki I Saito[1,3], MD, PhD

[1]Clinical Research Center, NHO Nagoya Medical Center, 4-1-1 Sannomaru, Naka-ku, Nagoya, Aichi, Japan

[2]Clinical Research Support Office, National Cancer Center Hospital East, Kashiwa, Chiba, Japan

[3]Clinical Research Center, NHO Headquarters, Meguro-ku, Tokyo, Japan

Corresponding Author:
Kaori Nagai, MSN
Clinical Research Center, NHO Nagoya Medical Center, 4-1-1 Sannomaru, Naka-ku, Nagoya, Aichi, Japan

Abstract

Background: The implementation of Clinical Data Interchange Standards Consortium (CDISC) standards is essential for accelerating clinical research and is mandated for new drug applications in Japan. However, the current status of their implementation and associated challenges in Japanese academic medical centers has not been comprehensively investigated.

Objectives: This study aimed to comprehensively clarify the current status, challenges, and opportunities associated with implementing CDISC standards in Japanese academic medical centers.

Methods: We conducted a questionnaire survey targeting 91 academic medical centers (83 university hospitals, 7 national centers for advanced and specialized medical care, and 1 national hospital organization) from June to August 2024. The survey assessed experience with contracted CDISC data creation, implementation status, barriers, and available resources. We performed Mann-Whitney *U* tests to assess the association between the number of data managers or biostatisticians and CDISC implementation status.

Results: Responses were received from 84 institutions (response rate: 92%). While 29% (26/91) had experience with contracted CDISC standards data creation, 22% (20/91) had implemented CDISC standards. The most frequently cited barrier to CDISC standards implementation was “significant human and financial effort and resource shortages” (62%, 56/91). A significant “supply and demand” gap was identified: while 66% (60/91) of institutions expected support (eg, materials, workshops) from other organizations, only 5% (5/91) were capable of providing such resources. Furthermore, 66% (60/91) of institutions had not yet decided on a future policy regarding CDISC compliance. Notably, institutions that had implemented CDISC standards had significantly higher numbers of data managers (P<.001) and biostatisticians (P<.001) compared to those that had not.

Conclusions: The implementation of CDISC standards in Japanese academia is limited, primarily due to resource shortages and a lack of specialized personnel. However, the discrepancy between the high demand for support and limited supply highlights a significant opportunity. Experienced academic research organizations, in cooperation with pharmaceutical companies and contract research organizations, can drive nationwide adoption by taking a strategic leadership role in providing educational resources and training, thereby addressing the critical shortage of specialized personnel and know-how.

(JMIR Med Inform 2026;14:e83774) doi:10.2196/83774

KEYWORDS

Clinical Data Interchange Standards Consortium; CDISC standards; academic research organization; ARO; Clinical Data Acquisition Standards Harmonization; CDASH; Study Data Tabulation Model; SDTM; Analysis Data Model; ADaM

Introduction

The Clinical Data Interchange Standards Consortium (CDISC) is a nonprofit organization dedicated to developing global electronic standards for clinical trial data. The “CDISC standards” refer to the set of standards developed by this consortium. Implementing these standards entails a series of technical activities throughout the clinical data lifecycle. Specifically, it involves designing case report forms based on Clinical Data Acquisition Standards Harmonization (CDASH), mapping collected raw data to Study Data Tabulation Model (SDTM) domains, and creating analysis-ready datasets according to Analysis Data Model (ADaM). These processes require writing programming scripts for data transformation, generating

XSL•FO
RenderX

metadata files such as define.xml, and rigorously validating the datasets and their conformance to the standards. In Japan, the Pharmaceuticals and Medical Devices Agency (PMDA) has been accepting electronic clinical trial data submissions compliant with CDISC standards for new drug marketing approval applications since October 2016 [1]. Furthermore, the Japan Agency for Medical Research and Development has expressed the view that compliance with CDISC standards from the planning and execution stages will become essential in academia-led clinical research and trials in the future [2].

Additionally, global data sharing platforms promote the sharing and reuse of clinical trial data [3-9], and several of these advance data standardization in collaboration with the CDISC [3-6,8].

The sharing of clinical trial data is expected to promote advancements in medicine and science [10,11]. Moreover, since July 1, 2018, the International Committee of Medical Journal Editors has mandated the inclusion of a data-sharing statement in manuscripts reporting the results of clinical trials submitted to International Committee of Medical Journal Editors member journals [12].

In 2017 in Japan, the University Hospital Medical Information Network Center and Japan Agency for Medical Research and Development cohosted the "CDISC Public Symposium" [2]. Furthermore, in 2018, University Hospital Medical Information Network, PMDA, and CDISC cohosted the "Workshop on CDISC Utilization in Academia" [13]. These activities aim to promote the dissemination of CDISC standards in Japanese academia.

The implementation of CDISC standards is expected to accelerate clinical research [14]. In particular, researchers and related institutions are beginning to recognize the importance of planning research and preparing case report forms based on the premise of electronic submissions compliant with CDISC standards throughout the processes of data collection, data management, and statistical analysis. These initiatives are expected to help reduce costs and workloads while maintaining data quality [15].

A previous study investigated the current status and challenges associated with the implementation of CDISC standards in Japanese academic medical centers [16]. However, in that study, the definition of "academia" was ambiguous.

Therefore, the present study aimed to comprehensively clarify the current status and challenges associated with implementing CDISC standards in Japanese academic medical centers.

Methods

Ethical Considerations

This study was a questionnaire survey targeting administrative personnel at academic medical centers regarding the operational status of CDISC standards. The study did not involve interventions on human participants or the collection of sensitive personal health information from patients. Therefore, an ethics review board assessment was not sought, in accordance with the ethical guidelines for medical and health research involving human subjects in Japan.

The purpose of the study was clearly explained in the invitation to the online questionnaire, and the completion and submission of the questionnaire were regarded as implied consent to participate. Participation was voluntary, and respondents could withdraw at any time by not submitting their responses.

To protect the privacy and confidentiality of the respondents, the collected data were stored securely and accessed only by the research team. The data were aggregated for analysis, and no personally identifiable information was reported. No compensation was provided to the participants for this study. This manuscript and the supplementary materials do not contain any images or data that could identify individual participants.

Participants and Survey Administration

In this study, "academia" is defined as institutions in Japan legally mandated to conduct research as part of their official duties. Based on this definition, the following 91 academic medical centers (hereinafter referred to as "institutions") were selected as survey targets: 83 university hospitals (43 national university hospitals, 8 public university hospitals, 31 private university hospitals, and 1 ministry-affiliated university hospital), 7 national centers for advanced and specialized medical care, and 1 national hospital organization. We contacted these institutions by email, requested their cooperation in the questionnaire survey, and sent them the questionnaire.

The survey period was from June 12 to August 16, 2024. The questionnaire survey was conducted online using Google Forms. As a general rule, 1 response per institution was accepted. No duplicate responses were received from any single institution; therefore, all submitted responses were included in the final analysis.

The survey was primarily distributed to the directors of clinical research centers or heads of data centers at each institution. In cases where direct contact information for these roles was unavailable, we identified the appropriate respondents through personal professional networks. For institutions where no direct contact could be established, the request was sent to the general administrative office of the Clinical Research Support Center, with instructions to forward the questionnaire to the staff member most knowledgeable about CDISC standards.

Questionnaire Items

The main questionnaire items were as follows:

Experience with contracted CDISC standards data creation

Implementation status of CDISC standards

Barriers to CDISC standards implementation

Future policies regarding CDISC standards-compliant data creation

Availability of CDISC standards-related documents and training

Ability to provide CDISC standards-related documents and training

Expectations for pharmaceutical companies, contract research organizations (CROs), and other academic research organizations (AROs)

XSL•FO
RenderX

Ability to provide to pharmaceutical companies, CROs, and other AROs

Number of data managers and biostatisticians

In this study, "implementation" was defined as CDISC data creation conducted internally, jointly with external partners, or externally with acceptance reviews performed by internal CDISC experts. "Experience with contracted CDISC standards data creation" was defined more broadly to encompass these implementation categories as well as external data creation performed without such internal expert-led acceptance procedures.

Further details regarding the questionnaire items are presented in Multimedia Appendix 1.

Statistical Analysis

Descriptive statistics were calculated using the total number of targeted institutions (n=91) as the denominator. This approach was adopted to establish a consistent baseline for future longitudinal surveys targeting the same population. Furthermore, using the total population as the denominator prevents the overestimation of implementation rates caused by selection bias—where institutions with greater interest in CDISC standards are more likely to respond—and ensures the results accurately reflect the status across all defined Japanese institutions. Categorical variables are presented as numbers and percentages. To assess the association of the number of data managers and biostatisticians with the CDISC implementation status, we performed the Mann-Whitney *U* test. In this analysis, the number of staff was treated as a continuous variable. Although staffing levels were categorized (0‐3, 4‐10, and ≥11) for visualization purposes, the statistical hypothesis testing was based on the continuous data. To examine potential confounders, we also analyzed the association between institution type (public/national vs private) and CDISC implementation using Fisher exact test. A *P* value <.05 was considered statistically significant. All statistical analyses were performed using R statistical software (version 4.4.1; R Foundation for Statistical Computing).

Results

Response Rate and Participant Characteristics

In this study, 91 institutions were targeted, among which responses were received from 84 (response rate: 92%). Of these, 7 (8%) institutions did not respond. The breakdown of the responding institutions was as follows: 42 national university hospitals, 27 private university hospitals, 7 public university hospitals, 7 national centers for advanced and specialized medical care, and 1 national hospital organization. No responses were received from ministry-affiliated university hospitals. The breakdown of respondents by job title is shown in Multimedia Appendix 2.

The percentages in these results were calculated with the total number of targeted institutions (N=91) as the denominator and rounded to the nearest integer, unless otherwise specified.

Experience With Contracted CDISC Standards Data Creation

Experience with contracted CDISC standards data creation refers to the track record of accepting projects for CDISC data creation. This includes cases where the actual data creation was outsourced to a third party. Regarding experience with contracted data creation using CDISC standards, 26 (29%) institutions reported having such experience, while 58 (64%) did not; 7 (8%) institutions did not respond to this question. Among the types of trials for which institutions had experience (multiple answers allowed), investigator-initiated clinical trials for drug approval were the most common, at 22 (24%), followed by industry-sponsored clinical trials for drug approval (n=5, 5%), specified clinical trials under Japan's Clinical Research Act [17] (n=5, 5%), and other clinical research (n=5, 5%) (Figure 1).

XSL•FO
RenderX

Figure 1. Experience with contracted Clinical Data Interchange Standards Consortium standards data creation (multiple responses allowed) (N=91).

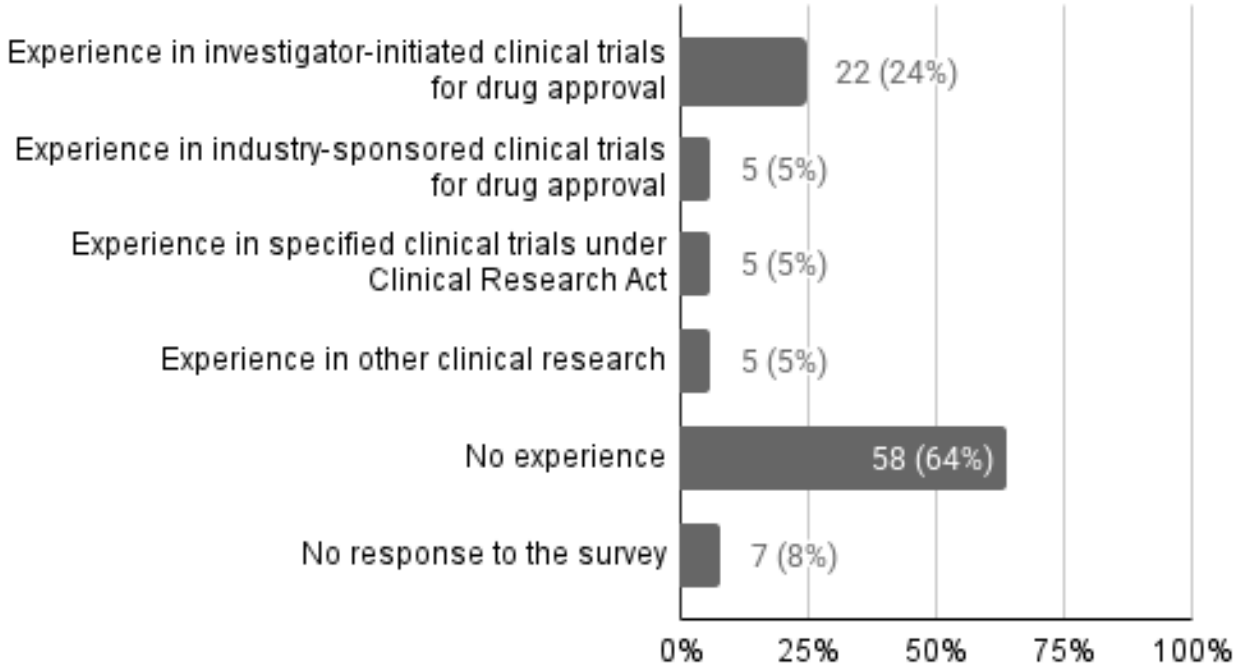

These results indicate that slightly less than 30% (26/91) of the institutions had experience with contracted data creation using CDISC standards. Notably, this experience extends beyond trials for drug approval to include specified clinical trials and other clinical research.

Implementation Status of CDISC Standards

Implementation of CDISC standards refers to creating CDISC data using internal resources or, in the case of outsourcing, conducting acceptance work by CDISC experts. Regarding the implementation status of CDISC standards, 20 institutions (22%) reported having implemented them, whereas 64 institutions (70%) reported not having implemented them; seven institutions (8%) did not respond.

Among the 20 institutions that had implemented CDISC standards, the most common combination of standards (multiple answers allowed) was the implementation of all three—CDASH, the SDTM, and the ADaM—reported by eight institutions (9% of the 91 institutions). This was followed by institutions implementing SDTM and ADaM (n=4, 4%), CDASH only (n=4, 4%), ADaM only (n=3, 3%), and SDTM only (n=1, 1%) (Figure 2).

XSL•FO
RenderX

Figure 2. Implementation status of the Clinical Data Interchange Standards Consortium standards (N=91). ADaM: Analysis Data Model; CDASH: Clinical Data Acquisition Standards Harmonization; SDTM: Study Data Tabulation Model.

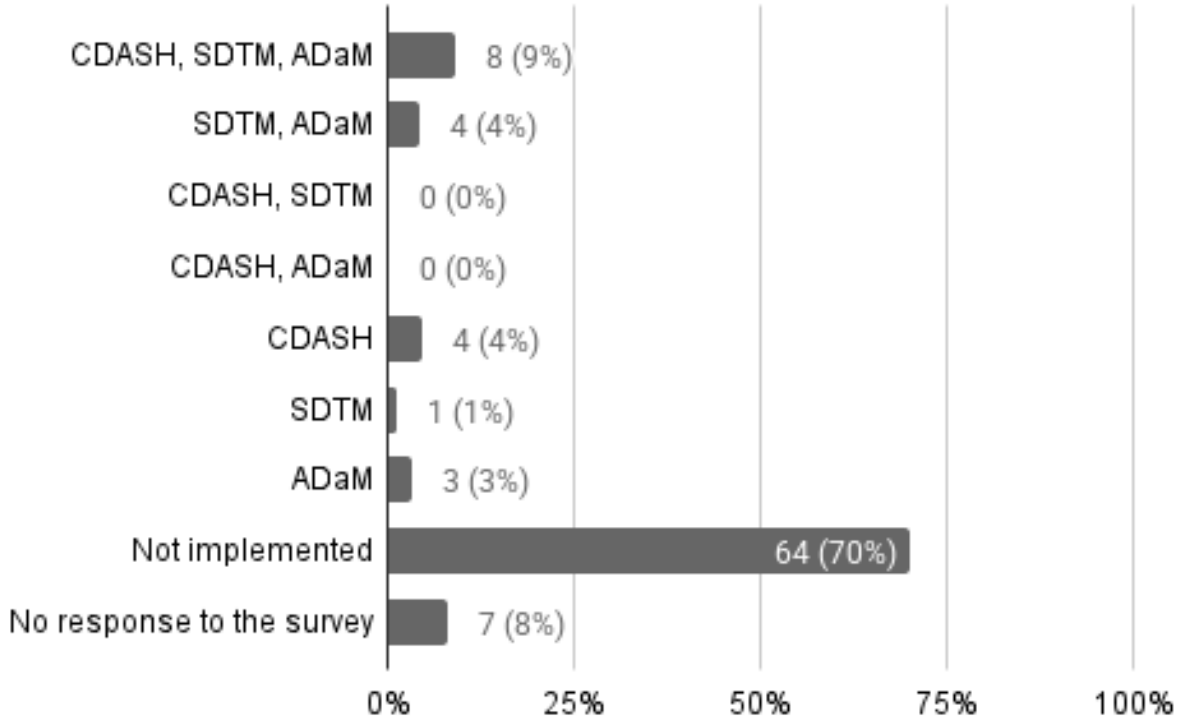

Regarding individual standards, ADaM was implemented by 15 (16%) institutions, SDTM by 13 (14%), and CDASH by 12 (13%).

These results indicate that while only 22% (20/91) of all institutions had implemented CDISC standards, many of these implementing institutions use multiple standards (CDASH, SDTM, and ADaM) in combination.

Barriers to CDISC Standards Implementation

Barriers with CDISC implementation refer to the obstacles or challenges that institutions face when attempting to adopt or maintain CDISC standards. Institutions cited the following items as barriers to CDISC standards implementation (multiple answers allowed). The most frequently cited barrier was “high human and financial effort and lack of resources” (n=56, 62%), followed by “lack of personnel knowledgeable in CDISC” (n=42, 46%), “no need to implement CDISC standards” (n=27, 30%), and “unsure how to implement CDISC standards” (n=27, 30%) (Figure 3).

XSL•FO
RenderX

Figure 3. Barriers to CDISC standards implementation (multiple responses allowed). Note: Percentages were calculated based on the total number of survey targets (N=91). "No response to the survey" indicates institutions that did not answer this survey entirely. CDISC: Clinical Data Interchange Standards Consortium.

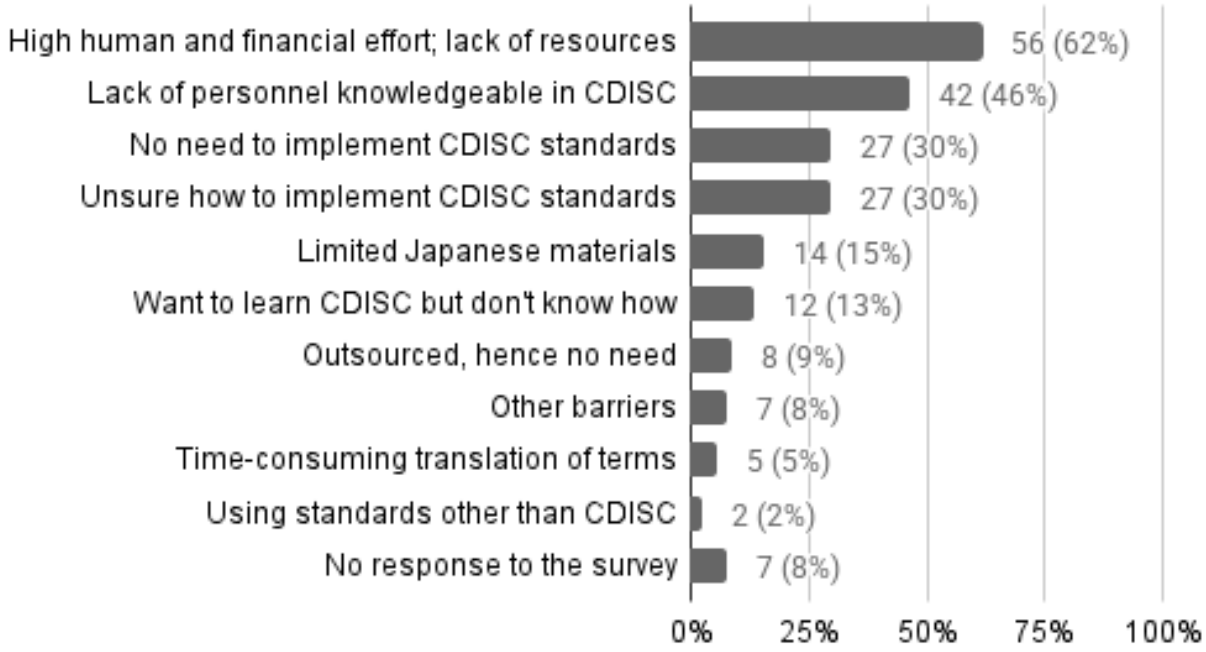

These results indicate that the main barriers to CDISC standards implementation are the significant human and financial effort required, resource shortages, and a lack of personnel knowledgeable about CDISC.

Future Policies Regarding CDISC Standards-Compliant Data Creation

Regarding future policies for CDISC standards-compliant data creation (single answer), the most common response, reported by 60 (66%) institutions, was "no decision made," followed by "will not undertake" (n=7, 8%), "will undertake, and external experts will perform the work with internal involvement" (n=6, 7%), "will undertake, and both internal and external personnel will perform the work" (n=5, 5%), "will undertake, but only external experts will perform the work without internal involvement" (n=5, 5%), and "will undertake, and the work will be performed internally" (n=1, 1%) (Table 1). These results indicated that 66% (60/91) of the institutions had not yet decided on their future policy; only 19% (17/91) had a clear policy for undertaking such work.

Table . Future policies regarding CDISC[a] standards-compliant data creation (N=91).[b]

Future policy regarding CDISC compliance	All institutions (N=91), n (%)	Currently implemented (n=20), n (%)	Currently not implemented (n=64), n (%)
Internal execution	1 (1)	1 (5)	0 (0)
Joint internal and external execution	5 (5)	3 (15)	2 (3)
External execution with internal involvement	6 (7)	5 (25)	1 (2)
External execution without internal involvement	5 (5)	1 (5)	4 (6)
Will not undertake	7 (8)	2 (10)	5 (8)
No decision made	60 (66)	8 (40)	52 (81)
No response to the survey	7 (8)	—[c]	—

[a]CDISC: Clinical Data Interchange Standards Consortium.

[b]Note: All values are n (%); percentages are calculated based on the total number of survey targets (N=91). "Implemented" and "not implemented" columns represent the current status at the time of the survey, where "implementation" is defined as internal CDISC data creation or expert-led acceptance work for outsourced tasks. "No response to the survey" refers to institutions that did not return the questionnaire.

[c]Not available.

The association between current implementation status and future policies is detailed in Table 1. Among the 20 institutions that had already implemented the standards, fewer than half (9 institutions, 45%) intended to continue "implementation"

XSL•FO
RenderX

(defined as work involving internal resources or internal expert-led acceptance). A similar lack of interest was observed among the 64 nonimplementing institutions, with only 3 (5%) planning for future implementation.

CDISC Standards Implementation Resources: Availability and Ability to Provide

Among all, 15 (16%) institutions reported having documents or training related to implementing CDISC standards. A breakdown of these resources (multiple answers allowed) indicated that "beginner-level training" was the most common, reported by 12 (13%) institutions, followed by "Japanese-language educational materials" (n=9, 10%), "documents on implementation know-how" (n=8, 9%), and "tools supporting CDISC" (n=8, 9%) (Table 2).

Table . Availability of and ability to provide CDISC[a] standards-related documents and training (multiple responses allowed) (N=91).[b]

Item	Availability, n (%)	Ability to provide, n (%)
Japanese-language educational materials on CDISC standards	9 (10)	4 (4)
Documents on implementation know-how for CDISC standards	8 (9)	4 (4)
Tools supporting CDISC standards implementation	8 (9)	4 (4)
Beginner-level training on CDISC standards	12 (13)	5 (5)
No response to the survey	7 (8)	7 (8)

[a]CDISC: Clinical Data Interchange Standards Consortium.

[b]Note: Percentages were calculated based on the total number of survey targets (N=91). "No response to the survey" indicates institutions that did not answer this survey entirely.

Next, regarding the question of whether these documents and training could be provided to other institutions, 5 (5%) institutions responded that they "could provide" them. A breakdown of providable resources is shown in Table 2.

These results indicate that while 16% (15/91) of institutions had CDISC standards implementation resources available, only 5% (5/91) were able to provide these resources to other institutions.

Support Expected From and Providable to Pharmaceutical Companies, CROs, and Other AROs

Regarding expectations for pharmaceutical companies, CROs, and other AROs (multiple answers allowed), 60 (66%) institutions responded that they had "some expectations." Among these 60 institutions, the most desired item was "materials and information on CDISC" (n=53, 58%), followed by "training sessions (seminars, workshops, etc) on CDISC" (n=45, 49%) and "on-the-job training related to CDISC" (n=33, 36%) (Table 3).

Table . Expectations for and ability to provide support to pharmaceutical companies, contract research organizations, and other academic research organizations (multiple responses allowed) (N=91).[a]

Item	Expectations, n (%)	Ability to provide, n (%)
Training sessions (seminars, workshops, etc) on CDISC[b]	45 (49)	2 (2)
On-the-job training related to CDISC	33 (36)	2 (2)
Materials and information on CDISC	53 (58)	4 (4)
No response to the survey	7 (8)	7 (8)

[a]Note: Percentages were calculated based on the total number of survey targets (N=91). "No response to the survey" indicates institutions that did not answer this survey entirely.

[b]CDISC: Clinical Data Interchange Standards Consortium.

Next, regarding support that could be provided to pharmaceutical companies, CROs, and other AROs (multiple answers allowed), 5 (5%) institutions responded that they "could provide" some support. A breakdown is shown in Table 3.

These findings revealed that 66% (60/91) of the institutions expected CDISC-related material provision, information sharing, and workshop hosting from pharmaceutical companies, CROs, and other AROs. On the other hand, only 5% (5/91) of the institutions were able to provide such support, indicating a limited capacity.

Number of Data Managers and Biostatisticians

Among the 84 responding institutions, the median number of data managers was 2 (mode: 0; range: 0 - 20) (Figure 4). Similarly, the median number of biostatisticians was 2 (mode: 1, range: 0 - 13) (Figure 5).

XSL•FO
RenderX

Figure 4. Number of data managers at responding facilities (n=84). Note: Analysis excluded the 7 institutions that did not respond to the survey.

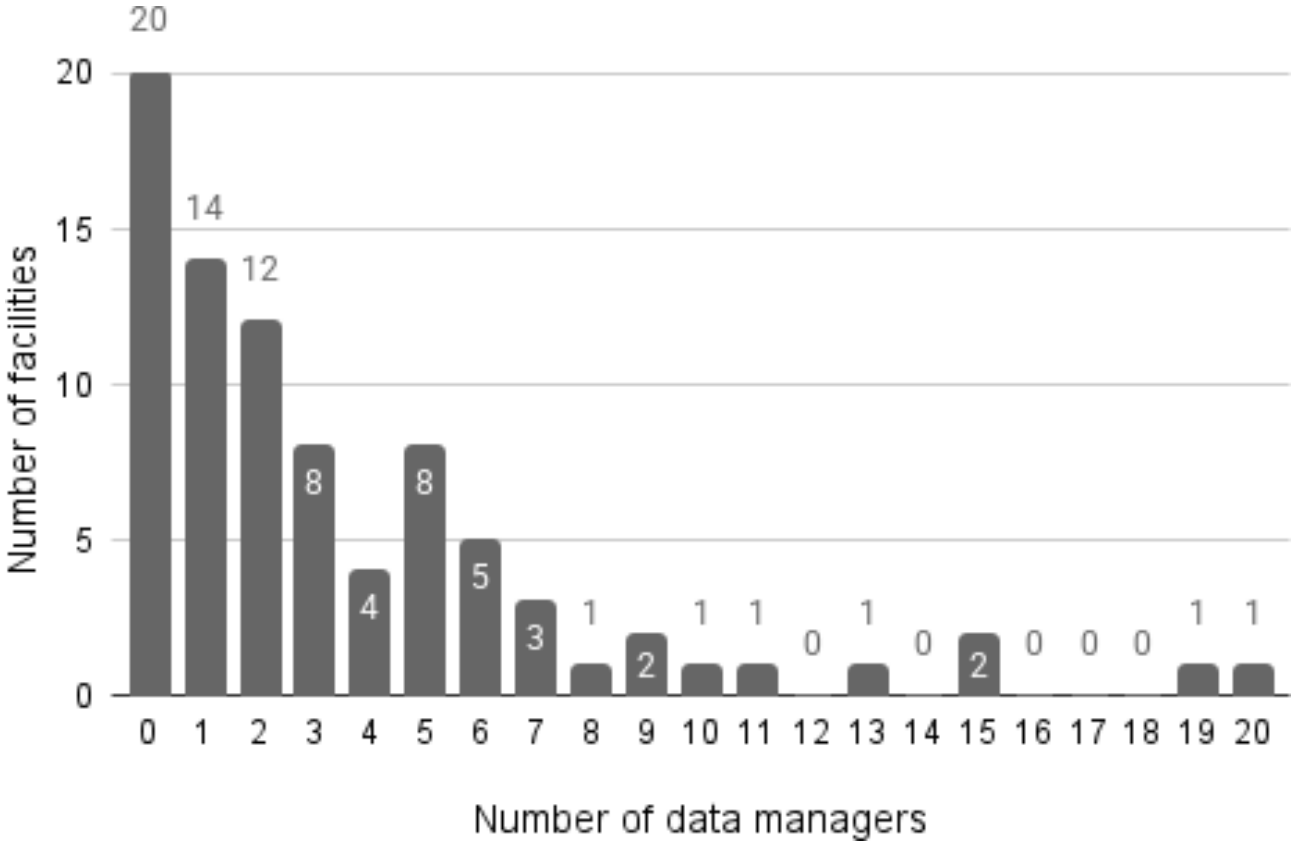

Figure 5. Number of biostatisticians at responding facilities (n=84). Note: Analysis excluded the 7 institutions that did not respond to the survey.

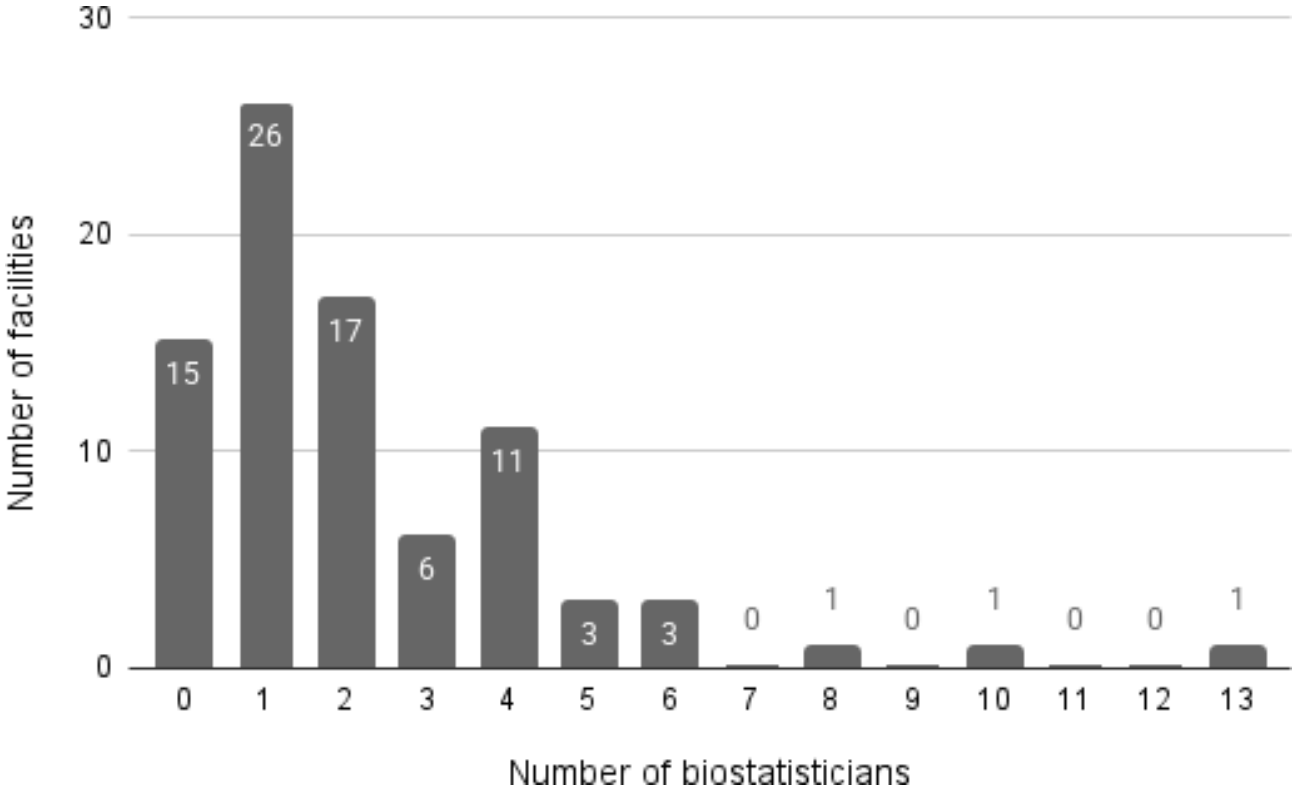

Association Between Staffing Levels and CDISC Standards Implementation Status

An analysis of the relationship between staffing levels and CDISC implementation showed that institutions with more data managers tended to be more advanced in their implementation (median 5, IQR 2 - 9.25 vs median 2, IQR 0 - 4; *P*<.001) (Figure 6). A similar trend was observed for biostatisticians (median 3.5, IQR 1.75 - 5 vs median 1, IQR 1-2; *P*<.001) (Figure 7).

XSL•FO
RenderX

Figure 6. Number of data managers and status of Clinical Data Interchange Standards Consortium standards implementation (n=84). Note: Analysis excluded the 7 institutions that did not respond to the survey. Data were categorized for visualization purposes, while the Mann-Whitney *U* test was performed on continuous variables (*P*<.001).

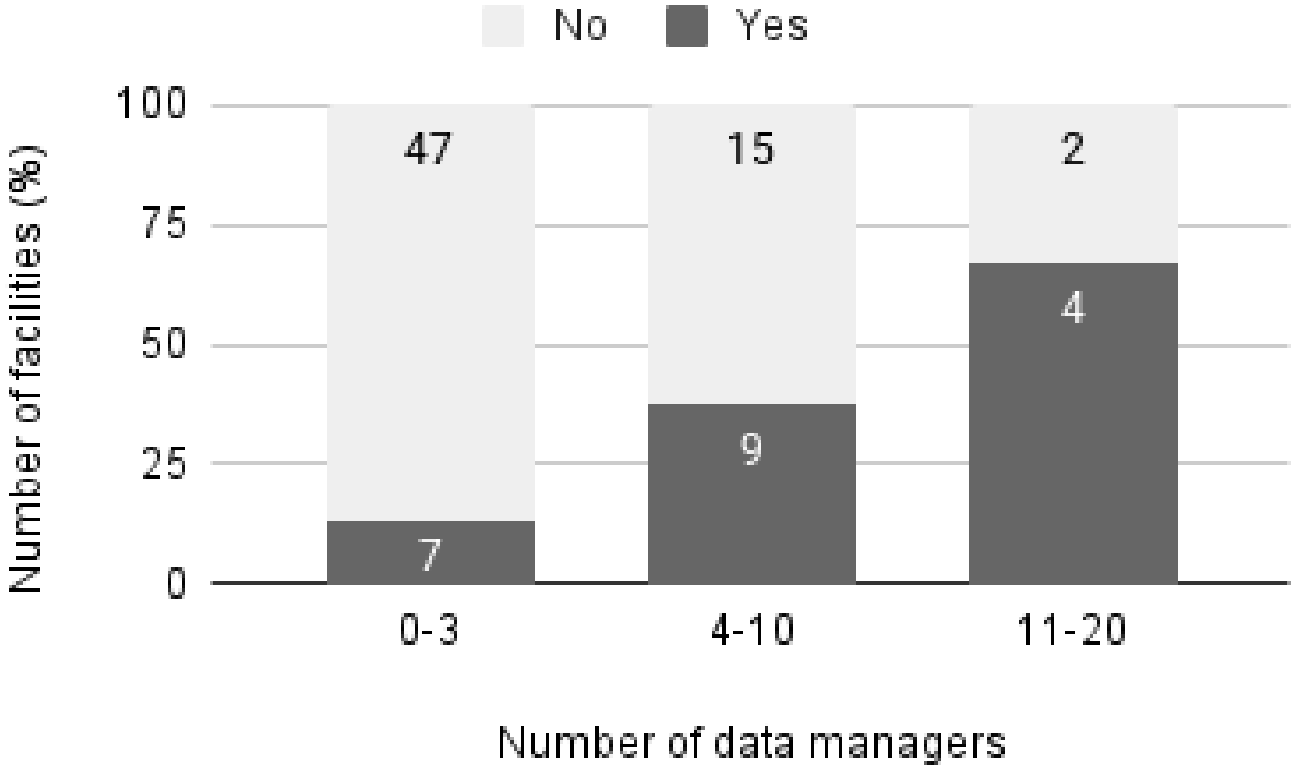

Figure 7. Number of biostatisticians and status of Clinical Data Interchange Standards Consortium standards implementation (n=84). Note: Analysis excluded the 7 institutions that did not respond to the survey. Data were categorized for visualization purposes, while the Mann-Whitney *U* test was performed on continuous variables (*P*<.001).

These findings suggest that institutions with more data managers and biostatisticians tend to be further along in implementing CDISC standards.

In addition to staffing levels, we evaluated the association between institution type and CDISC implementation. Implementation rates were 28.1% (16/57) in Public/National

XSL•FO
RenderX

institutions and 14.8% (4/27) in private institutions; however, no significant difference was observed (Fisher exact test, *P*=.27).

Discussion

Current Status and Significance of CDISC Standards Implementation

In a questionnaire survey conducted in 2020 to clarify the current status of and challenges associated with CDISC standards implementation in Japanese academic medical centers [16], the definition of "academia" was ambiguous, which posed challenges in interpreting the results and tracking changes over time. Therefore, in the present study, "academia" was more strictly defined to ensure the accuracy of longitudinal comparisons. By selecting institutions based on this clear definition, the present study could assess the current status and challenges associated with implementing CDISC standards more accurately, thereby providing foundational data to promote future adoption.

In a questionnaire survey conducted in 2020 to clarify the current status of and challenges associated with CDISC standards implementation in Japanese academic medical centers [16], the definition of "academia" was ambiguous, which posed challenges in interpreting the results and tracking changes over time. Therefore, in the present study, "academia" was more strictly defined to ensure the accuracy of longitudinal comparisons. By selecting institutions based on this clear definition, the present study could assess the current status and challenges associated with implementing CDISC standards more accurately, thereby providing foundational data to promote future adoption.

The findings revealed that only 29% (26/91) of institutions had experience with contracted CDISC standards data creation. Furthermore, institutions with experience in contracted data creation most frequently undertook investigator-initiated clinical trials for drug approval. This finding suggests that the application of CDISC standards in Japan, particularly that centered around investigator-initiated clinical trials for drug approval, is progressing. On the other hand, the present findings also confirmed that institutions had some experience in contracted CDISC standards data creation for specified clinical trials under the Clinical Research Act and other clinical research not intended for marketing approval applications. These findings suggest that CDISC standards are being used not only for regulatory submissions but also for standardizing and improving the efficiency of overall clinical research operations. In addition, it has been reported internationally that CDISC standards are also being used for Real-World Data [18]. We believe that clarifying the significance of standardization and efficiency and sharing practical case studies could lead to the promotion of CDISC standards implementation.

Regarding the implementation status of CDISC standards, the present study found that only 22% (20/91) of institutions had implemented them, indicating limited adoption. Notably, this study confirmed that while a high proportion of implementing institutions adopt multiple CDISC standards in combination, a certain number of institutions implement only individual standards. These results suggest that varying needs and resource situations at each institution may influence the form of CDISC standards implementation.

Barriers to CDISC Standards Implementation

Regarding implementation barriers, this study confirmed that "human and financial effort and resource shortages" remains the greatest challenge, followed by "a lack of personnel knowledgeable about CDISC." This finding suggests that securing human and financial resources and developing CDISC specialist personnel within institutions are crucial for promoting CDISC standards implementation. The findings also revealed that only 16% (15/91) of institutions possess documents or training related to CDISC standards, and furthermore, only 5% (5/91) of institutions can provide these resources to other institutions, which suggests that the expansion of CDISC-related educational resources within the country remains a challenge. We hypothesize that this discrepancy may stem from proprietary restrictions, copyright issues, or the lack of generalized templates that can be easily shared across institutions. In AROs in other countries as well, there is a demand not only for formal training by experts but also for open-source resources and "bite-sized" educational materials that are easily accessible online, such as the W3Schools model, as suggested by Jentoft et al [19]. Therefore, developing similar practical and accessible educational resources may serve as an important strategy for addressing the shortage of training materials in Japan.

Regarding barriers to implementation, 27 (30%) institutions cited "no need to implement CDISC standards." Within this group, some respondents cited "outsourced, hence no need." Furthermore, our detailed analysis revealed that the majority of these 27 (81%, 22/27) institutions selected "will not undertake" or "no decision made" regarding their future policies on CDISC standards-compliant data creation. The primary reason for these responses is likely that the PMDA requires CDISC compliance exclusively for new drug marketing approval applications, whereas many institutions primarily conduct research under the Clinical Research Act that falls outside this mandate. We included these institutions in our analysis to accurately reflect the current status of adoption, as excluding them would overlook the reality that a significant segment of academia operates outside the regulatory scope.

Regarding the respondents who cited outsourcing, it is important to distinguish this group from institutions that outsource but are considered to have "implemented" CDISC standards. As defined in our survey, "implementation" via outsourcing requires the institution to perform acceptance work using internal CDISC experts. In contrast, we interpret that respondents viewing outsourcing as a reason for nonimplementation may rely entirely on vendors without maintaining internal standards or oversight capabilities. However, as acknowledged in the Limitations section, the lack of explicit definitions in the survey may have led to variations in respondent interpretation regarding this distinction.

XSL•FO
RenderX

Future Policies and Opportunities for Strategic Support

Furthermore, the finding that a significant majority of institutions (66%, 60/91; Table 1) have made "no decision" regarding future CDISC policy suggests a deeper issue than mere resource constraints. Notably, this trend extends even to institutions that have already implemented CDISC standards. Half of these institutions (11/20) are uncertain about, or have decided against, continuing the implementation of CDISC-compliant data in the future, suggesting serious challenges in the sustainability of CDISC operations. This strategic inertia may indicate a systemic barrier, potentially stemming from the lack of regulatory incentives or clear mandates for the application of CDISC standards in clinical research not aimed at marketing approval. We considered that addressing this structural uncertainty is essential to enable institutions to commit to definitive standardization strategies.

While experienced AROs can play a pivotal role in driving adoption, the survey results indicate that 66% (60/91) of institutions specifically expect support from "pharmaceutical companies, CROs, and other AROs," with a primary desire for "materials and information." This highlights that academic institutions often cannot address the implementation gap on their own. Therefore, future strategies should not rely exclusively on peer-to-peer academic support but should also leverage industry resources. Active involvement and support from pharmaceutical companies and CROs were considered essential to provide the resources needed to bridge the gap between supply and demand.

Association Between Staffing Levels and Implementation

The present findings revealed significant variation among institutions in terms of the number of data managers and biostatisticians on staff. However, institutions with more of these specialists tended to be further along in regard to implementing CDISC standards. This result suggests that securing personnel with specialized knowledge is important for the effective implementation of CDISC standards, and as such, data managers and biostatisticians play a central role in the implementation process.

Limitations

A major limitation of this study is that adjustments for institutional resources such as hospital bed count or budget were not performed; these factors may be stronger determinants of CDISC adoption than staffing levels alone. The observed association between dedicated staffing and implementation may, therefore, be a reflection of overall institutional size or resource availability. Furthermore, the primary outcome variable, CDISC implementation status, was based solely on self-reported metrics from respondents and was not verified by external audit or inspection of the actual data standards used. This introduces the potential for response bias, such as the overestimation of institutional compliance. Finally, we acknowledge the nonresponse from specific institutional types; specifically, no responses were received from ministry-affiliated university hospitals. However, as this institutional category comprised only 1.1% (1/91) of the total institutions surveyed, the impact on the overall representativeness of Japanese academic medical centers is likely minimal. Furthermore, this study relies on self-reported data, which may be subject to respondent bias or misunderstanding of technical terms. For instance, a small number of sites reported implementing "ADaM only" without SDTM. Given that ADaM datasets are typically derived from SDTM, this discrepancy suggests a potential lack of accurate understanding of the standards among some respondents. Therefore, the results regarding technical proficiency should be interpreted with caution as they represent the respondents' subjective assessments rather than objectively verified capabilities. Furthermore, the questionnaire option labeled "outsourced, hence no need" was presented without explicit definitions distinguishing between outsourcing as a form of implementation and outsourcing as a reason for nonimplementation. Consequently, respondents may have selected this option based on their own interpretation. This lack of clarity may have led to misclassification, where institutions that had successfully implemented the system via outsourcing (with internal acceptance work) categorized themselves as having "no need."

Recommendations and Future Work

Therefore, developing these specialized human resources is likely essential for promoting their adoption. Expanding training opportunities and improving access to information regarding CDISC standards are key to promoting their wider adoption in Japanese academic medical centers.

Conclusions

The findings of the present study indicate that the implementation of CDISC standards in Japanese academic medical centers remains limited. The primary barrier identified was a lack of human and financial resources. On the other hand, many institutions are interested in implementing CDISC standards and seeking support such as workshops and the provision of materials. To bridge the gap between this high demand and the limited supply, future strategies should involve not only peer-to-peer academic support but also active resource sharing and cooperation from pharmaceutical companies and CROs. Notably, instances were observed where CDISC standards were being used even in clinical research not directly aimed at marketing approval applications, which is interpreted as a preliminary indication of the potential recognition within the research community of the operational efficiencies gained through standardization. Furthermore, the present findings suggest that the number of data managers and biostatisticians on staff is strongly associated with the implementation status of CDISC standards.

XSL•FO
RenderX

Acknowledgments

The authors would like to express their deep gratitude to the personnel of the 84 institutions that responded to the questionnaire, and also to the following individuals for their cooperation in this survey: Dr Hideki Hanaoka, Leader of TG3, National University Hospital Clinical Research Promotion Conference; Ms Mari Tsuchiya of its secretariat; and Ms Yoshiko Ito of the NHO Nagoya Medical Center. The authors used Google Gemini to assist in translating parts of the manuscript from Japanese to English. The authors thank FORTE Science Communications for English language editing.

Funding

This study was conducted as part of the Japan Agency for Medical Research and Development research and development project "Study of CDISC standards implementation in academia" (Principal Investigator: Toshiki Saito, NHO Nagoya Medical Center; Research Period: FY2022–FY2024) and supported by Japan Agency for Medical Research and Development under Grant Number JP22mk0101242 (https://www.amed.go.jp/koubo/11/03/1103C_00016.html). This study aims to comprehensively clarify the current status and challenges of implementing CDISC standards in Japanese academic medical centers.

Data Availability

The datasets generated or analyzed during this study are available from the corresponding author on reasonable request.

Authors' Contributions

Conceptualization: KN, NI, YI, TIS
Data curation: KN
Formal analysis: KN
Funding acquisition: TIS
Investigation: KN, NI, TIS
Methodology: KN, NI, YI, TIS
Project administration: TIS
Resources: KN, NI, YI, TIS
Supervision: TIS
Validation: NI
Visualization: KN
Writing – original draft: KN
Writing – review & editing: KN, NI, YI, TIS
All authors read and approved the final manuscript.

Conflicts of Interest

None declared.

Multimedia Appendix 1
Questionnaire content.
[DOCX File, 11 KB - medinform_v14i1e83774_app1.docx]

Multimedia Appendix 2
Breakdown of the survey participants—roles and professions.
[DOCX File, 1898 KB - medinform_v14i1e83774_app2.docx]

References

1. Basic principles on electronic submission of study data for new drug applications. : Pharmaceuticals and Medical Devices Agency; 2014 URL: https://www.pmda.go.jp/files/000160019.pdf [accessed 2025-06-08]
2. Joining the Clinical Data Interchange Standards Consortium (CDISC) and activity status. Japan Agency for Medical Research and Development. URL: https://www.amed.go.jp/en/aboutus/collaboration/cdisc.html [accessed 2025-06-08]
3. Lessons learned from sharing clinical trial data using Vivli. : Clinical Data Interchange Standards Consortium; 2023 URL: https://www.cdisc.org/sites/default/files/2023-07/2023_CDISC_Japan_Tsukida_Vivli.pdf [accessed 2025-06-08]
4. Yin PT, Desmond J, Day J. Sharing historical trial data to accelerate clinical development. Clin Pharmacol Ther 2019 Dec;106(6):1177-1178. [doi: 10.1002/cpt.1608] [Medline: 31538661]
5. National Academies of Sciences, Engineering, and Medicine; Health and Medicine Division; Board on Health Care Services; Board on Health Sciences Policy; Roundtable on Genomics and Precision Health; National Cancer Policy Forum; Forum on Neuroscience and Nervous System Disorders; Forum on Drug Discovery, Development, and Translation, Shore C, Hinners J, Khandekar E, Wizemann T. Data-sharing platforms. In: Reflections on Sharing Clinical Trial Data: Challenges

XSL•FO
RenderX

and a Way Forward: Proceedings of a Workshop: National Academies Press (US); 2020. URL: https://www.ncbi.nlm.nih.gov/books/NBK563333/ [accessed 2025-12-03]
6. ClinicalStudyDataRequest.com. URL: https://www.clinicalstudydatarequest.com/ [accessed 2025-12-03]
7. Green AK, Reeder-Hayes KE, Corty RW, et al. The project data sphere initiative: accelerating cancer research by sharing data. Oncologist 2015 May;20(5):464-e20. [doi: 10.1634/theoncologist.2014-0431] [Medline: 25876994]
8. Wold D, Walker S. CDISC BASIC Implementation Guide. Presented at: Presentation at CDISC 2022 US Interchange; Oct 26-27, 2022 URL: https://www.cdisc.org/sites/default/files/2022-11/2022-US-Interchange-Wold%2C%20Walker.pdf [accessed 2025-12-03]
9. Kato T. Clinical trial data sharing/utilization trends and company initiatives [Article in Japanese]. Clin Eval 2024;51(3):410-418 [FREE Full text]
10. For sharing individual participant/patient data (IPD) from clinical trials. : Japan Pharmaceutical Manufacturers Association; 2019 URL: https://www.jpma.or.jp/information/evaluation/results/allotment/lofurc000000b2pz-att/ctds_nl_2019.pdf [accessed 2025-06-08]
11. Lo B. Sharing clinical trial data: maximizing benefits, minimizing risk. JAMA 2015 Feb 24;313(8):793-794. [doi: 10.1001/jama.2015.292] [Medline: 25594500]
12. Taichman DB, Sahni P, Pinborg A, et al. Data sharing statements for clinical trials. BMJ 2017 Jun 5;357(24):j2372. [doi: 10.1136/bmj.j2372] [Medline: 28584025]
13. CDISC standards [Article in Japanese]. University Hospital Medical Information Network (UMIN) Center. URL: https://www.umin.ac.jp/cdisc [accessed 2025-06-08]
14. CDISC: a global approach to accelerating medical research. : CDISC; 2011 URL: https://www.diaglobal.org/productfiles/25849/20110515/w5/01%20w5_rebecca%20d.kush.pdf [accessed 2025-06-08]
15. Kiuchi T. The application of CDISC standards to clinical research in Japanese academia and its significance. J Natl Inst Public Health 2019;68(3):202-211. [doi: 10.20683/jniph.68.3_202]
16. Nagai K, Ikeda Y, Ohno M, Saito TI, Hinotsu S. Current status and issues of CDISC standards implementation among academia in Japan [Article in Japanese with English abstract]. Jpn Pharmacol Ther 2022;50(Suppl 1):s51-s61 [FREE Full text]
17. Clinical trials act [Report in Japanese]. : Ministry of Health, Labour and Welfare (MHLW) of Japan; 2017 URL: https://www.mhlw.go.jp/file/06-Seisakujouhou-10800000-Iseikyoku/0000213334.pdf [accessed 2025-07-21]
18. Facile R, Muhlbradt EE, Gong M, et al. Use of Clinical Data Interchange Standards Consortium (CDISC) standards for real-world data: expert perspectives from a qualitative Delphi survey. JMIR Med Inform 2022 Jan 27;10(1):e30363. [doi: 10.2196/30363] [Medline: 35084343]
19. Jentoft K, Tustison E, Yu H. CDISC implementation in an academic research organization. J Soc Clin Data Manag 2022;2:3 [FREE Full text] [doi: 10.47912/jscdm.164]

Abbreviations

ADaM: Analysis Data Model
ARO: academic research organization
CDASH: Clinical Data Acquisition Standards Harmonization
CDISC: Clinical Data Interchange Standards Consortium
CRO: contract research organization
PMDA: Pharmaceuticals and Medical Devices Agency
SDTM: Study Data Tabulation Model

Edited by A Coristine; submitted 06.Oct.2025; peer-reviewed by A Cheng, C Decker; accepted 29.Jan.2026; published 06.Mar.2026.

Please cite as:
Nagai K, Ito N, Ikeda Y, Saito TI
Current Status, Challenges, and Opportunities Associated With Implementing Clinical Data Interchange Standards Consortium Standards in Japanese Academic Medical Centers: Cross-Sectional Survey
JMIR Med Inform 2026;14:e83774
URL: https://medinform.jmir.org/2026/1/e83774
doi:10.2196/83774

© Kaori Nagai, Noriko Ito, Yuya Ikeda, Toshiki I Saito. Originally published in JMIR Medical Informatics (https://medinform.jmir.org), 6.Mar.2026. This is an open-access article distributed under the terms of the Creative Commons Attribution License (https://creativecommons.org/licenses/by/4.0/), which permits unrestricted use, distribution, and reproduction

XSL•FO
RenderX

in any medium, provided the original work, first published in JMIR Medical Informatics, is properly cited. The complete bibliographic information, a link to the original publication on https://medinform.jmir.org/, as well as this copyright and license information must be included.

XSL•FO
RenderX

Iterative Large Language Model–Guided Sampling and Expert-Annotated Benchmark Corpus for Harmful Suicide Content Detection: Development and Validation Study

Kyumin Park[1*], MS; Myung Jae Baik[2*], MD; YeongJun Hwang[3*], MS; Yen Shin[4], BS; HoJae Lee[4], BS; Ruda Lee[5], MA; Sang Min Lee[2], PhD; Je Young Hannah Sun[2], MD; Ah Rah Lee[2], PhD; Si Yeun Yoon[2], MA; Dong-ho Lee[1], PhD; Jihyung Moon[1], MS; JinYeong Bak[3], PhD; Kyunghyun Cho[6], PhD; Jong-Woo Paik[2], PhD; Sungjoon Park[1], PhD

[1]SoftlyAI, Seoul, Republic of Korea

[2]Department of Psychiatry, Kyung Hee University College of Medicine, Seoul, Republic of Korea

[3]Department of Artificial Intelligence, Sungkyunkwan University, Office 27306, Engineering Building 2, 2066 Seobu-ro Jangan-gu, Suwon-si, Gyeonggi-do, Republic of Korea

[4]KAIST, Daejeon, Republic of Korea

[5]Department of Psychology, University of Pennsylvania, Philadelphia, PA, United States

[6]Department of Computer Science, New York University, New York, NY, United States

[*]these authors contributed equally

Corresponding Author:
JinYeong Bak, PhD
Department of Artificial Intelligence, Sungkyunkwan University, Office 27306, Engineering Building 2, 2066 Seobu-ro Jangan-gu, Suwon-si, Gyeonggi-do, Republic of Korea

Abstract

Background: Harmful suicide content on the internet poses significant risks, as it can induce suicidal thoughts and behaviors, particularly among vulnerable populations. Despite global efforts, existing moderation approaches remain insufficient, especially in high-risk regions such as South Korea, which has the highest suicide rate among Organisation for Economic Co-operation and Development countries. Previous research has primarily focused on assessing the suicide risk of the authors who wrote the content rather than the harmfulness of content itself which potentially leads the readers to self-harm or suicide, highlighting a critical gap in current approaches. Our study addresses this gap by shifting the focus from assessing the suicide risk of content authors to evaluating the harmfulness of the content itself and its potential to induce suicide risk among readers.

Objective: This study aimed to develop an artificial intelligence (AI)–driven system for classifying online suicide-related content into 5 levels: illegal, harmful, potentially harmful, harmless, and non–suicide-related. In addition, the researchers construct a multimodal benchmark dataset with expert annotations to improve content moderation and assist AI models in detecting and regulating harmful content more effectively.

Methods: We collected 43,244 user-generated posts from various online sources, including social media, question and answer (Q&A) platforms, and online communities. To reduce the workload on human annotators, GPT-4 was used for preannotation, filtering, and categorizing content before manual review by medical professionals. A task description document ensured consistency in classification. Ultimately, a benchmark dataset of 452 manually labeled entries was developed, including both Korean and English versions, to support AI-based moderation. The study also evaluated zero-shot and few-shot learning to determine the best AI approach for detecting harmful content.

Results: The multimodal benchmark dataset showed that GPT-4 achieved the highest F_1-scores (66.46 for illegal and 77.09 for harmful content detection). Image descriptions improved classification accuracy, while directly using raw images slightly decreased performance. Few-shot learning significantly enhanced detection, demonstrating that small but high-quality datasets could improve AI-driven moderation. However, translation challenges were observed, particularly in suicide-related slang and abbreviations, which were sometimes inaccurately conveyed in the English benchmark.

Conclusions: This study provides a high-quality benchmark for AI-based suicide content detection, proving that large language models can effectively assist in content moderation while reducing the burden on human moderators. Future work will focus on enhancing real-time detection and improving the handling of subtle or disguised harmful content.

(JMIR Med Inform 2026;14:e73725) doi:10.2196/73725

XSL•FO
RenderX

KEYWORDS

artificial intelligence; dataset; suicide; suicide-related content; large language models

Introduction

Harmful suicide content on the internet poses a significant risk because it can induce suicidal thoughts in readers, potentially leading to self-harm or suicide [1,2]. The harmful suicide content includes materials that encourage or glorify suicide [3], making it appear as an attractive option and sharing suicide methods or instilling suicide knowledge in individuals with suicidal thoughts, thereby increasing the likelihood of actual suicide attempts [4]. In some cases, exposure to such harmful suicide content has led middle school students to commit suicide [5]. An analysis of adolescent suicide cases reveals that this age group, particularly female adolescents, is more vulnerable to the influence of triggering content [6,7]. Therefore, it is crucial to moderate such harmful suicide content before it spreads extensively.

Therefore, efforts to moderate harmful suicide content are intensifying. In the United States, initiatives focus on raising public awareness and safe content distribution, aligning with the World Health Organization guidelines [8]. Meanwhile, in 2022, the United Kingdom passed a law that makes such content illegal, emphasizing its serious commitment to addressing this issue [9]. In the Republic of Korea, which has the highest suicide rates among Organisation for Economic Co-operation and Development countries [10], the National Assembly of the Republic of Korea amended the Suicide Prevention Act, and the government has declared the dissemination of such content as illegal since 2019 [2]. Despite the increasing spread of harmful suicide content, its moderation is currently handled by only a single official and fewer than a thousand volunteers [11,12]. Considering the extensive use of social media in Korea [13], monitoring the large amounts of content is extremely challenging. In addition, moderating suicide content often leads to a high level of mental stress, hindering their ability to consistently and effectively monitor such content. Therefore, the need for an automatic harmful suicide content moderation system is urgent. The system can efficiently manage a growing volume of the content and ease the burden on human moderators.

However, previous research on online suicide content primarily focused on predicting the suicide risk of the authors who wrote the content. Zirikly et al [14] classified the suicide risk of authors based on content posted online (Reddit) into 4 levels. Similarly, Milne et al [15] and Yates et al [16] conducted research to predict the suicide and self-harm risks of online content authors. Subsequently, Yang et al [17] and Sawhney et al [18] used weakly supervised learning to enhance detection performance or collaborated with clinicians. Furthermore, Rawat et al [19] and Sawhney et al [20] performed tasks to detect suicide ideation and suicide events. All these studies focused on detecting the suicide risk of the author presented in the posts; they did not consider the potential propagation of suicide risk to readers by increasing their susceptibility to self-harm or suicidal behaviors. Other studies focused on understanding the negative effects of suicide content [6,21], or identifying the individuals who are most affected by the content [22-25]. Studies among Chinese adolescents have shown significant correlations between digital media usage and suicide or self-harm [23], and a meaningful relationship between suicide cases among Korean youths and searches related to suicide or self-harm [25]. In addition, three-quarters of young adults who have attempted suicide have reported using the internet for suicide or self-harm–related reasons [26], highlighting the risk posed by information that can induce suicide or self-harm.

Therefore, we introduce a *harmful suicide content detection* task that determines the level of harmfulness of the harmful suicide content to viewers. We then develop a multimodal *harmful suicide content detection benchmark* and a *task description document*. This document contains detailed instructions for annotators on how to assess the harmfulness of suicide-related content, which could also be useful for building instructions for large language models (LLMs). The benchmark and the document are developed by medical professionals, because such content might involve harmful visual language information that requires the judgment of the professionals (eg, self-harm photographs, or name of illegal drugs that can be used for suicide). Because labeling harmful suicide content causes mental stress, we focus on creating a small yet high-quality dataset. Furthermore, we demonstrate various methods using LLMs that can be effectively performed with few-shot examples.

Our contributions are as follows: (1) We propose a harmful suicide content detection task that classifies multimodal harmful suicide content as illegal, harmful, potentially harmful, harmless, or non–suicide-related. (2) We build a harmful suicide content detection benchmark that is multimodal and a Korean benchmark of 452 curated user-generated contents with corresponding medical expert annotations and a detailed task description document including the task details and instructions for annotators. (3) We create an English harmful suicide content detection benchmark translated from the Korean benchmark using a model (GPT-4) and analyze the quality and issues of translating suicide contents. (5) We demonstrate strategies to use LLMs to detect harmful suicide content by using the task description document and a small yet high-quality harmful suicide content detection benchmark. We test various closed and open-sourced LLMs using the machine-translated English benchmark. We observe that GPT-4 achieves F_1-scores of 66.46 and 77.09 in detecting illegal and harmful suicide content, respectively.

Methods

Study Design

In this section, we describe the design process for the harmful suicide content detection task and the steps to construct a harmful suicide content detection benchmark for this task. First, in the “Task Design” subsection, we outline the process of designing the task with emphasis on real-world implementation for detecting harmful suicide content in real time from online sources. This design phase includes detailed considerations for building the dataset.

XSL•FO
RenderX

Next, the "Data Processing Workflow" subsection describes the end-to-end process, from collecting harmful suicide content to developing the final harmful suicide content detection benchmark. Harmful suicide content is gathered from various online sources, and the preannotation process [27,28], which uses LLMs, is used to reduce annotators' exposure to vast quantities of harmful suicide content. Feedback generated from the annotation process by medical experts is used to update the task description document, which includes the categories and descriptions of harmful suicide content. This task description document is then used as an instruction for the preannotation process, creating an iterative process that builds and refines the harmful suicide content detection benchmark. Through this process, we ensure the inclusion of diverse, accurately labeled real-world harmful suicide content in the harmful suicide content detection benchmark while constructing a task description document that provides precise and comprehensive classification and explanations of the harmful suicide content.

As a result, from a collection of 43,244 harmful suicide content data points, we created a harmful suicide content detection benchmark consisting of 452 data points annotated by medical experts with suicide content categories, subcategories, and rationales for their classifications.

Ethical Considerations

We obtained institutional review board (IRB) approval (approval number: KHUH 2023-04-072) from the IRB of Kyung-Hee University Hospital, South Korea, based on the principles of the Declaration of Helsinki, ensuring adherence to ethical standards. The IRB approval includes the collection of suicide-related data, the development of guidelines for data classification, and data labeling. It also specifies the acquisition of data through the collection of publicly available posts from online spaces targeting the general public, and it outlines the development of an artificial intelligence model for detecting suicide-related content using these data. All personally identifiable information (PII) (eg, user IDs, names, addresses, and phone numbers) was anonymized and replaced with standardized tags. The benchmark contains extremely disturbing text and images, including self-harming photographs, blood, tools used for suicide and self-harm, and drug information. Even among medical professionals and researchers, prolonged exposure to such images can lead to severe mental stress. Therefore, we have deliberately chosen not to aim for the creation of a large-scale dataset but rather to limit the workload to prevent further intensifying mental stress. All these processes were conducted with IRB approval obtained prior to data collection. Given the nature of harmful suicide content and the legal restrictions against its unrestricted distribution, it is challenging to share the benchmark dataset openly. We understand the legal implications of distributing data containing information that potentially induces suicide. Despite these concerns, we believe that collecting such data to build a benchmark and conducting research to prevent its spread on the internet outweigh these legal issues. Access to the benchmark will be strictly limited, allowing only those researchers with IRB approval and a commitment not to distribute the content further, ensuring responsible use for research purposes only and adherence to legal standards. We believe that our work contributes significantly to the ongoing international effort against harmful suicide content and hope to aid in preventing its spread on the internet.

Task Design

Figure 1 illustrates the concept of using harmful suicide content detection in a real-world *moderation system*. The moderation system uses a model to automatically detect harmful suicide content and checks for illegal or harmful content and implements the appropriate *moderation policy* through a moderator's review. As this study introduces the harmful suicide content detection for the first time, our focus is on developing a model to automatically detect harmful suicide content rather than implementing an end-to-end moderation system. Therefore, this study focused on developing a harmful suicide content detection with this moderation system in mind, leaving the implementation of an end-to-end moderation system for future work. Specifically, we considered the inputs and outputs of harmful suicide content detection, considering the various real-world information on harmful suicide content that a moderation system might encounter as well as the moderation actions by a moderator.

XSL•FO
RenderX

Figure 1. Moderation system for harmful suicide content detection, categorizing online user-generated content into 5 classes by legality, harmfulness, and suicide relation. A moderator reviews content with potential illegality or harm, leading to legal reporting or content removal requests. No action is taken if no risks are found. "O" indicates that the corresponding value exists, and "X" indicates that the value does not exist. "O/X" denotes the potentiality of whether the corresponding value exists or not. LLM: large language model.

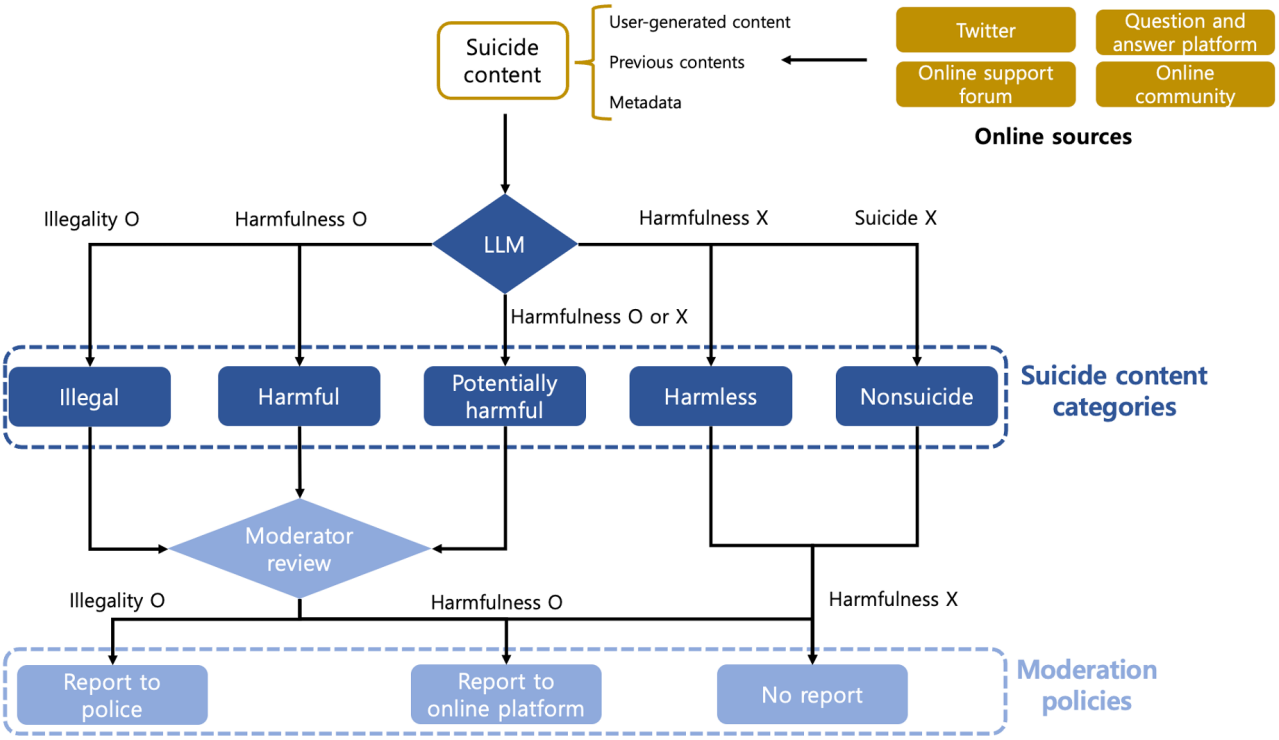

The model classifies the content into 5 distinct *suicide categories* based on illegality, harmfulness, and suicide-related aspects. For categories identified as having minimal harmfulness, a moderator validates the harmfulness through a review. Finally, the moderator moderates harmful suicide content using a moderation policy suitable for the identified harmfulness and illegality of the content, thereby minimizing human intervention and effectively moderating harmful suicide content.

To ensure that the detection system is applicable to real-world online data, the task targets various data from diverse sources to encompass a broad spectrum of user-generated content encountered on the internet. This approach ensures that the system effectively addresses the complexities and nuances of online posts ("Task Input" section).

The classification results produced by the harmful suicide content detection were crafted considering the functionality of a moderation system in mind. This means that the categories into which the content is sorted are specifically designed to facilitate the practical use of these results in moderating the content, ensuring that the system can serve as an effective tool for maintaining online safety and supporting mental well-being ("Task Output" section).

A moderator review was designed to validate the model's classification results and implement appropriate moderation. Specifically, for content categorized under the harmful categories, the process validates the harmfulness to ensure the reliability of the moderation system. In addition, because this process involves confirming the results of the model rather than newly identifying and classifying suicide content, it is more efficient in terms of reducing mental stress on moderators. Finally, suitable moderation policies were implemented based on the validation results. This system was developed to regulate suicide content and execute different moderation policies based on the illegality and harmfulness, thus preventing the spread of harmful suicide content online ("Moderator Review" section).

In summary, the entire process involves the model classifying online content into suicide categories, the moderator reviewing the results, and then implementing the corresponding moderation policy to ensure that the moderation system functions effectively. Throughout this process, multimodality information such as text and image data are used to reflect various aspects of the content in the model's input. Metadata from diverse sources and previous content serve as context. The model's output comprises 5 suicide categories, each differentiated by the presence or absence of illegality, harmfulness, and suicide-related aspects. Finally, the moderator review efficiently uses the model's classification results for validation, and effective moderation policies are implemented based on the content's illegality and harmfulness, thereby preventing the spread of harmful suicide content online.

Task Input

Considerations

We consider the following for designing the input of the task. (1) *Multimodality*: Because 50% of harmful suicide content contain images or videos [29], we consider text and images as inputs. (2) *Source diversity*: Harmful suicide content appears across various platforms, from social media to online communities [29]. We collected data from diverse sources for comprehensive coverage. (3) *Context information*: We also

XSL•FO
RenderX

incorporate previous content and metadata into our inputs. Previous content reveals the context of the target content, whereas metadata, such as user descriptions and view counts, provides additional insights, aiding in accurate harmfulness assessment.

Inputs

Given the considerations, the inputs for the task are as follows: (1) *User-generated content*: Contents created by users. The content includes text, and possibly images and URLs. Images and URLs are converted to text manually or using machine learning models (eg, image captioning and summarization). (2) *Previous content*: Previous content is often required because it provides context, clarifies references, and provides background information essential for the full comprehension of user-generated content. (3) *Metadata*: Other contextual information about the user-generated content such as view counts, like counts, creation time, user self-description, and so on.

Task Output

Considerations

We consider the following for designing the outputs of the task. (1) *Expert judgment*: Harmful suicide content involves specific terminology related to suicide, such as professional drug names, slang, and abbreviations. Thus, clinical expertise is required to accurately determine the legality and harmfulness of such suicide content and to decide on an appropriate response to the content. (2) *Moderation policy*: If an automatic harmful suicide content detection model is developed, it should be part of a moderation system and collaborate with human moderators or domain experts [18]. This implies that once the model detects harmful suicide content, it is necessary to consider appropriate actions. Therefore, the response of each output was considered when defining the output.

Outputs

We develop five harmful suicide content categories. Content should be mapped to one of the following categories: (1) *illegal* content that encourages or assists suicidal behavior; (2) *legal but harmful* content that, while not illegal, significantly induces suicide; (3) *potentially harmful* content that could be triggering for certain individuals, whereas it may be benign for others; (4) *harmless* content that is either neutral or positive for suicide; and (5) *nonsuicide* content that is not related to suicide.

Moderator Review

Moderator review includes the process of reexamining the suicide content classified by the model using moderator (eg, a clinical expert) and implementing the appropriate moderation policy. The moderation system identifies the harmfulness and illegality of suicide content and implements a corresponding moderation policy to block the spread of such content online. Thus, through moderator review, the moderator (1) verifies the classification result of the model and (2) implements the corresponding moderation policy. The moderator review is conducted for results classified as illegal, harmful, and potentially harmful because most online information is unrelated to suicide and reviewing all the information would increase moderator fatigue. Hence, reviews are conducted only for suicide information that may cause harm. The moderator verifies the illegality and harmfulness of content within these categories and conducts the corresponding moderation policy. Therefore, the moderator requires knowledge to comprehend and understand the content and distinctions of suicide content.

Moderation Policies

The moderator reviews the model's classification results and implements a corresponding moderation policy. The moderation policies are as follows: (1) *Report to police*: This is the strongest form of moderation policy intended to subject content creators to legal regulations by reporting to legal institutions. (2) *Report to online source*: Reporting the content to the online source where it is posted intends to prevent the spread of harmful information by requesting the deletion of the content. (3) *No report*: No additional actions, such as reporting the posts, are taken, allowing it to circulate online.

Report to police responds to content within the illegal suicide category containing illegal information. According to Korean law, certain types of content related to suicide are defined as illegal. Such content often includes illegal activities, such as the sale of illegal drugs; hence, reporting to legal institutions (eg, the police) imposes legal sanctions on the poster of such content.

Report to online source prevents the online spread of content containing or potentially containing harmful information related to suicide, such as illegal, harmful, and potentially harmful content. Because information spreads quickly online, it is reported to the online source where it was posted, and its removal is requested to prevent dissemination. For potentially harmful information, the harmfulness of which can vary depending on the reader, the moderator assesses the degree of harmfulness and reports whether it is severe.

No report is for harmless or nonsuicide content that poses no problem when posted online. Most online content is unrelated to suicide; therefore, it does not require reporting.

Table 1 shows the features of each category in terms of legality, harmfulness, and association with suicide. *Illegal suicide content* contains the most dangerous information, explicitly encouraging or facilitating suicidal behaviors. This category is critical for immediate intervention, embodying content that can actively propel individuals toward self-harm or suicide. *Harmful suicide content*, while not directly inciting suicide, significantly affects the audience by portraying suicide or self-harm in a manner that can trigger such actions among vulnerable individuals. The specificity of the depiction, whether through graphic imagery or detailed descriptions, amplifies its potential harm, making it a crucial target for moderating content. *Potentially harmful suicide content* traverses a gray area, with content that might not universally trigger harmful behaviors but could potentially do so in susceptible populations. This category underscores the complex challenge of content moderation, in which the impact of the content is not universally harmful and may vary significantly among individuals. *Harmless suicide content* focuses on providing support, hope, or neutral information regarding suicide without posing a risk of harm. This category

XSL•FO
RenderX

plays an essential role in suicide prevention by offering resources, support, and information to reduce suicide rates. Finally, *nonsuicide content* serves as a catchall for material that does not pertain to suicide or self-harm, highlighting the importance of distinguishing between genuinely harmful content and content unrelated to suicide.

Table . Illegality, harmfulness, and suicide relativity of categories and the moderation protocols[a].

Category	Illegality	Harmfulness	Suicide-related	Moderator review	Moderation policy
Illegal	O	O	O	O	Report to police and online source
Harmful	X	O	O	O	Report to online source
Potentially harmful	X	Δ	O	O	Report to online source or no report
Harmless	X	X	O	X	No report
Nonsuicide	X	N/A[b]	X	X	No report

[a]The (Δ) symbol represents a state that is in a gray area, indicating that the characteristic is neither fully present nor completely absent. "O" denotes the presence or applicability of a given attribute, whereas "X" denotes its absence. For instance, data categorized as "Harmful" are characterized by the absence of illegality (X), the presence of harmfulness (O), suicide-related (O), and the moderator review (O).

[b]N/A: not applicable.

Data Processing Workflow

This section describes the data processing workflow used to create a high-quality harmful suicide content detection benchmark for detecting harmful suicide content. As illustrated in Figure 2, the workflow starts from data collection, detailed in “Data Collections” subsection, and outlines the process to develop a robust and diverse benchmark for harmful suicide content detection, described in “Data Annotation” subsection. The primary goal is to create a small but high-quality benchmark that can comprehensively capture real-world scenarios and task description document that can be effectively used for LLM instruction. Key challenges include the stressful nature of the annotation process, the extremely low prevalence of illegal suicide content, and the need to ensure the benchmark’s completeness and use, given that this is a newly proposed task that must reflect various aspects of real-world data.

The methods used to address these challenges include (1) LLM sampling to reduce annotator exposure to a large volume of harmful suicide content while increasing the representation of rare, illegal suicide content; (2) an iterative annotation approach to continuously update the task description document and incorporate real-world scenarios, aiming to reflect diverse data until no further updates are required, while also considering modality (image and context) to adapt annotators effectively; and (3) filtering and validation, which involve updating the harmful suicide content detection benchmark to align with the latest task description document, categorizing and subcategorizing data accurately, and removing outliers such as incomprehensible content.

XSL•FO
RenderX

Figure 2. Overview of the data processing workflow, which consists of data collection, benchmark construction, and benchmark validation. We collect suicide content and annotate it with medical experts, leveraging LLM-based preannotation to balance categories, and we iteratively refine the task description document through feedback. We then construct the benchmark corpus with human-labeled data, an English-translated version, and the updated task description, and we validate it for applicability to LLMs. AI: artificial intelligence; LLM: large language model.

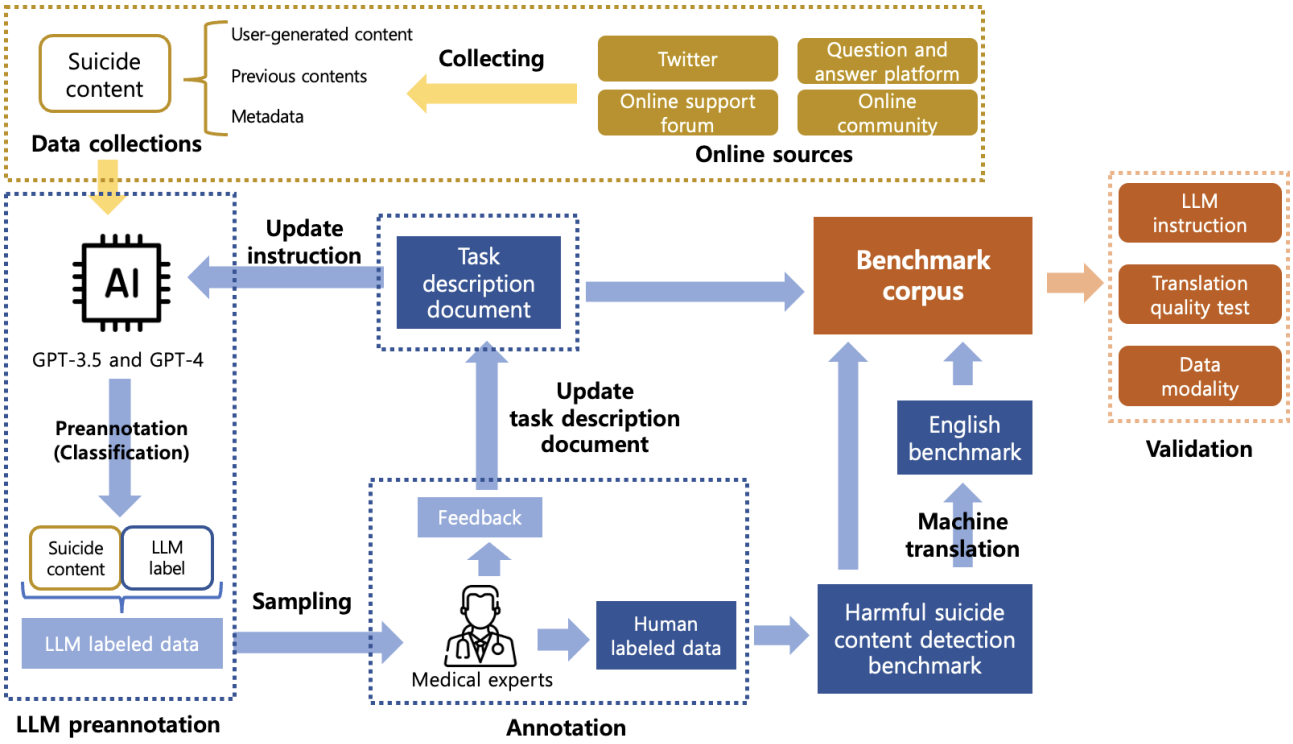

Data Collections

Developing a large-scale harmful suicide content dataset is highly challenging. Harmful suicide content is infrequently encountered in real-world scenarios [30], and the distressing nature of such content can cause mental strain for annotators. In addition, obtaining annotations from medical experts is expensive. Therefore, we focus on developing a high-quality curated benchmark dataset. Prior to the dataset collection, we obtained approval from the IRB of Kyung-Hee University Hospital, South Korea.

To cover the diverse source domains of the content, we collect user-generated content related to suicide from social media, Q&A platforms, online support forums, and online communities. Table 2 lists the number of raw data, benchmark data, descriptions of content, previous content, and metadata of each source.

Table . Number of collected harmful suicide content and harmful suicide content detection benchmark dataset for each domain[a].

Source	Raw data (no. of images)	Benchmark (no. of images)	Content	Previous content	Metadata
Twitter	12,125 (3,671)	359 (78)	Tweets written by users	Previous tweets in the thread where the content is written	User description, view count, like count, etc
Online community	794 (794)	48 (48)	Title and bodies of post written by users	N/A[b]	User nickname, view count
Q&A[c] platform	13,104 (0)	33 (0)	Question or answers written by users	Questions (if the content is an answer)	N/A
Online support forum	17,325 (0)	23 (0)	Counseling request posts or responses written by users or counselors	Counseling request posts (if the content is a response)	N/A
Total	43,244 (4,429)	452 (126)	N/A	N/A	N/A

[a]User-generated suicide content was collected along with source-specific metadata and previous content as context.

[b]N/A: not applicable.

[c]Q&A: question and answer.

XSL•FO
RenderX

Twitter

Twitter constitutes the majority of social media posts flagged for containing suicide-inducing information, with a substantial share of 74.69% [29]. To collect data related to suicide from Twitter, we used the Twitter application programming interface (API) v2 to gather posts that include suicide-related keywords in their text or hashtags. These suicide-related keywords were collected from previous research [31] and the guidelines of the "Korean Suicide Inducing Information Monitoring Group" [32]. We gathered 12,021 tweets, including 3635 with images, from May to August 2023 using the Twitter API. The suicide-related keywords used in the Twitter API are summarized in Table 3.

XSL•FO
RenderX

Table . Suicide-related keywords[a].

Classification of search terms	Search terms	Synonyms	Korean version of search terms	Korean version of synonyms
Suicide-related terms	Suicide	• Suicide	• 자살	• 자살
	Suicide method	• Suicide method • How to suicide • How to commit suicide	• 자살방법	• 자살방법 • 자살하는법 • 자살하는방법
	Dying method	• Dying method • How to die	• 죽는방법	• 죽는방법 • 죽는법
	Suicidal idea	• Suicidal idea • Suicidal thinking	• 자살충동	• 자살충동 • 자살생각
	Fall down	• Fall down • Suicide by jumping from a height	• 투신	• 투신 • 투신자살
	Hanging	• Hanging • Hanging suicide • Neck hanging	• 목맴	• 목맴 • 목맴자살 • 목매달기
	Will	• Will • ·How to write will	• 유서	• 유서 • 유서쓰는법
Self-harm–related terms	Self-harm	• Self-harm	• 자해	• 자해
	Self-harm method	• Self-harm method • How to self-harm	• 자해방법	• 자해방법 • 자해하는법
	Wrist cutting	• Wrist cutting • How to cut my wrist • Wrist cutting method	• 손목자해	• 손목자해 • 손목자해하는법 • 손목자해방법
	Self-harm wound	• Self-harm wound • Self-harm mark • Treatment for self-harm wound	• 자해흉터	• 자해흉터 • 자해자국 • 자해흉터치료
	Drug overdose	• Drug overdose • Drug lethal dose	• 약물과다복용	• 약물과다복용 • 약물치사량
	Acetaminophen	• Acetaminophen overdose • Acetaminophen lethal dose	• 타이레놀	• 타이레놀과다복용 • 타이레놀치사량

XSL•FO
RenderX

Classification of search terms	Search terms	Synonyms	Korean version of search terms	Korean version of synonyms
Suicide risk factor terms	Academic score	• Academic concern • Academic score	• 성적	• 성적 • 성적고민
	Bullying	• Bullying • Covert bullying • Outcast	• 왕따	• 왕따 • 은따 • 따돌림
	School violence	• School violence	• 학교폭력	• 학교폭력 • 학폭
	Family troubles	• Family troubles	• 가족문제	• 가족문제
	Domestic violence	• Domestic violence	• 가정폭력	• 가정폭력
	Dropout	• Dropout • How to drop out • Dropout method	• 자퇴	• 자퇴 • 자퇴하는법 • 자퇴방법
	Career	• Career • Career concern	• 진로	• 진로 • 진로고민
Suicide prevention terms	Suicide prevention	• Suicide prevention	• 자살예방	• ·자살예방
	Call for life	• Call for life • Call for life of Korea	• 생명의전화	• 생명의전화 • 한국생명의전화
	Suicide prevention center	• Suicide prevention center • 1393	• 자살예방센터	• 자살예방센터 • 1393
	Psychiatry	• ·Psychiatry • ·Neuropsychiatry • Psychiatry department • Mental hospital	• 정신과	• ·정신과 • ·신경정신과 • ·정신건강의학과 • 정신병원
	Mental health center	• Mental health center	• 정신건강복지센터	• 정신건강복지센터
Depression-related terms	Depression	• ·Depression • ·Depressed • ·Depressive disorder • ·Depressive symptom	• 우울증	• 우울증 • 우울 • ·우울장애 • ·우울증상

[a] Search terms and synonyms are defined in the study by Park et al [33].

Q&A Platform

On Q&A platforms, users often post questions about suicide-related issues, such as suicide methods, or respond to these queries. We collected questions and answers containing suicide-related keywords from Naver Knowledge In (a Korean Q&A platform) [33]. We collected data from March 2022 to March 2023, using the same keywords as those used for Twitter, resulting in 13,104 content items.

Online Support Forum

In online support forums, people write about their suicide-related concerns, and counselors provide responses to support them [31]. We collected posts from Lifeline Korea [34] and the Companions of Life Suicide Prevention Counselling [35]. We collected 17,325 pieces of content posted from March 2021 to June 2023.

Online Community

DCinside [36], a widely used online community in Korea comparable to Reddit, includes boards that function similarly to subreddits. We collected posts from 2 depression-focused boards (depression-minor and depression-mini boards) on the DCinside, known to contain suicide-related posts and where actual suicide incidents have been reported [37]. We collected posts including those containing images, resulting in a total of 794 data entries. Overall, we collected 43,244 entries of harmful suicide content, in total, from 4 online sources, with each harmful suicide content entry comprising content, previous content, and metadata.

Data Preprocessing

To remove private information from the benchmark and generate information that requires human intervention, such as link or image descriptions, we took the following steps. First, we

XSL•FO
RenderX

removed all PII. This involves replacing URLs, names, locations, phone numbers, emails, and IDs within the text with corresponding tags. Thereafter, we provided supplementary descriptions for the contents of the external links. Given that these links may contain significant information for accurately understanding the content, we manually reviewed the links and summarized their content. Third, we added text descriptions to the images whenever they were included in the content. We used GPT-4 to generate initial descriptions, which were subsequently reviewed and refined for accuracy by the researchers. Consequently, all PII values were removed from the text of the data, and we created link descriptions that summarized the content of any URLs present in the content text, along with text descriptions for the images.

Data Annotation

Task Description Document

The task description document was designed to explain the harmful suicide content detection and to provide guidance to the annotators. It contains vital information, including the purpose of identifying harmful suicide content and a detailed guide for annotating the content. In addition, it outlines the categories and subcategories of harmful suicide content, supplemented with real-world examples.

Our basis for understanding the definitions, categories, and examples of harmful suicide content was the “Korean Suicide Prevention Law” [2] and documents published by the “Korea Life Respect Hope Foundation’s suicide/harmful information monitoring team” [32]. We found that certain category names and descriptions were unclear or overlapped, thus requiring more distinct clarifications. To address this, we involved medical professionals in the data annotation process, which led to significant revisions and refinements of the categories and their descriptions, as well as the expansion of examples for each category. Following the studies by Fiesler et al [38] and Moon et al [39], we used an iterative coding process such that the medical experts individually annotate the real-world content, come together to refine the task description document, and then repeat the coding process individually. This updating process was iterative and performed 3 times to ensure comprehensive refinement. Further details of the iterative process are presented in the “Annotation Process” section. We demonstrate each category and its description in Table 4.

Table . Name and description of each suicide category.

Name	Description
Illegal suicide content	Content that can actively encourage others to commit suicide or assist suicide behavior.
Harmful suicide content	Harmful content that is not as harmful as illegal suicide content but clearly has the effect of causing suicide or self-harm in the general public.
Potentially harmful suicide content	Content that may trigger suicide or self-harm in some people but may not cause it in others or may rather have a positive effect in others.
Harmless suicide content	Content that is not harmful, such as content that helps prevent suicide to the general public or provides neutral information related to suicide.
Nonsuicide content	Content unrelated to suicide.

Annotation Process

The annotation process was divided into 3 phases. In each phase, medical experts (a clinical expert with an MD degree and a psychiatry professor with a PhD degree) annotated real-world harmful suicide content, using the task description document as a reference. At the end of each phase, the authors and annotators reviewed and enhanced the task description document through discussions, before proceeding to the next phase.

In the first phase, medical professionals annotated harmful suicide content by referring to the initial task description document. Before starting the annotation, we preannotated and sampled the contents to be annotated from the data collections, as illustrated in Figure 3. Although the contents are gathered using suicide-related keywords, only a small fraction is actually harmful suicide content that can cause harm to others. Therefore, we used the task description document as instruction for the LLMs, allowing them to preliminarily categorize the content into predefined categories. This approach enhances the efficiency of the annotation process for medical experts and reduces mental strain and costs. Consequently, we used the OpenAI GPT API to preannotation and sampled 196 harmful suicide content for human annotation from the collected 2272 Twitter data, 17,325 online forum data, and 13,104 Q&A data. Medical professionals then proceeded to annotate the sampled 196 harmful suicide content by following the annotation protocol and the initial task description document. The annotation protocol is described in the later part of this section. During the annotation process, they did not refer to the LLM labels generated by the LLM. Following the annotation, both the categories and subcategories were updated, leading to a revision of the task description document. Specifically, we refined 7 subcategories, added 2 new ones, and removed one.

In the second phase, we diversified the harmful suicide content in the benchmark and refined the task description document. Before annotation, we further preannotated and sampled 175 harmful suicide content for annotation from a pool of 8408 Twitter data points collected between May and June 2023. Similar to the first phase, we preannotated them using OpenAI GPT API with instructions written based on the task description document. Subsequently, medical professionals began the annotation of sampled harmful suicide content, strictly adhering to the annotation protocol and using the revised version of the

XSL•FO
RenderX

task description document as their guide. Once the annotation process was completed, we merged the 4 subcategories into 2.

In the final phase, we added multimodal (text and image) harmful suicide content to the benchmark dataset and included online communities as an additional source domain. For the image content, we initially generated textual descriptions of harmful images using visual language LLMs ("Data Preprocessing" subsection). These initial descriptions were then revised to correct any inaccuracies or fill in missing details. The refined descriptions were subsequently used to preannotate the content into categories and subcategories, as defined in the task description document from the second phase. Following this process, we preannotated and sampled 95 multimodal harmful suicide content items for annotation. Medical professionals then annotated based on the annotation protocol, and the task description document was finalized by revising the previous version.

Finally, we manually verified the entire benchmark dataset. This involved identifying and eliminating any remaining PIIs from all harmful suicide content and validating the final labels. During the finalization process, 14 content items were excluded from the benchmark. These contents deal with subcultures (such as games and comics) and, therefore, are incomprehensible to all annotators and cannot be categorized into any suicide category, leading to their exclusion. In addition, the task description document was completed, providing comprehensive information on the 5 categories and 25 subcategories, including their harmful category names, descriptions, and illustrative examples.

Figure 3. Illustration of the preannotation process. We construct prompts from the task description document, which includes categories, detailed descriptions, and subcategories (Table 4), and we use LLMs such as GPT-3.5 and GPT-4 to generate LLM-labeled data. We then sample the data to balance category distributions and have medical experts annotate them to build the human-labeled benchmark. AI: artificial intelligence; LLM: large language model.

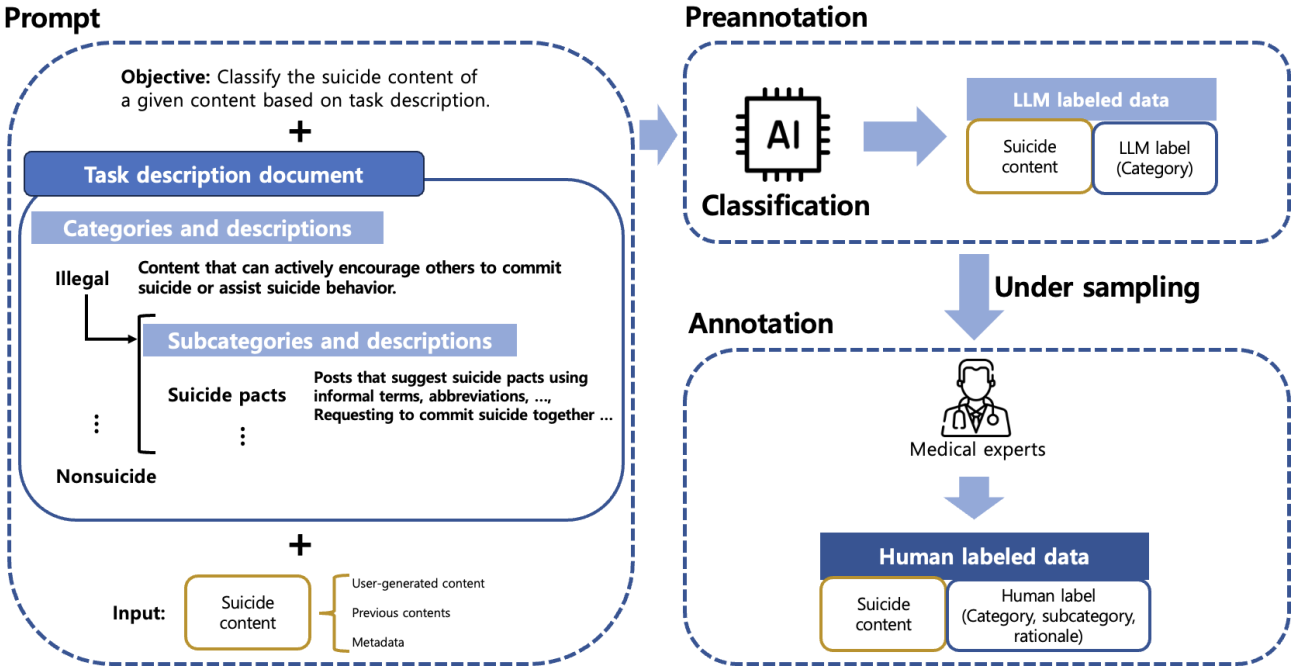

Annotation Protocol

In every phase, we adopted a consensus-based method for biomedical research and clinical practice [40,41]. For each harmful suicide content, 2 separate medical professionals (a clinical expert with an MD degree and a psychiatry professor with a PhD degree) independently labeled the category, subcategory, and rationale for their decisions regarding both the category and the subcategory. Each individual annotator assigned the label based on a comprehensive review of the user-generated content (text and image), previous content, and metadata associated with the harmful suicide content. The Inter-Annotator Agreement for category labels reached a high agreement of 0.77 (Cohen κ) after the second phase of the annotation process. In cases where there is a discrepancy in the category label assigned by individual annotators, a consensus is established through the input of 3 annotators, which includes an additional clinical expert (a psychiatry professor with a PhD degree). During this consensus, rationales written by the 2 individual annotators are combined into a single rationale. In addition, annotators comment on any data whose association with suicide content is uncertain, as well as on instances that imply a potential need to revise the task description. These comments were used at the end of each annotation phase to refine and update the task description document.

Construction of English Benchmark

We further created an English benchmark by translating all input attributes (content text, link or image descriptions, and metadata such as user descriptions). To enhance the usability of the Korean harmful suicide content detection benchmark, it was translated into English using machine translation with GPT-4 - 0613 for each attribute. As a result, we produced an English harmful suicide content detection benchmark containing the same 452 data entries as the original Korean harmful suicide content detection benchmark. The quality of the English

XSL•FO
RenderX

benchmark is evaluated in detail in the "English Benchmark Validation" subsection.

Results

Overview

After constructing the harmful suicide content detection benchmark through the data processing workflow, we evaluated the dataset from 3 perspectives. First, we assess whether the categories and descriptions of harmful suicide content outlined in the task description document are appropriate for providing sufficient information as instructions to LLMs to classify suicide contents ("Leveraging Task Description" subsection).

Next, we evaluate whether the data modalities included in the benchmark (eg, images) are suitable for classification by LLMs ("Leveraging Multimodality" subsection). In addition, we verify whether the LLMs can perform classification using only few-shot examples without further training through few-shot experiments ("Leveraging Few-shot Examples" subsection).

Finally, for the English harmful suicide content detection benchmark, we conduct experiments using various LLMs to compare performance with the original Korean benchmark to verify the use and carry out a direct analysis of data quality to verify the translation's quality ("Comparison Between LLMs" subsection and "English Benchmark Validation" subsection).

Setup

We used the GPT-3.5-turbo-16k API with a temperature of 0.0 and default hyperparameters, conducting 3-8 runs to calculate the average and standard error. For the few-shot experiments, we adopted an *N*-way *K*-shot approach by selecting *K* samples from each of the 5 classes (n=5) in the training dataset ("Data Annotation" subsection).

Metrics

We used the following metrics:

1. Macro F_1 measures the overall performance across the 5 categories.
2. *Mean Absolute Error (MAE) of Harmfulness* measures the model's deviation in predicting harmfulness and is categorized into four levels: 3 (most harmful: Illegal Suicide Content), 2 (harmful: Harmful Suicide Content), 1 (potentially harmful: Potentially Harmful Suicide Content), and 0 (not harmful: Harmless Suicide Content and Nonsuicide Content). This metric assesses the extent of the error in terms of harmfulness.
3. *Illegal* identifies illegal suicide content, and it is crucial for prompt regulation.
4. Harmful separates illegal or harmful suicide content from noncritical content, which is essential for moderating the content that poses harm.

In alignment with our objective of identifying and moderating as much harmful content as possible, our model is designed to initially detect harmful content, after which the results are carefully reviewed by a human moderator or expert. Hence, recall is prioritized over precision. This focus is particularly important for the Illegal and Harmful content categories, where missing instances of harmful suicide content pose a far greater risk than misclassifying content that is actually safe. Within our proposed framework, human moderators or clinical experts make the final judgment, ensuring that such misclassified cases can be corrected while minimizing the chance of harmful content going undetected. This design reflects how the system can function in real-world moderation scenarios, where recall is prioritized to maximize safety without disregarding precision.

Leveraging Task Description

We investigated the formulation of a task description document with diverse and extensive information into instructions because instruction construction significantly influences LLM performance [42-44]. The task description document for the harmful suicide content detection task contains crucial details, including the names and descriptions of 5 suicide categories as well as the names and explanations of 25 subcategories constituting up to 60% of the instruction at maximum. Category information includes detailed names and descriptions of the categories and subcategories. Thus, our experiments were designed to determine the details that most significantly impact performance by varying the granularity of the information.

Setup

We evaluate harmful suicide content detection performance by varying the detailed category information levels as follows: (1) category name; (2) category name and description; (3) category name with category description and subcategory name; and (4) category name with category description and subcategory name with subcategory description.

- Category name and description
- Category name with category description, and subcategory name
- Category name with category description, subcategory name with subcategory description

Results

Table 5 shows that the performance improves with more category information, with the most comprehensive level yielding the highest F_1-scores. Specifically, the macro F_1-score increases by 89% (from 18.86 to 35.75), and the illegal F_1 and harmful F_1-scores increase by 200% (from 11.87 to 35.80) and 57% (from 37.63 to 59.10), respectively, as compared with when using only the category name.

The increasing trend in macro F_1 and illegal or harmful F_1-scores suggests that more detailed information enhances the model's detection capabilities. However, adding only category descriptions decreased illegal or harmful recall (from 27.27 and 65.77 to 20.00 and 57.66, respectively).

XSL•FO
RenderX

Table . Results from the category and subcategory information detail experiment[a].

Category information	Subcategory information	Macro F_1	MAE[b]	Illegal F_1	Illegal recall	Harmful F_1	Harmful recall
Name	N/A[c]	18.86 (0.08)	1.4809 (0.0044)	11.87 (0.04)	27.27 (0.00)	37.63 (0.11)	65.77 (0.00)
Name and description	N/A	25.13 (0.16)	1.2173 (0.0042)	13.23 (0.17)	20.00 (0.00)	39.18 (0.04)	57.66 (0.00)
Name and description	Name	32.18 (0.06)	0.9867 (0.0016)	26.36 (0.00)	30.91 (0.00)	45.26 (0.08)	66.67 (0.00)
Name and description	Name and description	35.75 (0.29)[a]	0.8549 (0.0079)[a]	35.80 (0.87)[a]	58.79 (1.21)[a]	59.10 (0.41)[a]	86.79 (0.60)[a]

[a]A consistent increase in macro F_1, illegal F_1, and harmful F_1-scores is observed as the amount of information increases. Values are mean (SE). These values indicate the best performance in each column.

[b]MAE:mean absolute error.

[c]N/A: not applicable.

Formulating LLM Inputs

We assessed performance changes by incorporating images and training examples as inputs. We focused on the impact of images as multimodal data (“Leveraging Multimodality” subsection) and the effect of using training data with the annotation guide as postinstruction when combined with instruction (“Leveraging Few-shot Examples” subsection).

Leveraging Multimodality

Setup

The objective of this experiment was to determine the effect of image information on the classification performance of the model. We used 2 methods of conveying image information and compared their performances: the first method converts images into text descriptions, referred to as image description, whereas the second uses the images directly as inputs, referred to as vision. Three settings were tested for image descriptions: the first did not provide any image information, the second generated image descriptions using a model (gpt-4 - 1106), and the third involved human modifications to the descriptions created by the model. This allowed for a comparison of the performance of the models based on the generation of text-based image descriptions. In addition, we examined the impact of images (vision) when paired with the same image descriptions to observe their influence on performance. This involved adding the original image to each image description experiment for comparison. Overall, this setup evaluates the model’s performance in terms of the modality of suicide content through image descriptions and assesses the model’s multimodal capabilities through vision. Notably, during the annotation process, the annotators labeled the suicide category of the content based on both the text and the original images. We used GPT-4-turbo-2024-04-09, which can use both text and image inputs, for this experiment. We conducted an experiment on 113 test data entries that included images, among which only 3 belonged to the illegal suicide category; thus, illegal metrics were excluded from the results.

Results

Table 6 shows the impact of multimodal information on harmful suicide content detection tasks. In experiments regarding image descriptions without visual information, providing image details leads to superior performance compared with omitting them. Specifically, when using GPT-4–generated image descriptions, macro F_1 increased by 9.16% (from 50.46 to 55.08) and MAE decreased by 15.93% (from 0.3894 to 0.3333), indicating enhanced classification performance across all suicide categories. In addition, harmful F_1 and recall both increased by 8.00% (from 68.50 to 73.98 and from 75.76 to 81.82), suggesting that image information significantly aids in identifying harmfulness within suicide content. Comparing GPT-4 and human-modified image descriptions, using human-modified descriptions results in a reduction of macro F_1 by 3.55% (from 55.08 to 53.19) and increases MAE by 19.4% (from 0.3333 to 0.3982), although harmful F_1 increases by 2.61% (from 73.98 to 75.91) and harmful recall by 16.66% (from 81.82 to 95.45), indicating that human modifications enhance clarity and detection of harmfulness in content while decreasing overall category performance.

XSL•FO
RenderX

Table . Results of the input modality experiment on a subset of the benchmark that includes images[a].

Image description (text)	Vision (image)	Macro F_1	MAE[b]	Illegal F_1	Illegal recall	Harmful	Harmful recall
No description	X	50.46 (0.12)	0.3864 (0.0135)	N/A[c]	N/A	68.50 (0.21)	75.76 (0.26)
GPT-4 description	X	55.08 (0.09)[a]	0.3333 (0.0102)[a]	N/A	N/A	73.98 (0.09)	81.82 (0.00)
Human description	X	53.19 (0.13)	0.3982 (0.0154)	N/A	N/A	75.91 (0.08)[a]	95.45 (0.00)[a]
No description	O	47.78 (0.05)	0.4189 (0.0102)	N/A	N/A	67.42 (0.07)	90.91 (0.00)
GPT-4 description	O	50.08 (0.16)	0.3894 (0.0234)	N/A	N/A	69.22 (0.34)	83.33 (0.26)
Human description	O	46.55 (0.15)	0.4631 (0.0270)	N/A	N/A	69.37 (0.01)	90.91 (0.00)

[a]We compare 3 types of image descriptions (none, GPT-4-generated, and human-modified) with and without vision input. Without vision, GPT-4 descriptions achieve the best macro F_1 and MAE, while human descriptions perform best on harmful metrics. With vision, we observe an overall decrease in performance. Values are mean (SE). These values indicate the best performance in each column. "O" indicates that the column is used (vision) and "X" indicates that the column is not used.

[b]MAE: mean absolute error.

[c]N/A: not applicable.

In experiments using image information as visual input, we found a general decrease in overall performance across all settings, with reductions in macro F_1, MAE, and harmful F_1. Even in scenarios without image descriptions, macro F_1 decreased by 5.31% (from 50.46 to 47.78), and MAE increased by 8.41% (from 0.3864 to 0.4189). Particularly, the F_1-scores of potentially harmful content decreased significantly (from 54.46 to 42.77). This is owing to the model's sensitive reaction to certain images of potentially harmful suicide content, overestimating their harmfulness and classifying them as harmful.

However, in settings where we used images only as vision (no image description), the harmful recall score was 90.91, which was higher than when no image information was used (75.76); the score was 83.33 when using images with GPT-4 image description, which was higher than when using GPT-4 image description alone (81.82). This suggests that despite a decrease in the overall model performance owing to multimodality, using image information improves the identification of harmfulness in suicide content. In addition, vision can convey more information about harmfulness than text descriptions when human modification does not explicitly note the harmfulness of an image. Overall, the experiments with image descriptions confirmed that the information contained in an image enhances model performance in the harmful suicide content detection task, whereas adding vision information in a multimodal format decreases performance. However, the increase in harmful recall when using vision supports the potential of using vision as an effective tool for enhancing model capabilities in identifying harmful content, paving the way for future improvements in multimodal model performance.

Leveraging Few-Shot Examples

Few-shot refers to a setting where the model is provided with a small number of labeled examples as demonstrations before classifying new instances [45]. The goal of our few-shot experiments is to assess whether LLMs can effectively learn from only a handful of examples in high-stakes domains, where large-scale annotation is often insufficient to train models.

Setup

We examined 1- to 5-shot configurations, corresponding to 1-5 examples per category, totaling 5-25 examples. To construct the pool of demonstrations, medical experts who participated in the benchmark annotation selected 10 representative samples per category (50 in total). These expert-selected samples were used as the source for training demonstrations, while the remaining annotated data served as the test set. From the pool, 5 examples per category were randomly drawn for each experiment. To ensure robustness, we repeated the same experiment with 3 different random seeds, each sampling distinct few-shot samples, and we report the averaged results across these runs.

Results

Figure 4 shows how the performance metrics changed with the number of demonstration examples, with the standard error represented by vertical bars for each few-shot case. As the number of examples increased, macro F_1, MAE, and illegal metrics improved (Figure 4A), specifically illegal F_1 and recall in the 5-shot (Figure 4B). Although the F_1-score for harmful effects remained relatively stable, recall increased but plateaued after a certain threshold (2-shot) (Figure 4C).

XSL•FO
RenderX

Figure 4. Results from the few-shot example experiment. Increasing examples increases illegal F_1 and recall, with 5-shot setting achieving peak performance in the illegal metric. (A) Macro F_1 and mean absolute error; (B) illegal F_1 and recall; and (C) Harmful F_1 and recall. MAE: mean absolute error.

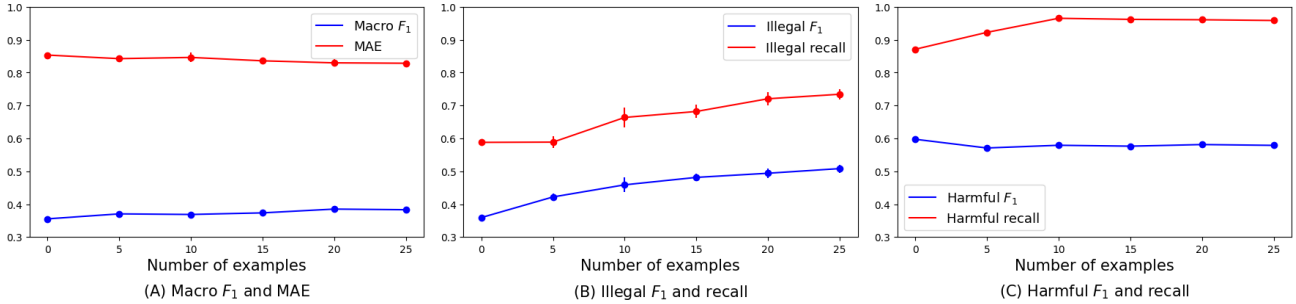

Comparison Between LLMs

We compared the performance of various LLMs in identifying harmful suicide content. Because open-sourced LLMs have instruction-following capabilities that depend on the language they have seen in the instruction tuning phase, we conducted experiments with different models for Korean and English benchmarks to address language barriers.

Setup

We categorized the selected LLMs into closed and open-sourced models. For the Korean benchmark, we used closed models because of the lack of open-source or multilingual LLMs that can properly follow the task's instructions in Korean. We also included a random baseline that arbitrarily categorized content into one of the 5 categories.

Closed Models

We used OpenAI's GPT-3.5 (gpt-3.5-turbo-16k-0613) and GPT-4 (gpt-4 - 1106-preview), which are accessed through the OpenAI API and capable of handling a context length of 1,28,000 characters. In addition, we experimented with Clova X, an LLM trained on Korean, using the Naver API [46].

Open-Sourced Models

We used the Zephyr-7B-beta model [47], an enhanced version of mistral-7B, which supports a context length of up to 32,000 characters. We also use LongChat-7B-16k [48] and Vicuna-7B-v1.5 - 16k [49], which are both fine-tuned Large Language Model Meta artificial intelligence (AI) models with a maximum context length of 16,000 characters.

To explore the model's adaptability of the model in few-shot learning contexts, we conducted experiments in both the zero-shot and 5-shot scenarios ("Leveraging Few-Shot Examples" subsection). However, for models unable to accept the context length of 12k tokens required for the 5-shot experiments, such as Clova X (4096), we limited our analysis to the zero-shot trials.

Results

Figure 5 shows the performance of the GPT models and Clova X on the Korean benchmark. GPT-4 outperformed all other models in every metric except for harmful recall (Figure 5A-E). GPT-3.5 follows GPT-4 in terms of performance across all metrics, except for harmful recall. Clova X showed lower performance than the GPT models but achieved the highest score in harmful recall (Figure 5F), indicating its high sensitivity to harmful content.

Figure 6 shows the performance of the GPTs and open-sourced LLMs on the translated English benchmark. GPT-4 exhibited the highest performance in differentiating categories in both the zero-shot and 5-shot settings across various metrics (Figure 6A-C and E). It leads the performance charts with macro F_1-scores of 46.37 in zero-shot and 52.59 in 5-shot. Notably, GPT-4 showed a significant MAE difference (0.5655 in zero-shot and 0.5755 in 5-shot), indicating that even when the category predictions were incorrect, they tended to be within similar levels of harmfulness.

GPT-3.5 ranked second to GPT-4 in category distinction performance (Figure 6A, B, and E) in zero-shot settings and showed comparable performance to open-sourced models in 5-shot settings. Its recall was relatively higher than GPT-4 in 5-shot settings (Figure 6C-F), indicating a more sensitive response to harmful information than the GPT-4.

Zephyr outperforms random in zero-shot settings with a macro F_1 of 20.99 and MAE of 1.2711; in addition, it achieves a comparable performance to GPT-3.5 in 5-shot settings with macro F_1 of 37.52 and MAE of 0.8217 (Figure 6A and B). LongChat exhibits the largest standard error in the illegal and harmful metrics (Figure 6C-F), indicating that few-shot examples significantly impact performance compared with other models. It recorded the highest standard errors in illegal F_1 and harmful F_1 at 4.09 and 1.67, respectively (Figure 6C and E). LongChat also showed the lowest recall for illegal and harmful content, particularly in harmful content, suggesting that it is less sensitive to harmful information (Figure 6D and F). Vicuna recorded the lowest performance in category classification (Figure 6A) among all models but achieved high recall for illegal and harmful content (Figure 6D and F). Notably, it scored the highest illegal recall of 76.36 and a harmful recall of 83.78, comparable with GPT-3.5's 85.89.

XSL•FO
RenderX

Figure 5. Results from the Korean benchmark experiment. Hatched bars indicate the Korean large language model (Clova X). Although Clova X has lower overall performance than generative pretrained transformers, it excels in harmful recall. (A) Macro F_1; (B) mean absolute error; (C) illegal F_1; (D) illegal recall; (E) harmful F_1; and (F) harmful recall. MAE: mean absolute error.

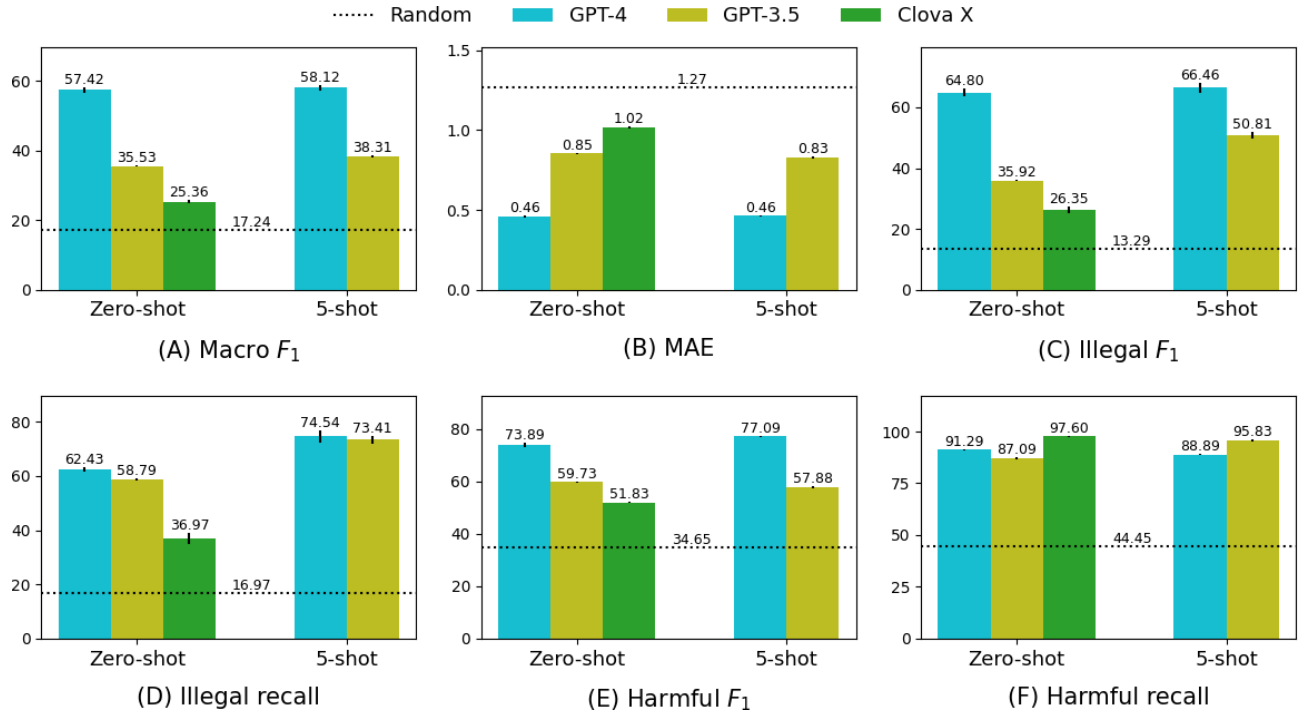

Figure 6. Results from the translated English benchmark experiment. Closed models (GPT-4 and GPT-3.5) show superior performance in the zero-shot setting compared with open-sourced models, whereas open-sourced models reach comparable performance to GPT-3.5 in 5-shot. (A) Macro F_1; (B) mean absolute error; (C) illegal F_1; (D) illegal recall; (E) harmful F_1; and (F) harmful recall. MAE: mean absolute error.

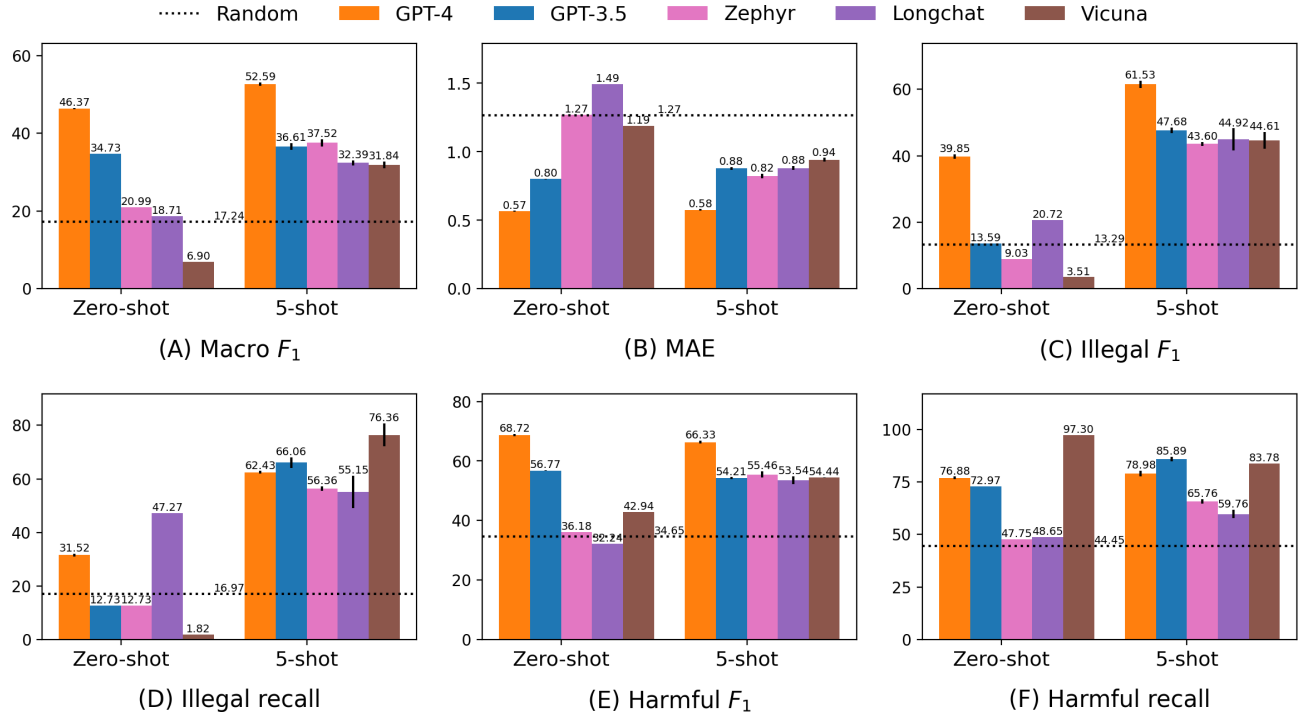

Analysis

Open-Sourced Versus Closed LLMs

GPT-4 recorded the highest performance across all accuracy metrics (macro F_1, MAE, illegal F_1, and harmful F_1) for all few-shot settings. In 5-shot settings, open-sourced models achieve a similar performance to GPT-3.5. However, in zero-shot settings, they struggled to understand lengthy instructions, resulting in random predictions (eg, LongChat) or biased predictions toward specific categories (eg, Vicuna), with Zephyr slightly outperforming random. In 5-shot scenarios, Zephyr matches GPT-3.5 in macro F_1, MAE, and harmful F_1, whereas LongChat and Vicuna show comparable performance in their respective metrics. Except for Vicuna, open-sourced

XSL•FO
RenderX

models generally showed lower recall than closed models in terms of illegal and harmful content.

Original Korean Versus Translated English

Figure 7 shows an analysis of GPT-3.5 and GPT-4's performance on the Korean and translated English benchmarks. Both models performed better on the Korean benchmark across all F_1 metrics (Figure 7A, C, and E). However, GPT-4 shows a decrease in macro F_1 from the English to the Korean benchmark by 19.24% in zero-shot (from 57.42 to 46.37) and 9.51% in 5-shot (from 58.12 to 52.59), with the largest decrease in illegal F_1 by 36.17% in zero-shot (from 64.80 to 39.85). GPT-3.5 also showed a considerable reduction in zero-shot illegal F_1 by 62.17% (from 35.92 to 13.59). Illegal recall decreases considerably, with GPT-4 decreasing by 49.51% (from 62.43 to 31.52) and GPT-3.5 by 78.34% in illegal recall (from 58.79 to 12.73), indicating a larger decrease than in F_1-scores (Figure 7D). The decrease in harmful F_1 is less significant, with GPT-4 decreasing by 7.00% (from 73.89 to 68.72) in zero-shot, and GPT-3.5 decreasing by 4.96% (from 59.73 to 56.77). This indicates that while translating the benchmark using GPT-4 does not significantly affect the overall quality, it may lead to issues in specific categories, notably illegal.

Figure 7. Performance comparison of closed models (GPT-3.5 and GPT-4) on the Korean and translated English benchmarks. Closed models exhibit better classification performance on the Korean benchmark than on the English benchmark, with the most significant difference noted in classifying the illegal category. (A) Macro F_1; (B) mean absolute error; (C) illegal F_1; (D) illegal recall; (E) harmful F_1; and (F) harmful recall. MAE: mean absolute error.

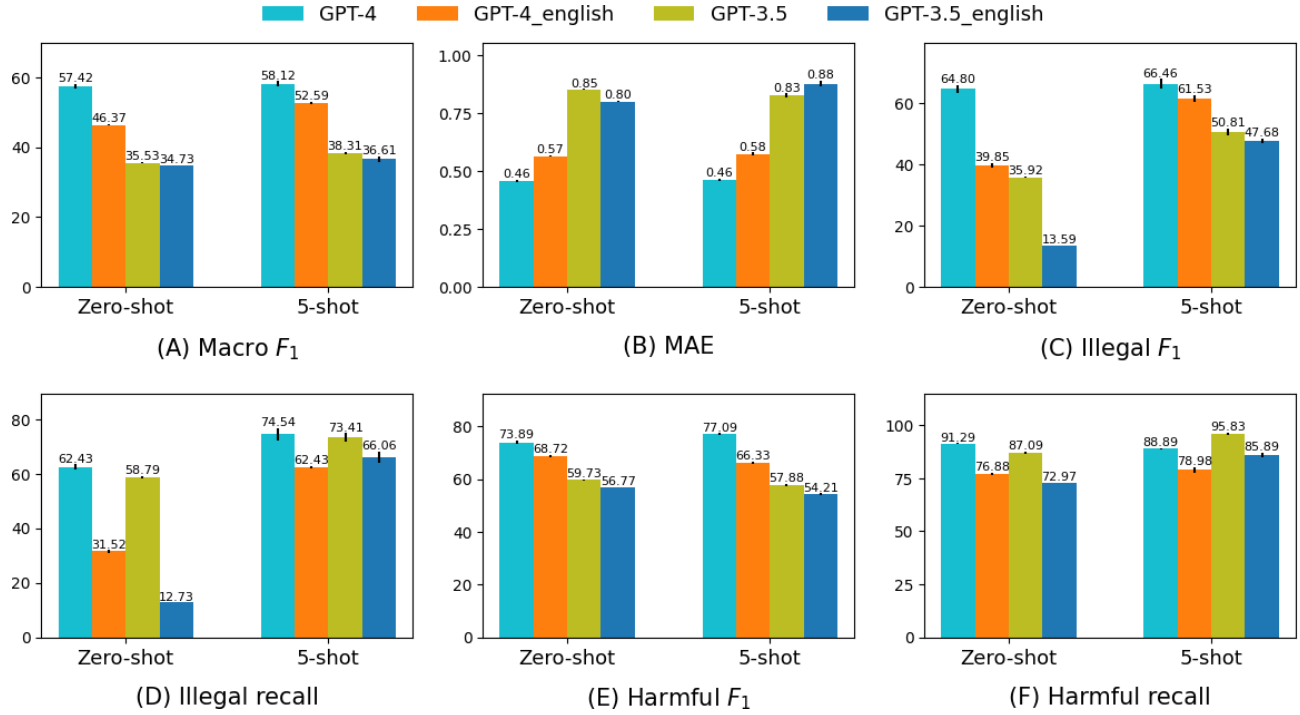

English Benchmark Validation

Considering the use of the English benchmark for experimenting with open-sourced models, it is necessary to evaluate the translation results. In particular, for content containing words related to suicide and harmful information, it is crucial to assess both the overall translation quality and how well the content has been translated. Because OpenAI's use policy potentially refuses to respond to harmful content, there may be instances in which proper translation has not been achieved. Therefore, we analyzed the following 2 aspects: (1) overall translation quality (quantitative analysis), and (2) translation of harmful content (qualitative analysis).

We evaluated the text content (CONTENT_TEXT) of every instance in the benchmark because every instance contains content text and it constitutes the largest proportion of text. We performed a quantitative analysis to assess translation quality using models (GPT-4 - 0613) and a qualitative analysis of the translation of harmful content by the authors.

Translation quality (quantitative analysis): Translation quality assesses how similar the translated content (in English) is to the original content (in Korean). We evaluated translation quality using Scalar Quality Metric (SQM) and Direct Assessment (DA) methods [50] through the GPT-4 - 0613 API, which aligns closely with human evaluations. SQM evaluates the translation quality of the source text (Korean) and target text (English) on a scale of 0-100, with descriptions provided for "no meaning preserved," "some meaning preserved," "most meaning preserved and few grammar mistakes," and "perfect meaning and grammar." DA, such as SQM, rates translation quality on a scale of 0-100 but provides descriptions only for "no meaning preserved" and "perfect meaning and grammar." On average, the translated contents scored 79.55 on SQM and 78.10 on DA, indicating that most instances of the benchmark translation results fall under "most meaning preserved and few grammar mistakes," successfully retaining the original meaning.

Translation of harmful content (qualitative analysis): Illegal and harmful suicide content includes harmful words and

XSL•FO
RenderX

expressions related to suicide and self-harm, encompassing abbreviations, drug names related to suicide, and expressions of methods for suicide and self-harm. Moreover, owing to OpenAI's use policy, there are cases in which harmful content is not translated or translation is refused. Thus, to determine how well such content was translated, we analyzed translation error cases for expressions related to suicide: (1) expressions related to suicide (abbreviations and words), and (2) OpenAI moderation.

Expressions related to suicide: After analyzing 55 instances of illegal suicide content and 56 instances of harmful suicide content, we identified the following types of translation errors: (1) abbreviation translation error, (2) translation of substances used for suicide, and (3) translation of slang related to suicide and self-harm.

Table 7 shows examples of translation errors for each category and error type. *Abbreviation translation error* occurs when abbreviations related to suicide and self-harm are incorrectly interpreted. To evade online platform moderation, abbreviations related to suicide are often used. In these cases, the translation process incorrectly translates these abbreviations into entirely different words. The Korean abbreviation means "commit double suicide and death leap"; however, the English translation misinterprets it entirely. In this study, 12 benchmark instances were identified. *Translation of Substances used for suicide* refers to cases in which drugs related to suicide and self-harm were incorrectly translated. Substances used for suicide are often referred to by abbreviations to avoid online platform moderation, and the actual drug names are often translated into general names for drugs during translation. In this example, the drug "zolpidem" was translated as "SleepingPill," which translates to the purpose of the drug (zolpidem is a type of sleeping pill) rather than the actual name of the drug. However, such translations result in the inability of the model to correctly identify the sale of specific drugs (illegal suicide category) during the category classification process. In this study, 15 instances were identified. *Translation of slang related to suicide and self-harm* refers to errors in the translation of clear expressions of suicide. For example, the Korean expression for "bloodletting self-harm" was incorrectly translated as "blood donation" in English, which changed the meaning of the text. Three instances were identified for this case.

Table . Qualitative analysis of benchmark translation results. The source text is the content text from the Korean benchmark data, and the proper translation is the result translated by a human while preserving the meaning. The translation result is obtained using a model and has been applied to the English benchmark. The underlined words indicate parts where translation errors occurred in the model's output.

Type	Content text
Translation error in the abbreviation (illegal suicide content)	
Source text	ㄷㅂㅈㅅㅌㅅ 하실 분 자차나 면허 있으신 분으로요
Proper translation (human)	Looking for someone who will commit double suicide and death leap, preferably someone with a car or a driver's license.
Translation result (model)	Looking for someone who can do delivery and sales, preferably someone with a car or a driver's license.
Translation error in substances that are used for suicide (illegal suicide content)	
Source text	정품#졸프ㅣ뎀판ㅁㅐ 하는곳 가짜없고 사기없는 솔직한 비밀상담 관심空 #여성최음ㅈㅔ ㄱㅜ입하는 곳. 라인: [ID] 카톡: [ID] 텔레: [ID]
Proper translation (human)	#GenuinezolpidemSellingPlace A place where there are no fakes, no scams, honest confidential consultation. Interested in #FemaleAphrodisiac Purchase place. Line: [ID] Kakaotalk: [ID] Telegram: [ID]
Translation result (model)	#GenuineSpleepingPillSellingPlace A place where there are no fakes, no scams, honest confidential consultation. Interested in #FemaleAphrodisiac Purchase place. Line: [ID] Kakaotalk: [ID] Telegram: [ID]
Translation of slang related to suicide or self-harm (harmful suicide content)	
Source text	사혈자해를 해보고싶다는 생각이 들어
Proper translation (human)	I'm thinking about wanting to try bleeding self-harm.
Translation result (model)	I'm thinking about wanting to try blood donation.

OpenAI Moderation

During the translation process of the benchmark data, we found a few instances where different translation errors occur from those related to expressions of suicide; some content are not translated at all. Unlike parts of the text that are translated incorrectly, the OpenAI API (gpt-4‐1106) refuses to translate and generates content (translated output) that has no relation to the original text (input text). Two instances occurred for this case; one involving content asking for help in committing suicide or self-harm and another involving direct sexual content.

XSL•FO
RenderX

Discussion

English Benchmark Integrity

The English benchmark was generated through machine translation using GPT-4. Quantitative evaluation showed relatively high scores (SQM: 79.55, DA: 78.10), indicating that most meanings were preserved. However, qualitative analysis revealed errors in suicide-related slang, abbreviations, and substance names (eg, bleeding self-harm translated as blood donation, zolpidem simplified to sleeping pill). Such inaccuracies may affect model performance and limit the benchmark's validity for multilingual generalization. Therefore, results on the English benchmark should be interpreted with caution. Future work will involve human validation of high-risk categories and improved translation methods for suicide-specific terminology.

Benchmark Size

Although the harmful suicide content benchmark is an essential step toward understanding and moderating online suicide-related content, it encompasses 452 data entries. This relatively small benchmark size is largely attributable to the fact that posts related to suicide comprise a small fraction of the total online content. In addition, filtering and deleting such content by online sources inherently limit the volume of data available for collection. Nevertheless, a carefully controlled annotation process that incorporates the knowledge of clinical experts supports the credibility of the benchmark and ensures a reliable set of labels. In addition, the task description document details 25 different subcategories of suicide content, and the benchmark comprises a wide array of suicide content, including actual data for each subcategory. Therefore, our detailed task description document and the data within our benchmark lay the groundwork for future efforts to create a large-scale suicide content dataset using the annotations described for the suicide content.

Dataset Usage

The harmful suicide content benchmark includes a task description document containing categories and subcategories of suicide content, along with a dataset of 452 annotated entries. Users can leverage the contents of the task description document as instructions for LLMs. In addition, data labeled for training within the benchmark can be used as few-shot examples, while data labeled for testing can serve as evaluation data.

Future Work

In clinical practice, detecting that a patient who has attempted suicide or self-harm has been exposed to suicide-related content can be highly valuable for preventing further self-harm or suicide attempts. This is because restricting harmful online content represents a relatively modifiable factor among the many risk factors associated with suicide and self-harm [51,52]. Building on this perspective, in future work, we plan to further validate the practical effectiveness of our suicide content detection model. Specifically, we aim to conduct a comparative study between individuals who have attempted suicide or self-harm and a control group of individuals without such experiences. By analyzing their online activity, we will investigate whether those with a history of suicidal or self-harming behaviors are more frequently exposed to harmful suicide-related content. Such a study would not only provide empirical evidence for the real-world use of our detection framework but also offer insights into the role of online harmful content in influencing vulnerable populations.

Funding

This research was partially supported by the Bio & Medical Technology Development Program of the National Research Foundation (NRF) and funded by the Korean government (MSIT) (NRF-2021M3A9E4080780 and 2021M3A9E4080784) and Institute of Information & communications Technology Planning & Evaluation (IITP) grant funded by the Korea government (MSIT) (RS-2019-II190421, AI Graduate School Support Program(Sungkyunkwan University), and Institute of Information & communications Technology Planning & Evaluation (IITP) grant funded by the Korea government (MSIT) (no. RS-2024 - 00509258 and no. RS-2024-00469482, Global AI Frontier Lab).

Data Availability

Our benchmark dataset contains sensitive and, in some cases, illegal information related to suicide. Due to the sensitivity of suicide-related content, the full benchmark dataset cannot be publicly released and is granted only through a controlled approval process [53]. In addition, since the dataset also contains illegal information, it cannot be made publicly available; however, it may be shared under appropriate requests and upon review by the authors [54]. We provide the website [55] to obtain the benchmark dataset and the codes used in the experiments. Applicants must follow the outlined process, after which the authors will review the requests and share the dataset as appropriate. This version includes only references to the original data (eg, tweet IDs, and URLs) and annotations by medical experts, ensuring that no legal or ethical violations occur upon public release.

Authors' Contributions

KP, MJB, RL, JM, JWP, and SP contributed to conception. KP, MJB, RL, JM, KC, JWP, and SP contributed to idea and theory. KP, MJB, YS, SML, YHS, ARL, SYY, JWP, and SP contributed to task design. KP, YH, YS, HL, and SP contributed to building data collections. MJB, RL, and JWP contributed to data annotation. KP, YH, YS, and SP contributed to data processing. KP, YH, YS, SML, YHS, ARL, SYY, and SP contributed to building the benchmark. KP, YH, DL, JB, KC, and SP contributed to technical validation. All authors contributed to the final manuscript and reviewed and approved the final manuscript. JB (jy.bak@skku.edu),

XSL•FO
RenderX

KC (kyunghyun.cho@nyu.edu), JWP (paikjw@khu.ac.kr), and SP (sungjoon.park@softly.ai, psj6512@gmail.com) are equal co-corresponding authors.

Conflicts of Interest

KP, DL, JM, and SP are affiliated with SoftlyAI. MJB and ARL are affiliated with Kyung Hee University Medical Center. YH and JB are affiliated with SungKyunKwan University. YS and HL are affiliated with KAIST. RL is affiliated with the University of Pennsylvania. MJB, SML, YHS, ARL, SYY, and JWP are affiliated with Kyung Hee University. KC is affiliated with New York University.

References

1. Understanding self-harm and suicide content online. Samaritans. 2020. URL: https://www.samaritans.org/about-samaritans/research-policy/internet-suicide/guidelines-tech-industry/understanding-self-harm-and-suicide-content/ [accessed 2025-12-20]
2. 자살예방 및 생명존중문화 조성을 위한 법률 [The act on the prevention of suicide and the creation of a culture of respect for life]. MOHW. 2019. URL: https://tinyurl.com/42xe7rwy [accessed 2025-12-20]
3. Zdanow C, Wright B. The representation of self injury and suicide on emo social networking groups. Afr Sociol Rev Afr de Sociol 2012;16:81-101 [FREE Full text]
4. Biddle L, Gunnell D, Owen-Smith A, et al. Information sources used by the suicidal to inform choice of method. J Affect Disord 2012 Feb;136(3):702-709. [doi: 10.1016/j.jad.2011.10.004]
5. Milmo D. 'The bleakest of worlds': how Molly Russell fell into a vortex of despair on social media. The Guardian. 2022. URL: https://www.theguardian.com/technology/2022/sep/30/how-molly-russell-fell-into-a-vortex-of-despair-on-social-media [accessed 2025-12-20]
6. Balt E, Mérelle S, Robinson J, et al. Social media use of adolescents who died by suicide: lessons from a psychological autopsy study. Child Adolesc Psychiatry Ment Health 2023 Apr 7;17(1):48. [doi: 10.1186/s13034-023-00597-9] [Medline: 37029395]
7. Twenge JM, Haidt J, Lozano J, Cummins KM. Specification curve analysis shows that social media use is linked to poor mental health, especially among girls. Acta Psychol (Amst) 2022 Apr;224:103512. [doi: 10.1016/j.actpsy.2022.103512]
8. National suicide prevention strategies. World Health Organization. 2018 URL: https://iris.who.int/server/api/core/bitstreams/9b9ea82a-b798-4c63-b90e-74bf8bdbf6b1/content [accessed 2025-12-20]
9. Donelan M. Secretary of State for Science, Innovation and Technology, the Lord Parkinson of Whitley Bay & Parliamentary Undersecretary of State for Arts and Heritage. Online Safety Act 2023. 2023. URL: https://www.legislation.gov.uk/ukpga/2023/50 [accessed 2025-12-20]
10. World health statistics 2023: monitoring health for the SDGS, sustainable development goals. World Health Organization. 2023. URL: https://www.who.int/publications/i/item/9789240074323 [accessed 2025-12-20]
11. Jung K. 처벌조항 유명무실 [Ministry of Health and Welfare requests zero investigations on suicide-inducing information on SNS, rendering punitive clauses ineffective]. 2022. URL: http://www.bosa.co.kr/news/articleView.html?idxno=2182323 [accessed 2025-12-20]
12. Min S. 자살유발정보 4년간 7배 늘었는데 · · · 모니터링 전담인력은 10년째 1명뿐 [Incidents of suicide-inducing information increase sevenfold in four years, yet monitoring staff remains solely one for a decade]. 2023. URL: https://www.khan.co.kr/article/202309241417001 [accessed 2025-12-20]
13. 2022 internet usage survey summary report (2022년도 인터넷이용실태조사 요약보고서). 2022 URL: https://www.msit.go.kr/bbs/view.do?sCode=user&bbsSeqNo=79&nttSeqNo=3173583 [accessed 2025-12-20]
14. Zirikly A, Resnik P, Uzuner Ö, Hollingshead K. CLPsych 2019 shared task: predicting the degree of suicide risk in reddit posts. In: Niederhoffer K, Hollingshead K, Resnik P, Resnik R, Loveys K, editors. 2019 Presented at: Proceedings of the Sixth Workshop on Computational Linguistics and Clinical Psychology; Jun 6, 2019; Minneapolis, Minnesota p. 24-33. [doi: 10.18653/v1/W19-3003]
15. Milne DN, Pink G, Hachey B, Calvo RA. CLPsych 2016 shared task: triaging content in online peer-support forums. In: Hollingshead K, Ungar L, editors. 2016 Presented at: Proceedings of the Third Workshop on Computational Linguistics and Clinical Psychology; Jun 16, 2016; San Diego, CA, USA p. 118-127. [doi: 10.18653/v1/W16-0312]
16. Yates A, Cohan A, Goharian N. Depression and self-harm risk assessment in online forums. In: Palmer M, Hwa R, Riedel S, editors. 2017 Presented at: Proceedings of the 2017 Conference on Empirical Methods in Natural Language Processing; Sep 9-11, 2017; Copenhagen, Denmark p. 2968-2978. [doi: 10.18653/v1/D17-1322]
17. Yang C, Zhang Y, Muresan S. Weakly-supervised methods for suicide risk assessment: role of related domains. Presented at: Proceedings of the 59th Annual Meeting of the Association for Computational Linguistics and the 11th International Joint Conference on Natural Language Processing (Volume 22: Short Papers); Aug 1-6, 2021. [doi: 10.18653/v1/2021.acl-short.133]
18. Sawhney R, Neerkaje A, Gaur M. A risk-averse mechanism for suicidality assessment on social media. In: Muresan S, Nakov P, Villavicencio A, editors. 2022 Presented at: Proceedings of the 60th Annual Meeting of the Association for Computational Linguistics (Volume 2: Short Papers); May 22-27, 2022; Dublin, Ireland p. 628-635. [doi: 10.18653/v1/2022.acl-short.70]

XSL•FO
RenderX

19. Rawat BPS, Kovaly S, Yu H, Pigeon W. ScAN: suicide attempt and ideation events dataset. Presented at: Proceedings of the 2022 Conference of the North American Chapter of the Association for Computational Linguistics; Jul 10-15, 2022; Seattle, United States p. 1029. [doi: 10.18653/v1/2022.naacl-main.75]
20. Sawhney R, Joshi H, Shah RR, Flek L. Suicide ideation detection via social and temporal user representations using hyperbolic learning. 2021 Presented at: Proceedings of the 2021 Conference of the North American Chapter of the Association for Computational Linguistics; Jun 6-11, 2021; Online p. 2176-2190 URL: https://aclanthology.org/2021.naacl-main [doi: 10.18653/v1/2021.naacl-main.176]
21. Marchant A, Hawton K, Stewart A, et al. A systematic review of the relationship between internet use, self-harm and suicidal behaviour in young people: the good, the bad and the unknown. PLoS One 2017;12(8):e0181722. [doi: 10.1371/journal.pone.0181722] [Medline: 28813437]
22. Sedgwick R, Epstein S, Dutta R, Ougrin D. Social media, internet use and suicide attempts in adolescents. Curr Opin Psychiatry 2019;32(6):534-541. [doi: 10.1097/YCO.0000000000000547]
23. Wang L, Liu X, Liu ZZ, Jia CX. Digital media use and subsequent self-harm during a 1-year follow-up of Chinese adolescents. J Affect Disord 2020 Dec;277:279-286. [doi: 10.1016/j.jad.2020.05.066]
24. Patchin JW, Hinduja S, Meldrum RC. Digital self-harm and suicidality among adolescents. Child Adolesc Ment Health 2023 Feb;28(1):52-59. [doi: 10.1111/camh.12574] [Medline: 35811440]
25. Choi WS, Han J, Hong HJ. Association Between internet searches related to suicide/self-harm and adolescent suicide death in South Korea in 2016-2020: secondary data analysis. J Med Internet Res 2023 Apr 20;25:e46254. [doi: 10.2196/46254] [Medline: 37079349]
26. Mars B, Heron J, Biddle L, et al. Exposure to, and searching for, information about suicide and self-harm on the Internet: prevalence and predictors in a population based cohort of young adults. J Affect Disord 2015 Oct;185:239-245. [doi: 10.1016/j.jad.2015.06.001]
27. Wang S, Liu Y, Xu Y, Zhu C, Zeng M. Want to reduce labeling cost? GPT-3 can help. In: Moens MF, Huang X, Specia L, Yih ST, editors. 2021 Presented at: Findings of the Association for Computational Linguistics; Nov 7-11, 2021; Punta Cana, Dominican Republic p. 4195-4205. [doi: 10.18653/v1/2021.findings-emnlp.354]
28. Wang X, Kim H, Rahman S, Mitra K, Miao Z. Human-LLM collaborative annotation through effective verification of LLM labels. 2024 May 11 Presented at: Proceedings of the CHI Conference on Human Factors in Computing Systems; May 11-16, 2024; Honolulu HI USA p. 1-21. [doi: 10.1145/3613904.3641960]
29. 온라인 자살유발정보, 국민이 직접 찾아내고 삭제한다! [Citizens directly identify and remove online suicide- inducing information!]. KPHN. 2020. URL: https://www.mohw.go.kr/board.es?mid=a10503010100&bid=0027&act=view&list_no=359157 [accessed 2025-12-20]
30. Markov T, Zhang C, Agarwal S, et al. A holistic approach to undesired content detection in the real world. AAAI 2023;37(12):15009-15018. [doi: 10.1609/aaai.v37i12.26752]
31. Lee D, Park S, Kang J, Choi D, Han J. Cross-lingual suicidal-oriented word embedding toward suicide prevention. 2020 Nov Presented at: Findings of the Association for Computational Linguistics; Nov 16-20, 2020 URL: https://www.aclweb.org/anthology/2020.findings-emnlp [doi: 10.18653/v1/2020.findings-emnlp.200]
32. 미디어 자살정보 모니터링 시스템 [Media suicide information monitoring system]. KFSP. 2023. URL: https://sims.kfsp.or.kr/ [accessed 2025-12-20]
33. Park S, Park K, Ahn J, Oh A. Suicidal risk detection for military personnel. Presented at: Proceedings of the 2020 Conference on Empirical Methods in Natural Language Processing (EMNLP); Nov 16-20, 2020 URL: https://www.aclweb.org/anthology/2020.emnlp-main [doi: 10.18653/v1/2020.emnlp-main.198]
34. 사이버상담 [cyber counselling]. Lifeline Korea. 2023. URL: https://www.lifeline.or.kr/business/opening_consult.php [accessed 2025-12-20]
35. 공개상담실 [public counselling room]. KSPCC. 2023. URL: http://auru.counselling.or.kr/contents/sub0201.php?PHPSESSID=4f99b850a26d94de69fe936d68006e51 [accessed 2025-12-20]
36. 디시인사이드 [DCinside]. DCInside. 2023. URL: https://www.dcinside.com/ [accessed 2025-12-20]
37. Jo J. 잇단 사고에 말 많은 '우울증 갤러리'‥"폐쇄는 안 한다"는 정부 [following a series of incidents, the government states it will not shut down the controversial 'depression gallery' despite the ongoing discussions]. MBC. 2023. URL: https://imnews.imbc.com/replay/2023/nwdesk/article/6490952_36199.html [accessed 2026-01-29]
38. Fiesler C, Jiang J, McCann J, Frye K, Brubaker JR. Reddit Rules! Characterizing an Ecosystem of Governance. ICWSM 2018;12(1). [doi: 10.1609/icwsm.v12i1.15033]
39. Moon J, Lee DH, Cho H, et al. Analyzing norm violations in live-stream chat. Presented at: Proceedings of the 2023 Conference on Empirical Methods in Natural Language Processing; Dec 6-10, 2023; Singapore p. 852-868. [doi: 10.18653/v1/2023.emnlp-main.55]
40. Gattrell WT, Hungin AP, Price A, et al. ACCORD guideline for reporting consensus-based methods in biomedical research and clinical practice: a study protocol. Res Integr Peer Rev 2022 Jun 7;7(1):3. [doi: 10.1186/s41073-022-00122-0] [Medline: 35672782]
41. Vakil N. Consensus guidelines: method or madness? Am J Gastroenterol 2011 Feb;106(2):225-227. [doi: 10.1038/ajg.2010.504] [Medline: 21301451]

XSL•FO
RenderX

42. Liu NF, Lin K, Hewitt J, et al. Lost in the middle: how language models use long contexts. Trans Assoc Comput Linguist 2024 Feb 23;12:157-173. [doi: 10.1162/tacl_a_00638]
43. Wu Y, Iso H, Pezeshkpour P, Bhutani N, Hruschka E. Less is more for long document summary evaluation by LLMs. 2023 Presented at: Proceedings of the 18th Conference of the European Chapter of the Association for Computational Linguistics (Volume 2; Mar 17-22, 2024; St Julian's, Malta p. 330-343. [doi: 10.18653/v1/2024.eacl-short.29]
44. Zhao Z, Wallace E, Feng S, Klein D, Singh S. Calibrate before use: improving few-shot performance of language models. In: Meila M, Zhang T, editors. Presented at: Proceedings of the 38th International Conference on Machine Learning; Jul 18-24, 2021; Virtual p. 12697-12706 URL: https://proceedings.mlr.press/v139/zhao21c.html [accessed 2025-12-20]
45. Brown T, et al. Language models are few-shot learners. Adv Neural Inf Process Syst 2020;33:1877-1901 [FREE Full text]
46. Kim B, Kim H, Lee SW, et al. What changes can large-scale language models bring? intensive study on hyperclova: billions-scale Korean generative pretrained transformers. In: Moens MF, Huang X, Specia L, Yih ST, editors. Presented at: Proceedings of the 2021 Conference on Empirical Methods in Natural Language Processing; Nov 7-11, 2021; Online and Punta Cana, Dominican Republic p. 3405-3424. [doi: 10.18653/v1/2021.emnlp-main.274]
47. Tunstall L, et al. Zephyr: direct distillation of LM alignment. arXiv. Preprint posted online on Oct 25, 2023. [doi: 10.48550/arXiv.2310.16944]
48. Li D, et al. How long can open-source llms truly promise on context length. LMSYS Org. 2023. URL: https://lmsys.org/blog/2023-06-29-longchat/ [accessed 2025-12-29]
49. Chiang WL, et al. Vicuna: an open-source chatbot impressing GPT-4 with 90%* ChatGPT quality. LMSYS Org. 2023. URL: https://lmsys.org/blog/2023-03-30-vicuna/ [accessed 2025-12-20]
50. Kocmi T, Federmann C. Large language models are state-of-the-art evaluators of translation quality. arXiv. Preprint posted online on Feb 28, 2023. [doi: 10.48550/arXiv.2302.14520]
51. Hawton K, Saunders KEA, O'Connor RC. Self-harm and suicide in adolescents. Lancet 2012 Jun 23;379(9834):2373-2382. [doi: 10.1016/S0140-6736(12)60322-5] [Medline: 22726518]
52. Skegg K. Self-harm. Lancet 2005;366(9495):1471-1483. [doi: 10.1016/S0140-6736(05)67600-3] [Medline: 16243093]
53. Shing HC, Nair S, Zirikly A, Friedenberg M, Daumé III H, Resnik P. Expert, crowdsourced, and machine assessment of suicide risk via online postings. 2018 Presented at: Proceedings of the Fifth Workshop on Computational Linguistics and Clinical Psychology: From Keyboard to Clinic; Jun 5, 2018; New Orleans, LA p. 25-36. [doi: 10.18653/v1/W18-0603]
54. Choshen L, Eldad D, Hershcovich D, Sulem E, Abend O. The language of legal and illegal activity on the darknet. 2019 Presented at: Proceedings of the 57th Annual Meeting of the Association for Computational Linguistics; Jul 28 to Aug 2, 2019; Florence, Italy p. 4271-4279. [doi: 10.18653/v1/P19-1419]
55. Bak J. Iterative large language model-guided sampling and expert-annotated benchmark corpus for harmful suicide content detection: development and validation study. GitHub. URL: https://github.com/Human-Language-Intelligence/Harmful-Suicide-Content-Detection [accessed 2025-12-20]

Abbreviations

AI: artificial intelligence
API: application programming interface
DA: Direct Assessment
IRB: institutional review board
MAE: mean absolute error
PII: Personally Identifiable Information
Q&A: question and answer
SQM: Scalar Quality Metric

Edited by A Benis; submitted 12.Mar.2025; peer-reviewed by A Gupta, L Wreyford, S Chowdhury, S Banerjee; accepted 16.Nov.2025; published 05.Feb.2026.

Please cite as:
Park K, Baik MJ, Hwang Y, Shin Y, Lee H, Lee R, Lee SM, Sun JYH, Lee AR, Yoon SY, Lee DH, Moon J, Bak J, Cho K, Paik JW, Park S
Iterative Large Language Model–Guided Sampling and Expert-Annotated Benchmark Corpus for Harmful Suicide Content Detection: Development and Validation Study
JMIR Med Inform 2026;14:e73725
URL: https://medinform.jmir.org/2026/1/e73725
doi:10.2196/73725

XSL•FO
RenderX

© Kyumin Park, Myung Jae Baik, YeongJun Hwang, Yen Shin, HoJae Lee, Ruda Lee, Sang Min Lee, Je Young Hannah Sun, Ah Rah Lee, Si Yeun Yoon, Dong-ho Lee, Jihyung Moon, JinYeong Bak, Kyunghyun Cho, Jong-Woo Paik, Sungjoon Park. Originally published in JMIR Medical Informatics (https://medinform.jmir.org), 5.Feb.2026. This is an open-access article distributed under the terms of the Creative Commons Attribution License (https://creativecommons.org/licenses/by/4.0/), which permits unrestricted use, distribution, and reproduction in any medium, provided the original work, first published in JMIR Medical Informatics, is properly cited. The complete bibliographic information, a link to the original publication on https://medinform.jmir.org/, as well as this copyright and license information must be included.

XSL•FO
RenderX

Original Paper

Development and Evaluation of SNOMED CT Automated Mapping Tool: Advancing Terminology Standardization and Semantic Interoperability

Youngsun Park[1], MSN; Hannah Kang[1], PhD; Jiwon Kim[1], BSN; Soo-Yong Shin[1], PhD; Dosang Cho[2], PhD; Sang Youl Rhee[3,4], PhD; Hong Seok Park[5], PhD; Kyung-Jae Lee[6], PhD; Sungchul Bae[1], PhD

[1]Kakao Healthcare Corp, Seongnam-si, Republic of Korea

[2]Department of Neurosurgery, Ewha Womans University Medical Center, Seoul, Republic of Korea

[3]Center for Digital Health, Kyung Hee University, Seoul, Republic of Korea

[4]Department of Endocrinology and Metabolism, Kyung Hee University College of Medicine, Seoul, Republic of Korea

[5]Department of Urology, Korea University College of Medicine, Seoul, Republic of Korea

[6]Department of Orthopedic Surgery, Keimyung University Dongsan Hospital, Daegu, Republic of Korea

Corresponding Author:
Sungchul Bae, PhD
Kakao Healthcare Corp
166, Pangyoyeok-ro, Bundang-gu, Gyeonggi-do
Seongnam-si, 13529
Republic of Korea
Phone: 82 1088569908
Email: utdwest13@gmail.com

Abstract

Background: Effective secondary use of healthcare data is hindered by fragmentation and a lack of semantic interoperability due to heterogeneous local terminologies. Standardizing clinical terms using SNOMED CT (Systematized Nomenclature of Medicine Clinical Terms) is essential but remains a manual, labor-intensive, and inconsistent process, especially across multiple institutions. Automated, scalable solutions are needed to support reliable mapping and new concept authoring for large-scale research.

Objective: We aimed to develop a large language model (LLM)-assisted tool that streamlines SNOMED CT terminology mapping and concept authoring, which enables seamless, standardized data integration across multi-institutional clinical datasets.

Methods: The mapping pipeline included preprocessing local terms, syntactic and LLM-based vector similarity mapping, and iterative enrichment based on validated results. Translation and semantic representation used GPT-4o (OpenAI). New concepts were authored through a structured postcoordination process, and both the efficiency and quality of authoring (including duplicate rate and Machine Readable Concept Model validation violations) were quantitatively evaluated. Performance was evaluated using diagnostic and surgical procedural terms from 4 major hospital networks (9 university hospitals) in South Korea, with additional usability feedback gathered from clinical terminologists.

Results: Using reference terms, top-5 accuracy for diagnostic mapping reached 98.7%, 89.7%, 98.5%, and 92.8% across the 4 institutions and 99.2%, 82.6%, 98.7%, and 84.7% for surgical procedural mapping. Implementation of the tool reduced manual mapping rates by 30% and overall manual workload by up to 90%. The proposed tool reduced average mapping and new concept creation time by approximately 75%, while decreasing the final mapping table processing time by 90%. New concept authoring errors also decreased, with duplicate concepts reduced by 83% and modeling rule violations by 72%.

Conclusions: This study developed and validated an automated, LLM-assisted SNOMED CT mapping tool that significantly improved efficiency, mapping accuracy, and new concept quality. Limitations include technical integration challenges and dependency on translation quality. Future directions involve leveraging SNOMED CT's ontology structure and knowledge graphs, enhancing sustainability through ongoing maintenance and quality assurance, and further advancing new concept authoring with automated Machine Readable Concept Model rule enforcement and inactivation processes to achieve robust and scalable terminology standardization.

XSL•FO
RenderX

(JMIR Med Inform 2026;14:e82670) doi:10.2196/82670

KEYWORDS

large language model; health information interoperability; systematized nomenclature of medicine; terminology; standardization

Introduction

Background

The secondary use of healthcare data holds tremendous promise for advancing medical research and improving patient outcomes [1,2]. However, several critical barriers—such as data fragmentation, the absence of standardized medical terminologies, and semantic interoperability—continue to impede its effective reuse, particularly across multiple institutions [3]. Data generated in different health care settings are often siloed and recorded using heterogeneous systems and local coding practices, resulting in substantial misinterpretation and incomplete integration [4]. Furthermore, these challenges are compounded by the unstructured nature of much clinical data and stringent privacy and security requirements [5,6].

Achieving semantic interoperability—the ability of systems and organizations to exchange data with unambiguous, shared meaning—is essential to overcoming these challenges and unlocking the true value of multi-institutional clinical research [7,8]. At the core of semantic interoperability is terminology standardization, which enables consistent representation and interpretation of clinical concepts across diverse sources [9]. Without such standardization, variations in medical terminology across institutions can lead to inconsistencies, miscommunications, and errors that ultimately undermine the quality and reliability of biomedical research [10]. This challenge has driven international efforts, such as the World Health Organization Digital Health Interoperability Frameworks and Centers for Disease Control and Prevention National Electronic Disease Surveillance System, to prioritize standardized terminologies and interoperable health data infrastructure on a global scale [11,12].

In line with these global initiatives and the growing demands for healthcare data interoperability, Kakao Healthcare has developed the Healthcare Data Research Suite (HRS)—a platform supporting multi-institutional research via standardized data models, advanced artificial intelligence (AI) tools, and robust data privacy features. Notably, HRS places terminology standardization at its core, reflecting both the operational realities and strategic priorities identified by international guidelines [11,12]. By integrating domain-specific standard terminologies, HRS aims to bridge the gaps between fragmented datasets and promote data sharing for research.

To realize this goal, HRS adopts SNOMED CT (Systematized Nomenclature of Medicine Clinical Terms) as its primary terminology. SNOMED CT is recognized worldwide as one of the most comprehensive clinical terminology systems, encompassing a wide range of domains including disorders and procedures [13,14]. Its hierarchical structure, postcoordination capabilities, and rich attribute relationships support the precise representation of clinical concepts and sophisticated querying across large datasets [15]. Despite these advantages, mapping local clinical terms to SNOMED CT remains a significant bottleneck: the process is labor-intensive, demands expertise, and often results in inconsistent mappings both within and across institutions [16].

Recent studies have explored automated SNOMED CT mapping using various AI approaches. Davidson et al [17], 2025, benchmarked SNOMED CT entity linking models by organizing a challenge using annotated clinical notes. Gehrmann et al [18], 2025, evaluated how variable formulation impacts MedCAT's SNOMED CT mapping performance. Kulyabin et al [19], 2024, developed and tested SNOBERT, a BERT-based entity linking model for clinical notes. While these solutions have made meaningful progress in the field, the requirements of multi-institutional research in our context further necessitated several key capabilities: (1) consistent mapping of diverse local terms, both within and across institutions; (2) management of bilingual language inputs, such as the simultaneous use of Korean and English; (3) incorporation of domain-specific curation rules; and (4) the ability to author new SNOMED CT concepts, to achieve accurate mapping that preserves the detailed meaning of source terms.

To meet these requirements and enable reliable standardization across multi-institutional studies, we have developed a large language model (LLM)–assisted terminology standardization tool that integrates automated SNOMED CT mapping and postcoordination in a unified workflow. This tool is specifically designed to overcome the challenges of mapping local terms from heterogeneous sources, handle multilingual data, and facilitate the flexible authoring of new concepts as required for large-scale clinical research.

Objectives

The objective of this work was to create an LLM-assisted tool that enhances terminology standardization for multi-institutional research by seamlessly integrating automated SNOMED CT mapping and postcoordination within a single solution.

Methods

Requirement Collection

The participants involved in user requirements collection included 10 experienced clinical terminologists and 3 data engineers. Participants were asked to provide feedback on essential features through an open-ended questionnaire.

System Architecture and Implementation

The overall process of automatic mapping is illustrated in Figure 1. The workflow consists of 2 main processes: auto-mapping and new concept authoring. The final mappings are progressively incorporated into the local term-SNOMED CT mapping database and integrated into the custom reference term database, which includes the previous mapping results of local codes.

XSL•FO
RenderX

Figure 1. Overall workflow of the LLM-assisted terminology standardization tool. LLM: large language model; MRCM: Machine Readable Concept Model; SNOMED CT: Systematized Nomenclature of Medicine Clinical Terms.

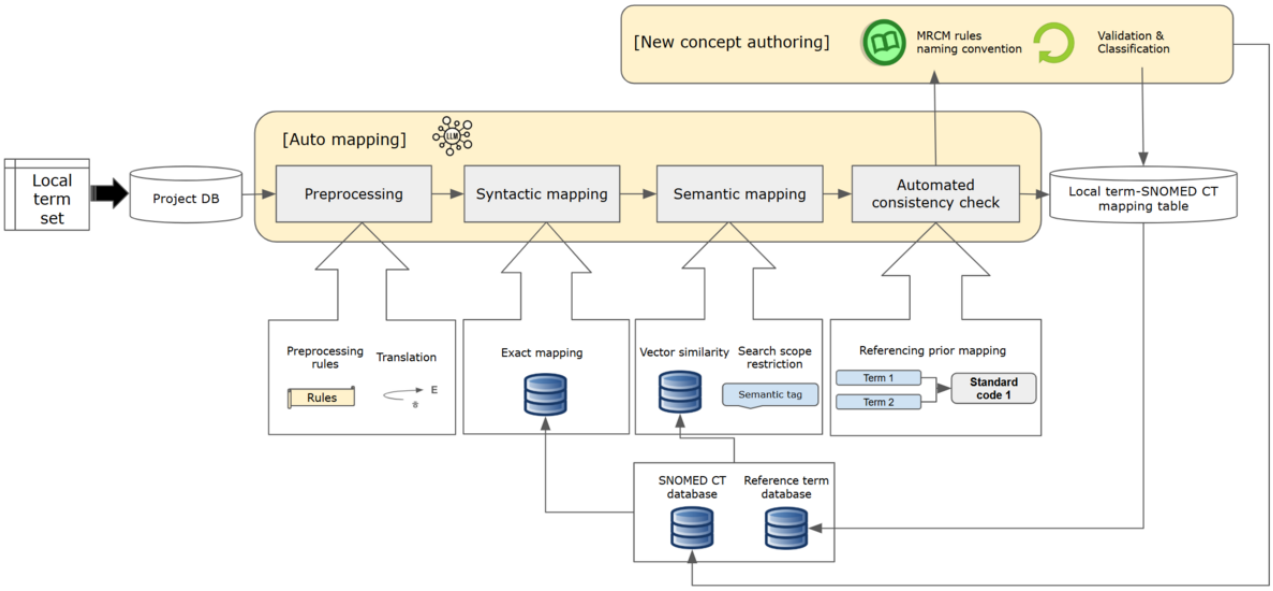

Auto-Mapping Method

Overview

The automated mapping process, as illustrated in Figure 2, begins with receiving a local term set and sequentially integrates four distinct components: (1) data preprocessing, (2) syntactic mapping, (3) semantic mapping, and (4) automated consistency check.

Figure 2. Overview of the LLM-assisted automated SNOMED CT mapping process for multi-institutional standardization. LLM: large language model; SNOMED CT: Systematized Nomenclature of Medicine Clinical Terms.

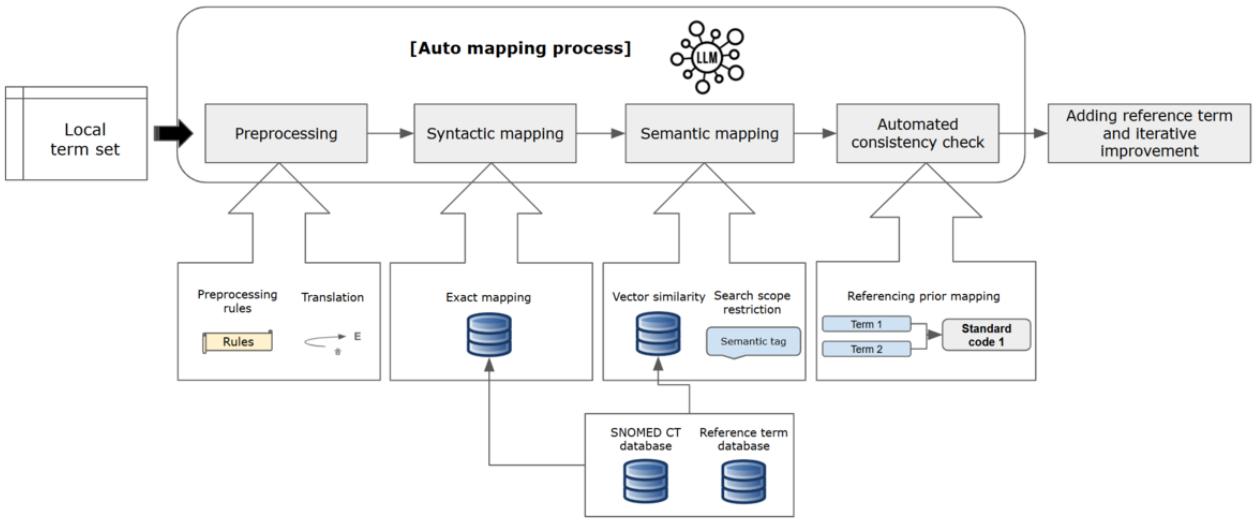

Data Preprocessing

Data preprocessing consists of three main steps: (1) removing unnecessary symbols, (2) expanding abbreviations to full terms, and (3) translating non-English terms such as Korean into English with LLM tools (eg, GPT-4o (OpenAI) or Gemini 2.0 Flash (Google)). In the first step, unnecessary symbols are removed based on professional review. Second, abbreviations are converted to their full forms through manual curation, as context-dependent abbreviations such as “MS” can have multiple meanings (“multiple sclerosis” in neurology or “mitral stenosis” in cardiology); automatic expansion is therefore avoided. Third, any local terms in Korean are translated to English using LLMs. Although GPT-4o was used in this study, the system is designed to flexibly substitute other models (eg, Gemini 2.0 Flash) to accommodate institutional IT or cloud service restrictions.

Furthermore, to maximize long-term accuracy, we implemented a postmapping rule-based refinement mechanism. This system analyzes the automated mapping output and removes nonessential terms or extraneous symbols that do not affect similarity scores. This quality assurance step ensures that these refined terms are immediately incorporated into the custom

XSL•FO
RenderX

reference term database for iterative use, thereby boosting subsequent mapping performance.

To enhance the reproducibility and institutional specificity, the system allows each participating institution to define and apply custom rule-based preprocessing before automated mapping. These user-defined rules are automatically applied within the mapping pipeline, allowing each site to enforce its own normalization standards as needed.

Syntactic Mapping

Following the data preprocessing steps, the syntactic mapping component performs exact mapping by identifying standard codes that are textually identical to the preprocessed local term. To achieve this, the component prioritizes a search that is restricted within the SNOMED CT description table. In addition, the search leverages custom reference terms, which function similarly to the SNOMED CT description and were developed based on previously confirmed mapping results. If a textual identity between the normalized local term and one of the entries in the reference corpus is found, it is recommended to the user as an exact match.

Semantic Mapping

The semantic mapping component is used when the syntactic mapping component fails to find an exact match, using vector similarity search techniques to automatically map local terms to standard codes. This process leverages LLM-based embedding models (such as the text-embedding-3-small model for OpenAI deployments) to encode all reference terms, which include SNOMED CT descriptions and previously mapped local terms. These reference embedding results are stored in the Faiss vector database [20].

To ensure the efficiency and domain relevance of semantic search, the component applies a crucial constraint developed from empirical insights. First, the search is restricted to the SNOMED CT description table and custom reference terms validated through previous mappings. This prioritizes exact and highly relevant matches within established terminology sources. Second, the results are further refined by limiting the search scope to specific semantic tags and datasets relevant to each domain. For instance, the imaging and functional test domain is limited to “Procedure” and “Regime/Therapy” semantic tags; the diagnosis domain exclusively uses “Disorder,” “Finding,” “Situation,” “Event,” and “Person” tags. Additionally, certain cases restricted searches to descendants of specific concepts, allowing for targeted searches within specific datasets. For example, when mapping datasets for culture medium, searches were limited not only to “substance” but specifically to descendants of the concept 421955000 |Culture medium (substance)|, enhancing both speed and accuracy.

Automated Consistency Check

The automated consistency check component serves as the final stage in the automated mapping process. Its primary function is to ensure consistency and adherence to established mapping principles across all mapping candidates generated by the preceding components. This component achieves its goal primarily through referencing a prior mapping rule. This rule is specifically designed to maintain consistency across terms. When duplicate source terms are present, a validated mapping for 1 instance is automatically applied to all others. This rule is applied across different institutions, increasing efficiency and ensuring uniformity, except when the datasets belong to different domains. A successful automated consistency check leads directly to the final system step: adding reference terms and iterative improvement enriching the knowledge base for future mapping runs.

New Concept Authoring Method

Our new concept authoring procedure closely follows the principles and steps outlined in the SNOMED CT Editorial Guide [21]. Subsequently, Figure 3 illustrates the process of the authoring of new concepts through postcoordination. The process consists of four steps: (1) the selection of a focus concept, supported by proximal primitive concept retrieval; (2) concept modeling performed in alignment with Machine Readable Concept Model (MRCM) rules [22], followed by terming; (3) classification and validation; and (4) integration with the mapping table.

Figure 3. New concept authoring process using postcoordination within the LLM-assisted terminology standardization tool. LLM: large language model; MRCM: Machine Readable Concept Model; SNOMED CT: Systematized Nomenclature of Medicine Clinical Terms.

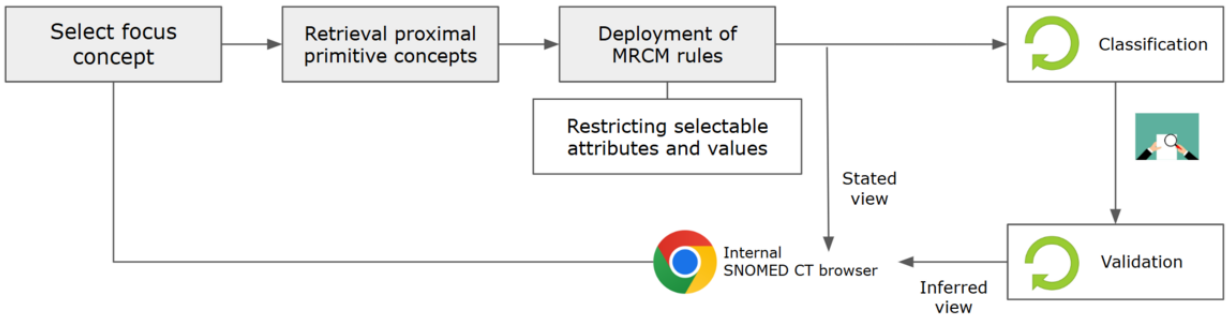

In the current version of our tool, we have operationalized 2 core rules from the editorial guide: the proximal primitive modeling principle and enforcement of MRCM rules. Other elements of the editorial guidance, such as cardinality, concept inactivation workflow, and modeling templates, are not yet implemented and are under consideration for future development.

The first implemented editorial rule is proximal primitive modeling. Adhering to this principle is recommended when

XSL•FO
RenderX

authoring new concepts in SNOMED CT [23]. The principle of proximal primitive modeling is vital for ensuring that classifiers accurately infer the most relevant proximal supertypes, which enhances precise subsumption [24,25]. When a user selects a focus concept required for modeling, not only the concept ID and fully specified name (FSN) of the focus concept, but also the corresponding proximal primitive concept are retrieved via the authoring-form API (Application Programming Interface) provided by Snowstorm [26].

The second implemented rule is the automated enforcement of MRCM rules. The MRCM defines the rules within the SNOMED CT concept model in a computer-readable format, allowing for validation of concept definitions and expressions to ensure compliance [27]. We have integrated these rules into the user interface (UI) by using the Snowstorm API. The tool restricts selectable attributes based on the domain of the focus concept. Using the GET /mrcm/{branch}/domain-attributes API, the focus concept ID is passed as parent IDs to retrieve only attributes relevant to the specific domain.

For naming guidance, our tool supports authors by automatically loading the FSN of the selected focus concept—retrieved via the authoring-form API—as a terming template. This allows users to customize the FSN, ensuring that the created concept precisely reflects the intended meaning, while maintaining overall consistency with SNOMED CT naming conventions.

Classification and validation are crucial steps in authoring new SNOMED CT terms for maintaining the precision and comprehensiveness of SNOMED CT and supporting accurate cohort queries over electronic health records [28]. We used the SNOMED (Systematized Nomenclature of Medicine) Release Validation Framework and the SNOMED OWL (Web Ontology Language) Toolkit in parallel to ensure the quality and consistency of our SNOMED CT editions, generate OWL expressions, and perform classification [29,30].

Once new concepts are authored, they are systematically stored in the mapping table, which is a structured database that includes the source terminology and corresponding target SNOMED CT identifiers [31]. We managed a Kakao Healthcare edition in our database that included all SNOMED International concepts, supplemented with new concepts assigned to a unique namespace identifier of the affiliated institution.

As the SNOMED CT Editorial Guide and modeling rules are subject to periodic updates, we monitor release notes and editorial guide updates on a monthly basis. While we conduct regular follow-up reviews each month, updates are applied to our edition on an annual basis through scheduled manual audits for the new concept authoring to comply with recent editorial changes.

System Implementation

To support the key functionalities of automatic mapping and new concept authoring, the system was implemented as 2 main components: a web application and an automatic mapping server. The web application, developed using Next.js (version 14; Vercel) and TypeScript (version 5; Microsoft), serves as the central platform that integrates various operations such as project management, data submission, mapping review, and concept authoring. React Query (version 5.28.14; TanStack) is used for managing asynchronous data interactions, and Tailwind CSS (version 3.3.0; Tailwind Labs) is used for styling. The application communicates with the backend services and the database to manage workflows and interface with the automatic mapping server. The automatic mapping server, built in Python (version 3.10; Python Software Foundation), performs the core mapping logic, including preprocessing of local terms, translation using LLM, and vector-based similarity search using FAISS (faiss-cpu version 1.9.0.post1; Meta AI Research). The server generates mapping results and stores them in a PostgreSQL (version 14.12; PostgreSQL Global Development Group) database. FastAPI (version 0.110.3; FastAPI framework) is used to serve the backend API.

Performance Evaluation

Method for Evaluating Accuracy

Dataset

The dataset for evaluating performance was collected from 4 hospital networks (a total of 9 university hospitals) in South Korea: Ewha Womans University Medical Center (EUMC) with 2 branches, Korea University Medical Center (KUMC) with 3 branches, DongSan Medical Center (DSMC) with 2 branches, and KyungHee University Medical Center (KHMC) with 2 branches. The selection of diagnostic and surgical procedure terms is strategically made due to their clear and distinct alignment with specific SNOMED CT semantic tags, such as “Disorder” and “Procedure,” which facilitates precise mapping. Furthermore, these codes encompass nearly all medical specialties, ensuring the heterogeneity of local medical practice in South Korea, thereby providing a robust dataset for evaluating the mapping tool’s performance. EUMC contributed 24,554 diagnostic and 8053 surgical procedure codes, KUMC provided 44,646 and 13,734, respectively, DSMC supplied 24,146 and 9432, while KHMC offered 27,842 diagnostic codes and 20,759 surgical procedure codes.

Preprocessing Rules

All performance evaluations were conducted using a common, standardized set of preprocessing rules applied uniformly across all 4 participating hospital networks (EUMC, KUMC, DSMC, and KHMC). The system’s “user-defined rules” functionality, while supported for production deployment, was intentionally not used during the formal testing in this study. This ensured that the comparison of mapping accuracy reflected the system’s performance under standardized, reproducible conditions.

LLM Configuration

All translation and concept generation tasks in this study were performed using GPT-4o (OpenAI, 2024) and its corresponding text-embedding-3-small embedding model for vector-based similarity mapping. The selection of GPT-4o was fixed across all institutions to ensure methodological consistency and reproducibility. All reported accuracy, efficiency, and usability metrics are therefore based exclusively on results generated from the GPT-4o-based pipeline.

XSL•FO
RenderX

Accuracy Assessment Strategy

The performance was measured by comparing its outputs against manually mapped results, which have been established as the gold standard. The manual mapping results were verified for accuracy and reliability through at least 2 rounds of internal review by 5 clinical terminology experts and 1 physician, and were further refined by external review with 2 physicians.

Accuracy was evaluated using both "top-1" and "top-5" approaches. The top-1 accuracy refers to the highest similarity score of a candidate being correct. The top-5 accuracy includes having the correct mapping among the 5 candidates with the highest similarity scores. Furthermore, to better characterize the contribution of the shared knowledge base versus the AI components, we stratified the "accuracy with reference terms" metric. We specifically calculated the "exact match" rate to distinguish successful mappings achieved via syntactic reference identity lookups (memorization from partner hospitals) from those achieved via vector-based semantic similarity search.

Specifically, we used a 2-pronged approach to measure mapping accuracy. First, we assessed the baseline performance at each participating hospital—EUMC, KUMC, DSMC, and KHMC—by using only the descriptions of the SNOMED CT Kakao Healthcare edition. The SNOMED CT Kakao Healthcare edition serves as the core internal database, managing all SNOMED International concepts and supplemented with new concepts assigned a unique namespace identifier of the affiliated institution. Crucially, the baseline analysis intentionally excludes any reference terms (previously confirmed mappings) that were accumulated or validated from the other participating hospital networks.

Second, we enhanced our analysis by adding reference terms from the other participating hospitals into the mapping process. For instance, when assessing EUMC, we introduced reference terms from KUMC, DSMC, and KHMC to gauge any changes in mapping accuracy. This comparative methodology was implemented in stages to allow us to compare the tool's performance before and after the addition of reference terms, as mapping data from other hospitals accumulated. The benefit measured in the subsequent metric, "accuracy with reference terms," therefore represents the isolated effect of integrating this shared, cross-institutional mapping knowledge.

Handling of "Not Mapped" Terms

To ensure comprehensive performance accounting, we clarified the treatment of local terms designated as "not mapped" within the accuracy calculation. These "not mapped" terms were established as part of the gold standard definition by the clinical terminology review committee. Such terms often represent local entries that human experts determined lacked a valid or appropriate SNOMED CT concept (eg, referencing only body structures or materials without a corresponding procedure).

Crucially, the system was not explicitly designed to predict a "not mapped" status. Therefore, when a term is validated by experts as "not mapped" (the gold standard outcome), the system's failure to provide any correct SNOMED CT prediction within the top-1 or top-5 candidates is inherently reflected in the overall accuracy calculation as a system prediction failure or error.

Method for Evaluating Efficiency

As a baseline, all processes were manually executed to assess the time required for each step. Data preprocessing time is the average time required for data cleaning and translation. New concept authoring time refers to the average time it takes for a person to author a new concept in compliance with SNOMED CT's principles. The final processing steps of the mapping table refer to the average time taken per dataset for integrating mapping tables and verifying data integrity. This observation is based on a 6-month operational period of a clinical terminology team consisting of 6 members. During this time, detailed logs and time-tracking data were collected across all stages of the terminology mapping process.

The results from the tool-based workflows were compared with the baseline data to evaluate the improvements: (1) efficiency gains are the reduction in time for each phase of the process, expressed as a percentage improvement over baseline; and (2) resource optimization evaluates the changes in human resource consumption.

Quality Assessment of New Concept Authoring

Quality was evaluated pre- and posttool adoption using 2 metrics derived from the full SNOMED CT authoring dataset as of August 27, 2024. First, the proportion of duplicate concepts was calculated by dividing the number of equivalent errors identified after classification by the total number of authored concepts at each time point. Second, the number of MRCM validation violations was measured by counting rule violations across all authored concepts before and after tool implementation.

System Usability Evaluation by Users

The system usability evaluation was conducted with 5 mappers who had previous experience with mapping methodologies before the tool development. These participants were introduced to the main features of the newly developed tool and were asked to perform approximately 100 sample mappings. After using the tool, they were encouraged to provide feedback in an open-ended format regarding their experience with the tool.

Ethical Considerations

This study was conducted as part of the research project "Development of an LLM-based Named Entity Recognition (NER) tool and a standardization support tool for using multicenter clinical free text." As no human participants or identifiable personal information were involved, institutional review board (IRB) approval was not required for this study itself. However, IRB approval or exemption was obtained from each institution for project administration purposes as follows: Ewha Womans University Medical Center (SEUMC IRB 2025-02-016, approved), DongSan Medical Center (DSMC IRB 2025-01-006, approved), Korea University Medical Center Anam (KUMC IRB 2025AN0239, approved), Guro (KUMC IRB 2025GR0222, approved), Ansan (KUMC IRB 2025AS0122, approved), and KyungHee University Medical Center (KHUH IRB 2025-01-047, exempted). This study was

XSL•FO
RenderX

conducted in compliance with institutional policies, the Korean Bioethics and Safety Act [32], and the Declaration of Helsinki [33]. Informed consent was not required due to the nature of the study.

Results

System Development and Deployment

System Development Requirements

Based on the users' survey, we found the following 11 key requirements as shown in Table 1. The UI of the auto-mapping enables users to map terms with a single click in a familiar table-based layout. Figure 4 displays the primary UI for the automated SNOMED CT mapping function. The interface is organized in a familiar table-based layout to facilitate the review and review of local diagnostic and surgical procedure terms. To maximize efficiency and minimize manual errors, the UI provides single-click mapping and automatic retrieval of FSNs immediately upon entering a standard concept ID. Furthermore, the interface supports essential collaborative functions for large-scale projects, including comprehensive filtering options and dedicated fields for review tracking and quality assurance by terminology experts.

Table 1. Key requirements for the LLM[a]-assisted automated SNOMED CT[b] mapping and new concept authoring tool, defined by clinical terminologists and data engineers for multi-institutional research environments.

Category	Key requirements
Project and dataset version management	• The ability to create projects and manage their versions for terminology datasets by institution and domain. • Support for uploading source files and downloading mapping table result files in the computable format (CSV and JSON)
Automated mapping and terminology support	• Automated mapping to eliminate the need for manual browser searches for each local term. • Translation functionalities to support multilingual datasets. • Management tools for mapping tables, including cross-checking mapping results.
New concept authoring and integration	• Functionality to author new concepts during the mapping process. • A user interface applying MRCM[c] rules during authoring. • Application of the classification of newly authored concepts. • Immediate incorporation of newly authored concepts into the browser. • Automatic integration of newly authored concepts into the mapping tables.
Review and quality assurance	• Features for human review of newly authored concepts for naming inconsistencies and semantic modeling errors.

[a]LLM: large language model.

[b]SNOMED CT: Systematized Nomenclature of Medicine Clinical Terms.

[c]MRCM: Machine Readable Concept Model.

Figure 4. User interface of the automated mapping page within the LLM-assisted terminology standardization tool. KHC: Kakao Healthcare; LLM: large language model.

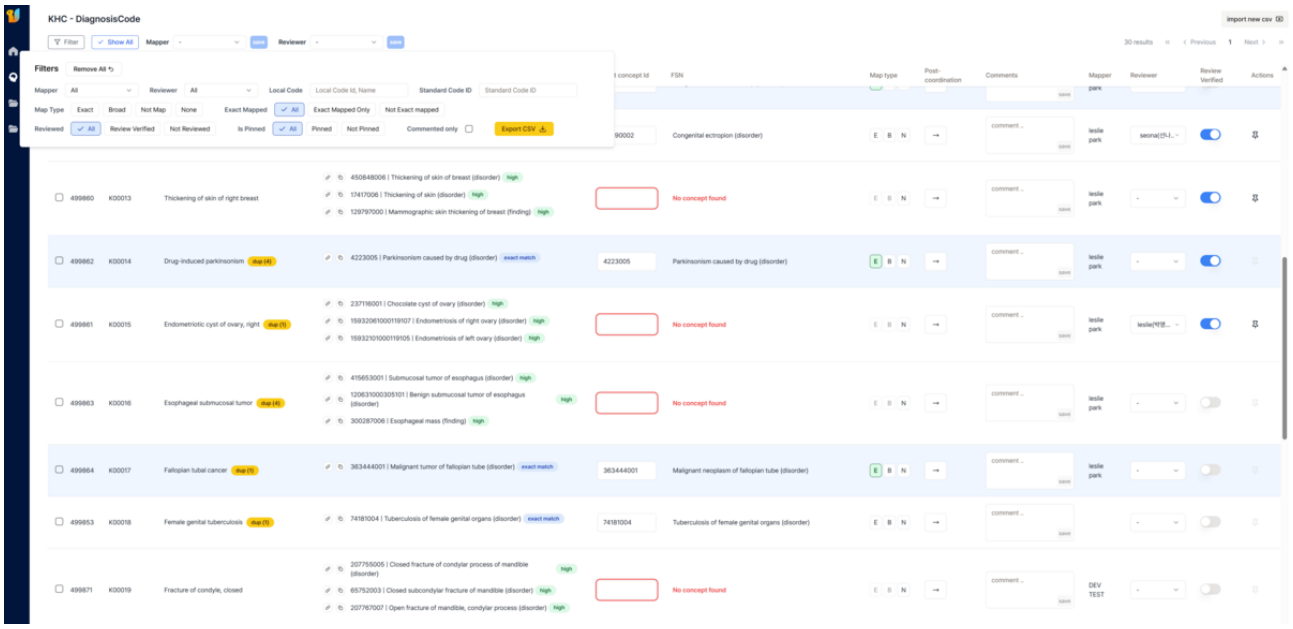

XSL•FO
RenderX

The new concept authoring tool, as shown in Figure 5, makes it easier to author new concepts with an intuitive visual editor that supports real-time updates. In illustrating Figure 5, the concept "254644003 |Hamartoma of lung (disorder)|" is used as the focus concept. Its modeling was cloned and then customized for the illustration, as duplicating the modeling of the focus concept is often an efficient and practical method when modeling new concepts. Then, the proximal primitive concept of selected focus concept, "64572001 |Disease (disorder)|," is automatically retrieved. Users can perform authoring within the UI through refinement or qualification methods.

Figure 5. User interface of the new concept authoring page within the LLM-assisted terminology standardization tool. FSN: fully specified name; LLM: large language model; PT: preferred term.

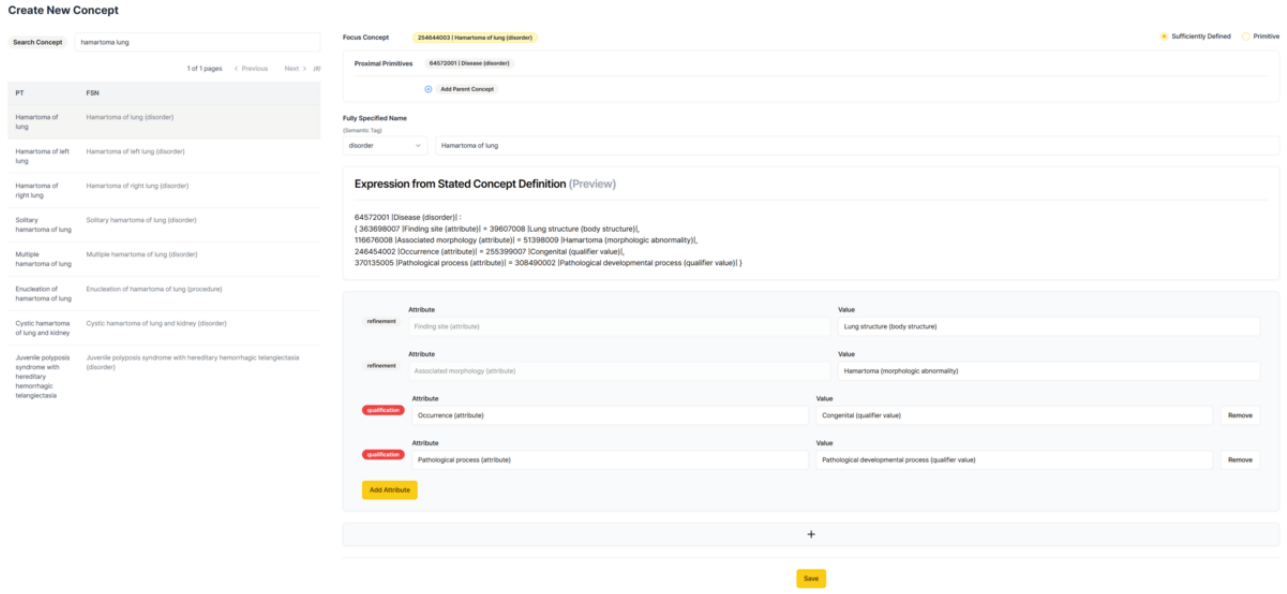

System Deployment

The system is actively deployed for terminology standardization at the Research Alliance participating hospitals, which is organized by Kakao Healthcare. To date, it has processed terminology from a total of 6 hospital networks, encompassing 12 university hospitals and 189,455 terms. The developed tool has been actively used to standardize terms across various domains, including diagnoses, surgical procedures, chief complaints, and laboratory tests.

System Evaluation

Result of Performance Evaluation

Table 2 displays the successful mappings achieved through syntactic matching (exact match lookups) using the custom reference database (baseline) vs those achieved after the iterative enrichment via shared reference terms (accuracy with reference terms) across 4 major hospital networks. The reported percentage represents the proportion of local terms that were successfully mapped by exact identity lookup. The analysis revealed that the inclusion of shared reference terms universally increased the proportion of terms resolved via exact match, reducing the reliance on vector-based search. However, the magnitude of this increase varied significantly across hospital networks.

XSL•FO
RenderX

Table 2. Syntactic mapping performance: exact match accuracy for diagnosis and surgical procedure domains.

Hospital networks, domain	Metric	Baseline accuracy (%)	Accuracy with reference terms (%)	Δ accuracy (%)
EUMC[a]				
Diagnosis	Exact match	36.3	94.5	58.2
Surgical procedure	Exact match	18.5	97.6	79.1
KUMC[b]				
Diagnosis	Exact match	23.4	36.6	13.2
Surgical procedure	Exact match	17.7	29.8	12.1
DSMC[c]				
Diagnosis	Exact match	34.9	94.9	60
Surgical procedure	Exact match	19.8	96.9	77.1
KHMC[d]				
Diagnosis	Exact match	21.9	55.2	33.3
Surgical procedure	Exact match	12.8	28.3	15.5

[a]EUMC: Ewha Womans University Medical Center.

[b]KUMC: Korea University Medical Center.

[c]DSMC: DongSan Medical Center.

[d]KHMC: KyungHee University Medical Center.

Notably, EUMC and DSMC exhibited a dramatic surge in exact match rates. For the diagnosis domain, exact match accuracy increased from 36.3% to 94.5% for EUMC and from 34.9% to 94.9% for DSMC. A similar trend was observed in the surgical procedure domain, where exact match rates reached 97.6% and 96.9%, respectively. In contrast, KUMC and KHMC showed more moderate increases. For the diagnosis domain, KUMC's exact match rate improved from 23.4% to 36.6%, and KHMC's improved from 21.9% to 55.2%. In the surgical domain, the exact match rates remained below 30% for both institutions (29.8% for KUMC and 28.3% for KHMC), though this still represented a gain of over 10% for each.

Table 3 summarizes the comparative performance evaluation of mapping accuracy for diagnostic and surgical procedure domains across 4 hospital networks. For each hospital and domain, mapping performance was measured as top-1 and top-5 accuracy, both at baseline (before incorporating reference terms) and after the inclusion of reference terms. To ensure statistical rigor, 95% CIs were calculated for all accuracy estimates. The absolute improvement in accuracy (Δ accuracy) was also calculated to quantify the benefit of leveraging shared reference mappings.

XSL•FO
RenderX

Table 3. Comparative performance evaluation of automated SNOMED CTa[a] mapping accuracy for diagnostic and surgical procedure domains across 4 South Korean multi-institutional networks. All improvements were statistically significant (McNemar test, $P<.01$ for all cases). 95% CIs were calculated using the Wald method.

Hospital network, domain, not mapped rate (%), metric	Baseline accuracy (%)	Accuracy with reference terms (95% CI)	Δ accuracy[b] (%)
EUMC[c]			
Diagnosis			
0			
Top-1	73.4	97.4 (97.2–97.6)	24.0
Top-5	88.9	98.7 (98.6–98.8)	9.8
Surgical procedure			
0			
Top-1	64.9	98.5 (98.2–98.8)	33.6
Top-5	84.7	99.2 (99.0–99.4)	14.5
KUMC [d]			
Diagnosis			
0.4			
Top-1	69.3	73.2 (72.8–73.6)	3.9
Top-5	87.0	89.7 (89.4–90.0)	2.7
Surgical procedure			
1.7			
Top-1	61.6	66.1 (65.3–66.9)	4.5
Top-5	79.0	82.6 (82.3–82.9)	3.6
DSMC [e]			
Diagnosis			
0			
Top-1	72.7	97.2 (97.0–97.4)	24.5
Top-5	88.2	98.5 (98.3–98.7)	10.3
Surgical procedure			
0			
Top-1	66.6	97.9 (97.6–98.2)	31.3
Top-5	85.2	98.7 (98.5–98.9)	13.5
KHMC [f]			
Diagnosis			
0			
Top-1	67.9	81.4 (80.9–81.9)	13.5
Top-5	85.5	92.8 (92.5–93.1)	7.3
Surgical procedure			
0			
Top-1	59.7	65.1 (64.5–65.7)	5.4
Top-5	81.1	84.7 (84.2–85.2)	3.6

[a]SNOMED CT: Systematized Nomenclature of Medicine Clinical Terms.

[b]Δ accuracy: accuracy with reference terms−baseline accuracy.

[c]EUMC: Ewha Womans University Medical Center.

[d]KUMC: Korea University Medical Center.

XSL•FO
RenderX

[e]DSMC: DongSan Medical Center.

[f]KHMC: KyungHee University Medical Center.

At baseline, top-5 accuracy for diagnosis was similar across hospitals, ranging from 85.5% to 88.9%. In contrast, surgical procedures showed greater variation, with baseline top-5 accuracy from 79% to 85.2%. After reference terms were incorporated, top-5 accuracy for diagnosis increased to between 89.7% and 98.7%, and for surgical procedures it rose to between 82.6% and 99.2%. EUMC and DSMC showed the highest postreference top-5 accuracy in both domains and achieved the largest absolute improvement in surgical procedures (up to 14.5% at EUMC and 13.5% at DSMC).

For top-1 accuracy, the improvement after reference terms addition was even more pronounced, especially in surgical procedures, with EUMC reaching a 33.6% increase. Top-5 accuracy remained consistently higher than top-1 in all hospitals and domains, but the relative improvement with reference terms was greater for top-1 than for top-5. All gains in accuracy were statistically significant (McNemar test, $P<.01$). In a supplementary evaluation, the exclusion of the syntactic mapping (exact match) step resulted in negligible variations in top-5 accuracy, suggesting that the vector-based semantic search effectively identifies these identical terms.

To provide context for performance ceilings, we analyzed the prevalence of unmappable terms. The gold standard dataset included terms categorized as "not mapped," representing local codes for which experts determined no valid SNOMED CT concept existed. These instances were treated as errors in the accuracy calculation. The prevalence of "not mapped" terms varied by institution and domain: EUMC (diagnosis: n=0, 0%; surgical procedure: n=0, 0%), KUMC (diagnosis: n=174, 0.4%; surgical procedure: n=219, 1.7%), DSMC (diagnosis: n=1, 0%; surgical procedure: n=0, 0%), and KHMC (diagnosis: n=0, 0%; surgical procedure: n=0, 0%).

Result of Efficiency Evaluation

Figure 6 clearly demonstrates the efficiency evaluation based on a 6-month operational period, showing significant reductions in manual workload across 4 key stages of the SNOMED CT mapping process. The manual mapping rate decreased from 100% to 70%, indicating a 30% reduction and highlighting the tool's effectiveness in enabling automated mapping. More broadly, the overall manual workload was significantly reduced, with marked enhancements in efficiency throughout the entire mapping process. Specifically, the average mapping time per item decreased from 10 to 2.4 minutes, representing a 76% reduction. The time required to create a new concept similarly dropped from 12 to 3 minutes (75% reduction), while the time needed to resolve errors during the review stage was reduced from 8 to 2 minutes (75% reduction). Most notably, the final processing time of the mapping table per dataset decreased from 30 to 3 minutes, achieving a 90% reduction.

Figure 6. Efficiency evaluation of the SNOMED CT mapping workflow, comparing manual baseline time to performance after adopting the LLM-assisted automated tool across 4 key stages: mapping, new concept authoring, error resolution, and final processing of the mapping table. LLM: large language model; SNOMED CT: Systematized Nomenclature of Medicine Clinical Terms.

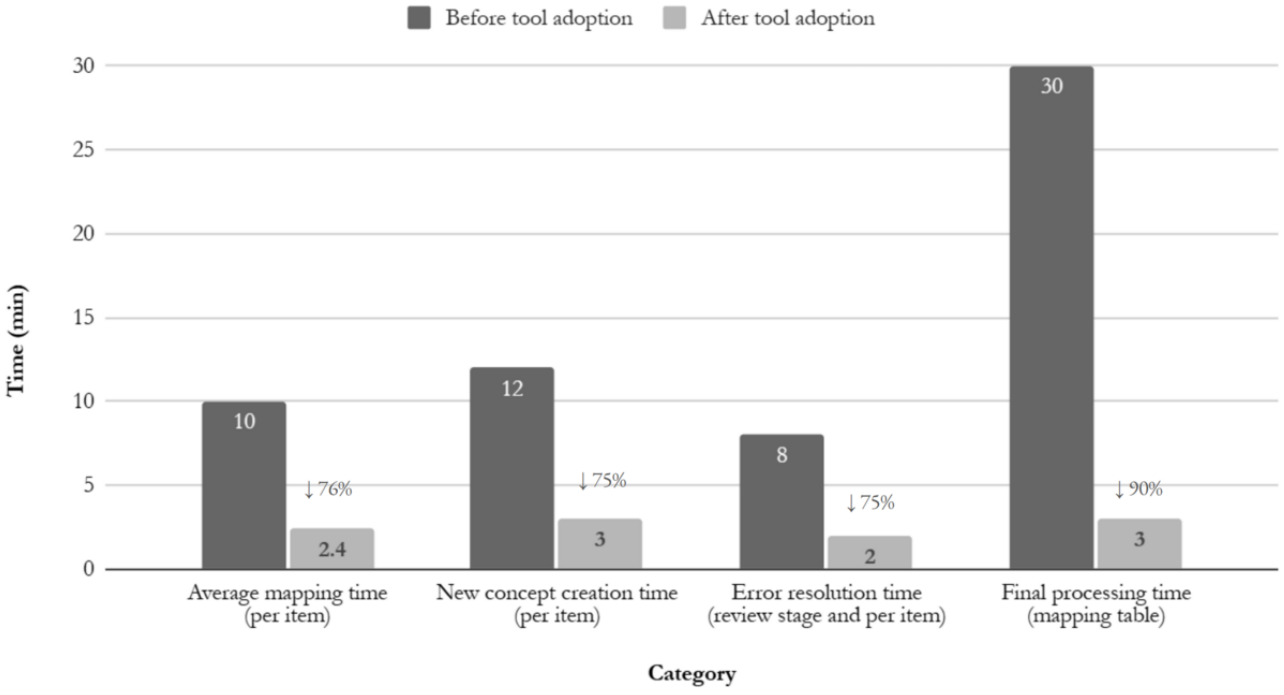

Results of New Concept Authoring Quality Evaluation

After implementation of the tool, both classification and MRCM validation errors decreased substantially, even as the total number of authored concepts increased. The proportion of duplicate concepts dropped from 0.8% (122/15,637) with manual authoring to 0.1% (46/34,401) with the tool, representing an 83% reduction. Likewise, MRCM validation violations

XSL•FO
RenderX

decreased by 72%, from 264 in the manual process to 75 with the tool-assisted workflow.

Result of System Usability Evaluation

Users highlighted several benefits of the system. First, the tool reduced effort during the mapping process by automatically suggesting candidate target concepts, which minimized the number of manual typing and clicking steps required. Second, users noted a significant decrease in errors, as the system eliminated mistakes that previously occurred when characters were deleted or data types were changed during manual copying and pasting of IDs or FSNs. The tool now conveniently enters the FSN when a valid ID is provided, further improving accuracy. Finally, the new system offered enhanced usability compared to the previous spreadsheet-based screens, which users found visually straining and inflexible. With the new interface, users reported a more comfortable and convenient experience.

Discussion

Principal Findings

This study developed an LLM-assisted SNOMED CT automatic mapping tool and evaluated it across multiple real-world hospital settings. Notably, the tool supports postcoordination, which minimizes semantic loss from source terms and leverages the strengths of SNOMED CT. In evaluation, the tool demonstrated high top-5 accuracy rates—92.6% for diagnostic concepts and 93.6% for surgical procedures. Incorporating reference mappings further increased accuracy by over 6% in both areas. Workflow efficiency was markedly enhanced, with mapping and concept authoring times reduced by approximately 75% and the proportion of cases requiring manual mapping dropping from 100% to 70%. Importantly, the tool reduced human modeling errors in new concept authoring, as evidenced by an 83% decrease in duplicate concept rate and a 72% reduction in MRCM validation violations. Error resolution and final processing of the mapping table were also significantly streamlined.

When evaluating site-specific performance, we found substantial variation across different hospital networks, especially after integrating the shared reference knowledge base. Performance in networks such as EUMC and DSMC was exceptionally high, with exact match rates exceeding 94% in diagnosis and 96% in surgical domains—likely reflecting the use of shared electronic medical record systems, which allowed most mappings to be resolved through simple identity lookups.

To analyze the actual contribution of the exact match step, we performed an internal assessment comparing mapping accuracy with and without the preliminary exact match stage. This assessment revealed that the difference in top-5 accuracy between the 2 configurations was negligible. Thus, the primary value of the exact match component lies not in enhancing end-to-end mapping quality but in workflow optimization: by quickly resolving about 30% of cases, it helps bypass computationally and financially intensive processes, contributing to pipeline efficiency and sustainability.

The accumulation and reuse of reference mappings across institutions is also central to our approach and reflects both the realities and strengths of terminology standardization initiatives in Korea; as more hospitals join and contribute to the shared repository, we anticipate continued improvements in mapping consistency and efficiency across various settings.

By contrast, KUMC and KHMC exhibited more modest improvements, as a substantial portion of their mappings could not be resolved through exact identity lookup alone. For these institutions, the shared knowledge base contributed to performance gains but was insufficient on its own; thus, many mappings still required the use of vector-based semantic similarity search. This highlights the ongoing need for advanced AI components when handling diverse or nonstandardized local terminologies that may not be well represented within a shared repository.

Further analysis of auto-mapping errors revealed 3 main sources of reduced accuracy: (1) the presence of local terms that reference only body structures or materials without an associated procedure—instances best categorized as “not mapped”; (2) terms requiring new concept creation via postcoordination—particularly in the surgical procedure domain, where postcoordination was frequently necessary; and (3) unresolved or ambiguous abbreviations. Understanding these error patterns provides important directions for future refinement of the system.

Comparison With Prior Work

A consistent set of challenges emerges across this and prior work, including the persistent difficulty of mapping rare or institution-specific terms, handling ambiguous abbreviations, and resolving semantically unclear expressions [17-19]. Beyond algorithmic advancements, real-world clinical deployment presents unique integration hurdles, such as harmonizing diverse IT infrastructures, maintaining synchronization between terminology servers and electronic medical record systems, and managing evolving local terminologies [18]. Importantly, our study reaffirms that, regardless of automation level, human review remains indispensable—not only for establishing and maintaining gold standard mappings that underpin system performance, but also for defining and updating mapping rules to reflect evolving clinical realities [17,18].

Limitations

First, we encountered various technical difficulties during implementation. The internal PostgreSQL database and the ElasticSearch (Elasticsearch B.V.) engine supporting SNOMED CT search (via SNOMED Snowstorm API and Browser) required frequent manual synchronization due to architectural differences. This was especially challenging since ElasticSearch lacks built-in transactional support. Accordingly, script-based data reconciliation was required to maintain consistency, but it remains to be fully automated.

Second, a significant limitation of our methodology involves the Korean-to-English translation step required for processing bilingual input data. As the accuracy of the subsequent vector similarity mapping is entirely dependent on the quality of the translated term, we acknowledge that the lack of gold-standard

XSL•FO
RenderX

comparisons or error analysis for this step is a methodological limitation.

Third, translation was handled as a fully automated preprocessing step to minimize human intervention and maximize efficiency within the mapping pipeline. To control quality when using models such as GPT-4o or Gemini 2.0 Flash, we used carefully designed, domain-specific prompts (Multimedia Appendix 1). These prompts enforced specific constraints: they defined clinical context (eg, diagnosis type), removed noise, and ensured that terms were translated strictly into the official medical vocabulary. However, the accuracy of subsequent mapping is entirely dependent on translation quality. Despite these controlled prompts, we currently lack external gold-standard metrics or formal error analysis for this critical phase.

We note that the volume of local terms requiring Korean translation was low, at approximately 1.5% of the total mapped terms. While this proportion is small, we acknowledge that translation inaccuracies in even a limited subset of terms could introduce minor bias into the overall mapping accuracy. Accordingly, we recognize the necessity of integrating translation-specific metrics into the overall evaluation framework.

Finally, while the gold standard for mapping underwent extensive review by experienced terminology experts both internally and externally, we did not collect or report an objective measure of interrater agreement, such as Cohen κ. Although this expert involvement likely improved reliability, the absence of a quantitative assessment remains a limitation and should be considered when interpreting our results.

Future Directions

Although retrieval-augmented generation was explored in our preliminary model, we observed limitations where the current general-purpose LLM failed to accurately leverage the inherent ontological structure of SNOMED CT, often yielding results identical to simple vector similarity search [34]. Therefore, further improvement is expected by using LLMs that are specifically designed to leverage both contextual information and the intrinsic structure of SNOMED CT in future research. Further, the use of SNOMED CT's ontology structure and knowledge graphs (eg, GraphRAG) is expected to enhance semantic retrieval and disambiguation capabilities, increasing accuracy and robustness across broader domains [35]. To improve authoring of new concepts, automation features applying detailed MRCM cardinality rules and an advanced inactivation process will be developed, reducing modeling errors and ensuring SNOMED CT compliance.

From a sustainability perspective, widespread adoption will require continued resource investment for tool maintenance and updates, as well as collaboration across clinicians, informaticians, terminology experts, and policymakers. Keeping standard codes current, ensuring ongoing quality assurance, and adapting to multilingual and ICD-11 (International Classification of Diseases, 11th Revision) or International Classification of Health Interventions-integrated environments—particularly for mapping complex surgical procedures—are essential for scalable and future-proof deployment. Despite concerns about the potential for increased operational costs when deploying commercial LLMs, our experimental results indicate that these expenses were negligible relative to the benefits achieved. For example, embedding 1.6 million tokens costs just US $0.03, and translating 1779 cases incurred only minimal costs based on standard token pricing. These findings highlight the economic viability and sustainability of incorporating LLM components into automated pipelines.

Our long-term vision is to deliver this solution as a cloud-based software-as-a-service platform, supporting agile terminology standardization across diverse medical institutions both domestically and worldwide. For effective adoption in new environments, local verification and adaptation may be necessary to address differences in data standards and clinical practices. Notably, the system's methodological approach aligns with the World Health Organization's and Centers for Disease Control and Prevention's international guidelines, supporting its potential generalizability across health systems worldwide [11,12].

Conclusions

We developed and validated the first large-scale, multi-institutional automatic terminology mapping tool supporting both pre- and postcoordinated SNOMED CT concepts. The tool substantially reduces manual workload, improves mapping accuracy, and enhances interoperability for clinical data across the evaluated sites. While our current evaluation was limited to internal implementation, further work will focus on advancing commercialization and expanding deployment. We anticipate that, with continued refinement and local verification, this tool could support terminology standardization and interoperability for broader national and international healthcare data integration in the future.

Acknowledgments

The authors would like to acknowledge the valuable contributions of the Ewha Womans University Medical Center, Kyung Hee University Medical Center, Korea University Medical Center, and Keimyung University DongSan Medical Center, particularly the IT departments at each hospital, for their cooperation. Our deepest gratitude goes to the Clinical Terminology Team and the Standards Technology Team at Kakao Healthcare for their outstanding support and technical expertise throughout the development of this study. We also used the generative artificial intelligence (AI) tool ChatGPT (GPT-4o, OpenAI; used in 2025) solely to assist with English language editing and grammar. The AI was not used to generate scientific content, analyze data, or create figures, tables, or references. All AI-assisted text was reviewed, verified, and edited by the authors, who take full responsibility for the content.

XSL•FO
RenderX

Data Availability

The datasets generated and analyzed during this study are not publicly available due to the hospital policies.

Funding

This work was supported by the Industrial Strategic Technology Development Program-Digital Healthcare (RS-2024-00467897, for the development of an LLM-based Named Entity Recognition [NER] tool and a standardization support tool for using multicenter clinical free text) funded by the Ministry of Trade, Industry and Energy (MOTIE, Korea). The funder was involved in this study's design and data collection, but had no role in the analysis, interpretation, or writing of this paper.

Authors' Contributions

Conceptualization: YP (equal), SB (equal)
Formal analysis: SB (lead)
Investigation: YP (lead), SB (lead), HK (supporting)
Methodology: YP (equal), SB (equal), HK (equal)
Project administration: S-YS (lead)
Resources: DC (equal), SYR (equal), HSP (equal), K-JL (equal)
Supervision: S-YS (lead)
Visualization: HK (lead)
Writing – original draft: YP (equal), SB (equal), HK (equal), JK (equal)
Writing – review & editing YP (lead), SB (lead), HK (supporting), JK (supporting), S-YS (supporting)
SB and JK developed the software.

Conflicts of Interest

Several authors (YP, SB, HK, JK, and S-YS) are employees of Kakao Healthcare Corp. The technology described in this paper is the subject of 2 pending Korean patent applications assigned to Kakao Healthcare Corp: (1) "Apparatus and Method for Mapping Local Term of Medical Institution Terms to Medical Standard Terms" (Korean patent application number 10-2024-0085332; filed June 28, 2024), and (2) "Apparatus and Method for Generating Medical Standard Terms" (Korean patent application number 10-2024-0085330; filed June 28, 2024). Some of the authors are named inventors on these applications and may be entitled to royalties or other financial benefits if the patents are granted.

Multimedia Appendix 1
GPT-4o translation prompt.
[PDF File (Adobe PDF File), 109 KB - medinform_v14i1e82670_app1.pdf]

References

1. Cascini F, Pantovic A, Al-Ajlouni YA, Puleo V, De Maio L, Ricciardi W. Health data sharing attitudes towards primary and secondary use of data: a systematic review. eClinicalMedicine 2024;71:102551 [FREE Full text] [doi: 10.1016/j.eclinm.2024.102551] [Medline: 38533128]
2. Premanandan S, Ahmad A, Jaranka A, Üreten E, Lee E, Gross J, Cajander, et al. Opportunities and challenges for designing in connected health: insights from an expert workshop. J Med Internet Res 2025;27:e72446 [FREE Full text] [doi: 10.2196/72446] [Medline: 41172290]
3. Dinov ID. Volume and value of big healthcare data. J Med Stat Inform 2016;4:3 [FREE Full text] [doi: 10.7243/2053-7662-4-3] [Medline: 26998309]
4. Ambalavanan R, Snead RS, Marczika J, Towett G, Malioukis A, Mbogori-Kairichi M. Challenges and strategies in building a foundational digital health data integration ecosystem: a systematic review and thematic synthesis. Front Health Serv 2025;5:1600689 [FREE Full text] [doi: 10.3389/frhs.2025.1600689] [Medline: 40621432]
5. Torab-Miandoab A, Samad-Soltani T, Jodati A, Akbarzadeh F, Rezaei-Hachesu P. A unified component-based data-driven framework to support interoperability in the healthcare systems. Heliyon 2024;10(15):e35036 [FREE Full text] [doi: 10.1016/j.heliyon.2024.e35036] [Medline: 39161828]
6. Prakash R, Dupre M, Østbye T, Xu H. Extracting critical information from unstructured clinicians' notes data to identify dementia severity using a rule-based approach: feasibility study. JMIR Aging 2024;7:e57926 [FREE Full text] [doi: 10.2196/57926] [Medline: 39316421]
7. Park HA, Hardiker N. Clinical terminologies: a solution for semantic interoperability. J Korean Soc Med Inform 2009;15(1):1. [doi: 10.4258/jksmi.2009.15.1.1]
8. Park HA, Kim HY, Min YH. Use of clinical terminology for semantic interoperability of electronic health records. J Korean Med Assoc 2012;55(8):720-728. [doi: 10.5124/jkma.2012.55.8.720]
9. Interoperability in healthcare. HIMSS. URL: https://nationalcapitalarea.himss.org/resources/interoperability-healthcare [accessed 2026-02-20]

XSL•FO
RenderX

10. Fennelly O, Grogan L, Reed A, Hardiker NR. Use of standardized terminologies in clinical practice: a scoping review. Int J Med Inform 2021;149:104431 [FREE Full text] [doi: 10.1016/j.ijmedinf.2021.104431] [Medline: 33713915]
11. Global Strategy on Digital Health 2020-2025. World Health Organization. URL: https://www.who.int/publications/i/item/9789240020924 [accessed 2026-02-13]
12. National Notifiable Diseases Surveillance System (NNDSS): Integrated surveillance information systems/NEDSS. CDC. URL: https://www.cdc.gov/nndss/what-is-case-surveillance/nedss.html [accessed 2026-02-13]
13. Park HA, Yu SJ, Jung H. Strategies for adopting and implementing SNOMED CT in Korea. Healthcare Inf Res 2021;27(1):3-10 [FREE Full text] [doi: 10.4258/hir.2021.27.1.3] [Medline: 33611871]
14. Donnelly K. SNOMED-CT: the advanced terminology and coding system for eHealth. Stud Health Technol Inform 2006;121:279-290. [Medline: 17095826]
15. Chang E, Mostafa J. The use of SNOMED CT, 2013-2020: a literature review. J Am Med Inform Assoc 2021;28(9):2017-2026 [FREE Full text] [doi: 10.1093/jamia/ocab084] [Medline: 34151978]
16. Isaradech N, Khumrin P. Auto-mapping clinical documents to ICD-10 using SNOMED-CT. AMIA Jt Summits Transl Sci Proc 2021;2021:296-304 [FREE Full text] [Medline: 34457144]
17. Davidson R, Hardman W, Amit G, Bilu Y, Della Mea V, Galaida A, et al. SNOMED CT entity linking challenge. J Am Med Inform Assoc Oxford University Press 2025;32(9):1397-1406. [doi: 10.1093/jamia/ocaf104] [Medline: 40657868]
18. Gehrmann J, Dogan A, Hagelschuer L, Quakulinski L, Koy A, Beyan O. Catnip for MedCAT: optimizing the input for automated SNOMED CT mapping of clinical variables. Stud Health Technol Inform 2025;331:142-152. [doi: 10.3233/SHTI251390] [Medline: 40899536]
19. Kulyabin M, Sokolov G, Galaida A, Maier A, Arias-Vergara T. SNOBERT: a benchmark for clinical notes entity linking in the SNOMED CT clinical terminology. Springer 2024:154-163. [doi: 10.1007/978-3-031-78119-3_11]
20. Douze M, Guzhva A, Deng C, Johnson J, Szilvasy G, Mazaré PE, et al. The Faiss library. arXiv. Preprint posted online on Oct 23, 2025 2025 Oct 23. [doi: 10.48550/arXiv.2401.08281]
21. SNOMED CT Editorial Guide. SNOMED International. URL: https://docs.snomed.org/snomed-ct-specifications/snomed-ct-editorial-guide [accessed 2026-02-13]
22. SNOMED CT machine readable concept model. SNOMED International. URL: https://docs.snomed.org/snomed-ct-specifications/snomed-ct-machine-readable-concept-model [accessed 2026-02-13]
23. Proximal primitive parent. SNOMED International. URL: https://docs.snomed.org/snomed-international-documents/snomed-ct-glossary/p/proximal-primitive-parent [accessed 2026-02-13]
24. Cimino JJ. Desiderata for controlled medical vocabularies in the twenty-first century. Methods Inf Med 1998;37(4-5):394-403 [FREE Full text] [Medline: 9865037]
25. Proximal primitive modeling. SNOMED CT Editorial Guide. URL: https://docs.snomed.org/snomed-ct-specifications/snomed-ct-editorial-guide/readme/authoring/general-modeling/proximal-primitive-modeling [accessed 2026-02-20]
26. IHTSDO/snowstorm. GitHub. URL: https://github.com/IHTSDO/snowstorm [accessed 2026-02-13]
27. Machine readable concept model (MRCM). SNOMED International. URL: https://docs.snomed.org/snomed-ct-user-guides/authoring-user-guide/faqs/machine-readable-concept-model-mrcm [accessed 2026-02-13]
28. Hao X, Li X, Huang Y, Shi J, Abeysinghe R, Tao C, et al. Quantitatively assessing the impact of the quality of SNOMED CT subtype hierarchy on cohort queries. J Am Med Inform Assoc 2025;32(1):89-96. [doi: 10.1093/jamia/ocae272] [Medline: 39520711]
29. IHTSDO/release-validation-framework. GitHub. URL: https://github.com/IHTSDO/release-validation-framework [accessed 2026-02-13]
30. IHTSDO/snomed-owl-toolkit. GitHub. URL: https://github.com/IHTSDO/snomed-owl-toolkit [accessed 2026-02-13]
31. HINS healthcare information standard. URL: https://www.hins.or.kr [accessed 2026-02-13]
32. Korean Law Information Center. URL: https://www.law.go.kr/LSW/eng/engLsSc.do?menuId=2&query=bioethics#liBgcolor0 [accessed 2026-02-27]
33. WMA Declaration of Helsinki – Ethical Principles for Medical Research Involving Human Participants. URL: https://www.wma.net/policies-post/wma-declaration-of-helsinki/ [accessed 2026-02-27]
34. Bratanič T. The limitations of text embeddings in RAG applications. neo4j. 2024. URL: https://neo4j.com/blog/developer/rag-text-embeddings-limitations/ [accessed 2026-02-20]
35. Choudhary S, Luthra T, Mittal A, Singh R. A survey of knowledge graph embedding and their applications. arXiv. Preprint posted online on Jul 16, 2021 2021 Jul 16. [doi: 10.48550/ARXIV.2107.07842]

Abbreviations

AI: artificial intelligence
API: application programming interface
DSMC: DongSan Medical Center
EUMC: Ewha Womans University Medical Center
FSN: fully specified name

XSL•FO
RenderX

HRS: Healthcare Data Research Suite
ICD-11: International Classification of Diseases, 11th Revision
IRB: institutional review board
KHMC: KyungHee University Medical Center
KUMC: Korea University Medical Center
LLM: large language model
MRCM: Machine Readable Concept Model
OWL: Web Ontology Language
SNOMED: Systematized Nomenclature of Medicine
SNOMED CT: Systematized Nomenclature of Medicine Clinical Terms
UI: user interface

Edited by A Coristine; submitted 20.Aug.2025; peer-reviewed by S Sung, K Adegoke, K Triep, D Chrimes; comments to author 27.Oct.2025; revised version received 21.Jan.2026; accepted 23.Jan.2026; published 09.Mar.2026.

Please cite as:
Park Y, Kang H, Kim J, Shin SY, Cho D, Rhee SY, Park HS, Lee KJ, Bae S
Development and Evaluation of SNOMED CT Automated Mapping Tool: Advancing Terminology Standardization and Semantic Interoperability
JMIR Med Inform 2026;14:e82670
URL: https://medinform.jmir.org/2026/1/e82670
doi:10.2196/82670
PMID:

©Youngsun Park, Hannah Kang, Jiwon Kim, Soo-Yong Shin, Dosang Cho, Sang Youl Rhee, Hong Seok Park, Kyung-Jae Lee, Sungchul Bae. Originally published in JMIR Medical Informatics (https://medinform.jmir.org), 09.Mar.2026. This is an open-access article distributed under the terms of the Creative Commons Attribution License (https://creativecommons.org/licenses/by/4.0/), which permits unrestricted use, distribution, and reproduction in any medium, provided the original work, first published in JMIR Medical Informatics, is properly cited. The complete bibliographic information, a link to the original publication on https://medinform.jmir.org/, as well as this copyright and license information must be included.

XSL•FO
RenderX

Design Principles for Interactive Dashboards in Drug Safety Surveillance: Design Science Research

Malwina Kotowicz, MSc; Mexhid Ferati, PhD; Soumitra Chowdhury, PhD; Cláudio Martins Pires, BSc

Department of Informatics, Faculty of Technology, Linnaeus University, Växjö, Sweden

Corresponding Author:
Mexhid Ferati, PhD
Department of Informatics, Faculty of Technology, Linnaeus University, Växjö, Sweden

Abstract

Background: Adverse drug reactions pose a serious threat to health care, leading to patient harm and substantial economic burden. Dashboards for drug safety surveillance are a valuable tool to tackle it.

Objective: This qualitative study aims to develop a dashboard for drug safety tracking with active and iterative involvement of end users. To support dashboard development, we formulate and iteratively refine design principles (DPs) for drug safety dashboards using the affordance theory.

Methods: Following a design science research approach, we conducted 3 cycles of iterative design and evaluation involving the end users. Four professional end users (with expertise in drug screening, drug discovery, and data science) and 6 nonprofessional end users (drug consumers) were engaged in the requirements gathering sessions through co-design workshops, usability testing through think-aloud sessions, and heuristic evaluation.

Results: The analysis resulted in a set of 8 DPs refined using the prototype's affordances (ie, actionable properties of the dashboard that guide user interaction and interpretation of data). Following themes emerged in the formulation and refinement of DPs: addressing the bootstrap problem through designing for immediate use (DP1a), allowing identification of patterns through visualizing causality while signalizing uncertainty (DP1b), tracking trends for relevant variables (DP1c), implementing user-controlled views (DP2a) and customizable levels of data granularity (DP2b), guiding user's visual attention through spatial layouts (DP2c), designing for higher public value (DP3a) and providing features to support decision-making for varied stakeholders' groups (DP3b). A high-fidelity dashboard prototype for drug safety surveillance was proposed as a result of applying the final set of DPs. Heuristic evaluation of the prototype revealed an overall usability score of 84%.

Conclusions: Applying DPs rooted in affordance theory led to a purposeful and user-relevant artifact that can improve understanding of drug safety data and potentially guide decision-making processes for professional users. Our theoretical contribution lies in providing refined DPs, while also demonstrating how affordances can aid dashboard development in pharmacovigilance. Our findings may be applicable to similar health information systems in related domains.

(JMIR Med Inform 2026;14:e75936) doi:10.2196/75936

KEYWORDS

drug safety surveillance; adverse drug reactions; pharmacovigilance; dashboard systems; medical informatics applications; design science research; decision support systems; user-centered design; clinical

Introduction

Overview

Adverse drug reactions (ADRs) pose a serious risk, leading to hospitalization of millions of patients every year, and the incidence of ADRs resulting in hospitalization has been consistently increasing in recent years [1-5]. ADRs are not only a major health concern, but also a tremendous economic burden, generating costs of several billion dollars each year [6,7]. Monitoring side effects associated with medicinal products is critical for regulatory bodies, health care providers, pharmacists, and, most importantly, drug consumers.

The rapid spread of health misinformation through online channels poses significant risks to public health [8,9]. Evidence suggests that many individuals, including physicians and medical students, resort to online searches for clinical information (ie, general web and social media queries rather than official pharmacovigilance portals). These channels frequently present user-generated or commercially sponsored content (eg, and influencer posts) that lacks expert review. Only a fraction of users consult credible resources (eg, specialized academic databases) [10,11]. Importantly, more than half of the online searches by health care professionals focus on drug safety and ADRs [12]. Relying on unverified sources for health information can be a major threat to public health, erode public trust, and can lead to severe consequences, including harm or

XSL•FO
RenderX

death [13]. Specialized platforms, such as interactive visualization dashboards for drug safety information at-a-glance, offer drug safety information in a trusted and concise way. Such platforms could be intended for professional users (ie, health care professionals, pharmacists, researchers, pharmaceutical companies, and regulatory agencies concerned with pharmacovigilance), as well as nonprofessional users (ie, patients, medical journalists, or lawyers protecting patient rights).

Dashboards in pharmacovigilance (DiPs), however, are scarce and often have complex interfaces resembling decision support systems rather than accessible designs. Additionally, most of the DiPs are not available online as open-source platforms, but are offered as proprietary software under license [14-17]. As a result, they have a limited audience and lack widespread availability. Moreover, DiP often lacks salient usability features, is poorly designed due to the absence of a structured design approach, or has functional deficiencies [17,18]. Several data mining techniques have been proposed as a valuable tool for early detection of potential safety signals (ie, indications or evidence that suggest a possible new ADR) in pharmacovigilance [19,20]. However, existing DiP rarely integrates data mining methods to enhance raw drug safety information and therefore offers limited insight [21-23]. Given the shortcomings of current platforms for drug safety surveillance and the scarcity of prescriptive knowledge regarding their design, we investigate the idea of finding more fitting designs for handling such data. In search of suitable design principles (DPs) that should lead the development of similar platforms, this study relies on the design science research (DSR) strategy and is guided by the following research question: what are the appropriate DPs for interactive dashboards in drug safety surveillance?

To address this question, we set out to develop and evaluate DPs for a class of dashboards in pharmacovigilance, following the DSR approach. We show that engaging in prototype creation reveals general DPs applicable to similar systems. Consequently, besides the artifact being developed, emergent DPs are proposed as transferable concepts for similar systems within the boundary conditions studied. To this end, we use the notion of affordances—properties of physical things or relationships between actors and these things—to support our research. Affordances help in exploring different designs in this study, since different physical features of the prototype can afford (ie, provide and bring about) the same functionality.

This study consists of the following steps. First, we identify general DPs for visual dashboards of drug safety data. Second, following the DSR methodology, we perform the requirements gathering session with a group of experts in drug screening, bioinformatics, and data science. Third, we create a prototype of an interactive dashboard, where we present drug safety data in a visually friendly manner, with the purpose of improving its general understandability. To this end, we also focus on finding suitable data mining techniques for knowledge extraction from publicly available data in pharmacovigilance. Fourth, we assess the prototype in demonstration and evaluation sessions with users to detect potential usability issues and receive feedback on possible improvements to the design. Altogether, we carry out 3 iterations of the DSR phases.

The aim of this research is thus to enhance the understanding of drug safety data and improve the potential for decision-making among intended users. Specifically, our objectives are to (1) formulate DPs, (2) re-evaluate these in 3 iterations of alternating phases of prototype development, demonstration, and evaluation, and (3) gain insight on how the notion of affordances and DPs can support the development of visualization tools in drug safety surveillance. It is important to mention that, in this study, by “professional users” we refer specifically to researchers in drug screening, bioinformatics, and data science; clinicians and pharmacists were not recruited in our sample. Accordingly, the DPs and evaluation results reported here are grounded in researcher workflows. While some principles are likely cross-cutting across stakeholder groups, we do not evaluate their applicability to clinician- or pharmacist-facing workflows in this study.

Current State of Drug Safety Surveillance Systems and Data Mining Standards

Three major global databases monitor drug safety: Food and Drug Administration (FDA) Adverse Events Reporting System (FAERS) database, VigiBase maintained by the Uppsala Monitoring Center (UMC) and World Health Organization (WHO), and EudraVigilance managed by the European Medicines Agency (EMA). FAERS, the world’s largest repository with more than 24 million reports as of March 2022, serves as a key postmarketing pharmacovigilance tool. EudraVigilance and VigiBase similarly collect ADR reports from the European Economic Area. These reports, submitted by manufacturers (mandatory) and health care professionals or consumers (voluntary), document suspected side effects from one or more drugs per patient case [20,24,25].

Although crucial for surveillance, these reports cannot establish direct causality because of factors such as comorbidities or concurrent medication [25]. To address this, database curators apply data mining to detect safety signals for expert review. The FDA encourages signal detection in drug development, as it positively impacts the process, while the WHO and UMC offer similar services to industry partners [20,26].

Several digital platforms exist for drug safety surveillance, but many, including FAERS, rely solely on reporting frequencies rather than integrated data mining [21]. According to Kumar [17], the FAERS dashboard is affected by limited awareness, unclear purpose, unintuitive navigation, and challenges in interpreting its data. Most reviewed platforms pose accessibility challenges, as they rely on proprietary databases, restricting access, reproducibility, and public transparency [16]. Many are outdated or limited in scope, relying on small datasets or alternative data sources instead of major repositories [14-16,27,28], while others focus only on ADR reporting rather than analysis and visualization [29-31].

Moreover, most platforms were not developed using the DSR process or participatory design methods and lack usability testing. Therefore, their complex interfaces often resemble expert decision support systems rather than accessible designs

XSL•FO
RenderX

[14-16], which can impact usability, hinder tool adoption, and compromise their practical impact [18,32]. These factors emphasize the need for open-source, user-centered drug safety tools that enhance accessibility and stakeholder engagement.

Data mining techniques are routinely used in pharmacovigilance to enhance the understanding of drug and vaccine safety profiles [33-36]. While no universal standard exists, guidelines provide statistical support for interpreting detected signals [37]. Disproportionality analysis (DPA) is currently the most common technique recommended by the FDA, UMC (WHO), and EMA, although the organizations deploy different statistical approaches [38]. Despite its importance, DPA results are seldom integrated into public dashboards, which continue to rely mainly on reporting frequencies [21-23]. This limitation may hinder a thorough understanding of the drug safety profiles and potentially lead to overlooking important trends, which further emphasizes the importance of incorporating safety signal assessments in public dashboards in pharmacovigilance.

New platforms have been developed in recent years primarily leveraging artificial intelligence (AI), machine learning, and real-world data integration for ADR detection in clinical practice. Specific new platforms include the PVClinical system using OMOP-CDM and Observational Health Data Sciences and Informatics (OHDSI) software stack for electronic health record integration [39] and established platforms such as Oracle Argus Safety, repClinical, PvNET, and ArisG for ADR administration and reporting [40]. AI-powered approaches show particular promise, with systematic reviews demonstrating effective natural language processing application across 16 studies for user-generated content analysis [41] and 12 studies showing deep learning models outperforming traditional machine learning for adverse event extraction [42]. However, challenges remain, including data quality, regulatory compliance, and the need for clinical validation of these emerging platforms [43].

Recent research on human-computer interaction (HCI) and user-centered design in pharmacovigilance dashboards is limited but emerging, with only a few directly relevant studies identified in the past few years. The strongest evidence comes from Yu et al [44] who developed a visualization platform for FDA adverse event data with usability demonstration through case studies and validated accuracy against manually processed data. In a study on integrating human-centered design of a public health data dashboard for sexually transmitted infections in the state of New York, Ansari and Martin [45] found that dashboards must reflect actual workflow needs, address data limitations transparently, and use design elements, such as clear notes and estimated data displays, to build user trust and handle common data quality issues. This process resulted in a highly functional design template. Malkani et al [46] identified and ranked key health care dashboard design attributes such as clarity, simplicity, visual hierarchy, responsiveness, and intuitive navigation as most critical for improving usability and user-centered decision-making. Gavriilidis et al [47] applied user-centered DPs to create the PVClinical platform for ADR investigation, identifying “actionability” as a key adoption factor and emphasizing needs for explainable, human-interpretable results. Broader context comes from patient safety dashboard research, where Murphy et al [48] found that among 33 studies, only 4 incorporated informatics or human factors principles in development or evaluation, highlighting a significant gap in rigorous HCI application.

The evidence base remains thin, with most pharmacovigilance visualization research focusing on technical implementation rather than systematic user-centered design evaluation. More rigorous HCI research is needed in this specialized domain [44,47,48]. Table 1 summarizes the limitations of available dashboards and shows the prototype features we explore in response to the identified gaps.

XSL•FO
RenderX

Table . Research gaps were identified through limitations to available dashboards for pharmacovigilance and prototype features were intended to address them.

Platform category (examples)	Key limitations noted in the literature	Intended prototype features
Regulatory public dashboards (FAERS[a]; EudraVigilance; VigiLyze)	Emphasize reporting frequencies; statistical signal detection (eg, DPA)[b] typically not available in the public UI[c]; access and reproducibility constraints (open access but not open source; VigiLyze requires membership). The FAERS public dashboard shows issues with awareness, navigation, and interpretability for nonspecialists [17,21-23]	Integrates DPA outputs in the UI; offers guided interactions; co-designed and usability-tested; open data and code with an open-access dashboard
Enterprise pharmacovigilance dashboards (Oracle Argus Safety; ArisG; repClinical; PvNET)	Proprietary, case-management and regulatory-reporting focus; limited public documentation of integrated analytics, no participatory design or formal usability evaluation; constrained transparency and reproducibility [40]	Offers exploratory analysis; transparent metrics (downloadable DPA files); hybrid-open model enabling inspection, reuse, and migration to a fully open-source stack
Clinical and EHR analytics on OMOP-CDM (PVClinical)	Integrates EHRs[d] via the OHDSI[e] stack and reports user-centered design; scope differs from spontaneous report dashboards; platform availability varies; continued need for clinical validation and regulatory alignment [39,43,47]	Complements PVClinical by focusing on FAERS spontaneous reports; reports outcomes of co-design, think-aloud usability (and its quantitative outcomes), and heuristic evaluation as a result of systematic user involvement in multicycle evaluation process
Academic or research visualization platforms	Often older or limited-scope implementations with small or alternative datasets; few report systematic user-centered design [14-16,28,44]	Built on open FAERS data—the largest, regularly updated public repository with API[f] access; applies recent visualization techniques via implementation of domain-informed design principles
Patient-facing ADR[g] reporting and medication information apps	Designed primarily for ADR submission or mobile information; not intended for exploratory signal analytics or integrated DPA visualization [27,29-31]	Analytic dashboard for exploring suspected drug-event patterns, supporting stakeholder decision contexts

[a]FAERS: Food and Drug Administration Adverse Events Reporting System.

[b]DPA: disproportionality analysis.

[c]UI: user interface.

[d]EHR: electronic health record.

[e]OHDSI: Observational Health Data Sciences and Informatics.

[f]API: application programming interface.

[g]ADR: adverse drug reaction.

Affordance as a Lens to Study DPs

Affordances are the action possibilities an artifact enables through its material features [49-51]. We use this lens operationally: each DP states (1) the intended user activity (affordance), (2) the dashboard features that enable it (material properties), and (3) the boundary conditions in which the principle applies. In this study, the artifact does not itself cause understanding or decisions; it supports them insofar as its features enable the specified affordances [52].

Formulating the DPs

DPs provide prescriptive guidance for constructing an artifact to meet stated objectives [50,53-55]. Drawing on literature on pharmacovigilance data literacy and dashboard design, we formulated DPs using the structure by Chandra et al [53] that ties (1) intended user activity (affordance), (2) enabling features (material properties), and (3) boundary conditions. We use the following template for DPs formulation:

Provide the system with (material property—in terms of form and function) in order for users to (activity of user or group of users—in terms of action) given that (boundary conditions—user group's characteristics or implementation settings) [53].

We consider drug safety surveillance as the boundary condition and analyze 2 user groups for this DSR prototype: (1) nonprofessionals (drug consumers) and (2) professional users as operationalized in this study (researchers in drug screening, bioinformatics, and data science). While health care professionals and pharmacists are central stakeholders for pharmacovigilance dashboards, they were not recruited in the present sample; consequently, findings and DPs are grounded in these boundary conditions.

We categorize the DPs into three classes: (1) DPs related to functionality that address the question of how well the dashboard serves its purpose, (2) DPs related to the mode of display that refer to the specific visualization techniques, and (3) DPs related to added value, which focus on the benefits the artifact provides to the public or end users.

We selected and refined DPs by applying an affordance alignment test: a principle was retained only when a target user

XSL•FO
RenderX

goal could be mapped to a concrete dashboard feature expected to enable the activity in the drug safety context [52,53]. Subsequent evaluation rounds confirmed and sharpened their scope.

DPs Related to Functionality

The value of new information infrastructures (IIs) lies in the users' community. However, since this community is initially small, the benefits of using the system may not be immediately apparent. Several authors emphasized the bootstrap problem that arises when the benefits of new IIs are perceived as indirect, delayed, or uncertain, which can lead to resistance in the system's adoption [56,57]. To address this issue, Hanseth and Lyytinen [57] recommend designing IIs for direct usefulness, that is, prioritizing immediate practical benefits for the users. This approach may enhance the perceived value of the system and help expand the user community. It may also create a positive feedback loop, where the use of the system leads to its further improvements, which in turn increase its usefulness and value. Consequently, we formulated the following DP: DP1a: it provides features to address the bootstrap problem, so that the system affords immediate use of the dashboard in drug safety surveillance.

Recker [58] investigates public dashboards related to the coronavirus pandemic, concluding that many present data through simple attributes (eg, number of cases, number of deaths, and number of recovered). Integrating state-tracking features that enable monitoring changes in states and events that trigger them (such as fluctuations in infection rates, or timelines of lockdowns and restrictions) could be a significant improvement, and the information presented in dashboards should answer the question how, instead of just how many. We formulated two DPs: (1) DP1b: it provides features to describe possible causality between variables, so that the system affords identification of patterns and trends in drug safety surveillance. (2) DP1c: it provides features to track changes in variables, so that the system affords tracking of the progression of relevant states in drug safety surveillance.

DPs Related to the Mode of Display

Matheus et al [59] suggest incorporating customizable views into decision-making dashboards, as this design strategy may help bypass the interpretation bias—"a single view might result in a limited picture of the situation." Expanding views to more than one view may lead to better understanding of the problem. Customized views help users to focus on relevant information and reduce the cognitive load associated with processing large volumes of data. We formulated the following DP: DP2a: it provides features to support customized views, so that the system affords examining various dimensions of data in drug safety surveillance.

Matheus et al [59] also suggest incorporating customizable features into decision-making dashboards, including the ability to toggle between detailed and high-level data visualizations. As these dashboards often contain a large volume of data, such features can help users understand the problem at hand by providing varying levels of detail. We formulated the following DP: DP2b: it provides overview and details, so that the system affords exploring data of different granularity levels in drug safety surveillance.

Toreini et al [60] follow a set of experiments to find ways to decrease task resumption failures. Tracking the real-time eye movements of the participants, they conclude that users start from and focus their attention on the upper left corner of the dashboard. Several authors suggest incorporating attention-augmenting features into dashboard elements (such as varied color, size, shape, and orientation) and visual cues (buttons and dials) to direct attention toward objects of higher importance [60,61] Consequently, DP2c: it provides features that stimulate attention and place important elements on the top-left area of the dashboard, so that the system affords improved attention management while using the dashboard in drug safety surveillance.

DPs Related to Added Value

Matheus et al [59] claim that creating dashboards should go beyond simply visualizing data. Creating public value should be embedded in the design process, as the data on its own is of little use. This way of thinking of the design process—through the prism of public value—transgresses the initial idea of merely finding the ways to present data in the best visual way. Data visualization should be the means, not the goal, and asking the question "what is the added value?" during the design process is necessary. Designers should prioritize generating public values such as engagement, transparency, and accountability, while also upholding public values such as privacy. Consequently: DP3a: it provides features to create public values, so that the system affords users' engagement in dashboard use in drug safety surveillance.

Embedding features that support decision-making is a crucial aspect of dashboard development [59]. Such features can be valuable for professional users, including health care professionals, pharmacists, researchers, and regulatory bodies in pharmacovigilance. We also expect the users would gain greater understanding and take up higher responsibility toward their own health, which would equip them better for decision-making. We formulated the following DP: DP3b: it provides features to support decision-making, so that the system affords users to evaluate what-if scenarios and consider different alternatives in drug safety surveillance. Initial DPs are shown in Table 2.

XSL•FO
RenderX

Table . Overview of initial design principles.

Design principle	Affordance	Material properties
DP1a	Obtaining immediate practical benefits while using the dashboard [56]	Features that respond to users' requirements, features that address actual user problems and offer solutions
DP1b	Identification of patterns and trends through exploration of DPA[a] analysis [58]	Features that enable identification and examination of patterns and trends in drug-ADR[b] evaluations
DP1c	Monitoring the progression of relevant states (how variables change over time) [58]	Features that allow tracking changes in relevant variables
DP2a	Exploring, analyzing, and interpreting data from different angles [59]	Features that enable analysis of data from multiple perspectives
DP2b	Exploring data from a broad and narrow perspective by switching between levels of granularity [59]	Features to adjust the level of detail depending on users' needs and the context of analysis
DP2c	Improved attention management while using the dashboard [60,61]	Features that stimulate attention, visual cues that direct attention toward important elements
DP3a	Active involvement in exploring the data, potentially increasing users' satisfaction [59]	Features with a potential to create public value (engagement, transparency, accountability, and adherence to privacy)
DP3b	Evaluating alternatives of actions, exploring what-if scenarios [59]	Features that support decision-making

[a]DPA: disproportionality analysis.

[b]ADR: adverse drug reaction.

Methods

Data Collection and Target Groups

We have considered 2 target groups for this work: professional users and nonprofessional users. We define professional users as those whose professional activities are concerned with drug safety surveillance and thus have extensive knowledge in the domain. For clarity, throughout the paper, "professional users" refers to this researcher group; the implications for clinician- and pharmacist-facing workflows lie outside this study's boundary conditions. In contrast, nonprofessional users are not professionally concerned by drug safety surveillance and in that sense are laymen in the domain of pharmacovigilance. Figure 1 depicts the user groups.

XSL•FO
RenderX

Figure 1. Professional (left) and nonprofessional (right) user groups. The broader professional stakeholder landscape includes health care professionals, pharmacists, researchers, regulatory agencies, and industry. In this study, the professional participants recruited were researchers in drug screening or drug development (E1-E4). Nonprofessional participants were drug consumers (C1-C6).

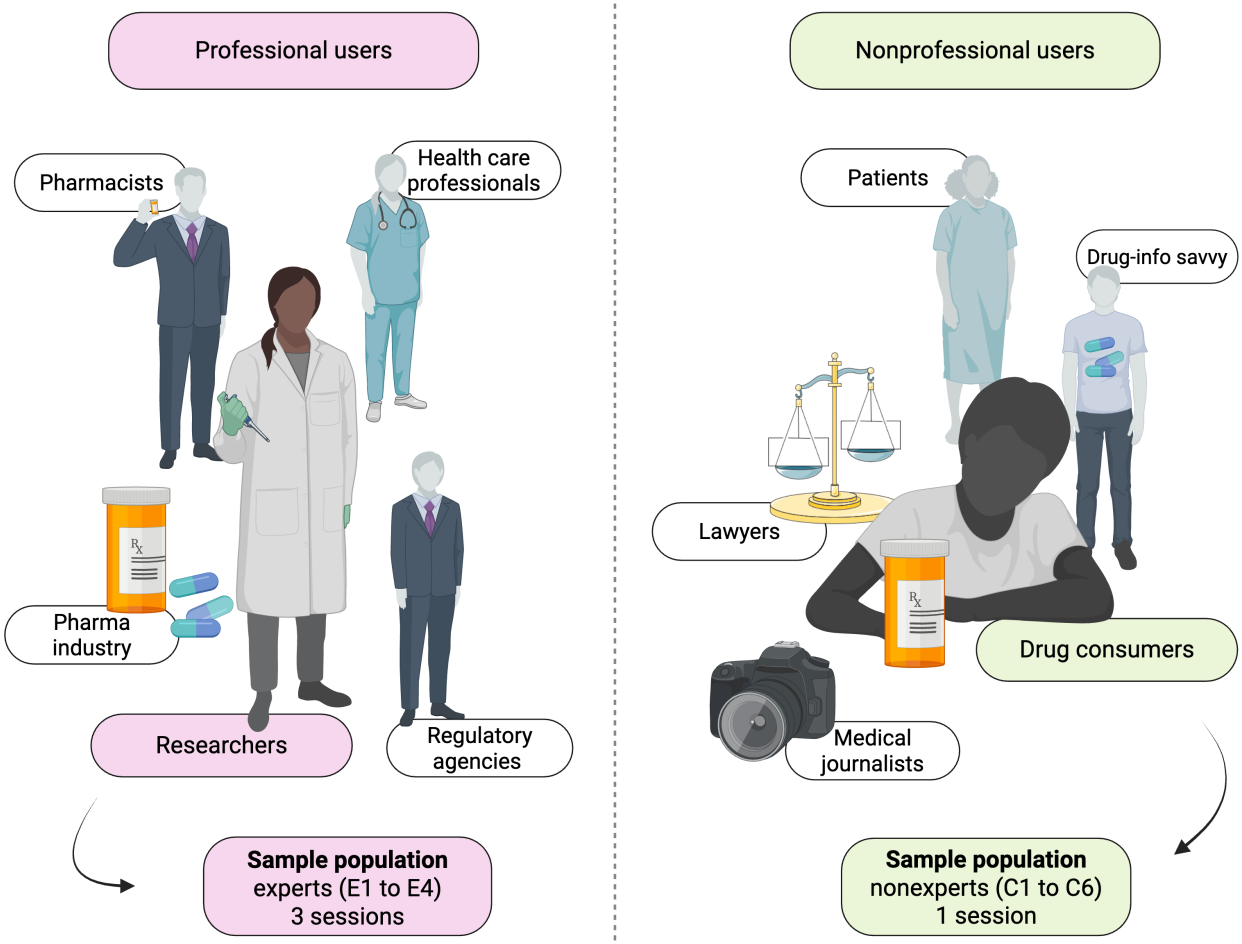

We have recruited a group of 4 expert users (referred to as experts, with participant IDs of E1 to E4) for this study. All experts were scientists of different academic degrees and expertise levels and were working on drug development and screening projects. Three out of 4 experts had extensive experience in data science and bioinformatics. In addition, all experts had many years of experience in data visualization and communication to the general and scientific community. Experts participated in the co-design workshop, pilot evaluation, and heuristic evaluation sessions.

For usability testing (think-aloud session), we have recruited a group of 6 nonexpert users (referred to as nonexperts, with participant ID of C1 to C6). All nonexperts were drug consumers and had a history of continuous medication therapy of at least 7 days at least once in the previous year. We assumed these users were potentially also drug safety information-savvy and might provide meaningful insights into which complex analyses are possible. Importantly, nonexperts were novices in the sense that they had no prior exposure to the tool in question or any other similar dashboards [62]. Although some nonexperts shared parts of professional experience with experts (eg, C4 and C5 had expertise in biomedical engineering and data science), they were not working on drug screening and discovery projects.

By design, think-aloud usability testing was conducted solely with nonprofessional "novice" users to evaluate first-time learnability and immediate practical use (DP1a) without prior-exposure effects from experts who had already interacted with the prototype during co-design and/or the pilot evaluation [62].

Overall, all participants were between 28 and 44 years old and were based in Germany, Sweden, France, Finland, and Portugal. A detailed description of participants recruited for this study is shown in Table S1 in Multimedia Appendix 1. Given the age range and the presence of multiple participants with advanced technical or professional backgrounds, this sample likely exhibits above-average digital and data literacy; while valuable for investigating complex interaction issues in early iterations, this may inflate task performance relative to older adults and users with lower digital health literacy.

DSR Approach

We followed a framework proposed by Sauro and Lewis [63] to quantitatively analyze the user experience. Furthermore, in heuristic evaluation, we quantitatively collected and analyzed data in line with the framework proposed by Dowding and Merrill [64]. Additionally, we qualitatively collected and analyzed data in all experimental sessions in this study.

We modified a staged DSR model, initially proposed by Peffers et al [65]. Thus, the DSR framework applied in this study consisted of the following stages: (1) problem definition and

XSL•FO
RenderX

objectives of the solution, (2) diagnosis phase, (3) data preparation phase, (4) design and development phase, and (5) demonstration and evaluation phase. Detailed descriptions of each phase are found in Multimedia Appendix 2.

A depiction of the DSR process is shown in Figure 2. v1-PowerPoint and v2-v4-Tableau prototypes were used in diagnosis and demonstration and evaluation phases, respectively. Blue boxes show individual phases and the order in which they occurred in DSR (yellow arrows). DPs emerged in the diagnosis phase and were then iteratively refined in the demonstration and evaluation phases.

Figure 2. Applied design science research model.

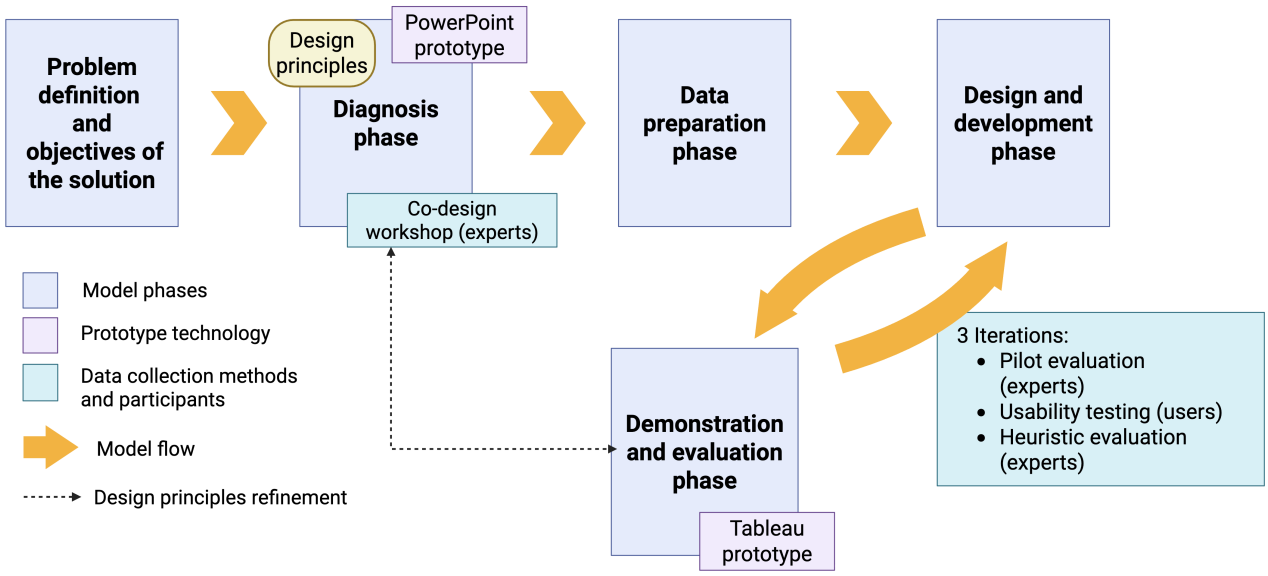

Data Collection in DSR Cycle

We have performed 3 iterations of the DSR cycle. That is, we started with the diagnosis phase, in which we first identified initial DPs by gathering secondary data available in the literature. Then, we proceeded with one requirement gathering session, in the form of a co-design workshop with experts. Next, we have engaged in the data preparation phase, where—after selecting a suitable drug safety data source—we have written Python scripts to get and process the data.

We then performed 3 iterations of alternating design and development and demonstration and evaluation phases. In the first iteration, we developed a prototype in Tableau software (v2; Tableau Software LLC) [66], and tested it in the pilot evaluation session with experts. The results obtained in this way fed the second DSR iteration. We have updated prototype features (v3) and proceeded with usability testing (in a think-aloud session) with nonexperts. Finally, in the last iteration, upon updating prototype features (v4), we performed heuristic evaluation with experts. A flowchart of research activities is shown in Figure 3.

Further details about the design and development phase are provided in Multimedia Appendix 2. In that appendix, we describe the diagnosis phase, including the development of DPs and requirements gathering. We also provide information on how we used Statista [67] and participant requests to inform the selection process of 5 drugs used for prototype development: ibuprofen, acetaminophen (paracetamol), prednisone, quetiapine, and morphine.

XSL•FO
RenderX

Figure 3. Overview of data collection activities.

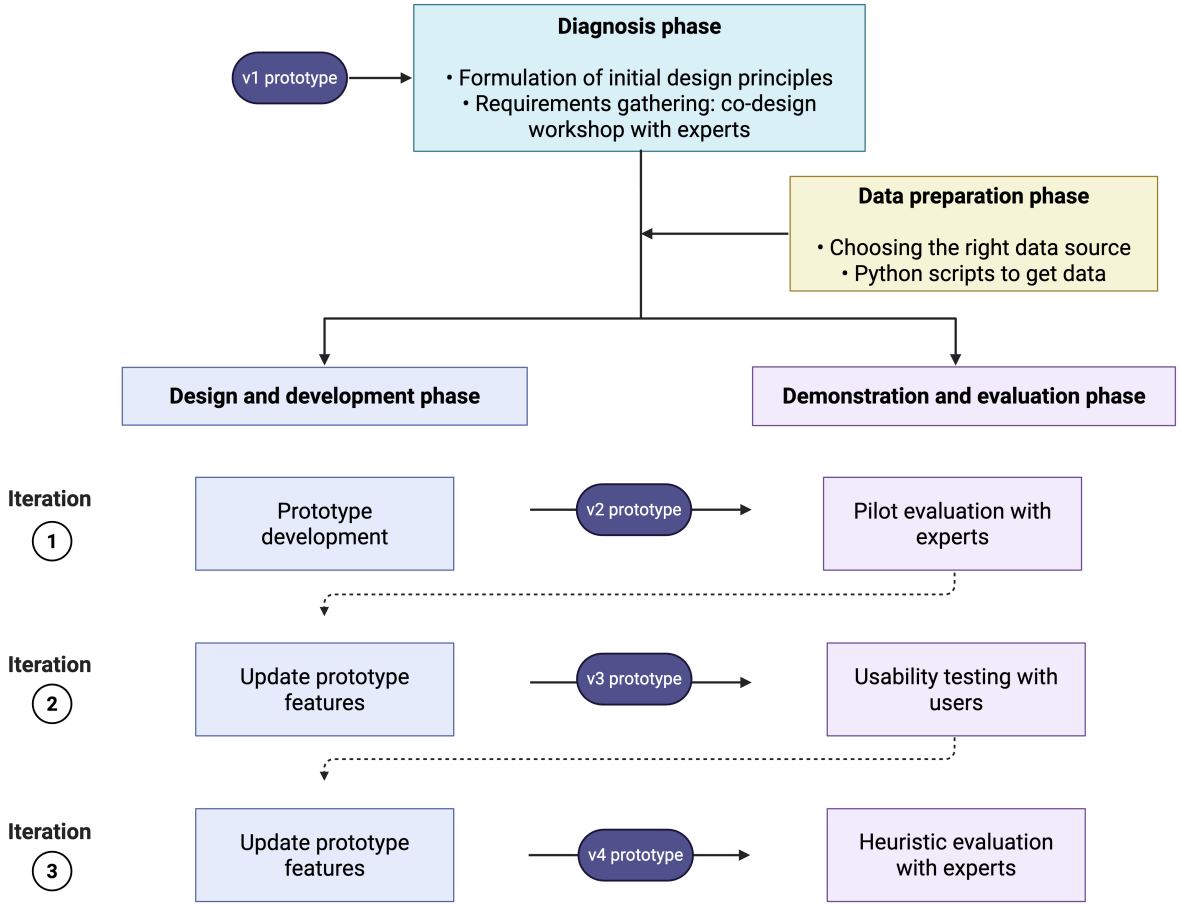

Demonstration and Evaluation Phase

Iteration 1: Pilot Evaluation

The researcher was moving through the dashboard by performing a set of predefined activities, while the participants controlled the navigation process by suggesting improvements whenever necessary. The session lasted 1 hour and was recorded with Otter.ai (Otter.ai, Inc) [68].

Iteration 2: Usability Testing

We have performed 6 usability tests with nonexpert users in think-aloud sessions. These included live meetings with 4 participants (C1, C2, C3, and C4) and virtual meetings with 2 participants (C5 and C6). Before the session, we have provided the users with a detailed protocol including introduction of the study, explanation on usability testing in the think-aloud session and a list with predefined tasks. These tasks required participants to do activities on the interface without the researchers' guidance. For the most part, researchers remained silent during users' task performance. Users were encouraged to express their thoughts while conducting the tasks. Additionally, 2 participants (C2 and C3) shared their thoughts on the usefulness of the dashboard and their interest in the tool in general. These short and unstructured discussions unfolded at the end of the sessions and were incorporated into findings. Each session lasted between 1.5 hours and 2.5 hours and was recorded with the same software, Otter.ai [68].

Experts were intentionally not included at this think-aloud stage to avoid learning effects from earlier sessions; their structured feedback was captured in the expert-focused co-design phase, pilot evaluation, and in the subsequent heuristic evaluation with 4 and 3 experts, respectively, which is within the 3 - 5 evaluator range known to uncover the majority of usability problems [69,70].

Iteration 3: Heuristic Evaluation

As originally suggested by Nielsen [71] and confirmed by other authors [62,69,72,73], 85% of usability violations can be detected by 3 to 5 evaluators in heuristic evaluation. We have performed heuristic evaluation with 3 experts (E1, E2, and E3).

Data Analysis

Overview

We used the framework method by Gale et al [74] to qualitatively analyze data in search of codes and themes. Importantly, and due to the specificity of DSR as a methodology (ie, when data are collected in iterations to repeatedly improve an artifact), codes and themes in this work refer to identified usability issues, dashboard features or elements undergoing evaluation and refinement, or any concept related to these (ie, the motivation behind the revision of DPs). Additionally, to prioritize the issues detected in usability testing and select appropriate solutions, we applied a method by Sauro and Lewis [63]. Finally, we analyzed the data from the heuristic evaluation through the assessment of 10 usability factors. These concepts

XSL•FO
RenderX

are discussed further below. Overall, we detected 33 themes (entities) in the co-design workshop session and 20 themes in the pilot evaluation session.

Usability Testing

For detecting usability issues, we applied a quantitative method by Sauro and Lewis [63]. We prioritized the usability issues according to their severity, considering the following factors: how much the issue has impacted the user trying to achieve the task, how critical the task was, and what was the frequency of the issue. Thus, the severity of issues was calculated by multiplying task criticality, impact, and frequency of occurrence. Overall, we detected 69 usability issues.

Each issue was then assigned one or more solutions. To choose the optimal solution to each usability issue, we considered 2 factors: complexity and effectiveness. Finally, a cost-benefit ratio (return on investment [ROI]) was calculated by dividing the effectiveness by the complexity. We decided which solutions to implement based on the following criteria: the solution had an ROI of 5 or more, was technically feasible, and was not solving the issue already covered by another solution with higher ROI. Overall, out of 56 conceptualized solutions, we arrived at 22 final solutions to be implemented. For a detailed description of the applied method, refer to Sauro and Lewis [63] and Rosemberg [75].

Heuristic Evaluation

Applying Dowding and Merrill's [64] heuristic evaluation, we assessed 10 usability factors using 49 close-ended questions. Usability factors had varying question counts; the maximum score per factor was calculated by summing questions assigned to it. Scores obtained per expert were calculated by summing the questions answered yes by each expert, per factor. A mean score was calculated by summing individual expert scores and dividing by the number of experts. The final result was the mean score divided by the maximum score (per factor and cumulatively). Next, overall severity rankings per usability factor were assigned, ranging from 0 (no usability problem) to 5 (usability catastrophe). Finally, qualitative analysis of comments per factor informed suggestions on future implementations. For a detailed description of the applied method, refer to Dowding and Merrill [64] and Nielsen [71].

Ethical Considerations

Informed consent was obtained from all participants prior to inclusion. Participation was voluntary, and participants were informed that they could opt out at any time. They were provided with information on how their data would be processed and that study data would be retained for no longer than 2 years from study start. No ethics or institutional review board approval was required for this work.

According to the Swedish Ethical Review Act (2003:460) [76], this study did not require formal ethical approval because it did not involve sensitive personal data, biological material, or any physical or psychological intervention. Only non-sensitive demographic information (country of residence, age, gender, profession) was collected. All participants were adults and data were pseudonymised using participant ID codes prior to analysis. Participants also provided consent for publication of the study results.

Results

Diagnosis Phase: DPs and Low-Fidelity Prototype

We have implemented DPs into a v1-low-fidelity prototype in PowerPoint. One dashboard element could be assigned to multiple DPs, but each assignment involved different functionalities of the element. Some DPs were action-oriented (DP1a and DP3a), and all material properties were assigned to them. We show how DPs shaped the v1-low-fidelity PowerPoint prototype in Table 3.

To afford exploration of data of varied granularity (DP2b), we created two dashboard sections: (1) an overview of common side effects for the chosen drug (the overview section) and (2) a detailed analysis of specific drug-side effect pairs (the detail section), split in separate pages where different visualization techniques were used (eg, a graph with age-gender distribution of affected populations). Additionally, we added drug and side effect search fields (Figure 4A–C).

To afford identification of patterns and trends (DP1b), the overview section displays a histogram of commonly reported side effects for a queried drug. Users could toggle between positive and negative side effects using buttons (Figure 4A). To afford monitoring the progression of relevant states (DP1c), a line graph with a year filter tracked reports for drug-side effect pairs over time (Figure 4C). Additionally, to afford improved attention management (DP2c), key graphs were positioned top-left, and warning messages were color-coded.

The system provided downloadable evaluation files containing detailed drug safety metrics (DA.csv, Figure 4A–C) to afford evaluating alternatives of actions (DP3b). Warning messages indicated whether an event was statistically significantly related to queried side effects and provided DPA information on mouse hover (Figure 4C). Two affordances, obtaining immediate practical benefits while using the dashboard (DP1a) and active involvement in exploring the data (DP3a) were expected to be enacted across all prototype features, as they aligned with the prototype's purpose.

XSL•FO
RenderX

Table . Instantiation of material properties.

Design principle	Instantiation of prototype features
DP1a	Initiated by all features and iteratively refined in response to users' input
DP1b	Graphs belonging to the overview section, warning messages with DPA[a] metrics on hover
DP1c	Line graph with the number of reports per drug-ADR[b] pairs, with year filters
DP2a	Interactivity of the graphs (eg, buttons to toggle between positive and negative ADRs), with year filters
DP2b	Splitting the dashboard into the overview and detail sections, with year filters
DP2c	Placing the graphs on the top-left, color-coded warning messages
DP3a	Initiated by all features expected to elicit values related to the transparency of drug safety data or the user engagement in health information tracking
DP3b	DPA metrics as downloadable files (DA.csv), warning messages with DPA information on hover

[a]DPA: disproportionality analysis.

[b]ADR: adverse drug reaction.

XSL•FO
RenderX

Figure 4. An excerpt from the v1-low-fidelity PowerPoint prototype. (A) The overview section. (B-C) The detail section.

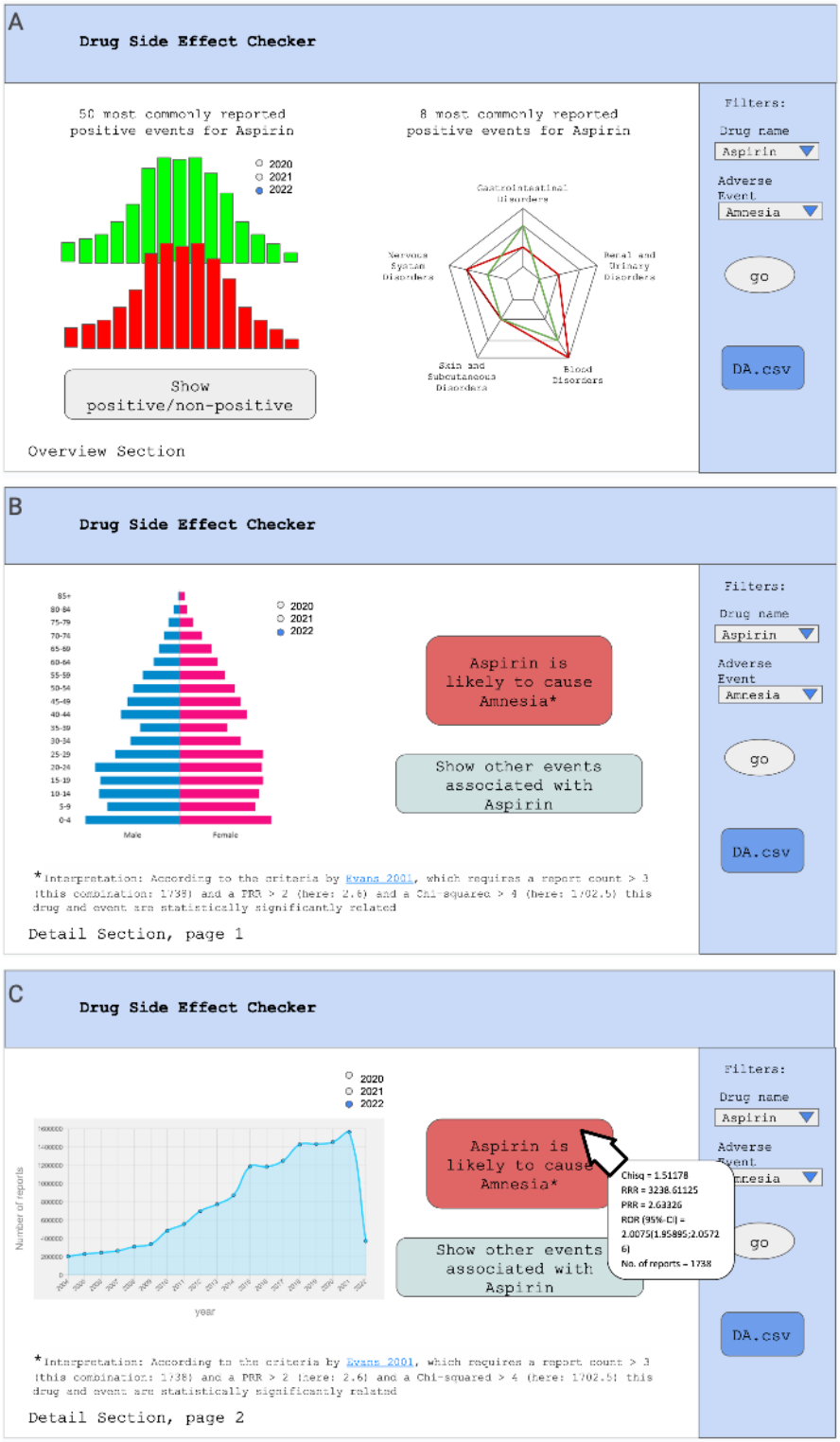

Diagnosis Phase: Requirements Gathering

Through a collaboration with a group of experts in a co-design workshop, we gathered the requirements for the prototype development. The v1-low-fidelity PowerPoint prototype was used in this session to visualize content of the dashboard, serving as a canvas for design activities. We summarize the principal findings in Table 4.

XSL•FO
RenderX

Table . Principal findings from the co-design workshop.

Feature or element	Related DPs[a]	Feedback
Indication graph	• DP2b (overview and details) • DP3b (decision-making support)	Offers details on common prescriptions for a queried drug, adding an extra variable to the displayed dataset.
Scrolling	• DP2c (attention stimulation)	Use scrolling instead of pagination, it is a preferred way for users to interact with the dashboards.
Drug and event search fields	• DP2b (overview and details)	Users seek information on potential side effects both before and after drug administration. Separate search fields allow users to look up a drug only (before an event occurs) or a drug and ADR[b] (after an event occurs).
DPA[c] metrics files	• DP3b (decision-making support) • DP2b (overview and details)	To influence decision-making of professional users, DPA files should include formulas and information on statistical models used for calculations, as well as the interpretation of calculated indicators.
Removing DPA info from the warning message's hover	• DP2b (overview and details)	While beneficial for researchers, high-level granularity data may confuse nonprofessional users. Access to DPA metrics is provided through downloadable files.
Age-gender distribution graph with modified age ranges, positioned top-left	• DP2b (overview and details) • DP3b (decision-making support) • DP2c (attention stimulation)	The graph provides information on common demographic attributes (age and gender). Using 10-year ranges provides optimal data granularity.
Histogram of most commonly reported side effects, positioned top-left	• DP2b (overview and details) • DP2c (attention stimulation) • DP2a (customized views) • DP1b (causality between variables)	The graph provides an overview of the most commonly reported ADRs, with the option to customize the display using a histogram filter (Related, Unrelated, All events). Limiting the bars to 20 provides optimal data granularity.
Per drug, there is a line graph showing the sum of side effects reported over time (the first line graph) and a second line graph illustrating specific side effects reported over time	• DP1c (state-tracking) • DP2a (customized views)	For researchers, viewing time series of drug-ADR report numbers is crucial. The second line graph helps identify, for example, specific events contributing to sudden increases in ADRs in selected years. The histogram filter is linked with line graphs, enhancing customization options.

[a]DP: design principle.

[b]ADR: adverse drug reaction.

[c]DPA: disproportionality analysis.

Adjusting Data Granularity

We found evidence that the dashboard supported the exploration of data of varied granularity (DP2b). Feedback from experts suggested adjusting the detail level on display. Some elements were considered too detailed, resulting in information overload, especially on the histogram and the age-gender distribution graph. Recommendations included fixing the histogram's displayed bars at 20 and setting age intervals on the age-gender distribution graph to 10 years (Figures 5A and 6A, respectively). Additionally, it was suggested that displaying detailed DPA metrics while hovering the warning message might confuse users unfamiliar with similar statistical methods, as per E1: this proportional reporting ratio and all that (...) Not super easy to interpret, right? This is greater than 2, but like, what is the upper bound? What is the lower bound? Like, how low can it go? (...) These values are not so easy to understand if you're not the professional who uses them.

Thus, the DPA information was removed from the warning message and added to downloadable DPA files, together with formulas for score calculation and interpretation of indicators. This was also in line with the suggested increase of data granularity on some occasions. Likewise, it has been proposed to implement a functionality to view the data by the condition for which a drug was prescribed. Finally, while initially considered, the BMI variable was ultimately excluded from the age-gender distribution graph. Although useful for analysis, BMI is rarely provided in the reports. Therefore, it was necessary to adjust the intended data granularity to what was available in the datasets. Considering all the above, we revised the following DP: DP2b: It provides an overview and details, while controlling overview-to-detail ratio, so that the system affords exploring data of different granularity levels in drug safety surveillance.

Accounting for different data granularity interest among various user groups, and considering that customizable level of detail

XSL•FO
RenderX

in displayed data can reduce distraction and potentially influence decision-making, we revised another DP: DP3b: It provides features to support decision-making and cluster them by the needs of distinct user groups, so that the system affords users to evaluate what-if scenarios and consider different alternatives in drug safety surveillance.

Figure 5. The first Tableau (v2-high-fidelity) prototype with analysis for ibuprofen (the overview section). (A) Modified histogram. (B) The first line graph. (C) The second line graph. (D) The histogram's filter.

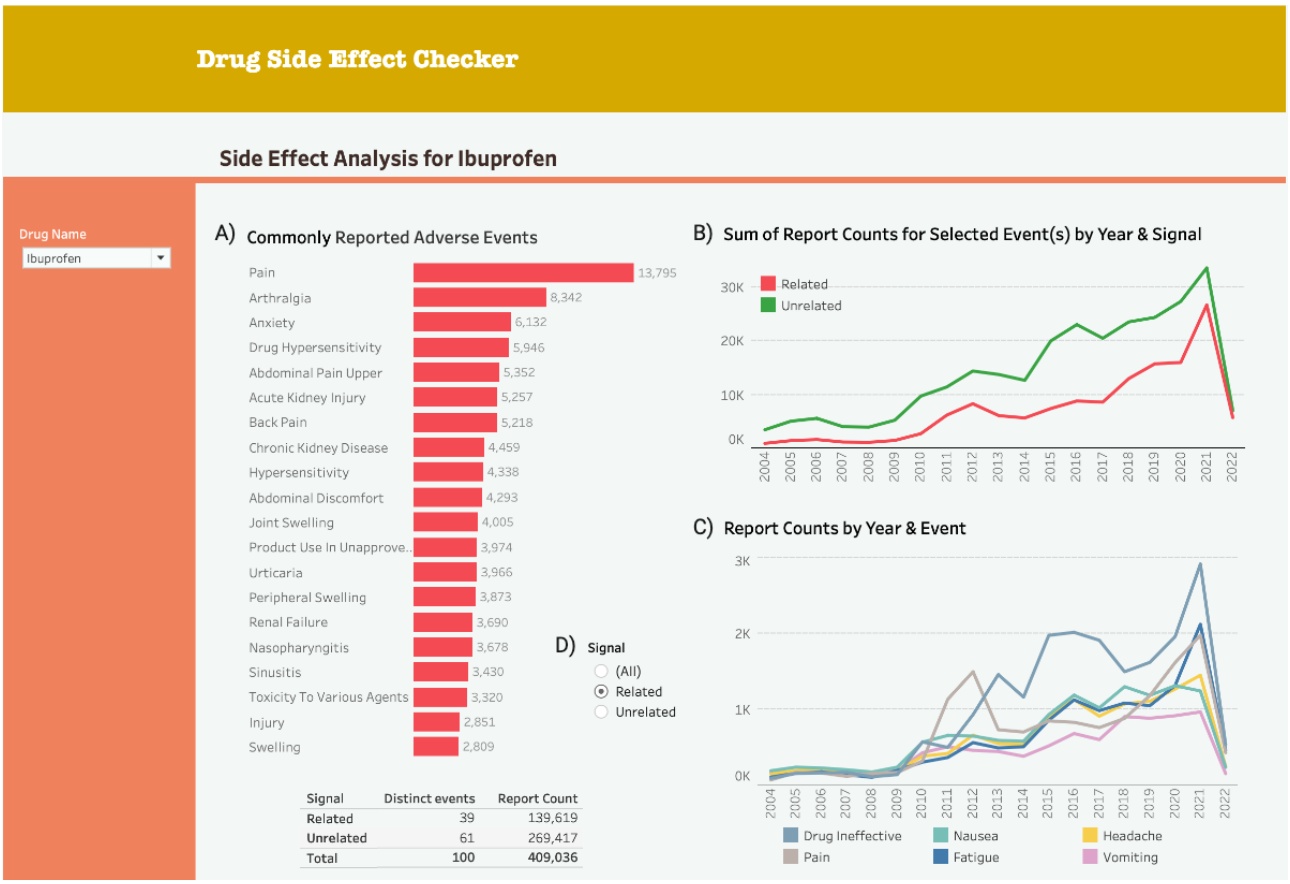

XSL•FO
RenderX

Figure 6. The first Tableau (v2-high-fidelity) prototype with analysis for ibuprofen and back pain (the detail section). (A) Modified age-gender distribution graph. (B) The reporter's type of occupation. (C) The indication graph. (D) The seriousness of the outcome. (E) The map with number of reports per country and the associated table. (F) Download buttons. (G) The event search field.

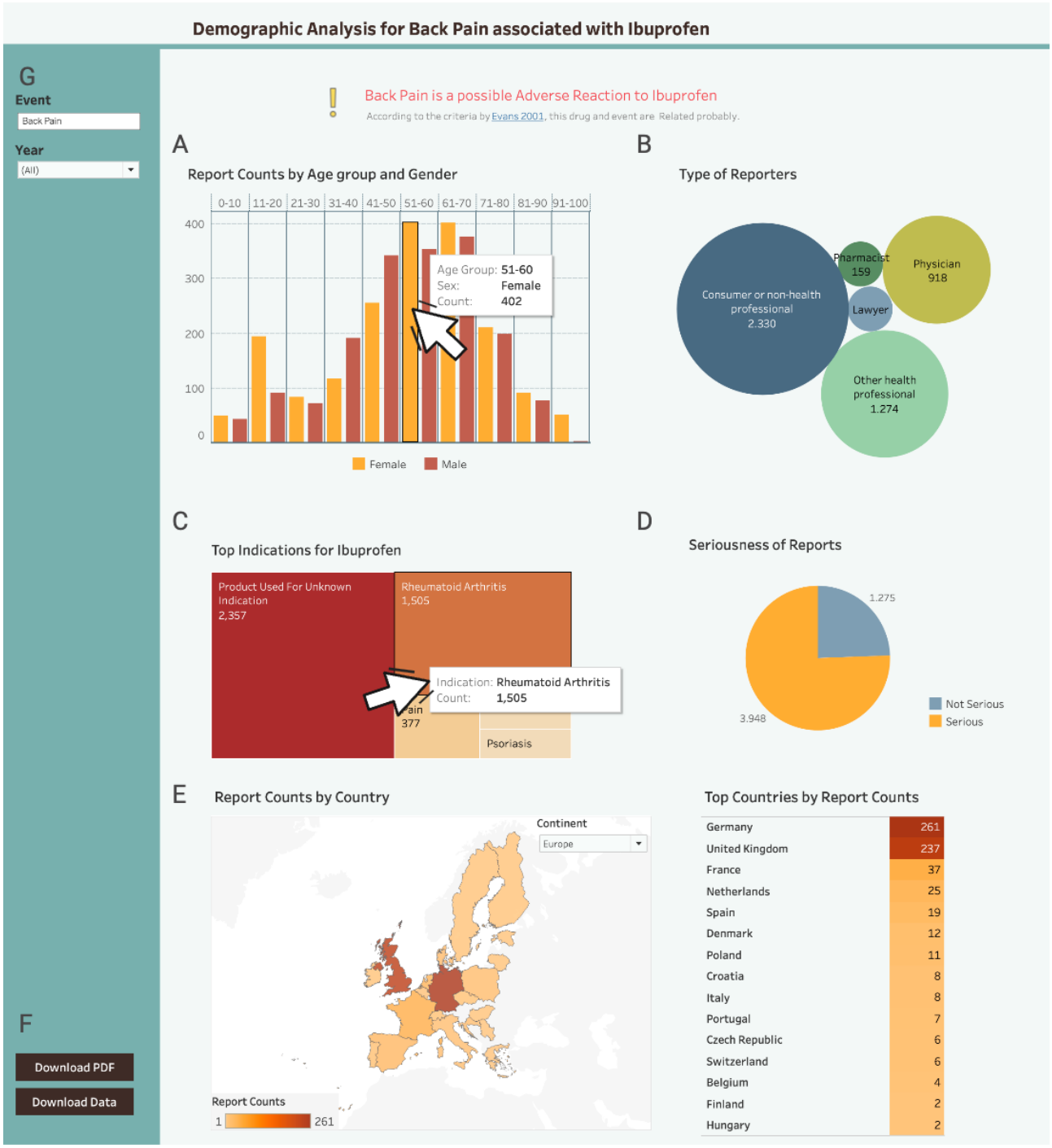

Scrolling Over Pagination

Feedback suggested changing from pagination to scrolling, as users often prefer to scroll, rather than having to navigate through multiple pages. Pagination is also considered more expensive in terms of browsing and might significantly slow the system down. Thus, we revised the DP: DP2c: it provides features that stimulate attention, place important elements on the top-left area of the dashboard, and promote scrolling over pagination, so that the system affords improved attention management while using the dashboard in drug safety surveillance.

Iteration 1

Design and Development: First Tableau Prototype

We transformed the v1-low-fidelity PowerPoint prototype into a v2-high-fidelity dashboard in Tableau, incorporating refined DPs based on the guidance from the co-design workshop. Figures 5 and 6 show the prototype after the first iteration.

After requirements analysis, to better afford monitoring the progression of relevant states (DP1c), we introduced 2 graphs: a line graph showing all side effect reports per drug per year

XSL•FO
RenderX

(Figure 5B) and a line graph showing specific side effect reports per drug per year (Figure 5C).

For exploration of data of varied granularity (DP2b), we added an indication graph showing the conditions for which the queried drug was prescribed when a side effect occurred (Figure 6C). In line with revised DP2b, we modified the age-gender distribution graph (Figure 6A). We also modified the histogram by reducing the number of bars to better afford identification of patterns and trends (DP1b). A map displayed side effect distribution per country with interactive continent selection and year filtering (Figure 6E).

With regard to improved attention management (DP2c), we positioned the histogram and the age-gender distribution graph on the top-left overview and detail sections, respectively. We replaced pagination with scrolling, aligning with DP2c. To better afford evaluating alternatives of actions (DP3b), we introduced safety signal reports with DPA information, displayed upon clicking the download data button (Figure S1 in Multimedia Appendix 3). To better afford exploring data from different angles (DP2a), all graphs in the overview section were made interactive: for example, selecting up to 6 histogram bars was reflected in the second line chart, where up to 6 individual events were displayed. It was also possible to limit the dataset by year ranges (Figure S2 in Multimedia Appendix 3).

Demonstration and Evaluation: Pilot Evaluation

While conducting a pilot evaluation, we were looking for suggestions on possible improvements to the prototype before embarking on usability testing. Overall, we received advice to implement a getting started tutorial containing screenshots of the dashboard elements with a short explanation on salient functionalities (eg, how to remove the selection and how to select using keyboard or mouse).

Importantly, expert E3 suggested implementing a feature related to selection-keeping—when the user chooses one or more side effects by clicking on the histogram bars, and then changes their drug selection, the dashboard should keep the selection of side effects. This feature can be useful to quickly compare drugs from the same drug classes (eg, ibuprofen and aspirin). According to E3: if you want to compare that one drug to another drug, to see if it (selected side effect) also occurs really often, then this makes sense (...) And you can see it (selected side effect) directly in the ranking.

This feature was in line with DP3b, potentially enhancing the decision-making of professional users.

Iteration 2

Design and Development: Updating Prototype Features

We updated the system by implementing selected findings from the pilot evaluation session. Thus, we introduced a getting started tutorial with informative screenshots that guided users through the dashboard functionalities (Figure 7).

Figure 7. An exemplary page from the getting started tutorial in the v3-updated prototype.

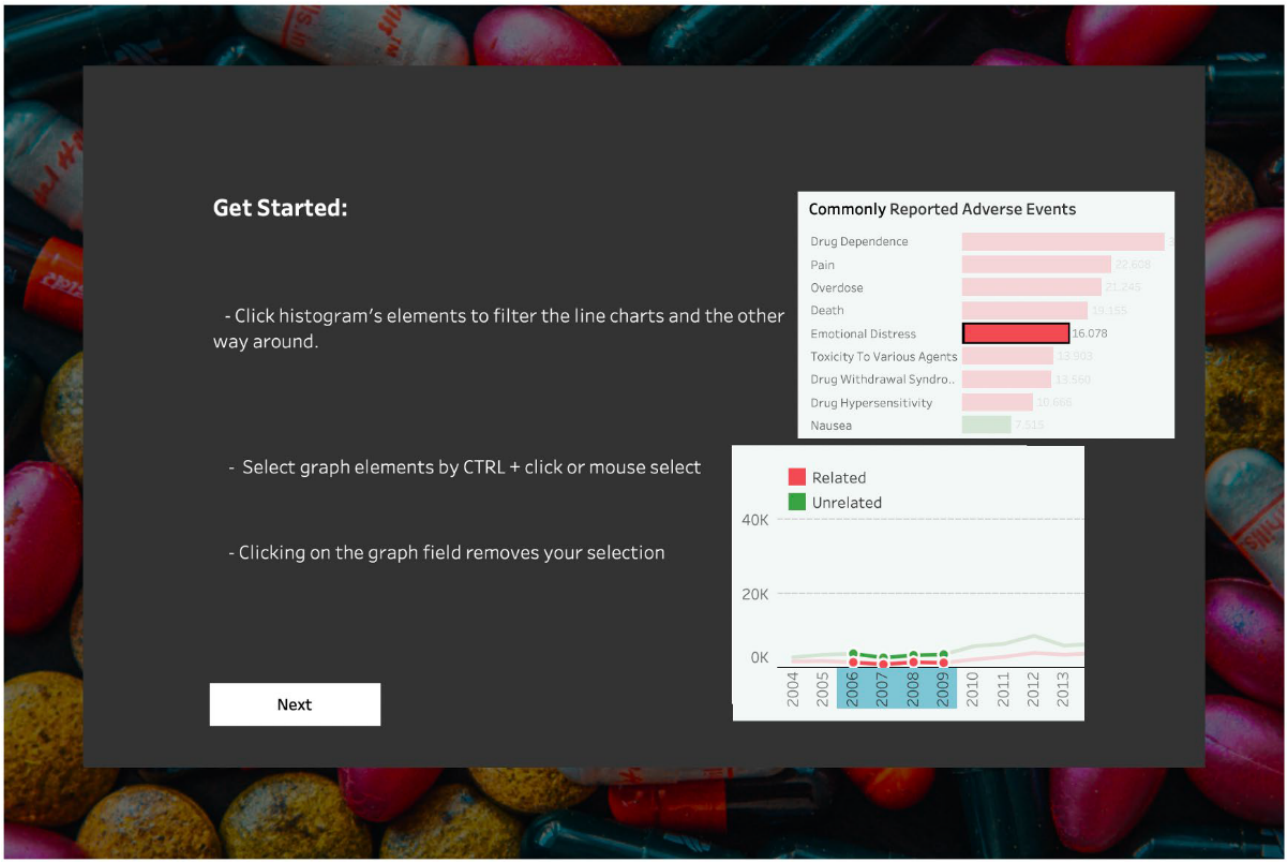

XSL•FO
RenderX

To better afford evaluating alternatives of actions (DP3b), we introduced the selection-keeping feature. For a detailed explanation, refer to Figure S3 in Multimedia Appendix 3, where we present a real-world scenario demonstrating the comparison of 2 commonly used pain-relieving drugs: ibuprofen and acetaminophen (also known as paracetamol).

Demonstration and Evaluation: Usability Testing

We conducted usability tests with nonprofessional users (refer to Multimedia Appendix 4 for details). We found several usability issues that could hinder obtaining immediate practical benefits while using the dashboard (DP1a). We grouped the issues according to the affected dashboard features or elements, and we discussed them in the corresponding order.

The getting started tutorial was hard to follow and long. Users struggled to grasp how the individual screenshots relate to the dashboard concepts. This confusion arose because the screenshots presented isolated dashboard elements instead of the dashboard as a whole. The inability to skip or revisit the tutorial was also a major issue. Regarding the histogram and associated filter**,** users had trouble understanding how to select bars by clicking or by dragging sections. Finding the histogram's filter (Figure 5D) took more than 15 seconds, which could hinder identification of patterns and trends (DP1b), as failing to use the filter could impede the thorough exploration of data.

Usability problems also arose for year selection across different dashboard sections. Users didn't fully explore year selection options and found deselecting elements challenging (Multimedia Appendix 4). The absence of a year selection field in the overview section could impede exploration of data of varied granularity (DP2b) and, in consequence, interfere with monitoring the progression of relevant states (DP1c).

Some dashboard elements lacked visibility and clear explanations of their utility. For example, the event search field was not visible enough (Figure 6G) and the utility of the second line graph was not clear to the users. Additionally, the dashboard language was too technical. We also found issues with download buttons, DPA metrics files, and safety signal reports. Multiple download buttons and files made downloads difficult. Moreover, the download dialog box was located beyond eye reach and the system failed to inform about the download status. Finally, safety signal reports were too detailed and specific. According to C2, the report provided "unnecessary information overload" in which the participant was not interested.

End questions revealed users' confusion about the data source and the meaning behind the evaluation of side effects as related or unrelated to a drug by data mining algorithms. This lack of understanding could constrain evaluating alternatives of actions (DP3b). However, users found the system attractive for exploring drug safety information (DP3b). They were often encouraged by its interactivity to explore data from different angles (DP2a) and expressed their interest in using the system as an auxiliary drug information source. C4 suggested that people generally search online for drug safety information, seeking medical advice on websites of compromised quality. The participant considered the dashboard a suitable information source even for users with no pharmacovigilance background, as long as it is supplementary to professional medical advice. Similarly, C3 suggested the system could be useful for direct comparison of drugs with the same active substance produced by different manufacturers. C3 often asks for a cheaper drug alternative at the pharmacy and could use the system to compare the safety information of equivalent drugs.

Iteration 3

Design and Development: Updating Prototype Features

Introducing the Video Tutorial

To better afford obtaining immediate practical benefits while using the dashboard (DP1a), we modified the tutorial. Usability testing revealed that users learn best by doing, but they require basic knowledge to get started. Well-designed tutorials allow users to uncover the true potential of the app and understand the associated benefits [77]. Following the idea that undiscovered features practically do not exist, we replaced the tutorial with the animated walkthrough video.

We recorded key features in a brief video (more than 1 minute) with subtitles explaining dashboard actions. We used icons (eg, pointing finger and large mouse cursor) to guide users and added a skip video button for more experienced users (Figure S5 in Multimedia Appendix 3). Finally, we included a help button allowing users to rewatch the tutorial (Figure 8).

XSL•FO
RenderX

Figure 8. A frame from the getting started video tutorial of the v4-updated prototype.

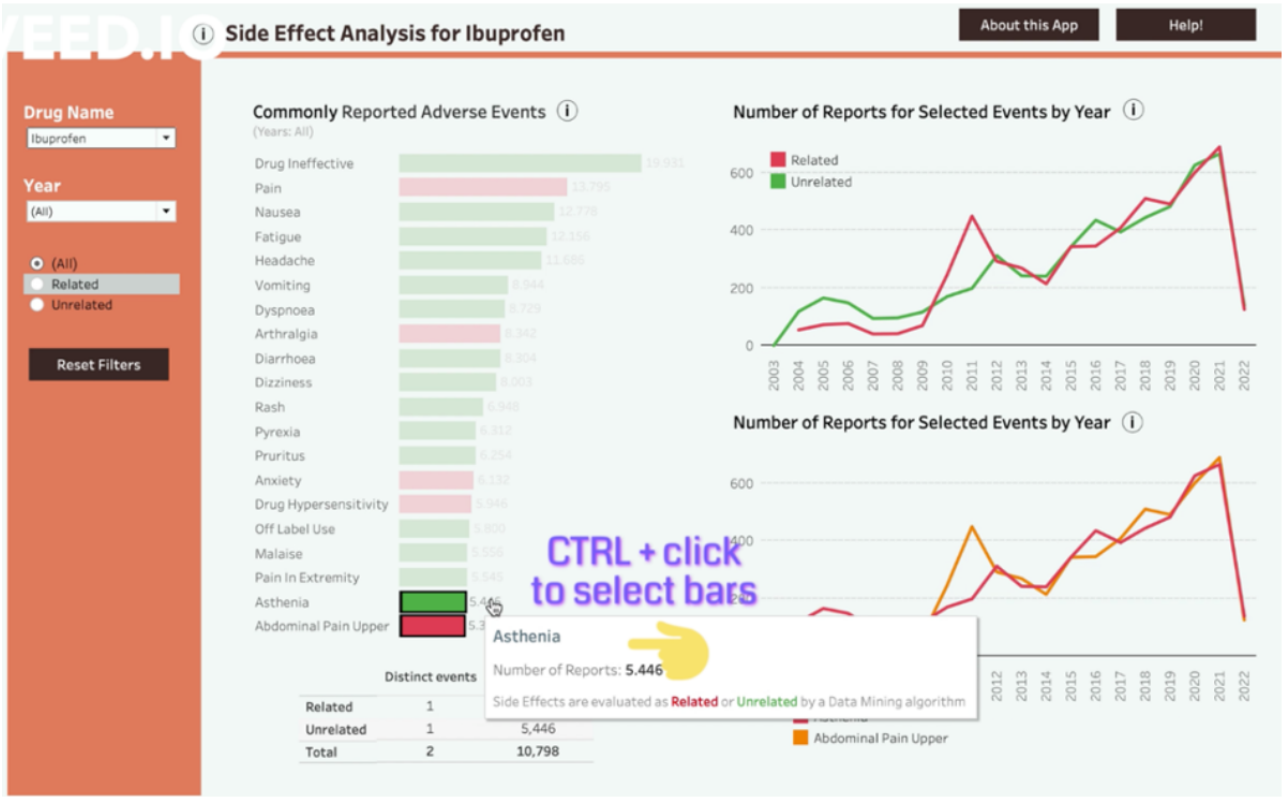

Emphasizing the Utility of Dashboard Elements

We addressed many usability issues by adding short labels to dashboard elements (Figures 9 and 10).

To better afford monitoring the progression of relevant states (DP1c), we included an info icon next to graphs and section headers. Users could see information about graph functionality and displayed data, as well as the explanation of complex terms. We also included information on the content of the overview and detail sections and explained how graphs interacted with each other.

Similarly, we expected the issue of insufficient visibility and unclear utility of some elements (eg, the event search field and the second line graph) would be addressed by including additional information in the tutorial (Figures S6 and S7 in Multimedia Appendix 3). Finally, we implemented the “About this App” section (Figure 11), where users could find information about the data source, safety signal evaluation, possible limitations to the tool, and external links.

Considering all the above, we refined the DPs: (1) DP1a: it provides features to address the bootstrap problem, add walkthrough videos, and explain dashboard elements**,** so that the system affords immediate use of the dashboard in drug safety surveillance. (2) DP1c: it provides features to track changes in the variables and highlight their utility, so that the system affords tracking of the progression of relevant states in drug safety surveillance.

XSL•FO
RenderX

Figure 9. Histogram with the info icon. Prototype v4.

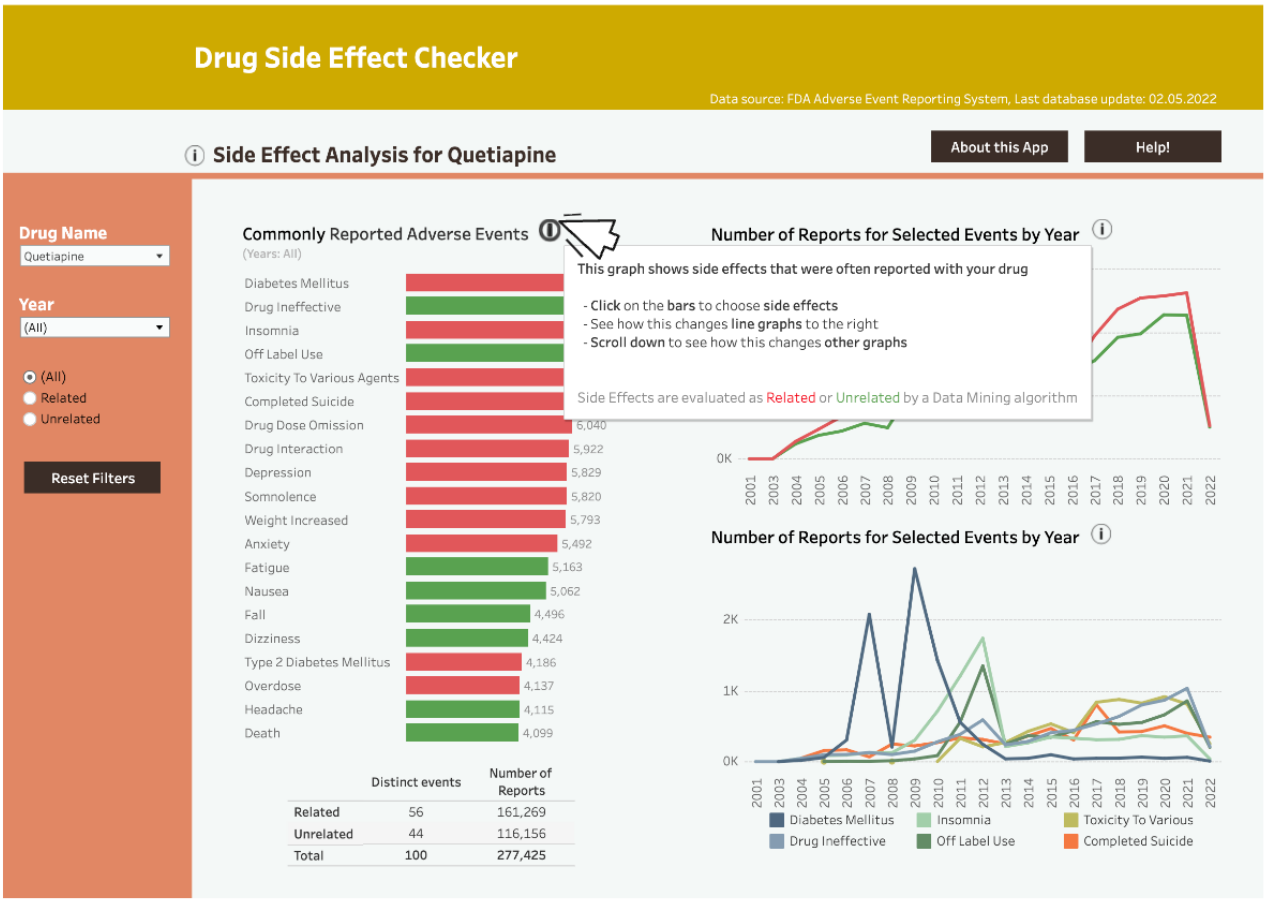

Figure 10. The overview section with the info icon. Prototype v4.

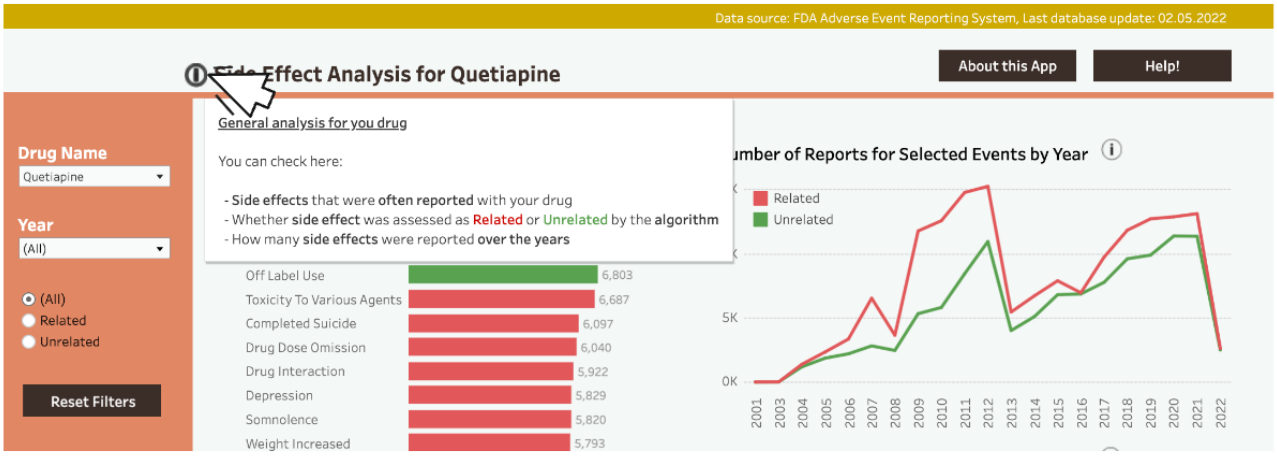

XSL•FO
RenderX

Figure 11. The About this App dashboard section. Prototype v4.

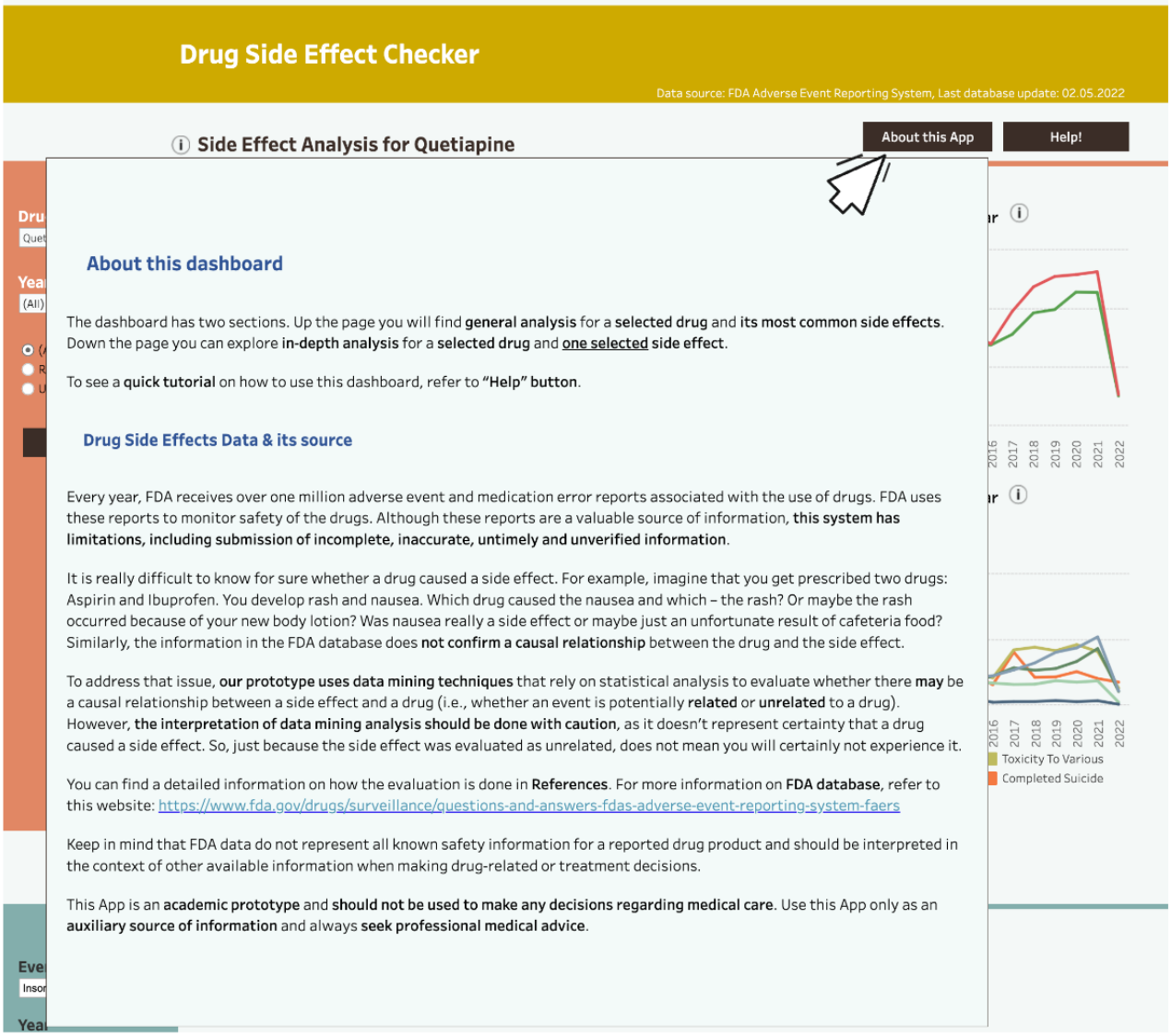

Signalizing the Uncertainty of Data Mining Results

To better afford identification of patterns and trends (DP1b), we added the information on the uncertainty behind DPA evaluation and advised caution when interpreting the results. Since safety signal detection can be used for hypothesis building, but not testing, we found it crucial to highlight these concepts. Safety signal detection is a starting point for further investigations, not a conclusion. Considering ethical and safety concerns, appropriate warnings are necessary.

We addressed all the above in several ways. First, we provided the explanation on the interpretation of DPA in a disclaimer (not shown) and in the About this App section. Accounting for users less familiar with the topic, we provided an illustrative real-world case scenario to explain the concepts. We also implemented the References button, providing the links to evaluation criteria and including similar information in the warning message (Figure 12). Finally, we added links to external resources on many occasions and further enriched DPA files in explanation. In line with the above, we refined the following DP: DP1b: it provides features to describe possible causality between variables and signalize uncertainty behind DPA results in different ways, so that the system affords identification of patterns and trends in drug safety surveillance.

Together, these changes replace specialist terminology with plain-language labels and confine full statistical detail to downloadable files, reducing cognitive load for lay users while preserving transparency for professional review.

XSL•FO
RenderX

Figure 12. (A) The warning message with the information on hover. (B) The References button with the information on hover. Prototype v4.

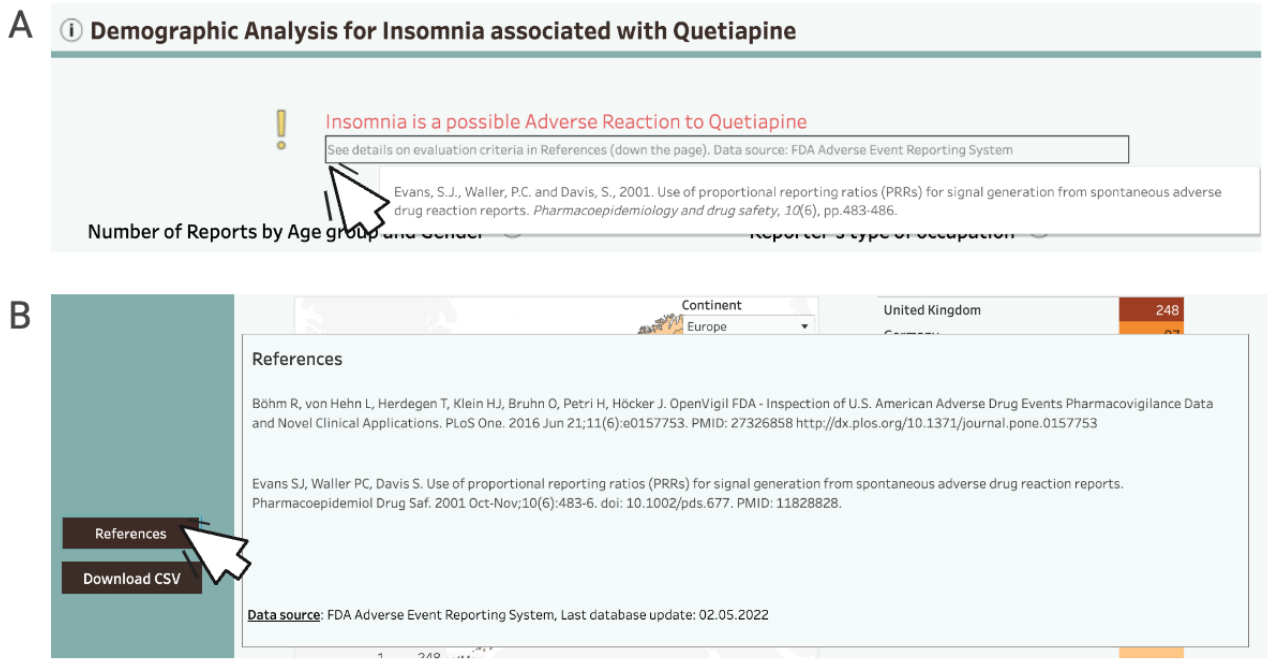

Improving the Usability of Other Elements

To address the usability issues related to the histogram, and to improve attention management while using the dashboard (DP2c), we relocated the histogram's filter to the upper-left corner, removed the confusing filter's name, and added a histogram's year filter with the information about the current year selection. We also implemented a Reset Filters button to unselect elements in the overview section (Figure 13).

To facilitate obtaining immediate practical benefits while using the dashboard (DP1a), we simplified the language and modified download options, removing redundant download buttons and files. With regard to evaluating alternatives of actions (DP3b), and considering different data granularity needs of users (DP2b), we removed safety signal reports from the background of the download page and simplified the view. Finally, we moved the download dialog box to the eye reach (Figure S8 in Multimedia Appendix 3).

The summary of all solutions implemented after usability testing is shown in Table S2 in Multimedia Appendix 4. The final version (v4) of the prototype was made available online [78]. We recommend using Google Chrome as a browser for a better experience.

XSL•FO
RenderX

Figure 13. Histogram with the side effect filter (All, Related, Unrelated), year filter, the Reset Filters button (bottom left), and information on current year selection (in fine print, gray). Prototype v4.

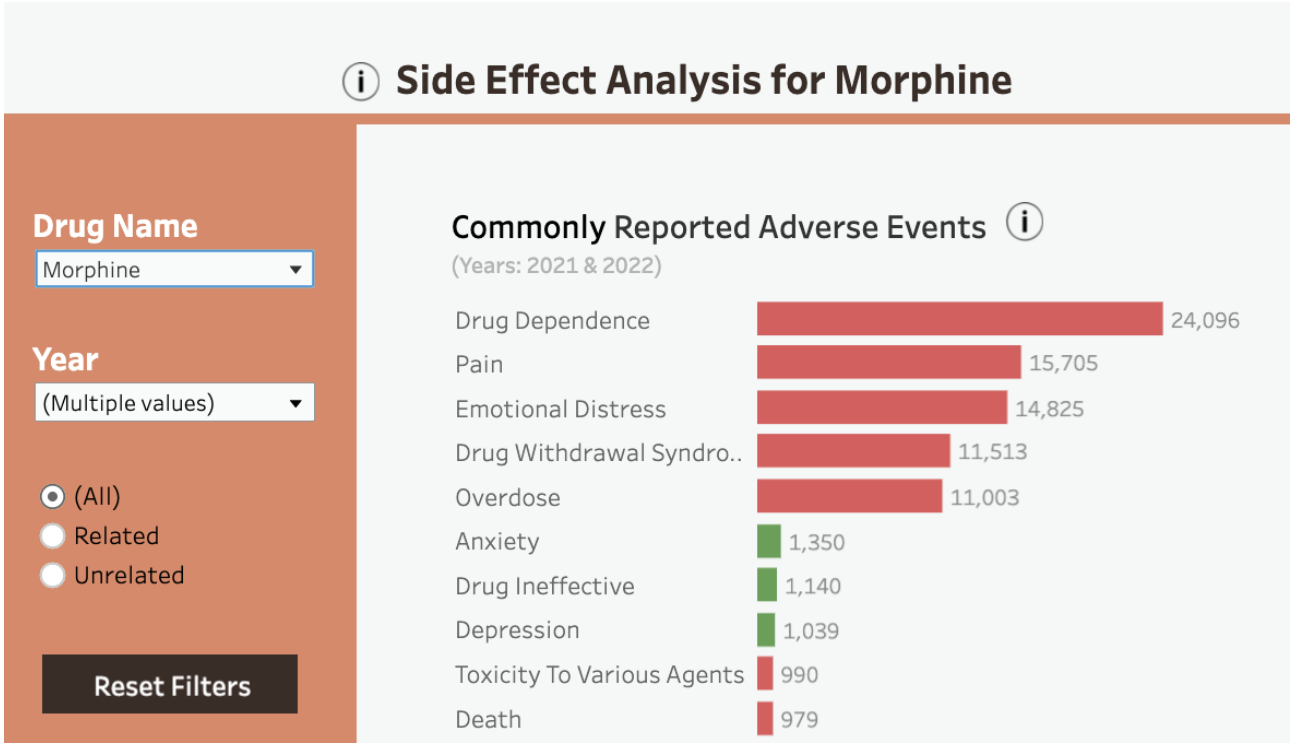

Demonstration and Evaluation: Heuristic Evaluation

We concluded the DSR cycle by performing heuristic evaluation (Figure 14). We identified 4 out of 10 usability factors with the lowest usability score: flexibility and efficiency of use (52%), user control and freedom (67%), visibility of system status (83%), and consistency and standards (83%). Two usability factors had the usability scores above 90%: recognition rather than recall (92%) and match between system and real world (93%), while 4 usability factors had the usability scores of 100%: aesthetic and minimalist design, orientation, spatial organization, and information coding, where the last 3 factors were related to dashboard visualization. The overall usability score was 84% (Table 5).

XSL•FO
RenderX

Figure 14. Usability scores per usability factor. Total is the overall usability score.

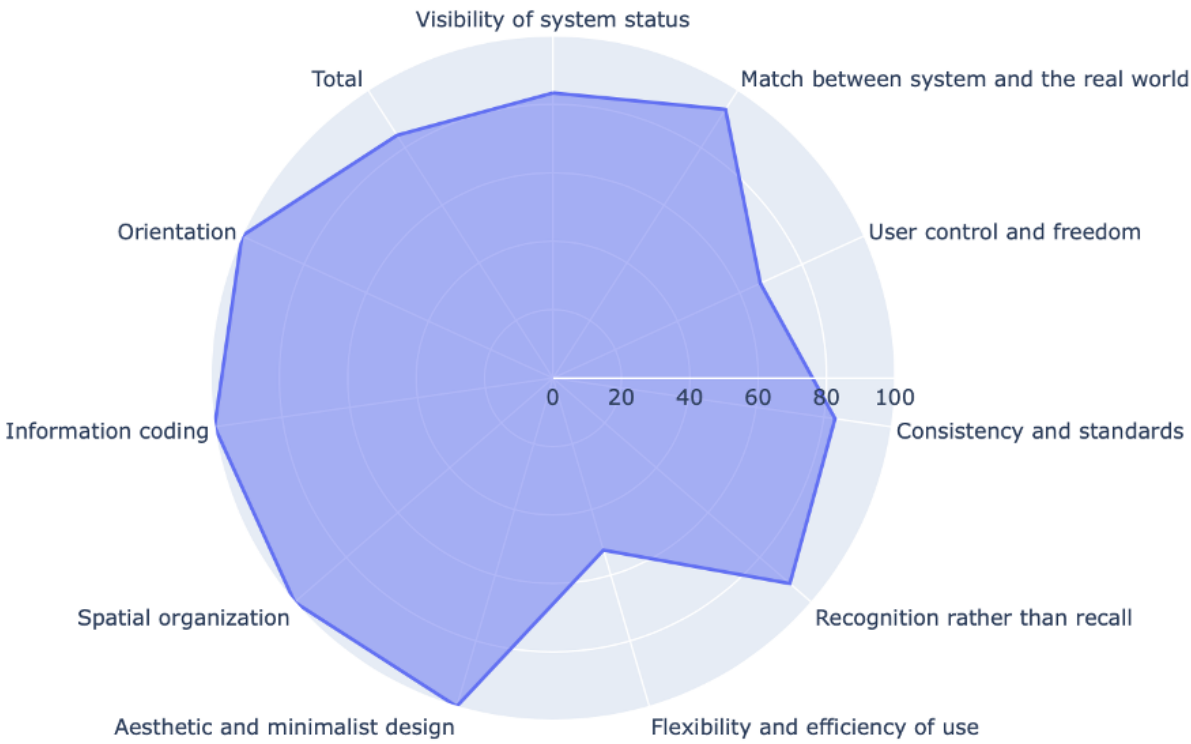

Table . A summary of usability factors with corresponding usability scores. Maximum score is a sum of close-ended questions per usability factor (eg, usability factor #9 had 2 questions, thus its maximum score was 2). E1, E2, and E3 are the scores assigned to each usability factor by each expert (ie, the sum of questions answered as yes by E1, E2, and E3). The result is the mean score divided by the maximum score, displayed as a percentage. Total is the overall usability score.

ID	Usability factor	Maximum score	E1	E2	E3	Mean score	Result (%)
1	Visibility of system status	6	5	5	5	5	83
2	Match between system and the real world	5	5	5	4	4.7	93
3	User control and freedom	5	4	3	3	3.3	67
4	Consistency and standards	6	5	4	6	5	83
5	Recognition rather than recall	4	4	3	4	3.7	92
6	Flexibility and efficiency of use	7	4	4	3	3.7	52
7	Aesthetic and minimalist design	7	7	7	7	7	100
8	Spatial organization	3	3	3	3	3	100
9	Information coding	2	2	2	2	2	100
10	Orientation	4	4	4	4	4	100
	Total	49	43	40	41	41	84

XSL•FO
RenderX

The overall severity ratings (Table 6) were in line with the obtained usability scores in most cases. Usability factor #3—user control and freedom was assigned the severity rating of 2 (minor usability problem), while the usability factor #1—visibility of system status was assigned the severity rating of 1 (cosmetic problem only) by all experts. Surprisingly, the usability factor #6—flexibility and efficiency of use, although it obtained the lowest overall usability score, was assigned the severity rating of 0 (no usability problem) by all experts. Several other usability factors were assigned the severity rating of 1 by some experts: usability factor #2—match between system and the real world (E3), usability factor #4—consistency and standards (E1), and usability factor #5—recognition rather than recall (E2). All remaining usability factors were evaluated as 0 (no usability problem).

The majority of usability issues referred to the flexibility and efficiency of use. We found evidence that the system lacked the ability to control display configurations and to hide unnecessary displays. Interestingly, although all participants noticed the lack of the option to hide unnecessary displays, it was not considered essential. According to E1: no buttons to hide or unhide panels, but not sure if the button is necessary. Information is well spread.

This could explain why this usability factor—although it obtained a relatively low usability score—was assigned an overall severity rating of 0 (no usability problem). Yet, as we saw a clear consensus regarding insufficient control of display configurations, we refined the following DP: DP2a: it provides features to support customized views and to control display configurations, so that the system affords examining different aspects of data in drug safety surveillance.

Table . Overall severity ratings assigned by experts (E1, E2, and E3) in heuristic evaluation.[a]

ID	Usability factor	Overall severity rating		
		E1	E2	E3
1	Visibility of system status	1	1	1
2	Match between system and the real world	0	0	1
3	User control and freedom	2	2	2
4	Consistency and standards	1	0	0
5	Recognition rather than recall	0	1	0
6	Flexibility and efficiency of use	0	0	0
7	Aesthetic and minimalist design	0	0	0
8	Spatial organization	0	0	0
9	Information coding	0	0	0
10	Orientation	0	0	0

[a] A score of 2: minor usability problem, 1: cosmetic problem only, 0: no usability problem.

Feedback also suggested that the system lacked clear exit options and a universal undo function, hindering user control and freedom. We also found support for the utility of the reset button; however, some participants noted that it did not deselect all elements when clicked. Regarding the visibility of system status**,** participants pointed out insufficient system feedback on its status. E3 identified a lack of visual feedback when selecting elements on some graphs. Although this action affected histograms, it was not communicated to the user. Similarly, E2 identified missing information on year selection in the detail section. Finally, concerning the consistency and standards**,** participants noted the absence of visual cues to identify active screens. E2 struggled to identify active screens when navigating between the main and download pages.

As a future agenda, we recommend implementing enhanced user control over display configurations, options to hide unnecessary displays, and adding a back or undo button. The functionality of the reset filters button should be improved to uniformly remove selections. Better feedback on the system status, like displaying selected years in the detail section, is crucial. Prompts and visual cues (eg, the event search box) should be placed where the eye is likely to be looking. Finally, all interactive elements (eg, the histogram and the first line graph) should provide feedback upon selection.

Discussion

DPs and the Value of Affordance Theory in This Study

Following the DSR methodology, we were able to empirically test and refine the initial, theory-driven DPs, by iteratively juxtaposing the results of experimental prototyping with theory-grounded, conceptual design recommendations. Consequently, we prove that the iterative translation of evaluation outcomes into prototype features results in refined design guidelines that could lead other practitioners in similar domains.

XSL•FO
RenderX

Throughout the study, we applied the affordance lens pragmatically: target affordances remained stable while prototype features were iteratively refined to instantiate them, which is in line with the view of Iivari [79] and Chandra et al [53]. Table 7 summarizes each principle in terms of user activity (affordance), enabling features (material properties), and the boundary conditions.

Table . The final list of refined design principles.

Design principle	Revised content
DP1a	Provide features to address the bootstrap problem, add walkthrough videos and explain dashboard elements, so that the system affords immediate use of the dashboard in drug safety surveillance
DP1b	Provide features to describe possible causality between variables and signalize uncertainty behind DPA[a] results in different ways, so that the system affords identification of patterns and trends in drug safety surveillance
DP1c	Provide features to track changes in the variables and highlight their utility, so that the system affords tracking of the progression of relevant states in drug safety surveillance
DP2a	Provide features to support customized views and to control display configurations, so that the system affords examining different aspects of data in drug safety surveillance
DP2b	Provide overview and details, while controlling overview-to-detail ratio, so that the system affords exploring data of different granularity levels in drug safety surveillance
DP2c	Provide features that stimulate attention, place important elements on the top-left area of the dashboard, and promote scrolling over pagination, so that the system affords improved attention management while using the dashboard in drug safety surveillance
DP3a	Provide features to create public values, so that the system affords users' engagement in dashboard use in drug safety surveillance
DP3b	Provide features to support decision-making and cluster them by the needs of distinct user groups, so that the system affords users to evaluate what-if scenarios and consider different alternatives in drug safety surveillance

[a]DPA: disproportionality analysis.

Addressing Existing Research Gaps

Our literature review identified pharmacovigilance systems that did not sufficiently incorporate user requirements, with resulting usability shortcomings [17,18,32]. We respond to this by using the DSR as a methodology. Additionally, this research gap was closely related to the bootstrap problem and DP1a (designing for direct use). We tackled the bootstrap problem in 2 ways: first, by including the requirements gathering phase in the design cycle, we increased the probability of addressing the real needs of users and therefore solving the right problem; second, by giving the users the opportunity to engage with the prototype in the initial stages of development, we initiated its use from the early versions. This positively affects the quality of the prototype and increases the chances of its successful adoption in the future. By iteratively responding to users' needs and targeting usability issues, we built a high-fidelity prototype that is usable for the evaluated tasks and user groups (overall usability score: 84%) and is designed to support sustained use; broader deployment remains future work.

We previously identified the lack of data mining techniques as a limitation of some of the systems for pharmacovigilance [17,21-23]. We suggested this was an important research gap to address, related directly to DP1b (causality between variables). We implemented DPA evaluation in the dashboard by including the information on potential safety signals [80]. We emphasized the uncertainty behind these results in multiple ways to make sure users were aware of their interpretation. Finally, the advantage of our prototype comes with improved visualization techniques. To that end, we followed the guidelines for visual dashboards by Bremser and Wagner [61] when deciding on visualization elements and features.

Consistent with DP3b ("cluster features by the needs of distinct user groups"), we view clinicians and pharmacists, researchers, and public users as distinct personas requiring layered functionality and language; our present DSR cycles cover the latter 2 groups (public users and research professionals), and clinician-facing tailoring should be undertaken in subsequent evaluations by others. In addition, regulatory decision-makers, policy analysts, and global health agencies represent further personas aligned with DP3b; though not evaluated here, they are recognized within our stakeholder scope and remain outside this study's boundary conditions.

Creating Public Value

Here, we articulate how the DPs and their instantiation can create public value when scaled and deployed in appropriate contexts; in this study, we assess feasibility and task-level usability rather than population-level impact.

XSL•FO
RenderX

We previously reviewed systems for pharmacovigilance that use proprietary databases or other data sources limited in diversity of stored information, volume, and availability [14-16,27,28]. To respond to this gap, related directly to DP3a (public value), we based the prototype on rich, open-access datasets with safety reports registered worldwide. In addition, both the code and the prototype are open-source and made available online, potentially contributing to the pharmacovigilance community. Moreover, through improved visualizations, we aim to enhance understanding and encourage users' active participation in interpreting the information.

To counter the misinformation during the COVID-19 pandemic, Murthy [81] recommends addressing information deficits where there is a high public interest but limited quality information available. Additionally, the author advocates for the modernization of public health communications by developing new, credible, and evidence-based online tools to effectively convey information to communities. By providing transparent and accurate drug safety data from reliable sources, our system may contribute to fighting misleading information and negative attitudes toward medication.

Our system is also a step forward in a higher degree of patient empowerment (the restoration of patients' access to public health data) and patient participation (the ability of patients to receive drug safety information and act upon it). In line with our findings, drug consumers could use the prototype for direct comparison of drugs with the same active compound, but produced by different manufacturers. Generic drugs (drug equivalents), although chemically the same as brand-name drugs (drugs produced by the pharmaceutical company that discovered them, protected by the patent), are often negatively perceived by drug consumers [82-84]. This is due to misbeliefs about brand-name drugs being better medicines per se.

There is strong evidence that, through a variety of incentives, medical doctors are influenced by pharmaceutical companies on which drugs to prescribe [85-88]. Physicians often enter contractual relationships with vendors, the latter being mostly representatives of brand-name drug companies, rather than cheaper generic drugs [89]. We suggest that by having a tool to directly compare primary safety profiles of drugs and their alternatives at hand, doctors may be encouraged to make more ethical decisions on their choice of collaboration with pharmaceutical companies.

Enhancing the Decision-Making

We integrated exportable DPA files into the prototype, considering them the main enabler of decision-making. When combined with data visualizations, this feature can significantly benefit pharmacovigilance professionals, including those affiliated with pharmaceutical industry or research institutes. These same affordances are pertinent to policy analysts and global health agencies, who require transparent, auditable summaries and cross-jurisdictional trend overviews. Detecting unusual or previously unknown drug-ADR associations is a first step in drug safety investigations [23,90]. Identified signals prompt further research, influencing actions such as product labelingchanges or potential drug withdrawal [91].

Regulatory bodies such as FDA, WHO, and EMA systematically monitor drug safety signals. Unusual associations undergo thorough scrutiny, involving literature reviews, clinical study revisions, and exploration of biochemical mechanisms. Results are compared with product information, and pharmaceutical companies are asked to provide relevant data, promoting higher industry accountability [91,92].

Contributions

Theoretical Contribution

Our work contributes to the prescriptive knowledge [93] by providing a list of refined, empirically-driven DPs. We suggest that, by delineating DPs, our work puts forward general design recommendations in similar solution domains. These can be extrapolated to a class of similar problems concerned with data visualization in pharmacovigilance. We do not claim the DPs are completely generalizable to other settings. Instead, they are put forward with the ambition to lead research on similar problems in wider contexts.

To our knowledge, there is no previous research that uses DSR methodology in designing dashboards for pharmacovigilance. By engaging in the DSR cycle, we were able to define affordances for similar systems, contributing to better understanding of the problem domain. These were (1) prompting users to engage with the dashboard (enabled by improved usability and attention management), (2) aiding analysis of what-if scenarios to support decision-making processes, (3) presenting data from different angles and at multiple granularity levels to examine its different facets, (4) showing changes in relevant variables over time, and (5) creating public value through generated insights.

Finally, we contribute to DSR by providing insights into how different requirements gathering and evaluation methods can support the development of visualization dashboards. While no claims can be made about the validity of these findings to other systems, we hope the techniques proposed here can be a useful instrument for identifying design issues early in the prototype development.

Practical Contribution

The practical contribution of our study lies in the developed artifact, publicly available online. Our system can be used by researchers and practitioners in pharmacovigilance, upon refinements. The code is open-source [94] and others can repurpose or reuse the scripts as partial solutions or inspiration for their projects. Though we confined our prototype to 5 drugs and 500 secondary events, the code can be adapted to an infinite number of drugs or secondary events to suit others' needs. For larger multisource deployments, the ETL and DPA steps can be executed in batches without altering the front end. Because the user interface consumes flat exports, the prototype can be reproduced in fully open-source dashboards or a custom front end.

The prototype is intended to demonstrate and operationalize the DPs. While usable for the studied tasks, broader public deployment requires the scale-up steps outlined in the next section. Any public-facing release by adopters would also

XSL•FO
RenderX

require clear plain-language disclaimers and risk communication for lay users, basic accessibility compliance, and a documented support pathway; these deployment activities are outside the scope of this study.

Our project however can be considered a hybrid open-source considering our reliance on the Tableau, which is a proprietary software. Table 8 provides an accurate description of the hybrid nature of our project with its respective components.

Finally, we do not claim full generalizability. The DPs are intended as reusable, prescriptive heuristics for similar dashboards within the stated boundary conditions; adaptation to clinician and pharmacist-facing workflows and additional user groups should be iteratively refined in those settings.

Table . Open-source status of project components.

Component	Status	Implication
Data	Open source	Fully accessible and usable by anyone
Code	Open source	All transformation and analysis code (eg, Python or R scripts) is on GitHub under an Open Source Initiative–approved license, allowing others to reuse and modify it
Dashboard prototype	Proprietary/Open access	The dashboard itself is viewable and accessible to anyone via Tableau Public (making it "open access"), but its dependency on proprietary Tableau software means others cannot easily reproduce, fork, or host a modified version without their own Tableau software or an equivalent proprietary viewer

Limitations and Future Research Agenda

This study has some limitations. First, drug safety surveillance can be viewed differently, leading to different affordances than those outlined here. Second, the DSR cycle could be extended to yet another phase. Iivari et al [95] proposes a framework for DPs evaluation in terms of their reusability: through the criteria of accessibility, importance, novelty, actability and effectiveness. Similarly, empirical testing of how revised DPs apply to other settings could be done through their repeated application in different boundary conditions [52]. Future research could address these issues to test the quality of the outcomes of this DSR project. Third, to support broader use, the prototype should be expanded to all FDA drugs and events via direct application programming interface calls [21].

Establishing readiness for broad public deployment of the prototype will require expanded datasets and multisite evaluations beyond the scope of this study. Moreover, including data from other databases (eg, EudraVigilance and VigiBase) would improve DPA evaluation, but requires (1) source-specific mapping into the common schema, (2) robust cross-repository deduplication, and (3) compliance with licensing and governance constraints. If further deployments are undertaken, evaluation can focus on user engagement, operational reliability, and decision support alignment with expert assessments, as these activities are beyond this study.

Relatedly, in the final prototype version, we keep shortcuts and advanced controls to a minimum to maintain clarity for nonprofessional users. This design choice explains the lower expert scores on flexibility, efficiency of use, and user control and freedom, which were nevertheless judged as low-severity issues. For expert-only deployments, future implementers can add more controls and configuration.

Importantly, our participant sample represented young and digitally proficient (late 20s to mid 40s), and several nonexpert participants held technical or professional roles (eg, data science, biomedical engineering, and humanitarian logistics). This sampling may limit generalizability to older adults and individuals with lower digital health literacy [96]. Older adults are more likely to experience polypharmacy [97] and may have distinct interaction needs (eg, larger text, higher contrast, simplified and error-tolerant interactions) [98], which we did not assess in this study. Future independent evaluations should specifically include older adults and lower-literacy users and consider accessibility guidance (eg, larger typographic scales, high-contrast palettes, and keyboard navigability) when adapting the dashboard for these groups.

Relatedly, some nonprofessional users found data mining terms challenging even when aided by tooltips and tutorials. The present prototype mitigates this by using plain-language labels, info icons, an "About this App" section, and by keeping advanced formulas in downloadable files; however, residual risk of misinterpretation remains. We therefore reiterate that DPA supports hypothesis generation rather than confirmation and should be interpreted cautiously by lay audiences. To reduce potential user anxiety, we emphasize this uncertainty in plain language and signpost users to seek professional advice for individual decisions. However, we did not evaluate affective outcomes (eg, worry and decisional conflict) among lay users; given the potential for spontaneous report dashboards to provoke anxiety, such outcomes should be assessed in independent evaluations by others.

Furthermore, it would be beneficial to implement a higher variety of data sources: scientific literature, clinical studies or data from text mining [20]. Also, the prototype would benefit from comprehensive benchmarking, such as head-to-head comparisons with existing pharmacovigilance tools on performance, cost, or user satisfaction. Future work could also

XSL•FO
RenderX

expand DPA methods to improve the validity of detected safety signals. Integrating and systematically evaluating additional machine learning approaches for ADR signal detection could enhance analytical breadth and validate performance across settings.

Finally, integration into health care IIs (eg, electronic health records) was outside the scope of this DSR prototype. The artifact targets public FDA data and does not process identifiable patient records. Any operational deployment by adopters would require institutional governance (eg, data use agreements, access control, auditability, and security increase) and, where applicable, compliance with jurisdictional regulations. The use of standard terminologies, decoupled Python scripts, and portability to open source (Multimedia Appendix 2) is intended to ease such translation, but we do not evaluate these deployment aspects here.

Conclusion

In this study, we applied the DSR cycle to investigate the design of visual dashboards to support activities within pharmacovigilance. To that end, we identified required affordances, developed corresponding DPs that satisfied them, and demonstrated their implementation, showing that they brought about expected outcomes. The developed DPs are anticipated to be applicable in various pharmacovigilance settings. Finally, we hope our research will be a catalyst of further research in similar domains.

Acknowledgments

All figures were created with BioRender [98].

Funding

No external financial support or grants were received from any public, commercial, or not-for-profit entities for the research, authorship, or publication of this article.

Data Availability

The datasets generated or analyzed during this study are available in the AdverseDrugEventPipeline repository [93].

Conflicts of Interest

None declared.

Multimedia Appendix 1
Demographics of the target groups.
[DOCX File, 15 KB - medinform_v14i1e75936_app1.docx]

Multimedia Appendix 2
Design science research approach details.
[DOCX File, 20 KB - medinform_v14i1e75936_app2.docx]

Multimedia Appendix 3
Prototype in Tableau.
[DOCX File, 6699 KB - medinform_v14i1e75936_app3.docx]

Multimedia Appendix 4
Usability testing and an overview of solutions implemented.
[DOCX File, 22 KB - medinform_v14i1e75936_app4.docx]

References

1. Das S. Predicting unknown adverse drug reactions using an unsupervised node embedding algorithm. : Massachusetts Institute of Technology; 2019 URL: https://dspace.mit.edu/handle/1721.1/124239 [accessed 2026-01-21]
2. Adedapo ADA, Adedeji WA, Adedapo IA, Adedapo KS. Cohort study on adverse drug reactions in adults admitted to the medical wards of a tertiary hospital in Nigeria: prevalence, incidence, risk factors and fatality. Br J Clin Pharmacol 2021 Apr;87(4):1878-1889. [doi: 10.1111/bcp.14577] [Medline: 32991765]
3. Giardina C, Cutroneo PM, Mocciaro E, et al. Adverse drug reactions in hospitalized patients: results of the FORWARD (Facilitation of Reporting in Hospital Ward) study. Front Pharmacol 2018;9:350. [doi: 10.3389/fphar.2018.00350] [Medline: 29695966]

XSL•FO
RenderX

4. Zaidi AS, Peterson GM, Bereznicki LRE, Curtain CM, Salahudeen MS. Ten-year trends in adverse drug reaction-related hospitalizations among people with dementia. Ther Adv Drug Saf 2022;13:20420986221080796. [doi: 10.1177/20420986221080796] [Medline: 35295667]
5. World Health Organization. In: Takanashi F, editor. WHO Pharmaceuticals Newsletter - No 1, 2022: World Health Organization; 2022:978-992.
6. Slight SP, Seger DL, Franz C, Wong A, Bates DW. The national cost of adverse drug events resulting from inappropriate medication-related alert overrides in the United States. J Am Med Inform Assoc 2018 Sep 1;25(9):1183-1188. [doi: 10.1093/jamia/ocy066] [Medline: 29939271]
7. Field TS, Gilman BH, Subramanian S, Fuller JC, Bates DW, Gurwitz JH. The costs associated with adverse drug events among older adults in the ambulatory setting. Med Care 2005 Dec;43(12):1171-1176. [doi: 10.1097/01.mlr.0000185690.10336.70] [Medline: 16299427]
8. Al Khaja KAJ, AlKhaja AK, Sequeira RP. Drug information, misinformation, and disinformation on social media: a content analysis study. J Public Health Policy 2018 Aug;39(3):343-357. [doi: 10.1057/s41271-018-0131-2] [Medline: 29795521]
9. Chou WYS, Oh A, Klein WMP. Addressing health-related misinformation on social media. JAMA 2018 Dec 18;320(23):2417-2418. [doi: 10.1001/jama.2018.16865] [Medline: 30428002]
10. Daei A, Soleymani MR, Ashrafi-Rizi H, Zargham-Boroujeni A, Kelishadi R. Clinical information seeking behavior of physicians: a systematic review. Int J Med Inform 2020 Jul;139:104144. [doi: 10.1016/j.ijmedinf.2020.104144] [Medline: 32334400]
11. O'Mathúna DP. How should clinicians engage with online health information? AMA J Ethics 2018 Nov 1;20(11):E1059-E1066. [doi: 10.1001/amajethics.2018.1059] [Medline: 30499435]
12. Dorfman S. What physicians want and need: insights from CMI/compas media vitals research. PM360. 2019. URL: https://www.pm360online.com/what-physicians-want-and-need-insights-from-cmi-compas-media-vitals-research/ [accessed 2026-01-21]
13. Swire-Thompson B, Lazer D. Public health and online misinformation: challenges and recommendations. Annu Rev Public Health 2020 Apr 2;41:433-451. [doi: 10.1146/annurev-publhealth-040119-094127] [Medline: 31874069]
14. Duke J, Faiola A, Kharrazi H. A novel visualization tool for evaluating medication side-effects in multi-drug regimens. In: Jacko JA, editor. Presented at: Human-Computer Interaction Interacting in Various Application Domains: 13th International Conference, HCI International 2009; Jul 19-24, 2009. [doi: 10.1007/978-3-642-02583-9_52]
15. Wei JX, Zhu YX, Sun J, Xu HM, Li M, Sun YH. ADRVis: an information visualization platform for adverse drug reactions. IJUNESST 2015 Oct 31;8(10):139-150. [doi: 10.14257/ijunesst.2015.8.10.14]
16. Shoshi A, Hoppe T, Kormeier B, Ogultarhan V, Hofestädt R. GraphSAW: a web-based system for graphical analysis of drug interactions and side effects using pharmaceutical and molecular data. BMC Med Inform Decis Mak 2015 Feb 28;15:15. [doi: 10.1186/s12911-015-0139-5] [Medline: 25881043]
17. Kumar A. The newly available FAERS public dashboard: implications for health care professionals. Hosp Pharm 2019 Apr;54(2):75-77. [doi: 10.1177/0018578718795271] [Medline: 30923396]
18. Vingen D, Andrews EJ, Ferati M. Usability in patient-oriented drug interaction checkers—a Scandinavian sampling and heuristic evaluation. Informatics (MDPI) 2020;7(4):42. [doi: 10.3390/informatics7040042]
19. Fukazawa C, Hinomura Y, Kaneko M, Narukawa M. Significance of data mining in routine signal detection: analysis based on the safety signals identified by the FDA. Pharmacoepidemiol Drug Saf 2018 Dec;27(12):1402-1408. [doi: 10.1002/pds.4672] [Medline: 30324671]
20. Duggirala HJ, Tonning JM, Smith E. Data mining at FDA – white paper. US Food and Drug Administration. 2018. URL: https://www.fda.gov/media/91848/download [accessed 2026-01-21]
21. FDA aes reporting system (FAERS) public dashboard. Food and Drug Administration. 2017 Sep. URL: https://www.fda.gov/Drugs/GuidanceComplianceRegulatoryInformation/Surveillance/AdverseDrugEffects/ucm070093.htm [accessed 2022-01-16]
22. VigiBase - the WHO global database. Uppsala Monitoring Centre. 2021 Dec. URL: https://who-umc.org/vigibase/vigibase-services/ [accessed 2022-08-07]
23. EudraVigilance. European Medicines Agency. 2022 Jun. URL: https://www.ema.europa.eu/en/human-regulatory/research-development/pharmacovigilance/eudravigilance [accessed 2022-08-08]
24. Duggirala HJ, Tonning JM, Smith E, et al. Use of data mining at the Food and Drug Administration. J Am Med Inform Assoc 2016 Mar;23(2):428-434. [doi: 10.1093/jamia/ocv063] [Medline: 26209436]
25. Guide on the interpretation of spontaneous case reports of suspected adverse reactions to medicines. inspections, human medicines pharmacovigilance and committees. European Medicines Agency. 2011. URL: https://www.ema.europa.eu/en/documents/report/guide-interpretation-spontaneous-case-reports-suspected-adverse-reactions-medicines_en.pdf [accessed 2026-01-21]
26. Signal management at UMC. Uppsala Monitoring Centre. 2022 Mar 23. URL: https://who-umc.org/signal-work/signal-detection/ [accessed 2022-03-23]
27. Roosan D, Li Y, Law A, et al. Improving medication information presentation through interactive visualization in mobile apps: human factors design. JMIR Mhealth Uhealth 2019 Nov 25;7(11):e15940. [doi: 10.2196/15940] [Medline: 31763991]

XSL•FO
RenderX

28. Sorbello A, Ripple A, Tonning J, et al. Harnessing scientific literature reports for pharmacovigilance. Prototype software analytical tool development and usability testing. Appl Clin Inform 2017 Mar 22;8(1):291-305. [doi: 10.4338/ACI-2016-11-RA-0188] [Medline: 28326432]
29. Defer G, Le Caignec F, Fedrizzi S, et al. Dedicated mobile application for drug adverse reaction reporting by patients with relapsing remitting multiple sclerosis (Vigip-SEP study): study protocol for a randomized controlled trial. Trials 2018 Mar 9;19(1):174. [doi: 10.1186/s13063-018-2560-4] [Medline: 29523169]
30. Delio J, Catalanotti JS, Marko K, et al. Integrating adverse event reporting into a free-text mobile application used in daily workflow increases adverse event reporting by physicians. Am J Med Qual 2020;35(5):374-379. [doi: 10.1177/1062860619891995] [Medline: 31795736]
31. Rubin DS, Pesyna C, Jakubczyk S, Liao C, Tung A. Introduction of a mobile adverse event reporting system is associated with participation in adverse event reporting. Am J Med Qual 2019;34(1):30-35. [doi: 10.1177/1062860618781920] [Medline: 29938520]
32. Corrao NJ, Robinson AG, Swiernik MA, Naeim A. Importance of testing for usability when selecting and implementing an electronic health or medical record system. J Oncol Pract 2010 May;6(3):120-124. [doi: 10.1200/JOP.200017] [Medline: 20808553]
33. Bae JH, Baek YH, Lee JE, Song I, Lee JH, Shin JY. Machine learning for detection of safety signals from spontaneous reporting system data: example of nivolumab and docetaxel. Front Pharmacol 2020;11:602365. [doi: 10.3389/fphar.2020.602365] [Medline: 33628176]
34. Lee H, Kim JH, Choe YJ, Shin JY. Safety surveillance of pneumococcal vaccine using three algorithms: disproportionality methods, empirical Bayes geometric mean, and tree-based scan statistic. Vaccines (Basel) 2020 May 22;8(2):242. [doi: 10.3390/vaccines8020242] [Medline: 32456068]
35. Omar NE, Fahmy Soliman AI, Eshra M, Saeed T, Hamad A, Abou-Ali A. Postmarketing safety of anaplastic lymphoma kinase (ALK) inhibitors: an analysis of the FDA Adverse Event Reporting System (FAERS). ESMO Open 2021 Dec;6(6):100315. [doi: 10.1016/j.esmoop.2021.100315] [Medline: 34864500]
36. Xiao C, Li Y, Baytas IM, Zhou J, Wang F. An MCEM framework for drug safety signal detection and combination from heterogeneous real world evidence. Sci Rep 2018 Jan 29;8(1):1806. [doi: 10.1038/s41598-018-19979-7] [Medline: 29379048]
37. Böhm R. Primer on disproportionality analysis. OpenVigil. 2018 Oct. URL: http://openvigil.sourceforge.net/doc/DPA.pdf [accessed 2022-02-07]
38. Caster O, Sandberg L, Bergvall T, Watson S, Norén GN. vigiRank for statistical signal detection in pharmacovigilance: first results from prospective real‐world use. Pharmacoepidemiol Drug Saf 2017 Aug;26(8):1006-1010 [FREE Full text] [doi: 10.1002/pds.4247]
39. Dimitriadis VK, Gavriilidis GI, Natsiavas P. Pharmacovigilance and clinical environment: utilizing OMOP-CDM and OHDSI software stack to integrate EHR data. Stud Health Technol Inform 2021 May 27;281:555-559. [doi: 10.3233/SHTI210232] [Medline: 34042637]
40. Budha MS, Khan J, Mujawar DT. Review on pharmacovigilance method, recent developments, future perspective and software. IJRASET 2024;12(2):251-255 [FREE Full text] [doi: 10.22214/ijraset.2024.58231]
41. Pilipiec P, Liwicki M, Bota A. Using machine learning for pharmacovigilance: a systematic review. Pharmaceutics 2022 Jan 23;14(2):266. [doi: 10.3390/pharmaceutics14020266] [Medline: 35213998]
42. Li Y, Tao W, Li Z, et al. Artificial intelligence-powered pharmacovigilance: a review of machine and deep learning in clinical text-based adverse drug event detection for benchmark datasets. J Biomed Inform 2024 Apr;152:104621. [doi: 10.1016/j.jbi.2024.104621] [Medline: 38447600]
43. R P, Andrews S D, GS N. Advancing drug safety surveillance: a review of AI techniques and strategies for improving pharmacovigilance and adverse event reporting. Int J Res Publ Rev 2024;5(5):13348-13351. [doi: 10.55248/gengpi.5.0524.1468]
44. Yu HM, Huang YM, Xiao J, et al. Establishment of a visualization platform for ADR query and analysis: an example of severe skin adverse reactions caused by sulfonylureas. Eur J Clin Pharmacol 2025 Jul;81(7):1055-1067. [doi: 10.1007/s00228-025-03842-6]
45. Ansari B, Martin EG. Integrating human-centered design in public health data dashboards: lessons from the development of a data dashboard of sexually transmitted infections in New York State. J Am Med Inform Assoc 2024 Jan 18;31(2):298-305. [doi: 10.1093/jamia/ocad102] [Medline: 37330670]
46. Malkani M, Madan E, Malkani D, et al. Rank ordered design attributes for health care dashboards including artificial intelligence: usability study. Online J Public Health Inform 2024 Nov 20;16(1):e58277. [doi: 10.2196/58277] [Medline: 39566038]
47. Gavriilidis GI, Dimitriadis VK, Jaulent MC, Natsiavas P. Identifying actionability as a key factor for the adoption of “Intelligent” systems for drug safety: lessons learned from a user-centred design approach. Drug Saf 2021 Nov;44(11):1165-1178. [doi: 10.1007/s40264-021-01103-w] [Medline: 34674190]
48. Murphy DR, Savoy A, Satterly T, Sittig DF, Singh H. Dashboards for visual display of patient safety data: a systematic review. BMJ Health Care Inform 2021 Oct;28(1):e100437. [doi: 10.1136/bmjhci-2021-100437] [Medline: 34615664]

XSL•FO
RenderX

49. Gibson JJ. The theory of affordances. In: Shaw R, Bransford J, editors. Perceiving, Acting, and Knowing: Toward an Ecological Psychology: Lawrence Erlbaum Associates; 1977:67-82.
50. Pan SL, Li M, Pee LG, Sandeep MS. Sustainability design principles for a wildlife management analytics system: an action design research. Eur J Inf Syst 2021 Jul 4;30(4):452-473. [doi: 10.1080/0960085X.2020.1811786]
51. Maier JRA, Fadel GM. Affordance based design: a relational theory for design. Res Eng Design 2009 Mar;20(1):13-27. [doi: 10.1007/s00163-008-0060-3]
52. Seidel S, Chandra Kruse L, Székely N, Gau M, Stieger D. Design principles for sensemaking support systems in environmental sustainability transformations. Eur J Inf Syst 2018 Mar 4;27(2):221-247. [doi: 10.1057/s41303-017-0039-0]
53. Chandra L, Seidel S, Gregor S. Prescriptive knowledge in IS research: conceptualizing design principles in terms of materiality, action, and boundary conditions. Presented at: 2015 48th Hawaii International Conference on System Sciences (HICSS); HI, USA p. 4039-4048. [doi: 10.1109/HICSS.2015.485]
54. Sein MK, Henfridsson O, Purao S, Rossi M, Lindgren R. Action Design Research1. MIS Q 2011 Mar 1;35(1):37-56. [doi: 10.2307/23043488]
55. Baskerville R, Baiyere A, Gergor S, et al. Design science research contributions: finding a balance between artifact and theory. J Assoc Iinform Syst 2018;19(5):358-376. [doi: 10.17705/1jais.00495]
56. Aanestad M, Jensen TB. Building nation-wide information infrastructures in healthcare through modular implementation strategies. J Strateg Inf Syst 2011 Jun;20(2):161-176. [doi: 10.1016/j.jsis.2011.03.006]
57. Hanseth O, Lyytinen K. Design theory for dynamic complexity in information infrastructures: the case of building internet. J Inf Technol 2010 Mar;25(1):1-19. [doi: 10.1057/jit.2009.19]
58. Recker J. Improving the state-tracking ability of corona dashboards. Eur J Inf Syst 2021 Sep 3;30(5):476-495. [doi: 10.1080/0960085X.2021.1907235]
59. Matheus R, Janssen M, Maheshwari D. Data science empowering the public: data-driven dashboards for transparent and accountable decision-making in smart cities. Gov Inf Q 2020 Jul;37(3):101284. [doi: 10.1016/j.giq.2018.01.006]
60. Toreini P, Langner M, Maedche A, et al. Designing attentive information dashboards. J Assoc Inform Syst 2022;22(2):521-552. [doi: 10.17705/1jais.00732]
61. Bremser W, Wagner WP. Developing dashboards for performance management. CPA J 2013;83(7):62-67.
62. Thyvalikakath TP, Monaco V, Thambuganipalle H, Schleyer T. Comparative study of heuristic evaluation and usability testing methods. Stud Health Technol Inform 2009;143:322-327. [Medline: 19380955]
63. Sauro J, Lewis JR. Quantifying the User Experience: Practical Statistics for User Research, 2nd edition: Morgan Kaufmann; 2016:356.
64. Dowding D, Merrill JA. The development of heuristics for evaluation of dashboard visualizations. Appl Clin Inform 2018 Jul;9(3):511-518. [doi: 10.1055/s-0038-1666842] [Medline: 29998455]
65. Peffers K, Tuunanen T, Rothenberger MA, Chatterjee S. A design science research methodology for information systems research. J Manag Inf Syst 2007 Dec;24(3):45-77. [doi: 10.2753/MIS0742-1222240302]
66. Beard L, Aghassibake N. Tableau (version 2020.3). J Med Libr Assoc 2021;109(1). [doi: 10.5195/jmla.2021.1135]
67. Statista OTC pharmaceuticals - worldwide. Statista. 2022. URL: https://www.statista.com/outlook/hmo/otc-pharmaceuticals/worldwide?srsltid=AfmBOoqOJV3dvb5VZaEczqUObuIS58T7fc9X1lQ43jIXDhkHj97tbJcK [accessed 2026-01-22]
68. Liang S, Fu Y. Voice meeting notes & real-time transcription. Otter.ai. 2016. URL: Otter.ai [accessed 2026-01-22]
69. Khanbhai M, Symons J, Flott K, et al. Enriching the value of patient experience feedback: web-based dashboard development using co-design and heuristic evaluation. JMIR Hum Factors 2022 Feb 3;9(1):e27887. [doi: 10.2196/27887] [Medline: 35113022]
70. Nielsen J. Finding usability problems through heuristic evaluation. 1992 Presented at: Proceedings of the SIGCHI Conference on Human Factors in Computing Systems - CHI '92. [doi: 10.1145/142750.142834]
71. Nielsen J. Usability Inspection Methods: John Wiley and Sons; 1994.
72. Georgsson M, Staggers N, Weir C. A modified user-oriented heuristic evaluation of a mobile health system for diabetes self-management support. Comput Inform Nurs 2016 Feb;34(2):77-84. [doi: 10.1097/CIN.0000000000000209] [Medline: 26657618]
73. Snyder ME, Jaynes H, Gernant SA, et al. Alerts for community pharmacist-provided medication therapy management: recommendations from a heuristic evaluation. BMC Med Inform Decis Mak 2019 Jul 16;19(1):135. [doi: 10.1186/s12911-019-0866-0] [Medline: 31311532]
74. Gale NK, Heath G, Cameron E, Rashid S, Redwood S. Using the framework method for the analysis of qualitative data in multi-disciplinary health research. BMC Med Res Methodol 2013 Sep 18;13:117. [doi: 10.1186/1471-2288-13-117] [Medline: 24047204]
75. Rosemberg C. Turning usability testing data into action. Toptal. 2017 Apr 20. URL: https://www.toptal.com/designers/usability-testing/turning-usability-testing-data-into-action [accessed 2022-09-10]
76. Sveriges riksdag. Lag (2003:460) om etikprövning av forskning som avser människor [swedish ethical review act]. SFS 2003:460. 2003. URL: https://www.riksdagen.se/sv/dokument-och-lagar/dokument/svensk-forfattningssamling/lag-2003460-om-etikprovning-av-forskning-som_sfs-2003-460/ [accessed 2026-02-27]

XSL•FO
RenderX

77. Balboni K. Creating app walkthroughs (+ 4 walkthrough examples). Appcues. 2022 Apr 20. URL: https://www.appcues.com/blog/the-5-best-walkthrough-examples [accessed 2022-09-05]
78. Drug side effect checker. Tableau Public. 2022. URL: https://public.tableau.com/app/profile/cl.udio.pires4914/viz/DrugSideEffectChecker/DrugSideEffectChecker [accessed 2026-01-22]
79. Iivari J. A paradigmatic analysis of information systems as a design science. Scand J Inf Syst 2007;19:39-64 [FREE Full text]
80. Evans SJ, Waller PC, Davis S. Use of proportional reporting ratios (PRRs) for signal generation from spontaneous adverse drug reaction reports. Pharmacoepidemiol Drug Saf 2001;10(6):483-486. [doi: 10.1002/pds.677] [Medline: 11828828]
81. Murthy V. Confronting Health Misinformation: The U.S. Surgeon General's Advisory on Building a Healthy Information Environment. : Office of the Surgeon General (U.S.); 2021. [Medline: 34283416]
82. Sanchez CK. Patient perceptions of generic drugs: dispelling misconceptions. US Pharm 2016;41(6):36-41 [FREE Full text]
83. Dunne SS, Dunne CP. What do people really think of generic medicines? A systematic review and critical appraisal of literature on stakeholder perceptions of generic drugs. BMC Med 2015 Jul 29;13:173. [doi: 10.1186/s12916-015-0415-3] [Medline: 26224091]
84. Aivalli PK, Elias MA, Pati MK, et al. Perceptions of the quality of generic medicines: implications for trust in public services within the local health system in Tumkur, India. BMJ Glob Health 2017;2(Suppl 3):e000644. [doi: 10.1136/bmjgh-2017-000644] [Medline: 29531844]
85. Fickweiler F, Fickweiler W, Urbach E. Interactions between physicians and the pharmaceutical industry generally and sales representatives specifically and their association with physicians' attitudes and prescribing habits: a systematic review. BMJ Open 2017 Sep 27;7(9):e016408. [doi: 10.1136/bmjopen-2017-016408] [Medline: 28963287]
86. DeJong C, Aguilar T, Tseng CW, Lin GA, Boscardin WJ, Dudley RA. Pharmaceutical industry-sponsored meals and physician prescribing patterns for medicare beneficiaries. JAMA Intern Med 2016 Aug 1;176(8):1114-1122. [doi: 10.1001/jamainternmed.2016.2765] [Medline: 27322350]
87. Wazana A. Physicians and the pharmaceutical industry: is a gift ever just a gift? JAMA 2000 Jan 19;283(3):373-380. [doi: 10.1001/jama.283.3.373] [Medline: 10647801]
88. Mitchell AP, Trivedi NU, Gennarelli RL, et al. Are financial payments from the pharmaceutical industry associated with physician prescribing?: a systematic review. Ann Intern Med 2021 Mar;174(3):353-361. [doi: 10.7326/M20-5665] [Medline: 33226858]
89. Lieb K, Scheurich A. Contact between doctors and the pharmaceutical industry, their perceptions, and the effects on prescribing habits. PLoS One 2014;9(10):e110130. [doi: 10.1371/journal.pone.0110130] [Medline: 25330392]
90. Analyse your data in Vigilyze. Uppsala Monitoring Centre. 2022 May 13. URL: https://who-umc.org/pv-products/vigilyze/ [accessed 2022-08-08]
91. Regulation and prequalification. World Health Organization. 2021 Dec 21. URL: https://www.who.int/teams/regulation-prequalification/regulation-and-safety/pharmacovigilance [accessed 2022-08-07]
92. Ventola CL. Big data and pharmacovigilance: data mining for adverse drug events and interactions. P T 2018 Jun;43(6):340-351. [Medline: 29896033]
93. Gregor S. The nature of theory in information systems1. MIS Q 2006 Sep 1;30(3):611-642. [doi: 10.2307/25148742]
94. AdverseDrugEventPipeline. GitHub. 2022. URL: https://github.com/Malwoiniak/AdverseDrugEventPipeline [accessed 2025-11-15]
95. Iivari J, Rotvit Perlt Hansen M, Haj-Bolouri A. A proposal for minimum reusability evaluation of design principles. Eur J Inf Syst 2021 May 4;30(3):286-303. [doi: 10.1080/0960085X.2020.1793697]
96. European Commission. Digital Decade: Report on the State of the Digital Decade 2023: Publications Office of the European Union; 2023. [doi: 10.2759/318547]
97. OECD. Health at a Glance 2023: OECD Indicators: OECD Publishing; 2023. [doi: 10.1787/7a7afb35-en]
98. Budiu R, Pernice K. UX guidelines for older adults (ages 65 and older). : Nielsen Norman Group; 2024 URL: https://www.nngroup.com/reports/senior-citizens-on-the-web/ [accessed 2026-01-31]
99. BioRender. BioRender. URL: https://www.biorender.com [accessed 2026-02-18]

Abbreviations

ADR: adverse drug reaction
AI: artificial intelligence
DiP: dashboard in pharmacovigilance
DP: design principle
DPA: disproportionality analysis
DSR: design science research
EMA: European Medicines Agency
FAERS: Food and Drug Administration Adverse Events Reporting System

XSL•FO
RenderX

FDA: Food and Drug Administration
HCI: human-computer interaction
II: information infrastructure
OHDSI: Observational Health Data Sciences and Informatics
ROI: return on investment
UMC: Uppsala Monitoring Centre
WHO: World Health Organization

Edited by C Perrin; submitted 13.Apr.2025; peer-reviewed by A Azizi, D Helminski, T Lima; accepted 03.Jan.2026; published 27.Feb.2026.

Please cite as:
Kotowicz M, Ferati M, Chowdhury S, Martins Pires C
Design Principles for Interactive Dashboards in Drug Safety Surveillance: Design Science Research
JMIR Med Inform 2026;14:e75936
URL: https://medinform.jmir.org/2026/1/e75936
doi:10.2196/75936

© Malwina Kotowicz, Mexhid Ferati, Soumitra Chowdhury, Cláudio Martins Pires. Originally published in JMIR Medical Informatics (https://medinform.jmir.org), 27.Feb.2026. This is an open-access article distributed under the terms of the Creative Commons Attribution License (https://creativecommons.org/licenses/by/4.0/), which permits unrestricted use, distribution, and reproduction in any medium, provided the original work, first published in JMIR Medical Informatics, is properly cited. The complete bibliographic information, a link to the original publication on https://medinform.jmir.org/, as well as this copyright and license information must be included.

XSL•FO
RenderX

Mild Cognitive Impairment Detection System Based on Unstructured Spontaneous Speech: Longitudinal Dual-Modal Framework

Yu-Shan Liao[1], MSc; Thiri Wai[2], MSc; Ting-Yun Liao[1], MSc; Ho-Ling Chang[1], MSc; Yu-Ling Chang[3], PhD; Li-Chen Fu[2,4], MSc, PhD

[1]Graduate Institute of Networking and Multimedia, National Taiwan University, Taipei, Taiwan

[2]Department of Computer Science and Information Engineering, National Taiwan University, No. 1, Sec 4, Roosevelt Rd, Taipei, Taiwan

[3]Department of Psychology, National Taiwan University, Taipei, Taiwan

[4]Center of Artificial intelligence Research, University of Tsukuba, Tsukuba, Ibaraki, Japan

Corresponding Author:
Li-Chen Fu, MSc, PhD
Department of Computer Science and Information Engineering, National Taiwan University, No. 1, Sec 4, Roosevelt Rd, Taipei, Taiwan

Abstract

Background: In recent years, the incidence of cognitive diseases has also risen with the significant increase in population aging. Among these diseases, Alzheimer disease constitutes a substantial proportion, placing a high-cost burden on health care systems. To give early treatment and slow the progression of patient deterioration, it is crucial to diagnose mild cognitive impairment (MCI), a transitional stage.

Objective: In this study, we use autobiographical memory (AM) test speech data to establish a dual-modal longitudinal cognitive detection system for MCI. The AM test is a psychological assessment method that evaluates the cognitive status of subjects as they freely narrate important life experiences.

Methods: Identifying hidden disease-related information in unstructured, spontaneous speech is more difficult than in structured speech. To improve this process, we use both speech and text data, which provide more clues about a person's cognitive state. In addition, to track how cognition changes over time in spontaneous speech, we introduce an aging trajectory module. This module uses local and global alignment loss functions to better learn time-related features by aligning cognitive changes across different time points.

Results: In our experiments on the Chinese dataset, the longitudinal model incorporating the aging trajectory module achieved area under the receiver operating characteristic curve of 0.85 and 0.89 on 2 datasets, respectively, showing significant improvement over cross-sectional, single time point models. We also conducted ablation studies to verify the necessity of the proposed aging trajectory module. To confirm that the model not only applies to AM test data, we used part of the model to evaluate the performance on the ADReSSo dataset, a single time point semistructured data for validation, with results showing an accuracy exceeding 0.88.

Conclusions: This study presents a noninvasive and scalable approach for early MCI detection by leveraging AM speech data across multiple time points. Through dual-modal analysis and the introduction of an aging trajectory module, our system effectively captures cognitive decline trends over time. Experimental results demonstrate the method's robustness and generalizability, highlighting its potential for real-world, long-term cognitive monitoring.

(JMIR Med Inform 2026;14:e80883) doi:10.2196/80883

KEYWORDS

mild cognitive impairment; longitudinal speech analysis; multimodal fusion; Alzheimer disease detection; deep learning; autobiographical memory test

Introduction

Alzheimer disease (AD) is a neurodegenerative disorder often associated with memory decline, language impairment, and a diminishing capacity to perform daily activities independently. However, AD remains incurable. Current research indicates that approximately 47 million people were diagnosed with dementia in 2015 [1], and it is expected that the number will triple by 2050 [2]. Such forecasts pose a significant burden on both patients' families and health care systems.

XSL•FO
RenderX

Within the spectrum of cognitive health, an intermediary stage exists between a state of normalcy and the onset of AD, denoted as mild cognitive impairment (MCI). Patients with MCI do not exhibit significant cognitive symptoms compared with those with AD. Those patients are still capable of performing daily activities independently. According to the study by Petersen et al [3], an estimated 16% of individuals with MCI progress to dementia within a year. Therefore, early identification of MCI holds significant value in instigating interventions aimed at impeding the advancement of dementia. However, the detection of MCI presents a notable challenge due to the subtle manifestation of its symptoms.

While biomarkers have demonstrated sensitivity in identifying MCI, such as positron emission tomography and magnetic resonance imaging [4,5], many of them necessitate invasive procedures. The associated costs of data collection for such methods are relatively high. Conversely, leveraging voice data for cognitive assessment offers a simpler and more suitable approach for long-term monitoring of cognitive status. Our approach relies on using autobiographical memory (AM) test data as the primary input [6], wherein interviewers engage participants in a series of questions and answers regarding their life experiences. This method, resembling a casual conversation, is more approachable than other psychological test methods because it reduces the testing stress experienced by participants.

Longitudinal analysis for MCI detection based on speech data remains relatively unexplored compared with other data types, such as magnetic resonance imaging, resulting in a scarcity of research in this area. The research proposed by Al-Hameed et al [7] focuses on extracting solely acoustic features from speech data collected across multiple visits from DementiaBank, which primarily pertains to speech associated with picture description tasks. They aim to predict participants' Mini-Mental State Examination scores and cognitive labels. Following feature selection, they used support vector machine or stochastic gradient descent for prediction. Integrating data from 3 visits achieved a 90% accuracy in distinguishing between healthy control (HC) and MCI in a binary classification task. However, due to label imbalance in the dataset, accuracy as a metric may not be entirely equitable. This study demonstrates that incorporating features from previous visits enhances prediction accuracy for subsequent visits.

Using the same dataset, another survey by Ammar et al [8] concentrates on extracting a wide range of linguistic features related to fluency and richness for Mini-Mental State Examination score prediction. However, unlike the former study, they do not leverage the correlation between previous visits. In the research proposed by Laguarta and Subirana [9], 16 physiological biomarkers were identified from speech data, represented in a personalized subject feature map. This feature map is capable of illustrating and monitoring cognitive changes over time. Achieving 93.6% accuracy in the ADReSS datasets, this study is the only one among them that visually depicts cognitive decline.

Yamada et al [10] used phone calls for long-term participant tracking, manually transcribing the conversations to extract linguistic features. They focused on extracting topic and word repetition features across different calls. Their model achieved an area under the receiver operating characteristic curve (AUROC) of 0.91 in classifying between AD and HC. In our previous work proposed by Chang et al [11], the author first extracted traditional acoustic feature sets, extended Geneva Minimalistic Acoustic Parameter Set [12], from AM audio files collected across multiple visits. The author then used TabNet [13] to learn the cognitive information embedded within these feature sets. To further enhance the model, an aging alignment loss was applied, encouraging cognitive representations in the latent space to be closer to each other. The approach achieved an accuracy of 0.66 and an F_1-score of 0.64.

In this work, we use AM data as the primary input for our model. We analyze the AM data from both linguistic and acoustic perspectives and further establish an aging trajectory module (ATM). By introducing the ATM, which captures cognitive decline across different time points through direction embeddings, our framework provides more representative modeling of longitudinal changes. The key contributions of this work are summarized as follows:

1. Unlike most studies focusing on single time point analysis, this work introduces a longitudinal framework using AM speech data to track cognitive changes over time.
2. The system jointly analyzes linguistic and acoustic features from unstructured AM speech, offering a richer representation of cognitive status than unimodal approaches.
3. Proposed ATM, which models cognitive decline by aligning temporal features across visits through a specially designed alignment loss applied to direction embeddings.

Methods

Problem Setting

There are 2 problem settings in this work: longitudinal type and cross-sectional type. The longitudinal problem setting is our main focus. The cross-sectional problem setting evaluates whether our model is general enough to tackle different tasks of detecting cognitive impairment disease detection tasks.

Longitudinal Problem Setting

In our problem setting, we have the dataset D={D1,D2,…,DV}with the corresponding label set L={L1,L2,…,LV}, where V means the total visit times, and D_k means the dataset at the kth visit. Each D_k is expressed as Dk={x1,k, x2,k, …, xN,k}, where N represents the number of the subjects involved in the test, andxi,k={xi,k1, xi,k2, …,xi,kM} represents the M stories provided by subject i at the kth visit; note that the number of M may vary across different visits. The corresponding labels set Lk={l1,k, l2,k, …, lN,k} shows the cognitive status of each subject, with each $l_{i,k}$ indicating whether the subject is an HC or has MCI.

During the data preprocessing, we extract the feature set {xi,km,a, xi,km,t, xi,km,l} from the raw audio xi,km, where xi,km,a, xi,km,t, xi,km,l represents the acoustic feature set, textual data, and linguistic feature set, respectively. Subsequently, the model input is the sequential visit data defined

XSL•FO
RenderX

in equation 1, where xi,1m1∈ xi,1, xi,2m2∈ xi,2, and xi,VmV∈ xi,V.

(0)m2, . . xmV={xm1m1,xm2m2, . . ,xmVmV}

It is worth noting that stories from each visit are randomly paired across visits within each subject. This design ensures that the model learns subject-level temporal progression rather than relying on similarities driven by specific story topics or linguistic content. Random pairing is not an arbitrary source of noise but a deliberate mechanism aligned with our longitudinal modeling objective. Because story content varies substantially across visits and participants, enforcing semantic matching or averaging all embeddings within a visit would bias the model toward topic-dependent features, flatten meaningful variability in linguistic complexity, and increase the risk of overfitting to specific story topics. In contrast, random pairing operates strictly within each subject, preserving the temporal order while exposing the model to multiple sampled transitions across training epochs. This provides a richer distribution of temporal transitions, enabling the framework to learn visit-level cognitive progression directions that remain robust to story content and reflect each subject's distribution of linguistic changes over time.

Formally, our model can be viewed as a mapping function fW, where *W* represents the set of learnable parameters. The function fWprojects the input sequence {xi,1m1,xi,2m2,…,xi,vmv} into the label of the last visit l(i,V). In this study, the maximum number of visits per subject, *V*, is 3, following the available structure of the dataset.

Cross-Sectional Problem Setting

In the cross-sectional problem setting, the primary difference from the longitudinal problem setting is that data collected from the same subject at different interview visits are treated as data from independent subjects. Thus, we have the dataset D={x1,x2, …, xCN} with the corresponding label set L={l1,l2, …, lCN}, where CN is the sum of all subjects from all visits, and x_i represents the raw audio for the subject *i* with the cognitive label l_i. The cognitive label l_i indicates that the subject is either an HC or under the targeted condition (MCI or AD). During the data preprocessing, we extract the feature set {xia,xit,xil} from the raw audio x_i. Our cross-sectional model aims to map the model input {xia,xit,xil} into the cognitive label l_i.

Overview

The system overview is shown in Figure 1. The goal of the system is to detect the cognitive condition of subjects, specifically whether they have MCI, using speech data. Before training, the speech data first undergo data preprocessing, which involves converting the audio files to text using automatic speech recognition (ASR), extracting additional linguistic features, and deep learning–based acoustic feature extraction. These steps generate additional text data and acoustic data, which are then intertwined to form dual-modal data pairs serving as the input for the model training. In addition, to effectively capture the features of aging and enhance the detection of potential MCI, the model input should have speech data for this time as well as points of follow-up data. This philosophy leads to our proposed longitudinal analysis for MCI detection.

Figure 1. Overall framework of the proposed longitudinal multimodal model. The model consists of two main modules: (1) encoder model, combining a CNN-based acoustic encoder and a BERT-based linguistic encoder to generate fused multimodal embeddings; and (2) aging trajectory module, which models longitudinal changes between consecutive visits using a direction encoder and cross-attention before classification. ASR: automatic speech recognition; BERT: bidirectional encoder representation for transformer; CLF: classifier; CNN: convolutional neural network; HC: healthy control; MCI: mild cognitive impairment.

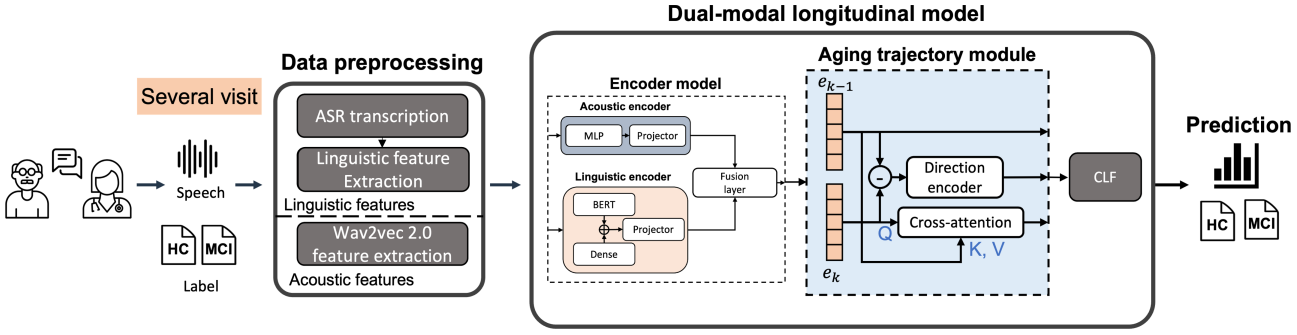

Data Preprocessing

Before the data are input into the model, they need to be preprocessed to ensure data quality and to extract useful features. After data collection is completed, given that the data are based on the entire interview process of each subject during a single visit, we first segment each story recording from the interview. To prepare the audio file of each subject, we segment the audio files based on the story topics provided by the subject, cutting the corresponding recall and probing audio files.

Acoustic Feature Extraction

The preprocessing of audio data is shown in Figure 2. First, the notation xi,km denotes a raw audio waveform, which means the *m*th audio file of the subject *i* collected at the *k*th interview visit undergoes basic processing, including normalization and resampling. Normalization is done using zero-mean unit-variance normalization. Next, the audio is segmented into *t*-second clips with a 5-second overlap. Each audio file can be denoted as xi,km={xi,km,1,xi,km,2,…,xi,km,seg_num}, where seg_num represents the number of clips to which the raw audio file can be divided, and the total number of segments varies for each audio file.

XSL•FO
RenderX

Figure 2. Overview of acoustic preprocessing. Each raw audio recording is divided into multiple fixed-length clips and processed by the wav2vec2.0 feature extractor to obtain frame-level representations. For each segment, the outputs from all clips are stacked and averaged to produce a single clip-level feature. The averaged clip features are then pooled across segments to generate the final visit-level wav2vec2.0 embedding, which is used as input to the acoustic encoder.

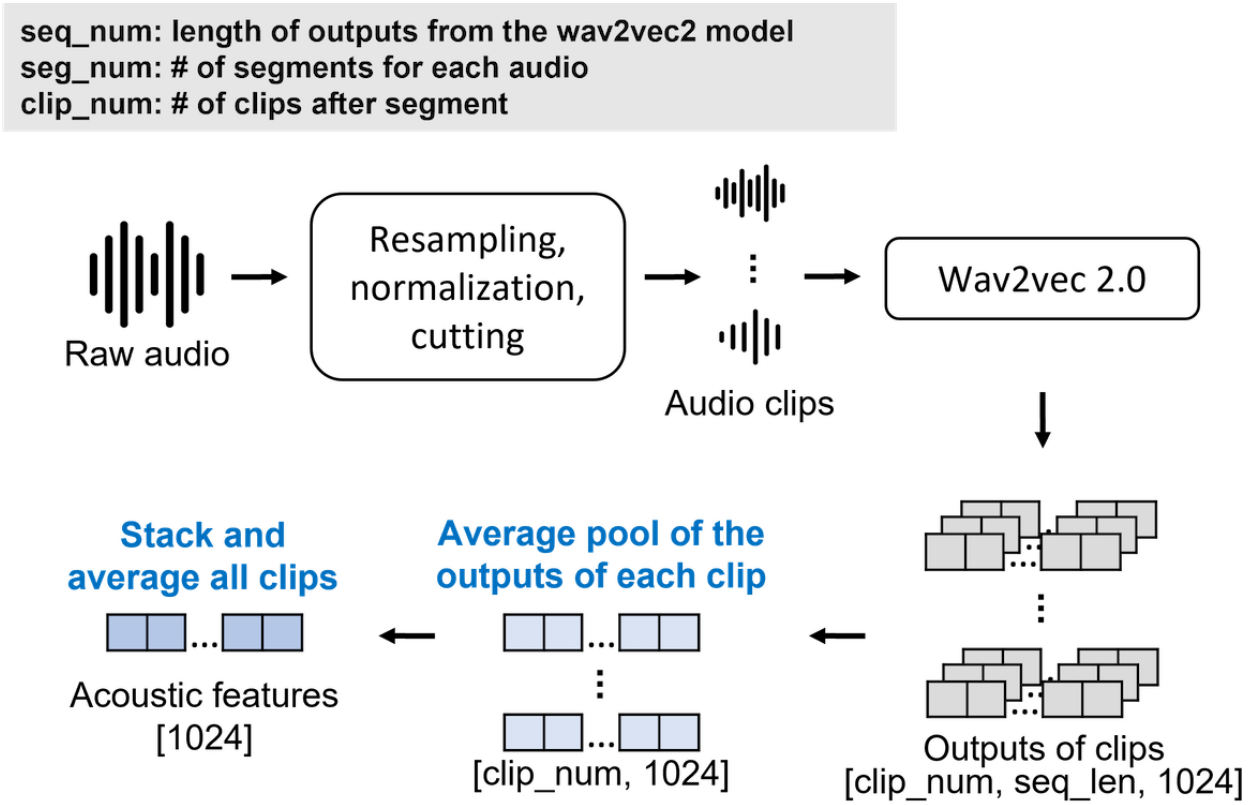

In our research, wav2vec 2.0 model [14] is used as an acoustic feature extractor, and we leverage the pretrained model available on Hugging Face. Using the wav2vec 2.0 model in advance to extract deep acoustic representation features offers the advantage of saving memory space and making the subsequent model structure lighter, thereby increasing training efficiency. Each clip is fed into the wav2vec 2.0 model, producing an output with dimensions [seq_len, 1024], where seq_len is determined by the convolution layer in wav2vec 2.0 and the clip length, which is computed by dividing the clip length and the multiplication of the stride length in the convolution layers. After obtaining the output of each clip, the first average pooling is performed, resulting in a 1024-dimensional acoustic feature for each clip. Then, all clip outputs are stacked together, and a final average pooling is conducted to obtain the final acoustic features xi,km,a of the entire raw audio file; hence, the dimension of xi,km,a is 1024.

Linguistic Feature Extraction

The preprocessing of linguistic data can be divided into 2 stages: generating the transcript and extracting features from the generated text. Since not all audio files in the dataset have manual transcripts, we use ASR to generate the transcripts for our research. We use the open-source tool kit "whisper-timestamped," which provides both timestamps and the corresponding text, as illustrated in Figure 3. Previous research [15-17] has confirmed that pauses are an indicator in AD-related diseases, where patients with MCI or AD tend to exhibit more frequent and longer pauses. In our study, we classify pauses based on the interval duration between sentences into 3 types: short pause (duration <0.5 seconds), medium pause (duration between 0.5 and 2 seconds), and long pause (duration >2 seconds) [18]. In addition to pauses, we calculate the mean length of utterance, which is defined as the average number of words spoken in a sentence. In this step, we will generate transcripts with pause information and 4 numerical linguistic features. Besides pause information, we provide additional syntax information to enrich the linguistic features. Previous research [19] has shown that the sentence structures used by individuals with AD and HC are different. Therefore, we use part-of-speech (POS) tagging in this study. After generating the text, we use the open-source tool kit "ckipnlp" for word parsing and POS tagging. The text segments are then categorized into 5 POS types: noun,

XSL•FO
RenderX

Figure 3. Example of how the result of whisper-timestamped, where the timestamp of the Mandarin speech is aligned with the transcript, is used for the temporal segmentation to extract linguistic features. MFCC: mel frequency cepstral coefficients.

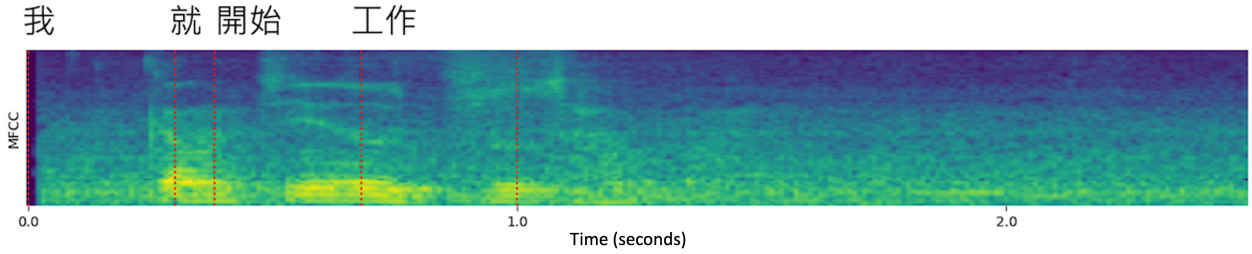

verb, adjective, pronoun, and other. In this step, we count the total number of these POS taggers.

In addition, due to the nature of the AM test, subjects can share stories on unrestricted topics. To facilitate the model to capture more meaningful information from the transcripts, we apply the topic insertion technique proposed by our previous work [11,18]. This technique is to add a sentence with the mentioned topic at the beginning of the transcript, such as “I’m going to share a story of...” The tester specifies the topic during data collection. This step helps ensure that the subsequent transcript is thematic. After the whole preprocessing of linguistic data, from the raw audio xi,km, we finally obtain the transcripts with topics and pauses xi,km,t, along with 9 additional linguistic features xi,km,l, which include mean length of utterance; the number of short, medium, and long pauses; and 5 types of POS tags.

Encoder Module

Acoustic Encoder

During the data preprocessing stage, 1024-dimensional deep learning–based acoustic features, denoted as xi,km,a, were extracted using the wav2vec 2.0 model. These high-level representations were then passed to a lightweight convolutional neural network–based acoustic encoder designed to capture hierarchical temporal-spectral patterns. The encoder consists of three 1D convolutional layers with kernel size 3 and stride 1, each followed by batch normalization, rectified linear unit activation, and max-pooling with a kernel size and stride of 2, progressively reducing the feature resolution by a factor of 8. The convolutional layers use 16, 32, and 64 filters, respectively, to model increasingly abstract local dependencies in the acoustic embedding. The resulting feature maps are flattened and projected through a fully connected layer that maps the representation to a 128-dimensional latent space. This projection enhances computational efficiency, mitigates overfitting, and provides a compact and informative acoustic embedding ai,km for multimodal fusion.

Linguistic Encoder

In the linguistic encoder, the ASR transcript xi,km,t and 9-dimension features xi,km,l generated during data preprocessing are sent to the BERT [20] model and a linear layer, respectively, for initial encoding. During data preprocessing, to ensure that the subjects’ speech has a thematic structure, we add a topic at the beginning of the transcript. In BERT, we borrow the concept of segment embeddings from the original paper [20]. Here, we refer to it as “context embedding” to enhance the model’s understanding of the topic and content. We divide the transcript into 2 parts: topic and context. The topic part is labeled as 0, and the context part as 1. These values are then encoded into context embeddings E_t and E_c through a learning embedding layer. This design helps the model determine whether there is a sufficient correlation between the topic and content. Research in AM tests indicates that episodic memory significantly declines in patients with cognitive impairments [21,22]. Therefore, we can assess the subject’s cognitive state by examining whether the subject’s story contains details related to the topic.

As illustrated in Figure 4, context embeddings are element-wise added to the original BERT token embeddings for further processing. A linear layer is used as a numerical encoder for linguistic features xi,km,l. Finally, the output from BERT and the learned numerical embeddings are concatenated and processed through a projector to obtain the final linguistic embedding ti,km.

Figure 4. Overview of the BERT embedding. Each input token is first mapped to a token embedding, which is combined with additional context embeddings to capture both semantic meaning and conversational context. BERT: bidirectional encoder representation for transformer.

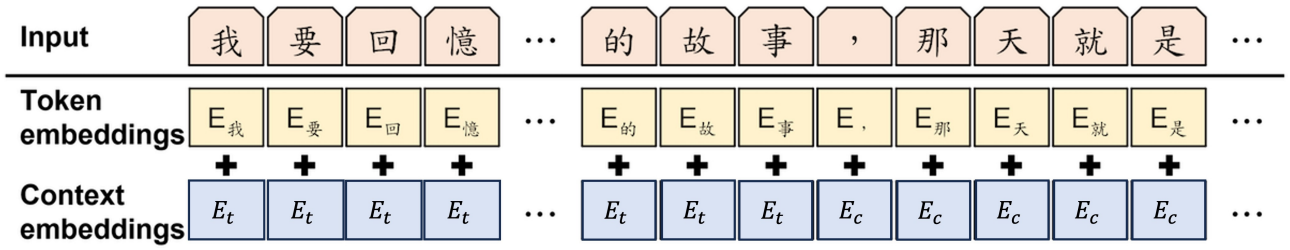

XSL•FO
RenderX

Fusion Layer

In this study, we adopt a self-attention fusion method to enable the model to capture information between different modalities more effectively. The concept is illustrated in Figure 5. After obtaining the acoustic embedding ai,km and the linguistic embedding ti,km, these 2 embeddings are added together to form a combined representation, which is then fed into a multihead self-attention layer. Through the calculations of the self-attention layer, we obtain the final integrated embedding ei,km. This design helps the model capture deeper interrelated information between different features.

Figure 5. Overview of the fusion layer. Acoustic and linguistic embeddings are integrated through a multihead attention mechanism, producing a joint embedding that captures cross-modal interactions and complementary cognitive cues.

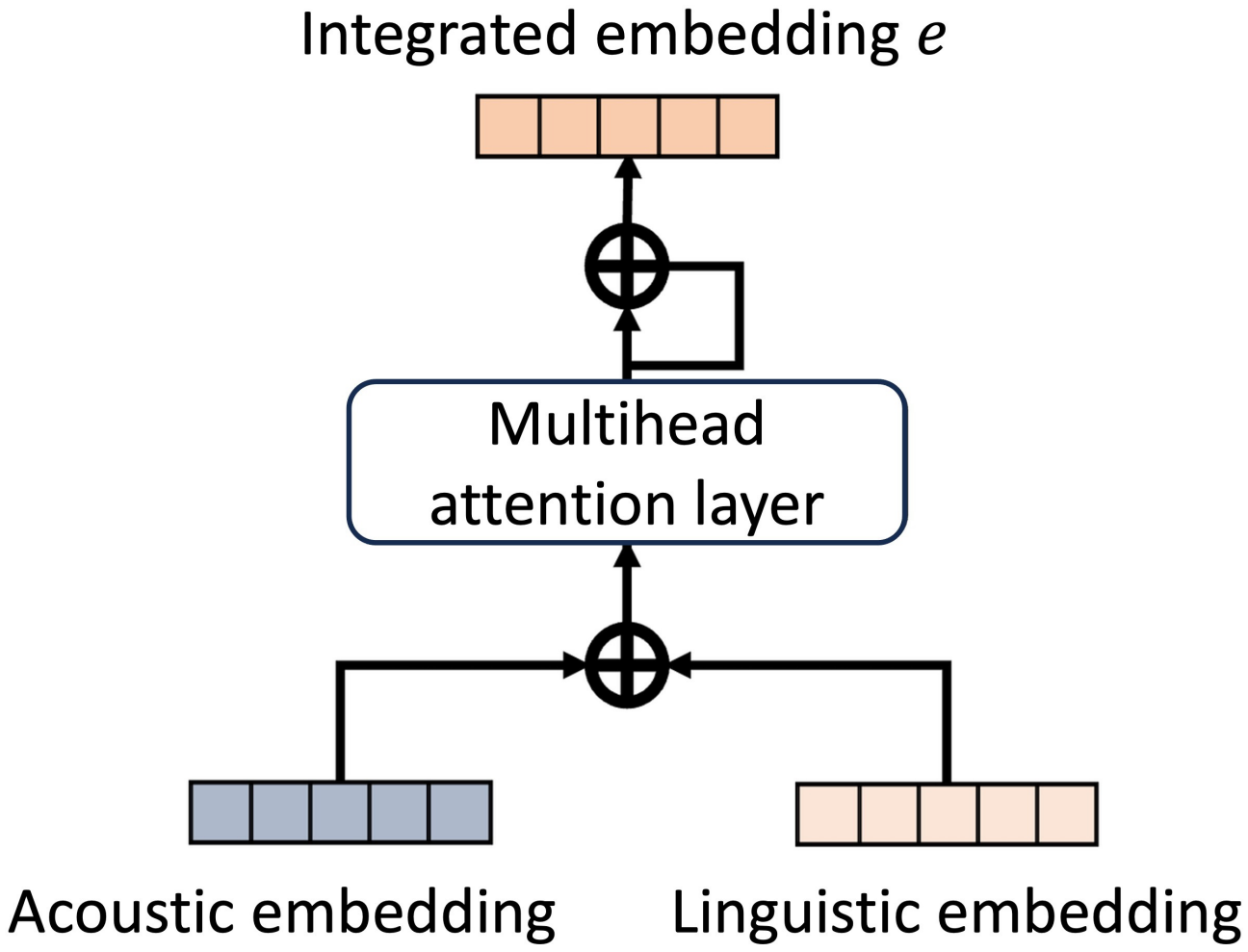

Aging Trajectory Module

The ATM is a key component of our longitudinal model, designed to capture cognitive changes across multiple visits. The structure is shown in Figure 6. In our study, each subject contributes up to 3 visits. Therefore, the model's initial input is in the form of a triplet, {xi,1m1, xi,2m2,xi,3m3}. After passing them through the encoder model process, this becomes the embedding triplet of the same form, {ei,1m1, ei,2m2,ei,3m3}. In this module stage, the embeddings are fed in pairs, such as {ei,1m1,ei,2m2}or {ei,2m2,ei,3m3}, so that the model focuses on learning the relationship between visits *k* and *k*-1. To model these relationships, we use a cross-attention mechanism, where the embedding from the *k*th visit serves as the query (*Q*), and the embedding from the (*k*-1)th visit serves as the key (*K*) and value (*V*). This mechanism allows us to capture the differences in feature values between 2 visits. The reason for using the *k*th visit embedding as the query and the (*k*-1)th visit embedding as the key and value is that, in practice, we can retrieve information only from the past data and not future data. This approach ensures that the model can access information only from the previous visits, reflecting a realistic scenario where future data are unavailable. By doing so, the model learns to focus on the most relevant past information that can be referenced by the current visit, enabling the tracking of changes and peeking of patterns of cognitive decline over time. This method effectively highlights the differences and similarities between visits, providing a more nuanced understanding of the subject's cognitive progression.

XSL•FO
RenderX

Figure 6. Overview of the aging trajectory module. Consecutive visit embeddings are compared through cross-attention and a direction encoder to capture cognitive differences between visits.

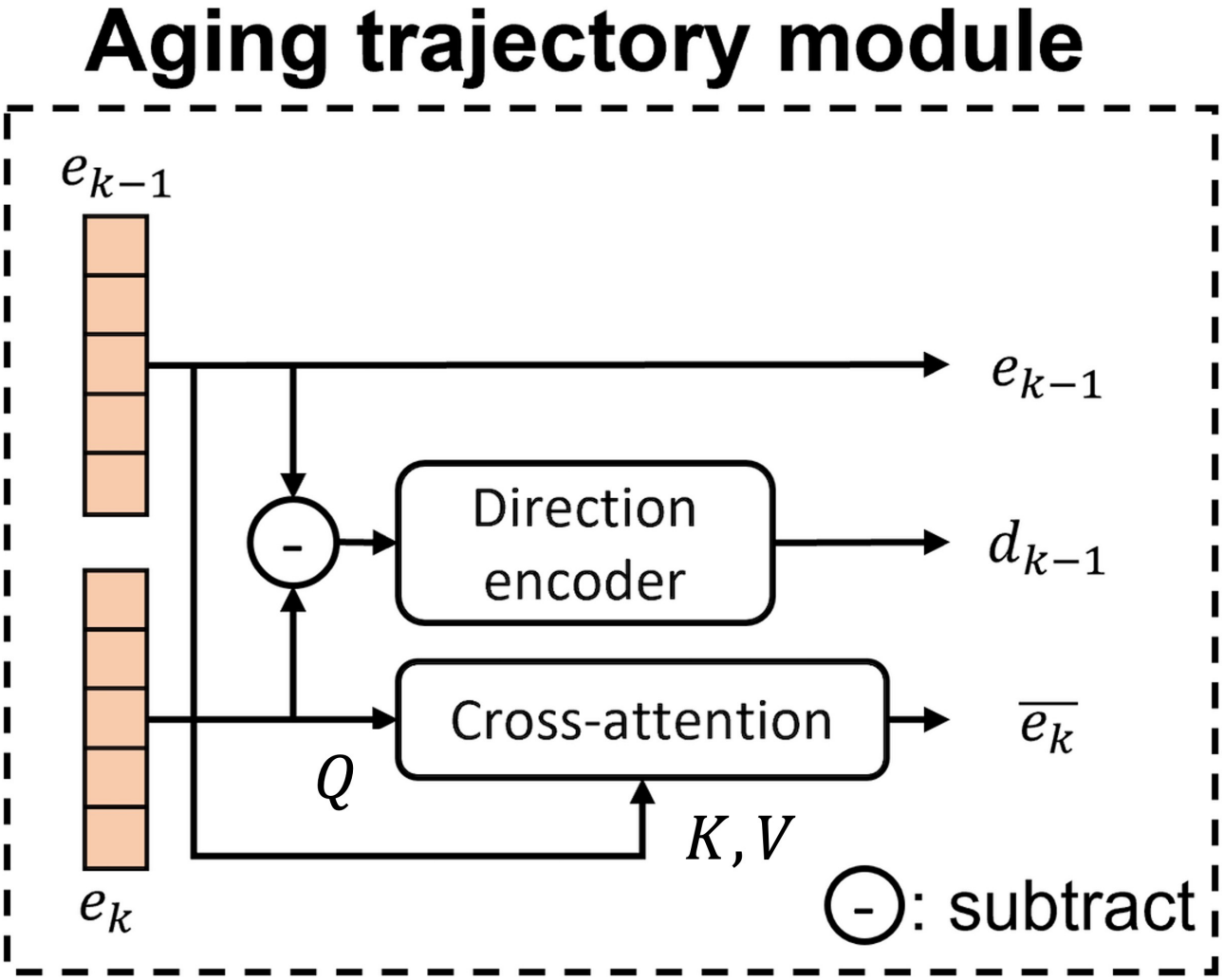

The concept of contrasts is quite straightforward. We aim to explore a deeper understanding of the relationship between the (*k*-1)th and *k*th visits. To achieve this, we use a cross-attention mechanism. In this setup, the embedding from the *k*th visit is used as the query (*Q*), whereas the embedding from the (*k*-1)th visit serves as the key (*K*) and value (*V*). This mechanism allows us to capture the differences in feature values between 2 visits. The reason for using the *k*th visit embedding as the query and the (*k*-1)th visit embedding as the key and value is that, in practice, we can retrieve information only from the past data and not future data. This approach ensures that the model can access information only from the previous visits, reflecting a realistic scenario where future data are unavailable. By doing so, the model learns to focus on the most relevant past information that can be referenced by the current visit, enabling the tracking of changes and peeking of patterns of cognitive decline over time. This method effectively highlights the differences and similarities between visits, providing a more nuanced understanding of the subject's cognitive progression.

To quantify the differences between visits, we introduce a direction encoder f_D, composed of several linear layers. The difference between embeddings is projected into a latent space to represent an aging-oriented change vector *d*, formulated as equation 2, where di,k−1mk−1,mk means the direction from mk-1th story in the (*k*-1)th visit to the mkth story in the *k*th visit. mk=1,2,…,Mi,k, where Mi,k is the total number of stories for subject *i* in the *k*th visit. Similarly, mk-1=1,2,…,Mi,k-1, where Mi,k-1 is the total number of stories for subject *i* in the (*k*-1)th visit.

(2)di,k−1mk−1,mk= fD(ei,kmk−ei,k−1mk−1)

In addition, during the training process, motivated by the research [11,23,24], we introduce 2 types of losses: subject alignment loss and group alignment loss. These alignment losses are designed to align both individual and group targets, helping the direction encoder learn more accurate aging-oriented changes. We expect that by applying these losses, the resulting direction *d* will carry more representative meaning, aiding the longitudinal model in accurately assessing the subject's cognitive condition.

Subject Alignment Loss

In the subject alignment loss L_S, the concept is to ensure that the same subject's internal directions are similar. In our problem setting, the stories of the input triplet are randomly paired in different visits. Therefore, it is expected that the directions from the same subject may vary in the latent space. However, the cognitive decline of a subject should be consistent. Figure 7 shows an illustration of the concept.

XSL•FO
RenderX

Figure 7. Illustration of the concept for subject alignment loss. It visualizes how the subject alignment loss ensures that the overall trajectory directions of the subject remain consistent, although the internal trajectory of story-level embeddings for the same subject may show slight variations across different visits.

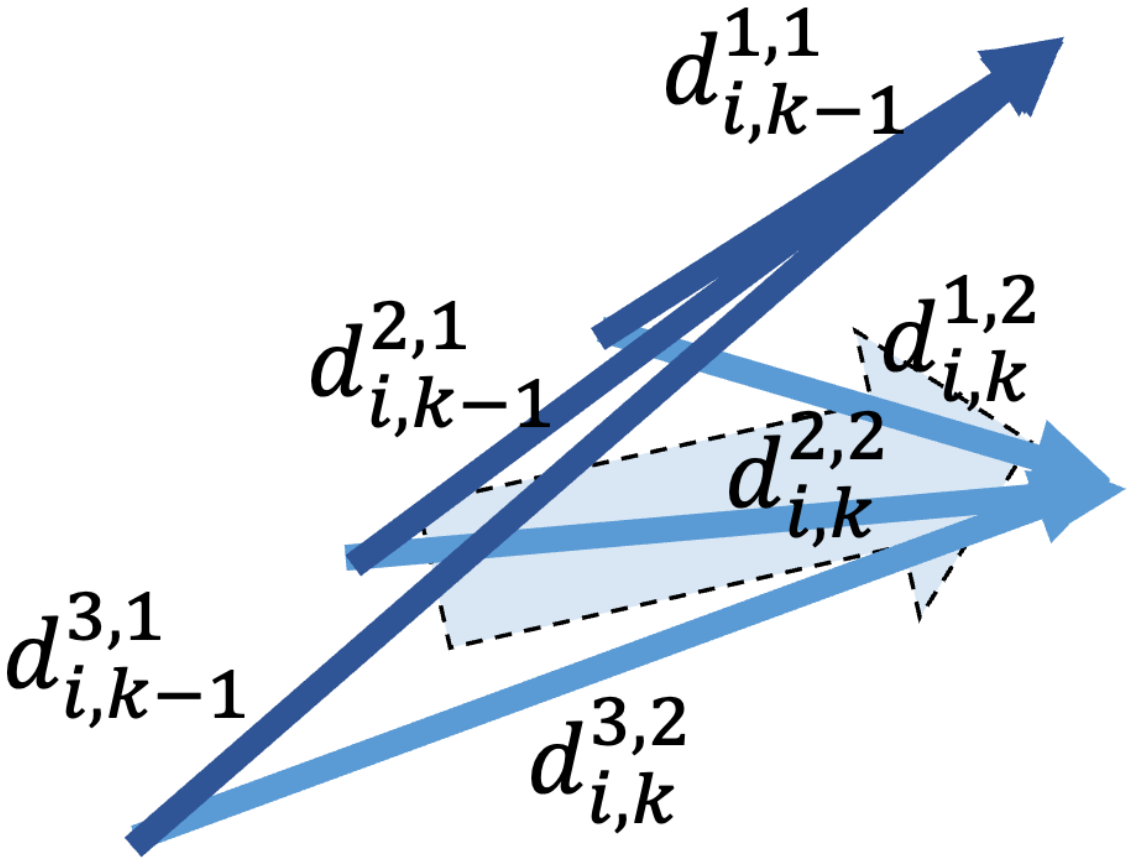

Therefore, subject alignment loss aims to reduce the differences in direction within the same subject. The loss used here is cosine similarity loss. The process of calculating the subject alignment loss is to first calculate the average subject direction for each visit as shown in equation 2. We then compute the subject alignment loss by summing the alignment loss of all subjects as defined in equation 3. The generalized subject alignment loss is defined as equation 3, where di,k−1− represents the average direction of every audio file in the (*k*-1)th visit to *k*th visit from the subject *i* in the latent space, and *N* represents the total number of subjects. $L_{S,i}$ represents the subject alignment loss for subject *i*, and cos θA,B=A.BAB is the cosine similarity function. In our case, since the dataset contains 3 visits, our *V* is 3, and the loss is applied to the pairs (first visit and second visit) and (second visit and third visit).

(3)di,k−1−=1Mi,k−1×Mi,k∑mk=1Mi,k∑mk−1=1Mi,k−1di,k−1mk−1,mk

LS=∑i=1NLS,i

(4) =∑i=1N∑k=2V∑mk=1Mi,k∑mk−1=1Mi,k−11−cosθ(di,k−1−,di,k−1mk−1,mk)

Group Alignment Loss

In the group alignment loss L_G, the concept is to ensure that subjects with the same cognitive label have similar cognitive progression changes as illustrated in Figure 8. Unlike the subject alignment loss, which focuses on the internal alignment of directions within a subject, the group alignment loss emphasizes the external alignment of directions between different subjects. Specifically, we compare the cognitive change directions of subjects with the same label transitions. Here, we use the Supervised Contrastive Loss (SupConLoss) [25] to encourage the directions of subjects with the same label changes to be closer to one another. The label transitions considered are HC to HC, HC to MCI, and MCI to MCI. The process of calculating the group alignment loss is using equations 5 and 6, where *N* represents the total number of subjects, and $L_{G,i}$ represents each group alignment loss for subject *i*. SupConLoss(·, ·) is the SupConLoss function. lk-1,ki is the label transition type of subject *i* from (*k* − 1)th visit to *k*th visit.

XSL•FO
RenderX

Figure 8. Illustration of the concept for group alignment loss. It visualizes how the group alignment loss enforces consistency in progression directions among subjects sharing the same cognitive label. Blue represents the group from healthy control (HC) to HC, yellow represents the group from HC to mild cognitive impairment (MCI), whereas orange represents the group from MCI to MCI.

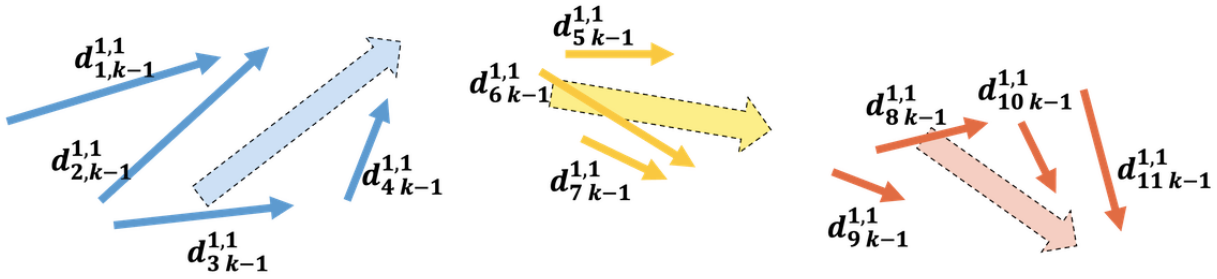

(6)LG=∑i=1NLG,i=∑i=1N∑k=2V∑mk=1Mk1Mk−1SupConLoss(ei,mk−1,mk,li)

(6)LG=∑i=1NLG,i=∑i=1N∑k=2V∑mk=1Mk1Mk−1SupConLoss(ei,mk−1,mk,li)

To summarize, group alignment loss L_G aims to minimize the distance between the cognitive progression directions of different subjects with the same cognitive label transitions types. This helps ensure that subjects exhibiting similar cognitive changes have consistent representations, thereby improving the model's ability to generalize across different subjects. By leveraging SupConLoss, we can effectively capture and align these progression patterns, leading to more accurate and robust cognitive state predictions.

Classifier and Overall Loss

After the ATM, we obtain the final outputs {e−i,1m1,e−i,2m2,e−i,3m3,di,1m1,m2, di,2m2,m3}, where e−i,kmk represents the enhanced latent representation after the cross-attention layer. These representations are then concatenated and fed into a classifier. The classifier comprises a batch normalization layer and a fully connected layer to produce the final prediction. Finally, the overall loss function can be formulated by equation 7, where Lclass is the binary classification loss, and α, δ, and γ are the hyperparameters of loss weight for L_E, L_G, and L_S, respectively. The hyperparameters are fine-tuned, and the optimal values are 0.01, 0.001, and 0.001.

(7)L= Lclass+αLE+δLG+γLS

The encoder loss L_E is a contrastive loss designed to enhance the representativeness of the embeddings generated by the encoder and is defined by equation 8, where N is the total number of the subjects, V is the total number of visits, and M_k is the total number of stories in the kth visit. This loss ensures that embeddings with the same cognitive status are closer to one another while pushing apart embeddings with different labels.

(8)LE=∑i=1NLE,i=∑i=1N∑k=2V∑mk=1MkSupConLoss(ei,mk,li)

Dataset

Dataset Collection

Our experiments primarily focus on comparisons using our self-collected National Taiwan University Autobiographical Memory Test (NTU-AM) dataset. Previous studies [6,11,26,27] have confirmed that the AM test effectively tracks changes in cognitive function by evaluating subjects' memory functions. It can be used as a tool for MCI testing. During the test, subjects are asked to recall important life stories from different periods in their past. Compared with formal memory testing methods, this process resembles a general conversation, which helps reduce the stress experienced by subjects.

For the collected data used in this study, professional psychologists conducted one-on-one interviews. During these interviews, a microphone is used to record the conversation between the subject and the interviewer. Furthermore, subjects are asked first to talk about the titles of the important events they want to share (eg, "I want to share the story about when I was admitted to college at the age of 18 and my test result were announced"). The process of describing the events can be divided into two stages, namely, recall and probing.

1. Recall: The subject is first asked to roughly describe the events leisurely and then is encouraged to share as many details of the event as possible.
2. Probing: The interviewer then asks even more detailed questions based on what the subject mentioned in the recall stage. These questions cover various categories, such as "what," "when," "where," emotion or thought, and time integration.

During a single interview, the same subject can share multiple stories as a matter of fact. To sum up, the overall process of the AM interview test can be described as follows: (1) the subject decides the number and content of stories to be shared, (2) shares the recall content of each story, and then (3) the interviewer probes each story with a series of detailed questions.

Moreover, to track the cognitive changes of subjects over a long term, they are invited to take the AM test again after at least 6 months. In our current research, our longitudinal data include up to 3 rounds of AM interview test data, that is, each subject has 1 test data and 2 follow-up data. All data were collected by professional psychologists with institutional review board approval, ensuring high-quality data.

The National Taiwan University Autobiographical Memory Test Cross-Sectional (NTU-AM-CS) dataset was collected under a cross-sectional scenario, with the demographic distribution of participants shown in Table 1. This dataset includes 111 subjects, consisting of 56 HC and 55 MCI participants. Each participant could provide multiple important life stories during a single visit.

XSL•FO
RenderX

Table . The demographic distribution of participants in the National Taiwan University Autobiographical Memory Test Cross-Sectional dataset.

Group	N	Male	Female	Age (years), mean (SD)	Years of education, mean (SD)	MMSE[a], mean (SD)
HC[b] (n=56)	56	18	38	71.3 (5.4)	16.2 (9.8)	28.7 (1.6)
MCI[c] (n=55)	55	17	38	70.7 (6.9)	13.1 (7.1)	27.1 (2.0)
Total (N=111)	111	35	76	71.0 (6.2)	14.6 (8.7)	27.9 (2.0)

[a]MMSE: Mini-Mental State Examination.

[b]HC: healthy control.

[c]MCI: mild cognitive impairment.

The longitudinal scenario dataset, National Taiwan University Autobiography Memory Test Longitudinal (NTU-AM-LG), involves 54 of the original 111 subjects who participated in follow-up studies, including 28 HC and 26 MCI participants. The types of data collected are the same as in the cross-sectional scenario, encompassing both recall and probing audio files. The key difference is that NTU-AM-LG includes story audio files from 3 visits. The demographic distribution for this dataset is also shown in Table 2.

Table . The demographic information of the National Taiwan University Autobiography Memory Test Longitudinal dataset.

Group (N=54)	Male	Female	Age (years), mean (SD)	Years of education, mean (SD)	MMSE[a], mean (SD)
HC[b] (n=28)	12	16	74.0 (5.9)	14.3 (2.7)	28.4 (1.5)
MCI[c] (n=26)	7	19	72.5 (6.4)	14.0 (9.6)	27.5 (1.9)
Total	19	35	73.3 (6.1)	14.1 (7.0)	28.0 (1.8)

[a]MMSE: Mini-Mental State Examination.

[b]HC: healthy control.

[c]MCI: mild cognitive impairment.

Ethical Considerations

The collection of experimental data from human participants was reviewed and approved by the National Taiwan University Hospital Research Ethics Committee B (protocol no. 202105013RINB, approved on June 18, 2021). All participants provided written informed consent prior to data collection. The original consent and institutional review board approval explicitly permitted the secondary analysis of deidentified recordings and transcripts for research purposes, without requiring additional consent. All data were fully deidentified before analysis, and no personal or identifiable information was retained in the research dataset. Participant privacy was protected by storing all files on secure, access-restricted servers, and only aggregated results are reported. Participants received NTD 160 (equivalent to US $5.09) per hour as compensation for their time and contribution. No identifiable participant images are included in this manuscript.

Experiment Dataset

The summary of the collected dataset can be provided. The total number of datasets is shown in Table 3, where the unit of measurement is the number of stories. Since each story includes both recall and probing phases, the quantities are identical for recall and probing data.

Table . Primary dataset statistics.

Dataset	Visit 1		Visit 2		Visit 3		Total	
	HC[a]	MCI[b]	HC	MCI	HC	MCI	HC	MCI
NTU-AM-CS[c]	134	122	N/A[d]	N/A	N/A	N/A	134	122
NTU-AM-LG[e]	44	30	50	40	76	54	170	124

[a]HC: healthy control.

[b]MCI: mild cognitive impairment.

[c]NTU-AM-CS: National Taiwan University Autobiography Memory Test Cross-Sectional.

[d]N/A: not applicable.

[e]NTU-AM-LG: National Taiwan University Autobiography Memory Test Longitudinal.

XSL•FO
RenderX

NTU-AM-CS is a cross-sectional dataset that includes a total of 111 subjects (56 HCs and 55 with MCI). Each subject participated in a single AM interview, during which they could share multiple stories. Therefore, NTU-AM-CS does not include repeated follow-up visits.

NTU-AM-LG is the longitudinal subset derived from NTU-AM-CS. A portion of participants agreed to return for additional follow-up interviews, resulting in up to 3 visits per subject. As shown in Table 3, the number of stories per visit varies because the volume of data depends on how many stories participants chose to share during each session. In some cases, more stories were collected in visit 3 than in earlier visits, which explains the higher data volume observed.

To further clarify disease progression patterns, the number of subjects transitioning across cognitive status categories between visits, including stable (HC→HC, MCI→MCI) and progressive or recovered (HC→MCI, MCI→HC) cases, is shown in Table 4.

Table . Cognitive status transitions between consecutive visits in the National Taiwan University Autobiography Memory Test Longitudinal dataset across visits 1 and 2 and visits 2 and 3.

Transition	Number of cases (subject based), n =108
HC[a] to HC	50
HC to MCI[b]	10
MCI to HC	8
MCI to MCI	40

[a]HC: healthy control.

[b]MCI: mild cognitive impairment.

For additional experiments, we primarily used a semistructured speech dataset. The National Taiwan University Hospital Picture Description Test (NTUH-PIC) and National Taiwan University Hospital Memory Test (NTUH-MEM) datasets, which we collected ourselves, include speech data from picture description and logical memory tests, respectively. Both datasets feature 2 cognitive labels: HC and MCI. In the picture description task, participants are required to describe the scenario depicted in a specific picture as accurately and detailed as possible. In the NTUH-PIC dataset, the well-known "cookie theft" picture [28] is used. For the logical memory test, participants first listen to a story and then must repeat it from memory. The third dataset, ADReSSo [29], was introduced as part of the cognitive challenge at INTERSPEECH 2020. This dataset also involves a picture description test, which also used "cookie theft" [28] but differs from the other datasets in that it includes only 2 cognitive labels: HC and AD. Due to data access limitations, we used only the training set for evaluation in this case. By incorporating these additional datasets, we aim to comprehensively evaluate the robustness and generalizability of our model across various types of speech data and cognitive assessments. The statistics of the additional dataset are shown in Table 5.

Table . Additional dataset statistics.

Dataset	Total	HC[a]	MCI[b]	Language	Test
NTUH-PIC[c]	80	40	40	Chinese	Picture Description Test
NTUH-MEM[d]	104	52	52	Chinese	Logical Memory Test
ADReSSo (Train)	166	79	87	English	Picture Description Test

[a]HC: healthy control.

[b]MCI: mild cognitive impairment.

[c]NTUH-PIC: National Taiwan University Hospital Picture Description Test.

[d]NTUH-MEM: National Taiwan University Hospital Memory Test.

Experiments

We conducted a series of experiments to evaluate our proposed longitudinal multimodal model under different data conditions and to verify the contribution of each model component.

Experiments on NTU-AM-LG

We evaluated the model on the longitudinal NTU-AM-LG dataset using 2 speaking tasks: recall and probing. For each task, we compared four variants of our model:

1. Ours (audio): acoustic branch only, wav2vec 2.0 to acoustic encoder to classifier.
2. Ours (text): linguistic branch only, BERT to linguistic encoder to classifier.
3. Ours (CS): cross-sectional problem setting
4. Ours (LG): full proposed longitudinal multimodal model with direction encoding and alignment losses.

XSL•FO
RenderX

These models were compared against standard baselines (BERT, wav2vec 2.0, and the prior AM-based work [11]), and the corresponding results are reported in the "Results" section.

An ablation study on NTU-AM-LG is made to examine the contribution of the ATM, direction embedding, and the 2 alignment losses, and we performed ablation experiments by removing (1) the direction, (2) the subject alignment loss, (3) the group alignment loss, and (4) both alignment losses.

Experiments on NTU-AM-CS

To demonstrate that the proposed encoders and fusion strategy also work without longitudinal information, we trained the same acoustic and linguistic encoders in the cross-sectional problem setting (Our [CS]) and compared them with BERT, wav2vec 2.0, and the prior AM method [11]. An ablation study is also conducted to highlight the importance of linguistic features and context embeddings.

Experiments on Additional Datasets

We further tested whether our proposed model transfers to other cognitive-speech datasets (NTUH-PIC and NTUH-MEM). We compared our method with that of Lin et al [18].

Finally, to enable comparison with existing AD or MCI speech work on a public dataset, we evaluated our model on the ADReSSo corpus.

Experimental Setup

In the subsequent experiments, due to the limitations of the dataset size, we will present the averaged performance of 10-fold cross-validation. To avoid data leakage, we will split the training set and validation set by subject for the NTU-AM-CS and NTU-AM-LG datasets. It ensures that audio files from different visits of the same subject will not appear in the training set and validation set simultaneously.

For the NTUH-PIC, NTUH-MEM, and ADReSSo datasets, since each subject provides only 1 audio file, there is no need to split the data by subject. We will perform down-sampling on the majority class in the training set during the experimental process to stabilize the model's learning capability. All experiments are conducted on an NVIDIA RTX 4090 GPU.

Evaluation Metrics

In the experimental section, we will use 6 different evaluation metrics to measure the performance of the model: accuracy, F_1-score, precision, sensitivity (recall), specificity, and AUROC. These are common indicators used to assess the predictive ability of a model. Each metric provides a different perspective on the effectiveness of the model.

In the NTU-AM dataset, since the dataset is split by subject, each evaluation set from every fold may have a similar number of subjects, but the number of audio files provided by each subject can vary. This can result in label imbalance in the final soft-voting results. Therefore, the most critical metrics in the subsequent experiments will be F_1-score and AUROC. These 2 metrics provide a fairer assessment in situations with label imbalance. As for other experiments, the primary metrics of interest will be accuracy and F_1-score.

Baseline

In the subsequent experiments in the NTU-AM dataset, we will use a fine-tuned BERT model and the wav2vec 2.0 model as baselines. Since these 2 models are the backbones of our proposed model, in the NTU-AM-LG dataset, the baseline model will be composed of these 2 main models as encoders. The embeddings generated from the 3 visits will be concatenated and passed through the same classifier. For the NTU-AM-CS dataset, the backbone model will serve as the encoder, followed by a classifier. However, these models will not have additional loss functions to assist training during the training process, relying only on the basic binary cross-entropy loss.

Implementation Details

The probing data are interview data, which include both the interviewer's and the subject's voices. Since our study aims to determine whether the subject has a tendency for MCI based on their audio data, the interviewer's speech is considered noise during training. To remove the interviewer's portion, we use the tool kit "pyannote" to split the audio into different speaker segments. This process results in audio files without the interviewer's voice. These cleaned files are then used to generate the linguistic features during the data preprocessing stage.

We used the "openai/whisper-large-v2" version from Hugging Face for the ASR tool. For data preprocessing, the pretrained Wav2vec 2.0 model used for the English dataset is "facebook/wav2vec2-base-960h," while for the Chinese dataset, we used "jonatasgrosman/wav2vec2-large-xlsr-53-chinese-zh-cn," which are also from HuggingFace. We used a 15-second clip segmentation with a 5-second overlap. Considering the limitations of the Wav2vec model, we resampled the audio files to 16,000 Hz and standardized them to mono-channel.

For the linguistic model, the BERT model used for the English dataset is "google-bert/bert-base-uncased," and for the Chinese dataset, it is "hfl/chinese-bert-wwm-ext," which is also the version used for the BERT baseline. In the Wav2vec baseline model, we used "jonatasgrosman/wav2vec2-large-xlsr-53-chinese-zh-cn." The hyperparameters used for implementing the proposed model are shown in Table 6.

XSL•FO
RenderX

Table . Hyperparameters used for implementation.

Hyperparameters	Value
BERT[a] attention dropout rate	0.3
BERT linear layer dropout rate	0.3
Maximum sentence (token) length	512
Dimension of audio embedding	128
Dimension of text embedding	128
Dimension of direction embedding	32
Learning rate	1e-5
Number of layers for attention-fusion	1
Number of layers for cross-attention	1
Batch size for training	8
Batch size for evaluation	8
Maximum epoch number	150
Early stop	10
α for encoder loss	0.01
δ for group alignment loss	0.001
γ for subject alignment loss	0.001

[a]BERT: bidirectional encoder representation for transformer.

Results

Results of NTU-AM-LG

We experiment with the model's effectiveness on both recall and probing data. Given the limited research on longitudinal speech, we primarily compare our model against baselines such as BERT, Wav2vec 2.0, and the unimodal model within our longitudinal framework. In addition, we present an ablation study to demonstrate the necessity of each component in our model. We discuss the results for recall data and probing data separately. It is important to note that both the cross-sectional (CS) and longitudinal (LG) models are trained on the same NTU-AM-LG dataset, sharing identical subjects and feature representations. The difference lies only in the problem formulation: the CS model performs single-visit classification, while the LG model performs a prognostic task that leverages prior visit embeddings to predict the final cognitive state. Thus, the performance difference reflects the use of incorporating longitudinal context rather than architectural or data disparities.

Table 7 shows the performance of our proposed model and the baselines for the recall data. First, when the input consists only of audio data, our proposed model "Ours (audio)" outperforms the previous work [11] on most metrics. Notably, there are improvements of 5% and 6% in F_1-score and AUROC, respectively.

XSL•FO
RenderX

Table . Results of recall data on National Taiwan University Autobiography Memory Test Longitudinal dataset.

Method	Accuracy	F_1-score	Precision	Sensitivity	Specificity	AUROC[a]
Audio only						
Chang et al [11]	0.66	0.64	0.74	0.67	0.65	0.63
Wav2Vec2	0.59	0.58	0.53	0.78[b]	0.43	0.60
Ours (audio)	0.67	0.69	0.73	0.73	0.66	0.69
Text only						
BERT[c]	0.73	0.65	0.77	0.64	0.82	0.73
Ours (text)	0.75	0.72	0.83	0.73	0.72	0.73
Text + Audio						
Ours (CS[d])	0.72	0.72	0.68[b]	0.76[b]	0.74	0.66
Ours (LG[e])	0.82[b]	0.78[b]	0.95[b]	0.72[b]	0.97[b]	0.85[b]

[a]AUROC: area under the receiver operating characteristic curve.

[b]Highest value for each metric.

[c]BERT: bidirectional encoder representation for transformer.

[d]CS: cross-sectional.

[e]LG: longitudinal.

As for the model using only linguistic data as input, our proposed linguistic longitudinal model, denoted as "Ours (text)," outperforms BERT, demonstrating that including extra-linguistic features and context embedding helps improve the model's performance with 7% increase in the F_1-score.

Finally, our model, which is denoted as "Ours (LG)" in Table 7, significantly outperforms other models across most metrics for the dual-modal longitudinal model that combines both data types. Specifically, there is up to a 16% improvement in accuracy, a 14% improvement in F_1-score, and a 22% improvement in AUROC. Since the previous work used only unimodal data, examining AM data from different perspectives benefits MCI detection. We also compare the cross-sectional setting results of NTU-AM-LG, denoted as "Ours (CS)" in Table 7, with the longitudinal settings, confirming that long-term tracking of subjects' cognitive trajectories in NTU-AM-LG helps improve the model's prediction accuracy. Specifically, there are improvements of 10% in accuracy, 6% in F_1-score, and 19% in AUROC.

Table 8 shows the results of the probing data. For the audio data, our proposed model outperforms wav2vec 2.0 in most metrics, with improvements of 9%, 18%, and 10% in accuracy, F_1-score, and AUROC, respectively. This indicates that instead of directly using wav2vec 2.0's output representation for classification, extracting features using wav2vec 2.0 followed by a convolutional neural network–based acoustic encoder structure can better capture the hidden cognitive patterns in audio data.

XSL•FO
RenderX

Table . Result of probing data on National Taiwan University Autobiography Memory Test Longitudinal dataset.

Method	Accuracy	F_1-score	Precision	Sensitivity	Specificity	AUROC[a]
Audio only						
Wav2vec2	0.76	0.53	0.60	0.53	0.87	0.70
Ours (audio)	0.85	0.71	0.67	0.78	0.83	0.80
Text only						
BERT[b]	0.85	0.72	0.83	0.71	0.94	0.82
Ours (text)	0.84	0.80	0.86	0.81	0.82	0.82
Text + Audio						
Ours (CS[c])	0.71	0.67	0.61	0.75	0.63	0.68
Ours (LG[d])	0.89[e]	0.83[e]	0.90[e]	0.82[e]	0.95[e]	0.89[e]

[a]AUROC: area under the receiver operating characteristic curve.

[b]BERT: bidirectional encoder representation for transformer.

[c]CS: cross-sectional.

[d]LG: longitudinal.

[e]Values in boldface are the highest values for each metric.

For the linguistic data results, our model performs comparably with BERT, with improvements of 8%, 3%, and 10% in F_1-score, precision, and sensitivity, respectively. This suggests that the inclusion of linguistic features and the context embedding layer can also aid in MCI detection on probing data.

Finally, in the dual-modal data tests, the proposed longitudinal model achieved the best performance, excelling in every metric. Specifically, it showed improvements of up to 13%, 30%, and 19% in accuracy, F_1-score, and AUROC, respectively. Comparing the longitudinal model with the cross-sectional model, it is evident that the longitudinal model continues to perform better. This indicates that incorporating input from multiple time points and considering the concept of aging direction can enhance the model's predictions, resulting in performance increases of 12%, 16%, and 21% in accuracy, F_1-score, and AUROC, respectively.

Ablation Study

In the longitudinal setting, the most crucial idea is the alignment loss we proposed. Therefore, this section examines the contribution of alignment loss by removing each loss individually. The results are shown in Table 9. In the table, "Without direction" refers to not including direction embedding as the classifier input; namely, the input would be ei,1m1, ei,2m2, ei,3m3 treating each time point's data as independent.

XSL•FO
RenderX

Table . Result of the ablation study for our proposed model on National Taiwan University Autobiography Memory Test Longitudinal dataset.

Method	Accuracy	F_1-score	Precision	Sensitivity	Specificity	AUROC[a]
Recall data						
Without direction	0.79	0.74	0.71	0.83	0.67	0.75
Ours (LG[b])	0.82[c]	0.78[c]	0.95[c]	0.72	0.97[c]	0.85[c]
Subject alignment loss	0.71	0.67	0.68	0.77	0.63	0.70
Group alignment loss	0.68	0.69	0.68	0.89[c]	0.47	0.68
Both alignment loss	0.65	0.59	0.64	0.62	0.63	0.63
Probing data						
Without direction	0.79	0.70	0.68	0.76	0.78	0.77
Ours (LG)	0.89[c]	0.83[c]	0.9[c]	0.82[c]	0.95[c]	0.89[c]
Subject alignment loss	0.78	0.59	0.61	0.59	0.92	0.75
Group alignment loss	0.69	0.54	0.63	0.55	0.8	0.68
Both alignment loss	0.65	0.53	0.60	0.53	0.87	0.70

[a]AUROC: area under the receiver operating characteristic curve.

[b]LG: longitudinal.

[c]Highest value for each metric in recall data and probing data, respectively.

The results show that incorporating alignment losses with direction embedding improves performance across both recall and probing data. For instance, on recall data, our full model improves AUROC by 10% (0.85 vs 0.75) and F_1-score by 4% compared with "Without direction." On probing data, the gains are even larger, with AUROC improved by 12% (0.89 vs 0.77) and F_1-score improved by 13% (0.83 vs 0.70). Importantly, removing the group alignment loss results in the sharpest performance drop, with AUROC decreasing by 17% (0.68 vs 0.85) and 21% (0.68 vs 0.89) for recall and probing data, respectively. Similarly, removing both alignment losses further reduces AUROC to 0.63 (recall) and 0.70 (probing), confirming their necessity.

Overall, these results highlight the complementary importance of both alignment losses that rely on the strong supervisory signal of ground-truth label transitions to capture temporal progression patterns in longitudinal settings. Removing either the subject alignment loss or the group alignment loss results in significant performance degradation, and removing both leads to the sharpest decline. This indicates that while the subject alignment loss stabilizes intrasubject trajectory consistency, the group alignment loss aligns intersubject cognitive progression trends across similar diagnostic groups.

Visualization

We visualize the latent space distribution of subjects across different visits to better interpret the role of the alignment loss. After passing through all modules, we extracted the final embeddings, applied principal component analysis for dimensionality reduction, and projected the results into a 2D space. The arrows in Figures 9 and 10 represent the trajectory of each subject's embeddings across consecutive visits, thereby illustrating how cognitive states evolve over time.

XSL•FO
RenderX

Figure 9. Principal component analysis projection of subject embeddings without alignment loss. The x- and y-axes represent the first 2 principal components. Colors denote diagnostic group and visit (blue tones = healthy control visits 1 - 3; red tones = mild cognitive impairment visits 1 - 3). Arrows illustrate the trajectory of each subject's embeddings. The scattered trajectories reflect high variability and weak temporal consistency without alignment loss.

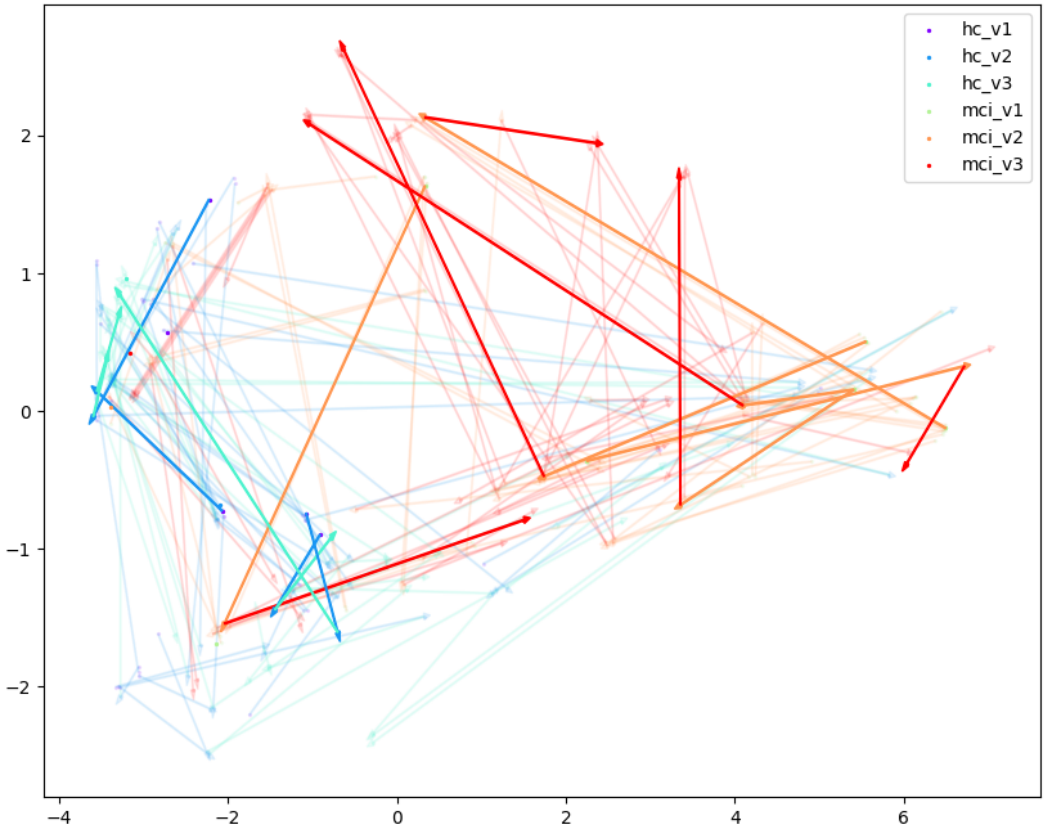

XSL•FO
RenderX

Figure 10. Principal component analysis projection of subject embeddings with alignment loss. The x- and y-axes show the first 2 principal components. Colors indicate diagnostic group and visit (blue tones = healthy control visits 1 - 3; red tones = mild cognitive impairment visits 1 - 3). Arrows illustrate the trajectory of each subject's embeddings. With alignment loss, trajectories become far more coherent and directionally consistent, indicating improved temporal stability and clearer separation between healthy control and mild cognitive impairment progression patterns.

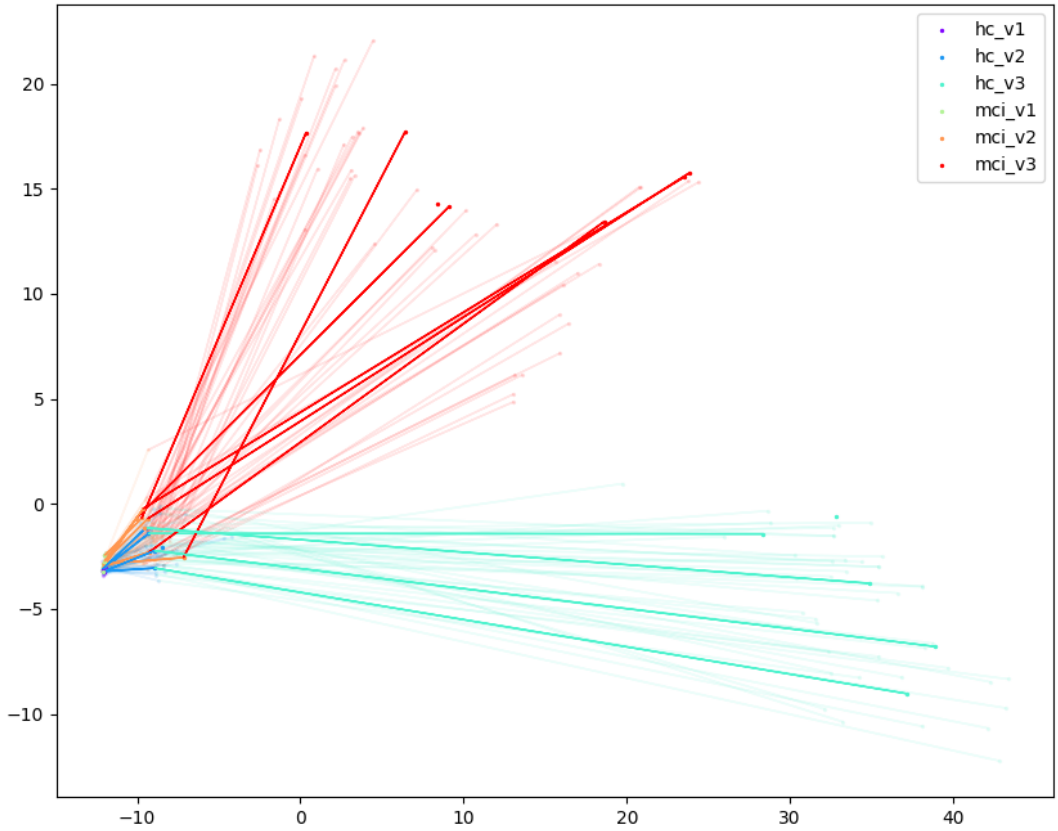

As shown in Figure 9 (without alignment loss), the trajectories are scattered and inconsistent, with large variability both within and across groups. This makes it difficult to distinguish between HC and MCI or to capture stable temporal patterns. In contrast, Figure 10 (with alignment loss) reveals more coherent trajectories: subjects within the same group (HC or MCI) show consistent progression directions across visits, while the separation between HC and MCI becomes clearer. Importantly, this indicates that the alignment loss encourages the model to capture cognitive progression trends rather than random variability in story content, reflecting interpretable patterns of decline (for MCI) and stability (for HC).

These results demonstrate that the alignment loss not only improves metrics but also enhances interpretability by aligning temporal trajectories in a way that reflects clinically meaningful differences in cognitive change. Feature-level analyses could provide even more intuitive examples of how the ATM aligns specific cognitive markers in speech. Future feature-level analyses could further enhance this by providing more intuitive illustrations of how the ATM captures and aligns specific cognitive markers in speech.

Results of NTU-AM-CS

In addition to the main longitudinal experiment, we conducted further evaluations in a cross-sectional setting to assess the performance of our proposed model. Here, the primary comparison is with our previous work [11], which also used audio and text data. However, a key difference is that the prior work relied on manual transcripts, which are less scalable and require special preprocessing for the transcripts. The results are shown in Tables 10 and 11.

XSL•FO
RenderX

Table . Results of recall data on National Taiwan University Autobiographical Memory Test Cross-Sectional dataset[c].

Method	Accuracy	F_1-score	Precision	Sensitivity	Specificity	AUROC[a]
Audio only						
Wav2vec2	0.65	0.42	0.41	0.48	0.47	0.51
Ours (audio)	0.57	0.60	0.52	0.72	0.45	0.58
Text only						
BERT[b]	0.67	0.56	0.62	0.61	0.67	0.64
Ours (text)	0.69	0.66	0.65	0.68	0.69	0.69[c]
Text + Audio						
Chang et al [11]	0.75[c]	0.61	0.76[c]	0.55	0.85[c]	0.68
Ours (CS[d])	0.74	0.72[c]	0.74	0.69[c]	0.83	0.68

[a]AUROC: area under the receiver operating characteristic curve.

[b]BERT: bidirectional encoder representation for transformer.

[c]Highest value of each evaluation metric.

[d]CS: cross-sectional.

Table . Results of probing data on National Taiwan University Autobiographical Memory Test Cross-Sectional dataset[c].

Method	Accuracy	F_1-score	Precision	Sensitivity	Specificity	AUROC[a]
Audio only						
Wav2vec2	0.55	0.49	0.65	0.43	0.66	0.61
Ours (audio)	0.61	0.65	0.56	0.84	0.43	0.64
Text only						
BERT[b]	0.69	0.64	0.66	0.72	0.67	0.69
Ours (text)	0.69	0.66	0.67	0.64	0.75[c]	0.65
Text + Audio						
Chang et al [11]	0.77[c]	0.64	0.62	0.73	0.68[c]	0.65
Ours (CS[d])	0.73	0.71[c]	0.67[c]	0.77[c]	0.68	0.72[c]

[a]AUROC: area under the receiver operating characteristic curve.

[b]BERT: bidirectional encoder representation for transformer.

[c]Highest value of each evaluation metric.

[d]CS: cross-sectional.

Our proposed method performs better or comparably on critical metrics such as F_1-score and AUROC in the results of recall data. Specifically, there is an 11% improvement in F_1-score. However, the precision is not as good as in the study by Chang et al [11]; our sensitivity metric performs better. For probing data, our method also yields better results in F_1-score and AUROC. However, the overall performance of the NTU-AM-CS dataset is not as promising as that of the NTU-AM-LG dataset. Detecting MCI features in AM data is challenging and reinforces the idea that long-term data relationships aid in model prediction.

Ablation Study

We investigated the contributions of linguistic features and context embedding in the encoder module for the prediction ability. The results are shown in Table 12. It demonstrates the impact of removing individual components on the model's predictions. For example, when linguistic features are removed, there is a noticeable decrease in specificity and a 6% drop in F_1-score. The most significant impact is seen when context embedding is removed, resulting in a 9% decrease in F_1-score and substantial declines in most other metrics. Only the sensitivity metric performs better, but overall, the original configuration still performs best in terms of F_1-score, which balances sensitivity and precision.

XSL•FO
RenderX

Table . Results of the ablation study for recall data on the National Taiwan University Autobiographical Memory Test Cross-Sectional dataset.

Method	Accuracy	F_1-score	Precision	Sensitivity	Specificity	AUROC[a]
Ours (CS[b])	0.74[c]	0.72[c]	0.74[c]	0.69[c]	0.83[c]	0.68[c]
Linguistic features	0.62	0.66	0.57	0.84[c]	0.45	0.62
Context embedding	0.59	0.63	0.53	0.80	0.45	0.60

[a]AUROC: area under the receiver operating characteristic curve.

[b]CS: cross-sectional.

[c]Highest values of each evaluation metric.

These results indicated that linguistic features provide auxiliary information that aids the model's decision-making, particularly in identifying negative samples. Context embedding supports the model's understanding of the story by distinguishing between the story topic and content through embeddings.

Result of Additional Dataset

In the experiment with an additional dataset, our main goal was to confirm whether the method our model uses to encode data is also applicable to other datasets related to cognitive tests. This means whether the way we encoded each data contributes to MCI detection. In Table 13, we present several results related to the detection of MCI. Our primary comparison targets in the NTUH-PIC and NTUH-MEM datasets are as per the study by Lin et al [18], which use textual information, including pauses, for MCI prediction. From the NTUH-PIC experimental results, there was an improvement of 11% in accuracy and 18% in F_1-score.

Table . Results of the National Taiwan University Hospital dataset.

Dataset	Method	Accuracy	F_1-score	Precision	Sensitivity	Specificity	AUROC[a]
NTUH-PIC[b]	Lin et al [18]	0.68	0.63	0.81[c]	0.58	0.78[c]	N/A[e]
	Ours (CS[d])	0.79[c]	0.81	0.80	0.88[c]	0.7	0.79
NTUH-MEM[f]	Lin et al [18]	0.68	0.66	0.75	0.7	0.65	N/A
	Ours (CS)	0.78[c]	0.76[c]	0.82[c]	0.73[c]	0.83[c]	0.78

[a]AUROC: area under the receiver operating characteristic curve.

[b]NTUH-PIC: National Taiwan University Hospital Picture Description Test.

[c]Highest values for each evaluation metric in its respective dataset.

[d]CS: cross-sectional.

[e]N/A: not applicable.

[f]NTUH-MEM: National Taiwan University Hospital Memory Test.

Similarly, in the NTUH-MEM dataset, a 10% improvement was observed in both accuracy and F_1-score compared with the study by Lin et al [18], indicating overall better performance. This experiment demonstrates that our data-encoding method effectively extracts latent representations suitable for MCI detection. Viewing data from multiple modalities provides consistent benefits for MCI detection. In addition, the performance differences observed in the NTU-AM-CS experiment indicate that using AM data for MCI detection is relatively challenging.

Due to the nature of the self-collected dataset, making comparisons with other works is challenging. Therefore, we present results on an open dataset in the final experiment. However, the ADReSSo dataset provides only HC and AD data. Table 14 shows our results alongside those of other state-of-the-art methods. Overall, our approach yields the best results, with a 4% improvement in both accuracy and F_1-score. In addition, our precision achieves the best performance. Once again, it confirms that our data-encoding method contributes to predictive outcomes in AD and MCI detection.

XSL•FO
RenderX

Table . Result of the ADReSSo dataset[a].

Method	Accuracy	F_1-score	Precision	Sensitivity	Specificity
Syed et al [30]	0.84	0.84	N/A[b]	0.79	0.90
Rohanian et al [31]	0.84	N/A	N/A	N/A	N/A
Zhu et al [32]	0.83	0.83	0.83	0.84[a]	N/A
Ying et al [33]	0.84	0.84	0.85	0.84[a]	N/A
Ours (CS[c])	0.88[a]	0.88[a]	0.93[a]	0.84[a]	0.92[a]

[a]Highest value in each evaluation metric.

[b]N/A: not applicable.

[c]CS: cross-sectional.

Discussion

Principal Results

In this study, we proposed a longitudinal framework for MCI detection using AM test speech data. The key innovation is the ATM, which leverages direction embeddings with subject and group alignment losses to model cognitive changes across multiple visits.

Our experiments demonstrate that the longitudinal framework substantially outperforms cross-sectional approaches. Compared with single-visit models, the longitudinal model achieved notable improvements, with AUROC gains of up to 21%, F_1-score increases of 16%, and accuracy improvements of 12%. These results confirm that incorporating multi–time point information provides a clearer picture of subtle cognitive trajectories that cannot be fully captured using only cross-sectional data.

The ablation studies further highlight the effectiveness of the alignment mechanisms. Removing the alignment losses led to considerable performance degradation, particularly a 17% - 21% drop in AUROC when the group alignment loss was excluded. This underscores the critical role of alignment in ensuring temporal consistency and improving the robustness of the framework.

In addition to evaluations on our self-collected dataset, we validated the framework on the publicly available ADReSSo dataset, which uses English picture description speech. Despite differences in language and task, our model achieved more than 88% accuracy, suggesting that the approach generalizes well across languages and cognitive assessment protocols.

In our analysis, the distribution of false positives and false negatives provides additional context for interpreting the model's sensitivity and specificity. False positives, which reduce specificity, were often linked to healthy subjects who displayed atypical speech characteristics such as disfluencies, pauses, or reduced lexical richness that mimicked early cognitive decline. On the other hand, false negatives, which lower sensitivity, were frequently observed in MCI subjects who retained strong narrative skills or enriched their responses with contextual details, thereby masking subtle impairments. These observations illustrate how individual variability in speech patterns can differentially impact sensitivity and specificity, underscoring both the strengths and the boundary conditions of the framework. While the alignment-based approach improves overall robustness, further refinement of feature representations and the inclusion of personalized modeling strategies may help balance sensitivity and specificity more effectively.

Taken together, these results highlight both the methodological and clinical significance of the proposed approach. Improvements in AUROC of 10% - 15% can translate into earlier identification of at-risk individuals and a reduction in false negatives in real-world screening. This demonstrates the potential of longitudinal, dual-modal speech analysis as a noninvasive, scalable tool for long-term cognitive monitoring, with the flexibility to be integrated into routine memory clinic assessments or used as a low-cost prescreening solution to complement standardized neuropsychological testing.

Limitations

Although the proposed framework shows promising performance for early MCI detection, several limitations remain. One major limitation of this study lies in the relatively small sample size of the NTU-AM-LG dataset, which includes only 54 subjects. Although each subject contributes multiple audio recordings across different visits, the limited number of unique participants poses inherent challenges for deep learning models, including a higher risk of overfitting, model instability, and low statistical power. As a result, while the proposed model demonstrates promising performance trends, its robustness and generalizability should be interpreted with caution. To mitigate these risks, we adopted strict subject-independent data splits and cross-validation to avoid data leakage and improve reliability. Nevertheless, future studies with larger and more diverse longitudinal datasets are essential to confirm the model's generalization capability and to further validate its clinical applicability. Furthermore, we also validate our approach on the publicly available ADReSSo dataset, although it is limited to a cross-sectional study. Cross-lingual robustness also presents a challenge, as our dataset is in Chinese while ADReSSo is in English. Linguistic and cultural factors such as narrative structure, emotional expression, and lexical choices may influence AM speech patterns and, in turn, affect model generalizability. Nevertheless, our results demonstrate encouraging cross-lingual generalizability. We highlight this as an open challenge and a direction for future work, where

XSL•FO
RenderX

cross-lingual adaptation and multilingual modeling will be crucial to improving robustness across diverse populations.

Moreover, the current longitudinal dataset includes 3 visits per participant, which restricts the ability to capture long-term trajectories of cognitive change. Collecting data across additional time points would allow the development of models better suited to characterizing the progression of cognitive decline.

This study also acknowledges potential confounding factors arising from the use of automatic speech processing tools. The *whisper-timestamped* model and *pyannote* diarization tool kit were used for transcription and speaker segmentation, respectively; however, the resulting ASR and diarization errors were not formally measured. Such errors, especially the higher ASR error rates likely to occur in participants with MCI due to disfluency or reduced articulation, and diarization inaccuracies that may introduce noise, could impact the extracted linguistic and acoustic features. These unaddressed confounders represent an inherent limitation of this study.

Further Studies

Based on the current findings, several directions can be explored in future work. First, extending the framework to multilingual settings will be essential for improving cross-lingual generalizability, as language and cultural factors strongly influence AM narratives. Second, adapting the model for low-resource scenarios will enhance its applicability in real-world clinical practice, where large-scale longitudinal datasets are often unavailable. Techniques such as transfer learning, data augmentation, and self-supervised pretraining could make the system more robust under such constraints.

Third, integrating AM speech analysis with other noninvasive modalities, such as wearable sensor data, offers the potential to capture complementary behavioral and physiological signals (eg, activity levels, sleep patterns, and heart rate variability). Such multimodal fusion could provide a more holistic view of cognitive health and improve early detection of decline. Finally, future studies should focus on personalized modeling of cognitive trajectories, acknowledging that the pace and pattern of decline vary across individuals. Personalized approaches may increase the clinical relevance of the framework and support tailored interventions.

Conclusions

We developed a dual-modal longitudinal analysis system to enhance the accuracy of diagnosing MCI. The system consists of an encoder and an ATM. We used a pretrained Wav2vec 2.0 model for speech data and BERT for text data to generate latent representations. Our proposed ATM generates significantly improved performance for MCI prediction, with F_1-scores of 0.78 and 0.83 on the recall and probing datasets, respectively. Combining data from both modalities improved understanding of the AM test data, with up to 19% and 12% improvements in F_1-score compared with unimodal models. In addition, ablation experiments verified the necessity of context embedding and linguistic features in the linguistic encoder. Our model's effectiveness was consistently superior across different datasets.

Acknowledgments

This research would not have been possible without the support of the

National Science and Technology Council of Taiwan and the Center of Artificial Intelligence and Advanced Robotics, National Taiwan University. We acknowledge that generative artificial intelligence was used solely to assist with improving grammar, clarity, and English language expression in the preparation of this manuscript. The authors reviewed and approved all edits to ensure accuracy and integrity of the scientific content.

Funding

This research was funded by the National Taiwan University (grant number NTU-ICRP-115L7505), National Science and Technology Council of Taiwan and the Center for Artificial Intelligence and Advanced Robotics, National Taiwan University (grant numbers NSTC 114-2634-F-002 -005, NSTC 114-2223-E-002 -002, and NSTC 112-2410-H-002-201-MY3).

Data Availability

The autobiographical memory speech data used in this study are not publicly available due to ethical and privacy restrictions involving patient privacy and informed consent. The ADReSSo dataset is publicly accessible for DementiaBank members.

Conflicts of Interest

None declared.

References

1. Prince M, Guerchet M, Prina M. The Epidemiology and Impact of Dementia-Current State and Future Trends: WHO Thematic Briefing; 2015. URL: https://hal.science/hal-03517019/document [accessed 2023-12-30]
2. World Alzheimer Report 2019: Attitudes to Dementia: Alzheimer's Disease International; 2019. URL: https://www.alzint.org/u/WorldAlzheimerReport2019.pdf [accessed 2024-01-19]

XSL•FO
RenderX

3. Petersen RC, Aisen PS, Beckett LA, et al. Alzheimer's Disease Neuroimaging Initiative (ADNI): clinical characterization. Neurology (ECronicon) 2010 Jan 19;74(3):201-209. [doi: 10.1212/WNL.0b013e3181cb3e25] [Medline: 20042704]
4. Chandra A, Dervenoulas G, Politis M, Initiative ADN. Magnetic resonance imaging in Alzheimer's disease and mild cognitive impairment. J Neurol 2019 Jun;266(6):1293-1302. [doi: 10.1007/s00415-018-9016-3] [Medline: 30120563]
5. Geda YE. Mild cognitive impairment in older adults. Curr Psychiatry Rep 2012 Aug;14(4):320-327. [doi: 10.1007/s11920-012-0291-x] [Medline: 22773365]
6. Levine B, Svoboda E, Hay JF, Winocur G, Moscovitch M. Aging and autobiographical memory: dissociating episodic from semantic retrieval. Psychol Aging 2002 Dec;17(4):677-689. [Medline: 12507363]
7. Al-Hameed S, Benaissa M, Christensen H. Detecting and predicting Alzheimer's disease severity in longitudinal acoustic data. Presented at: Proceedings of the 4th International Conference on Bioinformatics Research and Applications; Dec 8-10, 2017; Barcelona Spain p. 57-61. [doi: 10.1145/3175587.3175589]
8. Ben Ammar R, Ben Ayed Y. A language-based approach for predicting Alzheimer disease severity. In: International Conference on Research Challenges in Information Science: Springer; 2021:283-294. [doi: 10.1007/978-3-030-75018-3_19]
9. Laguarta J, Subirana B. Longitudinal speech biomarkers for automated Alzheimer's detection. Front Comput Sci 2021 Apr 8;3. [doi: 10.3389/fcomp.2021.624694]
10. Yamada Y, Shinkawa K, Shimmei K. Atypical repetition in daily conversation on different days for detecting Alzheimer disease: evaluation of phone-call data from regular monitoring service. JMIR Ment Health 2020 Jan 12;7(1):e16790. [doi: 10.2196/16790] [Medline: 31934870]
11. Chang HL, Wai T, Liao YS, Lin SY, Chang YL, Fu LC. A dual-modal fusion framework for detection of mild cognitive impairment based on autobiographical memory. IEEE J Biomed Health Inform 2025 Jun;29(6):4474-4485. [doi: 10.1109/JBHI.2025.3540207] [Medline: 40031689]
12. Eyben F, Scherer KR, Schuller BW, et al. The Geneva Minimalistic Acoustic Parameter Set (GeMAPS) for voice research and affective computing. IEEE Trans Affect Comput 2016 Apr 1;7(2). [doi: 10.1109/taffc.2015.2457417]
13. Arik S, Pfister T. TabNet: attentive interpretable tabular learning. AAAI 2021;35(8):6679-6687. [doi: 10.1609/aaai.v35i8.16826]
14. Baevski A, Zhou Y, Mohamed A, Auli M. wav2vec 2.0: a framework for self-supervised learning of speech representations. NIPS'20: Proceedings of the 34th International Conference on Neural Information Processing Systems 2020:12449-12460 [FREE Full text]
15. Yuan J, Cai X, Bian Y, Ye Z, Church K. Pauses for detection of Alzheimer's disease. Front Comput Sci 2021;2:624488. [doi: 10.3389/fcomp.2020.624488]
16. Pistono A, Pariente J, Bézy C, Lemesle B, Le Men J, Jucla M. What happens when nothing happens? An investigation of pauses as a compensatory mechanism in early Alzheimer's disease. Neuropsychologia 2019 Feb 18;124:133-143. [doi: 10.1016/j.neuropsychologia.2018.12.018] [Medline: 30593773]
17. Pastoriza-Domínguez P, Torre IG, Diéguez-Vide F, et al. Speech pause distribution as an early marker for Alzheimer's disease. Speech Commun 2022 Jan;136:107-117. [doi: 10.1016/j.specom.2021.11.009]
18. Lin SY, Chang HL, Wai T, Fu LC, Chang YL. Contrast-enhanced automatic cognitive impairment detection system with pause-encoder. Presented at: 2022 IEEE International Conference on Systems, Man, and Cybernetics (SMC); Oct 9-12, 2022; Prague, Czech Republic p. 2796-2801. [doi: 10.1109/SMC53654.2022.9945085]
19. Sangchocanonta S, Vongsurakrai S, Sroykhumpa K, et al. Development of Thai picture description task for Alzheimer's screening using part-of-speech tagging. Annu Int Conf IEEE Eng Med Biol Soc 2021 Nov:2104-2109. [doi: 10.1109/EMBC46164.2021.9629861]
20. Devlin J, Chang MW, Lee K, Toutanova K. BERT: pre-training of deep bidirectional transformers for language understanding. Proceedings of the 2019 Conference of the North American Chapter of the Association for Computational Linguistics: Human Language Technologies, Volume 1 (Long and Short Papers) 2019:4171-4186 [FREE Full text] [doi: 10.18653/v1/N19-1423]
21. Berna F, Schönknecht P, Seidl U, Toro P, Schröder J. Episodic autobiographical memory in normal aging and mild cognitive impairment: a population-based study. Psychiatry Res 2012 Dec 30;200(2-3):807-812. [doi: 10.1016/j.psychres.2012.03.022] [Medline: 22520853]
22. Irish M, Lawlor BA, O'Mara SM, Coen RF. Impaired capacity for autonoetic reliving during autobiographical event recall in mild Alzheimer's disease. Cortex 2011 Feb;47(2):236-249. [doi: 10.1016/j.cortex.2010.01.002] [Medline: 20153463]
23. Ouyang J, Zhao Q, Adeli E, Sullivan EV, Pfefferbaum A, Zaharchuk G, et al. Self-supervised longitudinal neighbourhood embedding. In: Medical Image Computing and Computer Assisted Intervention– MICCAI 2021: 24th International Conference 2021:80-89. [doi: 10.1007/978-3-030-87196-3_8]
24. Zhao Q, Liu Z, Adeli E, Pohl KM. Longitudinal self-supervised learning. Med Image Anal 2021 Jul;71:102051. [doi: 10.1016/j.media.2021.102051] [Medline: 33882336]
25. Khosla P, Teterwak P, Wang C, Sarna A, Tian Y, Isola P, et al. Supervised contrastive learning. arXiv. Preprint posted online on Apr 23, 2020. [doi: 10.48550/arXiv.2004.11362]

XSL•FO
RenderX

26. Leyhe T, Müller S, Milian M, Eschweiler GW, Saur R. Impairment of episodic and semantic autobiographical memory in patients with mild cognitive impairment and early Alzheimer's disease. Neuropsychologia 2009 Oct;47(12):2464-2469. [doi: 10.1016/j.neuropsychologia.2009.04.018] [Medline: 19409401]
27. Urbanowitsch N, Gorenc L, Herold CJ, Schröder J. Autobiographical memory: a clinical perspective. Front Behav Neurosci 2013 Dec 10;7:194. [doi: 10.3389/fnbeh.2013.00194] [Medline: 24339804]
28. Goodglass H, Kaplan E, Weintraub B. Boston Diagnostic Aphasia Examination: Lippincott Williams & Wilkins; 2001.
29. Luz S, Haider F, Fuente SDL, Fromm D, MacWhinney B. Detecting cognitive decline using speech only: The ADReSSo Challenge. MedRxiv. Preprint posted online on 2021. [doi: 10.1101/2021.03.24.21254263]
30. Syed ZS, Syed MSS, Lech M, Pirogova E. Tackling the ADRESSO challenge 2021: the MUET-RMIT system for Alzheimer's dementia recognition from spontaneous speech. Presented at: Interspeech 2021; Aug 30 to Sep 3, 2021; Brno, Czechia p. 3815-3819. [doi: 10.21437/Interspeech.2021-1572]
31. Rohanian M, Hough J, Purver M. Alzheimer's dementia recognition using acoustic, lexical, disfluency and speech pause features robust to noisy inputs. Presented at: Interspeech 2021; Aug 30 to Sep 3, 2021 URL: https://www.isca-archive.org/interspeech_2021/ [doi: 10.21437/Interspeech.2021-1633]
32. Zhu Y, Obyat A, Liang X, Batsis JA, Roth RM. WavBERT: exploiting semantic and non-semantic speech using Wav2vec and BERT for dementia detection. Interspeech 2021;2021:3790-3794. [doi: 10.21437/interspeech.2021-332] [Medline: 37063977]
33. Ying Y, Yang T, Zhou H. Multimodal fusion for Alzheimer's disease recognition. Appl Intell 2023 Jun;53(12):16029-16040. [doi: 10.1007/s10489-022-04255-z]

Abbreviations

AD: Alzheimer disease
AM: autobiographical memory
ASR: automatic speech recognition
ATM: aging trajectory module
AUROC: area under the receiver operating characteristic curve
BERT: bidirectional encoder representation for transformer
CS: cross-sectional
LG: longitudinal
MCI: mild cognitive impairment
NTU-AM: National Taiwan University Autobiographical Memory Test
NTU-AM-CS: National Taiwan University Autobiographical Memory Test Cross-Sectional
NTUH-MEM: National Taiwan University Hospital Memory Test
NTUH-PIC: National Taiwan University Hospital Picture Description Test
POS: part-of-speech

Edited by A Coristine; submitted 26.Jul.2025; peer-reviewed by B Jing, J Shi; revised version received 21.Nov.2025; accepted 25.Nov.2025; published 15.Jan.2026.

Please cite as:
Liao YS, Wai T, Liao TY, Chang HL, Chang YL, Fu LC
Mild Cognitive Impairment Detection System Based on Unstructured Spontaneous Speech: Longitudinal Dual-Modal Framework
JMIR Med Inform 2026;14:e80883
URL: https://medinform.jmir.org/2026/1/e80883
doi:10.2196/80883

© Yu-Shan Liao, Thiri Wai, Ting-Yun Liao, Ho-Ling Chang, Yu-Ling Chang, Li-Chen Fu. Originally published in JMIR Medical Informatics (https://medinform.jmir.org), 15.Jan.2026. This is an open-access article distributed under the terms of the Creative Commons Attribution License (https://creativecommons.org/licenses/by/4.0/), which permits unrestricted use, distribution, and reproduction in any medium, provided the original work, first published in JMIR Medical Informatics, is properly cited. The complete bibliographic information, a link to the original publication on https://medinform.jmir.org/, as well as this copyright and license information must be included.

XSL•FO
RenderX

Enhancing Anesthetic Depth Assessment via Unsupervised Machine Learning in Processed Electroencephalography Analysis: Novel Methodological Study

Po-Yu Huang[1], MD; Wei-Lun Hong[2], MS; Hui-Zen Hee[3], MD; Wen-Kuei Chang[1], MD; Ching-Hung Lee[2,4], PhD; Chien-Kun Ting[1,5], MD, PhD

[1]Department of Anesthesiology, Taipei Veterans General Hospital, No. 201, Sec 2, Shipai Rd, Beitou District, Taipei City, Taiwan

[2]Institute of Electrical and Control Engineering, National Yang Ming Chiao Tung University, Hsinchu City, Taiwan

[3]Department of Anesthesiology, Far Eastern Memorial Hospital, New Taipei City, Taiwan

[4]Department of Electrical Engineering, Chung Yuan Christian University, Taoyuan City, Taiwan

[5]Institute of Emergency and Critical Care Medicine, National Yang Ming Chiao Tung University, Taipei City, Taiwan

Corresponding Author:
Chien-Kun Ting, MD, PhD
Department of Anesthesiology, Taipei Veterans General Hospital, No. 201, Sec 2, Shipai Rd, Beitou District, Taipei City, Taiwan

Abstract

Background: General anesthesia comprises 3 essential components—hypnosis, analgesia, and immobility. Among these, maintaining an appropriate hypnotic state, or anesthetic depth, is crucial for patient safety. Excessively deep anesthesia may lead to hemodynamic instability and postoperative cognitive dysfunction, whereas inadequate anesthesia increases the risk of intraoperative awareness. Electroencephalography (EEG)-based monitoring has therefore become a cornerstone for evaluating anesthetic depth. However, processed electroencephalography (pEEG) indices remain vulnerable to various sources of interference, including electromyographic activity, interindividual variability, and anesthetic drug effects, which can yield inaccurate numerical outputs.

Objective: With recent advances in machine learning, particularly unsupervised learning, data-driven methods that classify signals according to inherent patterns offer new possibilities for anesthetic depth analysis. This study aimed to establish a methodology for automatically identifying anesthesia depth using an unsupervised, machine learning–based clustering approach applied to pEEG data.

Methods: Standard frontal EEG data from participants undergoing elective lumbar spine surgery were retrospectively analyzed, yielding more than 16,000 data points. The signals were filtered with a fourth-order Butterworth bandpass filter and transformed using the fast Fourier transform to estimate power spectral density. Normalized band power ratios for delta, high-theta, alpha, and beta frequencies were extracted as input features. Fuzzy C-Means (FCM) clustering (c=3, m=2) was applied to categorize anesthetic depth into slight, proper, and deep clusters.

Results: FCM clustering successfully identified 3 physiologically interpretable clusters consistent with EEG dynamics during progressive anesthesia. As anesthesia deepened, frontal alpha oscillations became more prominent within a delta-dominant background, while beta activity decreased with loss of consciousness. The fuzzy membership values quantified transitional states and captured the continuum of anesthetic depth. Visualization confirmed strong correspondence among cluster transitions, Patient State Index trends, and spectral density patterns.

Conclusions: This study demonstrates the feasibility of using unsupervised machine learning to enhance anesthetic depth assessment. By applying FCM clustering to pEEG data, this approach improves the understanding of anesthesia depth and integrates effectively with existing monitoring modalities. The proposed FCM-based method complements current EEG indices and may assist anesthesia practitioners and even nonanesthesia professionals in assessing anesthetic depth to enhance patient safety.

(JMIR Med Inform 2026;14:e77830) doi:10.2196/77830

KEYWORDS

artificial intelligence; cluster analysis; electroencephalography; general anesthesia; intraoperative monitoring; machine learning

XSL•FO
RenderX

Introduction

General anesthesia induces temporary loss of consciousness characterized by unconsciousness, immobility, and autonomic regulation of pain [1,2]. Maintaining an appropriate depth of anesthesia is essential for patient safety. Insufficient anesthesia may lead to intraoperative awareness, autonomic hyperactivity, and significant psychological distress [3]. Conversely, excessive anesthesia has been associated with neuroinflammation [4], neuronal injury, and postoperative cognitive dysfunction or delirium [5,6]. Therefore, continuous monitoring of anesthetic depth during surgery is of critical importance. Electroencephalography (EEG)-based monitoring serves as a valuable tool for this purpose. Real-time EEG analysis provides insight into anesthetic states, as oscillatory patterns vary with the anesthetic dose, type, and patient characteristics [7,8]. The Perioperative Quality Initiative 6 Workgroup, led by Chan, details the available EEG monitors [9]. Understanding perioperative neural activity enables anesthesiologists to optimize anesthesia delivery and enhance patient outcomes.

Artificial intelligence is revolutionizing anesthesiology, with techniques such as anesthesia depth monitoring [10]. Unsupervised machine learning operates without predefined hypotheses and identifies patterns and structures within datasets to classify patients, medications, and groups [11]. Unlike supervised machine learning, which correlates the input data with known outcomes, unsupervised machine learning categorizes instances based on inherent patterns. In EEG analyses, unsupervised machine learning methods such as fuzzy clustering have been used to analyze sleep stages [12], detect epileptic spikes [13], and identify significant elements in multichannel recordings [14].

Anesthesia management fundamentally involves 3 key components: hypnosis, analgesia, and muscle relaxation. During induction and maintenance, a reproducible spectral shift occurs in the EEG, wherein frontal alpha oscillations become prominent within a delta-dominant background, delta power progressively increases with deepening anesthesia, and beta activity decreases as consciousness is lost [8,15-17]. Power spectral metrics—including relative alpha, beta, and delta power, power ratios, and spectral entropy—have been shown to reliably distinguish between conscious and anesthetized states [18-20]. Inhalational agents such as sevoflurane and desflurane consistently produce dose-dependent increases in frontal alpha and delta power [17,21-23], providing a physiologic basis for categorizing anesthesia into light, proper, and deep stages. However, current perioperative EEG-based indices, such as the Bispectral Index (BIS) [24,25] and Patient State Index (PSi) [26,27], primarily reflect the hypnotic component but can be influenced by various factors, potentially leading to misleading processed numerical outputs. Therefore, this study aimed to enhance anesthetic depth assessment by focusing on the hypnosis dimension and applying unsupervised machine learning methods, specifically Fuzzy C-Means (FCM) clustering, to processed electroencephalography (pEEG) data.

The primary objective of this study was to establish a methodology for automatically identifying anesthesia depth through a visualized presentation, leveraging machine learning–based clustering techniques. By applying unsupervised learning to pEEG data, this approach aims to enhance the classification and understanding of anesthesia depth and facilitate patient-specific anesthesia management.

Methods

Recruitment

Data were collected at the Veterans General Hospital, Taipei, with the approval of the Institutional Review Board (number 2021-09-008BC). More than 16,000 data points were collected from 10 participants (Participants 1 - 10) who underwent elective lumbar spinal surgery in the prone position. The ages of the participants ranged from 44 to 78 years, with the American Society of Anesthesiologists' physical status classifications ranging from class I to class III. Participants with conditions such as pregnancy, neurological disorders, ongoing infections, a history of central nervous system medication use, respiratory failure, heart failure, or renal failure were excluded.

Masimo SedLine [28] brain function monitoring was performed with the participant in the supine position. Induction included fentanyl at 1 - 3 mcg/kg as an adjunct for intubation, followed by propofol at 1 - 3 mg/kg as an induction bolus. Rocuronium was administered at an intubation dose of 0.6 - 1 mg/kg for muscle relaxation. The participant was then intubated.

During maintenance, the inhalational agent sevoflurane was administered, with dosage adjustments titrated based on the PSi levels and pEEG density spectral array (DSA) patterns. The participant was then placed in a prone position for lumbar spinal surgery. After the completion of the surgery, the participant was returned to the supine position, and the inhalation agent was gradually titrated off. Rocuronium administration was reversed using sugammadex. Subsequently, the participants were extubated and transferred to the postanesthetic care unit for further monitoring and recovery.

Data Collection and Processing

Figure 1 outlines the preprocessing steps for the EEG data in our study.

XSL•FO
RenderX

Figure 1. Signal processing flow diagram. Flow diagram illustrating preprocessing and feature-extraction steps applied to processed electroencephalography data obtained from participants who underwent elective lumbar spine surgery at Taipei Veterans General Hospital. Raw frontal electroencephalography signals were filtered with a fourth-order Butterworth bandpass filter, and power spectral density was estimated using the Welch method with a 30-second window and 2-second overlap. Normalized delta, high-theta, alpha, and beta band power ratios were extracted as input features for unsupervised clustering using the Fuzzy C-Means (FCM) algorithm (*c=3*, *m=2*). EEG: electroencephalography.

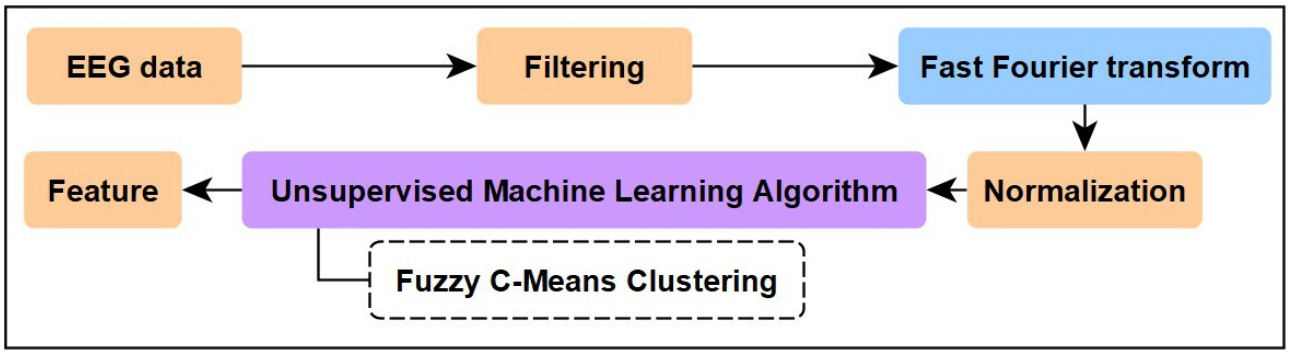

Signal Processing and Feature Extraction

EEG tracings from the 4 Masimo SedLine channels were averaged into 1-dimensional signals and synchronized for consistency. Each participant's EEG data were recorded at a sampling frequency of 178 Hz, with a data collection period ranging from 3 to 5 hours, depending on the duration of anesthesia. A fourth-order Butterworth bandpass filter (0.5 - 30 Hz) was applied to minimize the ripple and achieve a maximally flat response. Power spectral density was estimated using the Welch method implemented in Python (SciPy library), using a 30-second window with a 2-second sliding overlap to ensure both temporal continuity and frequency resolution. Additional preprocessing specifications are available in Multimedia Appendix 1. The Welch method and the fast Fourier transform were used to estimate the power spectral density, facilitating the extraction of alpha (8 - 12 Hz), beta (13 - 30 Hz), delta (0.5 - 4 Hz), and high-theta (6 - 8 Hz) band powers. Normalization was performed by calculating the ratio of each band's power to the sum of the power of these 4 specific bands (delta+high-theta+alpha+beta), ensuring that the sum of the feature vector elements equals 1. The 4 - 6 Hz and 12 - 13 Hz bands were excluded based on their limited variation across states. Removing these transitional zones established a "spectral buffer" to reduce noise, allowing the algorithm to prioritize the more discriminative delta and alpha and high-theta features. Manual artifact rejection was conducted by board-certified anesthesiologists and engineers to identify and exclude segments exhibiting abnormal, noisy epochs indicative of artifacts.

FCM Clustering Algorithm

FCM clustering categorizes data points into clusters with membership values between 0 and 1, accommodating the uncertainty in the cluster assignment. It was performed with 3 clusters (c=3), a fuzziness parameter (m) of 2, random initialization of cluster centers, and a convergence threshold of 0.005. The model iteratively updates the centroids and membership values until convergence, guided by a fuzziness parameter (m) that regulates cluster ambiguity. A global FCM model was established to generate fixed global cluster centroids. These fixed centroids were then applied to all participants to calculate membership values. Further implementation details are provided in Multimedia Appendix 1. This method extracts delta, alpha, high-theta, and beta band power ratios from pEEG signals to partition the data into 3 statistically distinct clusters. These clusters were subsequently labeled as "slight," "proper," and "deep" based on their physiological spectral characteristics. The capability of FCM to manage data ambiguity makes it suitable for nuanced depth assessments under general anesthesia.

Ethical Considerations

This study was conducted in accordance with the ethical principles outlined in the Declaration of Helsinki and was approved by the Institutional Review Board of Taipei Veterans General Hospital, Taiwan (number: 2021-09-008BC). Written informed consent was obtained from all participants prior to enrollment. The data used in this study were deidentified before analysis to ensure participant confidentiality and privacy. No identifiable personal information or images were included in the manuscript or supplementary materials. Participants did not receive any financial compensation for their participation in the study.

Results

Overview

In this study, an unsupervised learning method, FCM, was used to analyze the pEEG data from participants with complete datasets. Table 1 summarizes the demographic information and baseline characteristics of the participants. The analysis focused on a feature set comprising the delta-band power ratio and the sum of the alpha and high-theta band power ratios. The results revealed 3 distinct clusters. Based on the centroids' spectral features, we assigned post hoc clinical labels to these clusters representing different anesthesia depths: slight (green), proper (blue), and deep (red). This clustering approach was validated using visual representation to confirm the effectiveness of the feature set in differentiating anesthesia depths. Subsequently, the same method was applied to individual participant data, categorizing each participant's pEEG into 1 of the 3 clusters, thus providing a detailed estimation of the anesthesia depth for each individual.

XSL•FO
RenderX

Table . Demographic information and baseline characteristics. Demographic and intraoperative characteristics of 10 participants included in this retrospective observational study of processed electroencephalography–based anesthetic-depth assessment. All participants underwent elective lumbar spine surgery at Taipei Veterans General Hospital, Taiwan. Variables include age, sex, height, weight, BMI, American Society of Anesthesiologists classification, comorbidities, intraoperative blood loss, operation time, and postoperative hospital stay.

Participant	Age (years)	Sex	Height (cm)	Body weight (kg)	BMI (kg/m^2)	ASA[a] classification	Comorbidities	Blood loss (mL)	Operation time (minutes)	Postoperative stay (days)
1	63	F[b]	152.2	63.7	27.5	I	None	300	250	7
2	78	F	150.5	53.5	23.6	II	Hepatitis	200	280	6
3	65	M[c]	168	89.8	31.8	II	None	300	360	4
4	75	M	170	70	24.2	II	Hypertension, dementia	660	405	7
5	67	M	160	64	25.0	II	Hypertension	200	285	6
6	45	M	171	69.9	23.9	I	None	[d]—	170	2
7	61	M	160.3	77.7	30.2	II	Hypertension, diabetes mellitus	1300	195	6
8	68	F	157.7	71.1	28.6	II	Hypertension, diabetes mellitus	450	210	5
9	44	M	173.6	67.6	22.4	I	None	50	375	29
10	71	M	167	83	29.8	III	Hypertension, coronary artery disease	530	320	6

[a]ASA: American Society of Anesthesiologists.

[b]F: female.

[c]M: male.

[d]Not available.

FCM Clustering Analysis of pEEG Features

FCM clustering was applied to all participants, using alpha, beta, delta, and high-theta band power as the selected features for clustering. Figure 2 illustrates the FCM clustering results for all participants, with the delta band power ratio plotted on the *x*-axis and the sum of the alpha and high-theta band power ratios on the *y*-axis. Each data point represents a single time point of a participant's pEEG signal and is clustered into 3 distinct groups: slight anesthesia depth (green), proper anesthesia depth (blue), and deep anesthesia depth (red). The contribution of the beta band power ratio can be inferred as the sum of the delta, alpha, high-theta, and beta band power ratios equals 1, although not explicitly displayed. This visual depiction offers insights into the distribution of a participant's single time points within each anesthesia depth cluster.

After establishing the efficacy of the selected features and parameters through a collective analysis of the participants, our investigation shifted focus to the individual application of this methodology. The fixed global cluster centroids were then applied to the data of Participants 1 - 10 to calculate membership values and simplified estimation results. Following the methodology outlined, where all time indices share a common time scale, the pEEG data were combined with PSi data retrieved from the Masimo SedLine brain function monitoring system, and the time-frequency images were compared within the same figure, with each participant outputting a distinct figure. Within these figures, Participants 4 and 6 are described in the article. By incorporating this comprehensive approach, our study verified the applicability of the selected features and enhanced confidence in the adaptability of our methodology to diverse clinical scenarios and datasets, strengthening the reliability of our conclusions and paving the way for further exploration and validation within the anesthesia depth assessment domain.

XSL•FO
RenderX

Figure 2. Fuzzy C-Means clustering results for all participants. Two-dimensional clustering distribution of processed electroencephalography features from participants undergoing elective lumbar spine surgery. The *x*-axis represents the delta-power ratio and the *y*-axis the combined alpha and high-theta power ratios. Fuzzy C-Means clustering (*c=3*, *m=2*) identified 3 physiologically interpretable clusters corresponding to anesthesia-depth levels: slight (green), proper (blue), and deep (red). Each point denotes a 30-second windowed segment of electroencephalography data, demonstrating the continuum of anesthetic states observed across the study population.

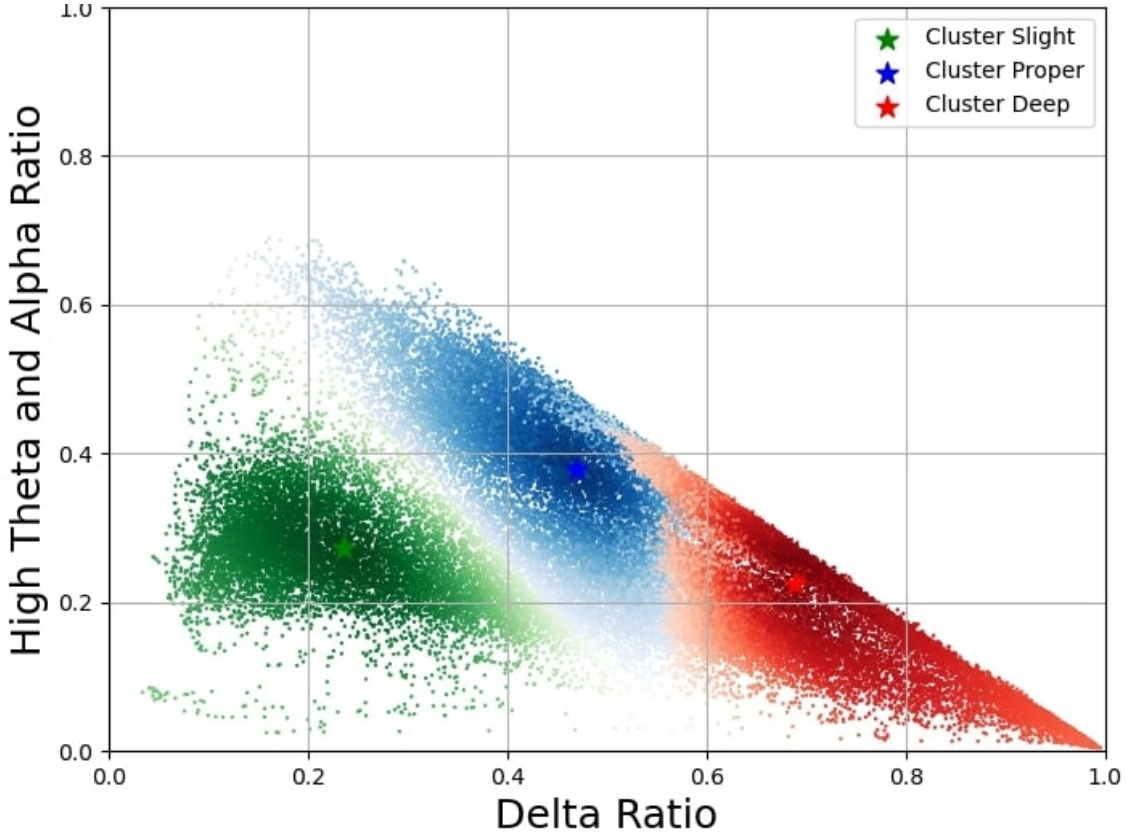

Participant 4 and Participant 6: FCM Clustering Analysis

Participant 4 underwent the same data retrieval and processing procedures as the other participants, with raw EEG data obtained from the Masimo SedLine brain function monitoring system. These data were subjected to filtering, fast Fourier transformation, normalization, and subsequent FCM clustering. The culmination of these processes is depicted in Figure 3, which comprises multiple panels, sharing a synchronized timescale on the *x*-axis.

Figure 3A shows the PSi of Participant 4 obtained from the Masimo SedLine brain function monitoring system. The *x*-axis represents the time scale, whereas the *y*-axis displays the PSi values, reflecting the PSi over time.

Figure 3B shows the results of FCM clustering for Participant 4. The *y*-axis illustrates the estimated membership values and denotes the degree of belongingness of each cluster. This belongingness quantifies the "fuzziness" of the FCM clustering, indicating the confidence level of each assignment of the data point to a particular cluster. It effectively quantifies the "color shading" shown in Figure 2, where darker shades represent higher confidence levels in cluster assignments. For example, a membership value of 1 signifies full belongingness to the cluster, and a value of 0.8 indicates 80% confidence in the assignment. This "soft" labeling approach allows for a more nuanced understanding of the clustering results, providing insights into the uncertainty associated with each classification of the data point.

Figure 3C represents a modified rendition of Figure 3B, specifically tailored to illustrate the anesthesia depth classification for Participant 4. Along the *y*-axis, this plot delineates the categorization into slight, proper, or deep anesthesia groups at individual time points. Figure 3B provides a detailed depiction of the continuous membership values, reflecting the degree of belonging to each cluster: slight, proper, and deep. However, this comprehensive display introduces the challenge of intuitively discerning the predominant cluster at a single point. While this approach offers a more complete dataset, it complicates the task of determining the cluster affiliations for each data point. Hence, the modified version in Figure 3C simplifies this interpretation by highlighting the cluster with the "higher value." This adaptation facilitates a more straightforward assessment of the anesthesia depth classification by presenting a clearer distinction. This clarity enhances the utility of visualization in aiding clinician decision-making during patient monitoring and management.

Figure 3D presents a time-frequency image derived from the raw EEG signal without processing, providing insights into the frequency components of the EEG signal over time. Overall, Figure 3 provides a comprehensive analysis of the EEG signals and anesthesia depth classification for Participant 4, contributing

XSL•FO
RenderX

to the understanding of brain function monitoring and anesthesia management.

Participant 6 then underwent identical signal processing and analysis procedures, resulting in Figure 4. This comprehensive Figures 4A-D underwent the same rigorous process as shown in Figures 3A-D.

Figure 3. Fuzzy C-Means clustering analysis of Participant 4. Representative analysis of Participant 4 (male, 75 years, American Society of Anesthesiologists class II) who underwent lumbar spine surgery at Taipei Veterans General Hospital. (**A**) shows the Patient State Index trend over time; (**B**) displays Fuzzy C-Means membership values representing the degree of belongingness to each cluster; (**C**) illustrates the simplified classification into slight, proper, and deep anesthesia levels; (**D**) presents the corresponding electroencephalography time-frequency spectrogram. These plots depict temporal transitions in anesthetic depth.

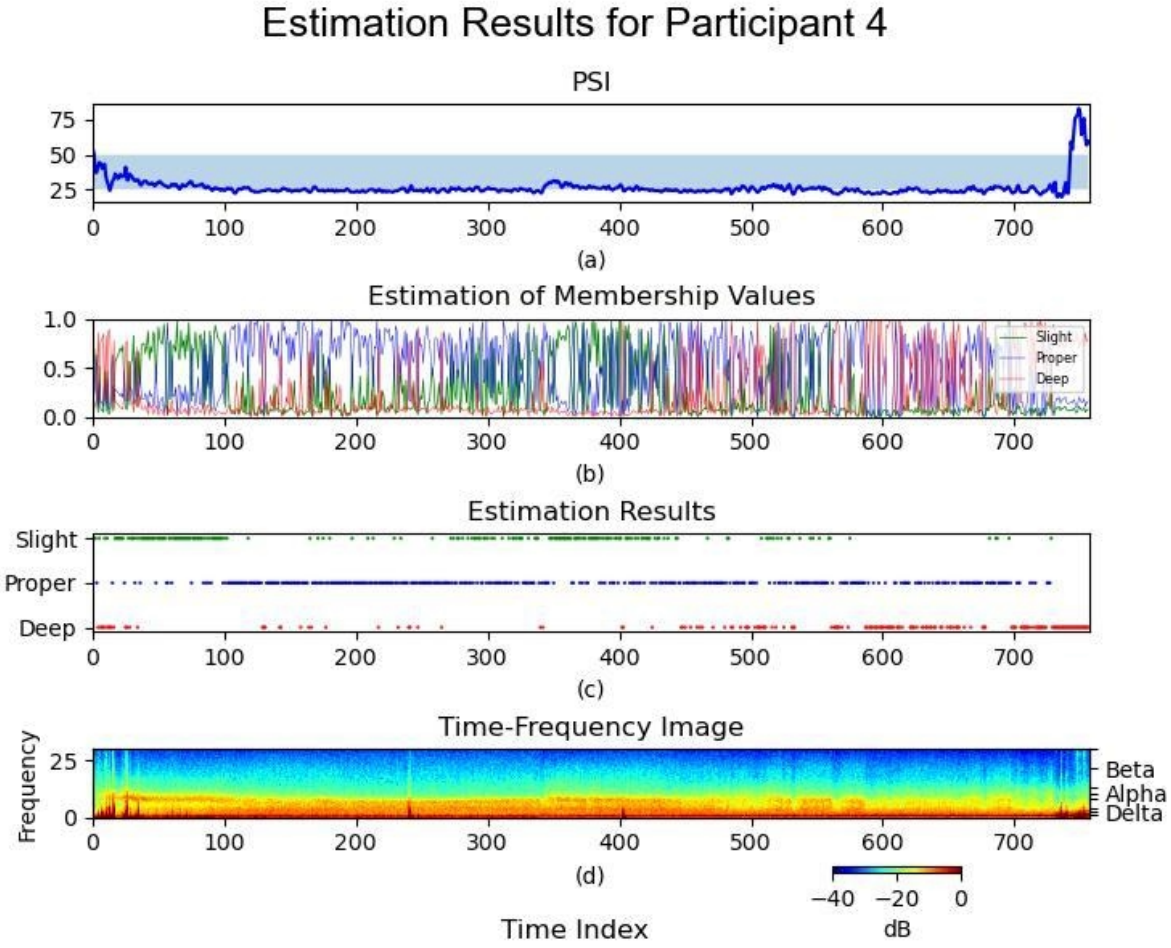

XSL•FO
RenderX

Figure 4. Fuzzy C-Means clustering analysis of Participant 6. Representative analysis of Participant 6 (male, 45 years, American Society of Anesthesiologists class I) who underwent elective lumbar spine surgery at Taipei Veterans General Hospital. (**A**) shows the Patient State Index trend over time. (**B**) displays Fuzzy C-Means membership values representing the degree of belongingness to each cluster. (**C**) illustrates the simplified classification into slight, proper, and deep anesthesia levels. (**D**) presents the corresponding electroencephalography time-frequency spectrogram. These plots depict temporal transitions in anesthetic depth. PSi: Patient State Index.

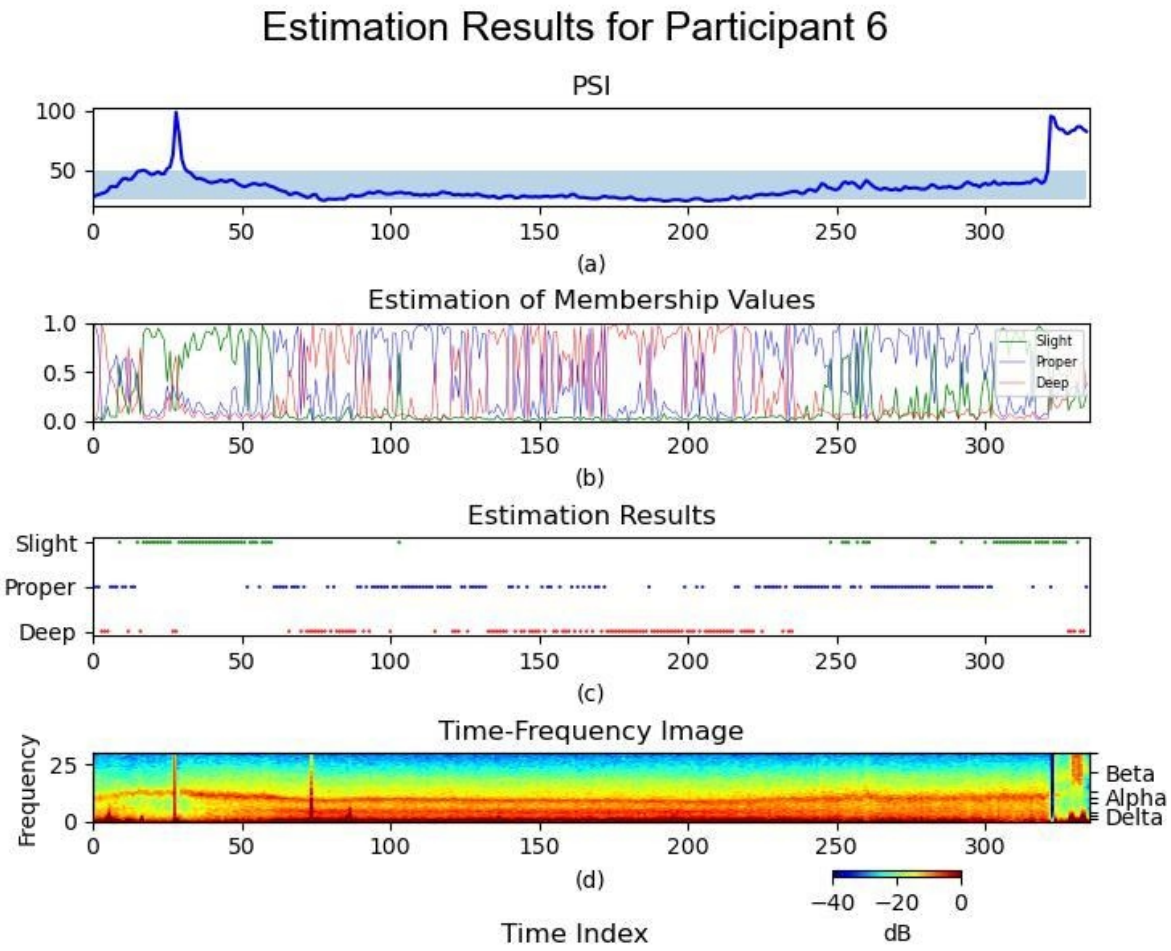

Discussion

Principal Findings

This study explored the feasibility of improving anesthetic depth assessment by applying unsupervised machine learning to pEEG data. EEG patterns vary with the depth of anesthesia [10]. PEEG-derived indices, such as the BIS and PSi, are susceptible to various influences, presenting limitations in their interpretation [24]. Purdon et al [8] characterized the EEG signatures of intravenous and inhaled anesthetics, providing additional insights into the depth of anesthesia. In Figure 2, the delta ratio quantifies cortical suppression, as delta oscillations reflect deep anesthesia and thalamocortical inhibition. The theta and alpha ratios were selected for their modulation by anesthetics in the frontal cortex. Alpha oscillations indicate stable unconsciousness under propofol and sevoflurane, correlating with GABAergic inhibition, while theta oscillations become prominent at higher anesthetic concentrations, particularly with sevoflurane, signaling transitions between moderate and deep anesthesia. Figures 3 and 4 depict Participants 4 and 6, respectively, demonstrating the combination of PSi values, anesthesia depth clustering values, simplified clustering results, and processed time-frequency images. These visual presentations illustrate patient-specific anesthesia depth, facilitating the automatic identification of anesthesia depth.

Postoperative delirium and neurocognitive complications after spinal surgery remain significant concerns [29], and perioperative EEG monitoring may contribute to their management [30]. In this study, one participant (Participant 4) had a history of cognitive dysfunction due to dementia. All participants underwent lumbar spinal surgery in the prone position with sevoflurane as the maintenance agent. The operation time ranged from 170 to 405 minutes. Most participants were discharged within 1 week, and no other cognitive impairments were documented.

Limitations

This study was constrained by a small sample size. While the extensive dataset of over 16,000 EEG epochs ensures high within-subject data density and supports the internal stability of the model for the analyzed participants, we acknowledge that the limited number of independent participants restricts the external generalizability of the findings. Previous studies have indicated that a sampling frequency of 100 Hz is sufficient for EEG-based analysis [31]. While a larger sample size could

XSL•FO
RenderX

further refine the FCM clustering results presented in Figure 1, the primary determinants of clustering effectiveness in single-subject EEG analysis are the duration and density of the data. With 3 to 5 hours of continuous EEG recordings per participant, our study provided sufficient granularity for meaningful intrasubject clustering, as demonstrated in Figures 3 and 4. Our primary objective was to explore the feasibility and establish the methodological framework for applying unsupervised machine learning to processed EEG data.

García et al [32] explored EEG activity and delineated an analgesia-related axis alongside hypnosis during general anesthesia, revealing distinct changes in EEG patterns. We acknowledge the limitation of a single-dimensional index in capturing the full spectrum of neural activity during anesthesia. However, our primary goal is to demonstrate the feasibility of unsupervised clustering within a clinical framework, focusing on the hypnosis axis—one of anesthesia's 3 key components. This study used frontal EEG signals, as used in processed systems such as BIS and SedLine. Frontal EEG monitoring inherently limits spatial coverage but remains the clinical standard due to its accessibility and reliability. The frontal cortex exhibits predictable EEG dynamics—α-spindle emergence and δ-wave dominance—with increasing anesthetic depth, correlating with loss of consciousness and hypnotic adequacy [33-35].

While this study does not include external validation or direct quantitative comparisons, this reflects the broader challenge in anesthetic depth classification, which lacks a universal standard. Although no intraoperative recall was observed, determining the optimal depth of anesthesia remains complex. Conventional monitors, such as BIS and SedLine, along with DSA visualization, aid clinical judgment but do not serve as definitive references. The study introduces a complementary tool to enhance anesthetic depth assessment. This is reflected in Figures 3 and 4, where multiple monitoring modalities are integrated to provide additional insights.

Finally, the frame-by-frame analysis maximizes temporal sensitivity but may result in rapid state transitions, or "flickering," as observed in Figure 3C. For clinical application, future iterations would likely require temporal smoothing algorithms to stabilize the output and minimize alarm fatigue. Despite strong visual correspondence with PSi trends, standardized quantitative metrics were not calculated due to methodological constraints. Specifically, the significant time delay inherent in the PSi algorithm [36] limits direct linear correlation with the frame-by-frame FCM method, and imposing rigid thresholds for concordance rates contradicts the continuous, fuzzy nature of anesthetic depth.

Comparison With Prior Work

Unsupervised learning involves algorithms that identify patterns or structures within a dataset, facilitating the discovery of novel classification methods [10]. Systematic reviews have highlighted the effectiveness of unsupervised clustering methods in various medical applications. Clustering analysis has revealed pivotal features underlying the progression from early stage to advanced Alzheimer disease [37]. Unsupervised learning models applied in cardiac resynchronization therapy can accurately discern patient clusters and are valuable for phenotyping and predicting treatment responses [38]. In amyotrophic lateral sclerosis research, the k-means score, a hierarchical clustering method, has emerged as the most widely used method for stratification and progression prediction [39]. We predefined 3 practical categories—slight, proper, and deep anesthesia—to emulate the structured reasoning process that governs intraoperative anesthetic management. Clinicians continuously evaluate anesthetic depth and determine whether to increase, maintain, or decrease anesthetic delivery. Each titration is typically incremental and followed by a brief observation period to allow pharmacokinetic redistribution and physiological stabilization before reevaluation. Although the equilibration interval varies among individuals, such judgments integrate both the instantaneous anesthetic state and its temporal evolution [36]. FCM clustering offers distinct advantages for modeling this continuum. It enables classification into clinically interpretable states while concurrently generating fuzzy membership values that quantify the degree to which a given epoch inclines toward a "lighter" or "deeper" level of anesthesia. This property captures the continuous and overlapping nature of anesthetic depth and mirrors the gradual, feedback-driven adjustments that characterize intraoperative anesthesia management.

In our continuous monitoring data, transitions between anesthetic states occurred gradually, consistent with the physiological continuum of anesthesia depth. Abrupt shifts from "light" directly to "deep" anesthesia were uncommon and, when observed, were generally attributable to identifiable physiological perturbations—such as bolus drug administration, intense noxious stimulation, or sudden hemodynamic changes—rather than modeling artifacts. Processed EEG indices may also be transiently affected by electromyographic [40], electrocardiographic [41], or mechanical vibration artifacts, particularly during spine surgery. These interferences are usually recognizable in the raw EEG tracing and can be excluded from analysis.

Near-equal memberships across clusters (≈33% each) are uncommon and typically occur when a feature vector lies between centroids or during transient noise, reflecting a transitional or indeterminate phase rather than a distinct anesthetic state. Interpretation of anesthetic depth is inherently pattern-based, as clinicians assess temporal trends and spectral features in the DSA—for instance, alpha dominance suggests adequate hypnosis, whereas delta and theta predominance or burst suppression indicate a deeper anesthetic level [42]. Therefore, a single epoch with near-equal memberships would not influence clinical judgment, which relies on the overall evolution of EEG patterns rather than isolated points.

Prior research has focused on developing and enhancing automated system controls, including closed-loop anesthesia. Components such as measurement devices, controllers, and actuators are central to these advancements [43]. pEEG-derived indices, such as the BIS [43,44] and PSi [45], frequently serve as key targets. This study introduced unsupervised learning clustering as a potential new approach for assessing anesthesia depth, offering additional avenues for improving automated anesthesia control systems.

XSL•FO
RenderX

The novel clustering approach provides an alternative method for assessing anesthesia depth, particularly focusing on the "hypnosis" axis, as depicted in Figure 3B and C. These figures illustrate the EEG density spectral array data from Participant 4, suggesting segmentation into slight, proper, and excessively deep anesthesia depths. Unlike traditional PSi values, which provide singular metrics, the representation of Figure 3B with fuzziness on the *y*-axis shows nuanced membership toward anesthesia depth clusters. The graphical depiction in Figure 3C highlights the peak values, indicating the period of deep anesthesia. This approach offers a novel tool for assisting clinical judgment in anesthesia depth assessment.

Among conventional unsupervised clustering paradigms, FCM, Gaussian Mixture Models (GMMs), and density-based algorithms such as Density-Based Spatial Clustering of Applications with Noise (DBSCAN) exhibit fundamentally distinct analytical mechanisms. FCM minimizes a distance-weighted objective function while permitting graded memberships across clusters—an essential property for anesthesia-related data in which EEG and physiological variables vary continuously and overlap across anesthetic states. In contrast, GMM represents data as a superposition of Gaussian components and assumes that each cluster conforms to an elliptical, symmetric distribution. However, anesthetic EEG features often display non-Gaussian characteristics, including skewness and heavy tails arising from nonlinear pharmacodynamic effects and interindividual variability, rendering GMM less robust and prone to boundary instability. Density-based algorithms such as DBSCAN, although effective in identifying discrete or spatially separated clusters, depend on fixed density thresholds and therefore perform poorly with continuous-depth data, where transitions between anesthetic states are gradual and density gradients evolve smoothly. Considering these properties, FCM provides a mathematically rigorous and physiologically consistent framework for delineating the smooth, overlapping transitions that define anesthetic depth.

Building upon these theoretical considerations, we initially explored k-means clustering but found it less flexible in classifying anesthetic depth. When visualizing frequency band proportions, k-means struggled to capture transition zones effectively, reinforcing our decision to use FCM for a more adaptable classification. The FCM algorithm stands out in unsupervised machine learning because of its adaptability and effectiveness in increasing data volumes. It iteratively adjusts centroids and clusters, creating personalized representations tailored to individuals, analogous to bespoke garments [46]. This adaptability ensures an accurate assessment of anesthesia depth dynamics, which is crucial for personalized healthcare.

Conclusions

In conclusion, this study established a machine learning–based methodology for anesthesia depth assessment, demonstrating its feasibility and providing preliminary insights into classification, visualization, and patient-specific management. By applying FCM clustering to processed EEG data, this novel approach enhances the understanding of anesthesia depth patterns and integrates with existing monitoring modalities, including PSi values and time-frequency image visualization for a more comprehensive assessment. Although preliminary, these findings lay the foundation for future research and refinement.

Acknowledgments

The authors declare the use of generative artificial intelligence in the writing process. According to the GAIDeT taxonomy (2025), the task of "Proofreading and editing" was delegated to ChatGPT (OpenAI) under full human supervision, specifically for grammatical error correction and phrasing improvements. The authors reviewed and edited the output as needed and take full responsibility for the content of the publication.

Funding

This work was supported by the National Science and Technology Council (NSTC), Taiwan [Grant number: NSTC 112-2314-B-A49 -068 -MY3].

Data Availability

The datasets generated or analyzed during this study are available from the corresponding author on reasonable request.

Authors' Contributions

Conceptualization: PYH, WLH, CHL, CKT
Methodology: PYH, WLH, HZH, CHL, CKT
Investigation: PYH, HZH, WLH
Formal analysis: PYH, WLH
Data curation: HZH
Writing – original draft: PYH
Writing – review and editing: CKT, CHL
Supervision: WKC, CKT, CHL
Project administration: WKC, CKT, CHL

XSL•FO
RenderX

Conflicts of Interest

None declared.

Multimedia Appendix 1

Detailed data preprocessing workflow and Fuzzy C-Means (FCM) parameter settings. Electromyography signals were processed via the Welch method (*30-s windows, 2-s overlap*). Normalized delta, high-theta, alpha, and beta band-power ratios were extracted as input features. The FCM algorithm ($c = 3$, $m = 2$) was applied with random initialization of cluster centers to identify three anesthesia depth clusters. Measures of dispersion for the delta band within each cluster are summarized in Table S1. Figures S1 and S2 show additional two-dimensional clustering distributions, demonstrating consistent three-cluster separation across different frequency-band pairings.

[PDF File, 304 KB - medinform_v14i1e77830_app1.pdf]

References

1. Brown EN, Lydic R, Schiff ND. General anesthesia, sleep, and coma. N Engl J Med 2010 Dec 30;363(27):2638-2650. [doi: 10.1056/NEJMra0808281] [Medline: 21190458]
2. Egan TD, Svensen CH. Multimodal general anesthesia: a principled approach to producing the drug-induced, reversible coma of anesthesia. Anesth Analg 2018 Nov;127(5):1104-1106. [doi: 10.1213/ANE.0000000000003743] [Medline: 30335656]
3. Ghoneim MM, Block RI, Haffarnan M, Mathews MJ. Awareness during anesthesia: risk factors, causes and sequelae: a review of reported cases in the literature. Anesth Analg 2009 Feb;108(2):527-535. [doi: 10.1213/ane.0b013e318193c634] [Medline: 19151283]
4. Zhou X, Dong S, Xu Y. Molecular mechanisms of propofol-induced cognitive impairment: suppression of critical hippocampal pathways. J Neurochem 2025 Apr;169(4):e70070. [doi: 10.1111/jnc.70070] [Medline: 40265596]
5. Aldecoa C, Bettelli G, Bilotta F, et al. Update of the European Society of Anaesthesiology and Intensive Care Medicine evidence-based and consensus-based guideline on postoperative delirium in adult patients. Eur J Anaesthesiol 2024 Feb 1;41(2):81-108. [doi: 10.1097/EJA.0000000000001876] [Medline: 37599617]
6. Da X, Li X, Dong A, Chen L, Ma Y, Li X. Effect of electroencephalogram-guided anesthesia on postoperative delirium in older adults after surgery: a systematic review and meta-analysis. Front Neurol 2025;16:1638282. [doi: 10.3389/fneur.2025.1638282] [Medline: 40948652]
7. Bennett C, Voss LJ, Barnard JPM, Sleigh JW. Practical use of the raw electroencephalogram waveform during general anesthesia: the art and science. Anesth Analg 2009 Aug;109(2):539-550. [doi: 10.1213/ane.0b013e3181a9fc38] [Medline: 19608830]
8. Purdon PL, Sampson A, Pavone KJ, Brown EN. Clinical electroencephalography for anesthesiologists: Part I: background and basic signatures. Anesthesiology 2015 Oct;123(4):937-960. [doi: 10.1097/ALN.0000000000000841] [Medline: 26275092]
9. Chan MTV, Hedrick TL, Egan TD, et al. American Society for Enhanced Recovery and Perioperative Quality Initiative Joint Consensus Statement on the role of neuromonitoring in perioperative outcomes: electroencephalography. Anesth Analg 2020 May;130(5):1278-1291. [doi: 10.1213/ANE.0000000000004502] [Medline: 31764163]
10. Hashimoto DA, Witkowski E, Gao L, Meireles O, Rosman G. Artificial intelligence in anesthesiology: current techniques, clinical applications, and limitations. Anesthesiology 2020 Feb;132(2):379-394. [doi: 10.1097/ALN.0000000000002960] [Medline: 31939856]
11. Choi RY, Coyner AS, Kalpathy-Cramer J, Chiang MF, Campbell JP. Introduction to machine learning, neural networks, and deep learning. Transl Vis Sci Technol 2020 Feb 27;9(2):14. [doi: 10.1167/tvst.9.2.14] [Medline: 32704420]
12. Nasibov E, Ozgören M, Ulutagay G, Oniz A, Kocaaslan S. On the analysis of BIS stage epochs via fuzzy clustering. Biomed Tech (Berl) 2010 Jun;55(3):147-153. [doi: 10.1515/BMT.2010.009] [Medline: 20156029]
13. Inan ZH, Kuntalp M. A study on fuzzy C-means clustering-based systems in automatic spike detection. Comput Biol Med 2007 Aug;37(8):1160-1166. [doi: 10.1016/j.compbiomed.2006.10.010] [Medline: 17145054]
14. Krajca V, Petránek S, Patáková I, Värri A. Automatic identification of significant graphoelements in multichannel EEG recordings by adaptive segmentation and fuzzy clustering. Int J Biomed Comput 1991;28(1-2):71-89. [doi: 10.1016/0020-7101(91)90028-d] [Medline: 1889908]
15. Fehrlin ES, Hight D, Kaiser HA, et al. A pilot investigation evaluating relative changes in fronto-occipital alpha and beta spectral power as measurement of anesthesia hypnotic depth. Anesth Analg 2023 Sep 1;137(3):656-664. [doi: 10.1213/ANE.0000000000006398] [Medline: 36961823]
16. Gutiérrez R, Maldonado F, Egaña JI, Penna A. Electroencephalographic alpha and delta oscillation dynamics in response to increasing doses of propofol. J Neurosurg Anesthesiol 2022 Jan 1;34(1):79-83. [doi: 10.1097/ANA.0000000000000733] [Medline: 33060553]
17. Koch S, Stegherr AM, Mörgeli R, et al. Electroencephalogram dynamics in children during different levels of anaesthetic depth. Clin Neurophysiol 2017 Oct;128(10):2014-2021. [doi: 10.1016/j.clinph.2017.07.417] [Medline: 28837907]

XSL•FO
RenderX

18. Liu Q, Chen YF, Fan SZ, Abbod MF, Shieh JS. Improved spectrum analysis in EEG for measure of depth of anesthesia based on phase-rectified signal averaging. Physiol Meas 2017 Feb;38(2):116-138. [doi: 10.1088/1361-6579/38/2/116] [Medline: 28033111]
19. Gu Y, Liang Z, Hagihira S. Use of multiple EEG features and artificial neural network to monitor the depth of anesthesia. Sensors (Basel) 2019 May 31;19(11):2499. [doi: 10.3390/s19112499] [Medline: 31159263]
20. Chen YF, Fan SZ, Abbod MF, Shieh JS, Zhang M. Electroencephalogram variability analysis for monitoring depth of anesthesia. J Neural Eng 2021 Nov 17;18(6):066030. [doi: 10.1088/1741-2552/ac3316] [Medline: 34695812]
21. Bruhn J, Röpcke H, Hoeft A. Approximate entropy as an electroencephalographic measure of anesthetic drug effect during desflurane anesthesia. Anesthesiology 2000 Mar;92(3):715-726. [doi: 10.1097/00000542-200003000-00016] [Medline: 10719951]
22. Bruhn J, Lehmann LE, Röpcke H, Bouillon TW, Hoeft A. Shannon entropy applied to the measurement of the electroencephalographic effects of desflurane. Anesthesiology 2001 Jul;95(1):30-35. [doi: 10.1097/00000542-200107000-00010] [Medline: 11465580]
23. Röpcke H, Rehberg B, Koenen-Bergmann M, Bouillon T, Bruhn J, Hoeft A. Surgical stimulation shifts EEG concentration-response relationship of desflurane. Anesthesiology 2001 Mar;94(3):390-399. [doi: 10.1097/00000542-200103000-00006] [Medline: 11374596]
24. Hajat Z, Ahmad N, Andrzejowski J. The role and limitations of EEG-based depth of anaesthesia monitoring in theatres and intensive care. Anaesthesia 2017 Jan;72 Suppl 1(Suppl 1):38-47. [doi: 10.1111/anae.13739] [Medline: 28044337]
25. Russell IF. The ability of bispectral index to detect intra-operative wakefulness during total intravenous anaesthesia compared with the isolated forearm technique. Anaesthesia 2013 May;68(5):502-511. [doi: 10.1111/anae.12177] [Medline: 23521699]
26. Prichep LS, Gugino LD, John ER, et al. The Patient State Index as an indicator of the level of hypnosis under general anaesthesia. Br J Anaesth 2004 Mar;92(3):393-399. [doi: 10.1093/bja/aeh082] [Medline: 14742326]
27. Obara S, Oishi R, Nakano Y, et al. Update on the SedLine® algorithm for calculating the Patient State Index of older individuals during general anesthesia: a randomized controlled trial. Minerva Anestesiol 2021 Jul;87(7):774-785. [doi: 10.23736/S0375-9393.21.14929-6] [Medline: 33938673]
28. Operator's manual: sedline sedation monitor. Masimo Corporation. 2018. URL: https://techdocs.masimo.com/globalassets/techdocs/pdf/lab-7373f_master.pdf [accessed 2026-01-16]
29. Müller J, Nowak S, Weidemeier M, et al. Duration of surgery and intraoperative blood pressure management are modifiable risk factors for postoperative neurocognitive disorders after spine surgery: results of the Prospective CONFESS Study. Spine (Phila Pa 1976) 2023 Aug 15;48(16):1127-1137. [doi: 10.1097/BRS.0000000000004722] [Medline: 37195031]
30. Seo JS, Park SW, Lee YS, Chung C, Kim YB. Risk factors for delirium after spine surgery in elderly patients. J Korean Neurosurg Soc 2014 Jul;56(1):28-33. [doi: 10.3340/jkns.2014.56.1.28] [Medline: 25289122]
31. Eagleman SL, Drover CM, Li X, MacIver MB, Drover DR. Offline comparison of processed electroencephalogram monitors for anaesthetic-induced electroencephalogram changes in older adults. Br J Anaesth 2021 May;126(5):975-984. [doi: 10.1016/j.bja.2020.12.042] [Medline: 33640118]
32. García PS, Kreuzer M, Hight D, Sleigh JW. Effects of noxious stimulation on the electroencephalogram during general anaesthesia: a narrative review and approach to analgesic titration. Br J Anaesth 2021 Feb;126(2):445-457. [doi: 10.1016/j.bja.2020.10.036] [Medline: 33461725]
33. Hagihira S. Changes in the electroencephalogram during anaesthesia and their physiological basis. Br J Anaesth 2015 Jul;115 Suppl 1(Suppl 1):i27-i31. [doi: 10.1093/bja/aev212] [Medline: 26174297]
34. Hight DF, Kaiser HA, Sleigh JW, Avidan MS. Continuing professional development module: an updated introduction to electroencephalogram-based brain monitoring during intended general anesthesia. Can J Anaesth 2020 Dec;67(12):1858-1878. [doi: 10.1007/s12630-020-01820-3] [Medline: 33190217]
35. Zhang Y, Wang Y, Cheng H, et al. EEG spectral slope: a reliable indicator for continuous evaluation of consciousness levels during propofol anesthesia. Neuroimage 2023 Dec;283:120426. [doi: 10.1016/j.neuroimage.2023.120426]
36. Obert DP, Schneider F, Schneider G, et al. Performance of the SEDLine monitor: age dependency and time delay. Anesth Analg 2023 Oct 1;137(4):887-895. [doi: 10.1213/ANE.0000000000006369] [Medline: 36727845]
37. Alashwal H, El Halaby M, Crouse JJ, Abdalla A, Moustafa AA. The application of unsupervised clustering methods to Alzheimer's disease. Front Comput Neurosci 2019;13:31. [doi: 10.3389/fncom.2019.00031] [Medline: 31178711]
38. Nazar W, Szymanowicz S, Nazar K, et al. Artificial intelligence models in prediction of response to cardiac resynchronization therapy: a systematic review. Heart Fail Rev 2024 Jan;29(1):133-150. [doi: 10.1007/s10741-023-10357-8] [Medline: 37861853]
39. Tavazzi E, Longato E, Vettoretti M, et al. Artificial intelligence and statistical methods for stratification and prediction of progression in amyotrophic lateral sclerosis: a systematic review. Artif Intell Med 2023 Aug;142:102588. [doi: 10.1016/j.artmed.2023.102588] [Medline: 37316101]
40. Lichtenfeld F, Kratzer S, Hinzmann D, García PS, Schneider G, Kreuzer M. The influence of electromyographic on electroencephalogram-based monitoring: putting the forearm on the forehead. Anesth Analg 2024 Jun 1;138(6):1285-1294. [doi: 10.1213/ANE.0000000000006652] [Medline: 37756246]

XSL•FO
RenderX

41. Tatum WO, Dworetzky BA, Freeman WD, Schomer DL. Artifact: recording EEG in special care units. J Clin Neurophysiol 2011 Jun;28(3):264-277. [doi: 10.1097/WNP] [Medline: 21633252]
42. Weyer C, Prötzl E, Kinateder T, et al. The strength of alpha oscillations in the electroencephalogram differently affects algorithms used for anesthesia monitoring. Anesth Analg 2021 Dec 1;133(6):1577-1587. [doi: 10.1213/ANE.0000000000005704] [Medline: 34543237]
43. Brogi E, Cyr S, Kazan R, Giunta F, Hemmerling TM. Clinical performance and safety of closed-loop systems: a systematic review and meta-analysis of randomized controlled trials. Anesth Analg 2017 Feb;124(2):446-455. [doi: 10.1213/ANE.0000000000001372] [Medline: 27482773]
44. Wang D, Song Z, Zhang C, Chen P. Bispectral index monitoring of the clinical effects of propofol closed-loop target-controlled infusion: systematic review and meta-analysis of randomized controlled trials. Medicine (Baltimore) 2021 Jan 29;100(4):e23930. [doi: 10.1097/MD.0000000000023930] [Medline: 33530193]
45. Castellanos Peñaranda C, Casas Arroyave FD, Gómez FJ, et al. Technical and clinical evaluation of a closed loop TIVA system with SEDLineTM spectral density monitoring: multicentric prospective cohort study. Perioper Med (Lond) 2020;9(1):1. [doi: 10.1186/s13741-019-0130-2] [Medline: 31921411]
46. Nayak J, Naik B, Behera HS. Fuzzy c-means (FCM) clustering algorithm: a decade review from 2000 to 2014. In: Computational Intelligence in Data Mining: New Delhi: Springer; 2015, Vol. 2:978-981. [doi: 10.1007/978-81-322-2208-8_14]

Abbreviations

BIS: Bispectral Index
DBSCAN: Density-Based Spatial Clustering of Applications with Noise
DSA: density spectral array
EEG: electroencephalography
EMG: electromyography
FCM: Fuzzy C-Means
GMM: Gaussian Mixture Model
pEEG: processed electroencephalography
PSi: Patient State Index

Edited by A Coristine; submitted 20.May.2025; peer-reviewed by CG Altintop, TP Kao; accepted 24.Dec.2025; published 06.Feb.2026.

Please cite as:
Huang PY, Hong WL, Hee HZ, Chang WK, Lee CH, Ting CK
Enhancing Anesthetic Depth Assessment via Unsupervised Machine Learning in Processed Electroencephalography Analysis: Novel Methodological Study
JMIR Med Inform 2026;14:e77830
URL: https://medinform.jmir.org/2026/1/e77830
doi:10.2196/77830

© Po-Yu Huang, Wei-Lun Hong, Hui-Zen Hee, Wen-Kuei Chang, Ching-Hung Lee, Chien-Kun Ting. Originally published in JMIR Medical Informatics (https://medinform.jmir.org), 6.Feb.2026. This is an open-access article distributed under the terms of the Creative Commons Attribution License (https://creativecommons.org/licenses/by/4.0/), which permits unrestricted use, distribution, and reproduction in any medium, provided the original work, first published in JMIR Medical Informatics, is properly cited. The complete bibliographic information, a link to the original publication on https://medinform.jmir.org/, as well as this copyright and license information must be included.

XSL•FO
RenderX

Machine Learning Prediction of Progression to Dialysis in Patients With Polycystic Kidney Disease: Population-Based Retrospective Cohort Study

Cheng-Hao Chang[1*], MD; Mingchih Chen[2,3*], PhD; Ming-Hsien Tsai[1,4], MD, PhD; Yen-Chun Huang[5], PhD; Hung-Hsiang Liou[6], MD; Ben-Chang Shia[2,3], MD, PhD; Chingying Liang[2,3], MD; Yu-Wei Fang[1,4], MD, PhD

[1]Division of Nephrology, Department of Internal Medicine, Shin-Kong Wu Ho-Su Memorial Hospital, No.95, Wen-Chang Road, Shih-lin District, Taipei, Taiwan

[2]Graduate Institute of Business Administration, College of Management, Fu Jen Catholic University, New Taipei City, Taiwan

[3]AI Development Center, Fu Jen Catholic University, New Taipei City, Taiwan

[4]Department of Medicine, Fu Jen Catholic University School of Medicine, New Taipei City, Taiwan

[5]Department of Artificial Intelligence, Tamkang University, New Taipei City, Taiwan

[6]Division of Nephrology, Department of Internal Medicine, Hsin-Jen Hospital, New Taipei City, Taiwan

[*]these authors contributed equally

Corresponding Author:
Yu-Wei Fang, MD, PhD
Division of Nephrology, Department of Internal Medicine, Shin-Kong Wu Ho-Su Memorial Hospital, No.95, Wen-Chang Road, Shih-lin District, Taipei, Taiwan

Abstract

Background: Autosomal dominant polycystic kidney disease (ADPKD), characterized by progressive cyst growth and renal decline, is the leading genetic cause of end‐stage renal disease.

Objective: This study aims to develop and validate machine learning (ML) models for predicting the risk of progression to dialysis in patients with ADPKD using a nationwide administrative database. Early identification of high-risk patients is critical for timely monitoring.

Methods: This retrospective cohort study used data from Taiwan's National Health Insurance Research Database (2007‐2018) to identify newly diagnosed patients with ADPKD. Six ML algorithms, including logistic regression, random forest, and extreme gradient boosting (XGBoost), were employed to predict progression to dialysis. Models were developed using 10-fold cross-validation, with the Synthetic Minority Oversampling Technique applied within training folds to address class imbalance. An ensemble-based feature selection strategy was implemented to identify the most robust predictors and optimize final model performance. Model evaluation was conducted using a strict temporal split.

Results: The study included 1856 patients with ADPKD, of whom 302 (16.27%) progressed to dialysis. Multivariable Cox regression identified several significant risk factors, including age 66 years and older (hazard ratio [HR] 4.63, 95% CI 2.71‐7.92; P<.001), anemia (HR 4.33, 95% CI 3.25‐5.78; P<.001), congestive heart failure (HR 1.81, 95% CI 1.29‐2.54; P<.001), and acute kidney injury (HR 1.69, 95% CI 1.19‐2.41; P=.003). Among the ML models, the XGBoost model, using an optimized set of 27 features, demonstrated the highest predictive performance on the held-out temporal test set (accuracy 98.3%; area under the curve 0.955; F_1-score 0.800; Brier score 0.022). The top predictors in the XGBoost model largely aligned with age, comorbidity burden, anemia, and cardiovascular disease markers. Medication use (eg, anticoagulants, loop diuretics, febuxostat) was also among the most influential predictors; however, medication-related predictors should be interpreted as proxies for disease complexity rather than direct risk modulators.

Conclusions: ML models can predict dialysis risk in patients with ADPKD using administrative data with temporal validation. This approach may support risk stratification by helping identify individuals at higher predicted risk who may warrant closer monitoring and further specialist evaluation.

(JMIR Med Inform 2026;14:e80343) doi:10.2196/80343

KEYWORDS

autosomal dominant polycystic kidney disease; ADPKD; artificial intelligence; machine learning; dialysis risk; predictive modeling

XSL•FO
RenderX

Introduction

Background

Polycystic kidney disease (PKD) is the leading genetic cause of end-stage renal disease (ESRD). The most common mutations in PKD occur in the *PKD1* or *PKD2* gene, which encode the proteins polycystin-1 and polycystin-2, respectively. These mutations result in abnormal cell proliferation, fluid secretion, and differentiation, leading to the formation and growth of cysts [1]. The progressive nature of renal cysts may cause structural and functional changes in the kidney. According to the latest guidelines, the estimated prevalence of PKD varies widely, ranging from approximately 2 to 14 per 10,000 individuals, depending on the study methodology and population characteristics [2].

Contemporary management of autosomal dominant polycystic kidney disease (ADPKD) has evolved to include both the management of associated complications and direct interventions aimed at the disease mechanism. A cornerstone of care remains the control of hypertension, a common and impactful complication. Angiotensin-converting enzyme inhibitors (ACEIs) and angiotensin II receptor blockers (ARBs) are widely recommended for their established efficacy in blood pressure control and proteinuria mitigation [3,4]. In addition, lifestyle interventions, such as dietary sodium restriction and weight management, play a crucial role in preserving renal function [5,6]. In parallel, disease-modifying therapies, such as the vasopressin V2 receptor antagonist tolvaptan, have been developed to slow cyst growth in select patients with rapidly progressing disease, who are often identified using prognostic markers such as genetic status or total kidney volume (TKV) [7]. Furthermore, other medications, such as statins and metformin, are frequently prescribed to manage concurrent conditions in this population, though their role as primary treatment options for ADPKD itself remains under investigation [8,9].

Study Objective

While risk stratification using advanced tools is crucial for guiding specialized treatments, a significant need remains for risk assessment methods based on accessible, routinely collected data. Currently, the gold-standard models for prognostication in ADPKD include the Mayo Imaging Classification, which utilizes height-adjusted TKV and patient age to predict the rate of estimated glomerular filtration rate (eGFR) decline, and the PROPKD score, which integrates genetic information (*PKD1* vs *PKD2* mutation type) with early clinical manifestations [2,10,11]. Although these models are invaluable, their broad implementation is often hindered by their dependence on specialized and resource-intensive evaluations. For instance, the Mayo Classification requires magnetic resonance imaging (MRI) or computed tomography to measure TKV, while the PROPKD score necessitates comprehensive genetic sequencing. These resources can be costly and are not universally available in all clinical settings, creating a gap for more scalable screening tools.

In parallel with these clinical tools, artificial intelligence (AI) has been increasingly used in ADPKD management. AI models have been developed to predict glomerular filtration rate decline, aiding in the early identification of high-risk patients and facilitating proactive management [12]. In imaging-based classifications, deep learning algorithms have been applied to automate ADPKD severity assessment, enhancing objectivity and reducing interobserver variability [13]. AI has also been instrumental in TKV quantification, a crucial prognostic marker in ADPKD. Deep learning-based segmentation models have demonstrated high accuracy in automated kidney segmentation from MRI and computed tomography images, significantly reducing manual workload [14,15]. While these advancements improve disease monitoring, they often still rely on the availability of imaging or detailed clinical data, leaving a gap for predictive models that can leverage more widely accessible administrative data to forecast hard clinical end points.

Therefore, this study aimed to develop and validate an AI-assisted model to identify significant predictors of progression to dialysis in patients with ADPKD using a nationwide administrative database. We evaluated multiple machine learning (ML) algorithms using a prespecified temporal split for model development and evaluation and summarized predictors to enhance interpretability and clinical usability. Our goal was to create a complementary tool for risk stratification, potentially aiding clinicians in monitoring patients and identifying those who may warrant more specialized evaluation.

Methods

Data Sources

This retrospective cohort study was based on the National Health Insurance Research Database (NHIRD), which is derived from Taiwan's universal compulsory health insurance system covering nearly 99% of the 23 million individuals in Taiwan since 1998 [16]. The database includes patients' hospitalization and outpatient visit records, and each individual was continuously followed. Disease diagnoses were coded according to the International Classification of Diseases, Ninth Revision, Clinical Modification (*ICD-9*-CM). The NHI Administration fully adopted *ICD-10*-CM for clinical records in 2016.

Ethical Considerations

This study was conducted in accordance with the principles of the Declaration of Helsinki and was reviewed and approved by the Ethics Review Board of Shin-Kong Wu Ho-Su Memorial Hospital (approval number 20211008R). The requirement for informed consent was waived by the review board because this study involved a secondary analysis of routinely collected administrative data, and no direct contact with individual participants occurred. The original data collection procedures and this secondary analysis were approved without the need for additional consent.

All data obtained from the NHIRD were fully deidentified prior to analysis. Personal identifiers were removed by the data holder, and the authors had no access to information that could be used to identify individual patients. Data access and analysis were conducted in compliance with relevant data protection regulations.

XSL•FO
RenderX

No financial or other compensation was provided to participants, as this study did not involve direct recruitment or interaction with human subjects.

The manuscript and all supplementary materials did not include any images or information that could lead to the identification of individual participants.

Study Design and Population

We identified new-onset ADPKD cases from the Catastrophic Illness Patient Registry between 2007 and 2018. To minimize potential misclassification bias from ICD coding, we implemented stringent validation criteria for both the primary diagnosis and comorbidities. The identification of patients with ADPKD followed a 2-step process: subjects were first identified using ICD diagnostic codes, and their diagnosis was then validated against Taiwan's Catastrophic Illness Patient Registry. A catastrophic illness certificate requires formal review and approval by physicians, ensuring a high degree of diagnostic accuracy for our study cohort [17-19].

The index date was defined as the first date on which a patient met the ADPKD case definition and had validation in the Catastrophic Illness Patient Registry. Baseline predictors were ascertained during the 365-day lookback period preceding the index date.

To construct a clean incident cohort and reduce reverse causation, we excluded individuals aged below 19 years or above 85 years, those with missing core administrative information (eg, sex, age, or index date), and those with evidence of ADPKD during the 2005 to 2006 washout period. We also excluded patients with any evidence of dialysis (hemodialysis or peritoneal dialysis) before the index date and those with kidney transplantation before the index date. Patients were followed from the index date until initiation of dialysis, death, or December 31, 2019, whichever occurred first.

Baseline Variables

The dataset includes a variety of demographic, clinical, and medication-related variables for individuals with ADPKD. The key demographic variables include sex and age. Clinical variables encompass a variety of diseases grouped as cerebrovascular (intracranial aneurysms, ischemic stroke, and hemorrhagic stroke), cardiovascular (hypertension, atrial fibrillation, congestive heart failure [CHF], peripheral vascular disease, arrhythmia, and ischemic heart disease), gastrointestinal (liver cirrhosis, peptic ulcer, diverticulosis, cholangitis, and acute pancreatitis), renal and urological (urinary tract infection [UTI] and acute kidney injury [AKI]), pulmonary (chronic obstructive pulmonary disease [COPD], pneumonia, and asthma), metabolic (dyslipidemia, diabetes mellitus, and gout), mental (dementia, anxiety, and depression), and other (glaucoma and anemia). Each comorbidity was confirmed if the corresponding diagnosis code appeared in at least 1 hospitalization record or at least 3 outpatient visit records within the 365-day lookback period preceding the index date.

Medication variables cover a broad spectrum, including antihypertensives (beta-blockers, alpha-blockers, ACEIs/ARBs, calcium channel blockers [CCBs], methyldopa, hydralazine, minoxidil, clonidine, potassium-sparing diuretics, thiazide diuretics, and loop diuretics), antidiabetic drugs (metformin, sulfonylureas, dipeptidyl peptidase-4 inhibitors, thiazolidinediones, other oral hypoglycemic agents, rapid-acting insulins, and long-acting insulins), antimetabolic agents (statins, fenofibrate, and other lipid-lowering agents), urate-lowering agents (benzbromarone, allopurinol, febuxostat), and other medications (nonsteroidal anti-inflammatory drugs [NSAIDs], sedative hypnotics, tranexamic acid, mammalian target of rapamycin inhibitors, sodium bicarbonate, anticoagulants, antiplatelet agents, and vitamin K). As with the definition of comorbidities, we adopted a widely used and validated approach to enhance specificity. Medication variables were quantified as the cumulative number of prescription days during the 365-day lookback period preceding the index date. This approach was used to capture exposure intensity beyond a binary indicator. The specific codes used to define all comorbidities and medications are detailed in Tables S1 and S2 in Multimedia Appendix 1, respectively.

Outcome Definition and Follow-Up

The primary end point was ESRD, defined as initiation of dialysis or receipt of kidney transplantation without prior dialysis. Patients were followed from the index date until ESRD, death, or December 31, 2019, whichever occurred first. For the ML classification models, the binary outcome was ESRD by the end of follow-up (event=1). In the ML analysis, the label reflects whether ESRD was observed by December 31, 2019, and does not represent a fixed-horizon risk. Patients without ESRD were labeled as nonevents (event=0), including those who died before reaching ESRD.

Data Preprocessing and Handling of Missing Data

Our strategy for handling missing data involved 2 stages. First, case-wise deletion was performed to exclude any patient records with missing core administrative data (eg, sex, age, or date of diagnosis), as indicated in the study flowchart. For the final cohort, predictor variables were constructed such that no missing values remained. The absence of a record for a specific variable was treated as meaningful data rather than as a missing value. For instance, if a patient had no prescriptions for a given medication, the cumulative exposure days were coded as 0. Similarly, if a patient did not meet the predefined criteria for a comorbidity, the variable was coded as 0, indicating absence.

Statistical Analysis

Categorical variables were presented as frequencies with percentages and compared using the chi-square test. Continuous variables were expressed as means with SDs and compared using the *t* test. Multivariable Cox proportional hazards regression models were used to estimate adjusted hazard ratios (HRs) and 95% CIs for the risk of dialysis initiation. A 2-tailed *P* value of <.05 was considered statistically significant. All statistical analyses were performed using SAS version 9.4 (SAS Institute Inc).

ML Model Development and Feature Selection

Given the extended accrual period, we used a temporal split to preserve chronological separation between model development and evaluation. Records from 2007 to 2016 (80%) were used

XSL•FO
RenderX

for model training, and records from 2017 to 2018 (20%) were reserved as an independent held-out test set for performance assessment.

Within the training set, we performed 10-fold cross-validation to improve robustness and reduce overfitting. To address class imbalance, Synthetic Minority Over-sampling Technique (SMOTE) was applied only within the training folds of each cross-validation iteration to avoid information leakage into the validation folds. Model performance was evaluated on the held-out test set using accuracy, Cohen κ, sensitivity, specificity, area under the curve (AUC), F_1 score, and Brier score, recognizing that multiple complementary metrics are needed under imbalanced outcome distributions.

The 6 ML algorithms were chosen to encompass a broad spectrum of modeling techniques, ranging from interpretable linear models to complex, high-performance ensembles. Logistic regression was selected as a conventional statistical method widely used in clinical research, serving as a robust and interpretable baseline for comparison. To capture complex nonlinear relationships, we included 2 distinct models: classification and regression trees, a foundational decision tree algorithm, and multivariate adaptive regression splines, a flexible model adept at identifying interactions between predictors. Finally, to leverage the superior predictive power of ensemble learning, 3 state-of-the-art algorithms were selected [20]. Random forest represents the bagging method, which builds independent trees to reduce variance, whereas CatBoost and eXtreme Gradient Boosting (XGBoost) are representatives of boosting methods that construct models sequentially to correct the errors of their predecessors and often yield high accuracy. This comprehensive selection allowed for a thorough evaluation of predictive performance across different algorithmic families, and these methods have been successfully applied in similar medical informatics contexts [21-23] (see Supplementary Methods in Multimedia Appendix 1 for detailed model descriptions). Hyperparameters for each model were optimized using random search within the training set under 10-fold cross-validation. The held-out temporal test set was used only for final performance evaluation. The specific hyperparameters for all models are detailed in Table S3 in Multimedia Appendix 1. All model construction was conducted using Python (version 3.9; Python Software Foundation).

We employed a 2-pronged feature selection approach to identify the most significant predictors. In the first approach, each model performed feature selection based on its own internal mechanism, and its performance was evaluated using this algorithm-specific feature set. In the second approach, we constructed an overall consensus ranking of predictors using rank aggregation across the 6 algorithms. We prespecified that the best-performing algorithm would be selected based on performance on the held-out temporal test set, considering discrimination, class-imbalance–sensitive metrics, and calibration. For the selected best-performing model, we additionally evaluated parsimony by sequentially adding predictors according to the consensus ordering and selecting the feature count that maximized test-set performance.

Results

Characteristics of the Study Population

From the NHIRD, 2677 incident ADPKD cases were identified between 2007 and 2018. After applying exclusion criteria (n=821), 1856 patients were included in the final cohort (Figure 1).

XSL•FO
RenderX

Figure 1. Study flowchart of patient selection and machine learning model development. The diagram shows the patient selection process from the NHIRD for the period 2007 - 2018 and the subsequent workflow for model development. Patients were split temporally into a training set (2007 - 2016) and a held-out test set (2017 - 2018). ESRD was ascertained through December 31, 2019. ADPKD: autosomal dominant polycystic kidney disease; CART: classification and regression trees; ESRD: end-stage renal disease; eXGB: extreme gradient boosting; LGR: logistic regression; MARS: multivariate adaptive regression splines; ML: machine learning; RF: random forest.

XSL•FO
RenderX

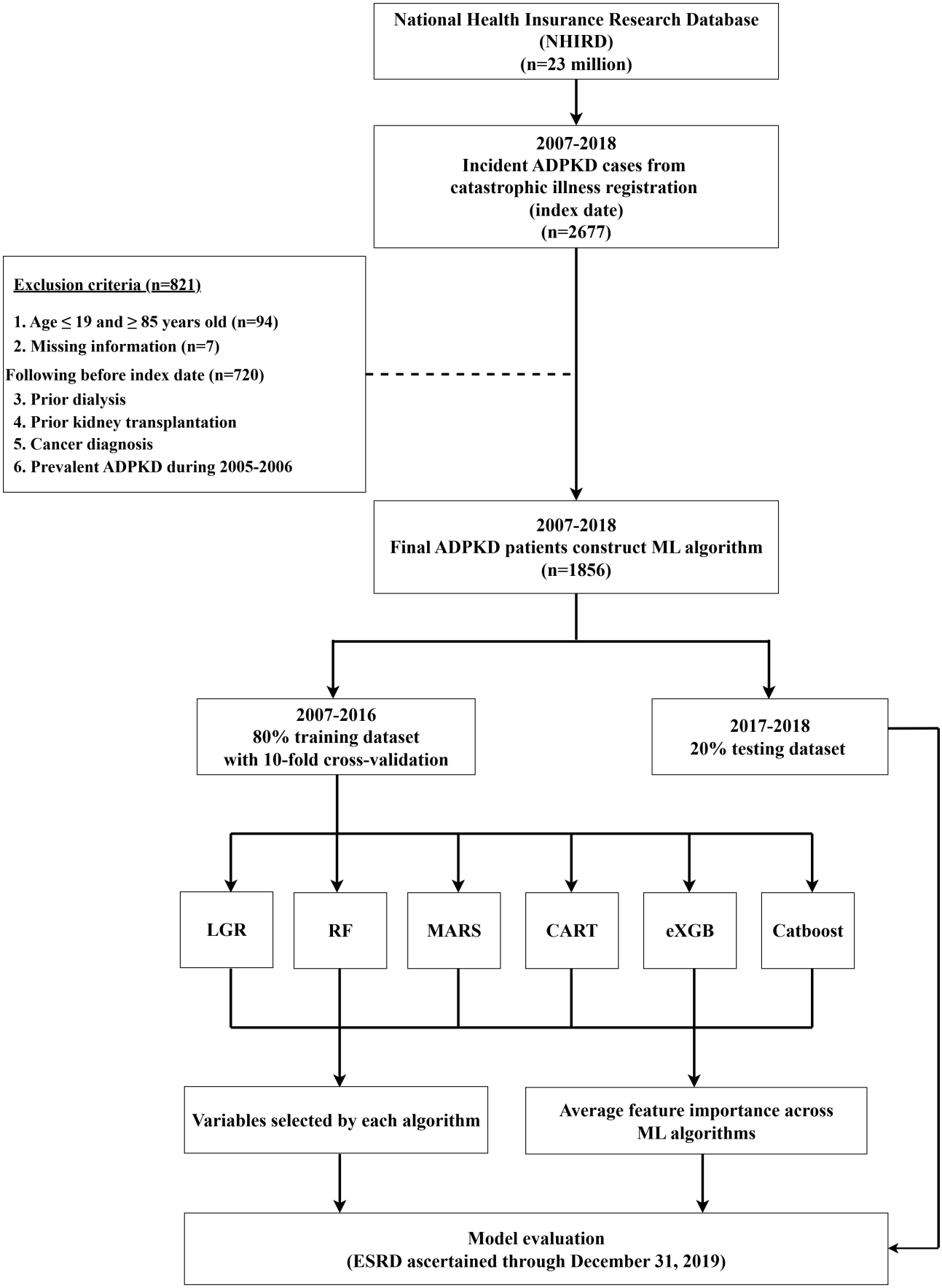

Table 1 summarizes baseline characteristics assessed during the 365-day lookback period preceding the index date. During follow-up through December 31, 2019, 302 patients (302/1856, 16.27%) initiated dialysis. Kidney transplantation without prior dialysis was observed in only 2 patients. Due to small cell size restrictions intended to protect patient privacy in the NHIRD

XSL•FO
RenderX

data release process, transplantation events could not be analyzed separately; therefore, ESRD outcomes are presented primarily in terms of dialysis initiation. The remaining 1554 patients (1554/1856, 83.73%) did not initiate dialysis and were censored at death or end of follow-up.

XSL•FO
RenderX

Table . Baseline characteristics of the cohort stratified by dialysis initiation during follow-up.

Baseline characteristic	Autosomal dominant PKD[a] (n=1856)	Dialysis initiation during follow-up	
		Yes	No
Sex , n (%)			
Male	1006 (54.20)	168 (55.63)	838 (53.93)
Female	850 (45.80)	134 (44.37)	716 (46.07)
Age group (y), n (%)			
≤40	687 (37.02)	56 (18.54)	631 (40.60)
41 - 55	754 (40.63)	152 (50.33)	602 (38.74)
56 - 65	265 (14.28)	56 (18.54)	209 (13.45)
≥66	150 (8.08)	38 (12.58)	112 (7.21)
Age, mean (SD)	45.85 (13.35)	50.94 (11.94)	44.86 (13.39)
CCI[b] group, n (%)			
1 - 2	1014 (54.63)	72 (3.88)	942 (50.75)
3 - 5	660 (35.56)	168 (9.05)	492 (26.51)
6+	182 (9.81)	62 (3.34)	120 (6.47)
CCI scores, mean (SD)	2.58 (2.34)	4.18 (2.27)	2.27 (2.22)
Underlying disease, n (%)			
Cerebrovascular diseases			
Intracranial aneurysms	20 (1.08)	4 (1.32)	16 (1.03)
Ischemic stroke	51 (2.75)	11 (3.64)	40 (2.57)
Hemorrhagic stroke	91 (4.90)	27 (8.94)	64 (4.12)
Cardiovascular diseases			
Hypertension	1164 (62.72)	203 (67.22)	961 (61.84)
AF[c]	34 (1.83)	15 (4.97)	19 (1.22)
CHF[d]	178 (9.59)	77 (25.50)	101 (6.50)
PVD[e]	71 (3.83)	26 (8.61)	45 (2.90)
Arrhythmia	214 (11.53)	69 (22.85)	145 (9.33)
Ischemic heart disease	344 (18.53)	105 (34.77)	239 (15.38)
Gastrointestinal diseases			
Liver cirrhosis	33 (1.78)	14 (4.64)	19 (1.22)
Peptic ulcer bleeding	84 (4.53)	25 (8.28)	59 (3.80)
Diverticulosis	32 (1.72)	10 (3.31)	22 (1.42)
Cholangitis	39 (2.10)	16 (5.30)	23 (1.48)
Acute pancreatitis	41 (2.21)	20 (6.62)	21 (1.35)
Renal and urological diseases			
UTI[f]	938 (50.54)	196 (64.90)	742 (47.57)
AKI[g]	173 (9.32)	71 (23.51)	102 (6.56)
Lung diseases			
COPD[h]	319 (17.19)	71 (23.51)	248 (15.96)
Pneumonia	543 (29.26)	121 (40.07)	422 (27.16)
Asthma	207 (11.15)	31 (10.26)	176 (11.33)

XSL•FO
RenderX

Baseline characteristic	Autosomal dominant PKD[a] (n=1856)	Dialysis initiation during follow-up	
		Yes	No
Metabolic diseases			
Dyslipidemia	706 (38.04)	124 (41.06)	582 (37.45)
DM[i]	277 (14.92)	73 (24.17)	204 (13.13)
Gout	427 (23.01)	122 (40.40)	305 (19.63)
Mental diseases			
Dementia	47 (2.53)	15 (4.97)	32 (2.06)
Anxiety	321 (17.30)	62 (20.53)	259 (16.67)
Depression	250 (13.47)	46 (15.23)	204 (13.13)
Others			
Glaucoma	88 (4.74)	18 (5.96)	70 (4.50)
Anemia	461 (24.84)	199 (65.89)	262 (16.86)
Medication, mean days of use during the 365-day pre-index period (SD)			
Antihypertension			
Beta-blockers	95.85 (107.05)	92.24 (91.14)	97.15 (112.30)
Alpha-blockers	94.40 (106.66)	101.10 (107.30)	90.89 (106.30)
ACEI[j]/ARB[k]	160.11 (132.18)	130.10 (102.30)	167.30 (137.50)
CCB[l]	157.80 (136.36)	162.20 (122)	156.50 (140.40)
Methyldopa	26.79 (37.29)	17.97 (28.55)	31.61 (41.78)
Hydralazine	51.68 (65.70)	46.13 (60.99)	56.27 (69.50)
Minoxidil	53.04 (70.99)	43.11 (51.21)	68.30 (94.18)
Clonidine	41.69 (49.51)	42.35 (38)	40.92 (61.88)
Potassium-sparing diuretics	54.94 (83.58)	31.52 (68.85)	60.38 (85.97)
Thiazide diuretics	66.84 (83.42)	45.18 (67.33)	73.30 (86.68)
Loops diuretics	59.35 (94.95)	60.11 (84.12)	58.75 (102.70)
Antidiabetic			
Metformin	122.29 (122.92)	44.17 (43.31)	130.20 (125.70)
Sulfonylureas	130.89 (120.83)	103.20 (117.20)	137.30 (121.40)
DPP4i[m]	120.03 (101.88)	100.40 (103)	125 (101.50)
Other OHAs	92.69 (102.37)	113.50 (126.70)	82.84 (88.87)
Rapid-acting insulins	14.71 (49.95)	2.12 (8.94)	27.31 (68.23)
Long-acting insulins	100.09 (88.53)	130 (109.90)	84.26 (73.73)
Antimetabolic			
Statin	121.32 (111.87)	124.60 (118.10)	120.60 (110.50)
Fenofibrate	57.96 (72.62)	56.79 (81.12)	58.42 (69.38)
Other lipid-lowering agents	75.24 (90.44)	6.19 (2.38)	92.50 (93.65)
Urate-lowering agents			
Benzbromarone	65.45 (79.37)	41.72 (49.69)	71.38 (84.22)
Allopurinol	82.52 (97.02)	78.39 (84.91)	85.45 (105)
Febuxostat	104.04 (101.03)	92.67 (79.03)	108.20 (107.80)
Other			

XSL•FO
RenderX

Baseline characteristic	Autosomal dominant PKD[a] (n=1856)	Dialysis initiation during follow-up	
		Yes	No
NSAID[n]	15.76 (34.22)	15.69 (29.67)	15.78 (35.12)
Sedative hypnotics	92.03 (158.68)	118.70 (188.30)	83.81 (147.50)
Tranexamic acid	5.05 (16.89)	6.59 (11.14)	4.59 (18.24)
mTOR[o] inhibitors	135.14 (148.87)	127.80 (140.60)	144 (174.70)
Sodium bicarbonate	9.50 (42.61)	20.52 (46.30)	7.25 (41.48)
Anticoagulants	110.46 (155.24)	113.10 (190.60)	109 (132.20)
Antiplatelet agents	211.22 (251.64)	204.20 (228.70)	214.30 (261.10)
Vitamin K	57.41 (91.58)	19.86 (43.90)	107.50 (114.30)

[a]PKD: polycystic kidney disease.
[b]CCI: Charlson Comorbidity Index.
[c]AF: atrial fibrillation.
[d]CHF: congestive heart failure.
[e]PVD: peripheral vascular disease.
[f]UTI: urinary tract infection.
[g]AKI: acute kidney injury.
[h]COPD: chronic obstructive pulmonary disease.
[i]DM: diabetes mellitus.
[j]ACEI: angiotensin-converting enzyme inhibitor.
[k]ARB: angiotensin II receptor blocker.
[l]CCB: calcium channel blocker.
[m]DPP4i: dipeptidyl peptidase-4 inhibitor.
[n]NSAID: nonsteroidal anti-inflammatory drug.
[o]mTOR: mechanistic target of rapamycin.

At baseline, the cohort had substantial cardiorenal comorbidity and medication use. The most prevalent comorbidities were hypertension (86.58%, 1606/1856) and UTI (50.38%, 935/1856), with pneumonia (29.26%, 543/1856), anemia (24.83%, 461/1856), and gout (23.01%, 427/1856) also common. Antihypertensive exposure was widespread (ACEI/ARB 161.30, SD 127.50 d; CCB 160.90, SD 133.70 d), and metabolic therapy was frequent (metformin 116.20, SD 137.10 d; long-acting insulin 91.71, SD 139.10 d).

Stratification by subsequent dialysis initiation highlighted clinically meaningful differences in baseline disease severity and management. Patients who later initiated dialysis were older (50.94, SD 11.94 vs 44.86, SD 13.39 y) and had higher comorbidity burden (Charlson Comorbidity Index [CCI] 4.18, SD 2.27 vs 2.27, SD 2.22; CCI≥6: 20.53% vs 7.72%), with the largest separations for anemia (65.89% vs 16.86%) and AKI (23.51% vs 6.56%). Baseline medication patterns were consistent with greater clinical complexity in the dialysis group, including lower metformin exposure (44.17, SD 95.41 vs 130.20, SD 148 d) and higher sodium bicarbonate exposure (20.52, SD 68.46 vs 7.25, SD 44.30 d).

Risk Analysis for Progression to Dialysis

Table 2 presents the multivariable Cox regression results. After adjustment for sex, age category, CCI category, and comorbidities, male sex was associated with a higher risk of dialysis initiation (aHR 1.55, 95% CI 1.13 - 2.11; *P*=.006). Age remained a strong predictor: compared with age younger than 55 years, the risk increased across categories. Among comorbidities, anemia showed the strongest association with dialysis initiation (aHR 4.33, 95% CI 3.25 - 5.78; *P*<.001). Congestive heart failure, AKI, and gout were also associated with a higher risk. Hypertension, COPD, and anxiety were associated with lower hazard in the adjusted model.

XSL•FO
RenderX

Table . Risk for entering dialysis in the patients with ADPKD[a].

	Cox model	
	aHR[b] (95% CI)	*P* value
Sex		
Ref=Female	1	—[c]
Male	1.55 (1.13 - 2.11)	.006
Age group		
Ref=<55	1	—
41 - 55	3.01 (2.12 - 4.30)	<.001
56 - 65	4.13 (2.63 - 6.50)	<.001
≥66	4.63 (2.71 - 7.92)	<.001
CCI[d] group		
Ref=12	1	—
345	1.42 (1.01 - 1.98)	.04
6+	1.28 (0.74 - 2.21)	.39
Underlying disease		
Cerebrovascular diseases		
Intracranial aneurysms	2.12 (0.71 - 6.31)	.18
Ischemic stroke	1.22 (0.59 - 2.49)	.59
Hemorrhagic stroke	1.03 (0.57 - 1.86)	.91
Cardiovascular diseases		
Hypertension	0.70 (0.53 - 0.94)	.02
AF[e]	0.66 (0.32 - 1.32)	.24
CHF[f]	1.81 (1.29 - 2.54)	<.001
PVD[g]	1.25 (0.79 - 2.00)	.34
Arrhythmia	0.98 (0.69 - 1.40)	.92
Gastrointestinal diseases		
Ischemic heart disease	1.09 (0.80 - 1.48)	.58
Liver cirrhosis	0.91 (0.48 - 1.72)	.77
Peptic ulcer bleeding	0.67 (0.42 - 1.09)	.11
Diverticulosis	0.82 (0.38 - 1.79)	.62
Cholangitis	1.10 (0.61 - 1.96)	.76
Acute pancreatitis	1.18 (0.69 - 2.04)	.55
Renal and urological diseases		
UTI[h]	0.84 (0.62 - 1.14)	.26
AKI[i]	1.69 (1.19 - 2.41)	.003
COPD[j]	0.61 (0.44 - 0.86)	.005
Pneumonia	0.86 (0.65 - 1.12)	.26
Asthma	0.74 (0.47 - 1.15)	.18
Metabolic diseases		
Dyslipidemia	0.78 (0.51 - 1.01)	.12
DM[k]	1.38 (0.97 - 1.96)	.07

XSL•FO
RenderX

	Cox model	
	aHR[b] (95% CI)	*P* value
Gout	1.49 (1.08 - 2.05)	.01
Mental diseases		
Dementia	0.71 (0.37 - 1.34)	.29
Anxiety	0.53 (0.34 - 0.82)	.004
Depression	1.33 (0.82 - 2.16)	.26
Others		
Glaucoma	1.02 (0.60 - 1.74)	.93
Anemia	4.33 (3.25 - 5.78)	<.001

[a]ADPKD: autosomal dominant polycystic kidney disease.
[b]aHR: adjusted hazard ratio.
[c]Not applicable.
[d]CCI: Charlson Comorbidity Index.
[e]AF: atrial fibrillation.
[f]CHF: congestive heart failure.
[g]PVD: peripheral vascular disease.
[h]UTI: urinary tract infection.
[i]AKI: acute kidney injury.
[j]COPD: chronic obstructive pulmonary disease.
[k]DM: diabetes mellitus.

Feature Importance Across ML Models

Figure 2 presents the relative importance of variables in predicting dialysis risk, as determined by the 6 ML models. A consensus emerged across the different algorithms, highlighting several key predictors. The top-ranked predictors spanned comorbidity burden and medication patterns, including anticoagulant use, hypertension, CCB use, higher CCI category, loop diuretics, sodium bicarbonate, anemia, and ACEI or ARB use, together with age and sex. Additional contributors included cardiorespiratory comorbidities, UTI, gout, and neuropsychiatric conditions and related medications.

XSL•FO
RenderX

Figure 2. Overall consensus feature ranking aggregated across 6 machine learning algorithms. Predictors were ranked within each algorithm using the model's native importance criterion; standardized ranks were then aggregated to generate an overall consensus ranking. ACEI: angiotensin-converting enzyme inhibitor; AF: atrial fibrillation; ARB: angiotensin II receptor blocker; CCB: calcium channel blocker; CCI: Charlson Comorbidity Index; COPD: chronic obstructive pulmonary disease; DM: diabetes mellitus; NSAID: nonsteroidal anti-inflammatory drug; PVD: peripheral vascular disease; UTI: urinary tract infection.

XSL•FO
RenderX

Performance Comparison of ML Models

Table 3 summarizes performance for 6 ML algorithms under 2 feature selection strategies: model-specific feature selection and a consensus feature set derived from rank aggregation. Using model-specific feature selection, XGBoost achieved the highest accuracy (0.9748) with specificity of 1, with an AUC of 0.9436 and a Brier score of 0.0254. Using the consensus feature set, performance improved across models. XGBoost achieved the highest accuracy (0.9832) and F_1-score (0.8), whereas MARS achieved the highest AUC (0.9762) and CatBoost achieved the lowest Brier score (0.0217), indicating strong discrimination with favorable calibration across top-performing models.

Table . The model predictions with six different machine learning algorithms.

Methods	Accuracy	Kappa	Sensitivity	Specificity	AUC[a]	F_1-score	Brier score
Variables selected by its own algorithm							
LGR[b]	0.9034	0.2552	0.4167	0.9292	0.7806	0.303	0.0771
RF[c]	0.9580	0.4790	0.4167	0.9867	0.9338	0.500	0.0352
MARS[d]	0.9664	0.6189	0.5833	0.9867	0.9558	0.6364	0.0260
CART[e]	0.9202	0.3037	0.4167	0.9469	0.9023	0.3448	0.0588
XGBoost[f]	0.9748	0.6551	0.5000	1	0.9436	0.6667	0.0254
CatBoost	0.9622	0.5521	0.5000	0.9867	0.9672	0.5714	0.0245
Variables selected based on the average results from six ML algorithms.							
LGR	0.9496	0.4735	0.5000	0.9735	0.9288	0.5000	0.0557
RF	0.9706	0.6174	0.5000	0.9956	0.9611	0.6316	0.0302
MARS	0.9790	0.7512	0.6667	0.9956	0.9762	0.7619	0.0232
CART	0.9454	0.4899	0.5833	0.9646	0.9399	0.5185	0.060
XGBoost	0.9832	0.7916	0.6667	1	0.9546	0.8000	0.0219
CatBoost	0.9790	0.7512	0.6567	0.9956	0.9676	0.7619	0.0217

[a]AUC: area under the curve.

[b]LGR: logistic regression.

[c]RF: random forest.

[d]MARS: multivariate adaptive regression splines.

[e]CART: classification and regression trees.

[f]XGBoost: extreme gradient boosting.

Optimization of the XGBoost Model via Feature Selection

Figure 3 shows the change in test set accuracy as top-ranked predictors from the consensus ranking were sequentially added to the XGBoost model. Accuracy increased rapidly as the highest-ranked predictors were included and reached its maximum with 27 predictors. This feature count was selected as the optimal balance between parsimony and predictive performance, and the 27-feature set was used for the final XGBoost model.

XSL•FO
RenderX

Figure 3. Optimization of extreme gradient boosting model performance by sequential feature addition. The plot shows the change in model accuracy (y-axis) as the number of top-ranked predictor variables (x-axis). The dashed vertical line indicates the point at which maximum accuracy was achieved with 27 variables.

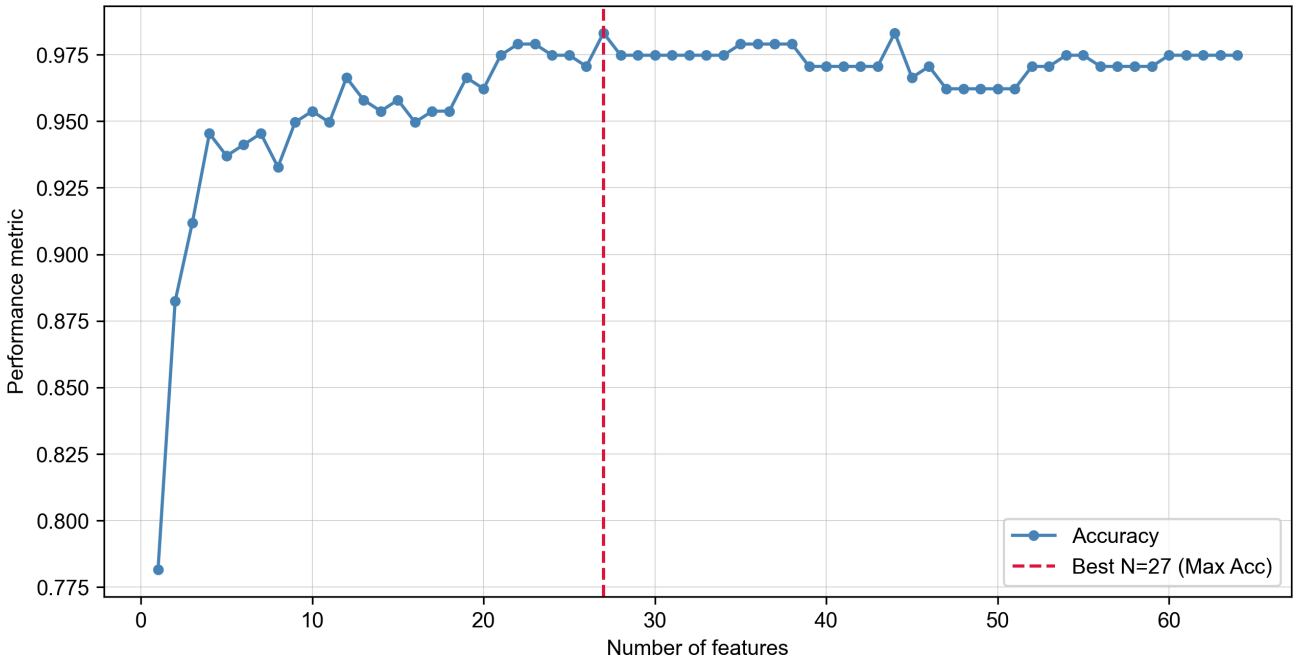

Key Predictors in the Final XGBoost Model

The final XGBoost model used 27 baseline predictors selected during feature optimization (Table 4). This set included demographic and comorbidity burden measures (age, sex, and CCI category), major clinical conditions linked to renal risk or frailty (anemia, hypertension, ischemic heart disease, gout, pneumonia, COPD, UTI, anxiety, and depression), and multiple medication exposures. Key medication predictors included antihypertensive classes (ACEI or ARB, CCB, beta-blockers, and alpha-blockers), agents reflecting advanced renal management or metabolic status (loop diuretics, sodium bicarbonate, potassium-sparing diuretics, and rapid-acting insulin), and medications that may relate to underlying diseases (anticoagulants, antiplatelet agents, NSAIDs, sedative hypnotics, tranexamic acid, febuxostat, and statins). It is crucial to note that these medication-related predictors should be interpreted as proxies for underlying disease severity and complexity (ie, confounding by indication), rather than as direct causal risk factors.

XSL•FO
RenderX

Table . The variables selected for the best accuracy result in XGBoost. The rank is the average ranking from the average results of LGR[a], RF[b], MARS[c], CART[d], XGBoost[e], and CatBoost.

Rank	Variable
1	Age
2	CCI[f] scores
3	Anticoagulants
4	Loops diuretics
5	Alpha-blockers
6	NSAID[g]
7	Sex
8	CCB[h]
9	Sedative hypnotics
10	Anemia
11	ACEI[i]/ARB[j]
12	Hypertension
13	Gout
14	Tranexamic acid
15	Febuxostat
16	Ischemic heart disease
17	Statin
18	Antiplatelet agents
19	Beta-blockers
20	Pneumonia
21	Sodium bicarbonate
22	Potassium-sparing diuretics
23	Rapid-acting insulins
24	Anxiety
25	COPD[k]
26	Depression
27	UTI[l]

[a]LGR: logistic regression.
[b]RF: random forest.
[c]MARS: multivariate adaptive regression splines.
[d]CART: classification and regression trees.
[e]XGBoost: extreme gradient boosting.
[f]CCI: Charlson Comorbidity Index.
[g]NSAID: nonsteroidal anti-inflammatory drug.
[h]CCB: calcium channel blocker.
[i]ACEI: angiotensin-converting enzyme inhibitors.
[j]ARB: angiotensin receptor blocker.
[k]COPD: chronic obstructive pulmonary disease.
[l]UTI: urinary tract infection.

XSL•FO
RenderX

Discussion

Principal Findings

This retrospective cohort study used data from the NHIRD to predict ESRD progression in ADPKD using 6 ML algorithms, with ESRD operationalized as initiation of maintenance dialysis. On the held-out temporal test set, XGBoost demonstrated the best overall performance after feature optimization (accuracy 0.9832; F_1 score 0.8). The final optimized XGBoost model was derived by sequentially adding top-ranked predictors and achieved peak accuracy with 27 variables. The most informative predictors reflected underlying disease severity and care intensity, including age, CCI, anemia, hypertension, ischemic heart disease, gout, pneumonia, COPD, UTI, anxiety, and depression, as well as medication exposures such as anticoagulants, loop diuretics, ACEI/ARB, CCB, and febuxostat.

Interpretation of Major Clinical Risk Factors

Hypertension is a common early manifestation of ADPKD, often developing before renal function declines. It affects up to 86.6% of patients with ADPKD, frequently appearing around 30 years of age, with up to 20% of them diagnosed before the age of 20 [24,25]. The underlying mechanisms involve intrarenal ischemia, renin-angiotensin-aldosterone system (RAAS) activation, and endothelial dysfunction. Progressive cyst expansion leads to renal hypoperfusion and sustained RAAS stimulation, further exacerbating hypertension and accelerating kidney damage [26,27]. This mechanistic framework is consistent with our results, where hypertension and cardiovascular comorbidity markers, including ischemic heart disease and related medication patterns, contributed meaningfully to dialysis risk prediction.

Age and overall comorbidity burden were among the highest-ranked predictors in both the consensus feature ranking and the final XGBoost feature set. This pattern suggests that administrative claims-based models capture the cumulative burden of systemic illness, frailty, and health care utilization that often accompanies advanced kidney disease trajectories [28,29]. In our cohort, ischemic heart disease and cardiovascular medication proxies (eg, anticoagulants, antiplatelet agents, beta-blockers, and loop diuretics) were repeatedly selected, indicating that cardiovascular disease severity and its treatment intensity provide informative signals of near-term dialysis risk [30,31].

In our cohort, anemia showed the strongest association with dialysis initiation in the adjusted Cox model and was consistently selected by the ML algorithms. A study conducted in Japan found that, despite higher hemoglobin levels in ADPKD than in other CKD types, anemia remains a key predictor of renal disease progression. In nondialysis patients with ADPKD, lower hemoglobin levels were associated with faster kidney function decline, with men with hemoglobin levels less than 12 g/dL and women with hemoglobin levels less than 11 g/dL at higher risk [32]. Together, these findings support anemia as a clinically accessible marker of advanced disease and progression risk in ADPKD.

AKI and infection-related diagnoses such as pneumonia and UTI also contributed to the prediction. These events may accelerate loss of residual kidney function through hemodynamic instability, inflammatory injury, or nephrotoxic exposures, and they may also serve as markers of vulnerability and more frequent clinical encounters. In parallel, medication predictors such as sodium bicarbonate and NSAIDs plausibly reflect clinically recognized metabolic acidosis and nephrotoxic exposure that often accompany advanced CKD and precede dialysis initiation [33].

Medication Predictors as Markers of Disease Severity

As highlighted earlier, a critical aspect of interpreting our findings is the potential for confounding by indication, particularly for medication-related predictors. In a retrospective cohort study, the use of a specific medication is often a marker of underlying disease severity rather than a cause of the outcome itself. Therefore, while these medications emerged as strong predictors in our model, they should be viewed primarily as indicators of a higher underlying risk profile, and our findings do not imply a causal relationship or recommend changes in prescribing practices. Consistent with prior work using administrative claims for kidney failure prediction, these medication patterns should be interpreted primarily as proxies for clinical complexity rather than as causal determinants of dialysis initiation [31].

Renin-angiotensin system inhibitors have been established as the first-line treatment due to their benefits in hypertension control [34]. In our model, the selection of additional antihypertensive classes (eg, alpha-blockers and CCB) and loop diuretics likely reflects difficult-to-control blood pressure, volume management needs, or concomitant cardiovascular disease rather than direct causal effects on renal decline. Similarly, anticoagulant and antiplatelet use may act as proxies for atrial fibrillation, vascular disease, or prior cardiovascular events, conditions that commonly cluster with advanced CKD and a higher risk of dialysis initiation.

Tranexamic acid was also selected among the final XGBoost predictors. In ADPKD, clinically significant gross hematuria is a common and clinically relevant event, and tranexamic acid has been used in small series for severe hematuria, although evidence remains limited [2,35]. Therefore, in claims-based modeling, tranexamic acid likely functions as a proxy for clinically significant hematuria or bleeding-related care that clusters with more advanced disease trajectories, rather than as a causal determinant of dialysis initiation.

Hyperuricemia is increasingly implicated in CKD progression, and our model identified gout and febuxostat as informative predictors of dialysis. This finding does not suggest a causal link but rather reflects prescribing patterns that align with both international guidelines and local reimbursement policies. Major clinical practice guidelines for ADPKD recommend allopurinol as the first-line urate-lowering therapy [2]. This standard is strictly reflected in Taiwan's National Health Insurance system, where reimbursement for the second-line agent, febuxostat, was restricted during our study period. These restrictions likely limited its use primarily to patients with substantial preexisting conditions, most notably advanced chronic kidney disease

XSL•FO
RenderX

(defined as eGFR <45 mL/min/1.73 m^2) or other complications such as urate nephrolithiasis or severe tophaceous gout. Consequently, the predictive signal from febuxostat in our model arises because it serves as a powerful proxy, identifying a patient subgroup with higher baseline renal risk and greater disease complexity. Further prospective studies are needed to determine if urate-lowering therapy itself modifies the disease course in ADPKD.

Statins, primarily known for their cholesterol-lowering effects, also possess anti-inflammatory and antioxidant properties that could be beneficial in PKD. Chronic inflammation and oxidative stress play roles in the pathophysiology of PKD, contributing to cyst growth and renal function decline. Evidence regarding the efficacy of statins in PKD is equivocal. Some cohort studies and animal research suggest that statins may slow the decline in renal function in patients with PKD by reducing inflammation and oxidative stress [9]. However, findings from definitive clinical trials in PKD populations, which are scarce, remain inconclusive.

Comparison With Existing Risk Stratification Tools

Our ML approach should be compared with existing clinical risk tools for ADPKD, such as the Mayo Imaging Classification and the PROPKD score. The primary advantage of our model lies in its broad accessibility. By leveraging nationwide administrative data, it bypasses the need for resource-intensive assessments, such as MRI for TKV measurement or genetic sequencing, making it a scalable and cost-effective tool for initial risk stratification across a large population. The main disadvantage, however, is the lack of direct pathophysiological data. Without TKV or genetic data, our model relies on surrogate markers of disease severity and cannot offer the same level of mechanistic insight or precision as the gold-standard tools. Therefore, our model should not be viewed as a replacement for these established methods but rather as a complementary instrument. Its optimal clinical role would be to serve as a first-line screening tool to efficiently identify high-risk patients who could then be prioritized for more definitive prognostic evaluations like imaging or genetic testing.

Strengths and Limitations

To our knowledge, this study represents the first nationwide ML-based analysis of dialysis risk in ADPKD using administrative data. It provides a scalable framework for population-level risk stratification. The use of the NHIRD, a large population-based dataset with long-term follow-up, ensures high generalizability to the nationwide population of Taiwan.

Several limitations of this study should be acknowledged. First, its retrospective design precludes the establishment of causality. Second, and most importantly, our study is constrained by the nature of the NHIRD, which lacks the gold-standard prognostic markers for ADPKD including genetic data (PKD1/PKD2 status) and imaging biomarkers like TKV, and key laboratory values such as eGFR or proteinuria. Without direct access to TKV or genetic data, our model inherently relies on surrogate markers such as comorbidity burden and medication patterns to infer underlying risk. Despite the use of a washout period and validation via the Catastrophic Illness Patient Registry, truly incident ADPKD cases cannot be fully guaranteed in claims-based data. We therefore wish to emphasize that our model is proposed as a complementary tool for broad-based risk stratification, not as a replacement for comprehensive clinical evaluation. Third, because observation windows vary by index year, the binary labeling framework may under-ascertain events among patients with shorter follow-up and can bias absolute risk interpretation. In addition, calibration curves were not presented, limiting assessment of absolute risk calibration. Fourth, because deaths occurring before ESRD were labeled as nonevents in the binary ML framework, patients with high competing mortality may be misclassified as having low renal risk. Fifth, the measurement of medication exposure, quantified by prescription days, is a proxy that does not capture actual patient adherence, dosage, or treatment adjustments. This limits our ability to make definitive conclusions about the role of specific pharmacological agents. Finally, our model was developed using a Taiwanese population, and its performance and the relative importance of predictors may vary across different ethnic and geographic groups, which may limit generalizability.

Future Work

Future studies should prioritize prospective validation in diverse external cohorts. Methodologically, fixed-horizon prediction and time-to-event approaches, including survival ML and competing-risk or multistate frameworks, should be evaluated to better align modeling with clinical trajectories. External validation datasets that include laboratory, genetic, and imaging biomarkers (eg, eGFR, proteinuria, PKD1/PKD2 status, and TKV) will enable integrated, multitiered risk stratification and more complete assessment of calibration and clinical utility. Moreover, instance-level explainability methods (eg, SHAP) can be explored to support clinical interpretability.

Conclusions

This study developed and evaluated 6 ML models to classify dialysis initiation risk in a nationwide ADPKD cohort using administrative claims data and a prespecified temporal validation design. On the held-out temporal test set, XGBoost showed the best overall performance. The most informative predictors primarily reflected disease severity and care intensity captured in claims data, including age, comorbidity burden, anemia, and hypertension, whereas medication variables should be interpreted as noncausal proxies of clinical complexity.

Acknowledgments

No generative artificial intelligence tools were used to generate the manuscript text, analyses, figures, tables, or multimedia appendix. All study design decisions, analyses, interpretations, and final wording were produced and verified by the authors.

XSL•FO
RenderX

Funding

This study was supported by the Shin-Kong Wu Ho-Su Memorial Hospital Research Foundation (2022SKHADR035) and The National Science and Technology Council, Taiwan (NSTC 112-2221-E-030 -009 -MY3). The funding source had no role in the study design, data collection, analysis, or interpretation of the results.

Data Availability

The dataset used in this study belongs to the Taiwan Ministry of Health and Welfare (MOHW). Due to data protection regulations, the dataset cannot be shared by the corresponding author upon request. However, researchers interested in accessing this dataset may apply for access through the website of the National Health Informatics Project of the MOHW [36].

Authors' Contributions

Conceptualization: MC, MHT, YWF
Data curation: MHT, HHL
Formal analysis: CHC, MC, YCH, CL
Funding acquisition: MC, YWF
Investigation: MHT, YWF
Methodology: CHC, MC, YCH, HHL, BCS, CL
Resources: MC, YCH
Software: MC, YCH
Supervision: MC, YWF
Validation: MHT, YCH, BCS
Writing – original draft: CHC, MC
Writing – review and editing: MHT, BCS, CL, YWF

Conflicts of Interest

None declared.

Multimedia Appendix 1
Supplementary methods and tables, including model implementation details for the six machine learning algorithms, ICD-9-CM/ICD-10-CM codes for comorbidities (Table S1), ATC codes and drug lists (Table S2), and tuned hyperparameters with software packages and versions (Table S3).
[DOCX File, 38 KB - medinform_v14i1e80343_app1.docx]

References

1. Harris PC, Torres VE. Polycystic kidney disease. Annu Rev Med 2009;60:321-337. [doi: 10.1146/annurev.med.60.101707.125712] [Medline: 18947299]
2. Kidney Disease: Improving Global Outcomes (KDIGO) ADPKD Work Group. KDIGO 2025 clinical practice guideline for the evaluation, management, and treatment of autosomal dominant polycystic kidney disease (ADPKD). Kidney Int 2025 Feb;107(2S):S1-S239. [doi: 10.1016/j.kint.2024.07.009] [Medline: 39848759]
3. Jafar TH, Stark PC, Schmid CH, et al. Progression of chronic kidney disease: the role of blood pressure control, proteinuria, and angiotensin-converting enzyme inhibition: a patient-level meta-analysis. Ann Intern Med 2003 Aug 19;139(4):244-252. [doi: 10.7326/0003-4819-139-4-200308190-00006] [Medline: 12965979]
4. Benck U, Krüger B, Schmitt WH. Blood pressure in early autosomal dominant polycystic kidney disease. N Engl J Med 2015 Mar 5;372(10):975-977. [doi: 10.1056/NEJMc1500332] [Medline: 25738679]
5. Kramers BJ, Koorevaar IW, Drenth JPH, et al. Salt, but not protein intake, is associated with accelerated disease progression in autosomal dominant polycystic kidney disease. Kidney Int 2020 Oct;98(4):989-998. [doi: 10.1016/j.kint.2020.04.053] [Medline: 32534051]
6. Nowak KL, Steele C, Gitomer B, Wang W, Ouyang J, Chonchol MB. Overweight and obesity and progression of ADPKD. Clin J Am Soc Nephrol 2021 Jun;16(6):908-915. [doi: 10.2215/CJN.16871020] [Medline: 34117082]
7. Torres VE, Chapman AB, Devuyst O, et al. Tolvaptan in patients with autosomal dominant polycystic kidney disease. N Engl J Med 2012 Dec 20;367(25):2407-2418. [doi: 10.1056/NEJMoa1205511] [Medline: 23121377]
8. Takiar V, Nishio S, Seo-Mayer P, et al. Activating AMP-activated protein kinase (AMPK) slows renal cystogenesis. Proc Natl Acad Sci U S A 2011 Feb 8;108(6):2462-2467. [doi: 10.1073/pnas.1011498108] [Medline: 21262823]
9. Fassett RG, Robertson IK, Ball MJ, Geraghty DP, Coombes JS. Effect of atorvastatin on kidney function in chronic kidney disease: a randomised double-blind placebo-controlled trial. Atherosclerosis 2010 Nov;213(1):218-224. [doi: 10.1016/j.atherosclerosis.2010.07.053] [Medline: 20810109]

XSL•FO
RenderX

10. Irazabal MV, Rangel LJ, Bergstralh EJ, et al. Imaging classification of autosomal dominant polycystic kidney disease: a simple model for selecting patients for clinical trials. J Am Soc Nephrol 2015 Jan;26(1):160-172. [doi: 10.1681/ASN.2013101138] [Medline: 24904092]
11. Cornec-Le Gall E, Audrézet MP, Rousseau A, et al. The PROPKD score: a new algorithm to predict renal survival in autosomal dominant polycystic kidney disease. J Am Soc Nephrol 2016 Mar;27(3):942-951. [doi: 10.1681/ASN.2015010016] [Medline: 26150605]
12. Niel O, Boussard C, Bastard P. Artificial intelligence can predict GFR decline during the course of ADPKD. Am J Kidney Dis 2018 Jun;71(6):911-912. [doi: 10.1053/j.ajkd.2018.01.051] [Medline: 29609979]
13. Kim Y, Bu S, Tao C, Bae KT, HALT Polycystic Kidney Disease Study Group. Deep learning-based automated imaging classification of ADPKD. Kidney Int Rep 2024 Jun;9(6):1802-1809. [doi: 10.1016/j.ekir.2024.04.002] [Medline: 38899202]
14. Sharma K, Rupprecht C, Caroli A, et al. Automatic segmentation of kidneys using deep learning for total kidney volume quantification in autosomal dominant polycystic kidney disease. Sci Rep 2017 May 17;7(1):2049. [doi: 10.1038/s41598-017-01779-0] [Medline: 28515418]
15. Taylor J, Thomas R, Metherall P, et al. An artificial intelligence generated automated algorithm to measure total kidney volume in ADPKD. Kidney Int Rep 2024 Feb;9(2):249-256. [doi: 10.1016/j.ekir.2023.10.029] [Medline: 38344736]
16. Lin LY, Warren-Gash C, Smeeth L, Chen PC. Data resource profile: the National Health Insurance Research Database (NHIRD). Epidemiol Health 2018;40:e2018062. [doi: 10.4178/epih.e2018062] [Medline: 30727703]
17. Kalatharan V, McArthur E, Nash DM, et al. Diagnostic accuracy of administrative codes for autosomal dominant polycystic kidney disease in clinic patients with cystic kidney disease. Clin Kidney J 2021 Feb;14(2):612-616. [doi: 10.1093/ckj/sfz184] [Medline: 33623686]
18. Nan-Ping Y, Yi-Hui L, Chi-Yu C, et al. Comparisons of medical utilizations and categorical diagnoses of emergency visits between the elderly with catastrophic illness certificates and those without. BMC Health Serv Res 2013 Apr 26;13:152. [doi: 10.1186/1472-6963-13-152] [Medline: 23622501]
19. Wang SW, Li LC, Su CH, Yang YH, Hsu TW, Hsu CN. Association of statin and its lipophilicity with cardiovascular events in patients receiving chronic dialysis. Clin Pharmacol Ther 2020 Jun;107(6):1312-1324. [doi: 10.1002/cpt.1722] [Medline: 31715017]
20. Hastie T, Tibshirani R, Friedman J. The Elements of Statistical Learning: Springer; 2009. [doi: 10.1007/978-0-387-84858-7]
21. Prokhorenkova L, Gusev G, Vorobev A, Dorogush AV, Gulin A. CatBoost: unbiased boosting with categorical features. Presented at: 32nd Conference on Neural Information Processing Systems (NeurIPS 2018); Dec 3-8, 2018 URL: https://proceedings.neurips.cc/paper_files/paper/2018/file/14491b756b3a51daac41c24863285549-Paper.pdf [accessed 2026-02-24]
22. Huang YC, Ho CW, Chou WR, Chen M. A framework to predict second primary lung cancer patients by using ensemble models. Ann Oper Res 2025 May;348(1):373-397. [doi: 10.1007/s10479-023-05691-x]
23. Chen KY, Huang YC, Liu CK, Li SJ, Chen M. Machine learning-driven prediction of medical expenses in triple-vessel PCI patients using feature selection. BMC Health Serv Res 2025 Jan 20;25(1):105. [doi: 10.1186/s12913-025-12218-6] [Medline: 39833782]
24. Rahbari-Oskoui F, Williams O, Chapman A. Mechanisms and management of hypertension in autosomal dominant polycystic kidney disease. Nephrol Dial Transplant 2014 Dec;29(12):2194-2201. [doi: 10.1093/ndt/gft513] [Medline: 24463189]
25. Helal I, Reed B, Mettler P, et al. Prevalence of cardiovascular events in patients with autosomal dominant polycystic kidney disease. Am J Nephrol 2012;36(4):362-370. [doi: 10.1159/000343281] [Medline: 23038404]
26. Chapman AB, Stepniakowski K, Rahbari-Oskoui F. Hypertension in autosomal dominant polycystic kidney disease. Adv Chronic Kidney Dis 2010 Mar;17(2):153-163. [doi: 10.1053/j.ackd.2010.01.001] [Medline: 20219618]
27. Schrier RW, Abebe KZ, Perrone RD, et al. Blood pressure in early autosomal dominant polycystic kidney disease. N Engl J Med 2014 Dec 11;371(24):2255-2266. [doi: 10.1056/NEJMoa1402685] [Medline: 25399733]
28. Kim DH, Schneeweiss S, Glynn RJ, Lipsitz LA, Rockwood K, Avorn J. Measuring frailty in Medicare data: development and validation of a claims-based frailty index. J Gerontol A Biol Sci Med Sci 2018 Jun 14;73(7):980-987. [doi: 10.1093/gerona/glx229] [Medline: 29244057]
29. Walker H, Day S, Grant CH, et al. Representation of multimorbidity and frailty in the development and validation of kidney failure prognostic prediction models: a systematic review. BMC Med 2024 Oct 11;22(1):452. [doi: 10.1186/s12916-024-03649-9] [Medline: 39394084]
30. Chuah A, Walters G, Christiadi D, et al. Machine learning improves upon clinicians' prediction of end stage kidney disease. Front Med 2022;9. [doi: 10.3389/fmed.2022.837232]
31. Li Y, Al-Sayouri S, Padman R. Towards interpretable end-stage renal disease (ESRD) prediction: utilizing administrative claims data with explainable AI techniques. AMIA Annu Symp Proc 2024;2024:664-673. [Medline: 40417492]
32. Ushio Y, Kataoka H, Sato M, et al. Association between anemia and renal prognosis in autosomal dominant polycystic kidney disease: a retrospective study. Clin Exp Nephrol 2020 Jun;24(6):500-508. [doi: 10.1007/s10157-020-01856-1] [Medline: 32036465]
33. Goraya N, Wesson DE. Clinical evidence that treatment of metabolic acidosis slows the progression of chronic kidney disease. Curr Opin Nephrol Hypertens 2019 May;28(3):267-277. [doi: 10.1097/MNH.0000000000000491] [Medline: 30681417]

XSL•FO
RenderX

34. Torres VE, Abebe KZ, Chapman AB, et al. Angiotensin blockade in late autosomal dominant polycystic kidney disease. N Engl J Med 2014 Dec 11;371(24):2267-2276. [doi: 10.1056/NEJMoa1402686] [Medline: 25399731]
35. Yao Q, Wu M, Zhou J, et al. Treatment of persistent gross hematuria with tranexamic acid in autosomal dominant polycystic kidney disease. Kidney Blood Press Res 2017;42(1):156-164. [doi: 10.1159/000474961] [Medline: 28395294]
36. National health informatics project of the MOHW. Ministry of Health and Welfare. URL: https://dep.mohw.gov.tw/DOS/mp-113.html [accessed 2026-02-27]

Abbreviations

ACEI: angiotensin-converting enzyme inhibitor
ADPKD: autosomal dominant polycystic kidney disease
AI: artificial intelligence
AKI: acute kidney injury
ARB: angiotensin II receptor blocker
AUC: area under the curve
CCB: calcium channel blocker
CCI: Charlson Comorbidity Index
COPD: chronic obstructive pulmonary disease
ESRD: end-stage renal disease
HR: hazard ratio
ML: machine learning
MRI: magnetic resonance imaging
NHIRD: National Health Insurance Research Database
NSAID: nonsteroidal anti-inflammatory drug
PKD: polycystic kidney disease
TKV: total kidney volume
UTI: urinary tract infection
XGBoost: extreme gradient boosting

Edited by A Coristine, A Benis; submitted 09.Jul.2025; peer-reviewed by SB Duan, SS Chai; revised version received 14.Feb.2026; accepted 17.Feb.2026; published 16.Mar.2026.

Please cite as:
Chang CH, Chen M, Tsai MH, Huang YC, Liou HH, Shia BC, Liang C, Fang YW
Machine Learning Prediction of Progression to Dialysis in Patients With Polycystic Kidney Disease: Population-Based Retrospective Cohort Study
JMIR Med Inform 2026;14:e80343
URL: https://medinform.jmir.org/2026/1/e80343
doi:10.2196/80343

© Cheng-Hao Chang, Mingchih Chen, Ming-Hsien Tsai, Yen-Chun Huang, Hung-Hsiang Liou, Ben-Chang Shia, Chingying Liang, Yu-Wei Fang. Originally published in JMIR Medical Informatics (https://medinform.jmir.org), 16.Mar.2026. This is an open-access article distributed under the terms of the Creative Commons Attribution License (https://creativecommons.org/licenses/by/4.0/), which permits unrestricted use, distribution, and reproduction in any medium, provided the original work, first published in JMIR Medical Informatics, is properly cited. The complete bibliographic information, a link to the original publication on https://medinform.jmir.org/, as well as this copyright and license information must be included.

XSL•FO
RenderX

Exploring Factors Associated With the Stalled Implementation of a Ground-Up Electronic Health Record System in South Africa: Qualitative Insights From the E-Tick Case Study Using the Consolidated Framework for Implementation Research (CFIR)

Campion Zharima[1], PhD; Frances Griffiths[2], PhD; Jane Goudge[1], PhD

[1]Centre for Health Policy, Faculty of Health Sciences, University of the Witwatersrand, Johannesburg, South Africa

[2]Centre for Primary Health Care Studies, Warwick Medical School, University of Warwick, Medical School Building, CV4 7AL, Coventry, United Kingdom

Corresponding Author:
Frances Griffiths, PhD
Centre for Primary Health Care Studies, Warwick Medical School, University of Warwick, Medical School Building, CV4 7AL, Coventry, United Kingdom

Abstract

Background: Electronic health records (EHRs) have the potential to improve service delivery through record keeping and monitoring health outcomes. As countries move toward universal health coverage, digital health tools such as EHRs are essential for achieving this goal. However, EHR implementation in middle-income countries like South Africa faces obstacles.

Objective: This study explores the reasons behind a stalled implementation of the electronic tick register (E-tick) system (an electronic version of a paper primary health care register to record services provided), using the Consolidated Framework for Implementation Research.

Methods: Using a qualitative design, in-depth interviews were conducted with 38 participants to explore their perceptions and experiences, and the factors surrounding the success and stalling of E-ticks. Participants included managers, stakeholders, implementers, and end users from the 3 implementation clinics. Data was collected using semistructured interview guides. The Thematic and Consolidated Framework for Implementation Research framework analysis (innovation, inner setting, individual characteristics, implementation process, and outer setting) was applied.

Results: The E-tick system was designed to improve data quality in paper health registers, addressing inaccuracies in reporting to district and provincial health departments (Innovation domain). Implementers iteratively developed the system through user input from managers and clinicians, and stakeholder engagement of software developers, funders, health managers, and decision-makers from the provincial health department (individual characteristics). Although the system was initially well adopted by end users, it stalled primarily due to outer setting factors, which included a change of developers, funding cuts, and limited support at the provincial health department level due to capacity gaps, political appointments, and mistrust stemming from corruption and abuse of the tender system. Moreover, resistance to leveraging lessons from locally developed small-scale systems further constrained institutional support for the E-tick.

Conclusions: Although successful implementation of EHRs can be facilitated by strong user engagement and co-design, outer setting factors such as governance, funding, and policy alignment can pose significant threats to sustainability. This underscores the importance of effective synergy between top-down and bottom-up processes for successful implementation.

(JMIR Med Inform 2026;14:e73831) doi:10.2196/73831

KEYWORDS

electronic health records; implementation; barriers; facilitators; Consolidated Framework for Implementation Research; CFIR

Introduction

Overview

Electronic health records (EHRs) hold the promise of improving service delivery, monitoring and evaluation of health interventions, and record-keeping for public health [1]. As more countries work towards universal health coverage, leveraging digital health tools like EHRs becomes more important for enhancing service delivery and improving quality of care [2,3]. The World Health Organization's global digital health strategy emphasizes the need for accelerated adoption of EHRs to achieve health goals [4]. However, EHR implementation in many middle-income countries remains slow due to financial and technological challenges [5].

XSL•FO
RenderX

Implementing EHRs is an evolving process that requires adaptive and context-specific policies to meet ever-changing needs [6], and a clear vision to move from pilot to scaled implementation [2]. In some high-income countries where implementation has occurred [7], a "top-down" approach has typically been used, where systems are preconfigured, and users must adapt. Although this offers coordination and central oversight, it can limit flexibility. In contrast, bottom-up approaches emphasize co-design with end users and adaptation to local workflows, which often enhances usability and adoption [8]. Research suggests that successful EHR implementation in complex health systems requires balancing national coordination with local innovation, as this allows centralized oversight, while engaging local health communities and tailoring systems to user needs [8,9].

South Africa has made policy advances, such as the National Digital Health Strategy (NDHS) (2019 - 2024) [10], with considerable resources as a middle-income country and sufficient technical expertise, but progress toward a national EHR has been slow. This is because policy direction and technical capacity are sometimes impeded by systemic and political barriers. Within this context, most primary health care facilities continue to rely on manual paper-based systems, which are labor-intensive and prone to errors in data collection [11,12]. However, bottom-up efforts have been made to improve data quality and accuracy. These include Tier.net, an electronic record system used with patients living with HIV and tuberculosis, and the electronic tick register (E-tick), the electronic record system we studied. The E-tick is a digital version of the tick register, a book in each health care facility for recording patient attendance and care delivered. In this paper, we use the Consolidated Framework for Implementation Research (CFIR) to explore an attempted implementation of the E-tick, a system conceptually similar to an EHR, examining how its implementation stalled despite a consultative approach in its implementation.

Background

Digital Health Policy in South Africa

As a middle-income country, South Africa has made policy strides in line with the global developments, which should facilitate the adoption of EHRs, such as the National Health Act 61 of 2003 and the NDHS (2019 - 2024) [10,13]. The Health Act outlines the role of the National Department of Health in coordinating health information systems across national, provincial, and district levels [10]. Although policy direction is set at the national level, the federal system means that provinces can independently determine their own health care spending. Therefore, implementation largely occurs at provincial and district levels, with each maintaining its own health information systems within the national framework. This provincial autonomy has contributed to fragmentation, as different provinces and regions develop EHR systems through separate procurement processes [14]. This fragmentation is further compounded by a political economy of procurement, in which tenders are prone to corruption, mismanagement, and the absence of oversight structures [15]. These factors directly affect which innovations are funded, how resources are distributed, and whether systems can successfully reach scale, as funding decisions often prioritize large-scale centralized systems.

South Africa uses 2 health information systems in the public sector: the Health Patient Registration System (HPRS) and the District Health Information Software (DHIS; developed through a collaboration between the University of the Western Cape and the University of Oslo), jointly developed by the University of the Western Cape and the University of Oslo [16]. The HPRS is a manual patient registry that records patient contact details as well as legal identification numbers, while the DHIS is an electronic system used to collect aggregated data on services provided to patients in public health facilities [17]. The DHIS data is first collected manually, then captured into the DHIS software, where it is submitted to the district, provincial, and national health departments. The method used to record primary health care data is a tick register, a manual paper-based system where clinicians mark or tick off the services provided in a large logbook with columns for dates and types of services offered (antenatal care, vaccinations, or chronic disease management). However, this process can be arduous, time-consuming, and prone to many recording errors. Studies evaluating the DHIS have confirmed persistent data gaps, citing poor documentation, manual entry under heavy workloads, and errors as major contributors to discrepancies [18].

South African Health System

South Africa plans to implement a National Health Insurance fund to facilitate better purchasing decisions through more formal contracting relationships rather than the historical allocation of budgets by provinces [19]. In this case, EHRs are key in monitoring patient outcomes and assessing the value of care purchased. Although most provinces have had some type of operational EHR system in public hospitals [20], there is no national EHR at the primary care level, and different architectures still pose a challenge to their integration for nationally coordinated use [21].

Provincial health departments in South Africa are often run by political appointees, who work under directives from their affiliated political party. This has led to pervasive corruption in the country's health system, which has been reported at various levels of government [22]. For example, 150 million rand awarded to a communications company during the COVID pandemic was misappropriated, and the health minister was suspended as a result [23]. In another case, the provincial chief financial officer who exposed a 1-billion-rand tender fraud was assassinated [24]. Such cases illustrate how poor financial management systems and political appointments enable corruption, which acts as an impediment to the public trust in the health system [25]. For digital health innovations, such dynamics increase the risk that systems are chosen for political or financial interests rather than their impact or merit, which affects the health department's ability to work with other stakeholders, or source funds for large-scale projects, including projects to implement EHRs. Moreover, the absence of countermeasures such as accountability and transparency makes it difficult to implement large-scale projects like EHRs.

XSL•FO
RenderX

The E-Tick System

An electronic version of the paper-based tick register (E-tick) was developed and piloted in 3 public health care facilities in the Ekurhuleni district between 2017 and 2021. Clinicians record services provided directly into the digital system on a patient's record, which also allows facility managers to monitor daily activities such as headcount and services offered. Although this is not a full EHR, the system can be expanded to include diagnosis and lab results and to integrate with other systems that are currently used in public health facilities. Against this backdrop, the E-tick system sought to provide an alternative that could improve data accuracy at the facility level while feeding directly into the existing provincial and national reporting systems. However, such progress is dependent on not only user adoption factors but also broader contextual dynamics [26]. Thus, by situating the E-tick in relation to both micro-level realities and macro-level policy and political economy, we aim to provide a more holistic understanding of why grassroots digital health interventions may stall or fail.

Consolidated Framework for Implementation Research (CFIR)

Implementation research seeks to understand why some implementation efforts succeed and others do not, and the role of the context [27]. To explore the key factors affecting implementation in our case study, we used the CFIR, which integrates existing theories of implementation and behavior change into a unified framework [28]. The CFIR is a meta-theoretical tool with standardized constructs to examine enablers and barriers to implementation across different stages (preimplementation, during implementation, and postimplementation) [29].

The CFIR was developed through a review of published theories and reports on factors influencing implementation [30]. Hence, its strength lies in its broad applicability and potential for generalizability, which are useful for informing practice across diverse settings. The framework has 5 broad domains (Table 1), which include: innovation domain, inner setting domain, outer setting domain, individuals domain, and the implementation process domain, which together capture multilevel determinants of implementation [31]. Due to the framework's flexibility, researchers can tailor it to specific interventions and contexts [32], and it has been widely adopted in research, applied across different research designs, and cited in over 300 published articles [29]. Recent updates have been made to the framework, using responses from authors who used the framework, leading to refined construct names and definitions to make them more encompassing [31]. In this paper, we draw on the updated CFIR to guide both our analysis and reporting of findings.

Table . Consolidated Framework for Implementation Research (CFIR) domains by Damschroder et al [28].

CFIR domains	Definition
Innovation	• The "thing" being implemented, such as a new treatment, program, or service. • Key factors that affect innovation include its source, evidence base, advantages over existing practices, adaptability, trialability, complexity, design, and cost.
Individuals	• The roles and characteristics of people involved in innovation. • Key roles include high-level leaders, mid-level leaders, opinion leaders, facilitators, and implementation teams who guide and support the innovation. • It also highlights innovation deliverers and recipients.
Inner setting	• The environment where an innovation is implemented, such as a hospital or school. • Key elements include structural characteristics like physical and IT infrastructure, work organization, and staffing levels.
Outer setting	• The broader context or setting within which an organization or project operates, such as a hospital system or school district. • Factors influencing implementation in the Outer Setting include large-scale disruptions, local attitudes, socioeconomic conditions, external partnerships, and regulatory policies.
Implementation process	• The activities and strategies to introduce and sustain an innovation. • Key components include forming teams to collaborate on tasks, assessing the needs of both innovation deliverers and recipients, and evaluating the context to identify barriers and facilitators. • Planning, tailoring strategies, engaging participants, testing small-scale changes, and reflecting on outcomes are critical steps.

XSL•FO
RenderX

Methods

This study adopted a qualitative design to explore the perceptions and experiences of external stakeholders, senior health managers, implementers, and end users of the E-tick system.

Participants and Sampling

We recruited a total of 38 participants, categorized into three groups: (1) managers and stakeholders, (2) implementation team, and (3) end users. The senior health managers and external stakeholders category included decision makers and higher-level people who were not directly involved in the system's implementation but provided insights into the context and the decisions impacting it. The implementation team comprised individuals who were responsible for initiating and deploying the system and introducing it to the users, while the end user team consisted of the clinicians and managers from 3 recipient facilities. Participants from the managers and stakeholders, as well as the implementation team, were purposively selected through referrals from key individuals and recruited via email. For end users, convenience sampling was used, with the researcher recruiting available users with the aid of gatekeepers during facility visits. Our sample intentionally included stakeholders from multiple levels of the health system to minimize elite bias, ensuring that the perspectives of senior health managers were balanced with those of frontline users and mid-level implementers. Below is a summary table of the participants in this study (Table 2).

Table . Study participants (N=38).

Category and roles	Count (n)
Senior managers and stakeholders	
National, provincial and district health managers	7
Parastatal staff	2
NGO[a] managers and staff	4
Academics	2
Private sector managers	2
Implementers	
Originators	2
IT Technician	1
Data capturers	3
End users	
Facility managers	3
Administrative officer	1
Nurses and midwives	9
Admin clerks	2

[a]NGO: Non-Governmental Organization.

Data Collection and Management

Data collection took place between November 2021 and June 2022, which was after the E-tick project had stalled. Thus, participants, particularly implementers and end users, reflected retrospectively on the system's development, piloting, and discontinuation. Due to COVID-19 health restrictions at the time, some of the interviews with senior health managers and the implementation team were conducted via web using video conferencing software. Interviews with end users were conducted in person in health care facilities during work hours and were conducted primarily in English, which is the standard working language in the facilities. However, participants were free to use local language terms or expressions, which were translated during transcription to preserve meaning.

Different semistructured interview guides were used for the 3 categories of participants. For the managers, we inquired about the broader digital health policy landscape, existing health information systems, government readiness, and feasibility for EHR implementation and the necessary next steps to advance EHR adoption in South Africa. For the implementation team and end users, the interview guides covered topics on the purpose and origins of the E-tick, its piloting rollout, experiences with implementation and daily use, training and support, perceived benefits and challenges, and overall recommendations for improvement. Interviews varied in length, ranging from 10 to 64 minutes. Shorter interviews (under 20 min) were mostly with busy frontline staff, including clerks and clinicians during clinic hours, who provided concise but relevant insights into system use. Longer interviews were with senior health managers with authority over policy alignment, resource allocation, and procurement processes, and implementers who facilitated implementation in the 3 health facilities. Despite these differences, data saturation was reached across stakeholder groups, as no new themes emerged in later interviews. All interviews were audio recorded, and recordings were stored in

XSL•FO
RenderX

a password-protected computer to ensure privacy. Audio recordings were transcribed using transcription software and checked for accuracy, and transcripts were anonymized by removing participant-identifying information.

Data Analysis

The first author led the coding, followed by regular debriefing meetings with coauthors, who are also academic supervisors, to review coding and theme development, which strengthened reliability. In this case, coauthors read all the transcripts, and discrepancies were discussed until consensus was reached. The interview transcripts were coded using NVivo qualitative analysis software (QSR International). Through this process, emergent issues were identified and used to develop the themes, following a 6-step thematic analysis process [33]. An inductive approach guided the thematic analysis, with broad topics derived from the interview guide, leading to the 4 stages of implementation reported in this study (Purpose and origins, Initial development, Piloting and expansion, and Halt). The accounts from the two originators formed the foundation, providing the background story and backbone of the implementation narrative, whose detailed recollections provided a chronological anchor for mapping implementation processes. These accounts were not taken at face value, but were supplemented by other participants' accounts, which were used to triangulate and integrate the information into a cohesive story.

After coding, the CFIR was applied to the analysis, linking the framework's 5 domains to the implementation process as reported in the study's findings (Table 3) [31]. The CFIR framework guided our analysis and reporting of findings. In this case, CFIR constructs were operationalized as sensitizing concepts to guide coding, with data excerpts being coded against relevant constructs, while leaving space for inductive subthemes to emerge. Thus, the analysis combined deductive coding (using CFIR constructs) with inductive coding to capture novel themes. Multiple coders reviewed transcripts, with regular team discussions to minimize confirmation bias.

Table . Implementation stages and applied Consolidated Framework for Implementation Research (CFIR) domains.

Stages of implementation	Description	Applied CFIR domains
Origins and purpose of the system (2015 - 2017)	Conception of E-tick[a] by system originators; designed to digitize the existing tick register and reduce errors.	• Innovation • Individuals • Inner setting • Outer setting
Initial development (2017 - 2019)	Early technical build and adaptation of the system, involving stakeholder input and limited resource mobilization.	• Individuals • Inner setting • Outer setting • Implementation process
Piloting (2019 - 2020)	Deployment of E-tick system in 3 health facilities.	• Individuals • Inner setting • Implementation process
Halt (2021)	Expansion beyond pilot sites stalled due to barriers to scale up and institutionalization.	• Inner setting • Outer setting

[a]E-tick: electronic tick register.

Ethical Considerations

Ethics approval for this study was granted by the University of the Witwatersrand Medical Human Research Ethics Committee (M210213). Additional permissions were obtained from the Ekurhuleni district research committee and the Gauteng Provincial Department of Health (GP_202106_035). The study was conducted in accordance with local, institutional, and national regulations governing research involving human participants, as well as the principles of the Declaration of Helsinki. All participants provided written informed consent prior to participation. The study purpose, procedures, potential risks, benefits, and participants' rights, including the right to withdraw at any time without penalty, were explained before consent was obtained. Participant privacy and confidentiality were maintained as interviews were conducted in private settings, and no identifying information was included in transcripts. All data were anonymized, securely stored on password-protected devices, and were only accessible to the research team. Participants did not receive any compensation for their participation.

Results

Overview

This section presents the findings, which are ordered according to the domains of the CFIR: innovation, inner setting, individual characteristics, implementation process, and outer setting. This structure allows us to highlight how factors at multiple levels and stages of implementation shaped the processes, outcomes, and ultimately the stalling of the E-tick system. To illustrate the distribution of themes across the framework, Multimedia Appendix 1 provides a summary of implementation stages, CFIR domains and applicable constructs, thematic findings, and illustrative quotes.

XSL•FO
RenderX

Origins and Purpose of the E-Tick: Innovation and Individuals Domains (2015-2017)

Identifying the Problem

The development and implementation of the E-tick was initiated and led by a senior district manager and supported by a senior technician who was employed by the funder, labeled as Originators 1 and 2. The senior manager explained the rationale behind the project:

> *Annually, the National Department of Health audits our data for accuracy, and we've always had poor audit reports. The biggest problem was the quality of the data. That's why we started the E-tick, to improve the data quality.* [Originator 1]

The source of poor data quality was traced back to the tick register: "The data was very poorly filled into the tick register, the services provided not counted properly." (Originator 1). This was the stage where most errors occurred: "The data issues started in the consultation room, and then the counting and the transferring of the data into the DHIS accounted for about eighty percent of the mistakes." (Originator 1). Some clinicians echoed these remarks as one shared: "The purpose was to reduce workload and be able to say, reduce patients' waiting time by doing away with pen and paper and to be able to keep our records digitally, which makes it easier to keep them." (Nurse 12 – AR).

The second originator further describes how decision makers often overlook the importance of effective data collection processes:

> *The problem in South Africa is that the people who decide where the funding goes don't take data management records management seriously. They want this wealth of data so they put in these big paper registers, but they don't look at the process it takes to get that data.* [Originator 2]

This includes having too many registers:

> *We had twenty-seven different registers, like the antenatal register for a mother and child, and a chronic disease register for HIV. The problem was that while completing all the registers, users were creating their own registers because some information was missing.* [Originator 1]

Nurses similarly described the burden, with one stating:

> *So with the E-tick it was one less writing system… our patients were registered, all the follow up visits are registered, and… it gave a clear history of the patient.* [Nurse 13 – MM]

Finding the Solution

Against this backdrop, the idea of the E-tick began with an invitation to a staff development project to discuss potential solutions to data quality problems:

> *We received an invitation because we already recognized a problem with data quality in our tick registers. They proposed several ways to enhance the system, involving different levels of information. While some suggestions were overly complex and resembled an Electronic Health System.* [Originator 1]

Eventually, the originators decided to make use of an Excel-based E-tick system:

> *The organization that developed the District Health Information System …had an Electronic Tick Register and we thought we can use that to improve the data quality. But the system was just an excel sheet.* [Originator 1]

Thus, the originators built on the Excel-based system:

> *We decided to improve the front end, the user interface for the clients. That's how we developed the E-tick. It was basically to collect the data electronically and to be able to feed it directly into the DHIS, in a way that is easy for the nurses in the consultation rooms.*
>
> *[Originator 1]*

End users confirmed that the system was simpler and helpful. One nurse explained:

> *It was user friendly. If only we would use E-tick only… we will definitely be perfect.* [Nurse 10 – AR]

Another shared:

> *And it was also user friendly. It wasn't like I'm talking from somebody that's not very computer literate, basically… it made it very easy, accessible.* [Nurse 13 – MM]

Initial Development of E-Tick System: Inner Setting and Individual Domains (2017-2019)

Stakeholder Engagement

The first originator approached a nonprofit organization for funding to get the project off the ground: "After our experience, we approached organization X for financial assistance and shared our ideas with them, as [they were already] our long-term funding partner deeply involved in data collection" (Originator 1). After the funders agreed, this was followed by meetings with software developers for planning: "Once the funders agreed, we met with [software] developers to explore system development possibilities, discussed utilizing the HPRS as our registration system." (Originator 1). It was at this point that the second originator, who worked for the funding organization, became involved. Together, the two originators represented 2 groups of stakeholders, one with the Department of Health and all staff at recipient facilities, and the other with the funding organization and developers:

> *[Originator 1] was very good on the clinician side and I was very good on the software side. I had been working with my team [funders] for many years before we started the E-tick, and I developed many systems with them.* [Originator 2]

As an iterative process, the originators worked closely between clinicians and developers:

XSL•FO
RenderX

> *In a normal software development cycle, you scope your business requirements, hand it over to the team, and they will go develop what they think you want and then return to show it to you. We took a different approach. We were involved in the development, sitting with them every step of the way instead of waiting for weeks for changes. This worked extremely well.* [Originator 2]

Several clinicians further confirmed this engagement, with one manager explaining:

> *The first early step was that we had meetings which included facility managers, other stakeholders and our partner [funder], to explain to us what wants to be introduced, which is when we were first given the idea of the E-tick and what it's supposed to do.* [Administrative officer 19 – RK]

The originators then selected the facilities for piloting involving managers in the process: "We used random selection and cluster sampling, through a session with all operational clinic managers, who actively participated in this process." (Originator 1). A manager from one of the facilities described their involvement: "We were called to a district meeting, and this was pitched, the intention was discussed with us... So the facilities that were going to be pilots were selected." (Assistant Director 17 – RK).

System Development

After selecting the facilities for piloting, the system was taken to the recipient facilities as one clinician recalls:

> *They called us for like a mini meeting to inform us about E-tick and told us that we were one of the only clinics currently using it, and they were piloting to see if it's going to work.* [Nurse 10 – AR]

In the meetings, one of the goals was to find ways to streamline the patient consultation:

> *We focused on what made it easy for clinicians to help the patients without them waiting too long. But a bonus that came out of the system is that the system was also able to retrieve a patient's entire history.* [Originator 2]

The clinicians provided feedback:

> *The clinicians had great ideas. The first time we had the screens ready, we took it back to the clinicians and asked them if this is what they wanted, they approved it and gave suggestions for changes, which we did.* [Originator 2]

Several engagements were made with the provincial Department of Health to gain support and input on issues such as data storage:

> *When we began the pilot, we engaged the Provincial office and kept them informed about the program. A provincial manager suggested storing the data on provincial servers instead. However, they weren't prepared to proceed at that time.* [Originator 1]

To ensure this was possible later, the developers ensured the system was compliant:

> *We looked at the Departments of Health security and ICT standards, we worked with the Department of Health ICT team as well, and their data team.* [Originator 2]

However, this did not go as planned, as the data center was not ready in time:

> *The idea was to eventually transfer the system and its data to the department's data center once it was established. However, when we developed it, there was no data center for us to put it in, and we had complied with all the national standards for the developing systems.* [Originator 2]

Piloting and Expansion: Inner Setting and Implementation Process Domains (2019-2020)

Planning and Configuration

In all 3 chosen facilities, the originators conducted an infrastructural assessment before beginning the pilot:

> *We had to check that all computers were working, and that they all had network. The developers didn't want to have a local server for each clinic because it's too complicated. So they changed the system to an online system that worked with the cloud.* [Originator 1]

Some of the existing infrastructure was from the Department of Health:

> *We only had to get the computers for the Provincial clinics. So that already made life much easier. Because every clinic, every clinician had a computer, or most of them.* [Originator 1]

A technician from the health department was involved in configuring them:

> *My role was to check infrastructure, to see if it's there. But they also installed some private infrastructure because of some policies with our network which would require a lot of approvals before we can run it.* [IT Technician]

This was further supplemented by the funding to improve the infrastructure:

> *They [funders] assisted us and made sure that each room had a network cable. Sometimes there were no plugs, so they put in the plugs. They put in the routers.* [Originator 1]

The planning and configurations also informed decisions on devices that were to be used:

> *We wanted to see what the nurses and the clinicians felt more comfortable with, the tablets or the desktops. Due to a lack of space in some consultation rooms, which were too small to put a big desktop, it was easier to mount a tablet onto the wall.* [Originator 2]

Training and Learning

A comprehensive user training was provided in recipient facilities, which was tailored for specific roles:

XSL•FO
RenderX

> *There were different training categories, because the roles were different like, clerks, clinicians and so on. It was [also] not just one training, it was several; this was because the facility was working on shifts, so they had to accommodate everyone. During rollout, there was another in-service training just to remind the staff.* [Nurse 17 – RK]

Moreover, the training was supplemented by regular visits for support and monitoring:

> *Then we had regular visits from [the originator], often enough for us to deal with whatever issues we were having on the system.* [Nurse 2 – MM]

The training was simple and accommodated varying levels of skills:

> *Some people could not use computers, but it was made as basic as possible to include those that are not computer literate.* [Nurse 17 – RK]

However, some users' competency and reactions to the training were influenced by age:

> *For the young ones, it was easy for them. For the old ones, it was a problem because they wanted to understand what they were ticking as they were pressing.* [Data capturer - 1]

In response, the originators sought assistance from data capturers, acting as an immediate source of help:

> *We had person in each clinic who would be there all day long. So for the first day or two they would sit with them [older users] when they completed it, until they became comfortable with it.* [Originator 1]

Support and Feedback Channels

To supplement the training, the originators had different people involved to provide support to end users, including IT technicians:

> *We provided desktop support, we were the first line of support. My role firstly was on all applications and IT projects running within the district.* [IT Technician]

While data capturers were already involved, especially in the early stages, admin people also assisted with various tasks:

> *We also had three admin people, one for each clinic that assisted in the clinic to help people with the training, setting up the system and checking that the computers are all working.* [Originator 1]

The originators also established communication channels to receive feedback from users:

> *We had a little book for users to report issues and to add anything, and an E-tick admin person was there. I also got information from data capturers and I would also go and check on everybody and they would give me feedback. We would report back to them monthly, usually.* [Originator 1]

Perceived Benefits of System Use

End users reported several benefits of the system, with some sharing how it improved continuity of care:

> *At times you find that the client may have been seen previously but the file could not be found. But if the client's details were captured on the previous visit, you could see it in the E-tick. So it helped with continuation of care.* [Nurse 11 – AR]

For other users, such as clerks, this reduced patient waiting times:

> *It also reduced the waiting period for the patient, because the first thing that we do is to register the patient and create a folder on the E-tick system. It's easier to use than retrieving the manual files, searching the files in the cabinets. When you're using an E-tick, you just search on the system.* [Admin Clerk 8 – AR]

Facility managers also found operational benefits, such as quicker service delivery:

> *The benefits were that the patient consultation times were shortened. It was a little bit faster. That was the best advantage that I've seen from the E-tick.* [Operations Manager 18 – RK]

Some users shared that the system improved data quality and access to it:

> *It improved the reporting of data. We had very reliable, consistent, and accurate data, at all times of the day.* [Administrative officer 19 – RK]

For some, the system enabled the monitoring of the clinic's performance:

> *We are able to evaluate ourselves on the number of patients that we are seeing. When our stats are sent to the DHIS, they can see that we are really performing.* [Nurse 4 – MM]

Perceived Challenges of System Use

Users reported several challenges with using the system, including the simultaneous use of the system with the manual:

> *To be brutal, they [users] were against it at first. They did not understand why we're implementing extra work for them.* [Administrative officer 19 – RK]

For some participants, the early days before mastering the system were difficult:

> *If you're not used to it yet, it takes time to get used to anything, especially if you're overloaded with a lot of patients.* [Nurse 14 – MM]

In some cases, short staffing led nurses to do administrative work, as one nurse shared:

> *I think it was mostly shortage of staff, sometimes I had to enter a new patient into the E-tick as a nurse, which would waste time and to delay the queue. You'd end up having to turn some patients back. So it needs us to be well staffed.* [Nurse 12 – AR]

XSL•FO
RenderX

In response, the originators designated roles for receptionists, clerks, and data capturers as the first point of contact for patient registrations.

There were concerns about the hardware and infrastructure that already existed in the facilities: "The [DOH's] ICT equipment was very outdated. Some of the computers are so old and they haven't been updated." (Originator 1 – R). Some users had challenges with the network infrastructure:

> *Our network system was failing us a lot. You'd be prepared to start the day and notice that you have no network.* [Nurse 12 – AR]

In response to this challenge, a back capture function was introduced, which allowed information to be captured into the system at a later stage. In one site, hardware was frequently stolen:

> *First disadvantage was theft. I'd say more than more than 70% of the tablets disappeared. All the rooms that had extension cords, but in less than two weeks, all the rooms had no extension cords. They also stole the chargers.* [Administrative officer 19 – RK]

In one clinic, the piloting coincided with ongoing protests by nurses:

> *When we were trying to start the system, the nurses and others would be outside complaining about the conditions in the clinic [a protest organized by unions]. Most of the nurses were not working. There were other issues in the clinic. I think they saw the E-tick as another thing that was worth protesting about, because it increased their workload.* [Originator 1 – R]

Halt and Barriers to Scale Up and Institutionalization: Outer Setting Domain (2021)

Changing Developers

Despite its relative success in implementation, several complications affected the continued use and development of the system. One of the complications came when there was a change in the software development company:

> *Originally [funders] were working with [a software developing company], who were helping with developing district programs. They were taken over by [another company] so the people that worked on our system were taken off the project, and a new team took over the development.* [Originator 1 – R]

This affected further developments:

> *We needed to update the system to make sure it's fine. Then it got stuck in that development phase because of the new developers that we have.* [Originator 1 – R]

Some of the previous work was undone by the new developers:

> *There were a lot of upgrades to the system, such as integration with the DHIS. But they removed some of the functionalities that were working well in the process. We were never happy with the final products that we got from them.* [Originator 1 – R]

Funding Cuts

The change of developers brought higher costs:

> *They [funders] agreed to pay for the additional development, but the new developers came with a lot of red tape and were quite expensive. The funding got cut and they could only give us a small amount to continue with the development.* [Originator 1 – R]

Moreover, the funders were eventually withdrawn from operating in the health district:

> *They [funders] moved out of the district, because their funding got canceled completely. So what's happening with their funding will affect our funding.* [Originator 1 – R]

This had an impact on keeping the system operational:

> *So because it's not open source, it was built on the Microsoft platform and the cost to keep it running is high. It's also web based so no offline capability, and we need constantly running servers.* [Originator 2 – T]

Thus, the system needed new funders:

> *We're looking for partners to fund the service, license costs and the implementation in facilities. To date, we haven't found anyone, so it's been put to sleep.* [Originator 2 – T]

Provincial and District Support

The originators had buy-in from district officials, who were in support of the system:

> *I had meetings with my chief director, and my director, and they are still very keen. The clinics are still very keen… So the buy-in is there, even after two to three years, but the funding is not there.* [Originator 1 – R]

However, the provincial health office's priority was to develop a new system, as the department technician explained:

> *Currently the department is rolling out an HIS platform where all other applications will be layered under and integrated into.* [IT Technician]

He further explained how locally developed systems were not as prioritized:

> *There were some contrasting and opposing views. The system was started from scratch but the department in most cases doesn't want that. They want to go on the market and buy something on the shelf. I don't think approvals were going to be granted.* [IT Technician]

The participant further mentions how the IT staff are often not seen as essential to the role of delivering care:

> *Sometimes different services compete for resources. They will say it's essential when it's a clinic, a doctor*

XSL•FO
RenderX

> *or medication, and then we [IT personnel] come last.* [IT Technician]

The originators also expressed their frustration with navigating such terrain:

> *So this is where we are stuck now. I think what is important to me is how difficult it is to roll out a system within the Department of Health, in the politics, the corruption and the agendas of people. It makes the story very complicated because we developed it the bottom up, seeing the need, with the buy-in from the district, and from all the role players.* [Originator 1 – R]

Broader Context (Outer Setting Domain)

Senior managers and external stakeholders shared insights into the Department of Health's challenges in implementing EHRs in South Africa. One manager notes how implementation requires a joint and collaborative effort of various stakeholders:

> *I think it's a complex sociotechnical project to do which requires many different role players and expertise and costs, which needs high level support from the National Department of Health which has been lacking.* [NPO manager]

The provincial health departments hold most of the decision-making power in digital health spending:

> *The national office can come up with guidelines and frameworks and ask for reports but the actual spending on health information systems is done at provincial.* [NPO manager]

In this case, the provincial health department had decided to prioritize an off-the-shelf system:

> *There is a provincial initiative and anything new that comes in has to talk to this one, there should be interoperability…I saw it [E-tick], it works. I tried to support it but we didn't get provincial support from the CIO.* [Provincial manager]

However, NGOs have been supporting and implementing local efforts to build systems (such as E-tick) in health care facilities:

> *NGOs are doing better than the districts and the provincial health in terms of implementing efficient systems. Most efficient systems are systems that have been introduced by NGO's instead of our provincial department.* [Provincial IT technician]

Some participants raised a concern over political appointments in key decision-making positions:

> *I don't believe that we have the right people in government with the right industry experience. They are just given the title and suddenly, they now have to make decisions. I think it's very wrong and it sets them up for failure.* [NGO Technician]

A health department technician added:

> *Most of our activities are driven by politicians while our head of department has his own strategies. We get our mandate from politicians.* [DoH Technician]

As a result, some decisions are made with bias:

> *There are bureaucratic officials in Department of Health national, provincial and local. If they do not like you and your project, they will say you have to go through SETA [a parastatal] which is extraordinarily slow, not particularly technically competent, and staggeringly expensive.* [NPO manager]

Moreover, one academic shared their experience with the Department of Health's reluctance:

> *I think there's not sufficient trust on the part of Government certainly in my experience. They are not coming to partner with us. In fact, they're pushing us away. We only get close when we work with NGO's and so on. The Government definitely keeps us at arms-length.* [Health Academic]

Corruption and inefficiencies have also created barriers, with the tender system being one of the issues:

> *It [corruption] is part of the tender system in South Africa, unfortunately the tender system is open to abuse.* [Provincial health manager - IT]

Moreover, past corruption scandals have tainted the reputation of the Department of Health:

> *The perception is that you can't trust the National Department any longer to do anything. No one is going to give the National Department a big pot of money to run a tender until it can show that it's got systems and people in place who can do it without squandering the money.* [National health manager]

This mistrust has also led to a reluctance to work within the department:

> *Now people are reluctant to work for the department for several reasons. They fear being embroiled in controversy and putting their personal integrity at stake.* [National health manager]

Discussions

Principal Findings

The E-tick system, an innovation, was developed to address the issue of poor data quality stemming from errors in data collection, which were common with the use of paper-based registers. The implementation process involved an iterative co-design process with input from all involved individuals, including end users and stakeholders, to ensure users' needs were met and to streamline the data entry process while supporting scalability and integration with other systems. Despite the system's successful piloting and user adoption in the inner setting, the outer setting posed challenges in funding, change of developers, and lack of support from the provincial health government, leading to the implementation stalling. Using the CFIR, we explored the interaction of different elements, actors, and stakeholders and how they facilitated or impeded implementation. As such, we organize this discussion using CFIR domains, highlighting both facilitators and barriers.

XSL•FO
RenderX

Innovation

Poor data quality is a problem that commonly affects routine monitoring of health outcomes [34]. The E-tick system had a clear relative advantage over paper-based registers to improve data quality and reporting, as errors that frequently compromised data quality and routine reporting were minimized, and users perceived the system as more streamlined than paper-based manual registers. At a national scale, this aligns with South Africa's policies that promote the digitization of record keeping and the establishment of a national EHR [10,35], a crucial component for strategic purchasing and health monitoring. The E-tick's co-design process enhanced usability and fostered buy-in, which is critical in adoption [36], yet innovation alone was insufficient to ensure sustainability.

Individuals

At the level of individuals, the originators showed strong commitment by providing vision, technical expertise, and persistence in driving the implementation of the E-tick system. Leadership practices are known to impact staff motivation, especially when they take a participatory approach [37,38]. Their leadership was instrumental in mobilizing resources, persuading managers and funders to support the system's adoption, acting as champions along with data capturers. Research shows how champions are crucial in promoting technology adoption through building enthusiasm and providing peer support [39]. End users also improved confidence in using the system as a result, especially after undergoing training, which sustained motivation during the pilot. However, while the successful adoption of the E-tick was due to the contribution of many actors, including external stakeholders, individuals in the inner setting were more affected by decisions in the outer setting. This reflects a broader challenge in digital health implementation in South Africa, that for locally developed systems to succeed, appropriate actors must be in place to provide leadership, vision, and sustained support, within an enabling environment that fosters continuity and long-term success [37,40].

Inner Setting

Within the inner setting, several facilitators supported early implementation, such as the co-design process and extensive user training. The originators successfully engaged a wide range of stakeholders, including senior managers and funders, which was pivotal in overcoming initial financial and political barriers. Involving end users was also crucial in enhancing the system's usability and promoting buy-in, an important aspect when ensuring effective user adoption [41,42]. Moreover, users' recognition of the system's value in improving data quality reinforced their motivation to adopt the system. Studies in other low- to middle-income countries show that organizational commitment is a critical success factor to sustain user motivation during piloting phases [43]. However, the sustained use of the E-tick required stable infrastructure, which often posed challenges for many users in the form of interrupted internet connectivity and power cuts. This mirrors challenges reported in other LMICs, where infrastructural fragilities, such as poor internet connectivity and unstable power supply, are common challenges to EHR adoption [44]. Moreover, without dedicated budgets to overcome these challenges, such as the use of mobile internet devices and backup power solutions, this creates uncertainty about sustained use.

Implementation Process

The implementation process revealed a mix of strengths and gaps, which were closely linked to the role of individuals and the inner setting. A key strength was the iterative co-design approach, which ensured that the system was not only technically functional but also responsive to user needs and compatible with existing workflows. Participatory design and user engagement are widely recognized in implementation science as best practice, as they enhance user ownership, adaptability, and long-term adoption, especially as most implementation efforts fail due to user resistance [45,46]. Thus, involving both clinicians and managers at early stages of the implementation process helped to align the E-tick system with user realities, reducing resistance to change. However, this process was undermined by a lack of a long-term financing mechanism and failed provincial support, despite the demonstrated proof of concept at the pilot phase. Therefore, while the implementation process was well executed, the system lacked the institutional anchoring and support for long-term use, a critical success factor of digital health efforts [47].

Outer Setting

We found that the most significant challenges were encountered in the outer setting, particularly the withdrawal of financial support, the change of developers, and the lack of support from the provincial health government due to its lack of capacity. Studies show that one of the main challenges to the initiation of digital health initiatives, including EHRs in South Africa, has been the poor governance and lack of political will [48,49]. For instance, the appointment of people without the required skills and competence has led to a chain of events that affect institutions such as the Gauteng provincial health department [50]. As a result, corruption has eroded the public's trust in the government. These issues are not isolated but rather reflective of the entrenched political economy dynamics that routinely affect digital health innovations in South Africa. Political appointments, who are put in place because they are easily manipulated, often make decisions driven by political interests rather than professional judgment, leading to the political control of government institutions and their spending [51]. As such, patronage networks often produce politically aligned rather than skilled appointments. This leaves room for corruption, irregular spending, fraud, and poor oversight to mitigate them, with procurement processes being vulnerable to perverse incentives, with contracts awarded to less qualified but politically connected vendors. Although efforts have been made to uncover large-scale corruption in South Africa, the necessary mechanisms have not yet been put in place to deal with the challenges [52,53]. Perverse incentives undermine sustainability as officials face pressure to launch new initiatives instead of sustaining existing ones to ensure full expenditure of budgets.

The administrative fragmentation can be seen as a product of South Africa's federal system, which means provinces can develop their own health information systems (bottom-up) or acquire them through separate procurement processes

XSL•FO
RenderX

(top-down) [8]. In this case, despite the provincial government's preference for a top-down approach by opting for an off-the-shelf system over the E-tick, they were unable to implement the former. High-income countries such as the United Kingdom, the United States, and Australia have taken top-down, bottom-up, and middle-out approaches, respectively, with varying outcomes [54]. Bottom-up approaches often build on existing systems, such as the E-tick, using interoperability standards to integrate them across facilities. In contrast, top-down approaches replace local systems with a centralized EHR, but this can be too complex, limiting flexibility and local adaptability, as in the case of the United Kingdom [55]. Therefore, our analysis shows that a single centralized model is not necessarily more effective, as lessons from these experiences, including Australia, suggest that a middle-out approach is more effective, as this blends both by offering central guidance while allowing for local systems to gradually align with national plans [56].

Implementing EHRs requires significant investment, vision, robust management systems, and strong oversight to sustain them, making effective leadership essential for success. Strong leadership plays an important role in guiding decision making, mobilizing the right expertise, and establishing mechanisms to prevent corruption, which increases the likelihood of successful implementation, particularly for large-scale EHRs [57]. Middle-income countries like South Africa and China have the capacity to finance and support EHR adoption, but such efforts can be undermined by corruption and poor governance [49,58]. In some cases, poor leadership and governance stand as significant barriers to achieving universal health coverage and strengthening health systems [59].

Implications for Policy and Practice

Our findings highlight several implications for policy and practice. One of them is the strengthening of accountability in health systems through transparent procurement systems and independent oversight to neutralize the effects of corruption and political patronage. In such cases, procurement frameworks could include pilot-to-scale pathways, where bottom-up innovations such as the E-tick could be formally assessed against national priorities and considered for integration with provincial and national systems. These steps could create a more enabling environment for similar innovations to scale sustainably. Moreover, while the E-tick system was locally hosted, it also incorporated cloud functionality, aligning with the cloud-based EHR architectures promoted in both the NDHS and the national data and cloud policy of South Africa [10,60]. Such policies can be leveraged to mitigate barriers such as reliance on facility servers or hardware failures, challenges already observed with the E-tick, which hold important lessons for similar middle-income country contexts.

Our findings also carry implications for digital health equity, a concept that examines how structural inequities shape the successes and challenges of digital health interventions [61]. In South Africa's dual health system, where private-sector facilities often have better infrastructure and resources than the public sector, grassroots innovations like E-tick are left to face compounded challenges, especially when implemented in low-resource contexts [62]. The stalled scale-up reflects not only outer system or structural barriers by the government but also the broader inequities in digital infrastructure, institutional support, and resourcing across the country's health system [63].

Limitations

Our study incorporates perspectives from a diverse range of stakeholders, including higher-level managers, decision makers, academics, and end users from recipient facilities. This diversity helped in capturing nuanced perspectives from different positions within the system and in closing information gaps through triangulation. A limitation of our study is that data collection from the implementation team, especially clinicians, occurred over a year after the system had halted. As a result, some participants struggled to accurately recall past events, while others had moved to different jobs by the time of data collection. As a result, formal member checking with participants was not possible due to staff turnover and the discontinuation of the E-tick project. However, we validated emerging findings through iterative review with coauthors who included experts in South African health systems and originators who led the implementation from the beginning and had contextual expertise.

Conclusions

In conclusion, the E-tick system is a valuable innovation that was developed from the ground up with user input. While the system showed promise, its long-term sustainability was undermined by external factors such as funding cuts and poor support, political appointments, and corruption, which led to the unwillingness of provincial officials to support local initiatives such as the E-tick. Such bureaucratic inefficiencies also affected the capacity to move forward with another system. This study demonstrates that without alignment to broader factors such as governance, corruption, and skilled leadership, innovative systems such as the E-tick will struggle to be implemented.

Acknowledgments

We would like to thank the study participants for generously sharing their time and experiences. We also acknowledge the support of the implementation team and the provincial and district health authorities for facilitating access to study sites.

XSL•FO
RenderX

Funding

This work is part of a PhD study funded by the South African National Research Foundation (NRF) through the SARChI programme for health systems and policy research at the Centre for Health Policy, School of Public Health, University of the Witwatersrand. Scholarship number: PMDS2205046516. The funders were not involved in writing this paper.

Conflicts of Interest

None declared.

Multimedia Appendix 1
Summary of findings by implementation stage, alignment with Consolidated Framework for Implementation Research (CFIR) domains, applicable constructs, thematic findings, and illustrative quotes.
[DOCX File, 22 KB - medinform_v14i1e73831_app1.docx]

References

1. Uslu A, Stausberg J. Value of the electronic medical record for hospital care: update from the literature. J Med Internet Res 2021 Dec 23;23(12):e26323. [doi: 10.2196/26323] [Medline: 34941544]
2. Kumar M, Mostafa J. Electronic health records for better health in the lower- and middle-income countries. LHT 2020 Mar 10;38(4):751-767. [doi: 10.1108/LHT-09-2019-0179]
3. Mehl G, Labrique A. Prioritizing integrated mHealth strategies for universal health coverage. Science 2014 Sep 12;345(6202):1284-1287. [doi: 10.1126/science.1258926] [Medline: 25214614]
4. Global Strategy on Digital Health 2020-2025, 1st edition: World Health Organization; 2021.
5. Kumar M, Mostafa J. Research evidence on strategies enabling integration of electronic health records in the health care systems of low- and middle-income countries: a literature review. Int J Health Plann Manage 2019 Apr;34(2):e1016-e1025. [doi: 10.1002/hpm.2754] [Medline: 30762907]
6. Wilson D, Sheikh A, Görgens M, Ward K, Bank W. Technology and universal health coverage: examining the role of digital health. J Glob Health 2021;11:16006. [doi: 10.7189/jogh.11.16006] [Medline: 34912559]
7. Fragidis LL, Chatzoglou PD. Implementation of a nationwide electronic health record (EHR). Int J Health Care Qual Assur 2018 Mar 12;31(2):116-130. [doi: 10.1108/IJHCQA-09-2016-0136] [Medline: 29504871]
8. Eason K, Dent M, Waterson P, Tutt D, Thornett A. Bottom-up and middle-out approaches to electronic patient information systems: a focus on healthcare pathways. J Innov Health Inform 2013 Dec 20;20(1):51-56. [doi: 10.14236/jhi.v20i1.47]
9. Robertson A, Cresswell K, Takian A, et al. Implementation and adoption of nationwide electronic health records in secondary care in England: qualitative analysis of interim results from a prospective national evaluation. BMJ 2010 Sep 1;341(sep01 3):c4564. [doi: 10.1136/bmj.c4564] [Medline: 20813822]
10. National Department of Health South Africa. National digital health strategy for South Africa 2019–2024. : Pretoria South Africa; 2019.
11. Horwood C, Luthuli S, Mapumulo S, et al. Challenges of using e-health technologies to support clinical care in rural Africa: a longitudinal mixed methods study exploring primary health care nurses' experiences of using an electronic clinical decision support system (CDSS) in South Africa. BMC Health Serv Res 2023 Jan 13;23(1):30. [doi: 10.1186/s12913-022-09001-2] [Medline: 36639801]
12. Masana N, Muriithi GM. Adoption of an integrated cloud-based electronic medical record system at public healthcare facilities in free-state, South Africa. Presented at: 2019 Conference on Information Communications Technology and Society (ICTAS); Mar 6-8, 2019; Durban, South Africa p. 1-6. [doi: 10.1109/ICTAS.2019.8703606]
13. Hassim A, Heywood M, Honermann B. The National Health Act 61 of 2003: a guide. : Siber Ink; 2008.
14. Chuma K, Sibiya P. Digital health ecosystem framework to address fragmentation of the health system in South Africa. AJNM 2022 Nov 10. [doi: 10.25159/2520-5293/11547]
15. Fourie D, Malan C. Public procurement in the South African economy: addressing the systemic issues. Sustainability 2020 Oct 20;12(20):8692. [doi: 10.3390/su12208692]
16. Garrib A, Stoops N, McKenzie A, et al. An evaluation of the district health information system in rural South Africa. S Afr Med J 2008 Jul;98(7):549-552. [Medline: 18785397]
17. English R, Masilela T, Barron P, Schönfeldt A. Health information systems in South Africa. In: Padarath A, English R, editors. South African Health Review 2011: Health Systems Trust; 2011:81-90.
18. Oyebola OG, Debra J, Thubelihle M. PMTCT data management and reporting during the transition phase of implementing the rationalised registers in Amathole District, Eastern Cape Province, South Africa. Int J Environ Res Public Health 2022 Nov 28;19(23):15855. [doi: 10.3390/ijerph192315855] [Medline: 36497931]
19. National department of health. national health insurance for south africa: towards universal health coverage. Gov Gaz. 2015 URL: https://www.gov.za/sites/default/files/gcis_document/201512/39506gon1230.pdf [accessed 2023-08-12]

XSL•FO
RenderX

20. Wright G, O'Mahony D, Cilliers L. Electronic health information systems for public health care in South Africa: a review of current operational systems. J Health Inform Afr 2017 Nov 5;4(1). [doi: 10.12856/JHIA-2017-v4-i1-164]
21. Olu O, Muneene D, Bataringaya JE, et al. How can digital health technologies contribute to sustainable attainment of universal health coverage in Africa? a perspective. Front Public Health 2019;7:341. [doi: 10.3389/fpubh.2019.00341] [Medline: 31803706]
22. Rispel LC, de Jager P, Fonn S. Exploring corruption in the South African health sector. Health Policy Plan 2016 Mar;31(2):239-249. [doi: 10.1093/heapol/czv047] [Medline: 26104821]
23. Zali M. Health department suspends officials over Digital Vibes contract. Mail Guard. 2021. URL: https://mg.co.za/news/2021-09-30-health-department-suspends-officials-over-digital-vibes-contract/ [accessed 2024-11-11]
24. Ndaba B. Babita Deokaran killed for exposing R1bn corruption at Tembisa Hospital, says Panyaza Lesufi. 2022. URL: https://www.iol.co.za/pretoria-news/news/babita-deokaran-killed-for-exposing-r1bn-corruption-at-tembisa-hospital-says-panyaza-lesufi-fbdb09a1-6e0e-4006-bbb3-a90f17b22279 [accessed 2024-11-11]
25. Adjekum A, Blasimme A, Vayena E. Elements of trust in digital health systems: scoping review. J Med Internet Res 2018 Dec 13;20(12):e11254. [doi: 10.2196/11254] [Medline: 30545807]
26. Marwaha JS, Landman AB, Brat GA, Dunn T, Gordon WJ. Deploying digital health tools within large, complex health systems: key considerations for adoption and implementation. NPJ Digit Med 2022 Jan 27;5(1):13. [doi: 10.1038/s41746-022-00557-1] [Medline: 35087160]
27. McAlearney AS, Walker DM, Livaudais-Toman J, Parides M, Bickell NA. Challenges of implementation and implementation research: learning from an intervention study designed to improve tumor registry reporting. SAGE Open Med 2016;4:2050312116666215. [doi: 10.1177/2050312116666215] [Medline: 27635248]
28. Damschroder LJ, Aron DC, Keith RE, Kirsh SR, Alexander JA, Lowery JC. Fostering implementation of health services research findings into practice: a consolidated framework for advancing implementation science. Implementation Sci 2009 Dec;4(1):50. [doi: 10.1186/1748-5908-4-50]
29. Kirk MA, Kelley C, Yankey N, Birken SA, Abadie B, Damschroder L. A systematic review of the use of the consolidated framework for implementation research. Implementation Sci 2015 Dec;11(1):72. [doi: 10.1186/s13012-016-0437-z]
30. Keith RE, Crosson JC, O'Malley AS, Cromp D, Taylor EF. Using the consolidated framework for implementation research (CFIR) to produce actionable findings: a rapid-cycle evaluation approach to improving implementation. Implement Sci 2017 Feb 10;12(1):15. [doi: 10.1186/s13012-017-0550-7] [Medline: 28187747]
31. Damschroder LJ, Reardon CM, Widerquist MAO, Lowery J. The updated consolidated framework for implementation research based on user feedback. Implement Sci 2022 Oct 29;17(1):75. [doi: 10.1186/s13012-022-01245-0] [Medline: 36309746]
32. Damschroder LJ, Lowery JC. Evaluation of a large-scale weight management program using the consolidated framework for implementation research (CFIR). Implement Sci 2013 May 10;8(1):51. [doi: 10.1186/1748-5908-8-51] [Medline: 23663819]
33. Braun V, Clarke V. Using thematic analysis in psychology. Qual Res Psychol 2006 Jan;3(2):77-101. [doi: 10.1191/1478088706qp063oa]
34. Radebe L, Haeri Mazanderani A, Sherman GG. Evaluating patient data quality in South Africa's national health laboratory service data warehouse, 2017-2020: implications for monitoring child health programmes. BMC Public Health 2022 Jun 29;22(1):1266. [doi: 10.1186/s12889-022-13508-y] [Medline: 35768861]
35. Kante M, Ndayizigamiye P. Internet of medical things, policies and geriatrics: an analysis of the national digital health strategy for South Africa 2019–2024 from the policy triangle framework perspective. Scientific African 2021 Jul;12:e00759. [doi: 10.1016/j.sciaf.2021.e00759]
36. Duffy A, Boroumandzad N, Sherman AL, Christie G, Riadi I, Moreno S. Examining challenges to co-design digital health interventions with end users: systematic review. J Med Internet Res 2025 Mar 14;27:e50178. [doi: 10.2196/50178] [Medline: 40085834]
37. Gilson L, Agyepong IA. Strengthening health system leadership for better governance: what does it take? Health Policy Plan 2018 Jul 1;33(suppl_2):ii1-ii4. [doi: 10.1093/heapol/czy052] [Medline: 30053034]
38. Open Mindsets: Participatory Leadership for Health: World Health Organization; 2016. URL: https://apps.who.int/iris/bitstream/handle/10665/251458/9789241511360-eng.pdf
39. Pettersen S, Eide H, Berg A. The role of champions in the implementation of technology in healthcare services: a systematic mixed studies review. BMC Health Serv Res 2024 Apr 11;24(1):456. [doi: 10.1186/s12913-024-10867-7] [Medline: 38605304]
40. Katurura MC, Cilliers L. Electronic health record system in the public health care sector of South Africa: a systematic literature review. Afr J Prim Health Care Fam Med 2018 Nov 20;10(1):e1-e8. [doi: 10.4102/phcfm.v10i1.1746] [Medline: 30456963]
41. Cresswell K, Morrison Z, Crowe S, Robertson A, Sheikh A. Anything but engaged: user involvement in the context of a national electronic health record implementation. Inform Prim Care 2011;19(4):191-206. [doi: 10.14236/jhi.v19i4.814] [Medline: 22828574]

XSL•FO
RenderX

42. Hartzler A, McCarty CA, Rasmussen LV, et al. Stakeholder engagement: a key component of integrating genomic information into electronic health records. Genet Med 2013 Oct;15(10):792-801. [doi: 10.1038/gim.2013.127] [Medline: 24030437]
43. Xiong S, Lu H, Peoples N, et al. Digital health interventions for non-communicable disease management in primary health care in low-and middle-income countries. NPJ Digit Med 2023 Feb 1;6(1):12. [doi: 10.1038/s41746-023-00764-4] [Medline: 36725977]
44. Hui CY, Abdulla A, Ahmed Z, et al. Mapping national information and communication technology (ICT) infrastructure to the requirements of potential digital health interventions in low- and middle-income countries. J Glob Health 2022 Dec 29;12:04094. [doi: 10.7189/jogh.12.04094] [Medline: 36579436]
45. Zharima C, Mhlanga S, Abdulla S, Goudge J, Griffiths F. What engagement strategies are useful in facilitating the implementation of electronic health records in health care settings? a rapid review of qualitative evidence synthesis using the normalization process theory. Digit Health 2024;10:20552076241291286. [doi: 10.1177/20552076241291286] [Medline: 39497787]
46. Voorheis P, Petch J, Pham Q, Kuluski K. Maximizing the value of patient and public involvement in the digital health co-design process: a qualitative descriptive study with design leaders and patient-public partners. In: König LM, editor. PLOS Digit Health 2023 Oct;2(10):e0000213. [doi: 10.1371/journal.pdig.0000213] [Medline: 37878566]
47. Bostan S, Johnson OA, Jaspersen LJ, Randell R. Contextual barriers to implementing open-source electronic health record systems for low- and lower-middle-income countries: scoping review. J Med Internet Res 2024 Aug 1;26:e45242. [doi: 10.2196/45242] [Medline: 39088815]
48. Rheeder R, Department of Moral Development of Society, Faculty of Theology, North-West University, Potchefstroom, South Africa. Corruption in the public health sector in South Africa: a global bioethical perspective. SAJBL 2021 Dec 31;14(3):79-83. [doi: 10.7196/SAJBL.2021.v14i3.693]
49. Zharima C, Griffiths F, Goudge J. Exploring the barriers and facilitators to implementing electronic health records in a middle-income country: a qualitative study from South Africa. Front Digit Health 2023;5:1207602. [doi: 10.3389/fdgth.2023.1207602] [Medline: 37600481]
50. Fana TE, Goudge J. Managing under austerity: a qualitative study of management-union relations during attempts to cut labour costs in three South African public hospitals. J Health Organ Manag 2024 Mar 5;38(9):89-105. [doi: 10.1108/JHOM-11-2022-0324] [Medline: 38448233]
51. Swanepoel PCF. The slippery slope to state capture: cadre deployment as an enabler of corruption and a contributor to blurred party-state lines. Law Democr Dev 2022;25(1):1-23. [doi: 10.17159/2077-4907/2021/ldd.v25.15]
52. Mcebisi J. South Africa needs these five fundamentals to change course and start rebuilding. Daily Maverick. 2022. URL: https://www.dailymaverick.co.za/article/2022-10-21-south-africa-needs-these-five-fundamentals-to-change-course-and-start-rebuilding/ [accessed 2024-06-18]
53. Kulati P. South Africans are sick to death of persistent corruption by politicians. Daily Maverick. 2025. URL: https://www.dailymaverick.co.za/opinionista/2025-07-21-south-africans-sick-to-death-of-persistent-corruption-by-politicians/ [accessed 2025-07-28]
54. Coiera E. Building a national health IT system from the middle out. J Am Med Inform Assoc 2009;16(3):271-273. [doi: 10.1197/jamia.M3183] [Medline: 19407078]
55. Cresswell KM, Worth A, Sheikh A. Comparative case study investigating sociotechnical processes of change in the context of a national electronic health record implementation. Health Informatics J 2012 Dec;18(4):251-270. [doi: 10.1177/1460458212445399] [Medline: 23257056]
56. Boudreau KJ. Let a Thousand Flowers Bloom? An Early Look at Large Numbers of Software App Developers and Patterns of Innovation. Organization Science 2012 Oct;23(5):1409-1427. [doi: 10.1287/orsc.1110.0678]
57. Alzghaibi HA, Hutchings HA. Exploring facilitators of the implementation of electronic health records in Saudi Arabia. BMC Med Inform Decis Mak 2022 Dec 7;22(1):321. [doi: 10.1186/s12911-022-02072-5] [Medline: 36476224]
58. Fu H, Lai Y, Li Y, Zhu Y, Yip W. Understanding medical corruption in China: a mixed-methods study. Health Policy Plan 2023 Apr 11;38(4):496-508. [doi: 10.1093/heapol/czad015] [Medline: 36798965]
59. Kodali PB. Achieving universal health coverage in low- and middle-income countries: challenges for policy post-pandemic and beyond. Risk Manag Healthc Policy 2023;16:607-621. [doi: 10.2147/RMHP.S366759] [Medline: 37050920]
60. National policy on data and cloud (notice 2533 of 2024, government gazette no50741). Government of South Africa.: Republic of South Africa: Department of Communications and Digital Technologies; 2024. URL: https://www.gov.za/sites/default/files/gcis_document/202406/50741gen2533.pdf [accessed 2024-09-21]
61. Gordon T, Booysen F, Mbonigaba J. Socio-economic inequalities in the multiple dimensions of access to healthcare: the case of South Africa. BMC Public Health 2020 Mar 4;20(1):289. [doi: 10.1186/s12889-020-8368-7] [Medline: 32131787]
62. Pillay Y, Motsoaledi PA. Digital health in South Africa: innovating to improve health. BMJ Glob Health 2018;3(Suppl 2):e000722. [doi: 10.1136/bmjgh-2018-000722] [Medline: 29713513]
63. Kim KK, Backonja U. Digital health equity frameworks and key concepts: a scoping review. J Am Med Inform Assoc 2025 May 1;32(5):932-944. [doi: 10.1093/jamia/ocaf017] [Medline: 39936843]

XSL•FO
RenderX

Abbreviations

CFIR: Consolidated Framework for Implementation Research
DHIS: District Health Information Software
E-tick: electronic tick register
EHR: electronic health record
HPRS: Health Patient Registration System
NDHS: National Digital Health Strategy

Edited by A Benis; submitted 13.Mar.2025; peer-reviewed by K Adegoke, Y Chu, Z Zhang; revised version received 29.Oct.2025; accepted 16.Nov.2025; published 12.Jan.2026.

Please cite as:
Zharima C, Griffiths F, Goudge J
Exploring Factors Associated With the Stalled Implementation of a Ground-Up Electronic Health Record System in South Africa: Qualitative Insights From the E-Tick Case Study Using the Consolidated Framework for Implementation Research (CFIR)
JMIR Med Inform 2026;14:e73831
URL: https://medinform.jmir.org/2026/1/e73831
doi:10.2196/73831

© Campion Zharima, Frances Griffiths, Jane Goudge. Originally published in JMIR Medical Informatics (https://medinform.jmir.org), 12.Jan.2026. This is an open-access article distributed under the terms of the Creative Commons Attribution License (https://creativecommons.org/licenses/by/4.0/), which permits unrestricted use, distribution, and reproduction in any medium, provided the original work, first published in JMIR Medical Informatics, is properly cited. The complete bibliographic information, a link to the original publication on https://medinform.jmir.org/, as well as this copyright and license information must be included.

XSL•FO
RenderX

Original Paper

Development of Quality Indicators for the Correct Use of Electronic Medical Records in Primary Care: Modified Delphi Study

Rico Paridaens[1], MD; Steve Van den Bulck[1,2], MD, PhD; Michel De Jonghe[3], MD; Benjamin Fauquert[4], MD; Liesbeth Meel[5], MSc; Willem Raat[1], MD, PhD; Bert Vaes[1], MD, PhD

[1]Academisch Centrum voor Huisartsgeneeskunde, Katholieke Universiteit Leuven (KU Leuven), Leuven, Flanders, Belgium

[2]Research Group Healthcare and Ethics, Hasselt University, Hasselt, Belgium

[3]Centre Académique de Médecine Générale, Université catholique de Louvain, Leuven, Belgium

[4]Unité de Recherche en Soins Primaires, Vrije Universiteit Brussel, Brussels, Belgium

[5]Belgian Centre for Evidence-Based Medicine (CEBAM), Leuven, Belgium

Corresponding Author:
Rico Paridaens, MD
Academisch Centrum voor Huisartsgeneeskunde
Katholieke Universiteit Leuven (KU Leuven)
Kapucijnenvoer 7
Block G, A and N/H, box 7001
Leuven, Flanders, 3000
Belgium
Phone: 32 16324010
Email: rico.paridaens@kuleuven.be

Abstract

Background: When used correctly, electronic medical records (EMRs) can support clinical decision-making, provide information for research, facilitate coordination of care, reduce medical errors, and generate patient health summaries. Studies have reported large differences in the quality of EMR data.

Objective: Our study aimed to develop an evidence-based set of electronically extractable quality indicators (QIs) approved by expert consensus to assess the good use of EMRs by general practitioners (GPs) from a medical perspective.

Methods: The RAND-modified Delphi method was used in this study. The TRIP and MEDLINE databases were searched, and a selection of recommendations was filtered using the specific, measurable, assignable, realistic, and time-bound principles. The panel comprised 12 GPs and 6 EMR developers. The selected recommendations were transformed into QIs as percentages.

Results: A combined list of 20 indicators and 30 recommendations was created from 9 guidelines and 4 review articles. After the consensus round, 20 (100%) indicators and 20 (67%) recommendations were approved by the panel. All 20 recommendations were transformed into QIs. Most (16, 40%) QIs evaluated the completeness and adequacy of the problem list.

Conclusions: This study provided a set of 40 EMR-extractable QIs for the correct use of EMRs in primary care. These QIs can be used to map the completeness of EMRs by setting up an audit and feedback system, and to develop specific (computer-based) training for GPs.

(JMIR Med Inform 2026;14:e80057) doi:10.2196/80057

KEYWORDS

electronic medical records; primary care; quality assessment; Delphi method; electronic audit and feedback

Introduction

With the advancement of digital technologies, electronic medical records (EMRs) have become the preferred method for recording, storing, and retrieving medical information [1]. The National Alliance for Health Information Technology defined the EMR as “an electronic record of health-related information on an individual that can be created, gathered, managed and consulted by authorised clinicians and staff within one health care organisation” [2,3]. Several studies have shown that the correct use of EMRs may improve the quality and efficiency of care and reduce mortality [4-6]. When used correctly, EMRs can support clinical decision-making (eg, monitoring medication safety) [7-9], facilitate care coordination, reduce medical errors,

XSL•FO
RenderX

and provide information for research [1,10]. EMR data can also be used to generate patient health summaries (PHSs). The PHS is a minimum set of clinically relevant data that can be transferred to other health care workers to support the continuity of care and deliver safe and high-quality care to patients [11,12].

Unfortunately, an observational analysis conducted by the Vlaams Agentschap Zorg en Gezondheid, based on approximately 2000 general practitioners' (GPs) consultations during weekends and holidays in Belgium between 2019 and 2020, revealed that only 32% of patients had a PHS. Several studies have shown that the amount of encoded data registered in EMRs is low (eg, the completeness of height and weight is <76%) [13-16]. Hamade et al [17] suggested that targeting EMR data quality or the use of EMR functions may significantly improve EMR use.

However, there remains a gap in knowledge regarding how to improve the correct use of EMRs [17]. Recently, Ngugi et al [18] developed and validated a set of indicators for the use of EMRs, focusing on the implementation of the EMR, in low- and middle-income countries. There are some guidelines on the good use of EMRs, but none are up to date [19,20]. Appropriate EMR training programs for health care workers and students can improve the use of EMRs; however, an exhaustive list of learning points is lacking [2,21]. Electronic audit and feedback (eA&F) can also be used to improve the correct use of the EMR and, more particularly, the quality of the data stored in the EMR [22]. Ivers et al [23] defined eA&F as "an electronic summary of the clinical performance of health care over a specified period of time aimed at providing information to health professionals to allow them to assess and adjust their performance." To this end, a validated set of quality indicators (QIs) is used. QIs are measurable items that refer to the structures, processes, and outcomes of care [24]. An evidence-based list of QIs, approved by expert consensus, could help develop appropriate training programs and eA&F interventions to improve EMR use [17,25,26]. This study aimed to develop an evidence-based set of electronically extractable QIs approved by expert consensus to assess the good use of EMRs by GPs from a medical perspective.

Methods

Study Design

The RAND-modified Delphi method was used to develop QIs for the use of EMRs from January 2024 to December 2024 based on the method used by Van den Bulck et al [27-29]. The process included the following: (1) development of a questionnaire based on recommendations and existing QIs from evidence-based guidelines and (2) rating procedure by an expert panel in 3 rounds, namely individual written questionnaire, online consensus meeting, and final appraisal.

Selection of Recommendations and Existing QIs

The TRIP database and MEDLINE were searched for guidelines and indicator sets using the following search terms: "Electronic medical records" AND ("Primary Health Care" OR "Primary Care" OR "General Practice") AND ("Standard of Care" OR "guideline" OR "recommendation" OR "quality indicator" OR "quality of health care" OR "quality of care"). The search was also extended to Google Scholar (accessed on April 2, 2024). The sources were selected by the primary researcher using the criteria specified in Textbox 1. Sources were not filtered based on the quality of the methodology because of the limited methodological information in any of the sources found in the first search. An exhaustive list of all indicators and recommendations relevant to EMR quality was compiled. For inclusion, indicators and recommendations were filtered using the specific, measurable, acceptable, realistic, and time-bound (SMART) principle [27-29]. A QI is defined by Grypdonck et al as "a measurable tool to assess the quality of care, including outcome-, process- and patient-oriented indicators" [30]. For recommendations, the following definition provided by the World Health Organization was used: "Recommendations are statements designed to help end-users make informed decisions on whether, when and how to undertake specific actions such as clinical interventions, diagnostic tests or public health measures, to achieve the best possible individual or collective health outcomes" [31]. Screening was performed by 2 independent researchers: a GP (primary researcher) and a methodologist. If there was a difference in the results for an indicator or recommendation between the 2 researchers, they discussed it until a consensus was reached. All remaining items (indicators and recommendations) were then categorized into topics according to the organization of the PHS in Belgium as explained by Domus Medica [19], and comparable with categories defined by Jabaaij et al [13] in the EMR scan for general practitioners: completeness and adequacy of the problem list, encoded registration in the EMR, completeness and actuality of medication list, risk factors and drug monitoring, patient identification and contact information, vaccination status, and patients' choices.

XSL•FO
RenderX

Textbox 1. Selection criteria used to filter articles in the literature.

Inclusion criteria

- Language: English, Dutch, or French
- Evaluation level: microlevel (evaluation at the patient level)
- Source age: indicator sets—any age; recommendations—maximum 10 years
- Target population: primary care providers

Exclusion criteria

- Language: other than English, Dutch, or French
- Evaluation level: mesolevel or macrolevel (regional, national, or other)
- Source age: recommendations published more than 10 years ago
- Target population: hospital physicians

Panel Selection

GPs and EMR developers were invited to participate in the panel via email. Using a purposive sampling technique, priority was given to representing all involved parties at the regional (Flanders, Wallonia, and Brussels) and occupational levels (solo GPs, GPs in group practices, programmers, and academic personnel). The final panel consisted of 18 participants: 11 (61%) Flemish-speaking participants and 7 (39%) French-speaking participants. There were 12 GPs (recently retired: n=1, 6%; worked in a community health center: n=1, 6%; had an individual practice: n=2, 11%; and worked in a group practice: n=8, 44%) and 6 (33%) EMR developers from different EMRs. They were provided with information about the aims and methodology of this study.

Written Questionnaire Round

Completion

An online LimeSurvey questionnaire was presented to a multidisciplinary expert panel (from August 2024 to November 2024) [32]. Each participant was asked to score each item for their capability to measure the quality of EMR use in primary care on a 9-point Likert scale (1=lowest score; 9=highest score). They were asked to base their assessment on the extractability of the indicator or recommendation from the EMR and its possible positive impact on the quality of care. Panel members could also label an item as “not assessable.” At the end of each topic, they were asked to give the top 5 (prioritization) of the items. If a topic did not contain enough items to create the top 5, participants were asked to order half of the indicators in the top X. Finally, all participants could write remarks and add new indicators.

Analysis

The results of the online survey were analyzed using a Node.js (OpenJS Foundation) script to subdivide each item into 3 categories: high, uncertain, or low potential as a QI [33]. The script generated a report for each participant with their responses, a general overview of the calculated parameters (Table 1), and a category based on these parameters (Table 2).

Table 1. Defined parameters to score each quality indicator and recommendation [28].

Parameter	Calculation
Total number of responses	N responses
Likert score	
For each score, the total number of responses	N responses for score
Median Likert score	Median Likert score of all responses
Highest ratings (%)	N responses with a score ≥7 divided by the total number of responses
Prioritization (top %)	Sum of the individual top X scores (eg, first place=score 3, second place=score 2, third place=score 1, and items not ranked in the top 3=score 0) divided by the maximum possible score (N responses × highest possible top score)

XSL•FO
RenderX

Table 2. Selection criteria for indicators and recommendations [28].

Criterion	Selection[a]	Discussion[a]	No selection[a]
Likert score: median	≥7	Any	Any
Likert score: distribution	≥70% with score ≥7	≥30% with score <3	Other
Prioritization (top %)	≥20%	≥1%	<1%

[a]Indicators and recommendations must fulfill all criteria, not only some, to be categorized as either "selection," "discussion," or "no selection."

Consensus Meeting Round

Each panel member received an individual feedback report 2 weeks before the consensus meeting. It also included new recommendations and comments. The report contained all items with a color code representing their potential to reach a consensus (Multimedia Appendix 1).

An online consensus meeting was held using Microsoft Teams [34]. To improve the efficiency of the consensus meeting, focus was given to the items categorized as "uncertain," together with the newly added indicators proposed by the panelists. Items with high potential were automatically selected for the final selection unless panel members requested a decision-making discussion. Items with low potential were excluded from the final selection unless the panel members requested deliberation.

All accepted indicators and recommendations were adjusted to the conclusions of the consensus meeting and conformed to the SMART criteria [27-29]. The recommendations were transformed into QIs as percentages. The final report was sent to the panel members for final acceptance in Dutch and French. The final indicator set was translated into English by the researchers.

Ethical Considerations

This study was approved on June 25, 2024, by the Social and Societal Ethics Committee of KU Leuven (G-2024-8020-R2(AMD)). The project was also vetted and approved by KU Leuven's Privacy and Ethics platform in view of the principles and obligations laid down in the General Data Protection Regulation of the European Parliament and the Council of 27 April 2016 [35]. Participants were asked to digitally sign an informed consent form before participation. All data were pseudonymized after the written questionnaire round using a unique identifier. Personal information was separated from other research data in a second file with password protection. The personal data was used to provide the participants the feedback report, to invite them for the consensus meeting round, and to approve the final report. All personal information was deleted after the study was finished. No compensation was provided to the participants.

Results

Extraction of QI and Recommendations

A total of 4 review articles listed QIs for the use of EMRs, containing 27 QIs [13,15,36-38]. Nine guidelines contained 53 QIs and 125 recommendations [11,19,20,39-42]. Where possible, duplicate items were removed, and indicators were linked to similar recommendations in the guidelines. This resulted in a combined list of 20 QIs and 30 recommendations (Figure 1 [11,13,15,19,20,36-42]; Multimedia Appendices 2-4).

Figure 1. Overview of the recommendation and indicator extraction. *Unique: repetitive recommendations were removed. ADEPD: NHG-Richtlijn Adequate dossiervorming met het elektronisch patiëntdossier; CIHI: Canadian Institute for Health Information; DM: Domus Medica; HASP: NHG Richtlijn Informatie-uitwisseling tussen huisarts en medisch specialist; HIQA: Health Information and Quality Authority; NCQA: National Committee for Quality Assurance; NHS: National Health Service; SSMG: Société Scientifique de Médecine Générale [11,14,16,20,21,38-44].

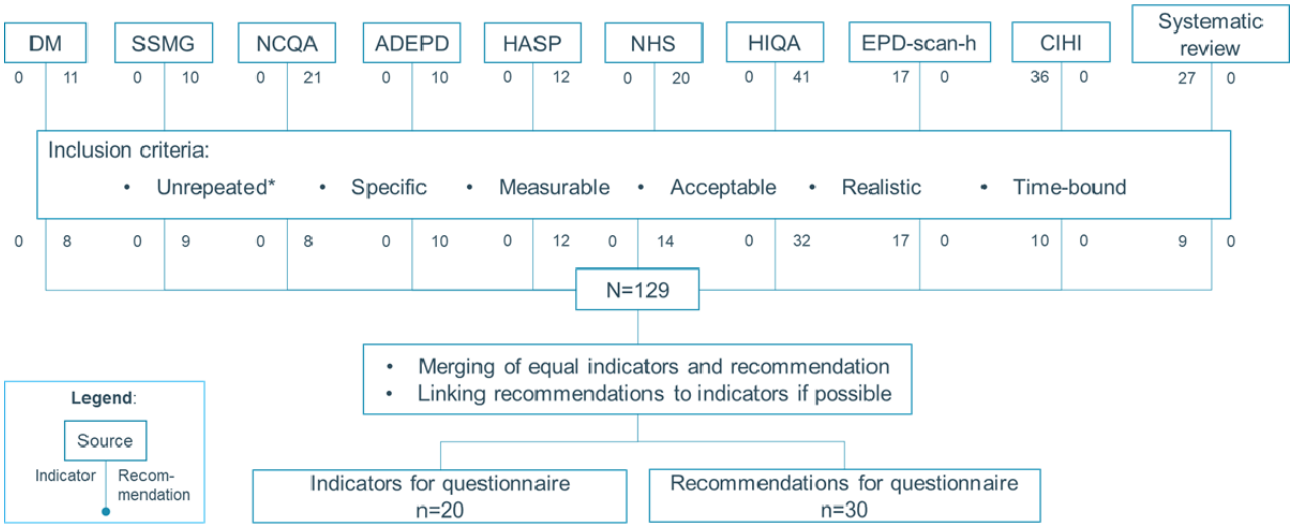

XSL•FO
RenderX

Questionnaire Round

All panel members (18/18, 100%) completed the questionnaire. On the basis of these categories, out of 50 items, 21 (42%) were selected, 27 (54%) required further discussion, and 2 (4%) were excluded.

Consensus Round

Of the 18 panel members, 13 (72%) were present for the consensus meeting—9 (50%) GPs and 4 (22%) EMR developers—8 (44%) of whom were Flemish speaking and 5 (28%) French speaking. In the panel round, none of the preselected indicators (n=7) or recommendations (n=14) were discarded. Of the 10 indicators labeled as "discussion," 7 (70%) were selected, and 1 (10%) indicator was further divided into 7 specific indicators (Multimedia Appendix 1; indicator 3). Of the 17 recommendations labeled as "discussion," 6 (35%) were selected. This resulted in a list of 20 indicators and 20 recommendations (Multimedia Appendix 1). During the consensus meeting, some items that were not yet extractable were included because the panel members felt that their clinical importance should prompt EMR providers to adapt their software.

Final Evaluation

The 20 recommendations were transformed into QIs and added to the 20 other QIs, resulting in 16 (40%) QIs regarding the completeness and adequacy of the problem list, 4 (10%) QIs regarding encoded registration in the EMR, 3 (8%) QIs regarding the completeness and actuality of the medication list, 6 (15%) QIs regarding risk factors and drug monitoring, 4 (10%) QIs regarding patient identification and contact information, 3 (8%) QIs regarding vaccination status, and 4 (10%) QIs regarding patient choices (Textbox 2; Multimedia Appendix 5). All panel members present in the consensus meeting (13/13, 100%) approved the final report.

XSL•FO
RenderX

Textbox 2. Quality indicators for the good use of electronic medical records (EMRs) in primary care.

Topic 1: completeness and adequacy of the problem list

1.1 The mean of active problem items listed on a patient's problem list

1.2 Percentage of items on the problem list that are linked to an encoded diagnosis

1.3 Percentage of patients with medication for thyroid disease in their medication list with an encoded diagnosis of thyroid disease on the problem list

1.4 Percentage of patients with medication for epilepsy in their medication list with an encoded diagnosis of epilepsy on the problem list

1.5 Percentage of patients with medication for Parkinson disease in their medication list with an encoded diagnosis of Parkinson disease on the problem list

1.6 Percentage of patients with medication for depression in their medication list with an encoded diagnosis of depression on the problem list

1.7 Percentage of patients with medication for cardiovascular disease in their medication list with an encoded diagnosis of cardiovascular disease on the problem list

1.8 Percentage of patients with medication for asthma or chronic obstructive pulmonary disease in their medication list with an encoded diagnosis of asthma or chronic obstructive pulmonary disease on the problem list

1.9 Percentage of patients with medication for diabetes in their medication list with an encoded diagnosis of diabetes on the problem list

1.10 Percentage of encoded items in the problem list with an additional description or comment

1.11 Percentage of encoded items in the problem list for which the estimated or actual date of onset has been registered

1.12 Percentage of inactive items on the problem list for which the estimated or actual date the condition was resolved has been registered

1.13 Percentage of surgeries and other procedures that have been registered as an encoded item

1.14 Percentage of surgeries and other procedures in the patient history that have been linked to the related episode of care

1.15 Percentage of surgeries and other procedures in the patient's history with an additional description or comment

1.16 Percentage of surgeries and other procedures in the patient summary for which the date and/or time on which the procedure was or is intended to be performed is registered

Topic 2: encoded registration in the EMR

2.1 The mean number of subcontacts created per contact during the observation period

2.2 Percentage of subcontacts during the observation period connected with an episode of care

2.3 Percentage of subcontacts (registered as consultation, home visit, or teleconsultation) with a subjective, objective, evaluation, and planning item

2.4 The number of patients with a global medical record in the practice with changes in the status of tasks (procedures or actions) over the total number of patients with a global medical record in the practice

Topic 3: completeness and actuality of the medication list

3.1 Percentage of medications on the medication list labeled as *active* that are no longer active

3.2 Percentage of active medications on the medication list that are linked to a health condition on the problem list

3.3 Percentage of active medications on the medication list for which the dosage and treatment regimen are complete

Topic 4: risk factors and drug monitoring

4.1 Percentage of patients with at least 1 registration for a drug allergy or intolerance

4.2 Percentage of patients with a registration for a risk factor; risk factors include clinical information that is imperative to know so that the life or health of the patient is not threatened, for example, prophylaxis for adrenal crisis (Addison disease), endocarditis, bleeding disorders, endoprosthesis, patients who are immunocompromised, (functional) asplenia, thrombosis, or particularly resistant microorganisms

4.3 Percentage of patients with at least 1 encoded registration for a physical examination (weight, height, blood pressure, and pulse)

4.4 Percentage of patients with at least 1 registration of an item for social history

4.5 Percentage of patients aged 12 years and older for whom there is at least 1 notation concerning the use of cigarettes, alcohol, and substances

4.6 Percentage of patients with at least 1 registration of an item for family medical history

Topic 5: patient identification and contact information

5.1 Percentage of patients with a registration for hospital preference

5.2 Percentage of patients with at least 1 registration of contact information for a contact person, caregiver, or person designated as representative

5.3 Percentage of patients with at least 1 registration of a health care professional in their care team

XSL•FO
RenderX

5.4 Percentage of patients with at least 1 registration for address, email, employer, home and work phone, marital status, registration status on patient platform (eg, Helena [43]), or cohousing people and animals

Topic 6: vaccination status

6.1 Percentage of patients aged 7 years and older who have a registration for all the recommended primary childhood vaccines

6.2 Percentage of patients aged 65 years and older who have a registration for a yearly influenza vaccine

6.3 Percentage of vaccinations for which the date the vaccination was administered is registered

Topic 7: patient choices

7.1 Percentage of patients with a registration of treatment preferences: euthanasia request or refusal for intubation, resuscitation, organ donation, vaccination, or blood transfusion

7.2 Percentage of patients with at least 1 contact with a subjective, objective, evaluation, or planning item linked to an encoded diagnosis regarding treatment preferences or end-of-life care

7.3 Percentage of patients with at least 1 registration of a goal for personalized care (goal-oriented care)

7.4 Percentage of patients with at least 1 registration regarding preferences for preventive health care

Discussion

Principal Findings and Comparison With Prior Work

This study used the RAND-modified Delphi method to validate a set of 40 QIs for the correct use of EMRs by GPs based on the indicators and recommendations found in the literature. These indicators are (potentially) EMR extractable and evaluate key aspects of EMR use by GPs: completeness and adequacy of the problem list, encoded registration, completeness and actuality of the medication list, risk factors and drug monitoring, patient identification and contact information, vaccination status, and patient choices. Using the SMART principle, we ensured that the QIs could be evaluated in clinical practice [27-29,44-46].

Previously, Jabaaij et al [38] developed the EMR scan for general practitioners in the Netherlands to evaluate EMR use. However, the method they used to define QIs was unclear. Ngugi et al [18] developed and validated a set of indicators for the use of EMRs in low- and middle-income countries. Their QIs mostly evaluated the general use of the EMRs (eg, indicator 7, "% of required data elements contained in EHRs"). Our study focuses on how data are registered and encoded in EMRs, focusing on which data are registered [18]. Other indicator sets were either outdated (aged >20 years) [36], focused on clinical performance instead of use of the EMR [15], or evaluated EMR use on the mesolevel or macrolevel instead of the microlevel [37]. Hamade et al [17] noted that while there are many studies on the implementation of EMR, there is a scarcity of studies on its use.

Most of the selected indicators evaluated the completeness and adequacy of the problem list. The problem list provides important information for decision-making [47]. Our indicators are primarily process indicators because they focus on the process of EMR registration (ie, use). However, these QIs cannot be directly linked to patient outcomes. Process indicators are useful for quality assessment. They are more sensitive to differences in quality than outcome measures and are easier to interpret [48]. Recent literature shows an interest in eA&F [22,29], dashboard interface features to support reflection on practice ("barometers") [27-29], and computer-based decision support in primary care [49]. The quality of data in EMRs impacts the effectiveness of these systems. Several studies have shown that improving data quality may improve the quality and efficiency of care and reduce mortality [4-6]. Unfortunately, data show that physicians spend approximately two-thirds of their work time interacting with EMRs in their offices. This administrative burden negatively impacts clinicians' wellness, leading to an increased chance of burnout. Recently, the interest in the use of artificial intelligence for analyzing data, identifying hidden information, identifying risks, and providing suggestions for diagnosis has increased rapidly. This can greatly facilitate the process for GPs to easily improve data quality without spending more time entering data in the EMR and less time interacting with patients [50]. GPs should not need to adapt their working habits to the capabilities of their medical software; rather, EMRs should be adapted to the needs of GPs to facilitate the correct registration of data [51]. An important lever to encourage EMR developers to align their software more closely with clinicians' data entry and retrieval needs lies in regulatory frameworks, such as homologation. This is a certification procedure to evaluate the mandatory standards and certification requirements that EMRs must fulfill to be approved for use within the health care system [52]. By embedding QIs derived through expert consensus, such as those developed in this study, into these frameworks, regulators can create explicit performance benchmarks that EMRs must meet. This alignment incentivizes developers to design functionalities that facilitate accurate, complete, and efficient data capture and reporting by clinicians [50].

Strengths and Limitations

Our panel included members working in all parts of Belgium and in all types of practices, giving it broad support. Because our panel included health professionals and EMR developers, we were able to define clinically relevant indicators that considered the technical requirements for extractability. During the consensus meeting, the EMR developers emphasized that these indicators could possibly stimulate GPs to use the features they have already developed more extensively. We are convinced that their opinion was a valuable addition to the panel. EMR developers were the most capable of assessing whether a QI could be automatically extracted from the EHR data. However, we cannot exclude a potential bias caused by their

XSL•FO
RenderX

inclusion (eg, the ease or cost of addressing a recommended QI outweighing the importance of making that QI available from a public health perspective). The scarcity of literature on the initial set of QIs and recommendations is a double-edged sword for our study. On the one hand, it limits the strengths of the initial set of QIs and recommendations because none of our sources used a systematic approach to evaluate the validity of their QIs and recommendations, had a well-explained methodology [13,15,36-38], or could be evaluated using the Appraisal of Guidelines for Research and Evaluation II method [11,19,20,39-42]. On the other hand, this allowed us to conduct a broad and general search on the topic, which could increase its universal applicability. There are many differences between countries in terms of how and which data are registered [11,19,20,39-42]. We attempted to generalize the QIs and recommendations as much as possible. However, adaptation to the local context is necessary. Another important limitation is that some indicators are not currently extractable. However, as mentioned earlier, these indicators reflect aspects of clinical practice that are important enough to warrant adaptation of EMRs to include this information.

Future Research Directions

This set of indicators is important for future research on EMR use. Developing a list of QIs is the first step in implementing a strategy and realizing a quality loop. The next essential step is to conduct practice testing for operational validity [29]. These results can be used to create an eA&F system [22,23]. This set of QIs can also be used to develop specific (computer based) training for GPs based on a set of learning goals [2]. It should be noted that our QIs can be used for the correct use of EMRs but cannot be used to quantify the quality of care provided by GPs. Further research is necessary to evaluate whether the correct use of the EMR, as proposed in this set of QIs, also affects the quality of care provided to patients and its possible effect on the data in the PHS.

Conclusions

This study provided a set of 40 EMR-extractable QIs for the correct use of EMRs in primary care based on international guidelines and approved by GPs and EMR developers. These QIs can be used as a framework to measure and improve the quality and completeness of EMRs in primary care.

Acknowledgments

The authors would like to thank all the participating panel members for the many hours they spent in this study.

Funding

This study was conducted by UZ Leuven and KU Leuven at the request of Rijksinstituut voor ziekte- en invaliditeitsverzekering–Institut national d’assurance maladie-invalidité and funded by Rijksinstituut voor ziekte- en invaliditeitsverzekering–Institut national d’assurance maladie-invalidité as part of a national project to improve medical care in Belgium.

Data Availability

The datasets generated or analyzed during this study are available from the corresponding author on reasonable request.

Authors' Contributions

RP conducted the literature search and organized each step of the Delphi procedure as part of his PhD project. LM assisted during each step of the Delphi procedure. SVdB oversaw the whole process and helped to draft the manuscript. BV and WR supervised the entire process from the beginning to the end and helped draft the manuscript. MDJ and BF were part of the panel during the Delphi procedure and helped draft the final manuscript. All the authors have read and approved the final manuscript.

Conflicts of Interest

None declared.

Multimedia Appendix 1
Example of the feedback report for panel members.
[PDF File (Adobe PDF File), 693 KB - medinform_v14i1e80057_app1.pdf]

Multimedia Appendix 2
Online questionnaire - Dutch version.
[PDF File (Adobe PDF File), 1776 KB - medinform_v14i1e80057_app2.pdf]

Multimedia Appendix 3
Online questionnaire - French version.
[PDF File (Adobe PDF File), 1722 KB - medinform_v14i1e80057_app3.pdf]

XSL•FO
RenderX

Multimedia Appendix 4
Online questionnaire - English version (automated generated translation by DeepL Translator; https://www.deepl.com/nl/translator).
[PDF File (Adobe PDF File), 2142 KB - medinform_v14i1e80057_app4.pdf]

Multimedia Appendix 5
Final indicator set.
[PDF File (Adobe PDF File), 182 KB - medinform_v14i1e80057_app5.pdf]

References

1. Hillestad R, Bigelow J, Bower A, Girosi F, Meili R, Scoville R, et al. Can electronic medical record systems transform health care? Potential health benefits, savings, and costs. Health Aff (Millwood) 2005;24(5):1103-1117. [doi: 10.1377/hlthaff.24.5.1103] [Medline: 16162551]
2. Samadbeik M, Fatehi F, Braunstein M, Barry B, Saremian M, Kalhor F, et al. Education and training on electronic medical records (EMRs) for health care professionals and students: a scoping review. Int J Med Inform 2020 Oct;142:104238. [doi: 10.1016/j.ijmedinf.2020.104238] [Medline: 32828034]
3. Defining key health information technology terms. Alliance. 2008. URL: https://tigerstandards.pbworks.com/f/HITTermsFinalReport.pdf [accessed 2025-01-25]
4. Zhang Y, Yu P, Shen J. The benefits of introducing electronic health records in residential aged care facilities: a multiple case study. Int J Med Inform 2012 Oct;81(10):690-704. [doi: 10.1016/j.ijmedinf.2012.05.013] [Medline: 22749424]
5. Chaudhry B, Wang J, Wu S, Maglione M, Mojica W, Roth E, et al. Systematic review: impact of health information technology on quality, efficiency, and costs of medical care. Ann Intern Med 2006 May 16;144(10):742-752 [FREE Full text] [doi: 10.7326/0003-4819-144-10-200605160-00125] [Medline: 16702590]
6. Bogale TN, Derseh L, Abraham L, Willems H, Metzger J, Abere B, et al. Effect of electronic records on mortality among patients in hospital and primary healthcare settings: a systematic review and meta-analyses. Front Digit Health 2024 Jun 26;6:1377826 [FREE Full text] [doi: 10.3389/fdgth.2024.1377826] [Medline: 38988733]
7. Kortteisto T, Raitanen J, Komulainen J, Kunnamo I, Mäkelä M, Rissanen P, et al. Patient-specific computer-based decision support in primary healthcare--a randomized trial. Implement Sci 2014 Jan 20;9:15 [FREE Full text] [doi: 10.1186/1748-5908-9-15] [Medline: 24444113]
8. Upshur RE, Tracy S. Chronicity and complexity: is what's good for the diseases always good for the patients? Can Fam Physician 2008 Dec;54(12):1655-1658 [FREE Full text] [Medline: 19074692]
9. Hasan S, Padman R. Analyzing the effect of data quality on the accuracy of clinical decision support systems: a computer simulation approach. AMIA Annu Symp Proc 2006;2006:324-328 [FREE Full text] [Medline: 17238356]
10. Wasserman RC. Electronic medical records (EMRs), epidemiology, and epistemology: reflections on EMRs and future pediatric clinical research. Acad Pediatr 2011;11(4):280-287 [FREE Full text] [doi: 10.1016/j.acap.2011.02.007] [Medline: 21622040]
11. National standard on information requirements for a national electronic patient summary. Health Information and Quality Authority. 2018 Dec. URL: https://www.hiqa.ie/sites/default/files/2019-01/PatientSummary_InfoReqs.pdf [accessed 2024-03-11]
12. Mathioudakis A, Rousalova I, Gagnat AA, Saad N, Hardavella G. How to keep good clinical records. Breathe (Sheff) 2016 Dec;12(4):369-373 [FREE Full text] [doi: 10.1183/20734735.018016] [Medline: 28210323]
13. Jabaaij L, Verheij R, Njoo K, van den Hoogen H, Tiersma W, Levelink H. Het meten van de kwaliteit van de registratie in elektronische patiënten dossiers van huisartsen met de EPD-scan-h. NIVEL. 2008. URL: https://www.nivel.nl/nl/publicatie/het-meten-van-de-kwaliteit-van-de-registratie-elektronische-patienten-dossiers-van [accessed 2025-04-23]
14. Terry AL, Stewart M, Cejic S, Marshall JN, de Lusignan S, Chesworth BM, et al. A basic model for assessing primary health care electronic medical record data quality. BMC Med Inform Decis Mak 2019 Feb 12;19(1):30 [FREE Full text] [doi: 10.1186/s12911-019-0740-0] [Medline: 30755205]
15. Nemeth LS, Ornstein SM, Jenkins RG, Wessell AM, Nietert PJ. Implementing and evaluating electronic standing orders in primary care practice: a PPRNet study. J Am Board Fam Med 2012;25(5):594-604 [FREE Full text] [doi: 10.3122/jabfm.2012.05.110214] [Medline: 22956695]
16. De Clercq E, Van Casteren V, Jonckheer P, Burggraeve P, Lafontaine MF. Electronic patient record data as proxy of GPs' thoughts. Stud Health Technol Inform 2008;141:103-110. [Medline: 18953130]
17. Hamade N, Terry A, Malvankar-Mehta M. Interventions to improve the use of EMRs in primary health care: a systematic review and meta-analysis. BMJ Health Care Inform 2019 May;26(1) [FREE Full text] [doi: 10.1136/bmjhci-2019-000023] [Medline: 31142493]
18. Ngugi P, Babic A, Kariuki J, Santas X, Naanyu V, Were MC. Development of standard indicators to assess use of electronic health record systems implemented in low-and medium-income countries. PLoS One 2021 Jan 11;16(1):e0244917 [FREE Full text] [doi: 10.1371/journal.pone.0244917] [Medline: 33428656]

XSL•FO
RenderX

19. Verdonck P, Strobbe J, Steenackers J, Van Royen J, De Naeyer P, Govaerts F, et al. Het Elektronisch Medisch Dossier: aanbeveling voor goede medische praktijkvoerin. Huisarts Nu 2004;33(2):58-70 [FREE Full text]
20. Organisation de la pratique. Société Scientifique de Médecine Générale (SSMG). URL: https://www.ssmg.be/organisation-pratique/ [accessed 2024-02-01]
21. Rajaram A, Hickey Z, Patel N, Newbigging J, Wolfrom B. Training medical students and residents in the use of electronic health records: a systematic review of the literature. J Am Med Inform Assoc 2020 Jan 01;27(1):175-180 [FREE Full text] [doi: 10.1093/jamia/ocz178] [Medline: 31592531]
22. Van Den Bulck S, Spitaels D, Vaes B, Goderis G, Hermens R, Vankrunkelsven P. The effect of electronic audits and feedback in primary care and factors that contribute to their effectiveness: a systematic review. Int J Qual Health Care 2020 Dec 15;32(10):708-720. [doi: 10.1093/intqhc/mzaa128] [Medline: 33057648]
23. Ivers NM, Sales A, Colquhoun H, Michie S, Foy R, Francis JJ, et al. No more 'business as usual' with audit and feedback interventions: towards an agenda for a reinvigorated intervention. Implement Sci 2014 Jan 17;9:14 [FREE Full text] [doi: 10.1186/1748-5908-9-14] [Medline: 24438584]
24. Kötter T, Blozik E, Scherer M. Methods for the guideline-based development of quality indicators--a systematic review. Implement Sci 2012 Mar 21;7(1):21 [FREE Full text] [doi: 10.1186/1748-5908-7-21] [Medline: 22436067]
25. Mottaghy FM, Hertel F, Beheshti M. Will we successfully avoid the garbage in garbage out problem in imaging data mining? An overview on current concepts and future directions in molecular imaging. Methods 2021 Apr;188:1-3. [doi: 10.1016/j.ymeth.2021.02.011] [Medline: 33592236]
26. Kim Y, Huang J, Emery S. Garbage in, garbage out: data collection, quality assessment and reporting standards for social media data use in health research, infodemiology and digital disease detection. J Med Internet Res 2016 Feb 26;18(2):e41 [FREE Full text] [doi: 10.2196/jmir.4738] [Medline: 26920122]
27. Dewaele S, Van den Bulck S, Gerne L, Vaes B. Development of primary care quality indicators for chronic obstructive pulmonary disease using a Delphi-derived method. NPJ Prim Care Respir Med 2022 Mar 18;32(1):12 [FREE Full text] [doi: 10.1038/s41533-022-00276-w] [Medline: 35304476]
28. Van den Bulck SA, Vankrunkelsven P, Goderis G, Van Pottelbergh G, Swerts J, Panis K, et al. Developing quality indicators for chronic kidney disease in primary care, extractable from the electronic medical record. A rand-modified Delphi method. BMC Nephrol 2020 May 05;21(1):161 [FREE Full text] [doi: 10.1186/s12882-020-01788-8] [Medline: 32370742]
29. Van den Bulck SA, Vankrunkelsven P, Goderis G, Broekx L, Dreesen K, Ruijten L, et al. Development of quality indicators for type 2 diabetes, extractable from the electronic health record of the general physician. A rand-modified Delphi method. Prim Care Diabetes 2020 Feb;14(1):75-84. [doi: 10.1016/j.pcd.2019.05.002] [Medline: 31204263]
30. Grypdonck L, Aertgeerts B, Luyten F, Wollersheim H, Bellemans J, Peers K, et al. Development of quality indicators for an integrated approach of knee osteoarthritis. J Rheumatol 2014 Jun 15;41(6):1155-1162. [doi: 10.3899/jrheum.130680] [Medline: 24737907]
31. WHO guidelines. World Health Organization. URL: https://www.who.int/publications/who-guidelines [accessed 2025-06-26]
32. LimeSurvey - free online survey tool. LimeSurvey. URL: https://www.limesurvey.org/ [accessed 2025-04-23]
33. Node.js - run JavaScript everywhere. OpenJS Foundation. URL: https://nodejs.org/en [accessed 2024-04-23]
34. Microsoft 365 Apps for enterprise. Microsoft. URL: https://www.microsoft.com/en-in/microsoft-365/enterprise/microsoft-365-apps-for-enterprise-product [accessed 2025-04-23]
35. General data protection regulation (GDPR). European Union. URL: https://eur-lex.europa.eu/legal-content/EN/TXT/?uri=legissum:310401_2 [accessed 2025-04-23]
36. De Lusignan S, Stephens PN, Adal N, Majeed A. Does feedback improve the quality of computerized medical records in primary care? J Am Med Inform Assoc 2002;9(4):395-401 [FREE Full text] [doi: 10.1197/jamia.m1023] [Medline: 12087120]
37. Pan-Canadian primary health care indicator - update report. Canadian Institute for Health Information. 2012. URL: https://publications.gc.ca/site/eng/444237/publication.html [accessed 2024-10-29]
38. Jabaaij L, Njoo K, Visscher S, van den Hoogen H, Levelink H, Verheij R. Verbeter uw verslaglegging, gebruik de EPD-scan-h. HUWE 2009;52:240-246. [doi: 10.1007/bf03085615]
39. Guidelines for medical record documentation. National Committee for Quality Assurance. 2018. URL: https://wpcdn.ncqa.org/www-prod/wp-content/uploads/2018/07/20180110_Guidelines_Medical_Record_Documentation.pdf [accessed 2024-02-24]
40. Summary care record. National Health Service England. URL: https://digital.nhs.uk/services/summary-care-records-scr [accessed 2024-02-01]
41. NHG-Richtlijn Adequate dossiervorming met het elektronisch patiëntendossier (ADEPD). Nederlands Huisartsen Genootschap. URL: https://www.nhg.org/praktijkvoering/informatisering/richtlijn-adequate-dossiervorming-epd/ [accessed 2024-10-29]
42. Richtlijn Informatie-uitwisseling tussen huisarts en medisch specialist (Richtlijn HASP). Nederlands Huisartsen Genootschap. 2017. URL: https://www.nhg.org/wp-content/uploads/2022/10/Richtlijn-Gegevensuitwisseling-Huisarts-en-Specialist-HASP.pdf [accessed 2024-10-29]
43. Helena voor patiënten. Helena. URL: https://nl-info.helena.care/helena-voor-patienten [accessed 2025-04-23]

XSL•FO
RenderX

44. Tichelaar J, Uil den SH, Antonini NF, van Agtmael MA, de Vries TP, Richir MC. A 'SMART' way to determine treatment goals in pharmacotherapy education. Br J Clin Pharmacol 2016 Jul 07;82(1):280-284 [FREE Full text] [doi: 10.1111/bcp.12919] [Medline: 26914983]
45. Smets M, Smeets M, Van den Bulck S, Janssens S, Aertgeerts B, Vaes B. Defining quality indicators for heart failure in general practice. Acta Cardiol 2019 Aug 27;74(4):291-298. [doi: 10.1080/00015385.2018.1492659] [Medline: 30261830]
46. Doran GT. There's a SMART way to write management's goals and objectives. J Manag Rev 1981;70:35-36 [FREE Full text]
47. Summerton N. The medical history as a diagnostic technology. Br J Gen Pract 2008;58(549):273-276. [doi: 10.3399/bjgp08x279779]
48. GBD 2017 Disease and Injury Incidence and Prevalence Collaborators. Global, regional, and national incidence, prevalence, and years lived with disability for 354 diseases and injuries for 195 countries and territories, 1990-2017: a systematic analysis for the Global Burden of Disease Study 2017. Lancet 2018 Nov 10;392(10159):1789-1858 [FREE Full text] [doi: 10.1016/S0140-6736(18)32279-7] [Medline: 30496104]
49. Donnelly C, Janssen A, Vinod S, Stone E, Harnett P, Shaw T. A systematic review of electronic medical record driven quality measurement and feedback systems. Int J Environ Res Public Health 2022 Dec 23;20(1):200 [FREE Full text] [doi: 10.3390/ijerph20010200] [Medline: 36612522]
50. Bednorz A, Mak JK, Jylhävä J, Religa D. Use of electronic medical records (EMR) in gerontology: benefits, considerations and a promising future. Clin Interv Aging 2023;18:2171-2183 [FREE Full text] [doi: 10.2147/CIA.S400887] [Medline: 38152074]
51. Wirth D, Senn O, Burgstaller JM, Djalali S, Muheim L, Rohrbasser A, et al. Acceptability of components for a mandatory quality improvement framework: a survey among Swiss general practitioners. Health Serv Insights 2025 Jun 21;18:11786329251346828 [FREE Full text] [doi: 10.1177/11786329251346828] [Medline: 40546342]
52. Elektronisch Medisch Dossier of EMD. Domus Medica. URL: https://www.domusmedica.be/expertisedomein/ict/het-elektronisch-medisch-dossier-emd [accessed 2025-11-06]

Abbreviations

eA&F: electronic audit and feedback
EMR: electronic medical record
GP: general practitioner
PHS: patient health summary
QI: quality indicator
SMART: specific, measurable, assignable, realistic, and time-bound

Edited by A Benis; submitted 03.Jul.2025; peer-reviewed by L Agrawal, M Jones; comments to author 23.Oct.2025; revised version received 12.Dec.2025; accepted 17.Dec.2025; published 19.Jan.2026.

Please cite as:
Paridaens R, Van den Bulck S, De Jonghe M, Fauquert B, Meel L, Raat W, Vaes B
Development of Quality Indicators for the Correct Use of Electronic Medical Records in Primary Care: Modified Delphi Study
JMIR Med Inform 2026;14:e80057
URL: https://medinform.jmir.org/2026/1/e80057
doi:10.2196/80057
PMID:

©Rico Paridaens, Steve Van den Bulck, Michel De Jonghe, Benjamin Fauquert, Liesbeth Meel, Willem Raat, Bert Vaes. Originally published in JMIR Medical Informatics (https://medinform.jmir.org), 19.Jan.2026. This is an open-access article distributed under the terms of the Creative Commons Attribution License (https://creativecommons.org/licenses/by/4.0/), which permits unrestricted use, distribution, and reproduction in any medium, provided the original work, first published in JMIR Medical Informatics, is properly cited. The complete bibliographic information, a link to the original publication on https://medinform.jmir.org/, as well as this copyright and license information must be included.

XSL•FO
RenderX

Original Paper

Multi-Institutional Drug Use Patterns in Hospitalized Older Patients: Retrospective Cross-Sectional Study

Chung Chun Lee[1*], MS; Grace Juyun Kim[2*], PharmD, PhD; Suhyun Kim[3,4], MS; Jee Young Hong[5], MD, PhD; Won Min Hwang[6], MD, PhD; Jong-Yeup Kim[1,7], MD, PhD; Kye Hwa Lee[8,9], MD, PhD; Kwangsoo Kim[3,10], PhD; Mingyu Kang[11], MD, PhD; Ju Han Kim[12], MD, PhD; Suehyun Lee[13], PhD

[1]Department of Biomedical Informatics, College of Medicine, Konyang University, Daejeon, Republic of Korea

[2]Asan Institute for Life Sciences, Asan Medical Center, Seoul, Republic of Korea

[3]Department of Transdisciplinary Medicine, Institute of Convergence Medicine with Innovative Technology, Seoul National University Hospital, Seoul, Republic of Korea

[4]Department of Clinical Medical Sciences, College of Medicine, Seoul National University, Seoul, Republic of Korea

[5]Department of Preventive Medicine, College of Medicine, Jeonbuk National University, Jeonju, Republic of Korea

[6]Division of Nephrology, Department of Internal Medicine, College of Medicine, Konyang University, Daejeon, Republic of Korea

[7]Healthcare Data Science Center, Konyang University Hospital, Daejeon, Republic of Korea

[8]Department of Information Medicine, Asan Medical Center, Seoul, Republic of Korea

[9]Department of Biomedical Informatics, College of Medicine, University of Ulsan, Ulsan, Republic of Korea

[10]Department of Medicine, College of Medicine, Seoul National University, Seoul, Republic of Korea

[11]Department of Internal Medicine, College of Medicine, Chungbuk National University, Cheongju, Republic of Korea

[12]Seoul National University Biomedical Informatics (SNUBI), Division of Biomedical Informatics, College of Medicine, Seoul National University, Seoul, Republic of Korea

[13]College of IT Convergence, Gachon University, Seongnam-si, Gyeonggi-do, Republic of Korea

[*]these authors contributed equally

Corresponding Author:
Suehyun Lee, PhD
College of IT Convergence
Gachon University
1342 Seongnamdaero
Sujeong-gu
Seongnam-si, Gyeonggi-do, 13120
Republic of Korea
Phone: 82 31 750 5333
Email: leesh@gachon.ac.kr

Abstract

Background: A rapidly aging population led to an increase in the number of patients with chronic diseases and polypharmacy. Although investigations on the appropriate number of drugs for older patients have been conducted, there is a shortage of studies on polypharmacy criteria in older inpatients from multiple institutions.

Objective: The aim of this study was to examine the patterns of polypharmacy and determine the criteria for the number of drugs defining polypharmacy in the geriatric inpatient population.

Methods: Electronic health records of 4 medical institutions for patients aged 65 years and older hospitalized between January 1, 2012, and December 31, 2020, were analyzed for the study. The maximum number of drugs prescribed was obtained for each patient and, along with a literature review, was used to determine the appropriate polypharmacy level for our population.

Results: We suggest a 4-level polypharmacy category system consisting of nonpolypharmacy, polypharmacy, major polypharmacy, and excessive polypharmacy based on a review of international guidelines and polypharmacy literature. Application of this system to our study population showed that the major polypharmacy category (use of 10-19 concurrent drugs) was an appropriate threshold for polypharmacy in hospitalized patients versus the traditional threshold of 5 or more concurrent drugs. The tendency of our study population to have a higher disease and drug count supports this threshold. Frequently prescribed therapeutic subgroups in this category were antibacterials for systemic use, anesthetics, and cardiac therapy.

XSL•FO
RenderX

Conclusions: This study proposes a polypharmacy categorization system for older inpatients, which differs from the common definition of the concomitant prescription of 5 or more drugs. The older population tends to have severe conditions including those requiring major surgeries; therefore, a drug count corresponding to the definition of major polypharmacy is appropriate.

(JMIR Med Inform 2026;14:e78353) doi:10.2196/78353

KEYWORDS

polypharmacy; older patients; medication; electronic health record; Common Data Model

Introduction

South Korea is reported to have the highest rate of aging among the Organisation for Economic Cooperation and Development countries, where 8.2 of 51.8 (15.7%) million people in 2020 were aged 65 years or older [1]. The prevalence of chronic diseases in this population was found to be 8481 of 10,097 (84%) individuals aged 65 years or older, making it highly likely that the cost of health care is increasing [2]. This requires close review and consideration of effective measures to prevent and treat chronic diseases and adverse events from polypharmacy.

With the increase in lifespan and aging population in South Korea, patients commonly have multiple concomitant diseases. Consequently, patients visit 1 or more health care institutions and are prescribed medications that expose them to polypharmacy [3]. In 2006, Intercontinental Marketing Statistics Korea found that an average of 4.16 medications were prescribed per health care appointment, which was the highest among the 10 countries studied [2]. A study using the South Korean health claims data of 2016-2019 reported that in 2016, a total of 1548 of 47,631 (3.3%) individuals aged 45 years or older experienced polypharmacy, defined as the use of 10 or more medications for at least 60 days, and this rate increased gradually up to 2019, where 2012 of 48,249 (4.2%) individuals aged 45 years or older were on polypharmacy [4]. To ensure that older adult patients receive appropriate drug therapy, the Korean Health Insurance Review & Assessment Service launched the Drug Utilization Review program. This provides real-time assessment of inappropriate patient drug therapy, including the use of duplicative drug ingredients or drugs of different therapeutic classes, inappropriate drugs for older adults, or drugs not to be used in combination [5].

Considering that older adults have decreased physiological functions and often have several chronic diseases, they are at a higher risk of polypharmacy and hospitalization. The use of at least 5-6 drugs is a definition widely used for polypharmacy in the ambulatory population, and several studies report 25% or more older adults on polypharmacy [2,6-9]. However, this definition may not be practical for the hospitalized older adult population, as this demographic tends to receive more treatments for multiple diseases. Previously reported definitions of polypharmacy in the geriatric hospitalized population were the prescription of 5-9 medications and that of hyper-polypharmacy were 10 or more medications [10,11]. There were also cases of using 5 or more drugs as the definition of polypharmacy for hospitalized patients [12,13]. Although definitions of polypharmacy applicable to older hospitalized patients exist, most studies use single-institution prescription data, making the findings difficult to generalize. Studies from multiple institutions are needed to determine and apply definitions of polypharmacy in the geriatric inpatient population.

Previous studies have used various data sources and methods to define polypharmacy. Data sources included health insurance claims, electronic medical records, spontaneous adverse drug event (ADE) reports, and surveys. The methods used to define polypharmacy include simple numeric definitions, numeric definitions with terms of duration in a therapy or health care setting, and nonnumeric descriptive definitions [14]. Definitions of polypharmacy are diverse due to differing patient age, underlying disease, and disease severity. Accordingly, it is necessary to review the existing definitions of polypharmacy to understand the categories used in various clinical settings and to apply the most appropriate method when assessing the status of polypharmacy in the study population.

Kim et al [2] reported that approximately 6.30 million patients aged 65 years or older in South Korea were prescribed drugs for at least 90 days during 2018, and among this population, 2.64 (41.9%) million were prescribed 5 or more drugs, and 0.77 (13.9%) million were prescribed 10 or more drugs. Cresswell et al [15] reported an increased risk of ADEs with a higher number of prescribed drugs. The older adults were especially at risk of serious long-term outcomes, including death and disability, from these ADEs [15]. Ensuring safer therapy for this population is important. Hanlon et al [16] found that in 167 adults aged 65 years and older, ADEs occurred in 58 (35%), and the most frequent ADEs were gastrointestinal disorders. This was followed by ADEs of the nervous, respiratory, endocrine, skin, and subcutaneous systems [16]. Among the 58 patients who had an ADE, 49 (84%) patients required medical care: 37 (63%) were examined by a physician, 7 (11%) were hospitalized, and 5 (10%) visited the emergency room [16]. Mabuchi et al [17] compared the number of drugs used in patients with a spontaneous ADE report to the overall patient population in Japan using real-world data. In both populations, the number of drugs used increased with age [17].

This study used anonymized electronic health record (EHR) data converted to the Observational Medical Outcomes Partnership (OMOP) Common Data Model (CDM) format, a standardized data structure that accommodates retrospective observational studies [18]. The OMOP CDM data content is generated by extracting EHR data recorded during patient care, removing personal identifiable information, transforming the data into a standardized structure, and mapping hospital-specific terms to standardized, controlled vocabularies. Each CDM in the 4 institutions included patient demographic, condition, measurement, procedure, and drug prescription information [19]. Overall, we examined the characteristics and patterns of polypharmacy in older hospitalized adults across 4 health care

XSL•FO
RenderX

institutions (presented as medical institutions A-D) and created a polypharmacy categorization system for this population. Specifically, for each polypharmacy category, we characterized the drugs and drug classes prescribed to the population of interest and examined their drug use patterns.

Methods

Study Participants and Observation Period

EHR data of 4 medical institutions converted to the OMOP CDM format were used to analyze polypharmacy patterns. The study participants were patients aged 20 years or older hospitalized at one of these 4 institutions between January 1, 2012, and December 31, 2020. The number of patients aged 20 years or older who visited the medical institutions in the study period ranged from 494,875 to 3,349,795. The number of hospitalized patients, hospitalization events, hospitalized patients aged 60 years and older, and the number of drug classes prescribed to the overall hospitalized patients are presented in Table 1.

To extract study participants, we consulted clinicians from medical departments who frequently encountered polypharmacy. The patient visit types were restricted to inpatients. The earliest date of patient admission was the patient study entry date; if the discharge date of this admission and the admission date of the next admission were within 30 days, the 2 admissions were treated as a single continuous admission period. To investigate the status of discharge drug use, drug exposure data from the outpatient setting were followed up for 7 days after patient discharge. For example, if the patient had 2 admission episodes, the total admission period would be the sum of the duration of admission 1 in days, 7 days after discharge from admission 1, the duration of admission 2 in days, and 7 days after discharge from admission 2 (Figure 1).

Table 1. Patient characteristics by medical institution.

	Medical institution A	Medical institution B	Medical institution C	Medical institution D
Patients, n (%)	602,483 (100)	1,944,140 (100)	3,349,795 (100)	494,875 (100)
Hospitalized patients, n (%)	169,931 (20.2)	405,956 (20.9)	419,460 (12.5)	128,700 (26)
Hospitalization events, n (%)	315,624 (100)	1,092,936 (100)	871,764 (100)	212,489 (100)
Older hospitalized adults aged ≥60 years, n (%)	48,512 (8.1)	166,071 (8.5)	113,573 (3.4)	33,997 (6.9)
Drug therapeutic subgroups (WHO[a] ATC[b] second-level codes [20]) prescribed, distinct n (%)	79 (84)	86 (91.5)	72 (76.6)	81 (81.2)

[a]WHO: World Health Organization.

[b]ATC: Anatomical Therapeutic Chemical.

Figure 1. Definition of patient observation period.

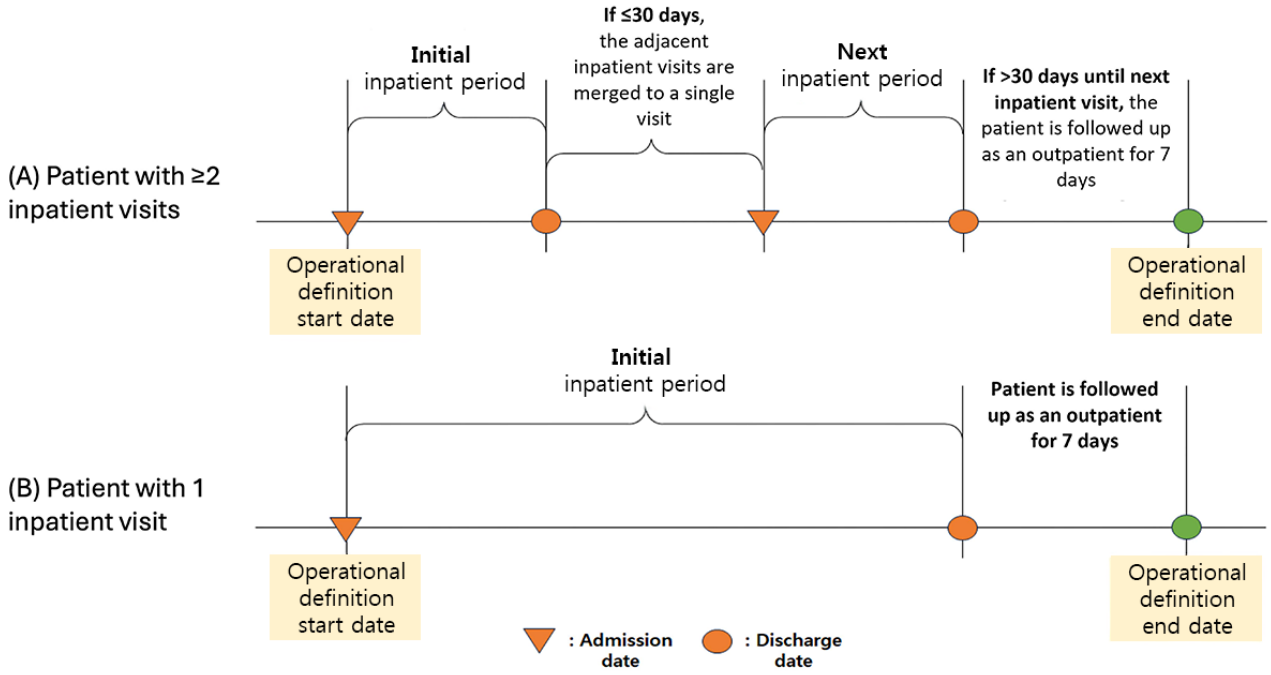

XSL•FO
RenderX

Polypharmacy Level

This study examined the distribution of patients by polypharmacy level for each medical institution. The polypharmacy levels increase by the number of concomitant drugs prescribed to the patient. The cutoff values for concomitant drug counts in each polypharmacy level were determined based on internationally recommended thresholds and existing literature on polypharmacy in older adults. The World Health Organization (WHO) and several countries defined the use of 5 or more drugs as polypharmacy [1,14]. WHO differentiates between appropriate and inappropriate polypharmacy by defining appropriate polypharmacy as evidence-based, personalized medication prescribing and inappropriate polypharmacy as irrational, excessive prescribing [21]. It emphasizes the importance of reducing inappropriate polypharmacy by continuously ensuring the appropriate, rational use of medications [21]. The European Geriatric Medicine Society states that polypharmacy patients should be closely managed through medication reviews to prevent inappropriate polypharmacy [22]. The National Institute for Health and Care Excellence recommends monitoring the benefits and harms of each drug taken by adults using 15 or more regular medications [23].

Masnoon et al [14] used concurrent drug counts, admission duration, and treatment duration to define polypharmacy, and Young et al [24] determined the category of polypharmacy by the number of concomitant drugs and the presence of high-risk drugs in the patient's drug regimen. Studies on hospitalized, older patients used polypharmacy levels other than the widespread definition of 5 or more drugs [25-27]. An investigation of the physical performance of hospitalized older patients defined polypharmacy as the use of 10 or more drugs during hospital stay [26]. A study analyzing risk factors of increased hospital stay in older adults defined polypharmacy as the concomitant use of 5 to 9 drugs and excessive polypharmacy as 10 or more drugs [25]. The polypharmacy definition for nursing home patients as well as older populations in general was also 5-9 concurrent drugs, and that of excessive polypharmacy was 10 or more concurrent drugs [27-29]. Kim et al [30] divided polypharmacy into 3 levels: concomitant use of 6 or more drugs as polypharmacy, 11 or more drugs as major polypharmacy, and 21 or more drugs as excessive polypharmacy [30].

Based on WHO recommendations and the literature search mentioned earlier, we suggested a polypharmacy categorization method to detect regimens, including an excessive number of drugs, with an aim to assist in detecting inappropriate polypharmacy (Table 2). Polypharmacy was defined as concomitant prescription of 5 or more drugs, which is consistent with the widespread definition [14] and based on previous studies on polypharmacy in older adults. The next severe polypharmacy level, which was major polypharmacy, was defined as the prescription of 10-19 drugs. This threshold was used, as it was commonly used in the older patient population [25-29]. The most severe polypharmacy level, excessive polypharmacy, was defined as the prescription of 20 or more drugs based on a previous study of polypharmacy use among older adults [30].

Table 2. Definition of polypharmacy based on the number of concomitant drugs.

Concomitant drugs, n	Polypharmacy category
<5	Nonpolypharmacy
5-9	Polypharmacy
10-19	Major polypharmacy
≥20	Excessive polypharmacy

Data Preprocessing and Data Analysis Environment

Preprocessing of the medical institution data was performed by converting the EHR to the OMOP CDM (version 5.3.1) format. We used the following inpatient data extracted from the CDM tables: person, drug_exposure, and visit_occurrence. The data for each CDM table were extracted for the years 2012-2020. Using drug_exposure OMOP CDM data, the severity of polypharmacy and drug use patterns in the patients were analyzed. Based on clinical professional consultation, the study patients were divided into those with 1 admission and those with 2 or more admissions. The operational definition of continuous admission was applied to the data of patients with multiple admissions within 30 days to obtain the final admission counts. Drug exposure data in the outpatient setting for 7 days after follow-up were extracted for each patient. We extracted the drug exposure data for all patients during their observation period and for each day of drug exposure and counted the number of drug ingredients exposed to the patient. The date of the maximum number of dispensed drug ingredients was determined. If the patient was exposed to this maximum number of drug ingredients for multiple days, the date closest to admission was used as the date of the maximum drug ingredient count. The drug ingredient count on that date was used to determine the patient's polypharmacy level. To perform the drug ingredient mapping process, we excluded patients without at least 7 days of drug exposure data after discharge.

Data processing and analyses were performed using R (version 4.1.3; R Foundation for Statistical Computing). Specifically, CDM data access, extraction, and conversion into variables were performed using R packages *RpostgreSql* (version 0.7-8) [31] and *sqldf* (version 0.4-11) [32]. R packages used for data preprocessing were *dplyr* (version 0.8.3) [33] and *data.table* (version 1.12.2) [34], and that used for descriptive analyses was *moonBook* (version 0.3.1) [35]. The *ggplot2* (version 3.2.1) [36] R package was used for data visualization. Medical institute A used 16 GB RAM in the Windows operating system (OS), medical institutes B and C used 64 GB RAM in the Windows

XSL•FO
RenderX

OS, and medical institute D used 128 GB RAM in the Windows OS.

Polypharmacy Pattern Analysis

For each patient, we mapped the WHO Anatomical Therapeutic Chemical (ATC) code to each drug exposure event in the OMOP CDM. Medical institutions A, C, and D assigned WHO ATC codes to drugs in the OMOP CDM using electronic data interchange (EDI) codes. This is possible because the EDI codes are loaded into the institutional CDM. Mapping the WHO ATC codes to EDI codes required a file with code information for drugs distributed in South Korea provided by the Korea Pharmaceutical Information Service [37]. Korea Pharmaceutical Information Service, operated by the Health Insurance Review & Assessment Service, assigns WHO ATC codes to drugs approved in South Korea. The code information file includes EDI, WHO ATC, and drug ingredient codes for each drug approved; therefore, assigning WHO ATC and drug ingredients to each drug in the OMOP CDM was possible. Traditional Korean medications and drugs without WHO-ATC, EDI, and drug ingredient codes were excluded from the mapping process.

Medical institution B did not have EDI codes available in the OMOP CDM; therefore, a different approach was used to assign WHO ATC codes to the drug concept IDs. This institution maps the WHO ATC code to each drug in the CDM drug_exposure table using the concept and concept_ancestor tables. If the drug_concept_id in the drug_exposure table was a descendant_concept_id of an ancestor_concept_id indicating a fifth-level WHO ATC code, then the concept_id and WHO ATC codes were mapped to the drug_concept_id. The concept table was used to determine if the ancestor_concept_id was a WHO ATC code, and the concept_ancestor table was used to determine if drug_concept_id was a descendant_concept_id of a WHO ATC code.

The maximum daily drug ingredient count was used to determine the polypharmacy level. A maximum drug ingredient count of less than 5 drugs was considered nonpolypharmacy, 5-9 drug ingredients as polypharmacy, 10-19 drug ingredients as major polypharmacy, and 20 drug ingredients or more as excessive polypharmacy.

Demographic characteristics were analyzed using the processed CDM data. The characteristics examined included the total number of inpatients and their admissions, patient age, precautionary drug use, proportion of older adults, admission duration, and drug ingredient exposure distribution for the years 2012-2020.

We performed single and combination drug class pattern analyses using the second ATC level as the unit for the drug class. This level was selected, as it represents clinically meaningful therapeutic groups, allowing the comparison of prescribing trends across multiple health care institutions. We excluded drugs in the ATC second-level B05 (blood substitutes and perfusion solutions) for the analyses, as these drugs have a low risk of interacting with other drugs, have little clinical significance, and are used in the majority of inpatients. [38]. The drug use patterns were visualized using the *ggplot2* R package. Single-drug class use patterns were analyzed by determining the number of patients using each drug class at least once. Combination drug class patterns were analyzed by first determining the date of the highest number of drugs prescribed for each patient and examining the drug classes used on that date. The workflow of the study is depicted in Figure 2.

Figure 2. Workflow for polypharmacy pattern determination. ATC: Anatomical Therapeutic Chemical; C03: diuretics; CDM: Common Data Model; EDI: electronic data interchange; J02: antimycotics for systemic use; M01: anti-inflammatories and antirheumatics; M05: drugs for treatment of bone diseases; N05: psycholeptics; OMOP: Observational Medical Outcomes Partnership.

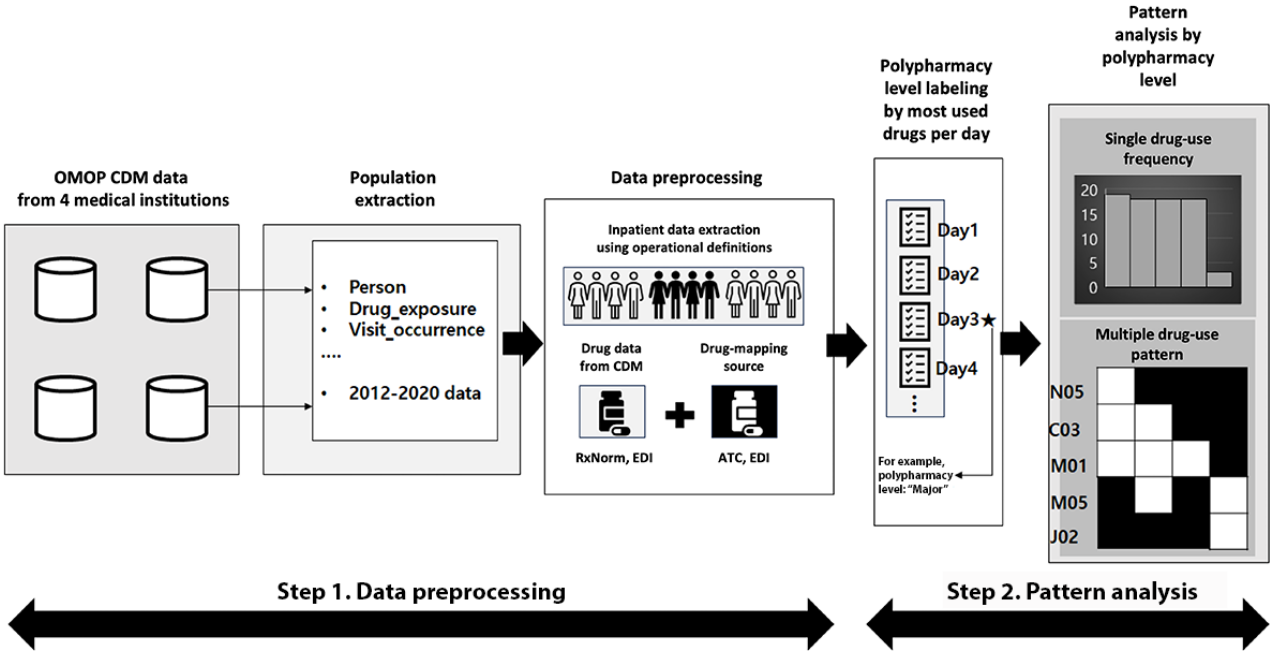

XSL•FO
RenderX

Ethical Considerations

The study was conducted in accordance with the Declaration of Helsinki and approved by the institutional review board of Konyang University Hospital (protocol code: KYUH2022-07-015-001, approved on September 21, 2022), Asan Medical Center (protocol code: 2022-0342, approved on October 21, 2022), Seoul National University Hospital (protocol code: E-2209-069-1358, approved on September 20, 2022), and Chungbuk University Hospital (protocol code: CBNUH2022-09-030, approved on October 18, 2022). Patient consent was waived, as the data were collected during the routine care of physicians and removed of personally identifiable information, therefore eliminating the risk of compromising patient privacy. There was no direct contact with any patients during the course of this study, and no compensation was provided to the participants.

Results

Polypharmacy Levels and Their Drug Use Patterns

The mean maximum daily drug counts in older adults aged 60-69, 70-79, and ≥80 years were highest in patients admitted to medical institution B followed by medical institution A. Duration of admission increased with higher age range in medical institution C. In all institutions except for institution A, the average hospitalization period of the population aged 70 years or older was longer than the population aged 60-69 years (Table 3).

Table 3. Multi-institutional maximum daily number of drugs prescribed and duration of hospitalization in older adults.

Age group (years)	Medical institution A		Medical institution B		Medical institution C		Medical institution D	
	Drugs, mean (SD)	Hospitalization period (days), mean (SD)	Drugs, mean (SD)	Hospitalization period (days), mean (SD)	Drugs, mean (SD)	Hospitalization period (days), mean (SD)	Drugs, mean (SD)	Hospitalization period (days), mean (SD)
60-69	21.3 (10.3)	24.0 (35.5)	24.6 (14.5)	19.3 (25.7)	15.9 (7.0)	17.3 (15.8)	20.0 (10.3)	15.2 (26.3)
70-79	21.5 (10.3)	25.3 (32.4)	25.2 (14.7)	19.7 (24.4)	16.1 (7.1)	18.5 (18.1)	20.3 (10.8)	18.0 (32.7)
≥80	20.9 (9.6)	22.8 (23.5)	24.5 (14.7)	19.3 (28.0)	15.5 (6.9)	19.1 (19.4)	19.8 (10.6)	18.1 (25.7)

Older Adult Polypharmacy Levels Based on Multi-Institutional CDM Data

The level of polypharmacy with the most patients was major polypharmacy in medical institutions A, C, and D, while for medical institution B, this was excessive polypharmacy (Table 4).

XSL•FO
RenderX

Table 4. Distribution of patients by polypharmacy level.

Medical institution and age group (years)	Nonpolypharmacy patients, n (%)	Polypharmacy patients, n (%)	Major polypharmacy patients, n (%)	Excessive polypharmacy patients, n (%)
Medical institution A				
60-69	730 (31.9)	2121 (24.9)	5002 (22.2)	3753 (24.7)
70-79	1123 (49.1)	4085 (48)	10,557 (46.9)	7251 (47.6)
≥80	436 (19)	2297 (27)	6936 (30.8)	4221 (27.7)
Total	2289 (100)	8503 (100)	22,495 (100)	15,225 (100)
Medical institution B				
60-69	4164 (61.4)	7975 (55.6)	22,847 (53.1)	55,016 (54)
70-79	2092 (30.8)	4887 (34.1)	15,422 (35.8)	37,130 (36.4)
≥80	528 (7.8)	1486 (10.4)	4756 (11.1)	9768 (9.6)
Total	6784 (100)	14,348 (100)	43,025 (100)	101,914 (100)
Medical institution C				
60-69	3657 (31.9)	8746 (30.9)	18,573 (31.6)	4777 (31.8)
70-79	5951 (51.9)	14,634 (51.7)	30,563 (52)	7977 (53.1)
≥80	1859 (16.2)	4927 (17.4)	9640 (16.4)	2269 (15.1)
Total	11,467 (100)	28,307 (100)	58,776 (100)	15,023 (100)
Medical institution D				
60-69	963 (26.6)	1954 (24.1)	3018 (22.8)	2173 (24.1)
70-79	1909 (52.7)	3991 (49.2)	6448 (48.7)	4609 (51.1)
≥80	752 (20.8)	2167 (26.7)	3775 (28.5)	2238 (24.8)
Total	3624 (100)	8112 (100)	13,241 (100)	9020 (100)

Multi-Institute CDM-Based Polypharmacy Pattern

The pattern of polypharmacy in the older adults was analyzed based on the use of single or combinations of drug therapeutic subgroups (WHO ATC second-level codes). The older population was defined as adults aged 65 years and older, based on the population grouping method of the National Statistical Office of Korea [1].

Single Drug Use Patterns

We examined frequently prescribed drug therapeutic subgroups using second-level WHO ATC codes as the subgroup unit. The 10 most frequently prescribed subgroups for each medical institution are presented in Figures 3-6. The horizontal axis represents the number of prescriptions for drugs included in the therapeutic subgroup specified on the vertical axis. According to the 10 most frequently prescribed therapeutic subgroups, the number of prescriptions tended to increase with higher levels of polypharmacy in all medical institutions, excluding institution C. The highest prescription frequency in this institution was observed at the major polypharmacy level.

For medical institution A, the antithrombotics (B01) therapeutic subgroup was frequently prescribed in patients in the nonpolypharmacy and polypharmacy levels compared to other levels and antibacterials for systemic use (J01) for the major and excessive polypharmacy levels. Notably, drugs in the anesthetic (N01) subgroup were most frequently prescribed to patients with excessive polypharmacy (Figure 3).

In medical institution B, patients in all polypharmacy levels except the excessive level were most frequently prescribed analgesics (N02). The most frequently prescribed therapeutic subgroups for patients with excessive polypharmacy included mineral supplements (A12) and antianemic preparations (B03). Patients in all polypharmacy levels were frequently prescribed antibacterial agents for systemic use (J01) and drugs for acid-related disorders (A02). Patients in the major polypharmacy level were frequently prescribed cardiac therapy (C01) and drugs for constipation (A06; Figure 4).

In medical institution C, the analgesic (N02) therapeutic subgroup was prescribed most frequently to patients in all polypharmacy levels. Cough and cold preparations (R05) were relatively frequently prescribed to patients in the nonpolypharmacy level, and lipid-modifying drugs (C10) and antithrombotics (B01) to patients in the polypharmacy level. Anesthetics (N01) were prescribed more frequently to patients in major and excessive polypharmacy levels than to those in other polypharmacy levels (Figure 5).

In medical institution D, antibacterials for systemic use (J01) and analgesics (N02) were prescribed frequently to patients across all polypharmacy levels. Drugs for acid-related disorders (A02) were frequently prescribed to patients in all polypharmacy levels, excluding the excessive level, whereas antihemorrhagics (B02) and anesthetics (N01) were most frequently prescribed to patients in the excessive level (Figure 6).

XSL•FO
RenderX

Figure 3. Single therapeutic subgroup (WHO ATC second-level) prescribing pattern in medical institution A. A02: acid-related disorder drug; A03: functional gastrointestinal disorder drug; A06: constipation drug; A10: antidiabetics; ATC: Anatomical Therapeutic Chemical; B01: antithrombotics; B02: antihemorrhagics; C01: cardiac therapy; C10: lipid-modifying agent; J01: systemic antibacterials; M03: muscle relaxant; N01: anesthetics; N02: analgesics; N05: psycholeptics; R05: cough and cold preparation; S01: ophthalmologicals; WHO: World Health Organization.

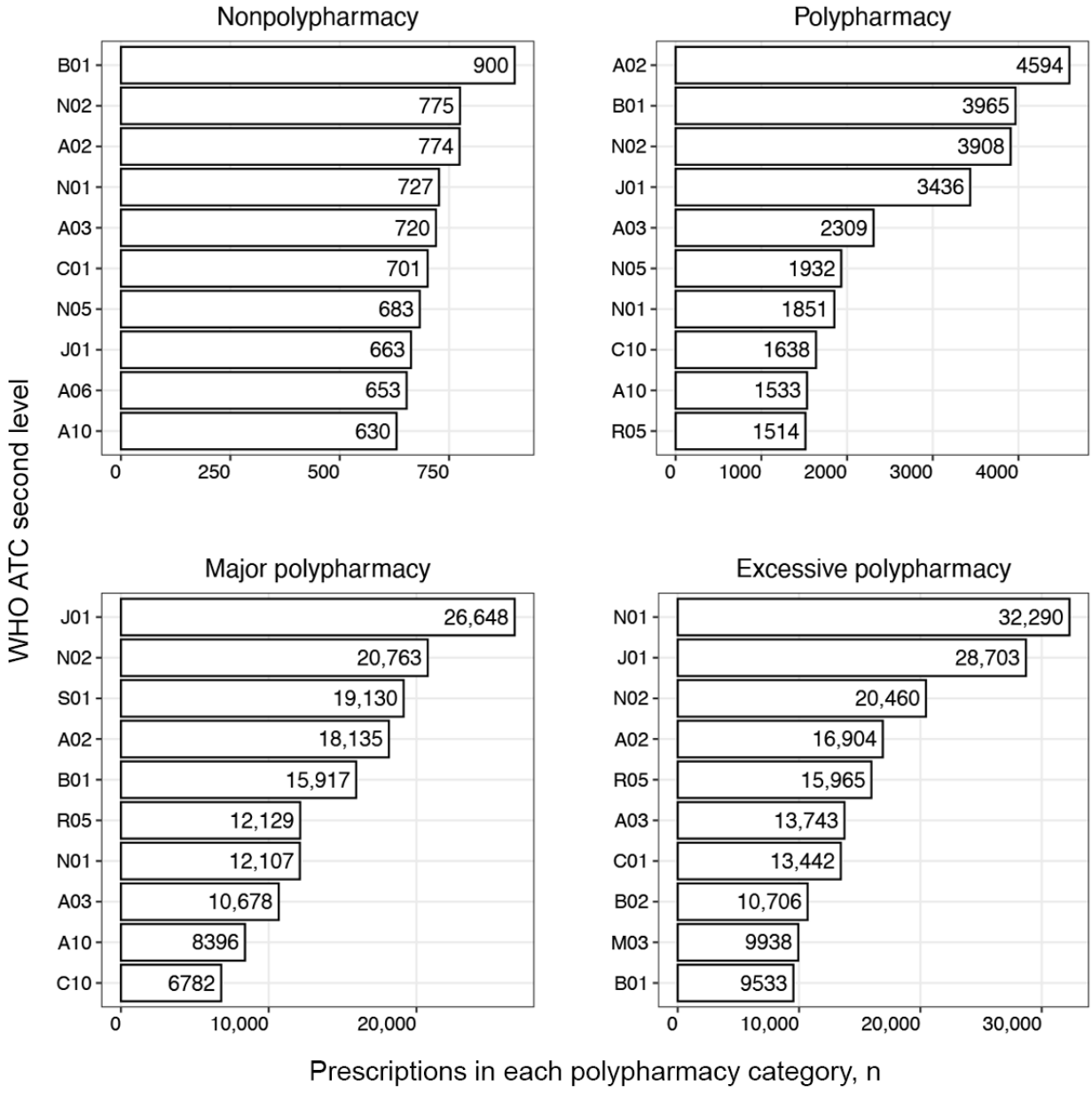

XSL•FO
RenderX

Figure 4. Single therapeutic subgroup (WHO ATC second-level) prescribing pattern in medical institution B. A02: acid-related disorder drug; A03: functional gastrointestinal disorder drug; A06: constipation drug; A10: antidiabetics; A12: mineral supplement; ATC: Anatomical Therapeutic Chemical; B01: antithrombotics; B02: antihemorrhagics; B03: antianemics; C01: cardiac therapy; C09: renin-angiotensin system agent; C10: lipid-modifying agent; H02: systemic corticosteroid; J01: systemic antibacterials; N01: anesthetics; N02: analgesics; N05: psycholeptics; V06: general nutrient; V08: contrast media; WHO: World Health Organization.

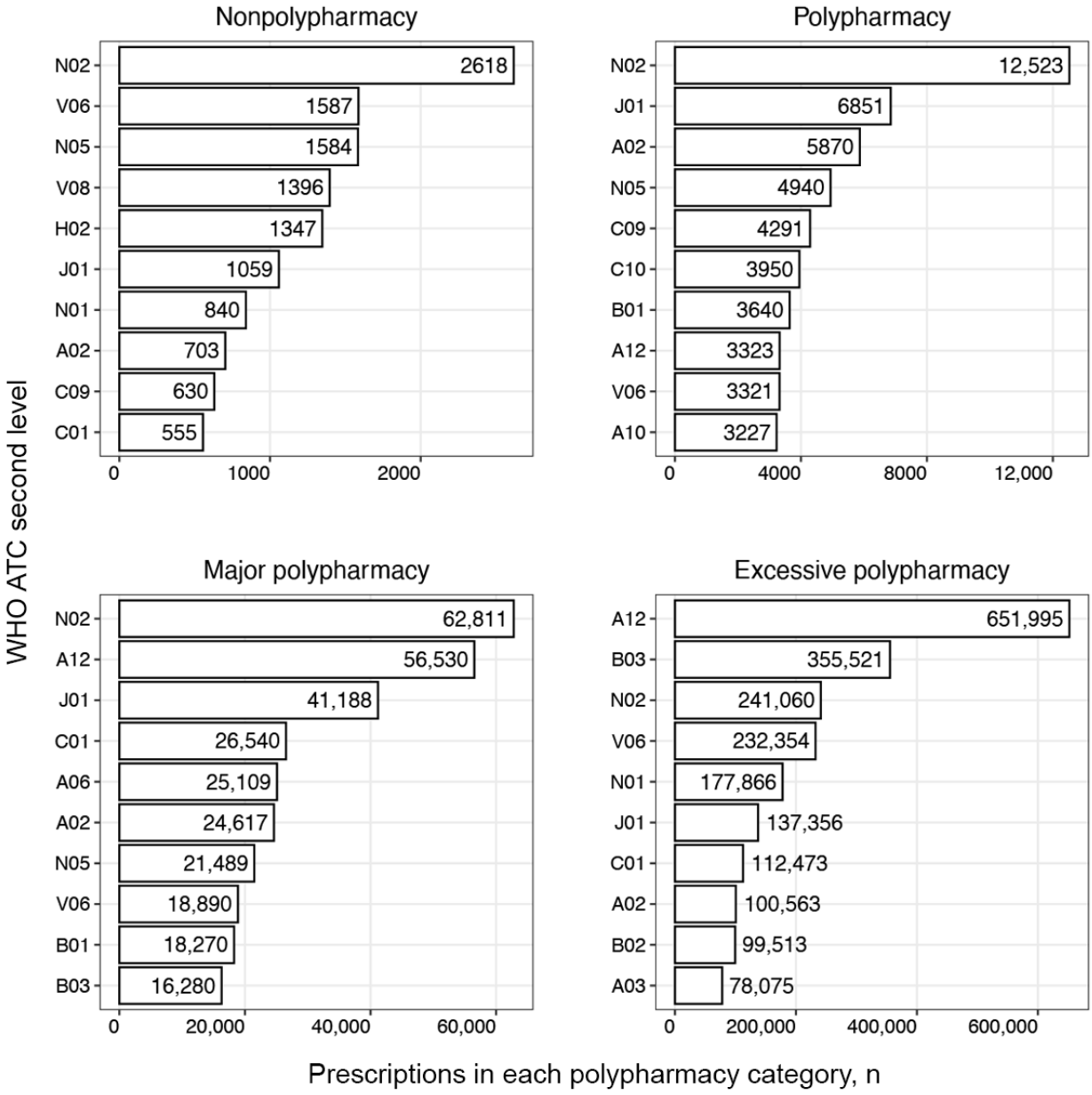

XSL•FO
RenderX

Figure 5. Single therapeutic subgroup (WHO ATC second-level) prescribing pattern in medical institution C. A02: acid-related disorder drug; A04: antiemetics and antinauseants; A10: antidiabetics; ATC: Anatomical Therapeutic Chemical; B01: antithrombotics; C01: cardiac therapy; C08: calcium channel blocker; C10: lipid-modifying agent; J01: systemic antibacterials; M03: muscle relaxant; N01: anesthetics; N02: analgesics; N05: psycholeptics; R05: cough and cold preparation; S01: ophthalmologicals; WHO: World Health Organization.

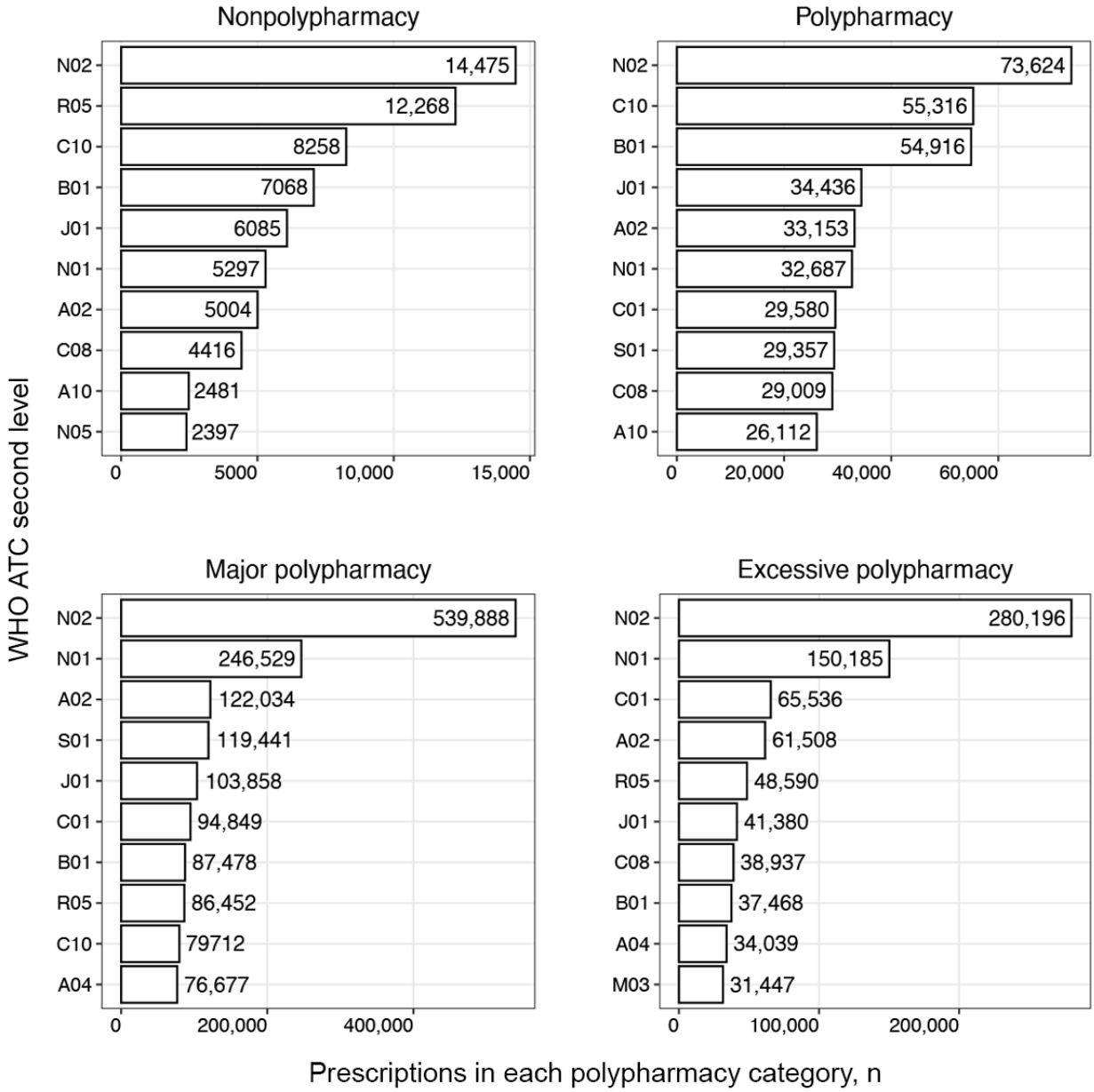

XSL•FO
RenderX

Figure 6. Single therapeutic subgroup (WHO ATC second-level) prescribing pattern in medical institution D. A02: acid-related disorder drug; A03: functional gastrointestinal disorder drug; A06: constipation drug; A10: antidiabetics; ATC: Anatomical Therapeutic Chemical; B01: antithrombotics; B02: antihemorrhagics; C01: cardiac therapy; C09: renin-angiotensin system agent; C10: lipid-modifying agent; J01: systemic antibacterials; M01: anti-inflammatories and antirheumatics; M03: muscle relaxant; N01: anesthetics; N02: analgesics; R03: obstructive airway disease drug; R05: cough and cold preparation; R06: systemic antihistamine; WHO: World Health Organization.

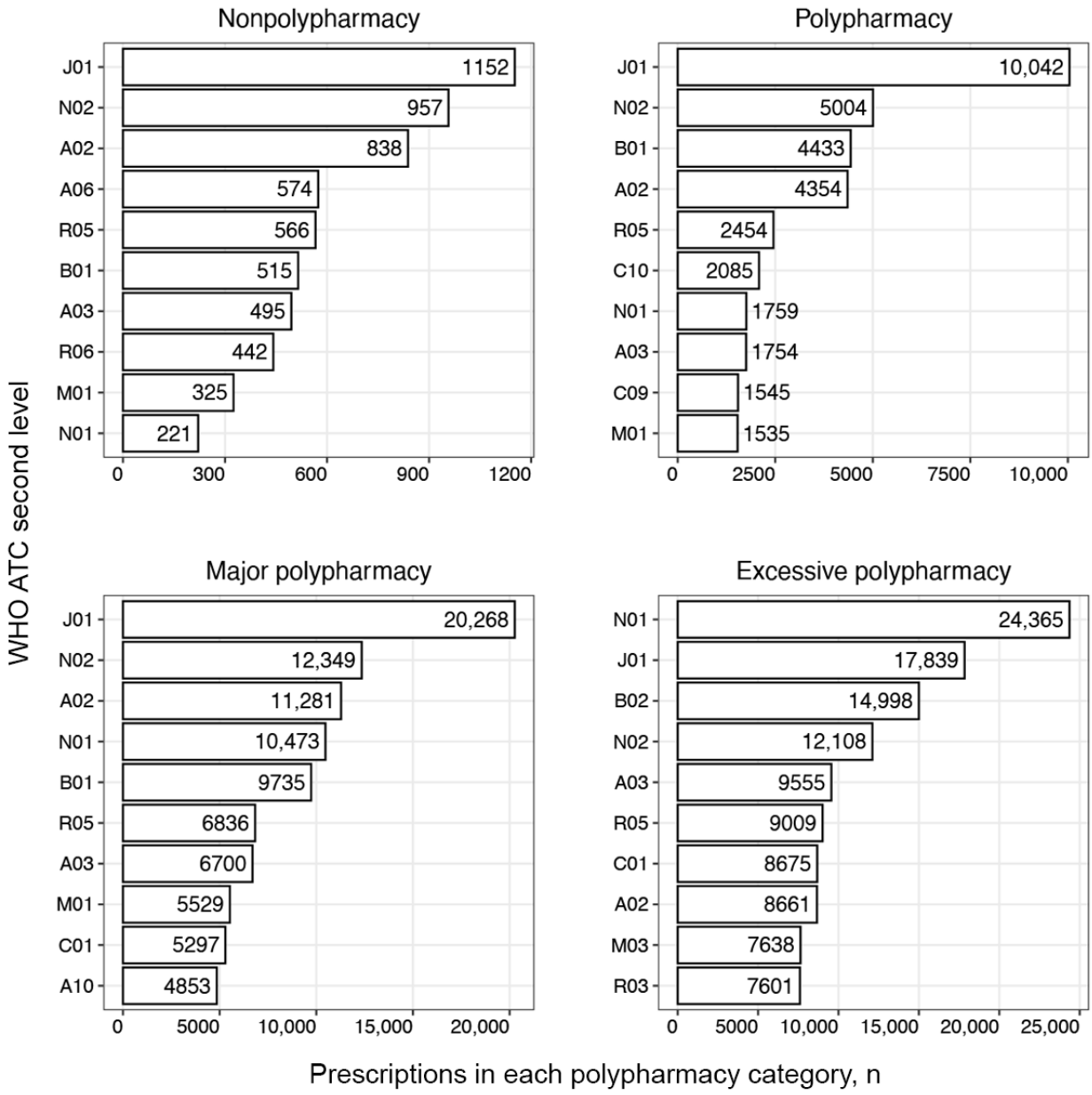

Concomitant Drug Use Patterns

Following the examination of single therapeutic subgroup patterns, concomitantly used therapeutic subgroups were analyzed to determine the trends in combination drug use in patients with polypharmacy. At medical institution A, the most frequently prescribed therapeutic subgroup combination for patients of the nonpolypharmacy level was B01 and N01. For patients in the polypharmacy level, A02-C01-N02-N05-V04 was the most frequently prescribed combination. Patients in the major polypharmacy level were most frequently prescribed with the therapeutic subgroup combination C01-H02-J01-M09-N01-N02-S01, while patients in the excessive polypharmacy group were most frequently prescribed the combination A02-A03-C01-H02-J01-M09-N01-N02-S01 (Figure 7). The full names for each of the therapeutic subgroups denoted as WHO ATC second-level codes are in Multimedia Appendix 1.

Results for medical institution B showed that patients in the nonpolypharmacy level were most frequently prescribed therapeutic subgroup combination N02-N05-V06, followed by combination H02-N01. The most frequent combination prescribed to patients at the polypharmacy level was B01-C01-C08-V08, followed by A02-G02-J01-M01-N01-V06 and A02-J01-N02. Patients in the major polypharmacy level were also most frequently prescribed the combination B01-C01-C08-V08. The second most frequently prescribed

XSL•FO
RenderX

combination at this level was A03-A06-N02-N05-R06-V06, and the third was A12-C01-J01-M09-N02-N05-V06. The most frequently prescribed subgroup combination for patients in the excessive polypharmacy level was A02-A03-B03-D10-N02-N05-V03, followed by A02-A12-B03-D10-N02-N05-V03 and A12-C01-J01-M09-N02-N05-S01-V06 (Figure 8).

In medical institution C, the 3 most frequent therapeutic subgroup combinations prescribed to patients at the nonpolypharmacy level each involved 1 subgroup: R05, N02, and J01. Patients in the polypharmacy level were most frequently prescribed therapeutic subgroup combination A03-M01-N01-S01. The most frequent subgroup combination prescribed for patients in the major polypharmacy level was A03-C01-M01-N01-S01, followed by A03-M01-N01-S01 and A02-A03-C01-N02-N05-V03. Patients in the excessive polypharmacy level were prescribed A02-A04-C01-J01-M03-N01-N02-R03-R05 most frequently. The second frequent combination was the same as the most frequent combination with the addition of subgroups A03 and A07. The third most frequent combination matched the second, excluding subgroup A02 (Figure 9).

In medical institution D, patients in the nonpolypharmacy level were prescribed therapeutic subgroup J01 most frequently, followed by individual subgroups A02, N02, and A06. Patients in the polypharmacy level were mostly prescribed the combination J01-N01-N02. Those in major polypharmacy level were prescribed B06-C01-H02-J01-N01-N02-S01, followed by J01-N02-R05-R06 and A02-J01-M01-N01-N05. Patients in the excessive polypharmacy level were prescribed combination A03-A04-B02-J01-M01-M03-N01-N02-N07-R05 most frequently, and the second and third most frequent combinations involved the addition of subgroup R03 and the removal of subgroup M01, respectively (Figure 10).

Figure 7. The most frequently prescribed 10 concomitant drug therapeutic subgroups (WHO ATC second-level combinations) used in each polypharmacy level at medical institution A. A02: acid-related disorder drug; A03: functional gastrointestinal disorder drug; A06: constipation drug; A12: mineral supplement; ATC: Anatomical Therapeutic Chemical; B01: antithrombotics; B02: antihemorrhagics; C01: cardiac therapy; C10: lipid-modifying agent; G04: urologicals; H02: systemic corticosteroid; J01: systemic antibacterials; M01: anti-inflammatories and antirheumatics; M03: muscle relaxant; M09: other musculo-skeletal system drug; N01: anesthetics; N02: analgesics; N05: psycholeptics; N07: other nervous system drug; R05: cough and cold preparation; S01: ophthalmologicals; V04: diagnostic agent; WHO: World Health Organization.

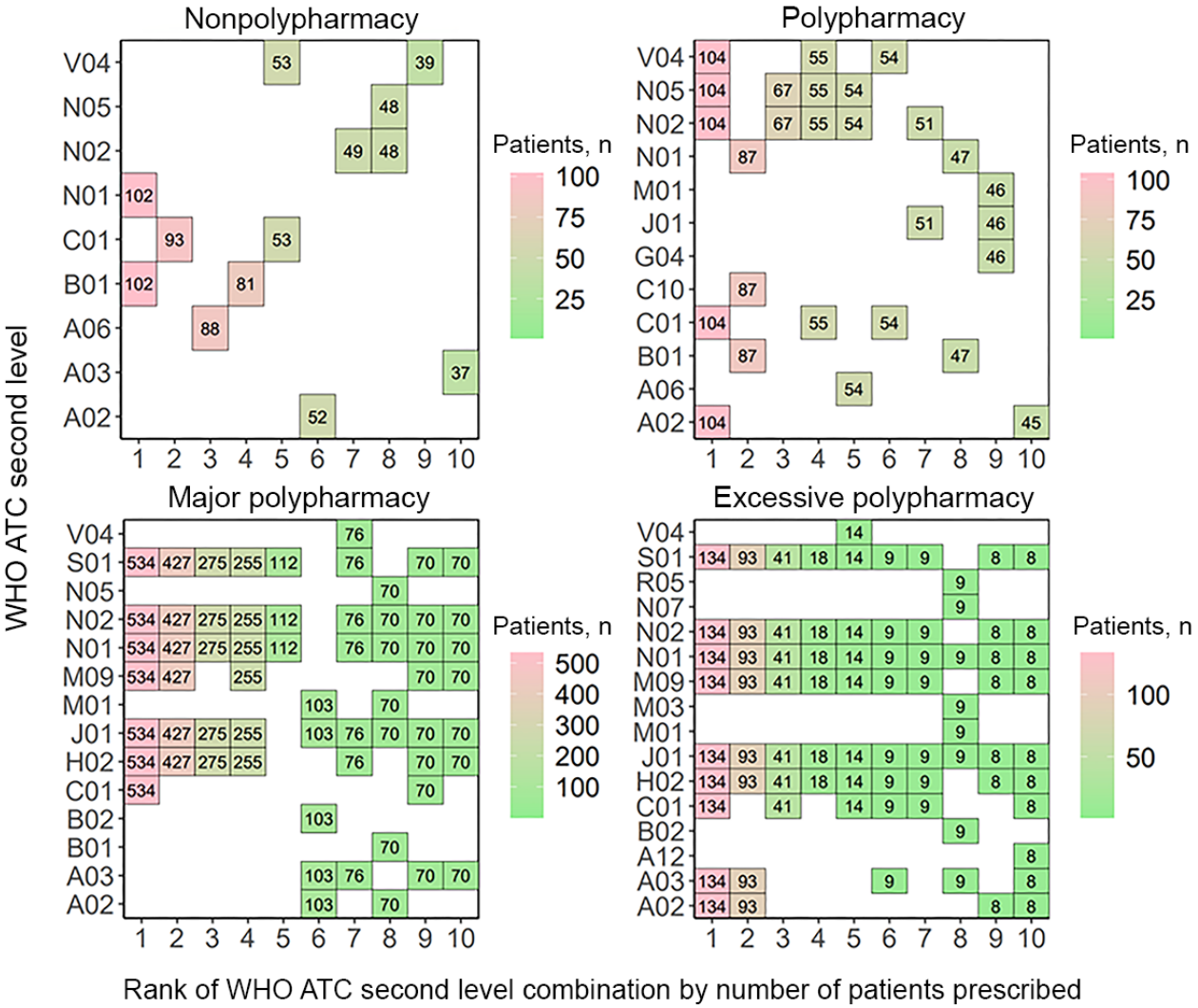

XSL•FO
RenderX

Figure 8. The most frequently prescribed 10 concomitant drug therapeutic subgroups (WHO ATC second-level combinations) used in each polypharmacy level at medical institution B. A02: acid-related disorder drug; A03: functional gastrointestinal disorder drug; A06: constipation drug; A12: mineral supplement; ATC: Anatomical Therapeutic Chemical; B01: antithrombotics; B03: antianemics; B06: other hematological agent; C01: cardiac therapy; C08: calcium channel blocker; C10: lipid-modifying agent; D06: dermatologic antibiotics and chemotherapeutics; D10: antiacne preparation; G02: other gynecologicals; H02: systemic corticosteroid; J01: systemic antibacterials; M01: anti-inflammatories and antirheumatics; M03: muscle relaxant; M09: other musculo-skeletal system drug; N01: anesthetics; N02: analgesics; N05: psycholeptics; N07: other nervous system drug; R05: cough and cold preparation; R06: systemic antihistamine; S01: ophthalmologicals; S03: ophthalmological and otological preparation; V03: other therapeutic product; V06: general nutrient; V08: contrast media; WHO: World Health Organization.

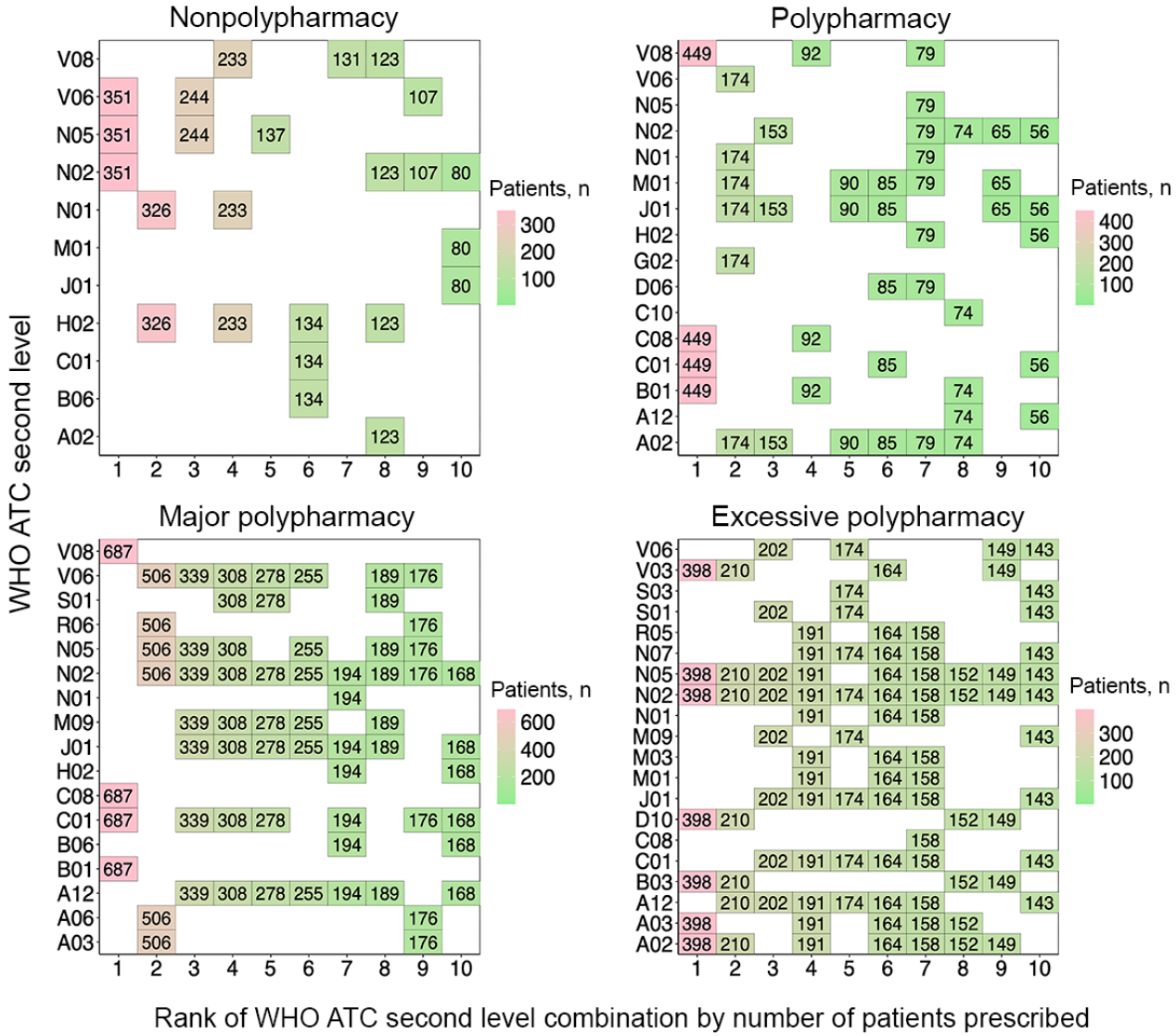

XSL•FO
RenderX

Figure 9. The most frequently prescribed 10 concomitant drug therapeutic subgroups (WHO ATC second-level combinations) used in each polypharmacy level at medical institution C. A02: acid-related disorder drug; A03: functional gastrointestinal disorder drug; A04: antiemetics and antinauseants; A06: constipation drug; ATC: Anatomical Therapeutic Chemical; B01: antithrombotics; B02: antihemorrhagics; C01: cardiac therapy; C08: calcium channel blocker; C10: lipid-modifying agent; H02: systemic corticosteroid; J01: systemic antibacterials; M01: anti-inflammatories and antirheumatics; M03: muscle relaxant; N01: anesthetics; N02: analgesics; N05: psycholeptics; N07: other nervous system drug; R02: throat preparation; R03: obstructive airway disease drug; R05: cough and cold preparation; S01: ophthalmologicals; V03: other therapeutic product; WHO: World Health Organization.

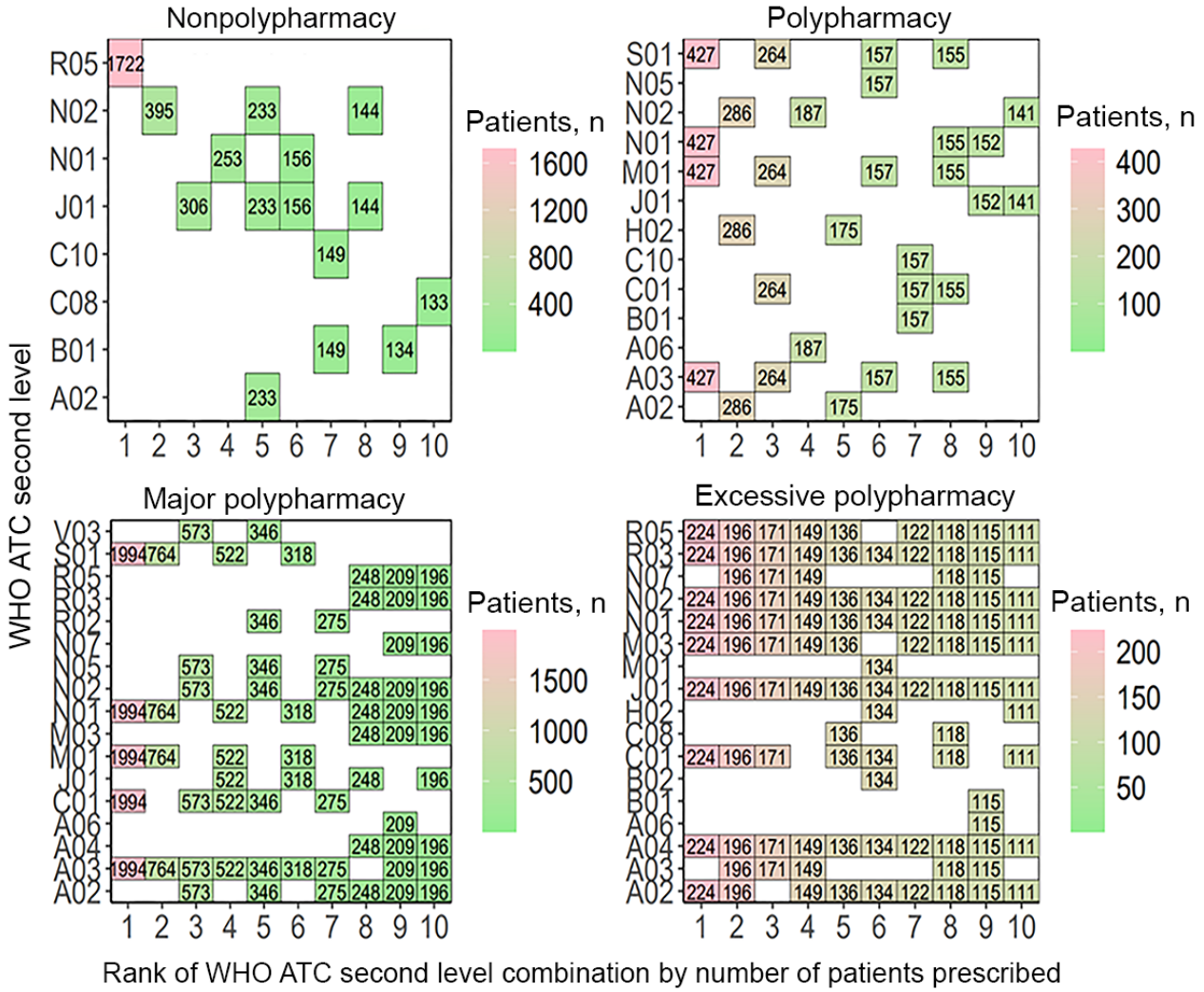

XSL•FO
RenderX

Figure 10. The most frequently prescribed 10 concomitant drug therapeutic subgroups (WHO ATC second-level combinations) used in each polypharmacy level at medical institution D. A02: acid-related disorder drug; A03: functional gastrointestinal disorder drug; A04: antiemetics and antinauseants; A06: constipation drug; ATC: Anatomical Therapeutic Chemical; B01: antithrombotics; B02: antihemorrhagics; B06: other hematological agent; C01: cardiac therapy; C07: beta-blocking agent; C08: calcium channel blocker; C09: renin-angiotensin system agent; C10: lipid-modifying agent; D06: dermatologic antibiotics and chemotherapeutics; H02: systemic corticosteriod; J01: systemic antibacterials; M01: anti-inflammatories and antirheumatics; M03: muscle relaxant; N01: anesthetics; N02: analgesics; N05: psycholeptics; N07: other nervous system drug; R03: obstructive airway disease drug; R05: cough and cold preparation; R06: systemic antihistamine; S01: ophthalmologicals; V03: other therapeutic product; WHO: World Health Organization.

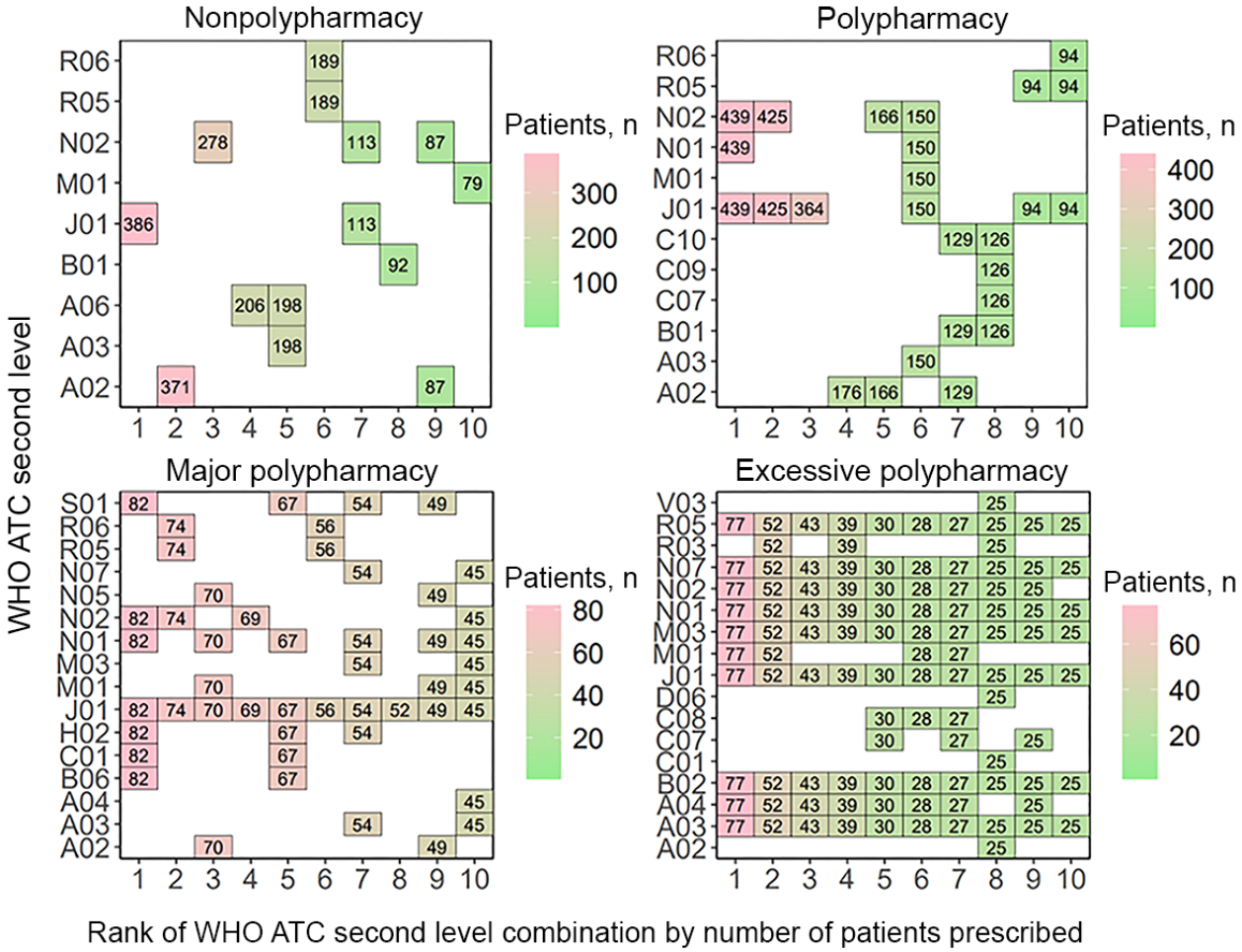

Discussion

Principal Findings

This study used EHR data converted to the OMOP CDM from 4 medical institutions for geriatric inpatients aged 65 years and older admitted over 9 years. Our study is the first to collect the EHR of patients and retrospectively study polypharmacy patterns over multiple institutions to determine a polypharmacy threshold in hospitalized older patients. The authors used data from 2 of the largest hospitals in the South Korean metropolitan area and 2 hospitals in the regional area to represent patients from distinct settings.

The use of OMOP CDM in all 4 study settings allowed the use of similar programming languages and software, thereby increasing the efficiency of the study. Although there were differences in the specific columns customized for each institution, the uniformity of the basic OMOP CDM tables and columns across institutions allowed for the distribution of a single analysis code customized for each institution, and the collection of analysis resulted in a standardized format.

We offer a possible definition of polypharmacy in hospitalized older adults. This was obtained by consulting clinical professionals to define the inpatient observation periods and reviewing previous studies [25,26,30] to determine the time point of drug exposure for polypharmacy level determination. We filtered out drugs that did not contribute to adverse events from polypharmacy (eg, WHO ATC code B05 and its lower-level codes), which improved the quality of our data.

The 4 health care institutions (A, B, C, and D) included in this study showed distinct differences in patient scale, proportion of older patients, sex and age distribution, and medication use patterns. Institution C had the largest patient population with 3,349,795 patients and demonstrated high proportions of older patients and excessive polypharmacy levels. Institution B had the next highest patient population with 1,944,140 patients and the highest number of hospitalization events with 1,092,936 events. This trend reflects that institutions located in metropolitan, urban settings had a higher patient population size and hospitalization event count than their rural counterparts. Institution A, despite having a relatively smaller scale with 602,483 patients, was characterized by the highest average

XSL•FO
RenderX

number of medications per age group and the longest hospital stays.

In terms of sex distribution, institution A showed higher male ratios in patients aged 5-60 years, but female patients were more prevalent in those aged 70 years and older. Institution C displayed higher female ratios in patients in their 50s and 80s or older, while male patients were more common in the 60- to 70-year age group. Institution D exhibited a unique pattern with higher female ratios in patients aged 80 years and older and higher male ratios in those aged 5-70 years. Overall, the proportion of female patients tended to increase in the older population, with sex ratios varying across institutions and age groups.

A tendency was observed for hospital length of stay to increase with advancing age across all institutions. Regarding polypharmacy prescriptions, institution B demonstrated the highest "excessive polypharmacy level" ratio across all age groups.

Comparison to Prior Work

The pattern of drug use among inpatients in the 4 medical institutions showed that patients in the major or excessive polypharmacy levels were most prevalent. This trend is consistent with the results of previous studies reporting 5-10 drugs or more as the polypharmacy threshold. A study using nationwide health care claims data found that hospital admission was significantly associated with polypharmacy (use of 5 or more drugs) and hyper-polypharmacy (use of 10 or more drugs) [39]. Another study reported an increase from 5.6 drugs taken per patient on average at admission to 7.6 drugs at discharge [40]. Considering that the number of drugs prescribed tended to increase during hospital admission, the use of 10-19 or more drugs (major polypharmacy or higher) as the threshold for inpatient polypharmacy was considered appropriate. All data were obtained and analyzed within the securely blocked environment of each medical institution.

The mean number of drugs used in medical institution B was higher than that used in other institutions by 3-10 drugs. The prescription frequency of drugs in the cardiac therapy (C01) WHO ATC therapeutic subgroups tended to increase with the severity of polypharmacy in all medical institutions, and the anti-inflammatory and antirheumatic product (M01) therapeutic subgroups increased across all institutions, excluding institution B. These results correspond with those of a study in which hypertension, osteoarthritis, and rheumatoid arthritis were reported to be prevalent in older individuals aged 65 years or older [41].

The patterns of concomitant therapeutic subgroups differed among the medical institutions. In the major polypharmacy category, medical institution A patients were frequently prescribed ophthalmologicals (WHO ATC second-level code S01), along with other therapeutic subgroups. This drug class has been consistently used in most prescribed combinations of therapeutic subgroups. Medical institution B prescribed drugs in various therapeutic categories including acid-related disorders (A02), functional gastrointestinal disorders (A03), antianemic preparations (B03), antithrombotics (B01), and cardiac therapies (C01) to patients in the major and excessive polypharmacy levels. Medical institution C, which had the highest number of study patients, prescribed drugs for WHO ATC second-level functional gastrointestinal disorders (A03), anti-inflammatory and antirheumatic products (M01), and ophthalmologicals (S01). These drug classes were in the 1-3 highest rank of concomitant drugs prescribed.

Distinct polypharmacy patterns in the polypharmacy group were that patients in all 4 institutions were more frequently prescribed lipid-modifying agents (C10), and in 3 institutions, antidiabetics (A10) were more frequently prescribed, compared to other polypharmacy groups (Figures 3-6). This reflects the increased prevalence of chronic diseases in the older population and their demand for multiple medications to treat the disease [42]. Furthermore, the result is consistent with a finding that older patients with diabetes have a high prevalence of polypharmacy, as these patients commonly have multiple concomitant diseases including cardiovascular, renal, and respiratory disorders [43]. The higher prescription frequencies of ophthalmic agents (S01) and anti-inflammatory and analgesic drugs (M01) observed in institution C reflect that this institution is highly specialized in ophthalmology or rheumatology. The major polypharmacy group was frequently prescribed cough and cold preparations (R05) compared to other polypharmacy groups (Figures 3-6). This trend was consistent with results of a previous study, which reported patients on 5 or more drugs having an odds ratio of 3.18 and 6 or more drugs having an odds ratio of 4.57 to receive prescriptions for cough and cold drugs [44].

Distinctive polypharmacy patterns observed in the excessive polypharmacy group were that cardiac drugs (C01) were frequently prescribed in all 4 institutions (Figures 3-6). This observation suggests that patients in the excessive polypharmacy group may have a higher burden of cardiovascular diseases or more severe cardiac comorbidities requiring complex medication regimens [45]. The frequent prescription of cardiac drugs in this group indicates that managing heart-related conditions—such as heart failure, arrhythmia, or ischemic heart disease—contributes substantially to the overall medication load. This reflects that the patients in the excessive polypharmacy group are clinically more fragile, thus requiring multiple medications for symptom control, prevention of complications, and comorbidity management. This group was also frequently prescribed functional gastrointestinal disorder drugs (A03), antihemorrhagics (B02), and muscle relaxants (M03; Figures 7-10). The reason for the high prevalence of antihemorrhagics prescribing indicates frequent surgeries or procedures in this population [46,47]. Muscle relaxants were found to be frequently prescribed in older polypharmacy patients and coprescribed with opioids [48]. This medication was shown to increase the risk of adverse outcomes including all-cause and cardiovascular mortality, warranting enhanced monitoring of drug therapy [48]. Gastrointestinal drugs may be used for the gastric protection caused by polypharmacy or due to the decreased physiological function of the gastrointestinal system [49].

Although each institution had a distinctive pattern, we observed that drugs related to surgeries, including those needed after the operation (eg, WHO ATC second-level codes C01, H02, J01,

XSL•FO
RenderX

N01, and N02), were commonly prescribed across institutions (Figures 7-10). This reflects the trend from 2011 to 2015, where 3,146,452 of 8,497,443 (37%) surgeries were performed in patients aged 65 years or older, and the surgeries were for high-risk conditions, such as glaucoma [50]. We observed that older inpatients frequently underwent surgeries and were prescribed several drugs during admission for these procedures. The high frequency of antibacterials (WHO ATC second-level code J01), anesthetics (N01), and analgesics (N02) in all polypharmacy levels in the older population reflects the complex clinical conditions of hospitalized older patients, who often require management of infections, surgeries or procedures, and pain control [51]. This population has a high prevalence of osteoarthritis, fractures, and cancer-related pain, increasing the risk of anesthetic and analgesic use [52].

Limitations

This study has several limitations. First, we included 4 medical institutions, which restricts the generalizability of the study results to the institutions of interest. Second, drugs without a mapped WHO ATC code were excluded; therefore, the prevalence of polypharmacy might have been underestimated. Third, we analyzed the pattern of polypharmacy using the second-level ATC code; thus, polypharmacy patterns at the ingredient level were not determined. Fourth, although we examined outpatient drug prescriptions up to 7 days after discharge, polypharmacy use in older outpatients was not comprehensively analyzed. This is a topic of interest for future studies. Fifth, we did not assess the appropriateness of polypharmacy based on linking prescribed drugs and their indications. Although an estimate of the drug-indication linkage is possible, the precise linkage is challenging, as the indications for the drugs were not explicitly recorded in the OMOP CDM database. Finally, the tables used for the analyses did not include the note table, which includes clinical results or interpretations in free-text format, and is a potential resource for detecting polypharmacy.

Conclusions

Based on well-established EHR-based CDM datasets in South Korea, we suggest a polypharmacy definition for older inpatients that is different from the commonly used definition of the concurrent prescription of 5 or more drugs. This is because, based on the severity of the patients' condition and the treatment they require, which includes major surgeries, the number of concomitant drugs used was higher than the commonly used definition of polypharmacy in the majority of patients in this study. Therefore, we suggest that 10 or more drugs is a more suitable definition of polypharmacy for geriatric inpatients. As the geriatric population increases, evaluating the appropriateness of existing polypharmacy definitions and serious outcomes of polypharmacy in this population, including renal failure, falls, and fractures, is necessary for future studies.

Acknowledgments

The authors appreciate the financial support provided by the Korea Health Industry Development Institute, Asan Medical Center, and the Korea Institute of Drug Safety and Risk Management. The authors thank Editage [53] for the English language editing.

Funding

This work was supported by a grant from the Korea Health Technology R&D Project through the Korea Health Industry Development Institute funded by the Ministry of Health & Welfare, Republic of Korea (grant HR21C0198 and RS-2022-KH125153), the Asan Institute for Life Sciences of Asan Medical Center (grant 2023IP0060), and the Korea Institute of Drug Safety and Risk Management in 2022.

Data Availability

The datasets generated or analyzed during this study are not publicly available due to privacy protection policies but are available after approval or exemption by the institutional review boards of the study institutions.

Authors' Contributions

Conceptualization: GJK, JHK, SL
Methodology: CCL, JYH, WMH, SL
Formal analysis: CCL, GJK, MK, SK
Data curation: CCL, GJK, MK, SK
Visualization: CCL, GJK, MK, SK
Writing—original draft preparation: CCL, KHL, GJK
Writing—review and editing: CCL, KHL, GJK, JYH, JYK, KK, SK, MK, WMH, JHK, SL

Conflicts of Interest

None declared.

Multimedia Appendix 1

XSL•FO
RenderX

World Health Organization Anatomical Therapeutic Chemical second-level codes and names.
[DOCX File , 31 KB - medinform_v14i1e78353_app1.docx]

References

1. Population projections for Korea (2020~2070). Ministry of Data and Statistics. 2021. URL: https://mods.go.kr/board.es?mid=a20108080000&bid=11748&act=view&list_no=416209 [accessed 2025-12-31]
2. Kim DS, Yun SH, Cho HJ, Chae J. Management of polypharmacy in the elderly. Health Insurance Review and Assessment Service Repository. 2022 Jan. URL: https://repository.hira.or.kr/handle/2019.oak/3039 [accessed 2025-12-31]
3. Faquetti ML, la Torre AM, Burkard T, Obozinski G, Burden AM. Identification of polypharmacy patterns in new-users of metformin using the Apriori algorithm: a novel framework for investigating concomitant drug utilization through association rule mining. Pharmacoepidemiol Drug Saf 2023 Mar;32(3):366-381. [doi: 10.1002/pds.5583] [Medline: 36579709]
4. Management of medications for elderly patients on polypharmacy. Seoul Metropolitan Council Secretariat. 2021. URL: https://books.google.co.kr/books?id=mdOgzwEACAAJ [accessed 2025-12-31]
5. Drug utilization review system of South Korea. Health Insurance Review & Assessment Service. 2022. URL: https://www.hira.or.kr/dummy.do?pgmid=HIRAA990001000330 [accessed 2025-12-31]
6. Ishizaki T, Mitsutake S, Hamada S, Teramoto C, Shimizu S, Akishita M, et al. Drug prescription patterns and factors associated with polypharmacy in >1 million older adults in Tokyo. Geriatr Gerontol Int 2020 Apr;20(4):304-311. [doi: 10.1111/ggi.13880] [Medline: 32048453]
7. George CJ, Verghese J, Izzetoglu M, Wang C, Holtzer R. The effect of polypharmacy on prefrontal cortex activation during single and dual task walking in community dwelling older adults. Pharmacol Res 2019 Jan;139:113-119 [FREE Full text] [doi: 10.1016/j.phrs.2018.11.007] [Medline: 30408573]
8. Jyrkkä J, Enlund H, Korhonen MJ, Sulkava R, Hartikainen S. Patterns of drug use and factors associated with polypharmacy and excessive polypharmacy in elderly persons: results of the Kuopio 75+ study: a cross-sectional analysis. Drugs Aging 2009;26(6):493-503. [doi: 10.2165/00002512-200926060-00006] [Medline: 19591524]
9. Aparasu RR, Mort JR, Brandt H. Polypharmacy trends in office visits by the elderly in the United States, 1990 and 2000. Res Social Adm Pharm 2005 Sep;1(3):446-459. [doi: 10.1016/j.sapharm.2005.06.004] [Medline: 17138489]
10. Li M, Wei N, Shi H, Jing X, Kan X, Gao H, et al. Prevalence and clinical implications of polypharmacy and potentially inappropriate medication in elderly patients with heart failure: results of six months' follow-up. J Geriatr Cardiol 2023 Jul 28;20(7):495-508 [FREE Full text] [doi: 10.26599/1671-5411.2023.07.002] [Medline: 37576481]
11. Zhao Y, Wang J, Zhu X, Zhang X, Zhang Y, Zhang W, et al. Multimorbidity and polypharmacy in hospitalized older patients: a cross-sectional study. BMC Geriatr 2023 Jul 11;23(1):423 [FREE Full text] [doi: 10.1186/s12877-023-04109-4] [Medline: 37434147]
12. Chavarro-Carvajal DA, Sánchez DC, Vargas-Beltran MP, Venegas-Sanabria LC, Muñoz OM. Clinical value of Hospital Admission Risk Profile (HARP) and the Identification of Seniors at Risk (ISAR) scales to predict hospital-associated functional decline in an acute geriatric unit in Colombia. Colomb Med (Cali) 2023;54(1):e2005304 [FREE Full text] [doi: 10.25100/cm.v54i1.5304] [Medline: 37440979]
13. Al Farsi RS, Al Alawi AM, Al Huraizi AR, Al-Saadi T, Al-Hamadani N, Al Zeedy K, et al. Delirium in medically hospitalized patients: prevalence, recognition and risk factors: a prospective cohort study. J Clin Med 2023 Jun 07;12(12):3897 [FREE Full text] [doi: 10.3390/jcm12123897] [Medline: 37373591]
14. Masnoon N, Shakib S, Kalisch-Ellett L, Caughey GE. What is polypharmacy? A systematic review of definitions. BMC Geriatr 2017 Oct 10;17(1):230 [FREE Full text] [doi: 10.1186/s12877-017-0621-2] [Medline: 29017448]
15. Cresswell KM, Fernando B, McKinstry B, Sheikh A. Adverse drug events in the elderly. Br Med Bull 2007;83:259-274. [doi: 10.1093/bmb/ldm016] [Medline: 17580312]
16. Hanlon JT, Schmader KE, Koronkowski MJ, Weinberger M, Landsman PB, Samsa GP, et al. Adverse drug events in high risk older outpatients. J Am Geriatr Soc 1997 Aug;45(8):945-948. [doi: 10.1111/j.1532-5415.1997.tb02964.x] [Medline: 9256846]
17. Mabuchi T, Hosomi K, Yokoyama S, Takada M. Polypharmacy in elderly patients in Japan: analysis of Japanese real-world databases. J Clin Pharm Ther 2020 Oct;45(5):991-996. [doi: 10.1111/jcpt.13122] [Medline: 31986233]
18. Standardized data: the OMOP Common Data Model. Observational Health Data Science and Informatics. URL: https://www.ohdsi.org/data-standardization/the-common-data-model [accessed 2024-03-31]
19. Voss EA, Makadia R, Matcho A, Ma Q, Knoll C, Schuemie M, et al. Feasibility and utility of applications of the common data model to multiple, disparate observational health databases. J Am Med Inform Assoc 2015 May;22(3):553-564 [FREE Full text] [doi: 10.1093/jamia/ocu023] [Medline: 25670757]
20. ATC/DDD Index 2025. Norwegian Institute of Public Health. URL: https://atcddd.fhi.no/atc_ddd_index [accessed 2022-10-12]
21. Mair A. Medication safety in polypharmacy: technical report. World Health Organization. 2019. URL: https://www.who.int/publications/i/item/medication-safety-in-polypharmacy-technical-report [accessed 2025-11-01]

XSL•FO
RenderX

22. van Poelgeest E, Seppala L, Bahat G, Ilhan B, Mair A, van Marum R, et al. Optimizing pharmacotherapy and deprescribing strategies in older adults living with multimorbidity and polypharmacy: EuGMS SIG on pharmacology position paper. Eur Geriatr Med 2023 Dec;14(6):1195-1209 [FREE Full text] [doi: 10.1007/s41999-023-00872-0] [Medline: 37812379]
23. Multimorbidity: clinical assessment and management. National Institute for Health and Care Excellence. 2016. URL: https://www.nice.org.uk/guidance/ng56 [accessed 2025-11-01]
24. Young EH, Pan S, Yap AG, Reveles KR, Bhakta K. Polypharmacy prevalence in older adults seen in United States physician offices from 2009 to 2016. PLoS One 2021;16(8):e0255642 [FREE Full text] [doi: 10.1371/journal.pone.0255642] [Medline: 34343225]
25. Vetrano DL, Landi F, De Buyser SL, Carfì A, Zuccalà G, Petrovic M, et al. Predictors of length of hospital stay among older adults admitted to acute care wards: a multicentre observational study. Eur J Intern Med 2014 Jan;25(1):56-62. [doi: 10.1016/j.ejim.2013.08.709] [Medline: 24054859]
26. Sganga F, Vetrano DL, Volpato S, Cherubini A, Ruggiero C, Corsonello A, et al. Physical performance measures and polypharmacy among hospitalized older adults: results from the CRIME study. J Nutr Health Aging 2014;18(6):616-621 [FREE Full text] [doi: 10.1007/s12603-014-0029-z] [Medline: 24950153]
27. Onder G, Liperoti R, Fialova D, Topinkova E, Tosato M, Danese P, et al. Polypharmacy in nursing home in Europe: results from the SHELTER study. J Gerontol A Biol Sci Med Sci 2012 Jun;67(6):698-704. [doi: 10.1093/gerona/glr233] [Medline: 22219520]
28. Chan DD, Hao Y, Wu S. Polypharmacy among disabled Taiwanese elderly: a longitudinal observational study. Drugs Aging 2009;26(4):345-354. [doi: 10.2165/00002512-200926040-00005] [Medline: 19476401]
29. Jyrkkä J, Enlund H, Korhonen MJ, Sulkava R, Hartikainen S. Polypharmacy status as an indicator of mortality in an elderly population. Drugs Aging 2009;26(12):1039-1048. [doi: 10.2165/11319530-000000000-00000] [Medline: 19929031]
30. Kim HA, Shin JY, Kim MH, Park BJ. Prevalence and predictors of polypharmacy among Korean elderly. PLoS One 2014;9(6):e98043 [FREE Full text] [doi: 10.1371/journal.pone.0098043] [Medline: 24915073]
31. Conway J, Eddelbuettel D, Nishiyama T, Prayaga S, Tiffin N. RPostgreSQL: R Interface to the 'PostgreSQL' Database System. 2025. URL: https://cran.r-project.org/web/packages/RPostgreSQL/index.html [accessed 2026-01-02]
32. Grothendieck G. sqldf: Manipulate R Data Frames Using SQL. 2017. URL: https://cran.r-project.org/web/packages/sqldf/index.html/ [accessed 2026-01-02]
33. Wickham H, François R, Henry L, Müller K, Vaughan D. dplyr: A Grammar of Data Manipulation. 2025. URL: https://cran.r-project.org/web/packages/dplyr/index.html/ [accessed 2026-01-02]
34. Barrett T, Dowle M, Srinivasan A, Gorecki J, Chirico M, Hocking T. data.table: Extension of 'data.frame'. 2025. URL: https://cran.r-project.org/web/packages/data.table/index.html [accessed 2026-01-02]
35. Moon K. R statistics and graphs for medical papers. 2015. URL: https://cran.r-project.org/web/packages/moonBook/index.html [accessed 2026-01-02]
36. Wickham H. ggplot2: Elegant Graphics for Data Analysis. New York, NY: Springer-Verlag New York; 2016. ISBN: 978-3-319-24277-4.
37. Drug code mapping information. Korea Pharmaceutical Information Service. 2019. URL: https://biz.kpis.or.kr/index.html [accessed 2022-10-01]
38. Ataei SM, Golestani A, Khosravi S, Tabatabaei-Malazy O, Malekpour M, Ebrahimpur M, et al. Medication use patterns and polypharmacy among elderly in Iran: a cross-sectional study using national health insurance claims data. BMJ Open 2025 Aug 21;15(8):e097863 [FREE Full text] [doi: 10.1136/bmjopen-2024-097863] [Medline: 40840984]
39. Cho HJ, Chae J, Yoon S, Kim D. Factors related to polypharmacy and hyper-polypharmacy for the elderly: a nationwide cohort study using National Health Insurance data in South Korea. Clin Transl Sci 2023;16(2):193-205 [FREE Full text] [doi: 10.1111/cts.13438] [Medline: 36401587]
40. Viktil KK, Blix HS, Eek AK, Davies MN, Moger TA, Reikvam A. How are drug regimen changes during hospitalisation handled after discharge: a cohort study. BMJ Open 2012;2(6):e001461 [FREE Full text] [doi: 10.1136/bmjopen-2012-001461] [Medline: 23166124]
41. Oh YH. The health status of older Koreans and policy considerations. Health and Welfare Policy Forum 2015;223:29-39. [doi: 10.23062/2015.05.4]
42. Kuribayashi R, Hasebe S, Ishida D, Hirose S, Mimori S, Takizawa T, et al. An age-stratified cross-sectional study of antidiabetic and non-antidiabetic drugs prescribed to Japanese outpatients with diabetes. Glob Health Med 2023 Oct 31;5(5):294-300 [FREE Full text] [doi: 10.35772/ghm.2023.01059] [Medline: 37908508]
43. Remelli F, Ceresini MG, Trevisan C, Noale M, Volpato S. Prevalence and impact of polypharmacy in older patients with type 2 diabetes. Aging Clin Exp Res 2022 Sep;34(9):1969-1983 [FREE Full text] [doi: 10.1007/s40520-022-02165-1] [Medline: 35723858]
44. Komagamine J. Characteristics of the use of cold combination products among older ambulatory patients at the National Hospital Organization Tochigi Medical Center in Japan: a retrospective single-center observational study. BMC Res Notes 2017 Dec 08;10(1):728 [FREE Full text] [doi: 10.1186/s13104-017-3070-2] [Medline: 29221489]

XSL•FO
RenderX

45. Sefera B, Sheleme T, Dechasa M, Ararame GG. Determinants of polypharmacy among ambulatory cardiovascular disease patients in Iluababora and Buno Bedele Zones, Ethiopia: prospective observational study. BMC Cardiovasc Disord 2025 Jul 04;25(1):468 [FREE Full text] [doi: 10.1186/s12872-025-04929-9] [Medline: 40615951]
46. Ockerman A, Vanassche T, Garip M, Vandenbriele C, Engelen MM, Martens J, et al. Tranexamic acid for the prevention and treatment of bleeding in surgery, trauma and bleeding disorders: a narrative review. Thromb J 2021 Aug 11;19(1):54 [FREE Full text] [doi: 10.1186/s12959-021-00303-9] [Medline: 34380507]
47. Gibbs VN, Champaneria R, Sandercock J, Welton NJ, Geneen LJ, Brunskill SJ, et al. Pharmacological interventions for the prevention of bleeding in people undergoing elective hip or knee surgery: a systematic review and network meta-analysis. Cochrane Database Syst Rev 2024 Jan 16;1(1):CD013295 [FREE Full text] [doi: 10.1002/14651858.CD013295.pub2] [Medline: 38226724]
48. Huang Y, Steptoe A, Wei L, Zaninotto P. The impact of high-risk medications on mortality risk among older adults with polypharmacy: evidence from the English Longitudinal Study of Ageing. BMC Med 2021 Dec 16;19(1):321 [FREE Full text] [doi: 10.1186/s12916-021-02192-1] [Medline: 34911547]
49. Pereira LB, Gonçalves AMRF, Fernandes CSE, Fontanella AT, Francisco PMSB, Mengue SS, et al. Use of drugs for gastrointestinal disorders: evidence from National Survey on Access, Use and Promotion of Rational Use of Medicines. Einstein (Sao Paulo) 2020;18:eAO5314 [FREE Full text] [doi: 10.31744/einstein_journal/2020ao5314] [Medline: 32785451]
50. Korean Statistical Information Service. Main surgery statistical yearbook. Statistical Database. 2016. URL: https://kosis.kr/eng/statisticsList/statisticsListIndex.do?menuId=M_01_01&vwcd=MT_ETITLE&parmTabId=M_01_01&parentId=F.1;F_10.2;#content-group [accessed 2025-12-24]
51. Al-Qurain AA, Gebremichael LG, Khan MS, Williams DB, Mackenzie L, Phillips C, et al. Prevalence and factors associated with analgesic prescribing in poly-medicated elderly patients. Drugs Aging 2020 Apr;37(4):291-300. [doi: 10.1007/s40266-019-00742-0] [Medline: 32016823]
52. Al-Qurain AA, Gebremichael LG, Khan MS, Williams DB, Mackenzie L, Phillips C, et al. Opioid prescribing and risk of drug-opioid interactions in older discharged patients with polypharmacy in Australia. Int J Clin Pharm 2021 Apr;43(2):365-374. [doi: 10.1007/s11096-020-01191-1] [Medline: 33206289]
53. Editage. URL: https://www.editage.co.kr/ [accessed 2024-04-10]

Abbreviations

ADE: adverse drug event
ATC: Anatomical Therapeutic Chemical
CDM: Common Data Model
EDI: electronic data interchange
EHR: electronic health record
OMOP: Observational Medical Outcomes Partnership
OS: operating system
WHO: World Health Organization

Edited by A Benis; submitted 01.Jun.2025; peer-reviewed by H Demir, YS Lo; comments to author 06.Oct.2025; revised version received 28.Nov.2025; accepted 17.Dec.2025; published 29.Jan.2026.

Please cite as:
Lee CC, Kim GJ, Kim S, Hong JY, Hwang WM, Kim JY, Lee KH, Kim K, Kang M, Kim JH, Lee S
Multi-Institutional Drug Use Patterns in Hospitalized Older Patients: Retrospective Cross-Sectional Study
JMIR Med Inform 2026;14:e78353
URL: https://medinform.jmir.org/2026/1/e78353
doi:10.2196/78353
PMID:

©Chung Chun Lee, Grace Juyun Kim, Suhyun Kim, Jee Young Hong, Won Min Hwang, Jong-Yeup Kim, Kye Hwa Lee, Kwangsoo Kim, Mingyu Kang, Ju Han Kim, Suehyun Lee. Originally published in JMIR Medical Informatics (https://medinform.jmir.org), 29.Jan.2026. This is an open-access article distributed under the terms of the Creative Commons Attribution License (https://creativecommons.org/licenses/by/4.0/), which permits unrestricted use, distribution, and reproduction in any medium, provided the original work, first published in JMIR Medical Informatics, is properly cited. The complete bibliographic information, a link to the original publication on https://medinform.jmir.org/, as well as this copyright and license information must be included.

XSL•FO
RenderX

Original Paper

Harmonizing Logical Observation Identifiers Names and Codes (LOINC) Codes and Units in Real-World Oncology Data: Method Development and Evaluation

Parvati Naliyatthaliyazchayil[1], PharmD, MS; Travis Stenerson[1], MHI, MD

ConcertAI, LLC, Cambridge, MA, United States

Corresponding Author:
Parvati Naliyatthaliyazchayil, PharmD, MS
ConcertAI, LLC
1120 Massachusetts Ave.
Cambridge, MA, 02138
United States
Phone: 1 317 985 7429
Email: parumenon.pm@gmail.com

Abstract

Background: The expanding use of multisource real-world electronic health record (EHR) and claims data offers major opportunities for research, drug discovery, and clinical decision support. While standards such as Logical Observation Identifiers Names and Codes (LOINC) can ensure semantic interoperability for laboratory observations, clinical documents, and other clinical terms, properly assigning these concepts remains a challenge. Studies show that 6% to 19% of laboratory tests cannot be accurately mapped to LOINC. Existing systems try to address this challenge but often depend on source data strings and other input features that may be absent, null, or incorrect. This underscores the need for a scalable approach to correct LOINC code assignments, standardize units, and ensure data integrity across multisource laboratory data.

Objective: This paper presents a universally applicable framework that identifies and corrects observable errors in quantitative laboratory results coded to LOINC and the Systematized Nomenclature of Medicine for the unit of measure without relying on raw source data strings. The process seeks to improve the accuracy, conformance, consistency, and completeness of laboratory data while maintaining complete provenance.

Methods: The proposed framework uses a 2-step process. First, LOINC codes are corrected using the associated unit of measure. Second, units are adjusted or populated to match a preferred unit for that LOINC code. In both steps, the quantitative result is checked against a predefined acceptable range to determine validity. The process is driven by 3 knowledge tables. The framework is applied to datasets derived from the ConcertAI database of approximately 10 million patients with cancer, evaluating improvements in LOINC code–unit conformance and unit completeness. Analyses are performed on 4 independently LOINC-coded datasets: the full ConcertAI dataset and 3 high-volume diverse subsets grouped by data source or EHR vendor.

Results: A total of 428 LOINC codes were observed across 6.34 billion records in the ConcertAI database. All 4 datasets were processed using the proposed framework. Before applying the framework, 73.1% (4,634,610,173/6,337,101,453) of records in the ConcertAI dataset had correctly assigned units based on the laboratory reasonable range table; after application, this increased to 99.7% (6,322,375,200/6,341,230,213). Similar improvements were observed across the 3 EHR-specific datasets, increasing from 78.5% (691,315,390/880,250,137) to 99.8% (879,626,472/881,157,852; source 1), 71.4% (2,132,455,936/2,985,465,124) to 99.8% (2,982,319,644/2,988,173,959; source 2), and 63.3% (2,936,710,502/4,640,432,294) to 99.6% (4,618,714,114/4,638,862,412; source 3). Unit completeness also improved substantially, increasing from 92.7% (5,879,071,858/6,341,230,213) to 99.8% (6,331,923,060/6,341,230,213) in the ConcertAI dataset and from 92.5% (814,867,241/881,157,852) to 100% (880,816,133/881,157,852), 94.4% (2,822,107,252/2,988,173,959) to 99.9% (2,986,624,027/2,988,173,959), and 91.7% (4,254,054,966/4,638,862,412) to 99.8% (4,632,935,919/4,638,862,412) in sources 1 to 3, respectively.

Conclusions: Laboratory data quality is crucial in oncology systems for therapy selection, monitoring, and disease progression assessment. This proposed solution is a first-of-its-kind, system-agnostic, and scalable normalization process that addresses key gaps in laboratory data quality across multiple dimensions.

XSL•FO
RenderX

(JMIR Med Inform 2026;14:e81254) doi:10.2196/81254

KEYWORDS

real-world data; laboratory data; harmonization; standardization; oncology; health care system; electronic health record; multisourced data; structured data; mapping; Fast Healthcare Interoperability Resources; FHIR; Logical Observation Identifiers Names and Codes; LOINC; Systematized Nomenclature of Medicine; SNOMED; unit conversion

Introduction

Background: Real-World Data in Health Care

Multisourced, comprehensive patient health data have seen a recent rise in prominence and utility in supporting research, drug discovery, pharmacovigilance, and clinical decision support [1]. These real-world data (RWD) are collected for individual patient care and reimbursement in often unconnected systems such as electronic health records (EHRs) and claims clearing houses [2]. Secondary use of RWD holds immense potential for improving health due to its volume, variety, and ubiquity [3].

The different source systems producing RWD bring individual challenges and opportunities, and it is often necessary to stitch together disparate sources to cover a complete patient journey [3]. For instance, medical claims may contain procedures and tests performed on a patient and their associated costs, but the results of those tests are only present in the EHR [4].

Data Quality and Semantic Interoperability Challenges

The path to a usable RWD dataset is fraught with challenges [2]. Errors can arise from any system or actor that generates, transmits, transforms, or persists the data during its lifetime [5]. Errors can be discernible from patterns observed in the data or can be hidden from downstream users when information is lost [6]. Information loss can result in incorrectness or missingness of variables, records, tables, or complete data sources [7]. Monitoring and minimizing information loss is a critical requirement of an RWD pipeline.

Semantic interoperability (SI), or the ability to ensure the same meaning and interpretation of data shared between systems [8], is a well-established and ongoing challenge in RWD [5]. It can manifest as redundant representations of the same concept, such as one EHR using the *International Classification of Diseases, 10th Revision, Clinical Modification*, and another using the Systematized Nomenclature of Medicine (SNOMED) to represent the same disease. Use of data standards and common ontologies can alleviate SI challenges but can also introduce errors if used incorrectly [5], which can commonly occur when a concept is assigned to a string by either a human or machine [9]. As health care data systems continue to evolve, the importance of SI is underscored by the increasing adoption of standards such as Fast Healthcare Interoperability Resources (FHIR) [10] with its associated code system bindings supported by the Food and Drug Administration, which are designed to ensure consistent data interpretation and improve interoperability across systems. Even FHIR-based representations may fall short in fully addressing semantic mismatches, particularly for complex domains such as laboratory data, in which variability in coding, units, and local conventions persists despite standardization efforts [11].

Laboratory Data and Logical Observation Identifiers Names and Codes Mapping Challenges

Laboratory result data are both valuable and particularly challenging in RWD [9]. To address SI, laboratory data primarily rely on codes from the Logical Observation Identifiers Names and Codes (LOINC) code system [12,13]. LOINC is the dominant global coding system for laboratory concepts but also extends to a broader range of clinical terms, including clinical questions and documents [12-15]. LOINC consists of concepts that have 6 attributes each. These include the analyte tested, how it is observed, the duration of observation, and the sample type that the observation is performed on [13]. Precoordinating that much information into a single concept makes it convenient for transmission by reducing the potential for misinterpretation but also makes it difficult to use when mapping to LOINC [14,15]. The complete information for LOINC mapping is rarely present in a single string, column, or record [15]. Relevant information may be spread across one or more fields in a record or laboratory information system, such as the observation's display string (eg, glucose), the data type of the result (numeric or categorical), the unit of measure (mass over volume or molarity), the associated order name or panel name (complete blood count or urinalysis), the associated sample (urine or blood), the device or equipment used to make the observation (urine dipstick or continuous glucose monitor), or other observations that occurred as part of the same panel of tests (Is the patient fasting?). Despite the abundance of resources, accurately translating these fields to the correct LOINC code remains a challenge.

This semantic and translational complexity means that laboratory results in RWD can frequently present with errors introduced during terminology binding to LOINC [16]. Prior studies have shown that LOINC codes could not be assigned for 6% to 19% of laboratory tests due to incomplete or incorrect information [17]. Systems have been proposed to reduce this error by coding via automated means in RWD [9,16,18] and clinical trial data [19]. These algorithms rely on source data strings and other input features that may be absent, null, or observably incorrect.

Unit of Measure and Normalization Challenges

The diversity of information required for LOINC mapping increases the likelihood of mapping difficulty [20] and significant information loss. If a result's unit of measure is absent or recorded in the wrong place or the associated panel name, order name, or sample type is missing from the data, it can mean insufficient information to properly assign the LOINC code [15]. Contextually appropriate filling in of absent units of measure has been shown to be effective in a system that extracts logical expressions from clinical trial inclusion criteria pertaining to quantitative laboratory results but not within RWD [21].

XSL•FO
RenderX

A laboratory result may present with a correct concept code, but it is possible to represent the same result using multiple scales (g or mg), and certain units are used interchangeably between sources (mg per day or mg per 24 hours). Unit normalization is necessary to ensure comparable results during data analysis and aggregation, and the variety of representation, the missingness, and the level of incorrectness can all lead to loss of utility of RWD. Even with a correct LOINC code, missing or inconsistent units have been shown to affect as much as 14% of laboratory records in some systems [22,23]. Mechanisms to normalize synonymous units exist, but these techniques do not handle situations in which the unit is incomplete, incorrect, or completely absent [24].

Proposed Framework and Objective: Correcting Quantitative Laboratory Results

In this paper, we present a framework to identify and correct observable errors in quantitative laboratory results that have already been coded to LOINC for the observation and SNOMED for the unit of measure without reliance on source data strings. This 2-step process first adjusts the LOINC code by using information contained in the associated unit of measure. Next, we use the quantitative result to inform whether we can safely populate a missing unit of measure or correct an erroneous unit of measure. Finally, all synonymous or related units are normalized to a single preselected unit for each LOINC code. We characterize the prevalence of these errors and then use this framework to correct laboratory results in a multisource RWD pipeline of oncology patient data from EHRs, laboratory information systems, and medical claims.

Methods

This section outlines the data collection and study design used to develop this framework.

Data Collection

Laboratory result data were extracted from the ConcertAI database, a US-based, deidentified, patient-level dataset from approximately 10 million patients with cancer aged ≥18 years during the period from 2015 to 2025. The data used in this study were sourced from EHRs, including oncology practices, hospitals, and academic medical centers. To evaluate the framework, we analyzed 4 laboratory datasets: the full ConcertAI database and 3 subsets corresponding to the individual EHR sources (represented as source 1, source 2, and source 3) that transmitted data to ConcertAI. These 3 subsets were selected because they were the top contributors of laboratory data by volume and represented a broad diversity of laboratory tests. Specifically, the ConcertAI database accounted for 6.34 billion records, source 1 included 880 million records, source 2 included 2.98 billion records, and source 3 included 4.64 billion records.

Data were contributed by multiple clinical sites and laboratories across the United States, representing a diverse group of care settings. Each dataset was standardized using LOINC codes for laboratory observations and SNOMED codes for units of measure. For records from the full ConcertAI database, LOINC codification was performed using ConcertAI's internal system; for EHR or data source–derived subsets, the LOINC codes that were delivered with those data were used. Only records with a numeric value were used in this study. All datasets used ConcertAI's unit codification that maps unit strings to SNOMED.

System Design

The laboratory correction framework was applied after standardization to LOINC and SNOMED. The laboratory correction system relies on 3 knowledge tables that have been manually created after careful examination of the ConcertAI laboratory data, as outlined below. Their role in supporting the logical framework is discussed later in this section. Below, we provide the formal definitions of these tables, including their constituent fields and primary keys. The procedures used to create each table and the column definitions are documented in Multimedia Appendix 1.

The LOINC conversion map (LCM) relates a LOINC concept and unit concept that are incongruous to a new LOINC code that is compatible with the unit of measure. The table structure incorporates the following computable fields: "old_loinc_code," "old_loinc_display," "old_loinc_system," "unit_code," "unit_display," "unit_system," "new_loinc_code," "new_loinc_display," and "new_loinc_system." The primary key for the table is defined as the composite of "old_loinc_code" and "unit_code." Examples are shown in Table 1, which has been formatted for readability. The complete computable version is available in Multimedia Appendix 1 and in the accompanying GitHub repository to support transparency and reproducibility.

Table 1. Logical Observation Identifiers Names and Codes (LOINC) conversion map.

LOINC code	Unit (SNOMED[a])	Corrected LOINC code
Platelets (#/volume) in blood (26515-7)	fL (258775009)	Platelet (entitic mean volume) in blood (28542-9)
Glucose (mass/volume) in blood (26515-7)	mEq/L (258865000)	Glucose (moles/volume) in blood (15074-8)
Glucose (mass/volume) in blood (26515-7)	mmol/L (258813002)	Glucose (moles/volume) in blood (15074-8)
Kappa light chains (mass/volume) in serum or plasma (11050-2)	Percentage (118582008)	Kappa lymphocytes/lymphocytes in blood (17096-9)

[a]SNOMED: Systematized Nomenclature of Medicine.

The reasonable range map defines metadata about a single LOINC code, including its assigned correct unit of measure, a minimum and maximum value that the laboratory test can reasonably take, and the mean and median of records with that LOINC code and unit across all 4 datasets. The correct unit of measure for each LOINC code was determined using the

XSL•FO
RenderX

"example_unit" supplied in the official LOINC distribution. These units were mapped to the corresponding SNOMED codes. For LOINC codes that listed more than one example unit, we examined the empirical distribution of units observed in our dataset and selected the unit with the highest frequency. This made the choice of the correct unit data driven and ensured that the process could be consistently reproduced in any system. If Unified Code for Units of Measure (UCUM) units are preferred, LOINC also provides "example_ucum_units," which can be incorporated similarly. Minimum and maximum reasonable values for each LOINC code were defined by estimating the empirical distribution of the data through quantiles of 0.005, 0.025, 0.16, 0.5 (median), 0.84, 0.975, and 0.995. The range was set at or near the highest and lowest of those quantiles, providing broad yet data-anchored thresholds for plausibility checking.

This knowledge table includes the following computable fields: "loinc_code, loinc_name," "unit_code," "unit_name," "min_reasonable," "max_reasonable," "mean," and "median." The primary key for this table is the "loinc_code." A readability-optimized version is shown in Table 2, whereas the complete computable version is provided in Multimedia Appendix 1 and the GitHub repository.

Table 2. Reasonable range map.

LOINC[a] code	Unit (SNOMED[b])	Reasonable range	Median	Mean
Platelets (#/volume) in blood (26515-7)	×10(3)/mcL (1287856009)	1-800	223.5	215.0
Glucose (mass/volume) in blood (2339-0)	mg/dL (258797006)	40-400	138.8	121
Kappa light chains (mass/volume) in serum or plasma (11050-2)	mg/L (258796002)	0.1-5000	68.7	25.9

[a]LOINC: Logical Observation Identifiers Names and Codes.

[b]SNOMED: Systematized Nomenclature of Medicine.

The unit multiplier map relates a correct unit to a synonymous, convertible, or incorrect unit along with a multiplier value, an additive scalar value, and a description of the relationship between the 2 units (eg, incorrect, synonym, or convertible). The scalar value is only used for temperature conversions. An empty "incorrect unit" represents a null unit field and is used to populate absent units. This knowledge table includes the following computable fields: "incorrect_unit_code," "incorrect_unit_name," "correct_unit_code," "correct_unit_name," "multiplier," "scalar_constant," and "multiplier_type." The primary key is the composite of "incorrect_unit_code," "correct_unit_code," and "multiplier_type." A readability-optimized version is shown in Table 3, with the full computable version available in Multimedia Appendix 1 and the GitHub repository.

Table 3. Unit multiplier map.

Incorrect unit (SNOMED[a])	Correct unit (SNOMED)	Multiplier	Scalar	Multiplier type (description)
<null>	×10(3)/mcL (1287856009)	1	0	"nullfill" (unit absent)
10*9/L (277288007)	×10(3)/mcL (1287856009)	1	0	"synonym"
cells/µL (258878000)	×10(3)/mcL (1287856009)	0.001	0	"unit_conversion" (convertible unit)
cells/µL (258878000)	×10(3)/mcL (1287856009)	1	0	"unit_typo" (known unit error)
g/dL (258795003)	mg/dL (258797006)	1000	0	"unit_conversion" (convertible unit)
g/dL (258795003)	mg/dL (258797006)	1	0	"unit_typo" (known unit error)
g/L (258794004)	mg/dL (258797006)	1	0	"unit_conversion" (convertible unit)

[a]SNOMED: Systematized Nomenclature of Medicine.

The framework logic is shown in Figure 1. Conformance to the selected "correct" unit is checked against the laboratory reasonable range (LRR) table entry. If the unit does not conform, the LCM provides a better LOINC code if one is known for the unit that is present in the record. In the second transformation, the unit is altered according to the unit multiplier map, normalized if it is a synonym, converted using a multiplier value, or swapped for the correct unit if it is a known error pattern or absent altogether. For example, the LOINC code 1920-8 (glucose [mass/volume] in blood) has the correct unit "mg/dL." If a record with this LOINC code has the unit "mmol/L," the LOINC code is changed using the LCM to 15074-8 (glucose [moles/volume] in blood). The process is only 2 steps, although not all records require both. Records may begin with LOINC code–unit conformance and skip the process altogether. Some require only LOINC conversion, some require only unit normalization, and many require LOINC conversion and then unit normalization.

XSL•FO
RenderX

Figure 1. Framework logic and knowledge table use. LCM: Logical Observation Identifiers Names and Codes (LOINC) conversion map; LRR: laboratory reasonable range; SNOMED: Systematized Nomenclature of Medicine; UMM: unit multiplier map.

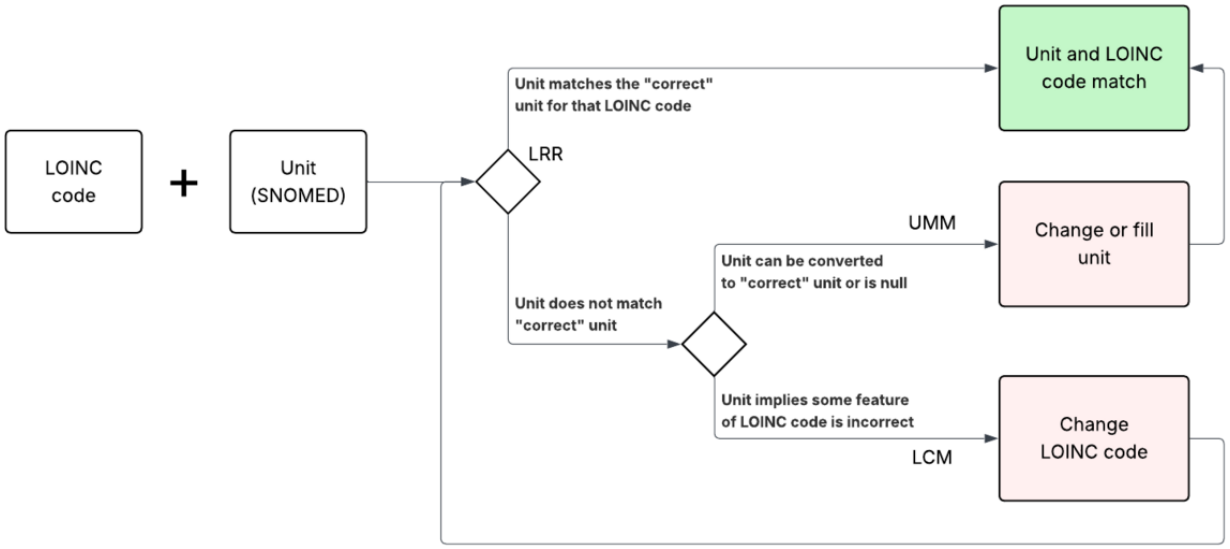

Each of these transformations only proceeds when the record's result value falls within the reasonable range associated with the LOINC code–unit pair that would appear in the transformed record. These ranges were selected using known correct data and designed to capture most possible values in that laboratory's value distribution.

In rare instances, the system must select between 2 possible transformations for the same record. This might occur in the situation visible in rows 5 and 6 in Table 3 when trying to convert from g/dL to mg/dL. We identified a common error in many records in which a unit's prefix was absent. A g/dL unit might be a simple data entry error at the source, or it may, in fact, require conversion by multiplying the result by 1000. The system uses the reasonable ranges to determine which of these 2 situations is more likely. If the reasonable ranges are not disparate enough to discern which transformation is required, proximity to the median of the target LOINC code–unit's distribution is compared. The transformation resulting in a record closer to that median is selected. If the compared laboratory results have medians of 0, distance from the mean is used.

To evaluate the success of each transformation, the value distribution of the output for any individual transformation was compared with the value distribution of known correct data with that LOINC code–unit pair. If the distribution of the numeric result of the transformed data matched that of known correct data, it was considered successful. If the distribution did not match, the discrepancy was investigated. These investigations led to the discovery of common error patterns that could then be accounted for in the next iteration by adding to the 3 knowledge tables.

To summarize, the precedence of the rules described above is as follows:

1. LRR conformance check—if the LOINC code–unit pair conforms to the LRR table, no transformation is applied.
2. LOINC conversion (LCM)—if the unit is incompatible with the LOINC code, the framework first selects the appropriate LOINC code.
3. Unit normalization or conversion (unit multiplier map)—after the LOINC code is finalized, unit normalization or conversion is applied.
4. Range validation—a transformation is only accepted if the resulting value falls within the target LOINC code's reasonable range.
5. Conflict resolution—when more than one unit transformation falls within the reasonable range, the system resolves this by checking proximity to the median of the known correct distribution or proximity to the mean when the distribution median is 0.

A few examples of LOINC code–unit incongruencies and framework processing are outlined in Multimedia Appendix 1.

Provenance is maintained within each transformed record in an attribute that acts as a ledger of each transformation that alters that record. This attribute is an array of objects that includes a descriptive string that details what features of the record were adjusted and what features were used to justify that adjustment for human readability. For computability, "object" includes the adjusted attribute names and preadjustment values for those attributes, ensuring transparency to downstream users and reversibility if necessary.

A summary of the steps for this framework is illustrated in Figure 2.

Figure 3 shows an example of LOINC code–unit pairs before transformation, each step of the transformation, and the final output after transformation.

XSL•FO
RenderX

Figure 2. Summary of the framework. LOINC: Logical Observation Identifiers Names and Codes; SNOMED: Systematized Nomenclature of Medicine.

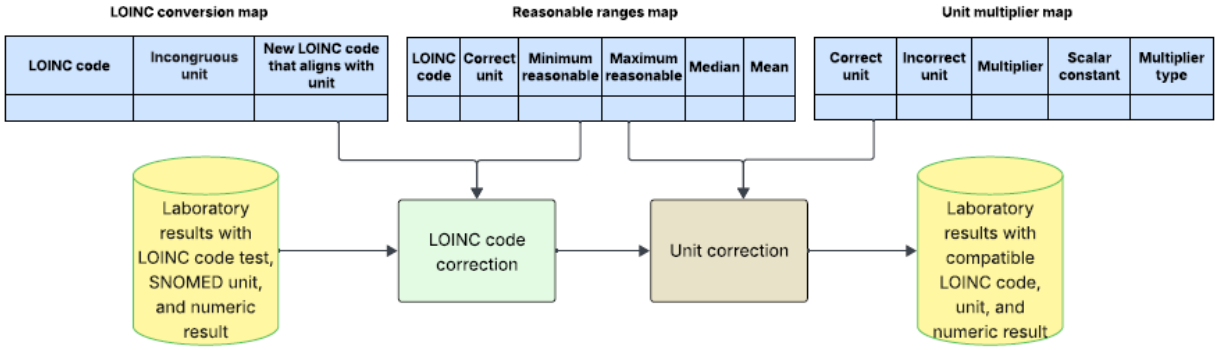

Figure 3. Example of Logical Observation Identifiers Names and Codes (LOINC) code–unit pairs before and after transformation.

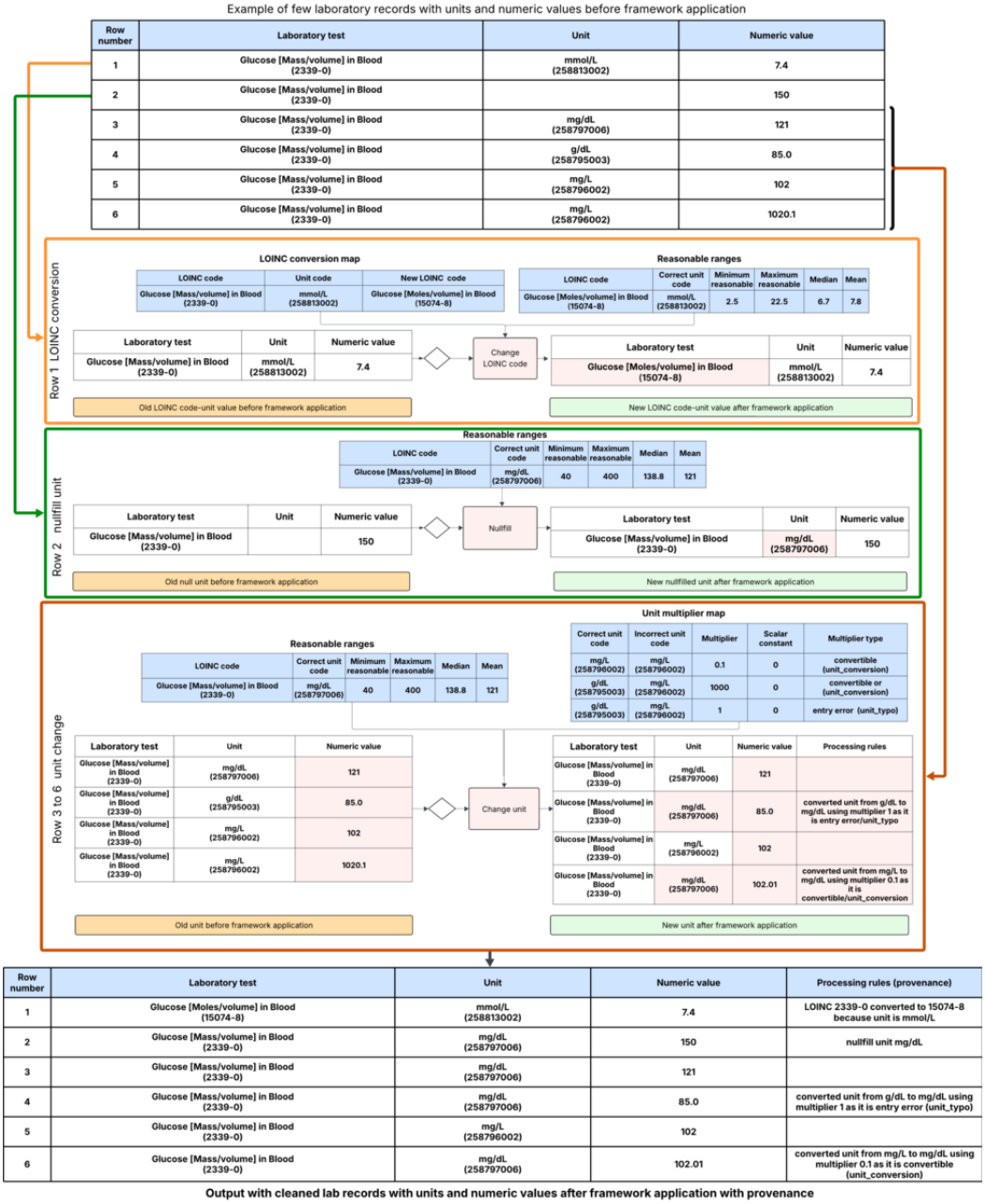

XSL•FO
RenderX

Ethical Considerations

This study used retrospective, deidentified data collected for clinical purposes. All data were fully anonymized before analysis, and unique patient identifiers were removed. Analysis of deidentified secondary data does not constitute human subjects research and does not require formal review or approval by an institutional review board, and thus, no institutional review board approval number was sought. Because only deidentified data were used, informed consent from individual patients was not required. Privacy and confidentiality were maintained throughout the study in accordance with all applicable regulations.

Results

Dataset Collection: Overview and LOINC Coverage

All 4 sets of laboratory data underwent the LOINC code and unit correction process, and the proportion of records exhibiting each LOINC code–unit pattern was calculated both before and after the framework execution. A total of 428 LOINC codes were included in this study, chosen based on their prevalence in the ConcertAI database. Not all datasets contained all 428 LOINC codes. These LOINC codes accounted for 6.34 billion records in the ConcertAI database and 880 million, 2.98 billion, and 4.64 billion records in the source-specific datasets from sources 1, 2, and 3, respectively.

System Design

Impact of Framework on Unit Correction

Before the application of the framework, 73.1% (4,634,610,173/6,337,101,453) records in the ConcertAI dataset with these LOINC codes had the correct unit as assigned by the LRR table. Following the application, this increased to 99.7% (6,322,375,200/6,341,230,213) of records. A similar trend was observed in each of the EHR-specific datasets: 78.5% (691,315,390/880,250,137) to 99.8% (879,626,472/881,157,852), 71.4% (2,132,455,936/2,985,465,124) to 99.8% (2,982,319,644/2,988,173,959), and 63.3% (2,936,710,502/4,640,432,294) to 99.6% (4,618,714,114/4,638,862,412) for sources 1, 2, and 3, respectively. The system increased the completion rate of units, defined as the proportion of records with nonmissing units, from 92.7% (5,879,071,858/6,341,230,213) to 99.8% (6,331,923,060/6,341,230,213) in the ConcertAI dataset and similarly in the other 3 datasets: 92.5% (814,867,241/881,157,852) to 100.0% (880,816,133/881,157,852), 94.4% (2,822,107,252/2,988,173,959) to 99.9% (2,986,624,027/2,988,173,959), and 91.7% (4,254,054,966/4,638,862,412) to 99.9% (4,632,935,919/4,638,862,412) for sources 1, 2, and 3, respectively. Because the framework assigns validated units to previously missing values, improvements in the correct unit rate reflect both corrections to misassigned units and the assignment of correct units to previously missing entries. As a result, the correct unit and completion rate metrics are related but not redundant: the correct unit rate captures accuracy among all populated units, whereas the completion rate captures overall presence of any unit.

LOINC-Level Quality Threshold

Not all LOINC codes start with the same degree of incorrectness. To evaluate the proportion of LOINC codes that reached specific data quality thresholds before and after framework application, records with each LOINC code were evaluated for unit correctness, and the number of LOINC codes passing certain unit correctness proportion thresholds was counted. These counts for each dataset are shown in Figure 4. Of the 428 LOINC codes, the number meeting the 99% threshold of unit correctness in the full ConcertAI dataset increased from 125 (29.2%) to 370 (86.4%). Similar improvements were observed across the 3 source datasets, which contained different total proportions of evaluated LOINC codes: 83.9% (359/428) of LOINC codes in source 1, a total of 93.2% (399/428) of LOINC codes in source 2, and 88.6% (379/428) of LOINC codes in source 3. In source 1, the proportion meeting the 99% threshold increased from 42.9% (154/359) to 86.4% (310/359); in source 2, it increased from 30.8% (123/399) to 87.7% (350/399); and in source 3, it increased from 16.9% (64/379) to 79.7% (302/379).

XSL•FO
RenderX

Figure 4. Number of Logical Observation Identifiers Names and Codes (LOINC)–coded records meeting unit correctness thresholds.

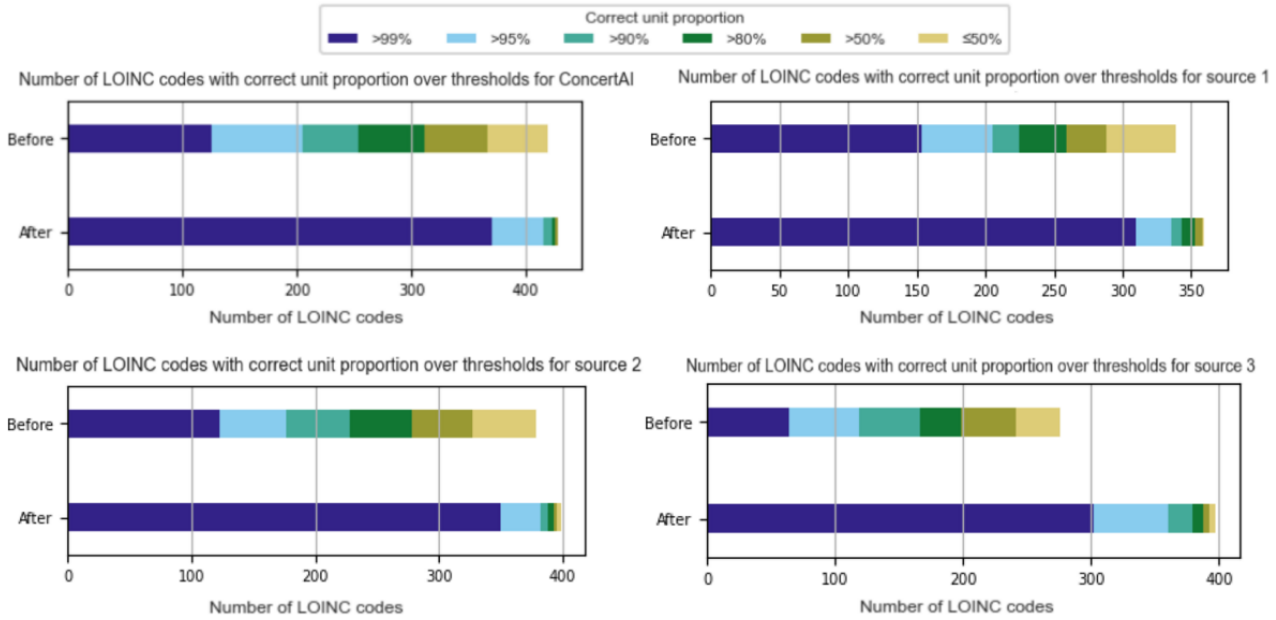

Illustrative Subset Analysis

To provide a more detailed view of the framework's impact, Figure 5 presents a closer look at 20 specific LOINC codes. These codes were selected for their varied domains and types of incongruencies in the starting data.

Records with each of these 20 LOINC codes had their unit classified as correct, synonymous to correct, absent, or incorrect. Incorrect units were subclassified as incorrect and suggestive of a LOINC change, incorrect but convertible to the correct unit through a multiplier, or incorrect but not convertible. These unit categories represent the types of errors that this system is designed to correct. The proportions in each category were calculated before and after the framework application and are shown in Figure 5 for each system.

A detailed report showing the proportion of correctness for each LOINC code across all 4 datasets before and after the framework application is available in Multimedia Appendix 2.

XSL•FO
RenderX

Figure 5. Error type proportions for specific Logical Observation Identifiers Names and Codes (LOINC) codes. GFR: glomerular filtration rate; HPF: high power field; MDRD: Modification of Diet in Renal Disease; SA: surface area; WBC: white blood cell.

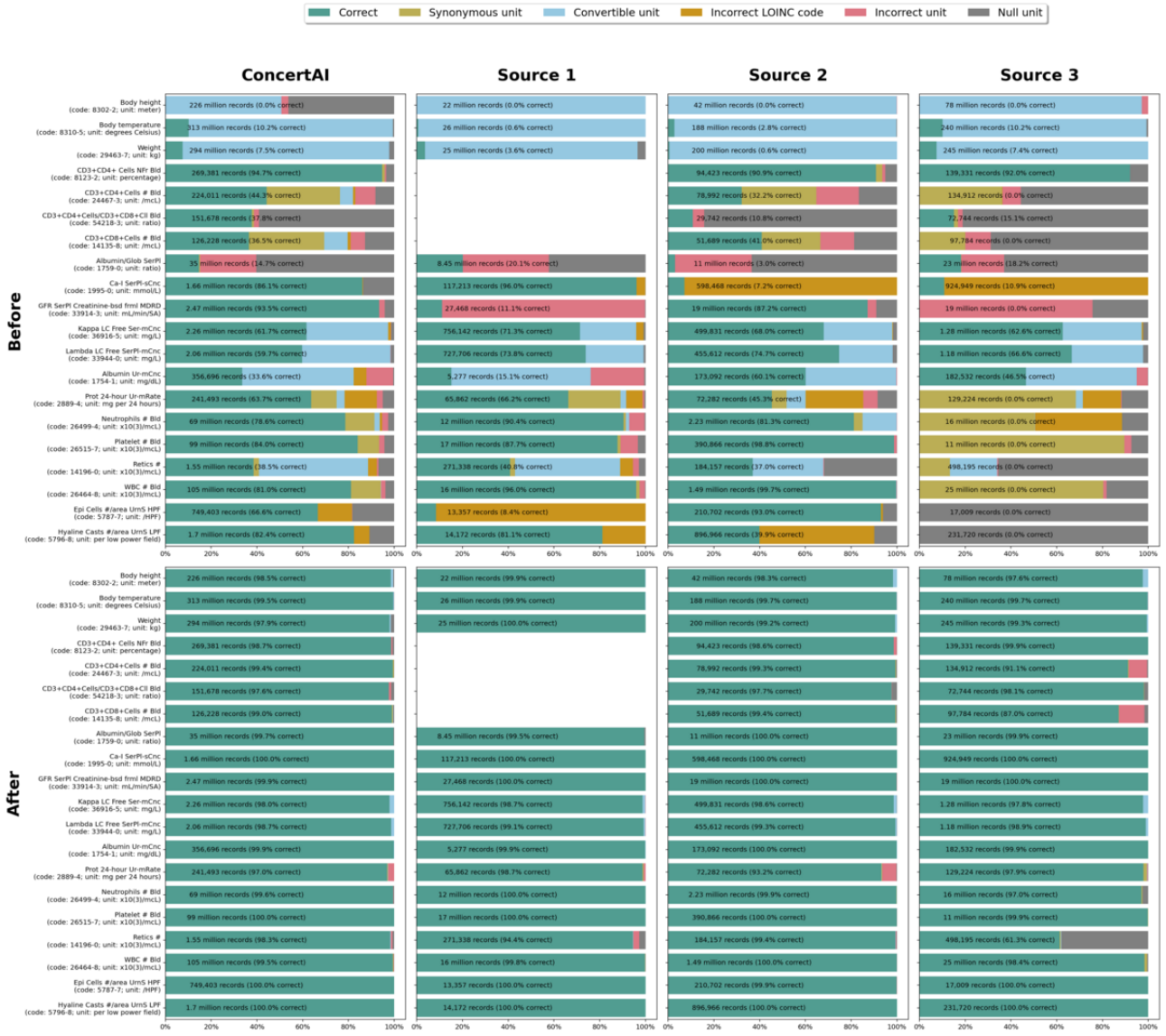

Discussion

Principal Findings

The proposed normalization framework significantly improved LOINC code–unit congruence and unit absentia across all evaluated datasets, demonstrating generalizability to any clinical data system using standard medical terminologies for observation and unit representation. The method improved LOINC code–unit congruence overall in the ConcertAI laboratory dataset from 73.1% (4,634,610,173/6,337,101,453) to 99.7% (6,322,375,200/6,341,230,213), with similar trends in the other 3 data sources. The method and knowledge tables were developed using the ConcertAI data and applied to these independent datasets to demonstrate generalizability. To the best of our knowledge, this framework is the first of its kind to address 2 key gaps: the absence of a system-agnostic process for cleaning multisource laboratory data for secondary use [18] and an approach tailored to RWD. RWD, where data quality is both challenging [25] and critical to data usability, may lack source-specific semantics such as the local observation concept display name. This would impede the use of a standardization process designed to take advantage of those strings [18].

Mechanism of Framework

The process, driven by 3 small, shareable knowledge tables, uses the observation concept (LOINC), the unit concept (SNOMED), and the numeric result as input. It first adjusts the LOINC code if the unit suggests a better LOINC code. It then normalizes the unit to a predetermined preferred unit for that LOINC code by filling null units, converting related units, or correcting units with overt errors. All transformations only proceed when the numeric result aligns with the predetermined distribution for the target LOINC code–unit pair. This “reasonable range” constraint addresses a shortcoming in existing proposed methodologies [19,21] that handle units without consideration of the numeric result. This range can be used to flag records that fall outside the reasonable distribution for exclusion from analysis or closer review.

XSL•FO
RenderX

Impact on Data Quality Dimensions

Ensuring that laboratory values fall within a reasonable distribution contributes to accuracy, or the degree to which the data represent the true value of what is intended to be measured, and plausibility, 2 prominent dimensions [25] of RWD quality. The results demonstrate improvements across a number of established quality dimensions [25] other than accuracy and plausibility, including conformance, consistency, completeness, and provenance [25-29]. The technique primarily addresses conformance to the approved LOINC code–unit pair set by the LRR table and consistency of semantic representation regardless of data source. Completeness is improved by populating the unit when null. This contextually appropriate population of absent units has not been addressed in prior studies of similar techniques [19,21].

Data Provenance

Data provenance is recognized as critical metadata for systems transmitting, storing, or using health data [30]. Records in RWD pipelines may undergo many transformations on their path to integration into a single dataset, and these transformations must all be tracked to enable error correction and improve trustworthiness with downstream consumers. Data provenance has been defined in many ways [31], and there are established specifications for recording provenance in health care data, such as the FHIR Provenance resource [32] based on the World Wide Web Consortium provenance specification [33]. Establishing the best method for provenance tracking within a system requires an assessment of the stakeholders for those data. The stakeholders for the transformations described in this paper were internal data analysts, informaticists, and quality assurance engineers. Provenance is maintained within each transformed record in an attribute that acts as a ledger of each transformation that altered that record. This attribute is an array of structures that include a descriptive, human-readable string detailing the transformation, as well as the altered attributes and preadjustment values that those attributes took. By consulting this array, transformations are fully reversible, original values are preserved, and a complete audit trail is available to support transparency and verification by downstream users.

Clinical and Research Relevance

Laboratory data quality and usability are critical in systems handling oncology data, where these results are used to select and monitor therapies and assess disease severity and progression [34]. LOINC code–unit incongruence, unit absentia, and lack of unit standardization put an undue burden on any analyst or application attempting to use laboratory data for clinical decision support, retrospective studies, or clinical trial eligibility [35,36]. Improving unit completeness at the source is challenging because units are often inconsistently documented or transmitted in EHR systems [37,38]. Potential upstream improvements could include enforcing unit capture at the point of entry, not allowing free-text entry of units, ensuring consistent transmission in Health Level Seven and FHIR messages, or applying unit standardization at the health system level before data export. However, such approaches depend on local workflows and vendor configurations and cannot be guaranteed for multisource RWD. Consequently, postcodification harmonization frameworks such as the one described in this paper provide a practical and reproducible solution. The technique outlined in this paper presents a minimal set of logical steps to correct these problems within the pipeline of a multisourced data system handling RWD. Enforcing semantic consistency between LOINC and unit improves data usability [24] but can also foster better data exchange [39] between systems by reducing semantic differences. Ultimately, this framework ensures that laboratory data are both accurate and complete, enabling faster data-driven decisions that can enhance patient care, data exchange, clinical trials, and RWD analysis.

Limitations and Future Work

The technique is presently limited by its capacity to correct the body system, which will reduce effectiveness for laboratory tests in which the potential body systems are relatively evenly distributed and share similar units when tested in either sample type. Information related to the body system can be present in the observation name but also in the panel name, the order name, discretely in another attribute in the laboratory result, or in other observations related to the result in question. Efforts are currently underway to evolve the process by incorporating panel or order-related information. The choice of SNOMED for unit may have been less ideal than UCUM [40,41], which is more flexible and more closely aligned with LOINC [42], which suggests a UCUM unit for some of its concepts. The FHIR [43] and Interoperability Standards Platform [44] also suggest that UCUM be used to represent units. However, the framework is easily adaptable by simply replacing the SNOMED codes used in the knowledge tables with UCUM codes without requiring any further changes in script. In addition, the steps described in this paper specifically address quantitative LOINC codes and require modification to be applicable to qualitative scale–type LOINC codes. Another limitation is that the creation of the knowledge tables requires clinical and terminologist expertise to recognize errors and prepare the tables, as well as a large dataset to prepare laboratory value distributions. This framework is designed for secondary use in RWD, where inconsistencies, missing values, and heterogeneous coding practices complicate analysis, and is not intended for integration into direct point-of-care clinical decision-making. Therefore, its use does not pose any direct safety risk to patients. The harmonization of LOINC code–unit combinations and the potential flagging of outlier values can influence downstream analyses such as cohort definitions or outlier detection. It enables data analysts to use laboratory data that would otherwise have required a significant time investment to clean. The primary aim of these corrections is to reduce inconsistencies and facilitate reliable data aggregation for secondary research purposes. Future work will focus on integrating the framework with emerging technologies such as artificial intelligence.

Practical Implementation

To support practical implementation, we have released a starter kit supporting normalization of 146 LOINC codes from blood or serum, covering the “Hematology and cell counts” class and “Chemistry” glucose codes. It has 3 knowledge tables and an accompanying Python script available via a public GitHub repository [45]. The knowledge tables incorporate LOINC and

XSL•FO
RenderX

SNOMED, which are maintained in multiple languages, allowing the tables to be used with datasets in different linguistic contexts. The numeric values in the tables are language independent and do not require conversion, supporting their generalizability to different languages. The Python script executing the rules takes FHIR Observation resources as input, and 6 example resources are provided.

Currently, the framework leverages SNOMED codes for units. However, the design is adaptable: implementers preferring UCUM codes can replace SNOMED codes with UCUM codes in the tables without any modification to the transformation script, allowing for seamless adoption of alternative unit standards. This flexibility ensures that the framework can be applied in diverse institutional or research contexts with minimal overhead.

A key component of the framework is its structured provenance tracking, which records all transformations applied to each laboratory record in a way that allows the original data to be reconstructed if needed. For each modification, information such as the applied rule, details of the transformation, which fields were changed, the original values, and the reference values used in the conversion is systematically captured. Collectively, these elements enable full traceability, providing a clear lineage from the transformed value back to the original measurement. This approach not only supports reproducibility and auditing but also ensures transparency, allowing researchers and data analysts to confidently interpret and validate the standardized data while retaining the ability to recover the source information.

By combining reproducible tables, adaptable unit standards, and robust provenance tracking, the framework provides a practical pathway for implementing consistent laboratory data harmonization in diverse settings while maintaining the transparency and traceability of each transformation.

Conclusions

As the demand for multisourced RWD datasets grows, ensuring data quality and semantic consistency becomes increasingly vital. Persistent challenges regarding SI in laboratory data continue to limit the full potential of these data assets. Common issues include missing or incorrect units and misassigned LOINC codes, all of which can hinder integration and analysis. This framework addresses these challenges by systematically identifying and correcting discrepancies in quantitative laboratory data and has been shown to improve unit accuracy to above 99% for all evaluated datasets. It enables scalable, system-agnostic normalization of laboratory data, addressing critical gaps in several data quality dimensions. By improving laboratory data quality at the foundational level, it strengthens the reliability of RWD for data analysis, insight generation, and utility in software applications.

Acknowledgments

The authors would like to express their sincere gratitude to the ConcertAI reviewers Sheenu Chandwani, Jannette Hanna, Jennifer Rider, and Jocelyn Benson for their constructive feedback and insightful comments, which greatly enhanced the quality of this paper.

Funding

ConcertAI, LLC, sponsored this study and provided financial support for the conduct of this research and preparation of this paper.

Data Availability

The datasets generated or analyzed during this study are not publicly available due to proprietary and licensing restrictions but may be available from ConcertAI, LLC, upon reasonable request and subject to applicable data use agreements and approval processes [46].

Conflicts of Interest

PN and TS are employed by ConcertAI, LLC.

Multimedia Appendix 1
Detailed process for building the 3 knowledge tables described in system design, that is, the reasonable range map, unit multiplier map, and Logical Observation Identifiers Names and Codes conversion map.
[DOCX File , 91 KB - medinform_v14i1e81254_app1.docx]

Multimedia Appendix 2
Detailed report on the proportion of correct units before and after application of the framework, stratified by Logical Observation Identifiers Names and Codes code and by data source.
[XLSX File (Microsoft Excel File), 112 KB - medinform_v14i1e81254_app2.xlsx]

References

XSL•FO
RenderX

1. Hao Y, Cheng C, Li J, Li H, Di X, Zeng X, et al. Multimodal integration in health care: development with applications in disease management. J Med Internet Res 2025 Aug 21;27:e76557 [FREE Full text] [doi: 10.2196/76557] [Medline: 40840463]
2. Liu F, Panagiotakos D. Real-world data: a brief review of the methods, applications, challenges and opportunities. BMC Med Res Methodol 2022 Nov 05;22(1):287 [FREE Full text] [doi: 10.1186/s12874-022-01768-6] [Medline: 36335315]
3. Dang A. Real-world evidence: a primer. Pharmaceut Med 2023 Jan 05;37(1):25-36 [FREE Full text] [doi: 10.1007/s40290-022-00456-6] [Medline: 36604368]
4. Wilson J, Bock A. The benefit of using both claims data and electronic medical record data in health care analysis. OPTUM. 2025. URL: https://www.optum.com/content/dam/optum/resources/whitePapers/Benefits-of-using-both-claims-and-EMR-data-in-HC-analysis-WhitePaper-ACS.pdf [accessed 2025-04-29]
5. An D, Lim M, Lee S. Challenges for data quality in the clinical data life cycle: systematic review. J Med Internet Res 2025 Apr 23;27:e60709 [FREE Full text] [doi: 10.2196/60709] [Medline: 40266662]
6. Abedjan Z, Chu X, Deng D, Fernandez RC, Ilyas IF, Ouzzani M, et al. Detecting data errors: where are we and what needs to be done? Proc VLDB Endow 2016 Aug 1;9(12):993-1004. [doi: 10.14778/2994509.2994518]
7. Munappy AR, Bosch J, Olsson HH. Data pipeline management in practice: challenges and opportunities. In: Morisio M, Torchiano M, Jedlitschka A, editors. Product-Focused Software Process Improvement. Cham, Switzerland: Springer; 2020:168-184.
8. de Mello BH, Rigo SJ, da Costa CA, da Rosa Righi R, Donida B, Bez MR, et al. Semantic interoperability in health records standards: a systematic literature review. Health Technol (Berl) 2022;12(2):255-272 [FREE Full text] [doi: 10.1007/s12553-022-00639-w] [Medline: 35103230]
9. Kelly J, Wang C, Zhang J, Das S, Ren A, Warnekar P. Automated mapping of real-world oncology laboratory data to LOINC. AMIA Annu Symp Proc 2021;2021:611-620 [FREE Full text] [Medline: 35308998]
10. FHIR® - Fast Healthcare Interoperability Resources®. eCQI Resource Center. URL: https://ecqi.healthit.gov/fhir?qt-tabs_fhir=about [accessed 2025-04-30]
11. Vorisek CN, Lehne M, Klopfenstein SA, Mayer PJ, Bartschke A, Haese T, et al. Fast Healthcare Interoperability Resources (FHIR) for interoperability in health research: systematic review. JMIR Med Inform 2022 Jul 19;10(7):e35724 [FREE Full text] [doi: 10.2196/35724] [Medline: 35852842]
12. Richesson RL, Campion TR, Knosp BM, Hanauer DA. LOINC implementation approaches in academic medical research centers - results from a survey of CTSA sites. J Clin Transl Sci 2025;9(1):e223. [doi: 10.1017/cts.2025.10151] [Medline: 41111944]
13. LOINC. URL: https://loinc.org [accessed 2025-04-29]
14. Drenkhahn C, Ingenerf J. The LOINC content model and its limitations of usage in the laboratory domain. Stud Health Technol Inform 2020 Jun 16;270:437-442. [doi: 10.3233/SHTI200198] [Medline: 32570422]
15. Lin MC, Vreeman DJ, Huff SM. Investigating the semantic interoperability of laboratory data exchanged using LOINC codes in three large institutions. AMIA Annu Symp Proc 2011;2011:805-814 [FREE Full text] [Medline: 22195138]
16. Fidahussein M, Vreeman DJ. A corpus-based approach for automated LOINC mapping. J Am Med Inform Assoc 2014;21(1):64-72 [FREE Full text] [doi: 10.1136/amiajnl-2012-001159] [Medline: 23676247]
17. Khan AN, Griffith SP, Moore C, Russell D, Rosario ACJ, Bertolli J. Standardizing laboratory data by mapping to LOINC. J Am Med Inform Assoc 2006;13(3):353-355 [FREE Full text] [doi: 10.1197/jamia.M1935] [Medline: 16501183]
18. Parr SK, Shotwell MS, Jeffery AD, Lasko TA, Matheny ME. Automated mapping of laboratory tests to LOINC codes using noisy labels in a national electronic health record system database. J Am Med Inform Assoc 2018 Oct 01;25(10):1292-1300 [FREE Full text] [doi: 10.1093/jamia/ocy110] [Medline: 30137378]
19. Wu CZ, Wales DL. Laboratory data standardization with SAS. PharmaSUG. 2017. URL: https://pharmasug.org/proceedings/2017/AD/PharmaSUG-2017-AD10.pdf [accessed 2025-04-30]
20. Vreeman DJ, Hook J, Dixon BE. Learning from the crowd while mapping to LOINC. J Am Med Inform Assoc 2015 Nov;22(6):1205-1211 [FREE Full text] [doi: 10.1093/jamia/ocv098] [Medline: 26224334]
21. Hao T, Liu H, Weng C. Valx: a system for extracting and structuring numeric lab test comparison statements from text. Methods Inf Med 2016 May 17;55(3):266-275 [FREE Full text] [doi: 10.3414/ME15-01-0112] [Medline: 26940748]
22. Results final report. AHRQ HCUP. URL: https://hcup-us.ahrq.gov/datainnovations/clinicaldata/3MSummaryResultsReportFinal.jsp [accessed 2025-04-29]
23. Abhyankar S, Demner-Fushman D, McDonald CJ. Standardizing clinical laboratory data for secondary use. J Biomed Inform 2012 Aug;45(4):642-650 [FREE Full text] [doi: 10.1016/j.jbi.2012.04.012] [Medline: 22561944]
24. Hauser RG, Quine DB, Ryder A, Campbell S. Unit conversions between LOINC codes. J Am Med Inform Assoc 2018 Feb 01;25(2):192-196 [FREE Full text] [doi: 10.1093/jamia/ocx056] [Medline: 28637208]
25. Castellanos EH, Wittmershaus BK, Chandwani S. Raising the bar for real-world data in oncology: approaches to quality across multiple dimensions. JCO Clin Cancer Inform 2024 Jan;8:e2300046 [FREE Full text] [doi: 10.1200/CCI.23.00046] [Medline: 38241599]
26. Data quality framework for EU medicines regulation. European Medicines Agency. 2023. URL: https://www.ema.europa.eu/en/documents/regulatory-procedural-guideline/data-quality-framework-eu-medicines-regulation_en.pdf [accessed 2025-04-30]

XSL•FO
RenderX

27. Real-world data: assessing electronic health records and medical claims data to support regulatory decision-making for drug and biological products. U.S. Food & Drug Administration. 2024 Jul. URL: https://www.fda.gov/regulatory-information/search-fda-guidance-documents/real-world-data-assessing-electronic-health-records-and-medical-claims-data-support-regulatory [accessed 2025-04-30]
28. NICE real-world evidence framework. National Institute for Health and Care Excellence. 2022. URL: https://www.nice.org.uk/corporate/ecd9/chapter/assessing-data-suitability#assessing-data-suitability [accessed 2025-04-30]
29. Daniel G, Silcox C, Bryan J. Characterizing RWD quality and relevancy for regulatory purposes. Duke-Margolis Center for Health Policy. 2018 Oct 1. URL: https://healthpolicy.duke.edu/sites/default/files/2020-03/characterizing_rwd.pdf [accessed 2025-04-28]
30. Ahmed M, Dar AR, Helfert M, Khan A, Kim J. Data provenance in healthcare: approaches, challenges, and future directions. Sensors (Basel) 2023 Jul 18;23(14):6495 [FREE Full text] [doi: 10.3390/s23146495] [Medline: 37514788]
31. Ram S, Liu J. A new perspective on semantics of data provenance. In: Proceedings of the First International Conference on Semantic Web in Provenance Management. 2009 Presented at: SWPM'09; October 25, 2009; Washington, DC URL: https://ceur-ws.org/Vol-526/InvitedPaper_1.pdf
32. Provenance. HL7 FHIR. URL: https://hl7.org/fhir/provenance.html [accessed 2025-11-30]
33. Groth P, Moreau L. PROV-overview: an overview of the PROV family of documents. W3C Working Group Note. 2013. URL: https://www.w3.org/TR/2013/NOTE-prov-overview-20130430/ [accessed 2025-11-30]
34. Cabalar I, Le TH, Silber A, O'Hara M, Abdallah B, Parikh M, et al. The role of blood testing in prevention, diagnosis, and management of chronic diseases: a review. Am J Med Sci 2024 Oct;368(4):274-286 [FREE Full text] [doi: 10.1016/j.amjms.2024.04.009] [Medline: 38636653]
35. Vesper HW, Myers GL, Miller WG. Current practices and challenges in the standardization and harmonization of clinical laboratory tests. Am J Clin Nutr 2016 Sep;104 Suppl 3(Suppl 3):907S-912S [FREE Full text] [doi: 10.3945/ajcn.115.110387] [Medline: 27534625]
36. Muñoz Monjas A, Rubio Ruiz D, Pérez Del Rey D, Palchuk MB. Enhancing real world data interoperability in healthcare: a methodological approach to laboratory unit harmonization. Int J Med Inform 2025 Jan;193:105665. [doi: 10.1016/j.ijmedinf.2024.105665] [Medline: 39500036]
37. Hajia M. Secondary use of laboratory data: potentialities and limitations. Iran J Pathol 2019;14(3):188-192 [FREE Full text] [doi: 10.30699/ijp.2019.95692.1942] [Medline: 31582994]
38. Khela H, Khalil J, Daxon N, Neilson Z, Shahrokhi T, Chung P, et al. Real world challenges in maintaining data integrity in electronic health records in a cancer program. Tech Innov Patient Support Radiat Oncol 2024 Mar;29:100233 [FREE Full text] [doi: 10.1016/j.tipsro.2023.100233] [Medline: 38293266]
39. Zayed AM, Sarikakis I, Delvaux N. Automated standardization and harmonization of laboratory units in large-scale clinical data using open-source R functions. Int J Med Inform 2026 Jan;205:106131 [FREE Full text] [doi: 10.1016/j.ijmedinf.2025.106131] [Medline: 41061385]
40. Bietenbeck A, Boeker M, Schulz S. NPU, LOINC, and SNOMED CT: a comparison of terminologies for laboratory results reveals individual advantages and a lack of possibilities to encode interpretive comments. J Lab Med 2018;42(6) [FREE Full text] [doi: 10.1515/labmed-2018-0103]
41. Schadow G, McDonald CJ. The unified code for units of measure. UCUM Organization. 2024. URL: https://ucum.org/ucum [accessed 2025-05-29]
42. Vogl K, Ingenerf J, Kramer J, Chantraine C, Drenkhahn C. LUMA: a mapping assistant for standardizing the units of LOINC-coded laboratory tests. Appl Sci 2022 Jun 08;12(12):5848 [FREE Full text] [doi: 10.3390/app12125848]
43. Datatypes. HL7 FHIR. URL: https://hl7.org/fhir/datatypes.html#Quantity [accessed 2025-05-29]
44. Representing units of measure (for use with numerical references and values). Assistant Secretary for Technology Policy. URL: http://www.healthit.gov/isp/representing-units-measure-use-numerical-references-and-values [accessed 2025-05-26]
45. PrecisionHealthIntelligence. GitHub. URL: https://github.com/PrecisionHealthIntelligence/loinc_unit_harmonization [accessed 2026-03-02]
46. ConcerAI. URL: https://www.concertai.com/contact-us/ [accessed 2026-03-02]

Abbreviations

EHR: electronic health record
FHIR: Fast Healthcare Interoperability Resources
LCM: Logical Observation Identifiers Names and Codes conversion map
LOINC: Logical Observation Identifiers Names and Codes
LRR: laboratory reasonable range
RWD: real-world data
SI: semantic interoperability
SNOMED: Systematized Nomenclature of Medicine
UCUM: Unified Code for Units of Measure

XSL•FO
RenderX

Edited by A Benis; submitted 25.Jul.2025; peer-reviewed by A Famotire, B Dixon; comments to author 11.Nov.2025; revised version received 23.Jan.2026; accepted 17.Feb.2026; published 09.Mar.2026.

Please cite as:
Naliyatthaliyazchayil P, Stenerson T
Harmonizing Logical Observation Identifiers Names and Codes (LOINC) Codes and Units in Real-World Oncology Data: Method Development and Evaluation
JMIR Med Inform 2026;14:e81254
URL: https://medinform.jmir.org/2026/1/e81254
doi:10.2196/81254
PMID:41802234

©Parvati Naliyatthaliyazchayil, Travis Stenerson. Originally published in JMIR Medical Informatics (https://medinform.jmir.org), 09.Mar.2026. This is an open-access article distributed under the terms of the Creative Commons Attribution License (https://creativecommons.org/licenses/by/4.0/), which permits unrestricted use, distribution, and reproduction in any medium, provided the original work, first published in JMIR Medical Informatics, is properly cited. The complete bibliographic information, a link to the original publication on https://medinform.jmir.org/, as well as this copyright and license information must be included.

XSL•FO
RenderX

Original Paper

Complete Blood Count–Derived Inflammation Indices to Predict 3-Year All-Cause Mortality in Patients With Diabetes and Acute Myocardial Infarction in Critical Care: Retrospective Cohort Study With Single-Center External Validation

Tong Zhou[1], MS; Kun Yang[1], PhD; Ying Yang[1], PhD; Song-Mei Liu[1], Prof Dr

Zhongnan Hospital of Wuhan University, Wuhan, China

Corresponding Author:
Song-Mei Liu, Prof Dr
Zhongnan Hospital of Wuhan University
No. 169, Donghu Road, Wuhan City, Hubei Province
Wuhan, 430071
China
Phone: 86 027 678 132 33
Email: smliu@whu.edu.cn

Abstract

Background: Inflammation plays a pivotal role in the progression of diabetes and its cardiovascular complications, particularly acute myocardial infarction (AMI). Patients with AMI often face high mortality and morbidity, making accurate prognosis crucial for clinical decision-making and outcome improvement.

Objective: This study aims to develop and validate a stacked predictive model using inflammation-related indices to predict 3-year all-cause mortality among patients with severe diabetes who experience acute myocardial infarction (AMI), aiming to improve patient prognosis.

Methods: We included 833 patients with severe diabetes combined with AMI from the Medical Information Mart for Intensive Care IV (MIMIC-IV) database (training/test cohort) and 166 cases from Zhongnan Hospital, China (external validation cohort with 3-year follow-up). A total of 5 inflammation-related indices (lymphocyte-to-monocyte ratio [LMR], neutrophil-to-lymphocyte ratio [NLR], neutrophil-to-platelet ratio [NPR], platelet-to-lymphocyte ratio [PLR], prognostic inflammatory value [PIV]) were analyzed for their association with mortality using Cox proportional hazards models. Kaplan-Meier curves and restricted cubic spline analysis explored survival probabilities and dose-response relationships. A stacked predictive model incorporating these indices was constructed, and its performance was evaluated using the area under the curve.

Results: LMR was a protective factor (hazard ratio [HR] 0.44, 95% CI 0.25-0.77; *P*<.001), while NLR (HR 1.78, 95% CI 1.19-2.65; *P*=.004) and PIV (HR 1.59, 95% CI 1.09-2.30; *P*=.01) were associated with increased mortality risk. Kaplan-Meier analysis showed mortality increased with decreasing LMR quartiles and increasing NLR, NPR, PLR, and PIV quartiles. Restricted cubic spline confirmed that decreasing LMR and increasing NLR, NPR, PLR, and PIV were associated with higher adverse event risk. The predictive model achieved an area under the curve of 0.803 (95% CI 0.736-0.871) in internal testing and 0.781 (95% CI 0.704-0.858) in the external validation cohort.

Conclusions: The stacked predictive model serves as a robust tool for predicting 3-year outcomes in patients with diabetes combined with AMI. Its reliance on routine, low-cost indices highlights its economic viability and potential for widespread clinical implementation, particularly for optimizing resource allocation in resource-limited settings. However, considering the single-center nature of the derivation data, future multicenter validation is essential to verify the model's generalizability across different health care systems before establishing it as a standard policy for risk stratification.

(JMIR Med Inform 2026;14:e83328) doi:10.2196/83328

KEYWORDS

3-year mortality; acute myocardial infarction; diabetes; inflammation-related indices; machine learning; prognosis

XSL•FO
RenderX

Introduction

Diabetes and its complications represent a growing global health challenge, affecting an increasing number of individuals worldwide. According to the International Diabetes Federation, an estimated 537 million individuals were living with diabetes in 2021, and this number is projected to 1.31 billion by 2050, underscoring the urgent need for effective prevention and management strategies [1].

Type 2 diabetes is characterized by systemic inflammation, driven by complex crosstalk between immune cells and β-cells, which plays a pivotal role in disease progression [2]. Importantly, inflammation not only contributes to the pathogenesis of diabetes itself but also plays a critical role in the development of its complications, including cardiovascular diseases (CVDs) such as atherosclerosis and acute myocardial infarction (AMI) [3-5].

CVD remains one of the leading causes of mortality in patients with diabetes, with AMI being one of the most devastating complications [6]. Patients with diabetes not only exhibit a higher incidence of AMI but also experience worse prognoses compared to individuals without diabetes [7]. Hyperglycemia has been implicated in these outcomes by promoting oxidative stress, endothelial dysfunction, and proinflammatory processes, including M1 macrophage polarization and enhanced monocyte adhesion to activated endothelial cells [8]. These inflammatory changes disrupt vascular homeostasis and contribute to microvascular damage [8]. Long-term prognosis in high-risk patients with diabetes combined with AMI plays a critical role in guiding clinical decision-making and improving outcomes. Prognostic studies provide valuable tools for identifying high-risk patients, enabling timely and targeted interventions to reduce mortality and improve survival rates.

Given the pivotal role of inflammation in both diabetes and AMI, there is growing interest in inflammatory markers as prognostic tools. Markers such as the lymphocyte-to-monocyte ratio (LMR), neutrophil-to-platelet ratio (NPR), platelet-to-lymphocyte ratio (PLR), neutrophil-to-lymphocyte ratio (NLR), and prognostic inflammatory value (PIV) have been widely used to reflect systemic inflammation and predict outcomes in CVDs and cancers [9-12]. Importantly, these indices derived from complete blood count (CBC) inherit its advantages of being stable, cost-effective, and widely accessible, making them potentially applicable for routine clinical use and large-scale prognostic studies. However, whether these inflammatory markers could be used for predicting clinical outcomes of patients with diabetes combined with AMI remains unclear. To address this gap, we leveraged data from the Medical Information Mart for Intensive Care IV (MIMIC-IV) database and the Department of Critical Care Medicine, Zhongnan Hospital of Wuhan University, China, to systematically compare and evaluate the prognostic utility of LMR, NPR, PLR, NLR, and PIV in predicting long-term mortality risk and clinical outcomes in this vulnerable population.

Methods

Ethical Considerations

This study adheres to the principles declared in the Declaration of Helsinki and STROBE (Strengthening the Reporting of Observational Studies in Epidemiology) guidelines and was approved by the Medical Ethics Committee of Zhongnan Hospital of Wuhan University (approval: 2020009). The Institutional Review Board of Beth Israel Deaconess Medical Center (BIDMC) granted a waiver of informed consent and approved the sharing of research resources. The authors obtained access to the MIMIC-IV database (certificate number: 65461627).

Source of Data

This study conducted a retrospective analysis using the large, publicly available intensive care database MIMIC-IV (version 3.0).

For external validation, data were obtained from Zhongnan Hospital of Wuhan University, China. This cohort included 166 patients admitted between January 1, 2021, and June 30, 2022. The final follow-up for outcome ascertainment was completed on July 22, 2025, by hospital record review and telephone interviews. During this period, 56 mortality events were recorded.

Case Inclusion and Exclusion Criteria

Patients diagnosed with both diabetes and AMI were included in this study. Patient identification was based on diagnostic codes from the *ICD-9* (*International Classification of Diseases, Ninth Revision*), and the *ICD-10* (*International Statistical Classification of Diseases, Tenth Revision*). AMI and diabetes mellitus were identified using *ICD-9* and *ICD-10* codes.

The exclusion criteria were as follows: (1) age <18 years; (2) an intensive care unit (ICU) stay of <24 hours; (3) multiple admissions, with only data from the first hospitalization included; and (4) missing data on lymphocyte, monocyte, neutrophil, or platelet count levels.

Data Extraction

The *psql* tool of PostgreSQL was used to extract the data. Laboratory variables were extracted from the first result recorded within 24 hours of ICU admission. Features with a missing data rate exceeding 30% were excluded, while multiple imputation was applied to those with a missing data rate below 30%. Missing data were handled using multiple imputation by chained equations. We used the predictive mean matching method with 5 imputations (m=5) and set the random seed to 1 for reproducibility. All predictor variables were included in the imputation model.

The LMR was calculated as lymphocyte count (10^9/L) / monocyte count (10^9/L), NPR as neutrophil count (10^9/L) / platelet count (10^9/L), the PLR as platelet count (10^9/L) / lymphocyte count (10^9/L), the NLR as neutrophil count (10^9/L) / lymphocyte count (10^9/L), and the PIV as lymphocyte count

XSL•FO
RenderX

(10^9/L) × platelet count (10^9/L) × monocyte count (10^9/L)/ lymphocyte count (10^9/L) [10-12].

Time-Zero Alignment

All predictor variables (including CBC components and inflammatory indices) were extracted as the first recorded value on admission to prevent any look-ahead bias. To ensure transportability, this identical protocol—using the admission baseline—was applied to the external validation cohort.

Outcomes

The start date of follow-up was defined as the date of hospital admission, and the study outcome was 3-year mortality.

Statistical Analysis

As this study is a retrospective analysis, sample size calculations were not performed. For categorical variables, the chi-square test or Fisher exact test was performed for analysis. Student 2-tailed *t* test and the Wilcoxon rank-sum test were used for continuous variables. Kaplan-Meier (K-M) curves and Cox proportional hazards models were used to determine the relationships between LMR, NPR, PLR, NLR, PIV, and the risk of mortality. In Model 1, adjustments were made for age, gender, BMI. In Model 2, further adjustments were made for age, gender, BMI, troponin T, creatine kinase isoenzymes (CK-MB), insulin, history of revascularization (percutaneous coronary intervention and coronary artery bypass grafting), hyperlipidemia, atrial fibrillation, and stroke. Subgroup analysis was performed to examine the relationship between the continuous inflammation index and 3-year mortality across different subgroups. Restricted cubic spline (RCS) analysis was conducted to explore the associations between the 5 indices and mortality in a dose–response manner.

Feature Selection

The variance inflation factor (VIF) was used to assess multicollinearity among features. Features with a VIF greater than 5 were removed due to concerns about multicollinearity (Table S1 in Multimedia Appendix 1).

To identify the most important features associated with prognosis, the Boruta (version 9.0.0; R packages) algorithm was used. As a robust feature selection method, Boruta identifies all relevant predictors by iteratively comparing the importance of real features with random shadow features. Features marked as important (green) were selected for subsequent machine learning model construction.

Construction and Validation of Predictive Models

To construct the predictive model, the important features were identified using the Boruta algorithm. Subsequently, the dataset was randomly split into a training set (666/833, 80%) and a testing set (176/833, 20%) with a fixed random seed of 123. Machine learning models were then developed using the H2O AutoML platform (version 3.44.0.3) in R (R Foundation for Statistical Computing). The AutoML process was configured with the following hyperparameters: maximum number of models = 200, maximum runtime = 24 hours, and class balancing enabled (balance_classes = TRUE) to address outcome imbalance. Finally, models were ranked based on the area under the curve (AUC), and a stacked ensemble model was generated using the top-performing base models.

Each base model was trained on prognostic outcomes derived from the training data, and prognostic scores for each patient were calculated and scaled to a range of 0 to 1, with higher scores indicated worse prognosis. An ensemble method was then applied by compiling the top 5 base models, ranked according to their area under the receiver operating characteristic curve, into a matrix of prognostic scores. A second-layer generalized linear model algorithm was then used to create the final model. Five-fold cross-validation was performed during model training to minimize overfitting and ensure the robustness of the results. A probability threshold of .5 was used to classify patients into high- and low-risk groups for the confusion matrix analysis.

Here, 5 inflammation-related indices—LMR, NPR, PLR, NLR, and PIV—were also selected as features for model construction. Separate models were built for each individual feature following the methodology described above. Additionally, a stacked ensemble model incorporating all 5 indices was constructed to explore their combined predictive performance.

Results

Baseline Characteristics

Following the inclusion and exclusion criteria, 833 patients with diabetes combined with AMI from the MIMIC-IV database were used as the training and test cohorts, and 166 cases from Zhongnan Hospital of Wuhan University, China, were enrolled as an external validation cohort. Figure 1 illustrates the flow of patient selection for this study.

XSL•FO
RenderX

Figure 1. Patient screening and feature selection. Inclusion and exclusion criteria for patients from the Medical Information Mart for Intensive Care IV (MIMIC-IV) database. AMI: acute myocardial infarction; ICU: intensive care unit.

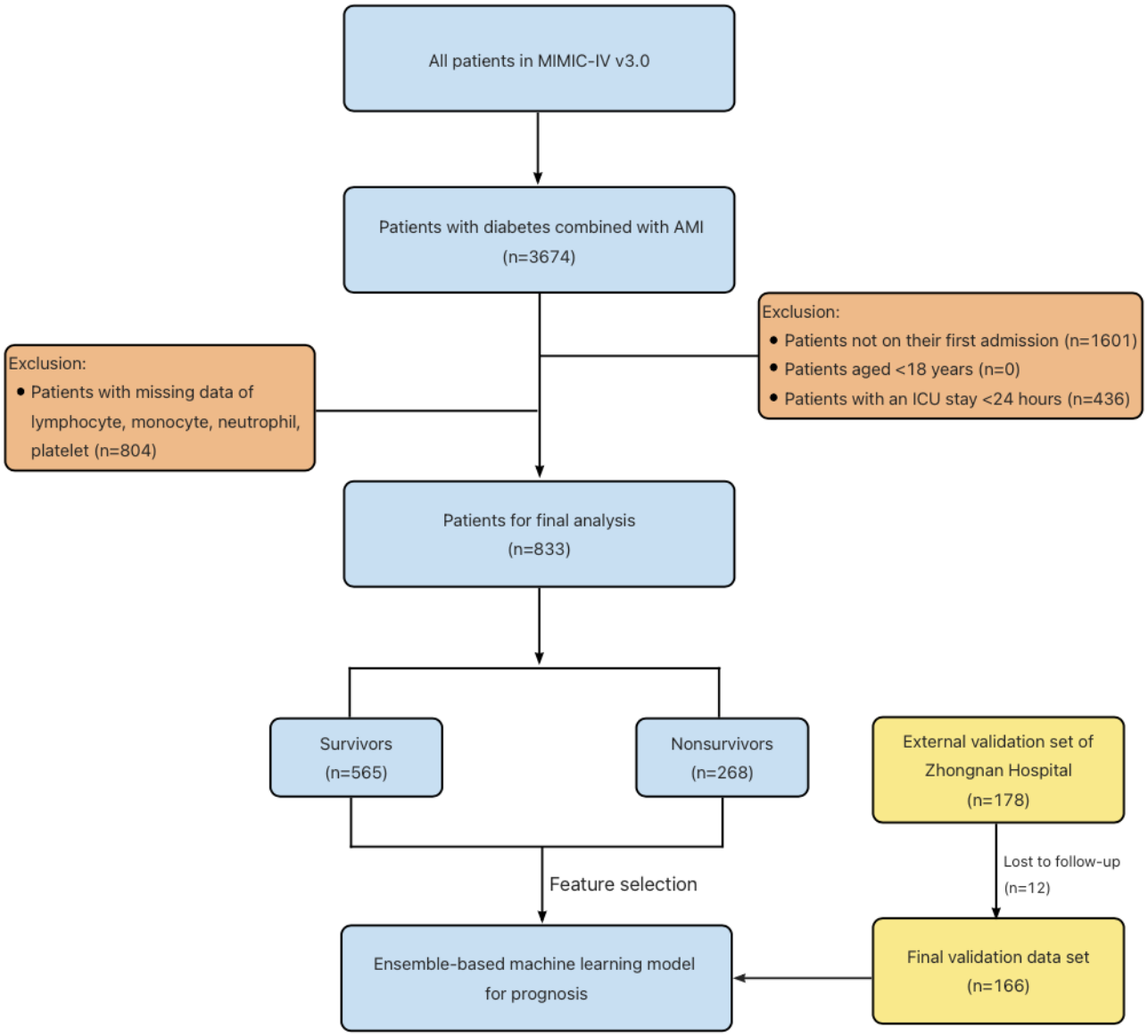

Table 1 provides a detailed comparison of baseline characteristics between survivors and nonsurvivors in the MIMIC-IV cohort (n=833), based on the 3-year mortality outcomes. Overall, the nonsurvivors were older and had a lower proportion of males compared with survivors. Among the comorbidities, the nonsurvivors exhibited significantly higher incidences of stroke, atrial fibrillation, and heart failure. Notably, the proportion of patients undergoing coronary artery bypass grafting was significantly lower in the nonsurvivor group. The nonsurvivors also exhibited significant differences in vital signs, including higher heart rate and respiratory rate, as well as higher diastolic blood pressure. As for laboratory parameters, the nonsurvivors had markedly elevated levels of mean corpuscular volume, red cell distribution width, white blood cells, phosphate, potassium, magnesium, alkaline phosphatase, creatinine, and urea nitrogen, suggesting metabolic and immune disturbance. Furthermore, inflammation-related indices also differed significantly between the 2 groups, with nonsurvivors exhibiting higher levels of NPR, PLR, NLR, and PIV, while LMR was lower. However, there was no significant change in troponin T or CK-MB between the survivors and nonsurvivors, demonstrating that these 2 markers typically show a significant increase during the acute phase of myocardial infarction and decrease rapidly during the recovery phase. These findings suggest that CBC-derived inflammation-related indices hold promise for predicting long-term prognosis in patients with diabetes combined with AMI.

XSL•FO
RenderX

Table 1. Baseline characteristics between survivors and nonsurvivors.

Characteristics	Total (n=833)	Survivors (n=565)	Nonsurvivors (n=268)	*P* value
Demographics				
Male, n (%)	576 (69.1)	408 (72.5)	168 (62.7)	.07
Age (years), mean (SD)	68.99 (11.10)	66.92 (10.64)	73.36 (10.81)	<.001
Weight (kg), mean (SD)	86.65 (23.09)	87.31 (22.07)	85.26 (25.11)	.23
BMI (kg/m^2)	29.87 (7.01)	29.85 (6.46)	29.93 (8.06)	.88
Vital signs, mean (SD)				
Heart rate (bpm)	86.82 (18.70)	83.80 (15.87)	93.21 (22.30)	<.001
Respiratory rate (breaths/min)	18.76 (6.86)	17.50 (5.75)	21.44 (8.14)	<.001
Systolic blood pressure (mm Hg)	118.67 (23.51)	117.55 (21.82)	120.93 (26.61)	.05
Diastolic blood pressure (mm Hg)	66.63 (15.75)	65.74 (14.51)	68.49 (17.90)	.02
Comorbidities, n (%)				
Hypertension	293 (35.2)	245 (43.4)	48 (17.9)	<.001
Stroke	71 (9)	27 (5)	44 (16)	<.001
Atrial fibrillation	61 (7)	33 (6)	28 (10)	<.001
Heart failure	457 (54.9)	271 (48)	186 (69.4)	<.001
Hyperlipidemia	601 (72.1)	438 (77.5)	163 (60.8)	<.001
Treatment, n (%)				
Insulin	809 (97.1)	552 (97.7)	257 (95.9)	.22
Percutaneous coronary intervention	94 (11)	53 (9)	41 (15)	.02
Coronary artery bypass grafting	439 (52.7)	396 (70.1)	43 (16)	<.001
Complete blood count, mean (SD)				
White blood cells ($10^9/L$)	11.66 (7.42)	10.60 (5.33)	13.89 (10.21)	<.001
Red cell distribution width (%)	14.41 (2.16)	13.95 (1.76)	15.39 (2.56)	<.001
Hemoglobin (g/dL)	11.61 (2.36)	12.13 (2.19)	10.51 (2.35)	<.001
Hematocrit (%)	35.71 (6.69)	37.00 (6.16)	33.01 (6.95)	<.001
Platelet count ($10^9/L$)	216.84 (81.65)	217.75 (77.27)	214.93 (90.31)	.64
Neutrophil count ($10^9/L$)	10.50 (5.78)	9.93 (5.12)	11.70 (6.82)	<.001
Lymphocyte count ($10^9/L$)	1.92 (4.34)	1.98 (1.20)	1.81 (7.46)	.61
Monocyte count ($10^9/L$)	0.78 (0.54)	0.67 (0.48)	0.99 (0.59)	<.001
Eosinophil count ($10^9/L$)	0.13 (0.19)	0.14 (0.18)	0.11 (0.20)	.02
Basophil Count ($10^9/L$)	0.04 (0.04)	0.04 (0.04)	0.04 (0.04)	.25
Mean corpuscular volume (fL)	90.43 (6.79)	89.84 (6.46)	91.68 (7.30)	.001
Mean corpuscular hemoglobin (pg)	29.32 (2.56)	29.42 (2.52)	29.11 (2.64)	.10
Mean corpuscular hemoglobin concentration (g/dL)	32.43 (1.50)	32.74 (1.43)	31.77 (1.43)	<.001
Immature granulocytes (%)	1.04 (0.92)	1.01 (0.90)	1.10 (0.95)	.17
Metabolic, mean (SD)				
Bicarbonate (mEq/L)	22.44 (4.40)	23.02 (3.94)	21.22 (5.04)	<.001
Phosphate (mg/dL)	3.95 (1.32)	3.75 (1.15)	4.38 (1.52)	<.001
Chloride (mEq/L)	101.03 (5.42)	100.99 (4.56)	101.13 (6.89)	.71
Potassium (mEq/L)	4.38 (0.73)	4.31 (0.65)	4.52 (0.84)	<.001

XSL•FO
RenderX

Characteristics	Total (n=833)	Survivors (n=565)	Nonsurvivors (n=268)	*P* value
Magnesium (mg/dL)	1.98 (0.36)	1.94 (0.34)	2.06 (0.40)	<.001
Calcium total (mg/dL)	8.70 (0.74)	8.76 (0.69)	8.58 (0.83)	.001
Aspartate aminotransferase (IU/L)	80.46 (131.84)	69.50 (117.58)	103.85 (155.73)	.001
Alanine aminotransferase (IU/L)	51.68 (94.95)	42.40 (71.36)	71.30 (129.58)	<.001
Albumin (g/dL)	3.45 (0.58)	3.61 (0.50)	3.13 (0.61)	<.001
Alkaline phosphatase (IU/L)	101.09 (104.40)	90.53 (52.22)	123.37 (165.74)	<.001
Glucose (mg/dL)	203.05 (105.71)	200.08 (102.18)	209.30 (112.72)	.24
Urea nitrogen (mg/dL)	31.57 (22.82)	25.91 (17.38)	43.49 (27.82)	<.001
Creatinine (mg/dL)	1.77 (1.68)	1.50 (1.44)	2.33 (1.99)	<.001
Troponin T (ng/mL)	1.18 (2.57)	1.08 (2.42)	1.39 (2.85)	.10
Creatine kinase isoenzymes (ng/mL)	28.73 (64.48)	28.48 (60.27)	29.26 (72.68)	.87
Coagulation, mean (SD)				
Partial thromboplastin time (sec)	48.09 (32.14)	48.73 (31.37)	46.73 (33.73)	.40
Inflammation-related indices, mean (SD)				
Lymphocyte-to-monocyte ratio	3.74 (4.28)	4.62 (4.76)	1.93 (2.11)	<.001
Neutrophil-to-platelet ratio	0.05 (0.05)	0.05 (0.05)	0.06 (0.05)	.001
Platelet-to-lymphocyte ratio	187.02 (184.20)	164.53 (169.65)	234.37 (203.96)	<.001
Neutrophil-to-lymphocyte ratio	9.55 (11.84)	7.63 (9.23)	13.61 (15.26)	<.001
Prognostic inflammatory value	2291.85 (3761.61)	1808.40 (2741.59)	3291.33 (5143.52)	<.001

For the external validation cohort (n=166), baseline analysis focused specifically on CBC data and indices in the prognostic model (LMR, NLR, NPR, PIV, and PLR). The detailed comparison between survivors and nonsurvivors based on the 3-year mortality outcomes are presented in Table S2 in Multimedia Appendix 1.

Associations Between the Inflammation-Related Indices and Mortality Risk

Cox proportional hazards analysis identified significant associations between inflammation-related indices (LMR, NPR, PLR, NLR, and PIV) and 3-year mortality risk (Table S3 in Multimedia Appendix 1). LMR was determined to be a protective factor, while NPR, PLR, NLR, and PIV were associated with an increased risk of mortality. These findings underscore the prognostic value of systemic inflammation markers in predicting long-term outcomes in this population.

LMR and Mortality Risk

Patients were stratified into quartiles based on LMR values: quartile 1 (LMR≤1.17; n=205), quartile 2 (1.17<LMR≤2.48; n=204), quartile 3 (2.48<LMR≤4.60; n=204), and quartile 4 (LMR>4.60; n=205). In Cox proportional hazards models, quartiles 2, 3, and 4 were significantly associated with reduced 3-year mortality risk compared to quartile 1, in both unadjusted and adjusted models (Table S3 in Multimedia Appendix 1). K-M survival analysis further demonstrated that patients in quartile 1 had the lowest 3-year survival probability, indicating the detrimental impact of low LMR (Figure 2A). RCS analysis revealed a decreasing trend between LMR and mortality risk, with a critical inflection point at LMR=2.44 (Figure 2B). Below this threshold, lower LMR values were strongly associated with increased mortality risk.

XSL•FO
RenderX

Figure 2. Kaplan Meier (K-M) survival analysis curves and restricted cubic spline (RCS) regression analysis of lymphocyte-to-monocyte ratio (LMR) for 3-year mortality. (A) K-M curves of LMR. (B) RCS analysis of LMR.

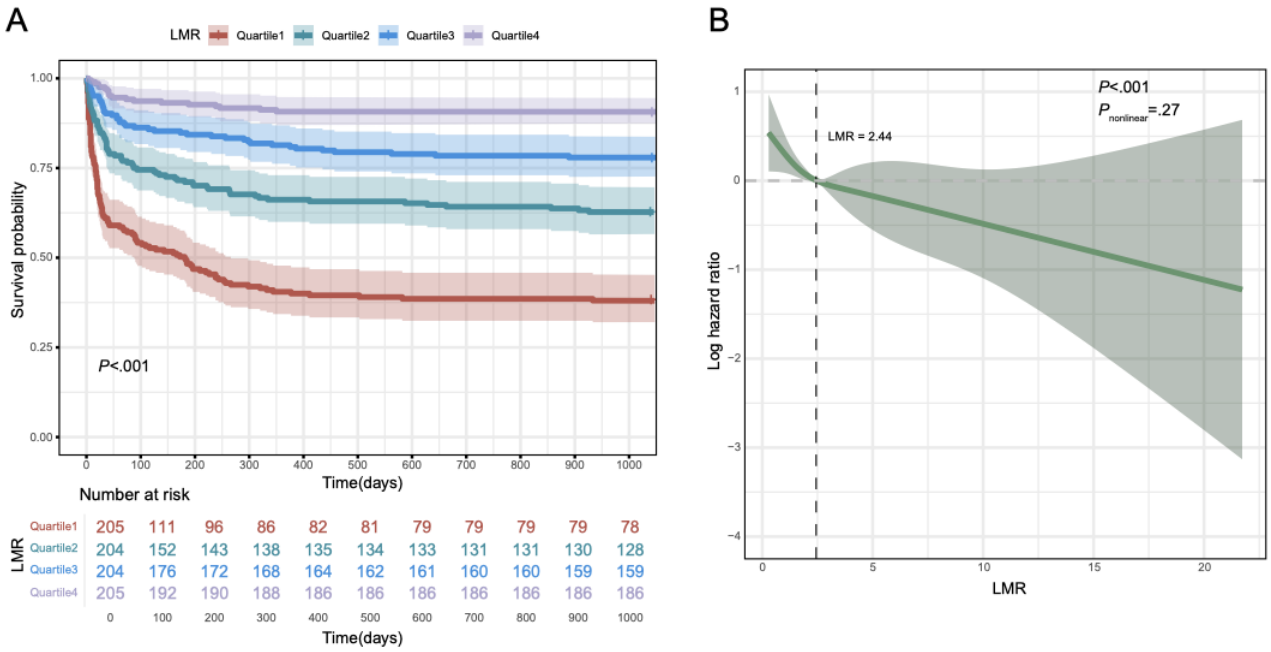

NPR and Mortality Risk

For NPR, patients were divided into 4 quartiles: quartile 1 (NPR≤0.033), quartile 2 (0.033<NPR≤0.046), quartile 3 (0.046<NPR≤0.064), and quartile 4 (NPR>0.064). In the unadjusted model, higher NPR values were significantly associated with increased mortality risk. However, this association was attenuated and lost statistical significance after adjustment for potential confounders (Table S3 in Multimedia Appendix 1). K-M survival analysis demonstrated that patients in quartile 4 (highest NPR) had the lowest 3-year survival probability compared with other quartiles, underscoring the detrimental impact of elevated NPR values (Figure 3A). RCS analysis revealed a nonlinear trend in the association between NPR and mortality risk, with a potential threshold observed around NPR=0.04. However, the test for nonlinearity did not reach statistical significance ($P_{\text{nonlinearity}}$=.27), suggesting that a linear relationship between these variables cannot be excluded (Figure 3B).

XSL•FO
RenderX

Figure 3. Kaplan-Meier (KM) survival analysis curves and restricted cubic spline (RCS) regression analysis of neutrophil-to-platelet ratio (NPR) and platelet-to-lymphocyte ratio (PLR) for 3-year mortality. (A) K-M curves of NPR. (B) RCS analysis of NPR. (C) K-M curves of PLR. (D) RCS analysis of PLR.

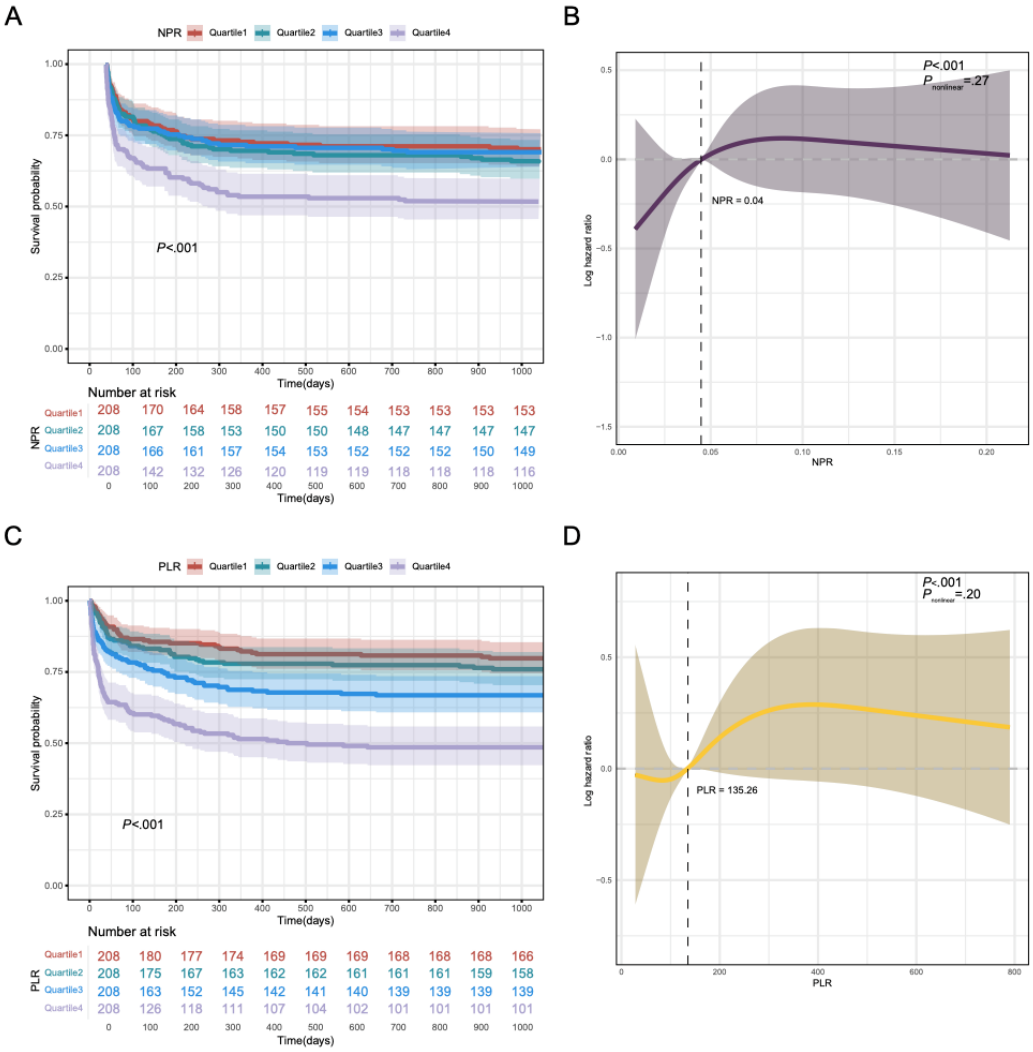

PLR and Mortality Risk

PLR was categorized into quartile 1 (PLR≤83.50), quartile 2 (83.50<PLR≤134.37), quartile 3 (134.37<PLR≤255.65), and quartile 4 (PLR>255.65). In the unadjusted model, higher PLR values were associated with increased mortality risk. However, after adjustment for confounding variables, this association was no longer statistically significant, suggesting potential confounding effects (Table S3 in Multimedia Appendix 1). K-M survival analysis demonstrated that patients in quartile 4 (highest PLR) had the lowest 3-year survival probability, consistent with the hypothesis that elevated PLR reflects a heightened inflammatory state (Figure 3C). RCS analysis indicated that as PLR increased, mortality risk also increased, with a notable value at PLR=135.26 (Figure 3D).

NLR and Mortality Risk

NLR quartiles were defined as follows: quartile 1 (NLR≤3.50), quartile 2 (3.50<NLR≤5.86), quartile 3 (5.86<NLR≤10.62), and quartile 4 (NLR>10.62). In both unadjusted and adjusted Cox proportional hazards models, patients in quartile 4 (highest NLR) exhibited a significantly increased risk of 3-year mortality compared with those in lower quartiles (Table S3 in Multimedia Appendix 1). K-M survival analysis further demonstrated that quartile 4 had the lowest 3-year survival probability, indicating the adverse prognostic impact of elevated NLR (Figure 4A). RCS analysis indicated that lower NLR values were associated with lower mortality risk, whereas higher NLR values significantly increased mortality risk, especially beyond a threshold of 5.75. Although the *P*=.07 suggests the nonlinear relationship was not fully significant, the trend between NLR and mortality risk is noteworthy (Figure 4B).

XSL•FO
RenderX

Figure 4. Kaplan-Meier (KM) survival analysis curves and restricted cubic spline (RCS) regression analysis of neutrophil-to-lymphocyte ratio (NLR) and prognostic inflammatory value (PIV) for 3-year mortality. (A) K-M curves of NLR. (B) RCS analysis of NLR. (C) K-M curves of PIV. (D) RCS analysis of PIV.

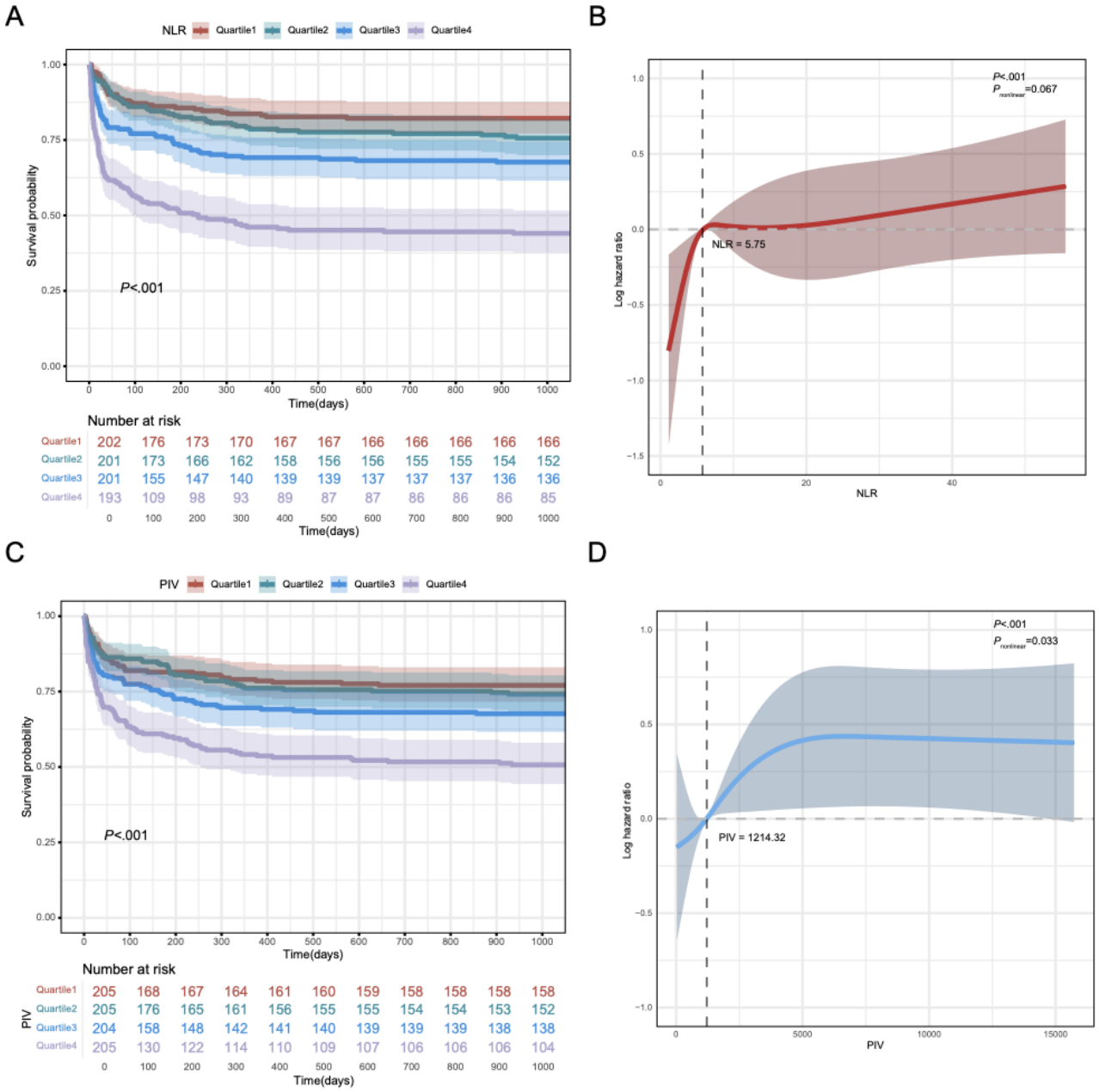

PIV and Mortality Risk

For PIV, the quartiles were defined as quartile 1 (PIV≤550.46), quartile 2 (550.46<PIV≤1207.40), quartile 3 (1207.40<PIV≤2619.32), and quartile 4 (PIV>2619.32). Similarly, in both unadjusted and adjusted Cox models, quartile 4 (highest PIV) was significantly associated with increased 3-year mortality risk compared with lower quartiles (Table S3 in Multimedia Appendix 1). K-M survival analysis demonstrated that patients in quartile 4 had the lowest 3-year survival probability (Figure 4C), suggesting an association between elevated PIV and poor outcomes. The RCS curve shows that 1214.32 is a risk turning point; beyond this value, risk increased significantly (Figure 4D).

Stratified Analyses

To further explore whether the relationship between inflammation-related indices and 3-year all-cause mortality persists under different conditions, subgroup analyses were conducted based on gender, age, BMI, hypertension, and hyperlipidemia. In the subgroup of patients aged ≥60 years, the hazard ratios (HRs) for all indices related to 3-year all-cause mortality were significant (Figures S1 and S2 in Multimedia Appendix 2). However, in the subgroup of patients aged <60 years, the HRs for NPR, PLR, and PIV did not show statistical significance. Furthermore, the HR for NPR was not statistically significant in the subgroup of patients with BMI<18 kg/m^2 and the subgroup of patients with hypertension. Similarly, the HRs for NPR and PIV were not statistically significant in the

XSL•FO
RenderX

subgroup of patients with BMI>28 kg/m^2 (Figures S1 and S2 in Multimedia Appendix 2).

Feature Selection

Initially, we compared the prognostic performance of individual CBC counts (lymphocyte, monocyte, neutrophil, and platelet counts) with inflammation-related indices using Cox regression models. The C-index values for individual cell counts ranged from 0.62 to 0.68, significantly lower than those of composite indices (0.72-0.79; Figure S3 in Multimedia Appendix 2). This disparity highlights the limited utility of isolated cell counts in capturing systemic inflammatory states. Given that the inflammation-related indices are derived from these individual cell counts, they inherently exhibit a higher degree of collinearity. Therefore, to focus more on the inflammation-related features themselves and minimize the impact of collinearity in the analysis, we excluded the individual immune cell counts before performing the VIF calculation.

We then examined the VIF to detect multicollinearity among variables, and features with a VIF>5 were removed (Table S1 in Multimedia Appendix 1). Subsequently, feature selection was performed using the Boruta algorithm, in which variables in the green area were identified as important features, whereas those in the red area were deemed unimportant (Figure S4 in Multimedia Appendix 2). Both CK-MB and troponin T were classified as unimportant (red box in Figure S4 in Multimedia Appendix 2), corroborating their limited prognostic value observed in baseline and Cox analysis (Table 1 and Figure S3 in Multimedia Appendix 2). This exclusion by the algorithm suggests that, although CK-MB and troponin T are critical for diagnosing acute myocardial injury, their transient elevation may not reflect the chronic inflammatory processes that drive long-term mortality in patients with diabetes combined with AMI.

Development and Validation of an Ensemble Machine Learning Model for Prognostic Prediction

After feature selection, we constructed a stacked model using all the important features, achieving an AUC of 0.862 in the test cohort (Figure 5A). To further explore the effectiveness of inflammation-related indices in predicting mortality risk in patients with diabetes combined with AMI, we built models based on individual inflammation-related indices, with AUCs of 0.782, 0.686, 0.598, 0.611, and 0.648 for LMR, NLR, NPR, PIV, and PLR, respectively, in the test cohort. We also combined these 5 indices into a stacked model, which achieved an AUC of 0.803 in the test cohort (Figure 5B; detailed parameters are shown in Figure 5D). Importantly, this combined inflammation-related indices model demonstrated robust generalizability, achieving an AUC of 0.781 in the external validation cohort (Figure 5C), with its predictive performance detailed in the confusion matrix (Figure 5E).

XSL•FO
RenderX

Figure 5. Receiver operating characteristic (ROC) curves of the machine learning prognostic models. (A) ROC curve for the model constructed using all important features in the test cohort. (B) ROC curves for models based on individual inflammation-related indices (lymphocyte-to-monocyte ratio [LMR], neutrophil-to-lymphocyte ratio [NLR], neutrophil-to-platelet ratio [NPR], prognostic inflammatory value [PIV], platelet-to-lymphocyte ratio [PLR]) and their combined model in the test cohort. (C) ROC curve for the combined inflammation-related indices model in the external validation cohort (area under the curve [AUC]=0.781). (D) Confusion matrix for the combined inflammation-related indices model in the test cohort. (E) Confusion matrix for the combined inflammation-related indices model in the external validation cohort.

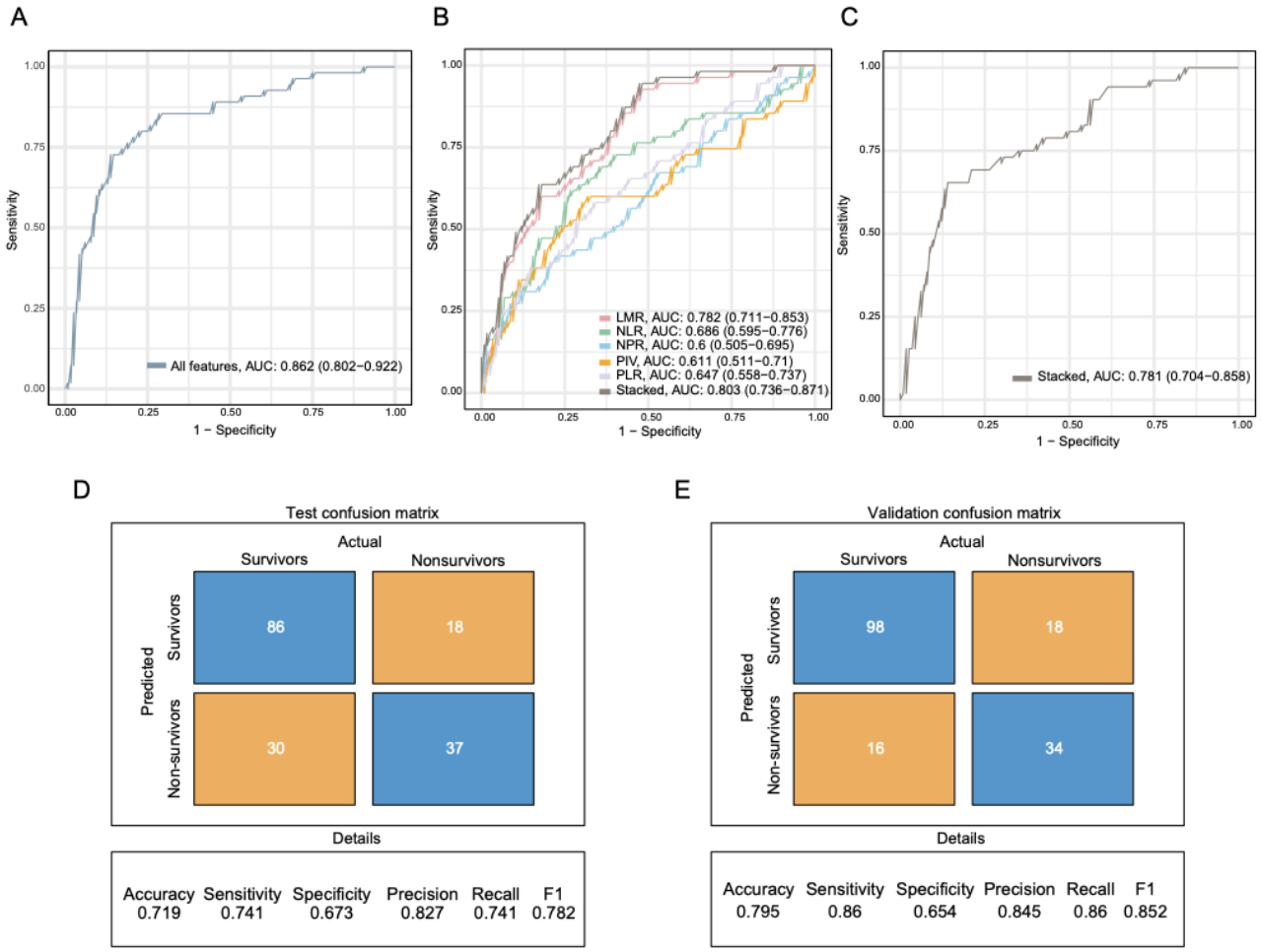

Although the combined model performed slightly worse than the model using all important features in the test cohort, it demonstrated comparable and generalizable prognostic ability. The combined inflammation-related indices model may contribute to future prognostic prediction by offering a simplified and cost-effective alternative for clinical applications.

Beyond discrimination, we evaluated the calibration and clinical utility of the model. The calibration plots displayed good agreement between predicted probabilities and observed outcomes, with Brier scores of 0.146 in the validation set and 0.155 in the external cohort (Figure S5 in Multimedia Appendix 2). Furthermore, decision curve analysis (DCA) indicated that the model provided a substantial net benefit over the "treat-all" or "treat-none" strategies across a wide range of threshold probabilities in both cohorts (Figure S5 in Multimedia Appendix 2).

In the external validation cohort, we also evaluated an enhanced model incorporating readily available vitals (age, heart rate, blood pressure, respiration rate). This "Indices + Vitals" model showed marginal improvement (AUC=0.788) and overlapping net benefit curves in DCA (Figure S6 in Multimedia Appendix 2), supporting the use of the 5-index model as a parsimonious stand-alone tool.

We further compared the stacked model with the best-performing single index LMR (Figure S8 in Multimedia Appendix 2). Although the improvements in net reclassification improvement and discrimination improvement were not statistically significant, the stacked model demonstrated superior overall performance. Specifically, it achieved a higher AUC (0.781 vs 0.771 in external validation) and, more importantly, better calibration (Brier score: 0.155 vs 0.183; calibration slope: 1.589 vs 3.147), suggesting that the multi-index approach provides more robust and accurate risk estimates than any single biomarker.

Application of the Model

Using the above model, we developed a web tool to predict the prognosis of patients with diabetes and acute myocardial infarction (Figure S9 in Multimedia Appendix 2). Users can get prediction results by directly inputting features on the web page [13].

XSL•FO
RenderX

Discussion

Overview

To the best of our knowledge, this study is the first to systematically compare 5 inflammation-related indices (LMR, NLR, NPR, PLR, and PIV) derived from CBC in relation to the 3-year mortality risk of patients with diabetes combined with AMI, and to explore their potential application in predicting long-term mortality risk. The findings indicate that inflammation may play a critical role in the long-term prognosis of patients with diabetes combined with AMI. By constructing both single-indicator models and combined predictive models, we demonstrated that these inflammation indices can effectively assess mortality risk while also providing a reference for rapid and straightforward clinical risk assessment methods. Interestingly, adding readily available vital signs to the inflammation-related indices provided limited incremental value in the external cohort, with minimal improvement. This suggests that the 5-index model may offer a streamlined tool for risk stratification (Figure S6 in Multimedia Appendix 2).

From a clinical perspective, the proposed model primarily relies on routine CBC components, which are widely available, rapid, and inexpensive. This accessibility could make the model a potentially useful tool for early risk stratification in settings such as emergency departments and ICUs, potentially helping clinicians to prioritize resource allocation.

The prognostic value of these CBC-derived inflammation-related indices likely stems from the synergistic pathophysiology of diabetes and AMI. The chronic hyperglycemia and insulin resistance unique to patients with diabetes induce low-grade chronic inflammation, which not only exacerbates cardiovascular damage but also drives disease progression through various mechanisms [14]. When AMI occurs, it triggers an acute stress response involving the sympathetic nervous system and the hypothalamic–pituitary–adrenal axis [15]. Both chronic metabolic inflammation and acute ischemic injury leads to a profound dysregulation of hematopoiesis, manifesting as the specific alterations in leukocytes and platelets observed in this study [16].

The elevated risk associated with high NLR, PLR, and PIV can be mechanically explained by the exacerbated proinflammatory and prothrombotic phenotype in patients with diabetes. Hyperglycemia and insulin resistance prime neutrophils to overreact during myocardial ischemia. A critical mechanism linking these cells to poor prognosis is the formation of neutrophil extracellular traps. In a diabetic environment, activated neutrophils release excessive neutrophil extracellular traps, which not only directly damage cardiomyocytes but also serve as a scaffold for platelet aggregation and thrombosis [17,18]. This interaction is particularly detrimental in AMI, as it contributes to microvascular obstruction and extends the infarct size [19]. Furthermore, diabetic platelets exhibit surface protein glycation and increased reactivity, making them more prone to adhering to leukocytes [20]. PIV (the systemic immune-inflammation index), which integrates neutrophils, platelets, and monocytes, essentially captures this extensive interplay between coagulation and inflammation, explaining its strong association with mortality in our cohort of patients with diabetes.

Conversely, the protective role of LMR highlights the importance of adaptive immunity in healing. Lymphocytes, particularly regulatory T cells, are essential for transitioning the immune response from the inflammatory phase to the reparative phase [21]. However, in patients with diabetes complicated by AMI, lymphocytes face dual suppression: chronic oxidative stress from hyperglycemia induces lymphocyte apoptosis, while the acute cortisol surge from AMI causes massive lymphopenia [22,23]. This severe depletion of lymphocytes impairs the containment of the inflammatory storm. Simultaneously, hyperglycemia promotes differentiation of monocytes into the proinflammatory M1 phenotype rather than the reparative M2 phenotype, further delaying scar healing and promoting adverse ventricular remodeling [24,25]. Therefore, a reduced LMR serves as a composite marker indicating an uncontrolled inflammatory response correlating with worse long-term survival.

The elevated levels of NLR, PLR, NPR, and PIV may reflect a proinflammatory state driven by interactions among platelets, neutrophils, and lymphocytes, which could be a critical driver of poor prognosis in patients with diabetes and CVDs. For instance, PIV, as an integrative inflammatory marker, captures the interplay between platelets, neutrophils, and lymphocytes. Studies have shown that elevated PIV levels are associated with worse outcomes in patients with hypertension [20]. Additionally, previous research has demonstrated that high NLR and PLR values are not only independent predictors of in-hospital mortality in patients with heart failure but are also closely associated with the risk of cardiac death [26,27]. Elevated NLR may indicate enhanced proinflammatory neutrophil activity and impaired lymphocyte function, whereas increased PLR may reflect both platelet activation and reduced lymphocyte-mediated immune function. In contrast, NPR primarily reflects the ratio between neutrophils and platelets, and its elevation has been associated with worse outcomes in patients with myocardial infarction with nonobstructive coronary arteries [28].

The protective role of LMR and the risk-associated roles of NLR, NPR, PLR, and PIV further underscore the critical importance of systemic inflammation and immune balance in the prognosis of patients with diabetes combined with AMI. These mechanisms suggest that protective and risk-related inflammatory markers may influence the prognosis of patients with diabetes combined with AMI through distinct pathways, providing a theoretical basis for future research on underlying mechanisms and advancements in diagnostic and therapeutic strategies.

In addition, the findings of this study highlight the significant value of inflammation-related indices in predicting the long-term prognosis of patients with diabetes combined with AMI.

Compared with traditional complex biomarkers or imaging techniques, these inflammation indices are derived from CBC, which is a widely available and affordable diagnostic tool. Furthermore, CBC results are highly stable and reproducible, making them reliable for both research and clinical practice [29]. These advantages highlight their practicality and feasibility

XSL•FO
RenderX

for preliminary prognostic assessment in patients with diabetes combined with AMI. The combined predictive model constructed based on these 5 indices (AUC=0.803) demonstrated a predictive ability comparable to that of the full importance features model (AUC=0.862). Moreover, our DCA confirmed that using this model to guide clinical decisions provides a higher net benefit than default strategies across a wide range of threshold probabilities (Figures 5A and B in Multimedia Appendix 2). By identifying high-risk patients, such prognostic models may facilitate early clinical interventions and potentially improve survival rates.

Limitations

Despite confirming the potential role of inflammation-related indices in predicting the long-term prognosis of patients with diabetes combined with AMI, this study has several limitations.

First, the regulatory mechanisms of inflammation in diabetes and AMI are highly complex, with different types of inflammatory cells potentially exerting bidirectional effects during disease progression. This intricate cellular regulation may not be fully captured by simplified inflammation-related indices.

Second, although 5 commonly used inflammation-related indices were analyzed, other potentially important inflammatory markers (eg, interleukin 6 and tumor necrosis factor α) were not included, which may underestimate the comprehensive impact of inflammation. Additionally, these indices primarily reflect systemic inflammation and may not adequately capture the influence of local immune microenvironments.

Third, a direct comparison with established scoring systems, such as the Global Registry of Acute Coronary Events or the Thrombolysis in Myocardial Infarction score, was not feasible in this study. Critical variables required for these scores—specifically cardiac arrest at admission, Killip classification, and coronary artery stenosis severity—were not systematically recorded or exhibited high levels of missingness in the structured electronic health records of the MIMIC-IV database. Regarding clinical utility, the DCA results suggest that using our model to guide clinical decisions would yield a net benefit over default strategies within a broad threshold range. However, the observed calibration drift in the external validation cohort highlights the heterogeneity between populations (Figures 5A and B in Multimedia Appendix 2). While the model's discriminative power remains robust, this finding emphasizes the necessity of model recalibration to adjust for baseline risk differences before local clinical implementation.

Fourth, the external validation was asymmetrical. While the primary 5-index model was successfully validated externally, we could not validate the full model containing ancillary covariates because these specific variables were not available in the external center's dataset. This limitation restricts the generalizability of the covariate-adjusted analysis to the derivation cohort.

Fifth, while MIMIC-IV provides a large-scale, high-quality dataset, it represents a single-center experience in the United States. Consequently, practice patterns, patient demographics, and admission criteria may differ from those in other institutions or countries, potentially limiting the direct generalizability of our findings. Although external validation was performed to assess transportability, future multicenter prospective studies are widely recommended.

Finally, regarding model transparency, while our model demonstrated excellent calibration in the internal validation, calibration drift was observed in the external validation cohort (Figures 5C and D in Multimedia Appendix 2), showing a tendency to underestimate risk in the new population. This suggests that while the model is effective for risk ranking, it may require recalibration using local data to optimize absolute probability estimates for different clinical settings.

Acknowledgments

During the preparation of this manuscript, the authors used DeepSeek (DeepSeek Inc) for grammar and language checking.

Funding

This work was supported by the National Natural Science Foundation of China (82172359, 82372338 and 81972009 to SML; 82402724 to KY; and 82202619 to YY) and the Translational Medicine and Interdisciplinary Research Joint Fund of Zhongnan Hospital of Wuhan University (ZNJC202302).

Data Availability

The datasets generated and/or analyzed during this study are available from the following sources. The Medical Information Mart for Intensive Care IV (MIMIC-IV) database is publicly available via PhysioNet [30], with access requiring completion of the Collaborative Institutional Training Initiative (CITI) Data or Specimens Only Research training and approval by the review board. The dataset from Zhongnan Hospital is not publicly available due to patient privacy and ethical restrictions; however, deidentified data may be available from the corresponding author upon reasonable request and with permission from the Ethics Committee of Zhongnan Hospital. To facilitate reproducibility, the code has been deposited in a public repository and is available at gitee [31].

XSL•FO
RenderX

Conflicts of Interest

None declared.

Multimedia Appendix 1
Additional tables.
[DOCX File , 31 KB - medinform_v14i1e83328_app1.docx]

Multimedia Appendix 2
Additional figures.
[DOCX File , 3211 KB - medinform_v14i1e83328_app2.docx]

References

1. GBD 2021 Diabetes Collaborators. Global, regional, and national burden of diabetes from 1990 to 2021, with projections of prevalence to 2050: a systematic analysis for the Global Burden of Disease Study 2021. Lancet 2023;402(10397):203-234 [FREE Full text] [doi: 10.1016/S0140-6736(23)01301-6] [Medline: 37356446]
2. Lee YS, Olefsky J. Chronic tissue inflammation and metabolic disease. Genes Dev 2021;35(5-6):307-328 [FREE Full text] [doi: 10.1101/gad.346312.120] [Medline: 33649162]
3. Wei X, Song H, Yin L, Rizzo MG, Sidhu R, Covey DF. Fatty acid synthesis configures the plasma membrane for inflammation in diabetes. Nature 2016;539(7628):294-298 [FREE Full text] [doi: 10.1038/nature20117] [Medline: 27806377]
4. Yang K, Sun J, Zhang Z, Xiao M, Ren D, Liu SM. Reduction of mRNA mA associates with glucose metabolism via YTHDC1 in human and mice. Diabetes Res Clin Pract 2023;198:110607. [doi: 10.1016/j.diabres.2023.110607] [Medline: 36878322]
5. Qin S, Yang K, Han S, Yuan Y, Mo J, Xiao M. N -methyladenine profiling of low-input multiplex clinical samples on transcriptome reveals RNA modifications implicated in type 2 diabetes and acute myocardial infarction. Clin Transl Med 2023;13(1):e1165. [doi: 10.1002/ctm2.1165] [Medline: 36631931]
6. Wong ND, Sattar N. Cardiovascular risk in diabetes mellitus: epidemiology, assessment and prevention. Nat Rev Cardiol 2023;20(10):685-695. [doi: 10.1038/s41569-023-00877-z] [Medline: 37193856]
7. Xia JG, Li B, Zhang H, Li QX, Lam SM, Yin CL. Precise metabolomics defines systemic metabolic dysregulation distinct to acute myocardial infarction associated with diabetes. Arterioscler Thromb Vasc Biol 2023;43(4):581-596. [doi: 10.1161/ATVBAHA.122.318871] [Medline: 36727520]
8. Edgar L, Akbar N, Braithwaite AT, Krausgruber T, Gallart-Ayala H, Bailey J. Hyperglycemia induces trained immunity in macrophages and their precursors and promotes atherosclerosis. Circulation 2021;144(12):961-982 [FREE Full text] [doi: 10.1161/CIRCULATIONAHA.120.046464] [Medline: 34255973]
9. Dentali F, Nigro O, Squizzato A, Gianni M, Zuretti F, Grandi AM. Impact of neutrophils to lymphocytes ratio on major clinical outcomes in patients with acute coronary syndromes: a systematic review and meta-analysis of the literature. Int J Cardiol 2018;266:31-37. [doi: 10.1016/j.ijcard.2018.02.116] [Medline: 29887466]
10. Trinh H, Dzul SP, Hyder J, Jang H, Kim S, Flowers J. Prognostic value of changes in neutrophil-to-lymphocyte ratio (NLR), platelet-to-lymphocyte ratio (PLR) and lymphocyte-to-monocyte ratio (LMR) for patients with cervical cancer undergoing definitive chemoradiotherapy (dCRT). Clin Chim Acta 2020;510:711-716. [doi: 10.1016/j.cca.2020.09.008] [Medline: 32919942]
11. Lin Y, Dai W, Chen Y, He X, Xu Y. Neutrophil-to-platelet ratio predicts mortality following percutaneous coronary intervention in patients with acute ST-elevation myocardial infarction. Front Physiol 2022;13:1011048. [doi: 10.3389/fphys.2022.1011048] [Medline: 36200052]
12. Guven DC, Sahin TK, Erul E, Kilickap S, Gambichler T, Aksoy S. The association between the pan-immune-inflammation value and cancer prognosis: a systematic review and meta-analysis. Cancers (Basel) 2022;14(11):2675. [doi: 10.3390/cancers14112675] [Medline: 35681656]
13. Prognostic tool for diabetic patients with acute myocardial infarction. URL: https://vigbly.shinyapps.io/shiny/ [accessed 2026-02-02]
14. Pradhan AD, Ridker PM. Do atherosclerosis and type 2 diabetes share a common inflammatory basis? Eur Heart J 2002;23(11):831-834. [doi: 10.1053/euhj.2001.3052] [Medline: 12042000]
15. Kun W, Jie Z, Shuai C, Xin WU, Guoqi Z, Shengbing WU, et al. Electroacupuncture ameliorates cardiac dysfunction in myocardial ischemia model rats: a potential role of the hypothalamic-pituitary-adrenal axis. J Tradit Chin Med 2023;43(5):944-954 [FREE Full text] [doi: 10.19852/j.cnki.jtcm.20230727.001] [Medline: 37679982]
16. Yamagishi S, Maeda S, Matsui T, Ueda S, Fukami K, Okuda S. Role of advanced glycation end products (AGEs) and oxidative stress in vascular complications in diabetes. Biochim Biophys Acta 2012;1820(5):663-671. [doi: 10.1016/j.bbagen.2011.03.014] [Medline: 21440603]
17. Döring Y, Soehnlein O, Weber C. Neutrophil extracellular traps in atherosclerosis and atherothrombosis. Circ Res 2017;120(4):736-743 [FREE Full text] [doi: 10.1161/CIRCRESAHA.116.309692] [Medline: 28209798]

XSL•FO
RenderX

18. Menegazzo L, Ciciliot S, Poncina N, Mazzucato M, Persano M, Bonora B. NETosis is induced by high glucose and associated with type 2 diabetes. Acta Diabetol 2015;52(3):497-503. [doi: 10.1007/s00592-014-0676-x] [Medline: 25387570]
19. Sreeramkumar V, Adrover JM, Ballesteros I, Cuartero MI, Rossaint J, Bilbao I. Neutrophils scan for activated platelets to initiate inflammation. Science 2014;346(6214):1234-1238 [FREE Full text] [doi: 10.1126/science.1256478] [Medline: 25477463]
20. Wu B, Zhang C, Lin S, Zhang Y, Ding S, Song W. The relationship between the pan-immune-inflammation value and long-term prognoses in patients with hypertension: National Health and Nutrition Examination Study, 1999-2018. Front Cardiovasc Med 2023;10:1099427 [FREE Full text] [doi: 10.3389/fcvm.2023.1099427] [Medline: 36937901]
21. Simões FC, Riley PR. Immune cells in cardiac repair and regeneration. Development 2022;149(8) [FREE Full text] [doi: 10.1242/dev.199906] [Medline: 35502777]
22. Gubser PM, Vasanthakumar A. Going sugar free: Treg cells avoid glucose to maintain functional fitness. Immunol Cell Biol 2021;99(6):558-560. [doi: 10.1111/imcb.12461] [Medline: 34013589]
23. Núñez J, Núñez E, Bodí V, Sanchis J, Mainar L, Miñana G. Low lymphocyte count in acute phase of ST-segment elevation myocardial infarction predicts long-term recurrent myocardial infarction. Coron Artery Dis 2010;21(1):1-7. [doi: 10.1097/mca.0b013e328332ee15] [Medline: 20050312]
24. Tapp LD, Shantsila E, Wrigley BJ, Pamukcu B, Lip GYH. The CD14++CD16+ monocyte subset and monocyte-platelet interactions in patients with ST-elevation myocardial infarction. J Thromb Haemost 2012;10(7):1231-1241 [FREE Full text] [doi: 10.1111/j.1538-7836.2011.04603.x] [Medline: 22212813]
25. van der Laan AM, Hirsch A, Robbers LF, Nijveldt R, Lommerse I, Delewi R. A proinflammatory monocyte response is associated with myocardial injury and impaired functional outcome in patients with ST-segment elevation myocardial infarction: monocytes and myocardial infarction. Am Heart J 2012;163(1):57-65.e2 [FREE Full text] [doi: 10.1016/j.ahj.2011.09.002] [Medline: 22172437]
26. Liu T, Wang B, Xiao S, Sun L, Zhu Z, Wang S. Correlation analysis between the static and the changed neutrophil-to-lymphocyte ratio and in-hospital mortality in critical patients with acute heart failure. Postgrad Med 2023;135(1):50-57. [doi: 10.1080/00325481.2022.2129177] [Medline: 36154549]
27. Tamaki S, Nagai Y, Shutta R, Masuda D, Yamashita S, Seo M. Combination of neutrophil-to-lymphocyte and platelet-to-lymphocyte ratios as a novel predictor of cardiac death in patients with acute decompensated heart failure with preserved left ventricular ejection fraction: a multicenter study. J Am Heart Assoc 2023;12(1):e026326 [FREE Full text] [doi: 10.1161/JAHA.122.026326] [Medline: 36565197]
28. Mohammed AA, Liu L, Mareai RM, Mohammed A, Yin G, Singh S. Combination of white blood cell count to mean platelet volume ratio and neutrophil-to-platelet ratio predicts long-term adverse events in patients with MINOCA. Mediators Inflamm 2022;2022:5642406 [FREE Full text] [doi: 10.1155/2022/5642406] [Medline: 36016662]
29. Doeleman MJH, Esseveld A, Huisman A, de Roock S, Tiel Groenestege WM. Stability and comparison of complete blood count parameters between capillary and venous blood samples. Int J Lab Hematol 2023;45(5):659-667. [doi: 10.1111/ijlh.14080] [Medline: 37128804]
30. MIMIC-IV. URL: https://physionet.org/content/mimiciv [accessed 2026-02-02]
31. ZhouTong202103/MIMIC. URL: https://gitee.com/zhoutong202103/mimic [accessed 2026-02-02]

Abbreviations

AMI: acute myocardial infarction
AUC: area under the curve
BIDMC: Beth Israel Deaconess Medical Center
CBC: complete blood count
CK-MB: creatine kinase isoenzymes
CVD: cardiovascular disease
DCA: decision curve analysis
HR: hazard ratio
ICD-10: International Statistical Classification of Diseases, Tenth Revision
ICD-9: International Classification of Diseases, Ninth Revision
ICU: intensive care unit
K-M: Kaplan-Meier
LMR: lymphocyte-to-monocyte ratio
MIMIC-IV: Medical Information Mart for Intensive Care IV
NLR: neutrophil-to-lymphocyte ratio
NPR: neutrophil-to-platelet ratio
PIV: prognostic inflammatory value
PLR: platelet-to-lymphocyte ratio
RCS: restricted cubic spline

XSL•FO
RenderX

STROBE: Strengthening the Reporting of Observational Studies in Epidemiology
VIF: variance inflation factor

Edited by A Benis; submitted 31.Aug.2025; peer-reviewed by M Al-Agil, Y Zhu, Y Chen; comments to author 11.Nov.2025; revised version received 06.Jan.2026; accepted 08.Jan.2026; published 12.Mar.2026.

Please cite as:
Zhou T, Yang K, Yang Y, Liu SM
Complete Blood Count–Derived Inflammation Indices to Predict 3-Year All-Cause Mortality in Patients With Diabetes and Acute Myocardial Infarction in Critical Care: Retrospective Cohort Study With Single-Center External Validation
JMIR Med Inform 2026;14:e83328
URL: https://medinform.jmir.org/2026/1/e83328
doi:10.2196/83328
PMID:

©Tong Zhou, Kun Yang, Ying Yang, Song-Mei Liu. Originally published in JMIR Medical Informatics (https://medinform.jmir.org), 12.Mar.2026. This is an open-access article distributed under the terms of the Creative Commons Attribution License (https://creativecommons.org/licenses/by/4.0/), which permits unrestricted use, distribution, and reproduction in any medium, provided the original work, first published in JMIR Medical Informatics, is properly cited. The complete bibliographic information, a link to the original publication on https://medinform.jmir.org/, as well as this copyright and license information must be included.

XSL•FO
RenderX

Original Paper

Neutrophil Percentage–to-Albumin Ratio as a Novel Prognostic Biomarker in Adult Diffuse Gliomas: Retrospective Study Integrating 3 Machine Learning Models and Cox Regression

Congcong Zhu[1,2], MD; Jiyang An[3], PhD; Lili Zhou[1], PhD

[1]Department of Oncology, The First Affiliated Hospital of Zhengzhou University, Zhengzhou, Henan, China

[2]Department of Oncology, The First Affiliated Hospital, and College of Clinical Medicine of Henan University of Science and Technology, Luoyang, Henan, China

[3]Department of Neurosurgery, The First Affiliated Hospital of Zhengzhou University, Zhengzhou, Henan, China

Corresponding Author:
Lili Zhou, PhD
Department of Oncology
The First Affiliated Hospital of Zhengzhou University
No. 1, East Jian She Road, Er Qi District
Zhengzhou, Henan, 450052
China
Phone: 86 176371002322
Email: zhoulili0@126.com

Abstract

Background: Adult-type diffuse glioma (ADG) is the most common primary malignant tumor of the central nervous system. Its highly invasive nature, marked heterogeneity, and resistance to therapy contribute to a high risk of recurrence and poor prognosis. At present, the lack of reliable prognostic tools poses a significant barrier to the development of individualized treatment strategies.

Objective: This study aimed to develop an effective prognostic model for ADG by integrating multiple machine learning algorithms, in order to enhance the precision of individualized clinical decision-making.

Methods: In this retrospective study, 160 newly diagnosed patients with ADG who underwent surgical resection and histopathological confirmation at our institution between June 2019 and September 2021 were included. A total of 32 variables, including clinical characteristics, molecular biomarkers, and preoperative hematological indicators, were collected. Overall survival (OS) and progression-free survival (PFS) were defined as the study endpoints. Feature selection was performed using least absolute shrinkage and selection operator regression, extreme gradient boosting, and random forest algorithms. Kaplan-Meier survival curves and log-rank tests were used for survival analysis. Multivariate Cox proportional hazards models were constructed to identify independent prognostic factors, and nomograms were developed accordingly. The model's discriminative ability, calibration, and clinical utility were evaluated using the concordance index, area under the receiver operating characteristic curve (area under the curve), calibration plots, and Kaplan-Meier analysis.

Results: Age, neutrophil percentage–to-albumin ratio (NPAR), and platelet-to-mean platelet volume ratio were identified as independent prognostic factors for OS, while age and NPAR were independent predictors for PFS (all $P<.001$). The prognostic models based on these variables demonstrated good predictive performance, with concordance index values of 0.731 and 0.763 for the training and validation cohorts in the OS model, respectively. The PFS model also showed robust performance. Area under the curve values and calibration curves further supported the models' accuracy and stability. Risk stratification analysis revealed clear survival differences between risk groups (all $P<.05$), indicating strong clinical applicability.

Conclusions: This study is the first to identify preoperative NPAR as a significant prognostic biomarker for ADG using machine learning approaches. The prognostic model incorporating NPAR, platelet-to-mean platelet volume ratio, and age demonstrated favorable predictive performance, offering a novel perspective for accurate risk stratification and personalized treatment in patients with ADG.

(JMIR Med Inform 2026;14:e79945) doi:10.2196/79945

XSL•FO
RenderX

KEYWORDS

adult-type diffuse glioma; machine learning; neutrophil percentage-to-albumin ratio; NPAR; prediction model; prognosis

Introduction

Glioma is the most common primary malignant tumor of the central nervous system, with an annual incidence of approximately 4.5 per 100,000 individuals [1]. Among its subtypes, adult-type diffuse glioma (ADG) constitutes the predominant pathological category, characterized by high invasiveness, frequent postoperative recurrence, and poor overall survival (OS) [2]. Epidemiological data indicate that ADG incidence exhibits age and sex specificity, with the highest prevalence observed in individuals aged 45-70 years (peak incidence at age 65-75 years) and a male predominance (male-to-female ratio: 1.3-1.6:1) [3].

Despite advances in multimodal treatment—including maximal surgical resection combined with radiochemotherapy—ADG survival outcomes have shown limited improvement over the past decade [4,5]. Novel therapies such as immune checkpoint inhibitors (eg, anti–PD-1 monoclonal antibodies) and targeted agents (eg, epidermal growth factor receptor inhibitors) offer promise, but their clinical benefits are restricted to specific molecular subgroups and are frequently accompanied by immune-related adverse events, such as pneumonitis (reported in 15%-20% of cases) and acquired resistance [6]. As such, there remains an urgent need for precise prognostic tools to identify treatment-sensitive subpopulations and guide individualized therapeutic decision-making.

Currently, prognostic evaluation of ADG largely depends on traditional clinicopathological parameters, including age, isocitrate dehydrogenase 1 (IDH1) mutation status, and O6-methylguanine-DNA methyltransferase (MGMT) promoter methylation [7,8]. However, these markers alone exhibit limited predictive accuracy for treatment response or survival. Emerging evidence suggests that inflammation within the tumor microenvironment (TME) plays a critical role in glioma progression by promoting angiogenesis and suppressing antitumor immune activity [9]. Peripheral blood–derived inflammatory biomarkers, such as the neutrophil-to-lymphocyte ratio (NLR), lymphocyte-to-monocyte ratio (LMR), and platelet-to-lymphocyte ratio (PLR), have demonstrated prognostic relevance in several malignancies, including breast and colorectal cancer [10,11]. However, their utility in ADG remains underinvestigated.

Recently, the neutrophil percentage-to-albumin ratio (NPAR)—a composite marker integrating systemic inflammation and nutritional status—has been proposed as a novel prognostic indicator in solid tumors [12]. Nevertheless, its prognostic value in ADG, particularly in the context of long-term survival and treatment response, remains unclear.

Moreover, most existing prognostic models in gliomas are based on conventional Cox regression analysis, which is limited in handling high-dimensional data and complex nonlinear interactions [13,14]. In contrast, machine learning algorithms such as least absolute shrinkage and selection operator (LASSO) regression, extreme gradient boosting (XGBoost), and random forest (RF) have shown superior performance in variable selection and pattern recognition [15-18]. However, no studies to date have integrated these 3 algorithms to enhance the robustness of prognostic modeling in ADG.

Therefore, this study proposes an innovative machine learning–based approach that integrates LASSO regression (for feature selection), XGBoost (a gradient-boosted decision tree method), and RF (an ensemble learning model) to develop a multidimensional prognostic tool based on clinical, molecular, and inflammatory parameters. The objective is to improve predictive accuracy and provide refined support for clinical decision-making in patients with ADG.

Methods

Ethical Considerations

This retrospective study was conducted in accordance with the Declaration of Helsinki and was approved by the Ethics Committee of The First Affiliated Hospital of Zhengzhou University (Approval No 2023-KY-0223-002). Given the retrospective nature of this study, the requirement for informed consent was waived by the ethics committee. All patient data were anonymized and deidentified prior to analysis. Personal identifiers were removed, and each patient was assigned a unique study code to ensure confidentiality throughout the research process. No financial compensation was provided to the participants.

Study Population

This retrospective study enrolled 160 treatment-naïve patients with ADG who underwent maximal safe surgical resection with histopathological confirmation at our institution between June 2019 and September 2021. The postoperative treatment regimen followed the standard protocol, consisting of concurrent chemoradiotherapy followed by adjuvant temozolomide chemotherapy. In cases of disease progression, targeted therapies such as bevacizumab or BRAF (B-Raf proto-oncogene, serine/threonine kinase) inhibitors (eg, for tumors harboring the BRAF V600E mutation) were administered based on clinical indications [19].

Inclusion criteria were as follows: (1) age ≥18 years, diagnosis of ADG in accordance with the 5th edition of the *WHO Classification of Tumors of the Central Nervous System* (World Health Organization [WHO] grade 3-4); (2) completion of preoperative magnetic resonance imaging or computed tomography evaluation; (3) no prior antitumor therapy; (4) receipt of standard treatment protocol; (5) availability of complete clinical data, including general characteristics, preoperative blood tests, cardiac, hepatic, and renal function assessments, as well as postoperative immunohistochemistry and molecular profiling; and (6) complete follow-up records.

Exclusion criteria were (1) postoperative mortality within 30 days due to surgical complications or nonneoplastic causes; (2) presence of severe systemic disease or active infection

XSL•FO
RenderX

potentially affecting study outcomes; (3) diagnosis of other concurrent malignancies; (4) significant cardiac, hepatic, or renal dysfunction; and (5) history of prior cranial surgery.

Postoperative follow-up included clinical and radiological evaluations every 3 months during the first year and every 6 months thereafter, until October 1, 2024. Progression-free survival (PFS) was defined as the time from diagnosis to radiographic or clinical disease progression or death from any cause. OS was defined as the time from diagnosis to death or the last follow-up.

Study Variables

Clinical data were collected from patients with ADG who met the inclusion and exclusion criteria. The variables analyzed in this study included: clinical characteristics, molecular biomarkers, genetic alteration markers, preoperative peripheral hematological indicators, and inflammation-related ratios.

Clinical Characteristics

Age, gender, preoperative tumor location, extent of tumor resection, maximum tumor diameter, and midline shift.

Molecular Biomarkers

Immunohistochemical markers included P53 protein (P53), oligodendrocyte transcription factor 2 (Olig-2), S100 calcium-binding protein (S100), epithelial membrane antigen (EMA), synuclein (SYN), alpha-thalassemia/mental retardation syndrome X-linked (ATRX), cluster of differentiation 34 (CD34), neuronal nuclei (NeuN), glial fibrillary acidic protein (GFAP), and proliferation cell nuclear antigen-67 (Ki-67).

Genetic Alteration Markers

IDH1 immunophenotype, telomerase reverse transcriptase (TERT) promoter region mutation, BRAF V600E point mutation, epidermal growth factor receptor (EGFR) amplification, MGMT promoter methylation status, 1p loss of heterozygosity (1pLOH), and 19q loss of heterozygosity (19qLOH).

Preoperative Peripheral Hematological Indicators

White blood cell (WBC), platelet (PLT), neutrophil (Neut), monocyte (Mono), lymphocyte (Lym), prothrombin time (PT), activated partial thromboplastin time (APTT), lactate dehydrogenase (LDH), and serum albumin (ALB). All preoperative peripheral hematological indicators, including NPAR, were measured from blood samples collected within 1 week prior to surgery, before the administration of any corticosteroids or other interventions that could significantly alter these values.

Inflammation-Related Ratios

According to international standards for inflammatory biomarkers, the following parameters were calculated and defined: PLR = PLT/Neut, NLR = Neut/Lym, LMR = Lym/Mono, monocyte-to-lymphocyte ratio (MLR) = Mono/Lym, prognostic nutritional index (PNI) = ALB + 5 × Lym, systemic inflammation response index (SIRI) = (Neut × Mono)/Lym, systemic immune-inflammation index (SII) = (PLT × Neut)/Lym, aggregate index of systemic inflammation (AISI) = (Neut × PLT × Mono)/Lym, NPAR = (Neut/WBC%)/ALB, neutrophil-lymphocyte-platelet ratio (NLPR) = Neut/(Lym × PLT).

Study Design and Statistical Analysis

The study design is illustrated in Figure 1.

A random seed was set to divide the 160 cases into a training cohort (n=112) and a validation cohort (n=48) at a 7:3 ratio. The primary endpoint was OS, and the secondary endpoint was PFS. A total of 32 variables were included, encompassing clinical characteristics (age, gender, tumor location, etc), molecular biomarkers (Ki-67, IDH1, R132H, etc), and inflammatory indicators (NPAR, NLR, etc).

Continuous variables were dichotomized using the median as the cutoff. This approach was chosen to simplify the clinical interpretation of the model and to facilitate risk stratification, while also mitigating the impact of potential outliers and meeting the model's assumption of proportional hazards for categorical predictors. Categorical variables were expressed as frequencies (percentages), and group comparisons were conducted using the chi-square test (expected frequency ≥5) or Fisher exact test (expected frequency <5). The Shapiro-Wilk test was used to assess the normality of continuous variables. For normally distributed data, comparisons between groups were performed using the 2-tailed independent-samples *t* test (2 groups) or 1-way ANOVA (3 or more groups), with data presented as mean (SD). For nonnormally distributed data, comparisons were performed using the Mann-Whitney *U* test (2 groups) or the Kruskal-Wallis H test (3 or more groups), with post hoc pairwise comparisons adjusted using the Bonferroni method. These data were reported as median (IQR). A 2-tailed *P* value <.05 was considered statistically significant for all analyses.

A total of 3 machine learning algorithms were applied: LASSO regression (using the *glmnet* package with 10-fold cross-validation to optimize λ), XGBoost (using the *xgboost* package with max depth=6 and learning rate=0.01), and RF (using the *randomForest* package with *ntree*=1000). Venn diagrams were used to identify overlapping important variables selected by all 3 algorithms. Survival differences between groups were visualized using Kaplan-Meier (KM) curves and compared using the log-rank test.

A Cox proportional hazards regression model was constructed to estimate hazard ratios (HRs) and 95% CIs. Based on multivariate Cox results, a nomogram was developed using the *rms* package. Time-dependent receiver operating characteristic (ROC) curves were generated, and the area under the curve (AUC) at 1, 3, and 5 years was calculated. The concordance index (C-index) was used to evaluate the model's discrimination ability. Calibration was assessed using calibration curves based on 1000 bootstrap resamples. KM survival analysis based on the median nomogram score was performed to evaluate clinical utility. The validation cohort was used to assess the model's predictive performance.

All statistical analyses were conducted using R software (version 4.4.1; R Foundation for Statistical Computing). A 2-sided *P* value <.05 was considered statistically significant.

XSL•FO
RenderX

Figure 1. Flowchart of the study design.

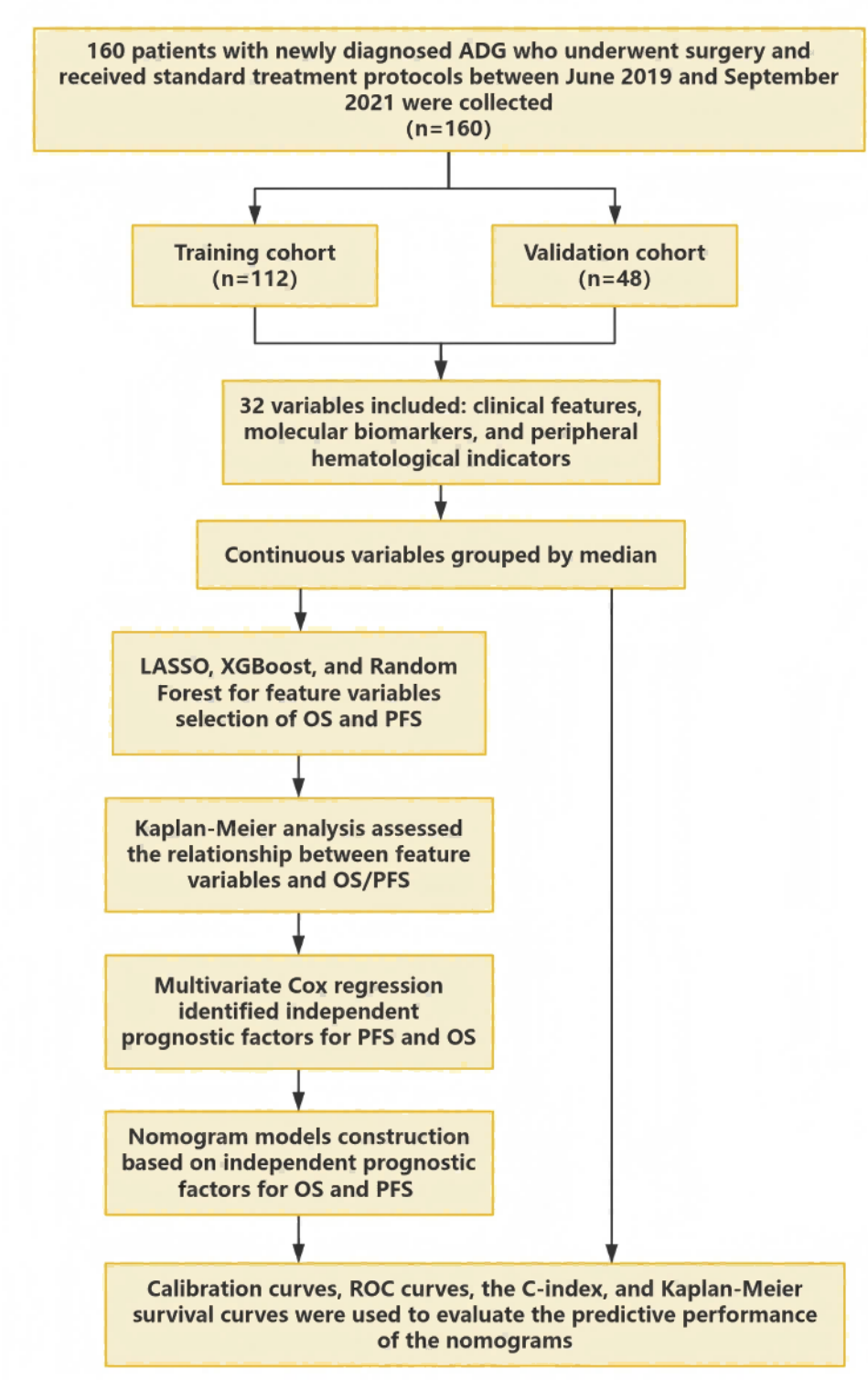

Results

Survival Outcomes

Among the 160 patients included in this study, a total of 132 (82.5%) experienced death events, and 152 (95%) experienced disease progression. The median OS was 23.0 months (IQR 15.0-38.3 months), while the median PFS was 10.5 months (IQR 6.8-17.5 months). The 1-, 3-, and 5-year OS rates were 85.6%, 27.1%, and 12.8%, respectively. The corresponding 1-, 3-, and 5-year PFS rates were 40.0%, 6.5%, and 3.4%, respectively. KM survival curves are presented in Figure 2.

XSL•FO
RenderX

Figure 2. Postoperative survival curves of 160 patients with adult-type diffuse glioma: (A) overall survival (OS) and (B) progression-free survival (PFS).

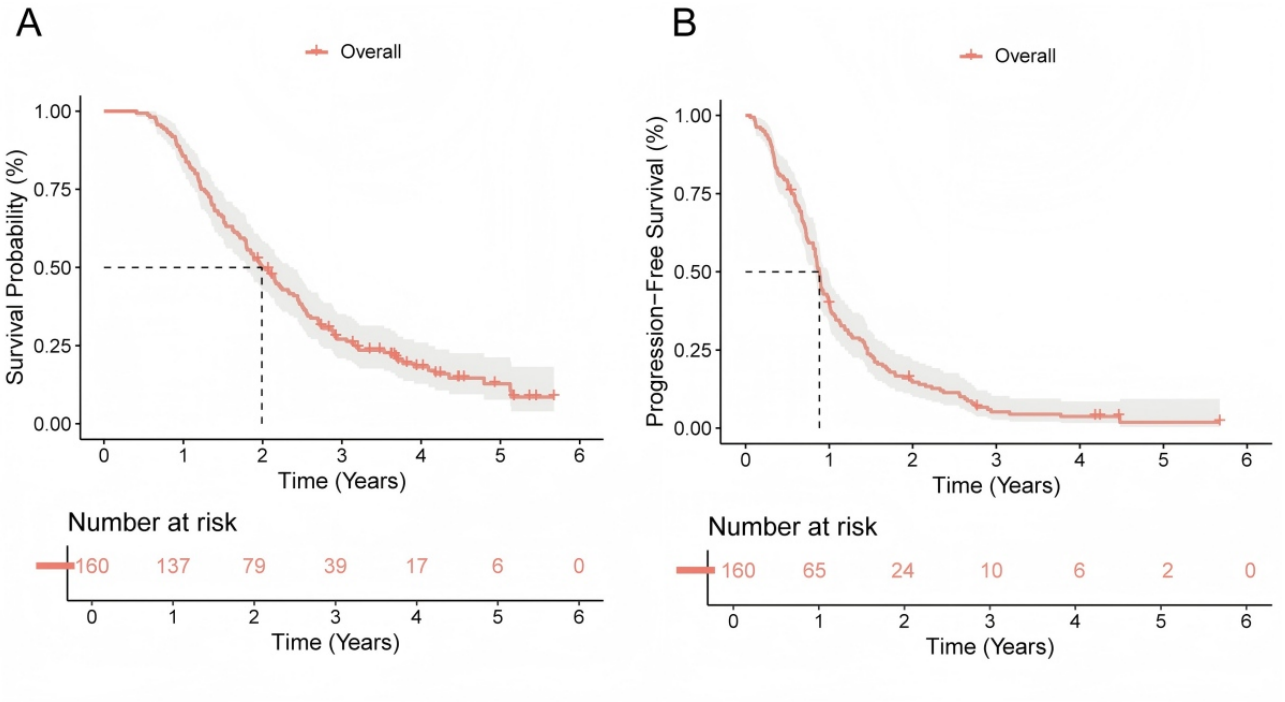

Baseline Characteristics

A total of 160 patients were included in this study, with a male-to-female ratio of approximately 1.4:1. The mean age was 51.3 (SD 13.6) years, and the median age was 53 (IQR 44-61) years. The maximum tumor diameter ranged from 1.0 to 9.5 cm, with a mean of 4.7 (SD 1.7) cm and a median of 5.0 cm (IQR 3.4-5.9 cm). Tumors were predominantly unilateral, with 76 cases (47.5%) on the left, 80 (50%) on the right, and 2 (2.5%) involving both sides. Midline shift was observed in 59.4% (95/160) of patients. All cases were classified as WHO grade 3-4. No significant differences in baseline characteristics were found between the training and validation cohorts (all P>.05). Detailed information is provided in Table 1.

XSL•FO
RenderX

Table 1. Baseline characteristics of 160 patients with adult-type diffuse glioma (ADG) stratified by group.

Variable	Training group, n (%)	Validation group, n (%)	*P* value
Age (years)			.58
<53	56 (50)	21 (44)	
≥53	56 (50)	27 (56)	
Sex			.06
Male	71 (63.4)	22 (46)	
Female	41 (36.6)	26 (54)	
Maximum tumor diameter (cm)			.89[a]
<5.0	55 (49.1)	23 (47)	
≥5.0	57 (50.9)	25 (52)	
Location			.74[b]
Left	54 (48.2)	22 (46)	
Right	56 (50.0)	24 (50)	
Double	2 (1.8)	2 (4)	
Midline shift			.16
No	41 (36.6)	24 (50)	
Yes	71 (63.4)	24 (50)	
Neutrophil percentage–to-albumin ratio			.92[b]
<1.578	55 (49.1)	24 (50)	
≥1.578	57 (50.9)	24 (50)	
Aggregate index of systemic inflammation			.60
<272.854	58 (51.8)	22 (46)	
≥272.854	54 (48.2)	26 (54)	
Immune-inflammation index			.86
<146.649	55 (49.1)	25 (52)	
≥146.649	57 (50.9)	23 (48)	
Lymphocyte-to-monocyte ratio			.39
<3.750	59 (52.7)	21 (44)	
≥3.750	53 (47.3)	27 (56)	
Neutrophil-to-lymphocyte ratio			.12
<2.677	51 (45.5)	29 (60)	
≥2.677	61 (54.5)	19 (40)	
Platelet-to-lymphocyte ratio			.23
<138.251	52 (46.4)	28 (58)	
≥138.251	60 (53.6)	20 (42)	
Monocyte-to-lymphocyte ratio			.39
<0.267	53 (47.3)	27 (56)	
≥0.267	59 (52.7)	21 (44)	
Prognostic nutritional index			.47
<50.55	52 (46.4)	26 (54)	
≥50.55	60 (53.6)	22 (46)	
Systemic inflammation response index			.86

XSL•FO
RenderX

Variable	Training group, n (%)	Validation group, n (%)	*P* value
<1.166	55 (49.1)	25 (52)	
≥1.166	57 (50.9)	23 (48)	
L actate dehydrogenase (IU/L)			.54
<174	53 (47.3)	26 (54)	
≥174	59 (52.7)	22 (46)	
Albumin (g/L)			.12
<42.35	51 (45.5)	29 (60)	
≥42.35	61 (54.5)	19 (40)	
Prothrombin time/Activated partial thromboplastin time			.39
<0.372	53 (47.3)	27 (56)	
≥0.372	59 (52.7)	21 (44)	
Platelet-to-mean platelet volume ratio			.12
<25.322	61 (54.5)	19 (40)	
≥25.322	51 (45.5)	29 (60)	
Proliferation cell nuclear antigen-67			.16
<30	28 (25)	18 (37)	
≥30	84 (75)	30 (63)	
Glial fibrillary acidic protein			>.99[b]
Positive	108 (96.4)	47 (98)	
Negative	4 (3.6)	1 (2)	
S100 calcium-binding protein			.74[b]
Positive	105 (93.8)	44 (92)	
Negative	7 (6.2)	4 (8)	
Oligodendrocyte transcription factor 2			>.99[b]
Positive	107 (95.5)	46 (96)	
Negative	5 (4.5)	2 (4)	
P53 protein			.09
Positive	103 (92)	39 (81)	
Negative	9 (8)	9 (19)	
Alpha-thalassemia/mental retardation syndrome X-linked			.27
Positive	96 (85.7)	37 (77)	
Negative	16 (14.3)	11 (23)	
Cluster of differentiation 34			.66
Positive	34 (30.4)	17 (35)	
Negative	78 (69.6)	31 (65)	
Epithelial membrane antigen			.56[b]
Positive	12 (10.7)	3 (6)	
Negative	100 (89.2)	45 (94)	
Synuclein			.40
Positive	22 (19.6)	13 (27)	
Negative	90 (80.4)	35 (73)	
Neuronal nuclei			>.99[b]

XSL•FO
RenderX

Variable	Training group, n (%)	Validation group, n (%)	*P* value
Positive	2 (1.9)	1 (2)	
Negative	110 (58.1)	47 (98)	
O6-methylguanine-DNA methyltransferase promoter methylation			>.99[b]
Methylated	6 (5.4)	2 (4)	
Unmethylated	106 (94.6)	46 (96)	
Isocitrate dehydrogenase 1 R132			.78[b]
Positive	12 (10.7)	4 (8)	
Negative	100 (89.2)	44 (92)	
1p loss of heterozygosity			.07[b]
Positive	2 (1.9)	4 (8)	
Negative	110 (58.1)	44 (92)	
19q loss of heterozygosity			.74[b]
Positive	7 (6.2)	4 (8)	
Negative	105 (93.8)	44 (92)	

[a]Indicates without continuity correction.

[b]Indicates Fisher exact test.

Differences in PFS and OS Between Groups

Since the measurement data did not meet the assumption of normality according to the Shapiro-Wilk test, the nonparametric Wilcoxon rank-sum test was applied to evaluate the impact of different clinical characteristics on PFS and OS. Data are presented as median (IQR).

Using PFS as the outcome variable, significant differences (all $P<.05$) were observed in the following 10 variables: age ($P<.001$), tumor location ($P=.03$), NPAR ($P=.002$), NLR ($P=.002$), PNI ($P=.01$), SYN ($P=.003$), MGMT promoter methylation ($P=.004$), IDH1 R132 ($P<.001$), 1pLOH ($P=.04$), and 19qLOH ($P<.001$).

Using OS as the outcome variable, a total of 12 variables showed significant associations (all $P<.05$): age ($P<.001$), NPAR ($P<.001$), LMR ($P=.03$), NLR ($P=.02$), MLR ($P=.03$), PNI ($P=.01$), LDH ($P=.04$), SYN ($P=.009$), MGMT ($P=.04$), IDH1 R132 ($P<.001$), 1pLOH ($P=.003$), and 19qLOH ($P<.001$). Detailed results are presented in Table 2.

XSL•FO
RenderX

Table 2. Comparison of progression-free survival (PFS) and overall survival (OS) among patients with glioblastoma between groups, median (IQR). The z and H values denote the test statistics for the Wilcoxon rank-sum test used in 2-group comparisons and the Kruskal-Wallis test used in multigroup comparisons, respectively.

Variable	Frequency, n	PFS (year), median (IQR)	z or H	*P* value	OS (year), median (IQR)	z or H	*P* value
Age (years)			4.42[a]	<.001		6.67[a]	<.001
<53	77	1.02 (0.74-2.37)			2.76 (1.96-3.67)		
≥53	83	0.73 (0.36-1.07)			1.36 (1.03-2.07)		
Sex			0.49[a]	.63		0.16[a]	.88
Male	93	0.90 (0.63-1.43)			2.03 (1.22-3.06)		
Female	67	0.84 (0.52-1.61)			1.95 (1.29-2.90)		
Maximum tumor diameter (cm)			–1.14[a]	.25		–1.04[a]	.30
<5.0	78	0.85 (0.59-1.45)			1.87 (1.21-2.91)		
≥5.0	82	0.92 (0.54-1.49)			2.13 (1.33-3.02)		
Location			7.050[b]	.03		3.26 [b]	.20
Left	76	0.90 (0.65-1.54)			2.05 (1.35-2.89)		
Right	80	0.86 (0.59-1.46)			1.98 (1.21-3.21)		
Double	4	0.33 (0.27-0.41)			1.13 (0.82-1.62)		
Midline-shift			–0.54[a]	.59		–0.86[a]	.39
No	65	0.85 (0.55-1.52)			1.80 (1.21-2.91)		
Yes	95	0.90 (0.58-1.45)			2.09 (1.33-3.00)		
Neutrophil percentage–to-albumin ratio			2.86[a]	.004		3.73[a]	<.001
<1.578	79	0.99 (0.67-1.74)			2.47 (1.53-3.58)		
≥1.578	81	0.83 (0.36-1.18)			1.72 (1.03-2.44)		
Aggregate index of systemic inflammation			1.35[a]	.18		1.28[a]	.20
<272.854	80	0.89 (0.67-1.47)			2.13 (1.32-3.38)		
≥272.854	80	0.88 (0.39-1.46)			1.91 (1.26-2.71)		
Immune-inflammation index			1.69[a]	.09		0.68[a]	.498
<146.649	80	0.89 (0.66-1.72)			2.07 (1.22-2.99)		
≥146.649	80	0.83 (0.50-1.24)			1.95 (1.30-2.90)		
Lymphocyte-to-monocyte ratio			–0.59[a]	.56		–2.13[a]	.03
<3.750	80	0.85 (0.53-1.43)			1.85 (1.22-2.52)		
≥3.750	80	0.89 (0.59-1.54)			2.45 (1.33-3.49)		
Neutrophil-to-lymphocyte ratio			2.83[a]	.005		2.41[a]	.02
<2.677	80	0.94 (0.67-1.81)			2.33 (1.35-3.56)		
≥2.677	80	0.83 (0.35-1.24)			1.85 (1.15-2.52)		
Platelet-to-lymphocyte ratio			0.85[a]	.40		0.47[a]	.64
<138.251	81	0.88 (0.61-1.54)			2.07 (1.22-3.13)		
≥138.251	79	0.88 (0.48-1.44)			1.94 (1.30-2.92)		
Monocyte-to-lymphocyte ratio			0.59[a]	.56		2.13[a]	.03
<0.267	80	0.89 (0.59-1.54)			2.45 (1.33-3.49)		
≥0.267	80	0.85 (0.53-1.43)			1.85 (1.22-2.52)		
Prognostic nutritional index			–2.26[a]	.02		–3.27[a]	.001

XSL•FO
RenderX

Variable	Frequency, n	PFS (year), median (IQR)	z or H	*P* value	OS (year), median (IQR)	z or H	*P* value
<50.55	78	0.83 (0.37-1.24)			1.79 (1.04-2.49)		
≥50.55	82	0.98 (0.64-1.61)			2.35 (1.51-3.21)		
Systemic inflammation response index			1.63[a]	.10		1.82[a]	.07
<1.166	80	0.90 (0.67-1.53)			2.39 (1.33-3.49)		
≥1.166	80	0.84 (0.38-1.46)			1.87 (1.22-2.56)		
Lactate dehydrogenase			1.04[a]	.30		2.11[a]	.04
<174	79	0.90 (0.51-1.79)			2.21 (1.34-3.21)		
≥174	81	0.85 (0.60-1.19)			1.80 (1.22-2.61)		
Albumin			–0.62[a]	.54		–1.61[a]	.11
<42.35	80	0.85 (0.64-1.27)			1.80 (1.21-2.63)		
≥42.35	80	0.92 (0.50-1.70)			2.15 (1.38-3.07)		
Prothrombin time/activated partial thromboplastin time			–0.12[a]	.91		0.52[a]	.60
<0.372	80	0.87 (0.51-1.47)			1.98 (1.21-3.56)		
≥0.372	80	0.88 (0.61-1.41)			2.00 (1.38-2.75)		
Platelet-to-mean platelet volume ratio			1.03[a]	.30		0.10[a]	.92
<25.322	80	0.88 (0.66-1.68)			1.96 (1.29-2.92)		
≥25.322	80	0.87 (0.50-1.31)			2.01 (1.26-2.97)		
Proliferation cell nuclear antigen-67			1.08[a]	.28		1.33[a]	.19
<30	46	0.92 (0.62-1.72)			2.36 (1.37-3.79)		
≥30	114	0.87 (0.52-1.43)			1.92 (1.24-2.74)		
Glial fibrillary acidic protein			0.21[a]	.84		1.09[a]	.28
Positive	155	0.88 (0.58-1.46)			1.96 (1.25-2.92)		
Negative	5	1.28 (0.21-2.76)			2.55 (2.22-4.35)		
S100 calcium-binding protein			–0.57[a]	.57		0.37[a]	.71
Positive	149	0.88 (0.59-1.46)			1.98 (1.22-2.92)		
Negative	11	0.88 (0.35-1.29)			2.55 (1.42-3.00)		
Oligodendrocyte transcription factor 2			–0.74[a]	.46		0.15[a]	.89
Positive	153	0.88 (0.58-1.46)			2.03 (1.22-2.92)		
Negative	7	0.83 (0.55-0.94)			1.89 (1.76-2.54)		
P53 protein			1.08[a]	.28		0.58[a]	.57
Positive	142	0.87 (0.58-1.43)			1.98 (1.22-2.89)		
Negative	18	1.13 (0.55-2.36)			1.97 (1.33-3.18)		
Alpha-thalassemia/mental retardation syndrome X-linked			1.71[a]	.09		1.48[a]	.14
Positive	133	0.85 (0.54-1.43)			1.94 (1.22-2.76)		
Negative	27	1.13 (0.70-2.35)			2.73 (1.40-3.55)		
Cluster of differentiation 34			–0.39[a]	.70		–0.47[a]	.64
Positive	51	0.85 (0.60-1.57)			2.07 (1.34-3.03)		
Negative	109	0.89 (0.51-1.43)			1.95 (1.22-2.89)		
Epithelial membrane antigen			–1.27[a]	.20		–0.51[a]	.61
Positive	15	1.02 (0.85-1.59)			1.81 (1.45-3.29)		

XSL•FO
RenderX

Variable	Frequency, n	PFS (year), median (IQR)	z or H	*P* value	OS (year), median (IQR)	z or H	*P* value
Negative	145	0.86 (0.54-1.46)			2.03 (1.22-2.92)		
Synuclein			2.86[a]	.004		2.63[a]	.009
Positive	35	0.67 (0.35-0.92)			1.44 (1.01-2.39)		
Negative	125	0.91 (0.64-1.54)			2.15 (1.35-3.14)		
Neuronal nuclei			–1.11[a]	.27		–0.35[a]	.73
Positive	3	1.72 (1.27-1.83)			1.96 (1.95-2.35)		
Negative	157	0.88 (0.55-1.46)			1.99 (1.22-2.94)		
O6-methylguanine-DNA methyltransferase promoter methylation			–2.86[a]	.004		–2.09[a]	.04
Positive	8	1.96 (1.25-2.44)			2.87 (2.16-3.63)		
Negative	152	0.86 (0.54-1.43)			1.94 (1.22-2.90)		
Isocitrate dehydrogenase 1 R132			–4.57[a]	<.001		–4.36[a]	<.001
Positive	16	1.88 (1.39-3.10)			3.34 (2.84-3.82)		
Negative	144	0.85 (0.51-1.23)			1.85 (1.21-2.72)		
1p loss of heterozygosity			–1.98[a]	.049		–3.00[a]	.003
positive	6	2.08 (1.19-2.52)			3.69 (3.31-4.27)		
negative	154	0.87 (0.56-1.43)			1.94 (1.22-2.89)		
19q loss of heterozygosity			–3.76[a]	<.001		–3.69[a]	<.001
positive	11	1.79 (1.32-3.73)			3.68 (2.63-4.19)		
negative	149	0.85 (0.53-1.42)			1.89 (1.21-2.84)		

[a]z values determined using the Wilcoxon rank sum test with two-group comparisons.

[b]H values determined using the Kruskal-Wallis test with multiple-group comparisons.

Construction and Validation of an OS-Based Prediction Model

Feature Variable Selection

Using OS as the outcome variable, a total of 3 machine learning algorithms—LASSO regression, XGBoost, and RF—were used to screen feature variables.

LASSO regression: based on the minimum λ value (λ_min), a total of 9 variables with nonzero coefficients were selected, including age, NPAR, platelet-to-mean platelet volume ratio (PMR), CD34 expression, SYN expression, EMA expression, IDH1 R132, 19qLOH, and MGMT promoter methylation (Figures 3A and B).

XGBoost model: according to feature importance scores, a total of 10 variables were selected, including age, PMR, SIRI, LMR, PNI, NPAR, maximum tumor diameter, PT/APTT, PLR, and LDH (Figure 3C).

RF: based on the mean decrease in Gini index, a total of 9 variables were selected, including age, PMR, NPAR, SIRI, NLR, PNI, LDH, SII, and PT/APTT (Figures 3D-F).

XSL•FO
RenderX

Figure 3. Feature variable selection based on 3 machine learning methods: (A) least absolute shrinkage and selection operator (LASSO) regression coefficient path plot: variable coefficients as a function of λ; (B) LASSO regression λ value tuning: 10-fold cross-validation to select the minimum λ value (λ_min); (C) extreme gradient boosting (XGBoost) feature importance: top 10 variables; (D) random forest (RF) error rate change: error rate as a function of the number of decision trees; (E) feature importance: assessed by Gini index; and (F) RF selected variables: top 9 variables. 19qLOH: 19q loss of heterozygosity; 1pLOH: 1p loss of heterozygosity; ALB: albumin; ATRX: alpha-thalassemia/mental retardation syndrome X-linked; CD34: cluster of differentiation 34; EMA: epithelial membrane antigen; GFAP: glial fibrillary acidic protein; IDH1R132: isocitrate dehydrogenase 1 R132; Ki-67: proliferation cell nuclear antigen-67; LDH: lactate dehydrogenase; LMR: lymphocyte-to-monocyte ratio; MGMT: O6-methylguanine-DNA methyltransferase; MLR: monocyte-to-lymphocyte ratio; NeuN: neuronal nuclei; NLR: neutrophil-to-lymphocyte ratio; NPAR: neutrophil percentage-to-albumin ratio; Olig-2: oligodendrocyte transcription factor 2; P53: P53 protein; PLR: platelet-to-lymphocyte ratio; PMR: platelet-to-mean platelet volume ratio; PNI: prognostic nutritional index; PT/APTT: prothrombin time/activated partial thromboplastin time; S100: S100 calcium-binding protein; SII: immune-inflammation index; SIRI: systemic inflammation response index; SYN: synuclein.

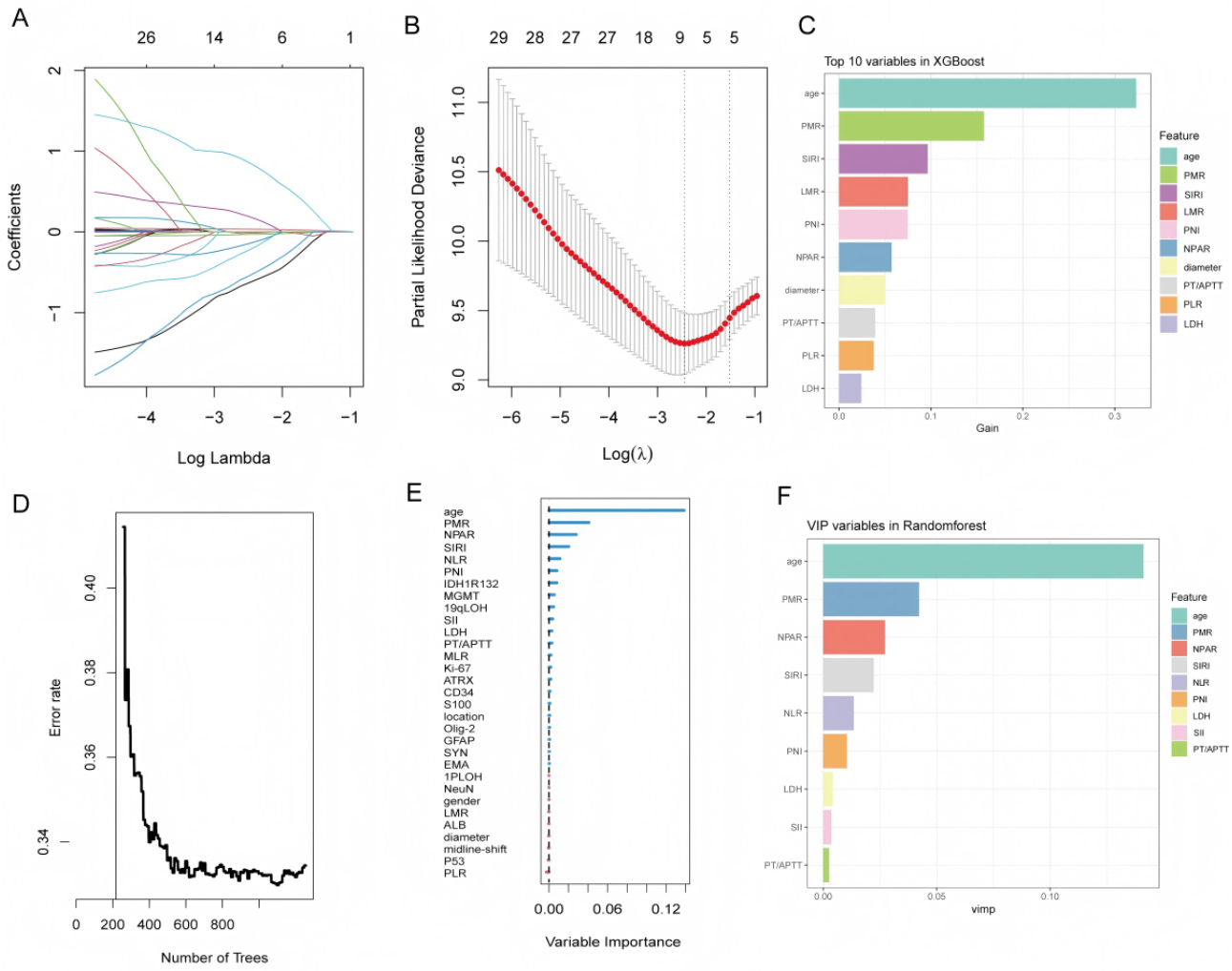

Survival Analysis

Based on the combined screening results from LASSO, XGBoost, and RF, Venn diagram intersection analysis identified age, NPAR, and PMR as key factors influencing OS (Figure 4A).

The prognostic impact of each individual variable was assessed using KM survival analysis (Figures 4B-D). Log-rank test results indicated that patients aged <53 years had significantly longer OS compared to those aged ≥53 years (P<.001), patients with NPAR <1.578 had significantly better OS than those with NPAR ≥1.578 (P<.001), while no significant difference in OS was observed between patients with PMR <25.322 and those with PMR ≥25.322 (P=.18).

Multivariate Cox proportional hazards regression analysis identified age (HR 1.05, 95% CI 1.03-1.07; P<.001), NPAR (HR 3.65, 95% CI 1.89-7.05; P<.001), and PMR (HR 0.96, 95% CI 0.93-0.98; P<.001) as independent prognostic factors for OS.

XSL•FO
RenderX

Figure 4. Identification of independent prognostic factors for overall survival (OS): (A) intersection analysis of feature variables from 3 models, (B) impact of age group on patient OS, (C) impact of neutrophil percentage-to-albumin ratio (NPAR) level on patient OS, (D) impact of platelet-to-mean platelet volume ratio (PMR) level on patient OS, and (E) forest plot of multivariate Cox regression analysis for OS. LASSO: least absolute shrinkage and selection operator.

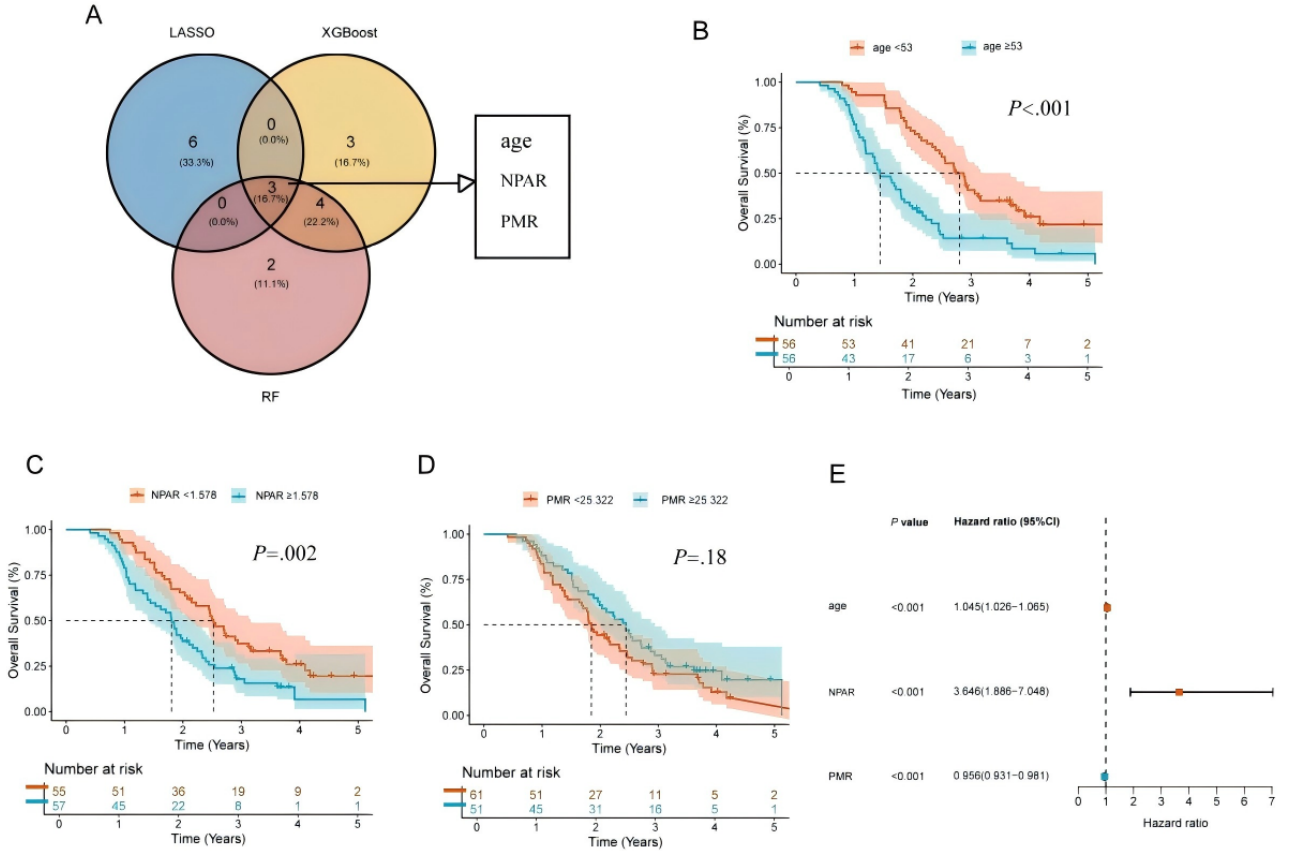

Construction and Validation of the OS Nomogram

Based on the multivariate Cox regression analysis, age, NPAR, and PMR were identified as independent prognostic factors for OS. A nomogram was constructed using these variables to predict 1-, 3-, and 5-year OS probabilities. Each variable was assigned a corresponding risk score, and the total score was used to estimate individual survival probability (Figure 5A). The calibration curve showed good agreement between the predicted and observed 1-, 3-, and 5-year OS rates (Figure 5B). Time-dependent ROC analysis demonstrated that the AUCs for 2-, 3-, and 4-year OS in the training cohort were 0.836, 0.820, and 0.801, respectively, indicating strong predictive performance across multiple timepoints (Figure 5C).

Patients were stratified into high- and low-risk groups based on the median nomogram score. KM survival analysis revealed that the high-risk group had significantly poorer OS compared with the low-risk group (P<.001), supporting the nomogram's utility in risk stratification (Figure 5D).

To further evaluate the discriminative ability of the nomogram score, a raincloud plot was used to visualize the score distribution between the survival and death groups. This plot, which integrates a density plot, box plot, and scatter plot, clearly illustrated the differences in score distribution, providing additional evidence of the nomogram's effectiveness in prognostic assessment (Figure 5E).

The calibration curve in the validation group indicated good predictive accuracy of the model for 1-, 2-, and 3-year survival in patients with ADG (Figure 6A). Time-dependent ROC analysis showed that the AUCs for 1-, 3-, and 4-year OS were 0.822, 0.797, and 0.722, respectively (Figure 6B). Risk stratification based on the nomogram score revealed a significant difference in score distribution between survivors and nonsurvivors. Patients in the high-risk group had significantly poorer OS compared with those in the low-risk group (P<.01), supporting the prognostic discriminatory power of the nomogram (Figure 6C). The C-index remained high in both the training and validation sets, suggesting robust and consistent predictive performance (Figure 6D).

XSL•FO
RenderX

Figure 5. Predictive performance of the overall survival (OS) nomogram: (A) prognostic nomogram integrating age, neutrophil percentage-to-albumin ratio (NPAR), and platelet-to-mean platelet volume ratio (PMR) to predict 1-, 3-, and 5-year OS probabilities through score conversion. For individual prediction, assign points for each variable, sum them to obtain a total score, and project this score downward to the bottom probability axes; (B) the calibration curve demonstrates the agreement between predicted and observed 1-, 3-, and 4-year OS probabilities in the training group; (C) time-dependent receiver operating characteristic (ROC) curves show area under the curve (AUC) values of 0.836, 0.820, and 0.801 for 2-, 3-, and 4-year OS, respectively; (D) survival analysis based on the median nomogram score reveals significant differences in OS between the high-risk and low-risk groups (P<.001); and (E) raincloud plot comparing the distribution of nomogram scores between the survival and death groups.

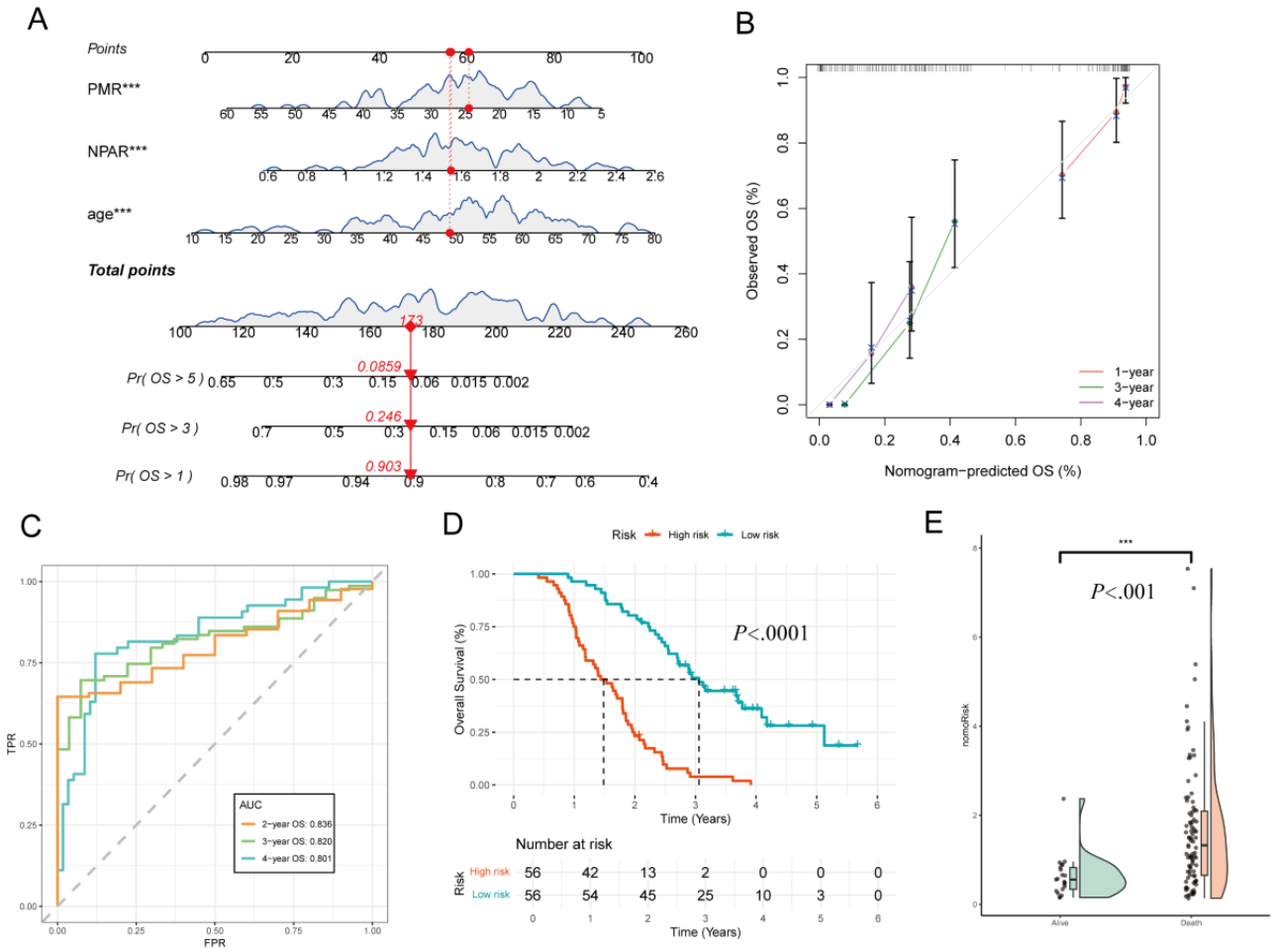

XSL•FO
RenderX

Figure 6. Validation of the overall survival (OS) nomogram: (A) the calibration curve demonstrates the agreement between predicted and observed 1-, 2-, and 3-year OS probabilities in the validation group; (B) time-dependent receiver operating characteristic (ROC) curves show area under the curve (AUC) values of 0.822, 0.797, and 0.722 for 1-, 3-, and 4-year OS, respectively; (C) survival analysis based on the median nomogram score reveals significant differences in OS between the high-risk and low-risk groups; and (D) comparison of the concordance index (C-index) between the training and validation groups.

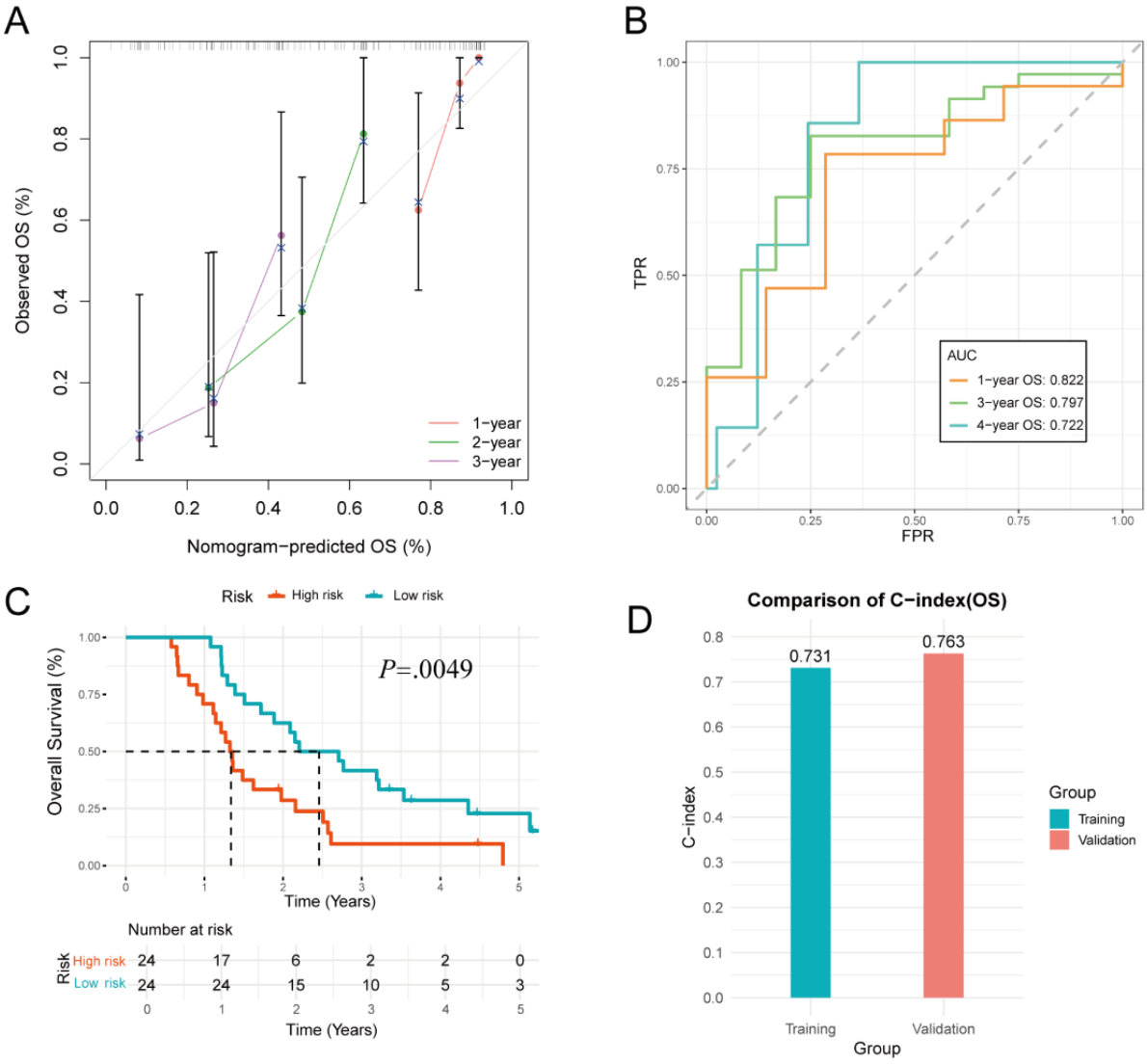

Construction and Validation of the PFS Prediction Model for ADG

Feature Variable Selection

Using PFS as the outcome variable, 3 machine learning algorithms—LASSO regression, XGBoost, and RF—were used to screen feature variables.

LASSO regression: based on the minimum λ value (λ_min), a total of 6 nonzero coefficient variables were selected, including age, NPAR, MLR, MGMT methylation, 1pLOH, and 19qLOH (Figure 7A and B).

XGBoost model: based on feature importance scores, a total of 10 variables were selected, including age, PT/APTT, PMR, SIRI, NPAR, NLR, maximum tumor diameter, PLR, SII, and Ki-67 expression (Figure 7C).

RF: based on the mean decrease in Gini index, a total of 9 variables were selected, including age, NPAR, ALB, tumor location, PNI, NLR, Ki-67, maximum tumor diameter, and LDH (Figures 7D and E).

XSL•FO
RenderX

Figure 7. Feature variable selection based on 3 machine learning methods: (A) least absolute shrinkage and selection operator (LASSO) regression coefficient path plot: variable coefficients as a function of λ, (B) LASSO regression parameter λ tuning based on the minimum criterion, (C) top 10 variables ranked by importance in the extreme gradient boosting (XGBoost) model, (D) change in error rate as a function of the number of decision trees during random forest (RF) model training, (E) RF feature importance: assessed by Gini index, and (F) RF selected variables: top 9 variables. 19qLOH: 19q loss of heterozygosity; 1pLOH: 1p loss of heterozygosity; ALB: albumin; ATRX: alpha-thalassemia/mental retardation syndrome X-linked; CD34: cluster of differentiation 34; EMA: epithelial membrane antigen; GFAP: glial fibrillary acidic protein; IDH1R132: isocitrate dehydrogenase 1 R132; Ki-67: proliferation cell nuclear antigen-67; LDH: lactate dehydrogenase; LMR: lymphocyte-to-monocyte ratio; MGMT: O6-methylguanine-DNA methyltransferase; MLR: monocyte-to-lymphocyte ratio; NeuN: neuronal nuclei; NLR: neutrophil-to-lymphocyte ratio; NPAR: neutrophil percentage-to-albumin ratio; Olig-2: oligodendrocyte transcription factor 2; P53: P53 protein; PLR: platelet-to-lymphocyte ratio; PMR: platelet-to-mean platelet volume ratio; PNI: prognostic nutritional index; PT/APTT: prothrombin time/activated partial thromboplastin time; S100: S100 calcium-binding protein; SII: immune-inflammation index; SIRI: systemic inflammation response index; SYN: synuclein.

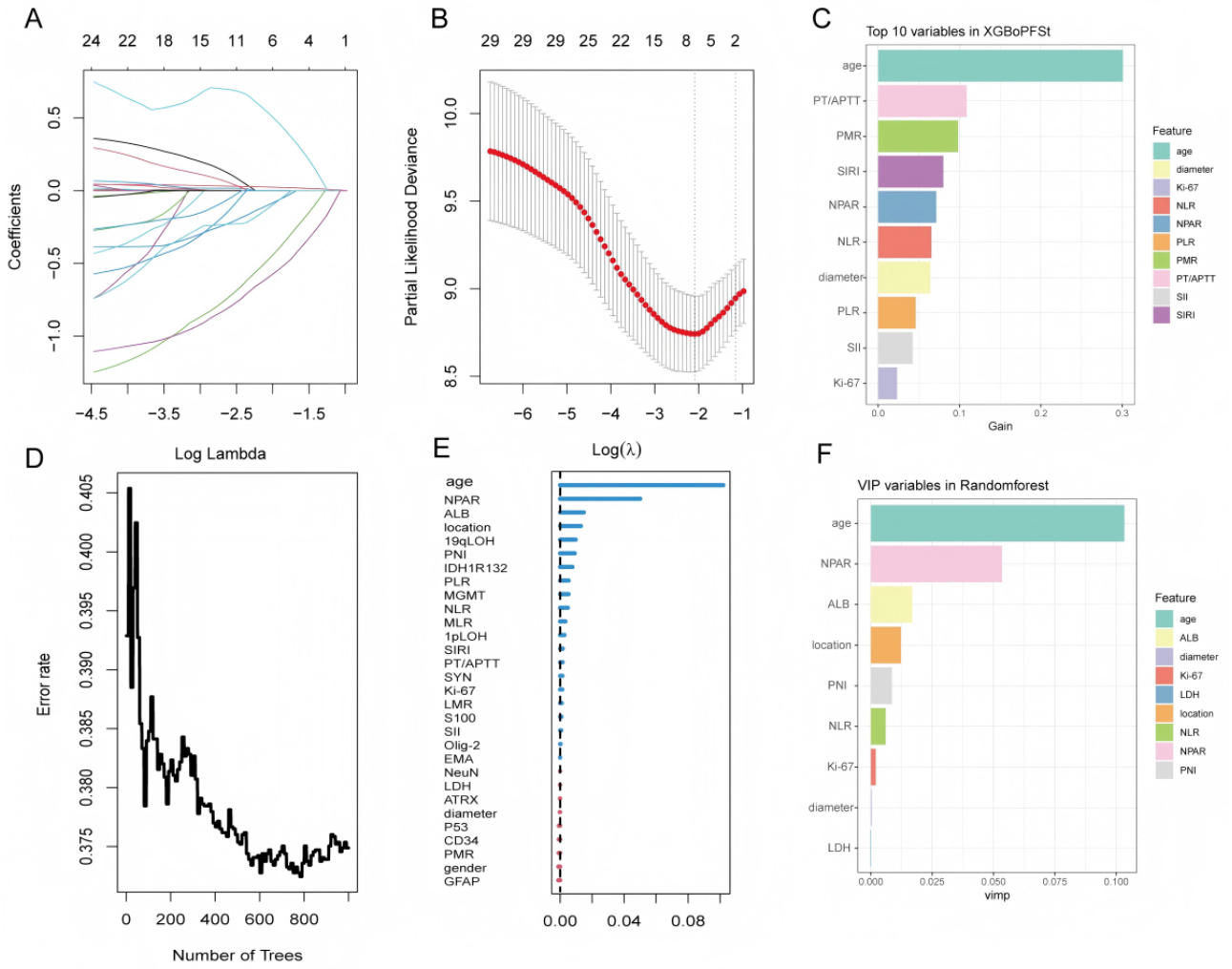

Survival Analysis

Based on the important variables screened by LASSO, XGBoost, and RF, Venn diagram intersection analysis identified age and NPAR as key factors influencing PFS (Figure 8A). The impact of each single factor on prognosis was assessed using KM survival analysis (Figures 8B and C). Log-rank test results showed that patients in the age <53 years group had significantly longer PFS than those in the age ≥53 years group (P<.001); patients in the NPAR <1.578 group had significantly longer PFS than those in the NPAR ≥1.578 group (P<.001). Multivariate Cox proportional hazards regression analysis revealed that age (HR 1.04, 95% CI 1.02-1.05; P<.001) and NPAR (HR 3.04, 95% CI 1.58-5.86; P<.001) were independent prognostic factors for PFS (Figure 8D).

XSL•FO
RenderX

Figure 8. Identification of independent prognostic factors for progression-free survival (PFS): (A) intersection analysis of feature variables from 3 models, (B) impact of age group on patient PFS, (C) impact of neutrophil percentage-to-albumin ratio (NPAR) level on patient PFS, and (D) forest plot of multivariate Cox regression analysis for PFS. LASSO: least absolute shrinkage and selection operator.

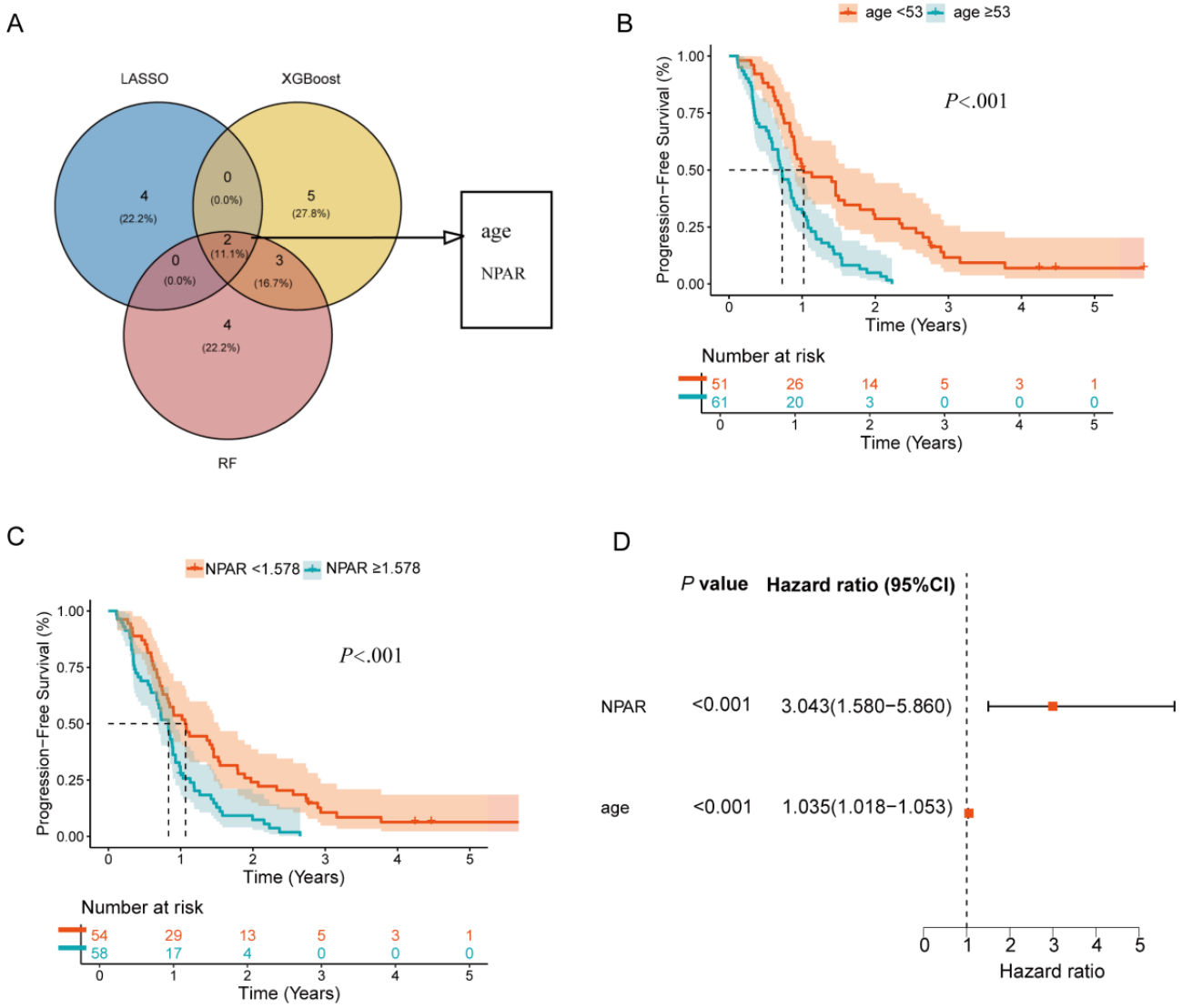

Construction and Validation of the PFS Nomogram

Based on multivariate Cox regression analysis, age and NPAR were identified as independent prognostic factors for PFS. A nomogram was constructed using these variables to predict 1-, 3-, and 5-year PFS rates. Each predictive variable was assigned a corresponding risk score, and the total score estimated the patient's probability of disease progression (Figure 9A).

The calibration curve demonstrated good agreement between the model-predicted and observed 12-, 24-, and 30-month PFS rates (Figure 9B). Time-dependent ROC curve analysis showed that the AUC for 1-, 2-, and 3-year PFS in the training group was 0.817, 0.864, and 0.873, respectively, indicating high predictive accuracy of the model at different timepoints (Figure 9C). Patients were divided into high-risk and low-risk groups based on the median nomogram score. KM survival curves revealed that the high-risk group had significantly lower PFS than the low-risk group (P<.001), demonstrating that the nomogram score effectively stratified patients' prognostic risk (Figure 9D).

The raincloud plot provides a visual representation of the score distribution differences between the 2 groups and further supporting the effectiveness of the nomogram score in prognostic assessment (Figure 9E).

Due to the high risk of patient recurrence, the calibration curve for the validation group demonstrated good predictive performance for 6-, 12-, and 18-month disease progression risk in patients with ADG (Figure 10A). Time-dependent ROC curve analysis showed that the AUC for 1-, 3-, and 5-year PFS in the validation group was 0.709, 0.843, and 0.953, respectively (Figure 10B). Based on the median nomogram score, patients in the validation group were divided into high-risk and low-risk groups. KM survival curves revealed significant differences in OS between the 2 groups (P<.05), further validating the prognostic discriminative ability of the nomogram score (Figure 10C).

The C-index of the model was excellent in both the training and validation groups, indicating stable predictive performance across different datasets (Figure 10D).

XSL•FO
RenderX

Figure 9. Predictive performance of the progression-free survival (PFS) nomogram: (A) prognostic nomogram integrating age and NPAR to predict 1-, 3-, and 5-year PFS probabilities through score conversion. For individual prediction, assign points for each variable, sum them to obtain a total score, and project this score downward to the bottom probability axes. (B) The calibration curve demonstrates the agreement between predicted and observed 12-, 24-, and 30-month PFS probabilities in the training group. (C) Time-dependent receiver operating characteristic (ROC) curves show area under the curve (AUC) values of 0.817, 0.864, and 0.873 for 1-, 2-, and 3-year PFS, respectively. (D) Survival analysis based on the median nomogram score reveals significant differences in PFS between the high-risk and low-risk groups (P<.001). (E) Raincloud plot comparing the distribution of nomogram scores between the survival (alive) and death (death) groups.

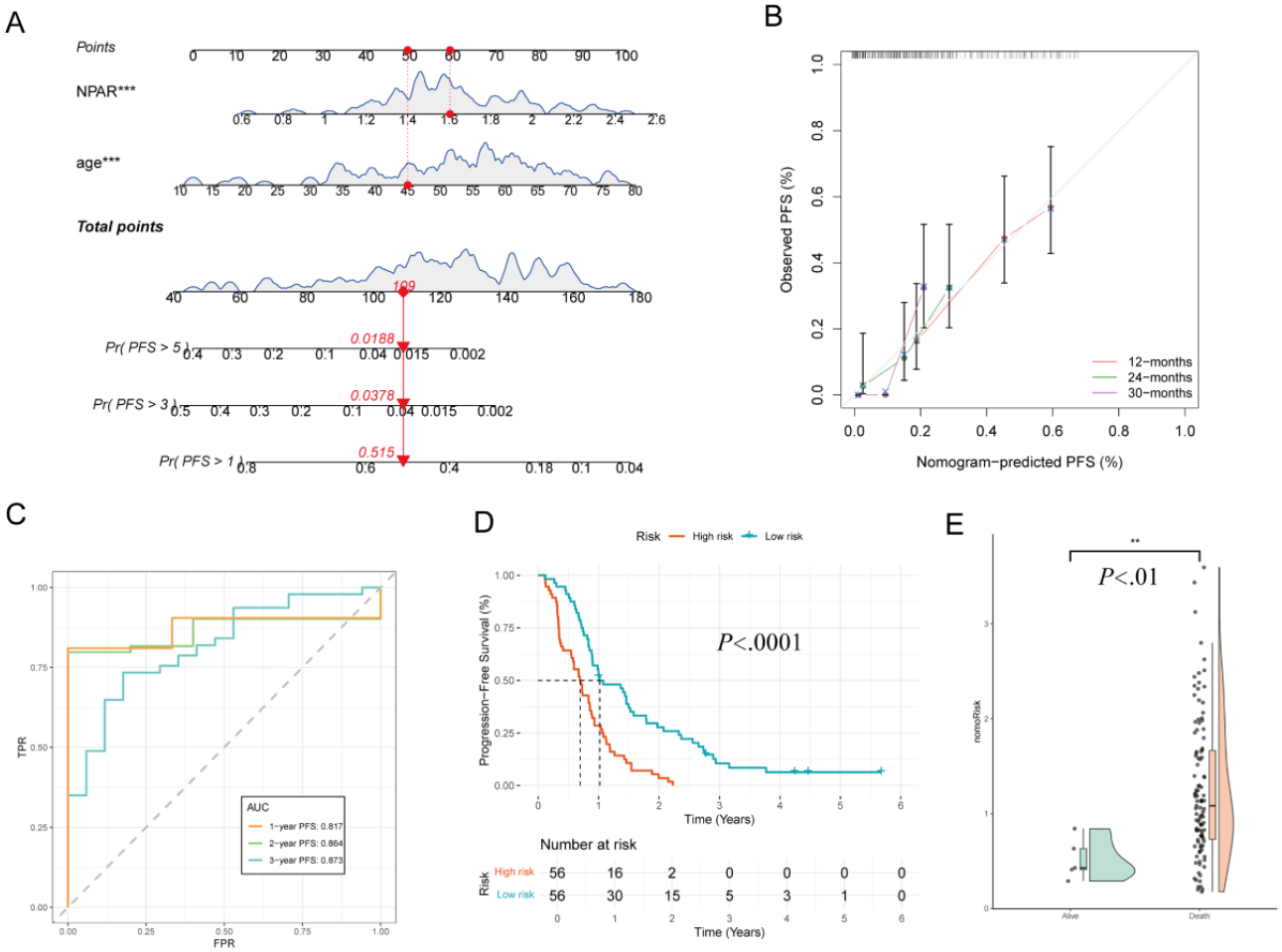

XSL•FO
RenderX

Figure 10. Validation of the progression-free survival (PFS) nomogram: (A) the calibration curve demonstrates the agreement between predicted and observed 6-, 12-, and 18-month PFS probabilities in the validation group; (B) time-dependent receiver operating characteristic (ROC) curves show area under the curve (AUC) values of 0.709, 0.843, and 0.953 for 1-, 3-, and 5-year PFS, respectively; (C) survival analysis based on the median nomogram score reveals significant differences in PFS between the high-risk and low-risk groups; and (D) comparison of the concordance index (C-index) between the training and validation groups.

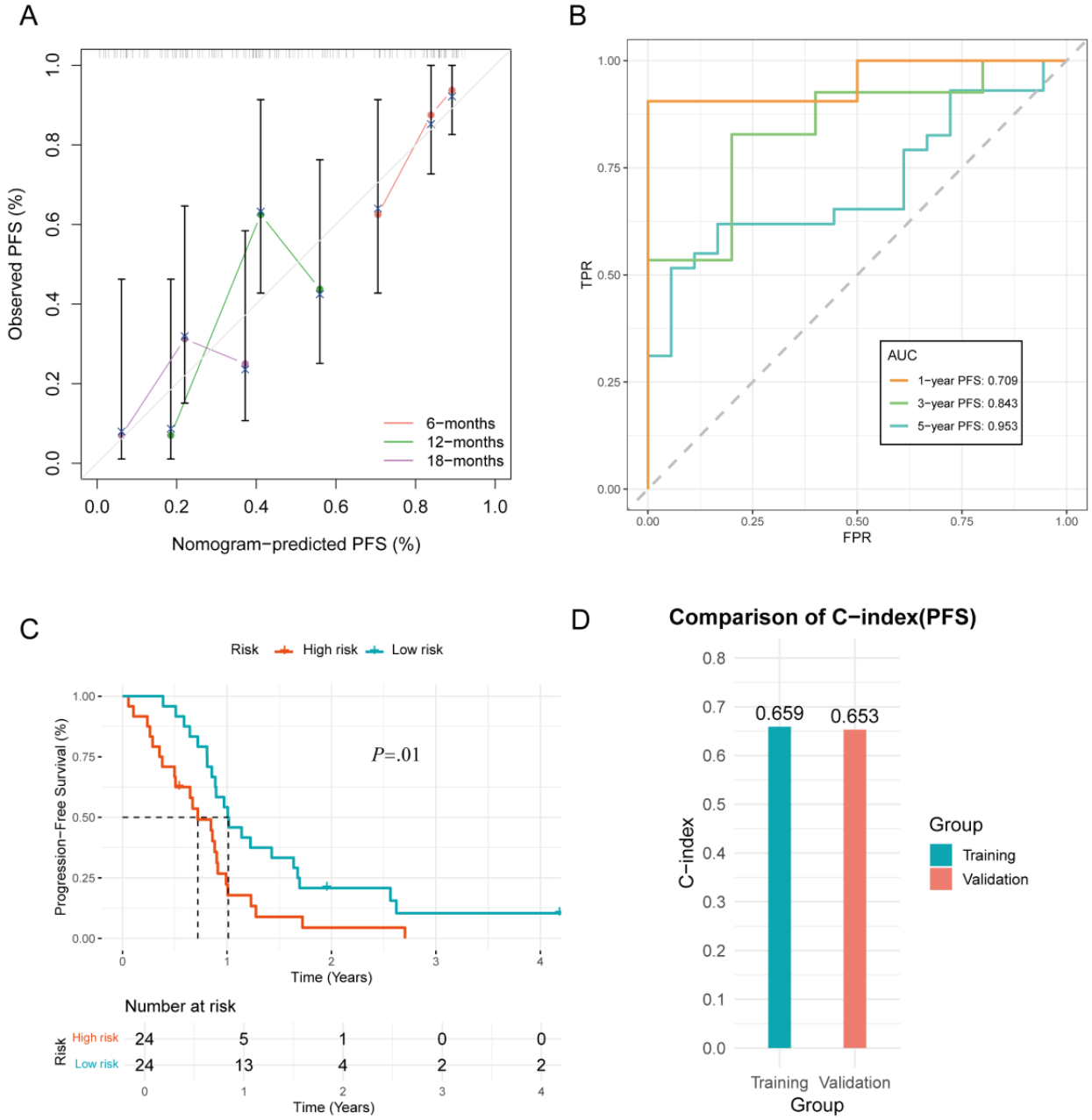

Discussion

Principal Results

ADG, characterized by high malignancy and strong invasiveness, accounts for 45% of all gliomas [20,21]. The tumor heterogeneity and infiltrative growth patterns of ADG often lead to progressive neurological impairment, posing significant challenges for clinical management [9,22]. This study demonstrated that standardized comprehensive treatment (surgery combined with concurrent chemoradiotherapy and temozolomide) extended the median overall survival (mOS) to 23.0 (IQR 15.0-38.3) months, which is superior to the approximately 15 months reported in previous studies [2,23,24]. However, 95% (152/160) of patients experienced postoperative recurrence, with a median progression-free survival (mPFS) of only 10.8 months and a 5-year PFS rate of merely 1.9% (3/160). Moreover, the long-term prognosis remains poor, with a 5-year OS rate of just 12.8% (20/160) [25]. Therefore, it is of great significance to further explore the key prognostic factors affecting patients with ADG, establish novel prognostic models, and develop effective preventive strategies.

The key methodological advance of our work lies in the robust feature selection achieved by integrating 3 distinct machine learning algorithms (LASSO, XGBoost, and RF) [26]. This integrative approach circumvents the inherent pitfalls of relying on a single method, be it traditional Cox regression or an

XSL•FO
RenderX

individual machine learning model [13,14]. Consequently, it ensures that the identified prognostic factors (age, NPAR, and PMR) are consistently salient across different modeling paradigms, thereby significantly strengthening the credibility of our results.

Compared to existing prognostic models for ADG, our model demonstrates superior predictive performance. While Kim et al [27] reported a C-index of 0.70 using a single machine learning approach, the OS model in this study achieved C-indices of 0.731 and 0.763 in the training and validation cohorts, respectively. Furthermore, the model maintained high time-dependent AUC values at multiple timepoints (AUCs of 0.836, 0.820, and 0.801 for 2-, 3-, and 4-year OS, respectively) along with favorable calibration. Importantly, our model innovatively incorporates readily accessible hematological biomarkers (NPAR and PMR). This provides a more cost-effective and clinically feasible prognostic assessment tool compared to traditional models that rely solely on clinical and molecular parameters [7,8].

Analysis of 32 variables showed that longer survival was observed in patients with canonical molecular markers such as IDH1 mutation and MGMT promoter methylation, implicating them as potential prognostic factors. IDH1 mutations play a critical role in suppressing tumor metabolism and proliferation [28,29]. Patients with IDH1-mutant astrocytoma included had an mOS of 40.0 (IQR 33.6–NA, NA is censored data—some patients remained alive at follow-up cutoff, so the upper quartile was not observed) months, markedly better than the 22.2 (IQR 14.4–34.7) months observed in IDH1 wild-type patients. Similarly, MGMT methylation enhances sensitivity of tumor cells to alkylating agents such as temozolomide by inhibiting MGMT transcription and reducing DNA repair capacity, thereby significantly prolonging both PFS and OS [29-31]. In this study, a 30-year-old patient with IDH-mutant astrocytoma and MGMT methylation achieved a survival period exceeding 64 months, demonstrating significant survival benefit [32].

Furthermore, by integrating multiple machine learning methods, the study systematically identified age, the inflammation-nutrition marker NPAR, and the platelet quantity and function marker PMR as independent prognostic factors for patients with ADG [16]. These variables demonstrated significant predictive power in forecasting the prognosis of patients with ADG [33,34].

Age was confirmed as a key prognostic factor in our model. Patients aged ≥53 years had a higher risk of disease progression and significantly shorter survival time compared with those aged <53 years. This finding aligns with previous research trends regarding the prognosis of older adults with ADG, which may be related to reduced treatment tolerance and alterations in tumor biological characteristics in older individuals. It suggests that clinicians should pay attention to age stratification and develop personalized treatment plans accordingly [28].

This study is the first to identify NPAR as an independent prognostic factor for ADG. Patients with high NPAR levels had significantly shorter mOS and mPFS, along with a markedly increased risk of disease recurrence and worse prognosis. As a novel indicator that comprehensively reflects systemic inflammation and nutritional status, the NPAR has increasingly been recognized for its prognostic value in various cancers such as pancreatic and urological cancers in recent years. The NPAR integrates both systemic inflammation (reflected by neutrophil percentage) and nutritional status (reflected by serum ALB), 2 key pathophysiological processes known to influence cancer prognosis. Neutrophils can impair immune surveillance by suppressing natural killer cell function and promote tumor cell proliferation and metastasis [12,35]. Serum ALB levels not only reflect the body's protein metabolic status but are also closely associated with immune dysfunction [36]. The prognostic value of NPAR may stem from its correlation with systemic inflammatory responses mediated by proinflammatory cytokines in the TME. This pathophysiological cascade can accelerate the progression of cachexia and facilitate the evolution of malignant tumor phenotypes by modulating the TME [37,38].

The prognostic value of NPAR stems from its integration of 2 pivotal pathophysiological pathways: protumor inflammation and host nutritional status. The neutrophil component reflects systemic inflammation. Within the glioma TME, neutrophils are polarized into tumor-associated neutrophils (TANs), which facilitate tumor progression by secreting matrix metalloproteinases to enhance invasion, releasing proangiogenic factors like vascular endothelial growth factor, and contributing to T-cell dysfunction [39]. Emerging evidence specifically links this protumorigenic neutrophil activity to glioma progression [40]. Conversely, hypoalbuminemia, indicative of poor nutritional status and diminished physiological reserve, is a well-established marker of impaired immune competence and poorer outcomes in patients with cancer [41]. Thus, NPAR comprehensively captures this detrimental interplay between a proinflammatory TME and a compromised host state.

Furthermore, this study identified a higher PMR as an independent prognostic factor for prolonged overall survival in patients with ADG. This finding is consistent with a study on angiosarcoma, which also reported that a high mean platelet volume–to–platelet count ratio served as an independent risk factor for patient mortality [42]. This consistent pattern across malignancies highlights the biological significance of composite indices based on platelet count and volume.

While studies have established that platelets can facilitate glioma progression by releasing factors like platelet-derived growth factor to stimulate proliferation [43] and by modulating the immune microenvironment to promote an M2 phenotype and immune escape [44], our discovery of PMR as a protective factor suggests a more nuanced role. We hypothesize that an elevated PMR reflects a distinct platelet phenotype characterized by a lower mean platelet volume which is generally associated with diminished platelet reactivity. Consequently, a high PMR may indicate a reduced capacity of platelets to engage in these documented protumorigenic processes, thereby explaining its association with improved survival in ADG.

The prognostic nomogram developed from the aforementioned factors demonstrates significant translational potential. This tool can be integrated into electronic medical record systems to enable automated risk stratification at the time of diagnosis. Consequently, high-risk patients could be considered for more

XSL•FO
RenderX

aggressive treatment strategies—such as intensified chemoradiation following maximal safe resection—or more intensive follow-up (eg, neuroimaging every 2-3 months), and even enrollment in novel clinical trials. Conversely, low-risk patients may be suitable candidates for treatment de-escalation, such as shortened adjuvant chemotherapy cycles or reduced radiation doses, aiming to preserve oncological control while enhancing quality of life. This nomogram-based decision-making model represents a constructive step toward precision neuro-oncology.

Limitations

This study is subject to several limitations, including its single-center retrospective design, which may limit generalizability, and a variable-to-sample size ratio that raises concerns about overfitting despite internal validation. These limitations underscore the necessity for external validation in independent multicenter cohorts as an essential next step. Moreover, the molecular mechanisms linking NPAR and PMR to glioma prognosis are not fully understood. To address these points and advance this research, future work must focus on multicenter prospective validation, augmenting the model's power through the integration of radiomics and genomics, and leveraging single-cell and multi-omics technologies to decipher the functional roles of these circulating biomarkers in glioma pathogenesis.

Conclusion

In conclusion, this study significantly improved the robustness of prognostic biomarkers through a multimodel cross-validation strategy. Among the numerous factors, age, the preoperative inflammation-nutrition composite indicator NPAR, and platelet quantity and function marker PMR were key prognostic factors. Patients with ADG with younger age and lower NPAR values had a lower risk of disease progression and better prognosis; meanwhile, patients with higher PMR exhibited longer survival. These biomarkers are not only easily accessible and cost-effective but also highly beneficial, offering a new perspective for personalized treatment of ADG.

Acknowledgments

We gratefully acknowledge the use of R statistical software and thank the funding agencies for their support of this research.

Authors' Contributions

CZ conceived the study concept, CZ and JA designed the study protocol and performed statistical analysis and interpretation, JA and LZ retrieved and selected the data, CZ and JA completed the draft writing and manuscript revision, and LZ oversaw the integration of the entire study and approved the final version. All authors have approved the submission of the final manuscript.

Conflicts of Interest

None declared.

References

1. Chen W, Guo S, Wang Y, Shi Y, Guo X, Liu D, et al. Novel insight into histological and molecular astrocytoma, IDH-mutant, grade 4 by the updated WHO classification of central nervous system tumors. Cancer Med 2023;12(18):18666-18678 [FREE Full text] [doi: 10.1002/cam4.6476] [Medline: 37667984]
2. Shaalan F, Ballout N, Chamoun WT. Insights into the role of Bmi-1 deregulation in promoting stemness and therapy resistance in glioblastoma: a narrative review. Cancer Med 2025;14(1):e70566 [FREE Full text] [doi: 10.1002/cam4.70566] [Medline: 39791545]
3. Sakly H, Said M, Seekins J, Guetari R, Kraiem N, Marzougui M. Brain tumor radiogenomic classification of O-methylguanine-DNA methyltransferase promoter methylation in malignant gliomas-based transfer learning. Cancer Control 2023;30:10732748231169149 [FREE Full text] [doi: 10.1177/10732748231169149] [Medline: 37078100]
4. Cen B, Zhang J, Pan X, Xu Z, Li R, Chen C, et al. Stimuli-responsive peptide/siRNA nanoparticles as a radiation sensitizer for glioblastoma treatment by co-inhibiting RELA/P65 and EGFR. Int J Nanomedicine 2024;19:11517-11537 [FREE Full text] [doi: 10.2147/IJN.S483252] [Medline: 39539970]
5. Schonfeld E, Choi J, Tran A, Kim LH, Lim M. The landscape of immune checkpoint inhibitor clinical trials in glioblastoma: a systematic review. Neurooncol Adv 2024;6(1):vdae174. [doi: 10.1093/noajnl/vdae174] [Medline: 39534539]
6. D'Aprile S, Denaro S, Gervasi A, Vicario N, Parenti R. Targeting metabolic reprogramming in glioblastoma as a new strategy to overcome therapy resistance. Front Cell Dev Biol 2025;13:1535073 [FREE Full text] [doi: 10.3389/fcell.2025.1535073] [Medline: 40078366]
7. Johnstad C, Reinertsen I, Thurin E, Dunås T, Bouget D, Sagberg LM, et al. The prognostic importance of glioblastoma size and shape. Acta Neurochir (Wien) 2024;166(1):450. [doi: 10.1007/s00701-024-06351-0] [Medline: 39531176]
8. Le Rhun E, Bink A, Felsberg J, Gramatzki D, Brandner S, Benhamida JK, et al. The clinical and molecular landscape of diffuse hemispheric glioma, H3 G34-mutant. Neuro Oncol 2025;27(6):1519-1535. [doi: 10.1093/neuonc/noaf015] [Medline: 39842935]
9. Sharma P, Aaroe A, Liang J, Puduvalli VK. Tumor microenvironment in glioblastoma: current and emerging concepts. Neurooncol Adv 2023;5(1):vdad009 [FREE Full text] [doi: 10.1093/noajnl/vdad009] [Medline: 36968288]

XSL•FO
RenderX

10. Attem J, Vemuganti GK. The role of small extracellular vesicles in retinoblastoma development and progression. Curr Eye Res 2025:1-15. [doi: 10.1080/02713683.2025.2457102] [Medline: 39905667]
11. Zhao Y, Wang Y, Jiang Y, Yang J, Zhang Y. The prognostic impact of neutrophil-to-lymphocyte ratio and platelet-to-lymphocyte ratio on patients with small cell lung cancer receiving first-line platinum-based chemotherapy: a systematic review and meta-analysis. BMC Pulm Med 2024;24(1):630 [FREE Full text] [doi: 10.1186/s12890-024-03447-2] [Medline: 39710633]
12. Li X, Wu M, Chen M, Liu R, Tao Q, Hu Y, et al. The association between neutrophil-percentage-to-albumin ratio (NPAR) and mortality among individuals with cancer: insights from National Health and Nutrition Examination Survey. Cancer Med 2025 Jan;14(2):e70527 [FREE Full text] [doi: 10.1002/cam4.70527] [Medline: 39831739]
13. Sun M, Li S, Guo Y, Zhou J, Fu D, Hua X, et al. Clinicopathological, immunohistochemical and therapeutic approaches on survival in patients with epithelioid glioblastoma: institutional experience in the management of 58 patients. Neurosurg Rev 2024;47(1):763. [doi: 10.1007/s10143-024-02957-1] [Medline: 39382734]
14. Zhang Z, Zhao Y, Ma Y, Chen C, Li Z, Wang Y, et al. Prediction of STAS in lung adenocarcinoma with nodules ≤ 2 cm using machine learning: a multicenter retrospective study. BMC Cancer 2025;25(1):417 [FREE Full text] [doi: 10.1186/s12885-025-13783-z] [Medline: 40055661]
15. Kurdi M, Alkhotani A, Alsinani T, Alkhayyat S, Katib Y, Jastaniah Z, et al. Effects of radiotherapy alone versus concomitant radiotherapy with temozolomide chemotherapy on the outcome of IDH-wildtype glioblastoma patients. Clin Oncol (R Coll Radiol) 2025;38:103741 [FREE Full text] [doi: 10.1016/j.clon.2024.103741] [Medline: 39742692]
16. Babajide Mustapha I, Saeed F. Bioactive molecule prediction using extreme gradient boosting. Molecules 2016;21(8):983 [FREE Full text] [doi: 10.3390/molecules21080983] [Medline: 27483216]
17. Hou W, Li C, Wang Z, Wang W, Wan S, Zou B. Predicting lymph node metastasis in rectal cancer: development and validation of a machine learning model using clinical data. JMIR Med Inform 2025;13:e73765 [FREE Full text] [doi: 10.2196/73765] [Medline: 40986886]
18. Alhumaidi NH, Dermawan D, Kamaruzaman HF, Alotaiq N. The use of machine learning for analyzing real-world data in disease prediction and management: systematic review. JMIR Med Inform 2025;13:e68898 [FREE Full text] [doi: 10.2196/68898] [Medline: 40537090]
19. Chu L, Sun Y, Tang X, Duan X, Zhao Y, Xia H, et al. The tumor-derived exosomes enhanced bevacizumab across the blood-brain barrier for antiangiogenesis therapy against glioblastoma. Mol Pharm 2025;22(2):972-983. [doi: 10.1021/acs.molpharmaceut.4c01227] [Medline: 39895311]
20. Incekara F, Smits M, van der Voort SR, Dubbink HJ, Atmodimedjo PN, Kros JM, et al. The association between the extent of glioblastoma resection and survival in light of MGMT promoter methylation in 326 patients with newly diagnosed IDH-wildtype glioblastoma. Front Oncol 2020;10:1087 [FREE Full text] [doi: 10.3389/fonc.2020.01087] [Medline: 32766140]
21. Kirishima M, Yokoyama S, Akahane T, Higa N, Uchida H, Yonezawa H, et al. Prognosis prediction via histological evaluation of cellular heterogeneity in glioblastoma. Sci Rep 2024;14(1):24955 [FREE Full text] [doi: 10.1038/s41598-024-76826-8] [Medline: 39438642]
22. Selvi H, Brüning-Richardson A, Danovi D. Systematic review of pre-clinical systems using artificial microenvironments and anti-migratory drugs to control migration of glioblastoma cells. Expert Rev Mol Med 2025;27:e6. [doi: 10.1017/erm.2024.33] [Medline: 39844377]
23. Bafiti V, Ouzounis S, Chalikiopoulou C, Grigorakou E, Grypari IM, Gregoriou G, et al. A 3-miRNA signature enables risk stratification in glioblastoma multiforme patients with different clinical outcomes. Curr Oncol 2022;29(6):4315-4331 [FREE Full text] [doi: 10.3390/curroncol29060345] [Medline: 35735454]
24. Sloan L, Sen R, Liu C, Doucet M, Blosser L, Katulis L, et al. Radiation immunodynamics in patients with glioblastoma receiving chemoradiation. Front Immunol 2024;15:1438044 [FREE Full text] [doi: 10.3389/fimmu.2024.1438044] [Medline: 39346903]
25. Su H, Peng Y, Wu Y, Zeng X. Overcoming immune evasion with innovative multi-target approaches for glioblastoma. Front Immunol 2025;16:1541467 [FREE Full text] [doi: 10.3389/fimmu.2025.1541467] [Medline: 39911397]
26. Yu C, Niu Z, Fang Q, Lei Q. Development and validation of a predictive model for severe tubular atrophy/interstitial fibrosis in patients with IgA nephropathy: multicenter retrospective study. JMIR Med Inform 2025;13:e78761 [FREE Full text] [doi: 10.2196/78761] [Medline: 41150862]
27. Kim Y, Kim KH, Park J, Yoon HI, Sung W. Prognosis prediction for glioblastoma multiforme patients using machine learning approaches: development of the clinically applicable model. Radiother Oncol 2023;183:109617. [doi: 10.1016/j.radonc.2023.109617] [Medline: 36921767]
28. Jeon YH, Choi KS, Lee KH, Jeong SY, Lee JY, Ham T, et al. Deep learning-based quantification of T2-FLAIR mismatch sign: extending IDH mutation prediction in adult-type diffuse lower-grade glioma. Eur Radiol 2025;35(9):5193-5202. [doi: 10.1007/s00330-025-11475-7] [Medline: 40050456]
29. Alnahhas I. Molecular testing in gliomas: what is necessary in routine clinical practice? Curr Oncol Rep 2024;26(11):1277-1282. [doi: 10.1007/s11912-024-01602-w] [Medline: 39361075]

XSL•FO
RenderX

30. Zhao B, Qi H, Ma W. MGMT promoter methylation and chemotherapy outcomes in low-grade and anaplastic gliomas. JAMA Oncol 2023;9(12):1734-1735. [doi: 10.1001/jamaoncol.2023.4736] [Medline: 37856142]
31. Sareen H, Ma Y, Becker TM, Roberts TL, de Souza P, Powter B. Molecular biomarkers in glioblastoma: a systematic review and meta-analysis. Int J Mol Sci 2022;23(16):8835 [FREE Full text] [doi: 10.3390/ijms23168835] [Medline: 36012105]
32. Butler M, Pongor L, Su Y, Xi L, Raffeld M, Quezado M, et al. MGMT status as a clinical biomarker in glioblastoma. Trends Cancer 2020;6(5):380-391 [FREE Full text] [doi: 10.1016/j.trecan.2020.02.010] [Medline: 32348734]
33. Neil ZD, Pierzchajlo N, Boyett C, Little O, Kuo CC, Brown NJ, et al. Assessing metabolic markers in glioblastoma using machine learning: a systematic review. Metabolites 2023;13(2):161 [FREE Full text] [doi: 10.3390/metabo13020161] [Medline: 36837779]
34. Mohammadzadeh I, Niroomand B, Hajikarimloo B, Habibi MA, Mortezaei A, Behjati J, et al. Can we rely on machine learning algorithms as a trustworthy predictor for recurrence in high-grade glioma? a systematic review and meta-analysis. Clin Neurol Neurosurg 2025;249:108762 [FREE Full text] [doi: 10.1016/j.clineuro.2025.108762] [Medline: 39884144]
35. Tingle SJ, Severs GR, Goodfellow M, Moir JA, White SA. NARCA: a novel prognostic scoring system using neutrophil-albumin ratio and Ca19-9 to predict overall survival in palliative pancreatic cancer. J Surg Oncol 2018;118(4):680-686. [doi: 10.1002/jso.25209] [Medline: 30196571]
36. Sasagasako T, Ueda A, Mineharu Y, Mochizuki Y, Doi S, Park S, et al. Postoperative Karnofsky performance status prediction in patients with IDH wild-type glioblastoma: a multimodal approach integrating clinical and deep imaging features. PLoS One 2024;19(11):e0303002 [FREE Full text] [doi: 10.1371/journal.pone.0303002] [Medline: 39527541]
37. Li R, Sun Z, Song S, He X, Shi X, Li Z, et al. NARFIB: a novel prognostic score based on the neutrophil-to-albumin ratio and fibrinogen can predict the prognosis of gastrointestinal stromal tumors. Cancer Manag Res 2020;12:11183-11190 [FREE Full text] [doi: 10.2147/CMAR.S281375] [Medline: 33177869]
38. Garcia-Martinez R, Andreola F, Mehta G, Poulton K, Oria M, Jover M, et al. Immunomodulatory and antioxidant function of albumin stabilises the endothelium and improves survival in a rodent model of chronic liver failure. J Hepatol 2015;62(4):799-806. [doi: 10.1016/j.jhep.2014.10.031] [Medline: 25450713]
39. Gao X, Xu M, Xiao H, Han Z, Wang Z, Sun G, et al. Tumor-associated neutrophils: a complex role in cancer. Clin Immunol 2025;280:110558. [doi: 10.1016/j.clim.2025.110558] [Medline: 40633742]
40. Sun C, Wang S, Ma Z, Zhou J, Ding Z, Yuan G, et al. Neutrophils in glioma microenvironment: from immune function to immunotherapy. Front Immunol 2024;15:1393173 [FREE Full text] [doi: 10.3389/fimmu.2024.1393173] [Medline: 38779679]
41. Yoo S, Chowell D, Valero C, Morris LGT, Chan TA. Pre-treatment serum albumin and mutational burden as biomarkers of response to immune checkpoint blockade. NPJ Precis Oncol 2022;6(1):23 [FREE Full text] [doi: 10.1038/s41698-022-00267-7] [Medline: 35393553]
42. Horisaki K, Taki T, Mori S, Okumura M, Akiyama M. Peripheral blood mean platelet volume and the ratio of mean platelet volume to platelet count as prognostic biomarkers in patients with cutaneous angiosarcoma of the head and neck: a retrospective cohort study. Acta Derm Venereol 2024;104:adv42227 [FREE Full text] [doi: 10.2340/actadv.v104.42227] [Medline: 39508501]
43. Mayr L, Neyazi S, Schwark K, Trissal M, Beck A, Labelle J, et al. Effective targeting of PDGFRA-altered high-grade glioma with avapritinib. Cancer Cell 2025;43(4):740-756.e8. [doi: 10.1016/j.ccell.2025.02.018] [Medline: 40086436]
44. Li X, Chen X, Gong S, Zhao J, Yao C, Zhu H, et al. Platelets promote CRC by activating the C5a/C5aR1 axis via PSGL-1/JNK/STAT1 signaling in tumor-associated macrophages. Theranostics 2023;13(6):2040-2056 [FREE Full text] [doi: 10.7150/thno.80555] [Medline: 37064877]

Abbreviations

19qLOH: 19q loss of heterozygosity
1pLOH: 1p loss of heterozygosity
ADG: adult-type diffuse glioma
AISI: aggregate index of systemic inflammation
ALB: albumin
APTT: activated partial thromboplastin time
ATRX: alpha-thalassemia/mental retardation syndrome X-linked
AUC: area under the curve
BRAF: B-Raf proto-oncogene, serine/threonine kinase
CD34: cluster of differentiation 34
C-index: concordance index
EGFR: epidermal growth factor receptor
EMA: epithelial membrane antigen
GFAP: glial fibrillary acidic protein

XSL•FO
RenderX

HR: hazard ratio
IDH1: isocitrate dehydrogenase 1
Ki-67: proliferation cell nuclear antigen-67
KM: Kaplan-Meier
LASSO: least absolute shrinkage and selection operator
LDH: lactate dehydrogenase
LMR: lymphocyte-to-monocyte ratio
Lym: lymphocyte
MGMT: O6-methylguanine-DNA methyltransferase
MLR: monocyte-to-lymphocyte ratio
Mono: monocyte
mOS: median overall survival
mPFS: median progression-free survival
NeuN: neuronal nuclei
Neut: neutrophil
NLPR: neutrophil-lymphocyte-platelet ratio
NLR: neutrophil-to-lymphocyte ratio
NPAR: neutrophil percentage–to-albumin ratio
Olig-2: oligodendrocyte transcription factor 2
OS: overall survival
P53: P53 protein
PFS: progression-free survival
PLR: platelet-to-lymphocyte ratio
PLT: platelet
PMR: platelet-to-mean platelet volume ratio
PNI: prognostic nutritional index
PT: prothrombin time
RF: random forest
ROC: receiver operating characteristic
S100: S100 calcium-binding protein
SII: immune-inflammation index
SIRI: systemic inflammation response index
SYN: synuclein
TAN: tumor-associated neutrophil
TERT: telomerase reverse transcriptase
TME: tumor microenvironment
WBC: white blood cell
WHO: World Health Organization
XGBoost: extreme gradient boosting

Edited by J Klann; submitted 01.Jul.2025; peer-reviewed by Z Zhang, Y Liu, Z Chen; comments to author 03.Nov.2025; accepted 25.Nov.2025; published 13.Jan.2026.

Please cite as:
Zhu C, An J, Zhou L
Neutrophil Percentage–to-Albumin Ratio as a Novel Prognostic Biomarker in Adult Diffuse Gliomas: Retrospective Study Integrating 3 Machine Learning Models and Cox Regression
JMIR Med Inform 2026;14:e79945
URL: https://medinform.jmir.org/2026/1/e79945
doi:10.2196/79945
PMID:

©Congcong Zhu, Jiyang An, Lili Zhou. Originally published in JMIR Medical Informatics (https://medinform.jmir.org), 13.Jan.2026. This is an open-access article distributed under the terms of the Creative Commons Attribution License (https://creativecommons.org/licenses/by/4.0/), which permits unrestricted use, distribution, and reproduction in any medium, provided the original work, first published in JMIR Medical Informatics, is properly cited. The complete bibliographic information, a link to the original publication on https://medinform.jmir.org/, as well as this copyright and license information must be included.

XSL•FO
RenderX

CT Radiomics–Based Machine Learning Model for Predicting Capsular and Neural Invasion in Thyroid Carcinoma: Diagnostic Accuracy Study

Fang-fang Cong[1*], MM; Ke Tian[2*], MM; Qian Gao[2*], MB; Fulin Wang[3], MM; Peng Sun[2], MM; Nan Xu[2], MD

[1]Department of MRI, Zhoukou Medical Science Research Center, Zhoukou Central Hospital, Zhoukou, China

[2]Department of Radiology, Air Force Medical Center, Air Force Medical University, Number 30 Fucheng Road, Haidian District, Beijing, China

[3]Department of CT, Zhoukou Medical Science Research Center, Zhoukou Central Hospital, Zhoukou, China

[*]these authors contributed equally

Corresponding Author:
Nan Xu, MD
Department of Radiology, Air Force Medical Center, Air Force Medical University, Number 30 Fucheng Road, Haidian District, Beijing, China

Abstract

Background: Thyroid carcinoma is the most prevalent endocrine malignancy, with a worldwide increasing incidence. Capsular invasion and neural invasion (NI) are pivotal prognostic factors for recurrence and survival; however, their preoperative noninvasive assessment remains challenging.

Objective: We aimed to identify computed tomography (CT) radiomic biomarkers associated with capsular invasion in thyroid carcinoma, construct machine learning models integrating radiomic and clinical data, and evaluate their utility for NI risk stratification.

Methods: In this retrospective cohort, 111 patients with thyroid carcinoma were divided into capsular invasion–positive (n=63) and capsular invasion–negative (n=48) groups, with 37 (33.3%) cases presenting concurrent NI. Radiomic features were extracted from arterial and venous phase CT images at original resolution, including 111 gray-level co-occurrence matrix features. Nine key radiomic features (A1-A9) were selected via least absolute shrinkage and selection operator regression (λ=0.017). To preserve the physical meaning of texture features (eg, spatial correlation and contrast reflecting tumor microstructural heterogeneity), no resampling or scaling was performed on the regions of interest during radiomic feature extraction. Nomogram models and random forest (RF) models were constructed based on clinical indicators (galectin-3, etc) and radiomic features, respectively. Additionally, a neural network (NN) model integrating multimodal data was developed. Model stability was verified using 5-fold cross-validation and 1000-time bootstrap resampling, while performance was evaluated via receiver operating characteristic curves, calibration curves, and decision curve analysis.

Results: Model performance analysis revealed that among the nomogram models, the clinical indicator-based nomogram achieved an internally estimated area under the curve (AUC) of 0.9418 (95% CI 0.892 - 0.976) in the capsular invasion prediction task. The radiomic-based nomogram had an internally estimated AUC of 0.9334 (95% CI 0.881 - 0.968) in the capsular invasion prediction task and 0.8001 (95% CI 0.663 - 0.898) in the cross-label association analysis task. In RF models, clinical indicator-based and radiomic-based RFs exhibited an AUC of 0.7646 (95% CI 0.651 - 0.857) and 0.8102 (95% CI 0.703 - 0.892) in the cross-label association analysis task, respectively. The NN model performed promisingly, with an AUC of 0.775 (95% CI 0.621 - 0.903) in the cross-label association analysis task and a mean absolute error of <0.05 on the calibration curve.

Conclusions: Capsular invasion is a strong predictor of NI risk in thyroid carcinoma. Radiomic models based solely on preoperative CT images show potential for preoperative NI risk stratification. Models incorporating clinical parameters (obtained from postoperative tissue), including the integrated multimodal model, are more accurately characterized as postoperative risk stratification tools. The NN model, which integrated raw CT images with clinical data, achieved an AUC of 0.775 (95% CI 0.621 - 0.903), underscoring the potential of such multimodal analysis to capture complex relationships between imaging phenotypes and tissue-level biomarkers for enhanced postoperative assessment. This framework's radiomic component points toward purely image-based, preoperative evaluation tools' development.

(JMIR Med Inform 2026;14:e77349) doi:10.2196/77349

XSL•FO
RenderX

KEYWORDS

thyroid carcinoma; capsular invasion; neural invasion; tadiomics; computed tomography; CT; artificial intelligence; machine learning

Introduction

Thyroid carcinoma represents the most prevalent malignancy of the endocrine system, with a worldwide increasing incidence in recent years [1]. The biological behavior of thyroid carcinoma varies considerably. Some patients experience favorable outcomes, while others face higher risks of recurrence and metastasis [2]. Accurate assessment of tumor aggressiveness and prognostic factors is critical for developing personalized therapeutic strategies and improving patients' quality of life. Capsular invasion and neural invasion (NI) are key prognostic determinants in thyroid carcinoma. Research has demonstrated that thyroid carcinoma patients with capsular invasion or NI exhibit significantly higher postoperative recurrence and mortality rates compared to those without such invasive features [3]. According to previous studies, thyroid carcinoma biomarkers galectin-3 (Gal-3), Hector Battifora Mesothelial Epitope-1 (HBME-1), and cytokeratin 19 (CK19) are often overexpressed in malignant tumors compared to benign lesions. However, whether they are related to capsular invasion and NI is unclear [4]. Radiomics, an emerging computational technology, enables high-throughput extraction of quantitative features from medical imaging data, which reflect multidimensional tumor characteristics, including morphology (eg, ranges of tumor boundaries), texture, and functional heterogeneity [5,6]. Computed tomography (CT)–based radiomic analysis holds promise for identifying imaging biomarkers closely associated with tumor biology and may provide novel insights for diagnosis and prognosis [7,8]. The development of CT-derived radiomic biomarkers linked to capsular invasion in thyroid carcinoma may facilitate early and precise prediction of tumor aggressiveness. Furthermore, clarifying the stratification value of these biomarkers for NI risk could empower clinicians to more accurately assess risk preoperatively and provide a reliable basis for targeted neuroprotective strategies [9]. Nevertheless, current research on molecular imaging biomarkers for capsular invasion in thyroid carcinoma remains in its exploratory phase, and their potential for stratifying NI risks needs further investigation. This study aims to systematically identify CT-based radiomic biomarkers associated with capsular invasion in thyroid carcinoma and comprehensively evaluate their risk stratification utility for NI, thereby advancing novel methodologies for precision oncology in thyroid carcinoma management.

Methods

Study Population

A total of 111 patients diagnosed with thyroid carcinoma and hospitalized were retrospectively enrolled. Based on the presence of capsular invasion, patients were categorized into a control group (capsular invasion–negative, n=48) and a study group (capsular invasion–positive, n=63). No significant differences in baseline characteristics were observed between the 2 groups (Table 1), ensuring comparability for subsequent analyses.

XSL•FO
RenderX

Table . Comparative analysis of baseline characteristics between patients with and without membrane invasion.[a]

		Control group (n=48)	Study group (n=63)	Statistics	*P* value
Gal-3[b], n (%)				9.3 (1)[c]	.002
	High expression	18 (37.5)	42 (66.67)		
	Low or no expression	30 (62.5)	21 (33.33)		
HBME-1[d], n (%)				1.7 (1)[c]	.19
	High expression	45 (93.75)	62 (98.41)		
	Low or no expression	3 (6.25)	1 (1.59)		
CK19[e], n (%)				29.3 (1)[c]	.001
	High expression	26 (54.17)	61 (96.83)		
	Low or no expression	22 (45.83)	2 (3.17)		
NI[f], n (%)				27.9 (1)[c]	<.001
	Yes	3 (6.25)	34 (53.97)		
	No	45 (93.75)	29 (46.03)		
CEA[g] (ng/mL), mean (SD)		31.66 (5.12)	34.91 (4.07)	−3.73（109）[h]	<.001
CCSA-2[i] (ng/mL), mean (SD)		19.26 (4.98)	19.86 (4.65)	−0.66（109）[h]	.51
CA199[j] (U/mL), mean (SD)		59.95 (11.03)	74.17 (10.07)	−7.07（109）[h]	<.001
CA125[k] (U/mL), mean (SD)		77.96 (13.75)	87.12 (14.87)	−3.32（109）[h]	.001
Age (y), mean (SD)		45.29 (12.37)	44.97 (10.83)	0.99（109）[h]	.64
BMI (kg/m^2), mean (SD)		21.83 (2.16)	22.51 (2.17)	−1.49（109）[h]	.14

[a]High expression was defined as ≥2-fold expression relative to peripheral blood mononuclear cell controls.
[b]Gal-3: galectin-3.
[c]Chi-square test.
[d]HBME-1: Hector Battifora Mesothelial Epitope-1.
[e]CK19: cytokeratin 19.
[f]NI: neural invasion.
[g]CEA: carcinoembryonic antigen.
[h]*t* test.
[i]CCSA-2: circulating cancer-specific antigen.
[j]CA199: carbohydrate antigen 199.
[k]CA125: carbohydrate antigen 125.

Inclusion criteria were as follows: (1) diagnosis of thyroid carcinoma confirmed by postoperative histopathological examination and compliance with the SEOM-GETNE-TTCC （ Spanish Society of Medical Oncology, Spanish Group for Neuroendocrine and Endocrine Tumors, and Spanish Group for Head and Neck Tumors） Clinical guideline for thyroid cancer (2023) [10]; (2) preoperative neck CT scan; (3) availability of complete clinical records, including postoperative histopathological reports explicitly documenting capsular invasion and NI status; and (4) high-quality imaging data with standardized acquisition protocols, clearly delineated tumor boundaries, and absence of motion artifacts. Exclusion criteria included having (1) concurrent diagnosis of other malignancies or (2) severe hepatic or renal dysfunction, active autoimmune diseases, or pregnancy or lactation.

Ethical Considerations

This study was approved by the Ethics Committee of Air Force Medical Center, Air Force Medical University (No. 2025‐47-YJ01) and adhered to the principles outlined in the Declaration of Helsinki. The ethics committee specifically evaluated and approved a waiver of informed consent for this retrospective study, considering the use of anonymized imaging and clinical data and the impracticability of obtaining individual consent. All data were anonymized and deidentified before analysis to ensure patient privacy and confidentiality. Participants did not receive any compensation.

Imaging Feature Extraction

CT scans were performed on 2 scanner models: a GE Discovery energy-spectrum CT (GE Healthcare) and a Siemens SOMATOM Definition Flash dual source CT (IncSiemens Healthineers). Scanner parameters were as follows: GE

XSL•FO
RenderX

parameters: 120 kV, automatic tube current (250 - 465 mA), 512 × 512 matrix, pitch 0.9. Siemens parameters: 120 kV, reference 210 mAs (CARE Dose4D), 512 × 512 matrix, pitch 0.8. All scans used iohexol contrast (2 mL/kg, 3 - 4 mL/s) with arterial/venous phases at 30/50 seconds. Contiguous 5 mm slices were acquired, and 1.25 mm thin-section reconstructions were generated for analysis.

For data harmonization, to mitigate interscanner variability, all images were reconstructed to a 1.25 mm slice thickness. For radiomic features (A1-A9), *z* score normalization was applied across the entire dataset. For deep learning input, minimum-maximum scaling to [0,1] was applied per scan.

Before feature extraction, raw CT images underwent preprocessing to enhance image quality and ensure accurate subsequent analyses. Thyroid cancer lesion boundaries were independently delineated by 2 associate chief physicians with 6 and 8 years of experience in head and neck imaging diagnosis, using ITK-SNAP (developed by the ITK-SNAP Development Team, University of Pennsylvania) software to manually delineate regions of interest (ROIs) on arterial phase CT images. For venous-phase features (A3, A5, A7, and A9), arterial-phase ROIs were propagated to venous-phase images using rigid image registration, followed by manual verification and adjustment. To verify consistency, CT images of 30 (27% of the cohort) randomly selected patients were analyzed. Intraclass correlation coefficients (ICC) were calculated to assess both ROI volume consistency and numerical consistency of core gray level cooccurrence matrix (GLCM) features (contrast, correlation, and energy; distance d=1, angle θ=0°, 45°, 90°, 135°). The ICC for ROI volume was 0.92 (95% CI 0.85 - 0.96, P<.001), and the ICC value range of GLCM core features was 0.88 - 0.94 (both P<.001), indicating excellent reproducibility. Discrepancies in 3 (10%) cases were resolved through consensus review with postoperative pathology as reference.

Dimensionality reduction was performed via principal component analysis (PCA) and linear discriminant analysis (LDA). Intensity-based features were concurrently extracted and subjected to least absolute shrinkage and selection operator (LASSO) regression to identify robust predictors. To mitigate interscan variability in gray-level intensity values caused by heterogeneous acquisition protocols, for the extraction of hand-crafted radiomic features (A1-A9), *z* score normalization was applied across the entire dataset to standardize the gray-scale distribution and eliminate interscan variability caused by heterogeneous CT acquisition protocols. It should be noted that applying normalization to the full dataset before cross-validation could lead to potential information leakage, as the mean and SD used for normalization may inadvertently include information from samples designated for validation. Although our primary aim was to compare the relative performance of different models rather than to provide absolute performance estimates, we acknowledge this methodological limitation and have further addressed its potential impact in the Discussion section. For the deep learning model (DenseNet121) input only: the original-resolution ROIs were first normalized to a [0, 1] range using minimum-maximum scaling, then resized to 224×224 pixels (to meet the fixed-size input requirement of the pretrained DenseNet121 backbone) and converted to 3-channel format by duplicating the grayscale image across RGB (red, green, and blue) channels. This 224×224 resizing step was exclusive to deep learning model training and did not involve radiomic feature extraction.

Notably on ROI resolution for feature extraction, a critical distinction was made between radiomic feature extraction and deep learning model input preparation in this study. All radiomic texture features (111 GLCM features and 9 LASSO-selected A1-A9 features) were extracted from original-resolution CT ROIs to avoid systematic scaling bias and retain the physical meaning of texture metrics. The resizing of ROIs to 224×224 pixels was a dedicated preprocessing step for the DenseNet121-based deep learning model, as pretrained convolutional neural networks (NN) typically require fixed-size inputs. This separation of technical processes ensures the reliability of both radiomic feature analysis and deep learning model training.

Model Development

Given the limited total sample size (111 patients), to maximize the use of data, a full-sample modeling approach was adopted.

Model construction: all 111 cases were used as the analysis cohort, with capsular invasion status (1=capsular invasion–positive, n=63; 0=capsular invasion–negative, n=48) as the labeling variable. Input features were tailored to each model type: a common set of clinical biomarkers (for the complete list, see Table 1) was used across all models, while pixel-level CT features A1-A9 (selected via LASSO regression from GLCM texture features of CT ROIs) were used specifically in the traditional radiomic models (nomogram and random forest [RF]).

The NN model used a multimodal input, comprising both raw arterial-phase CT ROI images and the suite of clinical biomarkers (for the complete list, see Table 1), to autonomously learn high-level spatial and clinical patterns associated with capsular invasion (Multimedia Appendix 1). It is crucial to note that the hand-crafted radiomic features (A1-A9) were not direct inputs to this NN model. For each patient, a single 2D axial slice with the largest tumor cross-section was selected, standardized to 224×224 pixels, and converted to 3-channel format. Rationale for arterial-phase only input: this single-phase design was implemented for two primary reasons: (1) to maintain model simplicity and mitigate overfitting risk given the limited sample size, and (2) because the arterial phase provides the most direct imaging correlate of tumor vascularity, a key biological process underlying invasion. We hypothesized that the convolutional NN could learn high-level features from the arterial phase that are informative for predicting outcomes potentially associated with venous-phase patterns. Rationale despite venous-phase radiomic feature importance: it is noteworthy that in our traditional radiomics analysis, a feature derived from the venous phase (A9) showed high importance. The decision to use only arterial-phase images for the deep learning model was based on a complementary hypothesis: that the convolutional NN could learn high-level, abstract features from the arterial phase that are biologically or spatially correlated with the tumor properties captured by the venous-phase radiomic signature (A9). This approach allowed

XSL•FO
RenderX

us to test whether a single, routinely acquired phase could provide sufficient information for the NN to make accurate predictions, thereby simplifying the model and its potential clinical translation.

Concerning model validation, NI status (1=NI-positive, n=37; 0=NI-negative, n=74) was used for a cross-label association analysis. The core goal was to evaluate whether the features associated with capsular invasion (as captured by our models) were also rank-informative for NI status within the same cohort. The full 111-case dataset was used for both (1) model training (with capsular invasion status as the label) and (2) cross-label association evaluation (with NI status as the label). It is crucial to note that this analysis evaluates the association between capsular invasion–related features and NI status on the same samples, primarily reflecting their strong pathological correlation rather than constituting an independent predictive validation on unseen data. The full 111-case cohort, labeled based on the presence or absence of capsular invasion, was used to construct 3 predictive models (nomogram, RF, and NN) to capture capsular invasion–associated features. The same full cohort, labeled based on the presence or absence of NI, was then used to evaluate the models' cross-predictive performance for NI risk stratification. To address potential concerns regarding the unconventional data usage design and to empirically validate our model's generalizability, we performed a supplementary traditional 7:3 hold-out validation.

For the nomogram development, clinically significant variables associated with capsular invasion were incorporated into a clinical nomogram, while gray-level features selected via LASSO regression were integrated into an imaging-based nomogram. Calibration curves (predicted probability vs observed probability) were generated to assess agreement between model predictions and observed outcomes, with internal validation performed using a bootstrap resampling method (B=1000 iterations).

The RF model architecture comprised 2 components: a clinical RF model incorporating capsular invasion–associated variables and an imaging RF model integrating LASSO-selected radiomic features. Hyperparameter optimization was conducted via 5-fold cross-validation using the caret package, with the number of trees (ntree) tuned from 50 to 500 (step size=5) and the minimum number of features per node split (mtry) ranging from 2 to 10. Model interpretability was enhanced through feature importance plots, decision tree visualization, receiver operating characteristic (ROC) curves, and out-of-bag error analysis.

For the input of the NN model (based on DenseNet121): to comply with the fixed-size input requirement of the pretrained DenseNet121 backbone, the original-resolution ROIs were first normalized to a [0, 1] range using minimum-maximum scaling, then resized to 224×224 pixels. The single-channel grayscale images were further converted to a 3-channel format by duplication across RGB channels. The first 10 convolution blocks of DenseNet121 were reserved for extracting high-level image features, and the feature map was compressed into fixed-length vectors through global average pooling. Image feature vectors (extracted by DenseNet121) and clinical feature vectors were normalized, respectively, and directly spliced into multimodal feature vectors. The spliced features were input to the fully connected layer and were finally classified (capsular invasion: positive or negative) through the Sigmoid output layer. The 9 radiomic features (A1-A9) were selected from GLCM features of the ROI via LASSO regression. The model was optimized using the Adam optimizer (learning rate=1×10^{4}) with binary cross-entropy loss over 50 training epochs (batch size=16). Early stopping was triggered if validation loss plateaued for 10 consecutive epochs (Multimedia Appendices 1 and 2).

The technical workflow is illustrated in Figure 1.

XSL•FO
RenderX

Figure 1. Workflow of CT imaging feature extraction and predictive model development. A9: venous-phase coefficient of variation; AUC: area under the curve; CA199: carbohydrate antigen 199; CEA: carcinoembryonic antigen; CK19: cytokeratin 19; CT: computed tomography; DCA: decision curve analysis; DICOM: Digital Imaging and Communications in Medicine; GE: General Electric; GLCM: gray-level co-occurrence matrix; LASSO: least absolute shrinkage and selection operator; LDA: linear discriminant analysis; OR: odds ratio; PCA: principal component analysis; ROC: receiver operating characteristic; ROI: regions of interest.

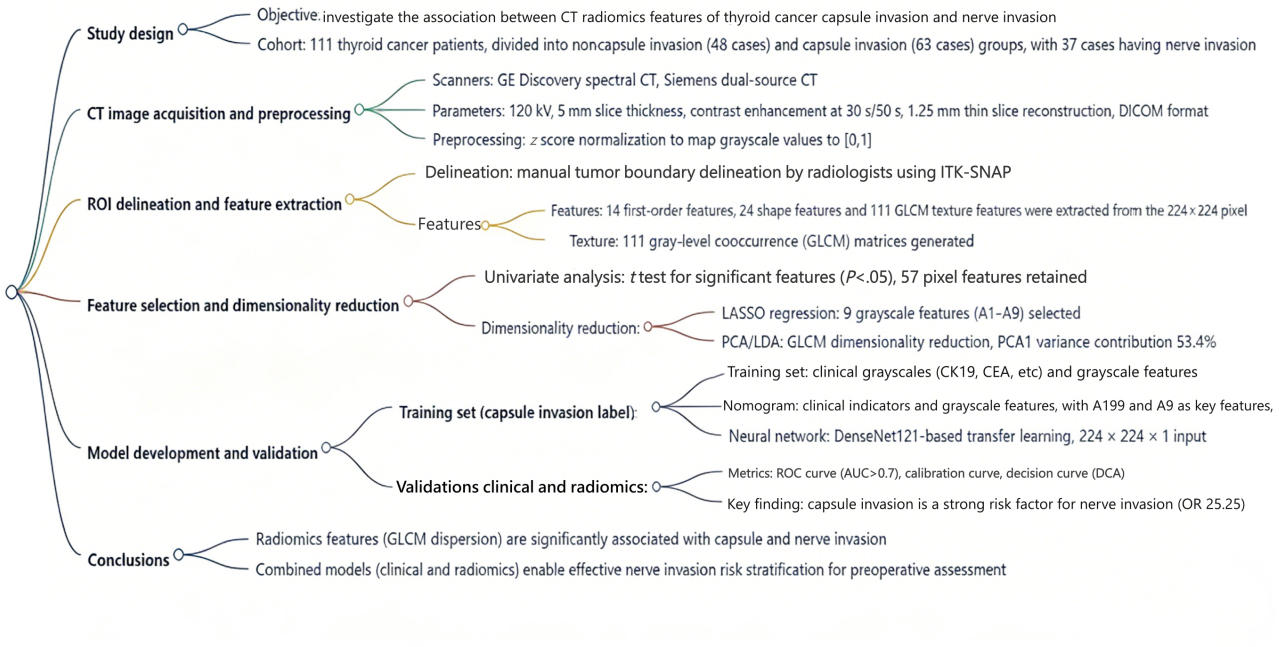

Model Interpretability Analysis

To interpret the NN's predictions and derive the importance scores in Figure 2B, we used Shapley Additive Explanations (SHAP). The analysis pipeline was as in the following paragraphs.

Concerning calculation for the validation set, SHAP values were computed for each input feature (clinical variables and the high-dimensional features extracted from raw CT images by DenseNet121). These values quantify a feature's contribution to a specific prediction.

Figure 2. Neural network model performance. (A) Mean training accuracy curves across the 5-fold cross-validation splits, plotted for different numbers of hidden units. (B) SHAP-based feature importance (normalized 0-100). Blue: clinical biomarkers (direct inputs); red: image patterns (learned from raw CT). (C) ROC curve for neural invasion prediction. Note for (B): normalized importance scores derived from SHAP analysis (see subsection in Methods: Model interpretability analysis). Imaging patterns were semantically annotated based on activation map visualizations. CA125: carbohydrate antigen 125; CA199: carbohydrate antigen 199; CCSA-2: circulating cancer-specific antigen; CEA: carcinoembryonic antigen; CK19: cytokeratin 19; CT: computed tomography; Gal-3: galectin-3; NI: neural invasion; NN: neural network; ROC: receiver operating characteristic; SHAP: Shapley Additive Explanations.

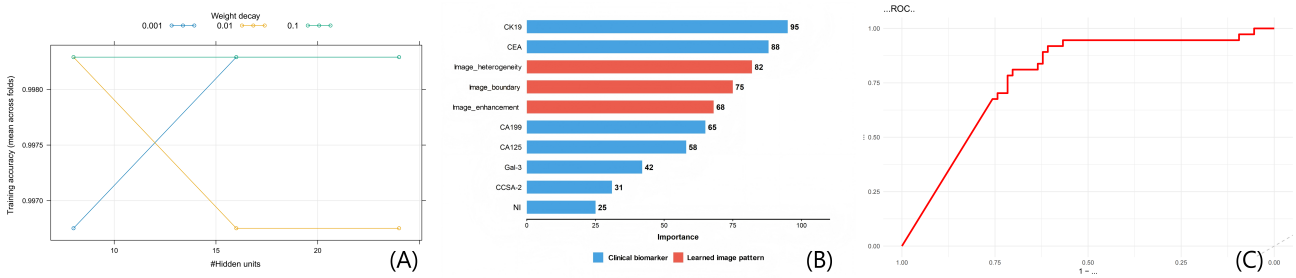

For aggregation and semantic mapping, global importance for each clinical variable was defined as its mean absolute SHAP value. For image features, activation maps corresponding to features with high mean absolute SHAP values were analyzed. Recurring visual patterns were inductively categorized into 3 semantic concepts: "Image_Heterogeneity," "Image_Boundary," and "Enhancement_Dynamics." The importance score for each concept was calculated as the mean absolute SHAP value of its constituent image feature dimensions.

In normalization, all resulting scores (for clinical variables and image concepts) were linearly normalized to a 0 - 100 scale for comparative visualization in Figure 2B.

Data Collection

All thyroid carcinoma tissue specimens were collected immediately after surgical resection, and 10% neutral buffered formalin was used for fixation within 30 minutes for morphological preservation. After paraffin embedding, 5-µm-thick sections were prepared, and tumor tissue areas (with

XSL•FO
RenderX

tumor cell content ≥80%, confirmed by 2 pathologists) were microdissected for quantitative polymerase chain reaction (qPCR) analysis. This ensured that the detected expression of Gal-3, HBME-1, and CK19 accurately reflected the biological characteristics of thyroid carcinoma cells.

Real-time fluorescence qPCR was performed to measure the levels of Gal-3, HBME-1, and CK19 in thyroid carcinoma tissue specimens from the 111 enrolled patients. Glyceraldehyde-3-phosphate dehydrogenase served as the endogenous reference gene for normalization. Peripheral blood mononuclear cells (PBMCs) from age- and sex-matched healthy individuals undergoing routine health screenings were used as the control group for qPCR analysis. Relative gene expression levels ≥2-fold compared to PBMC controls were pragmatically defined as high expression for subsequent categorical analysis. It is important to note that the use of PBMCs as a control group is a methodological consideration due to the practical and ethical challenges in obtaining matched healthy thyroid tissue samples. As PBMCs (of nonepithelial origin) and thyroid epithelial cells have fundamentally different baseline gene expression profiles, this comparison is intended to establish a highly sensitive detection threshold for identifying genes that are actively expressed at levels substantially above this technical background in tumor tissue, rather than to provide precise biological fold-change values across tissue types. The ≥2-fold threshold therefore serves as a pragmatic cutoff for distinguishing tumors with detectably high expression of the target genes. Therefore, it is crucial to emphasize that “high expression” as defined in this study indicates detectability above a nonepithelial (PBMC) baseline, and should not be interpreted as pathological overexpression relative to normal thyroid tissue.

Concurrently, baseline characteristics and serum levels of tumor biomarkers, including carcinoembryonic antigen (CEA), carbohydrate antigen 199 (CA199), and carbohydrate antigen 125 (CA125), and the second-generation assay for circulating cancer-specific antigen, were systematically collected.

Statistical Methods

All statistical analyses were performed using SPSS Statistics (version 27.0; IBM Corp) and R software (version 4.4.3; R Foundation). Continuous variables with normal distribution were expressed as mean ± SD ($x^{-}\pm s$), while categorical data were presented as n (%). Intergroup comparisons were conducted using independent samples *t* tests for continuous variables and chi-square tests for categorical variables. Multivariable binary logistic regression analysis was used to identify independent risk factors. The RF model was developed using the randomForestSRC, *ggRandomForests*, *pdp*, and *GGally* packages in R. Nomogram construction and calibration were implemented with the *rms*, *dcurves*, and *pROC* packages in R. NN architecture was built using the keras interface in R. Model accuracy was evaluated via the confusionMatrix() function from the *caret* package. All visualizations were generated using the *ggplot2* package in R. A *P* value <.05 was considered statistically significant.

Results

Overview

In this section, Table 1 presents the baseline characteristics of patients. The detailed multivariate logistic regression results (originally Tables 2 and 3) have been moved to the supplementary material; see Tables S1 and S2 in Multimedia Appendix 3.

Baseline Characteristics Comparison

The comparative analysis of baseline characteristics between patients with and without capsular invasion revealed statistically significant differences in the categorized expression levels (high vs low or no expression) of Gal-3 and CK19, as well as in the serum concentrations of tumor markers including CEA, CA199, and CA125 (*P*<.05, Table 1). Representative arterial-phase CT images and corresponding ROI delineations from patients with thyroid carcinoma are shown in Figure 3A-D.

XSL•FO
RenderX

Figure 3. Representative arterial-phase CT images of thyroid carcinoma. (A-C) A case with pathologically confirmed capsular invasion showing irregular tumor margins (arrow). (B-D) A case without NI demonstrating well-defined tumor boundaries. CT: computed tomography; NI: neural invasion; ROI: regions of interest.

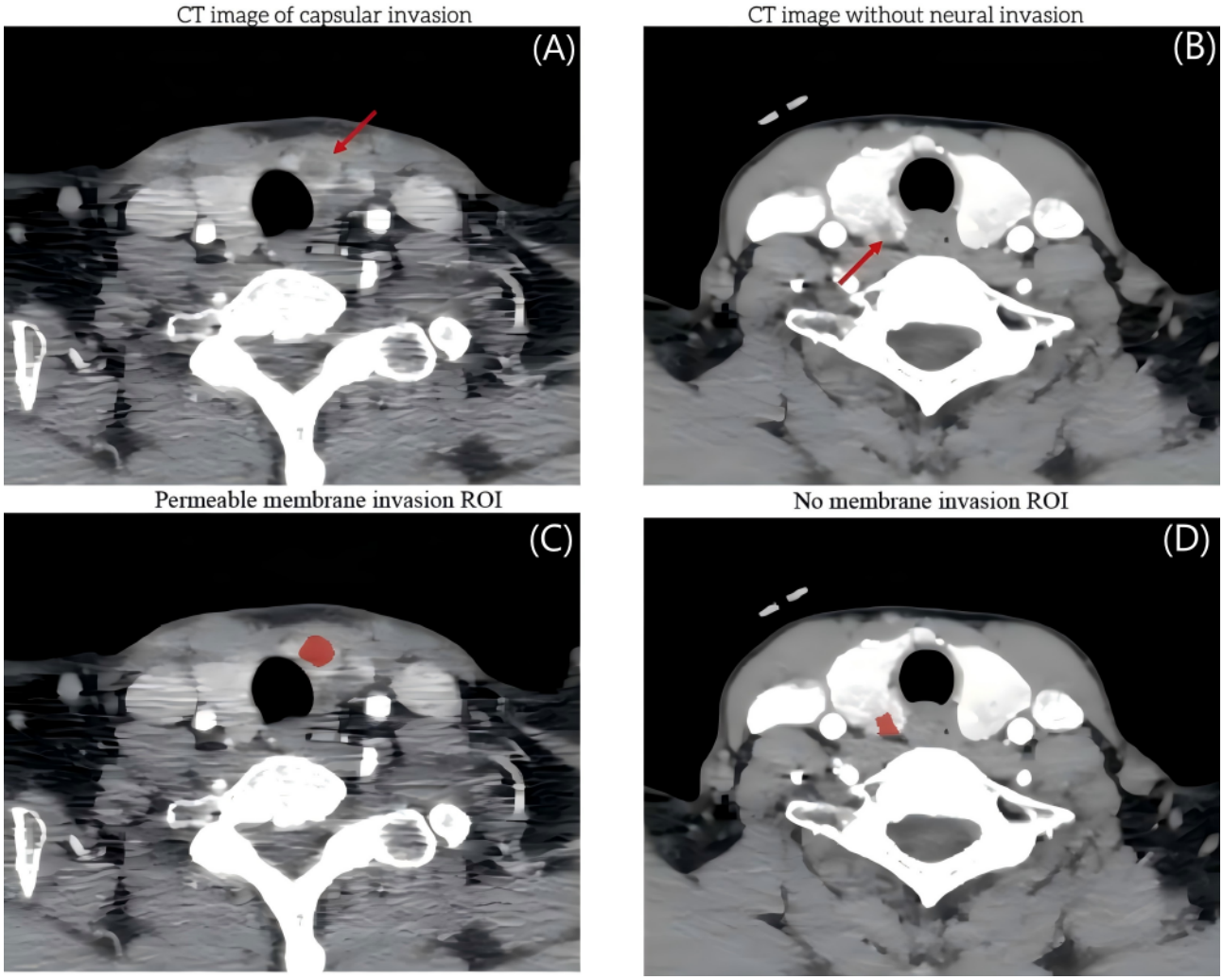

GLCM Analysis

The GLCM analysis yielded 111 texture features, which were subsequently subjected to dimensionality reduction via PCA and LDA. A total of 14 principal components were extracted for capsular invasion classification, with PCA1 and PCA2 accounting for 53.47% and 4.83% of the total variance, respectively. Significant intergroup differences were observed in PCA1 (t_{109}=11.671, P=.001, 2-tailed), where patients without capsular invasion exhibited greater dispersion in GLCM patterns, as evidenced by their larger Euclidean distance (6.98 vs 4.12 in the capsular invasion group). Similarly, NI analysis demonstrated significant differences in both PCA1 (t_{109}=10.339, P=.001) and PCA2 (t_{109}=−2.0187, P=.04). Non-NI cases again displayed greater GLCM dispersion, with Euclidean distances measuring 7.02 vs 4.05 in the NI group, a pattern consistent with the capsular invasion findings. LDA projections further corroborated this dispersion pattern, showing broader distribution clusters in noninvasion groups compared to their invasion counterparts. Visual representations of these analytical outcomes are provided in Figure 4.

XSL•FO
RenderX

Figure 4. Dimensionality reduction analysis. (A) PCA of capsular invasion status; (B) PCA of NI status; (C) LDA of capsular invasion status; (D) LDA of NI status. LD1: linear discriminant 1; LDA: linear discriminant analysis; LDA1: linear discriminant 1; NI: neural invasion; no-in: noninvasion; PC1: principal component 1; PC2: principal component 2; PCA: principal component analysis.

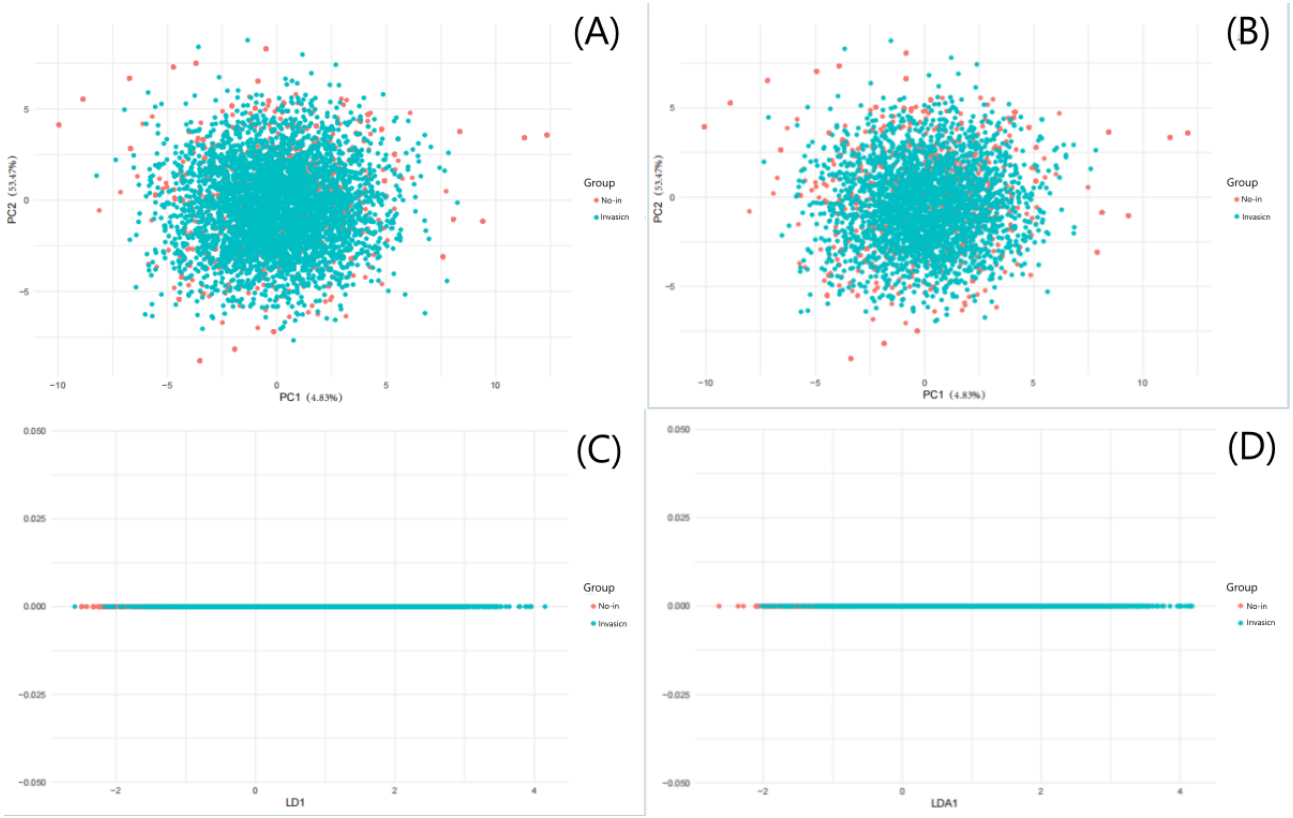

Multivariate Binary Logistic Regression Analysis Based on Clinical Indicators

It is important to emphasize that the following multivariate logistic regression analyses are intended to explore factors associated with the co-occurrence of pathological features, rather than to build preoperative predictive models. As both capsular invasion and NI are postoperative pathological diagnoses, their inclusion as variables in models predicting each other primarily reflects their strong pathological correlation, not a causal predictive relationship usable for preoperative assessment.

A multivariate binary logistic regression model was constructed with capsular invasion status as the dependent variable (1=presence, 0=absence). The analysis identified CK19, CEA, CA199, CA125, and NI as significant independent risk factors for capsular invasion. Notably, CK19 demonstrated an exceptionally strong association with capsular invasion, yielding an odds ratio (OR) of 60.491 (P<.05, see Table S1 in Multimedia Appendix 3).

A parallel analysis was performed with NI status as the dependent variable (1=presence, 0=absence). Among all clinical indicators, only capsular invasion emerged as a significant predictor of NI, with an OR of 25.25 (P<.05, Table S2 in Multimedia Appendix 3), underscoring the pronounced influence of capsular invasion on NI risk.

Gray-Level Feature Selection via LASSO Regression Analysis

A set of radiomic features was extracted from the pixels within the ROI. Following exclusion of features without significant differential expression, 57 discriminative features were retained for LASSO regression analysis. During variable selection, the penalty coefficient (λ) was iteratively adjusted to compress the initial 57 predictors. Optimal λ value (λ=0.017) was determined through cross-validation, achieving minimal model deviance while balancing parsimony and predictive accuracy. This process yielded a refined model incorporating 9 pivotal features (designated A1-A9), as presented in Figure 5. The 9 pixel-level features (A1-A9) selected in this study directly reflect the heterogeneity of contrast enhancement and tissue composition of thyroid carcinoma on CT images. Specifically: (1) differences in arterial-phase pixel intensity mean (A1) reflect variations in tumor vascular density: tumors with higher A1 values (stronger arterial enhancement) are more likely to have capsular invasion/NI, as increased angiogenesis provides conditions for tumor invasion; (2) variations in pixel intensity SD (A2) correspond to intratumoral necrosis: higher A2 values (uneven enhancement) often indicate necrotic foci, which are associated with poor differentiation (CK19 positivity) and higher NI risk; and (3) changes in venous-phase pixel percentile (A3 and A8) reflect capsule integrity: lower A3 or A8 values suggest capsule rupture, a direct marker of capsular invasion. These imaging phenotypes serve as quantifiable surrogates for pathological characteristics, such as vascular density, necrosis, and capsular status, enabling noninvasive preoperative assessment of tumor aggressiveness. Detailed feature definitions are provided in

XSL•FO
RenderX

Multimedia Appendix 2, with additional descriptions in Multimedia Appendix 1.

Figure 5. Cross-validated deviance profile versus log(λ) values.

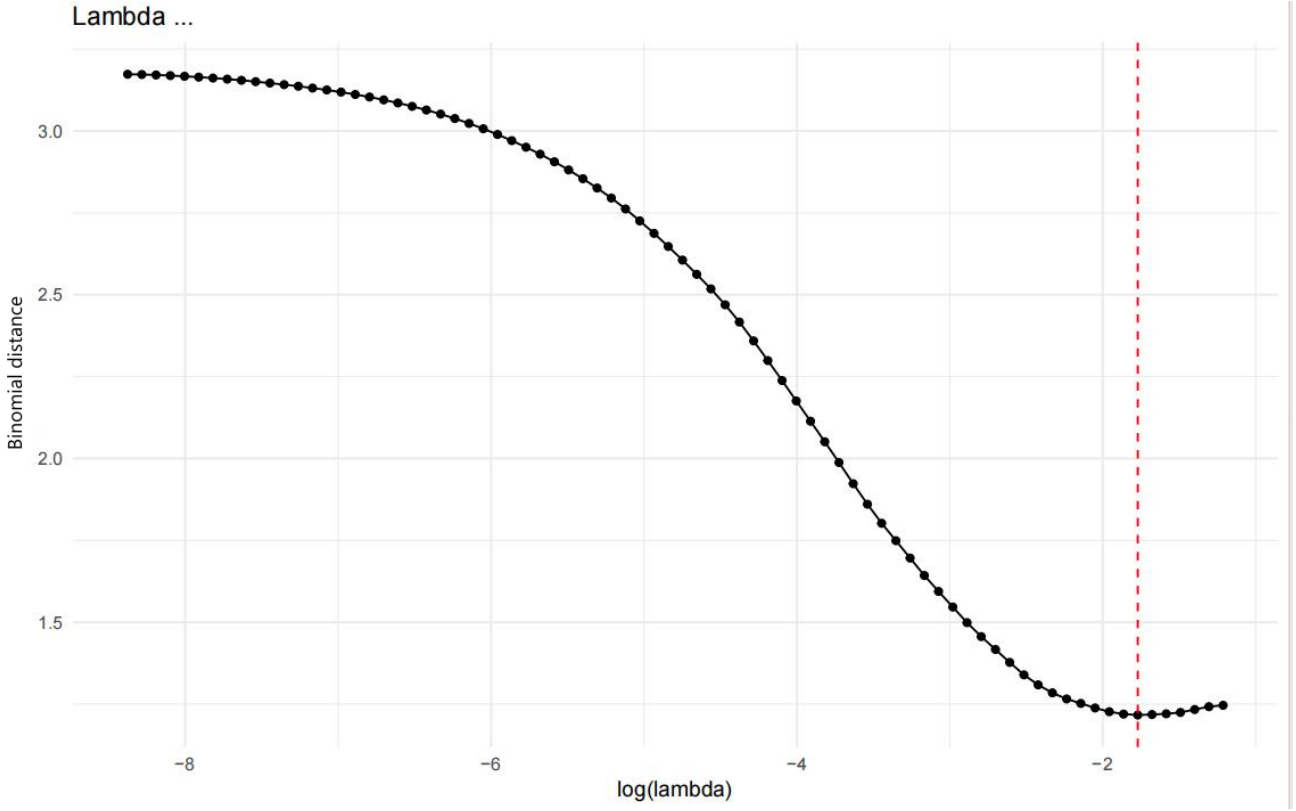

Development of Nomogram Models for Predicting NI Based on Capsular Invasion

A tumor biomarker-derived nomogram was constructed to assess the predictive value of capsular invasion for NI. ROC curve analysis demonstrated robust discriminative performance, with an internally estimated area under the curve (AUC) of 0.9418 for the capsular invasion-prediction task (modeled on the full 111-case dataset) and 0.7253 for the cross-label association analysis task (evaluated on the full 111-case dataset). Calibration curves indicated high consistency between predicted probabilities and observed outcomes across both tasks. Decision curve analysis further validated the clinical utility of the model, as its net benefit across all threshold probabilities outperformed the “treat-all” and “treat-none” strategies (Figure 6).

XSL•FO
RenderX

Figure 6. Clinically parameterized nomogram model for neural invasion prediction. (A) Nomogram integrating clinical biomarkers (Gal-3, CK19, CEA, CA199, and CA125) to predict NI risk, with key variables (CK19 and CA199) marked by "*" (high OR values from Tables S1 and S2 in Multimedia Appendix 3); red dashed lines guide point assignment for each variable. (B and C) Calibration curves for the capsular invasion–prediction task ((B) modeled on full 111-case dataset) and the cross-label association analysis task ((C) cross-prediction on full 111-case dataset), showing agreement between predicted NI probability (x-axis) and observed NI status (y-axis); 95% CI bands (light blue or red) and MAE are labeled. (D and E) DCA curves for both tasks (using the full 111-case dataset, with no traditional train or test split), comparing the net benefit of the nomogram (dark blue line) with "treat all" (red line) and "treat none" (gray line) strategies across different NI risk thresholds. (F and G) ROC curves for the capsular invasion-prediction task ((F) modeled on full 111-case dataset) and the cross-label association analysis task ((G) evaluated on full 111-case dataset), with exact AUC values and 95% CIs labeled; light blue or red bands represent 95% CIs. All analyses were based on the full 111-case cohort (capsular invasion–labeled modeling and NI-labeled evaluation). AUC: area under the curve; CA125: carbohydrate antigen 125; CA199: carbohydrate antigen 199; CCSA-2: circulating cancer-specific antigen; CEA: carcinoembryonic antigen; CK19: cytokeratin 19; DCA: decision curve analysis; Gal-3: galectin-3; MAE: mean absolute error; NI: neural invasion; OR: odds ratio; Prob: probability; RDATA: research data; ROC: receiver operating characteristic; .

XSL•FO
RenderX

A parallel nomogram model incorporating gray-level radiomic features achieved internally estimated AUC values of 0.9334 for the capsular invasion-prediction task (full 111-case dataset) and 0.8001 for the cross-label association analysis task (full 111-case dataset). Calibration curves similarly confirmed strong predictive accuracy for both tasks, and decision curve analysis revealed that the model achieved superior net clinical benefit across the entire spectrum of risk thresholds compared to reference strategies (Figure 7).

XSL•FO
RenderX

Figure 7. Gray-level feature-integrated nomogram model for neural invasion prediction. (A) Nomogram integrating LASSO-selected pixel-level features (A1-A9) to predict NI risk; footnotes define key features (A1 and A9) per the Gray-Level Feature Selection via LASSO Regression Analysis section. (B and C) Calibration curves for capsular invasion-prediction task ((B) modeled on full 111-case dataset) and cross-label association analysis task ((C) evaluated on full 111-case dataset); hollow circles (dark blue) and solid squares (coral red) represent data points, with 95% CI bands and MAE ((B) 0.05; (C) 0.049) labeled. (D and E) DCA curves, with the nomogram (dark blue line) showing higher net benefit than reference strategies across NI risk thresholds. (F and G) ROC curves for the capsular invasion-prediction task ((F) modeled on full 111-case dataset) and the cross-label association analysis task ((G) evaluated on full 111-case dataset); exact internally estimated AUC values (capsular invasion-prediction task: 0.9334; cross-label association analysis task: 0.8001) and 95% CIs are labeled, with light blue or red bands representing 95% CIs. All analyses used the full 111-case cohort (capsular invasion–labeled modeling and NI-labeled evaluation). AUC: area under the curve; DCA: decision curve analysis; LASSO: least absolute shrinkage and selection operator; MAE: mean absolute error; NI: neural invasion; Prob: probability; RDATA: research data.

XSL•FO
RenderX

RF Model Development

An RF model was constructed using tumor biomarkers, with CA199 demonstrating the highest feature importance (visualized in Figure 8A). A representative surrogate tree from the RF ensemble (visualized in Figure 8B) initiated classification through sequential partitioning: the root node split on "CA199<76," followed by a "yes" branch subdivided by "CK19=1," and further partitioned via "CEA<28." Out-of-bag error curves (visualized in Figure 8C) revealed stabilized misclassification rates for both training and validation sets as tree numbers increased, with training set errors consistently exceeding validation set values. The 5-fold cross-validation AUC (for capsular invasion prediction) was 0.782 (95% CI 0.671 - 0.874), and the out-of-bag error rate stabilized at 0.213 when ntree ≥300 (visualized in Figure 8D). When this model was used to predict NI (full-sample NI label), the model exhibited discriminative efficacy with an AUC of 0.7646, only 2.5% lower than the cross-validation AUC for capsular invasion, confirming no significant overfitting (Figure 8).

Figure 8. RF model based on clinical biomarkers. (A) Feature importance plot; (B) a representative surrogate tree from the RF ensemble; (C) out-of-bag error trajectories; and (D) ROC curve. CA125: carbohydrate antigen 125; CA199: carbohydrate antigen 199; CCSA2: colon cancer-specific antigen-2; CEA: carcinoembryonic antigen; CK19: cytokeratin 19; Gal3: galectin-3; RF: random forest; ROC: receiver operating characteristic.

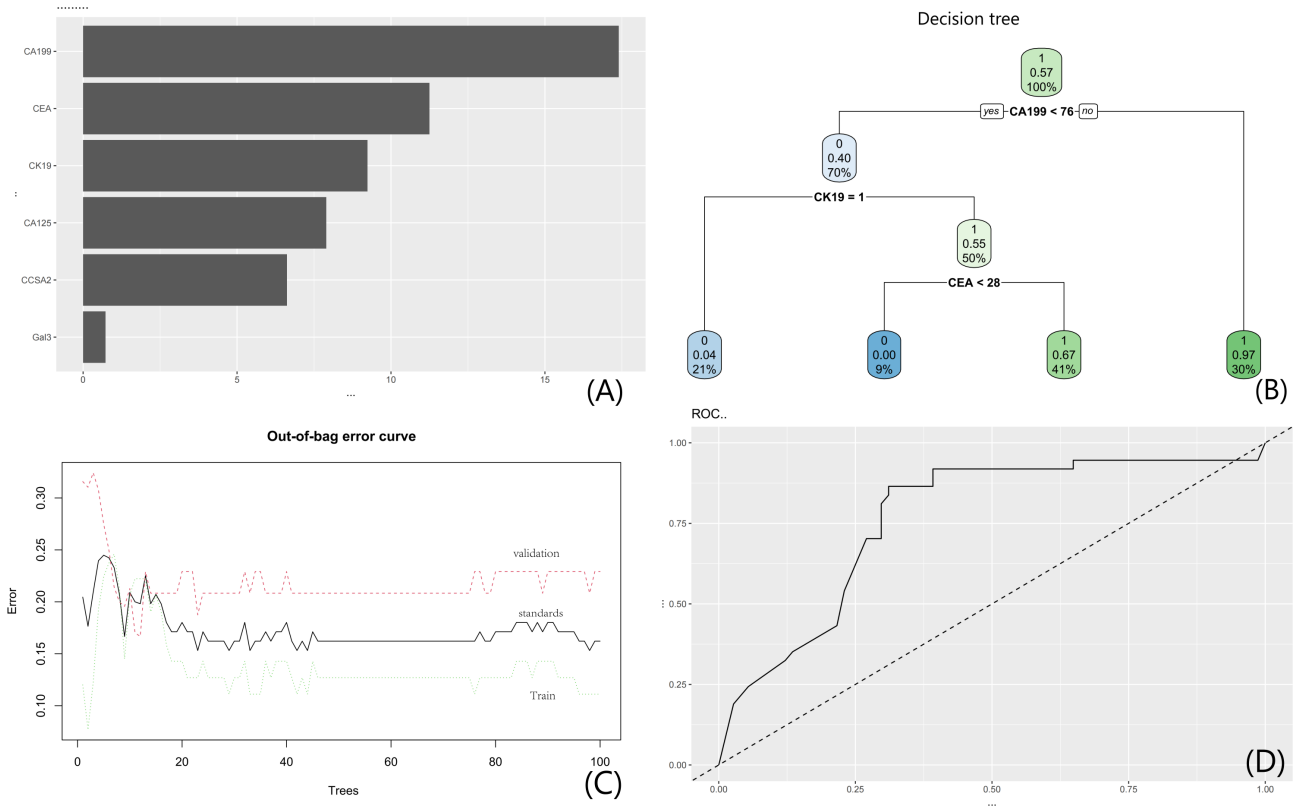

A parallel RF model incorporating gray-level features identified feature A9 as the primary contributor (corresponding to Figure 9A). A representative surrogate tree from the RF ensemble (corresponding to Figure 9B) partitioned data at "A9 <0.22," with subsequent splits at "A4 ≥0.25" and "A3 ≥0.22." Out-of-bag error curves mirrored the tumor biomarker-based model, showing convergence to stability with increasing tree numbers (corresponding to Figure 9C). The 5-fold cross-validation AUC (for capsular invasion prediction) was 0.825 (95% CI 0.723 - 0.906), and the out-of-bag error rate stabilized at 0.187 when ntree ≥350. ROC analysis confirmed enhanced predictive performance (corresponding to Figure 9D); its AUC for NI prediction was 0.8102% - 1.8% lower than the capsular invasion cross-validation AUC, further confirming low overfitting risk (Figure 9). These data collectively validate the clinical utility of both RF models.

XSL•FO
RenderX

Figure 9. RF model based on gray-level features. (A) Feature importance plot (features A1-A9 represent the 9 key radiomic grayscale features selected via LASSO regression from GLCM texture features of CT regions of interest. They quantify tumor heterogeneity in arterial and venous phases (eg, A1, A9); (B) a representative surrogate tree from the RF ensemble; (C) out-of-bag error trajectories; (D) ROC curve. A1: arterial-phase mean intensity; A9: venous-phase coefficient of variation; CT: computed tomography

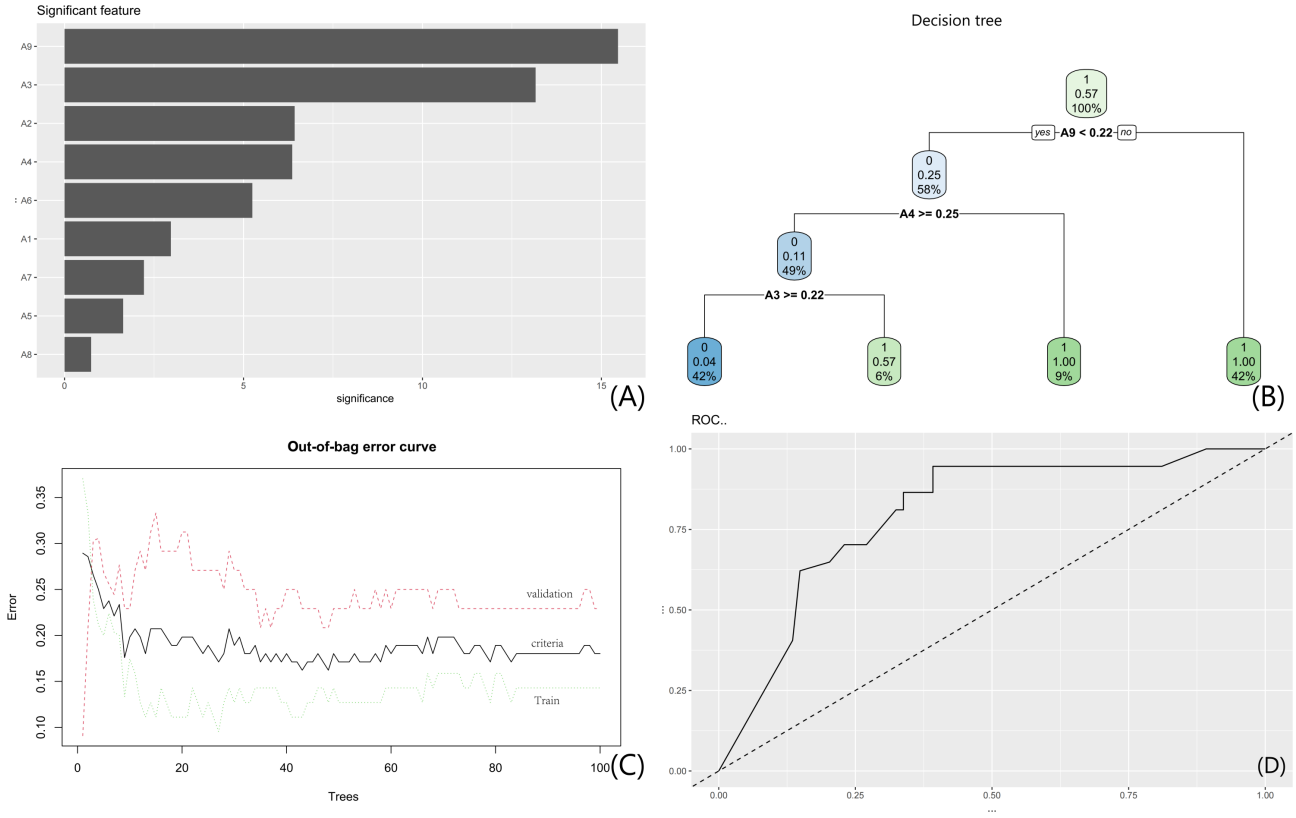

NN Model Development

The NN model used exclusively two input modalities: (1) raw arterial-phase CT ROI images and (2) clinical biomarkers. No hand-crafted radiomic features (A1-A9) were directly input to the NN.

An NN model integrating multimodal data demonstrated high learning efficiency, with training accuracy values exceeding 0.99 across learning curves (Figure 2A). It is important to note that Figure 2A displays the mean training accuracy across the 5-fold cross-validation splits, not a cross-validated test accuracy. The significant gap between the near-perfect training accuracy (>0.99) and the more moderate cross-validation AUC for the primary capsular invasion prediction task (0.798) is indicative of overfitting, a common challenge in training complex models on limited datasets. While early stopping was used to mitigate overtraining by halting training when validation loss plateaued, this gap suggests that the model still learned patterns highly specific to the training samples. The architecture used hidden units ranging from 10 to 30, where variations in hidden unit counts under distinct weight decay coefficients differentially influenced cross-validated accuracy values. Feature importance analysis based on SHAP values (as detailed in the Model Interpretability Analysis section) revealed that clinical biomarkers were the most influential predictors for NI risk, particularly CK19 (normalized importance score: 95) and CEA (normalized importance score: 88; Figure 2B). Concurrently, the semantically annotated image patterns—"Image_Heterogeneity" (score: 82), "Image_Boundary" (score: 75), and "Enhancement_Dynamics" (score: 68), which were autonomously learned and inductively summarized by the NN from the raw CT inputs, also contributed substantially to the predictions. Importantly, these image patterns were learned directly from raw CT images and are conceptually distinct from the hand-crafted radiomic features (A1-A9) used in traditional radiomic models. The model achieved an AUC of 0.775 in the validation set, confirming its satisfactory generalizability beyond the training cohort. The 5-fold cross-validation AUC (for capsular invasion prediction) of the integrated NN model was 0.798 (95% CI 0.695 - 0.883), with a coefficient of variation of 7.2% across folds—indicating stable performance. Early stopping was triggered at an average of 32 (SD 2.8, range: 28 - 35 epochs) across the 5 folds, effectively preventing overtraining. When predicting NI (full-sample NI label), the model achieved an AUC of 0.775 (95% CI 0.621 - 0.903)—only 2.3% lower than the capsular invasion cross-validation AUC, indicating that the model's predictive ability for NI remains robust despite some degree of overfitting on the primary capsular invasion task. Detailed architectural and performance metrics are illustrated in Figure 2. Feature importance analysis within the NN identified that its predictions were driven by several key learned representations: an image pattern capturing intratumoral heterogeneity, a feature related to venous-phase enhancement dynamics, and another reflecting textural uniformity, in conjunction with the clinical biomarkers CK19 and CEA. Feature importance analysis indicated that intratumoral heterogeneity was the most influential learned representation (importance score 0.82, full score=1.0).

XSL•FO
RenderX

About validation on an internal hold-out set, to further assess generalizability, a traditional 7:3 hold-out validation was performed. The RF model based on radiomic features (A1-A9) was trained on a subset of 78 cases and was subsequently evaluated on the separate, internal hold-out set of 33 cases. The observed AUC of 0.827 was promising, but the extremely wide 95% CI (0.652 - 0.981) indicates substantial uncertainty due to the small test sample size (n=33), necessitating cautious interpretation of the model's generalizability. This additional validation yielded a promising but variable performance (AUC=0.827, 95% CI 0.652 - 0.981) for NI prediction (see Multimedia Appendices 1 and 4 for details).

Discussion

Research Background and Basis

Thyroid carcinoma, the most prevalent malignancy of the head and neck region, has exhibited a rapid surge in incidence over the past decade, emerging as a critical threat to global human health [11]. Beyond its capacity to disrupt thyroid function and induce hormonal dysregulation, thyroid carcinoma frequently metastasizes to adjacent cervical tissues, lymph nodes, and even distant organs such as the lungs, liver, and bones, severely compromising physiological integrity [12]. Equally concerning are its profound psychosocial impacts, as patients endure debilitating fear, anxiety, and uncertainty regarding prognosis and treatment outcomes [13]. Current advances in thyroid carcinoma research have identified molecular markers such as *BRAF* (OMIM 164757) and *NRAS* (OMIM 164790) gene mutations, which have emerged as critical tools for diagnosis, prognostic stratification, and therapeutic decision-making [14]. Nevertheless, significant gaps persist in risk stratification for capsular invasion and NI, 2 pivotal prognostic determinants. Capsular invasion serves as a key predictor of lymph node metastasis, whereas NI directly correlates with postoperative survival quality and recurrence risk [3]. Elucidating the relationship between capsular invasion and NI is therefore essential for precise clinical assessment and optimized treatment planning. Therefore, the identification of radiogenomic biomarkers for capsular invasion using CT radiomics and the evaluation of their stratification value for NI are both scientifically imperative and clinically urgent.

Identification of Radiomic Signatures for Invasion Risk

In this study, GLCM analysis of CT images from thyroid carcinoma patients revealed distinct radiomic signatures between tumors with and without capsular invasion or NI. A total of 111 GLCM features were extracted and subjected to dimensionality reduction via PCA and LDA, which uncovered critical associations between key imaging biomarkers and invasion risk. The heterogeneous distribution of GLCM features in noninvasive cohorts, characterized by greater dispersion, reflects heightened spatial heterogeneity in gray-level pixel relationships within tumor microenvironments. This phenomenon may correlate with histopathological characteristics such as tumor boundary demarcation and cellular alignment integrity, a concept supported by the work of Wei et al [11], who demonstrated that radiomic features from multiparametric magnetic resonance imaging could effectively predict extrathyroidal extension in papillary thyroid carcinoma by capturing similar underlying tumor heterogeneity. In contrast, tumors with capsular invasion demonstrate enhanced propensity for boundary breaching [15], resulting in homogenization of imaging features. Noninvasive lesions, by comparison, maintained relatively intact tissue architecture [16,17], which manifests as increased textural complexity on imaging. This inverse relationship is further corroborated by a recent meta-analysis [18], which confirmed that textural homogenization in medical imaging often reflects the loss of normal tissue architecture due to invasive growth patterns. Thus, these findings suggest that GLCM feature dispersion may serve as a universal imaging biomarker of tumor invasiveness [19].

Mechanistically, tumors with NI exhibit the proliferative spread of malignant cells along nerve bundles [20], resulting in textural homogeneity on imaging. In contrast, noninvasive lesions present greater histological heterogeneity in interstitial architecture and cellular distribution [21]. Although direct radiomic studies on NI in thyroid carcinoma are scarce, the work of Mu et al [22] reinforces this biological rationale by showing that a radiomic signature on CT could effectively detect metastatic lymph nodes in thyroid carcinoma, demonstrating that imaging features can capture the tumor's propensity for local invasion and spread. LDA further corroborated these findings, demonstrating broader feature dispersion in noninvasive groups and supporting PCA findings, which suggest the utility of radiomic heterogeneity as a quantifiable biomarker for invasion risk in thyroid carcinoma [18].

Key Molecular Markers and Risk Pathways for Invasion

Notably, 3 (6.25%) patients in the capsular invasion–negative group were pathologically diagnosed with NI. This observation indicates that while capsular invasion is a dominant driver, NI can occur through alternative pathways (eg, direct perineural infiltration). Moreover, multivariate binary logistic regression identified CK19, CEA, CA199, CA125, and NI as independent risk factors for capsular invasion. Notably, CK19, a member of the cytokeratin family, exhibited an OR of 60.491, indicating that patients with significant CK19 expression had approximately 60.5 times the odds of having capsular invasion compared to those with nonsignificant expression. This finding is consistent with prior studies reporting CK19 overexpression in papillary thyroid carcinoma [23], where its upregulation enhances tumor cell proliferation and invasive potential via disruption of intercellular adhesion molecules, thereby facilitating tumor penetration through capsular barriers [24]. Laishram et al [25] further identified CK19 as a highly sensitive and specific immunohistochemical marker for thyroid carcinoma in a cross-sectional study using histopathology as the reference standard. Elevated serum levels of CEA, CA199, and CA125 further signify increased tumor burden and epithelial-mesenchymal transition, synergistically promoting invasive phenotypes [26,27]. Intriguingly, NI itself emerged as a covariate for capsular invasion, implying shared molecular pathways or microenvironmental crosstalk. Conversely, when NI was modeled as the dependent variable, only capsular invasion remained significant, underscoring its role as a

XSL•FO
RenderX

dominant predictor for NI. This finding is in line with the anatomical invasion pathway of thyroid carcinoma. Following capsular penetration, tumors demonstrate increased propensity for either direct NI (eg, recurrent laryngeal nerve involvement) or chemokine-mediated perineural infiltration through paracrine signaling modulation [28]. The resultant loss of tumor boundary integrity and disruption of the local microenvironment may jointly provide a structural basis and inflammatory background for NI. Importantly, the exclusion of variables such as age and tumor size from the model highlights the preeminence of capsular status in neural risk stratification, offering clinicians an actionable biomarker for preoperative assessment.

Predictive Model Construction and Clinical Translation Value

For preoperative assessment, the radiomic model prioritizes spatial heterogeneity derived from preoperative CT, enabling noninvasive risk prediction via texture features [6]. Such insights may guide surgical planning, such as the extent of resection or the consideration of intraoperative nerve monitoring. For postoperative stratification, the clinical biomarker-based nomogram and the integrated multimodal model use data available after surgery. They emphasize the biological aggressiveness associated with capsular invasion, aiding in postoperative pathological substaging and recurrence risk prediction. For instance, concurrent positivity for CA199 and CK19 in patients with capsular invasion could signal high-risk subgroups for NI, indicating the need for intensified adjuvant therapy. Specifically, by integrating quantitative molecular data with imaging phenotypes, these postoperative models could provide a supplementary risk assessment that might identify patients with occult invasive features or a higher propensity for recurrence, thereby adding prognostic granularity beyond standard histopathological examination alone. NN architectures further synergized clinical and imaging data, capturing nonlinear interactions between capsular invasion and neural risk [29]. Biological markers such as CEA may reflect intrinsic invasive potential, whereas radiomic features (eg, A9) represent its spatial manifestation. Notably, tumors with capsular invasion characterized by elevated CEA levels and disorganized textures (low A9 values) exhibited markedly increased NI rates, illustrating the model's ability to decode multifactorial invasion pathways. The high performance of all models in the cross-label association analysis (eg, AUCs ≈0.80) is largely concordant with the strong pathological correlation between capsular invasion and NI identified by logistic regression (OR=25.25). This indicates that the models effectively captured the shared features underlying both invasion types, rather than demonstrating independent predictive power for NI on entirely unseen data.

Concerning clinical translation and distinction between model types, it is crucial to distinguish the intended clinical context of the different models developed in this study. The radiomic models (nomogram and RF based on features A1-A9), derived solely from preoperative CT, hold promise as preoperative decision-support tools. They could inform surgical planning, such as the extent of resection or the need for intraoperative nerve monitoring, based on noninvasive imaging. In contrast, the clinical biomarker-based models and the multimodal NN model integrate data (Gal-3 and CK19) that are only available postoperatively from resected tissue. Therefore, their primary utility lies in postoperative risk stratification. They may help pathologists and clinicians identify high-risk subsets among patients already diagnosed with capsular invasion, potentially predicting the likelihood of concurrent or subsequent NI, and thus informing adjuvant therapy strategies or the intensity of follow-up. This postoperative application remains valuable, as it could refine prognostic assessment beyond standard histology.

Limitations and Future Directions

However, this study has several limitations. First, the multivariate logistic regression models (Tables S1 and S2 in Multimedia Appendix 3) are methodologically limited by circular reasoning. Using 1 postoperative pathological finding (eg, NI) to predict another (eg, capsular invasion) inflates the observed associations. The resultant astronomically high ORs with extremely wide CIs are classic signs of overfitting and multicollinearity within our dataset, rather than reliable measures of preoperative risk. These results should be interpreted as strong indicators of pathological co-occurrence, not as valid predictive effects.

Second, the single-center design, limited sample size (n=111), absence of external validation, and reliance on CT scanners from a single manufacturer may restrict generalizability and introduce selection bias.

Third, an additional limitation is the unconventional data usage design: the full dataset was used for both capsular invasion-modeling and cross-label association analysis without a separate held-out test set. Therefore, the reported AUCs for NI prediction are not directly comparable to studies using independent test sets. However, this design was necessary to maximize data use given the small sample size and to specifically test the cross-predictive value of capsular invasion–related features for NI, an exploratory goal that prioritizes verifying feature relevance across related clinical outcomes. Supplementary traditional 7:3 split validation confirmed consistent performance, mitigating concerns about overfitting to some extent (Multimedia Appendix 4).

Fourth is the sampling bias from single-slice analysis. Our NN model used only the single 2D slice with the largest cross-sectional tumor area. As capsular invasion predominantly occurs at the tumor boundaries or poles, this central slice may systematically exclude the imaging features most directly associated with capsular invasion, potentially limiting the model's sensitivity to capture these specific patterns. Consequently, the "Image_Boundary" pattern identified by the network (Figure 2B) likely reflects the general sharpness or regularity of the tumor-parenchyma interface on the central slice, rather than specific imaging signs of focal capsular penetration at the tumor periphery.

Fifth, there is a limitation regarding the control group for qPCR analysis. The use of PBMCs from healthy individuals as a control does not yield biologically precise fold-change values for epithelial markers such as CK19, due to their near absence in PBMCs. In this study, the ≥2-fold threshold was used primarily as a sensitive, technical cutoff to categorize tumors

XSL•FO
RenderX

into those with detectably high versus low or no expression of the target genes, facilitating subsequent clinical correlation analysis. This pragmatic approach should be distinguished from a biologically rigorous quantification of overexpression. Future studies should use paired adjacent normal thyroid tissue as the control to obtain accurate biological quantifications.

Sixth is the normalization-induced information leakage. The *z* score normalization of radiomic features was performed on the entire dataset before model development and cross-validation. This approach could theoretically allow information from validation samples (mean and SD) to leak into the training process, potentially inflating the model's performance estimates. While we used cross-validation and an independent hold-out set to mitigate overfitting, this methodological choice may still contribute to an optimistic bias in the reported metrics. Future studies should consider performing normalization within each fold of the cross-validation loop to provide a more rigorous and unbiased evaluation of model generalizability.

Seventh is feature selection bias. In this study, the LASSO regression was applied to the entire dataset to select the 9 key radiomic features (A1-A9) before model development and cross-validation. Performing feature selection outside the cross-validation loop can introduce selection bias, as the selection process is informed by data that would later serve for validation. This may lead to overfitting and an optimistic estimation of the model's generalizable performance. Consequently, the independence of the hold-out validation for the RF model is partially compromised. Future work should use a nested cross-validation framework, where feature selection is performed independently within each training fold, to obtain unbiased feature sets and more rigorous performance estimates.

Eighth is the potential misalignment from rigid registration. This study used rigid image registration to propagate arterial-phase ROIs to the venous-phase images for feature extraction (eg, feature A9, the venous-phase coefficient of variation). While efficient and commonly used, rigid registration assumes no tissue deformation between phases. Given that the thyroid is a soft organ susceptible to movement from swallowing or breathing, perfect alignment cannot be guaranteed. Any misalignment could cause venous-phase features to partially capture the texture of the tumor's immediate periphery or surrounding tissue rather than the tumor itself. This may introduce noise or bias, particularly for texture-based features such as A9. Therefore, the high importance score of A9 in our model may partially reflect registration artifacts (such as edge effects at the ROI boundaries) rather than solely genuine intratumoral heterogeneity. Although we performed manual verification and adjustment of the propagated ROIs, minor residual misalignments may persist. Future studies could consider using deformable (nonrigid) registration techniques or independent manual delineation on venous-phase images to ensure more accurate feature localization and interpretation.

Ninth is the resolution loss due to image resizing for deep learning. In this study, to comply with the input requirements of the pretrained DenseNet121 network, the entire ROI was resized as a whole from its original resolution to 224×224 pixels. This means that no prior cropping to a tumor-specific bounding box was performed. For smaller thyroid tumors, this global down-sampling can substantially reduce the number of pixels representing the tumor tissue, leading to a loss of fine spatial detail and high-frequency texture information. This process may diminish the model's ability to learn subtle textural patterns that are crucial for predicting capsular invasion, particularly in small lesions. Future studies could improve upon this by implementing a crop-to-bound-box step before resizing or by using NN architectures that support variable input sizes. Furthermore, the "learned image patterns" (eg, "Image_Heterogeneity" and "Image_Boundary") identified through our interpretability analysis (SHAP) may therefore reflect macrolevel structures or artifacts introduced by the global down-sampling process, rather than solely the fine, tumor-specific textural details that are theoretically of interest. For instance, patterns interpreted as heterogeneity could be influenced by the interpolation artifacts during resizing or by the inclusion of nontumoral perinodular tissues within the ROI. While these patterns still contributed to the model's predictive performance, their biological interpretability in relation to capsular invasion should be interpreted with this technical limitation in mind.

Tenth is the uncertainty in hold-out set performance. The performance of the NN model on the small independent hold-out set (n=33; AUC=0.827, 95% CI 0.652 - 0.981) showed a point estimate higher than that from the full-sample cross-validation (AUC=0.775). The wide 95% CI reflects the substantial uncertainty inherent in evaluating a model with such a limited test sample. While the hold-out set was constructed using stratified sampling to maintain a representative distribution of capsular invasion status, the observed difference in point estimates may be attributable to the small sample size and its associated variability. Therefore, the hold-out performance should be interpreted with caution, and the model's generalizability needs to be confirmed in larger, prospective cohorts.

Eleventh is the potential confounding in model comparison due to input differences. The radiomic RF model identified a venous-phase feature (A9) as highly predictive, while the NN was designed with arterial-phase-only inputs for simplicity and to mitigate overfitting. This design difference means that the lower AUC of the NN model (0.775) compared to the RF model (0.8102) may be partially attributable to the exclusion of venous-phase information rather than an inherent limitation of the deep learning architecture itself. Our study aimed to test whether a single phase (arterial) could provide a sufficient predictive signal for a deep learning model; however, this choice introduces a confounding factor when directly comparing performance across methodologies. Future studies could develop multimodal NN architectures incorporating both arterial and venous phases to enable a more equitable comparison and potentially enhance performance.

Future work will expand multicenter collaboration to include over 300 cases across diverse CT devices, incorporate data augmentation and explainable artificial intelligence methods, and establish standardized protocols to improve robustness. Most importantly, future models will focus on using exclusively

XSL•FO
RenderX

preoperative variables to achieve genuine preoperative risk stratification.

Conclusions

In conclusion, our exploratory analysis confirms a strong association between capsular invasion and NI in thyroid carcinoma. This study delineates complementary approaches for invasion risk assessment: (1) radiomic signatures from preoperative CT alone demonstrate potential for noninvasive, preoperative risk stratification; and (2) models incorporating postoperative tissue-derived biomarkers (eg, Gal-3 and CK19), including the multimodal model, provide a valuable framework for postoperative risk stratification. These postoperative tools could aid in identifying patients with high-risk pathological features, potentially guiding decisions on adjuvant therapy or surveillance intensity following surgery. The performance of the radiomic models lays the groundwork for future research toward fully preoperative predictive tools.

Acknowledgments

This study used traditional radiomics and machine learning methodologies for CT (computed tomography)-based capsular or neural invasion risk stratification in thyroid carcinoma. No generative artificial intelligence (GenAI) tools were used in data collection, preprocessing, feature extraction, model development, or interpretation. All analyses followed institutional ethics guidelines, with authors retaining full responsibility for methodological rigor and result validity.

Funding

This research received no specific grant from any funding agency in the public, commercial, or not-for-profit sectors.

Data Availability

The datasets used are available from the corresponding author upon reasonable request.

Authors' Contributions

FfC and KT designed this study. FW and QG collected and analyzed the data. PS and NX wrote and reviewed this paper. All authors have read and approved the final version.

Conflicts of Interest

None declared.

Multimedia Appendix 1
Detailed architecture of the neural network model for capsular invasion prediction.
[DOCX File, 15 KB - medinform_v14i1e77349_app1.docx]

Multimedia Appendix 2
Definitions and pathophysiological correlations of the 9 key radiomic features (A1-A9).
[DOCX File, 16 KB - medinform_v14i1e77349_app2.docx]

Multimedia Appendix 3
Detailed multivariate logistic regression analyses for capsular invasion (Table S1) and neural invasion (Table S2).
[DOCX File, 16 KB - medinform_v14i1e77349_app3.docx]

Multimedia Appendix 4
Hold-out validation results of the random forest model for neural invasion prediction.
[DOC File, 102 KB - medinform_v14i1e77349_app4.doc]

References

1. Mahkamova K, Latar NM, Aspinall S, Meeson A. Side population cells in anaplastic thyroid cancer and normal thyroid. Exp Cell Res 2019 Jan 1;374(1):104-113. [doi: 10.1016/j.yexcr.2018.11.012] [Medline: 30465733]
2. Latar NM, Mahkamova K, Elson J, et al. Impact of transforming growth factor beta 1 on normal and thyroid cancer side population cells. Endocrine 2022 May;76(2):359-368. [doi: 10.1007/s12020-022-02990-4] [Medline: 35118633]
3. Coca-Pelaz A, Shah JP, Hernandez-Prera JC, et al. Papillary thyroid cancer-aggressive variants and impact on management: a narrative review. Adv Ther 2020 Jul;37(7):3112-3128. [doi: 10.1007/s12325-020-01391-1] [Medline: 32488657]
4. Baloch Z, Mete O, Asa SL. Immunohistochemical biomarkers in thyroid pathology. Endocr Pathol 2018 Jun;29(2):91-112. [doi: 10.1007/s12022-018-9532-9] [Medline: 29744727]

XSL•FO
RenderX

5. Zhou Y, Zhou G, Zhang J, Xu C, Zhu F, Xu P. DCE-MRI based radiomics nomogram for preoperatively differentiating combined hepatocellular-cholangiocarcinoma from mass-forming intrahepatic cholangiocarcinoma. Eur Radiol 2022 Jul;32(7):5004-5015. [doi: 10.1007/s00330-022-08548-2] [Medline: 35128572]
6. Chen J, Xi J, Chen T, Yang L, Liu K, Ding X. Diagnostic performance of computed tomography-based artificial intelligence for early recurrence of cholangiocarcinoma: systematic review and meta-analysis. J Med Internet Res 2025 Sep 18;27:e78306. [doi: 10.2196/78306] [Medline: 40905766]
7. Stoyanova R, Takhar M, Tschudi Y, et al. Prostate cancer radiomics and the promise of radiogenomics. Transl Cancer Res 2016 Aug;5(4):432-447. [doi: 10.21037/tcr.2016.06.20] [Medline: 29188191]
8. Tao J, Liu D, Hu FB, et al. Development and validation of a computed tomography–based model for noninvasive prediction of the T stage in gastric cancer: multicenter retrospective study. J Med Internet Res 2024;26:e56851. [doi: 10.2196/56851]
9. Sollini M, Cozzi L, Chiti A, Kirienko M. Texture analysis and machine learning to characterize suspected thyroid nodules and differentiated thyroid cancer: where do we stand? Eur J Radiol 2018 Feb;99:1-8. [doi: 10.1016/j.ejrad.2017.12.004] [Medline: 29362138]
10. Alonso-Gordoa T, Jimenez-Fonseca P, Martinez-Trufero J, et al. SEOM-GETNE-TTCC clinical guideline thyroid cancer (2023). Clin Transl Oncol 2024 Nov;26(11):2902-2916. [doi: 10.1007/s12094-024-03736-6] [Medline: 39325263]
11. Wei R, Wang H, Wang L, et al. Radiomics based on multiparametric MRI for extrathyroidal extension feature prediction in papillary thyroid cancer. BMC Med Imaging 2021 Feb 9;21(1):20. [doi: 10.1186/s12880-021-00553-z] [Medline: 33563233]
12. Boucai L, Zafereo M, Cabanillas ME. Thyroid cancer: a review. JAMA 2024 Feb 6;331(5):425-435. [doi: 10.1001/jama.2023.26348] [Medline: 38319329]
13. Pitt SC, Zanocco K, Sturgeon C. The patient experience of thyroid cancer. Endocrinol Metab Clin North Am 2022 Dec;51(4):761-780. [doi: 10.1016/j.ecl.2022.04.002] [Medline: 36244692]
14. Nabhan F, Dedhia PH, Ringel MD. Thyroid cancer, recent advances in diagnosis and therapy. Int J Cancer 2021 Sep 1;149(5):984-992. [doi: 10.1002/ijc.33690] [Medline: 34013533]
15. Gritsenko PG, Ilina O, Friedl P. Interstitial guidance of cancer invasion. J Pathol 2012 Jan;226(2):185-199. [doi: 10.1002/path.3031] [Medline: 22006671]
16. Chapman JD. Measurement of tumor hypoxia by invasive and non-invasive procedures: a review of recent clinical studies. Radiother Oncol 1991;20 Suppl 1:13-19. [doi: 10.1016/0167-8140(91)90181-f] [Medline: 2020762]
17. Khan A, Hasana U, Nadeem IA, et al. Advances in colorectal cancer screening and detection: a narrative review on biomarkers, imaging and preventive strategies. J Egypt Natl Canc Inst 2025 Apr 11;37(1):20. [doi: 10.1186/s43046-025-00277-z] [Medline: 40214837]
18. Zhang L, Li D, Su T, Xiao T, Zhao S. Effectiveness of radiomics-based machine learning models in differentiating pancreatitis and pancreatic ductal adenocarcinoma: systematic review and meta-analysis. J Med Internet Res 2025 Jul 31;27:e72420. [doi: 10.2196/72420] [Medline: 40744488]
19. Liang C, Bian Z, Lv W, Chen S, Zeng D, Ma J. A computer-aided diagnosis scheme of breast lesion classification using GLGLM and shape features: combined-view and multi-classifiers. Phys Med 2018 Nov;55:61-72. [doi: 10.1016/j.ejmp.2018.10.016] [Medline: 30471821]
20. Pundavela J, Roselli S, Faulkner S, et al. Nerve fibers infiltrate the tumor microenvironment and are associated with nerve growth factor production and lymph node invasion in breast cancer. Mol Oncol 2015 Oct;9(8):1626-1635. [doi: 10.1016/j.molonc.2015.05.001] [Medline: 26009480]
21. Bilello M, Akbari H, Da X, et al. Population-based MRI atlases of spatial distribution are specific to patient and tumor characteristics in glioblastoma. Neuroimage Clin 2016;12:34-40. [doi: 10.1016/j.nicl.2016.03.007] [Medline: 27358767]
22. Mu J, Cao Y, Zhong X, Diao W, Jia Z. Prediction of cervical lymph node metastasis in differentiated thyroid cancer based on radiomics models. Br J Radiol 2024 Feb 28;97(1155):526-534. [doi: 10.1093/bjr/tqae010] [Medline: 38366237]
23. Dencic TI, Cvejic D, Paunovic I, Tatic S, Havelka M, Savin S. Cytokeratin19 expression discriminates papillary thyroid carcinoma from other thyroid lesions and predicts its aggressive behavior. Med Oncol 2013 Mar;30(1):362. [doi: 10.1007/s12032-012-0362-1] [Medline: 23269585]
24. Yan Q, Chen P, Chen X, et al. Expression of CK7, CK19 and p16 in HPV-mediated oropharyngeal squamous cell carcinoma. PeerJ 2024;12:e18286. [doi: 10.7717/peerj.18286] [Medline: 39619189]
25. Laishram H, Jagadale K, Shelke P, Bharadwaj R. Cross-sectional study to determine the diagnostic accuracy of cytokeratin-19 immunomarker in the diagnosis of thyroid malignancy with histopathology as gold standard. Niger Postgrad Med J 2025 Jan 1;32(1):61-67. [doi: 10.4103/npmj.npmj_3_25] [Medline: 40091473]
26. Chen J, Wang H, Zhou L, Liu Z, Tan X. A combination of circulating tumor cells and CA199 improves the diagnosis of pancreatic cancer. J Clin Lab Anal 2022 May;36(5):e24341. [doi: 10.1002/jcla.24341] [Medline: 35334495]
27. Ashi A, Al-Hajeili M, Almaghrabi S, et al. Prevalence of CEA, CA 125, and CA 15-3 serum tumour markers in different regions of Saudi Arabia. Saudi Med J 2024 Jun;45(6):565-571. [doi: 10.15537/smj.2024.45.6.20230878] [Medline: 38830664]
28. Chen SH, Zhang BY, Zhou B, Zhu CZ, Sun LQ, Feng YJ. Perineural invasion of cancer: a complex crosstalk between cells and molecules in the perineural niche. Am J Cancer Res 2019;9(1):1-21. [Medline: 30755808]

XSL•FO
RenderX

29. Sun P, Zhao Y, Men J, et al. Application of virtual and augmented reality technology in hip surgery: systematic review. J Med Internet Res 2023 Mar 10;25:e37599. [doi: 10.2196/37599] [Medline: 36651587]

Abbreviations

AUC: area under the curve
CA125: carbohydrate antigen 125
CA199: carbohydrate antigen 199
CCSA-2: circulating cancer-specific antigen
CEA: carcinoembryonic antigen
CK19: cytokeratin 19
CT: computed tomography
Gal-3: galectin-3
GLCM: gray-level co-occurrence matrix
HBME-1: Hector Battifora Mesothelial Epitope-1
ICC: intraclass correlation coefficient
LASSO: least absolute shrinkage and selection operator
LDA: linear discriminant analysis
MAE: mean absolute error
NI: neural invasion
NN: neural network
OR: odds ratio
PBMC: peripheral blood mononuclear cell
PCA: principal component analysis
qPCR: quantitative polymerase chain reaction
RF: random forest
RGB: red, green, and blue
ROC: receiver operating characteristic
ROI: regions of interest
SHAP: Shapley Additive Explanations
XAI: explainable artificial intelligence

Edited by A Coristine; submitted 12.May.2025; peer-reviewed by J Zhang, T Yusuff; revised version received 25.Jan.2026; accepted 26.Jan.2026; published 12.Mar.2026.

Please cite as:
Cong FF, Tian K, Gao Q, Wang F, Sun P, Xu N
CT Radiomics–Based Machine Learning Model for Predicting Capsular and Neural Invasion in Thyroid Carcinoma: Diagnostic Accuracy Study
JMIR Med Inform 2026;14:e77349
URL: https://medinform.jmir.org/2026/1/e77349
doi:10.2196/77349

© Fang-fang Cong, Ke Tian, Qian Gao, Fulin Wang, Peng Sun, Nan Xu. Originally published in JMIR Medical Informatics (https://medinform.jmir.org), 12.Mar.2026. This is an open-access article distributed under the terms of the Creative Commons Attribution License (https://creativecommons.org/licenses/by/4.0/), which permits unrestricted use, distribution, and reproduction in any medium, provided the original work, first published in JMIR Medical Informatics, is properly cited. The complete bibliographic information, a link to the original publication on https://medinform.jmir.org/, as well as this copyright and license information must be included.

XSL•FO
RenderX

Effects of Image Degradation on Deep Neural Network Classification of Scaphoid Fracture Radiographs: Comparison Study of Different Noise Types

Chihung Lin[1,2*], PhD; Alfred P Yoon[3*], MD; Chien-Wei Wang[4], MD; Tung Chao[1], MS; Kevin C Chung[4*], MS, MD; Chang-Fu Kuo[1,5,6,7*], MD, PhD

[1]Center for Artificial Intelligence in Medicine, Chang Gung Memorial Hospital, Taoyuan, Taiwan

[2]Department of Artificial Intelligence, Chang Gung University, Taoyuan, Taiwan

[3]Division of Plastic and Reconstructive Surgery, Section of Hand and Microvascular Surgery, University of California Davis Medical Center, Sacramento, CA, United States

[4]Comprehensive Hand Center, Michigan Medicine, Ann Arbor, MI, United States

[5]Division of Rheumatology, Allergy and Immunology, Center for Artificial Intelligence in Medicine, Chang Gung Memorial Hospital, No.5, Fuxing Street, Guishan District, Taoyuan City 333, Taoyuan, Taiwan

[6]College of Medicine, Chang Gung University, Taoyuan, Taiwan

[7]Division of Rheumatology, Orthopaedics and Dermatology, School of Medicine, University of Nottingham, Nottingham, United Kingdom

[*]these authors contributed equally

Corresponding Author:
Chang-Fu Kuo, MD, PhD
Center for Artificial Intelligence in Medicine, Chang Gung Memorial Hospital, Taoyuan, Taiwan

Abstract

Background: Deep learning models have shown strong potential for automated fracture detection in medical images. However, their robustness under varying image quality remains uncertain, particularly for small and subtle fractures, such as scaphoid fractures. Understanding how different types of image perturbations affect model performance is crucial for ensuring reliable deployment in clinical practice.

Objective: This study aimed to evaluate the robustness of a deep learning model trained to detect scaphoid fractures in radiographs when exposed to various image perturbations. We sought to identify which perturbations most strongly impact performance and to explore strategies to mitigate performance degradation.

Methods: Radiographic datasets were systematically modified by applying Gaussian noise, blurring, JPEG compression, contrast-limited adaptive histogram equalization, resizing, and geometric offsets. Model accuracy was evaluated across different perturbation types and levels. Image quality was quantified using peak signal-to-noise ratio and structural similarity index measure to assess correlations between degradation and model performance.

Results: Model accuracy declined with increasing perturbation severity, but the extent varied across perturbation types. Gaussian blur caused the most substantial performance drop, whereas contrast-limited adaptive histogram equalization increased the false-negative rate. The model demonstrated higher resilience to color perturbations than to grayscale degradations. A strong linear correlation was found between peak signal-to-noise ratio–structural similarity index measure and accuracy, suggesting that better image quality led to improved detection. Geometric offsets and pixel value rescaling had minimal influence, whereas resolution was the dominant factor affecting performance.

Conclusions: The findings indicate that image quality, especially resolution and blurring, substantially influences the robustness of deep learning–based fracture detection models. Ensuring adequate image resolution and quality control can enhance diagnostic reliability. These results provide valuable insights for designing more accurate and resilient medical imaging models under real-world variability.

(JMIR Med Inform 2026;14:e65596) doi:10.2196/65596

KEYWORDS

scaphoid fractures; contrast-limited adaptive histogram equalization; CLAHE; image quality; peak signal-to-noise ratio; PSNR; structural similarity index measure; SSIM; neural network.

XSL•FO
RenderX

Introduction

Significant advances in computer vision have led to remarkable improvements in deep neural network (DNN) performance on tasks such as medical image classification [1]. Despite these achievements, DNN-based systems exhibit limited robustness compared with human perception, especially in the context of image perturbations and corruption [2]. Adversarial attacks can cause substantial misclassifications, and even minor noise can adversely affect performance [3-5]. Nevertheless, state-of-the-art classifiers appear to exhibit some ability to overcome random noise [6].

In real-world medical imaging, DNN model robustness is critical because low-quality images and noise are not uncommon; these issues include radiographic underexposures and motion artifacts as well as downstream processing or transfer distortions that can alter image fidelity and affect artificial intelligence (AI) performance [7,8]. In addition, real-world clinical workflows may involve low-resolution screen recapturing or smartphone-captured radiographs in urgent or resource-limited settings, which introduce compounded degradations, such as resizing, compression, and display-related artifacts [9]. Our previous work on a DNN model that detected both visible and occult scaphoid fractures demonstrated that it was possible to reliably detect fractures of small bones and to assist in the radiographic detection of occult fractures that are not visible to human observers [10]. This experience indicated that image preprocessing, file formatting, and data storage could negatively impact model performance. We discovered that image processing techniques introduced noise into input files, potentially misleading the DNN model. Such noise, often imperceptible to the human eye, can significantly affect model performance and potentially lead to incorrect diagnoses [11]. Consequently, evaluation of performance is vital in convolutional neural network (CNN)–based models that process noisy images; this evaluation poses frequent challenges in clinical settings. Prior studies have revealed that neural networks are most accurate when the data to be classified exhibit quality similar to that of the model training data; it was recommended that noise be injected into the training data to increase model robustness [12]. However, the addition of many possible noises to a training dataset is both computationally expensive and impractical. To the best of our knowledge, no study has investigated the impacts of different types of noise on neural networks designed for fracture classification when radiographs serve as inputs.

This study investigated the robustness of our CNN-based scaphoid fracture classification model when various types of image noise were present. To comprehensively evaluate model performance, we simulated real-world conditions that yield low-quality clinical images. Using fine-tuning techniques to create noisy samples, we sought to enhance model performance under noisy or degraded conditions, thereby mitigating the adverse effects of image corruption [7]. Additionally, we examined the impacts of specific forms of image degradation on model performance; we explored particular model vulnerabilities that might warrant further refinement. Our goals were to ascertain model accuracy when processing low-quality clinical images and to identify the types of noise that most confounded the model, thereby providing valuable insights to aid the development of more resilient DNN-based medical image classifiers appropriate for real-world applications.

Methods

Ethical Considerations

The study protocol was approved by the institutional review board of Chang Gung Memorial Hospital (202202256B0).

Scaphoid Fracture Classification Model

As previously described in our earlier work [10], the scaphoid fracture classification model was built using an EfficientNetB1 [13] backbone and 240×240-pixel red, green, and blue (RGB) images with a classification threshold of 0.5. In a study by Yoon et al [10], the model was originally trained and validated using 3991 scaphoid fracture radiographs and 5542 normal scaphoid radiographs.

In this study, we adopted the same model architecture as in the study by Yoon et al [10] and initialized the network with the finalized pretrained weights from that study, as shown in Figure 1. We then further fine-tuned this model using the 5286 training radiographs from the dataset described in the “Dataset and Preprocessing” section and evaluated it on an independent test set. Fine-tuning was performed using the AdamW optimizer, with appropriate adjustments to the learning rate, weight decay, and batch size. The learning rate was reduced if the validation loss failed to improve over 6 epochs, and training was stopped early when model performance did not increase further after 15 epochs.

XSL•FO
RenderX

Figure 1. Complete pipeline for inference of a scaphoid fracture, including fracture (red box) and occult fracture. This report solely focuses on the performance of the fracture model.

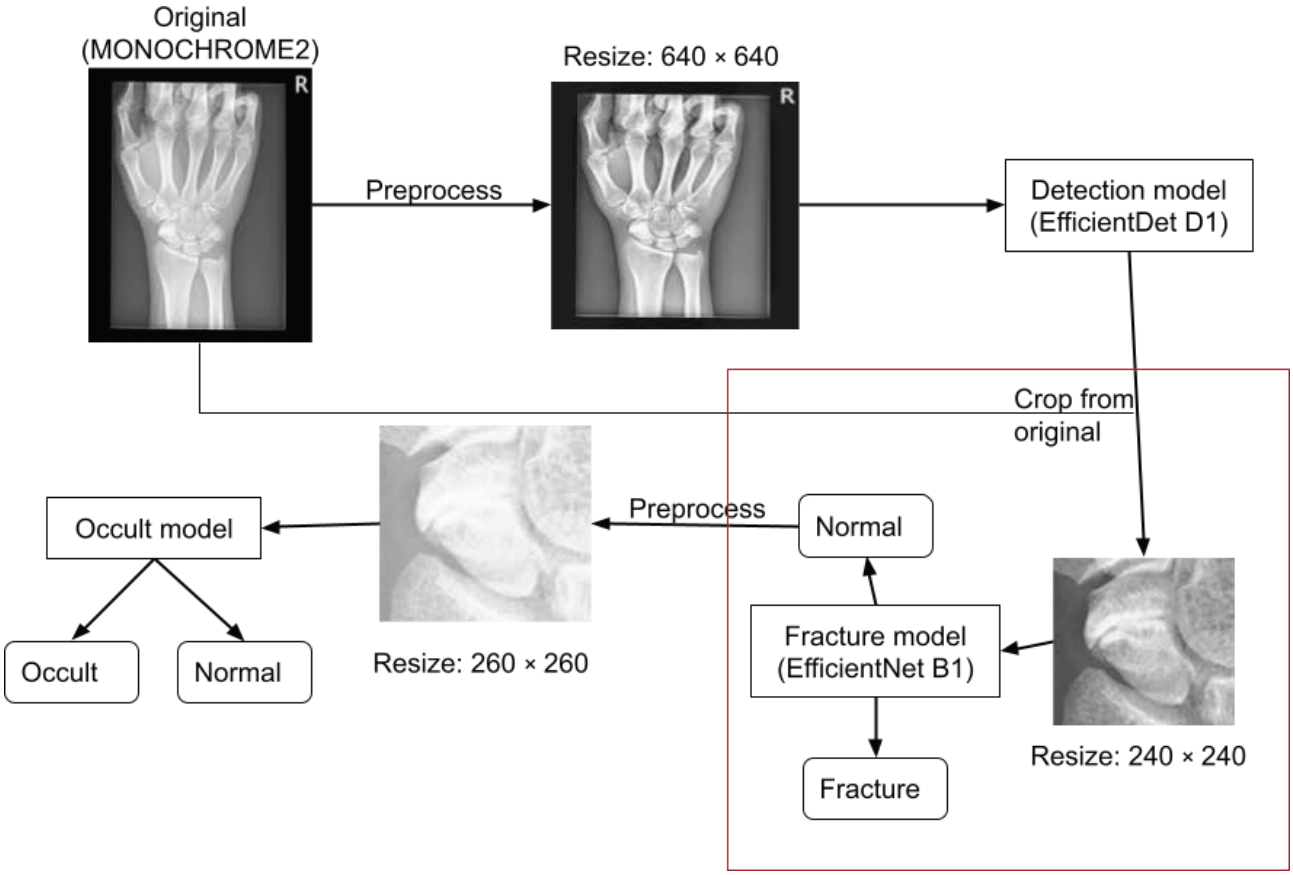

Dataset and Preprocessing

The scaphoid fracture classification model used in this study was fine-tuned and evaluated using 5954 radiographs stored in Chang Gung Memorial Hospital in Taiwan. Of these radiographs, 1483 were of fractured scaphoids, and the remaining 4471 were of normal scaphoids. Images were captured by commercially available x-ray machines from multiple manufacturers. All radiographs were reviewed by 3 experienced radiologists and labeled as *fractured* or *normal*. This dataset is distinct from the dataset used in our previous work [10], in which the model was originally developed using 3991 fracture and 5542 normal radiographs. In this study, we adopted the same model architecture as in the study by Yoon et al [10], initialized the network with the finalized pretrained weights from that study, and further fine-tuned the model using the 5286 training images described below before evaluating it on an independent test set.

The training dataset consisted of 5286 images, and the test dataset comprised 668 images. A total of 28 images were excluded for reasons including anatomical anomalies secondary to arthritis (12 images), 3 due to unclear laterality, 2 due to wrong-sided imaging, image artifacts introduced by the hardware (1 image), and imaging findings of likely previous fractures or chronic nonunion (10 images). Thus, the final test dataset contained 640 images. The images varied in size and position, but all were 12-bit grayscale images of posteroanterior views of the wrist. Most images were rectangular, with widths ranging from 1000 to 1600 pixels, and heights ranging from 1600 to 2200 pixels. If the photometric interpretation of an image was MONOCHROME1, the image was converted to MONOCHROME2. The scaphoid was isolated from each hand radiograph using a bounding box generated by a separate scaphoid detection model. This detector (not to be confused with the scaphoid fracture classifier) was not the focus of this study because its performance is robust against common perturbations.

Rescaling Images to 8-Bit Depth

All radiographs were 12-bit grayscale posteroanterior wrist views that varied in terms of size and position, with widths between 1000 and 1600 pixels, and heights between 1600 and 2200 pixels. The images were rescaled to 8-bit grayscale and compiled into RGB images using the value of interest (VOI) lookup table and windowing operations that were also used during model training.

The DICOM images were stored in 12-bit grayscale, but the model accepted only 24-bit RGB (color) images. Thus, the images were first rescaled to 8-bit grayscale (with pixel values ranging from 0 to 255) and then compiled into RGB images for interpretation. This rescaling process was based on the maximum and minimum values of the image, rather than the actual bit depth. A VOI lookup table and windowing operations were applied to all images to adjust the pixel values based on the DICOM VOI LUT and windowing tags (pydicom. pixel_data_handlers.apply_voi_lut, version 1.4, 2022).

Differences emerge when images do not contain the lowest and highest pixel values. For 12-bit grayscale images, these pixel

XSL•FO
RenderX

values are 0 and 4095, respectively. The resulting difference can brighten or darken the entire image. Furthermore, the use of a VOI lookup process may change the brightness and contrast. These differences are minor and usually imperceptible to the human eye.

Generating Datasets for Noise Testing

Overview

To assess model performance in the presence of distortions, we generated several low-quality datasets using different noise perturbations. First, we read the test images using method 1. Images were cropped to the scaphoid regions demarcated by the bounding boxes, resized to 240×240 pixels, converted to 8-bit grayscale, and saved in PNG format. We refer to these baseline images (without noise) as “clean” hereafter.

To systematically evaluate the robustness of our scaphoid fracture classification model, we created multiple “noisy” or “degraded” datasets by applying a variety of image perturbations to our *clean baseline test set* of 640 scaphoid radiographs. Each perturbation type and severity level corresponds to a row in Table 1, which lists the name of the treatment, the number of images, and the specific operation performed. Next, we describe the main categories of perturbations and their implementations.

XSL•FO
RenderX

Table . Information on all datasets, including the datasets from which they were modified, sample counts, and methods of modification.

Treatment name	Modified from	N	Operation
Clean dataset	Original DICOM file	640	Read original DICOM file with (1)
Gaussian blur_0.5	Scaphoid	640	Apply Gaussian blur (σ=0.5) to the cropped scaphoid
Gaussian blur_1.0	Scaphoid	640	Apply Gaussian blur (σ=1.0) to the cropped scaphoid
Gaussian blur_1.5	Scaphoid	640	Apply Gaussian blur (σ=1.5) to the cropped scaphoid
Gaussian blur_2.0	Scaphoid	640	Apply Gaussian blur (σ=2.0) to the cropped scaphoid
Gaussian blur_2.5	Scaphoid	640	Apply Gaussian blur (σ=2.5) to the cropped scaphoid
Gaussian blur_3.0	Scaphoid	640	Apply Gaussian blur (σ=3.0) to the cropped scaphoid
Gaussian noise (RGB)_1	Scaphoid	640	Add RGB Gaussian noise with SD 1.00 to the cropped scaphoid
Gaussian noise (RGB)_2	Scaphoid	640	Add RGB Gaussian noise with SD 2.00 to the cropped scaphoid
Gaussian noise (RGB)_3	Scaphoid	640	Add RGB Gaussian noise with SD 3.00 to the cropped scaphoid
Gaussian noise (RGB)_4	Scaphoid	640	Add RGB Gaussian noise with SD 4.00 to the cropped scaphoid
Gaussian noise (RGB)_5	Scaphoid	640	Add RGB Gaussian noise with SD 5.00 to the cropped scaphoid
Gaussian noise (RGB)_6	Scaphoid	640	Add RGB Gaussian noise with SD 6.00 to the cropped scaphoid
Gaussian noise (grayscale)_1	Scaphoid	640	Convert image to grayscale, add Gaussian noise with SD 1.00 to the cropped scaphoid
Gaussian noise (grayscale)_2	Scaphoid	640	Convert image to grayscale, add Gaussian noise with SD 2.00 to the cropped scaphoid
Gaussian noise (grayscale)_3	Scaphoid	640	Convert image to grayscale, add Gaussian noise with SD 3.00 to the cropped scaphoid
Gaussian noise (grayscale)_4	Scaphoid	640	Convert image to grayscale, add Gaussian noise with SD 4.00 to the cropped scaphoid
Gaussian noise (grayscale)_5	Scaphoid	640	Convert image to grayscale, add Gaussian noise with SD 5.00 to the cropped scaphoid
Gaussian noise (grayscale)_6.0	Scaphoid	640	Convert image to grayscale, add Gaussian noise with SD 6.00 to the cropped scaphoid
JPEG compression_10	Scaphoid	640	Degrade scaphoid images with compression strength=10 (slightest)
JPEG compression_30	Scaphoid	640	Degrade scaphoid images with compression strength=30
JPEG compression_50	Scaphoid	640	Degrade scaphoid images with compression strength=50
JPEG compression_70	Scaphoid	640	Degrade scaphoid images with compression strength=70
JPEG compression_90	Scaphoid	640	Degrade scaphoid images with compression strength=90 (strongest)

XSL•FO
RenderX

Treatment name	Modified from	N	Operation
CLAHE[a]_1	Scaphoid	640	Apply CLAHE (clip limit=1.0, tile grid size=[8, 8]) to the cropped scaphoid
CLAHE_2	Scaphoid	640	Apply CLAHE (clip limit=2.0, tile grid size=[8, 8]) to the cropped scaphoid
CLAHE_3	Scaphoid	640	Apply CLAHE (clip limit=3.0, tile grid size=[8, 8]) to the cropped scaphoid
CLAHE_4	Scaphoid	640	Apply CLAHE (clip limit=4.0, tile grid size=[8, 8]) to the cropped scaphoid
CLAHE_5	Scaphoid	640	Apply CLAHE (clip limit=5.0, tile grid size=[8, 8]) to the cropped scaphoid
Resize_400	Whole image	640	Resize whole images by width=400 while keeping the aspect ratio and crop out the scaphoid by projecting the recorded bounding box coordinates
Resize_600	Whole image	640	Resize whole images by width=600 while keeping the aspect ratio and crop out the scaphoid by projecting the recorded bounding box coordinates
Resize_800	Whole image	640	Resize whole images by width=800 while keeping the aspect ratio and crop out the scaphoid by projecting the recorded bounding box coordinates
Resize_1000	Whole image	640	Resize whole images by width=1000 while keeping the aspect ratio and crop out the scaphoid by projecting the recorded bounding box coordinates
Resize_1200	Whole image	640	Resize the whole images by width=1200 while keeping the aspect ratio and crop out the scaphoid by projecting the recorded bounding box coordinates
Resize_1400	Whole image	640	Resize whole images by width=1400 while keeping the aspect ratio and crop out the scaphoid by projecting the recorded bounding box coordinates
Geometrics_1	Whole image	5120	Modify the center point of bounding box (bbox) x,y coordinates by −20% and 0% and 20% of bbox length
Geometrics_2	Whole image	5120	Modify the center point of bbox x,y coordinates by −10% and 0% and 10% of bbox length
Geometrics_3	Whole image	10,240	Modify the 4 bbox x,y coordinates (xmin, xmax, ymin, ymax) by −10% and 10% of bbox length
Geometrics_4	Whole image	10,240	Modify the 4 bbox x,y coordinates (xmin, xmax, ymin, ymax) by −5% and 5% of bbox length

XSL•FO
RenderX

Treatment name	Modified from	N	Operation
12-bit-rescale_1	Original DICOM file	640	Read original DICOM file using method (2) and crop the scaphoid with the recorded bbox coordinates
12-bit-rescale_2	Original DICOM file	640	Read original DICOM file using method (2) and crop the scaphoid with the detector
Screenshot_MicroDicom_1	Original DICOM file	640	Read DICOM files using MicroDicom with the default settings, screenshoot the whole image at a resolution of 550×780, and crop the scaphoid with the detector
Screenshot_MicroDicom_2	Original DICOM file	640	Read DICOM files using MicroDicom with the default settings, enter fullscreen mode, screenshoot the whole image at a resolution of 900×1050 and crop the scaphoid with the detector
Screenshot_ImageJ	Original DICOM file	640	Read DICOM files using ImageJ, adjust contrast to 12-bit, screenshoot the whole image at a resolution width of 600 while retaining the height-width ratio, and crop the scaphoid with the detector

[a]CLAHE: contrast-limited adaptive histogram equalization.

Clean Dataset

We refer to the original 640 cropped scaphoid images (taken directly from DICOM files and converted to 8-bit depth) as the "clean" dataset (row 1 in Table 1). This set serves as our baseline for comparison.

Gaussian Blur

We simulated *blur* by convolving each scaphoid region with a Gaussian kernel using SDs (σ) ranging from 0.5 to 3.0 (rows 2-7 in Table 1). Specifically, we used a Python image-augmentation library (eg, *imgaug*; Python Software Foundation) to apply GaussianBlur(σ=x). Each σ setting generated a separate dataset of 640 images.

Gaussian Noise

For grayscale noise (rows 8-13 in Table 1), we converted each cropped scaphoid image to 8-bit grayscale, then added random Gaussian noise with SD values in the set {1, 2, 3, 4, 5, 6}. The resulting noised images were reconverted to RGB (by replicating the grayscale channel 3 times) to match the model's 3-channel input requirement.

For color (RGB) noise (rows 14-19 in Table 1), we similarly added Gaussian noise to the 3 RGB channels, resulting in "colored" noise. SD values were identical (1-6). Each level produced 640 modified images.

JPEG Compression

We degraded the quality of the cropped scaphoid images by JPEG compression (rows 20-24 in Table 1), with a compression strength of 10, 30, 50, 70, and 90 (higher values indicating more severe compression in our chosen library). Each compression level formed a dataset of 640 images.

This process simulates the impact of lossy image storage on fracture detection performance.

Contrast-Limited Adaptive Histogram Equalization

Contrast-limited adaptive histogram equalization (CLAHE; rows 25-29 in Table 1) enhances local contrast in radiographs, potentially exaggerating edges and intensifying noise. We generated 5 datasets by applying OpenCV's createCLAHE() with *cliplimit* in {1.0, 2.0, 3.0, 4.0, 5.0} and tileGridSize=(8,8). Each CLAHE setting yielded 640 images.

Resizing Whole Images

Before cropping the scaphoid region, we resized the *entire* original wrist radiograph (rows 30-35 in Table 1) to widths of 400, 600, 800, 1000, 1200, or 1400 pixels (preserving the aspect ratio), then reapplied our scaphoid bounding box coordinates to crop out the scaphoid. Finally, the cropped regions were resized to 240×240 pixels for model input. This procedure mimics variations in image resolution and scaling during clinical acquisition or display.

Geometric Offsets

To examine the robustness of our model to bounding box inaccuracies, we systematically shifted or distorted the bounding box coordinates by ±5%, 10%, or ±20% of the bounding box size. This sometimes resulted in only partial scaphoid capture. Four separate datasets (Geometrics_1 to Geometrics_4) covered different offset ranges (rows 36-39 in Table 1). Each row includes multiple transformations, so the total number of images can exceed 640.

Twelve-bit Rescaling

Instead of converting the DICOM images with our typical method (method 1), we used an alternative approach (method

XSL•FO
RenderX

2) that directly scales 12-bit raw pixel values (0-4095) into 8-bit (0-255). We generated 2 variations: (1) 12-bit-rescale_1: recorded bounding box coordinates were applied to these rescaled images; (2) 12-bit-rescale_2: we reran the scaphoid detection model on these rescaled images to obtain new bounding boxes.

Screenshot Datasets

We opened the original DICOM files in different DICOM viewing software (eg, MicroDicom; ImageJ developed by National Institutes of Health and the Laboratory for Optical and Computational Instrumentation), adjusted the default display or resolution, and took screenshots of the entire wrist X-ray. Screen resolutions varied (eg, 550×780 or 900×1050; rows 42-44 in Table 1). We then cropped out the scaphoid region using our detection model, resizing the final images to 240×240. Each screenshot setting introduced different display parameters, simulating suboptimal clinical scenarios where images may be shared or interpreted via screenshots instead of original DICOM files.

Each of these modifications produced a new dataset of 640 images (except when multiple bounding box transformations were applied, resulting in a large number of images). Collectively, these datasets allowed us to evaluate the effects of image degradations on the classification model's performance. Table 1 provides a concise summary of all transformations, whereas Multimedia Appendix 1 contains more detailed code snippets and pseudocode for each operation.

Additionally, 5 datasets were produced using the rescale method or by capturing screenshots from the original DICOM files on image viewers. Figure 2 and Table 1 detail all 44 perturbations. The details of noise introduction into the dataset are described in Multimedia Appendix 1.

Figure 2. Flowchart of the pipeline used to generate clean and noisy datasets. CLAHE: contrast-limited adaptive histogram equalization;

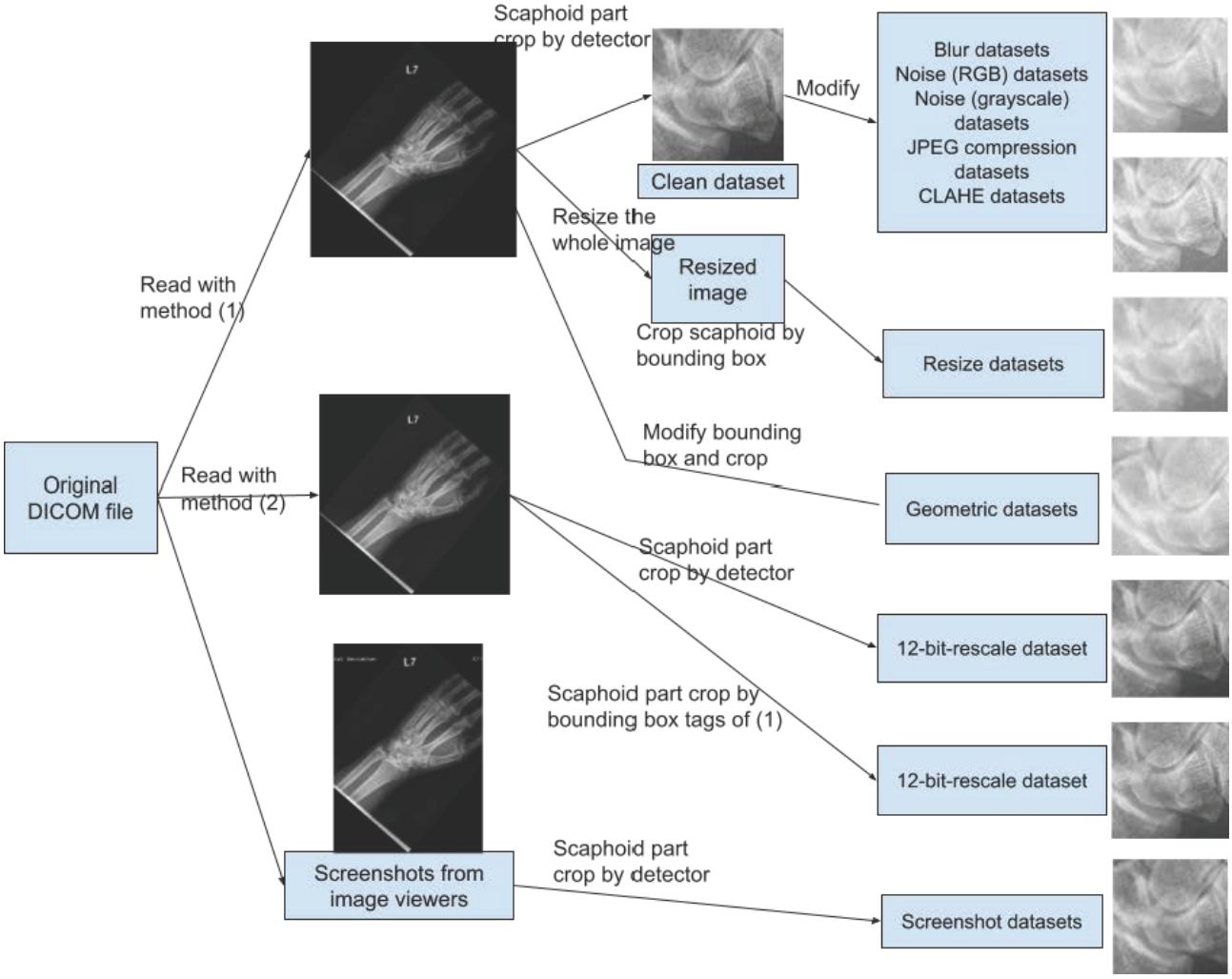

Image Quality Assessment

The peak signal-to-noise ratio (PSNR) and the structural similarity indexing method (SSIM) [14,15] were used as image quality assessment methods when gauging alterations in images. PSNR is a widely used metric that assesses the fidelity of an image compared with its original or uncompressed version. PSNR quantifies the difference between 2 images by calculating the ratio of the maximum possible power of the signal (the image) to the power of the noise (the error that is introduced). A higher PSNR value indicates better image quality because less noise is introduced during changes. In contrast, SSIM is a more advanced metric for measuring image quality that considers structural information, luminance, and contrast when comparing 2 images. SSIM calculates local similarities between the 2 images and combines them into a single score, ranging

XSL•FO
RenderX

from −1 to 1, where a higher value indicates greater similarity between the images. Both PSNR and SSIM values were calculated using TensorFlow image module (TensorFlow Module: tf.image), which allows efficient and accurate computations of both metrics. However, neither PSNR nor SSIM can be used for geometric transformations, such as affine and rotational adjustments, because both rely on pixel-by-pixel comparisons. Such comparisons become less meaningful when the spatial arrangement of image content is altered via geometric transformations. Consequently, datasets with modifications to the labeled scaphoid regions were excluded from comparison to maintain assessment integrity.

We calculated and compared PSNR and SSIM values for the clean and noisy images. Importantly, neither assessment is amenable to geometric transformations, such as affine and rotational adjustments. Therefore, the following datasets with modifications to the labeled scaphoid regions were excluded from the PSNR and SSIM comparisons: the 4 geometric datasets, the 12-bit rescale_2 datasets, and the 3 screenshot datasets. Both PSNR and SSIM were calculated using TensorFlow image functions (PSNR and SSIM).

Model Evaluation and Performance Metrics

The scaphoid fracture classification model was evaluated by analyzing its performance on various test datasets that included clean images and distorted images with diverse noise levels. Performance metrics, including model accuracy, sensitivity, specificity, and F_1-score, were calculated by comparing the model predictions with ground truth labels provided by experienced orthopedic and hand surgeons.

Robustness Against Image Quality Degradation

To assess model robustness against image quality degradation, model performances on distorted images were compared with model performances on clean images. This comparison sought to estimate fracture classification accuracy when perturbations were present, offering insights into potential real-world applications of the model and its robustness when image quality varies in clinical settings.

The Environment

Model inferences were executed on Linux Ubuntu 18.04 LTS (GPU: NVIDIA GeForce RTX 3080 (10 GB); Python version 3.7.13). Implementation was conducted with a TensorFlow backend and TensorFlow version 2.9.1.

Results

Performance of the Deep Learning Model With Varied Perturbations

We investigated the efficacy of a deep learning model designed to detect scaphoid fractures in radiographs, specifically when image quality had been deliberately compromised by adding perturbations. The primary datasets were altered using various methods: addition of Gaussian noise, blurring, JPEG compression, CLAHE, resizing, and geometric adjustments. Table 2 presents the quality assessment and model performance results across the evaluated datasets. Specifically, datasets that underwent blurring, Gaussian noise addition, JPEG corruption, CLAHE, or resizing are reported in rows 1–35; geometric datasets in rows 36–39; bit-rescaled datasets in rows 40–41; and screenshot datasets in rows 42–44. The model achieved an accuracy of 92.03% on the original unaltered dataset, which thus served as the performance benchmark for other evaluations.

XSL•FO
RenderX

Table . The quality assessment and model performance results across the evaluated datasets.

Treatment	PSNR[a], mean (SD)	Average SSIM[b], mean (SD)	Accuracy	Precision	Recall
Clean dataset	Inf	1.0000	0.9203	0.915	0.9119
Gaussian blur _0.5	52.5622 (2.6778)	0.9975 (0.0010)	0.9031	0.8896	0.9017
Gaussian blur _1.0	42.7419 (2.5447)	0.9758 (0.0096)	0.8422	0.7836	0.9085
Gaussian blur _1.5	39.9809 (2.5143)	0.9545 (0.0172)	0.8078	0.7299	0.9254
Gaussian blur _2.0	37.2251 (2.3945)	0.9183 (0.0272)	0.7625	0.6819	0.9085
Gaussian blur _2.5	35.4838 (2.3231)	0.8842 (0.0356)	0.7250	0.6530	0.8610
Gaussian blur _3.0	34.8328 (2.3077)	0.8674 (0.0399)	0.7203	0.6526	0.8407
Gaussian noise (grayscale)_1	47.7838 (0.1157)	0.9917 (0.0018)	0.9109	0.9190	0.8847
Gaussian noise (grayscale)_2	42.0190 (0.0432)	0.9697 (0.0066)	0.8906	0.8840	0.8780
Gaussian noise (grayscale)_3	38.5493 (0.0308)	0.9357 (0.0135)	0.8688	0.8436	0.8780
Gaussian noise (grayscale)_4	36.0689 (0.0271)	0.8929 (0.0216)	0.8422	0.7994	0.8780
Gaussian noise (grayscale)_5	34.1382 (0.0267)	0.8444 (0.0298)	0.8172	0.7602	0.8814
Gaussian noise (grayscale)_6	32.5600 (0.0276)	0.7932 (0.0376)	0.7734	0.7027	0.8814
Gaussian noise (RGB)_1	47.7851 (0.1134)	0.9917 (0.0018)	0.9156	0.9288	0.8847
Gaussian noise (RGB)_2	42.0211 (0.0368)	0.9697 (0.0065)	0.9094	0.9100	0.8915
Gaussian noise (RGB)_3	38.5487 (0.0225)	0.9357 (0.0135)	0.8969	0.8962	0.8780
Gaussian noise (RGB)_4	36.0686 (0.0180)	0.8929 (0.0215)	0.8891	0.8784	0.8814
Gaussian noise (RGB)_5	34.1376 (0.0173)	0.8444 (0.0299)	0.8547	0.8279	0.8644
Gaussian noise (RGB)_6	32.5599 (0.0168)	0.7931 (0.0376)	0.8219	0.7701	0.8746
JPEG compression_10 (slightest)	44.5076 (1.7566)	0.9829 (0.0046)	0.9141	0.9255	0.8847
JPEG compression_30	40.8137 (1.6190)	0.9619 (0.0091)	0.8922	0.9154	0.8441
JPEG compression_50	38.7102 (1.4519)	0.9411 (0.0119)	0.8688	0.8893	0.8169
JPEG compression_70	36.7313 (1.3293)	0.9125 (0.0150)	0.8609	0.8732	0.8169
JPEG compression_90 (strongest)	32.6132 (1.1419)	0.8146 (0.0233)	0.7656	0.6845	0.9119
CLAHE[c]_1	27.5678 (1.9698)	0.932 (0.0095)	0.8875	0.9176	0.8305
CLAHE_2	21.3350 (1.4853)	0.7836 (0.0182)	0.8250	0.9256	0.6746
CLAHE_3	18.7906 (1.3643)	0.6860 (0.0220)	0.7953	0.9457	0.5898
CLAHE_4	16.6896 (1.2363)	0.5904 (0.0262)	0.7812	0.9641	0.5458
CLAHE_5	15.6361 (1.1716)	0.5395 (0.0306)	0.7703	0.9353	0.5390
Resize_400	27.4436 (2.8561)	0.6578 (0.1013)	0.7188	0.6353	0.9153
Resize_600	29.2871 (3.0279)	0.7108 (0.1042)	0.8172	0.7514	0.9017
Resize_800	30.8330 (3.07574)	0.7651 (0.1007)	0.8516	0.8106	0.8847

XSL•FO
RenderX

Treatment	PSNR[a], mean (SD)	Average SSIM[b], mean (SD)	Accuracy	Precision	Recall
Resize_1000	32.3258 (3.6219)	0.8130 (0.0932)	0.8672	0.8454	0.8712
Resize_1200	33.3882 (3.8631)	0.8432 (0.08724)	0.8797	0.8682	0.8712
Resize_1400	34.5316 (3.6730)	0.8754 (0.0748)	0.8938	0.8874	0.8814
Geometrics_1	N/A[d]	N/A	0.8635	0.8524	0.8513
Geometrics_2	N/A	N/A	0.8949	0.9003	0.8682
Geometrics_3	N/A	N/A	0.8827	0.8765	0.8678
Geometrics_4	N/A	N/A	0.9021	0.9041	0.8809
12-bit-rescale_1	48.0188 (8.0564)	0.9945 (0.0181)	0.9188	0.9119	0.9119
12-bit-rescale_2	N/A	N/A	0.9141	0.9027	0.9119
Screenshot_MicroDicom_1	N/A	N/A	0.8281	0.7666	0.9017
Screenshot_MicroDicom_2	N/A	N/A	0.8625	0.8439	0.8610
Screenshot_ImageJ	N/A	N/A	0.7812	0.7123	0.8814

[a]PSNR: peak signal-to-noise ratio.

[b]SSIM: structural similarity index measure.

[c]CLAHE: contrast-limited adaptive histogram equalization.

[d]N/A: not applicable.

The Effects of Noise and Perturbations

This section discusses model performance on datasets directly modified from the cropped scaphoid radiographs and resized datasets without geometric modifications. Table 2 presents the quality assessment and model performance results across the evaluated datasets. Specifically, datasets that underwent blurring, Gaussian noise addition, JPEG corruption, CLAHE, or resizing are reported in rows 1–35; geometric datasets in rows 36-39; bit-rescaled datasets in rows 40-41; and screenshot datasets in rows 42-44. Further details can be found in Multimedia Appendix 1.

For datasets that included cropped scaphoid radiographs and resized images, if the severity of image degradation was minimal, the effect on model accuracy was negligible. An important observation was that the model exhibited varying degrees of resilience against different image perturbations. Even in some datasets with similar PSNR and SSIM values and comparable image quality, some discrepancies in model performances were observed. These findings underscore the nuanced robustness of the deep learning model against different image distortions.

On some noisy datasets, such as Gaussian blur_0.5, Gaussian noise (RGB)_1, Gaussian noise (grayscale)_1, and JPEG compression_10, the model performances were similar to that on the clean dataset. These datasets had the least severe distortions; the pixel values changed minimally, as indicated by the high PSNR and SSIM values. However, as the perturbations increased in severity, image features deteriorated further, and model performance declined. This trend was observed across all treatments, although the extent of performance decline varied according to the type of perturbation. We conclude that if the severity of a perturbation can be maintained below a specific level in degraded images, the model can maintain good performance.

Robustness Against Different Types of Perturbations

Next, we compared model robustness across different image perturbations. Although some datasets yielded similar average PSNR and SSIM assessments, model performances differed. This finding suggested that the model is more robust against certain types of distortions but more vulnerable to others.

Color and Grayscale Gaussian Noise

We expected that the PSNR and SSIM assessments would be similar after the introduction of Gaussian noise, regardless of whether the noise was in color or grayscale. This expectation was confirmed by the similar average PSNR and SSIM values of the corresponding RGB and grayscale Gaussian noise datasets. Nevertheless, model accuracy was considerably lower when grayscale noise was present, suggesting that the model solely enhanced resilience to color perturbations. This may be explained by the fact that the training set was exclusively composed of grayscale samples, although the model input layer accepted 3-channel color images.

Gaussian Blurring

Gaussian blurring substantially degraded model performance, comparatively more than other noises with similar image quality metrics. For images with PSNR values between 35 and 50, linear regression analysis revealed that Gaussian blurring was associated with a 5% to 12% decrease in accuracy compared with other nongeometric transformation techniques. Although blurring an image does not significantly decrease image quality, blurring likely affects fracture features and thus negatively

XSL•FO
RenderX

affects detection. This finding is consistent with the results of a previous study, which concluded that neural networks are very sensitive to blurring, probably because textures and edges are removed [16-18].

JPEG Compression

The effect of JPEG compression on model performance was similar to the effect of grayscale Gaussian noise. The neural network was surprisingly resilient to JPEG compression. Even after a 90% file size reduction via JPEG compression, the model achieved an accuracy of greater than 81%. This finding has important clinical implications: DICOM images, which are often larger than 20 MB, can be compressed by up to 70% via JPEG, but the model will maintain 90% accuracy in terms of detecting scaphoid fractures. This capability will render model implementation more computationally efficient.

Resizing

The resizing perturbations were designed to simulate a realistic low-resolution workflow in which radiographs may be downsampled before region extraction and later rescaled for AI inference; therefore, this setting reflects the combined effects of downscaling information loss and upscaling or interpolation artifacts from small cropped regions of interest (ROIs), rather than a purely isolated resolution test. The downscaling treatments required the new image to store information using fewer pixels than the original, which forced the image to compress its content. As a result, a substantial amount of information was lost when the number of available storage units was reduced, leading to blurry images and lowered image quality, as demonstrated by the PSNR and SSIM values. However, fracture detection accuracy did not significantly decline until the PSNR values fell below 30. Compared with other noise treatments, resizing an image may adequately preserve the features required for fracture detection.

Contrast-Limited Adaptive Histogram Equalization

CLAHE treatment enhances image contrast and thus dramatically alters the image [19,20]. A CLAHE-enhanced image can inadvertently mislead the model, especially if the model has not been trained with CLAHE-augmented data. Model accuracy decreased as the parameter “clip limit” (maximum limit of the adaptive histogram equalization) increased, considerably lowering the PSNR and SSIM values. However, the poor metric values do not necessarily imply that CLAHE transformation worsens the model performance more severely than that of other perturbations. Even at a cliplimit of 2, the PSNR declined to 21, lower than the PSNR after any Gaussian blur or JPEG treatment, and the model accuracy decreased to 83%. As the cliplimit was subsequently increased, the accuracy precipitously fell to 77% (Table 2). This finding differs from the result of a previous study, in which neural networks were resilient against changes in image contrast [17]. This discrepancy may be because Dodge and Karam [5] investigated contrast reduction only via grayscale image superimposition and assessed correct image classification (eg, a dog and a cat) using network models. In contrast, a scaphoid DNN must detect subtle linear features when identifying fractures, and CLAHE likely obscures contrast along the fracture line. CLAHE is useful when enhancing x-ray images before human interpretation, but it should only be used in neural networks that are trained via CLAHE augmentation. Additionally, if a chosen medical imaging software exhibits built-in CLAHE-enhancing features, the neural network must be trained with CLAHE-augmented data.

Differences in the Reductions of Precision and Recall Rates

The prevalence of scaphoid fractures in the test dataset was 46%. As all noisy datasets were derived from this dataset, the prevalences were identical. Accordingly, a decline in model accuracy can be attributed to either reduced precision or recall rates, with the former creating more false positives and the latter creating more false negatives.

In the last step of training, the model was fine-tuned to achieve precision and recall rates of 91%. We expected that these performance metrics would decrease when interpreting noisy datasets. Intriguingly, the severities of performance decline differed for precision and recall. Although most noisy datasets triggered declines in both precision and recall, the performance deteriorations exhibited by the precision rates were more pronounced. However, the recall rate was usually acceptable, even in heavily altered datasets. As the model seeks to identify all possibly useful scaphoid fractures, it remains clinically robust in terms of detecting fractures despite image perturbation, but at the cost of increased false-positive rates.

Only a few datasets showed the opposite, with a precision rate much greater than the recall rate; these were the JPEG compression_50, JPEG compression_70, and all CLAHE datasets. Conversely, the remaining JPEG compression datasets demonstrated a higher recall than precision rate, similar to other changes. Therefore, JPEG compression is likely not the principal explanation for such findings.

However, we found that CLAHE image treatment must be performed with caution. CLAHE primarily reduces recall (increasing false negatives) while precision tends to increase, indicating a heightened risk of missed fractures at higher clip limits (Table 2). If the images to be interpreted are of low quality and CLAHE enhancements are applied, machine learning scientists should be wary of inadvertently increasing the false-negative rates.

Relationship Between Image Quality Assessments and Model Performance

We combined all noisy datasets (excluding the CLAHE datasets, given their heterogeneity) into a single dataset with 18,560 samples exhibiting various perturbations. We used this combined dataset to investigate the relationship between image quality and model performance.

We calculated 25 quantiles of SSIM value distributions and grouped the images according to quantile; this approach yielded 25 groups with 742 or 743 samples each. Our grouping method effectively randomized the images and eliminated the effect of any particular degradation treatment when grouping images from different datasets by image quality. We regrouped images by SSIM quantiles, rather than PSNR quantiles, because the

XSL•FO
RenderX

distributions of SSIM values within each noisy dataset were wider and enabled easier stratification.

For each group, the average PSNR, average SSIM, and model accuracy were calculated (Figure 3). We found a strong linear relationship between average image quality and model accuracy. The model performed better on images with higher quality assessments.

XSL•FO
RenderX

Figure 3. The images were divided into 25 groups according to the structural similarity index measure (SSIM) value quantiles. PSNR: peak signal-to-noise ratio.

XSL•FO
RenderX

The average PSNR, average SSIM, and group accuracy for each were plotted; the accuracy exhibited strong linear relationships with both image quality assessments.

Both PSNR and SSIM regressions yielded high adjusted R-squared values (P<.001). As the PSNR and SSIM values are not independent, it is reasonable to expect that the 2 assessments would yield similar results for most image degradations [21]. However, the SSIM was normalized, whereas the PSNR was not. Robust linear associations between image quality evaluations and model performances were evident. Specifically, PSNR and SSIM, indicators of image quality, served as reliable independent tests that predicted AI performance under various perturbations. Higher image quality evaluations were invariably correlated with superior model performances. Although certain perturbations, such as geometric offsets or pixel value rescaling, did not appear to influence model performance, resolution was identified as a key factor, particularly in screenshot images. An enhanced focus on the ROI, such as zooming, effectively averted accuracy reduction. Recent research introduced a framework for the creation of Robust Medical Imaging AI models, which focuses on developing robust AI models for chest radiographs by addressing real-world sources of image degradation such as device heterogeneity, screen-captured inputs, and compression artifacts [22].

Effects of Geometric Offsets

CNN models extract hierarchical features from local regions of an image through convolution and pooling operations. In principle, a moderate change in object location within the image should therefore not drastically confuse the model. Our results generally reflected this expectation: the 4 geometrically modified datasets retained good overall accuracy when the scaphoid remained fully within the field of view. However, accuracy declined as the strength of the affine transformations increased. A likely explanation is that parts of the scaphoid were shifted outside the image boundaries, resulting in cropped or incomplete scaphoid regions being presented to the model. Such extreme geometric distortions are unlikely to occur under real-world clinical conditions.

To further assess whether the detection model contributed to performance degradation under realistic settings, we evaluated its robustness on the 3 real-world screenshot datasets and the 12-bit-rescale_2 dataset and compared these results with those from the 4 geometric offset datasets. As summarized in Table 3, the mean intersection over union (IoU) values for the screenshot and 12-bit-rescale_2 datasets (0.8728, SD 0.0679 to 0.9836, SD 0.0268) were consistently higher than those of the geometric offset datasets (0.5752, SD 0.0952 to 0.8530, SD 0.0222). The geometric offset datasets (Geometrics_1 - 4) were intentionally designed as synthetic baselines to simulate pure localization errors of the detector. The lower IoU values in Geometrics_1 - 3 (0.5752 - 0.7546) correspond to increasingly large artificial offsets, whereas Geometrics_4 (mean 0.8530, SD 0.0222) represents the least-modified geometric condition in which the scaphoid remains fully visible after offset treatment. Notably, Table 3 presents that the detector achieved IoU values exceeding Geometrics_4 on all screenshot datasets, suggesting that the detection model remains stable under realistic screenshot-related degradation.

Table . IoU values of the datasets which the detection model was involved with and the geometric datasets.

Datasets involve detection model	IoU[a], mean (SD)
Screenshot_MicroDicom_1	0.8768 (0.0625)
Screenshot_MicroDicom_2	0.8728 (0.0679)
Screenshot_ImageJ	0.8907 (0.0554)
12-bit-rescale_2	0.9836 (0.0268)
Geometric datasets[b]	
Geometrics_1	0.5752 (0.0952)
Geometrics_2	0.7546 (0.0662)
Geometrics_3	0.7063 (0.0529)
Geometrics_4	0.8530 (0.0222)

[a]IoU: intersection over union.

[b]Considering geometric datasets IoU as baseline, the detection model performed better on all the screenshot datasets, showing its robustness toward perturbations, and that the performance of the detection model would not be a major factor leading to failure of the classification model when image degradation occurs.

As the classification model still maintained reasonable accuracy across the geometric baselines, IoU values comparable to or higher than Geometrics_4 indicate that under real-world screenshot- and rescaling-related perturbations, the detector's localization accuracy is at least similar to its best geometric baseline performance and therefore is less likely to be a dominant contributor to the observed classification performance changes. Overall, these findings suggest that detector-related bounding box offsets likely play a limited role in the performance degradation observed in these realistic conditions.

Effects of Pixel Value Rescaling Methods

The 2 methods for rescaling images from 12-bit to 8-bit did not materially affect model performance. The 2 datasets derived from the alternative rescaling method, 12-bit-rescale_1 and 12-bit-rescale_2, showed only a minor decrease in accuracy

XSL•FO
RenderX

(<1%), although the rescaled images were nearly identical. Examination of the few inconsistent cases revealed that the classification confidence scores for "fracture" and "nonfracture" were much closer in these instances, with differences typically on the order of 10^2. In contrast, in most other cases, the confidence score gap exceeded 10^3, indicating stronger and more stable model decisions. These relatively uncertain confidence scores suggest that the inconsistent cases were inherently difficult for the model to judge, even without perturbation. As the model's decisions for such cases were already unstable, slight modifications introduced by the alternative rescaling algorithms—despite causing only minimal pixel value changes—could flip the predicted label. This likely explains the minor performance differences observed among the clean dataset and the 2 rescaled datasets (12-bit-rescale_1 and 12-bit-rescale_2).

Screenshot Datasets

Taking screenshots was the most complex perturbation of all the studied treatments. Resolution may be the factor that most strongly affects model performance. The only difference between the datasets Screenshot_MicroDicom_1 and Screenshot_MicroDicom_2 was the resolution; changing the resolution from 900×1050 to 550×780 pixels resulted in an accuracy reduction from 86.3% to 82.8%. The dataset Screenshot_ImageJ, the dataset with images resized to a width of 600 pixels while keeping the aspect ratio collected using ImageJ, exhibited the worst resolution and worst read accuracy (78.1%). Such declines in accuracy, precision rate, and recall rate were similar to declines observed in the corresponding resized datasets (Screenshot_MicroDicom_1 with Resize_600, Screenshot_MicroDicom_2 with Resize_1000, and Screenshot_ImageJ with Resize_600). Although the detection model had been involved in the preparation of these datasets, Table 3 implies that in these cases, scaphoids were correctly detected and cropped. In conjunction with the fact that the classification performance of screenshot datasets was worse than that of any of the geometric datasets, the degradation in model performance indeed stems from resizing effects. We also observed that although resolution deterioration was the major factor, the screenshot process did not impact model performance identically to pure resizing. Specifically, Screenshot_ImageJ showed a modest but consistent performance drop compared with its corresponding resized dataset (Resize_600) and also performed worse than another screenshot dataset (Screenshot_MicroDicom_1) collected at a similar resolution. This suggests that viewer-specific display or resampling algorithms during screenshot capture may also influence model performance.

On the basis of these results, one strategy that may prevent accuracy reduction after taking screenshots would be to zoom into the image and then take a screenshot at the 100% level. Although the radiographic image subsequently may not fit within the screen display, it is unnecessary to capture the entire image because the only ROI is the scaphoid.

Computational Cost and Inference Time

We evaluated the average inference time by running through the 640 whole-hand x-ray images from the clean testing dataset using the complete preprocessing, bounding box detection, and classification inference pipeline. We obtained a computation time of approximately 6 to 8 ms per image on an NVIDIA RTX 3080 (10 GB RAM), while warmup runs were not included. The end-to-end pipeline used less than 200 MB GPU memory per 240×240×3 input (including framework overhead), enabling near real-time inference on a single RTX 3080. Consequently, our approach is compatible with near-real-time applications, assuming a well-optimized implementation. Although resizing or blurring images may incur a minor preprocessing overhead, these operations add only approximately 1 ms to the total inference time, indicating that real-time usage in clinical workflow is feasible on a modern GPU.

Discussion

Principal Findings

Taken together, our findings highlight that the deep learning model's performance is inversely related to the severity of image degradation, with Gaussian blur, grayscale noise, and CLAHE standing out as the most disruptive factors. These types of distortions can destroy or obscure the crucial edge information that the network relies upon for detecting subtle fracture lines. In contrast, moderate JPEG compression, resizing, or color noise had a less pronounced effect. Notably, the resizing experiments in this study reflect a realistic low-resolution workflow involving downscaling, then cropping, and then upscaling, which is consistent with real-world recaptured or low-resolution imaging scenarios described in the literature [9]. While accuracy decreases were comparable between Screenshot_ImageJ and the corresponding Resize datasets, Screenshot_ImageJ showed a modest additional reduction in recall, suggesting that screenshot recapture can affect sensitivity beyond pure resizing.

From a clinical perspective, these results underscore the importance of maintaining sufficient image fidelity and avoiding overly aggressive postprocessing steps. If CLAHE-based enhancement or heavy contrast adjustments are used, training the model with matching augmentations may be necessary to preserve performance. Similarly, our analysis indicates that modest compression does not necessarily compromise diagnostic accuracy, suggesting an avenue for reducing file sizes without compromising model output.

Although the network proved fairly robust across various perturbations, investigators should remain cautious when applying transformations, such as extreme blurring, under or overexposure, or very low-resolution screenshots. In these scenarios, crucial details may be irretrievably lost, leading to significantly higher misclassification rates. Our results also emphasize that the precision rate is especially sensitive to noise, often dropping faster than recall. This behavior means that some perturbations can inflate false positives, which may still be acceptable in screening contexts that favor high recall but could impact workflows that depend on precise diagnoses.

XSL•FO
RenderX

In certain clinical scenarios, obtaining the original radiographic file may not be immediately feasible—such as in emergency settings, remote consultations, or when imaging systems have limited data access privileges. In such situations—particularly in emergency department workflows where the original radiographic DICOM file may not be readily accessible because of time pressure, remote consultation needs, or limited system privileges—clinicians or technicians may rely on on-screen screenshots or smartphone photographs for rapid review, sharing, or AI-assisted interpretation. Although practical, these recaptured images can introduce unintended degradation due to variations in capture resolution, scaling distortions, and secondary compression, which may obscure subtle fracture cues. This real-world practice motivated our inclusion of screenshot-based perturbations as a clinically relevant proxy for urgent or resource-limited conditions. To replicate such real-world conditions, our study incorporated a "screenshot" perturbation by capturing radiographs at different image sizes and resolutions. The resulting artifacts mimic the geometric and pixel-level distortions that may arise in urgent or resource-limited workflows, providing insight into how these factors influence model performance.

Although this study was conducted using data from a single institution, the dataset represents one of the largest and most diverse radiographic collections in Taiwan, drawn from multiple campuses within the Chang Gung Memorial Hospital system, with different scanners and protocols, introducing natural variability while maintaining consistent image quality and annotation standards. The main objective of this study was to test a methodological approach for evaluating model robustness to image degradation, rather than to claim broad generalization to all clinical environments. The single-institution design, therefore, provided a stable yet sufficiently varied dataset for controlled experimentation.

Comparison With Prior Work

Our findings are consistent with prior studies showing that CNNs are sensitive to image degradation and domain shifts in medical imaging. Recent research introduced the RoMIA framework, which aims to develop robust AI models for chest radiographs by addressing real-world sources of image degradation, such as device heterogeneity, screen-captured inputs, and compression artifacts. In parallel, previous studies have shown that AI can enhance image quality and improve diagnostic reliability across multiple imaging modalities, including computed tomography and radiography [1,7,23]. Moreover, real-world deployments have demonstrated that recaptured or smartphone-captured radiographs introduce compounded degradations (eg, scaling, compression, and display artifacts) that can alter AI outputs, underscoring the clinical relevance of evaluating robustness under such workflows [9]. Taken together, these studies highlight the growing emphasis on image fidelity and consistent acquisition parameters as key factors for ensuring robust and generalizable AI performance. Previous research [18] has demonstrated that blurring and contrast alteration primarily affect the high-frequency components essential for delineating structural boundaries—similar to the degradation patterns observed in this study. The alignment between our results and those of earlier works reinforces that these degradation effects are likely intrinsic to CNN-based architectures rather than model-specific artifacts.

Limitations

This study has several limitations. First, the robustness results reported here are relative to our standard clinical preprocessing pipeline. Specifically, the "clean" baseline was generated by detector-based cropping followed by resizing each scaphoid ROI to 240×240 pixels to match the fixed input size of EfficientNetB1. As this crop-and-resize step is itself a lossy operation, our robustness conclusions should be interpreted within this trained-and-deployed pipeline context, rather than as absolute performance relative to the raw, unprocessed DICOM images. Second, our analysis was confined to a single deep learning architecture, EfficientNetB1. Different backbones (eg, ResNet and DenseNet) may exhibit varying levels of robustness to specific noise types, such as Gaussian blur or CLAHE. Nevertheless, we expect that many of the general trends—such as vulnerability to edge-destroying blur—would hold true across CNN-based architectures. Third, all experiments were performed on retrospective datasets from a single institution and focused on controlled pixel-level perturbations. As a result, the data may not fully capture the diversity of real-world clinical acquisition conditions or additional artifacts, such as motion blur, partial occlusions, and multiview variability. Future prospective, multi-institutional studies incorporating these realistic factors would provide a more comprehensive assessment of model resilience and generalizability.

Future Directions

Future work could extend our methodology by evaluating multiple architectures under identical perturbations to quantify differences in susceptibility and to determine whether certain network designs are inherently more robust. Incorporating multiview data and realistic clinical artifacts (eg, motion blur and underexposure) may also help develop more generalizable models. Additionally, advanced data augmentation strategies that simulate image degradation during training could enhance robustness. Exploring hybrid or ensemble models that integrate texture- and shape-based cues, as well as integrating domain-specific priors, could further mitigate the impact of low-quality inputs.

Conclusions

Neural network models designed to complement radiographic interpretation in clinical practice will inevitably encounter image quality distortions due to variations in acquisition, processing, and storage. In this study, we systematically evaluated the effects of image degradation on the performance of a DNN for scaphoid fracture classification. We found a strong negative correlation between image quality and model accuracy, with Gaussian blur, grayscale Gaussian noise, and CLAHE exerting the greatest influence on performance.

Performance decline was primarily driven by decreases in precision, whereas recall remained relatively stable. When developing neural networks for fracture detection in clinical radiography, training with targeted perturbations—particularly

XSL•FO
RenderX

Gaussian blur, grayscale noise, and CLAHE—may improve the model robustness and ensure more reliable performance in diverse clinical environments.

Acknowledgments

No generative artificial intelligence was used in the preparation of this manuscript.

Funding

This work was supported by a grant from the Center for Artificial Intelligence in Medicine (grant CORPG3L0181, CORPG3M0231, CORPG3K0201, and CLRPG3H0015) at Chang Gung Memorial Hospital and National Science and Technology Council (112-2410-H-182A-001).

Data Availability

The datasets generated or analyzed during this study are not publicly available due to institutional review board regulations and patient privacy considerations but are available from the corresponding author upon reasonable request.

Authors' Contributions

Conceptualization: CFK, KCC, CL
Data curation: CFK, CWW
Formal analysis: CL, TC
Methodology: CL, APY
Project administration: CFK, KCC
Resources: CFK, CWW
Software: CL, TC
Supervision: CFK, KCC
Validation: CL, TC
Writing – original draft: CL, APY, TC
Writing – review & editing: APY, KCC, CWW
Co-first authors: CL, APY (corresponding author: CFK, KCC)

Conflicts of Interest

KC receives funding from the National Institutes of Health and book royalties from Wolters Kluwer and Elsevier. All other authors declare that they have no conflicts of interest related to this work.

Multimedia Appendix 1
Representative examples of all image perturbation types evaluated in this study.
[DOCX File, 16385 KB - medinform_v14i1e65596_app1.docx]

References

1. Gupta V, Erdal B, Ramirez C, et al. Current state of community-driven radiological AI deployment in medical imaging. JMIR AI 2024 Dec 9;3:e55833. [doi: 10.2196/55833] [Medline: 39653370]
2. Hendrycks D, Dietterich T. Benchmarking neural network robustness to common corruptions and perturbations. arXiv. Preprint posted online on Mar 28, 2019. [doi: 10.48550/arXiv.1903.12261]
3. Habibi Aghdam H, Jahani Heravi E, Puig D. Analyzing the stability of convolutional neural networks against image degradation. Presented at: International Conference on Computer Vision Theory and Applications; Feb 27-29, 2016; Rome, Italy p. 370-382. [doi: 10.5220/0005720703700382]
4. Hosseini H, Xiao B, Poovendran R. Google's cloud vision API is not robust to noise. 2017 Presented at: 2017 16th IEEE International Conference on Machine Learning and Applications (ICMLA); Dec 18-21, 2017. [doi: 10.1109/ICMLA.2017.0-172]
5. Dodge S, Karam L. A study and comparison of human and deep learning recognition performance under visual distortions. 2017 Presented at: 2017 26th International Conference on Computer Communication and Networks (ICCCN); Jul 31 to Aug 3, 2017; Vancouver, BC, Canada p. 1-7. [doi: 10.1109/ICCCN.2017.8038465]
6. Fawzi A, Moosavi-Dezfooli SM, Frossard P. Robustness of classifiers: from adversarial to random noise. Presented at: NIPS'16: Proceedings of the 30th International Conference on Neural Information Processing Systems; Dec 5-10, 2016; Barcelona, Spain p. 1632-1640. [doi: 10.5555/3157096.3157279]

XSL•FO
RenderX

7. Zhang S, Zhu Z, Yu Z, et al. Effectiveness of AI for enhancing computed tomography image quality and radiation protection in radiology: systematic review and meta-analysis. J Med Internet Res 2025 Feb 27;27:e66622. [doi: 10.2196/66622] [Medline: 40053787]
8. Javed H, El-Sappagh S, Abuhmed T. Robustness in deep learning models for medical diagnostics: security and adversarial challenges towards robust AI applications. Artif Intell Rev 2025;58(1):12. [doi: 10.1007/s10462-024-11005-9]
9. Kuo PC, Tsai CC, López DM, et al. Recalibration of deep learning models for abnormality detection in smartphone-captured chest radiograph. NPJ Digit Med 2021 Feb 15;4(1):25. [doi: 10.1038/s41746-021-00393-9] [Medline: 33589700]
10. Yoon AP, Lee YL, Kane RL, Kuo CF, Lin C, Chung KC. Development and validation of a deep learning model using convolutional neural networks to identify scaphoid fractures in radiographs. JAMA Netw Open 2021 May 3;4(5):e216096. [doi: 10.1001/jamanetworkopen.2021.6096] [Medline: 33956133]
11. Hena B, Wei Z, Castanedo CI, Maldague X. Deep learning neural network performance on NDT digital x-ray radiography images: analyzing the impact of image quality parameters—an experimental study. Sensors (Basel) 2023 Apr 27;23(9):4324. [doi: 10.3390/s23094324] [Medline: 37177528]
12. Nazaré TS, da Costa GBP, Contato W. A, Ponti M. Deep convolutional neural networks and noisy images. : Springer International Publishing; 2018 Presented at: Progress in Pattern Recognition, Image Analysis, Computer Vision, and Applications; Nov 7-10, 2017; Valparaíso, Chile. [doi: 10.1007/978-3-319-75193-1_50]
13. Tan M, Le Q. Efficientnet: rethinking model scaling for convolutional neural networks. 2019 Presented at: Proceedings of the 36th International Conference on Machine Learning; Jun 9-15, 2019; Long Beach, California, USA p. 6105-6114. [doi: 10.48550/arXiv.1905.11946]
14. Wang Z, Bovik AC, Sheikh HR, Simoncelli EP. Image quality assessment: from error visibility to structural similarity. IEEE Trans Image Process 2004 Apr;13(4):600-612. [doi: 10.1109/tip.2003.819861] [Medline: 15376593]
15. Wang Z. The SSIM index for image quality assessment. Laboratory for Computational Vision, New York University. URL: http://www.cns.nyu.edu/~lcv/ssim [accessed 2025-12-23]
16. Vernon D. Machine Vision: Automated Visual Inspection and Robot Vision: Prentice-Hall; 1991. URL: https://archive.org/details/machinevisionaut0000vern [accessed 2025-12-23]
17. Dodge S, Karam L. Understanding how image quality affects deep neural networks. Presented at: 2016 Eighth International Conference on Quality of Multimedia Experience (QoMEX); Jun 6-8, 2016; Lisbon, Portugal p. 1-6. [doi: 10.1109/QoMEX.2016.7498955]
18. Gonzalez RC, Woods RE. Digital Image Processing: Addison-Wesley Publishing Company; 1992.
19. Zuiderveld K. Contrast limited adaptive histogram equalization. In: Heckbert PS, editor. Graphics Gems IV: Academic Press Professional Inc; 1994:474-485. [doi: 10.1016/B978-0-12-336156-1.50061-6]
20. Pizer SM, Amburn EP, Austin JD, et al. Adaptive histogram equalization and its variations. Comput Vis Graph Image Process 1987 Sep;39(3):355-368. [doi: 10.1016/S0734-189X(87)80186-X]
21. Horé A, Ziou D. Image quality metrics: PSNR vs. SSIM. Presented at: 2010 20th International Conference on Pattern Recognition; Aug 23-26, 2010; Istanbul, Turkey p. 2366-2369. [doi: 10.1109/ICPR.2010.579]
22. Anand A, Krithivasan S, Roy K. RoMIA: A framework for creating robust medical imaging AI models for chest radiographs. Front Radiol 2023;3:1274273. [doi: 10.3389/fradi.2023.1274273] [Medline: 38260820]
23. Thirunavukarasu AJ, Elangovan K, Gutierrez L, et al. Democratizing artificial intelligence imaging analysis with automated machine learning: tutorial. J Med Internet Res 2023 Oct 12;25:e49949. [doi: 10.2196/49949] [Medline: 37824185]

Abbreviations

AI: artificial intelligence
CLAHE: contrast-limited adaptive histogram equalization
CNN: convolutional neural network
DNN: deep neural network
IoU: intersection over union
PSNR: peak signal-to-noise ratio
RGB: red, green, and blue
ROI: region of interest
SSIM: structural similarity index measure
VOI: value of interest

XSL•FO
RenderX

Edited by A Coristine; submitted 20.Aug.2024; peer-reviewed by AN Marginean, T Panboonyuen; revised version received 07.Dec.2025; accepted 08.Dec.2025; published 22.Jan.2026.

Please cite as:
Lin C, Yoon AP, Wang CW, Chao T, Chung KC, Kuo CF
Effects of Image Degradation on Deep Neural Network Classification of Scaphoid Fracture Radiographs: Comparison Study of Different Noise Types
JMIR Med Inform 2026;14:e65596
URL: https://medinform.jmir.org/2026/1/e65596
doi:10.2196/65596

© Chihung Lin, Alfred P Yoon, Chien-Wei Wang, Tung Chao, Kevin C Chung, Chang-Fu Kuo. Originally published in JMIR Medical Informatics (https://medinform.jmir.org), 22.Jan.2026. This is an open-access article distributed under the terms of the Creative Commons Attribution License (https://creativecommons.org/licenses/by/4.0/), which permits unrestricted use, distribution, and reproduction in any medium, provided the original work, first published in JMIR Medical Informatics, is properly cited. The complete bibliographic information, a link to the original publication on https://medinform.jmir.org/, as well as this copyright and license information must be included.

XSL•FO
RenderX

Original Paper

Exploring Self-Management–Based Mobile Health User Typologies and Associations Between User Types and Satisfaction With Key Mobile Health Functions: Comparative Study of Various Fitness and Weight Management App User Types

Tong Wang[1,2], PhD; Yiwen Fan[3], MD; Zheng Li[4], MSc; Xiaoyi Jiao[5,6], MSc; Qichuan Fang[7], MSc; Junhao Ma[8], MSc; Jianbo Lei[9,10,11], MD, PhD

[1]Department of Cardiology and Institute of Vascular Medicine, Peking University Third Hospital; State Key Laboratory of Vascular Homeostasis and Remodeling, Peking University, Beijing, China

[2]University of Health and Rehabilitation Sciences Qingdao Hospital (Qingdao Municipal Hospital), School of Health and Life Sciences, University of Health and Rehabilitation Sciences, Qingdao, Shandong, China

[3]Department of Oncology, The Affiliated Hospital of Southwest Medical University, Luzhou, China

[4]Department of Rehabilitation Medicine & Physical Therapy, The Affiliated Hospital of Southwest Medical University, Luzhou, China

[5]Center for Health Policy Studies, School of Public Health, Zhejiang University, Hangzhou, China

[6]Department of AI and IT, Second Affiliated Hospital, School of Medicine, Zhejiang University, Hangzhou, Zhejiang, China

[7]School of Medical Technology and Information Engineering, Zhejiang Chinese Medical University, Hangzhou, China

[8]School of Public Health, Hangzhou Medical College, Hangzhou, China

[9]Institute of Advanced Clinical Medicine, Center for Medical Informatics, Peking University, Beijing, China

[10]Clinical Research Center, Affiliated Hospital of Southwest Medical University, Luzhou, China

[11]The First Affiliated Hospital, Hainan Medical University, Haikou, China

Corresponding Author:
Jianbo Lei, MD, PhD
Institute of Advanced Clinical Medicine
Center for Medical Informatics
Peking University
38 Xueyuan Rd, Haidian District
Beijing, 100191
China
Phone: 86 8280 5901
Email: jblei@hsc.pku.edu.cn

Abstract

Background: Exploring user satisfaction is crucial for enhancing and ensuring the sustainable development of mobile health (mHealth) apps, particularly in the fitness and weight management sectors. Analyzing user types and developing user profiles are valuable for understanding differences in satisfaction. However, prior research lacks a classification of user types based on self-management characteristics and an analysis of satisfaction disparities among these types.

Objective: This study analyzes user heterogeneity from a self-management perspective among fitness and weight management app users by identifying user types and constructing profiles. It further explores differences in satisfaction with the functional design of these mHealth apps across user types.

Methods: First, 8 feature indicators were selected based on the Health Belief Model and the Behavior Change Wheel to evaluate users' levels of health knowledge and beliefs, as well as self-regulation related to self-management. Existing research was integrated to categorize mHealth app functional design into 5 categories: health guidance, health education, health monitoring, social features, and gamification. Second, a questionnaire survey was used to collect data on users' 8 health management characteristics and their satisfaction with the 5 functional design categories. A total of 2518 responses were collected, of which 1025 were included in the analysis. Cluster analysis was conducted to classify users into distinct types based on the 8 health management characteristics, and user profiles were constructed according to the distribution of these characteristics within each

XSL•FO
RenderX

type. Finally, the Kruskal-Wallis test was used to analyze differences in satisfaction across user types with respect to the 5 functional design categories of mHealth apps.

Results: Cluster analysis revealed that users could be categorized into 6 types based on the 8 self-management characteristics: positively proactive energizers, proactive intenders, negatively proactive energizers, low health management demanders, potential health management demanders, and passive attitude holders. Significant differences were observed across all 8 health management characteristics among the 6 user types (all P<.001). The Kruskal-Wallis test indicated significant variations in user satisfaction with the 5 functional designs of mHealth apps: H(4)=445.388, (P<.001). Overall, users reported the highest satisfaction with health guidance and health monitoring (median 4.00, IQR 1.00) and the lowest satisfaction with gamification (median 3.00, IQR 1.00). Positively proactive energizers, proactive intenders, and negatively proactive energizers demonstrated the highest satisfaction with health education and health guidance (median 4.00). Potential health management demanders, proactive intenders, positively proactive energizers, and negatively proactive energizers reported the highest satisfaction with health monitoring (median 4.00). Proactive intenders reported the highest satisfaction with social features and gamification (median 4.00).

Conclusions: Users of mHealth apps exhibit diverse types, with significant differences in health management characteristics and satisfaction with the 5 functional designs of fitness and weight management apps. This study clarifies individual-level differences in user satisfaction with mHealth apps.

(JMIR Med Inform 2026;14:e64860) doi:10.2196/64860

KEYWORDS

mHealth app; user satisfaction; self-management characteristics; user profile; unsupervised learning

Introduction

The poor continued use of mobile health (mHealth) apps poses a significant threat to the sustainability of the mHealth industry, while also weakening the benefits of health management for users. Approximately 40% of smartphone users utilize mHealth apps [1]. Research indicates that health management based on mHealth apps often requires continued use for over 3 weeks to demonstrate effective outcomes [2]. However, a real-world observational study revealed that only 2.58% of the 189,770 users who downloaded mHealth apps actively used them for at least one week [3], indicating that continued use of mHealth faces serious challenges. Furthermore, app uninstallations result in average monthly losses of US $57,000 for app companies [4], highlighting the negative impact of poor continued use on the industry. Therefore, it is necessary to research the usability of mHealth. Previous studies have shown that user satisfaction is a key determinant of acceptance and continued use [5].

User satisfaction is an important indicator for measuring the quality of mHealth services and has a significant impact on the continued usage and intention to use mHealth [6]. Exploring the factors related to user satisfaction has important reference value for promoting the use of mHealth. A review of existing research on mHealth satisfaction shows that studies mainly follow 3 perspectives: technology acceptance, functional design, and user characteristics. Research from the perspective of technology acceptance is primarily based on the technology acceptance model and its derivative theories, focusing on how users' perceived characteristics of mHealth technology influence satisfaction [7-11]. Studies on the influencing factors of satisfaction have gradually expanded from a practical dimension to multidimensional value [12], including perceived entertainment and other nonpractical characteristics [13]. Research from the perspective of functional design mainly focuses on how specific functional characteristics of mHealth meet user needs and improve satisfaction, such as data analysis, monitoring, and information sharing [14,15]. This line of research shows a trend of transition from overall evaluation to modular analysis, with the research focus shifting from overall satisfaction with mHealth to the exploration of multidimensional satisfaction [16-18].

Current research has conducted relatively in-depth explorations of mHealth satisfaction from the perspectives of technology acceptance and functional design; however, evidence regarding the relationship between heterogeneity in user characteristics and satisfaction remains limited [19]. A survey on the use of digital health tools among the US population revealed that there is no "one-size-fits-all" model in digital health, as consumers are not a homogeneous group [20]. However, digital health users cannot be classified solely based on sociodemographic characteristics, as each generation interacts with technology differently due to its unique experiences, needs, and levels of trust in the health care system [21]. Previous studies have confirmed that eHealth literacy [22], strong self-reporting capabilities [19], health needs [23], and poor health status [24] significantly influence mHealth satisfaction. Intrinsic characteristics, such as health knowledge, beliefs, and self-regulation skills and abilities, are central to self-management [25]. These findings suggest that self-management attributes provide important explanations for user heterogeneity and differences in satisfaction among users. Compared with traditional health care models, mHealth relies more heavily on self-management service models [26]. Systematic exploration of individual self-management–related characteristics can help construct user classifications that more deeply capture internal features, thereby promoting personalized and refined mHealth design [27]. However, there is a lack of research systematically integrating self-management characteristics and analyzing user-group heterogeneity based on combinations of these characteristics. In addition, empirical evidence on the differential distribution of satisfaction across different user types with respect to mHealth function design remains scarce, posing challenges for developers seeking to deliver mHealth services that meet the needs of diverse users.

XSL•FO
RenderX

To address the above limitations, this study, guided by self-management theory, analyzes relevant self-management characteristics based on the Health Belief Model (HBM) and Behavior Change Wheel (BCW) among users of fitness and weight management apps. A refined classification of these mHealth users is conducted based on characteristic attributes, and differences in satisfaction with mHealth functional design across user types are examined. Through this investigation, the study seeks to address the following research questions:

- Research question 1: User typology: How can users of fitness and weight management apps be systematically categorized using quantitative methods based on self-management characteristics? What are the defining attributes of each user type?
- Research question 2: Satisfaction differences. Do user groups with distinct self-management characteristics demonstrate statistically significant differences in satisfaction with various mHealth functional designs? What are the specific manifestations of these differences, and which factors are relevant?

Methods

Design

Guided by self-management theory, this study utilizes the HBM and BCW to select variables representing the self-management characteristics of mHealth users. Data were collected through a questionnaire survey, and unsupervised clustering analysis was used to identify user clusters. Subsequently, the characteristic distributions of different user clusters were analyzed to construct user profiles. Through intergroup difference analysis, this study compared satisfaction levels across user types with respect to various mHealth functional designs and examined the correlations between user characteristics and satisfaction with functional designs. The overall workflow of the study is illustrated in Figure 1.

Figure 1. Study flowchart. mHealth: mobile health.

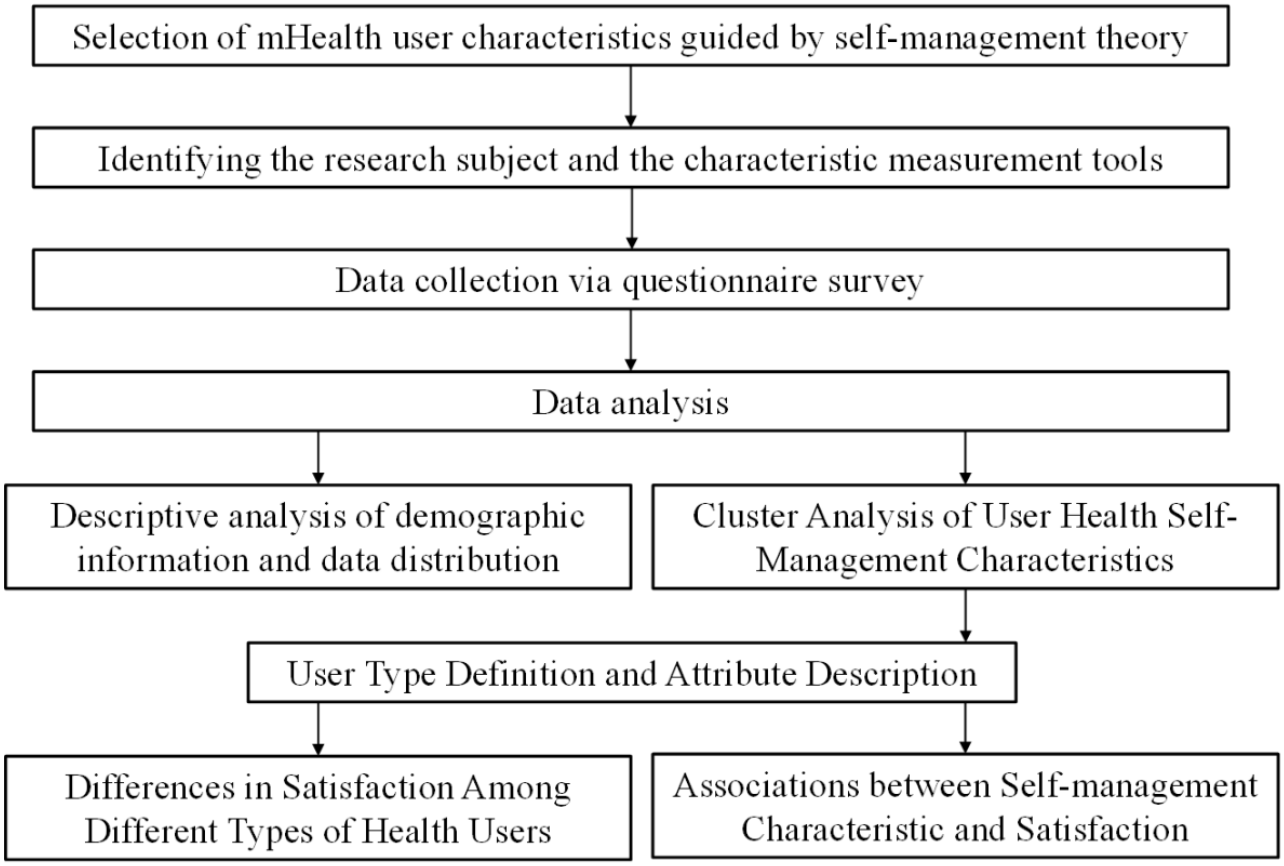

Selection of Self-Management–Related Characteristics

mHealth mainly improves health outcomes by empowering self-management abilities [28]. Therefore, this study selects variables representing user characteristics guided by self-management theory. In individual and family self-management theory [29], self-management refers to the process by which individuals and families use knowledge and beliefs, self-regulation skills and abilities, and social facilitation strategies to achieve health-related outcomes in their real-life environments. Among these components, knowledge and beliefs refer to information and perceptions related to a health condition or health behavior. The HBM is one of the most widely used models for explaining beliefs and perceptions underlying health behaviors [30]. HBM posits that individuals' perceptions of their susceptibility to a health issue and the potential severity of its consequences, together with perceived benefits of adhering to health recommendations and their intention and ability to engage in health management, are the most direct drivers of health behaviors [31]. HBM operationalizes these factors through perceived susceptibility, perceived severity, perceived benefits, perceived barriers, and self-efficacy [32]. Accordingly,

XSL•FO
RenderX

this study adopts these 5 variables from HBM to characterize the knowledge and beliefs component of self-management theory.

Self-regulation within self-management theory is an iterative process in which individuals utilize a variety of skills and abilities to achieve healthy behavior change [29]. The BCW, a classic theoretical model for explaining behavior change—particularly in the contexts of health promotion and disease prevention [33]—provides an important reference for selecting self-regulation–related characteristic variables in this study. The BCW posits that healthy behavior change can be achieved only when individuals possess capability, motivation, and opportunity [34]. Capability refers to the knowledge and skills required to engage in a particular behavior [35]. In the context of using mHealth for health management, essential knowledge and skills are reflected in 2 aspects: health management and the use of digital technology. eHealth literacy is among the most commonly used indicators for assessing an individual's ability to acquire health management information and utilize electronic health information to address health issues [36,37]. Accordingly, this study selects eHealth literacy to characterize self-regulation skills and abilities. In addition, motivation in the BCW refers to the beliefs that trigger behavioral change, encompassing reflective motivation and intrinsic motivation [34]. Motivation for health management can be divided into proactive health management intention and passive health management intention triggered by perceived health status, corresponding to reflective motivation and intrinsic motivation, respectively. Therefore, this study selects health management intention [38] and perceived health status [39] to further characterize the motivational dimension of self-management behavior. In summary, this study selects a total of 8 variables to analyze self-management characteristics among mHealth users. The definitions of each variable are presented in Table 1.

Table 1. mHealth[a] user self-management characteristics: a framework of 8 variables for user categorization.

User self-management characteristics	Definition
Perceived susceptibility	Beliefs about the likelihood of getting a disease or condition [31].
Perceived severity	Feelings about the seriousness of contracting an illness or of leaving it untreated, including evaluations of both medical and clinical consequences and possible social consequences [31].
Perceived benefits	Beliefs that engaging in health behaviors can help decrease the risk of diseases and health problems [40].
Perceived barriers	An individual's assessment of the difficulties and cost of adopting behaviors [32].
Health self-efficacy	The confidence individuals have in their ability to use their skills to complete health management tasks [41].
eHealth literacy	The ability to seek, find, evaluate, and use electronic health information from electronic resources to address health issues [36].
Perceived health status	The perception of one's own health status [39].
Health management intention	The degree of intention to engage in health protection [38].

[a]mHealth: mobile health.

Identification of Study Targets

The main purpose of this study is to delineate individuals' health management characteristics and classify users based on their levels of health management characteristics, and to further analyze differences in satisfaction with various mHealth app functional designs across user categories. Therefore, it is necessary to clarify the main functional designs of mHealth apps. Previous studies have summarized common mHealth app functional designs through systematic reviews and content analyses [42-44], categorizing functions according to their primary implementation purposes, such as education, tracking, social interaction, gamification, and motivational features [42]. Building on prior research, this study reorganizes the functional characteristics reported in the literature to propose a classification of mHealth app functional designs for analysis (see Table 2).

XSL•FO
RenderX

Table 2. Five functional designs and features of the mHealth[a] apps analyzed in this study

Functional designs	Definition	Features
Health guidance	Providing advice based on health plans and applications may provide real-time feedback and advice based on health plans and status [45], or offer strategies for behavior change that can contribute to improving health conditions [46].	Intelligent virtual assistants and communication with health care personnel [43]; interaction with medical staff [45]; and development of health plans and goal setting [46].
Health education	Offering necessary knowledge to achieve health behavior change [47].	Personalized education and general knowledge education [42]; image-based education, video education, and audio education [47].
Health monitoring	Recording past and current health statuses [47].	Health records and health diaries [43]; trackers, data entry, and data export [42]; and self-tracking [46].
Social function	Providing a platform for user interaction, communication, and maintaining connections [47].	Community forums and social media [42]; and social sharing [47].
Gamification	Integrating gaming mechanisms or elements into mHealth apps and enhancing the user experience with gamelike features [48].	Personalized avatars, challenges, tasks, health, and rewards [43]; points, badges, and levels [42].

[a]mHealth: mobile health.

To achieve the aforementioned research objectives, this study selected appropriate objects of study for empirical analysis. First, the comparability of different mHealth app functional designs was considered. To minimize the influence of differences in core service content across app types on comparability, this study selected a homogeneous category of apps as the empirical focus, thereby reducing potential confounding effects. Second, the application domains of different mHealth app categories were considered. Exercise, fitness, and weight management align with substantial health needs. These domains represent important modalities for primary prevention, and exercise therapy also serves as a key approach for tertiary prevention (disease management) in various conditions, such as cardiac rehabilitation, pulmonary rehabilitation, tumor rehabilitation, and metabolic disease management [49]. Given that exercise, fitness, and weight management apps account for more than half of all mHealth apps [50], and that these functions represent 48.37% of users' motivations for using mHealth apps [51], we selected exercise, fitness, and weight management apps as the units of analysis to represent a broader and more heterogeneous user population.

This study did not restrict respondents to users of a specific app for the following reasons. First, as the aim of this study is to examine the satisfaction of different user types with various mHealth functional designs in real-world contexts and to provide generalizable recommendations, the focus is on mHealth functional modules rather than on specific app design implementations. Accordingly, the research sample was not limited to users of a single app. Moreover, this questionnaire-based data collection approach captures multiple implementations of the same functional module (eg, health education), thereby enhancing sample diversity and improving the generalizability of the findings [52,53]. Second, this study was conducted in real-world settings, which differ from laboratory-based studies that examine factors influencing mHealth satisfaction. In laboratory environments, variables must be tightly controlled to quantify the idealized effects of specific factors, often requiring the use of a single app as the research object. By contrast, this study emphasizes user satisfaction with mHealth in real-world contexts, where the use of multiple similar apps by the same user is common. Analyzing such data provides real-world evidence that can inform future research and practical mHealth design.

Measurement Instrument

Based on the constructed User Health Management Characteristics Framework, this study measures 8 independent variables and 5 dependent variables reflecting satisfaction with mHealth functionalities. To achieve the aforementioned research objectives, it was necessary to select appropriate and measurable items corresponding to the characteristics defined within the framework. To ensure the rational design of the measurement scale, this study undertook a careful process of adapting previously validated scales, making nuanced adjustments to align them with the specific research objectives.

Specifically, the User Health Management Characteristics Framework includes 4 variables derived from the HBM (perceived severity, perceived susceptibility, perceived barriers, and perceived benefits), with measurement items adapted from HBM-related studies by Ahadzadeh et al [54], Saghafi-Asl et al [32], and McArthur et al [55]. Two variables were derived from the BCW (eHealth literacy and perceived health status), with measurement items drawn from BCW-related studies [39,56,57] and the Brief Health Literacy Screen scale [58]. In addition, 2 variables integrating both models (health self-efficacy and health management intention) were included, with measurement items adapted from health management–related studies, such as Zhou et al [59] and Li et al [38]. For the measurement of satisfaction with the 5 mHealth functional designs, this study first provided definitions and specific design examples of each function in the questionnaire, followed by item-based measurement. The satisfaction items were adapted from relevant studies on mHealth satisfaction [8]. All measurement items used a 5-point Likert scale, ranging from 1 (strongly disagree) to 5 (strongly agree).

A multistage validation and refinement process was implemented to ensure the conceptual accuracy and cultural

XSL•FO
RenderX

appropriateness of the English-originated scales within the Chinese context. First, the preliminary translation and adaptation of the scale items were collaboratively conducted by research team members proficient in both Chinese and English and with expertise in health informatics. Through group discussions, each item was refined to preserve the core meaning of the original construct while aligning with Chinese linguistic norms and the research context. Second, before the formal survey, 24 participants with backgrounds in medical informatics were invited to complete a pretest of the questionnaire. Participants were asked not only to respond to the questionnaire but also to provide feedback on the clarity and contextual appropriateness of the items. Based on this feedback, the wording of the questionnaire was further refined to eliminate ambiguities and improve readability, resulting in the final version used in the formal survey. Finally, during the data analysis phase, reliability and validity tests were conducted on the measurement model, thereby verifying the effectiveness and reliability of the measurement instrument from a data-driven perspective (see Multimedia Appendix 1).

Data Collection

The survey targeted individuals who had used exercise, fitness, or weight loss apps within the preceding 3 months. According to the N:q hypothesis [60], the ratio of sample size to item parameters in a scale should range from 20:1 to 10:1. In this study, a total of 51 items were included for measurement; therefore, applying the more conservative ratio of 20:1, the required sample size was approximately 1020.

From June 28, 2022, to September 8, 2022, a snowball sampling survey was conducted via the WeChat platform (Tencent Holdings Limited). The questionnaire link, generated using Wenjuanxing, was distributed through Moments (Tencent Holdings Limited) and various group chats. In total, 2518 questionnaires were collected. Of these, 902 respondents reported that they had not used the target apps within the preceding 3 months. A quality control item was included in the questionnaire: “This question is an attention test to ensure careful completion of the questionnaire. For this question, please select ‘strongly disagree’.” The correct response to this item was “1. strongly disagree.” Responses that answered this item incorrectly were considered to have failed the quality control check. In addition, given the length of the questionnaire, responses completed in less than 3 minutes or with identical answers across all scale items were deemed insufficiently attentive and were also excluded. Through this screening process, 591 responses were removed. Consequently, 1025 valid questionnaires remained for subsequent analysis. Before completing the questionnaire, all participants were informed of the study’s overall purpose and detailed procedures.

In this study, item-level missing data were addressed using mode imputation based on each respondent’s answers to other items within the same variable. Specifically, there were 3 missing values in total: 1 in perceived susceptibility, 1 in eHealth literacy, and 1 in gamification. As the questionnaire employed Likert scales, which represent ordinal rather than strictly continuous data, each missing value was replaced with the mode of the remaining items within the same scale for that respondent. The imputed values were 3, 5, and 3, respectively. Given that the dataset comprised a total of 45,100 item responses, the proportion of missing values was 0.0067%, which is negligible and unlikely to affect the results.

Data Analysis

To address the question “What are the common combinations of health management characteristics in users during the process of using mHealth?” we employed cluster analysis. Cluster analysis is an unsupervised machine learning technique that divides a set of observations into multiple clusters composed of similar objects and can identify the structural composition of different clusters. In clustering, similarity between observations within the same cluster is high, whereas similarity between observations from different clusters is low. Among various clustering methods, the k-means algorithm produces results that are easy to interpret, are suitable for clustering high-dimensional data, and demonstrate good scalability and efficiency when dealing with large datasets [61]. The clustering in this study was based on 8 health management characteristics (Table 1), and the sample size was moderate; therefore, k-means was appropriate for this study. The k-means algorithm requires the number of clusters to be predetermined. We determined the optimal number of clusters by integrating the Elbow Method and the Silhouette Coefficient. The Elbow Method identifies the inflection point by analyzing the relationship between the within-cluster sum of squared errors (SSE) and the number of clusters, while the Silhouette Coefficient is used to mathematically assess the compactness and separation of the clustering structure. The results showed that when the number of clusters was 6, an inflection point appeared in the SSE curve, and the Silhouette Coefficient reached a locally optimal value of 0.1514 (see Multimedia Appendix 2), indicating that this clustering solution maintains good within-cluster compactness while achieving favorable between-cluster separation. Therefore, we ultimately set the number of clusters to 6. To further verify the stability of this 6-cluster solution, we performed 10 repeated experiments with random initializations. The results showed a relative fluctuation rate of only 0.002% in the SSE values, demonstrating that the 6-cluster solution exhibits high repeatability and stability. We conducted the cluster analysis to determine the grouping of mHealth app users using sklearn.cluster in Python 3.8 (Python Foundation; see Multimedia Appendix 3).

To answer the question “Is there a difference in satisfaction with the functional design of mHealth apps among different types of users?” we performed rank sum tests to examine satisfaction and preferences regarding functionalities across user groups using SPSS 26 (IBM Corp). To address the question “How do health management characteristics affect users’ satisfaction and preferences for the functional design of mHealth apps?” we conducted a partial least squares analysis using SmartPLS 4 (SmartPLS GmbH). The significance level was set at $P<.05$ for 2-tailed tests.

The data collected for this study were analyzed to assess potential nonresponse bias. To accomplish this and examine nonresponse bias [11], the Mann-Whitney *U* test was used to compare responses from the first 20% (205/1025) and the last

XSL•FO
RenderX

20% (205/1025) of the sample. The results showed no significant differences between the 2 groups for the health guidance (z=−0.728, P=.47), health education (z=−1.171, P=.24), health monitoring (z=−0.857, P=.39), social function (z=−1.794, P=.07), and gamification (z=−0.260, P=.80) constructs. Therefore, nonresponse bias was not a concern in this study. This study followed the STROBE (Strengthening the Reporting of Observational Studies in Epidemiology) reporting standard (see Multimedia Appendix 4).

Ethical Considerations

This study utilized an online questionnaire survey. On the first page of the questionnaire, the research purpose, content, potential risks, data usage, confidentiality terms, and researcher contact information were clearly explained to participants. By checking a box, participants confirmed that they had read and understood the above information and voluntarily agreed to participate in the study, thereby providing informed consent. Participants who did not agree with the above content were directed to exit the online questionnaire. The questionnaire materials for this study were destroyed after the completion of quality control and transcription, within 6 months after the survey concluded. Any associated information, such as source IP addresses, collection time stamps, and serial numbers, was also destroyed to ensure privacy protection. Following transcription, the data were renumbered sequentially, starting from 1. All images and data presented in the manuscript or multimedia appendices are fully anonymized and cannot be used to identify any individual participant or user. No financial compensation was provided to participants. Approval was obtained from the Biomedical Ethics Committee of the Second Affiliated Hospital, School of Medicine, Zhejiang University, China (approval number IRB-2021-841).

Results

Demographic Information

The demographic characteristics of the included sample are presented in Table 3. The sample exhibited a balanced gender distribution (female: 553/1025, 53.95%; male: 472/1025, 46.05%), with participants predominantly aged 19-30 years (500/1025, 48.78%). In terms of education, most respondents held college degrees (519/1025, 50.63%), followed by master's degrees (269/1025, 26.24%). Income distribution showed that nearly one-quarter of participants (244/1025, 23.80%) earned ≤2500 RMB (1 RMB=US $0.14) monthly, whereas a smaller proportion (49/1025, 4.78%) reported incomes of 50,001 or higher. Regarding usage patterns, the largest group reported using the service 2-3 times per week (370/1025, 36.10%), while a minority were frequent users (>7 times per week: 59/1025, 5.76%). In terms of occupation, students constituted the largest subgroup (283/1025, 27.61%), followed by public servants/clerks (208/1025, 20.29%) and professional technical personnel (196/1025, 19.12%). Overall, 664 of 1025 (64.78%) users reported using 1 app.

XSL•FO
RenderX

Table 3. Descriptive statistics of demographic information for the analyzed sample (n=1025).

Characteristics	Values, n (%)
Gender	
Male	472 (46.05)
Female	553 (53.95)
Age (years)	
≤18	6 (0.59)
19-30	500 (48.78)
31-45	337 (32.88)
46-60	174 (16.98)
≥61	8 (0.78)
Education	
High school	37 (3.61)
Junior college education	111 (10.83)
College	519 (50.63)
Master's degree	269 (26.24)
Doctor's degree	89 (8.68)
Income (RMB[a])	
≤2500	244 (23.80)
2501-5000	159 (15.51)
5001-8000	178 (17.37)
8001-15,000	213 (20.78)
15,001-30,000	125 (12.20)
30,001-50,000	57 (5.56)
≥50,001	49 (4.78)
Frequency	
≤1 time per week	265 (25.85)
2-3 times per week	370 (36.10)
4-5 times per week	213 (20.78)
6-7 times per week	118 (11.51)
>7 times per week	59 (5.76)
Occupation	
Students	283 (27.61)
Medicine-related personnel	168 (16.39)
Public servants and clerks	208 (20.29)
Commercial and service personnel	107 (10.44)
Professional technical personnel	196 (19.12)
Manual workers	33 (3.22)
Unemployed and other personnel	30 (2.93)

[a]1 RMB=US $0.14.

Data Characteristics

A descriptive analysis of the 8 self-management characteristics and satisfaction with the 5 functional designs was conducted. First, we calculated the average score of multiple items measuring each characteristic variable to represent the level of that variable. However, because the distributions of the average

XSL•FO
RenderX

values for each variable were not normally distributed, medians and IQRs were used for presentation, as shown in Table 4.

Table 4. Descriptive statistics (median and IQR) of the 8 health management characteristics and satisfaction with the 5 functional designs for the analyzed sample (n=1025).

Characteristics	Median	First quartile (Q1)	Third quartile (Q3)	IQR
Health-specific determinants				
Perceived severity	4.25	3.75	5.00	1.25
Perceived susceptibility	3.50	3.00	4.00	1.00
Perceived barrier	2.50	2.00	3.50	1.50
Perceived benefit	4.75	4.00	5.00	1.00
Health self-efficacy	4.00	3.33	4.33	1.00
Perceived health status	3.67	3.00	4.00	1.00
eHealth literacy	4.00	3.50	4.50	1.00
Health management intention	4.00	3.33	4.33	1.00
Satisfaction				
Satisfaction with health guidance	4.00	3.00	4.00	1.00
Satisfaction with health education	3.67	3.00	4.00	1.00
Satisfaction with health monitoring	4.00	3.33	4.33	1.00
Satisfaction with social function	3.33	3.00	4.00	1.00
Satisfaction with gamification	3.00	3.00	4.00	1.00

Cluster Analysis of User Self-Management Characteristics and Determination of User Types

The determination of the optimal number of clusters in this study, which was set at 6, was based on the relationship between the within-cluster SSE and the number of clusters. Subsequently, cluster analysis was performed on the sample using *z* score–standardized values of the 8 health management indicators. The distribution across the 6 clusters was relatively uniform (140, 135, 189, 218, 180, and 163). Figure 2 shows the distribution of each indicator across the 6 clusters obtained from the analysis. A *z* score close to 0 indicates that the corresponding indicator in a given cluster approximates the overall average level, whereas a positive *z* score indicates that the indicator is above the average level in that cluster.

We further analyzed differences in each indicator across the 6 clusters using the Kruskal-Wallis test to assess the distinctiveness of each cluster. The results of the Kruskal-Wallis test demonstrated statistically significant differences in the *z* scores of all indicators across the 6 clusters (P<.001 for all). Specifically, significant differences were observed for the following: perceived severity, $H(5)=400.947$ (P<.001); perceived susceptibility, $H(5)=522.425$, (P<.001); perceived barrier, $H(5)=673.985$, (P<.001); perceived benefit, $H(5)=492.630$, (P<.001;) health self-efficacy, $H(5)=518.298$, (P<.001); perceived health status, $H(5)=490.411$, (P<.001); eHealth literacy, $H(5)=362.910$, (P<.001); and health management intention, $H(5)=390.573$, (P<.001). These findings indicate that the 6 clusters exhibit distinct patterns and magnitudes of health management characteristics, as reflected by the significant differences in the *z* scores of the respective indicators. The detailed *z* scores and pairwise comparison results for each indicator across the 6 clusters are presented in Table 5, allowing for a detailed examination of how each cluster differs from the others in terms of specific health management characteristics. Detailed test statistics are provided in Multimedia Appendix 5, which presents pairwise comparisons of health management characteristics among user groups.

The distribution of the 8 health management traits varied across individual users. To further understand user health management characteristics and provide references for personalized services in mHealth apps, this study categorized users based on combinations of their 8 current health management factors. Given the distinctiveness of each user group, the 6 types were named according to the indicator profiles within each cluster to reflect the main health management characteristics of users in each type. Cluster 1 was labeled “positively proactive energizers.” Users in this cluster exhibited higher perceived health status, health management self-efficacy, and health management intention than proactive intenders, along with substantially lower perceived barriers and perceived susceptibility.

Cluster 2 was labeled “proactive intenders,” characterized by users whose perceived health status, eHealth literacy, and health management intention are all above average, but who also report higher perceived barriers and perceived susceptibility. Proactive intenders (135/1025, 13.17%), the smallest group, represent users who demonstrate strong proactivity in health management, recognize their potential risk for health problems, and actively manage their health despite the presence of perceived barriers.

Cluster 3 was labeled “negatively proactive energizers.” Compared with positively proactive energizers, users in this cluster have slightly below-average perceived health status and

XSL•FO
RenderX

higher perceived susceptibility, yet they exhibit higher health management intention, health management self-efficacy, and eHealth literacy. Both positively proactive energizers (140/1025, 13.66%) and negatively proactive energizers (189/1025, 18.44%) represent groups with high levels of health management cognition, literacy, and capability, along with strong health management intention, making them the primary beneficiaries of current mHealth apps. The key difference between these 2 groups lies in perceived health status, which is higher among positively proactive energizers and below average among negatively proactive energizers. Cluster 4 was labeled "low health management demanders." Users in this cluster tend to have average perceived health status, with perceived susceptibility, perceived severity, and health management intention all below the average level. Low health management demanders constitute the largest proportion of users (218/1025, 21.27%) and represent a group with relatively good current health, limited emphasis on health management, insufficient awareness of health risks and potential harm, and consequently lower intention to engage in health management.

Cluster 5 was labeled "potential health management demanders." Users in this cluster have below-average perceived health status and, although their perceived benefits, perceived susceptibility, and perceived severity are above average, they exhibit lower health management intention and higher perceived barriers. Potential health management demanders (180/1025, 17.56%) represent individuals with poor current health status who are aware of the harms associated with health risks and recognize the benefits of health management for improving their condition, yet face substantial barriers to engaging in health management and therefore have a lower intention to do so. This group has both a clear recognition of the importance of health management and an objective need for it due to their poor health status.

Cluster 6 was labeled "passive attitude holders," comprising users whose perceived health status is below average and who report very low perceived benefits, health management self-efficacy, perceived severity, and health management intention. Passive attitude holders (163/1025, 15.90%) share similarities with low health management demanders, including low perceived benefits, health management self-efficacy, perceived severity, and intention for health management. However, they differ in that passive attitude holders perceive their health status as below average and face higher perceived barriers. This group perceives a decline in health status but lacks the willingness to improve it, placing them at high risk for illness.

From the perspective of age distribution, the 6 user categories exhibited distinct age-structure characteristics. Positively proactive energizers (n=140) comprised 48 (34.3%) aged 19-30 years, 48 (34.3%) aged 31-45 years, 42 (30.0%) aged 46-60 years, and 2 (1.4%) aged ≥61. Proactive intenders (n=135) consisted of 71 (52.6%) aged 19-30 years, 50 (37.0%) aged 31-45 years, 12 (8.9%) aged 46-60 years, and 2 (1.5%) aged ≥61. Negatively proactive energizers (n=189) included 2 (1.1%) aged ≤18, 65 (34.4%) aged 19-30 years, 79 (41.8%) aged 31-45 years, 41 (21.7%) aged 46-60 years, and 2 (1.1%) aged ≥61. Low health management demanders (n=218) comprised 1 (0.5%) aged ≤18, 103 (47.2%) aged 19-30 years, 69 (31.7%) aged 31-45 years, 44 (20.2%) aged 46-60 years, and 1 (0.5%) aged ≥61. Potential health management demanders (n=180) included 2 (1.1%) aged ≤18, 97 (53.9%) aged 19-30 years, 54 (30.0%) aged 31-45 years, 26 (14.4%) aged 46-60 years, and 1 (0.6%) aged ≥61. Passive attitude holders (n=163) were distributed as 1 (0.6%) aged ≤18, 116 (71.2%) aged 19-30 years, 37 (22.7%) aged 31-45 years, and 9 (5.5%) aged 46-60 years. Chi-square tests indicated that the associations between user clusters and both age (Cramer *V*=0.145) and education (Cramer *V*=0.116) groups were weak.

Figure 2. Cluster analysis–derived profiles of 6 user groups across 8 health management characteristics (*z* scores).

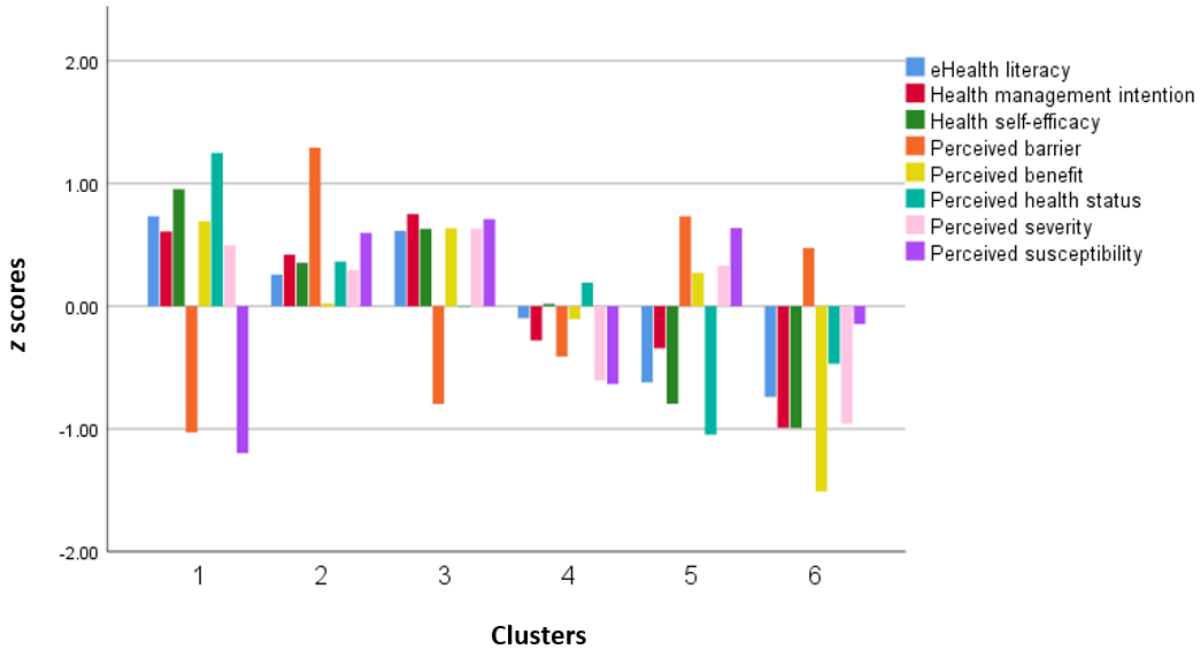

XSL•FO
RenderX

Table 5. Mean z scores and Kruskal-Wallis group comparisons of the 8 health management characteristics across the 6 user clusters.

Clustering variables	Cluster 1: positively proactive energizers (n=140)	Cluster 2: proactive intenders (n=135)	Cluster 3: negatively proactive energizers (n=189)	Cluster 4: low health management demanders (n=218)	Cluster 5: potential health management demanders (n=180)	Cluster 6: passive attitude holders (n=163)
Perceived severity	0.496[a,b,c]	0.294[b,e]	0.632[c]	–0.607[d]	0.331[a,e]	–0.956[f]
Perceived susceptibility	–1.197[a]	0.598[b,c,e]	0.709[c,e]	–0.634[d]	0.638[e]	–0.146[f]
Perceived barrier	–1.029[a,c]	1.292[b]	–0.796[c]	–0.410[d]	0.733[e,f]	0.476[f]
Perceived benefit	0.693[a,c]	0.022[b,d]	0.636[c]	–0.106[d]	0.273[e]	–1.510[f]
Health self-efficacy	0.955[a]	0.354[b,c]	0.630[c]	0.020[d]	–0.795[e,f]	–0.993[f]
Perceived health status	1.249[a]	0.363[b,d]	–0.004[c,d]	0.192[d]	–1.047[e]	–0.469[f]
eHealth literacy	0.733[a,c]	0.258[b]	0.615[c]	–0.097[d]	–0.621[e,f]	–0.740[f]
Health management intention	0.608[a,b,c]	0.419[b]	0.751[c]	–0.278[d,e]	–0.342[e]	–0.990[f]

[a-f]In the same row of data, if the same characteristic across the 6 clusters shares the same superscript (eg, "b"), it indicates that the difference between them is not statistically significant. Conversely, if the same characteristic across the 6 clusters does not share the same superscript, it suggests that the difference between them is statistically significant. For instance, cluster 1's perceived barrier is denoted as –1.029[a,c], and cluster 3's perceived barrier is denoted as –0.796[c]; the presence of the superscript "c" in both indicates that the Kruskal-Wallis test for the *z* scores of perceived barrier between cluster 1 and cluster 3 is not statistically significant. Conversely, cluster 2's perceived barrier is denoted as 1.292[b]. The absence of a common superscript implies that the Kruskal-Wallis test for the *z* scores of perceived barrier between cluster 1 and cluster 2 is statistically significant.

Differences in Satisfaction With mHealth App Functional Design Among Different Types of Health Users

First, the Kruskal-Wallis test was used to analyze differences in satisfaction with the 5 functional designs of the mHealth app among all users. The Kruskal-Wallis test indicated significant variations in user satisfaction with the 5 functional designs of mHealth apps—$H(4)=445.388$, $P<.001$. Specifically, the median satisfaction levels for the 5 functional dimensions among all users are presented in Table 6. Among these dimensions, health monitoring and health guidance exhibited the highest levels of satisfaction. Detailed satisfaction scores for the 5 functional designs, as well as pairwise comparisons of satisfaction among the 6 clusters, are also presented in Table 6. These results allow for a detailed examination of how each cluster differs from the others in terms of satisfaction with specific functional designs. Detailed test statistics are provided in Multimedia Appendix 6, which presents pairwise comparisons of satisfaction with the 5 functions across user groups.

Specifically, satisfaction with health guidance was higher in clusters 1, 2, 3, and 5 than in cluster 6. Pairwise comparisons revealed that clusters 1 ($z=6.246$, Bonferroni-adjusted $P<.001$), 2 ($z=8.404$, Bonferroni-adjusted $P<.001$), 3 ($z=6.887$, Bonferroni-adjusted $P<.001$), and 5 ($z=3.674$, Bonferroni-adjusted $P=.004$) differed significantly from cluster 6. Satisfaction with health education and health monitoring was significantly higher in clusters 1–3 than in clusters 4–6, with all 9 cross-group pairwise comparisons for each domain yielding statistically significant differences (health education: $z=2.77$-7.95, Bonferroni-adjusted $P<.001$ to .02 and health monitoring: $z=3.05$-7.88, Bonferroni-adjusted $P<.001$ to .03). With respect to social functions and gamification, users in cluster 2 reported higher satisfaction than those in the other 5 clusters. Pairwise comparisons revealed that cluster 2 differed significantly from cluster 1 ($z=–3.584$, Bonferroni-adjusted $P=.005$), cluster 3 ($z=4.599$, Bonferroni-adjusted $P<.001$), cluster 4 ($z=6.857$, Bonferroni-adjusted $P<.001$), cluster 5 ($z=7.392$, Bonferroni-adjusted $P<.001$), and cluster 6 ($z=5.992$, Bonferroni-adjusted $P<.001$) in social function; and from cluster 1 ($z=–3.999$, Bonferroni-adjusted $P=.001$), cluster 3 ($z=5.015$, Bonferroni-adjusted $P<.001$), cluster 4 ($z=5.880$, Bonferroni-adjusted $P<.001$), cluster 5 ($z=7.200$, Bonferroni-adjusted $P<.001$), and cluster 6 ($z=6.083$, Bonferroni-adjusted $P<.001$) in gamification.

XSL•FO
RenderX

Table 6. Median satisfaction and Kruskal-Wallis group comparisons regarding the 5 functional designs across the 6 user types.

Dependent variables	Median (IQR)						
	All users (n=1025)	Cluster 1: positively proactive energizers (n=140)	Cluster 2: proactive intenders (n=135)	Cluster 3: negatively proactive energizers (n=189)	Cluster 4: low health management demanders (n=218)	Cluster 5: potential health management demanders (n=180)	Cluster 6: passive attitude holders (n=163)
Satisfaction with health guidance	4.00 (1.00)	4.00[a,b,c,e] (1.67)	4.00[b,c] (1.00)	4.00[c] (1.00)	3.67[d,e,f] (1.00)	4.00[e] (1.00)	3.33[f] (1.00)
Satisfaction with health education	3.67 (1.00)	4.00[a,b,c] (1.67)	4.00[b,c] (1.33)	4.00[c] (1.33)	3.67[d,e] (1.00)	3.67[e,f] (1.00)	3.33[f] (1.00)
Satisfaction with health monitoring	4.00 (1.00)	4.00[a,b,c] (0.92)	4.00[b,c] (1.00)	4.00[c] (1.33)	3.67[d,e,f] (1.00)	4.00[e] (0.67)	3.67[f] (1.00)
Satisfaction with social function	3.33 (1.00)	3.33[a,f,c] (1.00)	4.00[b] (1.00)	3.33[c,d,f] (1.00)	3.00[d,e,f] (0.67)	3.00[e,f] (1.00)	3.33[f] (0.67)
Satisfaction with gamification	3.00 (1.00)	3.00[a,c,d,f] (1.00)	4.00[b] (1.33)	3.00[c,d,e,f] (1.33)	3.00[d,e,f] (0.67)	3.00[e,f] (1.33)	3.00[f] (0.33)

[a]In the same row of data, the group with a superscript "a" is statistically distinct from that with "b," "c," "d," and "e". However, the group with a superscript "b" is statistically not distinct from that with "b, c" because they share the superscript "b." Differing grouping labels indicate the heterogeneity across clusters.

Associations Between User Self-Management Characteristics and Satisfaction With mHealth App Functional Design

In this study, confirmatory factor analysis was used to test the reliability and validity of the questionnaire. The results, as shown in Multimedia Appendix 7, indicate that all constructs had Cronbach α and composite reliability values above 0.7; the average variance extracted for each construct was greater than 0.6; and the factor loadings for all items exceeded 0.7, demonstrating good reliability and convergent validity for all constructs. The heterotrait-monotrait ratio (HTMT) method was used to assess discriminant validity. The commonly accepted criterion for establishing discriminant validity is an HTMT value below 0.85. The results indicate that all construct pairs exhibited HTMT values below 0.85, supporting the discriminant validity of the measurement model. Using 8 health management characteristics as independent variables and satisfaction with 5 feature designs as dependent variables, partial least squares analysis was conducted to examine the impact of health management characteristics on satisfaction with the functional design of mHealth apps. The R^2 value represents the proportion of variance in the dependent variable explained by the independent variables and is used to interpret the goodness-of-fit of the regression equation, while β indicates the correlation between variables. Table 7 displays the β values and statistical significance of R^2 for the independent and dependent variables. Specifically, perceived barriers (β=.177, *z*=3.586, *P*<.001), perceived susceptibility (β=.076, *z*=2.056, *P*=.04), health self-efficacy (β=.140, *z*=3.307, *P*=.001), perceived health status (β=.111, *z*=2.967, *P*=.003), eHealth literacy (β=.153, *z*=3.947, *P*<.001), and health management intention (β=.148, *z*=3.966, *P*<.001) had a significant positive impact on satisfaction with health guidance; perceived barriers (β=0.143, *z*=3.130, *P*=.002), health self-efficacy (β=0.147, *z*=3.491, *P*<.001), perceived health status (β= 0.120, *z*=3.072, *P*=.002), eHealth literacy (β= 0.131, *z*=3.362, *P*=.001), and health management intention (β= 0.175, *z*=4.670, *P*<.001) had a significant positive impact on satisfaction with health education; perceived severity (β=.118, *z*=3.235, *P*=.001), perceived barriers (β=.107, *z*=2.194, *P*=.03), perceived benefits (β=.089, *z*=2.428, *P*=.02), perceived health status (β=.088, *z*=2.188, *P*=.03), eHealth literacy (β=.170, *z*=4.561, *P*<.001), and health management intention (β=.083, *z*=2.064, *P*=.04) had a significant positive impact on satisfaction with health monitoring; perceived susceptibility (β=.098, *z*=2.314, *P*=.02), perceived barriers (β=.150, *z*=3.032, *P*=.002), health self-efficacy (β=.195, *z*=4.598, *P*<.001), perceived health status (β=.135, *z*=3.391, *P*=.001), eHealth literacy (β=.118, *z*=2.805, *P*=.005), and health management intention (β=.139, *z*=3.396, *P*=.001) had a significant positive impact on satisfaction with social functions, whereas perceived benefits (β=–.210, *z*=5.906, *P*<.001) had a significant negative impact and perceived susceptibility (β=.099, *z*=2.200, *P*=.03), perceived barriers (β=.139, *z*=3.074, *P*=.002), health self-efficacy (β=.137, *z*=3.076, *P*=.002), perceived health status (β=.122, *z*=2.834, *P*=.005), eHealth literacy (β=.119, *z*=2.771, *P*=.006), and health management intention (β=.100, *z*=2.354, *P*=.02) had a significant positive impact on satisfaction with gamification, while perceived benefits (β=–.165, *z*=5.011, *P*<.001) had a significant negative impact. These results help explain why different types of users exhibit varying levels of satisfaction with different functional designs. The statistical analysis results for each path are presented in Multimedia Appendix 8.

XSL•FO
RenderX

Table 7. Results of partial least squares analyses for 8 health management characteristics on satisfaction of 5 functional designs (β value).

	Satisfaction with health guidance	Satisfaction with health education	Satisfaction with health monitoring	Satisfaction with social function	Satisfaction with gamification
Perceived severity	.058	.050	.118[a]	.034	–.012
Perceived susceptibility	.076[b]	.049	.046	.098[b]	.099[b]
Perceived barrier	.177[c]	.143[a]	.107[b]	.150[a]	.139[a]
Perceived benefit	.048	–.001	.089[b]	–.210[c]	–.165[c]
Health self-efficacy	.140[a]	.147[c]	.070	.195[c]	.137[a]
Perceived health status	.111[a]	.120[a]	.088[b]	.135[a]	.122[a]
eHealth literacy	.153[c]	.131[a]	.170[c]	.118[a]	.119[a]
Health management intention	.148[c]	.175[c]	.083[b]	.139[a]	.100[b]
R^2	.183	.168	.152	.144	.094

[a]$P<.01$.
[b]$P<.05$.
[c]$P<.001$.

Discussion

Principal Findings

Understanding the heterogeneity of mHealth users and analyzing distribution differences in satisfaction with mHealth function design among user groups with distinct characteristics have significant referential value for personalized mHealth design. Therefore, guided by self-management theory and driven by self-management characteristics, this study constructed mHealth user personas encompassing 6 categories, analyzed the main characteristics and attributes of these 6 types of mHealth users, and examined differences in satisfaction with various mHealth function designs across user types. The results show that levels of user self-management characteristics are unevenly distributed and that different combinations of self-management characteristics can explain user heterogeneity. Moreover, a clear correlation exists between user heterogeneity arising from self-management characteristics and satisfaction with specific function designs. The findings of this study mutually confirm and extend existing literature on differences in mHealth intervention effects, user participation motivation, and technology design principles.

User Profiles of Fitness and Weight Management Apps Based on Health Management Characteristics

This study categorizes mHealth users into 6 distinct groups based on their self-management characteristics, revealing a complex classification derived from self-management–related attributes such as knowledge, beliefs, self-regulation skills and abilities, and motivation. This classification system differs from traditional approaches that rely on broad demographic labels (such as age and education level), offering a more refined and interpretable psychographic user profile. Although the sample in this study is predominantly composed of young-to-middle-aged and highly educated users, comparison with the 50th Statistical Report on China's Internet Development (2022) [62] shows that while individuals aged 20-49 account for 56.6% of all Chinese internet users, only 28.5% have used online medical services. This indicates that even within the broadly age-eligible internet population, active adopters of digital health services constitute a specific subgroup. Accordingly, this study employed an online snowball sampling method to reach and recruit active users with genuine interest and engagement in mHealth management. The "young-to-middle-aged, well-educated" characteristics of the sample, to some extent, reflect the profile of individuals who pay close attention to such apps. However, chi-square test results show that the associations between user classification and age (Cramer V=0.145) and education level (Cramer V=0.116) are weak. Furthermore, analysis of the age composition of each user group revealed that every category spans multiple age layers, suggesting that single demographic labels are insufficient to capture the characteristics of the 6 user categories identified in this analysis. The uneven distribution of multiple features across different user categories indicates that there is no complete positive correlation between individuals' perceived health status and their health management abilities and motivations. The differentiation of users' characteristic attributes is consistent with relevant theories such as BCWs. Potential health management demanders and passive attitude holders both exhibit low health management intention, but their underlying mechanisms differ: the former perceive susceptibility and severity but face higher perceived barriers, whereas the latter generally lack recognition of the perceived benefits and health self-efficacy of health management. This is consistent with phenomena observed in studies of smoking cessation apps [63], namely that when users remain at the level of understanding health information but fail to convert it into personalized risk perception and action confidence, behavioral intentions are difficult to activate. Based on the results of this study, targeted interventions in mHealth management are needed according to individuals' motivation status and health perceptions, to facilitate the transformation of different perception characteristics into internal motivation and to address differences

XSL•FO
RenderX

in health management behaviors arising from varying motivation statuses [64]. In addition, although negatively proactive energizers perceive an average health status, they exhibit high health management intention and self-efficacy. This finding indicates that perceived health status alone is not the sole determinant of mHealth service use, which is also supported by existing studies [65], showing that patients' satisfaction with mHealth services may be influenced by individual differences in disease progression, perceived service attitudes, and understanding of diagnostic and treatment outcomes. Correspondingly, passive attitude holders exhibit low levels of perceived health status, perceived benefits, health self-efficacy, and health management intention, which aligns with a previous study [66] identifying lack of motivation and low perceived value as significant barriers to mHealth participation. In general, obtaining a positive mHealth service experience often depends on whether services can be personalized or adaptively adjusted to accommodate different user needs and motivations, and user heterogeneity is strongly correlated with self-management characteristics [67].

Satisfaction of Various User Types With mHealth App Functionality Design

There are significant differences in satisfaction with mHealth function designs among different user types, providing counterevidence to the "one-size-fits-all" function design strategy and underscoring the necessity of personalized design. This study found that proactive intenders and positively proactive energizers, characterized by high self-efficacy and strong health management intention, reported higher satisfaction with goal-oriented and interactive functions such as health guidance, health education, and health monitoring. This finding is consistent with multiple studies [63,68,69], indicating that users who actively focus on their own well-being demonstrate higher levels of engagement with mHealth. Features such as progress tracking, personalized feedback, and access to educational content are often welcomed and perceived as useful by these users.

Low health management demanders and passive attitude holders report lower satisfaction with most mHealth functions. This finding is consistent with a previous study [70], which indicated that for users with low intrinsic motivation or insufficient perceived value, complex functions or interfaces may act as barriers to use; such users require designs that are concise, intuitive, provide immediate and intuitive feedback, and involve low operational barriers. Notably, prior research has demonstrated a positive correlation between eHealth literacy and mHealth usage [71]. However, our findings offer a contrasting perspective, showing that potential health management demanders, despite having lower-than-average eHealth literacy, report high satisfaction with health guidance and health monitoring functions. This may be because this group's higher perceived benefits and perceived susceptibility compensate for their lower capability, thereby increasing their interest in tools that enhance health benefits and reduce health risks. This phenomenon may also be partially explained by the Dunning-Kruger effect, whereby users lacking specialized knowledge may be less able to critically evaluate application limitations, leading to inflated satisfaction ratings for mHealth. Individuals with low health literacy have been shown to report levels of confidence about their knowledge comparable to, or even higher than, those with high literacy [72]. Conversely, users with stronger health knowledge reserves tend to use educational materials and support functions in mHealth apps more frequently, thereby enhancing recognition and evaluation of specific functions [73]. The user-centered design concept, combined with the user types constructed in this study, can therefore provide valuable reference for mHealth designs that address the diverse needs of different user groups.

Recommendations

The findings of this study provide clear implications for the personalized design and practical application of mHealth. mHealth developers should adopt a user-centered design approach and, based on the user types constructed in this study, tailor functional modules accordingly. For positively proactive energizers, further development of data tracking, personalized goal setting, and systematic educational content can be pursued, alongside the appropriate introduction of gamification elements to enhance users' sense of enjoyment [74]. For potential health management demanders, design efforts should focus on lowering usage barriers, providing clear and step-by-step health guidance and monitoring tools, and strengthening health-related beliefs. For passive attitude holders, the primary objective may be to establish initial engagement and trust through simple designs and light-touch interventions, while incorporating social features to help this group build social support [75], increase awareness of health risks, and enhance beliefs in health management. Furthermore, the study's results suggest that when evaluating the effectiveness of mHealth functions, user heterogeneity must be considered, as overall average satisfaction may obscure substantial differences among user subgroups.

Limitations and Future Research

Although this study was carefully designed in terms of methodology and empirical analysis, several limitations should be acknowledged. First, to avoid comparability issues arising from differences in functional design across mHealth apps with different core service content, and to recruit as diverse a user sample as possible, this study selected exercise, fitness, and weight management apps as the objects of study. However, these apps cannot fully represent all types of mHealth apps. Nevertheless, by conducting empirical research on one of the most widely used and numerous categories of mHealth apps, this study verifies that individuals' self-management characteristics have important referential value for mHealth user classification. The results demonstrate significant differences in satisfaction with various functional designs across user types, and that the effects of self-management characteristics on satisfaction differ across functional design dimensions. These results provide direct empirical reference for the personalized design of fitness and weight loss apps, and the research conclusions may also offer inspiration for user classification–related studies in other types of mHealth apps. Second, although questionnaires are an effective research method, they cannot fully represent all users. Access to feedback data from the entire mHealth user population would enable a more refined classification of user types. At present, limited

XSL•FO
RenderX

research on mHealth apps has focused on users' health cognition and self-management abilities, which constrains the analysis of comprehensive user characteristics from a big data perspective. To mitigate sampling bias, data were collected from 34 regions across China, and the sample size was substantially larger than that of comparable studies, supporting the representativeness of the findings. Third, although empirical results indicate that 8 self-management characteristics significantly influence user satisfaction, these characteristics explain only a limited proportion of the variance in satisfaction with mHealth (R^2=0.094-0.183). Although the identified pathways were statistically significant, a substantial proportion of the variance in satisfaction remains unexplained by these characteristics. Given that the primary aim of this study was to examine whether the effects of heterogeneous user types on satisfaction differ—that is, to construct user profiles based on self-management characteristics and analyze differences in satisfaction across user types—we did not conduct an in-depth examination of other potential determinants of satisfaction (eg, usage context, service quality, and user experience). Future research on factors influencing mHealth satisfaction could incorporate additional predictive variables to improve the explanatory power of the model.

Conclusions

This study identified 6 distinct mHealth user typologies (fitness and weight management apps) derived from a comprehensive set of self-management characteristics. The results reveal an uneven distribution of multidimensional characteristics across different user categories. This granular classification provides a deeper understanding of user heterogeneity than traditional demographic-based approaches. Overall, the primary contribution of this work is an empirically validated framework that offers a structured approach to understanding mHealth user diversity. The identified user typologies and their differential functional satisfaction profiles yield actionable insights for the personalized design of fitness and weight management apps. Specifically, for health guidance and education features, proactive intenders, positively proactive energizers, and negatively proactive energizers report higher satisfaction. For health monitoring functions, potential health management demanders, proactive intenders, positively proactive energizers, and negatively proactive energizers demonstrate higher satisfaction. For social features and gamification design, proactive intenders exhibit significantly higher satisfaction than the other 5 user types. From a practical perspective, these findings underscore the importance of adapting mHealth features to the distinct self-management needs and preferences of specific user groups. Such adaptation is essential for enhancing user satisfaction, fostering sustained engagement, and ultimately improving the perceived usefulness of digital health solutions.

Funding

This work was funded by the National Natural Science Foundation of China (grants 72404112 and 72574006), the Municipal Natural Science Foundation of Beijing (grant 7222306), and the National TCM innovation team and talent support projects (grant ZYYCXTD-C-202210).

Data Availability

The data will be made available upon reasonable request to the corresponding author.

Authors' Contributions

Conceptualization: TW
Data curation: JL (lead), TW (equal)
Formal analysis: TW (lead)
Funding acquisition: JL (lead), TW (equal)
Investigation: JL (lead), TW (equal), YF (supporting), ZL (supporting), XJ (supporting), QF (supporting), JM (supporting)
Methodology: TW (lead), YF (supporting), ZL (supporting), XJ (supporting), QF (supporting)
Project administration: JL
Resources: JL
Supervision: JL
Writing – original draft: TW
Writing – review & editing: TW (lead), JL (equal)

Conflicts of Interest

None declared.

Multimedia Appendix 1
Measurement instrument.
[PDF File (Adobe PDF File), 298 KB - medinform_v14i1e64860_app1.pdf]

XSL•FO
RenderX

Multimedia Appendix 2
Cluster sum of squared errors values and silhouette coefficients.
[PDF File (Adobe PDF File), 121 KB - medinform_v14i1e64860_app2.pdf]

Multimedia Appendix 3
Clustering analysis code.
[PDF File (Adobe PDF File), 111 KB - medinform_v14i1e64860_app3.pdf]

Multimedia Appendix 4
STROBE checklist.
[PDF File (Adobe PDF File), 238 KB - medinform_v14i1e64860_app4.pdf]

Multimedia Appendix 5
Comparison of health management characteristics between pairs of user groups.
[PDF File (Adobe PDF File), 327 KB - medinform_v14i1e64860_app5.pdf]

Multimedia Appendix 6
Comparison of satisfaction across 5 functions between paired user groups.
[PDF File (Adobe PDF File), 230 KB - medinform_v14i1e64860_app6.pdf]

Multimedia Appendix 7
Reliability and validity analysis.
[PDF File (Adobe PDF File), 178 KB - medinform_v14i1e64860_app7.pdf]

Multimedia Appendix 8
Path coefficients.
[PDF File (Adobe PDF File), 131 KB - medinform_v14i1e64860_app8.pdf]

References

1. Khalil AA, Meyliana, Hidayanto AN, Prabowo H. Identification of factor affecting continuance usage intention of mHealth application: a systematic literature review. 2020 Dec 24 Presented at: The 4th International Conference on Informatics and Computational Sciences (ICICoS); November 10-11, 2020; Semarang, Indonesia p. 1-6. [doi: 10.1109/icicos51170.2020.9299038]
2. Wang Y, Xue H, Huang Y, Huang L, Zhang D. A systematic review of application and effectiveness of mHealth interventions for obesity and diabetes treatment and self-management. Adv Nutr 2017 May;8(3):449-462 [FREE Full text] [doi: 10.3945/an.116.014100] [Medline: 28507010]
3. Helander E, Kaipainen K, Korhonen I, Wansink B. Factors related to sustained use of a free mobile app for dietary self-monitoring with photography and peer feedback: retrospective cohort study. J Med Internet Res 2014 Apr 15;16(4):e109. [doi: 10.2196/jmir.3084] [Medline: 24735567]
4. AppsFlyer. The uninstall ThreatApp uninstall benchmarks. AppsFlyer. 2020. URL: https://www.appsflyer.com/infograms/2019-app-uninstall-benchmarks/ [accessed 2024-12-10]
5. Wang T, Wang W, Liang J, Nuo M, Wen Q, Wei W, et al. Identifying major impact factors affecting the continuance intention of mHealth: a systematic review and multi-subgroup meta-analysis. NPJ Digit Med 2022 Sep 15;5(1):145 [FREE Full text] [doi: 10.1038/s41746-022-00692-9] [Medline: 36109594]
6. Wang T, Zheng X, Liang J, An K, He Y, Nuo M, et al. Use of machine learning to mine user-generated content from mobile health apps for weight loss to assess factors correlated with user satisfaction. JAMA Netw Open 2022 May 02;5(5):e2215014 [FREE Full text] [doi: 10.1001/jamanetworkopen.2022.15014] [Medline: 35639374]
7. Yang M, Al Mamun A, Gao J, Rahman MK, Salameh AA, Alam SS. Predicting m-health acceptance from the perspective of unified theory of acceptance and use of technology. Sci Rep 2024 Jan 03;14(1):339 [FREE Full text] [doi: 10.1038/s41598-023-50436-2] [Medline: 38172184]
8. Wang T, Fan L, Zheng X, Wang W, Liang J, An K, et al. The impact of gamification-induced users' feelings on the continued use of mHealth apps: a structural equation model with the self-determination theory approach. J Med Internet Res 2021 Aug 12;23(8):e24546 [FREE Full text] [doi: 10.2196/24546] [Medline: 34387550]
9. Wang T, Wang W, Feng J, Fan X, Guo J, Lei J. A novel user-generated content-driven and Kano model focused framework to explore the impact mechanism of continuance intention to use mobile apps. Computers in Human Behavior 2024 Aug;157:108252. [doi: 10.1016/j.chb.2024.108252]

XSL•FO
RenderX

10. Hashemi P, Reychav I, Arora A, Sawaed N, Sabherwal R, Azuri J. How does information technology affect individuals' health behavior in a pandemic? Insights from mobile health application use during COVID-19. Computers in Human Behavior 2024 Feb;151:108005. [doi: 10.1016/j.chb.2023.108005]
11. Singh P, Malik G. From trial to triumph! A longitudinal design eliciting social impact perspective for sustained usage of gamified fitness apps. APJML 2024 Aug 20;37(2):382-402. [doi: 10.1108/APJML-03-2024-0315]
12. Han K, Zo H. Understanding the mobile healthcare applications continuance: the regulatory focus perspective. Int J Med Inform 2023 Sep;177:105161. [doi: 10.1016/j.ijmedinf.2023.105161] [Medline: 37544241]
13. Nam M, Song T, Kim D, Jang K, Kim J, Koo B, et al. Effects of content characteristics and improvement in user satisfaction on the reuse of home fitness application. Sustainability 2023 May 22;15(10):8371. [doi: 10.3390/su15108371]
14. He Y, Chen H, Xiang P, Zhao M, Li Y, Liu Y, et al. Establishing an evaluation indicator system for user satisfaction with hypertension management apps: combining user-generated content and analytic hierarchy process. J Med Internet Res 2024 Sep 03;26:e60773 [FREE Full text] [doi: 10.2196/60773] [Medline: 39226103]
15. Nuo M, Zheng S, Wen Q, Fang H, Wang T, Liang J, et al. Mining the influencing factors and their asymmetrical effects of mHealth sleep app user satisfaction from real-world user-generated reviews: content analysis and topic modeling. J Med Internet Res 2023 Jan 31;25:e42856 [FREE Full text] [doi: 10.2196/42856] [Medline: 36719730]
16. Luna-Perejon F, Malwade S, Styliadis C, Civit J, Cascado-Caballero D, Konstantinidis E, et al. Evaluation of user satisfaction and usability of a mobile app for smoking cessation. Comput Methods Programs Biomed 2019 Dec;182:105042 [FREE Full text] [doi: 10.1016/j.cmpb.2019.105042] [Medline: 31473444]
17. Lee H, Uhm KE, Cheong IY, Yoo JS, Chung SH, Park YH, et al. Patient satisfaction with mobile health (mHealth) application for exercise intervention in breast cancer survivors. J Med Syst 2018 Nov 06;42(12):254. [doi: 10.1007/s10916-018-1096-1] [Medline: 30402781]
18. Arensman R, Kloek C, Pisters M, Koppenaal T, Ostelo R, Veenhof C. Patient perspectives on using a smartphone app to support home-based exercise during physical therapy treatment: qualitative study. JMIR Hum Factors 2022 Sep 13;9(3):e35316 [FREE Full text] [doi: 10.2196/35316] [Medline: 36098993]
19. Fu HN, Adam TJ, Konstan JA, Wolfson JA, Clancy TR, Wyman JF. Influence of patient characteristics and psychological needs on diabetes mobile app usability in adults with type 1 or type 2 diabetes: crossover randomized trial. JMIR Diabetes 2019 Apr 30;4(2):e11462 [FREE Full text] [doi: 10.2196/11462] [Medline: 31038468]
20. Screenagers to silver surfers: how each generation clicks with care. Rock Health. 2025. URL: https://rockhealth.com/insights/screenagers-to-silver-surfers-how-each-generation-clicks-with-care/ [accessed 2025-05-07]
21. Conway N, Campbell I, Forbes P, Cunningham S, Wake D. mHealth applications for diabetes: user preference and implications for app development. Health Informatics J 2016 Dec;22(4):1111-1120 [FREE Full text] [doi: 10.1177/1460458215616265] [Medline: 26635324]
22. Nie L, Oldenburg B, Cao Y, Ren W. Continuous usage intention of mobile health services: model construction and validation. BMC Health Serv Res 2023 May 05;23(1):442 [FREE Full text] [doi: 10.1186/s12913-023-09393-9] [Medline: 37143005]
23. Lee J, Kim J. Can menstrual health apps selected based on users' needs change health-related factors? A double-blind randomized controlled trial. J Am Med Inform Assoc 2019 Jul 01;26(7):655-666 [FREE Full text] [doi: 10.1093/jamia/ocz019] [Medline: 30946478]
24. Jamison RN, Mei A, Ross EL. Longitudinal trial of a smartphone pain application for chronic pain patients: predictors of compliance and satisfaction. J Telemed Telecare 2016 Nov 10;24(2):93-100. [doi: 10.1177/1357633x16679049]
25. Ryan P, Sawin KJ. The individual and family self-management theory: background and perspectives on context, process, and outcomes. Nurs Outlook 2009 Jul;57(4):217-225.e6 [FREE Full text] [doi: 10.1016/j.outlook.2008.10.004] [Medline: 19631064]
26. Zhou Y, Li S, Huang R, Ma H, Wang A, Tang X, et al. Behavior change techniques used in self-management interventions based on mHealth apps for adults with hypertension: systematic review and meta-analysis of randomized controlled trials. J Med Internet Res 2024 Oct 22;26:e54978 [FREE Full text] [doi: 10.2196/54978] [Medline: 39437388]
27. Leziak K, Birch E, Jackson J, Strohbach A, Niznik C, Yee LM. Identifying mobile health technology experiences and preferences of low-income pregnant women with diabetes. J Diabetes Sci Technol 2021 Sep;15(5):1018-1026 [FREE Full text] [doi: 10.1177/1932296821993175] [Medline: 33605158]
28. Irfan Khan A, Gill A, Cott C, Hans PK, Steele Gray C. mHealth tools for the self-management of patients with multimorbidity in primary care settings: pilot study to explore user experience. JMIR Mhealth Uhealth 2018 Aug 28;6(8):e171 [FREE Full text] [doi: 10.2196/mhealth.8593] [Medline: 30154073]
29. Bauer W, Schiffman R, Ellis J, Erickson J, Polfuss M, Taani M, et al. An integrative review of the use of the individual and family self-management theory in research. Advances in Nursing Science 2025 Jun;48(2):E41. [doi: 10.1097/ans.0000000000000512]
30. Suess C, Maddock J, Dogru T, Mody M, Lee S. Using the Health Belief Model to examine travelers' willingness to vaccinate and support for vaccination requirements prior to travel. Tour Manag 2022 Feb;88:104405 [FREE Full text] [doi: 10.1016/j.tourman.2021.104405] [Medline: 34456412]
31. Glanz K, Rimer B, Viswanath K. Health Behavior and Health Education: Theory, Research, and Practice. San Francisco, CA: John Wiley & Sons; 2008:1-470.

XSL•FO
RenderX

32. Saghafi-Asl M, Aliasgharzadeh S, Asghari-Jafarabadi M. Factors influencing weight management behavior among college students: an application of the Health Belief Model. PLoS One 2020;15(2):e0228058 [FREE Full text] [doi: 10.1371/journal.pone.0228058] [Medline: 32032376]
33. Chauhan BF, Jeyaraman MM, Mann AS, Lys J, Skidmore B, Sibley KM, et al. Behavior change interventions and policies influencing primary healthcare professionals' practice-an overview of reviews. Implement Sci 2017 Jan 05;12(1):3 [FREE Full text] [doi: 10.1186/s13012-016-0538-8] [Medline: 28057024]
34. Michie S, Atkins L, West R. The Behaviour Change Wheel: A Guide to Designing Interventions. London, UK: Silverback Publishing; 2014:1-184.
35. Michie S, van SMM, West R. The Behaviour Change Wheel: a new method for characterising and designing behaviour change interventions. Implement Sci 2011;6:42 [FREE Full text] [doi: 10.1186/1748-5908-6-42] [Medline: 21513547]
36. Norman CD, Skinner HA. eHealth literacy: essential skills for consumer health in a networked world. J Med Internet Res 2006 Jun 16;8(2):e9 [FREE Full text] [doi: 10.2196/jmir.8.2.e9] [Medline: 16867972]
37. World Health Organization (WHO). Health promotion glossary of terms. WHO. Geneva, Switzerland: WHO; 2021. URL: https://apps.who.int/iris/handle/10665/350161 [accessed 2022-03-02]
38. Li W, Yuan K, Yue M, Zhang L, Huang F. Climate change risk perceptions, facilitating conditions and health risk management intentions: evidence from farmers in rural China. Climate Risk Management 2021;32:100283. [doi: 10.1016/j.crm.2021.100283]
39. Jeong H, Lee Y. Sex-based differences in the quality of life of elderly Koreans with chronic musculoskeletal pain. Int J Environ Res Public Health 2020 Jan 23;17(3):743 [FREE Full text] [doi: 10.3390/ijerph17030743] [Medline: 31979306]
40. Du J, Luo C, Shegog R, Bian J, Cunningham RM, Boom JA, et al. Use of deep learning to analyze social media discussions about the human papillomavirus vaccine. JAMA Netw Open 2020 Nov 02;3(11):e2022025 [FREE Full text] [doi: 10.1001/jamanetworkopen.2020.22025] [Medline: 33185676]
41. Williams DM, Rhodes RE. The confounded self-efficacy construct: conceptual analysis and recommendations for future research. Health Psychol Rev 2016 Dec;10(2):113-128 [FREE Full text] [doi: 10.1080/17437199.2014.941998] [Medline: 25117692]
42. Mendiola MF, Kalnicki M, Lindenauer S. Valuable features in mobile health apps for patients and consumers: content analysis of apps and user ratings. JMIR Mhealth Uhealth 2015 May 13;3(2):e40 [FREE Full text] [doi: 10.2196/mhealth.4283] [Medline: 25972309]
43. Gimpel H, Manner-Romberg T, Schmied F, Winkler TJ. Understanding the evaluation of mHealth app features based on a cross-country Kano analysis. Electron Markets 2021 Mar 24;31(4):765-794. [doi: 10.1007/s12525-020-00455-y]
44. Yoon S, Goh H, Nadarajan GD, Sung S, Teo I, Lee J, et al. Perceptions of mobile health apps and features to support psychosocial well-being among frontline health care workers involved in the COVID-19 pandemic response: qualitative study. J Med Internet Res 2021 May 31;23(5):e26282 [FREE Full text] [doi: 10.2196/26282] [Medline: 33979296]
45. Wilhide Iii CC, Peeples MM, Anthony Kouyaté RC. Evidence-based mHealth chronic disease mobile app intervention design: development of a framework. JMIR Res Protoc 2016 Feb 16;5(1):e25 [FREE Full text] [doi: 10.2196/resprot.4838] [Medline: 26883135]
46. Agarwal P, Gordon D, Griffith J, Kithulegoda N, Witteman HO, Sacha Bhatia R, et al. Assessing the quality of mobile applications in chronic disease management: a scoping review. NPJ Digit Med 2021 Mar 10;4(1):46 [FREE Full text] [doi: 10.1038/s41746-021-00410-x] [Medline: 33692488]
47. Wang Y, Collins WB. Systematic evaluation of mobile fitness apps: apps as the tutor, recorder, game companion, and cheerleader. Telematics and Informatics 2021 Jun;59:101552. [doi: 10.1016/j.tele.2020.101552]
48. Deterding S, Sicart M, Nacke L, O'Hara K, Dixon D, editors. Gamification: using game design elements in non-gaming contexts. 2011 Presented at: CHI 2011: The International Conference on Human Factors in Computing Systems; May 7-12, 2011; Vancouver, BC, Canada. [doi: 10.1145/1979742.1979575]
49. Lv H, Zeng N, Li M, Sun J, Wu N, Xu M, et al. Association between body mass index and brain health in adults: a 16-year population-based cohort and mendelian randomization study. Health Data Sci 2024 Mar 15;4:0087 [FREE Full text] [doi: 10.34133/hds.0087] [Medline: 38500551]
50. Serrano KJ, Yu M, Coa KI, Collins LM, Atienza AA. Mining health app data to find more and less successful weight loss subgroups. J Med Internet Res 2016 Jun 14;18(6):e154 [FREE Full text] [doi: 10.2196/jmir.5473] [Medline: 27301853]
51. Albarrak MM, Zakaria N, Meo SA. The role of mobile health applications (mHealth apps) in reshaping the body weight for better healthcare: a cross-sectional study. Pak J Med Sci 2024 Oct 11;40(9):1930-1936. [doi: 10.12669/pjms.40.9.9064] [Medline: 39416646]
52. Yin S, Cai X, Wang Z, Zhang Y, Luo S, Ma J. Impact of gamification elements on user satisfaction in health and fitness applications: a comprehensive approach based on the Kano model. Computers in Human Behavior 2022 Mar;128:107106. [doi: 10.1016/j.chb.2021.107106]
53. Mitchell R, Schuster L, Jin HS. Playing alone: can game design elements satisfy user needs in gamified mHealth services? Health Promot Int 2022 Apr 29;37(2):daab168 [FREE Full text] [doi: 10.1093/heapro/daab168] [Medline: 34651180]

XSL•FO
RenderX

54. Ahadzadeh AS, Pahlevan Sharif S, Ong FS, Khong KW. Integrating health belief model and technology acceptance model: an investigation of health-related internet use. J Med Internet Res 2015 Feb 19;17(2):e45 [FREE Full text] [doi: 10.2196/jmir.3564] [Medline: 25700481]
55. McArthur LH, Riggs A, Uribe F, Spaulding TJ. Health belief model offers opportunities for designing weight management interventions for college students. J Nutr Educ Behav 2018 May;50(5):485-493. [doi: 10.1016/j.jneb.2017.09.010] [Medline: 29097024]
56. Norman CD, Skinner HA. eHEALS: The eHealth Literacy Scale. J Med Internet Res 2006 Nov 14;8(4):e27 [FREE Full text] [doi: 10.2196/jmir.8.4.e27] [Medline: 17213046]
57. Austin JD, Allicock M, Atem F, Lee SC, Fernandez ME, Balasubramanian BA. A structural equation modeling approach to understanding pathways linking survivorship care plans to survivor-level outcomes. J Cancer Surviv 2020 Dec;14(6):834-846 [FREE Full text] [doi: 10.1007/s11764-020-00896-6] [Medline: 32474862]
58. Wallston KA, Cawthon C, McNaughton CD, Rothman RL, Osborn CY, Kripalani S. Psychometric properties of the brief health literacy screen in clinical practice. J Gen Intern Med 2014 Jan;29(1):119-126 [FREE Full text] [doi: 10.1007/s11606-013-2568-0] [Medline: 23918160]
59. Zhou C, Zheng W, Tan F, Lai S, Yuan Q. Influence of health promoting lifestyle on health management intentions and behaviors among Chinese residents under the integrated healthcare system. PLoS One 2022;17(1):e0263004 [FREE Full text] [doi: 10.1371/journal.pone.0263004] [Medline: 35077472]
60. Jackson DL. Revisiting sample size and number of parameter estimates: some support for the N:q hypothesis. Structural Equation Modeling: A Multidisciplinary Journal 2003 Jan;10(1):128-141. [doi: 10.1207/s15328007sem1001_6]
61. Lou N. Analysis of the intelligent tourism route planning scheme based on the cluster analysis algorithm. Comput Intell Neurosci 2022 Jun 28;2022:3310676-3310610 [FREE Full text] [doi: 10.1155/2022/3310676] [Medline: 35800698]
62. The 50th statistical report on China's internet development. China Internet Network Information Center. 2022. URL: https://www3.cnnic.cn/n4/2022/0914/c88-10226.html [accessed 2026-01-04]
63. Tudor-Sfetea C, Rabee R, Najim M, Amin N, Chadha M, Jain M, et al. Evaluation of two mobile health apps in the context of smoking cessation: qualitative study of cognitive behavioral therapy (CBT) versus non-CBT-based digital solutions. JMIR Mhealth Uhealth 2018 Apr 18;6(4):e98 [FREE Full text] [doi: 10.2196/mhealth.9405] [Medline: 29669708]
64. Prochaska JO, DiClemente CC. Stages and processes of self-change of smoking: toward an integrative model of change. Journal of Consulting and Clinical Psychology 1983;51(3):390-395. [doi: 10.1037/0022-006X.51.3.390]
65. Lu J, Zhao H, Ji Z, Dong Y. Effect of patient satisfaction on the utilization of mHealth services by patients with chronic disease. Digit Health 2025 Apr 15;11:20552076251333983 [FREE Full text] [doi: 10.1177/20552076251333983] [Medline: 40297355]
66. Alzghaibi H. Healthcare practitioners' perceptions of mhealth application barriers: challenges to adoption and strategies for enhancing digital health integration. Healthcare (Basel) 2025 Feb 25;13(5):494 [FREE Full text] [doi: 10.3390/healthcare13050494] [Medline: 40077056]
67. Wittmar S, Frankenstein T, Timm V, Frei P, Kurpiers N, Wölwer S, et al. User experience with a personalized mHealth service for physical activity promotion in university students: mixed methods study. JMIR Form Res 2025 Mar 28;9:e64384 [FREE Full text] [doi: 10.2196/64384] [Medline: 40153787]
68. Kowalski L, Finnes A, Koch S, Bujacz A. User engagement with organizational mHealth stress management intervention - a mixed methods study. Internet Interv 2024 Mar;35:100704 [FREE Full text] [doi: 10.1016/j.invent.2023.100704] [Medline: 38268709]
69. Monachelli R, Davis SW, Barnard A, Longmire M, Docherty JP, Oakley-Girvan I. Designing mHealth apps to incorporate evidence-based techniques for prolonging user engagement. Interact J Med Res 2024 Mar 26;13:e51974 [FREE Full text] [doi: 10.2196/51974] [Medline: 38416858]
70. Santos-Vijande ML, Gómez-Rico M, Molina-Collado A, Davison RM. Building user engagement to mHealth apps from a learning perspective: relationships among functional, emotional and social drivers of user value. Journal of Retailing and Consumer Services 2022 May;66:102956. [doi: 10.1016/j.jretconser.2022.102956]
71. Shaw G, Castro BA, Gunn LH, Norris K, Thorpe RJ. The association of eHealth literacy skills and mHealth application use among US adults with obesity: analysis of Health Information National Trends Survey Data. JMIR Mhealth Uhealth 2024 Jan 10;12:e46656 [FREE Full text] [doi: 10.2196/46656] [Medline: 38198196]
72. Canady BE, Larzo M. Overconfidence in managing health concerns: the Dunning-Kruger effect and health literacy. J Clin Psychol Med Settings 2023 Jun 29;30(2):460-468 [FREE Full text] [doi: 10.1007/s10880-022-09895-4] [Medline: 35768740]
73. Chua JYX, Choolani M, Chee CYI, Yi H, Lalor JG, Chong YS, et al. A mobile app–based intervention (Parentbot–a digital healthcare assistant) for parents: secondary analysis of a randomized controlled trial. J Med Internet Res 2025 Apr 17;27:e64882 [FREE Full text] [doi: 10.2196/64882] [Medline: 40245395]
74. Lin Y, Tudor-Sfetea C, Siddiqui S, Sherwani Y, Ahmed M, Eisingerich AB. Effective behavioral changes through a digital mHealth app: exploring the impact of hedonic well-being, psychological empowerment and inspiration. JMIR Mhealth Uhealth 2018 Jun 15;6(6):e10024 [FREE Full text] [doi: 10.2196/10024] [Medline: 29907557]

XSL•FO
RenderX

75. Nuseibeh BZ, Johns SA, Shih PC, Lewis GF, Gowan TM, Jordan EJ. Co-designing the MOSAIC mHealth app with breast cancer survivors: user-centered design approach. JMIR Form Res 2024 Dec 09;8:e59426 [FREE Full text] [doi: 10.2196/59426] [Medline: 39652855]

Abbreviations

BCW: Behavior Change Wheel
HBM: Health Belief Model
HTMT: heterotrait-monotrait ratio
mHealth: mobile health
SSE: sum of squared errors
STROBE: Strengthening the Reporting of Observational Studies in Epidemiology

Edited by A Coristine; submitted 29.Jul.2024; peer-reviewed by Y Yu, A Eisingerich; comments to author 30.Nov.2024; revised version received 10.Jan.2026; accepted 12.Jan.2026; published 10.Feb.2026.

Please cite as:
Wang T, Fan Y, Li Z, Jiao X, Fang Q, Ma J, Lei J
Exploring Self-Management–Based Mobile Health User Typologies and Associations Between User Types and Satisfaction With Key Mobile Health Functions: Comparative Study of Various Fitness and Weight Management App User Types
JMIR Med Inform 2026;14:e64860
URL: https://medinform.jmir.org/2026/1/e64860
doi:10.2196/64860
PMID:

©Tong Wang, Yiwen Fan, Zheng Li, Xiaoyi Jiao, Qichuan Fang, Junhao Ma, Jianbo Lei. Originally published in JMIR Medical Informatics (https://medinform.jmir.org), 10.Feb.2026. This is an open-access article distributed under the terms of the Creative Commons Attribution License (https://creativecommons.org/licenses/by/4.0/), which permits unrestricted use, distribution, and reproduction in any medium, provided the original work, first published in JMIR Medical Informatics, is properly cited. The complete bibliographic information, a link to the original publication on https://medinform.jmir.org/, as well as this copyright and license information must be included.

XSL•FO
RenderX

Original Paper

Balancing Privacy and Utility in Child and Adolescent Mental Health Services Research: Retrospective Cohort Study on Synthetic Data Generation

Mounir Haizoune[1], MSc; Bennett L Leventhal[2], MD; Dipendra Pant[3,4], MSc; Øystein Nytrø[3,4], PhD; Kaban Koochakpour[3,4], PhD; Roman A Koposov[5], MD, PhD; Lars Ravn Øhlckers[6], MSci; Norbert Skokauskas[3,7], MD, PhD

[1]Department of Analytics, Western Norway Regional Health Authority, Stavanger, Norway

[2]Department of Psychiatry and Behavioral Neuroscience, University of Chicago, Chicago, IL, United States

[3]Norwegian University of Science and Technology, Trondheim, Norway

[4]Department of Child and Adolescent Psychiatry, Clinic of Mental Health Care, St. Olav University Hospital Trondheim, Trondheim, Norway

[5]Regional Centre for Child and Youth Mental Health and Child Welfare, Faculty of Health Sciences, UiT The Arctic University of Norway, Tromsø, Norway

[6]Department of Child and Adolescent Psychiatry and Addiction, Stavanger University Hospital, Stavanger, Norway

[7]Regional Center for Child and Youth Mental Health and Child Welfare, Faculty of Medicine and Health Science, Trondheim, Norway

Corresponding Author:
Norbert Skokauskas, MD, PhD
Norwegian University of Science and Technology
Klostergata 46, 3. etasje
Campus Øya
Trondheim, 7030
Norway
Phone: 1 73558973
Email: norbert.skokauskas@ntnu.no

Abstract

Background: Electronic health records are essential for advancing research aimed at improving clinical outcomes. However, stringent data protection and privacy concerns severely limit the accessibility and use of real clinical data, particularly within Child and Adolescent Mental Health Services (CAMHS) involving vulnerable young individuals. This challenge can be effectively addressed through synthetic data generation, which safeguards individual privacy while facilitating comprehensive analyses of clinical information.

Objective: This study aims to investigate whether hierarchical synthetic data generators (SDGs) can effectively replicate the statistical properties, preserve the utility, and maintain the privacy of real CAMHS clinical data, thereby enabling data sharing and broader access to research-ready datasets.

Methods: This retrospective cohort study used electronic medical record data from 6924 distinct patients from CAMHS in Stavanger, Norway, comprising 7730 referral periods and 58,524 episodes of care. An 80%-20% split was used for training and testing. A hierarchical synthetic data generation model was trained to generate synthetic referral periods and associated episodes of care. Data quality was evaluated using SDMetrics for distribution (Kolmogorov-Smirnov Complement [KSC]/Total Variation Complement [TVC]), correlation (CorrelationSimilarity [CS]), and cardinality (CardinalityShapeSimilarity [CSS]) similarity. Privacy was evaluated using the Anonymeter library to simulate singling out, linkability, and inference reidentification attacks. Utility was assessed using the train synthetic test real (TSTR) pattern, comparing the predictive performance using precision-recall area under the curve [PRAUC] of models trained on synthetic vs real data for classifying the intensity of care.

Results: The hierarchical SDG created highly reproducible synthetic CAMHS data. The average statistical similarity scores were high across all metrics: KSC/TVC at 0.92, CS at 0.77 (intertable CS at 0.75), and CSS at 0.92. The synthetic data also demonstrated a low risk under simulated privacy attacks on a control dataset (n=1546): the average success rate was 6/1546 (0.39%) for singling out and 77/1546 (5%) for multivariate attacks. The average linkability risk was 54/1546 (0.5%), and the highest inference risk for a sensitive variable was 2/1546 (0.12%). The classification model trained on synthetic data (TSTR) produced comparable predictive performance (PRAUC=0.40) to the model trained on real data (PRAUC=0.43) for classifying

XSL•FO
RenderX

the intensity of care (low vs medium or higher). Shapley additive explanations analysis confirmed that the synthetic model's explanations aligned with real-world insights, validating its ability to capture fundamental predictive patterns.

Conclusions: Synthetic data can be used to build trust and promote collaboration among CAMHS researchers by offering access to extensive, representative samples with a low risk of patient identification. This approach expands the breadth of research while safeguarding patient privacy. Effective implementation of synthetic data generation depends on the model's ability to accurately identify and replicate the complex, sequential patterns present in real data.

(JMIR Med Inform 2026;14:e71819) doi:10.2196/71819

KEYWORDS

CAMHS; classification; length of referral; mental health; synthetic data generation

Introduction

The preservation of patient confidentiality is frequently identified as a significant barrier to conducting research with mental health care datasets [1]. Researchers appropriately face strict regulations and ethical considerations that limit access to real patient data. This is further complicated by selection bias [2], digital barriers [3], and high levels of sensitivity of mental health information, which, if disclosed, could lead to additional stigma, discrimination, and other negative consequences for individuals [4].

While these challenges are present across all mental health research, the use of large-scale data from patient records becomes significantly more complex with Child and Adolescent Mental Health Services (CAMHS) data. This is due to a set of problems associated with this vulnerable population. First, the variability in developmental stages among children and adolescents means that symptoms and diagnoses manifest differently across age groups (eg, anxiety in a 5-year-old compared to a 16-year-old), making data standardization and longitudinal analysis inherently difficult. Second, the necessity for age-appropriate interventions and evolving care pathways creates complex, nonlinear data structures that are challenging to model consistently [5]. Perhaps most critically, the ethical considerations surrounding privacy and consent for minors are far more stringent than for adult populations. Researchers must navigate nuanced consent processes involving both parents or guardians and the child's assent, often with varying legal requirements based on age and local jurisdiction [6,7]. This multilayered consent, coupled with heightened safeguarding responsibilities, severely restricts data sharing. Furthermore, due to their inherent nature, which includes stringent privacy regulations and the fragmented structure of care pathways, CAMHS datasets are typically smaller, exhibit greater structural fragmentation, and are consequently more challenging to access large-scale, generalizable research than adult health datasets.

These challenges can be effectively addressed by the generation of synthetic data. Synthetic data not only safeguard individual privacy but also permit comprehensive analyses of large-scale clinical data obtained directly from electronic medical records (EMRs) and other clinical data sources, even in sensitive areas such as CAMHS.

Previous studies have applied synthetic mental health data in data augmentation, privacy preservation, and fairness [8]. The SynthNotes framework, developed by Begoli et al [9], is notable for its ability to produce realistic and high-fidelity synthetic mental health documentation on a large scale. The framework facilitates benchmarking, optimization, and training for biomedical NLP, information extraction, and machine learning systems, all while ensuring strict privacy preservation. To ensure accurate and generalizable research results, synthetic data must accurately represent diverse minority subgroups. This is particularly important in addressing child and adolescent mental health inequities exacerbated by events like the COVID-19 pandemic [10]. Addressing these biases requires expertise in the underlying model and an understanding of fairness concepts like unawareness, demographic parity, and conditional fairness [8]. One approach involves directly de-biasing existing datasets to create "fair data," a process similar to synthetic data generation [11,12]. Alternatively, some researchers view data de-biasing as a "ground-up" generation problem, focusing on developing generative models that inherently incorporate fairness [13].

Predictive models trained on synthetic data for mental health have yielded encouraging findings in numerous studies, highlighting the critical importance of data quality, ethical considerations, and the necessity for ongoing research. A study by Rankin et al [14] used a deep learning approach to predict mental health quality using synthetic data derived from functional network connectivity data from resting-state functional magnetic resonance imaging, achieving high accuracy in classifying mental health quality. Using models trained on synthetic data, Ajith et al [15] combined data from multiple longitudinal mobile sensing studies to predict mental health symptoms, showing improved generalization across different datasets. While these models frequently failed to capture intricate patterns and subtleties, especially within diverse populations [16], their results highlight the potential of synthetic data to enhance predictive modeling in mental health, while addressing privacy and fairness concerns.

While prior synthetic health data studies focused on adult mental health, our research specifically examines how synthetic data generators (SDGs) effectively capture complex patterns and relationships in CAMHS data. We assess the essential trade-offs involving data quality, patient privacy, analytical utility, and optimal synthetic sample size to ensure generated data remains representative and valuable for research.

XSL•FO
RenderX

Methods

Data Source

This study was conducted using a retrospectively collected cohort from the Child and Adolescent Mental Health Department (CAMHD) at Stavanger University Hospital (SUS). The hospital functions as a referral center for about half a million inhabitants in the Rogaland metropolitan area and had an annual admission ranging from 17,000 to 19,000 during the study period. CAMHD at SUS provides assessment, diagnosis, and treatment for young people aged 18 years or younger, experiencing mental health issues such as depression, anxiety, trauma, developmental disorders like autism or attention-deficit/hyperactivity disorder (ADHD), and psychosis.

As detailed in Table 1, the dataset included 6924 distinct patients, 7730 referral periods, and a total of 58,524 episodes of care. Data extraction was performed using the electronic health record system (Distrubuert Informasjons og Pasientdatasystem i Sykehuset [DIPS]; Helse Vest IKT). The system provided access to administrative details like time of admission, department, and clinical personnel, as well as clinical information such as age, sex, and diagnosis for each episode of care.

Each episode is directly linked to a specific referral through a unique identifier. Allowing for comprehensive and continuous tracking of a patient's journey from their initial referral through all subsequent clinical interactions.

XSL•FO
RenderX

Table 1. Overview of the Child and Adolescent Mental Health Services dataset.

Variable	Entity	Description	Descriptive statistics
referralID	Consultation/stay	Unique identifier for each referral	• N/A[a]
Patientage	Referral	Age of the patient at referral	• Mean 11 (SD 4) • Median 12 (IQR 15)
Patientsex	Referral	Patient's sex (0=female; 1=male)	• Unique values=2 • Most frequent=male
referralStartDate	Referral	Date the referral was initiated	• Minimum=2014 • Maximum=2018
referralLength	Referral	The duration of the referral period in days	• Mean 58 (SD 41) • Median 30 (IQR 60)
stayID	Consultation/stay	Unique identifier for each consultation or stay	• N/A
staySartDate	Consultation/stay	Date when the consultation or stay began	• Minimum=2014 • Maximum=2018
StayLength	Consultation/stay	Duration of each stay in minutes	• Mean 58 (SD 41) • Median 30 (IQR 60)
personnelGrp	Consultation/stay	Category of medical personnel involved	• Unique values=4 • Most frequent="psychologist"
stayTypeGrp	Consultation/stay	Grouped type of consultation or stay	• Unique values=5 • Most frequent="treatment"
specialist	Consultation/stay	Indicates if the medical personnel is a specialist (yes/no)	• Unique values=2 • Most frequent="no"
roleGrp	Consultation/stay	Role of the clinical personnel during the consultation or stay	• Unique values=2 • Most frequent="contact"
cond1axisIGrp	Consultation/stay	*ICD-10*[b] Axis I (clinical syndromes)	• Unique values=8 • Most frequent="R40-R46"
cond1axisIIGrp	Consultation/stay	*ICD-10* Axis II (disabilities)	• Unique values=4 • Most frequent=N/A
cond1axisIIIGrp	Consultation/stay	*ICD-10* Axis III (intellectual developmental disorder)	• Unique values=4 • Most frequent=N/A
cond1axisIVGrp	Consultation/stay	*ICD-10* Axis IV (somatic diseases)	• Unique values=4 • Most frequent=N/A
cond1axisVGrp	Consultation/stay	*ICD-10* Axis V (psychiatric disorders and somatic diseases)	• Unique values=6 • Most frequent=N/A
cond1axisVIGrp	Consultation/stay	*ICD-10* Axis VI, global functioning (CGAS[c])	• Unique values=7 • Most frequent=6999

[a]N/A: not applicable.

[b]ICD-10: International Statistical Classification of Diseases, Tenth Revision.

[c]CGAS: Children Global Assessment Score.

Missing Data

The dataset contains *ICD-10* (*International Statistical Classification of Diseases, Tenth Revision*) diagnostic codes categorized across different axes or levels of detail. The *ICD-10* uses a multiaxial system for mental and behavioral disorders, including Axis I (clinical syndromes), Axis II (disabilities), and Axis III (environmental/lifestyle factors).

XSL•FO
RenderX

A key characteristic of the Axis columns is the high rate of missing data, which indicates "not applicable" rather than an error, as is common in clinical coding. For instance, the first condition in Axis I is nearly complete (0.7% missing), but subsequent codes within the same axis show drastically increased missingness (eg, 6th condition, 99.8% missing). This trend continues across other axes, like Axis II (eg, 3rd condition 99.6% missing). This consistent pattern of missing values signifies that a code was not relevant to a clinical episode, making data imputation inappropriate.

Ethical Considerations

The study is a quality assurance initiative directly building on the results of the "PILOT SYNDATA" project. The project was conducted as a collaboration between CAMHD SUS, the analytical department at SUS, and Helse Vest IKT (the regional IT service delivery company). The project's main purpose was to explore the safe use of synthetic data in mental health care.

The data for the "PILOT SYNDATA" project were collected from DIPS, and Helse Vest IKT performed the deidentification and aggregation procedures, with the resulting anonymized data then being used for synthetic data generation in the next phase. This entire process was conducted under a formal agreement that permits the secondary use of health data for research and quality assurance while ensuring patient privacy and confidentiality. Due to the complete deidentification and aggregation of the data, a waiver was not required to use the data in this study.

The study used a synthetic data generation process that creates entirely new, statistically representative data points. The process is fully compliant with HIPAA (Health Insurance Portability and Accountability Act) and GDPR (General Data Protection Regulation) regulations, significantly reducing the risk of an attacker reidentifying individuals or uncovering sensitive patient details from the original dataset.

As this was a retrospective analysis of existing data, no financial compensation was provided to participants. Additionally, it is not possible to identify any individual participants in the figures or supplementary materials. The images are illustrative and use a "real-like path" to represent an anonymized, generalized patient journey.

Synthetic Data Generation

We use HMASynthetiser, a multitable algorithm within the Synthetic Data Vault framework [17]. HMASynthetiser is a class model that implements a "hierarchical modeling algorithm" to analyze data structured in multiple levels, often called nested data. These models are particularly useful when dealing with complex datasets in which observations are grouped at different levels, such as referral periods and episodes of care (Multimedia Appendix 1).

The SDG systematically processes the real CAMHS dataset, examining how information is structured across the referrals and episodes of care tables. It uses a Gaussian copula to map the complex relationships between every data field. A Gaussian Copula [18] is a statistical model used to identify the dependency structure between the nested dataset (referrals/episodes). The approach ensures that the SDG process accurately mirrors the statistical patterns and distributions present in the original patient records, even for variables with nonstandard or highly dependent relationships. In addition, the parameters of the SDG are customized for each individual table in the hierarchy, allowing fine-tuning of the synthetic data generation process. Hierarchical modeling, combined with the statistical method, is essential for accurately capturing the complex dependency structures within CAMHS variables.

Data Modeling

To optimize data utility and patient privacy, the real CAMHS dataset underwent comprehensive preprocessing prior to synthetic data generation. This involved the systematic categorization of variables, such as age and admission type, into broader, analytically meaningful groupings. Specifically, age was discretized into decennial intervals, while variables, such as "performing personnel" and "admission type," were recorded by mapping their original granular values to more generalized, descriptive categories. Additionally, diagnostic Axes I-IV were grouped based on the *ICD-10* hierarchy, and Axis VI (Children's Global Assessment Score) underwent specific binning and categorization to abstract sensitive medical codes.

These comprehensive preprocessing steps ensured the data were optimally structured for generating high-fidelity synthetic data and accurately reflected real-world patterns while rigorously upholding patient data protection.

Experimental Setup

Figure 1 displays the experimental setup. The experiments performed in this study followed 3 structures: sample size, privacy risk assessment, and utility assessment.

XSL•FO
RenderX

Figure 1. General study design. AUC: area under the curve; TRTR: train real test real; TSTR: train synthetic test real.

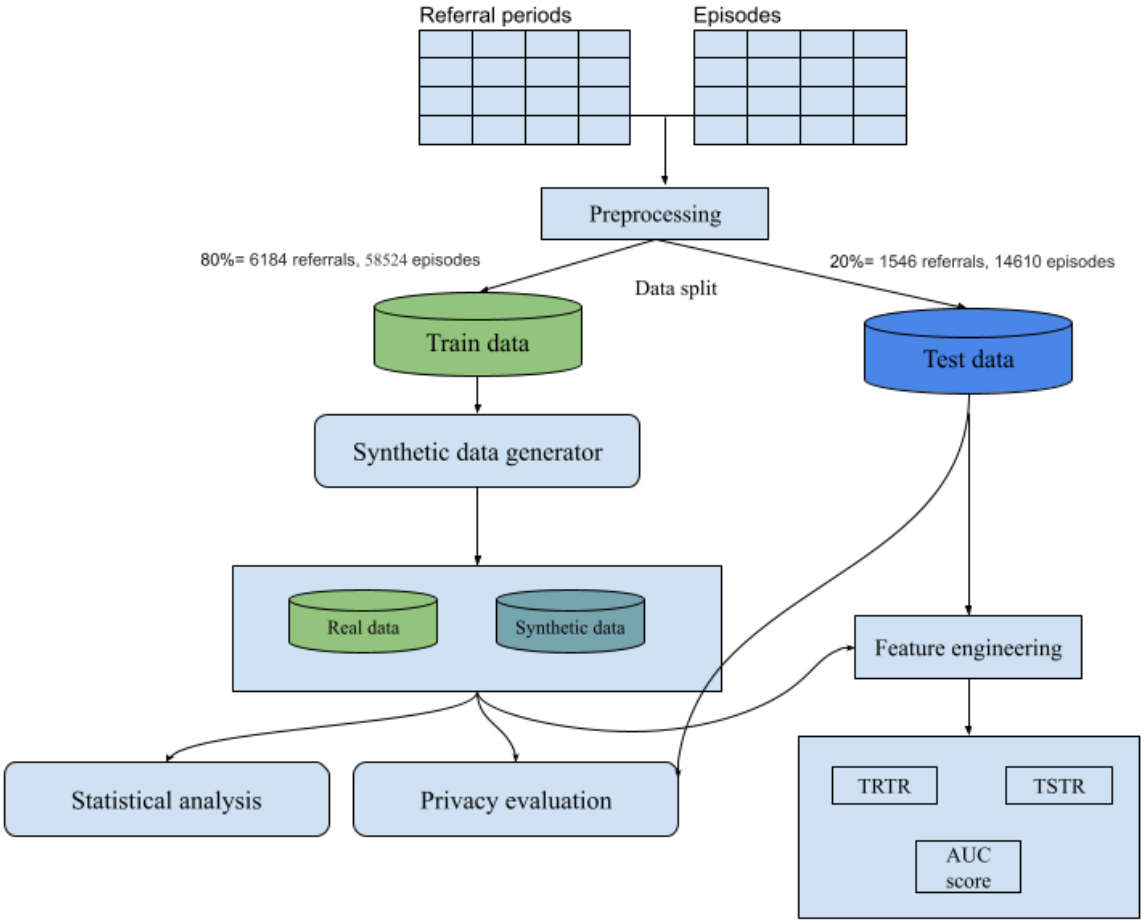

Sample Size

To evaluate the impact of sample size on predictive model performance (Multimedia Appendix 2), 4 distinct training sets (619, 1546, 3092, and 6184 referrals) were created from the real-world CAMHS data. For each of these sizes, a corresponding synthetic dataset was generated to enable a comparison of predictive model performance using both real and synthetic data across various data availability scenarios.

Privacy Risk Assessment

To measure the privacy risk in the generated synthetic data, we used the experimental approach via the Python library Anonymeter [19] (Multimedia Appendix 3). Initially, the attack uses synthetic data to create a series of guesses. The model then evaluates these guesses by comparing them to the values present in the original dataset, thereby assessing the effectiveness of the attack. The privacy model requires the adversary to conduct the same attack on a control dataset (records that were not used in the SDG). By contrasting the success rates of the attack on both training records and control records, a sensitive and significant measure of risk is established. Three types of privacy risk attacks were simulated and analyzed to evaluate the potential for reidentification: singling out, linkability, and inference risks.

Utility Assessment

Prediction tasks represent a robust and frequently used methodology for evaluating synthetic data utility, offering distinct advantages beyond conventional statistical comparisons. The method directly confirms the data's real-world applicability by assessing its capacity to replicate complex, nonlinear relationships for applications such as individualized mental health care planning or treatment pathway optimization. Furthermore, the approach validates the functional equivalence of synthetic data and provides a user-centric, interpretable metric of its inherent value, thereby facilitating the detection of subtle discrepancies overlooked by simpler analytical techniques [20]. To assess synthetic data utility, we formulated a downstream prediction task (Multimedia Appendix 4): classifying patient referral periods by intensity of care. Following Beckers et al [21], "intensity of care" was initially defined as low (<15 sessions/year), medium (15-51 sessions/year), or high (≥52 sessions/year). We extracted primary diagnosis of the first episode, sex, age, and total past referrals as predictor variables. Due to significant skewness (386/7730 high, 2087/7730 medium, and 5874/7730 low), the "medium intensity" and "high intensity" categories were merged into a "medium- or higher-intensity care" group. The combined group was selected to create a sufficiently sized positive class for stable model training, given the constraints of the severely skewed original distribution.

XSL•FO
RenderX

The dataset was then stratified by intensity and split into an 80% training set (6184 referral periods and 58,527 episodes) and a 20% independent test set (1546 referral periods and 14,610 episodes; Multimedia Appendix 5). The stratification ensured balanced distribution and kept all related patient data within either the training or test set; the test set was used solely for evaluation. A random forest model [22] was then trained using synthetic data generated at various scale factors (1, 2, 5, 10). The trained models were evaluated using the Train Synthetic, Test Real evaluation method [23], which involves training a model on synthetic data and testing it on real data.

Model performances were measured using precision-recall area under the curve (PRAUC), a robust metric particularly suited for imbalanced datasets [24,25]. We specifically chose PRAUC over the traditional area under the receiver operating characteristic curve because PRAUC is less susceptible to inflation from the majority (low intensity) class, providing a more accurate and rigorous measure of performance on the positive (medium- or higher-intensity care) class [24]. Results are presented as the median of a stratified 4-fold cross-validation.

Finally, SHAP (Shapley additive explanations) values [26] were computed for both models to assess variable interactions.

Statistical Analysis

To quantify the similarity between real and synthetic data, we used 4 key metrics from the SDMetrics Python library [23]. For numerical column distributions, we used the Kolmogorov-Smirnov Complement (KSC), while the Total Variation Complement (TVC) measured discrete column distributions. The preservation of intercolumn correlation patterns was evaluated using CorrelationSimilarity (CS), and CardinalityShapeSimilarity (CSS) was applied to assess the similarity in cardinality distributions within multitable datasets.

For privacy risk evaluation, we conducted 3 attack-based assessments focused on factual anonymization indicators: singling out determined the potential for identifying individual records; linkability assessed the risk of linking synthetic data back to the real dataset; and an inference attack was used to attempt to deduce sensitive individual information from seemingly nonsensitive data. A low inference risk means it is highly unlikely that an attacker could uncover specific, private details about individual patients from the original dataset.

Qualitative Visualization of Care Pathways

For the qualitative assessment, the specific “real patient path” was selected randomly from the overall real dataset after the synthetic data generation process was completed to ensure the visualization was not conditioned on the selected patient’s attributes prior to generation. This patient, a 12-year-old male diagnosed with “behavioral and emotional disorders” (F90-F98), represents a highly frequent and common clinical profile in our cohort. The corresponding “synthetic path” was then extracted from the synthetic data by identifying a synthetic patient with identical starting attributes (age, sex, and primary diagnosis) to provide a valid, anonymized, and attribute-matched comparison for event sequencing and density.

Results

Similarity and Quality Assessment of Synthetic CAMHS Data

As detailed in Table 2, the SDG produced CAMHS data that demonstrated high statistical similarity to the “real-world” CAMHS dataset. The result was evident across all reported metrics (KSC/TVC score=0.92; CS=0.75; CS (intertable)=0.73; CSS=0.9), with good fidelity remaining consistent regardless of the amount of “real-world” training samples provided to the algorithm.

Figure 2 presents 2 kernel density estimate plots, offering a visual comparison of feature distributions between real-world CAMHS data and synthetic data generated at various sample sizes. The left plot, illustrating “referral length,” reveals that the synthetic data distributions, particularly those derived from larger sample sizes (n=6184 and n=3092), closely align with the real test data’s distribution in the high-density range. While the synthetic data effectively captures the predominant patterns of referral lengths, there are minor deviations observed in the extreme tails, suggesting a slight challenge in perfectly replicating infrequent, very long referrals.

Similarly, the right plot, depicting “age,” demonstrates exceptionally high fidelity. All synthetic age distributions, regardless of the sample size, exhibit remarkable overlap with the real test data’s distribution. The peaks and overall shapes are nearly identical, indicating that the synthetic data generation process is highly successful in preserving the univariate statistical characteristics of patient age.

The observed high scores across the various quality metrics and kernel density estimates provide robust evidence that the synthetic data accurately replicates the original patient information’s characteristics and inherent relationships. Specifically, the significant KSC/TVC scores confirm that individual statistical distributions of each variable within the synthetic dataset demonstrate strong consistency with those observed in the real data, which implies that features like patient age ranges or referral lengths exhibit statistical properties consistent with their real-world counterparts. Furthermore, the high CS scores, including both intratable and intertable relationships, confirm the accurate preservation of complex dependencies and interactions between distinct variables. For example, critical correlational structures, such as the frequent association of specific diagnoses with treatment pathways or demographic profiles in the real data, are accurately maintained within the synthetic dataset. Finally, the high CSS scores confirm that the structural properties of the data, including the diversity of unique values within categorical fields and the overall shape of numerical distributions, are accurately replicated.

The consistent high scores underscore that the synthetic data not only replicates individual variable characteristics but also captures the intervariable relationships and the overall statistical integrity of the original, sensitive CAMHS patient information. The observed fidelity is critical for establishing synthetic data’s suitability for subsequent analytical and research applications.

XSL•FO
RenderX

Table 2. Average Kolmogorov-Smirnov Complement (KSC)/Total Variation Complement (TVC), CorrelationSimilarity (CS; single and intertable), and CardinalityShapeSimilarity (CSS) metrics from synthetic data evaluation experiments using different synthetic scale factor sizes.

	656 referrals	1546 referrals	3092 referrals	6184 referrals
KSC/TVC	0.91	0.92	0.92	0.92
CS	0.73	0.77	0.75	0.77
CS (intertable)	0.69	0.73	0.73	0.75
CSS	0.87	0.90	0.91	0.92

Figure 2. Visual comparison of the density distribution of the real and the derived synthetic Child and Adolescent Mental Health Services features. Density distributions for 2 selected features, “referral length” and “age,” and their synthetic derivatives are compared.

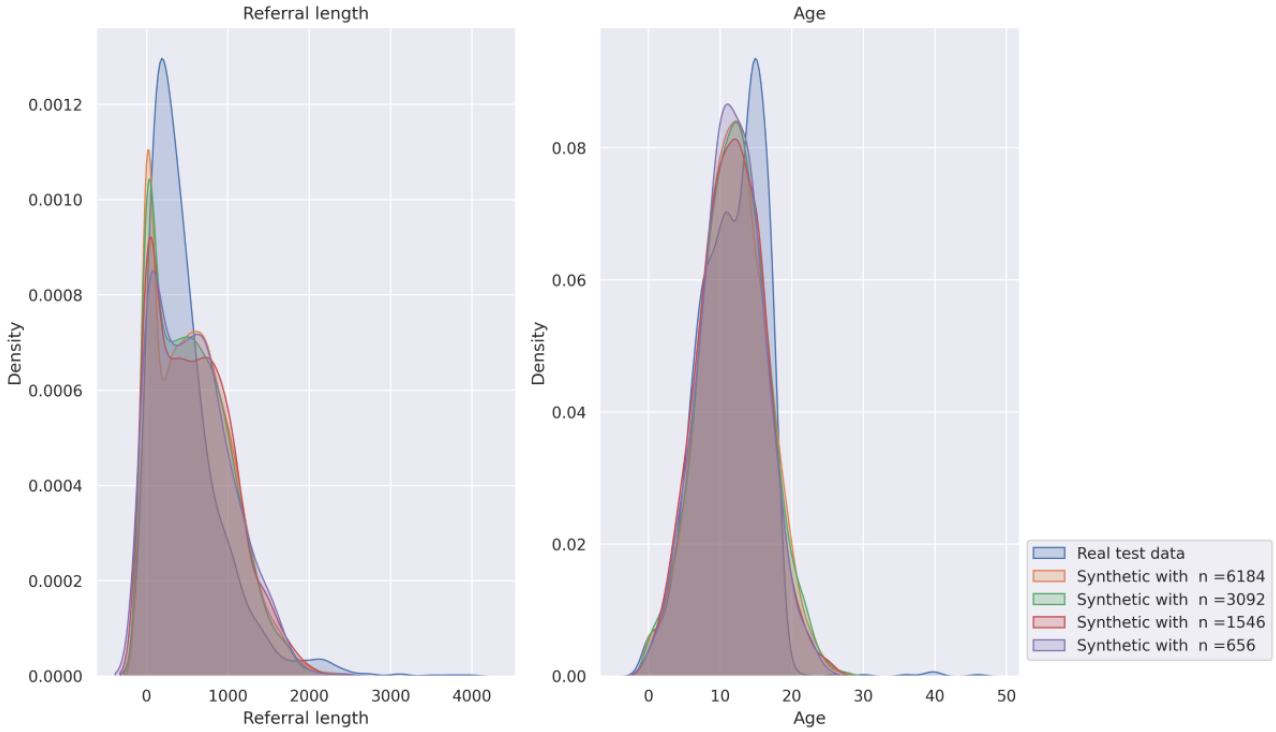

Synthetic Data Privacy Evaluation

To assess the potential for patient reidentification and information revelation, we performed 3 attack-based privacy evaluations: singling out, linkability, and attribute inference. Table 3 provides an overview of the success rate associated with the 3 simulated privacy attacks using synthetic data on a control real dataset (n=1546), highlighting the success rate achieved with various sample sizes. Specifically, the analysis reveals that both univariate and multivariate singling out attacks yield minimal average success rates, recorded at just 6/1546 (0.4%) and 77/1546 (5%), respectively. This indicates that the likelihood of successfully executing these types of attacks is low, regardless of the volume of data being analyzed. Furthermore, the table presents insights into the risk of linkability when using clinical and demographic variables as auxiliary data. The average risk of linkability is calculated to be 0.5% (8/1546), suggesting that while there is some potential for linking data to individuals, the overall risk remains quite low.

Similarly, inference risk of sensitive variables from patient age and sex was minimal for most attributes (Figure 3), with “admission week number” presenting the highest, yet still low, risk (2/1546, 0.12%).

A low percentage, for instance, a range of 0%-5%, indicates that an attacker’s capacity to deduce private details from the synthetic data is only marginally superior to random chance. To contextualize this, if Figure 3 reveals an inference risk of, for example, 2%, it signifies that an attacker possessing auxiliary nonsensitive information (eg, a patient’s age and gender from an external source) would still have only a 2% likelihood of accurately determining a specific sensitive attribute, such as a rare mental health diagnosis, from the synthetic dataset. The low probability demonstrates the robust privacy preservation achieved, reinforcing the suitability of this approach for sensitive health care data.

The results clearly demonstrate the robust capability of the synthetic data to effectively protect individual privacy. The protection is provided by the synthetic data generation process, which creates entirely new, statistically representative data points rather than simply masking or perturbing original records, thereby breaking any direct link to individual patients. As a result, it becomes highly unlikely for an attacker to reidentify specific individuals or uncover private, sensitive details about

XSL•FO
RenderX

patients from the original dataset, even if they possess some auxiliary information. This significantly mitigates risks associated with reidentification or attribute inference attacks, enabling a secure environment for data sharing.

Table 3. Success rate of singling out, linkability, and inference attacks on control data using various synthetic Child and Adolescent Mental Health Services data samples.

Risk type	6184 referrals, n/N (%)	3092 referrals, n/N (%)	1546 referrals, n/N (%)	619 referrals, n/N (%)
Singling out (univariate)[a] success rate	6/1546 (0.38)	6/1546 (0.38)	6/1546 (0.38)	7/1546 (0.43)
Singling out (multivariate)[b] success rate	46/1546 (3)	93/1546 (6)	62/1546 (4)	108/1546 (7)
Linkability[c] success rate	2/1546 (0.13)	5/1546 (0.34)	11/1546 (0.69)	13/1546 (0.84)

[a]Singling out (univariate) represents the percentage of successful attempts to uniquely identify an individual in the synthetic dataset using a single characteristic (based on 500 attacks). Lower values indicate better privacy.

[b]Singling out (multivariate) represents the percentage of successful attempts to uniquely identify an individual in the synthetic dataset using multiple combined characteristics (based on 100 attacks). Lower values indicate better privacy.

[c]Linkability represents the percentage of successful attempts to link synthetic records back to their original real records (based on 2000 attacks and 10 neighbors). Lower values indicate better privacy.

Figure 3. Inference risk.

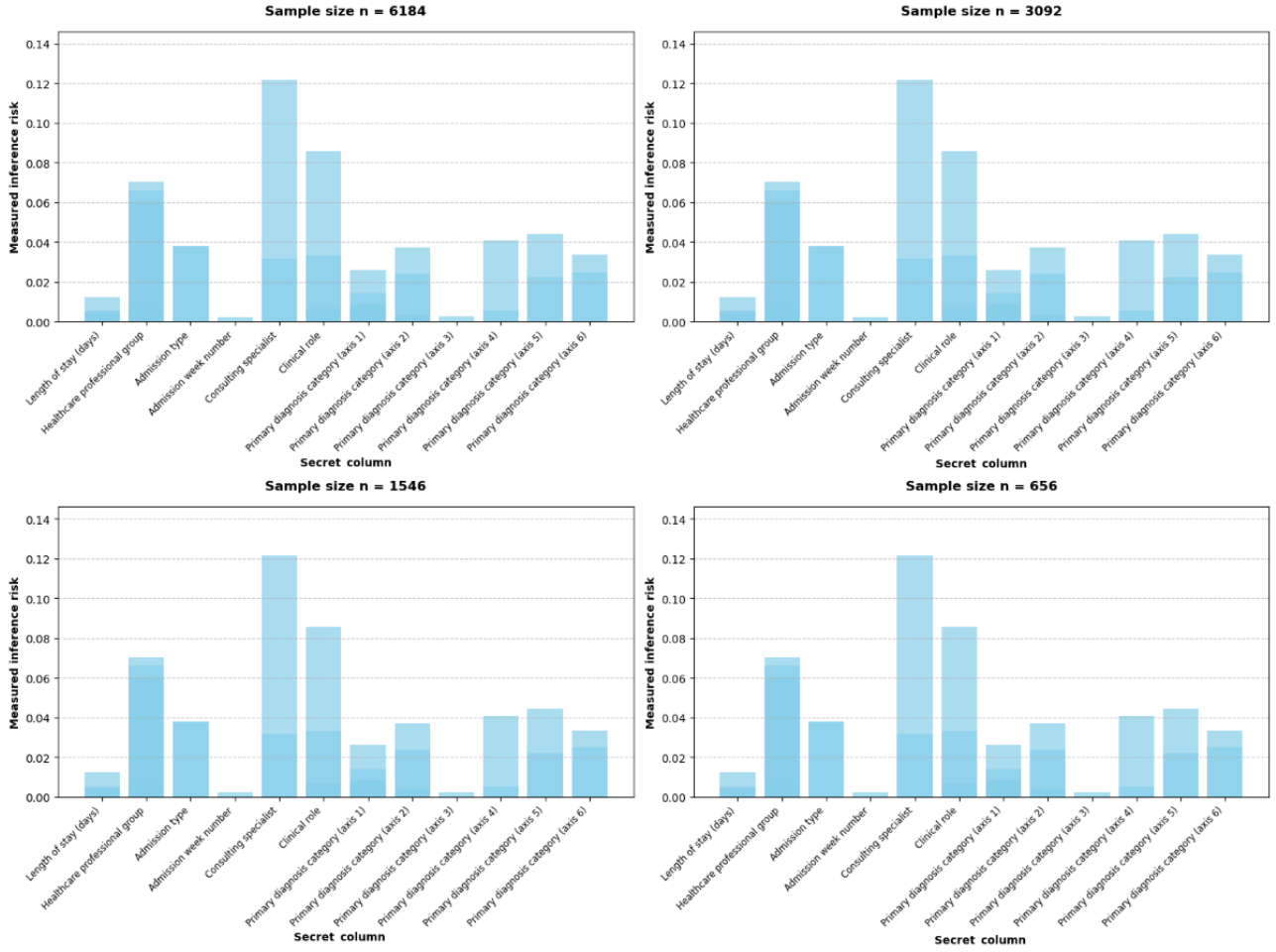

Synthetic Data Utility Evaluation

The target variable to be classified (intensity of care) in the utility evaluation was highly unbalanced in the real dataset, with 4111/6136 (67%) categorized as low intensity (<15 sessions annually), 2024/6136 (33%) as medium or higher intensity of care (>15 per year). We use the PRAUC metric to compare the predictive performance of machine learning models trained on real CAMHS data versus those trained on synthetic CAMHS data across different input sizes. Given the positive class prevalence of 33%, the random chance baseline (PRAUC baseline) is 0.33. As Table 4 illustrates, increasing sample size consistently improved predictive performance for both real and synthetic data models. In the most data-scarce setting (619 records), the random forest model's ability to classify medium-

XSL•FO
RenderX

or higher-intensity care patients was limited (real data: average PRAUC=0.39; synthetic data: PRAUC=0.32), However, when we increase the training set size to 6184 records, the model performance improved, with the average PRAUC for real data rising to 0.43 (a 30% increase over baseline) and for synthetic data to 0.40 (a 21% increase over baseline) demonstrating that the synthetic data preserves the analytical utility necessary to exceed the random threshold and capture real-world signals.

Our findings suggest that while privacy safeguards around children's data are paramount and often lead to smaller datasets, the value of more data in building accurate and robust predictive tools cannot be overstated. Simply put, the more comprehensive the data, the better equipped the models are to provide meaningful insights that can ultimately support patient care.

Table 4. Comparison of random forest–based prediction models trained on real, tested on real (TRTR) Child and Adolescent Mental Health Services (CAMHS) data alone versus those trained on synthetic, tested on real (TSTR) CAMHS data.

Sample size	TRTR, PRAUC[a] (range)	TSTR, PRAUC (range)
619 referrals	0.39 (0.34-0.44)	0.32 (0.28-0.38)
1546 referrals	0.40 (0.36-0.47)	0.33 (0.29-0.38)
3092 referrals	0.41 (0.37-0.47)	0.34 (0.30-0.39)
6184 referrals	0.43 (0.38-0.49)	0.40 (0.35-0.45)

[a]PRAUC: precision-recall area under the curve.

Reproducibility of Feature Interpretability (SHAP)

SHAP analysis, presented in Figure 4, provides an insight into how different patient characteristics impact the predicted intensity of care, both when the model is trained on real patient data and when it is trained on synthetic patient data.

The model consistently showed that a lower prevalence of "behavioral and emotional disorders" (F90-F98) led to a higher predicted intensity of care. This finding is a clinically meaningful observation rooted in the structure of CAMHS resource allocation; because F90-F98 diagnoses (eg, ADHD, externalizing difficulties) are highly prevalent and typically managed via lower-intensity, first-line support, their presence is not a strong predictor of high-intensity service use. Therefore, the absence of this common, low-intensity diagnosis in a patient referred for complex care suggests the presence of a less common, more severe, or highly comorbid condition that immediately necessitates the allocation of higher-intensity resources [27].

Conversely, a greater presence of "symptoms and signs (general)" (R40-R46) or "developmental disorders" (F80-F89) contributed to a lower predicted intensity of care. Patient age also presented a clear and consistent trend; younger patients were generally predicted to require higher intensity care, while older patients were associated with lower predicted intensity. On the plots, lower values for a feature are typically shown in gray, higher values in black; features increasing predicted intensity extend to the right, while those decreasing it extend to the left.

While the models showed consistent variable impact on the target prediction (intensity of care), we noted a significant difference in the strength of this impact between the synthetic and the real prediction models. The model trained on actual patient data showed a much wider range of impacts from individual features (SHAP values ranging from approximately –0.15 to 0.15), suggesting that real patient characteristics could lead to more pronounced shifts in the predicted intensity of care. In contrast, the model trained on synthetic data displayed a significantly narrower range of influence (approximately –0.03 to 0.03). The "flattening" of the variables' impact on the predicted intensity of care implies that while synthetic data helps the model learn the general direction of how patient characteristics relate to care intensity, it reduces the overall sensitivity of the model to the nuanced, individual variations found in real patient data. This effect, however, can be mitigated by using more advanced synthetic data generation techniques.

Despite the observed reduced variable impact in the synthetic model, the consistency in the direction of SHAP-based explanations remains clinically valuable. It effectively validates synthetic data's ability to capture fundamental predictive patterns in sensitive health care records, making synthetic datasets particularly useful for privacy-preserving exploratory research and facilitating hypothesis generation and validation. While acknowledging the continued need for further efforts to precisely replicate nuanced quantitative impacts for high-stakes clinical predictions, the qualitative fidelity of the result offers an effective tool for initial understanding and safe experimentation in CAMHS health research.

XSL•FO
RenderX

Figure 4. Shapley additive explanations (SHAP) values for intensity of care in (A) train real test real and (B) train synthetic test real models (n=6184).

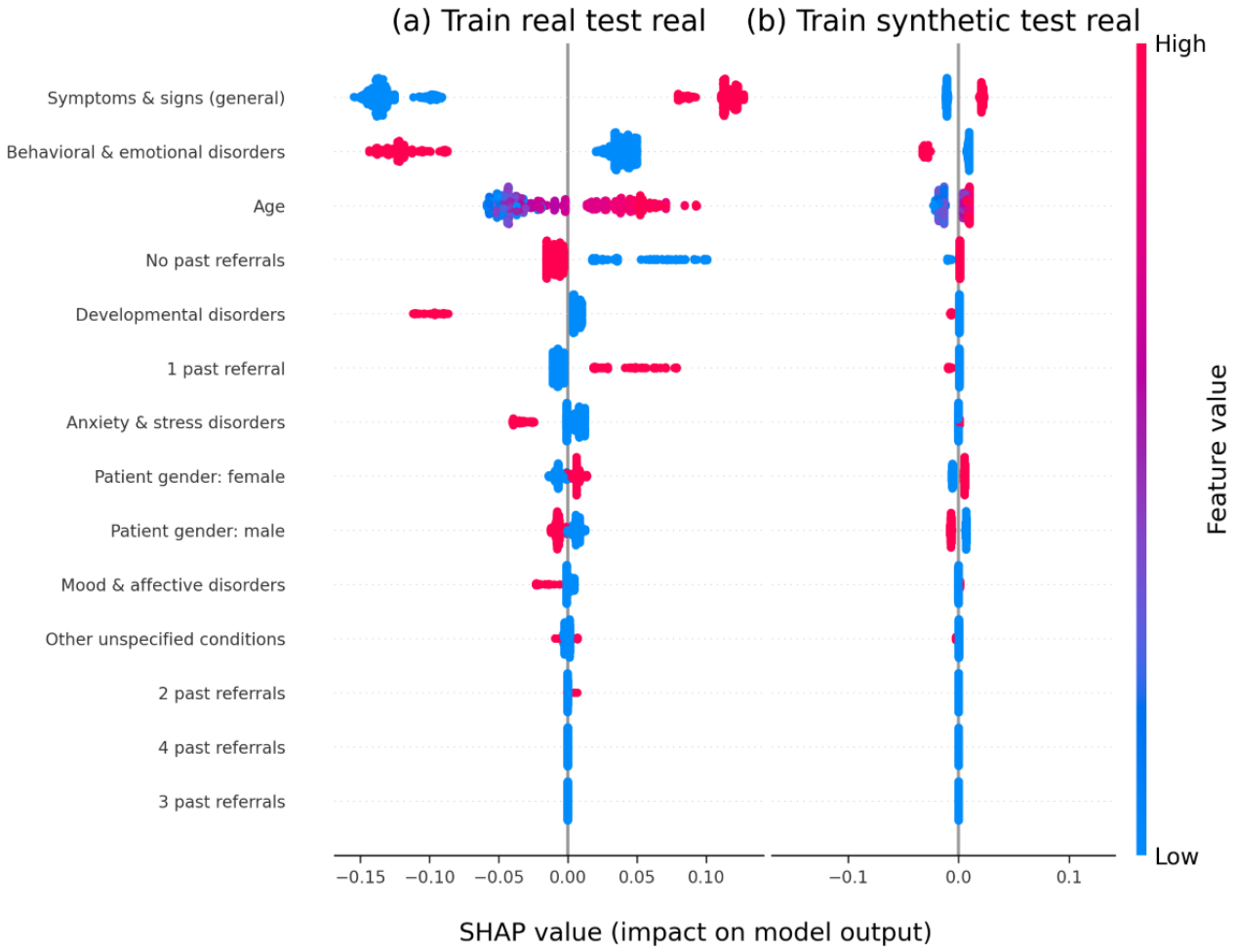

Synthetic and Real Individual Care Paths

Figure 5 compares 2 distinct care pathways for a 12-year-old male patient diagnosed with "behavioral and emotional disorders" (F90-F98). Both paths are presented on a shared timeline (x-axis) that has been aligned to start at a common point, allowing for direct comparison of event sequencing and density.

The figure serves as a comparative visualization, highlighting potential differences in the flow, types of interventions, and personnel involvement between a synthetic and a more real care path.

While synthetic CAMHS data successfully captures the overarching statistical patterns of the real CAMHS dataset, divergences at the individual patient level offer valuable insights. The differences result from synthetic data representing the most common trajectories, an average derived from the entire dataset that naturally filters out the unique noise and unobserved idiosyncratic factors influencing real-world care. Real CAMHS care is inherently nonlinear and dynamic, shaped by patient responses, unforeseen crises, resource constraints, and patient/family agency. These complexities, including feedback loops and real-world bottlenecks such as waiting lists, are challenging for synthetic data to perfectly replicate at an individual level, leading to the observed divergence.

XSL•FO
RenderX

Figure 5. Comparison of real-like and synthetic care paths for an attention-deficit/hyperactivity disorder (ADHD) patient. The x-axis (Date of stay [Aligned]) shows the progression of time. The y-axis separates the "Synthetic path" (top, solid line) from the "Real path" (bottom, dashed line). Individual markers represent stay events, annotated with stay types and personnel categories. The grey box (top left) indicates shared patient demographics for both trajectories.

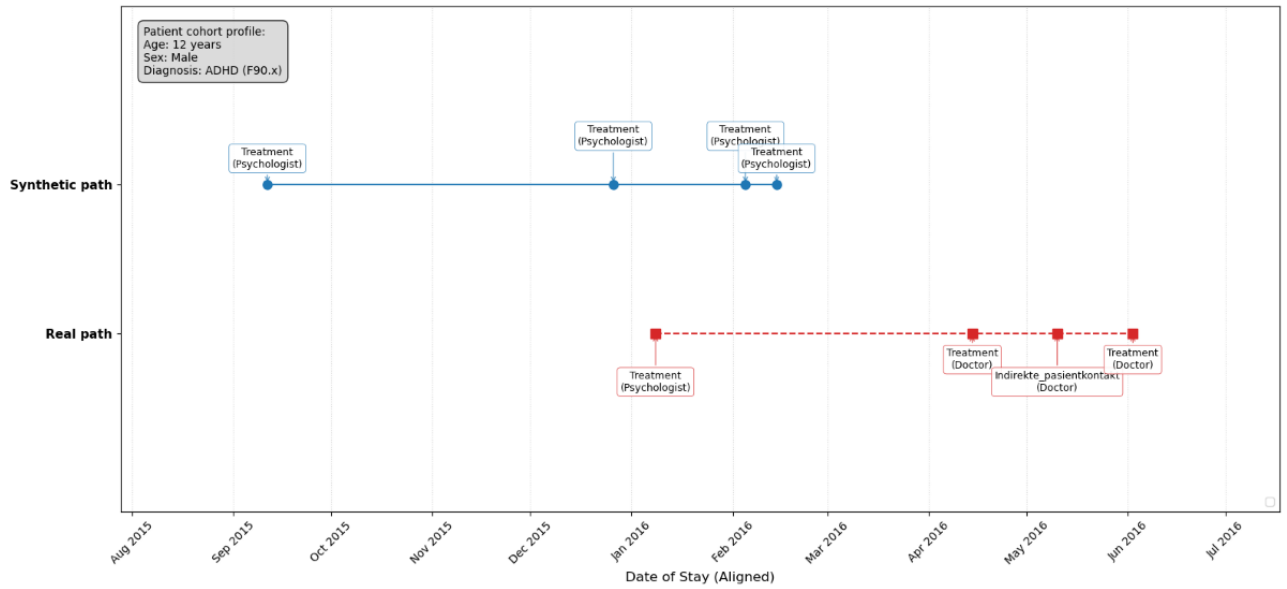

Discussion

Principal Findings

This study demonstrates the significant potential of synthetic data to enhance the utility of electronic health care records within CAMHS. Our methodology, using a hierarchical SDG, generated synthetic datasets that exhibited high statistical fidelity to real-world CAMHS data, as confirmed by various quality metrics (KSC/TVC, CS, CSS) and visual density comparisons. While minor quality variations were observed with decreasing sample sizes [28], the results confirm that our approach broadly preserves variable behaviors and dependencies between variables in the generated synthetic datasets [29]. However, identifying the precise minimum real data sample size for generating truly useful and high-fidelity synthetic CAMHS data is complex and highly dependent on the specific research scope and applications.

Models trained on synthetic data demonstrated predictive performance in classifying patient “intensity of care” (low vs medium or higher) that was comparable to models trained on real data. While the absolute predictive power of the model was modest (PRAUC=0.40-0.43 over a 0.33 random baseline), the key finding is the preservation of this utility in the synthetic data, as evidenced by the comparable scores**.**

The SHAP analysis confirmed that the synthetic model’s explainability aligned with real-world insights, underscoring the consistent importance of age and CAMHS diagnosis (eg, anxiety disorders, depression, ADHD, and autism spectrum disorder) in assessing care needs [30,31]. Furthermore, our findings provide strong evidence that synthetic data effectively protects individual privacy. The data generation process makes it highly unlikely for attackers to reidentify patients or uncover sensitive details from the original dataset, a critical requirement given the highly personal nature of CAMHS data.

The implications of high-fidelity, privacy-preserving synthetic CAMHS datasets are profound for children and adolescent mental health research and practice. Their availability removes critical barriers to data sharing and collaborative research, enabling more thorough investigations into mental health aspects across diverse populations [32], especially for vulnerable ones like those served by CAMHS. This capability facilitates a deeper understanding of mental disorder patterns and contributes to the development of more effective, personalized treatment methodologies [33]. Moreover, given that young adolescents often withhold important information from health care providers due to privacy concerns, which hinders effective diagnosis and treatment [34], synthetic data allows researchers to explore critical questions that would be impossible with real, incomplete data. These include understanding the impact of stigma on treatment adherence, evaluating novel personalized interventions, investigating the influence of “hidden” family dynamics, and simulating the effects of systemic barriers on access to care for vulnerable groups.

Furthermore, maintaining highly accurate long-term temporal and sequential relationships across numerous event types remains challenging in synthetic data generation. Most synthetic data quality metrics prioritize aggregate statistical properties over the exact fidelity of unique individual sequences. This means a synthetic dataset can be excellent at the population level but still show microlevel divergence in individual trajectories. Despite these differences, the divergence is valuable. It highlights that synthetic data, while not predicting exact individual pathways, excels at understanding general care models, developing system-level interventions via cohort simulations, and creating privacy-preserving case studies for training. It effectively complements the detailed study of highly personalized real-world clinical journeys.

XSL•FO
RenderX

Future Work

To improve upon the findings of this investigation, future research can focus on enhancing the synthetic data generation process. Conditional generative models, such as variational autoencoders [35] and generative adversarial networks [36], could be trained to produce synthetic data that reflects specific referral reasons or treatment modalities, conditioned on existing basic patient information. These advanced models are adept at learning complex data distributions, leading to higher-quality and more diverse synthetic outputs, which are crucial for capturing the varied presentations within CAMHS.

Beyond static data generation, further research can also explore integrating synthetic data with process mining techniques to enhance the modeling of complex care sequences. Specifically, synthetic process mining offers a powerful avenue for generating and analyzing event logs that mimic real patient journeys, but with full privacy control [37]. This would enable the creation of highly detailed, longitudinal synthetic care pathways, allowing researchers to simulate and analyze "what if" scenarios for process optimization without touching real patient data (eg, assessing the impact of adding a new therapy step or reducing wait times on patient flow). Furthermore, synthetic process mining could also generate diverse and comprehensive training data for predictive models focused on patient trajectories and outcomes, especially for rare events or complex multistage interventions where real CAMHS data are scarce or incomplete. This capability would significantly advance our understanding of care delivery dynamics and improve operational efficiency in CAMHS, ultimately benefiting young people awaiting and receiving support.

Limitations

It is important to recognize that our dataset had limitations in terms of clinical parameters. Our analysis revealed modest predictive power in the classification model (PRAUC approximately 0.43 on real data and 0.40 on synthetic data), necessitating caution in interpreting the absolute predictive accuracy. While the primary goal of this work was to establish the comparable utility between the synthetic and real datasets—which the similar PRAUC scores confirm—the absolute performance remains constrained. This constraint is likely attributable to 2 factors: severe class imbalance in the target variable (necessitating the aggregation of the rare high-intensity category into the 33% positive class) and the inherently limited, aggregated feature set available from administrative EMR. These limitations emphasize that the model should not be used in isolation for clinical prediction but rather that the synthetic data successfully preserves the utility inherent in the original feature space.

Furthermore, our dataset had limitations in terms of clinical parameters. Although we had access to basic data such as sex, age, and clinical primary diagnosis, our dataset lacked detailed information on the specific reason for the referral and the amount of additional care (eg, medication, group sessions, art therapy, physical therapy, and sheltered workshop). These clinical details are crucial for accurately assessing and classifying service intensity. The absence of these detailed clinical parameters may have impacted the accuracy of our analyses and the general applicability of our findings to a broader clinical context. Future research will benefit from a more comprehensive dataset that includes these key clinical parameters.

Regarding fairness evaluation, Norway's highly inclusive public health care system inherently minimizes selection bias. However, we acknowledge the potential for underrepresentation of underserved minorities and rare diagnoses. These issues can be effectively addressed by augmenting the data with synthetic samples of these specific groups and applying fairness measures tailored to the analytical goals of research aimed at serving these minority populations. While the methodology for creating synthetic CAMHS data is highly generalizable across different data environments and health care systems, it is crucial to recognize that the interpretation and applicability of findings derived from such synthetic data would always need to be contextualized within the specific health care system from which the original data was sourced. This underscores the need for localized validation and careful consideration of systemic differences when applying research findings across international borders.

Conclusions

This study provides evidence that synthetic data can be generated from CAMHS EMR that achieves a favorable balance between utility and privacy. The main findings confirm that the hierarchical synthetic data model produces datasets with high statistical fidelity and comparable predictive utility to real data, while simultaneously demonstrating a reduced risk of patient reidentification. This pilot study suggests that synthetic data, developed from standard EMR clinic records, offers a method compliant with HIPAA and GDPR regulations, facilitating clinical and administrative research that was previously unattainable. This advancement creates critical new opportunities for CAMHS research to progress despite confidentiality restrictions.

Acknowledgments

We gratefully acknowledge the invaluable help of the Individualized Digital Decision Assist System project, BUP Helse Stavanger, and Helse Vest IKT, Synnøve Olset, for bringing the collaborators together and providing valuable feedback in preparing this manuscript.

The authors confirm that generative artificial intelligence tools, specifically Gemini by Google, were used for three specific and limited purposes during the preparation of this manuscript and the revision process:

XSL•FO
RenderX

1. Language polishing: minor language refinement and grammatical correction throughout the manuscript text to improve readability and flow.

2. Structural drafting: generating the initial structural outline for the author's response emails to the academic editor during the peer-review process.

3. Content generation: generating the visual representation for Figure 5, based on the data and themes analyzed in this study. The authors take full responsibility for the content, integrity, and scientific accuracy of the research presented.

Data Availability

The underlying dataset can be shared upon reasonable request after signing a data transfer agreement with the receiving institution to ensure the protection of personal information. The code underlying these analyses is available from GitHub [38].

Authors' Contributions

Data curation and analysis: MH, LRØ
Check and investigation: MH, ØN
Methodology: MH
Project administration: MH
Writing—original draft: MH
Review and editing: DP, NS, ØN, BLL, KK, RAK, LRØ

Conflicts of Interest

None declared.

Multimedia Appendix 1
Entity-relationship diagram of the patient data schema. This diagram illustrates the relationship between the "referral" and "stay" entities, detailing the attributes and their data types (ID, datetime, numerical, categorical) for each, along with their respective primary and foreign keys.
[PNG File , 41 KB - medinform_v14i1e71819_app1.png]

Multimedia Appendix 2
Synthetic generation process. We used a constant input for the synthetic data generator HMSynthetiser (ie, a fixed subsample from the real dataset) to output 4 different synthetic CAMHS data. The similarity between each of the datasets was compared to the real training data by performing KSC/TVC, CS, and CSS metrics via the SDMetrics Python package.
[PNG File , 60 KB - medinform_v14i1e71819_app2.png]

Multimedia Appendix 3
Privacy evaluation. The Main attack (1) uses synthetic data to create a series of guesses. Anonymeter evaluates (2) these guesses by comparing them to the values present in the original dataset, to assess the effectiveness of the attack. Anonymeter requires the adversary to conduct the same attack on a control dataset (control attack), which consists of records that were not utilized in the generation of the synthetic data. Any insights the attacker gains regarding the control records from the synthetic dataset cannot be linked to privacy violations, as the design ensures that no information from the control dataset is incorporated into the synthetic dataset. By contrasting the success rates of the attack on both training records and control records, a sensitive measure of risk (3) is calculated.
[PNG File , 35 KB - medinform_v14i1e71819_app3.png]

Multimedia Appendix 4
Train synthetic test real. To evaluate model efficacy, the train synthetic test real (TSTR) approach was used. Two machine learning models were developed: one trained on real data and the other on synthetic data, both targeting patients with referral duration under 18 months to predict Child and Adolescent Mental Health Services (CAMHS) care intensity across three categories: fewer than 15 sessions, 15 or more sessions annually. The latter two categories were combined due to low occurrence of high intensity. Model performance was assessed using a 20% test subset from the real dataset, allowing comparison of synthetic and real data effectiveness. SHAP values were computed to analyze feature significance.
[PNG File , 63 KB - medinform_v14i1e71819_app4.png]

Multimedia Appendix 5

XSL•FO
RenderX

Characteristics of the training (n=6132) and test (n=1531) datasets. This table presents the distribution of demographic, clinical, and diagnostic variables across the training and test cohorts.
[PDF File (Adobe PDF File), 30 KB - medinform_v14i1e71819_app5.pdf]

References

1. Aboujaoude E. Protecting privacy to protect mental health: the new ethical imperative. J Med Ethics 2019;45(9):604-607. [doi: 10.1136/medethics-2018-105313]
2. Iflaifel M, Hall CL, Green HR, Willis A, Rennick-Egglestone S, Juszczak E, et al. Widening participation - recruitment methods in mental health randomised controlled trials: a qualitative study. BMC Med Res Methodol 2023;23(1):211 [FREE Full text] [doi: 10.1186/s12874-023-02032-1] [Medline: 37735627]
3. Berardi C, Antonini M, Jordan Z, Wechtler H, Paolucci F, Hinwood M. Barriers and facilitators to the implementation of digital technologies in mental health systems: a qualitative systematic review to inform a policy framework. BMC Health Serv Res 2024;24(1). [doi: 10.1186/s12913-023-10536-1] [Medline: 38408938]
4. Henderson C, Noblett J, Parke H, Clement S, Caffrey A, Gale-Grant O, et al. Mental health-related stigma in health care and mental health-care settings. Lancet Psychiatry 2014;1(6):467-482. [doi: 10.1016/S2215-0366(14)00023-6] [Medline: 26361202]
5. Sedlakova J, Daniore P, Horn Wintsch A, Wolf M, Stanikic M, Haag C, University of Zurich Digital Society Initiative (UZH-DSI) Health Community. Challenges and best practices for digital unstructured data enrichment in health research: a systematic narrative review. PLoS Digit Health 2023;2(10):e0000347 [FREE Full text] [doi: 10.1371/journal.pdig.0000347] [Medline: 37819910]
6. Waithira N, Mukaka M, Kestelyn E, Chotthanawathit K, Thi Phuong DN, Thanh HN, et al. Data sharing and reuse in clinical research: are we there yet? A cross-sectional study on progress, challenges and opportunities in LMICs. PLOS Glob Public Health 2024;4(11):e0003392. [doi: 10.1371/journal.pgph.0003392] [Medline: 39565766]
7. National Academies of Sciences, Engineering, and Medicine. Frontiers in Massive Data Analysis. Washington DC: The National Academies Press; 2013.
8. Bhanot K, Qi M, Erickson JS, Guyon I, Bennett KP. The problem of fairness in synthetic healthcare data. Entropy 2021;23(9):1165. [doi: 10.3390/e23091165]
9. Begoli E, Brown K, Srinivas S, Tamang S. SynthNotes: a generator framework for high-volume, high-fidelity synthetic mental health notes. 2022 Presented at: IEEE International Conference on Big Data (Big Data); 2018 Dec 10-13; Seattle, WA, USA. [doi: 10.1109/bigdata.2018.8621981]
10. Mori S, Ignat O, Lee A, Mihalcea R. Towards algorithmic fidelity: mental health representation across demographics in synthetic vs. human-generated data. arXiv. Preprint posted online on March 25, 2024 2024 [FREE Full text]
11. van Breugel B, Kyono T, Berrevoets J, van der Schaar M. Decaf: generating fair synthetic data using causally-aware generative networks. 2021 Presented at: Advances in Neural Information Processing Systems 34 (NeurIPS 2021); 2021 Dec 6-14; Online p. 10620-10632.
12. Kamiran F, Calders T. Classifying without discriminating. 2022 Presented at: 2nd International Conference on Computer, Control and Communication; 2009 Feb 17-18; Karachi, Pakistan p. 1-6. [doi: 10.1109/ic4.2009.4909197]
13. Ramachandranpillai R, Sikder MF, Bergström D, Heintz F. Bt-GAN: generating fair synthetic healthdata via bias-transforming generative adversarial networks. J Artif Intell Res 2024;79:1313-1341. [doi: 10.1613/jair.1.15317]
14. Rankin T, Gonzales M. Evaluating predictive models trained on synthetic data for mental health applications. Artif Intell Med 2022;123:102195. [doi: 10.1016/j.artmed.2022.102195]
15. Ajith M, Aycock DM, Tone EB. A deep learning approach for mental health quality prediction using functional network connectivity and assessment data. Brain Imaging Behav 2024;18:630-645. [doi: 10.1007/s11682-023-00801-4]
16. Lee K, Kim H. Machine learning for passive mental health symptom prediction: generalization across different longitudinal mobile sensing studies. PLoS One 2023;18(3):e0266516. [doi: 10.1371/journal.pone.0266516]
17. Patki N, Wedge R, Veeramachaneni K. The synthetic data vault. 2022 Presented at: IEEE International Conference on Data Science and Advanced Analytics (DSAA); 2016 Oct 17-19; Montreal, QC p. 2016. [doi: 10.1109/dsaa.2016.49]
18. Houssou R, Augustin M, Rappos E, Bonvin V, Robert-Nicoud S. Generation and simulation of synthetic datasets with copulas. arXiv. Preprint posted online on March 30, 2022 2022. [doi: 10.48550/arXiv.2203.17250]
19. Giomi M, Boenisch F, Wehmeyer C, Tasnádi B. A unified framework for quantifying privacy risk in synthetic data. arXiv. Preprint posted online on November 18, 2022 2022. [doi: 10.48550/arXiv.2211.10459]
20. Lu Y, Chen L, Zhang Y, Shen M, Wang H, Wang X. Machine Learning for Synthetic Data Generation: A Review. arXiv. Preprint posted online on February 8, 2023 2023. [doi: 10.48550/arXiv.2302.04062]
21. Beckers T, Koekkoek B, Tiemens B, Hutschemaekers G. Measuring the intensity of mental healthcare: Development of the Mental Healthcare Intensity Scale (MHIS). BMC Psychiatry 2023;23(1):377. [doi: 10.1186/s12888-023-04870-w]
22. Uddin S, Khan A, Hossain ME, Moni MA. Comparing different supervised machine learning algorithms for disease prediction. BMC Med Inform Decis Mak 2019;19(1):281 [FREE Full text] [doi: 10.1186/s12911-019-1004-8] [Medline: 31864346]

XSL•FO
RenderX

23. Esteban C, Hyland S, Rätsch G. Real-Valued (MEDICAL) time series generation with recurrent conditional GANs. arXiv. Preprint posted online on June 8, 2017 2017. [doi: 10.48550/arXiv.1706.02633]
24. Kiran A, Kumar S. Synthetic data and its evaluation metrics for machine learning. In: So-In C, Londhe ND, Bhatt N, Kitsing M, editors. Information Systems for Intelligent Systems. Smart Innovation, Systems and Technologies. Singapore: Springer; 2023:433-448.
25. Richardson E, Trevizani R, Greenbaum JA, Carter H, Nielsen M, Peters B. The receiver operating characteristic curve accurately assesses imbalanced datasets. Patterns (NY) 2024;5(6):100994. [doi: 10.1016/j.patter.2024.100994] [Medline: 39005487]
26. Lundberg S, Lee S. A unified approach to interpreting model predictions. 2017 Presented at: 31st Conference on Neural Information Processing Systems (NIPS 2017); 2017 Dec 4-9; Long Beach p. 4768-4777 URL: https://proceedings.neurips.cc/paper_files/paper/2017/file/8a20a8621978632d76c43dfd28b67767-Paper.pdf
27. Edbrooke-Childs J, Rashid A, Ritchie B, Deighton J. Predictors of amounts of child and adolescent mental health service use. Eur Child Adolesc Psychiatry 2023;32(11):2335-2342 [FREE Full text] [doi: 10.1007/s00787-022-02063-x] [Medline: 36114311]
28. McDermott MBA, Wang S, Marin N. A closer look at AUROC and AUPRC under class imbalance. 2020 Presented at: Proceedings of the 37th International Conference on Machine Learning; 2020 Jul 12-18; Online p. 6753-6763. [doi: 10.52202/079017-1400]
29. Marin J. Evaluating synthetic tabular data generated to augment small sample datasets. arXiv. Preprint posted online on November 19, 2022 2022. [doi: 10.48550/arXiv.2211.10760]
30. Benali F, Bodénès D, Labroche N, de RC. MTCopula synthetic complex data generation using copula. 2021 Presented at: 23rd International Workshop on Design, Optimization, Languages and Analytical Processing of Big Data (DOLAP); 2021 Mar 23; Nicosia, Cyprus URL: https://ceur-ws.org/Vol-2840/paper8.pdf
31. Smith J, Doe A. Age and Developmental Considerations in CAMHS. J Child Psychol Psychiatry 2023;64(2):123-134. [doi: 10.1111/jcpp.12345]
32. Brown L, Green P. Gender differences in mental health diagnoses and treatment. J Adolesc Health 2024;58(3):567-578. [doi: 10.1016/j.jadohealth.2024.01.002]
33. Rocks S, Stepney M, Glogowska M, Fazel M, Tsiachristas A. Understanding and evaluating new models of Child and Adolescent Mental Health Services in South-East England: a study protocol for an observational mixed-methods study. BMJ Open 2018;8(12):e024230 [FREE Full text] [doi: 10.1136/bmjopen-2018-024230] [Medline: 30518588]
34. Improvements ahead: how humansAI might evolve together in the next decade. Pew Research Center. 2018. URL: https://www.pewresearch.org/internet/2018/12/10/improvements-ahead-how-humans-and-ai-might-evolve-together-in-the-next-decade/ [accessed 2026-01-26]
35. Wan Z, Zhang Y, He H. Variational autoencoder based synthetic data generation for imbalanced learning. 2017 Presented at: 2017 IEEE Symposium Series on Computational Intelligence (SSCI); Honolulu, HI, USA; 2017 Nov 27-Dec 1; Honolulu. [doi: 10.1109/ssci.2017.8285168]
36. Guo J, Jin S, Wang M, Han C. Generating synthetic mixed-type longitudinal electronic health records for artificial intelligent applications. NPJ Digit Med 2023;6(1):68. [doi: 10.1038/s41598-023-33049-7]
37. Bullward A, Aljebreen A, Coles A. Process mining and synthetic health data: reflections and lessons learnt. 2022 Presented at: 4th International Conference on Process Mining (ICPM 2022); 2022 Oct 23-28; Bozen-Bolzano p. 4. [doi: 10.1007/978-3-031-27815-0_25]
38. mounirHai/SynthCAMH. GitHub. URL: https://github.com/mounirHai/SynthCAMH [accessed 2026-12-05]

Abbreviations

ADHD: attention-deficit/hyperactivity disorder
CAMHD: Child and Adolescent Mental Health Department
CAMHS: Child and Adolescent Mental Health Services
CS: CorrelationSimilarity
CSS: CardinalityShapeSimilarity
DIPS: Distrubuert Informasjons og Pasientdatasystem i Sykehuset
EMR: electronic medical record
GDPR: General Data Protection Regulation
HIPAA: Health Insurance Portability and Accountability Act
ICD-10: International Statistical Classification of Diseases, Tenth Revision
KSC: Kolmogorov-Smirnov Complement
PRAUC: precision-recall area under the curve
SDG: synthetic data generator
SHAP: Shapley additive explanations
SUS: Stavanger University Hospital

XSL•FO
RenderX

TVC: Total Variation Complement

Edited by A Coristine; submitted 27.Jan.2025; peer-reviewed by W Farr, X Ding; comments to author 12.May.2025; accepted 23.Oct.2025; published 26.Feb.2026.

Please cite as:
Haizoune M, Leventhal BL, Pant D, Nytrø Ø, Koochakpour K, Koposov RA, Øhlckers LR, Skokauskas N
Balancing Privacy and Utility in Child and Adolescent Mental Health Services Research: Retrospective Cohort Study on Synthetic Data Generation
JMIR Med Inform 2026;14:e71819
URL: https://medinform.jmir.org/2026/1/e71819
doi:10.2196/71819
PMID:

©Mounir Haizoune, Bennett L Leventhal, Dipendra Pant, Øystein Nytrø, Kaban Koochakpour, Roman A Koposov, Lars Ravn Øhlckers, Norbert Skokauskas. Originally published in JMIR Medical Informatics (https://medinform.jmir.org), 26.Feb.2026. This is an open-access article distributed under the terms of the Creative Commons Attribution License (https://creativecommons.org/licenses/by/4.0/), which permits unrestricted use, distribution, and reproduction in any medium, provided the original work, first published in JMIR Medical Informatics, is properly cited. The complete bibliographic information, a link to the original publication on https://medinform.jmir.org/, as well as this copyright and license information must be included.

XSL•FO
RenderX

Developing a Thai User Interface Terminology for Systematized Nomenclature of Medicine Clinical Terms Implementation in Primary Care: Cross-Sectional Content Coverage Analysis

Nat Tangchitnob[1], MD; Wanchana Ponthongmak[1], PhD; Boonchai Kijsanayotin[1,2], MD, PhD; Oraluck Pattanaprateep[1], PhD; Sithakom Phusanti[3], MD; Pongsakorn Atiksawedparit[3], MD, PhD; Kamonporn Suwanthaweemeesuk[3], MSc, MD; Jirayus Siangfu[4], MD; Gareth J McKay[5], PhD; John Attia[6], MD, PhD; Ammarin Thakkinstian[1], PhD

[1]Department of Clinical Epidemiology and Biostatistics, Faculty of Medicine, Ramathibodi Hospital, Mahidol University, Rama 6 Road, Ratchathewi, Bangkok, Thailand

[2]Thai Health Information Standards Development Center, Health Systems Research Institute, Ministry of Public Health, Bangkok, Thailand

[3]Chakri Naruebodindra Medical Institute, Faculty of Medicine Ramathibodi Hospital, Mahidol University, Bangkok, Thailand

[4]Chulabhorn Hospital, Chulabhorn Royal Academy, Bangkok, Thailand

[5]Centre for Public Health, Queen's University Belfast, Belfast, United Kingdom

[6]Centre for Clinical Epidemiology and Biostatistics, School of Medicine and Public Health, University of Newcastle Australia, Newcastle, Australia

Corresponding Author:
Wanchana Ponthongmak, PhD
Department of Clinical Epidemiology and Biostatistics, Faculty of Medicine, Ramathibodi Hospital, Mahidol University, Rama 6 Road, Ratchathewi, Bangkok, Thailand

Abstract

Background: Primary care in Thailand often uses mixed Thai-English free-text documentation for diagnoses and clinical problems, limiting standardization, interoperability, and secondary data use. Clinical terminologies like Systematized Nomenclature of Medicine Clinical Terms (SNOMED CT), a comprehensive reference terminology, can bridge this gap through the use of structured clinical data. Developing and mapping a local user interface terminology (UIT) is one of the key strategies for implementing SNOMED CT in real-world clinical settings.

Objective: This study aimed to develop a Thai UIT derived from frequently used terms in real-world primary care practice, map these terms to SNOMED CT concepts, and evaluate the extent of concept coverage.

Methods: Frequently used clinical terms were extracted from outpatient medical records from the family, emergency, and internal medicine departments using a customized tokenization method, N-gram analysis, and expert review. This process yielded 2054 Thai-specific terms. All terms were normalized and mapped to SNOMED CT through manual expert-driven and semiautomated tools. Unmapped terms were subsequently analyzed to identify mapping barriers and solutions.

Results: Of the 2054 Thai-specific terms, 2012 were successfully mapped to 2041 (97.98%) SNOMED CT concepts, including 1781 (85.50%) fully, 123 (5.90%) broader, 56 (2.69%) narrower, 81 (3.89%) inexact mappings, and 42 (2.02%) remained unmapped. Most mappings were one-to-one (1984), with 28 terms mapped to multiple concepts (57), covering 1486 unique SNOMED CT concepts. The remaining 42 unmapped terms were mostly due to culturally specific expressions or concepts not yet represented in SNOMED CT. These were categorized for potential postcoordination, exclusion, or national extension development.

Conclusions: This study demonstrates the feasibility of developing a Thai UIT mapped to SNOMED CT and describes mapping challenges. The resulting UIT enhances semantic clarity in clinical documentation and supports better interoperability, clinical decision-making, and health data analytics within Thailand's health care system.

(JMIR Med Inform 2026;14:e80039) doi:10.2196/80039

KEYWORDS

standards and interoperability; Systematized Nomenclature of Medicine Clinical Terms; SNOMED CT; eHealth infrastructure; clinical terminology; natural language processing; concept coverage

XSL•FO
RenderX

Introduction

Health care provision is a knowledge-intensive industry, but the quality and accessibility of health care data often fail to adequately meet these needs [1]. This is partly due to the data collection process, which commonly takes place in a fast-paced, high-pressure point-of-care environment [2], leading to the generation of data sufficient to meet the immediate clinical tasks but often lacking the completeness, standardization, and structure necessary for secondary use, for example, research, that drives health care improvement [3,4]. This limitation may compromise patient safety, care quality, and the ability to generate actionable insights [2,5]. To harness the full potential of health care data, it is essential to prioritize structured data collection that supports timely and effective use across the health care ecosystem [3,4]. Standardized clinical terminology, structured representations of clinical concepts understandable to both humans and computer systems, is an essential technology improvement required for developing reusable data that enables interoperable health care delivery [6].

Because clinical terminology must be comprehensive and support multilingual use, the Systematized Nomenclature of Medicine Clinical Terms (SNOMED CT) has been widely adopted internationally as a reference terminology standard that is indispensable for standardized information exchange across clinical care and research settings [7]. SNOMED CT adopts a concept-oriented structure; each unique clinical idea is represented by a concept identified by a language-independent, machine-readable unique identifier.

SNOMED CT consists of 3 core components, including concepts, descriptions, and relationships. Concepts represent the underlying clinical meaning; descriptions provide human-readable terms in multiple languages; and relationships define how concepts are linked within the ontology. A single concept can have multiple descriptions, enabling flexible, precise, and multilingual representation of clinical ideas. Relationships form a poly-hierarchical graph structure to express, distinguish, and connect each clinical concept, maximizing practicality while minimizing ambiguity [8]. For example, the concept “Nodule of lung (disorder)” can be described by multiple terms across languages (eg, English, French, and Swedish), and its meaning is defined through relationships as the child of both “Lesion of lung (disorder)” and “Lung mass (finding),” the associated morphology “Nodule (morphologic abnormality),” and the finding site “Lung structure (body structure).” This structure enables consistent clinical data representation and supports semantic interoperability. Successfully implementing SNOMED CT not only improves data quality and standardization of clinical data but also enhances the quality of health care through more efficient data use for both clinical and research applications [9,10]. While SNOMED CT offers a robust, language-independent conceptual framework, it does not automatically capture the variability of clinical expressions used in routine practice, particularly in multilingual or mixed-language documentation environments.

User interface terminology (UIT) refers to the set of terms clinicians use during routine clinical documentation. It consists of user-friendly and context-specific expressions that reflect the natural phrasing and cognitive patterns of clinical practice [11]. UITs are typically designed to be used by a defined user group and certain settings, prioritizing efficiency and usability [12]. Within the Open Medical Record System (OpenMRS; OpenMRS Inc) ecosystem, many implementations rely on Columbia International eHealth Laboratory (CIEL), an openly maintained UIT that serves as a common starting point for clinical data capture in OpenMRS deployments [13]. CIEL supports user-friendly clinical data capture while providing mappings to international reference terminologies (including SNOMED CT) [14], enabling the harmonization of locally meaningful data for use with global standards, facilitating secondary data use, interoperability, and research usability [3,4]. Combining the advantages of both terminologies leverages their complementary strengths, enhancing communication accuracy, data quality, and adoption among clinicians, while providing semantic precision, computability, and cross-system interoperability [10,11]. Together, they facilitate the standardization of a clinical narrative into more structured data [15,16].

Despite its advantages, implementing SNOMED CT presents challenges, particularly in non–English-speaking contexts [7,10,17]. Studies investigating the performance of SNOMED CT in multilingual contexts report 2 important indicators. Concept coverage refers to the proportion of source clinical ideas that can be represented by a concept, while term coverage refers to the proportion of source terms included in the SNOMED CT description, reflecting comprehensiveness of concept and the usability of descriptions, respectively [18]. For example, European-based studies demonstrate varying degrees of success in translation and implementation efforts. A fully translated Swedish version of SNOMED CT achieved good concept coverage (87%) but lower term coverage (47%), reflecting limited alignment with real-world clinical language [19]. In contrast, a German UIT without the use of SNOMED CT reached comparable term coverage (46%) despite the lack of codes in some key semantic areas, such as procedures, devices, or genes [16,19]. These findings suggest that constructing or adopting language-specific UITs, linked to SNOMED CT’s richer semantics and logical structure, is urgently needed and more effective than simply relying on direct translation [10,15].

Thailand became a member of SNOMED International in 2022, signaling a national commitment to adopt SNOMED CT as the reference terminology for addressing the country’s interoperability and health care data quality challenges [20]. Since joining, SNOMED CT codes have been incorporated into the national reporting and reimbursement datasets for diagnostic data. In clinical practice, a few health care institutes have begun integrating SNOMED CT’s abundant descriptions into their diagnosis entry systems. This approach complements the previous process, in which physicians manually selected *International Classification of Diseases (ICD)* codes. However, the potential benefits of adopting SNOMED CT (eg, improved data granularity, semantic interoperability, and enhanced secondary data use) have yet to be fully realized across the country [9,10]. A prior study in Thailand attempted to auto-map

XSL•FO
RenderX

Thai discharge summary terms to *ICD* codes through SNOMED CT descriptions but excluded all non-English characters, limiting its ability to interpret locally used abbreviations and mixed-language expressions common in Thai clinical documentation [21].

This study was conducted with the following 3 main objectives. First, to develop a Thai-language UIT derived from real-world clinical practice. Using a dynamic corpus of clinical texts, we apply a term collection methodology that integrates clinical expertise with natural language processing (NLP) techniques. The resulting UIT is expected to facilitate and support standardized data entry, enhance data quality, and improve user acceptance of SNOMED CT within Thailand's health care system.

Second, to evaluate the content coverage of SNOMED CT, defined as the proportion of clinical ideas in the Thai context that can be represented through international reference terminology.

Third, to perform mapping analysis of partially mapped and unmapped terms in order to identify potential areas where SNOMED CT or the Thai national extension may need further refinement to better represent Thai health care data.

Methods

Data Source

Data used for the development of the UIT were retrospectively retrieved from the chief complaint and present illness sections of electronic medical records (EMRs) at Chakri Naruebodindra Medical Institute, Ramathibodi Hospital, Mahidol University, covering the period from January 2019 to April 2023. Data were obtained from outpatient clinics in the family medicine (FM) and emergency departments, representing primary care settings. To enhance lexical diversity and coverage, additional data were obtained from the high-volume internal medicine (IM) department. Records lacking both the chief complaint and present illness sections were excluded from the study.

UIT

In this study, UIT was defined as a set of clinically relevant terms used by clinicians to express their clinical ideas within the EMRs. These terms can be presented in either the semistructured or unstructured free-text entries. To qualify as UIT, the terms must contain adequate meaning, clarity, and clinical specificity to support accurate documentation and enable secondary uses, as assessed by medical doctors (eg, " " [chest pain], " " [vomiting blood], " " [ischemic heart disease]), whereas terms that were vague or noninformative (eg, "1 pta" [1 month prior to admission] or "without evidence of") were not considered UIT.

The content of the UIT was harvested from the free-text documents produced during actual patient encounters. Clinician-entered free-text data (chief complaint and present illness) from the EMRs were preprocessed and transformed into clinical terms using NLP techniques, including cleaning, tokenization using our customized method, and N-gram generation. Term frequencies were then calculated, and terms meeting predefined threshold criteria were included in the UIT. The overall process is illustrated as follows (see Figure 1):

XSL•FO
RenderX

Figure 1. Summary overview of the mapping process. Collecting data from all sources (left upper box). Turning free text to N-gram using a customized dictionary from 5 sources (middle upper box). Interface terms selected by term frequency and experts (right upper box). Indexing the interface terms (pink). Mapping to the semantically equivalent SNOMED CT concept (blue). OA: osteoarthritis; SNOMED CT: Systematized Nomenclature of Medicine Clinical Terms.

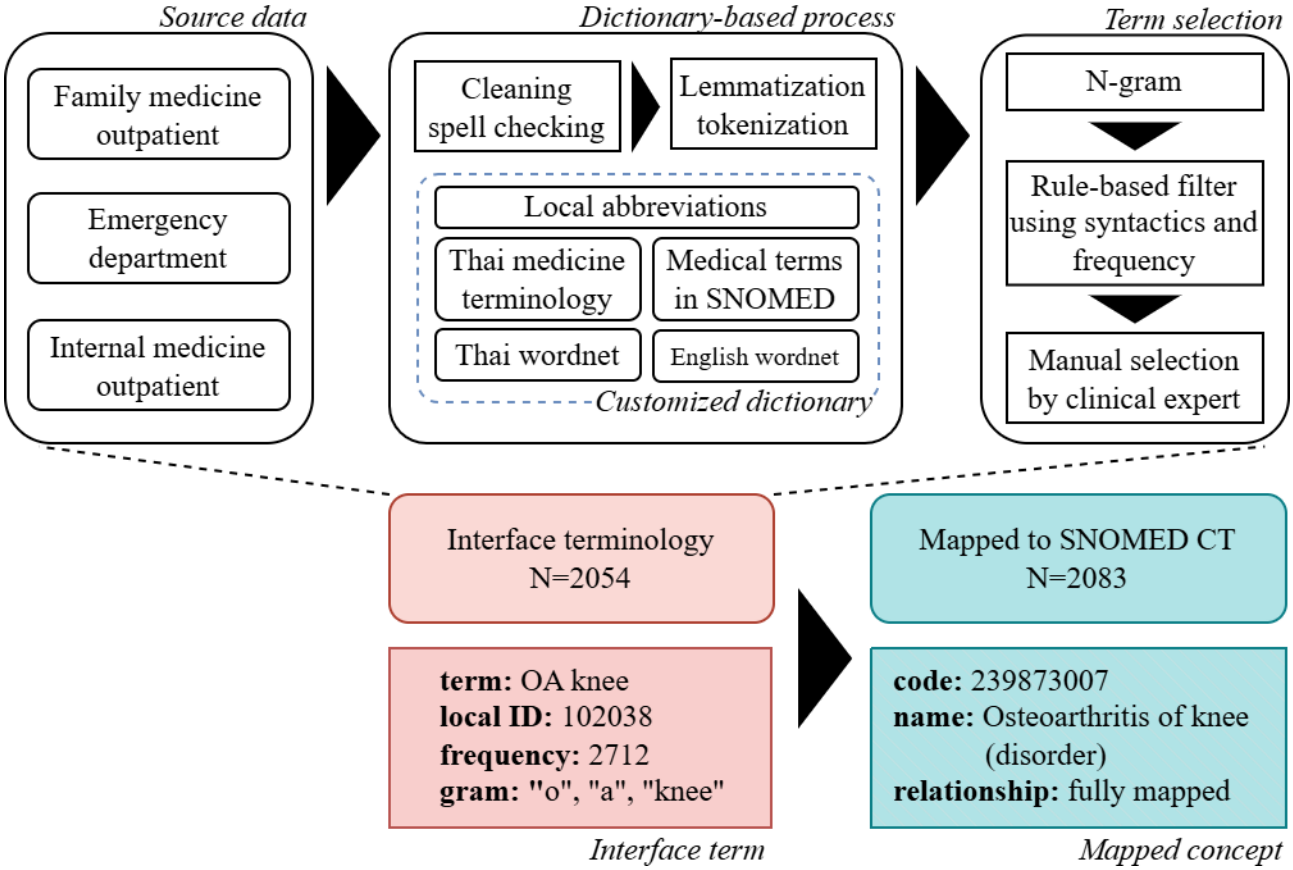

Text Preprocessing and Tokenization

Free-text data were preprocessed using the Python library for Thai NLP (ie, PyThaiNLP version 4.0.2) [22], which normalized texts by applying case normalization, correcting misplaced Thai tone marks and vowels, removing punctuation, and eliminating duplicate entries (eg, repeated sentences from prior visits). This process removed approximately 11.4% of the total characters, improving data consistency and validity. The code used for implementing text preprocessing and tokenization is provided in the GitHub repository [23].

Because Thai is a continuous-script language, which has no word and sentence boundaries (eg, “ ” [ischemic heart disease] consists of 4 lexical units: “ ”(disease), “ ”(heart), “ ”(deficiency), “ ”(blood)), standard Thai tokenizers trained on general Thai corpora perform poorly, particularly for medical text [24]. We therefore used a customized maximum matching algorithm, a greedy approach that segments text by repeatedly choosing the longest possible valid term from a dictionary that matches the current position. The dictionary was expanded to include medical jargon, drug names, and local abbreviations to optimize tokenization accuracy for clinical narratives.

Formally, given an input string S and a dictionary D, at each position j, the algorithm identifies all candidate substrings of S beginning at j that appear in D, and selects the candidate with the maximum length. This substring is then appended to the output sequence of tokens, and the process continues from the next unmatched character until the entire string is segmented.

This left-to-right longest-match strategy enables more accurate tokenization of Thai medical terms.

The custom dictionary D integrated five sources (Figure 1) (1) English WordNet; (2) Thai WordNet; (3) SNOMED CT descriptions (providing English clinical terms and medical jargon); (4) Thai medicine terminology (the national medicine database contains drug ingredients, generic names, trade names, and herbal medicine); and (5) a manually curated abbreviation dictionary (Multimedia Appendix 1), comprising abbreviations with ≥2 capital letters occurring >100 times in the dataset. These abbreviations were reviewed by physicians, validated using 5 random samples of medical records, and mapped to SNOMED CT. This custom dictionary was also used to spell-check before tokenization, ensuring that incorrect or nonstandard spellings were corrected before segmentation (Figure 1).

The N-grams of length 1 - 5, representing continuous sequences of N tokens (or grams), were generated to identify meaningful patterns and construct candidate terms or phrases.

For example, words contained unigram to 5-grams were: “ ” (fever) for unigram, “ ” (abdominal pain) for bigram, “ ” (oral cavity wound) for trigram, “ ” (both legs are swelled) for 4-gram, and “ ” (abnormal bleeding from vagina) for 5-gram. Syntactically irrelevant N-grams (ie, those containing >50% stop words, punctuation,

XSL•FO
RenderX

or numbers; or terms beginning or ending with stop words or prepositions) were excluded. The remaining N-grams were ranked by frequency and carefully reviewed by experienced clinicians. Clinically relevant terms were defined as those that conveyed sufficient meaning for documenting patient conditions.

In the first round, medical doctors reviewed intervals of ranked lists (Multimedia Appendix 1), marked the terms that are clinically meaningful and appropriate for representing as structured data, and selected the terms by applying the following inclusion criteria: (1) frequency rank within the top 70th percentile or (2) absolute frequency ≥300 occurrences, thresholds that reflected diminishing returns in identifying clinically relevant terms (Figure 2). After the second round, 2054 terms were selected from the pool of 10,260 candidate terms for inclusion in the interface terminology, representing commonly used clinical expressions across EMRs.

Figure 2. Numbers of included clinical terms per interval of rank-frequency categorized by the N of N-gram. Blue vertical lines indicate the cut point where term frequency was 300. Red vertical lines indicate the cut point where the percentile of rank-frequency reaches 70.

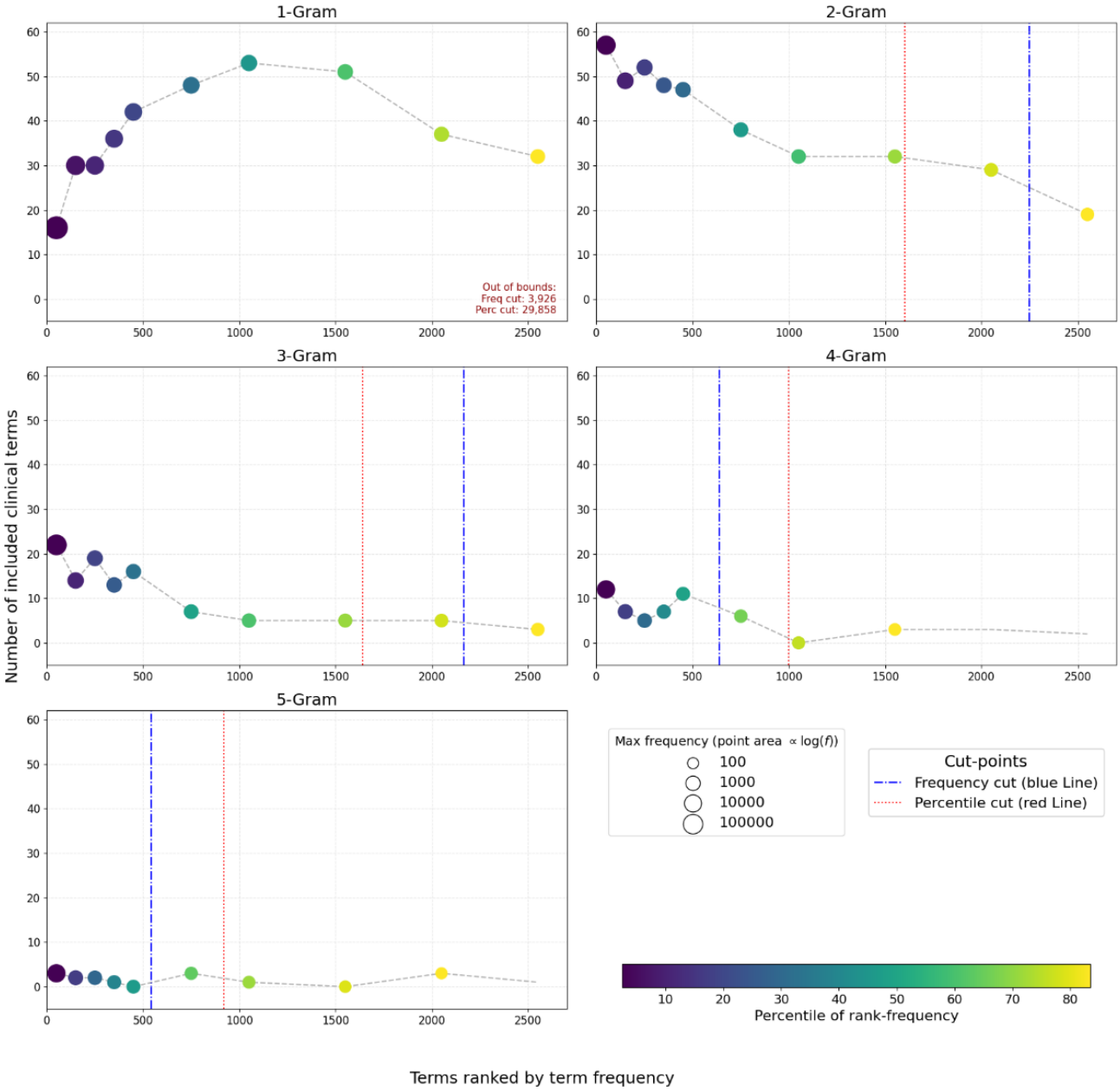

Mapping to SNOMED CT

Each UIT term was mapped to a semantically equivalent SNOMED CT concept using Snap2SNOMED, an open-source, publicly available mapping tool developed and maintained by SNOMED International. The tool provides key functionalities, including a built-in SNOMED CT browser, versioning, and automated lexical mapping (applicable to English-language terms only). Because automated mapping requires English input, 946 Thai terms were translated into English using Google Translate (Google LLC), and these translated terms were used as source terms for mapping. The automated mapping results were manually reviewed and validated by 2 clinical domain experts (NT and JS). To ensure semantic equivalency to the original Thai terms, 5 clinical usage contexts were supplied to the mappers for each term, selected at random from different patients. Manual mappings were guided by semantic equivalence

XSL•FO
RenderX

criteria recommended in the Snap2SNOMED User Guide, prioritizing alignment for meaning, clinical intent, and hierarchical appropriateness. Disagreements between mappers were resolved through iterative discussion and consensus-based remapping.

Mapping results were classified into three categories, as illustrated in Figure 1: (1) fully mapped: SNOMED CT concepts that fully captured the semantics of the source term (eg, "valvular heart disease" mapped to "Heart valve disorder [disorder]"); (2) partially mapped: SNOMED CT concepts that were close but not fully semantically equivalent to the source term (eg, "home SBP" mapped to the narrower concept "Average home systolic blood pressure [observable entity]"); and (3) unmapped: source terms that lacked sufficient representation in existing SNOMED CT concepts.

A single source term could be potentially mapped to multiple SNOMED CT concepts (referred to as one-to-many mapping), resulting in more mapping pairs than source terms. This arose from one of two scenarios (1) homonyms, terms carried multiple distinct meanings, each represented by different SNOMED CT concepts following guidelines from SNOMED CT managing conventions and (2) ambiguous terms explicitly excluded from SNOMED CT due to insufficient contextual specificity (eg, "fundus" referring to either a hollow organ apex or the eye's interior surface). These ambiguous terms were conservatively classified as unmapped to preserve terminological clarity and precision.

Partially mapped pairs were further classified into broader, narrower, and inexact relationships to quantify mapping quality. The broader referred to the SNOMED CT concept, which encompasses the meaning of the source term. Narrower referred to when the SNOMED CT concept represented only part of the source term's meaning. In cases where semantic equivalence required postcoordination with multiple SNOMED CT concepts, we selected a single precoordinated concept in the same hierarchy as the narrower one. For example, "nodule at right upper lung" was mapped to the broader concept "Nodule of lung (disorder)" rather than combining a finding with "Upper lobe of right lung (body structure)." Inexact referred to mappings where the best available SNOMED CT concept differed in lexical and semantic characteristics but provided a clinically relevant approximation. For example, "over-the-counter drug use" was inexactly mapped to "Patient on self-medication (finding)."

Mapping Analysis

Terms unable to be mapped by mappers were discussed and categorized into either partially mapped or unmapped terms, including ambiguous terms and terms for which no semantic equivalency was found in SNOMED CT. For the terms that can be represented using postcoordination of 2 or more concepts from the same hierarchy, for example, " " (sweating and palpitation), we decided to categorize them as unmapped terms for further analysis. Partially mapped and unmapped terms were analyzed to assess their potential for practical implementation within our research team. Specifically, the analysis examined whether these terms could be adequately represented through SNOMED CT postcoordination or should be proposed for inclusion in an updated national edition of SNOMED CT. This evaluation helped identify specific content areas where concept expansion would better align the terminology with local clinical practice and ensure comprehensive coverage in the national edition.

Ethical Considerations

The study protocol was reviewed and approved by the Ramathibodi Human Research Ethics Committee (Approval number COA.MURA2023/469). The informed consent was waived due to the retrospective nature of the dataset and minimal risk to participants. All personally identifiable information (eg, names, surnames, dates of birth, addresses, hospital numbers, and visit dates) was removed from the dataset prior to analysis to ensure privacy and confidentiality.

Results

Dataset Characteristics

A total of 1,88,468 documents were initially retrieved from the EMRs during the study period. After excluding records with missing data, 1,83,557 documents from 53,142 patients were included in the analysis to develop the interface terminology. Characteristics of the 53,142 patients are described in Table 1. IM patients were the oldest (mean 59.3, SD 16.9), followed by FM (mean 54.4, SD 15.2), and emergency department (mean 43.4, SD 28.0). The percentage of males was highest in emergency (44.3%), followed by IM (39.7%) and FM (36.94%).

At the document level, the IM department contributed the largest volume (1,18,382/1,83,557, 64.5%), followed by the emergency (34,829/1,83,557, 19.0%) and FM departments (30,346/1,83,557, 16.5%). The median number of documents per patient (IQR) was 2 (1-5) for IM, 1 (1-2) for emergency, and 1 (1-3) for FM (Table 1).

Text-level analysis of 1,83,557 documents yielded 14,946,559 total words. IM contributed the majority (10,471,768/14,946,559, 70.1%), followed by emergency (2,750,896/14,946,559, 18.4%) and FM (1,723,895/14,946,559, 11.5%). Median (IQR) words per document were 107 (62-175) for IM, 74 (44-125) for ER, and 60 (38-99) for FM. Thai words were varied by department. Emergency department documents had the highest proportion of Thai words (1,752,756/2,750,896, 63.7%), followed by FM (1,016,914/1,723,895, 59.0%), while IM contained the lowest proportion (4,154,255/10,471,768, 39.7%).

XSL•FO
RenderX

Table . Characteristics of data from the 3 outpatient departments.

Characteristics	FM[a]	ER[b]	IM[c]	Total
Patient-level				
Number of patients (n)	12,128	22,878	29,985	53,142
Age (years), mean (SD)	54.37 (15.21)	43.42 (27.97)	59.31 (16.91)	53.98 (15.42)
Male (sex), n (%)	4480 (36.94)	10,137 (44.31)	11,892 (39.66)	21,821 (41.06)
Document level				
Number of documents (n)	30,346	34,829	1,18,382	1,83,557
Documents per patient, median (IQR)	1 (1-3)	1 (1-2)	2 (1-5)	2 (1-4)
Text-level				
Unique words (n)	20,070	25,055	33,286	41,755
Unique Thai words, n (%)	10,475 (52.19)	12,647 (50.78)	15,216 (45.71)	20,407 (48.87)
Total words (n)	1,723,895	2,750,896	10,471,768	14,946,559
Total Thai words, n (%)	1,016,914 (58.99)	1,752,756 (63.72)	4,154,255 (39.67)	6,923,925 (46.32)
Word per document, median (IQR)	60 (38 - 99)	74 (44 - 125)	107 (62 - 175)	81 (43 - 141)

[a]FM: family medicine.

[b]ER: emergency room.

[c]IM: internal medicine.

Coverage

A total of 2054 frequently used clinical source terms met the inclusion criteria and were integrated into the interface terminology. Of these, 2012 terms were successfully mapped to 2041 SNOMED CT concepts. Most terms were mapped one-to-one (1984 terms), while 28 terms were mapped to 57 multiconcepts through one-to-many mappings, yielding a total of 2083 entries while covering 1486 unique SNOMED CT codes. The final mappings are provided in Multimedia Appendix 2. Mapping characteristics are as follows:

- Language: English (1140 out of 2083 terms [54.73%]) and Thai (943 out of 2083 terms [45.27%]).
- N-gram: unigrams (1098 terms), bigrams (741 terms), trigrams (189 terms), 4-grams (45 terms), and 5-grams (10 terms).
- Equivalency: 1781 (85.50%) fully mapped terms, 123 (5.90%) mapped to broader concepts, 56 (2.69%) mapped to narrower concepts, and 81 (3.89%) inexactly mapped terms (Table 2). The remaining 42 terms (2.02%) could not be mapped due to culturally specific expressions or clinical concepts not yet represented in any SNOMED CT concept.
- Overall, the concept coverage was 85.50%. Combining fully and partially mapped terms yielded an overall concept coverage of 97.98%.

Term coverage is defined as the percentage of local clinical terms that can be accurately mapped to an existing SNOMED CT description. Among 1140 English terms, 656 terms (31.49%) had direct lexical matches with English SNOMED CT descriptions, including simple variations of writing, for example, “wound dressing” versus “Dressing wound.” The remaining 484 English terms (23.24%) did not have an exact lexical match and were still mappable through contextual interpretation, such as local abbreviations (eg, “f/u” → “Follow-up visit [procedure]”), or variation in writing style (eg, “contact tb” → “Exposure to tuberculosis [situation]”). As expected, no Thai terms were considered direct lexical matches because SNOMED CT descriptions are not yet translated into Thai.

Table . Concept coverage of Systematized Nomenclature of Medicine Clinical Terms (SNOMED CT) for Thai interface terminology.

Concept equivalency	English	Thai	Total
Fully mapped, n (%)	973 (46.71)	808 (38.79)	1781 (85.50)
Partially mapped, n (%)	140 (6.72)	120 (5.75)	260 (14.48)
Broader	65 (3.12)	58 (2.78)	123 (5.90)
Narrower	38 (1.82)	18(0.86)	56 (2.69)
Inexact	37 (1.78)	44 (2.11)	81 (3.89)
Unmapped, n (%)	27 (1.30)	15 (0.72)	42 (2.02)
Total, n (%)	1140 (54.73)	943 (45.27)	2083 (100)

XSL•FO
RenderX

Mapping Analysis

Mapping analysis of the 260 partially mapped terms revealed linguistic and semantic challenges. All 123 broader (5.90%) and 56 narrower (2.69%) pairs comprised of concepts differed in granularity, where terms belonged to the same semantic domain, but they were at different levels of clinical detail or abstraction. On the other hand, inexact terms arose when clinical intention aligned, but lexical or cultural expression differed. For example, “ ” (sleep with multiple pillows) was used to indicate the situation when a patient cannot sleep lying down due to shortness of breath; it was inexactly mapped to “Orthopnea (finding)” and “ (taking medicine regularly)” and its variations were the patient-reported concept “Drug compliance good (finding).”

We also observed that culture and linguistic characteristics contributed to mismatches. Some Thai expressions convey complex clinical scenarios through idiomatic phrasing, complicating alignment with SNOMED CT. For example, “over-the-counter drug use” in the Thai context often implies access to medications that would require prescriptions in many other countries. After deliberation in our team, although this was mapped to “Patient on self-medication (finding),” this concept does not fully capture its implications within Thailand’s health care system.

Forty-two unmapped terms (2.02%) were further categorized into 3 categories based on their characteristics (see Table 3).

Ambiguous terms (23/42, 54.76%) violated SNOMED CT naming conventions and required additional contexts for appropriate representation (eg, “lobe,” “node,” and “septum”).

Multiple clinical concepts (10/42, 23.81%) represented multiple distinct findings or events (eg, “s1 s2” [heart sounds], “ ” [sweating and palpitation], “ ” [fall and head collision]). Many terms reflect Thai-specific linguistic constructions and could potentially be addressed through postcoordination.

Clinically meaningful terms without SNOMED CT equivalents (9/42, 21.43%). Some terms were (locally) nationally specific (eg, “ ” [fear of heights or a feeling of butterflies in the stomach]) while others were universally applicable but absent from SNOMED CT (eg, “ ” [antipyretic medicine] and “DOI” [date of infection]). The terms were exhaustively searched using both lexical and graph properties of SNOMED CT through the use of SNOMED CT Expression Constraint Language.

Table . Categories for unmapped concepts.

Characteristics	Ambiguous terms	Multiconcept terms	No concept terms
Value, n (%)	23 (54.76)	10 (23.81)	9 (21.43)
Further intervention	Exclusion from terminology or addition of contextual information	Postcoordination or separation to multiple distinct concepts	Creation of new concept
Examples	• Lobe • Node • Septum	• S1S2 (Heart sounds) • (sweating and palpitation) • (fall and head collision)	• DOI (Date of Infection) • (Antipyretic medicine) • (fear of heights or a feeling of butterflies in the stomach)

Discussion

Principal Findings

This study developed a multilingual UIT derived from real-world clinical documents across the FM, emergency, and IM departments and evaluated its alignment with SNOMED CT. The resulting UIT reflects a nearly balanced linguistic composition (54.49% English terms and 45.51% Thai terms). Consistent with the bilingual nature of Thai medical records. SNOMED CT demonstrated strong concept coverage with 85.50% full and 97.98% full plus partial coverage, confirming its suitability as a reference terminology even in the setting where nearly half of the source terms are non-English. However, term coverage remained modest (31.49%) because SNOMED CT descriptions have not yet been translated into Thai, making exact lexical matches possible only for English-language terms.

The source data also showed different patterns in clinical documentation practices. For instance, IM generated the highest volume of text but had the lowest proportion of Thai words, consistent with its more technical and specialty-oriented clinical activities. In contrast, emergency and FM documents contained more Thai narrative language, which may reflect more direct patient-provider interaction, brief encounters, and patient-reported symptoms. These differences emphasize the need for UITs that can accommodate both biomedical language and colloquial Thai expressions.

We also found that only a small proportion of terms remained unmapped (2.02%), underscoring that the majority of local expressions can be integrated into SNOMED CT without major structural changes. These relatively small, unmapped concepts may help identify where efforts should be strategically concentrated at the national level. Moreover, the moderate-term coverage (31.49%), driven entirely by English lexical matches, reinforces the need for localized terminology tools and translation strategies if Thailand aims to scale SNOMED CT adoption nationwide.

Comparison With Previous Work

Despite differences in term extraction methods, particularly our focus on commonly used clinical terms and the use of a more recent SNOMED CT release, our findings generally align with previous evaluations of SNOMED CT concept coverage. Prior studies have reported a strong preference for high coverage in

XSL•FO
RenderX

the English-language international edition (86% fully mapped and 92% partially mapped) and similar strong performance in the fully translated Swedish edition when applied to Swedish clinical datasets (87% fully mapped and 92% partially mapped) [19]. In comparison, our findings showed 85.50% full and 97.98% full plus partial coverage, demonstrating that SNOMED CT remains robust even in bilingual and partially non-English documentation environments.

Comparable evidence has also been observed in low- and middle-income country settings. For example, an evaluation from Argentina reported 83% coverage based on user feedback during real-world implementation [12]. Other specific domains targeting nationwide data collection and surveillance objectives have very high coverage, 99% precoordinated and 100% postcoordinated concept coverage for AIDS-defining illnesses in Kenya [25], and high correspondence for tuberculosis-related terminology, although the latter did not include a formal concept coverage analysis [14].

In Thailand, a prior study mapped Thai discharge summary notes to SNOMED CT but removed non-English content and did not report concept coverage [21]. Our study extends this work by incorporating both English and Thai clinical terms from 3 departments, performing concept coverage, term coverage, and mapping analysis, and examining implications for national UIT development. This provides a more comprehensive and representative assessment of SNOMED CT's applicability for Thai primary care and hospital settings.

Partially mapped terms frequently reflect homonyms (eg, " " meaning both abdominal colic and a cigarette unit), mismatches in granularity (eg, "hypoglycemic symptom" mapped to hypoglycemia [disorder]), or culturally shaped usage patterns. These challenges are consistent with those reported in other multilingual SNOMED CT mapping studies [10,26]. In the Thai language, many biomedical concepts and terms are not readily expressed in Thai. Unlike languages that share linguistic roots (eg, English, French, and Swedish), Thai lacks direct lexical equivalents for some medical terms, creating communication barriers between clinicians, patients, and even health care providers. To ensure mutual understanding, clinicians need to phrase simple questions that patients can comprehend, allowing information to be collected accurately. For example, "compliance" is simply conveyed as "taking medicine regularly" or "never miss a dose," which is reflected in how these terms appeared in the EMRs. This observation has also been reported in other languages, not from the same roots as the English language [27].

Term coverage in our dataset was modest (31.49%), driven entirely by English lexical matches. The observed term coverage is comparable with countries whose SNOMED CT editions are only partially translated, for example, Dutch (35%) and French (39%) [19]. A considerable proportion of our Thai clinical terms were synonymous with globally common English medical jargon, reflecting Thailand's long-standing integration of English terminology in medical education and clinical communication. As shown in Table 1, Thai language use was more prevalent in primary care departments (FM and emergency), while IM documents contained more specialized English terminology, consistent with previous reports [28].

Challenges in Expressing Clinical Concepts in the Thai Context

Our mapping analysis of partially mapped terms highlighted several challenges in representing Thai clinical concepts within SNOMED CT. Many partially mapped terms require determining whether they should (1) be represented through postcoordination with existing SNOMED CT concepts (thereby supporting international interoperability) or (2) be introduced as new concepts in the Thai national extension to preserve locally specific meaning.

Postcoordination can be beneficial for international interoperability but may lose nuanced local semantics. Conversely, creating new concepts preserves the locally used expression but introduces a long-term maintenance burden and requires clear criteria for inclusion. No standardized national guidelines currently exist; decisions must consider clinical relevance, documentation frequency, clinical importance, and anticipated use cases within Thailand's EMR ecosystem. A representative example from our study is "over-the-counter drug use," which frequently appeared in our dataset and reflects a long-standing public health challenge in unsupervised medication access in Thailand [29], which contributes to national issues such as antimicrobial resistance and drug misuse [30]. While "Patient on self-medication (finding)" is the most relevant concept in SNOMED CT, it does not fully represent Thailand's regulatory distinctions and safety concerns. If more granular differentiation is required in Thailand for surveillance or policy purposes, a new child concept under "Patient on self-medication (finding)" may be warranted.

The analysis of unmapped terms also highlighted the role of language-specific and culturally specific expressions that are not directly translatable into English (see Table 3). In our data, 20.93% of unmapped terms reflected culturally unique, ambiguous, or context-dependent meanings. These findings suggested three key strategies for terminology management and strengthening (1) exclude ambiguous terms or add contextual information to the context-dependent terms. For example, the Thai term " " has multiple meanings (fear of heights or a feeling of butterflies in the stomach). Instead of mapping it directly, adding the more specific term " " (giddiness in the heart) mapped to "Palpitations (finding)" can ensure clarity and avoid misclassification. (2) Use postcoordination for multiconcept or idiomatic expressions. This pattern was also found in the English context, for example, the concept "Nausea and vomiting (finding)," which exists as a precoordinated concept within the international edition of SNOMED CT. However, since separated distinct concepts are presented, we suggest mapping to separate entities to preserve legacy information and also interoperability with the international context. (3) Recommend new concepts for national extension or international inclusion for globally relevant but unsupported terms. This should be done with a well-established concept with clear practical implications. One example we found was a local abbreviation, "DOI (Date of Infection)," which we believe has seen an increase in occurrences during the pandemic, particularly

XSL•FO
RenderX

in cases where infectious history has been thoroughly collected. Additionally, some of these represent global clinically relevant concepts insufficiently addressed by SNOMED CT, indicating areas for future expansion [7].

Overall, these challenges highlight the need for national governance structures, clearly defined criteria for new concept creation, and a systematic strategy for translation and localization to ensure accurate, consistent, and interoperable representation of Thai clinical terminology. Regional guidance from the Asia eHealth Information Network (AeHIN) similarly emphasizes that successful and sustainable interoperability depends not only on the technical standards but also on governance, architecture, workforce capacity, and institutional processes [31]. Centralized governance through a national health data dictionary and terminology services, as described in many interoperability architectures, like Open Health Information Exchange (OpenHIE; Linux Foundation Public Health), can standardize terminological assets and reduce fragmentation across implementation sites [32]. Such services can support the controlled use of postcoordination and governed concept creation and enable local expressiveness while preserving semantic consistency and international interoperability. Importantly, these functions are best managed at the terminology service level rather than within individual EMR implementations, thereby reducing duplication and implementation burden. In addition, mappings between shared UITs and reference terminologies or classification systems (eg, the *ICD* family) should be centrally maintained, versioned, and routinely updated. For example, the OpenMRS ecosystem also adopts the similar implementation pattern, where many deployments rely on the CIEL interface terminology, centrally managed and distributed via Open Concept Lab, supporting reuse and reducing divergence across implementations [13].

Strengths and Limitations

To our knowledge, this is the first study in Thailand—and among the few resource-limited countries—to develop a UIT and evaluate both concept- and term-level coverage of SNOMED CT in a real-world clinical setting. A key strength of this study lies in its data source, free-text entries from actual clinical encounters, which ensures that the extracted terms are grounded in real-world usage. Moreover, the terminology development process integrated clinical expertise with NLP techniques in a resource-limited setting, offering valuable insights for similar environments. The final UIT is composed of the commonly used clinical term. Although it is small in numbers, we believe this terminology to be generally applicable for use within Thailand. Although SNOMED CT concept coverage has been examined in a few resource-limited country settings, evidence remains scarce. This study extends the discussion to Southeast Asia by evaluating Thai-language primary care data, constructing a UIT mapped to SNOMED CT, and reporting concept coverage.

Several limitations should be acknowledged. First, source data were collected from a single hospital, which may limit the generalizability of the developed UIT. Consequently, the developed UIT may not fully capture the diversity of expression terms used across Thailand's broader health care system, particularly in regions where distinct dialects or documentation styles prevail. Nevertheless, this study achieved its goal of constructing a realistic UIT to inform national implementation strategies and evaluate the feasibility of adopting SNOMED CT as a national standard. As new clinical terms and concepts emerge, the UTI can be continuously expanded through routine monitoring, domain-expert review, and integration of automated extraction tools to ensure incremental improvement over time. Second, although the mapping and term extraction processes were performed by clinically trained physicians, the subjective nature of manual mapping introduces the potential for interpretation bias or human error. An interannotator agreement score was not assessed due to constraints in available personnel and resources; consequently, only one mapper and one reviewer contributed to the final mapping. Third, the coverage results may be overestimated compared to those reported in previous studies because our term list was developed from commonly used clinical expressions and mapped to a more recent SNOMED CT release. At the same time, the mapping tool Snap2SNOMED does not support postcoordination at the time of this writing, which may lead to a potential underestimation of full SNOMED CT content coverage. However, since postcoordination has not been generally performed in previous studies, the results remain broadly comparable with existing evidence [19].

Recommendation for Future Research

Future research should expand the evaluation of concept and term coverage across hospitals of varying sizes and settings, including northern, northeastern, and southern regions of Thailand, where specific dialects may influence clinical documentation practices. Extending these methods beyond a single institution will help determine the generalizability of the UIT and support efforts toward national standardization.

Automated methods should also be explored. Advanced NLP techniques and large language models may substantially improve the efficiency and accuracy of term extraction, disambiguation, and SNOMED CT mapping, particularly as our team is already beginning to implement these tools in parallel methodological work. Additional studies should examine how postcoordination can be operationalized in real-world EMRs, with the goal of identifying best practices that maintain semantic precision without burdening clinicians during documentation.

Finally, future research should include more diverse document types (eg, operative notes, procedure reports, and specialty consults) and a broader population. Doing such improves characterization of locally used clinical concepts, strengthens coverage estimates, and supports the development of a more comprehensive national UIT that accurately reflects the linguistic and clinical diversity of Thailand's health care system.

Conclusions

In conclusion, SNOMED CT represents most common clinical concepts but lacks sufficient local language coverage. With the interpretation of local clinical terms, a Thai UIT mapped to SNOMED CT can serve as a comprehensive standard for clinical documentation. This hybrid approach can enhance data quality, promote interoperability, and facilitate better use of health care

XSL•FO
RenderX

data, contributing to improved patient care and creating opportunities for international collaboration.

Acknowledgments

This manuscript is a part of the thesis of Nat Tangchitnob, MD, within the international Ph.D. program in Data Science for Healthcare and Clinical Informatics, conducted at the Department of Clinical Epidemiology and Biostatistics, Faculty of Medicine, Ramathibodi Hospital, Mahidol University, Bangkok, Thailand.

Funding

The authors received no specific funding for this work.

Data Availability

All terminology data generated or analyzed during this study are included in this published article and its supplementary information files. The developed codes for this study are available at GitHub [23].

Authors' Contributions

Conceptualization: NT, WP, BK, OP, AT
Data curation: SP, PA, KS
Formal analysis: NT, WP, OP, AT
Funding acquisition: OP, AT
Investigation: NT, JS
Methodology: NT, WP, BK, GJM, JA, AT
Project administration: WP, OP
Resources: OP
Software: NT, WP
Supervision: WP, BK, OP, AT
Validation: WP, BK, AT
Visualization: NT
Writing – original draft: NT, WP, OP, JS
Writing – review & editing: NT, BK, SP, PA, KS, GJM, JA, AT

Conflicts of Interest

None declared.

Multimedia Appendix 1
Top 10 frequency of the most common abbreviations and First-round results of interface term selection.
[DOCX File, 26 KB - medinform_v14i1e80039_app1.docx]

Multimedia Appendix 2
Interface Terminology mapped to SNOMED CT (Systematized Nomenclature of Medicine Clinical Terms).
[XLSX File, 234 KB - medinform_v14i1e80039_app2.xlsx]

References

1. Lewis AE, Weiskopf N, Abrams ZB, et al. Electronic health record data quality assessment and tools: a systematic review. J Am Med Inform Assoc 2023 Sep 25;30(10):1730-1740. [doi: 10.1093/jamia/ocad120] [Medline: 37390812]
2. Linder JA, Schnipper JL, Middleton B. Method of electronic health record documentation and quality of primary care. J Am Med Inform Assoc 2012;19(6):1019-1024. [doi: 10.1136/amiajnl-2011-000788] [Medline: 22610494]
3. Liu F, Panagiotakos D. Real-world data: a brief review of the methods, applications, challenges and opportunities. BMC Med Res Methodol 2022 Nov 5;22(1):287. [doi: 10.1186/s12874-022-01768-6] [Medline: 36335315]
4. Botsis T, Hartvigsen G, Chen F, Weng C. Secondary use of EHR: data quality issues and informatics opportunities. Summit Transl Bioinform 2010 Mar 1;2010(1-5):1-5. [Medline: 21347133]
5. Bowman S. Impact of electronic health record systems on information integrity: quality and safety implications. Perspect Health Inf Manag 2013;10(Fall):1c. [Medline: 24159271]
6. Cimino JJ. Desiderata for controlled medical vocabularies in the twenty-first century. Methods Inf Med 1998 Nov;37(4-5):394-403. [doi: 10.1055/s-0038-1634558] [Medline: 9865037]

XSL•FO
RenderX

7. Millar J. The need for a global language - SNOMED CT introduction. Stud Health Technol Inform 2016;225(683-5):683-685. [doi: 10.3233/978-1-61499-658-3-683] [Medline: 27332304]
8. Rector A, Schulz S, Rodrigues JM, Chute CG, Solbrig H. On beyond Gruber: “Ontologies” in today’s biomedical information systems and the limits of OWL. J Biomed Inform 2019;100S:100002. [doi: 10.1016/j.yjbinx.2019.100002] [Medline: 34384571]
9. Thiel R, Birov S, Piesche K, et al. The costs and benefits of SNOMED CT implementation: an economic assessment model. Stud Health Technol Inform 2016;228(441-5):441-445. [doi: 10.3233/978-1-61499-678-1-441] [Medline: 27577421]
10. Vuokko R, Vakkuri A, Palojoki S. Systematized Nomenclature of Medicine-Clinical Terminology (SNOMED CT) clinical use cases in the context of electronic health record systems: systematic literature review. JMIR Med Inform 2023 Feb 6;11:e43750. [doi: 10.2196/43750] [Medline: 36745498]
11. Rosenbloom ST, Miller RA, Johnson KB, Elkin PL, Brown SH. Interface terminologies: facilitating direct entry of clinical data into electronic health record systems. J Am Med Inform Assoc 2006;13(3):277-288. [doi: 10.1197/jamia.M1957] [Medline: 16501181]
12. Osornio AL, Luna D, Gambarte ML, Gomez A, Reynoso G, de Quirós FGB. Creation of a local interface terminology to SNOMED CT. Stud Health Technol Inform 2007;129(Pt 1):765-769. [Medline: 17911820]
13. Kanter AS, Borland R, Barasa M, et al. The importance of using open source technologies and common standards for interoperability within eHealth: perspectives from the millennium villages project. Adv Health Care Manag 2012;12(189-204):189-204. [doi: 10.1108/s1474-8231(2012)0000012013] [Medline: 22894051]
14. Halland K, Britz K, Gerber A. Investigations into the use of Snomed CT to enhance an OpenMRS health information system. SACJ 2011;47(1):33-45. [doi: 10.18489/sacj.v47i0.14]
15. Schulz S, Rodrigues JM, Rector A, Chute CG. Interface terminologies, reference terminologies and aggregation terminologies: a strategy for better integration. Stud Health Technol Inform 2017;245(940-4):940-944. [doi: 10.3233/978-1-61499-830-3-940] [Medline: 29295238]
16. Hashemian Nik D, Kasáč Z, Goda Z, Semlitsch A, Schulz S. Building an experimental German user interface terminology linked to SNOMED CT. Stud Health Technol Inform 2019 Aug 21;264(153-7):153-157. [doi: 10.3233/SHTI190202] [Medline: 31437904]
17. Park HA, Yu SJ, Jung H. Strategies for adopting and implementing SNOMED CT in Korea. Healthc Inform Res 2021 Jan;27(1):3-10. [doi: 10.4258/hir.2021.27.1.3] [Medline: 33611871]
18. Rosenbloom ST, Miller RA, Johnson KB, Elkin PL, Brown SH. A model for evaluating interface terminologies. J Am Med Inform Assoc 2008;15(1):65-76. [doi: 10.1197/jamia.M2506] [Medline: 17947616]
19. Miñarro-Giménez JA, Cornet R, Jaulent MC, et al. Quantitative analysis of manual annotation of clinical text samples. Int J Med Inform 2019 Mar;123(37-48):37-48. [doi: 10.1016/j.ijmedinf.2018.12.011] [Medline: 30654902]
20. Thailand. SNOMED International. 2025 Oct 22. URL: https://www.snomed.org/members/thailand [accessed 2026-02-27]
21. Isaradech N, Khumrin P. Auto-mapping clinical documents to ICD-10 using SNOMED-CT. AMIA Jt Summits Transl Sci Proc 2021;2021:296-304. [Medline: 34457144]
22. Phatthiyaphaibun W, Chaovavanich K, Polpanumas C, et al. PyThaiNLP: thai natural language processing in python. Presented at: Proceedings of the 3rd Workshop for Natural Language Processing Open Source Software (NLP-OSS 2023); Jul 13, 2023 URL: https://aclanthology.org/2023.nlposs-1 [accessed 2026-02-05] [doi: 10.18653/v1/2023.nlposs-1.4]
23. Chirurgo/terminology2snomed [internet]. GitHub. URL: https://github.com/Chirurgo/terminology2snomed [accessed 2026-02-05]
24. Damrongkamoltip K, Ruenlek K, Limprasert W, Boonkwan P. Comparing a Thai words segmentation methods in the LST20 dataset. J Comput Creat Technol 2024;2(2):61-70. [doi: 10.14456/jcct.2024.7]
25. Oluoch T, de Keizer N, Langat P, et al. A structured approach to recording AIDS-defining illnesses in Kenya: a SNOMED CT based solution. J Biomed Inform 2015 Aug;56(387-94):387-394. [doi: 10.1016/j.jbi.2015.07.009] [Medline: 26184057]
26. Miñarro-Giménez JA, Martínez-Costa C, Karlsson D, Schulz S, Gøeg KR. Qualitative analysis of manual annotations of clinical text with SNOMED CT. PLoS ONE 2018;13(12):e0209547. [doi: 10.1371/journal.pone.0209547] [Medline: 30589855]
27. Perez-de-Viñaspre O, Oronoz M. SNOMED CT in a language isolate: an algorithm for a semiautomatic translation. BMC Med Inform Decis Mak 2015;15 Suppl 2(Suppl 2):S5. [doi: 10.1186/1472-6947-15-S2-S5] [Medline: 26100112]
28. Yusuff KB, Tayo F. Does a physician’s specialty influence the recording of medication history in patients’ case notes? Br J Clin Pharmacol 2008 Aug;66(2):308-312. [doi: 10.1111/j.1365-2125.2008.03202.x] [Medline: 18537964]
29. Cooper RJ. Over-the-counter medicine abuse - a review of the literature. J Subst Use 2013 Apr;18(2):82-107. [doi: 10.3109/14659891.2011.615002] [Medline: 23525509]
30. Chautrakarn S, Khumros W, Phutrakool P. Self-medication with over-the-counter medicines among the working age population in metropolitan areas of Thailand. Front Pharmacol 2021;12(726643):726643. [doi: 10.3389/fphar.2021.726643] [Medline: 34456738]
31. Marcelo AB, Pascual KC, Udayasankaran JG, Allaudin FS, Kijsanayotin B. A framework for regional health information systems interoperability: the asia ehealth information network (AeHIN) experience. In: Roadmap to Successful Digital Health Ecosystems: Elsevier; 2022:399-414. [doi: 10.1016/B978-0-12-823413-6.00005-7]

XSL•FO
RenderX

32. Mamuye AL, Yilma TM, Abdulwahab A, et al. Health information exchange policy and standards for digital health systems in africa: a systematic review. PLOS Digit Health 2022 Oct;1(10):e0000118. [doi: 10.1371/journal.pdig.0000118] [Medline: 36812615]

Abbreviations

AeHIN: Asia eHealth Information Network
CIEL: Columbia International eHealth Laboratory
EMR: electronic medical record
FM: family medicine
***ICD*:** *International Classification of Diseases*
IM: internal medicine
NLP: natural language processing
OpenHIE: Open Health Information Exchange
OpenMRS: Open Medical Record System
SNOMED CT: Systematized Nomenclature of Medicine Clinical Terms
UIT: user interface terminology

Edited by A Benis; submitted 03.Jul.2025; peer-reviewed by AS Kanter, T Ohlsen; accepted 08.Jan.2026; published 09.Mar.2026.

Please cite as:
Tangchitnob N, Ponthongmak W, Kijsanayotin B, Pattanaprateep O, Phusanti S, Atiksawedparit P, Suwanthaweemeesuk K, Siangfu J, McKay GJ, Attia J, Thakkinstian A
Developing a Thai User Interface Terminology for Systematized Nomenclature of Medicine Clinical Terms Implementation in Primary Care: Cross-Sectional Content Coverage Analysis
JMIR Med Inform 2026;14:e80039
URL: https://medinform.jmir.org/2026/1/e80039
doi:10.2196/80039

© Nat Tangchitnob, Wanchana Ponthongmak, Boonchai Kijsanayotin, Oraluck Pattanaprateep, Sithakom Phusanti, Pongsakorn Atiksawedparit, Kamonporn Suwanthaweemeesuk, Jirayus Siangfu, Gareth J McKay, John Attia, Ammarin Thakkinstian. Originally published in JMIR Medical Informatics (https://medinform.jmir.org), 9.Mar.2026. This is an open-access article distributed under the terms of the Creative Commons Attribution License (https://creativecommons.org/licenses/by/4.0/), which permits unrestricted use, distribution, and reproduction in any medium, provided the original work, first published in JMIR Medical Informatics, is properly cited. The complete bibliographic information, a link to the original publication on https://medinform.jmir.org/, as well as this copyright and license information must be included.

XSL•FO
RenderX

Original Paper

Large Language Models for Psychiatric Diagnosis Based on Multicenter Real-World Clinical Records: Comparative Study

Maoqian Sun[1,2], MD; Jia Yu[3], MD; Zhuhong Long[2], MD; Yun Yang[2], MD; Tao Xiao[4], MD; Jiaquan Liang[5], MD; Jun Feng[6], MD; Huaili Deng[7], MD; Guoping Huang[2], MD, PhD

[1]Mental Health Center, University-Town Hospital of Chongqing Medical University, Chongqing, China
[2]Sichuan Mental Health Center, The Third Hospital of Mianyang, Mianyang, China
[3]Third People's Hospital of Panzhihua, Panzhihua, China
[4]The Third People's Hospital of Ganzhou, Ganzhou, China
[5]The Third People's Hospital of Foshan, Foshan, China
[6]Lanzhou Third People's Hospital, Lanzhou, China
[7]Shanxi Provincial Mental Health Center, Taiyuan, China

Corresponding Author:
Guoping Huang, MD, PhD
Sichuan Mental Health Center
The Third Hospital of Mianyang
No. 190, East Section of Jiannan Road
Youxian District
Mianyang, 621000
China
Phone: 86 0816 2282249
Email: xyhuanggp@126.com

Abstract

Background: Psychiatric disorders are diagnostically challenging and often rely on subjective clinical judgment, particularly in resource-limited settings. Large language models (LLMs) have demonstrated potential in supporting psychiatric diagnosis; however, robust evidence from large-scale, real-world clinical data remains limited.

Objective: This study aimed to evaluate and compare the diagnostic performance of multiple LLMs for psychiatric disorders using multicenter real-world electronic health records (EHRs).

Methods: We retrospectively analyzed 9923 inpatient EHRs collected from 6 psychiatric centers across China, encompassing all ICD-10 (International Statistical Classification of Diseases, Tenth Revision) psychiatric categories. In total, 3 LLMs—GPT-4.0 (OpenAI), GPT-3.5 (OpenAI), and GLM-4-Plus (Zhipu AI)—were evaluated against physician-confirmed discharge diagnoses. Diagnostic performance was assessed using strict accuracy criteria and lenient classification metrics, with subgroup analyses conducted across diagnostic categories and age groups.

Results: GPT-4.0 achieved the highest overall strict diagnostic accuracy (71.7%) and the highest weighted F1-score under lenient evaluation (0.881), particularly for high-prevalence disorders, such as mood disorders and schizophrenia spectrum disorders. Diagnostic performance varied across age groups, with the highest accuracy observed in older adult patients (up to 79.5%) and lower accuracy in adolescents. Across centers, model performance remained stable, with no significant intercenter differences.

Conclusions: LLMs—especially GPT-4.0—demonstrate promising capability in supporting psychiatric diagnosis using real-world EHRs. However, diagnostic performance varies by age group and disorder category. LLMs should be regarded as assistive tools rather than replacements for clinical judgment, and further validation is needed before routine clinical implementation.

(JMIR Med Inform 2026;14:e77699) doi:10.2196/77699

KEYWORDS

psychiatric disorders; large language models; artificial intelligence; multicenter study; real-world data

XSL•FO
RenderX

Introduction

Mental disorders are a significant public health concern worldwide; they have high prevalence rates, which are continuously increasing each year [1]. About 20% of the global population is estimated to experience mental illness in their lifetime, placing a substantial burden on both society and health care systems [2]. However, there is an acute scarcity of psychiatric professionals. Many countries have fewer than 5 psychiatrists per 100,000 individuals; this results in delays in providing timely, high-quality diagnostic and therapeutic services for patients with mental health disorders, particularly in resource-limited regions, including China [3]. This medical resource shortage further underscores the urgent need to increase the accuracy and efficiency of psychiatric diagnoses. In addition, psychiatric diagnoses are inherently complex and challenging. Complex etiologies and high symptom heterogeneity characterize mental disorders. The symptom descriptions of patients often depend on subjective expression, with physicians' medical records and clinical diagnoses also based on their subjective experience [4]. This subjectivity makes diagnoses susceptible to variation among physicians, leading to inconsistent diagnostic outcomes. Therefore, in psychiatry, there is a crucial need to use modern technologies to increase diagnostic efficiency and accuracy [5].

Recently, the widespread adoption of electronic health records (EHRs) has provided a wealth of unstructured data to support the application of artificial intelligence technologies in medical diagnostics, offering new opportunities for diagnosing psychiatric disorders [6]. Large language models (LLMs), including the GPT series, exhibit powerful capabilities in natural language processing and semantic understanding. They can efficiently process unstructured text and have shown great potential in medical diagnostic assistance [7-10].

At present, studies on the application of LLMs in other medical fields have further confirmed their clinical potential. For example, Hasani et al [11] assessed the performance of GPT-4.0 (OpenAI) in standardizing radiology reports; they reported that it generates high-quality standardized radiology reports and significantly improves the efficiency of report generation and data analysis capabilities. Liu et al [12] compared GPT-4.0 with senior neurosurgeons and reported that the performance of GPT-4.0 in complex medical tasks is comparable with that of experienced experts, demonstrating its value in facilitating the diagnosis of complex cases. In addition, Horiuchi et al [13] reported that GPT-4.0 has demonstrated superior diagnostic accuracy in challenging neuroradiology cases, suggesting that generative artificial intelligence technologies can serve as important supplements to physician cognition in complex diagnostic scenarios. Overall, these studies demonstrate the potential application of GPT-4.0 in multidomain diagnostic tasks.

In psychiatry, LLMs have also begun to garner attention. Because psychiatric diagnoses heavily depend on textual descriptions of patient complaints and medical history, LLMs naturally possess significant application advantages in this field. Previous studies have revealed that ChatGPT-4 (OpenAI) can achieve an accuracy rate of 96.1% in the diagnosis of obsessive-compulsive disorder, significantly outperforming that of clinical psychologists (81.5%) and primary care physicians (49.5%) [14]. In 1 study, researchers used the UTH-BERT model and reported that its diagnostic accuracy for medical history in EHRs (74.3%) surpassed that of psychiatrists with intermediate experience (71.5%) [15]. Despite these advances, prior studies on LLM-based psychiatric diagnosis have several limitations. First, the scope of diseases in previous LLM research has often been narrow, with most studies focusing on a single or a small subset of psychiatric disorders (eg, major depressive disorder and obsessive-compulsive disorder) [16]. In contrast, our study simultaneously included all major *ICD-10* (*International Statistical Classification of Diseases, Tenth Revision*) psychiatric categories (F00-F99), thereby providing broader coverage than previous studies. Nevertheless, our analysis was conducted at the level of primary diagnoses within each category, without explicitly addressing comorbidity patterns, which remains an important direction for future research. Second, data sources are often single and lack validation in real-world clinical settings. Current studies rely primarily on simulated cases or data from a single institution [17], making it challenging to capture patient characteristics across diverse regions and health care practices. In the Chinese context, several studies have begun to explore the use of LLMs for psychiatric diagnosis and Chinese-language medical records; however, comprehensive, large-scale validation in real-world psychiatric EHRs—especially with direct comparisons between international and Chinese models—remains limited. Third, the diagnostic performance across age groups has not been thoroughly investigated, with most studies focusing solely on overall accuracy without examining differences in diagnostic performance across age groups (eg, adolescents and older adult patients). Symptoms, disease progression, and treatment plans for psychiatric disorders significantly differ across different age groups. Whether LLMs can adapt to these differences remains unexplored.

To address the aforementioned issues, this study optimized 3 key aspects: data sources, disease coverage, and population segmentation. First, we incorporated real-world EHR data from 6 representative provincial and municipal psychiatric centers across different regions of China. By directly using clinical records to evaluate the model, this approach is better aligned with real-world medical settings, filling the gap left by previous studies that lacked real-world data validation in the Chinese language. Second, we covered all psychiatric disorders listed in the *ICD-10* classification (F0-F9), overcoming the limitations of previous studies, which focused primarily on a single or a few disease types. This design allowed us to evaluate the model's generalization ability across a broad range of clinical diagnostic tasks. In addition, we conducted fine-grained age stratification, systematically comparing the model's diagnostic performance across 4 age groups: adolescents, young adults, middle-aged individuals, and older adult patients. This allowed the identification of the model's adaptation differences across different age groups. In summary, our study, based on large-scale, multicenter real-world data, is the first to comprehensively evaluate the clinical potential of LLMs for psychiatric diagnosis in China.

XSL•FO
RenderX

Methods

Research Design and Data Sources

The study data were sourced from 6 provincial and municipal psychiatric centers in China. These centers are located in Sichuan, Gansu, Shanxi, Guangdong, Jiangxi, and other regions, covering Southwest China, Northwest China, North China, South China, and East China, thereby ensuring good regional representation. The dataset included the EHRs of psychiatric inpatients between July 2017 and July 2024. In total, 12,819 cases were initially screened. Among them, 2896 cases were excluded owing to incomplete records or unclear diagnoses. Therefore, 9923 eligible cases were included. The EHR data used in this study consisted exclusively of unstructured narrative text fields, including chief complaints, history of present illness, and psychiatric examination notes. Structured data, such as laboratory test results, medication prescriptions, vital signs, nursing notes, and imaging reports, were not included, as psychiatric diagnosis primarily depends on descriptive symptomatology and mental status examination rather than auxiliary tests. All records included in the model were noted down by attending psychiatrists at the time of admission only. Clinical notes taken during hospitalization were not included, ensuring that the model received only information available at the initial diagnostic encounter and preventing potential temporal information leakage.

Ethical Considerations

The Ethics Committee of the Sichuan Provincial Mental Health Center approved this study (approval 202460). Considering the retrospective nature of the study, the Ethics Committee exempted the need for informed consent from the patients. All EHR data were fully deidentified in accordance with the Health Insurance Portability and Accountability Act safe harbor method (45 CFR 164.514(b)), with direct identifiers (eg, names, addresses, contact details, and hospital IDs) removed before analysis. In addition, because narrative clinical text can contain residual indirect identifiers, a stratified manual audit of 500 randomly sampled EHR narratives (approximately 5% of the dataset) was conducted to further minimize reidentification risk. Among these 500 records, 7 (1.4%) instances of potential indirect identifiers were identified and corrected before model inference. No direct identifiers were detected in the sampled records.

Model queries were transmitted through encrypted API calls (HTTPS/TLS) rather than public chat interfaces. Although no formal data processing agreement was established with the external provider, the institutional review board explicitly approved the use of deidentified clinical narratives for inference on external LLM servers. It was assured that the procedure complied with local data governance regulations and did not include identifiable personal information. Only deidentified free text—without metadata, patient identifiers, or institutional information—was transmitted, and no protected health information left the institution.

The study adhered to relevant international and domestic privacy frameworks, including General Data Protection Regulation Article 46 for cross-border data transfer, China's Personal Information Protection Law, and ISO/IEC 27018 guidelines for the protection of personal data in public cloud environments. Nevertheless, we acknowledge that narrative EHR text has inherent deidentification limitations, and we minimized data transmission to mitigate privacy risks.

Data Preprocessing

To closely replicate real-world clinical settings, the admission diagnosis names were removed from the medical history; no other data were modified, thereby preserving the integrity of the original data [18]. The diagnoses were classified into 11 categories by extracting only the first letter and the 10-digit *ICD-10* codes from Chapter V (Mental and Behavioral Disorders; F0-F9) and other related codes. Specifically, F0 includes organic mental disorders such as dementia; F1 includes substance-related disorders such as alcohol addiction; F2 includes schizophrenia and associated psychotic conditions; F3 includes mood disorders such as depression; F4 includes anxiety and stress-related disorders; F5 includes disorders associated with physiological conditions, such as eating disorders; F6 includes personality and behavioral disorders in adults; F7 includes intellectual disabilities; F8 includes developmental disorders such as autism; and F9 includes behavioral and emotional conditions beginning in childhood, including attention-deficit or hyperactivity disorders [19]. For subgroup analysis, patients were stratified into 4 age groups: adolescents (≤17 years), young adults (18-35 years), middle-aged adults (36-59 years), and older adult individuals (≥60 years). The thresholds at 18 and 60 years follow established conventions in psychiatric and geriatric research [20]. The adult group was further subdivided into young and middle-aged categories to capture differences in onset age, symptom presentation, and comorbidity patterns of major psychiatric disorders across life stages.

Research Tools and Model Setup

In total, 3 LLMs were selected for evaluation: GPT-4.0 and GPT-3.5 (OpenAI) and GLM-4-Plus (Zhipu AI). GPT-3.5 was chosen as a widely used baseline model because of its broad accessibility and extensive application in previous medical natural language processing tasks, providing a reference point for evaluation [21]. GPT-4.0, a more advanced successor in the GPT series, was included to assess performance improvements driven by enhanced semantic understanding and reasoning capabilities [22]. GLM-4-Plus is one of the most advanced Chinese-optimized LLMs [23]. It was selected to examine the adaptability and potential of domestic LLMs in psychiatric diagnosis using Chinese-language EHRs and to compare their performance with that of international mainstream models under localized application scenarios.

In addition, a unified prompt was used: "请根据以下患者信息给出最可能的诊断。" ("Please provide the most likely diagnosis based on the following patient information"). Because the clinical input consisted of Chinese-language EHR narratives, the instruction prompt was also written in Chinese to maintain monolingual consistency and avoid potential cross-lingual prompting effects. This prompt was intentionally selected to ensure methodological consistency and fair comparability across all LLMs, as varying prompt strategies may introduce

XSL•FO
RenderX

model-specific advantages. Zero-shot prompts also reflect a realistic clinical scenario in which clinicians typically expect the model to provide a diagnostic impression directly without additional examples. No English prompt or mixed-language prompt was used at any stage. No prompt engineering or chain-of-thought prompting was applied, as the study aimed to evaluate each model's baseline diagnostic capability under identical input conditions. The preprocessed data included the patient's sex, age, chief complaints, medical history, and psychiatric examination results. The psychiatric examination results included narrative descriptions of key mental status domains, such as appearance and behavior, mood and affect, thought process and content, cognitive function, and insight, which were documented in a standardized format across all participating centers to ensure structural consistency and data comparability. These inputs were provided to the model to generate diagnostic results. All diagnostic analyses by the LLMs were completed between January 1 and January 31, 2025. The discharge diagnosis served as the reference standard and was confirmed by a senior associate chief physician with over 10 years of clinical experience.

Model outputs were evaluated using a 0-2 point scoring system: 2 points for a completely correct diagnosis (exact *ICD-10* match), 1 point for a partially correct diagnosis, and 0 points for an incorrect diagnosis. "Partially correct" was operationally defined as cases in which the predicted diagnosis was clinically close to, but not an exact, *ICD-10* match. Examples included (1) misclassification within the schizophrenia spectrum (eg, schizotypal disorder scored as schizophrenia), (2) assigning a broader category within mood disorders without specifying the exact episode (eg, manic episode scored as mood disorder), or (3) capturing the correct diagnostic domain at a broader level of granularity (eg, generalized anxiety disorder scored as anxiety disorder). Predictions that did not meet these criteria were considered incorrect.

To ensure reliability and minimize bias, multiple 2-rater groups were formed, each comprising 2 attending psychiatrists with more than 5 years of independent clinical experience. Both raters independently scored each case after the model outputs were anonymized and randomized, which blinded them to the source model. Disagreements were resolved by consensus with a senior psychiatrist. Interrater reliability was assessed using Cohen κ coefficient, which demonstrated substantial agreement (Cohen κ=0.82).

Data Analysis

Statistical analyses were conducted using SPSS Statistics (version 27.0; IBM Corp). Descriptive statistics were used to present the demographic characteristics and distributions of disease categories. Model performance was evaluated by comparing the predicted diagnoses with the discharge diagnoses, which served as the reference standard. Accuracy was calculated as the proportion of correct predictions (score=2). In this study, strict evaluation criteria were used as the primary analytic framework. Under this explicit definition, only exact matches between the model-predicted *ICD-10* diagnosis and the discharge diagnosis (score=2) were considered correct, whereas partially correct predictions (score=1) were treated as incorrect.

For the classification performance metrics—namely, precision, recall, and F_1-score—we also applied a lenient evaluation. Under this lenient definition, both exact matches (score=2) and partially correct predictions (score=1) were treated as correct and counted as true positives (TPs). In this framework, TPs were predictions that were exactly or partially consistent with the true diagnosis (score=2 or score=1); false positives (FPs) were predictions for a class when the true diagnosis belonged to another class; and false negatives (FNs) were cases in which the true diagnosis belonged to a class, but the model prediction did not. Predictions with score=0 were always treated as incorrect. These lenient metrics were used exclusively for the classification performance results and are clearly labeled as such. All other analyses throughout the manuscript relied solely on the strict evaluation criteria. In addition, performance metrics, including precision, recall, and F_1-score, were computed under a strict definition: only exact matches between the model-predicted *ICD-10* diagnosis and the discharge diagnosis were considered correct. In this framework, TPs are cases where the prediction exactly matches the true diagnosis; FPs are predictions for a class when the true diagnosis belongs to another class; and FNs are cases where the true diagnosis belongs to a class, but the model prediction does not. Partially correct outputs (score=1) were treated as incorrect predictions and classified as FPs or FNs depending on the prediction-reference mismatch; only score=2 outputs were counted as TPs.

The macro- and weighted-average F_1-scores were calculated to measure overall performance. Because the F8 category contained only 8 cases (0.1% of the dataset), macroaverage F_1-scores were additionally reported, both including and excluding this extremely rare category, to provide a more stable estimate of overall performance. Tests of normality and homogeneity of variance were conducted. The Shapiro-Wilk test indicated that the score data significantly deviated from normality across all model groups, and the Levene test confirmed unequal variances (Table S1 in Multimedia Appendix 1). Therefore, nonparametric rank-sum tests were applied for intergroup comparisons. In addition, Kruskal-Wallis tests were used to examine whether diagnostic accuracy differed across the 6 centers for each model (Table S2 in Multimedia Appendix 1). A P value of <.05 indicated significance. To further compare diagnostic performance across LLMs, an ordinal logistic regression analysis was conducted. Because the diagnostic outcome was an ordered 0-2 score (0=incorrect, 1=partially correct, and 2=correct), a proportional odds model was applied to estimate the likelihood of achieving a higher diagnostic score for each model. GPT-3.5 served as the reference category. Odds ratios (ORs) and 95% CIs were calculated to quantify differences in diagnostic performance. The results of this analysis are presented in Table S3 in Multimedia Appendix 1.

Results

Demographic Characteristics and Disease Category Distribution

In total, 9923 patients (3665, 36.93% males and 6258, 63.07% females) were included in this study. Across age groups, 1881 (18.96%) were adolescents (≤17 years), 2468 (24.87%) were

XSL•FO
RenderX

young adults (18-35 years), 3695 (37.24%) were middle-aged adults (36-59 years), and 1879 (18.94%) were older adults (≥60 years). The disease categories were distributed as follows (Table 1): mood disorders (F3) were the most common, accounting for 36.7% (3646/9923) of the cases, followed by schizophrenia, schizotypal, and delusional disorders (F2, 2470/9923, 24.9%), and neurotic disorders (F4, 1991/9923, 20.1%). The distribution of other disorders was relatively low.

Table 1. Demographic data and clinical characteristics.

Characteristics	Value
Sex, n (%)	
Male	3665 (36.93)
Female	6258 (63.07)
Age (y), mean (SD)	40.5 (20.03)
Age category, n (%)	
Adolescent (≤17 y)	1881 (19)
Young adult (18-35 y)	2468 (24.9)
Middle-aged (36-59 y)	3695 (37.2)
Older adult (≥60 y)	1879 (18.9)
Disorder category, n (%)	
F0 (Organic disorders)	597 (6)
F1 (Substance use disorders)	243 (2)
F2 (Schizophrenia, schizotypal, and delusional disorders)	2470 (24.9)
F3 (Mood disorders)	3646 (36.7)
F4 (Neurotic disorders)	1991 (20.1)
F5 (Eating disorders, etc)	70 (0.7)
F6 (Personality disorders)	86 (0.9)
F7 (Mental retardation)	177 (1.8)
F8 (Autism, etc)	8 (0.1)
F9 (Behavioral disorders)	635 (6.4)

Diagnostic Accuracy of the 3 Models

Overall, GPT-4.0 achieved an overall accuracy of 71.7%, outperforming GLM-4-Plus (69.3%) and GPT-3.5 (68.8%). In terms of category-specific performance, GPT-4.0 exhibited higher overall accuracy than the other models in the F1, F3, and F6 categories. However, in the F2 and F4 categories, the diagnostic accuracy rates of the 3 models were similar, with no significant differences. Among the different age groups, diagnostic accuracy was higher in the older adult group (with an overall accuracy rate of 74.3%-79.5%). Additional analysis using the rank-sum test revealed significant differences between adolescents and middle-aged adults, adolescents and older adults, young adults and middle-aged adults, and young adults and older adults (P<.001). The results are summarized in Tables 2 and 3, and the category-level diagnostic score patterns across the 3 models are visualized in Figure 1.

XSL•FO
RenderX

Table 2. Diagnostic accuracy.

Category	GPT-4.0, n (%)			GPT-3.5, n (%)			GLM-4-Plus, n (%)		
	Correct	Partially correct	Incorrect	Correct	Partially correct	Incorrect	Correct	Partially correct	Incorrect
Disorder category									
F0	394 (66)	152 (25.5)	51 (8.5)	338 (56.6)	143 (24)	116 (19.4)	415 (69.5)	94 (15.7)	88 (14.7)
F1	208 (85.6)	22 (9.1)	13 (5.3)	182 (74.9)	25 (10.3)	36 (14.8)	206 (84.8)	14 (5.8)	23 (9.5)
F2	1906 (77.2)	460 (18.6)	104 (4.2)	1834 (74.3)	531 (21.5)	105 (4.3)	1890 (76.5)	475 (19.2)	105 (4.3)
F3	2738 (75.1)	561 (15.4)	347 (9.5)	2654 (72.8)	489 (13.4)	503 (13.8)	2576 (70.7)	773 (21.2)	297 (8.1)
F4	1347 (67.6)	310 (15.6)	334 (16.8)	1368 (68.7)	308 (15.5)	315 (15.8)	1281 (64.3)	323 (16.2)	387 (19.4)
F5	48 (68.6)	2 (2.9)	20 (28.6)	41 (58.6)	0 (0)	29 (41.4)	50 (71.4)	1 (1.4)	19 (27.1)
F6	59 (68.6)	3 (3.5)	24 (27.9)	20 (23.3)	11 (12.8)	55 (64)	36 (41.9)	0 (0)	50 (58.1)
F7	123 (69.5)	22 (12.4)	32 (18.1)	83 (46.9)	9 (5.1)	85 (48)	131 (74)	6 (3.4)	40 (22.6)
F8	8 (100)	0 (0)	0 (0)	7 (87.5)	0 (0)	1 (12.5)	6 (75)	0 (0)	2 (25)
F9	285 (44.9)	85 (13.4)	265 (41.7)	296 (46.6)	78 (12.3)	261 (41.1)	282 (44.4)	79 (12.4)	274 (43.1)
Age category									
Adolescent (≤17 y)	1148 (61)	367 (19.5)	366 (19.5)	1116 (59.3)	341 (18.1)	424 (22.5)	1010 (53.7)	497 (26.4)	374 (19.9)
Young adult (18-35 y)	1727 (70)	480 (19.4)	261 (10.6)	1638 (66.4)	456 (18.5)	374 (15.2)	1654 (67)	534 (21.6)	280 (11.3)
Middle-aged (36-59 y)	2759 (74.7)	530 (14.3)	406 (11)	2672 (72.3)	551 (14.9)	472 (12.8)	2715 (73.5)	540 (14.6)	440 (11.9)
Older adult (≥60 y)	1482 (78.9)	240 (12.8)	157 (8.4)	1397 (74.3)	246 (13.1)	236 (12.6)	1494 (79.5)	194 (10.3)	191 (10.2)
Total	7116 (71.7)	1617 (16.3)	1190 (12)	6823 (68.8)	1594 (16.1)	1506 (15.2)	6873 (69.3)	1762 (17.8)	1285 (12.9)

Table 3. Comparison of diagnostic scores based on age.

Age category	*P* value		
	GPT-4.0	GPT-3.5	GLM-4-Plus
Adolescent[a] vs young adult[b]	<.001	<.001	<.001
Adolescent vs middle-aged[c]	<.001	<.001	<.001
Adolescent vs older adult[d]	<.001	<.001	<.001
Young adult vs middle-aged	<.001	<.001	<.001
Young adult vs older adult	<.001	<.001	<.001
Middle-aged vs older adult	<.001	.15	<.001

[a]Adolescent: ≤17 years.

[b]Young adult: 18-35 years.

[c]Middle-aged: 36-59 years.

[d]Older adult: ≥60 years.

XSL•FO
RenderX

Figure 1. Heatmap of the diagnostic scores. The color intensity indicates the model's diagnostic score (on a 2-point scale), with darker colors indicating higher scores. This reflects the diagnostic accuracy of the models in each category.

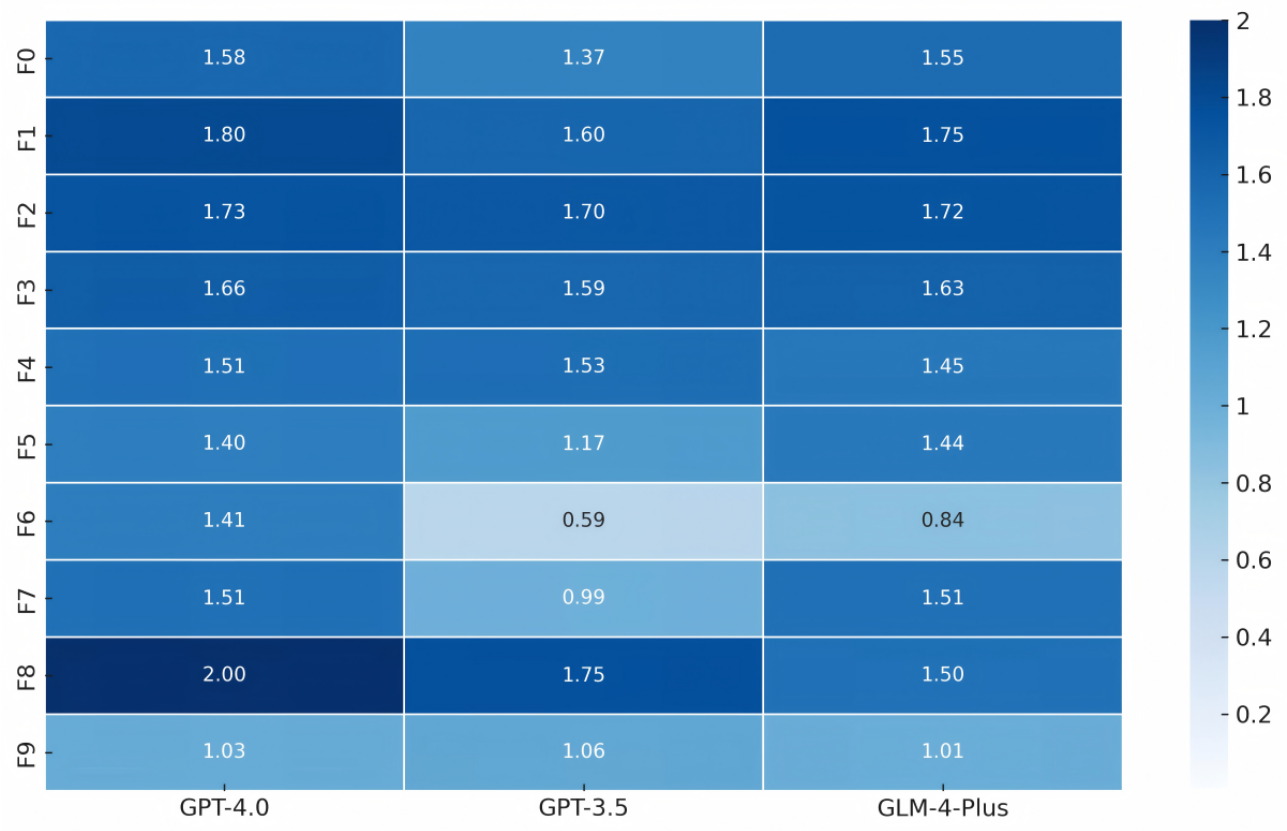

Center-Level Diagnostic Performance

To evaluate whether model performance varied across institutions, a supplementary center-level analysis was conducted. The diagnostic accuracies of all 3 models demonstrated only minor numerical fluctuations across the 6 centers. Importantly, the Kruskal-Wallis test indicated no statistically significant differences for any of the models (GPT-4.0: P=.52; GPT-3.5: P=.47; and GLM-4-Plus: P=.61). The detailed results for each center are provided in Table S2 in Multimedia Appendix 1.

Analysis of Differences in Scoring Distribution of 3 Models

The rank-sum test was used to compare differences in the scoring distributions of GPT-4.0, GPT-3.5, and GLM-4-Plus across various *ICD-10* categories. We observed that GPT-4.0 had higher scores than GPT-3.5 in the F0 (P<.001), F6 (P<.001), and F7 (P<.001) categories. Furthermore, GLM-4-Plus exhibited differences in its scoring distribution compared with GPT-3.5 in the F0 (P<.001) and F7 (P<.001) categories. Overall, the score distribution of GPT-4.0 was superior to that of both GPT-3.5 (P<.001) and GLM-4-Plus (P<.001). However, the difference in the scoring distribution between GPT-3.5 and GLM-4-Plus was not statistically significant (P=.09). Table 4 summarizes the results.

XSL•FO
RenderX

Table 4. Comparison of the diagnostic scores of the different large language models.

Disorder category	*P* value		
	GPT-4.0 vs GPT-3.5	GPT-4.0 vs GLM-4-Plus	GPT-3.5 vs GLM-4-Plus
F0	<.001	.69	<.001
F1	.002	.67	.008
F2	.02	.60	.08
F3	.002	<.001	.77
F4	.43	.02	.002
F5	.17	.75	.098
F6	<.001	<.001	.14
F7	<.001	.63	<.001
F8	.38	.17	.59
F9	.65	.72	.42
Total	<.001	<.001	.09

Comparison of the Classification Performance of 3 Models

Table 5 summarizes the precision, recall, and F_1-scores of the GPT-4.0, GPT-3.5, and GLM-4-Plus models across various *ICD-10* disease categories. To enhance interpretability, these classification metrics were computed using a lenient evaluation framework, in which both exact matches (score=2) and partially correct predictions (score=1) were treated as correct. GPT-4.0 achieved the highest F_1-scores in the F0 (0.915), F1 (0.926), and F2 (0.929) categories. GLM-4-Plus achieved the highest precision in the F2 category (0.951), whereas GPT-4.0 had a superior recall rate (0.959). Small-sample categories exhibited significant fluctuations, including the F8 category, where GPT-4.0's recall rate reached 1.00, while its precision was only 0.308. This phenomenon reflects class imbalance and overprediction in rare categories. The macroaverage F_1-scores (including F8) were 0.655, 0.410, and 0.712 for GPT-4.0, GPT-3.5, and GLM-4-Plus, respectively. The weighted average F_1-score of GPT-4.0 (0.881) was superior to that of both GPT-3.5 (0.849) and GLM-4-Plus (0.873). To mitigate the instability caused by the extremely small F8 category, macroaverage F_1-scores were also calculated after excluding F8. The exclusion yielded more stable macrolevel estimates: 0.821 for GPT-4.0, 0.745 for GPT-3.5, and 0.806 for GLM-4-Plus.

To further complement this evaluation, we also performed an ordinal logistic regression analysis using the 0-2 scoring system (0=incorrect, 1=partially correct, and 2=correct) as the outcome variable, accounting for its ordinal nature. The results were consistent with the overall performance patterns observed in the main analysis. GPT-4.0 was significantly more likely to achieve a higher diagnostic score compared with GPT-3.5 (OR 1.18, 95% CI 1.11-1.25; *P*<.001). In contrast, GLM-4-Plus showed slightly lower odds of achieving a higher score relative to GPT-3.5 (OR 0.95, 95% CI 0.90-1.01). Although this difference did not reach statistical significance (*P*=.09; Table S3 in Multimedia Appendix 1).

XSL•FO
RenderX

Table 5. Precision, recall, and F1-scores of the different large language models (lenient evaluation).

Category[a]	GPT-4.0			GPT-3.5			GLM-4-Plus		
	Precision	Recall	F_1-score	Precision	Recall	F_1-score	Precision	Recall	F_1-score
Disorder category									
F0	0.916	0.915	0.915	0.897	0.814	0.853	0.857	0.929	0.891
F1	0.906	0.947	0.926	0.924	0.852	0.887	0.880	0.961	0.919
F2	0.902	0.959	0.929	0.850	0.961	0.902	0.951	0.876	0.912
F3	0.857	0.906	0.881	0.849	0.864	0.856	0.884	0.862	0.873
F4	0.913	0.835	0.872	0.859	0.843	0.851	0.863	0.867	0.865
F5	0.549	0.714	0.621	0.519	0.586	0.550	0.785	0.607	0.685
F6	0.554	0.721	0.626	0.405	0.372	0.388	0.750	0.409	0.529
F7	0.973	0.819	0.890	0.979	0.525	0.684	0.820	0.913	0.864
F8	0.308	1.000	0.471	0.159	0.875	0.269	0.667	0.500	0.571
F9	0.962	0.592	0.733	0.971	0.589	0.733	0.576	0.960	0.720
Macro average	0.653	0.701	0.655	0.436	0.428	0.410	0.730	0.717	0.712
Macro average (excluding F8)	—[b]	—	0.821	—	—	0.745	—	—	0.806
Weighted average	0.888	0.882	0.881	0.859	0.851	0.849	0.882	0.871	0.873

[a]A lenient evaluation framework was used for all metrics in this table. Both score=2 (exact match) and score=1 (partially correct) predictions were considered as correct.

[b]Not applicable.

Discussion

Principal Findings

This multicenter real-world study is the first to systematically evaluate the diagnostic performance of 3 LLMs—GPT-4.0, GPT-3.5, and GLM-4-Plus—across the full spectrum of *ICD-10* psychiatric categories via Chinese psychiatric EHRs. The results demonstrate that GPT-4.0 achieved the highest overall strict diagnostic accuracy (71.7%), followed by GLM-4-Plus (69.3%) and GPT-3.5 (68.8%), showing a clear performance gradient across model generations. In addition to strict accuracy, GPT-4.0 also achieved a higher lenient F_1-score (0.881), indicating performance when partially correct predictions are counted as correct. These complementary metrics highlight different aspects of diagnostic ability under distinct evaluation frameworks.

Consistent with these findings, the ordinal logistic regression provided a quantitative estimate of these differences: GPT-4.0 was significantly more likely to achieve a higher diagnostic score compared with GPT-3.5 (OR 1.18, 95% CI 1.11-1.25; P<.001). In contrast, GLM-4-Plus demonstrated ORs comparable with those of GPT-3.5 (OR 0.95, 95% CI 0.90-1.01), indicating no statistically significant difference in performance between the 2 models. These results further support the interpretation that GPT-4.0 provides a measurable performance advantage, whereas GLM-4-Plus and GPT-3.5 exhibit broadly similar diagnostic capability.

Significant differences were observed across most age groups, with diagnostic accuracy generally increasing with age. Older adult patients exhibited notably better diagnostic performance than adolescents and young adults. For GPT-4.0 and GLM-4-Plus, all pairwise adjacent age-group comparisons were statistically significant (all P<.001). For GPT-3.5, accuracy also increased with age overall; however, the comparison between middle-aged and older adult patients did not reach statistical significance (P=.15). This trend likely reflects several clinical and documentation-related factors: older adults typically present with more stable symptom trajectories, longer disease histories, and more structured and complete EHR documentation, whereas younger patients often exhibit heterogeneous and fluctuating emotional and behavioral symptoms, which increase diagnostic uncertainty.

Across diagnostic categories, GPT-4.0 consistently showed stronger contextual reasoning ability and more accurate extraction of relevant diagnostic cues. It performed particularly well in mood disorders (F3), personality disorders (F6), and several neurotic and stress-related disorders (F4). GLM-4-Plus demonstrated strong performance in schizophrenia spectrum disorders (F2), suggesting an advantage in identifying disorders with clearly structured symptom patterns. GPT-3.5 exhibited the highest rate of misclassification, particularly between disorders with overlapping emotional or behavioral symptoms.

In low-prevalence categories, such as pervasive developmental disorders (F8), all 3 models showed instability in performance. GPT-4.0 achieved perfect recall but exhibited low precision, suggesting overidentification in categories with limited diagnostic cues. These patterns highlight the ongoing challenge

XSL•FO
RenderX

for general-purpose LLMs in identifying rare psychiatric conditions.

Beyond model comparison, this study demonstrates the overall feasibility of applying large-scale language models to real-world psychiatric EHRs covering all *ICD-10* categories. The results indicate that GPT-4.0 can extract diagnostically relevant information efficiently and generate multidimensional diagnostic suggestions, thereby supporting initial clinical screening, reducing physician workload, and improving efficiency in high-volume psychiatric settings. However, LLM-based diagnosis remains dependent on the quality of EHRs, symptom clarity, and physician interpretation, and cannot be used as a substitute for clinical expertise or individualized assessment.

Overall, GPT-4.0 demonstrated the strongest, most stable, and most clinically meaningful diagnostic performance across age groups and psychiatric categories, supporting its potential value as a diagnostic assistance tool within real-world psychiatric workflows.

Center-Level Consistency and Its Implications

Although the 6 centers differed in documentation habits, patient demographics, and narrative styles, all 3 LLMs demonstrated stable diagnostic performance across sites. This consistency suggests that the models rely primarily on core clinical symptom patterns rather than center-specific narrative conventions, which may explain their robustness in real-world settings. The absence of center-level variability also indicates that LLM-based diagnostic support may generalize well across institutions with heterogeneous clinical workflows—a critical requirement for real-world deployment. From an implementation perspective, these findings imply that LLM-assisted diagnostic tools may not require site-specific retraining or local optimization, substantially reducing the technical and operational burden associated with clinical adoption. Collectively, these observations highlight the scalability and practical utility of LLMs in psychiatric diagnostic workflows.

Misclassification Patterns in the F8 Category

The extreme imbalance between recall and precision in the F8 category warrants further clinical interpretation. Although GPT-4.0 successfully identified all true F8 cases, its low precision indicates a substantial number of FP predictions. Upon reviewing these cases, we found that most FPs originated from F9 (behavioral and attention-deficit/hyperactivity disorder–related disorders), with a smaller proportion from F7 (intellectual disabilities). These diagnostic groups share overlapping behavioral and neurodevelopmental characteristics with F8—including impulsivity, irritability, social dysfunction, and developmental impairment—which may lead the model to rely on broad behavioral descriptors when more specific differentiating features are not explicitly documented in the narrative EHR. This overdiagnosis pattern suggests that GPT-4.0 is sensitive to general behavioral dysregulation but is less effective in distinguishing between rare neurodevelopmental disorders with partially overlapping phenotypes. Understanding this tendency toward misclassification is essential for evaluating the model's safety profile when applied to clinically rare categories.

Comparison With Previous Work

The superior diagnostic performance of GPT-4.0 observed in this study is consistent with previous evaluations, which report that newer-generation LLMs outperform earlier versions in clinical reasoning tasks [24-26]. This performance advantage has been attributed to the enhanced ability of GPT-4.0 to capture semantic associations and long-range contextual patterns in complex textual inputs [27]. Previous studies have demonstrated that GPT-4.0 provides higher diagnostic accuracy, better contextual understanding, and more stable reasoning patterns than does GPT-3.5 across diverse clinical applications. Our findings extend this body of evidence to the domain of psychiatric diagnosis via Chinese-language EHRs in real-world settings.

A major distinction between our study and earlier work is the use of multicenter real-world psychiatric EHR narratives rather than simulated vignettes or single-institution datasets. The complexity and variability of real-world clinical documentation allow for a more realistic assessment of LLM behavior in routine psychiatric practice, thereby providing stronger ecological validity.

Consistent with the broader literature, earlier-generation models, such as the GPT-3.5, tend to perform less reliably in disorders characterized by overlapping emotional or behavioral symptoms [24-26]. In our study, this general pattern was reflected in GPT-3.5's tendency to misclassify personality disorders (F6) as mood disorders (F3), likely due to the similarity and ambiguity of symptom descriptions in these categories within real-world psychiatric EHRs. This observation aligns with the known challenges faced by earlier LLMs in distinguishing clinically overlapping symptom domains. In contrast, GLM-4-Plus demonstrated strong performance in schizophrenia spectrum disorders (F2), suggesting that models trained on Chinese corpus characteristics may perform well in categories with clear and structured symptom patterns.

Beyond diagnostic accuracy, prior studies have highlighted the potential role of LLMs as clinical decision support tools capable of improving workflow efficiency and reducing clinician workload in real-world health care settings [28]. In psychiatry, recent evaluations have summarized the diagnostic accuracy of LLMs and emphasized their potential utility in assisting clinicians with complex diagnostic decisions [29]. More broadly, advances in deep learning–based electronic health record analytics have demonstrated the feasibility of extracting clinically meaningful information from narrative EHRs to support timely screening and downstream decision-making processes [30].

Taken together, our findings reinforce the performance advantages of GPT-4.0 observed in previous work and highlight the importance of evaluating both international and domestic LLMs in localized, real-world psychiatric contexts.

Limitations

This study has several limitations. First, although we used multicenter real-world psychiatric EHRs, differences in documentation style—including variability in narrative structure, terminology, completeness of information, and implicit

XSL•FO
RenderX

diagnostic cues—may have influenced model performance. These inconsistencies can alter the prominence, clarity, and temporal linkage of symptom descriptions, potentially affecting diagnostic outputs. Broader validation in institutions with diverse linguistic and cultural backgrounds is needed to assess cross-system and cross-national generalizability more fully [31].

Second, this study adopted a single unified prompting strategy to ensure consistent comparability across models. However, previous research has shown that more advanced prompting techniques can improve diagnostic reasoning. For example, Savage et al [32] reported that diagnostic reasoning prompts enhance LLMs' ability to emulate stepwise clinical reasoning compared with standard prompts. In our setting, a small exploratory pilot study using chain-of-thought prompts on 200 randomly selected cases suggested a modest improvement in exact-match accuracy (about 2-3 percentage points), particularly for mood and anxiety disorder categories. Although this was not a full comparative experiment, the results suggest that the prompting strategy may influence diagnostic performance. Future studies should systematically evaluate zero-shot, few-shot, and chain-of-thought prompt approaches across diagnostic categories and age groups.

Third, the study used a single-label classification framework based on primary discharge diagnoses. While this reflects routine clinical practice, it does not capture psychiatric comorbidities, which are common and clinically important. Multilabel diagnostic frameworks may be necessary to better reflect the real-world complexity of diagnosis.

Fourth, our analysis relied on static EHR text and did not incorporate longitudinal or multimodal clinical information. Real-world psychiatric care involves dynamic symptom progression and treatment trajectories, which cannot be fully captured in static narratives. Integrating time series EHR data, imaging, or laboratory results may increase the diagnostic robustness of LLMs [33].

Fifth, the dataset did not include key socioeconomic variables—such as education level, employment or income status, or urban versus rural residence—which limited our ability to examine potential algorithmic bias or fairness across different social strata. These factors can shape health care access, diagnostic pathways, and linguistic characteristics of clinical documentation, and their absence prevented a systematic assessment of whether model performance varied across sociodemographic groups. Future studies incorporating richer socioeconomic status–related demographic information will be essential for evaluating equity in LLM-assisted diagnostic workflows.

Sixth, although admission diagnoses were removed from model inputs, sections, such as the history of present illness, may still include implicit diagnostic tendencies embedded within physicians' narrative styles. To address this concern, we manually reviewed a subset of correctly and incorrectly classified cases to determine whether the model relied on "giveaway" phrases or diagnosis-specific linguistic cues. We did not identify consistent or systematic patterns—such as psychopharmacological keywords, standardized phrasing, or clinician-specific formulations—that uniquely pointed to a specific diagnosis. When such terms occurred (eg, references to antidepressants or antipsychotics), they were typically nonspecific and appeared across multiple diagnostic categories.

However, certain unmasked psychotropic medications—particularly lithium and clozapine, which function as strong diagnostic proxies—may have allowed the models to infer diagnoses through medication extraction rather than full clinical reasoning, potentially inflating accuracy in specific categories. These observations suggest that while soft leakage cannot be entirely eliminated in narrative EHRs, its impact on model performance in this dataset was likely limited. Future studies should consider masking medication names or evaluating model behavior under medication-removed conditions to better isolate true diagnostic reasoning.

In addition, this study has privacy-related limitations. Although all EHR narratives were deidentified before transmission to external LLM servers, narrative clinical text carries inherent challenges for complete anonymization. Despite multiple safeguards, the possibility of residual identifiers cannot be entirely eliminated, and future research should prioritize on-premise or institution-governed LLM deployment to avoid external data transmission fully. Moreover, because the manual deidentification audit was conducted on a sampled subset of 500 records rather than the full dataset, a small risk of undetected residual identifiers cannot be completely excluded.

Furthermore, the study did not include a human benchmark for comparison, such as the diagnostic accuracy of junior clinicians, admitting psychiatrists, or structured admission diagnoses. Without this comparative context, it is difficult to ascertain whether the observed strict accuracy of 71.7% represents a clinically meaningful performance threshold. Future research should incorporate human-model comparison frameworks or prospective reader studies to more clearly establish the clinical utility of LLM-assisted diagnostic workflows.

Finally, although multicenter data improved external validity, further validation through prospective observational designs or randomized controlled trials is necessary to robustly establish the real-world clinical utility of LLMs in psychiatric diagnostic workflows [31].

Future Directions

Future research should expand the diversity of data sources to evaluate the generalizability of LLMs across different health care systems, linguistic environments, and cultural contexts. The incorporation of longitudinal EHR data, time series symptom trajectories, and multimodal clinical information—such as laboratory tests and imaging—may further enhance the ability of LLMs to capture dynamic clinical changes and improve diagnostic robustness.

Furthermore, more sophisticated strategies warrant systematic investigation. Comparative evaluations of zero-shot, few-shot, and chain-of-thought prompts across different psychiatric categories and age groups may help optimize the integration of LLMs into clinical workflows. Future studies should also explore multilabel diagnostic frameworks to capture psychiatric comorbidities better and reflect the complexity of real-world clinical presentations.

XSL•FO
RenderX

Finally, prospective validation—particularly through observational studies or randomized controlled trials—will be essential for establishing the real-world clinical utility, reliability, and safety of LLM-assisted diagnostic tools in psychiatric practice.

Conclusions

This multicenter real-world study systematically evaluated the diagnostic performance of the GPT-4.0, GPT-3.5, and GLM-4-Plus across all *ICD-10* psychiatric categories using Chinese psychiatric EHRs. GPT-4.0 demonstrated the strongest and most stable diagnostic performance in this study across age groups and diagnostic categories and showed clear advantages in interpreting complex psychiatric narratives. All models performed less reliably in low-prevalence categories, and diagnostic accuracy varied substantially across age groups, with lower accuracy observed in adolescents and young adults.

These findings confirm the feasibility of applying LLMs to real-world psychiatric EHRs and highlight the potential value of GPT-4.0 as a diagnostic support tool. However, the diagnostic outputs of LLMs remain constrained by the quality of documentation, symptom clarity, and the limitations of the models. LLMs should therefore be viewed as complementary tools that can assist clinicians but cannot replace clinical expertise, individualized assessment, or professional decision-making in psychiatric practice.

Acknowledgments

Generative artificial intelligence tools (ChatGPT and OpenAI) were used to assist with language refinement and editing. All content was reviewed and verified by the authors.

Funding

No external financial support or grants were received from any public, commercial, or not-for-profit entities for the research, authorship, or publication of this article.

Data Availability

The datasets generated and analyzed during this study are not publicly available due to patient privacy, but are available from the corresponding author on reasonable request.

Authors' Contributions

Conceptualization: MS, JY, GH
Methodology: MS, JY
Data curation: MS, JY, ZL, YY, TX
Formal analysis: MS, JY
Investigation: MS, JY, ZL, YY, TX
Writing – original draft: MS, JY, JL
Writing – review & editing: MS, JY, JF, HD, GH
Supervision: GH
Project administration: GH
All authors read and approved the final manuscript.

Conflicts of Interest

None declared.

Multimedia Appendix 1
Instrument and additional tables.
[DOCX File , 19 KB - medinform_v14i1e77699_app1.docx]

References

1. Freeman M. The world mental health report: transforming mental health for all. World Psychiatry 2022;21(3):391-392 [FREE Full text] [doi: 10.1002/wps.21018] [Medline: 36073688]
2. Murray CJL, GBD 2021 Collaborators. Findings from the global burden of disease study 2021. Lancet 2024;403(10440):2259-2262. [doi: 10.1016/S0140-6736(24)00769-4] [Medline: 38762327]
3. Jacob KS. Mental health services in low-income and middle-income countries. Lancet Psychiatry 2017;4(2):87-89. [doi: 10.1016/S2215-0366(16)30423-0] [Medline: 28063878]
4. First MB. Diagnostic and statistical manual of mental disorders, 5th edition, and clinical utility. J Nerv Ment Dis 2013;201(9):727-729. [doi: 10.1097/NMD.0b013e3182a2168a] [Medline: 23995026]

XSL•FO
RenderX

5. Bzdok D, Meyer-Lindenberg A. Machine learning for precision psychiatry: opportunities and challenges. Biol Psychiatry Cogn Neurosci Neuroimaging 2018;3(3):223-230. [doi: 10.1016/j.bpsc.2017.11.007] [Medline: 29486863]
6. Afshar M, Adelaine S, Resnik F, Mundt MP, Long J, Leaf M, et al. Deployment of real-time natural language processing and deep learning clinical decision support in the electronic health record: pipeline implementation for an opioid misuse screener in hospitalized adults. JMIR Med Inform 2023;11:e44977 [FREE Full text] [doi: 10.2196/44977] [Medline: 37079367]
7. Brown TB, Mann B, Ryder, N, Subbiah, M. Language models are few-shot learners. 2020 Presented at: NIPS'20: Proceedings of the 34th International Conference on Neural Information Processing Systems; 2020 December 6 - 12; Vancouver BC Canada p. 1877-1901.
8. Thirunavukarasu AJ, Ting DSJ, Elangovan K, Gutierrez L, Tan TF, Ting DSW. Large language models in medicine. Nat Med 2023;29(8):1930-1940. [doi: 10.1038/s41591-023-02448-8] [Medline: 37460753]
9. Huo B, Cacciamani GE, Collins GS, McKechnie T, Lee Y, Guyatt G. Reporting standards for the use of large language model-linked chatbots for health advice. Nat Med 2023;29(12):2988. [doi: 10.1038/s41591-023-02656-2] [Medline: 37957381]
10. Liang H, Tsui BY, Ni H, Valentim CCS, Baxter SL, Liu G, et al. Evaluation and accurate diagnoses of pediatric diseases using artificial intelligence. Nat Med 2019;25(3):433-438. [doi: 10.1038/s41591-018-0335-9] [Medline: 30742121]
11. Hasani AM, Singh S, Zahergivar A, Ryan B, Nethala D, Bravomontenegro G, et al. Evaluating the performance of Generative Pre-trained Transformer-4 (GPT-4) in standardizing radiology reports. Eur Radiol 2024;34(6):3566-3574. [doi: 10.1007/s00330-023-10384-x] [Medline: 37938381]
12. Liu J, Zheng J, Cai X, Wu D, Yin C. A descriptive study based on the comparison of ChatGPT and evidence-based neurosurgeons. iScience 2023;26(9):107590 [FREE Full text] [doi: 10.1016/j.isci.2023.107590] [Medline: 37705958]
13. Horiuchi D, Tatekawa H, Oura T, Oue S, Walston SL, Takita H, et al. Comparing the diagnostic performance of GPT-4-based ChatGPT, GPT-4V-based ChatGPT, and radiologists in challenging neuroradiology cases. Clin Neuroradiol 2024;34(4):779-787. [doi: 10.1007/s00062-024-01426-y] [Medline: 38806794]
14. Kim J, Leonte KG, Chen ML, Torous JB, Linos E, Pinto A, et al. Large language models outperform mental and medical health care professionals in identifying obsessive-compulsive disorder. NPJ Digit Med 2024;7(1):193 [FREE Full text] [doi: 10.1038/s41746-024-01181-x] [Medline: 39030292]
15. Otsuka N, Kawanishi Y, Doi F, Takeda T, Okumura K, Yamauchi T, et al. Diagnosing psychiatric disorders from history of present illness using a large-scale linguistic model. Psychiatry Clin Neurosci 2023;77(11):597-604 [FREE Full text] [doi: 10.1111/pcn.13580] [Medline: 37526294]
16. Hua Y, Na H, Li Z, Liu F, Fang X, Clifton D, et al. A scoping review of large language models for generative tasks in mental health care. NPJ Digit Med 2025;8(1):230 [FREE Full text] [doi: 10.1038/s41746-025-01611-4] [Medline: 40307331]
17. Reichenpfader D. Simulating Diverse Patient Populations Using Patient Vignettes and Large Language Models. 2024 Presented at: Proceedings of the First Workshop on Patient-Oriented Language Processing (CL4Health) @ LREC-COLING 2024; 2025 17 December; Torino, Italia.
18. Fernandes AC, Cloete D, Broadbent MT, Hayes RD, Chang C, Jackson RG, et al. Development and evaluation of a de-identification procedure for a case register sourced from mental health electronic records. BMC Med Inform Decis Mak 2013;13:71 [FREE Full text] [doi: 10.1186/1472-6947-13-71] [Medline: 23842533]
19. First MB, Pincus HA. Classification in psychiatry: ICD-10 v. DSM-IV. A response. Br J Psychiatry 1999 Sep;175:205-209. [doi: 10.1192/bjp.175.3.205] [Medline: 10645319]
20. Zhang H, Ji J. Prevalence of mental disorders in China. Lancet Psychiatry 2019;6(3):188-189. [doi: 10.1016/S2215-0366(19)30034-3] [Medline: 30792113]
21. Perera Molligoda Arachchige AS. Role of ChatGPT 3.5 in emergency radiology, with a focus on cardiothoracic emergencies: proof with examples. iRADIOLOGY 2024;2(5):510-521. [doi: 10.1002/ird3.65]
22. Achiam J, Adler S, Agarwal S. Gpt-4 technical report. arXiv:2303.08774 2024 [FREE Full text]
23. He Y. Chinese simpleqa: A chinese factuality evaluation for large language models. In: arXiv preprint. 2025 Presented at: Proceedings of the 63rd Annual Meeting of the Association for Computational Linguistics (Volume 1: Long Papers); 2025 17 December; Vienna, Austria p. 19182-19208. [doi: 10.18653/v1/2025.acl-long.941]
24. Taloni A, Borselli M, Scarsi V, Rossi C, Coco G, Scorcia V, et al. Comparative performance of humans versus GPT-4.0 and GPT-3.5 in the self-assessment program of American Academy of Ophthalmology. Sci Rep 2023;13(1):18562 [FREE Full text] [doi: 10.1038/s41598-023-45837-2] [Medline: 37899405]
25. Hoppe JM, Auer MK, Strüven A, Massberg S, Stremmel C. ChatGPT with GPT-4 outperforms emergency department physicians in diagnostic accuracy: retrospective analysis. J Med Internet Res 2024;26:e56110 [FREE Full text] [doi: 10.2196/56110] [Medline: 38976865]
26. Barile J, Margolis A, Cason G, Kim R, Kalash S, Tchaconas A, et al. Diagnostic accuracy of a large language model in pediatric case studies. JAMA Pediatr 2024;178(3):313-315. [doi: 10.1001/jamapediatrics.2023.5750] [Medline: 38165685]
27. Bubeck S, Chandrasekaran V, Eldan R, Gehrke J, Horvitz E, Kamar E, et al. Sparks of artificial general intelligencearly: early experiments with GPT-4. arXiv:2303.12712 2023 [FREE Full text]

XSL•FO
RenderX

28. Lee D, Yoon SN. Application of artificial intelligence-based technologies in the healthcare industry: opportunities and challenges. Int J Environ Res Public Health 2021;18(1) [FREE Full text] [doi: 10.3390/ijerph18010271] [Medline: 33401373]
29. Gargari OK, Fatehi F, Mohammadi I, Firouzabadi SR, Shafiee A, Habibi G. Diagnostic accuracy of large language models in psychiatry. Asian J Psychiatr 2024;100:104168. [doi: 10.1016/j.ajp.2024.104168] [Medline: 39111087]
30. Shickel B, Tighe PJ, Bihorac A, Rashidi P. Deep EHR: a survey of recent advances in deep learning techniques for electronic health record (EHR) analysis. IEEE J. Biomed. Health Inform 2018;22(5):1589-1604. [doi: 10.1109/jbhi.2017.2767063]
31. Lotter W, Hassett MJ, Schultz N, Kehl KL, Van Allen EM, Cerami E. Artificial intelligence in oncology: current landscape, challenges, and future directions. Cancer Discov 2024;14(5):711-726. [doi: 10.1158/2159-8290.CD-23-1199] [Medline: 38597966]
32. Savage T, Nayak A, Gallo R, Rangan E, Chen JH. Diagnostic reasoning prompts reveal the potential for large language model interpretability in medicine. NPJ Digit Med 2024;7(1):20 [FREE Full text] [doi: 10.1038/s41746-024-01010-1] [Medline: 38267608]
33. Volinsky-Fremond S, Horeweg N, Andani S, Barkey Wolf J, Lafarge MW, de Kroon CD, et al. Prediction of recurrence risk in endometrial cancer with multimodal deep learning. Nat Med 2024;30(7):1962-1973. [doi: 10.1038/s41591-024-02993-w] [Medline: 38789645]

Abbreviations

EHR: electronic health record
FP: false positive
FN: false negative
ICD-10: International Statistical Classification of Diseases, Tenth Revision
LLM: large language model
OR: odds ratio
TP: true positive

Edited by A Coristine; submitted 25.May.2025; peer-reviewed by KH Jung, HJ Kim, J Wang; comments to author 17.Aug.2025; accepted 11.Dec.2025; published 13.Jan.2026.

Please cite as:
Sun M, Yu J, Long Z, Yang Y, Xiao T, Liang J, Feng J, Deng H, Huang G
Large Language Models for Psychiatric Diagnosis Based on Multicenter Real-World Clinical Records: Comparative Study
JMIR Med Inform 2026;14:e77699
URL: https://medinform.jmir.org/2026/1/e77699
doi:10.2196/77699
PMID:41408781

©Maoqian Sun, Jia Yu, Zhuhong Long, Yun Yang, Tao Xiao, Jiaquan Liang, Jun Feng, Huaili Deng, Guoping Huang. Originally published in JMIR Medical Informatics (https://medinform.jmir.org), 13.Jan.2026. This is an open-access article distributed under the terms of the Creative Commons Attribution License (https://creativecommons.org/licenses/by/4.0/), which permits unrestricted use, distribution, and reproduction in any medium, provided the original work, first published in JMIR Medical Informatics, is properly cited. The complete bibliographic information, a link to the original publication on https://medinform.jmir.org/, as well as this copyright and license information must be included.

XSL•FO
RenderX

Identifying and Analyzing Bot-Generated Responses in Online Health Care Surveys: Methodological Study

Emily Hamovitch[1], MSW, MPH; Kaileah McKellar[1], MPH, PhD; Walter P Wodchis[1,2], MA, PhD

[1]Institute of Health Policy, Management and Evaluation, University of Toronto, 155 College Street, Toronto, ON, Canada

[2]Institute for Better Health, Trillium Health Partners, Mississauga, ON, Canada

Corresponding Author:
Emily Hamovitch, MSW, MPH
Institute of Health Policy, Management and Evaluation, University of Toronto, 155 College Street, Toronto, ON, Canada

Abstract

Background: The increasing reliance on online surveys for collecting patient-reported feedback for health care research has led to growing concerns over fraudulent responses generated by bots. These automated responses threaten data integrity by fabricating survey results, distorting statistical analyses, and potentially misguiding policy decisions. Addressing this issue is critical for maintaining the validity of research findings that inform health care practice and policy.

Objective: This study aimed to develop a robust set of criteria for identifying bot-generated responses in online health care surveys and to examine how these responses impact data quality. We then explored differences in survey results between probable human and suspected bot respondents in a survey assessing patient-reported outcome measures and patient-reported experience measures within a geographic region in Ontario, Canada.

Methods: A survey was conducted from July to October 2023 using Research Electronic Data Capture (REDCap; Vanderbilt University), distributed with a generic link via email, and later shared on social media. The survey collected data on health care use, patient experiences, health outcomes, digital health care engagement, and demographics. A 3-tier classification system was developed to detect bot responses based on predefined "red flags," including duplicate open-ended responses, inconsistent demographic reporting, identical timestamps, and location discrepancies. Quantitative analysis included chi-square tests to assess differences between probable human and suspected bot responses and Spearman correlation tests to examine relationships among health care indicators.

Results:: Analysis included 1154 responses, with 58% (n=668) classified as suspected bot-generated. The most frequent suspected bot-identification criterion was duplicated open-ended responses (293/668, 44%). Chi-square tests revealed statistically significant differences (P<.05) between suspected bots and probable humans across most survey items. Suspected bots demonstrated response patterns concentrated in the middle of Likert scales, whereas probable humans were more likely to select extreme values. Correlation analyses showed that expected relationships between key health indicators (eg, depression symptoms) were present in probable human responses but reversed in suspected bot-generated data, highlighting the potential for compromised validity in unfiltered survey datasets.

Conclusions: The findings underscore the necessity of implementing bot prevention and detection methods in online health care surveys to preserve data integrity. Failure to do so risks distorting research conclusions, particularly in health equity studies where demographic misclassification may bias results. The study highlights effective bot detection strategies, including open-text analysis, timestamp evaluation, and geographic validation, and recommends integrating these techniques into survey design. As bots continue to evolve, ongoing advancements in bot prevention and detection will be crucial to maintaining the reliability of digital health research.

(JMIR Med Inform 2026;14:e73622) doi:10.2196/73622

KEYWORDS

bots; online surveys; data integrity; patient-reported outcome measures; patient-reported experience measures; health care research; digital health; survey validity

Introduction

Patient-reported outcome measures (PROMs) and patient-reported experience measures (PREMs) are invaluable tools for understanding and improving health care from the patient's perspective. PROMs assess health status, functional abilities, symptoms, and quality of life directly from patients, often through self-reported questionnaires, providing insights into the impact of interventions and overall care quality [1-3]. PREMs, on the other hand, capture patients' perceptions of their health care experience, focusing on whether key processes

XSL•FO
RenderX

occurred and how care was delivered [2]. These measures are essential for implementing person-centered care, as they enable health care providers to align their practices with patient needs and experiences [4]. PROMs and PREMs have also been incorporated into care routines to support quality improvement initiatives [4]. By prioritizing patient-reported data, health care systems can address inequities, promote patient-centered and value-based care, and ensure that care delivery aligns with the priorities and needs of diverse patient populations [4].

A common approach to collecting PROMs and PREMs is through online surveys. Online surveys have become an increasingly prominent tool for research, particularly in social and behavioral health fields, due to their efficiency, cost-effectiveness, and ability to overcome challenges faced by traditional data collection methods such as face-to-face, mail, or telephone surveys [5,6]. These challenges include declining response rates, rising costs, and the need for social distancing during events like the COVID-19 pandemic [5,7-10]. Internet-based platforms such as Qualtrics (Qualtrics International) Inc., SurveyMonkey (Momentive Inc.), and Research Electronic Data Capture (REDCap; Vanderbilt University) have enabled researchers to collect data remotely, making it possible to reach large general populations [5,7,10]. These tools reduce the resources required for data collection, minimize participant burden, and offer greater anonymity, encouraging honest disclosure of personal or sensitive information [7,10]. Additionally, the limited availability of a sampling frame with accurate contact information has necessitated the use of distribution methods involving generic survey links and promotion through online platforms and social media. Unfortunately, recruiting participants through generic links creates susceptibility to data quality issues [11].

While early guidance on online surveys for health research warned of the risk of hoax responses [12], the increasing use of online surveys has been accompanied by a growing concern over fraudulent responses, particularly from bots - applications that automatically complete surveys – producing insincere data and inaccurate results [13]. These bots are capable of mimicking human behavior by selecting multiple-choice answers and generating plausible open-ended responses, making them difficult to detect. Bots can submit hundreds of fabricated responses within hours, potentially overwhelming researchers with invalid data and causing significant financial loss if participant incentives are misallocated [8]. Their presence threatens data quality, which can distort statistical analyses and compromise research findings [10]. Researchers, evaluators, and program analysts also face challenges in identifying fraudulent responses due to the increasing sophistication of bots and the anonymity of online participants [14]. Despite the implementation of data protection mechanisms to prevent bot responses, such as reCAPTCHA (Google LLC), bot programmers easily bypass these safeguards using virtual private networks or servers [7]. As bots become more prevalent and capable, addressing this issue is critical to ensuring data integrity and the validity of research findings that inform policy and practice.

This study adds to this literature by proposing a structured 3-tier classification system that integrates multiple indicators of responses by suspected bots, offering a robust and transparent protocol for identifying suspected bot responses. Additionally, this study goes beyond merely identifying suspected bot-generated responses in online surveys; it systematically examines how suspected bots influence response patterns in a health care experience survey. While existing research has focused on detecting fraudulent responses, fewer studies have examined how suspected bot-generated data may distort patient-reported experience and outcome measures in health care contexts. Our study extends this work by analyzing discrepancies between suspected bot and probable human responses in a survey of PROMs and PREMs. Such differences provide an assessment of potential bias and the relative importance of detection.

Methods

Survey

This study was undertaken within a broader evaluation of Ontario Health Teams (OHT), focusing on patient experiences and outcomes. A patient survey was implemented to support planning and evaluation of integrated care for attributed populations in Ontario, Canada. Consent was obtained from all respondents included in the analysis. The survey was intended for patients from a large OHT, gathering data on PREMs and PROMs. Questions included Likert scale items on health care use, health outcomes, accessing care, having someone to count on, being heard, managing health, safety, care transitions, digital health care use, demographics; as well as an open-text section to provide additional feedback. Six timestamps were programmed throughout the survey at multiple points to track survey progress. Data were collected between July 2023 and October 2023 using REDCap. REDCap is a web-based platform designed for research data capture, widely used in academic and clinical studies. The survey was distributed through the OHT's email lists and social media platforms. Social media distribution occurred primarily through Facebook (Meta), which was the OHT's main platform. Posts containing the survey link and QR code were shared periodically between July and October 2023, and a paid Facebook advertisement was implemented in early October to boost participation. Participants were invited to enter a draw for a $25 CAD (US $18.62) gift card as an incentive. Entry into the draw was voluntary and completed through a separate form linked on the survey's thank-you page, allowing respondents to opt out and ensuring that contact information was stored separately from survey responses. A copy of the survey is provided in Multimedia Appendix 1.

Suspected Bot Identification

Upon reviewing the qualitative responses and timestamp data, the research team identified clear evidence of suspected bot-generated responses in the survey. Many responses were duplicative, contained overly formal or generic language, or were nonsensical. The response patterns, combined with irregular timestamp data, confirmed the presence of suspected bots. As a result, the team developed specific criteria to systematically identify and remove suspected bot-generated responses from the dataset.

XSL•FO
RenderX

Criteria to identify suspected bots were developed using the following themes: generic and duplicative open-ended responses; concerns with location as determined by postal code (including postal codes that were invalid or nonsensical); timing irregularities; identical timestamps to other participants; illogical demographic reporting; and discrepancies in reporting health care use. In addition, a "bot takeover day" (October 10 onward) was included as a criterion, reflecting the sudden influx of suspicious responses observed on or after that date.

To identify bots in the survey data, we developed a 3-tier classification system based on specific "red flags" (concerning or questionable features or responses in the data). This approach builds on prior research that has typically relied on individual indicators or sets of criteria considered in parallel to flag fraudulent responses [5,7-9]. By combining multiple indicators into a structured, tiered framework, our system increases the robustness and transparency of suspected bot identification. Tier 1 criteria identified a respondent as a suspected bot if any single criterion occurred on its own (eg, duplicate open-ended responses that were exact full-text matches, not brief "No"-type replies, invalid postal codes, or identical timestamps). Tier 2 classified a respondent as a suspected bot if 2 or more criteria from its list were observed. For example, one tier 2 criterion included having a valid postal code outside of the region where participants received health care services. This criterion was not sufficient on its own to categorize a respondent as a suspected bot, as some participants may legitimately live elsewhere and receive care in the area where the participants were sampled. However, when combined with other criteria, it strengthened the likelihood of being a suspected bot-generated response. Finally, tier 3 flagged respondents as suspected bots if any tier 3 criterion was combined with at least 2 additional criteria from either tier 2 or tier 3, resulting in a total of 3 or more issues. One Tier 3 indicator reflected a sudden influx of suspicious responses observed on October 10, 2023 ("bot takeover day"). This indicator was not used as a standalone criterion and had minimal influence on classification: more than 99% of suspected bot responses were already identified using Tier 1 and/or Tier 2 criteria alone, with only 3 additional responses flagged through the use of this indicator. Demographic characteristics such as race or ethnicity, gender, and sexual orientation were not used as criteria for suspected bot identification. Demographic variables were analyzed only after classification to describe group-level differences between suspected bots and probable humans.

One criterion for identifying suspected bots was the presence of open-text responses that were deemed to be either (1) generic or informal, or (2) had a similar sentence structure to other responses. To evaluate this more subjective criterion, 2 reviewers (LC and SU) independently coded open-ended responses based on these criteria. Responses were categorized as suspected bots if reviewers agreed they met either criterion. When reviewers disagreed on whether open-ended responses should be classified as generic or informal, a third member of the research team (KM) provided the final determination. Interrater reliability between the 2 independent coders was substantial (Cohen κ=0.63, P<.001).

Although this study applied the identification criteria for a survey implemented on the REDCap platform, the 3-tier system is designed to be adaptable across different survey platforms, including Qualtrics, SurveyMonkey, and other online tools. The criteria used (such as duplicated open-text responses, timestamp irregularities, and geographic inconsistencies) are not platform-specific.

Suspected Bot Response Analysis

To examine differences in survey responses between probable humans and suspected bots, bar charts were created to visually compare response patterns. Chi-square tests were conducted to identify significant differences in the proportions of responses between the 2 groups. For select-all-that-apply items, including "Who did you receive care from?," responses were summarized into a mutually exclusive categorical variable prior to analysis. Respondents selecting more than 1 option were classified as having received care from "multiple providers," while those selecting a single option were classified according to that provider type.

To account for multiple comparisons across survey items, a Bonferroni correction was applied (adjusted α=.05/59=0.00085) to control for Type I error. We quantified the magnitude of group differences by calculating effect sizes for each chi-square test. Cramer V was computed for all categorical comparisons, along with 95% CIs.

Additionally, Spearman correlation tests were conducted to evaluate significant relationships between 2 health indicators, analyzed separately for probable humans and suspected bots, to identify patterns that align with or deviate from expected human perception and behavior. Two sets of correlations were examined: (1) the correlation between "little interest or pleasure in doing things" and "feeling down, depressed, or hopeless," and (2) the correlation between self-rated health and the frequency of interaction with the health system. The first pair represents the 2 core items of the Patient Health Questionnaire–2 (PHQ-2), a validated depression screener in which these items are strongly and positively correlated with one another [15]. The second pair was selected because extensive literature has shown that poorer self-rated health is associated with increased health care use, including higher rates of hospitalization and outpatient visits [16,17]. These 2 pairs, therefore, provide theoretically justified validity checks.

Ethical Considerations

This study received approval from the University of Toronto Research Ethics Board (#38072). All procedures were conducted in accordance with institutional ethical standards and the principles of the Declaration of Helsinki. Participants provided informed consent electronically prior to beginning the survey. The consent form outlined the purpose of the study, the voluntary nature of participation, potential risks and benefits, and data management procedures. Participants were informed that they could decline to answer any question or withdraw at any time prior to survey submission. To protect privacy and confidentiality, survey responses were collected anonymously. Any contact information provided for entry into the incentive draw was submitted through a separate form and stored

XSL•FO
RenderX

separately from survey data. Data were stored on secure, password-protected institutional servers accessible only to authorized members of the research team.

Results

Frequency of Suspected Bot Identification

Table 1 illustrates the final criteria for identifying suspected bots and the frequency with which each criterion was met among respondents ultimately classified as suspected bots or probable humans. While some probable human respondents exhibited isolated red flags, they did not meet the necessary combination of criteria required for suspected bot classification. After removing survey responses where substantive questions were not answered (n=231), 1154 survey respondents remained. Among them, 58% (n=668) were categorized as suspected bots, and 42% (n=486) were categorized as probable humans. Table 1 illustrates the number of respondents who met the eligibility criteria for each identification criterion. Overall, 529 survey respondents met the criteria for Tier 1, 570 respondents met the criteria for Tier 2 (136 of whom did not meet the criteria for Tier 1), and 551 respondents met the criteria for Tier 3 (3 of whom did not meet the criteria for Tier 1 or Tier 2).

XSL•FO
RenderX

Table . Frequency of each suspected bot identification criteria. Percentages within each tier sum to greater than 100% because a single respondent may meet multiple identification criteria.

Criteria	Assessed categories		
	Suspected bot (n)	Probable human (n)	Respondents identified as suspected bots who met criteria, n (%)
Tier 1			
Had an identical open-ended question response identical to at least one other respondent (Duplicate open-ended responses that were exact full-text matches, not brief "No"-type replies)	293	0	(293/668) 44%
Open text is generic, informal, or similar sentencing structure	49	0	(49/668) 7%
Duplicate invalid postal codes that were completed on the same day	189	0	(189/668) 28%
Duplicate out-of-province postal codes (excluding Quebec) that were completed on the same day	152	0	(152/668) 23%
Tier 2			
Identical open-ended question marked as "no" that also fell within the same day and similar time frame	80	0	(80/668) 12%
2 or more survey respondents entered their surveys within 30 seconds of one another (but not identical), and this is the case in 3 or more timestamps	340	2	(340/668) 51%
Had an identical timestamp (identical hours, minutes, and seconds) with at least one other respondent on the following timestamps:			
First timestamp	114	0	(114/668) 17%
Second timestamp	93	0	(93/668) 14%
Third timestamp	75	1	(75/668) 11%
Fourth timestamp	80	0	(80/668) 12%
Fifth timestamp	69	2	(69/668) 10%
Sixth timestamp	75	0	(75/668) 11%
Survey was completed between 1 AM and 5:00 AM Eastern Time (as identified on any of the timestamps)	154	7	(154/668) 23%
Time spent on survey is 3 minutes or less (among respondents who completed the survey)	42	11	(42/668) 6%
Invalid postal code (gibberish or numeric)	189	0	(189/668) 28%
Valid postal code but outside of Ontario	153	0	(153/668) 23%
Valid Ontario postal code but outside of the region of the primary care center in which respondents were recruited	165	5	(165/668) 25%

XSL•FO
RenderX

Criteria	Assessed categories		
	Suspected bot (n)	Probable human (n)	Respondents identified as suspected bots who met criteria, n (%)
Discrepancy in reporting ED[a] visits	347	55	(347/668) 52%
Between the ages of <18 - 44 years but reported living in a retirement home or long-term care facility.	123	1	(123/668)18%
Tier 3			
Bot takeover day of October 10 or after	618	94	(618/668) 93%
Postal code from neighboring province	55	3	(55/668) 8%

[a]ED: emergency department.

In tier 1, the most commonly reported “red flag” was having an identical open-ended response to another survey respondent. In tier 2, the most common ’red flag’ was a discrepancy in reporting an emergency department visit, where respondents indicated they had received care from the emergency department in 1 question but later reported that they had not been to the emergency department in the past 12 months. There was also a high frequency of respondents completing their surveys within similar timeframes (completing 3 or more of the same sections within 30 s of another respondent).

Differences in Responses Between Suspected Bots and Probable Humans

Overall, probable humans had a higher average percentage of missingness on all questions (mean 13% [for probable humans vs mean 5% for suspected bots).

Chi-square tests revealed significant differences ($P<.05$) in response distributions between probable humans and suspected bots for 55 out of 59 survey questions. After Bonferroni correction for multiple comparisons (adjusted $\alpha=.00085$), 50 of 59 valid comparisons remained statistically significant (Table S1 in Multimedia Appendix 2). The magnitude of effect sizes ranged from Cramer V=0.01 (“When you left the hospital were you provided with easy to follow instructions on whom to contact if you had a question about your treatment or if your condition became worse?”) to Cramer V=0.72 (“In general, do your health care providers encourage you to bring someone with you to your appointments?”), with a mean Cramer V of 0.31 (Table S1 in Multimedia Appendix 2). Among the 9 survey questions that showed no statistically significant difference between probable humans and suspected bots, most items were binary (yes or no) questions that followed branching logic and were therefore presented only to a subset of respondents. The remaining non-significant items were measured on a 5-point response scale, where probable humans tended to provide slightly less positively skewed responses (for example, being more likely to select experiencing “slight pain or discomfort” rather than “no pain or discomfort”).

In terms of demographics (Figure 1), suspected bots more often reported younger ages (under 18–44 years) and being male, while probable humans more often reported being female. Both groups most frequently identified as heterosexual and White, but suspected bots more often selected minority sexual orientations (eg, bisexual, queer, and two-spirit) and racial or ethnic categories (eg, Black, Asian, Latin, and Indigenous).

XSL•FO
RenderX

Figure 1. Distribution of demographics for suspected bots versus probable humans.

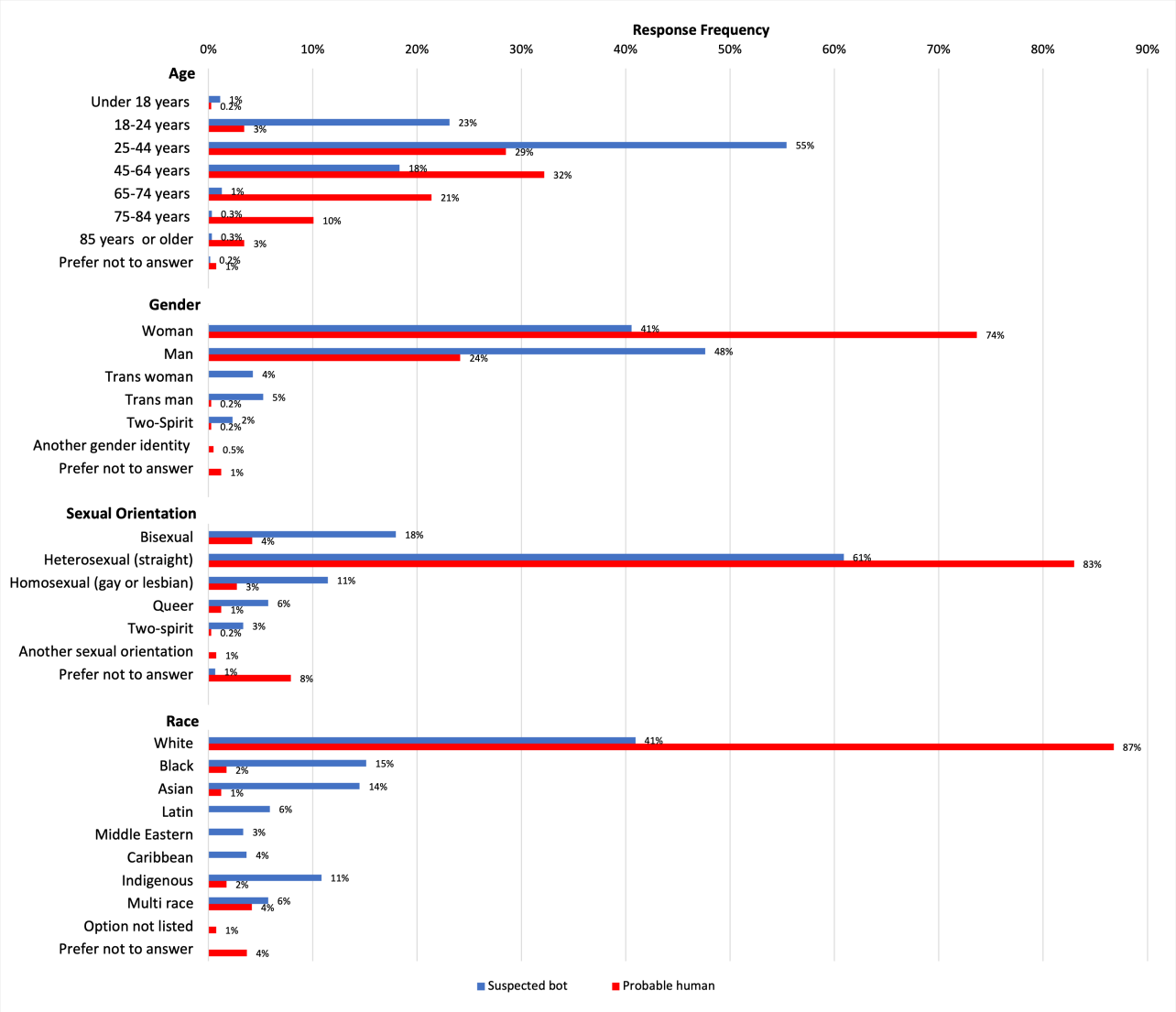

Visualizations (Figures 2 and 3) showed that suspected bots tended to cluster at mid-scale responses, while probable humans more often selected extreme values. For PROMs, probable humans were more likely to report the most favorable outcomes (eg, “no problems walking about”) and the least favorable (eg, “nearly every day” feeling depressed), whereas suspected bots gravitated toward midpoints (eg, “slight problems,” “several days”). Similar patterns appeared in PREMs, where suspected bots more frequently selected “somewhat” responses (eg, “somewhat easy” to access supports, “somewhat too long” to get care), while probable humans showed a greater spread across extremes.

XSL•FO
RenderX

Figure 2. Distribution of probable human and suspected bot responses for patient-reported outcome measures.

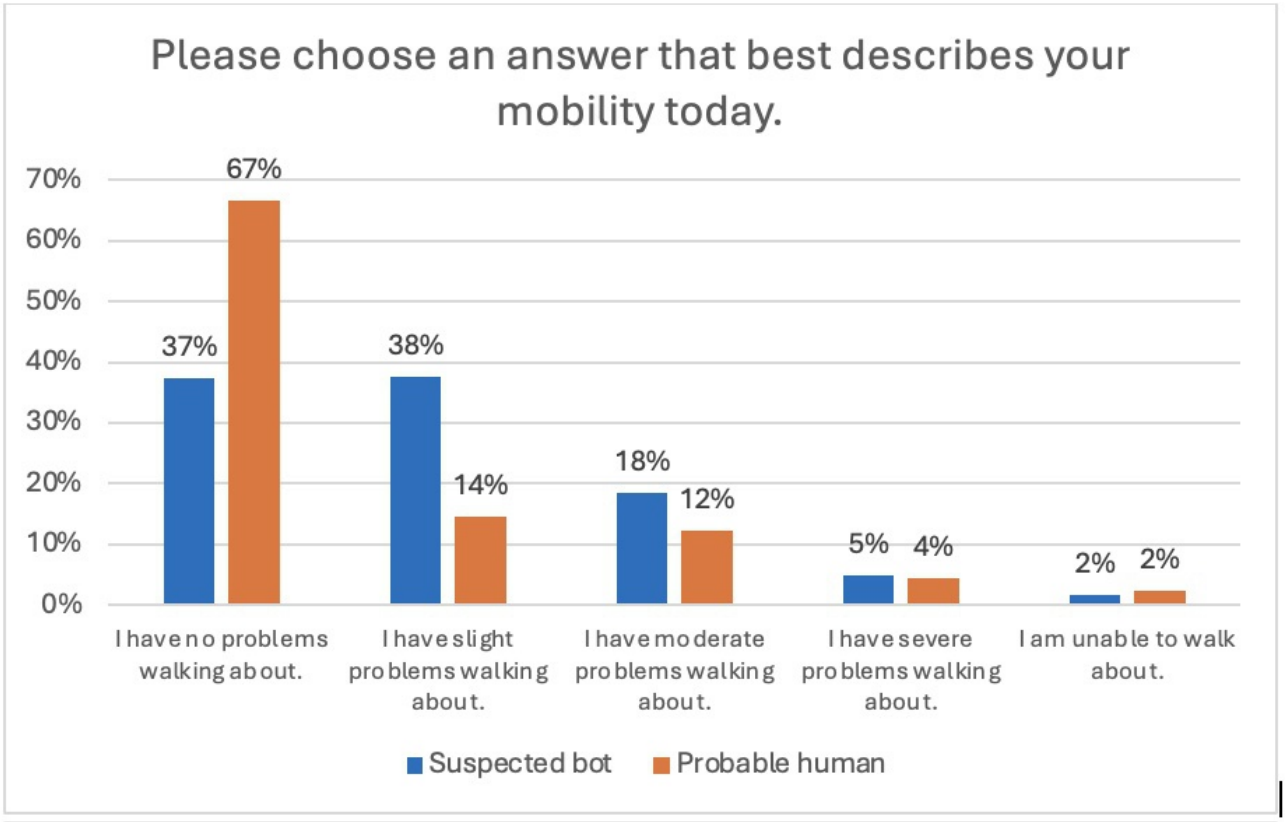

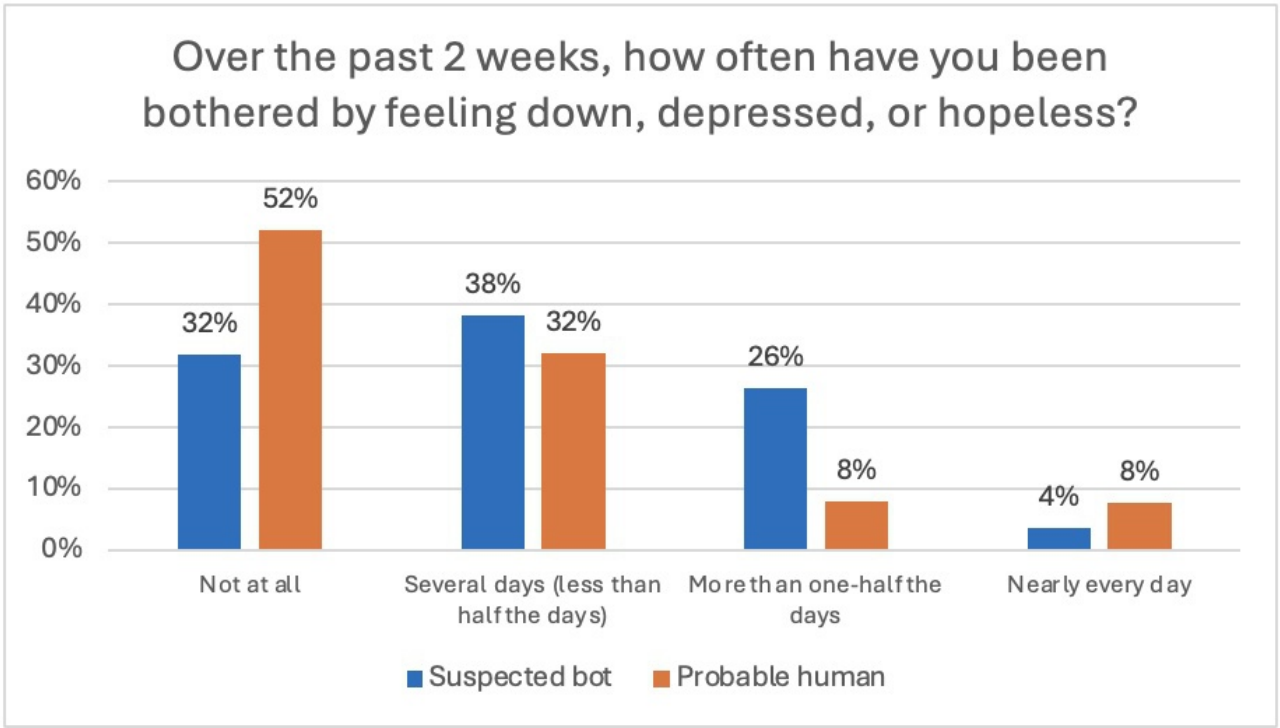

The survey also assessed health service use, including emergency department visits, hospitalizations, and specialist care in the past year. Suspected bots more frequently reported using the emergency department and being hospitalized compared to probable humans. When asked yes or no questions about these services (such as whether an emergency department visit could have been managed by a regular provider, whether their provider was informed after hospital discharge, or whether a specialist had relevant medical information), suspected bots were more likely to respond "yes" than probable humans. This was consistent with other patterns, such as reporting "somewhat confident" when asked about managing health post-emergency department visit, while probable humans were more likely to select "very confident" or "not at all confident."

The survey included 1 nominal question, which asked about the main reason participants had not looked at their medical records online (for those who indicated this to be the case). There did not appear to be any trend or pattern for the distribution of

XSL•FO
RenderX

responses. Ironically, a substantially higher percentage of suspected bots (compared to probable humans) indicated that a reason for not having looked at medical records online was not having reliable access to the internet.

Figure 3. Distribution of probable human and suspected bot responses for patient-reported experience measures.

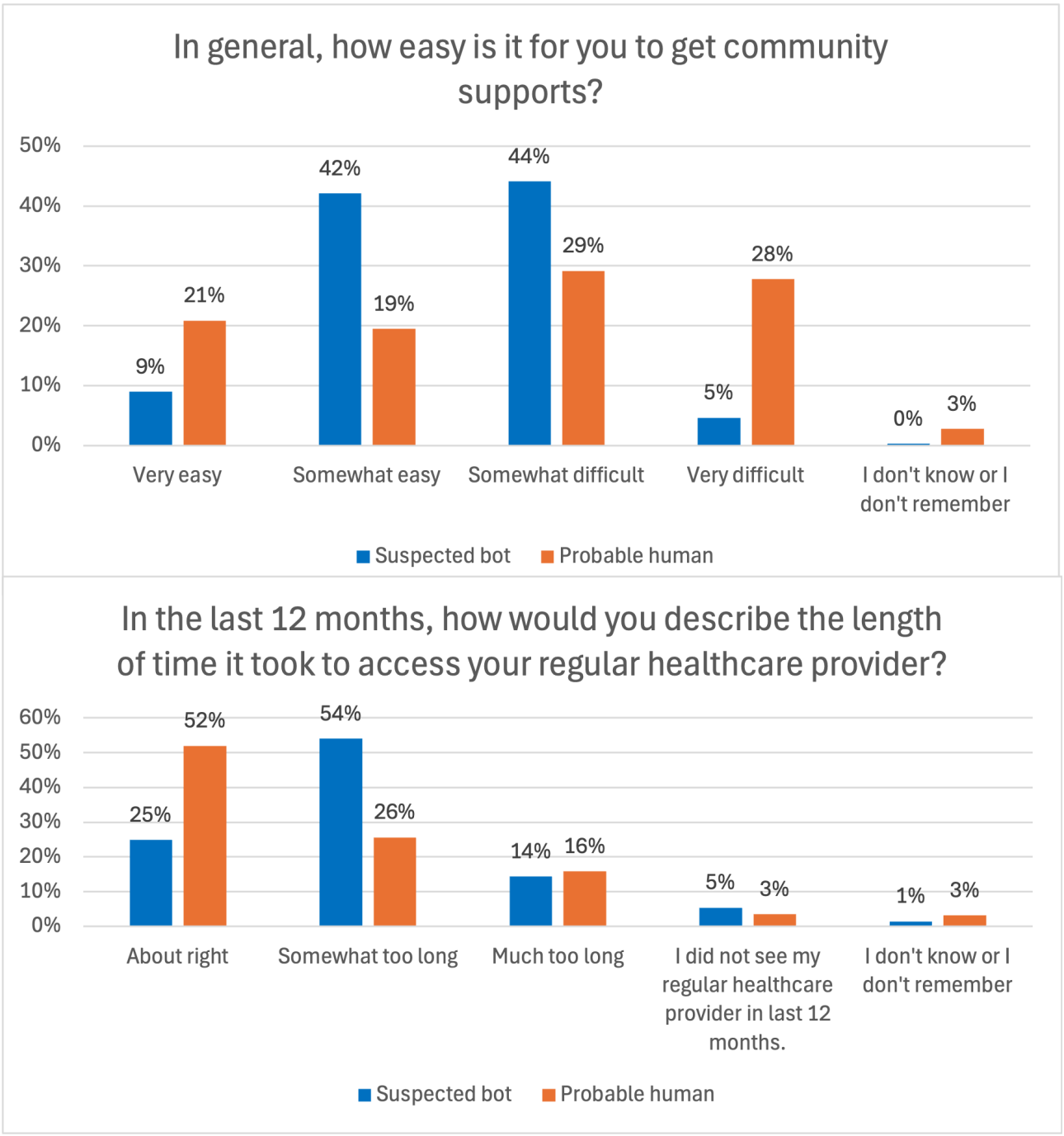

Correlations

Spearman correlations indicated significant correlations between the indicators of having "little interest or pleasure in doing things" and "feeling down, depressed, or hopeless," both of which are indicators of depression. For probable humans, the Spearman correlation was 0.48 (P<.001), indicating a moderate positive correlation between the 2 variables, whereas for suspected bots, the Spearman correlation of −0.33 (P<.001) indicated a moderate negative correlation between the 2 variables.

When analyzing the correlation between self-rated health ("how do you rate your own health?") and frequency of interacting with the health system ("how often do you interact with the health system?"), a Spearman correlation of −0.07 for probable humans indicated a weak negative correlation; however, this was not significant (P=.15). For suspected bots, the Spearman correlation was 0.06, indicating a weak positive correlation; however, this was also not significant (P=.15).

XSL•FO
RenderX

Discussion

Principal Findings

The results of this study demonstrate the imperative need for researchers, evaluators, and program analysts in the health care field to recognize and address the potential threats posed by bots in online survey research. Failure to detect and remove bot-generated responses can lead to compromised data quality and incorrect inferences. Implementing robust data screening strategies is important for reducing fraudulent responses and improving the likelihood that valid data are retained. These responses respect the integrity of genuine participants whose experiences deserve to be accurately reported.

Implications of Including Bot Data in Health Care Surveys

Our findings extend prior work on bot response patterns by demonstrating how these differences manifest in PROMs and PREMs, with implications for health care survey research. Across multiple survey domains—health outcomes, health care access, and experiences—probable humans were more likely than suspected bots to select the most favorable outcomes (or in some cases, the least favorable response options). In contrast, suspected bots exhibited a tendency to select responses clustered around the middle of the scale. As a result, the presence of bot-generated data could dilute the strength of human responses, skewing average scores toward the midpoint and diminishing the ability to detect meaningful trends. This issue extends beyond scaled responses; even in nominal questions, such as the reason for not accessing medical records online, suspected bots disproportionately selected specific response options, such as lacking reliable internet access. This discrepancy suggests that bot-generated data may introduce artificial patterns in categorical variables, leading to inaccurate estimates of barriers to health care access and potentially misinforming policy decisions. This distortion may undermine construct validity, as the data fail to capture real-world experiences. Additionally, probable humans demonstrated a higher level of missingness compared to suspected bots. This likely reflects natural variation in survey completion behavior (such as skipped or unanswered questions). In contrast, the lower level of missingness among suspected bots may indicate automated completion rather than a marker of higher data quality. This difference underscores the importance of evaluating missing data patterns alongside other indicators when assessing data integrity.

Beyond response patterns, the inclusion of bot-generated data introduces a significant risk of bias, particularly in research focusing on health equity. The demographics of suspected bot responses differed notably from those of probable human participants. These patterns may reflect random bot response patterns inflating less common categories; however, this pattern may be partially driven by the ordering of the race or ethnicity response options. In the survey, several minority categories appear in the middle of the list, whereas “White” appears at the bottom. Given the tendency of suspected bots to select middle-of-the-scale responses, the positioning of race or ethnicity response options likely contributed to the higher selection of minority categories among bots. We also acknowledge the possibility that some marginalized respondents were misclassified as suspected bots. This discrepancy poses a major threat to the validity of studies that examine health care use and outcomes among specific demographic subgroups. In equity-focused research, where accurate representation of marginalized populations is crucial, failing to filter out bots could lead to misleading conclusions and inappropriate policy recommendations.

The impact of suspected bot interference is further underscored when examining the relationship between key indicators of depression. Among probable human respondents, the correlation between “having little interest or pleasure in doing things” and “feeling down, depressed, or hopeless” aligned with established patterns in the literature, reflecting a logical association between these 2 related constructs. However, among suspected bot-generated responses, this relationship was unexpectedly reversed, indicating a negative correlation that does not align with theoretical expectations. Notably, a moderate negative correlation suggests a systematic response pattern (such as contradictory response selection) rather than a pattern consistent with genuine symptom co-occurrence. This inconsistency suggests that suspected bot responses do not accurately reflect underlying psychological constructs, reinforcing the need to identify and eliminate suspected bots from survey research. The inconsistency also provides face validity to our bot-detection algorithm.

Bot Detection Strategies

Several methods to identify suspected bots that were used in this study align with those used in similar research. These include: analyzing open-ended responses for nonsensical, duplicative, or inconsistent data [5,8,10,18]; tracking survey completion times [5,7,8,13,19,20]; flagging surveys that were completed at unusual times of the day [8]; and identifying suspicious patterns related to zip codes and geographic location [20]. We applied all applicable bot detection strategies for which we had data available. There are additional bot detection techniques that were not used in this study but have been used in prior research. These include: checking participants' responses to questions that are asked in 2 ways [8,14,19], (such as “how old are you?” and “what y were you born?”); using IP addresses to check for responses that were completed in the same household or very close to one another in relation to the time the survey was submitted [5,14]; and examining email addresses for suspicious wording or similar content [8,20]. Another strategy involves external validation of participant information, such as verifying names, addresses, phone numbers, and birth dates to ensure responses are unique and legitimate [21]. Investigators can also cross-reference participants’ details using publicly available databases, social media, or professional networking sites to further confirm authenticity, although ethical considerations must be weighed when implementing such approaches [21]. While these strategies may help reduce fraudulent responses, they can also create additional burdens and reduce anonymity for legitimate participants.

Among the bot detection strategies used in this study, some were particularly effective in identifying suspected bot-generated responses. Notably, open-ended responses provided valuable

XSL•FO
RenderX

insight, as suspected bot-generated answers often contained repetitive, illogical, or off-topic content across multiple responses. Unusual quantitative responses alone can be difficult to interpret, as they might seem plausible despite being artificially generated. However, open-ended responses can provide valuable context that may help in assessing the authenticity of data. Unlike structured response options, which bots can randomly or systematically select, qualitative responses require coherence and reasoning, making them a powerful tool for distinguishing between genuine participants and automated responses. That said, recent advances in generative artificial intelligence mean that open-text answers are becoming increasingly sophisticated and may no longer be a fully reliable safeguard against fraud [22]. Geographic inconsistencies, such as invalid or duplicate postal codes, or locations outside the intended survey region, were also strong indicators of suspected bot activity, although individual respondents may misreport to preserve anonymity. Additionally, anomalies in time-related metrics, including extremely short survey completion times, completion at unusual hours, or multiple surveys submitted at identical timestamps, further helped differentiate suspected bots from probable human respondents. Based on these findings, we recommend collecting postal or ZIP codes and incorporating multiple timestamps within surveys to enhance suspected bot detection. While no single strategy is universally effective across all surveys, we recommend using a combination of detection methods tailored to the specific survey and target population.

While several strategies are outlined to detect bots, it is also important to prevent bots from entering surveys in the first place. Tools such as Completely Automated Public Turing test to tell Computers and Humans Apart (CAPTCHA) have been developed to offer an additional level of security against bot infiltration [23]. However, research has shown that these tools can be bypassed, as bots are increasingly programmed to recognize and circumvent such challenges [7,20,24]. Similarly, honeypot questions (hidden prompts designed to engage only automated respondents) have also proven ineffective, as more sophisticated bots can now avoid these traps [8,20]. Indeed, researchers who have used this method have reported that bots did not provide responses to these questions [8]. Given the growing complexity of automated survey fraud, it is essential for technology companies to continue developing advanced bot detection solutions. Survey platforms such as REDCap and Qualtrics should integrate these technologies to automate bot prevention, reducing the burden on researchers and ensuring more consistent data quality measures.

Recommendations

It is recommended that bot detection strategies be implemented at multiple stages in the research process. This includes prior to data collection (eg, using targeted recruitment with specific distribution lists), during data collection (eg, monitoring data daily to identify potential fraud), and following data collection (eg, implementing a systemic check of potential fraud) [18]. Finally, increasing awareness among researchers about the impact of bots in survey research is crucial. We recommend that training in bot prevention and detection be incorporated into research methods and survey design coursework to equip researchers with the necessary skills to safeguard data integrity. There will continue to be a value and need to reach out with surveys to broad groups of public and enabling survey research in this context will continue to be important.

As internet-based research (and survey research in particular) continues to expand, there is a growing opportunity for researchers across disciplines to contribute to the development of comprehensive bot detection methodologies. Moving forward, greater efforts should be directed toward developing universal technologies and initiatives for bot detection. Standardized approaches that can be seamlessly integrated across different research platforms will help safeguard the validity of online data collection and ensure that digital survey research remains a trusted tool for generating meaningful insights.

Limitations

While this study offers valuable insights, several limitations must be acknowledged. Since bot detection methods were applied to a single case study, their effectiveness has yet to be evaluated across different datasets, which may limit generalizability. Additionally, the data were collected within one region of Ontario, and the characteristics of the probable human responses, and their differences from suspected bot responses, may not be representative of broader populations. As response patterns may vary across settings, researchers working in other regions or with different populations should assess whether similar differences between suspected bot and probable human data are observed. However, the bot identification framework is adaptable, as criteria, such as postal or ZIP code validation, open-text analysis, and completion times can be tailored to reflect local contexts. Differences observed between probable human and suspected bot responses may also partially reflect differences between recruitment channels, such as respondents reached through email lists versus social media postings. Survey respondents recruited via open online platforms may differ systematically in demographics or response behaviors, independent of bot activity. Although some degree of misclassification is therefore possible, our detection framework was deliberately conservative and assumed responses were human unless sufficient evidence across multiple indicators suggested otherwise. Despite using various suspected bot detection strategies, there is also potential for undetected sophisticated bots, which could still impact the dataset's validity. Furthermore, the study was conducted at a specific point in time, and as automated response technologies evolve, the effectiveness of these detection methods may diminish. The study relied on assumed response patterns to identify suspected bots, but without absolute verification, such as IP tracking or manual validation, there remains some uncertainty in classification. Finally, while we observed that suspected bot responses reversed an expected positive correlation between depression-related items, this pattern was not incorporated into our 3-tier classification framework. Such a pattern would align conceptually with a Tier 3 criterion, as it represents a complex and context-dependent anomaly that would require corroboration from additional indicators to support classification. Future research should examine whether anomalies in response patterns, in addition to structural indicators, can serve as reliable markers of fraudulent responses.

XSL•FO
RenderX

Conclusions

This study provides criteria for identifying bots in online surveys. In comparing survey results from the suspected bots and probable humans, identified by the developed criteria, we found important differences in response patterns that would jeopardize data validity if bots were not correctly identified. By incorporating robust data validation protocols early in the research process, researchers can minimize bias and prevent the inclusion of inauthentic data, strengthening the reliability of findings. This study should be interpreted as a cautionary case rather than a prescriptive template. Without verified contact lists or other forms of participant validation, open online surveys will remain vulnerable to contamination despite the use of screening methods.

Acknowledgments

Artificial intelligence tools were used to assist with technical tasks such as formatting tables and supporting code refinement during data analysis. All analytic decisions, code implementation, result verification, and manuscript content were developed and reviewed by the authors.

Funding

This research was supported by a grant from the Ontario Ministry of Health to the Health System Performance Network (#694). The funders had no role in data analysis, decision to publish, or preparation of the report.

Data Availability

The datasets that were created and analyzed during this study are not publicly available, as public data sharing was not included in the original research ethics approval and participant consent form. Deidentified data may be made available for research purposes upon reasonable request to the corresponding author, subject to institutional approvals and data-sharing agreements, and provided that participant confidentiality can be maintained.

Authors' Contributions

EH and KM contributed to the conceptualization and methodology of the study, curated the data, and developed and implemented the coding criteria to identify suspected bots (with oversight from WW). EH completed the analysis and drafted the manuscript. KM and WW provided critical revision and editing of the manuscript.

Conflicts of Interest

None declared.

Multimedia Appendix 1
Ontario Health Team Patient Survey (full survey instrument used in the study).
[DOCX File, 1252 KB - medinform_v14i1e73622_app1.docx]

Multimedia Appendix 2
Chi-square test results comparing survey responses between probable humans and suspected bots, with Bonferroni-adjusted *P* values and Cramer V effect sizes.
[DOCX File, 98 KB - medinform_v14i1e73622_app2.docx]

References

1. Gibbons C, Porter I, Gonçalves-Bradley DC, et al. Routine provision of feedback from patient-reported outcome measurements to healthcare providers and patients in clinical practice. Cochrane Database Syst Rev 2021 Oct 12;10(10):CD011589. [doi: 10.1002/14651858.CD011589.pub2] [Medline: 34637526]
2. Donald EE, Whitlock K, Dansereau T, Sands DJ, Small D, Stajduhar KI. A codevelopment process to advance methods for the use of patient-reported outcome measures and patient-reported experience measures with people who are homeless and experience chronic illness. Health Expect 2022 Oct;25(5):2264-2274. [doi: 10.1111/hex.13489] [Medline: 35411709]
3. Kingsley C, Patel S. Patient-reported outcome measures and patient-reported experience measures. BJA Education 2017 Apr;17(4):137-144. [doi: 10.1093/bjaed/mkw060]
4. Casaca P, Schäfer W, Nunes AB, Sousa P. Using patient-reported outcome measures and patient-reported experience measures to elevate the quality of healthcare. Int J Qual Health Care 2023 Dec 26;35(4):mzad098. [doi: 10.1093/intqhc/mzad098] [Medline: 38113907]
5. Thompson AD, Utz RL. Online surveys: lessons learned in detecting and protecting against insincerity and bots. Qual Quant 2025 Feb;59(S1):23-39. [doi: 10.1007/s11135-024-01973-z]

XSL•FO
RenderX

6. Singh S, Sagar R. A critical look at online survey or questionnaire-based research studies during COVID-19. Asian J Psychiatr 2021 Nov;65:102850. [doi: 10.1016/j.ajp.2021.102850] [Medline: 34534919]
7. Griffin M, Martino RJ, LoSchiavo C, et al. Ensuring survey research data integrity in the era of internet bots. Qual Quant 2022;56(4):2841-2852. [doi: 10.1007/s11135-021-01252-1] [Medline: 34629553]
8. Storozuk A, Ashley M, Delage V, Maloney EA. Got bots? Practical recommendations to protect online survey data from bot attacks. TQMP 2020;16(5):472-481. [doi: 10.20982/tqmp.16.5.p472]
9. Dewitt J, Capistrant B, Kohli N, et al. Addressing participant validity in a small internet health survey (the restore study): protocol and recommendations for survey response validation. JMIR Res Protoc 2018 Apr 24;7(4):e96. [doi: 10.2196/resprot.7655] [Medline: 29691203]
10. Guy AA, Murphy MJ, Zelaya DG, Kahler CW, Sun S. Data integrity in an online world: demonstration of multimodal bot screening tools and considerations for preserving data integrity in two online social and behavioral research studies with marginalized populations. Psychol Methods 2024 Sep 9. [doi: 10.1037/met0000696] [Medline: 39250292]
11. Pozzar R, Hammer MJ, Underhill-Blazey M, et al. Threats of bots and other bad actors to data quality following research participant recruitment through social media: cross-sectional questionnaire. J Med Internet Res 2020 Oct 7;22(10):e23021. [doi: 10.2196/23021] [Medline: 33026360]
12. Eysenbach G, Wyatt J. Using the Internet for surveys and health research. J Med Internet Res 2002;4(2):E13. [doi: 10.2196/jmir.4.2.e13] [Medline: 12554560]
13. Chen AT, Komi M, Bessler S, Mikles SP, Zhang Y. Integrating statistical and visual analytic methods for bot identification of health-related survey data. J Biomed Inform 2023 Aug;144:104439. [doi: 10.1016/j.jbi.2023.104439] [Medline: 37419375]
14. Xu Y, Pace S, Kim J, et al. Threats to online surveys: recognizing, detecting, and preventing survey bots. Soc Work Res 2022 Nov 14;46(4):343-350. [doi: 10.1093/swr/svac023]
15. Dadfar M, Lester B. Psychometric characteristics of Patient Health Questionnaire-2 (PHQ-2) in Iranian psychiatric open access outpatients. Austin J Psychiatry Behav Sci 2017;4(1) [FREE Full text]
16. Xu F, Johnston JM. Self-rated health and health service utilization: a systematic review. Int J Epidemiol 2015 Oct;44(suppl_1):i180-i180. [doi: 10.1093/ije/dyv096.267]
17. Tamayo-Fonseca N, Nolasco A, Quesada JA, et al. Self-rated health and hospital services use in the Spanish National Health System: a longitudinal study. BMC Health Serv Res 2015 Nov 4;15(1):492. [doi: 10.1186/s12913-015-1158-8] [Medline: 26537822]
18. Johnson MS, Adams VM, Byrne J. Addressing fraudulent responses in online surveys: insights from a web ‐ based participatory mapping study. People and Nature 2024 Feb;6(1):147-164. [doi: 10.1002/pan3.10557]
19. King-Nyberg B, Thomson E, Morris-Reade J, Borgen R, Taylor C. The bot toolbox: an accidental case study on how to eliminate bots from your online survey. J Soc Thought 2023;7 [FREE Full text]
20. Goodrich B, Fenton M, Penn J, Bovay J, Mountain T. Battling bots: experiences and strategies to mitigate fraudulent responses in online surveys. Applied Eco Perspectives Pol 2023 Jun;45(2):762-784. [doi: 10.1002/aepp.13353]
21. Teitcher JEF, Bockting WO, Bauermeister JA, Hoefer CJ, Miner MH, Klitzman RL. Detecting, preventing, and responding to “fraudsters” in internet research: ethics and tradeoffs. J Law Med Ethics 2015;43(1):116-133. [doi: 10.1111/jlme.12200] [Medline: 25846043]
22. Pinzón N, Koundinya V, Galt RE, et al. AI-powered fraud and the erosion of online survey integrity: an analysis of 31 fraud detection strategies. Front Res Metr Anal 2024;9:1432774. [doi: 10.3389/frma.2024.1432774] [Medline: 39687573]
23. Loebenberg G, Oldham M, Brown J, et al. Bot or not? Detecting and managing participant deception when conducting digital research remotely: case study of a randomized controlled trial. J Med Internet Res 2023 Sep 14;25(5):e46523. [doi: 10.2196/46523] [Medline: 37707943]
24. Lebrun B, Temtsin S, Vonasch A, Bartneck C. Detecting the corruption of online questionnaires by artificial intelligence. Front Robot AI 2023;10:1277635. [doi: 10.3389/frobt.2023.1277635] [Medline: 38371744]

Abbreviations

CAPTCHA: Completely Automated Public Turing test to tell Computers and Humans Apart
OHT: Ontario Health Team
PHQ-2: Patient Health Questionnaire-2
PREM: patient-reported experience measure
PROM: patient-reported outcome measure
REDCap: Research Electronic Data Capture

XSL•FO
RenderX

Edited by A Coristine; submitted 07.Mar.2025; peer-reviewed by C Falk, N Pinzón, SP Uppu; revised version received 20.Jan.2026; accepted 21.Jan.2026; published 05.Mar.2026.

Please cite as:
Hamovitch E, McKellar K, Wodchis WP
Identifying and Analyzing Bot-Generated Responses in Online Health Care Surveys: Methodological Study
JMIR Med Inform 2026;14:e73622
URL: https://medinform.jmir.org/2026/1/e73622
doi:10.2196/73622

© Emily Hamovitch, Kaileah McKellar, Walter P Wodchis. Originally published in JMIR Medical Informatics (https://medinform.jmir.org), 5.Mar.2026. This is an open-access article distributed under the terms of the Creative Commons Attribution License (https://creativecommons.org/licenses/by/4.0/), which permits unrestricted use, distribution, and reproduction in any medium, provided the original work, first published in JMIR Medical Informatics, is properly cited. The complete bibliographic information, a link to the original publication on https://medinform.jmir.org/, as well as this copyright and license information must be included.

XSL•FO
RenderX

Original Paper

Chatbot Outreach in Value-Based Preventive Care: Retrospective Analysis

Jincy Chacko[1,2*], DHI; Yuane Jia[3*], PhD; Kimon Stathakos[1*], MBA; Kathleen Mazza[1*], PhD; Doran Kim[1*], MSM; Michael Diefenbach[1*], PhD; Lorena Carlo[2*], PhD

[1]Northwell Health, New Hyde Park, NY, United States

[2]Department of Health Informatics, School of Health Professions, Rutgers University, Piscataway, NJ, United States

[3]Department of Interdisciplinary Studies, School of Health Professions, Rutgers University, Newark, NJ, United States

[*]all authors contributed equally

Corresponding Author:
Jincy Chacko, DHI
Northwell Health
2000 Marcus Avenue, Suite 300
New Hyde Park, NY, 11042-1069
United States
Phone: 1 9863946
Email: chackoj.informatics@gmail.com

Abstract

Background: As health care delivery shifts toward value-based care, proactive strategies to close preventive care gaps are essential. However, patient engagement remains suboptimal due to logistical, behavioral, and socioeconomic barriers. Traditional outreach methods, such as phone calls, emails, and postal mail, have long been used, but emerging digital approaches, such as chatbot-based messaging, offer potential advantages in scalability and personalization. Their comparative effectiveness, however, remains underexplored.

Objective: This study aimed to evaluate the effectiveness of chatbot outreach compared with traditional communication methods (phone, email, mail, and multichannel) in promoting compliance with preventive screenings and wellness visits defined by the Healthcare Effectiveness Data and Information Set and the Centers for Medicare & Medicaid Services guidelines.

Methods: This retrospective study evaluated patient outreach campaigns conducted from 2021 to 2023 across an integrated health system in New York. The final analytic sample included 50,145 care gaps from 41,959 eligible participants, predominantly female (29,989/50,145, 60%), White (31,857/50,145, 64%), with mean age ranging from 49.36 to 72.81 years over the study period. All participants were residents of New York state, and 81% (40,553/50,145) maintained an active relationship with a primary care provider during the participation year. Outreach modalities included automated chatbot SMS text messages, nonautomated phone calls, and organization-led email or mail campaigns. Participant data were enriched with social vulnerability scores to account for community-level disadvantages. Exposure was defined as the outreach method (chatbot, phone, email, mail, or multichannel), with assignment based on engagement history and operational protocols. The primary outcome was care-gap closure or compliance with identified measure gaps annually. Logistic regression and chi-square analyses examined associations between outreach method, patient demographics, primary care physician relationship, social vulnerability index (SVI), and compliance.

Results: Phone outreach consistently achieved higher compliance than chatbot or multichannel outreach across most groups and years. Chatbot messages outperformed phone calls only in diabetes care in 2023 (odds ratio [OR] 1.81, 95% CI 1.48-2.21; $P<.001$). Primary care physician continuity remained a strong predictor of gap closure, especially in primary care (ORs ranged 1.36-2.61; $P<.001$). Higher SVI quartiles were associated with lower compliance in blood pressure, cancer care, and diabetes care groups; however, primary care outcomes showed higher odds of compliance in the third quartile of SVI, contradicting the typical linear-deprivation narrative. Women, Hispanic or Latino individuals, and Asian patients demonstrated higher odds of compliance in some groups and years.

Conclusions: Outreach modality is an important, modifiable factor in preventive care adherence. While phone-based outreach remains the most effective overall approach, chatbot-based strategies may have targeted applications in digitally engaged

XSL•FO
RenderX

populations such as the diabetic group. Segmented, equity-informed outreach strategies that integrate technology, patient preferences, and primary care continuity are essential to achieving high-impact, scalable outcomes in value-based care settings.

(JMIR Med Inform 2026;14:e81370) doi:10.2196/81370

KEYWORDS

chatbot outreach; digital health; health communications; health equity, preventive care gaps; value-based care

Introduction

Background and Rationale

The development of health care delivery in the United States over the past decade has increasingly centered on value-based care (VBC), which emphasizes quality, outcomes, and cost-effectiveness over service volume. Promoted by the Centers for Medicare & Medicaid Services (CMS), the value-based preventive care concept represents a focused application of the VBC framework that prioritizes proactive prevention and early disease detection, aligning financial incentives with population health goals [1,2]. This approach is particularly relevant for managing chronic diseases and addressing preventive care needs in large, diverse patient populations [3].

Despite widespread consensus on the benefits of preventive services such as annual wellness visits, cancer screenings (CXs), diabetes care (DB), and blood pressure (BP) monitoring, patient adherence remains suboptimal [4-6]. Barriers to engagement include socioeconomic challenges, low health literacy, lack of awareness, and fragmented communication between care providers [7,8]. Health systems have historically used outreach methods such as telephone calls, emails, and postal mail to notify and engage patients with gaps in preventive care. However, these approaches can be resource-intensive and vary in their reach and effectiveness, particularly among hard-to-engage populations [9].

Emerging digital outreach tools, including automated chatbots and SMS text messaging, may offer a promising alternative for improving engagement at scale. These technologies can support bidirectional communication, personalize patient interactions, and reduce administrative burdens [10]. Several public health campaigns, particularly during the COVID-19 pandemic, have demonstrated the feasibility of chatbot-based outreach in promoting vaccine uptake and disseminating timely health information. However, the use of these tools for broader preventive care engagement, particularly in chronic disease management and CX, remains underexplored [11].

Based on a previous systematic review conducted on this topic by Chacko et al [11], the current state indicates a limited body of evidence on chatbot outreach beyond immunization programs, highlighting a need for further research into their effectiveness, cost-efficiency, and equity impact. Studies reporting on outreach mechanisms for preventive care have varied in their implementation approaches and study methodologies. Therefore, drawing a generalizable conclusion is not possible. It is uncertain if benefits of chatbot outreach apply uniformly across various demographic and clinical groups. Moreover, the integration of these tools into large health systems workflows may present unique challenges that remain underexplored in the literature [11].

Objectives

To address these gaps, this study aims to evaluate the impact of emerging technology, such as chatbot-based outreach, on preventive screening uptake compared to conventional methods, such as outreach via phone calls and email communications. The authors posited that the use of chatbots in preventive care will significantly increase the uptake of screening for annual wellness visits, hypertension, diabetes, and CXs compared to traditional methods of communication. Conducted at a large integrated delivery network in New York, the study focused on patients identified as having care gaps using the Healthcare Effectiveness Data and Information Set (HEDIS) and CMS preventive screening criteria. This study builds upon recent findings that suggest automated outreach tools may offer scalable and equitable solutions for preventive health engagement [11]. By evaluating their effectiveness across multiple screening domains, which included CXs, DB, and hypertension screening, along with primary care (PC) measures such as annual wellness visits, the study contributes to the growing body of evidence informing digital outreach strategies in VBC-aligned care delivery. Findings from this evaluation may help guide future investments in digital health infrastructure and support the implementation of targeted, technology-enabled outreach programs.

Methods

Study Design

This study retrospectively evaluated data collected from VBC outreach activities conducted over a 3-year period, from 2021 to 2023. Members identified by their insurance carrier as having care gaps, attributed to the health system, were targeted for outreach. Outreach was conducted using phone calls, web-based chatbots, email messages, mailed letters, and sometimes a combination of these methods. The strategy for outreach method allocation was dependent on operational capacity and technology adoption. During year 1 (2021), due to reduced operational capacity following the 2020 pandemic year, new technology was piloted to aid in outreach. The subsequent years' attribution strategy was adjusted to maintain a balance between outreach methods with increased volume of gaps, capacity in the workforce, and efficiencies found in technology adoption. Multichannel outreach involves the sequential use of 2 or more methods within the same measurement year when initial outreach attempts fail to result in engagement. Due to the inability to attribute the outcome to any single method alone, outreach using multiple methods was grouped into 1 category. Outreach method assignments followed operational protocols

XSL•FO
RenderX

and capacities that varied each year, rather than being randomized. Therefore, this study is exploratory in nature, focused on understanding trends that may drive empirical decisions about the modality of outreach in the future.

Data Sources

Participant demographic information was collected from the health system's electronic medical record (EMR). Outreach process measures and final compliance data were collected 3 months post each study year from the respective operational teams performing outreach. These data included an indicator for participant relationship with primary care provider (PCP) within the health system and the total number of care gaps for the given year per participant. Deidentification was completed before the data were shared with researchers. The social vulnerability index (SVI) was acquired from the 2022 dataset compiled by the Centers for Disease Control and Prevention [12]. The census tract level SVI was mapped to participant zip code with the aid of cross-mapping from the Department of Housing and Urban Development, accessed in June 2024 [13].

Inclusion Criteria

Participant eligibility for the identified gap measures was a primary inclusion criterion. Clinical criteria for eligibility are industry-defined guidelines (electronic Clinical Quality Measures), maintained by CMS [14], or HEDIS specifications provided by the National Committee for Quality Assurance [15], with changes published each year publicly. These define the required age ranges, diagnosis inclusion, and completion intervals for preventive services such as wellness visits, CX, BP, and DB. The other important criterion determining inclusion in the final analysis was having at least one outreach attempt using a phone, chatbot, email, or letter during the measurement year. As the study focused on understanding the efficiency of outreach methods, the population that received no outreach was outside the scope of this study.

Exclusion Criteria

Preventive measure groups and individual measures with an insufficient sample size (n<10) were excluded due to the need for valid statistical and comparative testing. Records with unknown outcomes (ie, unverified or missing documentation of care gap closure) or missing demographic variables (age, gender, race, ethnicity, and address [needed for SVI grouping]) were excluded. For example, if there was no known address for the patient documented, it would not be possible to map an SVI and include the participant in the stratified analysis, and therefore, such participants' data were removed from all study datasets before any analysis was conducted. Process measures such as documented patient engagement steps (eg, message opened or call answered) were collected and used to define successful outreach delivery. Unsuccessful outreach deliveries (eg, in case of erroneous contact information) were excluded.

The dataset remained representative of the population served by the health system and met eligibility criteria for each measure throughout this process. Four measure groups remained eligible for analysis after the applied exclusions: PC, BP, CX, and DB. Multimedia Appendix 1 provides the distribution of participants and measure gaps within each group.

Data Management

Deidentified data were aggregated at the patient-gap-year granularity using Microsoft Power BI [16]. Individual preventive measures were grouped into care domains (eg, PC, CX, etc) based on clinical relevance and alignment with HEDIS and CMS quality measurement categories. The grouping was determined by the study team using established measure definitions to facilitate domain-level comparisons. The case of multiple SVIs mapped to a single participant due to geographic overlap in the data was resolved by assigning the SVI from the most populous county to the participant, which is a common approach in health care research. Figure 1 shows the flow of participants and gaps volume through the applied exclusions.

XSL•FO
RenderX

Figure 1. Participant and measure gap flow diagram for each year in the study, listing participant volume first and gaps (n) in parentheses. NY: New York.

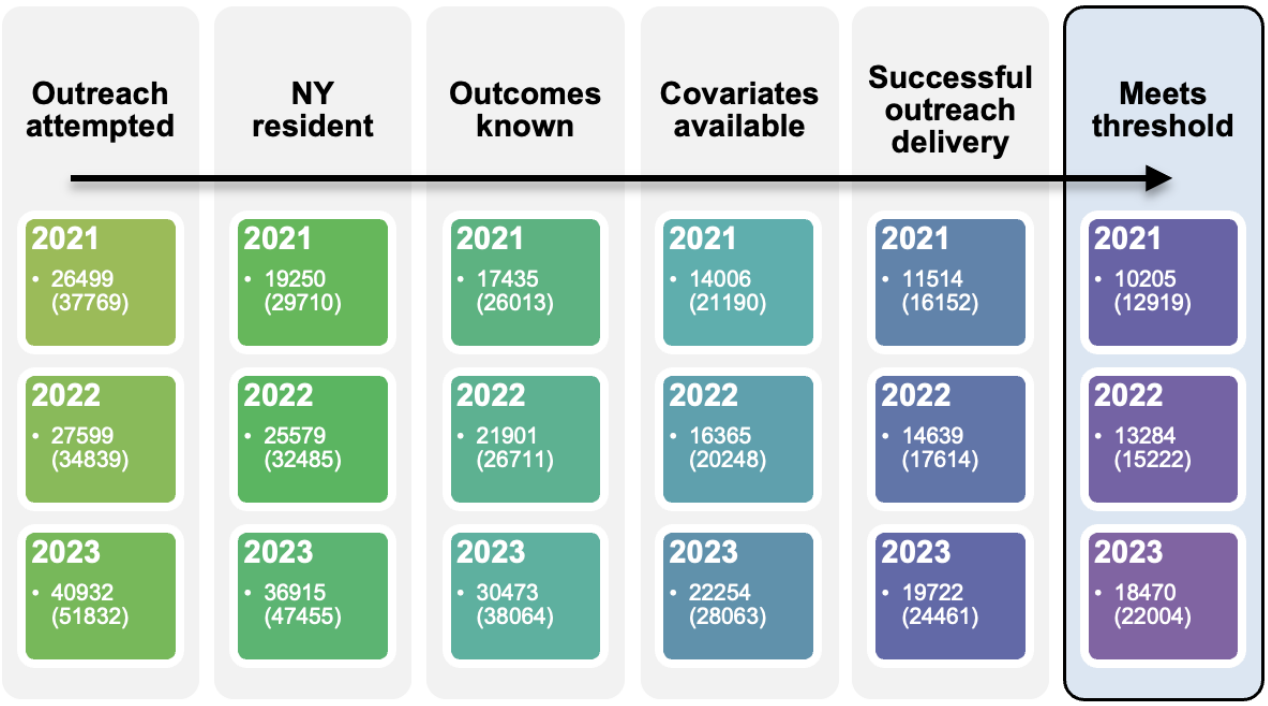

Study Variables

The primary independent variable, also referred to as the outreach method or intervention, was coded as 1 of the 4 single-channel methods (phone, chatbot, email, and mail) or multichannel to indicate any combination of these methods. Multichannel methods were grouped because the sample sizes in individual groups did not meet the statistical validity requirements for comparison.

The primary outcome or dependent variable evaluated was the completion of or compliance with the identified measure, measured 3 months following each study year (eg, March 2022 for the study year of 2021). It was documented separately for each year of the study, 3 months post end of year, and represented as a binary variable, indicated by 1 for "yes" and 0 for "no." The primary outcome was collected as part of the operational process of verifying completion of or compliance with the measure gap within the reporting period. This may include a verification by patient report, EMR validation, or a confirmation by payor data sharing. The authors collected this information retrospectively from data reported to governing agencies for each year.

Demographic data, including age, gender, race, ethnicity, and the SVI, were used to study covariates that could potentially impact the outcomes of outreach. Additionally, covariates included the presence of an active relationship with a PCP (defined as having a designated PCP of record within the health system and at least 1 documented encounter with that provider or associated practice within the preceding 18 months) and the burden of unmet care (defined as the total count of gaps for each participant per year).

Among the continuous variables, age was capped at 89 years to prevent reidentification. The count of gaps variable was used to assess potential imbalances in record weighting within the grouped measure files, as the datasets were analyzed at a gap level (n=1 gap per participant) rather than at a participant level. Tables S1-S4 in Multimedia Appendix 2 demonstrate the range and mean of the count of gaps per year for each measure group.

Categorical variables included demographic factors, gender, race group, ethnicity, socioeconomic factors, SVI, and active PCP relationship. Gender was coded into male/female as collected in the EMR. Race was grouped into White, Black or African American, Asian, and other. The other race group included Pacific Islander, Alaskan, and Native Americans, as well as patient self-reported "other" race identity. Ethnicity was only collected as a bivariate containing options for Hispanic and Latino or not Hispanic or Latino. Each participant was assigned an SVI quartile (1-4), where quartile 1 was the group with the least social vulnerability, and quartile 4 was the group with the most social vulnerability.

Statistical Analysis

All statistical analyses were conducted using IBM SPSS Statistics for Windows (version 29.0) [17]. The dataset was divided into measure-group files for each year. Analysis was performed for each measure group, with BP as an exception because it contained only 1 measure. Textbox 1 provides a list of subgroups (measures) within each measure group that were included in the final analysis. Descriptive statistics and contingency tables verified adequate cell counts (n≥10) for bivariate analyses per measure group, and any variables not meeting the threshold were excluded from final analysis for the respective measure group [18,19]. Notably, SVI quartile 2 often did not meet the valid n threshold, as was the case when the outreach method was email only. These were excluded from statistical analysis. This conservative approach ensured the robustness of the reported associations while maintaining data

XSL•FO
RenderX

integrity across all measure groups. Effect sizes are reported as odds ratios (ORs) with 95% CI and *P* values. Categorical variables were converted into dummy variables using reference coding (eg, phone outreach, male, White, non-Hispanic/Latino, SVI quartile 1, and no active PCP as baseline categories) before logistic regression analysis.

Textbox 1. Measure groups and subgroups 2021-2023.

Primary care

- Annual wellness visit
- Pediatric well-care visit

Blood pressure (single measure only)

Cancer screening

- Breast cancer screening
- Cervical cancer screening
- Colorectal cancer screening

Diabetes care

- Hemoglobin A1c control <8.0% in diabetes
- Hemoglobin A1c poor control >9.0% in diabetes
- Hemoglobin A1c testing in diabetes
- Nephropathy assessment
- Retinal eye examination
- Kidney health evaluation for participants with diabetes

Collinearity was assessed between included variables, which led to the exclusion of the insurance group from the final analysis due to its high correlation with age in this dataset. Chi-square tests identified preliminary predictors among the categorical variables, after which a 2-step backward stepwise logistic regression was performed. Step 1 entered all demographic variables and PCP relationship. Step 2 introduced outreach modality to quantify its independent association with the final compliance outcome, that is, gap closure after controlling significant covariates in the previous step. A chi-square test was also conducted between the PCP relationship variable and outreach methods to examine any existing associations before both were included in the regression model. Statistical significance was set at α=.05.

Ethical Considerations

The Northwell Institutional Review Board reviewed this study protocol and approved it on August 15, 2024 (HSRD24-0151), with a waiver of consent requirements in accordance with research involving deidentified secondary data. No patient contact or intervention occurred as part of the study, and all data were fully anonymized prior to analysis. To minimize analytic bias, eligibility and exclusion criteria were applied consistently using standardized definitions from HEDIS and CMS electronic Clinical Quality Measures.

Results

Participant Characteristics and Descriptive Statistics

After applying exclusions, the analytic dataset contained 12,919, 15,222, and 22,004 care gaps for 2021, 2022, and 2023, respectively, bringing the overall volume of gaps to 50,145. Gap volumes increased by approximately 18% (15,222/12,919) in 2022 and 45% (22,004/15,222) in 2023, with PC accounting for 47% (23,481/50,145) of gaps, CX 31% (15,335/50,145), BP 12% (5891/50,145), and DB 11% (5438/50,145). A total of 81% (40,553/50,145) of gaps came from participants who had an active relationship with the PCP during the participating year. Women predominated in all groups except diabetes in 2021-2022, and the cancer cohort showed an expected skew due to female-targeted measures. Among the 50,145 gaps, participants mostly belonged to the White racial group at 64% (31,857), followed by other 18% (8812), Black at 12% (6230), Asian at 6% (3246), and Hispanic/Latino at 16% (8199). The mean age for the PC group declined from 72.8 (SD 11.6) years in 2021 to 60.2 (SD 27.1) years and 49.4 (SD 30.5) years in 2022 and 2023, respectively, resulting from the gradual inclusion of the pediatric subgroup. All other measure groups had a mean age range from 56.4 to 66.3 years. The average gaps per participant were below 2 for all measures except DB, which had 2.9 gaps per participant in 2021, 2 in 2022, and 2.2 in 2023. See Multimedia Appendix 2 (Tables S1-S4) for detailed distribution for all 3 years.

Outreach included phone, chat, email, and multichannel approaches. Email was only valid for PC in 2021 and DB in 2023. Multichannel cohort met criteria in PC and CX across all years and DB and BP in 2023. Outreach shifted from phone-dominated in 2021 to greater chatbot and multichannel use by 2023. Multimedia Appendix 2 displays this trend with detailed values for each group.

XSL•FO
RenderX

Compliance Trends and Bivariate Associations

Multimedia Appendix 3 indicates the compliance rate for all 3 years across the measure groups. All measure groups indicate the highest compliance rate in 2021 and a subsequent decrease in 2022. While other measure groups have increased compliance in 2023, possibly indicating a postpandemic stabilization, compliance in the BP group continues to decrease this year. This decrease, however, is relative, as BP continues to be the group with the highest compliance rate each year (1042/1486, 70% to 1440/2550, 56%), while CX is the group with the lowest compliance rate (1698/4264, 40% to 1600/7656, 21%).

Across all measure groups, the outreach method showed a significant association with compliance. The PC group demonstrated the strongest relationship in 2021 with a large effect size (χ^2_3=1767.8; *P*<.001; V=0.57). Though this association persisted for all 3 years, its magnitude decreased, showing a moderate effect size in 2022 (χ^2_2 =220.3; *P*<.001; V=0.16) and 2023 (χ^2_2=409.5; *P*<.001; V=0.21). A significant but weak association was observed for the DB group in 2021 (χ^2_1=10.1; *P*=.001; ϕ=0.08) and a moderate effect size emerged in 2023 (χ^2_3=41.3; *P*<.001; V=0.14). The CX group showed a significant association in 2022 (χ^2_2=14.1; *P*<.001; V=0.10) and 2023 (χ^2_2=70.2; *P*<.001; V=0.10), though effect sizes remained weak throughout. BP had significant but weak associations between intervention and outcome for all 3 years. All significant chi-square test results are listed in Table 1, along with the analytic sample size. A complete report on all variables is available in Multimedia Appendix 4.

XSL•FO
RenderX

Table 1. Significant associations between covariates and outcome.

Measure and variable	Year	n	Chi-square (*df*)	*P* value	Effect size (ϕ or V)	Interpretation
Primary care						
Active PCP[a] relationship	2021	5415	270.8 (1)	<.001	ϕ=0.22	Moderate
Active PCP relationship	2022	8445	14.1 (1)	<.001	ϕ=0.04	Weak
Active PCP relationship	2023	9544	265.7 (1)	<.001	ϕ=0.17	Weak
Ethnicity	2022	8445	41.4 (1)	<.001	ϕ=0.07	Weak
Ethnicity	2023	9544	46.8 (1)	<.001	ϕ=0.07	Weak
Gender	2021	5415	8.7 (1)	.003	ϕ=0.04	Weak
Gender	2022	8445	8.7 (1)	.003	ϕ=0.03	Weak
Gender	2023	9544	5.4 (1)	.02	ϕ=0.02	Weak
Intervention	2021	5415	1767.8 (3)	<.001	V=0.57	Large
Intervention	2022	8445	220.3 (2)	<.001	V=0.16	Moderate
Intervention	2023	9544	409.5 (2)	<.001	V=0.21	Moderate
Race group	2021	5415	8.8 (3)	.03	V=0.04	Weak
Race group	2022	8445	54.9 (3)	<.001	V=0.08	Weak
Race group	2023	9544	20.5 (3)	<.001	V=0.05	Weak
SVI[b] quartile	2021	5415	25.2 (2)	<.001	V=0.07	Weak
SVI quartile	2022	8445	10.4 (2)	.006	V=0.04	Weak
D iabetes care						
Active PCP relationship	2021	1737	29.9 (1)	<.001	ϕ=0.13	Weak
Active PCP relationship	2022	1470	7.2 (1)	.007	ϕ=0.07	Weak
Gender	2022	1470	11.1 (1)	<.001	ϕ=0.09	Weak
Intervention	2021	1737	10.1 (1)	.001	ϕ=0.08	Weak
Intervention	2023	2216	41.3 (3)	<.001	V=0.14	Moderate
SVI quartile	2023	2216	18.6 (2)	<.001	V=0.09	Weak
Cancer screening						
Active PCP relationship	2021	4252	8.2 (1)	.004	ϕ=0.03	Weak
Active PCP relationship	2023	7571	4.4 (1)	.04	ϕ=0.02	Weak
Ethnicity	2022	3407	15.4 (1)	<.001	ϕ=0.07	Weak
Ethnicity	2023	7571	6.1 (1)	.01	ϕ=0.03	Weak
Gender	2021	4252	35.0 (1)	<.001	ϕ=0.09	Weak
Gender	2022	3407	5.1 (1)	.02	ϕ=0.04	Weak
Intervention	2022	3407	14.1 (2)	<.001	V=0.10	Weak
Intervention	2023	7571	70.2 (2)	<.001	V=0.10	Weak
Race group	2022	3407	22.7 (3)	<.001	V<0.01	Weak
SVI quartile	2023	7571	17.0 (2)	<.001	V=0.05	Weak
Blood pressure						
Active PCP relationship	2021	1484	6.8 (1)	.009	ϕ=0.07	Weak
Active PCP relationship	2022	1852	135.7 (1)	<.001	ϕ=0.27	Moderate
Gender	2022	1852	10.4 (1)	.001	ϕ=0.08	Weak
Intervention	2021	1484	17.0 (1)	<.001	ϕ=0.11	Weak
Intervention	2022	1852	41.0 (1)	<.001	ϕ=0.15	Weak

XSL•FO
RenderX

Measure and variable	Year	n	Chi-square (*df*)	*P* value	Effect size (ϕ or V)	Interpretation
Intervention	2023	2542	58.1 (2)	<.001	V=0.03	Weak
SVI quartile	2021	1484	14.2 (2)	<.001	V=0.10	Weak
SVI quartile	2022	1852	21.7 (3)	<.001	V=0.11	Moderate
SVI quartile	2023	2542	34.3 (2)	<.001	V=0.12	Weak

[a]PCP: primary care provider.

[b]SVI: social vulnerability index.

The PCP relationship was significantly associated with preventive care gap closure across several measure groups. In the PC group, a moderate association was observed in 2021 (χ^2_1=270.8; *P*<.001; ϕ=0.22), with significance maintained through 2023 (*P*<.001; ϕ=0.17). In the BP group, associations were significant in 2021 (χ^2_1=6.8; *P*=.009; ϕ=0.07) and stronger in 2022 (χ^2_1=135.7; *P*<.001; ϕ=0.27) but not sustained in 2023. The DB group followed a similar pattern, showing small but significant associations in 2021 (χ^2_1=29.9; *P*<.001; ϕ=0.13) and 2022 (χ^2_1=7.2; *P*=.007; ϕ=0.07), which was not sustained in 2023. The CX group showed inconsistent results, with weak associations in 2021 (χ^2_1=8.2; *P*=.004; ϕ=0.03) and 2023 (χ^2_1=4.4; *P*=.04; ϕ=0.02).

The association between SVI and compliance showed dynamic patterns across years. SVI demonstrated a consistent association with compliance in the BP group for all 3 years, peaking in 2022 with the strongest effect size (χ^2_3=21.7; *P*<.001; V=0.11). In contrast, the CX group (χ^2_2=17.0; *P*<.001; V=0.05) and the DB group (χ^2_2=18.6; *P*<.001; V=0.09) showed this association in 2023 only, both with small effect sizes. The same association weakened over time in the PC group, with significant, weak associations observed in 2021 (χ^2_2=25.2; *P*<.001; V=0.07) and 2022 (χ^2_2=10.4; *P*=.006; V=0.04), and no significant association detected in 2023.

Race was significantly associated with compliance in the PC group across all years, but effect sizes were negligible (Cramer V ranged from 0.04 to 0.08). A similar near-zero association was observed for the CX group (V=0.004) in 2022 only. Ethnicity demonstrated small but consistent associations with PC compliance in 2022 (χ^2_1=41.4; *P*<.001; ϕ=0.07) and 2023 (χ^2_1=46.8; *P*<.001; ϕ=0.07). In the CX group, ethnicity was associated in 2022 (χ^2_1=15.4; *P*<.001; ϕ=0.07) with a small effect, and in 2023 with a weaker effect (χ^2_1=6.1; *P*=.01; ϕ=0.03). No significant associations with race or ethnicity were observed in the DB or BP groups.

A significant but small and diminishing association between gender and compliance was noted in the PC group across all 3 years, with effect sizes ranging from 0.02 to 0.04. For the BP and DB groups in 2022 only, gender was significantly associated with compliance with weak effect sizes. Gender associations in the CX group are not reported because most measures in this group specifically targeted women.

Regression Analysis of Compliance Predictors

After adjusting for other significant predictors, the outreach method remained significantly associated with compliance. Compared with phone call outreach, chatbot outreach consistently reduced the odds of gap closure across PC, BP, and CX measures, with a 30%-65% decrease in likelihood, as shown in Figures 2-4. An exception was observed in the DB group in 2023, where chatbot outreach outperformed phone calls (OR 1.81, 95% CI 1.48-2.21; *P*<.001). Multichannel campaigns were generally less effective than phone calls and chatbot outreach, except in the CX group in 2021, where multichannel outreach increased the odds of gap closure compared with phone calls (OR 2.12, 95% CI 1.01-4.44; *P*=.047). This was likely a reflection of the relatively smaller sample size that year, whereas subsequent years had greater representation of multichannel outreach, yielding narrower CIs.

XSL•FO
RenderX

Figure 2. Odds ratio and 95% CI by significant predictors and measure group in 2021. BP: blood pressure; CX: cancer screening; DB: diabetes care; OR: odds ratio; PC: primary care; PCP: primary care provider; SVI: social vulnerability index.

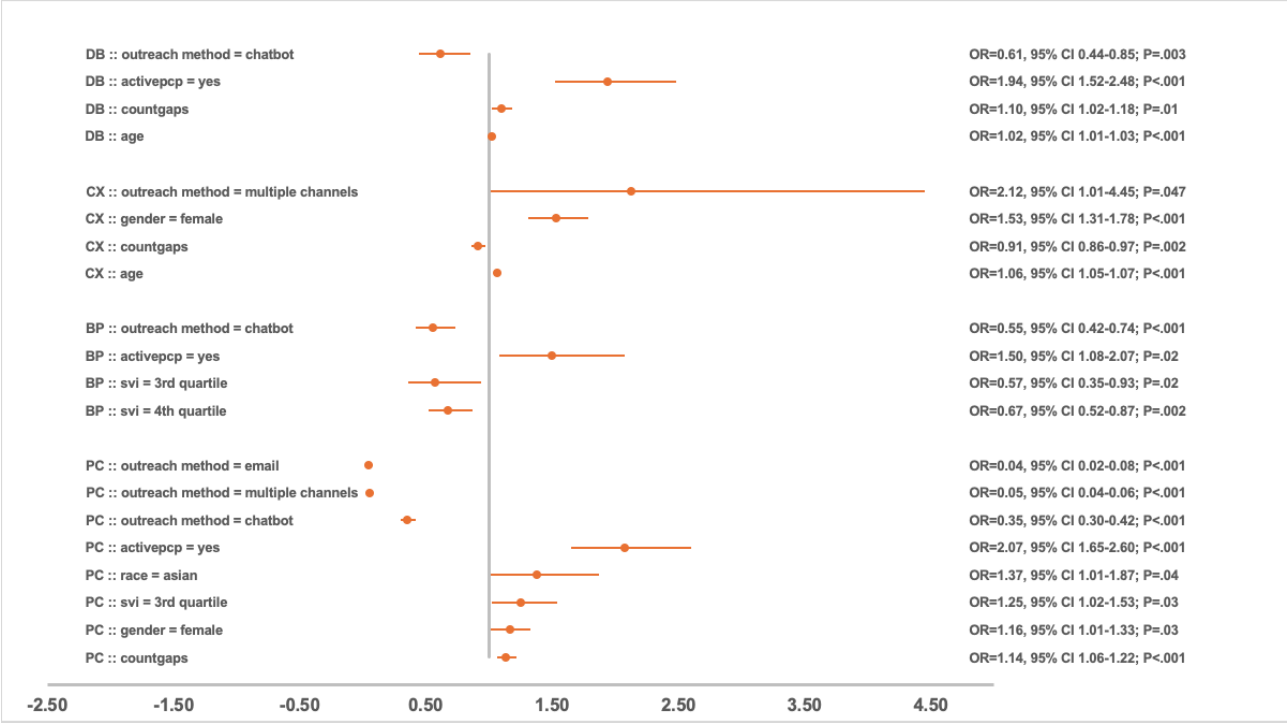

Figure 3. Odds ratio and 95% CI by significant predictors and measure group in 2022. BP: blood pressure; CX: cancer screening; DB: diabetes care; OR: odds ratio; PC: primary care; PCP: primary care provider; SVI: social vulnerability index.

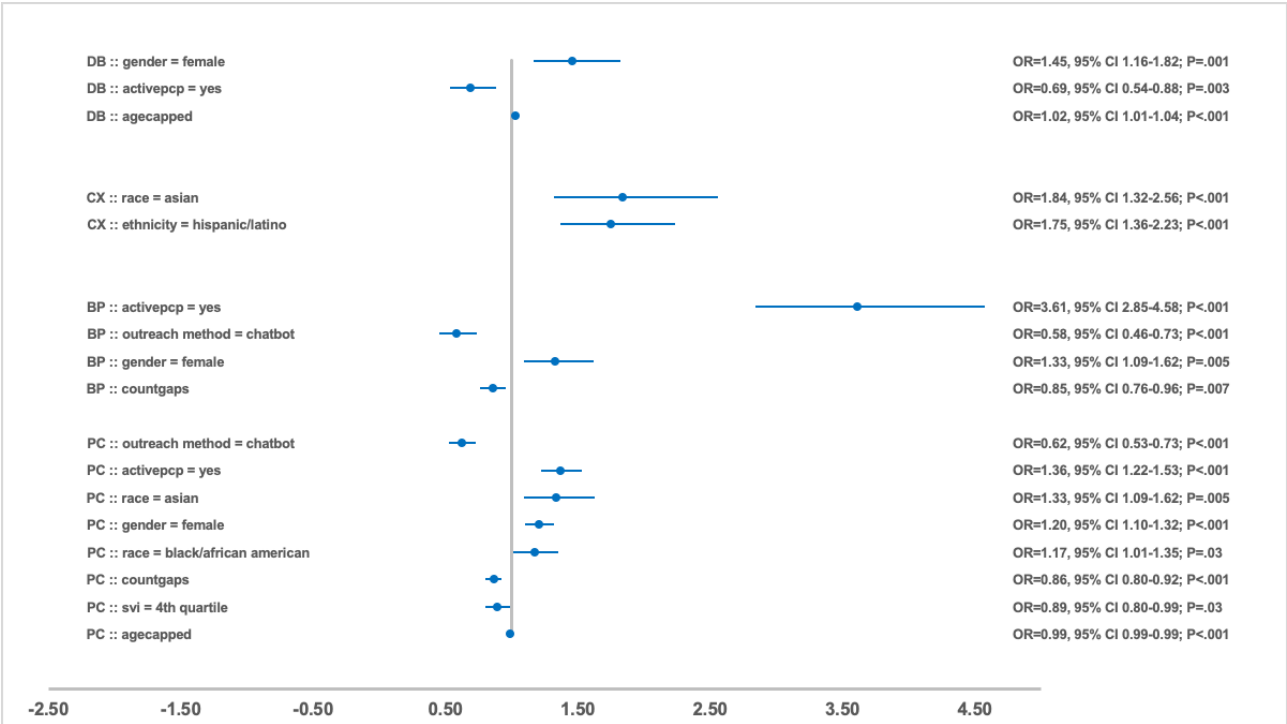

Taking account of other covariates, having a PCP relationship was the strongest predictor (*P*<.001) for care gaps compliance in the PC measure group, with ORs 2.07 (95% CI 1.65-2.60), 1.36 (95% CI 1.22-1.53), and 2.61 (95% CI 2.31-2.94) for 2021, 2022, and 2023 respectively. BP and DB had similarly significant associations in 2021 (BP: OR 1.50, 95% CI 1.08-2.07; *P*=.02; DB: OR 1.94, 95% CI 1.52-2.48; *P*<.001) and 2022 (BP: OR 3.61, 95% CI 2.85-4.58; *P*<.001; DB: OR 0.69, 95% CI 0.54-0.88; *P*=.003), but this association was not sustained in 2023. The final model for the CX group did not surface the PCP relationship as a predictor.

The SVI quartile demonstrated a complex relationship with compliance in the PC group. Participants in the third quartile were more likely to close gaps in 2021 (OR 1.25, 95% CI 1.02-1.53; *P*=.03) and 2023 (OR 1.70, 95% CI 1.49-1.95; *P*<.001) compared with the less vulnerable first quartile. In

XSL•FO
RenderX

contrast, in 2022, participants in the fourth quartile were less likely to close gaps (OR 0.89, 95% CI 0.80-0.99; *P*=.03) relative to the first quartile group. For the BP group, lower odds of gap closure were observed among the third quartile (OR 0.57, 95% CI 0.35-0.93; *P*=.02) and fourth quartile (OR 0.67, 95% CI 0.52-0.87; *P*=.002) in 2021, as well as the fourth quartile in 2023 (OR 0.61, 95% CI 0.50-0.73; *P*<.001). Similar patterns were noted for the CX and DB groups in 2023, where participants in the fourth quartile had reduced odds of closing gaps (CX: OR 0.79, 95% CI 0.70-0.91; *P*<.001; DB: OR 0.62, 95% CI 0.51-0.76; *P*<.001).

Women in the PC group had higher odds of compliance than men across all years, with ORs of 1.16 (95% CI 1.01-1.33; *P*=.03) in 2021, 1.20 (95% CI 1.10-1.32; *P*<.001) in 2022, and 1.18 (95% CI 1.08-1.28; *P*<.001) in 2023. Higher odds of gap closure for women were also observed in 2022 for the BP group (OR 1.33, 95% CI 1.09-1.62; *P*=.005) and DB group (OR 1.45, 95% CI 1.16-1.82; *P*=.001).

Asians were more likely to close gaps in PC group during 2021 (OR 1.37, 95% CI 1.01-1.87; *P*=.04) and 2022 (OR 1.33, 95% CI 1.09-1.62; *P*=.005) compared with White participants. They also showed higher odds of compliance in the CX group in 2022 (OR 1.84, 95% CI 1.32-2.56; *P*<.001). Race and ethnicity were not retained in the final model for BP and DB across all 3 years. However, ethnicity had a positive influence compliance in the CX group in 2022 (OR 1.75, 95% CI 1.36-2.23; *P*<.001) and 2023 (OR 1.32, 95% CI 1.14-1.53; *P*<.001), as well as in the PC group in 2023 (OR 1.29, 95% CI 1.16-1.44; *P*<.001).

Increasing age (capped at 89 years) showed a small, diminishing association with compliance. In the DB group, each additional year of age was associated with 1%-2% higher likelihood of gap closure, while in the CX group, the increased likelihood was 6% in 2021 and 2% in 2023. In contrast, in the PC group, older age was associated with a 1% lower likelihood of closing gaps in 2022 and 2023. Age was not a significant predictor in the final BP models across all 3 years. All percentage values for likelihood are reported based on the OR values in Figures 2-4.

Figure 4. Odds ratio and 95% CI by significant predictors and measure group in 2023. BP: blood pressure; CX: cancer screening; DB: diabetes care; OR: odds ratio; PC: primary care; PCP: primary care provider; SVI: social vulnerability index.

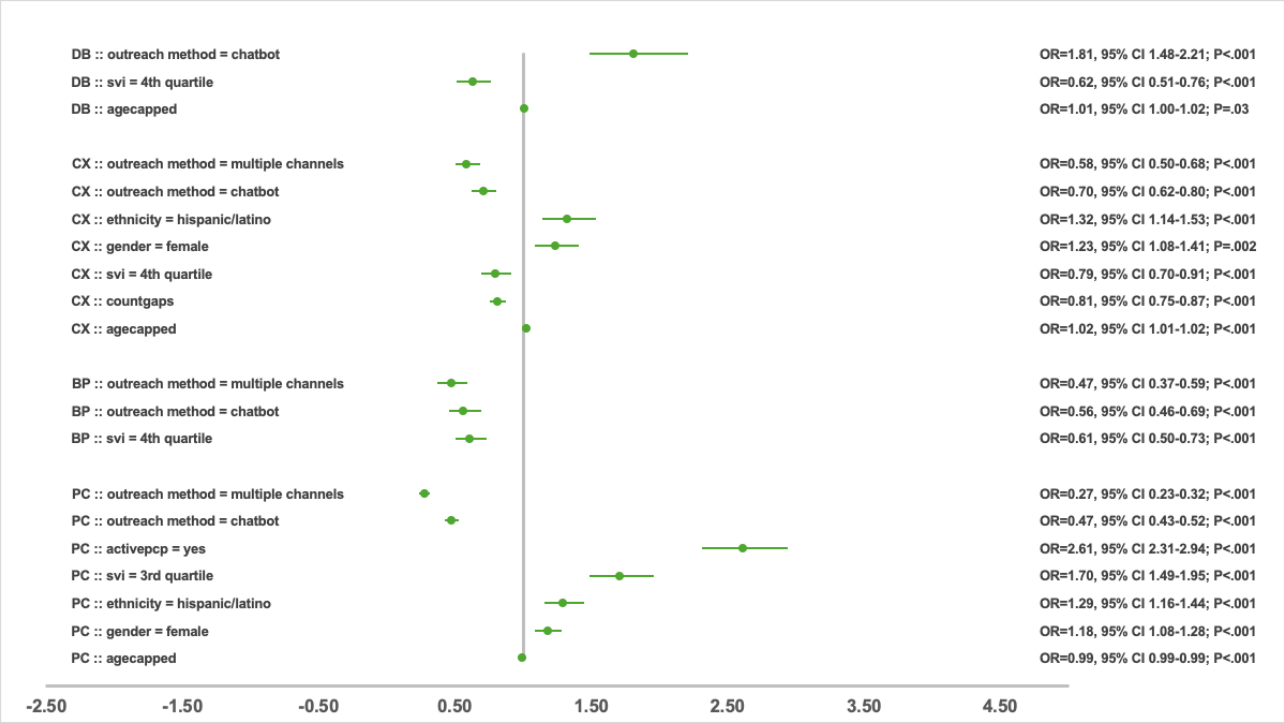

An increase in the number of gaps was associated with a higher likelihood of gap closure in the DB group only in 2021 (OR 1.10, 95% CI 1.02-1.18; *P*=.01), with no significant effects observed in later years. Unlike the DB group, BP and CX groups showed an inverse relationship, where each additional gap decreased the likelihood of compliance (BP 2022: OR 0.85, 95% CI 0.76-0.96; *P*=.007; CX 2021: OR 0.91, 95% CI 0.86-0.97; *P*=.002; CX 2023: OR 0.81, 95% CI 0.75-0.87; *P*<.001). The PC group demonstrated inconsistency, with more gaps increasing the odds of compliance in 2021 (OR 1.14, 95% CI 1.06-1.22; *P*<.001) but decreasing them in 2022 (OR 0.86, 95% CI 0.80-0.92; *P*<.001). ORs, 95% CIs, and *P* values for all variables with significant association in the final regression models are presented in Figures 2-4 across the 3 years. Each point in these figures represents the OR for the listed cohort and variable group on the left, and the line through the point represents the CI. The actual numbers for OR, CI, and *P* value are listed on the right side. Reference values for each category include male, White, non-Hispanic/Latino, SVI first quartile, no active PCP, and phone outreach. Any subgroups excluded due to low volume (<10) for the year are not included in the regression analysis.

Model discrimination, as assessed by the area under the receiver operating characteristic curve (AUC), was highest for the PC measure group in 2021 (AUC=0.82), indicating good

XSL•FO
RenderX

discriminatory ability. Other measure groups demonstrated modest discrimination, with AUCs ranging from 0.59 to 0.68 across years. In 2021, the model also achieved the highest classification accuracy for the PC group (78.6%), while the classification accuracy for other groups varied, ranging from 70.6% (BP) to 63.5% (CX) and 67% (DB).

Across all models, chi-square statistics were significant (P<.001), suggesting that the models were statistically associated with the outcomes. Nagelkerke R^2 values, reflecting the proportion of variance explained, were highest in 2021 for the PC group (R^2=0.41) and lower for other models, ranging from 0.02 to 0.13. Calibration, as assessed by the Hosmer-Lemeshow goodness-of-fit test, showed acceptable fit for some models (eg, CX in 2022 and 2023: P=.85 and P=.98; DB in 2022 and 2023: P=.34), but poorer fit in others (eg, PC in 2023: P<.001), indicating room for improvement in predicted versus observed outcomes alignment. Complete model diagnostics are provided in Table 2.

Table 2. Final regression model metrics for each measure group, 2021-2023.

Year and measure group	Chi-square (*df*)	*P* value	Nagelkerke R^2	*P* value (Hosmer–Lemeshow)	Overall classification accuracy, %	AUC[a]
2021						
PC[b]	1942.15 (9)	<.001	0.41	.02	78.6	0.82
BP[c]	37.44 (5)	<.001	0.04	.10	70.6	0.59
CX[d]	244.08 (6)	<.001	0.08	.002	63.5	0.65
DB[e]	71.39 (4)	<.001	0.06	<.001	67.0	0.60
2022						
PC	408.45 (10)	<.001	0.06	<.001	59.3	0.63
BP	180.73 (4)	<.001	0.13	.21	67.7	0.68
CX	48.79 (8)	<.001	0.02	.85	83.2	0.59
DB	37.00 (4)	<.001	0.04	.34	69.3	0.60
2023						
PC	882.59 (9)	<.001	0.12	<.001	60.7	0.67
BP	90.76 (6)	<.001	0.05	.09	58.1	0.61
CX	145.14 (7)	<.001	0.03	.98	78.9	0.60
DB	68.64 (6)	<.001	0.04	.34	55.6	0.60

[a]AUC: area under the receiver operating characteristic curve.

[b]PC: primary care.

[c]BP: blood pressure.

[d]CX: cancer screening.

[e]DB: diabetes care.

Discussion

Key Findings

Outreach modality remains the key modifiable lever for influencing preventive care gap closure strategies. However, its impact is declining in the PC group across the 3 years, is marginal in the BP and CX group, and needs continued studies in the DB group to establish a trend and sustained evidence of association. In VBC, where outreach for gaps in care is conducted at scale, even smaller effect sizes are worth noting, as they highlight the need for ongoing research to further understand nuances between measure groups and outreach technology preferences for optimizing operational efficiencies.

Among the outreach methods, phone calls demonstrated a stronger positive impact on outcomes compared to chatbots. This may be attributed to the chatbot's deterministic, rule-based design, which lacks the interactivity and adaptability of more advanced artificial intelligence (AI)–powered conversational agents. These results are also in agreement with the recent findings from McDowell et al [20], who presented health communication preferences from their study to show that while the majority of participants preferred SMS text messaging communication in interactions with family and friends, their preference in communicating with health care providers was primarily by use of the phone call. Even though the chatbot design for this study was a web-based chat conversation, it was initiated through an SMS text message seeking consent for further communication. As noted by Fanaroff [21], SMS text messaging–based communication, though universally accessible, may face barriers in health communications due to privacy laws such as the HIPAA (Health Insurance Portability and Accountability Act)–related security constraints imposed during implementation, which can create barriers like requiring multiple clicks to get to the core of the message. This can erode patient trust in digital health technologies, especially as incidences of

XSL•FO
RenderX

SMS text message phishing attacks have increased in the last 5 years [22]. The 2023 diabetes group exception may point to a self-management culture within DB, suggesting potential for enhanced impact through digital engagement. It certainly points to a need for segmentation by measure groups when designing outreach strategies, as well as a need for further exploration of the underlying factors driving these emerging behavioral patterns.

Sustained PCP relationships more than doubled the odds of closing gaps in PC, reinforcing the understanding that it facilitates preventive measures and use in agreement with previous findings [23]. However, the effect reversed for diabetes in 2022, suggesting disease-specific pathways (eg, endocrinology follow-up may supplant the PCP role for glycemic monitoring). The lack of association between PCP relationships and BP, DB, and CX in the 2023 regression models suggests that outreach strategies should be customized by measure and specifically address the distinct impact of PCP relationships within each measure group.

Socioeconomic vulnerability appears to be an emerging barrier. The strengthening association and effect size for this covariate in the BP group over time suggest that an equity-focused resource allocation for hypertension is warranted. The association that emerged in the CX and DB groups in 2023 cannot be ignored. These results are consistent with evidence that shows neighborhood-level disadvantage suppresses screening adherence, with Montgomery et al [24] presenting one recent example of such evidence in a cancer cohort. However, the differential effect between third and fourth quartile participants in the PC group contradicts the usual linear-deprivation narrative. This highlights the need to study community-level resilience factors and changing attitudes toward PC since the 2020 pandemic.

Other demographic predictors had a relatively smaller impact. Race and ethnicity became significant variables for PC and CX outcomes in 2022 and 2023 with small effect sizes. Specifically, the positive direction of the OR for minority groups like Asians and Hispanics is surprising and suggests the need for further targeted research into culture-based practices that promote positive outcomes, so outreach strategies can be culturally tailored for better effectiveness. Gender effects in the PC group are consistently small but show higher odds of compliance among women, agreeing with prior findings [11]. In contrast, gender effects in the BP and DB groups are inconsistent across the 3 years, while interpretation within the CX group is limited due to 2 of its 3 measures being restricted to female participants.

The overall compliance rate difference between the various measure groups does indicate some weight for the burden of completion. For example, the BP measure can be completed with a single PCP visit during the year, whereas CX measures require multiple engagements with health care, which may include imaging appointments or laboratory work in addition to follow-up visits. Complex measures should be complemented with additional support or touchpoints for optimal outreach strategies.

Limitations

This study has several limitations that should be considered when interpreting the findings. First, although the analysis draws from a large sample of individuals with preventive care gaps, the retrospective observational design limits the explanatory power of the findings. Additionally, the outreach method distribution was not uniform across measure groups; for instance, email-only and multichannel outreach cohorts did not consistently meet inclusion thresholds, restricting comparative analyses within certain subgroups. Because outreach assignments followed operational workflows rather than randomization, some selection bias may exist. Exclusions for incomplete or low-volume subgroups were applied to ensure valid statistical testing and consistent data quality. While these steps may modestly limit generalizability, the retained sample remained representative of the health system's attributed population, supporting the internal validity of findings. Generalizability is therefore most applicable to similar real-world VBC settings.

An additional limitation of this study was the presence of unmeasured variables that may account for differences in the efficiency of outreach methods. Factors such as participants' language preference, digital literacy, barriers to completion, comorbidities, and other psychosocial or contextual influences were not consistently captured across all outreach methods, likely contributing to the limited variance explained by several models. Although classification accuracy was acceptable in some cases (eg, 78.6% for PC in 2021), lower performance metrics, including the area under the receiver operating characteristic curve (eg, 0.59 for CX in 2022), indicate potential model under specification. Future research should incorporate more granular clinical, behavioral, and sociodemographic variables to enhance understanding and optimization of outreach effectiveness.

Recommendations for Practice

Even though this is not a randomized trial, the findings from this study apply to a large representative population, therefore several practical recommendations can be made to enhance the design and implementation of outreach strategies for value-based cohorts. Phone calls consistently outperformed chatbots and multichannel campaigns in driving preventive care gap closure across most measure groups and years. Health systems should continue to prioritize phone-based outreach, particularly for high-impact measure groups such as PC, while evaluating digital methods as supplementary rather than primary channels until they are more effective or better personalized. The study highlights meaningful variations in outreach effectiveness by measure group and socioeconomic status. To maximize effectiveness, outreach strategies should be customized according to the specific clinical area and complexity of the care gap, such as differentiating approaches for PC, chronic disease management, and more complex screening measures. For example, the stronger performance of chatbot outreach in the DB group in 2023 suggests that measure-specific digital readiness may guide outreach channel selection.

We also recommend enhancing chatbots for better engagement. Chatbots are an emerging technology that offers better

XSL•FO
RenderX

scalability than phone calls. The rule-based design of the chatbot used in this study likely limited its effectiveness. Transitioning to more advanced, AI-powered conversational agents that support interactive dialogue and user personalization could improve patient engagement and outcomes [25].

Socioeconomic vulnerability was a significant and increasing barrier to care gap closure, particularly in the BP group. Health systems should adopt equity-focused outreach strategies that prioritize high-SVI communities for additional support, such as community health worker involvement or tailored messaging. This is especially important in measure groups with heavier burdens of completion, like CX or chronic disease monitoring.

The relatively low explanatory power of the models underscores the need to expand the range of included variables. Incorporating clinical data (eg, comorbidities and medication adherence), behavioral factors (eg, health beliefs and prior screening history), and social determinants of health (eg, transportation access and housing stability) could significantly enhance the precision of predictive models used to guide outreach prioritization.

Conclusion

In conclusion, this study found that there is variability in the effectiveness of chatbots in outperforming traditional outreach methods for preventive screenings. The findings confirm that outreach modality continues to be a key, modifiable factor in closing preventive care gaps, with phone-based outreach consistently outperforming chatbots and multichannel strategies across most measure groups. However, the effectiveness of each outreach method varied notably by clinical context and patient subgroup, highlighting the need for a segmented outreach design that accounts for differences in patient preferences, health conditions, and burden of gap completion. The limited effectiveness of deterministic, rule-based chatbots points to the potential value of transitioning to more adaptive, AI-enabled engagement tools, particularly those capable of personalized communication and responsiveness to digital literacy. Socioeconomic vulnerability remained a key barrier, with differing trends between the third and fourth SVI quartiles indicating that vulnerability is not a linear predictor of behavior. Incorporating structured data on preferences, barriers, and comorbidities will improve model accuracy. Future research using prospective, randomized designs should further evaluate outreach modality, language, and communication preferences to guide inclusive, high-impact preventive care.

Acknowledgments

The authors would like to recognize the contributions of Mathew Sabu for data cleaning, deidentification, and analysis support during the early stages of this study.

The authors would also like to acknowledge the use of artificial intelligence tools, such as the built-in Microsoft text editor and Grammarly, to refine and clarify text that was primarily written by humans in the preparation of this manuscript.

Funding

This study did not receive external funding. The analysis was conducted as part of an operational quality improvement initiative at Northwell Health and as a component of the author’s doctoral dissertation at Rutgers University, with academic oversight provided by faculty advisors.

Data Availability

The datasets analyzed in this study were derived from health system operational data and accessed under applicable data use agreements that restrict public dissemination, even in deidentified form. Due to such contractual, ethical, and governance constraints, the data are not publicly available. Access may be considered upon reasonable request to the corresponding author and is subject to approval by the data-owning institution and execution of an appropriate data use agreement.

Authors' Contributions

JC led the conceptualization and project administration of the study and was responsible for data curation, formal analysis, visualization, and writing of the original draft. Conceptualization and methodology were jointly contributed by JC, YJ, KS, KM, DK, MD, and LC. Investigation and interpretation of findings were conducted by JC, YJ, KS, and LC. Data curation and resources were supported by KS and DK. Supervision and methodological oversight were provided by YJ, LC, KM, and MD. Writing, review, and editing were performed by all authors. All authors reviewed and approved the final manuscript and agree to be accountable for all aspects of the work in accordance with the International Committee of Medical Journal Editors and CRediT taxonomy guidelines.

Conflicts of Interest

Some authors are employed by Northwell Health, which supported this study as part of internal evaluation and quality improvement activities. Other authors are affiliated with Rutgers University as doctoral student or faculty and contributed to the study

XSL•FO
RenderX

independently as part of academic research. None of the authors reports any financial conflicts of interest or competing interests related to the content of this manuscript.

Multimedia Appendix 1
Measure group volume of participants and gaps per year of study. Each cell lists participant volume with measure gaps volume in brackets (n).
[PNG File , 53 KB - medinform_v14i1e81370_app1.png]

Multimedia Appendix 2
Table S1: Distribution table for final analysis of PC group 2021-2023. Table S2: Distribution table for final analysis of BP group 2021-2023. Table S3: Distribution table for final analysis of CX group 2021-2023. Table S4: Distribution table for final analysis of DB group 2021-2023.
[XLSX File (Microsoft Excel File), 17 KB - medinform_v14i1e81370_app2.xlsx]

Multimedia Appendix 3
Compliance rate by measure group 2021-2023.
[PNG File , 25 KB - medinform_v14i1e81370_app3.png]

Multimedia Appendix 4
Table A: All Associations between covariates and outcome.
[XLSX File (Microsoft Excel File), 13 KB - medinform_v14i1e81370_app4.xlsx]

Multimedia Appendix 5
Eligibility criteria for each included measure for 2021-2023.
[DOCX File , 21 KB - medinform_v14i1e81370_app5.docx]

Multimedia Appendix 6
Distribution (%) of gaps by outreach method and measure group 2021-2023.
[PNG File , 29 KB - medinform_v14i1e81370_app6.png]

References

1. Value-based care. CMS. URL: https://www.cms.gov/priorities/innovation/key-concepts/value-based-care [accessed 2025-07-13]
2. Preventive health services. HealthCare.gov. 2025. URL: https://www.healthcare.gov/coverage/preventive-care-benefits/ [accessed 2025-07-13]
3. Figueroa JF, Duggan CE, Joynt Maddox KE. Value-based payment in Medicare: progress, challenges, and future directions. J Health Polit Policy Law 2025;50(6):1059-1079. [doi: 10.1215/03616878-11995200] [Medline: 40538335]
4. Seither R, Yusuf OB, Dramann D, Calhoun K, Mugerwa-Kasujja A, Knighton CL. Coverage with selected vaccines and exemption from school vaccine requirements among children in kindergarten - United States, 2022-23 school year. MMWR Morb Mortal Wkly Rep 2023;72(45):1217-1224 [FREE Full text] [doi: 10.15585/mmwr.mm7245a2] [Medline: 37943705]
5. Mykyta L, Cohen RA. Characteristics of adults aged 18-64 who did not take medication as prescribed to reduce costs: United States, 2021. NCHS Data Brief 2023(470):1-8 [FREE Full text] [Medline: 37314379]
6. Ma Z, Richardson LC. Cancer screening prevalence and associated factors among US adults. Prev Chronic Dis 2022;19:E22 [FREE Full text] [doi: 10.5888/pcd19.220063] [Medline: 35446757]
7. Murugesu L, Heijmans M, Rademakers J, Fransen MP. Challenges and solutions in communication with patients with low health literacy: perspectives of healthcare providers. PLoS One 2022;17(5):e0267782 [FREE Full text] [doi: 10.1371/journal.pone.0267782] [Medline: 35507632]
8. Coombs NC, Campbell DG, Caringi J. A qualitative study of rural healthcare providers' views of social, cultural, and programmatic barriers to healthcare access. BMC Health Serv Res 2022;22(1):438 [FREE Full text] [doi: 10.1186/s12913-022-07829-2] [Medline: 35366860]
9. Lieu TA, Elkin EP, Escobar PR, Finn L, Klein NP, Durojaiye C, et al. Effect of electronic and mail outreach from primary care physicians for COVID-19 vaccination of black and Latino older adults: a randomized clinical trial. JAMA Netw Open 2022;5(6):e2217004 [FREE Full text] [doi: 10.1001/jamanetworkopen.2022.17004] [Medline: 35713906]
10. Bickmore TW, Picard RW. Chatbots in health care: connecting patients to information. In: Health Technology and Informatics. Bethesda, MD: National Library of Medicine (US); 2023.
11. Chacko J, Mazza K, Stathakos K, Kim D, Carlo L. Evaluating technology-driven strategies for enhancing patient outreach for preventive care: a systematic review. Cureus 2025;17(2):e79467. [doi: 10.7759/cureus.79467] [Medline: 40130097]

XSL•FO
RenderX

12. Social Vulnerability Index. ATSDR. 2024. URL: https://www.atsdr.cdc.gov/place-health/php/svi/index.html [accessed 2026-01-22]
13. HUD USPS ZIP code crosswalk files. HUD USPS. URL: https://www.huduser.gov/portal/datasets/usps_crosswalk.html [accessed 2024-06-24]
14. Measures inventory. CMS.gov. 2025. URL: https://www.cms.gov/priorities/innovation/key-concepts/value-based-care [accessed 2025-07-13]
15. HEDIS measures. National Committee for Quality Assurance. 2025. URL: https://www.ncqa.org/hedis/measures/ [accessed 2025-07-13]
16. Microsoft Power BI desktop. Microsoft. 2025. URL: https://www.microsoft.com/en-us/power-platform/products/power-bi/desktop [accessed 2027-01-22]
17. IBM SPSS Statistics for Windows. IBM. Armonk, NY: IBM Corp URL: https://www.ibm.com/products/spss-statistics [accessed 2026-01-22]
18. McHugh ML. The chi-square test of independence. Biochem Med (Zagreb) 2013;23(2):143-149 [FREE Full text] [doi: 10.11613/bm.2013.018] [Medline: 23894860]
19. Peduzzi P, Concato J, Kemper E, Holford TR, Feinstein AR. A simulation study of the number of events per variable in logistic regression analysis. J Clin Epidemiol 1996;49(12):1373-1379 [FREE Full text] [doi: 10.1016/s0895-4356(96)00236-3] [Medline: 8970487]
20. McDowell B, Dumais KM, Gary ST, de Gooijer I, Ward T. Preferences and attitudes towards digital communication and symptom reporting methods in clinical trials. Patient Prefer Adherence 2025;19:255-263 [FREE Full text] [doi: 10.2147/PPA.S474535] [Medline: 39901901]
21. Fanaroff J. A high-tech wreck: HIPAA roadblocks to texting patients. J Perinatol 2025;45(2):271-272. [doi: 10.1038/s41372-024-02131-x] [Medline: 39354212]
22. Lindsey D, Sinkey R, Travers C, Budhwani H, Richardson M, Quinney R, et al. When HIPAA hurts: legal barriers to texting may reinforce healthcare disparities and disenfranchise vulnerable patients. J Perinatol 2025;45(2):278-281. [doi: 10.1038/s41372-024-02080-5] [Medline: 39147791]
23. Ibrahim R, Sainbayar E, Pham HN, Shahid M, Saleh AA, Javed Z, et al. Social Vulnerability Index and cardiovascular disease care continuum: a scoping review. JACC Adv 2024;3(7):100858 [FREE Full text] [doi: 10.1016/j.jacadv.2024.100858] [Medline: 39130018]
24. Montgomery KB, McLeod MC, DePalo DK, Dugan MM, Zager JS, Elleson KM, et al. Impact of social determinants of health on melanoma nodal surveillance in a multi-institutional cohort. Ann Surg Oncol 2025;32(3):1453-1462. [doi: 10.1245/s10434-024-16498-w] [Medline: 39576454]
25. Bhimani M, Baker RH, Ausin MS, Meixiong G, Lasko R, Raglow-Defranco M, et al. Using a multilingual AI care agent to reduce disparities in colorectal cancer screening for higher fecal immunochemical test adoption among Spanish-speaking patients: retrospective analysis. J Med Internet Res 2025;27:e71211 [FREE Full text] [doi: 10.2196/71211] [Medline: 40561471]

Abbreviations

AI: artificial intelligence
AUC: area under the receiver operating characteristic curve
BP: blood pressure
CMS: Centers for Medicare & Medicaid Services
CX: cancer screening
DB: diabetes care
EMR: electronic medical record
HEDIS: Healthcare Effectiveness Data and Information Set
HIPAA: Health Insurance Portability and Accountability Act
OR: odds ratio
PC: primary care
PCP: primary care provider
SVI: social vulnerability index
VBC: value-based care

XSL•FO
RenderX

Edited by A Benis; submitted 01.Aug.2025; peer-reviewed by C Wang, PS Olson; comments to author 07.Oct.2025; revised version received 07.Jan.2026; accepted 08.Jan.2026; published 12.Feb.2026.

Please cite as:
Chacko J, Jia Y, Stathakos K, Mazza K, Kim D, Diefenbach M, Carlo L
Chatbot Outreach in Value-Based Preventive Care: Retrospective Analysis
JMIR Med Inform 2026;14:e81370
URL: https://medinform.jmir.org/2026/1/e81370
doi:10.2196/81370
PMID:

©Jincy Chacko, Yuane Jia, Kimon Stathakos, Kathleen Mazza, Doran Kim, Michael Diefenbach, Lorena Carlo. Originally published in JMIR Medical Informatics (https://medinform.jmir.org), 12.Feb.2026. This is an open-access article distributed under the terms of the Creative Commons Attribution License (https://creativecommons.org/licenses/by/4.0/), which permits unrestricted use, distribution, and reproduction in any medium, provided the original work, first published in JMIR Medical Informatics, is properly cited. The complete bibliographic information, a link to the original publication on https://medinform.jmir.org/, as well as this copyright and license information must be included.

XSL•FO
RenderX

Development of a Practical Nomogram for Depression Risk Stratification in Older Adults With Hypertension and Diabetes: Retrospective Analysis of Data From the China Health and Retirement Longitudinal Study

Ting Peng, MD; Ying Zhang, MD; Rujia Miao*, MD; Jiangang Wang*, Prof Dr

Health Management Center, The Third Xiangya Hospital, Central South University, 138 Tongzipo Road, Yuelu District, Changsha, Hunan, China
*these authors contributed equally

Corresponding Author:
Jiangang Wang, Prof Dr
Health Management Center, The Third Xiangya Hospital, Central South University, 138 Tongzipo Road, Yuelu District, Changsha, Hunan, China

Abstract

Background: Depression affects over 40% of middle-aged and older Chinese adults living with both hypertension and diabetes, amplifying cardiovascular risk, functional decline, and mortality. Existing screening instruments—such as the 10-item Center for Epidemiologic Studies Depression Scale—focus narrowly on mood symptoms and are rarely feasible in busy primary care consultations. They also omit routine functional, cognitive, and social data that may jointly drive depressive states in cardiometabolic populations.

Objective: This study aimed to develop and validate a concise, clinically actionable nomogram that quantifies individual depression risk using readily available information in Chinese adults aged ≥45 years who have diagnosed hypertension and type 2 diabetes.

Methods: We analyzed anonymized wave 5 China Health and Retirement Longitudinal Study data collected between July 2020 and August 2020. Of 1504 eligible participants, 635 (42.2%) met the Center for Epidemiologic Studies Depression Scale cutoff score of >10 for probable depression. A total of 42 candidate predictors spanning demographics, laboratory values, comorbidities, functional status, and socioenvironmental factors were screened. Least absolute shrinkage and selection operator regression with 10-fold cross-validation identified the most parsimonious set. A multivariable logistic model was built on a 70% training set (n=1052) and evaluated on a 30% testing set (n=452). Performance was assessed using the area under the receiver operating characteristic curve (AUC), calibration plots, decision curve analysis, and Shapley additive explanations for interpretability. Multiple imputation was used to handle <20% missingness.

Results: Nine nonredundant predictors entered the final nomogram: activity of daily living score, memory impairment, number of pain sites, sleep duration, life satisfaction score, self-rated health score, social activity engagement score, retirement status, and memory test score. The model achieved excellent discrimination (training AUC=0.819; testing AUC=0.825) and calibration (mean absolute error ≤0.018). Decision curves demonstrated positive net clinical benefit across clinically relevant threshold probabilities. Shapley additive explanations analysis revealed a 3-fold increase in depression odds per 1-point increase in activity of daily living score, whereas retirement conferred substantial protection (prevalence of depression: 103/635, 16.2% in the retired group vs 269/869, 31.0% in the nonretired group; *P*<.001), mediated by greater social participation.

Conclusions: The 9-item nomogram enables <3-minute depression risk stratification in resource-limited primary care settings for adults with hypertension and diabetes. Functional decline, affective-cognitive burden, and socioeconomic disengagement constitute the dominant causal pathway. Prospective trials should examine whether interventions targeting postretirement social engagement and functional rehabilitation can reduce incident depression in this high-risk population.

(JMIR Med Inform 2026;14:e81529) doi:10.2196/81529

KEYWORDS

depression risk prediction; hypertension; diabetes; activities of daily living; nomogram

XSL•FO
RenderX

Introduction

Depression imposes an additional burden on people living with chronic conditions, especially among middle-aged and older adults who are trying to manage both high blood pressure and diabetes [1]. These physical illnesses often appear together with depressive symptoms, making treatment harder and speeding up the loss of daily function [2]. Studies have shown that, in this group, the rate of depression can reach more than 40% in some samples, and it is linked to poorer treatment adherence, higher heart-related risks, and greater chances of early death [3,4]. Even though depression is clearly important, it is still missed in many primary care visits [5]. The screening tools we have are reliable on paper, but they are hard to fit into busy clinics because of limited time and other practical barriers. The 10-item version of the Center for Epidemiologic Studies Depression Scale (CESD-10), widely used in Chinese-speaking populations, is a good example: when used alone, it cannot draw on the wider set of clinical, behavioral, and social clues that would help physicians spot depression earlier [6,7].

Most earlier models for predicting depression were built for people receiving psychiatric care or used general risk factors, so they do not work well for people who also have long-term illnesses [8,9]. A key weakness is that these models rarely include measures of daily function, such as the ability to bathe, dress, cook, and handle money, together with behavioral and social factors [10]. This omission matters because poor physical function can be both an early sign of depression and a result of uncontrolled blood pressure or blood sugar, making it hard to know which came first [11]. For these reasons, we set out to create a simple, practical tool to estimate depression risk in middle-aged and older adults with hypertension and diabetes. Using data from the China Health and Retirement Longitudinal Study (CHARLS), we examined 42 possible predictors covering medical, psychological, and social areas. Using a logistic regression model improved through machine learning and checked through several validation steps, we carried out 3 tasks: choosing the smallest set of predictors that still separates high-risk from low-risk individuals; turning these predictors into a clear, easy-to-use score that can be applied in busy, low-resource clinics; and showing, with numbers, how much heart- and metabolism-related functional problems act as a link between illness and depression. Rather than focusing only on symptoms, our approach places depression risk within the patient's overall health picture. The resulting model can guide clinicians and also point to potentially modifiable risk factors.

Methods

Ethical Considerations

This study used anonymized data from the fifth wave of the CHARLS. The project was approved by the Peking University Biomedical Ethics Committee in June 2008 (approval IRB00001052–11015). All personal identifiers were removed before our analysis. Patients and the public were not involved in the design, conduct, reporting, or dissemination of this research. All participants provided written informed consent, and the study followed the ethical principles set out in the Declaration of Helsinki. No financial or material compensation was offered to study participants.

Study Population

We carried out a retrospective study using data from the fifth wave of the CHARLS collected between July 2020 and August 2020. Participants had to be aged at least 45 years and have both hypertension and diabetes. We excluded anyone who was missing key details such as CESD-10 score, diagnosis of hypertension or diabetes, or age. After these exclusions, 1504 people were left for the analysis. Depression status was based on the CESD-10, a brief questionnaire that mixes positively and negatively worded statements. Each item is scored from 0 to 3, yielding total scores from 0 to 30; higher scores mean more severe depressive symptoms [12,13]. In Chinese older adults, a score above 10 is generally taken to indicate possible depression, and this cutoff has been shown to work well in previous studies and in latent profile analyses [13,14]. Using this cutoff, of the 1504 participants, we labeled 635 (42.2%) as the depression group and 869 (57.8%) as the nondepression group.

Candidate Predictor Variables

Guided by earlier studies and clinical practice, we chose 42 factors that might relate to depression risk [15-17]. These factors cover basic personal details, overall health, daily habits, blood test results, and how well people manage daily tasks. The full list is as follows: sex, age, marital status, smoking status, drinking status, cancer, lung disease, heart disease, stroke, mental illness, arthritis, high blood fat, liver disease, kidney disease, stomach disease, asthma, memory problems, hip fracture, number of painful body sites, exercise level, sleep hours, social activity engagement, whether the patient was retired, medical insurance, pension insurance, years of schooling, household size, number of living children, household income, recent physician visits, memory test score, activity of daily living (ADL) score, instrumental ADL (IADL) score, self-rated health, and satisfaction with life. Regarding "social activity engagement," it was categorized into the following eight types: (1) interacted with friends (visiting friends or socializing with friends); (2) played mahjong, played chess, played cards, or went to community clubs; (3) provided help to family members, friends, or neighbors who do not live with the participant and who did not pay them for the help; (4) went to a sports, social, or other type of club; (5) took part in community-related organization activities; (6) did voluntary or charity work; (7) attended an educational or training course; and (8) other.

Participants completed the questionnaire based on their actual situation: participation in 1 type of the above activities was recorded as "1," participation in 2 types was recorded as "2," and a higher count indicated a higher level of social activity engagement of the participant. For "life satisfaction," the CHARLS survey asked respondents about their overall satisfaction with their lives, with 5 response options: "extremely satisfied," "very satisfied," "relatively satisfied," "not very satisfied," and "not satisfied at all." For the convenience of statistical analysis, we assigned numerical values to these levels: "1" represented "not satisfied at all," "5" represented "extremely

XSL•FO
RenderX

satisfied," and so on, with each level corresponding to a specific number.

Model Construction Methods

We used least absolute shrinkage and selection operator (LASSO) regression to pick out the most useful risk factors while keeping the list short. Ten-fold cross-validation helped us find the best penalty value (λ). We then split the data into a training set (1052 people) and a testing set (452 people) in a 7:3 ratio. The training set was used to find the key factors linked to depression. These factors were entered into a standard logistic regression, and we drew a simple chart (nomogram) to show how each one affected the risk of depression. To keep the model easy to use, we removed predictors with little impact, reran the logistic regression with the remaining ones, and built the final nomogram.

Model Evaluation Methods

To check how well the model performed, we used receiver operating characteristic curves and the area under these curves (AUC) to measure overall ability to separate people with and without depression, calibration plots to check whether the predicted chances matched what really happened, and decision curve analysis to weigh the benefits of true positive predictions against the harms of false ones, giving a clear picture of both accuracy and clinical value.

Model Interpretation Methods

To make the model easier to understand, we used Shapley additive explanations (SHAP) values to show how much each factor mattered. We drew 4 simple charts (an overall importance plot, a swarm plot, a waterfall plot, and a force plot) that displayed how every factor pushed the risk of depression up or down. These pictures help readers see which factors carry the most weight and how they work together in the model.

Data Processing Methods

All statistical analyses and figure generation were performed using R (R Foundation for Statistical Computing). When less than 20% of the data were missing, we used the *mice* package to run 5 rounds of imputation and kept the set that best matched the overall pattern. We report counts and percentages for categorical variables and means with SDs for continuous variables. We compared groups using 2-tailed *t* tests, chi-square tests, or nonparametric tests as needed; the latter were chosen when the data did not follow the rules for parametric tests. A *P* value <.05 was considered statistically significant.

Results

Flowchart

The study flowchart is presented in Figure 1.

XSL•FO
RenderX

Figure 1. Study flowchart. Analysis of China Health and Retirement Longitudinal Study (CHARLS) wave 5 participants with hypertension and diabetes comorbidity (aged ≥45 years). DCA: decision curve analysis; LASSO: least absolute shrinkage and selection operator; ROC: receiver operating characteristic; SHAP: Shapley additive explanations.

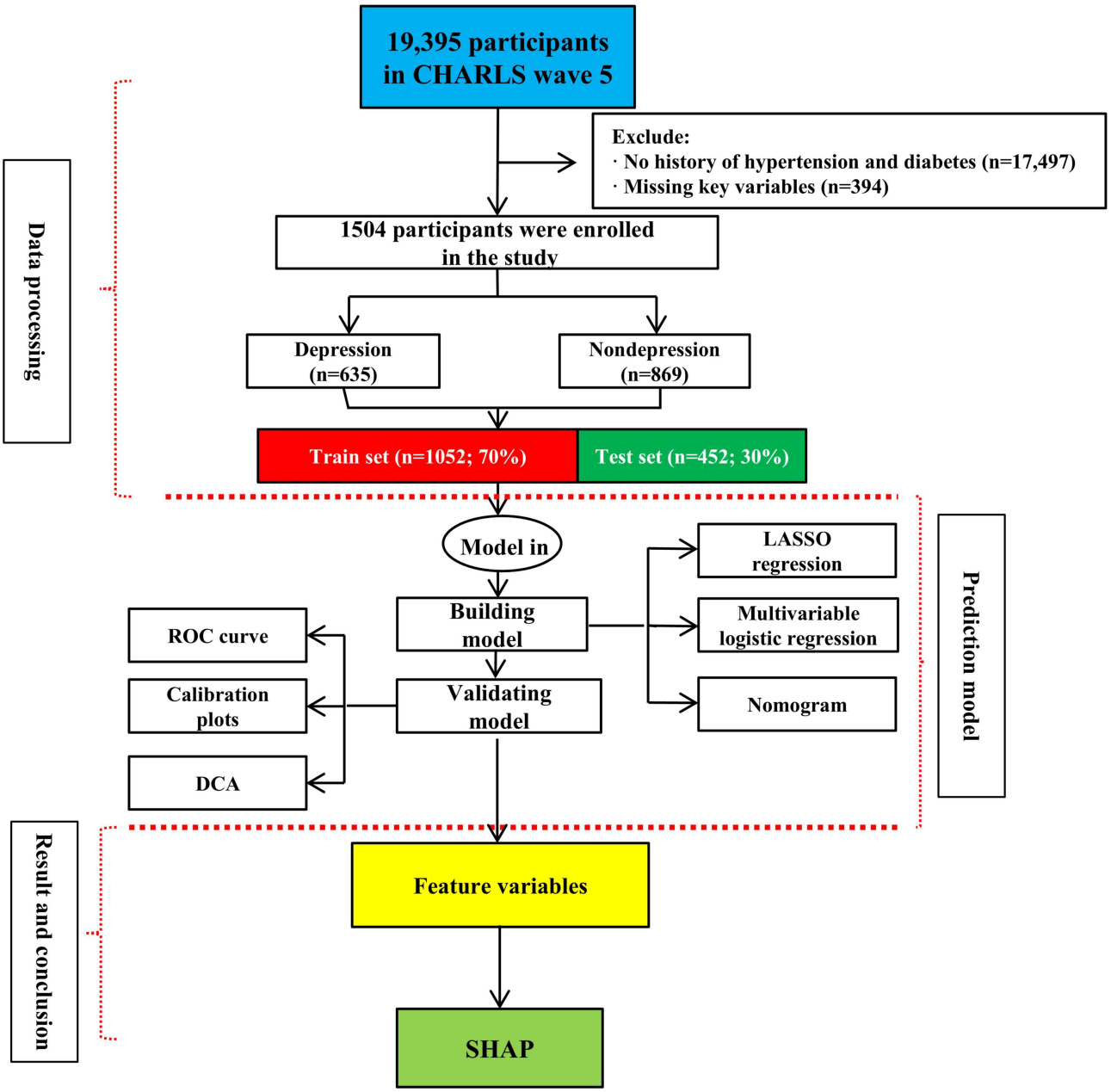

Baseline Characteristics

We included 1504 adults with an average age of 65.99 (SD 8.28) years and 64.93 (SD 8.72) years for those with and without depression, respectively; 678 (45.1%) were men, and 826 (54.9%) were women. Of these 1504 participants, 635 (42.2%) were classed as having possible depression, and 869 (57.8%) were classed as nondepressed. Table 1 shows that the 2 groups differed on many key points. Those with possible depression were more often women, widowed or separated, and less active and reported more illnesses, such as lung disease, heart disease, stroke, arthritis, mental illness, liver disease, kidney disease, stomach disease, asthma, hip fracture, and memory problems. They also had more pain sites; poorer sleep; lower income; fewer years of schooling; smaller households; more physician visits; fewer social activities; and lower scores on memory, daily activities, self-rated health, and life satisfaction (P<.05 in all cases).

XSL•FO
RenderX

Table . Baseline characteristics of study participants by depression status. *P* values were calculated using *t* tests, chi-square tests, or nonparametric tests as appropriate. A *P* value of <.05 was considered statistically significant.

Characteristic	Nondepression (n=869)	Depression (n=635)	*P* value
Medical insurance, n (%)	834 (96.0)	608 (95.7)	.93
Pension insurance, n (%)	765 (88.0)	543 (85.5)	.17
Exercise, n (%)	793 (91.3)	548 (86.3)	.003
Retired, n (%)	269 (31.0)	103 (16.2)	<.001
Sex (male), n (%)	463 (53.3)	215 (33.9)	<.001
Married, n (%)	746 (85.8)	504 (79.4)	.001
Hip fracture, n (%)	9 (1.0)	13 (2.0)	.16
Cancer, n (%)	30 (3.5)	24 (3.8)	.84
Lung disease, n (%)	120 (13.8)	156 (24.6)	<.001
Heart disease, n (%)	326 (37.5)	339 (53.4)	<.001
Stroke, n (%)	98 (11.3)	136 (21.4)	<.001
Psychiatric disease, n (%)	25 (2.9)	58 (9.1)	<.001
Arthritis, n (%)	324 (37.3)	389 (61.3)	<.001
Dyslipidemia, n (%)	572 (65.8)	457 (72.0)	.01
Liver disease, n (%)	90 (10.4)	107 (16.9)	<.001
Kidney disease, n (%)	144 (16.6)	174 (27.4)	<.001
Stomach disease, n (%)	261 (30.0)	265 (41.7)	<.001
Asthma, n (%)	55 (6.3)	85 (13.4)	<.001
Memory problems, n (%)	47 (5.4)	97 (15.3)	<.001
Vigorous physical activity, n (%)	237 (27.3)	193 (30.4)	.21
Moderate physical activity, n (%)	474 (54.5)	319 (50.2)	.11
Light physical activity, n (%)	727 (83.7)	482 (75.9)	<.001
Drinking, n (%)	318 (36.6)	142 (22.4)	<.001
Smoking, n (%)	203 (23.4)	95 (15.0)	<.001
Hospitalization in the previous year, n (%)	241 (27.7)	266 (41.9)	<.001
Recent physician visits, n (%)	227 (26.1)	220 (34.6)	<.001
Total income, mean (SD)	¥54,055.20 (US $7858.73; ¥79,512.32 [US $10,687.50])	¥32,470.65 (US $4720.71; ¥88,119.77 [US $12,811.20])	<.001
Family size (number of individuals), mean (SD)	2.88 (1.56)	2.58 (1.40)	<.001
Number of healthy children, mean (SD)	2.37 (1.25)	2.69 (1.21)	<.001
Financial support from children to parents, mean (SD)	¥6984.23 (US $1015.40; ¥15,871.02 [US $2307.39])	¥5448.44 (US $792.12; ¥8541.60 [US $1241.81])	.03
Financial support from parents to children, mean (SD)	¥9176.07 (US $1334.05; ¥49,285.04 [US $7165.26])	¥4270.93 (US $620.93; ¥21,830.53 [US $3173.81])	.02
Self-rated health score (1-5), mean (SD)	2.82 (0.90)	2.18 (0.89)	<.001
Life satisfaction score (1-5), mean (SD)	3.41 (0.66)	2.87 (0.87)	<.001
Number of pain sites, mean (SD)	2.11 (3.01)	4.53 (4.35)	<.001
Sleep duration (h), mean (SD)	6.21 (1.68)	5.27 (2.06)	<.001

XSL•FO
RenderX

Characteristic	Nondepression (n=869)	Depression (n=635)	*P* value
Social activity engagement (number of activities participated in), mean (SD)	0.94 (1.14)	0.65 (0.90)	<.001
Age (y), mean (SD)	64.93 (8.72)	65.99 (8.28)	.02
Educational level[a], mean (SD)	2.26 (1.11)	1.85 (1.02)	<.001
Total MET[b] (min), mean (SD)	4627.13 (4936.56)	4832.40 (5150.61)	.43
Memory score (0-11), mean (SD)	4.51 (1.74)	3.61 (1.84)	<.001
ADL[c] score (0-6), mean (SD)	0.34 (0.85)	1.20 (1.60)	<.001
IADL[d] score (0-5), mean (SD)	0.32 (0.84)	1.18 (1.50)	<.001

[a]Educational level was scored as follows: 1=illiterate; 2=below junior high school; 3=junior high school and above, below university; 4=university and above.

[b]MET: metabolic equivalent of task.

[c]ADL: activity of daily living.

[d]IADL: instrumental ADL.

Results of Model Construction

As the regularization strength (λ) increases, the model error initially decreases and then increases. We chose the simplest model within 1 SE of the minimum error. This left 16 variables whose coefficients stayed above 0 (Figure 2A). Each line in the plot shows one variable's coefficient; as λ grows (moving right), many lines drop to 0 and are removed. In the end, 16 factors remained: life satisfaction score, sleep hours, self-rated health score, IADL score, memory score, pain sites, ADL score, retirement status, arthritis, sex, memory problems, social activity engagement type, recent physician visits, stroke, years of schooling, and heart disease, listed from most to least important (Figure 2C). Figure 2D shows the direction of each factor: red bars mean higher risk, and blue bars mean lower risk.

Figure 2. Predictor selection using least absolute shrinkage and selection operator (LASSO) regression. (A) Cross-validation plot showing the relationship between the regularization parameter (λ) and model deviance. The vertical dashed line indicates the optimal λ value (minimum λ+1 SE). (B) LASSO coefficient path plot showing how variable coefficients shrink toward 0 as λ increases. (C) Ranking of the 16 selected predictors based on their standardized regression coefficients. (D) Coefficient direction plot indicating risk (red=positive coefficient) and protective (blue=negative coefficient) factors for depression. Act: social activity engagement; ADL: activity of daily living; DA: number of pain sites; IADL: instrumental ADL; memrye: memory problems; satlife: life satisfaction score; SRH: self-rated health score.

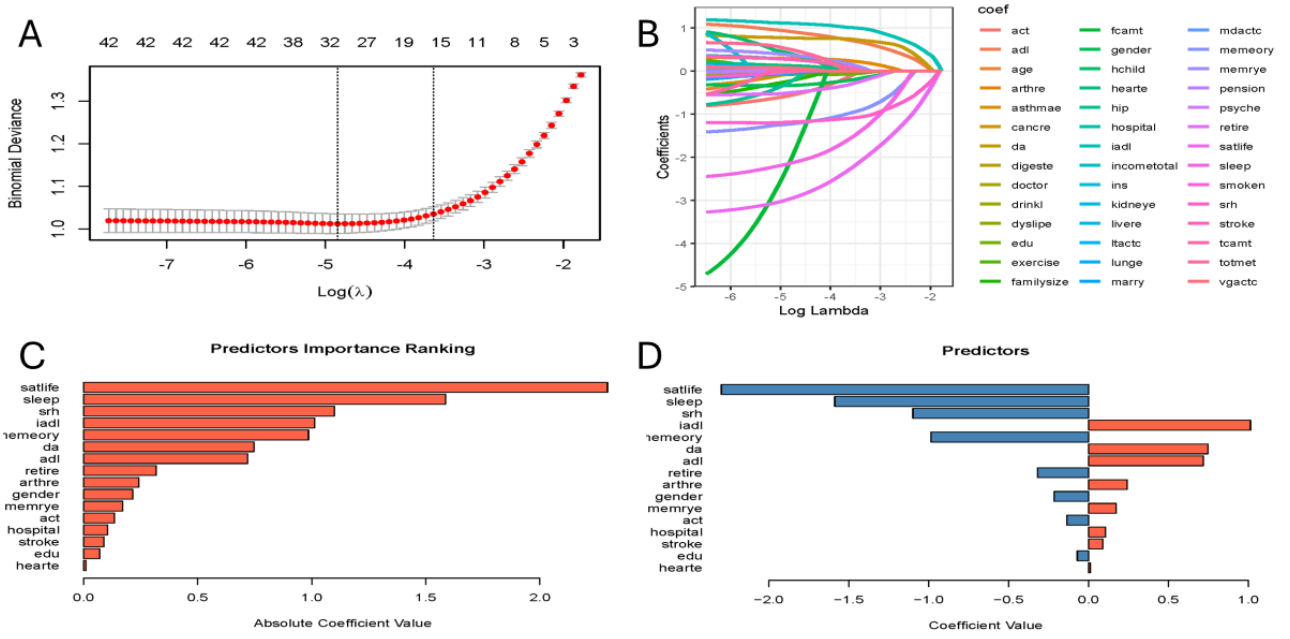

We took the 16 variables and ran them together in a new regression model and then drew a simple point chart (nomogram). The chart showed which factors mattered the most so that we could drop the weaker ones. After this step, 9 factors remained: retirement status, self-rated health score, life satisfaction score, number of pain sites, sleep hours, social activity engagement type, memory score, ADL score, and memory-related disease. We put these 9 factors into a final regression and built the last nomogram (Figure 3). On the chart, each line shows how many points a person obtains for that

XSL•FO
RenderX

factor; the bottom scale turns the total points into the chance of depression. Higher total points mean higher risk.

Figure 3. Nomogram for predicting depression risk. The nomogram was constructed using 9 predictors selected from multivariate logistic regression. Each predictor is assigned a point value based on its regression coefficient. The total score corresponds to the predicted probability of depression in the bottom scale. Higher total scores indicate a higher risk of depression. Act: social activity engagement; ADL: activity of daily living; DA: number of pain sites; memrye: memory problems; satlife: life satisfaction score; SRH: self-rated health score.

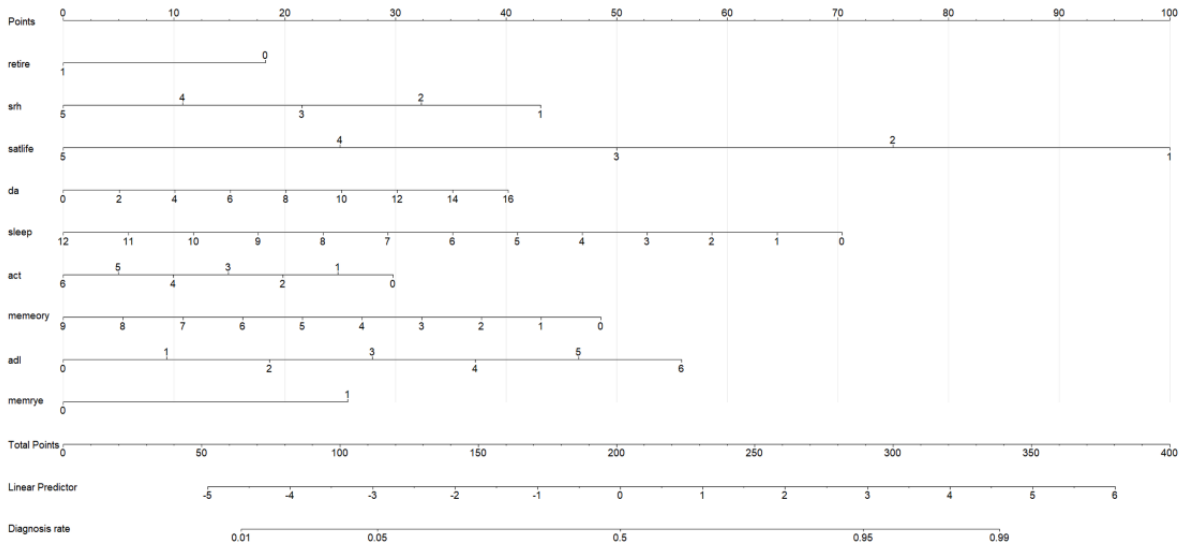

Results of Model Evaluation

We tested how well the model separated people with and without depression using the AUC. In the training data (Figure 4A), the AUC was 0.819, and in the testing data (Figure 4D), it was 0.825, showing good discrimination. The predicted probabilities matched the real outcomes closely in both sets; the average error was only 0.006 in training (Figure 4B) and 0.018 in testing (Figure 4E). Decision curve analysis (Figures 4C and 4F) also showed clear clinical benefit: the model yielded much larger net benefits than the "treat all" or "treat none" approaches. Overall, the nomogram was accurate and clinically useful.

Figure 4. Evaluation of the predictive model. (A) Receiver operating characteristic (ROC) curve and area under the curve (AUC) value in the training set (AUC=0.819). (B) Calibration plot in the training set (mean absolute error=0.006). (C) Decision curve analysis (DCA) in the training set. (D) ROC curve and AUC value in the testing set (AUC=0.825). (E) Calibration plot in the testing set (mean absolute error=0.018). (F) DCA in the testing set. The model demonstrates strong discriminative ability, good calibration, and high clinical utility in both datasets.

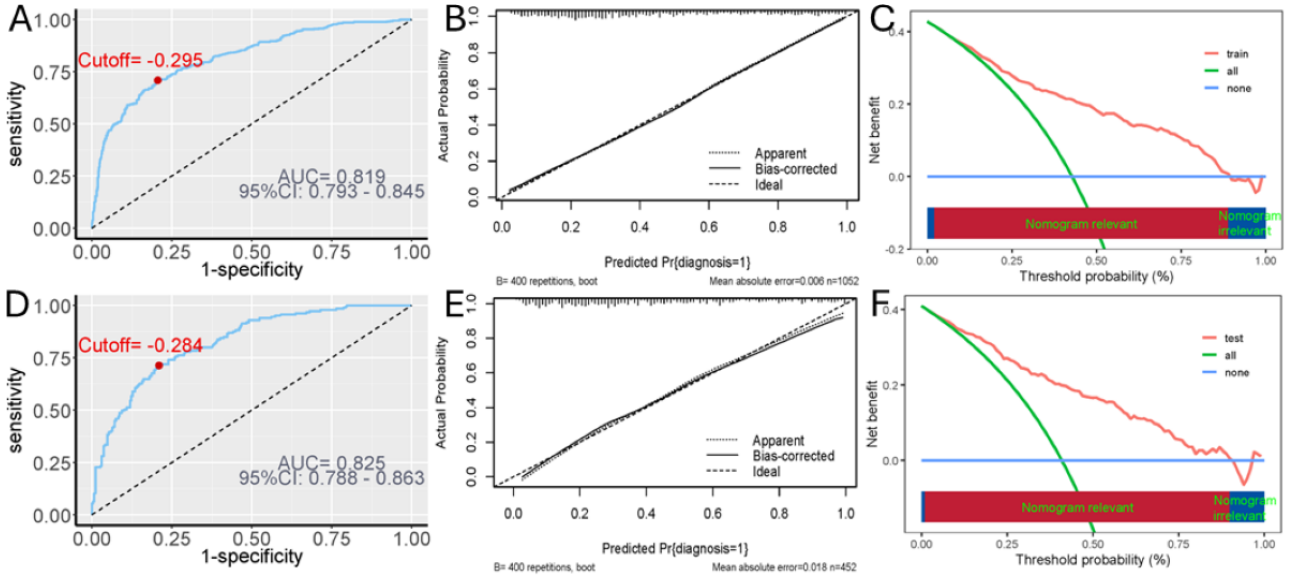

Results of Model Interpretation

We used SHAP values to look at the 9 main variables. Global and swarm plots (Figure 5A-B) show how each variable affects the entire sample. ADL score, memory problems, and number of pain sites pushed the risk upward, whereas retirement status, social activity engagement type, sleep hours, life satisfaction score, self-rated health score, and memory score pushed it

XSL•FO
RenderX

downward. To see how these factors worked for individual people, we picked 2 participants at random and used waterfall and force plots (Figure 5C-D) to show each factor's exact contribution.

Figure 5. Shapley additive explanations (SHAP) analysis of the final model. (A) Global SHAP importance plot showing the average impact of each feature on model predictions. (B) SHAP swarm plot illustrating the distribution of SHAP values for each feature across all participants (red=increased risk; blue=decreased risk). (C) Waterfall plot for a randomly selected individual showing the contribution of each feature to the final prediction. (D) Force plot for another individual, highlighting the cumulative effect of features on the predicted probability of depression. Positive SHAP values (red) increase the risk of depression, whereas negative values (blue) decrease it. Act: social activity engagement; ADL: activity of daily living; DA: number of pain sites; memrye: memory problems; satlife: life satisfaction score; SRH: self-rated health score.

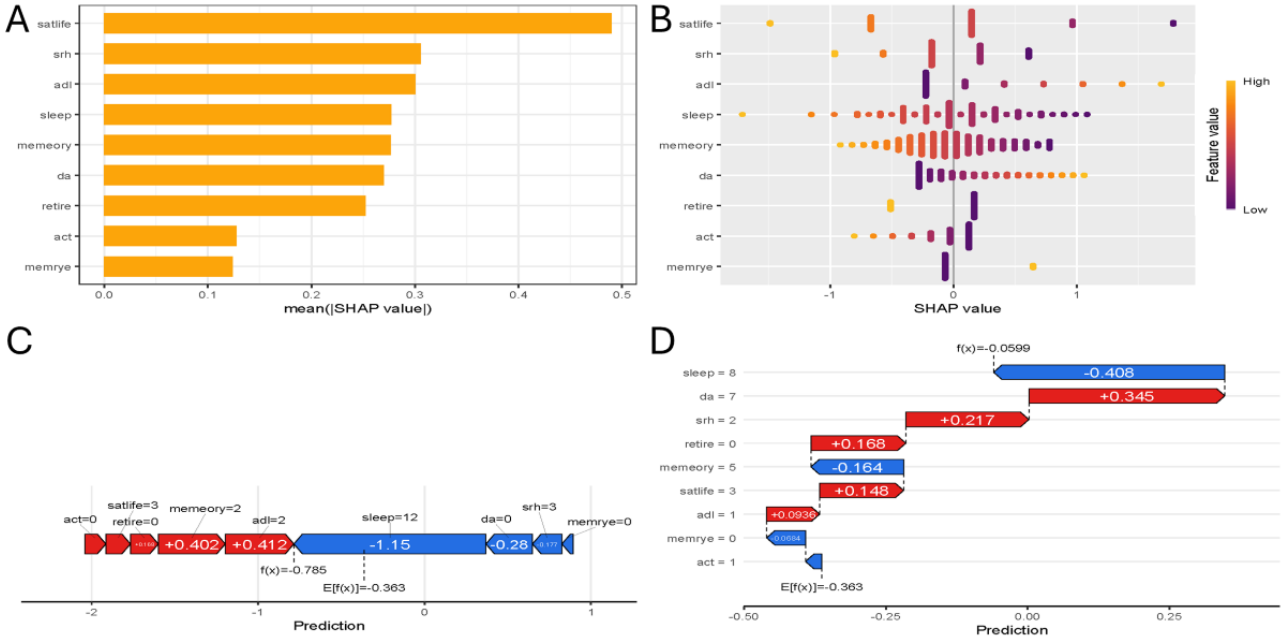

Discussion

Principal Findings

This study establishes a clinically operable prediction model for depression risk among middle-aged and older patients with hypertension and diabetes, leveraging multidimensional predictors to achieve robust discrimination (AUC=0.819 - 0.825) and calibration (mean absolute error≤0.018). Nine core variables emerged as significant predictors in the final nomogram: ADL score, memory disorders, number of pain sites, sleep duration, life satisfaction score, self-rated health score, social activity engagement, retirement status, and memory score. The centrality of functional impairment as a mechanistic pathway is underscored by the ADL score's dominant predictive role [18,19], where individuals with depression exhibited markedly elevated scores (mean 1.20, SD 1.60 vs mean 0.34, SD 0.85; *P*<.001). Each unit increase in ADL score corresponded to a 3-fold increase in depression risk, particularly at critical thresholds beyond ADL score ≥2. Retirement status provided substantial protection against depression [19,20], with prevalence rates nearly halved among retirees (103/635, 16.2%) compared to nonretirees (269/869, 31.0%; *P*<.001) mediated by significantly greater social participation (mean activity score 0.94, SD 1.14 vs mean 0.65, SD 0.90; *P*<.001). SHAP value distributions (Figure 5A-B) corroborated a triadic pathogenesis framework. First, functional autonomy erosion (ADL and IADL decline interacting with multisite pain) imposes physical constraints that amplify helplessness [21,22]. Second, affective-cognitive burden manifests through memory disorders (there were memory disorders in 97/635, 15.3% vs 47/869, 5.4% of participants with and without depression, respectively; *P*<.001), and reduced life satisfaction (mean score 2.87, SD 0.87 vs mean score 3.41, SD 0.66 among participants with and without depression; *P*<.001) depletes emotional reserves [23]. Third, socioeconomic disengagement was evidenced by significantly lower household incomes among participants with depression (mean ¥32,470.65 [US $4720.71], SD ¥88,119.77 [US $12,811.20] vs mean ¥54,055.20 [US $7858.73], SD ¥79,512.32 [US $10,687.50], respectively; *P*<.001), constraining access to health-promoting resources [24,25]. The nonlinear inflection point observed in the ADL-depression relationship indicates that moderate functional decline triggers disproportionately severe psychological sequelae, offering an identifiable intercept for targeted interventions [26].

These findings advance beyond prior depression prediction paradigms in several critical dimensions. Traditional screening instruments reliant on mood-based symptomatology such as the Patient Health Questionnaire series demonstrate limited applicability in cardiometabolic populations due to diagnostic circularity: they cannot resolve whether fatigue or anhedonia stems from depression vs underlying chronic disease pathology [27,28]. Our model effectively dissociates these confounds by operationalizing ADLs as an independent construct validated through SHAP's feature dissociation capability. For instance, while arthritis prevalence was markedly higher among participants with depression (389/635, 61.3% vs 324/869, 37.3%; *P*<.001), LASSO selected number of pain sites rather than arthritis diagnosis as the principal pain predictor due to its ability to quantify functional impact severity [29]. When

XSL•FO
RenderX

benchmarked against models with similar AUC values to those of the model evaluated in this study, such as the depressive symptom predictor by Zheng et al [30,31], our algorithm demonstrates superior translational efficiency by using information already captured in routine chronic disease management ADL documentation during nursing assessments, medication review for memory issues, and social history documenting retirement status. This obviates the need for additional screening instruments, reducing assessment time to under 3 minutes. Moreover, we identify novel modifiable pathways absent in prior frameworks. The protective effect of retirement when linked to sustained social activity engagement reveals life transitions as windows for resilience-building interventions [32]. Enhancing life satisfaction emerged as another actionable leverage point given its strong negative association with depression (β=−0.63 via LASSO), suggesting that psychosocial enrichment may disrupt pathogenic cascades more effectively than purely biomedical approaches [33].

Methodologically, the integration of LASSO regression with SHAP value interpretation constitutes a primary strength. LASSO refined the predictor pool from 42 candidates to 9 nonredundant variables, efficiently eliminating noncontributory markers such as cancer or lung disease. SHAP analysis then transformed statistical coefficients—for example, the negative β value for retirement (−0.89)—into clinically interpretable narratives. At an individual level (Figure 5D), retirees maintaining active social roles exhibited an 18-fold depression risk reduction compared to their socially isolated counterparts. The CHARLS cohort's population representativeness further enhances generalizability to China's aging cardiometabolic patient demographic. Four principal limitations warrant acknowledgment. Due to the cross-sectional nature of wave 5 CHARLS data, causal precedence between functional decline and depression could not be definitively established. However, the biological gradient observed in ADL risk proportionality (higher scores predicting depression probability stepwise) lends credibility to functional deterioration as a driver rather than a secondary consequence [34,35]. Second, depression ascertainment using a CESD-10 score >10 may overlook subsyndromal presentations, potentially underestimating risk in highly functional individuals [36]. Third, unmeasured variables influencing both pathways, particularly medication adherence patterns or pharmacodynamic interactions between psychotropics and antihypertensives, were unaccounted for. Finally, sociocultural proxies unique to Chinese aging populations' children's financial support demonstrating borderline significance (*P*=.02-.03) were excluded from the final model despite their potential clinical relevance [37]. Future iterations should address this through culturally adapted predictor sets.

This study was conducted based on statistical data from the CHARLS database. Therefore, the results of this study have limitations in terms of applicability to young and middle-aged populations, as well as populations from different regions and ethnic groups. In future research, we may consider combining data from public databases in the Americas, Europe, and other regions to conduct joint modeling, thereby improving the generalization performance of the model. These findings suggest priority areas for future research and clinical application. Longitudinal analyses using multiwave CHARLS data should test the proposed retirement–social engagement–protection pathway, examining whether weekly social activity sustains resilience to depressive symptoms. A 3-tier risk stratification protocol based on nomogram scores may guide care: individuals scoring ≤150 can continue annual screening; those scoring 150 to 250 should receive functional preservation strategies, including task-oriented exercise and cognitive behavioral approaches to improve ADLs, sleep, and social engagement; and those scoring ≥250 would require multidisciplinary management due to high comorbidity. Embedding this algorithm into electronic health records within China's National Essential Public Health Service Package could enable automated alerts when thresholds are met. Pilot programs should focus on communities where the baseline ADL score is ≥1.5; in this study, 51.2% (325/635) of participants with depression were in this category. Randomized trials are needed to evaluate mediator-targeted interventions, including combined ADL and pain management, structured postretirement social role adaptation, and hemoglobin A_{1c}–stratified memory screening in diabetes. Targeting domain-specific vulnerabilities rather than symptoms alone may reduce depression incidence while optimizing primary care resources.

Conclusions

We developed and validated a depression risk model for middle-aged and older adults with hypertension and diabetes. The nomogram, integrating 9 routinely collected predictors, including ADL score, memory impairment, and pain burden, showed strong discrimination and calibration. Depression risk rose 3-fold for each unit increase in ADL score, whereas retirement was protective. Functional impairment, emotional cognitive burden, and socioeconomic disadvantage formed the dominant risk pathway. LASSO-SHAP integration streamlined predictor selection, enabling screening in under 3 minutes. Prospective trials should test interventions targeting postretirement social engagement and functional rehabilitation, alongside implementing a 3-tier risk stratification protocol in primary care. Targeting these domain-specific risks could reduce depression incidence.

Acknowledgments

The authors are grateful to all the participants and staff of the China Health and Retirement Longitudinal Study.

XSL•FO
RenderX

Funding

This study was funded by the Chinese Cardiovascular Association-ASCVD Fund (2023-CCA-ASCVD-018), the Project of State Key Clinical Department (Z2023058), and the Natural Science Foundation of Hunan Province (2025JJ90208).

Data Availability

The datasets generated or analyzed during this study are available from the corresponding author on reasonable request.

Authors' Contributions

TP contributed to data curation and writing—original draft. YZ managed writing—review and editing. JW and RM managed writing—review and editing.

Conflicts of Interest

None declared.

References

1. Bi YH, Pei JJ, Hao C, Yao W, Wang HX. The relationship between chronic diseases and depression in middle-aged and older adults: a 4-year follow-up study from the China Health and Retirement Longitudinal Study. J Affect Disord 2021 Jun 15;289:160-166. [doi: 10.1016/j.jad.2021.04.032] [Medline: 33984686]
2. Hairi NN, Bulgiba A, Mudla I, Said MA. Chronic diseases, depressive symptoms and functional limitation amongst older people in rural Malaysia, a middle income developing country. Prev Med 2011 Oct;53(4-5):343-346. [doi: 10.1016/j.ypmed.2011.07.020] [Medline: 21864564]
3. Lam MI, Chen P, Xie XM, et al. Heart failure and depression: a perspective from bibliometric analysis. Front Psychiatry 2023 Mar 2;14:1086638. [doi: 10.3389/fpsyt.2023.1086638] [Medline: 36937736]
4. Hare DL, Toukhsati SR, Johansson P, Jaarsma T. Depression and cardiovascular disease: a clinical review. Eur Heart J 2014 Jun 1;35(21):1365-1372. [doi: 10.1093/eurheartj/eht462] [Medline: 24282187]
5. Mitchell AJ, Vaze A, Rao S. Clinical diagnosis of depression in primary care: a meta-analysis. Lancet 2009 Aug 22;374(9690):609-619. [doi: 10.1016/S0140-6736(09)60879-5] [Medline: 19640579]
6. Zhang Y, Ting RZW, Lam MHB, et al. Measuring depression with CES-D in Chinese patients with type 2 diabetes: the validity and its comparison to PHQ-9. BMC Psychiatry 2015 Aug 18;15:198. [doi: 10.1186/s12888-015-0580-0] [Medline: 26281832]
7. Chin WY, Choi EPH, Chan KTY, Wong CKH. The psychometric properties of the Center for Epidemiologic Studies Depression Scale in Chinese primary care patients: factor structure, construct validity, reliability, sensitivity and responsiveness. PLoS ONE 2015 Aug 7;10(8):e0135131. [doi: 10.1371/journal.pone.0135131] [Medline: 26252739]
8. Tan J, Ma C, Zhu C, et al. Prediction models for depression risk among older adults: systematic review and critical appraisal. Ageing Res Rev 2023 Jan;83:101803. [doi: 10.1016/j.arr.2022.101803] [Medline: 36410622]
9. Jin H, Wu S, Di Capua P. Development of a clinical forecasting model to predict comorbid depression among diabetes patients and an application in depression screening policy making. Prev Chronic Dis 2015 Sep 3;12:E142. [doi: 10.5888/pcd12.150047] [Medline: 26334714]
10. Karpouzian-Rogers T, Dworak EM, Bucko P, et al. Measures of decision-making ability and functional outcomes in older adults: results from a scoping review in the ARMCADA study. Front Psychol 2025 Mar 21;16:1540493. [doi: 10.3389/fpsyg.2025.1540493] [Medline: 40191575]
11. Pietrzak B, Kujawa J, Lipert A. Depressive disorders, cognitive and physical function of older people in early dementia detection. Life (Basel) 2023 Oct 4;13(10):2010. [doi: 10.3390/life13102010] [Medline: 37895392]
12. Andresen EM, Malmgren JA, Carter WB, Patrick DL. Screening for depression in well older adults: evaluation of a short form of the CES-D (Center for Epidemiologic Studies Depression Scale). Am J Prev Med 1994;10(2):77-84. [Medline: 8037935]
13. Fu H, Si L, Guo R. What is the optimal cut-off point of the 10-item Center for Epidemiologic Studies Depression Scale for screening depression among Chinese individuals aged 45 and over? An exploration using latent profile analysis. Front Psychiatry 2022 Mar 14;13:820777. [doi: 10.3389/fpsyt.2022.820777] [Medline: 35360127]
14. Zhao Z, Chu Y, Chen X, Liu T. Association between outdoor and indoor air pollutant exposure and depression among middle-aged and older adults in China. Sci Rep 2025 Jul 1;15(1):22162. [doi: 10.1038/s41598-025-07185-1] [Medline: 40594657]
15. Wu Q, Feng J, Pan CW. Risk factors for depression in the elderly: an umbrella review of published meta-analyses and systematic reviews. J Affect Disord 2022 Jun 15;307:37-45. [doi: 10.1016/j.jad.2022.03.062] [Medline: 35351490]
16. Bottomley C, Nazareth I, Torres-González F, et al. Comparison of risk factors for the onset and maintenance of depression. Br J Psychiatry 2010 Jan;196(1):13-17. [doi: 10.1192/bjp.bp.109.067116] [Medline: 20044653]

XSL•FO
RenderX

17. Morelli D, Dolezalova N, Ponzo S, Colombo M, Plans D. Development of digitally obtainable 10-year risk scores for depression and anxiety in the general population. Front Psychiatry 2021 Aug 13;12:689026. [doi: 10.3389/fpsyt.2021.689026] [Medline: 34483986]
18. Zhu X, Wang Y, Luo Y, Ding R, Shi Z, He P. Bidirectional, longitudinal associations between depressive symptoms and IADL/ADL disability in older adults in China: a national cohort study. BMC Geriatr 2024 Aug 6;24(1):659. [doi: 10.1186/s12877-024-05248-y] [Medline: 39107705]
19. Arayici ME, Kose A, Dolu S, et al. Epidemiological assessment of depression, activities of daily living and associated factors in elderly individuals aged 65 years and older: evidence from a population-based study. J Clin Med 2025 Apr 21;14(8):2853. [doi: 10.3390/jcm14082853] [Medline: 40283685]
20. Zhan Y, Ning H, Zhang Y. From work to community: how social participation and retirement can benefit older adults' depression. Front Psychiatry 2025 Mar 3;16:1522222. [doi: 10.3389/fpsyt.2025.1522222] [Medline: 40099148]
21. Liu P, Chen H, Tong B, Zhu D, Cong X, Shang S. Association between multisite musculoskeletal pain and disability trajectories among community-dwelling older adults. Aging Clin Exp Res 2024 May 23;36(1):115. [doi: 10.1007/s40520-024-02764-0] [Medline: 38780859]
22. Denkinger MD, Lukas A, Nikolaus T, Peter R, Franke S, ActiFE study group. Multisite pain, pain frequency and pain severity are associated with depression in older adults: results from the ActiFE Ulm study. Age Ageing 2014 Jul;43(4):510-514. [doi: 10.1093/ageing/afu013] [Medline: 24603284]
23. Hallford DJ, Rusanov D, Yeow JJE, Barry TJ. Overgeneral and specific autobiographical memory predict the course of depression: an updated meta-analysis. Psychol Med 2021 Apr;51(6):909-926. [doi: 10.1017/S0033291721001343] [Medline: 33875023]
24. Ridley M, Rao G, Schilbach F, Patel V. Poverty, depression, and anxiety: causal evidence and mechanisms. Science 2020 Dec 11;370(6522):eaay0214. [doi: 10.1126/science.aay0214] [Medline: 33303583]
25. Campbell D, Green MJ, Davies N, et al. Effects of depression on employment and social outcomes: a Mendelian randomisation study. J Epidemiol Community Health 2022 Jun;76(6):563-571. [doi: 10.1136/jech-2021-218074] [Medline: 35318279]
26. Yan W, Wang L, Li C, Meng Y, Guo Q, Li H. Bidirectional association between ADL disability and depressive symptoms among older adults: longitudinal evidence from CHARLS. Sci Rep 2025 Feb 28;15(1):7125. [doi: 10.1038/s41598-025-91680-y] [Medline: 40021702]
27. Nouwen A, Deschênes SS, Balkhiyarova Z, Albertorio-Díaz JR, Prokopenko I, Schmitz N. Measurement invariance testing of the Patient Health Questionnaire-9 (PHQ-9) across people with and without diabetes mellitus from the NHANES, EMHS and UK Biobank datasets. J Affect Disord 2021 Sep 1;292:311-318. [doi: 10.1016/j.jad.2021.05.031] [Medline: 34139403]
28. Cheng HT, Ho MC, Hung KY. Affective and cognitive rather than somatic symptoms of depression predict 3-year mortality in patients on chronic hemodialysis. Sci Rep 2018 Apr 12;8(1):5868. [doi: 10.1038/s41598-018-24267-5] [Medline: 29651018]
29. Hawker GA, Gignac MAM, Badley E, et al. A longitudinal study to explain the pain-depression link in older adults with osteoarthritis. Arthritis Care Res (Hoboken) 2011 Oct;63(10):1382-1390. [doi: 10.1002/acr.20298] [Medline: 20662042]
30. Zheng Y, Zhang C, Liu Y. Risk prediction models of depression in older adults with chronic diseases. J Affect Disord 2024 Aug 15;359:182-188. [doi: 10.1016/j.jad.2024.05.078] [Medline: 38768825]
31. Zheng Y, Zhang T, Yang S, Wang F, Zhang L, Liu Y. Using machine learning to predict the probability of incident 2-year depression in older adults with chronic diseases: a retrospective cohort study. BMC Psychiatry 2024 Dec 2;24(1):870. [doi: 10.1186/s12888-024-06299-6] [Medline: 39623372]
32. Settels J, Böckerman P. Impact of retirement on quality of life: role of changes in social network involvement. Res Aging 2025;47(7-8):375-391. [doi: 10.1177/01640275251324871] [Medline: 40073282]
33. Koivumaa-Honkanen H, Kaprio J, Honkanen R, Viinamäki H, Koskenvuo M. Life satisfaction and depression in a 15-year follow-up of healthy adults. Soc Psychiatry Psychiatr Epidemiol 2004 Dec;39(12):994-999. [doi: 10.1007/s00127-004-0833-6] [Medline: 15583908]
34. Lin F, Liu C, Liu H. Development and validation of a predictive model for activities of daily living dysfunction in older adults: retrospective analysis of data from the China Health and Retirement Longitudinal Study. JMIR Med Inform 2025 Jun 19;13:e73030. [doi: 10.2196/73030] [Medline: 40537082]
35. Zhang F, Yang W. Interaction between activities of daily living and cognitive function on risk of depression. Front Public Health 2024 Feb 7;12:1309401. [doi: 10.3389/fpubh.2024.1309401] [Medline: 38384887]
36. Björgvinsson T, Kertz SJ, Bigda-Peyton JS, McCoy KL, Aderka IM. Psychometric properties of the CES-D-10 in a psychiatric sample. Assessment 2013 Aug;20(4):429-436. [doi: 10.1177/1073191113481998] [Medline: 23513010]
37. Wangliu Y. Does intergenerational support affect older people's social participation? An empirical study of an older Chinese population. SSM Popul Health 2023 Feb 21;22:101368. [doi: 10.1016/j.ssmph.2023.101368] [Medline: 36873267]

Abbreviations

ADL: activity of daily living
AUC: area under the receiver operating characteristic curve

XSL•FO
RenderX

CESD-10: 10-item Center for Epidemiologic Studies Depression Scale
CHARLS: China Health and Retirement Longitudinal Study
IADL: instrumental activity of daily living
LASSO: least absolute shrinkage and selection operator
SHAP: Shapley additive explanations

Edited by A Benis; submitted 30.Jul.2025; peer-reviewed by H Luo, H Liu, M Zhou; revised version received 05.Jan.2026; accepted 17.Feb.2026; published 12.Mar.2026.

Please cite as:
Peng T, Zhang Y, Miao R, Wang J
Development of a Practical Nomogram for Depression Risk Stratification in Older Adults With Hypertension and Diabetes: Retrospective Analysis of Data From the China Health and Retirement Longitudinal Study
JMIR Med Inform 2026;14:e81529
URL: https://medinform.jmir.org/2026/1/e81529
doi:10.2196/81529

© Ting Peng, Ying Zhang, Rujia Miao, Jiangang Wang. Originally published in JMIR Medical Informatics (https://medinform.jmir.org), 12.Mar.2026. This is an open-access article distributed under the terms of the Creative Commons Attribution License (https://creativecommons.org/licenses/by/4.0/), which permits unrestricted use, distribution, and reproduction in any medium, provided the original work, first published in JMIR Medical Informatics, is properly cited. The complete bibliographic information, a link to the original publication on https://medinform.jmir.org/, as well as this copyright and license information must be included.

XSL•FO
RenderX

Two-Minute Deep Learning–Powered Brain Quantitative Mapping: Accelerating Clinical Imaging With Synthetic Magnetic Resonance Imaging

Yawen Liu[1,2], PhD; Hongxia Yin[2,3], MEng; Zuofeng Zheng[4], MD; Wenjuan Liu[5], MD; Tingting Zhang[2], MEng; Linkun Cai[6], PhD; Haijun Niu[6], PhD; Han Lv[1,2], MD; Zhenghan Yang[2], MD; Zhenchang Wang[1,2], MD; Pengling Ren[1,2], PhD

[1]Precision and Intelligence Medical Imaging Lab, Beijing Friendship Hospital, Capital Medical University, No.95 Yongan Road, Xicheng District, Beijing, China

[2]Department of Radiology, Beijing Friendship Hospital, Capital Medical University, Beijing, China

[3]Department of Medical Engineering, Beijing Friendship Hospital, Capital Medical University, Beijing, China

[4]Department of Radiology, Beijing Anzhen Hospital, Capital Medical University, Beijing, China

[5]Department of Radiology, Aerospace Center Hospital, Beijing, China

[6]School of Biological Science and Medical Engineering, Beihang University, Beijing, China

Corresponding Author:
Pengling Ren, PhD
Precision and Intelligence Medical Imaging Lab, Beijing Friendship Hospital, Capital Medical University, No.95 Yongan Road, Xicheng District, Beijing, China

Abstract

Background: Quantitative magnetic resonance imaging (MRI) is an advanced technique that can map the physical properties (T1, T2, and proton density [PD]) of different tissues, offering crucial insights for disease diagnosis. Nonetheless, the practical application of this technology is indeed constrained by several factors, with the most notable being the protracted scanning duration.

Objective: This study aimed to explore whether deep learning (DL)–based superresolution reconstruction of ultrafast whole brain synthetic MRI can obtain quantitative T1/T2/PD maps that are closely approximated to those from routine clinical scans, while substantially shortening scan time and preserving diagnostic image quality.

Methods: A total of 151 healthy adults and 7 individuals with different pathologies were prospectively enrolled. Each individual was examined twice on a 3.0T scanner using routine and fast synthetic MRI protocols. The routine scans (acquisition matrix: 320×256) were interpolated to 512 by 512 for clinical display and served as reference images. The fast scans (acquisition matrix: 192×128) were preprocessed to 256 by 256 and used as inputs to a superresolution generative adversarial network (SRGAN), which reconstructed them to the same 512 by 512 interpolated resolution as the reference. For each quantitative chart, 120 (75.95%) healthy individuals' images were used for training, and 38 (24.05%) individuals' images (healthy individuals: n=31, 19.62%; patients: n=7, 4.43%) were used for testing. Agreement was assessed with a paired *t* test, two 1-sided tests, Bland-Altman analysis, and coefficients of variation.

Results: DL reconstructed and reference T1/T2/PD values were strongly correlated (T1: R^2=0.98; T2: R^2=0.97; and PD: R^2=0.99). The slopes of the linear regression were near 1.0 both for T1 (0.9418) and PD (0.9946), whereas T2 values were moderate, as the slope of the linear regression was 0.8057. Additionally, the average biases of T1, T2, and PD values were small (0.93%, −0.85%, and 0.31%, respectively). The intra- and intergroup coefficient of variation for most of the brain regions stayed below 5%, especially for PD values, and after DL reconstruction, it still has quantitative accuracy for lesions. Quantitative and qualitative analyses of image quality also indicate that SRGAN markedly suppressed noise and artifacts in fast acquisitions, restoring structural fidelity (structural similarity image measure) and signal fidelity (peak signal-to-noise ratio) close to the level of routine scans while substantially improving perceptual naturalness over fast scans (as measured by the naturalness image quality evaluator), although not yet matching that of routine imaging.

Conclusions: SRGAN superresolution applied to ultrafast synthetic MRI yields whole brain T1, T2, and PD maps that show strong correlation with routine synthetic MRI while halving acquisition time and maintaining diagnostic image quality. Although T1 and PD values exhibit near-ideal agreement, and T2 values demonstrate a moderate systematic underestimation, this approach represents a promising step toward accelerating clinical deployment of quantitative brain imaging.

XSL•FO
RenderX

(JMIR Med Inform 2026;14:e79389) doi:10.2196/79389

KEYWORDS

magnetic resonance imaging; qMRI; fast MRI; deep learning; brain imaging

Introduction

Quantitative magnetic resonance imaging (qMRI) can reflect the inherent properties of human tissue relaxation times and proton density (PD), providing valuable support for verifying visual assessments of structures and tissues against a normal quantitative standard, thereby holding significant clinical diagnostic value [1]. Nevertheless, the extended scan time of qMRI imposes limitations on its practical use. Synthetic MRI, based on multidynamic, multiecho sequences, can provide multiple quantitative information and multicontrast images in a single scan, enabling fast qMRI scans [2,3]. It has been proven to have comparable diagnostic value to conventional scanning methods, with the generated quantitative data being valuable for disease identification [4-7]. However, the single scan time of this imaging method still typically ranges from 4 to 7 minutes, particularly for brain MRI imaging, which can lead to individual discomfort and potentially impact image quality. Therefore, improving the imaging speed of synthetic MRI is the key to realizing ultrafast qMRI.

It is also crucial to ensure the quality of qMRI and the reliability of quantitative values while accelerating imaging. Usually, fast imaging methods such as parallel acquisition and compressed sensing may result in a loss of image quality [8]. The reconstruction technology based on deep learning (DL) has been applied in various medical image reconstruction tasks, and its development makes it possible to solve the trade-off between image quality and scan time. Generative adversarial networks, renowned for generating high-fidelity superresolution images, have been successfully used in MRI [9]. Many researchers have implemented the concept of generative adversarial networks for MRI image reconstruction, achieving high-quality reconstruction from highly undersampled data [10-14]. In addition, the generative adversarial approach can be used for tasks, such as artifact correction and denoising in MRI [15,16]. In clinical practice, in addition to focusing on image quality, it is more important to determine whether the DL-based reconstruction method can provide less bias and consistent quantitative data [17].

To shorten synthetic MRI quantitative acquisitions and increase clinical throughput, we hypothesized that DL superresolution can generate T1/T2/PD maps that are close to routine long acquisition quantitative values while maintaining image quality, thereby providing faster yet equally reliable neuroimaging and ultimately enhancing diagnostic precision and patient comfort.

Methods

Participants

This study was approved by the Medical Research Ethics Committees of the Beijing Friendship Hospital, Capital Medical University (2020-P2-122-02). Written informed consent was obtained from all participants prior to enrollment. A total of 151 healthy individuals were prospectively recruited at 1 institution for this study. The inclusion criteria were as follows: (1) the age of the individual was greater than or equal to 18 years, (2) the individual showed no structural changes or signs of disease in brain MRI, and (3) the individual showed no contraindications or adverse reactions to MRI examination. The exclusion criteria were as follows: (1) there were obvious artifacts in the images, and (2) the individual failed to complete all MRI examinations. In addition, we also collected images from 7 individuals with different pathologies (white matter [WM] hyperintensities, cerebral infarcts, and encephalomalacia) to evaluate the potential for clinical application.

Synthetic MRI Acquisition

All MRI examinations were performed using a SIGNA Pioneer 3.0 T MRI scanner (GE Healthcare). All individuals underwent two synthetic MRI scans using the multidynamic multiecho sequence (MDME sequence, named MAGiC in the GE scanner): a routine scan protocol and a fast scan protocol. The routine scan uses commonly used clinical acquisition parameters: TR=4000 ms; TE1=18.3 ms; TE2=91.4 ms; TI=28.2 ms; thickness=5 mm; FOV=220×220 mm; acquisition matrix=320×256; echo-train length=16; bandwidth=31.25 kHz; delay times=170, 670, 1840, and 3840 ms; and acceleration factors=2, 24 slices, with a pixel size of 0.7×0.8 and an acquisition time of 4 minutes 55 seconds. Fast scan modifies the acquisition matrix and acceleration factor, which affect the acquisition time, by changing the acquisition matrix to 192×128 and the acceleration factor to 3. The remaining parameters remained the same as those of the routine scan, with a pixel size of 1.1×1.7 and an acquisition time of 1 minute 52 seconds.

Data Preprocessing

The same method was used to retrieve the quantitative maps (T1 maps, T2 maps, and PD maps) as mentioned in a previous study [18]. In this study, quantitative maps from the routine scan (reconstruction matrix=512×512, 0.43×0.43 mm² pixel) served as the high-resolution (HR) reference, whereas those from the fast scan (reconstruction matrix=256×256, 0.86×0.86 mm² pixel) were used as low-resolution (LR) inputs. DICOM images were directly read and prepared for network training. It should be noted that the maximum image intensities of T1 maps, T2 maps, and PD maps are 43,000, 20,000, and 1600, respectively, which correspond to 10 times the actual values. This scaling is due to the rescaling slope value of 0.1 specified in the DICOM header file.

Network Architecture

The detailed generator network structure is shown in Figure 1A. It starts with a 9 by 9 convolutional filter and connects to 5 residual blocks, each of which consists of two 3 by 3 convolutional layers alternating with batch normalization layers, and activation is performed using a rectified linear unit (ReLU) function. After the residual network, a 3 by 3 convolution and a 1 by 1 convolution are connected, and a subpixel convolutional

XSL•FO
RenderX

layer is used to upsample the image. In the generator network, except for the last layer that uses tanh as the activation function, all other layers use ReLU as the activation function. The discriminator network structure is shown in Figure 1B. In the discriminator network D, our model first uses an architecture comprising eight 3×3 convolutional layers and Leaky ReLU function activation. All convolutional layers except the first have batch normalization layers. The Sigmoid activation function is applied to the last fully connected layer, which outputs the probability of discriminating whether the input HR image is a real HR image or an image generated by the generator. The network architecture includes a pretrained VGG-19 network, which is used for feature extraction and loss function calculation.

Figure 1. The architecture of the superresolution generative adversarial network. BN: batch normalization; DL: deep learning; HR: high resolution; ReLU: rectified linear unit.

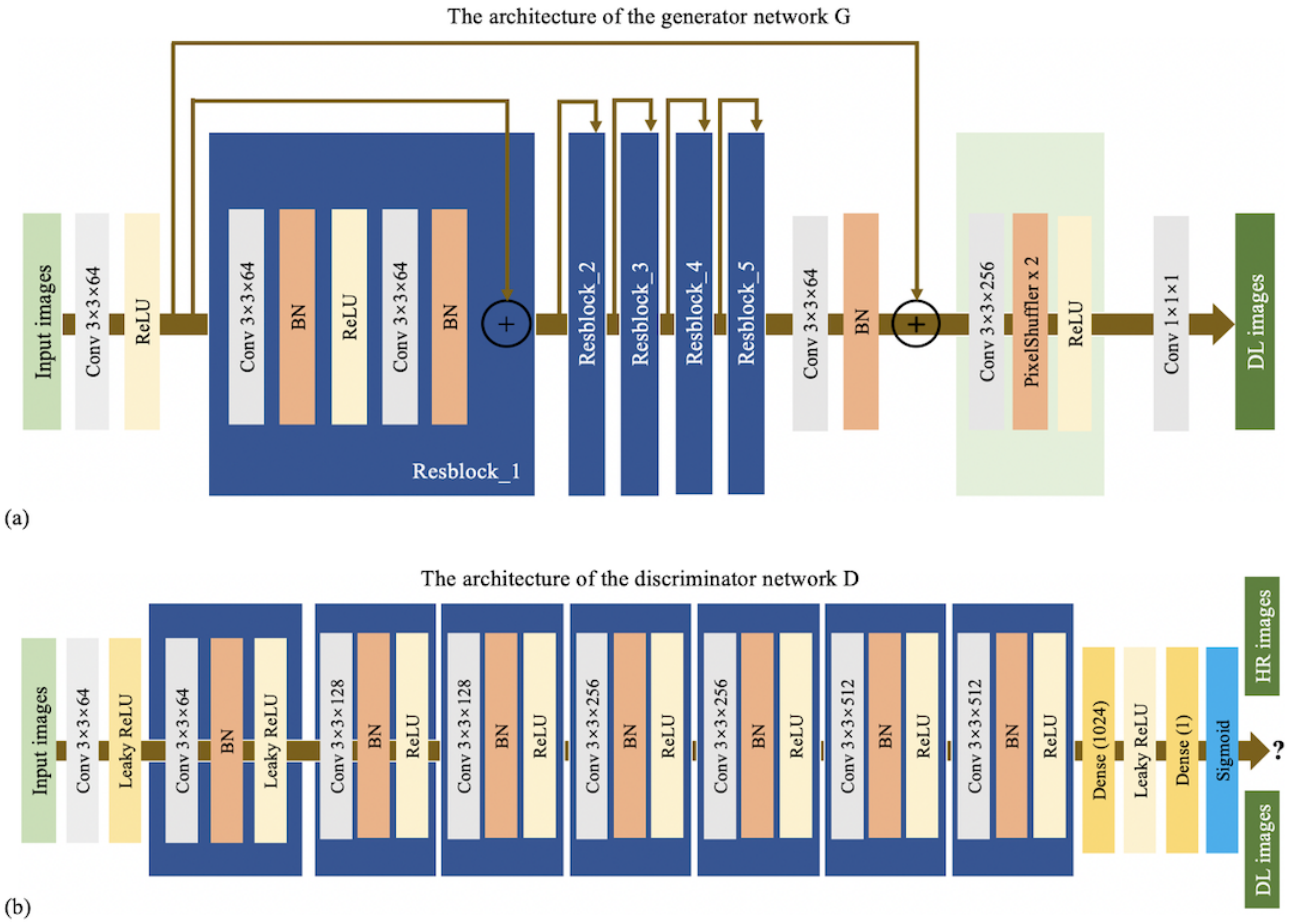

Loss Function

The pixel-by-pixel error method used is the L1 loss function, also known as the mean absolute error, which is calculated using equation 1. Although SRGAN completely discards the pixel-by-pixel error, we still add this error in a certain proportion during the actual training process to amplify the difference and guide the optimization of the model. The cross-entropy loss function of the discriminator is used as the adversarial error of the network, and the calculation method is expressed using equation 2. In addition to using the adversarial error, SRGAN also uses a content error, which is defined as the Euclidean distance between the superresolved image and the feature map of the reference image, and the calculation method is expressed using equation 3. The content error is used to align the content of LR images and HR images, which plays the same role as the mean square error. In this network, the pretrained VGG-19 network is used to extract the feature parameter map. Therefore, the loss function for the generator in this network is described using equation 4.

$$(1) L_{mae} = \frac{1}{CHW}\sum_{i,j,k} |I_{i,j,k}^{DL} - I_{i,j,k}^{GT}|$$

where I^{DL} is the output image of the generator and I^{GT} is the input reference image.

$$(2) L_{gan} = -\sum_{i} \log D(G(I^{DL}))$$

where G and D are the generative network and the discriminative network, respectively.

$$(3) L_{VGG} = \frac{1}{C_j H_j W_j}\sum_{x=1}^{W_j}\sum_{y=1}^{H_j}\sum_{c=1}^{C_j}(\phi_j(G(I^{DL}))_{x,y,c} - \phi_j(G(I^{GT}))_{x,y,c})^2$$

where $(\varnothing j)$ is the feature map obtained from the jth convolutional layer of the VGG-19 network, C_j, H_j, and W_j are the number of channels and height and width of the feature map, respectively, I^{DL} is the output image of the generator, and I^{GT} is the input reference image.

$$(4) L_{total} = L_{mae} + 10^{-3} L_{gan} + 2 \times 10^{-6} L_{VGG}$$

Implementation

Approximately 80% (120 healthy individuals) of the dataset were allocated to training, and the remaining individuals (healthy individuals: 31, 19.62%; and patients: 7, 4.43%) were used for

XSL•FO
RenderX

testing. Slices from each individual were pooled and randomly shuffled within their respective sets to prevent any sequential bias and improve the performance of the model. Before training, all quantitative maps (T1, T2, and PD) underwent intensity normalization to match the output range of the generator network, that is, imagenorm=(pixelvalue/normalizepara)×2−1, where normalize_para is set to 45,000, 22,000, and 1800 for T1, T2, and PD maps, respectively.

The DL models for T1, T2, and PD maps were trained separately but with identical hyperparameters. Each model was implemented using the TensorLayer framework [19] and optimized via the adaptive moment estimation (Adam) optimizer with a learning rate of 1×10^{3} and step-wise decay every 1000 iterations. Training was performed on an NVIDIA Tesla V100 GPU with a batch size of 8 and a total of 200 epochs. All other parameters were kept at their default settings.

Quantitative Value Measurements

The flowchart illustrating the process of quantitative value measurements is presented in Figure 2.

For healthy participants, quantitative value analysis of brain tissue and brain regions was conducted. First, brain tissue segmentation was performed on each individual's quantitative map using the New Segment tool within SPM [20] software. Then, quantitative value extraction of gray matter (GM) and WM was performed using self-written programs in the MATLAB (The MathWorks Inc.) platform.

Figure 2. The process of quantitative value measurements for healthy participants. AAL: anatomical automatic labeling; GM: gray matter; JHU: Johns Hopkins University; WM: white matter.

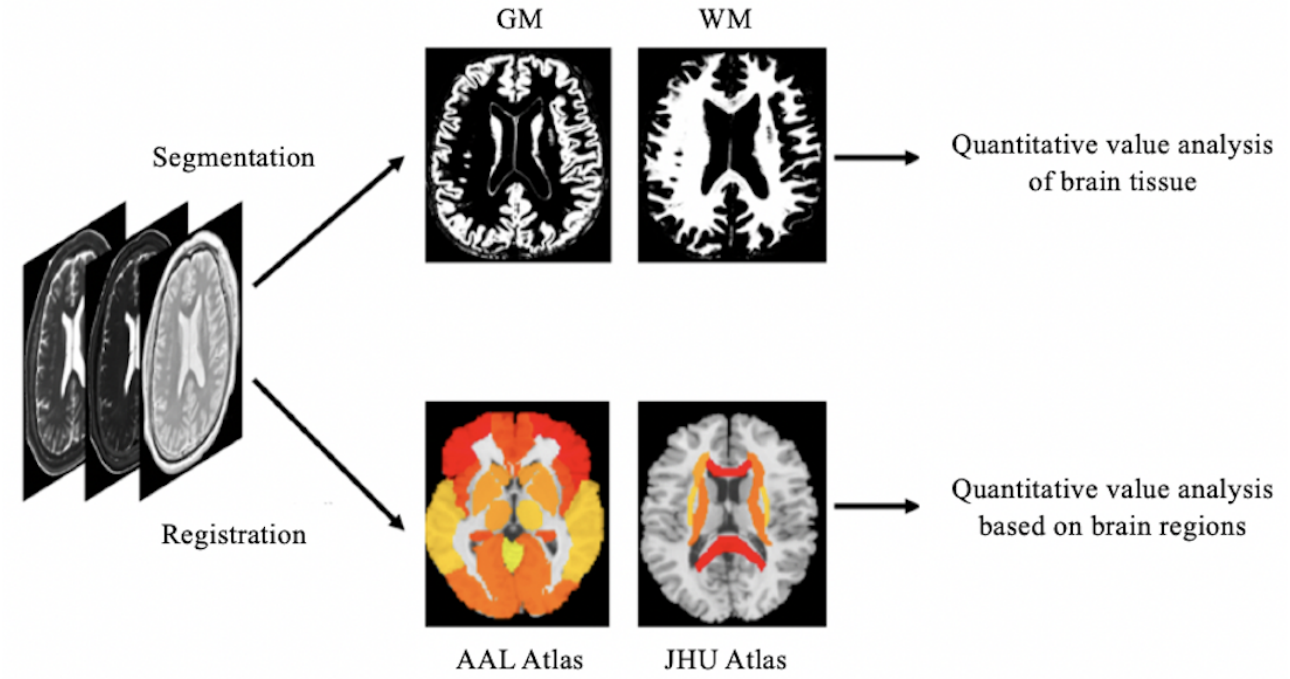

In addition to analyzing quantitative values for both GM and WM tissue, analysis was also performed by different brain regions for clinical evaluation and application. Using the anatomical automatic labeling atlas of the Montreal Neurological Institute (MNI), 10 GM regions of interest (ROIs) were created on anatomical structures, including frontal cortex, temporal cortex, parietal cortex, occipital cortex, insula, hippocampus, caudate nucleus, putamen, pallidum, and thalamus. Additionally, using the JHU-WhiteMatter-48 atlas, 9 WM ROIs were generated, including the middle cerebellar peduncle, genu of corpus callosum, splenium of corpus callosum, cerebral peduncle, internal capsule, anterior corona radiata, superior corona radiata, posterior corona radiata, and external capsule [21]. In all analyses, right and left quantitative data were averaged. The quantitative value of the corresponding brain region in the quantitative map reconstructed by DL and from routine scans was obtained for each individual for subsequent statistical analysis.

For the images of individuals with pathologies, an experienced radiologist used the ITK-SNAP software (version 3.8.0; [22]) to delineate the ROI of typical lesions manually and acquired the mean value of the signal in the ROI. To ensure paired comparison, identical ROI size and location were replicated on the DL reconstructed and reference routine scan images. A total of 12 ROIs were obtained from 7 (4.43%) patients (individual 3: 3 ROIs, individual 5: 3 ROIs, individual 7: 2 ROIs, and the remaining 4 individuals: 1 ROI each).

Image Quality Evaluation

Two full-reference evaluation indices—peak signal-to-noise ratio (PSNR) and structural similarity image measure (SSIM)—were used in this study for image quality assessment [23]. The larger the value of the 2 indices, the better the image quality. The PSNR was defined by equation 5:

$$MSE=\sum_{m=1}^{M}\sum_{n=1}^{N}[R(m,n)-I(m,n)]^{2}M\times N$$

$$(5)PSNR=20\log L^{2}MSE$$

The calculation method of SSIM is given by equation 6:

$$,$$

$$(6)SSIM(X,Y)=(2\mu X\mu Y+C1)(2\sigma XY+C2)(\mu X^{2}+\mu Y^{2}+C1)(\sigma X^{2}+\sigma Y^{2}+C2)$$

XSL•FO
RenderX

$C1=(K1L)2, C2=(K2L)2$

where μ and μ, σ and σ, and σ are the local means, SDs, and cross-covariance for the DL quantitative images and routine scans, respectively, and C1 and C2 are 2 quantities used to stabilize the division in the case of a weak denominator, with L=65,535, K1 = 0.01, and K2= 0.03.

In addition, a no-reference image quality assessment method, the naturalness image quality evaluator (NIQE), was used to evaluate the quality of quantitative images reconstructed by DL, with fast scan and with routine scan, respectively [24]. Unlike PSNR and SSIM, the lower the value of NIQE, the less distortion and higher image quality.

Statistical Analysis

For the quantitative analysis of brain tissue in healthy participants, Paired *t*-test was used to compare the differences in quantitative values between DL and routine scans, and equivalence was confirmed using two one-sided tests (TOST). Linear regression analysis and Bland-Altman analysis were used in the study, and we combined GM and WM to comprehensively evaluate overall bias. This method captures the overall trends and variability of different tissue types, which is crucial for evaluating the performance of DL reconstruction in clinically relevant contexts. For the region-based quantitative value analysis in healthy participants, coefficients of variation (CVs) were calculated within each imaging method (intragroup CV) and across each imaging method (intergroup CV). Intergroup CV was calculated using the average of the quantitative values from each method. For the images of individuals with pathologies, Paired *t*-test was used to compare quantitative values in different ROIs between groups. All statistical analyses were performed using SPSS 22.0 and GraphPad Prism 9. A *P* value <.05 was considered statistically significant.

Ethical Considerations

This study was approved by the Medical Research Ethics Committees of Beijing Friendship Hospital, Capital Medical University (2020-P2-122-02). All participants provided informed consent before participating. Participants' privacy and confidentiality were protected, with all data being deidentified during analysis. No compensation was provided for participation. No identifiable information of participants was included in the paper or supplementary materials in Multimedia Appendix 1. All procedures adhered to ethical guidelines for participant autonomy, safety, and confidentiality.

Results

Time Consumption

The average whole brain acquisition time was 4 minutes 55 seconds for routine scans, with an additional 1 minute for vendor postprocessing. Fast scans were completed in 1 minute 52 seconds; applying the SRGAN network trained in this study then reconstructed, the 512 by 512 quantitative T1/T2/PD maps were completed in approximately 1 second. Thus, the combined acquisition and reconstruction time was reduced from 5 minutes 55 seconds to 1 minute 53 seconds, promoting the wider clinical application of quantitative neuroimaging and synthetic MRI.

Quantitative Value Accuracy

A paired *t* test showed significant differences in GM tissue values between DL and fast scans (T1: *P*<.001, PD: *P*=.002), while there was no significant difference in GM tissue values between DL and routine scans at T1 (*P*=.66) and PD (*P*=.18). However, compared with routine scans, T2 values still showed significant differences after DL (*P*<.001). For WM, compared with routine scans, there was no significant difference in T2 after DL (*P*=.11). Although there were still significant differences in T1 and PD, the differences were reduced compared with fast scans (Table 1).

Table . The quantitative value of brain tissue obtained by fast scan, deep learning (DL), and routine scan.

	Fast, mean (SD)	DL, mean (SD)	Routine, mean (SD)	*P* value[a]	*P* value[b]
GM[c]					
T1 (ms)	1200.03 (36.01)	1230.17 (34.12)	1232.65 (34.98)	<.001	.66
T2 (ms)	97.87 (2.07)	91.36 (2.60)	93.33 (3.50)	<.001	<.001
PD (%)	79.69 (2.35)	80.29 (1.51)	80.11 (1.23)	.002	.18
WM[d]					
T1 (ms)	814.88 (35.78)	855.06 (32.12)	837.86 (35.88)	<.001	<.001
T2 (ms)	84.57 (2.17)	80.23 (1.61)	79.92 (2.05)	<.001	.11
PD (%)	67.55 (1.94)	68.49 (1.44)	68.21 (1.29)	<.001	.01

[a]*t* test results between DL and fast scans.

[b]*t* test results between DL and routine scans.

[c]GM: gray matter.

[d]WM: white matter.

Setting the clinically acceptable brain tissue quantification value limit to ±5% of the mean values from the routine scans (T1_GM epsilon: 61.63 ms, T2_GM epsilon: 4.67 ms, PD_GM epsilon: 4.01%, T1_WM epsilon: 41.89 ms, T2_GM epsilon: 4.00 ms, and PD_WM epsilon: 3.41%), the 90% TOST CI for the brain tissue in 3 quantitative maps (T1_GM: −11.88 to 6.91, T2_GM:

XSL•FO
RenderX

−2.48 to−1.46, PD_GM: −0.04 to 0.41, T1_WM: 10.94 to 23.46, T2_WM: −0.01 to 0.03, and PD_WM: 0.10 to 0.45) were all within the predefined margins (P<.001).

Figure 3 shows the relationship and Bland-Altman plots between the T1, T2, and PD values obtained by DL and routine scans (reference). The correlations to the reference value were excellent, as the R^2 for the T1, T2, and PD values of DL compared to the reference value was 0.98, 0.97, and 0.99, respectively. The slopes of the linear regression were near 1.0 both for T1 (0.9418) and PD (0.9946). In contrast, the T2 values were moderate, as the slope of the linear regression was 0.8057 (Figure 3A,C,E). In addition, the average percentage bias for T1, T2, and PD was 0.93%, −0.85%, and 0.31%, respectively. The 95% limits of agreement were 6.20% to −4.34% for T1, 3.00% to −4.70% for T2, and 1.98% to −1.35% for PD (Figure 3B,D,F). Similarly, Figure 4 shows the relationship and Bland-Altman plots of the T1, T2, and PD acquired by DL and fast scans. The results of linear regression analysis also showed a strong correlation between the 2 methods in T1 and PD (T1: R^2=0.99 and PD: R^2=0.98), with a slightly lower correlation in T2 (R^2=0.80). The slopes of the linear regression were near 1.0 both for T1 (0.9680) and PD (0.9381). In contrast, the T2 values were moderate, as the slope of the linear regression was 0.7755 (Figure 4A,C,E). The results of the bias trend of T1, T2, and PD between these 2 methods also showed similar results, that is, the mean percentage difference for T1 and PD was smaller (3.66% and 1.09%, respectively), whereas the mean percentage difference for T2 was slightly higher (−6.32%) (Figure 4B,D,F).

XSL•FO
RenderX

Figure 3. Scatterplots and Bland-Altman plot results for deep learning versus routine scans. The linear regression lines represent a strong linear relationship with a robust fit between the tissue value measurements of T1, T2, and proton density (PD) obtained from the 2 magnetic resonance imaging methods. Bland-Altman plots show mean percentage differences (solid red line) and the 95% CIs (dashed black line). SRGAN: superresolution generative adversarial network.

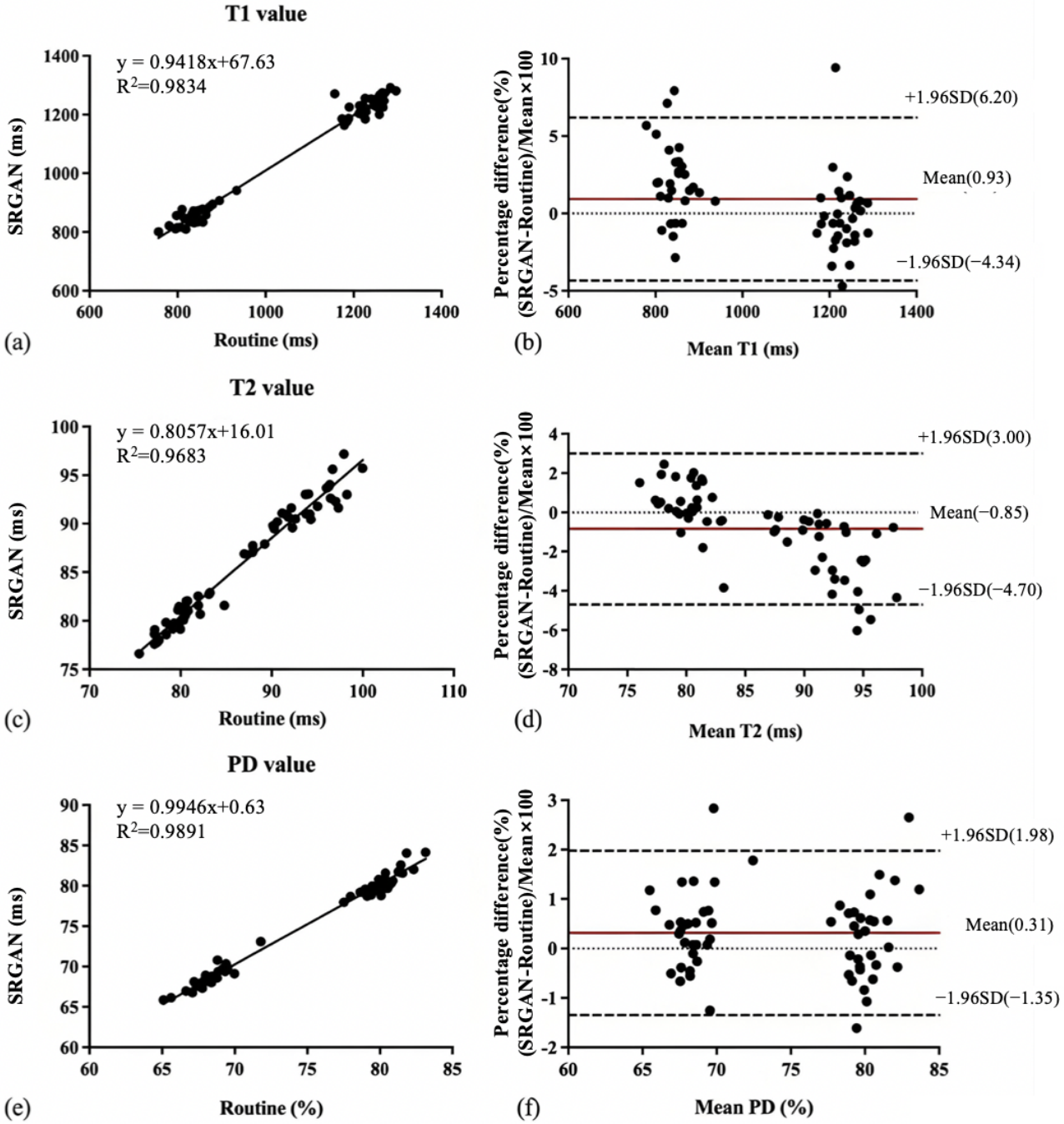

XSL•FO
RenderX

Figure 4. Scatterplots and Bland-Altman plot results for deep learning versus fast scans. The linear regression lines represent a strong linear relationship with a robust fit between the tissue value measurements of T1, T2, and proton density (PD) obtained from the 2 magnetic resonance imaging methods. Bland-Altman plots show mean percentage differences (solid red line) and the 95% CIs (dashed black line). SRGAN: superresolution generative adversarial network.

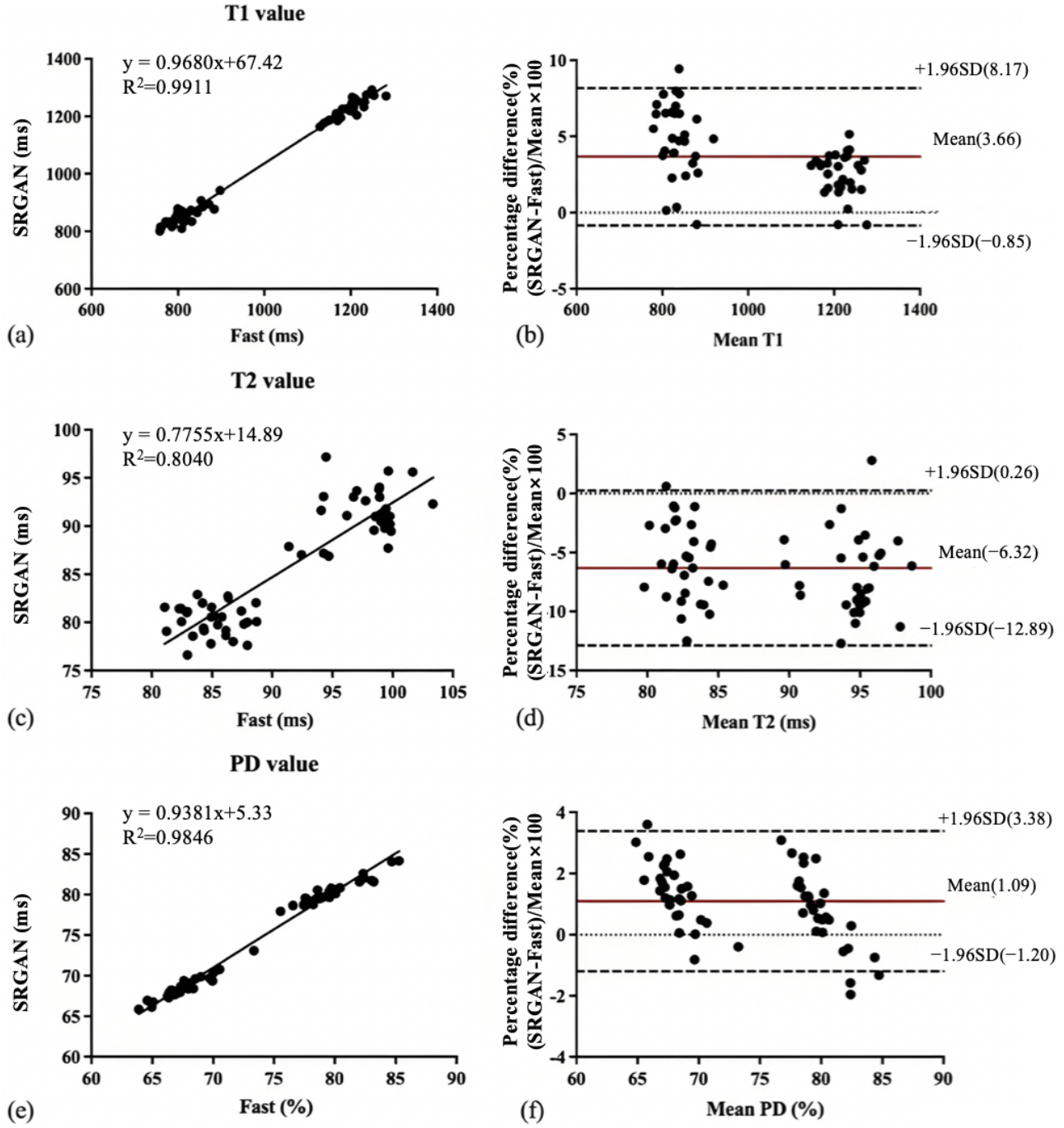

Table 2 presents the intragroup CV and intergroup CV of brain regions' quantitative values acquired by DL and routine scans. The intragroup variability of the quantitative values obtained by these 2 methods is small, as the intragroup CV for the routine scan's PD values ranges from 1.64% to 6.44%, and the PD values for DL range from 1.98% to 5.84%. The highest intragroup CV of T1 and T2 values was noted in the pallidum (T1: 18.77% vs 17.25%; and T2: 17.00% vs 16.33%). The intergroup CV was lower than the intragroup CV for all brain regions. For intergroup CV, there were no significant differences in the quantitative values of T1, T2, and PD for the WM region after DL reconstruction. However, significant differences in T2 values were observed in the GM regions, including the frontal cortex, temporal cortex, parietal cortex, occipital cortex, insula, and hippocampus.

Table 3 presents the quantitative values in ROI of typical lesions acquired by DL and routine scans. Compared with the quantitative values under routine scans, there were no significant differences in the quantitative values reconstructed by deep learning (T1, *P*=.67; T2, *P*=.73; and PD, *P*=.75).

XSL•FO
RenderX

Table . Intragroup and intergroup coefficient of variation (CV) for T1, T2, and proton density (PD) based on anatomical automatic labeling (AAL) and Johns Hopkins University (JHU) atlas in healthy individuals.

Brain region	Intragroup CV (%)		Intergroup CV (%) (T1/T2/PD)	*P* value (T1/T2/PD)
	DL[a] (T1/T2/PD)	Routine (T1/T2/PD)		
AAL atlas				
Frontal	7.41/7.28/3.62	8.20/7.14/3.44	2.07/5.17/0.61	.29/.001/.94
Temporal	5.10/8.00/3.31	5.50/8.62/3.27	1.65/4.98/0.40	.38/.003/.83
Parietal	9.32/14.40/3.02	9.08/15.90/2.97	1.30/8.11/0.45	.38/<.001/.42
Occipital	7.43/11.07/2.15	7.19/13.32/2.41	1.72/5.10/0.47	.60/.005/.55
Insula	9.03/15.23/2.39	9.86/13.44/2.53	1.80/7.12/0.72	.95/.02/.36
Hippocampus	8.95/11.43/2.53	9.02/14.30/2.71	2.62/6.08/0.72	.22/.005/.34
Caudate	13.69/16.20/5.29	14.65/17.14/5.37	2.60/5.32/0.76	.70/.35/.92
Putamen	13.48/12.37/2.62	14.48/17.33/3.47	2.04/5.44/0.73	.99/.11/.92
Pallidum	18.77/16.33/2.26	17.25/17.00/2.61	3.54/3.37/0.85	.51/.56/.50
Thalamus	13.37/12.39/2.38	13.99/13.96/3.00	1.69/4.05/0.88	.77/.27/.67
JHU atlas				
MCP[b]	7.28/7.04/1.72	5.89/8.13/1.64	1.67/2.79/0.51	.50/.08/.28
GCA[c]	15.33/9.77/5.84	15.22/9.11/6.44	1.99/2.89/0.76	.87/.52/.55
SCA[d]	6.44/3.70/1.98	6.00/4.64/1.94	1.74/1.71/0.63	.19/.05/.13
CP[e]	10.16/7.81/4.77	9.62/7.54/5.01	2.73/2.55/1.08	.41/.14/.55
IC[f]	9.55/4.29/3.95	9.63/4.52/4.20	1.30/1.74/0.68	.83/.21/.45
ACR[g]	9.01/5.62/2.94	9.78/6.91/3.86	1.97/1.34/0.91	.92/.97/.98
SCR[h]	9.95/4.68/3.73	8.35/4.95/3.07	2.16/1.31/1.03	.27/.14/.28
PCR[i]	14.19/3.72/4.25	12.20/4.59/3.69	2.60/2.49/0.96	.42/.03/.23
EC[j]	11.32/5.02/2.82	11.23/4.89/3.36	1.38/0.92/0.95	.65/.69/.21

[a]DL: deep learning.
[b]MCP: middle cerebellar peduncle.
[c]GCA: genu of corpus callosum.
[d]SCA: splenium of corpus callosum.
[e]CP: cerebral peduncle.
[f]IC: internal capsule.
[g]ACR: anterior corona radiata.
[h]SCR: superior corona radiata.
[i]PCR: posterior corona radiata.
[j]EC: external capsule.

XSL•FO
RenderX

Table . Quantitative value in the region of interest (ROI) of typical lesions acquired by deep learning (DL) and routine scan.

ROI	Description	T1[a] (ms)		T2[b] (ms)		PD[c,d] (%)	
		DL	Routine	DL	Routine	DL	Routine
1	WMH[e]	1019.68	1052.20	100.84	112.9	80.70	79.16
2	WMH	1034.41	1052.78	96.32	96.71	75.21	77.09
3	WMH	955.68	1013.20	94.78	104.52	70.77	72.97
4	CI[f]	1217.30	1398.16	126.53	149.71	80.00	81.26
5	Encephalomalacia	3597.26	3683.45	310.67	276.99	102.83	106.59
6	WMH	1088.41	1214.51	109.50	121.23	82.11	84.70
7	CI	1832.00	1679.00	136.10	133.80	90.50	90.90
8	Encephalomalacia	3719.04	3892.54	292.16	272.32	101.31	104.98
9	WMH	1734.53	1517.03	163.45	182.01	85.14	86.37
10	WMH	1171.00	1238.00	110.60	124.70	80.70	81.10
11	Encephalomalacia	3666.00	3469.00	350.20	295.80	107.80	106.30
12	WMH	1253.00	1285.00	113.20	105.20	78.70	83.00

[a]*P*=.67.

[b]*P*=.73.

[c]PD: proton density.

[d]*P*=.75.

[e]WMH: white matter hyperintensities.

[f]CI: cerebral infarcts.

Image Quality

Figure 5 and Tables 4 and 5 compare image quality among the 3 protocols. After SRGAN reconstruction, DL maps simultaneously preserved quantitative accuracy and outperformed fast acquisitions in every objective metric, demonstrating high image quality.

XSL•FO
RenderX

Figure 5. Representative results of the proposed method. Results of fast scans (left), deep learning (DL) reconstruction (middle), and routine scans (right) are displayed for T1 map, T2 map, and proton density (PD) map.

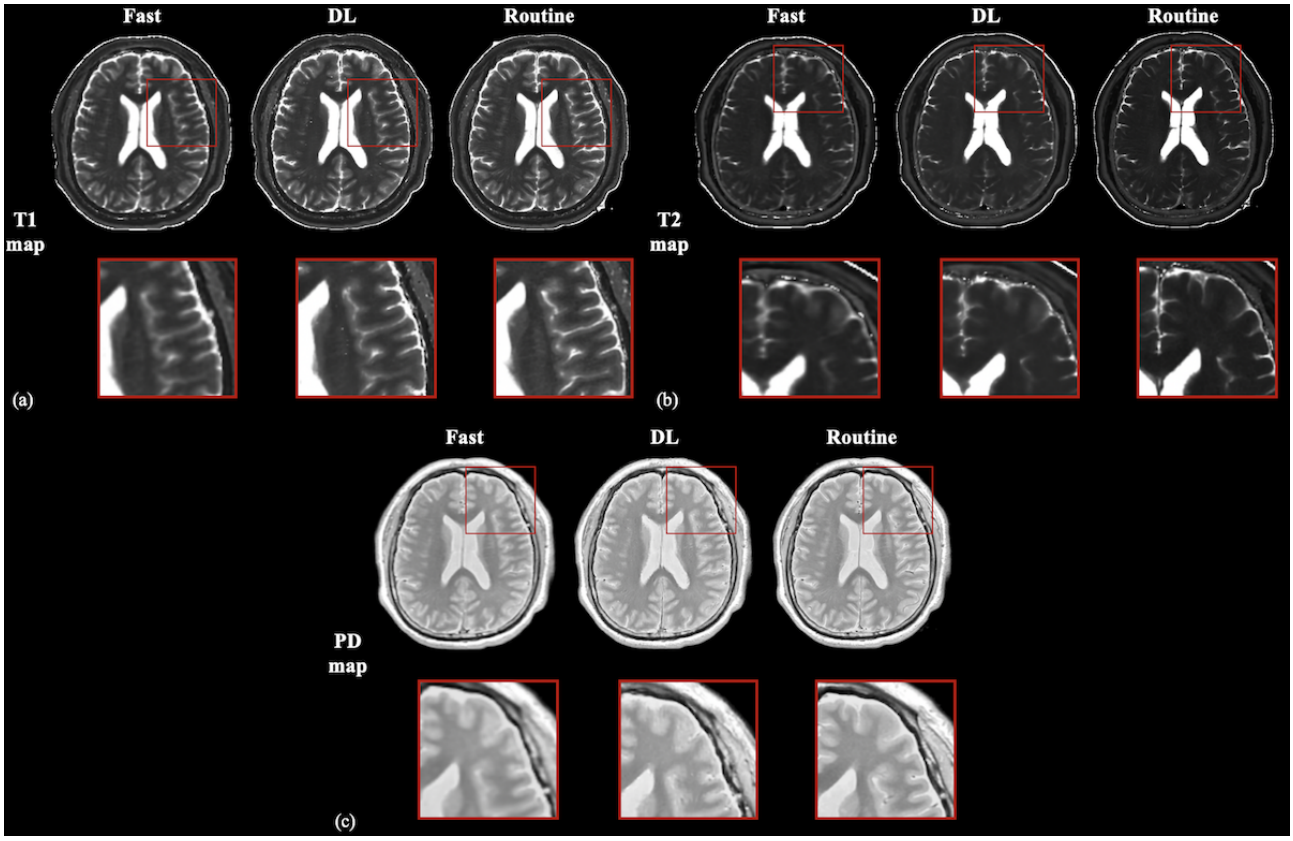

Table . Comparison of image quality between the deep learning quantitative maps and routine scans using the structural similarity image measure (SSIM) and peak signal-to-noise ratio (PSNR).

	PSNR, mean (SD)	SSIM, mean (SD)
T1 maps	21.94 (2.36)	0.82 (0.08)
T2 maps	29.14 (1.81)	0.93 (0.03)
PD[a] maps	58.01 (3.15)	0.99 (0.01)

[a]PD: proton density.

Table . The naturalness image quality evaluator of quantitative maps under fast scan, deep learning (DL), and routine scan.

	Fast scan, mean (SD)	DL, mean (SD)	Routine, mean (SD)
T1 maps	29.46 (6.42)	13.36 (1.88)	10.90 (1.84)
T2 maps	30.56 (5.57)	18.79 (1.46)	15.21 (1.78)
PD[a] maps	34.66 (2.99)	11.74 (2.17)	10.85 (2.53)

[a]PD: proton density.

Discussion

Principal Findings

In this paper, we trained an SRGAN network to reconstruct whole brain T1, T2, and PD maps from accelerated synthetic MRI data. Experimental results show that the application of DL for reconstruction can generate quantitative maps from fast scans with a 50% reduction in acquisition time. The quantitative instability caused by LR acquisition is reduced, with no significant difference between the reconstructed and routine scan values, and intra- and inter-CVs are small in most brain regions. Our study also found that the resulting maps still allow clear visual detection of common pathologies, thereby helping to shorten clinical scanning time.

Comparison With Prior Work

In previous studies, the use of commercial algorithms for fast image reconstruction resulted in a total brain acquisition time exceeding 3 minutes [25]. Our research further reduces the collection time to less than 2 minutes while maintaining accuracy. DICOM raw data were used as input and output for

XSL•FO
RenderX

the network, which conforms to the standard practice of DICOM image processing, where metadata (including rescaled slopes) are crucial for accurate image analysis and quantitative measurement. By adhering to these specifications, the study maintains the integrity of the qMRI data, facilitating a reliable evaluation of the DL reconstruction techniques' impact on the accuracy of quantitative brain tissue values.

The MDME sequence was used to acquire the quantitative maps, and several studies have investigated the repeatability and reproducibility of quantitative values using this sequence. In this study, we applied multiple quantitative metrics and statistical methods to analyze differences among DL reconstructed, fast scan, and routine scan values. The results of our study, as indicated by the paired *t* tests, provide valuable insights into the performance of DL reconstruction and demonstrate that it improves the accuracy of fast quantitative MRI scans, bringing tissue-specific T1, T2, and PD values closer to those of routine clinical acquisitions. In GM, the method achieved no statistically significant difference compared to routine scans. However, a small but statistically significant underestimation in T2 remained. A previous study examining the influence of parameter modifications on MDME-derived quantitative values reported that alterations in acquisition matrix or acceleration factor induced negligible variance in measured constants, with the exception of CSF T2 estimation [26,27]. Notably, this investigation was performed on an isolated, homogeneous phantom; consequently, partial volume effects and other anatomical confounders were absent. The present fast scan protocol, in contrast, simultaneously varies both matrix size and acceleration factor without a commensurate increase in the number of echo times. This divergence in experimental design may compromise the accuracy of T2 mapping—particularly through reduced sampling density in echo space—thereby introducing systematic bias into the fitted relaxation constants. However, TOST analysis further indicates that the 90% CIs of all brain tissue parameters in the 3 quantitative maps are within clinically acceptable ranges, providing the possibility for the clinical applications of DL quantitative reconstruction.

In our quantitative analysis, the linear regression slope for T2 values (DL vs routine) was 0.8057, which deviates from the ideal value of 1.0. Clinically, this may affect the diagnostic accuracy of high T2 lesions, leading to misdiagnosis or delayed intervention. Most of the samples in this study were healthy volunteers, and the accuracy of DL for T2 values under specific pathological manifestations was not validated. Such bias may arise primarily from the L1 loss component, which enforces pixel-wise fidelity at the expense of high-frequency details and can lead to oversmoothing—particularly in regions with high tissue contrast or rapid T2 decay. Consequently, although the average T2 error across healthy tissue may satisfy TOST criteria, it may reduce the accuracy of this method in extreme cases of dynamic range that often occur in pathology. Despite this limitation, the SRGAN model demonstrated good performance in overall image quality metrics, indicating its practicality in routine clinical workflows, although it requires appropriate attention.

Linear regression and Bland-Altman plots also demonstrated that the vast majority of quantitative parameters exhibited high correlation and agreement between the DL and routine scans, with 95% of data points lying within the limits of agreement, which is in line with previous research [28,29]. In contrast, T2 estimates derived from the DL exhibited a marked bias relative to the reference (Figure 3 vs Figure 4). These findings indicate that the DL model successfully compensates for systematic errors introduced by the fast scan, yielding quantitative values that closely approximate those obtained under routine scans. Such error mitigation directly supports the primary objective of this study: to establish the feasibility of using DL for accurate, ultrafast quantitative MR reconstruction.

In addition to measuring the quantitative values of gray and WM, the study also applied classic atlases from brain science analysis: the anatomical automatic labeling and the Johns Hopkins University atlases [30]. These atlases divide the brain into regions based on structure or function, which allows for a more comprehensive characterization of the accuracy and reliability of the quantitative values. Generally, the intragroup CV should ideally be below 10%, and the intergroup CV should remain under 15%, yet a significant intragroup CV was observed in deep GM nucleus regions, such as pallidum. This may be due to the inhomogeneity of B1 and differences in data acquisition parameters or variations in the age and gender of the individuals, which have also been shown and analyzed in previous studies [31-33]. Additionally, these numerical disparities may stem from spatial registration errors between individual quantitative maps and brain region templates, potentially affecting the extraction of quantitative values. Our study also observed significant differences in the T2 CVs between DL and routine scans in some GM brain regions. This difference indicates that although the SRGAN model has good consistency at the overall organizational level, it may introduce variability at the regional scale, which may be due to the model's sensitivity to local texture or noise, potentially limiting its practicality in precise quantitative neuroimaging applications. However, the intra- and inter-group CV for the remaining brain regions remained below 5%, especially for PD values, which show minimal intragroup and intergroup variation across all brain regions. This implies that T2 is relatively sensitive in quantitative analysis and should be a key focus in disease analysis.

The outlined lesion areas in the study are predominantly distributed in the WM. The average T1, T2, and PD quantitative values within these lesion areas exceed 1000 milliseconds, 100 milliseconds, and 80 milliseconds, respectively, which are higher than the ranges observed in the healthy participants' quantitative values. Furthermore, different types of lesions exhibit distinct quantitative values. WM hyperintensities and acute-phase cerebral infarction have similar quantitative values. In contrast, the quantitative values in encephalomalacia are significantly higher than those in the other 2 types of lesions, particularly the T1 values within encephalomalacia (approaching 4000 ms), which are similar to the T1 value of cerebrospinal fluid because the components of encephalomalacia are similar to cerebrospinal fluid. These findings align with clinical knowledge, indicating that lesion areas generally have longer T1 and T2 relaxation

XSL•FO
RenderX

times. Importantly, the quantitative values obtained through DL still maintain diagnostic efficacy. Through careful examination of quantitative values, it was found that with a small amount of lesion data, although the difference in quantitative values between DL and routine scans did not reach statistical significance, 5 reconstructed T2 values were lower than those of the routine scan in 7 WMH and infarct ROIs. Given that these lesions have already exhibited high T2 relaxation times (usually >100 ms), any systematic underestimation may weaken their abnormal manifestations. This may be because superresolution networks are only trained on quantitative images of healthy adults and do not include any pathological cases. Therefore, the model has not yet learned the characteristic diastolic curves of common brain injuries, such as significant prolongation of WM hyperintensities on T2. This lack of exposure may lead to the network interpreting high T2 values in lesions as outliers or reconstruction artifacts, thereby regressing these values to the healthy tissue distribution. Therefore, the sample size will continue to be expanded in the future to verify the quantitative accuracy of DL reconstruction in various neurological diseases.

While the DL maps have basically met the predefined quantitative equivalence margins, the no-reference NIQE metric reveals a residual perceptual gap: compared with fast scanning, the DL image quality has significantly improved (as indicated by a decreased NIQE score), but compared with routine scans, the NIQE scores of the 3-parameter images are slightly higher. This suggests that the current model ensures the accuracy of clinical quantification and significantly improves accuracy on the basis of fast scans, but further improvement is needed to achieve complete perceptual equality with routine HR imaging.

Limitations

This study still has some limitations. First, the study adopted the widely validated SRGAN framework and focused on quantitative agreement and image quality comparison; however, emerging architectures such as ESRGAN or SwinIR were not compared, nor were traditional non-DL upsampling methods used as baselines. Second, the network was trained exclusively on data acquired with a GE 3.0 T scanner and entirely on normal-appearing brain tissue (only 7 patients with 3 common lesion types were used for testing), so the performance of the method on pathological tissue is a preliminary proof of concept rather than evidence of clinical equivalence. The small number of pathology cases limits statistical power and generalizability to diverse or high-contrast lesions, which may pose a barrier to routine clinical deployment. Third, based on the current amount of data, using the training set and testing set with a single subject-level split of 8:2 may prevent data leakage from related slices but may not fully capture the variability between multiple random partitions. Due to limited training data, the model runs on 2D slices instead of 3D volumes, which may result in a loss of spatial continuity between slices. Fourth, acceleration was limited to an R of 3, reconstruction was performed on postprocessed quantitative maps, raw k-space data were not used, and weighted images generated from the quantitative maps were not evaluated. Additionally, the ground truth images have been reconstructed from a matrix of 320 by 256 to a matrix of 512 by 512, and thus, the model learns to reproduce the interpolated image content rather than recovering genuine high-frequency details that would be present in a natively HR acquisition. Finally, evaluation was performed based on quantitative metrics without introducing a qualitative visual assessment by radiologists.

Future Directions

Future research should focus on the following improvements: systematically compare the current SRGAN implementation with newer superresolution networks and quantify the individual contributions of perceptual and adversarial losses to quantitative accuracy, and compare them with non-DL baseline reconstruction methods to better illustrate the benefits of DL. A prospective cohort including demyelinating disease, tumor edema, and microhemorrhages will be enrolled, and the model will be fine-tuned or retrained if necessary before wider clinical deployment. To improve robustness, we will collect both k-space and image-domain data and develop a dual-domain joint reconstruction framework. Future work will explore 3D or slice-aware architectures based on richer training data and computing resources and attempt to use different data partitioning methods to validate generalization further. Finally, the weighted images derived from the superresolved quantitative maps will be generated and assessed for diagnostic quality.

Conclusions

In conclusion, accelerating synthetic MRI is pivotal for its broader clinical adoption in neuroimaging. In this study, we undertook the optimization and enhancement of images acquired through fast synthetic MRI via DL-based reconstruction techniques. Our efforts may result in a remarkable 50% reduction in clinical scan time, all the while achieving better image quality. Importantly, reconstructed T1 and PD maps show excellent agreement with reference scans, supporting their potential for reliable quantification, although T2 values exhibit a consistent underestimation at higher intensities. Despite this limitation, the overall strong correlations and low average biases suggest that using DL methods to mitigate biases in quantitative values is feasible. Furthermore, the shortened scan time not only enhances patient comfort but also reduces the likelihood of motion artifacts. This optimization streamlines the scanning workflow, minimizes redundancy, and maximizes the efficient use of MRI machines.

Acknowledgments

The authors are grateful to Dr Yi Zhu and Dr Rong Wei for their assistance with debugging the deep learning models. The authors also thank Dr Qi Sun for his help with the statistical methods.

XSL•FO
RenderX

Funding

This study was supported by the Space Medical Experiment Project of China Manned Space Program (HYZHXMH01005), Beijing Scholar 2015 (Zhenchang Wang), Beijing Friendship Hospital, Capital Medical University (YYZZ202351), and State Key Laboratory of Digestive Health (25ZX-QN05).

Data Availability

The datasets generated or analyzed during this study are available from the corresponding author on reasonable request.

Authors' Contributions

Conceptualization: YL (lead), HY (equal), PR (equal)
Data curation: YL
Formal analysis: YL (lead), ZZ (supporting)
Funding acquisition: ZW (lead), PR (equal)
Investigation: YL (lead), TZ (supporting)
Methodology: YL, ZZ (supporting), WL (supporting), TZ (supporting), LC (supporting), HL (supporting)
Project administration: PR
Resources: YL (lead), HL (supporting)
Supervision: HY (lead), ZW (equal), ZY (supporting)
Validation: YL
Visualization: YL
Writing – original draft: YL (lead), HY (supporting), HN (supporting)
Writing – review & editing: YL (lead), ZY (supporting), ZW (supporting), PR (supporting)

Conflicts of Interest

None declared.

Multimedia Appendix 1
The details of network structure and loss function.
[DOCX File, 15 KB - medinform_v14i1e79389_app1.docx]

References

1. Cashmore MT, McCann AJ, Wastling SJ, McGrath C, Thornton J, Hall MG. Clinical quantitative MRI and the need for metrology. Br J Radiol 2021 Apr 1;94(1120):20201215. [doi: 10.1259/bjr.20201215] [Medline: 33710907]
2. Warntjes JBM, Dahlqvist O, Lundberg P. Novel method for rapid, simultaneous T1, T2*, and proton density quantification. Magn Reson Med 2007 Mar;57(3):528-537. [doi: 10.1002/mrm.21165] [Medline: 17326183]
3. Blystad I, Warntjes JBM, Smedby O, Landtblom AM, Lundberg P, Larsson EM. Synthetic MRI of the brain in a clinical setting. Acta Radiol 2012 Dec 1;53(10):1158-1163. [doi: 10.1258/ar.2012.120195] [Medline: 23024181]
4. Gao W, Yang Q, Li X, et al. Synthetic MRI with quantitative mappings for identifying receptor status, proliferation rate, and molecular subtypes of breast cancer. Eur J Radiol 2022 Mar;148(157):110168. [doi: 10.1016/j.ejrad.2022.110168] [Medline: 35078137]
5. Zhang Z, Li S, Wang W, et al. Synthetic MRI for the quantitative and morphologic assessment of head and neck tumors: a preliminary study. Dentomaxillofac Radiol 2023 Sep;52(6):20230103. [doi: 10.1259/dmfr.20230103] [Medline: 37427697]
6. Ma L, Lian S, Liu H, et al. Diagnostic performance of synthetic magnetic resonance imaging in the prognostic evaluation of rectal cancer. Quant Imaging Med Surg 2022 Jul;12(7):3580-3591. [doi: 10.21037/qims-22-24] [Medline: 35782274]
7. Li M, Fu W, Ouyang L, et al. Potential clinical feasibility of synthetic MRI in bladder tumors: a comparative study with conventional MRI. Quant Imaging Med Surg 2023 Aug 1;13(8):5109-5118. [doi: 10.21037/qims-22-1419] [Medline: 37581035]
8. Bauer S, Markl M, Honal M, Jung BA. The effect of reconstruction and acquisition parameters for GRAPPA-based parallel imaging on the image quality. Magn Reson Med 2011 Aug;66(2):402-409. [doi: 10.1002/mrm.22803] [Medline: 21381100]
9. Goodfellow I, Pouget-Abadie J, Mirza M, et al. Generative adversarial networks. Commun ACM 2020 Oct 22;63(11):139-144. [doi: 10.1145/3422622]
10. Mardani M, Gong E, Cheng JY, et al. Deep generative adversarial neural networks for compressive sensing MRI. IEEE Trans Med Imaging 2019 Jan;38(1):167-179. [doi: 10.1109/TMI.2018.2858752] [Medline: 30040634]
11. Quan TM, Nguyen-Duc T, Jeong WK. Compressed sensing MRI reconstruction using a generative adversarial network with a cyclic loss. IEEE Trans Med Imaging 2018 Jun;37(6):1488-1497. [doi: 10.1109/TMI.2018.2820120] [Medline: 29870376]

XSL•FO
RenderX

12. Yang G, Yu S, Dong H, et al. DAGAN: deep de-aliasing generative adversarial networks for fast compressed sensing MRI reconstruction. IEEE Trans Med Imaging 2018 Jun;37(6):1310-1321. [doi: 10.1109/TMI.2017.2785879] [Medline: 29870361]
13. Liu Y, Liu Y, Vanguri R, et al. 3D isotropic super-resolution prostate MRI using generative adversarial networks and unpaired multiplane slices. J Digit Imaging 2021 Oct;34(5):1199-1208. [doi: 10.1007/s10278-021-00510-w] [Medline: 34519954]
14. Su PY, Shih HJ, Xu JL. Rapid liver fibrosis evaluation using the UNet-ResNet50-32 × 4d model in magnetic resonance elastography: retrospective study. JMIR Med Inform 2025 Oct 20;13:e80351. [doi: 10.2196/80351] [Medline: 41115237]
15. Ran M, Hu J, Chen Y, et al. Denoising of 3D magnetic resonance images using a residual encoder-decoder Wasserstein generative adversarial network. Med Image Anal 2019 Jul;55:165-180. [doi: 10.1016/j.media.2019.05.001] [Medline: 31085444]
16. Latif S, Asim M, Usman M, Qadir J, Rana R. Automating motion correction in multishot MRI using generative adversarial networks. arXiv. Preprint posted online on Nov 24, 2018. [doi: 10.48550/arXiv.1811.09750]
17. Qiu S, Chen Y, Ma S, et al. Multiparametric mapping in the brain from conventional contrast-weighted images using deep learning. Magn Reson Med 2022 Jan;87(1):488-495. [doi: 10.1002/mrm.28962] [Medline: 34374468]
18. Liu Y, Niu H, Ren P, et al. Generation of quantification maps and weighted images from synthetic magnetic resonance imaging using deep learning network. Phys Med Biol 2022 Jan 17;67(2). [doi: 10.1088/1361-6560/ac46dd] [Medline: 34965516]
19. Don H, Supratak A, Mai L, et al. Tensorlayer: a versatile library for efficient deep learning development. Presented at: MM '17: Proceedings of the 25th ACM international conference on Multimedia; Oct 23-27, 2017; Mountain View, CA p. 1201-1204. [doi: 10.1145/3123266.3129391]
20. SPM8. UCL: Department of Imaging Neuroscience. URL: https://www.fil.ion.ucl.ac.uk/spm/software/spm8/ [accessed 2026-01-14]
21. Zheng Z, Liu Y, Yin H, et al. Evaluating T1, T2 relaxation, and proton density in normal brain using synthetic MRI with fast imaging protocol. Magn Reson Med Sci 2024 Oct 1;23(4):514-524. [doi: 10.2463/mrms.tn.2022-0161] [Medline: 37690836]
22. itk-SNAP. URL: http://www.itksnap.org/pmwiki/pmwiki.php [accessed 2026-01-14]
23. Wang Z, Bovik AC, Sheikh HR, Simoncelli EP. Image quality assessment: from error visibility to structural similarity. IEEE Trans Image Process 2004 Apr;13(4):600-612. [doi: 10.1109/tip.2003.819861] [Medline: 15376593]
24. Saad MA, Bovik AC, Charrier C. Blind image quality assessment: a natural scene statistics approach in the DCT domain. IEEE Trans on Image Process 2012 Aug;21(8):3339-3352. [doi: 10.1109/TIP.2012.2191563]
25. Kim E, Cho HH, Cho SH, et al. Accelerated synthetic MRI with deep learning-based reconstruction for pediatric neuroimaging. AJNR Am J Neuroradiol 2022 Nov;43(11):1653-1659. [doi: 10.3174/ajnr.A7664] [Medline: 36175085]
26. Zheng Z, Yang J, Zhang D, et al. The effect of scan parameters on T1, T2 relaxation times measured with multi-dynamic multi-echo sequence: a phantom study. Phys Eng Sci Med 2022 Jun;45(2):657-664. [doi: 10.1007/s13246-022-01128-0] [Medline: 35553390]
27. Hirano Y, Ishizaka K, Sugimori H, et al. Assessment of accuracy and repeatability of quantitative parameter mapping in MRI. Radiol Phys Technol 2024 Dec;17(4):918-928. [doi: 10.1007/s12194-024-00836-4] [Medline: 39198352]
28. McAllister A, Leach J, West H, Jones B, Zhang B, Serai S. Quantitative synthetic MRI in children: normative intracranial tissue segmentation values during development. AJNR Am J Neuroradiol 2017 Dec;38(12):2364-2372. [doi: 10.3174/ajnr.A5398] [Medline: 28982788]
29. Saccenti L, Andica C, Hagiwara A, et al. Brain tissue and myelin volumetric analysis in multiple sclerosis at 3T MRI with various in-plane resolutions using synthetic MRI. Neuroradiology 2019 Nov;61(11):1219-1227. [doi: 10.1007/s00234-019-02241-w] [Medline: 31209528]
30. Rolls ET, Huang CC, Lin CP, Feng J, Joliot M. Automated anatomical labelling atlas 3. Neuroimage 2020 Feb 1;206:116189. [doi: 10.1016/j.neuroimage.2019.116189] [Medline: 31521825]
31. Hagiwara A, Fujimoto K, Kamagata K, et al. Age-related changes in relaxation times, proton density, myelin, and tissue volumes in adult brain analyzed by 2-dimensional quantitative synthetic magnetic resonance imaging. Invest Radiol 2021 Mar 1;56(3):163-172. [doi: 10.1097/RLI.0000000000000720] [Medline: 32858581]
32. Hagiwara A, Hori M, Cohen-Adad J, et al. Linearity, bias, intrascanner repeatability, and interscanner reproducibility of quantitative multidynamic multiecho sequence for rapid simultaneous relaxometry at 3 T: a validation study with a standardized phantom and healthy controls. Invest Radiol 2019 Jan;54(1):39-47. [doi: 10.1097/RLI.0000000000000510] [Medline: 30300164]
33. Zheng Z, Liu Y, Wang Z, Yin H, Zhang D, Yang J. Evaluating age-and gender-related changes in brain volumes in normal adult using synthetic magnetic resonance imaging. Brain Behav 2024 Jul;14(7):e3619. [doi: 10.1002/brb3.3619] [Medline: 38970221]

Abbreviations

AAL: anatomical automatic labeling

XSL•FO
RenderX

CV: coefficient of variation
DL: deep learning
GM: gray matter
HR: high resolution
LR: low resolution
MRI: magnetic resonance imaging
NIQE: naturalness image quality evaluator
PD: proton density
PSNR: peak signal-to-noise ratio
ReLU: rectified linear unit
ROI: region of interest
SRGAN: superresolution generative adversarial network
SSIM: structural similarity image measure
TOST: two 1-sided tests
WM: white matter

Edited by A Coristine; submitted 20.Jun.2025; peer-reviewed by B Feige, J Bao; accepted 23.Dec.2025; published 23.Jan.2026.

Please cite as:
Liu Y, Yin H, Zheng Z, Liu W, Zhang T, Cai L, Niu H, Lv H, Yang Z, Wang Z, Ren P
Two-Minute Deep Learning–Powered Brain Quantitative Mapping: Accelerating Clinical Imaging With Synthetic Magnetic Resonance Imaging
JMIR Med Inform 2026;14:e79389
URL: https://medinform.jmir.org/2026/1/e79389
doi:10.2196/79389

© Yawen Liu, Hongxia Yin, Zuofeng Zheng, Wenjuan Liu, Tingting Zhang, Linkun Cai, Haijun Niu, Han Lv, Zhenghan Yang, Zhenchang Wang, Pengling Ren. Originally published in JMIR Medical Informatics (https://medinform.jmir.org), 23.Jan.2026. This is an open-access article distributed under the terms of the Creative Commons Attribution License (https://creativecommons.org/licenses/by/4.0/), which permits unrestricted use, distribution, and reproduction in any medium, provided the original work, first published in JMIR Medical Informatics, is properly cited. The complete bibliographic information, a link to the original publication on https://medinform.jmir.org/, as well as this copyright and license information must be included.

XSL•FO
RenderX

Original Paper

Nomograms Based on X-Ray Radiomics for Predicting Pain Progression in Knee Osteoarthritis Using Data From the Foundation for the National Institutes of Health: Development and Validation Study

Yingwei Sun[1*], MD; Jing Liu[2*], MSc; Chunbo Deng[3*], MD; Chengbao Peng[2], MSc; Shinong Pan[4], MD; Xueyong Liu[5], MD

[1]Department of Radiology, Affiliated Hospital of Liaoning University of Traditional Chinese Medicine, Shenyang, China
[2]Platform Engineering Research Center, Neusoft Research Institute of Healthcare Technology, Shenyang, China
[3]Department of Sports and Trauma, Central Hospital Affiliated to Shenyang Medical College, Shenyang, China
[4]Department of Radiology, Shengjing Hospital of China Medical University, Shenyang, China
[5]Department of Rehabilitation, Shengjing Hospital of China Medical University, Shenyang, China
[*]these authors contributed equally

Corresponding Author:
Xueyong Liu, MD
Department of Rehabilitation
Shengjing Hospital of China Medical University
No.16 Puhe Road, Shenbei New District
Shenyang, 110134
China
Phone: 86 2418940112266
Email: liusjh@sj-hospital.org

Abstract

Background: Knee osteoarthritis (KOA) is one of the most prevalent chronic musculoskeletal disorders among the older adult population. Screening populations at risk of rapid progression of osteoarthritis and implementing appropriate early intervention strategies is advantageous for the treatment and prognosis of affected patients.

Objective: This study aimed to construct and validate a nomogram model based on x-ray radiomics to effectively identify individuals experiencing progression of KOA pain.

Methods: The Foundation for the National Institutes of Health Biomarkers Consortium included a total of 600 participants who were classified as pain progressors (n=297, 49.5%) and non–pain progressors (n=303, 50.5%) according to an increase in the Western Ontario and McMaster Universities Osteoarthritis Index pain score of ≥9 points (on a scale from 0 to 100) during the follow-up period of 24 to 48 months. X-rays that lacked defined spacing in the DICOM image were excluded. Fully automatic selection of subchondral bone regions on the inner and outer edges of the tibia and femur as regions of interest and extraction of radiomics features for different combinations of regions of interest were conducted. Least absolute shrinkage and selection operator regression was used to select features and generate a radiomics score using Shapley additive explanations for interpretability. The radiomics score, along with clinical indicators, was incorporated into nomograms using a multivariable logistic regression model. The subgroup analysis focused solely on the progression of pain and cases with no progression at all. The receiver operating characteristic curve, along with calibration and decision curves, was used to assess the discriminative performance.

Results: A total of 450 participants were included in the study. Shapley additive explanations analysis identified Wavelet-HH_gldm_HighGrayLevelEmphasis as the primary radiomics feature. Nomogram 1 and nomogram 2 for predicting KOA pain progression achieved area under the curve values of 0.766 and 0.753, respectively, with mean absolute errors of 0.012 and 0.008, respectively, in the calibration curves. Decision curve analysis showed a positive net benefit across a range of threshold probabilities. In subgroup analyses, nomogram 3 and nomogram 4 yielded areas under the curve of 0.795 and 0.740, respectively.

Conclusions: The nomograms based on x-ray radiomics demonstrated excellent predictive capability and accuracy in forecasting the progression of KOA pain.

XSL•FO
RenderX

(JMIR Med Inform 2026;14:e78338) doi:10.2196/78338

KEYWORDS

radiomics; osteoarthritis; knee; nomogram; artificial intelligence

Introduction

Osteoarthritis (OA) is one of the most common joint disorders affecting the older adult population. With the aging of the population, its incidence has been increasing year by year, imposing a significant burden on both individuals and society [1]. Knee OA (KOA) has the highest incidence among all types of OA. The etiology of KOA is multifactorial, and its pathogenesis remains unclear. KOA can be categorized into various clinical phenotypes and molecular subtypes, including metabolic, inflammatory, mechanical, and genetic [2]. The current treatment guidelines are not suitable for the early diagnosis of KOA and do not distinguish patients who may experience rapid progression [3]. Identifying patients at high risk of rapid progression of KOA will assist in patient education and in the prioritization and allocation of health care resources [4].

The subchondral bone is essential for knee joint structure. Its degeneration disrupts the homeostasis of the intra-articular environment, potentially triggering cartilage degeneration and injury. Furthermore, it is associated with the incidence and progression of OA [5,6]. X-ray imaging continues to be the most prevalent, convenient, and cost-effective modality for evaluating KOA. However, it can only provide a rough estimate of disease severity without quantitative analysis or predicting disease progression [7]. With the application of artificial intelligence in KOA, x-rays can now predict the progression of KOA [3]. Leung et al [8] developed a deep learning predictive model to assess the risk of progression in KOA using knee x-ray images. The findings of their study indicated that this deep learning model surpassed traditional binary outcome models, which are based on standard scoring systems, in predicting the likelihood of total knee arthroplasty among patients with OA [8]. Although deep learning technology is regarded as the most sophisticated image classification technique currently available, its inherent lack of interpretability poses challenges for users in comprehending the model's decision-making outcomes [9].

Radiomics is a novel approach that harnesses advanced image analysis tools and the rapid development of medical imaging data. By integrating artificial intelligence, it enables high-throughput extraction of information from standard medical images and applies the extracted data to clinical decision support systems to enhance the accuracy of diagnosis, prognosis, and prediction [10]. Radiomics has been gradually applied in the field of KOA. Current research primarily focuses on using radiomics to diagnose KOA and predict its radiological progression [11-14]. However, studies on radiomics for predicting the pain progression of KOA are still relatively scarce. A recent study that used magnetic resonance imaging (MRI) radiomics to predict pain progression in KOA demonstrated that the constructed radiomics model achieved an area under the receiver operating characteristic curve (AUC) of 0.79 to 0.86 for KOA pain progression prediction [15]. Nevertheless, the study incorporated 200 radiomics parameters and included omics data from 12- and 24-month follow-ups, resulting in high model complexity and limited practical applicability.

Therefore, this study aimed to develop a nomogram model integrating x-ray subchondral radiomics features and clinical characteristics to predict pain progression in KOA. The Shapley additive explanations (SHAP) method was incorporated to offer a comprehensive explanation and intuitive visualization of the model's predictive mechanisms. This approach allows for the identification of high-risk individuals with rapid pain progression among patients with KOA using cost-effective detection methods, thereby providing clinicians with evidence-based guidance for early intervention strategies.

Methods

Participants

This study involved participants from the Foundation for the National Institutes of Health (FNIH) Osteoarthritis Biomarkers Project. The design of this research is detailed in previously published literature [16,17]. In brief, the FNIH Osteoarthritis Biomarkers Project includes 600 participants with KOA of Kellgren-Lawrence grades 1 to 3. According to the results of the follow-up, the 600 participants at baseline were categorized into four distinct subgroups: (1) participants exhibiting both radiological and pain progression (n=194, 32.3%), (2) participants with only radiological progression (n=103, 17.2%), (3) participants experiencing only pain progression (n=103, 17.2%), and (4) participants who exhibited neither radiological nor pain progression (n=200, 33.3%). Radiological progression was defined as a loss of minimum joint space width of ≥0.7 mm in the medial femorotibial compartment between baseline and follow-up at 24, 36, or 48 months. Pain progression was characterized by a sustained increase in the Western Ontario and McMaster Universities Osteoarthritis Index (WOMAC) pain subscale (≥9 on a scale from 0 to 100) based on the minimum clinically important difference during the same time frame. In the Digital Imaging and Communications in Medicine (DICOM) standard, pixel spacing is a critical factor for converting image pixels into physical dimensions. Spacing ensures the reliability and reproducibility of medical images in diagnosis, research, and treatment planning [18]. However, some datasets lack or contain erroneous spacing information. They use default values (1.0, 1.0), which result in calculated knee dimensions significantly exceeding normal human anatomical ranges. Such data can be defined as "DICOM data with invalid spacing information." In the standardization process for the Osteoarthritis Initiative (OAI) knee x-ray images, cases with unspecified pixel spacing were excluded. As the pixel spacing of 0.2 mm was predominant in the dataset, all retained images were calibrated to this value to ensure consistent spatial scaling [19]. The specific process of normalization is described in Multimedia Appendix 1 [20-22]. Groups 1 and 3, which

XSL•FO
RenderX

showed pain progression, were combined as the case group, whereas groups 2 and 4, with no pain progression, served as the control group for analysis. Additionally, we conducted subgroup analyses on group 3 (with only pain progression) and group 4 (without both pain and radiological progression). The study flow diagram is shown in Figure 1.

Figure 1. Flowchart of the study. The x-ray images of the knee joint were normalized, and the regions of interest were automatically identified and selected. Subsequently, imaging omics parameters were extracted, followed by a screening process for feature parameters. Imaging omics labels were then constructed to evaluate clinical features, ultimately leading to the generation of a nomogram and an assessment of its performance.

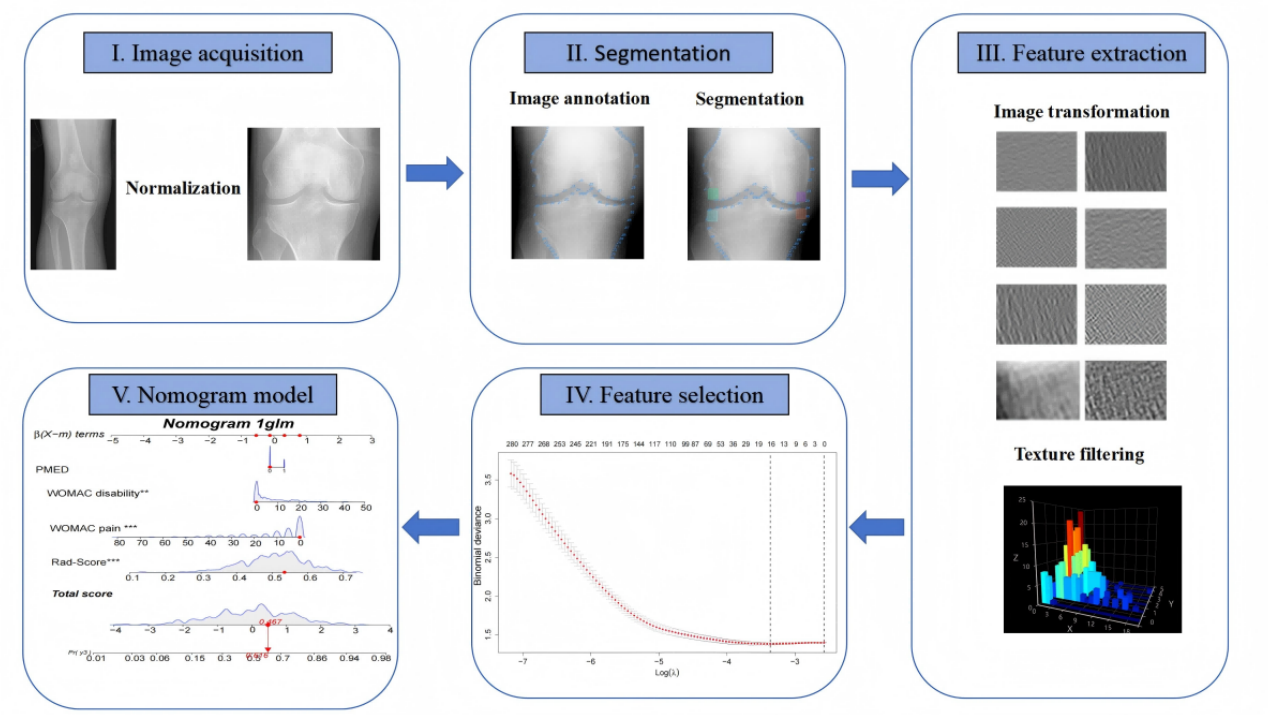

Segmentation and Region of Interest Annotation

BoneFinder (The University of Manchester) is a fully automated software tool designed to outline and segment skeletal structures from 2D radiographs by placing a series of points along bone contours or at key anatomical landmarks. In brief, BoneFinder uses a random forest voting mechanism to precisely determine the optimal placement of model feature points, enabling robust and accurate shape model matching. The system can accurately identify and segment bones not previously present in new images. This method demonstrates exceptional robustness and precision across various skeletal applications, with its generated point data being widely applicable to morphometric analyses, including the construction of statistical morphological models and automatic derivation of standard geometric measurement parameters [23], resulting in 74 markers per image (Figure 2). The fully automatic BoneFinder knee module achieves a mean point-to-curve error of less than 1.0 mm for 99% of 500 images (ie, in 99% of images, the error is less than 1.0 mm) without considering knee size [24].

Four vertical lines are constructed at the marked points 64, 58, 54, and 48 on the knee joint x-ray image, as identified by BoneFinder. These lines are sequentially designated as line 1, line 2, line 3, and line 4. The distance between line 1 and line 2 is denoted as R1, whereas the distance between line 3 and line 4 is referred to as R2. With point 64 designated as the vertex and a side length of R1/4, a square encompassing the medial tibia was defined as the region of interest (ROI). With marker point 64 designated as the vertex and a quarter of R1 as the side length, a square encompassing the medial tibia was defined as the ROI. First, using marker point 48 as the vertex and a quarter of R2 as the side length, a square area on the lateral tibia was selected to define ROI. Second, the selection process for the femur ROI differs from that of the tibia ROI. ROI 3 is defined with the line intersecting marker 24 as its lower boundary, while the line intersecting marker point 26 serves as the side boundary of this ROI. ROI 4 of the lateral femur uses the line indicated at point 14 as the lower boundary of the ROI and the column line marked at point 12 as its vertical boundary. Then, squares with side lengths of a quarter of R1 and a quarter of R2 are constructed. To assess the repeatability of ROI delineation, a total of 40 cases were randomly selected from the collected dataset. Two senior musculoskeletal radiologists (YWS and SNP) conducted manual segmentation of ROIs. Dice similarity coefficients were used to assess manual and automated segmentation agreement. Image annotation was performed using Neusoft Darts [25].

XSL•FO
RenderX

Figure 2. Schematic diagram of the automated region of interest segmentation process.

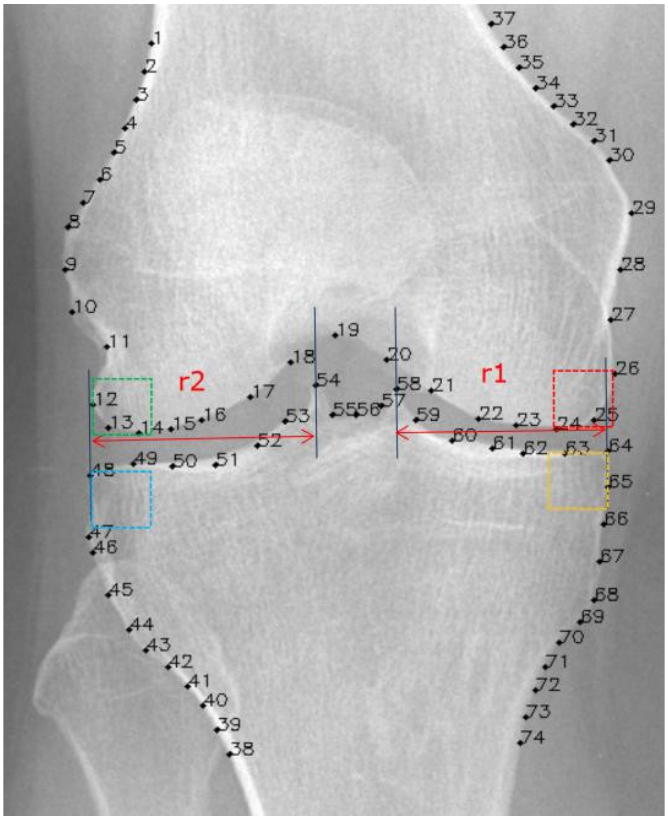

Radiomics Feature Extraction

The extraction of radiomics features was based on Neusoft Discovery [25]. The features that were extracted can be categorized into 3 distinct groups. First-order features were derived from the gray values of images, reflecting the distribution and heterogeneity of intensity within the ROI, typically including maximum, minimum, mean, median, range, variance, kurtosis, skewness, and entropy. The second-order features refer to the extracted texture characteristics, which include texture feature values derived from the gray-level co-occurrence matrix, gray-level run-length matrix, gray-level connected region size matrix, neighborhood difference matrix, and gray-level correlation matrix. The texture features can quantify the distribution of textures within the ROI that are difficult to perceive visually. Third, features were extracted after log transformation, first-level wavelet decomposition, and gradient transformation were applied to the ROI. All features were normalized using the following formula: $Z=(x–\mu)/\sigma$.

Radiomics Feature Selection and Radiomics Signature Construction

The Spearman correlation was used to remove the redundant features. The feature subset was optimized using the least absolute shrinkage and selection operator (LASSO) method in logistic regression. A 10-fold cross-validation approach was used to identify the optimal model that minimizes the mean squared error, and the correlation coefficients of the features selected by the best LASSO model were calculated. According to the coefficients derived from LASSO regression, a weighted calculation was performed to obtain the radiomics score (rad-score). Radiomics parameters from 4 ROIs (ROIs 1-4) were extracted individually, and rad-score 1 was developed following LASSO screening of the nonzero parameters. The radiomics parameters were applied to ROI 1 and ROI 3, leading to the development of rad-score 2. In subgroup analysis, rad-score 3, obtained from extracted and screened nonzero parameters from ROIs 1 to 4, and rad-score 4, obtained from extracted and screened nonzero parameters from ROI 1 and ROI 3, predicted pain progression only and no progression at all, respectively. SHAP analysis was used to mitigate the “black-box” effect of machine learning, enabling feature prioritization and interpretability of individual radiomics features on the rad-score. Feature maps were used to visualize the results of the rad-score.

Development and Evaluation of Nomograms

The analysis used stepwise backward multivariable logistic regression to identify clinical risk factors at baseline and construct nomograms. The Akaike information criterion likelihood ratio test was used as the stopping rule for the backward stepwise logistic regression analysis. Clinical information from patients at baseline included age, sex, history of injury, BMI, the minimum joint space width of the medial tibial-femoral compartment, Kellgren-Lawrence grade, WOMAC pain score and WOMAC disability score, medicine for pain in the previous 12 months, and race. The nomograms were developed based on the prediction probability value of the optimal radiomics models and clinical independent risk factors. The discriminative ability of the nomogram was evaluated using the AUC and accuracy. Calibration of the nomogram was performed through calibration curves, with optimal calibration indicated by alignment with the diagonal line. Internal validation was conducted using a bootstrap method involving 1000

XSL•FO
RenderX

resampling iterations, and the mean absolute error was used to assess model calibration. Additionally, decision curve analysis (DCA) quantified net benefits at various threshold probabilities to evaluate the clinical effectiveness of the nomograms.

Statistical Analysis

The comparison of categorical variables was conducted using the Pearson chi-square test. Continuous variables were expressed as mean and SD and analyzed using either the 2-tailed *t* test or Mann-Whitney *U* test. The normality of continuous data was assessed using the Kolmogorov-Smirnov test; measurements that followed a normal distribution were subjected to the *t* test, whereas those that did not conform to a normal distribution underwent the Mann-Whitney *U* test. The DeLong test was used for comparing 2 models. *P* values were calculated using a 2-tailed *z* test, with $P<.05$ considered statistically significant. All statistical analyses were performed using the EmpowerStats software (X&Y Solutions, Inc) and the R software (version 4.2.2; R Foundation for Statistical Computing).

Ethical Considerations

This study was conducted in accordance with the Declaration of Helsinki (as revised in 2013). The Institutional Review Board of the University of California, San Francisco (approval 10-00532), and the 4 clinical centers of the OAI project recognized the study as HIPAA (Health Insurance Portability and Accountability Act) compliant. All participants provided written informed consent. Patient-identifiable information (including names and hospital ID numbers) was carefully removed from the x-ray images and reports before analysis. Due to the retrospective design of this study, participants received no compensation.

Results

Baseline Clinical Characteristics

Due to the lack of spacing in DICOM images, a total of 450 participants were ultimately included in the study, with 227 (50.4%) and 223 (49.6%) in the control and case groups, respectively. The baseline characteristics of participants in both the case and control groups were frequency matched for factors including age, BMI, WOMAC functional scores, Kellgren-Lawrence grade, pain medication history, and race. Notably, a statistically significant difference was observed in WOMAC pain scores ($P=.04$) and medication history ($P=.02$) between the 2 groups (Table 1). In subgroup analysis, 18% (n=81) of the individuals demonstrated only pain progression during the follow-up period, whereas 32.9% (n=148) of the individuals exhibited neither pain progression nor radiographic deterioration. The baseline characteristics of participants across both groups were well matched, with no statistically significant differences observed (Table S1 in Multimedia Appendix 2).

Table 1. Baseline characteristics of the study population.

Characteristic	Control group (n=223)	Case group (n=227)	*P* value
Demographics			
Age (years), mean (SD)	62.14 (8.91)	61.48 (8.79)	.38
Female sex, n (%)	131 (58.7)	136 (59.9)	.80
Race, n (%)			.44
Asian	3 (1.3)	2 (0.9)	
Black or African American	21 (9.4)	32 (14.1)	
White	196 (87.9)	191 (84.1)	
Other non-White race	3 (1.3)	2 (0.9)	
Clinical measures			
BMI (kg/m^2), mean (SD)	30.36 (4.85)	30.50 (4.71)	.75
WOMAC[a] pain score (0-20), mean (SD)	2.70 (3.40)	1.87 (2.47)	.04
WOMAC function score (0-68), mean (SD)	8.15 (10.98)	8.13 (9.18)	.15
History of knee injury, n (%)	77 (34.5)	83 (36.6)	.65
Use of pain medication, n (%)	49 (22.0)	73 (32.2)	.02
Radiographic measures			
Kellgren-Lawrence grade, n (%)			.70
1	29 (13.0)	29 (12.8)	
2	112 (50.2)	106 (46.7)	
3	82 (36.8)	92 (40.5)	
Minimum medial joint space width (mm), mean (SD)	3.77 (1.10)	3.80 (1.32)	.87

[a]WOMAC: Western Ontario and McMaster Universities Osteoarthritis Index.

XSL•FO
RenderX

Segmentation and Feature Extraction

The automated segmentation dataset was used for radiomics feature extraction as the Dice similarity coefficients between automatic and manual segmentation were excellent (0.800; Table S2 in Multimedia Appendix 2). We used 10-fold cross-validation to identify the optimal tuning parameter (alpha). In total, 16 nonzero coefficient features were derived from the optimal tuning parameters in rad-score 1. Rad-score 2 comprised 12 nonzero coefficient features. In subgroup analysis, rad-score 3 included 11 nonzero feature parameters, whereas rad-score 4 consisted of 3 nonzero features (Tables S3-S6 in Multimedia Appendix 2 and Figures S1-S4 in Multimedia Appendix 2). The correlation among features was analyzed using Spearman correlation analysis, and heat maps are presented in Figures S1 to S4 in Multimedia Appendix 2.

Development and Evaluation of Radiomics Signatures

Table 2 shows the diagnostic proficiency of 4 radiomics signatures. The AUC value for rad-score 1 was 0.728 (95% CI 0.681-0.774), the AUC value for rad-score 2 was 0.716 (95% CI 0.635-0.736), the AUC value for rad-score 3 was 0.775 (95% CI 0.714-0.837), and the AUC value for rad-score 4 was 0.679 (95% CI 0.604-0.755; Table 2). The SHAP plot in Figure 3 visually illustrates how radiomics features influenced model predictions in terms of magnitude and direction. Features are sorted vertically by global importance. Each point represents the SHAP value of each feature for a specific patient plotted horizontally and stacked vertically to show density distribution. The color of the point reflects the feature value, from low (blue) to high (red; Figures 3A and C). The bar chart illustrates the impact of various imaging features on the rad-score. Wavelet-HH_gldm_HighGrayLevelEmphasis showed significant effects on both rad-score 1 and rad-score 2 (Figures 3B and D). The SHAP values of each feature in rad-score 3 and rad-score 4 are shown in Figure S5 in Multimedia Appendix 2. Figure 4 shows representative participants with x-ray subchondral bone feature maps from 4 ROIs. The case group participant demonstrated higher ROI heterogeneity than the control group participant, with a higher score (0.58 vs 0.44).

Table 2. Diagnostic efficacy of the 4 radiomics scores.

Radiomics score	AUC[a] (95% CI)	Accuracy	Sensitivity	Specificity
1	0.728 (0.681-0.774)	0.684	0.797	0.570
2	0.716 (0.635-0.736)	0.668	0.683	0.677
3	0.775 (0.714-0.837)	0.742	0.753	0.716
4	0.679 (0.604-0.755)	0.694	0.580	0.757

[a]AUC: area under the receiver operating characteristic curve.

Figure 3. Shapley additive explanations (SHAP) summary plots of the radiomics score. The plot illustrates the feature relevance and attributions of the model's predictive performance: (A) rad-score 1 and (B) rad-score 2. The bar chart illustrates the impact of various imaging features on the rad-score: (C) rad-score 1 and (D) rad-score 2.

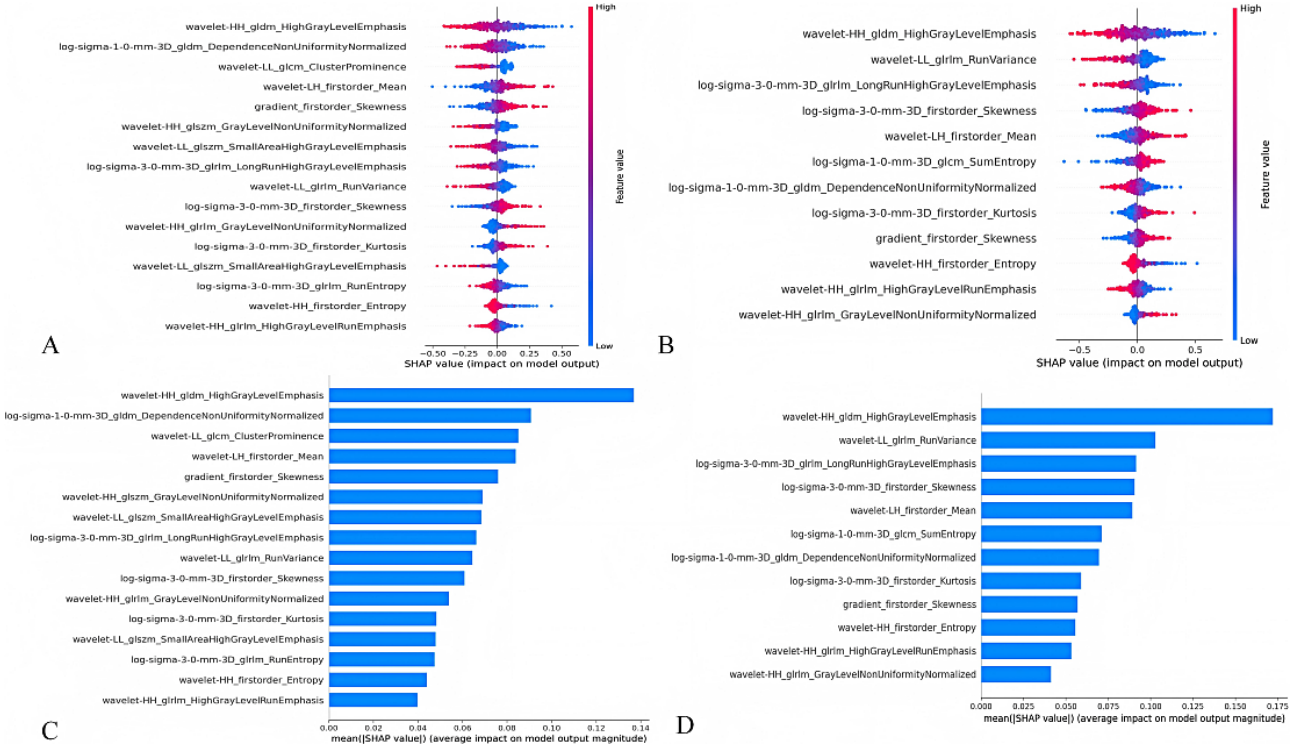

XSL•FO
RenderX

Figure 4. Visualization of radiomics signatures. The case group participant demonstrated higher region of interest heterogeneity than the control group participant, with a higher score.

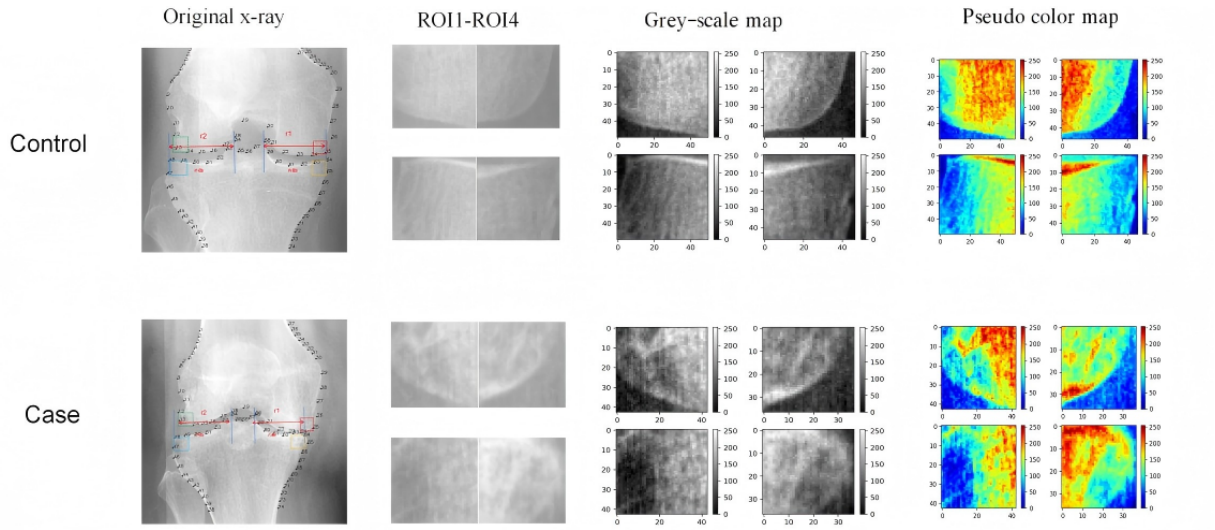

Construction and Testing of Nomograms

Through multiple regression analysis, the WOMAC disability score, pain medication history, and WOMAC pain score were found to be risk factors for KOA pain progression. We constructed visual nomograms by integrating the score with selected clinical risk factors. The AUC of nomogram 1 was 0.766 (95% CI 0.722-0.809), and the AUC of nomogram 2 was 0.753 (95% CI 0.708-0.797). The comparison of AUC between the 2 models showed no statistically significant difference (DeLong test; *P*>.05; Figure 3). The calibration curve demonstrated that all cohorts were accurately aligned with the actual observations. The internal validation was conducted using the bootstrap method, with a resampling count set to 1000. The mean absolute errors of the calibration curves for the 2 models were found to be 0.012 and 0.008, indicating that the model demonstrated a high level of calibration accuracy (Figure 5 and Table 3). The DCA demonstrated that, if the threshold probability in the clinical decision was in the range of 10% to 70%, both nomogram 1 and nomogram 2 could yield more net benefits compared with either the treat-all-patients strategy or the treat-none strategy.

Figure 5. Development and validation of the nomogram to predict pain progression in knee osteoarthritis (A: nomogram 1; B: nomogram 2), the receiver operating characteristic curves of nomogram 1 and nomogram 2(C), the calibration curves of nomogram 1 and nomogram 2 (D and E, respectively), and decision curves for nomogram 1 and nomogram 2 (F). PMED: Use of pain medication.

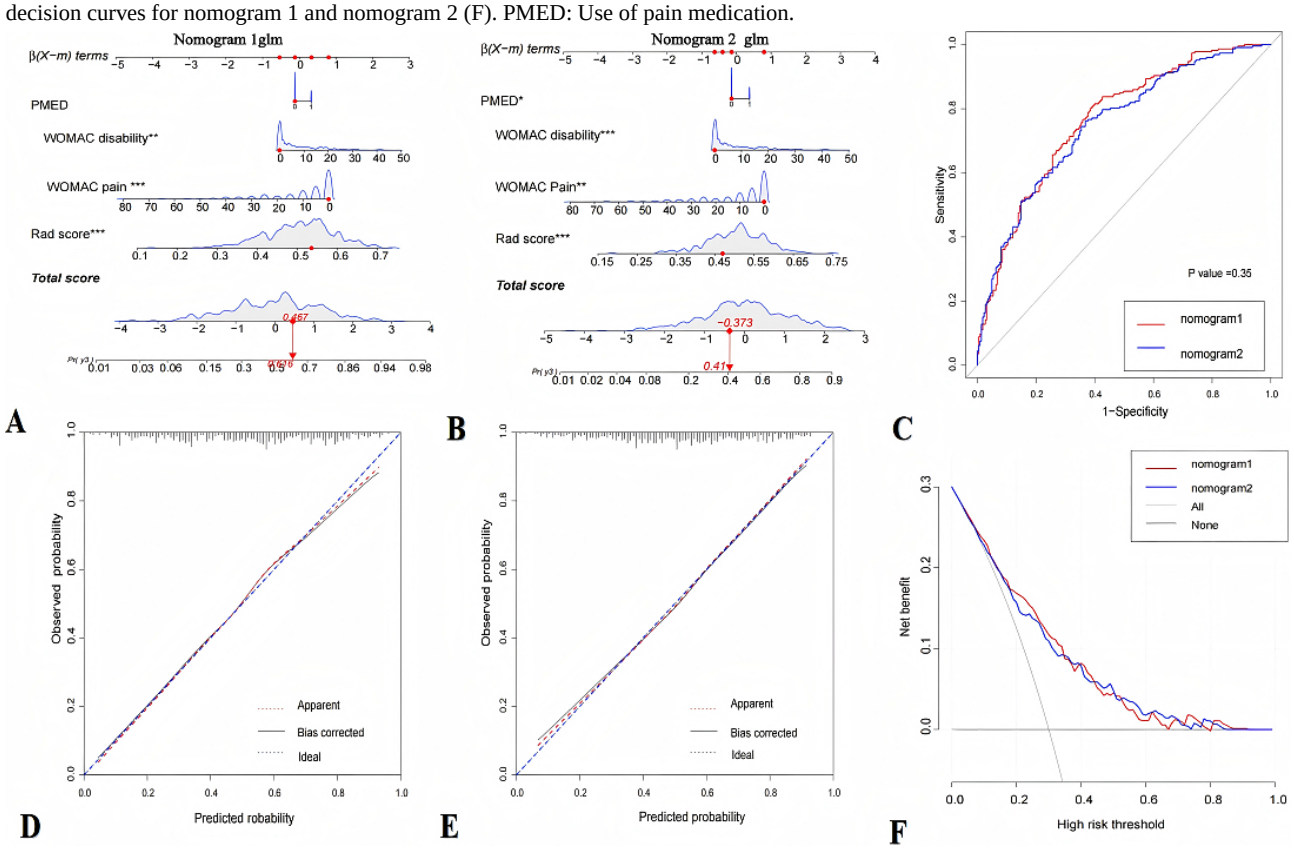

XSL•FO
RenderX

Table 3. Diagnostic efficacy of the 4 nomogram models.

Model	AUC[a] (95% CI)	Accuracy	Sensitivity	Specificity	MAE[b]
Nomogram 1	0.766 (0.722-0.809)	0.709	0.692	0.726	0.012
Nomogram 2	0.753 (0.708-0.797)	0.693	0.648	0.740	0.008
Nomogram 3	0.795 (0.734-0.865)	0.760	0.691	0.797	0.011
Nomogram 4	0.740 (0.673-0.808)	0.686	0.740	0.695	0.013

[a]AUC: area under the receiver operating characteristic curve.

[b]MAE: mean absolute error.

Subgroup Analyses

The AUC of nomogram 3 was 0.795 (95% CI 0.734-0.865), and the AUC of nomogram 4 was 0.740 (95% CI 0.673-0.808). The comparison of the AUC between the 2 models showed a statistically significant difference (DeLong test; $P<.05$). The calibration curve demonstrated a robust concordance between the probabilities predicted and the actual observed outcomes. The DCAs demonstrated that, if the threshold probability in the clinical decision was within the range of 10% to 65%, the curve corresponding to nomogram 3 was above nomogram 4, and the AUC that it formed with the "treat none" and "treat all" lines was relatively larger. The net benefit of nomogram 3 was superior to that of nomogram 4, making it the better model (Table 3 and Figure 6).

Figure 6. Development and validation of the nomogram to predict pain progression in knee osteoarthritis (A: nomogram 3; B: nomogram 4), the receiver operating characteristic curves of nomogram 3 and nomogram 4 (C), the calibration curves of nomogram 3 and nomogram 4 (D and E, respectively), and decision curves for nomogram 3 and nomogram 4 (F). PMED: Use of pain medication.

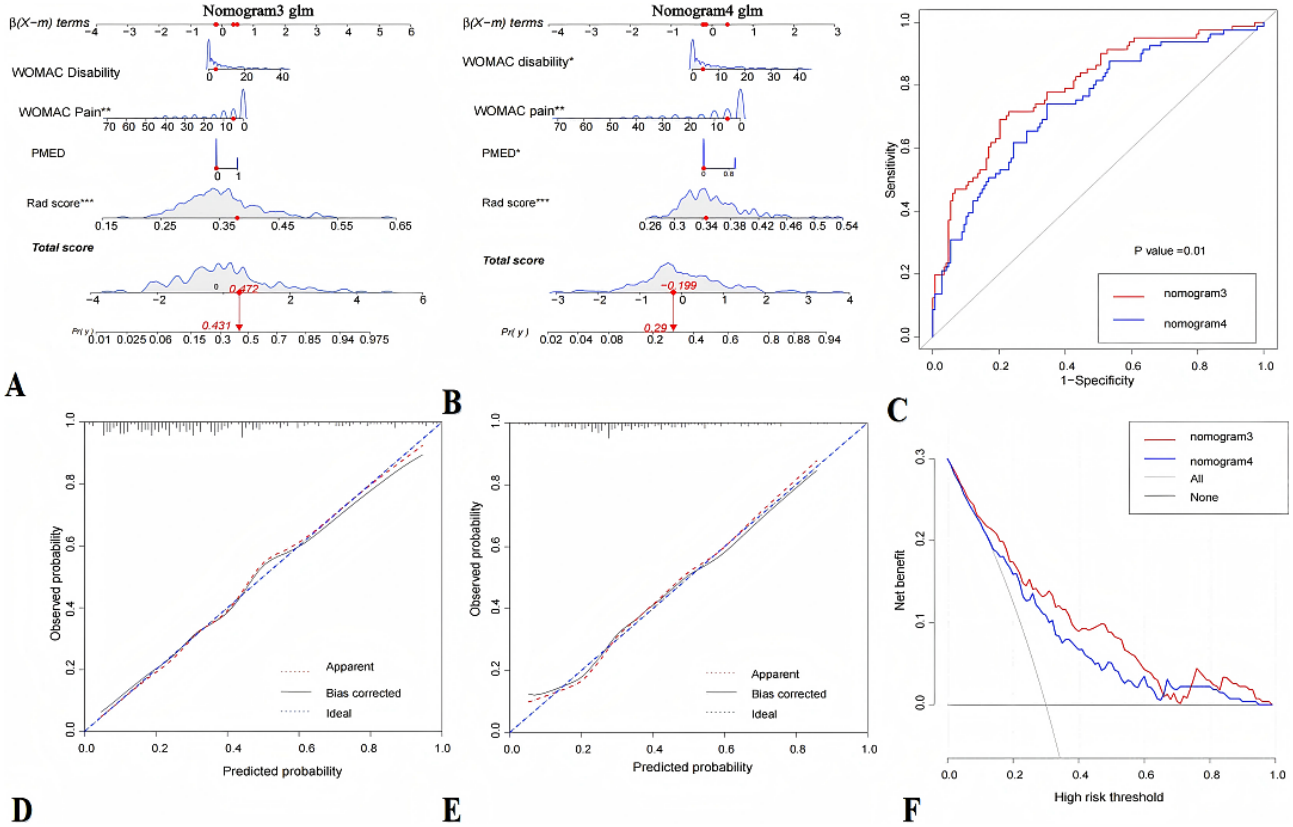

Discussion

Principal Findings

Our study developed a nomogram integrating x-ray radiomics features and clinical variables to predict pain progression in KOA. The resulting baseline-based, cost-effective nomogram demonstrated commendable accuracy and reproducibility in forecasting KOA pain progression, offering significant potential for guiding early intervention strategies in at-risk populations. The application of advanced artificial intelligence to widely available and cost-effective x-ray imaging represents a feasible and promising approach for predicting KOA pain progression. Radiomics models can automatically classify KOA [26], and texture analysis of the subchondral bone, particularly in the tibia, has shown predictive value for radiographic KOA incidence [27,28]. Given the complex etiology of KOA and the frequent discrepancy between clinical symptoms and radiological severity, we focused on subchondral bone remodeling—a process linked to pain pathogenesis through

XSL•FO
RenderX

molecules such as netrin-1 and PEG2, which promote sensory nerve innervation [29,30]. This rationale supported our use of subchondral bone radiomics for predicting symptomatic progression. Radiomics enables high-throughput extraction of quantitative features from medical images, providing data for clinical decision support systems [10]. The selection of key ROIs is critical as different image areas contain varying levels of information relevant to disease progression [31]. While the medial subchondral bone often shows a stronger correlation with OA [32] and the medial tibial margin is recognized as highly informative due to its role in absorbing uneven mechanical loads [33], the optimal ROI selection remains debated. Some deep learning studies for KOA pain progression have also concentrated on the medial joint space and osteophytes [8], whereas other radiomics research suggests that including the entire tibial subchondral bone may yield better outcomes than focusing solely on specific compartments [17].

In this study, we systematically evaluated the impact of ROI selection on model accuracy by constructing radiomics signatures both from 4 ROIs encompassing the entire knee joint and from the 2 medial ROIs alone. Our findings revealed that incorporating lateral ROIs did not improve the overall model AUC compared to using medial ROIs only. However, subgroup analysis indicated that models combining medial and lateral ROIs achieved significantly higher AUC values in specific contexts. The primary cause of this discrepancy may stem from disease heterogeneity. Notably, in the main analysis, both the pain progression group and the nonprogression group included participants with radiological progression. Pathological changes in the lateral subchondral bone may accelerate the radiological progression of the knee joint [34-36]. Therefore, the role of radiomics features in lateral ROIs during pain progression was likely diluted or masked by features from radiologically progressive participants in the control group.

When compared to prior studies, our model demonstrated competitive predictive performance. For instance, Kraus et al [16] applied 3 texture parameters to predict KOA pain progression, achieving AUCs ranging from 0.603 to 0.649. Our rad-score yielded AUCs between 0.679 and 0.775, representing a substantial improvement. This aligns with the understanding that multivariable models integrating multiple risk factors generally provide more reliable estimates than those based on single parameters [37]. The superior performance of our baseline-based model is particularly notable compared to previously reported predictive capabilities relying solely on baseline biomarkers [38]. A recent study using MRI-based radiomics to predict KOA pain progression reported high predictive accuracy, with AUC values ranging from 0.79 to 0.86 [15]. This performance is commendable. However, it is important to note that their model incorporated a substantially larger set of 200 radiomics parameters and, crucially, relied on omics data extracted from 12- and 24-month follow-up MRI scans. While this approach yields high accuracy, the model's complexity and its dependence on longitudinal imaging data significantly limit its practicality and scalability in routine clinical settings. In contrast, our study deliberately pursued a more streamlined and clinically translatable strategy. By using only baseline x-ray images and constructing a parsimonious model using key radiomics features and clinical variables, our baseline-based model eliminates the need for costly follow-up MRI scans and complex feature sets, making it more feasible for immediate clinical application and potential widespread adoption.

Research using deep learning methods to predict KOA pain progression remains scarce. A study using OAI data demonstrated that deep learning models achieved an AUC of 0.77 for predicting KOA pain progression, significantly higher than the 0.692 of traditional models [39]. By integrating demographic, clinical, and imaging risk factors with a deep learning model incorporating baseline knee x-rays, the highest diagnostic efficacy (AUC=0.807) was achieved in predicting pain progression. However, the original study failed to provide specific feature information. In contrast, our study visually presented each feature parameter's impact on the rad-score using Shapley summaries. Wavelet-HH_gldm_HighGrayLevelEmphasis, a gray-level correlation matrix feature derived from high-frequency (HH) subbands of wavelet-transformed images, reflects the concentration of high–gray value regions and emphasizes texture variations in these areas. By quantifying texture changes in knee images, this feature effectively captures tissue degeneration differences caused by pain progression, indirectly reflecting pathological changes and potentially enabling prediction of knee pain progression.

The nomogram was selected for its ability to simplify complex statistical models into user-friendly graphical interfaces that generate individualized risk estimates [40]. While nomograms have been applied in OA contexts such as predicting outcomes after total knee replacement [41,42], their application specifically for predicting KOA pain progression represents a novel contribution. Our nomogram uniquely integrates radiomics signatures with key clinical variables: baseline WOMAC pain scores, WOMAC disability scores, and analgesic use. Interestingly, the baseline WOMAC pain score served as a negative predictor in our model, potentially reflecting the development of tolerance to chronic pain in patients with KOA [43]. The inclusion of WOMAC disability scores and analgesic use is supported by their established roles as risk factors in KOA phenotypic and prognostic models [44,45].

Limitations

This study has several limitations. First, the relatively small sample size may affect statistical power and generalizability. Second, the use of data from previous nested case-control studies could introduce selection bias. Third, our analysis relied solely on internal validation because it was difficult to find an equivalent external cohort. Although the data were sourced from the well-established FNIH Osteoarthritis Biomarkers Project, external validation using independent datasets, such as those from the PROGRESS OA study (phase 2 of the FNIH Biomarkers consortium), was not feasible as these data have not been publicly released [46]. To our knowledge, no other studies have explored the specific pain progression patterns defined by the FNIH [15], and other studies using FNIH data have similarly been unable to perform external validation.

XSL•FO
RenderX

Conclusions

A nomogram based on baseline x-ray radiomics signatures can effectively predict the progression of pain in KOA. This has significant implications for supporting health care professionals in tailoring treatment plans for individuals experiencing rapid pain progression, as well as in reducing health care costs, and these findings need further validation in future trials.

Acknowledgments

The data for this study were obtained and analyzed from the controlled-access datasets distributed from the Osteoarthritis Initiative, a data repository housed within the National Institute of Mental Health Data Archive. The Osteoarthritis Initiative represents a public-private partnership consisting of 5 contracts funded by the National Institutes of Health.

Funding

This study received funding from Liaoning Province Science and Technology Plan Joint Program (2024012243-JH4/4800) and Liaoning Province Science and Technology Plan Joint Technical Breakthrough Plan Project (2024JH2/10 2600325).

Data Availability

The datasets generated or analyzed during this study are available in the Osteoarthritis Initiative repository [47].

Authors' Contributions

Conceptualization: YS, XL
Data curation: YS
Funding acquisition: YS, XL
Investigation: SP
Methodology: JL, CD, XL
Project administration: JL, XL
Resources: JL
Software: CP
Supervision: CP, SP, XL
Validation: YS, XL
Visualization: YS, XL
Writing—original draft: YS, CD
Writing—review and editing: YS, CD, XL

Conflicts of Interest

None declared.

Multimedia Appendix 1
Size normalization and pixel normalization of the x-ray.
[DOCX File , 198 KB - medinform_v14i1e78338_app1.docx]

Multimedia Appendix 2
Baseline characteristics of the subgroup population, radiomic characteristics, and Dice and Shapley additive explanations summary plots of the radiomic score.
[DOCX File , 1921 KB - medinform_v14i1e78338_app2.docx]

References

1. Safiri S, Kolahi AA, Smith E, Hill C, Bettampadi D, Mansournia MA, et al. Global, regional and national burden of osteoarthritis 1990-2017: a systematic analysis of the Global Burden of Disease Study 2017. Ann Rheum Dis 2020 Jun;79(6):819-828. [doi: 10.1136/annrheumdis-2019-216515] [Medline: 32398285]
2. Fan X, Sun AR, Young RS, Afara IO, Hamilton BR, Ong LJ, et al. Spatial analysis of the osteoarthritis microenvironment: techniques, insights, and applications. Bone Res 2024 Feb 04;12(1):7 [FREE Full text] [doi: 10.1038/s41413-023-00304-6] [Medline: 38311627]
3. Jamshidi A, Pelletier JP, Martel-Pelletier J. Machine-learning-based patient-specific prediction models for knee osteoarthritis. Nat Rev Rheumatol 2019 Jan;15(1):49-60. [doi: 10.1038/s41584-018-0130-5] [Medline: 30523334]
4. Atukorala I, Pathmeswaran A, Makovey J, Metcalf B, Bennell KL, March L, et al. Can pain flares in knee osteoarthritis be predicted? Scand J Rheumatol 2021 May;50(3):198-205. [doi: 10.1080/03009742.2020.1829035] [Medline: 33467963]

XSL•FO
RenderX

5. Hu W, Chen Y, Dou C, Dong S. Microenvironment in subchondral bone: predominant regulator for the treatment of osteoarthritis. Ann Rheum Dis 2021 Apr;80(4):413-422 [FREE Full text] [doi: 10.1136/annrheumdis-2020-218089] [Medline: 33158879]
6. Hu Y, Chen X, Wang S, Jing Y, Su J. Subchondral bone microenvironment in osteoarthritis and pain. Bone Res 2021 Mar 17;9(1):20 [FREE Full text] [doi: 10.1038/s41413-021-00147-z] [Medline: 33731688]
7. Roemer FW, Demehri S, Omoumi P, Link TM, Kijowski R, Saarakkala S, et al. State of the art: imaging of osteoarthritis-revisited 2020. Radiology 2020 Jul;296(1):5-21. [doi: 10.1148/radiol.2020192498] [Medline: 32427556]
8. Leung K, Zhang B, Tan J, Shen Y, Geras KJ, Babb JS, et al. Prediction of total knee replacement and diagnosis of osteoarthritis by using deep learning on knee radiographs: data from the osteoarthritis initiative. Radiology 2020 Sep;296(3):584-593 [FREE Full text] [doi: 10.1148/radiol.2020192091] [Medline: 32573386]
9. Guan B, Liu F, Haj-Mirzaian A, Demehri S, Samsonov A, Neogi T, et al. Deep learning risk assessment models for predicting progression of radiographic medial joint space loss over a 48-MONTH follow-up period. Osteoarthritis Cartilage 2020 Apr;28(4):428-437 [FREE Full text] [doi: 10.1016/j.joca.2020.01.010] [Medline: 32035934]
10. Lambin P, Leijenaar RT, Deist TM, Peerlings J, de Jong EE, van Timmeren J, et al. Radiomics: the bridge between medical imaging and personalized medicine. Nat Rev Clin Oncol 2017 Dec;14(12):749-762. [doi: 10.1038/nrclinonc.2017.141] [Medline: 28975929]
11. Jiang H, Peng Y, Qin SY, Chen C, Pu Y, Liang R, et al. MRI-based radiomics and delta-radiomics models of the patella predict the radiographic progression of osteoarthritis: data from the FNIH OA biomarkers consortium. Acad Radiol 2024 Apr;31(4):1508-1517. [doi: 10.1016/j.acra.2023.10.003] [Medline: 37923575]
12. Lin T, Peng S, Lu S, Fu S, Zeng D, Li J, et al. Prediction of knee pain improvement over two years for knee osteoarthritis using a dynamic nomogram based on MRI-derived radiomics: a proof-of-concept study. Osteoarthritis Cartilage 2023 Feb;31(2):267-278 [FREE Full text] [doi: 10.1016/j.joca.2022.10.014] [Medline: 36334697]
13. Almhdie-Imjabbar A, Podsiadlo P, Ljuhar R, Jennane R, Nguyen KL, Toumi H, et al. Trabecular bone texture analysis of conventional radiographs in the assessment of knee osteoarthritis: review and viewpoint. Arthritis Res Ther 2021 Aug 06;23(1):208 [FREE Full text] [doi: 10.1186/s13075-021-02594-9] [Medline: 34362427]
14. Li W, Feng J, Zhu D, Xiao Z, Liu J, Fang Y, et al. Nomogram model based on radiomics signatures and age to assist in the diagnosis of knee osteoarthritis. Exp Gerontol 2023 Jan;171:112031 [FREE Full text] [doi: 10.1016/j.exger.2022.112031] [Medline: 36402414]
15. Wang T, Liu H, Zhao W, Cao P, Li J, Chen T, et al. Predicting knee osteoarthritis progression using neural network with longitudinal MRI radiomics, and biochemical biomarkers: a modeling study. PLoS Med 2025 Aug 21;22(8):e1004665 [FREE Full text] [doi: 10.1371/journal.pmed.1004665] [Medline: 40839548]
16. Kraus VB, Collins JE, Charles HC, Pieper CF, Whitley L, Losina E, et al. Predictive validity of radiographic trabecular bone texture in knee osteoarthritis: The Osteoarthritis Research Society International/Foundation for the National Institutes of Health Osteoarthritis Biomarkers Consortium. Arthritis Rheumatol 2018 Jan;70(1):80-87 [FREE Full text] [doi: 10.1002/art.40348] [Medline: 29024470]
17. Almhdie-Imjabbar A, Toumi H, Lespessailles E. Performance of radiological and biochemical biomarkers in predicting radio-symptomatic knee osteoarthritis progression. Biomedicines 2024 Mar 16;12(3):666 [FREE Full text] [doi: 10.3390/biomedicines12030666] [Medline: 38540279]
18. Chen B, Duan X, Yu Z, Leng S, Yu L, McCollough C. Technical Note: development and validation of an open data format for CT projection data. Med Phys 2015 Dec;42(12):6964-6972 [FREE Full text] [doi: 10.1118/1.4935406] [Medline: 26632052]
19. Swiecicki A, Li N, O'Donnell J, Said N, Yang J, Mather RC, et al. Deep learning-based algorithm for assessment of knee osteoarthritis severity in radiographs matches performance of radiologists. Comput Biol Med 2021 Jun;133:104334. [doi: 10.1016/j.compbiomed.2021.104334] [Medline: 33823398]
20. Singh A, Horng H, Roshkovan L, Weeks JK, Hershman M, Noël P, et al. Development of a robust radiomic biomarker of progression-free survival in advanced non-small cell lung cancer patients treated with first-line immunotherapy. Sci Rep 2022 Jun 15;12(1):9993 [FREE Full text] [doi: 10.1038/s41598-022-14160-7] [Medline: 35705618]
21. Almhdie-Imjabbar A, Nguyen KL, Toumi H, Jennane R, Lespessailles E. Prediction of knee osteoarthritis progression using radiological descriptors obtained from bone texture analysis and Siamese neural networks: data from OAI and MOST cohorts. Arthritis Res Ther 2022 Mar 08;24(1):66 [FREE Full text] [doi: 10.1186/s13075-022-02743-8] [Medline: 35260192]
22. Tiulpin A, Thevenot J, Rahtu E, Lehenkari P, Saarakkala S. Automatic knee osteoarthritis diagnosis from plain radiographs: a deep learning-based approach. Sci Rep 2018 Jan 29;8(1):1727 [FREE Full text] [doi: 10.1038/s41598-018-20132-7] [Medline: 29379060]
23. Lindner C, Thiagarajah S, Wilkinson JM, arcOGEN Consortium, Wallis GA, Cootes TF. Fully automatic segmentation of the proximal femur using random forest regression voting. IEEE Trans Med Imaging 2013 Aug;32(8):1462-1472. [doi: 10.1109/TMI.2013.2258030] [Medline: 23591481]
24. Lindner C, Thiagarajah S, Wilkinson JM, Wallis GA, Cootes TF, arcOGEN Consortium. Accurate bone segmentation in 2D radiographs using fully automatic shape model matching based on regression-voting. Med Image Comput Comput Assist Interv 2013;16(Pt 2):181-189. [doi: 10.1007/978-3-642-40763-5_23] [Medline: 24579139]

XSL•FO
RenderX

25. Li Y, Chen D, Liu S, Lin J, Wang W, Huang J, et al. Supervised training models with or without manual lesion delineation outperform clinicians in distinguishing pulmonary cryptococcosis from lung adenocarcinoma on chest CT. Mycoses 2024 Jan;67(1):e13692. [doi: 10.1111/myc.13692] [Medline: 38214431]
26. Li W, Liu J, Xiao Z, Zhu D, Liao J, Yu W, et al. Automatic grading of knee osteoarthritis with a plain radiograph radiomics model: combining anteroposterior and lateral images. Insights Imaging 2024 Jun 13;15(1):143 [FREE Full text] [doi: 10.1186/s13244-024-01719-3] [Medline: 38867121]
27. Janvier T, Jennane R, Toumi H, Lespessailles E. Subchondral tibial bone texture predicts the incidence of radiographic knee osteoarthritis: data from the Osteoarthritis Initiative. Osteoarthritis Cartilage 2017 Dec;25(12):2047-2054 [FREE Full text] [doi: 10.1016/j.joca.2017.09.004] [Medline: 28935435]
28. Pishgar F, Guermazi A, Roemer FW, Link TM, Demehri S. Conventional MRI-based subchondral trabecular biomarkers as predictors of knee osteoarthritis progression: data from the Osteoarthritis Initiative. Eur Radiol 2021 Jun;31(6):3564-3573 [FREE Full text] [doi: 10.1007/s00330-020-07512-2] [Medline: 33241511]
29. Jiang W, Jin Y, Zhang S, Ding Y, Huo K, Yang J, et al. PGE2 activates EP4 in subchondral bone osteoclasts to regulate osteoarthritis. Bone Res 2022 Mar 09;10(1):27 [FREE Full text] [doi: 10.1038/s41413-022-00201-4] [Medline: 35260562]
30. Zhu S, Zhu J, Zhen G, Hu Y, An S, Li Y, et al. Subchondral bone osteoclasts induce sensory innervation and osteoarthritis pain. J Clin Invest 2019 Mar 01;129(3):1076-1093 [FREE Full text] [doi: 10.1172/JCI121561] [Medline: 30530994]
31. Jiang T, Lau SH, Zhang J, Chan LC, Wang W, Chan PK, et al. Radiomics signature of osteoarthritis: current status and perspective. J Orthop Translat 2024 Mar 16;45:100-106 [FREE Full text] [doi: 10.1016/j.jot.2023.10.003] [Medline: 38524869]
32. Hirvasniemi J, Klein S, Bierma-Zeinstra S, Vernooij MW, Schiphof D, Oei EH. A machine learning approach to distinguish between knees without and with osteoarthritis using MRI-based radiomic features from tibial bone. Eur Radiol 2021 Nov;31(11):8513-8521 [FREE Full text] [doi: 10.1007/s00330-021-07951-5] [Medline: 33884470]
33. Egloff C, Hügle T, Valderrabano V. Biomechanics and pathomechanisms of osteoarthritis. Swiss Med Wkly 2012 Jul 19;142:w13583 [FREE Full text] [doi: 10.4414/smw.2012.13583] [Medline: 22815119]
34. Lim YZ, Wang Y, Wluka AE, Davies-Tuck ML, Teichtahl A, Urquhart DM, et al. Are biomechanical factors, meniscal pathology, and physical activity risk factors for bone marrow lesions at the knee? A systematic review. Semin Arthritis Rheum 2013 Oct;43(2):187-194. [doi: 10.1016/j.semarthrit.2013.03.002] [Medline: 24157092]
35. Hunter DJ, Niu J, Felson DT, Harvey WF, Gross KD, McCree P, et al. Knee alignment does not predict incident osteoarthritis: the Framingham osteoarthritis study. Arthritis Rheum 2007 Apr;56(4):1212-1218. [doi: 10.1002/art.22508] [Medline: 17393450]
36. Sharma L, Song J, Felson DT, Cahue S, Shamiyeh E, Dunlop DD. The role of knee alignment in disease progression and functional decline in knee osteoarthritis. JAMA 2001 Jul 11;286(2):188-195. [doi: 10.1001/jama.286.2.188] [Medline: 11448282]
37. Huang Y, Liu Z, He L, Chen X, Pan D, Ma Z, et al. Radiomics signature: a potential biomarker for the prediction of disease-free survival in early-stage (I or II) non-small cell lung cancer. Radiology 2016 Dec;281(3):947-957. [doi: 10.1148/radiol.2016152234] [Medline: 27347764]
38. Hunter DJ, Deveza LA, Collins JE, Losina E, Katz JN, Nevitt MC, et al. Multivariable modeling of biomarker data from the phase I Foundation for the National Institutes of Health Osteoarthritis Biomarkers Consortium. Arthritis Care Res (Hoboken) 2022 Jul;74(7):1142-1153 [FREE Full text] [doi: 10.1002/acr.24557] [Medline: 33421361]
39. Guan B, Liu F, Mizaian AH, Demehri S, Samsonov A, Guermazi A, et al. Deep learning approach to predict pain progression in knee osteoarthritis. Skeletal Radiol 2022 Feb;51(2):363-373 [FREE Full text] [doi: 10.1007/s00256-021-03773-0] [Medline: 33835240]
40. Iasonos A, Schrag D, Raj GV, Panageas KS. How to build and interpret a nomogram for cancer prognosis. J Clin Oncol 2008 Mar 10;26(8):1364-1370. [doi: 10.1200/JCO.2007.12.9791] [Medline: 18323559]
41. Paz-González R, Balboa-Barreiro V, Lourido L, Calamia V, Fernandez-Puente P, Oreiro N, et al. Prognostic model to predict the incidence of radiographic knee osteoarthritis. Ann Rheum Dis 2024 Apr 11;83(5):661-668 [FREE Full text] [doi: 10.1136/ard-2023-225090] [Medline: 38182405]
42. Sun H, You Y, Jiang Q, Ma Y, Huang C, Liu X, et al. Radiomics-based nomogram for predicting total knee replacement in knee osteoarthritis patients. Eur J Radiol 2025 Jan;182:111854 [FREE Full text] [doi: 10.1016/j.ejrad.2024.111854] [Medline: 39626336]
43. Li X, Li C, Zhang P. Predictive models of radiographic progression and pain progression in patients with knee osteoarthritis: data from the FNIH OA biomarkers consortium project. Arthritis Res Ther 2024 May 30;26(1):112 [FREE Full text] [doi: 10.1186/s13075-024-03346-1] [Medline: 38816759]
44. Huang Z, Bucklin MA, Guo W, Martin JT. Disease progression and clinical outcomes in latent osteoarthritis phenotypes: data from the Osteoarthritis Initiative. Research Square. Preprint posted online on January 26, 2024 2024 Jan 26:rs.3.rs-3855831 [FREE Full text] [doi: 10.21203/rs.3.rs-3855831/v1] [Medline: 38343849]
45. Li HH, Chan LC, Chan PK, Wen C. An interpretable knee replacement risk assessment system for osteoarthritis patients. Osteoarthr Cartil Open 2024 Feb 16;6(2):100440 [FREE Full text] [doi: 10.1016/j.ocarto.2024.100440] [Medline: 38385105]

XSL•FO
RenderX

46. Collins JE, Robinson D, Arden N, Bay-Jensen AC, Deveza LA, Karsdal M, et al. Biochemical biomarkers of knee osteoarthritis progression: results from the FNIH biomarkers consortium progress OA study. Osteoarthr Cartil Open 2025 Sep 05;7(4):100677 [FREE Full text] [doi: 10.1016/j.ocarto.2025.100677] [Medline: 41050370]
47. The Osteoarthritis Initiative. National Institute of Mental Health Data Archive. URL: https://nda.nih.gov/oai [accessed 2026-01-05]

Abbreviations

AUC: area under the receiver operating characteristic curve
DCA: decision curve analysis
DICOM: Digital Imaging and Communications in Medicine
FNIH: Foundation for the National Institutes of Health
HIPAA: Health Insurance Portability and Accountability Act
KOA: knee osteoarthritis
LASSO: least absolute shrinkage and selection operator
MRI: magnetic resonance imaging
OA: osteoarthritis
OAI: Osteoarthritis Initiative
rad-score: radiomics score
ROI: region of interest
SHAP: Shapley additive explanations
WOMAC: Western Ontario and McMaster Universities Osteoarthritis Index

Edited by A Benis; submitted 03.Jun.2025; peer-reviewed by HD Zuo, G Tang; comments to author 11.Nov.2025; accepted 17.Dec.2025; published 14.Jan.2026.

Please cite as:
Sun Y, Liu J, Deng C, Peng C, Pan S, Liu X
Nomograms Based on X-Ray Radiomics for Predicting Pain Progression in Knee Osteoarthritis Using Data From the Foundation for the National Institutes of Health: Development and Validation Study
JMIR Med Inform 2026;14:e78338
URL: https://medinform.jmir.org/2026/1/e78338
doi:10.2196/78338
PMID:

©Yingwei Sun, Jing Liu, Chunbo Deng, Chengbao Peng, Shinong Pan, Xueyong Liu. Originally published in JMIR Medical Informatics (https://medinform.jmir.org), 14.Jan.2026. This is an open-access article distributed under the terms of the Creative Commons Attribution License (https://creativecommons.org/licenses/by/4.0/), which permits unrestricted use, distribution, and reproduction in any medium, provided the original work, first published in JMIR Medical Informatics, is properly cited. The complete bibliographic information, a link to the original publication on https://medinform.jmir.org/, as well as this copyright and license information must be included.

XSL•FO
RenderX

Linking Electronic Health Records for Multiple Sclerosis Research: Comparative Study of Deterministic, Probabilistic, and Machine Learning Linkage Methods

Ohoud Almadani[1*], MSHI; Yasser Albogami[2*], PhD; Adel Alrwisan[1*], PhD

[1]Saudi Food and Drug Authority, 4904 northern ring branch rd, 13513, Hittin Dist, Unit number : 1, Riyadh, Saudi Arabia

[2]Department of Clinical Pharmacy, College of Pharmacy, King Saud University, Riyadh, Saudi Arabia

[*]all authors contributed equally

Corresponding Author:
Ohoud Almadani, MSHI
Saudi Food and Drug Authority, 4904 northern ring branch rd, 13513, Hittin Dist, Unit number : 1, Riyadh, Saudi Arabia

Abstract

Background: Data linkage in pharmacoepidemiological research is commonly employed to ascertain exposures and outcomes or to obtain additional information on confounding variables. However, to protect patient confidentiality, unique patient identifiers are not provided, which makes data linkage across multiple sources challenging. The Saudi Real-World Evidence Network (SRWEN) aggregates electronic health records from various hospitals, which may require robust linkage techniques.

Objective: We aimed to evaluate and compare the performance of deterministic, probabilistic, and machine learning (ML) approaches for linking deidentified data of patients with multiple sclerosis (MS) from the SRWEN and Ministry of National Guard Health Affairs electronic health record systems.

Methods: A simulation-based validation framework was applied before linking real-world data sources. Deterministic linkage was based on predefined rules, whereas probabilistic linkage was based on a similarity score–based matching. For ML, both similarity score–based and classification approaches were applied using neural networks, logistic regression, and random forest models. The performance of each approach was assessed using confusion matrices, focusing on sensitivity, positive predictive value, F_1 score, and computational efficiency.

Results: The study included linked data of 2247 patients with MS from 2016 to 2023. The deterministic approach resulted in an average F_1 score of 97.2% in the simulation and demonstrated varying match rates in real-world linkage: 1046/2247 (46.6%) to 1946/2247 (86.6%). This linkage was computationally efficient, with run times of <1 second per rule. The probabilistic approach provided an average F_1 score of 93.9% in the simulation, with real-world match rates ranging from 1472/2247 (65.5%) to 2144/2247 (95.4%) and processing times ranging from approximately 0.1 to 5 seconds per rule. ML approaches achieved high performance (F_1 score reached 99.8%) but were computationally expensive. Processing times ranged from approximately 13 to 16,936 seconds for the classification-based approaches and from approximately 13 to 7467 seconds for the similarity score–based approaches. Real-world match rates from ML models were highly variable depending on the method used; the similarity score–based approach identified 789/2247 (35.1%) matched pairs, whereas the classification-based approach identified 2014/2247 (89.6%).

Conclusions: Probabilistic linkage offers high linkage capacity by recovering matches missed by deterministic methods and proved to be both flexible and efficient, particularly in real-world scenarios where unique identifiers are lacking. This method achieved a great balance between recall and precision, enabling better integration of various data sources that could be useful in MS research.

(JMIR Med Inform 2026;14:e79869) doi:10.2196/79869

KEYWORDS

EHR; MS; probabilistic; deterministic; ML; multiple sclerosis; electronic health record; machine learning

Introduction

Real-world data (RWD) derived from routine clinical care provide remarkable potential for generating pharmacoepidemiological studies related to medication safety, effectiveness, and utilization [1-4]. The recent emergence of electronic health records (EHRs) in the Kingdom of Saudi Arabia led to the foundation of the Saudi Real-world Evidence Network (SRWEN) by the Saudi Food and Drug Authority [5-8]. This central network plans to integrate and harmonize EHRs from various hospitals, primarily to maximize the efficacy

XSL•FO
RenderX

of RWD in contributing to drug regulatory policymaking and understanding disease dynamics in the Saudi population [6,7].

Common data models (CDMs), such as the observational medical outcomes partnership model, incorporate consolidated formats necessary for data standardization across multiple clinical data sources to perform large-scale observational studies [9-11]. CDMs enable researchers to pool multiple EHR datasets and perform federated data analyses through standardized data architectures, formats, and terminologies [10,11]. The observational medical outcomes partnership CDM, developed as part of the observational health data sciences and informatics, offers a systematic framework of clinical data across diverse subdomains such as demographics, diagnoses, medications, procedures, and laboratory results. It uses standardized terminologies, mitigating inherent variability, customized formats, or inconsistent coding in raw EHR data [9,11].

While CDMs are in place to standardize structures in collecting and evaluating clinical data, many are built on deidentified datasets that may not hold vital contextual information or complete patient histories [9-11]. Thus, restricting the ability to solve such limitations of CDM as incomplete data mapping, the lack of direct mappings for some clinical or medication concepts, laboratory or narrative data gaps, which necessitate going back to the data to retrieve context-specific information that may not be contained in the standardized model [9-11]. Therefore, EHR linkage offers a powerful solution addressing this limitation by enabling researchers to link patient records across various databases and reconstruct comprehensive longitudinal health trajectories [12-14]. Common linkage approaches are deterministic, probabilistic, and machine learning (ML) linkage, each with advantages and challenges [14-16]. For instance, the deterministic linkage is based on an exact matching across predefined variables, achieving high precision; however, sensitivity may be compromised in this case, particularly when matching data that contain errors in a given variable. Probabilistic linkage overcomes this weakness by using weighted matching, enhancing sensitivity at the cost of reduced precision in specific applications [12,13]. ML techniques, such as gradient boosting and neural networks (NNs), can achieve high levels of accuracy [12,13]. These models are particularly successful when integrating a dataset with large volumes of missing and errant data, identifying more links than deterministic and probabilistic approaches [16].

With a growing number of multiple sclerosis (MS) cases among the Saudi population—from 25 per 100,000 in 1998 to 40.4 per 100,000 in 2020—the linkage of data pertaining to MS is of priority, especially given the complexity of MS treatment management, both within Saudi Arabia and globally [17]. SRWEN contains a complex variety of data sources, reference standards, and case definitions, highlighting the intrinsic complexity associated with the reliability of RWD in health care settings [7]. Therefore, accurate linkage of EHRs is paramount for addressing the complexities associated with defining patient outcomes with MS, such as disease progression, relapse rate, and treatment response. This analysis requires frequent validation by clinical expertise and enhancement of the validity and robustness of the SRWEN[17]. To achieve this, we compared different EHR linkage methods, including deterministic, probabilistic, and ML approaches. The findings from this study may have implications for the value and design of future longitudinal studies using linked MS data.

Methods

Ethical Considerations

This study was approved by the institutional review board of Saudi Food and Drug Authority with approval number 2024_17 and by the King Abdullah International Medical Research Center with approval number ROMJ/WE/WS/059/2023. Because the data were extracted from the EHR system as part of routine clinical care, patients are required to provide consent to receive treatment within the institution. Separate study-specific consent was considered waived in accordance with institutional policies. Patient privacy and confidentiality were granted through de-identification of all records prior to data exchange, such that no direct identifiers were available to the research team.

Study Population and Data Sources

In this study, we used 2 datasets from 2 different sources. First, we included SRWEN data of patients with MS between 2016 and 2023. The SRWEN functions as a repository of longitudinal health care information and incorporates diverse EHR data, such as demographics, medical history, medication use, laboratory outcomes, hospitalizations, and clinical outcomes. Information is gathered from diverse EHRs from multiple hospitals in Saudi Arabia, including the Ministry of National Guard Health Affairs (MNGHA). Subsequently, these collected data are standardized through a CDM to ensure consistency and streamline analysis [6]. Furthermore, an anonymization process is implemented prior to exchanging data to ensure patient privacy [6]. For the purposes of this study, we focused exclusively on extracting and analyzing MNGHA data within SRWEN.

Similarly, we collected MNGHA EHR data from King Abdullah International Medical Research Center, identifying patients with MS using the International Classification of Diseases 10th version (*ICD10*: G35) for the same period of (2016 - 2023). MNGHA EHRs contain routinely collected data, including patient characteristics, diagnostic history, medications history, and visit records (ie, admissions, outpatient clinical visits, or emergency visits; Table S1 in Multimedia Appendix 1).

While SRWEN collects data already from the MNGHA, the benefit of the direct link between these 2 entities is advantageous. Data within SRWEN are organized and standardized within a CDM, providing for multi-institutional data analysis at the risk of some loss in source detail. By linking the primary MNGHA EHRs to their corresponding RERN representations, we were able to recover additional clinical granularity from narrative diagnosis notes and reports. This linkage also allowed validation of data consistency between SRWEN and its original source, resulting in a larger and more accurate longitudinal profile of patients with MS.

XSL•FO
RenderX

Simulation-Based Validation

Overview

We first cloned and deidentified the original dataset to address the challenge of linking deidentified records from the targeted database (ie, SRWEN) with original records (ie, MNGHA EHRs). This process ensured a realistic framework testing and that the dataset resembled the deidentified target dataset. Simulating the conditions of the intended linkage objective, we linked records to themselves using these deidentified cloned records, employing deterministic, probabilistic, and ML approaches. Following this self-linkage phase, we assessed each approach's performance using computational efficiency metrics. Consequently, the best-performing linkage method was used to link the original records to the target dataset, thereby maximizing the accuracy and reliability of the final linkage. This methodology enabled a rigorous, performance-based selection of the optimal linkage approach for secure and accurate record linkage of deidentified datasets [13].

Deterministic Approach

Deterministic EHR linkage is a rule-based approach that relies on exact matches between specific patient identifiers across different EHR systems [12,14,15,18]. Given the lack of patient identifiers in SRWEN, we implemented multiple matching criteria (ie, rules) based on a range of available variables, each considered both independently and in unique combinations (Table S2 in Multimedia Appendix 1). We explored different variable groupings in some detail to determine how various linkage methods perform under conditions with differing degrees of completeness and complexity of data encountered in real-world settings. This approach generates pairs of records classified as match or nonmatches. For each pair, we included multiple linkage variables, including demographic characteristics (eg, gender, date of birth, nationality, eligibility), and health care–related fields (eg, *ICD-10* codes, diagnosis description and date, medication order details, visit type and date, and facility information) [12,14,15,18]. Additional derived variables were generated from these data elements, including coverage, which was derived from eligibility and indicated a patient's treatment eligibility, the first MS diagnosis date, derived from the diagnosis data, and inpatient admission status, derived from visit records.

Probabilistic Approach

In this approach, patient records were grouped into blocks based on shared variables (eg, date of birth, initial MS diagnosis date, received medications, or admission events) to reduce the number of pairwise comparisons required for linkage [12,14,19]. Subsequently, each record pair within a block was compared across diverse fields, including gender, coverage (ie, eligibility), region, nationality, facility name, or diagnostic codes other than MS [12,14,19]. A similarity score was assigned to each record pair corresponding to the level of agreement on predefined variables. Variable weights were estimated as match probabilities (ie, m-probability)—the probability that two field values match, given that the records refer to the same individual—and unmatch probability (ie, u-probability)—the probability that 2 field values match given that the records refer to different individuals. These probabilities were computed using the expectation-maximization algorithm [12-14,19]. An overall similarity score for each pair was computed by summing the weighted scores across all variables [12,14,19].

Pairs were categorized as matches or nonmatches using a one-to-one linkage approach. This method was implemented using the "select_n_to_m" function from the rclin package, which maximizes total similarity score under the constraint that each record is linked only once [20]. This probabilistic approach incorporates imperfect matches caused by inaccuracies or missing data, thereby enhancing the quality and reliability of linked EHR datasets in clinical studies [19].

ML Approach

In the ML approach, record linkage was performed in 2 methods. First, we generated pairs of records using common variables in the cloned data to limit the number of comparisons, creating a grouped set of pairs [20] Similarity scores were computed for each pair across different selected variables 20[]. Pairs were labeled as matches or nonmatches for training using the known true matches. The pairs were then fed into different models for training, and we fitted the model on variables that had the higher impact based on each variable similarity score, allowing the model to learn patterns that accurately identify true matches [20].

Second, a classification-based ML approach was implemented by training models on a labeled training dataset comprising 75% of all possible record pairs derived from the original dataset. Match and nonmatch labels were derived from the reference dataset. The remaining 25% of the record pairs were used for the testing dataset to evaluate the classifier performance [16].

Four ML algorithms—K-nearest neighbor, logistic regression (LR), NN, and random forest (RF)—were used in both methods to evaluate their linkage accuracy [16]. Internal validation was reinforced using a 100-replication bootstrap approach in each method for more robust performance estimates and to ensure stability across repeated sampling iterations [16]

Real-World Record Linkage

In the real-world matching scenario, we linked data from SRWEN and MNGHA to identify patients diagnosed with MS between 2016 and 2023. Because the SRWEN and MNGHA datasets lack a unique common identifier, no reference standard was available to evaluate the performance of each matching algorithm [13]. Therefore, model performance was compared based on the number of matched record pairs identified.

Statistical Analysis

Descriptive analyses of both datasets, including diseases, demographics, and facilities, were tabulated and presented by counts and percentages. Using original identifiers as the reference standard, accurate matches and true nonmatches were defined for the simulation [13]. True matches were record pairs agreeing on identifiers, whereas true nonmatches were record pairs conflicting on identifiers [13]. Sensitivity and positive predictive value (PPV) were calculated along with their corresponding 95% CI. Additionally, the F_1 score was calculated as a measure of balanced accuracy between sensitivity and PPV

XSL•FO
RenderX

(equation 1) [19]. Computational time required by the ML model to complete the record linkage process.

$$F1score=2\times\frac{Sensitivity\times PPV}{Sensitivity+PPV} \quad (1)$$

Results

Descriptive Analysis

The MNGHA dataset contained 2642 patients with MS, whereas 2247 were identified from SRWEN. Because only MNGHA-related dataset within SRWEN was used, 395/2642 (14.9%) patients with MS from the original MNGHA dataset were not captured in the SRWEN data. The distribution of demographic data between the 2 data sources was comparable. For instance, the mean age of patients in the MNGHA dataset was 34.4 (SD 11) years, which was similar to the mean age of 34.6 (SD 11.3) years in SRWEN.

Deterministic Approach

The highest number of pairwise comparisons (3,854,740) was observed in the "sex" variable, compared with a significant precise pairwise comparisons (6212) using the "date of birth (DOB)" or "nationality" variables. Sensitivity was consistent with a perfect score across the variables. However, the specificity rate varied, with the highest (99.9%) observed using "DOB" and the lowest (5%) observed using "nationality." Conversely, precision was considerably low across different variables, with the highest (42.5%) observed using "DOB." Moreover, both "DOB" and "MS Date" had relatively high F_1 scores of 59.7% and 48.8%, respectively (Table 1).

Table . Results of deterministic matching in % based on an individual variable.

Metric	Sex	DOB[a]	Nationality	Coverage	Facility	Region	MS[b] date[c]	Admissions	Other diagnoses	Medications
Accuracy	44.45	99.95	5.09	69	62.92	58.06	99.92	88.15	64.37	99.73
Sensitivity (recall)	100	100	100	100	100	100	100	100	100	100
Specificity	44.43	99.95	5.05	68.99	62.91	58.04	99.92	88.14	64.36	99.73
PPV[d] (precision)	0.07	42.53	0.04	0.12	0.10	0.09	32.28	0.32	0.11	12.45
F_1 score	0.14	59.68	0.08	0.25	0.21	0.18	48.81	0.64	0.21	22.14

[a]DOB: date of birth.

[b]MS: multiple sclerosis.

[c]MS date: first multiple sclerosis diagnosis.

[d]PPV: positive predictive value.

A sequence of deterministic linkage rules was applied to evaluate data matching using a set of variables instead of a single variable (Table 1). The number of correctly matched pairs remained consistent across most rules, with 2642 pairs correctly matched for each rule. Likewise, almost all of the linkage rules resulted in a nearly perfect score across the metrics. The average F_1 score for the deterministic approach was 97.2% (Table S3 in Multimedia Appendix 1). In terms of computing time, deterministic linkage was completed in less than one second for each criterion (Table S3 in Multimedia Appendix 1).

Probabilistic Approach

To ensure a manageable dataset for analysis, we first reduced the number of comparisons by blocking records based on exact matches on DOB (6212 pairs). Precision remained consistently perfect regardless of the variables used across diverse combinations of matching criteria in the probabilistic approach. Both specificity and sensitivity increased with more variables, as the combination of sex, nationality, and coverage was 76%. Further, adding the facility name and the MS diagnosis date led to a perfect score. A similar observation was found for the F_1 score, which began at 69.9% with sex only, increased to 94.6% after adding facility name and region, and reached a perfect score of 100% with the inclusion of MS diagnosis date.

By using a combination of the best-performing variables derived from the deterministic approach to improve match accuracy further, in addition to examining different blocking criteria, precision was constantly at 100%. Sensitivity and specificity rates were high, considerably assisted by combining specific clinical variables. Likewise, the F_1 score ranged from 82% to 99.9% (Table S3 in Multimedia Appendix 1). In terms of computing time, probabilistic linkage required 0.1 to 5 seconds for each criterion (Table S3 in Multimedia Appendix 1).

Using this probabilistic approach with the one-to-one linkage (ie, select_n_to_m from the reclin package) matching criterion, the linkage models achieved perfect performance for all the metrics evaluated. In addition, m-probabilities and u-probabilities were compared across the variables under different matching criteria (Table S4 in Multimedia Appendix 1).

ML Approach

In the similarity-score method, models trained on combinations of DOB, MS diagnosis date, and medications, after being blocked (ie, exact match) on admission, performed best overall. NN, RF, and LR models demonstrated comparable performance, with slightly higher accuracy using NN (99.37% vs 99.36%). However, computational time analysis showed that LR presented a combination of high performance and acceptable processing time (15 - 766 s). In contrast, both RF and NN, while having

XSL•FO
RenderX

comparable results to LR, were less practical for large-scale linkage tasks due to their longer training times (15 - 7467 s) associated with their complexity (Table S5 in Multimedia Appendix 1).

In the classification approach, despite the blocking variable or combination of matching criteria, performance was constantly high among the three models, ranging from 91.7% to 100%, while computational efficiency varied depending on the blocking strategy and applied comparison criteria. Moreover, the classification is usually more computationally expensive (13 - 16,936 s) compared with the similarity-score approach, affecting scalability for larger datasets. However, K-nearest neighbor demonstrated an excellent trade-off between computational efficiency and linkage performance (Table S5 in Multimedia Appendix 1).

Record Linkage

The deterministic approach produced the fewest matched pairs. Increasing the number of variables (eg, adding admissions or medications) made the linkage criteria stricter, resulting in gradually fewer matched pairs, ranging from 1046/2247 (46.6%) to 1946/2247 (86.6%). The probabilistic approach achieved more pairs ranging from 1472/2247 (65.5%) to 2144/2247 (95.4%) based on the combination of variables. The ML approach, using similarity scoring or classification with an NN model, generated 789/2247 (35.1%) pairs and 2014/2247 (89.6%) pairs, respectively (Table S5 in Multimedia Appendix 1).

Discussion

Principal Results

Through the simulated scenario and after using a mixture of variables without identifiers, we determined that the deterministic method was the most efficient data linkage algorithm. Although this approach had limited generality, it accomplished 100% scores across all metrics without incurring high computational times. Therefore, the deterministic approach is practical when we need absolute certainty in matched pairs. In contrast, the probabilistic method also demonstrated efficient performance with a similar mixture of variables. Initially, the recall and specificity metrics exhibited low performances. However, when we applied one-to-one linkages, the performance of the probabilistic method improved significantly, yielding a 100% score. Furthermore, the core benefit of this approach is retrieving a higher number of matched pairs, signifying its advantage when maximum generalization and thorough data retrieval are required. In the case of ML methods like NN models, we attained perfect performance scores at the expense of higher computational costs, limiting their feasibility in real-world scenarios. Among all methods, the probabilistic approach provided the highest number of patients, signifying its flexibility in real-world healthcare scenarios. These outcomes give a reproducible framework for appropriate EHR record linkages, underscoring its efficacy in practical patient care situations.

Considering the average F_1 score for the different models in each approach, the deterministic approach achieved the highest average (97.2%), followed by the probabilistic approach (93.9%). Noteworthy, the probabilistic approach using one-to-one linkage achieved an average of 100%, and in both probabilistic and ML approaches, an initial blocking step based on exact matching was performed. Examining the criteria without applying any blocking led to poor performance in the probabilistic method and was infeasible for ML. Figure 1 shows a comparison between deterministic and probabilistic approaches, while Figure 2 shows a comparison between similarity score and classification ML approaches.

Figure 1. Performance comparison of deterministic and probabilistic approaches. PPV: positive predictive value.

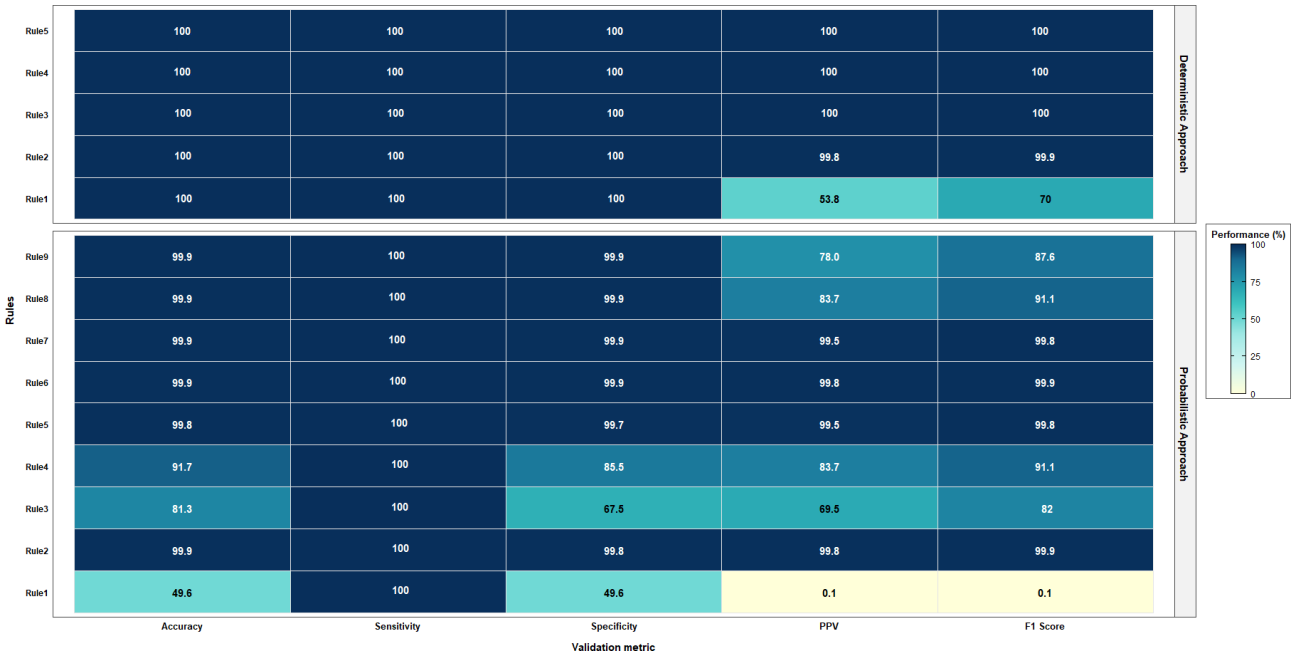

XSL•FO
RenderX

Figure 2. Performance comparison of machine learning models. KNN: K-nearest neighbor; LR: logistic regression; NN: neural network; PPV: positive predictive value; RF: random forest.

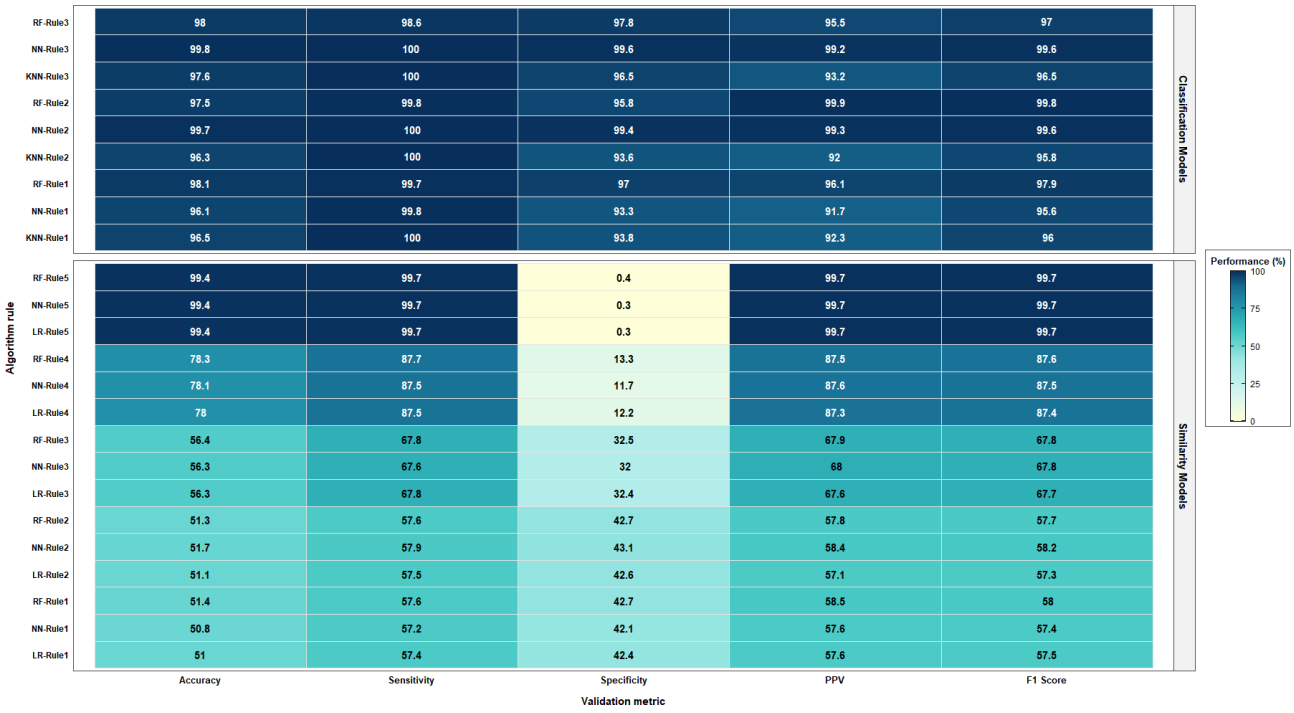

Comparison with Prior Work

Despite the application of a straightforward deterministic algorithm requiring exact matching among all variables of linkage rule, our deterministic solution outperformed the probabilistic method, in contrast to findings from previous studies [21,22]. For instance, Gomatam et al [21] used a forward stepwise deterministic method to evaluate variables independently before constructing matching rules. We used a similar approach and observed high specificity and recall, achieving a perfect score, using this method [21]. The probabilistic linkage was implemented similarly to prior research, and we only allowed for exact matches in the deterministic approach. However, unlike previous studies' findings where probabilistic linkage outperformed deterministic linkage in most scenarios, our results are comparable, with slightly better performance of the deterministic approach when linkage rules (rather than individual variables) were employed [19,21-23]. Implementing a one-to-one linkage method proposed by the reclin package further improved the probabilistic approach to exceed the performance of the deterministic approach when using similar matching rules [20]. Compared with Röchner et al [16], our ML approach exhibited a lower performance than the deterministic approach using a similar combination of rules. Furthermore, even though NN in the classification method achieved a near-perfect score, it required significantly more computational time than the deterministic approach. Nonetheless, we reached a similar finding to Röchner et al [16] in identifying the NN as the highest-performing algorithm in record linkage.

Computational benchmarking was performed on a standard workstation featuring an Intel Core i7 processor, 16 GB of RAM, and 2 GB of GPU (64-bit Windows OS). From a computational perspective, the most efficient method of linkage was the deterministic approach: each run finished in under one second, F_1 scores were between 70% and 100%, and memory requirements were low (<2 GB). The probabilistic approach required 0.1 to 4.88 seconds (F_1 score 82% - 99.9%), while maintaining moderate memory requirements (<8 GB) and achieving excellent accuracy. In contrast, machine-learning-based methodologies were very computationally intensive requiring: 12 to 7467 seconds (~0.2 - 124 min; F_1 score 57.3% - 99.7%, similarity-based models), and 13 to 16,936 seconds (~0.2 - 282 min; F_1 score 95% - 99.8%, classification-based models), both at a maximum memory requirement of 12 to 14 GB. These data demonstrate that the deterministic and probabilistic approaches are ideal for large scale and routine linkage tasks where the computational efficiency of the method is crucial, while ML-based methods, though highly accurate, demand greater resources and are better suited for smaller or high-value analytic linkages where accuracy outweighs runtime considerations.

Clinical and Regulatory Implications

Beyond demonstrating methodological aspects, this study supports the assertion that EHR linkage of original sources with their standardized mapping has clinical importance of linking the fragmented data of MS into a multi-institutional timeline that supports relapse reconstruction, mapping of treatment trajectories, and assessment of long-term outcomes. Importantly, this linkage addresses the challenges of RWD in MS by enabling the validation of deidentified records and matching the structured components (diagnoses, labs, prescriptions, utilization) with unstructured data (notes by physicians and radiology reports) to improve phenotype definition when ICD codes are ineffectively applied. The linked dataset supports earlier case identification (using utilization surrogates as proxies when standard scales are not available), risk stratification and

XSL•FO
RenderX

compliance monitoring across care sites, and provides more frequent and expandable data for pharmacoepidemiologic and safety surveillance that will be more robust than values obtained from trial groups. At the same time, addressing challenges related to the lack of data sufficiency, burdens related to the gaining of patient-reported outcomes data, evolving criteria for diagnosis, and the need for consistent harmonization and resourcing across systems. This linkage produces an analytically reproducible and available dataset for the practical and generalizable studies related to MS and in support of decisions concerning it, changing otherwise unstructured clinical data into actionable knowledge connecting to clinicians, regulators, and health-system leaders.

With the growing availability of large-scale clinical datasets, opportunities to create more comprehensive patient care pathways through data linkage are expanding. The findings of this study suggest that probabilistic linkage of anonymized datasets using indirect identifiers can substantially improve linkage capacity, minimize computational cost, and maintain patient privacy. Probabilistic linkage has demonstrated a greater ability to recover more pairs that may be missed by deterministic methods (1472-2144 vs 1046-1946) due to its flexibility, highlighting its potential as a complementary method to deterministic linkage. Furthermore, to ensure transparency, we examined the contributions of each linkage variable before developing the matching criteria. This approach allowed us to identify the most influential variables for effective linkage. More particularly, the date of birth and first MS diagnosis date achieved F_1 scores of 59.7% and 48.8%, respectively, suggesting strong linkage capabilities with balanced precision and recall. Moreover, incorporating both variables in the matching rules of the deterministic approach resulted in a perfect record linkage across all performance metrics. This improved linkage capability is beneficial for patients with MS by enabling data integration across different providers and supports an even more unified and comprehensive record of each patient's journey. Such a broad linkage helps researchers and clinicians track the progression of diseases over time, evaluate treatment effects on symptoms, and track long-term health outcomes.

The study findings are significant for regulatory requirements, especially when conducting policymaking and postmarketing surveillance. The low computational costs of the deterministic approach enable the regulators to evaluate its treatment outcomes and specify any safety issues, whereas the flexibility and open-ended retrieval of the probabilistic approach is remarkable, especially in the case of comprehensive data retrieval from anonymized records. Therefore, using both deterministic and probabilistic approaches is significant for creating a comprehensive clinical data source for policymaking, postmarketing assessments, and monitoring of the healthcare industry. Ultimately, a combination of these approaches can lead to excellent patient outcomes regarding safety and treatment accuracy.

Limitations

Several limitations must be acknowledged in this study. First, our selection of methods was affected by computational constraints, which highlighted the need for advanced optimization and more powerful hardware for ML models. Discrepancies in patient records count between datasets could also affect generalizability, highlighting the importance of complete data capture in future studies. In our linkage of RWD, we standardized both datasets in terms of variable names and value structure, perhaps influencing the performance of algorithms when linking across different data quality in a real-world application. Furthermore, one patient in SRWEN had an inaccurate date of birth, while 4 patients in both data sets had an unknown nationality. Also, 44 patients in MNGHA and 11 patients in SRWEN had an unknown coverage status. Variables such as other diagnoses, admissions (visits), and medications contain null values (no value), but we believe that these nulls refer to the absence of a clinical event rather than missing entries. Lastly, the lack of an identifier limited our ability to validate the results against a reference standard for the real-world linkage section. Consequently, we could not accurately evaluate the retrieval of matched pairs. Therefore, we used the number of matches solely to describe the linkage performance in real-world linkage.

Conclusion

The findings of this study demonstrate how probabilistic linkage with indirect identifiers can enhance data integration, particularly for MS research and patient care. In real-world situations where we lack unique identifiers, probabilistic linkage proved to be both flexible and efficient as a complement to traditional approaches. These results provide a more holistic overview of patients with MS care and afford researchers access to an inclusive dataset for studying disease progression, treatment outcomes, and monitoring medication safety. In conclusion, applying probabilistic linkage techniques can be expected to facilitate more informed, data-driven clinical and research practices in managing MS.

Acknowledgments

The views expressed in this paper are those of the author(s) and do not necessarily reflect those of the Saudi Food and Drug Authority or its stakeholders. Guaranteeing the accuracy and the validity of the data is a sole responsibility of the research team.

Data Availability

The data that support the study findings are not publicly available due to confidentiality restrictions.

XSL•FO
RenderX

Authors' Contributions

Conceptualization: OA, YA, AA
Methodology: OA, YA, AA
Formal analysis: OA
Data curation: YA, AA
Investigation: OA, YA, AA
Project administration: OA
Validation: OA, YA, AA
Visualization: OA
Writing – original draft: OA
Writing – review & editing: YA, AA

Conflicts of Interest

None declared.

Multimedia Appendix 1
Supplementary tables.
[DOCX File, 40 KB - medinform_v14i1e79869_app1.docx]

References

1. Hernán MA. Methods of public health research — strengthening causal inference from observational data. N Engl J Med 2021 Oct 7;385(15):1345-1348. [doi: 10.1056/NEJMp2113319] [Medline: 34596980]
2. Li M, Chen S, Lai Y, et al. Integrating real-world evidence in the regulatory decision-making process: a systematic analysis of experiences in the US, EU, and China using a logic model. Front Med (Lausanne) 2021;8:669509. [doi: 10.3389/fmed.2021.669509] [Medline: 34136505]
3. Beaulieu-Jones BK, Finlayson SG, Yuan W, et al. Examining the use of real-world evidence in the regulatory process. Clin Pharmacol Ther 2020 Apr;107(4):843-852. [doi: 10.1002/cpt.1658] [Medline: 31562770]
4. Yoshida S, Takeuchi M, Tanaka-Mizuno S, et al. Clinical epidemiology and pharmacoepidemiology studies with real-world databases. Proc Jpn Acad Ser B Phys Biol Sci 2022;98(10):517-528. [doi: 10.2183/pjab.98.026] [Medline: 36504194]
5. Samra H, Li A, Soh B, Zain MA. Utilisation of hospital information systems for medical research in Saudi Arabia: a mixed-method exploration of the views of healthcare and IT professionals involved in hospital database management systems. Health Inf Manag 2020;49(2-3):117-126. [doi: 10.1177/1833358319847120] [Medline: 31046465]
6. Alnofal FA, Alrwisan AA, Alshammari TM. Real-world data in Saudi Arabia: current situation and challenges for regulatory decision-making. Pharmacoepidemiol Drug Saf 2020 Oct;29(10):1303-1306. [doi: 10.1002/pds.5025] [Medline: 32458499]
7. Althunian TA, Alrasheed MM, Alnofal FA, et al. Recording type 2 diabetes mellitus in a standardised central Saudi database: a retrospective validation study. BMJ Open 2023 Mar 21;13(3):e065468. [doi: 10.1136/bmjopen-2022-065468] [Medline: 36944455]
8. Alharbi RA. Adoption of electronic health records in Saudi Arabia hospitals: knowledge and usage. J King Saud Univ Sci 2023 Feb;35(2):102470. [doi: 10.1016/j.jksus.2022.102470]
9. Hripcsak G, Shang N, Peissig PL, et al. Facilitating phenotype transfer using a common data model. J Biomed Inform 2019 Aug;96:103253. [doi: 10.1016/j.jbi.2019.103253] [Medline: 31325501]
10. Garza M, Del Fiol G, Tenenbaum J, Walden A, Zozus MN. Evaluating common data models for use with a longitudinal community registry. J Biomed Inform 2016 Dec;64:333-341. [doi: 10.1016/j.jbi.2016.10.016] [Medline: 27989817]
11. Papez V, Moinat M, Payralbe S, et al. Transforming and evaluating electronic health record disease phenotyping algorithms using the OMOP common data model: a case study in heart failure. JAMIA Open 2021 Feb;4(3):ooab001. [doi: 10.1093/jamiaopen/ooab001] [Medline: 34514354]
12. Blake HA, Sharples LD, Harron K, van der Meulen JH, Walker K. Probabilistic linkage without personal information successfully linked national clinical datasets. J Clin Epidemiol 2021 Aug;136:136-145. [doi: 10.1016/j.jclinepi.2021.04.015] [Medline: 33932483]
13. Avoundjian T, Dombrowski JC, Golden MR, et al. Comparing methods for record linkage for public health action: matching algorithm validation study. JMIR Public Health Surveill 2020 Apr 30;6(2):e15917. [doi: 10.2196/15917] [Medline: 32352389]
14. Ruppert LP, He J, Martin J, et al. Linkage of Indiana State Cancer Registry and Indiana Network for patient care data. J Registry Manag 2016;43(4):174-178. [Medline: 29595920]
15. Conway RBN, Armistead MG, Denney MJ, Smith GS. Validating the matching of patients in the linkage of a large hospital system's EHR with state and national death databases. Appl Clin Inform 2021 Jan;12(1):82-89. [doi: 10.1055/s-0040-1722220] [Medline: 33567463]

XSL•FO
RenderX

16. Röchner P, Rothlauf F. Using machine learning to link electronic health records in cancer registries: on the tradeoff between linkage quality and manual effort. Int J Med Inform 2024 May;185:105387. [doi: 10.1016/j.ijmedinf.2024.105387] [Medline: 38428200]
17. Al-Saeed OM, Albogami MF, Hatem M. Multiple sclerosis in Saudi Arabia: a literature review. Saudi J Health Sci 2021;10(3):160-164. [doi: 10.4103/sjhs.sjhs_163_21]
18. Grannis SJ, Williams JL, Kasthuri S, Murray M, Xu H. Evaluation of real-world referential and probabilistic patient matching to advance patient identification strategy. J Am Med Inform Assoc 2022 Jul 12;29(8):1409-1415. [doi: 10.1093/jamia/ocac068] [Medline: 35568993]
19. Zhu Y, Matsuyama Y, Ohashi Y, Setoguchi S. When to conduct probabilistic linkage vs. deterministic linkage? A simulation study. J Biomed Inform 2015 Aug;56:80-86. [doi: 10.1016/j.jbi.2015.05.012] [Medline: 26004791]
20. van der Laan J. Record linkage using machine learning. 2024. URL: https://htmlpreview.github.io/?https://github.com/djvanderlaan/reclin2/blob/master/inst/doc/record_linkage_using_machine_learning.html [accessed 2026-01-21]
21. Gomatam S, Carter R, Ariet M, Mitchell G. An empirical comparison of record linkage procedures. Stat Med 2002 May 30;21(10):1485-1496. [doi: 10.1002/sim.1147] [Medline: 12185898]
22. Tromp M, Ravelli AC, Bonsel GJ, Hasman A, Reitsma JB. Results from simulated data sets: probabilistic record linkage outperforms deterministic record linkage. J Clin Epidemiol 2011 May;64(5):565-572. [doi: 10.1016/j.jclinepi.2010.05.008] [Medline: 20952162]
23. Joffe E, Byrne MJ, Reeder P, et al. A benchmark comparison of deterministic and probabilistic methods for defining manual review datasets in duplicate records reconciliation. J Am Med Inform Assoc 2014;21(1):97-104. [doi: 10.1136/amiajnl-2013-001744] [Medline: 23703827]

Abbreviations

CDM: common data model
EHR: electronic health record
ICD10: International Classification of Diseases 10th version
LR: logistic regression
ML: machine learning
MNGHA: Ministry of National Guard Health Affairs
MS: multiple sclerosis
NN: neural network
RERN: Real-world Evidence Network
RF: random forest
RWD: Real-world data

Edited by A Benis; submitted 01.Jul.2025; peer-reviewed by D Chrimes, J Li; revised version received 29.Dec.2025; accepted 29.Dec.2025; published 04.Feb.2026.

Please cite as:
Almadani O, Albogami Y, Alrwisan A
Linking Electronic Health Records for Multiple Sclerosis Research: Comparative Study of Deterministic, Probabilistic, and Machine Learning Linkage Methods
JMIR Med Inform 2026;14:e79869
URL: https://medinform.jmir.org/2026/1/e79869
doi:10.2196/79869

© Ohoud Almadani, Yasser Albogami, Adel Alrwisan. Originally published in JMIR Medical Informatics (https://medinform.jmir.org), 4.Feb.2026. This is an open-access article distributed under the terms of the Creative Commons Attribution License (https://creativecommons.org/licenses/by/4.0/), which permits unrestricted use, distribution, and reproduction in any medium, provided the original work, first published in JMIR Medical Informatics, is properly cited. The complete bibliographic information, a link to the original publication on https://medinform.jmir.org/, as well as this copyright and license information must be included.

XSL•FO
RenderX

Knowledge-Guided Explainable Recommendation Tool for Cancer Risk Prediction Models Using Retrieval-Augmented Large Language Models: Development and Validation Study

Shumin Ren[1,2*], PhD; Xin Zheng[1*], MSc; Jing Zhao[1], MSc; Jiale Du[1], MSc; Yuxin Zhang[1], MSc; Cheng Bi[1], MSc; Jie Song[1], MSc; Jinyi Zhang[2], MSc; Hongmei Lang[2], MD; Fan Zhang[3], MD; Bairong Shen[1], Prof Dr

[1]Institutes for Systems Genetics, West China Hospital of Sichuan University, Frontiers Science Center for Disease-related Molecular Network, Chengdu, Sichuan, China

[2]West China School of Medicine, Sichuan University, Sichuan University affiliated Chengdu Second People's Hospital, Chengdu Second People's Hospital, Chengdu, Sichuan, China

[3]Health Management Center, General Practice Medical Center, West China Hospital, Sichuan University, Chengdu, Sichuan, China

[*]these authors contributed equally

Corresponding Author:
Bairong Shen, Prof Dr
Institutes for Systems Genetics, West China Hospital of Sichuan University, Frontiers Science Center for Disease-related Molecular Network, Chengdu, Sichuan, China

Abstract

Background: Cancer risk prediction models are vital for precision prevention, enabling individualized assessment of cancer susceptibility based on genetic, clinical, environmental, and lifestyle factors. However, the practical use of these models is hindered by fragmented resources, heterogeneous reporting, and the absence of transparent, structured systems for systematic discovery and comparison.

Objective: This study aimed to develop a retrieval-augmented, knowledge-guided system that provides accurate recommendations for cancer risk prediction models.

Methods: We developed CanRisk-RAG, a recommendation platform underpinned by a precisely constructed knowledge base comprising more than 800 peer-reviewed cancer risk prediction models spanning diverse cancer types, modeling approaches, and predictive variables. The system integrates (1) large language model (LLM)–based semantic tag extraction, (2) embedding vectorization of structured metadata and abstracts, (3) a multifactor ranking algorithm combining semantic similarity with multiple quality indicators, and (4) LLM-generated literature summarization to support rapid user interpretation. Performance was evaluated across 4 types of representative queries. Eight domain experts independently assessed retrieval quality. CanRisk-RAG was benchmarked against PubMed, ChatGPT-4o, ScholarAI, and Gemini 1.5 Flash.

Results: On the independent validation set, CanRisk-RAG consistently outperformed all 4 baseline applications, achieving the highest overall relevance (8.30 [SD 0.59]) and reliability (7.62 [SD 0.76]) scores on a 10-point scale (P<.05). It also demonstrated high authenticity, data completeness, and consistency. Baseline applications frequently returned incomplete, inconsistent, or fabricated results, especially for complex, multifactorial queries, whereas CanRisk-RAG delivered accurate and structured recommendations grounded in validated evidence.

Conclusions: CanRisk-RAG presents a transparent, domain-specific, and semantically enriched framework for discovering cancer risk prediction models, addressing several limitations of existing keyword-based search tools and general-purpose LLMs. By integrating structured knowledge, multifactor ranking, and LLM-based reasoning, the system aims to improve the precision, reproducibility, and usability of model selection in cancer risk prediction. While our evaluation demonstrates encouraging performance compared with baseline systems, further validation in broader clinical contexts and real-world applications is warranted. The framework's general design may also be adaptable to other clinical model domains, providing a potential foundation for advancing evidence-based model discovery in precision medicine.

(JMIR Med Inform 2026;14:e78519) doi:10.2196/78519

KEYWORDS

cancer risk prediction models; large language models; LLMs; retrieval-augmented generation; RAG; personalized medicine; biomedical information retrieval

XSL•FO
RenderX

Introduction

Cancer risk prediction models are increasingly recognized as essential components of precision medicine, offering clinicians and researchers the ability to estimate an individual's likelihood of developing cancer based on diverse risk factors. These models integrate genetic markers, clinical data, environmental exposures, and lifestyle behaviors, thereby enabling more personalized approaches to prevention and screening [1-4]. These heterogeneous factors are not independent but often interact in complex and nonlinear ways. For example, genetic susceptibility may amplify the carcinogenic effects of smoking or obesity, while lifestyle interventions can partially mitigate inherited risk [5,6]. Understanding and modeling these interdependencies is therefore crucial for accurate cancer risk prediction.

Statistical approaches such as logistic regression, Cox proportional hazards models, and Bayesian networks have traditionally been used to analyze correlations and interactions among these predictors. More recently, advanced machine learning techniques, including random forests, gradient boosting, and deep neural networks, have enabled the modeling of higher-order, nonlinear, and cross-domain relationships between genetic, clinical, and environmental factors [7-10]. These methods can capture subtle patterns that traditional regression frameworks may overlook, thus improving predictive accuracy and interpretability when properly validated.

By identifying individuals at elevated risk, cancer risk prediction models facilitate earlier interventions, targeted monitoring, and ultimately reductions in cancer incidence and mortality [11,12]. Recent advances have demonstrated that combining heterogeneous risk determinants can substantially improve predictive accuracy. For instance, multivariate models that combine germline mutations (eg, BRCA1/2), hormonal and reproductive history, and lifestyle exposures have achieved strong discriminative power in breast cancer risk prediction [13,14], while integrative models linking smoking intensity, air pollution exposure, and genomic markers have improved lung cancer risk stratification [15,16]. Together, these developments highlight both the promise and the complexity of synthesizing genetic, clinical, environmental, and behavioral information into actionable tools for precision prevention.

Despite the promise of cancer risk prediction models, their practical impact is limited by barriers related to accessibility and adoption. A fundamental problem lies in the fragmentation of available models, which vary widely in methodological approach, target population, and predictive variables. Clinicians and researchers often struggle to identify the most appropriate model for a given use case, a challenge compounded by the lack of centralized, structured resources for systematic discovery. General medical retrieval systems are ill-suited to this task, as they are designed primarily to locate literature rather than extract or recommend specialized prediction tools. As a result, existing models are underutilized, research efforts are frequently duplicated, and the translational pathway from model development to clinical implementation remains inefficient. Indeed, it has been observed that most published prediction models are never adopted in clinical practice, highlighting a persistent gap between academic research and implementation [17]. Reviews further emphasize that although many models have been developed, only a small fraction have been successfully translated into clinical or public health practice, largely due to limitations in validation, usability, and acceptability [18,19].

To date, most users seeking cancer risk prediction models have relied on mainstream biomedical databases such as PubMed [20]. While PubMed provides broad access to scientific publications, its keyword-based search mechanisms often generate an overwhelming number of results, many of which are irrelevant for model identification. Moreover, critical details regarding model structure, predictive variables, validation cohorts, or performance metrics are typically buried in unstructured text, making systematic retrieval difficult.

In parallel, institutional platforms have been developed to provide more direct access to specific risk prediction tools. The US National Cancer Institute's Division of Cancer Epidemiology and Genetics offers a set of statistical macros and online calculators covering selected cancer types [21], while the Memorial Sloan Kettering Cancer Center provides nomograms tailored to particular clinical scenarios [22]. Although these resources represent valuable contributions, their scope remains restricted to only several (typically fewer than a dozen) tools, employ relatively narrow modeling methodologies, and lack detailed metadata regarding model characteristics or generalizability.

Large language models (LLMs) have recently been explored as potential solutions to improve medical information access. Their ability to integrate knowledge and process complex clinical text holds significant promise for bridging gaps between scattered information and practical decision-making [23-26]. However, empirical studies highlight critical weaknesses in LLMs, including limited precision, the generation of fabricated or irrelevant outputs, and the opacity of reasoning processes [23,27,28]. Retrieval-augmented generation (RAG) has been proposed as a mechanism to mitigate these shortcomings by grounding model outputs in external knowledge sources [29,30]. Several initiatives illustrate the potential of this approach. RefAI [31], for instance, combines PubMed retrieval with a GPT-4–based summarization system, enabling more effective access to recent biomedical publications. Similarly, WeiseEule [32] integrates keyword-driven retrieval from PubMed with LLM-based responses to improve query precision. However, these systems largely depend on user-defined search terms and ad hoc knowledge construction, leading to inconsistent coverage and limited reproducibility. Moreover, they are not designed to handle structured, model-specific metadata, such as predictive variables, validation cohorts, or performance metrics, that are critical for evidence-based model selection.

To address these challenges, the present study introduces CanRisk-RAG, a knowledge-guided and LLM-enhanced recommendation system designed to systematically retrieve, rank, and summarize cancer risk prediction models. Built on a knowledge base that we systematically constructed to consolidate validated cancer risk prediction models across

XSL•FO
RenderX

multiple cancer types, predictive variables, and methodological frameworks, CanRisk-RAG provides a structured foundation for model discovery and reuse. By combining domain-curated knowledge with LLM-driven semantic reasoning, the system bridges the gap between unstructured user queries and structured model metadata. Furthermore, a multi-factor ranking algorithm integrates semantic similarity with evidence-based indicators, such as publication quality, model performance, and timeliness, ensuring that recommended models are both relevant and scientifically robust. To enhance interpretability and usability, CanRisk-RAG also generates concise LLM-based summaries that highlight key model characteristics.

In essence, CanRisk-RAG aims to provide a scalable, transparent, and domain-aware retrieval framework that supports both research and clinical decision-making in cancer risk assessment. By facilitating the efficient reuse of existing models and improving accessibility for diverse user needs, including population-level screening and high-risk cohorts defined by genetic predisposition or family history, it represents a step toward operationalizing precision prevention in oncology.

This paper is organized as follows: We first introduce the data sources and system development workflow. Next, we describe the design of the evaluation tasks and the specific evaluation metrics used. We then present the performance results of CanRisk-RAG in terms of model recommendation and tool usability, along with comparative analyses against four baseline applications. Finally, we discuss the implications of the findings and explore potential directions for extending the system to other cancer research or medical domains.

Methods

Overview

The Methods section outlines the construction of CanRisk-RAG, covering data preparation, semantic vectorization, tag extraction via LLM, hybrid ranking with multiple quality indicators, literature summarization, and comparative evaluation. For more implementation details and technical specifications, please refer to Supplemental Information 1.1 in Multimedia Appendix 1.

Dataset

Data Preparation

We constructed a knowledge base containing peer-reviewed cancer risk prediction models, consolidating clinically developed and validated cancer risk prediction models extracted from PubMed. The detailed search criteria and the inclusion and exclusion standards used for model collection are provided in Supplemental Information 1.2 and 1.3 in Multimedia Appendix 1.

Following this procedure, a total of 808 cancer risk prediction models were included. Each model is uniquely identified by a model ID (MID). Each model was comprehensively described using metadata covering 3 major categories, namely basic information, sample information, and model information, across a total of 36 fields. To facilitate structured storage and interpretation, an Entity–Relationship (ER) diagram was constructed (see Supplemental Information 1.4 in Multimedia Appendix 1). In addition, as illustrated in Figure 1, the knowledge base organizes data across more than 10 cancer types (see Supplemental Information 2.1 in Multimedia Appendix 2 for the full distribution), over 13 methodological frameworks (eg, logistic regression, Cox regression, nomograms), and 3095 predictive factors, including age, body mass index, sex, and family history.

Figure 1. Distribution of cancer types, model types, and predictive factors in the CanRisk-RAG.

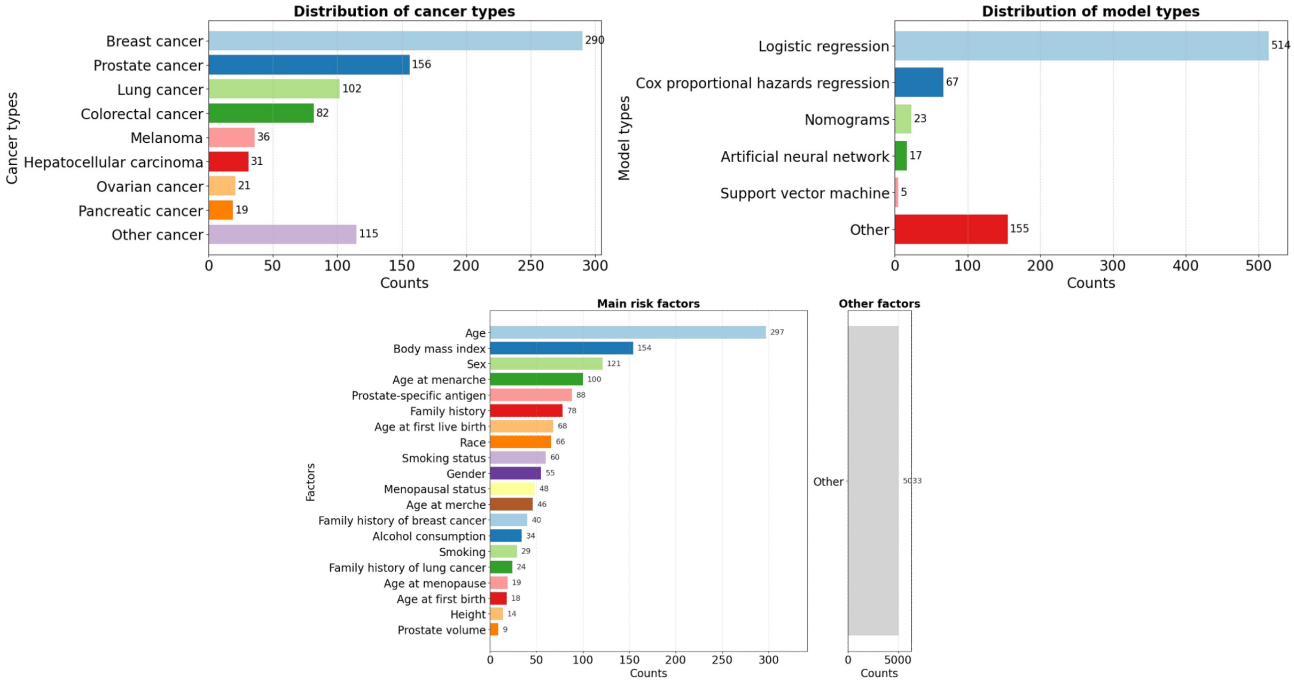

XSL•FO
RenderX

Data Segmentation and Vectorization

To enable semantic retrieval, data from the knowledge base were transformed into structured vector representations. Key attributes of each model, including cancer type, methodological approach, research stage, predictive factors, and geographic context were integrated to form composite descriptors that reflect the essential semantic characteristics of the models. These descriptors were then encoded using advanced sentence embedding techniques to generate dense vector representations, ensuring that key semantic meaning was preserved.

In parallel, the textual abstracts of the model research were independently embedded to capture complementary contextual details not fully represented by structured metadata. The combination of structured semantic vectors and unstructured textual embeddings provided a comprehensive representation of each model (see Supplemental Information 1.1 in Multimedia Appendix 1 for details). This dual encoding strategy established the basis for subsequent similarity search and model ranking, allowing the system to align user queries with the most relevant prediction models in a context-aware and interpretable manner.

Workflow of CanRisk-RAG

System Architecture

The overall workflow of CanRisk-RAG comprises a multistage pipeline that transforms unstructured model resources into structured model recommendations (Figure 2). The system integrates several key components: (1) semantic tag extraction, in which user queries are parsed by a LLM into predefined biomedical fields; (2) semantic embedding and vectorization, which encode both structured metadata and unstructured abstracts into dense representations for similarity computation; (3) multifactor ranking, combining semantic similarity with quality indicators such as the journal impact factor (JIF), the area under the curve (AUC), and publication recency to ensure reliable prioritization; and (4) LLM-based summarization, which synthesizes retrieved content into concise and readable outputs. Together, these stages enable CanRisk-RAG to perform context-aware retrieval, interpret complex user intents, and deliver transparent, evidence-based model recommendations supported by structured domain knowledge.

Figure 2. Pipeline of CanRisk-RAG construction. This figure presents the full pipeline of CanRisk-RAG, a retrieval-augmented framework designed to identify and summarize validated cancer risk prediction models from peer-reviewed resources. The workflow proceeds from user query interpretation to model recommendation: (1) users enter a natural language query describing desired model features; (2) a large language model (LLM)–based semantic tag extractor converts the query into structured fields (eg, cancer type, model type, predictive factors, study region); (3) the query is matched against a knowledge base constructed from PubMed containing over 800 cancer risk models and 3000 predictive variables; (4) structured metadata and text are vectorized using optimized sentence embeddings; (5) semantic similarity between query and models is computed; (6) a multifactor ranking algorithm integrates similarity, journal impact factor (JIF), model area under the curve (AUC), and publication recency into a composite score; and (7) top-ranked models are presented with metadata and an LLM-generated summary.

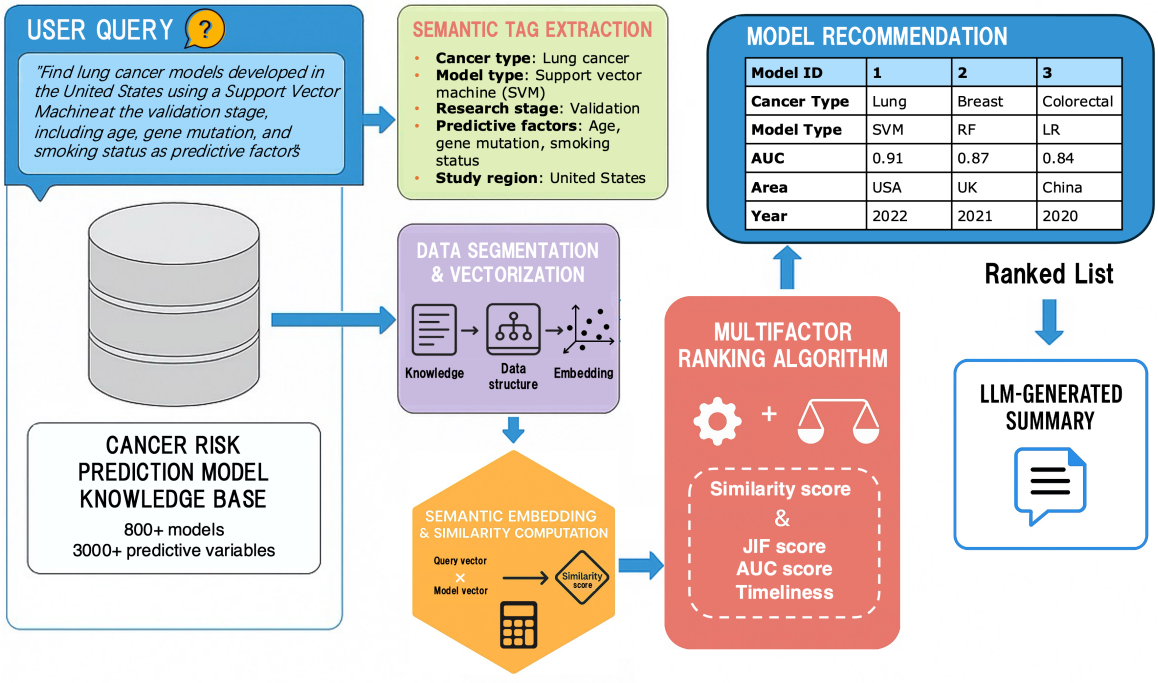

Tag Extraction for Enhanced Semantic Matching

To support efficient retrieval, user queries were first transformed from free text into structured semantic representations. This process was facilitated by a LLM (DeepSeek-V3) [33], chosen for its open-source nature and ability to support scalable deployment. Rather than directly matching raw text against the database, the model extracted predefined semantic fields, including cancer type, model type, research stage, predictive factors, and study region, thereby aligning user intent with structured knowledge (see Supplemental Information 1.5 in Multimedia Appendix 1 for the prompt contents).

XSL•FO
RenderX

An evaluation set of 40 queries (Supplemental Information 1.6 in Multimedia Appendix 1) was constructed to evaluate the tag extraction process. The queries were designed to cover diverse cancer types, model types, predictive factor combinations, geographic contexts, and noisy inputs (eg, typos and incomplete descriptions). Two independent annotators created gold labels following the predefined schema (Cancer_Type, Model_Type, Research_Type, Involved_Factors, Country), and disagreements were adjudicated by a third expert. Precision, recall, and F_1-score were calculated per category and additionally provided uncertainty estimates using Wilson 95% CIs for precision (Supplemental Information 1.7 in Multimedia Appendix 1).

Embedding Model Selection

To prioritize relevant models, CanRisk-RAG employs a ranking strategy primarily driven by semantic similarity. User queries are semantically aligned with database entries through embedding-based similarity, which captures both structured tags and contextual meaning. The similarity score serves as the main determinant, reflecting the degree of correspondence between user intent and model characteristics.

Before performing multifactor ranking, to determine which embedding model achieved the best semantic representation performance, we evaluated four widely used sentence-embedding architectures [34-36], including all-MiniLM-L6-v2, all-MiniLM-L12-v2, all-mpnet-base-v2, and all-distilroberta-v1. Each model's output was assessed by 2 independent evaluators across 12 predefined recommendation queries derived from 4 thematic categories (Textbox 1). For each model, average relevance and reliability scores were calculated. All-distilroberta-v1 achieved the highest overall performance, with statistically significant advantages in both relevance and reliability metrics (see Supplemental Information 2.2 in Multimedia Appendix 2). Therefore, all-distilroberta-v1 was selected as the optimal embedding model for subsequent tool development and deployment.

Textbox 1. Evaluation themes and representative queries used for CanRisk-RAG development.

Model recommendation tasks based on cancer type

- Breast cancer
- Lung cancer
- Prostate cancer

Model recommendation tasks based on model type

- Logistic regression
- Support vector machine
- Neural network

Model recommendation tasks based on predictive factors

- Age, gene mutation, and family history
- PSA level, digital rectal examination, and prior biopsy
- Sex, smoking status, emphysema, and pulmonary nodule

Comprehensive model recommendation tasks

- Gastric cancer; logistic regression; predictive factors: age, family history, and BMI
- Colorectal cancer; Cox proportional hazards regression; predictive factors: prior biopsy, alcohol intake, and height
- Bladder cancer; nomogram models; predictive factors: race, gene mutation, smoking status, and education

Multifactor Ranking Algorithm

To enhance credibility and practical utility, 3 additional factors were integrated into the ranking: the JIF as an indicator of publication quality [31], the AUC as a measure of model performance, and publication recency to emphasize timely contributions. The AUC was treated as a continuous metric using a smoothed compression function, while JIF values were normalized through a log-smoothing transformation to mitigate right-skewed distributions [37]. The publication year was linearly normalized to yield a continuous timeliness score. These components were then combined into a unified weighted scoring function (Equation 1).

(1)Total score=α×similarity score+β×journal impact factor score+γ×AUC score+δ×timeliness score

LLM-Based Literature Summarization

To support user interpretation, CanRisk-RAG incorporates an automated summarization component that synthesizes the content of retrieved studies into concise, coherent overviews. By integrating information across multiple abstracts, the system highlights key findings and methodological features, enabling users to rapidly grasp the essential contributions of relevant models.

XSL•FO
RenderX

Assessment Experiments

Benchmarking and Evaluation Design

To optimize the performance of CanRisk-RAG, we conducted a comprehensive comparative evaluation using 12 representative queries spanning 4 thematic areas, including cancer types, modeling approaches, predictive factors, and integrated multicomponent queries. Each theme was further divided into subthemes to reflect major research directions in cancer risk prediction [38-47] (see Textbox 1). Eight domain experts, including 3 clinical cancer researchers and 5 biomedical informatics specialists, independently assessed the outputs for all themes, with each query evaluated by 2 experts. In parallel, multiple ablation experiments on the training dataset (Table 1) examining alternative weighting schemes enabled the optimization of the final ranking configuration, ensuring balanced and robust system performance.

Table . Weight configurations for multifactor ranking algorithm used in ablation experiments.

Group	α (Similarity)	β (JIF)[a]	γ (AUC)[b]	δ (Timeliness)
G1 (Proposed)	0.85	0.05	0.05	0.05
G2 (Similarity only)	1	0	0	0
G3 (AUC+)	0.7	0.05	0.2	0.05
G4 (Recency+)	0.7	0.05	0.05	0.2
G5 (JIF+)	0.7	0.2	0.05	0.05
G6 (Similarity + Recency)	0.85	0	0	0.15
G7 (Similarity + AUC)	0.85	0	0.15	0
G8 (Similarity + JIF)	0.85	0.15	0	0
G9 (Similarity + Recency + AUC)	0.8	0	0.1	0.1
G10 (Similarity + Recency + JIF)	0.8	0.1	0	0.1
G11 (Similarity + AUC + JIF)	0.8	0.1	0.1	0

[a]JIF: journal impact factor.

[b]AUC: area under the curve.

At the application level, CanRisk-RAG was benchmarked against PubMed, ChatGPT-4o [48], ScholarAI [49], and Gemini 1.5 Flash [50], each accessed through their respective application programming interfaces under standardized query conditions. Prompts were standardized across systems to maintain fairness in comparison (see Supplemental Information 1.8 in Multimedia Appendix 1).

This stage was evaluated by domain experts. Performance was scored on 5 key dimensions: relevance, reliability, authenticity, data completeness, and consistency (0 - 10 scale). Table 2 summarizes the evaluation types, metrics, and definitions used to assess the 5 applications, including CanRisk-RAG (see Supplemental Information 1.9 in Multimedia Appendix 1 for the scoring criteria of the 5 evaluation metrics).

XSL•FO
RenderX

Table . Evaluation metrics and definitions used for model recommendation and tool usability assessment.

Evaluation metrics type and metric names		Definition
Model recommendation performance evaluation		
	Relevance	The purpose of the relevance assessment is to determine the extent to which the recommended models match the user's specified criteria.
	Reliability	The reliability assessment examines the authority of the sources where the models were published and evaluates the performance of the models themselves.
	Authenticity	Authenticity checks whether the sources of the models are genuine and can be verified in various journal databases.
	Data completeness	Data completeness evaluates the thoroughness of the model information provided by each application, including metadata, cancer type, modeling type, model performance, predictive factors, and more.
	Consistency	Consistency evaluation measures how consistently the model recommendation results align when the same search conditions or prompts are used in 2 separate instances.
Tool usability evaluation		
	User goal achievement	This metric evaluates whether the tool meets users' specific needs and expectations under open-ended, self-defined query scenarios. Participants independently formulated queries based on their own research or clinical information needs. The score reflects the extent to which users were able to successfully locate relevant cancer risk prediction models that satisfied their personalized model recommendation requirements.
	Operative accessibility	Operative accessibility refers to the overall ease of using the tool and encompasses aspects such as deployment complexity, interface design, navigation intuitiveness, and loading speed. A user-friendly tool should minimize operational complexity and cognitive load while offering clearly structured content, intuitive workflows, and comprehensive help pages.

Validation and Usability

To prevent data leakage between hyperparameter tuning and final performance assessment, we strictly separated the datasets used for weight optimization and for comparative evaluation. Weight optimization and ablation analyses were conducted solely on the development dataset, whereas the final benchmarking against baseline applications (PubMed, ChatGPT-4o, ScholarAI, and Gemini 1.5 Flash) was performed on an independent, held-out evaluation set. This evaluation set consisted of 20 carefully designed queries (Supplemental Information 1.10 in Multimedia Appendix 1) covering previously unseen cancer types, modeling approaches, and multifactorial scenarios that jointly specified cancer type, model type, and predictive factors. Recommendation outputs were independently assessed by eight domain experts using the predefined five evaluation dimensions.

In addition, usability was assessed by 10 potential end users, including clinicians and biomedical informatics researchers, based on 2 criteria: goal achievement and operative accessibility (see Supplemental Information 1.11 in Multimedia Appendix 1 for the scoring criteria). Inclusion criteria of potential end users required participants to be able to independently complete retrieval tasks. To mitigate potential conflict-of-interest bias, individuals involved in system development or dataset curation were excluded from usability scoring. None of the evaluators were members of the development team.

This multiperspective evaluation enabled a systematic assessment of CanRisk-RAG's retrieval quality and practical applicability in comparison to existing systems. Table 2 summarizes the evaluation types, metrics, and definitions used for the assessment of CanRisk-RAG.

XSL•FO
RenderX

Statistical Analysis

The evaluation was conducted in 2 phases: first, the embedding models were assessed, then the 5 applications were evaluated. Descriptive statistics on the scores were given by the evaluators, including the mean and SD. To determine the consistency among evaluators for every metric assessed, we conducted a 2-way intraclass correlation coefficient analysis.

For the evaluation of different applications, the Shapiro-Wilk test was employed to determine whether the scores assigned by different evaluators for a specific metric followed a normal distribution. Due to the departure of the scores from normality, the Mann-Whitney *U* test was selected to compare the overall performance scores. To explore variations in performance across the five applications and various subthemes, the Kruskal-Wallis rank-sum test was employed. When significant differences were identified by the Kruskal-Wallis test, Dunn post hoc multiple comparisons test was used to evaluate the performance of the different baselines in relation to CanRisk-RAG. Cliff delta was reported for all pairwise comparisons. Multiplicity control across post hoc tests was handled using Benjamini–Hochberg adjustments (α=.05). A significance level of P<.05 was applied to all statistical tests. All statistical tests were performed using Python (version 3.12).

Ethical Considerations

This study did not involve human or animal subjects; therefore, an ethics review board assessment was not required in accordance with institutional and national guidelines of Sichuan University. All analyses were conducted on publicly available, nonidentifiable data, consistent with regional research ethics policies [51].

Results

Tool Interface

As shown in Figure 3, the homepage of CanRisk-RAG features an interactive input form (Figure 3A) that allows users to specify any retrieval criteria related to cancer risk prediction models. Users may define the desired number of recommended results through a customizable selection option. Additionally, users can directly access the data source associated with the homepage by clicking the “CRPMKB” link in the main navigation bar. After entering the desired model criteria in the input field and clicking the “Search” button, the system displays the results page (Figure 3B), which presents a list of recommended models retrieved based on the user’s specified conditions. In the table result, each recommended model is presented with detailed information, including attributes such as MID, PMID, Journal, Model Name, Model Type, AUC, Research Type, Involved Factors, Year, Country, Cancer Type, Total Score. Each model entry is hyperlinked to its corresponding detailed record (Figure 3C). Furthermore, for all recommended models, the tool automatically generates a summary of the corresponding research abstract (Figure 3B), providing a concise overview of these studies to support rapid understanding and comparison.

Figure 3. CanRisk-RAG tool interfaces. (A) Homepage query form. (B) Recommendation results page. (C) Detailed model information page.

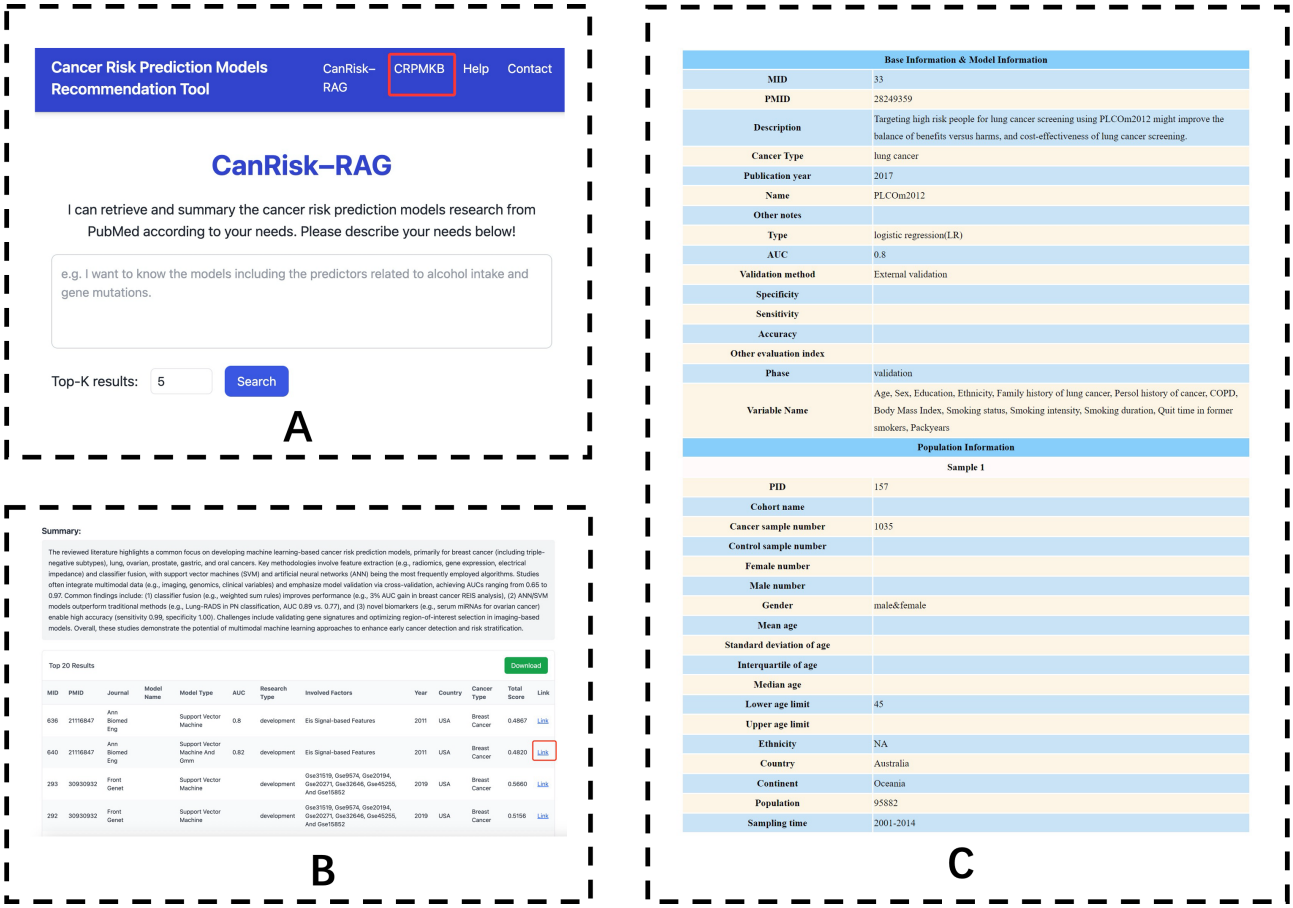

XSL•FO
RenderX

Model Recommendation Evaluation Results

Weight Configuration

We systematically evaluated eleven alternative weighting configurations (G1-G11) that varied the relative contributions of similarity (α), JIF (β), model AUC (γ), and publication timeliness (δ) (Table 3). Each configuration was tested on the same dataset of representative queries, and the average scores for relevance, reliability, and total performance were calculated.

A nonparametric Kruskal–Wallis *H* test revealed a statistically significant overall difference among the eleven configurations (H=47.916, P<6.430 × 10 , see Supplemental Information 2.3 in Multimedia Appendix 2).

The proposed configuration (G1: α=.85, β=.05, γ=0.05, δ=0.05) achieved the highest overall score, significantly outperforming variants such as SimOnly and Recency+ (P_{Holm}<.01). G1 consistently yielded higher scores across all configurations, demonstrating a robust performance on relevance and reliability.

Table . Performance comparison of different weighting configurations (mean [SD] for relevance, reliability, and total scores).

Group	Avg_Relevance, mean (SD)	Avg_Reliability, mean (D)	Avg_Total, mean (SD)
G1 (Proposed)	9.50 (0.78)	8.88 (0.85)	18.38 (1.44)
G8 (Similarity + JIF[a])	8.50 (0.66)	9.21 (0.78)	17.71 (1.16)
G7 (Similarity + AUC[b])	8.92 (0.97)	8.75 (0.85)	17.67 (1.55)
G6 (Similarity + Recency)	9.25 (0.74)	8.04 (0.81)	17.29 (1.12)
G3 (AUC+)	7.96 (0.96)	9.25 (0.90)	17.21 (1.59)
G5 (JIF+)	8.17 (0.92)	8.67 (0.96)	16.83 (1.37)
G10 (Similarity + Recency + JIF)	8.08 (0.78)	8.25 (0.79)	16.33 (0.87)
G9 (Similarity + Recency + AUC)	8.17 (1.05)	8.08 (0.93)	16.25 (1.51)
G11 (Similarity + AUC + JIF)	7.83 (0.64)	7.92 (0.72)	15.75 (0.79)
G2 (Similarity only)	9.42 (0.65)	5.46 (0.72)	14.88 (1.08)
G4 (Recency+)	7.33 (0.96)	7.08 (0.72)	14.42 (1.06)

[a]JIF: journal impact factor.

[b]AUC: area under the curve.

Performance Comparison of Applications

In the comparative evaluation across 5 applications, CanRisk-RAG consistently achieved the highest relevance and reliability across all 4 themes of the validation set (Table 4, see Supplemental Information 2.4 and 2.5 in Multimedia Appendix 2 for detailed statistics), delivering markedly superior retrieval precision compared with existing applications. For relevance, the average score was 8.30 (SD 0.59; 95% CI 8.02-8.58), indicating that the retrieved models closely matched the intended cancer types, modeling approaches, and predictive factors specified in the queries. In terms of reliability, the average score reached 7.62 (SD 0.76; 95% CI 7.27-7.98), reflecting strong consistency with authoritative and well-validated literature sources. These results confirm that, when applied to independent validation themes, CanRisk-RAG maintains robust generalization and stable interpretability, effectively extending to unseen data while preserving retrieval accuracy and quality consistency, thereby underscoring its scalability and real-world applicability. PubMed showed reasonable accuracy for straightforward cancer-type queries but struggled when tasks involved modeling approaches or specific predictive factors, often returning incomplete or no usable results. Scholar AI performed moderately in simpler recommendation tasks, but its accuracy dropped sharply for more complex, integrative queries. ChatGPT-4o occasionally retrieved relevant cancer-type models but frequently missed methodological or variable-level details. Gemini 1.5 Flash repeatedly failed to interpret user intent or generate sufficient recommendations, underscoring its limited capability for structured retrieval.

XSL•FO
RenderX

Table . Comparative evaluation of relevance and reliability on the test set across 5 applications.

Applications	Relevance, mean (SD)	P_{bh} [a]	Reliability, mean (SD)	P_{bh}
Topic 1				
CanRisk-RAG	8.70 (0.45)	—[b]	8.10 (0.55)	—
ChatGPT-4o	5.90 (1.24)	<.05	3.50 (0.35)	<.05
Gemini 1.5 Flash	2.40 (0.42)	<.05	1.80 (0.57)	<.05
PubMed	5.70 (0.97)	<.05	7.20 (1.04)	ns[c]
ScholarAI	7.90 (1.02)	ns	6.60 (0.96)	ns
Topic 2				
CanRisk-RAG	8.50 (0.50)	—	7.80 (0.76)	—
ChatGPT-4o	1.30 (0.84)	<.05	1.00 (0.35)	<.05
Gemini 1.5 Flash	1.20 (0.45)	<.05	1.80 (0.27)	<.05
PubMed	2.40 (1.14)	<.05	6.50 (1.00)	ns
ScholarAI	6.10 (0.74)	<.05	5.20 (1.30)	<.05
Topic 3				
CanRisk-RAG	8.40 (0.42)	—	7.20 (0.76)	—
ChatGPT-4o	1.80 (0.27)	<.05	1.10 (0.42)	<.05
Gemini 1.5 Flash	1.10 (0.42)	<.05	0.90 (0.55)	<.05
PubMed	1.20 (0.57)	<.05	5.60 (2.90)	ns
ScholarAI	5.10 (0.89)	<.05	4.70 (1.82)	ns
Topic 4				
CanRisk-RAG	7.60 (0.42)	—	7.40 (0.82)	—
ChatGPT-4o	2.20 (0.57)	<.05	1.10 (0.55)	<.05
Gemini 1.5 Flash	1.90 (0.22)	<.05	1.70 (0.57)	<.05
PubMed	0.10 (0.22)	<.05	0.40 (0.42)	<.05
ScholarAI	1.80 (1.15)	<.05	1.20 (1.04)	<.05
Average score				
CanRisk-RAG	8.30 (0.59)	—	7.62 (0.76)	—
ChatGPT-4o	2.80 (2.01)	<.05	1.68 (1.15)	<.05
Gemini 1.5 Flash	1.65 (0.65)	<.05	1.55 (0.60)	<.05
PubMed	2.35 (2.28)	<.05	4.92 (3.13)	<.05
ScholarAI	5.22 (2.44)	<.05	4.42 (2.37)	<.05

[a]P_{bh}: Benjamini–Hochberg adjusted significance levels, representing statistical comparisons against the corresponding CanRisk-RAG scores within the same topic or in the overall average.

[b]Not applicable.

[c]Not significant.

As a structured and knowledge-grounded recommendation system, CanRisk-RAG achieved high performance in authenticity, data completeness, and consistency, and was therefore used as the benchmark for evaluating other applications (Figure 4). PubMed, while fully reliable in authenticity and consistency due to its literature-based retrieval, showed only moderate data completeness, particularly failing in the comprehensive recommendation task. The 3 LLM-based tools, Scholar AI, ChatGPT-4o, and Gemini 1.5 Flash, performed less reliably overall and often generated incomplete or inconsistent metadata (see Supplemental Information 2.6 in Multimedia Appendix 2). Scholar AI displayed partial strength across themes but still suffered from missing model details, while Gemini 1.5 Flash showed some consistency in recommending models based on cancer types and modeling approaches yet frequently fabricated or cited nonscientific sources such as blogs or online news (see relevant examples in Supplemental Informations 1.12 and 1.13 in Multimedia Appendix 1).

XSL•FO
RenderX

Figure 4. Comparative evaluation of authenticity, data completeness, and consistency among 4 baseline applications in cancer risk prediction model recommendation tasks.

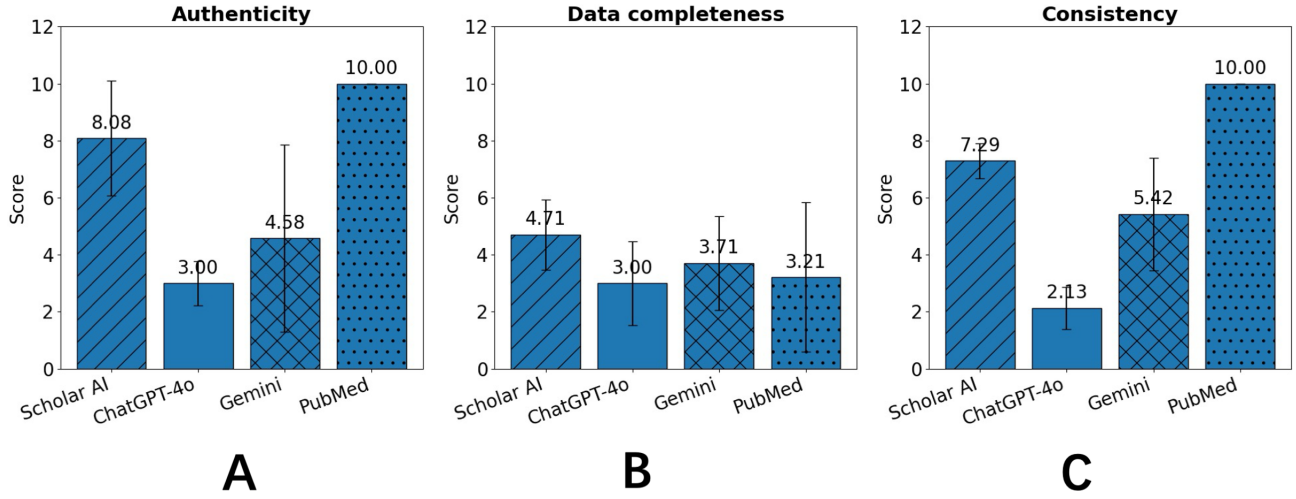

Overall, these findings demonstrate that CanRisk-RAG effectively bridges structured domain knowledge with LLM-driven semantic reasoning, achieving both high retrieval precision and reproducibility. Across all evaluation metrics, CanRisk-RAG consistently outperformed PubMed, Scholar AI, ChatGPT-4o, and Gemini 1.5 Flash, attaining markedly higher relevance and reliability alongside near-perfect scores in authenticity, data completeness, and consistency. In contrast, the baseline systems frequently struggled with complex, multifactorial queries, often returning incomplete, inconsistent, or fabricated information.

Usability Evaluation Results

The usability scores are summarized in Supplemental Information 14 in Multimedia Appendix 1. On a 3-point scale, CanRisk-RAG achieved a mean score of 2.7 (SD 0.48) for user goal achievement, indicating that the system was generally effective in meeting users' personalized retrieval needs. In addition, the tool demonstrated good operative accessibility, with an average score of 2.5 (SD 0.53), suggesting that users found the interface and overall operation intuitive and easy to use. Taken together, these results indicate that CanRisk-RAG is user-friendly, enabling most users to accomplish their intended tasks efficiently with minimal operational burden.

Discussion

Principal Findings

The results highlight CanRisk-RAG's clear advantages in recommending cancer risk prediction models, outperforming general-purpose LLM tools and traditional systems like PubMed. By combining an organized knowledge base, which provides rich metadata including cancer types, modeling methods, and performance metrics with a RAG framework, CanRisk-RAG enables high-quality personalized recommendations and advances beyond keyword-based retrieval toward expert-level semantic recommendation. Unlike ChatGPT-4o, Scholar AI, and Gemini 1.5 Flash, which often hallucinate content or misinterpret domain-specific queries, CanRisk-RAG delivers accurate recommendations with structured information grounded in validated literature. It should be noted that as a peer-reviewed, specialized biomedical literature database, PubMed achieved near-perfect scores in authenticity and consistency, which should be interpreted as a reference baseline rather than an algorithmic achievement. While PubMed inherently ensures authenticity through direct literature indexing, it lacks the semantic parsing capabilities required for complex, multifactorial queries, thereby underscoring the value of domain-specific systems that integrate structured knowledge with semantic understanding. It should also be acknowledged that a degree of circularity exists between the system design of CanRisk-RAG and the reliability evaluation. Specifically, JIF is incorporated as a low-weight auxiliary signal in the ranking algorithm, while the reliability metric used in expert evaluation partially reflects publication in authoritative journals. Consequently, the high reliability scores achieved by CanRisk-RAG should be partly interpreted as evidence that the system adheres to its predefined design principles, namely prioritizing models supported by established, higher-reputation peer-reviewed sources, rather than being overinterpreted as direct indicators of clinical effectiveness.

The system adopts a dual-embedding strategy that fuses tag-level semantic representations with embeddings of the original user query, allowing it to jointly capture structured domain constraints and broader user intent. This design enables effective semantic matching even in the absence of exact keyword overlap. Building on this representation, a multi-factor ranking algorithm integrates semantic similarity with complementary quality indicators—including JIF, model AUC, and publication recency—to enhance the credibility and practical usefulness of the recommended models. This is particularly beneficial for model comparison and systematic review scenarios, where both relevance and evidential strength are critical. In addition, our tag-extraction evaluation demonstrates that DeepSeek-V3 achieves high overall accuracy (micro-F_1=0.994), with only two omission cases observed in the 40-query test set. These rare errors were primarily attributable to implicit semantic descriptors or typographical issues rather than systematic extraction failures. Importantly, the fused embedding framework provides partial robustness to such upstream imperfections, as the original-query embedding channel can still encode missing concepts even when a structured tag is not completely extracted.

XSL•FO
RenderX

With respect to the comparative evaluation strategy, baseline LLM systems, namely ChatGPT-4o, ScholarAI, and Gemini 1.5 Flash, were evaluated using static zero-shot prompts to ensure standardized and reproducible conditions across tools. Although this design choice reduces prompt engineering bias and enhances fairness, it may underestimate the upper bound performance of general purpose LLMs, which can benefit from chain of thought prompting, multiround clarification, or interactive refinement. However, incorporating adaptive and tool-specific prompt optimization would compromise reproducibility and comparability, as performance would then depend on prompt engineering expertise rather than intrinsic system capability. Importantly, CanRisk-RAG does not rely on iterative user clarification. Instead, it embeds domain knowledge and semantic constraints directly into the retrieval pipeline, reflecting a distinct design philosophy that shifts cognitive and procedural burden from the user to the system. This property is particularly important in clinical and translational research settings. Moreover, unlike interactive LLM-based tools, CanRisk-RAG produces deterministic and reproducible outputs for identical inputs, which is essential for evidence-based model discovery and systematic research workflows.

Although the superior performance of CanRisk-RAG highlights the advantage of integrating structured domain knowledge with retrieval-augmented generation, its effectiveness largely depends on the built-in knowledge base, which supplies high-quality, expert-verified model information. Consequently, the "extensibility" of the framework depends on the sustainable expansion of such constructed resources. To address this scalability challenge, we developed a semiautomated update pipeline that combines automated literature retrieval, rule-based metadata extraction, and LLM-assisted knowledge extraction in a workflow [52]. This tool substantially improves data update efficiency while reducing manual workload. Nevertheless, essential human review and expert supplementation are retained to ensure the accuracy of curated content. The knowledge base is planned to be updated every six months to maintain both recency and reliability.

In addition, although currently focused on cancer risk prediction models, the CanRisk-RAG framework is adaptable to other disease domains and scenarios, including prognosis and treatment response models, underscoring its potential as a universal platform for the discovery and application of clinical prediction models.

Limitations

Despite the encouraging performance of CanRisk-RAG, several limitations should be acknowledged.

First, although CanRisk-RAG offers enhanced flexibility and effective retrieval, its performance is inevitably shaped by multiple structured layers of uncertainty spanning internal (algorithmic) and external (evidence-base) factors. Internally, reliance on semantic similarity may reduce field-level specificity; LLM-based tag extraction can over-generalize factors (eg, interpreting "family history of breast cancer" as "family history" or generalizing a specific genetic factor such as BRCA1/2 mutation into a broad category like "genetic risks") and changes in multi-factor weights (eg, raising "Recency" weight from 0.05 to 0.15) can alter rankings. These factors introduce algorithmic uncertainty, which we partially mitigated through ablation experiments and iterative weighting optimization. Externally, heterogeneity in study design, sample size, population, and reporting limits comparability and generalizability. For instance, lung cancer survival models from small regional cohorts may not generalize to multi-institutional datasets, and models trained on East Asian populations may underperform in Western populations due to demographic and healthcare-system differences. Even established models (eg, Gail) exhibit cohort-dependent AUC and calibration, highlighting cross-dataset variability as an important uncertainty layer. Future work will incorporate domain adaptation and uncertainty quantification methods to reduce these effects.

Second, the current ranking strategy relies on a limited set of quality-related indicators. JIF is included as a low-weight auxiliary signal and is normalized to mitigate its influence; however, it remains a coarse, venue-level metric that does not directly reflect study-level methodological rigor. Important indicators such as sample size, calibration reporting, and the extent of external validation are not yet uniformly available across the curated literature and therefore could not be systematically incorporated as first-class ranking features in the present version. As a result, residual bias may be introduced when finer-grained quality signals are missing or inconsistently reported, even though JIF is used only to refine the ordering among semantically similar candidates. In addition, the ranking strategy incorporates reported AUC values as a quantitative indicator of model performance without explicitly differentiating or weighting AUCs derived from model development versus external validation stages. This design choice may inadvertently favor development studies that report optimistic performance over rigorously validated models with stronger generalizability. Future versions of CanRisk-RAG will aim to integrate validation-aware performance stratification and explicit study-level quality indicators, such as cohort size, validation design, and calibration metrics, to better balance apparent accuracy with real-world applicability and progressively reduce reliance on venue-level signals.

Third, the present study relied on a single LLM (DeepSeek-V3) for semantic tag extraction and literature summarization. While this design choice ensured internal consistency and reproducibility across experiments, it inevitably limited robustness to model-specific variability and potential biases inherent to a single LLM. In addition, baseline comparisons with general-purpose LLMs were conducted under a static zero-shot prompting setting without access to external retrieval, web browsing, or tool invocation capabilities. As a result, these baselines were constrained to parametric-only knowledge, which may underestimate their performance in more interactive or retrieval-augmented configurations. In this context, the evaluation primarily highlights the hallucination risks and structural limitations of ungrounded LLM responses when external knowledge is unavailable, rather than serving as an exhaustive benchmark of the full capabilities of modern LLM ecosystems. Future work will extend this evaluation framework by incorporating multi-model ensemble strategies for tag extraction and summarization to enhance robustness and

XSL•FO
RenderX

stability. In parallel, more comprehensive comparisons will be conducted against LLM-based systems equipped with web browsing, tool use, or fully integrated RAG workflows, including multi-turn and interactive prompting strategies.

Fourth, expert scoring was performed manually, introducing subjectivity despite inter-rater consistency checks. Future studies will incorporate automated evaluation methods, such as rule-based matching and semantic alignment metrics, to improve reproducibility and reduce dependence on manual assessments.

Fifth, although CanRisk-RAG includes an LLM-based literature summarization module, the current evaluation is primarily centered on retrieval and recommendation performance. The adopted metrics assess the relevance and reliability of retrieved models and metadata but do not explicitly quantify the factual accuracy or hallucination rate of the generated summaries. The summarization component is intended to serve as an assistive tool for facilitating user comprehension and synthesizing key information from retrieved literature, rather than to provide precise quantitative data; future work will incorporate dedicated evaluation protocols to systematically assess the quality and faithfulness of the generative component.

Finally, a key limitation of the present study is that the CanRisk-RAG knowledge base was constructed using literature retrieved prior to December 2022, and therefore does not include cancer risk prediction models published from 2023 onward. This temporal constraint may temporarily place CanRisk-RAG at a relative disadvantage when compared with contemporary LLMs that potentially have access to more recent biomedical literature. Beyond general concerns regarding data currency, this cutoff has specific implications for users seeking state-of-the-art computational or deep learning–based cancer risk prediction models, as recent years have witnessed a rapid proliferation of AI-driven approaches incorporating deep neural networks and multimodal data integration. As a result, the current version of CanRisk-RAG may be less suitable for users whose primary objective is to identify the most recent model architectures. To address this limitation and enhance temporal coverage, we have developed a semiautomated update pipeline that integrates automated literature retrieval, rule-based metadata extraction, and LLM-assisted curation, while retaining expert review to ensure data quality. The knowledge base is planned to be updated on a semiannual basis. Future evaluations will incorporate newly published models to assess how expanded temporal coverage influences retrieval performance, and to enable more temporally aligned comparisons with evolving LLM-based systems, particularly in the context of rapidly advancing AI-driven cancer risk modeling.

Conclusion

This study introduced CanRisk-RAG, a knowledge-driven retrieval framework for cancer risk prediction models that integrates structured knowledge with semantic reasoning. Through systematic evaluation, CanRisk-RAG demonstrated superior performance in relevance, reliability, and data consistency compared with existing retrieval systems. These results indicate that combining structured knowledge representation with LLM-based reasoning can substantially improve the precision and transparency of model discovery in biomedical research, supporting reproducible and evidence-based applications in precision oncology.

Acknowledgments

The authors used ChatGPT (OpenAI, GPT-4) for language editing purposes during the preparation of this manuscript. The authors confirm that all final manuscript decisions, including content approval and submission, were made exclusively by the authors.

Funding

This work was supported by the National Natural Science Foundation of China (32570773, 32270690) and the Medical Research Projects in Chengdu City (2025434).

Data Availability

The source code for data processing is available at GitHub [52,53].

Authors' Contributions

Conceptualization: BS (lead), SR (equal)
Data curation: SR
Formal analysis: SR (lead), XZ (supporting)
Funding acquisition: BS (lead), SR (supporting)
Investigation: SR
Methodology: BS (lead), SR (equal), J Zhang (supporting)
Project administration: BS (lead), SR (equal)
Resources: BS
Supervision: BS
Validation: SR (lead), XZ (supporting), JD (supporting), YZ (supporting), CB (supporting)
Visualization: SR (lead), J Zhao (supporting)
Writing—original draft: SR (lead), XZ (supporting)

XSL•FO
RenderX

Writing—review & editing: SR (lead), JS (supporting), J Zhang (supporting), HL (supporting), ZF (supporting)

Conflicts of Interest

None declared.

Multimedia Appendix 1
Supplementary methods and details.
[DOCX File, 1745 KB - medinform_v14i1e78519_app1.docx]

Multimedia Appendix 2
Raw scores of experiments.
[XLSX File, 73 KB - medinform_v14i1e78519_app2.xlsx]

References

1. Vickers AJ. Prediction models in cancer care. CA Cancer J Clin 2011;61(5):315-326. [doi: 10.3322/caac.20118] [Medline: 21732332]
2. Lophatananon A, Usher-Smith J, Campbell J, et al. Development of a cancer risk prediction tool for use in the UK primary care and community settings. Cancer Prev Res (Phila) 2017 Jul;10(7):421-430. [doi: 10.1158/1940-6207.CAPR-16-0288] [Medline: 28559460]
3. Engel C, Fischer C. Breast cancer risks and risk prediction models. Breast Care (Basel) 2015 Feb;10(1):7-12. [doi: 10.1159/000376600] [Medline: 25960719]
4. Tutsoy O, Sumbul HE. A novel deep machine learning algorithm with dimensionality and size reduction approaches for feature elimination: thyroid cancer diagnoses with randomly missing data. Brief Bioinform 2024 May 23;25(4):bbae344. [doi: 10.1093/bib/bbae344] [Medline: 39007597]
5. Chen X, Jansen L, Guo F, Hoffmeister M, Chang-Claude J, Brenner H. Smoking, genetic predisposition, and colorectal cancer risk. Clin Transl Gastroenterol 2021 Mar 1;12(3):e00317. [doi: 10.14309/ctg.0000000000000317] [Medline: 33646204]
6. Byrne S, Boyle T, Ahmed M, Lee SH, Benyamin B, Hyppönen E. Lifestyle, genetic risk and incidence of cancer: a prospective cohort study of 13 cancer types. Int J Epidemiol 2023 Jun 6;52(3):817-826. [doi: 10.1093/ije/dyac238] [Medline: 36651198]
7. Su YR, Sakoda LC, Jeon J, et al. Validation of a genetic-enhanced risk prediction model for colorectal cancer in a large community-based cohort. Cancer Epidemiol Biomarkers Prev 2023 Mar 6;32(3):353-362. [doi: 10.1158/1055-9965.EPI-22-0817] [Medline: 36622766]
8. Bruno V, Betti M, D'Ambrosio L, et al. Machine learning endometrial cancer risk prediction model: integrating guidelines of European Society for Medical Oncology with the tumor immune framework. Int J Gynecol Cancer 2023 Nov 6;33(11):1708-1714. [doi: 10.1136/ijgc-2023-004671] [Medline: 37875322]
9. Choi J, Ha TW, Choi HM, et al. Development of a breast cancer risk prediction model incorporating polygenic risk scores and nongenetic risk factors for Korean women. Cancer Epidemiol Biomarkers Prev 2023 Sep 1;32(9):1182-1189. [doi: 10.1158/1055-9965.EPI-23-0064] [Medline: 37310812]
10. Tutsoy O, Koç GG. Deep self-supervised machine learning algorithms with a novel feature elimination and selection approaches for blood test-based multi-dimensional health risks classification. BMC Bioinformatics 2024 Mar 8;25(1):103. [doi: 10.1186/s12859-024-05729-2] [Medline: 38459463]
11. Hassan FH, Wye AYK, Yusof SSS, Xiang TY. Predicting risk of getting smoking-related cancer: a comparison of three prediction models. Presented at: LOPAL '18: Proceedings of the International Conference on Learning and Optimization Algorithms: Theory and Applications; May 2-5, 2018. [doi: 10.1145/3230905.3230950]
12. Bae CY, Kim BS, Jee SH, Lee JH, Nguyen ND. A study on survival analysis methods using neural network to prevent cancers. Cancers (Basel) 2023 Sep 27;15(19):4757. [doi: 10.3390/cancers15194757] [Medline: 37835451]
13. Mertens E, Barrenechea-Pulache A, Sagastume D, Vasquez MS, Vandevijvere S, Peñalvo JL. Understanding the contribution of lifestyle in breast cancer risk prediction: a systematic review of models applicable to Europe. BMC Cancer 2023 Jul 21;23(1):687. [doi: 10.1186/s12885-023-11174-w] [Medline: 37480028]
14. Lee CPL, Irwanto A, Salim A, et al. Breast cancer risk assessment using genetic variants and risk factors in a Singapore Chinese population. Breast Cancer Res 2014 Jun 18;16(3):R64. [doi: 10.1186/bcr3678] [Medline: 24941967]
15. Liang H, Zhou X, Zhu Y, et al. Association of outdoor air pollution, lifestyle, genetic factors with the risk of lung cancer: a prospective cohort study. Environ Res 2023 Feb 1;218:114996. [doi: 10.1016/j.envres.2022.114996] [Medline: 36481370]
16. Li Y, Xiao X, Han Y, et al. Genome-wide interaction study of smoking behavior and non-small cell lung cancer risk in Caucasian population. Carcinogenesis 2018 Mar 8;39(3):336-346. [doi: 10.1093/carcin/bgx113] [Medline: 29059373]
17. Markowetz F. All models are wrong and yours are useless: making clinical prediction models impactful for patients. NPJ Precis Oncol 2024 Feb 28;8(1):54. [doi: 10.1038/s41698-024-00553-6] [Medline: 38418530]

XSL•FO
RenderX

18. Colditz GA, Wei EK. Risk prediction models: applications in cancer prevention. Curr Epidemiol Rep 2015 Dec;2(4):245-250. [doi: 10.1007/s40471-015-0057-1]
19. Waters EA, Taber JM, McQueen A, Housten AJ, Studts JL, Scherer LD. Translating cancer risk prediction models into personalized cancer risk assessment tools: stumbling blocks and strategies for success. Cancer Epidemiol Biomarkers Prev 2020 Dec;29(12):2389-2394. [doi: 10.1158/1055-9965.EPI-20-0861] [Medline: 33046450]
20. White J. PubMed 2.0. Med Ref Serv Q 2020;39(4):382-387. [doi: 10.1080/02763869.2020.1826228] [Medline: 33085945]
21. Risk assessment macros, software programs, and tools. National Cancer Institute. URL: https://dceg.cancer.gov/tools/risk-assessment [accessed 2025-09-13]
22. Prediction tools - a tool for doctors and patients. Memorial Sloan Kettering Cancer Center. URL: https://www.mskcc.org/nomograms [accessed 2025-09-13]
23. Clusmann J, Kolbinger FR, Muti HS, et al. The future landscape of large language models in medicine. Commun Med (Lond) 2023 Oct 10;3(1):141. [doi: 10.1038/s43856-023-00370-1] [Medline: 37816837]
24. Peng C, Yang X, Chen A, et al. A study of generative large language model for medical research and healthcare. NPJ Digit Med 2023 Nov 16;6(1):210. [doi: 10.1038/s41746-023-00958-w] [Medline: 37973919]
25. Kasneci E, Sessler K, Küchemann S, et al. ChatGPT for good? On opportunities and challenges of large language models for education. Learn Individ Differ 2023 Apr;103:102274. [doi: 10.1016/j.lindif.2023.102274]
26. Li Y, Tao W, Li Z, et al. Artificial intelligence-powered pharmacovigilance: a review of machine and deep learning in clinical text-based adverse drug event detection for benchmark datasets. J Biomed Inform 2024 Apr;152:104621. [doi: 10.1016/j.jbi.2024.104621] [Medline: 38447600]
27. Jin Q, Leaman R, Lu Z. Retrieve, summarize, and verify: how will ChatGPT affect information seeking from the medical literature? J Am Soc Nephrol 2023 Aug 1;34(8):1302-1304. [doi: 10.1681/ASN.0000000000000166] [Medline: 37254254]
28. Day T. A preliminary investigation of fake peer-reviewed citations and references generated by ChatGPT. Prof Geogr 2023 Nov 2;75(6):1024-1027. [doi: 10.1080/00330124.2023.2190373]
29. Gao Y, Xiong Y, Gao X, et al. Retrieval-augmented generation for large language models: a survey. arXiv. Preprint posted online on Dec 18, 2023. [doi: 10.48550/arXiv.2312.10997]
30. Liu S, McCoy AB, Wright A. Improving large language model applications in biomedicine with retrieval-augmented generation: a systematic review, meta-analysis, and clinical development guidelines. J Am Med Inform Assoc 2025 Apr 1;32(4):605-615. [doi: 10.1093/jamia/ocaf008] [Medline: 39812777]
31. Li Y, Zhao J, Li M, et al. RefAI: a GPT-powered retrieval-augmented generative tool for biomedical literature recommendation and summarization. J Am Med Inform Assoc 2024 Sep 1;31(9):2030-2039. [doi: 10.1093/jamia/ocae129] [Medline: 38857454]
32. Aftab W, Apostolou Z, Bouazoune K, Straub T. Optimizing biomedical information retrieval with a keyword frequency-driven prompt enhancement strategy. BMC Bioinformatics 2024 Aug 27;25(1):281. [doi: 10.1186/s12859-024-05902-7] [Medline: 39192204]
33. Liu A, Feng B, Xue B, et al. Deepseek-v3 technical report. arXiv. Preprint posted online on Dec 27, 2024. [doi: 10.48550/arXiv.2412.19437]
34. Galli C, Donos N, Calciolari E. Performance of 4 pre-trained sentence transformer models in the semantic query of a systematic review dataset on peri-implantitis. Information 2024;15(2):68. [doi: 10.3390/info15020068]
35. Lis S, Kubkowski M, Borkowska O, Serwa D, Kuparnik J. Analyzing credit risk model problems through natural language processing-based clustering and machine learning: insights from validation reports. J Risk Model Valid 2024;18. [doi: 10.21314/JRMV.2024.006]
36. Wilianto D, Suganda Girsang A. Automatic short answer grading onhigh school's e-learning using semantic similarity methods. TEM Journal 2023 Feb 27:297-302. [doi: 10.18421/TEM121-37]
37. Kiesslich T, Beyreis M, Zimmermann G, Traweger A. Citation inequality and the Journal Impact Factor: median, mean, (does it) matter? Scientometrics 2021 Feb;126(2):1249-1269. [doi: 10.1007/s11192-020-03812-y]
38. Pockett RD, Castellano D, McEwan P, Oglesby A, Barber BL, Chung K. The hospital burden of disease associated with bone metastases and skeletal-related events in patients with breast cancer, lung cancer, or prostate cancer in Spain. Eur J Cancer Care (Engl) 2010 Nov;19(6):755-760. [doi: 10.1111/j.1365-2354.2009.01135.x] [Medline: 19708928]
39. Bray F, Ferlay J, Soerjomataram I, Siegel RL, Torre LA, Jemal A. Global cancer statistics 2018: GLOBOCAN estimates of incidence and mortality worldwide for 36 cancers in 185 countries. CA Cancer J Clin 2018 Nov;68(6):394-424. [doi: 10.3322/caac.21492] [Medline: 30207593]
40. Kim G, Bahl M. Assessing risk of breast cancer: a review of risk prediction models. J Breast Imaging 2021;3(2):144-155. [doi: 10.1093/jbi/wbab001] [Medline: 33778488]
41. Lee A, Mavaddat N, Cunningham A, et al. Enhancing the BOADICEA cancer risk prediction model to incorporate new data on RAD51C, RAD51D, BARD1 updates to tumour pathology and cancer incidence. J Med Genet 2022;59(12):1206-1218. [doi: 10.1136/jmedgenet-2022-108471] [Medline: 36162851]
42. Louro J, Posso M, Hilton Boon M, et al. A systematic review and quality assessment of individualised breast cancer risk prediction models. Br J Cancer 2019 Jul;121(1):76-85. [doi: 10.1038/s41416-019-0476-8] [Medline: 31114019]

XSL•FO
RenderX

43. Lee YCA, Al-Temimi M, Ying J, et al. Risk prediction models for head and neck cancer in the US population from the INHANCE consortium. Am J Epidemiol 2020 Apr 2;189(4):330-342. [doi: 10.1093/aje/kwz259] [Medline: 31781743]
44. Katki HA, Kovalchik SA, Petito LC, et al. Implications of nine risk prediction models for selecting ever-smokers for computed tomography lung cancer screening. Ann Intern Med 2018 Jul 3;169(1):10-19. [doi: 10.7326/M17-2701] [Medline: 29800127]
45. Zhang X, Rice M, Tworoger SS, et al. Addition of a polygenic risk score, mammographic density, and endogenous hormones to existing breast cancer risk prediction models: a nested case-control study. PLoS Med 2018 Sep;15(9):e1002644. [doi: 10.1371/journal.pmed.1002644] [Medline: 30180161]
46. Khor S, Haupt EC, Hahn EE, Lyons LJL, Shankaran V, Bansal A. Racial and ethnic bias in risk prediction models for colorectal cancer recurrence when race and ethnicity are omitted as predictors. JAMA Netw Open 2023 Jun 1;6(6):e2318495. [doi: 10.1001/jamanetworkopen.2023.18495] [Medline: 37318804]
47. Guan Z, Huang T, McCarthy AM, et al. Combining breast cancer risk prediction models. Cancers (Basel) 2023 Feb 8;15(4):1090. [doi: 10.3390/cancers15041090] [Medline: 36831433]
48. Törnberg P. Chatgpt-4 outperforms experts and crowd workers in annotating political Twitter messages with zero-shot learning. arXiv. Preprint posted online on Apr 13, 2023. [doi: 10.48550/arXiv.2304.06588]
49. ScholarAI. 2024. URL: https://scholarai.io [accessed 2024-08-04]
50. Waisberg E, Ong J, Masalkhi M, et al. Google's AI chatbot "Bard": a side-by-side comparison with ChatGPT and its utilization in ophthalmology. Eye 2024 Mar;38(4):642-645. [doi: 10.1038/s41433-023-02760-0]
51. Ethical Review Measures for Life Science and Medical Research Involving Human Subjects (National Health and Family Planning Commission Document No. 4 [2023]). Sichuan University. URL: https://kyy.scu.edu.cn/info/1416/5946.htm [accessed 2026-03-03]
52. Shuminren/llms_clinicalriskmodel_tool. GitHub. URL: https://github.com/Shuminren/LLMs_ClinicalRiskModel_Tool [accessed 2026-02-16]
53. Shuminren/CanRisk-RAG. GitHub. URL: https://github.com/Shuminren/CanRisk-RAG [accessed 2026-03-02]

Abbreviations

AUC: area under the curve
JIF: journal impact factor
LLM: large language model
MID: model ID
RAG: retrieval-augmented generation

Edited by A Coristine; submitted 04.Jun.2025; peer-reviewed by M Al-Agil, O Tutsoy, Z Li; revised version received 27.Jan.2026; accepted 29.Jan.2026; published 09.Mar.2026.

Please cite as:
Ren S, Zheng X, Zhao J, Du J, Zhang Y, Bi C, Song J, Zhang J, Lang H, Zhang F, Shen B
Knowledge-Guided Explainable Recommendation Tool for Cancer Risk Prediction Models Using Retrieval-Augmented Large Language Models: Development and Validation Study
JMIR Med Inform 2026;14:e78519
URL: https://medinform.jmir.org/2026/1/e78519
doi:10.2196/78519

© Shumin Ren, Xin Zheng, Jing Zhao, Jiale Du, Yuxin Zhang, Cheng Bi, Jie Song, Jinyi Zhang, Hongmei Lang, Fan Zhang, Bairong Shen. Originally published in JMIR Medical Informatics (https://medinform.jmir.org), 9.Mar.2026. This is an open-access article distributed under the terms of the Creative Commons Attribution License (https://creativecommons.org/licenses/by/4.0/), which permits unrestricted use, distribution, and reproduction in any medium, provided the original work, first published in JMIR Medical Informatics, is properly cited. The complete bibliographic information, a link to the original publication on https://medinform.jmir.org/, as well as this copyright and license information must be included.

XSL•FO
RenderX

Original Paper

Impact of Age on Hospital Outcomes Following Minimally Invasive Posterior Lumbar Interbody Fusion: Retrospective Analysis of the Nationwide Inpatient Sample Database from 2016 to 2020

Yu-Jun Lin[1,2], MD; Fu-Yuan Shih[1,2], MD; Jin-Fu Huang[1], MD; Chun-Wei Ting[1], MD; Yu-Chin Tsai[1], MD, PhD; Lin Chang[1], MD; Yu-Hua Huang[1], MD, PhD; Ming-Jung Chuang[1], MD

[1]Department of Neurosurgery, Kaohsiung Chang Gung Memorial Hospital and Chang Gung University College of Medicine, Kaohsiung City, Taiwan, Taiwan

[2]Department of Neurosurgery, Kaohsiung Municipal Ta-Tung Hospital, Kaohsiung City, Taiwan

Corresponding Author:
Yu-Jun Lin, MD
Department of Neurosurgery
Kaohsiung Chang Gung Memorial Hospital and Chang Gung University College of Medicine
Number 123, Da-Pei Road
Niao-Song District
Kaohsiung City, Taiwan, 83301
Taiwan
Phone: 886 7 7317123 ext 8011
Fax: 886 7 7318762
Email: linyujun1022@gmail.com

Abstract

Background: Minimally invasive posterior lumbar interbody fusion (MIS-PLIF) is commonly performed to treat degenerative lumbar spinal conditions. Patients of advanced age often present with multiple comorbidities and reduced physiological reserves, influencing surgical risks and recovery. The growing aging population has led to a rising demand for care for older adults, posing significant challenges for health care systems worldwide.

Objective: This study aimed to identify the associations between different age groups and MIS-PLIF outcomes.

Methods: This study retrospectively analyzed data from the United States Nationwide Inpatient Sample collected between 2016 and 2020. Patients aged ≥60 years who underwent MIS-PLIF were eligible for inclusion in this study. Patients were categorized into age groups (60-69, 70-79, and ≥80 y). Logistic and linear regressions were used to determine the associations between the study variables and outcomes, including in-hospital mortality, complications, nonroutine discharge, and length of stay.

Results: A total of 785 patients aged ≥60 (mean age 69.4, SD 0.2) years who underwent MIS-PLIF were included in the analysis, and 18.7% (147/785) experienced at least one complication. After adjustment, compared with patients aged 60 to 69 years, the risk of nonroutine discharge was significantly increased in patients aged 70 to 79 years (adjusted odds ratio 2.33, 95% CI 1.57-3.46; *P*<.001) and ≥80 years (adjusted odds ratio 4.79, 95% CI 2.64-8.67; *P*<.001). No significant differences in the risk of complications or length of hospital stay were observed across the age groups.

Conclusions: In older patients undergoing MIS-PLIF, advanced age is an independent predictor of nonroutine discharge. Furthermore, our findings suggest that age alone is not an independent risk factor for complications or extended hospital stays among older patients. These findings underscore that MIS-PLIF is a viable option for older patients, for whom extra attention may still be needed for postoperative care. Implementing age-stratified management for older patients undergoing MIS-PLIF may have important clinical policy implications.

(JMIR Med Inform 2026;14:e76424) doi:10.2196/76424

KEYWORDS

age; minimally invasive posterior lumbar interbody fusion; MIS-PLIF; Nationwide Inpatient Sample; NIS; in-hospital outcome

XSL•FO
RenderX

Introduction

Minimally invasive posterior lumbar interbody fusion (MIS-PLIF) represents a surgical cornerstone in addressing lumbar spine pathology [1,2]. This innovative procedure accesses the lumbar spine through a posterior approach to treat damaged intervertebral discs and fuse adjacent vertebrae [3]. The procedure can achieve results similar to those of open procedures while minimizing disruption to the surrounding tissues.

With the increase in population age, the incidence of degenerative spine disorders has also increased, leading to an increased demand for surgical treatments. Conditions such as osteoarthritis, spinal stenosis, and degenerative disc disease are more common in older individuals, resulting in a growing need for procedures such as spinal fusion, laminectomy, and discectomy to manage pain and improve mobility [4]. The relationship between advancing age and spinal health is paramount, given the potential implications of age-related changes in bone density [5,6]. These changes may not only influence the procedural success of MIS-PLIF but also impact the overall safety and effectiveness of the procedure.

Surgery for degenerative spinal conditions presents specific challenges in the older population seeking relief from symptoms [7,8]. Beyond the structural considerations of bone density, older patients often have additional health concerns and comorbidities, adding increased risk to the surgical procedure and the subsequent recovery process [9]. Understanding the relationship between age and surgical outcomes is important for tailoring surgical approaches to ensure optimal outcomes and postoperative recovery in the older population.

Despite MIS-PLIF being a common and generally well-tolerated procedure, limited research has specifically focused on the impact of age on postoperative outcomes [10,11]. The increasing prevalence of degenerative spinal diseases in older individuals makes it important to understand how age may influence the success and safety of MIS-PLIF. Furthermore, age-stratified management is becoming increasingly important due to the rapidly growing older population worldwide. This study aimed to deepen the understanding of the effect of age on outcomes by analyzing the relationship between advancing age and postoperative outcomes of MIS-PLIF using a large, nationally representative dataset from the United States [12]. Using a large, nationally representative dataset, this study provides the statistical power necessary to detect clinically meaningful differences across age groups that smaller studies may have missed. This study may offer valuable implications for both clinical practice and policy development.

Methods

Ethical Considerations

This study was conducted in accordance with the principles of the Declaration of Helsinki (1975) and its amendments. The protocol for this study was submitted for review to the Institutional Review Board of Chang Gung Medical Foundation (202301168B0), which granted an exemption from formal Institutional Review Board oversight. This study complies with the terms of the Nationwide Inpatient Sample (NIS) data-use agreement. The data used in this study were obtained through the Online Health Care Cost and Utilization Project (HCUP) Central Distributor. Given the anonymized nature of the data, the requirement for informed consent was consequently waived. No compensation was provided to participants.

Data Source

This investigation drew upon data extracted from the NIS for the period of 2016 to 2020. The NIS, an initiative of the HCUP under the aegis of the Agency for Healthcare Research and Quality [13], encompasses a 20% stratified sample of inpatient admissions across 45 states and 1051 participating hospitals. The database meticulously records a wealth of patient information at the time of discharge, including primary and secondary diagnoses and procedures, dates of admission and discharge, discharge status, demographic details, and duration of hospital stay. Moreover, the NIS is equipped with statistical weights designed to facilitate the extrapolation of these findings to national patient volumes.

Study Design

This study was designed as a population-based, retrospective analysis. All data were sourced through a request to the Online HCUP Central Distributor, which manages the database [14] (certificate HCUP-4T28I74JW). This research strictly adhered to the data-use protocols stipulated by the NIS under the HCUP. The investigation used deidentified secondary data from the NIS database; hence, there was no direct involvement of patients or the public.

Study Population

The NIS database was searched for patients aged ≥60 years who underwent MIS-PLIF during the study period. The exclusion criteria were (1) traumatic injury; (2) injury in traffic accidents; and (3) missing values for weight, outcomes of interest, and covariates. All diagnoses and procedures were identified by the *International Classification of Diseases, Ninth Revision and Tenth Revision, Clinical Modification* (*ICD-9-CM* and *ICD-10-CM*) codes, as detailed in Table S1 in Multimedia Appendix 1. Following previous literature, we stratified age into 3 groups (ie, 60-69 y, 70-79 y, and ≥80 y) to perform comparative analyses across these categories [15,16].

Main Outcomes and Variables

The primary outcomes included in-hospital mortality, nonroutine discharge (ie, discharged to long-term care facilities), prolonged length of stay (LOS; defined as ≥75th percentile of LOS in the study population), and complications. Complications assessed included surgical (eg, infection, dural tear, hemorrhage, hematoma or seroma, and postoperative anemia) and medical complications (eg, pneumonia, pulmonary embolism, acute kidney injury, acute myocardial infarction, and urinary retention) based on insights from our literature review and clinical experience.

Demographic variables analyzed in this study encompassed patient age, sex, race or ethnicity (categorized as White, Black, Hispanic, and other), household income, insurance status

XSL•FO
RenderX

(identified by the primary payer), and whether admission occurred over a weekend. Household income quartiles were derived from the NIS, which estimates income based on the ZIP code of each patient's residence [17]. Comorbidities were identified using *ICD-9* and *ICD-10* codes and included diabetes mellitus, osteoporosis, obesity (defined as a BMI ≥30 kg/m²), chronic obstructive pulmonary disease, renal disease, hypertension, coronary artery disease, and heart failure. Relevant codes for each comorbidity are provided in Table S1 in Multimedia Appendix 1. Charlson Comorbidity Index was calculated from individual comorbidities to represent patients' overall severity of comorbid conditions.

Additionally, characteristics related to the hospital, such as bed size, location and teaching status, and regional location, were also collected as part of the extensive dataset available for all patients.

Statistical Analysis

The NIS database comprises a 20% stratified sample of US annual inpatient admissions, using weighted samples, strata, and clusters to facilitate national estimates in all analyses. Data analysis was conducted using the SURVEY procedure in SAS, which is optimized for sample survey data. Descriptive statistics for patients are presented as counts (n) and weighted percentages (%) or as means with SEs. Group comparisons for categorical variables were conducted using the Rao-Scott chi-square test, whereas weighted mean differences for continuous variables were analyzed using survey methods that account for stratification, clustering, and sampling weights, ensuring valid and robust statistical inferences within the context of complex survey designs. Logistic regression analyses were performed to assess the associations between study variables and binary outcomes, with results presented as odds ratios (ORs) and 95% CI. Linear regression was performed to assess the associations between the study variables and LOS. Multivariable regression was adjusted for variables that were significant (P<.05) in the univariate analysis. All statistical tests were 2-sided, with P<.05, deemed to indicate statistical significance. The analyses were conducted using SAS (version 9.4; SAS Institute Inc).

Results

Patient Selection

The patient selection process is illustrated in Figure 1. Between 2016 and 2020, 863 patients aged ≥60 years who underwent MIS-PLIF were identified from the NIS database. After excluding 29 patients with traumatic injuries, 1 patient with a traffic accident injury, and 48 patients with missing information on race, ethnicity, and household income, 785 patients were included in the study. Using the sample weight from the NIS database, this cohort corresponds to a total of 3925 hospitalized patients across the United States, as illustrated in Figure 1.

Figure 1. Flow diagram of patient selection. MIS-PLIF: minimally invasive posterior lumbar interbody fusion; NIS: Nationwide Inpatient Sample.

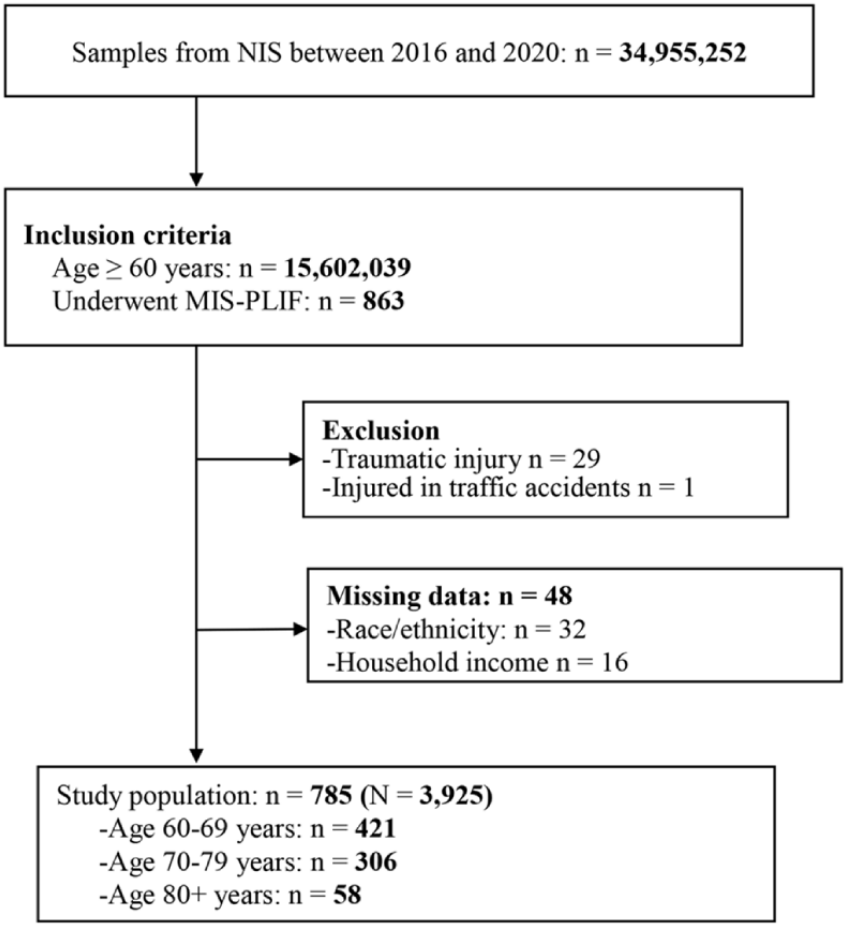

XSL•FO
RenderX

Characteristics of the Study Population

In the study population, the mean age was 69.4 (SD 0.2) years, 60.9% (478/785) were female individuals, 79.2% (622/785) were White, and 72.9% (572/785) had insurance covered by Medicare or Medicaid. A total of 66% (518/785) of the patients were diagnosed with spondylolisthesis. Patients aged 60 to 69 years had a significantly higher percentage of obesity, patients aged 70 to 79 years had a significantly higher frequency of diabetes mellitus and heart failure than the other age groups, and patients aged ≥80 years had the highest frequency of renal disease and hypertension (Table 1).

XSL•FO
RenderX

Table 1. Characteristics of the study population by age group.

Characteristics	All patients (N=785)	Age (y)			*P* value
		60-69 (n=421)	70-79 (n=306)	≥80 (n=58)	
Patient characteristics					
Age (y), mean (SD)	69.4 (0.2)	64.5 (0.1)	73.6 (0.1)	82.7 (0.1)	*<.001*[a]
Sex, n (%)					.95
Male	307 (39.1)	163 (38.7)	121 (39.5)	23 (39.7)	
Female	478 (60.9)	258 (61.3)	185 (60.5)	35 (60.3)	
Race and ethnicity, n (%)					*<.001*[a]
Black	93 (11.8)	63 (15)	29 (9.5)	1 (1.7)	
Hispanic	41 (5.2)	26 (6.2)	13 (4.2)	2 (3.4)	
White	622 (79.2)	314 (74.6)	256 (83.7)	52 (89.7)	
Other	29 (3.7)	18 (4.3)	8 (2.6)	3 (5.2)	
Household income, n (%)					*<.001*[a]
Q1[b]	196 (25)	117 (27.8)	63 (20.6)	16 (27.6)	
Q2	203 (25.9)	98 (23.3)	96 (31.4)	9 (15.5)	
Q3	198 (25.2)	113 (26.8)	67 (21.9)	18 (31)	
Q4	188 (23.9)	93 (22.1)	80 (26.1)	15 (25.9)	
Medicare or Medicaid insurance, n (%)					*<.001*[a]
No	213 (27.1)	182 (43.2)	29 (9.5)	2 (3.4)	
Yes	572 (72.9)	239 (56.8)	277 (90.5)	56 (96.6)	
Admission type, n (%)					.62
Elective	713 (90.8)	383 (91)	279 (91.2)	51 (87.9)	
Emergent	72 (9.2)	38 (9)	27 (8.8)	7 (12.1)	
Spondylolisthesis, n (%)					.71
No	267 (34)	147 (34.9)	100 (32.7)	20 (34.5)	
Yes	518 (66)	274 (65.1)	206 (67.3)	38 (65.5)	
Hospital characteristics					
Hospital bed size, n (%)					.31
Small	158 (20.1)	87 (20.7)	61 (19.9)	10 (17.2)	
Medium	267 (34)	149 (35.4)	102 (33.3)	16 (27.6)	
Large	360 (45.9)	185 (43.9)	143 (46.7)	32 (55.2)	
Hospital location or teaching status, n (%)					.11
Rural	45 (5.7)	22 (5.2)	18 (5.9)	5 (8.6)	
Urban nonteaching	174 (22.2)	91 (21.6)	67 (21.9)	16 (27.6)	
Urban teaching	566 (72.1)	308 (73.2)	221 (72.2)	37 (63.8)	
Hospital region, n (%)					.27
Northeast	155 (19.7)	79 (18.8)	63 (20.6)	13 (22.4)	
Midwest	160 (20.4)	86 (20.4)	59 (19.3)	15 (25.9)	
South	387 (49.3)	216 (51.3)	148 (48.4)	23 (39.7)	
West	83 (10.6)	40 (9.5)	36 (11.8)	7 (12.1)	
Comorbidities, n (%)					
Diabetes mellitus	199 (25.4)	100 (23.8)	91 (29.7)	8 (13.8)	*.003*[a]

XSL•FO
RenderX

Characteristics	All patients (N=785)	Age (y)			*P* value
		60-69 (n=421)	70-79 (n=306)	≥80 (n=58)	
Osteoporosis	50 (6.4)	23 (5.5)	22 (7.2)	5 (8.6)	.33
Obesity	198 (25.2)	116 (27.6)	72 (23.5)	10 (17.2)	*.03*[a]
Chronic obstructive pulmonary disease	74 (9.4)	40 (9.5)	29 (9.5)	5 (8.6)	.96
Renal disease	66 (8.4)	20 (4.8)	29 (9.5)	17 (29.3)	*<.001*[a]
Hypertension	574 (73.1)	284 (67.5)	243 (79.4)	47 (81)	*<.001*[a]
Coronary heart disease	116 (14.8)	54 (12.8)	50 (16.3)	12 (20.7)	.06
Heart failure	26 (3.3)	9 (2.1)	15 (4.9)	2 (3.4)	*<.001*[a]
Charlson Comorbidity Index, n (%)					*<.001*[a]
0	372 (47.4)	205 (48.7)	142 (46.4)	25 (43.1)	
1	212 (27)	128 (30.4)	74 (24.2)	10 (17.2)	
2	111 (14.1)	52 (12.4)	45 (14.7)	14 (24.1)	
≥3	90 (11.5)	36 (8.6)	45 (14.7)	9 (15.5)	

[a]*P*<.05.

[b]Quartiles (Q1-Q4) were derived by dividing the distribution of the variable into four equal parts, with Q1 representing the lowest and Q4 the highest range.

In-Hospital Outcomes

Only 0.1% (1/785) of the study population died in the hospital, whereas 18.7% (147/785) had at least one complication, of which 13.8% (108/785) had a least one surgical complication, and 7.3% (57/785) had at least one medical complication. Among the 3 age groups, patients aged ≥80 years had a significantly higher frequency of nonroutine discharge (20/58, 35% in the ≥80 y age group vs 52/421, 12.4% in the 60-69 y age group and 76/306, 24.9% in the 70-79 y age group; *P*<.001). There were no significant differences in complications (*P*=.68) and LOS (*P*=.11) between the 3 age groups (Table 2).

XSL•FO
RenderX

Table 2. In-hospital outcomes of the study population by age group.

Outcomes	All patients (N=785)	Age groups (y)			*P* value
		60-69 (n=421)	70-79 (n=306)	≥80 (n=58)	
All-cause in-hospital mortality, n (%)	1 (0.1)	0 (0)	1 (0.3)	0 (0)	—[a]
Any complications, n (%)	147 (18.7)	72 (17.1)	63 (20.6)	12 (20.7)	.31
Any surgical complication, n (%)	108 (13.8)	57 (13.5)	43 (14.1)	8 (13.8)	.97
Infection	15 (1.9)	11 (2.6)	4 (1.3)	0 (0)	—
Dural tear	12 (1.5)	4 (1)	6 (2)	2 (3.4)	.22
Hemorrhage, hematoma, and seroma	2 (0.3)	2 (0.5)	0 (0)	0 (0)	—
Postoperative anemia	81 (10.3)	41 (9.7)	34 (11.1)	6 (10.3)	.77
Any medical complication, n (%)	57 (7.3)	25 (5.9)	27 (8.8)	5 (8.6)	.10
Pneumonia	3 (0.4)	1 (0.2)	1 (0.3)	1 (1.7)	.01[b]
Pulmonary embolism	2 (0.3)	1 (0.2)	1 (0.3)	0 (0)	—
Acute kidney injury	13 (1.7)	8 (1.9)	5 (1.6)	0 (0)	—
Acute myocardial infarction	2 (0.3)	0 (0)	1 (0.3)	1 (1.7)	—
Retention of urine	43 (5.5)	17 (4)	22 (7.2)	4 (6.9)	.04[b]
Nonroutine discharge[c], n (%)	148 (18.9)	52 (12.4)	76 (24.9)	20 (34.5)	<.001[b]
Length of stay (d), mean (SD)	2.9 (0.1)	2.7 (0.1)	3.2 (0.2)	3.1 (0.1)	.11

[a]Not applicable.

[b]*P*<.05.

[c]Excluding patients who died in the hospital.

Associations Between Age and Inpatient Outcomes

Table 3 shows the univariate and multivariable analyses of the associations between patient and in-hospital outcomes. After adjustment, the multivariable analysis showed that compared with patients aged 60 to 69 years, those aged 70 to 79 years (adjusted OR 2.33, 95% CI 1.57-3.46; *P*<.001) and those aged ≥80 years (adjusted OR 4.79, 95% CI 2.64-8.67; *P*<.001) had a significantly higher risk of nonroutine discharge (Table 3).

Table 3. Associations between any surgical or medical complication, nonroutine discharge, and age.

Outcomes	Age (y)							
	70-79 vs 60-69				≥80 vs 60-69			
	OR[a] (95% CI)	*P* value	Adjusted OR (95% CI)	*P* value	OR (95% CI)	*P* value	Adjusted OR (95% CI)	*P* value
Any surgical complication[b]	1.04 (0.71-1.54)	.83	1.05 (0.72-1.55)	.79	1.02 (0.55-1.90)	.95	0.98 (0.53-1.83)	.95
Any medical complication[c]	1.53 (0.99-2.38)	.06	1.16 (0.69-1.94)	.57	1.49 (0.75-2.96)	.25	0.81 (0.28-2.33)	.69
Nonroutine discharge[d,e]	2.36 (1.66-3.34)	*<.001* [f]	2.33 (1.57-3.46)	*<.001* [f]	3.73 (2.17-6.43)	*<.001*	4.79 (2.64-8.67)	*<.001*

[a]OR: odds ratio.

[b]Adjusted for variables that were significant (*P*<.05) in the univariate analysis, including sex, admission type, spondylolisthesis, hospital location, teaching status, and hospital region.

[c]Adjusted for variables that were significant (*P*<.05) in the univariate analysis, including sex, Medicare or Medicaid, admission type, spondylolisthesis, hospital location, teaching status, renal disease, heart failure, and Charlson Comorbidity Index (CCI).

[d]Adjusted for variables that were significant (*P*<.05) in the univariate analysis, including race, Medicare or Medicaid, admission type, spondylolisthesis, hospital location, teaching status, hospital region, diabetes mellitus, obesity, chronic obstructive pulmonary disease, renal disease, hypertension, coronary heart disease, heart failure, and CCI.

[e]Excluding patients who died in the hospital.

[f]*P*<.05.

XSL•FO
RenderX

In addition, compared to patients aged 60 to 69 years, the LOS was not significantly different in the other 2 age groups after adjustment for confounders in the multivariable analysis (70-79 vs 60-69, adjusted β=0.33, *P*=.14; ≥80 vs 60-69, adjusted β=0.14, *P*=.61). Similar findings were observed when the LOS analysis was restricted to home-discharge patients (Table S2 and S3 in Multimedia Appendix 1). Similar outcome patterns were observed when age was modeled as a continuous variable (Tables S4 and S5 in Multimedia Appendix 1).

Discussion

Principal Findings

This study used the NIS data to determine the impact of age on outcomes following MIS-PLIF in patients aged ≥60 years. The results revealed a low in-hospital mortality rate (only 0.1%) and a complication rate of 18.7%, with no significant differences across age groups and a similar LOS between the 3 age groups. Nonroutine discharge is a binary variable that indicates a deviation from the standard discharge pathway, such as transfer to another hospital with better medical resources, and is often associated with greater clinical severity. Notably, older age was associated with an increased risk of nonroutine discharge, with a 2.3-fold increase in patients aged 70 to 79 years and a 4.8-fold increase in those aged ≥80 years. However, older age did not significantly influence LOS or complication risk. These findings offer valuable insights into the relationship between age and postoperative outcomes after MIS-PLIF, suggesting that while MIS-PLIF is a viable and generally safe option for older patients, extra attention should be given to postoperative care, especially for those aged >70 years.

Minimally invasive procedures have become the method of choice due to decreased surgical trauma and faster recovery. Studies have compared the outcomes of MIS-PLIF with those of open procedures. For example, Mimura et al [18] compared adjacent segment pathology in patients who received a minimally invasive procedure and those who received an open approach for degenerative spondylolisthesis. The results showed that compared to conventional open PLIF, MIS-PLIF was associated with a higher disease-free survival rate and a lower incidence of adjacent segment pathology. Goldstein et al [19] performed a systematic review and meta-analysis examining adverse events of minimally invasive versus open posterior lumbar fusion. All outcomes of interest were similar between the 2 groups, although patients who underwent the minimally invasive procedures had a slightly lower rate of postoperative medical complications. However, the authors noted that the overall quality of the evidence was low.

Among the various outcomes assessed in our study, only nonroutine discharge was significantly associated with older age. Other studies have also reported that increasing age is associated with higher rates of nonroutine discharge in patients undergoing lumbar fusion; however, these studies did not further stratify older patients by age [20,21]. While there can be many reasons for this association, a possible reason is that older patients are in general more likely to be transferred to specialized care facilities after discharge because they have greater needs than their younger counterparts [22]. In addition, patients with a more advanced age may need more care than family members can provide at home or specialized rehabilitation services that are available in such facilities.

While advanced age is associated with adverse events for many surgical procedures [12,23], our results clearly showed that increased age did not significantly affect LOS or complication rate following MIS-PLIF. Luo et al [24] compared the surgical outcome of multilevel anterior cervical discectomy and fusion in older and younger patients with myelopathy. Overall, outcomes were similar between different age groups, although the older patients tended to have a lower recovery rate and higher short-term complication rate. Liu et al [25] reported that in patients undergoing PLIF, factors associated with the need for a perioperative blood transfusion were 3 or more fusion segments, low hemoglobin preoperatively, hypertension, lower BMI, and more advanced age. Our results challenge common perceptions about the risks associated with surgical procedures in older populations and highlight the potential viability of MIS-PLIF for patients of advanced age, even for those aged >80 years.

Clinical Implications

The findings of this study have important clinical implications for the management of older patients undergoing MIS-PLIF. Notably, while MIS-PLIF is generally safe for older adults, the increased likelihood of nonroutine discharges in patients aged ≥70 years underscores the need for tailored postoperative care plans. Clinicians should consider enhanced recovery protocols and more comprehensive discharge planning to address the specific needs of older patients. This could involve early involvement of multidisciplinary teams, including geriatric specialists, physical therapists, and social workers, to facilitate smoother transitions to either home or rehabilitative settings.

Strengths and Limitations

The primary strength of this study lies in its analysis of a large and nationally representative patient database, which enhances the generalizability of the conclusions to the broader population in the United States. This extensive scope ensures that the findings reflect a wide demographic profile, providing valuable insights applicable to the general population. The study's relatively large sample size enabled the assessment of various complications, including infrequent complications.

Nevertheless, this study has several limitations. This was a retrospective study, which may have introduced selection bias. As with other studies relying on *ICD* coding systems, this study may have been affected by potential coding inaccuracies. Additionally, it lacks long-term postdischarge follow-up data and preadmission status information, which are essential for a comprehensive assessment of outcomes. Furthermore, comorbidities may vary in severity; however, the NIS database lacks detailed clinical parameters, such as glomerular filtration rate, glycated hemoglobin levels, and precise BMI values, limiting our ability to assess severity or perform precise staging for conditions such as diabetes, chronic kidney disease, and obesity. Complications were identified throughout the hospitalization period, without the ability to distinguish between intraoperative and postoperative events. Preoperative physical

XSL•FO
RenderX

performance status, such as the American Society of Anesthesiologists Physical Status Classification, was not available. We could not confirm the timing of postoperative infections due to the absence of time-stamped data. Certain outcomes, such as changes in neurological function, altered mental status, or pain, are not captured in this administrative database, as it lacks such granular clinical and laboratory details. Minor complications, such as intolerance to pain medication, are also difficult to accurately identify, as they may not be consistently coded in electronic medical records. Although this study provides a broad overview of the outcomes using a large cohort, these limitations warrant cautious interpretation of the findings and highlight the need for future clinical studies to address more detailed outcome measures.

Conclusions

In conclusion, this study on the impact of age on MIS-PLIF outcomes demonstrated that the procedure is relatively safe for patients aged ≥60 years, as evidenced by the low in-hospital mortality rate and low complication rate, regardless of age. However, patients aged ≥70 years had a higher risk of nonroutine discharge. Although age alone did not significantly affect LOS and complications, targeted postoperative care for older patients, particularly those aged ≥70 years, is still recommended.

These findings support the notion that MIS-PLIF is a viable surgical option for older adults, including those aged ≥80 years. Importantly, age alone should be viewed as a factor that necessitates tailored postoperative strategies. Implementing age-stratified management pathways—including early engagement of geriatric care teams, customized rehabilitation plans, and structured discharge protocols—may optimize recovery, reduce health care burden, and enhance patient outcomes.

Funding

No external financial support or grants were received from any public, commercial, or not-for-profit entities for the research, authorship, or publication of this paper.

Data Availability

All data generated or analyzed during this study are included in this published article and its supplementary information files.

Authors' Contributions

Conceptualization: YJL
Data curation: YJL, FYS
Formal analysis: JFH
Funding acquisition: YJL
Investigation: CWT
Methodology: YJL, FYS, JFH
Project administration: YCT, LC
Resources: YJL
Software: JFH, CWT
Supervision: YHH, MJC
Validation: YJL, LC
Visualization: YCT, LC
Writing – original draft: YJL, FYS, JFH, CWT
Writing – review and editing: YHH, MJC
All authors approved the final version of the manuscript.

Conflicts of Interest

None declared.

Multimedia Appendix 1
Supplementary Tables S1 to S5.
[DOCX File , 24 KB - medinform_v14i1e76424_app1.docx]

References

1. Logroscino CA, Proietti L, Pola E, Scaramuzzo L, Tamburrelli FC. A minimally invasive posterior lumbar interbody fusion for degenerative lumbar spine instabilities. Eur Spine J 2011 May 29;20 Suppl 1(Suppl 1):S41-S45 [FREE Full text] [doi: 10.1007/s00586-011-1762-1] [Medline: 21445617]

XSL•FO
RenderX

2. Sidhu GS, Henkelman E, Vaccaro AR, Albert TJ, Hilibrand A, Anderson DG, et al. Minimally invasive versus open posterior lumbar interbody fusion: a systematic review. Clin Orthop Relat Res 2014 Jun;472(6):1792-1799. [doi: 10.1007/s11999-014-3619-5] [Medline: 24748069]
3. Xu DS, Walker CT, Godzik J, Turner JD, Smith W, Uribe JS. Minimally invasive anterior, lateral, and oblique lumbar interbody fusion: a literature review. Ann Transl Med 2018 Mar;6(6):104. [doi: 10.21037/atm.2018.03.24] [Medline: 29707553]
4. Wu PH, Kim HS, Jang IT. Intervertebral disc diseases PART 2: a review of the current diagnostic and treatment strategies for intervertebral disc disease. Int J Mol Sci 2020 Mar 20;21(6):2135 [FREE Full text] [doi: 10.3390/ijms21062135] [Medline: 32244936]
5. Grote C, Reinhardt D, Zhang M, Wang J. Regulatory mechanisms and clinical manifestations of musculoskeletal aging. J Orthop Res 2019 Jul 03;37(7):1475-1488 [FREE Full text] [doi: 10.1002/jor.24292] [Medline: 30919498]
6. Sharma N, Reche A. Unraveling the relationship between osteoporosis, treatment modalities, and oral health: a comprehensive review. Cureus 2023 Nov;15(11):e49399 [FREE Full text] [doi: 10.7759/cureus.49399] [Medline: 38146583]
7. Agarwal N, Goldschmidt E, Taylor T, Roy S, Dunn SC, Bilderback A, et al. Impact of frailty on outcomes following spine surgery: a prospective cohort analysis of 668 patients. Neurosurgery 2021 Feb 16;88(3):552-557. [doi: 10.1093/neuros/nyaa468] [Medline: 33372214]
8. Al Jammal OM, Shahrestani S, Delavar A, Brown NJ, Gendreau JL, Lien BV, et al. Demographic predictors of treatments and surgical complications of lumbar degenerative diseases: an analysis of over 250,000 patients from the National Inpatient Sample. Medicine (Baltimore) 2022 Mar 18;101(11):e29065 [FREE Full text] [doi: 10.1097/MD.0000000000029065] [Medline: 35356929]
9. Damluji AA, Forman DE, van Diepen S, Alexander KP, Page RL2, Hummel SL, et al. Older adults in the cardiac intensive care unit: factoring geriatric syndromes in the management, prognosis, and process of care: a scientific statement from the American Heart Association. Circulation 2020 Jan 14;141(2):e6-32 [FREE Full text] [doi: 10.1161/CIR.0000000000000741] [Medline: 31813278]
10. Mohan S, Cha ED, Lynch CP, Geoghegan CE, Jadczak CN, Singh K. Impact of advanced age on postoperative outcomes following transforaminal lumbar interbody fusion. J Am Acad Orthop Surg 2021 May 17;29(17):e869-e879. [doi: 10.5435/jaaos-d-20-01382]
11. Tong Y, Fernandez L, Bendo JA, Spivak JM. Enhanced recovery after surgery trends in adult spine surgery: a systematic review. Int J Spine Surg 2020 Aug 31;14(4):623-640 [FREE Full text] [doi: 10.14444/7083] [Medline: 32986587]
12. Watt J, Tricco AC, Talbot-Hamon C, Pham B, Rios P, Grudniewicz A, et al. Identifying older adults at risk of harm following elective surgery: a systematic review and meta-analysis. BMC Med 2018 Jan 12;16(1):2 [FREE Full text] [doi: 10.1186/s12916-017-0986-2] [Medline: 29325567]
13. Healthcare cost and utilization project user support. Overview of the Nationwide Inpatient Sample (NIS). URL: https://hcup-us.ahrq.gov/nisoverview.jsp [accessed 2023-12-12]
14. HCUP-US central distributor availability of databases. Agency for Healthcare Research and Quality. URL: https://hcup-us.ahrq.gov/db/availability_public.jsp [accessed 2025-05-29]
15. Garfein AJ, Herzog AR. Robust aging among the young-old, old-old, and oldest-old. J Gerontol B Psychol Sci Soc Sci 1995 Mar 01;50(2):S77-S87. [doi: 10.1093/geronb/50b.2.s77] [Medline: 7757843]
16. Reinert SS, Kinney AL, Jackson K, Diestelkamp W, Bigelow K. Age stratification and sample entropy analysis enhance the limits of stability tests for older adults. J Appl Biomech 2017 Dec 01;33(6):419-423. [doi: 10.1123/jab.2016-0019] [Medline: 28605220]
17. NIS Description of data elements. Agency for Healthcare Research and Quality. URL: https://hcup-us.ahrq.gov/db/vars/zipinc_qrtl/nisnote.jsp [accessed 2025-05-29]
18. Mimura T, Tsutsumimoto T, Yui M, Takahashi J, Kuraishi S, Misawa H. Adjacent segment pathology following posterior lumbar interbody fusion for lumbar degenerative spondylolisthesis: a comparison between minimally invasive and conventional open approach. Spine J 2021 Aug;21(8):1297-1302. [doi: 10.1016/j.spinee.2021.03.027] [Medline: 33785474]
19. Goldstein CL, Macwan K, Sundararajan K, Rampersaud YR. Perioperative outcomes and adverse events of minimally invasive versus open posterior lumbar fusion: meta-analysis and systematic review. J Neurosurg Spine 2016 Mar;24(3):416-427. [doi: 10.3171/2015.2.SPINE14973] [Medline: 26565767]
20. Best MJ, Buller LT, Falakassa J, Vecchione D. Risk factors for nonroutine discharge in patients undergoing spinal fusion for intervertebral disc disorders. Iowa Orthop J 2015;35:147-155 [FREE Full text] [Medline: 26361458]
21. Cabrera A, Bouterse A, Nelson M, Razzouk J, Ramos O, Bono CM, et al. Accounting for age in prediction of discharge destination following elective lumbar fusion: a supervised machine learning approach. Spine J 2023 Jul;23(7):997-1006. [doi: 10.1016/j.spinee.2023.03.015] [Medline: 37028603]
22. Sokas CM, Cowan J, Dalton MK, Coogan K, Bader A, Bernacki R, et al. Association between patient-reported frailty and non-home discharge among older adults undergoing surgery. J Am Geriatr Soc 2020 Dec 08;68(12):2909-2913. [doi: 10.1111/jgs.16846] [Medline: 33031587]
23. Massarweh NN, Legner VJ, Symons RG, McCormick WC, Flum DR. Impact of advancing age on abdominal surgical outcomes. Arch Surg 2009 Dec 21;144(12):1108-1114. [doi: 10.1001/archsurg.2009.204] [Medline: 20026827]

XSL•FO
RenderX

24. Luo CA, Lim AS, Lu ML, Chiu PY, Lai PL, Niu CC. The surgical outcome of multilevel anterior cervical discectomy and fusion in myelopathic elderly and younger patients. Sci Rep 2022 Mar 16;12(1):4495 [FREE Full text] [doi: 10.1038/s41598-022-08243-8] [Medline: 35296700]
25. Liu B, Pan J, Zong H, Wang Z. Establishment and verification of a perioperative blood transfusion model after posterior lumbar interbody fusion: a retrospective study based on data from a local hospital. Front Surg 2021 Aug 30;8:695274. [doi: 10.3389/fsurg.2021.695274] [Medline: 34527694]

Abbreviations

HCUP: Health Care Cost and Utilization Project
ICD-9-CM: International Classification of Diseases, Ninth Revision
ICD-10-CM: International Classification of Diseases, Tenth Revision, Clinical Modification
LOS: length of stay
MIS-PLIF: minimally invasive posterior lumbar interbody fusion
NIS: Nationwide Inpatient Sample
OR: odds ratio

Edited by A Benis; submitted 23.Apr.2025; peer-reviewed by T Asada, P Menon Naliyatthaliyazchayil; comments to author 16.Jun.2025; revised version received 31.Jul.2025; accepted 30.Nov.2025; published 06.Jan.2026.

Please cite as:
Lin YJ, Shih FY, Huang JF, Ting CW, Tsai YC, Chang L, Huang YH, Chuang MJ
Impact of Age on Hospital Outcomes Following Minimally Invasive Posterior Lumbar Interbody Fusion: Retrospective Analysis of the Nationwide Inpatient Sample Database from 2016 to 2020
JMIR Med Inform 2026;14:e76424
URL: https://medinform.jmir.org/2026/1/e76424
doi:10.2196/76424
PMID:

©Yu-Jun Lin, Fu-Yuan Shih, Jin-Fu Huang, Chun-Wei Ting, Yu-Chin Tsai, Lin Chang, Yu-Hua Huang, Ming-Jung Chuang. Originally published in JMIR Medical Informatics (https://medinform.jmir.org), 06.Jan.2026. This is an open-access article distributed under the terms of the Creative Commons Attribution License (https://creativecommons.org/licenses/by/4.0/), which permits unrestricted use, distribution, and reproduction in any medium, provided the original work, first published in JMIR Medical Informatics, is properly cited. The complete bibliographic information, a link to the original publication on https://medinform.jmir.org/, as well as this copyright and license information must be included.

XSL•FO
RenderX

Machine Learning–Based Risk Prediction for Coronary Heart Disease Complicated by Hyperhomocysteinemia: Retrospective Study

Ming-Yuan Du[1,2,3], MMD; Meng-Ke Lyu[3], MMD; Hai-long Liu[1,2,3], MMD; Yi-zhuo Li[1,2,3], MD; Hai-feng Yan[1,2,3], MD; Xiao-hui Li[1,2,3], MD

[1]Heart Center, The First Affiliated Hospital of Henan University of Chinese Medicine, National Regional (TCM) Cardiovascular Diagnosis and Treatment Center, Zhengzhou, China

[2]Collaborative Innovation Center of Prevention and Treatment of Major Diseases by Chinese and Western Medicine, Zhengzhou, China

[3]The First Affiliated Hospital of Henan University of Traditional Chinese Medicine, No. 19 Renmin Road, Jinshui District, Henan Province, Zhengzhou, China

Corresponding Author:
Meng-Ke Lyu, MMD
The First Affiliated Hospital of Henan University of Traditional Chinese Medicine, No. 19 Renmin Road, Jinshui District, Henan Province, Zhengzhou, China

Abstract

Background: Hyperhomocysteinemia (HHcy) is recognized as an independent risk factor for coronary heart disease (CHD), yet accurately predicting CHD risk in patients with HHcy remains a challenge. This study aimed to develop and validate multiple machine learning models for predicting CHD risk in patients with HHcy and elucidate key predictors using Shapley Additive Explanation (SHAP) algorithms.

Objective: This study aims to develop and validate machine learning models for predicting the risk of coronary heart disease in individuals with normal homocysteine levels, aiming to improve early risk stratification and clinical decision-making.

Methods: This single-center retrospective study collected data from patients who were diagnosed with HHcy through electronic medical records, which were randomly divided into training (n=364, 70%), validation (n=78, 15%), and test (n=78, 15%) sets. Seven machine learning models were constructed, including logistic regression, k-nearest neighbor, decision tree, random forest, extreme gradient boost, light gradient boosting machine (LightGBM), and stacking. Six core variables (age, weight, hypertension, continuous drinking history, activated partial thromboplastin time, and carotid plaque) were utilized as inputs, with performance evaluation metrics encompassing area under the receiver operating characteristic curve, accuracy, F_1-score, calibration curve, Brier score, and decision curve analysis. Additionally, SHAP interpretation was conducted on the optimal LightGBM model.

Results: The LightGBM model exhibited superior performance in the test set (area under the receiver operating characteristic curve=0.807, F_1-score=0.606), demonstrated good calibration (Brier score=0.2415), and yielded high clinical net benefit. SHAP analysis revealed age and activated partial thromboplastin time as the most influential predictors, followed by hypertension, weight, carotid plaque, and continuous drinking history. The correlation heat map illustrated low collinearity among variables, ensuring model stability.

Conclusions: The LightGBM model demonstrated high accuracy and interpretability in forecasting CHD risk among patients with HHcy. The integration of machine learning and interpretable artificial intelligence methods holds promise for delivering personalized early risk assessment and intervention strategies in clinical settings.

(JMIR Med Inform 2026;14:e80809) doi:10.2196/80809

KEYWORDS

retrospective study; hyperhomocysteinemia; coronary heart disease; machine learning; predictive model

Introduction

Hyperhomocysteinemia (HHcy) predisposes individuals to heightened and premature susceptibility to coronary heart disease (CHD) [1,2]. Existing research has substantiated that HHcy expedites atherosclerosis progression via various mechanisms, including vascular endothelial impairment, pro-oxidative stress, and disrupted coagulation pathways, establishing it as a stand-alone CHD risk factor [3-5]. Nevertheless, the CHD risk profile in HHcy cohorts is heterogeneous, potentially modulated by a confluence of factors

XSL•FO
RenderX

encompassing age, biochemical milieu, lifestyle choices, and vascular morphology.

The current assessment tools for CHD risk in patients with HHcy are limited [6]. Traditional models, such as Cox or logistic regression, are typically based on a small number of variables and struggle to capture the intricate nonlinear interactions among variables in real clinical settings. Furthermore, these models often rely on predictors that necessitate specialized knowledge or image interpretation, hindering their widespread adoption among noncardiovascular specialist clinicians [7]. Given that HHcy is a common condition and many patients are initially diagnosed in primary or nonspecialist clinics, there is a pressing need for a predictive tool that offers predictability, universality, and interpretability to facilitate early risk assessment and intervention in clinical practice.

Machine learning technology holds potential for predicting the likelihood of diabetes, arrhythmia, and various cardiovascular diseases by effectively capturing intricate multidimensional patterns [8]. Ensemble models, such as light gradient boosting machine (LightGBM) and extreme gradient boosting (XGBoost), excel in automatically discerning key features and enhancing predictive accuracy [9]. Nevertheless, there is a scarcity of dedicated modeling research on CHD risk among individuals with HHcy. Moreover, the clinical interpretability of numerous machine learning models remains inadequate, constraining their reliability and utility in medical settings [10,11].

This study seeks to develop CHD risk prediction models for individuals with HHcy using real-world electronic health record data from a single center [12]. The study aims to compare the performance of 7 mainstream machine learning algorithms in terms of discriminative power, calibration, and clinical net benefit. To improve clinical interpretability, the Shapley Additive Explanation (SHAP) method was used to assess model decision-making and identify key variables. Emphasis was placed on the generalizability of variable selection and form, prioritizing standardized biochemical and lifestyle indicators that are routinely accessible to avoid reliance on specific specialties or complex imaging techniques. The objective is to create a practical model that can be easily implemented across various clinical settings, balancing predictability and interpretability. This model aims to serve as an early risk assessment tool for high-risk HHcy populations and establish a basis for future multicenter external validation studies.

Methods

Research Materials

A comprehensive workflow of the study, including data collection, feature selection, model development, evaluation, and interpretation, is illustrated in Figure 1.

Figure 1. Flowchart of developing and validating machine learning–based models for predicting coronary heart disease (CHD) risk in patients with hyperhomocysteinemia. This flowchart outlines the entire process of constructing and evaluating risk prediction models for CHD in patients with hyperhomocysteinemia. AUC: area under the receiver operating characteristic curve; CV: cross-validation, DCA: decision curve analysis; KNN: k-nearest neighbor; LightGBM: light gradient boosting machine; XGBoost: extreme gradient boosting.

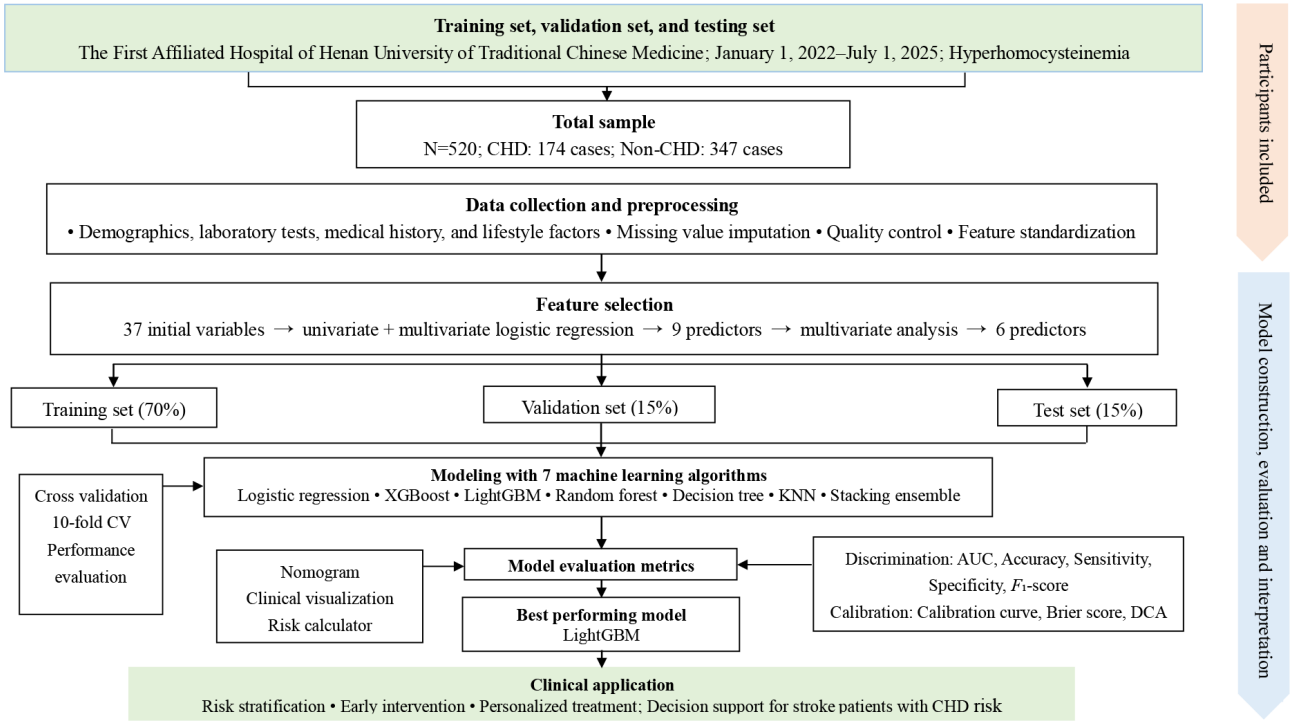

General Information

This retrospective registry study examines patients with HHcy treated at the First Affiliated Hospital of Henan University of Traditional Chinese Medicine between January 1, 2022, and July 1, 2025.

Patients were categorized into either the CHD group or the non-CHD group based on clinical diagnoses. Subsequent to

XSL•FO
RenderX

admission, demographic features, laboratory values, medical history, familial history, and additional indicators were gathered for statistical assessment.

Ethical Considerations

Ethical approval was obtained from the Ethics Committee of the First Affiliated Hospital of Henan University of Chinese Medicine (approval number: 2025HL-202‐01). The data used were fully deidentified, and no personally identifiable information was accessible to the researchers. The requirement for informed consent was waived by the ethics committee in accordance with national regulations, citing the retrospective nature of the study. No compensation was provided to participants.

Diagnostic Criteria

The patient was diagnosed with stable CHD in accordance with the 2025 American College of Cardiology/American Heart Association (ACC/AHA) guideline for chronic coronary syndromes [13]. Acute coronary syndromes were identified following the criteria outlined in the 2023 ESC and 2021 ACC/AHA guidelines for non–ST-elevation acute coronary syndrome [14,15].

Inclusion and Exclusion Criteria

Inclusion Criteria

Participants were required to meet the diagnostic criteria for HHcy, be aged between 18 and 80 years, and have complete baseline clinical data available for analysis.

Exclusion Criteria

Participants excluded from the study encompass those with comorbid severe organic conditions (eg, advanced tumors, hepatorenal insufficiency), nonatherosclerotic heart ailments (eg, congenital heart disease, myocarditis), individuals with mental illness or cognitive deficits hindering study cooperation, pregnant or lactating women, and those engaged in other clinical trials within the preceding 3 months.

Observation Indicators

This study utilized data collected through a standardized case report form, encompassing five key categories of core indicators: (1) demographics and basic information, such as age, gender, height, weight, BMI, educational level, and marital status; (2) medical history and lifestyle factors, including a history of diseases, such as hypertension, diabetes, transient ischemic attack, as well as lifestyle habits, such as persistent smoking and alcohol consumption; (3) laboratory examination indicators, comprising blood routine parameters (red blood cell, white blood cell, and platelet counts), biochemical markers (total cholesterol, triglycerides, and creatinine), and coagulation function tests (activated partial thromboplastin time [APTT], prothrombin time, and fibrinogen); (4) imaging examination indicators, specifically the presence or absence of carotid plaques as determined by ultrasound or computed tomography angiography; and (5) quality control measures involving the uniform extraction of all data by trained researchers through the electronic medical record system and laboratory information system. A double-person review system was implemented to ensure data accuracy. Following the integrity assessment, no missing values were identified in the variables included, thus obviating the need for imputation or data elimination procedures. The detailed data extraction workflow and quality control procedures are provided in Multimedia Appendix 1.

Machine Learning Modeling and Related Statistical Methods

Statistical analysis was performed using SPSS Statistics 27. Machine learning modeling utilized R 4.5 (caret package) and Python 3.13 (scikit-learn, xgboost, lightgbm) libraries. Quantitative data were reported as mean (SD). Group differences were assessed using independent-sample 2-tailed *t* tests (for normal distribution) or Mann-Whitney *U* tests (for nonnormal distribution), based on data distribution. Categorical data were presented as n (%), with group differences analyzed using the chi-square test or Fisher exact probability method.

Variable Screening and Dataset Division

Variable screening involved a 2-step dimensionality reduction approach utilizing “univariate+multivariate logistic regression.” Initially, 9 variables exhibiting significant differences ($P<.05$) between the CHD and non-CHD groups were selected for the candidate pool. Subsequently, multivariate analysis was conducted using stepwise regression (backward method, inclusion criterion $\alpha=.05$, exclusion criterion $\alpha=.10$), resulting in the retention of 6 independent predictors: age, body weight, hypertension, history of continuous alcohol consumption, APTT, and carotid artery plaque. The variance inflation factors for all variables were less than 5, indicating the absence of significant multicollinearity.

The data were stratified based on the presence of CHD comorbidity, resulting in division into a training set (n=364), a validation set (n=78), and a test set (n=78) at a ratio of 7:1.5:1.5. To ensure result reproducibility, a random seed (random_state=2024) was set. The training set was used for model training and initial parameter optimization, the validation set for fine-tuning model parameters and classification threshold optimization, and the test set as an independent dataset for the final model performance assessment.

Machine Learning Model Construction

Seven classification models were developed to forecast the risk of CHD, categorized into traditional models (logistic regression, decision tree, and k-nearest neighbors [KNNs]) and ensemble models (random forest, XGBoost, LightGBM, and stacking). Hyperparameter optimization was performed on all models using grid search (GridSearchCV) on the training set to enhance the area under the receiver operating characteristic curve (AUC) on the validation set.

Logistic regression employs L2 regularization and class weight balancing (class_weight='balanced') with a regularization strength of C=0.1. The decision tree and random forest models optimize the max_depth, which is ultimately determined to be 7, with min_samples_split set to 2 for the decision tree and n_estimators set to 50 for the random forest. KNN utilizes the Euclidean distance metric, with the number of neighbors ultimately set to 9.

XSL•FO
RenderX

In the context of boosting models, both XGBoost and LightGBM were configured with a scale_pos_weight of 2 to address class imbalance. Parameter optimization yielded the following settings: XGBoost (max_depth=3 and learning_rate=0.3) and LightGBM (max_depth=3 and learning_rate=0.01). The stacking model used the aforementioned 6 models as base learners, with logistic regression serving as the meta-learner. The integration of outputs was achieved through 5-fold cross-validation.

All parameter tuning details are listed in Table S2 in Multimedia Appendix 2 to enhance reproducibility.

Model Evaluation and Validation

A multidimensional index is used to thoroughly assess the model's performance, with the subsequent metrics computed on the training, validation, and test sets, respectively:

Discrimination is primarily assessed using the AUC, computed through "sklearn.metrics.roc_auc_score." Additionally, metrics, such as accuracy, recall, specificity, and F_1-score, are documented. To provide a comprehensive evaluation of classification performance, the precision-recall (PR) curve is generated, and the PR-AUC is determined.

Calibration is assessed through a calibration curve generated using the sklearn.calibration.calibration_curve function. An optimal calibration curve closely aligns with the diagonal line. The Brier score quantifies the accuracy of predicted probabilities by measuring the mean squared error between predicted probabilities and true labels. A lower Brier score signifies more precise predicted probabilities.

We used a 10-fold cross-validation method on the training set to assess model stability, recording the mean AUC and standard deviation. To evaluate generalization capability, we considered the metrics of the test set as the reference standard. A significant decrease in the test set's AUC compared to the training set (eg, ΔAUC<0.1) suggested potential overfitting.

Sample Imbalance Processing and Threshold Optimization

To address the 1:2 sample imbalance between the CHD and non-CHD groups, the following strategies were implemented to enhance the model's ability to identify the minority class (CHD group):

For models supporting weight parameters (eg, logistic regression, XGBoost, LightGBM, and random forest), class_weight='balanced' or scale_pos_weight=2 was set. Specifically, class_weight='balanced' automatically calculates class weights inversely proportional to class frequencies, amplifying the contribution of CHD samples in the loss function. Meanwhile, scale_pos_weight=2 directly sets the weight of positive samples (CHD group) to twice that of negative samples (non-CHD group), aligning with the 1:2 sample ratio and mitigating the model's bias toward the majority class caused by imbalance.

Although class weight adjustment balances class importance during training, the default classification threshold (0.5) may not meet the clinical demand for high sensitivity in CHD screening. Therefore, further threshold optimization was performed on the best-performing LightGBM model. Based on predicted probabilities from the validation set, candidate thresholds ranging from 0.1 to 0.6 (stepping at 0.05) were evaluated, with sensitivity, specificity, and F_1-score calculated for each threshold. The optimal threshold was determined by balancing these metrics—prioritizing high sensitivity (to identify as many true CHD patients as possible) while maintaining acceptable specificity. This approach breaks the limitation of a fixed threshold, enabling the model to better align with the practical goal of "reducing missed diagnoses" in imbalanced scenarios (see Figure S1 in Multimedia Appendix 3).

Analysis of Model Interpretability

The LightGBM model's optimal performance was assessed using the SHAP algorithm for both global and local interpretability analyses. Globally, the SHAP summary plot illustrated the average contribution of each variable to the model prediction, identifying key factors influencing the risk of CHD. Locally, the SHAP dependence plot depicted the functional relationship between each feature and the model output, highlighting the positive and negative effects of variables, such as age and APTT, on the predicted value. Additionally, a Pearson correlation heatmap was generated to assess collinearity among features, confirming that no strong correlations (r<0.5) existed among the model variables. This analysis ensured the model's stability and bolstered the credibility of its interpretation.

Sample Size Estimation

Based on the recommendations by van Smeden et al [16,17] and Riley et al [18,19], we estimated the minimum sample size required to develop a reliable multivariable prediction model using 5 candidate predictors. Assuming an outcome prevalence of approximately 30%, a shrinkage factor of 0.9, and an expected Cox-Snell R^2 of 0.15, the minimum required sample size was calculated to be approximately 218. This study developed models with a larger sample size, thus mitigating the potential for major overestimation bias based on these parameters.

External Benchmark Models

For comparative purposes, Framingham risk score [20] and the ACC/AHA pooled cohort equations (ASCVD score) [21] were calculated for all patients using baseline clinical parameters. These scores were included as benchmark models to evaluate the incremental value of the model.

Results

Comparison of Clinical Data Between the 2 Groups

This study comprised 520 patients with HHcy, with 174 in the CHD group and 347 in the non-CHD group, resulting in a CHD detection rate of 33.46%. The analysis of baseline data revealed significant differences in 9 variables between the 2 groups, all with P<.05, as detailed in Table 1.

XSL•FO
RenderX

Table . Comparison of baseline characteristics between patients with hyperhomocysteinemia with and without coronary heart disease (CHD)[a].

Characteristic	Control group (n=347)	Case group (n=174)	*P* value
Demographic and general information			
Age (y), mean (SD)	65.30 (10.36)	70.49 (8.76)	<.001[b]
Sex, n (%)			<.001[b]
Male	263 (0.71)	107 (0.29)	
Female	83 (0.55)	67 (0.45)	
Height (cm), mean (SD)	167.89 (7.29)	167.62 (7.30)	.78
Weight (kg), mean (SD)	66.96 (10.60)	71.52 (9.91)	.04[b]
BMI, mean (SD)	24.73 (3.22)	25.12 (3.06)	.07
Education level, n (%)			.86
Junior high school or below	224 (0.66)	114 (0.34)	
High school and above	122 (0.67)	60 (0.33)	
Household annual income (RMB 10,000 yuan[c]), n (%)			.13
<8	280 (0.67)	150 (0.33)	
≤8	66 (0.73)	24 (0.27)	
Occupation in the 6 months prior to onset, n (%)			.66
Mental workers	43 (0.64)	24 (0.36)	
Physical workers	303 (0.74)	105 (0.26)	
Payment type, n (%)			.12
Basic medical care	232 (0.69)	102 (0.31)	
Urban medical care	113 (0.61)	72 (0.39)	
Marital status, n (%)			.65
Married	333 (0.67)	166 (0.33)	
Separated	13 (0.62)	8 (0.32)	
Body temperature	36.46 (0.29)	36.45 (0.22)	.85
Respiratory rate	18.95 (4.67)	18.68 (1.76)	.82
Heart rate	77.14 (12.62)	77.41 (12.64)	.88
Systolic blood pressure	143.87 (21.69)	141.49 (21.09)	.16
Diastolic blood pressure	84.19 (13.92)	81.67 (14.37)	.05
Medical history, n (%)			
Hypertension	209 (0.61)	134 (0.39)	<.001[b]
Diabetes mellitus	176 (0.70)	76 (0.30)	.14
Hyperlipidemia	79 (0.70)	36 (0.30)	.58
History of TIA[d]	20 (0.56)	16 (0.44)	.15
Continuous smoking history	135 (0.75)	44 (0.25)	<.001[b]
Continuous drinking history	82 (0.78)	20 (0.22)	<.001[b]
Carotid plaque	275 (0.64)	154 (0.36)	.01[b]
Blood biochemical indicators, mean (SD)			
Red blood cell count	4.46 (0.48)	4.43 (0.52)	.32
White blood cell count	6.90 (4.28)	6.61 (1.93)	.80
Platelet count	207.82 (60.41)	211.49 (53.30)	.32

XSL•FO
RenderX

Characteristic	Control group (n=347)	Case group (n=174)	*P* value
Hemoglobin concentration	141.76 (29.06)	143.21 (38.77)	.15
Total cholesterol	4.42 (1.27)	4.39 (1.24)	.63
Triglycerides	1.73 (1.59)	1.65 (1.10)	.39
Low-density lipoprotein	2.63 (0.87)	2.53 (0.98)	.11
High-density lipoprotein	1.14 (0.29)	1.20 (0.30)	.06
Prothrombin time	11.37 (2.76)	10.86 (2.96)	.84
Fibrinogen content	3.15 (0.95)	3.19 (0.75)	.11
Activated partial thromboplastin time	30.52 (4.95)	29.44 (3.82)	.01[b]
Thrombin time	18.67 (64.39)	15.23 (1.89)	.34
Glycated hemoglobin	6.50 (1.63)	6.44 (1.28)	.17
Creatinine	74.44 (70.07)	65.23 (21.57)	.04[b]
Uric acid	313.56 (92.76)	310.13 (90.29)	.64

[a]The table includes demographic information, clinical history, lifestyle factors, and laboratory indicators for a total of 520 patients. Quantitative variables are presented as mean (SD), while categorical variables are shown as counts and percentages. Group differences were assessed using independent-sample *t* tests for normally distributed data, Mann-Whitney *U* tests for nonnormally distributed data, and chi-square tests for categorical data.

[b]P<.05.

[c]Conversion based on an exchange rate of 1 US $≈7 RMB.

[d]TIA: transient ischemic attack.

Univariate Regression Analysis of Risk Factors for CHD in HHcy Patients

Nine statistically significant factors were selected as independent variables for logistic regression analysis to predict the occurrence of CHD. The results revealed that 6 variables—age, weight, hypertension, continuous drinking history, APTT, and carotid plaque—significantly influenced the occurrence of CHD (all *P*<.05), as shown in Table 2.

Table . Logistic regression analysis of risk factors for coronary heart disease (CHD) in patients with hyperhomocysteinemia.[a]

Factor	OR[b]	SE	Wald statistics	*P* value	95% CI
Age	1.06	0.01	22.68	<.001	1.08-1.03
Gender	0.69	0.26	2.12	.15	1.14-0.42
Weight	1.04	0.01	13.90	<.001	1.06-1.02
Hypertension	1.99	0.23	9.26	<.001	3.09-1.28
Continuous smoking history	0.90	0.27	0.14	.71	1.54-0.53
Continuous drinking history	0.51	0.33	4.03	.045	0.99-0.27
APTT[c]	0.95	0.02	5.82	.02	0.99-0.90
Cr[d]	0.99	0.01	1.96	.16	1.00-0.98
Carotid plaque	1.79	0.29	3.99	.046	3.18-1.01

[a]The table presents the outcomes of univariate logistic regression analysis that pinpoint factors linked to the incidence of coronary heart disease in patients with hyperhomocysteinemia. It encompasses odds ratios, SE, Wald statistics, and 95% CI for each factor.

[b]OR: odds ratio.

[c]APTT: activated partial thromboplastin time.

[d]Cr: creatinine.

XSL•FO
RenderX

Establishment and Evaluation of 7 Machine Learning Models for CHD Risk Prediction in Patients With HHcy

This study utilized 7 machine learning algorithms, namely logistic regression, XGBoost, LightGBM, random forest, decision tree, KNNs, and stacking ensemble, to develop risk prediction models for CHD in patients with HHcy based on 6 core predictors: age, weight, hypertension, continuous drinking history, APTT, and carotid plaque. In the training set assessment, each model exhibited distinct performance characteristics. Notably, the decision tree, random forest, and XGBoost models achieved perfect discrimination (AUC=1.000) and classification metrics (accuracy, sensitivity, specificity, and F_1-score=1.000), indicating potential overfitting, unlike the logistic regression and KNN models. The LightGBM model displayed strong performance with an AUC of 0.987, accuracy of 0.854, and F_1-score of 0.818. Conversely, the stacking ensemble model yielded an AUC of 0.933, accuracy of 0.810, and F_1-score of 0.660, demonstrating inferior performance compared to the aforementioned potentially overfitting models.

During the validation phase, model performance varied notably among different algorithms. The XGBoost model exhibited the highest AUC of 0.802 and an F_1-score of 0.689. The stacking model outperformed others with an AUC of 0.800, the highest accuracy of 0.769, and an F_1-score of 0.625. The LightGBM model achieved an AUC of 0.780 and an F_1-score of 0.648. In comparison, the logistic model yielded an AUC of 0.755 and an F1-score of 0.639. The random forest model attained an AUC of 0.777; however, it demonstrated low sensitivity at 0.355 and an F_1-score of 0.489. The decision tree model, with an AUC of 0.679 and an F_1-score of 0.613, displayed limited generalization ability and was notably impacted by overfitting during training.

During testing, the LightGBM model demonstrated the highest AUC of 0.807, a sensitivity of 0.913, and an F_1-score of 0.636, indicating promising performance. The logistic model yielded an AUC of 0.796, an F_1-score of 0.603, a sensitivity of 0.826, and a specificity of 0.618, striking a balance between prediction accuracy and clinical relevance. In contrast, the stacking model achieved an AUC of 0.802 but exhibited lower sensitivity at 0.478 and an F_1-score of 0.564, suggesting limited generalizability. Although the random forest model achieved the highest accuracy at 0.769, its F_1-score was 0.571. The XGBoost model's performance notably decreased, with an AUC of 0.757 and an F_1-score of 0.523 (Table 3).

XSL•FO
RenderX

Table . Performance metrics of the 7 machine learning models for predicting coronary heart disease (CHD) risk in patients with hyperhomocysteinemia across different datasets.

Model and stage	AUC[a]	Accuracy	Sensitivity	Specificity	F_1-score
Training					
Decision tree	1.000	1.000	1.000	1.000	1.000
KNN[b]	0.795	0.734	0.475	0.861	0.540
LightGBM[c]	0.987	0.854	0.992	0.787	0.818
Logistic	0.701	0.646	0.683	0.627	0.560
Random forest	1.000	1.000	1.000	1.000	1.000
Stacking	0.933	0.810	0.558	0.934	0.660
XGBoost[d]	1.000	1.000	1.000	1.000	1.000
Validation					
Decision tree	0.679	0.692	0.613	0.745	0.613
KNN	0.751	0.731	0.452	0.915	0.571
LightGBM	0.780	0.679	0.742	0.638	0.648
Logistic	0.755	0.667	0.742	0.617	0.639
Random forest	0.777	0.705	0.355	0.936	0.489
Stacking	0.800	0.769	0.484	0.957	0.625
XGBoost	0.802	0.756	0.677	0.809	0.689
Testing					
Decision Tree	0.656	0.615	0.696	0.582	0.516
KNN	0.768	0.744	0.565	0.818	0.565
LightGBM	0.807	0.692	0.913	0.600	0.636
Logistic	0.796	0.679	0.826	0.618	0.603
Random Forest	0.765	0.769	0.522	0.873	0.571
Stacking	0.802	0.782	0.478	0.909	0.564
XGBoost	0.757	0.603	0.739	0.545	0.523

[a]AUC: area under the receiver operating characteristic curve.

[b]KNN: k-nearest neighbors.

[c]LightGBM: light gradient boosting machine.

[d]XGBoost: extreme gradient boosting.

In conclusion, both the LightGBM and logistic regression models demonstrated consistent performance across the validation and testing phases, indicating their heightened clinical utility.

The performance of the 7 machine learning models (decision tree, KNN, LightGBM, logistic regression, random forest, stacking, and XGBoost) in predicting CHD in patients with hyperhomocysteinemia was evaluated. Performance metrics, such as area under the receiver operating characteristic (ROC) curve (AUC), accuracy, sensitivity, specificity, and F_1-score, were assessed on the training, validation, and test sets. The results indicate consistent discriminative ability and stability across different data partitions, with LightGBM demonstrating superior performance in the test set (AUC=0.807, F_1-score=0.636).

Model Performance Evaluation

Upon analyzing the ROC curves, it was evident that within the training set, the random forest (AUC=0.961), XGBoost (AUC=0.953), stacking (AUC=0.933), and LightGBM (AUC=0.890) models displayed exceptional discriminatory capabilities, indicating potential overfitting. Conversely, the logistic regression model exhibited a comparatively lower AUC of 0.697, while the KNN and decision tree models achieved AUC values of 0.776 and 0.833, respectively (Figure 2A). In the validation set, the stacking model maintained superior performance (AUC=0.800), closely followed by LightGBM (AUC=0.796), XGBoost (AUC=0.792), and random forest (AUC=0.792). The logistic model also demonstrated satisfactory performance (AUC=0.740), surpassing the decision tree (AUC=0.734) and KNN (AUC=0.764) models (Figure 2B). Within the testing set, the LightGBM (AUC=0.807) and stacking (AUC=0.802) models achieved the highest AUC values, trailed

XSL•FO
RenderX

by KNN (AUC=0.768), random forest (AUC=0.765), and XGBoost (AUC=0.757). The logistic regression model also displayed robust discriminatory ability (AUC=0.796), while the decision tree model exhibited the lowest AUC (0.656; Figure 2C).

Figure 2. Receiver operating characteristic (ROC) curves of coronary heart disease (CHD) risk prediction models constructed by 7 machine learning algorithms in Hyperhomocysteinemia patients ROC) curves were utilized to assess the discriminative performance of 7 distinct machine learning models, including logistic regression, k-nearest neighbors (KNN), decision tree, random forest, extreme gradient boosting (XGBoost), light gradient boosting machine (LightGBM), and stacking, on various datasets: the training set, validation set, and test set denoted as (A), (B), and (C) respectively. The area under the receiver operating characteristic curve (AUC) was employed as a metric to quantify the models' performance, where increased values are indicative of enhanced capability in discriminating between individuals with CHD and those without.

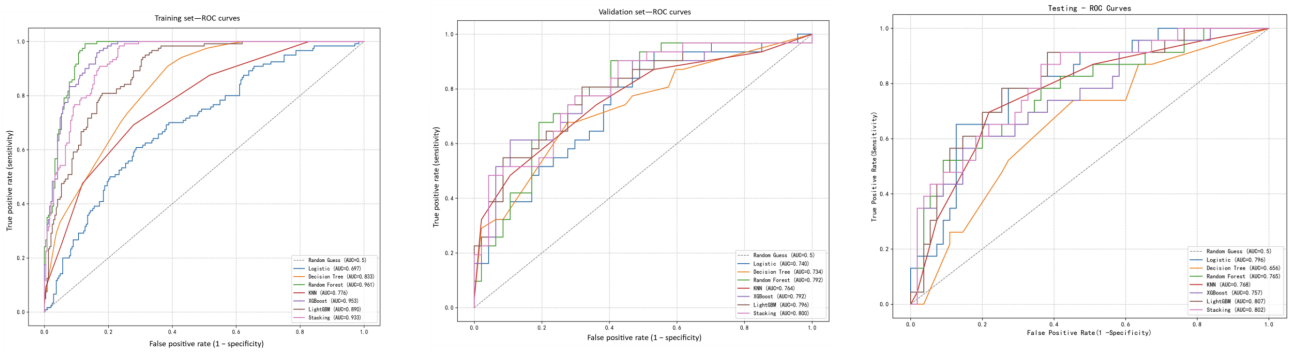

A B C

Upon analyzing the PR curves, distinct variations in model efficacy were evident across the three datasets. In the training dataset, the random forest model exhibited the highest PR-AUC value of 0.904, outperforming XGBoost (0.890), stacking (0.853), and LightGBM (0.770), underscoring its robust classification capability on the internal data. Conversely, the Logistic model displayed limited discriminatory power with an AUC of 0.494, while the decision tree and KNN models achieved PR-AUCs of 0.699 and 0.645, respectively (Figure 3A).

Figure 3. Precision-recall (PR) curves of coronary heart disease (CHD) risk prediction models constructed by the 7 machine learning algorithms. PR curves evaluate model performance in imbalanced datasets, emphasizing precision (positive predictive value) and recall (sensitivity). The results for the training set are displayed in (A), the validation set in (B), and the test set in (C). The PR-AUC (area under the precision-recall curve) is reported for each model, with greater values denoting better classification performance for the positive class (CHD). KNN: k-nearest neighbor; LightGBM: light gradient boosting machine; XGBoost: extreme gradient boosting.

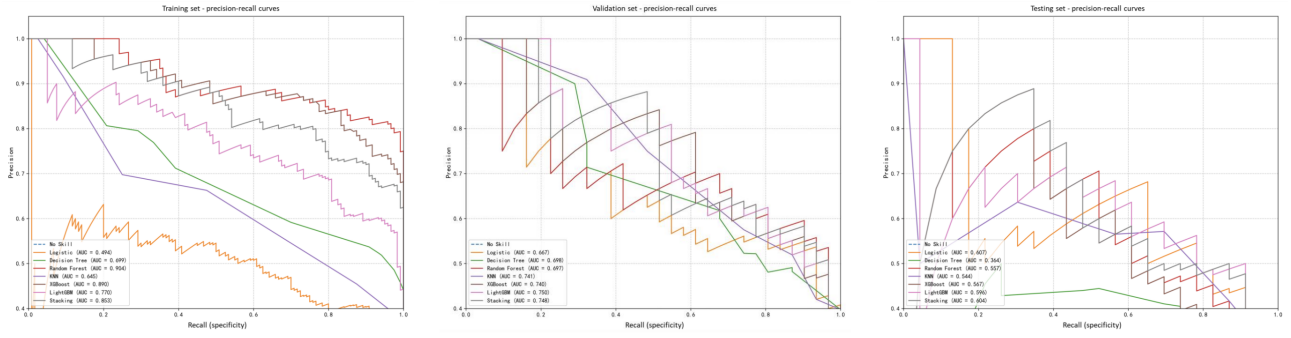

A B C

In the validation dataset, the LightGBM model demonstrated the highest PR-AUC of 0.750, followed closely by stacking (0.748) and KNN (0.741). The XGBoost and random forest models performed comparably with AUCs of 0.740 and 0.697, respectively, whereas the logistic model yielded a PR-AUC of 0.667, and the decision tree model slightly lagged behind with an AUC of 0.698 (Figure 3B).

In the testing dataset, the LightGBM (AUC=0.596) and stacking (AUC=0.604) models exhibited moderate PR performance. The logistic model followed with an AUC of 0.607. Conversely, XGBoost (0.567), random forest (0.557), and KNN (0.544) demonstrated slightly lower PR-AUCs, with the decision tree model displaying the weakest performance (AUC=0.364; Figure 3C).

ROC Curve Analysis of Risk Prediction Models Based on 10-Fold Cross-Validation

ROC analysis using 10-fold cross-validation was used to assess the efficacy of 3 leading models: logistic regression, LightGBM, and stacking. As depicted in Figure 4A, during the training phase, the LightGBM model demonstrated the highest average AUC of 0.691, marginally surpassing logistic regression (AUC=0.679) and stacking (AUC=0.677), underscoring its superior discriminatory capability. Additionally, as illustrated in Figure 4B, following hyperparameter optimization, LightGBM's performance was further bolstered, with its mean AUC escalating from 0.689 (0.025) to 0.701 (0.074). This enhancement substantiates LightGBM's resilience across iterations. Consequently, LightGBM was ultimately designated as the preferred model for subsequent analyses.

XSL•FO
RenderX

Figure 4. Receiver operating characteristic (ROC) curve analysis of risk prediction models based on 10-fold cross-validation. (A) ROC curves were generated for the 3 best-performing models, namely logistic regression, light gradient boosting machine (LightGBM), and stacking, through 10-fold cross-validation on the training dataset. LightGBM demonstrated the highest average area under the receiver operating characteristic curve (AUC) of 0.691, with logistic regression and stacking following closely at 0.679 and 0.677, respectively. (B) A comparison of LightGBM performance prehyperparameter and posthyperparameter optimization revealed enhancements. The optimized model exhibited a higher mean AUC of 0.701 (SD 0.074), surpassing the original model's performance of 0.689 (SD 0.025), thus validating its increased stability.

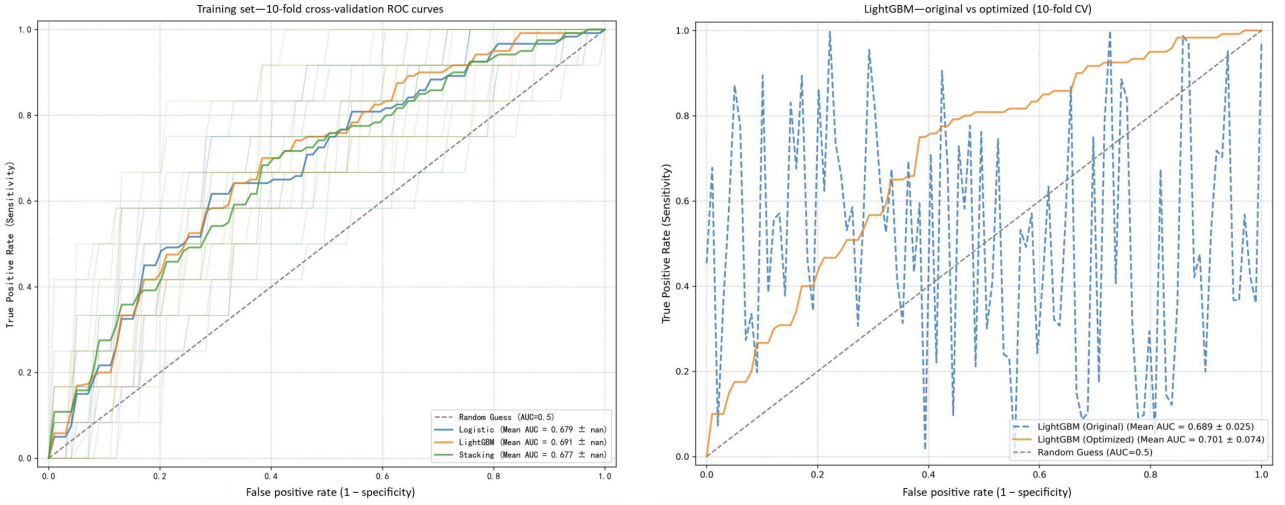

A B

Calibration Curves and Brier Score Analysis

Calibration curves and Brier scores were utilized to assess the alignment between predicted probabilities and observed outcomes across various datasets. In the training set (Figure 5A), all models exhibited moderate calibration performance. The KNN model displayed the lowest Brier score (0.2134), closely trailed by random forest (0.240), logistic regression (0.2482), and XGBoost (0.2487). Within the validation set (Figure 5B), random forest exhibited favorable calibration (Brier score=0.2614), with XGBoost (0.2662) and KNN (0.2758) also demonstrating relatively strong performance. In the test set (Figure 5C), logistic regression demonstrated the most accurate calibration (Brier score=0.2507), followed by XGBoost (0.2737) and KNN (0.2629). While the Brier scores indicated acceptable calibration for multiple models, no single model consistently outperformed others across all 3 datasets. Nevertheless, XGBoost and KNN showcased consistent and favorable calibration performance.

Figure 5. Calibration curves and Brier scores of 6 machine learning models. Calibration curves were utilized to evaluate the concordance between predicted probabilities and observed outcomes of coronary heart disease (CHD) across 3 sets: the training set, validation set, and test set. The diagonal dotted line in the graphs symbolizes ideal calibration, with Brier scores (inset) serving as a measure of prediction accuracy (lower scores indicating improved calibration). Both extreme gradient boosting (XGBoost) and k-nearest neighbors (KNN) models demonstrated consistent calibration performance across all datasets.

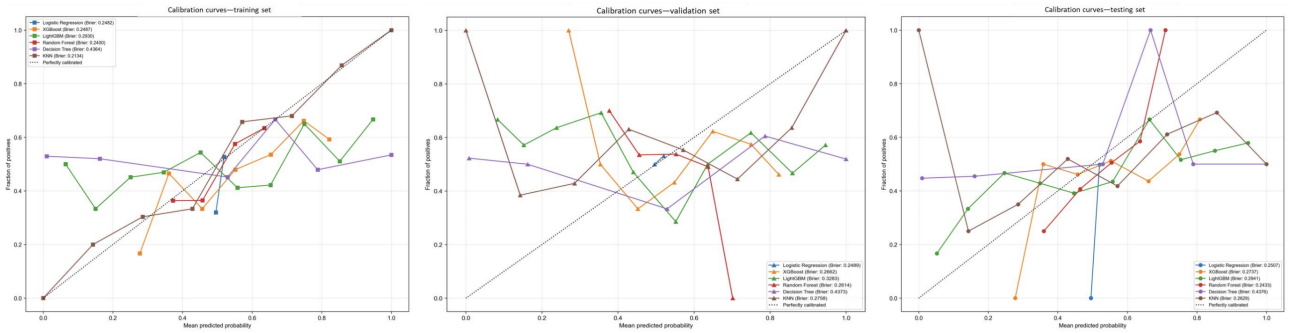

A B C

Clinical Utility Evaluation Based on Decision Curve Analysis

Decision curve analysis was used to assess the clinical efficacy of various machine learning models on the training, validation, and test sets. Figure 6 illustrates that the KNN model yielded the highest average net benefit across all 3 datasets (training: 0.2984, validation: 0.2974, and test: 0.281), closely trailed by LightGBM (training: 0.3262, validation: 0.264, and test: 0.2415) and XGBoost (train: 0.3084, validation: 0.2615, and test: 0.2383). These models consistently outperformed the "Treat None" and "Treat All" strategies in terms of net benefit over a broad range of probability thresholds. Notably, LightGBM and KNN consistently demonstrated superior clinical utility, particularly within the 0.3 - 0.7 threshold range, suggesting their potential for guiding personalized preventive interventions in practical healthcare settings.

XSL•FO
RenderX

Figure 6. Decision curve analysis (DCA) of 6 machine learning models. The clinical utility of models is assessed by DCA through the calculation of net benefit at different probability thresholds in the training, validation, and test sets. Net benefit is determined as the difference between the proportion of correctly identified cases of coronary heart disease (CHD) and the proportion of unnecessary interventions. K-nearest neighbors (KNN), light gradient boosting machine (LightGBM), and extreme gradient boosting (XGBoost) consistently exhibited superior net benefit compared to strategies of treating all or treating none, especially within the 0.3 - 0.7 threshold range.

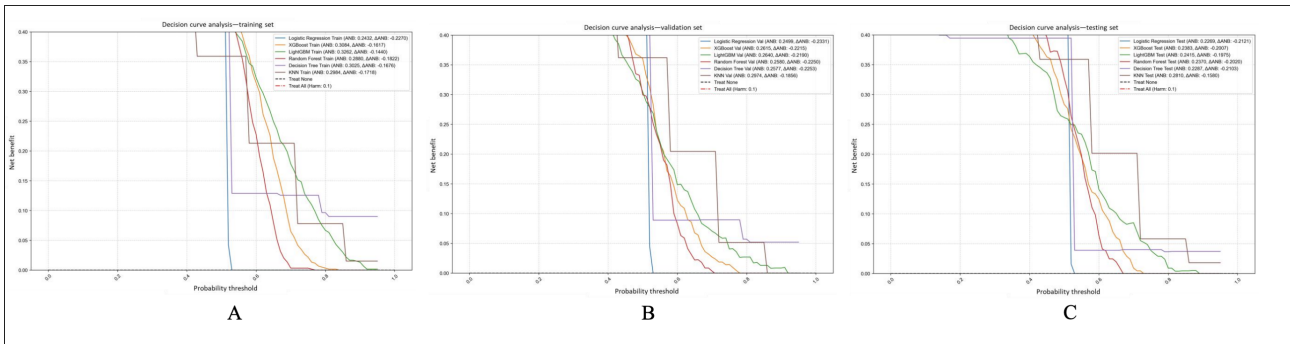

SHAP-Based Interpretation of the Optimal LightGBM Model

To enhance the interpretability of the LightGBM model, SHAP values were utilized to assess the significance of individual features on the model's predictions. The feature importance summary plot, derived from the mean absolute SHAP values, identified age, APTT, hypertension, weight, carotid plaque, and continuous drinking history as the primary predictors influencing the risk of CHD in patients with HHcy (Figure 7A). Notably, age and APTT exhibited the most substantial average impact, underscoring their pivotal roles in the model's predictive capabilities.

Figure 7. Shapley Additive Explanation (SHAP)–based interpretation and feature correlation analysis of the light gradient boosting machine (LightGBM) model. (A) A SHAP summary plot displays the average absolute impact of individual features on the prediction of coronary heart disease (CHD) risk, highlighting age and activated partial thromboplastin time (APTT) as the most influential factors. (B) A SHAP dependence plot illustrates the direction (positive or negative) and strength of feature effects on the model's output, indicating that higher age and APTT levels are associated with an increased risk of CHD. (C) A Pearson correlation heatmap of key features demonstrates minimal multicollinearity ($|r|$<0.5 for all features except continuous drinking or smoking history, where r=0.54), thereby ensuring the stability of the model. Cr: creatinine.

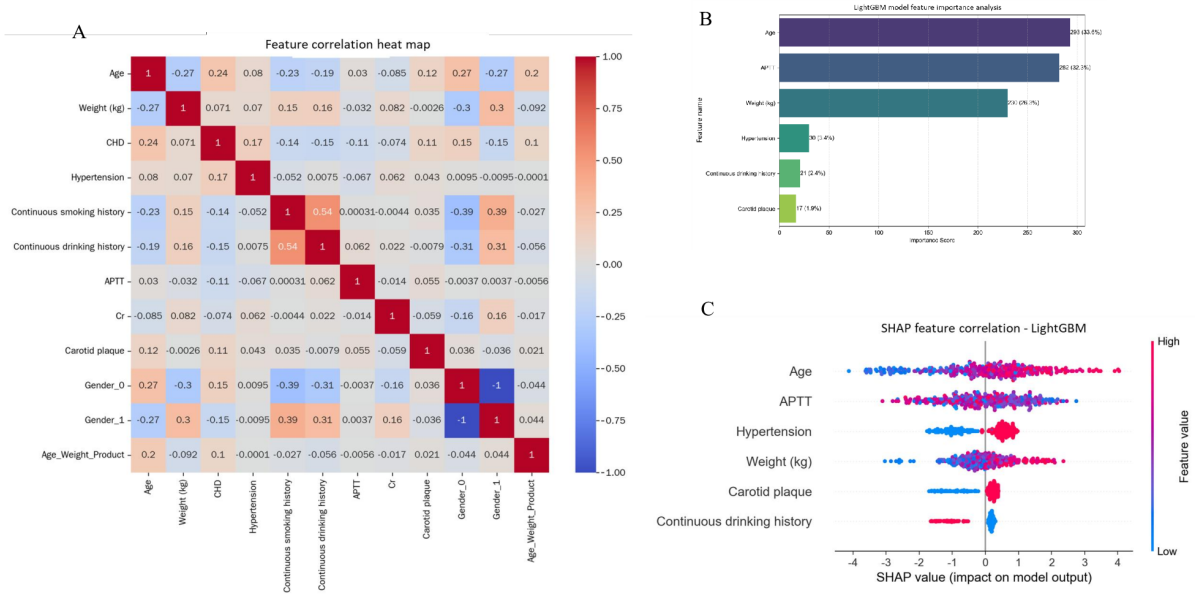

The SHAP dependence plot (Figure 7B) illustrates the impact of each feature on the model output in terms of both direction and magnitude. The elevated values of age and APTT were consistently linked to a higher predicted risk of CHD, with hypertension and carotid plaque presence also notably increasing the SHAP value. Notably, the influence of continuous drinking history exhibited variability across individual patient profiles, suggesting potential interactions with other variables.

A feature correlation heatmap (Figure 7C) was generated to evaluate multicollinearity and the interplay among essential features. The heatmap reveals a moderate positive correlation between continuous drinking history and continuous smoking history (r=0.54) and a slight negative correlation between age

XSL•FO
RenderX

and weight (r=–0.27). These findings endorse the incorporation of these variables into the LightGBM model without introducing unnecessary redundancy.

These results demonstrate that the LightGBM model offers both superior predictive accuracy and the ability to reveal the significance and interplay of clinical features. This capability can enhance personalized risk evaluation and targeted preventive measures for coronary heart disease in individuals with HHcy.

Discussion

This research conducted a comparative analysis of 7 machine learning algorithms to forecast the likelihood of CHD in patients with HHcy using authentic single-center electronic health records. The models were developed utilizing 6 fundamental variables (age, weight, hypertension, history of sustained alcohol consumption, APTT, and carotid artery plaque), and their discriminatory capacity, calibration, and clinical applicability were thoroughly assessed across training, validation, and test datasets. The findings revealed that the LightGBM model exhibited superior overall performance, demonstrating the highest AUC (0.807) and a relatively elevated F_1-score (0.636) in the test set, underscoring its promising clinical predictive capability.

A significant discovery is that the model does not depend on variables specific to CHD or HHcy. Instead, it opts for indicators that are commonly available and extensively standardized in routine clinical settings, including coagulation function (activated partial thromboplastin time), arterial structure markers (presence of carotid artery plaques), basal metabolism (body weight), and behavioral aspects (alcohol consumption history). These variables do not necessitate expert image analysis or sophisticated molecular assays, thereby augmenting the model's practicality in primary health care facilities or noncardiovascular disciplines.

Upon applying the SHAP algorithm to interpret the model, we validated that age and APTT are the most impactful variables within the model. Notably, the predictive significance of APTT warrants special consideration. Serving as a marker for the intrinsic coagulation pathway, it could potentially signify a hypercoagulable state within the HHcy population. This pathological characteristic has been identified as a key factor contributing to accelerated atherosclerosis [22]. The SHAP dependence plot and correlation heatmap provided additional confirmation of the minimal collinearity among variables, thereby augmenting the interpretive clarity and reliability of the model.

The stacking model exhibits a high AUC of 0.800 in the validation set; however, its F_1-score decreases to 0.33 in the test set, with a sensitivity of only 0.26, indicating limited generalization ability and a predisposition toward overfitting. Conversely, the LightGBM model demonstrates consistent performance across the training, validation, and test sets, underscoring its robustness in diverse sample scenarios. While the logistic regression model shows a slightly lower AUC, its balanced F_1-score, sensitivity, and specificity underscore its reliability in terms of generalization stability.

In this study, we aim to streamline variable processing by avoiding artificial binning, segmentation, high-dimensional mapping transformations, and the creation of interaction terms. This approach is intended to enhance the model's generalizability across different datasets by minimizing reliance on specific data structures. Additionally, we refrain from using oversampling methods, such as synthetic minority over-sampling technique, to mitigate issues related to feature distribution drift resulting from synthetic sample generation. Instead, we tackle data imbalance by adjusting category weights and optimizing thresholds.

However, this study is subject to several limitations. First, the data were sourced from a singular medical institution, potentially introducing regional, health care–seeking motivation, or detection biases. For instance, individuals with high homocysteine levels who consented to coagulation function tests may exhibit distinct health awareness and disease profiles compared to those who declined the tests. Second, the retrospective design of the study resulted in the exclusion of crucial variables that could impact CHD risk, such as dietary patterns, nutritional status, and renal function. Consequently, the interpretation of changes in serum markers remains inconclusive. Furthermore, the study solely predicted the present CHD status of patients documented in electronic health records. The absence of longitudinal follow-up data precluded the modeling of event timing or disease progression. To address these limitations, future research should integrate prospective cohorts and long-term follow-up data to validate the model's reliability and establish a dynamic risk assessment framework.

In conclusion, the LightGBM model developed in this study exhibits exceptional predictive accuracy and interpretability in individuals with HHcy, offering a robust basis for real-world implementation. We propose its consideration as a potential tool for early CHD risk stratification to aid clinicians in promptly identifying high-risk patients. Subsequent investigations may concentrate on external validation and model refinement in a multicenter context.

Funding

This research was supported by the National Natural Youth Science Foundation of China (grant numbers 82205021 and 82405290) and the Science and Technology Innovation Guidance Plan Project in the Medical and Health Field of Zhengzhou City (grant number 2024YLZDJH075).

Data Availability

The datasets produced and/or scrutinized in this study are not publicly accessible to safeguard patient confidentiality and comply with institutional guidelines. However, interested parties may obtain the data from the corresponding author upon request.

XSL•FO
RenderX

Authors' Contributions

The study was designed by and data analysis was supervised by MKL and MYD. Data collection was conducted by HL, HY, XL, and YL. MKL and MYD contributed to manuscript writing and revision. All authors have reviewed and approved the final manuscript.

Conflicts of Interest

None declared.

Multimedia Appendix 1
Detailed data extraction and quality-control protocols.
[DOCX File, 18 KB - medinform_v14i1e80809_app1.docx]

Multimedia Appendix 2
Grid search ranges and final hyperparameters for all machine learning models.
[DOCX File, 18 KB - medinform_v14i1e80809_app2.docx]

Multimedia Appendix 3
Threshold optimization curve for the light gradient boosting machine (LightGBM) model.
[PDF File, 223 KB - medinform_v14i1e80809_app3.pdf]

References

1. Guéant JL, Guéant-Rodriguez RM, Oussalah A, Zuily S, Rosenberg I. Hyperhomocysteinemia in cardiovascular diseases: revisiting observational studies and clinical trials. Thromb Haemost 2023 Mar;123(3):270-282. [doi: 10.1055/a-1952-1946] [Medline: 36170884]
2. Tinelli C, Di Pino A, Ficulle E, Marcelli S, Feligioni M. Hyperhomocysteinemia as a risk factor and potential nutraceutical target for certain pathologies. Front Nutr 2019;6:49. [doi: 10.3389/fnut.2019.00049] [Medline: 31069230]
3. Balint B, Jepchumba VK, Guéant JL, Guéant-Rodriguez RM. Mechanisms of homocysteine-induced damage to the endothelial, medial and adventitial layers of the arterial wall. Biochimie 2020 Jun;173:100-106. [doi: 10.1016/j.biochi.2020.02.012] [Medline: 32105811]
4. Herrero-Fernandez B, Gomez-Bris R, Somovilla-Crespo B, Gonzalez-Granado JM. Immunobiology of atherosclerosis: a complex net of interactions. Int J Mol Sci 2019 Oct 24;20(21):5293. [doi: 10.3390/ijms20215293] [Medline: 31653058]
5. Cetin E, Raby AC. Understanding atherosclerotic plaque cellular composition: recent advances driven by single cell omics. Cells 2025 May 23;14(11):770. [doi: 10.3390/cells14110770] [Medline: 40497946]
6. Alaa AM, Bolton T, Di Angelantonio E, Rudd JHF, van der Schaar M. Cardiovascular disease risk prediction using automated machine learning: a prospective study of 423,604 UK Biobank participants. PLoS One 2019;14(5):e0213653. [doi: 10.1371/journal.pone.0213653] [Medline: 31091238]
7. Wysocki A, Fułek M, Macek P, et al. Ultrasound carotid plaque score and severity of coronary artery disease assessed by computed tomography angiography in patients with arterial hypertension. Diagnostics (Basel) 2024 May 25;14(11):1101. [doi: 10.3390/diagnostics14111101] [Medline: 38893628]
8. Pal P, Singh HV, Grover V, Manikandan R, Karimi R, Khishe M. Interactive cardiovascular disease prediction system using learning techniques: Insights from extensive experiments. Results Control Optim 2025 Jun;19:100560. [doi: 10.1016/j.rico.2025.100560]
9. Hajihosseinlou M, Maghsoudi A, Ghezelbash R. A novel scheme for mapping of MVT-type Pb–Zn prospectivity: LightGBM, a highly efficient gradient boosting decision tree machine learning algorithm. Nat Resour Res 2023 Dec;32(6):2417-2438. [doi: 10.1007/s11053-023-10249-6]
10. Gulum MA, Trombley CM, Ozen M, Esen E, Aksamoglu M, Kantardzic M. Why are explainable AI methods for prostate lesion detection rated poorly by radiologists? Appl Sci (Basel) 2024;14(11):4654. [doi: 10.3390/app14114654]
11. Obeagu EI, Ezeanya CU, Ogenyi FC, Ifu DD. Big data analytics and machine learning in hematology: transformative insights, applications and challenges. Medicine (Baltimore) 2025;104(10):e41766. [doi: 10.1097/MD.0000000000041766] [Medline: 40068020]
12. Weng SF, Reps J, Kai J, Garibaldi JM, Qureshi N. Can machine-learning improve cardiovascular risk prediction using routine clinical data? PLoS One 2017;12(4):e0174944. [doi: 10.1371/journal.pone.0174944] [Medline: 28376093]
13. Williams MS, Levine GN, Kalra D, et al. Correction to: 2025 AHA/ACC clinical performance and quality measures for patients with chronic coronary disease: a report of the American College of Cardiology/American Heart Association joint committee on performance measures. Circ Cardiovasc Qual Outcomes 2025 Jul;18(7):e000141. [doi: 10.1161/HCQ.0000000000000141] [Medline: 40663623]

XSL•FO
RenderX

4. Byrne RA, Rossello X, Coughlan JJ, et al. 2023 ESC Guidelines for the management of acute coronary syndromes. Eur Heart J 2023 Oct 12;44(38):3720-3826. [doi: 10.1093/eurheartj/ehad191] [Medline: 37622654]
15. Visseren FLJ, Mach F, Smulders YM, et al. 2021 ESC Guidelines on cardiovascular disease prevention in clinical practice. Eur J Prev Cardiol 2022 Feb 19;29(1):5-115. [doi: 10.1093/eurjpc/zwab154] [Medline: 34558602]
16. van Smeden M, de Groot JAH, Moons KGM, et al. No rationale for 1 variable per 10 events criterion for binary logistic regression analysis. BMC Med Res Methodol 2016 Nov 24;16(1):163. [doi: 10.1186/s12874-016-0267-3] [Medline: 27881078]
17. van Smeden M, Moons KG, de Groot JA, et al. Sample size for binary logistic prediction models: beyond events per variable criteria. Stat Methods Med Res 2019 Aug;28(8):2455-2474. [doi: 10.1177/0962280218784726] [Medline: 29966490]
18. Riley RD, Snell KI, Ensor J, et al. Minimum sample size for developing a multivariable prediction model: part II—binary and time-to-event outcomes. Stat Med 2019 Mar 30;38(7):1276-1296. [doi: 10.1002/sim.7992] [Medline: 30357870]
19. Riley RD, Snell KIE, Ensor J, et al. Minimum sample size for developing a multivariable prediction model: part I—continuous outcomes. Stat Med 2019 Mar 30;38(7):1262-1275. [doi: 10.1002/sim.7993] [Medline: 30347470]
20. D'Agostino RB Sr, Vasan RS, Pencina MJ, et al. General cardiovascular risk profile for use in primary care: the Framingham Heart study. Circulation 2008 Feb 12;117(6):743-753. [doi: 10.1161/CIRCULATIONAHA.107.699579] [Medline: 18212285]
21. Goff DC Jr, Lloyd-Jones DM, Bennett G, et al. 2013 ACC/AHA guideline on the assessment of cardiovascular risk: a report of the American College of Cardiology/American Heart Association Task Force on Practice Guidelines. Circulation 2014 Jun 24;129(25 Suppl 2):S49-S73. [doi: 10.1161/01.cir.0000437741.48606.98] [Medline: 24222018]
22. Yin H, Cheng X, Liang Y, et al. High perceived stress may shorten activated partial thromboplastin time and lead to worse clinical outcomes in patients with coronary heart disease. Front Cardiovasc Med 2021;8:769857. [doi: 10.3389/fcvm.2021.769857] [Medline: 34912866]

Abbreviations

ACC/AHA: American College of Cardiology/American Heart Association
APTT: activated partial thromboplastin time
AUC: area under the receiver operating characteristic curve
CHD: coronary heart disease
HHcy: hyperhomocysteinemia
KNN: k-nearest neighbor
LightGBM: light gradient boosting machine
PR: precision-recall
ROC: receiver operating characteristic
SHAP: Shapley Additive Explanation
XGBoost: extreme gradient boosting

Edited by J Klann; submitted 17.Jul.2025; peer-reviewed by L Hou, Y Zhou; revised version received 17.Jan.2026; accepted 20.Jan.2026; published 19.Mar.2026.

Please cite as:
Du MY, Lyu MK, Liu HL, Li YZ, Yan HF, Li XH
Machine Learning–Based Risk Prediction for Coronary Heart Disease Complicated by Hyperhomocysteinemia: Retrospective Study
JMIR Med Inform 2026;14:e80809
URL: https://medinform.jmir.org/2026/1/e80809
doi:10.2196/80809

© Ming-Yuan Du, Meng-Ke Lyu, Hai-long Liu, Yi-zhuo Li, Hai-feng Yan, Xiao-hui Li. Originally published in JMIR Medical Informatics (https://medinform.jmir.org), 19.Mar.2026. This is an open-access article distributed under the terms of the Creative Commons Attribution License (https://creativecommons.org/licenses/by/4.0/), which permits unrestricted use, distribution, and reproduction in any medium, provided the original work, first published in JMIR Medical Informatics, is properly cited. The complete bibliographic information, a link to the original publication on https://medinform.jmir.org/, as well as this copyright and license information must be included.

XSL•FO
RenderX

Bridging Population Patterns and Individual Prediction: Framework for Prospective Multimorbidity Study

Qianyao Zhang[1], BBA; Runtong Zhang[1], Prof Dr; Weiguang Ma[1], MSc; Butian Zhao[2], PhD; Xiaomin Zhu[3], Prof Dr

[1]Department of Information Management, School of Economics and Management, Beijing Jiaotong University, No.3 Shangyuancun, Haidian District, Beijing, China

[2]School of Management, Beijing University of Chinese Medicine, Beijing, China

[3]School of Mechanical, Electronic and Control Engineering, Beijing Jiaotong University, Beijing, China

Corresponding Author:
Runtong Zhang, Prof Dr
Department of Information Management, School of Economics and Management, Beijing Jiaotong University, No.3 Shangyuancun, Haidian District, Beijing, China

Abstract

Background: Multimorbidity has become a major global public health challenge. However, existing research primarily emphasizes the identification of disease patterns at the population level and lacks the capacity to provide predictive insights into individual future pattern membership. Bridging this gap is crucial for personalized prevention and management.

Objective: This study aims to propose an innovative framework that integrates population-level multimorbidity pattern recognition with individual-level predictive modeling, thus advancing multimorbidity research from descriptive analysis to prospective multimorbidity pattern prediction.

Methods: Using longitudinal health follow-up data, we first applied latent transition analysis (LTA) to identify temporally stable multimorbidity patterns. These patterns were subsequently transformed into predictive labels to construct a novel deep learning model, CLA-Net (Cross-Lag Attention Network). CLA-Net is designed to predict individual future multimorbidity patterns by leveraging the complementary strengths of Gated Recurrent Units (GRU) and transformer architectures. It introduces a bitemporal directed cross-attention mechanism to simultaneously capture temporal dependencies and complex feature interactions. We compared CLA-Net against several advanced baselines and conducted ablation studies to validate its architectural components.

Results: In terms of pattern recognition, the LTA identified 5 clinically meaningful multimorbidity patterns: Cardiometabolic-Multisystem, Hypertension-Arthritis, Respiratory-Musculoskeletal, Metabolic Syndrome, and Gastritis-Arthritis. In terms of prediction, experimental results demonstrated that CLA-Net significantly outperformed all baseline models. CLA-Net achieved an accuracy of 0.8352 (SD 0.0048), a precision of 0.8326 (SD 0.0053), a recall of 0.8312 (SD 0.0056), and an F_1-score of 0.8319 (SD 0.0051). Notably, it achieved an area under the curve of 0.9293, surpassing baseline models. Ablation studies confirmed the necessity of the dual-branch architecture and the directed cross-attention mechanism, as removing these components resulted in performance declines ranging from 0.93% to 2.50%.

Conclusions: This study extends the scope of LTA beyond descriptive statistical modeling and establishes the scientific value of multimorbidity pattern prediction as an independent research task. By bridging population-level insights with individual-level prediction, the proposed framework provides a data-driven tool for the prospective prediction of future multimorbidity pattern membership conditional on survival, thereby supporting stratified disease management and care planning, rather than general risk stratification for acute or end-stage deterioration. This offers new methodological and practical value for precision medicine and public health policymaking.

(JMIR Med Inform 2026;14:e84261) doi:10.2196/84261

KEYWORDS

multimorbidity; latent transition analysis; LTA; deep learning; population-level patterns; personalized medicine

Introduction

Multimorbidity, commonly defined as the coexistence of 2 or more chronic conditions within a single individual [1], has emerged as one of the most pressing public health challenges of the 21st century amid the accelerating global trend of population aging [2]. Worldwide, approximately one-third of adults have 2 or more chronic diseases, and the proportion exceeds 50% among individuals aged 60 years and older [3]. Multimorbidity not only substantially increases health care resource consumption and imposes a heavy burden on health systems, but also severely compromises patients' quality of life, leading to a markedly higher risk of functional disability and

XSL•FO
RenderX

premature mortality, thereby greatly increasing the complexity of chronic disease management and clinical decision-making [4,5]. Previous studies have demonstrated that the co-occurrence of chronic diseases is not a random phenomenon but tends to manifest as distinct multimorbidity patterns, in which specific combinations of diseases frequently occur in particular populations [6,7]. This suggests the potential existence of shared pathophysiological mechanisms, risk factors, or lifestyle determinants underlying these patterns [8]. Therefore, systematically identifying, understanding, and predicting these multimorbidity patterns holds strategic importance for the early detection of high-risk individuals, the advancement of precision medicine, and the optimization of health care resource allocation [9,10].

Although various methods for identifying multimorbidity patterns have been proposed, such as factor analysis, cluster analysis, latent class analysis (LCA), and network analysis [11-15], they share significant limitations and fall short of meeting the clinical demand for personalized and prospective management. First, most approaches group populations primarily based on disease prevalence or epidemiological characteristics, assuming homogeneity within groups while overlooking the inherent heterogeneity among individuals [14,16]. Such population-level stratification can facilitate the identification of common multimorbidity patterns at a macrolevel but fails to uncover microlevel differences within patterns, which is particularly inadequate for supporting fine-grained individualized management in clinical practice. In reality, even among patients belonging to the same multimorbidity pattern, disease trajectories may differ substantially. For example, some patients experience slow progression and remain stable over a long period, whereas others may rapidly develop multisystem dysfunction [17]. Neglecting such heterogeneity may directly result in biased risk assessments and inefficient resource allocation, thereby severely constraining the practical implementation of precision medicine. In addition, existing studies have mainly focused on static multimorbidity pattern mining [16,18], and the methods used often struggle to maintain consistency of pattern meanings in longitudinal data. This instability not only reduces the comparability of research findings but also weakens the ability to capture disease progression, thereby limiting the clinical interpretability and practical value of the conclusions.

To address the above challenges, latent transition analysis (LTA), a longitudinal latent variable model, has been introduced into health research. LTA can identify stable latent health states across multiple time points and ensure their consistency and comparability over time [19]. Compared to other longitudinal modeling approaches, LTA offers distinct advantages for identifying multimorbidity evolution. Unlike growth mixed models or latent growth curve models, which primarily characterize continuous trajectories of a single variable (eg, functional decline over time), LTA is specifically designed to model transitions between discrete, qualitative latent statuses, aligning perfectly with the categorical nature of multimorbidity patterns. Furthermore, in contrast to standard Markov chain models that rely on observed states, LTA separates measurement error from true structural transitions by inferring latent classes from multiple observed indicators, thereby ensuring more robust and clinically meaningful pattern identification. By modeling follow-up data, LTA can effectively capture heterogeneity within populations and provide new perspectives for understanding the dynamic evolution of multimorbidity patterns [20,21]. However, LTA is essentially a descriptive statistical method, with its primary focus on identifying and summarizing patterns from historical or current data, while lacking the capacity to predict individual future health states. This limitation hinders its ability to meet urgent clinical needs, such as providing precise early warnings for high-risk individuals, developing timely intervention strategies, and guiding personalized treatment planning. Therefore, constructing predictive models that can accurately forecast individuals' future multimorbidity patterns carries substantial clinical value and practical significance.

Predicting individual future multimorbidity patterns requires accounting for both the temporal evolution of health states and the complex interactions among multidimensional health features. On the one hand, the progression of chronic diseases exhibits marked and highly nonlinear temporal dependencies. A patient's current health status not only reflects their immediate physiological condition but also embodies the evolution from the previous health state, reflecting the staged characteristics of disease progression [22]. Ignoring such sequential state transitions weakens a model's ability to capture disease progression trends, thereby limiting its capacity to deliver reliable forward-looking predictions. On the other hand, multidimensional health features, including lifestyle factors, preexisting conditions, and functional indicators, are interconnected through intricate nonlinear couplings and synergistic effects. These dynamic interactions drive the formation and evolution of multimorbidity patterns [23]. Many conventional statistical methods, such as logistic regression, support vector machines, random forests, gradient boosting trees, and k-nearest neighbors (KNN), perform well in modeling static feature associations [24,25]. However, when confronted with high-dimensional, nonlinear, and temporally dependent medical data, their modeling capacity is limited, making it difficult to simultaneously capture nonlinear state transitions and deep couplings among features. Therefore, there is an urgent need to develop a model that overcomes these limitations by effectively integrating sequential health state changes and feature coupling effects in longitudinal data, thus enabling precise and prospective prediction of individual future multimorbidity patterns and providing robust data support for clinical decision-making.

Based on the above discussion, this study proposes an innovative framework that integrates population-level multimorbidity pattern recognition with precise prediction of individual future states, thereby advancing multimorbidity research from macrolevel description to prospective application. Specifically, the framework first uses LTA to identify population-level multimorbidity patterns with temporal consistency and clinical stability from longitudinal follow-up data, and then transforms these patterns into individual predictive labels. On this basis, we designed the Cross-Lag Attention Network (CLA-Net), which leverages immediate longitudinal context to model

XSL•FO
RenderX

short-term, nonlinear state transitions and complex feature interactions among health variables, thereby enabling accurate prediction of individual future multimorbidity patterns.

The contributions of this study can be summarized in 3 aspects. First, we propose a novel cross-paradigm framework that bridges a statistical latent-variable modeling approach with deep representation learning for longitudinal multimorbidity research. Specifically, population-level multimorbidity patterns identified through LTA are leveraged as clinically interpretable supervisory signals for individual-level prediction. By integrating latent structure discovery with prospective modeling, this framework overcomes the limitation of traditional multimorbidity studies that are largely restricted to retrospective pattern characterization and establishes multimorbidity pattern prediction as a distinct and clinically meaningful research task.

Second, we propose a novel hybrid neural network architecture, CLA-Net, for multimorbidity pattern prediction. CLA-Net integrates the inherent strength of Gated Recurrent Units (GRU) in efficiently modeling short-term, nonlinear state transitions with the powerful representational capacity of the transformer architecture in capturing complex feature interactions. This design surpasses the capacity of traditional linear models, enabling deep modeling of the intricate couplings within medical data. Furthermore, CLA-Net incorporates a bitemporal directed cross-attention mechanism, which establishes directional information channels between the preceding and current health states. This mechanism facilitates feature extraction across time steps and dynamic association modeling, allowing the network to simultaneously perceive and effectively integrate dynamic state changes and feature coupling effects within complex longitudinal medical data.

Third, the experimental results demonstrate that the proposed CLA-Net model significantly outperforms other mainstream baseline models. Further ablation studies confirm that the synergistic integration of GRU and transformer, together with the bitemporal directed cross-attention mechanism, is the key factor driving the performance improvement. These findings not only provide strong evidence for the superiority of CLA-Net and the soundness of its design but also offer new insights and paradigms for model development in the field of multimorbidity pattern prediction.

Methods

Overview

We designed a novel research framework that integrates multimorbidity pattern recognition with individualized prediction. The overarching idea is to first identify population-level latent multimorbidity patterns with temporal consistency from longitudinal health data, and then build a deep learning model to predict each individual's future pattern membership, thereby establishing a unified framework that bridges population-level recognition and individual-level prediction. As illustrated in Figure 1, the proposed framework consists of 3 stages. In the first stage, LTA is applied to longitudinal health records to identify latent multimorbidity patterns at the population level, ensuring that these patterns maintain consistent clinical meaning and comparability across different time points, thus providing a stable and reliable label basis for subsequent individual prediction tasks. In the second stage, based on the LTA-derived pattern labels, we design and construct the CLA-Net, which integrates temporal dependencies and complex feature interactions to enable accurate prediction of individual future pattern membership. In the third stage, we conduct a comprehensive performance evaluation and validation of the prediction model.

XSL•FO
RenderX

Figure 1. Proposed framework for multimorbidity pattern recognition and prediction. CLA-Net: Cross-Lag Attention Network; LTA: latent transition analysis.

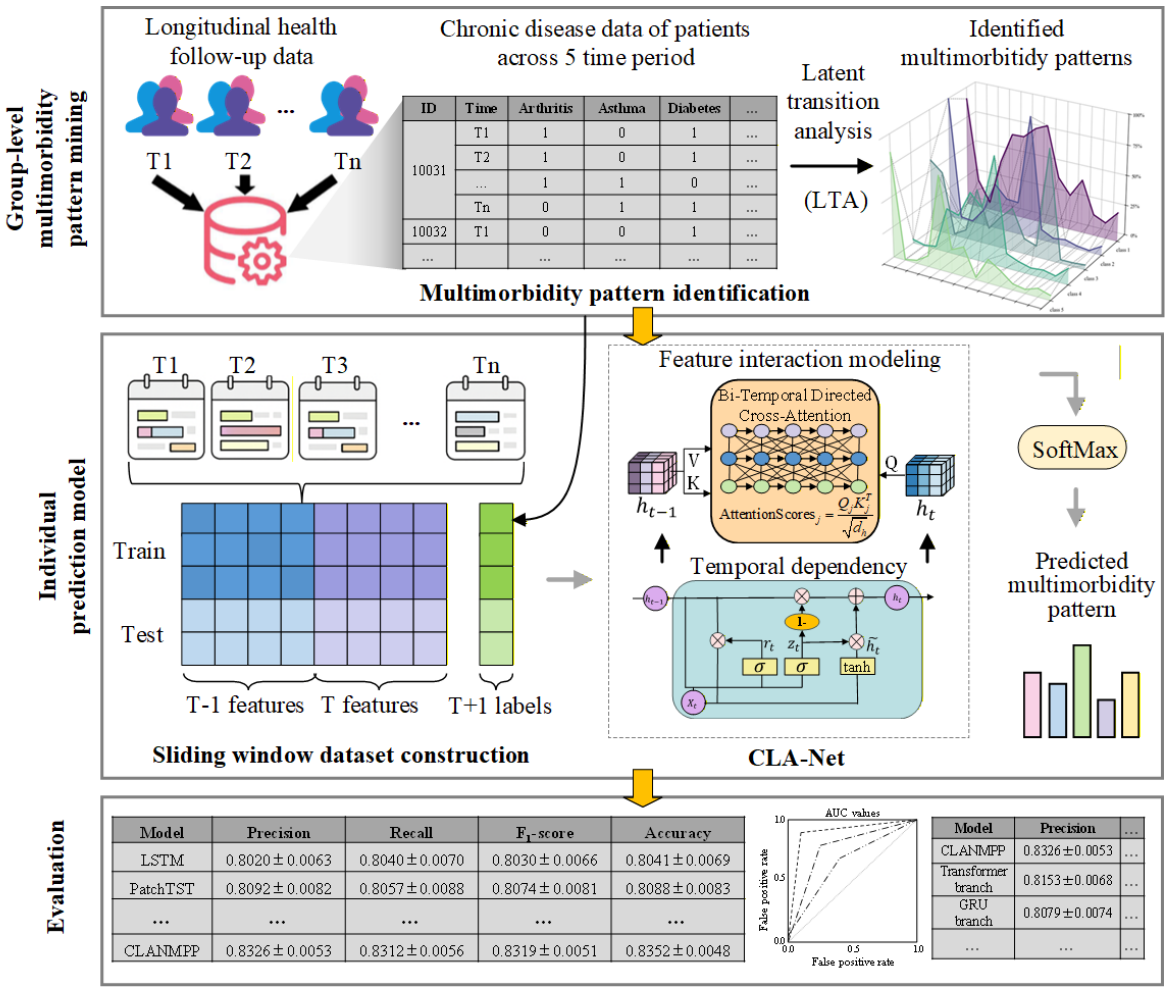

Multimorbidity Pattern Identification

This study used SAS 9.4 (SAS Institute) to apply LTA for identifying the latent class structures of population-level multimorbidity patterns across 5 waves of China Health and Retirement Longitudinal Study (CHARLS) data. LTA is a longitudinal analytic method based on finite mixture models, which can detect unobserved health subgroups (latent statuses) within the sample across multiple time points. By imposing measurement invariance constraints, LTA ensures temporal consistency and stability of the latent classes [20], thereby guaranteeing that the identified classes maintain comparable and clinically meaningful interpretations across different time points. This provides stable and reliable classification labels for subsequent individual prediction modeling tasks. To control classification error and enhance model stability, we adopted a 2-step analytic strategy [26]. The detailed procedure is as follows: in step 1, we first conducted LCA separately at each time point to explore the optimal number of latent class partitions. In the model specification process, we considered different numbers of latent classes (ranging from 2 to 6) [26]. Model fit was evaluated using the Akaike Information Criterion (AIC), Bayesian Information Criterion (BIC), sample-size adjusted BIC (SaBIC), and entropy, to determine the optimal class solution.

Specifically, the AIC balances model fit and complexity, with smaller values indicating better fit [27]. The BIC adds a penalty for sample size, favoring more parsimonious models and thus being more conservative in class determination, particularly in large samples [28]. The SaBIC further adjusts BIC for sample size, offering greater robustness in large-sample contexts [29]. Entropy (ranging from 0 to 1) measures the certainty of individual classification, with values above 0.80 generally indicating high classification accuracy [30]. In addition, we used the Bootstrap Likelihood Ratio Test (BLRT) to compare log-likelihood differences between adjacent class models, in order to assess whether adding an extra class significantly improves model fit [31,32].

In step 2, after determining the optimal number of classes, we conducted chi-square tests on the log-likelihood values of each model [31] and performed invariance testing of class structures across different measurement time points, in order to verify whether the meanings of multimorbidity classes remained consistent over time [31]. This step is a critical prerequisite for ensuring that classes retain the same interpretive meaning across time points, thereby enhancing the interpretability and stability of the model [33].

In this study, LTA is used as a population-level structure discovery tool to identify clinically stable multimorbidity phenotypes, rather than as a component optimized for

XSL•FO
RenderX

downstream predictive performance. The primary objective of LTA in our framework is to define a consistent and interpretable latent outcome space that reflects the underlying disease co-occurrence structure at the population level. Accordingly, LTA was estimated using the full longitudinal dataset across all available survey waves to maximize phenotype stability and clinical interpretability by leveraging the complete temporal information within the observed follow-up window. Within this 5-wave longitudinal design, the use of all waves enables the identified latent classes and transition patterns to reflect the evolution of multimorbidity structures across the entire observed period, rather than being driven by partial or wave-specific information. This design choice allows the latent class definitions to be less sensitive to sampling variability across individual waves and ensures that the resulting multimorbidity patterns are representative of the population dynamics observed within the study timeframe, rather than tailored to a specific subsample.

Proposed CLA-Net Framework

Multimorbidity Pattern Prediction Dataset

This study constructed a task-oriented dataset for prospective prediction of multimorbidity patterns based on the CHARLS, a nationally representative longitudinal survey in China. To bridge the gap between population-level pattern discovery and individual-level prediction, we constructed a supervised learning task using LTA-derived latent classes as predictive targets. Since LTA is a probabilistic model, it outputs the posterior probability of an individual belonging to each latent class rather than a deterministic category. To transform these probabilistic outputs into deterministic prediction labels for CLA-Net, we used a maximum posterior probability assignment strategy. Specifically, for each individual n at time step t, the LTA model calculates a posterior probability vector $\boldsymbol{P}_{n,t} = [p_1, p_2,\ldots, p_K]$, where K is the number of latent patterns. The ground truth label $y_{n,t}$ is assigned to the class with the highest probability:

$$(1)\text{yn,t=arg maxk}\in\{1,...,K\}(\text{Pn,t(k)})$$

These deterministic labels ($y_{n,t}$) serve as the supervisory signals (ground truth) for training the CLA-Net.

We used 2 consecutive follow-up waves as the input window to predict the multimorbidity pattern at the subsequent wave. In CHARLS, the intervals between survey waves are 2‐3 years, which align with the slow evolution and long-term accumulation process of chronic diseases. Although the intervals vary slightly, the progression of chronic conditions is characterized by slow variables (ie, gradual progression, stable trends, and limited abrupt changes), making 2‐3 years sufficient to capture substantial changes in individual health status while reducing noise from short-term fluctuations. This temporal span is clinically reasonable for modeling chronic disease progression. According to the study objectives, we reorganized the raw data using a sliding-window approach to construct 3 temporally progressive subdatasets, each corresponding to a "past–current → future" window structure:

- Subdataset 1: 2011 features as early input ($\mathbf{x}_{t-1}$), 2013 features as current input ($\mathbf{x}_t$), and 2015 LTA-derived multimorbidity patterns as prediction labels (y_{t+1})
- Subdataset 2: 2013 features as ($\mathbf{x}_{t-1}$), 2015 features as ($\mathbf{x}_t$), and 2018 multimorbidity patterns as (y_{t+1})
- Subdataset 3: 2015 features as ($\mathbf{x}_{t-1}$), 2018 features as ($\mathbf{x}_t$), and 2020 multimorbidity patterns as (y_{t+1})

The 3 subdatasets were concatenated by rows to form a unified prediction dataset, structured as triplets ($\mathbf{x}_{t-1}$,$\mathbf{x}_t$, y_{t+1}), where $\mathbf{x}_{t-1}$ and $\mathbf{x}_t$ represent feature vectors from 2 consecutive time points, and y_{t+1} denotes the LTA-identified future multimorbidity pattern label. This construction preserves the natural temporal evolution of disease states without relying on long-sequence assumptions, while effectively augmenting the training data. It enables the model to learn multistage health state transitions within the same population, thereby providing a robust data foundation for subsequent individual-level prospective prediction.

Overview of the Model Architecture

This study proposes an innovative deep learning model, named the CLA-Net. CLA-Net integrates the sequential state encoding capability of GRU with the global feature interaction advantages of an improved transformer architecture, enabling fine-grained cross-time feature interactions through a bitemporal directed cross-attention mechanism. The model is composed of 4 core modules: an input embedding layer, a temporal GRU encoder, a transformer encoding layer based on the bitemporal directed cross-attention mechanism, and a classifier layer. An overview of the model architecture is shown in Figure 2.

XSL•FO
RenderX

Figure 2. The architecture of the Cross-Lag Attention Network.

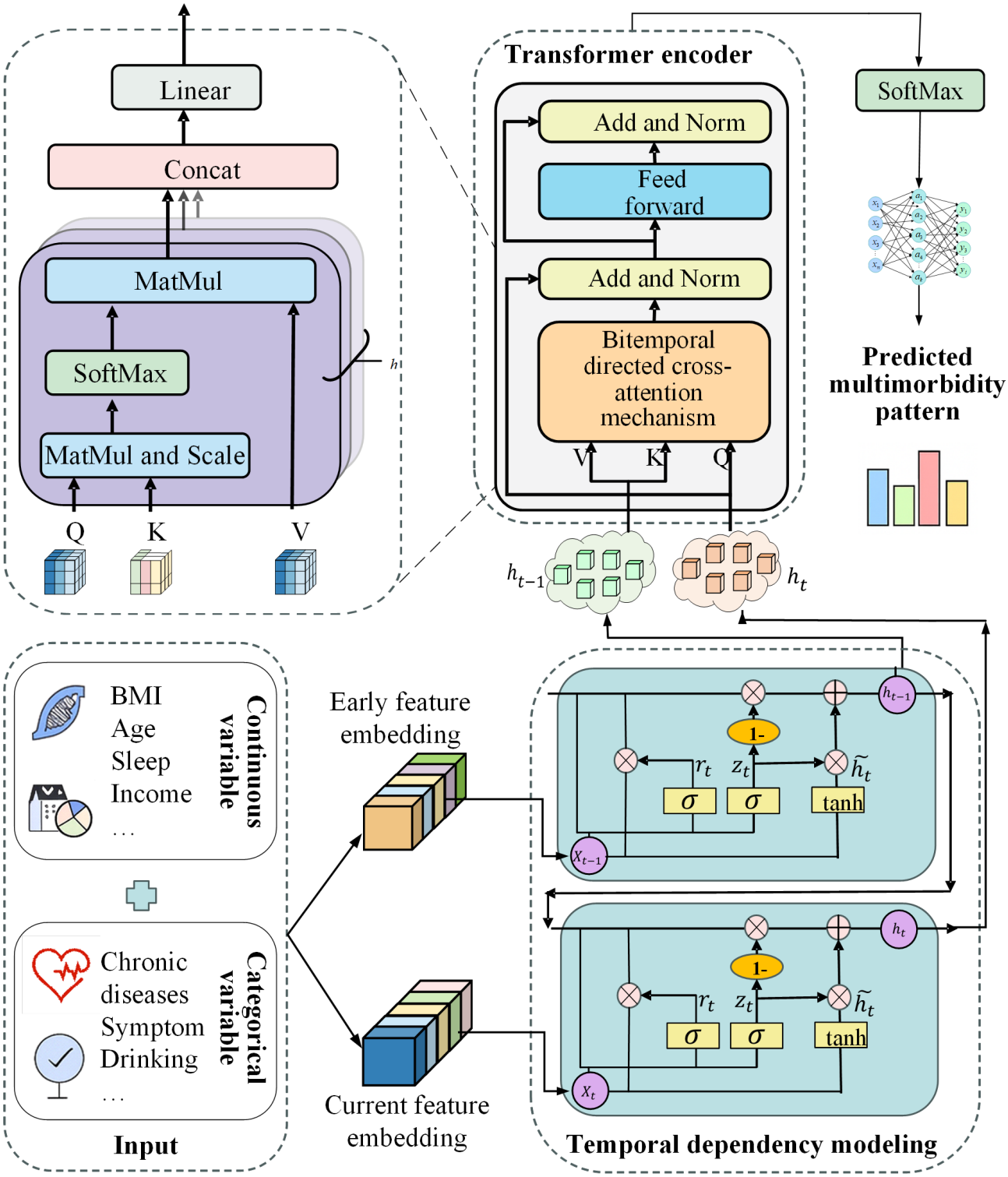

Components of CLA-Net

Feature Embedding Layer

The input features include continuous variables (eg, biomarkers and cognitive scores) and binary indicator variables (eg, disease diagnoses and medication use). Socioeconomic variables, including total household income and per capita household consumption, were inspected for extreme values prior to normalization. Given the heavy-tailed distributions of these variables, a percentile-based outlier handling strategy was applied to mitigate the undue influence of extreme observations while preserving the original scale of the data. Min-max normalization was then used to rescale these variables to a common range, ensuring numerical stability and consistency with the scaling of other continuous inputs used in the model. Binary features were kept unchanged. Subsequently, heterogeneous features are mapped into a unified representation space through learnable linear transformations:

(2)Xt−1Wext−1+be∈ Rd

(3)Xt=WeXt+be∈ Rd

XSL•FO
RenderX

where xt∈ RD denotes the raw input features, Xt∈ Rddenotes the embedded representation, We∈ Rd×Dand be∈ Rdare shared parameters, *D* denotes the input dimension, and *d* represents the hidden space dimension.

Temporal GRU Encoder

After feature embedding, the representations of features from the earlier time point ($\mathbf{X}_{t-1}$) and the current time point ($\mathbf{X}_t$) are concatenated into a 2-step sequence, which is then fed into a GRU for temporal modeling. Through the update mechanism of its hidden states, the GRU efficiently captures the sequential evolution of the disease process, ensuring that the nonlinear dynamics of health state transitions are explicitly modeled. This design enables the network to capture the critical short-term progression from *t*–1 to *t* and to explicitly model the nonlinear dynamics underlying near-term health state transitions.

(4)ht−1=GRU(Xt−1,hinit)

(5)ht=GRU(Xt,ht−1)

where $\mathbf{h}_{init}$ denotes the initial hidden state, and $\mathbf{h}_{t-1}$ and $\mathbf{h}_t$ represent the hidden state outputs at the 2 time steps. The internal computational mechanism of the GRU is defined as follows:

(6)rt=σ(WrXt+Urht−1+br)

(7)zt=σ(WzXt+Uzht−1+bz)

(8)h~t=tanh (WhXt+Uh(rt⊙ht−1)+bh)

(9)ht=(1−zt)⊙ht−1+zt⊙h~t

Here, $\mathbf{X}_t$ denotes the input at time step *t*. $\mathbf{r}_t$ is the reset gate, which controls how much information from the previous time step is retained. $\mathbf{z}_t$ is the update gate, which determines the proportion of information to be updated at the current time step. ht~ represents the candidate's hidden state. σis the sigmoid activation function, and ⊙ denotes elementwise multiplication. $\mathbf{W}_*$ and $\mathbf{U}_*$ are learnable weight matrices, and $\mathbf{b}_*$ is the bias vector.

Transformer Encoding Layer

Bitemporal Directed Cross-Attention Mechanism

Although GRUs are effective at encoding immediate longitudinal context via gated state updates, they have limited capacity to explicitly characterize fine-grained interactions among heterogeneous features, especially when the predictive signal arises from short-term, nonlinear state transitions rather than long-range history. In our setting, an individual's future multimorbidity pattern is shaped not only by the recent state representation but also by complex cross-feature influences that operate across adjacent time points. To address this, we adopt an asymmetric attention paradigm, in which features from the current time point are used as the query vector **Q**, while features from the earlier time point serve as the keys (**K**) and values (**V**) in the attention computation, enabling the model to attend to historical representations when updating the current state. This design reflects the directional interactions between features across time. For each attention head $j \in \{1,...,H\}$, the GRU outputs are first projected into the **Q**, **K**, and **V** spaces:

(10){Qj=htWQ(j)Kj=ht−1WK(j)Vj=ht−1WV(j)

where Q_j, K_j, and V_j denote the query, key, and value representations of the *j*th attention head, which are vector-valued representations derived from the input hidden states. WQ(j), WK(j), WV(j)∈ Rd×dh denotes the projection matrix of the *j*th head, *d* is the input dimension, and $d_h=d/H$ is the dimension of each attention head. The attention scores are computed using scaled dot-product attention:

(11)Attention scoresj=QjKjTdh

The scaling factor 1/dh is critical for maintaining gradient stability. Without scaling, the dot-product values increase with feature dimensionality, which may push the SoftMax function into regions with extremely small gradients. The computation for each attention head is defined as

(12)headj=Attention(Qj,Kj,Vj)=SoftMax (QjKjTdh)Vj

After concatenating the outputs of all attention heads, a linear transformation is applied to obtain the multi-head cross-attention output:

(13)MultiHeadCrossAttn(ht−1,ht)=Concat(head1,…,headH)Wo

where $\mathbf{W}_O$ denotes the output projection matrix. Through the multihead mechanism, the model can learn distinct attention patterns in different representation subspaces, allowing it to attend to diverse types of feature relationships simultaneously and thereby enhancing its expressive capacity.

Stacked Transformer Encoder Architecture

To capture the hierarchical patterns of disease progression, we use a stack of *L* transformer encoder layers. Each layer builds upon the representations from the previous one, thereby progressively modeling more complex temporal dependencies. Each layer, $l \in \{1,..,L\}$ consists of 2 sublayers with residual connections. Specifically, Equation 14 corresponds to the bitemporal directed cross-attention mechanism sublayer, while Equation 15 represents the positionwise feed-forward network (FFN) sublayer:

(14)z^(l)=LayerNorm(z(l−1)+Dropout(MultiHeadCrossAttn(ht−1,z(l−1))))

(15)z(l)=LayerNorm (z^(l)+Dropout(FFN(z^(l))))

Here, the positionwise FFN uses the ReLU activation function and incorporates dropout to prevent overfitting, defined as

(16)FFN(x)=ReLU(xW1+b1)W2+b2

where $\mathbf{W}_1$ is the weight matrix of the first feed-forward layer, which expands the feature dimension by a factor of 4 to enhance nonlinear representational capacity. $\mathbf{W}_2$ is the weight matrix of the second feed-forward layer, which projects the expanded dimension back to the original size *d*. $\mathbf{b}_1$ and $\mathbf{b}_2$ denote the bias vectors for the first and second layers, respectively. After passing through *L* stacked layers, we obtain the final fused representation $\mathbf{z}^{(L)}$, which simultaneously encodes early and later temporal information of patients and is further enriched through direct cross-time feature interactions.

Classifier Layer

The fused features $\mathbf{z}^{(L)}$ output by the transformer encoder are fed into a 2-layer fully connected neural network as the classifier. This classifier consists of a linear layer, a ReLU

XSL•FO
RenderX

activation function, a dropout layer, and a final linear output layer, which maps the fused features into probability distributions over multimorbidity patterns.

First Layer: Linear Mapping and Nonlinear Activation

The first layer of the classifier consists of a linear mapping followed by a nonlinear activation function. This step is crucial for transforming the fused features into a more complex representation. The output of this layer is computed as follows:

(17)o=ReLU (z(L)W1(c)+b1(c))

where W1(c)∈ Rd×d and b1(c)∈ Rd are the weight matrix and bias vector of the first layer, respectively, and ReLU denotes the activation function. A dropout regularization is applied after this layer to reduce the risk of overfitting.

Second Layer: Output Mapping

The second layer of the classifier maps the transformed features to output logits, representing the class scores. This layer computes the logits as follows:

(18)ylogits=o W2(c)+b2(c)

where W2(c)∈ Rd×C and b2(c)∈ RC represent the weight matrix and bias vector of the second layer, respectively, and *C* denotes the number of output classes. The final prediction $\mathbf{y}_{\text{logits}}$ is obtained by applying the SoftMax function to transform the outputs into probabilities:

(19)y^=SoftMax(ylogits)=exp (ylogits, c)∑c′=1Cexp (ylogits, c′)

Loss Function

We trained the model using the standard cross-entropy loss function for multiclass, single-label classification. Based on the predicted probability distribution y^ output by the classifier, the cross-entropy loss is defined as

(20)L=−1N∑i=1N∑c=1Cyi(c)log (y^i(c))

where *C* denotes the number of classes, yi(c)is the one-hot encoded true label of the *i*th sample for class *c*, and yi(c)represents the predicted probability that the *i*th sample belongs to class *c*. The objective is to minimize the average loss across all training samples. Cross-entropy is particularly suitable for our multiclass single-label task because it encourages the network to assign high probability to the correct class while penalizing confident but incorrect predictions. Since the dataset has a relatively balanced class distribution, no class weighting was applied in the loss function. The use of SoftMax outputs with cross-entropy is equivalent to maximizing the likelihood of the correct class and is a standard choice for neural network classifiers.

Algorithm 1 in Textbox 1 presents the pseudocode of the CLA-Net model. The algorithm details how each component is sequentially executed on each batch of data.

XSL•FO
RenderX

Textbox 1. Algorithm 1: CLA-Net (Cross-Lag Attention Network) model.

Input:

xt: Features at time *t* (continuous features xtcont , discrete features xtdisc)

x_{t-1}: Features at time t–1 (continuous features xt−1cont , discrete features xt−1disc)

y: Label (5-class classification)

Output: Predicted probability distribution **p**, cross-entropy loss *L*

Process:

1: // *1. Feature preprocessing and embedding*

2: et−1←Embedding (xt−1disc)*// Embedding of discrete features*

3: et←Embedding (xtdisc)

4: ct−1←LayerNorm (xt−1cont)*// Normalization of continuous features*

5: ct←LayerNorm (xtcont)

6:xt−1←Linear (Concat(et−1, ct−1))*// Concatenation of features at time t−1*

7: xt←Linear (Concat(et, ct))*// Concatenation of features at time t*

8: Xt−1←We xt−1+be

9: Xt←We xt+be

10: *// 2. GRU-based temporal encoding*

11:ht−1←GRU (Xt−1, hinit)*// Hidden state at time t−1*

12: ht←GRU (Xt, ht−1)*// Hidden state at time t*

13: *// 3. Transformer encoder based on the bitemporal directed cross-attention mechanism*

14: for do

15: for head i=1,…,Ha do

16: Q(i)←WQ(i)ht, K(i)←WK(i)ht−1, V(i)←WV(head)ht−1

17: A(i)←Softmax (Q(i)(K(i)) dk)*// Attention weights*

18:head(i)←A(i)V(i)*// Context vector*

19: end for

20: Z←Concat (head(1),…,head(H))Wo

21: U←LayerNorm (ht+Dropout(Z))*// Residual connection and normalization*

22: ht←LayerNorm (U+Dropout (FFN(U)))

23: end for

24: Let z←ht*// final fused representation*

25: *// 4. Classification and prediction*

26: o←Flatten(z)

27: p←Softmax (Wfc o+bfc)*// Output probability distribution*

28: L←−∑i=15yilog pi*// Cross-entropy loss*

29: return **p**, *L*

Training Configuration and Implementation Details

All experiments were conducted using PyTorch v1.7.0 (Facebook AI Research, Meta Platforms) and Python 3.8 (Python Software Foundation) on Ubuntu 18.04 (Canonical Ltd), with an NVIDIA RTX 4090 GPU (24 GB memory) and 32 GB RAM (CUDA 11.0). The proposed model and all baselines were trained under identical configurations and hyperparameters (Table 1). The main settings were 60 training epochs, mini-batch size of 64, embedding and GRU hidden dimensions set to 128, Adam optimizer with a learning rate of 0.0001 (determined via grid search), cross-entropy loss, and a dropout rate of 0.3 applied to both transformer layers and the classifier. Model weights were initialized using PyTorch defaults. During data preprocessing, feature normalization was fitted only on the training set and then applied to the validation and test sets. The dataset was partitioned into 80% training and 20% testing sets using a subject-wise splitting strategy based on unique individual identifiers. This approach ensures that all

XSL•FO
RenderX

longitudinal observations from the same participant were assigned exclusively to a single subset, thereby preventing potential data leakage. From the training set, 20% (n/N) of the individuals were further held out as a validation set. During training, the macro-F_1-score on the validation set was used as the criterion for early stopping and model selection. Only the best-performing model on the validation set was retained, and a final evaluation was conducted on the independent test set.

Table . Training hyperparameters.

Parameters or hyperparameters	Value
Epoch	60
Learning rate	0.0001
Dropout	0.3
Random seed	42
Batch size	64
Hidden dimension	128

Evaluation Metrics

To evaluate the performance of the model in the multiclass classification task, we used commonly used metrics, including accuracy, precision, recall, and F_1-score, and reported their macroaveraged values. Macroaveraging assigns equal weight to each class, thereby avoiding the bias of microaveraging, which tends to favor majority classes in imbalanced datasets. This provides a more comprehensive and balanced assessment of the model's ability to identify all 5 multimorbidity patterns. The formulas for these evaluation metrics are as follows:

$$\text{Accuracy}=\sum_{c=1}^{C}TP_c\Big/\sum_{c=1}^{C}(TP_c+FP_c+FN_c+TN_c) \quad (21)$$

$$\text{Precision}_c=TP_c/(TP_c+FP_c) \quad (22)$$

$$\text{Recall}_c=TP_c/(TP_c+FN_c) \quad (23)$$

$$F1=2\times\text{Precision}_c\times\text{Recall}_c/(\text{Precision}_c+\text{Recall}_c) \quad (24)$$

where TP_c, FP_c, FN_c, and TN_c denote the true positives, false positives, false negatives, and true negatives for class c, respectively. Accuracy represents the proportion of correctly predicted samples to the total number of samples. Precision measures the proportion of samples predicted as a given class that actually belong to that class. Recall indicates the proportion of samples that are correctly identified among those that truly belong to a given class. The F_1-score, defined as the harmonic mean of precision and recall, provides a balanced measure of the model's classification performance for a given class. Macroaveraging is obtained by taking the arithmetic mean of the metric values across all classes. The formulas are defined as follows:

$$\text{Macro-Precision}=\frac{1}{C}\sum_{c=1}^{C}\text{Precision}_c,\ \text{Macro-Recall}=\frac{1}{C}\sum_{c=1}^{C}\text{Recall}_c,\ \text{Macro-F1}=\frac{1}{C}\sum_{c=1}^{C}F1_c \quad (25)$$

In addition, we further introduced the receiver operating characteristic (ROC) curve and the area under the curve (AUC) as complementary evaluation metrics. While accuracy focuses on the correctness of class predictions, AUC assesses the ranking quality of predicted probabilities. Particularly in multiclass problems, a higher macroaveraged AUC together with higher accuracy provides stronger evidence that the model can achieve good discrimination across all classes, rather than merely benefiting from class size distributions. The ROC curve is plotted with the false positive rate (FPR) on the x-axis and the true positive rate (TPR) on the y-axis and is mathematically defined as:

$$\text{FPR}=FP/(FP+TN),\ \text{TPR}=TP/(TP+FN) \quad (26)$$

AUC measures the overall discriminative ability of a model, with values ranging from 0 to 1, where values closer to 1 indicate stronger separation between positive and negative classes. Commonly, AUC >0.9 is considered excellent, 0.8‐0.9 good, 0.7‐0.8 acceptable, and <0.7 poor. For multiclass prediction, we adopted a one-vs-rest strategy, treating each class as positive against all others to compute class-specific ROC curves and AUC values. To validate the effectiveness of the proposed model, we compared it with multiple baselines under identical test conditions and reported AUC as a key performance metric. The evaluation procedures followed recommended practices for multiclass classification to ensure reliable assessment of predictive performance.

In addition to AUC-ROC, we also reported AU-PRC (area under the precision-recall curve), which provides a complementary evaluation of model performance by emphasizing the trade-off between precision and recall. AU-PRC is particularly informative in settings with class imbalance, as it focuses on the model's ability to correctly identify positive instances without being overly influenced by true negatives. Similar to the ROC-based evaluation, AU-PRC was computed using a one-vs-rest strategy for multiclass prediction, and class-specific precision-recall (PR) curves were aggregated to assess overall performance.

Baseline Models

Logistic Regression

A linear classification model that estimates class probabilities through a logistic function, serving as a simple and interpretable baseline to assess the benefit of nonlinear feature interactions [34].

Support Vector Machine

A margin-based classifier that constructs an optimal separating hyperplane in the feature space, enabling the evaluation of nonlinear decision boundaries through kernel-based learning [34].

XSL•FO
RenderX

Random Forest

An ensemble learning method that aggregates multiple decision trees trained on bootstrapped samples, capturing nonlinear feature relationships and improving robustness against overfitting [35].

XGBoost

A gradient boosting framework that builds additive tree-based models in a stagewise manner, designed to optimize predictive performance by modeling complex nonlinear interactions among features [36].

Convolutional Neural Network

Extracts local temporal features via convolutional kernels without explicitly modeling temporal order, serving to test the importance of temporal structure [37].

Long Short-Term Memory

Captures long-term dependencies through gating mechanisms, used to compare different recurrent units for short-sequence modeling [38].

Transformer

Models relationships across time steps using self-attention, with concatenated features fed into a standard transformer encoder [39].

PatchTST

Reduces computational complexity through a "patching" strategy, improving efficiency for long-sequence prediction [40].

iTransformer

Applies attention along the feature dimension rather than the temporal dimension, better capturing inter-variable relationships in multivariate time series [41].

Mamba

Mamba uses a selective state space mechanism to model long-term dependencies with linear complexity [42].

MambaTS

An enhanced variant of Mamba that incorporates improved state space mechanisms to further boost long-sequence prediction performance [43].

Long Short-Term Memory+Transformer

A variant of CLA-Net that replaces the GRU encoder with a long short-term memory (LSTM), used to compare the effects of different recurrent units.

To ensure a fair comparison with the deep learning models, the input configuration for all traditional machine learning baselines (logistic regression, support vector machine, random forest, and XGBoost) was aligned with the dual-time-point setup of CLA-Net. Specifically, the feature vectors from the historical time point (Xt-1) and the current time point (Xt) were concatenated to form a single flattened input vector [Xt-1, Xt]. This ensures that all models use the exact same longitudinal information, preventing any performance bias due to information asymmetry.

Ethical Considerations

Ethical approval for the original data collection in the CHARLS project was granted by the Biomedical Ethics Review Committee of Peking University (approval number: IRB00001052-11015). All participants provided written informed consent at the time of enrollment. As this study involves a secondary analysis of publicly available, deidentified data, the requirement for additional informed consent was waived. To ensure privacy and confidentiality, all direct identifiers were removed from the dataset by the CHARLS team prior to public release. Furthermore, this paper and its supplementary materials do not contain any images or information that could identify individual participants.

Results

Dataset

This study adopted a longitudinal cohort design using publicly available data from the CHARLS. CHARLS is a nationally representative longitudinal survey covering 28 provinces, 150 counties and districts, and 450 communities, and provides extensive demographic, chronic disease, and other health-related information. Using 2011 as the baseline, we included respondents with at least 2 chronic conditions and complete demographic data who participated in all 5 waves, yielding 3644 individuals and 18,220 person-wave observations. The sample selection process is shown in Figure 3. Attrition during follow-up occurred due to both mortality and nonmortality loss to follow-up. Specifically, the without-follow-up observations (30,483 person-wave observations) corresponded to 1617 person-wave observations attributable to death and 28,866 person-wave observations attributable to other reasons for nonparticipation.

Data preprocessing included logical error correction and outlier removal. Regarding missing value treatment, to strictly prevent data leakage, we adhered to a rigorous "split-then-impute" strategy. The dataset was first partitioned into training and independent test sets. Subsequently, missing values were handled using the MiceForest method for multiple imputation [44]. Crucially, the imputation model was fitted exclusively on the training set. The MiceForest method is based on random forests and predictive mean matching, allowing it to capture nonlinear relationships and improve imputation accuracy [45,46]. To ensure data quality, variables with more than 50% missingness were excluded, and only those with relatively low missingness were retained [45].

The final dataset variables are summarized in Table S1 in Multimedia Appendix 1 and include (1) individual identifiers and survey time (ID and year); (2) 14 chronic disease variables used for LTA-based identification and transition modeling of multimorbidity patterns, which also served as target variables in the prediction task; and (3) symptom variables along with demographic, behavioral, psychological, socioeconomic, and macropolicy features, which were used as input features for the prediction model. A final cohort of 3644 individuals with multimorbidity who maintained participation across all 5 survey waves was included in the analysis. Table 2 presents the baseline sociodemographic characteristics of the participants (recorded

XSL•FO
RenderX

in 2011). The cohort was predominantly female (n=2132, 58.51%) and comprised mainly middle-aged and older adults, with 93.33% (n=3401) of participants aged between 45 and 74 years. In terms of socioeconomic status, the sample was characterized by relatively low educational attainment, as 90.12% (n=3284) of participants had an education level below junior high school. The majority were married (n=3283, 90.09%) and resided in rural areas (n=2306, 63.28%), while less than half (n=1550, 42.54%) were covered by pension insurance.

Figure 3. Participant selection flowchart. CHARLS: China Health and Retirement Longitudinal Study.

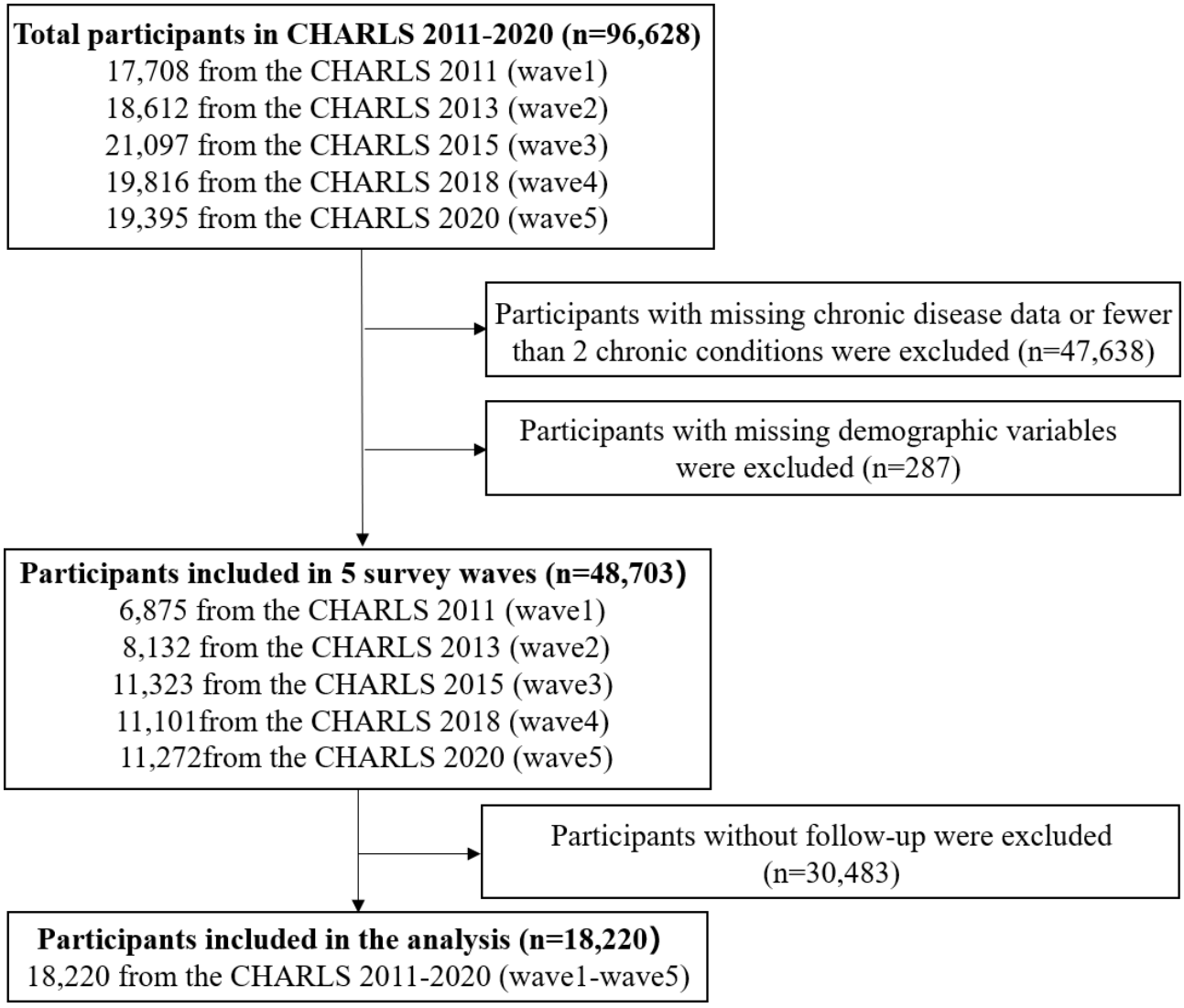

XSL•FO
RenderX

Table . Demographic characteristics.

Variables	Values
Gender, n (%)	
Men	1512 (41.49)
Women	2132 (58.51)
Age (years), n (%)	
<18	1 (0.03)
18 - 44	65 (1.78)
45 - 59	1881 (51.62)
60 - 74	1520 (41.71)
≥75	177 (4.86）
Education level, n (%)	
Below junior high school	3284 (90.12)
High school or vocational training	313 (8.59)
Higher education	47 (1.29)
Marital status, n (%)	
Unmarried	361 (9.91)
Married	3283 (90.09)
Residence, n (%)	
Rural	2306 (63.28)
Urban	1338 (36.72)
Pension coverage, n (%)	
No	2094 (57.46)
Yes	1550 (42.54)

LTA-Based Identification of Multimorbidity Patterns

To clarify the consistency and heterogeneity of multimorbidity pattern structures across different time points, we first conducted LCA at each wave to provide the basis for subsequent LTA. The model fit results (Table 3) indicated that the 5-class solution performed best across multiple criteria: at T1, T2, T3, and T5, it achieved the lowest AIC and SaBIC values with good classification quality (entropy=0.838 - 0.926); at T4, although the 4-class and 5-class solutions showed comparable entropy, the 5-class model outperformed in AIC, BIC, and SaBIC. The BLRT consistently supported the 5-class solution across all time points (all P<.001). Moreover, the class distributions of the 5-class solution were relatively stable and clinically plausible across waves. Taken together, the 5-class model was selected as the optimal solution for the LTA.

After establishing the 5-class structure at each time point, we tested measurement invariance to ensure the validity of cross-time comparisons. As shown in Table 4, constraining item-response probabilities to be equal across time did not significantly worsen model fit compared to the freely estimated model ($\Delta\chi^2_{75}$=88.7; P=.14). This nonsignificant likelihood ratio test confirmed measurement invariance, indicating that the latent classes maintained consistent meanings across all 5 waves.

XSL•FO
RenderX

Table . Latent class analysis results for multimorbidity patterns at 5 time points based on the CHARLS (China Health and Retirement Longitudinal Study) database.

Time and class		Percent (%)	AIC[a]	BIC[b]	SaBIC[c]	Entropy	BLRT[d]
T1							
	2	40.5/59.5	4196.03	4375.85	4283.70	0.720	—[e]
	3	47.8/16.5/35.8	3598.93	3871.77	3731.96	0.802	<0.001
	4	21.4/15.6/34.8/28.2	3378.95	3744.80	3557.32	0.839	<0.001
	5	11.6/15.3/39.8/9.4/23.9	3230.96	3782.83	3500.03	0.926	<0.001
	6	17.1/15.0/32.5/19.4/14.4/1.6	3293.62	3752.49	3517.35	0.856	<0.001
T2							
	2	37.7/62.3	4083.43	4263.25	4171.11	0.711	—
	3	46.0/15.3/38.6	3498.78	3771.62	3631.81	0.803	<0.001
	4	10.7/15.1/40.3/33.8	3285.65	3651.50	3464.03	0.860	<0.001
	5	11.1/13.6/39.5/2.1/33.7	3197.59	3656.45	3421.32	0.889	<0.001
	6	14.7/12.8/34.9/7.4/27.6/2.6	3167.49	3719.36	3436.56	0.878	<0.001
T3							
	2	36.6/63.4	4199.14	4378.97	4286.82	0.701	—
	3	39.5/12.7/47.8	3603.58	3876.42	3736.61	0.800	<0.001
	4	20.5/12.0/35.6/32.0	3446.95	3812.80	3625.33	0.802	<0.001
	5	5.0/9.6/33.0/24.1/28.3	3238.82	3697.68	3462.54	0.838	<0.001
	6	2.4/8.1/0.2/30.1/16.8/13.6/4.6	3218.26	3770.13	3487.33	0.884	<0.001
T4							
	2	41.3/58.7	5174.42	5354.24	5262.09	0.687	—
	3	18.4/42.2/39.4	4448.84	4721.68	4581.87	0.798	<0.001
	4	11.2/44.0/35.8/9.0	4034.00	4399.85	4212.37	0.849	<0.001
	5	8.7/9.8/29.9/26.8/24.7	3869.07	4327.93	4092.79	0.842	<0.001
	6	8.0/9.9/30.8/19.4/27.6/4.2	3832.77	4384.64	4101.84	0.834	<0.001
T5							
	2	49.0/51.0	5576.80	5756.62	5664.47	0.694	—
	3	22.7/35.5/41.8	4771.20	5044.04	4904.23	0.812	<0.001
	4	11.8/34.9/43.4/9.9	4272.68	4638.53	4451.05	0.848	<0.001
	5	9.8/12.5/32.2/37.2/8.2	4087.68	4639.55	4356.75	0.849	<0.001
	6	13.2/9.0/30.6/3.4/8.8/36	4135.51	4594.37	4359.23	0.839	<0.001

[a]AIC: Akaike Information Criterion.

[b]BIC: Bayesian Information Criterion.

[c]SaBIC: sample-size adjusted Bayesian Information Criterion.

[d]BLRT: Bootstrap Likelihood Ratio Test.

[e]Not applicable.

XSL•FO
RenderX

Table . Likelihood ratio tests for measurement invariance of the latent transition analysis model.

Model	LogLik[a]	−2LL[b]	Chi-square[c] (*df*)[d]	*P* value
M_free[e]	−97100	194,200	—[f]	—
M_invariant[g]	−97144.4	194,288.7	88.7 (75)	.14

[a] LogLik: log-likelihood.

[b]−2LL: −2 log-likelihood.

[c]$\Delta\chi^2$: chi-square difference test.

[d]Δdf: difference in degrees of freedom.

[e]M_free: model with all parameters freely estimated across time.

[f]Not applicable.

[g]M_invariant: model with item-response probabilities constrained to be equal across time points.

The LTA clustering results for the 5-class model are shown in Figure 4. Class 1 (19.8%) had the highest overall disease burden, with nearly universal hypertension (82.7%), accompanied by high prevalence of heart disease (78.1%), dyslipidemia (69.3%), gastritis (68.9%), diabetes (43.9%), arthritis (90.4%), lung disease (44.3%), and stroke (24.1%). This class represented severe multisystem involvement [47] and was labeled the "Severe Cardiometabolic-Multisystem Pattern."

Class 2 (22.3%) was characterized by extremely high probabilities of hypertension (99.7%) and arthritis (99.6%). Gastritis showed a moderate prevalence (37.5%), while dyslipidemia (27.3%) and heart disease (26.6%) were present in about one-quarter of individuals. Other conditions were rare (<13%), indicating a pattern primarily dominated by hypertension and joint disease. This class was labeled the "Hypertension-Arthritis Pattern."

Class 3 (15.6%) was dominated by lung disease (90.8%), with co-occurrence of arthritis (58.7%), asthma (50.4%), gastritis (43.4%), and hypertension (35.3%). This class was labeled the "Respiratory-Musculoskeletal Pattern."

Class 4 (24.1%) exhibited typical metabolic syndrome features, including high prevalence of hypertension (88.3%), dyslipidemia (54.5%), and heart disease (44.4%), with moderate diabetes (36.3%) and gastritis (33.4%). Other diseases were less common (<14%), indicating a primarily cardiometabolic profile without extensive multisystem involvement. This class was labeled the "Metabolic Syndrome Pattern."

Class 5 (18.2%) had the lowest overall disease burden, dominated by arthritis (85.2%) and gastritis (76.4%), with all other diseases below 25%. This class was labeled the "Gastritis-Arthritis Pattern." The naming of latent multimorbidity patterns was guided by the dominant disease combinations and their clinical interpretation, following conventions widely used in epidemiologic and multimorbidity-cluster studies [19,48-52].

XSL•FO
RenderX

Figure 4. Disease probabilities in the 5 multimorbidity patterns.

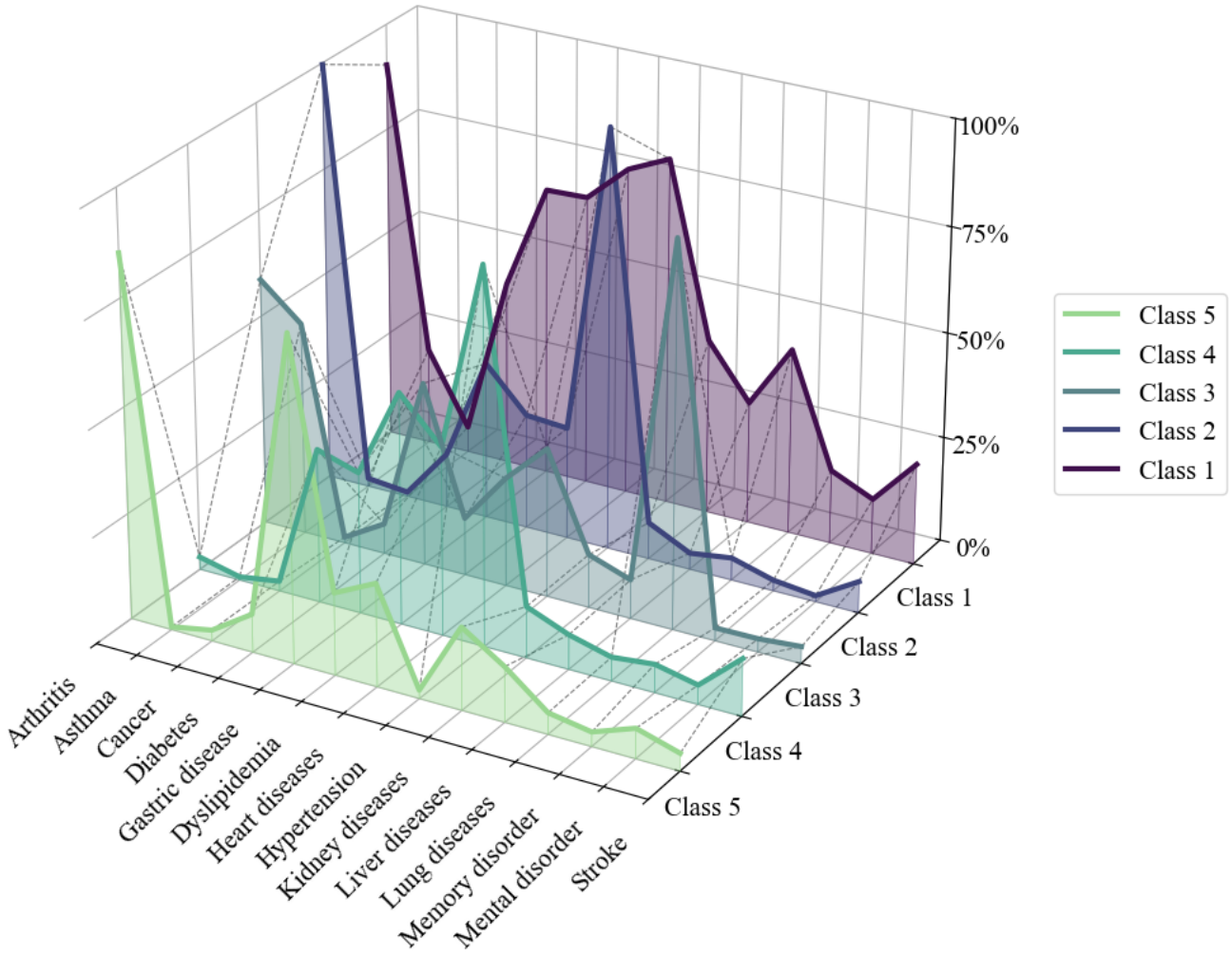

Performance Evaluation Results of CLA-Net

In the experiments, the proposed method was trained on the training set and evaluated on an independent test set. To ensure robustness, the entire process was repeated 50 times, and the mean and SD of all evaluation metrics across these runs were reported as the final performance results. The comparative performance of all models on the multimorbidity pattern prediction task is summarized in Table 5, the ROC curves are presented in Figures 5 and 6, and the detailed results of the ablation study are shown in Table 6.

As shown in Table 5, CLA-Net consistently outperformed all baseline models in multimorbidity pattern prediction. Traditional machine learning approaches perform relatively poorly, while deep learning models designed for temporal modeling yield substantial improvements. Among the baselines, Mamba performed best overall, while convolutional neural network (CNN) performed the worst, underscoring the importance of temporal feature modeling in longitudinal health data. The hybrid LSTM+transformer model achieved relatively high accuracy, highlighting the benefits of combining sequential modeling with attention mechanisms. Nevertheless, CLA-Net surpassed all baselines across accuracy, precision, recall, and F_1-score, with low SDs confirming its stability and robustness.

We further conducted formal statistical significance testing to assess whether the observed performance gains of CLA-Net over baseline models were statistically robust. Specifically, 2-sided Wilcoxon signed-rank tests were applied to paired performance scores obtained from 50 repeated experimental runs for each evaluation metric. To account for multiple comparisons across baseline models and metrics, *P* values were adjusted using the Holm step-down procedure. The Wilcoxon signed-rank test results are given in Table 7. The results indicate that CLA-Net achieves statistically significant performance improvements over all baseline models. The consistent significance across repeated experiments confirms that the observed gains are robust rather than driven by random fluctuations.

XSL•FO
RenderX

Table . The results of the performance comparison.[a]

Types of models and models	Precision	Recall	F_1-score	Accuracy
Machine learning models, mean (SD)				
Logistic regression	0.7385 (0.0075)	0.7350 (0.0080)	0.7320 (0.0082)	0.7335 (0.0079)
SVM[b]	0.7540 (0.0069)	0.7510 (0.0074)	0.7480 (0.0076)	0.7495 (0.0072)
Random forest	0.7650 (0.0062)	0.7620 (0.0068)	0.7590 (0.0070)	0.7605 (0.0066)
XGBoost	0.7856 (0.0059)	0.7820 (0.0062)	0.7835 (0.0060)	0.7892 (0.0052)
Deep learning models, mean (SD)				
CNN[c]	0.7835 (0.0090)	0.7779 (0.0084)	0.7807 (0.0086)	0.7860 (0.0082)
LSTM[d]	0.8020 (0.0063)	0.8040 (0.0070)	0.8030 (0.0066)	0.8041 (0.0069)
Transformer	0.8138 (0.0079)	0.8074 (0.0076)	0.8106 (0.0072)	0.8120 (0.0069)
iTransformer	0.8167 (0.0074)	0.8189 (0.0078)	0.8178 (0.0071)	0.8184 (0.0070)
PatchTST	0.8092 (0.0082)	0.8057 (0.0088)	0.8074 (0.0081)	0.8088 (0.0083)
MambaTS	0.8191 (0.0061)	0.8214 (0.0067)	0.8202 (0.0062)	0.8210 (0.0064)
Mamba	0.8226 (0.0062)	0.8258 (0.0068)	0.8242 (0.0061)	0.8242 (0.0064)
LSTM + Transformer	0.8234 (0.0060)	0.8256 (0.0065)	0.8245 (0.0062)	0.8247 (0.0058)
CLA-Net (our model)	*0.8326 (0.0053)*	*0.8312 (0.0056)*	*0.8319 (0.0051)*	*0.8352 (0.0048)*

[a]The italicized values represent the best performance of each data handling strategy on the evaluation metrics. These italicized values are used to highlight the most outstanding results among the different strategies.

[b]SVM: support vector machine.

[c]CNN: convolutional neural network.

[d]LSTM: long short-term memory.

Figure 5. The area under the receiver operating characteristic curve of the Cross-Lag Attention Network and baseline models. AUC: area under the curve; CLA-Net: Cross-Lag Attention Network; CNN: convolutional neural network; LSTM: long short-term memory; SVM: support vector machine.

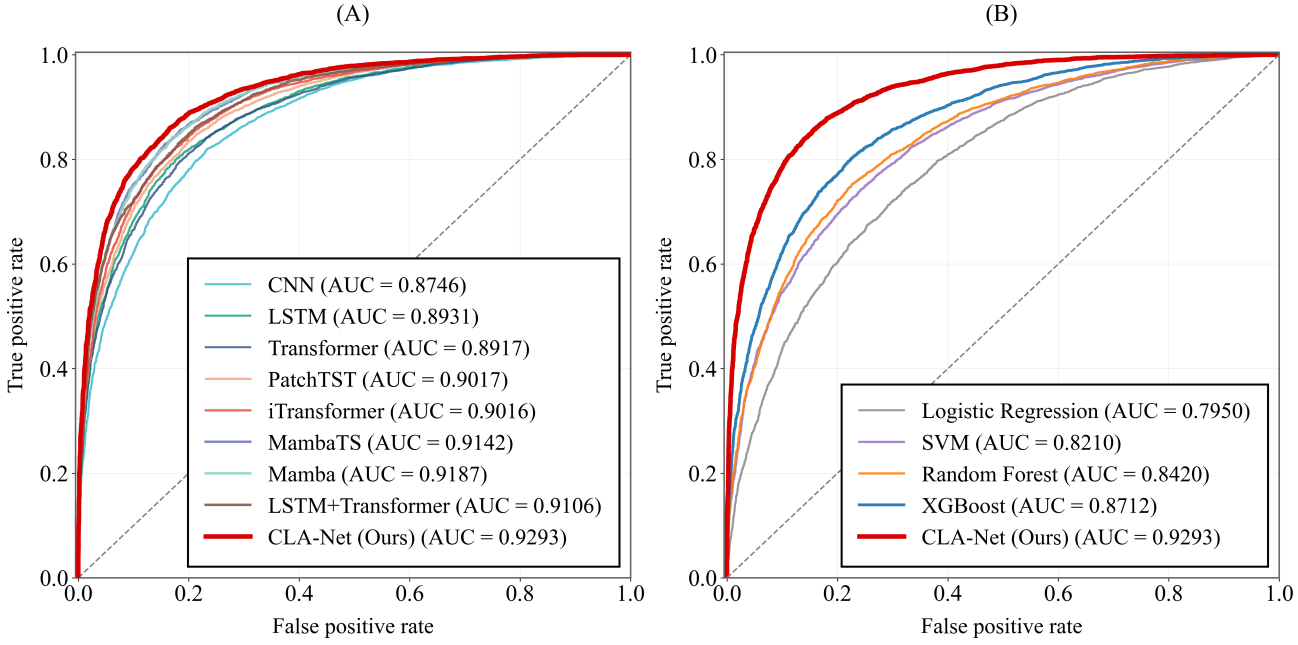

XSL•FO
RenderX

Figure 6. The area under the precision-recall curve of the Cross-Lag Attention Network and baseline models. AU -PRC: area under the precision-recall curve; CLA-Net: Cross-Lag Attention Network; CNN: convolutional neural network; LSTM: long short-term memory; SVM: support vector machine.

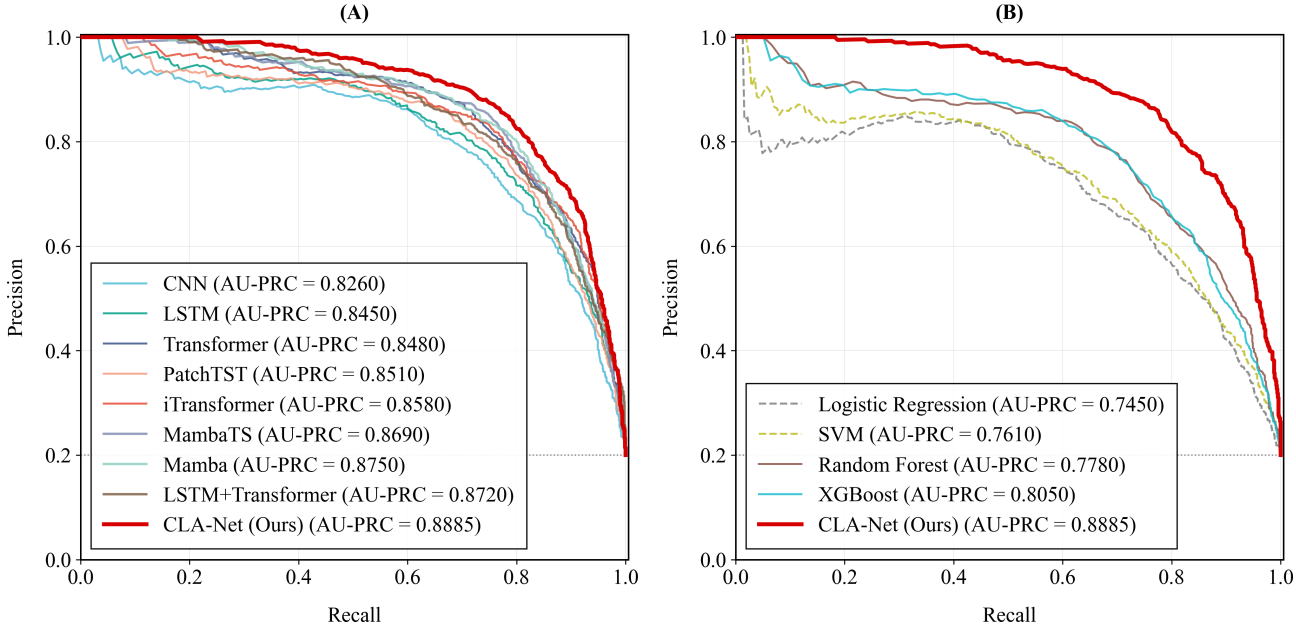

Table . Results of the ablation study.[a]

Type and ablation setup		Precision, mean (SD)	Recall, mean (SD)	F_1-score, mean (SD)	Accuracy, mean (SD)
Full model					
	CLA-Net[b] (our model)	*0.8326 (0.0053)*	*0.8312 (0.0056)*	*0.8319 (0.0051)*	*0.8352 (0.0048)*
Module ablation					
	Transformer branch	0.8153 (0.0068)	0.8116 (0.0071)	0.8134 (0.0069)	0.8166 (0.0065)
	GRU[c] branch	0.8079 (0.0074)	0.8067 (0.0078)	0.8073 (0.0075)	0.8102 (0.0072)
	Replacing the bitemporal directed cross-attention mechanism with self-attention	0.8218 (0.0059)	0.8196 (0.0062)	0.8207 (0.0060)	0.8244 (0.0057)
Input configuration ablation					
	Single-time-point input	0.7982 (0.0083)	0.7964 (0.0087)	0.7973 (0.0085)	0.7985 (0.0082)
	Three-time-point input	*0.8338 (0.0055)*	0.8265 (0.0058)	0.8301 (0.0056)	0.8311 (0.0053)
	Four-time-point input	0.8251 (0.0057)	*0.8316 (0.0061)*	0.8283 (0.0059)	0.8287 (0.0056)
Architecture design					
	Reversing the order of transformer and GRU components	0.8230 (0.0061)	0.8208 (0.0064)	0.8219 (0.0062)	0.8235 (0.0059)

[a]The italicized values represent the best performance of each data handling strategy on the evaluation metrics.

[b]CLA-Net: Cross-Lag Attention Network.

[c]GRU: Gated Recurrent Unit.

XSL•FO
RenderX

Table . Statistical test results.[a]

Baseline	Precision *W*	Recall *W*	F_1-score *W*	Accuracy *W*
Logistic regression	0***	0***	0***	0***
SVM[b]	0***	0***	0***	0***
Random forest	0***	0***	0***	0***
XGBoost	0***	0***	0***	0***
CNN[c]	0***	0***	0***	0***
LSTM[d]	0***	0***	0***	0***
Transformer	1***	0***	0***	1***
iTransformer	13***	68***	20***	15***
PatchTST	0***	0***	0***	0***
MambaTS	27***	82***	39***	0***
Mamba	52***	258***	101***	11***
LSTM+transformer	80***	227***	126***	11***

[a]Two-sided Wilcoxon signed-rank tests were conducted on paired metric scores obtained from 50 repeated runs (n=50) to compare Cross-Lag Attention Network against each baseline model; Reported W corresponds to the Wilcoxon test statistic; To control for multiple comparisons across 12 baselines and 4 metrics, *P* values were adjusted using the Holm procedure; ***: $P<.001$.

[b]SVM: support vector machine.

[c]CNN: convolutional neural network.

[d]LSTM: long short-term memory.

Figure 5 presents the AUC-ROC curves comparing CLA-Net with a range of baseline models. As shown in Figure 5A, among deep learning approaches, CLA-Net achieves the highest AUC of 0.9293, demonstrating superior discriminative ability in multimorbidity pattern prediction. Models explicitly designed for temporal modeling, such as Mamba (AUC=0.9187), MambaTS (AUC=0.9142), PatchTST (AUC=0.9017), and iTransformer (AUC=0.9016), outperform conventional CNN-based architectures, highlighting the importance of capturing long-range temporal dependencies in longitudinal health data. The hybrid LSTM+transformer model attains an AUC of 0.9106, ranking among the strongest deep learning baselines, while CNN yields the lowest AUC (0.8746) within this group.

To further assess performance under class imbalance, Figure 6 reports the PR curves and corresponding AUC-PRC values. As shown in Figure 6, CLA-Net achieves the highest AUC-PRC among deep learning models (0.8885), indicating a superior PR trade-off across recall levels. Temporal models such as Mamba, iTransformer, and LSTM+transformer also perform competitively, whereas CNN shows relatively weaker performance. Figure 6 demonstrates that CLA-Net substantially outperforms traditional machine learning baselines, including logistic regression, support vector machine, random forest, and XGBoost. Overall, the PRC results complement the ROC analysis and further confirm the robustness of CLA-Net in identifying future multimorbidity patterns under imbalanced conditions.

As summarized in Table 6, the full CLA-Net consistently outperformed all ablation variants, underscoring the importance of integrating both GRU and the bitemporal directed cross-attention mechanism. Removing either component or replacing cross-attention with self-attention led to clear performance drops, confirming the effectiveness of the original design.

Regarding input configurations, single-time-point input resulted in the largest decline, while 3-time-point and 4-time-point settings provided only marginal gains but reduced overall accuracy, indicating that the 2-time-point design achieves the optimal balance, efficiently capturing the most relevant temporal signals without introducing the complexity or noise associated with longer historical windows. These results indicate that, under the current architecture, incorporating immediate temporal context is critical for prediction, whereas extending the input window beyond 2 time points yields diminishing or even negative returns. In addition, reversing the order of transformer and GRU also impaired performance, supporting the strategy of “temporal encoding before interaction.”

Figures 7 and 8 show the class-specific ROC and PR curves for the 5 multimorbidity patterns. All classes achieved consistently high ROC performance, with AUCs ranging from 0.9198 to 0.9426 and a macroaverage of 0.9293. The PRC analysis yielded AUC-PRC values between 0.8310 and 0.8620 (macroaverage=0.8429), indicating stable precision-recall trade-offs across classes. Overall, CLA-Net demonstrates robust and balanced predictive performance for all multimorbidity patterns.

To complement this threshold-free evaluation, Table 8 reports classwise precision, recall, and F_1-scores, indicating consistently good predictive performance across patterns, with F_1-scores ranging from 0.7906 to 0.8508. As further illustrated by the confusion matrix in Figure 9, classification errors are primarily

XSL•FO
RenderX

concentrated among clinically related multimorbidity patterns, suggesting that residual misclassifications arise from intrinsic overlap between multimorbidity profiles rather than systematic model failure.

Figure 7. Multiclass area under the receiver operating characteristic curve of the Cross-Lag Attention Network. AUC: area under the curve.

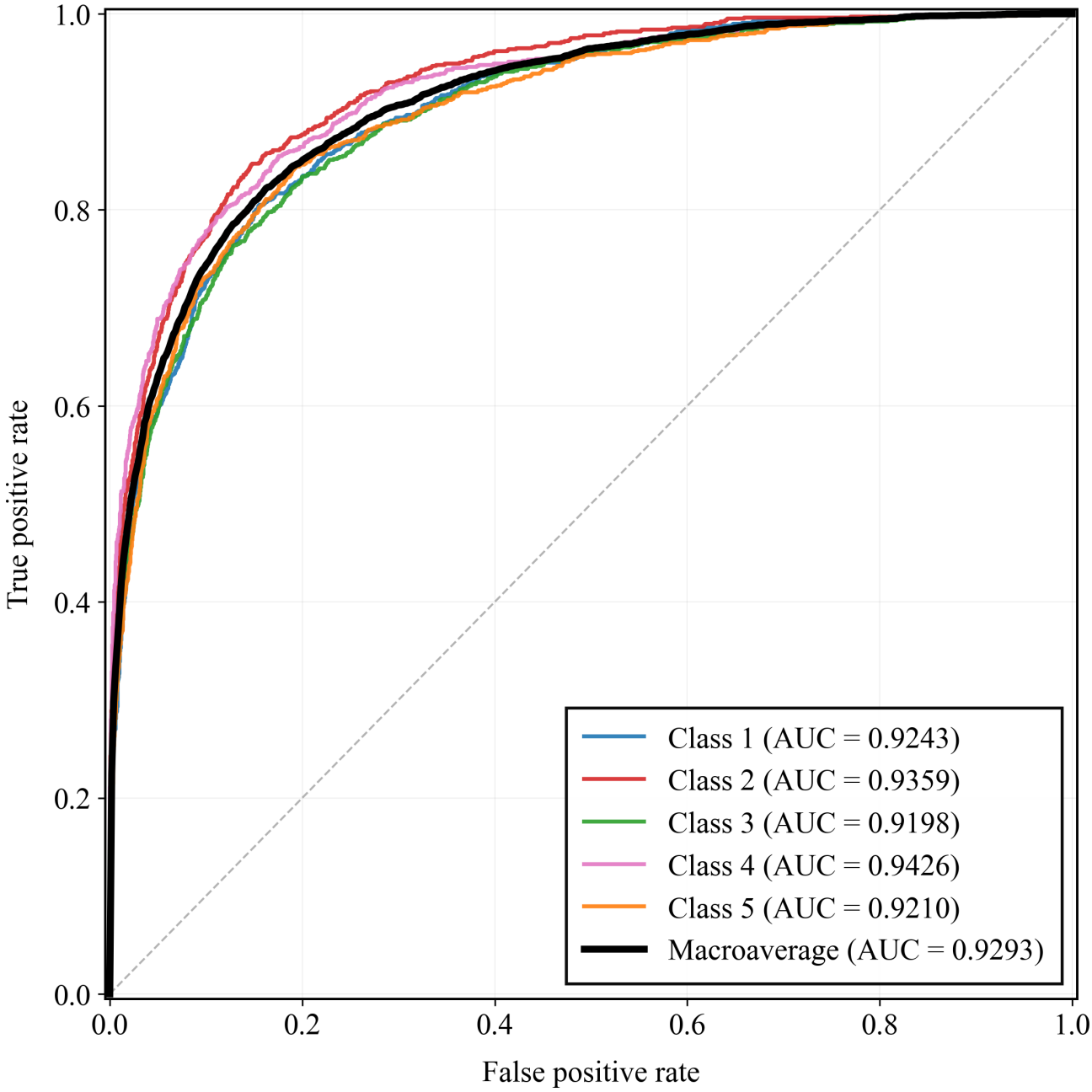

XSL•FO
RenderX

Figure 8. Multiclass area under the precision-recall curve of Cross-Lag Attention Network. AU-PRC: area under the precision-recall curve.

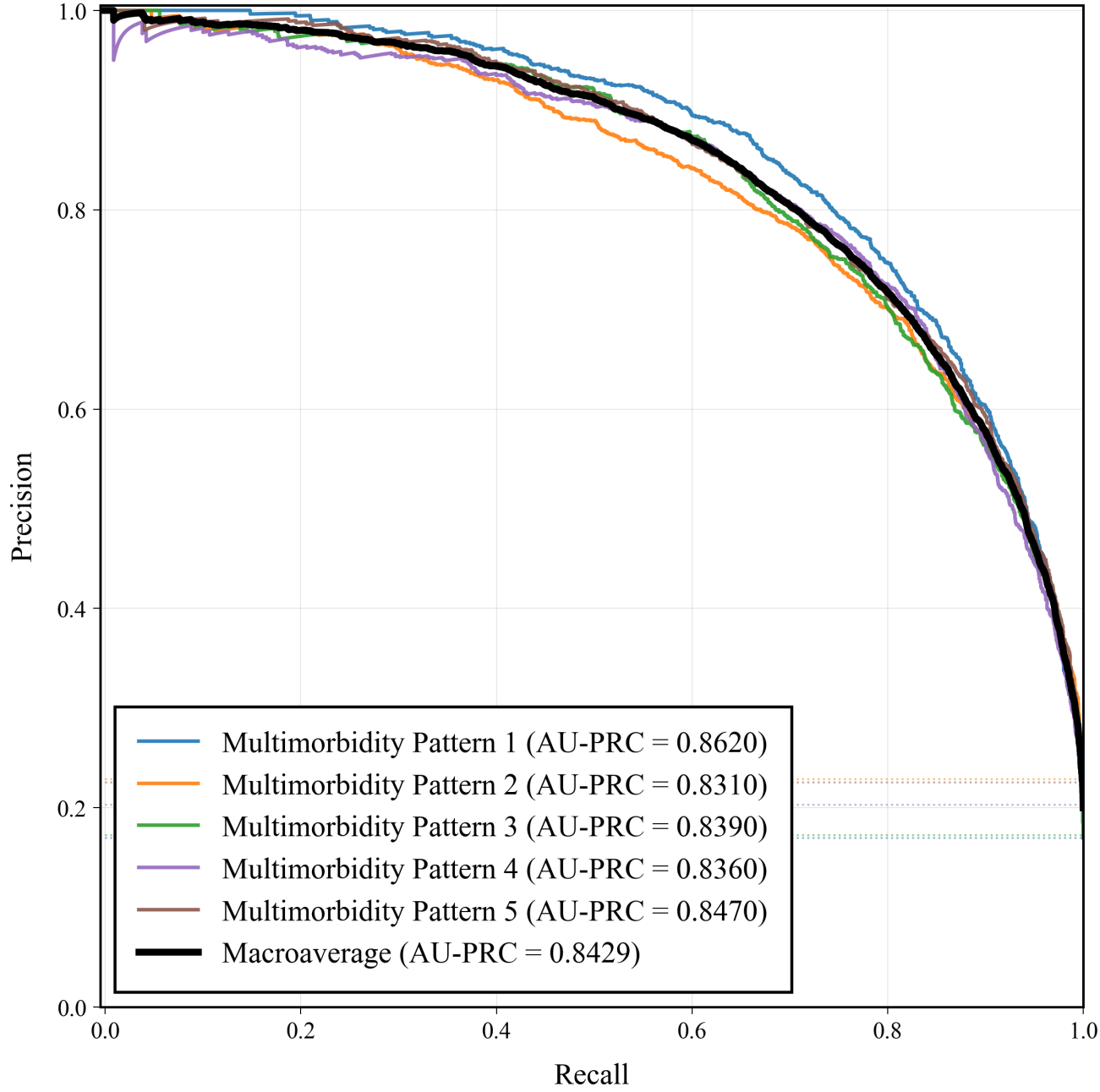

Table . Detailed classwise performance metrics of Cross-Lag Attention Network.

Multimorbidity pattern (class)	Prevalence (%)	Precision, mean (SD)	Recall, mean (SD)	F_1-score, mean (SD)
C1: Severe Cardiometabolic-Multisystem	19.80	0.8403 (0.006)	0.8314 (0.007)	0.8359 (0.006)
C2: Hypertension-Arthritis	22.30	0.8402 (0.005)	0.8515 (0.006)	0.8458 (0.005)
C3: Respiratory-Musculoskeletal	15.60	0.8002 (0.009)	0.7813 (0.010)	0.7906 (0.009)
C4: Metabolic Syndrome	24.10	0.8480 (0.006)	0.8535 (0.006)	0.8508 (0.006)
C5: Gastritis-Arthritis	18.20	0.8221 (0.007)	0.8194 (0.008)	0.8207 (0.007)
Macroaverage	—[a]	0.8303 (0.007)	0.8274 (0.008)	0.8288 (0.007)
Weighted average (overall)	100	0.8326 (0.006)	0.8312 (0.007)	0.8319 (0.006)

[a]Not applicable.

XSL•FO
RenderX

Figure 9. Confusion matrix across the 5 multimorbidity patterns.

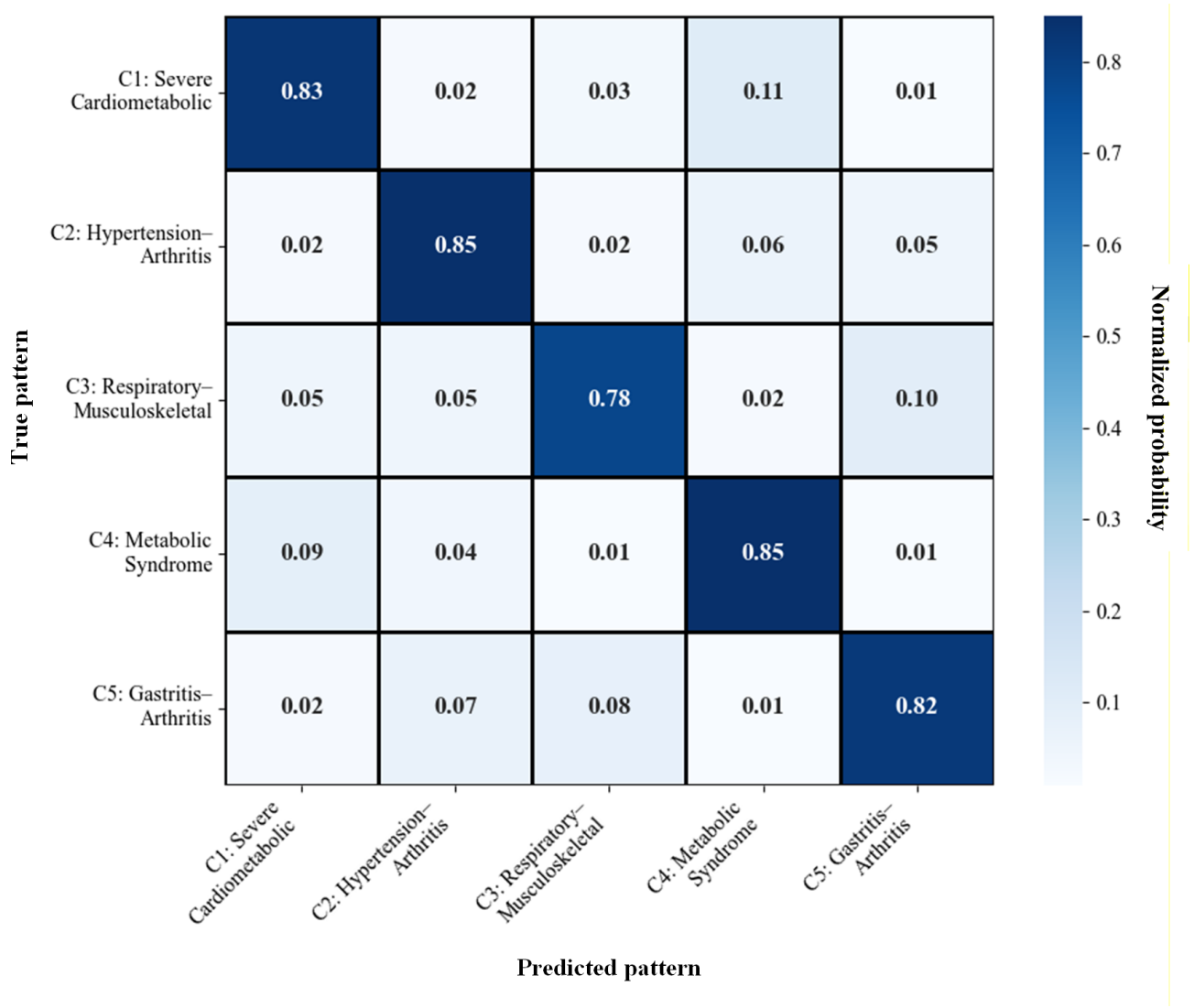

Sensitivity Analysis: Robustness of Class Stability

To address concerns regarding potential information leakage and the temporal robustness of latent class definitions, we conducted a comprehensive sensitivity analysis in which the LTA was reestimated using only the training-period waves (2011 - 2015), thereby excluding all future observations used as prediction targets in the main analysis. This analysis was designed to evaluate whether the multimorbidity pattern structure identified in the full longitudinal dataset was inherently stable, rather than being driven by information from later waves.

We first reassessed the optimal number of latent classes by fitting LTA models with 2 to 6 classes under a free-parameter specification using the training-period data only. As shown in Table 9, information criteria (AIC, BIC, and SaBIC) consistently improved as the number of classes increased from 2 to 5, while a marginal deterioration in fit was observed when moving from 5 to 6 classes. The BLRT strongly supported the 5-class solution over the 4-class solution (P<.001), whereas the improvement from 5 to 6 classes was only marginal (P=.03), suggesting diminishing returns with increased model complexity.

XSL•FO
RenderX

Table . Model fit of latent transition analysis based on training-period waves (2011 - 2015).

Models (waves used) and number of classes	AIC[a]	BIC[b]	SaBIC[c]	Entropy	BLRT[d] (*P* value)
LTA[e] (free parameters; 2011-2015)					
2	6128.4	6316.2	6201.7	0.72	—[f]
3	5486.9	5759.8	5594.3	0.8	<.001
4	5142.6	5500.7	5284.9	0.84	<.001
5	4926.8	5369.9	5104.2	0.87	<.001
6	4954.1	5482.4	5166.5	0.85	.03
Selected model (2011-2015)					
5	4926.8	5369.9	5104.2	0.87	—
LTA (invariant)					
5	4968.3	5389.6	5136.8	0.86	—

[a]AIC: Akaike Information Criterion.

[b]BIC: Bayesian Information Criterion.

[c]SaBIC: sample-size adjusted Bayesian Information Criterion.

[d]BLRT: Bootstrap Likelihood Ratio Test.

[e]LTA: latent transition analysis.

[f]Not applicable.

In addition, classification quality, as reflected by entropy, reached its highest value under the 5-class solution (entropy=0.87), indicating satisfactory class separation despite the reduced number of waves and observations compared with the full-sample model. Taken together, these results demonstrate that the 5-class structure remained the optimal and most parsimonious representation of multimorbidity patterns even when the analysis was restricted to the training-period data.

To ensure consistency of class interpretation across time, measurement invariance constraints were imposed on the selected 5-class model. Although imposing invariance resulted in a modest increase in information criteria and a slight reduction in entropy (from 0.87 to 0.86), the overall classification quality remained high, indicating that the core latent structure was robust to parameter constraints and not dependent on future observations.

Beyond overall model fit, we directly examined the stability of class definitions by comparing disease-specific item-response probabilities between the full-sample LTA model and the training-period-only LTA model. For each latent class, the top 4 representative chronic conditions were retained, and their conditional probabilities were contrasted across the 2 modeling strategies (Table 10).

XSL•FO
RenderX

Table . Concordance of class definitions between full-sample latent transition analysis and training-only latent transition analysis.

Multimorbidity pattern (class) and top 4 representative conditions[a]	Probability (full model)[b]	Probability (training period only)[c]	Difference (bias)	Pearson correlation coefficient (r)[d]
Class 1: Cardiometabolic-Multisystem				0.954
Arthritis	0.904	0.774	−0.130	
Hypertension	0.827	0.854	0.027	
Heart disease	0.781	0.781	0.000	
Dyslipidemia	0.693	0.662	−0.031	
Class 2: Hypertension-Arthritis				0.983
Hypertension	0.997	0.917	−0.080	
Arthritis	0.996	0.958	−0.038	
Gastric disease	0.374	0.446	0.072	
Dyslipidemia	0.273	0.331	0.058	
Class 3: Respiratory-Musculoskeletal				0.970
Lung disease	0.908	0.783	−0.125	
Arthritis	0.587	0.604	0.017	
Asthma	0.504	0.540	0.036	
Gastric disease	0.434	0.466	0.032	
Class 4: Metabolic Syndrome				0.973
Hypertension	0.883	0.841	−0.042	
Dyslipidemia	0.545	0.646	0.101	
Heart disease	0.444	0.346	−0.098	
Diabetes	0.363	0.308	−0.055	
Class 5: Gastritis-Arthritis				0.965
Arthritis	0.852	0.892	0.040	
Gastric disease	0.764	0.818	0.054	
Heart disease	0.242	0.302	0.060	
Kidney disease	0.194	0.253	0.059	
Overall stability				
Average across all classes	—[g]	—	0.048[e]	0.969[f]

[a]To ensure consistency, the top 4 conditions with the highest prevalence in the full model were selected for comparison for each pattern.

[b]Derived from the complete dataset, including Waves 1 through 5 (2011 - 2020).

[c]Derived exclusively from the training dataset (Waves 1 through 3, 2011 - 2015), blinding the model to future test data.

[d]Pearson correlation coefficient calculated based on the probability vectors of all 14 chronic conditions for the corresponding class.

[e]Mean absolute deviation value.

[f]Mean value.

[g]Not applicable.

Across all 5 classes, the composition and relative ordering of dominant conditions remained highly consistent. The cardiometabolic-multisystem class continued to be characterized by a high prevalence of arthritis, hypertension, heart disease, and dyslipidemia; the hypertension-arthritis class preserved its defining dual dominance of hypertension and arthritis; the respiratory-musculoskeletal class remained anchored by lung disease and asthma; the metabolic syndrome class retained its core metabolic features; and the gastritis-arthritis class continued to reflect co-occurring gastrointestinal and musculoskeletal conditions. Importantly, no class exhibited a change in its defining disease constellation when future waves were excluded from model estimation.

Quantitatively, the similarity between item-response probability profiles was high across all classes, with Pearson correlation coefficients ranging from 0.954 to 0.983 and a mean correlation

XSL•FO
RenderX

of 0.969. These correlations were computed using the full set of disease-specific probabilities, indicating strong structural concordance rather than superficial agreement limited to a subset of conditions [53]. Differences in absolute probabilities were generally modest, with a mean absolute deviation of 0.048 across classes, reflecting only minor shifts in disease prevalence rather than substantive changes in class meaning.

Taken together, these findings provide strong evidence that the multimorbidity class structure identified in the main analysis is stable and not driven by information from future observations. Even when latent classes were defined exclusively using training-period data, both the optimal number of classes and their clinical interpretations remained highly consistent with those derived from the full-sample model. The observed differences were limited to modest shifts in absolute disease probabilities, while the underlying pattern structure and relative disease importance were preserved.

We acknowledge that, under a strictly unbiased evaluation framework, latent class definitions could alternatively be derived exclusively from training-period data and then applied to the test set, for example, by projecting test observations onto a training-derived latent space. In this study, however, we adopted a population-level LTA fitted on all available waves to define stable multimorbidity patterns, which were subsequently treated as fixed targets for prediction. Importantly, as demonstrated in Table 9, the latent class structures derived from training-period data and from the full dataset exhibited a high degree of concordance (mean r=0.969), indicating that the class definitions were not driven by any single wave or subset of the data. Therefore, the use of the full-sample LTA model to generate predictive targets does not introduce meaningful bias into the evaluation. The "ground truth" labels for the test set would remain virtually unchanged even if they were generated by projecting test data onto a latent space fitted strictly to training parameters. The reported predictive performance of CLA-Net reflects a genuine ability to forecast future multimorbidity states rather than an artifact of information leakage in the target generation process.

To explicitly assess whether the use of full-sample LTA targets introduces any optimistic bias in predictive evaluation, we conducted an additional experiment in which the LTA model was estimated exclusively on training-period data, with all model parameters fixed thereafter. The downstream prediction pipeline was then fully repeated using these training-only LTA-derived targets, and the CLA-Net model was retrained and reevaluated accordingly.

As summarized in Table 11, the predictive performance obtained under training-only LTA targets remains highly consistent with the original results based on full-sample LTA targets. Specifically, the differences in accuracy, precision, recall, and F_1-score are all below 0.3%, and all metrics remain well within 1 SD of the original estimates. The slight performance reductions observed are expected and can be attributed to minor numerical variations in latent class assignment, rather than to any systematic bias arising from information leakage.

Table . Comparison of predictive performance under full-sample and training-only LTA[a] targets.

Metric	Full-sample LTA targets, mean (SD)	Training-only LTA targets, mean (SD)	Difference
Accuracy	0.8352 (0.0048)	0.8338 (0.0050)	−0.0014 (−0.17%)
Precision	0.8326 (0.0053)	0.8315 (0.0055)	−0.0011 (−0.13%)
Recall	0.8312 (0.0056)	0.8290 (0.0060)	−0.0022 (−0.26%)
F_1-score	0.8319 (0.0051)	0.8302 (0.0054)	−0.0017 (−0.20%)

[a]LTA: latent transition analysis.

Transition-Focused Evaluation of Multimorbidity Class Prediction

To disentangle the prediction of genuine multimorbidity progression from trivial class persistence, we conducted a stratified evaluation by separating individuals into those whose multimorbidity class remained unchanged between consecutive waves (stayer-only) and those who experienced a true class transition (transition-only). Performance was assessed using macroaveraged precision, recall, F_1-score, and overall accuracy for each subset.

To further account for chance agreement and the high prevalence of class persistence, we additionally report chance-adjusted performance metrics. Across the full sample, CLA-Net achieved a Cohen κ of 0.7935 (SD 0.0055) and a Matthews correlation coefficient of 0.7968 (SD 0.0058), reflecting substantial chance-adjusted concordance between predicted and observed class labels. These values are consistent with the maintained performance on the transition-only subset, confirming that CLA-Net possesses robust discriminative power to identify genuine multimorbidity evolution rather than merely replicating static baselines.

As shown in Table 12, the model retained substantial discriminative ability on the transition-only subset, where individuals experienced a true change in multimorbidity class between tand t+1. On this subset, macroaveraged precision, recall, and F_1-score reached 0.7615 (SD 0.0106), 0.7632 (SD 0.0112), and 0.7623 (SD 0.0102), respectively, with an overall accuracy of 0.7654 (SD 0.0096). Although performance on the transition-only subset was lower than that observed in the full-sample and stayer-only evaluations, this reduction is expected given the increased complexity of predicting off-diagonal class transitions. Because multimorbidity patterns tend to remain relatively stable across adjacent waves in populations with largely irreversible chronic conditions, the transition-only subset represents a smaller and more

XSL•FO
RenderX

heterogeneous group, which inherently increases prediction difficulty and performance variability, as reflected by the larger SDs observed.

Table . Performance evaluation on different dynamic subsets.

Evaluation subset	Precision, mean (SD)	Recall, mean (SD)	F_1-score, mean (SD)	Accuracy, mean (SD)
Full sample	0.8326 (0.0053)	0.8312 (0.0056)	0.8319 (0.0051)	0.8352 (0.0048)
Transition-only ($Y_t \neq Y_{t+1}$; 23.47%)	0.7615 (0.0106)	0.7632 (0.0112)	0.7623 (0.0102)	0.7654 (0.0096)
Stayer-only ($Y_t = Y_{t+1}$; 76.53%)	0.8544 (0.0049)	0.8521 (0.0052)	0.8533 (0.0047)	0.8566 (0.0044)

As an important clinical benchmark, we further evaluated a naive persistence model that simply predicts class($t+1$)=class(t). On the test set, the naive model obtained an overall accuracy of 0.7653, substantially below CLA-Net (0.8352, SD 0.0048). Notably, on the transition-only subset, the naive model achieves 0% accuracy by definition, whereas CLA-Net maintains 0.7654 accuracy, demonstrating its added value in identifying genuine transitions rather than merely reproducing stable states. Together, these results indicate that the overall performance gain is not driven by trivial persistence, but by the model's capacity to capture progression-related signals associated with changes in multimorbidity structure.

To further account for chance agreement and the high prevalence of class persistence, we additionally report chance-adjusted performance metrics. Across the full sample, CLA-Net achieved a Cohen κ of 0.7935 (SD 0.0055) and a Matthews correlation coefficient of 0.7968 (SD 0.0058), reflecting substantial chance-adjusted concordance between predicted and observed class labels. These values are consistent with the maintained performance on the transition-only subset, confirming that CLA-Net possesses robust discriminative power to identify genuine multimorbidity evolution rather than merely replicating static baselines.

Sensitivity Analysis of Data Imputation Methods

To strictly verify the validity and robustness of the imputation strategy used in this study (ie, MiceForest), we conducted a comparative experiment to assess how different missing data handling methods affect the final predictive performance of CLA-Net. In this experiment, the standard MiceForest algorithm was replaced by 4 alternative strategies: complete case analysis (CCA; directly discarding samples with missing values), random imputation (filling missing values with randomly selected observed values), mean imputation (filling with the variable mean), and KNN imputation. The comparative results are presented in Table 13.

Table . Performance comparison of Cross-Lag Attention Network using different missing data handling strategies.[a]

Imputation strategy	Precision, mean (SD)	Recall, mean (SD)	F_1-score, mean (SD)	Accuracy, mean (SD)
Complete case analysis	0.8015 (0.0072)	0.7980 (0.0078)	0.7995 (0.0075)	0.8050 (0.0070)
Random imputation	0.8080 (0.0085)	0.8050 (0.0090)	0.8065 (0.0088)	0.8110 (0.0082)
Mean imputation	0.8150 (0.0065)	0.8120 (0.0069)	0.8135 (0.0066)	0.8180 (0.0062)
KNN[b] imputation	0.8265 (0.0058)	0.8240 (0.0062)	0.8252 (0.0060)	0.8290 (0.0055)
MiceForest (ours)	*0.8326 (0.0053)*	*0.8312 (0.0056)*	*0.8319 (0.0051)*	*0.8352 (0.0048)*

[a]The italicized values represent the best performance of each data handling strategy on the evaluation metrics. These italicized values are used to highlight the most outstanding results among the different strategies.

[b]KNN: k-nearest neighbors.

As shown in Table 13, the model using MiceForest for data imputation achieved the best performance across all metrics (accuracy=0.8352, F_1-score=0.8319). In contrast, CCA resulted in the lowest performance (accuracy=0.8050). It is important to note that the CCA metrics were evaluated on a reduced test set (subset of individuals with complete data only), whereas imputation methods were evaluated on the full test set. Despite being tested on this potentially "cleaner" subset, CCA still underperformed. This confirms that the substantial reduction in training sample size caused by discarding data severely compromises the model's ability to learn robust patterns, thereby limiting its generalizability. Random imputation also performed poorly (accuracy=0.8110), primarily because randomly assigned values introduce significant noise and disrupt the true correlation structure between variables. While mean imputation (accuracy=0.8180) and KNN imputation (accuracy=0.8290) showed improvements over random methods, they still lagged behind MiceForest.

These results indicate that MiceForest, which leverages iterative random forests to model non-linear interactions, effectively preserves the underlying data structure better than stochastic (random) or distance-based (KNN) methods, confirming it as the optimal choice for our framework.

XSL•FO
RenderX

Discussion

Principal Results

This study proposes an innovative research framework that integrates population-level multimorbidity pattern recognition with individual-level future prediction, achieving a key transition in multimorbidity research from descriptive statistics to prospective prediction.

In terms of multimorbidity pattern recognition, this study identified 5 clinically meaningful classes using LTA: Cardiometabolic-Multisystem, Hypertension-Arthritis, Respiratory-Musculoskeletal, Metabolic Syndrome, and Gastritis-Arthritis. Patients in the Cardiometabolic-Multisystem pattern bore the heaviest overall disease burden, with widespread hypertension, heart disease, dyslipidemia, diabetes, gastritis, arthritis, lung disease, and kidney disease, while the coexistence of stroke further indicated advanced vascular damage. The interactions and cascading effects among these chronic conditions have been confirmed in multiple studies. For instance, cardiometabolic diseases such as hypertension, diabetes, dyslipidemia, and heart disease frequently co-occur and significantly increase the risk of cardiovascular events and mortality [50]. Inflammatory arthritis (eg, rheumatoid arthritis) has also been associated with elevated cardiovascular risk [54]. This multisystem involvement highlights the importance of comprehensive and integrated management for such patients. The Hypertension-Arthritis pattern was characterized by the strong co-occurrence of hypertension and arthritis. This pattern is well supported by prior studies showing that hypertension is a common multimorbidity of osteoarthritis, potentially linked through shared mechanisms such as inflammation, oxidative stress, and vascular dysfunction, with arthritis treatments possibly influencing blood pressure [51,55]. The Respiratory-Musculoskeletal pattern was defined by a high prevalence of lung disease, arthritis, and asthma, often accompanied by gastritis and hypertension. This finding is consistent with previous clinical evidence [52,56]. The Metabolic Syndrome class exhibited high rates of hypertension, dyslipidemia, heart disease, and diabetes, without significant multisystem involvement. This aligns with the classical definition of metabolic syndrome and its strong association with increased risks of cardiovascular disease and type 2 diabetes [57]. Finally, the Gastritis-Arthritis pattern showed the lowest overall disease burden, primarily involving arthritis and gastritis. This finding is supported by prior medical studies reporting comorbidities such as enteropathic arthritis in patients with inflammatory bowel disease or gastrointestinal complications related to arthritis medications [58].

In multimorbidity pattern prediction, this study introduces CLA-Net, a novel deep learning framework specifically designed to forecast multimorbidity patterns from longitudinal health data with short temporal lags. Our comprehensive evaluation demonstrated that CLA-Net consistently outperformed all baseline methods, achieving an accuracy of 0.8352 and an AUC of 0.9293. Several strong deep learning baselines included in the comparison, such as Mamba, PatchTST, and iTransformer, were originally developed for long-sequence time series forecasting and are optimized to exploit long-range temporal dependencies through mechanisms such as selective state-space modeling or patch-based representations. In the present task, the input sequence consists of 2 adjacent time points $t-1$ and t, which may limit the extent to which these architectures can fully leverage their design strengths. In contrast, CLA-Net explicitly focuses on modeling short-lag transitions through a dual-branch architecture and a bitemporal directed cross-attention mechanism, enabling more effective capture of immediate disease-state dependencies. Compared with the best-performing baseline Mamba model, CLA-Net improved accuracy by 1.10% (0.8352 vs 0.8242) and by 1.05% over the hybrid LSTM+transformer architecture (0.8352 vs 0.8247). More notably, CLA-Net increased AUC by 1.87% relative to LSTM+transformer (0.9293 vs 0.9106), indicating superior discriminative ability across decision thresholds, which is particularly important for clinical applications requiring flexible risk stratification strategies.

Our ablation experiments revealed the critical contributions of individual components and validated the soundness of the architectural design. Only the transformer branch reduced accuracy to 0.8166 (−1.86%), highlighting its essential role in capturing global cross-temporal dependencies. Retaining only the GRU branch further decreased accuracy to 0.8102 (−2.50%), indicating that while GRU effectively models temporal dynamics, the absence of global feature interactions severely limits its ability to capture complex multimorbidity patterns. The performance gap between the 2 branches (0.8166 vs 0.8102) also suggests that global interactions are slightly more important than local temporal dependencies, yet their integration is necessary to achieve optimal performance. Replacing the bitemporal directed cross-attention with standard self-attention reduced accuracy to 0.8244 (−0.93%), with precision and F_1-scores declining by 1.08% and 1.12%, respectively. This underscores the importance of the directed mechanism in maintaining predictive stability and balance. Unlike standard self-attention, which may cause “future information leakage,” the dual-window design enforces a “history-to-current” information flow that better aligns with the clinical logic of predicting future risk based on historical data.

In terms of input configuration, single-time-point input resulted in a sharp drop in accuracy to 0.7985 (−3.67%) and recall to 0.7964 (−3.48%), indicating that the absence of historical information causes the model to miss many true multimorbidity cases, likely because early signals of certain patterns can only be detected through temporal evolution. Interestingly, adding more historical time points (3 or 4) did not improve overall performance: with 3 time points, precision slightly increased (0.8355 vs 0.8334) but accuracy dropped to 0.8228 and recall to 0.8185; with 4 time points, recall reached its highest (0.8360), but accuracy (0.8268) and F_1-score (0.8262) fell below the 2-time-point configuration. This empirical finding suggests that for this specific multimorbidity prediction task, immediate history is significantly more predictive than long-term history. Including more distant waves (eg, from 6‐8 years prior) appears to introduce noise or weaker relevance that obscures the strong signals from the most recent health state transition. Therefore, the 2-time-point configuration effectively captures

XSL•FO
RenderX

the critical "immediate" evolution while minimizing interference from outdated information, thus striking the best balance between information richness and model complexity. Importantly, this temporal design also has clear implications for practical clinical use. By leveraging a "past–current" window spanning approximately 2 - 3 years to predict multimorbidity patterns 2 - 3 years into the future, CLA-Net is not intended for short-term clinical decision-making (eg, acute care), but rather for midterm risk stratification and early intervention planning. In real-world settings, such predictions could be used to identify individuals who are likely to transition into more complex or higher-burden multimorbidity patterns within the next few years, thereby providing a clinically meaningful window for intervention. Finally, reversing the order of GRU and transformer (GRU-transformer) lowered accuracy to 0.8235 (−1.17%), confirming the effectiveness of the "temporal encoding before interaction" design. GRU provides temporally aware representations that serve as more suitable inputs for subsequent attention mechanisms, enabling more effective cross-temporal interactions, whereas applying attention without temporal context may lead to suboptimal feature modeling.

Considering the chronic and partially irreversible nature of many included conditions, class persistence is expected to be high. Consistent with this, approximately 76.53% of test instances were stayers. While the naive model achieves high accuracy on stable patients, it has zero clinical utility for risk warning, as it fails to identify any patient whose health state is deteriorating or changing (0% accuracy on the transition subset). In contrast, CLA-Net successfully identifies 76.54% of the patients who undergo pattern transitions. From a clinical perspective, the primary value of a predictive model lies in its ability to provide early warnings for high-risk transitions rather than merely confirming stability. Therefore, the complexity of the deep learning approach is justified by its ability to capture these critical, nonlinear disease progressions that a simple persistence rule completely misses.

Regarding generalizability, the proposed framework is designed to be transferable to other longitudinal electronic health record (EHR) datasets. The LTA component relies on routinely collected chronic disease diagnoses, which are widely available across EHR systems, allowing population-level pattern structures to be reestimated or adapted to different health care contexts. Meanwhile, the CLA-Net architecture operates on generic temporal feature representations and does not depend on dataset-specific coding schemes. This modular design facilitates scalability to larger cohorts and longer observation periods and enables potential transfer learning scenarios in which a pretrained representation model can be fine-tuned using locally derived multimorbidity structures. These properties suggest that the framework has the potential for broader application beyond the present dataset. However, due to the inherent survivorship bias of longitudinal follow-up cohorts, the current model is primarily applicable to chronic disease management in surviving, community-dwelling populations. Importantly, it should not be applied to high-acuity clinical settings (eg, emergency or Intensive Care Unit populations) where mortality risk is a competing outcome and may dominate near-term trajectories. In such contexts, mortality-aware endpoints and competing-risk modeling would be required prior to any clinical deployment.

Practical Implications

The ability of CLA-Net to anticipate future multimorbidity pattern membership offers important implications for the longitudinal management of patients with established chronic conditions. Rather than responding to isolated disease events, clinicians can leverage pattern-based forecasts to organize care around expected configurations of coexisting conditions, thereby supporting a more coordinated and forward-looking approach to chronic disease management.

First, knowledge of an individual's likely future multimorbidity pattern can inform proactive care planning within patients with multimorbidity. For example, individuals predicted to enter the metabolic syndrome pattern may benefit from earlier emphasis on lifestyle modification, metabolic regulation, and adherence support, with the aim of slowing progression toward more complex cardiometabolic profiles. Similarly, those expected to belong to the cardiometabolic-multisystem pattern can be prioritized for closer surveillance and integrated management across cardiovascular, metabolic, and musculoskeletal domains, helping to mitigate cumulative disease burden over time.

Second, pattern-level prediction provides a practical framework for structuring multidisciplinary collaboration. Instead of relying on uniform or reactive referral pathways, health care providers may tailor multidisciplinary team composition according to the anticipated constellation of conditions. For instance, the respiratory-musculoskeletal pattern underscores the value of coordinated input from pulmonology, rheumatology, and rehabilitation services to jointly address respiratory impairment and functional limitation. Likewise, the gastritis-arthritis pattern highlights the need for alignment between gastroenterology and pain management to balance long-term anti-inflammatory therapy with gastrointestinal protection.

At the organizational level, pattern-based predictions can facilitate more efficient allocation of follow-up intensity, monitoring priorities, and supportive services for patients with multimorbidity within long-term chronic care systems. Consistent with its design scope, the proposed framework does not seek to model acute deterioration, end-stage progression, or mortality-related outcomes. Rather, it functions as a scalable decision-support layer to identify patients who may benefit from anticipatory, pattern-oriented management strategies in settings focused on sustained multimorbidity care.

Limitations and Future Direction

Although this study has made significant progress in multimorbidity pattern prediction, several areas remain for improvement. First, although CLA-Net demonstrated strong predictive performance on a longitudinal cohort, the current evaluation was conducted using a single data source. Differences in population characteristics, disease coding systems, and follow-up structures across EHR datasets may affect model behavior and warrant further investigation. Future work will focus on validating the framework across diverse EHR datasets, exploring transfer learning strategies, and extending the model to other chronic disease domains and health care systems.

XSL•FO
RenderX

Second, this study does not explicitly incorporate medication-related information into the modeling framework. Chronic conditions were therefore represented as binary indicators of presence or absence, without distinguishing between actively treated and untreated disease states. This abstraction is appropriate for predicting future multimorbidity pattern membership at the population level, but it may obscure clinically relevant differences in disease control achieved through pharmacological management. Consequently, the predicted pattern assignments should be interpreted as reflecting disease co-occurrence status rather than treatment-adjusted clinical responses. Future work integrating longitudinal medication data may further enhance the clinical granularity of multimorbidity pattern prediction.

Third, the model's predictive performance reflects a combined but functionally distinct reliance on objective disease history and subjective self-assessment measures, such as self-rated health and self-rated memory. While objective disease variables anchor predictions to diagnosed multimorbidity status, subjective assessments provide higher-level summaries of perceived health and functional burden and may contribute more strongly for individuals with borderline or heterogeneous disease profiles. Although the proposed framework demonstrates strong overall predictive performance, the relative contributions of subjective versus objective inputs cannot be fully disentangled within the current framework without dedicated interpretability analyses, such as feature attribution or attention visualization. Addressing this limitation and providing greater transparency regarding the sources of predictive power will be a key focus of future work.

Fourth, although the proposed framework demonstrates strong predictive performance, incorporating detailed interpretability analyses, such as SHAP (Shapley Additive Explanations) values or attention weight visualizations, may further enhance its practical utility. Owing to the complexity of the model architecture, such analyses are beyond the scope of this study. Future research will focus on developing tailored interpretability strategies to better elucidate the learned multimorbidity representations and support clinical interpretation.

Fifth, regarding temporal granularity, the survey waves in the CHARLS dataset are separated by nonuniform intervals, ranging from approximately 2 to 3 years. In the current CLA-Net architecture, transitions between adjacent waves are modeled as equidistant steps, without explicitly encoding the varying time intervals. This simplification may introduce temporal noise into the estimation of transition dynamics, particularly when interpreting changes across waves with heterogeneous follow-up durations. Future work could address this limitation by incorporating time-aware representations or modeling strategies explicitly designed for irregular temporal intervals.

Another methodological consideration concerns the transformation of probabilistic latent class assignments into deterministic labels for supervised prediction. In this study, posterior class probabilities obtained from the LTA were converted into hard labels using a maximum posterior probability assignment strategy. While this approach provides a clear and stable supervisory signal for training the prediction model, it inevitably discards information regarding classification uncertainty. In particular, individuals with ambiguous or borderline posterior distributions are treated as belonging entirely to a single class, which may encourage overconfident predictions. Future work could address this limitation by leveraging soft targets, such as full posterior probability vectors, within the learning objective. Incorporating probabilistic supervision through distribution-based loss functions or uncertainty-aware architectures may enable a more nuanced representation of multimorbidity structure and further improve predictive robustness.

Finally, to ensure the integrity of longitudinal trajectory modeling and the stability of LTA patterns, this study included participants present in all 5 waves (2011‐2020). We acknowledge that excluding individuals who died or dropped out due to severe illness may introduce survivorship bias, potentially skewing the dataset toward a "healthier survivor" cohort. However, this inclusion criterion was a necessary methodological trade-off to accurately capture the continuous evolution of multimorbidity patterns. It is worth noting that the primary goal of this framework is to support chronic disease management and secondary prevention in the general population, rather than predicting acute mortality risk in end-stage patients. To address this limitation, future research could incorporate advanced strategies such as joint longitudinal-survival modeling, inverse probability-of-censoring weighting, or competing-risk frameworks to explicitly account for nonrandom attrition and mortality, thereby extending the model's generalizability to high-risk clinical populations.

Conclusion

This study addresses the complex challenges of multimorbidity management in the context of population aging by proposing an innovative framework that bridges population-level pattern recognition and individual risk prediction. Using LTA, we identified multimorbidity patterns with temporal consistency and clinical stability (ie, Cardiometabolic-Multisystem, Hypertension-Arthritis, Respiratory-Musculoskeletal, Metabolic Syndrome, and Gastritis-Arthritis), which were then transformed into predictive labels to develop the CLA-Net deep learning model. CLA-Net integrates the sequential modeling capacity of GRU with the feature interaction advantages of a bitemporal directed cross-attention mechanism, achieving superior performance in capturing both temporal dependencies and complex feature interactions in chronic disease progression. Experimental results demonstrated that CLA-Net significantly outperformed existing methods across accuracy, recall, precision, F_1-score, and AUC.

Acknowledgments

This work is supported by the Beijing Logistics Informatics Research Base. We used ChatGPT-5 for language polishing.

XSL•FO
RenderX

Funding

This work was supported by the National Social Science Foundation of China (grant number 18ZDA086), the National Natural Science Foundation of China (grant number 62173025), the Fundamental Research Funds for the Central Universities (grant number 2025-JYB-XJSJJ-022), and Beijing Logistics Informatics Research Base.

Data Availability

The datasets generated or analyzed during this study are available from the corresponding author on reasonable request.

Authors' Contributions

Conceptualization: QZ, WM
Data curation: QZ, WM
Formal analysis: QZ
Funding acquisition: RZ
Investigation: QZ
Methodology: QZ, WM, BZ
Project administration: RZ, WM, XZ
Resources: RZ, WM
Software: QZ
Validation: QZ, WM, BZ
Writing – original draft: QZ
Writing – review & editing: QZ, RZ, WM, BZ, XZ

Conflicts of Interest

None declared.

Multimedia Appendix 1
Final dataset variables.
[DOCX File, 22 KB - medinform_v14i1e84261_app1.docx]

References

1. MacMahon S, Calverley P, Chaturvedi N, et al. Multimorbidity: a priority for global health research. : The Academy of Medical Sciences; 2018 URL: https://acmedsci.ac.uk/file-download/82222577 [accessed 2026-02-20]
2. Skou ST, Mair FS, Fortin M, et al. Multimorbidity. Nat Rev Dis Primers 2022 Jul 14;8(1):48. [doi: 10.1038/s41572-022-00376-4] [Medline: 35835758]
3. Du Y, de Bock GH, Vonk JM, et al. Lifestyle factors and incident multimorbidity related to chronic disease: a population-based cohort study. Eur J Ageing 2024 Nov 28;21(1):37. [doi: 10.1007/s10433-024-00833-x] [Medline: 39609306]
4. Nunes BP, Flores TR, Mielke GI, Thumé E, Facchini LA. Multimorbidity and mortality in older adults: a systematic review and meta-analysis. Arch Gerontol Geriatr 2016;67:130-138. [doi: 10.1016/j.archger.2016.07.008] [Medline: 27500661]
5. Fortin M, Lapointe L, Hudon C, Vanasse A, Ntetu AL, Maltais D. Multimorbidity and quality of life in primary care: a systematic review. Health Qual Life Outcomes 2004 Sep 20;2(1):51. [doi: 10.1186/1477-7525-2-51] [Medline: 15380021]
6. Violan C, Foguet-Boreu Q, Flores-Mateo G, et al. Prevalence, determinants and patterns of multimorbidity in primary care: a systematic review of observational studies. PLoS One 2014;9(7):e102149. [doi: 10.1371/journal.pone.0102149] [Medline: 25048354]
7. Prados-Torres A, Calderón-Larrañaga A, Hancco-Saavedra J, Poblador-Plou B, van den Akker M. Multimorbidity patterns: a systematic review. J Clin Epidemiol 2014 Mar;67(3):254-266. [doi: 10.1016/j.jclinepi.2013.09.021] [Medline: 24472295]
8. Dong X, Ma Y, Zhang H, Wang P. Individual-level transitions between chronic disease multimorbidity clusters and the risk of five-year mortality in longitudinal cohort of Chinese middle-aged and older adults. Aging Clin Exp Res 2025 Jul 9;37(1):216. [doi: 10.1007/s40520-025-03078-5] [Medline: 40632375]
9. Muth C, Blom JW, Smith SM, et al. Evidence supporting the best clinical management of patients with multimorbidity and polypharmacy: a systematic guideline review and expert consensus. J Intern Med 2019 Mar;285(3):272-288. [doi: 10.1111/joim.12842] [Medline: 30357955]
10. Zhang J, Zhou J, Zhou L, Ba Z. Extracting multifaceted characteristics of patients with chronic disease comorbidity: framework development using large language models. JMIR Med Inform 2025 May 15;13(1):e70096. [doi: 10.2196/70096] [Medline: 40373298]
11. Held FP, Blyth F, Gnjidic D, et al. Association rules analysis of comorbidity and multimorbidity: the concord health and aging in men project. J Gerontol A Biol Sci Med Sci 2016 May;71(5):625-631. [doi: 10.1093/gerona/glv181]

XSL•FO
RenderX

12. Hu Y, He H, Ou Q, et al. Prevalence of common chronic disease and multimorbidity patterns in Guangdong province with three typical cultures: analysis of data from the Diverse Life-Course Cohort study. Front Public Health 2023 May 4;11:1163791. [doi: 10.3389/fpubh.2023.1163791]
13. Ng SK, Tawiah R, Sawyer M, Scuffham P. Patterns of multimorbid health conditions: a systematic review of analytical methods and comparison analysis. Int J Epidemiol 2018 Oct 1;47(5):1687-1704. [doi: 10.1093/ije/dyy134] [Medline: 30016472]
14. Zhang Z, He P, Yao H, et al. A network-based study reveals multimorbidity patterns in people with type 2 diabetes. iScience 2023 Oct;26(10):107979. [doi: 10.1016/j.isci.2023.107979]
15. Nicolet A, Assouline D, Le Pogam MA, et al. Exploring patient multimorbidity and complexity using health insurance claims data: a cluster analysis approach. JMIR Med Inform 2022 Apr 4;10(4):e34274. [doi: 10.2196/34274] [Medline: 35377334]
16. Wang X, Zhang R, Zhu X. What can we learn from multimorbidity? A deep dive from its risk patterns to the corresponding patient profiles. Decis Support Syst 2024 Nov;186:114313. [doi: 10.1016/j.dss.2024.114313]
17. Zhu J, Wu Y, Lin S, Duan S, Wang X, Fang Y. Identifying and predicting physical limitation and cognitive decline trajectory group of older adults in China: a data-driven machine learning analysis. J Affect Disord 2024 Apr 1;350:590-599. [doi: 10.1016/j.jad.2024.01.095] [Medline: 38218258]
18. Strauss VY, Jones PW, Kadam UT, Jordan KP. Distinct trajectories of multimorbidity in primary care were identified using latent class growth analysis. J Clin Epidemiol 2014 Oct;67(10):1163-1171. [doi: 10.1016/j.jclinepi.2014.06.003] [Medline: 25063556]
19. Zacarías-Pons L, Vilalta-Franch J, Turró-Garriga O, Saez M, Garre-Olmo J. Multimorbidity patterns and their related characteristics in European older adults: a longitudinal perspective. Arch Gerontol Geriatr 2021;95:104428. [doi: 10.1016/j.archger.2021.104428] [Medline: 33991948]
20. Collins LM, Lanza ST. Latent Class and Latent Transition Analysis: With Applications in the Social, Behavioral, and Health Sciences: John Wiley & Sons; 2009.
21. Wang Y, Xu X, Liu J, et al. Latent transition analysis of instrumental activities of daily living in Chinese elderly: based on the 2014–2018 wave of the Chinese Longitudinal Healthy Longevity Survey. BMC Geriatr 2024 Jan 22;24(1):83. [doi: 10.1186/s12877-023-04631-5]
22. Paukner M, Ladner DP, CAPriCORN Team, Zhao L. Measuring disease burden with individual cumulative incidence in patients with cirrhosis. J Biomed Inform 2025 Sep;169:104883. [doi: 10.1016/j.jbi.2025.104883] [Medline: 40752671]
23. Zeng H, Miao C, Wang R, et al. Influence of comorbidity of chronic diseases on basic activities of daily living among older adults in China: a propensity score-matched study. Front Public Health 2024;12:1292289. [doi: 10.3389/fpubh.2024.1292289] [Medline: 38638478]
24. Uddin S, Wang S, Lu H, Khan A, Hajati F, Khushi M. Comorbidity and multimorbidity prediction of major chronic diseases using machine learning and network analytics. Expert Syst Appl 2022 Nov;205:117761. [doi: 10.1016/j.eswa.2022.117761]
25. Yang D, Kim J, Yoo J, Cha WC, Paik H. Identifying the risk of sepsis in patients with cancer using digital health care records: machine learning-based approach. JMIR Med Inform 2022 Jun 15;10(6):e37689. [doi: 10.2196/37689] [Medline: 35704364]
26. Nylund-Gibson K, Grimm R, Quirk M, Furlong M. A latent transition mixture model using the three-step specification. Struct Equ Modeling 2014 Jul 3;21(3):439-454. [doi: 10.1080/10705511.2014.915375]
27. Vrieze SI. Model selection and psychological theory: a discussion of the differences between the Akaike information criterion (AIC) and the Bayesian information criterion (BIC). Psychol Methods 2012 Jun;17(2):228-243. [doi: 10.1037/a0027127] [Medline: 22309957]
28. Lorah J, Womack A. Value of sample size for computation of the Bayesian information criterion (BIC) in multilevel modeling. Behav Res 2019 Feb;51(1):440-450. [doi: 10.3758/s13428-018-1188-3]
29. Sclove SL. Application of model-selection criteria to some problems in multivariate analysis. Psychometrika 1987 Sep;52(3):333-343 [FREE Full text] [doi: 10.1007/BF02294360]
30. Larose C, Harel O, Kordas K, Dey DK. Latent class analysis of incomplete data via an entropy-based criterion. Stat Methodol 2016 Sep;32:107-121. [doi: 10.1016/j.stamet.2016.04.004] [Medline: 27695391]
31. Park J, Kim HJ, Duffy RD. Using latent transition analysis to explore changes in decent work across time. J Couns Psychol 2025 Jan;72(1):80-91. [doi: 10.1037/cou0000773] [Medline: 39680017]
32. Dziak JJ, Lanza ST, Tan X. Effect size, statistical power and sample size requirements for the bootstrap likelihood ratio test in latent class analysis. Struct Equ Modeling 2014 Jan 1;21(4):534-552. [doi: 10.1080/10705511.2014.919819] [Medline: 25328371]
33. Rinne LF, Ye A, Jordan NC. Development of fraction comparison strategies: a latent transition analysis. Dev Psychol 2017 Apr;53(4):713-730. [doi: 10.1037/dev0000275] [Medline: 28221051]
34. Kalantar B, Pradhan B, Naghibi SA, Motevalli A, Mansor S. Assessment of the effects of training data selection on the landslide susceptibility mapping: a comparison between support vector machine (SVM), logistic regression (LR) and artificial neural networks (ANN). Geomat Nat Hazards Risk 2018 Jan 1;9(1):49-69. [doi: 10.1080/19475705.2017.1407368]

XSL•FO
RenderX

35. Belgiu M, Drăguţ L. Random forest in remote sensing: a review of applications and future directions. ISPRS J Photogramm Remote Sens 2016 Apr;114:24-31. [doi: 10.1016/j.isprsjprs.2016.01.011]
36. Ogunleye A, Wang QG. XGBoost model for chronic kidney disease diagnosis. IEEE/ACM Trans Comput Biol Bioinform 2020;17(6):2131-2140. [doi: 10.1109/TCBB.2019.2911071] [Medline: 30998478]
37. Lecun Y, Bottou L, Bengio Y, Haffner P. Gradient-based learning applied to document recognition. Proc IEEE 1998;86(11):2278-2324. [doi: 10.1109/5.726791]
38. Hochreiter S, Schmidhuber J. Long short-term memory. Neural Comput 1997 Nov 15;9(8):1735-1780. [doi: 10.1162/neco.1997.9.8.1735] [Medline: 9377276]
39. Vaswani A, Shazeer N, Parmar N, et al. Attention is all you need. Presented at: 31st Conference on Neural Information Processing Systems (NIPS 2017); Dec 4-9, 2017 URL: https://proceedings.neurips.cc/paper_files/paper/2017/hash/3f5ee243547dee91fbd053c1c4a845aa-Abstract.html [accessed 2025-09-09]
40. Nie Y, Nguyen NH, Sinthong P, Kalagnanam J. A time series is worth 64 words: long-term forecasting with transformers. arXiv. Preprint posted online on 2023. [doi: 10.48550/arXiv.2211.14730]
41. Liu Y, Hu T, Zhang H, et al. ITransformer: inverted transformers are effective for time series forecasting. arXiv. Preprint posted online on 2024. [doi: 10.48550/arXiv.2310.06625]
42. Gu A, Dao T. Mamba: linear-time sequence modeling with selective state spaces. arXiv. Preprint posted online on 2024. [doi: 10.48550/arXiv.2312.00752]
43. Cai X, Zhu Y, Wang X, Yao Y. MambaTS: improved selective state space models for long-term time series forecasting. arXiv. Preprint posted online on 2024. [doi: 10.48550/arXiv.2405.16440] [Medline: 38800661]
44. Stekhoven DJ, Bühlmann P. MissForest--non-parametric missing value imputation for mixed-type data. Bioinformatics 2012 Jan 1;28(1):112-118. [doi: 10.1093/bioinformatics/btr597] [Medline: 22039212]
45. Lee T, Shi D. A comparison of full information maximum likelihood and multiple imputation in structural equation modeling with missing data. Psychol Methods 2021 Aug;26(4):466-485. [doi: 10.1037/met0000381] [Medline: 33507765]
46. Zhao B, Zhang R, Chen D, et al. A machine-learning-based approach for identifying diagnostic errors in electronic medical records. IEEE Trans Rel 2024 Jun;73(2):1172-1186. [doi: 10.1109/TR.2023.3330733]
47. Wang S, Li Z, Wang X, et al. Bioinformatics analysis of comorbid mechanisms between ischemic stroke and end stage renal disease. Sci Rep 2025 May 16;15(1):17060. [doi: 10.1038/s41598-025-01049-4]
48. Xi J, Miao M, Li PWC, Yu DSF. Prognostic effects of multimorbidity clusters on health outcomes in adults: a systematic review and meta-analysis. Ageing Res Rev 2025 Dec;112:102897. [doi: 10.1016/j.arr.2025.102897] [Medline: 40934974]
49. Garin N, Koyanagi A, Chatterji S, et al. Global multimorbidity patterns: a cross-sectional, population-based, multi-country study. J Gerontol A Biol Sci Med Sci 2016 Feb;71(2):205-214. [doi: 10.1093/gerona/glv128] [Medline: 26419978]
50. Canoy D, Tran J, Zottoli M, et al. Association between cardiometabolic disease multimorbidity and all-cause mortality in 2 million women and men registered in UK general practices. BMC Med 2021 Oct 28;19(1):258. [doi: 10.1186/s12916-021-02126-x] [Medline: 34706724]
51. Ching K, Houard X, Berenbaum F, Wen C. Hypertension meets osteoarthritis - revisiting the vascular aetiology hypothesis. Nat Rev Rheumatol 2021 Sep;17(9):533-549. [doi: 10.1038/s41584-021-00650-x] [Medline: 34316066]
52. Katz J, Bartels CM. Multimorbidity in rheumatoid arthritis: literature review and future directions. Curr Rheumatol Rep 2024 Jan;26(1):24-35. [doi: 10.1007/s11926-023-01121-w] [Medline: 37995046]
53. Adler J, Parmryd I. Quantifying colocalization by correlation: the Pearson correlation coefficient is superior to the Mander's overlap coefficient. Cytometry A 2010 Aug;77(8):733-742. [doi: 10.1002/cyto.a.20896] [Medline: 20653013]
54. Nurmohamed MT, Heslinga M, Kitas GD. Cardiovascular comorbidity in rheumatic diseases. Nat Rev Rheumatol 2015 Dec;11(12):693-704. [doi: 10.1038/nrrheum.2015.112] [Medline: 26282082]
55. Lu K, Ma F, Yi D, Yu H, Tong L, Chen D. Molecular signaling in temporomandibular joint osteoarthritis. J Orthop Translat 2022 Jan;32:21-27. [doi: 10.1016/j.jot.2021.07.001] [Medline: 35591935]
56. Cielen N, Maes K, Gayan-Ramirez G. Musculoskeletal disorders in chronic obstructive pulmonary disease. Biomed Res Int 2014;2014:965764. [doi: 10.1155/2014/965764] [Medline: 24783225]
57. Bozkurt B, Aguilar D, Deswal A, et al. Contributory risk and management of comorbidities of hypertension, obesity, diabetes mellitus, hyperlipidemia, and metabolic syndrome in chronic heart failure: a scientific statement from the American Heart Association. Circulation 2016 Dec 6;134(23):e535-e578. [doi: 10.1161/CIR.0000000000000450] [Medline: 27799274]
58. Zohar A, Cohen AD, Bitterman H, et al. Gastrointestinal comorbidities in patients with psoriatic arthritis. Clin Rheumatol 2016 Nov;35(11):2679-2684. [doi: 10.1007/s10067-016-3374-y] [Medline: 27530409]

Abbreviations

AIC: Akaike Information Criterion
AU-PRC: area under the precision-recall curve
AUC: area under the curve
BIC: Bayesian Information Criterion
BLRT: Bootstrap Likelihood Ratio Test

XSL•FO
RenderX

CCA: complete case analysis
CHARLS: China Health and Retirement Longitudinal Study
CLA-Net: Cross-Lag Attention Network
CNN: convolutional neural network
EHR: electronic health record
FFN: feed-forward network
FPR: false positive rate
GRU: Gated Recurrent Unit
KNN: k-nearest neighbors
LCA: latent class analysis
LSTM: long short-term memory
LTA: latent transition analysis
PR: precision-recall
ROC: receiver operating characteristic
SaBIc: sample-size adjusted Bayesian Information Criterion
SHAP: Shapley Additive Explanations
TPR: true positive rate

Edited by A Coristine; submitted 16.Sep.2025; peer-reviewed by J Wang, L Dong, MZ Hossain, Q Lu, W Niu, X Shi; accepted 29.Jan.2026; published 10.Mar.2026.

Please cite as:
Zhang Q, Zhang R, Ma W, Zhao B, Zhu X
Bridging Population Patterns and Individual Prediction: Framework for Prospective Multimorbidity Study
JMIR Med Inform 2026;14:e84261
URL: https://medinform.jmir.org/2026/1/e84261
doi:10.2196/84261

© Qianyao Zhang, Runtong Zhang, Weiguang Ma, Butian Zhao, Xiaomin Zhu. Originally published in JMIR Medical Informatics (https://medinform.jmir.org), 10.Mar.2026. This is an open-access article distributed under the terms of the Creative Commons Attribution License (https://creativecommons.org/licenses/by/4.0/), which permits unrestricted use, distribution, and reproduction in any medium, provided the original work, first published in JMIR Medical Informatics, is properly cited. The complete bibliographic information, a link to the original publication on https://medinform.jmir.org/, as well as this copyright and license information must be included.

XSL•FO
RenderX

Enhanced Prediction of Atrial Fibrillation in Patients With Ischemic Stroke Through Electronic Medical Records and Text Mining: Algorithm Development and Validation

Yu-Wei Chen[1,2,3*], MD, PhD; Sheng-Feng Sung[4,5*], MD, PhD; Ya-Han Hu[6,7], PhD; Yu-Hsuan Yang[6], MBA

[1]Department of Neurology, Landseed International Hospital, Taoyuan City, Taiwan

[2]Department of Neurology, National Taiwan University Hospital, Taipei, Taiwan

[3]Center for General Education, National Central University, Taoyuan City, Taiwan

[4]Division of Neurology, Department of Internal Medicine, Ditmanson Medical Foundation Chia-Yi Christian Hospital, Chiayi, Taiwan

[5]Department of Nursing, Fooyin University, Kaohsiung, Taiwan

[6]Department of Information Management, National Central University, No. 300, Zhongda Rd, Zhongli District, Taoyuan City, Taiwan

[7]Asian Institute for Impact Measurement and Management, National Central University, Taoyuan City, Taiwan

[*]these authors contributed equally

Corresponding Author:
Ya-Han Hu, PhD
Department of Information Management, National Central University, No. 300, Zhongda Rd, Zhongli District, Taoyuan City, Taiwan

Abstract

Background: Stroke remains one of the leading causes of mortality and long-term disability worldwide. Atrial fibrillation (AF) is a major and often underdiagnosed risk factor for ischemic stroke as it is frequently asymptomatic and may remain undetected until a catastrophic cerebrovascular event occurs. The lack of timely identification and preventive treatment for AF substantially increases stroke risk. Although previous studies have proposed various predictive models for AF detection, many rely primarily on structured clinical variables and are developed using data from a single institution, which limits their generalizability and real-world applicability across different health care settings.

Objective: The objective of this study was to develop a robust and generalizable AF risk prediction model for patients with stroke using electronic medical records. By integrating structured clinical variables with features derived from unstructured clinical text, this study aimed to construct a more comprehensive representation of patient health status. Furthermore, this study emphasized systematic internal and external validation, along with calibration assessment, to evaluate model stability and generalizability across multiple hospital datasets, thereby supporting its potential use in routine clinical practice.

Methods: This study analyzed datasets from 2 hospitals in Taiwan: Landseed International Hospital (LIH), with 3988 patients, and Chia-Yi Christian Hospital (CYCH), with 5821 patients. We applied 5 feature engineering techniques to extract features from unstructured electronic medical record data, addressed data imbalance using 6 distinct resampling methods, and used 9 classification algorithms to compare model performance across both internal and external validation sets. This study identified the top 20 most important features from the best-performing models for both the LIH and CYCH datasets.

Results: The optimal predictive model for LIH was based solely on structured variables, whereas the model for CYCH achieved superior results by integrating structured variables with text-derived variables obtained from unstructured clinical notes using term frequency–inverse document frequency. Notably, feature importance analysis consistently identified the ratio of E- to A-wave velocities, left atrial size, and age as the top 3 predictive factors across both datasets, underscoring their critical role in AF risk assessment among patients with stroke.

Conclusions: This study demonstrated the development of predictive models for AF in patients with ischemic stroke. Notably, the integration of structured variables with variables derived from unstructured clinical text improved predictive performance in selected model configurations. Rigorous internal and external validation processes confirmed the superior performance of ensemble learning–based machine learning models compared with alternative algorithms, underscoring the potential of this approach for AF risk prediction.

(JMIR Med Inform 2026;14:e78117) doi:10.2196/78117

KEYWORDS

atrial fibrillation; stroke; electronic medical records; text mining; clinical decision support

XSL•FO
RenderX

Introduction

Stroke ranks as the second leading cause of death and the third leading cause of disability worldwide, with both related mortality rates and the global disease burden continuing to rise [1,2]. The most common types of recurrent stroke are acute ischemic stroke (AIS) and transient ischemic attack (TIA) [3]. Within 1 year following an ischemic stroke, the risk of recurrence exceeds 7% [4-6]. Moreover, patients who experience a recurrent stroke within 10 years face more than twice the risk of death or disability compared with those who experience a first stroke [7].

Atrial fibrillation (AF) is a common sustained or paroxysmal cardiac arrhythmia [8,9]. Treatment may often be delayed as AF can be asymptomatic or episodic, making it challenging to detect [10]. AF is closely associated with cerebrovascular disease: irregular heartbeats over time can impair efficient blood contraction and clearance, potentially leading to blood clot formation. These clots may then travel to the brain and cause a stroke if AF remains untreated, increasing the risk of acute complications [11,12]. Patients with AF have twice the risk of dying from cardiovascular disease and up to a 5-fold increased risk of stroke [13]. Consequently, AF impacts patients with stroke significantly in terms of risk, treatment, and daily care requirements [14-17]. Regarding medication, for patients with stroke and AF, oral anticoagulants (eg, factor IIa and Xa inhibitors and warfarin) have been shown to reduce mortality by one-quarter and the risk of recurrent stroke by two-thirds [12]. Comparatively, antiplatelet drugs can reduce the risk of recurrent stroke by three-fifths [18]. Newer direct oral anticoagulants such as apixaban, rivaroxaban, edoxaban, and dabigatran are considered relatively safer and more effective, with a reduced risk of major bleeding compared with warfarin [19,20]. Physicians should find more underdiagnosed patients with AF, mostly paroxysmal AF, among those with AIS and TIA to administer appropriate safe and effective treatment for stroke prevention [21].

Risk assessment scales such as CHA2DS2-VASc [22] and its 2024 updated CHA2DS2-VA version [23] are widely used as clinical tools for evaluating AF risk based on variables collected from patient data. However, these assessments often require additional time or supplementary screening items to thoroughly identify associated risks. Long-term screening studies reveal that the diagnosis rate of AF, particularly paroxysmal AF, tends to increase with extended electrocardiographic (electrocardiogram; ECG) monitoring, although this also raises costs. Furthermore, collecting ECG data is time-intensive and can be cumbersome. Some researchers advocate for the use of continuous ECG monitoring (eg, Holter monitors) for AF detection, noting that recordings exceeding 24 hours may improve detection rates. However, given limited medical resources [7], the presence or absence of AF in patients with stroke significantly influences both treatment outcomes and subsequent risk levels. Thus, it is crucial to develop an efficient screening method that enables physicians to more accurately identify high-risk patients [10].

Electronic medical records (EMRs) contain rich structured and unstructured information that can be leveraged to support risk stratification and early detection of AF among patients with ischemic stroke [24]. While prior studies have demonstrated the potential of machine learning models for AF prediction, many have relied primarily on structured variables and data from a single institution, which may limit model generalizability and real-world applicability across different clinical settings [25-27]. In addition, the incremental value of incorporating unstructured clinical text into predictive models has not been systematically evaluated using rigorous external validation.

The aim of this study was to develop and validate a robust and generalizable machine learning model for predicting AF during hospitalization among patients with ischemic stroke using EMRs. Specifically, we sought to (1) integrate structured clinical variables with features derived from unstructured clinical text; (2) systematically evaluate multiple feature extraction methods, resampling strategies, and classification algorithms; and (3) assess model performance and calibration through rigorous internal and external validation across 2 independent hospital datasets. By emphasizing generalizability and real-world applicability, this study aimed to provide an effective decision support tool to facilitate early identification of high-risk patients and support clinical screening strategies for AF after stroke.

Methods

Study Population

This retrospective study was conducted using EMR datasets from 2 hospitals in Taiwan. The study population included all inpatients who were diagnosed with or suspected of having ischemic stroke by a physician during hospitalization, as well as those who presented with stroke-related symptoms. The dataset from Landseed International Hospital (LIH) covered the period from 2018 to 2022 and included a total of 3988 patients, while the dataset from Chia-Yi Christian Hospital (CYCH) spanned 2007 to 2020 and comprised 5821 patients. In total, 9809 patients were initially identified across the 2 hospitals.

Because the objective of this study was to develop predictive models for AF among patients with ischemic stroke without a prior history of AF, several exclusion criteria were applied. Consistent with prior studies, patients with documented AF prior to the index stroke were classified as having known AF before stroke and were excluded from model development. Known AF before stroke was defined as an AF diagnosis recorded in the medical history at the time of admission, indicating that AF had been identified through outpatient visits or cardiac monitoring before the current hospitalization. In addition, patients with AF detected on admission were excluded. AF detected on admission was identified based on the initial ECG, admission records, or documentation in the present illness or past medical history.

After applying the inclusion and exclusion criteria, the LIH dataset consisted of 1969 inpatients with unstructured clinical records, 2032 inpatients with structured clinical data, and 1226 inpatients with both structured and unstructured data. Similarly, the CYCH dataset included 3319 inpatients with unstructured

XSL•FO
RenderX

data, 1441 inpatients with structured data, and 1072 inpatients with both data types.

Patients with both structured and unstructured data were defined as the intersecting cohort, representing overlapping patients across the 2 data sources. This intersecting cohort constituted the final analytic population used for model development and evaluation to ensure consistent feature availability across all included patients. Patients with data available in only 1 data source were not included in the final modeling analyses.

In the LIH intersecting cohort, 7% (86/1226) of the patients were identified as having AF during hospitalization following ischemic stroke. In contrast, in the CYCH intersecting cohort, 32.6% (350/1072) of the patients met the criteria for AF. Therefore, both cohorts exhibited class imbalance with notably different proportions of AF cases, which motivated the use of resampling strategies in subsequent model development.

Ethical Considerations

The study protocol was approved by the institutional review boards of LIH (IRB-22-049) and Ditmanson Medical Foundation Chia-Yi Christian Hospital (IRB2022071). As this was a retrospective study using de-identified medical records, the requirement for informed consent was waived by both institutional review boards. To ensure patient confidentiality, all personal identifiers were removed and replaced with unique study identification numbers prior to analysis. No participants received any financial compensation, as no direct contact or intervention was involved.

Outcome Variable

The primary outcome variable in this study was the occurrence of AF during hospitalization following ischemic stroke among patients in the intersecting cohort. AF status was determined using a predefined set of criteria that integrated multiple data sources from the EMRs, as summarized in Table 1. Specifically, AF was ascertained based on evidence from structured diagnostic information, unstructured clinical text, and medication records. Structured data included *International Classification of Diseases* diagnosis codes indicative of AF, whereas unstructured sources comprised textual mentions of AF in clinical narratives and examination reports, such as Holter monitoring reports; cardiac ultrasound reports; ECG reports, excluding the first ECG on admission; and general medical records, including discharge summaries. Keyword-based text searches were conducted using commonly used terms referring to AF. In addition, prescriptions of antiarrhythmic agents and oral anticoagulants were incorporated as supportive evidence for AF identification [28]. A patient was classified as having AF if any one of the criteria listed in Table 1 was satisfied.

Table . Criteria used to ascertain atrial fibrillation (AF) status in the intersecting cohort.

Criterion	Conditions
AF-1	AF documented in the stroke registry during hospitalization
AF-2	AF-related keywords identified in Holter monitoring report text
AF-3	AF-related keywords identified in cardiac ultrasound report text
AF-4	AF-related keywords identified in ECG[a] report text, excluding the first ECG on admission
AF-5	AF-related keywords identified in clinical narratives, including hospital discharge summaries
AF-6	Presence of an AF-related *ICD*[b] diagnosis code (*ICD-9-CM*[c] 427.31 or *ICD-10-CM*[d] I48.91)
AF-7	Prescription of antiarrhythmic medications, including amiodarone, propafenone, or dronedarone
AF-8	Prescription of oral anticoagulants, including warfarin, apixaban, edoxaban, rivaroxaban, or dabigatran

[a]ECG: electrocardiogram.

[b]*ICD*: *International Classification of Diseases.*

[c]*ICD-9-CM*: *ICD, Ninth Revision, Clinical Modification.*

[d]*ICD-10-CM*: *ICD, 10th Revision, Clinical Modification.*

Predictor Variables and Text Preprocessing

Predictor variables comprised data obtained within 72 hours of admission. After excluding patients with a history of AF or diagnosed with AF upon admission, all variables were standardized across both hospitals.

The structured variables, detailed in Multimedia Appendix 1, comprised a comprehensive set of clinical predictors that are routinely available at hospital admission and during early hospitalization. These structured predictors included demographic characteristics (sex, age, height, and weight); vascular imaging findings derived from carotid duplex sonography; echocardiographic parameters reflecting cardiac structure and function (eg, aortic diameter, left atrial size, ventricular dimensions, ejection fraction, and diastolic function indexes); vital signs (body temperature, heart rate, respiratory rate, and blood pressure); and laboratory measurements covering hepatic function, renal function, coagulation profiles, inflammatory markers, lipid profiles, and hematological indexes. In addition, neurological severity was captured using individual

XSL•FO
RenderX

National Institutes of Health Stroke Scale (NIHSS) subitems, as well as the overall NIHSS score, enabling fine-grained representation of stroke-related neurological deficits. Family medical history variables related to hypertension, diabetes mellitus, stroke, and ischemic heart disease were also included as nominal predictors. Together, these structured variables provided a multidimensional characterization of patients' demographic profiles, cardiovascular status, metabolic conditions, neurological severity, and familial risk factors.

Unstructured data encompassed magnetic resonance imaging results, chief concerns, and present illness. Text preprocessing of variables derived from unstructured clinical text involved Chinese-English translation, spell-checking, abbreviation expansion, nonword symbol removal, AF-suggestive word deletion, lowercase conversion, word form reduction, negation marking as "_NEG" using additional negation words [29,30] and the Natural Language Toolkit's (Team NLTK) *mark_negation* function, and stop word removal.

For text feature extraction, we used bidirectional encoder representations from transformers (BERT) [31,32], Doc2Vec [33,34], term frequency–inverse document frequency (TF-IDF) [35,36], and MetaMap [37,38]. These 4 methods were selected to represent complementary paradigms in clinical natural language processing, ranging from deep contextualized language models to traditional statistical and knowledge-based approaches. BERT has demonstrated strong performance in modeling contextual semantics and capturing complex linguistic patterns in clinical narratives and has been widely adopted in biomedical and clinical natural language processing tasks. Doc2Vec was included as a representative neural embedding method that captures document-level semantics with lower computational complexity, making it suitable for large-scale clinical text analysis. TF-IDF remains a widely used and robust baseline in clinical text mining due to its interpretability and effectiveness in high-dimensional sparse representations. MetaMap was incorporated to leverage domain-specific medical knowledge by mapping clinical text to standardized concepts in the Unified Medical Language System, which has been shown to enhance semantic normalization and downstream clinical prediction tasks.

Medical concepts (concept unique identifiers) were identified via MetaMap and subsequently transformed into feature vectors using TF-IDF applying a term frequency threshold with maximum and minimum values set to 0.9 and 0.1, respectively. In addition, Chinese text translation and spell-checking were conducted using *googletrans* (version 3.1.0a0) and *pyspellchecker* (version 0.8.1) to improve text consistency prior to feature extraction.

Prediction Model Development and Evaluation

Figure 1 delineates a comprehensive machine learning model validation workflow encompassing both internal and external validation phases. The internal validation phase uses the LIH dataset and a 10-fold cross-validation strategy. During this process, various combinations of resampling methods and modeling techniques are evaluated, with the top 3 best-performing combinations (totaling 9 configurations) selected for further analysis. This step is crucial for identifying the most appropriate models and parameter settings for the given data.

Figure 1. The process of machine learning model construction. ADASYN: adaptive synthetic sampling; BERT: bidirectional encoder representations from transformers; CatBoost: categorical boosting; CYCH: Chia-Yi Christian Hospital; DT: decision tree; KNN: k-nearest neighbor; LightGBM: light gradient-boosting machine; LIH: Landseed International Hospital; LR: logistic regression; NB: naive Bayes; RF: random forest; SMOTE: synthetic minority oversampling technique; SMOTENC: SMOTE for nominal and continuous features; SVM: support vector machine; TF-IDF: term frequency–inverse document frequency; XGB: extreme gradient boosting.

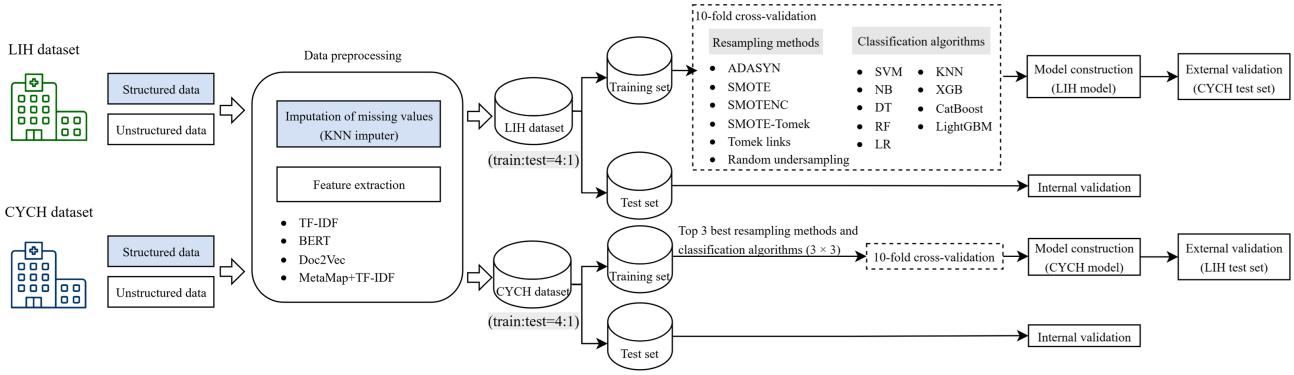

The external validation phase leverages an independent dataset from CYCH. In this stage, the optimal model and resampling method combinations identified during internal validation are used to train models, which are subsequently evaluated on the external dataset. This phase is essential for assessing the models' generalizability, ensuring their robustness and efficacy when applied to novel, unseen data. This rigorous 2-stage validation approach enhances the reliability and external validity of the developed predictive models, providing a robust framework for clinical application in AF risk assessment among patients with stroke. For both the internal and external validation phases, we used k-nearest neighbor imputation to address missing values within structured data. Additionally, we applied multiple feature extraction techniques to the unstructured text, including TF-IDF, BERT, Doc2Vec, and MetaMap combined with TF-IDF, followed by subsequent evaluations to compare model performance. To comprehensively evaluate the predictive power of different data types, we constructed and compared three distinct model configurations: (1) models using only structured variables, (2) models using only variables derived from unstructured clinical text (ie, text-derived variables), and (3) models combining both structured and text-derived variables.

XSL•FO
RenderX

To address the class imbalance present in the datasets from both hospitals, we implemented various resampling techniques during the model training phase, including adaptive synthetic sampling, synthetic minority oversampling technique (SMOTE), SMOTE for nominal and continuous features, SMOTE-Tomek, Tomek links, and random undersampling. We stratified and split the data into training and test sets with a 4:1 ratio using the parameter *stratify=df[['AF']]* to maintain consistent class ratios across sets.

We evaluated multiple classifiers, including support vector machine, Gaussian naïve Bayes, k-nearest neighbor, decision tree, random forest, logistic regression, Extreme Gradient Boosting (XGBoost), categorical boosting (CatBoost), and light gradient-boosting machine (LightGBM). The training process incorporated 10-fold cross-validation with stratification (*stratify=df[['AF']]*) to obtain robust performance estimates. We assessed model performance using multiple evaluation metrics, including the area under the receiver operating characteristic curve (AUC), sensitivity, specificity, and expected calibration error. Following the identification of optimal model combinations, we conducted both internal and external validation. The final results reflected the outcomes of the test set.

To enhance model interpretability, we used Shapley values (using *shap* version 0.45.0) to explain the best-performing models in both the LIH and CYCH datasets. This approach provides insights into the relative importance of different features in the prediction task.

Baseline Models

The baseline model was compared with machine learning models using traditional risk-scoring models (AS5F [age, stroke severity NIHSS>5 to find atrial fibrillation] [39-41] and CHASE-LESS [coronary, heart failure, age, stroke severity–lipidemia, sugar, and prior stroke] [15,42,43]). CHASE-LESS was developed using data derived from a Taiwanese population, which is consistent with the population of this study, and its variables include age, NIHSS score, coronary heart disease, congestive heart failure, hyperlipidemia, diabetes mellitus, and prior stroke or TIA. The threshold value of CHASE-LESS was set to 6, and the scoring items were based on the variables in the EMR at the time of admission. The AS5F score is designed to determine the need for long-term ECG monitoring in patients with AIS or TIA.

Results

We conducted modeling and prediction using both structured and text-derived variables from the two hospitals. In the internal validation for LIH (Table 2), the combination of structured variables with logistic regression yielded the best performance, achieving an AUC of 0.896. For text-derived variables, the model using Doc2Vec, random undersampling, and LightGBM achieved an AUC of 0.674. When integrating both structured and text-derived variables, the model incorporating Doc2Vec, SMOTE, and CatBoost performed well, with an AUC of 0.885. Some models showed enhanced performance when integrating both types of variables. For instance, in the LightGBM model implementation, the integration of structured and text-derived variables, coupled with the adaptive synthetic sampling technique, demonstrated superior performance, with an AUC of 0.876. This feature-integrated approach substantially outperformed both models using only structured variables (AUC=0.850) and those using only text-derived variables (AUC=0.468). However, not all combined approaches demonstrated such improvement.

XSL•FO
RenderX

Table . Comparative analysis of Landseed International Hospital (LIH) models for atrial fibrillation prediction for the area under the receiver operating characteristic curve (AUC) metric: internal validation using the LIH dataset.

Model	Structured variables, AUC	Text-derived variables, AUC				Structured+text-derived variables, AUC			
		BERT[a]	Doc2Vec	MetaMap	TF-IDF[b]	BERT	Doc2Vec	MetaMap	TF-IDF
AS5F[c]	0.597	—[d]	—	—	—	—	—	—	—
CHASE-LESS[e]	0.657	—	—	—	—	—	—	—	—
SVM[f]									
Imbalanced	0.835	0.403	0.496	0.499	0.64	0.654	0.837	0.809	0.862
Undersampling	0.778	0.579	0.61	0.48	0.595	0.482	0.76	0.779	0.841
ADASYN[g]	0.812	0.548	0.514	0.466	0.602	0.504	0.846	0.81	0.868
SMOTE[h]	0.803	0.54	0.511	0.51	0.672	0.504	0.824	0.783	0.796
Gaussian NB[i]									
Imbalanced	0.52	0.439	0.604	0.572	0.466	0.404	0.535	0.566	0.468
Undersampling	0.763	0.495	0.671	0.483	0.574	0.616	0.764	0.551	0.599
ADASYN	0.455	0.402	0.533	0.534	0.643	0.452	0.456	0.545	0.52
SMOTE	0.458	0.507	0.532	0.55	0.525	0.477	0.42	0.547	0.609
KNN[j]									
Imbalanced	0.618	0.463	0.47	0.519	0.666	0.486	0.642	0.58	0.567
Undersampling	0.646	0.398	0.451	0.491	0.527	0.526	0.576	0.628	0.648
ADASYN	0.627	0.529	0.45	0.483	0.506	0.421	0.603	0.691	0.625
SMOTE	0.594	0.446	0.427	0.511	0.548	0.405	0.577	0.582	0.608
DT[k]									
Imbalanced	0.542	0.529	0.512	0.535	0.503	0.613	0.576	0.531	0.553
Undersampling	0.621	0.433	0.509	0.49	0.539	0.673	0.634	0.501	0.531
ADASYN	0.666	0.439	0.584	0.521	0.448	0.723	0.631	0.567	0.675
SMOTE	0.545	0.45	0.599	0.574	0.439	0.713	0.673	0.604	0.548
RF[l]									
Imbalanced	0.815	0.548	0.535	0.533	0.586	0.627	0.758	0.757	0.756
Undersampling	0.846	0.376	0.658	0.553	0.523	0.609	0.838	0.738	0.829
ADASYN	0.82	0.523	0.532	0.487	0.476	0.6	0.832	0.79	0.821
SMOTE	0.86	0.502	0.539	0.522	0.565	0.621	0.845	0.815	0.851
LR[m]									
Imbalanced	0.896	0.523	0.659	0.504	0.641	0.798	0.862	0.819	0.805

XSL•FO
RenderX

Model	Structured variables, AUC	Text-derived variables, AUC				Structured+text-derived variables, AUC			
		BERT[a]	Doc2Vec	MetaMap	TF-IDF[b]	BERT	Doc2Vec	MetaMap	TF-IDF
Undersampling	0.84	0.462	0.664	0.492	0.558	0.769	0.783	0.805	0.827
ADASYN	0.865	0.463	0.635	0.537	0.621	0.752	0.847	0.789	0.804
SMOTE	0.866	0.471	0.624	0.543	0.644	0.757	0.833	0.803	0.787
XGB[n]									
Imbalanced	0.845	0.402	0.541	0.571	0.653	0.813	0.812	0.822	0.822
Undersampling	0.829	0.408	0.617	0.537	0.547	0.797	0.787	0.824	0.826
ADASYN	0.849	0.41	0.5	0.46	0.504	0.865	0.868	0.86	0.874
SMOTE	0.856	0.449	0.591	0.474	0.581	0.882	0.868	0.857	0.819
CatBoost[o]									
Imbalanced	0.869	0.41	0.609	0.517	0.652	0.774	0.85	0.778	0.849
Undersampling	0.868	0.407	0.657	0.536	0.573	0.772	0.854	0.806	0.835
ADASYN	0.864	0.524	0.522	0.481	0.558	0.809	0.875	0.857	0.864
SMOTE	0.855	0.46	0.567	0.529	0.564	0.833	0.885	0.84	0.866
LightGBM[p]									
Imbalanced	0.829	0.524	0.46	0.619	0.538	0.801	0.75	0.837	0.798
Undersampling	0.783	0.361	0.674	0.435	0.513	0.777	0.79	0.783	0.81
ADASYN	0.85	0.471	0.642	0.604	0.468	0.852	0.843	0.773	0.876
SMOTE	0.858	0.488	0.665	0.616	0.525	0.811	0.873	0.845	0.837

[a]BERT: bidirectional encoder representations from transformers.

[b]TF-IDF: term frequency–inverse document frequency.

[c]AS5F: age, stroke severity National Institutes of Health Stroke Scale >5 to find atrial fibrillation.

[d]Not applicable.

[e]CHASE-LESS: coronary, heart failure, age, stroke severity–lipidemia, sugar, and prior stroke.

[f]SVM: support vector machine.

[g]ADASYN: adaptive synthetic sampling.

[h]SMOTE: synthetic minority oversampling technique.

[i]NB: naïve Bayes.

[j]KNN: k-nearest neighbor.

[k]DT: decision tree.

[l]RF: random forest.

[m]LR: logistic regression.

[n]XGB: extreme gradient boosting.

[o]CatBoost: categorical boosting.

[p]LightGBM: light gradient-boosting machine.

In the external validation of the LIH model using the CYCH dataset (Table 3), the best performance was achieved using a combination of BERT and SMOTE, with an AUC of 0.795, which exceeded the AUC for models using only structured variables (AUC=0.781) and those using only text-derived variables. In the internal validation for CYCH (Table 4), the best-performing model was a combination of BERT with undersampling and XGBoost, achieving an AUC of 0.861. In the external validation, the optimal combination involved an imbalanced technique with CatBoost, resulting in an AUC of

XSL•FO
RenderX

0.832. These findings suggest that combining structured and text-derived variables can improve predictive performance in some models, highlighting the importance of selecting appropriate models and resampling techniques to enhance model outcomes.

Figure 2 presents the external validation results from the 2 hospitals, indicating that the combination of CatBoost and SMOTE ranked third in both cases as determined by the AUC metric. Overall, ensemble learning demonstrated superior performance throughout the validation process. While the incorporation of text-derived variables did not consistently yield the highest AUC values in both internal and external validation, it is noteworthy that their inclusion generally resulted in improved outcomes based on the expected calibration error during external validation.

Table . Performance of the top 3 Landseed International Hospital models incorporating structured and unstructured feature combinations: external validation using the Chia-Yi Christian Hospital dataset.

Model	AUC[a]	Sensitivity	Specificity	ECE[b]
XGB[c]				
Structured	0.781	0.651	0.776	0.187
Structured+MRI[d]	0.771	0.549	0.843	0.174
Structured+CC[e]	0.776	0.623	0.796	0.171
Structured+PI[f]	0.773	0.597	0.798	0.178
Structured+MRI+CC+PI	0.775	0.571	0.821	0.168
CatBoost[g]				
Structured	0.789	0.463	0.892	0.09
Structured+MRI	0.781	0.311	0.942	0.147
Structured+CC	0.788	0.483	0.895	0.093
Structured+PI	0.79	0.46	0.91	0.104
Structured+MRI+CC+PI	0.788	0.443	0.911	0.107
LightGBM[h]				
Structured	0.781	0.611	0.81	0.161
Structured+MRI	0.794	0.509	0.889	0.111
Structured+CC	0.772	0.5	0.864	0.124
Structured+PI	0.784	0.509	0.873	0.124
Structured+MRI+CC+PI	0.795	0.574	0.855	0.133

[a]AUC: area under the receiver operating characteristic curve.

[b]ECE: expected calibration error.

[c]XGB: extreme gradient boosting.

[d]MRI: magnetic resonance imaging.

[e]CC: chief concern.

[f]PI: present illness.

[g]CatBoost: categorical boosting.

[h]LightGBM: light gradient-boosting machine.

XSL•FO
RenderX

Table . Performance of the top 3 Chia-Yi Christian Hospital (CYCH) models incorporating structured and unstructured (magnetic resonance imaging+chief concerns+present illness) feature combinations.

Model	Internal validation (CYCH dataset), AUC[a]	External validation (LIH[b] dataset)	
		AUC	ECE[c]
XGB[d]			
Imbalanced	0.858	0.816	0.08
Undersampling	0.861	0.776	0.176
ADASYN[e]	0.852	0.73	0.338
SMOTE[f]	0.845	0.692	0.334
CatBoost[g]			
Imbalanced	0.851	0.832	0.129
Undersampling	0.859	0.816	0.253
ADASYN	0.843	0.76	0.363
SMOTE	0.843	0.776	0.305
LightGBM[h]			
Imbalanced	0.84	0.764	0.225
Undersampling	0.816	0.769	0.366
ADASYN	0.789	0.726	0.37
SMOTE	0.778	0.662	0.409

[a]AUC: area under the receiver operating characteristic curve.

[b]LIH: Landseed International Hospital.

[c]ECE: expected calibration error.

[d]XGB: extreme gradient boosting.

[e]ADASYN: adaptive synthetic sampling.

[f]SMOTE: synthetic minority oversampling technique.

[g]CatBoost: categorical boosting.

[h]LightGBM: light gradient-boosting machine.

XSL•FO
RenderX

Figure 2. Ranking of the top 3 model and resampling method combinations for external validation: validation of the Landseed International Hospital (LIH) model using the Chia-Yi Christian Hospital (CYCH) dataset (A) and validation of the CYCH model using the LIH dataset (B). ADASYN: adaptive synthetic sampling; AUC: area under the receiver operating characteristic curve; CatBoost: categorical boosting; ECE: expected calibration error; LightGBM: light gradient-boosting machine; SMOTE: synthetic minority oversampling technique; XGB: extreme gradient boosting.

XSL•FO
RenderX

Discussion

Summary of Main Findings

This study developed and validated machine learning–based prediction models for identifying AF during hospitalization among patients with ischemic stroke by leveraging EMRs from 2 independent hospitals. The main findings can be summarized in 3 points. First, models trained on structured clinical variables achieved strong predictive performance, and the integration of unstructured clinical text further improved discrimination and calibration in selected model configurations, particularly in the external validation setting. Second, ensemble learning methods, including CatBoost, XGBoost, and LightGBM, consistently outperformed traditional risk scores and conventional classifiers across internal and external validation. Third, feature importance analysis using SHAP revealed that echocardiographic parameters, including the ratio of E- to A-wave velocities, left atrial size, and age, were among the most influential predictors across both datasets. Together, these findings demonstrate the feasibility and generalizability of incorporating structured and unstructured EMR data to support early risk stratification for AF after ischemic stroke.

Implications of Integrating Structured and Text-Derived Variables

Although the integration of structured variables with variables derived from unstructured clinical text improved predictive performance in several model configurations, the results in Table 2 indicate that such integration did not uniformly outperform models based solely on structured variables. This finding warrants careful interpretation rather than being viewed as a limitation of the proposed framework. In this study, structured clinical variables already encompassed well-established and highly discriminative predictors of AF, including echocardiographic parameters such as the ratio of E- to A-wave velocities, left atrial size, and age. When such strong predictors are present, models trained exclusively on structured variables may achieve near-optimal performance, leaving limited room for additional gains from text-derived variables.

Moreover, variables derived from unstructured clinical text are inherently high-dimensional and potentially noisy, particularly when generated using representation techniques such as TF-IDF or Doc2Vec. For certain classifiers that are sensitive to feature dimensionality or redundancy, the inclusion of text-derived variables may dilute the contribution of strong structured predictors, resulting in marginal or inconsistent performance gains. This phenomenon is consistent with prior observations in studies integrating clinical text with structured EMR data.

Importantly, our results suggest that the benefit of feature-level integration is highly model dependent. Ensemble learning–based algorithms, including LightGBM, XGBoost, and CatBoost, demonstrated a greater capacity to exploit complementary information from heterogeneous feature sources, particularly when combined with appropriate resampling strategies. In contrast, simpler or less flexible classifiers did not consistently benefit from the inclusion of text-derived variables. These findings indicate that integrating unstructured clinical text should be viewed as a complementary strategy whose effectiveness depends on the interaction among feature representation, classifier architecture, and imbalance-handling methods.

In addition, Table 2 indicates that resampling did not consistently improve performance for all classifiers as some models achieved comparable results when trained on the original imbalanced data. This finding suggests that the necessity of resampling is model dependent. Ensemble learning–based classifiers may inherently mitigate class imbalance effects, whereas other models benefit more substantially from resampling techniques. Therefore, resampling should be considered a robustness-oriented strategy rather than a mandatory preprocessing step.

Significant Features

Figure 3 illustrates the 20 most significant features identified for the LIH and CYCH datasets using shap (version 0.45.0). In Figure 3, features are ranked according to their mean absolute Shapley values, which quantify the global importance of each feature in relation to the model's output. Figure 3A presents the feature ordering for LIH, whereas Figure 3C depicts the ordering for CYCH. Figure 3 shows beeswarm plots that visualize the Shapley values for each patient concerning these features. The beeswarm plots convey the contribution of each feature to the model's output based on the magnitude and direction of the Shapley values. Figure 3B represents the contributions of LIH patients, whereas Figure 3D illustrates those of CYCH patients. Notably, the graphs reveal that the top 3 features consistently identified across both datasets were ratio of E- to A-wave velocities, left atrial size, and age.

XSL•FO
RenderX

Figure 3. The top 20 most important features identified by the model based on structured variables. Panels A and C display bar charts representing the mean absolute Shapley values, which indicate the average contribution of each feature to the model's output. Panels B and D present beeswarm plots of individual Shapley values for each feature across patients, where the position of each dot on the x-axis reflects that feature's contribution to the prediction for a given patient. The color of each dot corresponds to the relative value of the associated feature. BUN: blood urea nitrogen; CRP: C-reactive protein; E/A: ratio of E- to A-wave velocities; HbA_{1c}: hemoglobin A_{1c}; HDL: high-density lipoprotein; HR: heart rate; INR: international normalized ratio; LA: left atrial size; LVEF: left ventricular ejection fraction; LVIDd: left ventricular internal dimension in diastole; LVPWd: left ventricular posterior wall in diastole; N1A: level of consciousness responsiveness; N1C: level of consciousness commands; N2: best gaze; N3: visual fields; N8: sensory; N10: dysarthria; N11: extinction and inattention; PTTControl: partial thromboplastin time control; RR: respiratory rate; SBP: systolic blood pressure; SHAP: Shapley additive explanations; TG: triglyceride.

XSL•FO
RenderX

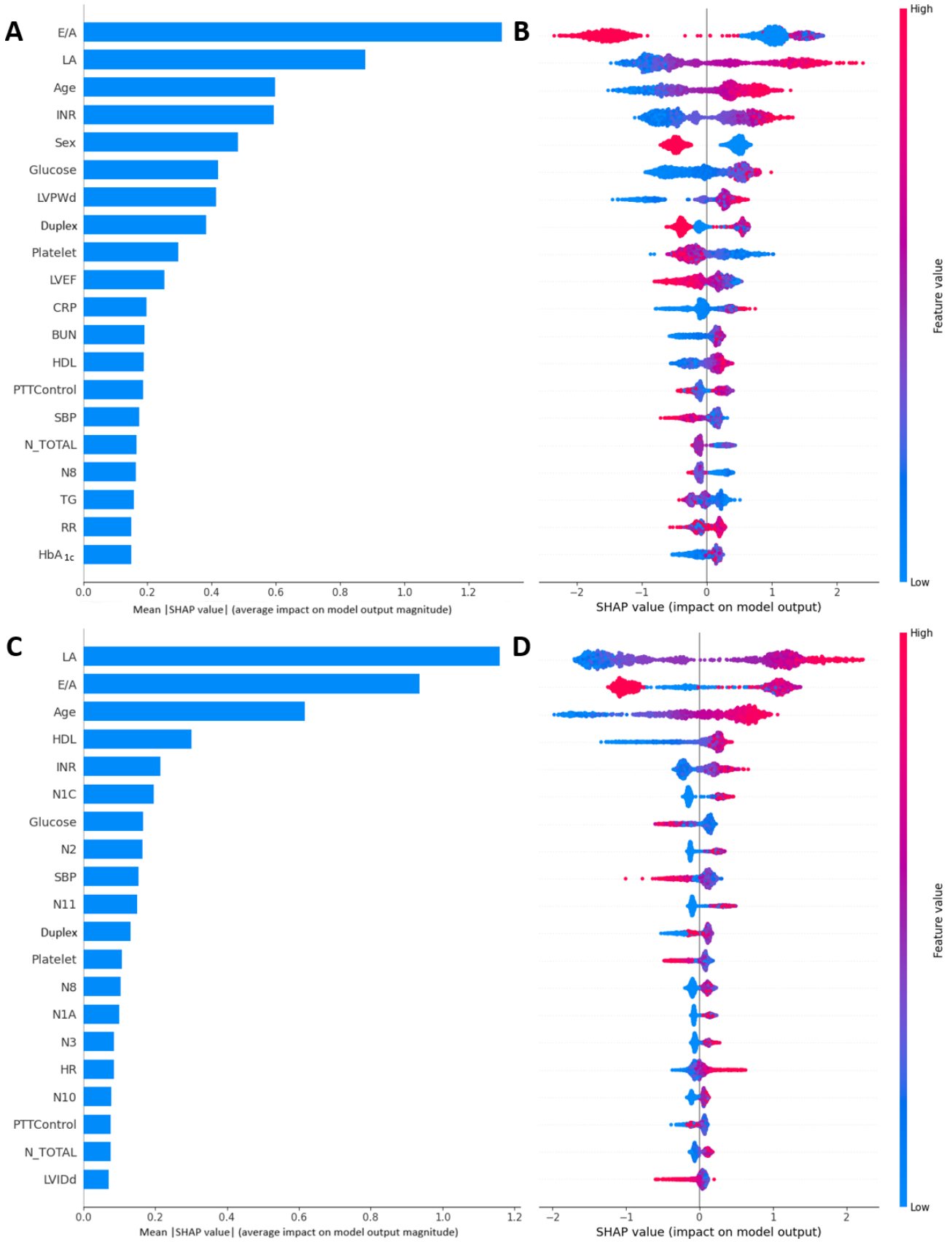

Clinical Applications and Significance

Predicting AF following a stroke is critical for effective secondary stroke prevention as it directly influences medical decision-making and patient outcomes. Given the constraints of health care resources, it is essential to optimize their use by incorporating efficient screening protocols. In this context, machine learning offers a highly effective approach. This study identified the optimal combination of variables derived from unstructured clinical text through rigorous external validation

XSL•FO
RenderX

supplemented by internal validation using the LIH dataset and further validated using EMR data from CYCH. Although models built on internal data are often preferred for clinical applications, our experiments revealed that models developed using the CYCH data occasionally outperformed those based on LIH data. This discrepancy may be attributed to missing information and the relatively small sample size of the LIH dataset. The models developed in this study aim to support clinicians by identifying high-risk patients who would benefit from additional screening measures, such as ECG, ultimately reducing the risk of missed diagnoses and ensuring timely and appropriate treatment.

Limitations

This study has several limitations that should be acknowledged. First, the data source poses a potential issue as the data were derived from EMRs within the hospitals. It is possible that patients were diagnosed with AF outside these institutions, introducing bias, particularly given the older age demographic of the hospital population. Second, regarding the data themselves, while generalizability was tested across 2 different hospitals, the variability in clerical styles between the hospitals may affect the consistency of the variables derived from unstructured clinical text. For structured variables, a high proportion of missing values in factors known to be associated with stroke or AF (eg, smoking history), uncertainties about the accuracy of the records, and the small and variable sample size could all impact the overall efficacy of the model. Finally, it should be noted that the predictors contributing to the model in this study do not imply causality.

Conclusions

This study demonstrates the feasibility of developing machine learning–based predictive models to identify AF in patients with ischemic stroke using EMR data. The integration of structured variables with variables derived from unstructured clinical text, including medical history and magnetic resonance imaging findings extracted from free-text sources, showed potential to improve predictive performance in selected model configurations. Internal and external validation results indicate that ensemble learning–based models performed favorably compared with other algorithmic approaches, supporting their potential utility for AF risk prediction in clinical settings.

Funding

This research was supported in part by the National Central University–Landseed Hospital Research and Development Office (NCU-LSH-111-B-008) and the Ministry of Science and Technology of the People's Republic of China (grant MOST 111-2410-H-008-026-MY2).

Data Availability

The datasets generated or analyzed during this study are not publicly available due to patient privacy and institutional data protection regulations but are available from the corresponding author on reasonable request.

Authors' Contributions

Conceptualization: YWC, YHH, SFS
Data curation: YWC, SFS
Formal analysis: YWC, YHH, SFS, YHY
Investigation: YWC, SFS
Methodology: YWC, YHH, SFS
Supervision: YHH
Validation: YWC, YHH, SFS, YHY
Writing—original draft: YWC, YHH, SFS, YHY
Writing—review and editing: YWC, YHH, SFS, YHY
All authors had full access to all the data in the study and take responsibility for the integrity of the data and the accuracy of the data analysis.

Conflicts of Interest

None declared.

Multimedia Appendix 1
Detailed definitions and summary statistics of structured clinical variables extracted from electronic medical records at Landseed International Hospital and Chia-Yi Christian Hospital, including variable descriptions, data types, distributions, and proportions of missing values.
[DOCX File, 31 KB - medinform_v14i1e78117_app1.docx]

References

1. Feigin VL, Brainin M, Norrving B, et al. World Stroke Organization (WSO): global stroke fact sheet 2022. Int J Stroke 2022 Jan;17(1):18-29. [doi: 10.1177/17474930211065917] [Medline: 34986727]

XSL•FO
RenderX

2. Feigin VL, Forouzanfar MH, Krishnamurthi R, et al. Global and regional burden of stroke during 1990–2010: findings from the Global Burden of Disease Study 2010. Lancet 2014 Jan 18;383(9913):245-254. [doi: 10.1016/s0140-6736(13)61953-4] [Medline: 24449944]
3. Pennlert J, Eriksson M, Carlberg B, Wiklund PG. Long-term risk and predictors of recurrent stroke beyond the acute phase. Stroke 2014 Jun;45(6):1839-1841. [doi: 10.1161/STROKEAHA.114.005060] [Medline: 24788972]
4. Bergström L, Irewall AL, Söderström L, Ögren J, Laurell K, Mooe T. One-year incidence, time trends, and predictors of recurrent ischemic stroke in Sweden from 1998 to 2010: an observational study. Stroke 2017 Aug;48(8):2046-2051. [doi: 10.1161/STROKEAHA.117.016815] [Medline: 28706114]
5. Feigin VL, Norrving B, Mensah GA. Global burden of stroke. Circ Res 2017 Feb 3;120(3):439-448. [doi: 10.1161/CIRCRESAHA.116.308413] [Medline: 28154096]
6. Lee M, Wu YL, Ovbiagele B. Trends in incident and recurrent rates of first-ever ischemic stroke in Taiwan between 2000 and 2011. J Stroke 2016 Jan;18(1):60-65. [doi: 10.5853/jos.2015.01326] [Medline: 26687123]
7. Lip GYH, Hunter TD, Quiroz ME, Ziegler PD, Turakhia MP. Atrial fibrillation diagnosis timing, ambulatory ECG monitoring utilization, and risk of recurrent stroke. Circ Cardiovasc Qual Outcomes 2017 Jan;10(1):e002864. [doi: 10.1161/CIRCOUTCOMES.116.002864] [Medline: 28096204]
8. Lee SR, Choi EK, Han KD, Cha MJ, Oh S. Trends in the incidence and prevalence of atrial fibrillation and estimated thromboembolic risk using the CHA2DS2-VASc score in the entire Korean population. Int J Cardiol 2017 Jun 1;236:226-231. [doi: 10.1016/j.ijcard.2017.02.039] [Medline: 28233629]
9. Ball J, Carrington MJ, McMurray JJ, Stewart S. Atrial fibrillation: profile and burden of an evolving epidemic in the 21st century. Int J Cardiol 2013 Sep 1;167(5):1807-1824. [doi: 10.1016/j.ijcard.2012.12.093] [Medline: 23380698]
10. Jones NR, Taylor CJ, Hobbs FD, Bowman L, Casadei B. Screening for atrial fibrillation: a call for evidence. Eur Heart J 2020 Mar 7;41(10):1075-1085. [doi: 10.1093/eurheartj/ehz834] [Medline: 31811716]
11. Huang CK, Wang JC, Chung CH, Chen SJ, Liao WI, Chien WC. The risk and timing of acute ischemic stroke after electrical cardioversion for atrial fibrillation in Taiwan: a nationwide population-based cohort study. Int J Cardiol 2022 Mar 15;351:55-60. [doi: 10.1016/j.ijcard.2021.12.035] [Medline: 34954280]
12. Mtwesi V, Amit G. Stroke prevention in atrial fibrillation: the role of oral anticoagulation. Med Clin North Am 2019 Sep;103(5):847-862. [doi: 10.1016/j.mcna.2019.05.006] [Medline: 31378330]
13. Lee E, Choi EK, Han KD, et al. Mortality and causes of death in patients with atrial fibrillation: a nationwide population-based study. PLoS ONE 2018 Dec 26;13(12):e0209687. [doi: 10.1371/journal.pone.0209687] [Medline: 30586468]
14. Chao TF, Liu CJ, Tuan TC, et al. Lifetime risks, projected numbers, and adverse outcomes in Asian patients with atrial fibrillation: a report from the Taiwan nationwide AF cohort study. Chest 2018 Feb;153(2):453-466. [doi: 10.1016/j.chest.2017.10.001] [Medline: 29017957]
15. Hsieh CY, Kao HM, Sung KL, Sposato LA, Sung SF, Lin SJ. Validation of risk scores for predicting atrial fibrillation detected after stroke based on an electronic medical record algorithm: a registry-claims-electronic medical record linked data study. Front Cardiovasc Med 2022 Apr 29;9:888240. [doi: 10.3389/fcvm.2022.888240] [Medline: 35571191]
16. Hsieh FI, Lien LM, Chen ST, et al. Get with the guidelines-stroke performance indicators: surveillance of stroke care in the Taiwan stroke registry: get with the guidelines-stroke in Taiwan. Circulation 2010 Sep 14;122(11):1116-1123. [doi: 10.1161/CIRCULATIONAHA.110.936526] [Medline: 20805428]
17. Hsieh FI, Chiou HY. Stroke: morbidity, risk factors, and care in Taiwan. J Stroke 2014 May;16(2):59-64. [doi: 10.5853/jos.2014.16.2.59] [Medline: 24949310]
18. Garg N, Kumar A, Flaker GC. Antiplatelet therapy for stroke prevention in atrial fibrillation. Mo Med 2010;107(1):44-47. [Medline: 20222295]
19. Själander S, Sjögren V, Renlund H, Norrving B, Själander A. Dabigatran, rivaroxaban and apixaban vs. high TTR warfarin in atrial fibrillation. Thromb Res 2018 Jul;167:113-118. [doi: 10.1016/j.thromres.2018.05.022] [Medline: 29803981]
20. Yang L, Brooks MM, Glynn NW, Zhang Y, Saba S, Hernandez I. Real-world direct comparison of the effectiveness and safety of apixaban, dabigatran, rivaroxaban, and warfarin in Medicare beneficiaries with atrial fibrillation. Am J Cardiol 2020 Jul 1;126:29-36. [doi: 10.1016/j.amjcard.2020.03.034] [Medline: 32359718]
21. Granger CB, Alexander JH, McMurray JJV, et al. Apixaban versus warfarin in patients with atrial fibrillation. N Engl J Med 2011 Sep 15;365(11):981-992. [doi: 10.1056/NEJMoa1107039] [Medline: 21870978]
22. Lip GY, Nieuwlaat R, Pisters R, Lane DA, Crijns HJ. Refining clinical risk stratification for predicting stroke and thromboembolism in atrial fibrillation using a novel risk factor-based approach: the Euro Heart Survey on atrial fibrillation. Chest 2010 Feb;137(2):263-272. [doi: 10.1378/chest.09-1584] [Medline: 19762550]
23. Van Gelder IC, Rienstra M, Bunting KV, et al. 2024 ESC Guidelines for the management of atrial fibrillation developed in collaboration with the European Association for Cardio-Thoracic Surgery (EACTS). Eur Heart J 2024 Sep 29;45(36):3314-3414. [doi: 10.1093/eurheartj/ehae176] [Medline: 39210723]
24. Karnik S, Tan SL, Berg B, et al. Predicting atrial fibrillation and flutter using electronic health records. Annu Int Conf IEEE Eng Med Biol Soc 2012;2012:5562-5565. [doi: 10.1109/EMBC.2012.6347254] [Medline: 23367189]
25. Chamberlain AM, Roger VL, Noseworthy PA, et al. Identification of incident atrial fibrillation from electronic medical records. J Am Heart Assoc 2022 Apr 5;11(7):e023237. [doi: 10.1161/JAHA.121.023237] [Medline: 35348008]

XSL•FO
RenderX

26. Hulme OL, Khurshid S, Weng LC, et al. Development and validation of a prediction model for atrial fibrillation using electronic health records. JACC Clin Electrophysiol 2019 Nov;5(11):1331-1341. [doi: 10.1016/j.jacep.2019.07.016] [Medline: 31753441]
27. Verhaeghe J, De Corte T, Sauer CM, et al. Generalizable calibrated machine learning models for real-time atrial fibrillation risk prediction in ICU patients. Int J Med Inform 2023 Jul;175:105086. [doi: 10.1016/j.ijmedinf.2023.105086] [Medline: 37148868]
28. Khurshid S, Keaney J, Ellinor PT, Lubitz SA. A simple and portable algorithm for identifying atrial fibrillation in the electronic medical record. Am J Cardiol 2016 Jan 15;117(2):221-225. [doi: 10.1016/j.amjcard.2015.10.031] [Medline: 26684516]
29. Hu M, Liu B. Mining and summarizing customer reviews. : ACM Presented at: Proceedings of the Tenth ACM SIGKDD International Conference on Knowledge Discovery and Data Mining; Aug 22-25, 2004; Seattle, WA. [doi: 10.1145/1014052.1014073]
30. Liu B, Hu M, Cheng J. Opinion observer: analyzing and comparing opinions on the web. Presented at: Proceedings of the 14th International Conference on World Wide Web; May 10-14, 2005. [doi: 10.1145/1060745.1060797]
31. Devlin J, Chang MW, Lee K, Toutanova K. BERT: pre-training of deep bidirectional transformers for language understanding. Presented at: Proceedings of the 2019 Conference of the North American Chapter of the Association for Computational Linguistics: Human Language Technologies; Jun 2-7, 2019. [doi: 10.18653/v1/N19-1423]
32. Gardazi NM, Daud A, Malik MK, Bukhari A, Alsahfi T, Alshemaimri B. BERT applications in natural language processing: a review. Artif Intell Rev 2025;58(6):166. [doi: 10.1007/s10462-025-11162-5]
33. Le Q, Mikolov T. Distributed representations of sentences and documents. Proc Mach Learn Res 2014;32(2):1188-1196 [FREE Full text]
34. Getzen E, Ruan Y, Ungar L, Long Q. Mining for health: a comparison of word embedding methods for analysis of EHRs data. In: Zhao Y, Chen DG, editors. Statistics in Precision Health: Theory, Methods and Applications: Springer International Publishing; 2024:313-338. [doi: 10.1007/978-3-031-50690-1_13]
35. Sparck Jones K. A statistical interpretation of term specificity and its application in retrieval. J Doc 1972 Jan;28(1):11-21. [doi: 10.1108/eb026526]
36. Salton G, Buckley C. Term-weighting approaches in automatic text retrieval. Inf Process Manag 1988;24(5):513-523. [doi: 10.1016/0306-4573(88)90021-0]
37. Aronson AR, Lang FM. An overview of MetaMap: historical perspective and recent advances. J Am Med Inform Assoc 2010;17(3):229-236. [doi: 10.1136/jamia.2009.002733] [Medline: 20442139]
38. Bodenreider O. The Unified Medical Language System (UMLS): integrating biomedical terminology. Nucleic Acids Res 2004 Jan 1;32(Database issue):D267-D270. [doi: 10.1093/nar/gkh061] [Medline: 14681409]
39. Uphaus T, Weber-Krüger M, Grond M, et al. Development and validation of a score to detect paroxysmal atrial fibrillation after stroke. Neurology 2019 Jan 8;92(2):e115-e124. [doi: 10.1212/WNL.0000000000006727] [Medline: 30530796]
40. Zheng X, Wang F, Zhang J, et al. Using machine learning to predict atrial fibrillation diagnosed after ischemic stroke. Int J Cardiol 2022 Jan 15;347:21-27. [doi: 10.1016/j.ijcard.2021.11.005] [Medline: 34774886]
41. Sung SF, Sung KL, Pan RC, Lee PJ, Hu YH. Automated risk assessment of newly detected atrial fibrillation poststroke from electronic health record data using machine learning and natural language processing. Front Cardiovasc Med 2022 Jul 29;9:941237. [doi: 10.3389/fcvm.2022.941237] [Medline: 35966534]
42. Hsieh CY, Lee CH, Sung SF. Development of a novel score to predict newly diagnosed atrial fibrillation after ischemic stroke: the CHASE-LESS score. Atherosclerosis 2020 Feb;295:1-7. [doi: 10.1016/j.atherosclerosis.2020.01.003] [Medline: 31972497]
43. Ratajczak-Tretel B, Lambert AT, Al-Ani R, et al. Prediction of underlying atrial fibrillation in patients with a cryptogenic stroke: results from the NOR-FIB Study. J Neurol 2023 Aug;270(8):4049-4059. [doi: 10.1007/s00415-023-11680-8] [Medline: 37162578]

Abbreviations

AF: atrial fibrillation
AIS: acute ischemic stroke
AS5F: age, stroke severity National Institutes of Health Stroke Scale>5 to find atrial fibrillation
AUC: area under the receiver operating characteristic curve
BERT: bidirectional encoder representations from transformers
CatBoost: categorical boosting
CHASE-LESS: coronary, heart failure, age, stroke severity–lipidemia, sugar, and prior stroke
CYCH: Chia-Yi Christian Hospital
ECG: electrocardiogram
EMR: electronic medical record
LightGBM: light gradient-boosting machine

XSL•FO
RenderX

LIH: Landseed International Hospital
NIHSS: National Institutes of Health Stroke Scale
SHAP: Shapley additive explanations
SMOTE: synthetic minority oversampling technique
TF-IDF: term frequency–inverse document frequency
TIA: transient ischemic attack
XGBoost: extreme gradient boosting

Edited by A Benis; submitted 02.Jun.2025; peer-reviewed by PJ Lee, SY Lin; revised version received 10.Jan.2026; accepted 19.Jan.2026; published 10.Mar.2026.

Please cite as:
Chen YW, Sung SF, Hu YH, Yang YH
Enhanced Prediction of Atrial Fibrillation in Patients With Ischemic Stroke Through Electronic Medical Records and Text Mining: Algorithm Development and Validation
JMIR Med Inform 2026;14:e78117
URL: https://medinform.jmir.org/2026/1/e78117
doi:10.2196/78117

© Yu-Wei Chen, Sheng-Feng Sung, Ya-Han Hu, Yu-Hsuan Yang. Originally published in JMIR Medical Informatics (https://medinform.jmir.org), 10.Mar.2026. This is an open-access article distributed under the terms of the Creative Commons Attribution License (https://creativecommons.org/licenses/by/4.0/), which permits unrestricted use, distribution, and reproduction in any medium, provided the original work, first published in JMIR Medical Informatics, is properly cited. The complete bibliographic information, a link to the original publication on https://medinform.jmir.org/, as well as this copyright and license information must be included.

XSL•FO
RenderX

Research on the Prediction of Coal Workers' Pneumoconiosis Based on Easily Detectable Clinical Data: Machine Learning Model Development and Validation Study

Haiquan Li[1,2], PhD; Jiaqi Jia[3], ME; Xu Shi[2], MM; Yudie Dong[3], ME; Songquan Wang[3], PhD; Yuming Cui[3], PhD; Wenlu Hang[2], PhD; Dekun Zhang[1], PhD

[1]School of Chemical Engineering & Technology, China University of Mining and Technology, Xuzhou, Jiangsu, China

[2]Department of Respiratory and Critical Care Medicine, Second Affiliated Hospital of Xuzhou Medical University, 32 Meijian Road, Xuzhou, Jiangsu, China

[3]School of Mechatronic Engineering, Jiangsu Normal University, Xuzhou, Jiangsu, China

Corresponding Author:
Wenlu Hang, PhD
Department of Respiratory and Critical Care Medicine, Second Affiliated Hospital of Xuzhou Medical University, 32 Meijian Road, Xuzhou, Jiangsu, China

Abstract

Background: Coal workers' pneumoconiosis (CWP) is the most prevalent occupational disease that causes irreversible lung damage. Early prediction of CWP is the key to blocking the irreversible process of pulmonary fibrosis. The prediction of CWP based on imaging data and biomarker detection is constrained due to high cost and poor convenience.

Objective: The study aimed to use easily detectable clinical data to construct a prediction model for CWP through machine learning (ML) methods.

Methods: A prediction framework was established using a moderate-sized dataset and multidimensional clinical features, including occupational information, lung function parameters, and blood indicators. Six ML algorithms (light gradient boosting machine, random forest, extreme gradient boosting, categorical boosting, support vector machine, and logistic regression) were trained and evaluated using a stratified 5-fold cross-validation and a held-out test set. Hyperparameter optimization was performed using a unified Optuna-based strategy to ensure fair comparison across models. Model interpretability was assessed using Shapley Additive Explanation on top-performing models. In addition, an ablation analysis was conducted by retraining models after excluding job type to assess the independent predictive value of clinical biomarkers.

Results: All 6 models achieved consistently high predictive performance, and the differences among the top-performing models were small on the test set. After Optuna-based optimization, light gradient boosting machine and categorical boosting achieved high test-set area under curve values (0.974 and 0.975, respectively), while extreme gradient boosting achieved the highest recall (0.926) and F_1-score (0.952). Compared with the baseline models, hyperparameter optimization resulted in only minor performance changes, indicating robust prediction under the current feature set and evaluation protocol. Shapley Additive Explanation analysis consistently identified age, forced expiratory volume/forced vital capacity, and platelet count as key contributors to CWP risk prediction. The ablation analysis further showed that model performance remained strong after removing job type, supporting the independent predictive value of clinical features beyond occupational history.

Conclusions: The research results have confirmed the potential of combining simple multidimensional features with ML algorithms for predicting CWP and provided new ideas for early diagnosis and intervention of patients with CWP.

(JMIR Med Inform 2026;14:e80156) doi:10.2196/80156

KEYWORDS

coal workers' pneumoconiosis; disease prediction; machine learning; clinical data; job-type

Introduction

As a traditional fossil energy source, coal has long held an important position in the global energy system. A large amount of respiratory coal dust can be generated during coal mining, processing, loading, and transportation and enter the human lungs through diffusion and sedimentation, inducing the occurrence of coal workers' pneumoconiosis (CWP) [1]. The pathogenesis of CWP is complex, characterized by strong concealment in the early stage, high mortality rate in the later stage, and poor quality of life for patients. Once diagnosed, the course of the disease is irreversible and there is currently no

XSL•FO
RenderX

effective cure in clinical practice [2,3]. Early identification of CWP can delay the deterioration of the condition and prevent it from developing into progressive mass fibrosis or respiratory failure.

High kilovoltage X-ray examination is the gold standard for CWP diagnosis. To avoid the problem of overlapping and occlusion of tissue and organ images, computed tomography detection technology has also been used for CWP diagnosis [4,5]. However, the imaging differences among early patients with CWP are not significant, and there are also issues such as high cost, high radiation risk, and convenient equipment use, which collectively constrain the early identification of patients with CWP. At present, the development of biomarker detection technology has significantly improved the clinical feasibility of CWP early screening [6,7]. As a measurable biological indicator, biomarkers can objectively reflect the physiological and pathological status of the body, such as proteins, genes, and metabolites, etc. The research on the expression levels of biomarkers in the serum of patients with CWP is the most extensive, including transforming growth factor-α [8], interleukin-8 [9], noncoding RNA (such as microRNA) [10], and common lipid metabolites such as phosphatidylethanolamines and free fatty acids [11], all of which have been proven to have important guiding significance for early identification of CWP. On the other hand, the occurrence and development of lung diseases usually have an impact on changes in lung microbiota and respiratory flora. MicroRNA expression profiles [12], surfactant-associated protein A and surfactant-associated protein D [13] in bronchoalveolar lavage fluid, and transforming growth factor-β, interleukin-1β, and matrix metalloproteinase-9 in sputum [14], as well as benzene and aldehydes in volatile organic compounds of exhaled breath [15], are also commonly used for early identification of CWP. However, metabolic processes are regulated by multiple factors. The lower specificity and sensitivity reduce the reliability of early screening of CWP through a single biomarker. Meanwhile, the high cost of detecting specific biomarkers also limits the early identification of patients with CWP.

Previous studies have shown that blood routine examination, as an economical, efficient, and easy-to-operate screening method in clinical practice, has important guiding significance for early identification and risk assessment of diseases, especially in mining areas where medical resources are relatively scarce [16,17]. CWP usually leads to lung infections or the occurrence of inflammatory diseases, which are often reflected in lung function, coagulation function, inflammatory markers, etc. This provides the possibility for early identification of patients with CWP [18]. At present, there is a relative lack of research on CWP prediction based on routine clinical blood data. This study aims to develop a low-cost CWP early screening tool based on machine learning (ML) models. By establishing a 3D feature space of occupational exposure history, lung function parameters, and routine blood indicators, and combining 6 algorithms including light gradient boosting machine (LightGBM), random forest (RF), extreme gradient boosting (XGBoost), categorical boosting (CatBoost), support vector machine (SVM), and logistic regression (LR) for comparative analysis of predictive performance. In addition, an Optuna-based hyperparameter optimization strategy was applied to tune the models under a unified evaluation protocol. Finally, the Shapley Additive Explanation (SHAP) method was used to interpret model predictions and analyze the contributions of key parameters such as lung function indicators and blood indicators. The high-precision and interpretable prediction model constructed can provide theoretical basis for early screening of CWP.

Methods

Ethical Considerations

This study was approved by the Second Affiliated Hospital of Xuzhou Medical University ([2024] 082701). Due to the retrospective nature of the study and the use of deidentified data, the requirement for informed consent was waived by the institutional review board. To ensure privacy and confidentiality, all personal identifiers, such as names and national identification numbers, were removed and replaced with unique study IDs before data analysis. No financial compensation was provided to the participants as the data were extracted from routine clinical and physical examination records. Furthermore, we confirm that no identifiable information or images of individual participants are included in this manuscript or its supplementary materials.

Data Sources

Two hundred eighty-seven patients with CWP were admitted to a large tertiary hospital from June 28, 2022, to September 20, 2024. Dust-exposed workers undergoing annual occupational health examinations at the same hospital from 2022 to 2024 were considered as controls. Considering some workers attended examinations in multiple years, records were deduplicated using a unique personal identifier, and only the most recent examination record per worker was retained, yielding 2446 unique controls. These data were retrospectively extracted from the hospital's electronic medical records system and physical examination database. All participants were male, aged between 22 and 90 years, and were employees of a certain mining group. The testing report included common demographic information, job types, and routine biochemical indicators.

The clinical test data of dust-exposed workers and patients with CWP were intersected, and 17 indicators were selected as candidate features. These indicators included job type, age, forced expiratory volume/forced vital capacity (FEV1/FVC), white blood cell count (WBC), absolute neutrophil count (ANC), absolute lymphocyte count (ALC), absolute monocyte count (AMC), absolute eosinophil count (AEC), red blood cell count, hemoglobin, platelet count (PLT), alanine aminotransferase (ALT), glucose, triglycerides, cholesterol, high-density lipoprotein, and low-density lipoprotein. The raw dataset initially comprised 36 job types. However, when categorized by disease status, a highly significant class imbalance was observed that the number of healthy individuals exposed to dust was approximately 8 times that of patients with CWP. This severe imbalance phenomenon can cause the model to lean toward the majority class during training, thereby reducing its ability to recognize diseased samples and affecting the model's generalization performance [19]. Therefore, the original 36 job

XSL•FO
RenderX

titles were first merged into 11 broader job categories based on similarity in work environment and job tasks. And then examined the distribution of CWP cases across these categories and found substantial imbalance (eg, only 1 CWP case among vehicle drivers vs 218 cases among mixed excavation and coal mining workers). To avoid unstable estimates driven by rare categories and to ensure adequate case representation for modeling, we restricted the analytic cohort to 5 job categories with sufficient CWP case counts, including mixed excavation and coal mining workers, excavation workers, coal miners, winch operators, and conveyor operators. After this restriction, the final dataset included 1085 dust-exposed healthy individuals and 271 participants with CWP.

Data Preprocessing

After verification, it was found that FEV1/FVC and low-density lipoprotein had missing values, accounting for 3.68% (50/1356) and 1.48% (20/1356), respectively. In order to avoid the impact of missing values on subsequent analysis and model training, the *k*-nearest neighbor (KNN) algorithm was used to fill in the missing value variables. The KNN imputation was performed within the training data for each fold in cross-validation, ensuring that the test data remained unseen during preprocessing. The specific calculation method is shown in equation (1).

$$(1)d(xi,xj)\sum k=1p(xik-xjk)2$$

Among them, x_i and x_j, respectively, represent the feature vectors of 2 samples, and x_{ik} and x_{jk}, respectively, represent the *k*th feature of these 2 samples.

The categorical variable job type was processed using one-hot encoding, which converts each category into a binary feature column. Categories include mixed excavation and coal mining, excavation workers, winch operators, conveyor operators, and coal miners. The remaining 15 continuous feature variables were standardized, and each feature was transformed into a distribution with a mean 0 (SD 1) for the model to analyze. Standardization was performed only on the training data, with the same scaling applied to the validation and test sets. The calculation method for the standard score of each feature is shown in equation (2).

$$(2)Z=x-\mu\sigma$$

Among them, x is a certain value of the feature in the original data, μ is the mean of the feature, and σ is the SD of the feature.

Statistical Analysis and Feature Selection

Statistical analysis was conducted using SPSS Statistics (version 26.0; IBM Corp). The normality of quantitative data was tested using the *K-S* test, and the homogeneity of variance was tested using the Levene test. Data with normal distribution were represented by mean (SD), and intergroup comparison was tested using 2 independent samples *t* test. The data with nonnormal distribution were represented by median (P25-P75), and Mann-Whitney *U* test was used for intergroup comparison. Categorical variables were represented by the number of examples (%), and comparison between groups was conducted using the chi-square test. The difference was statistically significant with $P<.05$. The Least Absolute Shrinkage and Selection Operator (LASSO) algorithm, an embedded feature selection method, was used for regression analysis to identify key feature variables associated with CWP, thereby reducing model complexity and enhancing generalization capability. LASSO regression achieved feature selection by performing α regularization on coefficients, shrinking the coefficients of less important features to 0 [20]. To ensure no information leakage, LASSO feature selection was performed within each fold's training data, and the same selected features were applied to the validation data within each fold. This method was combined with correlation analysis in filtering methods to comprehensively select features.

Construction and Evaluation of ML Models

Six representative ML models including tree-based ensemble learning models (LightGBM, XGBoost, RF, and CatBoost) and traditional classification algorithms (LR and SVM) were used for constructing CWP prediction models. A brief overview of each model's key characteristics and its relevance to this study is provided below.

For tree-based ensemble learning models, XGBoost uses second-order Taylor expansion for high accuracy and speed, incorporates regularization to prevent overfitting, and supports parallel computing for efficient training [21]. LightGBM uses a leaf-wise growth strategy and histogram-based feature discretization for efficiency, with built-in class weight adjustments beneficial for imbalanced datasets [22]. CatBoost uses an ordered boosting strategy for better generalization, directly handles categorical features, and uses a symmetric tree structure to reduce overfitting [23]. RF builds multiple decision trees from bootstrapped samples, randomly selects features at each split, and aggregates predictions through voting for robust classification [24].

To compare model performance on imbalanced datasets, 2 traditional models were also selected for comparison with the ensemble models. LR as a generalized linear model predicts probabilities using a sigmoid function [25]. SVM finds an optimal hyperplane to separate classes, using slack variables and a radial basis function kernel for inseparable data. Class weights were also incorporated into its objective function for imbalance handling [26]. In this study, class weights were applied in the loss functions of both traditional models to effectively handle the class imbalance issue.

Python (version 3.8.0; Python Software Foundation) software was used for model training and evaluation, randomly dividing the dataset into training and test set in an 8:2 ratio. To further assess model stability, 5-fold stratified cross-validation within the training data was used. In this procedure, the dataset was randomly divided into 5 nonoverlapping subsets. In each fold, 4 subsets were used as the training set, and the remaining 1 subset was used for validation. This process was repeated 5 times, and the average performance across all folds was taken as the evaluation metric. The test set was only used for the final model evaluation, ensuring it remained unseen during model training and hyperparameter tuning. In the process of model training and evaluation, based on the confusion matrix, the performance of the model was comprehensively judged through accuracy, precision, recall, F_1-score value, and the area under

XSL•FO
RenderX

curve (AUC) of the subjects. The corresponding calculation formulas are as follows:

(3)Accuracy=TN+FNTP+FP

(4)Precision=TPTP+FP

(5)Recall=TPTP+FN

(6)F1=2∗precision∗recallprecision+recall

Among them, *TP* represents true positive, *TN* represents true negative, *FP* represents false positive, and *FN* represents false negative. Figure 1 shows the technical roadmap of this study.

Figure 1. The technical roadmap of this study. AUC: area under the curve; CatBoost: categorical boosting; LightGBM: light gradient boosting machine; LR: logistic regression; RF: random forest; SHAP: Shapley Additive Explanation; SVM: support vector machine; XGBoost: extreme gradient boosting.

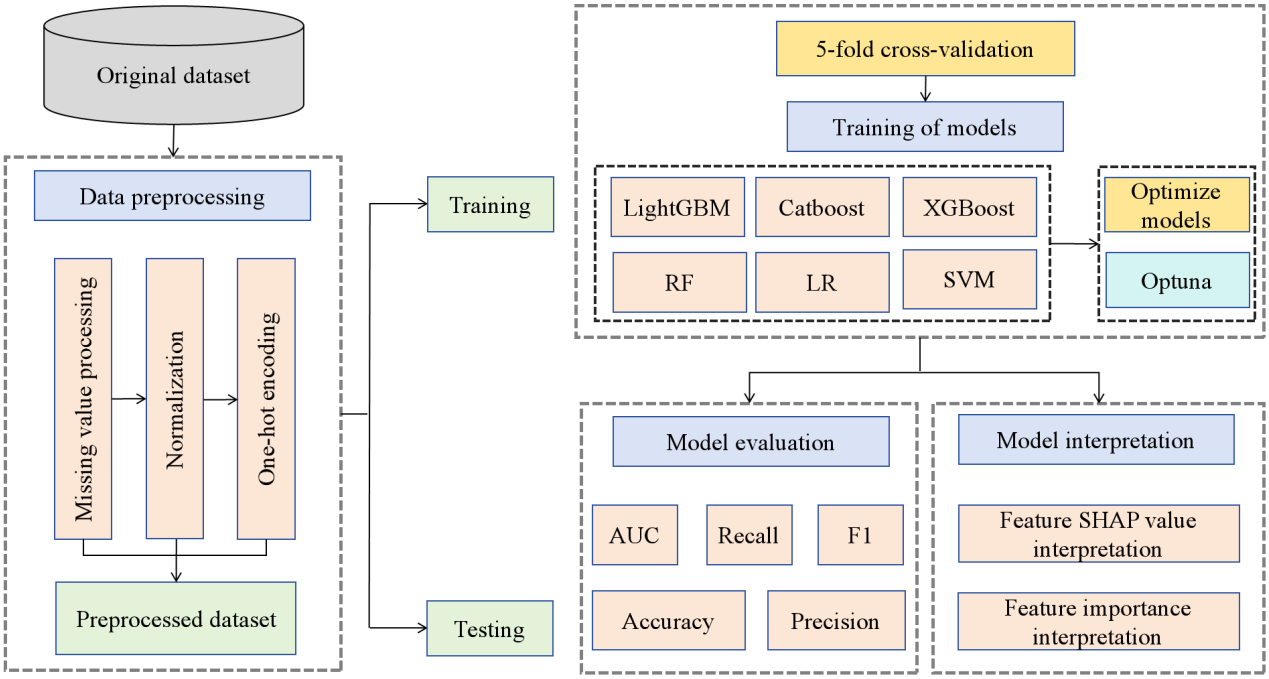

Results

Results of Statistical Analysis and Feature Selection

Table 1 shows the comparison of basic characteristics between the dust-exposed workers and the patients with CWP. It is found that 13 indicators, including job type, age, FEV1/FVC, WBC, ANC, ALC, AMC, AEC, hemoglobin, PLT, ALT, cholesterol, and glucose, have statistical significance (P<.05) compared between the 2 groups.

XSL•FO
RenderX

Table . Comparison of basic characteristics between the dust-exposed workers and the patients with coal workers' pneumoconiosis.

	Healthy	Disease	Test	Statistic	*P* value
Job type/Case	1085	271	Pearson χ^2	—[a]	<.001
Mixed workers for excavation and coal mining, n (%)	160 (14.7)	219 (80.8)	—	—	—
Excavator workers, n (%)	253 (23.3)	35 (12.9)	—	—	—
Winch operator, n (%)	260 (24)	3 (1.1)	—	—	—
Conveyor operator, n (%)	234 (21.6)	6 (2.2)	—	—	—
Coal miners, n (%)	178 (16.4)	8 (3)	—	—	—
Age, median (IQR)	48 (39-52)	69 (62-77)	Mann-Whitney *U*	*U*=11,900, *Z*=−23.43	<.001
FEV1/FVC[b] (%), median (IQR)	90 (86-97)	75.86 (68-89)	Mann-Whitney *U*	*U*=177,046, *Z*=12.02	<.001
WBC[c] ($\times 10^9$ /L), median (IQR)	6.36 (5.42-7.60)	5.84 (4.92-6.96)	Mann-Whitney *U*	*U*=177,670, *Z*=5.32	<.001
ANC[d] ($\times 10^9$ /L), median (IQR)	3.53 (2.86-4.39)	2.97 (2.21-3.98)	Mann-Whitney *U*	*U*=185,504, *Z*=6.67	<.001
ALC[e] ($\times 10^9$ /L), median (IQR)	2.21 (1.82-2.69)	2.01 (1.58-2.72)	Mann-Whitney *U*	*U*=163,138, *Z*=2.80	.005
AMC[f] ($\times 10^9$ /L), median (IQR)	0.39 (0.33-0.48)	0.47 (0.38-0.68)	Mann-Whitney *U*	*U*=94,124, *Z*=−9.17	<.001
AEC[g] ($\times 10^9$ /L), median (IQR)	0.16 (0.10-0.25)	0.13 (0.07-0.19)	Mann-Whitney *U*	*U*=174,854, *Z*=4.83	<.001
RBC[h] ($\times 10^{12}$ /L), median (IQR)	4.89 (4.64-5.12)	4.85 (4.46-5.33)	Mann–Whitney *U*	*U*=150,982, *Z*=0.69	.49
HB[i] (g/L), median (IQR)	151 (144-158)	148 (136-160)	Mann-Whitney *U*	*U*=161,103, *Z*=2.44	.01
PLT[j] ($\times 10^9$ /L), median (IQR)	244 (211-276)	200 (158.50-240)	Welch t	*U*=208,796, *Z*=10.71	<.001
ALT[k] (U/L), median (IQR)	20 (15-27)	17 (12-24)	Mann-Whitney *U*	*U*=180,185, *Z*=5.75	<.001
GLU[l] (mmol/L), median (IQR)	5.25 (4.85-5.75)	4.91 (4.41-5.62)	Mann-Whitney *U*	*U*=180,125, *Z*=6.14	<.001
TG[m] (mmol/L), median (IQR)	1.42 (0.99-2.33)	1.28 (0.96-2.01)	Mann-Whitney *U*	*U*=157,897, *Z*=1.89	.06
CHOL[n] (mmol/L), median (IQR)	4.86 (4.29-5.52)	4.48 (3.67-5.22)	Mann-Whitney *U*	*U*=181,528, *Z*=5.98	<.001
HDL[o] (mmol/L), median (IQR)	1.27 (1.12-1.47)	1.23 (1.05-1.54)	Mann-Whitney *U*	*U*=150,479, *Z*=0.60	.55
LDL[p] (mmol/L), median (IQR)	2.67 (2.29-3.11)	2.69 (2.13-3.21)	Mann-Whitney *U*	*U*=129,398, *Z*=0.67	.50

[a]Not available.

[b]FEV1/FVC: forced expiratory volume/forced vital capacity.

[c]WBC: white blood cell.

[d]ANC: absolute neutrophil count.

[e]ALC: absolute lymphocyte count.

[f]AMC: absolute monocyte count.

XSL•FO
RenderX

[g]AEC: absolute eosinophil count.
[h]RBC: red blood cell count.
[i]HB: hemoglobin.
[j]PLT: platelet count.
[k]ALT: alanine aminotransferase.
[l]GLU: glucose.
[m]TG: triglycerides.
[n]CHOL: cholesterol.
[o]HDL: high-density lipoprotein.
[p]LDL: low-density lipoprotein.

Figure S1 in Multimedia Appendix 1 showed the cross-validation curve of LASSO regression. When the α value is low, the model may contain too many irrelevant features, resulting in significant errors (overfitting). When the α value is large, the model may remove too many important features, which also leads to an increase in error (underfitting). At the optimal α value, the cross-validation error is minimized. The LASSO coefficient plot was shown in Figure S2 in Multimedia Appendix 1, which showed that the coefficients of 9 features, including job-type mixed excavation coal, job-type excavation worker, job-type conveyor operator, job-type winch operator, age, FEV1/FVC, AMC, PLT, and ANC, were not 0 at the optimal α value. This indicated the criticality of these features and their significant explanatory power for the target variable; therefore, they should be retained in the final model for prediction.

In order to avoid the problem of multicollinearity caused by strong correlation between features, this study used correlation analysis in a filtering method to comprehensively select features based on the 17 features selected through statistical analysis and LASSO regression screening in the early stage. By calculating the Spearman correlation coefficient matrix (Figure 2), the threshold was set to an absolute value of *r* greater than 0.8, and highly correlated terms in the feature pairs were selected. Based on the absolute value of LASSO regression weights, the features that contribute more to the target were retained, thereby eliminating redundant variables. Specifically, a Spearman correlation matrix was computed on the training data, and pairs with an absolute value of *r* greater than 0.8 were considered highly correlated. For each highly correlated pair, the feature with the larger absolute LASSO coefficient was retained and the other feature was removed. In the current dataset, WBC and ANC showed high correlation (r=0.833); thus, WBC was removed and ANC was retained. After redundancy filtering, 16 nonredundant features were used as inputs for subsequent model development, including job-type mixed excavation coal, job-type excavation worker, job-type conveyor operator, job-type winch operator, job-type coal miner, age, FEV1/FVC, ANC, ALC, AMC, AEC, hemoglobin, PLT, ALT, cholesterol, and glucose.

XSL•FO
RenderX

Figure 2. Spearman correlation coefficient matrix. AEC: absolute eosinophil count; ALC: absolute lymphocyte count; ALT: alanine aminotransferase; AMC: absolute monocyte count; ANC: absolute neutrophil count; CHOL: cholesterol; FEV1/FVC: forced expiratory volume/forced vital capacity; GLU: glucose; HB: hemoglobin; PLT: platelet count; WBC: white blood cell count.

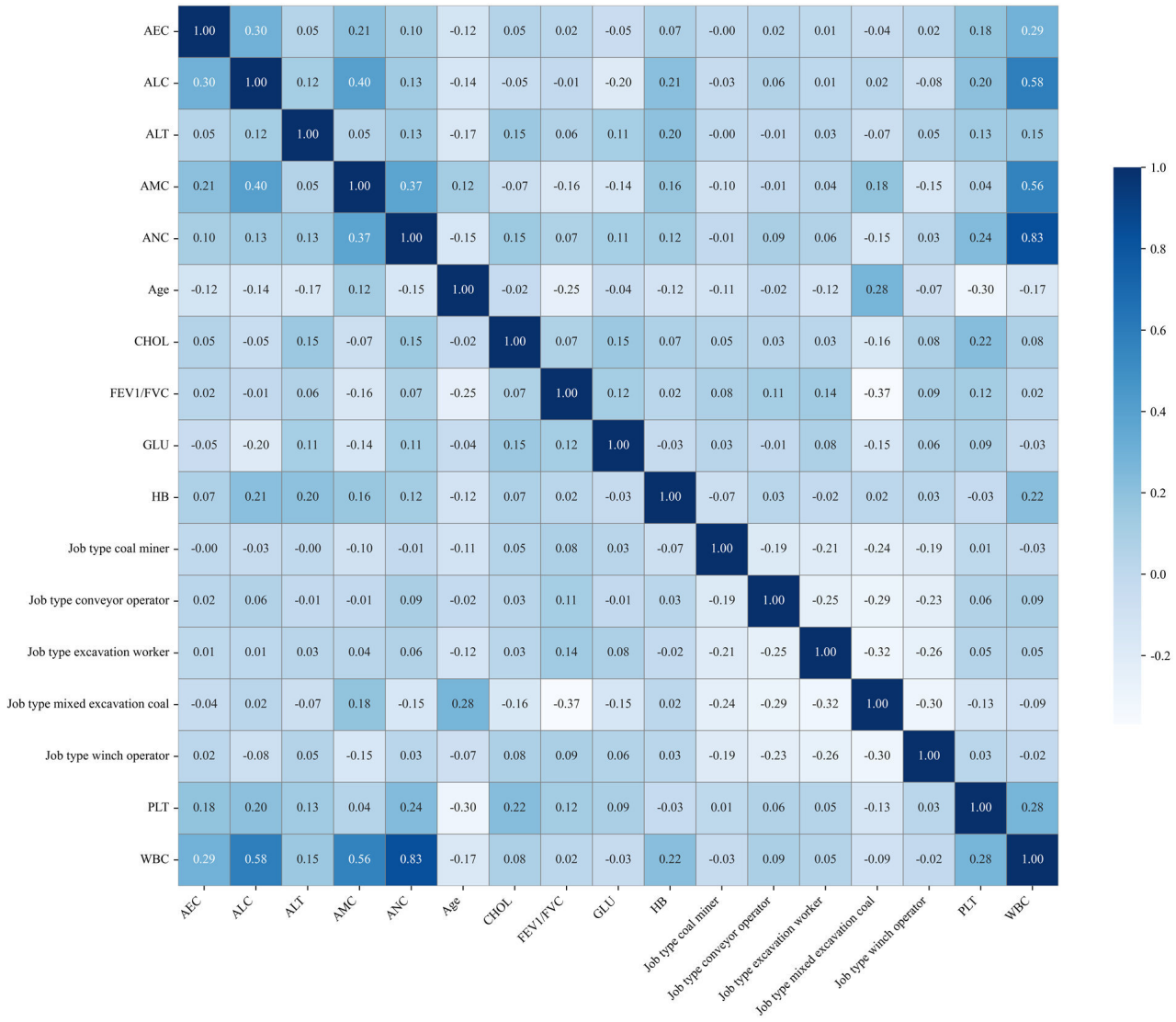

Evaluation of the CWP Prediction Model

The selected 16 clinical features were input as feature variables into 6 ML models, and 5-fold cross-validation was performed for each model during training. The performance of each model was comprehensively evaluated based on the test-set data, and the output results of each model were organized and are summarized in Table 2. Meanwhile, the visualized results of the data in Table 2 are shown in Figure S3 in Multimedia Appendix 1. From the figure, it can be seen that the AUC of each fold of the 6 models in cross-validation was consistently high (all folds >0.90), indicating that the generalization ability of the 6 models is strong and stable. The AUC values of the 6 models were ranked in descending order as CatBoost (0.979), LightGBM (0.978), XGBoost (0.976), RF (0.972), SVM (0.968), and LR (0.967). This result indicated that the performance of ensemble learning models on imbalanced datasets was superior to traditional models, verifying the advantages of ensemble learning models in dealing with such problems [27]. Taking into account accuracy, precision, recall, and F_1-score, both the LightGBM and RF models achieved the highest accuracy (0.982), precision (1), and F_1-score (0.951), while the LR model had the highest recall (0.926). Therefore, based on the overall performance across multiple evaluation indicators, LightGBM and RF were preliminarily considered as top-performing predictive models.

XSL•FO
RenderX

Table . Evaluation of predictive performance of different models[b].

Model	Accuracy	Precision	Recall	F_1-score	AUC[a]
LightGBM[c]	0.982[b]	1.000[b]	0.907	0.951[b]	0.978
CatBoost[d]	0.978	0.980	0.907	0.942	0.979[b]
XGBoost[e]	0.978	0.980	0.907	0.942	0.976
RF[f]	0.982[b]	1.000[b]	0.907	0.951[b]	0.972
LR[g]	0.956	0.862	0.926[b]	0.893	0.967
SVM[h]	0.963	0.907	0.907	0.907	0.968

[a]AUC: area under the curve.

[b] Significant values.

[c]LightGBM: light gradient boosting machine.

[d]CatBoost: categorical boosting.

[e]XGBoost: extreme gradient boosting.

[f]RF: random forest.

[g]LR: logistic regression.

[h]SVM: support vector machine.

In order to further improve the predictive performance and to ensure a fair comparison among candidate models, this study used the Optuna algorithm to optimize the hyperparameters of all 6 ML models (LightGBM, CatBoost, XGBoost, RF, LR, and SVM) under the same optimization budget, and also conducted 5-fold cross-validation during training. The output results of each optimized model were summarized in Table 3, and the visualized results were shown in Figure S4 in Multimedia Appendix 1. The results showed that the AUC of each fold in cross-validation was consistently high (all folds >0.90), indicating that the generalization ability of the 6 models was strong and stable. After applying an equivalent hyperparameter optimization strategy, the overall performance of the 6 models remains high and the differences among the top-performing models were small. Specifically, CatBoost and LightGBM achieved high test-set AUC values (0.975 and 0.974, respectively). In addition, XGBoost achieved the highest recall (0.926) and F_1-score (0.952) on the test set. Compared with the baseline results, hyperparameter optimization led to only small changes in performance. Overall, the 6 models maintained consistently high performance under the current evaluation protocol.

Table . Performance evaluation of optimized models.

Model	Accuracy	Precision	Recall	F_1-score	AUC[a]
LightGBM[b]-Optuna	0.982	1	0.907	0.951	0.974
CatBoost[c]-Optuna	0.982	1	0.907	0.951	0.975
XGBoost[d]-Optuna	0.982	0.98	0.926	0.952	0.969
RF[e]-Optuna	0.974	0.961	0.907	0.933	0.968
LR[f]-Optuna	0.952	0.847	0.926	0.885	0.968
SVM[g]-Optuna	0.967	0.925	0.907	0.916	0.962

[a]AUC: area under the curve.

[b]LightGBM: light gradient boosting machine.

[c]CatBoost: categorical boosting.

[d]XGBoost: extreme gradient boosting.

[e]RF: random forest.

[f]LR: logistic regression.

[g]SVM: support vector machine.

Model Interpretability

In order to gain a deeper understanding of the impact of various clinical features on the model's prediction results, this study used the SHAP method to conduct interpretability analysis on the 2 representative top-performing models LightGBM-Optuna and CatBoost-Optuna. The calculation method was shown in Equation 7.

$$(7)\text{SHAP}(y)= \text{SHAP}(\text{base})+\sum_{i=1}^{n}\text{SHAP}(xi)$$

XSL•FO
RenderX

Among them, *SHAP (base)* is the baseline value of the entire model, and *SHAP* (x_i) is the contribution of each sample to the final prediction result.

The summary results of SHAP values are shown in Figure 3, which displayed the distribution of SHAP values for 17 input feature variables. Each point in the figure represented a feature, and the position of the point represented the SHAP value of the feature, which was the contribution of the feature to the model output. If the SHAP value is positive, it indicates that the feature increases the risk of disease and has a positive impact on the output results. Conversely, if it is negative, it indicates that the feature reduces the risk of disease and has a negative impact on the output results. In addition, the color range from blue to red reflects the actual value of the feature, with red indicating high values and blue indicating low values. The darker the color, the stronger the impact of the feature on the target variable. Overall, both models showed consistent patterns in feature effects. Age is the most influential variable, and higher age values were mainly associated with positive SHAP values, suggesting that older individuals tended to have a higher predicted disease risk. In contrast, higher values of FEV1/FVC were mostly distributed on the negative side, indicating that better lung function (higher FEV1/FVC) was related to a lower predicted risk. PLT showed a similar tendency, with higher values generally corresponding to negative SHAP values. On the other hand, higher AMC values tended to correspond to positive SHAP values, indicating a positive association with increased predicted risk. These results suggested that the model predictions were largely driven by age-related factors and lung function indicators, together with selected hematological and biochemical variables.

Figure 3. Summary chart of SHAP values. (a) LightGBM-Optuna; (b) CatBoost-Optuna. AEC: absolute eosinophil count; ALC: absolute lymphocyte count; ALT: alanine aminotransferase; AMC: absolute monocyte count; ANC: absolute neutrophil count; CHOL: cholesterol; FEV1/FVC: forced expiratory volume/forced vital capacity; GLU: glucose; HB: hemoglobin; PLT: platelet count; SHAP: Shapley Additive Explanations.

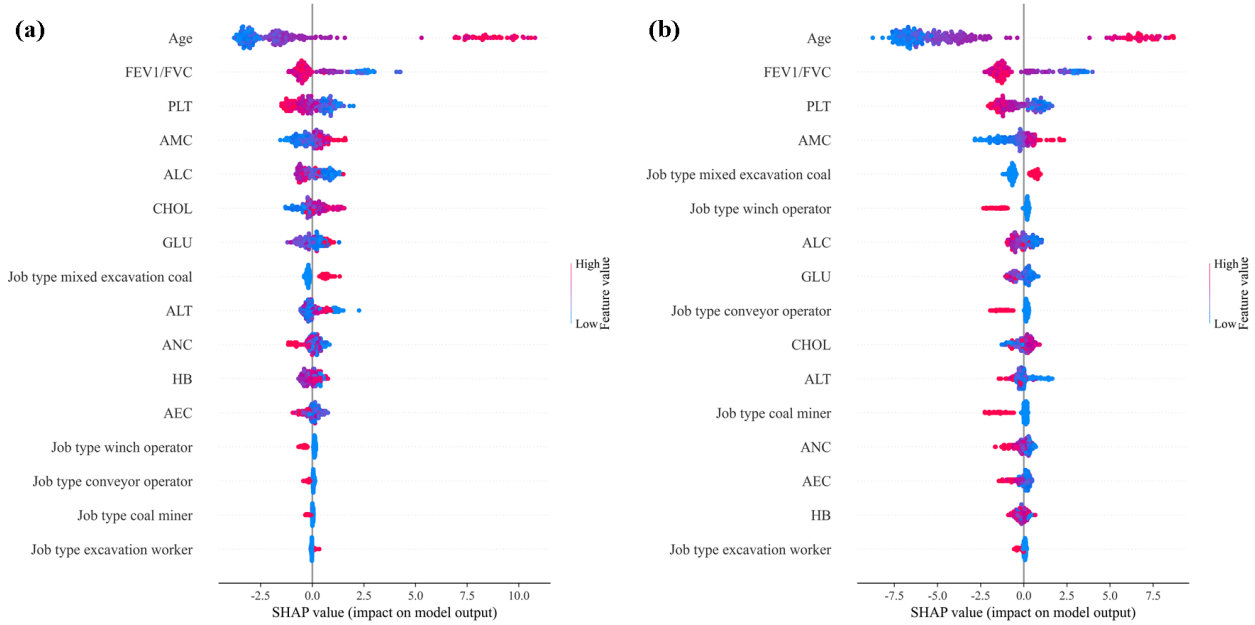

Figure 4 showed the SHAP feature importance matrix, which arranged the average SHAP absolute value of each feature from high to low. The horizontal axis represented the contribution value, and the larger the value, the greater the contribution to the model results. In both the Optuna-tuned LightGBM and CatBoost models, age showed the highest contribution, followed by FEV1/FVC and PLT, which indicates that these variables play the most important roles in the prediction of CWP risk.

XSL•FO
RenderX

Figure 4. Matrix diagram of SHAP feature importance. (a) LightGBM-Optuna; (b) CatBoost-Optuna. AEC: absolute eosinophil count; ALC: absolute lymphocyte count; ALT: alanine aminotransferase; AMC: absolute monocyte count; ANC: absolute neutrophil count; CHOL: cholesterol; FEV1/FVC: forced expiratory volume/forced vital capacity; GLU: glucose; HB: hemoglobin; PLT: platelet count; SHAP: Shapley Additive Explanation.

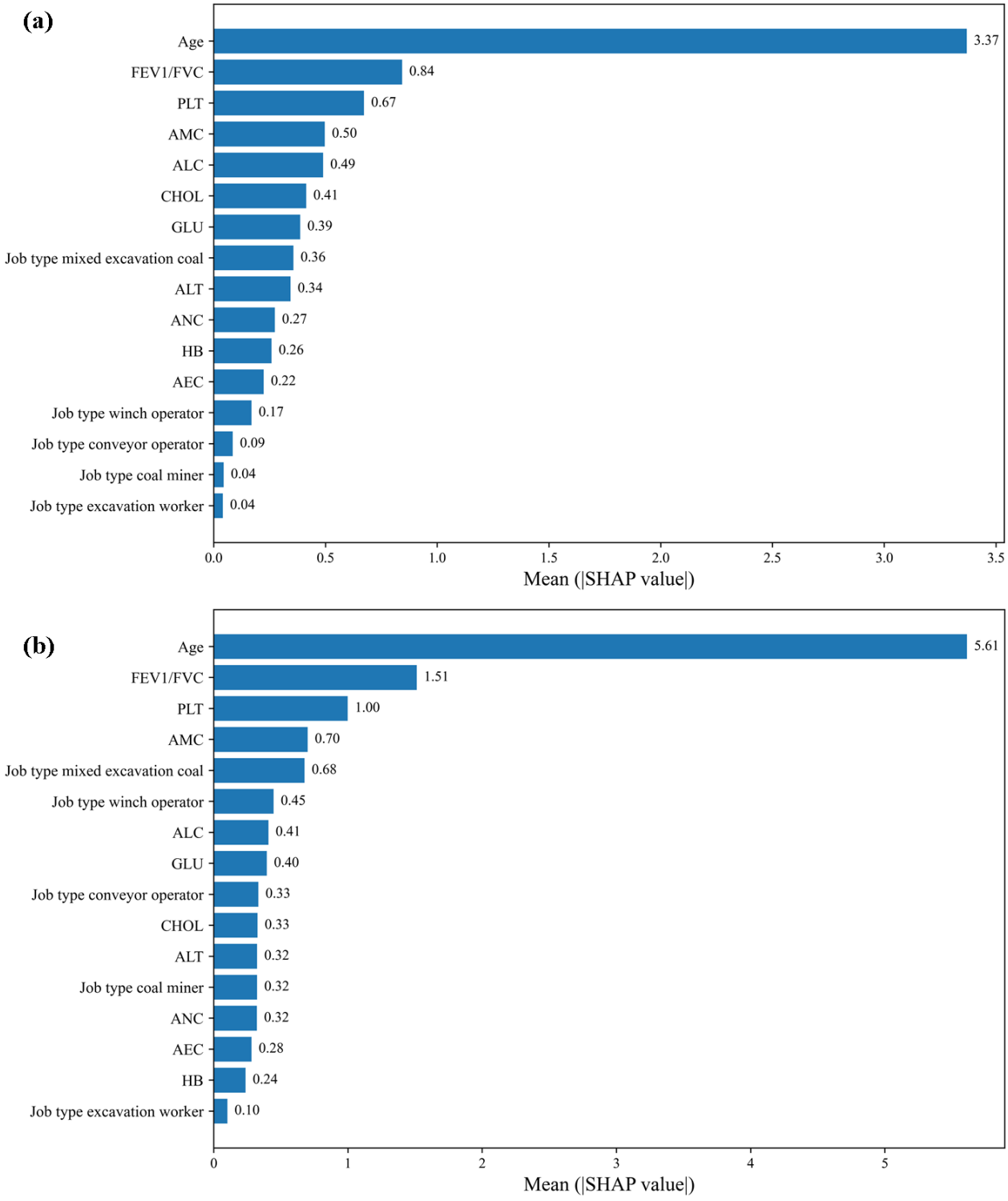

To further examine how the top 3 influential features affect the model output, SHAP dependence plots were generated (Figure S5 in Multimedia Appendix 1). As shown in the dependence plot for age, the SHAP values generally increase with age, and the risk contribution became more pronounced after approximately 55 - 60 years, suggesting that older age was associated with a higher predicted disease risk. For FEV1/FVC, lower values correspond to higher SHAP values, indicating an increased risk, whereas higher values (approximately 85% - 100%) were associated with SHAP values close to zero or negative, suggesting a lower predicted risk. Similarly, the PLT dependence plot showed that lower PLT levels tended to contribute positively to disease risk, while higher PLT values (approximately 250 - 350×10^9/L) were more often associated with negative SHAP values, indicating a reduced predicted risk.

XSL•FO
RenderX

Discussion

Principal Findings

In clinical research, it is very common for medical records to have missing values in a certain examination due to the complexity of data collection and individual differences among different patients. By calculating the Euclidean distance between samples, KNN interpolation can identify *K*-neighboring samples that are most similar to missing values and then use the average feature information of neighboring samples to fill in the missing values, effectively restoring the integrity of the data [28]. As a categorical variable, the values of job type do not have a sequential relationship, and categories with larger values do not necessarily have greater weights than categories with smaller values. In order to enable ML models to better capture the relationship between feature variables and target variables, single hot encoding was applied to categorical features in this study [29]. The remaining 15 characteristic variables are all continuous features, but their units and ranges of values vary greatly. For example, PLT is measured in unit ×10^9/L and has a wide range of variable values, while glucose is measured in unit mmol/L and has a smaller range of values. This inconsistent scale may lead to the model being more sensitive to certain features with larger numerical ranges during training and ignoring other features with smaller scales, thereby affecting the training effectiveness of the model. Standardizing irregular continuous variables is often the key to solving such problems [30].

Feature selection is a crucial step in ML applications, aimed at selecting the most relevant features to the target variable in order to improve model performance and interpretability [31]. The common feature selection methods mainly include embedded, wrapped, and filtered methods [32]. As an embedded feature selection method, LASSO uses regression analysis to screen out key feature variables related to CWP, reducing model complexity and improving model generalization ability. In this study, LASSO regression analysis is applied to compress the coefficients of some unimportant features to 0 by performing α regularization on the coefficients, thereby achieving feature selection [20]. The preprocessed dataset still suffers from class imbalance, with the number of dust-exposed workers without CWP being about 4 times that of patients with CWP. Regarding the issue of class imbalance, commonly used methods in model construction include data sampling and ensemble learning [33]. In order to preserve the distribution characteristics of the original data as much as possible and avoid the bias and noise that may be introduced by data oversampling methods [34], ensemble learning models were used to handle imbalanced data in this study. Specifically, we selected decision tree-based ensemble learning models such as LightGBM, RF, CatBoost, and XGBoost and compared them with traditional LR and SVM models.

To ensure a fair comparison among candidate models, this study adopted a unified hyperparameter optimization strategy based on Optuna. Optuna is a Bayesian optimization framework that uses a tree-structured Parzen estimator to efficiently explore the hyperparameter space by prioritizing promising regions. Under the same optimization budget and the same stratified *k*-fold cross-validation protocol, all 6 models were tuned and evaluated consistently. The results show that after optimization, all models achieved consistently high cross-validated performance, while the differences among the top-performing models remained small on the held-out test set. This finding suggests that the current feature set and evaluation setting already provide strong predictive ability, and further improvements are more likely to depend on feature refinement or decision strategy rather than extensive hyperparameter tuning. In addition, the top-performing models show comparable overall performance, but each presents advantages under different evaluation priorities. Specifically, models such as LightGBM and CatBoost demonstrate stronger overall discrimination, whereas XGBoost tends to perform better when recall- or F_1-related sensitivity is emphasized. Therefore, LightGBM and CatBoost were both retained as top-performing models for subsequent interpretability analysis. Job type reflects different dust exposure scenarios in coal mining and therefore contributes to CWP risk prediction, which is consistent with epidemiological evidence [35]. The concentration, particle size, and composition of coal dust have a significant impact on the pathogenesis and prevalence of CWP [36,37]. The different working scenarios in coal mines in the same region also have a significant impact on the prevalence of CWP. The excavator workers are mainly responsible for developing tunnels, and the cut rocks are rich in free silica. The pathogenicity of silica dust is much higher than that of coal dust, which can lead to more severe pulmonary fibrosis (silicosis) and a shorter onset period [38,39]. Coal miners mainly come into contact with coal dust (carbon-based dust), which has relatively weaker pathogenicity compared to silica dust and slower disease progression. At the same time, the excavation face is a temporary work site, and the ventilation and dust removal facilities are usually not as complete as those in the coal mining face, resulting in greater difficulty in dust control [40]. Mixed workers for excavation and coal mining are exposed to silica dust and coal dust simultaneously, and the synergistic effect of the 2 types of dust may accelerate lung damage [41,42].

To examine whether the clinical variables provide predictive value beyond occupational history, we conducted an ablation analysis by retraining the baseline models after removing the job-type variable. Because hyperparameter tuning led to only minor changes in performance, using baseline models for this analysis was sufficient to evaluate the independent contribution of clinical variables. The results of each model are summarized in Table 4, which showed that model performance remained highly robust. For example, the AUC of LightGBM only slightly changed from 0.978 (with job type) to 0.973 (without job type), indicating that the physiological signals captured by clinical features and biomarkers are major contributors to the model's predictive capability.

XSL•FO
RenderX

Table . Ablation analysis of model performance without job type.

Model	Accuracy	Precision	Recall	F_1-score	AUC[a]
LightGBM[b]	0.982	1	0.907	0.951	0.973
CatBoost[c]	0.978	0.98	0.907	0.942	0.977
XGBoost[d]	0.982	1	0.907	0.951	0.978
RF[e]	0.982	1	0.907	0.951	0.976
LR[f]	0.963	0.893	0.926	0.909	0.969
SVM[g]	0.974	0.98	0.889	0.932	0.971

[a]AUC: area under curve.

[b]LightGBM: light gradient boosting machine.

[c]CatBoost: categorical boosting.

[d]XGBoost: extreme gradient boosting.

[e]RF: random forest.

[f]LR: logistic regression.

[g]SVM: support vector machine.

This finding is also supported by the SHAP interpretation results. The decrease in FEV1/FVC reflects impaired lung function, while the corresponding increase in SHAP value suggests that ventilation function may be an important feature of CWP. This is consistent with the results of existing studies suggesting that alveolar-arterial oxygen gradient in lung function can be used as a predictor of CWP [43]. Platelets, as important cells for hemostasis and coagulation, play a role by participating in systemic inflammatory and immune responses, providing new therapeutic targets for inflammatory diseases [44]. For example, a previous study found that lower PLT levels were associated with a higher risk of developing severe *mycoplasma pneumoniae* pneumonia [45]. Due to the important role of platelets in inflammation and tissue repair, this phenomenon may be related to inflammation or weakened immune function leading to lung damage. These findings emphasize the importance of clinical features in CWP risk assessment and provide new perspectives for a deeper understanding of the pathogenesis of CWP.

Despite its contributions, this study has several limitations. First, the cohort was derived from a single center and a specific occupational group, which may introduce regional or selection bias and limit generalizability to other settings. Second, although model performance was evaluated rigorously, interpretability remains limited and warrants further investigation. Most importantly, smoking history was not available in the retrospective physical examination records. Because smoking is a major confounder for both lung function and inflammatory biomarkers, part of the observed discrimination may reflect unmeasured differences in smoking behavior rather than CWP status alone. Furthermore, differences in physical demands and lifestyle factors associated with distinct job roles could potentially influence certain biomarkers. While our analysis indicates strong independent predictive value for the biomarkers, future studies should consider more granular lifestyle adjustments.

Conclusions

This study developed a ML-based model for CWP prediction using multidimensional clinical features. The 6 candidate models achieved consistently high performance, and Optuna-based tuning resulted in only small changes, suggesting robust prediction under the current protocol. SHAP analysis identified age, FEV1/FVC, and PLT as key contributors to CWP risk prediction. Moreover, ablation analysis showed that the models remained highly accurate even without job type, indicating that clinical biomarkers provide strong predictive signals beyond occupational information. These results support the potential of routine clinical data for early CWP screening and intervention.

Funding

This study was supported by the National Natural Science Foundation of China (82405130) and the Natural Science Foundation of Jiangsu Province (BK20220236).

Data Availability

The datasets analyzed during this study are available from the corresponding author upon reasonable request.

XSL•FO
RenderX

Authors' Contributions

HL, YC, WH, and DZ were responsible for the conceptualization and design of the study. JJ, XS, and YD performed the data extraction and the data analysis. HL and WH provided clinical advice and recommendations on usability and clinical relevance. HL, JJ, and SW drafted the original manuscript. All authors critically reviewed and approved the final manuscript.

Conflicts of Interest

None declared.

Multimedia Appendix 1
Cross-validation curve of least absolute shrinkage and selection operator regression, least absolute shrinkage and selection operator coefficient chart, cross-validation of 6 models and receiver operating characteristic curves of the final model, receiver operating characteristic curves of optimized model, and Shapley Additive Explanation dependency graph.
[DOCX File, 17478 KB - medinform_v14i1e80156_app1.docx]

References

1. Vanka KS, Shukla S, Gomez HM, et al. Understanding the pathogenesis of occupational coal and silica dust-associated lung disease. Eur Respir Rev 2022 Sep 30;31(165):210250. [doi: 10.1183/16000617.0250-2021] [Medline: 35831008]
2. Blackley DJ, Hall NB, Flattery J, Harris DA, Cummings KJ, Laney AS. Rise in lung transplants for coal workers' pneumoconiosis and silicosis. Am J Respir Crit Care Med 2025 Apr;211(4):642-644. [doi: 10.1164/rccm.202409-1767RL] [Medline: 39805092]
3. Wang Z, Zhang J, Yang Y, et al. Current status, trends, and predictions in the burden of coal worker's pneumoconiosis in 204 countries and territories from 1990 to 2019. Heliyon 2024 Oct 15;10(19):e37940. [doi: 10.1016/j.heliyon.2024.e37940] [Medline: 39381106]
4. Akira M, Suganuma N. Imaging diagnosis of pneumoconiosis with predominant nodular pattern: HRCT and pathologic findings. Clin Imaging 2023 May;97:28-33. [doi: 10.1016/j.clinimag.2023.02.010] [Medline: 36878176]
5. Mandrioli D, Schlünssen V, Ádám B, et al. WHO/ILO work-related burden of disease and injury: protocol for systematic reviews of occupational exposure to dusts and/or fibres and of the effect of occupational exposure to dusts and/or fibres on pneumoconiosis. Environ Int 2018 Oct;119:174-185. [doi: 10.1016/j.envint.2018.06.005] [Medline: 29958118]
6. Deng H, Chen Y, Wu M, Zhang T. ERCC1 which affects lipids metabolism and actin dynamics in coal workers' pneumoconiosis is a candidate biomarker for early warning and diagnosis. PLoS One 2024;19(9):e0308082. [doi: 10.1371/journal.pone.0308082] [Medline: 39283905]
7. Yu X, Xiong T, Yu L, et al. Gut microbiome and metabolome profiling in coal workers' pneumoconiosis: potential links to pulmonary function. Microbiol Spectr 2024 Nov 5;12(11):e0004924. [doi: 10.1128/spectrum.00049-24] [Medline: 39283109]
8. Lee JS, Shin JH, Lee KM, et al. Serum levels of TGF-β1 and MCP-1 as biomarkers for progressive coal workers' pneumoconiosis in retired coal workers: a three-year follow-up study. Ind Health 2014;52(2):129-136. [doi: 10.2486/indhealth.2013-0112] [Medline: 24464026]
9. Lee JS, Shin JH, Choi BS. Serum levels of IL-8 and ICAM-1 as biomarkers for progressive massive fibrosis in coal workers' pneumoconiosis. J Korean Med Sci 2015 Feb;30(2):140-144. [doi: 10.3346/jkms.2015.30.2.140] [Medline: 25653483]
10. Huang R, Yu T, Li Y, Hu J. Upregulated has-miR-4516 as a potential biomarker for early diagnosis of dust-induced pulmonary fibrosis in patients with pneumoconiosis. Toxicol Res 2018;7(3):415-422. [doi: 10.1039/C8TX00031J]
11. Chen Z, Shi J, Zhang Y, et al. Lipidomics profiles and lipid metabolite biomarkers in serum of coal workers' pneumoconiosis. Toxics 2022 Aug 26;10(9):496. [doi: 10.3390/toxics10090496] [Medline: 36136461]
12. Song J, Xu M, Wang T, et al. Exosomal miRNAs contribute to coal dust particle-induced pulmonary fibrosis in rats. Ecotoxicol Environ Saf 2023 Jan 1;249:114454. [doi: 10.1016/j.ecoenv.2022.114454] [Medline: 38321673]
13. Zhou Y, Wang H, Xing J, et al. Expression levels of surfactant-associated proteins and inflammation cytokines in serum and bronchoalveolar lavage fluid among coal miners: a case-control study. J Occup Environ Med 2014 May;56(5):484-488. [doi: 10.1097/JOM.0000000000000169] [Medline: 24806560]
14. Prince P, Boulay ME, Pagé N, Desmeules M, Boulet LP. Induced sputum markers of fibrosis and decline in pulmonary function in asbestosis and silicosis: a pilot study. Int J Tuberc Lung Dis 2008 Jul;12(7):813-819. [Medline: 18544209]
15. Xuan W, Zheng L, Bunes BR, Crane N, Zhou F, Zang L. Engineering solutions to breath tests based on an e-nose system for silicosis screening and early detection in miners. J Breath Res 2022 Apr 7;16(3). [doi: 10.1088/1752-7163/ac5f13] [Medline: 35303733]
16. Shi H, You M, Li X, et al. Evaluation of factors associated with adult skeletal fluorosis in coal-burning type of endemic fluorosis and initial screening model based on machine learning in Guizhou, Southwest China. Ecotoxicol Environ Saf 2025 Mar 15;293:118018. [doi: 10.1016/j.ecoenv.2025.118018] [Medline: 40073783]

XSL•FO
RenderX

17. Qian X, Li Y, Zhang X, et al. A cardiovascular disease prediction model based on routine physical examination indicators using machine learning methods: a cohort study. Front Cardiovasc Med 2022;9:854287. [doi: 10.3389/fcvm.2022.854287] [Medline: 35783868]
18. Hang W, Bu C, Cui Y, et al. Research progress on the pathogenesis and prediction of pneumoconiosis among coal miners. Environ Geochem Health 2024 Jul 16;46(9):319. [doi: 10.1007/s10653-024-02114-z] [Medline: 39012521]
19. Mrad AB, Lahiani A, Mefteh-Wali S, Mselmi N. Correction: a comparative analysis of machine learning techniques for imbalanced data. Ann Oper Res 2024 Oct;341(2-3):1349-1349. [doi: 10.1007/s10479-024-06079-1]
20. Zheng H, Zhu W, Niu Z, et al. A novel nutrition-based nomogram to predict prognosis after curative resection of gastric cancer. Front Nutr 2021;8:664620. [doi: 10.3389/fnut.2021.664620] [Medline: 34760907]
21. Bentéjac C, Csörgő A, Martínez-Muñoz G. A comparative analysis of gradient boosting algorithms. Artif Intell Rev 2021 Mar;54(3):1937-1967. [doi: 10.1007/s10462-020-09896-5]
22. Hajihosseinlou M, Maghsoudi A, Ghezelbash R. A novel scheme for mapping of MVT-type Pb–Zn prospectivity: LightGBM, a highly efficient gradient boosting decision tree machine learning algorithm. Nat Resour Res 2023 Dec;32(6):2417-2438. [doi: 10.1007/s11053-023-10249-6]
23. Hancock JT, Khoshgoftaar TM. CatBoost for big data: an interdisciplinary review. J Big Data 2020;7(1):94. [doi: 10.1186/s40537-020-00369-8] [Medline: 33169094]
24. Breiman L. Random forests. Mach Learn 2001 Oct;45(1):5-32. [doi: 10.1023/A:1010933404324]
25. Mirbagheri B, Alimohammadi A. Improving urban cellular automata performance by integrating global and geographically weighted logistic regression models. Trans GIS 2017 Dec;21(6):1280-1297 [FREE Full text] [doi: 10.1111/tgis.12278]
26. Chen W, Pourghasemi HR, Naghibi SA. A comparative study of landslide susceptibility maps produced using support vector machine with different kernel functions and entropy data mining models in China. Bull Eng Geol Environ 2018 May;77(2):647-664. [doi: 10.1007/s10064-017-1010-y]
27. Rahmatinejad Z, Dehghani T, Hoseini B, et al. A comparative study of explainable ensemble learning and logistic regression for predicting in-hospital mortality in the emergency department. Sci Rep 2024 Feb 10;14(1):3406. [doi: 10.1038/s41598-024-54038-4] [Medline: 38337000]
28. Xiao JL. SVM and KNN ensemble learning for traffic incident detection. Physica A Stat Mech Its Appl 2019 Mar;517:29-35. [doi: 10.1016/j.physa.2018.10.060]
29. Budholiya K, Shrivastava SK, Sharma V. An optimized XGBoost based diagnostic system for effective prediction of heart disease. J King Saud Univ Comput Inf Sci 2022 Jul;34(7):4514-4523. [doi: 10.1016/j.jksuci.2020.10.013]
30. Thorjussen CBH, Liland KH, Måge I, Solberg LE. Computational test for conditional independence. Algorithms ;17(8):323. [doi: 10.3390/a17080323]
31. Khan F, Tarimer I, Alwageed HS, et al. Effect of feature selection on the accuracy of music popularity classification using machine learning algorithms. Electronics (Basel) 2022;11(21):3518. [doi: 10.3390/electronics11213518]
32. Senbagamalar L, Logeswari S. Genetic clustering algorithm-based feature selection and divergent random forest for multiclass cancer classification using gene expression data. Int J Comput Intell Syst 2024;17(1):23. [doi: 10.1007/s44196-024-00416-9]
33. Yuan X, Sun C, Chen S. A clustering-based adaptive undersampling ensemble method for highly unbalanced data classification. Appl Soft Comput 2024 Jul;159:111659. [doi: 10.1016/j.asoc.2024.111659]
34. van den Goorbergh R, van Smeden M, Timmerman D, Van Calster B. The harm of class imbalance corrections for risk prediction models: illustration and simulation using logistic regression. J Am Med Inform Assoc 2022 Aug 16;29(9):1525-1534. [doi: 10.1093/jamia/ocac093] [Medline: 35686364]
35. Cool CD, Murray J, Vorajee NI, et al. Pathologic findings in severe coal workers' pneumoconiosis in contemporary US coal miners. Arch Pathol Lab Med 2024 Jul 1;148(7):805-817. [doi: 10.5858/arpa.2022-0491-OA] [Medline: 37852172]
36. Peng H, Tang A, Cheng Y, et al. Study of dust deposition pattern in the respiratory tract of dust particles less than 10 μm in size. Powder Technol 2024 Aug;444:120033. [doi: 10.1016/j.powtec.2024.120033]
37. Sun Y, Kinsela AS, Cen X, et al. Impact of reactive iron in coal mine dust on oxidant generation and epithelial lung cell viability. Sci Total Environ 2022 Mar 1;810:152277. [doi: 10.1016/j.scitotenv.2021.152277] [Medline: 34902414]
38. Yang B, Liu X, Peng C, Meng X, Jia Q. Silicosis: from pathogenesis to therapeutics. Front Pharmacol 2025;16:1516200. [doi: 10.3389/fphar.2025.1516200] [Medline: 39944632]
39. Keles C, Sarver E. A study of respirable silica in underground coal mines: particle characteristics. Minerals 2022;12(12):1555. [doi: 10.3390/min12121555]
40. Wang Z, Li S, Ren T, Wu J, Lin H, Shuang H. Respirable dust pollution characteristics within an underground heading face driven with continuous miner: a CFD modelling approach. J Clean Prod 2019 Apr;217:267-283. [doi: 10.1016/j.jclepro.2019.01.273]
41. Zhang Y, Yan J, Ren Y, et al. Coal dust particles can upregulate the expression of NLRP3 inflammasome components in rat alveolar macrophages through phagocytosis. Sci Rep 2025 Mar 15;15(1):8989. [doi: 10.1038/s41598-025-93946-x] [Medline: 40089559]

XSL•FO
RenderX

42. Sun Y, Kinsela AS, Waite TD. Elucidation of alveolar macrophage cell response to coal dusts: role of ferroptosis in pathogenesis of coal workers' pneumoconiosis. Sci Total Environ 2022 Jun 1;823:153727. [doi: 10.1016/j.scitotenv.2022.153727] [Medline: 35149061]
43. Dong H, Zhu B, Kong X, Zhang X. Efficient clinical data analysis for prediction of coal workers' pneumoconiosis using machine learning algorithms. Clin Respir J 2023 Jul;17(7):684-693. [doi: 10.1111/crj.13657] [Medline: 37380332]
44. Bo Y, Lu Q, Li B, Sha R, Yu H, Miao C. The role of platelets in central hubs of inflammation: a literature review. Medicine (Baltimore) 2024 May 10;103(19):e38115. [doi: 10.1097/MD.0000000000038115] [Medline: 38728509]
45. Ye Y, Gao Z, Zhang Z, Chen J, Chu C, Zhou W. A machine learning model for predicting severe mycoplasma pneumoniae pneumonia in school-aged children. BMC Infect Dis 2025 Apr 21;25(1):570. [doi: 10.1186/s12879-025-10958-8] [Medline: 40259232]

Abbreviations

AEC: absolute eosinophil count
ALC: absolute lymphocyte count
ALT: alanine aminotransferase
AMC: absolute monocyte count
ANC: absolute neutrophil count
AUC: area under curve
CatBoost: categorical boosting
CWP: coal workers' pneumoconiosis
FEV1/FVC: forced expiratory volume/forced vital capacity
KNN: k-nearest neighbor
LASSO: Least Absolute Shrinkage and Selection Operator
LightGBM: light gradient boosting machine
LR: logistic regression
ML: machine learning
PLT: platelet count
RF: random forest
SHAP: Shapley Additive Explanation
SVM: support vector machine
WBC: white blood cell count
XGBoost: extreme gradient boosting

Edited by A Coristine, A Benis; submitted 05.Jul.2025; peer-reviewed by XC Wang, X Liang, Z Yang; revised version received 04.Jan.2026; accepted 08.Jan.2026; published 13.Feb.2026.

Please cite as:
Li H, Jia J, Shi X, Dong Y, Wang S, Cui Y, Hang W, Zhang D
Research on the Prediction of Coal Workers' Pneumoconiosis Based on Easily Detectable Clinical Data: Machine Learning Model Development and Validation Study
JMIR Med Inform 2026;14:e80156
URL: https://medinform.jmir.org/2026/1/e80156
doi:10.2196/80156

© Haiquan Li, Jiaqi Jia, Xu Shi, Yudie Dong, Songquan Wang, Yuming Cui, Wenlu Hang, Dekun Zhang. Originally published in JMIR Medical Informatics (https://medinform.jmir.org), 13.Feb.2026. This is an open-access article distributed under the terms of the Creative Commons Attribution License (https://creativecommons.org/licenses/by/4.0/), which permits unrestricted use, distribution, and reproduction in any medium, provided the original work, first published in JMIR Medical Informatics, is properly cited. The complete bibliographic information, a link to the original publication on https://medinform.jmir.org/, as well as this copyright and license information must be included.

XSL•FO
RenderX

Assessing the Impact of Sociodemographic Factors on Artificial Intelligence Models in Predicting Dementia: Retrospective Cohort Study

Xingyi Liu[1], PhD; Muskan Garg[1], PhD; Maria Vassilaki[2], MD, PhD; Jennifer St Sauver[2], PhD; Ronald C Petersen[3], MD, PhD; Momin M Malik[4], PhD; Chung Il Wi[4], MD; Young J Juhn[4], MD, PhD; Sunghwan Sohn[1], PhD

[1]Department of Artificial Intelligence and Informatics, Mayo Clinic, Harwick Building, 7th Fl., 205 3rd Ave SW, Rochester, MN, United States

[2]Department of Quantitative Health Sciences, Mayo Clinic, Rochester, MN, United States

[3]Department of Neurology, Mayo Clinic, Rochester, MN, United States

[4]Department of Pediatric and Adolescent Medicine, Mayo Clinic, Rochester, MN, United States

Corresponding Author:
Sunghwan Sohn, PhD
Department of Artificial Intelligence and Informatics, Mayo Clinic, Harwick Building, 7th Fl., 205 3rd Ave SW, Rochester, MN, United States

Abstract

Background: Artificial intelligence (AI) is increasingly applied to health care, yet concerns about fairness persist, particularly in relation to sociodemographic disparities. Previous studies suggest that socioeconomic status (SES) and sex may influence AI model performance, potentially affecting groups that are historically underserved or understudied.

Objective: This study aimed to (1) assess algorithmic bias in AI-driven dementia prediction models based on SES and sex (biological sex), (2) compare the utility of an individual-level SES measure (the Housing-Based Socioeconomic Status [HOUSES] Index) versus an area-level measure (the Area Deprivation Index) for bias detection, and (3) evaluate the effectiveness of an oversampling technique (the Synthetic Minority Oversampling Technique for Nominal and Continuous features) for bias mitigation.

Methods: This study used data from two population-based cohorts: the Mayo Clinic Study on Aging (n=3041) and the Rochester Epidemiology Project (n=19,572). Four AI models (random forest, logistic regression, support vector machine, and Naïve Bayes) were trained using a 5-year observation window of structured electronic health record data to predict dementia onset within the subsequent 1-year window. Fairness and model performance were assessed using the balanced error rate (BER) across intersecting SES-sex subgroups. The Synthetic Minority Oversampling Technique for Nominal and Continuous features algorithm was applied to the training data to balance the representation of SES groups.

Results: Across both cohorts, individuals with lower SES generally exhibited higher BERs (worse performance) than high SES groups, confirming the presence of bias. In the MCSA cohort, males with high SES, as indicated by the HOUSES Index, consistently exhibited the lowest BERs across all evaluated models. Balancing the training data based on a specific SES measure showed a trend toward reducing the BER disparity when evaluated using that same measure. However, this targeted improvement demonstrated nonuniversal benefits; in some cases, it exacerbated disparities when evaluated using other, unbalanced SES measures. This pattern suggests that fairness interventions are not universally beneficial across different definitions of the protected attribute. While the balancing approach improved fairness in model performance for lower SES groups, it often came at the cost of a slight reduction in overall model performance. However, an exception was observed in the MCSA cohort when balancing based on the HOUSES Index using logistic regression, support vector machine, and Naïve Bayes, where the performances of both the high and low SES groups improved.

Conclusions: This research highlights the importance of incorporating sociodemographic context into AI modeling in health care. The choice of SES measure may lead to different assessments of algorithmic bias. The HOUSES Index, as a validated individual-level SES measure, may be more effective for bias mitigation than area-level measures. Future AI development should integrate bias mitigation strategies to ensure models do not reinforce existing disparities in health outcomes.

(JMIR Med Inform 2026;14:e80405) doi:10.2196/80405

KEYWORDS

artificial intelligence; AI bias; dementia; Area Deprivation Index; socioeconomic status; machine learning

XSL•FO
RenderX

Introduction

In 2024, Alzheimer dementia affected approximately 6.9 million people in the United States, and this number is projected to escalate to 13.8 million by 2060. This growth places an immense burden on patients and their families, society, and the health care system, manifesting in an estimated 18.4 billion hours of unpaid care annually, valued at US $346.6 billion [1]. Despite this considerable prevalence, cognitive impairment, including mild cognitive impairment (MCI) and dementia, often goes undetected in clinical settings. Diagnoses frequently come late in the cognitive decline process, reducing opportunities to enhance patients' quality of life and exacerbating existing health disparities. Ongoing research in health care seeks to leverage artificial intelligence (AI) to enhance dementia prediction.

The rapid advancements in computing power, data storage, and predictive analytics have significantly accelerated the integration of AI tools into the US health care system [2]. By 2014, 97% of nonfederal acute care hospitals had adopted a certified electronic health record (EHR) [3]. As of January 2025, the US Food and Drug Administration has approved more than 1000 clinical AI applications [4]. This foundational shift has enabled the widespread adoption of AI. AI-powered solutions have already demonstrated transformative potential in health care.

Beyond diagnostics, AI research continues to explore ways to address health disparities, such as reducing unexplained pain disparities through image-based algorithms in underserved populations [5]. However, alongside these advancements lies the critical challenge of mitigating biases inherent in AI systems. Studies have revealed that AI algorithms trained on biased data can perpetuate health disparities, particularly among underresourced and understudied populations [6-9]. For example, a race-based algorithm for estimating kidney function produced higher estimates for Black patients than for White patients, resulting in delayed referrals for organ transplants among Black individuals [10]. Such findings underscore the ethical imperative to scrutinize differential model performance by socioeconomic status (SES) and other social determinants of health (SDOH), which have profound implications for underserved populations and care delivery. SES, as a core component of SDOH, plays a pivotal role in shaping health outcomes through biological, behavioral, and environmental pathways [11-20].

Recent studies have highlighted the pervasive issue of bias in health care AI systems, particularly SES. For instance, a 2019 study [21] defines algorithmic bias in health care as the application of an algorithm that compounds the challenges affecting underserved groups across SES, race, background, religion, sex, or disability, thereby amplifying disparities in health systems. The authors discuss how AI can inadvertently perpetuate and exacerbate challenges faced by underserved populations if not carefully designed and implemented. Another study outlines various elements of potential bias in the development and implementation of AI algorithms in health care. It emphasizes that such biases can propagate stereotypes and discrimination, further marginalizing underserved populations and contributing to socioeconomic health care disparities [22]. Similarly, research indicates that lower SES is associated with poorer predictive model performance, potentially due to incomplete or inaccurate EHR data [23].

In addition to SES disparities, sex differences have emerged as a critical factor influencing AI model performance in dementia prediction. Research indicates that females often exhibit more severe cognitive impairment and experience a faster rate of cognitive decline compared to males at the onset of Alzheimer disease [24]. Sociodemographic factors, such as lower education levels and SES, disproportionately affect older female individuals, increasing their risk for dementia [25-27]. Predictive models for cognitive decline, such as Cox regression, demonstrate varying performances across sexes, indicating potential biases in predictive accuracy [28]. Additionally, transfer learning approaches have revealed that cognitive deficits in female individuals, once detected at the MCI stage, tend to deteriorate more consistently over time, whereas male participants exhibit a wider variety of declines across multiple cognitive functions [29].

Despite these findings, there remains a significant gap in strategies to mitigate biases in AI models. While some studies have proposed methods to detect and quantify such biases, comprehensive approaches to address and correct them are limited [30]. Our study seeks to fill this gap by not only examining the relationship between SES, sex, and AI model performance in dementia prediction but also implementing oversampling techniques to ensure adequate representation of socioeconomically disadvantaged groups. By doing so, we aim to reduce disparities in model performance across different SES groups, thereby enhancing fairness in AI-driven health care solutions.

Methods

Study Population

In our study, we used 2 cohorts. First, we studied individuals participating in the Mayo Clinic Study on Aging (MCSA) [31]. The MCSA, which commenced in 2004, is a population-based research study focused on investigating the epidemiology of MCI, dementia, and related biomarkers (N=5890; dementia, n=682, 11.6%; and non-dementia, n=5208, 88.4%). Participants for the study were chosen randomly from among persons living in Olmsted County, Minnesota, at the time of recruitment. These participants completed detailed cognitive assessments, including the Clinical Dementia Rating scale, a full-scale neurological evaluation, and various neuropsychological tests. Using established criteria, a consensus committee made diagnoses, classifying participants as cognitively unimpaired, having MCI, or having dementia. MCI diagnostic criteria have been disclosed in previous publications [32], and dementia diagnoses adhered to the criteria laid out in the *Diagnostic and Statistical Manual of Mental Disorders, Fourth Edition* [33].

Second, we studied a larger cohort of persons living in Olmsted County, MN, between 2004 and 2020, derived from the Rochester Epidemiology Project (REP) medical records linkage system (N=290,528; dementia, n=8,205, 2.8%; and non-dementia, n=282,323, 97.2%) [34]. The onset of dementia

XSL•FO
RenderX

was identified by the date of the first diagnosis code (*International Classification of Diseases [ICD], Ninth or Tenth Revision code*) received between 2004 and 2020.

Socioeconomic Measures

We assessed potential biases in model performance using two residence-based SES measures: the Area Deprivation Index (ADI) [35] and the Housing-Based Socioeconomic Status (HOUSES) Index [36]. The ADI is a multidimensional evaluation of a person's socioeconomic conditions at the census block group level. We used both national-level and state-level ADI rankings. The national-level ADI rankings were used to divide participants into two groups: those in the higher ADI quartile group (76-100) were considered to reside in an area with high socioeconomic deprivation (hereafter, low SES), and those in the ADI group (0 - 75) were considered the referent group (hereafter, high SES). Similarly, the state-level ADI ranking was categorized into two groups: ADI (8-10) for low SES and ADI (0 - 7) for high SES. The HOUSES Index is a housing-based SES indicator, derived from an analysis of 4 specific variables related to a housing unit. The bottom quartile was considered low SES, and the remaining quartiles were considered high SES. The HOUSES Index was only used in the MCSA cohort because it is not available for the REP cohort. By incorporating both the HOUSES Index and ADI measures, our study aimed to evaluate and compare their effectiveness in identifying SES-related biases in the performance of AI models. In addition to quantifying bias in model performance based on SES, our study also considered sex.

Prediction Timeline Window

Our goal was to use records from the past 5 years (observation window) to forecast whether a patient would be diagnosed with dementia in the following year (prediction window).

For both cohorts, we applied consistent inclusion and exclusion criteria. For patients with dementia (case), the incident date was the date of dementia onset. We excluded patients whose age at the incident date was less than 50 years. The index date (point for prediction) is set to 1 year before the dementia incident date. We performed frequency matching for age between participants with dementia and participants without dementia. For patients without dementia (control), we assigned index dates to match age with cases—that is, patients without dementia at the index date have a similar age distribution to patients with dementia at their index dates. As shown in Figure 1, the 5-year period preceding the index date serves as the observation window. The 1-year period following the index date is the prediction window for both groups. We exclude patients with no record within the observation window. We also exclude patients without dementia who do not have at least 1 year of follow-up after their index date (whose last record date is not at least 1 year after the index date).

Figure 1. Timeline overview for dementia and non-dementia patients. For patients with dementia (cases), the index date is set 1 year before their diagnosis. For patients without dementia (controls), the index date is assigned to match the age distribution of the cases. The model uses a 5-year observation window preceding the index date to predict the onset of dementia within the subsequent 1-year prediction window.

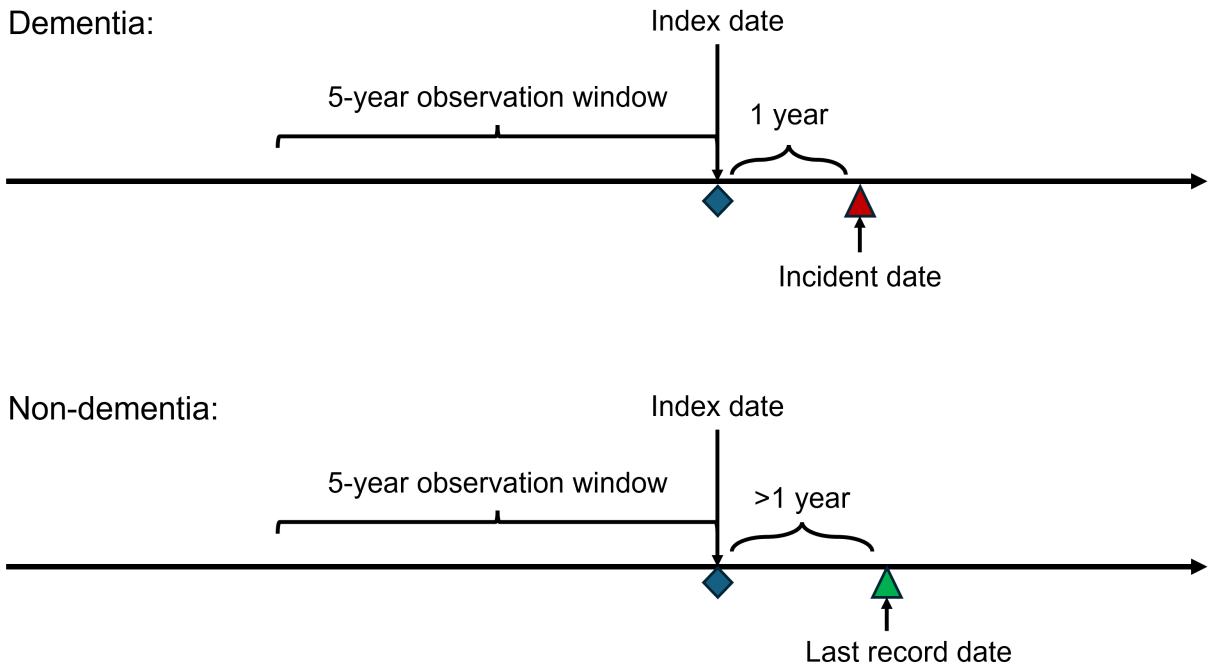

Assessing AI Bias Across Different SES and Sex Categories

Four machine learning algorithms were selected to capture a variety of model classes commonly used in clinical prediction tasks, allowing for an assessment of whether observed bias patterns were robust across different algorithmic assumptions and complexities. The selected models were (1) logistic regression (LR), a well-established, interpretable linear model that serves as a standard baseline in clinical research; (2) support vector machine (SVM), a powerful kernel-based method capable of learning complex, nonlinear decision boundaries; (3) random

XSL•FO
RenderX

forest (RF), a nonlinear ensemble of decision trees that is robust to overfitting and can implicitly capture complex interactions between features; and (4) Naïve Bayes (NB), a simple yet efficient probabilistic classifier based on Bayes' theorem with strong independence assumptions. This selection enables a more comprehensive evaluation of how algorithmic bias manifests across linear, nonlinear, ensemble, and probabilistic modeling paradigms. We trained and tested the 4 AI models to predict the incidence of dementia in the following year.

The experimental process begins with preprocessing the data. The 5-year observation period is divided into five 1-year windows. During each 1-year window, patients may have multiple visits. For each visit, we extracted ICD-9 and ICD-10 codes, categorized the codes using the Clinical Classifications Software (CCS) [37], which groups diagnoses and procedures into clinically relevant categories and then generated a one-hot–encoded vector representing the CCS categories for the visit. We computed the element-wise sum of all visit vectors within each 1-year window. To robustly distinguish between years with no visit and years with visits but no relevant diagnoses, we used a missing indicator method. For 1-year windows where a patient had no visits, the corresponding annual vector was filled with zeros. Concurrently, we introduced 5 binary features, one for each year of the observation window, setting the feature to "1" to explicitly flag a year with no visits and "0" otherwise. Finally, we formed the final input vector by concatenating the 5 annual vectors, sex, age at the index date, and the 5 created binary visit-indicator features. Our primary objective was to assess the baseline performance and bias of models built only on the most common, structured data elements that are widely available for nearly all patients within a standard EHR system.

In this study, we developed and evaluated 4 AI models for each cohort. We randomly partitioned the dataset into two subsets: 70% for training and 30% for testing. Within the training set, we used a 5-fold cross-validation strategy to identify the optimal parameters for each model, thereby ensuring robust performance estimates and minimizing the risk of overfitting. After determining the best-performing configuration for each model, we retrained the model on the entire training set and subsequently evaluated its performance using the 30% test set. All model development and evaluation procedures were conducted independently within each of the 2 cohorts. We did not perform cross-cohort validation.

Within each cohort, and for each model, we then conducted subgroup analyses by comparing performance across different sex groups and among various SES-sex subgroups. This approach was used to identify potential differences in predictive bias.

To assess the fairness of these models, we used the balanced error rate (BER) [23], defined as the unweighted mean of the false-positive rate (FPR) and the false-negative rate (FNR), as follows:

$$BER=\frac{FPR+FNR}{2}$$

The FPR, also referred to as 1−specificity, represents the proportion of negative instances that are incorrectly classified as positive. Formally,

$$FPR=\frac{\text{False positive (FP)}}{\text{True negative (TN)}+\text{False positive (FP)}}$$

The FNR, also referred to as 1−sensitivity, represents the proportion of positive instances that are incorrectly classified as negative. Formally,

$$FNR=\frac{\text{False negative (FN)}}{\text{True positive (TP)}+\text{False negative (FN)}}$$

By incorporating both the FPR and FNR, BER captures imbalances in how models treat positively and negatively labeled individuals, allowing us to identify potential disparities or biases in the predictive performance.

To assess the variability and reliability of the BER estimates, we calculated bootstrap CIs for each SES-sex group:

1. Bootstrapping procedure: We generated 1000 bootstrap samples by randomly resampling with replacement from the original test datasets.
2. BER calculation: For each bootstrap sample, we calculated the BER.
3. CI estimation: The distribution of the bootstrap BERs was used to compute the 95% CI, providing an estimate of the uncertainty around the BER.

To assess statistical differences in model performance (BER) between SES-sex groups, we conducted a series of pairwise 2-tailed *t* tests with a significance threshold of 0.05. The Levene test was used to assess variance homogeneity, with the Welch *t* test applied for unequal variances and the standard *t* test for equal variances. Each test was performed independently to evaluate a specific contrast (eg, low vs high SES within a sex group). To correct for the increased risk of type 1 errors (false positives) due to multiple comparisons, we applied the Benjamini-Hochberg procedure. For each of the 4 AI models, we collected the *P* values from all pairwise *t* tests performed for that model and applied the Benjamini-Hochberg correction to this complete set of *P* values. This method controls the false discovery rate at our chosen significance level of 0.05. All reported statistical significances for pairwise comparisons are based on the results of this false discovery rate correction.

In addition to these pairwise comparisons, a separate baseline analysis was conducted to contextualize the performance of all subgroups relative to a single reference point. For this analysis, the "male in high SES" subgroup was designated as the baseline category. We then calculated the difference in BER for all other sociodemographic subgroups by comparing their BERs to the BER of this baseline group. This method provides a consistent benchmark for evaluating the performance disparities relative to the reference group.

Reducing SES-Related Bias

To address disparities in AI model performance related to SES, we implemented the Synthetic Minority Oversampling Technique for Nominal and Continuous features (SMOTE-NC) [38]. SMOTE-NC is a variant of an oversampling technique designed to generate synthetic examples in datasets that include both continuous and categorical variables. This method is

XSL•FO
RenderX

particularly useful in addressing imbalances in datasets, which can lead to biased model performance.

In the context of our study, we applied SMOTE-NC to balance the representation of understudied SES groups within our training dataset. This process preserved the ratio of dementia cases and controls in the cohort (Tables 1 and 2). We set the number of neighbors parameter to 5 and used a fixed random seed of 42. This process ensured that the distribution of SES groups in the training dataset was balanced, without introducing synthetic examples into the test set. Following the oversampling, the AI models were retrained on the balanced dataset using the same cross-validation strategy. To assess the effectiveness of SES balancing, we compared the performance (BER) of models trained on the oversampled datasets with those trained on the original, imbalanced datasets.

Table . Participant characteristics in Mayo Clinic Study on Aging (MCSA; N=3041), stratified by dementia cases (n=679, 22.3%) and non-dementia controls (n=2362, 77.7%).

MCSA	Case	Control
Age (y; at index date), n (%)		
55 - 64	1 (0)	3 (0)
65 - 74	32 (5)	112 (5)
75 - 84	259 (38)	906 (38)
85 - 94	364 (54)	1261 (53)
≥95	23 (3)	80 (4)
Sex, n (%)		
Male	353 (52)	1192 (51)
Female	326 (48)	1170 (49)
Race, n (%)		
Native American or Alaska Native	0 (0)	0 (0)
Asian	8 (1)	11 (1)
Hawaiian or Pacific Islander	0 (0)	1 (0)
Black or African American	1 (0)	5 (0)
White	666 (98)	2337 (99)
More than one	3 (1)	5 (0)
Missing	1 (0)	3 (0)
Background, n (%)		
Hispanic	2 (0)	6 (0)
Non-Hispanic	674 (99)	2350 (100)
Missing	3 (1)	6 (0)
HOUSES[a] Index, n (%)		
Q1 (low SES[b])	146 (22)	506 (21)
Q2-Q4 (high SES)	533 (78)	1856 (79)
National-level ADI[c], n (%)		
76 - 100 (low SES)	35 (5)	94 (4)
0 - 75 (high SES)	644 (95)	2268 (96)
State-level ADI, n (%)		
8 - 10 (low SES)	202 (30)	572 (24)
0 - 7 (high SES)	477 (70)	1790 (76)
Number of visits, mean (SD)	93.3 (65.0)	79.5 (62.7)

[a]HOUSES: Housing-Based Socioeconomic Status.

[b]SES: socioeconomic status.

[c]ADI: Area Deprivation Index.

XSL•FO
RenderX

Table . Participant characteristics in Rochester Epidemiology Project (REP; N=19,572), stratified by dementia cases (n=7335, 37.5%) and nondementia controls (n=12,237, 62.5%).

REP	Case	Control
Age (y; at index date), n (%)		
50 - 54	97 (1)	194 (1)
55 - 64	405 (6)	810 (7)
65 - 74	1199 (16)	2398 (20)
75 - 84	2830 (39)	5660 (46)
85 - 94	2485 (34)	3016 (25)
≥95	319 (4)	159 (1)
Sex, n (%)		
Male	3040 (41)	5298 (43)
Female	4295 (59)	6939 (57)
Race, n (%)		
Black	80 (1)	123 (1)
Asian	118 (2)	229 (2)
Hawaiian or Pacific Islander	3 (0)	4 (0)
American Indian	3 (0)	11 (0)
Other or mixed	58 (1)	121 (1)
White	7049 (96)	11,681 (96)
Refusal	11 (0)	24 (0)
Unknown	13 (0)	44 (0)
Background, n (%)		
Hispanic	105 (1)	238 (2)
Non-Hispanic	6504 (89)	10,536 (86)
Missing	726 (10)	1463 (12)
National-level ADI[a], n (%)		
76 - 100 (low SES[b])	444 (6)	651 (5)
0 - 75 (high SES)	6891 (94)	11,586 (95)
State-level ADI, n (%)		
8 - 10 (low SES)	2098 (29)	3176 (26)
0 - 7 (high SES)	5237 (71)	9061 (74)
Number of visits, mean (SD)	76.2 (70.4)	55.8 (52.2)

[a]ADI: Area Deprivation Index.

[b]SES: socioeconomic status.

Ethical Considerations

The study was approved by the institutional review boards (IRBs) of the Mayo Clinic (20 - 004498) and the Olmsted Medical Center (028-OMC-20). The need for informed consent was waived for the study. Approval for the MCSA (IRB number 14 - 004401) was also obtained from the IRBs of the Mayo Clinic and Olmsted Medical Center in Rochester, Minnesota. Participants of the MCSA provided written informed consent before participation. The MCSA informed consent and the study's IRB protocol allow secondary analysis without additional consent. All data were accessed and analyzed within secure and institutionally approved computing environments. No individual identifiers were presented in the manuscript. The results are reported only in aggregate form, ensuring that patients cannot be identified. No compensation was provided to participants, as this study involved the retrospective analysis of medical records.

XSL•FO
RenderX

Results

Cohort Characteristics

Table 1 presents the participant characteristics for the MCSA cohort. Approximately 21% (652/3041) of cases were categorized as low SES based on the HOUSES Index, 4% (129/3041) were categorized based on the national-level ADI, and 25% (774/3041) were categorized based on the state-level ADI. To understand the relationship between SES measures, we assessed the concordance between the HOUSES Index and both ADI measures in the MCSA cohort. There was limited overlap between the classifications. Among those identified as low SES by the HOUSES Index, only 12.0% (78/652) were concurrently classified as low SES by the national-level ADI, and 40.0% (261/652) were concurrently classified as low SES by the state-level ADI. This lack of concordance indicates that while these metrics all aim to measure disadvantage, they identify distinct subpopulations.

Table 2 summarizes the participant characteristics for the REP cohort. SES analyses indicate that approximately 6% (1095/19,572) of cases were classified as low SES using the national-level ADI, and 27% (5274/19,572) of cases were classified as low SES using the state-level ADI (the HOUSES Index is not available in the REP cohort). SES measure distributions were similar for controls in both populations.

The average number of visits during the 5-year observation window was 93.3 (SD 65.0) for patients with dementia and 79.5 (SD 62.7) for patients without dementia in the MCSA cohort, and 76.2 (SD 70.4) and 55.8 (SD 52.2), respectively, in the REP cohort. We also assessed data completeness by calculating the average number of years missed, defined as the count of years within the 5-year observation window where a patient had no recorded visits. When analyzing the combined population of patients with dementia and patients without dementia, most SES measures indicated that the low SES group exhibited a higher average number of years missed compared to the high SES group. In the MCSA cohort, the high SES group averaged 0.12 missed years compared to 0.17 missed years for the low SES group based on the HOUSES Index. Similarly, the national-level ADI showed 0.13 missed years for the high SES group and 0.16 missed years for the low SES group, while the state-level ADI showed a divergent pattern, with 0.14 missed years for the high SES group compared to 0.11 missed years for the low SES group. A consistent pattern emerged in the REP cohort, where the national-level ADI showed averages of 0.54 missed years for the high SES group and 0.71 for the low SES group, and the state-level ADI showed 0.54 for the high SES group compared to 0.59 for the low SES group.

Figures 2 and 3 show the top 20 CCS categories that appear among cases versus controls, ordered by the percentage of patients who had those CCS categories in the MCSA cohort and the REP cohort, respectively. In both cohorts, more patients with dementia visited for “essential hypertension” than patients without dementia during the 5-year observation period (MCSA: 85.4% vs 78.4%; and REP: 76.2% vs 67.0%). Similarly, more patients with dementia visited for “other nervous system disorders” than patients without dementia during the same period (MCSA: 70.0% vs 54.6%; and REP: 61.3% vs 38.4%).

Figure 2. Top 20 Clinical Classifications Software (CCS) categories that appear among cases versus controls during the 5-year observation period, ordered by the percentage of patients who had those CCS categories in the Mayo Clinic Study on Aging cohort.

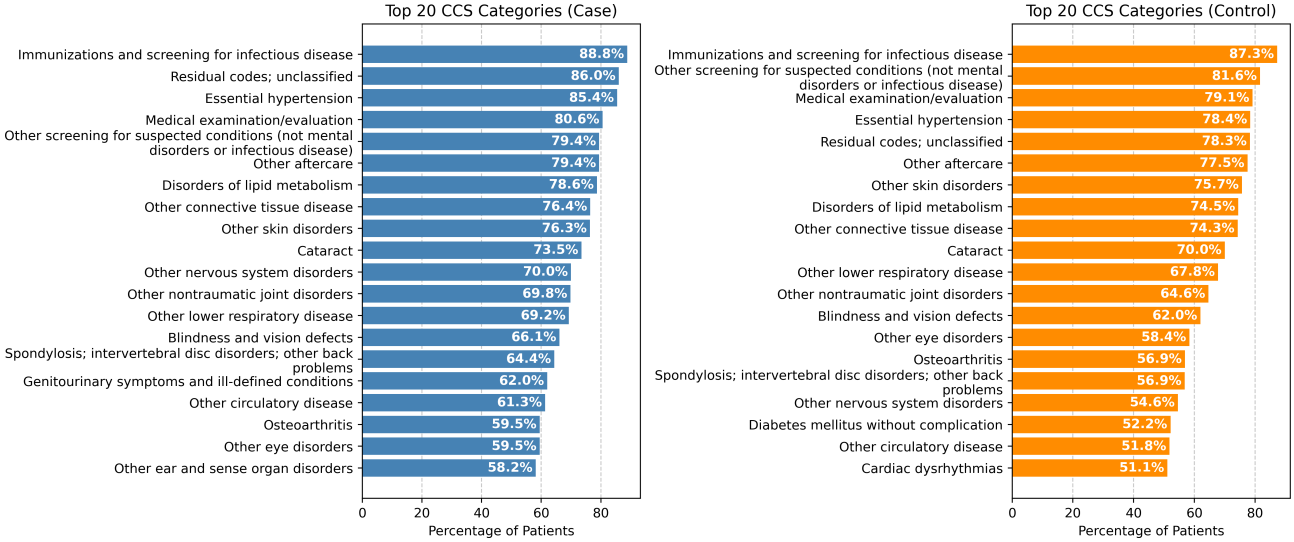

XSL•FO
RenderX

Figure 3. Top 20 Clinical Classifications Software (CCS) categories that appear among cases versus controls during the 5-year observation period, ordered by the percentage of patients who had those CCS categories in the Rochester Epidemiology Project cohort.

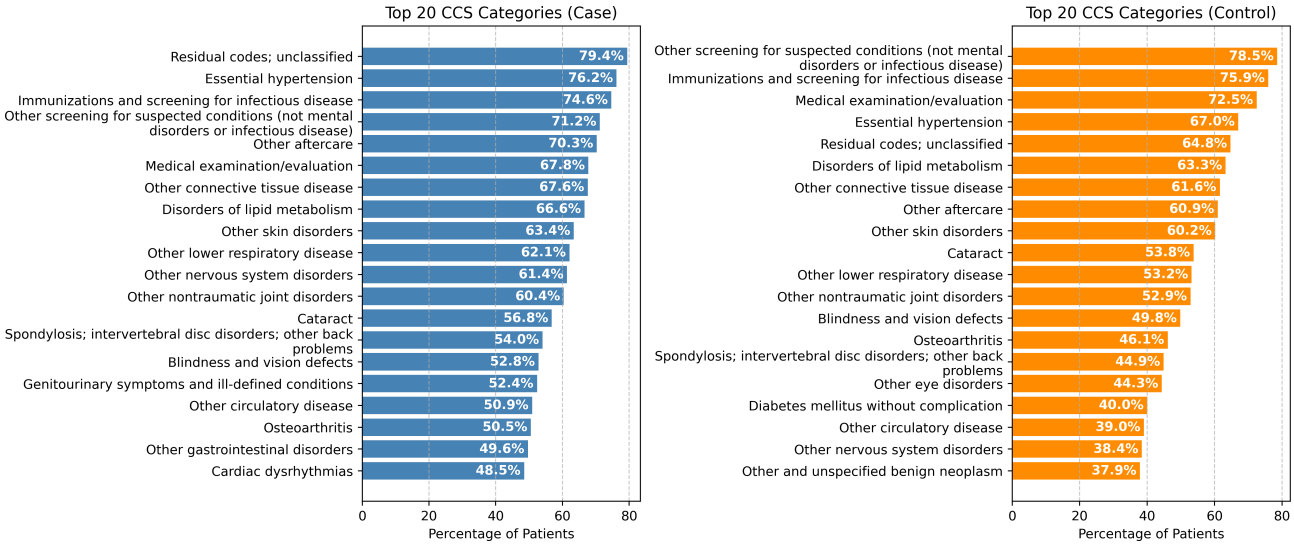

Bias Measurement

Table 3 presents a comparison of BERs for AI-based dementia prediction models stratified by SES, as indicated by both the ADIs and the HOUSES Index in the MCSA cohort. The first 2 rows compare BERs among males, the next 2 rows compare BERs among females, and the final 2 rows compare BERs for both males and females combined. Between each pair of rows, superscript letters denote statistically significant differences in BER for the low SES group compared to the high SES group (based on Benjamini-Hochberg–corrected $P<.05$): “h” indicates a significantly lower BER, “i” indicates a significantly higher BER, and “j” indicates no statistically significant difference. Across all evaluated models, individuals (males and females combined) with low SES, as measured by both the ADIs and the HOUSES Index, consistently exhibited higher BERs. When focusing on males only, those with low SES similarly demonstrated higher or equal BERs across models. However, for females, the patterns differed: in nearly all evaluated models, females with low SES, as indicated by the national-level ADI, consistently showed higher BERs, while female participants with low SES, as indicated by the state-level ADI, showed comparable BERs. In contrast, those with low SES as measured by the HOUSES Index consistently exhibited lower or equal BERs.

Table 4 compares BERs within each AI-based dementia prediction model among SES-sex subgroups in the MCSA cohort. We selected “male in high SES” as the baseline category. For each model, the table displays how the BERs for “male in low SES,” “female in high SES,” and “female in low SES” compare to this baseline. “Lower” indicates a lower BER than the baseline, “higher” indicates a higher BER, and empty cells signify no statistically significant difference. From the table, it is evident that males with high SES, as indicated by the HOUSES Index, consistently exhibited the lowest BERs across all evaluated models. Furthermore, males with high SES measured by the 2 ADIs showed the lowest BERs in almost all models, with the exception of the RF when using the national-level ADI and the NB model when using either the state-level or national-level ADI.

Table 5 presents a comparison of BERs for AI-based dementia prediction models stratified by SES—as indicated by both ADIs—in the REP cohort (the HOUSES Index was not available in the REP cohort). In every evaluated model except NB, individuals (combining both males and females) with low SES, as determined by both ADIs, consistently exhibited higher BERs. When focusing on females only, those with low SES similarly demonstrated higher BERs across almost all models, with the exception of the NB model when using the state-level ADI. Furthermore, males with high SES showed lower BERs in almost all models, with the exception of the NB model when using either the state-level or national-level ADI.

XSL•FO
RenderX

Table . Comparison of balanced error rates (BERs) for artificial intelligence–based dementia prediction models in the Mayo Clinic Study on Aging (MCSA) cohort.[a]

MCSA (sex and SES group)	National-level ADI[m], BER (95% CI)				State-level ADI, BER (95% CI)				HOUSES[c] Index, BER (95% CI)			
	RF[d]	LR[e]	SVM[f]	NB[g]	RF	LR	SVM	NB	RF	LR	SVM	NB
Male												
High	0.2827[h] (0.23-0.33)	0.3598[h] (0.30-0.41)	0.4419[h] (0.40-0.48)	0.4207[h] (0.37-0.47)	0.2546[h] (0.20-0.31)	0.3368[h] (0.28-0.40)	0.4334[h] (0.39-0.48)	0.4151[h] (0.36-0.47)	0.2688[h] (0.22-0.32)	0.3404[h] (0.28-0.40)	0.4273[h] (0.38-0.47)	0.3907[h] (0.33-0.44)
Low	0.5408[i] (0.17-0.88)	0.5378[i] (0.21-0.88)	0.4531[i] (0.12-0.67)	0.5247[i] (0.20-0.80)	0.3957[i] (0.29-0.50)	0.4482[i] (0.34-0.56)	0.4651[i] (0.38-0.54)	0.4447[i] (0.34-0.54)	0.3767[i] (0.26-0.49)	0.4591[i] (0.33-0.58)	0.4996[i] (0.44-0.54)	0.5708[i] (0.50-0.63)
Female												
High	0.3157[i] (0.26-0.37)	0.3661[h] (0.31-0.42)	0.4790[h] (0.44-0.51)	0.3822[h] (0.33-0.43)	0.3053[h] (0.24-0.37)	0.3709[j] (0.31-0.43)	0.4745[i] (0.44-0.51)	0.3867[h] (0.33-0.45)	0.3269[i] (0.26-0.39)	0.3775[i] (0.31-0.45)	0.4908[i] (0.45-0.53)	0.3964[i] (0.33-0.46)
Low	0.2419[h] (0.10-0.42)	0.4646[i] (0.27-0.67)	0.5147[i] (0.36-0.64)	0.5436[i] (0.33-0.72)	0.3221[i] (0.23-0.42)	0.3715[j] (0.27-0.47)	0.4424[h] (0.36-0.52)	0.4104[i] (0.31-0.51)	0.2750[h] (0.18-0.38)	0.3573[h] (0.25-0.46)	0.4555[h] (0.38-0.52)	0.3921[h] (0.29-0.49)
Male and female												
High	0.3006[h] (0.26-0.34)	0.3625[h] (0.32-0.40)	0.4586[h] (0.43-0.48)	0.4036[h] (0.37-0.44)	0.2784[h] (0.24-0.32)	0.3525[h] (0.31-0.39)	0.4537[h] (0.39-0.51)	0.4012[h] (0.36-0.45)	0.2943[h] (0.25-0.34)	0.3579[h] (0.32-0.40)	0.4558[h] (0.42-0.49)	0.3925[h] (0.35-0.43)
Low	0.3258[i] (0.18-0.49)	0.4844[i] (0.31-0.66)	0.4902[i] (0.35-0.62)	0.5437[i] (0.37-0.69)	0.3627[i] (0.29-0.44)	0.4074[i] (0.34-0.48)	0.4620[i] (0.43-0.49)	0.4292[i] (0.36-0.50)	0.3181[i] (0.24-0.39)	0.3971[i] (0.32-0.48)	0.4721[i] (0.42-0.52)	0.4617[i] (0.39-0.53)

[a]Superscript alphabets indicate a statistically significant difference in BER for the low socioeconomic status (SES) group compared to the high SES group within that stratum, based on Benjamini-Hochberg–corrected $P<.05$.

[b]ADI: Area Deprivation Index.

[c]HOUSES: Housing-Based Socioeconomic Status.

[d]RF: random forest.

[e]LR: logistic regression.

[f]SVM: support vector machine.

[g]NB: Naïve Bayes.

[h]BER significantly lower.

[i]BER significantly higher.

[j]No statistically significant difference.

XSL•FO
RenderX

Table . Balanced error rate (BER) difference for male in high socioeconomic status (SES) as a baseline for Table 3.

MCSA[a] (sex and SES group)	National-level ADI[b], BER				State-level ADI[b], BER				HOUSES[c] Index, BER			
	RF[d]	LR[e]	SVM[f]	NB[g]	RF	LR	SVM	NB	RF	LR	SVM	NB
Male												
High	Base	Base	Base	Base	Base	Base	Base	Base	Base	Base	Base	Base
Low	Higher[h]	Higher[h]	Higher[h]	Higher[h]	Higher[h]	Higher[h]	Higher[h]	Higher[h]	Higher[h]	Higher[h]	Higher[h]	Higher[h]
Female												
High	Higher[h]	Higher[h]	Higher[h]	Lower[i]	Higher[h]	Higher[h]	Higher[h]	Lower[i]	Higher[h]	Higher[h]	Higher[h]	Higher[h]
Low	Lower[i]	Higher[h]	Higher[h]	Higher[h]	Higher[h]	Higher[h]	Higher[h]	Lower[i]	Higher[h]	Higher[h]	Higher[h]	—[j]

[a]MCSA: Mayo Clinic Study on Aging.

[b]ADI: Area Deprivation Index.

[c]HOUSES: Housing-Based Socioeconomic Status.

[d]RF: random forest.

[e]LR: logistic regression.

[f]SVM: support vector machine.

[g]NB: Naïve Bayes.

[h]Higher: BER significantly higher than baseline.

[i]Lower: BER significantly lower than baseline.

[j]No statistically significant difference from baseline.

XSL•FO
RenderX

Table . Comparison of balanced error rates (BERs) for artificial intelligence–based dementia prediction models in the Rochester Epidemiology Project (REP) cohort.

REP (sex and SES[a] group)	National-level ADI[b], BER (95% CI)				State-level ADI, BER (95% CI)			
	RF[c]	LR[d]	SVM[e]	NB[f]	RF	LR	SVM	NB
Male								
High	0.2550[g] (0.24-0.27)	0.2922[g] (0.27-0.31)	0.3138[g] (0.29-0.33)	0.3500[h] (0.33-0.37)	0.2500[g] (0.23-0.27)	0.2839[g] (0.25-0.32)	0.3415[g] (0.32-0.36)	0.3551[h] (0.33-0.38)
Low	0.3001[h] (0.21-0.39)	0.3113[h] (0.23-0.40)	0.3378[h] (0.25-0.44)	0.3165[g] (0.24-0.40)	0.2756[h] (0.24-0.32)	0.2943[h] (0.27-0.33)	0.3458[h] (0.31-0.38)	0.3302[g] (0.29-0.36)
Female								
High	0.2606[g] (0.24-0.28)	0.2988[g] (0.28-0.32)	0.3266[g] (0.31-0.35)	0.3585[g] (0.34-0.37)	0.2335[g] (0.21-0.26)	0.2815[g] (0.26-0.30)	0.3341[g] (0.32-0.35)	0.3682[h] (0.35-0.39)
Low	0.2648[h] (0.20-0.33)	0.3123[h] (0.25-0.38)	0.3688[h] (0.29-0.42)	0.4067[h] (0.34-0.47)	0.2560[h] (0.23-0.29)	0.2962[h] (0.27-0.33)	0.3584[h] (0.33-0.39)	0.3478[g] (0.32-0.38)
Male and female								
High	0.2581[g] (0.25-0.27)	0.2958[g] (0.28-0.31)	0.3163[g] (0.29-0.33)	0.3547[g] (0.34-0.37)	0.2478[g] (0.23-0.27)	0.2827[g] (0.27-0.30)	0.3376[g] (0.32-0.35)	0.3626[h] (0.35-0.38)
Low	0.2772[h] (0.23-0.33)	0.3124[h] (0.27-0.36)	0.3437[h] (0.29-0.39)	0.3752[h] (0.33-0.42)	0.2637[h] (0.24-0.29)	0.2955[h] (0.28-0.32)	0.3547[h] (0.33-0.38)	0.3411[g] (0.32-0.36)

[a]SES: socioeconomic status.

[b]ADI: Area Deprivation Index.

[c]RF: random forest.

[d]LR: logistic regression.

[e]SVM: support vector machine.

[f]NB: Naïve Bayes.

[g]BER significantly lower.

[h]BER significantly higher.

Table 6 compares BERs within each AI-based dementia prediction model among SES-sex subgroups (using the same approach as Table 4) in the REP cohort; we selected "male in high SES" as the baseline category. From the table, most of both males and females with low SES exhibit higher BER compared to males with high SES. Furthermore, females with high SES, as indicated by the national-level ADI, exhibited higher BER compared to males with high SES. However, females with high SES, as indicated by the state-level ADI, exhibited the lowest BERs across almost all the evaluated models except for the NB model.

XSL•FO
RenderX

Table . Balanced error rate (BER) difference for male high socioeconomic status (SES) as a baseline for Table 5.

REP[a] (sex and SES group)	National-level ADI[b], BER				State-level ADI, BER			
	RF[c]	LR[d]	SVM[e]	NB[f]	RF	LR	SVM	NB
Male								
High	Base	Base	Base	Base	Base	Base	Base	Base
Low	Higher[g]	Higher[g]	Higher[g]	Lower[h]	Higher[g]	Higher[g]	Higher[g]	Lower[h]
Female								
High	Higher[g]	Higher[g]	Higher[g]	Higher[g]	Lower[h]	Lower[h]	Lower[h]	Higher[g]
Low	Higher[g]	Higher[g]	Higher[g]	Higher[g]	Higher[g]	Higher[g]	Higher[g]	Lower[h]

[a]REP: Rochester Epidemiology Project.

[b]ADI: Area Deprivation Index.

[c]RF: random forest.

[d]LR: logistic regression.

[e]SVM: support vector machine.

[f]NB: Naïve Bayes.

[g]Higher: BER significantly higher than baseline.

[h]Lower: BER significantly lower than baseline.

Table 7 presents a comparison of the relative differences in BERs between low and high SES groups, as indicated by both the ADIs and the HOUSES Index, across the 4 AI-based dementia prediction models in the MCSA cohort. The relative difference (value close to 0 is perfectly balanced between low and high SES groups), calculated as (low SES' BER−high SES' BER)/high SES' BER, was first shown for the baseline case with no dataset balancing. Subsequently, the relative differences after balancing the training dataset (separately using national-level ADI, state-level ADI, and the HOUSES Index) are displayed. Within each model and SES measure, if the difference postbalancing was lower than the baseline, the corresponding cell is marked with "i"; otherwise, it is marked with "j". As indicated by "h" in the table, balancing the training dataset using any one of the 3 SES measures was associated with narrower BER differences between high and low SES groups when stratified by that same SES measure. However, in several cases, most notably with the LR and RF models under national-level ADI balancing, the relative difference shifted from positive to negative. This shift indicates an inversion of the disparity, whereby the low SES group achieved a lower BER than the high SES group. Furthermore, when the training dataset was balanced using one SES measure but performance was stratified by another SES measure, BER differences were similarly reduced across nearly all cases. The exceptions occurred when SES was stratified by national-level ADI and the training dataset was balanced by state-level ADI or the HOUSES Index under the RF model or when the training dataset was balanced by national-level ADI but evaluated using the HOUSES Index with the SVM and NB models. For instance, balancing the training data on the HOUSES Index increased the BER disparity measured by the national-level ADI from 8.38% to 30.37% with the RF model. This pattern suggests that fairness interventions are not universally beneficial across different definitions of the protected attribute.

Table 8 presents the same comparison as in Table 7 but for the REP cohort. Similarly, as indicated by footnote "g" in the table, balancing the training dataset using any one of the 3 SES measures consistently reduced the BER differences between high and low SES groups when stratified by that same SES measure. A similar pattern of disparity inversion was observed, where balancing on the national-level ADI for the RF model and the state-level ADI for the SVM model also resulted in negative relative differences.

XSL•FO
RenderX

Table . Comparison of balanced error rate (BER) differences between low and high socioeconomic status (SES) groups under various data balancing strategies in artificial intelligence (AI)–based dementia prediction models (Mayo Clinic Study on Aging [MCSA] cohort).

MCSA (sex and balance on)	National-level ADI[a], (low SES' BER−high SES' BER)/high SES' BER (percentile)				State-level ADI, (low SES' BER−high SES' BER)/high SES' BER (percentile)				HOUSES[b] Index, (low SES' BER−high SES' BER)/high SES' BER (percentile)			
	RF[c]	LR[d]	SVM[e]	NB[f]	RF	LR	SVM	NB	RF	LR	SVM	NB
Male and female												
N/A[g]	8.38%	33.63%	6.89%	34.71%	30.28%	15.57%	1.83%	6.98%	8.09%	10.95%	3.58%	17.63%
National-level ADI	−5.84%[h,i]	−7.27%[h,i]	3.49%[h,i]	5.11%[h,i]	2.53%[i]	2.14%[i]	1.13%[i]	2.94%[i]	4.27%[i]	9.79%[i]	5.90%[j]	18.13%[j]
State-level ADI	−30.37%[j]	−28.64%[i]	−5.31%[i]	−22.96%[i]	3.91%[h,i]	1.11%[h,i]	−0.27%[h,i]	−1.12%[h,i]	−1.95%[i]	−0.20%[i]	1.03%[i]	−9.75%[i]
HOUSES Index	25.13%[j]	−14.89%[i]	−2.33%[i]	1.15%[i]	15.89%[i]	2.45%[i]	1.52%[i]	−0.50%[i]	2.24%[h,i]	3.43%[h,i]	−0.86%[h,i]	3.83%[h,i]

[a]ADI: Area Deprivation Index.

[b]HOUSES: Housing-Based Socioeconomic Status.

[c]RF: random forest.

[d]LR: logistic regression.

[e]SVM: support vector machine.

[f]NB: Naïve Bayes.

[g]Not applicable.

[h]Results corresponding to models trained on datasets balanced using the same SES measure by which performance is stratified.

[i]Relative BER difference lower.

[j]Relative BER difference higher.

Table . Comparison of balanced error rate (BER) differences between low and high socioeconomic status (SES) groups under various data balancing strategies in artificial intelligence–based dementia prediction models (Rochester Epidemiology Project [REP] cohort).

REP (sex and balance on)	National-level ADI[a],(low SES' BER−high SES' BER)/high SES' BER [percentile])				State-level ADI, (low SES' BER−high SES' BER)/high SES' BER [percentile])			
	RF[b]	LR[c]	SVM[d]	NB[e]	RF	LR	SVM	NB
Male and female								
N/A[f]	7.40%	5.61%	8.66%	5.78%	6.42%	4.53%	5.07%	−5.93%
National-level ADI	−1.80%[g,h]	2.37%[g,h]	3.28%[g,h]	2.63%[g,h]	−4.25%[h]	6.75%[i]	3.11%[h]	−2.70%[h]
State-level ADI	−4.14%[h]	9.26%[i]	−0.05%[h]	6.73%[i]	1.62%[g,h]	0.16%[g,h]	−0.52%[g,h]	−3.28%[g,h]

[a]ADI: Area Deprivation Index.

[b]RF: random forest.

[c]LR: logistic regression.

[d]SVM: support vector machine.

[e]NB: Naïve Bayes.

[f]Not applicable.

[g]Results corresponding to models trained on datasets balanced using the same socioeconomic status (SES) measure by which performance is stratified.

[h]Relative BER difference lower.

[i]Relative BER difference higher.

XSL•FO
RenderX

Discussion

Principal Findings

Our study demonstrates socioeconomic bias in AI-driven dementia prediction models. Across both the research cohort (MCSA) and the real-world cohort (REP), the combined male and female population with lower SES consistently exhibited higher BERs compared to their higher SES counterparts, except when using the NB model in the REP cohort. This discrepancy suggests that AI models, when trained on imbalanced SES datasets, may not generalize well across different socioeconomic groups, potentially reinforcing existing health care disparities. The findings highlight important differences in bias detection across SES measures. Both the ADI and the HOUSES Index were effective in identifying disparities, but they capture different aspects of socioeconomic disadvantage. The HOUSES Index, which is based on housing data, identified a more nuanced variation in model performance. In contrast, the ADI (both national-level and state-level rankings), which is derived from census block group–level data, showed broader disparities but may be less sensitive to individual economic conditions.

One important factor contributing to the observed differences in performance between high and low SES groups is the imbalance in their representation within both cohorts. Individuals from higher SES groups significantly outnumber those from lower SES groups. This skewed distribution can have a direct impact on model performance, as AI algorithms trained on predominantly high SES individuals may not adequately capture the health-related patterns of populations with low SES.

A key implication of this imbalance is that AI models become optimized for the majority (high SES) group, leading to lower accuracy and higher BERs for the understudied (low SES) group. Machine learning models inherently learn patterns based on the data they are exposed to, and if the majority of training samples come from high SES individuals, the model is likely to develop a bias toward their health characteristics and health care access patterns. This bias can manifest in the form of increased BER for participants with low SES. Furthermore, disparities in health care access and utilization between SES groups can compound these biases. Traditionally, it is argued that individuals from higher SES backgrounds have more comprehensive and consistent health records, whereas individuals with lower SES may experience gaps in care that lead to incomplete medical histories [23]. Our findings support this view: the low SES group exhibited a higher average number of years with missed visits compared to the high SES group, as reported in the Results section.

Another important observation is the interaction between SES and sex. In the MCSA cohort, high SES male participants generally exhibited the lowest BERs. In the REP cohort, however, the results depended on the specific SES measure used: high SES female individuals tended to have the lowest BERs when stratified by the state-level ADI, whereas this pattern was not observed with the national-level ADI. This discrepancy between cohorts may result from MCSA's active recruitment and retention process, which likely selected for a subgroup of male participants with higher health literacy and more complete records than the general population—a selection bias less present in the passive data collection of the REP cohort. Furthermore, within the REP cohort, the fact that high SES female individuals did not exhibit this advantage under the national-level ADI highlights the differential validity of SES measures. Broader metrics such as the national-level ADI may fail to capture localized resource variations that drive health outcomes for female participants, nuances that are better reflected by more granular measures such as the state-level ADI.

To address these disparities, we applied the SMOTE-NC to balance the SES representation in the training data. This approach narrowed the observed SES-related disparities in BERs, demonstrating that balanced data distributions can improve AI model fairness. However, the effectiveness of this technique varied across SES measures—while balancing based on the HOUSES Index and state-level ADI consistently reduced BER disparities, national-level ADI balancing sometimes led to unintended increases in BER differences for certain models. This may indicate that the national-level ADI lacks the necessary resolution to distinguish SES levels within specific states effectively. Unlike the state-level ADI or the HOUSES Index, the national-level ADI may not adequately represent the local socioeconomic context required for effective data balancing. Furthermore, the limited concordance observed between the HOUSES Index and the ADI measures may explain why oversampling based on one measure resulted in disparities in the others.

While our balancing approach improved fairness in model performance for lower SES groups, it often came at the cost of a slight reduction in overall model performance. In some cases, this intervention led to an inversion of bias, resulting in the models performing better on the low SES group than the high SES group. The trade-off between fairness and predictive accuracy is a known challenge in AI-driven health care apps, and our results highlight this issue. Most balancing strategies led to improved performance for the low SES group while slightly decreasing overall predictive accuracy. However, an exception was observed in the MCSA cohort when balancing based on the HOUSES Index using LR, SVM, and NB, where both the high and low SES group performances improved. This suggests that housing-based SES metrics, such as the HOUSES Index, may be more effective for bias mitigation than area-level measures such as the ADI.

Beyond statistical significance, it is crucial to consider the clinical importance of these performance disparities. For instance, in the MCSA cohort, the NB model using the HOUSES Index yielded a BER of 39.3% for the high SES group compared to 46.2% for the low SES group. While this represents a modest absolute difference of 6.9 percentage points, its impact at a population level is substantial. In a hypothetical clinical screening scenario involving 1000 patients from each SES group, this disparity would translate to an additional 69 patients from low SES backgrounds being misclassified compared to their high SES counterparts. Such a systematic difference in accuracy, when deployed at scale, could further disadvantage already underserved populations in clinical care. Patients from socioeconomically disadvantaged backgrounds would be

XSL•FO
RenderX

disproportionately subject to the consequences of misclassification, including delayed diagnosis and intervention in the case of false negatives, or unnecessary, costly, and anxiety-inducing follow-up procedures in the case of false positives. This quantification highlights how seemingly small statistical biases can manifest as meaningful clinical harms.

Limitations

While this study provides valuable insights, it is important to recognize limitations. First, although our study cohorts (MCSA and REP) represent Midwestern populations with a dominant White demographic, they are not representative of the broader US population [39]. Therefore, the findings regarding SES- and sex-based bias warrant validation in more representative populations. Second, our AI models do not include certain important clinical factors, such as cognitive test scores, functional assessments, or advanced biomarkers, in dementia prediction. Instead, we focused on commonly available variables in real-world clinical settings because the primary goal of this study was to investigate AI bias rather than to maximize predictive accuracy. Third, relying on ICD codes to identify dementia cases in the REP cohort introduces potential ascertainment bias. In real-world settings, socioeconomic barriers to care may prevent low SES individuals from obtaining a formal diagnosis despite the presence of disease. Consequently, these undiagnosed individuals are liable to be misclassified as not having dementia. This specific form of label noise likely inflates the apparent error rates (specifically false negatives) for low SES groups independent of algorithmic performance. Fourth, the requirement for a 5-year observation window and subsequent follow-up may inadvertently exclude individuals with fragmented care. This selection factor suggests that the performance disparities reported here may underestimate the full extent of algorithmic bias. Additionally, while SMOTE-NC consistently reduced numerical BER disparities, the statistical significance of this reduction was not formally tested. These findings should be interpreted as descriptive evidence of fairness improvement. Finally, we did not consider temporal validation of the AI models over time, particularly in the REP cohort (real-world data). Health care systems are dynamic, and evolving diagnostic criteria for dementia and changes in ICD coding practices may lead to concept drift. Consequently, the models' utility for predicting dementia risk in future patient populations requires further investigation. Nonetheless, our main objective was to assess the SES-driven AI model bias rather than to optimize prediction performance, and our findings successfully demonstrate the influence of SES on AI bias in dementia prediction.

Future Work

In this study, BER was selected as the primary metric for evaluating model performance and fairness. This metric is particularly well suited for classification tasks with imbalanced classes, such as dementia prediction, because it gives equal importance to errors made on the understudied and majority classes, unlike standard accuracy. Our use of BER aligns with a fairness goal of achieving parity in overall error rates between demographic subgroups. However, it is important to acknowledge that "fairness" is a multifaceted concept, and no single metric can capture all its dimensions. Alternative fairness criteria could have been used, each with different implications. Future work should extend this analysis by evaluating these models against a broader suite of fairness metrics to provide a more holistic assessment of their performance trade-offs. We should also investigate whether differences in health care utilization patterns contribute to these variations, as female individuals may engage with health care services differently than male participants, potentially influencing AI model predictions.

Our further research should explore advanced fairness-aware algorithms that optimize both fairness and predictive accuracy, ensuring that model improvements do not disproportionately benefit or disadvantage any subgroup. Additionally, our future work should evaluate alternative debiasing strategies beyond oversampling, such as model recalibration and adversarial learning, to address structural biases inherent in the data.

Conclusions

This study underscores the biases in AI models predicting dementia, with performance disparities observed across SES and sex groups. Individuals from lower SES backgrounds consistently experienced less accurate predictions, as reflected in higher BERs. These disparities suggest that AI models trained on real-world health care data may inadvertently reinforce patterns of underservice among certain populations, underscoring the need for fairness-aware modeling approaches.

Comparisons between SES measures revealed that the HOUSES Index and ADI capture different aspects of socioeconomic disadvantage, with the HOUSES Index potentially offering more granularity at the individual level. The observed sex-based disparities in model bias further emphasize the intersectionality of SDOH, highlighting the importance of multidimensional fairness evaluations in AI-driven health care applications.

Ultimately, this research reinforces the ethical imperative to integrate sociodemographic factors into AI model development and evaluation. Addressing these biases is essential for promoting fair AI-driven solutions in dementia risk prediction, where early and accurate diagnosis is critical for patient outcomes.

Funding

This study was supported by National Institutes of Health R01 AG068007, R01 HL171508, and RF1 AG090341. The Mayo Clinic Study of Aging was supported by National Institutes of Health grants (U01 AG006786, P30 AG062677, R37 AG011378, R01 AG041851, and R01 NS097495), the Alexander Family Alzheimer's Disease Research Professorship of the Mayo Clinic, the Mayo Foundation for Medical Education and Research, the Liston Award, the GHR Foundation, and the Schuler Foundation

XSL•FO
RenderX

and used the resources of the Rochester Epidemiology Project (REP) medical records linkage system, which is supported by the National Institute on Aging (AG 058738), by the Mayo Clinic Research Committee, and by fees paid annually by REP users. The content is solely the responsibility of the authors and does not necessarily represent the official views of the National Institutes of Health.

Data Availability

The datasets generated or analyzed during this study are not publicly available due to privacy and legal reasons. The Mayo Clinic Study on Aging and Rochester Epidemiology Project studies provide data to qualified researchers upon reasonable request.

Authors' Contributions

XL: Methodology, Software, Formal analysis, Investigation, Writing – original draft, Writing – review & editing, Visualization.
MV: Validation, Resources, Data Curation, Writing – review & editing.
JSS: Validation, Resources, Data Curation, Writing – review & editing.
MG: Validation, Writing – review & editing.
RCP: Validation, Writing – review & editing.
MMM: Validation, Writing – review & editing.
CW: Validation, Writing – review & editing.
YJJ: Validation, Writing – review & editing.
SS: Conceptualization, Supervision, Project administration, Funding acquisition, Writing – review & editing.

Conflicts of Interest

MV consulted for F. Hoffmann-La Roche Ltd, unrelated to this manuscript; she currently receives research funding from the National Institutes of Health and has equity ownership in Johnson and Johnson, Merck, Medtronic, and Amgen. RCP serves as a consultant for Roche, Inc.; Eisai, Inc.; Genentech, Inc.; Eli Lilly, Inc.; and Nestle, Inc.; served on a Data Safety Monitoring Board for Genentech; receives royalties from Oxford University Press and UpToDate; and receives National Institutes of Health funding.

References

1. 2024 Alzheimer's disease facts and figures. Alzheimers Dement 2024 May;20(5):3708-3821. [doi: 10.1002/alz.13809] [Medline: 38689398]
2. Sage growth partners. The state of healthcare automation: urgent need, growing awareness and tremendous potential. 2021. URL: https://go.sage-growth.com/state-of-healthcare-automation [accessed 2026-02-04]
3. National trends in hospital and physician adoption of electronic health records. ASTP - Assistant Secretary for Technology Policy. 2025. URL: https://www.healthit.gov/data/quickstats/national-trends-hospital-and-physician-adoption-electronic-health-records [accessed 2026-01-22]
4. Artificial intelligence-enabled medical devices. US Food and Drug Administration (FDA). 2024. URL: https://www.fda.gov/medical-devices/software-medical-device-samd/artificial-intelligence-and-machine-learning-aiml-enabled-medical-devices [accessed 2026-01-22]
5. Pierson E, Cutler DM, Leskovec J, Mullainathan S, Obermeyer Z. An algorithmic approach to reducing unexplained pain disparities in underserved populations. Nat Med 2021 Jan;27(1):136-140. [doi: 10.1038/s41591-020-01192-7] [Medline: 33442014]
6. Steinwachs DM, Stratton K, Kwan LY. Accounting for social risk factors in medicare payment. : National Academies Press; 2017 URL: https://www.nationalacademies.org/read/23635/chapter/1 [accessed 2026-01-22]
7. Obermeyer Z, Powers B, Vogeli C, Mullainathan S. Dissecting racial bias in an algorithm used to manage the health of populations. Science 2019 Oct 25;366(6464):447-453. [doi: 10.1126/science.aax2342] [Medline: 31649194]
8. Nelson A. Unequal treatment: confronting racial and ethnic disparities in health care. J Natl Med Assoc 2002 Aug;94(8):666-668. [Medline: 12152921]
9. Dzau VJ, McClellan MB, McGinnis JM, et al. Vital directions for health and health care: priorities from a National Academy of Medicine initiative. JAMA 2017 Apr 11;317(14):1461-1470. [doi: 10.1001/jama.2017.1964] [Medline: 28324029]
10. Vyas DA, Eisenstein LG, Jones DS. Hidden in plain sight—reconsidering the use of race correction in clinical algorithms. N Engl J Med 2020 Aug 27;383(9):874-882. [doi: 10.1056/NEJMms2004740] [Medline: 32853499]
11. Warnecke RB, Oh A, Breen N, et al. Approaching health disparities from a population perspective: the National Institutes of Health Centers for Population Health and Health Disparities. Am J Public Health 2008 Sep;98(9):1608-1615. [doi: 10.2105/AJPH.2006.102525] [Medline: 18633099]
12. Roberts ET, Zaslavsky AM, Barnett ML, Landon BE, Ding L, McWilliams JM. Assessment of the effect of adjustment for patient characteristics on hospital readmission rates: implications for pay for performance. JAMA Intern Med 2018 Nov 1;178(11):1498-1507. [doi: 10.1001/jamainternmed.2018.4481] [Medline: 30242346]

XSL•FO
RenderX

13. Sills MR, Hall M, Colvin JD, et al. Association of social determinants with children's hospitals' preventable readmissions performance. JAMA Pediatr 2016 Apr;170(4):350-358. [doi: 10.1001/jamapediatrics.2015.4440] [Medline: 26881387]
14. Franks P, Fiscella K. Effect of patient socioeconomic status on physician profiles for prevention, disease management, and diagnostic testing costs. Med Care 2002 Aug;40(8):717-724. [doi: 10.1097/00005650-200208000-00011] [Medline: 12187185]
15. Baker DW, Chassin MR. Holding providers accountable for health care outcomes. Ann Intern Med 2017 Sep 19;167(6):418-423. [doi: 10.7326/M17-0691] [Medline: 28806793]
16. Bernheim SM, Ross JS, Krumholz HM, Bradley EH. Influence of patients' socioeconomic status on clinical management decisions: a qualitative study. Ann Fam Med 2008;6(1):53-59. [doi: 10.1370/afm.749] [Medline: 18195315]
17. Bach PB, Pham HH, Schrag D, Tate RC, Hargraves JL. Primary care physicians who treat Blacks and Whites. N Engl J Med 2004 Aug 5;351(6):575-584. [doi: 10.1056/NEJMsa040609] [Medline: 15295050]
18. Jha AK, Zaslavsky AM. Quality reporting that addresses disparities in health care. JAMA 2014 Jul 16;312(3):225-226. [doi: 10.1001/jama.2014.7204] [Medline: 25027134]
19. Snyder-Mackler N, Burger JR, Gaydosh L, et al. Social determinants of health and survival in humans and other animals. Science 2020 May 22;368(6493):eaax9553. [doi: 10.1126/science.aax9553] [Medline: 32439765]
20. Adler NE, Newman K. Socioeconomic disparities in health: pathways and policies. Health Aff (Millwood) 2002;21(2):60-76. [doi: 10.1377/hlthaff.21.2.60] [Medline: 11900187]
21. Panch T, Mattie H, Atun R. Artificial intelligence and algorithmic bias: implications for health systems. J Glob Health 2019 Dec;9(2):010318. [doi: 10.7189/jogh.09.020318] [Medline: 31788229]
22. Nazer LH, Zatarah R, Waldrip S, et al. Bias in artificial intelligence algorithms and recommendations for mitigation. PLOS Digit Health 2023 Jun;2(6):e0000278. [doi: 10.1371/journal.pdig.0000278] [Medline: 37347721]
23. Juhn YJ, Ryu E, Wi CI, et al. Assessing socioeconomic bias in machine learning algorithms in health care: a case study of the HOUSES index. J Am Med Inform Assoc 2022 Jun 14;29(7):1142-1151. [doi: 10.1093/jamia/ocac052] [Medline: 35396996]
24. Cadena-Hernandez AG, Trejo-Castro AI, Celaya-Padilla JM, Tamez-Pena J, Martinez-Torteya A. Longitudinal gender-specific differences in the conversion from mild cognitive impairment to Alzheimer's disease. Presented at: 2018 IEEE EMBS International Conference on Biomedical & Health Informatics (BHI); Mar 4-7, 2018. [doi: 10.1109/BHI.2018.8333404]
25. Gamberger D, Ženko B, Mitelpunkt A, Shachar N, Lavrač N. Clusters of male and female Alzheimer's disease patients in the Alzheimer's Disease Neuroimaging Initiative (ADNI) database. Brain Inform 2016 Sep;3(3):169-179. [doi: 10.1007/s40708-016-0035-5] [Medline: 27525218]
26. Aditya CR, Pande MBS. Devising an interpretable calibrated scale to quantitatively assess the dementia stage of subjects with Alzheimer's disease: a machine learning approach. Informatics in Medicine Unlocked 2017;6:28-35. [doi: 10.1016/j.imu.2016.12.004]
27. Puaschitz NG, Jacobsen FF, Mannseth J, et al. Factors associated with access to assistive technology and telecare in home-dwelling people with dementia: baseline data from the LIVE@Home.Path trial. BMC Med Inform Decis Mak 2021 Sep 15;21(1):264. [doi: 10.1186/s12911-021-01627-2] [Medline: 34525979]
28. Twait EL, Andaur Navarro CL, Gudnason V, Hu YH, Launer LJ, Geerlings MI. Dementia prediction in the general population using clinically accessible variables: a proof-of-concept study using machine learning. The AGES-Reykjavik study. BMC Med Inform Decis Mak 2023 Aug 28;23(1):168. [doi: 10.1186/s12911-023-02244-x] [Medline: 37641038]
29. Liu Z, Garg M, Fu S, et al. Harnessing transfer learning for dementia prediction: leveraging sex-different mild cognitive impairment prognosis. Presented at: 2023 IEEE International Conference on Bioinformatics and Biomedicine (BIBM); Dec 5-8, 2023. [doi: 10.1109/BIBM58861.2023.10385516]
30. Wu H, Sylolypavan A, Wang M, Wild S. Quantifying health inequalities induced by data and AI models. 2022 Presented at: Proceedings of the Thirty-First International Joint Conference on Artificial Intelligence; Jul 23-29, 2022. [doi: 10.24963/ijcai.2022/721]
31. Roberts RO, Geda YE, Knopman DS, et al. The Mayo Clinic Study of Aging: design and sampling, participation, baseline measures and sample characteristics. Neuroepidemiology 2008;30(1):58-69. [doi: 10.1159/000115751] [Medline: 18259084]
32. Petersen RC. Mild cognitive impairment as a diagnostic entity. J Intern Med 2004 Sep;256(3):183-194. [doi: 10.1111/j.1365-2796.2004.01388.x] [Medline: 15324362]
33. Guze SB. Diagnostic and Statistical Manual of Mental Disorders, 4th ed. (DSM-IV). AJP 1995 Aug;152(8):1228-1228. [doi: 10.1176/ajp.152.8.1228]
34. Rocca WA, Yawn BP, St Sauver JL, Grossardt BR, Melton LJ 3rd. History of the Rochester Epidemiology Project: half a century of medical records linkage in a US population. Mayo Clin Proc 2012 Dec;87(12):1202-1213. [doi: 10.1016/j.mayocp.2012.08.012] [Medline: 23199802]
35. Kind AJH, Buckingham WR. Making neighborhood-disadvantage metrics accessible - the Neighborhood Atlas. N Engl J Med 2018 Jun 28;378(26):2456-2458. [doi: 10.1056/NEJMp1802313] [Medline: 29949490]
36. Juhn YJ, Beebe TJ, Finnie DM, et al. Development and initial testing of a new socioeconomic status measure based on housing data. J Urban Health 2011 Oct;88(5):933-944. [doi: 10.1007/s11524-011-9572-7] [Medline: 21499815]

XSL•FO
RenderX

37. Cohen JW, Cohen SB, Banthin JS. The medical expenditure panel survey: a national information resource to support healthcare cost research and inform policy and practice. Med Care 2009 Jul;47(7 Suppl 1):S44-S50. [doi: 10.1097/MLR.0b013e3181a23e3a] [Medline: 19536015]
38. Chawla NV, Bowyer KW, Hall LO, Kegelmeyer WP. SMOTE: synthetic minority over-sampling technique. J Artif Intell Res 2002;16:321-357. [doi: 10.1613/jair.953]
39. St Sauver JL, Grossardt BR, Leibson CL, Yawn BP, Melton LJ 3rd, Rocca WA. Generalizability of epidemiological findings and public health decisions: an illustration from the Rochester Epidemiology Project. Mayo Clin Proc 2012 Feb;87(2):151-160. [doi: 10.1016/j.mayocp.2011.11.009] [Medline: 22305027]

Abbreviations

ADI: Area Deprivation Index
AI: artificial intelligence
BER: balanced error rate
DEM: dementia
HOUSES: Housing-Based Socioeconomic Status
LR: logistic regression
MCI: mild cognitive impairment
MCSA: Mayo Clinic Study on Aging
NB: Naïve Bayes
REP: Rochester Epidemiology Project
RF: Random Forest
SES: socioeconomic status
SMOTE-NC: Synthetic Minority Oversampling Technique for Nominal and Continuous features
SVM: support vector machine

Edited by A Coristine; submitted 09.Jul.2025; peer-reviewed by J Dai, LM Diaz; accepted 07.Jan.2026; published 17.Feb.2026.

Please cite as:
Liu X, Garg M, Vassilaki M, St Sauver J, Petersen RC, Malik MM, Wi CI, Juhn YJ, Sohn S
Assessing the Impact of Sociodemographic Factors on Artificial Intelligence Models in Predicting Dementia: Retrospective Cohort Study
JMIR Med Inform 2026;14:e80405
URL: https://medinform.jmir.org/2026/1/e80405
doi:10.2196/80405

© Xingyi Liu, Muskan Garg, Maria Vassilaki, Jennifer St Sauver, Ronald C Petersen, Momin M Malik, Chung Il Wi, Young J Juhn, Sunghwan Sohn. Originally published in JMIR Medical Informatics (https://medinform.jmir.org), 17.Feb.2026. This is an open-access article distributed under the terms of the Creative Commons Attribution License (https://creativecommons.org/licenses/by/4.0/), which permits unrestricted use, distribution, and reproduction in any medium, provided the original work, first published in JMIR Medical Informatics, is properly cited. The complete bibliographic information, a link to the original publication on https://medinform.jmir.org/, as well as this copyright and license information must be included.

XSL•FO
RenderX

Screening for Clinically Significant Nephrolithiasis Based on Simple Health Checkup Clinical and Urine Parameters in General Populations: Multicenter Machine Learning Study

Hao-Wei Chen[1,2,3], MD, PhD; Pei-Siou Wei[4,5], MS; Yu-Chen Chen[1,2,6], MD; Jeng-Yih Wu[7,8,9], MD; Chia-I Lin[8], MD; Yii-Her Chou[1,2], MD, PhD; Yung-Shun Juan[1,2], MD, PhD; Wen-Jeng Wu[1,2], MD, PhD; Chung-Yao Kao[4], PhD; Jung-Ting Lee[10], PhD

[1]Department of Urology, Kaohsiung Medical University Chung-Ho Memorial Hospital, Kaohsiung, Taiwan
[10]School of Medicine, National Sun Yat-sen University, 70 Lien-Hai Road, Kaohsiung, Taiwan
[2]Graduate Institute of Clinical Medicine, College of Medicine, Kaohsiung Medical University, Kaohsiung, Taiwan
[3]Center for Big Data Research, Kaohsiung Medical University, Kaohsiung, Taiwan
[4]Department of Electrical Engineering, National Sun Yat-sen University, Kaohsiung, Taiwan
[5]United Kaohsiung AI Medical Technology Co, Ltd., Kaohsiung, Taiwan
[6]Regenerative Medicine and Cell Therapy Research Center, Kaohsiung Medical University, Kaohsiung, Taiwan
[7]Department of Internal Medicine, Kaohsiung Medical University Chung-Ho Memorial Hospital, Kaohsiung, Taiwan
[8]Health Management Center, Kaohsiung Medical University Chung-Ho Memorial Hospital, Kaohsiung, Taiwan
[9]College of Medicine, Kaohsiung Medical University, Kaohsiung, Taiwan

Corresponding Author:
Jung-Ting Lee, PhD
School of Medicine, National Sun Yat-sen University, 70 Lien-Hai Road, Kaohsiung, Taiwan

Abstract

Background: Nephrolithiasis affects approximately 15% of the population and often remains undetected in asymptomatic individuals. Current diagnostic approaches rely on imaging tools, such as ultrasound or computed tomography, which are costly, operator dependent, or involve radiation, making them unsuitable for large-scale screening. A standardized, practical, and low-cost screening strategy for early identification of clinically significant kidney stones is still lacking.

Objective: This study aimed to develop a low-cost, rapid screening model for clinically significant nephrolithiasis using machine learning (ML) and simple clinical parameters.

Methods: We conducted a multihospital retrospective study using data from 3 hospitals in Kaohsiung, Taiwan (2012 - 2021). Adults without renal colic were included. ML models were trained and tested using 10 routine variables: sex, age, BMI, gout, diabetes, estimated glomerular filtration rate, urine pH, red blood cell count, specific gravity, and bacteriuria. Multiple ML algorithms were trained and evaluated, and the best-performing model was selected based on the area under the receiver operating characteristic curve and the area under the precision-recall curve. To assess model interpretability, Shapley value analysis was performed to determine the relative importance and contribution of each variable to the model's predictive performance.

Results: Among 6528 participants, the best-performing model achieved an area under the receiver operating characteristic curve of 0.968 (95% CI 0.956 - 0.980), an area under the precision-recall curve of 0.936 (95% CI 0.918 - 0.953), a sensitivity of 0.873 (95% CI 0.841 - 0.904), and a specificity of 0.947 (95% CI 0.935 - 0.959). Shapley value analysis identified urine red blood cell count, estimated glomerular filtration rate, and urine specific gravity as the 3 most influential predictors.

Conclusions: This ML-based model enables efficient, noninvasive, and large-scale kidney stone screening using routine health data. It can be integrated into health checkups or telemedicine platforms to facilitate early detection and proactive management. Although the model was developed using an Asian population, future validation in diverse cohorts is warranted to confirm its generalizability.

(JMIR Med Inform 2026;14:e80764) doi:10.2196/80764

KEYWORDS

machine learning; nephrolithiasis; health services; software as a medical device; computer-aided diagnosis

XSL•FO
RenderX

Introduction

Approximately 10% of the global population faces a lifetime risk of developing kidney stones [1], and the prevalence of this disease has been steadily rising over the past two decades [2,3]. The most common symptoms include flank pain and hematuria, and kidney and ureteral stones are significant risk factors for chronic kidney disease [4]. A study reported that in the year 2000 alone, the total medical expenditure for treating kidney and ureteral stones in the United States reached US $2.1 billion [5].

Currently, there is no effective tool available for kidney stone screening. Renal ultrasonography is the most commonly used method for detecting kidney stones in clinical settings and emergency departments [5]. While it is a convenient and radiation-free technique, its accuracy is highly dependent on the operator's skill, thus requiring trained medical professionals for both operation and interpretation. As a result, its use in large-scale screening would demand substantial health care manpower [6,7]. In contrast, abdominal computed tomography (CT) is considered the gold standard for diagnosing kidney and ureteral stones [8]. However, due to its high radiation exposure and limited accessibility for routine or large-scale screening, CT is not suitable for asymptomatic populations or frontline outpatient use [9]. Therefore, existing imaging tools are impractical for large-scale screening of kidney stones. Developing a simple, cost-effective, and accessible screening tool would be highly beneficial for the early detection of kidney stones and for timely medical decision-making.

We previously developed an artificial intelligence (AI) algorithm that uses routine health checkup data, including urine routine and blood creatinine, to preliminarily predict the presence of kidney stones larger than 2 mm in overweight individuals (BMI ≥25 kg/m^2) [6]. This tool has shown potential for use in kidney stone screening. In this study, we aimed to build upon our prior success by leveraging machine learning (ML) techniques and routine health data to further develop a clinically applicable AI model that can predict clinically significant kidney stones in all patients—not limited to those with BMI >24 kg/m^2. The models will be validated using patient cohorts from multiple hospitals.

Methods

Description of Participants

In this cohort study, clinical data were retrospectively collected from three hospitals located in Kaohsiung, Taiwan: Kaohsiung Medical University Hospital, Kaohsiung Municipal Ta-Tung Hospital, and Kaohsiung Municipal Siaogang Hospital. The data collection period spanned from January 2012 to March 2021.

Patients were categorized into 2 groups based on the presence or absence of nephrolithiasis measuring ≥2 mm. This classification followed the methodology of our previously published ML-based nephrolithiasis screening model developed for overweight and obese individuals [6]. In accordance with prior urological literature, stone fragments smaller than 2 mm are considered clinically insignificant, as they are unlikely to cause stone-related events or require intervention [7]. Therefore, a cutoff of 2 mm was adopted in this study to define clinically significant nephrolithiasis. The presence of stones of 2 mm or larger was confirmed using abdominal CT or a combination of renal ultrasonography and plain abdominal radiography (KUB: kidney, ureter, and bladder), consistent with our prior study protocol [6]. Patients were excluded if they experienced renal colic at the time of data collection, had undergone kidney transplantation, had indwelling foreign bodies in the upper urinary tract (eg, ureteral stents or percutaneous nephrostomy tubes), were receiving renal replacement therapy (hemodialysis or peritoneal dialysis), were aged younger than 18 years, or lacked complete medical records. For model development, data from January 2012 to December 2019 were used for training and validation. An independent test cohort comprising data collected between January 2020 and March 2021 was used for the clinical evaluation of model performance.

Ethical Considerations

This study was approved by the Institutional Review Board of Kaohsiung Medical University Hospital (KMUHIRB-E(I)-20210331) and conducted in accordance with the principles outlined in the Declaration of Helsinki. The requirement for informed consent was waived due to the retrospective nature of the study and the minimal risk to participants. All data were obtained from existing electronic health records and were fully deidentified before analysis. No personally identifiable information was accessed by the researchers, and data access was restricted to authorized study personnel only. No compensation was provided to participants, as no direct contact or intervention was involved in this retrospective study.

Variables and Data Processing

A total of 10 predictor variables were included for model development, categorized into sociodemographic, health-related, and clinical domains. The categorical response variable indicated the presence (1) or absence (0) of nephrolithiasis ≥2 mm. Sociodemographic variables included age (numeric) and sex (categorical: male=1 and female =0). Health-related variables comprised BMI (numeric with 2 decimals) and a history of diabetes mellitus and gout (both categorical: with=1 and without=0).

Clinical variables included five parameters derived from urine and blood tests:

1. Urine specific gravity (SG; numeric with 3 decimals)
2. Urine pH (numeric with 1 decimal)
3. Bacteriuria (categorical: present =1, absent =0)
4. Urine red blood cell (RBC) count (treated as a numeric variable; details described as follows): In Taiwan, urine RBC counts are commonly reported in terms of a range (eg, 6 - 10 RBCs per high-power field [HPF]), with the lowest range being "0 to 2 RBCs per HPF." In this study, the urine RBC data we collected consist of the following ranges: 0 to 2, 3 to 5, 6 to 10, 11 to 25, 26 to 50, 51 to 99, and 100 or greater. As such, it may be treated as a categorical variable in this study. However, to accommodate various range scales used by different hospitals and make the model

XSL•FO
RenderX

universally applicable, we adopted the mean of the reported ranges (eg, 8 for the range 6 - 10 RBCs per HPF) as the corresponding urine RBC count and treated the variable as numeric (continuous). The exceptions to the rule are the range of "0 to 2" and the ranges whose mean values exceed 100. For the 0 to 2 range, the value 0 is assigned. This is due to an American Urological Association guideline, which defines microhematuria as "3 or more RBCs per HPF on microscopic examination." Therefore, 0 to 2 RBCs per HPF is generally considered as no hematuria. On the other hand, patients with macroscopic hematuria generally have their urine RBC counts reported as "100 or more RBCs per HPF," or a range with a mean value exceeding 100, or something equivalent to that effect. As such, for ranges whose mean values exceed 100 RBCs per HPF, we applied the capped value of 200 to maintain consistency across the dataset [10].

5. Estimated glomerular filtration rate (eGFR), numeric with 1 decimal, calculated using the Isotope Dilution Mass Spectrometry–traceable Modification of Diet in Renal Disease equation: eGFR (mL/min/1.73 m^2)=175×$(Scr)^{-1.154}$×$(age)^{-0.203}$×(0.742 if female) [8]

For descriptive statistics, the Fisher exact test was used for categorical variables (eg, sex, history of diabetes mellitus, and history of gout), and the Mann-Whitney *U* test was applied for numeric variables (eg, age, BMI, eGFR, urine SG, urine RBC count, and urine pH) between patients with and without nephrolithiasis. To verify the similarity between the training and testing datasets, we compared feature distributions by calculating category percentages for categorical variables and means with SDs for continuous variables. All statistical analyses were performed using the Statistical Package for the Social Sciences for Windows (version 24.0; IBM), and *P* values of less than .05 were considered statistically significant.

Model Development, Fitting, and Evaluation

ML methods were used to build the models [9]. The logistic regression, the k-nearest neighbors algorithm, the support vector machine, and the random forest (RF) algorithm were used as the standard methods for comparison, while an artificial neural network (ANN) model was developed for deep learning classification. All standard models were implemented in Python using the scikit-learn library (version 1.1.3; scikit-learn developers) with recommended settings. The respective algorithms for each method were run using the recommended parameters [11,12].

For the ANN, implemented in Python, the 10-fold cross-validation protocol was performed on the training set to produce 10 models, each structured as a 9-layer fully connected neural network. These models were averaged into 1 final model. To address the imbalance between stone-positive and stone-negative cohorts, the synthetic minority over-sampling technique, as well as the approach of assigning different weights to the 2 patient groups, was adopted when training our models. In addition, a pronounced sex imbalance among the patient cohorts was observed. To ensure equitable accuracy for the 2 gender groups, 2 separate cutoff thresholds were identified for male and female patients. The 2 thresholds were then standardized to 0.5 by applying gender-specific rescalers to the averaged outputs. The resulting combined structure served as the final ANN model with a unified threshold of 0.5. Additional information is provided in Figure S1 in Multimedia Appendix 1.

Data between January 2012 and December 2019 were used for model training and validation. The data were randomly divided into a training dataset (75%) and a validation dataset (25%). Model training was performed using the training data, while validation data helped identify overfitting or bias. Data registered after January 1, 2020, formed the testing dataset (ie, the holdout dataset) for independent evaluation of model performance. Performance on the testing data was assessed by various metrics, including the area under the receiver operating characteristic (ROC) curve (AUROC), the area under the precision-recall (PR) curve (AUPRC), and net benefit by the decision curve analysis. The optimal thresholds for standard models were based on the Youden index [13] from their respective training ROC curves. For the ANN, the classification threshold was preset at 0.5. These thresholds were used to calculate sensitivity, specificity, positive predictive value, and negative predictive value on the validation and testing sets. Model calibration analysis was also performed to assess how accurately the output probabilities of the models reflect the true likelihood of outcomes.

To examine model stability and fairness across different patient subgroups, additional analyses were performed by individual variables (eg, sex, diabetes, gout, bacteriuria, urine RBC count, age, BMI, and eGFR), where model performance metrics (area under the curve [AUC] and accuracy) were calculated independently for each subgroup.

Importance of Feature Variables

To evaluate the predictive power of each feature variable, their relative impact on the ANN model output was assessed by applying the Shapley value analysis [14]. Features with notably high impact were selected, and an ANN model was trained using only these variables. The performance of the model was compared with that of the full-variable ANN model to assess whether key features alone provided sufficient predictive power.

Results

Characteristics of Study Participants

In the training dataset, 1243 (33.11%) participants had nephrolithiasis, and 2511 (66.89%) participants were without nephrolithiasis of 2 mm or greater, among a total of 3754 (100.0%) participants. The validation dataset had 414 (33.09%) participants with and 837 (66.91%) participants without nephrolithiasis of 2 mm or greater, among a total of 1251 (100.0%) participants. The testing dataset had 400 (26.26%) participants with and 1123 (73.74%) participants without nephrolithiasis of 2 mm or greater, among a total of 1523 (100.0%) participants. The characteristics of the participants in these 3 sets are described in detail in Tables 1 and 2. Statistical similarity among the 3 sets was observed. It is also observed that the mean values (or the "percentages," in the case of binary variables) of the variables we selected are statistically different between participants with and without nephrolithiasis. The

XSL•FO
RenderX

Fisher exact and Mann-Whitney *U* tests were applied to verify the statistical significance of these differences, and the resulting *P* values are also reported in Tables 1 and 2.

XSL•FO
RenderX

Table . Descriptive analysis of the training, validation, and testing datasets.

	Training set, n (%)				Validation set, n (%)				Testing set, n (%)			
	w/neph[a] (n=1243, 33.1%)	wo/neph[b] (n=2511, 66.9 %)	Total (N=3754)	*P* value	w/neph (n=414, 33.1%)	wo/neph (n=837, 66.9%)	Total (N=1251)	*P* value	w/neph (n=400, 26.3%)	wo/neph (n=1123, 73.7%)	Total (N=1523)	*P* value
Gender				.02				.19				<.001
Male	820 (66.0)	1750 (69.7)	2570 (68.5)		273 (65.9)	584 (69.8)	857 (68.5)		250 (62.5)	433 (38.6)	683 (44.8)	
Female	423 (34.0)	761 (30.3)	1184 (31.5)		141 (34.1)	253 (30.2)	394 (31.5)		150 (37.5)	690 (61.4)	840 (55.2)	
Diabetes				<.001				<.001				<.001
With	220 (17.7)	148 (5.9)	368 (9.8)		86 (20.8)	59 (7.1)	145 (11.6)		94 (23.5)	15 (1.3)	109 (7.2)	
Without	1023 (82.3)	2363 (94.1)	3386 (90.2)		328 (79.2)	778 (92.9)	1106 (88.4)		306 (76.5)	1108 (98.7)	1414 (92.8)	
Gout				<.001				<.001				<.001
With	49 (3.9)	16 (0.6)	65 (1.7)		20 (4.8)	3 (0.4)	23 (1.8)		12 (3.0)	4 (0.4)	16 (1.1)	
Without	1194 (96.1%)	2495 (99.4)	3689 (98.3)		394 (95.2)	834 (99.6)	1228 (98.2)		388 (97.0)	1119 (99.6%)	1507 (98.9)	
BAC[c]				<.001				<.001				<.001
With	191 (15.4)	249 (9.9)	440 (11.7)		47 (11.4)	78 (9.3)	125 (10.0)		49 (12.3)	145 (12.9)	194 (12.7)	
Without	1052 (84.6)	2262 (90.1)	3314 (88.3)		367 (88.6)	759 (90.7)	1126 (90.0)		351 (87.7)	978 (87.1)	1329 (87.3)	
Urine RBC count[d]				<.001				<.001				<.001
0-2	219 (17.6)	2265 (90.2)	2484 (66.2)		80 (19.3)	752 (89.8)	832 (66.5)		84 (21.0)	921 (82.0)	1005 (66.0)	
3-5	128 (10.3)	169 (6.7)	297 (7.9)		36 (8.7)	63 (7.52)	99 (7.9)		41 (10.3)	138 (12.3)	179 (11.7)	
6-10	104 (8.4)	44 (1.8)	148 (3.9)		35 (8.5)	13 (1.6)	48 (3.8)		35 (8.8)	30 (2.7)	65 (4.3)	
11-25	153 (12.3)	23 (0.9)	176 (4.7)		56 (13.5)	6 (0.72)	62 (5.0)		43 (10.7)	19 (1.7)	62 (4.1)	
26-50	141 (11.3)	5 (0.2)	146 (3.9)		38 (9.2)	2 (0.24)	40 (3.2)		33 (8.2)	6 (0.5)	39 (2.5)	
51-99	121 (9.7)	1 (0.04)	122 (3.3)		47 (11.4)	0 (0.0)	47 (3.8)		32 (8.0)	3 (0.3)	35 (2.3)	
≥100	377 (30.4)	4 (0.16)	381 (10.1)		122 (29.4)	1 (0.12)	123 (9.8)		132 (33.0)	6 (0.5)	138 (9.1)	

[a]w/neph: with nephrolithiasis.

[b]wo/neph: without nephrolithiasis.

[c]BAC: bacteriuria.

[d]RBC: red blood cell.

XSL•FO
RenderX

Table . Characteristics about age, BMI, urine pH, estimated glomerular filtration rate (eGFR), and urine red blood cell (RBC) count of patients in the training, validation, and testing datasets.

	Training set, mean (SD) [95% CI]			Validation set, mean (SD) [95% CI]			Testing set, mean (SD) [95% CI]		
	w/neph[a]	wo/neph[b]	*P* value	w/neph	wo/neph	*P* value	w/neph	wo/neph	*P* value
Age	55.92 (13.30) [55.15 - 56.68]	50.92 (10.10) [50.51 - 51.33]	<.001	55.53 (13.47) [54.34 - 56.71]	51.36 (10.07) [50.73 - 51.98]	<.001	57.31 (13.80) [55.95 - 58.66]	45.52 (9.32) [44.97 - 46.07]	<.001
eGFR	74.67 (29.23) [72.98 - 76.35]	86.31 (17.83) [85.58 - 87.03]	<.001	73.38 (30.44) [70.70 - 76.06]	85.95 (17.64) [84.86 - 87.04]	<.001	69.47 (26.74) [66.84 - 72.10]	95.03 (19.18) [93.90 - 96.15]	<.001
BMI	25.77 (3.81) [25.55 - 25.99]	24.64 (3.63) [24.50 - 24.79]	<.001	25.91 (4.02) [25.56 - 26.27]	24.67 (3.59) [24.45 - 24.89]	<.001	26.65 (4.82) [26.18 - 27.13]	23.68 (3.86) [23.45 - 23.90]	<.001
Urine pH	6.03 (0.79) [5.98 - 6.07]	6.03 (0.74) [6.00 - 6.06]	.93	6.07 (0.80) [5.99 - 6.15]	6.01 (0.75) [5.96 - 6.06]	.21	6.11 (0.84) [6.02 - 6.19]	6.02 (0.79) [5.97 - 6.06]	.06
Urine RBC count	75.42 (84.64) [70.55 - 80.30]	1.03 (8.83) [0.67 - 1.39]	<.001	74.93 (84.60) [67.48 - 82.38]	0.83 (6.82) [0.41 - 1.26]	<.001	78.18 (87.85) [69.54 - 86.82]	2.48 (15.48) [1.58 - 3.39]	<.001
Urine SG[c]	1.014 (0.006) [1.0137 - 1.0144]	1.018 (0.007) [1.018 - 1.0185]	<.001	1.014 (0.007) [1.013 - 1.0145]	1.018 (0.007) [1.018 - 1.0185]	<.001	1.015 (0.008) [1.014 - 1.0154]	1.018 (0.006) [1.018 - 1.0187]	<.001

[a]w/neph: with nephrolithiasis.

[b]wo/neph: without nephrolithiasis.

[c]SG: specific gravity.

Model Performance

The ANN model we developed demonstrated strong discriminatory power in identifying participants with kidney or ureteral stones, using only limited information typically collected at an initial clinical visit. It achieved validation and testing AUROCs of 0.970 and 0.968 and validation and testing AUPRCs of 0.960 and 0.936, respectively. Using a cutoff value of 0.5, the model showed high sensitivity, specificity, positive predictive value, and negative predictive value in both validation and testing sets, with overall correction rates of 92.3% and 92.7%, respectively. These performance measures indicate that the model achieved a good balance in identifying both positive and negative cases and is able to render both high precision and high recall.

The performance of models obtained using standard methods appeared to be somewhat inferior to that of the ANN model, with the exception of the RF algorithm, which performed equally well. The logistic regression, k-nearest neighbors, and support vector machine (linear kernel) models had testing AUROCs of 0.933, 0.916, and 0.910, respectively, and testing AUPRCs of 0.822, 0.876, and 0.790, respectively. The RF model achieved AUROC and AUPRC of 0.965 and 0.934, which are almost the same as those of the ANN model. The overall correction rate was 90.5%. Despite the high AUROC and AUPRC scores, the RF model showed unbalanced performance between sensitivity and specificity, a pattern also observed in the other conventional models.

Table 3 summarizes the performance data of these 5 models. Figure 1A-C presents their training, validation, and testing ROC curves, while Figure 2A-C presents the respective PR curves.

XSL•FO
RenderX

Figure 1. The receiver operating characteristic (ROC) curves of the artificial neural network (ANN), random forest, k-nearest neighbor (KNN), support vector machine (SVM), and logistic regression models. (A) Training ROC curves. (B) Validation ROC curves. (C) Testing ROC curves. AUROC: area under the receiver operating characteristic curve.

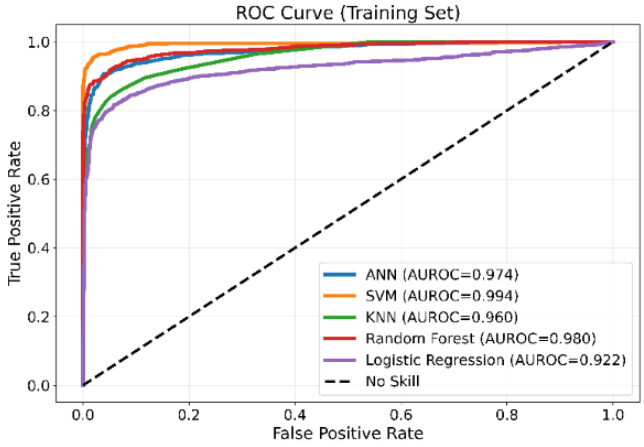

Fig. 1A

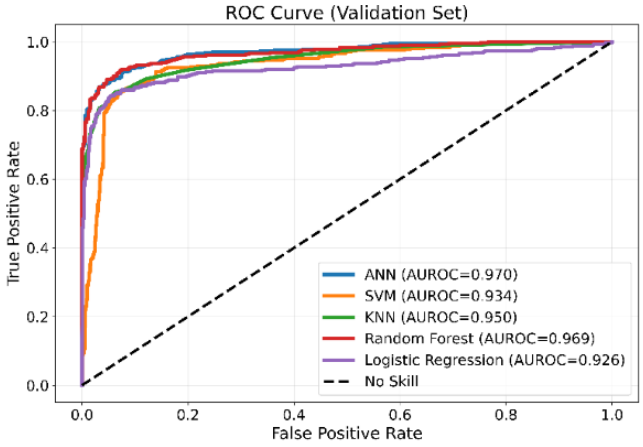

Fig. 1B

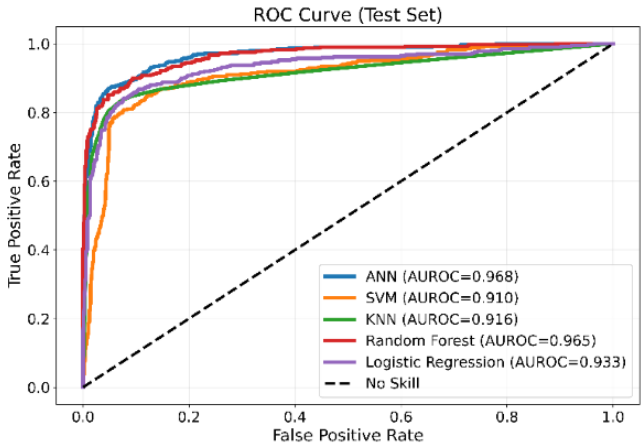

Fig. 1C

XSL•FO
RenderX

Figure 2. Precision-recall (PR) curves of the artificial neural network (ANN), random forest, k-nearest neighbor (KNN), support vector machine (SVM), and logistic regression models. (A) Training PR curves. (B) Validation PR curves. (C) Testing PR curves. AUPRC: area under the precision-recall curve.

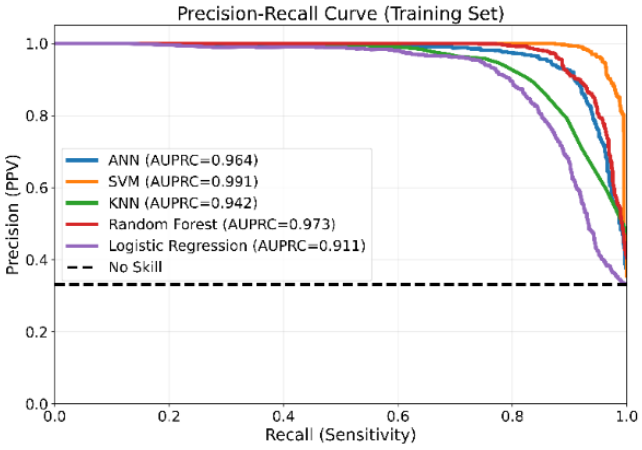

Fig. 2A

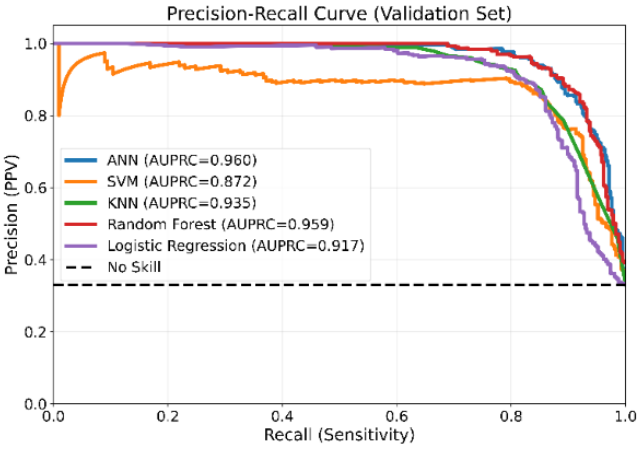

Fig. 2B

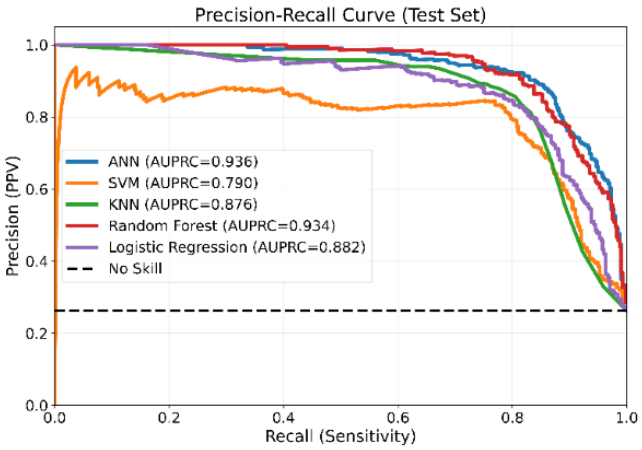

Fig. 2C

XSL•FO
RenderX

Table . Summary of model performances.

Model and dataset	AUROC[a] (95% CI)	AUPRC[b] (95% CI)	Accuracy (95% CI)	Sensitivity (95% CI)	Specificity (95% CI)	PPV[c] (95% CI)	NPV[d] (95% CI)
ANN[e]							
Training	0.974 (0.968 - 0.980)	0.964 (0.956 - 0.971)	0.943 (0.935 - 0.951)	0.907 (0.890 - 0.923)	0.961 (0.954 - 0.968)	0.920 (0.903 - 0.937)	0.954 (0.946 - 0.963)
Validation	0.970 (0.958 - 0.982)	0.960 (0.946 - 0.973)	0.923 (0.908 - 0.937)	0.889 (0.860 - 0.918)	0.939 (0.923 - 0.956)	0.878 (0.846 - 0.911)	0.945 (0.928 - 0.962)
Testing	0.968 (0.956 - 0.98)	0.936 (0.918 - 0.953)	0.927 (0.915 - 0.939)	0.873 (0.841 - 0.904)	0.947 (0.935 - 0.959)	0.853 (0.819 - 0.888)	0.954 (0.941 - 0.968)
LR[f]							
Training	0.922 (0.911 - 0.934)	0.911 (0.899 - 0.922)	0.900 (0.891 - 0.910)	0.817 (0.796 - 0.839)	0.942 (0.932 - 0.951)	0.874 (0.855 - 0.893)	0.912 (0.902 - 0.923)
Validation	0.926 (0.906 - 0.945)	0.917 (0.897 - 0.936)	0.908 (0.892 - 0.924)	0.843 (0.808 - 0.878)	0.940 (0.924 - 0.956)	0.875 (0.842 - 0.907)	0.924 (0.906 - 0.942)
Testing	0.933 (0.916 - 0.949)	0.882 (0.859 - 0.904)	0.909 (0.895 - 0.924)	0.800 (0.761 - 0.839)	0.948 (0.935 - 0.961)	0.847 (0.810 - 0.883)	0.930 (0.915 - 0.945)
KNN[g]							
Training	0.960 (0.954 - 0.966)	0.942 (0.932 - 0.951)	0.905 (0.896 - 0.914)	0.861 (0.842 - 0.880)	0.927 (0.917 - 0.937)	0.853 (0.834 - 0.873)	0.931 (0.921 - 0.941)
Validation	0.950 (0.936 - 0.963)	0.935 (0.918 - 0.952)	0.899 (0.882 - 0.915)	0.862 (0.829 - 0.896)	0.916 (0.898 - 0.935)	0.836 (0.801 - 0.871)	0.931 (0.914 - 0.948)
Testing	0.916 (0.896 - 0.936)	0.876 (0.853 - 0.899)	0.892 (0.876 - 0.907)	0.848 (0.812 - 0.883)	0.907 (0.890 - 0.924)	0.765 (0.726 - 0.805)	0.944 (0.930 - 0.957)
SVM[h]							
Training	0.994 (0.991 - 0.996)	0.991 (0.987 - 0.994)	0.972 (0.966 - 0.977)	0.957 (0.946 - 0.969)	0.979 (0.973 - 0.984)	0.957 (0.945 - 0.968)	0.979 (0.973 - 0.985)
Validation	0.934 (0.917 - 0.949)	0.872 (0.848 - 0.895)	0.828 (0.807 - 0.849)	0.930 (0.905 - 0.955)	0.778 (0.750 - 0.806)	0.674 (0.636 - 0.713)	0.957 (0.942 - 0.973)
Testing	0.910 (0.891 - 0.929)	0.790 (0.761 - 0.818)	0.722 (0.700 - 0.745)	0.920 (0.893 - 0.947)	0.652 (0.624 - 0.680)	0.485 (0.449 - 0.520)	0.958 (0.944 - 0.972)
RF[i]							
Training	0.980 (0.975 - 0.984)	0.973 (0.966 - 0.979)	0.939 (0.931 - 0.946)	0.919 (0.904 - 0.934)	0.949 (0.940 - 0.957)	0.899 (0.882 - 0.915)	0.959 (0.952 - 0.967)
Validation	0.969 (0.958 - 0.979)	0.959 (0.945 - 0.972)	0.924 (0.909 - 0.939)	0.918 (0.891 - 0.944)	0.927 (0.910 - 0.945)	0.862 (0.830 - 0.894)	0.958 (0.944 - 0.972)
Testing	0.965 (0.954 - 0.975)	0.934 (0.916 - 0.951)	0.905 (0.890 - 0.920)	0.900 (0.871 - 0.929)	0.907 (0.890 - 0.924)	0.774 (0.736 - 0.812)	0.962 (0.951 - 0.974)

[a]AUROC: area under the receiver operating characteristic curve.

[b]AUPRC: area under the precision-recall curve.

[c]PPV: positive predictive value.

[d]NPV: negative predictive value.

[e]ANN: artificial neural network.

[f]LR: logistic regression.

[g]KNN: k-nearest neighbor.

[h]SVM: support vector machine.

[i]RF: random forest.

XSL•FO
RenderX

Regarding the practical relevance of models' predicted probabilities, the results of decision curve analysis and model calibration analysis are shown in Figure 3A-C and Figure 4A-C, respectively. Figure 3 indicates that all models rendered higher net benefits than those of the baseline strategies ("treat all" and "treat none") over a large range of threshold probabilities. Among them, the performance of the ANN and RF models appeared to be superior to the others over the validation and testing datasets. Figure 4 indicates that the predicted probabilities of all models were somewhat deviated from the actual events. As such, despite exhibiting good performance for identifying nephrolithiasis, further calibration of the model outputs appears to be required. To further evaluate the robustness and generalizability of the ANN model, subgroup analyses were conducted based on demographic and clinical characteristics.

Figure 3. Decision curve analysis for the artificial neural network (ANN), random forest, k-nearest neighbor (KNN), support vector machine (SVM), and logistic regression models. (A) Net benefits over the training set. (B) Net benefits over the validation set. (C) Net benefits over the testing set.

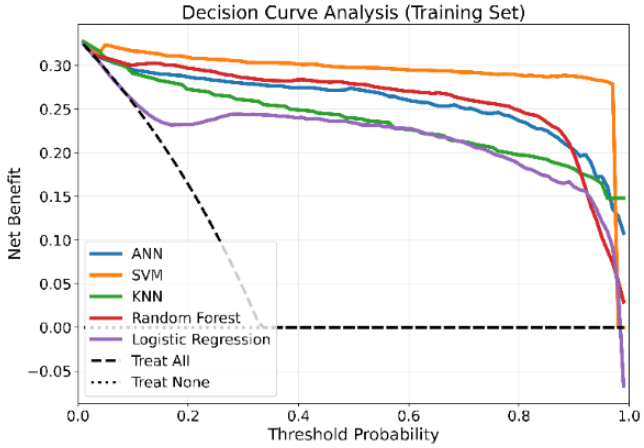

Fig. 3A

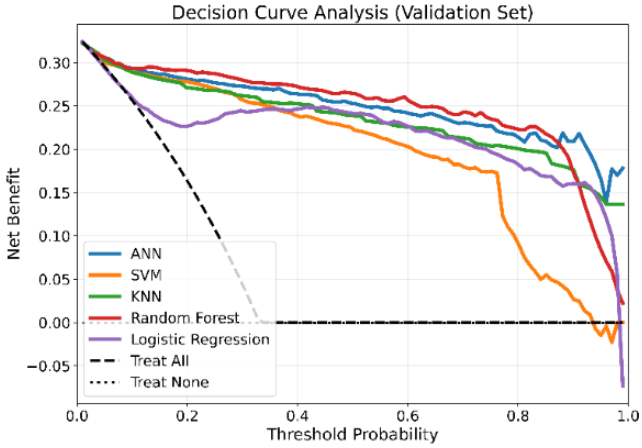

Fig. 3B

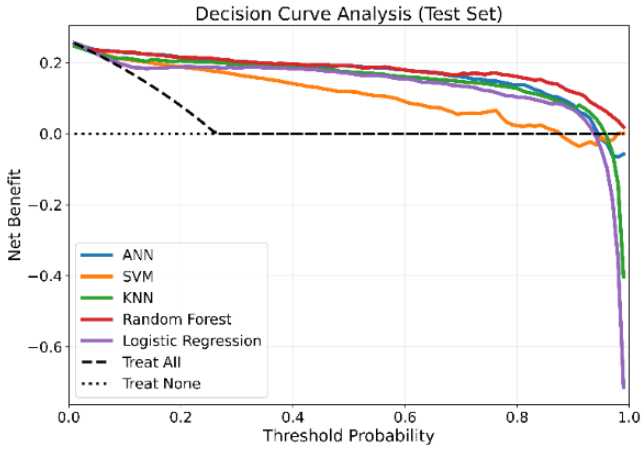

Fig. 3C

XSL•FO
RenderX

Figure 4. Model calibration analysis for the artificial neural network (ANN), random forest, k-nearest neighbor (KNN), support vector machine (SVM), and logistic regression (LR) models. (A) Over the training set. (B) Over the validation set. (C) Over the testing set.

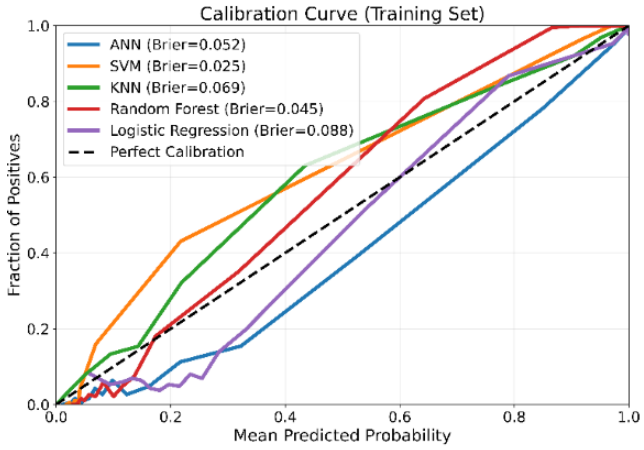

Fig. 4A

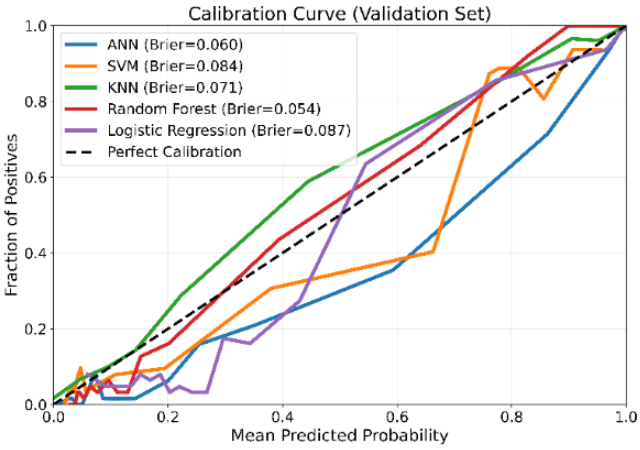

Fig. 4B

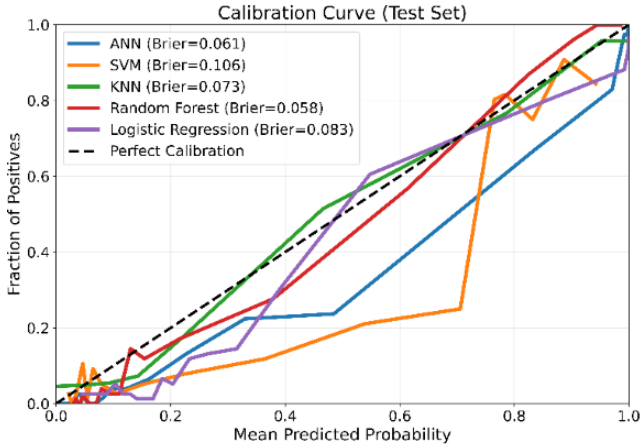

Fig. 4C

In the subgroup analysis, the ANN model achieved an AUC of 0.965 and an accuracy of 0.917 in male patients and an AUC of 0.970 and an accuracy of 0.936 in female patients. Similar consistent performances were observed across other subgroups. In patients with diabetes, the model achieved an AUC of 0.961 and an accuracy of 0.890, whereas in those without diabetes, the AUC and accuracy were 0.963 and 0.930, respectively. In patients with gout, the model reached an AUC of 1.000 and accuracy of 1.000, while in those without gout, the AUC was 0.967, and the accuracy was 0.926. For patients with bacteriuria, the AUC was 0.967, and the accuracy was 0.926, compared with 0.968 and 0.929 in those without bacteriuria. Among urine RBC subgroups, the AUC and accuracy were 0.915 and 0.942 for 0 to 2 RBCs, 0.936 and 0.866 for 3 to 5 RBCs, 0.950 and 0.908 for 6 to 10 RBCs, and 0.936 and 0.916 for 10 or more RBCs. By age category, the AUC and accuracy were 0.972 and 0.949 for patients aged 18 to 40 years, 0.956 and 0.923 for those aged 40 to 65 years, and 0.916 and 0.907 for those older than 65 years. For BMI subgroups, the model achieved 0.966 and 0.934 for BMI less than 25 kg/m^2, 0.961 and 0.918 for BMI of 25 to 30 kg/m^2, and 0.964 and 0.913 for BMI of 30 kg/m^2 or greater. Finally, among patients with eGFR less than 60, the AUC and accuracy were 0.992 and 0.981, compared with 0.953 and 0.921 for those with eGFR greater than 60.

Importance of Feature Variables

The results of the Shapley value analysis for the ANN model are shown in Figure 5A, which indicates that the predictive power of the model was predominantly driven by three features: urine RBC count, eGFR, and urine SG. An ANN model trained using only these 3 predictors (referred to as “ANN-3P” thereafter, as opposed to “ANN-10P” for the original 10-predictor ANN model) achieved validation and testing AUROCs of 0.954 and 0.943, and validation and testing AUPRCs of 0.938 and 0.891, respectively; the performance is competitive with that of the ANN-10P model. Figure 5B-E displays the ROC and PR curves of the 2 models, and a comprehensive performance comparison is summarized in Table 4. The outstanding performance of the ANN-3P model confirms the predictive power rendered by the 3 key feature variables.

XSL•FO
RenderX

Figure 5. Results of the Shapley value analysis and receiver operating characteristic (ROC), precision-recall curves of the artificial neural network (ANN) models. (A) Summary plot of the Shapley values. (B) Validation ROC curves. (C) Validation PR curves. (D) Testing ROC curves. (E) Testing PR curves. AUROC: area under the receiver operating characteristic curve; AUPRC: area under the precision-recall curve; eGFR: estimated glomerular filtration rate; SG: specific gravity; SHAP: Shapley Additive Explanations; urineRBC: urine red blood cell.

XSL•FO
RenderX

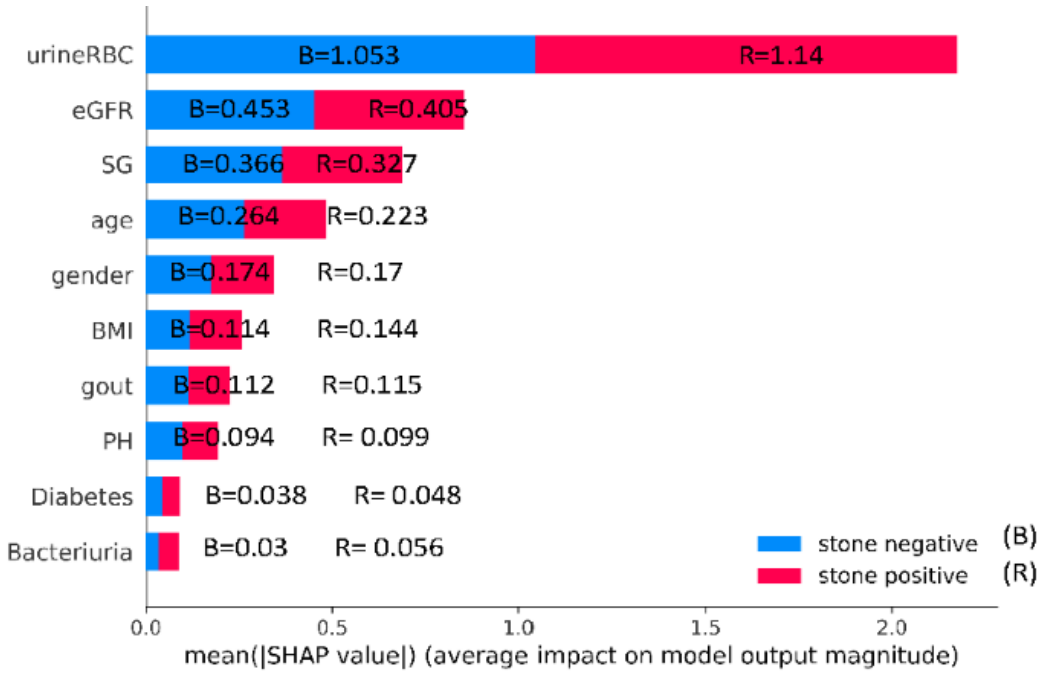

Fig. 5A

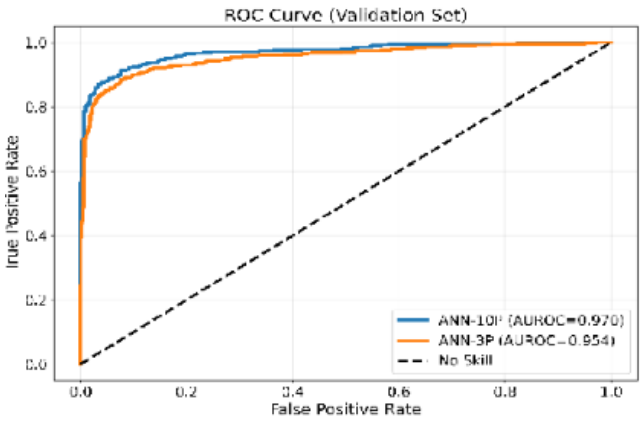

Fig. 5B

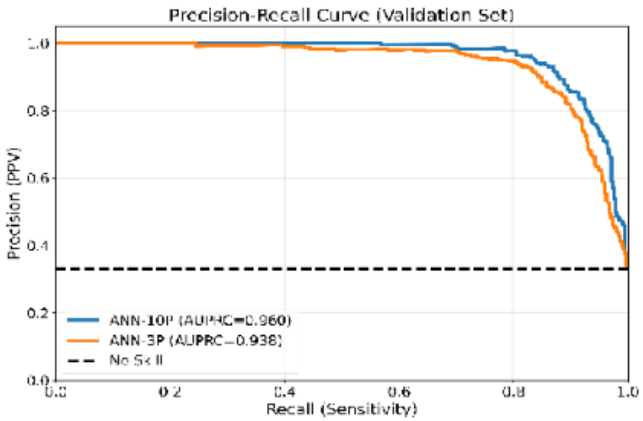

Fig. 5C

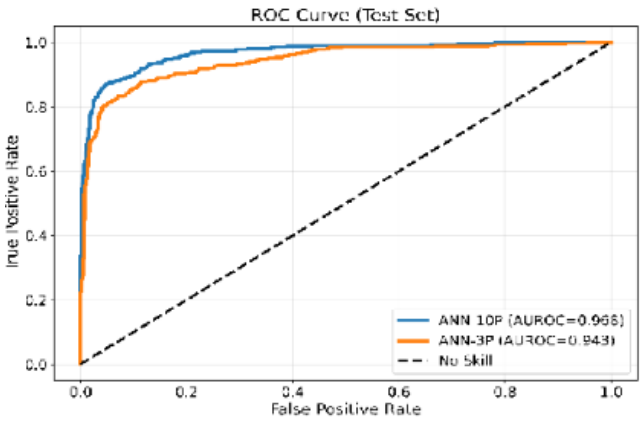

Fig. 5D

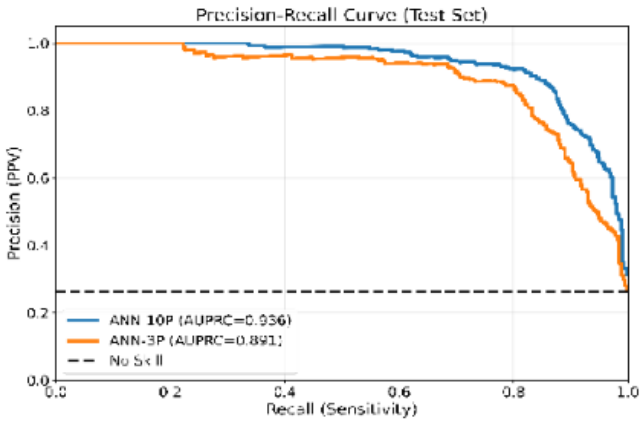

Fig.5E

XSL•FO
RenderX

Table . Performance comparison between artificial neural network (ANN)-3P and ANN-10P models.

Model and dataset	AUROC[a] (95% CI)	AUPRC[b] (95% CI)	Accuracy (95% CI)	Sensitivity (95% CI)	Specificity (95% CI)	PPV[c] (95% CI)	NPV[d] (95% CI)
ANN-10P							
Training	0.974 (0.968 - 0.980)	0.964 (0.956 - 0.971)	0.943 (0.935 - 0.951)	0.907 (0.890 - 0.923)	0.961 (0.954 - 0.968)	0.920 (0.903 - 0.937)	0.954 (0.946 - 0.963)
Validation	0.970 (0.958 - 0.982)	0.960 (0.946 - 0.973)	0.923 (0.908 - 0.937)	0.889 (0.860 - 0.918)	0.939 (0.923 - 0.956)	0.878 (0.846 - 0.911)	0.945 (0.928 - 0.962)
Testing	0.968 (0.956 - 0.98)	0.936 (0.918 - 0.953)	0.927 (0.915 - 0.939)	0.873 (0.841 - 0.904)	0.947 (0.935 - 0.959)	0.853 (0.819 - 0.888)	0.954 (0.941 - 0.968)
ANN-3P							
Training	0.953 (0.945 - 0.960)	0.934 (0.924 - 0.943)	0.910 (0.901 - 0.919)	0.866 (0.846 - 0.885)	0.932 (0.922 - 0.942)	0.863 (0.843 - 0.883)	0.934 (0.923 - 0.943)
Validation	0.954 (0.906 - 0.945)	0.938 (0.921 - 0.954)	0.908 (0.892 - 0.924)	0.892 (0.864 - 0.918)	0.916 (0.899 - 0.933)	0.841 (0.809 - 0.872)	0.945 (0.930 - 0.959)
Testing	0.943 (0.927 - 0.956)	0.891 (0.869 - 0.913)	0.883 (0.867 - 0.899)	0.878 (0.845 - 0.909)	0.885 (0.866 - 0.903)	0.731 (0.691 - 0.771)	0.953 (0.940 - 0.965)

[a]AUROC: area under the receiver operating characteristic curve.

[b]AUPRC: area under the precision-recall curve.

[c]PPV: positive predictive value.

[d]NPV: negative predictive value.

Discussion

Principal Findings

Epidemiological studies indicate that approximately 10% of the global population faces a lifetime risk of developing kidney stones [1], and approximately 80% of those affected experience recurrence after stone treatment [15]. Although kidney stones are not malignant such as cancers, they can cause severe flank pain that often drives patients to seek emergency care [16]. In more serious cases, stones may lead to urinary tract infections, sepsis, and even hospitalization. Furthermore, recent studies have reported a strong association between nephrolithiasis and the development of chronic kidney disease [4]. Despite these risks, most kidney stones are only diagnosed after patients present with symptoms and undergo imaging-based evaluations in clinical settings [17]. Currently, there is no widely adopted, large-scale, low-cost, and simple screening tool available for the early detection of kidney stones [18,19].

In 2024, our team developed an AI-based model using routine health checkup data to screen for kidney stones in overweight and obese individuals. The model achieved excellent performance (AUC=0.96), and its advantages include low cost, rapid computation, minimal computational power requirements, and no need for physician involvement [6]. This enables its application in frontline health screenings to identify high-risk individuals for further evaluation. Building on the success of our previous work, this study extends the application of our AI framework to the general population. Our findings suggest the potential for a scalable, accessible, and noninvasive tool to detect clinically significant kidney stones across diverse patient groups, providing a much-needed advancement in the proactive management of urolithiasis.

In some regions, certain high-end health screening programs incorporate renal ultrasound (US), plain abdominal radiography (KUB), or even CT to detect asymptomatic kidney stones. While US is a fast, user-friendly, and radiation-free imaging modality, its accuracy is highly operator dependent. Studies comparing US with CT have reported widely varying sensitivity (24% - 69%) and specificity (53% - 90%) levels [20-22]. This variability limits its reliability, especially in large-scale screening, as it requires experienced physicians and access to ultrasound equipment, both of which are resource intensive. Plain x-rays or KUB, although useful in identifying some kidney stones, expose patients to radiation (0.7 mSv per scan) [20]. Plain abdominal x-rays (KUB) can identify some radiopaque stones but have limited sensitivity and expose patients to ionizing radiation (~0.7 mSv per scan) [22] . For women of reproductive age, pregnancy status must be considered before imaging. Furthermore, the interpretation of KUB relies on trained radiologists, making it less practical for community-based screening. Currently, abdominal CT is the gold standard for diagnosing kidney and ureteral stones. However, it has notable drawbacks, including significant radiation exposure (10 mSv for standard noncontrast CT and 1 - 3 mSv for low-dose CT) [20,23] and high medical cost [24]. These factors make CT unsuitable for large-scale or repeated screening, particularly in asymptomatic populations. Given the limitations of traditional imaging modalities in mass screening contexts, our AI-based approach offers a compelling alternative. Using only routine clinical parameters from standard health checkups, our model provides a rapid, low-cost, and accessible method for the early detection of kidney stones without the need

XSL•FO
RenderX

for imaging, radiation, or specialized personnel. This has significant implications for population-level screening and preventive nephrology.

To the best of our knowledge, this study is the first to use a large-scale dataset that integrates simple clinical information from both patients with and without kidney stones, applying ML techniques to develop a computer-aided screening tool for detecting stones of various compositions. This approach reflects real-world clinical scenarios and aims to support early detection and decision-making for further diagnostic evaluation. In this study, we expanded upon our previous work by incorporating 10 easily accessible clinical variables to construct an AI-based model capable of identifying individuals at high risk for kidney stones [6]. These variables, readily available during routine health checkups, emergency visits, or outpatient consultations, can be collected and analyzed quickly, with no additional burden on patients or health care resources.

One of the key advantages of this tool lies in its simplicity and cost-effectiveness. Unlike imaging-based diagnostics, which require expensive equipment and specialized interpretation, our AI model only needs a standard internet-connected computer and does not rely on urologists or radiologists for execution. This enhances its feasibility and scalability, particularly in resource-limited settings or rural areas. Conceptually, our AI screening model functions similarly to the fecal occult blood test used for colorectal cancer screening [25]—offering a rapid, noninvasive, and low-cost method to identify high-risk individuals who would then proceed to confirmatory imaging tests such as ultrasound, x-rays, or CT scans.

Furthermore, because our model relies on only 10 standard health checkup parameters, patients do not require any additional testing. This makes the tool highly compatible with existing clinical workflows. Given its accessibility and minimal operational requirements, it could be readily implemented in annual health screenings or even in the follow-up of patients who have undergone treatment for kidney stones [26,27]. By enabling earlier detection of stones—even when they are still small and asymptomatic—the model could facilitate timely intervention, reduce the risk of complications, and simplify surgical management.

Importantly, this approach also holds significant potential for use in telemedicine. By leveraging basic clinical data and our AI software, health care providers could remotely screen for kidney stones in patients living far from medical centers, enabling early identification and reducing the likelihood of emergency presentations. Overall, this screening tool may serve as a practical and scalable solution for improving access to care, minimizing disease burden, and promoting proactive management of urolithiasis across diverse health care settings.

Our AI model is designed as a practical screening tool to identify kidney stones using only routine blood and urine data collected during health checkups. In real-world workflows, it can be seamlessly integrated into existing laboratory information systems, allowing automated risk predictions once test results are available. For individuals with a high predicted probability of nephrolithiasis, clinicians can proceed with confirmatory imaging such as ultrasonography or CT for diagnosis, while those with low risk can safely avoid unnecessary imaging. This stepwise approach facilitates early detection and appropriate resource allocation. Furthermore, it should be noted that the algorithm only uses laboratory data from routine urinalysis and no additional (expensive) tests are required. As such, the extra cost for using our algorithm is minimal, making it highly affordable. Early identification enables timely lifestyle interventions or pharmacologic prevention, potentially reducing emergency visits and treatment costs associated with advanced stone disease.

The variables selected in our model were based on previously validated clinical factors strongly associated with nephrolithiasis. Although several of these factors showed significant differences (P<.001) between cases and controls, which may contribute to potential overestimation of model performance, we minimized this bias by applying stratified sampling and reweighting techniques during model training. Consistently high AUC and accuracy values across all subgroups further support the robustness and generalizability of our model.

As every participant in this study underwent imaging confirmation to verify the presence or absence of stones, conducting multiethnic and cross-national validation would require substantial resources and logistical coordination. Therefore, this work focuses on an Asian cohort as an initial step. Although our dataset was comprehensive—comprising a large number of patients from multiple hospitals—and we further validated the model using an independent testing cohort in a clinical trial setting, one important limitation must be acknowledged. All patients included in this study were of Asian ethnicity. As a result, the predictive performance of our AI model may be limited when applied to populations of different racial or ethnic backgrounds. Differences in genetics, diet, and environmental factors could potentially affect the clinical presentation and risk profiles of kidney stone disease. To reduce racial and environmental bias, variables known to vary with ethnicity or diet—such as urinary calcium, oxalate, citrate, or lifestyle factors—were excluded. Instead, our model incorporated clinically relevant indicators of stone risk, including hematuria, bacteriuria, and serum creatinine. These features are biologically plausible and less population dependent, suggesting that the model may be applicable across diverse groups, although future international validation is warranted to confirm its performance. Future research should focus on collecting and integrating data from diverse populations to further refine and recalibrate the model. This will be essential to enhance the generalizability and global applicability of the AI-based kidney stone screening tool.

Conclusions

In this multihospital study, we developed an ML-based model that accurately identifies clinically significant kidney stones using only 10 routine clinical and urine parameters. This low-cost, noninvasive tool enables large-scale, manpower-free screening and can be readily integrated into health checkups or telemedicine, offering a practical solution for early detection and proactive management of nephrolithiasis.

XSL•FO
RenderX

Funding

This work was supported in part by the National Science and Technology Council of Taiwan (NSTC 112-2221-E-037-006, NSTC 113-2221-E-037-006, NSTC 113-2222-E-110-007, and NSTC 114-2221-E-037-006) and Kaohsiung Medical University Hospital (KMUH113-R006 and KMUH114-4R60). The funders do not have any role in the writing of the manuscript or the decision to submit it for publication.

Data Availability

The datasets generated and/or analyzed during this study are available from the corresponding author upon reasonable request.

Authors' Contributions

HWC: Conceptualization, methodology, data curation, funding acquisition, validation, writing – original draft, writing – review & editing
JTL: Conceptualization, funding acquisition, formal analysis, validation, visualization, writing – original draft, writing – review & editing
PSW: Data curation, methodology, software, formal analysis, validation, writing – review & editing
YCC: Project administration, resources, investigation, writing – review & editing
JYW: Resources, investigation, writing – review & editing
CIL: Resources, investigation, writing – review & editing
YHC: Resources, investigation, writing – review & editing
YSJ: Resources, investigation, writing – review & editing
WJW: Supervision, resources, investigation, writing – review & editing
CYK: Conceptualization, methodology, formal analysis, validation, writing – original draft, writing – review & editing

Conflicts of Interest

PSW reports serving as CEO and shareholder of United Kaohsiung AI Medical Technology Co. Ltd., which has been licensed the intellectual properties partly developed via his doctoral work at National Sun Yat-sen University. In this study, he was only involved in developing and training the AI model and did not participate in patient data collection, data labeling, or the independent validation of the testing cohort. These procedures were conducted by separate clinical teams to maintain objectivity and minimize potential bias. All related institutional and ICMJE conflict of interest policies were followed, and measures were taken to ensure objectivity, confidentiality, and transparency throughout the research and commercialization processes. All other authors declare no conflicts of interest.

Multimedia Appendix 1
Details regarding the construction of the artificial neural network model.
[DOCX File, 30 KB - medinform_v14i1e80764_app1.docx]

References

1. Raheem OA, Khandwala YS, Sur RL, Ghani KR, Denstedt JD. Burden of urolithiasis: trends in prevalence, treatments, and costs. Eur Urol Focus 2017 Feb;3(1):18-26. [doi: 10.1016/j.euf.2017.04.001] [Medline: 28720363]
2. Roberson D, Sperling C, Shah A, Ziemba J. Economic considerations in the management of nephrolithiasis. Curr Urol Rep 2020 Mar 31;21(5):18. [doi: 10.1007/s11934-020-00971-6] [Medline: 32236700]
3. Abufaraj M, Xu T, Cao C, et al. Prevalence and trends in kidney stone among adults in the USA: analyses of National Health and Nutrition Examination Survey 2007–2018 data. Eur Urol Focus 2021 Nov;7(6):1468-1475. [doi: 10.1016/j.euf.2020.08.011] [Medline: 32900675]
4. Chuang TF, Hung HC, Li SF, Lee MW, Pai JY, Hung CT. Risk of chronic kidney disease in patients with kidney stones-a nationwide cohort study. BMC Nephrol 2020 Jul 22;21(1):292. [doi: 10.1186/s12882-020-01950-2] [Medline: 32698782]
5. Pearle MS, Calhoun EA, Curhan GC, Urologic Diseases of America Project. Urologic diseases in America project: urolithiasis. J Urol 2005 Mar;173(3):848-857. [doi: 10.1097/01.ju.0000152082.14384.d7] [Medline: 15711292]
6. Chen HW, Lee JT, Wei PS, et al. Machine learning models for screening clinically significant nephrolithiasis in overweight and obese populations. World J Urol 2024 Mar 9;42(1):128. [doi: 10.1007/s00345-024-04826-4] [Medline: 38460023]
7. Rippel CA, Nikkel L, Lin YK, et al. Residual fragments following ureteroscopic lithotripsy: incidence and predictors on postoperative computerized tomography. J Urol 2012 Dec;188(6):2246-2251. [doi: 10.1016/j.juro.2012.08.040] [Medline: 23083650]
8. Levey AS, Stevens LA, Schmid CH, et al. A new equation to estimate glomerular filtration rate. Ann Intern Med 2009 May 5;150(9):604-612. [doi: 10.7326/0003-4819-150-9-200905050-00006] [Medline: 19414839]

XSL•FO
RenderX

9. Goodfellow I, Bengio Y, Courville A. Deep Learning: MIT press; 2016. URL: http://www.deeplearningbook.org [accessed 2026-01-23]
10. Barocas DA, Boorjian SA, Alvarez RD, et al. Microhematuria: AUA/SUFU guideline. J Urol 2020 Oct;204(4):778-786. [doi: 10.1097/JU.0000000000001297] [Medline: 32698717]
11. Pedregosa F, Varoquaux G, Gramfort A, et al. Scikit-learn: machine learning in python. J Mach Learn Res 2011;12:2825-2830 [FREE Full text] [doi: 10.5555/1953048.2078195]
12. Kramer O. Machine Learning for Evolution Strategies: Springer; 2016. [doi: 10.1007/978-3-319-33383-0]
13. Ruopp MD, Perkins NJ, Whitcomb BW, Schisterman EF. Youden Index and optimal cut-point estimated from observations affected by a lower limit of detection. Biom J 2008 Jun;50(3):419-430. [doi: 10.1002/bimj.200710415] [Medline: 18435502]
14. Kamath U, Liu J. Explainable artificial intelligence: an introduction to interpretable machine learning: Springer; 2021. [doi: 10.1007/978-3-030-83356-5]
15. Fisang C, Anding R, Müller SC, Latz S, Laube N. Urolithiasis--an interdisciplinary diagnostic, therapeutic and secondary preventive challenge. Dtsch Arztebl Int 2015 Feb 6;112(6):83-91. [doi: 10.3238/arztebl.2015.0083] [Medline: 25721435]
16. Scales CD Jr, Lin L, Saigal CS, et al. Emergency department revisits for patients with kidney stones in California. Acad Emerg Med 2015 Apr;22(4):468-474. [doi: 10.1111/acem.12632] [Medline: 25779695]
17. Rule AD, Lieske JC, Pais VM Jr. Management of kidney stones in 2020. JAMA 2020 May 19;323(19):1961-1962. [doi: 10.1001/jama.2020.0662] [Medline: 32191284]
18. Ellison JS, Tasian GE. Engaging patients in clinical trials on kidney stones: lessons learned. Eur Urol Focus 2025 Sep;11(5):712-715. [doi: 10.1016/j.euf.2025.03.005] [Medline: 40113514]
19. Chen HW, Chen YC, Lee JT. Re: Jonathan S. Ellison, Gregory E. Tasian. Engaging patients in clinical trials on kidney stones: lessons learned Eur Urol Focus. In press. https://doi.org/10.1016/j.euf.2025.03.005. Eur Urol Focus 2025 May 23:S2405-4569(25)00120-8. [doi: 10.1016/j.euf.2025.04.034] [Medline: 40413156]
20. Fulgham PF, Assimos DG, Pearle MS, Preminger GM. Clinical effectiveness protocols for imaging in the management of ureteral calculous disease: AUA technology assessment. J Urol 2013 Apr;189(4):1203-1213. [doi: 10.1016/j.juro.2012.10.031] [Medline: 23085059]
21. Ulusan S, Koc Z, Tokmak N. Accuracy of sonography for detecting renal stone: comparison with CT. J Clin Ultrasound 2007 Jun;35(5):256-261. [doi: 10.1002/jcu.20347] [Medline: 17373690]
22. Fowler KAB, Locken JA, Duchesne JH, Williamson MR. US for detecting renal calculi with nonenhanced CT as a reference standard. Radiology 2002 Jan;222(1):109-113. [doi: 10.1148/radiol.2221010453] [Medline: 11756713]
23. Hamm M, Knopfle E, Wartenberg S, Wawroschek F, Weckermann D, Harzmann R. Low dose unenhanced helical computerized tomography for the evaluation of acute flank pain. J Urol 2002 Apr;167(4):1687-1691. [Medline: 11912388]
24. Quhal F, Seitz C. Guideline of the guidelines: urolithiasis. Curr Opin Urol 2021 Mar 1;31(2):125-129. [doi: 10.1097/MOU.0000000000000855] [Medline: 33399368]
25. Hewitson P, Glasziou P, Irwig L, Towler B, Watson E. Screening for colorectal cancer using the faecal occult blood test, Hemoccult. Cochrane Database Syst Rev 2007 Jan 24;2007(1):CD001216. [doi: 10.1002/14651858.CD001216.pub2] [Medline: 17253456]
26. Tzelves L, Geraghty R, Lombardo R, et al. Duration of follow-up and timing of discharge from imaging follow-up, in adult patients with urolithiasis after surgical or medical intervention: a systematic review and meta-analysis from the European Association of Urology Guideline Panel on urolithiasis. Eur Urol Focus 2023 Jan;9(1):188-198. [doi: 10.1016/j.euf.2022.06.016] [Medline: 35851252]
27. Tzelves L, Juliebø-Jones P, Skolarikos A, Somani BK. Imaging follow-up for patients with kidney stones: European Association of Urology versus American Urological Association guidelines. Eur Urol Focus 2025 Sep;11(5):733-735. [doi: 10.1016/j.euf.2025.03.015] [Medline: 40175244]

Abbreviations

AI: artificial intelligence
ANN: artificial neural network
AUC: area under the curve
AUPRC: area under the precision-recall curve
AUROC: area under the receiver operating characteristic curve
CT: computed tomography
eGFR: estimated glomerular filtration rate
HPF: high-power field
KUB: kidney, ureter, and bladder
ML: machine learning
RBC: red blood cell
RF: random forest
ROC: receiver operating characteristic curve

XSL•FO
RenderX

SG: specific gravity
US: ultrasound

Edited by A Benis; submitted 18.Jul.2025; peer-reviewed by M Jaradat, SB Duan; revised version received 27.Oct.2025; accepted 01.Jan.2026; published 19.Feb.2026.

Please cite as:
Chen HW, Wei PS, Chen YC, Wu JY, Lin CI, Chou YH, Juan YS, Wu WJ, Kao CY, Lee JT
Screening for Clinically Significant Nephrolithiasis Based on Simple Health Checkup Clinical and Urine Parameters in General Populations: Multicenter Machine Learning Study
JMIR Med Inform 2026;14:e80764
URL: https://medinform.jmir.org/2026/1/e80764
doi:10.2196/80764

© Hao-Wei Chen, Pei-Siou Wei, Yu-Chen Chen, Jeng-Yih Wu, Chia-I Lin, Yii-Her Chou, Yung-Shun Juan, Wen-Jeng Wu, Chung-Yao Kao, Jung-Ting Lee. Originally published in JMIR Medical Informatics (https://medinform.jmir.org), 19.Feb.2026. This is an open-access article distributed under the terms of the Creative Commons Attribution License (https://creativecommons.org/licenses/by/4.0/), which permits unrestricted use, distribution, and reproduction in any medium, provided the original work, first published in JMIR Medical Informatics, is properly cited. The complete bibliographic information, a link to the original publication on https://medinform.jmir.org/, as well as this copyright and license information must be included.

XSL•FO
RenderX

Prediction of First and Multiple Antiretroviral Therapy Interruptions in People Living With HIV: Comparative Survival Analysis Using Cox and Explainable Machine Learning Models

Donald Salami[1], PhD; Emily Koech[2], MD; Janet M Turan[3], PhD; Kristen A Stafford[1], PhD; Lilly Muthoni Nyagah[4], PhD; Stephen Ohakanu[1], BEng; Anthony K Ngugi[5], PhD; Manhattan Charurat[1], Prof Dr

[1]Center for International Health, Education and Biosecurity, Institute of Human Virology, School of Medicine, University of Maryland, 725 W Lombard St, Baltimore, MD, United States

[2]Center for International Health, Education, and Biosecurity, Kenya, Nairobi, Kenya

[3]Department of Health Policy and Organization, School of Public Health, The University of Alabama, Birmingham, AL, United States

[4]Department of Strategic Information, Ministry of Health's National AIDS and STI Control Program Kenya, Nairobi, Kenya

[5]Department of Population Health, Aga Khan University Nairobi, Nairobi, Kenya

Corresponding Author:
Donald Salami, PhD
Center for International Health, Education and Biosecurity, Institute of Human Virology, School of Medicine, University of Maryland, 725 W Lombard St, Baltimore, MD, United States

Abstract

Background: The Cox proportional hazards (CPH) model is a common choice for analyzing time-to-treatment interruptions in patients on antiretroviral therapy (ART), valued for its straightforward interpretability and flexibility in handling time-dependent covariates. Machine learning (ML) models have increasingly been adapted for handling temporal data, with added advantages of handling complex, nonlinear relationships and large datasets, and providing clear practical interpretations.

Objective: This study aims to compare the predictive performance of the traditional CPH model and ML models in predicting treatment interruptions among patients on ART, while also providing both global and individual-level explanations to support personalized, data-driven interventions for improving treatment retention.

Methods: Using data from 621,115 patients who started ART between 2017 and 2023, in Kenya, we compared the performance of the CPH with the following ML models—gradient boosting machine, extreme gradient boosting, regularized generalized linear models (Ridge, Lasso, and Elastic-Net), and recursive partitioning—in predicting first and multiple treatment interruptions. Explainable surrogate technique (model-agnostic) was applied to interpret the best performing model's predictions globally, using variable importance and partial dependence profiles, and at individual level, using breakdown additive, Shapley Additive Explanations, and ceteris paribus.

Results: The recursive partitioning model achieved the best performance with a predictive concordance index score of 0.81 for first treatment interruptions and 0.89 for multiple interruptions, outperforming the CPH model, which scored 0.78 and 0.87 for the same scenarios, respectively. Recursive partitioning's performance can be attributed to its ability to model nonlinear relationships and automatically detect complex interactions. The global model-agnostic explanations aligned closely with the interpretations offered by hazard ratios in the CPH model, while offering additional insights into the impact of specific features on the model's predictions. The breakdown additive and Shapley Additive Explanations explainers demonstrated how different variables contribute to the predicted risk at the individual patient level. The ceteris paribus profiles further explored the time-varying model to illustrate how changes in a patient's covariates over time could impact their predicted risk of treatment interruption.

Conclusions: Our results highlight the superior predictive performance of ML models and their ability to provide patient-specific risk predictions and insights that can support targeted interventions to reduce treatment interruptions in ART care.

(JMIR Med Inform 2026;14:e78964) doi:10.2196/78964

KEYWORDS

antiretroviral therapy; explainable machine learning; machine learning; recursive partitioning; treatment interruptions.

XSL•FO
RenderX

Introduction

The Cox proportional hazards (CPH) model has long been a foundational tool for time-to-event analysis, widely used in health care research to examine treatment interruptions, including among patients on antiretroviral therapy (ART). The CPH model is a favorable choice due to its straightforward interpretability; its coefficients can be easily understood as hazard ratios, which quantify the relative effect of each covariate on the likelihood of an event, offering clear insights for clinical decision-making and risk assessment [1,2]. In addition, its flexibility in handling time-dependent covariates allows it to incorporate variables that change over time, providing a more accurate reflection of patient dynamics [3-5]. Our previous work [6] focused on using time-dependent covariates within the CPH model to enhance its application in modeling the complex patterns of multiple treatment interruptions in patients on ART, aiming to capture the nuanced and changing influences on treatment adherence.

Despite its popularity, the CPH model has limitations. A key disadvantage is its handling of high-dimensional data with many covariates, as it can be prone to overfitting and may yield unreliable results due to multicollinearity [4]. This risk is particularly pronounced in time-dependent CPH models, where changing covariates can amplify the potential for erroneous inferences [4]. In addition, as a semiparametric model, it does not fully specify the baseline hazard function, potentially limiting its ability to capture complex, nonlinear relationships [7]. These limitations highlight the need for more flexible modeling approaches, especially when working with complex health care datasets with nonlinear, time-varying, or high-dimensional characteristics.

Machine learning (ML) models are increasingly used in time-to-event analysis due to their ability to capture complex, nonlinear relationships at scale. In HIV and ART research, however, most survival ML applications such as random survival forests and gradient boosting primarily rely on baseline or time-invariant covariates, limiting their ability to reflect the dynamic nature of ART care. Although some methods, including recursive partitioning (RP), have been adapted to incorporate temporal structures and time-varying effects [8-10], support for fully time-varying covariates remains limited in many survival ML frameworks. RP provides a flexible alternative by modeling nonlinear effects and interactions with time-varying covariates, yet its application to large-scale, longitudinal ART cohorts has been limited. In addition, advances in model interpretability have made ML models more explainable, helping to bridge the gap between predictive accuracy and practical applicability. Through methods such as permutation importance, partial dependence plots, and Shapley Additive Explanations (SHAP) values [11-13], ML models now provide insights into variable importance and individual predictions, making them increasingly useful for clinical decision-making and patient-centered care.

The aim of this paper is first to compare the performance of traditional CPH model and ML models in predicting treatment interruptions among patients on ART. This comparison aims to evaluate whether ML models, with their flexibility in handling nonlinear relationships and time-dependent covariates, can provide more accurate and reliable predictions than the CPH model. Second, provide clear, intuitive explanations for the predictions at both the global level to understand overall patterns and key risk factors and the local level for individualized predictions for a patient. By combining predictive accuracy with interpretability, this study aims to support health care providers in identifying patients at high risk for treatment interruption and in implementing personalized interventions to enhance treatment retention.

Methods

Study Population and Data

The analysis used longitudinal, deidentified electronic medical record (EMR) data from patients initiated on ART between January 1, 2017, and November 30, 2023, across 2156 facilities in all 47 counties of Kenya. Eligible patients had at least 2 follow-up visits or drug pickups after ART initiation, were followed for more than 28 days postinitiation, and had returned to care if they had experienced an initial treatment interruption.

Data Preprocessing and Definitions

The preprocessing, cleaning, feature engineering, and covariate definitions are detailed in our previous work [6]. Treatment interruption was defined as no ART drug pickup and no clinical contact for greater than 28 days after the last expected contact [14]. Time-invariant covariates included age, gender, education, marital and employment status, noncommunicable disease, baseline regimen, and ART initiation year, while time-varying covariates were adherence, alcohol intake, World Health Organization stage, viral load, clinical stability assessment, regimen line, multimonth dispensing (MMD), differentiated service delivery (DSD) model, and prevention with positives package. Full list of covariates and description is included in Table S1 in Multimedia Appendix 1. A key preprocessing step included creating an “unknown” category for categorical variables with missing data. Engineered features included the COVID-19 pandemic period—dummy variable to indicate the COVID-19 pandemic; missed appointment—failure to attend a scheduled visit within 1-3 days of the scheduled date; defaulted appointment—failure to attend a scheduled visit within 4-28 days; and the duration of treatment interruption—average duration of any treatment interruption before a patient returned to care.

Analysis and Models

We performed 2 sets of modeling, that is, time-invariant model, for first-ever treatment interruption, and a time-varying model, for multiple interruptions. The data structure differs between the models: in a time-invariant model, covariates were fixed, with 1 row per patient containing the time to interruption and interruption status. In a time-varying model, covariates change over time, with multiple rows per patient representing different time intervals and multiple interruption statuses.

Our base reference model was the traditional CPH model. The time-invariant CPH assessed the effect of fixed covariates on time to first interruption, with an assumption that the hazard ratio remains constant over time, while the time-varying allowed

XSL•FO
RenderX

covariates to change over time, capturing the dynamic effects of these covariates on the hazard at different intervals.

Our choice of ML models was based on algorithms with the ability to fit time-varying covariates and their computational feasibility at scale. We evaluated 3 classes of algorithms: boosting methods for their efficiency and predictive performance, regularized shrinkage models for handling multicollinearity and improving generalization, and RP for its ability to capture nonlinear relationships and interactions while remaining interpretable. Although random survival forests are widely used in survival analysis, their computational demands and limited support for fully time-varying covariates constrained their applicability in this study. The trained models are as described:

- Gradient boosting machine (GBM): an ensemble learning method that builds a series of decision trees, where each new tree corrects the errors of the previous ones. It is powerful for time-invariant survival analysis due to its ability to handle complex, nonlinear relationships and improve predictive accuracy by minimizing loss iteratively.
- Extreme gradient boosting (XGBoost): an optimized version of GBM, known for its speed and performance, especially with large datasets. It is well suited for our analysis due to its efficiency, scalability, and ability to manage missing data, offering robust predictions in survival tasks. The Accelerated Failure Time model was trained for a time-varying dataset.
- Regularized generalized linear models: Extends traditional regression models with regularization techniques—Ridge (L2), Lasso (L1), and Elastic Net (a combination of both)—to prevent overfitting and handle multicollinearity. These models are beneficial in time-invariant survival analysis for selecting relevant covariates while improving model generalization, especially with high-dimensional data.
- Recursive partitioning (LTRCtrees/Rpart): Uses decision trees to model survival data, splitting the dataset based on covariates to form homogeneous subgroups. It is advantageous due to its interpretability and ability to handle nonlinear relationships without making parametric assumptions.

We initially trained each model using default hyperparameters as a baseline, followed by hyperparameter tuning through a 10-fold cross-validation over a grid of parameter combinations. The optimal set of hyperparameters was selected based on the highest Harrell's concordance index (C-index) score, reflecting the study's primary objective of ranking patients by treatment interruption risk. The optimal parameter sets were then used for final model training. All analysis and modeling were performed using R Statistical Software (version 4.4.0; R Foundation for Statistical Computing).

Model Evaluation

We evaluated model performance using an 80:20 train-test split (including the Cox models to ensure comparability). Likewise, a 10-fold cross-validation was performed on the train set, and models were trained on k-1 folds and validated on the remaining fold, repeating this process 10 times, with each fold serving as the validation set once.

Final model evaluation and comparison were performed using the C-index, a widely used metric for assessing the performance of survival models. The C-index measures the model's ability to correctly rank pairs of observations based on survival times, with values ranging from 0.5 (random prediction) to 1.0 (perfect ranking). We calculated the C-index for each model on both the training and test sets to evaluate predictive accuracy. This approach ensured that the models performed well during training and on validation data, providing a reliable measure of generalizability. Furthermore, to assess the sensitivity and uncertainty of the predictive performance measures, we conducted 200 bootstrap resampling iterations to estimate the IQR distribution of the scores for our best performing model.

Model Interpretability

To interpret our model predictions, we used the DALEX package in R [15] and applied 2 levels of model-agnostic explanation, that is, model level global explanations—using permutation variable importance and partial dependence plots, and individual-level explanations—using variable attribution—breakdown and SHAP values and ceteris paribus (CP) analysis.

Global-Level Explanations

The global-level explanations are listed as follows:

1. Variable importance: Using a permutation-based approach, we assessed how removing the effect of selected variables through multiple permutations impacts model performance.
2. Partial dependence profiles: We explored the effects of selected variables by examining how the model's predicted values change as a function of individual variables, based on randomly selected observations.

Individual-Level Explanations

The individual-level explanations are listed as follows:

1. Variable attributions: This explains how a model's prediction for a single observation differs from the average prediction and distributes the difference among explanatory variables. We applied two methods: (1) Breakdown additive attribution, a procedure that decomposes the model's prediction into contributions from each explanatory variable. (2) SHAP, the averaging of variable attribution values over all (or several) possible orderings to show their individual impacts.
2. CP profiles: This explores how the model's prediction changes when the value of a single explanatory variable is altered, while keeping all other variables constant.

Ethical Considerations

This study was reviewed and approved as nonhuman subject research by the institutional review boards of the University of Maryland, Baltimore (HP-00108126), and the Aga Khan University Nairobi (2023/ISERC-94 (v2)). The analysis used secondary EMR data that were fully deidentified prior to receipt by the study team in accordance with Kenya's Data Protection

XSL•FO
RenderX

Act and institutional guidelines; therefore, written informed consent was not required.

Results

Our dataset comprised 621,115 unique patients on ART, with 432,041 first treatment interruption events and 959,170 multiple treatment interruption events. Data were split into an 80:20 ratio for the training and test sets, respectively. The hyperparameters for each model, along with the final parameter combinations used in the final model, are shown in Table 1. The predictive performance of ML models and their comparison with the CPH are shown in Table 2 and Figure 1, summarized by the estimated C-index scores and 95% CIs for both the train and test sets.

XSL•FO
RenderX

Table . Hyperparameters for the machine learning models.

Model (R package) and parameter	Chosen value (time-invariant model)	Chosen value (time-varying model)
Cox proportional hazards (survival)		
N/A[a]	N/A	N/A
Gradient boosting machine (gbm3)		
distribution	coxPH (ties = Efron)	coxph (ties = Efron)
n.trees	100	3000
interaction.depth	3	3
n.minobsinnode	5	20
shrinkage	0.01	0.001
bag.fraction	1	0.5
cv.folds	10	10
id	Unique value of patient ID	Unique value of patient ID
Extreme gradient boosting (xgboost)		
Objective	survival:cox	survival:aft—accelerated failure time
eval_metric	cox-nloglik	aft-nloglik
max_depth	5	6
eta	0.2	0.3
colsample_bytree	0.8	1
min_child_weight	5	1
subsample	1	1
n_folds	10	10
best nrounds	99	N/A
aft_loss_distribution	N/A	normal
aft_loss_distribution_scale	N/A	1
Regularized generalized linear models (glmnet)		
lambda	Length of 100, ranging logarithmically from 10^{10} to 10^{-2}. With minimum lambda = c (Ridge: 0.01, Lasso: 0.023, Elastic Net: 0.01748)	Length of 100, ranging logarithmically from 10^{10} to 10^{-2}. With minimum lambda=c (Ridge: 0.01, Lasso: 0.01, Elastic Net: 0.01)
type.measure	"C"—Harrel's concordance measure	"C"—Harrel's concordance measure
nfolds	10	10
maxit	1.00E+05	1.00E+05
alpha	c (0, 0.5, 1) where 0—Ridge penalty, L2 regularization only[b]. 0.5—Elastic-Net, L1 and L2 regularization[c]. 1—Lasso, L1 regularization only[d].	c (0, 0.5, 1) where 0—Ridge penalty, L2 regularization only[b]. 0.5—Elastic-Net, L1 and L2 regularization[c]. 1—Lasso, L1 regularization only[d].
Recursive partition (LTRCtrees/rpart)		
complexity parameter	0.0001	0.0214
xval (cross validations)	10	10
maxsurrogate	5	0
maxdepth	20	30
minsplit	20	10
maxcompete	4	4

XSL•FO
RenderX

[a]N/A: not applicable.

[b]Ridge—applies L2 regularization which penalizes the sum of the squared coefficients and is effective in cases where multicollinearity is present in the predictor variables.

[c]Elastic-Net regression—applies a combination of L1 and L2 regularization.

[d]Lasso—applies L1 regularization which can shrink some coefficients to zero, effectively performing feature selection.

Figure 1. Models' comparison: C-Index with 95% CIs. (A) C-Index comparison for the time-invariant models. (B) C-Index comparison for the time-varying models.

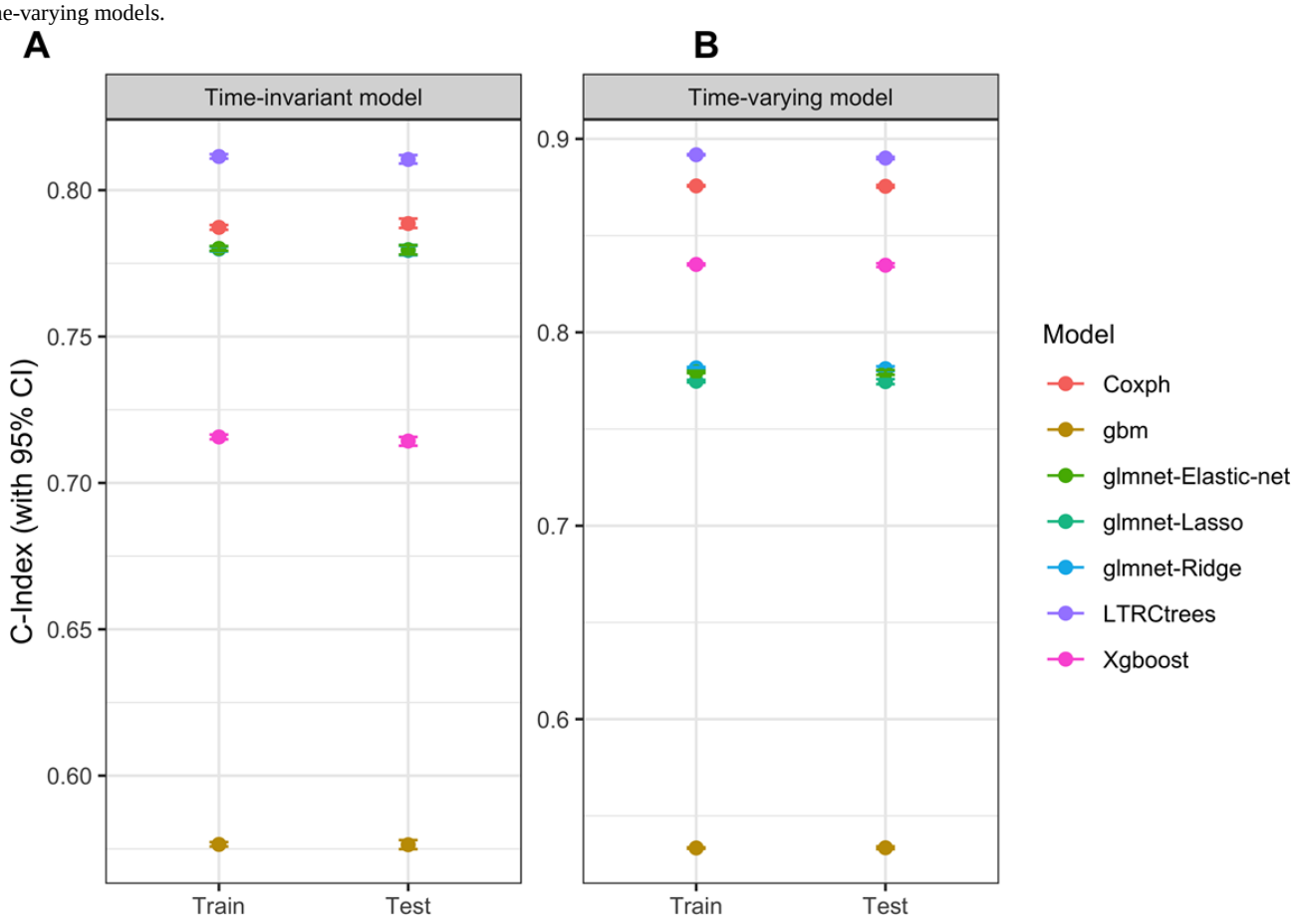

Table . Models' comparison of the time-invariant and time-varying models, using C-index scores for train and test sets.

	Time-invariant model		Time-varying model	
Model	C-Index—train (95% CI)	C-Index—test (95% CI)	C-Index—train (95% CI)	C-Index—test (95% CI)
Coxph	0.7873 (0.7865 - 0.7881)	0.7886 (0.7871 - 0.7903)	0.8757 (0.8754 - 0.8761)	0.8755 (0.8748 - 0.8762)
glmnet—Lasso	0.7801 (0.7793 - 0.7809)	0.7797 (0.7780 - 0.7813)	0.7747 (0.7741 - 0.7754)	0.7745 (0.7732 - 0.7758)
glmnet—Ridge	0.7799 (0.7791 - 0.7807)	0.7794 (0.7778 - 0.7810)	0.7816 (0.7810 - 0.7821)	0.7812 (0.7800 - 0.7824)
glmnet—Elastic-net	0.7801 (0.7793 - 0.7809)	0.7796 (0.7780 - 0.7812)	0.7795 (0.7789 - 0.7801)	0.7793 (0.7780 - 0.7805)
gbm	0.5765 (0.5758 - 0.5773)	0.5764 (0.5749 - 0.5780)	0.5334 (0.5330 - 0.5337)	0.5335 (0.5328 - 0.5342)
Xgboost	0.7157 (0.7149 - 0.7165)	0.7143 (0.7127 - 0.7157)	0.8351 (0.8346 - 0.8356)	0.8347 (0.8338 - 0.8357)
LTRCtrees	0.8115 (0.8108 - 0.8123)	0.8105 (0.8091 - 0.8120)	0.8918 (0.8915 - 0.8921)	0.8901 (0.8895 - 0.8907)

In the time-invariant analysis, the glmnet models—Lasso, Ridge, and Elastic-Net—produced comparable results to the CPH model, with train C-index values ranging from 0.7799 to 0.7801 and test C-index values ranging from 0.7794 to 0.7796. XGBoost performed slightly worse than the CPH model, while the GBM model had the lowest performance. The LTRCtrees model outperformed all other ML models and the CPH model with a C-index value of 0.8115 for the train set and 0.8105 for the test set. The LTRCtrees model remained the top performer in the time-varying analysis with a C-index of 0.8918 for the train set and 0.8901 for the test set. XGBoost was the next best performing ML model and slightly comparable with the CPH model. We further evaluated the best-performing model (ie, LTRCtrees), using a 200-bootstrap resamples; the C-index interquartile range remained stable across resamples.

XSL•FO
RenderX

Figures 2 and 3 show the permutation-based variable importance for the top 10 variables in both the time-invariant and time-varying models. MMD emerged as the most important variable in the time-invariant model, while the duration of treatment interruption was most important in the time-varying model. In addition, variables such as viral load, ART start year, stability assessment, baseline regimen, and occupation were consistently ranked among the top 10 most influential variables in both models. The permutation-based variable importance results were similar to the ranking of the absolute values of the coefficients of the CPH models (Table 3). MMD, missed and defaulted appointments, year of ART initiation, occupation, and stability assessment consistently ranked among the top 10 variables in both the time-invariant LTRCtree and CPH models. In the time-varying models, duration of interruption, MMD, year of ART initiation, baseline regimen, and occupation were consistently top influencers in both LTRCtree and CPH models.

Figure 2. LTRCtree time-invariant model top 10 most important variables. ART: antiretroviral therapy; MMD: multimonth dispensing; PwP: prevention with positives package.

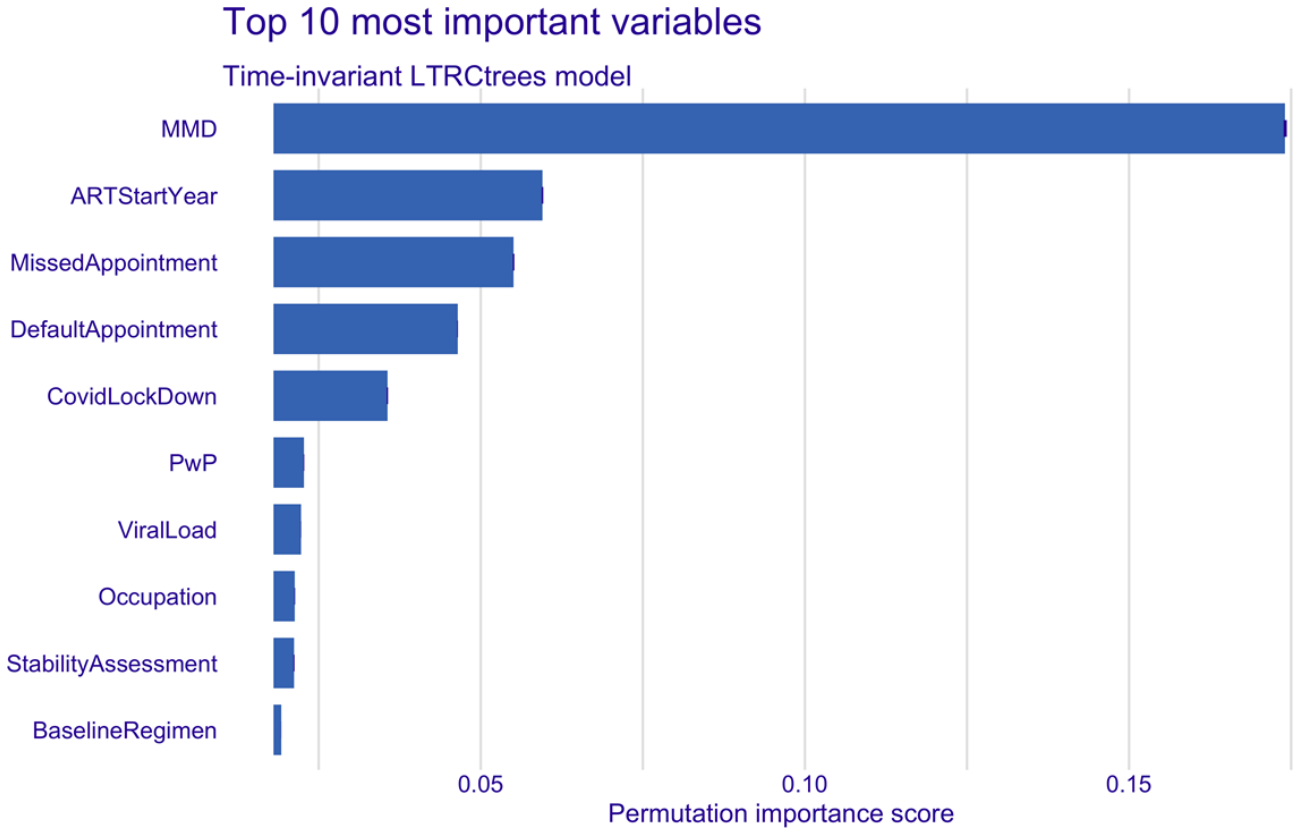

XSL•FO
RenderX

Figure 3. LTRCtree time-varying model top 10 most important variables. ART: antiretroviral therapy; MMD: multimonth dispensing.

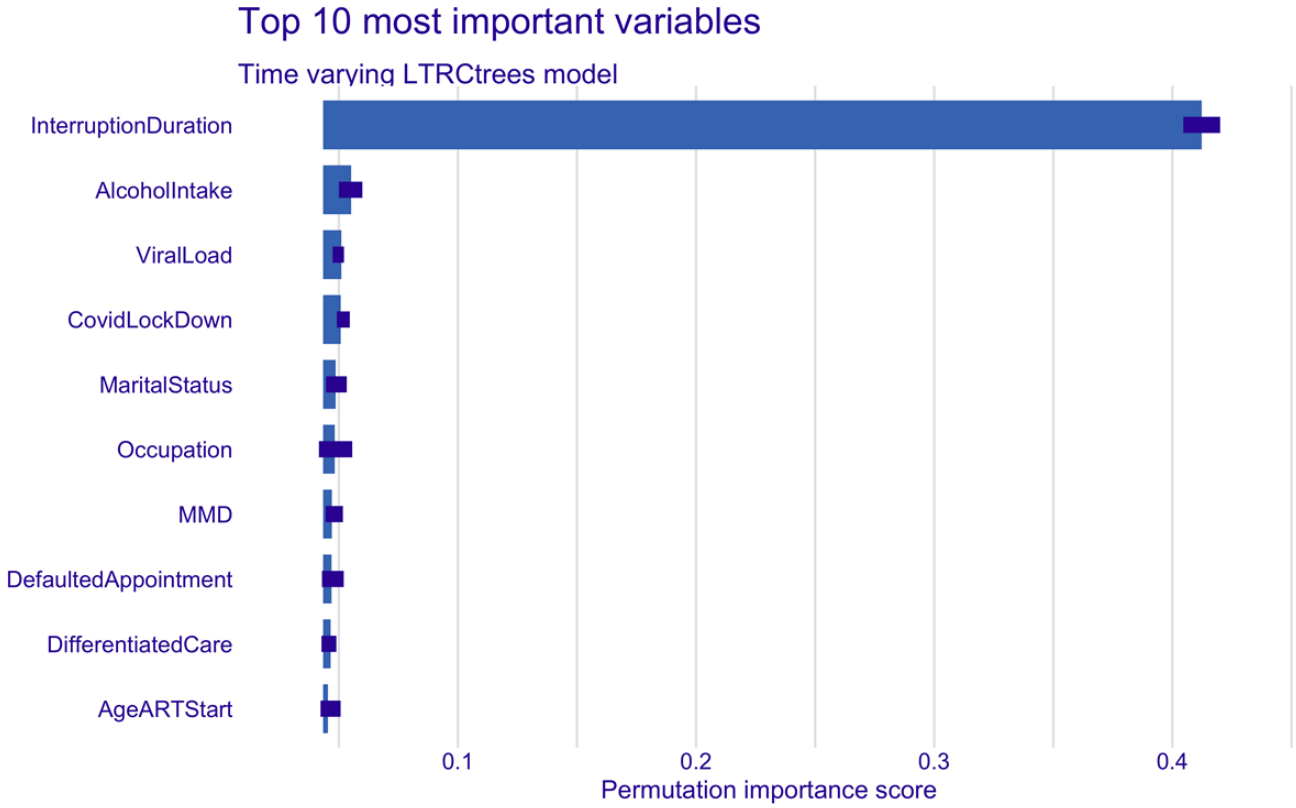

XSL•FO
RenderX

Table . Hazard ratio of the top 10 variables from the time-invariant and time-varying Cox proportional hazards models.

Covariates	Time invariant—first treatment interruption N=497,208; events=346,118[a]		Time varying—multiple treatment interruption N=7,352,030; events=842,500	
	Hazard ratio (95% CI)[b]	*P* value	Hazard ratio (95% CI)[c]	*P* value
Marital status				
Other	Reference category		Reference category	
Cohabiting	1.02 (0.97-1.07)	.39	1.02 (0.99-1.05)	.26
Divorced	1.00 (0.95-1.04)	.91	0.98 (0.95-1.01)	.21
Married, monogamous	1.00 (0.95-1.05)	.89	0.99 (0.96-1.02)	.45
Married, polygamous	1.07 (1.02-1.12)	.01	0.86 (0.84-0.89)	<.001
Separated	1.10 (1.03-1.18)	<.001	1.18 (1.13-1.23)	<.001
Single	1.06 (1.01-1.11)	.02	1.01 (0.98-1.04)	.45
Widowed	1.07 (1.02-1.13)	<.001	1.00 (0.97-1.03)	.91
Employment status				
Employed	Reference category		Reference category	
Unemployed	1.00 (0.99-1.01)	.72	1.00 (0.99-1.01)	.75
Unknown	1.34 (1.33-1.36)	<.001	1.24 (1.23-1.25)	<.001
Adherence				
Good	Reference category		Reference category	
Fair	1.26 (1.23-1.29)	<.001	0.97 (0.95-0.99)	<.001
Bad	1.81 (1.69-1.94)	<.001	1.09 (1.03-1.15)	<.001
Unknown	1.13 (1.10-1.17)	<.001	0.95 (0.93-0.97)	<.001
Alcohol intake				
Never	Reference category		Reference category	
Monthly or less	0.93 (0.89-0.97)	<.001	0.98 (0.95-1.00)	.08
2-4 times a month	0.95 (0.89-1.02)	.13	1.02 (0.98-1.07)	.26
2-3 times a week	0.99 (0.94-1.05)	.85	1.02 (0.98-1.05)	.36
4 or more times a week	0.96 (0.91-1.01)	.09	1.01 (0.98-1.04)	.59
Unknown	0.99 (0.95-1.03)	.53	1.18 (1.15-1.21)	<.001
Viral load				
<200	Reference category		Reference category	
200 - 999	1.10 (1.09-1.11)	<.001	1.00 (1.00-1.01)	.27
>1000	1.14 (1.12-1.16)	<.001	1.10 (1.09-1.11)	<.001
Unknown	0.82 (0.81-0.83)	<.001	1.11 (1.10-1.11)	<.001
Clinical stability assessment				
Stable	Reference category		Reference category	
Unstable	1.31 (1.30-1.32)	<.001	1.09 (1.08-1.09)	<.001
Baseline ART[d] regimen				
Other	Reference category		Reference category	
2NRTIs[e] + Boosted PI[f].	0.85 (0.83-0.87)	<.001	0.89 (0.88-0.91)	<.001
2NRTIs + INSTI[g].	1.11 (1.08-1.13)	<.001	1.02 (1.01-1.04)	<.001
2NRTIs + NNRTI[h]	1.59 (0.79-3.17)	.19	0.99 (0.71-1.39)	.97
NRTI + INSTI	1.14 (1.04-1.25)	.01	1.30 (1.24-1.36)	<.001

XSL•FO
RenderX

Covariates	Time invariant—first treatment interruption N=497,208; events=346,118[a]		Time varying—multiple treatment interruption N=7,352,030; events=842,500	
	Hazard ratio (95% CI)[b]	*P* value	Hazard ratio (95% CI)[c]	*P* value
Multimonth dispensing (months)				
1	Reference category		Reference category	
2	0.57 (0.57-0.58)	<.001	0.75 (0.75-0.76)	<.001
3 - 5	0.28 (0.28-0.28)	<.001	0.46 (0.46-0.46)	<.001
6	0.15 (0.14-0.15)	<.001	0.27 (0.27-0.28)	<.001
6+	0.04 (0.04-0.05)	<.001	0.22 (0.21-0.22)	<.001
Prevention with positives package				
0	Reference category		Reference category	
1	0.86 (0.85-0.86)	<.001	0.93 (0.92-0.94)	<.001
2	0.61 (0.60-0.62)	<.001	0.85 (0.84-0.86)	<.001
3 or more	0.59 (0.59-0.60)	<.001	0.85 (0.84-0.85)	<.001
ART initiation year				
2017	Reference category		Reference category	
2018	1.21 (1.20-1.22)	<.001	1.20 (1.19-1.21)	<.001
2019	1.50 (1.48-1.52)	<.001	1.48 (1.47-1.49)	<.001
2020	1.68 (1.66-1.71)	<.001	1.83 (1.82-1.85)	<.001
2021	2.02 (1.99-2.05)	<.001	2.22 (2.20-2.25)	<.001
2022	2.08 (2.05-2.12)	<.001	2.64 (2.61-2.68)	<.001
2023	0.63 (0.61-0.65)	<.001	3.51 (3.42, 3.60)	<.001
COVID-19 pandemic period				
Non–COVID-19 period	Reference category		Reference category	
COVID-19 period	1.17 (1.16-1.18)	<.001	0.92 (0.91-0.92)	<.001
Prior missed appointment				
No	Reference category		N/A[i]	N/A
Yes	0.35 (0.34-0.35)	<.001	N/A	N/A
Prior default appointment				
No	Reference category		N/A	N/A
Yes	0.52 (0.51-0.53)	<.001	N/A	N/A
Missed appointments				
0	N/A	N/A	Reference category	
1-3	N/A	N/A	0.93 (0.93-0.94)	<.001
4-6	N/A	N/A	0.81 (0.80-0.82)	<.001
7+	N/A	N/A	0.73 (0.72-0.75)	<.001
Default appointments				
0	N/A	N/A	Reference category	
1-3	N/A	N/A	1.00 (1.00-1.01)	.1
4-6	N/A	N/A	0.97 (0.96-0.98)	<.001
7+	N/A	N/A	0.95 (0.94-0.96)	<.001

XSL•FO
RenderX

Covariates	Time invariant—first treatment interruption N=497,208; events=346,118[a]		Time varying—multiple treatment interruption N=7,352,030; events=842,500	
	Hazard ratio (95% CI)[b]	*P* value	Hazard ratio (95% CI)[c]	*P* value
Duration of treatment interruptions				
0 (No interruptions)	N/A	N/A	Reference category	
<30 days	N/A	N/A	29.94 (29.63-30.26)	<.001
30-197 days	N/A	N/A	19.63 (19.51-19.75)	<.001
180-364 days	N/A	N/A	8.15 (8.08-8.23)	<.001
365 days or more	N/A	N/A	2.85 (2.82-2.88)	<.001

[a]N=number of observations in the train dataset, that is, 80% of the entire dataset; events=number of treatment interruptions.

[b]Concordance=0.79 (se=0).

[c]Concordance=0.88 (se=0).

[d]ART: antiretroviral therapy.

[e]NRTIs: nucleoside analog reverse transcriptase inhibitors.

[f]PI: protease inhibitor.

[g]INSTI: integrase strand transfer inhibitor.

[h]NNRTI: nonnucleoside analog reverse transcriptase inhibitor.

[i]N/A: not applicable.

The full results of the time-invariant and time-varying CPH models are included in Table S2 in Multimedia Appendix 1. The partial dependence plots for the top 4 variables from both models are displayed in Figures 4 and 5. These plots show the average predicted risk for each of these variables. Short dispensing interval (MMD of 1 month), initiating ART in 2021, and having not missed or defaulted on an appointment were associated with higher predicted risks of first treatment interruption. Conversely, longer dispensing intervals (6+ months MMD), initiating ART in 2023, and having missed or defaulted on an appointment had a lower predicted risk of first treatment interruption. Short interruption durations (<30 days), unknown viral load, separated marital status, and unspecified alcohol use were all associated with higher predicted risk of multiple treatment interruption, while having no prior interruptions (ie, interruption duration of zero), lower viral load (<200), and no alcohol consumption showed lower predicted risk of multiple treatment interruption.

XSL•FO
RenderX

Figure 4. Time-invariant model; partial dependence plots for top 4 variables. Panels show the marginal effect of each variable on the average predicted risk of treatment interruption. (A) Multimonth dispensing duration, (B) ART initiation year, (C) missed appointment, and (D) defaulted appointment. ART: antiretroviral therapy; MMD: multimonth dispensing.

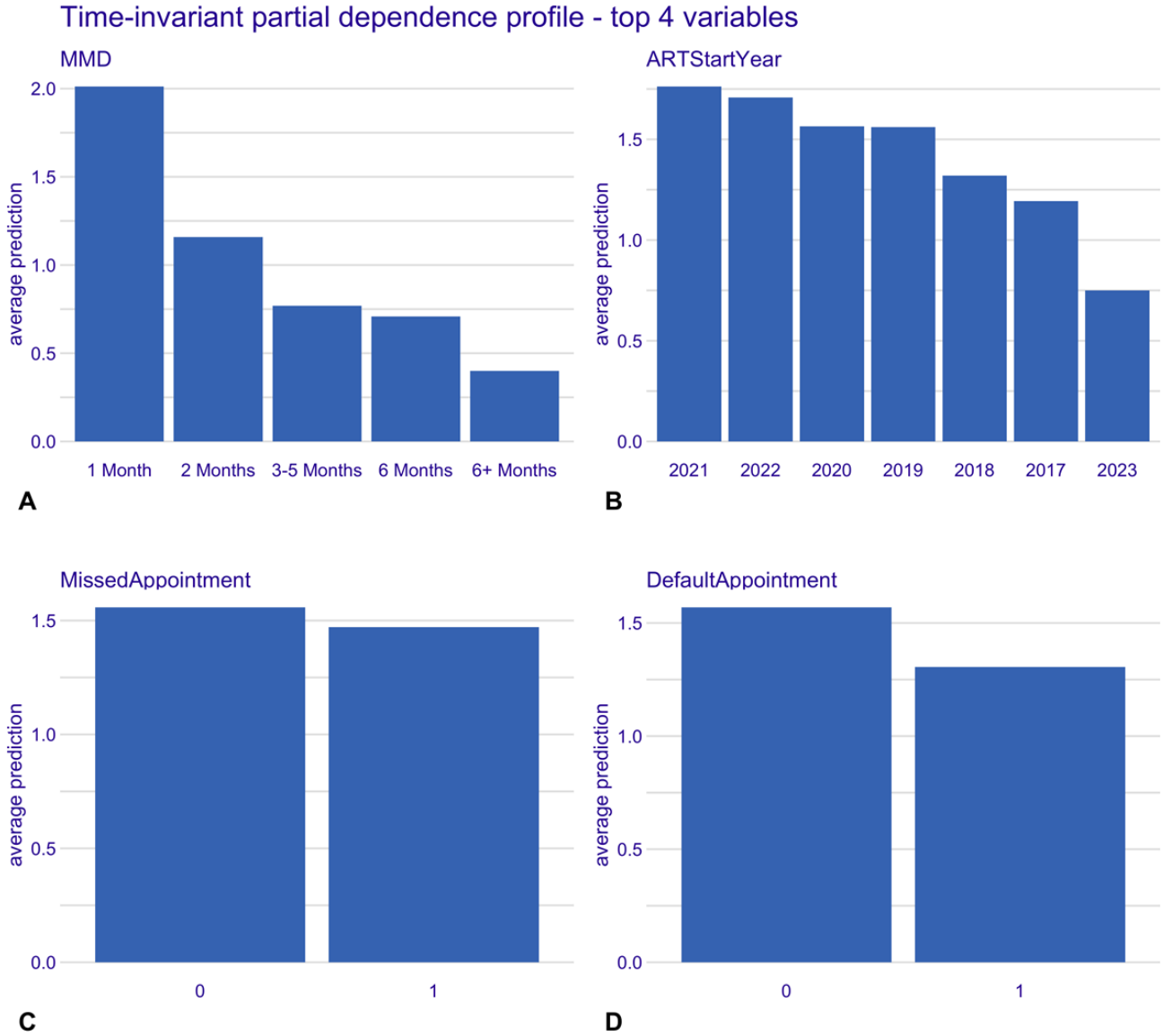

XSL•FO
RenderX

Figure 5. Time-varying model; partial dependence plots for top 4 variables. Panels show the marginal effect of each variable on the average predicted risk of treatment interruption. (A) Treatment interruption duration, (B) viral load count, (C) alcohol use, and (D) marital status.

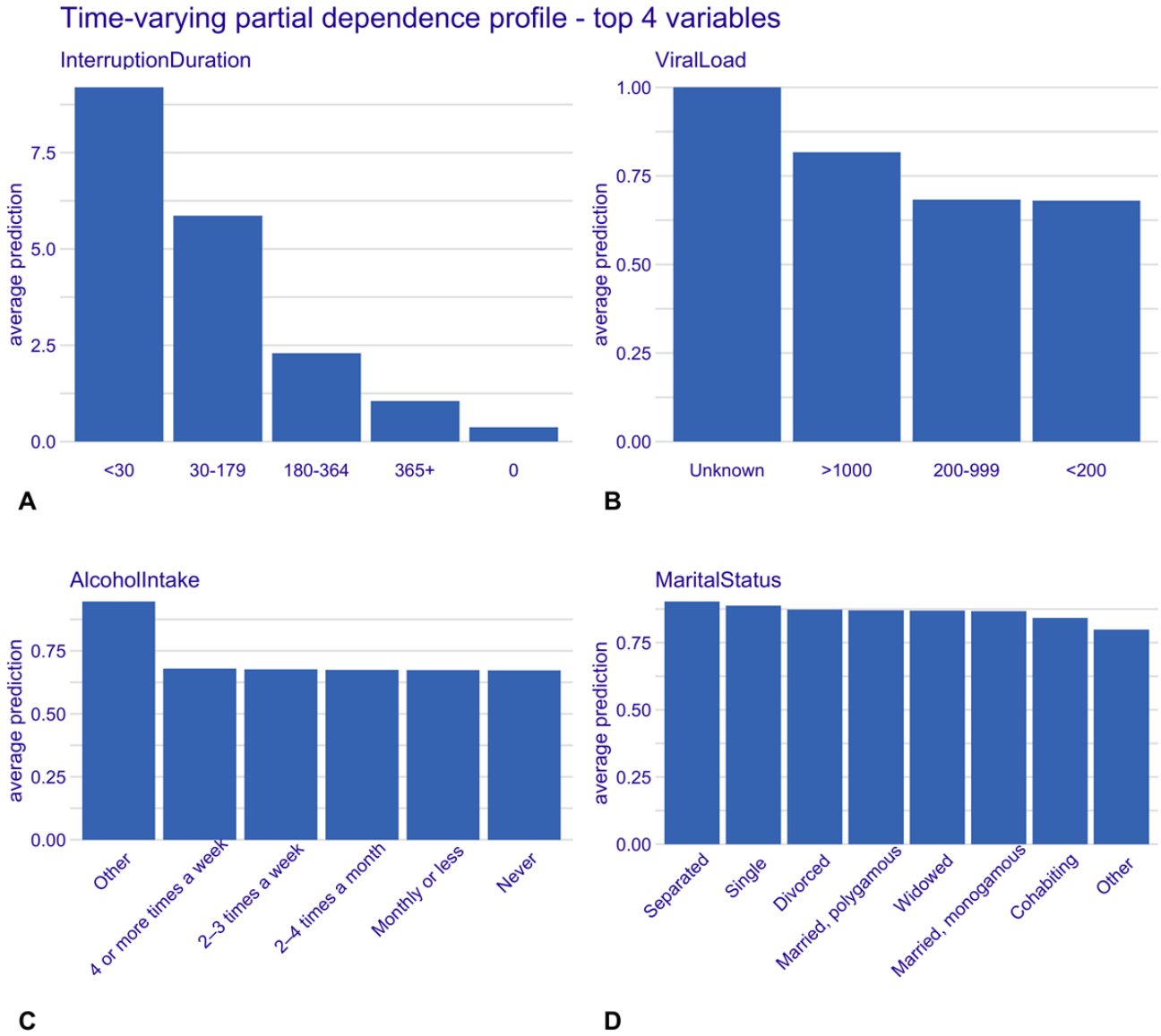

To examine individual-level predictions for the time-invariant model, we randomly selected 2 observations from the dataset: one representing a patient (labeled "patient A") who experienced a first treatment interruption, and another representing a patient (labeled "patient B") who did not experience an interruption by the end of the follow-up period.

The row labeled "intercept" represents the overall average prediction value (1.516) for the model—baseline prediction (Figure 6A). The subsequent rows show how the mean prediction changes when a specific covariate is fixed. Green bars indicate an increase in the risk of treatment interruption, while red bars show a decrease in the risk. The final row (prediction), shown with a blue bar, displays the overall mean value and change, giving the final predicted risk of treatment interruption for the patient. Patient A had a high predicted risk of treatment interruption, with a risk score of 2.051, which is 0.535 points higher than the model's average prediction (Figure 6). Covariates influencing this prediction are short MMD intervals (1 month), viral load of 200 - 999, did not receive a prevention with positive package, not defaulted on appointment, non–COVID-19 pandemic period, aged 25 - 34 years at the start of ART, and baseline regimen of 2NRTIs + NNRTI. Patient B, on the other hand, had a low predicted risk (0) of interruption, largely driven by the long MMD interval (6+ months), enrolled in the DSD fast-track model, and had prior missed and defaulted appointments contributing to a reduced risk (Figure 7).

XSL•FO
RenderX

Figure 6. Time-invariant model breakdown and SHAP attribution plots for patient A. **(A)** Breakdown plot decomposing the model prediction into cumulative covariate contributions. Intercept—model's overall average prediction value; green bars, with (+) sign indicate increased risk of treatment interruption; red bars, with (−) sign indicate decreased risk of interruption; and blue bar, "prediction" is the individual predicted risk of interruption for the patient. **(B)** SHAP plot summarizing the direction and magnitude of individual covariate effects on the predicted risk of treatment interruption. Note: variable labels shown in the plots represent categorical levels of the corresponding covariates; see Table S1 in Multimedia Appendix 1 for full description. ART: antiretroviral therapy; MMD: multimonth dispensing; NNRTI: nonnucleoside analog reverse transcriptase inhibitor; NRTIs: nucleoside analog reverse transcriptase inhibitors; PwP: prevention with positives package; SHAP: Shapley Additive Explanations.

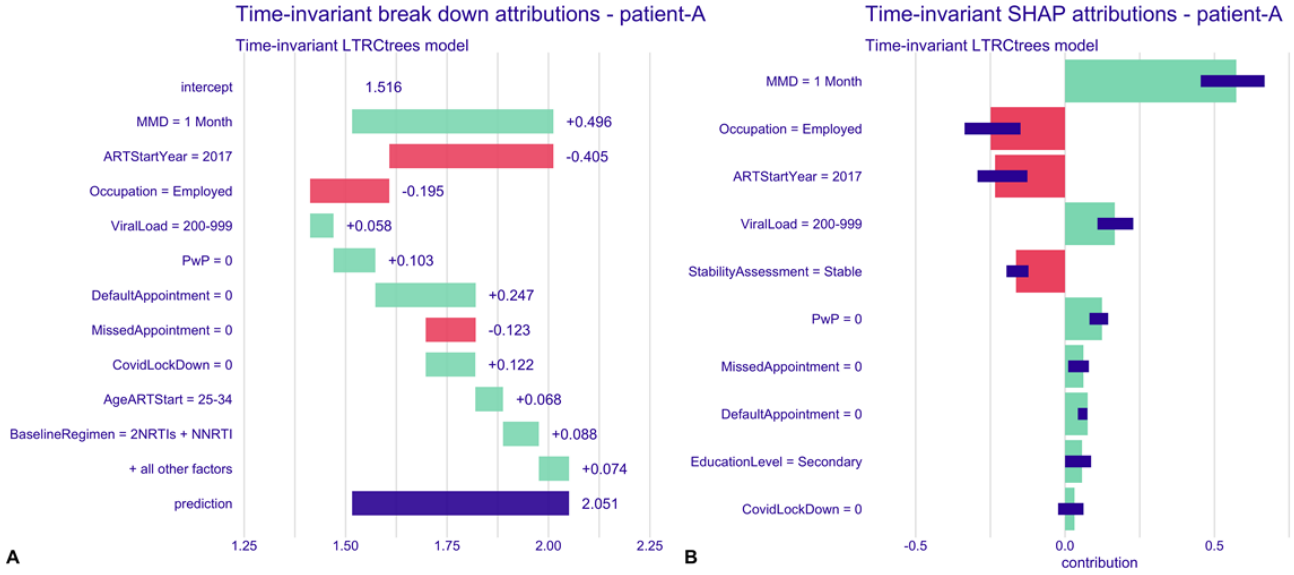

Figure 7. Time-invariant model breakdown and SHAP attribution plots for patient B. **(A)** Breakdown plot decomposing the model prediction into cumulative covariate contributions. Intercept—model's overall average prediction value; green bars, with (+) sign indicate increased risk of treatment interruption; red bars, with (−) sign indicate decreased risk of interruption; and blue bar, "prediction" is the individual predicted risk of interruption for the patient. **(B)** SHAP plot summarizing the direction and magnitude of individual covariate effects on the predicted risk of treatment interruption. ART: antiretroviral therapy; MMD: multimonth dispensing; PwP: prevention with positives package; SHAP: Shapley Additive Explanations.

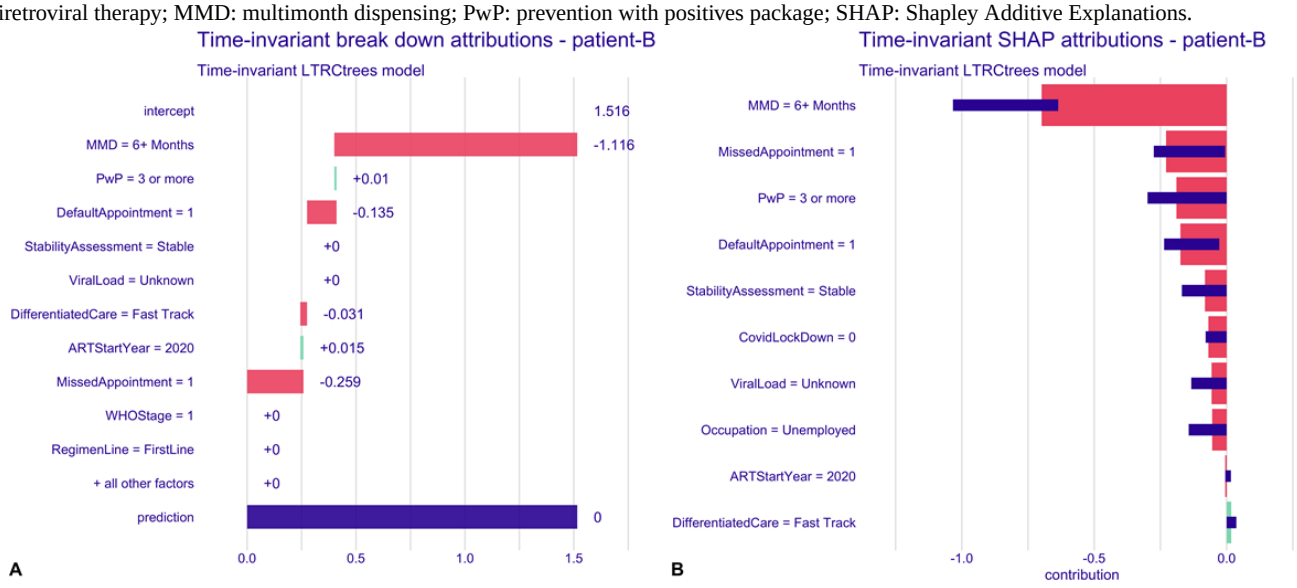

The right plots of both Figures 6 and 7 show the SHAP plots for the patients, where the SHAP values represent the computed mean attribution across 25 random orderings of the explanatory variables. The red bars indicate an average increase in risk, while the green bars show a decrease in risk. The violet box plots summarize the distribution of the attributions over the 25 orderings. The plots reveal similar influential variables as in the breakdown attributions, with a slight reordering of importance and the inclusion of additional variables—such as education level and stability assessment for patient A, and COVID-19 pandemic period for patient B.

To examine the time-varying model's prediction for a single time-interval instance for a patient, we randomly selected 2 patients: patient C, who had experienced 1 or more interruptions and subsequently returned to care; patient D, who had no history of treatment interruption. Figure 6 shows the breakdown and SHAP attribution plots for a single time interval for patient C. After considering all variable contributions, the final predicted risk of subsequent treatment interruption for this patient was 2.43, which is 1.614 points above the average prediction. The key covariate contributing to this risk prediction is the patient's previous interruption duration (duration of 30 - 179 days). In contrast, being on a 6-month MMD interval and having not

XSL•FO
RenderX

missed or defaulted on any appointments were associated with a lower risk of subsequent interruptions. The SHAP plot reflects similar variable contributions (Figure 8B). The predicted risk of treatment interruption for patient D was 0.181, which is 0.635 lower than the average model prediction (Figure 9A). Key covariates contributing to this reduced risk include no prior treatment interruptions (interruption duration of zero), being on a 3 - to 5-month MMD interval, having a viral load between 200 and 999 cp/mL, the COVID-19 pandemic period, no defaulted appointments, good adherence, and starting ART between the ages of 35 and 44 years. SHAP plots (Figure 9B) further highlighted covariates associated with a lower risk for this patient.

Figure 8. Time-varying model, breakdown, and SHAP attribution plots for patient C. **(A)** Breakdown plot decomposing the model prediction into cumulative covariate contributions. Intercept—model's overall average prediction value; green bars, with (+) sign indicate increased risk of treatment interruption; red bars, with (−) sign indicate decreased risk of interruption; and blue bar, "prediction" is the individual predicted risk of interruption for the patient. **(B)** SHAP plot summarizing the direction and magnitude of individual covariate effects on the predicted risk of treatment interruption. ART: antiretroviral therapy; MMD: multimonth dispensing; PwP: prevention with positives package; SHAP: Shapley Additive Explanations.

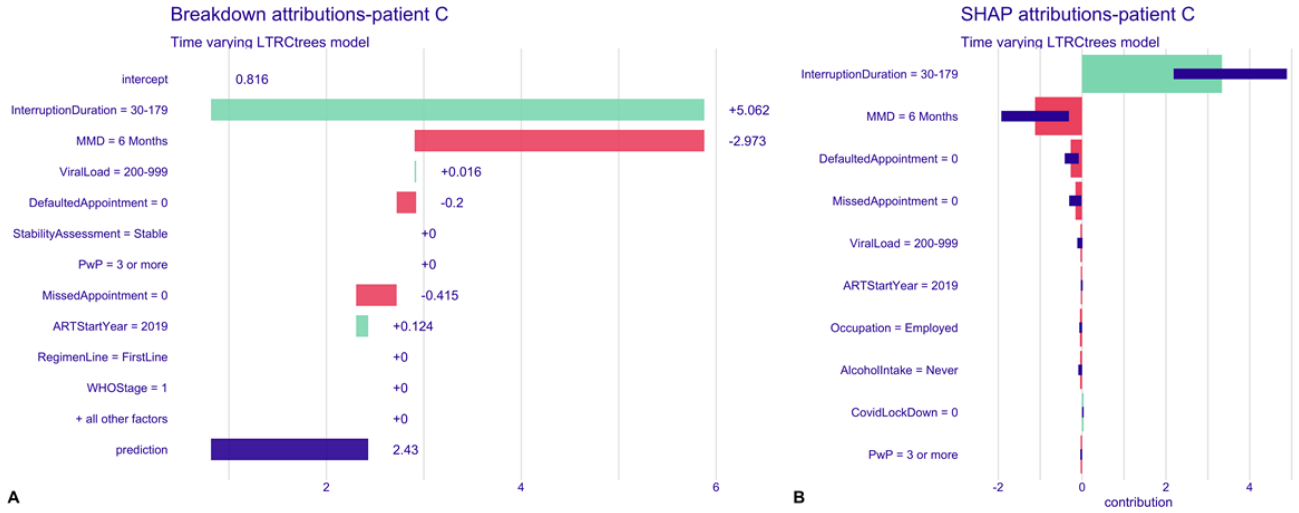

Figure 9. Time-varying model, breakdown, and SHAP attribution plots for patient D. **(A)** Breakdown plot decomposing the model prediction into cumulative covariate contributions. Intercept—model's overall average prediction value; green bars, with (+) sign indicate increased risk of treatment interruption; red bars, with (−) sign indicate decreased risk of interruption; and blue bar, "prediction" is the individual predicted risk of interruption for the patient. **(B)** SHAP plot summarizing the direction and magnitude of individual covariate effects on the predicted risk of treatment interruption. ART: antiretroviral therapy; MMD: multimonth dispensing; NNRTI: nonnucleoside analog reverse transcriptase inhibitor; NRTIs: nucleoside analog reverse transcriptase inhibitors; SHAP: Shapley Additive Explanations.

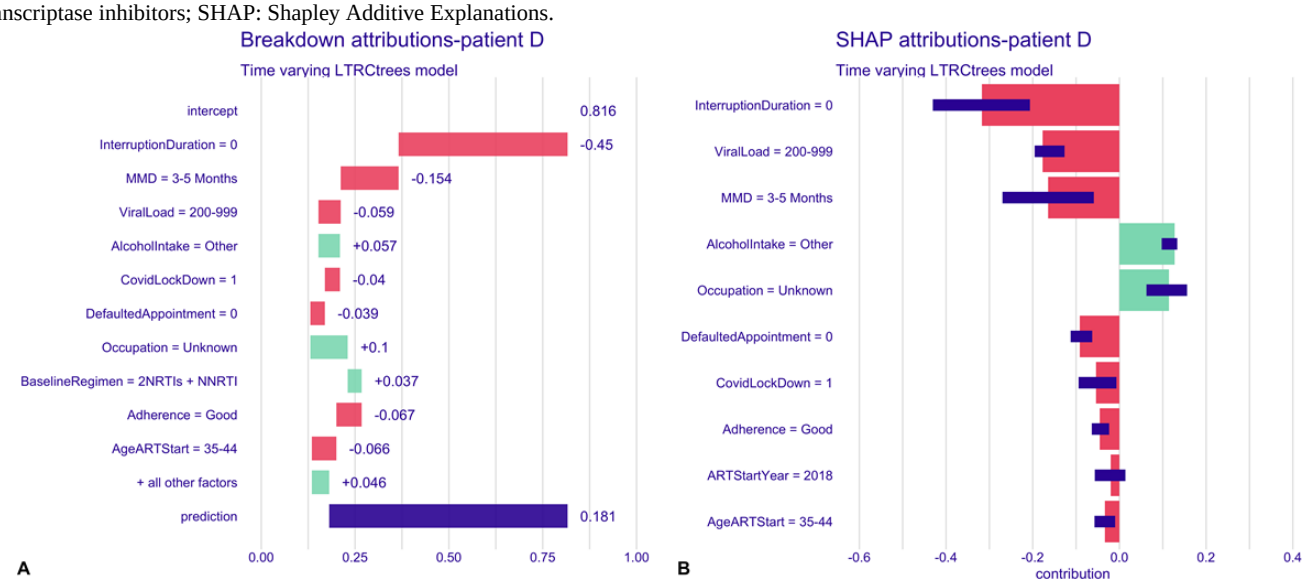

Using CP profile plots, we further examined how the model's predictions for these patients would shift if key covariates—such as the duration of the previous interruption, viral load, DSD model, MMD, missed appointments, and defaulted appointments—were altered. This allowed us to explore how changes in time-varying covariates impact the risk of multiple treatment interruptions. The blue dot and dotted line in the CP plot (Figures 10 and 11) represent the values of the covariates and the corresponding prediction for the patient. Each green bar in the plot shows the predicted change in value and direction for a specific covariate, with bars pointing to the right of the dotted line indicating an increased risk of interruption and bars pointing to the left indicating a decreased risk.

XSL•FO
RenderX

Figure 10. Ceteris paribus profile plots for patient C. Panels show the marginal effect of changes of each variable on the predicted risk of treatment interruption. (A) Defaulted appointments, (B) differentiated care model, (C) interruption duration, (D) missed appointments, (E) multimonth dispensing duration, and (F) viral load. Blue dot is the value of the covariate; blue dotted line corresponding prediction for the patient; green bars—predicted change in value and direction for a specific covariate; and bars right of the dotted line indicate increased risk, while those to the left indicate decreased risk. ART: antiretroviral therapy; HCW: health care worker; MMD: multimonth dispensing.

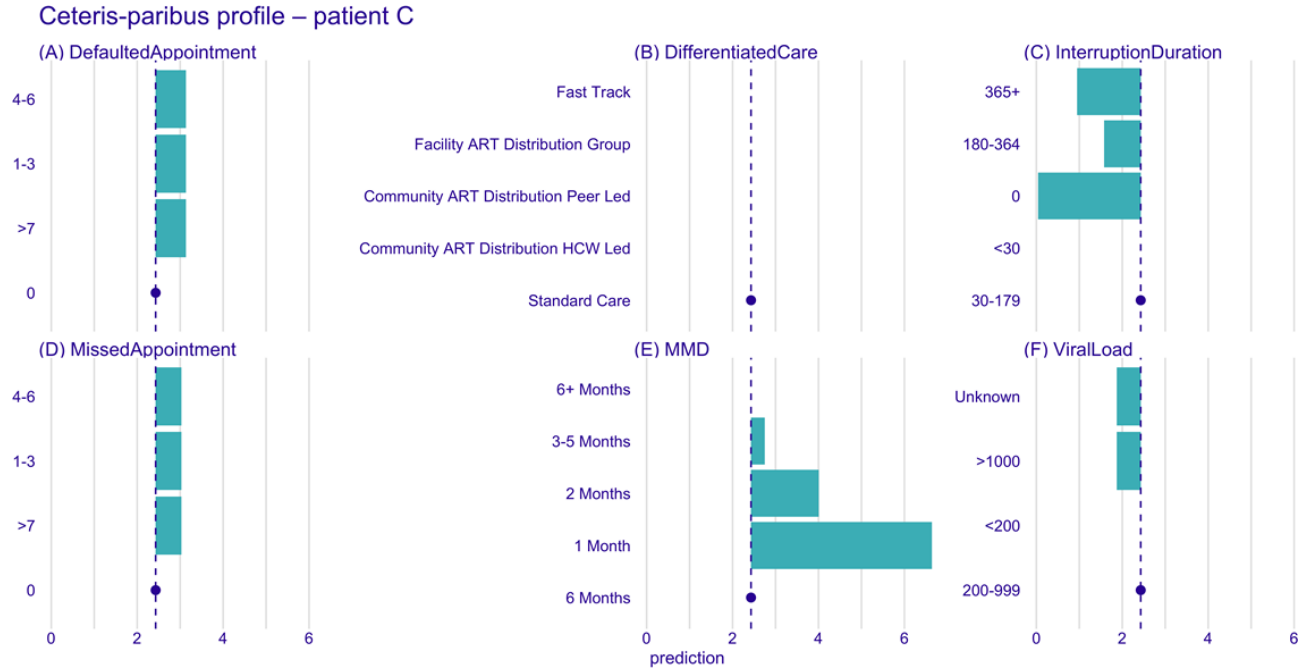

Figure 11. Ceteris paribus profile plots for patient D. Panels show the marginal effect of changes of each variable on the predicted risk of treatment interruption. (A) Defaulted appointments, (B) differentiated care model, (C) interruption duration, (D) missed appointments, (E) multimonth dispensing duration, and (F) viral load. Blue dot is the value of the covariate; blue dotted line corresponding prediction for the patient; green bars—predicted change in value and direction for a specific covariate; and bars right of the dotted line indicate increased risk, while those to the left indicate decreased risk. ART: antiretroviral therapy; HCW: health care worker; MMD: multimonth dispensing.

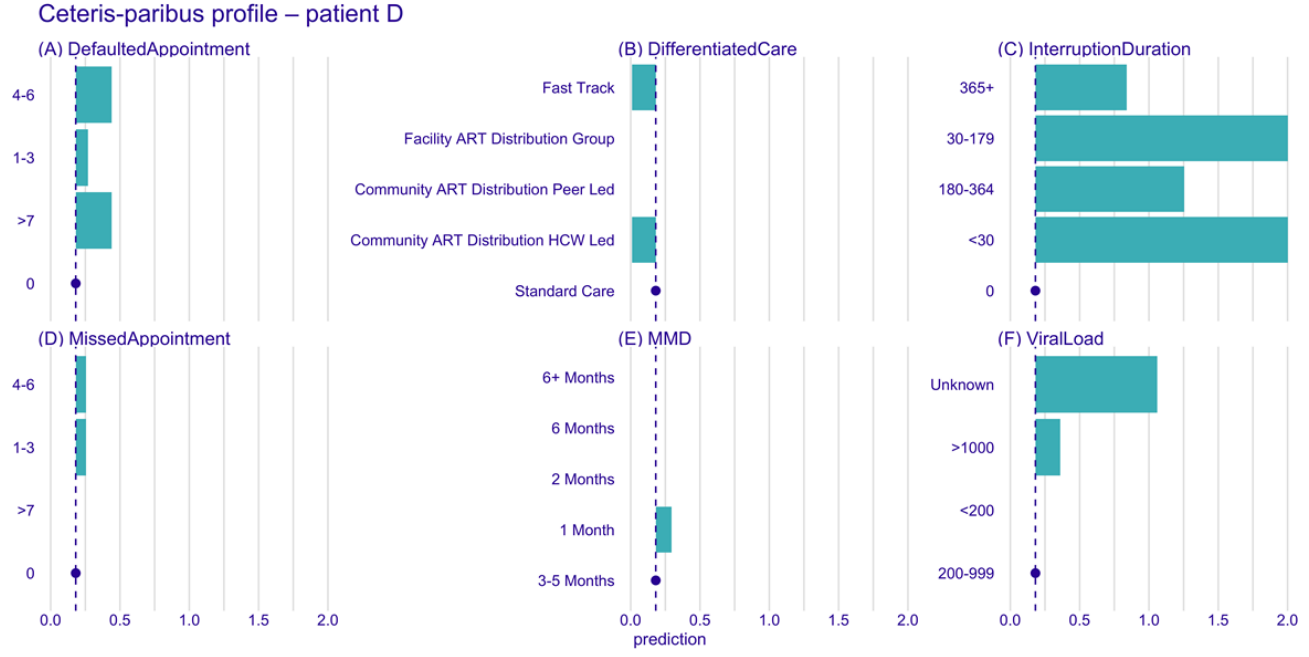

The CP plot (Figure 10) for patient C indicates that their risk of future treatment interruptions would increase significantly if they were to miss or default on an appointment or be placed on a shorter MMD interval. However, the predicted risk remains unchanged if they were to transition across different DSD models. The future risk of treatment interruption would increase for patient D if they miss or default on an appointment, had an increase in their viral load, were placed on a 1-month MMD interval, or experienced a treatment interruption, irrespective of how long it took to return to care (Figure 11). Transitioning from their current standard care DSD model to fast track or community ART distribution health care worker–led models would slightly reduce the risk of interruption.

XSL•FO
RenderX

Discussion

Principal Findings

We compared the traditional CPH model with 6 different ML models to predict the risk of treatment interruption in 621,115 patients receiving ART in 256 facilities across all 47 counties in Kenya. The analysis was conducted in 2 parts: time-invariant models for predicting time-to-first treatment interruptions and time-varying models for predicting time-to-multiple treatment interruptions. Model evaluation was performed using an 80:20 train-test split, and Harrell's C-index was applied to compare the performance of the models on both the train and test sets. Prediction from the best-performing model was then interpreted at both global and individual levels.

The RP model outperformed all other models in both the time-invariant and time-varying analyses. It achieved C-index values of 0.8115 for the train set and 0.8105 for the test set in the time-invariant model, and 0.8918 for the train set and 0.8901 for the test set in the time-varying model. These results align with findings from previous studies that have compared CPH models with ML models, demonstrating the effectiveness of RP models in survival analysis. Previous studies have reported C-index values ranging from 0.63 to 0.96, primarily from ML models such as GBM, random survival forest, and survival support vector machines in predicting survival for patients with cancer [16-19]. Other studies that focused on predicting treatment interruptions in patients on ART had typically reported metrics such as sensitivity, specificity, and area under the curve, with values ranging between 61.9% and 76.0% [20-24]. Few of these studies have incorporated time-varying covariates [16,25]. Even when compared with prior studies that evaluated ML models against CPH [17], our RP approach achieved higher discrimination, with C-index values of 0.8105 and 0.8901 compared with reported XGBoost performance of approximately 0.73. Notably, our study stands out as one of the few to apply RP within a time-varying survival framework, effectively constructing a survival tree that accommodates time-varying covariates.

The RP method offers flexibility in detecting complex interactions without assuming proportional hazards. They automatically select covariates and split points, allowing more adaptive modeling of survival times [26]. This method is advantageous for identifying nonlinear relationships and interactions, making it particularly useful in our case where covariate effects changed over time. The RP model also had the advantage of simple hyperparameter tuning and faster computational times compared with the other ML models we evaluated. We attempted to train a random survival forest model but were unsuccessful due to the large computational resources and extensive time required to handle our large dataset. Likewise, the widely used randomForestSRC R package does not currently support time-varying covariates directly. While random forests are known for their high predictive performance, their significant computational requirements make them less practical for real-world applications [16].

To ensure that our results were fully comparable with the traditional CPH, we implemented a cohesive framework for explaining the ML predictions with meaningful insights. Using a model-agnostic [15] explainer framework, we gained detailed insights into how specific variables influenced individual-level predictions and overall global outcomes, similar to the interpretations provided by hazard ratios in the CPH model. The explainer framework offers additional advantages by capturing complex, nonlinear relationships that traditional CPH may overlook.

On a global level, the permutation-based variable importance from the RP model was similar to the ranking of the absolute values of the coefficients of the CPH model for both time-invariant and time-varying models. In addition, the effects of the selected covariates we considered in the partial dependence plots were consistent with the direction of hazard ratios in the CPH model. This combination of techniques offers diverse insights into our model predictive performance. They reveal the most significant effects and risks associated with treatment interruption across various covariates without the assumptions of linearity, hence capturing potential nonlinear effects that traditional CPH models might overlook. Overall, these methods provide more comprehensive global explanations, particularly for complex variable interactions.

Further exploration using breakdown attribution and SHAP plots reveals how individual variables influence each patient's predicted risk within specific time intervals. On a global level, the time-invariant model was primarily influenced by MMD. Considering this at the patient level, the breakdown and SHAP plots provide detailed insights into how MMD increases or decreases risk, explaining why patient A was at a higher risk than patient B based on MMD. In addition, these plots highlight the most influential covariates for predicting the risk of a first treatment interruption for each patient, emphasizing individual variability in risk factors. For the time-varying model, we furthered the instance-level exploration using CP profiles. These plots provided insights into how a patient's predicted risk would change if certain variables were adjusted. For example, with patient C—who has no history of treatment interruption—we explored the predicted risk of an interruption if the patient were to miss or default on an appointment, transition to a less intensive DSD model, or receive a different drug-dispensing interval. In contrast, for patient D—a patient with a history of interruptions—the focus was on understanding how the predicted risk of another interruption might change if they transitioned to a less intensive care model, adjusted their dispensing interval, or missed an appointment. The changes highlighted for each patient provide actionable insights to guide transitions between DSD models and targeted interventions to prevent treatment interruptions. Following ART initiation, CP profiles can identify patients whose interruption risk under standard care would decrease with earlier DSD enrollment or longer dispensing intervals. For patients returning to care after an interruption, CP profiles quantify how changes in follow-up intensity or MMD duration influence recurrent interruption risk, supporting tailored rather than routine care. These scenario-based insights align with recent World Health Organization and global guidance [27,28] emphasizing person-centered, targeted care packages for patients reengaging in treatment.

XSL•FO
RenderX

Bringing the various components together, our model could be integrated into an EMR system to predict a patient's risk of treatment interruption in real time. This integration would allow the model to continuously process each patient's historical data, current visit date, and next scheduled visit date, creating a new data point for each interaction. With each visit, the EMR system would automatically update risk predictions, enabling health care providers to proactively identify high-risk patients before interruptions occur. The Kenya EMR currently includes an ML module that generates interruption risk scores based on a limited set of patient-centric covariates. By leveraging our model's broader range of covariates, the current system can be optimized for improved prediction accuracy and comprehensive risk assessment.

Limitations

Our study had some limitations. First is the issue of missing data, as highlighted in our previous work [6]. This was addressed by creating an "unknown" category for affected variables, given that the data were not missing at random. Variables with more than 60% missingness, such as baseline and follow-up CD4 counts, were excluded, which may have introduced bias. Sensitivity analyses comparing complete-case models with alternative "unknown" category specifications were conducted in prior work [6] and showed consistent results. Multiple imputation was not considered, given data were not missing at random. Second, while the explainer we used is model-agnostic, it lacks built-in support for survival-specific metrics such as Brier score and area under the curve. Survex explainer is specifically designed for survival models, but it currently does not support the LTRCtrees package or time-varying survival models. A potential work-around could be treating the model as a classification task, focusing on whether there was an interruption or not within a specified fixed time, although this approach will sacrifice the temporal dimension of survival analysis or future studies can consider implementing other Survex-supported algorithms with the ability to fit time-varying covariates. Finally, generating breakdown and SHAP attribution profiles for individual predictions was computationally intensive, particularly for SHAP, which may limit real-time EMR use. However, subsampling across observations or feature permutations can substantially reduce computational cost while preserving accurate SHAP approximations.

Conclusions

Our study compared the predictive performance of the traditional Cox model with 6 different ML models for predicting the risk of treatment interruptions in patients on ART. Overall, our results demonstrate that ML models outperform the traditional Cox model, with RP, in particular, effectively capturing nonlinear effects and complex interactions without relying on proportional hazards assumptions, making it well suited for time-varying survival analyses. Our model-agnostic explanation aligns well with the Cox model results while also offering additional, patient-specific insights for targeted interventions. The combination of enhanced predictive performance and interpretability demonstrates how ML models can effectively support patient-centered care strategies to reduce the likelihood of treatment interruptions in ART.

Acknowledgments

The authors acknowledge the technical inputs of Davies Kimanga (Centers for Disease Control and Prevention—Kenya) and Jacob Odhiambo (The Palladium Group Kenya) during the early phases of the study design. The authors also acknowledge the following staff of The Palladium Group Kenya, that is, Mary Gikura, Kennedy Muthoka, Ashley Odhiambo, and Evans Munene, for their support with data access and validation. Finally, the authors also thank members of the INSIGHT technical working group from CIHEB Kenya—Sam Wafula, Rebecca Wangusi, Patrick Awuor, Violet Makokha, Dinah Nakhanu Mamai, Sarah Nzioka, and Emmah Momanyi—for their valuable contribution and insights into the Kenya treatment program.

Funding

This work was supported by the National Institutes of Health (NIH) D43 Fogarty Global health research training program and Integrated Networks of Scholars in Global Health Research Training (INSIGHT D43TW012274). The findings and conclusions in this paper are solely those of the authors and do not reflect the official positions of their respective institutions. All authors take full responsibility for the decision to submit this manuscript for publication.

Conflicts of Interest

None declared.

Multimedia Appendix 1
Full list of covariates and descriptions.
[DOCX File, 66 KB - medinform_v14i1e78964_app1.docx]

References

1. Cox DR. Regression models and life-tables. J R Stat Soc Series B 1972 Jan 1;34(2):187-202. [doi: 10.1111/j.2517-6161.1972.tb00899.x]

XSL•FO
RenderX

2. Kalbfleisch JD, Schaubel DE. Fifty years of the Cox model. Annu Rev Stat Appl 2023 Mar 10;10(1):1-23. [doi: 10.1146/annurev-statistics-033021-014043]
3. Cox DR, Oakes D. Analysis of Survival Data: Chapman and Hall; 1987. URL: https://www.routledge.com/Analysis-of-Survival-Data/Cox-Oakes/p/book/9780412244902?srsltid=AfmBOop9h4oTLfhsnPee_a42cacTol4DIAPZfcQtE7YWoTGaGLqw_ai1 [accessed 2025-02-11]
4. Fisher LD, Lin DY. Time-dependent covariates in the Cox proportional-hazards regression model. Annu Rev Public Health 1999;20(1):145-157. [doi: 10.1146/annurev.publhealth.20.1.145] [Medline: 10352854]
5. Zhang Z, Reinikainen J, Adeleke KA, Pieterse ME, Groothuis-Oudshoorn CGM. Time-varying covariates and coefficients in Cox regression models. Ann Transl Med 2018 Apr;6(7):121. [doi: 10.21037/atm.2018.02.12] [Medline: 29955581]
6. Salami D, Koech E, Turan JM, et al. Using big data to evaluate the impact of differentiated care on first and recurrent HIV treatment interruptions in Kenya. SSRN. Preprint posted online on Dec 23, 2025. [doi: 10.2139/ssrn.5954474]
7. Andersen PK. Fifty years with the Cox proportional hazards regression model. J Indian Inst Sci 2022 Oct;102(4):1135-1144. [doi: 10.1007/s41745-021-00283-9]
8. Ishwaran H, Kogalur UB, Blackstone EH, Lauer MS. Random survival forests. Ann Appl Stat 2008 Sep;2(3):841-860. [doi: 10.1214/08-AOAS169]
9. Bender A, Rügamer D, Scheipl F, Bischl B. A general machine learning framework for survival analysis. Presented at: Joint European Conference on Machine Learning and Knowledge Discovery in Databases; Sep 14-18, 2020. [doi: 10.1007/978-3-030-67664-3_10]
10. Nagpal C, Jeanselme V, Dubrawski A. Deep parametric time-to-event regression with time-varying covariates. Presented at: Proceedings of AAAI Spring Symposium on Survival Prediction - Algorithms, Challenges, and Applications 2021; Mar 22-24, 2021 URL: https://proceedings.mlr.press/v146/nagpal21a.html [accessed 2026-01-22]
11. Breiman L. Random forests. Mach Learn 2001 Oct;45(1):5-32. [doi: 10.1023/A:1010933404324]
12. Friedman JH. Greedy function approximation: a gradient boosting machine. Ann Statist 2001 Oct;29(5):1189-1232. [doi: 10.1214/aos/1013203451]
13. Lundberg S, Lee SI. A unified approach to interpreting model predictions. arXiv. Preprint posted online on May 22, 2017. [doi: 10.48550/arXiv.1705.07874]
14. Monitoring, evaluation, and reporting indicator reference guide MER 2.0. : PEPFAR US President's Emergency Plan for AIDS Relief; 2024 URL: https://www.state.gov/wp-content/uploads/2025/01/FY25-MER-v2.8-Indicator-Reference-Guide_508-Compliant.pdf [accessed 2024-12-19]
15. Maksymiuk S, Gosiewska A, Biecek P. Landscape of R packages for explainable artificial intelligence. arXiv. Preprint posted online on Sep 24, 2020. [doi: 10.48550/arXiv.2009.13248]
16. Cygu S, Seow H, Dushoff J, Bolker BM. Comparing machine learning approaches to incorporate time-varying covariates in predicting cancer survival time. Sci Rep 2023 Jan 25;13(1):1370. [doi: 10.1038/s41598-023-28393-7]
17. Moncada-Torres A, van Maaren MC, Hendriks MP, Siesling S, Geleijnse G. Explainable machine learning can outperform Cox regression predictions and provide insights in breast cancer survival. Sci Rep 2021 Mar 26;11(1):6968. [doi: 10.1038/s41598-021-86327-7]
18. Tran TT, Lee J, Gunathilake M, et al. A comparison of machine learning models and Cox proportional hazards models regarding their ability to predict the risk of gastrointestinal cancer based on metabolic syndrome and its components. Front Oncol 2023;13:1049787. [doi: 10.3389/fonc.2023.1049787] [Medline: 36937438]
19. Xu L, Cai L, Zhu Z, Chen G. Comparison of the Cox regression to machine learning in predicting the survival of anaplastic thyroid carcinoma. BMC Endocr Disord ;23(1):129. [doi: 10.1186/s12902-023-01368-5]
20. Esra RT, Carstens J, Estill J, et al. Historical visit attendance as predictor of treatment interruption in South African HIV patients: extension of a validated machine learning model. PLOS Global Public Health 2023;3:e0002105. [doi: 10.1371/journal.pgph.0002105]
21. Ogbechie MD, Fischer Walker C, Lee MT, et al. Predicting treatment interruption among people living with HIV in Nigeria: machine learning approach. JMIR AI 2023 May 12;2(1):e44432. [doi: 10.2196/44432] [Medline: 38875546]
22. Maskew M, Sharpey-Schafer K, De Voux L, et al. Applying machine learning and predictive modeling to retention and viral suppression in South African HIV treatment cohorts. Sci Rep 2022 Jul 26;12(1):12715. [doi: 10.1038/s41598-022-16062-0] [Medline: 35882962]
23. Pettit AC, Bian A, Schember CO, et al. Development and validation of a multivariable prediction model for missed HIV health care provider visits in a large US clinical cohort. Open Forum Infect Dis 2021 Jul;8(7):ofab130. [doi: 10.1093/ofid/ofab130] [Medline: 34327249]
24. Ramachandran A, Kumar A, Koenig H, et al. Predictive analytics for retention in care in an urban HIV clinic. Sci Rep 2020 ;10(1):6421. [doi: 10.1038/s41598-020-62729-x]
25. Suresh K, Severn C, Ghosh D. Survival prediction models: an introduction to discrete-time modeling. BMC Med Res Methodol 2022 Jul 26;22(1):207. [doi: 10.1186/s12874-022-01679-6] [Medline: 35883032]
26. Fu W, Simonoff JS. Survival trees for left-truncated and right-censored data, with application to time-varying covariate data. Biostatistics 2017 Apr 1;18(2):352-369. [doi: 10.1093/biostatistics/kxw047] [Medline: 28025180]

XSL•FO
RenderX

27. Supporting re-engagement in HIV treatment services. World Health Organization. 2024. URL: https://www.who.int/publications/i/item/9789240097339 [accessed 2026-01-22]
28. Differentiation at re-engagement in HIV care: a multi-country workshop. International AIDS Society (IAS). 2024. URL: https://www.differentiatedservicedelivery.org/resources/differentiation-at-re-engagement-in-hiv-care-a-multi-country-workshop/ [accessed 2025-11-17]

Abbreviations

ART: antiretroviral therapy
C-index: concordance index
CP: ceteris paribus
CPH: Cox proportional hazards
DSD: differentiated service delivery
EMR: electronic medical record
GBM: gradient boosting machine
ML: machine learning
MMD: multimonth dispensing
RP: recursive partitioning
SHAP: Shapley Additive Explanations
XGBoost: extreme gradient boosting

Edited by A Benis; submitted 16.Jun.2025; peer-reviewed by RS A, Y Shi; revised version received 24.Dec.2025; accepted 29.Dec.2025; published 04.Feb.2026.

Please cite as:
Salami D, Koech E, Turan JM, Stafford KA, Nyagah LM, Ohakanu S, Ngugi AK, Charurat M
Prediction of First and Multiple Antiretroviral Therapy Interruptions in People Living With HIV: Comparative Survival Analysis Using Cox and Explainable Machine Learning Models
JMIR Med Inform 2026;14:e78964
URL: https://medinform.jmir.org/2026/1/e78964
doi:10.2196/78964

© Donald Salami, Emily Koech, Janet M Turan, Kristen A Stafford, Lilly Muthoni Nyagah, Stephen Ohakanu, Anthony K Ngugi, Manhattan Charurat. Originally published in JMIR Medical Informatics (https://medinform.jmir.org), 4.Feb.2026. This is an open-access article distributed under the terms of the Creative Commons Attribution License (https://creativecommons.org/licenses/by/4.0/), which permits unrestricted use, distribution, and reproduction in any medium, provided the original work, first published in JMIR Medical Informatics, is properly cited. The complete bibliographic information, a link to the original publication on https://medinform.jmir.org/, as well as this copyright and license information must be included.

XSL•FO
RenderX

Prospective Diagnostic Accuracy and Technical Feasibility of Artificial Intelligence-Assisted Rib Fracture Detection on Chest Radiographs: Observational Study

Shu-Tien Huang[1,2,3], MSc, MD; Liong-Rung Liu[1,2,3], MSc, MD; Ming-Feng Tsai[2,3,4], MD; Ming-Yuan Huang[1,3*], MSc, MD; Hung-Wen Chiu[2,5*], PhD

[1]Department of Emergency Medicine, Mackay Memorial Hospital, Taipei, Taiwan

[2]Graduate Institute of Biomedical Informatics, College of Medical Science and Technology, Taipei Medical University, 9F, Education & Research Building, Shuang-Ho Campus, No. 301, Yuantong Rd., Zhonghe Dist., New Taipei City, Taiwan

[3]College of Medicine, Mackay Medical University, New Taipei City, Taiwan

[4]Division of Plastic Surgery, Mackay Memorial Hospital, Taipei, Taiwan

[5]Clinical Big Data Research, Taipei Medical University Hospital, Taipei City, Taiwan

[*]these authors contributed equally

Corresponding Author:
Hung-Wen Chiu, PhD
Graduate Institute of Biomedical Informatics, College of Medical Science and Technology, Taipei Medical University, 9F, Education & Research Building, Shuang-Ho Campus, No. 301, Yuantong Rd., Zhonghe Dist., New Taipei City, Taiwan

Abstract

Background: Rib fractures are present in 10% - 15% of thoracic trauma cases but are often missed on chest radiographs, delaying diagnosis and treatment. Artificial intelligence (AI) may improve detection and triage in emergency settings.

Objective: This study aims to evaluate diagnostic accuracy, processing speed, and technical feasibility of an artificial intelligence–assisted rib fracture detection system using prospectively collected data within a real-world, high-volume emergency department workflow.

Methods: We conducted an observational feasibility study with prospective data collection of a faster region-based convolutional neural network–based AI model deployed in the emergency department to analyze 23,251 real-world chest radiographs (22,946 anteroposterior; 305 oblique) from April 1 to July 2, 2023. This study was approved by the Institutional Review Board of MacKay Memorial Hospital (IRB No. 20MMHIS483e). AI operated passively, without influencing clinical decision-making. The reference standard was the final report issued by board-certified radiologists. A subset of discordant cases underwent post hoc computed tomography review for exploratory analysis.

Results: AI achieved 74.5% sensitivity (95% CI 0.708-0.780), 93.3% specificity (95% CI 0.930-0.937), 24.2% positive predictive value, and 99.2% negative predictive value. Median inference time was 10.6 seconds versus 3.3 hours for radiologist reports (paired Wilcoxon signed-rank test W=112 987.5, P<.001). The analysis revealed peak imaging demand between 08:00 and 16:00 and Thursday-Saturday evenings. A 14-day graphics processing unit outage underscored the importance of infrastructure resilience.

Conclusions: The AI system demonstrated strong technical feasibility for real-time rib fracture detection in a high-volume emergency department setting, with rapid inference and stable performance during prospective deployment. Although the system showed high negative predictive value, the observed false-positive and false-negative rates indicate that it should be considered a supportive screening tool rather than a stand-alone diagnostic solution or a replacement for clinical judgment. These findings support further clinician-in-the-loop studies to evaluate clinical feasibility, workflow integration, and impact on diagnostic decision-making. However, interpretation is limited by reliance on radiology reports as the reference standard and the system's passive, non-interventional deployment.

(JMIR Med Inform 2026;14:e77965) doi:10.2196/77965

KEYWORDS

artificial intelligence; chest radiograph; clinical decision support; digital health; emergency radiology; feasibility study; faster R-CNN; real-world data; rib fracture

XSL•FO
RenderX

Introduction

Digital health technologies, particularly artificial intelligence (AI), are increasingly used to address diagnostic delays in high-acuity clinical settings. In emergency departments, timely identification of injuries is essential, yet radiographic interpretation remains constrained by heavy workloads and the inherent complexity of imaging—especially for subtle findings such as rib fractures.

Rib fractures are a frequent consequence of thoracic trauma, occurring in 10% - 15% of trauma patients and often indicating more serious underlying injuries [1-3]. When missed, they may lead to inadequate pain management, delayed respiratory support, pneumonia, or even preventable intensive care unit admissions. Beyond clinical harm, undetected fractures also carry medicolegal implications and increase health care costs.

Despite their significance, rib fractures are notoriously difficult to detect on chest radiographs (CXRs)—the first-line imaging modality in most emergency departments—due to overlapping anatomical structures and subtle fracture lines. Reported sensitivities for radiologist detection can be as low as 15%, with up to half of fractures potentially missed in high-volume settings [4,5]. Although computed tomography (CT) and ultrasound can improve accuracy, they are resource-intensive and not always feasible for frontline triage [6-8]. These limitations highlight an urgent need for AI-driven tools that can assist clinicians by rapidly identifying suspected rib fractures in routine CXRs, enabling more effective prioritization and timely intervention.

Recent advances in AI, particularly deep learning, have demonstrated strong potential in automating image analysis tasks across medical domains, including dermatology, ophthalmology, and pulmonary imaging [9-11]. Deep learning models, especially convolutional neural networks, can automatically extract complex image features and have shown superior performance compared to traditional machine learning methods in various image classification tasks [11-13]. Transfer learning further enables the adaptation of pretrained convolutional neural networks—originally developed for natural images—for medical image classification tasks, including bone fracture detection [14,15].

Although prior studies have applied deep learning to rib fracture detection with promising results, most were retrospective, limited in scale, and did not assess feasibility in operational emergency department workflows [7,16,17]. These proof-of-concept efforts did not address the practical barriers to integrating AI into emergency radiology workflows, such as inference latency, system interoperability, or artifact handling.

To address this gap, we conducted an observational feasibility study with prospective data collection, evaluating an AI model for rib-fracture detection on CXRs. The system was passively deployed in parallel with routine emergency department imaging workflows using real-world data, without influencing clinical decisions. This design allowed the assessment of diagnostic performance, processing speed, and operational characteristics within standard clinical workflows.

Methods

Study Design

The observational feasibility study protocol was reviewed and approved by the Institutional Review Board of MacKay Memorial Hospital (IRB No. 20MMHIS483e) prior to the initiation of data collection. MacKay Memorial Hospital is a tertiary referral and level 1 trauma center in northern Taiwan. The AI system functioned passively in real time without influencing clinical decisions or patient management. As the system functioned in a noninterventional, observational manner, prospective trial registration was not required.

From April 1 to July 2, 2023, all chest and rib radiographs acquired in the emergency department were automatically processed by the AI system in near-real-time. Both standard CXRs and rib-only views acquired during the study period were automatically analyzed, as both modalities are routinely used for suspected thoracic trauma. During the study period, a temporary 14-day graphics processing unit (GPU) hardware outage occurred, during which radiographs were not processed in real time; these examinations were excluded from turnaround time analysis but retained for diagnostic accuracy, as formal radiology reports were available. No additional exclusion criteria were applied beyond the 14-day system outage; all eligible emergency radiographs during the study period were included in the analysis. The system operated passively alongside routine clinical workflows, without influencing clinical decisions. AI-identified suspected rib fractures were highlighted using bounding boxes on a backend interface, which was accessible only for research evaluation and remained hidden from the clinical care team (Figure 1).

XSL•FO
RenderX

Figure 1. Study workflow of a prospective observational feasibility study evaluating an artificial intelligence–assisted rib fracture detection system using chest radiographs in patients admitted to the emergency department at a high-volume tertiary medical center (April 1-July 2, 2023). GPU: graphics processing unit.

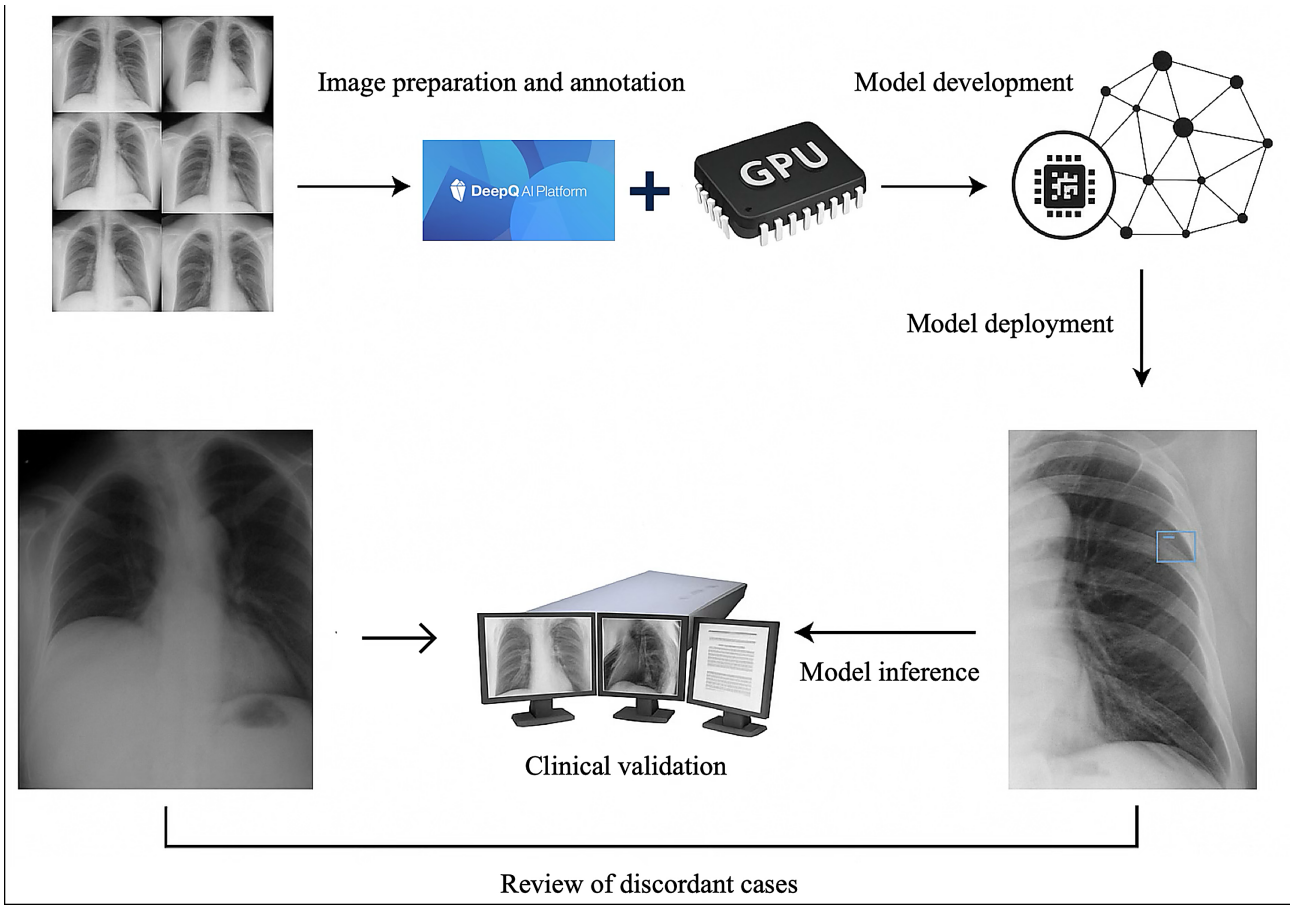

Ethical Considerations

This study was approved by the Institutional Review Board of MacKay Memorial Hospital (IRB No. 20MMHIS483e) and conducted in accordance with the Declaration of Helsinki. Informed consent was waived because the study involved secondary analysis of routinely acquired, deidentified clinical imaging data, and the AI system operated passively without influencing patient management.

All data were deidentified prior to analysis and processed on secure institutional servers with access limited to authorized research personnel. No compensation was provided to participants. All images included in the manuscript were fully anonymized, and no identifiable patient information is disclosed.

Consistent with the approved observational study design, all AI outputs—including discordant cases—were withheld from treating clinicians and did not influence patient management.

AI Model Development

CXRs were retrospectively collected from the hospital picture archiving and communication system (PACS) for model training. All images were deidentified and preprocessed using histogram equalization and image inversion to improve fracture conspicuity. Fracture locations were annotated using bounding boxes by a board-certified emergency physician with 18 years of clinical experience via the DeepQ AI platform [18].

A deep learning model was developed using PyTorch (v1.13) with GPU acceleration. The architecture was based on faster region-based convolutional neural network (R-CNN) [19], incorporating a ResNet-50 backbone for feature extraction, a region proposal network for candidate region generation, and a classification head for fracture detection.

The dataset comprised 2079 CXRs (1065 fracture-positive and 1014 normal) collected between 2010 and 2020. Images were randomly divided into training (80%) and validation (20%) sets at the image level, as each radiograph represented an independent study. When multiple images were obtained from the same patient encounter, each radiograph was treated as an independent sample. Data augmentation—including random rotation, flipping, brightness, and contrast adjustment—was applied to improve generalization. To address the inherent class imbalance given the low fracture prevalence, class-weighted loss and oversampling of fracture-positive images were employed.

Model Validation

Model performance was assessed on a hold-out test set of 262 CXRs containing 724 expert-annotated rib fractures. Evaluation metrics were reported at both the case and object levels.

At the case level, the unit of analysis was the radiographic study. A study was considered positive if at least 1 rib fracture was detected, regardless of the number of fractures present. The model correctly identified fractures in 230 of 257

XSL•FO
RenderX

fracture-positive studies, achieving a sensitivity of 89.5%. With only 8 false-positive cases, precision reached 96.6%, yielding an overall F_1-score of 0.93.

At the object level, performance reflected per-lesion detection accuracy. The model correctly localized 680 of 724 annotated rib fractures (recall=94.0%) and generated 55 false-positive boxes. The mean average precision at an intersection-over-union threshold of ≥0.5 was 0.65, indicating robust lesion-level localization (Table 1).

Table . Dataset composition and performance of the artificial intelligence (AI) model using retrospective emergency department chest radiographs, including case-level detection and object-level localization (intersection-over-union [IoU]≥0.50).

Category and metric	Value
Dataset	
Total images	262
Ground-truth boxes	724
Case-level detection (%)	
Sensitivity (recall)	89.6
Precision	96.6
F_1-score	0.93
Object-level localization	
Recall	94.0%
mAP[a] (IoU≥0.5)	0.65

[a]mAP: mean average precision.

Curve-based analyses further characterized the model's detection behavior (Figure 2). The precision-recall curve (Figure 2A) maintained precision ≥0.90 until recall fell below 0.55 (precision-recall area under the curve=0.65), demonstrating high reliability across a broad sensitivity range. The free-response receiver operating characteristic (FROC) curve (Figure 2B) showed true-positive rates of 0.77 at 1 false positive per image and 0.88 at three, representing practical trade-offs between sensitivity and alert frequency in potential clinical deployment.

Figure 2. The performance of the artificial intelligence (AI)–assisted rib fracture detection model was evaluated in the retrospective model development and validation dataset using emergency department chest radiographs. (A) Precision-recall curve demonstrating case-level detection performance at an intersection-over-union (IoU) threshold of ≥0.50 (area under the curve=0.65). (B) Free-response receiver operating characteristic (FROC) curve showing lesion-level sensitivity as a function of false positives per image, with localization performance assessed at the same IoU threshold (mean average precision=0.65; recall=94%).

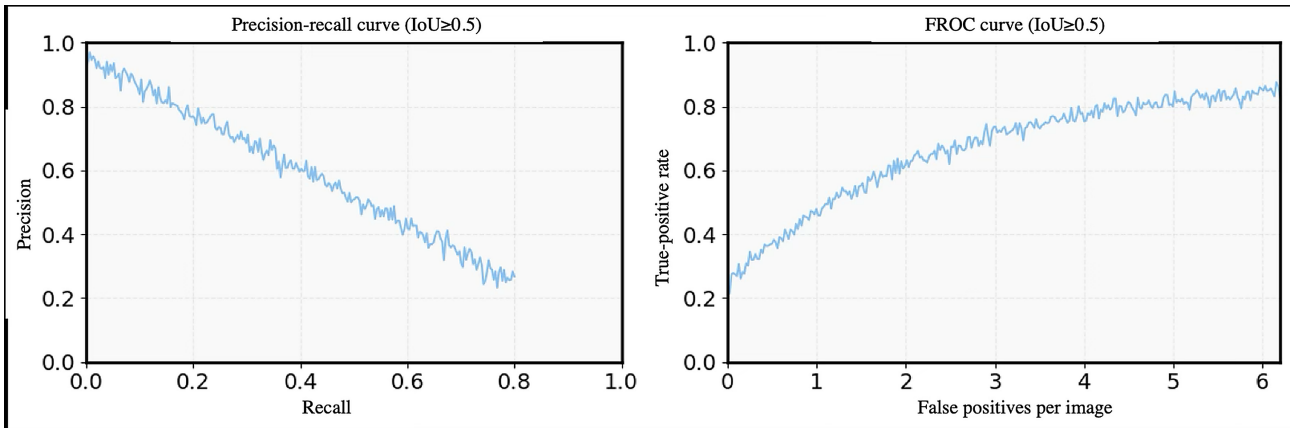

Prospective Evaluation of AI Model in Emergency Department Workflow

The trained model was prospectively evaluated in parallel with clinical workflow, performing automated inference on incoming emergency radiographs. During the automated inference process, all incoming radiographs were standardized and resized to a fixed resolution of 512×512 pixels. The prospective evaluation cohort (April-July 2023) was temporally and operationally independent from the retrospective training and validation dataset (2010-2020), and no patient overlap existed between the 2 cohorts. During the prospective evaluation phase, all chest and rib radiographs from emergency department encounters were automatically processed by the AI system without disrupting clinical workflows. The bounding box outputs were logged for research analysis but were not disclosed to radiologists or used for patient management.

XSL•FO
RenderX

Performance Assessment Using NLP-Derived Labels

To evaluate AI performance in the real-world setting, output was compared to formal radiology reports issued by board-certified radiologists. A rule-based natural language processing (NLP) pipeline was developed to extract structured rib fracture labels (positive, negative, or ambiguous) from free-text reports. The algorithm combined keyword detection (eg, “rib fracture,” “fx”) and negation handling (eg, “no evidence of,” “no definite fracture”).

To validate NLP accuracy, a random sample of 200 radiology reports was manually reviewed by 2 emergency physicians blinded to both NLP and AI results. The NLP classification achieved 96.5% agreement (193/200) with manual review, with a Cohen κ of 0.91, indicating excellent concordance. Most discrepancies were due to ambiguous language or complex negation structures (Table 2).

Table . Confusion matrix comparing natural language processing (NLP)–extracted radiology report labels with manual expert review in a randomly selected subset of 200 emergency department chest radiographs, used to assess labeling accuracy in the retrospective dataset.

Manual review	Fracture present	Fracture absent	Ambiguous	Total (NLP prediction)
NLP: fracture present	95	2	1	98
NLP: fracture absent	3	90	2	95
NLP: ambiguous	1	2	4	7
Total (manual review)	99	94	7	200

Formal radiology reports served as the primary reference standard for AI evaluation. This approach may have underestimated AI sensitivity because CT confirmation was not performed systematically. In select discordant cases—where the AI flagged fractures not documented in the reports—subsequent CT scans confirmed some of these findings. These discrepancies were retrospectively reviewed to investigate potential underreporting by radiologists. While informative, these exploratory adjudications were not used as a universal reference standard due to inconsistent CT availability. Nonetheless, radiology reports remained the definitive benchmark for all performance metrics. Additionally, the selected misclassified cases were examined to identify recurring patterns of diagnostic oversight among frontline physicians.

Targeted Adjudication of Discordant Cases

To further explore potential underreporting within the report-based reference standard, we performed a focused review of discordant cases in which the AI system flagged suspected rib fractures not documented in the corresponding formal radiology reports. Because not all discordant cases had confirmatory CT imaging, an illustrative subset of 11 cases was selected based on the availability of same-encounter chest CT and clinical relevance for qualitative adjudication. Each case was reviewed to determine whether the AI-predicted fractures corresponded to true fractures confirmed on CT. These adjudications were exploratory and intended to contextualize the potential clinical value of AI detection beyond the report-based benchmarking.

Data Analysis

Case-level performance was assessed at the radiographic study (accession) level by comparing AI outputs to NLP-derived labels from radiology reports. A study was considered positive if at least 1 image within the same examination was flagged as having a rib fracture by the AI system; otherwise, the study was classified as negative. Key metrics included sensitivity, specificity, accuracy, positive predictive value, negative predictive value (NPV), and F_1-score. Ninety-five percent CIs were calculated using nonparametric bootstrap resampling (1000 iterations). The results were summarized in confusion matrices and diagnostic performance plots.

Statistical Analysis

All statistical analyses were performed using Python 3.11 (pandas v2.2, scikit-learn v1.4) and R 4.3.2. Continuous variables were reported as mean (SD) or median with IQR. Categorical variables were summarized as counts and percentages. A 2-tailed $P<.001$ was considered statistically significant.

This study was reported in accordance with the Checklist for Artificial Intelligence in Medical Imaging (CLAIM) guideline, with the completed checklist provided as Checklist 1.

Results

Study Cohort

From April 1 to July 2, 2023, all chest and dedicated rib radiographs acquired in the emergency department were automatically processed by the AI system in a parallel workflow, yielding 23,251 imaging studies from 20,908 unique patient visits. Population demographics are summarized in Table 3. The mean age was 55.9 years (SD 22.3; range 0 - 106), with 10,770 (51.5%) male and 10,138 (48.5%) female patients. A radiologist review identified 589 rib-fracture cases (prevalence 2.8%).

XSL•FO
RenderX

Table . Demographic and clinical characteristics of patients in the emergency department included in a prospective observational study of artificial intelligence (AI)–assisted rib fracture detection (April 1-July 2, 2023).

Characteristic	Value
Total cases	20,908
Age (y), mean (SD; range)	55.9 (22.3; 0 - 106)
Sex, n (%)	
Male	10,770 (51.5)
Female	10,138 (48.5)
Radiologist-confirmed rib fractures, n (%)	589 (2.8)

AI Model Performance

AI model outputs were compared on a per-case basis against structured rib-fracture labels derived from board-certified radiology reports. At the selected operating point—corresponding to approximately one false-positive per image on the FROC curve—the system achieved a sensitivity of 0.745 (95% CI 0.708 - 0.780) and specificity of 0.933 (95% CI 0.930 - 0.937). Positive predictive value was 0.242 (95% CI 0.223 - 0.262), and negative predictive value was 0.992 (95% CI 0.991 - 0.994). The overall F_1-score was 0.365 (95% CI 0.340 - 0.390) with an accuracy of 0.928 (Table 4).

Table . Case-based diagnostic performance of an artificial intelligence–assisted rib fracture detection system in a prospective observational emergency department study[a].

Metric	Estimate (95% CI)
Sensitivity	0.745 (0.708 - 0.780)
Specificity	0.933 (0.930 - 0.937)
PPV[b]	0.242 (0.223 - 0.262)
NPV[c]	0.992 (0.991 - 0.994)
F_1-score	0.365 (0.340 - 0.390)
Accuracy	0.928 (N/A[d])

[a]Performance metrics are reported with 95% CIs using final radiologist reports as the reference standard.

[b]PPV: positive predictive value.

[c]NPV: negative predictive value.

[d]N/A: not available.

As shown in Figure 3, the AI system correctly identified 431 (74.5%) fracture-positive cases while producing 1357 (6.1%) false positives and 148 (0.7%) false negatives across 23,251 studies. This distribution demonstrates the model's high true-negative count (n=18,972, 93.3%) and its strong negative predictive value during deployment in the emergency department. No temporal drift or learning curve effects were observed, as the deployed model remained fixed throughout the study period.

XSL•FO
RenderX

Figure 3. Case-level confusion matrix of the artificial intelligence (AI)–assisted rib fracture detection system during prospective emergency department deployment, using final radiologist reports as the reference standard. Darker blue indicates a higher number of cases (count), as shown in the color bar.

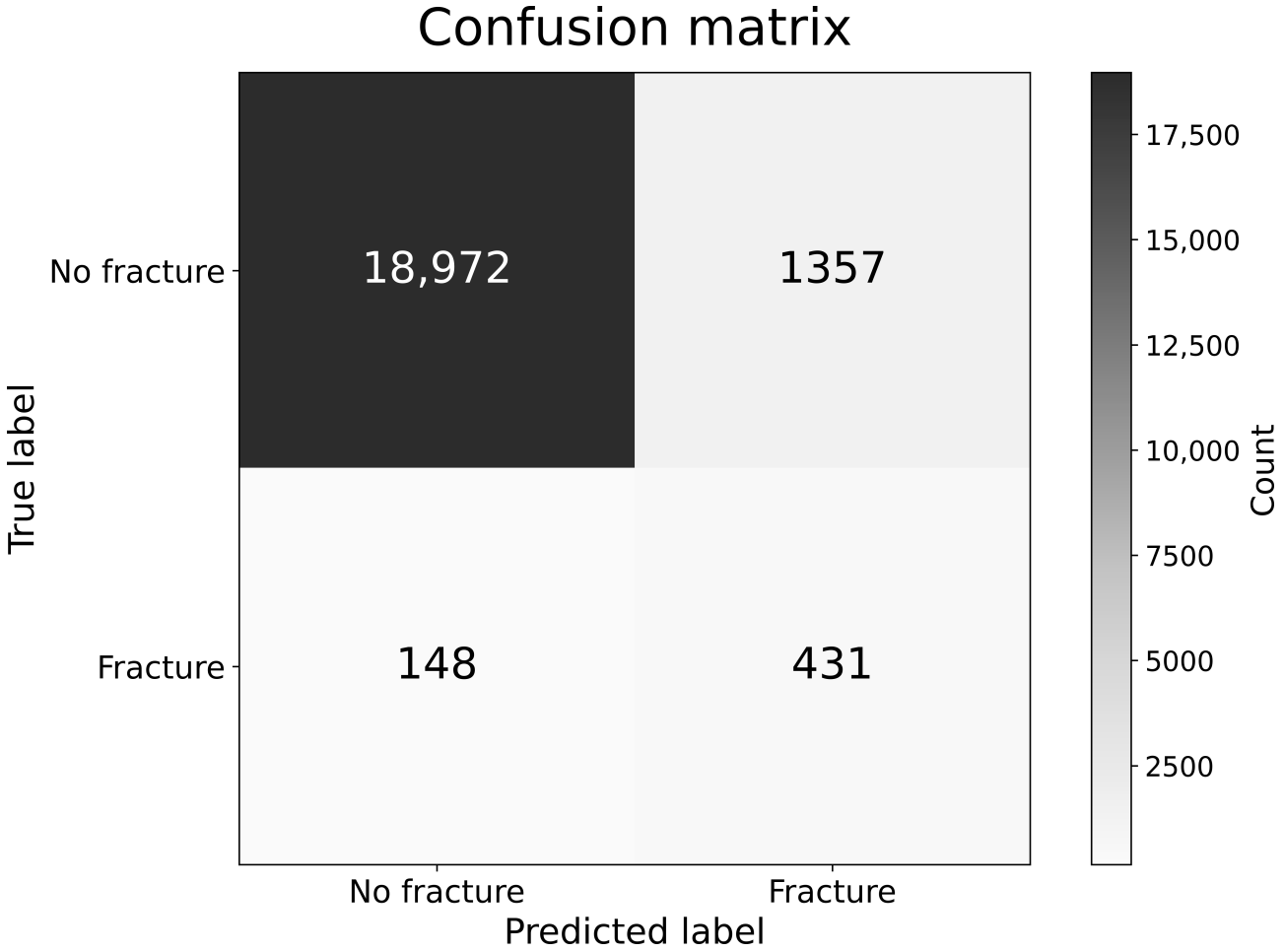

Imaging Workload Patterns

Analysis of imaging demand revealed predictable diurnal and weekly patterns, with peak volumes between 08:00 and 16:00 daily and secondary surges on Thursday to Saturday evenings. Demand was the lowest between 00:00 and 07:00 across all days of the week (Figure 4).

XSL•FO
RenderX

Figure 4. Heatmap illustrating the temporal distribution of chest radiograph imaging workload by hour of day and weekday during prospective emergency department deployment. Color intensity represents the number of chest radiographs acquired per hour, highlighting peak imaging periods across weekdays and weekends.

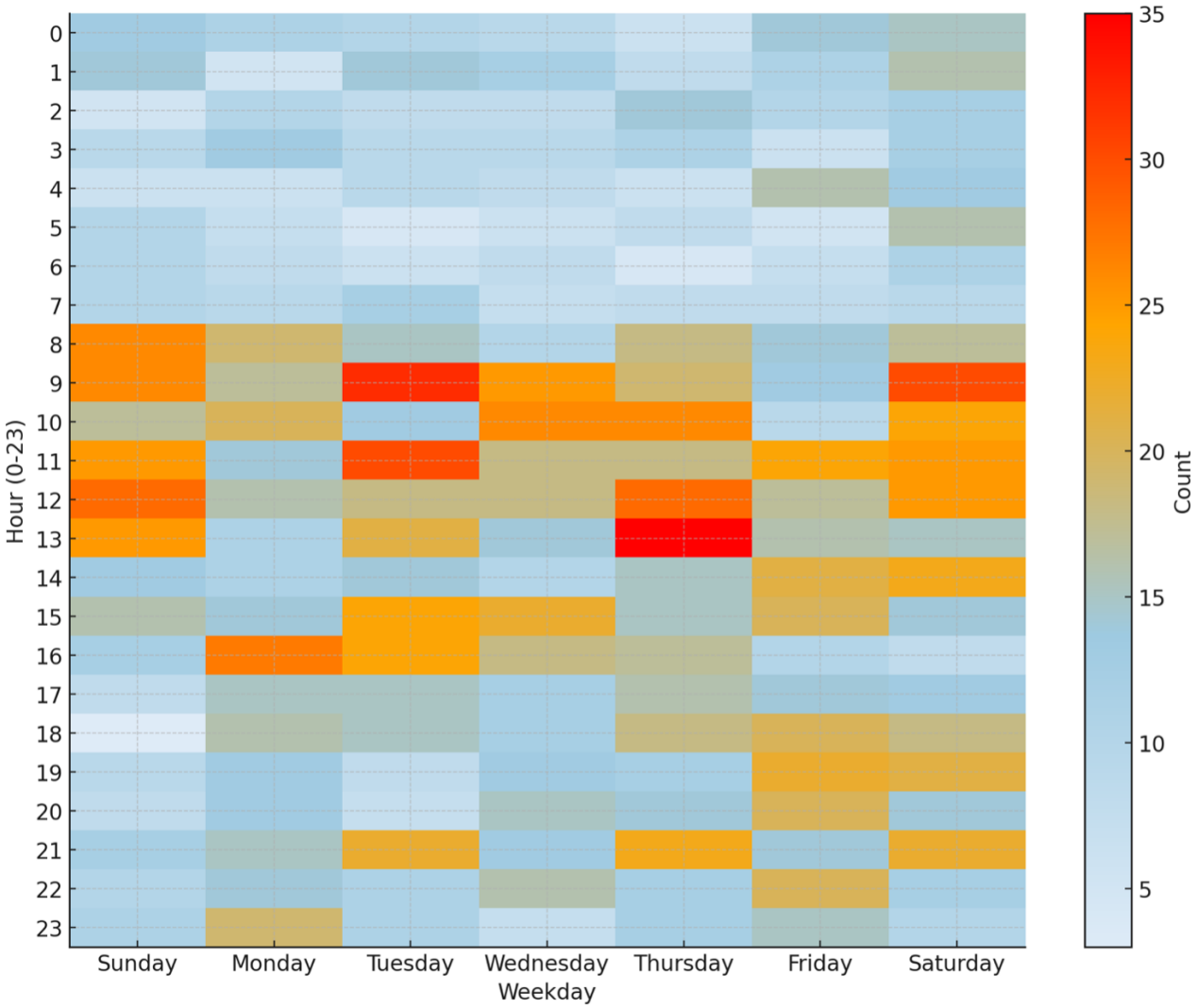

Inference Turnaround Time

A total of 19,641 paired cases were included to compare AI inference and radiologist report turnaround times. As shown in Table 5, the AI system achieved a median processing time of 10.6 seconds per image (IQR 9.0 - 14.0; range 3 - 35 s), compared with a median of 3.3 hours (IQR 1.31 - 4.80; range 0.08 - 72 h) for radiologist reports. This represents a more than 1000-fold reduction in turnaround time. Figure 5 illustrates this disparity using boxplots on a logarithmic scale. A paired Wilcoxon signed-rank test confirmed that AI inference was significantly faster than radiologist reporting (W=112,987.5; P<.001). This median reporting time reflects the full clinical workflow, including overnight and backlog delays typical of high-volume emergency radiology settings.

Table . Turnaround times for artificial intelligence (AI) inference versus radiologist reporting during prospective emergency department deployment (n=19,641)[a].

Metric	AI inference time (s)	Radiologist report time (s)
Mean	10.9	10,877
Standard deviation	3.0	4008
Median (50%)	10.6	11,880
IQR (25% - 75%)	9.0 - 14.0	4728 - 17,280
Min	3.0	300
Max	35.0	259,200

[a]Times are summarized using descriptive statistics, including median and interquartile range.

XSL•FO
RenderX

Figure 5. Comparison of turnaround times between artificial intelligence (AI) inference and radiologist reporting during prospective emergency department deployment (April 1-July 2, 2023). Boxplots on a logarithmic scale illustrate differences in processing time distributions between real-time AI inference and routine clinical reporting.

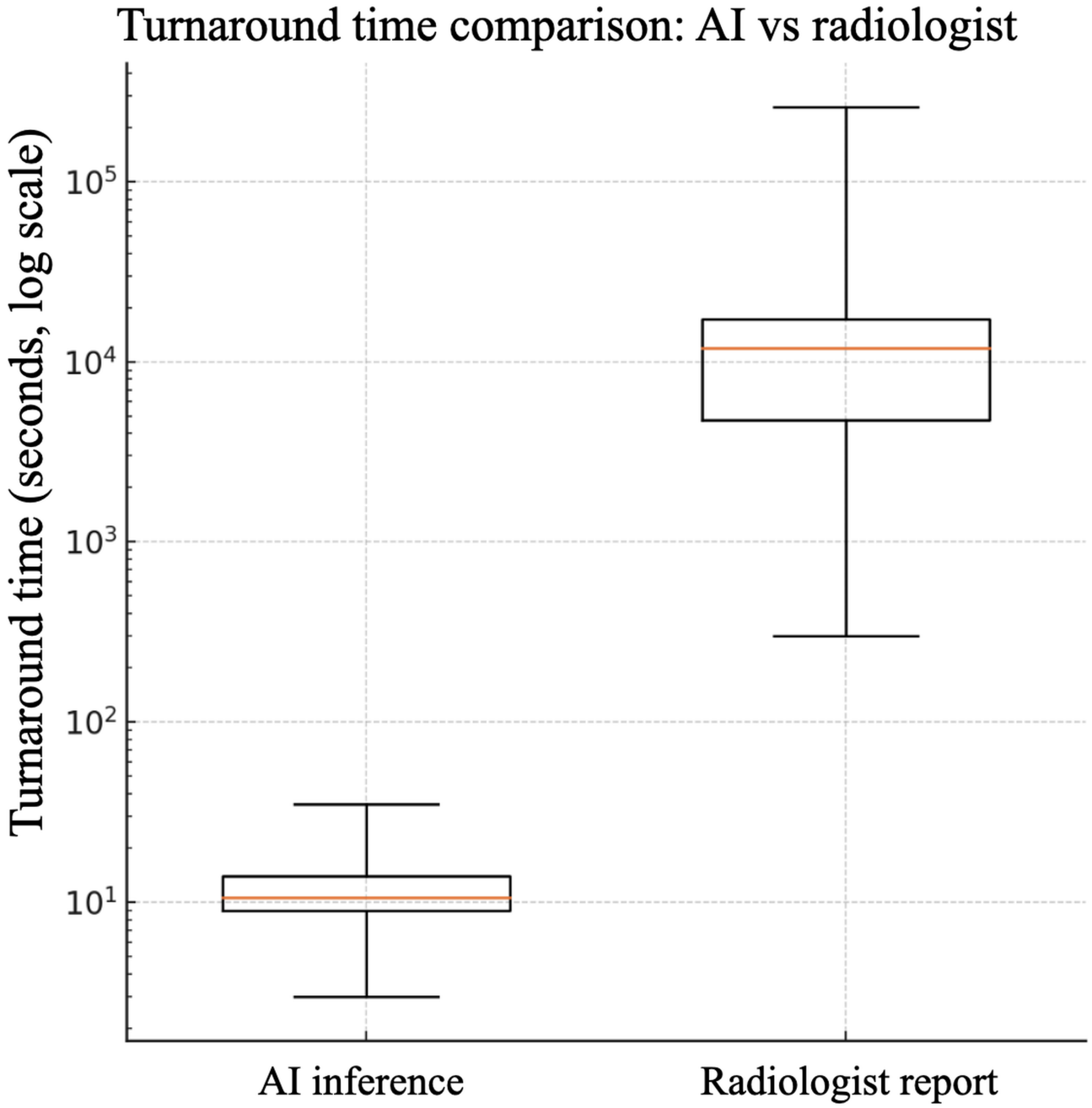

This processing speed highlights the potential of AI-assisted triage systems to complement radiology workflows by rapidly identifying cases for prioritized review, especially in high-volume emergency settings.

System Reliability

During the prospective evaluation of the AI system operating in a parallel clinical workflow, the AI platform experienced 1 service interruption—from 27 April to 10 May 2023—caused by GPU overload that halted all inference operations. A total of 3610 studies acquired during this 14-day outage were excluded from the turnaround time analysis but retained in the diagnostic accuracy evaluation (their formal radiology reports remained available). Following hardware replacement, full functionality was restored on 11 May, and no further outages occurred over the remainder of the study period.

Illustrative Review of Discordant Cases

To further evaluate the AI system's potential diagnostic value beyond report-based benchmarking, a targeted adjudication was conducted on 11 representative discordant cases in which the AI system flagged suspected rib fractures not described in the corresponding radiology reports (Table 6). Among these, 7 cases (cases 1 - 7) were subsequently confirmed as true fractures on CT ("AI-CT concordant"), indicating that several AI-labeled false positives in the report-based analysis represented true fractures missed in the reference standard. The remaining 4 cases (cases 8 - 11) were confirmed negative on CT, primarily attributable to nonfracture anatomical structures or imaging

XSL•FO
RenderX

artifacts. Including these CT-confirmed fractures as true positives would modestly increase the model's effective sensitivity and positive predictive value, highlighting the underestimation inherent in report-based benchmarking.

Table . Targeted post hoc computed tomography (CT) adjudication of representative discordant cases in which artificial intelligence (AI) flagged suspected rib fractures not described in the corresponding radiology reports during prospective emergency department deployment.

Case	AI output	Radiologist report	Emergency physician	Outcome	Note (AI significance)
1	Flagged right rib fracture	No fracture	Noted with POCUS[a]	CT-confirmed	Triage value, prompting clinicians to perform US[b]
2	Flagged right rib fracture	No fracture	Missed	CT-confirmed	AI-CT concordance
3	Flagged left fifth rib fracture	No fracture	Missed	CT-confirmed	AI-CT concordance
4	Flagged rib fracture post chest tube	No fracture	Missed	CT-confirmed	Chest tube artifact did not impair detection
5	Flagged lower-rib fracture	No fracture	Missed	CT-confirmed	AI-CT concordance
6	Flagged fracture near hardware	No fracture	Missed	CT-confirmed	Detected fracture adjacent to surgical hardware
7	Flagged fracture under scapular shadow	No fracture	Missed	CT-confirmed	AI-CT concordance
8	Flagged fracture at scapula border	No fracture	No fracture	False positive	Scapular margin misidentified
9	Flagged rib fracture at bra clasp	No fracture	No fracture	False positive	Bra hardware artifact
10	Flagged fracture at chest tube marker	No fracture	No fracture	False positive	Chest tube marker misinterpreted
11	Flagged fracture (image noise)	No fracture	No fracture	False positive	Image noise

[a]POCUS: point-of-care ultrasound.

[b]US: ultrasound.

In one representative case (Case 3), the AI system correctly identified a subtle nondisplaced fracture of the left fifth rib that was not documented in the radiology report but later verified on 3D CT reconstruction (Figure 6). In contrast, Figure 7 illustrates the main sources of false positives, including scapular margin misinterpretation, chest-tube hardware artifacts, and motion-induced noise.

XSL•FO
RenderX

Figure 6. Representative true-positive rib fracture detected by artificial intelligence (AI) and confirmed by computed tomography (CT) during prospective emergency department deployment. (A) Chest radiograph showing an AI-flagged fracture of the left fifth rib that was not described in the initial radiology report. (B) Corresponding CT image confirming the fracture at the same anatomical location.

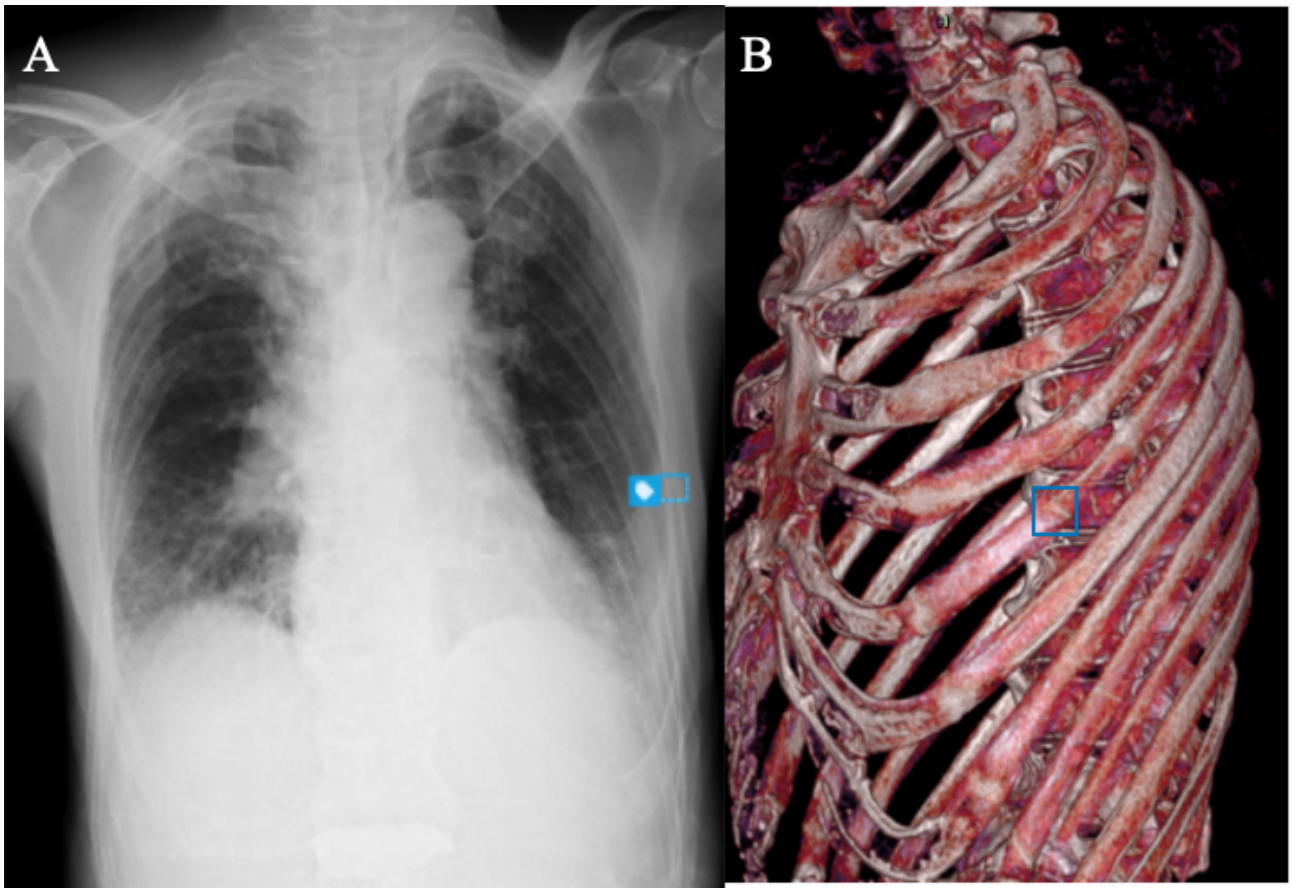

Figure 7. Representative false-positive detections generated by an artificial intelligence (AI)–assisted rib fracture detection system during prospective emergency department deployment. The examples illustrate common sources of false-positive signals on chest radiographs. (A) Scapular margin overlap misinterpreted as a rib fracture. (B) Chest tube marker misidentified as a rib discontinuity. (C) Bra hardware producing a linear opacity mimicking a fracture. (D) Image noise and low-contrast regions leading to spurious detection.

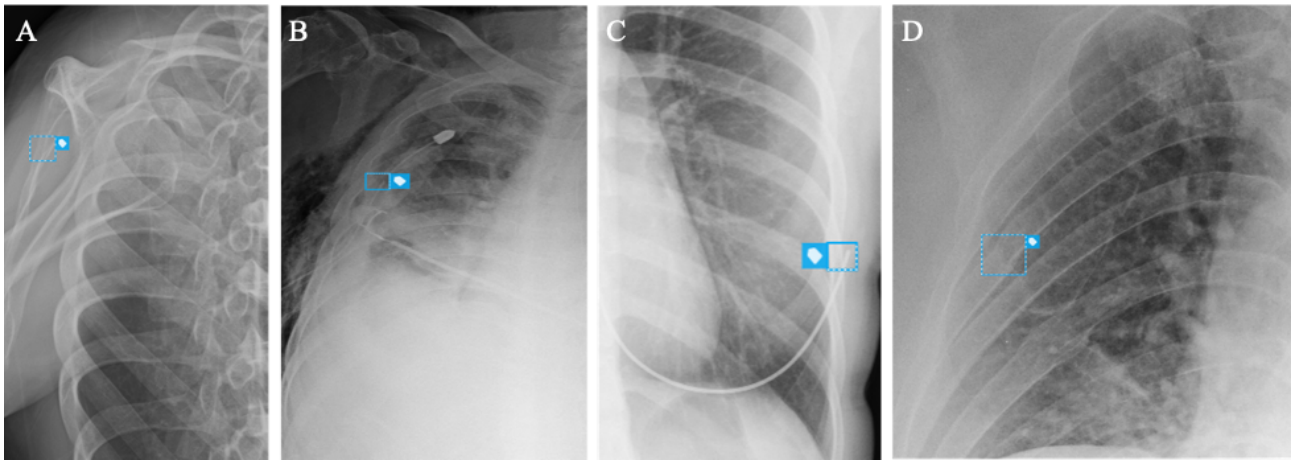

This targeted CT adjudication underscores the potential of AI-assisted screening to augment clinical vigilance by identifying subtle or overlooked fractures, while also emphasizing the need to improve artifact robustness and optimize false-positive suppression for practical clinical integration.

Common Pitfalls in Frontline Rib Fracture Detection

Our review of discordant cases identified 3 principal drivers of missed rib fractures by emergency physicians: first, non-thoracic presenting complaints (eg, catheter malfunction or abdominal pain) led interpreters to focus on unrelated findings and overlook subtle rib breaks; second, the absence of classic chest pain—patients describing only mild discomfort or a vague “pop”—lowered clinical vigilance for nondisplaced fractures; and third, competing urgent injuries (facial, limb, or soft-tissue

XSL•FO
RenderX

trauma) diverted attention from the chest, resulting in underappreciated fractures.

Discussion

Principal Findings

In this observational feasibility study using real-world emergency department imaging data, we demonstrated that a faster R-CNN–based AI system can operate in parallel with routine clinical workflows to provide near-instantaneous rib fracture triage without influencing patient care. During a 3-month evaluation period, the model automatically processed 23,251 CXRs with a median inference time of 10.6 seconds per image, achieving a turnaround time reduction exceeding 3 orders of magnitude compared with formal radiologist reporting, while maintaining 74.5% sensitivity and 93.3% specificity. These findings position AI as a potential automated screening aid capable of rapidly identifying low-risk examinations and generating signals that could inform future prioritization strategies. The observed discrepancy between the 10.6-second AI inference time and the 3.3-hour radiologist turnaround time reflects a critical clinical bottleneck in busy emergency departments. Although these metrics represent different stages—technical processing versus final clinical documentation—the delay in official reporting highlights the diagnostic gap AI aims to address. In this context, near-instantaneous AI alerts may support case prioritization before formal reporting, although no clinician-facing alerts were implemented in this study.

However, the current findings primarily demonstrate technical feasibility rather than full clinical feasibility, as the AI system operated passively without direct clinician interaction. Future clinician-in-the-loop evaluations will be necessary to assess workflow integration, usability, and impact on diagnostic behavior or patient outcomes.

Although the system's positive predictive value was relatively low (24.2%), this trade-off aligns with its design as a triage support tool rather than a stand-alone diagnostic system. In high-volume emergency departments, the ability to rapidly identify examinations with a low likelihood of fracture is crucial. The model's high NPV of 99.2% allows clinicians to focus on a smaller, higher-risk subset of cases, thereby improving efficiency and reducing cognitive load. Given the observed sensitivity of 74.5%, false-negative cases remain possible, and the system should not be used as a stand-alone rule-out mechanism or as a substitute for clinical judgment.

Comparison to Prior Work

Similar findings have been reported by Yao et al [20], who demonstrated that deep learning systems with high NPV on chest CT can reduce radiologists' workload by effectively identifying nonfracture cases. A recent systematic review by van den Broek et al [21] further emphasized the triage value of AI in fracture detection, underscoring its potential across multiple imaging modalities.

Our AI system also demonstrated robust performance across circadian and weekly imaging surges, with peak volumes observed between 08:00 and 16:00 and during Thursday to Saturday evenings. However, a 14-day GPU hardware outage during the study period highlighted a real-world challenge of maintaining the AI system's reliability in clinical environments. This incident underscores the need for infrastructure redundancy, real-time monitoring, and failover protocols—key considerations for sustainable AI deployment. These practical aspects of AI deployment remain underreported in most published studies [22].

Compared with prior approaches such as the PACS-AI platform [23], our system offered full automation, operating continuously in real time and without the need for manual image selection. This better reflects the demands of frontline emergency radiology. Herpe et al [24] demonstrated improved diagnostic accuracy with PACS-integrated AI for limb fractures; however, their study did not evaluate scalability or autonomous triage capability under high-throughput conditions. In contrast, our study incorporated prospective data collection within a real-world emergency department workflow, allowing the assessment of AI performance, reliability, and operational feasibility under authentic clinical conditions.

Focused adjudication of discordant cases revealed that the AI system correctly identified rib fractures that were missed by both radiologists and emergency physicians in 7 cases, all subsequently confirmed on follow-up CT ("AI-CT concordant"). These findings highlight the potential of AI to strengthen diagnostic vigilance in complex clinical scenarios. While prior studies—such as Zhou et al [25]—have shown that AI can detect rib fractures overlooked in initial CT interpretations, with confirmation on follow-up imaging, these investigations have largely centered on CT-based workflows. Although CT is highly sensitive, its routine use is limited by concerns over radiation, cost, and logistics. In contrast, our CXR-focused approach targets the most widely used imaging modality in acute care, offering a more scalable and practical solution for real-world emergency triage. Notably, Brady et al [26] have emphasized that diagnostic errors and discrepancies are not uncommon in radiology, with daily error rates estimated at 3% - 5%, reinforcing the importance of AI as a complementary tool to enhance diagnostic accuracy.

Four false-positive cases revealed predictable pitfalls, including the misinterpretation of scapular margins, chest-tube hardware, and motion artifacts. Similar findings were reported by Sun et al [27], who noted frequent false positives in an AI model for rib fracture detection on CXR, often due to anatomical overlap and imaging artifacts. These results support the need for artifact-aware retraining and preprocessing optimization to reduce false alerts and improve clinical integration.

This targeted CT adjudication further highlights the complementary role of AI in identifying subtle or overlooked fractures and underscores the inherent limitation of using report-based labels as the reference standard in real-world studies.

Future Directions

In addition, integrating AI-generated alerts into emergency radiology workflows will require careful calibration of alert thresholds to minimize false positives and prevent alert fatigue

XSL•FO
RenderX

among clinicians. Human-centered design, interface refinement, and iterative feedback from end users will be critical to achieving effective and sustainable adoption.

While most prior prospective studies have emphasized diagnostic performance or radiologist feedback, our findings extend beyond these metrics to include diagnostic efficacy, operational resilience, and system failure contingencies. These real-world insights support the feasibility and clinical value of embedding AI into routine emergency department workflows. Recent work has highlighted the importance of not only measuring accuracy but also assessing robustness across patient and workflow variability [28]. Furthermore, the need for deployment frameworks that address hardware resilience, continuous quality monitoring, and interpretability safeguards is increasingly recognized as essential for sustainable AI adoption in high-acuity settings [29].

Recent reports and position statements have highlighted a persistent gap between the promising diagnostic performance of AI systems and their limited demonstrated clinical benefit. Robust, prospective, and randomized clinical studies remain urgently needed to justify large-scale implementation [30,31]. Even high-performing AI models (area under the curve≈0.85) have failed to surpass standard clinical practice in improving patient outcomes [32,33]. These findings reinforce ongoing concerns that most AI or machine learning devices, despite regulatory authorization, are primarily validated using retrospective data and therefore remain susceptible to selection bias, distributional shift, and overestimation of generalizability [34,35].

Clinical decision-making in emergency care is inherently multimodal: physicians integrate imaging findings with the mechanism of injury, examination, and vital signs to guide judgment. In contrast, this AI system analyzes images in isolation and is designed not to replace but to support clinicians as a rapid screening aid—enhancing vigilance in high-volume, high-pressure environments where missed fractures may occur. Incorporating multimodal clinical data in future models could further improve diagnostic relevance and workflow integration.

Although this was an observational feasibility study, it represents one of the largest evaluations of an AI-assisted rib fracture detection system in real-world emergency radiology. The findings demonstrate that such a system can provide meaningful diagnostic support, maintain consistent performance at scale, and potentially enhance patient safety. Future implementation should therefore shift from technical to clinical feasibility, focusing on clinician-in-the-loop impact studies, PACS-integrated trials, and workflow efficiency assessments. Although user perception was not formally assessed, informal feedback from emergency physicians indicated strong interest in AI-supported flagging—particularly for subtle fractures and during periods of high patient volume.

Future research should prioritize prospective, multicenter studies to validate generalizability and quantify AI impact on workflow, resource utilization, and patient outcomes. Model improvements—including artifact-aware retraining, expanded fracture coverage in challenging scenarios such as subtle or anatomically obscured fractures, and continuous learning—will be critical to enhance diagnostic precision. Finally, building infrastructure resilience and integrating effective alert management into radiologist workflows are essential for sustainable clinical adoption.

Limitations

First, this single-center observational study may limit generalizability to other institutions with different imaging protocols, patient populations, or workflow environments. Second, during retrospective model development, training and validation were performed at the image level rather than the patient level. This may have resulted in optimistic internal validation estimates due to potential within-patient similarity, which likely contributes to the observed performance gap between retrospective validation and prospective real-world deployment. Additionally, stratified performance analyses by age group and sex were not performed due to the low prevalence of rib fractures in certain subgroups, particularly pediatric patients. Similarly, the small fraction of oblique views (approximately 1.3%) prevented a dedicated analysis by imaging view, as the limited sample size would yield unstable estimates for these specific cohorts.

The prospective evaluation period also did not include winter months. Seasonal variation in trauma mechanisms or imaging artifacts may influence fracture detectability in certain settings; therefore, caution is warranted when generalizing these findings across different seasonal contexts.

Additionally, the use of a 512×512 resolution for model inference represents a technical trade-off; while it facilitates rapid processing, the associated downsampling may limit the detection of very subtle cortical disruptions.

Third, using radiology reports as the reference standard—while pragmatic—may underestimate the AI system's true performance, as subtle or occult fractures can be underreported in clinical practice. A focused CT review of representative discordant cases further supported this concern, revealing instances where AI-predicted fractures were subsequently confirmed as true fractures on CT. This approach likely yielded conservative performance estimates, since NLP-derived labels may not capture subtle fractures identified by AI or CT.

Regarding the study design, although post hoc adjudication is generally more appropriate for hypothesis generation than for definitive performance reassessment, modifying the reference standard after study completion may introduce bias. Accordingly, in this study, performance evaluation was anchored to the contemporaneous clinical reference standard used in routine practice. More comprehensive adjudication strategies—such as consensus radiologist review of AI-positive, report-negative cases—may provide additional insights when implemented within a separately designed study.

Finally, because AI predictions were not disclosed to clinicians, we did not assess downstream clinical outcomes, including changes in diagnostic behavior, time to intervention, or patient management. As for the data pipeline, although we used NLP to extract rib fracture labels from radiology reports, which may introduce misclassification in ambiguous cases, the pipeline demonstrated high agreement with manual review (κ=0.91).

XSL•FO
RenderX

Given the observed 3.5% discrepancy rate, any residual label noise propagating through the large-scale dataset may introduce modest uncertainty into performance estimates. However, the substantial sample size (n=23,251) is expected to attenuate the impact of such noise, supporting the stability of the resulting confidence intervals for large-scale clinical benchmarking.

Conclusions

In this observational feasibility study, we evaluated a faster R-CNN–based AI system deployed in parallel with clinical workflows to automatically detect rib fractures on CXRs using real-world emergency department data. Although AI outputs were not visible to clinicians, the system processed over 23,000 studies with high throughput, achieving 74.5% sensitivity and 93.3% specificity and delivering results within seconds—over 1000 times faster than formal radiologist reports.

These findings demonstrate strong technical feasibility of real-time AI-assisted rib fracture detection in emergency radiology. While clinical decisions remained unaffected during this observational phase, future studies should validate clinical feasibility through clinician-in-the-loop evaluation, PACS integration, and workflow optimization to address potential alert fatigue and false-positive management.

Acknowledgments

We thank the emergency department, radiology department, and information technology teams for their support during system deployment and data extraction. Generative artificial intelligence tools were used solely for language editing and grammar checking. All scientific content, analyses, interpretations, and conclusions were developed by the authors. The artificial intelligence system evaluated in this study was deployed on the DeepQ AI platform as a technical deployment environment. The authors have no financial, employment, or equity relationship with DeepQ Technology or HTC, and the platform was used solely for noncommercial research purposes.

Funding

This research was financially supported by National Science and Technology Council, Taiwan, under Grant No. NSTC113-2221-E-038 - 006

Data Availability

The imaging data analyzed in this study are not publicly available due to institutional regulations and patient privacy protections. Deidentified data may be made available from the corresponding author upon reasonable request and subject to institutional review board approval.

Authors' Contributions

Conceptualization: H-WC, S-TH
Methodology: H-WC, S-TH
Data curation: M-YH, S-TH
Formal analysis: M-YH, S-TH
Investigation: M-YH, S-TH
Writing – original draft: M-YH, S-TH
Writing – review & editing: H-WC, L-RL, M-FT, M-YH, S-TH
Supervision: CH-W

Conflicts of Interest

None declared.

Checklist 1
CLAIM (Checklist for Artificial Intelligence in Medical Imaging).
[PDF File, 3 KB - medinform_v14i1e77965_app1.pdf]

References

1. Tignanelli CJ, Rix A, Napolitano LM, Hemmila MR, Ma S, Kummerfeld E. Association between adherence to evidence-based practices for treatment of patients with traumatic rib fractures and mortality rates among US trauma centers. JAMA Netw Open 2020 Mar 2;3(3):e201316. [doi: 10.1001/jamanetworkopen.2020.1316] [Medline: 32215632]
2. Colling KP, Goettl T, Harry ML. Outcomes after rib fractures: more complex than a single number. J Trauma Inj 2022 Dec;35(4):268-276. [doi: 10.20408/jti.2021.0096] [Medline: 39380934]
3. Sharma OP, Oswanski MF, Jolly S, Lauer SK, Dressel R, Stombaugh HA. Perils of rib fractures. Am Surg 2008 Apr;74(4):310-314. [doi: 10.1177/000313480807400406] [Medline: 18453294]

XSL•FO
RenderX

4. Griffith JF, Rainer TH, Ching AS, Law KL, Cocks RA, Metreweli C. Sonography compared with radiography in revealing acute rib fracture. AJR Am J Roentgenol 1999 Dec;173(6):1603-1609. [doi: 10.2214/ajr.173.6.10584808] [Medline: 10584808]
5. Tomas X, Facenda C, Vaz N, et al. Thoracic wall trauma-misdiagnosed lesions on radiographs and usefulness of ultrasound, multidetector computed tomography and magnetic resonance imaging. Quant Imaging Med Surg 2017 Aug;7(4):384-397. [doi: 10.21037/qims.2017.08.02] [Medline: 28932697]
6. Chapman BC, Overbey DM, Tesfalidet F, et al. Clinical utility of chest computed tomography in patients with rib fractures CT chest and rib fractures. Arch Trauma Res 2016 Dec;5(4):e37070. [doi: 10.5812/atr.37070] [Medline: 28144607]
7. Huang ST, Liu LR, Chiu HW, Huang MY, Tsai MF. Deep convolutional neural network for rib fracture recognition on chest radiographs. Front Med 2023;10. [doi: 10.3389/fmed.2023.1178798]
8. Pishbin E, Ahmadi K, Foogardi M, Salehi M, Seilanian Toosi F, Rahimi-Movaghar V. Comparison of ultrasonography and radiography in diagnosis of rib fractures. Chin J Traumatol 2017 Aug;20(4):226-228. [doi: 10.1016/j.cjtee.2016.04.010] [Medline: 28687342]
9. Gulshan V, Peng L, Coram M, et al. Development and validation of a deep learning algorithm for detection of diabetic retinopathy in retinal fundus photographs. JAMA 2016 Dec 13;316(22):2402-2410. [doi: 10.1001/jama.2016.17216] [Medline: 27898976]
10. Rajpurkar P, Irvin J, Zhu K, et al. CheXNet: radiologist-level pneumonia detection on chest x-rays with deep learning. arXiv. Preprint posted online on Nov 14, 2017. [doi: 10.48550/arXiv.1711.05225]
11. Esteva A, Kuprel B, Novoa RA, et al. Dermatologist-level classification of skin cancer with deep neural networks. Nature 2017 Feb 2;542(7639):115-118. [doi: 10.1038/nature21056] [Medline: 28117445]
12. Litjens G, Kooi T, Bejnordi BE, et al. A survey on deep learning in medical image analysis. Med Image Anal 2017 Dec;42:60-88. [doi: 10.1016/j.media.2017.07.005] [Medline: 28778026]
13. Lundervold AS, Lundervold A. An overview of deep learning in medical imaging focusing on MRI. Z Med Phys 2019 May;29(2):102-127. [doi: 10.1016/j.zemedi.2018.11.002] [Medline: 30553609]
14. Kora P, Ooi CP, Faust O, et al. Transfer learning techniques for medical image analysis: a review. Biocybern Biomed Eng 2022 Jan;42(1):79-107. [doi: 10.1016/j.bbe.2021.11.004]
15. Olczak J, Fahlberg N, Maki A, et al. Artificial intelligence for analyzing orthopedic trauma radiographs. Acta Orthop 2017 Dec;88(6):581-586. [doi: 10.1080/17453674.2017.1344459] [Medline: 28681679]
16. Wu J, Liu N, Li X, et al. Convolutional neural network for detecting rib fractures on chest radiographs: a feasibility study. BMC Med Imaging 2023 Jan 30;23(1):18. [doi: 10.1186/s12880-023-00975-x] [Medline: 36717773]
17. Lee K, Lee S, Kwak JS, Park H, Oh H, Koh JC. Development and validation of an artificial intelligence model for detecting rib fractures on chest radiographs. J Clin Med 2024 Jun 30;13(13):3850. [doi: 10.3390/jcm13133850] [Medline: 38999416]
18. Chang EY. DeepQ: advancing healthcare through artificial intelligence and virtual reality. Presented at: MM '17: Proceedings of the 25th ACM international conference on Multimedia New York; Oct 23-27, 2017. [doi: 10.1145/3123266.3130875]
19. Ren S, He K, Girshick R, Sun J. Faster R-CNN: towards real-time object detection with region proposal networks. arXiv. Preprint posted online on Jun 4, 2015. [doi: 10.48550/arXiv.1506.01497]
20. Yao L, Guan X, Song X, et al. Rib fracture detection system based on deep learning. Sci Rep 2021 Dec 6;11(1):23513. [doi: 10.1038/s41598-021-03002-7] [Medline: 34873241]
21. van den Broek MCL, Buijs JH, Schmitz LFM, Wijffels MME. Diagnostic performance of artificial intelligence in rib fracture detection: systematic review and meta-analysis. Surgeries 2024;5(1):24-36. [doi: 10.3390/surgeries5010005]
22. Kelly CJ, Karthikesalingam A, Suleyman M, Corrado G, King D. Key challenges for delivering clinical impact with artificial intelligence. BMC Med 2019 Oct 29;17(1):195. [doi: 10.1186/s12916-019-1426-2] [Medline: 31665002]
23. Theriault-Lauzier P, Cobin D, Tastet O, et al. A responsible framework for applying artificial intelligence on medical images and signals at the point of care: the PACS-AI platform. Can J Cardiol 2024 Oct;40(10):1828-1840. [doi: 10.1016/j.cjca.2024.05.025] [Medline: 38885787]
24. Herpe G, Nelken H, Vendeuvre T, et al. Effectiveness of an artificial intelligence software for limb radiographic fracture recognition in an emergency department. J Clin Med 2024 Sep 20;13(18):5575. [doi: 10.3390/jcm13185575] [Medline: 39337062]
25. Zhou Q, Qin P, Luo J, et al. Evaluating AI rib fracture detections using follow-up CT scans. Am J Emerg Med 2023 Oct;72:34-38. [doi: 10.1016/j.ajem.2023.07.018] [Medline: 37478635]
26. Brady AP. Error and discrepancy in radiology: inevitable or avoidable? Insights Imaging 2017 Feb;8(1):171-182. [doi: 10.1007/s13244-016-0534-1] [Medline: 27928712]
27. Sun H, Wang X, Li Z, et al. Automated rib fracture detection on chest X-ray using contrastive learning. J Digit Imaging 2023 Oct;36(5):2138-2147. [doi: 10.1007/s10278-023-00868-z] [Medline: 37407842]
28. Hong WS, Haimovich AD, Taylor RA. Predicting hospital admission at emergency department triage using machine learning. PLoS ONE 2018;13(7):e0201016. [doi: 10.1371/journal.pone.0201016] [Medline: 30028888]
29. Moskalenko V, Kharchenko V. Resilience-aware MLOps for AI-based medical diagnostic system. Front Public Health 2024;12:1342937. [doi: 10.3389/fpubh.2024.1342937] [Medline: 38601490]

XSL•FO
RenderX

30. Khera R, Butte AJ, Berkwits M, et al. AI in medicine-JAMA's focus on clinical outcomes, patient-centered care, quality, and equity. JAMA 2023 Sep 5;330(9):818-820. [doi: 10.1001/jama.2023.15481] [Medline: 37566406]
31. Armoundas AA, Narayan SM, Arnett DK, et al. Use of artificial intelligence in improving outcomes in heart disease: a scientific statement from the American Heart Association. Circulation 2024 Apr 2;149(14):e1028-e1050. [doi: 10.1161/CIR.0000000000001201] [Medline: 38415358]
32. Mazor T, Farhat KS, Trukhanov P, et al. Clinical trial notifications triggered by artificial intelligence-detected cancer progression: a randomized trial. JAMA Netw Open 2025 Apr 1;8(4):e252013. [doi: 10.1001/jamanetworkopen.2025.2013] [Medline: 40257799]
33. Mandair D, Elia MV, Hong JC. Considerations in translating AI to improve care. JAMA Netw Open 2025 Apr 1;8(4):e252023. [doi: 10.1001/jamanetworkopen.2025.2023] [Medline: 40257804]
34. Habib AR, Gross CP. FDA regulations of AI-driven clinical decision support devices fall short. JAMA Intern Med 2023 Dec 1;183(12):1401-1402. [doi: 10.1001/jamainternmed.2023.5006] [Medline: 37812411]
35. Chouffani El Fassi S, Abdullah A, Fang Y, et al. Not all AI health tools with regulatory authorization are clinically validated. Nat Med 2024 Oct;30(10):2718-2720. [doi: 10.1038/s41591-024-03203-3] [Medline: 39187696]

Abbreviations

AI: artificial intelligence
AP: anteroposterior
CLAIM: Checklist for Artificial Intelligence in Medical Imaging
CT: computed tomography
CXR: chest radiograph
FROC: free-response receiver operating characteristic
GPU: graphics processing unit
NLP: natural language processing
NPV: negative predictive value
PACS: picture archiving and communication system
R-CNN: region-based convolutional neural network

Edited by A Coristine, A Benis; submitted 22.May.2025; peer-reviewed by D Yoo, E Bai, J Zhang; revised version received 30.Dec.2025; accepted 01.Jan.2026; published 29.Jan.2026.

Please cite as:
Huang ST, Liu LR, Tsai MF, Huang MY, Chiu HW
Prospective Diagnostic Accuracy and Technical Feasibility of Artificial Intelligence-Assisted Rib Fracture Detection on Chest Radiographs: Observational Study
JMIR Med Inform 2026;14:e77965
URL: https://medinform.jmir.org/2026/1/e77965
doi:10.2196/77965

© Shu-Tien Huang, Liong-Rung Liu, Ming-Feng Tsai, Ming-Yuan Huang, Hung-Wen Chiu. Originally published in JMIR Medical Informatics (https://medinform.jmir.org), 29.Jan.2026. This is an open-access article distributed under the terms of the Creative Commons Attribution License (https://creativecommons.org/licenses/by/4.0/), which permits unrestricted use, distribution, and reproduction in any medium, provided the original work, first published in JMIR Medical Informatics, is properly cited. The complete bibliographic information, a link to the original publication on https://medinform.jmir.org/, as well as this copyright and license information must be included.

XSL•FO
RenderX

Machine Learning Prediction of Pharmacogenetic Testing Uptake Among Opioid-Prescribed Patients Using Electronic Health Records: Retrospective Cohort Study

Mohammad Yaseliani[1], MSc; Je-Won Hong[2], PharmD; Jiang Bian[3,4], MS, PhD; Larisa Cavallari[2,5], PharmD; Julio D Duarte[2,5], PharmD, PhD; Danielle Nelson[6], MPH, MD; Wei-Hsuan Lo-Ciganic[7,8,9], MSPharm, MS, PhD; Khoa Anh Nguyen[2*], PharmD; Md Mahmudul Hasan[1,10*], PhD

[1]Department of Pharmaceutical Outcomes and Policy, College of Pharmacy, University of Florida, 1889 Museum Road, Malachowsky Hall, Suite 6300, Gainesville, FL, United States

[10]Department of Information Systems and Operations Management, Warrington College of Business, University of Florida, Gainesville, FL, United States

[2]Department of Pharmacotherapy and Translational Research, College of Pharmacy, University of Florida, Gainesville, FL, United States

[3]Department of Biostatistics and Health Data Science, School of Medicine, Indiana University, Indianapolis, IN, United States

[4]Center for Biomedical Informatics, Regenstrief Institute, Indianapolis, IN, United States

[5]Center for Pharmacogenomics and Precision Medicine, University of Florida, Gainesville, FL, United States

[6]College of Medicine, University of Florida, Gainesville, FL, United States

[7]Division of General Internal Medicine, School of Medicine, University of Pittsburgh, Pittsburgh, PA, United States

[8]Center for Pharmaceutical Policy and Prescribing, University of Pittsburgh, Pittsburgh, PA, United States

[9]Geriatric Research Education and Clinical Center, North Florida/South Georgia Veterans Health System, Gainesville, FL, United States

[*]these authors contributed equally

Corresponding Author:
Md Mahmudul Hasan, PhD
Department of Pharmaceutical Outcomes and Policy, College of Pharmacy, University of Florida, 1889 Museum Road, Malachowsky Hall, Suite 6300, Gainesville, FL, United States

Abstract

Background: Opioids are a widely prescribed class of medication for pain management. However, they have variable efficacy and adverse effects among patients, due to the complex interplay between biological and clinical factors. Pharmacogenetic testing can be used to match patients' genetic profiles to individualize opioid therapy, improving pain relief and reducing the risk of adverse effects. Despite its potential, the pharmacogenetic testing uptake (use of pharmacogenetic testing) remains low due to a range of barriers at the patient, health care provider, infrastructure, and financial levels. Since testing typically involves a shared decision between the provider and patient, predicting the likelihood of a patient undergoing pharmacogenetic testing and understanding the factors influencing that decision can help optimize resource use and improve outcomes in pain management.

Objective: This study aimed to develop machine learning (ML) models, identifying patients' likelihood of pharmacogenetic uptake based on their demographics, clinical variables, medication use, and social determinants of health.

Methods: We used electronic health record data from a single center health care system to identify patients prescribed opioids. We extracted patients' demographics, clinical variables, medication use, and social determinants of health, and developed and validated ML models, including a neural network, logistic regression, random forest, extreme gradient boosting (XGB), naïve Bayes, and support vector machines for pharmacogenetic testing uptake prediction based on procedure codes. We performed 5-fold cross-validation and created an ensemble probability-based classifier using the best-performing ML models for pharmacogenetic testing uptake prediction. Various performance metrics, uptake stratification analysis, and feature importance analysis were used to evaluate the performance of the models.

Results: The ensemble model using XGB and support vector machine–radial basis function classifiers had the highest *C*-statistics at 79.61%, followed by XGB (78.94%), and neural network (78.05%). While XGB was the best-performing model, the ensemble model achieved a high accuracy (32,699/48,528, 67.38%), recall (537/702, 76.50%), specificity (32,162/47,826, 67.25%), and negative predictive value (32,162/32,327, 99.49%). The uptake stratification analysis using the ensemble model indicated that it can effectively distinguish across uptake probability deciles, where those in the higher strata are more likely to undergo pharmacogenetic testing in the real world (320/4853, 6.59% in the highest decile compared to 6/4853, 0.12% in the lowest).

XSL•FO
RenderX

Furthermore, Shapley Additive Explanations value analysis using the XGB model indicated age, hypertension, and household income as the most influential factors for pharmacogenetic testing uptake prediction.

Conclusions: The proposed ensemble model demonstrated a high performance in pharmacogenetic testing uptake prediction among patients using opioids for pain. This model can be used as a decision support tool, assisting clinicians in identifying patients' likelihood of pharmacogenetic testing uptake and guiding appropriate decision-making.

(JMIR Med Inform 2026;14:e81048) doi:10.2196/81048

KEYWORDS

ensemble model; ML; machine learning; opioids; opioid prescription; pain management; pharmacogenetic testing

Introduction

Opioid prescribing presents a complex therapeutic challenge due to variable efficacy and the risk of adverse effects, often resulting in a trial and error approach for prescription. These variations in opioid response often arise from interindividual differences in pharmacokinetics and pharmacodynamics, influenced in part by genetic variations [1]. Over recent decades, pharmacogenetic testing has emerged as a promising strategy to tailor opioid therapy to an individual genetic profile, with the goal of enhancing pain relief, minimizing adverse effects, and improving overall patient outcomes. Several opioids, including codeine, tramadol, hydrocodone, and oxycodone, are metabolized to varying extents by cytochrome P450 family 2 subfamily D member 6 (CYP2D6), which is an enzyme involved in the metabolism of many drugs [2]. A pragmatic trial demonstrated improved composite pain intensity outcomes with CYP2D6-guided pain management, highlighting the potential benefits of personalized therapy based on pharmacogenetic testing [2]. Based on the current evidence, the Clinical Pharmacogenetics Implementation Consortium (CPIC) provides guidelines on using CYP2D6 genotype results for prescribing tramadol, hydrocodone, and codeine [2]2 yet their real-world impact depends on whether patients offered pharmacogenetic testing actually complete it. In opioid prescribing contexts, uptake hinges on perceived use and timing, out-of-pocket costs, health literacy, trust, social context, and clinician offering practices, as well as workflow constraints that differ across acute, perioperative, and chronic pain settings.

Electronic health records (EHRs) contain rich information relevant to testing acceptance: prior and current opioid exposures, pain diagnoses, comorbidity burden, care setting, prescriber specialty, monitoring and follow-up patterns, previous laboratory or genetic testing, and engagement with the health system. Machine learning (ML) such as neural network (NN), random forest (RF), and logistic regression (LR) can synthesize these heterogeneous and high-dimensional features [3] to produce calibrated, patient-level probability estimates of pharmacogenetic testing uptake at the moment testing is offered. Such predictions could help health systems, including patient care teams and insurers, tailor communication (eg, language, framing, and channel), select appropriate clinical checkpoints (such as before initiating certain opioids or at dose escalation), and allocate resources where they are most likely to improve test uptake without adding unnecessary burden. These predictions may be especially valuable for patients who are expected to benefit most from testing (though this was not the focus of this study), enabling patient care teams to dedicate additional resources to support uptake in this population.

Prior work has developed ML predictive models to support uptake for vaccines [4], cancer screening [5], and genetic counseling [6]; however, pharmacogenetics-specific models for opioid-related testing are scarce, and few studies evaluate calibration, clinical use, fairness, and workflow integration together. In this study, we aimed to predict the likelihood that patients receiving opioid prescriptions will undergo pharmacogenetic testing after an offer in routine care. We hypothesized that ML models could accurately predict the likelihood of pharmacogenetic testing uptake among opioid-prescribed patients by identifying patterns in demographic, clinical, and health care use factors associated with testing behavior under current practice conditions. Our objectives were to achieve strong discrimination and predictive performance of the ML models, and reliable model calibration through patients' stratification in subgroups based on the predicted probability of test uptake. We emphasized model explainability to support clinician understanding and sought to identify factors influencing the likelihood of pharmacogenetic testing uptake in opioid therapy. Ultimately, we aimed to complement, rather than replace, clinical judgment, potentially facilitating better use of pharmacogenetic testing for precision pain management. By focusing on actionable predictions at the point of offer, this paper may help programs deliver the right message through the right channel at the right time: improving test uptake, informing safer opioid prescribing, and advancing equitable delivery of pharmacogenetic testing.

Methods

Overview

The overall ML pipeline for pharmacogenetic testing uptake prediction is shown in Figure 1. The pipeline involves 4 steps, including study design, data preprocessing and feature selection, model development, and comprehensive evaluation. Each step involves several tasks that are critical to building and evaluating the final predictive model. The details of each step are described in this section.

XSL•FO
RenderX

Figure 1. Overall machine learning pipeline for pharmacogenetic testing uptake prediction. CPIC: Clinical Pharmacogenetics Implementation Consortium; ROC: receiver operating characteristic; SDoH: social determinants of health; SHAP: Shapley Additive Explanations; SVM: support vector machine; SVM-RBF: support vector machine–radial basis function; XGBoost: extreme gradient boosting.

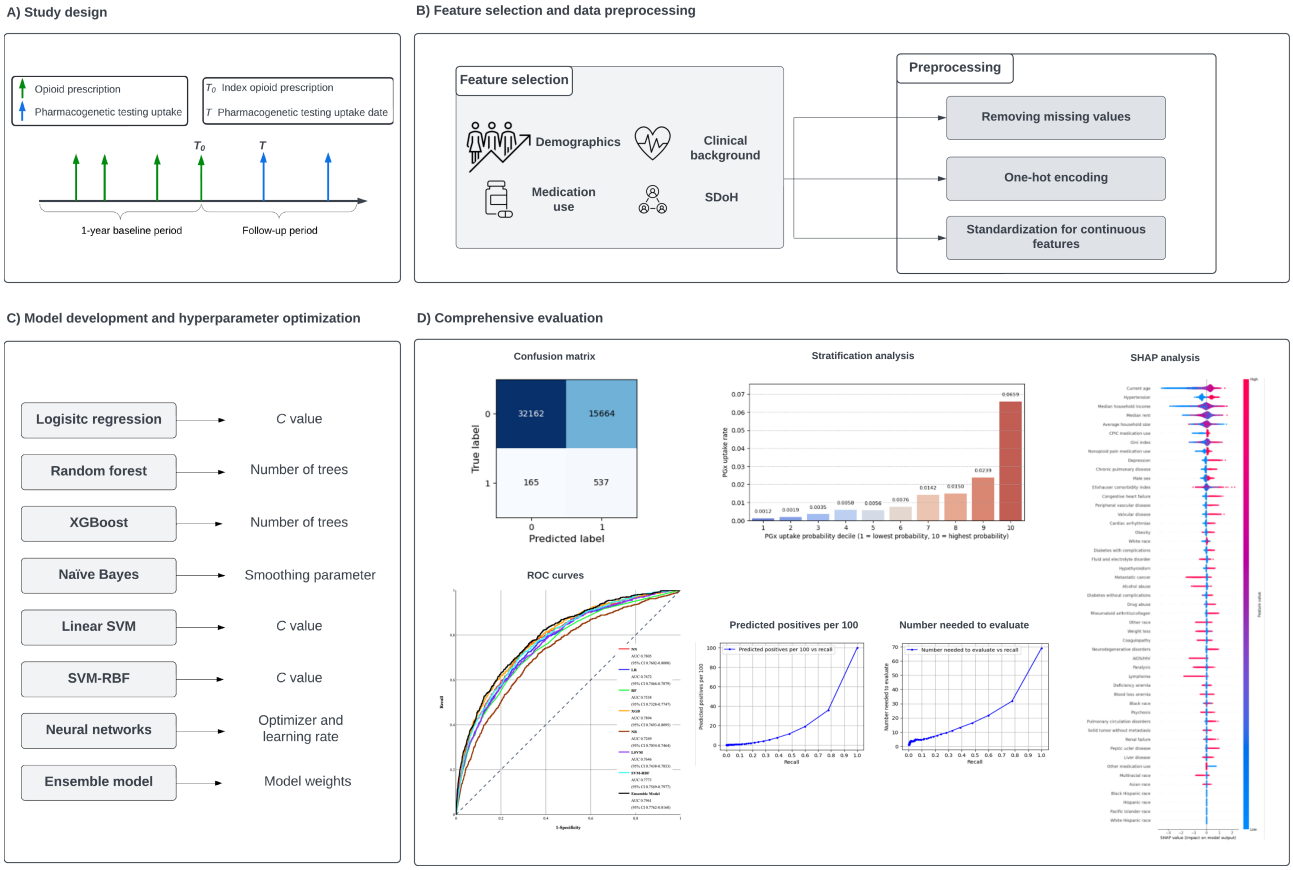

Ethical Considerations

We used real-world deidentified EHR data available from the University of Florida Health Integrated Data Repository (IDR) to develop the models. These data included information on patients' demographics, clinical variables, and medication use from 2011 to 2023. The study was conducted in compliance with ethical standards and was approved by the University of Florida Institutional Review Board under the reference number IRB202301927. This study is a secondary analysis of existing deidentified EHR data, and the approved IRB covers secondary analyses without additional consent. Therefore, no informed consent was obtained.

Study Design

Patients' age range was 1 to 89 years, and we did not exclude any patients based on age. Patients were included if they were aged between 18 and 89 years and had an opioid prescription order for noncancer treatment from 2011 to 2023. Patients were stratified into an intervention group (patients with a minimum of one pharmacogenetic testing order) and a control group (those with no history of pharmacogenetic testing order). We used current procedural terminology codes to determine patients' pharmacogenetic testing. To create the cohort for ML model development, we defined the index dates separately for intervention and control groups. The index date for the intervention group was defined as the most recent date of an opioid prescription prior to pharmacogenetic testing. The index date for the control group was defined as the earliest date of opioid prescription. All baseline covariates were collected in the 1-year period prior to the index date. The outcome was a binary target variable, indicating whether the patient was in the intervention or control group based on their pharmacogenetic testing record. If a patient was in the intervention group, their outcome value was encoded as 1 and otherwise 0.

Feature Selection and Data Preprocessing

We selected four different categories of features for our study sample: (1) demographics, (2) clinical history, (3) medication use, and (4) social determinants of health (SDoH). Demographics included age, sex, and race, where age was continuous, sex was binary, and race was multicategory which was one-hot-encoded to get separate binary inputs for each racial group and prevent the ordinality assumption by the model. We used the *International Classification of Diseases, Ninth Revision* (*ICD-9*) and *International Classification of Diseases, Tenth Revision* (*ICD-10*) codes to determine the clinical history variables, including a diagnosis of AIDS/HIV, alcohol abuse, blood loss anemia, cardiac arrhythmias, chronic pulmonary disease, coagulopathy, systolic (congestive) heart failure, deficiency anemia, depression, diabetes with complications, diabetes without complications, drug abuse, fluid and electrolyte disorder, hypertension, hypothyroidism, liver disease, lymphoma, metastatic cancer, neurodegenerative disorders, obesity, paralysis, peptic ulcer disease, peripheral vascular disease, psychosis, pulmonary circulation disorders, renal failure, rheumatoid arthritis or collagen, solid tumor without metastasis, valvular disease, and weight loss. Furthermore, we

XSL•FO
RenderX

included the Elixhauser comorbidity index [7] to calculate the overall health care burden for each patient. In addition, the SDoH information included the average household size, Gini index as a measure of income inequality, median household income, and median gross rent, all linked to the University of Florida Health EHR based on year and ZIP code using the Agency for Healthcare Research and Quality SDoH database [8]. We removed all the missing data, so all patients had complete information for model development.

Model Development and Hyperparameter Optimization

We adopted a comprehensive strategy for model development using LR, extreme gradient boosting (XGB) [9], RF [10], support vector machine (SVM) [11] with linear and radial basis function (RBF) kernels (ie, linear support vector machine [LSVM] and SVM-RBF), and NN to capture predictive performance across a wide range of models for pharmacogenetic testing uptake prediction. LR was first developed due to its ability to capture linear relationships in the data and providing baseline performance. Similarly, the naïve Bayes (NB) model was developed due to its simplicity and effectiveness in high-dimensional spaces. However, considering LR's and NB's limitations in capturing complex nonlinear relationships, we trained tree-based models, including XGB and RF, given their ability to capture nonlinear interactions that may be critical to accurately predicting the pharmacogenetic testing uptake. LSVM and SVM-RBF were developed to capture high-dimensional complex interactions among input features. Finally, the NN was trained to explore more complex interactions among features that may be missed by traditional models.

To train the models, we randomly partitioned the data with a stratified 80/20 train/test split. To mitigate the risk of overfitting and get the best performance out of ML models, we conducted 5-fold cross-validation. For LR, we tuned the hyperparameter *C* with values of 0.01, 0.1, 1, and 10. To tune NB, we used smoothing parameters ranging from 10^{-9} to 10^{-5} with 10x increments. Both XGB and RF models were tuned with 100, 200, 300, 400, and 500 trees to explore the effect of different numbers of trees on performance. LSVM and SVM-RBF were optimized with *C* values equal to 0.01, 0.1, 1, and 10. Finally, NNs were trained with all possible combinations of various optimizers and learning rates. The optimizers included stochastic gradient descent [12], Adam [13], and Nadam [14], and learning rates ranged from 10^{-5} to 10^{-1} with 10x increases. The best hyperparameters were selected based on the highest area under the receiver operating characteristic curve (AUC) or *C*-statistics achieved on the training set during the cross-validation process.

We trained all the models using the best-performing hyperparameters and evaluated their performance on the test set. Notably, we used a balanced class weighting approach, assigning proportionally higher weights to the minority class, to decrease the risk of overfitting when training each of the models. As an additional analysis, we used the synthetic minority over-sampling technique (SMOTE) [15] with a 1:1 class ratio between minority and majority samples, creating a balanced dataset for model training and evaluation. To improve the performance and enhance generalizability of the models, we created a weighted probability-based ensemble classifier. We used a grid search optimization procedure, searching for the best combination of model weights, conditioned on having a total sum of weights equal to 1. The ensemble model achieving the highest AUC or *C*-statistics was selected as the final best model for pharmacogenetic testing uptake prediction.

Comprehensive Evaluation

We followed TRIPOD+AI (Transparent Reporting of a Multivariable Prediction Model for Individual Prognosis or Diagnosis + Artificial Intelligence) guidelines [16] to evaluate the performance of ML models. AUC or *C*-statistics demonstrates the discriminative ability of the model, considering the trade-off between sensitivity and specificity at different threshold values. DeLong test [17,18] is used to identify whether there is a statistically significant difference between AUC values. Accuracy provides the overall performance of the model by calculating the proportion of true negative and true positive cases compared to all the samples in the data. However, this measure may be misleading for rare events and not suitable for highly imbalanced datasets. To address this, we calculated specificity, which measures the model's ability to correctly identify true negative cases and recall or sensitivity, indicating the model's performance for identifying true positive cases. Since model performance may not be optimal, we used the Youden index [19-21] to obtain the best performing classification threshold for each model, where the highest value of "specificity+sensitivity-1" is achieved. To further evaluate model performance for real-world applications, we calculated the number needed to evaluate and predictive positives per 100 patients, showing how many predictions must be made to identify 1 actual positive case and the number of pharmacogenetic testing uptake predictions per 100 individuals, respectively. Moreover, we did stratification analysis, where pharmacogenetic testing uptake probabilities were categorized into 10 deciles in ascending order and the percentage of actual pharmacogenetic testing uptake in the data was identified in each decile to evaluate the ability of the model in identifying more uptakes in the higher strata. In addition, we used the Shapley Additive Explanations (SHAP) [22] analysis to report feature importance and identify the features that are most influential to pharmacogenetic testing uptake.

Results

Patient Characteristics

We used data from the University of Florida Health IDR with patients from a wide range of demographic and clinical backgrounds. The data included a total of 455,773 patients, 7645 (1.68%) with a recorded pharmacogenetic testing and 448,128 (98.32%) without. After removing 160,914 further patients who had no opioid prescription, there were 294,859 patients using opioids in the cohort. We further excluded patients with no race information and SDoH variables (after matching with the Agency for Healthcare Research and Quality database). Overall, the final cohort included 242,640 patients, where 3510 (1.45%) had a recorded pharmacogenetic testing uptake and 239,130 (98.55%) did not. The cohort had an average age of 58 (SD 17.47) years, a gender distribution comprising 41.49%

XSL•FO
RenderX

(100,670/242,640) as male participants and 58.51% (141,970/242,640) as female participants, and a racial distribution of 64.94% (157,567/242,640) White individuals, 28.77% (69,810/242,640) Black individuals, and 6.29% (15,263/242,640) belonging to other racial groups (ie, Hispanic, White Hispanic, Black Hispanic, Asian, Pacific Islander, American Indian, Multiracial, and other). In addition, the cohort had an average household size of 2.58 (SD 0.28), a Gini index of 0.45 (SD 0.05), and an average median income of US $46,324. Table 1 presents the key sociodemographic characteristics of patients in the cohort. Moreover, the distribution of patient characteristics in the training and test sets is provided in Table 2.

Table . Sociodemographic summary of patients.

Characteristics	Pharmacogenetic testing	Nonpharmacogenetic testing	*P* value[a]
Number of individuals, n (%)	3510 (1.45)	239,130 (98.55)	—[b]
Sex, n (%)			<.001
Male	1627 (46.35)	99,043 (41.42)	
Female	1883 (53.65)	140,087 (58.58)	
Race, n (%)			<.001
American Indian	12 (0.34)	346 (0.14)	
Asian	30 (0.85)	2345 (0.98)	
Black	1010 (28.77)	68,800 (28.77)	
Black Hispanic	0 (0.00)	1 (0.00)	
Hispanic	1 (0.03)	168 (0.07)	
Multiracial	13 (0.37)	1165 (0.49)	
Pacific Islander	0 (0.00)	109 (0.05)	
White	2346 (66.84)	155,221 (64.91)	
White Hispanic	0 (0.00)	45 (0.02)	
Other	98 (2.79)	10,930 (4.57)	
Age (y), mean (SD)	66.04 (12.99)	58.24 (17.51)	<.001
Average household size, mean (SD)	2.60 (0.27)	2.58 (0.28)	<.001
Gini index[c], mean (SD)	0.454 (0.051)	0.451 (0.052)	<.001
Median household income (US $), mean (SD)	46,093.44 (15,015.22)	46,328.29 (15,538)	.374
Median gross rent[d], mean (SD)	898.12 (213.45)	905.81 (223.60)	.034

[a]*P* values were calculated using a chi-square test for categorical variables and independent 2-tailed *t* test with equality of variance analysis for continuous variables.

[b]Not applicable.

[c]The Gini index ranges from 0 to 1, where 0 represents perfect equality and 1 represents perfect inequality.

[d]The median gross rent is per month in US $ and is based on rented cash-paid housing units.

XSL•FO
RenderX

Table . Distribution of patient characteristics in the training and test sets.

Characteristics	Training (n=194,112)	Testing (n=48,528)
Sex, n (%)		
Male	80,519 (41.48)	20,151 (41.52)
Female	113,593 (58.52)	28,377 (58.48)
Race, n (%)		
American Indian	273 (0.14)	85 (0.18)
Asian	1877 (0.97)	498 (1.03)
Black	55,993 (28.85)	13,817 (28.47)
Black Hispanic	1 (0.00)	0 (0.00)
Hispanic	128 (0.07)	41 (0.08)
Multiracial	919 (0.47)	259 (0.53)
Pacific Islander	89 (0.05)	20 (0.04)
White	125,938 (64.88)	31,629 (65.18)
White Hispanic	33 (0.02)	12 (0.02)
Other	8861 (4.56)	2167 (4.47)
Age, mean (SD)	58.36 (17.48)	58.32 (17.45)
Average household size, mean (SD)	2.58 (0.28)	2.58 (0.28)
Gini index, mean (SD)	0.45 (0.05)	0.45 (0.05)
Median household income (US $), mean (SD)	46,327.05 (15,529.07)	46,316.28 (15,536.70)
Median rent (US $), mean (SD)	905.64 (223.38)	905.92 (223.78)

Model Performance

The ROC curves of all models and their corresponding AUC or *C*-statistics with 95% CIs are provided in Figure 2. The ensemble model achieved the highest *C*-statistics of 79.61% using 0.7 and 0.3 weights for XGB and SVM-RBF, respectively. In contrast, NB achieved the lowest *C*-statistics at 72.49%. Other models had comparable *C*-statistics, equal to 75.38% (RF), 76.72% (LR), 76.46% (LSVM), 77.73% (SVM-RBF), 78.05% (NN), and 78.94% (XGB). Additionally, the DeLong test results indicated that there was a statistically significant difference ($P<.05$) between the *C*-statistics of the ensemble model and all other classifiers, showing its higher performance is less likely to be due to chance.

XSL•FO
RenderX

Figure 2. Receiver operating characteristic curves of developed models. AUC: area under the receiver operating characteristic curve, LR: logistic regression, LSVM: linear support vector machine, NB: naïve Bayes, NN: neural network, RF: random forest, SVM-RBF: support vector machine–radial basis function, XGB: extreme gradient boosting.

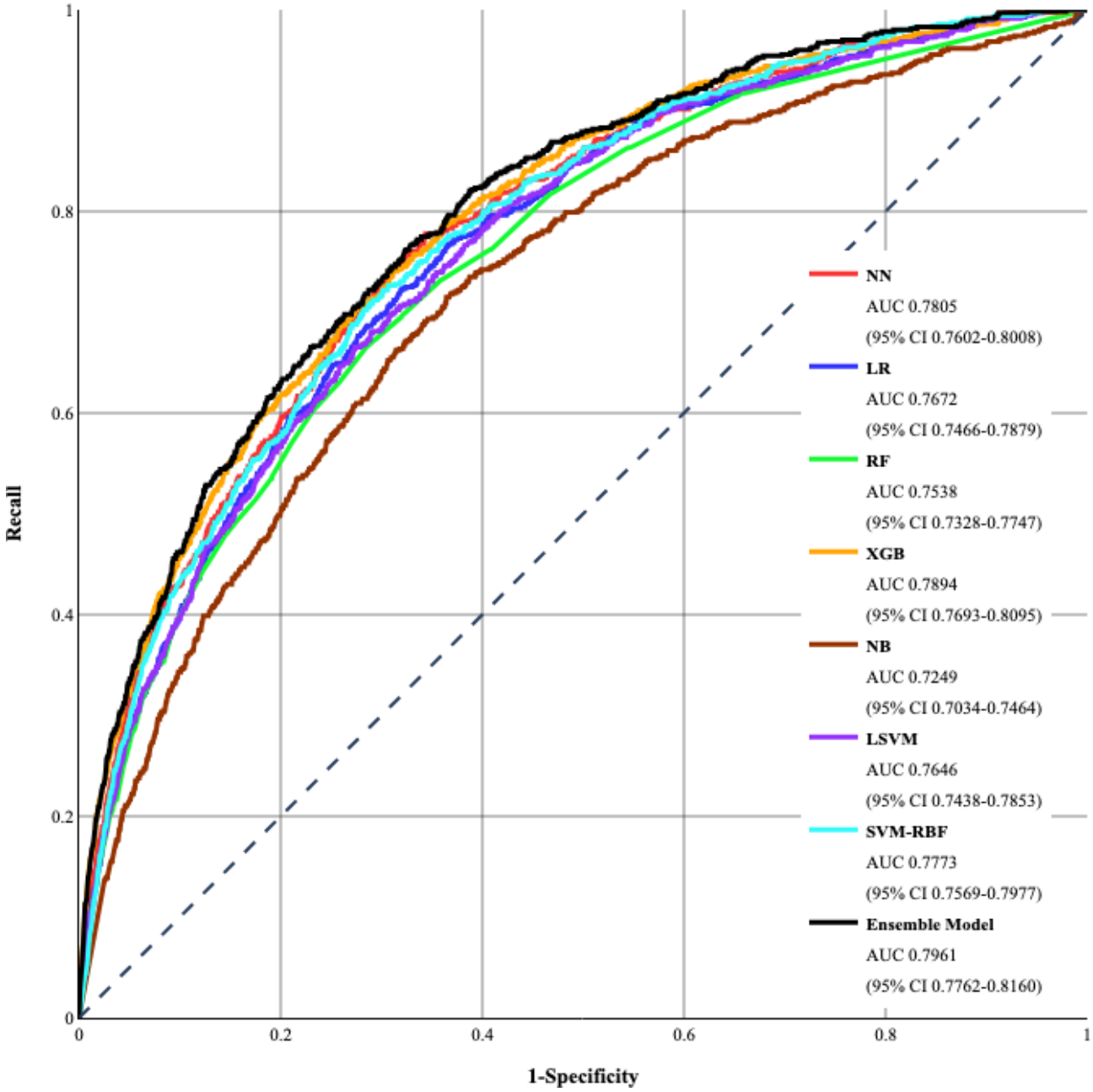

Since model performance was not optimal, we used the Youden index [19-21] to obtain the best performing classification threshold for each model. Figure 3 portrays the confusion matrices for all developed models based on their Youden index threshold. Table 3 provides a summary of performance for all developed models. Accuracy representing the proportion of correctly classified cases was highest for XGB (35,201/48,528, 72.54%), followed by RF (34,603/48,528, 71.31%), LSVM (34,504/48,528, 71.10%), and SVM-RBF (34,260/48,528, 70.60%). Other classifiers had 65% to 70% accuracy with the ensemble model having an accuracy of 67.38% (32,699/48,528).

XSL•FO
RenderX

Figure 3. Confusion matrix of models based on Youden index: (A) neural network; (B) logistic regression; (C) random forest; (D) gradient boosting; (E) naïve Bayes; (F) linear support vector machine; (G) support vector machines-radial basis function; and (H) Ensemble model.

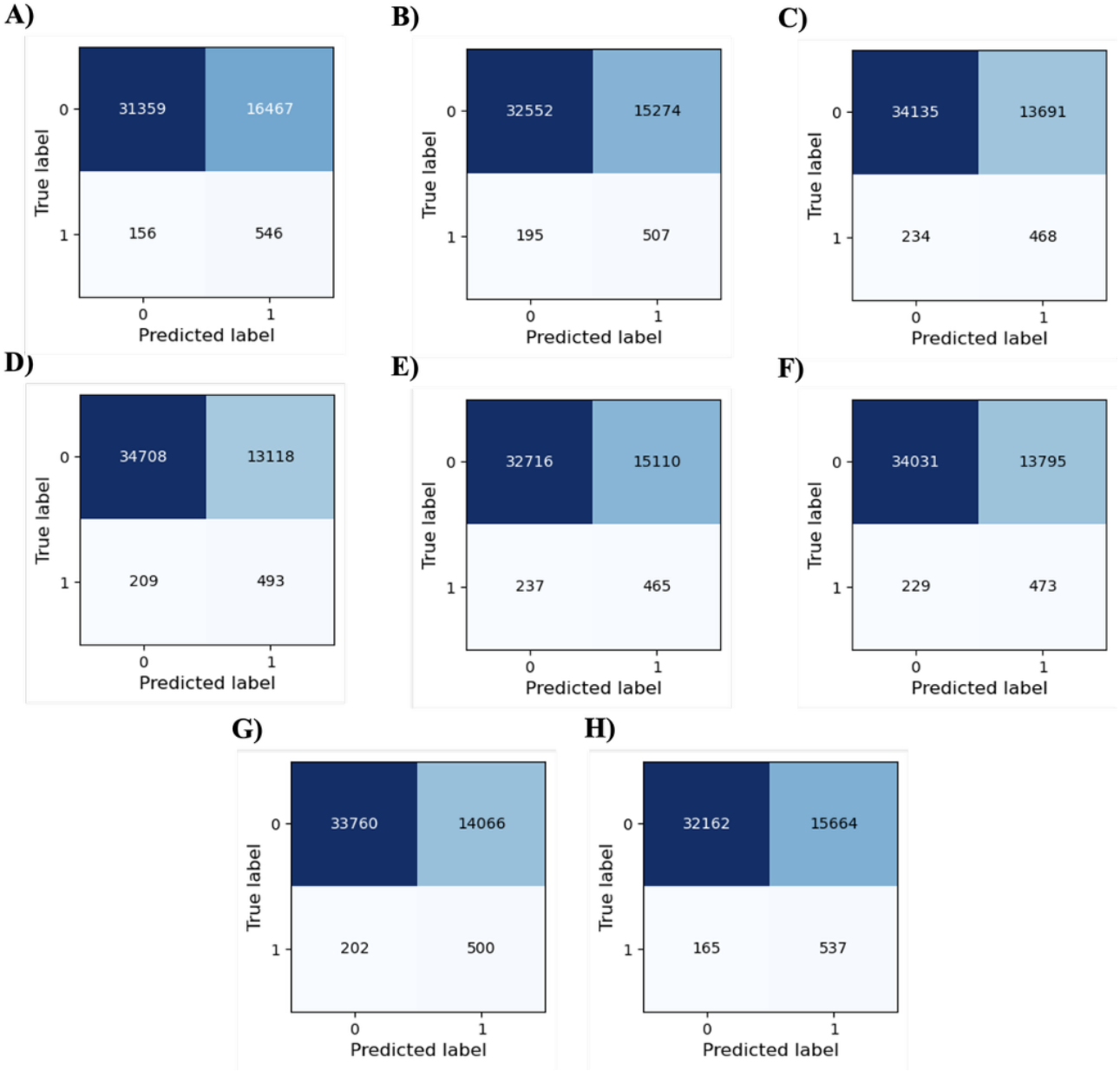

XSL•FO
RenderX

Table . Performance metrics of developed models based on Youden index.

Model	Accuracy	Recall	Specificity	NPV[a]	PPV[b]	AUC[c]
NN[d]	65.75	77.78	65.57	99.51	3.21	78.05
LR[e]	68.12	72.22	68.06	99.40	3.21	76.72
RF[f]	71.31	66.67	71.37	99.32	3.31	75.38
XGB[g]	72.54	70.23	72.57	99.40	3.62	78.94
NB[h]	68.38	66.24	68.41	99.28	2.99	72.49
LSVM[i]	71.10	67.38	71.16	99.33	3.32	76.46
SVM-RBF[j]	70.60	71.23	70.59	99.41	3.43	77.73
Ensemble	67.38	76.50	67.25	99.49	3.31	79.61

[a]NPV: negative predictive value.

[b]PPV: positive predictive value.

[c]AUC: area under the receiver operating characteristic curve.

[d]NN: neural network.

[e]LR: logistic regression.

[f]RF: random forest.

[g]XGB: extreme gradient boosting.

[h]NB: naïve Bayes.

[i]LSVM: linear support vector machine.

[j]SVM-RBF: support vector machine–radial basis function.

To assess the model performance in identifying true positive cases (ie, those with a recorded pharmacogenetic testing uptake) and true negative cases (ie, those without a recorded pharmacogenetic testing uptake), recall and specificity were calculated. Recall values ranged from 66.24% (465/702) to 77.78% (546/702) with the NN model achieving the highest recall and the ensemble model achieving 76.50% (537/702). Specificity values ranged from 65.57% (31,359/47,826) to 72.57% (34,708/47,826), with the XGB model achieving the highest specificity. To further assess models' performance in distinguishing between true positives and true negatives, negative predictive value (NPV) and positive predictive value (PPV) were calculated. NPV values ranged from 99.28% (32,716/32,953) to 99.51% (31,359/31,515) with the NN model having the highest NPV, while PPV values ranged from 2.99% (456/15,575) to 3.62% (493/13,611) with XGB achieving the highest value. To evaluate model fairness, we used the ensemble model to calculate the performance metrics across different racial groups (Table 4). All the metrics, except NPV, exhibited notable variations across different racial groups with AUC ranging from 74.31% to 83.29%, and accuracy from 65.11% (20,592/31,629) to 79.15% (205/259).

Table . Performance metrics of developed models across racial groups[a].

Race group	Accuracy	Recall	Specificity	NPV[b]	PPV[c]	AUC[d]
White	65.11	75.27	64.95	99.44	3.11	77.73
Black	70.34	81.59	70.18	99.61	3.88	83.29
Multiracial	79.15	75.00	79.22	99.51	5.36	74.31
Asian	74.90	66.67	75.00	99.46	3.15	82.69
Other	78.27	60.87	78.45	99.47	2.94	82.32

[a]The performance metrics were reported using the testing data for the racial groups with at least 4 samples in the positive class (ie, pharmacogenetic testing uptake)

[b]NPV: negative predictive value.

[c]PPV: positive predictive value.

[d]AUC: area under the receiver operating characteristic curve.

The SMOTE results, including ROC curves and performance metrics measured at the Youden index are provided in Multimedia Appendix 1. The results did not show any improvement, and the overall performance significantly reduced. The best-performing model was the ensemble model with 73.63% AUC, which is lower than the AUC without SMOTE (ie, 79.61%). All other models demonstrated a notable decrease

XSL•FO
RenderX

in AUC and other performance metrics, especially accuracy, specificity, and NPV.

Stratification analysis results are presented in Figure 4. The analysis was performed by dividing the predicted probabilities of pharmacogenetic testing uptake into deciles and calculating observed uptake rates within each to assess performance across the probability groups. The lowest decile was decile 1 with the lowest probability values, while decile 10 represented the highest probability values. Within each decile, observed uptake rates were calculated to plot against the probability deciles. The observed event rates demonstrated an increasing trend across the probability deciles (except for the 5th). The event rate in the highest probability decile was 6.59% (320/4853) while 0.12% (6/4853) in the lowest decile.

Figure 4. Stratification analysis for the probability of pharmacogenetic testing uptake.

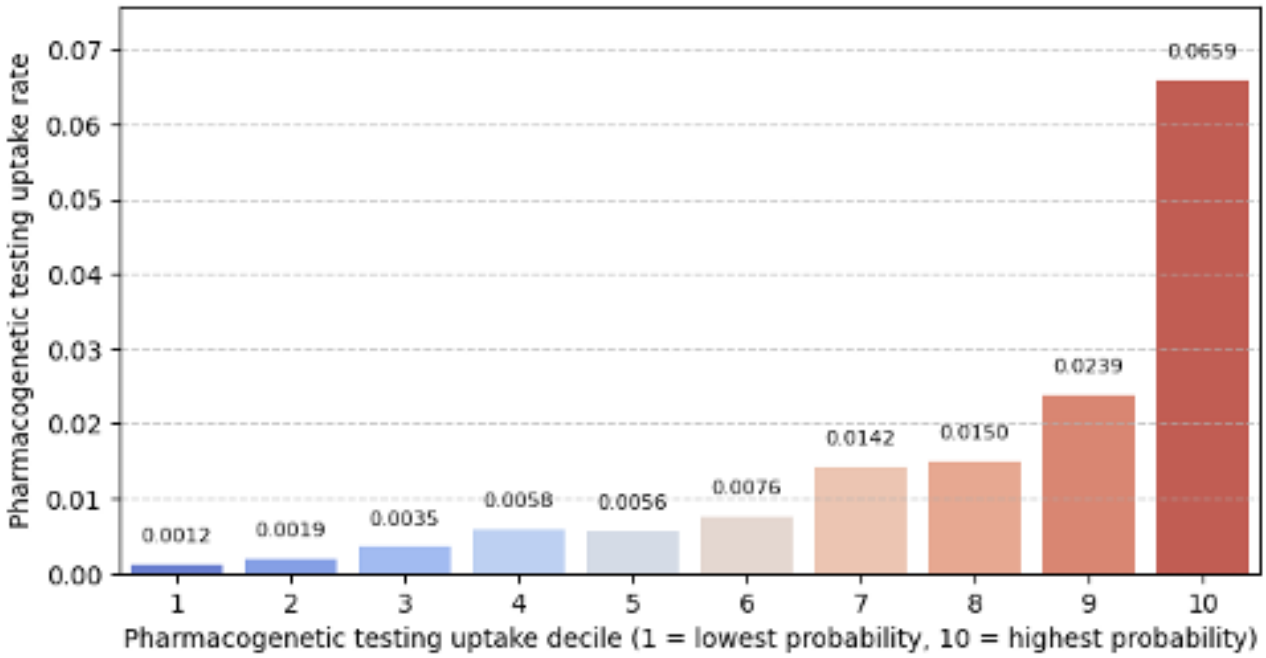

Figure 5 demonstrates the plots of recall values against predictive positives per 100 and the number needed to evaluate. Predictive positives per 100 represent the number of individuals per 100 who are predicted to undergo pharmacogenetic testing across different recall values. The number needed to evaluate indicates the number of individuals that need to be assessed by the model to find 1 true positive (ie, recorded pharmacogenetic testing uptake).

Figure 5. Recall versus (A) predicted positives per 100 and (B) number needed to evaluate.

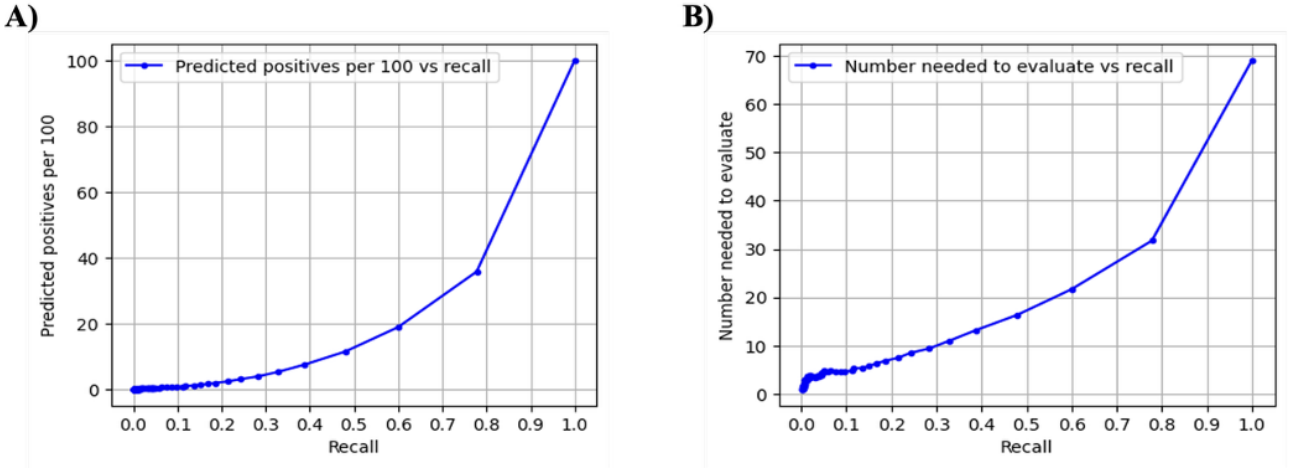

SHAP analysis for feature importance using the XGB model has been shown in Figure 6. Age had the highest impact on pharmacogenetic testing uptake, where older patients are more likely to undergo pharmacogenetic testing. Hypertension and median household income were the next most important features, both associated with a higher likelihood of pharmacogenetic testing uptake. Other SDoH factors were among the top 7 important factors for pharmacogenetic testing uptake. In contrast, racial group variables (ie, Hispanic, Pacific Islander, and White Hispanic) had the lowest influence on the outcome.

XSL•FO
RenderX

Figure 6. Shapley Additive Explanations (SHAP) analysis for feature importance (the x-axis shows the impact on prediction and the color represents the feature value, ie, red for high and blue for low). CPIC: Clinical Pharmacogenetics Implementation Consortium.

XSL•FO
RenderX

Discussion

Principal Findings

ML has widely been used in pharmacogenetics, where investigations focused on using genetic information to predict drug response [23,24]. However, this is the first study to develop ML models for predicting probability of the use of pharmacogenetic testing using clinical and nonclinical factors such as demographics, comorbidities, medication history, and SDoH. It highlighted the potential of using ML methods to improve the use of pharmacogenetic testing, especially in pain management with opioid medications. The results of this study demonstrated that the ensemble model achieved the highest AUC compared to other models for pharmacogenetic testing uptake prediction. Although the XGB model, when evaluated at its Youden index, performed better than other models in terms of accuracy, recall, specificity, and NPV, we selected the ensemble model as the final classifier. This was because the ensemble model harnesses the strengths of both high-performing XGB and SVM-RBF models for prediction, ultimately improving the performance for pharmacogenetic testing uptake prediction. Overall, the ensemble model proves to be a viable tool for accurately predicting pharmacogenetic testing uptake, supporting more informed, data-driven decision-making.

Several methodological considerations must be addressed when interpreting these promising results. The primary goal of our study was to predict pharmacogenetic testing uptake, which is a clinically favorable outcome. In this scenario, NPV represents the ability of the model to correctly predict no pharmacogenetic testing uptake out of all no-uptake predictions. While our study showed a very high NPV (32,162/32,327; 99.49%), a low NPV could lead to negative consequences, including resource misallocation, alert fatigue, and missed clinical opportunities for those who need pharmacogenetic testing uptake for more effective treatment. In contrast, PPV represents the accuracy of the model in correctly predicting pharmacogenetic testing uptake out of all positive predictions. Thus, a lower PPV leads to lower trustworthiness of positive predictions and inadequate resource allocation to patients who are wrongly predicted to undergo pharmacogenetic testing. Since our data was highly imbalanced with a low percentage of patients having a recorded pharmacogenetic testing uptake, we used a balanced class weighting approach for final model development, assigning proportionally higher weights to the minority class (ie, pharmacogenetic testing uptake). However, the model achieved a much lower PPV compared to NPV. To address this issue, threshold moving was used as a strategy to balance clinical context and consequences of false positives compared to false negatives. Since lowering and raising the threshold can decrease or increase PPV and NPV, the optimal threshold should be selected based on the trade-off between minimizing the consequences of misallocated interventions (ie, higher NPV) and maximizing clinical opportunities for patient care (ie, higher NPV). Overall, the high NPV in our study based on the Youden index could be advantageous in decision-making, as it allows for the allocation of more resources and encouragement plans for patients predicted not to undergo pharmacogenetic testing.

We conducted a comprehensive feature importance analysis to enhance model interpretability and clinical acceptance. The SHAP value analysis using the XGB model highlighted the contribution of each feature to individual predictions, enhancing the model's clinical credibility and trustworthiness. The most influential features were age, hypertension, and household income, suggesting that these features require more attention for increasing pharmacogenetic testing uptake among patients. As mentioned, pharmacogenetic testing uptake is not necessarily due to opioid prescribing and could be due to prescribing of other medications and participation in a research project, potentially affecting the study results. Thus, although the results demonstrate the model's transparency and clinical use, more research is needed before integrating the model into a real-world decision support system. While the SHAP diagram ranks features based on their overall importance, it is crucial to examine critical factors for each patient on a case-by-case basis when making decisions.

Beyond individual prediction, we evaluated the model's ability to stratify patients into meaningful pharmacogenetic testing uptake categories. The uptake stratification analysis showed that the ensemble model effectively differentiated patients across pharmacogenetic testing uptake deciles, with higher uptake probabilities corresponding to higher observed uptake rates. Such an analysis can assist decision-makers in categorizing patients into different deciles based on their likelihood of pharmacogenetic testing uptake and prioritize those in lower deciles (less likely for the pharmacogenetic testing uptake) for optimal resource allocation and improved access to testing. It is important to recognize that stratification analysis often relies on predefined thresholds (ie, 10% in this study) to categorize probabilities into deciles, which may not be optimal for real-world decision-making.

The implementation of the pharmacogenetic testing uptake prediction model addresses the barriers to pharmacogenetic testing in opioid therapy. Our models accurately predict the likelihood of pharmacogenetic testing uptake but do not identify patients who clinically require or should receive testing (this was not the objective of this study). The models capture associations between demographic, clinical, and social determinants with testing behavior under current practice patterns, not clinical appropriateness. This distinction is important as the predictions reflect existing health care access and use patterns rather than evidence-based treatment recommendations. The predictive patterns we observed, favoring older patients with multiple comorbidities and greater health care access, largely reflect existing health care use behaviors and socioeconomic factors rather than clinical need or potential for improved outcomes. Consequently, this model should not be interpreted as a clinical decision support tool for determining which patients should receive pharmacogenetic testing. Rather, the primary applications of this model lie in health care operations and policy rather than direct clinical care. By providing the probability of pharmacogenetic testing uptake at the individual patient level, health systems can identify patients less likely to receive guideline-recommended testing and target barrier-reduction efforts. Insurers can use uptake predictions to forecast costs, allocate resources to underserved populations,

XSL•FO
RenderX

and design coverage policies that promote equitable access to precision medicine. Such predictions could be particularly useful for patients predicted to benefit from testing (not the focus of this study), allowing care teams to prioritize resources to promote uptake in this population. By quantifying uptake likelihood, the model supports data-driven decisions about resource allocation and coverage policies to move beyond trial-and-error opioid prescribing toward more systematic, evidence-based pain management.

Our study has several limitations. First, it is notable that although the study used PPV as a performance metric, it is highly dependent on outcome prevalence and may not generalize across different patient populations or clinical settings, reducing its applicability in decision-making. Second, this study used various clinical and demographic variables to develop more-informed ML models. However, the underrepresentation of certain racial groups, such as Hispanic and Pacific Islander, could potentially affect models' outcomes. This raises concerns about the bias and fairness issues, as ML models may exhibit lower performance for these groups compared to others. Third, while the study incorporated SDoH information as potential predictors of pharmacogenetic testing uptake, this information was based on ZIP code-level data, which may lack the necessary granularity required for precise prediction. Detailed individual-level data on variables such as income, education, and household size could enhance the model's reliability and improve the accurate identification of each feature's contribution to the outcome. Fourth, the model's performance may not directly translate to external populations with varying demographic and clinical backgrounds. Specifically, the model was trained on data from a single EHR system, including minority racial groups, and the results may not be applicable to other racial groups. Therefore, caution is warranted when interpreting the model's outcomes for these populations. Finally, some of the patients in the data who had a recorded pharmacogenetic testing uptake were part of a clinical trial where the cost of testing was covered. This would potentially influence the ability of the model to identify the true impact of patients' economic and income status on undergoing pharmacogenetic testing. To demonstrate the model's broader applicability, future work should focus on external validation using independent datasets from different health systems and identification of patients who are more likely to benefit from testing. This would help evaluate the model's robustness and clinical use for real-world decision-making.

Conclusions

Pharmacogenetic testing is a viable tool for matching patients' genetic profiles to suitable opioids for pain treatment. This study proposed ML models for pharmacogenetic testing uptake prediction using data from an EHR system. Results demonstrated that the ensemble ML model combining XGB and SVM-RBF classifiers achieved the highest AUC at 79.61%, making it a reliable prediction model for pharmacogenetic testing uptake prediction. Additionally, the uptake stratification and feature importance analysis using SHAP values further indicated the model's use for real-world applications. Following further validation using an external dataset, this model can be integrated into a data-driven decision support system, enabling health systems and insurers in resource planning and health equity assessment to optimize pain management and improve patient outcomes.

Conflicts of Interest

None declared.

Multimedia Appendix 1
Synthetic minority over-sampling technique results.
[DOCX File, 174 KB - medinform_v14i1e81048_app1.docx]

References

1. Dale O, Moksnes K, Kaasa S. European palliative care research collaborative pain guidelines: opioid switching to improve analgesia or reduce side effects. a systematic review. Palliat Med 2011 Jul;25(5):494-503. [doi: 10.1177/0269216310384902] [Medline: 21708856]
2. Crews KR, Monte AA, Huddart R, et al. Clinical pharmacogenetics implementation consortium guideline for CYP2D6, OPRM1, and COMT genotypes and select opioid therapy. Clin Pharmacol Ther 2021 Oct;110(4):888-896. [doi: 10.1002/cpt.2149] [Medline: 33387367]
3. Deo RC. Machine learning in medicine. Circulation 2015 Nov 17;132(20):1920-1930. [doi: 10.1161/CIRCULATIONAHA.115.001593] [Medline: 26572668]
4. Vike NL, Bari S, Stefanopoulos L, et al. Predicting COVID-19 vaccination uptake using a small and interpretable set of judgment and demographic variables: cross-sectional cognitive science study. JMIR Public Health Surveill 2024 Mar 18;10:e47979. [doi: 10.2196/47979] [Medline: 38315620]
5. Zhang B, Shi H, Wang H. Machine learning and AI in cancer prognosis, prediction, and treatment selection: a critical approach. J Multidiscip Healthc 2023;16:1779-1791. [doi: 10.2147/JMDH.S410301] [Medline: 37398894]
6. Nguyen MH, Applegate CD, Murray B, et al. Assessing genetic counseling efficiency with natural language processing. J Am Med Inform Assoc 2025 Nov 10:ocaf190. [doi: 10.1093/jamia/ocaf190] [Medline: 41211696]

XSL•FO
RenderX

7. van Walraven C, Austin PC, Jennings A, Quan H, Forster AJ. A modification of the Elixhauser comorbidity measures into a point system for hospital death using administrative data. Med Care 2009 Jun;47(6):626-633. [doi: 10.1097/MLR.0b013e31819432e5] [Medline: 19433995]
8. Social determinants of health database. Agency for Healthcare Research and Quality. URL: https://www.ahrq.gov/sdoh/data-analytics/sdoh-data.html#download [accessed 2025-04-04]
9. Chen T, Guestrin C. XGBoost: a scalable tree boosting system. Presented at: KDD '16: Proceedings of the 22nd ACM SIGKDD International Conference on Knowledge Discovery and Data Mining; Aug 13-17, 2016. [doi: 10.1145/2939672.2939785]
10. Breiman L. Random forests. Mach Learn 2001 Oct;45(1):5-32. [doi: 10.1023/A:1010933404324]
11. Cervantes J, Garcia-Lamont F, Rodríguez-Mazahua L, Lopez A. A comprehensive survey on support vector machine classification: Applications, challenges and trends. Neurocomputing 2020 Sep;408:189-215. [doi: 10.1016/j.neucom.2019.10.118]
12. Ruder S. An overview of gradient descent optimization algorithms. arXiv. Preprint posted online on Sep 15, 2016. [doi: 10.48550/arXiv.1609.04747]
13. Kingma DP, Ba LJ. Adam: a method for stochastic optimization. Presented at: International Conference on Learning Representations; May 7-9, 2015 URL: https://dare.uva.nl/search?identifier=a20791d3-1aff-464a-8544-268383c33a75 [accessed 2025-12-18]
14. Dozat T. Incorporating Nesterov momentum into Adam. Presented at: International Conference on Learning Representations (ICLR 2016); May 2-4, 2016 URL: https://openreview.net/pdf?id=OM0jvwB8jIp57ZJjtNEZ [accessed 2026-01-07]
15. Chawla NV, Bowyer KW, Hall LO, Kegelmeyer WP. SMOTE: synthetic minority over-sampling technique. jair 2002;16:321-357. [doi: 10.1613/jair.953]
16. Collins GS, Moons KGM, Dhiman P, et al. TRIPOD+AI statement: updated guidance for reporting clinical prediction models that use regression or machine learning methods. BMJ 2024 Apr 16;385:e078378. [doi: 10.1136/bmj-2023-078378] [Medline: 38626948]
17. DeLong ER, DeLong DM, Clarke-Pearson DL. Comparing the areas under two or more correlated receiver operating characteristic curves: a nonparametric approach. Biometrics 1988 Sep;44(3):837-845. [Medline: 3203132]
18. Sun X, Xu W. Fast implementation of DeLong's algorithm for comparing the areas under correlated receiver operating characteristic curves. IEEE Signal Process Lett 2014;21(11):1389-1393. [doi: 10.1109/LSP.2014.2337313]
19. Youden WJ. Index for rating diagnostic tests. Cancer 1950 Jan;3(1):32-35. [doi: 10.1002/1097-0142(1950)3:1<32::aid-cncr2820030106>3.0.co;2-3] [Medline: 15405679]
20. Fluss R, Faraggi D, Reiser B. Estimation of the Youden index and its associated cutoff point. Biom J 2005 Aug;47(4):458-472. [doi: 10.1002/bimj.200410135] [Medline: 16161804]
21. Schisterman EF, Faraggi D, Reiser B, Hu J. Youden index and the optimal threshold for markers with mass at zero. Stat Med 2008 Jan 30;27(2):297-315. [doi: 10.1002/sim.2993] [Medline: 17624866]
22. Lundberg SM, Lee SI. A unified approach to interpreting model predictions. Presented at: NIPS'17: Proceedings of the 31st International Conference on Neural Information Processing Systems; Dec 4-9, 2017. [doi: 10.5555/3295222.3295230]
23. Firoozbakht F, Yousefi B, Schwikowski B. An overview of machine learning methods for monotherapy drug response prediction. Brief Bioinform 2022 Jan 17;23(1):bbab408. [doi: 10.1093/bib/bbab408] [Medline: 34619752]
24. Adam G, Rampášek L, Safikhani Z, Smirnov P, Haibe-Kains B, Goldenberg A. Machine learning approaches to drug response prediction: challenges and recent progress. NPJ Precis Oncol 2020;4(1):19. [doi: 10.1038/s41698-020-0122-1] [Medline: 32566759]

Abbreviations

AUC: area under the receiver operating characteristic curve
CPIC: Clinical Pharmacogenetics Implementation Consortium
CYP2D6: cytochrome P450 family 2 subfamily D member 6
EHR: electronic health record
***ICD-10*:** *International Classification of Diseases, Tenth Revision*
***ICD-9*:** *International Classification of Disease, Ninth Revision*
IDR: Integrated Data Repository
LR: logistic regression
LSVM: linear support vector machine
ML: machine learning
NB: naïve Bayes
NN: neural network
NPV: negative predictive value
PPV: positive predictive value
RF: random forest

XSL•FO
RenderX

SDoH: social determinants of health
SHAP: Shapley Additive Explanations
SMOTE: synthetic minority over-sampling technique
SVM: support vector machine
SVM-RBF: support vector machine–radial basis function
TRIPOD+AI: Transparent Reporting of a Multivariable Prediction Model for Individual Prognosis or Diagnosis + Artificial Intelligence
XGB: extreme gradient boosting

Edited by J Klann; submitted 21.Jul.2025; peer-reviewed by A Berihun, R Mpofu; revised version received 13.Nov.2025; accepted 26.Nov.2025; published 21.Jan.2026.

Please cite as:
Yaseliani M, Hong JW, Bian J, Cavallari L, Duarte JD, Nelson D, Lo-Ciganic WH, Nguyen KA, Hasan MM
Machine Learning Prediction of Pharmacogenetic Testing Uptake Among Opioid-Prescribed Patients Using Electronic Health Records: Retrospective Cohort Study
JMIR Med Inform 2026;14:e81048
URL: https://medinform.jmir.org/2026/1/e81048
doi:10.2196/81048

© Mohammad Yaseliani, Je-Won Hong, Jiang Bian, Larisa Cavallari, Julio Duarte, Danielle Nelson, Wei-Hsuan Lo-Ciganic, Khoa Anh Nguyen, Md Mahmudul Hasan. Originally published in JMIR Medical Informatics (https://medinform.jmir.org), 21.Jan.2026. This is an open-access article distributed under the terms of the Creative Commons Attribution License (https://creativecommons.org/licenses/by/4.0/), which permits unrestricted use, distribution, and reproduction in any medium, provided the original work, first published in JMIR Medical Informatics, is properly cited. The complete bibliographic information, a link to the original publication on https://medinform.jmir.org/, as well as this copyright and license information must be included.

XSL•FO
RenderX

Development of Venous Thromboembolism Risk Prediction Models Based on Whole Blood Gene Expression Profiling Using 20 Machine Learning Algorithms: Comprehensive Analysis Study

Yedong Huang[1*], MD, PhD; Xiaoyun Chen[2*], MD, PhD; Guannan Bai[3], MD; Yajun Zhao[4], MD; Dapeng Kuang[5], MD; Lin Zhang[6,7], Prof Dr; Wei Lu[8], Prof Dr

[1]Department of Radiation Oncology, Clinical Oncology School of Fujian Medical University, Fujian Cancer Hospital, Fuzhou, Fujian, China

[2]The School of Clinical Medicine, Fujian Medical University; Department of Respiratory and Critical Care Medicine, Fujian Provincial Geriatric Hospital, No. 147 Beihuan Middle Road, Fuzhou, China

[3]Children's Hospital, Zhejiang University School of Medicine, Hangzhou, China

[4]Department of Health Management Centre, Zhongshan Hospital, Fudan University, Shanghai, China

[5]Department of Emergency and Critical Care, Shanghai General Hospital, Shanghai Jiao Tong University School of Medicine, Shanghai, China

[6]Department of Epidemiology and Preventive Medicine, The School of Public Health and Preventive Medicine, Monash University, Victoria, Australia

[7]Suzhou Industrial Park Monash Research Institute of Science and Technology, Monash University, Suzhou, China

[8]Department of Cardiovascular Surgery, The Quzhou Affiliated Hospital of Wenzhou Medical University, Quzhou People's Hospital, Quzhou City, No.100 of Minjiang Road, Wenzhou, China

[*]these authors contributed equally

Corresponding Author:
Wei Lu, Prof Dr
Department of Cardiovascular Surgery, The Quzhou Affiliated Hospital of Wenzhou Medical University, Quzhou People's Hospital, Quzhou City, No.100 of Minjiang Road, Wenzhou, China

Abstract

Background: There is a lack of venous thromboembolism (VTE) risk prediction models based on gene expression information.

Objective: This study aimed to construct a VTE prediction model based on whole blood gene expression profiling, by performing a comprehensive analysis of 20 machine learning (ML) algorithms.

Methods: Two transcriptome datasets containing patients with VTE and healthy controls were obtained by searching the Gene Expression Omnibus database and used as the training and validation sets, respectively. Feature selection for model construction was performed on the training set using the least absolute shrinkage and selection operator and random forest, followed by the selection of the intersection of the chosen features. Subsequently, recursive feature elimination was applied to further refine the selected features. The selected features underwent model construction using 20 ML algorithms. The performance of the models was evaluated using various methods such as receiver operating characteristic and confusion matrix. The validation set was used for external model validation.

Results: The final results demonstrated that all algorithm models, except for k-nearest neighbor, exhibited good performance in VTE prediction. External validation data indicated that 9 algorithm models had an area under the curve greater than 0.75. The confusion matrix analysis revealed that the algorithm models maintained high specificity in the external validation cohort.

Conclusions: This study used 20 ML algorithms to construct VTE prediction models based on whole blood gene expression information, with 9 of these models demonstrating good diagnostic performance in external validation cohorts. The above models, when used in conjunction with D-dimer, may provide more valuable references for VTE diagnosis.

(JMIR Med Inform 2026;14:e75565) doi:10.2196/75565

KEYWORDS

venous thromboembolism; gene expression profiling; machine learning; biomarkers; predictive models; ROC; receiver operating characteristic curve; transcriptome

Introduction

Venous thromboembolism (VTE) is a prevalent thrombotic disorder in clinical practice, consisting primarily of deep venous thrombosis and pulmonary embolism. VTE remains a major global health burden, affecting approximately 10 million people annually and ranking among the most common vascular diseases worldwide [1]. The pathogenesis of VTE is considered to be

XSL•FO
RenderX

multifaceted and intricate, encompassing a multitude of factors, including but not limited to congenital genetic factors, malignancies, pregnancy in women, surgical trauma, and the use of oral contraceptives [2,3]. Despite the existence of relatively comprehensive prevention and assessment systems, the high mortality rate associated with VTE remains a significant concern among clinical practitioners. According to a study by Heit et al [4], the short-term (30-d) survival rate for deep vein thrombosis is approximately 94.5%, whereas the short-term survival rate for pulmonary embolism is only 66.8%.

In clinical practice, the diagnostic modalities most frequently used for VTE include D-dimer measurement, ultrasonography, and venography [5]. Among these methods, venography is considered the gold standard for diagnosing VTE. However, due to its invasive nature and the potential risk of contrast-induced renal impairment and allergic reactions, its clinical application is limited [6]. The limitations of ultrasonography include its subjectivity and difficulty in detecting deep venous thrombosis [7]. D-dimer testing is known to lack specificity, as elevated D-dimer levels may be caused by conditions such as infection, autoimmune diseases, pregnancy, and childbirth, leading to a higher likelihood of false positive results [8]. Therefore, it is crucial to construct a VTE risk prediction model with high performance.

With the advancement of science and technology, artificial intelligence (AI) has become a widely studied and highly regarded field in recent years, particularly in the medical domain. As one of the methods for achieving AI, machine learning (ML) algorithms have tremendous potential in medical research [9-11]. The aim of this study was to construct a VTE risk prediction model based on whole blood gene expression information, using a comprehensive analysis of 20 ML algorithms and external validation, with the goal of providing a reference for clinical decision-making and VTE prevention. These models are not only designed to differentiate between existing VTE cases and controls, but also intended to detect high-risk patients in early or asymptomatic stages, thereby serving as predictive tools that may assist in clinical decision-making before definitive diagnostic imaging is performed.

Methods

Data and Source

The gene expression data of patients with VTE and healthy controls were retrieved and downloaded from the Gene Expression Omnibus (GEO) database and used as the training and validation groups, respectively, in this study. The GSE19151 dataset was used as the training set, while the GSE48000 dataset served as the validation set. Both datasets were generated using the Affymetrix Human Genome U133 Plus 2.0 microarray platform (GPL570). Table 1 shows the basic information of the 2 datasets, GSE19151 and GSE48000. The GSE19151 dataset comprises gene expression data from 70 patients with VTE and 63 healthy controls [12]; the GSE48000 dataset contains gene expression data from 107 patients with VTE and 25 healthy controls [13]. Data analysis was performed using the *Scikit-learn* (sklearn) module in Python (version 3.6; Python Software Foundation).

Table . Details of the Gene Expression Omnibus (GEO)[a] datasets used in this study.

Dataset	GEO ID	Sample size (n)	PubMed ID	Number of genes	Country
Training set	GSE19151	133	21737128	13,515	USA
Validation set	GSE48000	132	25684211	31,412	USA

[a]GEO: Gene Expression Omnibus.

Feature Selection

Least absolute shrinkage and selection operator (LASSO) regression analysis method was developed by Robert Tibshirani [14]. The principle of this method is to construct a penalty function to achieve the goal of shrinking regression coefficients and refining the model. While the principle of feature selection using random forest (RF) is mainly based on evaluating the contribution of each feature in the RF on each tree. In this study, we used the mean decrease in Gini impurity to measure feature importance in the RF model. The above 2 methods were used to select modeling features in the training set, and the intersection analysis was subsequently performed to reveal the features selected by both methods. This intersection strategy was designed to combine the strengths of both linear (LASSO) and nonlinear (RF) approaches and to reduce potential selection bias by focusing on consistently selected features. Although this intersection approach may sacrifice sensitivity, it enhances stability and reduces overfitting risk in high-dimensional settings. All feature selection procedures were performed exclusively on the training dataset to prevent information leakage from the validation data. The results were then visualized by a Venn plot.

Recursive Feature Elimination for Model Simplification

The main idea of the recursive feature elimination (RFE) method is to repeatedly construct models and remove the most significant features, ranking the features according to the order in which they are eliminated. To achieve a more streamlined model without compromising performance, the features selected by the aforementioned method were further screened and simplified using the RFE method in our study.

Construction of a VTE Risk Prediction Model Using 20 ML Algorithms

After completing the feature selection process, this study constructed the model using commonly used ML algorithms in the field, which included the following: adaptive boosting, artificial neural network, bagging, Bayesian ridge, decision tree, elastic net, extra tree (extremely randomized trees), gradient boosting, k-nearest neighbors (KNN) algorithm, LASSO, linear

XSL•FO
RenderX

LASSO, linear regression, logistic regression, naïve Bayes, RF, ridge regression, ridge cross-validation (ridge regression with cross-validation), stochastic gradient descent, support vector machine, and voting (voting classifier). The algorithm code is taken from the sklearn website [15]. All models were constructed using 5-fold cross-validation.

External Validation of the Model

In this study, GSE48000 was used as the external validation cohort to evaluate the generalization ability of the 20 ML models, ensuring the reproducibility of the model. The performance of the external validation was evaluated by the receiver operating characteristic (ROC) curve. All feature selection and model training were exclusively performed on the training dataset. The final trained models were then directly applied to the validation dataset without any retraining or adjustment, thereby ensuring a true external validation.

Decision Curve Analysis

To evaluate the potential clinical use of the constructed models, we performed decision curve analysis (DCA) across both internal and external evaluation settings. The net benefit for each model was calculated using the standard formula:

NetBenefit=TPN-FPN*PT1-PT

where TP and FP denote the numbers of true and false positives at a given threshold probability, and *n* is the total number of samples. DCA was conducted over a range of clinically relevant threshold probabilities from 0.05 to 0.5. The decision curves were generated using Python with appropriate packages compatible with sklearn.

Ethical Considerations

This study involved secondary analysis of publicly available, deidentified transcriptomic datasets obtained from the GEO database. As per institutional and GEO data usage policies, such analysis does not require ethical approval or informed consent. For more information, please refer to the GEO data policy [16].

Results

The Features Selected by LASSO Regression and RF

To determine the optimal regularization strength in LASSO regression, we used 5-fold cross-validation to identify the λ value corresponding to the “one standard error rule” (λ_1 se), which balances model simplicity and predictive performance. The regularization path was explored using the LASSO cross-validation function in sklearn, which automatically tests a logarithmic range of λ values. We selected 24 features corresponding to λ=−3.38.

The process of feature selection using LASSO regression is illustrated in Figure 1A and B and Figure 1C illustrates the 24 features selected by LASSO regression and their corresponding coefficients. The screening results of the RF are shown in Figure 1D, where the lollipop plot displays the 20 features selected by RF, with the length of the horizontal axis representing the corresponding importance of each gene. The Venn diagram in Figure 1E shows the intersection of the features selected by LASSO regression and RF methods. The 8 features selected by the intersection analysis are as follows: *TRMT5*, *TGFB1*, *SRSF5*, *RAB5C*, *MYH9*, *LSP1*, *GBP1*, and *DICER1*.

XSL•FO
RenderX

Figure 1. The process of selecting modeling features using least absolute shrinkage and selection operator (LASSO) and random forest methods.

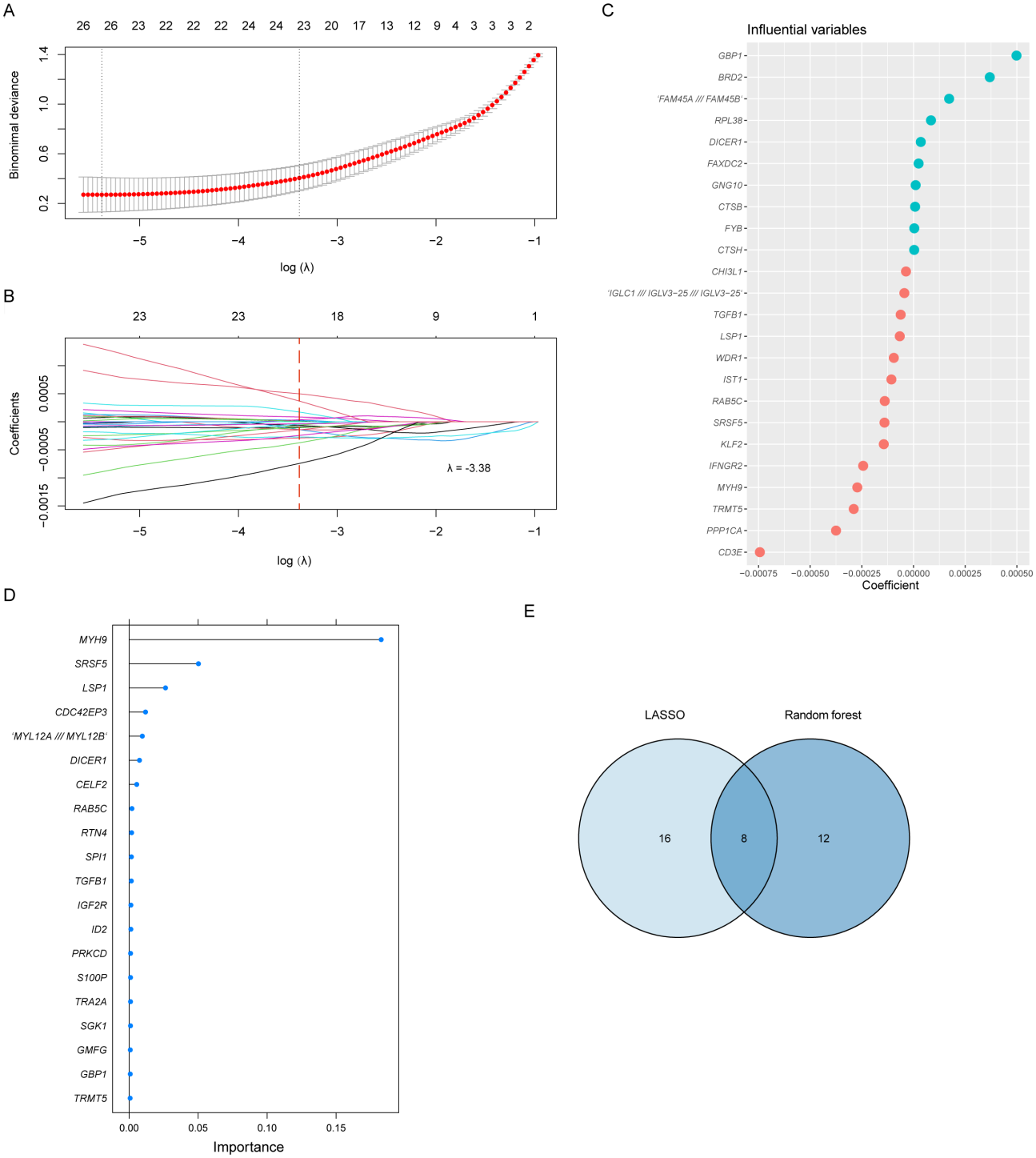

Recursive Feature Elimination to Simplify the Model

The above 8 features were further simplified using the RFE algorithm, which reduces costs and improves the generalizability of the model while removing redundant features. Figure 2 displays the results of the RFE calculations using a line graph. The results indicate that the accuracy of the model in cross-validation no longer significantly changes when the number of features is reduced to 7. The features further refined by the RFE algorithm include 7 genes: *SRSF5*, *MYH9*, *LSP1*, *RAB5C*, *TGFB1*, *DICER1*, and *GBP1*.

XSL•FO
RenderX

Figure 2. The process of simplifying modeling features using recursive feature elimination.

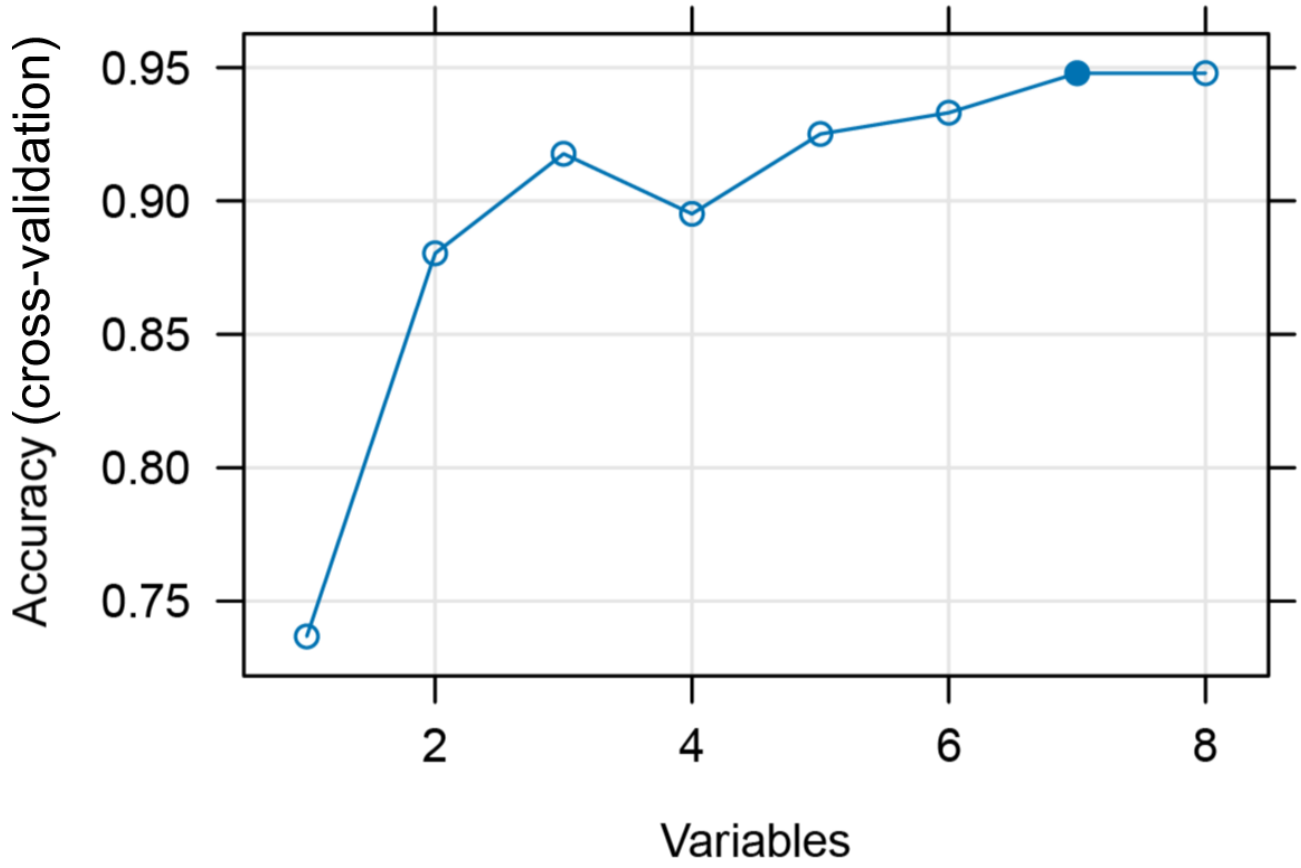

Construction of VTE Risk Prediction Models Using 20 ML Algorithms

Based on the 7 features selected, our study used 20 commonly used ML algorithms to construct the models and used 5-fold cross-validation to improve the accuracy of model evaluation and reduce random error. Figure 3A displays the ROC curves and corresponding area under the curve (AUC) values of the 20 ML models using different colored lines. Figure 3B depicts a radar chart showcasing the accuracy, F_1-score, precision, and recall for 20 ML algorithms. The accuracy reflects the proportion of correctly predicted samples; precision reflects the proportion of actual VTE cases among samples classified as VTE by the model; recall represents the proportion of VTE cases correctly classified by the model among all VTE samples; the F_1-score is a value used to comprehensively evaluate both recall and precision. As illustrated in Figure 3, most models exhibit an AUC value greater than 0.9, and the radar chart based on 4 parameters evaluation indicates that, except for the KNN model, all other ML models can make relatively accurate predictions for VTE.

XSL•FO
RenderX

Figure 3. Performance comparison of 20 machine learning models using receiver operating characteristic (ROC) curves and radar plots. (**A**) ROC curves and area under the curve values based on 20 machine learning models. (**B**) Radar plots comparing accuracy, F_1-score, precision, and recall across models. AdaBoost: adaptive boosting; ANN: artificial neural network; KNN: k-nearest neighbor; LASSO: least absolute shrinkage and selection operator; SGD: stochastic gradient descent; SVM: support vector machine.

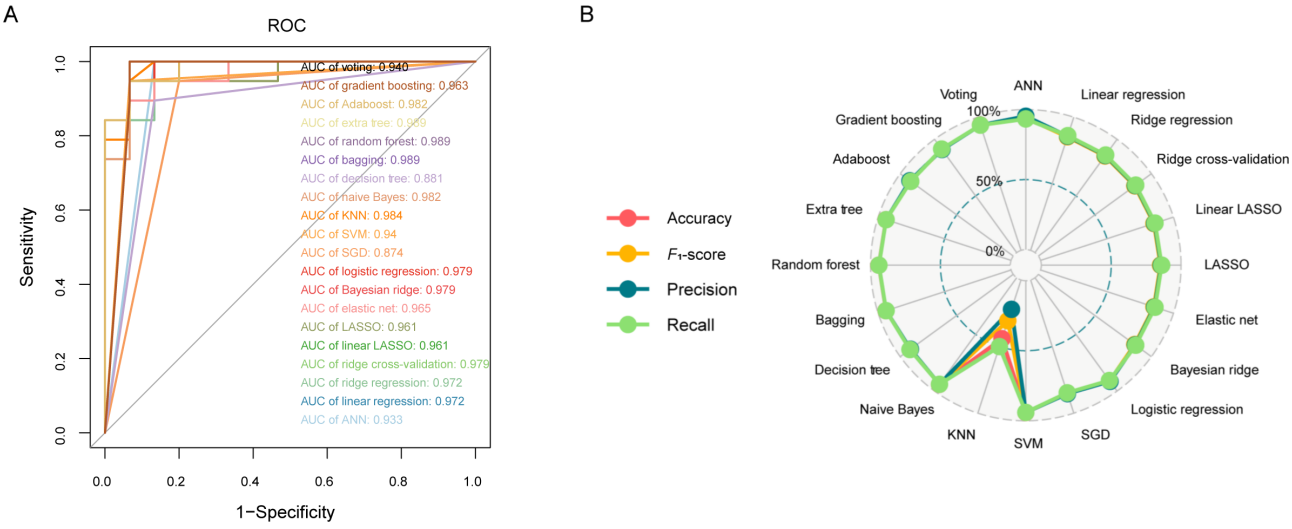

Figure 4 presents the confusion matrices for 20 ML algorithms, among which the sensitivity of all models except for the KNN fluctuated between 87% and 93%, and the specificity fluctuated between 79% and 100%. The findings above indicate that, with the exception of the KNN model, the remaining 19 ML models possess favorable predictive efficacy for VTE. Multimedia Appendix 1 presents the DCA for 20 ML algorithms.

Figure 4. Confusion matrices for 20 machine learning algorithms. The top-left cell indicates the true positive, top-right indicates the false negative, bottom-left indicates the false positive, and bottom-right indicates the true negative. AdaBoost: adaptive boosting; ANN: artificial neural network; KNN: k-nearest neighbor; LASSO: least absolute shrinkage and selection operator; SGD: stochastic gradient descent; SVM: support vector machine.

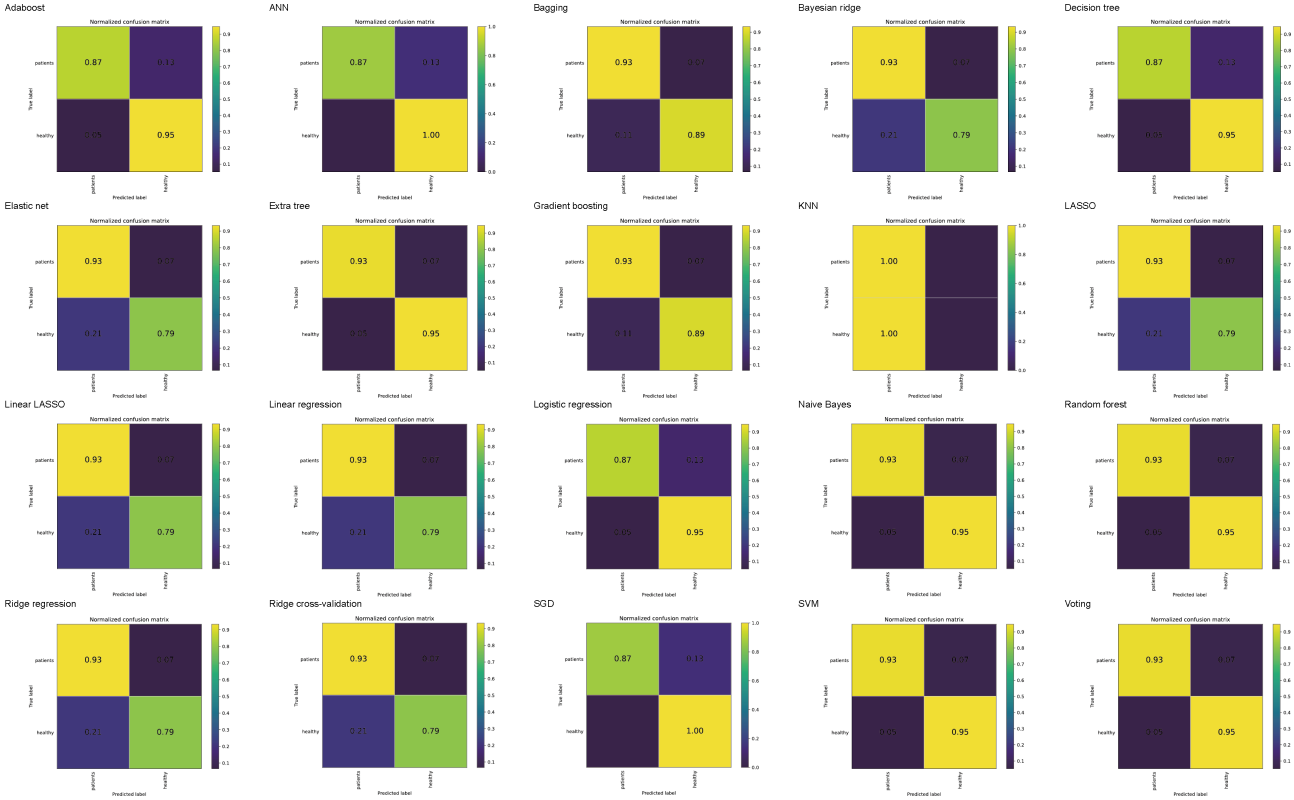

External Validation of the Models

To ensure the reproducibility and generalizability of the model, this study performed external validation of the 20 ML models using the GSE48000 dataset. Figure 5 illustrates the ROC curves and the corresponding AUC based on the external validation dataset. The results revealed a significant decrease in the AUC of all models during external validation, but the AUC of the following 9 models remained above 0.75: extra tree, RF, Bayesian ridge, elastic net, LASSO, linear LASSO, ridge cross-validation, ridge regression, and linear regression. This result indicates that the predictive performance of the models

XSL•FO
RenderX

corresponding to the 9 ML algorithms is relatively stable, and they exhibit strong generalizability.

Figure 5. The external validation receiver operating characteristic (ROC) curve plot for the 20 machine learning models. AdaBoost: adaptive boosting; ANN: artificial neural network; KNN: k-nearest neighbor; LASSO: least absolute shrinkage and selection operator; SGD: stochastic gradient descent; SVM: support vector machine.

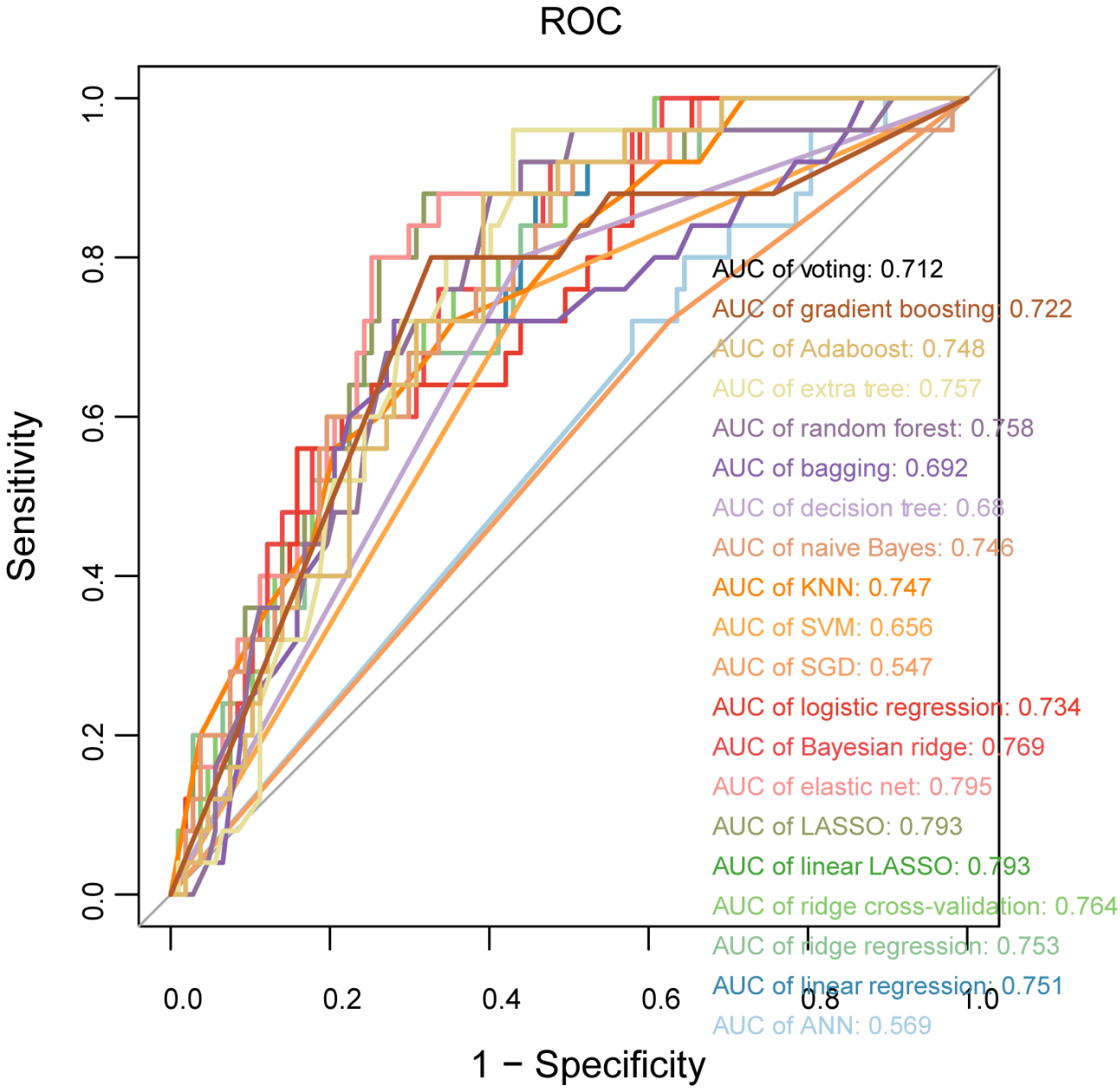

Figure 6 displays the confusion matrices of 20 ML algorithms during external validation. The sensitivity of all models decreased significantly, ranging from 37% to 62%, whereas the specificity remained relatively stable, fluctuating between 72% and 96%. These findings suggest that the models still possess high specificity in the external validation dataset. Multimedia Appendix 2 displays the DCA for 20 ML algorithms in external validation.

XSL•FO
RenderX

Figure 6. Confusion matrices of 20 machine learning algorithms during external validation. The top-left cell indicates the true positive, top-right indicates the false negative, bottom-left indicates the false positive, and bottom-right indicates the true negative. AdaBoost: adaptive boosting; ANN: artificial neural network; KNN: k-nearest neighbor; LASSO: least absolute shrinkage and selection operator; SGD: stochastic gradient descent; SVM: support vector machine.

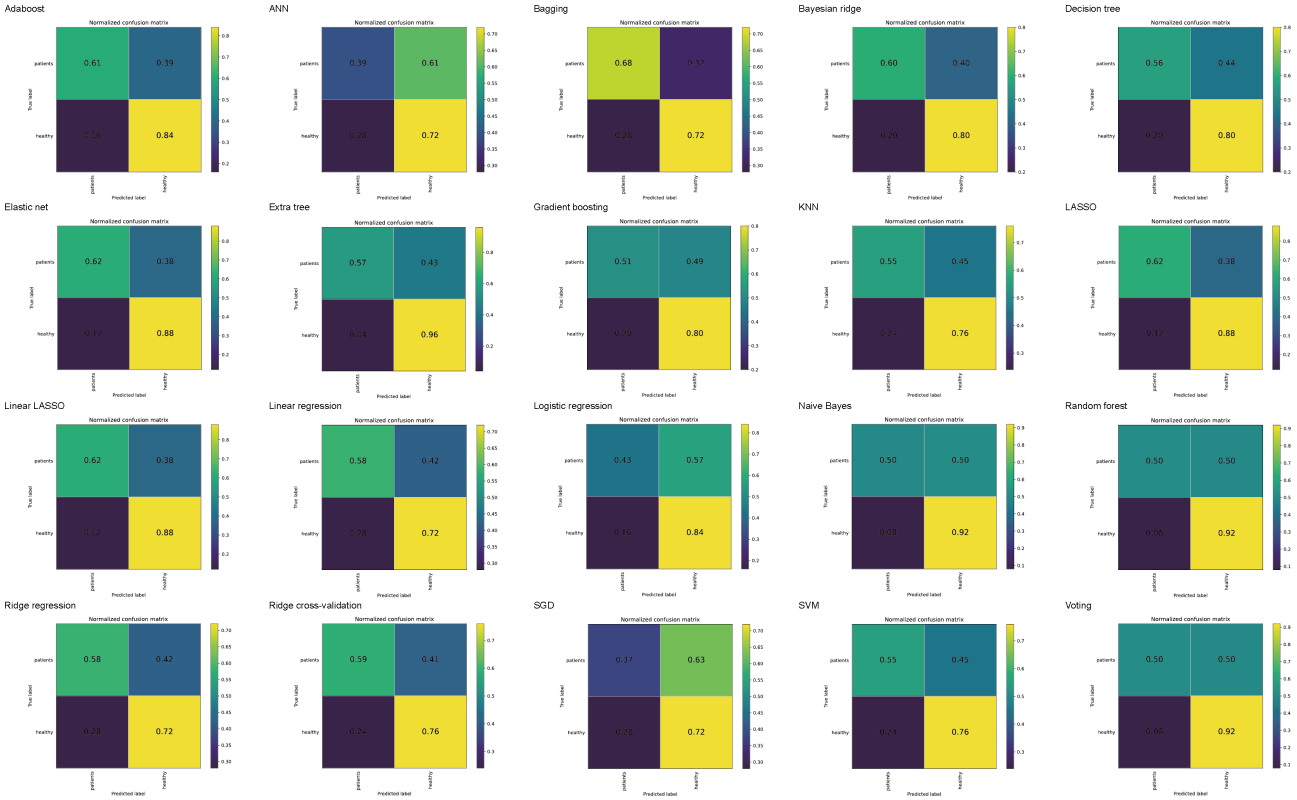

Discussion

Principal Findings

As a rapidly advancing field in computer science, AI has the ability to process vast and intricate medical data for the diagnosis and prediction of potential clinical outcomes [17]. ML, as a component of AI, can extract valuable information and patterns from vast amounts of data through learning and analysis, thereby achieving AI [18]. In the medical field, ML is predominantly used for medical image analysis, disease prediction and risk assessment, health care management, decision support, and drug development, among other applications [19-21]. As the first study to construct a VTE risk prediction model based on whole blood gene expression information, the present research aims to empower the diagnosis of VTE through the use of ML algorithms. It is important to note that the current model was trained and validated only on healthy controls versus patients with VTE and does not assess its discriminative ability in populations with other inflammatory or thrombotic conditions. On the other hand, the external validation results indicate that the models developed in this study are characterized by low sensitivity and high specificity. According to the "No free lunch" theory proposed by Wolpert et al [22], a perfect model does not exist. In other words, if a certain ML model outperforms other algorithms in a particular evaluation metric, it must inevitably sacrifice some performance in other metrics as a trade-off. As a result of this constraint, it is not feasible to determine a flawless ML model as the conclusive outcome. Rather, a more fitting model is chosen by taking into account a comprehensive evaluation of diverse metrics.

At present, the models used for predicting the risk of VTE occurrence are predominantly built upon clinical features. Darzi et al [23] conducted a meta-analysis that included 17 studies, which indicated that VTE may be associated with the following factors: advanced age, elevated C-reactive protein levels, increased D-dimer and fibrinogen levels, tachycardia, thrombocytosis, leukocytosis, fever, leg swelling, malignancy, immobility, infection, and so on. In 2021, Pandor et al [24] conducted a systematic review of 24 VTE risk assessment models to evaluate their predictive performance. The results showed that the *C*-statistic was generally less than 0.7 for all models, with only a few models having favorable *C*-statistics (>0.8). Among these models, sensitivity fluctuated between 12% and 100%, while specificity varied between 7.2% and 100%. Based on the aforementioned findings, the study suggests that the existing VTE risk prediction models have generally weak predictive ability and high heterogeneity, and thus, does not recommend the use of any specific prediction model. Our study is an exciting and innovative attempt to discover modeling features based on gene expression analysis. In the internal validation, most of the models developed in this study exhibited good performance (AUC >0.90), while in the external validation, the data showed that 9 models had an AUC greater than 0.75. Considering clinical applicability, we note that models such as LASSO, ridge regression, and linear regression not only performed well in external validation (AUC >0.75), but also offer the advantages of simplicity, computational efficiency, and interpretability. In contrast, while ensemble models such

XSL•FO
RenderX

as RF and extra trees demonstrated strong predictive power, their black-box nature may pose challenges for clinical interpretation. As such, we believe interpretable models like LASSO may be better suited as candidates for further clinical translation.

The current clinical diagnostic techniques for VTE primarily consist of D-dimer testing, ultrasonography, and venography [5]. Each of the aforementioned 3 diagnostic methods has their own limitations to varying degrees. In 2016, Crawford et al [25] conducted a meta-analysis of 1585 patients from 4 studies and reported that the sensitivity and specificity of D-dimer for diagnosing VTE were 80% to 100% and 23% to 63%, respectively. Although the sensitivity and specificity of D-dimer for diagnosing VTE may vary slightly across different studies, they generally exhibit high sensitivity and low specificity. The main reason for this phenomenon is that various conditions, including trauma, malignancy, and inflammation, can cause an elevation in D-dimer levels, leading to high sensitivity but low specificity in diagnosing VTE using D-dimer testing [26]. In summary, an isolated increase in D-dimer levels is insufficient to establish a diagnosis of VTE. The VTE risk prediction model developed in this study complements D-dimer well in terms of diagnostic performance. Moreover, since both tests use blood samples, they are highly compatible with each other in combination. The high specificity of the developed models, when used in combination with D-dimer testing, can assist clinicians in excluding false-positive cases that may be misdiagnosed as VTE by D-dimer alone. Furthermore, the joint use of the models and D-dimer has the potential to improve the diagnostic accuracy of VTE in patients. This patient population should be regarded as a priority for VTE prevention by clinicians to optimize VTE prevention measures, avoid wastage of medical resources, and achieve greater precision in VTE prevention. A potential clinical application of the gene expression-based models could be in a 2-step diagnostic pathway. For instance, the models may be used as a secondary triage tool following a positive D-dimer result to improve specificity and reduce unnecessary imaging procedures. Alternatively, they could be selectively applied to high-risk subpopulations (eg, older patients, postoperative individuals, or those with cancer) where D-dimer alone may be insufficiently specific. On the other hand, despite encouraging AUC values and specificity in external validation, we acknowledge that the observed sensitivity levels (ranging from 37%-62%) limit the standalone diagnostic capability of the models. This performance pattern may partly result from the significant class imbalance in the validation dataset and potential dataset shift. Importantly, the models are not intended to replace established diagnostic tools, but rather to serve as adjunctive decision aids. Their high specificity may be particularly valuable in ruling out false positives among D-dimer positive patients. Future work may consider ensemble approaches, risk stratification frameworks, or combining these models with clinical parameters to improve sensitivity while preserving specificity.

This study has several limitations. First, the modeling and external validation data were obtained from 2 sequencing cohorts in the GEO database (n=133; n=132), which may be considered a relatively small sample size, and the external validation set also exhibited a notable class imbalance (107 VTE vs 25 controls), which may have contributed to the observed reduction in sensitivity. Second, as the model has not yet been implemented in clinical practice, and both datasets were derived from US populations without detailed ethnicity annotations in the GEO records, its predictive performance in real-world clinical settings and across diverse ethnic backgrounds remains unverified. Third, we used a sequential feature selection strategy combining LASSO, RF, and RFE, aiming to enhance robustness and reduce dimensionality. However, we acknowledge that this approach may introduce complexity and the potential risk of overfitting, particularly when applied to algorithms that already incorporate internal regularization mechanisms. This redundancy could limit generalizability. Moreover, although some of the best-performing models in this study are inherently nontransparent, several interpretable models (eg, LASSO and logistic regression) were also included to ensure interpretability and practical applicability. In future work, we aim to further improve the explainability of complex models by using Shapley Additive Explanations or Local Interpretable Model-Agnostic Explanations–based interpretation frameworks, thereby enhancing their clinical interpretability and reliability. Future studies may benefit from alternative feature selection strategies, such as embedded or end-to-end feature learning methods within specific model frameworks, and from incorporating formal calibration analyses to improve clinical interpretability and reliability.

Conclusions

The current study used ML algorithms to construct 20 VTE risk prediction models based on whole blood gene expression information. Notably, 9 of these models displayed favorable diagnostic performance in the external validation dataset. Thus, these models, in conjunction with D-dimer, have the potential to serve as a valuable reference for the clinical diagnosis of VTE.

Acknowledgments

The authors acknowledge the efforts of the Gene Expression Omnibus database in providing high-quality open resources for researchers.

Funding

This study was supported by the Research Innovation Fund for Chinese Universities (Grant No. 2025XH113).

XSL•FO
RenderX

Data Availability

The data that support the findings of this study are available from the corresponding author upon reasonable request.

Authors' Contributions

YH, LZ, and WL conceptualized the study and developed the methodology. YH and XC curated the data and performed the formal analysis. YH and XC wrote the original draft. GB, YZ, and DK visualized the results. LZ and WL supervised and administered the project and reviewed and edited the manuscript. All authors have directly accessed and verified the underlying data reported in the manuscript. All authors critically reviewed the manuscript for important intellectual content and had final responsibility for the decision to submit for publication.

Conflicts of Interest

None declared.

Multimedia Appendix 1
Decision curve analysis (DCA) for 20 machine learning algorithms.
[ZIP File, 210 KB - medinform_v14i1e75565_app1.zip]

Multimedia Appendix 2
Decision curve analysis (DCA) for 20 machine learning algorithms in external validation.
[ZIP File, 221 KB - medinform_v14i1e75565_app2.zip]

References

1. Khan F, Tritschler T, Kahn SR, Rodger MA. Venous thromboembolism. Lancet 2021 Jul 3;398(10294):64-77. [doi: 10.1016/S0140-6736(20)32658-1] [Medline: 33984268]
2. Heit JA. Epidemiology of venous thromboembolism. Nat Rev Cardiol 2015 Aug;12(8):464-474. [doi: 10.1038/nrcardio.2015.83] [Medline: 26076949]
3. Phillippe HM. Overview of venous thromboembolism. Am J Manag Care 2017 Dec;23(20 Suppl):S376-S382. [Medline: 29297660]
4. Heit JA, Silverstein MD, Mohr DN, Petterson TM, O'Fallon WM, Melton LJ 3rd. Predictors of survival after deep vein thrombosis and pulmonary embolism: a population-based, cohort study. Arch Intern Med 1999 Mar 8;159(5):445-453. [doi: 10.1001/archinte.159.5.445] [Medline: 10074952]
5. Muñoz Rodríguez FJ. Diagnosis of deep vein thrombosis. Rev Clin Esp 2020 Jun 27:S0014-2565(20)30132-6. [doi: 10.1016/j.rce.2020.03.009] [Medline: 32600570]
6. Righini M, Robert-Ebadi H, Le Gal G. Diagnosis of acute pulmonary embolism. J Thromb Haemost 2017 Jul;15(7):1251-1261. [doi: 10.1111/jth.13694] [Medline: 28671347]
7. Varrias D, Palaiodimos L, Balasubramanian P, et al. The use of point-of-care ultrasound (POCUS) in the diagnosis of deep vein thrombosis. J Clin Med 2021 Aug 30;10(17):17. [doi: 10.3390/jcm10173903] [Medline: 34501350]
8. Johnson ED, Schell JC, Rodgers GM. The D-dimer assay. Am J Hematol 2019 Jul;94(7):833-839. [doi: 10.1002/ajh.25482] [Medline: 30945756]
9. Choi RY, Coyner AS, Kalpathy-Cramer J, Chiang MF, Campbell JP. Introduction to machine learning, neural networks, and deep learning. Transl Vis Sci Technol 2020 Feb 27;9(2):14. [doi: 10.1167/tvst.9.2.14] [Medline: 32704420]
10. Deo RC. Machine learning in medicine. Circulation 2015 Nov 17;132(20):1920-1930. [doi: 10.1161/CIRCULATIONAHA.115.001593] [Medline: 26572668]
11. Wang H, Chen B, Sun H, Zhang Y. Carbon-based molecular properties efficiently predicted by deep learning-based quantum chemical simulation with large language models. Comput Biol Med 2024 Jun;176:108531. [doi: 10.1016/j.compbiomed.2024.108531] [Medline: 38728991]
12. Lewis DA, Stashenko GJ, Akay OM, et al. Whole blood gene expression analyses in patients with single versus recurrent venous thromboembolism. Thromb Res 2011 Dec;128(6):536-540. [doi: 10.1016/j.thromres.2011.06.003] [Medline: 21737128]
13. Lewis DA, Suchindran S, Beckman MG, et al. Whole blood gene expression profiles distinguish clinical phenotypes of venous thromboembolism. Thromb Res 2015 Apr;135(4):659-665. [doi: 10.1016/j.thromres.2015.02.003] [Medline: 25684211]
14. Tibshirani R. The lasso method for variable selection in the Cox model. Stat Med 1997 Feb 28;16(4):385-395. [doi: 10.1002/(sici)1097-0258(19970228)16:4<385::aid-sim380>3.0.co;2-3] [Medline: 9044528]
15. Scikit-learn. Machine Learning in Python. URL: https://scikit-learn.org/stable/ [accessed 2026-01-14]
16. GEO: gene expression omnibus. URL: https://www.ncbi.nlm.nih.gov/geo/info/disclaimer.html [accessed 2026-01-16]

XSL•FO
RenderX

17. Hamet P, Tremblay J. Artificial intelligence in medicine. Metab Clin Exp 2017 Apr;69S:S36-S40. [doi: 10.1016/j.metabol.2017.01.011] [Medline: 28126242]
18. Haug CJ, Drazen JM. Artificial intelligence and machine learning in clinical medicine, 2023. N Engl J Med 2023 Mar 30;388(13):1201-1208. [doi: 10.1056/NEJMra2302038] [Medline: 36988595]
19. Shehab M, Abualigah L, Shambour Q, et al. Machine learning in medical applications: a review of state-of-the-art methods. Comput Biol Med 2022 Jun;145:105458. [doi: 10.1016/j.compbiomed.2022.105458] [Medline: 35364311]
20. Currie G, Hawk KE, Rohren E, Vial A, Klein R. Machine learning and deep learning in medical imaging: intelligent imaging. J Med Imaging Radiat Sci 2019 Dec;50(4):477-487. [doi: 10.1016/j.jmir.2019.09.005] [Medline: 31601480]
21. Gupta R, Srivastava D, Sahu M, Tiwari S, Ambasta RK, Kumar P. Artificial intelligence to deep learning: machine intelligence approach for drug discovery. Mol Divers 2021 Aug;25(3):1315-1360. [doi: 10.1007/s11030-021-10217-3] [Medline: 33844136]
22. Wolpert DH, Macready WG. No free lunch theorems for optimization. IEEE Trans Evol Computat 1997 Apr;1(1):67-82. [doi: 10.1109/4235.585893]
23. Darzi AJ, Karam SG, Charide R, et al. Prognostic factors for VTE and bleeding in hospitalized medical patients: a systematic review and meta-analysis. Blood 2020 May 14;135(20):1788-1810. [doi: 10.1182/blood.2019003603] [Medline: 32092132]
24. Pandor A, Tonkins M, Goodacre S, et al. Risk assessment models for venous thromboembolism in hospitalised adult patients: a systematic review. BMJ Open 2021 Jul 29;11(7):e045672. [doi: 10.1136/bmjopen-2020-045672] [Medline: 34326045]
25. Crawford F, Andras A, Welch K, Sheares K, Keeling D, Chappell FM. D-dimer test for excluding the diagnosis of pulmonary embolism. Cochrane Database Syst Rev 2016 Aug 5;2016(8):CD010864. [doi: 10.1002/14651858.CD010864.pub2] [Medline: 27494075]
26. Chopard R, Albertsen IE, Piazza G. Diagnosis and treatment of lower extremity venous thromboembolism: a review. JAMA 2020 Nov 3;324(17):1765-1776. [doi: 10.1001/jama.2020.17272] [Medline: 33141212]

Abbreviations

AI: artificial intelligence
AUC: area under the curve
DCA: decision curve analysis
GEO: Gene Expression Omnibus
KNN: k-nearest neighbors algorithm
LASSO: least absolute shrinkage and selection operator
ML: machine learning
RF: random forest
RFE: recursive feature elimination
ROC: receiver operating characteristic
VTE: venous thromboembolism

Edited by J Klann; submitted 07.Apr.2025; peer-reviewed by B Chen, L Raymond Guo, Z Ren; revised version received 11.Nov.2025; accepted 25.Nov.2025; published 16.Jan.2026.

Please cite as:
Huang Y, Chen X, Bai G, Zhao Y, Kuang D, Zhang L, Lu W
Development of Venous Thromboembolism Risk Prediction Models Based on Whole Blood Gene Expression Profiling Using 20 Machine Learning Algorithms: Comprehensive Analysis Study
JMIR Med Inform 2026;14:e75565
URL: https://medinform.jmir.org/2026/1/e75565
doi:10.2196/75565

© Yedong Huang, Xiaoyun Chen, Guannan Bai, Yajun Zhao, Dapeng Kuang, Lin Zhang, Wei Lu. Originally published in JMIR Medical Informatics (https://medinform.jmir.org), 16.Jan.2026. This is an open-access article distributed under the terms of the Creative Commons Attribution License (https://creativecommons.org/licenses/by/4.0/), which permits unrestricted use, distribution, and reproduction in any medium, provided the original work, first published in JMIR Medical Informatics, is properly cited. The complete bibliographic information, a link to the original publication on https://medinform.jmir.org/, as well as this copyright and license information must be included.

XSL•FO
RenderX

Automated Classification of Lymphoma Subtypes From Histopathological Images Using a U-Net Deep Learning Model: Comparative Evaluation Study

Jin Zhao*, MM; Xiaolian Wen*, MM; Li Ma, MD; Liping Su, MD

Department of Hematology, Cancer Hospital Affiliated to Shanxi Medical University, Shanxi Province Cancer Hospital, Shanxi Hospital Affiliated to Cancer Hospital, Chinese Academy of Medical Sciences, No. 3, Zhigong New Street, Taiyuan, China

*these authors contributed equally

Corresponding Author:
Liping Su, MD
Department of Hematology, Cancer Hospital Affiliated to Shanxi Medical University, Shanxi Province Cancer Hospital, Shanxi Hospital Affiliated to Cancer Hospital, Chinese Academy of Medical Sciences, No. 3, Zhigong New Street, Taiyuan, China

Abstract

Background: Accurate classification and grading of lymphoma subtypes are essential for treatment planning. Traditional diagnostic methods face challenges of subjectivity and inefficiency, highlighting the need for automated solutions based on deep learning techniques.

Objective: This study aimed to investigate the application of deep learning technology, specifically the U-Net model, in classifying and grading lymphoma subtypes to enhance diagnostic precision and efficiency.

Methods: In this study, the U-Net model was used as the primary tool for image segmentation integrated with attention mechanisms and residual networks for feature extraction and classification. A total of 620 high-quality histopathological images representing 3 major lymphoma subtypes were collected from The Cancer Genome Atlas and the Cancer Imaging Archive. All images underwent standardized preprocessing, including Gaussian filtering for noise reduction, histogram equalization, and normalization. Data augmentation techniques such as rotation, flipping, and scaling were applied to improve the model's generalization capability. The dataset was divided into training (70%), validation (15%), and test (15%) subsets. Five-fold cross-validation was used to assess model robustness. Performance was benchmarked against mainstream convolutional neural network architectures, including fully convolutional network, SegNet, and DeepLabv3+.

Results: The U-Net model achieved high segmentation accuracy, effectively delineating lesion regions and improving the quality of input for classification and grading. The incorporation of attention mechanisms further improved the model's ability to extract key features, whereas the residual structure of the residual network enhanced classification accuracy for complex images. In the test set (N=1250), the proposed fusion model achieved an accuracy of 92% (1150/1250), a sensitivity of 91.04% (1138/1250), a specificity of 89.04% (1113/1250), and an F_1-score of 90% (1125/1250) for the classification of the 3 lymphoma subtypes, with an area under the receiver operating characteristic curve of 0.95 (95% CI 0.93 - 0.97). The high sensitivity and specificity of the model indicate strong clinical applicability, particularly as an assistive diagnostic tool.

Conclusions: Deep learning techniques based on the U-Net architecture offer considerable advantages in the automated classification and grading of lymphoma subtypes. The proposed model significantly improved diagnostic accuracy and accelerated pathological evaluation, providing efficient and precise support for clinical decision-making. Future work may focus on enhancing model robustness through integration with advanced algorithms and validating performance across multicenter clinical datasets. The model also holds promise for deployment in digital pathology platforms and artificial intelligence–assisted diagnostic workflows, improving screening efficiency and promoting consistency in pathological classification.

(JMIR Med Inform 2026;14:e72679) doi:10.2196/72679

KEYWORDS

deep learning; lymphoma; U-Net; pathological subtype; automated diagnosis; medical image analysis; artificial intelligence; AI

Introduction

Lymphoma is a malignant tumor originating in the lymphatic system, with a steadily increasing global incidence. On the basis of its clinical features and histological characteristics, lymphoma can be classified into various subtypes, with Hodgkin lymphoma and non-Hodgkin lymphoma being the most prevalent [1,2]. Accurate classification and grading of lymphoma are critical for clinical treatment and prognostic evaluation [3]. Conventional diagnostic approaches rely on the visual

XSL•FO
RenderX

examination of tissue sections by pathologists under a microscope, a process that is labor-intensive and influenced by subjective judgment. Diagnostic accuracy is often limited by the pathologist's expertise and technical proficiency and by sample quality [4,5]. With the advancements in medical imaging and computational technology, artificial intelligence (AI) techniques such as deep learning have been gradually introduced into medical image analysis [6], showing great potential in automated image segmentation, feature extraction, and disease diagnosis [7].

Deep learning, particularly convolutional neural networks (CNNs), has achieved significant success in medical image analysis, offering new approaches for automated lymphoma diagnosis [8,9]. Among them, the U-Net architecture, a specialized form of convolutional neural network, has demonstrated notable effectiveness in segmentation tasks by enabling precise delineation of lesion areas and producing high-quality inputs for subsequent classification and grading [7,10]. Despite these advancements, several challenges persist in the automated analysis of lymphoma histopathology images [11]. Minimal morphological differences between subtypes and the inherent complexity of lesion regions increase classification difficulty [12]. Moreover, the performance of existing deep learning models remains highly dependent on large volumes of annotated data. Limited datasets and overfitting remain a pressing challenge [13,14]. Therefore, developing a deep learning model that can effectively improve the accuracy of lymphoma pathological image classification and grading has become a critical research direction in medical image analysis [15].

Recent studies have shown that pathological diagnosis of lymphoma is associated with considerable interobserver variability, with consistency coefficients (κ values) ranging between 0.55 and 0.70. Misclassification frequently occurs among morphologically similar subtypes, including follicular lymphoma (FL) and mantle cell lymphoma (MCL). Previous research has applied CNNs and other machine learning models for automatic classification of pathological images, such as Inception-V3–based models for breast cancer image analysis or residual network (ResNet)–based models for predicting lung cancer types and molecular features. These studies highlight the substantial potential of AI in assisting pathological diagnosis. However, research specifically focused on the classification of lymphoma pathological subtypes remains limited and often restricted to individual subtypes or single-model architectures. There is still a lack of systematic validation of hybrid deep learning models for fine-grained classification across multiple lymphoma subtypes.

This study aimed to achieve automated segmentation, subtype classification, and grading of lymphoma pathological images by integrating deep learning techniques, including the U-Net model, attention mechanisms, and residual networks (ResNet), all of which are established deep learning approaches [4]. This research has significant clinical and practical implications. Deep learning models have the potential to significantly improve the accuracy of lymphoma pathological diagnosis, reduce human-related diagnostic errors, and provide more objective and consistent diagnostic results [16]. Automated systems can also process large volumes of pathological slides at high speed, offering an efficient auxiliary tool for pathologists, accelerating the lymphoma diagnostic workflow, and reducing patient waiting times. Moreover, precise identification and grading of lymphoma subtypes may contribute to the development of personalized treatment strategies, allowing for more tailored treatment plans and improving treatment outcomes and survival rates [17].

The primary objective of this study was to explore and evaluate the application of deep learning techniques in classifying and grading lymphoma pathological subtypes. An automated image analysis system was constructed based on the U-Net architecture. Through deep learning methods such as image segmentation, feature extraction, and classification prediction, this study sought to accurately identify different lymphoma subtypes and achieve effective grading. In addition, this study used cross-validation techniques to assess the stability and accuracy of the proposed model. A comparative analysis with traditional pathological diagnostic methods was conducted to verify the model's clinical feasibility. Ultimately, this study aimed to provide effective technical support for the early diagnosis of lymphoma, advancing the application and development of AI into the field of medical pathology.

Methods

Data Collection and Preprocessing

A total of 620 high-quality histopathological images representing 3 major lymphoma subtypes were collected from The Cancer Genome Atlas (TCGA) and The Cancer Imaging Archive (TCIA). The number of samples per subtype was approximately balanced. Inclusion criteria required complete pathological annotations and clearly defined tissue structures. Images exhibiting severe artifacts, incomplete labeling, or low resolution were excluded. All slides were stained with hematoxylin and eosin and resized to 512 × 512 pixels to ensure model compatibility. No stain normalization was applied.

The image data in this study primarily consisted of standardized lymphoma tissue section images captured using high-resolution digital scanners and stored in TIFF or PNG format. Image preprocessing steps included denoising, contrast enhancement, and image normalization. Gaussian filtering was used to reduce noise, whereas histogram equalization was used to enhance contrast and improve the visibility of lesion regions. All images were uniformly cropped and resized to ensure consistent input data quality for the network. These preprocessing procedures were implemented to improve data quality and model classification accuracy (Figure S1 in Multimedia Appendix 1).

Feature Extraction From Image Data

This study used the U-Net architecture to conduct image segmentation, enabling precise identification of lesion areas and the generation of high-quality segmentation maps. Subsequently, ResNet was used for feature extraction and classification. The residual learning structure in ResNet enabled the capture of deep pathological features from the segmented images, thereby improving classification accuracy and supporting automated grading of lymphoma subtypes. During

XSL•FO
RenderX

training, 5-fold cross-validation was used to optimize model hyperparameters and reduce the risk of overfitting. The Adam optimization algorithm was used in conjunction with a learning rate decay strategy to enhance training stability and convergence (Figure S2 in Multimedia Appendix 1). The training dataset was randomly divided into 3 subsets, with 70% allocated to the training set and 15% each allocated to the validation and test sets.

Model Construction and Training

The model used in this study was based on the standard U-Net architecture, enhanced by integrating ResNet residual modules and attention mechanisms. To achieve subtype classification and grading of lymphoma, the combined use of U-Net and ResNet allowed for effective image segmentation and deep feature extraction. The cross-entropy loss function was used, and the Adam optimizer with an initial learning rate of 0.001 was adopted to ensure stable model convergence. A learning rate decay mechanism was applied to progressively adjust the learning rate, improving model convergence and training stability (Figure S3 in Multimedia Appendix 1). The model can automatically extract and learn features of different lymphoma subtypes and grades from images through this training process, enabling efficient classification and accurate grading of new images.

To further justify the selected model architecture, a comparative evaluation was conducted against several classic CNN frameworks widely used in medical image analysis (Table S1 in Multimedia Appendix 1). Fully convolutional networks offered advantages in simplicity and computational efficiency but demonstrated limited sensitivity in detecting small lesions and boundary structures in pathological images. SegNet achieved reliable semantic segmentation performance but often resulted in detail loss during the upsampling stage due to its deconvolutional design. DeepLabv3+, which uses atrous convolution and multiscale feature fusion, significantly improved segmentation accuracy but introduced increased model complexity, computational cost, and reduced interpretability in clinical settings. In contrast, the hybrid deep learning framework proposed in this study—featuring a U-Net backbone, ResNet residual connections, and attention mechanisms—achieved a better balance among segmentation accuracy, training stability, and interpretability. It is particularly well-suited for the classification and grading of lymphoma images characterized by blurry boundaries and high subtype heterogeneity.

Model Evaluation and Optimization

Model performance was evaluated using multiple metrics, including accuracy, recall, precision, and F_1-score, to assess classification effectiveness. The receiver operating characteristic curve and the area under the curve (AUC) were used to further evaluate the model's discriminative ability. To prevent overfitting and enhance generalization capability, the model incorporated dropout layers and data augmentation techniques. Augmentation strategies included image rotation, translation, and flipping, which increased the diversity of the training data and improved model robustness. During training, the performance on the validation set was monitored in real time to identify and preserve the model with the best generalization ability for subsequent testing (Figure S4 in Multimedia Appendix 1).

Traditional Pathology Baseline and Metric Sources

To establish a reproducible baseline for comparison with traditional pathological diagnosis, we conducted a randomized crossover washout reading study. Six board-certified pathologists with ≥5 years of professional experience were enrolled. From the 620 cases included in this study, a subset of 180 (29%) was stratified by subtype, center, and diagnostic difficulty to form the reading set. The reference standard (ground truth) was determined by 2 senior pathologists independently, with any discrepancies resolved by a third expert adjudicator. Each reader completed case interpretation under 2 study arms: unassisted and AI-assisted (with U-Net–generated segmentation masks and posterior probability and attention cues displayed). The order of arms and case sequence was computer randomized, with a washout period of at least 2 weeks, and the readers were blinded to previous assessments. The primary endpoint was case-level accuracy. Secondary endpoints included sensitivity, specificity, F_1-score, AUC, mean average precision (mAP), weighted κ, and single-case reading time. Segmentation performance was evaluated using case-level dice coefficient and intersection over union (macro- and microaveraged). Classification and grading were assessed at the whole-slide image level; patch-level probabilities were aggregated via attention pooling, and classification thresholds were determined on the validation set using the Youden index and subsequently fixed for the test set. For statistical analyses, the DeLong test was used to compare AUCs, whereas the McNemar test was applied to paired proportions (accuracy, sensitivity, and specificity). The 95% CIs were estimated via the bias-corrected and accelerated bootstrap method (1000 iterations), and Holm-Bonferroni correction was used for multiple comparisons.

Image Data Analysis Methods

Image data analysis focused on 2 primary tasks: image classification and subtype grading. First, deep CNNs based on U-Net and ResNet were used to analyze histopathological slide images. These architectures effectively captured cellular morphology and tissue-level structural features, enabling accurate differentiation among lymphoma subtypes. For subtype grading, the analysis extended beyond subtype identification to include the evaluation of lymphocyte distribution, morphological variation, and lesion heterogeneity within the image (Figure S5 in Multimedia Appendix 1). To ensure accuracy in classification and grading, the image analysis methods integrated traditional medical imaging analysis techniques with deep learning approaches using automated and manual annotation strategies.

Statistical Analysis and Result Validation

Following model construction, statistical methods were used to validate its performance comprehensively. In addition to conventional classification evaluation metrics, a confusion matrix was used to analyze the model's prediction results in detail, identifying errors such as false positives and false negatives. The average accuracy of the model was calculated through multiple repeated experiments, and k-fold cross-validation was used to ensure the robustness of the results.

XSL•FO
RenderX

Furthermore, 2-tailed *t* tests or ANOVA were conducted to analyze differences among models, ensuring that the selected model demonstrated superior performance in lymphoma subtype classification and grading tasks (Figure S6 in Multimedia Appendix 1).

Feature Analysis and Subtype Differentiation

Feature analysis was conducted using the U-Net and ResNet architectures to extract and differentiate cellular and tissue-level characteristics from histopathological images. Key features, including tumor cell morphology, tissue architecture, and cellular distribution, were effectively captured to support the accurate identification of lymphoma subtypes and enhance understanding of histological variation among them.

U-Net provided precise segmentation of lesion regions, whereas ResNet enabled efficient feature extraction and supported deeper network training. The combination of these 2 architectures facilitated the recognition of complex spatial relationships between cells and tissues, contributing to improved classification accuracy.

In addition, statistical analysis methods are crucial in evaluating model performance. Metrics such as sensitivity, specificity, precision, and recall were calculated to comprehensively assess the performance of different models in classifying lymphoma pathological subtypes. Confusion matrices and receiver operating characteristic curve analyses were also used to evaluate each model's predictive effectiveness, providing deeper insights into the strengths and limitations of the models in identifying various subtypes.

Ethical Considerations

All histopathological images used in this study were obtained from publicly available databases (TCGA project and TCIA). All datasets underwent strict anonymization procedures before public release and complied with the relevant ethical policies and data sharing regulations. No new patient samples were collected during the course of this research. Therefore, additional ethics approval was not required. This study adhered to the ethical principles outlined in the Declaration of Helsinki and its subsequent amendments. Access to the image data is available under the open access policies of TCGA and TCIA or upon request from the corresponding author.

Results

Effect Analysis of Data Preprocessing and Image Quality Enhancement

In this study, the quality of lymphoma pathological slide images directly affected the performance of the deep learning model. Therefore, multiple image preprocessing techniques, including Gaussian filtering for noise reduction, histogram equalization, and image normalization, were applied to improve image quality. Figure 1 illustrates the visual differences between raw and preprocessed images. In the preprocessed images, background noise was substantially reduced, edges appeared sharper, and lesion regions became more prominent. These enhancements facilitated clearer visualization of pathological features and improved input consistency for model training. During subsequent deep learning model training, the preprocessed images exhibited higher segmentation accuracy and lower error rates. A detailed dataset analysis was also conducted to assess sample distribution. Table 1 presents the number of samples in the training, validation, and test sets, along with the specific distribution of each class, providing crucial data support for subsequent model training.

Figure 1. Visualization of data preprocessing effects. This figure showcases the effects of different preprocessing stages on the same lymphoma image slide: (A) the original image; (B) the denoised image processed through Gaussian filtering; (C) the contrast-enhanced image after histogram equalization; and (D) the normalized image, showing clearer edges and details.

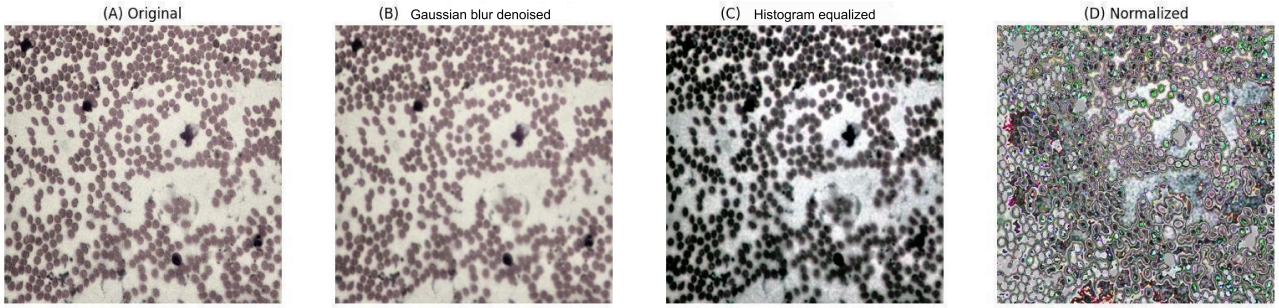

Table . Distribution of dataset samples—the number of samples in the training, validation, and test sets along with their corresponding categories.

Dataset	Number of immune cell samples	Number of epithelial cell samples	Number of matrix cell samples	Total
Training set	4000	3000	2500	9500
Validation set	500	400	350	1250
Test set	500	400	350	1250
Total	5000	3800	3200	12,000

XSL•FO
RenderX

To evaluate the impact of image preprocessing on model performance, a comparative experiment was conducted using both unprocessed and preprocessed images. The results showed that unprocessed images achieved only 77.12% (964/1250) accuracy in the segmentation task, with poor edge detection quality, slower model convergence, and a substantially higher error rate. In contrast, preprocessed images achieved a segmentation accuracy of 84.4% (1055/1250), demonstrating clearer delineation of lesion boundaries and exhibiting a noticeably faster training speed (Table S2 in Multimedia Appendix 1). These findings highlight the importance of preprocessing steps such as Gaussian filtering, histogram equalization, and normalization in significantly enhancing segmentation performance.

Performance of the U-Net Model in Image Segmentation

The application of the U-Net architecture in image segmentation demonstrated strong performance in accurately segmenting lesion areas in lymphoma pathological slides, significantly outperforming traditional methods. Figure 2 illustrates the performance of the U-Net model in segmentation tasks. During training and validation, the U-Net model achieved a segmentation accuracy exceeding 85.04% (1063/1250) on the test set, with a recall rate of 88% (1100/1250). These results confirmed the capability of U-Net in handling complex medical images, particularly lymphoma pathological slides. Effective segmentation of lesion areas provided high-resolution input data for downstream tasks, including subtype classification and pathological grading.

Figure 2. U-Net image segmentation results. This figure shows the performance of the U-Net model on the image segmentation task for lymphoma pathological slides. Segmented regions are marked in different colors to distinguish lesion areas from healthy tissue.

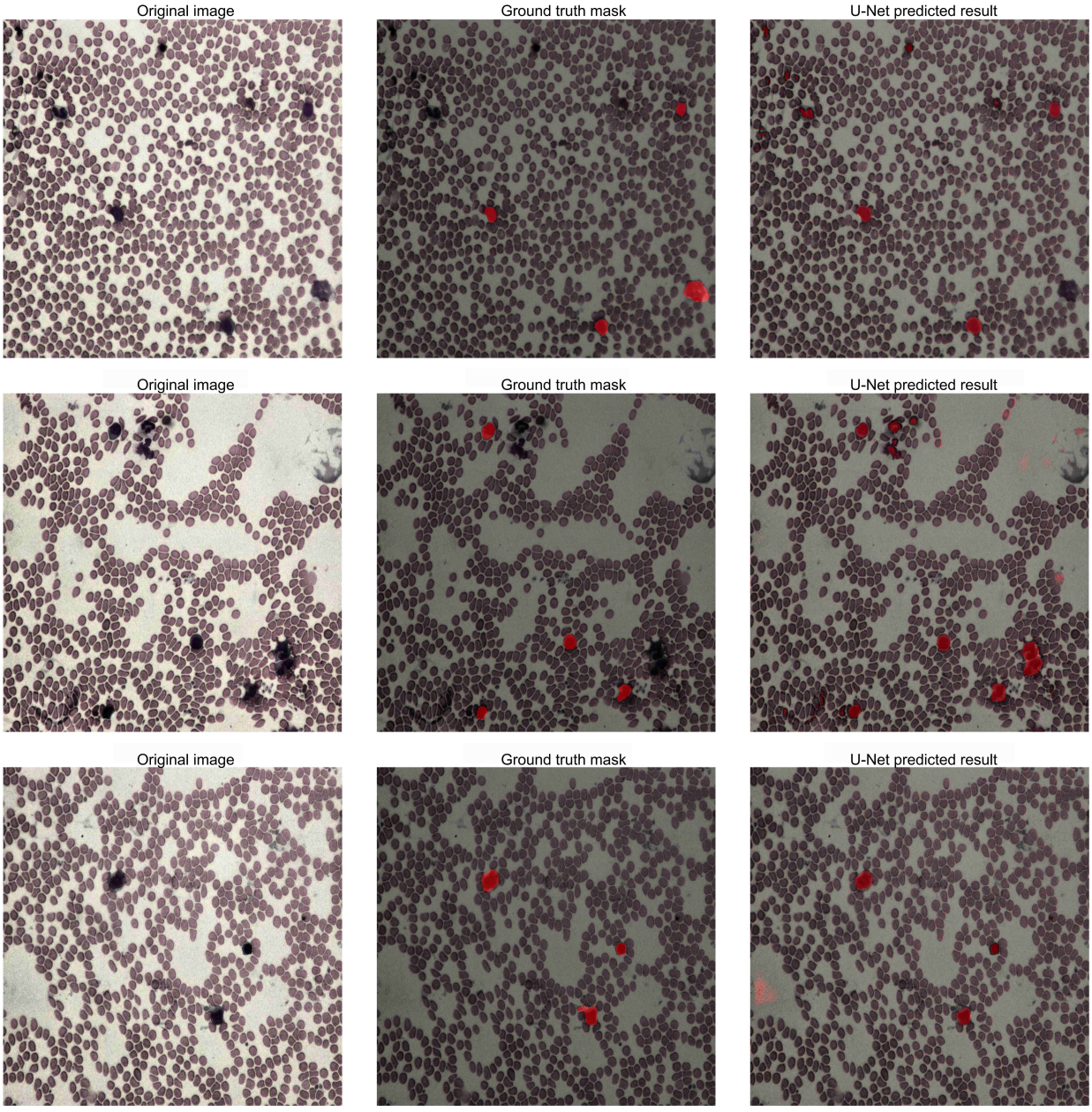

XSL•FO
RenderX

Analysis of the Synergistic Effects of Attention Mechanisms and ResNet

Integrating attention mechanisms with ResNet for feature extraction and classification markedly enhanced model performance. Figure 3 shows the results of lymphoma subtype classification using the combined model. Incorporating the attention mechanism enabled the network to concentrate on diagnostically relevant image regions, thereby reducing errors in differentiating morphologically similar subtypes. Meanwhile, the residual structure of ResNet effectively mitigated the vanishing gradient problem and facilitated the learning of complex image features. Compared with traditional CNNs, the classification accuracy of the proposed deep learning model increased from 81.04% (1013/1250) to 91.04% (1138/1250), representing an improvement of approximately 10 percentage points.

Figure 3. Analysis of attention mechanism and residual network (ResNet) synergy. This figure compares model performance in subtype classification tasks: (A) results of a traditional convolutional neural network and (B) results after incorporating attention mechanisms and ResNet, showing significant improvement in accuracy. CLL: chronic lymphocytic leukemia; FL: follicular lymphoma; MCL: mantle cell lymphoma.

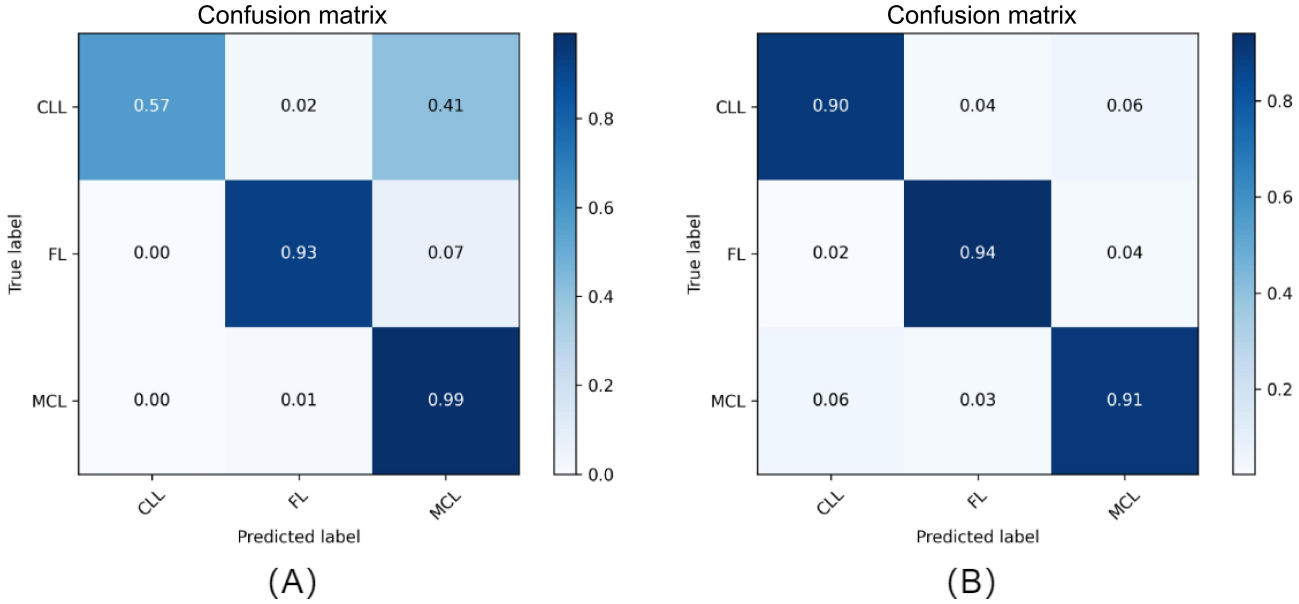

Evaluation of Model Stability and Generalization Capability

To evaluate the stability and generalization capability of the model, 5-fold cross-validation was performed. The model demonstrated high consistency across the 5 independently partitioned training-validation subsets with only minor fluctuations in accuracy (Figure 4). During cross-validation (N=10,750 samples), the model achieved an average accuracy of 90% (9675/10,750), confirming its robustness and reliability. Even under small-sample conditions, the model maintained high predictive accuracy, indicating good generalization ability and strong resistance to overfitting.

XSL•FO
RenderX

Figure 4. Analysis of model stability and generalization capability. This figure shows the accuracy changes during 5-fold cross-validation. The blue line represents the training set, and the red line represents the validation set. The figure shows stable and minimal fluctuations in model performance across different data splits.

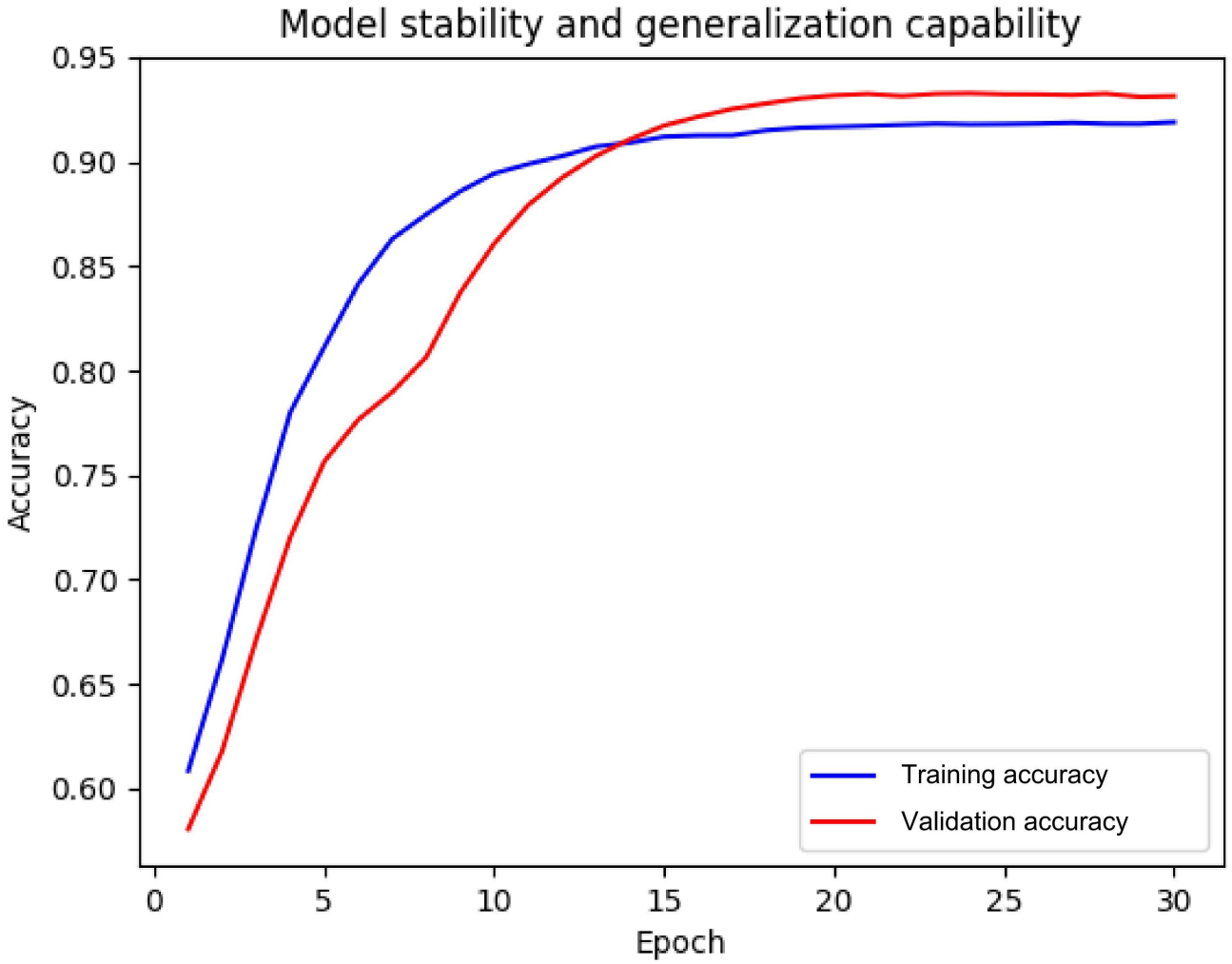

Analysis of Lymphoma Subtype Classification Results

To evaluate the performance of the deep learning model in lymphoma subtype classification, classification results on the test set were analyzed using accuracy, precision-recall curves, and mAP as evaluation metrics. The results showed that the model achieved a classification accuracy of 98% (1225/1250) when distinguishing FL, chronic lymphocytic leukemia, and MCL. Additionally, the precision-recall curve demonstrated a high AUC, and the mAP reached 97%, indicating strong overall classification performance. Multiclass analysis revealed that most classification errors occurred between subtypes with similar morphological characteristics, such as FL and MCL (Figure 5). The incorporation of a feature enhancement module significantly improved the model's ability to extract critical features from key regions, leading to a nearly 5% increase in classification performance.

XSL•FO
RenderX

Figure 5. Evaluation of lymphoma subtype classification performance. This figure shows the model's performance in subtype classification, including (A) accuracy, (B) precision-recall curve, and (C) mean average precision (mAP), reflecting comprehensive performance in multiclass classification tasks. CLL: chronic lymphocytic leukemia; FL: follicular lymphoma; MCL: mantle cell lymphoma.

XSL•FO
RenderX

Under 5-fold cross-validation (total sample size: n=10,750), the model achieved an average classification accuracy of 90% (9675/10,750; SD 1.9%), an F_1-score of 90% (9673/10750; SD 2.3%), and an AUC of 0.95 (SD 0.015) across the 3 lymphoma subtypes, all statistically significant (=0.004). In terms of subtype performance, the model demonstrated the highest sensitivity for FL at 94.2% (393/417), followed by chronic lymphocytic leukemia at 90.6% (378/417), whereas the performance for MCL was relatively lower at 87.3% (363/416), which may be attributed to the blurred boundaries and higher heterogeneity typically observed in MCL images. As this study primarily focused on model architecture and performance evaluation, interpretability tools such as gradient-weighted class activation mapping were not incorporated. Future work will include model interpretability analyses to enhance its clinical applicability.

To evaluate the superiority of the proposed model across different deep learning architectures, we systematically compared the fusion model with several mainstream CNN-based frameworks (Table S3 in Multimedia Appendix 1). The results showed that traditional fully convolutional networks and SegNet underperformed in the detection of small lesions and boundary delineation, with overall accuracies of 81.04% (1013/1250) and 83.52% (1044/1250), respectively—significantly lower than those of U-Net and its improved variants (P=0.006). DeepLabv3+ achieved improved segmentation accuracy (dice coefficient=83.9%) but suffered from increased training complexity and limited interpretability. In contrast, U-Net demonstrated stable performance in both segmentation and classification tasks (dice coefficient=85.5%; accuracy=1099/1250, 87.92%). The further incorporation of attention mechanisms and ResNet led to continuous performance gains, and the final fusion model achieved the best results in segmentation dice coefficient, classification accuracy, and AUC (dice coefficient=89.7%; accuracy=1150/1250, 92%; AUC=0.95), with statistically significant differences (P<). These findings indicate that the proposed fusion model provides a significant advantage in multisubtype classification and grading tasks.

Comparative Analysis With Traditional Pathological Diagnosis Methods

Compared to traditional pathologists' manual slide review methods, the deep learning model in this study demonstrated significant advantages in classification and grading tasks of lymphoma pathology images. Figure S7 in Multimedia Appendix 1 shows a comparison of accuracy between the deep learning model and the average accuracy of pathologists. Under conditions involving small sample sizes or diagnostically complex subtypes, the model maintained consistent performance and achieved higher classification accuracy than pathologists. Particularly in images with rich details or blurred edges, the deep learning model reduced human error and improved diagnostic efficiency, highlighting its potential application in clinical practice. To ensure fairness in comparison, all participating pathologists were mid- to senior-level professionals with more than 5 years of diagnostic experience in hematopathology (Figure S7 in Multimedia Appendix 1). Diagnoses were conducted in accordance with the World Health Organization classification guidelines and the expert consensus on pathological diagnosis of lymphoma. Each pathologist independently reviewed the same set of blinded slide images, and no communication was allowed during the review process. Final diagnostic results were determined through majority consensus. This selection protocol was designed to reflect the average diagnostic level of experienced pathologists in routine clinical practice.

Model Optimization and Accuracy Improvement Strategies

To improve model accuracy and stability, a series of optimization strategies were implemented, including learning rate decay, data augmentation, and dropout regularization, which significantly improved model performance. Figure 6 illustrates the performance changes of the model under different optimization strategies. The model gained greater diversity during training through the use of data augmentation, effectively improving its generalization capability. The incorporation of dropout layers effectively mitigated overfitting by reducing model reliance on specific neurons, allowing the network to maintain high accuracy on new datasets.

XSL•FO
RenderX

Figure 6. Effects of model optimization on accuracy improvement. This figure illustrates the impact of optimization strategies (learning rate decay, data augmentation, and dropout regularization) on model training: (A) changes in the loss function before and after optimization and (B) changes in accuracy before and after optimization, showing improved accuracy.

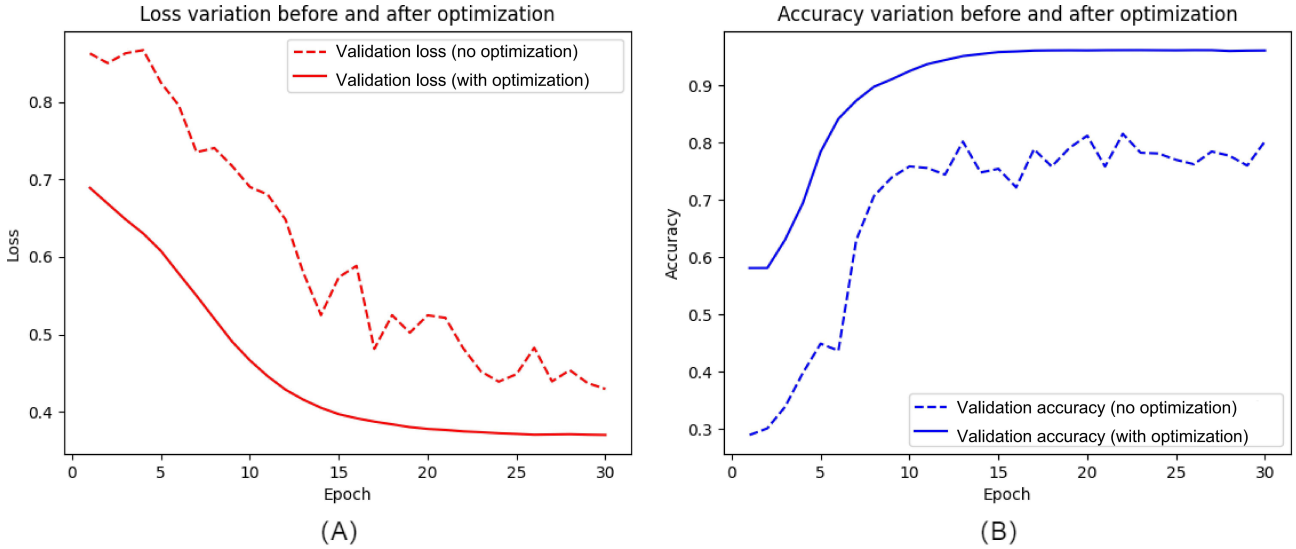

Discussion

Principal Findings

This study explored the application of deep learning techniques, particularly the U-Net model, in classifying and grading lymphoma pathological subtypes. The results showed that deep learning models significantly improved the efficiency and accuracy of automated lymphoma diagnosis. By integrating U-Net for image segmentation with ResNet for feature extraction, a robust diagnostic system was developed capable of differentiating Hodgkin lymphoma from non-Hodgkin lymphoma and accurately predicting lesion grades. Notably, the proposed deep learning model demonstrated significant advantages in segmentation accuracy, classification accuracy, and model stability. These results validated the potential of deep learning in medical image analysis, especially in disease diagnosis and clinical decision support systems.

U-Net exhibited outstanding performance in image segmentation tasks. Its precision in delineating lesion regions highlighted its ability to process complex pathological features. Lymphoma lesion regions often display irregular morphology and poorly defined boundaries, which limit the effectiveness of conventional manual segmentation methods. U-Net, through the hierarchical feature extraction capabilities of CNNs [15], enabled automated and accurate segmentation of lesion areas while minimizing subjective variability. The model achieved an accuracy exceeding 85.04% (1063/1250) on the test set, significantly improving the efficiency of lesion recognition and extraction [9].

However, despite the excellent performance of the deep learning model, several challenges were encountered, particularly regarding data scarcity and annotation quality. The acquisition of pathological images of lymphoma remains difficult, particularly for high-quality annotated data, which may impact model training effectiveness and generalization ability [7]. To address this issue, this study used strategies such as data augmentation and cross-validation [18] to improve the robustness and accuracy of the model. Nevertheless, inconsistencies in data quality, particularly the subjective differences among pathologists during annotation [19], may still affect model training and prediction. Future work could benefit from the development of standardized annotation protocols and the construction of larger, high-quality datasets to further refine model performance.

To optimize model accuracy and stability, several techniques were incorporated, including attention mechanisms, ResNet-based residual learning, and comprehensive data augmentation. The use of attention modules enabled the model to more precisely focus on diagnostically relevant regions within the pathological images, thereby reducing the influence of irrelevant features and enhancing subtype classification accuracy. ResNet's residual structure effectively mitigated the common issue of vanishing gradients in deep networks, enhancing the model's ability to learn complex pathological features. These optimization strategies significantly improved the model's performance in lymphoma subtype classification, achieving a classification accuracy of 92% (1150/1250) and a grading accuracy of 89.04% (1113/1250).

Compared to traditional pathological diagnostic methods, deep learning models offer distinct advantages. Traditional pathology relies on pathologists' experience and technical expertise, making the diagnostic process vulnerable to subjectivity and relatively inefficient when analyzing complex histological images [20]. In contrast, deep learning models can process large volumes of images quickly and provide efficient and objective diagnostic results [21]. Comparative analysis with manual slide review by pathologists revealed that deep learning models exhibited higher accuracy in handling complex and detail-rich images. Specifically, deep learning models reduced human error and improved diagnostic efficiency in lesion segmentation and subtype differentiation [6,22,23].

Despite the robust performance of deep learning models, several technical limitations remain. First, deep learning models' "black-box" nature presents a significant challenge, especially

XSL•FO
RenderX

in clinical settings, where physicians tend to favor interpretable diagnostic methods. Future research should focus on enhancing model interpretability by using visualization techniques and traceability analysis, allowing clinicians to better understand the rationale behind model predictions. Second, although the model achieved high accuracy in feature extraction and classification tasks, minor errors may still occur in subtype classification and grading, particularly when morphological differences between subtypes are subtle. Improving the model's performance in analyzing complex pathological images remains a key direction for future research.

In summary, this study confirmed the immense potential of deep learning technologies in lymphoma pathological image analysis and provides robust technical support for the automated diagnosis of clinical lymphoma. With ongoing advancements in computational methods, the application of deep learning in medical imaging analysis will become more extensive and profound. Such progress will play a vital role in developing personalized treatment plans, evaluating therapeutic efficacy, and improving patient survival rates, thereby providing substantial clinical value. The successful application of the proposed approach not only accelerated the diagnostic workflow but also provided clinicians with precise and efficient diagnostic tools, promoting greater automation and enhanced analytical capability in pathological image analysis.

Conclusions

This study demonstrated the significant potential of deep learning techniques, particularly the U-Net model, in lymphoma pathological subtype classification and grading. By combining U-Net for image segmentation and ResNet for feature extraction, an efficient and accurate diagnostic framework was developed capable of distinguishing Hodgkin lymphoma from non-Hodgkin lymphoma and precisely predicting the grades of lesions. The proposed model achieved strong performance in segmentation accuracy, classification accuracy, and model stability, validating the potential of deep learning technologies in medical imaging analysis, especially in disease diagnosis and clinical decision support.

As the core of this research, the U-Net model exhibited exceptional performance in segmenting pathological regions, effectively addressing challenges such as irregular morphology and blurred boundaries in lymphoma tissues. These capabilities significantly improved segmentation efficiency and accuracy, providing high-quality input data for subsequent classification and grading tasks. Additionally, integrating attention mechanisms and ResNet further optimized feature extraction and classification capabilities, achieving a classification accuracy of 92% (1150/1250) and a grading accuracy of 89.04% (1113/1250).

Despite the encouraging results, certain limitations remain. The limited availability of annotated lymphoma pathological images and inconsistencies in labeling quality may affect the model's training effectiveness and generalizability. Although data augmentation and cross-validation were used to improve robustness, variability in annotation and the scarcity of high-quality labeled data continue to pose challenges. In addition, the deep learning model's "black-box" nature limits its interpretability, which affects clinical acceptance and the transparency of decision-making. Moreover, the dataset used in this study was primarily derived from publicly available databases with a relatively limited sample size and without multicenter or real-world clinical validation, which may introduce sampling bias and increase the risk of overfitting. The model also exhibited relatively lower recognition performance for morphologically ambiguous subtypes such as MCL, suggesting that further optimization is needed to address highly heterogeneous lesions. Future work should focus on expanding the dataset with multicenter cohorts, integrating the model into digital pathology workflows as a clinical decision support tool, enhancing interpretability through visualization-based modules, and addressing ethical and regulatory challenges to ensure the safe and responsible application of AI technologies in health care settings.

In summary, this study demonstrated the outstanding performance of U-Net–based deep learning models in analyzing lymphoma pathological images. These techniques significantly improved diagnostic efficiency and accuracy while offering clinicians effective and reliable decision support tools. As AI technology continues to evolve, deep learning models are expected to play an increasingly important role in medical imaging analysis, offering robust support for developing personalized treatment plans and enhancing patient outcomes, thereby advancing medical imaging analysis toward greater automation and intelligence as shown in Multimedia Appendix 2.

Funding

This study was supported by the Fundamental Research Program of Shanxi Province (202203021222388).

Data Availability

The datasets generated or analyzed during this study are available from the corresponding author on reasonable request.

Authors' Contributions

LS conceived and designed the study. JZ, XW, and LM performed the experiments and analyzed the data. JZ and XW wrote the manuscript. All authors reviewed and approved the final version of the manuscript.

Conflicts of Interest

None declared.

XSL•FO
RenderX

Multimedia Appendix 1
Supplementary figures and tables.
[DOCX File, 523 KB - medinform_v14i1e72679_app1.docx]

Multimedia Appendix 2
Visual abstract.
[DOCX File, 357 KB - medinform_v14i1e72679_app2.docx]

References

1. Pichler AS, Amador C, Fujimoto A, et al. Advances in peripheral T cell lymphomas: pathogenesis, genetic landscapes and emerging therapeutic targets. Histopathology 2025 Jan;86(1):119-133. [doi: 10.1111/his.15376] [Medline: 39679758]
2. Al-Maghrabi H, Al-Maghrabi J. Non-Hodgkin's primary lymphoma involving the genitourinary tract: histopathological experience from two tertiary hospitals, western region, Saudi Arabia. Am J Clin Exp Urol 2024;12(5):288-295. [doi: 10.62347/GFNJ2400] [Medline: 39584011]
3. Qiu L, Medeiros LJ, Li S. High-grade B-cell lymphomas: double hit and non-double hit. Hum Pathol 2025 Feb;156:105700. [doi: 10.1016/j.humpath.2024.105700] [Medline: 39603365]
4. Doeleman T, Hondelink LM, Vermeer MH, van Dijk MR, Schrader AM. Artificial intelligence in digital pathology of cutaneous lymphomas: a review of the current state and future perspectives. Semin Cancer Biol 2023 Sep;94:81-88. [doi: 10.1016/j.semcancer.2023.06.004] [Medline: 37331571]
5. Kuker RA, Lehmkuhl D, Kwon D, et al. A deep learning-aided automated method for calculating metabolic tumor volume in diffuse large B-cell lymphoma. Cancers (Basel) 2022 Oct 25;14(21):5221. [doi: 10.3390/cancers14215221] [Medline: 36358642]
6. Haghofer A, Fuchs-Baumgartinger A, Lipnik K, et al. Histological classification of canine and feline lymphoma using a modular approach based on deep learning and advanced image processing. Sci Rep 2023 Nov 9;13(1):19436. [doi: 10.1038/s41598-023-46607-w] [Medline: 37945699]
7. Naji H, Sancere L, Simon A, et al. HoLy-Net: segmentation of histological images of diffuse large B-cell lymphoma. Comput Biol Med 2024 Mar;170:107978. [doi: 10.1016/j.compbiomed.2024.107978] [Medline: 38237235]
8. Yang YF, Zhao E, Shi Y, Zhang H, Yang YY. Multicenter investigation of preoperative distinction between primary central nervous system lymphomas and glioblastomas through interpretable artificial intelligence models. Neuroradiology 2024 Nov;66(11):1893-1906. [doi: 10.1007/s00234-024-03451-7] [Medline: 39225815]
9. Shi T, Jiang H, Wang M, Diao Z, Zhang G, Yao YD. Metabolic anomaly appearance aware U-net for automatic lymphoma segmentation in whole-body PET/CT scans. IEEE J Biomed Health Inform 2023 May;27(5):2465-2476. [doi: 10.1109/JBHI.2023.3248099] [Medline: 37027631]
10. Weisman AJ, Kieler MW, Perlman S, et al. Comparison of 11 automated PET segmentation methods in lymphoma. Phys Med Biol 2020 Nov 27;65(23):235019. [doi: 10.1088/1361-6560/abb6bd] [Medline: 32906088]
11. Isavand P, Aghamiri SS, Amin R. Applications of multimodal artificial intelligence in non-Hodgkin lymphoma B cells. Biomedicines 2024 Aug 5;12(8):1753. [doi: 10.3390/biomedicines12081753] [Medline: 39200217]
12. Steinbuss G, Kriegsmann M, Zgorzelski C, et al. Deep learning for the classification of non-Hodgkin lymphoma on histopathological images. Cancers (Basel) 2021 May 17;13(10):2419. [doi: 10.3390/cancers13102419] [Medline: 34067726]
13. Tran KA, Kondrashova O, Bradley A, Williams ED, Pearson JV, Waddell N. Deep learning in cancer diagnosis, prognosis and treatment selection. Genome Med 2021 Sep 27;13(1):152. [doi: 10.1186/s13073-021-00968-x] [Medline: 34579788]
14. Schmidt-Barbo P, Kalweit G, Naouar M, et al. Detection of disease-specific signatures in B cell repertoires of lymphomas using machine learning. PLoS Comput Biol 2024 Jul;20(7):e1011570. [doi: 10.1371/journal.pcbi.1011570] [Medline: 38954728]
15. Jiang C, Chen K, Teng Y, et al. Deep learning-based tumour segmentation and total metabolic tumour volume prediction in the prognosis of diffuse large B-cell lymphoma patients in 3D FDG-PET images. Eur Radiol 2022 Jul;32(7):4801-4812. [doi: 10.1007/s00330-022-08573-1] [Medline: 35166895]
16. Jiang H, Diao Z, Shi T, et al. A review of deep learning-based multiple-lesion recognition from medical images: classification, detection and segmentation. Comput Biol Med 2023 May;157:106726. [doi: 10.1016/j.compbiomed.2023.106726] [Medline: 36924732]
17. Hamdi M, Senan EM, Jadhav ME, Olayah F, Awaji B, Alalayah KM. Hybrid models based on fusion features of a CNN and handcrafted features for accurate histopathological image analysis for diagnosing malignant lymphomas. Diagnostics (Basel) 2023 Jul 4;13(13):2258. [doi: 10.3390/diagnostics13132258] [Medline: 37443652]
18. Srisuwananukorn A, Salama ME, Pearson AT. Deep learning applications in visual data for benign and malignant hematologic conditions: a systematic review and visual glossary. haematol 2023;108(8):1993-2010. [doi: 10.3324/haematol.2021.280209]
19. Huang Z, Guo Y, Zhang N, et al. Multi-scale feature similarity-based weakly supervised lymphoma segmentation in PET/CT images. Comput Biol Med 2022 Dec;151:106230. [doi: 10.1016/j.compbiomed.2022.106230] [Medline: 36306574]

XSL•FO
RenderX

20. Schoenpflug LA, Chatzipli A, Sirinukunwattana K, et al. Tumour purity assessment with deep learning in colorectal cancer and impact on molecular analysis. J Pathol 2025 Feb;265(2):184-197. [doi: 10.1002/path.6376] [Medline: 39710952]
21. Huang H, Yan Z, Li B, et al. LungPath: artificial intelligence-driven histologic pattern recognition for improved diagnosis of early-stage invasive lung adenocarcinoma. Transl Lung Cancer Res 2024 Aug 31;13(8):1816-1827. [doi: 10.21037/tlcr-24-258] [Medline: 39263012]
22. Ning X, Liu R, Wang N, et al. Development of a deep learning-based model to diagnose mixed-type gastric cancer accurately. Int J Biochem Cell Biol 2023 Sep;162:106452. [doi: 10.1016/j.biocel.2023.106452]
23. Khalid M, Deivasigamani S, V S, Rajendran S. An efficient colorectal cancer detection network using atrous convolution with coordinate attention transformer and histopathological images. Sci Rep 2024 Aug 17;14(1):19109. [doi: 10.1038/s41598-024-70117-y] [Medline: 39154091]

Abbreviations

AI: artificial intelligence
AUC: area under the curve
CNN: convolutional neural network
FL: follicular lymphoma
mAP: mean average precision
MCL: mantle cell lymphoma
ResNet: residual network
TCGA: The Cancer Genome Atlas
TCIA: The Cancer Imaging Archive

Edited by A Benis; submitted 15.Feb.2025; peer-reviewed by O Pitsun, S Vasavi; revised version received 11.Oct.2025; accepted 13.Oct.2025; published 06.Jan.2026.

Please cite as:
Zhao J, Wen X, Ma L, Su L
Automated Classification of Lymphoma Subtypes From Histopathological Images Using a U-Net Deep Learning Model: Comparative Evaluation Study
JMIR Med Inform 2026;14:e72679
URL: https://medinform.jmir.org/2026/1/e72679
doi:10.2196/72679

© Jin Zhao, Xiaolian Wen, Li Ma, Liping Su. Originally published in JMIR Medical Informatics (https://medinform.jmir.org), 6.Jan.2026. This is an open-access article distributed under the terms of the Creative Commons Attribution License (https://creativecommons.org/licenses/by/4.0/), which permits unrestricted use, distribution, and reproduction in any medium, provided the original work, first published in JMIR Medical Informatics, is properly cited. The complete bibliographic information, a link to the original publication on https://medinform.jmir.org/, as well as this copyright and license information must be included.

XSL•FO
RenderX

Original Paper

Deep Learning for Dynamic Prognostic Prediction in Minimally Invasive Surgery for Intracerebral Hemorrhage: Model Development and Validation Study

Jingxuan Wang[1*], MD; Jian Shi[2*], PhD; Qing Ye[3], MD; Danyang Chen[1], MD; Yuhao Sun[1], MD; Chao Pan[1], MD; Yingxin Tang[1], MD; Ping Zhang[1], MD; Zhouping Tang[1,4], MD

[1]Department of Neurology, Tongji Hospital, Tongji Medical College, Huazhong University of Science and Technology, Wuhan City, China

[2]State Key Laboratory of Intelligent Manufacturing Equipment and Technology, Huazhong University of Science and Technology, Wuhan City, China

[3]Big Data and Artificial Intelligence Office, Tongji Hospital, Tongji Medical College, Huazhong University of Science and Technology, Wuhan City, China

[4]Key Laboratory for Diagnosis and Treatment of Severe Zoonotic Infectious Diseases, Huazhong University of Science and Technology, Wuhan city, China

[*]these authors contributed equally

Corresponding Author:
Zhouping Tang, MD
Department of Neurology
Tongji Hospital, Tongji Medical College
Huazhong University of Science and Technology
No. 1095, Jiefang Avenue
Wuhan City, 430030
China
Phone: 86 83663337
Email: ddjtzp@163.com

Abstract

Background: The pathological and physiological state of patients with intracerebral hemorrhage (ICH) after minimally invasive surgery (MIS) is a dynamic evolution, and the traditional models cannot dynamically predict prognosis. Clinical data at multiple time points often show the characteristics of different categories, different numbers, and missing data. The existing models lack methods to deal with imbalanced data.

Objective: This study aims to develop and validate a dynamic prognostic model using multi–time point data from patients with ICH undergoing MIS to predict survival and functional outcomes.

Methods: In this study, 287 patients who underwent MIS for ICH were retrospectively collected on the day of surgery, days 1, 3, 7, and 14 after surgery, and the day of drainage tube removal. Their general information, vital signs, laboratory test findings, neurological function scores, head hematoma volume, and MIS-related indicators were collected. In addition, this study proposes a multistep attention model, namely the MultiStep Transformer. The model can simultaneously output 3 types of prediction probabilities for 30-day survival probability, 180-day survival probability, and 180-day favorable functional outcome (modified Rankin Scale [mRS] 0-3) probability. Five-fold cross-validation was used to evaluate the performance of the model and compare it with mainstream models and traditional scores. The main evaluation indexes included accuracy, precision, recall, and F_1-score. The predictive performance of the model was evaluated using receiver operating characteristic (ROC) curves; its calibration was assessed via calibration curves; and its clinical utility was examined using decision curve analysis (DCA). Attributable value analysis was conducted to assess the key predictive features.

Results: The 30-day survival rate, 180-day survival rate, and 180-day favorable functional outcome rate among 287 patients were 92.3%, 88.8%, and 52.3%, respectively. In terms of predictive efficacy for survival and functional outcomes, the MultiStep Transformer model showed a remarkable superiority over traditional scoring systems and other deep learning models. For these three outcomes, the model achieved areas under the receiver operating characteristic curves (AUROCs) of 0.87 (95% CI 0.82-0.92), 0.85 (95% CI 0.77-0.93), and 0.75 (95% CI 0.72-0.78), with corresponding Brier scores of 0.1041, 0.1115, and 0.231. DCA confirmed that the model provided a definite clinical net benefit when threshold probabilities ranged within 0.06-0.26, 0.04-0.5, and 0.21-0.71.

XSL•FO
RenderX

Conclusions: The MultiStep Transformer model proposed in this study can effectively use imbalanced data to construct a model. It possesses good dynamic prediction ability for short-term and long-term survival and functional outcome of patients with ICH undergoing MIS, providing a novel tool for individualized assessment of prognosis among patients with ICH undergoing MIS.

(JMIR Med Inform 2026;14:e86327) doi:10.2196/86327

KEYWORDS

intracerebral hemorrhage; minimally invasive surgery; dynamic features; prognosis prediction; deep learning

Introduction

Intracerebral hemorrhage (ICH) accounts for 10%-15% of all stroke cases [1,2]. It is the leading cause of death and disability worldwide [3], characterized by [4] high morbidity, disability, and mortality rates. Conservative medical treatment of ICH exhibits limited efficacy [5]. Surgery for the removal of hematoma may improve the functional outcome of patients [6]. However, Surgical Trial in Intracerebral Haemorrhage (STICH) [7] and Surgical Trial in Intracerebral Haemorrhage II (STICH II) [8] confirmed the failure of craniotomy in improving functional outcomes among patients with ICH.

Recently, minimally invasive surgery (MIS), characterized by limited trauma, rapid recovery, and other advantages, has received increasing attention. Minimally Invasive Surgery Plus Alteplase for Intracerebral Hemorrhage Evacuation Phase 3 (MISTIE Ⅲ) [9] demonstrated the safety of minimally invasive hematoma evacuation combined with alteplase thrombolysis. The Early Minimally Invasive Removal of Intracerebral Hemorrhage (ENRICH) [10] trial reported that MIS can improve the functional outcomes of patients with lobar ICH at 180 days. Although the ENRICH trial provided encouraging evidence regarding the efficacy of MIS, not all patients with ICH can benefit from this approach. The uncertainty surrounding the therapeutic efficacy of MIS poses challenges for assessing the prognosis of patients.

Moreover, the condition of patients with ICH is a dynamic process. Although some tools have been used to predict death or functional outcome in patients with ICH [11-17], these predictions are mostly based on data at admission or a single time point, which cannot reflect the dynamic changes of the disease and also limit the accuracy of prognostic assessment. Electronic health records (EHRs) containing abundant data reflect the pathological and physiological state of dynamic changes in patients with ICH undergoing MIS. However, data extracted from EHR, without systematic organization, exhibits characteristics such as variable quality, high dimensionality, heterogeneity, temporality, and incompleteness [18], posing significant challenges for predictive modeling. Therefore, this study aimed to leverage multitime point, imbalanced data from patients undergoing MIS for ICH to develop a dynamic prognostic model and validate its performance in predicting survival and functional outcomes.

Methods

Study Design and Population

Patients with ICH who underwent MIS for ICH in the Department of Neurology, Tongji Hospital, Tongji Medical College, Huazhong University of Science and Technology were enrolled in this study. Clinical and imaging data were collected retrospectively on the day of surgery, 1, 3, 7, and 14 days after surgery, and on the day of drainage tube removal. A deep learning algorithm was used to construct a dynamic prognostic model and validate the effect of the model.

In total, 372 patients undergoing MIS for ICH between May 2012 and May 2024 were selected. Among them, 11 cases of ICH caused by cerebrovascular malformation and coagulopathy, 25 cases with a history of neurological deficit and renal failure, and 49 patients with missing outcome data were excluded, and data from 287 patients were analyzed. A flowchart for the patient selection process is shown in Figure 1.

The inclusion criteria were as follows: (1) patients with spontaneous acute ICH in basal ganglia or lobar regions based on cranial computed tomography (CT), who underwent stereotactic intracranial hematoma puncture and drainage surgery after admission; (2) ICH hematoma volume 20-100 mL; (3) age 18-80 years old; (4) surgery within 1 week of onset; and (5) survival for at least 7 days after admission.

The exclusion criteria were as follows: (1) coagulation disorders, such as thrombocytopenia and significant abnormal coagulation indexes caused by hepatitis; (2) traumatic ICH; (3) intracranial infection and other diseases leading to a significant increase in intracranial pressure; (4) previous severe heart, liver, kidney, or lung diseases or functional failure; (5) previous history of neurological dysfunction; (6) ICH was caused by structural abnormalities of the cerebral blood vessels (eg, arteriovenous malformations, intracranial aneurysms, vasculitis, and moyamoya disease); and (7) ICH was caused by brain tumor or cerebral infarction and was treated with thrombolytic therapy.

The model was developed and validated in accordance with the TRIPOD-AI (Transparent Reporting of a multivariable prediction model for Individual Prognosis Or Diagnosis–Artificial Intelligence) checklist.

XSL•FO
RenderX

Figure 1. Patient selection flowchart. ICH: intracerebral hemorrhage; MIS: minimally invasive surgery.

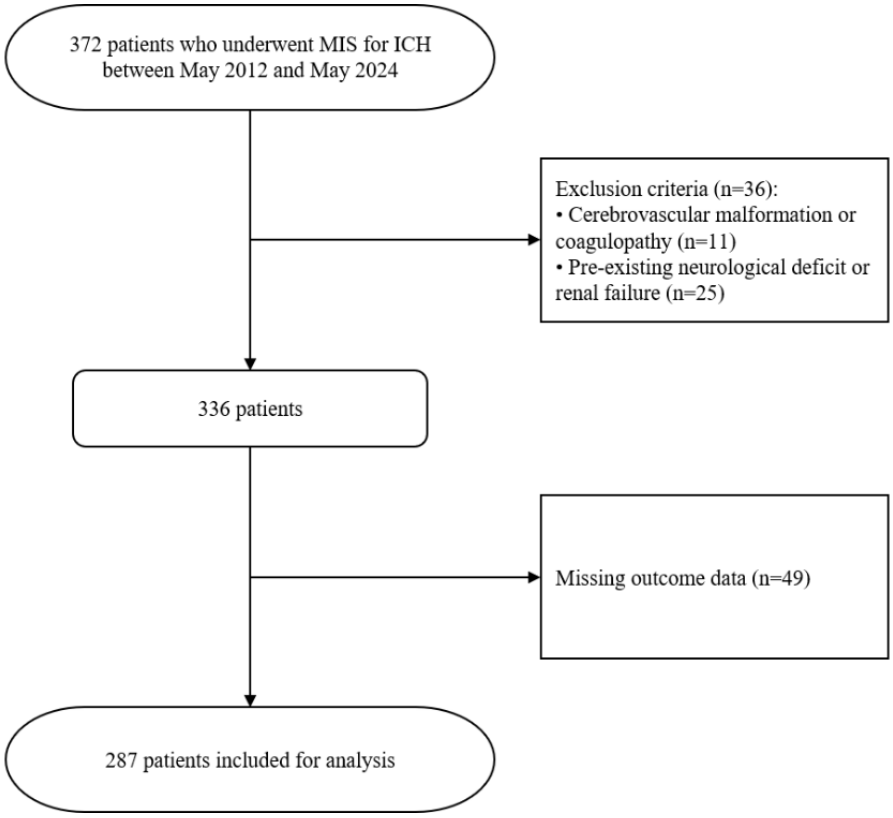

Data Sources and Collection

We electronically extracted clinical data from the EHR of Tongji Hospital, Tongji Medical College, Huazhong University of Science and Technology. Data were collected on general information, vital signs, laboratory test findings, neurological function scores, and MIS-related metrics, such as the time from onset to surgery and the duration of drainage tube placement, along with established neurological scales: the ICH score, Glasgow Coma Scale (GCS), National Institutes of Health Stroke Scale (NIHSS), and the functional outcome in patients with primary intracerebral hemorrhage (FUNC) score. Rapid segmentation and volume calculation of hematomas on cranial CT images were conducted using 3D Slicer.

Follow-up and Clinical Outcomes

Follow-up was conducted via telephone call. The primary outcome was all-cause mortality at 30 days. Secondary outcomes included all-cause mortality at 180 days and functional outcome at 180 days. The outcomes were assessed using the modified Rankin Scale (mRS), which was transformed into a binary variable, favorable functional outcome (mRS 0-3) and unfavorable functional outcome (mRS 4-6) [19,20]. The assessment was conducted by 2 medical doctors (JW and YS), with discrepancies being resolved through arbitration by a senior physician (PZ).

Data Processing and Statistical Analysis

Missing values in this study were predominantly attributed to the absence of imaging features at certain time points, whereas clinical features (vital signs, laboratory studies, etc) were fully documented. Instead of imputing the missing imaging features, the model automatically ignored the corresponding time points via an attention mechanism and completed representation learning and outcome prediction solely based on available temporal imaging features and comprehensive clinical features. To ensure a consistent input structure across patients and time points, we adopted a simple zero-imputation strategy during preprocessing. For patients with missing measurements at specific time points (eg, when certain laboratory tests or clinical assessments were not performed on a given day), the corresponding feature values were set to zero. All features were standardized before model training so that zero-imputed values lie within a well-defined range and are distinguishable from typical observed values.

For continuous variables, intergroup comparisons were conducted using the *t* test. The chi-square test was used for categorical variables. Data are presented as median (IQR), mean (SD), and range. A *P* value of <.05 was considered statistically significant.

Model Development and Training

Modeling Strategy

The changes of clinical indicators after MIS for ICH reflect the dynamic changes of individual status. Reasonable modeling of time series data dependence and cross-time point information interaction is of high importance for survival and prognosis prediction. We collected a data series of patients' multidimensional clinical measures: , where x^{1d}, x^{3d}, x^{7d}, x^{14d} denote the characteristics at 1, 3, 7, and 14 days after surgery, respectively. x^{ft} denotes fixed features (eg, gender and age) that do not change over time. x^{op}denotes the characteristics of the day of surgery. In particular, since not all individuals had

XSL•FO
RenderX

the same drainage tube removal time, the corresponding characteristics were introduced separately.

Our objective was to learn a mapping function $f: X \rightarrow \gamma$, where γ {0,1}represents the survival and prognosis labels, specifically defined as 30-day survival, 180-day survival, and 180-day favorable functional outcome. Crucially, we aimed to establish a mapping function capable of predicting both future data and the final labels from postoperative data of any given day. For instance, when input with first-day postoperative data x^{1d}, the model was meant to successfully predict subsequent data x^{3d}, x^{7d}, x^{14d} and the final ternary label γ. The problem was a multistage, multi–time point, and multivariate time series classification task.

Since the clinical indicators at each time point in X were not entirely consistent, it was not feasible to establish a unified model for cyclic prediction at each time point. Available machine learning or deep learning models exhibit limited capability in handling variable dimensional feature data [21].

To address this, we proposed a MultiStep Transformer model designed to capture nonlinearly evolving clinical features over time and manage the cross-influences existing between different time points.

MultiStep Transformer Model Architecture

In the MultiStep Transformer model, we introduced a multistage feature prediction module and a time-sharing embedding mechanism. It cooperated with the transformer encoder to realize the reinforcement modeling of multi–time point sequences. Specifically, we constructed a multilayer feature prediction module to predict and train each prognostic data separately. Finally, the Transformer encoder was used to predict 30-day survival probability, 180-day survival probability, and 180-day favorable prognosis probability. The overall process of the model is shown in Figure 2.

The MultiStep Transformer model was able to receive data at any time point as input and output for 3 types of prediction probabilities. The model framework is as follows:

Figure 2. Model diagram.

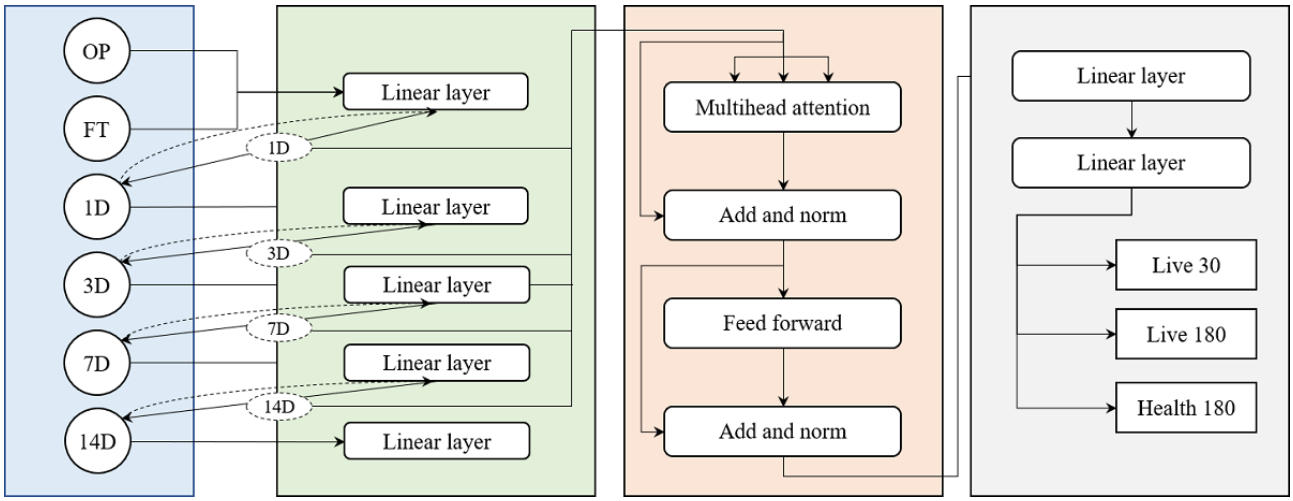

Multistage Feature Cycle Prediction Module

The core idea of the multistage feature cycle prediction module was to use the information of current and previous time points to recursively infer the feature expression of missing or future time points, which was formulated as

Here, $LR_t(\cdot)$represents a linear mapping layer specific to the t-th time point, responsible for establishing recursive dependencies among the time-series features. This design effectively mitigated the challenges of incomplete clinical data and the isolation of temporal features, thereby enhancing the ability of the model to capture temporal evolutionary trends.

Time-Sharing Feature Embedding

In view of the large difference of input data dimensions and strong heterogeneity of feature distribution at different time points, an independent linear mapping layer was designed:

The high-dimensional projection of the input at each time point was conducted to eliminate the difference in input dimensions and ensure the consistency of the sequence dimensions of the input of the transformer encoder. In addition, the independent mapping parameters W_t and d_t captured the unique statistical characteristics of time points and improved the adaptability of the model to the information of different stages.

Transformer Encoder Structure and Time-Series Dependence Modeling

Through the self-attention mechanism, the transformer encoder flexibly modeled the interactive dependencies between all positions in a sequence. It overcame the limitations of traditional recurrent neural networks and possessed the capabilities of parallel computation and long-range dependency capture. In our framework, the same temporal feature sequence was used simultaneously as the query, key, and value in the self-attention operation. This design allows feature extraction to be performed directly on the observed sequence without forcing all patients to have the same number of time points and therefore naturally supports variable-length temporal inputs.

XSL•FO
RenderX

Input sequence: concatenate the embedding vectors at all time points to form an input sequence:

Here, t= 6 represents the number of input feature layers, and B denotes the batch size for each training or inference step. The experimental framework supports arbitrary combinations of time points as input, for example using only Day-1 data or Days 1, 3, 7, and 14, depending on data availability and clinical requirements.

Encoding process: the multilayer stacked transformer encoder consisted of multihead self-attention and a feed-forward network. A single layer was formulated as

Where the same sequence serves as Q, K, and V in the self-attention module. The model performs multistep, progressive computation; features from earlier time points are encoded first, and then information from subsequent time points is gradually integrated. After multilayer coding, the model comprehensively considered the influence between different time points and its feature correlation, and the output sequence was expressed as:

$$Z = \text{TransformerEncoder}(H) \quad (6)$$

The encoding vector Z^d at the final time point of the sequence was taken as the representation of the comprehensive temporal dynamic state of patients.

Survival Prediction Head

The final classification layer was mapped using single-layer linearity:

Here, σ denotes the sigmoid activation function for generating binary classification probability outputs. The output data format was (30 live, 180 live, and 180 heal), representing the probability of 30-day survival, 180-day survival, and 180-day favorable functional outcome, respectively.

Training and Prediction Processes

For model training, data were input uniformly, and the model was trained step by step. Specifically, features from all time points $X = \{x^{ft}, x^{op}, x^{1d}, x^{3d}, x^{7d}, x^{14d}\}$were input into the model. The model first processed the features $[x^{ft}, x^{op}]$ through the linear layer LR_{1d} to compute , and calculate the loss using x^{1d}, followed by backpropagation to optimize LR_{1d}. Subsequently, stepwise prediction and optimization were conducted sequentially based on the mapping layers in the multistage feature prediction module. All features, including known inputs and predicted outputs, were combined into a complete feature sequence . Finally, the transformer encoded all temporal features to obtain the patient's dynamic state representation Z, which was then classified using a linear layer.

During inference, given the first i temporal features X_i (eg, $X_i = \{x^{ft}, x^{op}, x^{1d}, x^{3d}\}$), the model applied masking to the existing feature time points based on the number of feature layers and directly computed subsequent features , finally predicting survival and prognosis (30 live, 180 live, and 180 heal).

Model hyperparameters were selected empirically based on preliminary experiments on the training folds. The network was optimized using the Adam optimizer with a fixed learning rate of 0.001 and trained for 200 epochs per fold. We used the cross-entropy loss for outcome prediction, combined with the feature prediction loss for intermediate temporal features in the multistage prediction module. The batch size, number of transformer layers, hidden dimensions, and dropout rate were tuned within a reasonable range to balance model performance and overfitting risk.

Model Evaluation

The predictive performances of different models and scores were compared using accuracy, precision, recall, and F_1-score. The predictive performance of the model was evaluated by the area under the receiver operating characteristic curve (AUROC). Calibration curves were plotted to assess the consistency between the predicted probabilities and the observed outcomes of the model. In addition, decision curve analysis (DCA) was performed to evaluate the clinical utility of the model.

Model Interpretation

To gain insight into the decision-making process of the model, we used attribution values, a technique used to quantify how much each input feature contributes to the output of the model. Attribution values revealed the importance of clinical characteristics in predicting the outcome and helped us determine which characteristics had the greatest impact on the model's decision-making process.

Ethical Considerations

This study was approved by the Medical Ethics Committee of Tongji Hospital, Tongji Medical College, Huazhong University of Science and Technology (TJ-IRB202502129). Given the retrospective nature of the study and the absence of any direct interaction with participants, informed consent was exempted by the ethics committee, and no compensation of any form was provided. This study adheres to the ethical principles outlined in the Declaration of Helsinki.

Results

Baseline Characteristics of the Study Population

The mean age of the 287 patients was 53.2 (10.6) years, and 67.9% of the patients were male. Their 30-day survival rate was 92.3%, their 180-day survival rate was 87.8%, and the rate of favorable functional outcome at 180 days was 52.3%. The presence of intraventricular hemorrhage, GCS, NIHSS, ICH score, and FUNC score showed significant differences across the 3 groups of patients (Tables S1-S3 in Multimedia Appendices 1-3).

XSL•FO
RenderX

Evaluation of the Model Performance

Due to variations in clinical assessment items across different time points, the feature categories at each time point were not entirely consistent. In the collected dataset, there were 48 features on the day of surgery, 47 features on postoperative days 1 and 3, a total of 46 features on postoperative day 7, a total of 10 features on postoperative day 14, and 15 features on the day of drainage tube removal (feature labels are in Multimedia Appendix 4). Based on feature dimensions of the patients, we constructed a MultiStep Transformer model with 4 feature prediction modules.

Given the limited sample size (287 patients) and single-center design, we adopted a 5-fold cross-validation scheme for internal validation. The entire cohort was randomly partitioned into 5 approximately equal subsets. In each iteration, one subset was held out as the validation (test) set, and the remaining 4 subsets were used for model training. This process was repeated 5 times so that each subset served as the validation set exactly once. Model performance metrics were averaged across the 5 folds and reported together with their SDs, providing an estimate of variability and robustness. The outcome labels were not evenly distributed across classes. To mitigate the impact of class imbalance, we ensured that the proportion of outcome categories in each fold of the cross-validation was approximately consistent with that of the full cohort by using stratified splitting according to the target labels. In addition, class weights inversely proportional to class frequencies in the training data were applied in the loss function to reduce bias toward the majority class. This strategy helped the model to learn more balanced decision boundaries across different outcome categories.

We calculated the confusion matrices of the results to obtain accuracy, precision, recall, and F_1-score. Regarding the prediction results, actual labels were defined as follows: true positive (TP), positive labels correctly predicted; false positive (FP), negative labels incorrectly predicted; true negative (TN), negative labels correctly predicted; false negative (FN), positive labels incorrectly predicted. The evaluation metrics were calculated as follows:

For comparison, we selected the commonly used deep learning models, including temporal convolutional network (TCN), gated recurrent unit (GRU), and transformer. Table 1 presents the comparison of prediction performance between the MultiStep Transformer model and each deep learning model.

Table 1. Comparison of model performance.

Model and scene	Accuracy (%), mean (SD)	Precision (%), mean (SD)	Recall (%), mean (SD)	F_1-score (%), mean (SD)
GRU[a]				
live_30	77.34 (28.89)	100 (0)	75.66 (30.88)	81.17 (28.30)
live_180	66.5 (27.68)	98.1 (0.99)	63.39 (31.91)	70.24 (33.74)
heal_180	73.70 (7.20)	75.61 (6.44)	71.92 (10.52)	73.49 (8.05)
TCN[b]				
live_30	85.55 (19.8)	100 (0)	84.49 (21.23)	89.83 (15.30)
live_180	74.04 (19)	97.92 (2.55)	71.57 (21.23)	80.96 (15.30)
heal_180	74.68 (5.86)	77.09 (2.51)	71.94 (12.72)	73.90 (8.03)
Transformer				
live_30	88.83 (12.53)	100 (0)	88 (13.40)	93.01 (8.50)
live_180	76.33 (15.52)	98.18 (2.28)	74.16 (16.59)	83.54 (12.12)
heal_180	78.95 (5.91)	81.75 (3.65)	76.43 (13.4)	78.28 (7.81)
MultiStepTransformer (Ours)				
live_30	92.43 (1.68)	96.47 (2.15)	95.37 (1.83)	95.89 (0.92)
live_180	88.80 (3.24)	93.99 (1.68)	93.22 (3.90)	93.55 (1.20)
heal_180	80.13 (3.68)	81.16 (2.13)	82.02 (6.05)	81.42 (2.82)

[a]GRU: gated recurrent unit.

[b]TCN: temporal convolutional network.

The proposed method achieved the best performance in terms of accuracy, recall, and F_1-score for the 3 categories of outcomes. The accuracy of the MultiStep Transformer model was 92.43 (1.68) for 30-day survival, 88.80 (3.24) for 180-day survival, and 80.13 (3.68) for 180-day favorable functional outcome, respectively.

Furthermore, we separated the 4 scores (GCS, NIHSS, ICH score, and FUNC score) from the data to predict the three categories of outcomes. The FUNC score is associated with the volume of hematoma, but there were some missing data, and it could not be combined with the other scores for classification. We compared the single-score classification and the combined classification of scores (ICH score, GCS, and NIHSS),

XSL•FO
RenderX

respectively. We also used support vector machine (for classification). Using the same 5-fold cross validation, their confusion matrices were calculated to obtain the corresponding indicators (Table 2).

As can be seen, the NIHSS predicts the best results of the traditional scores for 30-day survival. The FUNC score was superior to the other 2 scores in the accurate classification of 180-day survival and 180-day favorable functional outcome. It significantly improved the prediction of 180-day favorable functional outcome, indicating that the FUNC score was better at predicting the long-term prognosis of patients. The combination of the ICH score, GCS, and NIHSS features significantly improved 30-day survival prediction, but the FUNC score still exhibited some advantages in long-term prediction.

Figure 3 presents a comparison of classification accuracy between the MultiStep Transformer model, traditional scoring methods, and other deep learning models. The results indicated that compared to either traditional scoring methods or other deep learning models, our proposed method offers superior performance in both short-term and long-term predictions of the 3 outcome categories. Furthermore, the MultiStep Transformer model yielded the smallest SD (eg, mean 92.43, SD 1.68 for accuracy in 30-day survival prediction), reflecting its consistent performance across different data subsets, enhanced stability, and strong generalization capability.

Figures 4A, D, and G present the receiver operating characteristic (ROC) curves of the model for different outcomes, namely 30-day survival, 180-day survival, and 180-day favorable functional outcome. The model achieved AUROCs of 0.87 (95% CI 0.82-0.92), 0.85 (95% CI 0.77-0.93), and 0.75 (95% CI 0.72-0.78) for these 3 outcomes, respectively.

Furthermore, the calibration curves demonstrated good calibration performance of the model (Figures 4B, E, and H), with corresponding Brier scores of 0.1041, 0.1115, and 0.231, respectively. DCA indicated that the model yielded a net benefit when the threshold probabilities ranged within 0.06-0.26, 0.04-0.5, and 0.21-0.71, respectively (Figures 4C, F, and I). The above findings confirm that this model exhibits favorable generalizability.

XSL•FO
RenderX

Table 2. Comparison of traditional scores.

Score and scene	Accuracy (%), mean (SD)	Precision (%), mean (SD)	Recall (%), mean (SD)	F_1-score (%), mean (SD)
ICH[a] score				
live_30	73.36 (16.52)	56.56 (4.66)	66.00 (11.4)	54.22 (10.68)
live_180	71.07 (15.30)	55.96 (4.90)	58.51 (7.03)	53.88 (9.33)
heal_180	60.52 (5.78)	66.05 (6.37)	59.67 (3.89)	55.65 (5.53)
GCS[b]				
live_30	78.61 (3.63)	55.27 (5.30)	63.4 (12.93)	55.47 (6.98)
live_180	76.96 (2.85)	57.64 (7.18)	61.71 (8.53)	57.92 (8.23)
heal_180	57.92 (3.74)	58.73 (4.62)	56.89 (4.59)	54 (5.61)
NIHSS[c]				
live_30	83.22 (1.60)	58.03 (4.79)	67.72 (11.77)	59.60 (6)
live_180	78.31 (2.72)	55.88 (7.82)	61.67 (11.79)	56.94 (9.08)
heal_180	56.92 (2.45)	57.43 (4.79)	55.31 (3.29)	52.36 (4.51)
FUNC[d] score				
live_30	81.57 (16.08)	70 (24.81)	66.58 (27.95)	67.46 (26.83)
live_180	79.56 (18.99)	68.75 (25.62)	65.75 (28.37)	65.99 (27.79)
heal_180	71.56 (23.01)	74.40 (20.49)	70.83 (19.43)	68.10 (23.25)
Combination of the ICH score, GCS, and NIHSS				
live_30	85.86 (1.61)	60.67 (6.36)	70.98 (13.28)	62.93 (8.07)
live_180	79.29 (3.12)	58.39 (5.30)	63.17 (10.61)	59.02 (6.64)
heal_180	57.58 (3.75)	57.37 (6.33)	56.00 (5.09)	52.91 (6.86)
MultiStep Transformer (ours)				
live_30	92.43 (1.68)	96.47 (2.15)	95.37 (1.83)	95.89 (0.92)
live_180	88.80 (3.24)	93.99 (1.68)	93.22 (3.90)	93.55 (1.20)
heal_180	80.13 (3.68)	81.16 (2.13)	82.02 (6.05)	81.42 (2.82)

[a]ICH: intracerebral hemorrhage.

[b]GCS: Glasgow Coma Scale.

[c]NIHSS: National Institutes of Health Stroke Scale.

[d]FUNC: functional outcome in patients with primary intracerebral hemorrhage.

XSL•FO
RenderX

Figure 3. Comparison of classification accuracy across models and traditional scoring methods. FUNC: functional outcome in patients with primary intracerebral hemorrhage; GCS: Glasgow Coma Scale; GRU: gated recurrent unit; ICH: intracerebral hemorrhage; NIHSS: National Institutes of Health Stroke Scale; TCN: temporal convolutional network.

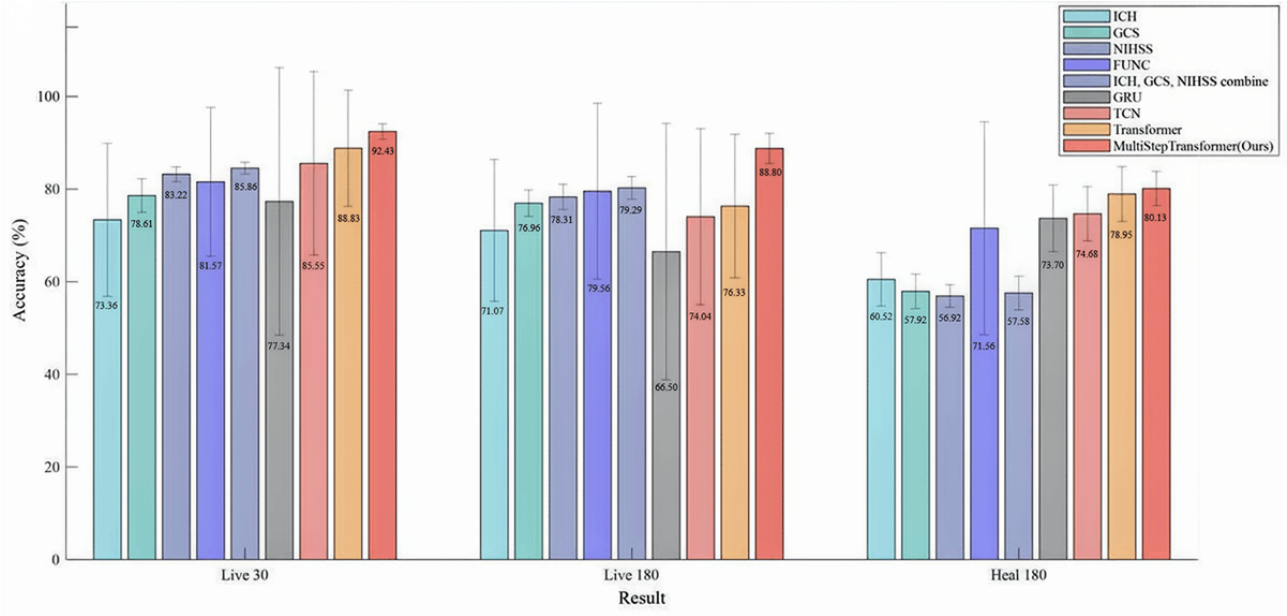

Figure 4. Results of 5-fold cross-validation: Panels A-C depict the ROC curve, calibration curve, and decision curve for 30-day survival, respectively; panels D-F represent those for 180-day survival; and panels G-I denote those for 180-day favorable functional outcome. AUC: area under the curve; ROC: receiver operating characteristic.

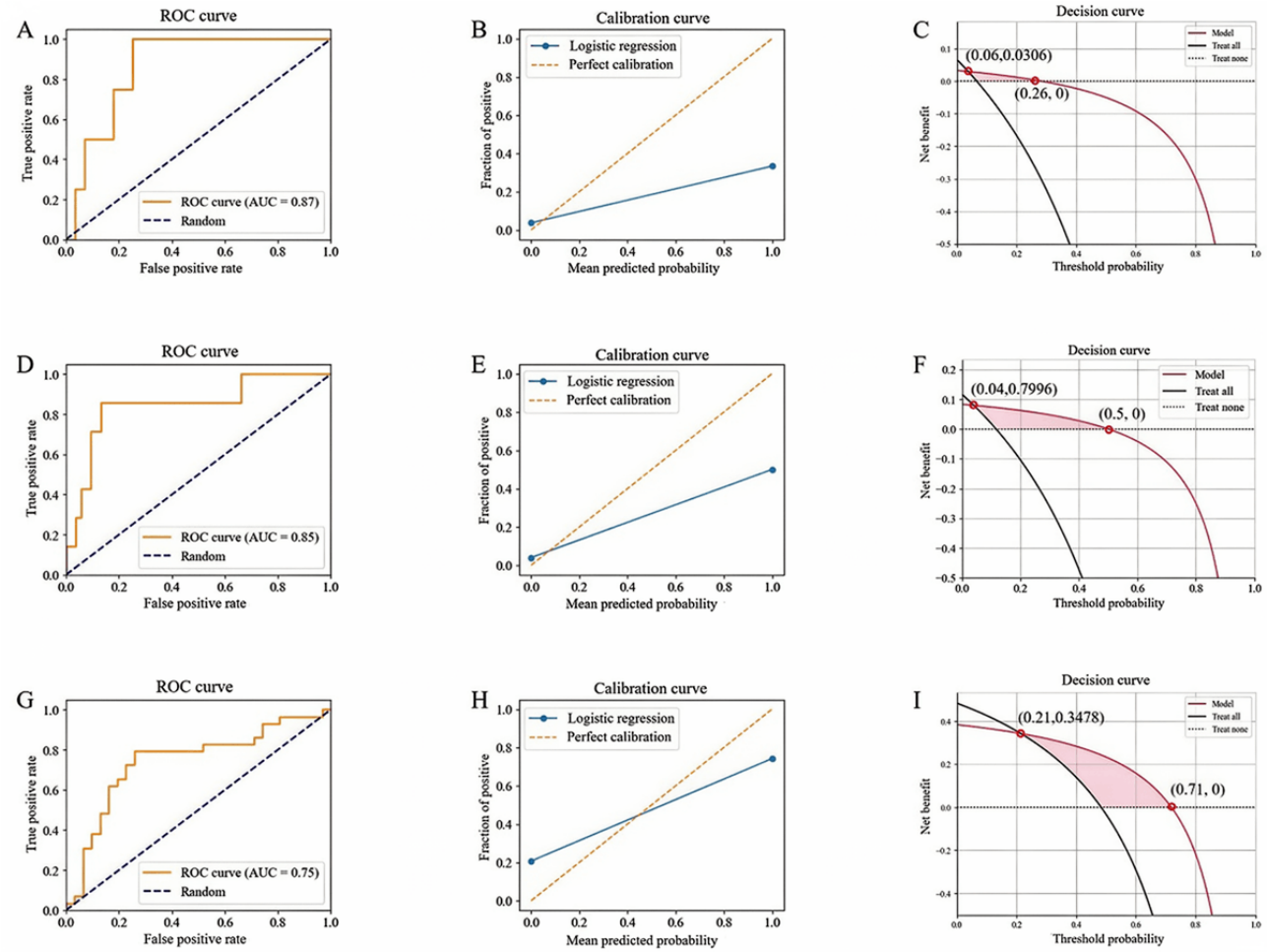

XSL•FO
RenderX

Model Interpretation

In this study, we used deep neural networks to classify clinical data for predicting patients' outcomes. Specifically, we visualized the attribution values calculated by the model alongside the corresponding input feature values in the same diagram to interpret the model's decision-making mechanism.

The attribution values indicated the contribution of each clinical feature to the model's output. The feature importance was relatively similar between postoperative day 1 and day 3, while some changes emerged in the key clinical features affecting predictions by days 7 and 14 (Figure 5).

The horizontal axis in Figure 5 represents the indices of the input features as discrete integers, facilitating the identification of specific features. The left vertical axis denotes the attribution values, displayed with blue bars that illustrate each feature's relative contribution to the output. The right vertical axis corresponds to the original feature values, plotted as a red dashed line to visualize the correspondence between attributions and raw data. This integrated plot helps identify the most influential features on the model's predictions, enabling a more comprehensive understanding of the model's behavior.

Figure 5. Visualization of attribution values of features.

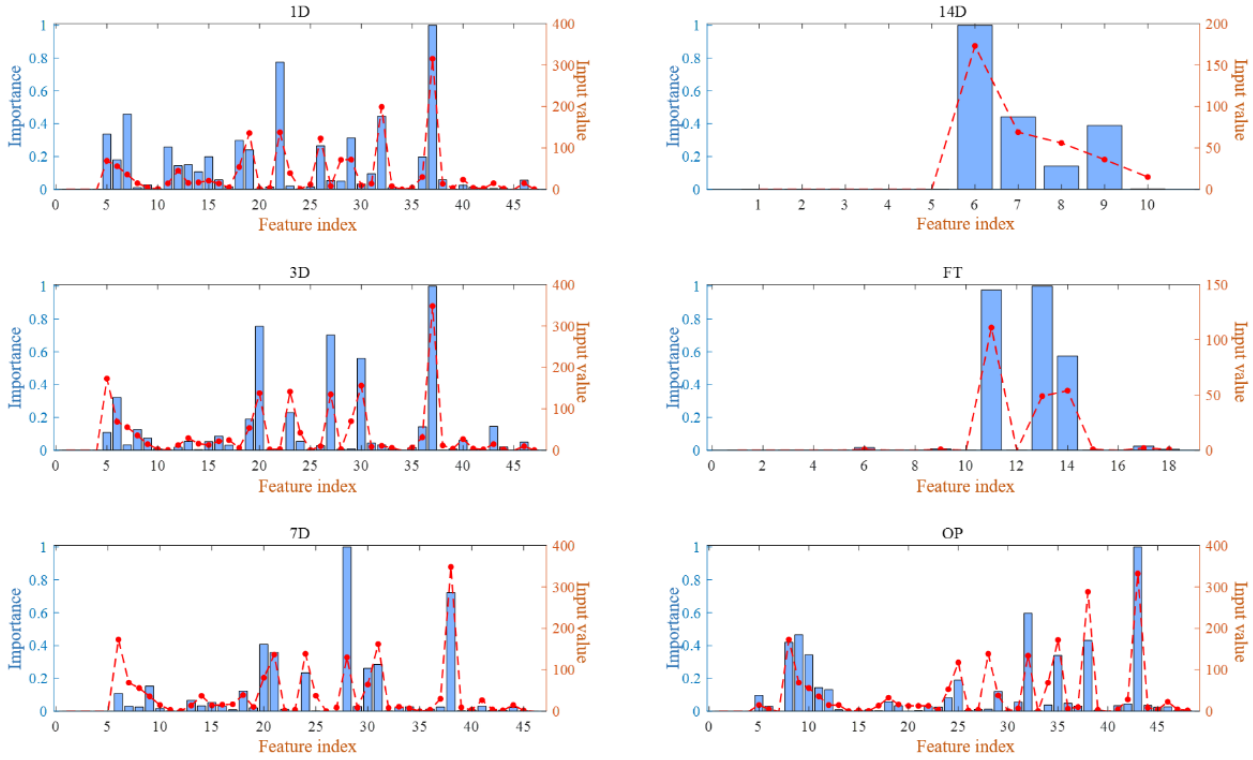

Discussion

Principal Findings

This study reports the construction process and model performance of the MultiStep Transformer model, a novel deep learning model that can dynamically predict short-term and long-term survival and functional outcome in patients with ICH undergoing MIS. The experimental results showed that the model significantly outperformed the mainstream deep learning models (GRU, TCN, and transformer) and traditional clinical scores (GCS, NIHSS, ICH score, and FUNC score) on the 3 prediction tasks of 30-day survival, 180-day survival, and 180-day favorable functional outcome.

In patients undergoing MIS for ICH, neurological functions, vital signs, imaging findings, and laboratory parameters are subjected to continuous changes, generating substantial clinical data. However, temporal data in EHR present challenges, including irregular recording intervals and variable sequence lengths across individuals. Meanwhile, most of the previous studies have conducted predictions at fixed time points, whereas many clinical scenarios necessitate continuous outcome updates with the emergence of new data [22]. Therefore, it is essential to develop a dynamic model to process variably dimensional features. This approach not only addresses the needs of clinical practice but also allows personalized management of patients.

The MultiStep Transformer model incorporates innovative designs to address common challenges in real-world clinical data, such as missing time points, heterogeneous feature dimensions, and inconsistent sampling frequencies.

First, multistage feature prediction addresses data missingness. Through layered stepwise linear mapping, the model not only imputes missing values at certain time points but also enhances temporal dependencies among features, thereby improving the accuracy of predictions.

Second, time point–specific embedding resolves dimensionality inconsistency. Independent linear embedding layers ensure unified representation of heterogeneous input data, strengthening the generalizability of the model.

XSL•FO
RenderX

Third, the self-attention mechanism of the transformer captures long-range dependencies. Compared to traditional recurrent neural networks, the transformer architecture more effectively learns complex nonlinear dependencies and interactions across several time points.

Finally, we visualized feature importance through attribution values. The values revealed which clinical features played a pivotal role in the final predictions. A higher attribution value of a feature suggested a greater influence on the model's decision-making. The MultiStep Transformer model successfully captured the dynamic shifts of key perioperative features during MIS, thereby enhancing the interpretability of the model and its credibility in clinical practice.

Comparison With Prior Work

TCN is a feedforward network architecture that models time series by stacking convolutional layers [23]. Under the constraint of convolutional layers, it can effectively prevent information leakage. Multilayer convolution can also capture local time dependence and short-term dynamic changes in multi–time point clinical data. GRU is a type of recurrent neural network, which uses a gating unit to control the memory and forgetting of information. It has a relatively small number of parameters and high training stability and can model the dependence from local to global. For clinical data with multiple time points, GRU can better extract cross-temporal global features [24]. With the attention mechanism as the core, Transformer can model the relationships between any time points in a sequence in a global scope [25], making it suitable for dealing with long sequences and complex temporal patterns. In addition, it has good parallel computing ability and can effectively use global information.

Compared to the mainstream deep learning models, the MultiStep Transformer model offers full usage and efficient modeling of complex imbalanced time-series data by introducing a multistage feature cycle prediction module, time-sharing embedding mechanism, and transformer encoder structure. Besides, the modular design of the MultiStep Transformer model enables adaptation to flexible inputs, supports dynamic input time points, and is suitable for clinical scenarios with different monitoring frequencies, thereby improving its practicability.

In 30-day survival prediction, GRU, TCN, and transformer achieved 100% precision, indicating rare false positive errors, but their low recall suggests many missed diagnoses. The MultiStep Transformer exhibited a significant improvement in recall and F_1-score, suggesting a more accurate identification ability while avoiding excessive conservatism. The performance of all models decreased with the prolongation of prediction time, but the MultiStep Transformer still showed a high F_1-score in 180-day survival prediction, with greatly improved recall. These findings imply that it is more sensitive in long-term prediction and not overly conservative. In the prediction of a favorable functional outcome at 180 days, all models performed worse compared to their performance in survival prediction, highlighting the challenges in predicting functional outcomes. The MultiStep Transformer was the only model with a recall of more than 80%, indicating that it was more advantageous in identifying patients with a greater chance of recovery.

Traditional scoring systems are widely used in clinical practice due to their simplicity and have demonstrated considerable value in predicting the outcomes of ICH. For predicting mortality, the ICH score achieved AUROCs of 0.83-0.84, while the FUNC score showed AUROCs of 0.79-0.83. In predicting functional outcomes, the ICH score attained AUROCs of 0.77-0.82, compared to 0.76-0.78 for the FUNC score [26]. When predicting death or severe disability, the NIHSS score yielded an AUROC of 0.796, the GCS score achieved an AUROC of 0.650, and the ICH score revealed an AUROC of 0.674 [27]. By comparison, the model developed in this study demonstrated superior predictive performance. For the prediction of 30-day survival, 180-day survival, and 180-day favorable functional outcome, the model achieved AUROCs of 0.87 (95% CI 0.82-0.92), 0.85 (95% CI 0.77-0.93), and 0.75 (95% CI 0.72-0.78), respectively. Meanwhile, calibration curves and DCA confirmed that this model has excellent calibration performance and definite clinical benefit. Furthermore, the inherent limitations of traditional scoring systems are becoming increasingly apparent. McCracken et al. indicated that nearly two decades after its introduction, the predictive accuracy of the ICH score may no longer be sufficient for contemporary clinical practice, necessitating adjustments and optimization [28]. More importantly, the clinical guideline "Guidelines for Neuroprognostication in Critically Ill Adults with Intracerebral Hemorrhage" emphasizes that no single score or clinical variable should be used as the sole basis for prognostic judgment at 3 months or beyond [29]. Accordingly, factors such as preoperative functional status, surgical complications, and intervention timing should be comprehensively considered when developing assessment tools for patients undergoing surgery [30]. The dynamic prognostic model developed in this study aligns with this philosophy. From a clinical perspective, accurate prediction of long-term functional outcomes is crucial for rehabilitation planning and patient communication. For predicting 180-day functional outcomes, the most challenging task, our model achieved an F_1-score of 81.42%, significantly surpassing traditional scoring systems (maximum 71.56%), suggesting its substantial potential in guiding rehabilitation strategies.

Limitations

There are some limitations to this study. First, this study was a single-center retrospective study with a small sample size, which constitutes the most critical methodological limitation. Population heterogeneity, treatment variability, and fluctuations in data quality may potentially compromise model performance. Although our dataset, spanning over ten years and including medical records from both local and nonlocal patients, confers a certain degree of representativeness, and despite rigorous cross-validation for model performance evaluation, single-center data are inevitably influenced by institutional clinical protocols and inherent biases of retrospective data collection. This poses a distinct challenge for dynamic models, whose generalizability is limited by institutional variations in feature distributions and missing patterns. Second, the puncture needle used in MIS leads to artifacts in CT images, which will affect the accurate calculation of hematoma volume. Third, the model only predicted binary outcomes, such as survival or death, favorable

XSL•FO
RenderX

prognosis, and unfavorable prognosis, but could not predict the specific mRS score. The prediction ability of the functional outcome was not comprehensive enough. Finally, we collected clinical data at a few time points, which may have affected the performance of the model. In the future, more clinical data at more time points can help train the model more effectively.

Future Work

All features incorporated into this model are derived from routine clinical practice in MIS for ICH, eliminating the need for additional data collection efforts. Meanwhile, the model supports continuous integration of the latest data and dynamic updating of prediction outcomes, which can precisely match the time-varying characteristics of ICH progression and the clinical decision-making needs of MIS. Leveraging these advantages, the ideal application of the dynamic prediction model developed in this study is to be embedded in the EHR system, thereby providing clinicians with real-time individualized prognostic predictions to support accurate decision-making. However, its implementation faces obstacles such as technical integration and workflow adaptation. Future work will advance in multiple directions. First, more time-point data will be incorporated to improve the model's performance, and external validation of the model will be conducted in multicenter, prospective cohorts. This is a key step to evaluate its real-world generalizability and promote clinical translation. Second, standardized interfaces will be developed to achieve seamless integration of the model with different EHR systems and ensure real-time data updates. Third, the actual impact of the model on clinical decision-making and final clinical outcomes will be evaluated in real clinical settings, and a replicable workflow solution will be formulated.

Conclusions

Based on clinical data, the MultiStep Transformer model uses deep learning methods to achieve the goal of dynamic, comprehensive, and accurate prediction. It can stably output multiple prediction results in a single prognostic model at the same time. This study explored the individualized management of patients with ICH undergoing MIS, providing a new method for predicting short-term and long-term survival and functional outcomes and bringing a reference for the diagnosis and treatment of ICH in clinical practice.

Data Availability

The datasets used during the current study are available from the corresponding author upon reasonable request.

Funding

This work was supported by the Major Program (JD) of Hubei Province (grant number 2023BAA005); Fundamental Research Funds for the Central Universities (grant number YCJJ20251401); the National Natural Science Foundation of China (grant numbers 92148206, 82571528); the Key Research and Development Program of Wuhan (grant number 2024020702030123); the Huazhong University of Science and Technology (grant number 2024JCYJ044); and the Research Fund of Tongji Hospital (grant numbers 2022ZHFY01, AI2024B03).

Authors' Contributions

JW and JS performed investigation, data curation, formal analysis, validation, and wrote the original draft. QY, DC, CP, and YT contributed to conceptualization. YS performed investigation. PZ and ZT handled project administration, supervision, and funding acquisition, and contributed to writing—review and editing. All authors reviewed the manuscript.

Conflicts of Interest

None declared.

Multimedia Appendix 1
Baseline Characteristics of Patients Classified by 30-day Survival or Mortality.
[DOCX File , 24 KB - medinform_v14i1e86327_app1.docx]

Multimedia Appendix 2
Baseline Characteristics of Patients Classified by 180-day Survival or Mortality.
[DOCX File , 24 KB - medinform_v14i1e86327_app2.docx]

Multimedia Appendix 3
Baseline Characteristics of Patients Classified by 180-day Favorable or Unfavorable Functional Outcome.
[DOCX File , 24 KB - medinform_v14i1e86327_app3.docx]

Multimedia Appendix 4
Feature labels.

XSL•FO
RenderX

[DOCX File , 17 KB - medinform_v14i1e86327_app4.docx]

References

1. Qureshi AI, Tuhrim S, Broderick JP, Batjer HH, Hondo H, Hanley DF. Spontaneous intracerebral hemorrhage. N Engl J Med 2001 May 10;344(19):1450-1460 [FREE Full text] [doi: 10.1056/NEJM200105103441907] [Medline: 11346811]
2. Sheth KN. Spontaneous Intracerebral Hemorrhage. N Engl J Med 2022 Oct 27;387(17):1589-1596 [FREE Full text] [doi: 10.1056/NEJMra2201449] [Medline: 36300975]
3. Zille M, Farr TD, Keep RF, Römer C, Xi G, Boltze J. Novel targets, treatments, and advanced models for intracerebral haemorrhage. EBioMedicine 2022 Feb 11;76:103880 [FREE Full text] [doi: 10.1016/j.ebiom.2022.103880] [Medline: 35158309]
4. Duan T, Li L, Yu Y, Li T, Han R, Sun X, et al. Traditional Chinese medicine use in the pathophysiological processes of intracerebral hemorrhage and comparison with conventional therapy. Pharmacol Res 2022 May;179:106200 [FREE Full text] [doi: 10.1016/j.phrs.2022.106200] [Medline: 35367344]
5. Bruno C, Cesta CE, Hjellvik V, Ulrichsen SP, Bjørk MH, Esen B, et al. Corrigendum to Antipsychotic use during pregnancy and risk of specific neurodevelopmental disorders and learning difficulties in children: a multinational cohort study [eClinicalMedicine 70 (2024) 102531/DOI: 10.1016/j.eclinm.2024.102531]. EClinicalMedicine 2025 Feb 28;81:103139 [FREE Full text] [doi: 10.1016/j.eclinm.2025.103139] [Medline: 40104086]
6. Wilting FN, Sondag L, Schreuder FH, Dammers R, Klijn CJ, Boogaarts HD. Surgery for spontaneous supratentorial intracerebral haemorrhage. Cochrane Database Syst Rev 2025 Jul 17;7(7):CD015387 [FREE Full text] [doi: 10.1002/14651858.CD015387.pub2] [Medline: 40673401]
7. Mendelow AD, Gregson BA, Fernandes HM, Murray GD, Teasdale GM, Hope DT, STICH investigators. Early surgery versus initial conservative treatment in patients with spontaneous supratentorial intracerebral haematomas in the International Surgical Trial in Intracerebral Haemorrhage (STICH): a randomised trial. Lancet 2005 Jan 29;365(9457):387-397 [FREE Full text] [doi: 10.1016/S0140-6736(05)17826-X] [Medline: 15680453]
8. Mendelow AD, Gregson BA, Rowan EN, Murray GD, Gholkar A, Mitchell PM, STICH II Investigators. Early surgery versus initial conservative treatment in patients with spontaneous supratentorial lobar intracerebral haematomas (STICH II): a randomised trial. Lancet 2013 Aug 03;382(9890):397-408 [FREE Full text] [doi: 10.1016/S0140-6736(13)60986-1] [Medline: 23726393]
9. Hanley DF, Thompson RE, Rosenblum M, Yenokyan G, Lane K, McBee N, MISTIE III Investigators. Efficacy and safety of minimally invasive surgery with thrombolysis in intracerebral haemorrhage evacuation (MISTIE III): a randomised, controlled, open-label, blinded endpoint phase 3 trial. Lancet 2019 Mar 09;393(10175):1021-1032 [FREE Full text] [doi: 10.1016/S0140-6736(19)30195-3] [Medline: 30739747]
10. Pradilla G, Ratcliff JJ, Hall AJ, Saville BR, Allen JW, Paulon G, ENRICH trial investigators, ENRICH Trial Investigators. Trial of Early Minimally Invasive Removal of Intracerebral Hemorrhage. N Engl J Med 2024 Apr 11;390(14):1277-1289 [FREE Full text] [doi: 10.1056/NEJMoa2308440] [Medline: 38598795]
11. Hemphill JC, Farrant M, Neill TA. Prospective validation of the ICH Score for 12-month functional outcome. Neurology 2009 Oct 06;73(14):1088-1094 [FREE Full text] [doi: 10.1212/WNL.0b013e3181b8b332] [Medline: 19726752]
12. Hemphill JC, Bonovich DC, Besmertis L, Manley GT, Johnston SC. The ICH score: a simple, reliable grading scale for intracerebral hemorrhage. Stroke 2001 Apr 1;32(4):891-897 [FREE Full text] [doi: 10.1161/01.str.32.4.891] [Medline: 11283388]
13. Gregório T, Pipa S, Cavaleiro P, Atanásio G, Albuquerque I, Chaves PC, et al. Prognostic models for intracerebral hemorrhage: systematic review and meta-analysis. BMC Med Res Methodol 2018 Nov 20;18(1):145 [FREE Full text] [doi: 10.1186/s12874-018-0613-8] [Medline: 30458727]
14. Matsumoto K, Ishihara K, Matsuda K, Tokunaga K, Yamashiro S, Soejima H, et al. Machine Learning-Based Prediction for In-Hospital Mortality After Acute Intracerebral Hemorrhage Using Real-World Clinical and Image Data. J Am Heart Assoc 2024 Dec 17;13(24):e036447 [FREE Full text] [doi: 10.1161/JAHA.124.036447] [Medline: 39655759]
15. Zhao X, Zhou B, Luo Y, Chen L, Zhu L, Chang S, et al. CT-based deep learning model for predicting hospital discharge outcome in spontaneous intracerebral hemorrhage. Eur Radiol 2024 Jul;34(7):4417-4426 [FREE Full text] [doi: 10.1007/s00330-023-10505-6] [Medline: 38127074]
16. Huang X, Wang D, Zhang Q, Ma Y, Li S, Zhao H, et al. Development and Validation of a Clinical-Based Signature to Predict the 90-Day Functional Outcome for Spontaneous Intracerebral Hemorrhage. Front Aging Neurosci 2022 May 09;14:904085 [FREE Full text] [doi: 10.3389/fnagi.2022.904085] [Medline: 35615596]
17. Chen Y, Rivier CA, Mora SA, Torres Lopez V, Payabvash S, Sheth KN, et al. Deep learning survival model predicts outcome after intracerebral hemorrhage from initial CT scan. Eur Stroke J 2025 Mar;10(1):225-235 [FREE Full text] [doi: 10.1177/23969873241260154] [Medline: 38880882]
18. Si Y, Du J, Li Z, Jiang X, Miller T, Wang F, et al. Deep representation learning of patient data from Electronic Health Records (EHR): A systematic review. J Biomed Inform 2021 Mar 16;115:103671 [FREE Full text] [doi: 10.1016/j.jbi.2020.103671] [Medline: 33387683]

XSL•FO
RenderX

19. Hall AN, Weaver B, Liotta E, Maas MB, Faigle R, Mroczek DK, et al. Identifying Modifiable Predictors of Patient Outcomes After Intracerebral Hemorrhage with Machine Learning. Neurocrit Care 2021 Feb;34(1):73-84 [FREE Full text] [doi: 10.1007/s12028-020-00982-8] [Medline: 32385834]
20. Schneider H, Huynh TJ, Demchuk AM, Dowlatshahi D, Rodriguez-Luna D, Silva Y, PREDICT/Sunnybrook ICH CTA Study Group. Combining Spot Sign and Intracerebral Hemorrhage Score to Estimate Functional Outcome: Analysis From the PREDICT Cohort. Stroke 2018 Jun;49(6):1511-1514 [FREE Full text] [doi: 10.1161/STROKEAHA.118.020679] [Medline: 29720436]
21. Zhang Z, Zhang R, Xiao K, Sun X. G4Beacon: An In Vivo G4 Prediction Method Using Chromatin and Sequence Information. Biomolecules 2023 Feb 03;13(2):292 [FREE Full text] [doi: 10.3390/biom13020292] [Medline: 36830661]
22. Bashiri FS, Carey KA, Martin J, Koyner JL, Edelson DP, Gilbert ER, et al. Development and external validation of deep learning clinical prediction models using variable-length time series data. J Am Med Inform Assoc 2024 May 20;31(6):1322-1330 [FREE Full text] [doi: 10.1093/jamia/ocae088] [Medline: 38679906]
23. Zheng Z, Zhang X, Yu J, Guo R, Zhangzhong L. Deep Neural Networks for the Classification of Pure and Impure Strawberry Purees. Sensors (Basel) 2020 Feb 23;20(4):1223 [FREE Full text] [doi: 10.3390/s20041223] [Medline: 32102254]
24. Aihara S, Shibata R, Mizukami R, Sakai T, Shionoya A. Deep Learning-Based Myoelectric Potential Estimation Method for Wheelchair Operation. Sensors (Basel) 2022 Feb 18;22(4):73-84 [FREE Full text] [doi: 10.3390/s22041615] [Medline: 35214514]
25. Dirgová Luptáková I, Kubovčík M, Pospíchal J. Wearable Sensor-Based Human Activity Recognition with Transformer Model. Sensors (Basel) 2022 Mar 01;22(5):1911 [FREE Full text] [doi: 10.3390/s22051911] [Medline: 35271058]
26. Gregório T, Pipa S, Cavaleiro P, Atanásio G, Albuquerque I, Chaves PC, et al. Assessment and Comparison of the Four Most Extensively Validated Prognostic Scales for Intracerebral Hemorrhage: Systematic Review with Meta-analysis. Neurocrit Care 2019 Apr;30(2):449-466 [FREE Full text] [doi: 10.1007/s12028-018-0633-6] [Medline: 30426449]
27. You S, Zheng D, Yoshimura S, Ouyang M, Han Q, Wang X, INTERACT Investigators. Optimum Baseline Clinical Severity Scale Cut Points for Prognosticating Intracerebral Hemorrhage: INTERACT Studies. Stroke 2024 Jan;55(1):139-145 [FREE Full text] [doi: 10.1161/STROKEAHA.123.044538] [Medline: 38018833]
28. McCracken DJ, Lovasik BP, McCracken CE, Frerich JM, McDougal ME, Ratcliff JJ, et al. The Intracerebral Hemorrhage Score: A Self-Fulfilling Prophecy? Neurosurgery 2019 Mar 01;84(3):741-748 [FREE Full text] [doi: 10.1093/neuros/nyy193] [Medline: 29762777]
29. Hwang DY, Kim KS, Muehlschlegel S, Wartenberg KE, Rajajee V, Alexander SA, et al. Guidelines for Neuroprognostication in Critically Ill Adults with Intracerebral Hemorrhage. Neurocrit Care 2024 Apr;40(2):395-414 [FREE Full text] [doi: 10.1007/s12028-023-01854-7] [Medline: 37923968]
30. Zyck S, Du L, Gould G, Latorre JG, Beutler T, Bodman A, et al. Scoping Review and Commentary on Prognostication for Patients with Intracerebral Hemorrhage with Advances in Surgical Techniques. Neurocrit Care 2020 Aug;33(1):256-272 [FREE Full text] [doi: 10.1007/s12028-020-00962-y] [Medline: 32270428]

Abbreviations

AUROC: area under the receiver operating characteristic curve
CT: computer tomography
DCA: decision curve analysis
EHR: electronic health record
ENRICH: Early Minimally Invasive Removal of Intracerebral Hemorrhage
FN: false negative
FP: false positive
FUNC: Functional Outcome in Patients with Primary Intracerebral Hemorrhage
GCS: Glasgow Coma Scale
GRU: gated recurrent unit
ICH: intracerebral hemorrhage
MIS: minimally invasive surgery
MISTIE Ⅲ: Minimally Invasive Surgery Plus Alteplase for Intracerebral Hemorrhage Evacuation Phase 3
mRS: modified Rankin Scale
NIHSS: National Institute of Health Stroke Scale
ROC: receiver operating characteristic
STICH: Surgical Trial in Intracerebral Haemorrhage
STICH II: Surgical Trial in Intracerebral Haemorrhage II
TCN: temporal convolutional network
TN: true negative
TP: true positive

XSL•FO
RenderX

TRIPOD-AI: Transparent Reporting of a multivariable prediction model for Individual Prognosis Or Diagnosis–Artificial Intelligence

Edited by M Focsa; submitted 22.Oct.2025; peer-reviewed by M Chen, K Zhang; comments to author 25.Nov.2025; accepted 20.Dec.2025; published 07.Jan.2026.

Please cite as:
Wang J, Shi J, Ye Q, Chen D, Sun Y, Pan C, Tang Y, Zhang P, Tang Z
Deep Learning for Dynamic Prognostic Prediction in Minimally Invasive Surgery for Intracerebral Hemorrhage: Model Development and Validation Study
JMIR Med Inform 2026;14:e86327
URL: https://medinform.jmir.org/2026/1/e86327
doi:10.2196/86327
PMID:

©Jingxuan Wang, Jian Shi, Qing Ye, Danyang Chen, Yuhao Sun, Chao Pan, Yingxin Tang, Ping Zhang, Zhouping Tang. Originally published in JMIR Medical Informatics (https://medinform.jmir.org), 07.Jan.2026. This is an open-access article distributed under the terms of the Creative Commons Attribution License (https://creativecommons.org/licenses/by/4.0/), which permits unrestricted use, distribution, and reproduction in any medium, provided the original work, first published in JMIR Medical Informatics, is properly cited. The complete bibliographic information, a link to the original publication on https://medinform.jmir.org/, as well as this copyright and license information must be included.

XSL•FO
RenderX

Original Paper

Ranking-Aware Multiple Instance Learning for Histopathology Slide Classification: Development and Validation Study

Ho Heon Kim[1,2*], MS; Gisu Hwang[1*], MS; Won Chan Jeong[1], BS; Young Sin Ko[1,3], MD, PhD

[1]AI R&D Center, Seegene Medical Foundation, Seoul, Republic of Korea

[2]Department of Medical Sciences, Graduate School, The Catholic University of Korea, Seoul, Republic of Korea

[3]Pathology Center, Seegene Medical Foundation, Seoul, Republic of Korea

[*]these authors contributed equally

Corresponding Author:
Young Sin Ko, MD, PhD
AI R&D Center, Seegene Medical Foundation
17F, Seegene Medical Tower, 288 Dapsimni-ro, Dongdaemun-gu
Seoul, 02637
Republic of Korea
Phone: 82 2 2228 9349
Email: noteasy@mf.seegene.com

Abstract

Background: Multiple instance learning (MIL) is widely used for slide-level classification in digital pathology without requiring expert annotations. However, even partial expert annotations offer valuable supervision; few studies have effectively leveraged this information within MIL frameworks.

Objective: This study aims to develop and evaluate a ranking-aware MIL framework, called rank induction, that effectively incorporates partial expert annotations to improve slide-level classification performance under realistic annotation constraints.

Methods: We developed rank induction, a MIL approach that incorporates expert annotations using a pairwise rank loss inspired by RankNet. The method encourages the model to assign higher attention scores to annotated regions than to unannotated ones, guiding it to focus on diagnostically relevant patches. We evaluated rank induction on 2 public datasets (Camelyon16 and DigestPath2019) and an in-house dataset (Seegene Medical Foundation-stomach; SMF-stomach) and tested its robustness under 3 real-world conditions: low-data regimes, coarse within-slide annotations, and sparse slide-level annotations.

Results: Rank induction outperformed existing methodologies, achieving an area under the receiver operating characteristic curve (AUROC) of 0.839 on Camelyon16, 0.995 on DigestPath2019, and 0.875 on SMF-stomach. It remained robust under low-data conditions, maintaining an AUROC of 0.761 with only 60.2% (130/216) of the training data. When using coarse annotations (with 2240-pixel padding), performance slightly declined to 0.823. Remarkably, annotating just 20% (18/89) of the slides was enough to reach near-saturated performance (AUROC of 0.806, vs 0.839 with full annotations).

Conclusions: Incorporating expert annotations through ranking-based supervision improves MIL-based classification. Rank induction remains robust even with limited, coarse, or sparsely available annotations, demonstrating its practicality in real-world scenarios.

(JMIR Med Inform 2026;14:e84417) doi:10.2196/84417

KEYWORDS

multiple instance learning; learning to rank; digital pathology; whole slide image; weakly supervised learning; mixed supervision; data-efficient training

Introduction

With the rise of digital pathology, whole slide images (WSIs) have become essential for computer-assisted diagnosis tasks such as tumor detection, subtype classification, and prognosis prediction [1-3]. Due to their extremely high resolution, WSIs are typically divided into smaller patches before being used in deep learning models. In fully supervised learning settings, this requires patch-level labels—an annotation process that is time consuming and labor intensive due to the scarcity of lesion-containing patches. To reduce the burden of exhaustive labeling, the multiple instance learning (MIL) framework has

XSL•FO
RenderX

emerged as the dominant approach for slide-level prediction. MIL operates in a weakly supervised setting, using only slide-level labels and eliminating the need for detailed patch annotations. Despite this advantage, MIL models still require large datasets to achieve generalizable performance due to a weak supervision signal [4]. In data-constrained settings, MIL training often becomes unstable, leading to a significant reduction in predictive accuracy. To address the limitations of weak supervision, recent studies can be broadly categorized based on the strength of supervision into three main streams: (1) slide-level approaches relying solely on slide labels, (2) pseudolabel-based methods that infer patch-level labels, and (3) expert-guided methods leveraging direct annotations.

Slide-level approaches operate solely with slide-level supervision but aim to improve performance through semisupervised learning, self-supervised learning, or multiresolution architectures [5-12]. For instance, dual-stream multiple instance learning (DS-MIL) introduced a dual-stream architecture that models relationships between high- and low-attention instances to mitigate attention collapse and improve feature discrimination [11]. Hierarchical image pyramid transformer (HIPT) leveraged hierarchical self-supervised vision transformers to capture multiscale contextual information across gigapixel WSIs, demonstrating that strong representation learning can alleviate weak supervision limitations [12]. However, because these approaches still rely only on slide-level labels, the supervision signal remains weak and cannot fully guide the model toward diagnostically relevant regions.

Pseudolabel-based methods generate inferred patch-level labels from attention maps to strengthen the weak supervision signal. A prominent data-efficient training using pseudolabel is clustering-constrained attention multiple instance learning (CLAM), which selects high- and low-attention instances within each slide to form pseudopositive or pseudonegative sets and trains an auxiliary instance classifier [13]. Iterative multiple instance learning proposed an iterative framework that refines both instance and slide representations by retraining the feature extractor with attention-derived pseudolabels, though its performance depends on the stability of the initial MIL attention [14]. In general, pseudolabeling techniques aim to fill the gap in patch-level labels by generating inferred annotations [13-18]. Despite their utility, pseudolabels are inherently noisy, as they are inferred rather than observed. Consequently, MIL pipelines that solely rely on pseudolabels often suffer from degraded performance.

In contrast, expert-guided methods offer a promising way to improve both performance and supervision quality by directly integrating expert annotations. Nevertheless, this approach remains relatively underexplored compared to other categories. A notable study described the attention induction model, which uses pathologist-drawn lesion annotations to guide model attention [19]. However, by enforcing attention scores proportional to the size of the annotated regions, this method inherently biases the model toward larger areas, increasing the risk of overlooking small but clinically critical diagnostic features.

To overcome this limitation, we propose rank induction, a novel MIL framework that introduces a pathology-informed inductive bias. Rather than constraining attention based on region size, rank induction assumes that annotated regions should carry higher diagnostic importance than unannotated ones. By learning relative ranks between patches, our method provides finer-grained supervision, guiding the model to focus on diagnostically relevant areas even when annotations are sparse or training data are limited.

Methods

Problem Definition

We extend the standard MIL framework by incorporating patch-level annotations from pathologists as explicit instance labels, either across all training slides or only a subset. In a typical MIL setting, each WSI is divided into K patches $\{x_1,\ldots,x_K\}$, and only a slide-level label, indicating disease presence, is provided. A slide is labeled positive if at least 1 patch contains a lesion and negative if all patches are normal (for simplicity, we assume a fixed K across slides).

In our extended setting, we additionally use binary labels $\{y_1,\ldots,y_k\}$ at the patch level, where $y_k \in \{0,1\}$, $y_k=1$, if a patch overlaps with a pathologist-annotated region, and $y_k=0$ otherwise. The core inductive bias we introduce is simple but clinically grounded: patches overlapping annotated regions should receive higher attention than unannotated ones. This reflects the assumption that tumor-confirmed regions are more relevant to slide-level diagnosis than those confirmed to be normal.

Rank Induction

As illustrated in Figure 1, rank induction consists of 2 key components: pairwise rank comparison derived from rich annotation supervision and attention thresholding to filter out residual noninformative patches. To implement our ranking-aware attention mechanism, we first define the computation of patch-wise attention. Let z_k denote the feature vector of patch x_k extracted by a backbone feature encoder. We compute a raw attention score s_k from z_k using an attention layer and normalize it using softmax: . Inspired by RankNet [20], rank induction introduces a ranking constraint that encourages higher attention scores for annotated patches than for nonannotated ones, such that $s_i > s_j$, where s_i is the attention score for an annotated patch and s_j for a nonannotated patch.

XSL•FO
RenderX

Figure 1. Overview of rank induction.

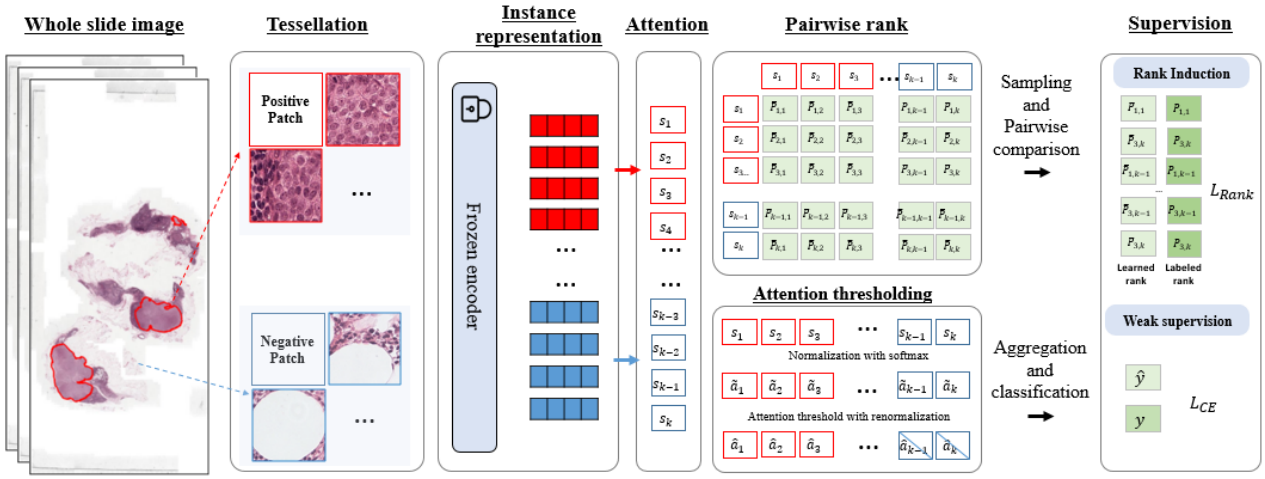

To avoid the normalization constraint of softmax ( ), we apply the ranking loss directly on the raw attention scores $s_i \in R$. We define the pairwise ranking preference using a sigmoid function:

Here, *m* is a margin parameter that enforces separation between positive and negative patches and σ is a scaling factor. We exclude same-class pairs (eg, lesion-lesion or normal-normal) and define the valid pair set: $P = \{(i,j)|y_i = 1, y_j = 0\}$. Let be the ground truth ranking label. The rank loss is defined as:

We jointly optimize the slide-level binary cross-entropy loss and the rank loss:

$$L = L_{BCE} + \lambda L_{rank}$$

where λ is a weighting hyperparameter. For slides without annotated lesions (ie, negative slides), we omit the ranking loss and only apply the slide-level loss.

To mitigate slide-level representation dilution, where a few high-attention lesion patches are overwhelmed by numerous low-attention nonlesion patches during the attention-weighted summation, we apply an attention thresholding strategy during training. Specifically, we threshold the normalized attention weights and then renormalize all (including zero-valued) weights as follows:

Here, *T* is a predefined threshold and *K* is the number of patches. The threshold *T* is introduced to prevent the slide-level representation from being dominated by the large number of negative instances when the bag size is large. For example, in a slide containing 2000 instances with only 10 lesion patches, even if attention is highly concentrated on those few positives, the aggregate contribution from thousands of near-zero attention weights of negative patches can still overshadow the lesion signal, leading to degraded slide representations. By applying *T*, we effectively suppress these noise-like weights and maintain a more balanced representation across instances.

Datasets

We evaluated rank induction on 2 public datasets (Camelyon16 [21] and DigestPath2019 [22]) and an in-house dataset (Seegene Medical Foundation-stomach; SMF-stomach). Textbox 1 provides a detailed description of the datasets used in this study, with sample count statistics summarized in Table 1, which presents the statistics for the 3 datasets.

XSL•FO
RenderX

Textbox 1. Description of the datasets used in this study.

- Camelyon16: this dataset consists of 399 hematoxylin and eosin-stained whole slide images (WSIs) of lymph node sections for breast cancer metastasis detection. It is originally split into 67.7% (270/399) training slides and 32.3% (129/399) test slides. For model development and hyperparameter tuning, we further split the 270 training WSIs into 216 (80%) training slides and 54 (20%) validation slides (an 8:2 split). Each slide includes a slide-level diagnosis and polygon-based lesion annotations provided by expert pathologists. In this study, slides containing metastasis were labeled as abnormal, while negative slides were labeled as normal.
- DigestPath2019: we used the colonoscopy tissue segmentation dataset from the DigestPath Challenge 2019. The dataset originally includes 660 training images and 212 test images with slide-level labels (benign or malignant). However, because the test set is not publicly available, we used only the 660 labeled WSIs. We allocated 20% (132/660) of the slides as the test set and used the remaining 80% (528/660) for training and validation. Specifically, we split the 528 slides into 422 (79.9%) for training and 106 (20.1%) for validation. Each WSI is a JPEG image with an average resolution of approximately 5000×5000 pixels. For consistency, we mapped malignant samples to the abnormal class and benign samples to the normal class.
- SMF-stomach (in-house): we constructed an in-house gastric pathology dataset at Seegene Medical Foundation (SMF). Slide preparation and digitization followed standard operating procedures described by Kim et al [23]. A distinct feature of this dataset, as illustrated in Multimedia Appendix 1, is that at least 3 consecutive tissue sections are placed on a single glass slide; however, pixel-level annotations were not exhaustively applied to every section. A single board-certified pathologist reviewed the slides and provided polygon-based annotations only for representative regions; thus, unannotated tissue sections may coexist within the same WSI. Following the diagnostic criteria of Ko et al [24], lesions were originally categorized as malignant, dysplasia, negative, and uncategorized. We excluded the uncategorized class due to its high heterogeneity. For the binary classification task, we mapped malignant and dysplasia to the abnormal class and negative to the normal class. The final dataset comprised 209 slides, allocated as 120 (57.4%) for training, 30 (14.4%) for validation, and 59 (28.2%) for testing.

Table 1. Dataset statistics (whole slide images).

Dataset	Train		Validation		Test	
	Abnormal	Normal	Abnormal	Normal	Abnormal	Normal
Camelyon16	89	127	22	32	49	80
DigestPath2019	160	262	40	66	50	82
SMF-stomach[a]	81	39	20	10	39	20

[a]SMF-stomach: Seegene Medical Foundation-stomach.

Data Preprocessing

We applied the same preprocessing pipeline to all datasets. First, we performed tissue-background segmentation using the multilevel Otsu algorithm. Each WSI was converted to grayscale and thresholded to generate a binary mask that separated tissue from the white background. We retained only the foreground tissue regions and discarded blank or irrelevant areas.

Next, we tessellated each foreground region into nonoverlapping patches of size 224×224 pixels. For Camelyon16 and SMF-stomach, we extracted patches at 20× magnification, whereas for DigestPath2019, we used the original image resolution.

After tessellation, we computed the tissue coverage ratio for each patch and discarded patches containing less than 5% tissue, as these were considered mostly empty. Finally, we used a ResNet-50 [24] pretrained on ImageNet-1k [25] to extract features from each patch. Specifically, we used the output of the third residual block and applied an adaptive average pooling layer to obtain a 2048-dimensional feature vector.

Statistical Methods

To evaluate rank induction, we designed a series of experiments targeting performance, data efficiency, and annotation use. Our evaluation included 6 different experiment types, which are discussed in the following subsections.

Model Comparison

We trained and evaluated 7 different MIL models on 3 datasets: the baseline attention-based MIL (AB-MIL), the attention induction method, 2 variants of CLAM (single-branch [SB]; multibranch [MB]), DS-MIL, HIPT, and the proposed rank induction method.

Low-Data Regime

To test data efficiency, we trained models on subsets of the training data at 20%, 40%, 60%, 80%, and 100% of the full set. For each fraction, we trained all 7 models (AB-MIL, attention induction, CLAM-SB, CLAM-MB, DS-MIL, HIPT, and rank induction) from scratch and evaluated them on a common held-out test set.

Annotation Granularity

To simulate real-world coarse annotations, we degraded annotation precision by expanding the original lesion masks on Camelyon16 slides. At 40× magnification, we added symmetric paddings of 0, 448, 896, 1344, 1792, and 2240 pixels to each polygon annotation. For instance, a 448-pixel padding at 40× resolution adds 1 patch-width around the lesion, which corresponds to a 224-pixel patch at 20× magnification—potentially including normal tissue and simulating noisy annotations.

XSL•FO
RenderX

Subset-Annotated Slide Setting

In real-world clinical settings, not all slides can be exhaustively annotated. We tested rank induction under partial supervision by varying the proportion of positive slides with patch-level annotations (5%, 10%, 20%, 40%, 60%, and 80%) in the Camelyon16 training set (111 positive slides in total). The remaining positive slides were treated with slide-level labels only. Negative slides, by definition, had no lesion annotations.

Ablation Test

To assess the contribution of attention thresholding, we performed an ablation study with threshold values $T \in \{0,0.25,0.5,1,2,5\}$. The case of $T=0$ served as the reference condition (ie, without attention thresholding). We compared WSI classification performance and the cumulative attention weight assigned to nonlesion patches on the test set to examine how different thresholds affect model behavior.

Attention Localization

To assess interpretability, we compared how different MIL models spatially focus on tumor regions in Camelyon16. This is not a dense pixel-wise segmentation map; rather, it is a ranking over discrete patches, with scores defined for all patches in the slide [13]. Because no established gold standard protocol exists for evaluating such attention maps, we quantified spatial alignment between attention and expert lesion annotations using 3 metrics: intersection over union (IoU), Dice score, and pointing game [25]. For each WSI, we ranked all patches by attention weight and then selected only the top α% relative to the number of tumor-annotated patches in that slide ($\alpha \in \{1, 5, 10, 20, 50, 75, 100\}$). To ensure that the ideal case could always achieve a score of 1, IoU and Dice score were computed by sampling up to the number of tumor-annotated patches, whereas the pointing game was evaluated by sampling from all patches in the slide. We then computed IoU and Dice score between the selected high-attention patches and the tumor-annotated patches, averaged over positive test slides. We also measured the pointing game by calculating a hit rate, defined as whether at least 1 of the top α highest attention patches fell within the annotated tumor region (classified as a hit). For all malignant test slides, localization accuracy was defined as hits divided by the sum of hits and misses.

For model evaluation, we computed area under the receiver operating characteristic curve (AUROC), area under the precision-recall curve (AUPRC), and accuracy for slide-level classification. All results were averaged over a 10-fold Monte Carlo cross-validation. We assessed statistical significance using the Mann-Whitney *U* test, with *P* values <.05 considered statistically significant.

Experiment Details

We implemented the models in Python using the PyTorch deep learning framework. WSI data preprocessing was carried out with OpenSlide, OpenCV, and Pillow libraries. Visualization of attention maps and result plots was generated using Seaborn and Matplotlib libraries (specific version information for each library can be found in the GitHub repository). The training and experiments were run on a computing system with a pair of NVIDIA A100 graphics processing units (80 GB memory each) and an Intel Xeon Gold 6338N central processing unit (128 cores, 2.20 GHz) with 512 GB of RAM. Additionally, because the original implementation of attention induction was not publicly available, we reimplemented the method based on the descriptions provided in the paper. Our implementation is available to facilitate reproducibility [26].

For optimization, we used the Adam optimizer with a learning rate of 2×10^{-4} and a weight decay of 1×10^{-5}. We trained each model for up to 200 epochs using an early stopping criterion: if the validation loss did not improve for 7 consecutive epochs (after an initial 20-epoch warmup period), training was stopped. In practice, most models converged well before 200 epochs under this criterion. For all MIL benchmarks, the ResNet-50 backbone was frozen during training. Crucially, we used a frozen ResNet-50 backbone for all MIL benchmarks. Although methods such as DS-MIL and HIPT typically leverage self-supervised pretraining or hierarchical encoders, we used ResNet-50 as the feature extractor for this experiment. This ensured a direct comparison of the MIL aggregation strategies themselves, isolating their performance from the variations in pretrained feature representations.

We set the rank loss hyperparameters as follows: the scaling factor $\sigma=1$ and margin $m=1$ in the pairwise probability formula, and the rank loss weight $\lambda=1$. In each training iteration, to limit memory use and ensure computational efficiency when computing the rank loss, we randomly sampled up to 1024 positive and 1024 negative patches per slide. The attention threshold *T* was set to 1.

Ethical Considerations

This study used both publicly available deidentified datasets (Camelyon16 and DigestPath2019) and a private clinical dataset (SMF-stomach). The Camelyon16 and DigestPath2019 datasets consist of fully deidentified WSIs, publicly released for research under their respective challenge licenses; therefore, no institutional review board (IRB) approval or informed consent was required for their use. For the SMF-stomach dataset, this study was approved by the IRB of the Seegene Medical Foundation (SMF-IRB-2024-015). Given the anonymous and deidentified nature of the retrospective pathological images, informed consent was not required.

Results

Model Performance

We compared rank induction against 6 representative MIL benchmarks: AB-MIL, attention induction, CLAM, DS-MIL, and HIPT, regarding slide-level classification performance. On Camelyon16, rank induction achieved an AUROC of 0.839 (SD 0.050) and an AUPRC of 0.850 (SD 0.042), outperforming all baseline methods with consistently low variance (Table 2). We observed similar performance trends on the DigestPath2019 dataset. Although all models performed well due to the dataset's relative simplicity, rank induction achieved the best results (AUROC=0.995; AUPRC=0.993) with stable variance. On the SMF-stomach dataset, rank induction demonstrated the best performance, achieving an AUROC of 0.875 (SD 0.008) and an AUPRC of 0.937 (SD 0.006). Due to space constraints, the

XSL•FO
RenderX

full accuracy comparison for all datasets is reported in Multimedia Appendix 2.

Table 2. Comparison of model performance across methods on 2 public datasets and an in-house dataset.

Model	Camelyon16		DigestPath2019		SMF[a]-stomach	
	AUROC[b], mean (SD)	AUPRC[c], mean (SD)	AUROC, mean (SD)	AUPRC, mean (SD)	AUROC, mean (SD)	AUPRC, mean (SD)
AB-MIL[d]	0.741 (0.146)	0.730 (0.183)	0.993 (0.003)	0.990 (0.005)	0.864 (0.031)	0.928 (0.016)
Attention induction	0.742 (0.142)	0.727 (0.179)	0.994 (0.002)	0.990 (0.003)	0.868 (0.031)[e]	0.930 (0.016)[e]
CLAM-SB[f]	0.732 (0.137)	0.700 (0.179)	0.977 (0.019)	0.965 (0.026)	0.837 (0.023)	0.919 (0.013)
CLAM-MB[g]	0.794 (0.128)[e]	0.767 (0.168)[e]	0.976 (0.019)	0.963 (0.026)	0.838 (0.032)	0.916 (0.025)
DS-MIL[h]	0.690 (0.170)	0.666 (0.223)	0.995 (0.004)[e]	0.993 (0.006)[e]	0.839 (0.031)	0.915 (0.016)
HIPT[i]	0.483 (0.103)	0.416 (0.136)	0.962 (0.058)	0.947 (0.091)	0.676 (0.064)	0.751 (0.060)
Rank induction	*0.839 (0. 050)* [j,k, l,m, o ,p]	*0.850 (0. 042)* [j,k, l,m, o ,p]	*0.995 (0. 002)* [j,k, l,m,n,p]	*0.993 (0. 002)* [j,k, l,m,n, p]	*0.875 (0. 008)* [j,m, n,o,p]	*0.937 (0. 006)* [j,m, n,o,p]

[a]SMF: Seegene Medical Foundation.

[b]AUROC: area under the receiver operating characteristic curve.

[c]AUPRC: area under the precision-recall curve.

[d]AB-MIL: attention-based multiple instance learning.

[e]Second-best result.

[f]CLAM-SB: clustering-constrained attention multiple instance learning, single-branch.

[g]CLAM-MB: clustering-constrained attention multiple instance learning, multibranch.

[h]DS-MIL: dual-stream multiple instance learning.

[i]HIPT: hierarchical image pyramid transformer.

[j]Italicization indicates the best result.

[k]$P<.05$ vs attention-based multiple instance learning.

[l]$P<.05$ vs attention induction.

[m]$P<.05$ vs clustering-constrained attention multiple instance learning, single-branch.

[n]$P<.05$ vs clustering-constrained attention multiple instance learning, multibranch.

[o]$P<.05$ vs dual-stream multiple instance learning.

[p]$P<.05$ vs hierarchical image pyramid transformer.

Data-Efficient Learning With Expert Annotation

To investigate data-efficient training with expert annotation under low-data regimes reflecting real-world constraints, we assessed model performance on Camelyon16 by varying the proportion of training data (Figure 2). With only 20% of the slides, all methods achieved AUROC scores in the range of 0.4 to 0.6, and statistically significant differences were observed between rank induction and the other benchmarks. Among them, rank induction achieved the highest AUROC. At 40% and 60% of the training data size, rank induction significantly outperformed other MIL methods. When trained with 80% of the data, rank induction achieved an AUROC of 0.786 (SD 0.042), surpassing HIPT (AUROC=0.464, SD 0.076), DS-MIL (AUROC=0.709, SD 0.154), AB-MIL (AUROC=0.707, SD 0.186), attention induction (AUROC=0.714, SD 0.193), CLAM-SB (AUROC=0.721, SD 0.180), and CLAM-MB (AUROC=0.847, SD 0.042).

XSL•FO
RenderX

Figure 2. Area under the receiver operating characteristic curve (AUROC) performance across different training set sampling ratios on Camelyon16. AB-MIL: attention-based multiple instance learning; DS-MIL: dual-stream multiple instance learning; CLAM-MB: clustering-constrained attention multiple instance learning, multibranch; CLAM-SB: clustering-constrained attention multiple instance learning, single-branch; HIPT: hierarchical image pyramid transformer. Asterisks indicate statistical significance based on the Mann-Whitney U test: *P<.05, **P<.001, ***P<.0001, and ****P<.00001.

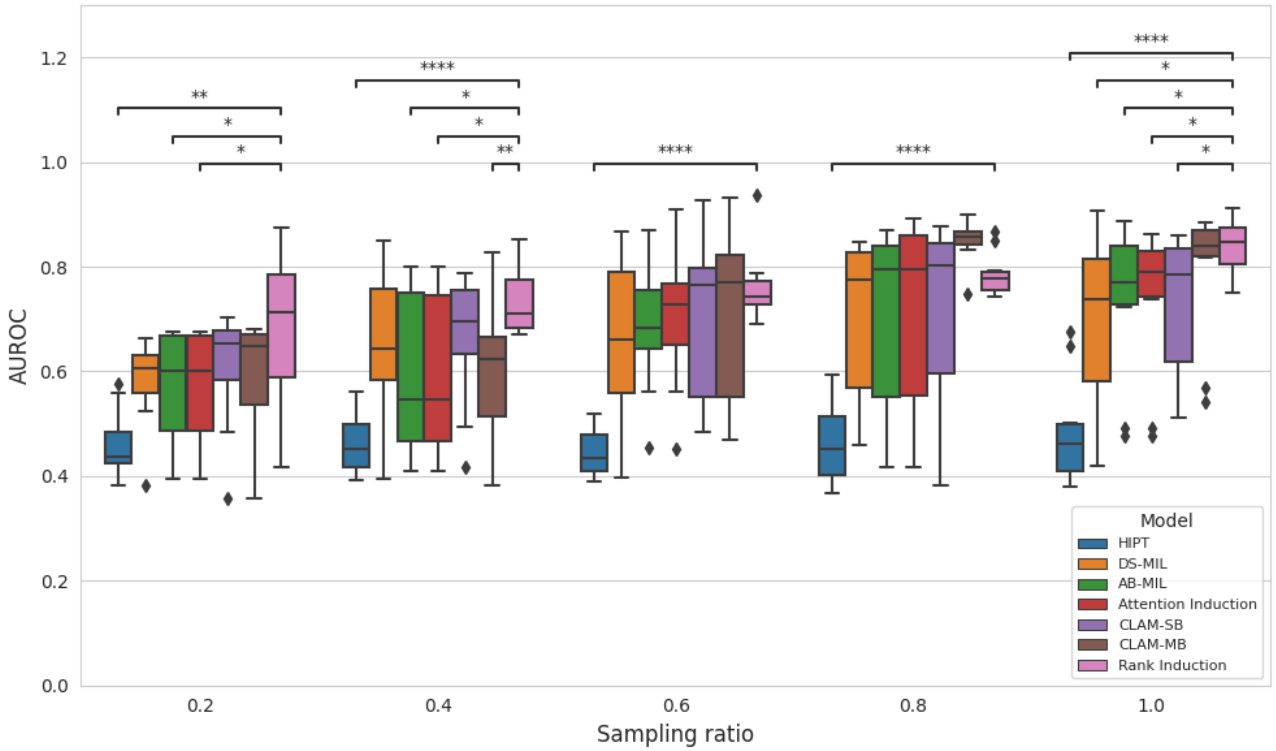

Annotation Granularity

We evaluated model robustness to noisy or imprecise annotations by progressively padding the pathologist-drawn tumor regions on Camelyon16 to simulate coarse lesion markings. Both rank induction and attention induction were trained under each noise condition. With the original annotations (0-pixel padding), rank induction achieved an AUROC of 0.839 (SD 0.050). Even at the highest padding level, its performance declined only slightly to an AUROC of 0.823 (SD 0.050; Figure 3). In comparison, attention induction dropped from an AUROC of 0.742 (SD 0.142) to 0.723 (SD 0.134) as annotation noise increased. Across all levels of annotation coarseness, rank induction consistently outperformed attention induction, although the differences were not statistically significant at some padding levels.

XSL•FO
RenderX

Figure 3. Annotation granularity experiment on Camelyon16. (A) Comparison of slide-level classification performance (area under the receiver operating characteristic curve [AUROC]) between attention induction and rank induction. (B) Representative visualization of the artificially expanded annotations used in the experiment. The thin inner red line indicates the original precise lesion annotation provided by the pathologist (ground truth), while the bold outer red line represents the artificially expanded annotation boundary simulating coarser supervision granularity.

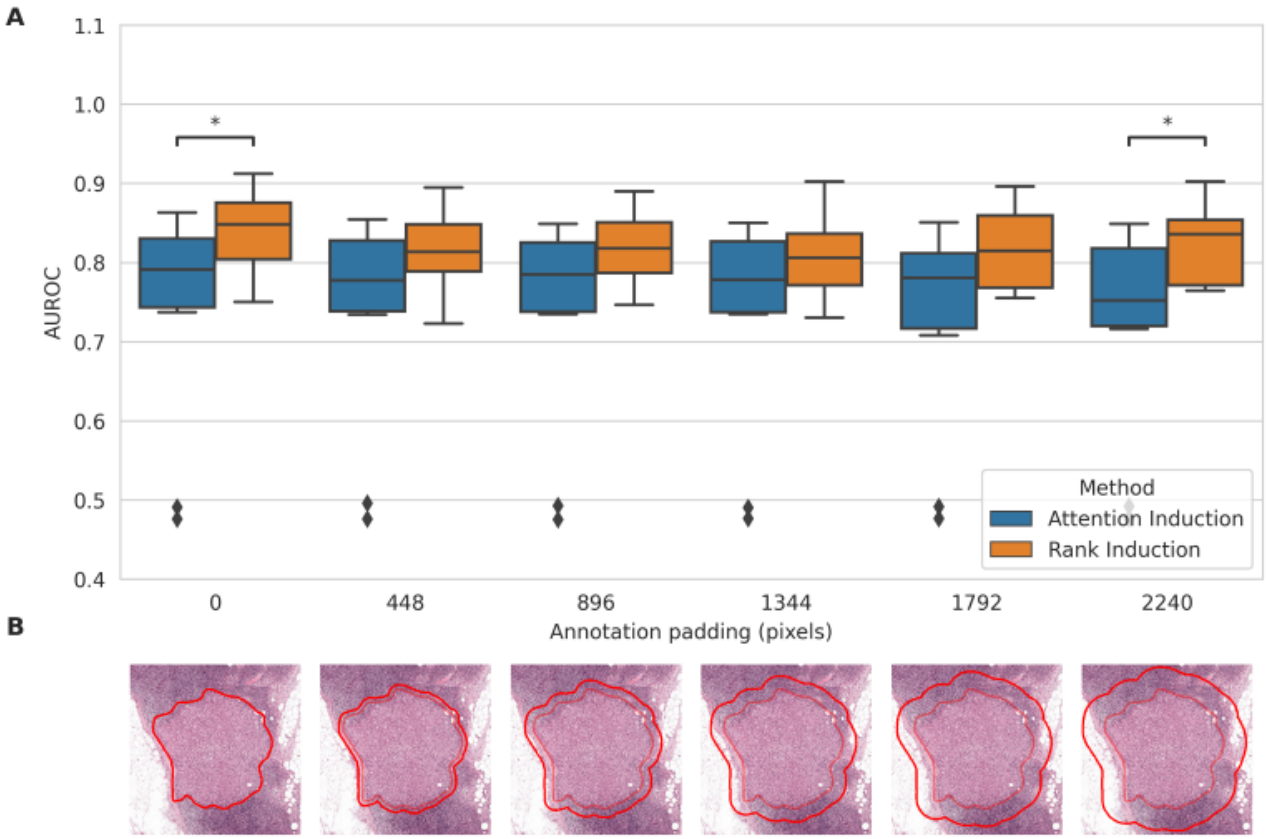

Fraction of Expert Annotation

To simulate real-world scenarios in which annotating all WSIs is infeasible, we evaluated model performance by varying the proportion of annotated positive WSIs in the training set. As a baseline (0% annotation), AB-MIL achieved an average AUROC of 0.741 (SD 0.146; Figure 4). With only 10% (9/89) of positive WSIs annotated in the train dataset, rank induction boosted the performance to an average AUROC of 0.782 (SD 0.070). Increasing the annotation coverage to 20% (18/89) raised the AUROC to 0.807 (SD 0.070), while using all available positive WSIs (N=89) yielded a final AUROC of 0.839 (SD 0.050). Notably, rank induction achieved near-saturated performance with 20% of the annotated data, demonstrating high data efficiency. Moreover, the introduction of even minimal annotation significantly reduced performance variance compared to the unannotated baseline. The performance curve began to plateau beyond approximately 20% annotation coverage, indicating diminishing returns in AUROC gains, while maintaining low variability.

XSL•FO
RenderX

Figure 4. Impact of annotation fraction on area under the receiver operating characteristic curve (AUROC). WSI: whole slide image.

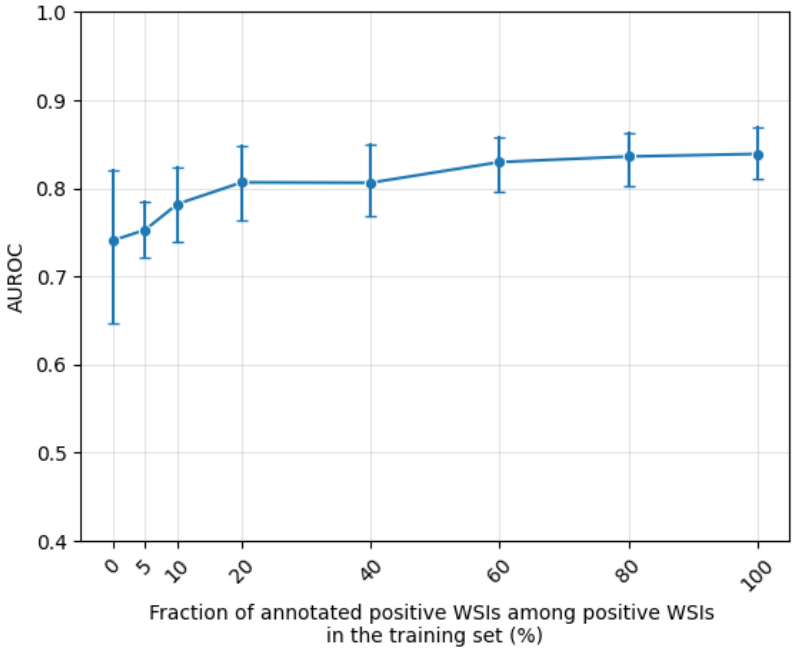

Ablation Test

The impact of varying the attention threshold *T* on model performance and attention distribution is presented in Table 3. As *T* increased from 0 to 2, both AUROC and AUPRC improved steadily, accompanied by a marked reduction in the average sum of attention assigned to nonlesion patches.

Table 3. Effect of attention threshold *T* on whole slide image (WSI) classification performance and sum of attention weight for nonlesion patches.

Threshold	Test dataset (n=129)		Positive WSI in the test dataset (n=49; sum of nonlesion attention), mean (SD)
	AUROC[a]	AUPRC[b]	
0	0.830	0.846	0.465 (0.420)
0.25	0.853	0.878	0.411 (0.434)
0.5	0.869	0.881	0.362 (0.423)
1	0.894	0.905	0.269 (0.387)
2	0.916	0.922	0.178 (0.354)
5	0.909	0.914	0.105 (0.339)

[a]AUROC: area under the receiver operating characteristic curve.

[b]AUPRC: area under the precision-recall curve.

With no thresholding (*T*=0) or low thresholds (*T*<1, where attention distributions remain nearly uniform), the AUROC remained relatively low. This suggests that weakly attended nonlesion patches diluted the slide-level representation. The best performance was observed at *T*=2 (AUROC=0.916; AUPRC=0.922), indicating that moderate thresholding effectively suppresses noise-like, low-value attention weights while preserving discriminative focus. Excessively high thresholds (eg, *T*=5) yielded a slight decline, reflecting an optimal balance near *T*=2.

Attention Localization and Qualitative Analysis

To evaluate the effect of rank induction on attention localization, we examined whether the attention weights were concentrated within expert-annotated regions. Across all 3 localization metrics, rank induction consistently demonstrated greater focus on the annotated areas compared to other MIL methods. At α=5, AB-MIL, attention induction, and rank induction achieved IoU scores of 0.029, 0.023, and 0.031 and Dice scores of 0.056, 0.045, and 0.059, respectively. When α increased to 75, the performance gap between rank induction and the baseline models became more pronounced (Figures 5A and 5B). A similar trend was observed in pointing game accuracy (Figure 5C). Qualitatively, both AB-MIL and attention induction produced noisy attention maps that highlighted not only tumor regions but also large areas of normal tissue, resulting in frequent false positives. In contrast, rank induction generated sharp and well-localized attention maps, accurately delineating lesion areas with minimal off-target activation—closely matching the ground truth annotations. This distinct separation between tumor and normal regions explains rank induction's

XSL•FO
RenderX

superior performance and enhances the interpretability of its predictions (Figure 6).

Figure 5. Attention localization performance of attention-based multiple instance learning (AB-MIL), attention induction, and rank induction. (A) Intersection over union (IoU) score according to the top α% of patches. (B) Dice score according to the top α% of patches. (C) Average pointing game score. WSI: whole slide image.

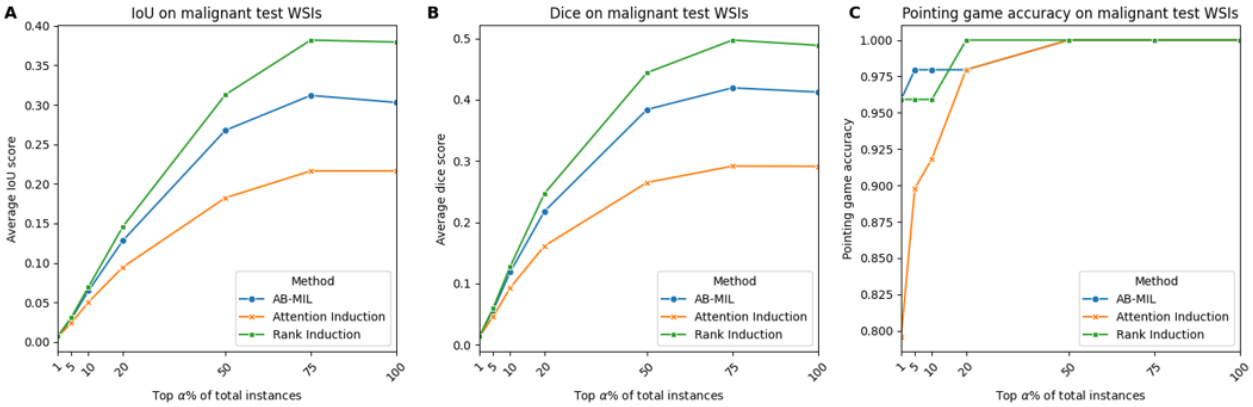

Figure 6. Qualitative visualization of patch selection for attention-based multiple instance learning (AB-MIL), attention induction, and rank induction. (A) A positive WSI thumbnail. (B) Attention distributions from each model in the lesion (red box) and nonlesion (blue box) regions in (A). (C) Another positive WSI thumbnail. (D) Attention distributions from each model in the lesion and nonlesion regions in (C).

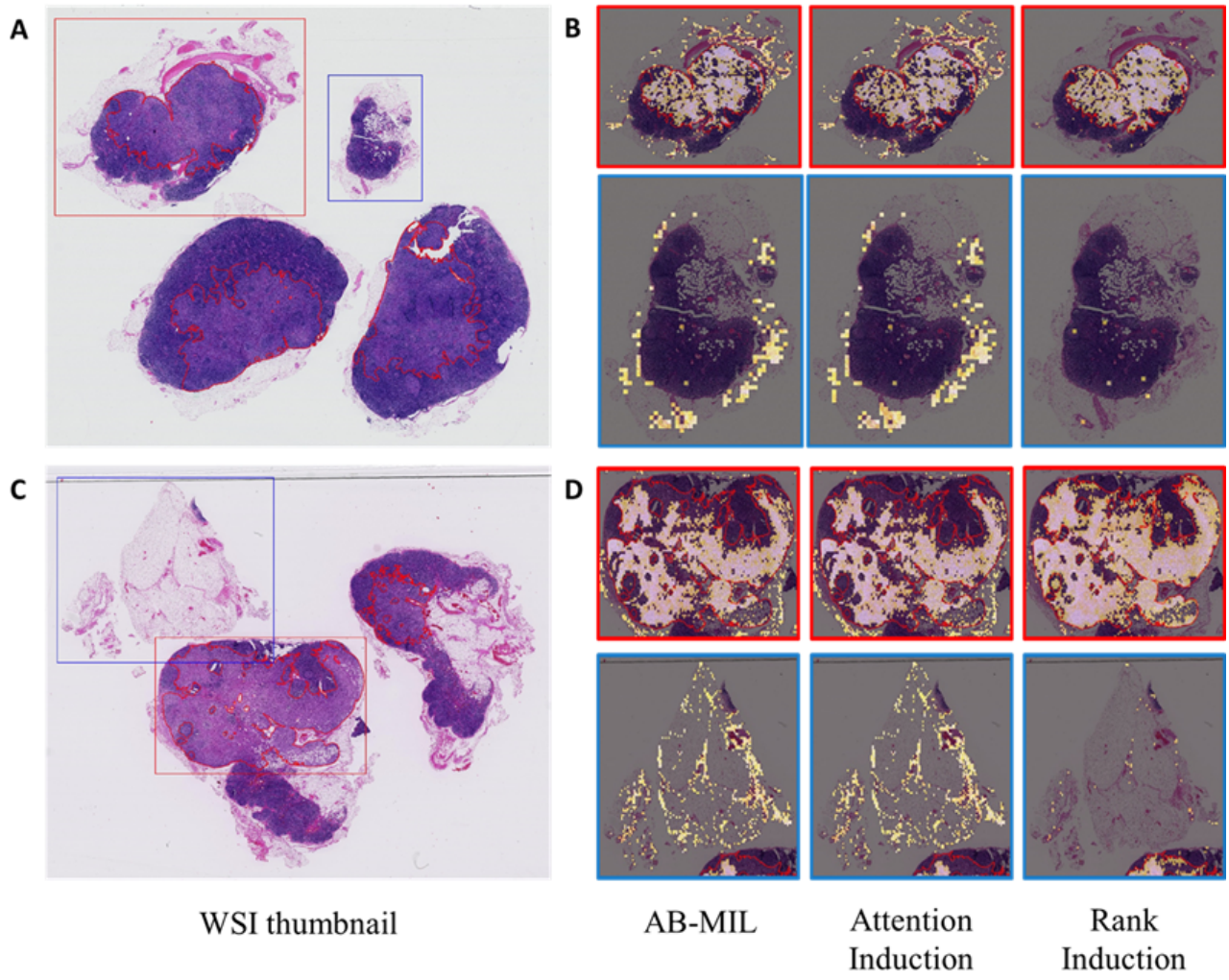

XSL•FO
RenderX

Discussion

Principal Findings

In this work, we present rank induction, the first method to integrate MIL with expert annotations using pairwise rank constraints. By enforcing a ranking loss that encourages higher attention scores for annotated patches than for nonannotated ones, our approach effectively strengthens the weak supervision signal inherent to MIL frameworks.

We validated rank induction through comprehensive experiments on 2 public datasets and 1 in-house dataset, covering 5 key scenarios: full-data classification, low-data regimes, varying annotation granularity, subset annotation settings, and qualitative visualization. Across all settings, rank induction consistently outperformed baseline methods, including pseudo-labeling approaches and attention induction, while producing more faithful and interpretable attention heat maps.

Notably, the proposed ranking mechanism is model-agnostic and can be used as a versatile module within other MIL architectures. As demonstrated in Multimedia Appendix 3, integrating rank induction into existing methods such as DS-MIL and HIPT consistently improved their performance. In our main experiments, these baseline models (DS-MIL and HIPT) exhibited lower performance than that reported in their original studies. This discrepancy arises because we used a standard ImageNet-pretrained ResNet-50 backbone across all models to ensure a fair comparison of the MIL aggregation strategies themselves, rather than relying on the self-supervised pretraining typically required by those methods. However, even under this constrained setting, incorporating rank induction significantly boosted their classification accuracy, demonstrating the robustness and generalizability of our ranking-based supervision.

Ultimately, these performance improvements stem from bridging weak and strong supervision through informative pairwise constraints that approximate expert guidance. Rank induction is grounded in a simple yet clinically intuitive assumption: models should prioritize annotated regions over nonannotated ones. This inductive bias aligns naturally with domain knowledge in pathology, establishing rank induction as an effective and practical solution for real-world applications.

Real-World Application With Expert Annotations

The pairwise ranking approach in rank induction addresses key challenges associated with expert annotations in real-world settings. In practice, tumor regions often exhibit irregular and heterogeneous morphology with poorly defined boundaries, making precise annotations difficult. Consequently, annotations are frequently coarse or incomplete. Despite this, rank induction maintained robust classification performance even with noisy annotations (Figure 3). This resilience likely stems from the pairwise training mechanism: although some comparisons may involve incorrectly labeled patches, most pairwise relationships remain valid, enabling the model to suppress noise and learn effectively.

Moreover, due to time and resource limitations, only a subset of positive WSIs can typically be annotated in clinical workflows. In such scenarios, extracting maximum value from limited expert input is critical. Unlike attention induction, which relies on assigning exact attention weights to individual patches, rank induction leverages a larger number of patch-pair comparisons from the valid pair set P, which grows quadratically with the number of annotated patches. This design allows the model to achieve near-saturated performance even with partial annotations (Figure 4).

Although pseudolabeling offers an alternative when expert annotations are unavailable, as seen in methods such as CLAM, it introduces uncertainty by relying on the model's own predictions. These pseudolabels are inherently noisier than expert supervision and can lead to cascading errors. In contrast, rank induction avoids this risk by grounding supervision in verified expert annotations, leading to more stable and accurate slide-level predictions, especially in low-data or noisy-label conditions.

Comparison of Fully Supervised Learning and Rank Induction

In scenarios where exhaustive patch-level annotations are available for all WSIs, fully supervised learning remains a strong baseline. Using the same training settings as our MIL models, a patch-level convolutional neural network with a fine-tuned ResNet-50 backbone and max-pooling aggregation achieved an AUROC of 0.892 on Camelyon16. This result outperformed the AUROC of 0.839 achieved by rank induction, which utilizes a frozen backbone and MIL-based aggregation. This result illustrates the upper bound of fully supervised performance given complete expert annotations and domain-specific fine-tuning (Multimedia Appendix 4).

However, in realistic clinical environments, exhaustive annotation is rarely feasible. When only 10% (9/89) of positive WSIs were annotated in the train dataset, the fully supervised model trained on this subset achieved an AUROC of 0.729. In contrast, rank induction, using the same 10% of patch-level annotations and leveraging slide-level labels from the remaining 90%, achieved a higher AUROC of 0.775. The key difference lies in how each method handles unannotated slides. Fully supervised models are limited to the annotated subset and cannot benefit from weak labels. Rank induction, by integrating both patch- and slide-level supervision through pairwise ranking constraints, makes effective use of all available data, even with sparse annotations.

These findings highlight a clear trade-off: while fully supervised learning performs best under ideal, fully annotated conditions, rank induction offers a more practical and annotation-efficient alternative. Its ability to generalize from partial supervision makes it especially suitable for real-world digital pathology applications, where annotations are incomplete or expensive.

Limitations

Our study has several limitations. First, although we validated our method on 3 datasets, including 1 in-house dataset (SMF-stomach), the diversity of organs and pathologies remains limited. Specifically, the SMF-stomach dataset was collected from a single institution, which may introduce biases related to specific staining protocols or scanner characteristics. To fully assess cross-domain robustness, future work should include

XSL•FO
RenderX

evaluation on larger, multicenter cohorts with diverse scanners. Nonetheless, the inclusion of Camelyon16 partially addresses this concern, as it contains slides from multiple medical institutions, providing evidence of generalization.

Conclusions

In summary, rank induction provides a practical and effective solution for improving slide-level classification in digital pathology by bridging weak and strong supervision via pairwise ranking constraints. By leveraging only sparse expert annotations, it achieves a strong balance between annotation efficiency and model performance, outperforming traditional MIL and pseudolabeling approaches, particularly in low-data or noisy-label settings.

Although fully supervised learning may yield higher accuracy when exhaustive annotations are available, rank induction offers a more scalable and annotation-efficient alternative for real-world use. Its robustness with limited annotations and its ability to highlight diagnostically relevant regions underscore the potential of rank-based supervision to improve both model interpretability and generalizability across diverse clinical environments.

Conflicts of Interest

None declared.

Multimedia Appendix 1
Example of a partially annotated whole slide image from the Seegene Medical Foundation-stomach dataset.
[PNG File , 511 KB - medinform_v14i1e84417_app1.png]

Multimedia Appendix 2
Comparison of slide-level classification accuracy across different multiple instance learning methods on 3 datasets.
[DOCX File , 30 KB - medinform_v14i1e84417_app2.docx]

Multimedia Appendix 3
Impact of integrating rank induction into existing multiple instance learning architectures (dual-stream multiple instance learning and hierarchical image pyramid transformer).
[DOCX File , 31 KB - medinform_v14i1e84417_app3.docx]

Multimedia Appendix 4
Performance comparison between fully supervised learning and rank induction under varying proportions of annotated positive whole slide images.
[PNG File , 41 KB - medinform_v14i1e84417_app4.png]

References

1. Song AH, Jaume G, Williamson DF, Lu MY, Vaidya A, Miller TR, et al. Artificial intelligence for digital and computational pathology. Nat Rev Bioeng 2023 Oct 02;1(12):930-949. [doi: 10.1038/s44222-023-00096-8]
2. Saltz J, Gupta R, Hou L, Kurc T, Singh P, Nguyen V, Cancer Genome Atlas Research Network, et al. Spatial organization and molecular correlation of tumor-infiltrating lymphocytes using deep learning on pathology images. Cell Rep 2018 Apr 03;23(1):181-93.e7 [FREE Full text] [doi: 10.1016/j.celrep.2018.03.086] [Medline: 29617659]
3. van der Laak J, Litjens G, Ciompi F. Deep learning in histopathology: the path to the clinic. Nat Med 2021 May 14;27(5):775-784. [doi: 10.1038/s41591-021-01343-4] [Medline: 33990804]
4. Campanella G, Hanna MG, Geneslaw L, Miraflor A, Werneck Krauss Silva V, Busam KJ, et al. Clinical-grade computational pathology using weakly supervised deep learning on whole slide images. Nat Med 2019 Aug 15;25(8):1301-1309 [FREE Full text] [doi: 10.1038/s41591-019-0508-1] [Medline: 31308507]
5. Zhang H, Meng Y, Zhao Y, Qiao Y, Yang X, Coupland SE, et al. DTFD-MIL: double-tier feature distillation multiple instance learning for histopathology whole slide image classification. In: Proceedings of the IEEE/CVF Conference on Computer Vision and Pattern Recognition. 2022 Presented at: CVPR 2022; June 18-24, 2022; New Orleans, LA URL: https://ieeexplore.ieee.org/document/9880112?denied= [doi: 10.1109/cvpr52688.2022.01824]
6. Zhou Y, Lu Y. Multiple instance learning with critical instance for whole slide image classification. In: Proceedings of the IEEE 20th International Symposium on Biomedical Imaging. 2023 Presented at: ISBI 2023; April 18-21, 2023; Cartagena, Colombia URL: https://ieeexplore.ieee.org/abstract/document/10230595/ [doi: 10.1109/isbi53787.2023.10230595]
7. Zhou Y, Lu Y. Deep hierarchical multiple instance learning for whole slide image classification. In: Proceedings of the IEEE 19th International Symposium on Biomedical Imaging. 2022 Presented at: ISBI 2022; March 28-31, 2022; Kolkata, India URL: https://ieeexplore.ieee.org/abstract/document/9761678/ [doi: 10.1109/isbi52829.2022.9761678]

XSL•FO
RenderX

8. Qu L, Li S, Luo X, Liu S, Guo Q, Wang M, et al. Weakly semi-supervised whole slide image classification by two-level cross consistency supervision. ArXiv. Preprint posted online on April 16, 2025 2026 [FREE Full text] [doi: 10.48550/arXiv.2504.12132]
9. Ouyang M, Fu Y, Yan R, Shi S, Ling X, Zhu L, et al. MergeUp-augmented semi-weakly supervised learning for WSI classification. ArXiv. Preprint posted online on August 23, 2024 2026 [FREE Full text] [doi: 10.48550/arXiv.2408.12825]
10. Lu MY, Chen RJ, Wang J, Dillon D, Mahmood F. Semi-supervised histology classification using deep multiple instance learning and contrastive predictive coding. ArXiv. Preprint posted online on October 23, 2019 2026 [FREE Full text] [doi: 10.48550/arXiv.1910.10825]
11. Li B, Li Y, Eliceiri KW. Dual-stream multiple instance learning network for whole slide image classification with self-supervised contrastive learning. ArXiv. Preprint posted online on November 17, 2020 2026 [FREE Full text] [doi: 10.48550/arXiv.2011.08939]
12. Chen RJ, Chen C, Li Y, Chen TY, Trister AD, Krishnan RG, et al. Scaling vision transformers to gigapixel images via hierarchical self-supervised learning. ArXiv. Preprint posted online on June 6, 2022 2026 [FREE Full text] [doi: 10.1109/cvpr52688.2022.01567]
13. Lu MY, Williamson DF, Chen TY, Chen RJ, Barbieri M, Mahmood F. Data-efficient and weakly supervised computational pathology on whole-slide images. Nat Biomed Eng 2021 Jun 01;5(6):555-570. [doi: 10.1038/s41551-020-00682-w] [Medline: 33649564]
14. Zhou Y, Che S, Lu F, Liu S, Yan Z, Wei J, et al. Iterative multiple instance learning for weakly annotated whole slide image classification. Phys Med Biol 2023 Jul 19;68(15). [doi: 10.1088/1361-6560/acde3f] [Medline: 37311470]
15. Zhou Y, Lu Y. Multiple instance learning with task-specific multi-level features for weakly annotated histopathological image classification. In: Proceedings of the 2022 IEEE International Conference on Acoustics, Speech and Signal Processing. 2022 Presented at: ICASSP 2022; May 23-27, 2022; Singapore, Singapore URL: https://ieeexplore.ieee.org/abstract/document/9747121/ [doi: 10.1109/icassp43922.2022.9747121]
16. Myronenko A, Xu Z, Yang D, Roth HR, Xu D. Accounting for Dependencies in Deep Learning Based Multiple Instance Learning for Whole Slide Imaging. In: de Bruijne M, Cattin PC, Cotin S, Padoy N, Speidel S, Zheng Y, et al, editors. Medical Image Computing and Computer Assisted Intervention – MICCAI 2021. Cham, Switzerland: Springer International Publishing; 2021:329-338.
17. Lerousseau M, Vakalopoulou M, Classe M, Adam J, Battistella E, Carré A, et al. Weakly supervised multiple instance learning histopathological tumor segmentation. In: Martel AL, Abolmaesum P, Stoyanov D, Mateus D, Zuluaga MA, Zhou SK, et al, editors. Medical Image Computing and Computer Assisted Intervention – MICCAI 2020. Cham, Switzerland: Springer International Publishing; 2020:470-479.
18. Qu L, Luo X, Liu S, Wang M, Song Z. DGMIL: distribution guided multiple instance learning for whole slide image classification. In: Wang L, Dou Q, Fletcher PT, Speidel S, Li S, editors. Medical Image Computing and Computer Assisted Intervention – MICCAI 2022. Cham, Switzerland: Springer; 2022:24-34.
19. Koga R, Yokota T, Arihiro K, Hontani H. Attention induction based on pathologist annotations for improving whole slide pathology image classifier. J Pathol Inform 2025 Jan;16:100413. [doi: 10.1016/j.jpi.2024.100413] [Medline: 39845979]
20. Burges C. From RankNet to LambdaRank to LambdaMART: an overview. Microsoft Research. 2010. URL: https://www.microsoft.com/en-us/research/wp-content/uploads/2016/02/MSR-TR-2010-82.pdf [accessed 2026-01-11]
21. Ehteshami Bejnordi B, Veta M, Johannes van Diest P, van Ginneken B, Karssemeijer N, Litjens G, the CAMELYON16 Consortium, et al. Diagnostic assessment of deep learning algorithms for detection of lymph node metastases in women with breast cancer. JAMA 2017 Dec 12;318(22):2199-2210. [doi: 10.1001/jama.2017.14585] [Medline: 29234806]
22. Da Q, Huang X, Li Z, Zuo Y, Zhang C, Liu J, et al. DigestPath: a benchmark dataset with challenge review for the pathological detection and segmentation of digestive-system. Med Image Anal 2022 Aug;80:102485 [FREE Full text] [doi: 10.1016/j.media.2022.102485] [Medline: 35679692]
23. Kim HH, Ko YS, Jeong WC, Yun S, Kim K. Evaluating the robustness of slide-level AI predictions on out-of-focus whole slide images: a retrospective observational study. J Pathol Inform 2025 Nov;19:100518 [FREE Full text] [doi: 10.1016/j.jpi.2025.100518] [Medline: 41146682]
24. Ko YS, Choi YM, Kim M, Park Y, Ashraf M, Quiñones Robles WR, et al. Improving quality control in the routine practice for histopathological interpretation of gastrointestinal endoscopic biopsies using artificial intelligence. PLoS One 2022;17(12):e0278542 [FREE Full text] [doi: 10.1371/journal.pone.0278542] [Medline: 36520777]
25. Zhang J, Bargal SA, Lin Z, Brandt J, Shen X, Sclaroff S. Top-down neural attention by excitation backprop. Int J Comput Vis 2017 Dec 23;126:1084-1102. [doi: 10.1007/s11263-017-1059-x]
26. JMIR: Official repository for "Ranking-Aware Multiple Instance Learning for Histopathology Slide Classification: Development and Validation Study". GitHub. URL: https://github.com/SMF-AI/rank_induction_JMIR [accessed 2026-01-20]

Abbreviations

AB-MIL: attention-based multiple instance learning
AUPRC: area under the precision-recall curve

XSL•FO
RenderX

AUROC: area under the receiver operating characteristic curve
CLAM: clustering-constrained attention multiple instance learning
CLAM-MB: clustering-constrained attention multiple instance learning, multibranch
CLAM-SB: clustering-constrained attention multiple instance learning, single-branch
DS-MIL: dual-stream multiple instance learning
HIPT: hierarchical image pyramid transformer
IoU: intersection over union
IRB: institutional review board
MIL: multiple instance learning
SMF-stomach: Seegene Medical Foundation-stomach
WSI: whole slide image

Edited by A Benis; submitted 19.Sep.2025; peer-reviewed by Y Zhou, Y Lu; comments to author 23.Oct.2025; revised version received 14.Dec.2025; accepted 01.Jan.2026; published 04.Feb.2026.

Please cite as:
Kim HH, Hwang G, Jeong WC, Ko YS
Ranking-Aware Multiple Instance Learning for Histopathology Slide Classification: Development and Validation Study
JMIR Med Inform 2026;14:e84417
URL: https://medinform.jmir.org/2026/1/e84417
doi:10.2196/84417
PMID:

©Ho Heon Kim, Gisu Hwang, Won Chan Jeong, Young Sin Ko. Originally published in JMIR Medical Informatics (https://medinform.jmir.org), 04.Feb.2026. This is an open-access article distributed under the terms of the Creative Commons Attribution License (https://creativecommons.org/licenses/by/4.0/), which permits unrestricted use, distribution, and reproduction in any medium, provided the original work, first published in JMIR Medical Informatics, is properly cited. The complete bibliographic information, a link to the original publication on https://medinform.jmir.org/, as well as this copyright and license information must be included.

XSL•FO
RenderX

Original Paper

Early Prediction of Delirium in Postcardiac Surgery Patients: Machine Learning Model Development and External Validation

Huixiu Hu[1,2,3*], MMed; Yuxiang Wang[4*], BSc; Houfeng Li[5*], MMed; Qinglai Zang[6,7*], MSc; Jing Huang[8], MMed; Ying Zhang[3], MMed; Jinjing Wu[4], MSc; Long Liu[4], MSc; Zhen Xing[3*], MMed; Yaohua Yu[1,2*], BMed

[1]The Graduate School of Fujian Medical University, Fuzhou, Fujian, China

[2]Department of Anesthesiology, The First Hospital of Putian City, Putian, China

[3]Department of Anesthesiology, The First Affiliated Hospital of Hebei North University, Zhangjiakou, Hebei, China

[4]School of Health Science and Engineering, University of Shanghai for Science and Technology, Shanghai, Shanghai, China

[5]Department of Anesthesiology, Changhai Hospital, the Second Military Medical University, Shanghai, China

[6]School of Anesthesiology, Second Military Medical University, Shanghai, China

[7]Information Center, The Second Affiliated Hospital of Naval Medical University, Shanghai, China

[8]Graduate School, Wannan Medical College, Wuhu, Anhui, China

[*]these authors contributed equally

Corresponding Author:
Yaohua Yu, BMed
The Graduate School of Fujian Medical University
No.1 Xuefu North Road, Shangjie Town, Minhou County
Fuzhou, Fujian, 351022
China
Phone: 86 139 5956 1579
Email: yyh.8@163.com

Abstract

Background: Delirium is a frequent postoperative complication among patients who have undergone cardiac surgery and is associated with prolonged hospitalization, cognitive decline, and increased mortality. Early prediction of delirium is therefore critical for initiating timely interventions.

Objective: This study proposes the development and validation of a machine learning–based model to predict postoperative delirium in patients undergoing cardiac surgery during intensive care unit (ICU) care, facilitating the early detection of individuals at high risk of delirium and supporting clinicians in the deployment of targeted preventive strategies.

Methods: This study extracted data on postoperative cardiac surgery patients who remained in the ICU for more than 24 hours from the Medical Information Mart for Intensive Care IV version 2.0 (MIMIC-IV 2.0) database and the eICU Collaborative Research Database (eICU-CRD). The MIMIC-IV 2.0 cohort was randomly divided into a training set and an internal validation set in a 7:3 ratio, whereas the eICU-CRD functioned as an independent validation cohort. We used data from the first 24 hours of ICU monitoring to model the likelihood of delirium over the entire ICU admission period. Delirium was identified by a positive Confusion Assessment Method for the Intensive Care Unit evaluation (ie, score ≥4). We built predictive models by using logistic regression, support vector classifier, extreme gradient boosting (XGB), and random forest classifiers. Their performance was assessed via the area under the receiver operating characteristic curve, accuracy, sensitivity, positive predictive value, negative predictive value, and F_1-score.

Results: The analysis involved 2124 patients from the MIMIC-IV 2.0 database and 2406 from the eICU-CRD. A set of 57variables was selected to construct the predictive models. Among the various machine learning models tested, the XGB model demonstrated the best performance for delirium prediction during internal validation. As for external validation, the model achieved an area under the receiver operating characteristic curve of 0.75, indicating strong discriminatory ability. The most important predictive features identified by the model included hospital length of stay, minimum Glasgow Coma Scale score, mean blood pressure, Sequential Organ Failure Assessment score, weight, urine output, heart rate, and age.

Conclusions: The XGB model with strong predictive capability for ICU delirium after cardiac surgery was developed and externally validated. This model offers essential technical support for building real-time delirium alert systems and enables ongoing risk stratification and evidence-based decision-making within the ICU environment.

XSL•FO
RenderX

(JMIR Med Inform 2026;14:e73283) doi:10.2196/73283

KEYWORDS

prediction model; machine learning; cardiac surgery; intensive care unit; delirium; Medical Information Mart for Intensive Care IV version 2.0 database; MIMIC-IV 2.0 database; eICU Collaborative Research Database; eICU-CRD

Introduction

Delirium is an acute neuropsychiatric syndrome commonly associated with encephalopathy, acute cerebral dysfunction, and states of confusion, particularly following surgical procedures [1-4]. In patients undergoing cardiac surgery, the incidence of postoperative delirium has been reported to range from 10% to 40% [5-7]. This condition is linked to a variety of adverse outcomes, including heightened pain perception, depression, cognitive impairment, and increased mortality [8,9]. Currently, the assessment of patients' arousal can be conducted using standardized tools such as the Richmond Agitation-Sedation Scale and the Confusion Assessment Method for the Intensive Care Unit (CAM-ICU) to identify different types of delirium with distinct characteristics [10-12]. Despite the existence of standardized instruments, the diagnosis of delirium frequently depends on the patient's subjective assessment of their condition. If the occurrence of delirium in patients could be predicted within a short period, it will substantially reduce the aforementioned risks.

Machine learning (ML), a branch of artificial intelligence, has driven notable progress across numerous domains of health care [13,14]. One such area where ML has shown its potential is in the postoperative surveillance with cardiac surgery, offering more information to predict delirium [15,16]. It has the potential to improve patient health care outcomes [17,18]. Compared to traditional data analysis techniques, ML models can provide more intricate predictions and perform real-time monitoring using objective data from all patients [19-21]. Furthermore, recent research has also used ML to forecast the near-term mortality rates of patients after cardiac operations. For example, Nistal-Nuño [22] constructed an extreme gradient boosting (XGB)–based predictive model to estimate 24-hour postoperative mortality following cardiac surgery. The outcome demonstrated that XGB attained an area under the receiver operating characteristic curve (AUC) of 87.5%, signifying the model's exceptional performance in forecasting intensive care unit (ICU) mortality, notably surpassing other models. Zhang et al [23] assessed an ML model, comparing it to existing severity-of-illness systems to develop a real-time tool for predicting death. However, no correlation-predictive models using ML have been developed for patients who experience delirium after cardiac surgery.

In this study, we created and verified 4 models using ML techniques to anticipate the occurrence of delirium and facilitate identification. Furthermore, we enhanced the interpretability of the results by prioritizing the independent variables according to their predictive significance.

Methods

Ethical Considerations

This study used data from 2 publicly available critical care databases: Medical Information Mart for Intensive Care IV version 2.0 (MIMIC-IV 2.0) database and eICU Collaborative Research Database (eICU-CRD). Both databases were approved by the institutional review boards of the Beth Israel Deaconess Medical Center and the Massachusetts Institute of Technology. As all data were fully deidentified before release, the requirement for individual informed consent was waived in accordance with the Declaration of Helsinki and applicable regulations. All team members underwent certified training in "Data or Specimens Only Research" to comply with ethical regulations governing dataset access.

Study Population

This study used 2 publicly available critical care databases to develop and validate a predictive model. The training dataset was sourced from MIMIC-IV 2.0, which includes 76,943 ICU admissions recorded at Beth Israel Deaconess Medical Center (Boston, Massachusetts, United States) between 2008 and 2019 [24]. For external validation, we used the eICU-CRD, which contains deidentified data for over 200,000 patients admitted to 208 US hospitals between 2014 and 2015 [25]. Both databases contain structured clinical data, including demographics, vital signs, laboratory test results, procedures, medications, and outcomes. We included adult patients (aged ≥18 years) who underwent major cardiovascular surgeries, such as coronary artery bypass grafting, heart valve repair or replacement, combined procedures, or other surgeries involving cardiopulmonary bypass.

We applied consistent inclusion and exclusion criteria across both datasets to ensure cohort comparability and data quality. Inclusion criteria required patients to meet the age threshold and have documented cardiovascular surgery. We excluded patients who had ICU stays shorter than 24 hours (to ensure sufficient observation data), missing essential demographic or outcome variables, or delirium recorded within the first 24 hours of ICU admission (to preserve the prediction time window). Although the 2 datasets differ in time range and hospital coverage, we aligned the study population by applying uniform definitions for surgical type and using a standardized 24-hour observation window. Figure 1 summarizes the baseline characteristics of the 2 cohorts.

XSL•FO
RenderX

Figure 1. Schematic representation of the study design. eICU-CRD: eICU Collaborative Research Database; ICU: intensive care unit; MIMIC-IV 2.0: Medical Information Mart for Intensive Care IV version 2.0.

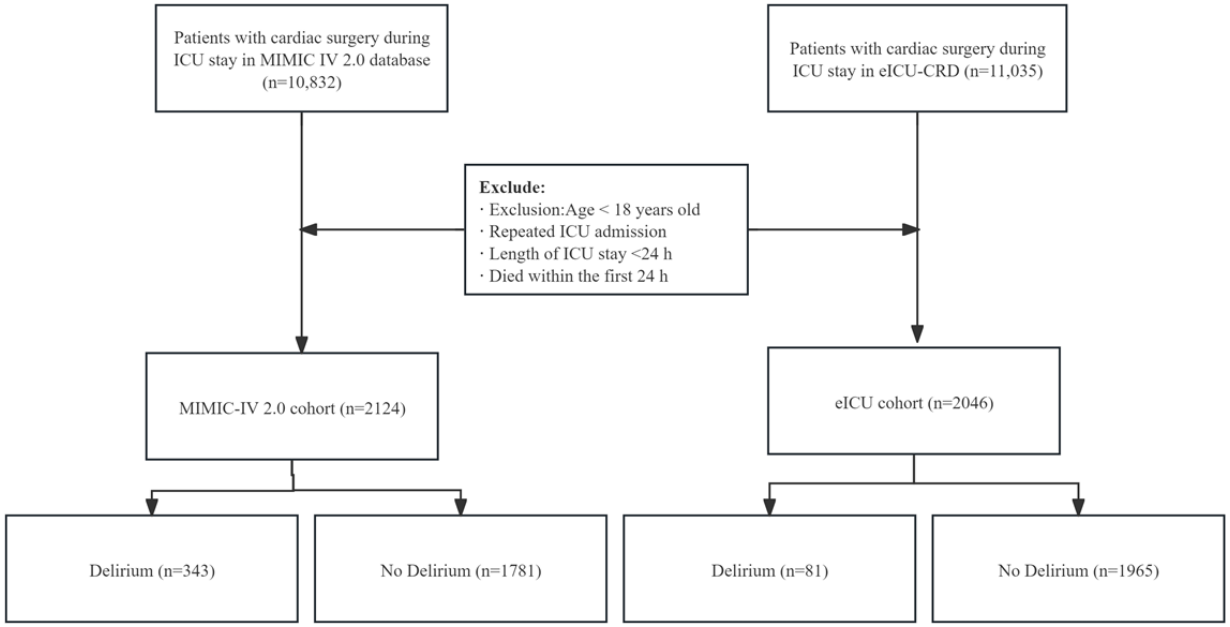

Delirium Assessment

Delirium served as the primary outcome, identified on the basis of a positive CAM-ICU assessment (score ≥4) and consistent diagnostic coding. The observation window was the first 24 hours after ICU admission, during which patient data were collected for modeling. If at least one positive delirium assessment occurred at the time of prediction, the patient was considered delirious.

Data Extraction and Processing

The clinical data were retrieved and extracted using the structured query language, with pgAdmin 4 serving as the administrative platform for PostgreSQL. The prediction model included just clinical and laboratory characteristics that were accessible on the initial day of admission to the ICU, with patients being recognized by their unique ID numbers. The predictors consisted of the following variables— (1) demographics: age, gender, ethnicity and weight; (2) vital signs: heart rate, mean blood pressure, respiratory rate, systolic blood pressure, and temperature; (3) laboratory analysis: hemoglobin level, platelet count, white blood cell count, lactate and urine output; (4) severity scoring: Glasgow Coma Scale (GCS) and Sequential Organ Failure Assessment (SOFA) scores; (5) comorbidities: myocardial infarction, congestive heart failure, peripheral vascular disease, cerebrovascular disease, dementia, chronic pulmonary disease, rheumatic disease, peptic ulcer disease,diabetes (with control, without control), paraplegia, renal disease, malignant cancer, severe liver disease, and AIDS; (6) medications: opioids, barbiturates, benzodiazepines, acetaminophen, antipsychotics, anticoagulant, antihistamines, diuretics, anesthesia, and anticholinergics; (7) treatment measures: emergency admission, first care unit, last care unit, renal replacement therapy, invasive ventilation, length of ICU stay.

Missing Data Management

Variables exhibiting a missing value rate exceeding 10% were omitted to prevent potential bias. Variables with less than 10% missing values were subjected to multivariable imputations [26].

Data Balance

The dataset showed a marked imbalance, with notably fewer positive delirium cases compared with negative ones, which caused the model to lean toward predicting the majority (negative) class. To mitigate this issue, we used the Synthetic Minority Oversampling Technique to artificially augment the number of positive samples, thereby achieving a more balanced class distribution and enhancing the model's ability to generalize.

Feature Selection

The feature selection process involved using the recursive elimination of features approach of the random forest [27]. This method was used to identify the most optimal combinations of predictive variables. By examining the weight of features and their correlation and after stratified 10-fold cross-validation, final features were selected based on importance scores, correlation analysis, and cross-validation results. This process reduced dimensionality while preserving predictive power.

Model Development and Hyperparameter Tuning

The MIMIC-IV 2.0 dataset (N=2124) was randomly split into a training set (1487/2124, 70%) and a testing set (637/2124, 30%), whereas the eICU-CRD dataset was used as an external validation cohort. We developed prediction models using 4 widely adopted ML algorithms. Logistic regression was implemented for binary classification using maximum likelihood estimation [28]. Random forest, an ensemble learning method, combined multiple decision trees through majority voting to

XSL•FO
RenderX

enhance predictive performance [29]. XGB used a gradient boosting framework to iteratively build strong learners from weak ones [30]. Support vector classifier aimed to find the optimal hyperplane in a high-dimensional space for classification [31]. Bayesian optimization was used to identify optimal hyperparameters for each model, improving training efficiency and performance [32].

Model Performance Evaluation

To comprehensively assess the discriminatory performance of the prediction models, we used the receiver operating characteristic (ROC) as the primary evaluation metric. Additional metrics included accuracy, positive predictive value, negative predictive value, and sensitivity. We also reported the F_1-score, the harmonic mean of precision and sensitivity, to reflect the balance between these two metrics. Together, these indicators were used to evaluate the clinical applicability of each model in stratifying the risk of postoperative delirium among cardiac surgery patients. Shapley Additive Explanations (SHAP) was used to investigate the interpretability of the final predictive model.

Statistical Analysis

All statistical analyses were conducted using Stata 17.0 and SPSS (version 27.0; IBM Corp). Frequencies and percentages were used to summarize categorical variables, with comparisons made via the chi-square test. The distribution of continuous variables was assessed using the Shapiro-Wilk test. Normally distributed data were reported as mean (SD) and compared using independent 2-tailed *t* tests. Skewed data were summarized as median and IQR and analyzed using the Mann-Whitney U or Kruskal-Wallis test, based on group composition. Statistical significance was determined using 2-sided tests, with a threshold of $P<.05$.

Results

Baseline Characteristics

A total of 2124 patients from the MIMIC-IV 2.0 database were included in the final analysis. Among them, 16.1% (343/2124) of cardiac surgery patients were diagnosed with delirium during their hospital stay, occurring after the first day of ICU admission. In the external validation cohort, an analysis was conducted on 2046 cases obtained from the eICU-CRD, of whom 3.81% (81/2046) developed delirium during the same postoperative period, also defined as after the first ICU day. In these patients with delirium, maximum heart rate, minimum mean blood pressure, minimum hemoglobin level, minimum platelet count, maximum white blood cell count, urine output, minimum GCS score, SOFA, and length of ICU stay showed a notable disparity between the two different groups. Tables 1-3 present a concise summary of the comparison of fundamental traits, vital signs, and laboratory analysis between patients with and without delirium. According to the data, patients with delirium are predominantly male, typically older, and have longer hospital stays with higher severity scores upon admission. Additionally, factors such as weight loss, decreased urine output, and decreased mean arterial pressure may all exacerbate the likelihood of delirium in patients.

XSL•FO
RenderX

Table 1. Characteristics of patients and controls from the development dataset for the first 24-hour model cohort: demographics and vital signs.

Patient characteristics	MIMIC-IV 2.0[a] cohort			eICU-CRD[b] cohort		
	No delirium (n=1781)	Delirium (n=343)	*P* value	No delirium (n=1965)	Delirium (n=81)	*P* value
Gender, n (%)			.10			.09
Male	1144.0 (64.2)	195.0 (56.9)		937.0 (49.5)	46 (57)	
Female	637.0 (35.8)	148.0 (43.1)		992.0 50.5)	35 (43)	
Race, n (%)			.80			.62
Asian	47.0 (2.6)	6.0 (1.7)		29.0 (1.5)	6.0 (1.4)	
Black	80.0 (4.5)	19.0 (5.5)		475.0 (24.2)	18.0 (22.5)	
Hispanic	126.0 (7.1)	42.0 (12.2)		1227.0 (62.4)	53.0 (65)	
White	1391.0 (78.1)	219.0 (63.8)		132.0 (6.7)	12.0 (14.8)	
Unknown	29.0 (1.6)	47.0 (13.7)		96.0 (4.9)	10.0 (2.3)	
Other	108.0 (6.1)	10.0 (2.)		6.0 (0.3)	2.0 (2.5)	
Age (y), median (IQR)	70.0 (61.0-79.0)	75.0 (64.0-81.0)	<.001	68.0 (57.0-77.0)	71.0 (61.0-79.8)	<.001
Weight (kg), median (IQR)	83.8 (70.8-96.7)	80.0 (60.0-95.4)	.02	85.2 (70.0-102.0)	84.5 (67.9-103.4)	.31
Vital signs, median (IQR)						
Heart rate min (bpm)	67.0 (60.0-74.0)	68.0 （59.0-77.0）	.12	69.0（59.0-80.0）	70.0（60.0-80.0）	.29
Heart rate max (bpm)	94.0 (86.0-106.0)	97.0 （88.0-110.0）	<.001	101.0（88.0-116.0）	107.0 (92.2-124.5)	<.001
Heart rate mean (bpm)	80.2 (73.3-87.5)	82.7 (75.6-89.3)	<.001	83.6 (75.7-94.4)	86.3 (75.7-97.9)	.007
Mean blood pressure min (mm Hg)	57.0 (53.0-62.0)	55.0 (49.5-60.0)	<.001	62.0 (54.0-72.0)	60.0 (52.0-68.0)	<.001
Mean blood pressure max (mm Hg)	97.0 (89.0-107.0)	95.0 (88.0-108.0)	.33	103.0 (99.0-118.0）	104.0 (91.0-122.0)	.31
Mean blood pressure mean (mm Hg)	74.6 (70.3-79.4)	73.3 (69.3-78.8)	.02	80.0 (76.6-90.4)	78.2 (70.3-88.2)	.02
Respiratory rate min (bpm)	12.0 (10.0-14.0)	12.0 (9.0-14.0)	.75	13.0 (11.0-16.0)	13.0 (11.0-16.0)	.63
Respiratory rate max (bpm)	26.0 (23.0-29.0)	26.0 (23.00-30.0)	.69	27.0 (24.0-32.00)	28.0 (24.0-33.00)	.42
Respiratory rate mean (bpm)	17.8 (16.2-19.6)	18.1 (16.2-20.2)	.23	19.2 (17.1-21.9)	19.2 (16.9-22.9)	.76
Systolic blood pressure min (mm Hg)	93.0 (91.0-95.0)	93.0 (91.00-96.0)	.85	97.0 (95.6-98.4)	97.1 (95.34-98.63)	.001
Systolic blood pressure max (mm Hg)	91.0 (93.0-95.0)	93.0 (91.0-96.0)	.003	92.0 (89.0-94.0)	91.0 (86.3-94.0)	.15
Systolic blood pressure mean (mm Hg)	97.7 (96.5-98.7)	97.9 (96.7-99.0)	.14	100.0 (99.0-100.0)	100.0 (100.0-100.0)	.92
Temperature mean (˚C)	36.7 (36.5-36.9)	36.72 (36.5-37.0)	.48	36.7 (36.6-37.0)	36.8 (36.9-36.5)	.007

[a]MIMIC-IV Medical Information Mart for Intensive Care IV version 2.0.

[b]eICU-CRD: eICU Collaborative Research Database.

XSL•FO
RenderX

Table 2. Characteristics of patients and controls from the development dataset for the first 24-hour model cohort: laboratory test results and comorbidities.

Patient characteristics	MIMIC-IV 2.0[a] cohort			eICU-CRD[b] cohort		
	No delirium (n=1781)	Delirium (n=343)	*P* value	No delirium (n=1965)	Delirium (n=81)	*P* value
Laboratory results, median (IQR)						
Hemoglobin min (g/100 mL)	8.4 (7.5-9.6)	9.0 (7.9-10.3)	<.001	8.4 (7.3-9.4)	9.0 (7.9-10.3)	<.001
Hemoglobin max (g/100 mL)	11.5 (10.0-12.9)	11.4 (10.4-14.2)	.64	11.4 (10.4-12.9)	11.4 (10.4-20.1)	.62
Platelet min (10^9/L)	147.0 (111.0-198.0)	130.0 (95.0-179.0)	<.001	145.0 (109.0-197.0)	128.0 (96.0-178.0)	<.001
Platelet count max (10^9/L)	125.0 (151.0-245.0)	188.0 (149.0-242.0)	.57	128.0 (97.0-235.0)	186.0 (153.0-245.0)	.55
White blood cell min (10^9/L)	8.8 (6.3-11.7)	9.5 (6.9-12.3)	.12	9.2 (6.3-12.0)	9.6 (7.0-12.4)	.14
White blood cell max (10^9/L)	13.1 (10.0-17.3)	14.8 (11.3-19.6)	<.001	14.0 (10.0-17.3)	14.7 (11.4-20.0)	<.001
Lactate min (mmol/L)	1.2（0.9-1.5）	1.2（0.9-1.6）	.21	1.4 (1.0-2.1)	1.3 (0.9-1.9)	.18
Urine output (mL)	1832.0 (1290.0-2617.0)	1575.0 (1002-2321.0)	<.001	1496.0 (796.3-2600.0)	1229.5 (600.0-2056.0)	<.001
Comorbidity, n (%)						
Myocardial infarction	30 (1.7)	3 (0.9)	.37	181 (9.2)	30 (6.8)	.11
Congestive heart failure	724 (40.7)	184 (53.6)	<.001	1251 (63.7)	51 (63)	.78
Peripheral vascular disease	281 (15.8)	84 (24.5)	<.001	14 (0.7)	1.0 (1.1)	.36
Cerebrovascular disease	186 (10.4)	65 (19.0)	<.001	90 (4.6)	6 (7.3)	.02
Chronic pulmonary disease	498 (28)	125 (36.4)	.002	303 (15.4)	11 (13.6)	.35
Renal disease	387 (21.7)	96 (28.0)	.01	321 (16.3)	13 (15.7)	.74
Diabetes with control	1538 (7.7)	30 (8.7)	.53	155 (7.9)	7 (8.5)	.58
Diabetes without control	495 (27.8)	97 (28.3)	.85	503 (30.2)	24 (29.5)	.84
Rheumatic disease	78 (4.4)	23 (6.7)	.06	82.0 (4.6)	5 (6.5)	.06
Peptic ulcer disease	13 (0.7)	7 (2)	.02	9.0 (0.5)	1 (1.5)	.02
Severe liver disease	16 (0.9)	7 (2)	.06	18.0 (1.0)	2 (2.3)	.07
Dementia	11 (0.6)	3 (0.9)	.59	13.0 (0.7)	1 (0.9)	.61
Paraplegia	15 (0.8)	12 (3.5)	<.001	16.0 (0.9)	3 (3.7)	<.001
Malignant cancer	103 (5.8)	16 (4.7)	.41	181.0 (9.2)	5 (6.8)	.11
AIDS	4 (0.2)	5 (3)	.38	1964.00 (99.0)	1 (1.2)	.04

[a]MIMIC-IV Medical Information Mart for Intensive Care IV version 2.0.

[b]eICU-CRD: eICU Collaborative Research Database.

XSL•FO
RenderX

Table 3. Characteristics of patients and controls from the development dataset for the first 24-hour model cohort: score, drug, and treatment measures.

Patient characteristics	MIMIC-IV 2.0[a] cohort			eICU-CRD[b] cohort		
	No delirium (n=1781)	Delirium (n=343)	*P* value	No delirium (n=1965)	Delirium (n=81)	*P* value
Score, median (IQR)						
GCS[c] (min)	14.0 (14.0-15.0)	11.0 (6.0-14.0)	<.001	15.0 (14.0-15.00)	12.0 (8.0-14.0)	<.001
SOFA[d]	4.0 (2.0-7.0)	8.0 (6.0-11.0)	<.001	5.0 (3.0-7.0)	7.0 (5.0-10.0)	<.001
Drug, n (%)						
Acetaminophen	1005 (56.4)	164 (47.8)	.003	1104 (56.2)	41 (50.6)	.054
Anesthesia	38 (2.1)	5 (1.5)	.002	35 (1.9)	1 (1.2)	.02
Anticholinergics	1062 (59.6)	221 (64.4)	.10	387 (19.7)	19 (23.5)	.03
Anticoagulant	519 (29.1)	92 (26.8)	.39	539 (27.4)	36 (44.4)	.41
Antipsychotics	18 (1.0)	11 (3.2)	.001	21 (1.1)	17 (3.9)	<.001
Barbiturates	2.0 (0.1)	343 (100)	.54	3 (0.1)	81 (100)	.54
Benzodiazepines	138 (7.7)	32 (9.3)	.32	142 (8)	35 (9.5)	.34
Diuretics	694 (39)	131 (38.2)	.79	854 (43.5)	29 (35.5)	.008
Opioids	1040 (58.4)	201 (58.6)	.94	981 (49.9)	38 (46.9)	.28
Treatment measures, n (%)						
Emergency admission	1121 (62.9)	231 (67.3)	.12	380 (19.3)	17 (20.9)	.52
First care unit	1724 (96.8)	321 (93.6)	.004	1779 (90.5)	75 (92.6)	.04
Last care unit	42 (2.4)	16 (4.7)	.02	453 (23)	36 (44.4)	<.001
Renal Replacement Therapy	15 (0.8)	11 (3.2)	<.001	719 (36.6)	46 (56.8)	.047
Invasive ventilation	1179 (66.2)	298 (86.9)	<.001	1699 (86.5)	77 (95.1)	<.001
Length of ICU[e] stay, median (IQR)	2.4 (2.0-3.4)	5.9（4.0-10.3）	<.001	3.20 (3.0-5.5)	6.7 (5.3-12.5)	<.001

[a]MIMIC-IV Medical Information Mart for Intensive Care IV version 2.0.

[b]eICU-CRD: eICU Collaborative Research Database.

[c]GCS: Glasgow Coma Scale.

[d]SOFA: Sequential Organ Failure Assessment.

[e]ICU: intensive care unit.

Model Performance Evaluation

Using 4 ML algorithms, we developed predictive models to assess the risk of postoperative delirium in cardiac surgery patients, leveraging electronic health record data for early identification of high-risk individuals. Figure 2 presents ROC curves of all models, allowing a systematic comparison of their discriminative performance. Among the models, XGB demonstrated the best overall predictive performance, achieving the highest AUC for identifying patients at risk of delirium. The random forest classifiers also exhibited strong performance, although slightly lower than that of the XGB model. Notably, both XGB and random forest classifiers maintained high predictive accuracy, indicating good model generalizability. In contrast, support vector classifier and logistic regression models showed substantially lower discriminative power. To further validate the clinical applicability of the XGB model, model performance was assessed using several evaluation metrics,including accuracy, sensitivity, positive predictive value, and negative predictive value (Table 4). Furthermore, the corresponding confusion matrices illustrating these metrics are displayed in Figure 3.

The model was externally validated using the eICU-CRD, a large-scale critical care dataset incorporating records from 208 hospitals, to assess its performance on independent data. The XGB model maintained strong discriminative performance in ROC analysis, with high AUC values confirming its reliability across institutions (Figure 4). The model was further rigorously validated through precision-recall analysis and calibration curves (Figures 5A and B).

XSL•FO
RenderX

Figure 2. Receiver operating characteristic curves of different machine learning algorithms evaluated on the internal validation set. LR: logistic regression; SVC: support vector classifier; RFC: random forest classifier; XGB: extreme gradient boosting.

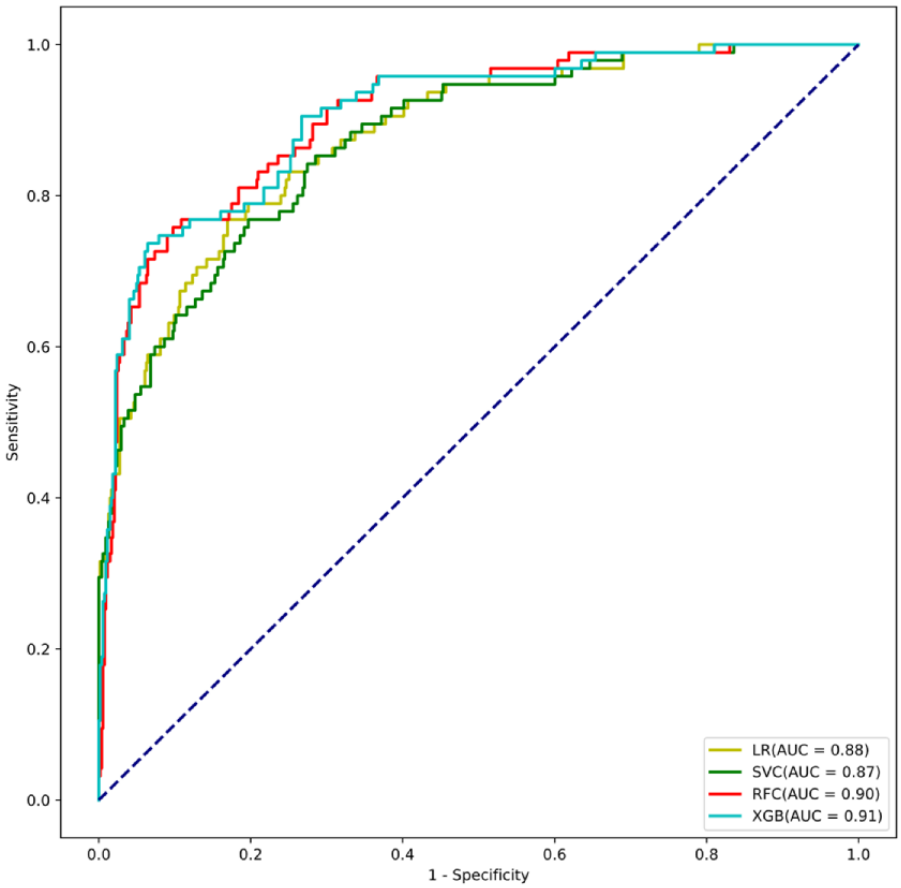

Table 4. Test set evaluation of machine learning model performance.

Model	Accuracy	Sensitivity	AUC[a]	PPV[b]	NPV[c]	F_1-score
LR[d]	0.82	0.73	0.88	0.44	0.95	0.55
XGB[e]	0.83	0.77	0.91	0.47	0.95	0.58
SVC[f]	0.83	0.67	0.87	0.45	0.94	0.54
RFC[g]	0.88	0.75	0.90	0.58	0.95	0.65

[a]AUC: area under the receiver operating characteristic curve.

[b]PPV: positive predictive value.

[c]NPV: negative predictive value.

[d]LR: logistic regression.

[e]XGB: extreme boosting gradient.

[f]SVC: support vector classifier.

[g]RFC: random forest classifier.

XSL•FO
RenderX

Figure 3. Confusion matrix for binary classification. (A) Logistic regression (LR), (B) extreme gradient boosting (XGB), (C) support vector classifier (SVC), (D) random forest classifier (RFC).

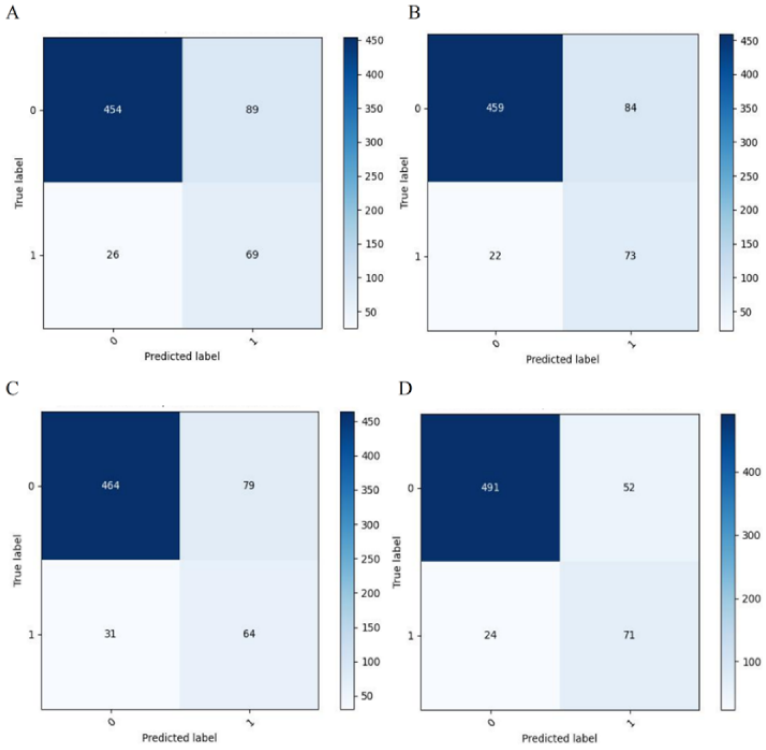

Figure 4. Receiver operating characteristic curves of various machine learning models evaluated on the external validation cohort. LR: logistic regression; RFC: random forest classifier; SVC: support vector classifier; XGB: extreme gradient boosting.

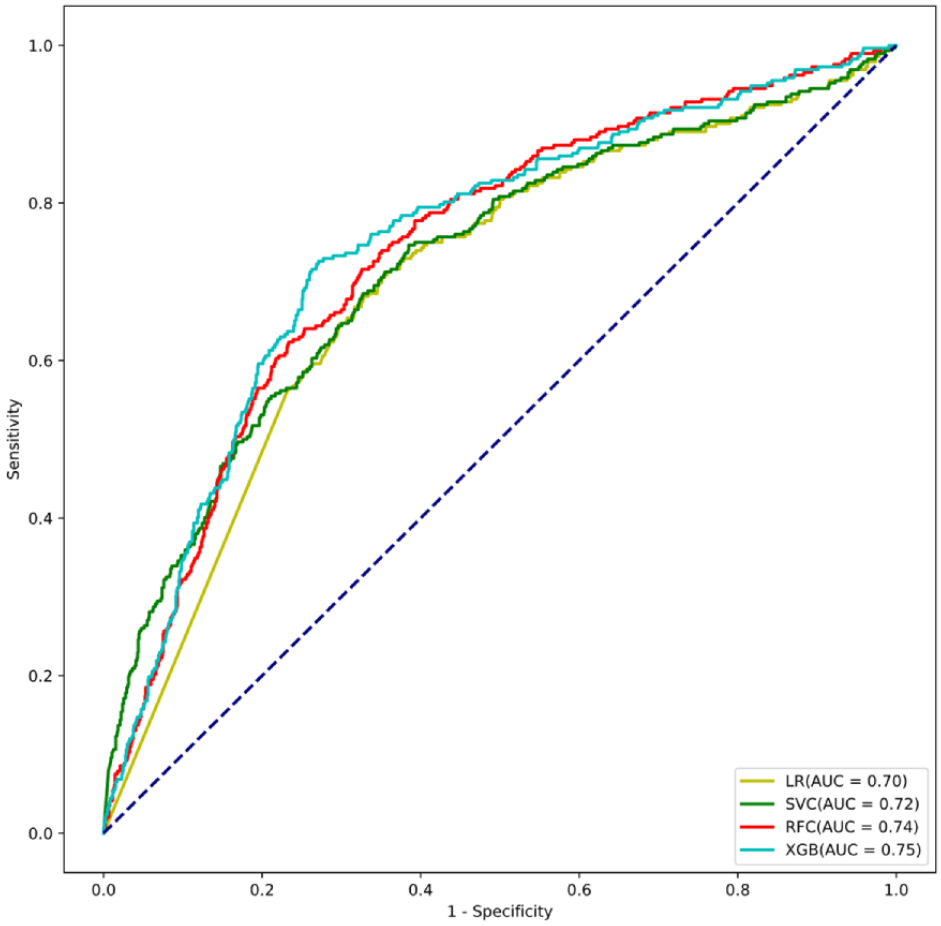

XSL•FO
RenderX

Figure 5. (A) Precision-recall curve. (B) Calibration curves and calculated Brier scores. LR: logistic regression; RFC: random forest classifier; SVC: support vector classifier;XGB: extreme gradient boosting.

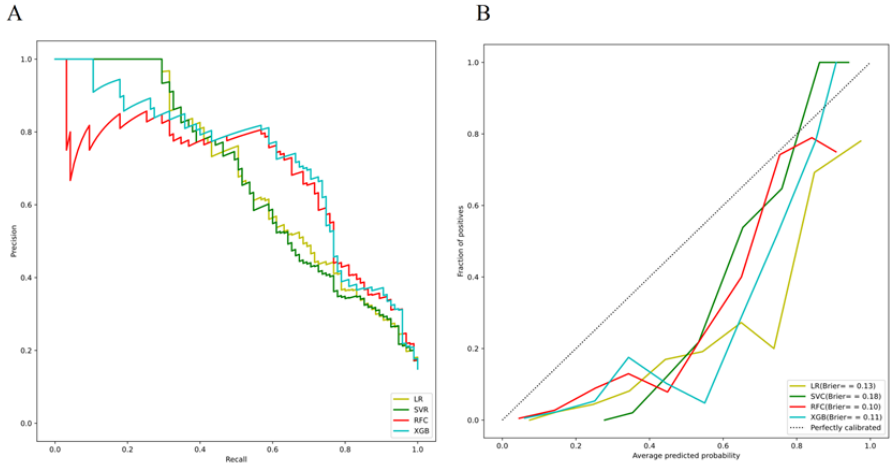

Variable Importance

The predictive contribution of each variable to postoperative delirium varied among cardiac surgery ICU patients. The XGB algorithm was used to estimate variable importance and highlight the top predictors influencing model accuracy. The top predictors included length of stay in ICU, lowest GCS score, age, mean blood pressure, SOFA score, weight, heart rate and urine output (Figure 6). To further interpret the influence and directionality of these features on model predictions, we generated SHAP summary plots (Figure 7). These visualizations provide a detailed explanation of how individual features contributed to the model output, offering insights into their relative impact and potential clinical relevance.

Figure 6. Variable contribution rankings estimated using the XGB model. GCS: Glasgow Coma Scale; ICU_los: the length time of ICU; MBP: mean blood pressure; SOFA: Sequential Organ Failure Assessment.

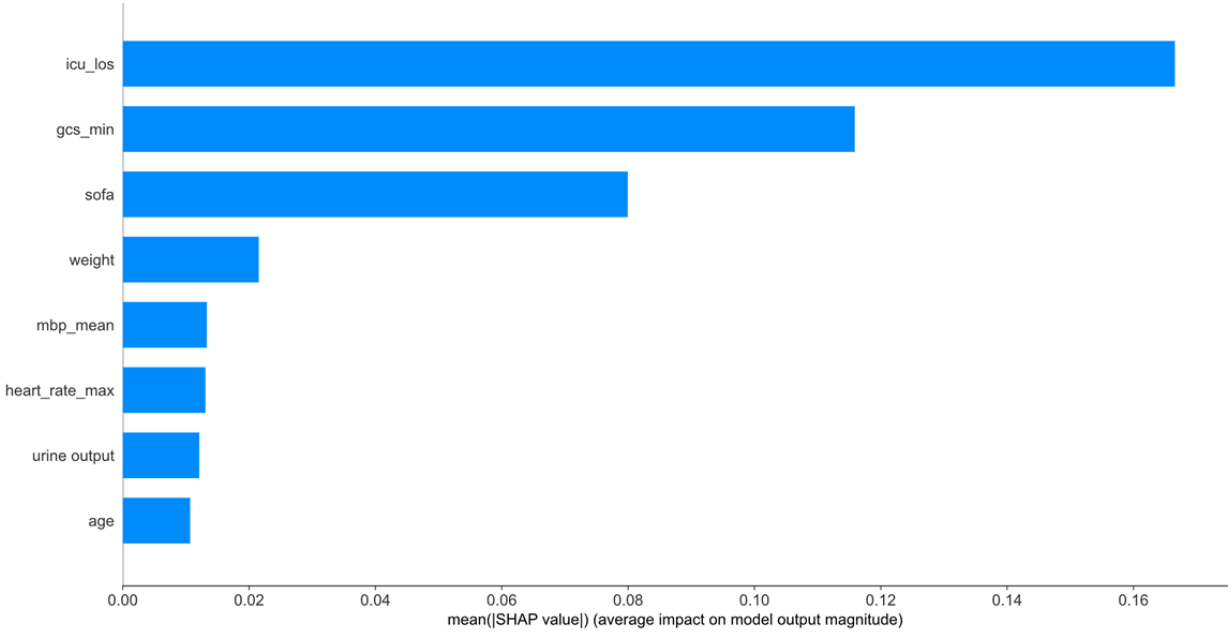

XSL•FO
RenderX

Figure 7. Shapley Additive Explanations (SHAP) summary plots illustrating feature contributions in the extreme gradient boosting (XGB) model. GCS: Glasgow Coma Scale; ICU_los: length of stay in the intensive care unit; MBP: mean blood pressure; SOFA: Sequential Organ Failure Assessment.

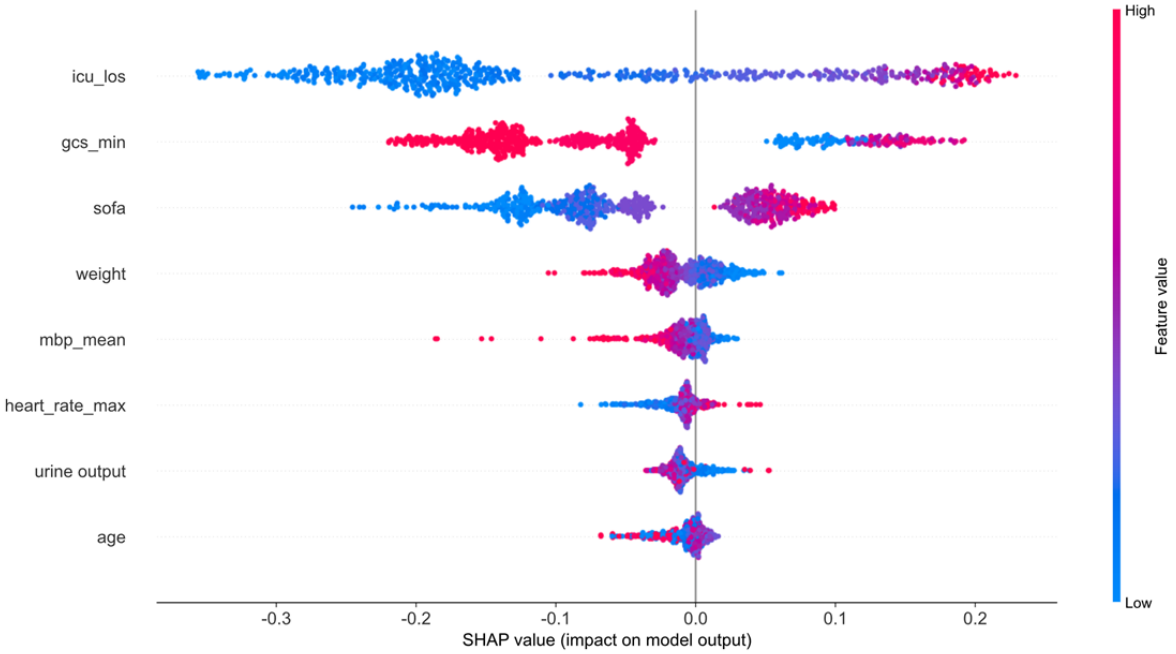

Discussion

Principal Findings

In this large-scale retrospective study, we developed and validated an ML model to predict postoperative delirium, a common and burdensome complication after cardiac surgery, with reported incidence rates ranging from 18% to 52% [33-35]. The XGB-based model, trained on the MIMIC-IV 2.0 dataset, demonstrated excellent performance in internal validation (AUC=0.91) and maintained strong discriminative power in external validation using the eICU-CRD dataset (AUC=0.75). Key predictors identified by the model included length of stay in ICU, min GCS score, mean blood pressure, SOFA score, weight, urine output, heart rate, and age. As far as we are aware, this study presents one of the earliest ML models that are developed to predict delirium in a diverse population of cardiac surgery patients. Importantly, our model relies on routinely available clinical data from the first 24 hours of ICU admission, enabling early identification of high-risk patients throughout their ICU stay. This early-warning capability offers a critical window for timely intervention, allowing clinicians to implement targeted strategies at the earliest stages of delirium onset. The model's high temporal relevance and wide applicability support its potential use in guiding personalized care plans and improving patient outcomes.

Comparison With Previous Work

Among existing tools for predicting postoperative cognitive complications, the CAM-ICU score remains the most widely used [36-38]. However, its applicability may be limited in certain surgical contexts or patient subgroups. Some individual populations require more tailored analysis, and it is important to note that CAM-ICU may not capture the full spectrum of delirium severity, potentially compromising its construct validity [12,39,40]. Therefore, balancing feasibility and validity in specific clinical settings is essential. Our ML approach addresses these limitations by offering a data-driven, individualized risk assessment that adapts to patient heterogeneity and enables broader clinical applicability.

Furthermore, this study incorporated SHAP to enhance the interpretability of the XGB model. SHAP provides a transparent and traceable explanation framework for individualized risk prediction of delirium, allowing visualization of how each feature influences the model's output in both direction and magnitude [41,42]. This helps clinicians better understand the rationale behind specific predictions. Through SHAP analysis, we identified a set of clinically relevant predictors closely associated with patient deterioration, including length of stay in ICU, lowest GCS score, age, mean blood pressure, SOFA score, weight, urine output, and heart rate.

The XGB model demonstrated superior predictive performance, its clinical value extends beyond accuracy—it lies in its ability to inform real-time decision-making. Future research should focus on integrating these key features into dynamic clinical monitoring and intervention workflows. For instance, early abnormalities in high-impact variables, such as lowest GCS score, mean blood pressure, or urine output could trigger automated alerts within electronic health record systems, enabling real-time risk stratification. Additionally, individualized SHAP-based explanations could support patient-centered clinical strategies, facilitating a closed-loop "early warning–targeted intervention" model. This approach may ultimately enhance early prevention and improve outcomes in postoperative delirium management.

Strengths and Limitations

This study has several notable strengths. First, model development was based on large scale, real-world data from 2

XSL•FO
RenderX

publicly available critical care databases (MIMIC-IV 2.0 and eICU-CRD), which offer extensive clinical information and robust sample sizes, thereby increasing the trustworthiness and general applicability of our findings. Second, as far as we are aware, this is the earliest known study to apply ML techniques for predicting postoperative delirium in a broad cardiac surgery cohort. This tailored approach enables more accurate risk stratification by accounting for individual variability across surgical subtypes. One notable strength of our model lies in its exclusive use of routinely available clinical data obtained within the first day of ICU stay, eliminating the need for additional or specialized testing. The use of early time-series features to quantify dynamic changes in key physiological indicators allows real-time risk estimation with high clinical practicality and timeliness. From a translational perspective, the model demonstrated a sensitivity of 77% in identifying high-risk patients early, providing a valuable window for initiating preventive interventions. These proactive measures have the potential to reduce ICU length of stay, lower per-patient hospitalization costs, and minimize readmission risk, ultimately interrupting the cascade of adverse outcomes often associated with postoperative delirium. Finally, by focusing on the first day of ICU data, the model creates a strategic opportunity for timely clinical action, supporting the implementation of early, targeted strategies aimed at mitigating symptom progression and reducing complication rates.

Our study has several limitations. First, we acknowledge that our findings may be racially biased against White patients and the applicability to other populations may be limited due to the database being derived from Western countries. Second, the use of open public databases to obtain data may introduce missing data bias, which is unavoidable. Third, as this study is retrospective and observational in nature, selection bias is inevitable. Specifically, the collection of retrospective data depends on existing medical records that may vary in completeness and accuracy due to differences in clinical documentation practices and data entry habits. Such inconsistencies can result in missing or inaccurate key clinical information, which in turn affects the quality of data used for model training. Moreover, retrospective studies lack the ability to actively intervene in or control the research process, making it difficult to eliminate the influence of confounding variables. This limitation weakens the strength of causal inferences drawn from the analysis. Additionally, our model has not yet undergone prospective clinical validation, which limits its current applicability in real-world clinical practice. Prospective validation, ideally conducted under well-controlled trial conditions and standardized workflows, is essential for evaluating the predictive performance and robustness of the model in diverse clinical settings. Without this step, there remains a risk that the model's actual performance may deviate from the retrospective findings, particularly when applied to different health care systems or patient populations.

Conclusions

We constructed and assessed an effective predictive model targeting postoperative delirium in patients admitted to the ICU after cardiac surgery. This model leverages routinely available patient information from the initial 24-hour ICU stay to estimate the risk of delirium throughout the hospitalization period. Given its reliance on readily available early-stage variables, the model has the potential to serve as a practical and accessible risk stratification tool for health care professionals and patients when selecting optimal cardiac treatment strategies.

Acknowledgments

The authors gratefully acknowledge the institutional review boards of Beth Israel Deaconess Medical Center and the Massachusetts Institute of Technology for providing authorization to use data from the Medical Information Mart for Intensive Care IV version 2.0 database and eICU Collaborative Research Database.

Funding

The authors have not declared a specific grant for this research from any funding agency in the public, commercial, or not-for-profit sectors.

Data Availability

The datasets used and analyzed during this study are available from the corresponding author on reasonable request.

Authors' Contributions

HH contributed to study design, data extraction, methods, data analysis, and manuscript preparation. YW, QZ, JW, and LL contributed to data interpretation and data analysis. HL, JH, and YZ contributed to data extraction and data interpretation. YY and ZX directed the project. YY is the guarantor of this study.

Conflicts of Interest

None declared.

References

XSL•FO
RenderX

1. Li T, Li J, Yuan L, Wu J, Jiang C, Daniels J, RAGA Study Investigators. Effect of regional vs general anesthesia on incidence of postoperative delirium in older patients undergoing hip fracture surgery: the RAGA randomized trial. JAMA 2022 Jan 04;327(1):50-58 [FREE Full text] [doi: 10.1001/jama.2021.22647] [Medline: 34928310]
2. Chen M, Zhang L, Shao M, Du J, Xiao Y, Zhang F, et al. E4BP4 coordinates circadian control of cognition in delirium. Adv Sci (Weinh) 2022 Jun 17;9(23):e2200559 [FREE Full text] [doi: 10.1002/advs.202200559] [Medline: 35713240]
3. Wu YC, Tseng PT, Tu YK, Hsu CY, Liang CS, Yeh TC, et al. Association of delirium response and safety of pharmacological interventions for the management and prevention of delirium: a network meta-analysis. JAMA Psychiatry 2019 May 01;76(5):526-535 [FREE Full text] [doi: 10.1001/jamapsychiatry.2018.4365] [Medline: 30810723]
4. Brown KN, Soo A, Faris P, Patten SB, Fiest KM, Stelfox HT. Association between delirium in the intensive care unit and subsequent neuropsychiatric disorders. Crit Care 2020 Jul 31;24(1):476 [FREE Full text] [doi: 10.1186/s13054-020-03193-x] [Medline: 32736572]
5. Tschernatsch M, Juenemann M, Alhaidar F, El Shazly J, Butz M, Meyer M, et al. Epileptic seizure discharges in patients after open chamber cardiac surgery-a prospective prevalence pilot study using continuous electroencephalography. Intensive Care Med 2020 Jul;46(7):1418-1424 [FREE Full text] [doi: 10.1007/s00134-020-06073-8] [Medline: 32405742]
6. Li Q, Shen J, Lv H, Liu Y, Chen Y, Zhou C, et al. Incidence, risk factors, and outcomes in electroencephalographic seizures after mechanical circulatory support: a systematic review and meta-analysis. Front Cardiovasc Med 2022 Aug 03;9:872005 [FREE Full text] [doi: 10.3389/fcvm.2022.872005] [Medline: 35990978]
7. Hawkins RB, Mehaffey JH, Guo A, Charles EJ, Speir AM, Rich JB, Virginia Cardiac Services Quality Initiative. Postoperative atrial fibrillation is associated with increased morbidity and resource utilization after left ventricular assist device placement. J Thorac Cardiovasc Surg 2018 Oct;156(4):1543-9.e4 [FREE Full text] [doi: 10.1016/j.jtcvs.2018.03.169] [Medline: 29801690]
8. Sáez de Asteasu ML, Martínez-Velilla N, Zambom-Ferraresi F, Casas-Herrero Á, Cadore EL, Galbete A, et al. Assessing the impact of physical exercise on cognitive function in older medical patients during acute hospitalization: secondary analysis of a randomized trial. PLoS Med 2019 Jul 05;16(7):e1002852 [FREE Full text] [doi: 10.1371/journal.pmed.1002852] [Medline: 31276501]
9. Fan G, Zhong M, Su W, An Z, Zhu Y, Chen C, et al. Effect of different anesthetic modalities on postoperative delirium in elderly hip fractures: a meta-analysis. Medicine (Baltimore) 2024 Jun 07;103(23):e38418 [FREE Full text] [doi: 10.1097/MD.0000000000038418] [Medline: 38847680]
10. Pun BT, Badenes R, Heras La Calle G, Orun OM, Chen W, Raman R, COVID-19 Intensive Care International Study Group. Prevalence and risk factors for delirium in critically ill patients with COVID-19 (COVID-D): a multicentre cohort study. Lancet Respir Med 2021 Mar;9(3):239-250 [FREE Full text] [doi: 10.1016/S2213-2600(20)30552-X] [Medline: 33428871]
11. Berger M, Terrando N, Smith SK, Browndyke JN, Newman MF, Mathew JP. Neurocognitive function after cardiac surgery: from phenotypes to mechanisms. Anesthesiology 2018 Oct;129(4):829-851 [FREE Full text] [doi: 10.1097/ALN.0000000000002194] [Medline: 29621031]
12. Young M, Holmes N, Kishore K, Marhoon N, Amjad S, Serpa-Neto A, et al. Natural language processing diagnosed behavioral disturbance vs confusion assessment method for the intensive care unit: prevalence, patient characteristics, overlap, and association with treatment and outcome. Intensive Care Med 2022 May;48(5):559-569 [FREE Full text] [doi: 10.1007/s00134-022-06650-z] [Medline: 35322288]
13. Li RC, Asch SM, Shah NH. Developing a delivery science for artificial intelligence in healthcare. NPJ Digit Med 2020 Aug 21;3:107 [FREE Full text] [doi: 10.1038/s41746-020-00318-y] [Medline: 32885053]
14. Talpur N, Abdulkadir SJ, Alhussian H, Hasan MH, Aziz N, Bamhdi A. Deep Neuro-Fuzzy System application trends, challenges, and future perspectives: a systematic survey. Artif Intell Rev 2023;56(2):865-913 [FREE Full text] [doi: 10.1007/s10462-022-10188-3] [Medline: 35431395]
15. Deeken F, Sánchez A, Rapp MA, Denkinger M, Brefka S, Spank J, PAWEL Study Group. Outcomes of a delirium prevention program in older persons after elective surgery: a stepped-wedge cluster randomized clinical trial. JAMA Surg 2022 Feb 01;157(2):e216370 [FREE Full text] [doi: 10.1001/jamasurg.2021.6370] [Medline: 34910080]
16. Humeidan ML, Reyes JC, Mavarez-Martinez A, Roeth C, Nguyen CM, Sheridan E, et al. Effect of cognitive prehabilitation on the incidence of postoperative delirium among older adults undergoing major noncardiac surgery: the neurobics randomized clinical trial. JAMA Surg 2021 Feb 01;156(2):148-156 [FREE Full text] [doi: 10.1001/jamasurg.2020.4371] [Medline: 33175114]
17. Xue B, Li D, Lu C, King CR, Wildes T, Avidan MS, et al. Use of machine learning to develop and evaluate models using preoperative and intraoperative data to identify risks of postoperative complications. JAMA Netw Open 2021 Mar 01;4(3):e212240 [FREE Full text] [doi: 10.1001/jamanetworkopen.2021.2240] [Medline: 33783520]
18. Heilbroner SP, Few R, Mueller J, Chalwa J, Charest F, Suryadevara S, et al. Predicting cardiac adverse events in patients receiving immune checkpoint inhibitors: a machine learning approach. J Immunother Cancer 2021 Oct;9(10):e002545 [FREE Full text] [doi: 10.1136/jitc-2021-002545] [Medline: 34607896]
19. Dara S, Dhamercherla S, Jadav SS, Babu CM, Ahsan MJ. Machine learning in drug discovery: a review. Artif Intell Rev 2022;55(3):1947-1999 [FREE Full text] [doi: 10.1007/s10462-021-10058-4] [Medline: 34393317]

XSL•FO
RenderX

20. Zhong Y, Brooks MM, Kennedy EH, Bodnar LM, Naimi AI. Use of machine learning to estimate the per-protocol effect of low-dose aspirin on pregnancy outcomes: a secondary analysis of a randomized clinical trial. JAMA Netw Open 2022 Mar 01;5(3):e2143414 [FREE Full text] [doi: 10.1001/jamanetworkopen.2021.43414] [Medline: 35262718]
21. Sumner SA, Bowen D, Holland K, Zwald ML, Vivolo-Kantor A, Guy GP, et al. Estimating weekly national opioid overdose deaths in near real time using multiple proxy data sources. JAMA Netw Open 2022 Jul 01;5(7):e2223033 [FREE Full text] [doi: 10.1001/jamanetworkopen.2022.23033] [Medline: 35862045]
22. Nistal-Nuño B. Machine learning applied to a cardiac surgery recovery unit and to a coronary care unit for mortality prediction. J Clin Monit Comput 2022 Jun;36(3):751-763. [doi: 10.1007/s10877-021-00703-2] [Medline: 33860407]
23. Zhang L, Xu F, Han D, Huang T, Li S, Yin H, et al. Influence of the trajectory of the urine output for 24 h on the occurrence of AKI in patients with sepsis in intensive care unit. J Transl Med 2021 Dec 20;19(1):518 [FREE Full text] [doi: 10.1186/s12967-021-03190-w] [Medline: 34930308]
24. Shi Y, Stornetta DS, Reklow RJ, Sahu A, Wabara Y, Nguyen A, et al. A brainstem peptide system activated at birth protects postnatal breathing. Nature 2021 Jan;589(7842):426-430 [FREE Full text] [doi: 10.1038/s41586-020-2991-4] [Medline: 33268898]
25. Davidson S, Villarroel M, Harford M, Finnegan E, Jorge J, Young D, et al. Day-to-day progression of vital-sign circadian rhythms in the intensive care unit. Crit Care 2021 Apr 22;25(1):156 [FREE Full text] [doi: 10.1186/s13054-021-03574-w] [Medline: 33888129]
26. Murphy MS, Ducharme R, Hawken S, Corsi DJ, Petrcich W, El-Chaâr D, et al. Exposure to intrapartum epidural analgesia and risk of autism spectrum disorder in offspring. JAMA Netw Open 2022 May 02;5(5):e2214273 [FREE Full text] [doi: 10.1001/jamanetworkopen.2022.14273] [Medline: 35616937]
27. Proix T, Delgado Saa J, Christen A, Martin S, Pasley BN, Knight RT, et al. Imagined speech can be decoded from low- and cross-frequency intracranial EEG features. Nat Commun 2022 Jan 10;13(1):48 [FREE Full text] [doi: 10.1038/s41467-021-27725-3] [Medline: 35013268]
28. Schober P, Vetter TR. Logistic regression in medical research. Anesth Analg 2021 Jan 14;132(2):365-366 [FREE Full text] [doi: 10.1213/ANE.0000000000005247] [Medline: 33449558]
29. Rhodes JS, Cutler A, Moon KR. Geometry- and accuracy-preserving random forest proximities. IEEE Trans Pattern Anal Mach Intell 2023 Sep;45(9):10947-10959. [doi: 10.1109/TPAMI.2023.3263774] [Medline: 37015125]
30. Li Q, He Y, Pan J. CrossFuse-XGBoost: accurate prediction of the maximum recommended daily dose through multi-feature fusion, cross-validation screening and extreme gradient boosting. Brief Bioinform 2023 Nov 22;25(1):bbad511 [FREE Full text] [doi: 10.1093/bib/bbad511] [Medline: 38216539]
31. Que Z, Lin CJ. One-class SVM probabilistic outputs. IEEE Trans Neural Netw Learn Syst 2025 Apr;36(4):6244-6256. [doi: 10.1109/TNNLS.2024.3395148] [Medline: 38717884]
32. Chen Y, Ou Z, Zhou D, Wu X. Advancements and challenges of artificial intelligence-assisted electroencephalography in epilepsy management. J Clin Med 2025 Jun 16;14(12):4270 [FREE Full text] [doi: 10.3390/jcm14124270] [Medline: 40566015]
33. Wang YY, Yue JR, Xie DM, Carter P, Li QL, Gartaganis SL, et al. Effect of the tailored, family-involved hospital elder life program on postoperative delirium and function in older adults: a randomized clinical trial. JAMA Intern Med 2020 Jan 01;180(1):17-25 [FREE Full text] [doi: 10.1001/jamainternmed.2019.4446] [Medline: 31633738]
34. Brown CH, Neufeld KJ, Tian J, Probert J, LaFlam A, Max L, Cerebral Autoregulation Study Group, et al. Effect of targeting mean arterial pressure during cardiopulmonary bypass by monitoring cerebral autoregulation on postsurgical delirium among older patients: a nested randomized clinical trial. JAMA Surg 2019 Sep 01;154(9):819-826 [FREE Full text] [doi: 10.1001/jamasurg.2019.1163] [Medline: 31116358]
35. Leone M, Einav S, Chiumello D, Constantin JM, De Robertis E, De Abreu MG, Guideline contributors. Noninvasive respiratory support in the hypoxaemic peri-operative/periprocedural patient: a joint ESA/ESICM guideline. Intensive Care Med 2020 Apr;46(4):697-713 [FREE Full text] [doi: 10.1007/s00134-020-05948-0] [Medline: 32157356]
36. Gélinas C, Bérubé M, Puntillo KA, Boitor M, Richard-Lalonde M, Bernard F, et al. Validation of the critical-care pain observation tool-neuro in brain-injured adults in the intensive care unit: a prospective cohort study. Crit Care 2021 Apr 13;25(1):142 [FREE Full text] [doi: 10.1186/s13054-021-03561-1] [Medline: 33849619]
37. Honarmand K, Lalli RS, Priestap F, Chen JL, McIntyre CW, Owen AM, et al. Natural history of cognitive impairment in critical illness survivors. A systematic review. Am J Respir Crit Care Med 2020 Jul 15;202(2):193-201 [FREE Full text] [doi: 10.1164/rccm.201904-0816CI] [Medline: 32078780]
38. Rosas IO, Bräu N, Waters M, Go RC, Malhotra A, Hunter BD, et al. Tocilizumab in patients hospitalised with COVID-19 pneumonia: efficacy, safety, viral clearance, and antibody response from a randomised controlled trial (COVACTA). EClinicalMedicine 2022 May;47:101409 [FREE Full text] [doi: 10.1016/j.eclinm.2022.101409] [Medline: 35475258]
39. Madrigal C, Kim J, Jiang L, Lafo J, Bozzay M, Primack J, et al. Delirium and functional recovery in patients discharged to skilled nursing facilities after hospitalization for heart failure. JAMA Netw Open 2021 Mar 01;4(3):e2037968 [FREE Full text] [doi: 10.1001/jamanetworkopen.2020.37968] [Medline: 33724390]

XSL•FO
RenderX

40. Saczynski JS, Koethe B, Fick DM, Vo QT, Devlin JW, Marcantonio ER, et al. Cognitive and functional change in skilled nursing facilities: differences by delirium and Alzheimer's disease and related dementias. J Am Geriatr Soc 2024 Nov;72(11):3501-3509. [doi: 10.1111/jgs.19112] [Medline: 39171670]
41. Huang HL, Lee JY, Lo YS, Liu IH, Huang SH, Huang YW, et al. Whole-blood 3-gene signature as a decision aid for rifapentine-based tuberculosis preventive therapy. Clin Infect Dis 2022 Sep 14;75(5):743-752 [FREE Full text] [doi: 10.1093/cid/ciac003] [Medline: 34989801]
42. McKenna M, Shackelford D, Pontes C, Ball B, Nance E. Multiple particle tracking detects changes in brain extracellular matrix and predicts neurodevelopmental age. ACS Nano 2021 May 25;15(5):8559-8573 [FREE Full text] [doi: 10.1021/acsnano.1c00394] [Medline: 33969999]

Abbreviations

AUC: area under the receiver operating characteristic curve
CAM-ICU: Confusion Assessment Method for the Intensive Care Unit
eICU-CRD: eICU Collaborative Research Database
GCS: Glasgow Coma Scale
ICU: intensive care unit
MIMIC-IV 2.0: Medical Information Mart for Intensive Care IV version 2.0
ML: machine learning
ROC: receiver operating characteristic
SHAP: Shapley Additive Explanations
SOFA: Sequential Organ Failure Assessment
XGB: extreme gradient boosting

Edited by J Klann; submitted 01.Mar.2025; peer-reviewed by P Tekkali, A Özel; comments to author 30.Apr.2025; accepted 26.Sep.2025; published 11.Feb.2026.

Please cite as:
Hu H, Wang Y, Li H, Zang Q, Huang J, Zhang Y, Wu J, Liu L, Xing Z, Yu Y
Early Prediction of Delirium in Postcardiac Surgery Patients: Machine Learning Model Development and External Validation
JMIR Med Inform 2026;14:e73283
URL: https://medinform.jmir.org/2026/1/e73283
doi:10.2196/73283
PMID:

©Huixiu Hu, Yuxiang Wang, Houfeng Li, Qinglai Zang, Jing Huang, Ying Zhang, Jinjing Wu, Long Liu, Zhen Xing, Yaohua Yu. Originally published in JMIR Medical Informatics (https://medinform.jmir.org), 11.Feb.2026. This is an open-access article distributed under the terms of the Creative Commons Attribution License (https://creativecommons.org/licenses/by/4.0/), which permits unrestricted use, distribution, and reproduction in any medium, provided the original work, first published in JMIR Medical Informatics, is properly cited. The complete bibliographic information, a link to the original publication on https://medinform.jmir.org/, as well as this copyright and license information must be included.

XSL•FO
RenderX

Original Paper

Ensemble Machine Learning Models for Predicting Patients With High Usage: Model Validation and Economic Impact Analysis

Joshua Kuan Tan[1*], MSc, MBBS; Le Quan[2*], MSc; Hao Yi Tan[1*], MPH, MD; Su-Yen Goh[3*], MBBS; Julian Thumboo[1*], MBBS; Marianne Au[4*], BBus; Yong Mong Bee[5*], MBBS; Jen Hong Tan[2*], PhD

[1]Health Services Research Unit, Singapore General Hospital, Singapore, Singapore

[2]Data Science and Artificial Intelligence Laboratory, Singapore General Hospital, Singapore, Singapore

[3]Future Health Systems Department, Singapore General Hospital, Singapore, Singapore

[4]Group Finance, SingHealth, Singapore, Singapore

[5]Department of Endocrinology, Singapore General Hospital, Singapore, Singapore

[*]all authors contributed equally

Corresponding Author:
Joshua Kuan Tan, MSc, MBBS
Health Services Research Unit
Singapore General Hospital
Outram Road
Singapore, 169608
Singapore
Phone: 65 223322
Email: joshua.tan.kuan@singhealth.com.sg

Abstract

Background: Machine learning models are increasingly used to predict patients at risk of high health care usage for targeted interventions.

Objective: This study aimed to evaluate the predictive performance of multiclass ensemble models across different levels of health care usage and assess their potential application through real-world economic impact analysis.

Methods: A total of 4 previously developed binary classification models (base learners)—boosted trees, multivariate adaptive regression splines, multilayer perceptron, and logistic regression—were extended using a stacking ensemble approach. These base learner models generated individual-level predicted probabilities, which were used as inputs to build multiclass prediction models forecasting usage across defined strata: length of stay (LOS) of <7, 7-13, 14-29, and ≥30 days, and emergency department (ED) visits of <3, 3-4, 5-9, and ≥10 visits. In total, 3 ensemble algorithms were evaluated: random forest, boosted trees, and linear support vector machines. Ensemble models were trained on registry data from 2020-2021 and temporally validated on 2021-2022 data. Performance was assessed using multiclass area under the receiver operating curve, accuracy, and confusion matrix–derived metrics. Economic impact was estimated via Monte Carlo simulations using inpatient billing data, assuming a 20% cost reduction in the following year.

Results: The models were trained on 108,886 patients and validated on 111,004 patients. Among all ensemble configurations, boosted tree models regardless of base learner achieved the highest performance, with multiclass area under the receiver operating curve scores of 0.6877 (95% CI 0.6927-0.7255) for LOS and 0.7601 (95% CI 0.7301-0.7654) for ED visits, and corresponding accuracies of 0.6522 (95% CI 0.6465-0.6579) and 0.7457 (95% CI 0.7405-0.7508), respectively. In the validation set, these models correctly assigned 30.3% of inpatient LOS and 39.8% of ED visits to the correct class, identifying 77% of future inpatient users and 73.9% of future ED users. Economic impact analysis for LOS identified the boosted tree model with logistic regression base learner as dominant, achieving a simulated average cost reduction of SGD $152 million (US $111 million), SGD $2.4 million (US $1.75 million; 1.5%) more than the next best model using a multilayer perceptron base learner.

Conclusions: Ensemble models can effectively predict multilevel health care usage and potentially generate meaningful cost savings when applied to real-world settings. These models may support targeted interventions and guide planning and budgeting in diabetes-related population health programs.

(JMIR Med Inform 2026;14:e77202) doi:10.2196/77202

XSL•FO
RenderX

KEYWORDS

diabetes mellitus; healthcare utilization; population health management, machine learning; artificial intelligence; economic analysis; decision analysis; Monte Carlo simulation

Introduction

Health care expenditure in high-income countries is rising [1], with chronic diseases (specifically diabetes mellitus) being a leading contributor. Diabetes accounts for approximately 15% of health care expenditure in the United States [2], 9% in the European Union [3], and 11% in Singapore [4]. It is a significant cause of cardiovascular disease, kidney failure, eye disease, peripheral vascular disease, and neuropathy, all associated with substantial morbidity, mortality, and higher health care costs.

Health care spending is also highly skewed, with a small proportion of patients incurring most costs [5]. Efforts to identify high-need, high-cost (HNHC) patients—typically the top 5% of usage or cost—have led to predictive models using regression and machine learning [6]. However, the clinical utility of these models remains uncertain, as few studies assess their net benefit compared with not using them [6-8]. Furthermore, the potential to reduce costs among the top decile or 5% of high-cost patients is smaller than commonly assumed [9], possibly due to heterogeneity in patient characteristics and usage patterns, variability in group membership over time, and a small proportion who are amenable to cost-reducing interventions [5,9,10]. Focusing narrowly on the highest users may also overlook many individuals with future health care needs outside this group.

Building on these insights, our previous study expanded the predictive focus beyond traditional HNHC patients by developing binary classification models to predict inpatient and emergency department (ED) usage across various thresholds for patients in the Singapore Health Services Diabetes Registry (SDR), a clinical database of over 130,000 patients with diabetes [11]. In this study, we extended that work by creating separate multiclass ensemble models for inpatient bed days and ED visits. We validated these models, evaluated their relevance for population health program development, and analyzed their potential economic impact using real-world financial data [7,8]. Our goal is to develop clinically actionable predictive models that can be integrated into broader diabetes-related population health initiatives.

Methods

Study Design and Population

This study used data from the SDR spanning 2020-2022, comprising 2 datasets: 2020-2021 and 2021-2022. The 2019-2020 dataset, previously used to develop the binary classification models [11], was excluded from the current analysis to prevent overfitting. Each dataset (2019-2020, 2020-2021, and 2021-2022) was constructed as a cross-sectional snapshot based on a fixed 1-year prediction window. Patients could appear in multiple datasets across years if they continued to meet inclusion criteria for entry into the registry [12]; however, within each dataset, only 1 record per patient per year was used. Multiple visits within the same year were aggregated to derive annual service-level usage metrics (eg, total inpatient bed days and total ED visits).

Predictor Variables

Individual-level predicted probabilities from the binary classification models, which reflect the predicted likelihood of future usage, were used as predictor variables in the corresponding ensemble models (ie, length of stay [LOS] probabilities for the LOS ensemble model and ED probabilities for the ED ensemble model). Additionally, current-year LOS or ED visits were also included as predictors. Full details on predictor variables for the binary models are provided in Table S1 in Multimedia Appendix 1 and our previous publication [11]; briefly, they include age, gender, ethnicity, housing type, comorbidities (eg, hypertension, hyperlipidemia, and chronic kidney disease), diabetes-related complications, and mean glycated hemoglobin.

Outcome Variables

Multiclass ensemble models were developed to predict usage for LOS and ED visits across 4 classes each. For LOS, the classes were <7 days, 7-13 days, 14-29 days, and ≥30 days. For ED visits, the classes were <3 visits, 3-4 visits, 5-9 visits, and ≥10 visits.

Inclusion and Exclusion Criteria

Patients aged 18 years or older with type 2 diabetes mellitus were included. Patients with missing variables were excluded, as data imputation was not performed, and most machine learning algorithms used in this study do not natively support missing values.

Handling Unbalanced Data

Class imbalance negatively affected model performance in previous studies, and random upsampling outperformed the synthetic minority oversampling technique [11]. We applied random upsampling using the ‘upSample’ function from the *caret* package [13] to achieve equal representation across all classes in the training dataset (ie, an equal number of patients across all classes).

Machine Learning Models

Previously developed binary classification models from the multi-institutional SDR were used to predict total inpatient LOS and ED visits over a calendar year [11]. Predictions were made across 3 thresholds in the 2 outcomes: LOS of ≥7, ≥14, and ≥30 days; and ED attendance of ≥3, ≥5, and ≥10 visits.

We used the best-performing binary classification models from our previous work, which were trained using the 2019-2020 dataset as base learners: boosted trees, multivariate adaptive regression splines, multilayer perceptron, and logistic regression [11]. For each base learner type, 3 separate binary models were developed to predict inpatient LOS of ≥7, ≥14, and ≥30 days, and ED attendance of ≥3, ≥5, and ≥10 visits, respectively. The

XSL•FO
RenderX

individual-level predicted probabilities from these binary models were then used as inputs (meta-features) in a stacking ensemble model designed to classify patients into 4 mutually exclusive outcome categories (LOS: <7, 7-13, 14-29, ≥30 days, and ED: <3, 3-4, 5-9, ≥10 visits).

Stacking was selected over voting-based methods for its ability to learn optimal weights for combining base learner outputs, rather than treating all models equally or assigning manual weights [14]. Furthermore, 3 algorithms were tested as meta-learners: random forest, boosted trees, and linear support vector machines (SVMs). All models were developed in R (version 4.3.1; R Core Team) using the *tidymodels* package [15].

The 2020-2021 dataset was used to train and test the ensemble models, with a 75:25 split. Models were then temporally validated on an unseen 2021-2022 dataset. Each dataset represented a patient-year observation with a fixed 1-year prediction horizon. All predictor variables, including inpatient bed days and ED visits, were derived exclusively from the preceding calendar year to predict usage in the subsequent year, ensuring that no future information was used at the time of prediction and avoiding look-ahead bias. While patients could appear in multiple datasets across years, training and validation were temporally separated to ensure that predictions were evaluated on future, unseen patient-year data, consistent with real-world deployment for chronic disease management. To ensure consistency and reproducibility, we used default hyperparameters for all base learners and meta-learners.

Explainability

We did not conduct explainability analysis for the ensemble models, as previous analyses of the base learner models with model-specific variable importance scores, permutation feature importance plots, and partial dependence plots demonstrated consistent and predictable behavior [11]. The ensemble models' transparent construction from base learner outputs rendered additional explainability analysis unnecessary.

Performance Indicators

Model performance was assessed using multiclass area under the receiver operating curve (AUROC; one-vs-rest approach), and accuracy (95% CI) was calculated using the DeLong method (via the pROC package) for AUROC and the confusionMatrix function (from the caret package) for accuracy. Confusion matrices were analyzed, and new metrics specific to our 4-class prediction task were developed for population health programs (Figure 1). Additional metrics, including sensitivity, specificity, positive predictive value, negative predictive value, and balanced accuracy, are detailed in the Multimedia Appendix 1.

These new metrics were designed for population-level interventions using the prediction models. Our priorities were maximizing correct predictions, followed by identifying users, and minimizing unnecessary predictions (ie, patients predicted to have usage but who ultimately did not). Maximizing correct predictions minimizes underpredictions, overpredictions, and missed cases. Increasing identified users enables interventions to reach more patients with future needs, while minimizing unnecessary predictions enhances program efficiency by reducing resources spent on patients unlikely to use services.

Figure 1. Confusion matrix in a 4-class problem and related evaluation variables.

Prediction \ Actual	0	1	2	3
0	A	B	C	D
1	E	F	G	H
2	I	J	K	L
3	M	N	O	P

Labels	Inpatient bed days	Emergency Department Visits
0	< 7 days	< 2 visits
1	7 - 13 days	3 - 4 visits
2	14 - 29 days	5 - 9 visits
3	≥ 30 days	≥ 10 visits

Variable	Description	Formula
Total	All patients in the prediction	$= A + B + \cdots + P$
Users	All actual users	$=$ Total $- (A + E + I + M)$
Correct predictions	Ratio of correct predictions (*among patients with actual usage*) to all users	$= \frac{F + K + P}{\text{Utilizers}}$
Underprediction	Ratio of underpredictions (*among patients with actual usage*) to all users	$= \frac{G + H + L}{\text{Utilizers}}$
Overprediction	Ratio of overprediction (*among patients with actual usage*) to all users	$= \frac{J + N + O}{\text{Utilizers}}$
Unnecessary predictions	Ratio of predicted users (*among patients with **no** actual usage*) to all patients with ***no*** usage	$= \frac{E + I + M}{A + E + I + M}$
Missed cases	Ratio of predicted nonusers (*among patients with actual usage*) to all users	$= \frac{B + C + D}{\text{Utilizers}}$
Identified users	Ratio of predicted users (*among patients with actual usage*) to all users	$=$ Correct predictions + Underprediction + Overprediction

XSL•FO
RenderX

Economic Impact Analysis of the Models

We assessed the potential economic impact of the top 5 ensemble models with the largest proportion of correct predictions for inpatient bed days. Using individual-level inpatient cost data, we modeled hypothetical cost reductions to simulate the financial implications of targeted intervention. These simulations assume that accurately predicted patients would receive effective interventions that reduce future inpatient costs. Cost savings were not attributed to the prediction alone, but to downstream programs triggered by the prediction.

In total, 2 key parameters were incorporated—reach and benefits, both factors important to population-level impact. Reach was defined as the proportion of patients within a predicted usage class who would receive the intervention [16], while benefits referred to the hypothetical percentage reduction in future inpatient costs among those reached, attributable to the intervention.

We used total inpatient costs (in Singapore dollars and the equivalent United States dollars [US $], presubsidies) for each calendar year, using the conversion rate of SGD $1=US $1.370, which is accurate as of 1 June 2022. We assessed model performance using fixed effects and Monte Carlo simulations with 10,000 iterations to account for random effects. “Total benefit” was defined as the simulated reduction in inpatient costs in the following year, enabling us to compare models and identify the dominant one. A schematic of the economic impact analysis model is provided in Figure 2, with parameters detailed in Table S2 in Multimedia Appendix 1.

In the fixed effects model, we modeled the benefit at a uniform 50% cost reduction for all identified patients—an optimistic scenario to benchmark maximum potential impact. In contrast, the Monte Carlo simulations modeled a more conservative and realistic benefit at an average cost reduction of 20% across all classes, with stochastic variation applied using a normal distribution.

Real-world programmatic use was further simulated by varying reach across usage tiers: average reach levels were set at 90% for the highest usage class, 70% for the middle class, and 50% for the lowest classes, each with a 5% variance. For example, the reach for the highest users ranged from 85% to 95% across simulations. This tiered approach reflects potential operational realities: patients predicted in the highest usage class are fewer in number and more likely to be prioritized and successfully engaged by targeted interventions. In contrast, lower usage classes include larger populations, making it less feasible to reach all patients in practice. To account for individual variability in intervention uptake, reach levels were also modeled using a binomial probability distribution.

From the Monte Carlo simulations, we identified the dominant model as the one with the highest median cost savings. To explore uncertainty and assess the robustness of this selection, we performed parameter sensitivity analysis stratified by usage class. Specifically, we varied the reach and benefit parameters in 10% intervals (ranging from 10% to 90%), resulting in 81 unique parameter combinations. For each combination, 1000 Monte Carlo runs were conducted to account for stochastic variability. The distribution of cost savings across simulations was analyzed, and results were visualized using the *plotly* package [17] to provide an interactive and detailed view of model performance under different programmatic scenarios.

Figure 2. Schematic of economic impact analysis model.

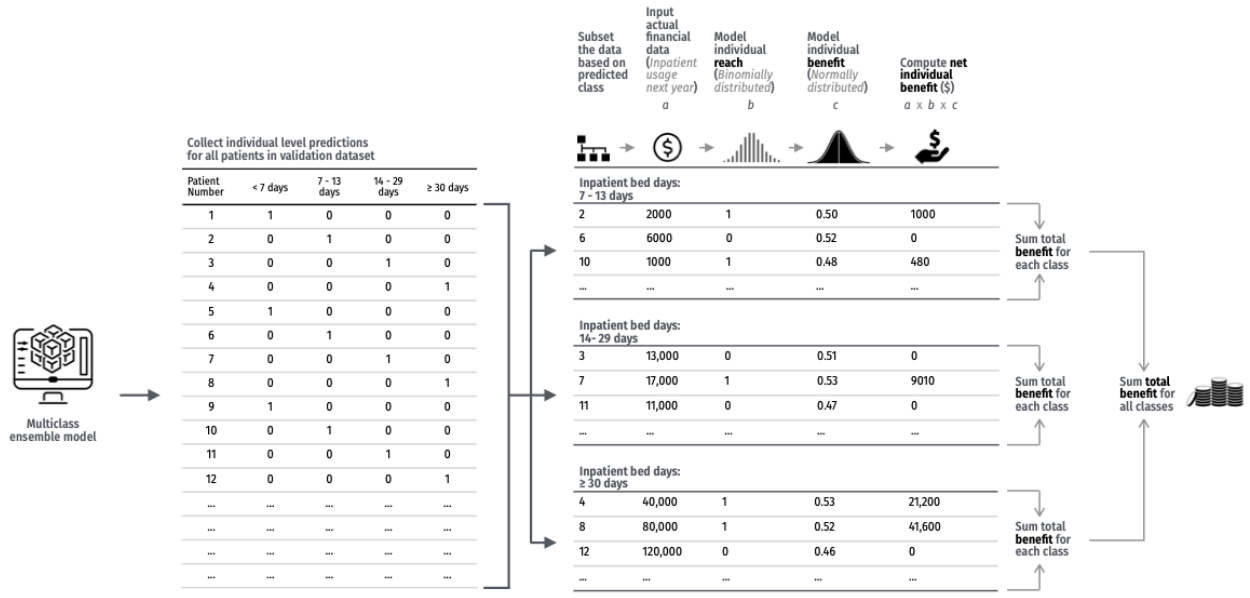

Reporting Checklist

We reported our study using the Transparent Reporting of a multivariable prediction model for Individual Prognosis or Diagnosis + Artificial Intelligence (TRIPOD+AI) checklist (Multimedia Appendix 2) [18].

XSL•FO
RenderX

Ethical Considerations

Ethics approval was obtained from the Singapore Health Services Centralized Institutional Review Board before initiating this study (reference 2022/2133). As all participant data were deidentified, a waiver for participant consent was also obtained. All procedures were performed in compliance with relevant laws and institutional guidelines.

Results

Characteristics of the Datasets

The demographics, comorbidities, and usage characteristics of the datasets have been previously described [11]. The 2020-2021 and 2021-2022 datasets included 108,886 of 140,859 (77.3%) patients and 111,004 of 137,584 (80.7%) patients from the total SDR cohort, respectively. Total inpatient costs (presubsidies) per annum are summarized in Table 1, and inpatient LOS distributions are illustrated in Figures S1-S3 in Multimedia Appendix 1.

Inpatient usage showed an increasing trend, with gross inpatient bills (unadjusted for inflation) rising from a nominal value of SGD $808 (US $590) million in 2019 to SGD $1.01 billion (US $737 million) in 2022. The proportion of patients with inpatient usage increased from 46,686 of 134,670 (34.7%) in 2019 to 51,228 of 137,627 (37.2%) in 2022, while the average cost per patient rose from SGD $17,321 to SGD $19,704 (US $12,643 to US $14,382). Total inpatient costs were heavily right-skewed (Table S3 in Multimedia Appendix 1) and followed a Pareto distribution (Figure S1 in Multimedia Appendix 1), with the top 10% of patients accounting for 80% of cumulative health care costs and inpatient bed days annually (Figures S1 and S2 in Multimedia Appendix 1). A strong correlation was observed between gross inpatient bills and inpatient bed days (Figure S3 in Multimedia Appendix 1).

XSL•FO
RenderX

Table 1. Performance metrics of the top 5 best-performing ensemble models.

Model characteristics	Accuracy (95% CI)	Multiclass AUROC[a] (95% CI)	Correct predictions, %	Underpredictions, %	Overpredictions, %	Unnecessary predictions, %	Identified users, %	Missed cases, %
Best performing ensemble models on test dataset (2021-2022)								
Predicting inpatient bed days category								
Boosted tree with MARS[b] as base learner	0.6522 (0.6465-0.6579)	0.6877 (0.6927-0.7255)	30.5	23.2	24.1	31.3	77.8	22.2
Boosted tree with MLP[c] as base learner	0.6685 (0.6629-0.6741)	0.6832 (0.6875-0.7202)	30.2	20.3	25.5	29.6	76	24
Boosted tree with logistic regression as base learner	0.6495 (0.6438-0.6552)	0.6696 (0.6896-0.722)	30.2	20	26	31.7	76.1	23.9
Boosted tree with boosted tree as base learner	0.6654 (0.6598-0.671)	0.6776 (0.6936-0.7259)	29.7	21.2	24.1	29.9	75.1	24.9
Linear SVM[d] with MLP as base learner	0.7300 (0.7246-0.7352)	0.6758 (0.6757-0.7089)	26.8	19.7	22.6	22.6	69.1	30.9
Predicting emergency department visits category								
Boosted tree with MARS as base learner	0.7457 (0.7405-0.7508)	0.7601 (0.7301-0.7654)	39.5	10.7	24.8	24	75	25
Boosted tree with logistic regression as base learner	0.7205 (0.7151-0.7258)	0.7569 (0.7294-0.7641)	39.3	11	24.9	26.6	75.2	24.8
Boosted tree with MLP as base learner	0.7432 (0.738-0.7484)	0.7557 (0.731-0.7664)	37.9	10.4	25.8	24.2	74	26
Boosted tree with Boosted tree as base learner	0.7425 (0.7372-0.7476)	0.7527 (0.7016-0.7378)	37.1	14.7	18.3	24.2	70.1	29.9
Linear SVM using MARS as base learner	0.7849 (0.7800-0.7898)	0.7722 (0.7316-0.7681)	30.3	6.6	34.8	19.6	71.8	28.2
Best performing ensemble models on validation datasets								
Predicting inpatient bed days category								
Boosted tree with MARS as base learner	0.6405 (0.6377-0.6434)	0.6811 (0.6986-0.714)	30.3	21.1	25.6	32.1	77	23
Boosted tree with boosted tree as base learner	0.6496 (0.6468-0.6524)	0.6828 (0.6966-0.712)	29.9	21.9	24.7	31.1	76.4	23.6
Boosted tree with logistic regression as base learner	0.6357 (0.6329-0.6385)	0.6767 (0.6929-0.7082)	29.4	20.2	27.6	32.6	77.1	22.9
Boosted tree with MLP as base learner	0.6558 (0.6530-0.6586)	0.6782 (0.6957-0.7111)	29.2	19.2	27.4	30.3	75.8	24.2
Linear SVM with MLP as base learner	0.71 (0.7073-0.7127)	0.6742 (0.6851-0.7004)	26.5	19.3	24.5	24	70.4	29.6
Predicting emergency department visits category								
Boosted tree with logistic regression as base learner	0.7053 (0.7026-0.7079)	0.7669 (0.7199-0.7359)	39.8	10.4	23.7	27.9	73.9	26.1
Boosted tree with boosted tree as base learner	0.7317 (0.7290-0.7343)	0.7577 (0.7139-0.73)	39.7	12.5	19	25.1	71.1	28.9
Boosted tree with MLP as base learner	0.7269 (0.7243-0.7295)	0.7563 (0.7158-0.732)	36.9	10.5	23.9	25.5	71.3	28.7
Boosted tree using MARS as base learner	0.7266 (0.7239-0.7292)	0.7664 (0.7169-0.7332)	36.7	10.2	24.7	25.5	71.5	28.5
Linear SVM using MARS as base learner	0.7656 (0.7631-0.7681)	0.7818 (0.7204-0.7368)	30.1	6.7	32.2	21	69	31

[a]AUROC: area under the receiver operating curve.

XSL•FO
RenderX

[b]MARS: multivariate adaptive regression splines.

[c]MLP: multilayer perceptron.

[d]SVM: support vector machine.

Multiclass Model Performance

We developed 12 ensemble models by combining 4 base learner models with 3 ensemble algorithms: random forest, boosted trees, and linear SVM. Detailed performance metrics for all 12 models on the test dataset are provided in Table S4-S6 in Multimedia Appendix 1. We then selected top 5 models for each prediction task based on the highest percentages of correct predictions and identified users (Table 1 and Table S4 in Multimedia Appendix 1), and their performance was temporally validated on the unseen dataset from 2021 to 2022; detailed performance metrics for these models on the test dataset are provided in Tables S7 and S8 in Multimedia Appendix 1.

Boosted tree models outperformed other ensemble algorithms across metrics, including multiclass AUROC, correct predictions, and identified users. While linear SVM models had comparable multiclass AUROC scores to boosted tree models, they showed significantly lower correct predictions, fewer identified users, and more missed cases. Random forest models performed poorly across all metrics.

Boosted tree models demonstrated consistent performance on test and validation datasets, indicating robustness on unseen data (Table 1 and Table S4 in Multimedia Appendix 1). For inpatient bed days, these models correctly assigned approximately 30% of future users to the appropriate category, identified >75% of future users, and generated 30%-32% unnecessary predictions among nonusers. For ED visits, they correctly assigned 36%-39% of future users, identified 70%-75% of users, and generated approximately 25% unnecessary predictions among nonusers.

Economic Impact Analysis of the Models

Results from the fixed effects and Monte Carlo simulations are presented in Table 2 and Figure S4 in Multimedia Appendix 1. The boosted tree ensemble model with logistic regression as the base learner emerged as the dominant model, although other boosted tree models performed similarly. In the fixed effects simulation, the dominant model generated an estimated benefit of SGD $210 (US $153) million. In the Monte Carlo simulations, it produced a median benefit of SGD $152 (US $110) million. Notably, nearly half of the simulations for the dominant model exceeded the 75th percentile of simulations from other models (Table 2 and Figure S4 in Multimedia Appendix 1).

Table 2. Results of fixed effects and Monte Carlo simulations.

Variables	Models				
	Boosted tree with logistic regression as base learner	Boosted tree with MLP[a] as base learner	Boosted tree with MARS[b] as base learner	Boosted tree with boosted tree as base learner	Linear SVM[c] with MLP as base learner
Results for the fixed effects simulation (SGD $)					
Total simulated reduction in inpatient bill	210,220,829	205,184,563	209,535,576	206,000,929	189,308,087
Results for the Monte Carlo simulations (SGD $)					
Mean (SD)	152,794,862 (6,001,058)	150,437,894 (5,816,301)	149,408,731 (5,959,678)	147,699,501 (5,809,931)	136,692,927 (7,365,761)
Median (IQR)	152,854,645 (8,656,193)	150,468,563 (8,399,851)	149,405,404 (8,402,405)	147,756,137 (8,198,816)	136,722,177 (12,202,993)
Range (minimum-maximum)	134,202,838-170,594,658	133,162,981-167,868,627	131,679,740-167,051,047	129,415,870-165,742,786	118,420,401-153,678,680
Q25	148,510,936	146,256,897	145,189,862	143,596,095	130,577,413
Q75	157,167,129	154,656,748	153,592,267	151,794,911	142,780,406

[a]MLP: multilayer perceptron.

[b]MARS: multivariate adaptive regression splines.

[c]SVM: support vector machine.

Parameter Sensitivity Analysis

We evaluated the dominant model's performance across various permutations of reach and benefit (Figure 3 and interactive plots available on GitHub [19]). As expected, the net benefit increased with higher individual cost reductions (Figures 3A-3C) and program reach. For predicting LOS of 14-29 days (Figure 3B), with a constant 50% cost reduction, the simulated net benefit ranged from SGD $5.95 to SGD $9.62 (US $4.34 to US $7.02) million at 10% reach, SGD $35.6 to SGD $40.7 (US $26.0 to US $29.7) million at 50% reach, and SGD $66.6 to SGD $70.0 (US $48.6 to US $51.1) million at 90% reach.

With increasing program reach, the range of simulated average benefit per patient narrowed. For LOS of 14-29 days (Figure 3D), with a 50% cost reduction, the average benefit per patient

XSL•FO
RenderX

ranged from SGD $3708 to SGD $5814 (US $2707 to US $4244) at 10% reach and from SGD $4656 to SGD $4389 (US $3399 to US $3204) at 90% reach. The implications of these findings are further discussed in the Discussion section.

Figure 3. 3D scatterplot for Monte Carlo simulations across various permutations of reach and benefit for the boosted tree with logistic regression as base learner ensemble. (A) Simulated net benefit for prediction 7-13 days; (B) simulated net benefit for prediction 14-29 days; (C) simulated net benefit for prediction ≥30 days; (D) simulated average benefit per patient for prediction 7-13 days; (E) simulated average benefit per patient for prediction 14-29 days; and (F) simulated average benefit per patient for prediction ≥30 days. Readers can refer to the interactive plots on GitHub for higher resolution interactive images.

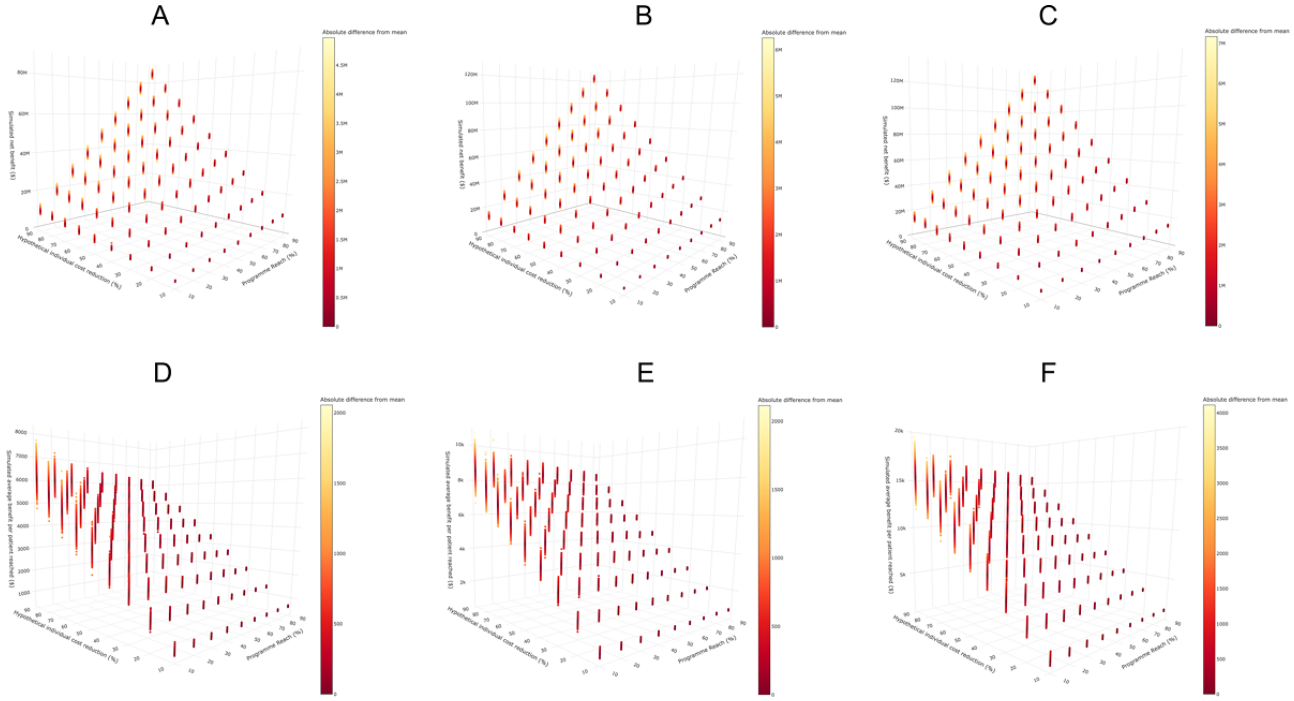

Discussion

Principal Findings

In this study, we expanded on our previous work by developing multiclass ensemble machine learning models to predict future inpatient LOS and ED visits. The models were evaluated using public health program objectives, analyzing predictions through confusion matrices and performance metrics to identify the best-performing models. Economic impact analysis, incorporating inpatient cost data and program-related simulations, identified the boosted tree ensemble algorithm with logistic regression as the base learner as dominant for LOS. Further testing across analytical parameters confirmed its robustness and practical applicability.

While previous studies focused on binary outcomes with limited evaluation of clinical utility [6,20], our study reframes high health care usage as a multiclass problem, enabling more nuanced predictions across different health care events. By incorporating financial data into the economic impact analysis with Monte Carlo simulations, we model the potential benefits of the model, enhancing its relevance for real-world applications [7,8]. This novel approach to economic impact analysis represents a significant contribution to machine learning in health care and the design of resource-efficient health programs.

Advancing High User Prediction Through Multiclass Modeling and Economic Impact Analysis

Our study advances the prediction and targeting of patients with high health care usage by moving beyond binary classification. While many previous studies have focused on predicting binary outcomes—such as identifying HNHC patients in the top 5% or 10% of usage—this strategy has limited practical utility, as most high users do not remain so over time [9,21,22]. Consequently, there is growing recognition of the need to predict risk across multiple levels of usage, enabling stratified interventions tailored to predicted resource needs [9].

To the best of our knowledge, few studies have applied machine learning to predict health care usage across multiple discrete classes. One recent study using Louisiana Department of Health records built multinomial models to predict clinical service usage (ie, number of clinic visits across 5 classes), and found that tree-based ensemble methods, such as extreme gradient boosting and random forest, consistently outperformed logistic regression, neural networks, and naïve Bayes models—likely due to their capacity to model complex nonlinear interactions in heterogeneous data [23]. Another study within the New York City safety net system developed multiple models to predict acute care usage as both binary and continuous outcomes. Their best-performing model, which predicted the number of acute care days as a continuous variable, successfully identified approximately half of the patients who would go on to have very high acute care use [24].

XSL•FO
RenderX

Our study builds on these approaches in several novel ways. First, we applied a stacking ensemble framework to a multiclass prediction problem, enabling stratification across 4 tiers of inpatient bed days and ED visits. This allows for more granular predictions and targeted interventions, unlike previous work focused solely on binary or continuous outcomes. Second, we introduced custom evaluation metrics derived from confusion matrices (Figure 1) that are directly relevant to population health program planning. Third, we conducted a Monte Carlo–based economic impact analysis, incorporating real-world inpatient cost data to estimate potential cost savings under varying assumptions of reach and benefit. This coupling of predictive modeling with economic simulation offers a practical and policy-relevant contribution to the literature on machine learning for health care resource optimization.

Practical Usage of Ensemble Prediction Models for Future Inpatient Bed Days and ED Visits

Our study predicted LOS and ED usage across 4 tiers, rather than focusing on a specific percentile as is the case in many previous studies [6]. This approach enables tailored interventions based on predicted resource use. The distribution of predictions in the confusion matrix (Tables S4 and S5 in Multimedia Appendix 1), with more predictions in the lower usage tier and fewer in the highest usage tier, suggests that low-cost, scalable interventions (eg, clinical flags, EMR risk prompts, or light-touch monitoring) may be suitable for the lower tier (7-13 inpatient days or 3-4 ED visits) [9,10]. For the middle tier (14-29 inpatient days or 5-9 ED visits), moderately scalable interventions, such as programs involving community nurses or care coordinators, may be effective. Higher-cost, intensive interventions are needed for the highest tier (≥30 inpatient days or ≥10 ED visits), although the scalability is limited.

The new model evaluation metrics we developed address the varying costs of misclassification [25]. Models achieving high correct predictions and low unnecessary predictions enhance program efficiency, while those with more identified users allow interventions to reach more patients, although subsequent recalibration of the intervention may be required downstream. Future health programs using these models should assess patient characteristics and clinical needs at enrollment and during follow-up to ensure appropriate intervention assignment. These metrics may also be adapted for other multiclass problems in health care.

Balancing trade-offs between correct and unnecessary predictions is crucial when selecting the best model. Models with higher correct predictions often had more unnecessary predictions (Tables S4-S6 in Multimedia Appendix 1). Similarly, models with more identified users showed higher unnecessary predictions. This trade-off highlights the need to balance these metrics. Although unnecessary predictions may reduce program efficiency, prioritizing correct predictions and identified users led to greater economic benefits, as shown in our economic impact analyses (Table 2 and Figure S4 in Multimedia Appendix 1). Boosted tree ensemble models, which had higher correct predictions, identified users and unnecessary predictions, and significantly outperformed linear SVM ensemble models.

An important feature of our ensemble models is the tiered distribution of predictions (Tables S4-S7 in Multimedia Appendix 1), with the fewest in the highest tier, followed by the middle, and most in the lower tier. This distribution supports efficient resource allocation: low-cost, scalable interventions can be directed to lower tiers, while high-cost, intensive interventions are reserved for the highest tier—ensuring sustainable deployment of resources.

This stratified output also enables a graduated intervention pathway, starting with risk-appropriate outreach and followed by clinical reassessment to adjust intervention intensity. This flexibility is essential given the modest positive predictive value (13%-14%), even in the highest usage group—a reflection of the complexity and unpredictability of health care use, driven by diverse clinical and social factors.

Nevertheless, our best models identified more than 75% of future high users (≥7 inpatient days), offering valuable opportunities for early engagement. Even if further triage is needed, this early identification is a key step in proactive population health management. Future implementations should incorporate qualitative review or clinical vetting to further optimize targeting and minimize risks of overintervention or alert fatigue.

Implications of Economic Impact Analysis and Parameter Sensitivity Analysis

To our knowledge, this is the first study to conduct an economic impact analysis of predictive models for identifying patients at risk of high health care usage. We selected the best-performing ensemble model for inpatient LOS, leveraging inpatient billing data to assess its real-world potential. The boosted tree ensemble algorithm with logistic regression as its base learner emerged as the dominant model (Table 2 and Figure 3), demonstrating superior performance in both fixed effects and Monte Carlo simulations. Notably, the median simulation outcome for the dominant model exceeded the 75th percentile of other models, indicating that its typical performance surpassed even the best-case scenarios (upper quartile) of the alternatives. This highlights the dominant model's consistency and reliability, despite similar AUROC, accuracy, and evaluation metrics across models.

Findings from the parameter sensitivity analysis provide health care planners with insights into the potential cost savings on different combinations of reach and benefit. Our results show that increasing program reach significantly boosts total benefit, while reducing variability in benefit per patient, especially when more high-cost patients (typically those found in the top cost percentiles) are included. This reflects the Pareto distribution of inpatient costs (Figure S1 in Multimedia Appendix 1), where maximizing program reach is essential for capturing high-cost patients and maximizing the overall net benefit.

While the parameter sensitivity analysis does not explicitly incorporate intervention costs, it serves as a useful planning tool by simulating the financial space available for intervention. For example, in a conservative scenario targeting patients predicted to stay 14-29 days, assuming a 30% cost reduction and 50% reach, projected savings reach SGD $21.0 (US $15.3)

XSL•FO
RenderX

million in a year. This estimate can guide budget planning, allowing programs to allocate resources up to this amount while maintaining a positive return on investment. Future iterations of this analysis could incorporate cost parameters and extend to multiyear projections, enhancing its utility for implementation planning.

Limitations

We acknowledge the potential for selection bias arising from the exclusion of patients with missing variables. Complete case analysis was used because data imputation was not performed, and several of the machine learning algorithms applied in this study do not natively support missing values. Nevertheless, a substantial proportion of the registry was retained: 74.6% (100,500/134,670) of eligible patients were included in training the binary base learners, 77.3% (108,886/140,859) in training the stacking ensemble models, and 80.7% (111,004/137,584) in the validation dataset as detailed in our previous study [11]. Patients excluded due to missing data were more likely to have limited interaction with the health care system (eg, no inpatient, ED, or primary care visits), and their exclusion is unlikely to materially affect model performance for predicting higher levels of usage. However, we acknowledge that missingness may be informative, and future work could explore multiple imputation strategies or algorithms that explicitly handle missing data to further assess the robustness and generalizability of the findings.

A methodological limitation is the potential for logical inconsistencies in the predicted probabilities generated by independently trained binary classifiers used as inputs to the stacking ensemble model. For instance, a patient may receive a higher predicted probability for LOS≥14 days than for LOS≥7 days, which violates logical ordering. While these probabilities were not used directly to assign final classes, serving instead as features for a stacking ensemble meta-learner, such inconsistencies could still affect interpretability and calibration. We did not formally assess the prevalence of these inconsistencies in this study. However, we acknowledge this limitation and plan to explore ordinal-consistent modeling strategies in future work, such as classifier chains or ordinal regression frameworks that preserve monotonicity across outcome thresholds.

Additionally, we did not benchmark against simpler baselines, such as heuristic rules (eg, previous year usage) or native multiclass algorithms. Future work could explore these comparisons to better understand the incremental benefits of ensemble architectures in terms of complexity, predictive performance, and operational interpretability.

Another methodological consideration is the absence of hyperparameter tuning, which may have improved absolute model performance. Our objective in this study was to evaluate relative model performance across ensemble strategies and to develop a transparent and reproducible framework. Default hyperparameters were used to ensure consistency and comparability. We acknowledge that in real-world deployment, targeted hyperparameter tuning would likely be performed to further optimize predictive accuracy, and we identify this as a direction for future work.

Relatedly, we did not perform standard decision curve analysis as our multiclass models output discrete class labels corresponding to stratified intervention tiers rather than risk probabilities used for binary decisions. Future work could explore ordinal or multiclass extensions of decision curve analysis that may better reflect stratified care models and potentially enhance decision support performance.

Additionally, in our economic simulations, we also assumed normally distributed variation in intervention benefit; while this was suitable for benchmarking, we acknowledge that future work could explore log-normal or gamma distributions.

A further consideration is the potential impact of pandemic-related disruptions during the study period, which coincided entirely with the COVID-19 pandemic (2020-2022). As the ensemble models were trained and validated on temporally distinct datasets from this period, unmeasured shifts in disease burden and health care delivery—such as deferred elective care, changes in admission criteria, infection control protocols, ED triage processes, and inpatient discharge practices—may have influenced LOS and ED usage patterns. While a detailed exploration of these pandemic-related dynamics is beyond the scope of this study, we acknowledge that they may have affected model performance and limited generalizability to nonpandemic settings. We intend to validate the models using postpandemic data (eg, 2024 onwards) in future work to assess robustness under more stable health care conditions.

Another important limitation is the real-world variability in health care usage among high users; the best models could correctly assign only about 30% of future users to the appropriate category. This variability, likely influenced by regression to the mean and the inherent complexity of the prediction task, highlights the need for additional program measures, such as downstream assessments of predicted patients.

From a pragmatic perspective, not all high users may respond to interventions, and real-world efficacy is likely to vary depending on clinical or social drivers [6]. Our economic impact analyses assumed average cost reductions across usage tiers to facilitate comparative evaluation of ensemble models, but we acknowledge this simplification may not capture the full heterogeneity of intervention effects. Future work could explore stratified modeling based on clinical or social risk profiles when such data becomes available. However, by predicting varying levels of resource use, our models allow for interventions to target patients who may be more amenable to them [9]. This remains an area requiring further research to pinpoint patients with modifiable trajectories [26]. It has been suggested that prediction models should combine quantitative prediction modeling with qualitative assessment for better case identification [6]. In line with this, we plan to explore the use of large language models to analyze unstructured clinical text and better understand social determinants of health [27], supporting a more tailored and prescriptive approach to patient management.

XSL•FO
RenderX

Conclusions

We used binary classification machine learning algorithms to develop ensemble models predicting future health care usage, focusing on inpatient LOS and ED visits. These models were evaluated using metrics relevant to population health programs. Economic and parameter sensitivity analyses of the best-performing models offered valuable insights for designing effective health initiatives. Our ensemble model could be integrated into a diverse decision-making framework, providing tailored recommendations for patients with predicted high health care usage.

Acknowledgments

The authors declare the use of generative artificial intelligence (GenAI) in the research and writing process. According to the Generative Artificial Intelligence Delegation taxonomy (2025), proofreading and editing tasks were delegated to GenAI tools under full human supervision. The GenAI tool used was ChatGPT-4o (OpenAI). However, responsibility for the final manuscript lies entirely with the authors. GenAI tools are not listed as authors and do not bear responsibility for the final outcomes.

Funding

No external financial support or grants were received from any public, commercial, or not-for-profit entities for the research, authorship, or publication of this article.

Data Availability

The datasets generated and/or analyzed during this study are not publicly available due to Singapore Health Services Cluster Data Policy on data sharing restrictions. Data are available from the Singapore Health Services Diabetes Registry Disease Registry Committee for researchers who meet the criteria for access to confidential data. The criteria include institutional review board approval, data use approval, and a research collaboration agreement. The point of contact for the Singapore Health Services Diabetes Registry Disease Registry Committee is Lee Thong Shuen (email: lee.thong.shuen@singhealth.com.sg).

The underlying code for this study is not publicly available for proprietary reasons but may be made available to qualified researchers on reasonable request from the corresponding author.

Authors' Contributions

JKT: Study design, statistical analyses, model development, data interpretation, data visualization, manuscript drafting, and review.
LQ: Study design, model development, data interpretation, and manuscript review
HYT: Data interpretation and manuscript review.
S-YG: Study design, data interpretation, and manuscript review.
JT: Study design, data interpretation, manuscript drafting, and review.
MA: Data collection, data interpretation, manuscript drafting, and review.
YMB: Study design, data interpretation, manuscript drafting, and review.
JHT: Study design, model development, data interpretation, data visualization, and manuscript review.

Conflicts of Interest

None declared.

Multimedia Appendix 1
Additional tables and figures.
[DOCX File , 14757 KB - medinform_v14i1e77202_app1.docx]

Multimedia Appendix 2
TRIPOD+AI checklist.
[PDF File (Adobe PDF File), 3799 KB - medinform_v14i1e77202_app2.pdf]

References

1. OECD Health Statistics 2023 - OECD. OECD. URL: https://www.oecd.org/health/health-data.htm [accessed 2024-01-19]
2. Parker ED, Lin J, Mahoney T, Ume N, Yang G, Gabbay RA, et al. Economic costs of diabetes in the U.S. in 2022. Diabetes Care 2024;47(1):26-43. [doi: 10.2337/dci23-0085] [Medline: 37909353]

XSL•FO
RenderX

3. MEPs Mobilising for Diabetes Blueprint for Action on Diabetes in the European Union by 2030. MEPs Mobilising for Diabetes. URL: https://www.mepinterestgroupdiabetes.eu/wp-content/uploads/2021/03/MMD-BLUEPRINT-FOR-ACTION-ON-DIABETES.pdf [accessed 2024-09-25]
4. Percentage of spending on mental health, diabetes and ageing versus total healthcare spending in 2018 against amount budgeted for 2019. Ministry of Health Singapore. 2019. URL: https://www.moh.gov.sg/news-highlights/details/percentage-of-spending-on-mental-health-diabetes-and-ageing-versus-total-healthcare-spending-in-2018-against-amount-budgeted-for-2019/ [accessed 2024-09-25]
5. Wammes JJG, van der Wees PJ, Tanke MAC, Westert GP, Jeurissen PPT. Systematic review of high-cost patients' characteristics and healthcare utilisation. BMJ Open 2018 Sep 08;8(9):e023113 [FREE Full text] [doi: 10.1136/bmjopen-2018-023113] [Medline: 30196269]
6. de Ruijter UW, Kaplan ZLR, Bramer WM, Eijkenaar F, Nieboer D, van der Heide A, et al. Prediction models for future high-need high-cost healthcare use: a systematic review. J Gen Intern Med 2022;37(7):1763-1770 [FREE Full text] [doi: 10.1007/s11606-021-07333-z] [Medline: 35018571]
7. Steyerberg EW, Vickers AJ, Cook NR, Gerds T, Gonen M, Obuchowski N, et al. Assessing the performance of prediction models: a framework for traditional and novel measures. Epidemiology 2010;21(1):128-138 [FREE Full text] [doi: 10.1097/EDE.0b013e3181c30fb2] [Medline: 20010215]
8. Steyerberg EW, Vergouwe Y. Towards better clinical prediction models: seven steps for development and an ABCD for validation. Eur Heart J 2014;35(29):1925-1931 [FREE Full text] [doi: 10.1093/eurheartj/ehu207] [Medline: 24898551]
9. Madvig P, Pearl R. Managing the Most Expensive Patients. Harv Bus Rev 2020;5(February). URL: https://hbr.org/2020/01/managing-the-most-expensive-patients [accessed 2020-02-05]
10. Crowley C, Perloff J, Stuck A, Mechanic R. Challenges in predicting future high-cost patients for care management interventions. BMC Health Serv Res 2023;23(1):992 [FREE Full text] [doi: 10.1186/s12913-023-09957-9] [Medline: 37710262]
11. Tan JK, Quan L, Salim NNM, Tan JH, Goh S, Thumboo J, et al. Machine learning-based prediction for high health care utilizers by using a multi-institutional diabetes registry: model training and evaluation. JMIR AI 2024;3:e58463 [FREE Full text] [doi: 10.2196/58463] [Medline: 39418089]
12. Lim DYZ, Chia SY, Abdul Kadir H, Mohamed Salim NN, Bee YM. Establishment of the singhealth diabetes registry. Clin Epidemiol 2021;13:215-223 [FREE Full text] [doi: 10.2147/CLEP.S300663] [Medline: 33762850]
13. Max K, Jed W, Steve W, Andre W, Chris K. caret: Classification and Regression Training. URL: https://cran.r-project.org/web/packages/caret/caret.pdf [accessed 2026-01-17]
14. Zhi-Hua Z. Ensemble Methods: Foundations and Algorithms 1st Ed. Hall/CRC: Chapman; 2012.
15. Max K, Hadley W. Tidymodels: a collection of packages for modeling and machine learning using tidyverse principles. URL: https://www.tidymodels.org/ [accessed 2026-01-17]
16. Moore GF, Audrey S, Barker M, Bond L, Bonell C, Hardeman W, et al. Process evaluation of complex interventions: Medical Research Council guidance. MRC Population Health Science Research Network 2015;350:h1258 [FREE Full text] [doi: 10.1136/bmj.h1258] [Medline: 25791983]
17. Plotly Technologies Inc. Collaborative Data Science. Montreal: Plotly Technologies Inc; 2015.
18. Collins GS, Moons KGM, Dhiman P, Riley RD, Beam AL, Van Calster B, et al. TRIPOD+AI statement: updated guidance for reporting clinical prediction models that use regression or machine learning methods. BMJ 2024;385:e078378 [FREE Full text] [doi: 10.1136/bmj-2023-078378] [Medline: 38626948]
19. Monte-Carlo-Simulations-using-Ensemble-Model-for-Population-Health. Github. URL: https://joshuatankuan.github.io/Monte-Carlo-Simulations-using-Ensemble-Model-for-Population-Health/ [accessed 2026-01-26]
20. Tan JK, Zhang X, Cheng D, Leong IYO, Wong CS, Tey J, et al. Using the johns hopkins ACG case-mix system for population segmentation in a hospital-based adult patient population in singapore. BMJ Open 2023;13(3):e062786 [FREE Full text] [doi: 10.1136/bmjopen-2022-062786] [Medline: 36997258]
21. Ng SH, Rahman N, Ang IYH, Sridharan S, Ramachandran S, Wang DD, et al. Characterization of high healthcare utilizer groups using administrative data from an electronic medical record database. BMC Health Serv Res 2019;19(1):452 [FREE Full text] [doi: 10.1186/s12913-019-4239-2] [Medline: 31277649]
22. Johnson TL, Rinehart DJ, Durfee J, Brewer D, Batal H, Blum J, et al. For many patients who use large amounts of health care services, the need is intense yet temporary. Health Aff (Millwood) 2015;34(8):1312-1319. [doi: 10.1377/hlthaff.2014.1186] [Medline: 26240244]
23. Rahman Y, Dua P. A machine learning framework for predicting healthcare utilization and risk factors. Healthcare Analytics 2025;8:100411. [doi: 10.1016/j.health.2025.100411]
24. Li Z, Gogia S, Tatem K, Cooke C, Singer J, Chokshi D, et al. Developing a Model to Predict High Health Care Utilization Among Patients in a New York City Safety Net System. Med Care 2022;61(2):102-108 [FREE Full text] [doi: 10.1097/MLR.0000000000001807] [Medline: 36472326]
25. Theissler A, Thomas M, Burch M, Gerschner F. ConfusionVis: Comparative evaluation and selection of multi-class classifiers based on confusion matrices. Knowledge-Based Systems 2022;247:108651. [doi: 10.1016/j.knosys.2022.108651]

XSL•FO
RenderX

26. Berkman ND, Chang E, Seibert J, Ali R. Characteristics of High-Need, High-Cost Patients : A "Best-Fit" Framework Synthesis. Ann Intern Med 2022;175(12):1728-1742 [FREE Full text] [doi: 10.7326/M21-4562] [Medline: 36343343]
27. Guevara M, Chen S, Thomas S, Chaunzwa TL, Franco I, Kann BH, et al. Large language models to identify social determinants of health in electronic health records. NPJ Digit Med 2024;7(1):6 [FREE Full text] [doi: 10.1038/s41746-023-00970-0] [Medline: 38200151]

Abbreviations

AUROC: area under the receiver operating characteristic curve
ED: emergency department
HNHC: high-need, high-cost
LOS: length of stay
SDR: Singapore Health Services Diabetes Registry
SVM: support vector machine
TRIPOD+AI: Transparent Reporting of a multivariable prediction model for Individual Prognosis or Diagnosis + Artificial Intelligence

Edited by A Coristine, A Benis; submitted 09.May.2025; peer-reviewed by E Bai, G Lim; comments to author 06.Oct.2025; revised version received 02.Jan.2026; accepted 02.Jan.2026; published 20.Feb.2026.

Please cite as:
Tan JK, Quan L, Tan HY, Goh SY, Thumboo J, Au M, Bee YM, Tan JH
Ensemble Machine Learning Models for Predicting Patients With High Usage: Model Validation and Economic Impact Analysis
JMIR Med Inform 2026;14:e77202
URL: https://medinform.jmir.org/2026/1/e77202
doi:10.2196/77202
PMID:

©Joshua Kuan Tan, Le Quan, Hao Yi Tan, Su-Yen Goh, Julian Thumboo, Marianne Au, Yong Mong Bee, Jen Hong Tan. Originally published in JMIR Medical Informatics (https://medinform.jmir.org), 20.Feb.2026. This is an open-access article distributed under the terms of the Creative Commons Attribution License (https://creativecommons.org/licenses/by/4.0/), which permits unrestricted use, distribution, and reproduction in any medium, provided the original work, first published in JMIR Medical Informatics, is properly cited. The complete bibliographic information, a link to the original publication on https://medinform.jmir.org/, as well as this copyright and license information must be included.

XSL•FO
RenderX

Original Paper

Enhanced Magnetic Resonance Imaging–Based Knee Cartilage Segmentation Using a Swin-UNet Conditional Generative Adversarial Network: Development and Validation Study

Jun Young Park[1*], MD, PhD; Ji-Hoon Nam[2,3,4*], MSc; Shakhboz Abdigapporov[3], MSc; Jong-Keun Kim[5], MD, PhD; Yong-Gon Koh[6], MD; Byung Woo Cho[7], MD, PhD; Hyuck Min Kwon[8], MD, PhD; Kwan Kyu Park[8], MD, PhD; Kyoung-Tak Kang[2,3,4], PhD

[1]Department of Orthopaedic Surgery, Yonsei University College of Medicine, Yongin Severance Hospital, Yongin-si, Gyeonggi-do, Republic of Korea

[2]Department of Mechanical Engineering, Yonsei University, Seoul, Seoul, Republic of Korea

[3]Clevion Co., Ltd., Seoul, Republic of Korea

[4]Skyve R&D LAB, Skyve Co., Ltd., Seoul, Republic of Korea

[5]Department of Orthopaedic Surgery, HeungK Hospital, Seoul, Republic of Korea

[6]Department of Orthopaedic Surgery, Joint Reconstruction Center, Yonsei Sarang Hospital, Seoul, Republic of Korea

[7]Department of Orthopaedic Surgery, Yonsei University College of Medicine, Gangnam Severance Hospital, Seoul, Republic of Korea

[8]Department of Orthopaedic Surgery, Yonsei University College of Medicine, Severance Hospital, Seoul, Republic of Korea

[*]these authors contributed equally

Corresponding Author:
Kyoung-Tak Kang, PhD
Department of Mechanical Engineering
Yonsei University
50 Yonsei-ro
Seodaemun-gu
Seoul, 03722
Republic of Korea
Phone: 82 2 2123 4827
Fax: 82 2 362 2736
Email: tagi1024@gmail.com

Abstract

Background: Accurate segmentation of cartilage from magnetic resonance imaging (MRI) is crucial for the diagnosis and surgical planning of knee osteoarthritis. However, manual segmentation is time-consuming, and conventional computed tomography–based surgical systems are limited by their inability to visualize cartilage.

Objective: This study aimed to develop a clinically targeted deep learning framework, the Swin-UNet conditional generative adversarial network (cGAN), for the automatic segmentation of femoral and tibial cartilage in MRI. We then evaluated its performance against conventional UNet, UNet cGAN, and Swin-UNet baseline models.

Methods: Our dataset comprised 232 knee MRI scans. We conducted quantitative experiments on the proposed Swin-UNet cGAN model and compared the results with those of widely used UNet, UNet cGAN, and Swin-UNet models for femoral and tibial cartilage segmentation, using the Dice similarity coefficient, mean intersection over union, 95th percentile Hausdorff distance, and average symmetric surface distance. All performance metrics were statistically analyzed. In addition, the performance of the Swin-UNet cGAN model was evaluated on an external validation dataset.

Results: The proposed Swin-UNet cGAN achieved the highest mean Dice similarity coefficient and intersection over union scores for both femoral and tibial cartilage segmentation, demonstrating performance statistically comparable to the best-performing baseline (UNet) in the tibia. Regarding distance metrics (average symmetric surface distance and 95th percentile Hausdorff distance), the proposed model significantly outperformed all baselines in the tibia while achieving results comparable to the UNet cGAN in the femur. It also maintained consistently high segmentation performance on both the internal test set and an external validation dataset.

XSL•FO
RenderX

Conclusions: These findings indicate that the proposed Swin-UNet cGAN achieves more accurate knee cartilage segmentation than UNet, UNet cGAN, and Swin-UNet, particularly in terms of boundary accuracy, while maintaining promising generalizability performance across both internal testing and external validation cohorts. This MRI-based deep learning approach addresses critical limitations of computed tomography–based patient-specific instrumentation systems by providing cartilage visualization, potentially improving surgical precision and outcomes in total knee arthroplasty.

(JMIR Med Inform 2026;14:e86155) doi:10.2196/86155

KEYWORDS

cartilage; deep learning; generative adversarial network; knee cartilage segmentation; magnetic resonance imaging; MRI; segmentation; swim-UNet

Introduction

Knee joint osteoarthritis is a progressive degenerative disorder affecting the articular cartilage, underlying subchondral bone, and surrounding periarticular tissues. It presents with pain, stiffness, and reduced mobility, ranking among the leading causes of disability in adults [1,2]. Timely identification and precise quantification of alterations in cartilage structure and composition are essential for optimal management of knee osteoarthritis [3].

An extensive array of imaging modalities is used in clinical and research settings to deepen understanding of osteoarthritis pathogenesis [4]. Magnetic resonance imaging (MRI) offers superior visualization of cartilage structure and is the modality of choice for assessing cartilage damage and morphological alterations. In addition, MRI provides a noninvasive, radiation-free examination and excels at evaluating overall knee pathology, owing to its superior soft-tissue contrast relative to X-ray and computed tomography (CT) [5].

Quantitative analysis of cartilage morphology depends on accurate medical-image segmentation and visualization of the articular cartilage, with subsequent 3D reconstruction enabling measurement of thickness, volume, and surface area [6]. However, this process is complex and time-consuming, as each image slice must be segmented individually using manual segmentation software [7]. In recent years, deep learning (DL)–based artificial intelligence models, particularly convolutional neural network (CNN) architectures, have been adopted as a cutting-edge solution for knee cartilage segmentation and osteoarthritis diagnosis [8]. CNN-based models have shown strong potential for accurately segmenting cartilage and bone across imaging modalities [9].

Toit et al [9] studied a modified UNet algorithm to automatically segment the femoral articular cartilage in 3D ultrasound images of healthy volunteer knees. Wang et al [10] proposed a novel network, Patch Attention UNet, to enhance knee cartilage segmentation by applying an attention mechanism; it was evaluated on multiple datasets. Recently, generative adversarial networks (GANs) have captivated the research community, with several studies demonstrating that GAN-generated delineations can match manual tracings and materially enhance segmentation performance [11]. Gaj et al [11] developed a conditional generative adversarial network (cGAN) model built on the UNet architecture that delivers fully automated, highly accurate segmentation of knee cartilage and meniscus.

Therefore, our objective was to develop a Swin-UNet cGAN, a tailored adversarial framework merging a hierarchical Swin-UNet generator with a pixel-wise CNN discriminator for 2D segmentation of knee joint cartilage, and to evaluate its performance on both an internal test set and an external validation dataset. We compared the segmentation performance of our proposed model with traditional UNet, UNet cGAN, and Swin-UNet models using the Dice similarity coefficient (DSC), mean Intersection over Union (IoU), average symmetric surface distance (ASSD), and 95th percentile Hausdorff distance (HD95).

We hypothesized that the Swin-UNet cGAN model would achieve the highest performance in segmenting femoral and tibial cartilage.

Methods

Ethical Considerations

This study was approved by the Institutional Review Board (IRB) of Yonsei Sarang Hospital (IRB number 2025-11-002) and Yongin Severance Hospital (IRB number 9-2025-0189). The requirement for informed consent was waived by the IRB owing to the retrospective nature of this study and the use of deidentified imaging data. All procedures involving human participants were conducted in accordance with institutional ethical standards and approved by the relevant IRBs. All patient data were fully anonymized prior to analysis, with no possibility of individual patient identification. Patients received no compensation for the use of their deidentified MRI data in this research. No identifiable patient information or images are included in this manuscript or its supplementary materials.

Dataset

The internal dataset was collected from Yonsei Sarang Hospital and consisted of 232 MRI scans from patients with knee osteoarthritis scheduled for patient-specific instrument (PSI)–guided total knee arthroplasty (TKA) from October 2023 through December 2024. All internal examinations were performed on a 3.0 T system (uMR 770; United Imaging Healthcare) using a 3D high-resolution T2*-weighted gradient-echo sequence (repetition time [TR]/echo time [TE]=17/9.3 ms; flip angle=25°), with a 20-cm field of view and 1-mm thick sagittal slices oriented relative to the posterior femoral condyles. This imaging protocol is commonly used when fabricating PSI [12]. Each scan comprised 90-110 slices. A medical imaging specialist manually segmented cartilage on every slice. The 232 scans were randomly split at the case level:

XSL•FO
RenderX

a total of 162 (70%) scans were assigned to the training set, 35 (15%) scans to the validation set, and 35 (15%) scans to the testing set. For model development, the original 512 × 512 pixel images and their corresponding masks were down-sampled to 224 × 224 pixels.

For external validation, an independent dataset was obtained from Yongin Severance Hospital, consisting of 25 consecutive PSI-guided TKA cases. All external validation knee MRI examinations were performed on a 3.0 T system (SIGNA Premier; GE Healthcare) with a 20-cm field of view and 2-mm thick sagittal slices oriented relative to the posterior femoral condyles. TR and TE were automatically adjusted by the scanner to optimize image quality, with nominal target values of TR/TE=30/11 ms.

Swin-UNet–Based cGAN Model

GAN-based networks usually consist of 2 parts: a generator model that produces synthetic samples from noise with a prior distribution and a discriminator model that acts as a binary classifier to differentiate real data from generated synthetic samples. In this study, the widely used cGAN [13] was adopted for MRI knee bone and cartilage segmentation. In this work, the generator is a mapping function from a source domain image into a segmentation mask, rather than mapping noise to real data as in the original GAN model, and predicts a manual segmentation mask. The cGAN-based model uses the discriminator to judge the quality of segmentation given the source image from the dataset. The binary classifier distinguishes the differences between the manual segmentation mask and the synthetic segmentation mask generated by the generator model, designating them as real and fake samples, respectively. This study introduces a Swin-UNet–based cGAN for knee MRI segmentation [14] to create synthetic masks and a PatchGAN discriminator [15] that learns discriminative features to distinguish generated masks from manual annotations.

Generator of the Swin-UNet–Based cGAN Model

The generator of the knee cartilage segmentation model is a hierarchical Swin Transformer architecture integrated into a UNet-like encoder-decoder structure, as shown in Figure 1. The input image size and patch size are set as 224 × 224 and 4, respectively. The C-dimensional (C=32) tokenized inputs with a resolution of H/4 × W/4 are fed into 2 consecutive Swin Transformer blocks (using a 7 × 7 attention window) to perform representation learning, and the feature dimension and resolution remain unchanged. The patch merging layer reduces the number of tokens (down-samples by 2×) and increases the feature dimension to 2× the original dimension. The encoder repeats this procedure 3 times. The patch merging layer in the encoder divides the input patches into 4 parts and concatenates them together. The feature resolution is down-sampled by 2×, and because the concatenate operation increases the feature dimension by 4×, a linear layer is applied on the concatenated features to unify the feature dimension to 2× the original dimension. The bottleneck consists of 2 Swin Transformer blocks and is used to learn deep feature representation. In the bottleneck, the feature resolution and dimension remain unchanged.

XSL•FO
RenderX

Figure 1. Overall architecture of the proposed network.

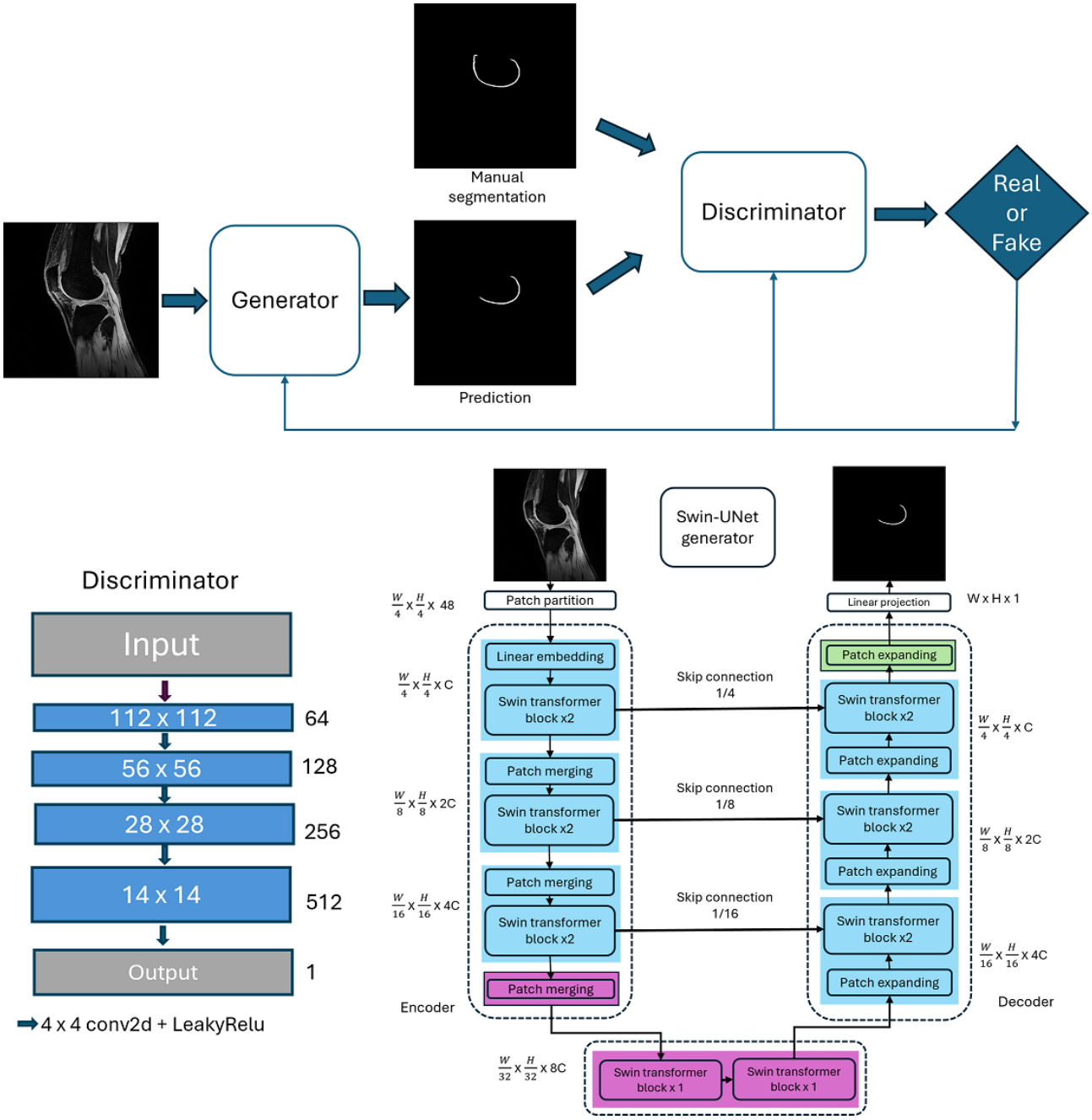

The decoder has a symmetrical architecture to the encoder, based on the Swin Transformer blocks. The patch expanding layer in the decoder is used to up-sample the extracted deep features. The patch expanding layer reshapes the feature maps of adjacent dimensions into higher-resolution feature maps, up-sampling by 2×, and reduces the feature dimension to half of the original dimension.

Skip connections are used to fuse the multiscale features from the encoder with the up-sampled features. Both shallow and deep features are concatenated together to reduce the loss of spatial information caused by down-sampling.

Discriminator of the Swin-UNet–Based cGAN Model

The discriminator of the proposed model is a PixelGAN-style convolutional binary classifier of “fake” predicted segmented masks and “real” manually segmented masks. The network input has 2 channels (image + mask) and spatial size H × W. The discriminator network architecture consists of four 4 × 4 convolutional layers with LeakyRelu activation function. Normalization is applied to stabilize the training samples, and Dropout2d prevents the discriminator from overpowering the generator in the early stages and encourages robust feature learning. The final layer is a 4 × 4 stride convolution, which produces a grid of real or fake logits. With 224 × 224 input, the discriminator produces a 13 × 13 authenticity map.

In the proposed model, a linearly increasing adversarial weight schedule was used, with λ starting at 0 after pretraining and gradually increasing to 1×10^{-4} over the GAN training epochs. This prevented gradient shocks and was selected as the most stable λ based on validation stability. Prior to selecting λ, larger values of 5×10^{-4} and 1×10^{-3} were empirically explored;

XSL•FO
RenderX

although these values increased the adversarial influence, they led to unstable training.

Loss Function of the Swin-UNet–Based cGAN Model

The proposed knee cartilage segmentation model uses a combination of supervised segmentation loss and adversarial losses. If segmentation performance mainly relies on adversarial loss, the output segmentation mask might not always share the same global structure as the manually segmented mask [16-19]. For traditional segmentation losses, the DSC and cross-entropy can be applied as loss functions for the generator network to improve performance by decreasing the distance between generated "fake" and manually segmented "real" masks. The proposed model uses multiple loss functions during training because the training experiments were conducted in multiple stages: generator model pretraining for segmentation mask predictions and overall training of the developed Swin-UNet cGAN–based knee segmentation model. During both the pretraining and overall model training phases, binary cross-entropy (BCE) with logits loss is adopted as the primary segmentation loss.

where yi is the ground truth mask of the real samples and is the mask predicted by the generator network. For adversarial loss, a hinge loss formulation is applied to improve training stability.

The discriminator network is trained using hinge loss to improve classification of real and fake sample data. For real mask samples, the discriminator is set to output values greater than 1; for fake samples, output are less than –1. The overall loss is computed as the mean of the 2 hinge components. The overall discriminator loss can be written as follows.

In the proposed model training, a gradient penalty was implemented to stabilize training by penalizing deviations in gradient norm from 1. Finally, the generator's overall loss is composed of the total segmentation loss and a weighted adversarial loss.

For the proposed model training, the Adam optimizer was used with a learning rate of 1×10^{-4} for the transformer-based generator and 5×10^{-5} for the patch-based discriminator networks, with a weight decay of 1×10^{-5}. To maximize the prediction results of the segmentation model, the generator was first pretrained for 30 epochs using only the segmentation loss (BCE with logits loss). After pretraining, adversarial training was performed for 40 epochs using a combination of segmentation and adversarial losses. During overall model training, adversarial weight λ_{adv} increased linearly until it reached the final value of 1×10^{-4}. Training of all experimented models was performed using an NVIDIA GeForce RTX 4090 24 GB graphics processing unit.

Evaluation Metrics

The performance of the knee cartilage segmentation models was compared with that of the Swin-UNet segmentation model, the UNet-based GAN segmentation model [11], and the traditional CNN-based UNet model using the DSC, IoU, HD95, and ASSD. The DSC represent the overlap between the predicted and ground truth masks. A DSC of 1 (or 100%) represents perfect overlap, whereas a value of 0 indicates no overlap between the ground truth and predicted masks.

The mean IoU metric is calculated by dividing the area of intersection of the predicted and ground truth masks by the area of the union of 2 masks.

The Hausdorff distance (HD) measures the extent to which 2 subsets of a metric space differ. Because HD is sensitive to outliers, the 95th percentile (HD95) is frequently used instead. By considering the 95th percentile of distances, HD95 provides a more robust measure of boundary conformity, effectively ignoring the most extreme 5% of outliers.

where A and B denote the sets of boundary points for the predicted and ground truth segmentations, respectively; ||a – b|| represents the Euclidean distance between points a and b; and P_{95} denotes the 95th percentile of the accumulated distances.

The ASSD measures the average distance between boundary points, making it highly sensitive to the precise alignment of contours.

where |A| and |B| denote the cardinality of the boundary sets A and B, respectively. All surface metrics (ASSD and HD95) were computed on 224 × 224 masks, the same resolution used for training and inference. Distances were converted to millimeters using the effective in-plane spacing of 0.89 mm/pixel.

Reliability of Manual Segmentation

For consistent and reliable manual labeling of our dataset, DSC and IoU metrics were calculated for intra- and interrater comparisons across femur and tibia segmentations. Two experienced manual data labeling experts, rater A and rater B, segmented the entire dataset. For reliability assessment, MRI data from 30 randomly selected patients were labeled a second time by both raters at a different time of day than the first labeling session. For the final training and test datasets, segmentation masks created by a single expert rater were used for each slice.

XSL•FO
RenderX

Ablation Study

To empirically validate the architectural decisions and hyperparameter configurations of the proposed Swin-UNet cGAN framework, a comprehensive ablation study was designed focusing on 3 critical components. First, model sensitivity to the magnitude of the adversarial loss was evaluated by testing varying adversarial weights ranging from 0.0001 to 0.1 to determine the optimal balance between pixel-wise segmentation accuracy and adversarial shape refinement. Second, to assess the impact of training stability, a constant weight schedule was compared against a linear warm-up strategy, in which adversarial weights increased linearly from zero to the target value over the training epochs. Third, to identify the most effective objective function for segmenting fine cartilage structures within the adversarial framework, standard BCE loss alone was compared with a hybrid objective combining BCE and Dice loss.

Statistical Analysis

Statistical analyses were performed using R (version 4.3.1; R Foundation for Statistical Computing). For multiple comparisons of the results, the normality of the data distribution was first assessed. Data following a normal distribution were analyzed using repeated measures ANOVA, whereas nonnormally distributed data were analyzed using the Friedman test. Post hoc comparisons were conducted using the Bonferroni correction. Inter- and intrarater reliability were evaluated using the DSC. A *P* value of less than .05 was considered statistically significant.

Results

Cartilage Segmentation Results

DSC, mean IoU, ASSD, and HD95 results for femoral and tibial cartilage segmentation are summarized in Table 1.

Table 1. Knee cartilage segmentation results.

Structure and metric	Model, mean (SD)				*P* value
	UNet	UNet cGAN[a]	Swin-UNet	Proposed (Swin-UNet cGAN)	
Femur					<.001
DSC[b] (%)	78.6 (3.1)[c]	80.2 (1.2)[d]	76.5 (4.5)[e]	82 (1.5)[f]	
IoU[g] (%)	69.4 (3.9)[c]	69.9 (1.8)[c]	65.3 (5.2)[e]	71.9 (2.1)[d]	
ASSD[h] (mm)	1.34 (0.32)[e]	0.24 (0.05)[d]	0.58 (0.17)[c]	0.22 (0.08)[d]	
HD95[i] (mm)	5.14 (1.64)[e]	1.25 (0.21)[d]	2.94 (0.96)[c]	1.31 (0.27)[d]	
Tibia					<.001
DSC (%)	79.2 (6.3)[cd]	80 (1.8)[c]	70.5 (8.6)[e]	81 (1.7)[d]	
IoU (%)	69.7 (7.3)[cd]	70.1 (2.5)[c]	59.5 (8.5)[e]	71.1 (2.1)[d]	
ASSD (mm)	1.05 (1.46)[e]	0.32 (0.27)[d]	0.83 (0.83)[c]	0.23 (0.15)[f]	
HD95 (mm)	3.62 (5.62)[e]	1.46 (1.13)[d]	3.33 (2.89)[c]	1.25 (0.53)[f]	

[a]cGAN: conditional generative adversarial network.

[b]DSC: Dice similarity coefficient.

[c-f]Footnotes c, d, e, and f indicate significant differences between models based on post hoc pairwise comparisons (*P*<.05). Superscript letters follow the journal style (alphabetical order by first appearance) and do not represent a rank order of performance. Means sharing the same footnote are not significantly different.

[g]IoU: intersection over union.

[h]ASSD: average symmetric surface distance.

[i]HD95: 95th percentile Hausdorff distance.

For femoral cartilage, the baseline UNet achieved a mean DSC of 78.6% (SD 3.1%) and an IoU of 69.4% (SD 3.9%), with an ASSD of 1.34 (SD 0.32) mm and an HD95 of 5.14 (SD 1.64) mm. Adding adversarial training in UNet cGAN slightly improved overlap (DSC 80.2%, SD 1.2%; IoU 69.9%, SD 1.8%; *P*<.001 vs UNet) and markedly reduced surface errors (ASSD 0.24, SD 0.05 mm; HD95 1.25, SD 0.21 mm; *P*<.001 vs UNet). Swin-UNet without adversarial training underperformed both UNet and UNet cGAN in overlap metrics (DSC 76.5%, SD 4.5%; IoU 65.3%, SD 5.2%) and showed only intermediate surface accuracy (ASSD 0.58, SD 0.17 mm; HD95 2.94, SD 0.96 mm). The proposed Swin-UNet cGAN achieved the best femoral cartilage segmentation, with a DSC of 82% (1.5%) and an IoU of 71.9% (SD 2.1%; *P*<.001 vs all other models), and significantly lower ASSD and HD95 than UNet and Swin-UNet (*P*<.001), while maintaining surface accuracy comparable to UNet cGAN.

For tibial cartilage, the baseline UNet yielded a DSC of 79.2% (SD 6.3%) and an IoU of 69.7% (SD 7.3%), with an ASSD of 1.05 (SD 1.46) mm and an HD95 of 3.62 (SD 5.62) mm. UNet cGAN preserved similar overlap (DSC 80%, SD 1.8%; IoU 70.1%, SD 2.5%) but substantially reduced surface errors (ASSD 0.32, SD 0.27 mm; HD95 1.46, SD 1.13 mm). Swin-UNet again

XSL•FO
RenderX

showed the weakest performance (DSC 70.5%, SD 8.6%; IoU 59.5%, SD 8.5%; ASSD 0.83, SD 0.83 mm; HD95 3.33, SD 2.89 mm). The proposed Swin-UNet cGAN yielded the highest overall tibial performance, achieving a DSC of 81% (SD 1.7%) and an IoU of 71.1% (SD 2.1%). While it showed significantly higher overlap than both Swin-UNet and UNet cGAN (P<.001), the difference compared with the standard UNet was not statistically significant. Importantly, it yielded the lowest ASSD (0.23, SD 0.15 mm) and HD95 (1.25, SD 0.53 mm) among all models (P<.001 vs all baselines). Taken together, the progression from UNet to UNet cGAN, Swin-UNet, and Swin-UNet cGAN effectively serves as an ablation series that disentangles the contributions of adversarial training and the Swin-Transformer backbone.

The proposed Swin-UNet cGAN achieved highly efficient inference performance. On an NVIDIA GeForce RTX 4090, the average inference time was 16.9 ms per 2D slice, culminating in a total processing time of 1.68 seconds per patient volume. This corresponds to a throughput of approximately 59 slices per second, demonstrating the model's suitability for near-real-time clinical workflows.

Qualitative Comparison of Segmentation Outputs

Figure 2 illustrates qualitative segmentation outputs of the models on unseen test data. The rows correspond to the femur, tibia, and overlaps (segmentation masks overlaid on the input MRI), respectively. The columns display the Input image, ground truth, and predictions from UNet, UNet cGAN, Swin-UNet, and our proposed Swin-UNet cGAN (Ours). As shown in the "Overlaps" row, the proposed model produces the most visually accurate segmentation for both bone and cartilage compared with the baseline models.

Figure 2. Qualitative comparison results of our proposed model and baseline models on the knee cartilage segmentation dataset.

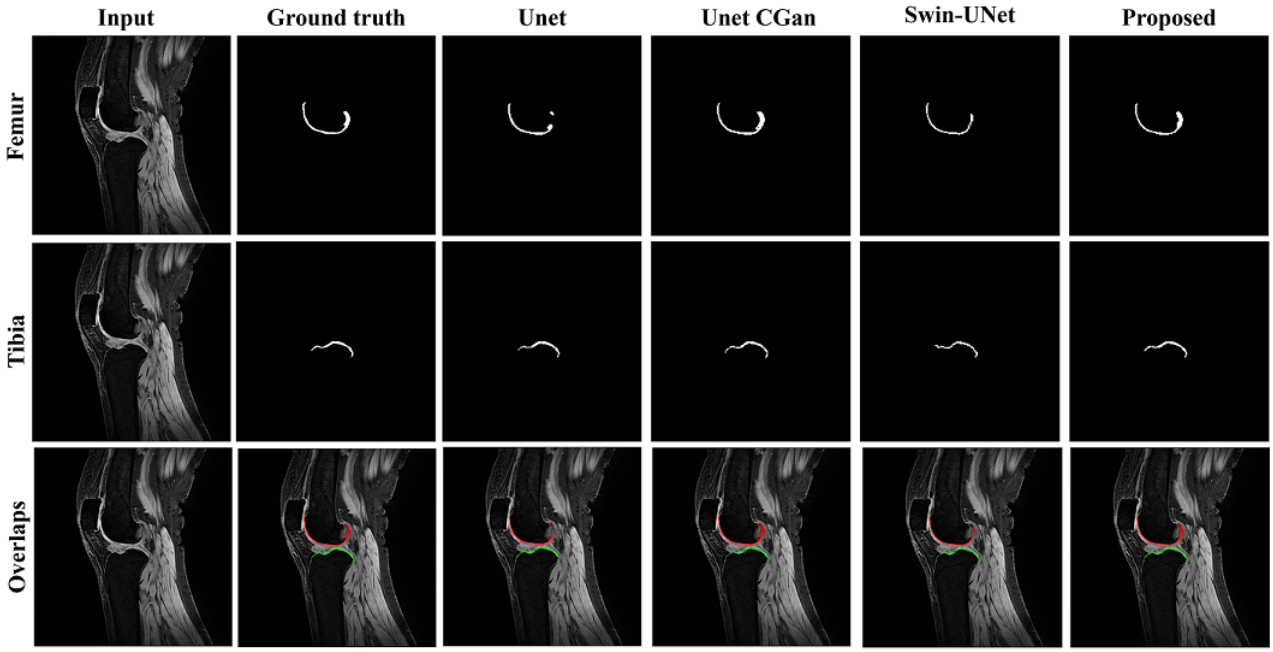

Reliability of Manual Segmentation

Inter- and intrarater agreement calculations for DSC and IoU scores comparing overlap between labeled masks showed high reliability on the original dataset. For intrarater agreement, DSCs for rater 1 and rater 2 averaged 98.9% and 99%, respectively, across femur and tibia. The IoU scores also were high at 98% and 98.3%, demonstrating excellent internal consistency for labeling MRI data. For interrater agreement, the DSC was 95.5% and the mean IoU was 91.9%, indicating greater than 90% agreement between the 2 raters.

External Validation

Quantitative evaluation results on the external validation dataset are summarized. The proposed model demonstrated consistent segmentation performance across both femoral and tibial structures. For the femur, the model achieved a DSC of 73.1% (SD 6.9%) and an IoU of 65% (SD 6.9%). In terms of boundary delineation accuracy, ASSD was 1.30 (SD 0.70) mm and the HD95 was 5.91 (SD 2.93) mm. For the tibia, the model yielded a DSC of 69.7% (SD 7.4%) and an IoU of 62.6% (SD 7.2%). The distance-based metrics showed similar precision to the femur, with an ASSD of 2.16 (SD 0.94) mm and an HD95 of 7.18 (SD 2.64) mm.

Ablation Study on Model Component

A comprehensive ablation study was conducted to optimize the Swin-UNet cGAN configuration, as summarized in Table 2. First, regarding the adversarial weight, a value of 0.0001 yielded the best performance, whereas increasing the weight led to instability and performance degradation. Second, the linear warm-up strategy outperformed the constant schedule, improving tibial metrics and training stability. Although femoral surface errors were marginally higher with warm-up, this trade-off was negligible given the overall gains. Finally, BCE loss alone outperformed the combined BCE + Dice loss, likely because the discriminator sufficiently enforces global shape constraints, making the additional geometric guidance from Dice loss redundant.

XSL•FO
RenderX

Table 2. Ablation study results of the proposed Swin-UNet conditional generative adversarial network framework analyzing the impact of adversarial weight, scheduling strategies, and segmentation loss functions on segmentation performance.

Component and configuration	Femoral cartilage, mean (SD)				Tibial cartilage, mean (SD)			
	DSC[a] (%)	IoU[b] (%)	ASSD[c] (mm)	HD95[d] (mm)	DSC (%)	IoU (%)	ASSD (mm)	HD95 (mm)
Adversarial weight								
0.0001	81.67 (1.3)	71.52 (1.9)	0.21 (0.05)	1.25 (0.2)	80.55 (1.9)	70.62 (2.3)	0.27 (0.2)	1.35 (0.75)
0.001	80.01 (3.06)	69.58 (3.4)	0.24 (0.05)	1.30 (0.22)	78.63 (2.05)	68.47 (2.5)	0.38 (0.26)	1.64 (0.99)
0.01	76.75 (2.5)	65.53 (3.03)	0.3 (0.05)	1.41 (0.2)	69.61 (3.3)	58.25 (3.8)	0.83 (0.32)	2.9 (1.01)
0.1	55.48 (2.6)	43.02 (2.3)	2.21 (0.53)	3.25 (1.22)	42.92 (3.14)	30.6 (2.8)	3.51 (1.03)	9.79 (3.43)
Scheduling								
Constant	81.67 (1.3)	71.52 (1.9)	0.21 (0.05)	1.25 (0.2)	80.55 (1.9)	70.62 (2.3)	0.27 (0.2)	1.35 (0.75)
Warm-up	82 (1.5)	71.9 (2.1)	0.22 (0.08)	1.31 (0.27)	81 (1.7)	71.1 (2.1)	0.23 (0.15)	1.25 (0.53)
Segmentation loss								
BCE[e]	82 (1.5)	71.9 (2.1)	0.22 (0.08)	1.31 (0.27)	81 (1.7)	71.1 (2.1)	0.23 (0.15)	1.25 (0.53)
BCE + Dice	81.28 (1.5	70.88 (2.2)	0.27 (0.04)	1.43 (0.2)	79.17 (2.28)	68.84 (2.8)	0.39 (0.32)	1.73 (1.3)

[a]DSC: Dice similarity coefficient.

[b]IoU: intersection over union.

[c]ASSD: average symmetric surface distance.

[d]HD95: 95th percentile Hausdorff distance.

[e]BCE: binary cross-entropy.

Discussion

The most important finding of this study is that the proposed Swin-UNet cGAN model provided overall strong knee cartilage segmentation compared with the baseline UNet, UNet cGAN, and Swin-UNet models. Specifically, our model achieved higher DSC and IoU while maintaining tibial mask overlap comparable to UNet, and demonstrated markedly lower ASSD and HD95 while maintaining femoral surface accuracy comparable to UNet cGAN. These findings confirm our hypothesis that the Swin-UNet cGAN model achieves the highest performance in segmenting femoral and tibial cartilage.

Our results demonstrate that combining hierarchical Swin self-attention with adversarial refinement effectively captures the fine-grained pixel information needed for segmentation of knee cartilage. By embedding the Swin-UNet generator into a cGAN framework, we achieve superior cartilage delineation: the hierarchical self-attention mechanism—leveraging windowed self-attention rather than relying solely on skip connections—accurately traces cartilage boundaries and anatomically curved regions. Moreover, the Swin transformer backbone constructs a multiscale feature hierarchy through patch merging and expansion, enabling the network to integrate both detailed structural cues and broader contextual information more effectively than CNN-based encoders such as UNet.

For femoral cartilage, the proposed Swin-UNet cGAN model showed a statistically significant improvement over all baseline models, including UNet, UNet cGAN, and Swin-UNet, with higher DSC and IoU and markedly lower ASSD and HD95 (P<.05), while maintaining comparable surface accuracy to UNet-cGAN. Notably, for tibial cartilage, UNet-cGAN showed a statistically significant improvement over plain UNet, whereas the difference between the proposed Swin-UNet cGAN and UNet, although numerically larger, did not reach statistical significance. This finding is likely related to the relatively large intercase variability of the UNet baseline and the limited sample size, which reduce statistical power to detect small additional gains. Nevertheless, the proposed model consistently achieved the highest mean performance and the lowest ASSD and HD95, indicating the best overall balance between volumetric overlap and surface accuracy. From a clinical perspective, MRI-based PSI relies on accurate 3D surface reconstruction rather than volumetric overlap alone. Therefore, the substantial reductions in ASSD and HD95 achieved by the proposed Swin-UNet cGAN are particularly meaningful, as they indicate more precise cartilage boundaries that are directly relevant for the design and fit of PSI cutting guides.

An interesting finding of this study is that the plain Swin-UNet achieved lower DSC and IoU than UNet for both femoral and tibial cartilage. This may be explained by the inherent structural advantages of convolutional architectures such as UNet, which are highly effective at extracting local image features and can be trained stably even with relatively small datasets. In contrast, transformer-based architectures such as Swin-UNet are designed to capture long-range global context but typically require large-scale training data to fully learn these relationships. Under the limited knee MRI dataset used in this study, plain Swin-UNet appears to have suffered from overfitting and unstable convergence, resulting in lower performance (76.5%) than UNet (79.2%).

XSL•FO
RenderX

In this context, the effectiveness of the proposed Swin-UNet cGAN becomes more evident. As shown in Table 1, although the standalone Swin-UNet performed poorly, its performance markedly improved to 82% when used as the generator within a cGAN framework, surpassing that of UNet (79.2%). This suggests that adversarial learning, through the discriminator, imposes strong anatomical shape constraints on the generator, thereby compensating for the data dependency of the transformer architecture and enabling more accurate cartilage segmentation.

The disproportionate improvement in surface metrics (ASSD and HD95) compared with overlap metrics (DSC and IoU) can be attributed to the fundamental differences in their sensitivity. While DSC and IoU measure volumetric overlap and are relatively insensitive to minor boundary fluctuations, distance-based metrics such as ASSD and HD95 directly quantify contour delineation precision. Adversarial training in the proposed framework explicitly optimizes boundary realism through the discriminator, thereby yielding substantial gains in boundary precision even when volumetric improvements appear modest.

To benchmark our method against the current state of the art, we evaluated nnUNet on the same dataset (Table S1 in Multimedia Appendix 1). While nnUNet provided competitive volumetric overlap, the Swin-UNet cGAN achieved statistically significant improvements in both DSC (P=.02) and IoU (P=.04). Crucially, nnUNet struggled with boundary precision in severe osteoarthritis cases, yielding high HD95 values (2.55 mm and 2.75 mm for femur and tibia, respectively). In contrast, the proposed model markedly reduced surface errors, achieving HD95 values of 1.31 mm and 1.25 mm (P<.001) and significantly lower ASSD (P<.001). This demonstrates that the adversarial framework offers superior robustness in capturing the fine, irregular boundaries of degenerated cartilage compared with the self-configuring UNet approach.

Previous research by Chen et al [20] demonstrated that using Segmentation of Knee Images 2010 (SKI10) data, their model achieved a 1% to 2% DSC improvement over nnUNet, with results of 89% for femur cartilage and 88% for tibia cartilage. Guo et al [21] created a dataset of 700 MRI scans by pooling data from Osteoarthritis Initiative (OAI; n=200), fastMRI (n=175), SKI10 (n=100), and an internal hospital database (n=225). They trained 4 distinct DL models—UNet, UNet++, residual UNet (ResUNet), and transformer UNet (TransUNet)—on this dataset with corresponding labeled cartilage. Among these, TransUNet showed superior performance, achieving DSCs of 82.3% for femur cartilage and 80.3% for tibia cartilage. Further innovation came from Gaj et al [11], who developed a DL model for cartilage and meniscus segmentation by integrating a conditional GAN with UNet. This approach led to notable performance improvements, with femur cartilage segmentation increasing from 84.2% to 89.7% (a greater than 5% gain) compared with traditional UNet. For tibia cartilage, the method increased medial cartilage segmentation from 77% to 86.1% and lateral cartilage from 86.2% to 91.8%, using OAI data. Gaj et al's [11] work clearly illustrates that cGANs can significantly enhance the capabilities of established models like UNet. A quantitative benchmarking table summarizing the datasets, methods, and metrics of these existing studies is presented in Table 3.

XSL•FO
RenderX

Table 3. Comparison of segmentation performance with previous methods.

Study (year) and method	Dataset	Performance
Liu et al [22] (2019)		
SUSAN	SKI10[a] (n=50) and internal (n=120)	• Femur (DSC[b]=81%; ASSD[c]=0.65 mm) • Tibia (DSC=75%; ASSD=0.73 mm)
Gaj et al [11] (2020)		
UNet cGAN[d]	OAI[e] (n=176)	• Femur (DSC=89.7%) • Tibia (DSC=91.8%)
Chen et al [20] (2022)		
3D DNN[f] with adversarial loss	SKI10 (n=100)	• Femur (DSC=89%) • Tibia (DSC=88%)
Guo et al [21] (2024)		
TransUNet[g]	OAI (n=200), fastMRI (n=175), SKI10 (n=100), and internal (n=225)	• Femur (DSC=82.3%) • Tibia (DSC=80.3%)
Wang et al [10] (2025)		
PA-UNet[h] (2D)	OAI-ZIB[i] (n=507)	• Femur (DSC=88.8%; HD95[j]=9.1 mm) • Tibia (DSC=82.7%; HD95=11.7 mm)
PA-UNet[h] (2D)	SKI10 (n=100)	• Femur (DSC=78.2%; HD95=16.4 mm) • Tibia (DSC=71.6%; HD95=18.7 mm)
Proposed framework		
Swin-UNet cGAN	Internal (n=232)	• Femur (DSC=82%; ASSD=0.22 mm; HD95=1.31 mm) • Tibia (DSC=81%; ASSD=0.23 mm; HD95=1.25 mm)

[a]SKI10: Segmentation of Knee Images 2010.

[b]DSC: Dice similarity coefficient.

[c]ASSD: average symmetric surface distance.

[d]cGAN: conditional generative adversarial network.

[e]OAI: Osteoarthritis Initiative.

[f]DNN: deep neural network.

[g]TransUNet: transformer UNet.

[h]PA-UNet: patch attention UNet.

[i]OAI-ZIB: Osteoarthritis Initiative–Zuse Institute Berlin.

[j]HD95: 95th percentile Hausdorff distance.

Beyond spatial overlap assessed by DSC, evaluating boundary precision is crucial for clinical applications such as PSI. Liu et al [22] reported ASSD values of 0.65 mm and 0.73 mm for femoral and tibial cartilage, respectively, using their SUSAN framework. Most recently, Wang et al [10] applied a patch attention UNet (PA-UNet) to the Osteoarthritis Initiative–Zuse Institute Berlin (OAI-ZIB) and SKI10 datasets. Although they achieved competitive DSCs, they reported HD values ranging from 9.1 mm to 18.7 mm, indicating potential challenges in handling outlier boundary pixels.

In this study, the proposed Swin-UNet cGAN demonstrated high surface accuracy, achieving ASSD values of 0.22 mm and 0.23 mm and HD95 values of 1.31 mm and 1.25 mm for femoral and tibial cartilage, respectively. Although direct quantitative comparison is challenging due to differences in datasets, these low error rates suggest that integrating the Swin Transformer with adversarial learning effectively refines segmentation boundaries and may offer superior precision for clinical workflows.

A common limitation observed in prior studies is the use of mixed datasets that combine MRI scans from both healthy individuals and patients without explicitly accounting for osteoarthritis progression. Because knee MRI segmentation is most frequently applied in the context of arthroplasty, we trained our DL model using MRI data from patients diagnosed with Kellgren-Lawrence Grades 3-4 who were already scheduled for TKA. This targeted methodology ensures that our model's findings are highly relevant and directly applicable to real-world clinical scenarios, particularly for patients with advanced osteoarthritis, for whom accurate segmentation is critical for surgical planning and improved patient outcomes.

In addition, a recently published study demonstrated that, compared with training on mixed datasets containing both

XSL•FO
RenderX

healthy participants and patients, training primarily on patient data reduced femoral cartilage DSC from 88.8% to 78.2% and tibial cartilage DSC from 82.7% to 71.6% [10].

In terms of clinical relevance, our results are expected to bring significant advancements not only in quantitative diagnostics during knee arthroscopy but also in computer-assisted surgery, including robotic-assisted TKA. Most contemporary robotic‐assisted procedures are predicated almost entirely on image‐based workflows using CT [23]. However, the patient-specific model is generated exclusively from CT data and includes only the bony anatomy; thus, all registration landmarks must be acquired directly on bone during robot-assisted TKA. Intraoperatively, this requirement necessitates a sharp probe to penetrate the overlying cartilage until the underlying bone surface is reached, ensuring accurate alignment. However, an MRI-derived model inherently preserves the cartilage in its segmentation, facilitating a more straightforward and intuitive registration process.

The clinical impact of incorporating cartilage information has been quantified in several comparative studies [24,25]. Additionally, recent meta-analyses have confirmed that MRI-based PSI demonstrates fewer alignment outliers and superior accuracy compared with CT-based techniques, especially in knees with irregular or worn cartilage [26,27]. The practical implications of the inability of CT to visualize cartilage have led to compensatory measures, such as assuming uniform cartilage thickness or manually removing residual cartilage intraoperatively, potentially compromising surgical precision. In addition, recent studies have shown that CT-based PSI can result in inaccurate alignment in varus deformity knees [28]. According to their study, the authors recommended adding approximately 2 mm of cartilage thickness to the planned lateral tibial resection value in CT-based PSI workflows for patients with varus deformity [28]. However, because cartilage thickness can vary substantially between individuals and across different regions of the joint, artificially increasing the resection thickness by a fixed 2 mm only on the lateral side may introduce design challenges and potential inaccuracies in PSI planning. In contrast, MRI-based PSI directly incorporates patient-specific cartilage thickness, thereby eliminating the need for such heuristic adjustments and potentially overcoming these limitations. Our Swin-UNet cGAN model directly addresses these well-documented limitations by providing accurate, automated segmentation of both femoral and tibial cartilage. This advancement has the potential to eliminate the alignment errors associated with CT-based PSI, representing a significant step toward more precise, reproducible surgical outcomes in TKA.

This study has several limitations. First, we performed segmentation of only the knee joint (distal femur and proximal tibia) cartilage. Future research should expand to include the ligaments and menisci. However, the MRI protocol optimized for PSI fabrication provides a suboptimal evaluation of ligamentous and meniscal structures. Second, the primary training and internal test datasets were acquired on a single 3.0 T MRI system (uMR 770; United Imaging Healthcare) using 1 PSI-optimized 3D T2*-weighted gradient-echo sequence. Although this relatively homogeneous acquisition protocol reduces within-study variability, it may limit the generalizability of our model to other scanner vendors, field strengths, coil configurations, and cartilage-focused imaging protocols beyond those used in this study. External validation was performed on a separate 3.0 T MRI system (SIGNA Premier; GE Healthcare), where segmentation performance was slightly lower than on the internal test set, likely reflecting a degree of domain shift related to differences in slice thickness (2 mm for the external dataset vs 1 mm for the internal dataset), with reduced through-plane resolution and increased partial-volume effects. Nevertheless, the model maintained reasonably high performance on this external cohort, indicating partial robustness to protocol variation. Larger multicenter studies with more heterogeneous MRI protocols and scanner types, together with additional training on datasets acquired with thicker slices and/or explicit domain-adaptation strategies, are needed to further narrow this performance gap and fully establish robustness across diverse clinical environments. Third, the current model uses a downsampled input resolution of 224 × 224 and performs slice-wise 2D segmentation, without explicitly leveraging full 3D spatial context, which is important for volumetric MRI analysis. This resolution choice was primarily driven by the need to manage the high memory complexity of the Swin Transformer backbone within a dual-network GAN framework during training, rather than solely by inference speed constraints. We acknowledge that this downsampling results in an approximate pixel spacing of 0.89 mm, which is relatively coarse compared with thin cartilage structures and may limit the capture of extremely fine details. However, contemporary PSI design workflows for TKA, including most commercial systems, are typically based on sagittal 2D cartilage contours that are subsequently reconstructed into 3D surfaces, making a 2D architecture practically compatible with current clinical and industrial pipelines. While our use of surface-based metrics (ASSD and HD95) provides an indirect assessment of 3D geometric accuracy, future work should extend the framework to 2.5D or 3D architectures with high resolution and directly evaluate interslice consistency and PSI template fit. Fourth, although our proposed model is more advanced than those in previous studies, it exhibited a slightly lower DSC. However, as noted above, this limitation can be attributed to our dataset, which consists of patients (Kellgren-Lawrence grades 3-4) awaiting TKA, where extensive cartilage damage hinders segmentation compared with that in a previous study [11]. Nonetheless, we demonstrated that our Swin-UNet cGAN outperforms the UNet cGAN used in previous studies, even when evaluated on this highly challenging dataset. Future work will explore self-supervised pretraining or advanced augmentation to further improve data efficiency and push performance on small‐sample domains.

The Swin-UNet cGAN integrates hierarchical shifted-window attention into its UNet-style transformer generator and uses a pixel-level CNN discriminator to refine outputs, enabling overall more effective segmentation of fine cartilage structures than the standard UNet, the UNet cGAN, and the Swin-UNet, and this advantage was consistently preserved on an external validation dataset. Clinically, this MRI-based segmentation approach has the potential to address key limitations of current CT-based PSI and robotic-assisted TKA workflows by providing

XSL•FO
RenderX

accurate visualization of femoral and tibial cartilage, enabling more anatomically faithful preoperative models, reducing alignment errors related to unmodeled cartilage thickness, and supporting more intuitive intraoperative registration on the articular surface.

Acknowledgments

During the preparation of this work, the authors used Gemini 3 in order to improve readability and language editing. After using this tool/service, the authors reviewed and edited the content as needed and take full responsibility for the content of the publication.

Funding

No external financial support or grants were received from any public, commercial, or not-for-profit entities for the research, authorship, or publication of this article.

Data Availability

The datasets generated or analyzed during this study are not publicly available due to institutional review board restrictions but are available from the corresponding author on reasonable request.

Authors' Contributions

Conceptualization: KTK
Methodology: JHN, SA
Formal analysis: SA
Data curation: JKK, YGK
Writing – original draft: JYP
Writing – review & editing: BWC, HMK
Supervision: KKP, KTK

Conflicts of Interest

KTK is the chief executive officer of Skyve and Clevion Co Ltd, but this did not influence the results of this study. JHN is an employee of Skyve and Clevion Co Ltd, but this also did not affect the results of this study. YGK is a shareholder of Skyve. The remaining authors declare no conflicts of interest.

Multimedia Appendix 1
Quantitative comparison of segmentation performance between nnUNet and the proposed Swin-UNet cGAN.
[DOCX File , 25 KB - medinform_v14i1e86155_app1.docx]

References

1. Koh YG, Lee JA, Kim YS, Lee HY, Kim HJ, Kang KT. Optimal mechanical properties of a scaffold for cartilage regeneration using finite element analysis. J Tissue Eng 2019;10:1-10 [FREE Full text] [doi: 10.1177/2041731419832133] [Medline: 30834102]
2. Koh YG, Lee JA, Lee HY, Kim HJ, Kang KT. Biomechanical evaluation of the effect of mesenchymal stem cells on cartilage regeneration in knee joint osteoarthritis. Appl Sci (Basel) 2019;9(9):1868. [doi: 10.3390/app9091868]
3. Zhang Q, Geng J, Zhang M, Kan T, Wang L, Ai S. Cartilage morphometry and magnetic susceptibility measurement for knee osteoarthritis with automatic cartilage segmentation. Quant Imaging Med Surg 2023;13(6):3508-3521. [doi: 10.21037/qims-22-1245] [Medline: 37284124]
4. Hafezi-Nejad N, Demehri S, Guermazi A, Carrino JA. Osteoarthritis year in review 2017: updates on imaging advancements. Osteoarthritis Cartilage 2018;26(3):341-349 [FREE Full text] [doi: 10.1016/j.joca.2018.01.007] [Medline: 29330100]
5. Blumenkrantz G, Majumdar S. Quantitative magnetic resonance imaging of articular cartilage in osteoarthritis. Eur Cell Mater 2007;13:76-86 [FREE Full text] [doi: 10.22203/ecm.v013a08] [Medline: 17506024]
6. Eck BL, Yang M, Elias JJ, Winalski CS, Altahawi F, Subhas N. Quantitative MRI for evaluation of musculoskeletal disease: cartilage and muscle composition, joint inflammation, and biomechanics in osteoarthritis. Invest Radiol 2023;58(1):60-75 [FREE Full text] [doi: 10.1097/RLI.0000000000000909] [Medline: 36165880]
7. Pham DL, Xu C, Prince JL. Current methods in medical image segmentation. Annu Rev Biomed Eng 2000;2(1):315-337. [doi: 10.1146/annurev.bioeng.2.1.315] [Medline: 11701515]
8. Bousson V, Benoist N, Guetat P, Attané G, Salvat C, Perronne L. Application of artificial intelligence to imaging interpretations in the musculoskeletal area: where are we? Where are we going? Joint Bone Spine 2023;90(1):105493. [doi: 10.1016/j.jbspin.2022.105493] [Medline: 36423783]

XSL•FO
RenderX

9. du Toit C, Orlando N, Papernick S, Dima R, Gyacskov I, Fenster A. Automatic femoral articular cartilage segmentation using deep learning in three-dimensional ultrasound images of the knee. Osteoarthr Cartil Open 2022;4(3):100290 [FREE Full text] [doi: 10.1016/j.ocarto.2022.100290] [Medline: 36474947]
10. Wang X, Shi C. Patch attention U-Net for knee cartilage segmentation in magnetic resonance images. Biomed Signal Process Control 2025;106:107754. [doi: 10.1016/j.bspc.2025.107754]
11. Gaj S, Yang M, Nakamura K, Li X. Automated cartilage and meniscus segmentation of knee MRI with conditional generative adversarial networks. Magn Reson Med 2020;84(1):437-449. [doi: 10.1002/mrm.28111] [Medline: 31793071]
12. Kwon OR, Kang KT, Son J, Suh DS, Heo DB, Koh YG. Patient-specific instrumentation development in TKA: 1st and 2nd generation designs in comparison with conventional instrumentation. Arch Orthop Trauma Surg 2017;137(1):111-118. [doi: 10.1007/s00402-016-2618-2] [Medline: 28005167]
13. Hamghalam M, Simpson AL. Medical image synthesis via conditional GANs: application to segmenting brain tumours. Comput Biol Med 2024;170:107982 [FREE Full text] [doi: 10.1016/j.compbiomed.2024.107982] [Medline: 38266466]
14. Cao H, Wang Y, Chen J, Jiang D, Zhang X, Tian Q. Swin-Unet: Unet-like pure transformer for medical image segmentation. Computer Vision – ECCV 2022 Workshops (Lecture Notes in Computer Science) 2023;13764:205-218 [FREE Full text] [doi: 10.1007/978-3-031-25066-8_9]
15. Demir U, Unal G. Patch-based image inpainting with generative adversarial networks. ArXiv. Preprint posted online on March 20, 2018 2018 [FREE Full text] [doi: 10.48550/arXiv.1803.07422]
16. Xue Y, Xu T, Huang X. Adversarial learning with multi-scale loss for skin lesion segmentation. 2018 Presented at: IEEE 15th international symposium on biomedical imaging (ISBI 2018); April 4-7, 2018; Washington. [doi: 10.1109/isbi.2018.8363707]
17. Jaemin S, Sang J, Kyu-Hwan J. Retinal vessel segmentation in fundoscopic images with generative adversarial networks. ArXiv. Preprint posted online on June 26, 2017 2017 [FREE Full text] [doi: 10.48550/arXiv.1706.09318]
18. Isola P, Zhu JY, Zhou T, Efros AA. Image-to-image translation with conditional adversarial networks. 2017 Presented at: Proceedings of the IEEE Conference on Computer Vision and Pattern Recognition (CVPR 2017); July 21-26, 2017; Honolulu. [doi: 10.1109/cvpr.2017.632]
19. Armanious K, Jiang C, Fischer M, Küstner T, Hepp T, Nikolaou K, et al. MedGAN: medical image translation using GANs. Comput Med Imaging Graph 2020;79:101684. [doi: 10.1016/j.compmedimag.2019.101684] [Medline: 31812132]
20. Chen H, Zhao N, Tan T, Kang Y, Sun C, Xie G. Knee bone and cartilage segmentation based on a 3D deep neural network using adversarial loss for prior shape constraint. Front Med (Lausanne) 2022;9:792900 [FREE Full text] [doi: 10.3389/fmed.2022.792900] [Medline: 35669917]
21. Guo J, Yan P, Qin Y, Liu M, Ma Y, Li J. Automated measurement and grading of knee cartilage thickness: a deep learning-based approach. Front Med (Lausanne) 2024;11:1337993 [FREE Full text] [doi: 10.3389/fmed.2024.1337993] [Medline: 38487024]
22. Liu F. SUSAN: Segment unannotated image structure using adversarial network. Magn Reson Med 2019;81(5):3330-3345 [FREE Full text] [doi: 10.1002/mrm.27627] [Medline: 30536427]
23. Hong HT, Koh YG, Cho BW, Kwon HM, Park KK, Kang KT. An Image-Based augmented reality system for achieving accurate bone resection in total knee arthroplasty. Cureus 2024;16(4):e58281 [FREE Full text] [doi: 10.7759/cureus.58281] [Medline: 38752081]
24. Pfitzner T, Abdel MP, von Roth P, Perka C, Hommel H. Small improvements in mechanical axis alignment achieved with MRI versus CT-based patient-specific instruments in TKA: a randomized clinical trial. Clin Orthop Relat Res 2014;472(10):2913-2922 [FREE Full text] [doi: 10.1007/s11999-014-3784-6] [Medline: 25024031]
25. Frye BM, Najim AA, Adams JB, Berend KR, Lombardi AV. MRI is more accurate than CT for patient-specific total knee arthroplasty. Knee 2015;22(6):609-612. [doi: 10.1016/j.knee.2015.02.014] [Medline: 25813758]
26. An VVG, Sivakumar BS, Phan K, Levy YD, Bruce WJM. Accuracy of MRI-based vs CT-based patient-specific instrumentation in total knee arthroplasty: a meta-analysis. J Orthop Sci 2017;22(1):116-120. [doi: 10.1016/j.jos.2016.10.007] [Medline: 27823847]
27. Schotanus MGM, Thijs E, Heijmans M, Vos R, Kort NP. Favourable alignment outcomes with MRI-based patient-specific instruments in total knee arthroplasty. Knee Surg Sports Traumatol Arthrosc 2018;26(9):2659-2668. [doi: 10.1007/s00167-017-4637-0] [Medline: 28698929]
28. Kang DG, Kim KI, Bae JK. MRI-based or CT-based patient-specific instrumentation in total knee arthroplasty: how do the two systems compare? Arthroplasty 2020;2(1):1 [FREE Full text] [doi: 10.1186/s42836-019-0020-6] [Medline: 35236432]

Abbreviations

ASSD: average symmetric surface distance
BCE: binary cross-entropy
cGAN: conditional generative adversarial network
CNN: convolutional neural network
CT: computed tomography

XSL•FO
RenderX

DL: deep learning
DSC: Dice similarity coefficient
GAN: generative adversarial network
HD: Hausdorff distance
HD95: 95th percentile Hausdorff distance
IoU: intersection over union
IRB: Institutional Review Board
MRI: magnetic resonance imaging
OAI: Osteoarthritis Initiative
PSI: patient-specific instrument
ResUNet: residual UNet
SKI10: Segmentation of Knee Images 2010
TE: echo time
TKA: total knee arthroplasty
TR: repetition time
TransUNet: transformer UNet

Edited by A Coristine; submitted 20.Oct.2025; peer-reviewed by AM Hasan, YH Kwak, A Humayun; comments to author 17.Nov.2025; revised version received 12.Jan.2026; accepted 30.Jan.2026; published 02.Mar.2026.

Please cite as:
Park JY, Nam JH, Abdigapporov S, Kim JK, Koh YG, Cho BW, Kwon HM, Park KK, Kang KT
Enhanced Magnetic Resonance Imaging–Based Knee Cartilage Segmentation Using a Swin-UNet Conditional Generative Adversarial Network: Development and Validation Study
JMIR Med Inform 2026;14:e86155
URL: https://medinform.jmir.org/2026/1/e86155
doi:10.2196/86155
PMID:

©Jun Young Park, Ji-Hoon Nam, Shakhboz Abdigapporov, Jong-Keun Kim, Yong-Gon Koh, Byung Woo Cho, Hyuck Min Kwon, Kwan Kyu Park, Kyoung-Tak Kang. Originally published in JMIR Medical Informatics (https://medinform.jmir.org), 02.Mar.2026. This is an open-access article distributed under the terms of the Creative Commons Attribution License (https://creativecommons.org/licenses/by/4.0/), which permits unrestricted use, distribution, and reproduction in any medium, provided the original work, first published in JMIR Medical Informatics, is properly cited. The complete bibliographic information, a link to the original publication on https://medinform.jmir.org/, as well as this copyright and license information must be included.

XSL•FO
RenderX

Original Paper

Leveraging Naturalistic Driving Digital Biomarkers for Early Mild Cognitive Impairment Detection: Deep Learning Strategies

Firas Al-Hindawi[1,2], PhD; Teresa Wu[3,4], PhD; Yutong Wen[3,4], MSc; Peter Serhan[5,6], MS; Erica Forzani[6,7], PhD; Francis Tsow[8], PhD; Yonas E Geda[9], MSc, MD

[1]Industrial & Systems Engineering Department, King Fahd University of Petroleum and Minerals, Dhahran, Saudi Arabia

[2]Interdisciplinary Research Center for Smart Mobility and Logistics, King Fahd University of Petroleum and Minerals, Dhahran, Saudi Arabia

[3]School of Computing and Augmented Intelligence, Arizona State University, Tempe, AZ, United States

[4]ASU Mayo Center for Innovative Imaging, Arizona State University, Tempe, AZ, United States

[5]School of Electrical, Computer and Energy Engineering, Arizona State University, Tempe, AZ, United States

[6]Center for Bioelectronics and Biosensors, Biodesign Institute, Arizona State University, Tempe, AZ, United States

[7]School of Engineering for Matter, Transport and Energy, Arizona State University, Tempe, AZ, United States

[8]TF Health Corporation, Phoenix, AZ, United States

[9]Barrow Neurological Institute, Phoenix, AZ, United States

Corresponding Author:
Teresa Wu, PhD
School of Computing and Augmented Intelligence
Arizona State University
Tempe
699 S. Mill Ave.
Tempe, AZ, 85281
United States
Phone: 1 4809655172
Email: teresa.wu@asu.edu

Abstract

Background: Alzheimer disease and related dementias are increasing worldwide, with early detection during the mild cognitive impairment (MCI) stage critical for timely intervention. Driving behavior, which reflects everyday cognitive functioning, has emerged as a promising, noninvasive, and inexpensive digital biomarker when paired with machine learning. However, prior research has often relied on controlled settings, high-level features, or assumptions that fail to capture the sporadic nature of MCI, leaving a gap in modeling naturalistic driving data for robust early detection.

Objective: This study aims to address the limitations of prior work by developing deep learning strategies that leverage driving data collected in a naturalistic setting as digital biomarkers for early detection of MCI.

Methods: Clinically classified participants (8 with MCI and 14 cognitively normal; N=22) drove their personal vehicles under naturalistic conditions for several consecutive days. A total of 3 participants (2 cognitively normal and 1 MCI) withdrew before completing the experiments. In-vehicle sensors recorded GPS, accelerometer, and gyroscope signals, which were segmented into full trips and turning maneuvers. Three modeling strategies were compared: (1) single-view, (2) feature-level fusion, and (3) model-level late fusion. Classification models were trained and evaluated to assess their accuracy, discriminative ability, and participant-level performance.

Results: Models using full-trip data consistently outperformed turn-only inputs, with the best-performing model achieving 78% accuracy and an area under the receiver operating characteristic curve of 77%. Turn-based inputs alone demonstrated limited discriminative power; however, combining them with trip data through late fusion improved performance, though not beyond the full-trip baseline. Participant-level analysis indicated that classification accuracy improved with increased data volume, and trip-wise modeling more effectively captured the episodic nature of MCI than majority-vote aggregation. A frequency-based risk score was proposed as an interpretable and flexible output, enabling practical application in clinical and community settings.

Conclusions: Naturalistic driving behavior offers a scalable and noninvasive approach for early cognitive screening. Deep learning models using full-trip naturalistic driving data show promise for detecting MCI, with fusion strategies providing

XSL•FO
RenderX

supplementary insights. This framework supports proactive, real-world monitoring of cognitive decline, laying the foundation for digital health interventions in dementia prevention.

(JMIR Med Inform 2026;14:e83622) doi:10.2196/83622

KEYWORDS

aging; Alzheimer's disease; mild cognitive impairment; smart driving; machine learning; deep learning; data fusion

Introduction

Alzheimer disease (AD) and AD-related dementias are a growing public health concern. In the United States, cases are projected to reach 13.2 million by 2050, placing a significant strain on health care systems and caregivers [1-6]. Worldwide, over 55 million people are affected, with numbers expected to rise to 152 million by 2050 [5,7-9]. The disease progresses gradually, beginning with an asymptomatic phase, followed by mild cognitive impairment (MCI) and eventually dementia [10]. MCI is a transitional stage between normal aging and dementia, involving cognitive but not functional decline [11,12]. Accurate diagnosis at this stage is vital, as early detection allows timely intervention to slow progression and manage symptoms [13-16].

Identifying MCI early is challenging. Current tools, such as neuropsychological tests or biomarkers such as magnetic resonance imaging and positron emission tomography, are clinic-bound, offer only brief cognitive snapshots, and could be invasive, costly, or impractical for large-scale screening [5,6,17]. These methods often miss early MCI, as markers appear later in disease progression [18], highlighting the need for noninvasive, cost-effective biomarkers that support frequent monitoring in real-life settings [5,6,17,19-22]. Recently, spatial navigation deficits and driving behavior have emerged as potential early biomarkers for preclinical AD [23,24]. Tasks such as driving engage multiple cognitive functions in real-world contexts, and even mild impairments can lead to detectable changes in driving patterns [5,6,19,25]. Research shows that older adults with preclinical AD or MCI may limit their driving range, make more navigation errors, and drive more cautiously than cognitively normal peers [25,26]. These driving changes have been linked to AD biomarkers such as elevated amyloid and tau, even when standard cognitive tests are normal [25,27,28]. Notably, such changes can be detected by machine learning (ML) models using in-vehicle sensor data, as demonstrated in studies such as LongROAD [25] and GPS driving [19]. These studies show that ML can accurately identify individuals with MCI or preclinical AD by analyzing patterns in driving behavior such as speed, acceleration, and route choice, often outperforming conventional tools [5,6,19,25], while showing potential for real-time cognitive monitoring through everyday driving.

Despite encouraging progress, ML-based driving diagnostic systems still face key challenges. Many studies rely on simple, high-level features such as trip frequency and duration [19,25], overlooking nuanced indicators such as turn velocity, acceleration patterns, and path deviations that more directly reflect cognitive function. Furthermore, monthly driving records are treated as independent, even when from the same driver, risking data leakage and inflating performance by allowing driver-specific patterns to appear in both training and testing sets. Although recent work has incorporated richer features such as metabolic rate and ensured proper train-test separation [5,6], those studies were conducted in controlled settings with predefined routes, limiting real-world applicability. Additionally, most approaches rely on summary statistics and classical ML models, missing the potential of more powerful deep learning time-series classification techniques. Finally, conventional evaluation frameworks assume MCI symptoms appear consistently across trips, whereas studies have shown that cognitive performance in MCI can vary markedly from day to day, highlighting its sporadic nature [29-31]. Individuals with MCI may only show impairment in a minority of trips, leading models to misclassify them as cognitively normal, yet even occasional MCI-like trips could still serve as an early indicator of cognitive decline.

To address these limitations, this study proposes a new framework that improves both data representation and model evaluation. It shifts from artificial test settings to naturalistic driving by equipping participants' personal vehicles with tracking devices and allowing several days of normal driving, capturing real-world cognitive function. Instead of treating each participant's data as a uniform whole and relying on majority-based classification, the model adopts a granular, context-aware approach, evaluating each trip and turn individually to detect episodic impairments, consistent with the sporadic nature of MCI. Rather than delivering a binary diagnosis, it identifies subtle changes over time and flags individuals for further evaluation, enabling proactive cognitive health monitoring. The framework aggregates binary trip- and turn-level classifications over time to enable longitudinal monitoring and transforms them into a continuous, participant-level risk score (eg, the proportion of trips flagged as impaired). This frequency-based risk score provides a nonbinary, dynamic measure that reflects gradual cognitive change and supports proactive follow-up rather than a 1-time diagnostic label. Specifically, the framework includes a targeted feature-extraction pipeline that segments time-series data from full trips and cognitively demanding turning maneuvers, producing 2 complementary multivariate inputs. Deep learning architectures are then evaluated under 3 paradigms: (experiment 1) single-view modeling of trips and turns, (experiment 2) feature-level fusion, and (experiment 3) model-level late fusion using dual encoders. This design is guided by 3 key research questions.

For research question 1 (RQ1), effectiveness in naturalistic settings, can driving-based digital-biomarker strategies that showed promise in previous controlled environments [5,6] remain effective amid the noise and variability of day-to-day, real-world driving?

XSL•FO
RenderX

For research question 2 (RQ2), data handling and representation, what preprocessing and feature-extraction pipeline best transforms raw multisensor driving streams into informative inputs for deep learning?

For research question 3 (RQ3), optimal modeling strategy under data constraints, given current dataset limitations, but also anticipating richer data in future studies, which learning paradigm offers the most robust path forward? To answer this, we decompose this question into three comparative subquestions:

1. Single-view baselines: How well can early MCI be detected when trips and turns are modeled independently?
2. Early (data-level) fusion: Does combining trip and turn data at the feature level improve over the best single-view model?
3. Late (model-level) fusion: Can merging latent representations from trip and turn encoders outperform both single-view and early-fusion models?

The remainder of this paper is organized as follows. The Methods section describes this study's design, materials, and methods used to develop the framework, and the experimental methodology. The Results section presents the outcomes of the conducted experiments. The Discussion section discusses the findings and concludes the paper.

Methods

Study Design

Figure 1 presents an overview of the proposed methodology, which includes participant recruitment with expert cognitive classification, sensor-based driving data collection, preprocessing, feature engineering, and model training and evaluation. Raw sensor streams were cleaned, synchronized, and segmented into 2 complementary multivariate time-series datasets: full-trip sequences and turning maneuvers, used as inputs for subsequent experiments.

Figure 1. Overview of the adopted methodology, illustrating the sequential steps from participant recruitment to model training and evaluation. N denotes the number of samples (trips or turns), C the number of sensor channels, and L_1 and L_2 the interpolated sequence lengths for the trip and turn time-series inputs, respectively. MCI: mild cognitive impairment; MTS: multivariate time series.

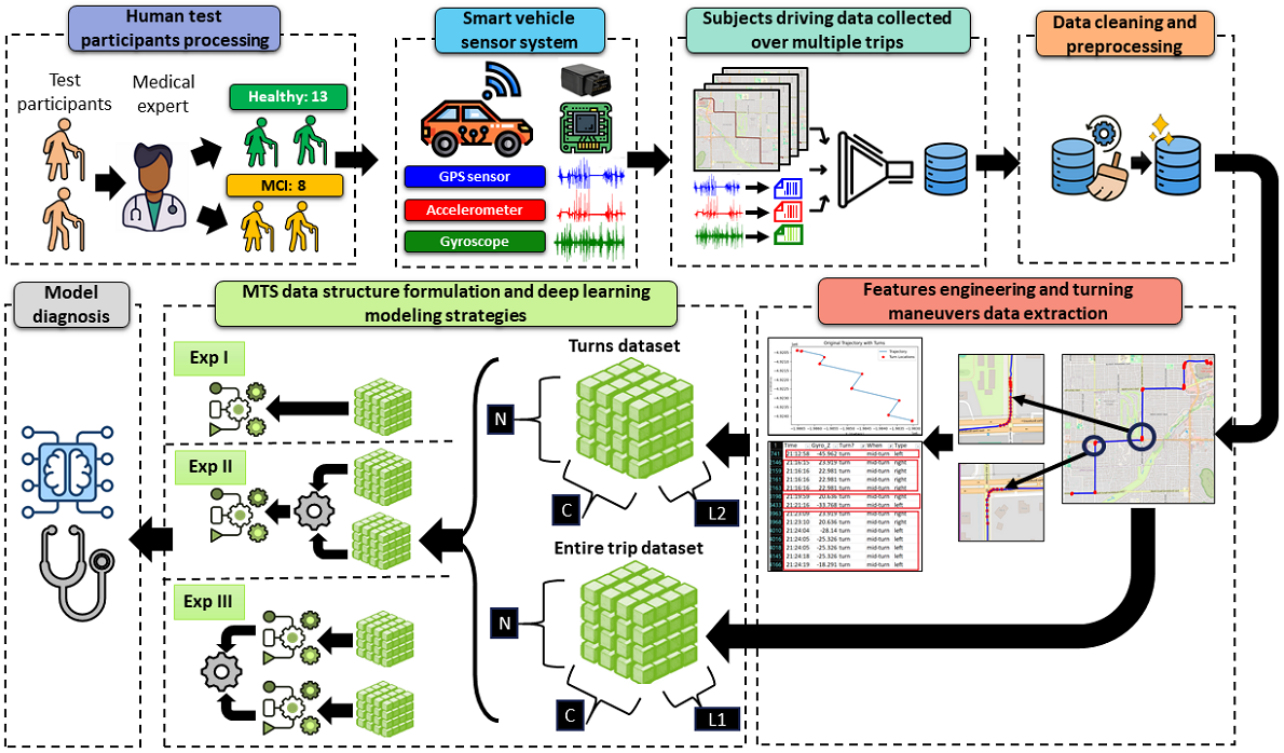

Study Participants

To ensure accurate data interpretation, participant diagnoses were conducted in collaboration with a neurologist specializing in AD. Based on cognitive assessments, 13 participants were classified as cognitively healthy and 8 as having MCI. This grouping enabled structured comparison of driving behavior between cognitively normal and impaired individuals. Table 1 summarizes the demographic and medical diagnoses of the participants.

XSL•FO
RenderX

Table 1. Participant demographics and group classification: this study included 21 older adults (ages 65-85 y), with 11 male and 10 female participants. Medical evaluations classified 13 as cognitively healthy and 8 as having MCI[a].

Participant numbers	Age (y)	Sex	Clinical condition
Participant 1	78	Male	MCI
Participant 2	80	Male	Healthy
Participant 3	70	Male	Healthy
Participant 4[b]	72	Female	Healthy
Participant 5	73	Female	Healthy
Participant 6	74	Male	MCI
Participant 7	77	Female	Healthy
Participant 8	87	Female	Healthy
Participant 9	85	Female	Healthy
Participant 10	82	Female	MCI
Participant 11	71	Female	Healthy
Participant 12	72	Female	MCI
Participant 13	65	Male	MCI
Participant 14[b]	75	Male	Healthy
Participant 15[b]	71	Female	MCI
Participant 16	76	Male	Healthy
Participant 17	75	Female	MCI
Participant 18	83	Male	Healthy
Participant 19	76	Male	MCI
Participant 20	80	Female	Healthy
Participant 21	79	Male	Healthy
Participant 22	75	Male	Healthy

[a]MCI: mild cognitive impairment.

[b]Participants withdrew before completing the experiment, leaving insufficient data for their inclusion in the final analysis.

As shown in the table, this study focused on naturalistic driving performance in adults aged 65-85 years, a group at higher risk for cognitive decline. Further, 21 participants were initially recruited, but 3 participants (participants 4, 14, and 15) withdrew before completing the driving experiment, leaving insufficient data for analysis.

Smart Vehicle Telematics System

Each participant's personal vehicle was fitted with a BitBrew on-board diagnostics (OBD) data logger to continuously record naturalistic driving behavior (Figure 2). This advanced telematics device integrates 3 sensors: GPS, accelerometer, and gyroscope. Together, they capture vehicle location, movement, and dynamic behavior, enabling comprehensive real-world driving analysis.

The GPS module tracks the vehicle's location and speed, recording longitude and latitude coordinates and measuring speed in meters per second (m/s) at a frequency of 1 Hz (1 update per second). The accelerometer captures linear acceleration along 3 axes: longitudinal (forward and backward), lateral (side to side), and vertical (up and down), in m/s^2. It detects events such as harsh braking, rapid acceleration, and sharp turns, operating at 24 Hz for high-resolution motion detection. The gyroscope measures angular velocity in radians per second (rad/s) around 3 axes: pitch (tilting forward and backward), roll (tilting side to side), and yaw (rotational movement around the vertical axis). This sensor operates at 24 Hz and provides data on lane changes, skidding, and rollovers.

Participants drove their vehicles freely with no specific instructions, allowing for natural capture of daily driving behavior. Table 2 summarizes the driving periods for each participant, including start and end dates and total duration. All data from the OBD logger was transmitted to an AWS S3 (Amazon Web Services Simple Storage Service) bucket for cloud-based storage and analysis.

XSL•FO
RenderX

Figure 2. Overview of the data collection system used in the naturalistic driving study. AWS S3: Amazon Web Services Simple Storage Service; OBD: on-board diagnostics.

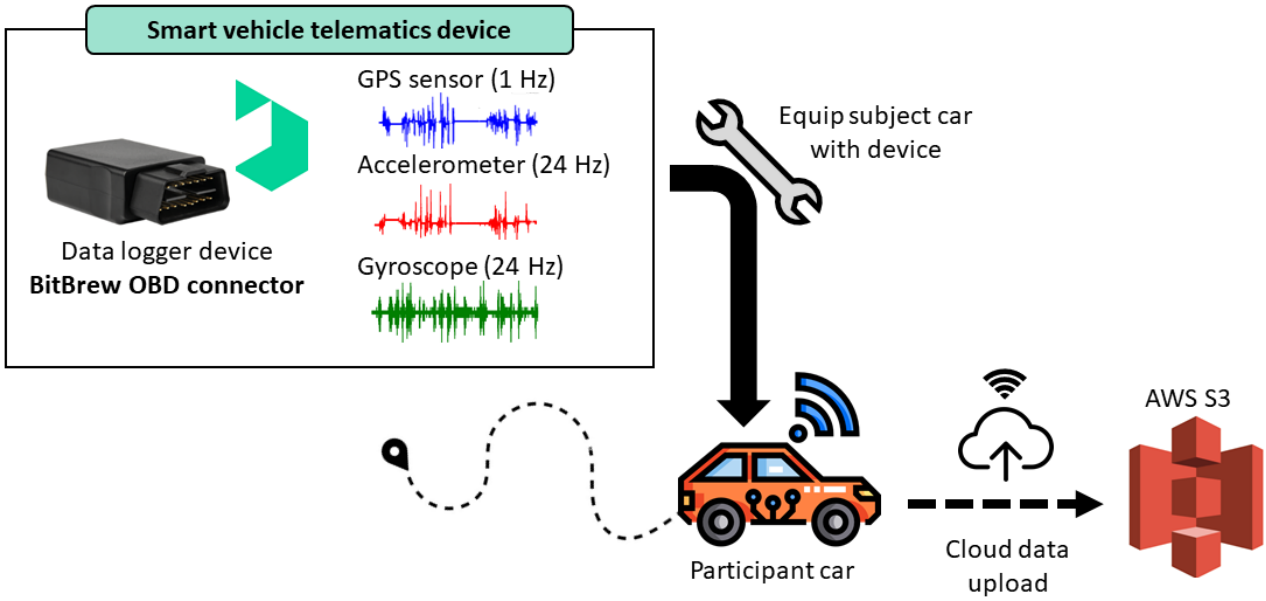

Table 2. Naturalistic driving test periods for study participants, detailing the start and end dates along with the duration (in days) for each observation period.

Participant number	Start date	End date	Duration (d)
Participant 1	March 29, 2023	April 7, 2023	9
Participant 2	April 13, 2023	April 20, 2023	7
Participant 3	May 4, 2023	May 11, 2023	7
Participant 4	__[a]	—	—
Participant 5	May 19, 2023	May 26, 2023	7
Participant 6	May 26, 2023	June 2, 2023	7
Participant 7	June 2, 2023	June 9, 2023	7
Participant 8	June 30, 2023	July 7, 2023	7
Participant 9	July 7, 2023	July 14, 2023	7
Participant 10	July 14, 2023	July 21, 2023	7
Participant 11	July 21, 2023	July 28, 2023	7
Participant 12	August 15, 2023	August 21, 2023	6
Participant 13	September 15, 2023	September 22, 2023	7
Participant 14	—	—	—
Participant 15	—	—	—
Participant 16	August 25, 2023	September 8, 2023	14
Participant 17	August 25, 2023	September 8, 2023	14
Participant 18	September 22, 2023	September 29, 2023	7
Participant 19	September 29, 2023	October 6, 2023	7
Participant 20[b]	October 10, 2023	January 20, 2024	86
Participant 21	October 10, 2023	October 27, 2023	17
Participant 22	October 27, 2023	November 3, 2023	7

[a]Not available.

[b]Participants did the experiment over 2 periods (October 10, 2023, to October 27, 2023, and November 12, 2023, to January 20, 2024).

XSL•FO
RenderX

Naturalistic Driving Data Collection, Cleaning, and Preprocessing

This naturalistic driving study was conducted in Tempe, Arizona, and extended to nearby cities, including Phoenix, Glendale, Chandler, Scottsdale, and Mesa. Participants drove their personal vehicles, each equipped with a BitBrew OBD data logger, which passively recorded real-world driving behavior. The system continuously captured GPS location, accelerometer, and gyroscope data during each session, enabling a comprehensive analysis of driving patterns without imposing specific instructions or restrictions.

Recorded routes spanned a wide range of road types such as residential streets, highways, and urban roads. The dataset included a variable number of trips per participant, with differences in trip length, duration, and driving conditions reflecting the complexity of real-world behavior. However, sensor data was not always consistent across modalities for the same participant due to device malfunctions, intermittent failures, or temporary disconnections. These issues sometimes caused sensors to stop mid-trip, fail to initiate, or record out of sync, resulting in incomplete or misaligned data. To address these challenges, a structured preprocessing pipeline was applied to ensure that only high-quality, reliable, and synchronized driving records were retained for subsequent analysis.

The first step in preprocessing involved segmenting individual trips from the continuous sensor data stream. Timestamps from the accelerometer, GPS, and gyroscope were analyzed to identify gaps between recordings. If the time difference between consecutive points was less than 1 minute, the data was treated as part of the same trip. Gaps exceeding 1 minute marked the start of a new trip. After segmentation, the data were organized into participant-specific folders, with separate subfolders for each sensor and individual CSV files representing distinct trips.

Although segmentation provided structure, several data quality issues emerged. Sensor malfunctions led to missing data, and differences in recording frequency created synchronization challenges. The accelerometer and gyroscope recorded at 24 Hz, while the GPS operated at 1 Hz, resulting in mismatched data lengths. To resolve this, a cleaning process was applied. A mismatch check flagged any case where the number of trips differed across sensors. When discrepancies were found, the system logged debugging information and excluded incomplete trips. Data from all sensors was merged using shared time attributes such as day, month, hour, and minute. Trips with missing values were flagged, stored separately, and excluded from further analysis. Only complete and synchronized trips were retained. Table 3 shows the number of trips kept for each participant after preprocessing.

XSL•FO
RenderX

Table 3. Number of trips retained per participant after data cleaning and synchronization. Due to sensor malfunctions, missing data, and synchronization issues, the total number of trips was reduced.

Participant number	Number of trips recorded by each sensor		
	Accelerometer	GPS	Gyroscope
Participant 1	28	28	28
Participant 2	18	18	18
Participant 3	30	30	30
Participant 4	—[a]	—	—
Participant 5	46	46	46
Participant 6	21	21	21
Participant 7	39	39	39
Participant 8	6	6	6
Participant 9	11	11	11
Participant 10	11	11	11
Participant 11	21	21	21
Participant 12	3	3	3
Participant 13	13	13	13
Participant 14	—	—	—
Participant 15	—	—	—
Participant 16	10	10	10
Participant 17	11	11	11
Participant 18	11	11	11
Participant 19	4	4	4
Participant 20	126	126	126
Participant 21	6	4	6
Participant 22	24	24	24

[a]Not available.

Features, Engineering, and Turning Maneuvers Data Extraction

Turning Maneuvers Data Extraction

Turning a vehicle is a cognitively demanding task involving decision-making, divided attention, working memory, processing speed, and spatial orientation. These functions are often impaired in individuals with MCI and may serve as early biomarkers for AD. Following prior studies [5,6], this work focuses on turning maneuvers, which have shown potential in detecting cognitive decline in standardized controlled experiments. Unlike previous research, this study uses naturalistic driving, where participants follow their routine behavior without instructions. This introduces additional noise into the data, allowing us to test whether turning-related features remain informative under real-world conditions.

Turning detection required converting GPS coordinates from latitude and longitude into Cartesian coordinates for accurate geometric and kinematic analysis. The transformations used are shown in equations 1 and 2. Given a point on the Earth's surface with latitude ∅ and longitude λ, the x and y coordinates were calculated as:

where R is the Earth's radius (approximately 6371 km), and ∅ and λ are expressed in radians.

To identify turning maneuvers, the peak point of each arc path was detected by analyzing the rate of change in x and y rectangular coordinate arrays. By computing the first derivative (dy/dx), the directional changes were captured, with abrupt gradient shifts indicating deviations from straight paths. To filter out gradual curves, various thresholds were tested. It was found that a gradient of 10 degrees (0.174533 radians) reliably captured meaningful turns. However, relying on the gradient alone produced occasional errors. Points where dx=0, resulting in undefined gradients, were discarded. Additionally, turn stamp points with 0 speed, which typically corresponded to stationary periods rather than active maneuvers, were also excluded. Further refinement addressed redundant peak detections within a single turn. In some cases, multiple nearby peaks were

XSL•FO
RenderX

incorrectly classified as separate turns. To resolve this, a smoothing approach was applied. Sequential turn points were merged and replaced by their median index, reducing overlap and ensuring 1 peak per turn event. Once peaks were identified, all surrounding points were extracted by applying a temporal window. Based on empirical observations, a turn maneuver was identified by including all sensor readings occurring 15 seconds before and after the peak point. Accelerometer and gyroscope readings were downsampled to align with the 1 Hz GPS rate by averaging every 24 readings from the higher frequency sensors. Figure 3 illustrates an example of turns extracted from a sample trip.

Figure 3. Illustration of the turn maneuver detection process. The leftmost map represents the original trip path recorded using GPS data. The middle section highlights detected turning maneuvers, marked by red dots, which were identified based on changes in trajectory. The rightmost section zooms in on extracted turn segments, showing detailed turning paths.

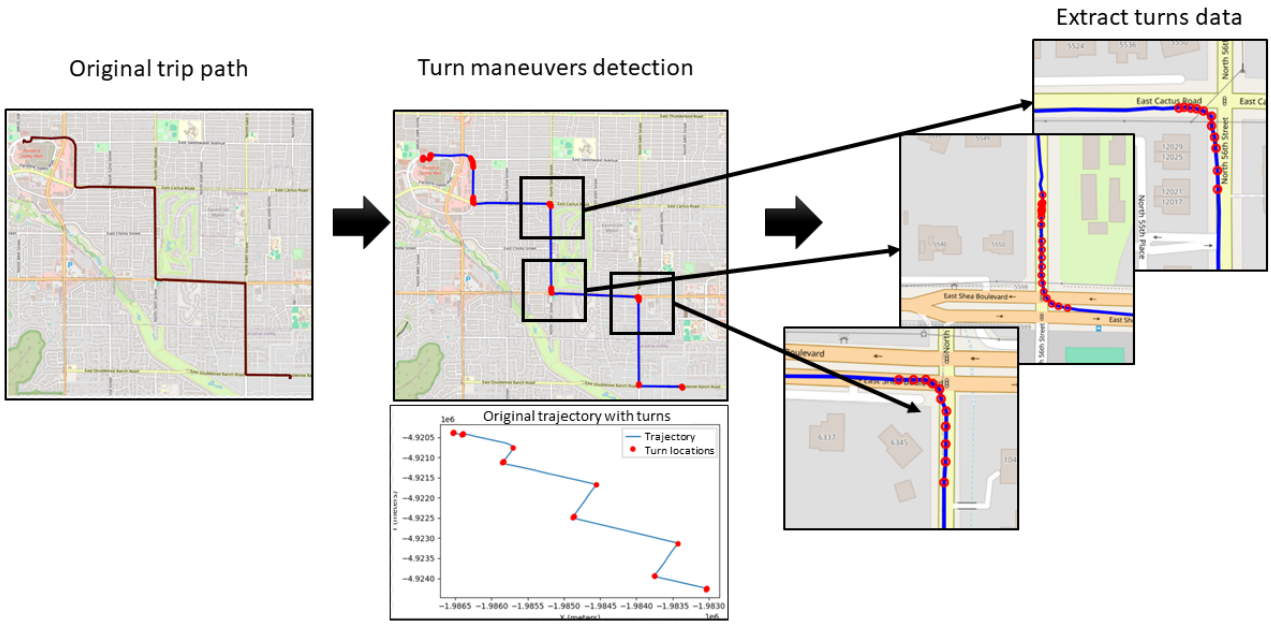

Features Engineering (Radial Acceleration)

An additional engineered feature was radial acceleration, which captures how sharply and assertively a driver navigates turns. Higher radial acceleration values may indicate sharper bends or faster speeds, while rapid fluctuations within a maneuver suggest frequent microadjustments in steering and speed. These patterns can reflect reduced motor control and cognitive instability. Radial acceleration was computed by taking the temporal gradient of the gyroscope data along the X, Y, and Z axes. This provided a continuous measure of changes in angular velocity over time, enriching the representation of driver motion. Equations 3-5 show the computation for each axis:

Table 4 summarizes the final set of 10 features used in the input tensor for all models. Each feature represents a specific aspect of motion captured by the GPS, accelerometer, or gyroscope sensors. The Gyro_X_Acc, Gyro_Y_Acc, and Gyro_Z_Acc variables correspond to the angular accelerations derived from the temporal derivatives of the gyroscope signals.

XSL•FO
RenderX

Table 4. Final set of sensor-based features used in the dataset. The table lists the 10 input channels used across all experiments. Each feature captures a different dimension of vehicle motion using raw or derived signals from speed, accelerometer, and gyroscope sensors.

Feature or channel	Description
Speed	Vehicle speed measured in meters per second (m/s)
Acc_X	Linear acceleration along the vehicle's longitudinal axis (forward/backward)
Acc_Y	Linear acceleration along the lateral axis (side-to-side motion)
Acc_Z	Linear acceleration along the vertical axis (up or down motion)
Gyro_X	Angular velocity around the x-axis (roll rate)
Gyro_Y	Angular velocity around the y-axis (pitch rate)
Gyro_Z	Angular velocity around the z-axis (yaw rate or heading change)
Gyro_X_Acc	Angular acceleration around the x-axis, derived from Gyro_X
Gyro_Y_Acc	Angular acceleration around the y-axis, derived from Gyro_Y
Gyro_Z_Acc	Angular acceleration around the z-axis, derived from Gyro_Z

Multivariate Time Series Data Formulation

This study used 2 datasets: one capturing entire trip readings and another focused on turning maneuvers. Both were formatted as multivariate time series to preserve the sequential nature of driving behavior. Depending on the dataset, each row represented either a full trip or a turn, and each sensor served as a separate time-dependent variable. To standardize input lengths for model training, sequences were aligned and resampled through interpolation, ensuring uniform temporal resolution across samples.

Time Series Alignment and Interpolation

Trip and turn durations varied widely across drivers, requiring a preprocessing step to standardize time series lengths. Without it, inconsistent sequence sizes would hinder the model's ability to learn temporal patterns. To address this, interpolation was applied to resample all sequences to a fixed number of time points. To select the optimal length, different resolutions were tested by plotting samples and evaluating the balance between data redundancy and information loss. Alignment and interpolation were applied separately to the trip and turn datasets to maintain consistency within each.

For the trip dataset, the distribution of raw sequence lengths (Figure 4) was analyzed, and a target that preserved most trips without excessive compression was selected. This choice was further validated by visually inspecting sensor signals before and after resampling, confirming that key temporal patterns were retained. Based on this process, a fixed length of 1200 points was selected for the trip dataset.

Figure 4. Distribution of trip lengths in the raw dataset. Each bar represents the number of trips with a given sequence length (in time steps). The histogram was used to inform the selection of a standardized interpolation length that balances coverage and temporal resolution.

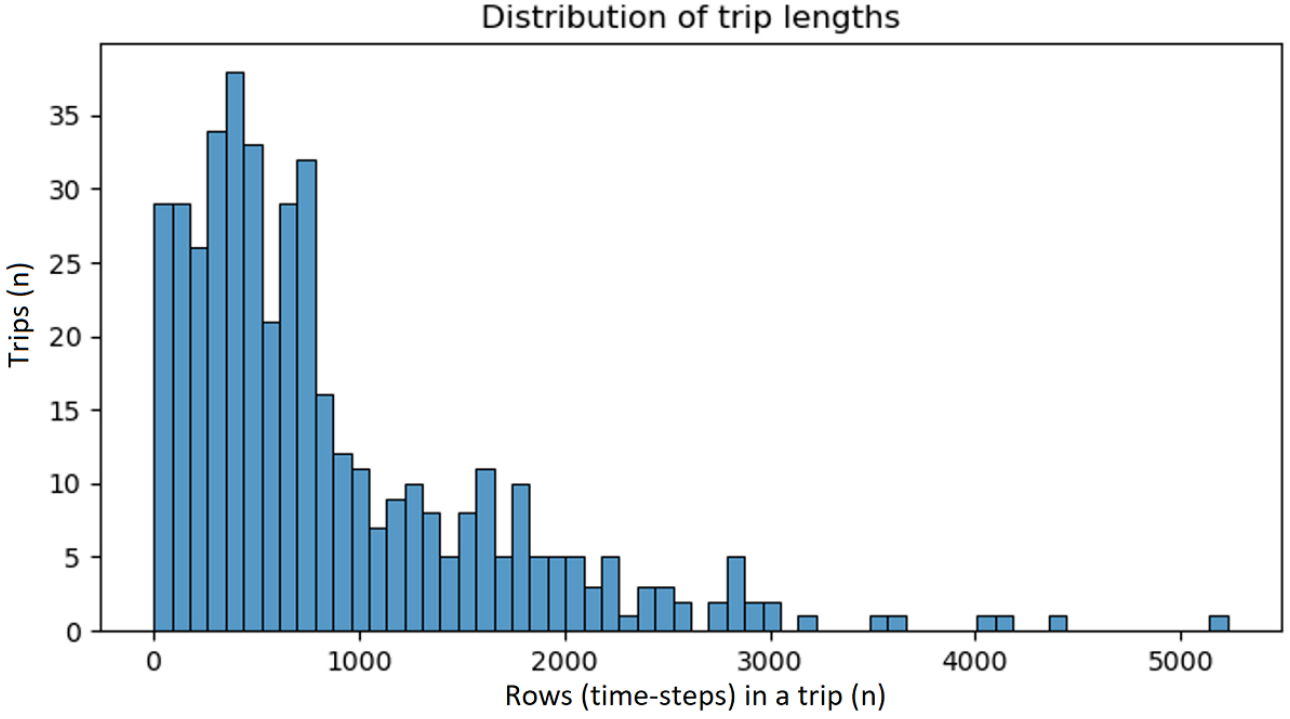

XSL•FO
RenderX

For the turning maneuvers dataset, the extraction process described in Turning Maneuvers Data Extraction produced segments with a standardized length of 31-time steps by centering each around the turn midpoint and including a fixed number of points before and after. In most cases, this window was fully available, making interpolation unnecessary. However, in rare edge cases, such as turns at the very start or end of a trip, the available context was limited, resulting in shorter segments. These were interpolated to ensure consistency across the dataset.

Final Data Representation

After interpolation, all sensor streams were consolidated into a single structured format. Each trip or turn was represented as a 3D tensor with dimensions N × C × L, where N is the number of trips or turns, C is the number of channels (sensors), and L is the standardized sequence length. Each row corresponds to a distinct trip or turn, columns represent the sensor channels (eg, speed), and the entries hold the sequential readings for the interpolated time steps. Figure 5 shows how all sensor data were aligned and merged into this final format.

Figure 5. Representation of the MTS dataset structure used. Each row corresponds to either an entire trip or a turn, depending on the dataset. The dataset is formatted as a 3D tensor with dimensions (trip or turn, channels [sensors], and sensor readings). MTS: multivariate time series.

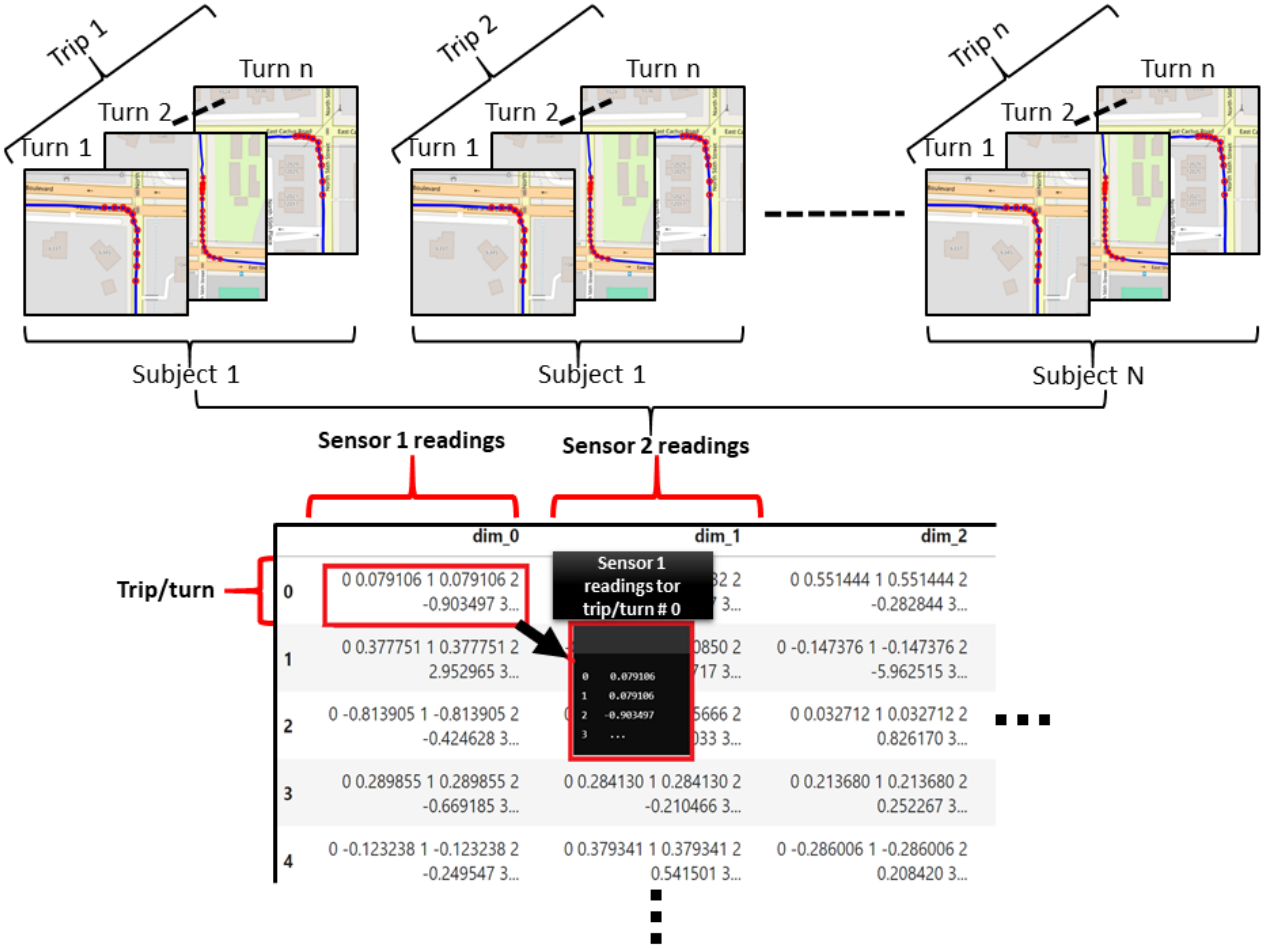

Experiments

This section describes the experimental setup and methods used to analyze driving behavior and classify participants based on cognitive status. We hypothesize that naturalistic driving contains digital signatures that can support early MCI detection. The central question is how to best process and model this data to maximize predictive performance. To explore this, we designed 3 experiments based on the same source of driving data but varying in input representation and modeling strategy. By decomposing the problem along 2 dimensions, what part of the data to use (entire trip vs turns) and how to architect the model (single vs multiple inputs or models), we aim to identify which configurations most effectively preserve behaviorally relevant information.

Three main architecture families were used: 1D convolutional neural networks (1D-CNNs), recurrent neural networks (RNNs), and temporal convolutional networks (TCNs); because they align well with the characteristics of naturalistic driving data, which are multivariate, sequential, and temporally dependent. 1D-CNNs were selected for their ability to detect short, localized motion patterns such as rapid accelerations or turning dynamics; RNNs were included to capture longer behavioral trends that unfold over an entire trip; and TCNs were chosen for their ability to model both short- and long-range dependencies efficiently and robustly. Variants within each family (eg, lightweight 1D-CNNs and attention-based RNNs) were explored to identify which architectural style best captures early MCI-related temporal signatures in real-world driving behavior.

XSL•FO
RenderX

All models were trained using a unified configuration to ensure comparability across experiments. The loss function was standard cross-entropy with class weighting applied when needed to address class imbalance. Standard scaling normalization was applied where indicated in the tables. Optimization was performed with AdamW using a learning rate of 1×10^{-3} and a weight decay of 1×10^{-4}. A cosine annealing learning-rate scheduler with T_{max} equal to the number of epochs was used to promote stable convergence. Training was conducted with a batch size of 32 for 200 epochs (reduced from 500 after observing convergence before epoch 200). Dropout was applied only when specified by the architecture variant, as detailed in the appendices.

Table 5 summarizes the details of the experiments, while Figure 6 illustrates the modeling strategies in each.

Table 5. Summary of experimental setups showcasing the data source, feature representation, and modeling paradigm. Sensor channels include speed, linear accelerations (X/Y/Z), angular velocities (X/Y/Z), and derived angular accelerations (X/Y/Z).

Experiment	Data source	Feature representation (input to model)	Predictive-modeling strategy
1(a)	Entire trip only	Multivariate time series (10 raw sensor channels)	Single-view deep models (1D-CNN[a], RNN[b], and TCN[c] variants)
1(b)	Turning maneuvers only	Multivariate time series (same 10 channels, windowed around turns)	Single-view deep models (1D-CNN, RNN, and TCN variants)
2	Trip and turn signals (concatenated)	Feature-level fusion (20-channel time series)	Single model (1D-CNN, RNN, and TCN) trained on fused input
3	Trip and turn signals (separate)	Two parallel 10-channel time series	Dual encoders with late fusion

[a]1D-CNN: 1D convolutional neural network.

[b]RNN: recurrent neural network.

[c]TCN: temporal convolutional network.

Figure 6. Overview of the data formulation and experimental paradigms. The left side shows the data formulation that produces the 2 multivariate inputs used in this study: the entire-trip sensor readings (green) and concatenated turn-segment readings (blue). The right side summarizes how the produced data are used in our experiment, which consists of 3 modeling paradigms: Exp 1 (single-view models trained on trips or turns separately), Exp 2 (feature-level fusion of the 2 inputs), and Exp 3 (dual encoders with late fusion).

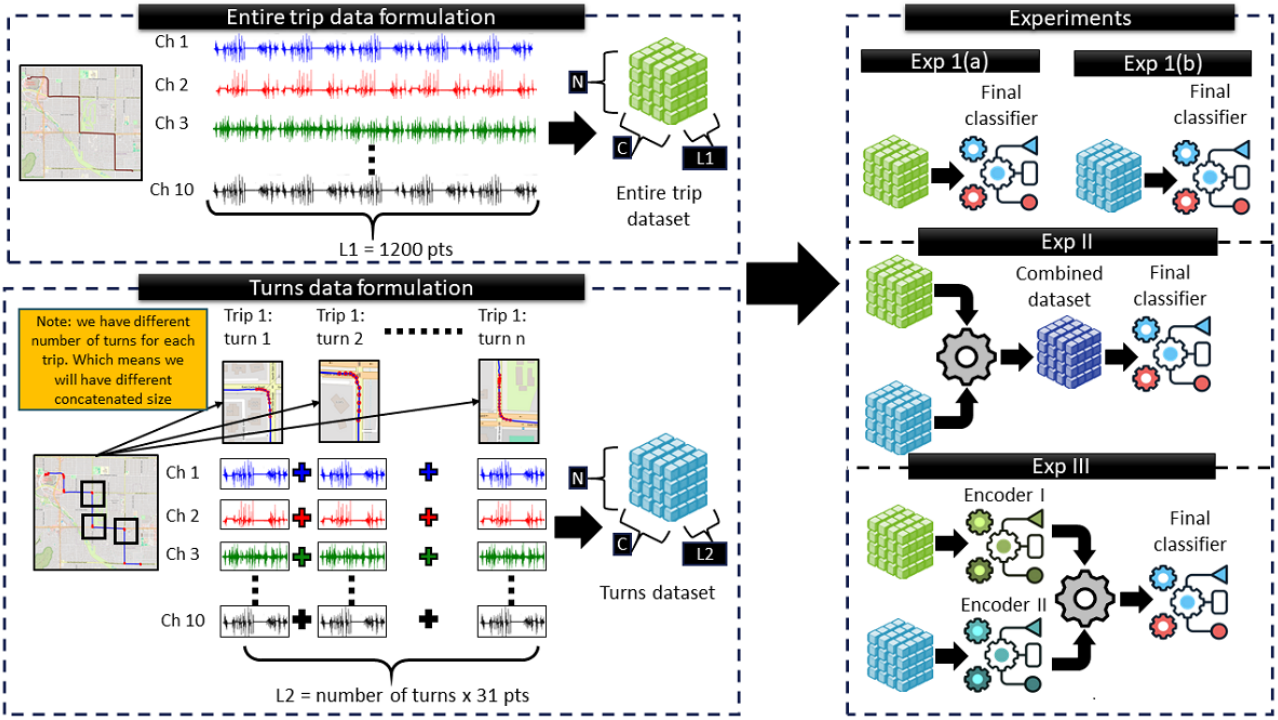

Experiment 1: Single Data Representation With Single Model

This experiment evaluates the effectiveness of using a single type of input, either full trips or turn segments, modeled independently (Figure 6). All input data was treated as a multivariate time series and interpolated to a fixed length using 10 sensor channels. For each data type, various model architectures were tested, including 1D-CNNs, RNNs, and TCNs (details in Multimedia Appendix 1). In the full-trip setting (experiment 1(a)), each trip was used as a standalone sequence to capture broad driving behavior. In contrast, the turn-only setting (experiment 1(b)) focused on concatenated turn segments. This experiment isolated a specific behavior

XSL•FO
RenderX

substructure to examine whether it holds predictive power on its own.

Experiment 2: Combined Input With Single Model (Data Fusion)

In this experiment, feature-level fusion was explored by combining full-trip and turn-based inputs into a single tensor, as illustrated in Figure 6. Sensor readings from 10 channels were extracted for the entire trip and interpolated to a fixed length of 1200 time points (L_1) to ensure consistency. Separately, all turn segments from each trip were concatenated and interpolated to the same length (L_1 =1200), despite variability in the number of turns across trips. After alignment, both sequences were concatenated along the channel dimension, resulting in a unified tensor with shape (N, C=20, and L=1200), where N denotes the number of trips and C includes 10 channels from the trip data and 10 from the turn data. As in experiment 1, a range of model architectures was evaluated, including 1D-CNNs, RNNs, and TCNs, using the fused input. The objective was to assess whether the joint modeling of global and localized driving behavior could improve classification performance. Further architectural details are provided in Multimedia Appendix 2.

Experiment 3: Separate Inputs and Models With Late Fusion (Model Fusion)

In the final experiment, a model fusion approach was adopted. Separate models were trained independently on the trip-level and turn-level data. As shown in Figure 6, a total of 2 distinct datasets were prepared for each trip. In the upper branch, the complete 10-channel sensor stream was resampled to a fixed length of L_1 points and passed to encoder 1, where a latent representation of global driving behavior was learned. In the lower branch, all turning maneuvers for the same trip were concatenated, and the resulting sequence was standardized to L_2 points (which differed from L_1) before being input to encoder 2.

Encoders were selected from 3 architectural families, 1D-CNN, RNN, or TCN (for example, DualTinyFCN, DualGRU, and DualTCN), and were trained with separate weights. The latent vectors from both encoders were combined using a late fusion classifier. This allowed the model to integrate complementary global and local driving features while maintaining the independence of each encoder. Further model details are provided in Multimedia Appendix 3.

Model Training Framework

The training framework for all experiments followed a structured procedure. The process began with data preprocessing, where the turning maneuvers dataset was transformed into a 3D tensor representation with dimensions (N, C, and L). To evaluate the model's performance in distinguishing between cognitively healthy individuals and those with MCI, a 7-fold interparticipant cross-validation strategy was implemented. Given the limited sample size, no independent test set was used. Instead, interparticipant cross-validation was adopted to maximize data use while ensuring that the evaluation remained unbiased. Each fold contained a unique set of participants for testing, with the remaining participants used for training, ensuring that no individual appeared in both sets and thereby eliminating any risk of data leakage across folds.

Stratification was handled at the participant level. Each fold maintained an equal ratio of cognitively normal to MCI participants in the validation set. As the models operated on trip or turn-level data (rather than directly on participants), it was not possible to simultaneously stratify the trip or turn samples and preserve strict participant separation. We therefore prioritized participant-level stratification, as it provides a more reliable measure of generalization to unseen drivers, even though the resulting number of trips or turns per class could become imbalanced across folds. To mitigate any resulting class imbalance, balanced accuracy was reported alongside overall accuracy, area under the receiver operating characteristic curve (AUC), precision, and recall to provide a fairer assessment of performance across both diagnostic groups.

Once the dataset was partitioned, each model was trained on the training folds and evaluated on unseen participants in the validation fold. The average metrics across all 7 folds were used to report the final performance.

Evaluation Metrics

To assess the performance of the ML models, multiple evaluation metrics were used. Given the class imbalance in the dataset, relying solely on accuracy could be misleading. Therefore, we used a combination of accuracy, balanced accuracy, AUC, precision, and recall to provide a comprehensive evaluation of model effectiveness.

Accuracy measures the overall proportion of correctly classified instances, but can be biased when the dataset is imbalanced. Balanced accuracy addresses this issue by computing the average recall across both classes, making it a more reliable metric for evaluating performance in cases where 1 class is underrepresented. AUC provides an indication of the model's ability to distinguish between the 2 classes, with higher values indicating better separability. Precision quantifies the proportion of positive classifications that are actually correct, which is particularly important in minimizing false positives. Recall, on the other hand, measures the model's ability to correctly identify positive instances, ensuring that individuals with MCI are accurately detected. The formulas used for computing these metrics are summarized in Table 6.

XSL•FO
RenderX

Table 6. Evaluation metrics and their mathematical formulations.

Metric	Formula[a]	Description
Accuracy		Proportion of correctly classified instances out of all cases.
Balanced accuracy		Average recall for both classes, accounting for imbalances.
AUC[b]	Computed from the ROC[c] curve	Measures the model's ability to distinguish between classes.
Precision		Proportion of correctly identified positive cases among predicted positives.
Recall (sensitivity)		Proportion of actual positives correctly classified by the model.

[a]FN: false negative, FP: false positive, TN: true negative, TP: true positive.

[b]AUC: area under the receiver operating characteristic curve.

[c]ROC: receiver operating characteristic.

Ethical Considerations

A total of 22 participants were initially recruited, informed about the study, and provided written consent. This study was approved by the Institutional Review Board at Arizona State University (STUDY00006547).

Participant privacy and confidentiality were strictly maintained throughout this study. All data were deidentified using unique participant identification codes, and no personally identifiable information was included in any analyses or publications.

Participants received no financial compensation for their participation.

Results

This section reports the performance of the 3 experimental paradigms, single-view modeling (experiment 1), feature-level data fusion (experiment 2), and model-level fusion (experiment 3), evaluated with 7-fold, participant-stratified cross-validation. For every experiment, we averaged accuracy, balanced accuracy, AUC, precision, recall, and F_1-score across folds.

Experiment 1 Results

Experiment 1 examined whether early MCI signals could be more effectively captured from full-trip data or from isolated turning maneuvers when modeled independently. To provide a performance reference, a nontemporal baseline model was first implemented using summarized trip-level statistics from the raw sensor data. For each trip, the mean and SD of the accelerometer (X, Y, and Z), gyroscope (X, Y, and Z), and speed signals were computed, resulting in 14 static features. These features were used to train a random forest classifier, representing a simple benchmark based on conventional telematics features used in earlier driving and cognitive-monitoring studies [19,25]. Table 7 summarizes the cross-validated results for 21 single-view models. The full-trip experiment (1(a)) consistently outperformed the turn-only experiment across all tested architectures. The best performance was achieved by a lightweight convolutional model (TinyFCN without normalization but with class weighting), reaching 78.3% accuracy, 73.6% balanced accuracy, and an AUC of 76.7%. Other strong performers included deeper convolutional models (InceptionTimeSmall) and attention-enhanced recurrent networks (gated recurrent unit, GRU + Attn), suggesting that both paradigms can leverage the extended temporal context of full trips. Channel normalization was found to make results worse.

XSL•FO
RenderX

Table 7. Cross-validation results for all experiments. Metrics are averaged over 8 folds.

Experiment	Model	Normalize	Weights	Accuracy (%)	BA[a] (%)	AUC[b] (%)	Precision (%)	Recall (%)	F_1-score (%)
Baseline	RF[c]	Yes	—[d]	55	49	52	33	20	25
1(a)	1D-CNN[e]	No	No	73	63	62	57	72	63
1(a)	GRU[f]	No	Yes	73	69[g]	73[g]	63	75	60
1(a)	GRU and attention	No	Yes	77	69	66	64	79	69[g]
1(a)	GRU and multiattention	No	Yes	71	69	65	57	83[h]	64
1(a)	Inception lite	Yes	Yes	59	61	56	47	80	54
1(a)	Inception lite	No	Yes	68	65	60	63	64	53
1(a)	InceptionTimeSmall	Yes	Yes	69	69	69	65[h]	67	58
1(a)	InceptionTimeSmall	No	Yes	78[g]	66	64	69[g]	71	65[h]
1(a)	LSTM[i]	No	Yes	69	69	64	56	78	59
1(a)	ResNet TSC[j]	Yes	Yes	65	66	64	52	82	60
1(a)	ResNet TSC	No	Yes	77[h]	67	65	57	73	63
1(a)	TCN[k]	No	Yes	71	60	59	52	68	57
1(a)	TCN and attention	No	Yes	58	58	62	47	86[g]	56
1(a)	TinyFCN	Yes	No	73	63	62	57	72	63
1(a)	TinyFCN	Yes	Yes	72	66	64	65	73	62
1(a)	TinyFCN	No	Yes	78[g]	74[g]	77[g]	65[h]	66	64
1(a)	Tiny TCN	Yes	Yes	63	64	65	51	76	57
1(a)	Tiny TCN	No	Yes	64	60	58	48	82	57
1(b)	1D-CNN	No	No	63	54	53	44	30	34
1(b)	TinyFCN	Yes	Yes	63	56	58	44	53	46
1(b)	TinyFCN	No	Yes	59	57	59	42	64	47

[a]BA: balanced accuracy.

[b]AUC: area under the receiver operating characteristic curve.

[c]RF: random forest.

[d]Not available.

[e]1D-CNN: 1D convolutional neural network.

[f]GRU: gated recurrent unit.

[g]The second best values.

[h]The best values.

[i]LSTM: long short-term memory.

[j]TSC: time series classification.

[k]TCN: temporal convolutional network.

In contrast, the turn-only experiment 1(b) showed significantly lower performance. The best model in this setting, TinyFCN with normalization, reached only 62.7% accuracy and 56.3% balanced accuracy, a decline of about 16 percentage points compared to its trip-level counterpart. Precision dropped below 45% in most turn-only models, indicating insufficient discriminative power in short maneuver windows. Some architectures (eg, TCN + Attn) achieved high recall (up to 86.4%) by overpredicting the positive class, but at the cost of precision and balanced accuracy. Due to the weak performance of turn-only models, subsequent experiments focused on configurations that included turn data only in combination with full-trip data, either through feature-level fusion (experiment 2) or model-level fusion (experiment 3). This decision avoided further computational investment in a setting that showed limited utility for early AD detection under naturalistic conditions.

Overall, experiment 1 demonstrates that global driving behavior across full trips offers substantially more predictive information than isolated turning maneuvers. Among all architectures,

XSL•FO
RenderX

compact convolutional models such as TinyFCN provided the best balance of performance and efficiency, while recurrent models with attention were also competitive. The performance of full-trip TinyFCN (accuracy ≈78%, AUC ≈77%) serves as the baseline for subsequent fusion experiments.

It is important to note that earlier studies [5,6] identified turn-specific kinematic features as promising biomarkers for MCI. However, those findings were obtained in controlled environments, where participants drove short, predefined routes under standardized conditions. In such settings, turn segments are clearly defined, confounding variables are minimized, and behavioral comparisons are more reliable. In contrast, the present study analyzed turning maneuvers within naturalistic, long-distance trips that varied widely in road conditions, traffic, and route design. As a result, turn segments were shorter, noisier, and occasionally truncated by sensor limitations. These factors contributed to the limited performance of turn-only models and motivated the shift toward combining turn data with richer trip-level context in the remaining experiments.

Experiment 2 Results

In experiment 2, trip and turn signals were concatenated at the feature level, and a single model was trained on the resulting 20-channel input. A total of 4 architectures (TinyFCN, GRU, long short-term memory, and TCN) were evaluated. Their cross-validated performance is reported in Table 8.

Table 8. Cross-validated performance of feature-level data-fusion models (experiment 2). Trip and turn signals were concatenated into a single 20-channel input and evaluated with 7-fold participant-stratified cross-validation.

Experiment	Model	Normalize	Weights	Accuracy (%)	BA[a] (%)	AUC[b] (%)	Precision (%)	Recall (%)	F_1-score (%)
2	TinyFCN	No	Yes	62	59	52	44	86[c]	56[c]
2	GRU[d]	No	Yes	68[e]	63	63[e]	52[e]	62	53
2	LSTM[f]	No	Yes	67	67[c]	64[c]	55[c]	69[e]	55[e]
2	TCN[g]	No	Yes	70[c]	63[e]	63	50	62	53

[a]BA: balanced accuracy

[b]AUC: area under the receiver operating characteristic curve.

[c]The best values.

[d]GRU: gated recurrent unit.

[e]The second best is only underlined.

[f]LSTM: long short-term memory.

[g]TCN: temporal convolutional network.

Overall, performance improved over the turn-only models from experiment 1(b), confirming that global trip context can offset the sparsity of turn data. However, none of the fusion models outperformed the best full-trip baselines from experiment 1(a). The highest accuracy (70%) was achieved by TCN, though its AUC (63%) and balanced accuracy (63%) fell short of the full-trip TinyFCN benchmark. Long short-term memory delivered the highest balanced accuracy (67%), while GRU achieved similar accuracy and recall but lower precision. TinyFCN, which had previously performed best on full trips, dropped to 62% accuracy and 52% AUC, suggesting that feature-level concatenation may impair its ability to model trip dynamics effectively.

These results indicate that early fusion does not offer a reliable method for combining localized and global driving features. While a modest gain in recall was observed, it came at the cost of precision and overall discriminative power. This degradation likely results from the mismatch in temporal characteristics between trips and turns when merged into a single input. These findings support the need for a late-fusion strategy, as explored in experiment 3, where each data type is modeled independently before integration.

Experiment 3 Results

In the final experiment, the trip and turn streams were treated as complementary modalities. Each was processed by a dedicated encoder, and their latent vectors were merged in a late-fusion classifier. Table 9 summarizes the cross-validated results for 7 dual-branch architectures. The dual-encoder strategy outperformed the feature-level fusion models from experiment 2 across all metrics and approached the performance of the best full-trip baselines from experiment 1(a). The highest overall accuracy (75%) was achieved by DualTinyFCN, which also recorded the best AUC (68%) and matched the highest recall (74%). DualTCN with self-attention produced the strongest balanced accuracy (72%) and recall (77%), while maintaining 75% accuracy. DualGRU with a single attention head offered a solid alternative at 73% accuracy and 65% balanced accuracy; its multihead variant improved recall to 84% but at the cost of precision.

XSL•FO
RenderX

Table 9. Cross-validation results for model-level fusion (experiment 3). Each architecture comprises separate trip and turn encoders whose outputs are combined by either concatenation (DualTinyFCN) or a learned gating mechanism (all others).

Experiment	Model	Normalize	Weights	Accuracy (%)	BA[a] (%)	AUC[b] (%)	Precision (%)	Recall (%)	F_1-score (%)
3	Dual GRU[c]	No	Yes	63	62	58	47	67	50
3	Dual GRU Attn	No	Yes	73	65[d]	63	56[d]	76	62[d]
3	Dual GRU Multi-Head	No	Yes	66	63	66	52	84[e]	60
3	Dual LSTM[f]	No	Yes	65	62	64	51	61	50
3	DualTCN	No	Yes	66	60	67[d]	47	79[d]	57
3	DualTCN Attn	No	Yes	75[d]	72[e]	66	57[e]	77	63[e]
3	Dual Tiny FCN[g]	No	Yes	75[e]	65	68[e]	53	74	61

[a]BA: balanced accuracy

[b]AUC: area under the receiver operating characteristic curve.

[c]GRU: gated recurrent unit.

[d]The second best values.

[e]The best values.

[f]LSTM: long short-term memory

[g]FCN: fully convolutional network

Relative to experiment 2, balanced accuracy improved by 6 to 8 percentage points, and AUC increased by about 5 points, suggesting that separate feature extraction for trips and turns reduced the interference observed with early fusion. While none of the dual-branch models surpassed the single-view TinyFCN baseline from experiment 1(a), the performance gap was reduced to within 4 points, with noticeably stronger recall and class balance.

These results indicate that turning behavior carries useful complementary information, which becomes effective when modeled independently before fusion. However, the late-fusion models still fell short of the trip-only baseline, unlike in earlier studies conducted under controlled driving conditions. A likely explanation is the greater behavioral variability in naturalistic turn maneuvers, where factors such as traffic, shallow bends, truncated segments, and GPS inconsistencies introduce noise that diminishes signal quality. To overcome this, 2 improvements are proposed. First, a more selective turn-extraction method could be implemented to filter out low-information maneuvers (eg, shallow curves or stop-sign rolls) and retain only cognitively demanding turns. Second, the use of an adaptive fusion mechanism, such as a trainable gating or context-aware attention layer, could allow the model to dynamically weigh turn features based on context, rather than relying on fixed integration. These enhancements may help future late-fusion models surpass the trip-only benchmark.

Participant-Level Performance of the Best-Performing Model

To further evaluate model effectiveness, participant-level performance was analyzed using the best-performing model from experiment 1(a), which achieved the highest average accuracy (78%). Figure 7 shows the percentage of correctly classified trips per participant, color-coded by diagnostic group.

XSL•FO
RenderX

Figure 7. Per-subject trip classification accuracy of the best performance model, color-coded by cognitive status (green=healthy, red=MCI). MCI: mild cognitive impairment.

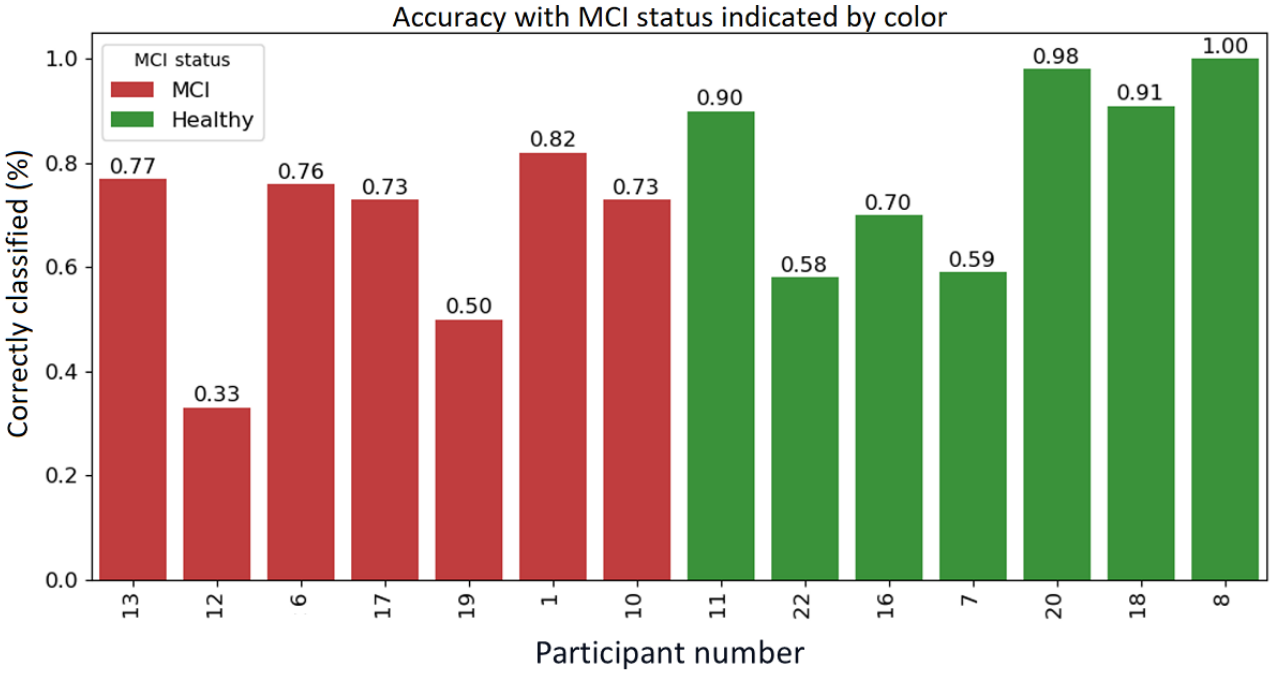

This analysis revealed that trips from cognitively healthy participants were classified more accurately than those from the MCI group. Within the MCI cohort, classification accuracy appeared to correlate with the number of available trips. Participants 12 and 19, who contributed only 3 and 4 trips respectively, showed the lowest accuracies (33% and 50%). In contrast, participant 1, also in the MCI group, provided 28 trips and achieved over 80% accuracy, suggesting that greater data volume improves participant-specific classification performance. These findings support the decision to evaluate trips individually rather than applying a majority-vote rule per participant, as done in previous work. As MCI symptoms tend to appear episodically, a majority-vote approach may misclassify participants with sporadic impairments. For instance, participant 12, clinically diagnosed with MCI, was misclassified on 2 of 3 trips. A majority-vote method would incorrectly label this participant as healthy, masking the sporadic but clinically meaningful deviations this framework aims to detect.

The granular trip-wise approach captures the variability that defines mild impairment and provides a more sensitive early warning mechanism than binary participant-level labels. This variability can be expressed as a frequency-based risk score based on the proportion of trips classified as impaired for each driver. Rather than producing a fixed “MCI” or “healthy” label, the score outputs a continuous risk value between 0 and 1, allowing clinicians to define thresholds for follow-up assessment. The choice of such a threshold will have practical implications. A low threshold (eg, flagging drivers if 10% or more of their trips are classified as impaired) increases sensitivity and supports early detection but may lead to more false positives and unnecessary follow-up. A high threshold (eg, 50%) reduces false positives but risks missing individuals with sporadic lapses (precisely the pattern seen in early MCI). As the risk score is continuous, thresholds can be tailored to specific clinical contexts. For example, high sensitivity may be prioritized in population-level screening, while higher precision may be preferred in specialist clinics. By presenting performance curves across thresholds or reporting AUC values alongside confusion matrices at clinically relevant cutoffs, these trade-offs can be made explicit and support informed deployment of the model in practice.

Trip count was also found to influence the stability of those episodic signals. With fewer than 5 trips, a single misclassified journey can flip a driver’s apparent status, explaining the wide swings in accuracy for participants 12 and 19. As the dataset grows (through additional participants, extended monitoring, or data augmentation), the law of large numbers should attenuate this volatility and sharpen the distinction between truly unimpaired drivers and those with early cognitive change. Overall, these results reinforce the importance of context-aware, trip-level evaluation for detecting early MCI. Rather than relying on binary labels, future implementations should adopt frequency-based risk scoring to translate trip-level outputs into longitudinal, clinically actionable indicators.

Discussion

This study demonstrated the potential of naturalistic driving data as a digital biomarker for early MCI detection. Prior limitations, such as controlled test settings, reliance on summary statistics, and rigid evaluation protocols, were addressed through a framework that embraces real-world variability and context-aware analysis, structured around the 3 research questions posed in the Introduction section.

First, the robustness of driving-based biomarkers under naturalistic conditions was assessed (RQ1). Models trained on full-trip data achieved 78% accuracy (AUC 77%) despite variations in routes, traffic, and sensor noise, while turn-only

XSL•FO
RenderX

inputs underperformed by approximately 16 percentage points. These results affirm that early cognitive change is detectable through naturalistic driving; however, short turning maneuvers alone were found to be too noisy to provide reliable indicators.

Second, to address RQ2, a multistage pipeline was developed to transform raw, noisy, multisensor data into structured model inputs. Signals of varying frequencies were aligned, trips segmented, and interpolation applied to ensure consistency. Turn maneuvers were extracted using a targeted method, yielding maneuver-level data while preserving temporal and sensor fidelity for deep learning.

Third, modeling strategies were compared under current data limitations (RQ3). Single-view models on full-trip data remained strongest. While early fusion of trip and turn data failed to outperform this baseline, late fusion using dual encoders significantly improved balanced accuracy and recall, suggesting that turn cues become useful when learned in a dedicated branch. As larger, cleaner turn datasets are acquired, late fusion is expected to surpass trip-only models, especially with mechanisms that emphasize turns only when informative.

In addition, the participant-level analysis revealed that most misclassifications occurred among MCI drivers with few recorded trips, underscoring the effects of behavioral noise and data scarcity. As MCI is marked by sporadic impairments, traditional aggregate predictions may miss subtle signs. By evaluating each trip and maneuver individually, the proposed approach enables detection of episodic lapses, offering a practical early warning system for clinical follow-up.

Future improvements should focus on refining turn extraction through context-aware filtering, enhancing late-fusion models with adaptive gating or attention mechanisms, and enriching the dataset via increased participation and targeted augmentation. Prospective validation and integration of complementary modalities (eg, eye-tracking and in-cabin audio) may yield a more comprehensive behavioral signature of early cognitive decline. Furthermore, given the relatively small dataset, future work could explore the use of transfer learning from models pretrained on large-scale sensor-based time-series datasets. Models trained on motion, activity recognition, or physiological sensing data capture general temporal and kinematic patterns that overlap with vehicle dynamics such as acceleration and rotation. Fine-tuning such pretrained encoders on naturalistic driving data could improve feature extraction, reduce dependence on large labeled cohorts, and enhance generalization to new drivers or sensing platforms. Incorporating transfer learning in this way would be a practical step toward building more data-efficient and scalable cognitive monitoring systems. Collectively, these efforts may further establish naturalistic driving as a viable and nuanced platform for proactive cognitive health monitoring.

Acknowledgments

We want to thank the support of BitBrew Inc (Danlaw Inc)’s colleagues who supported our work by providing the on-board diagnostics. Along this line, we want to express special thanks to Christa Lomazzo, Sudhir Sagi, Priya Gomatham, John Highberg, Mike Carrol, and Larry Dimitrievski for the great product, product support, and collaboration. We also note that TF Health Corporation conducts business under the trade name Breezing Co.

We want to deeply thank the financial and management support of the National Institutes of Health, National Institute of Aging (R43AG078063, R01AG057708, and 2R44AG078063); Wear Tech Center, Partnership for Economic Innovation, Arizona Commerce Authority; and A. J. and Sigismunda Palumbo Charitable Trust. We want to thank the late Ezra Geda, who diligently worked on this project and supported the team with his unforgettable kindness and persistence. Ezra, you are missed, but we will carry forward this project in your honor.

Data Availability

The datasets presented in this paper are not readily available because the data are part of an ongoing study. Requests to access the datasets should be directed to the corresponding author. The underlying code for this study (and training or validation datasets) is not publicly available but may be made available to qualified researchers on reasonable request to the corresponding author.

Funding

This work was supported by the National Institutes of Health (R43AG078063), National Institute of Aging (R01AG057708 and 2R44AG078063), Wear Tech Center, Partnership for Economic Innovation, Arizona Commerce Authority, and Palumbo Charitable Trust.

Authors' Contributions

Conceptualization: FA-H, FT, YEG, TW, EF
Data curation: FA-H, PS
Formal analysis: FA-H, PS
Funding acquisition: TW, EF, FT
Investigation: FA-H, TW
Methodology: FA-H, FT, TW, EF
Project administration: TW, EF

XSL•FO
RenderX

Resources: YEG, FT
Supervision: TW, EF
Validation: FA-H
Visualization: FA-H
Writing - original draft: FA-H, TW, YW, EF, FT, YEG
Writing - review and editing: FA-H, TW, YW, EF, FT, YEG
Software: FA-H
All authors have read and agreed to the published version of this paper.

Conflicts of Interest

None declared.

Multimedia Appendix 1
Experiment 1.
[DOCX File , 15 KB - medinform_v14i1e83622_app1.docx]

Multimedia Appendix 2
Experiment 2.
[DOCX File , 15 KB - medinform_v14i1e83622_app2.docx]

Multimedia Appendix 3
Experiment 3.
[DOCX File , 15 KB - medinform_v14i1e83622_app3.docx]

References

1. Better MA. 2023 Alzheimer's disease facts and figures. Alzheimers Dement 2023;19(4):1598-1695. [doi: 10.1002/alz.13016] [Medline: 36918389]
2. Bennett DA, Schneider JA, Arvanitakis Z, Kelly JF, Aggarwal NT, Shah RC, et al. Neuropathology of older persons without cognitive impairment from two community-based studies. Neurology 2006;66(12):1837-1844. [doi: 10.1212/01.wnl.0000219668.47116.e6] [Medline: 16801647]
3. Knopman DS, Parisi JE, Salviati A, Floriach-Robert M, Boeve BF, Ivnik RJ, et al. Neuropathology of cognitively normal elderly. J Neuropathol Exp Neurol 2003;62(11):1087-1095. [doi: 10.1093/jnen/62.11.1087] [Medline: 14656067]
4. Casey DA, Antimisiaris D, O'Brien J. Drugs for Alzheimer's disease: are they effective? P T 2010;35(4):208-211 [FREE Full text] [Medline: 20498822]
5. Al-Hindawi F, Serhan P, Geda YE, Tsow F, Wu T, Forzani E. LiveDrive AI: a pilot study of a machine learning-powered diagnostic system for real-time, non-invasive detection of mild cognitive impairment. Bioengineering (Basel) 2025;12(1):86 [FREE Full text] [doi: 10.3390/bioengineering12010086] [Medline: 39851360]
6. Serhan P, Victor S, Osorio Perez O, Abi Karam K, Elghoul A, Ransdell M, et al. Smart driving technology for non-invasive detection of age-related cognitive decline. Sensors (Basel) 2024;24(24):8062 [FREE Full text] [doi: 10.3390/s24248062] [Medline: 39771798]
7. Plassman BL, Langa KM, Fisher GG, Heeringa SG, Weir DR, Ofstedal MB, et al. Prevalence of dementia in the United States: the aging, demographics, and memory study. Neuroepidemiology 2007;29(1-2):125-132 [FREE Full text] [doi: 10.1159/000109998] [Medline: 17975326]
8. Shin JH. Dementia epidemiology fact sheet 2022. Ann Rehabil Med 2022;46(2):53-59 [FREE Full text] [doi: 10.5535/arm.22027] [Medline: 35508924]
9. World Alzheimer Report 2019: Attitudes to Dementia. Alzheimer's Disease International. 2019. URL: https://www.alzint.org/resource/world-alzheimer-report-2019/ [accessed 2026-02-05]
10. Dubois B, Feldman HH, Jacova C, Hampel H, Molinuevo JL, Blennow K, et al. Advancing research diagnostic criteria for Alzheimer's disease: the IWG-2 criteria. Lancet Neurol 2014;13(6):614-629. [doi: 10.1016/S1474-4422(14)70090-0] [Medline: 24849862]
11. Albert MS, DeKosky ST, Dickson D, Dubois B, Feldman HH, Fox NC, et al. The diagnosis of mild cognitive impairment due to Alzheimer's disease: recommendations from the National Institute on Aging-Alzheimer's Association workgroups on diagnostic guidelines for Alzheimer's disease. Alzheimers Dement 2011;7(3):270-279 [FREE Full text] [doi: 10.1016/j.jalz.2011.03.008] [Medline: 21514249]
12. Davatzikos C, Resnick SM, Wu X, Parmpi P, Clark CM. Individual patient diagnosis of AD and FTD via high-dimensional pattern classification of MRI. Neuroimage 2008;41(4):1220-1227 [FREE Full text] [doi: 10.1016/j.neuroimage.2008.03.050] [Medline: 18474436]

XSL•FO
RenderX

13. Crous-Bou M, Minguillón C, Gramunt N, Molinuevo JL. Alzheimer's disease prevention: from risk factors to early intervention. Alzheimers Res Ther 2017;9(1):71 [FREE Full text] [doi: 10.1186/s13195-017-0297-z] [Medline: 28899416]
14. Leifer BP. Early diagnosis of Alzheimer's disease: clinical and economic benefits. J Am Geriatr Soc 2003;51(5 Suppl Dementia):S281-S288. [doi: 10.1046/j.1532-5415.5153.x] [Medline: 12801384]
15. Kishore P, Usha Kumari C, Kumar M, Pavani T. Detection and analysis of Alzheimer's disease using various machine learning algorithms. Mater Today: Proc 2021;45:1502-1508. [doi: 10.1016/j.matpr.2020.07.645]
16. Misra C, Fan Y, Davatzikos C. Baseline and longitudinal patterns of brain atrophy in MCI patients, and their use in prediction of short-term conversion to AD: results from ADNI. Neuroimage 2009;44(4):1415-1422 [FREE Full text] [doi: 10.1016/j.neuroimage.2008.10.031] [Medline: 19027862]
17. Gunes S, Aizawa Y, Sugashi T, Sugimoto M, Rodrigues PP. Biomarkers for Alzheimer's disease in the current state: a narrative review. Int J Mol Sci 2022;23(9):4962 [FREE Full text] [doi: 10.3390/ijms23094962] [Medline: 35563350]
18. Jack CR, Knopman DS, Jagust WJ, Shaw LM, Aisen PS, Weiner MW, et al. Hypothetical model of dynamic biomarkers of the Alzheimer's pathological cascade. Lancet Neurol 2010;9(1):119-128 [FREE Full text] [doi: 10.1016/S1474-4422(09)70299-6] [Medline: 20083042]
19. Bayat S, Babulal GM, Schindler SE, Fagan AM, Morris JC, Mihailidis A, et al. GPS driving: a digital biomarker for preclinical Alzheimer disease. Alzheimers Res Ther 2021;13(1):115 [FREE Full text] [doi: 10.1186/s13195-021-00852-1] [Medline: 34127064]
20. de la Paz Scribano Parada M, Palau FG, Rodríguez SV, Rincon M, Rico Barroeta MJ, García Rodriguez M, et al. Preclinical cognitive markers of Alzheimer disease and early diagnosis using virtual reality and artificial intelligence: literature review. JMIR Med Inform 2025;13:e62914 [FREE Full text] [doi: 10.2196/62914] [Medline: 39881486]
21. Oh SS, Kang B, Hong D, Kim JI, Jeong H, Song J, et al. A multivariable prediction model for mild cognitive impairment and dementia: algorithm development and validation. JMIR Med Inform 2024;12(1):e59396 [FREE Full text] [doi: 10.2196/59396] [Medline: 39576972]
22. van den Berg RL, van der Landen SM, Keijzer MJ, van Gils AM, van Dam M, Ziesemer KA, et al. Smartphone- and tablet-based tools to assess cognition in individuals with preclinical Alzheimer disease and mild cognitive impairment: scoping review. J Med Internet Res 2025;27:e65297 [FREE Full text] [doi: 10.2196/65297] [Medline: 40424609]
23. Coughlan G, Laczó J, Hort J, Minihane A, Hornberger M. Spatial navigation deficits - overlooked cognitive marker for preclinical Alzheimer disease? Nat Rev Neurol 2018;14(8):496-506. [doi: 10.1038/s41582-018-0031-x] [Medline: 29980763]
24. Allison SL, Fagan AM, Morris JC, Head D. Spatial navigation in preclinical Alzheimer's disease. J Alzheimers Dis 2016;52(1):77-90 [FREE Full text] [doi: 10.3233/JAD-150855] [Medline: 26967209]
25. Di X, Shi R, DiGuiseppi C, Eby DW, Hill LL, Mielenz TJ, et al. Using naturalistic driving data to predict mild cognitive impairment and dementia: preliminary findings from the Longitudinal Research on Aging Drivers (LongROAD) study. Geriatrics (Basel) 2021;6(2):45. [doi: 10.3390/geriatrics6020045] [Medline: 33922735]
26. Bennett JM, Chekaluk E, Batchelor J. Cognitive tests and determining fitness to drive in dementia: a systematic review. J Am Geriatr Soc 2016;64(9):1904-1917. [doi: 10.1111/jgs.14180] [Medline: 27253511]
27. Roe CM, Barco PP, Head DM, Ghoshal N, Selsor N, Babulal GM, et al. Amyloid imaging, cerebrospinal fluid biomarkers predict driving performance among cognitively normal individuals. Alzheimer Dis Assoc Disord 2017;31(1):69-72 [FREE Full text] [doi: 10.1097/WAD.0000000000000154] [Medline: 27128959]
28. Roe CM, Babulal GM, Mishra S, Gordon BA, Stout SH, Ott BR, et al. Tau and amyloid positron emission tomography imaging predict driving performance among older adults with and without preclinical Alzheimer's disease. J Alzheimers Dis 2017;61(2):509-513 [FREE Full text] [doi: 10.3233/JAD-170521] [Medline: 29171997]
29. Cerino ES, Katz MJ, Wang C, Qin J, Gao Q, Hyun J, et al. Variability in cognitive performance on mobile devices is sensitive to mild cognitive impairment: results from the Einstein aging study. Front Digit Health 2021;3:758031 [FREE Full text] [doi: 10.3389/fdgth.2021.758031] [Medline: 34927132]
30. Gorus E, De Raedt R, Lambert M, Lemper J, Mets T. Reaction times and performance variability in normal aging, mild cognitive impairment, and Alzheimer's disease. J Geriatr Psychiatry Neurol 2008;21(3):204-218. [doi: 10.1177/0891988708320973] [Medline: 18838743]
31. Zdanowski S, Tieks A, Jeronimus BF, Zuidersma M. Intra-individual variability in cognitive performance can befuddle the study of cognitive impairments and decline. J Alzheimers Dis 2022;85(2):519-525 [FREE Full text] [doi: 10.3233/JAD-210304] [Medline: 34864656]

Abbreviations

1D-CNN: 1D convolutional neural network
AD: Alzheimer disease
AUC: area under the receiver operating characteristic curve
AWS S3: Amazon Web Services Simple Storage Service
GRU: gated recurrent unit
MCI: mild cognitive impairment

XSL•FO
RenderX

ML: machine learning
OBD: on-board diagnostics
RNN: recurrent neural network
TCN: temporal convolutional network

Edited by A Benis; submitted 05.Sep.2025; peer-reviewed by Y Cheng, SB Celebi; comments to author 13.Oct.2025; revised version received 18.Nov.2025; accepted 01.Jan.2026; published 06.Mar.2026.

Please cite as:
Al-Hindawi F, Wu T, Wen Y, Serhan P, Forzani E, Tsow F, Geda YE
Leveraging Naturalistic Driving Digital Biomarkers for Early Mild Cognitive Impairment Detection: Deep Learning Strategies
JMIR Med Inform 2026;14:e83622
URL: https://medinform.jmir.org/2026/1/e83622
doi:10.2196/83622
PMID:

©Firas Al-Hindawi, Teresa Wu, Yutong Wen, Peter Serhan, Erica Forzani, Francis Tsow, Yonas E Geda. Originally published in JMIR Medical Informatics (https://medinform.jmir.org), 06.Mar.2026. This is an open-access article distributed under the terms of the Creative Commons Attribution License (https://creativecommons.org/licenses/by/4.0/), which permits unrestricted use, distribution, and reproduction in any medium, provided the original work, first published in JMIR Medical Informatics, is properly cited. The complete bibliographic information, a link to the original publication on https://medinform.jmir.org/, as well as this copyright and license information must be included.

XSL•FO
RenderX

Enhancing Predictive Accuracy of Mood Symptoms Using Wearable Devices and Machine Learning in Bipolar Disorder

P Keerthana Nair*, MBBS; Priyanka Renita D'Souza*, MBBS, MD

Department of Psychiatry, Kasturba Medical College Mangalore, Manipal Academy of Higher Education, Manipal, India

*all authors contributed equally

Corresponding Author:
Priyanka Renita D'Souza, MBBS, MD
Department of Psychiatry, Kasturba Medical College Mangalore, Manipal Academy of Higher Education, Manipal, India

Related Article:

https://medinform.jmir.org/2025/1/e66277

(JMIR Med Inform 2026;14:e92172) doi:10.2196/92172

KEYWORDS

machine learning; wearable device; bipolar disorder; mood disorder; digital mental health

We read the paper "Using Wearable Device and Machine Learning to Predict Mood Symptoms in Bipolar Disorder: Development and Usability Study" by Wu et al [1] with great interest. The integration of wearable data with machine learning to predict mood symptoms is clinically relevant and holds significant potential for real-world applications. However, we would like to highlight specific methodological aspects and possible future directions that could significantly enhance clinical reliability.

Our primary observation concerns the use of weekly mood assessments with backfilling. The authors acknowledged that their labeling method relied on self-rated questionnaires with backfilled mood symptoms for the preceding 7 days, and the participants may not complete these promptly as symptoms emerged, which could affect the accuracy of mood labels. In line with this, we appreciate the intent to minimize patient burden, but using retrospective entry to accurately capture daily mood fluctuations may not be reliable in the context of bipolar disorder. A patient feeling particularly low at the time of filling the weekly scale may unknowingly project that state onto the entire week, and that single net rating may not reflect the preceding days. This may create a risk of labeling daily physiological data with an inaccurate mood state, especially as the wearable data (sleep, activity, heart rate) are collected daily. To address this, future study designs may incorporate ecological momentary assessment, similar to the studies by Schwartz et al [2] and Li et al [3] that used digital biomarkers in studies on mood disorders. Implementing a quick visual check-in once or twice a day, for instance, a 5-point emoji scale with an optional short note, would reduce recall bias and ensure that daily wearable data are mapped against actual daily mood.

Furthermore, physiological markers such as average heart rate and total sleep hours are nonspecific and easily influenced by external stressors, including daily conflicts, work pressure, or life events. Without accounting for these confounding factors, the model risks interpreting situational stress as mood signals. As noted by the authors, heart rate is an index of sympathetic and parasympathetic influences of the autonomic nervous system in both stress and resting states, highlighting the overlap between stress response and mood states. Therefore, including a brief daily measure in future models to capture perceived daily stress would help in differentiating reactive distress from endogenous mood changes.

In conclusion, the integration of wearable biosensors is a promising development. However, we believe that a shift in study design from retrospective weekly aggregates to real-time, context-sensitive monitoring would further maximize the clinical utility of these models.

Acknowledgments

We used the generative artificial intelligence tool Gemini to make minor edits to the manuscript to improve language clarity, which were further reviewed and revised by the authors. The authors take full responsibility for the content of the publication.

Funding

The authors declare that no financial support was received for this work.

XSL•FO
RenderX

Data Availability

Data sharing is not applicable to this paper as no datasets were generated or analyzed during this study.

Authors' Contributions

Conceptualization: PKN, PRD
Formal analysis: PKN
Writing – original draft: PKN
Writing – review & editing: PRD
Supervision: PRD
Both authors approved the final manuscript.

Conflicts of Interest

None declared.

Editorial Notice

The corresponding author of "Using Wearable Device and Machine Learning to Predict Mood Symptoms in Bipolar Disorder: Development and Usability Study" was given the opportunity to respond to this letter but did not respond.

References

1. Wu CT, Hsieh MH, Chen IM, et al. Using wearable device and machine learning to predict mood symptoms in bipolar disorder: development and usability study. JMIR Med Inform 2025 Sep 16;13(1):e66277. [doi: 10.2196/66277] [Medline: 40957006]
2. Schwartz S, Schultz S, Reider A, Saunders EFH. Daily mood monitoring of symptoms using smartphones in bipolar disorder: a pilot study assessing the feasibility of ecological momentary assessment. J Affect Disord 2016 Feb;191:88-93. [doi: 10.1016/j.jad.2015.11.013] [Medline: 26655117]
3. Li H, Mukherjee D, Krishnamurthy VB, et al. Use of ecological momentary assessment to detect variability in mood, sleep and stress in bipolar disorder. BMC Res Notes 2019 Dec 4;12(1):791. [doi: 10.1186/s13104-019-4834-7] [Medline: 31801608]

Edited by A Coristine; submitted 26.Jan.2026; this is a non–peer-reviewed article;accepted 27.Feb.2026; published 12.Mar.2026.

Please cite as:
Nair PK, D'Souza PR
Enhancing Predictive Accuracy of Mood Symptoms Using Wearable Devices and Machine Learning in Bipolar Disorder
JMIR Med Inform 2026;14:e92172
URL: https://medinform.jmir.org/2026/1/e92172
doi:10.2196/92172

© P Keerthana Nair, Priyanka Renita D'Souza. Originally published in JMIR Medical Informatics (https://medinform.jmir.org), 12.Mar.2026. This is an open-access article distributed under the terms of the Creative Commons Attribution License (https://creativecommons.org/licenses/by/4.0/), which permits unrestricted use, distribution, and reproduction in any medium, provided the original work, first published in JMIR Medical Informatics, is properly cited. The complete bibliographic information, a link to the original publication on https://medinform.jmir.org/, as well as this copyright and license information must be included.

XSL•FO
RenderX

Correction: Comprehensive Pediatric Health Risk Stratification Using an AI-Driven Framework in Children Aged 2 to 8 Years: Design and Validation Study

Jundan Chen*, PhD; Zhihe Mao*, BA

School of Physical Education, Hunan University of Arts and Science, 3150 Dongting Road, Changde, Hunan, China

*all authors contributed equally

Corresponding Author:
Zhihe Mao, BA
School of Physical Education, Hunan University of Arts and Science, 3150 Dongting Road, Changde, Hunan, China

Related Article:

Correction of: https://medinform.jmir.org/2026/1/e80163

Abstract

(JMIR Med Inform 2026;14:e92491) doi:10.2196/92491

In “Comprehensive Pediatric Health Risk Stratification Using an AI-Driven Framework in Children Aged 2 to 8 Years: Design and Validation Study” [1], the authors noted two errors.

The author list has been corrected from the following:

Zhihe Mao, PhD; Jundan Chen, PhD

The author list now reads:

Jundan Chen, PhD; Zhihe Mao, BA

Author ZM’s contact information has been corrected to the following:

Phone: 86 13789072016

Fax: 86 07367283047

The correction will appear in the online version of the paper on the JMIR Publications website, together with the publication of this correction notice. Because this was made after submission to PubMed, PubMed Central, and other full-text repositories, the corrected article has also been resubmitted to those repositories.

Reference

1. Chen J, Mao Z. Comprehensive pediatric health risk stratification using an AI-driven framework in children aged 2 to 8 years: design and validation study. JMIR Med Inform 2026 Jan 26;14:e80163. [doi: 10.2196/80163] [Medline: 41587023]

Submitted 30.Jan.2026; this is a non–peer-reviewed article;accepted 05.Feb.2026; published 27.Feb.2026.

Please cite as:
Chen J, Mao Z
Correction: Comprehensive Pediatric Health Risk Stratification Using an AI-Driven Framework in Children Aged 2 to 8 Years: Design and Validation Study
JMIR Med Inform 2026;14:e92491
URL: https://medinform.jmir.org/2026/1/e92491
doi:10.2196/92491

© Jundan Chen Jr, Zhihe Mao Jr. Originally published in JMIR Medical Informatics (https://medinform.jmir.org), 27.Feb.2026. This is an open-access article distributed under the terms of the Creative Commons Attribution License (https://creativecommons.org/licenses/by/4.0/), which permits unrestricted use, distribution, and reproduction in any medium, provided the original work, first published in JMIR Medical Informatics, is properly cited. The complete bibliographic information, a link to the original publication on https://medinform.jmir.org/, as well as this copyright and license information must be included.

XSL•FO
RenderX

Corrigenda and Addenda

Correction: Exploring the Potential of Claude 3 Opus in Renal Pathological Diagnosis: Performance Evaluation

JMIR Publications Editorial Office

Related Article:

Correction of: https://medinform.jmir.org/2024/1/e65033

(JMIR Med Inform 2026;14:e88845) doi:10.2196/88845

Following the publication of "Exploring the Potential of Claude 3 Opus in Renal Pathological Diagnosis: Performance Evaluation" [1], concerns were raised regarding a potential conflict of interest between reviewer X Liu and members of the author list. After review, it was determined that the authors and the reviewer were both affiliated with Sichuan University West China Hospital. This conflict of interest was not disclosed to the editorial office as per journal policy.

This article has been subsequently reassessed by the *JMIR Medical Informatics* editor in chief, who determined that the content of this review did not unduly influence the decision to accept the article. The decision to accept the submission was based primarily on the remaining reviewers' comments and the previous editor in chief's contemporary appraisal of the manuscript.

As such, the JMIR Publications Editorial Office issues this corrigendum to update the Conflicts of Interest statement as follows:

> *Reviewer X Liu was found to have undisclosed conflicts of interest with members of the author list under the terms of JMIR Publications policy. The editor in chief determined that the content of the reviews did not unduly influence the decision to accept the article. The decision to accept the submission was based primarily on the remaining reviewers' comments and the editor in chief's contemporary appraisal of the manuscript.*

We regret that these issues were not identified before publication.

The correction will appear in the online version of the paper on the JMIR Publications website together with the publication of this correction notice. Because this was made after submission to PubMed, PubMed Central, and other full-text repositories, the corrected article has also been resubmitted to those repositories.

Reference

1. Li X, Liu K, Lang Y, Chai Z, Liu F. Exploring the potential of claude 3 opus in renal pathological diagnosis: performance evaluation. JMIR Med Inform 2024 Nov 15;12:e65033 [FREE Full text] [doi: 10.2196/65033] [Medline: 39547661]

Submitted 02.Dec.2025; this is a non–peer-reviewed article;accepted 02.Dec.2025; published 23.Feb.2026.

Please cite as:
Editorial Office JMIRP
Correction: Exploring the Potential of Claude 3 Opus in Renal Pathological Diagnosis: Performance Evaluation
JMIR Med Inform 2026;14:e88845
URL: https://medinform.jmir.org/2026/1/e88845
doi:10.2196/88845
PMID:

©JMIR Publications Editorial Office. Originally published in JMIR Medical Informatics (https://medinform.jmir.org), 23.Feb.2026. This is an open-access article distributed under the terms of the Creative Commons Attribution License (https://creativecommons.org/licenses/by/4.0/), which permits unrestricted use, distribution, and reproduction in any medium, provided the original work, first published in JMIR Medical Informatics, is properly cited. The complete bibliographic information, a link to the original publication on https://medinform.jmir.org/, as well as this copyright and license information must be included.

XSL•FO
RenderX

Patient Experiences With Outpatient Pharmacy Services in Hospitals Using Automated Pharmacy Systems: Cross-Sectional Study

Ali Jasem Buabbas[1], MSc, PhD; Fatemah Mohammad Alsaleh[2], MSc, PhD; Mariam Alsanafi[2], MSc, PhD; Maryam Ali Safar[3], BMedSc, DMD; Ahmad T Al-Sultan[1], MSc, PhD; Talal Ahmad Zaman[4]

[1]Department of Community Medicine and Behavorial Sciences, College of Medicine, Kuwait University, Hawalli, Jabriya, Kuwait

[2]Department of Pharmacy Practice, College of Pharmacy, Kuwait University, Jabriya, Kuwait

[3]Ministry of Health, Kuwait, Kuwait

[4]College of Medicine, University of Alexandria, Alexandria, Egypt

Corresponding Author:
Ali Jasem Buabbas, MSc, PhD
Department of Community Medicine and Behavorial Sciences, College of Medicine, Kuwait University, Hawalli, Jabriya, Kuwait

Abstract

Background: Advancements in health technology and the adoption of electronic systems in hospital pharmacies have transformed pharmacy practice and service delivery, with patients and health care providers reporting perceived benefits related to patient care and safety. Therefore, it is of paramount importance to seek patients' opinions based on their experiences in receiving outpatient pharmacy services through automated pharmacy systems.

Objective: This study aimed to investigate patients' experiences and explore their satisfaction with outpatient pharmacy services in hospitals using automated pharmacy systems.

Methods: This cross-sectional study used an online questionnaire to assess patients' experiences of outpatient pharmacy services in governmental hospitals in Kuwait where automated pharmacy systems are implemented.

Results: Almost 95% (393/416) of the participants either agreed or strongly agreed that they were totally satisfied with the services delivered through the automated pharmacy systems. Participants reported the perceived benefits of these outpatient pharmacy services, including perceived prevention of medication errors (211/416, 50.7%), time savings (356/416, 85.6%), and easier access to prescription information at any time (249/416, 59.9%).

Conclusions: Patients' experiences with outpatient pharmacy services in automated pharmacy settings were generally positive, reflecting satisfaction with medication collection and service quality.

(JMIR Med Inform 2026;14:e80963) doi:10.2196/80963

KEYWORDS

automated pharmacy; pharmacy practice; patient experience; patient satisfaction; e-dispensing; e-prescribing

Introduction

Over the past years, pharmacy practice has undergone significant transformation with the adoption of electronic prescribing (e-prescribing) and electronic dispensing (e-dispensing; hospital information system [HIS]) systems, resulting in numerous advantages within professional practice settings. Notable examples include reductions in medication errors [1-4], time savings [5,6], and increased work efficiency [1,2,6]. However, such systems also present certain challenges. Reported drawbacks include risks to medication safety (eg, unclear or incorrect dosage instructions or strength) [4], technical issues [1,5], and resistance to adoption among staff [1]. Difficult adoption of automated systems has been reported in previous studies and has been attributed to their incapability to execute some functions that were previously completed manually [2,5,6]. The implementation of e-prescribing and/or e-dispensing systems has been extensively examined in the literature, with a focus on evaluating whether their intended purposes have been achieved and whether the anticipated benefits have been realized.

A systematic review of the literature on the barriers and facilitators to implementing an e-prescribing system highlighted the importance of identifying the perceptions of user groups, including pharmacists, managers, and patients [7]. Patients' involvement in the assessment process is essential because the quality of outpatient pharmacy service delivery is ultimately perceived by them; therefore, patient satisfaction can be considered an indicator of success [8,9]. Previous studies have supported the need for future research to evaluate the impact of

XSL•FO
RenderX

integrated e-prescribing and e-dispensing systems [8,10], as the combination of these 2 domains has the potential to improve various aspects of pharmacy schemes and practice [10].

In this study, the term "automated pharmacy" encompasses 2 key domains. The first is the receipt of prescriptions via an e-prescribing system, also referred to as a "pharmacy information system," which is a subset of a much greater HIS. Within such a system, patient data and medication lists are stored electronically. The second component of the "automated pharmacy" concept involves an e-dispensing system, in which electronic cabinets with the drugs on the shelves (most of which are prepackaged) are used to deliver the prescribed medications to the dispensing area. Briefly, the pharmacist receives the prescription from the patient, reviews it to ensure that the medications are accurately prescribed, and uses the e-prescribing system to send the order to the electronic or automated cabinet. The cabinet prepares the medications and delivers them to the pharmacist, who then dispenses them and provides patient counseling.

In Kuwait, there are 6 general governmental hospitals, all of which have transitioned their outpatient pharmacies from manual processes to automated systems. However, the extent of implementation varies across institutions. In some settings, automated dispensing systems are not fully connected to the e-prescribing platform, while in others, the e-prescribing system functions as a stand-alone tool that is not integrated with the HIS or electronic health records.

Following implementation, several challenges arise for staff operating integrated e-prescribing and automated dispensing systems, despite the technological advancements they offer. These challenges include technical difficulties, workflow and organizational issues, and factors related to users' attitudes, adaptation, and readiness to use technology. Such issues can affect the quality of the outpatient pharmacy services delivered to patients, particularly regarding waiting times, the adequacy of medication counseling, availability of medications, and the accuracy of medication dispensing. These challenges highlight the need to explore patients' experiences to understand their perceptions and satisfaction with outpatient pharmacy care in hospitals, which can help identify areas for improving and optimizing service quality.

Within this context, previous studies in Kuwait have examined the perspectives of health care providers regarding the use of HISs in primary care settings [11,12] or secondary care settings [13]. Patients' satisfaction with e-prescribing and electronic health records has also been explored [14,15]. In the existing literature, there is no research in Kuwait that examined patients' satisfaction based on their experiences with integrated automated outpatient pharmacy services. Thus, this study aimed to assess patients' satisfaction with their experiences in receiving outpatient pharmacy services through integrated e-prescribing and e-dispensing systems in the outpatient pharmacies of secondary care governmental hospitals. This enabled the development of recommendations to improve pharmacy practice in Kuwait.

Methods

Study Design, Sample, and Setting

The design of this study was a cross-sectional survey, using a questionnaire developed in Google Forms that was electronically administered to collect data from patients at their convenience between June and July 2024 at the outpatient pharmacies of 4 governmental hospitals in the state of Kuwait. The selected hospitals were Adan, Jahra, Farwaniya, and Jaber Al-Ahmad, which had all adopted and implemented the concept of automated pharmacy, which is using an integrated e-prescribing and e-dispensing system in the outpatient pharmacies.

A Survey Questionnaire

The items of the questionnaire were taken from previous validated studies [16]. Content validity was evaluated by the research team, which included 2 academic staff members from the Pharmacy Practice Department at the College of Pharmacy, Kuwait University, who are experts in their field, and 1 academic staff member from the College of Medicine with expertise in health informatics. This evaluation involved reviewing the questionnaire items to ensure their relevance to the study objectives and their clarity. Several modifications were made to ensure compatibility and appropriateness for the research aim, sample, and setting. The term "medication teaching" was replaced with "medication counseling," as this terminology is commonly used and understood by patients and pharmacy staff in Kuwait. The section "pharmacy place" was removed because it addressed the physical layout of the pharmacy, which was unrelated to the study's aim and objectives. Additionally, 1 item was excluded, which was about "the availability of a private area for counseling," because this service is not consistently provided across outpatient pharmacies in Kuwait and is not applicable to the local setting. A new section was added, which was about "dispensing medications," and was developed from previous studies [17,18] to explore aspects of communication between pharmacists and patients.

Questionnaire Structure

The questionnaire consisted of 40 items and seven sections: (1) time of prescription dispensing (3 items), (2) pharmacist attitudes (5 items), (3) medication supply (5 items), (4) medication counseling (5 items), (5) dispensing medications (5 items), (6) overall impact of automated pharmacy on outpatient pharmacy services (7 items), and (7) sociodemographic characteristics (10 items).

Inclusion and Exclusion Criteria

This study included secondary care hospitals that offer integrated automated outpatient pharmacy services. Patients and/or caregivers who provide close, hands-on care to the patient are familiar with the patient's experiences with outpatient pharmacy services and can offer valuable insights alongside the patients themselves. Eligible participants were those who were able to complete the questionnaire and were therefore invited to take part in the study. Private hospitals and private pharmacies were excluded from this study because they operate under different policies and procedures and do not use integrated e-prescribing

XSL•FO
RenderX

and e-dispensing systems within their outpatient pharmacy services.

Pilot Study

A pilot study was conducted to ensure clarity and readability with 25 patients who were waiting to receive their medications from outpatient pharmacies. The results demonstrated that the questionnaire was easy to understand and well received, confirming its readiness for full-scale distribution.

Recruitment and Data Collection

Patients waiting to receive their medications in the outpatient pharmacy areas were approached and invited to participate voluntarily. The questionnaire was administered to patients using a QR code or via a tablet device, providing direct access to the online questionnaire. No identifying patient information was collected, and responses could not be linked to individual patients. Pharmacy staff were not present while participants completed the survey, which helped maintain anonymity and reduce potential social desirability bias. For patients unable to complete the questionnaire themselves, a next of kin who was familiar with their experience (eg, a spouse, son, or sister) was permitted to respond on their behalf (Figure 1).

The questionnaire was offered in 2 languages, Arabic and English, to accommodate a diverse patient population. The original English version of the questionnaire was translated into Arabic, and the translation was validated using a back-translation method to ensure accuracy and clarity. All patients who met the inclusion criteria were invited to participate. Data collection was undertaken by a group of pharmacy students (n=6) from the College of Pharmacy, Kuwait University. They were available in the waiting areas of the outpatient pharmacies to share the online questionnaire with patients.

Figure 1. The recruitment protocol of the study participants.

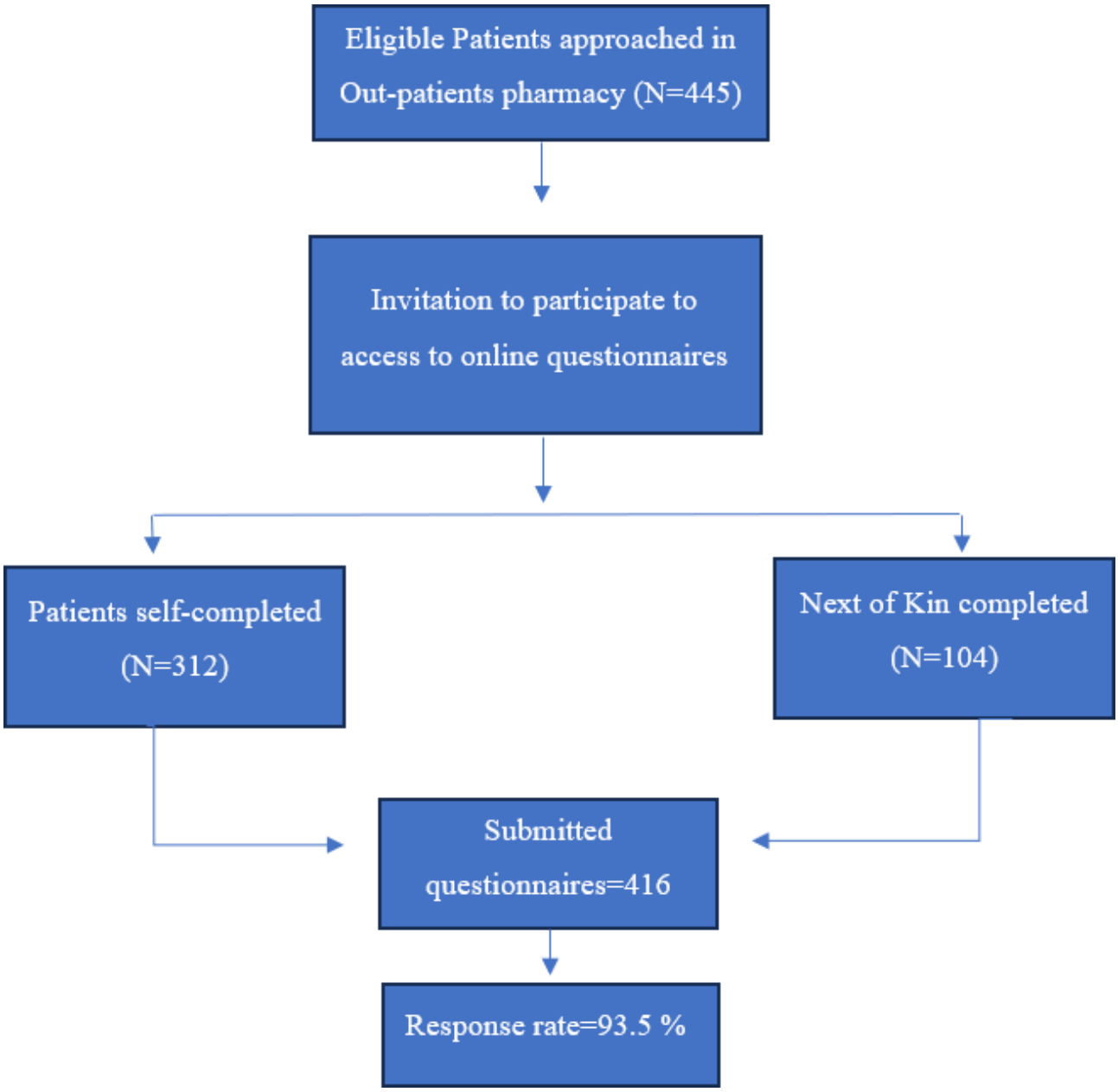

XSL•FO
RenderX

Construct Validation Using Factor Analysis and Reliability Assessment

The Kaiser-Meyer-Olkin (KMO) test and Bartlett's test of sphericity were used to evaluate sampling adequacy [19]. These tests help determine whether data are suitable for factor analysis. Data factorability was confirmed with a KMO value above 0.50 and a significant Bartlett's test value (P<.05) [19]. Principal component analysis with Promax rotation, an oblique method, was used. Promax was selected because it permits factors to correlate, which aligns with the expected relationships among the constructs [20]. The number of factors was decided based on eigenvalues, scree plots, and explained variance. Exploratory factor analysis was performed with a factor loading cutoff of 0.40 to extract scale dimensions [19,21].

Internal consistency reliability was assessed using Cronbach α coefficient based on a 4-point Likert scale (time of prescription dispensing, pharmacist attitudes, medication supply, medication counseling, and dispensing medications). A Cronbach α value of ≥0.70 was regarded as satisfactory evidence of internal consistency for the new instrument [19,20,22].

Ethical Considerations

Ethical approval for this study was obtained from the The Standing Committee for Coordinating Medical and Health Research prior to data collection (reference number 2352). Participation was voluntary, and informed consent was obtained from all participants before administering the survey. To protect privacy and confidentiality, no personally identifiable information was collected. Surveys were completed anonymously in the outpatient pharmacy waiting area, and participants were informed that they could decline to answer any question or withdraw at any time without any impact on their care or pharmacy services. All collected data were kept confidential, stored securely, and accessible only to the research team. Study findings are reported in aggregate form, ensuring that no individual participant can be identified.

Statistical Data Analysis

Statistical analyses were conducted using IBM SPSS Statistics (version 29; IBM Corp). Descriptive statistics were used to present the data. Categorical variables were presented as frequencies and percentages. To summarize the patients' perspective scores, responses for the questionnaire items were averaged across all items within the category. As an initial exploratory comparison, patient and caregiver perspective scores were compared using the Mann-Whitney U test due to nonnormal score distributions and unequal group sizes.

A normality test for the component scores was undertaken using the Shapiro-Wilk test, which indicated that the data were not normally distributed. Accordingly, results are presented as minimum, maximum, median, and IQR. Nonparametric statistical tests were used to assess associations between component scores and variables of interest, including the Mann-Whitney U test for binary comparisons, the Kruskal-Wallis test for comparisons across multiple groups, Spearman rank correlation for continuous variables, and the chi-square test for trend for ordinal categorical variables.

For analyses based on a priori hypotheses involving comparisons across multiple groups, post hoc pairwise comparisons were conducted following statistically significant Kruskal-Wallis tests, with P values adjusted for multiple comparisons using the Dunn-Bonferroni method. These analyses were planned and considered confirmatory. Effect sizes were reported as rank-biserial correlation coefficients (r_rb) for binary comparisons, epsilon squared (ε^2) for multigroup comparisons, and Spearman correlation coefficient (ρ) for continuous variables.

Multiple linear regression analyses were performed to identify independent factors associated with the overall score across domains of patients' perspectives on automated pharmacy services. Additional association analyses not specified a priori were treated as exploratory and were not adjusted for multiple comparisons; these results are presented for hypothesis generation. Ordinal survey responses were averaged across items within each component to generate composite scores for inferential analyses. Statistical significance was set at P value of <.05.

A sensitivity analysis was conducted to assess the results to potential selection bias arising from voluntary participation and convenience sampling. This analysis examined the possible impact of underrepresentation of less satisfied patients on the study outcomes. Specifically, the patients' perspective score was systematically reduced by 0.3, 0.5, and 1.0 SDs, representing mild, moderate, and severe dissatisfaction scenarios, respectively. These thresholds were selected based on established effect size conventions for continuous outcomes and their application in patient-reported outcome research [23]. For each scenario, the multiple linear regression analyses were repeated using the adjusted outcome variable, while all predictor variables and model specifications remained unchanged.

Results

Sociodemographic Characteristics of the Study Participants

A total of 445 patients were approached, of whom 416 completed the questionnaire, producing a response rate of 93.5%. The sociodemographic characteristics of the study participants are illustrated in Table 1.

XSL•FO
RenderX

Table . Sociodemographic characteristics of participants (N=416).

Characteristics	Values, n (%)
Total	416 (100.0)
Hospital	
Adan	111 (26.7)
Jahra	95 (22.8)
Farwaniya	100 (24.0)
Jaber Al-Ahmad	110 (26.4)
Age (years)	
<29	142 (34.3)
30-39	108 (26.1)
40-49	105 (25.4)
≥50	59 (14.3)
Nationality	
Kuwaiti	351 (84.4)
Non-Kuwaiti	65 (15.6)
Sex	
Male	117 (28.1)
Female	299 (71.9)
Marital status	
Single	158 (38.0)
Married	258 (62.0)
Education	
High school or less	76 (18.3)
Diploma	108 (26.0)
Bachelor	208 (50.0)
Higher education	24 (5.8)
Estimated number of pharmacy visits in the last year	
Once to twice	92 (22.1)
3-4 times	155 (37.3)
Monthly	161 (38.7)
Weekly	8 (1.9)
Dispense medications	
Personally	312 (75.0)
Someone else	104 (25.0)
The time I have waited to receive my medication	
≤5 minutes	136 (35.5)
6-15 minutes	167 (43.6)
>15 minutes	80 (20.9)
The number of medications in my prescription	
1-5 items	331 (79.6)
6-10 items	62 (14.9)
>10 items	23 (5.5)

XSL•FO
RenderX

Most participants were female (299/416, 71.9%), Kuwaiti nationals (351/416, 84.4%), younger than 29 years (142/416, 34.3%), and married (258/416, 62.0%). Half of the participants (208/416, 50%) held a bachelor's degree. Regarding pharmacy visits, approximately one-third of the participants visited the pharmacy monthly (161/416, 38.7%), while another third reported visiting 3 or 4 times per year (155/416, 37.3%). Most participants were collecting medications for themselves (312/416, 75%) and had between 1 and 5 medications in their prescriptions (331/416, 79.6%). Dispensing waiting times varied, with the majority of participants waiting 6 - 15 minutes (167/416, 40.1%), followed by those waiting less than 5 minutes (136/416, 32.7%), and those waiting more than 15 minutes (80/416, 19.2%).

Based on the exploratory factor analysis results shown in Table 2, each item with a value greater than 0.40 was assigned to an extracted factor. The KMO value of 0.914 indicated that the data were appropriate for factor analysis, and the value of Bartlett's test of sphericity was significant (χ^2_{231}=5140.38; P<.001). The scree plot indicated a 5-component solution, with all items showing acceptable communalities, and eigenvalues greater than 1.0 were extracted, accounting for 67.27% of the total variance. The reliability of the 22-item factored scale was obtained. The overall Cronbach α for the scale showed excellent reliability (α=0.92).

Table . Results of the exploratory factor analysis.

Component	Item	Factor loadings[a]	Eigenvalue	VE[b] (%)	CVE[c] (%)
Time of prescription dispensing			1.79	8.12	8.12
	1.00	0.83			
	2.00	0.90			
Pharmacist attitude			4.03	18.32	26.44
	3.00	0.74			
	4.00	0.74			
	5.00	0.83			
	6.00	0.80			
	7.00	0.75			
Medication supply			3.56	16.18	42.62
	8.00	0.67			
	9.00	0.62			
	10.00	0.72			
	11.00	0.73			
	12.00	0.71			
Medication counseling			3.05	13.84	56.46
	13.00	0.52			
	14.00	0.40			
	15.00	0.84			
	16.00	0.85			
	17.00	0.68			
Dispensing medication			2.38	10.81	67.27
	18.00	0.43			
	19.00	0.79			
	20.00	0.69			
	21.00	0.79			
	22.00	0.54			

[a]Extraction method: principal component analysis. Rotation method: Promax. Factor loading cutoff: >0.40.

[b]VE: variance explained.

[c]CVE: cumulative variance explained.

XSL•FO
RenderX

Time of Prescription Dispensing

The results showed that most respondents agreed or strongly agreed that their prescriptions were dispensed within a reasonable time (364/416, 87.5%; Table 3).

XSL•FO
RenderX

Table . Perceptions of e-prescription and automated dispensing systems in outpatient pharmacies at secondary care hospitals (N=416).

Item	Values, n (%)								Range	Overall median score (IQR)[a]
	Strongly agree	Agree	Disagree	Strongly disagree	Never	Rarely	Sometimes	Many times		
Time of prescription dispensing									1.0-4.0	3.0 (0.5)
1. Receive medications within a reasonable time	136 (32.7)	228 (54.8)	38 (9.1)	14 (3.4)	—[b]	—	—	—		
2. Waiting time is acceptable considering the quantity of prescription medication	115 (27.6)	226 (54.3)	63 (15.1)	12 (2.9)	—	—	—	—		
Pharmacist attitude									4.0-1.2	3.4 (1.0)
3. Pharmacist helped me to get the medications	201 (48.3)	201 (48.3)	9 (2.2)	5 (1.2)	—	—	—	—		
4. Pharmacist helped to solve any problem while getting the medication	168 (40.4)	211 (50.7)	33 (7.9)	4 (1.0)						
5. Pharmacist answered my questions	197 (47.4)	200 (48.1)	18 (4.3)	1 (0.2)						
6. Pharmacist understood the medical case	172 (41.3)	222 (53.4)	21 (5.0)	1 (0.2)						
7. Pharmacist treated me with respect	254 (61.1)	153 (36.8)	5 (1.2)	4 (1.0)						
Medication supply									4.0-1.8	3.2 (0.8)
8. Medication quantity was sufficient	178 (42.8)	214 (51.4)	19 (4.6)	5 (1.2)						

XSL•FO
RenderX

Item	Values, n (%)								Range	Overall median score (IQR)[a]
	Strongly agree	Agree	Disagree	Strongly disagree	Never	Rarely	Sometimes	Many times		
9. All my medications were available in the pharmacy	131 (31.5)	180 (43.3)	87 (20.9)	18 (4.3)						
10. Medication name was clear and easy to read	197 (47.4)	200 (48.1)	14 (3.4)	5 (1.2)						
11. Medication label or sticker instructions were clear	192 (46.2)	202 (48.6)	18 (4.3)	4 (1.0)						
12. Medication appearance and quality was good	195 (46.9)	211 (50.7)	10 (2.4)	0 (0.0)						
Medication counseling									4.0-1.0	3.0 (0.8)
13. Pharmacist explained the reason of my medication	169 (40.6)	187 (45.0)	44 (10.6)	16 (3.8)						
14. Pharmacist told me how to take the correct medication dose	189 (45.4)	192 (46.2)	27 (6.5)	8 (1.9)						
15. Pharmacist explained my medication's possible side effects	84 (12.5)	159 (38.2)	159 (38.2)	52 (12.5)						
16. Pharmacist explained how to store my medication	82 (12.5)	128 (30.8)	154 (37.0)	52 (12.5)						
17. I had enough time with the pharmacist	123 (29.6)	194 (46.6)	77 (18.5)	22 (5.3)						
Dispensing medication									4.0-1.0	3.8 (0.4)

XSL•FO
RenderX

Item	Values, n (%)								Range	Overall median score (IQR)[a]
	Strongly agree	Agree	Disagree	Strongly disagree	Never	Rarely	Sometimes	Many times		
18. The communication with the pharmacist and/or the doctor was challenging	—	—	—	—	218 (52.4)	111 (26.7)	71 (17.1)	16 (3.8)		
19. The prescription was sent to the wrong pharmacy	—	—	—	—	349 (83.9)	53 (12.7)	12 (2.9)	2 (0.5)		
20. The wrong medication was dispensed to me	—	—	—	—	384 (92.3)	26 (6.3)	4 (1.0)	2 (0.5)		
21. I received wrong instructions regarding the drugs dispensed for me	—	—	—	—	371 (89.2)	31 (7.5)	12 (2.9)	2 (0.5)		
22. My medical prescription or information was not received by the pharmacy	—	—	—	—	294 (70.7)	79 (19.0)	32 (7.7)	11 (2.6)		

[a]For each perspective score, responses for the questionnaire items were averaged across all items within the category.

[b]Not applicable.

Most participants (341/416, 82.0%) also found the waiting time acceptable, considering the number of medications prescribed. A statistically significant association (P=.006; chi-square test) was found between the number of medications prescribed and the reported waiting time (Table 4). Patients prescribed 1 - 5 medications were more likely to experience shorter waiting times: 38.8% (118/304) received their medications within 5 minutes, 41.8% (127/304) waited 6 - 15 minutes, and 19.4% (59/304) waited more than 15 minutes.

Table . Association between the number of medications and the waiting time to receive the medications (P=.006[a]; chi-square for trend).

Number of medications	Waiting time		
	≤5 minutes	6-15 minutes	>15 minutes
1-5 items, n (raw %)	118 (38.8)	127 (41.8)	59 (19.4)
6-10 items, n (raw %)	14 (24)	31 (53)	13 (22)
>10 items, n (raw %)	4 (19)	9 (43)	8 (38)

[a]Chi-square test for trend.

XSL•FO
RenderX

In contrast, patients prescribed 6 - 10 medications experienced longer waiting times. Only 24% (14/58) received their medications within 5 minutes, while 53% (31/58) waited 6 - 15 minutes, and 22% (13/58) waited more than 15 minutes. Among those prescribed more than 10 medications, few (4/21, 19%) received their medications within 5 minutes or less, while many (9/21, 43%) waited 6 - 15 minutes, and a similar proportion (8/21, 38%) waited more than 15 minutes, as shown in Table 4.

Pharmacist Attitudes

As shown in Table 3, the results indicated that most participants had positive perceptions of pharmacist attitudes. The majority agreed or strongly agreed that the pharmacists helped obtain their medications (401/416, 96.5%) and assisted them in resolving issues related to medication access (379/416, 91.1%). In addition, a large proportion reported that the pharmacists answered their questions (397/416, 95.5%) and demonstrated knowledge and understanding toward their medical cases (394/416, 94.7%). Furthermore, most participants shared the perspective that the pharmacists treated them with respect and dignity (407/416, 97.9%).

Medication Supply

Most participants found the quantities of medications dispensed to be sufficient (392/416, 94.2%). Additionally, nearly three-quarters (311/416, 74.8%) reported that all their prescribed medications were available in the pharmacy (Table 3). However, a subset of participants (105/416, 25.2%) encountered instances where 1 or more prescribed medications were unavailable. Medication labels were clear and easy to read for most participants (397/416, 95.5%), and the usage instructions were clear and understandable (394/416, 94.8%). Furthermore, the majority expressed satisfaction with the appearance and quality of the medications provided (406/416, 97.6%).

Medication Counseling

The results revealed that the pharmacists performed well in several key areas of patient counseling (Table 3), which included explaining the purpose of medication use (356/416, 85.6%), providing instructions on correct medication dosage (381/416, 91.6%), and dedicating sufficient time to patients during consultations (317/416, 76.2%). However, notable gaps were identified in some specific aspects of counseling. Only half of the participants reported receiving information about the potential side effects of their medications (211/416, 50.7%). Similarly, counseling on proper medication storage was lacking, with approximately half of the participants not receiving such explanations (206/416, 49.5%).

Dispensing Medications

As shown in Table 3, most participants reported that communication challenges with pharmacists and/or physicians rarely or never occurred (329/416, 79.1%). Similarly, errors in the e-prescribing and e-dispensing process were uncommon. Specifically, the majority of participants agreed that rarely or never were prescriptions sent to the wrong pharmacy (402/416, 96.6%), the wrong medication was dispensed (410/416, 98.6%), incorrect instructions were received regarding the medications dispensed (402/416, 96.7%), or the prescription information was not received by the pharmacy (373/416, 89.7%).

Impact of Automated Pharmacy and Overall Satisfaction With Outpatient Pharmacy Services

The participants identified several perceived benefits of the integrated e-prescribing and e-dispensing systems, reflecting their positive impact on outpatient pharmacy services (Multimedia Appendix 1). These perceived benefits included time savings (356/416, 85.6%), perceived prevention of medication errors (211/416, 50.7%), and convenient access to prescription information at any time (249/416, 59.9%).

Also, the results showed high overall satisfaction with the automated outpatient pharmacy services, as 94.5% (393/416) of participants either agreed or strongly agreed that they were satisfied with the services delivered through the automated systems (Multimedia Appendix 2).

The overall median score for the time of prescription dispensing section was 3.0, while the median score for pharmacist attitudes was 3.4. The median scores for the medication supply, medication counseling, and dispensing medications domains were 3.2, 3.0, and 3.8, respectively (Table 3).

Tables 5 and 6 demonstrate the relationships between sociodemographic characteristics and the overall median scores for each questionnaire component. There were significant differences among hospitals, with small effect sizes for the time of prescription dispensing and the dispensing medications scores (ε^2=0.05 and ε^2=0.02, respectively). The median time of prescription dispensing score for Farwaniya hospital was significantly higher than for Adan hospital (3.2 vs 3.0; adjusted P=.03) and Jaber Al-Ahmad hospital (3.2 vs 3.0; adjusted P<.001). The median dispensing medications score for Jaber Al-Ahmad hospital was significantly higher than for Adan hospital (4.0 vs 3.8; adjusted P=.02) and Jahra hospital (4.0 vs 3.8; adjusted P=.04).

XSL•FO
RenderX

Table . Component scores for a survey assessing e-prescribing and e-dispensing systems in outpatient pharmacies at secondary care hospitals according to sociodemographic characteristics (N=416).

Characteristics	Median score (IQR)[a]				
	Time of prescription dispensing	Pharmacist attitude	Medication supply	Medication counseling	Dispensing medication
Hospital					
Adan	3.0 (0.5)	3.4 (1.0)	3.2 (0.8)	3.0 (0.8)	3.8 (0.6)
Jahra	3.0 (1.0)	3.4 (1.0)	3.2 (1.0)	3.0 (1.0)	3.8 (0.6)
Farwaniya	3.2 (1.0)	3.4 (1.0)	3.3 (1.0)	3.0 (1.2)	3.8 (0.4)
Jaber Al-Ahmad	3.0 (1.5)	3.6 (1.0)	3.4 (0.8)	3.0 (0.9)	4.0 (0.4)
Age (years)					
<29	3.0 (0.6)	3.4 (1.0)	3.2 (1.0)	3.0 (1.0)	3.8 (0.6)
30-39	3.0 (1.0)	3.6 (1.0)	3.3 (0.8)	3.0 (0.9)	3.8 (0.4)
40-49	3.0 (0.5)	3.4 (1.0)	3.2 (0.8)	3.0 (0.8)	3.8 (0.4)
≥50	3.0 (0.5)	3.4 (0.8)	3.2 (0.8)	2.6 (1.0)	4.0 (0.4)
Nationality					
Kuwaiti	3.0 (0.5)	3.4 (1.0)	3.2 (0.8)	3.0 (1.0)	3.8 (0.6)
Non-Kuwaiti	3.0 (0.8)	3.6 (1.0)	3.2 (0.9)	3.0 (1.1)	3.8 (0.4)
Sex					
Male	3.0 (1.0)	3.6 (1.0)	3.4 (1.0)	3.0 (1.2)	3.8 (0.6)
Female	3.0 (0.5)	3.4 (1.0)	3.2 (0.8)	3.0 (0.8)	3.8 (0.4)
Marital status					
Single	3.0 (0.5)	3.5 (1.0)	3.2 (0.8)	3.0 (0.8)	3.8 (0.6)
Married	3.0 (0.5)	3.4 (1.0)	3.2 (0.8)	3.0 (1.0)	3.8 (0.4)
Education					
High school or less	3.0 (1.0)	3.6 (1.0)	3.2 (1.0)	3.0 (1.0)	4.0 (0.4)
Diploma	3.0 (0.5)	3.2 (1.0)	3.4 (0.8)	3.0 (1.4)	3.8 (0.6)
Bachelor	3.0 (0.5)	3.4 (1.0)	3.2 (0.8)	3.0 (0.8)	3.8 (0.6)
Higher education	3.0 (1.9)	3.7 (0.9)	3.6 (1.0)	3.1 (1.6)	3.9 (0.9)
Estimated number of pharmacy visits in the last year					
Once to twice	3.0 (1.4)	3.4 (1.0)	3.1 (1.0)	3.0 (1.0)	4.0 (0.6)
3-4 times	3.0 (0.5)	3.4 (1.0)	3.4 (0.8)	3.0 (0.8)	3.8 (0.4)
Monthly	3.0 (0.5)	3.6 (1.0)	3.2 (0.8)	3.0 (1.0)	3.8 (0.6)
Weekly	3.0 (1.0)	3.3 (1.4)	3.0 (1.1)	2.5 (1.8)	3.6 (0.9)
Dispense medications					
Personally	3.0 (0.5)	3.4 (1.0)	3.2 (0.8)	3.0 (0.8)	3.8 (0.4)
Someone else	3.0 (0.5)	3.3 (1.0)	3.2 (0.9)	2.9 (1.0)	3.8 (0.8)
The time I have waited to receive my medication					
≤5 minutes	3.5 (1.0)	3.6 (0.9)	3.6 (1.0)	3.0 (1.0)	4.0 (0.4)
6-15 minutes	3.0 (0.5)	3.4 (0.8)	3.2 (0.6)	2.8 (0.6)	3.8 (0.6)
>15 minutes	2.8 (1.0)	3.2 (1.0)	3.1 (1.0)	2.8 (1.0)	3.6 (0.6)
The number of medications in my prescription					
1-5 items	3.0 (0.5)	3.4 (1.0)	3.4 (0.8)	3.0 (0.8)	3.8 (0.4)
6-10 items	3.0 (0.5)	3.5 (1.0)	3.0 (1.0)	3.0 (0.9)	3.8 (0.6)

XSL•FO
RenderX

Characteristics	Median score (IQR)[a]				
	Time of prescription dispensing	Pharmacist attitude	Medication supply	Medication counseling	Dispensing medication
11-15 items	3.0 (1.0)	3.0 (0.6)	3.2 (0.8)	3.0 (1.0)	3.8 (0.6)

[a]For each perspective score, responses for the questionnaire items were averaged across all items within the category.

Table . Relationships between sociodemographic variables and component scores for a survey assessing e-prescribing and e-dispensing systems in outpatient pharmacies at secondary care hospitals (N=416).

Characteristics	Time of prescription dispensing		Pharmacist attitude		Medication supply		Medication counseling		Dispensing medication	
	Effect size[a]	*P* value[b]	Effect size[a]	*P* value[b]	Effect size[a]	*P* value[b]	Effect size[a]	*P* value[b]	Effect size[a]	*P* value[b]
Hospital	0.055	<.001	0.004	.71	0.004	.73	0.003	.60	0.018	.02
Age (years)	−0.050	.31	−0.050	.34	−0.003	.96	−0.130	.007	0.040	.46
Nationality	0.370	.72	−0.120	.90	0.150	.89	1.370	.17	0.450	.65
Gender	0.219	.13	0.225	.12	0.105	.09	0.053	.39	0.112	.06
Marital status	0.028	.61	0.008	.89	0.019	.74	0.057	.33	0.052	.35
Education	0.110	.03	0.010	.87	0.040	.43	−0.070	.15	0.090	.07
Number of visits (last year)	−0.010	.89	0.030	.54	0.001	.98	0.030	.63	−0.060	.22
Dispense medications	0.281	.12	0.242	.46	0.266	.22	0.272	.190	0.299	.06
Time waited	−0.460	<.001	−0.150	.003	−0.150	.003	−0.220	<.001	−0.170	.001
Number of medications	−0.110	.03	−0.030	.51	−0.090	.06	−0.020	.77	−0.050	.33

[a]Rank-biserial correlation (r_{rb}) for 2-group comparisons, epsilon squared (ε^2) for multigroup comparisons, and Spearman correlation coefficient for continuous variables. Interpretation thresholds: r_{rb}≈0.10=small, ≈0.30=moderate, and ≥0.50=large; ε^2≈0.01=small, ≈0.06=moderate, and ≥0.14=large; and value of P ranges from −1 to +1, P<.1=small, .1-.3=medium, and >.5=large.

[b]Mann-Whitney *U* tests (2 groups), Kruskal-Wallis tests (≥3 groups), or Spearman rank correlation test (continuous variables).

An indirect correlation coefficient of r=−0.13 was present between age and medication counseling score (P=.007). Likewise, there was an indirect correlation between dispensing medications score and education level (r=−0.11; P=.03). All 4 other domains of the questionnaire had scores that were significantly related to the amount of time it took to receive prescriptions (P<.05), with indirect Spearman rank correlation coefficients ranging from −0.15 to −0.46. Furthermore, a significant indirect correlation coefficient of r=−0.11 was found between number of medications and dispensing medications score (P=.03). For other patient characteristics, no statistically significant differences or associations were observed across any of the 5 perspective domains (all P>.05).

All 5 domains of the questionnaire were significantly related to each other (P≤.001), with Spearman rank correlation coefficients ranging from 0.30 to 0.62 (Table 7). The number of medications a patient was prescribed and the amount of time they waited to obtain those prescriptions had a significant association (P=.006), as seen in Table 4. In other words, the amount of waiting time rises as the number of medications increases (from 1 - 5 items to 6 - 10 items or 10 items or more).

XSL•FO
RenderX

Table . Spearman rank correlations between domains in a survey assessing e-prescribing and e-dispensing systems in outpatient pharmacies at secondary care hospitals (N=416).

Component	Time of prescription dispensing		Pharmacist attitude		Medication supply		Medication counseling		Dispensing medication	
	R	*P* value	*R*	*P* value	*R*	*P* value	*R*	*P* value	*R*	*P* value
Time of prescription dispensing	N/A[a]	N/A	0.48	<.001	0.47	<.001	0.44	<.001	0.3	<.001
Pharmacist attitude	0.48	<.001	N/A	N/A	0.62	<.001	0.62	<.001	0.39	<.001
Medication supply	0.47	<.001	0.62	<.001	N/A	N/A	0.62	<.001	0.48	<.001
Medication counseling	0.44	<.001	0.62	<.001	0.62	<.001	N/A	N/A	0.48	<.001
Dispensing medication	0.3	<.001	0.39	<.001	0.48	<.001	0.48	<.001	N/A	N/A

[a]Not applicable.

The results showed that there is an inverse relationship between medication dispensing waiting time and patient perceptions of automated outpatient pharmacy services, whereas increased waiting times were associated with less satisfaction of pharmacists' attitudes, medication counseling, and dispensing practices.

Table 8 shows the results of the multiple regression model examining patients' perceptions toward automated outpatient pharmacy services, with total perception scores modeled as a function of sociodemographic and other relevant variables. All variables were entered simultaneously to estimate their independent associations. The model was statistically significant (F_{231}=2.32; *P*=.001) and explained 11% of the variance in patients' perceptions. Compared with patients who waited 5 minutes or less, those who waited 6-15 minutes and more than 15 minutes reported significantly lower perception scores (β=−3.70, 95% CI −5.76 to −1.65, *P*<.001 and β=−6.19, 95% CI −8.82 to −3.56, *P*< .001, respectively).

XSL•FO
RenderX

Table . Multivariable linear regression predicting the total score across all key domains of patients' perspectives on automated pharmacy, adjusted for sociodemographic and other variables.

Characteristics	Regression coefficient (β)[a]	95% CI	SE	*t* statistic (*df*)	*P* value
Constant	78.69	74.42 to 82.96	2.17	36.22 (395)	<.001
Hospital					
Adan	N/A[b]	N/A	N/A	N/A	N/A
Jahraa	−1.57	−4.20 to 1.07	1.34	−1.17 (395)	.24
Farwaniya	−1.27	−3.95 to 1.41	1.36	−0.93 (395)	.35
Jaber AlAhmad	0.69	−1.88 to 3.25	1.30	0.53 (395)	.59
Age (years)					
<29	N/A	N/A	N/A	N/A	N/A
30 - 39	−0.08	−2.61 to 2.46	1.29	−0.06 (395)	.95
40 - 49	−1.40	−4.14 to 1.34	1.39	−1.01 (395)	.32
≥50	−1.83	−5.15 to 1.49	1.69	−1.08 (395)	.28
Nationality					
Kuwaiti	−0.95	−3.50 to 1.60	1.30	−0.73 (395)	.47
Non-Kuwaiti	N/A	N/A	N/A	N/A	N/A
Sex					
Male	N/A	N/A	N/A	N/A	N/A
Female	−0.68	−2.69 to 1.34	1.03	−0.66 (395)	.51
Marital status					
Single	N/A	N/A	N/A	N/A	N/A
Married	1.11	−1.14 to 3.36	1.15	0.97 (395)	.33
Education					
High school and less	N/A	N/A	N/A	N/A	N/A
Diploma	−1.23	−3.97 to 1.52	1.40	−0.88 (395)	.38
Bachelor	−2.16	−4.66 to 0.34	1.27	−1.70 (395)	.09
Higher education	−0.62	−4.93 to 3.69	2.19	−0.28 (395)	.78
Estimated number of pharmacy visits in the last year					
Once to twice	N/A	N/A	N/A	N/A	N/A
3-4 times	0.75	−1.64 to 3.13	1.21	0.62 (395)	.54
Monthly	1.74	−0.71 to 4.19	1.25	1.39 (395)	.16
Weekly	−2.96	−9.78 to 3.86	3.47	−0.85 (395)	.39
Dispense medications					
Personally	N/A	N/A	N/A	N/A	N/A
Someone else	−1.86	−3.94 to 0.21	1.06	−1.76 (395)	.08
The time I have waited to receive my medication					
≤5 minutes	N/A	N/A	N/A	N/A	N/A
6 - 15 minutes	−3.70	−5.76 to −1.65	1.04	−3.55 (395)	<.001
>15 minutes	−6.19	−8.82 to −3.56	1.34	−4.63 (395)	<.001
The number of medications in my prescription					
1 - 5 items	N/A	N/A	N/A	N/A	N/A
6 - 10 items	−0.23	−2.81 to 2.34	1.31	−0.18 (395)	.86

XSL•FO
RenderX

Characteristics	Regression coefficient (β)[a]	95% CI	SE	*t* statistic (*df*)	*P* value
>10 items	−2.58	−6.58 to 1.42	2.03	−1.27 (395)	.21

[a]Results from multivariable linear regression using the total score across all key components of patients' perspectives on automated pharmacy as a continuous outcome variable, along with hospital location, age, nationality, gender, marital status, education, number of pharmacy visits in the last year, dispensed medications, time waited to receive medication, and number of medications in the prescription. The regression coefficients (β) represent the mean difference in the overall patients' perspective score associated with each category increase, holding all other variables constant. The 95% CIs and *P* values are reported.

[b]Not applicable.

The results of the sensitivity analyses are shown in Table 9. Across all simulated dissatisfaction scenarios (−0.3 SD, −0.5 SD, and −1.0 SD), the direction, magnitude, and statistical significance of the regression coefficients remained consistent with those observed in the primary analysis (Table 8). In particular, the association between longer waiting times and lower patient perspective scores persisted across all scenarios, with nearly identical regression coefficients and 95% CIs. As expected, the model intercept decreased progressively with increasing downward shifts, reflecting lower assumed overall patient perspectives under more conservative assumptions. The results showed that there were no remarkable changes in the estimated effects of individual predictors, and no variables changed their significance status across the sensitivity analyses.

XSL•FO
RenderX

Table . Sensitivity analysis of multivariable linear regression outcomes across different dissatisfaction assumptions.

Characteristics	Mild (SD −0.3)			Moderate (SD −0.5)			Severe (SD −1.0)		
	B	95% CI	*P* value	*B*	95% CI	*P* value	*B*	95% CI	*P* value
Constant	75.9	71.6 to 80.1	<.001	74.0	69.7 to 78.3	<.001	69.3	65.0 to 73.6	<.001
Hospital									
Adan	N/A[a]	N/A	N/A	N/A	N/A	N/A	N/A	N/A	N/A
Jahraa	−1.6	−4.2 to 1.1	.24	−1.6	−4.2 to 1.1	.24	−1.6	−4.2 to 1.1	.24
Farwaniya	−1.3	−3.9 to 1.4	.35	−1.3	−3.9 to 1.4	.35	−1.3	−3.9 to 1.4	.35
Jaber AlAhmad	0.7	−1.9 to 3.3	.59	0.7	−1.9 to 3.3	.59	0.7	−1.9 to 3.3	.59
Age (years)									
<29	N/A	N/A	N/A	N/A	N/A	N/A	N/A	N/A	N/A
30 - 39	−0.1	−2.6 to 2.5	.95	−0.1	−2.6 to 2.5	.95	−0.1	−2.6 to 2.5	.95
40 - 49	−1.4	−4.1 to 1.3	.32	−1.4	−4.1 to 1.3	.32	−1.4	−4.1 to 1.3	.32
≥50	−1.8	−5.1 to 1.5	.28	−1.8	−5.1 to 1.5	.28	−1.8	−5.1 to 1.5	.28
Nationality									
Kuwaiti	−0.9	−3.5 to 1.6	.47	−0.9	−3.5 to 1.6	.47	−0.9	−3.5 to 1.6	.47
Non-Kuwaiti	N/A	N/A	N/A	N/A	N/A	N/A	N/A	N/A	N/A
Sex									
Male	N/A	N/A	N/A	N/A	N/A	N/A	N/A	N/A	N/A
Female	−0.7	−2.7 to 1.3	.51	−0.7	−2.7 to 1.3	.51	−0.7	−2.7 to 1.3	.51
Marital status									
Single	N/A	N/A	N/A	N/A	N/A	N/A	N/A	N/A	N/A
Married	1.1	−1.1 to 3.4	.33	1.1	−1.1 to 3.4	.33	1.1	−1.1 to 3.4	.33
Education									
High school and less	N/A	N/A	N/A	N/A	N/A	N/A	N/A	N/A	N/A
Diploma	−1.2	−4.0 to 1.5	.38	−1.2	−4.0 to 1.5	.38	−1.2	−4.0 to 1.5	.38
Bachelor	−2.2	−4.7 to 0.3	.09	−2.2	−4.7 to 0.3	.09	−2.2	−4.7 to 0.3	.09
Higher education	−0.6	−4.9 to 3.7	.78	−0.6	−4.9 to 3.7	.78	−0.6	−4.9 to 3.7	.78
Estimated number of pharmacy visits in the last year									
Once to twice	N/A	N/A	N/A	N/A	N/A	N/A	N/A	N/A	N/A
3-4 times	0.7	−1.6 to 3.1	.54	0.7	−1.6 to 3.1	.538	0.7	−1.6 to 3.1	.54
Monthly	1.7	−0.7 to 4.2	.16	1.7	−0.7 to 4.2	.164	1.7	−0.7 to 4.2	.16
Weekly	−3.0	−9.8 to 3.9	.39	−3.0	−9.8 to 3.9	.394	−3.0	−9.8 to 3.9	.39
Dispense medications									
Personally	N/A	N/A	N/A	N/A	N/A	N/A	N/A	N/A	N/A
Someone else	−1.9	−3.9 to 0.2	.08	−1.9	−3.9 to 0.2	.08	−1.9	−3.9 to 0.2	.08
The time I have waited to receive my medication									
≤5 minutes	N/A	N/A	N/A	N/A	N/A	N/A	N/A	N/A	N/A

XSL•FO
RenderX

Characteristics	Mild (SD −0.3)			Moderate (SD −0.5)			Severe (SD −1.0)		
	B	95% CI	*P* value	*B*	95% CI	*P* value	*B*	95% CI	*P* value
6 - 15 minutes	−3.7	−5.8 to −1.7	<.001	−3.7	−5.8 to −1.7	<.001	−3.7	−5.8 to −1.7]	<.001
>15 minutes	−6.2	−8.8 to −3.6	<.001	−6.2	−8.8 to −3.6	<.001	−6.2	−8.8 to −3.6]	<.001
The number of medications in my prescription									
1 - 5 items	N/A	N/A	N/A	N/A	N/A	N/A	N/A	N/A	N/A
6 - 10 items	−0.2	−2.8 to 2.3	.86	−0.2	−2.8 to 2.3	.86	−0.2	−2.8 to 2.3	.86
>10 items	−2.6	−6.6 to 1.4	.21	−2.6	−6.6 to 1.4	.21	−2.6	−6.6 to 1.4	.21

[a]Not applicable.

Discussion

Principal Findings

Studying patients' opinions and satisfaction provides a clear picture of the perceived impact and success of implementing automated pharmacy systems in the real world. Patient feedback can help determine whether the system meets their needs, improves the quality of outpatient pharmacy services, and achieves its intended goals in practice.

The existing literature has shown numerous advantages of using such technology in pharmacy practice. In this context, this study revealed that patients perceived integrated e-prescribing and e-dispensing systems as beneficial to outpatient pharmacy services and expressed overall satisfaction with their experiences of care, as reported by 95% (393/416) of the participants. Participants cited several key perceived benefits, including time savings, perceived prevention of medication errors, convenient access to prescription information at any time, and effective communication between pharmacists and physicians. These findings are consistent with previous studies, which have similarly reported a perceived reduction in medication errors [1-3], time savings in the prescribing and dispensing process [5,6], and increased work efficiency [1,2,6] following the adoption of automated pharmacy systems.

Influence of Sociodemographic Data on Participant Satisfaction

The findings revealed that the satisfaction levels of the participants varied across several sociodemographic groups. This study found an indirect association between age and medication counseling and between dispensing medications score and educational level. This could be explained by the notion that people with higher education levels could have higher expectations of health care services, which could lead to dissatisfaction when these are unmet [24]. Similar findings were found in a previous study [25], which assessed patient satisfaction toward outpatient pharmacy services among outpatients attending public health clinics in Malaysia. The findings revealed that demographic factors (eg, age, education level, self-perceived health status, and general knowledge of pharmacists) significantly influenced patients' perceptions of health care services. Notably, older age and higher education levels were associated with a lower patient satisfaction mean score [25]. Similarly, a study conducted in Pakistan [26] reported that male patients were significantly more satisfied with community outpatient pharmacy services than females. Younger patients (aged 18 - 27 years) exhibited greater satisfaction than older age groups. Illiterate and less-educated individuals showed greater satisfaction levels, while those with higher education levels were less satisfied, likely due to higher expectations. Marital status and occupation also played a potential role, with married individuals showing greater satisfaction and government employees showing less satisfaction. No significant association was observed among students after statistical adjustment [26].

Patients' Satisfaction With Dispensing Time, Pharmacists' Attitudes, and Medication Supply

Although most patients in this study agreed that their prescriptions were dispensed in a reasonable time, the findings revealed that the patients with more medications experienced longer waiting times, suggesting challenges in processing large or complex orders using the automated pharmacy systems.

These findings aligned with those of a previous study into primary health care settings in Kuwait [27], which found that patients' satisfaction was strongly influenced by the timeliness of prescription fulfillment by physicians. Numerous studies have demonstrated that e-prescription systems reduce dispensing times and improve pharmacy workflow [28]. In this context, a study assessed the impact of e-prescription systems on pharmacy workflow and practice in Finland and found a reduction in both median and average delivery times across various prescription types [29]. In particular, the maximum dispensing time with the adoption of e-prescribing systems was shorter in 2012 (6 minutes and 22 seconds) than the time with the use of non–e-prescribing systems in 2006 (12 minutes and 40 seconds). The study concluded that e-prescribing systems significantly improved the efficiency of prescription processing in Finnish community pharmacies [29]. Additionally, a study conducted in Sweden into the impact of integrated e-prescribing systems on pharmacists' practice found that the pharmacists perceived the system as expediting prescription processing and reducing the risk of medication errors [1]. The results showed a positive

XSL•FO
RenderX

correlation between the perceived usefulness of the electronic system for improving work efficiency and medication safety.

This study revealed that the participants were highly satisfied with the pharmacists' attitudes. Nearly all the participants agreed that the pharmacists helped obtain their medications, effectively resolved issues related to medication access, answered their questions, demonstrated knowledge of their medical conditions, and treated them with dignity and respect. These findings were supported by previous studies showing that e-prescribing systems enhance communication between patients and pharmacists [7], patients and prescribers [5], and pharmacists and other health care providers [30,31]. Similarly, a study conducted in Qatar reported comparable levels of satisfaction among participants regarding pharmacists' empathy and communication skills [16]. Furthermore, effective communication, regardless of whether systems are manual or electronic, has been found to significantly contribute to overall patient satisfaction [7,32].

The findings of this study demonstrated statistically significant differences in patient satisfaction across outpatient pharmacies in the 4 general hospitals, particularly regarding medication dispensing speed and pharmacists' attitudes. These site-level variations may reflect differences in staffing levels, staff competencies, workload, maturity of automation, or local operational workflows. For instance, the higher satisfaction with medication dispensing speed observed at Farwaniya Hospital compared with Adan Hospital may be attributable to shorter waiting times, fewer medications per prescription, or more efficient dispensing practices. While patient satisfaction is an important indicator of service performance, it should be interpreted alongside technical and organizational factors to provide a comprehensive understanding of the effectiveness and efficiency of digital pharmacy systems.

The findings of this study indicated that approximately one-quarter of the surveyed participants experienced medication unavailability. Similar findings have been reported by previous studies [33-36], highlighting the need for improved inventory integration to overcome such issues and enhance patient satisfaction. In this context, a study showed that automated drug-dispensing systems carry advantages over traditional systems in improving inventory control and reducing storage errors, resulting in better patient satisfaction [37,38].

The participants in this study were satisfied with the perceived accuracy of the pharmacy's handling of medical prescription information. In support of the claim that prescription accuracy contributes to patient satisfaction, a systematic review study revealed that the integration of e-prescription and e-dispensing systems significantly reduced pharmacy errors [39]. This indicates that the adoption of automated systems may enhance perceived accuracy and is associated with higher levels of patient satisfaction and perceived safety.

Patients' Satisfaction With Medication Counseling and the Dispensing Process

Despite the growing use of e-prescription and e-dispensing systems, challenges remain in their utilization. The findings of this study indicated that the patients reported high levels of satisfaction with medication counseling overall. Specifically, pharmacists were commended for clearly explaining the purpose of medication use, providing accurate dosage instructions, and allocating sufficient time for patients during consultations. However, approximately half of the participants expressed dissatisfaction with the counseling received regarding potential drug side effects and proper medication storage.

A US study into outpatient use of electronic prescriptions found that the use of an e-prescribing system led to lower rates of adverse drug events among patients, suggesting that appropriate counseling on side effects and storage could further reduce such risks [40]. Therefore, in this study, the lack of counseling regarding the side effects of medications and storage conditions indicates a potential gap in quality of practice. This may pertain to numerous reasons, such as a long queue of patients waiting, leading to time pressures, or pharmacists' limited counseling skills, which would affect the quality of the counseling. This shortcoming may reflect the need for additional pharmacist training to improve their counseling skills and not neglect any important information from patient education. Previous research has shown that training physicians in e-prescribing significantly reduces errors and improves workflow, thus indicating that e-prescription systems alone do not resolve counseling-related challenges unless supplemented by targeted education [41]. Addressing these aspects could significantly enhance both patient satisfaction and medication safety.

In addition, despite the automation of the dispensing process, the findings of this study reported longer waiting times for patients with prescribed multiple medications. This association suggests that prolonged waiting times may negatively influence patients' overall perception of outpatient pharmacy domains, including pharmacists' attitudes, medication counseling, medication supply, and dispensing medications. The literature showed that previous studies are consistent with the findings of this study, indicating that waiting time is a critical determinant of patient satisfaction, irrespective of whether outpatient pharmacy services are delivered through conventional or automated systems [38,42,43]. Therefore, the findings revealed that the success of automated outpatient pharmacy services relies not only on technology use but also on efficient workflow that led to suitable time medication dispensing.

This finding highlights the need for process optimization within pharmacy workflows. As with counseling gaps, delays in dispensing may diminish the perceived benefits of automation. Similar studies conducted in Saudi Arabia [38,44] emphasized the value of integrated pharmacy systems while acknowledging the need for region-specific improvements. These studies support the idea that continuous pharmacist education and the implementation of structured feedback mechanisms are essential for identifying and addressing system inefficiencies. By incorporating such strategies, pharmacies can better meet patient expectations and improve the outpatient pharmacy services.

Impact of E-Prescribing and E-Dispensing Systems on Outpatient Pharmacy Services

This study found that most patients reported a positive impact based on their experiences with the medication dispensing process, with pharmacist communication emerging as a key

XSL•FO
RenderX

contributor to patient satisfaction. These findings are consistent with those of a study in Qatar in 2013, which emphasized the importance of pharmacist-patient communication [16]. While pharmacy staff provide irreplaceable expertise in prescription monitoring and dispensing, the integration of electronic systems may help alleviate workload and reduce cognitive burden. Participants perceived that reducing manual tasks enhanced efficiency and contributed to improved patient safety by minimizing the risk of human error [45]. Pharmacists and pharmacy technicians are susceptible to fatigue, stress, and other human limitations, which may compromise dispensing accuracy. In this context, e-prescription systems serve as a valuable support tool that may help mitigate such risks [18,45]. By providing an additional layer of safety and reliability, these systems can contribute to patients' perceptions of positive outcomes and higher satisfaction levels.

The absence of a comparison group involving nonautomated outpatient pharmacies is considered a key methodological limitation of this study. Consequently, the findings cannot isolate the specific effects of automation from other contextual or organizational factors and should be interpreted as reflecting patient experiences within automated pharmacy settings only, which limits their generalizability to other pharmacy models. Future studies using comparative or quasi-experimental designs are needed to evaluate the incremental impact of automation on patient experience and service performance.

Limitations

This study has several limitations. First, it focused exclusively on patients in Kuwait. While the findings provide valuable insights into local users of outpatient pharmacy services, the generalizability of the results to other populations and health care systems may be limited. In addition, the absence of a comparison group involving nonautomated outpatient pharmacies limits the ability to isolate the specific impact of automation.

Second, patient satisfaction data were self-reported, which may have introduced recall or self-reporting bias and may not accurately reflect the actual quality or safety of outpatient pharmacy services. Third, the presence of pharmacy students in the waiting area may have introduced courtesy or social desirability bias, which may have potentially inflated satisfaction scores (approximately 95% agreement), despite private survey completion. The consistently high levels of agreement observed may therefore partly reflect response tendencies rather than true satisfaction levels. Accordingly, future studies should consider alternative data collection approaches or comparative analyses across sites or time periods to better assess this potential bias. Fourth, despite the sensitivity analyses conducted, voluntary participation and convenience sampling may have introduced selection bias, as patients who were more satisfied or more engaged with automated outpatient pharmacy services may have been more likely to participate. Although the sensitivity analyses suggest that potential underrepresentation of less satisfied patients is unlikely to have materially altered the study conclusions, the findings may not be fully representative of all users of automated outpatient pharmacy systems in Kuwait, particularly individuals who actively avoid or disengage from these systems. Fifth, the study was conducted in 4 governmental hospitals and did not include private hospitals or pharmacies, which may differ in service quality, system implementation, and operational policies. Sixth, the cross-sectional design captured perceptions at a single point in time, limiting the ability to assess changes in patient-reported satisfaction over time.

Finally, although responses were obtained from both patients and caregivers, caregivers represented a smaller proportion of the sample (104/416, 25%). An exploratory comparison using the Mann-Whitney *U* test did not detect statistically significant differences between the 2 groups; therefore, further subgroup analyses were not pursued.

Future Research

Future research should link patient-reported perceptions with objective safety and quality indicators, such as medication dispensing error rates, adverse drug events, dispensing accuracy, workflow measures, and prescription turnaround time, to determine whether perceived benefits correspond to measurable improvements in patient outcomes. Longitudinal and mixed methods designs, including qualitative interviews, may provide deeper insight into how and why perceived benefits evolve over time and whether anticipated benefits are realized in routine practice. Methodologically, probability-based sampling approaches should be considered to improve representativeness and reduce selection bias. In addition, remote or independent survey administration and comparative designs across data collection settings may help assess and minimize social desirability bias. Comparative studies involving governmental and private sector hospitals or pharmacies are also warranted, given potential differences in implementation maturity, staffing, workflows, and service policies. Finally, future studies specifically powered to compare patient and caregiver perspectives, alongside technical and organizational assessments, would provide a more comprehensive evaluation of system effectiveness and help identify actionable improvement strategies.

Conclusions

This study demonstrated that integrated e-prescribing and e-dispensing systems offer clear perceived benefits in outpatient pharmacies within governmental hospitals in Kuwait. This is reflected in the positive experiences reported by patients, reflecting overall perceived satisfaction and perceived service performance within the operating systems.

However, the findings also highlight areas requiring improvement to maximize patients' satisfaction toward pharmacy automation systems. The following clinical implications are made:

1. Workflow design optimization: operational strategies should be implemented to improve pharmacy workflow design within automated pharmacy settings to enhance work efficiency, especially for processing lengthy prescriptions and managing drug inventories to reduce dispensing delays, as well as making sure that a counseling area is available for patient education.

XSL•FO
RenderX

2. E-prescribing system enhancement: counseling prompts should be integrated to ensure that important information is delivered completely and properly to patients.
3. Automated inventory management: enhanced inventory control should be implemented, including proactive stock monitoring to clarify what is available and what is near expiry to improve the supply chain management. This is essential because the results showed that approximately 25% (105/416) of patients reported medication unavailability.
4. Staff training: pharmacy staff should receive comprehensive training on best practices for using integrated e-prescription and e-dispensing systems. This would improve patient counseling, interprofessional communication, patient safety, and overall patient satisfaction.
5. Feedback mechanisms: regular collection of feedback from both patients and pharmacy staff should be instituted to identify and address issues related to waiting times, medication availability, and the quality of counseling services.

By addressing these identified gaps, pharmacists can enhance patient satisfaction and improve the overall performance of outpatient pharmacy services supported by integrated digital systems. Strengthening the digital infrastructure and workflow integration would enable hospitals to optimize outpatient pharmacy services and move toward patient-centered digital pharmacy models that support efficient, reliable, and safe medication services. These findings have relevance beyond the study setting and may inform the development of digital outpatient pharmacy services across hospitals in the Arabian Gulf region.

Acknowledgments

The authors would like to thank the students from the College of Pharmacy at Kuwait University who undertook the data collection: Yousef Bahman, Ritaj Alawadhi, Sadeem Almubarak, Nourah Alshammeri, Zainab Moradi, and Sara Alorf.

Funding

No external financial support or grants were received from any public, commercial, or not-for-profit entities for the research, authorship, or publication of this article.

Conflicts of Interest

None declared.

Multimedia Appendix 1
The impact of integrated e-prescribing and e-dispensing systems on outpatient pharmacy services.
[PNG File, 49 KB - medinform_v14i1e80963_app1.png]

Multimedia Appendix 2
Overall satisfaction with automated outpatient pharmacy services.
[PNG File, 5 KB - medinform_v14i1e80963_app2.png]

References

1. Rahimi B, Timpka T. Pharmacists' views on integrated electronic prescribing systems: associations between usefulness, pharmacological safety, and barriers to technology use. Eur J Clin Pharmacol 2011 Feb;67(2):179-184. [doi: 10.1007/s00228-010-0936-9] [Medline: 21069521]
2. Abdel-Qader DH, Cantrill JA, Tully MP. Satisfaction predictors and attitudes towards electronic prescribing systems in three UK hospitals. Pharm World Sci 2010 Oct;32(5):581-593. [doi: 10.1007/s11096-010-9411-z] [Medline: 20593237]
3. Bright HR, Peter JV, Chandy SJ. Electronic prescribing system in a Teaching Hospital-user satisfaction and factors affecting successful implementation. Der Pharmacia Letter 2019;11(2):10-24 [FREE Full text]
4. Kauppinen H, Ahonen R, Timonen J. The impact of electronic prescriptions on medication safety in Finnish community pharmacies: a survey of pharmacists. Int J Med Inform 2017 Apr;100:56-62. [doi: 10.1016/j.ijmedinf.2017.01.014] [Medline: 28241938]
5. Hammar T, Nyström S, Petersson G, Rydberg T, Åstrand B. Swedish pharmacists value ePrescribing: a survey of a nationwide implementation. J Phara Health Ser Res 2010 Mar;1(1):23-32. [doi: 10.1211/jphsr.01.01.0012]
6. McLeod M, Karampatakis GD, Heyligen L, McGinley A, Franklin BD. The impact of implementing a hospital electronic prescribing and administration system on clinical pharmacists' activities—a mixed methods study. BMC Health Serv Res 2019 Mar 12;19(1):156. [doi: 10.1186/s12913-019-3986-4] [Medline: 30866925]
7. Gagnon MP, Nsangou É, Payne-Gagnon J, Grenier S, Sicotte C. Barriers and facilitators to implementing electronic prescription: a systematic review of user groups' perceptions. J Am Med Inform Assoc 2014;21(3):535-541. [doi: 10.1136/amiajnl-2013-002203] [Medline: 24130232]

XSL•FO
RenderX

8. Beard RJ. Electronic prescribing and robotic dispensing: the impact of integrating together on practice and professionalism. In: Dekoulis G, editor. Robotics—Legal, Ethical and Socioeconomic Impacts: Intech Open; 2017. [doi: 10.5772/intechopen.69769]
9. Tsyben A, Gooding N, Kelsall W. Assessing the impact of a newly introduced electronic prescribing system across a paediatric department— lessons learned. Arch Dis Child 2016 Sep;101(9):e2. [doi: 10.1136/archdischild-2016-311535.20] [Medline: 27540199]
10. Marotti R. Can we translate the UK automation experience? Pharm Pract Res 2016 Sep;46(3):253-255. [doi: 10.1002/jppr.1184]
11. Almutairi BA, Potts HWW, Al-Azmi SF. Physicians' perceptions of electronic prescribing with electronic medical records in Kuwaiti primary healthcare centres. Sultan Qaboos Univ Med J 2019;18(4):e476-e482. [doi: 10.18295/squmj.2018.18.04.008]
12. Buabbas A, Al-shawaf H, editors. Pharmacists perspectives on the effectiveness of primary care information system on pharmacy practice in Kuwait health care centres. Presented at: Proceedings of the 6th International Symposium on Health Informatics and Bioinformatics; May 2-5, 2011. [doi: 10.1109/HIBIT.2011.6450800]
13. Al-Otaibi J, Tolma E, Alali W, Alhuwail D, Aljunid SM. The factors contributing to physicians' current use of and satisfaction with electronic health records in Kuwait's public health care: cross-sectional questionnaire study. JMIR Med Inform 2022 Oct 7;10(10):e36313. [doi: 10.2196/36313] [Medline: 36206039]
14. Al-Jafar E. Exploring patient satisfaction before and after electronic health record (EHR) implementation: the Kuwait experience. Perspect Health Inf Manag 2013;10(Spring):1c. [Medline: 23805063]
15. Al-Azmi SF, Mohammed AM, Hanafi MI. Patients' satisfaction with primary heath care in Kuwait after electronic medical record implementation. J Egypt Public Health Assoc 2006;81(5-6):277-300. [Medline: 18706302]
16. Khudair IF, Raza SA. Measuring patients' satisfaction with pharmaceutical services at a public hospital in Qatar. Int J Health Care Qual Assur 2013;26(5):398-419. [doi: 10.1108/IJHCQA-03-2011-0025] [Medline: 23905301]
17. Frail CK, Kline M, Snyder ME. Patient perceptions of e-prescribing and its impact on their relationships with providers: a qualitative analysis. J Am Pharm Assoc (2003) 2014 Nov;54(6):630-633. [doi: 10.1331/JAPhA.2014.13176]
18. Odukoya OK, Stone JA, Chui MA. E-prescribing errors in community pharmacies: exploring consequences and contributing factors. Int J Med Inform 2014 Jun;83(6):427-437. [doi: 10.1016/j.ijmedinf.2014.02.004] [Medline: 24657055]
19. Polit DF, Beck CT. Nursing Research Generating and Assessing Evidence for Nursing Practice, 10th edition: Wolters Kluwer; 2017.
20. Moridi M, Pazandeh F, Hajian S, Potrata B. Development and psychometric properties of Midwives' Knowledge and Practice Scale on Respectful Maternity Care (MKP-RMC). PLoS One 2020;15(11):e0241219. [doi: 10.1371/journal.pone.0241219] [Medline: 33141835]
21. Fu E, White MA, Hughto JMW, Steiner B, Willis EA. Development of the physical activity tracking preference questionnaire. Int J Exerc Sci 2019;12(5):297-309. [doi: 10.70252/WEJR4154] [Medline: 31156755]
22. Ekolu SO, Quainoo H. Reliability of assessments in engineering education using Cronbach's alpha, KR and split-half methods. Global J Eng Educ 2019;21(1):24-29 [FREE Full text]
23. Cohen J. Statistical Power Analysis for the Behavioral Sciences, 2nd edition: Routledge; 1988.
24. Jackson JL, Chamberlin J, Kroenke K. Predictors of patient satisfaction. Soc Sci Med 2001 Feb;52(4):609-620. [doi: 10.1016/s0277-9536(00)00164-7] [Medline: 11206657]
25. Ismail A, Gan YN, Ahmad N. Factors associated with patient satisfaction towards pharmacy services among out-patients attending public health clinics: questionnaire development and its application. PLoS One 2020;15(11):e0241082. [doi: 10.1371/journal.pone.0241082] [Medline: 33170854]
26. Alanazi AS, Shah S, Abbas G, et al. Assessing patient satisfaction with community pharmacy services: a large regional study at Punjab, Pakistan. Patient Prefer Adherence 2023;17:13-22. [doi: 10.2147/PPA.S389053] [Medline: 36636289]
27. Alhashem AM, Alquraini H, Chowdhury RI. Factors influencing patient satisfaction in primary healthcare clinics in Kuwait. Int J Health Care Qual Assur 2011;24(3):249-262. [doi: 10.1108/09526861111116688] [Medline: 21938970]
28. Porterfield A, Engelbert K, Coustasse A. Electronic prescribing: improving the efficiency and accuracy of prescribing in the ambulatory care setting. Perspect Health Inf Manag 2014;11(Spring):1g. [Medline: 24808808]
29. Peltoniemi T, Suomi R, Peura S, Lähteenoja MNY. Electronic prescription as a driver for digitalization in Finnish pharmacies. BMC Health Serv Res 2021 Sep 27;21(1):1017. [doi: 10.1186/s12913-021-07003-0] [Medline: 34565354]
30. Campbell C, Morris C, McBain L. Electronic transmission of prescriptions in primary care: transformation, timing and teamwork. J Prim Health Care 2021 Dec;13(4):340-350. [doi: 10.1071/HC21050] [Medline: 34937647]
31. Darwesh BM, Machudo SY, John S. The experience of using an automated dispensing system to improve medication safety and management at King Abdul Aziz University Hospital. J Pharm Pract Community Med 2017 Jun 15;3(3):114-119. [doi: 10.5530/jppcm.2017.3.26]
32. Callaway Kim K, Rothenberger SD, Tadrous M, et al. Drug shortages prior to and during the COVID-19 pandemic. JAMA Netw Open 2024 Apr 1;7(4):e244246. [doi: 10.1001/jamanetworkopen.2024.4246] [Medline: 38578641]
33. Paulo Mário Elobo M. Factors influencing drug stock-outs at health facilities—Mocuba. MOJ Biol Med 2024;9(1):8-10. [doi: 10.15406/mojbm.2024.09.00209]

XSL•FO
RenderX

34. Phuong JM, Penm J, Chaar B, Oldfield LD, Moles R. The impacts of medication shortages on patient outcomes: a scoping review. PLoS One 2019;14(5):e0215837. [doi: 10.1371/journal.pone.0215837] [Medline: 31050671]
35. Atif M, Malik I, Mushtaq I, Asghar S. Medicines shortages in Pakistan: a qualitative study to explore current situation, reasons and possible solutions to overcome the barriers. BMJ Open 2019 Sep 4;9(9):e027028. [doi: 10.1136/bmjopen-2018-027028] [Medline: 31488466]
36. Amirthalingam P, Alruwaili AS, Albalawi OA, et al. Comparing patient satisfaction with automated drug dispensing system and traditional drug dispensing system: a cross-sectional study. Patient Prefer Adherence 2024;18:2337-2345. [doi: 10.2147/PPA.S492802] [Medline: 39583135]
37. Oldland AR, Golightly LK, May SK, Barber GR, Stolpman NM. Electronic inventory systems and barcode technology: impact on pharmacy technical accuracy and error liability. Hosp Pharm 2015 Jan;50(1):34-41. [doi: 10.1310/hpj5001-34] [Medline: 25684799]
38. Momattin H, Arafa S, Momattin S, Rahal R, Waterson J. Robotic pharmacy implementation and outcomes in Saudi Arabia: a 21-month usability study. JMIR Hum Factors 2021 Sep 1;8(3):e28381. [doi: 10.2196/28381] [Medline: 34304149]
39. Osmani F, Arab-Zozani M, Shahali Z, Lotfi F. Evaluation of the effectiveness of electronic prescription in reducing medical and medical errors (systematic review study). Ann Pharm Fr 2023 May;81(3):433-445. [doi: 10.1016/j.pharma.2022.12.002] [Medline: 36513154]
40. Gabriel MH, Powers C, Encinosa W, Bynum JPW. E-prescribing and adverse drug events: an observational study of the Medicare part D population with diabetes. Med Care 2017 May;55(5):456-462. [doi: 10.1097/MLR.0000000000000684] [Medline: 28060051]
41. Craxford S, Taylor L, Duguid A, Shivji F, Pickering S. The learning curve of electronic prescribing. Br J Hosp Med 2015 Sep 2;76(9):538-540. [doi: 10.12968/hmed.2015.76.9.538]
42. Leemanza Y, Kristin E. Effectiveness of wait time targets and patient satisfaction feedback in decreasing wait times for prescription services in an outpatient pharmacy. Can J Hosp Pharm 2024;77(1):e3438. [doi: 10.42112/cjhp.3438] [Medline: 38204510]
43. Yulia R, Hartono R, Indrayanti M, Ayumuyas NP, Herawati F. Studying waiting time in pharmacy: a strategy for improving patient satisfaction. MethodsX 2025 Jun;14:103282. [doi: 10.1016/j.mex.2025.103282] [Medline: 40230556]
44. Almaghaslah D, Alsayari A, Almaghaslah S, Alsanna H. Patients' satisfaction with e-prescribing (Wasfaty) in Saudi Arabia: a survey of country-level implementation. Healthcare (Basel) 2022 Apr 27;10(5):806. [doi: 10.3390/healthcare10050806] [Medline: 35627943]
45. Whitaker M, Lester C, Rowell B. Handing off electronic prescription data from prescribers to community pharmacies: a qualitative analysis of pharmacy staff perspectives. J Patient Saf 2024 Sep 1;20(6):397-403. [doi: 10.1097/PTS.0000000000001244] [Medline: 38742931]

Abbreviations

e-dispensing: electronic dispensing
e-prescribing: electronic prescribing
HIS: hospital information system
KMO: Kaiser-Meyer-Olkin

Edited by A Sen; submitted 19.Jul.2025; peer-reviewed by C Duclos, H Rajesh, M Hany; revised version received 22.Jan.2026; accepted 23.Jan.2026; published 06.Mar.2026.

Please cite as:
Buabbas AJ, Alsaleh FM, Alsanafi M, Safar MA, Al-Sultan AT, Zaman TA
Patient Experiences With Outpatient Pharmacy Services in Hospitals Using Automated Pharmacy Systems: Cross-Sectional Study
JMIR Med Inform 2026;14:e80963
URL: https://medinform.jmir.org/2026/1/e80963
doi:10.2196/80963

© Ali Jasem Buabbas, Fatemah Mohammad Alsaleh, Mariam Alsanafi, Maryam Ali Safar, Ahmad T Alsultan, Talal Ahmad Zaman. Originally published in JMIR Medical Informatics (https://medinform.jmir.org), 6.Mar.2026. This is an open-access article distributed under the terms of the Creative Commons Attribution License (https://creativecommons.org/licenses/by/4.0/), which permits unrestricted use, distribution, and reproduction in any medium, provided the original work, first published in JMIR Medical Informatics, is properly cited. The complete bibliographic information, a link to the original publication on https://medinform.jmir.org/, as well as this copyright and license information must be included.

XSL•FO
RenderX

AI Scribes: Are We Measuring What Matters?

Enrico Coiera, PhD; David Fraile-Navarro, PhD

Australian Institute of Health Innovation, Macquarie University, Level 6, 75 Talavera Road, Sydney, NSW, Australia

Corresponding Author:
Enrico Coiera, PhD
Australian Institute of Health Innovation, Macquarie University, Level 6, 75 Talavera Road, Sydney, NSW, Australia

Abstract

Artificial intelligence (AI) scribes, software that can convert speech into concise clinical documents, have achieved remarkable clinical adoption at a pace rarely seen for digital technologies in health care. The reasons for this are understandable: the technology works well enough, it addresses a genuine pain point for clinicians, and it has largely sidestepped regulatory requirements. In many ways, clinical adoption of AI scribes has also occurred well ahead of robust evidence of their safety and efficacy. The papers in this theme issue demonstrate real progress in the technology and evidence of its benefit: documentation times are reported to decrease when using scribes, clinicians report feeling less burdened, and the notes produced are often of reasonable quality. Yet as we survey the emerging evidence base, there remains one outstanding and urgent unanswered question: Are AI scribes safe? We need to know the clinical outcomes achievable when scribes are used compared to other forms of note taking.

(JMIR Med Inform 2026;14:e89337) doi:10.2196/89337

KEYWORDS

artificial intelligence; AI; digital scribes; medical scribes; electronic documentation; patient safety; error prevention

Beyond Efficiency

Early evaluation of any technology naturally focuses on its primary promise, in the case of scribes [1], reducing documentation burden. The studies in this collection confirm that artificial intelligence (AI) scribes deliver on this front. Kanaparthy and colleagues' [2] rapid review found a general trend toward reduced self-reported documentation time and improvements in clinician satisfaction. The comparative analysis by Ha and colleagues [3] demonstrates that current commercial systems can generate reasonable-quality SOAP (subjective, objective, assessment, and plan) notes in about a minute after a 15-minute encounter. These are meaningful findings. Having shown that scribes likely save time in the settings they have so far been evaluated in (eg, primary care and outpatient settings), we can turn to harder questions of safety, clinical reasoning, and wider system-level effects.

Toward Systematic Harm Measurement

How safe are clinical scribes? Do they make errors, what type of errors might see when using digital scribes, and are these errors clinically consequential? What are the causes of errors, and what then are the harm mitigations we need to put into place?

Several papers in this collection begin this work. Ha and colleagues [3] highlight that none of the systems they evaluated are error free. Biro and colleagues [4] have developed and validated an instrument specifically designed to assess the accuracy and safety of AI scribe outputs, an essential foundation since, without standardized measurement, we cannot compare across systems or track changes over time. Their early work confirms that AI scribes do make errors, and some have patient safety implications.

Digital technologies have the capacity to both reduce human error and generate new error classes [5]. This raises another question worthy of further investigation: Are digital scribe errors equivalent to human errors, or do they have different risk profiles? A human might lose attention momentarily; a digital scribe will not fatigue but may misrecognize words through speech recognition errors. An AI might confidently fabricate a medication or symptom that was never mentioned or omit clinically significant details in the pursuit of conciseness, each reshaping the clinical narrative in different ways.

Equally, we should recognize that the status quo carries its own safety risks: clinician burnout and cognitive overload contribute to errors that scribes may help reduce. A complete safety evaluation must weigh new risks introduced by AI against existing risks that the technology may mitigate and consider what analogous error-detection and correction mechanisms we need to build for AI-generated documentation.

Clinical Reasoning When Using a Digital Scribe: An Underexplored Frontier

Perhaps the richest opportunity for future research relates to the quality of clinical care when documentation is outsourced to AI. Note-taking is not merely administrative work. When a clinician summarizes their thoughts into a document, they are actively processing information, prioritizing what matters, and forming and testing hypotheses in real time. The clinical note

XSL•FO
RenderX

is not just a record of the consultation; it is a cognitive artifact that supports clinical reasoning [6].

What happens to this human sense-making process when documentation is delegated to an AI? We may be freeing the attention of clinicians to be more present with patients, or we may be altering how they would normally think. The Y-KNOT (Your-Knowledgeable Navigator of Treatment) implementation study offers an intriguing signal: expert ratings suggested that while most AI-generated drafts were rated positively, around 1 in 6 preanesthetic assessments were judged to have a negative impact on clinical decision-making [7]. As we document faster, are we also documenting differently? Does that difference matter for patient care? If so, can we mitigate the potential for harm, for example, through clinical training or redesigning the user interaction with a scribe to bring clinicians back into the document-and-reason loop?

Ecosystem Perspectives

AI scribes sit at a critical position within a clinical workflow. They determine what gets recorded and how it is structured, which in turn shapes what downstream systems, including other AI tools, will see and act on. In this sense, scribes are a gateway technology, creating data layers that propagate through the health system. As we have argued elsewhere in the context of generative AI more broadly, it is helpful to view these technologies through an ecosystem lens that emphasizes system-level properties over isolated components [8]. With this perspective, we can evaluate the broader scribe ecosystem against system-level dimensions: resilience (how does care adapt when the scribe fails?), sustainability (what happens when cloud-based systems change or disappear?), and service interactions (does optimizing documentation affect other aspects of care?).

The patients in Leiserowitz and colleagues' [9] survey were generally open to an AI scribe when it was framed as supporting clinician focus. Their study also showed one interaction worth monitoring: a meaningful proportion of patients indicated they might withhold sensitive information if an always-listening device was present. Understanding these broader system effects will require looking beyond the scribe itself to the clinical environment it inhabits.

Regulatory Evolution

There are several reasons why we still lack safety evidence. AI scribes have proliferated [10] in part because they sit outside traditional medical device classification [11]. Many commercial scribes skirt the software as a medical device definition of a decision support system and so have evaded regulation. With no regulatory demands for robust safety evaluation, there is little commercial value, it seems, in publishing commercial safety data. The evidence in this collection suggests that we may need new regulatory thinking, not because current systems are demonstrably unsafe, but because they are different. These systems do influence clinical decisions, and unlike traditional medical devices, they are not static; the large language model underlying a scribe may be updated or retrained over time. Regulatory frameworks designed for deterministic, frozen technologies may need to evolve alongside the technology itself. The question is not whether to regulate but how to do so in ways that preserve innovation while ensuring ongoing safety. Potential mechanisms might include postmarket surveillance requirements, mandatory incident reporting for generative medical AI, or periodic re-evaluation as underlying models are updated.

Conclusion

The papers in this theme issue represent important progress. AI scribes appear to deliver on their core promise of reducing documentation burden, and the field is developing increasingly rigorous evaluation approaches. Building on this foundation, we see an opportunity to expand what we measure: systematic assessment of errors and harms, investigation of effects on clinical reasoning, and attention to ecosystem-level dynamics. Documentation burden is real, and technologies that address it are welcome. The next chapter of research can help ensure that the time saved translates into better care.

Funding

This work was supported by the National Health and Medical Research Council (NHMRC) Centre for Research Excellence in Digital Health. EC and DF-N are supported by an NHMRC investigator grant (GNT2008645). The funders had no role in this manuscript. A large language model (Claude, Anthropic) was used to assist with editing this manuscript.

Authors' Contributions

Conceptualization: EC
Writing – original draft: EC, DF-N
Writing – review & editing: EC, DF-N

Conflicts of Interest

None declared.

References

1. Coiera E, Kocaballi B, Halamka J, Laranjo L. The digital scribe. NPJ Digit Med 2018;1(1):58. [doi: 10.1038/s41746-018-0066-9] [Medline: 31304337]

XSL•FO
RenderX

2. Kanaparthy NS, Villuendas-Rey Y, Bakare T, et al. Real-world evidence synthesis of digital scribes: rapid review. JMIR AI 2025 Oct 10;4:e76743. [doi: 10.2196/76743] [Medline: 41071988]
3. Ha E, Choon-Kon-Yune I, Murray L, et al. Evaluating the usability, technical performance, and accuracy of artificial intelligence (AI) scribes for primary care: a competitive analysis. JMIR Hum Factors 2025 Jul 23;12:e71434. [doi: 10.2196/71434] [Medline: 40700466]
4. Biro J, Handley JL, Cobb NK, et al. Accuracy and safety of AI-enabled scribe technology: instrument validation study. J Med Internet Res 2025 Jan 27;27:e64993. [doi: 10.2196/64993] [Medline: 39869899]
5. Magrabi F, Ong MS, Runciman W, Coiera E. An analysis of computer-related patient safety incidents to inform the development of a classification. J Am Med Inform Assoc 2010;17(6):663-670. [doi: 10.1136/jamia.2009.002444] [Medline: 20962128]
6. Leung TI, Coristine AJ, Benis A. AI scribes in health care: balancing transformative potential with responsible integration. JMIR Med Inform 2025 Aug 1;13:e80898. [doi: 10.2196/80898] [Medline: 40749188]
7. Kim J, Lee SY, You SC, et al. A bilingual on-premises AI agent for clinical drafting: implementation report (Y-KNOT project). JMIR Med Inform 2025 Nov 24;13:e76848. [Medline: 41284981]
8. Coiera E, Fraile-Navarro D. AI as an ecosystem — ensuring generative AI is safe and effective. NEJM AI 2024 Aug 22;1(9). [doi: 10.1056/AIp2400611]
9. Leiserowitz G, Mansfield J, MacDonald S, Jost M. Patient attitudes toward ambient voice technology to support an AI scribe program. JMIR Med Inform 2025 Nov 27;13:e77901. [doi: 10.2196/77901] [Medline: 41308194]
10. Henry TA. 2 in 3 physicians are using health AI—up 78% from 2023. American Medical Association. 2025 Feb 26. URL: https://www.ama-assn.org/practice-management/digital-health/2-3-physicians-are-using-health-ai-78-2023 [accessed 2026-01-28]
11. Digital scribes. Australian Therapeutic Goods Administration. 2025. URL: https://www.tga.gov.au/products/medical-devices/software-and-artificial-intelligence/manufacturing/artificial-intelligence-ai-and-medical-device-software/digital-scribes [accessed 2025-12-08]

Abbreviations

AI: artificial intelligence
SOAP: subjective, objective, assessment, and plan
Y-KNOT: Your-Knowledgeable Navigator of Treatment

Edited by A Coristine; submitted 10.Dec.2025; this is a non–peer-reviewed article;accepted 14.Jan.2026; published 06.Feb.2026.

Please cite as:
Coiera E, Fraile-Navarro D
AI Scribes: Are We Measuring What Matters?
JMIR Med Inform 2026;14:e89337
URL: https://medinform.jmir.org/2026/1/e89337
doi:10.2196/89337

© Enrico Coiera, David Fraile-Navarro. Originally published in JMIR Medical Informatics (https://medinform.jmir.org), 6.Feb.2026. This is an open-access article distributed under the terms of the Creative Commons Attribution License (https://creativecommons.org/licenses/by/4.0/), which permits unrestricted use, distribution, and reproduction in any medium, provided the original work, first published in JMIR Medical Informatics, is properly cited. The complete bibliographic information, a link to the original publication on https://medinform.jmir.org/, as well as this copyright and license information must be included.

XSL•FO
RenderX

Identification and Localization of Breast Tumor Components via a Convolutional Neural Network Based on High-Frequency Ultrasound Combined With Histopathologic Registration: Prospective Study

Jia-Qian Yao[1*], MD; Wen-Wen Zhou[1,2*], MD; Zhi-Fei Chai[3], ME; Fei Ren[3], PhD; Tong-Yi Huang[1], MD; Tian-Tian Zhen[4], MD; Hui-Juan Shi[4], MD, PhD; Xiao-Yan Xie[1], MD, PhD; Ze Zhao[3], PhD; Ming Xu[1], MD, PhD

[1]Department of Medical Ultrasonics, The First Affiliated Hospital, Sun Yat-sen University, 58 Zhongshan 2nd Road, Guangzhou, China

[2]Department of Medical Ultrasonics, Suzhou Municipal Hospital Affiliated with Nanjing Medical University, Suzhou, China

[3]Institute of Computing Technology, Chinese Academy of Sciences, Beijing, China

[4]Department of Pathology, The First Affiliated Hospital, Sun Yat-sen University, Guangzhou, China

[*]these authors contributed equally

Corresponding Author:
Ming Xu, MD, PhD
Department of Medical Ultrasonics, The First Affiliated Hospital, Sun Yat-sen University, 58 Zhongshan 2nd Road, Guangzhou, China

Abstract

Background: Given the highly heterogeneous biology of breast cancer, a more effective noninvasive diagnostic tool that unravels microscopic histopathology patterns is urgently needed.

Objective: This study aims to identify cancerous regions in ultrasound images of breast cancer via convolutional neural network based on registered grayscale ultrasound images and readily accessible biopsy whole slide images (WSIs).

Methods: This single-center study prospectively included participants undergoing ultrasound-guided core needle biopsy procedures for Breast Imaging Reporting and Data System category 4 or 5 breast lesions for whom breast cancer was pathologically confirmed from July 2022 to February 2023 consecutively. The basic information, ultrasound image data, biopsy tissue specimens, and corresponding WSIs were collected. After core needle biopsy procedures, the stained breast tissue specimens were sliced and coregistered with an ultrasound image of a needle tract. Convolutional neural network models for identifying breast cancer cells in ultrasound images were developed using FCN-101 and DeepLabV3 networks. The image-level predictive performance was evaluated and compared quantitatively by pixel accuracy, Dice similarity coefficient, and recall. Pixel-level classification was illustrated through confusion matrices. The cancerous region in the testing dataset was further visualized in ultrasound images. Potential clinical applications were qualitatively assessed by comparing the automatic segmentation results and the actual pathological tissue distributions.

Results: A total of 105 participants with 386 ultrasound images of breast cancer were included, with 270 (70%), 78 (20.2%), and 38 (9.8%) images in the training, validation, and test datasets, respectively. Both models performed well in predicting the cancerous regions in the biopsy area, whereas the FCN-101 model was superior to the DeepLabV3 model in terms of pixel accuracy (86.91% vs 69.55%; P=.002) and Dice similarity coefficient (77.47% vs 69.90%; P<.001). The two models yielded recall values of 54.64% and 58.46%, with no significant difference between them (P=.80). Furthermore, the FCN-101 model had an advantage in predicting cancerous regions, while the DeepLabV3 model achieved more accurate predictive pixels in normal tissue (both P<.05). Visualization of cancerous regions on grayscale ultrasound images demonstrated high consistency with those identified on WSIs.

Conclusions: The technique for spatial registration of breast WSIs and ultrasound images of a needle tract was established. Breast cancer regions were accurately identified and localized on a pixel level in high-frequency ultrasound images via an advanced convolutional neural network with histopathologic WSI as the reference standard.

(JMIR Med Inform 2026;14:e81181) doi:10.2196/81181

KEYWORDS

breast; neoplasms; biopsy; ultrasonography; registration

XSL•FO
RenderX

Introduction

Breast cancer heterogeneity has induced challenges in treatment planning and follow-up management, which leads to unfavorable outcomes [1,2]. Currently, ultrasound is a widely used diagnostic tool for breast cancer management, particularly valuable in screening, positive diagnosis, and treatment response assessment [3]. However, the biological heterogeneity of breast cancers leads to varied morphological features on ultrasound [4], often resulting in malignancy underestimation and overestimation. Furthermore, there is a heterogeneous response to treatment among patients with breast cancer [5-7]. Curative effect assessment secondary to preoperative neoadjuvant treatment is largely based on cancer volume changes [8], as well as biopsy for further validation [9]. A more accurate noninvasive diagnostic tool that indicates living cancer cells in breast cancer is urgently needed [10-12].

Hematoxylin and eosin (H&E) staining of breast tissue captured via core needle biopsy (CNB) has been introduced to reflect the underlying cellular and molecular information [13-15]. Preoperative diagnosis and curative effect assessment of breast cancer can be undermined by insufficient and nonrepresentative tissue owing to the heterogeneous distribution of breast cancer [16]. Likewise, the partial samples obtained by CNB may not represent the entire lesion [17]. There remains a need for standardized methods or imaging biomarkers available for accurately localizing histopathological cancerous subregions.

The convolutional neural network (CNN), a developed type of deep learning algorithm, has shown remarkable performance in correlating macroscopic imaging and microscopic histopathologic microstructure. A previous study showed that a multimodal radiomics model combining ultrasound and whole slide image (WSI) can effectively distinguish between luminal and nonluminal breast cancers [18]. Other studies have explored using the deep learning algorithm for correlation between magnetic resonance imaging (MRI) and whole-mount specimen images to localize prostate cancer [19]. Theoretically, these approaches may also be applicable in the ultrasound identification and localization of cancerous regions in breast cancer. Nonetheless, few studies have focused on this aspect. The correlation of ultrasound modality and readily accessible biopsy WSI remains open to question.

Therefore, this study aims to identify and localize cancerous regions in breast cancer based on a CNN algorithm that integrates high-frequency ultrasound (HFUS) images with WSI histopathology. The predictive performance of the model will be assessed.

Methods

Study Population

Consenting participants were recruited between July 2022 and February 2023 and were included as the training, validation, and test population. The eligibility criteria included the following: (1) index lesion was defined as category 4 or 5 according to the fifth edition of the American College of Radiology Breast Imaging Reporting and Data System (BI-RADS) of ultrasound [20]; (2) index lesion was visible on HFUS, and complete imaging data were stored; (3) underwent ultrasound-guided breast lesion biopsy and the histopathology indicated breast cancer. Participants were excluded if (1) the biopsy specimen was incomplete or inaccessible; (2) the breast ultrasound images were incomplete; (3) there was a history of treatment for breast cancer (surgery, antihormonal therapy, immunotherapy, and radiation therapy); (4) the pathologic diagnosis was incomplete. The study sample included 163 consecutive participants undergoing ultrasound-guided breast biopsy for suspicion of cancer. Of these, three participants whose ultrasound images had poor quality and one who did not provide research consent were excluded. Participants with incomplete, fractional tissue specimens (n=2) and benign histology reports (n=52) were also excluded.

Ultrasound and CNB Examination

The overall design of this study is shown in Figure 1. Expert radiologists with at least 10 years of experience performed breast ultrasound examinations and ultrasound-guided CNB procedures following the standard practice protocol. Location, number, and morphologic characteristics (size, shape, orientation, margin, echo pattern, vascularity, and calcifications) of lesions were identified and categorizations were assigned by the expert radiologists according to the fifth edition of ultrasound BI-RADS [20]. An Aplio i900 Ultrasound System (Canon) with an i24LX8 high-frequency linear probe (frequency range: 8.0 - 18.0 MHz) was used to generate breast ultrasound images. All images were stored in DICOM format for subsequent analysis.

WSI Acquisition

When breast cancer was suspected, an ultrasound-guided CNB procedure was performed by expert radiologists to determine the diagnosis. MAGNUM biopsy instruments (BARD) with disposable core tissue biopsy needles (16G, 22 mm, MN1620, BARD) were adopted. During the procedure, the needle tip was positioned approximately 0.5 cm from the target biopsy region. The radiologists aligned the ultrasound probe and needle to visualize the entire needle tract. Subtle needle deflections were occasionally observed. These deflections were dynamically corrected in real time by adjusting the needle trajectory. The radiologists captured two B-mode HFUS images per biopsy for subsequent registration, including one pre-fire and one post-fire. To ensure the specimens were representative, biopsies were taken by the radiologist from different regions of the lesion, typically 4 - 6 samples, focusing on solid areas on B-mode ultrasound or areas with abundant vascularity on color Doppler flow imaging. When multiple lesions were encountered, the most suspicious lesion for malignancy was chosen for analysis. To facilitate the follow-up spatial registration of ultrasound and histopathologic images, the needle tip side of the biopsy specimen from the index lesion was stained with biological tissue dye (BIOGNOST), depicted in Figure S1 in Multimedia Appendix 1. After 2 to 5 minutes of coloration, the biopsy specimens were placed in 10% neutral buffered formalin for fixation and sent for histopathologic examination.

XSL•FO
RenderX

Figure 1. Workflow of the proposed cancerous regions identification protocol in this study. First, we got cropped HFUS images and corresponding spatially aligned biopsy WSIs. Second, a registration process was applied to achieve anatomic correlation. Third, the segmentation model was constructed using the FCN-101 and DeepLabV3 architectures. AI: artificial intelligence; HFUS: high-frequency ultrasound; ROI: region of interest; WSI: whole slide image.

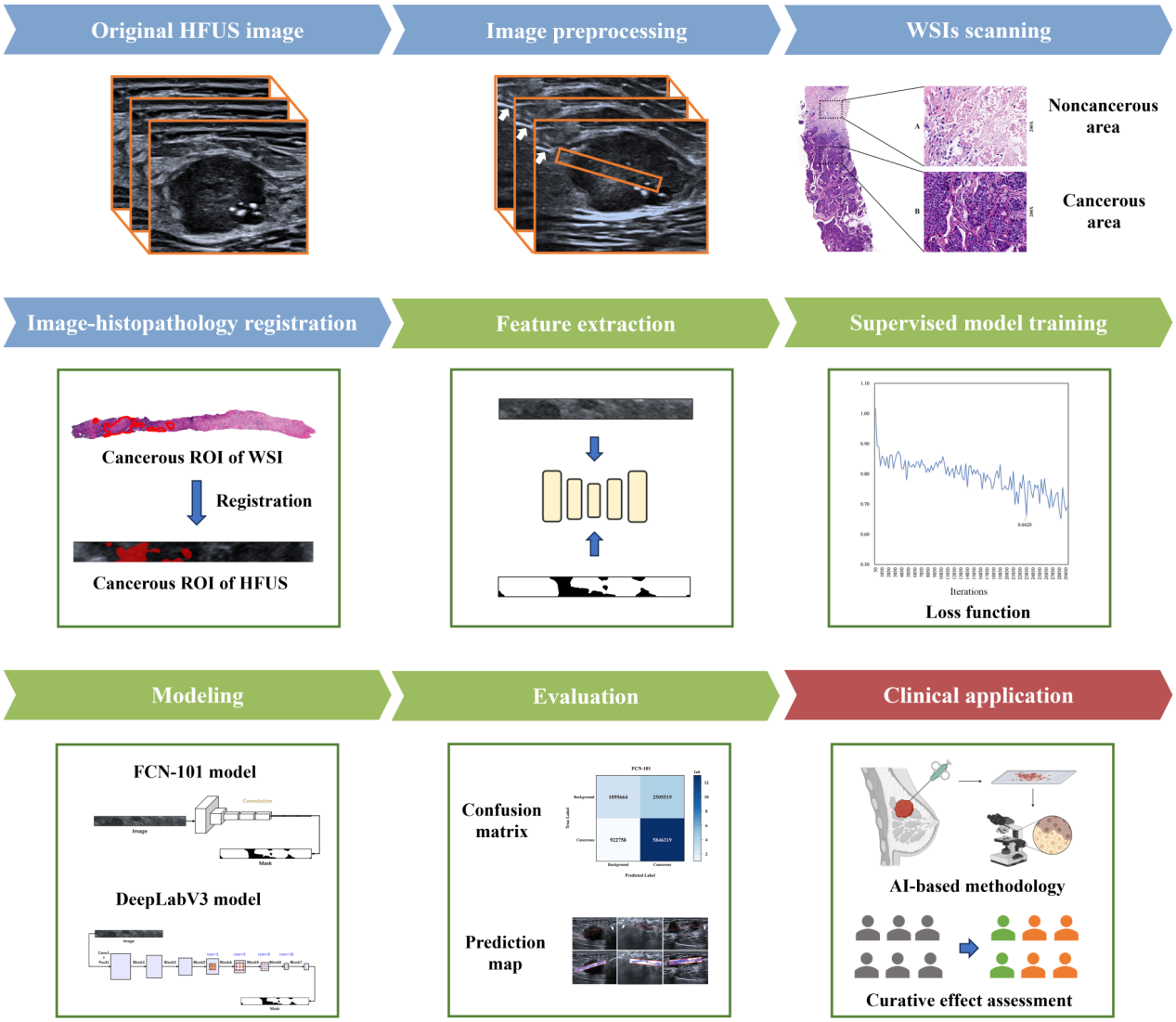

The tissue samples were fixed and oriented during the embedding process to preserve the longitudinal axis. Each 3 µm histological slide was then sectioned parallel to the initial needle trajectory, thereby ensuring that the analyzed WSI represented the same gross anatomical plane captured by HFUS. The tissue strips were very small, thus the dimensional changes and distortion introduced by histological processing were assumed to be limited. Each section was stained with H&E. For each participant, all slides stained with H&E were reviewed by two experienced breast pathologists (with 5 y and 10 y of experience), and the histopathologic type was reported. Scanning of the H&E slides was performed using a KFBIO Digital Pathology Slide Scanner (KF-PRO-020) with a 200X objective lens. Representative heterogeneous cancer cell distribution of breast cancer in biopsy WSI is depicted in Figure S2 in Multimedia Appendix 1.

Imaging Registration

The expert pathologist with 10 years of experience used the open-source software QuPath (version 0.4.0) for digital histopathology analysis. The maximal cross-section of the extracted core was used for analysis. Cancer cells were identified based on nuclear atypia and mitotic figures. The regions of interest (ROIs) of cancerous regions were manually outlined on all high-resolution WSI slices, generating a per-pixel cancer cell labeling (Figure 2).

For 4 - 6 samples from one lesion, the expert pathologist selected 1 - 4 specimens for further registration processing. The method for selecting was based on three criteria: (1) intact and well-formed; (2) length matches the needle notch (22 mm); (3) clear and distinguishable staining. For each selected tissue sample, one radiologist with at least 5 years of experience correlated the WSI to two captured B-mode HFUS images. To ensure the spatial registration from WSI to the HFUS images, the radiologist compares the pre-fire and post-fire HFUS images using Photoshop software (version CC 2019; Adobe Inc). In the software, the needle tip position in the pre-fire image was taken as the starting point; actual length of the biopsy specimen was determined by the needle projection distance in the post-fire

XSL•FO
RenderX

image. Then, the radiologist cropped the biopsy area in the pre-fire image for subsequent annotation and analysis. The detailed image cropping process is demonstrated in Figure 2. The HFUS image of the needle tract was then saved in JPG format. The ROIs outlined in WSIs were converted to correlated HFUS images via Labelme software, an open-source image annotation tool (version 5.1.0).

Figure 2. Spatial registration and mapping protocol between HFUS and WSI. We compared the pre-fire image and post-fire image to crop the needle tract in HFUS images. An experienced pathologist manually outlined the cancerous cells on WSI images using QuPath software (version 0.4.0 [21]), which were transferred to the cropped HFUS images, creating the labeled dataset for training. HFUS: high-frequency ultrasound; ROI: region of interest; WSI: whole slide image.

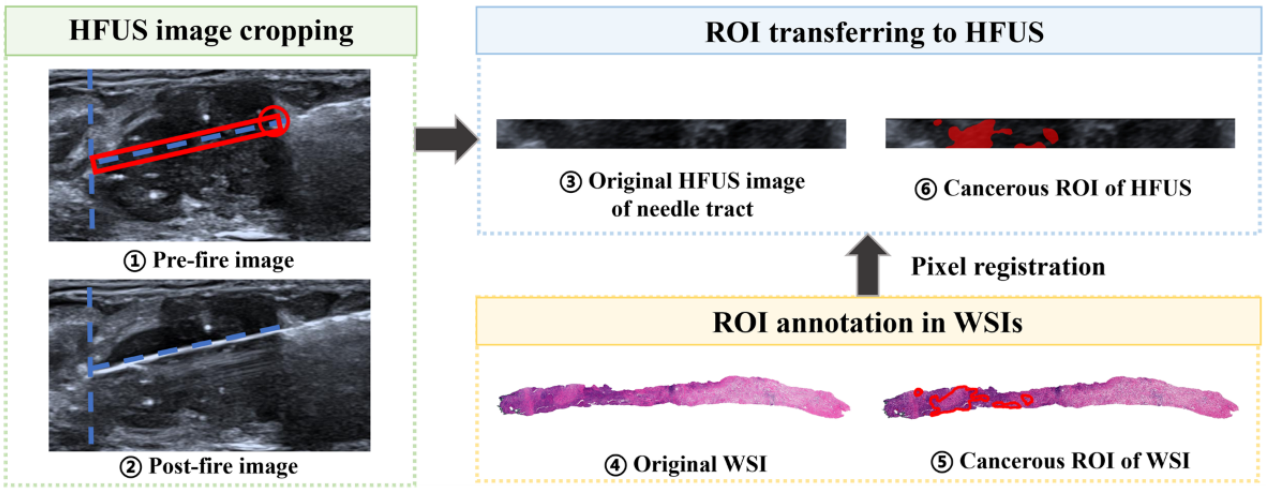

Data Preprocessing

The HFUS images and their ROIs annotation were obtained to establish the CNN prediction model. Open-source libraries including Python (version 3.8.11; Python Software Foundation), Imgviz (version 1.5.1), and Numpy (version 1.21.6) were used to convert the dataset into the standard VOC format. To enhance the robustness and generalization capability of the model, data augmentation strategies, such as random horizontal flipping, rotation, and pixel transformations, were used to increase the generalizability of the model. The dataset was randomly divided into training (n=270, 70%), validation (n=78, 20.2%), and test (n=38, 9.8%) subsets using a 7:2:1 ratio with no overlap between the subsets. Image pixel values were normalized using the *z*-score method to reduce computation burden and accelerate model convergence.

Model Development

The fully automated segmentation CNN model was designed to identify cancerous regions in breast cancer based on HFUS images, with the ROIs in WSI as the reference standard. The independent CNN model was trained with advanced FCN-101 [22] and DeepLabV3 [23] networks as the backbone, separately. During training, the models were adapted using the AdamW optimized algorithm and CosineAnnealing learning rate adjustment curve to improve efficiency. The weighted Dice loss function was used to mitigate the data imbalance during the training process, as plotted in Figure S3 in Multimedia Appendix 1. The iteration parameters with the lowest loss values were chosen, which were 0.6626 for the FCN-101 model and 0.7285 for the DeepLabV3 model. In the fine-tuned process, parameters were selected to construct the segmentation model when the best performance on the test dataset was achieved. Finally, cancerous regions in breast cancer were localized. More details on the CNN model are provided in Multimedia Appendix 1. The source code for our CNN models is available on GitHub [24].

Statistical Analysis

All statistical analysis was conducted with IBM SPSS Statistics 25.0 (version 25.0; IBM Corp), Python (version 3.8.11; Python Software Foundation), and R software (version 4.2.1, R Foundation for Statistical Computing). Continuous variables were exhibited as means (SDs) or medians and IQRs and compared using a 1-sample *t* test or Mann-Whitney *U* test where appropriate. Categorical variables were expressed as counts and percentages and compared through χ^2 tests. To assess and compare the segmentation performance of CNN models based on independent networks, pixel accuracy (PA), Dice similarity coefficient (DSC), mean Intersection over Union, precision, and recall were calculated. These metrics were computed separately for each test image, and the final performance values were obtained by averaging the image-level results across the entire dataset. To avoid inflated degrees of freedom arising from multiple images per participant, a paired-sample *t* test was performed at the participant level to compare the performance of FCN-101 and DeepLabV3 models. Normality of the paired differences was confirmed using the Shapiro-Wilk test. Detailed evaluation metrics were demonstrated in the Supplementary Methods in Multimedia Appendix 1. The confusion matrices were adopted to show the pixel-level classification of cancerous regions and normal tissue based on aggregated raw pixel counts. Two-tailed $P<.05$ was considered statistically significant.

Ethical Considerations

This single-center prospective study involving human participants was approved by the local institutional review board of the First Affiliated Hospital of Sun Yat-sen University (Ethics [2023]842). Written informed consent was obtained from all

XSL•FO
RenderX

participants prior to their inclusion in the study. This study was conducted in accordance with the Declaration of Helsinki and its subsequent amendments. All data were deidentified before analysis to ensure participant privacy. Participants did not receive any financial or material compensation, as all procedures were part of routine clinical care, and the analytical use of the resulting data was clearly explained to participants during enrollment. No identifiable images or personal information are included.

Results

Participant Characteristics

A total of 163 individual participants received ultrasound-guided breast biopsy, and 58 participants were excluded (Figure 3). The final prospective dataset contained 105 participants (mean age, 53.7, SD 11.3 y old; all female) diagnosed as breast cancer with 386 HFUS images of the needle tract. All biopsies ultimately achieved successful targeting and adequate sampling in the 105 participants. Among them, 64 (87.7%), 19 (95%), and 9 (75%) invasive breast cancer and 9 (12.3%), 1 (5%), and 3 (25%) ductal carcinomas in situ were identified in the training, validation, and test subsets, respectively. Characteristics were compared between three subsets in Table 1 and no evidence of a statistical difference was observed, except for vascularity, where internal vascularity of breast lesions was observed in the training dataset (P=.03).

Figure 3. Flowchart showing inclusion and exclusion criteria of participants. BI-RADS: Breast Imaging Reporting and Data System; US: ultrasound; WSI: whole slide image.

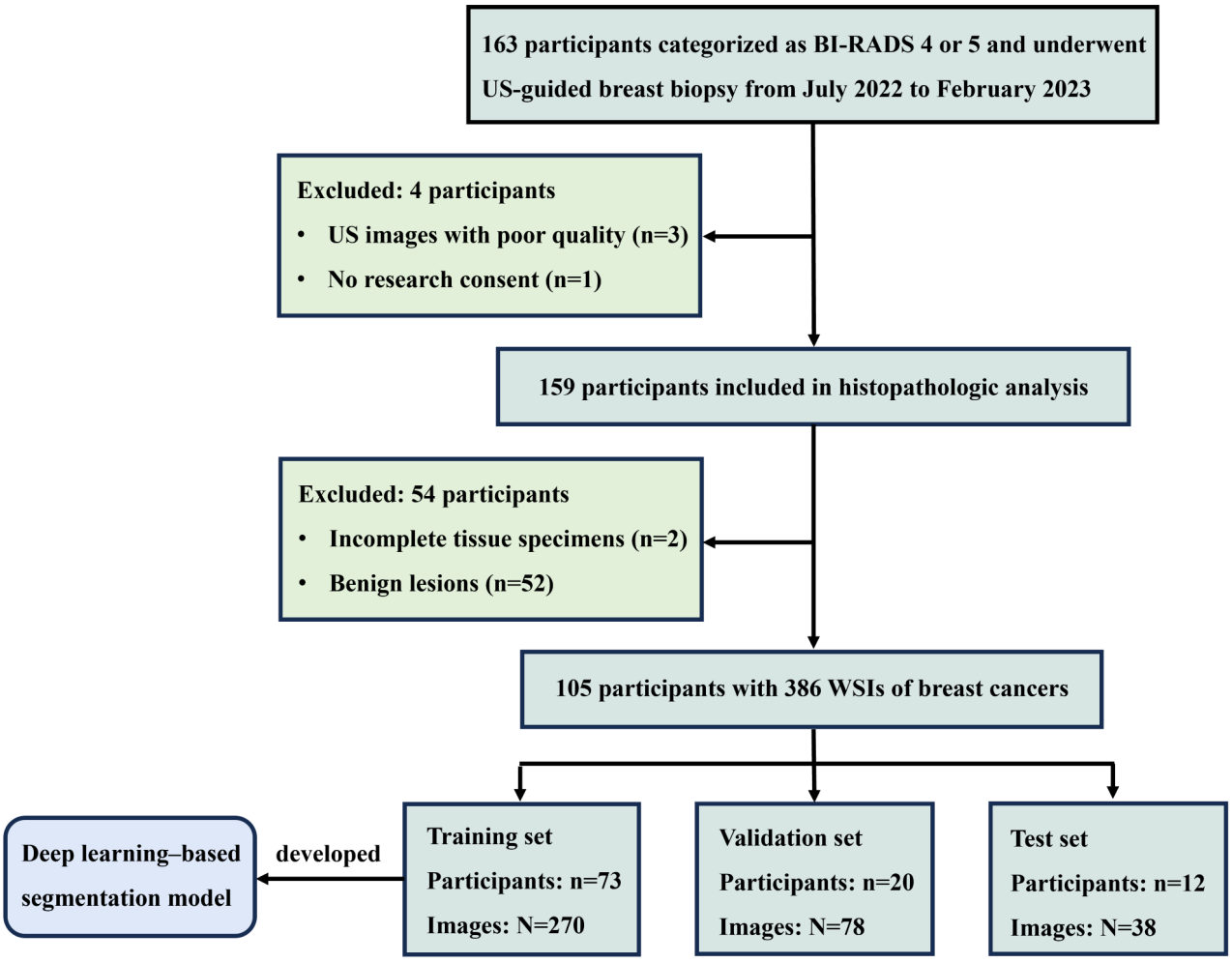

XSL•FO
RenderX

Table . Participants and breast cancer characteristics. Unless otherwise indicated, data are numbers of lesions, with the percentages in parentheses.

Characteristic	Training set (n=73)	Validation set (n=20)	Testing set (n=12)	*P* value
Age (y), mean (SD)	52.7 (SD 11.2)	57.8 (SD 13.2)	52.8 (SD 7.4)	.21
Lesion number, n (%)				.08
Solitary	64 (87.7)	19 (95)	8 (66.7)	
Numerous	9 (12.3)	1 (5)	4 (33.3)	
BI-RADS[a] categorization, n (%)				.96
BI-RADS 4a	5 (6.8)	1 (5)	1 (8.3)	
BI-RADS 4b	9 (12.3)	3 (15)	1 (8.3)	
BI-RADS 4c	18 (24.7)	3 (15)	2 (16.7)	
BI-RADS 5	40 (54.8)	13 (65)	8 (66.7)	
Lesion location, n (%)				.68
Left breast	32 (43.8)	11 (55)	6 (50)	
Right breast	41 (56.2)	9 (45)	6 (50)	
Quadrant, n (%)				.30
Upper outer quadrant	45 (61.6)	9 (45)	5 (41.7)	
Lower outer quadrant	10 (13.7)	1 (5)	2 (16.7)	
Upper inner quadrant	12 (16.4)	6 (30)	3 (25)	
Lower inner quadrant	6 (8.2)	4 (20)	2 (16.7)	
Volume (mm^3), mean (SD)	4.1 (SD 5.1)	3.4 (SD 2.8)	4.3 (SD 7.0)	.82
Orientation, n (%)				.22
Parallel	82 (89.1)	15 (75)	11 (91.7)	
Not parallel	10 (10.9)	5 (25)	1 (8.3)	
Echo pattern, n (%)				.78
Hypoechoic	86 (93.5)	20 (100)	12 (100)	
Heterogeneous	6 (6.5)	0 (0)	0 (0)	
Margin, n (%)				.52
Circumscribed	6 (8.2)	2 (10)	2 (16.7)	
Not circumscribed	67 (91.8)	18 (90)	10 (83.3)	
Shape, n (%)				.47
Oval/Round	3 (4.1)	0 (0.0)	1 (8.3)	
Irregular	70 (95.9)	20 (100.0)	11 (91.7)	
Calcification, n (%)				.40
Absence	36 (49.3)	25 (59.5)	8 (66.7)	
Calcification in a mass	37 (50.7)	17 (40.5)	4 (33.3)	
Vascularity, n (%)				.03
Absent	11 (15.1)	7 (35)	2 (16.7)	
Internal vascularity	56 (76.7)	11 (55)	7 (58.3)	
Vessels in rim	6 (18.2)	2 (10)	4 (33.3)	
Histopathologic pattern, n (%)				.13
Invasive breast cancer	64 (87.7)	19 (95)	9 (75)	
Ductal carcinoma in situ	9 (12.3)	1 (5)	3 (25)	

[a]BI-RADS: Breast Imaging Reporting and Data System.

XSL•FO
RenderX

Model Evaluation

The segmentation capacity of the image-based CNN model based on FCN-101 and DeepLabV3 in the test dataset is provided in Table 2. The table presents image-level descriptive statistics, while all inferential comparisons were conducted at the participant level (n=12). In the test dataset, FCN-101 showed higher accuracy (PA: 86.91% vs 69.55%, *P*=.002), similarity (DSC: 77.47% vs 69.90%, *P*<.001), mean Intersection over Union (67.47% vs 60.29%, *P*<.001), and precision (66.01% vs 56.15%, *P*<.001) compared to DeepLabV3. There was no evidence of a difference in recall (54.64% vs 58.46%, *P*=.80) between the two algorithms.

Table . Comparison of prediction performance of FCN-101 and DeepLabV3 models in predicting cancerous regions in breast cancer in the test dataset. All metrics reflect image-level performance and are expressed as percentages. Statistical comparisons (*P* values) were performed at the participant level using paired analyses.

Evaluation metric	FCN-101, % (95% CI)	DeepLabV3, % (95% CI)	*P* value
PA[a]	86.91 (80.30-94.77)	69.55 (65.82-73.99)	.002
DSC[b]	77.47 (70.74-85.88)	69.90 (63.43-75.02)	<.001
mIoU[c]	67.47 (59.70-75.54)	60.29 (54.19-66.57)	<.001
Precision	66.01 (55.69-73.45)	56.15 (48.12-64.17)	<.001
Recall	54.64 (45.57-63.75)	58.46 (49.03-65.66)	.80

[a]PA: pixel accuracy.

[b]DSC: Dice similarity coefficient.

[c]mIoU: mean Intersection over Union.

The confusion matrix presented in Figure 4 evaluates the pixel categorization capacity, providing further insight into the per-pixel predictions of each model. The results indicated that the FCN-101 model successfully predicted the majority of cancerous pixels (5,846,319 vs 4,649,445 pixels; *P*<.05). However, the DeepLabV3 model demonstrated more accurate predictive pixels in background components (2,440,670 vs 1,895,664 pixels; *P*<.05). Based on the pixel-wise confusion matrices, the recall and specificity of FCN-101 were 86.37% and 43.07%, while those of DeepLabV3 reached 68.69% and 55.46%.

Figure 4. Confusion matrices for predicting cancerous regions. Confusion matrices were applied to summarize pixel-level classification outcomes aggregated across the entire test dataset for (A) FCN-101 and (B) DeepLabV3, indicating discordance or concordance with the ground truth (cancerous cell/background) from WSI results. WSI: whole slide image.

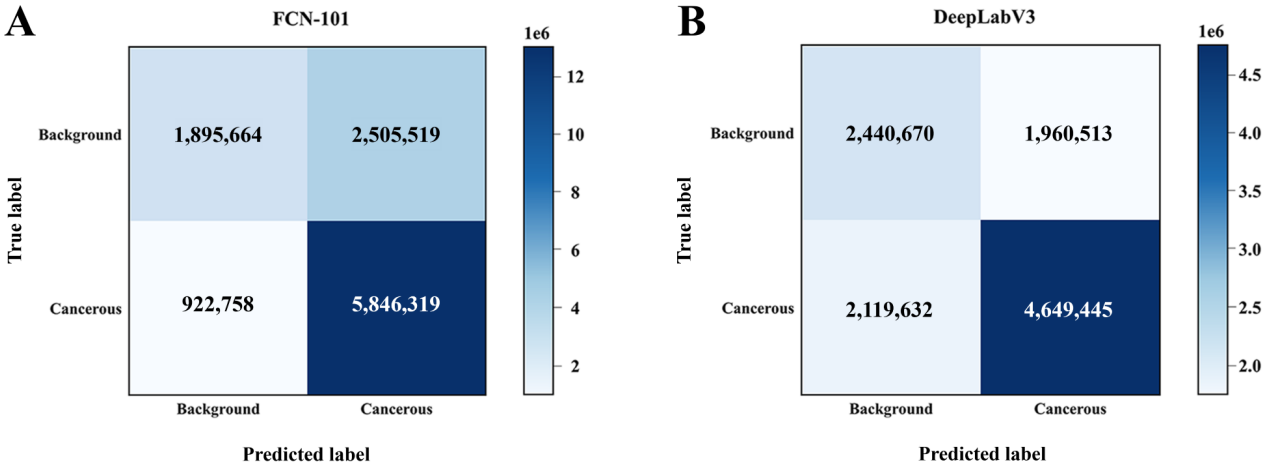

Model Visualization

In the test dataset, the automatic segmentation results of cancerous regions based on the two networks were visually displayed and qualitatively compared with the gold standard to evaluate the predictive performance of the models. Cancerous regions in the CNB biopsy area of three different participants' breast HFUS images were identified and localized in Figure 5, as generated by the FCN-101 and DeepLabV3 models. Cancerous region predictions by the two CNN models align closely with the actual histopathology. Additionally, even in challenging cases with unclear boundaries and mixed internal echoes, as represented in Example 2, both models were able to accurately predict the specific distribution of cancerous regions within the lesions.

XSL•FO
RenderX

Figure 5. Examples of identifying cancerous regions in three participants with invasive breast cancer. (**A**) Original HFUS images, with biopsy needle (white arrow) pointing to the needle tract area (red frame). (**B**) Annotation of ground truth labels by an expert pathologist. (**C**) Prediction results of the FCN-101 model (gray area). (**D**) Prediction results of the DeepLabV3 model (gray area). HFUS: high-frequency ultrasound.

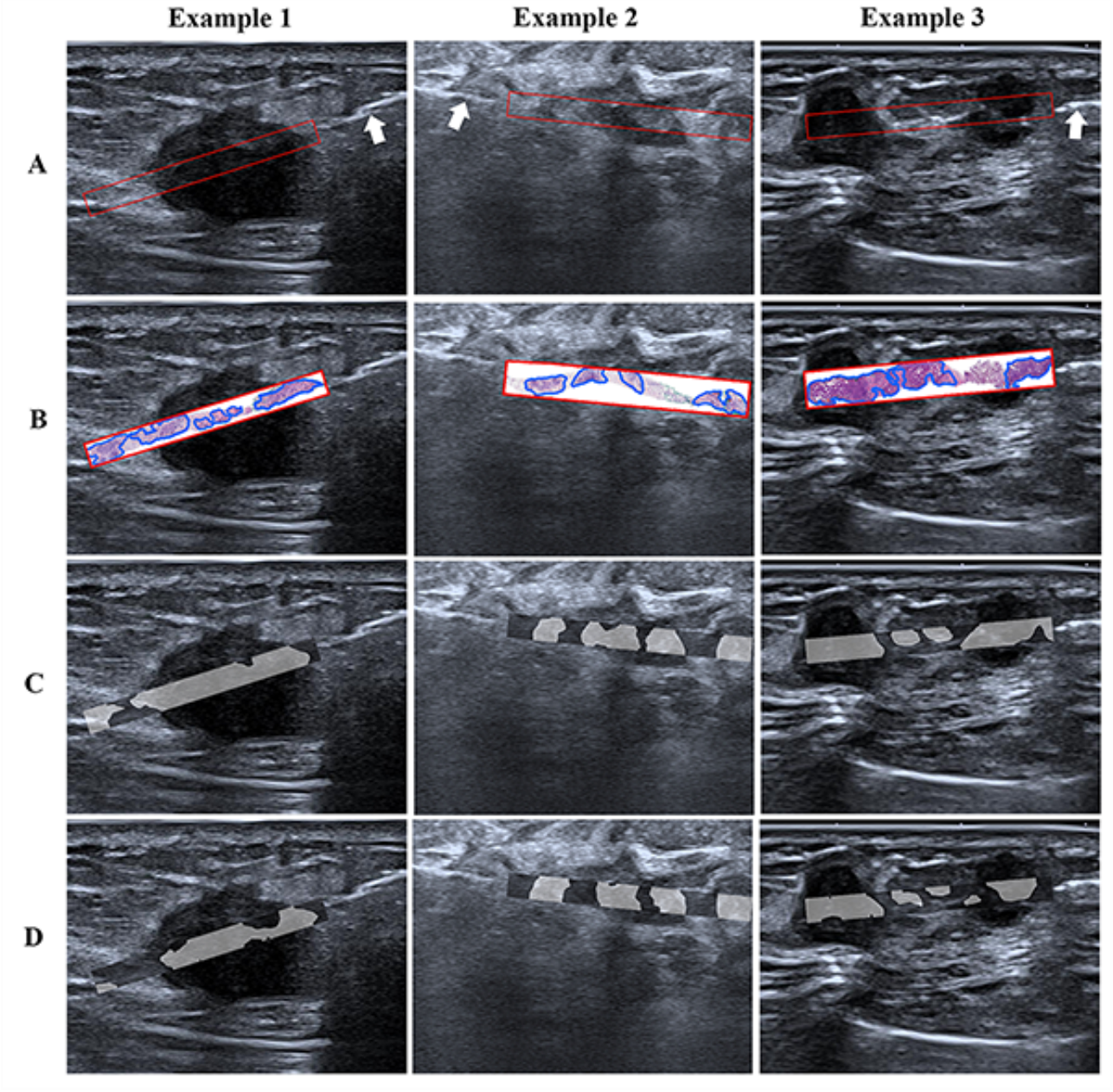

Discussion

Principal Results

Breast cancer is a group of highly heterogeneous diseases with varying imaging features. Thus, differential diagnosis through imaging is limited [25,26]. Development and validation of a fast and noninvasive method equal to histologic results is urgently needed. Here, we developed a cancerous region classifier using a deep learning network with true labels from radiology-pathology registration. The FCN-101 model was superior to the DeepLabV3 model in terms of PA (86.91% vs 69.55%; *P*=.002) and DSC (77.47% vs 69.90%; *P*<.001). Recall values were 54.64% and 58.46%, with no significant difference observed between them (*P*=.80). The FCN-101 model excelled in identifying cancerous regions (5,846,319 vs 4,649,445 pixels; *P*<.05), whereas DeepLabV3 was more accurate for normal tissue (2,440,670 vs 1,895,664 pixels; *P*<.05) in pixel-level predictions. In the clinical workflow, the model could segment cancerous regions in grayscale ultrasound images of the breast. The results highlight the model's potential for advancing breast cancer assessment at the microscopic level via ultrasound imaging.

Efforts have been made to establish a methodology pertaining to image-histopathology registration [27-32]. For example, Ward et al [27] and Kwak et al [28] demonstrated accurate alignment between MRIs and digital histopathologic analyses in patients with prostate cancer. In addition, Wildeboer et al [29] established a multiparametric machine learning on ultrasound for histopathology localization of prostate cancer. However, similar research in breast imaging remains limited. In our study, WSIs from CNB provided accessible clinical data suitable for state-of-the-art deep learning algorithms.

XSL•FO
RenderX

Thus, a strength of this study is that we combined accessible CNB tissue samples with real-time ultrasound imaging to facilitate the registration process. The biopsy needle targeted the desired section plane while the tissue sample was obtained at the same level, which was crucial for registration. Moreover, HFUS offers spatial tissue distribution data, enhancing dynamic biopsy procedures and clinical utility. However, subtle registration errors existed; for example, the biopsy needle was deflected when encountering small breast tumors or rigid glandular tissue [33]. To address this, our skilled operators actively mitigated needle deflections. Pre-fire and post-fire ultrasound images were compared to ensure that the extracted tissue precisely corresponded to the visualized ultrasound plane.

Studies have investigated the biopsy efficacy between existing methods. Currently, three image-guided breast biopsy techniques are used: stereotactic-, ultrasound-, and MRI-guided biopsies. Stereotactic biopsy is indicated for calcifications, and MRI-guided biopsy is indicated for lesions visible only on MRI; both primarily assess ductal proliferative lesions. Ultrasound-guided biopsy, however, applies to a broader range of breast lesions [34]. Yashima et al [35] retrospectively compared the positive biopsy rate in 453 patients with 500 lesions that underwent ultrasound-guided core needle biopsy or vacuum-assisted biopsy and reported positive biopsy rates of 61.9% and 72.4% (P=.032), respectively. Unrepresentative CNB specimens might not fully reflect the overall characteristics of the tumor [17]. Although multipoint sampling and repetitive biopsy increased the detection rate, they also increased complications like bleeding, infection, and tumor spreading [36]. Based on this, our model may generate real-time cancer prediction heatmaps, where suspicious regions are highlighted to assist biopsy site selection during CNB sampling. However, prior to clinical use, the proposed approach should undergo rigorous supervision and ethical evaluation to ensure its safety and reliability in guiding biopsy decisions.

The visualized cancerous map was used to enhance the interpretability of the model. Here, we found that distribution maps facilitated the assessment of cancerous regions by highlighting the hypoechoic area in HFUS images (illustrated in Figure 5), which is in accordance with clinical routine. Furthermore, areas of abnormal echogenicity or edges of lesions often corresponded to cancerous regions identified in histopathology, which was also correctly predicted by the deep learning models. Guided by the ultrasound-based CNN algorithm, doctors could identify suspicious regions based on predicted cancerous regions, even in small lesions, helping to ensure sufficient and representative CNB samples for accurate histopathological assessment. However, the model is intended to assist clinicians and cannot replace their judgment in biopsy decision-making.

Notably, there is a discrepancy between the per-image recall and the pixel-level aggregated recall, which can be explained by the scale-dependent nature of these two evaluation strategies. This scale-dependent discrepancy indicates that the current model achieves higher sensitivity for larger tumors, while the detection of small lesions remains more challenging. It highlights an important direction for future optimization aimed at improving detection stability across different tumor sizes.

Although the two models had advantages in predicting cancerous regions, the confusion matrix analysis revealed a relatively low specificity, particularly for the FCN-101 model (43.07%). This indicates the presence of false-positive segmentation, with a proportion of normal background pixels being incorrectly segmented as cancerous. Such oversegmentation may be acceptable in identifying suspicious regions when emphasizing sensitivity. However, in the context of biopsy guidance, such behavior highlights the need for further optimization toward more precise boundary discrimination. Future work will focus on improving specificity through better loss function design, boundary-aware learning, and postprocessing strategies.

Limitations

This study combined registered WSIs and HFUS images to enhance cancerous region recognition in breast cancer, which has not been well-established in the literature. Still, we acknowledge the limitations of this study. First, it is a single-center prospective study with a small and potentially homogenous dataset, which undermines the model's generalizability and heightens the risk of overfitting. Besides, the small sample size in the test set limits statistical power and the generalizability of the prospective findings. To address this, we plan to incorporate data from multiple centers for robust external validation and conduct prospective studies to explore the models' role in assisting breast biopsy and postoperative follow-up after neoadjuvant therapy. Second, the relatively low recall indicates that some malignant regions may be missed; future studies will focus on improving model sensitivity through ensemble and data balancing approaches. Besides, benchmarking against widely adopted baseline models (eg, U-Net) could be performed in future research. Third, there is an absence of molecular subtype or pathological classification analysis and an imbalance of specific subtypes with small sample sizes (ductal carcinoma in situ in the test set). Given that different subtypes and cancer types exhibit distinct morphological features, a subtype-specific analysis could reveal performance differences and lead to refined models optimized for specific subtypes. Fourth, other imaging modalities such as color Doppler flow imaging, elastography, and contrast-enhanced ultrasound also play paramount roles in breast cancer diagnosis. For example, the lower prevalence of internal vascularity in the test set compared with the training set may have influenced model performance. Combining the information from multiple modalities could potentially further improve the performance of the CNN model. Fifth, the ultrasound-histopathology registration was based on biopsy WSIs and ultrasound images of the needle tract. Spatial correspondence should be regarded as approximate, and pixel-level metrics may overestimate the physical precision, which necessitates further refinement and validation via the whole-mount specimen.

Conclusion

In conclusion, we have proposed and evaluated deep learning models to identify cancerous regions in breast cancer in HFUS images through spatial registration of breast biopsy WSIs and HFUS images. This technique is potentially useful in conventional ultrasound examinations and ultrasound-guided breast biopsy procedures.

XSL•FO
RenderX

Acknowledgments

During drafting and revision of the manuscript, we used ChatGPT 5.0 (OpenAI) to polish the work to refine the language and improve readability. The authors reviewed and edited the content to ensure accuracy and take full responsibility for the content of the publication.

Funding

This study was supported by the National Scientific Foundation Committee of China (grants 82071951, 82102057, 82402297) and the Major Research Plan of the National Natural Science Foundation of China (grant 92059201). The funders had no role in the study design, data collection and analysis, decision to publish, or preparation of the manuscript.

Data Availability

All data supporting the findings are available from the corresponding author on reasonable request. Source code for our convolutional neural network models is deposited on GitHub [37].

Authors' Contributions

JQY contributed to conceptualization, formal analysis, investigation, methodology, and writing – original draft. WWZ contributed to data curation, formal analysis, investigation, methodology, and writing – original draft. ZFC contributed to formal analysis, software, and validation. FR contributed to software, methodology, and supervision. TYH contributed to data curation, investigation, and methodology. TTZ contributed to data curation and investigation. HJS contributed to data curation and supervision. XYX contributed to conceptualization, funding acquisition, and supervision. ZZ contributed to conceptualization, methodology, software, supervision, and visualization. MX contributed to conceptualization, funding acquisition, project administration, and writing – review and editing. JQY and WWZ are cofirst authors. ZZ and MX are cocorresponding authors.

Conflicts of Interest

None declared.

Multimedia Appendix 1
Supplementary figures and notes illustrating the modeling framework and statistical evaluation methodologies used in this study.
[DOCX File, 3635 KB - medinform_v14i1e81181_app1.docx]

References

1. Zardavas D, Irrthum A, Swanton C, Piccart M. Clinical management of breast cancer heterogeneity. Nat Rev Clin Oncol 2015 Jul;12(7):381-394. [doi: 10.1038/nrclinonc.2015.73] [Medline: 25895611]
2. Lüönd F, Tiede S, Christofori G. Breast cancer as an example of tumour heterogeneity and tumour cell plasticity during malignant progression. Br J Cancer 2021 Jul;125(2):164-175. [doi: 10.1038/s41416-021-01328-7] [Medline: 33824479]
3. Berg WA, Bandos AI, Mendelson EB, Lehrer D, Jong RA, Pisano ED. Ultrasound as the primary screening test for breast cancer: analysis from ACRIN 6666. J Natl Cancer Inst 2016 Apr;108(4):djv367. [doi: 10.1093/jnci/djv367] [Medline: 26712110]
4. Kutasovic JR, McCart Reed AE, Sokolova A, Lakhani SR, Simpson PT. Morphologic and genomic heterogeneity in the evolution and progression of breast cancer. Cancers (Basel) 2020 Mar 31;12(4):848. [doi: 10.3390/cancers12040848] [Medline: 32244556]
5. Haque W, Verma V, Hatch S, Suzanne Klimberg V, Brian Butler E, Teh BS. Response rates and pathologic complete response by breast cancer molecular subtype following neoadjuvant chemotherapy. Breast Cancer Res Treat 2018 Aug;170(3):559-567. [doi: 10.1007/s10549-018-4801-3] [Medline: 29693228]
6. Fayanju OM, Ren Y, Thomas SM, et al. The clinical significance of breast-only and node-only pathologic complete response (pCR) after neoadjuvant chemotherapy (NACT): a review of 20,000 breast cancer patients in the National Cancer Data Base (NCDB). Ann Surg 2018 Oct;268(4):591-601. [doi: 10.1097/SLA.0000000000002953] [Medline: 30048319]
7. Romeo V, Accardo G, Perillo T, et al. Assessment and prediction of response to neoadjuvant chemotherapy in breast cancer: a comparison of imaging modalities and future perspectives. Cancers (Basel) 2021 Jul 14;13(14):3521. [doi: 10.3390/cancers13143521] [Medline: 34298733]
8. Fowler AM, Mankoff DA, Joe BN. Imaging neoadjuvant therapy response in breast cancer. Radiology 2017 Nov;285(2):358-375. [doi: 10.1148/radiol.2017170180] [Medline: 29045232]
9. Kuerer HM, Smith BD, Krishnamurthy S, et al. Eliminating breast surgery for invasive breast cancer in exceptional responders to neoadjuvant systemic therapy: a multicentre, single-arm, phase 2 trial. Lancet Oncol 2022 Dec;23(12):1517-1524. [doi: 10.1016/S1470-2045(22)00613-1] [Medline: 36306810]

XSL•FO
RenderX

10. Shi Z, Huang X, Cheng Z, et al. MRI-based quantification of intratumoral heterogeneity for predicting treatment response to neoadjuvant chemotherapy in breast cancer. Radiology 2023 Jul;308(1):e222830. [doi: 10.1148/radiol.222830] [Medline: 37432083]
11. Fatayer H, Sharma N, Manuel D, et al. Serial MRI scans help in assessing early response to neoadjuvant chemotherapy and tailoring breast cancer treatment. Eur J Surg Oncol 2016 Jul;42(7):965-972. [doi: 10.1016/j.ejso.2016.03.019] [Medline: 27260848]
12. Ali HR, Jackson HW, Zanotelli VRT, et al. Imaging mass cytometry and multiplatform genomics define the phenogenomic landscape of breast cancer. Nat Cancer 2020 Feb;1(2):163-175. [doi: 10.1038/s43018-020-0026-6] [Medline: 35122013]
13. Shamai G, Binenbaum Y, Slossberg R, Duek I, Gil Z, Kimmel R. Artificial intelligence algorithms to assess hormonal status from tissue microarrays in patients with breast cancer. JAMA Netw Open 2019 Jul 3;2(7):e197700. [doi: 10.1001/jamanetworkopen.2019.7700] [Medline: 31348505]
14. Liu H, Xu WD, Shang ZH, et al. Breast cancer molecular subtype prediction on pathological images with discriminative patch selection and multi-instance learning. Front Oncol 2022;12:858453. [doi: 10.3389/fonc.2022.858453]
15. Park KH, Loibl S, Sohn J, et al. Pan-Asian adapted ESMO Clinical Practice Guidelines for the diagnosis, treatment and follow-up of patients with early breast cancer. ESMO Open 2024 May;9(5):102974. [doi: 10.1016/j.esmoop.2024.102974] [Medline: 38796284]
16. Tasoulis MK, Lee HB, Yang W, et al. Accuracy of post-neoadjuvant chemotherapy image-guided breast biopsy to predict residual cancer. JAMA Surg 2020 Dec 1;155(12):e204103. [doi: 10.1001/jamasurg.2020.4103] [Medline: 33026457]
17. Brogi E, Krystel-Whittemore M. Papillary neoplasms of the breast including upgrade rates and management of intraductal papilloma without atypia diagnosed at core needle biopsy. Mod Pathol 2021 Jan;34(Suppl 1):78-93. [doi: 10.1038/s41379-020-00706-5] [Medline: 33106592]
18. Huang Y, Yao Z, Li L, et al. Deep learning radiopathomics based on preoperative US images and biopsy whole slide images can distinguish between luminal and non-luminal tumors in early-stage breast cancers. EBioMedicine 2023 Aug;94:104706. [doi: 10.1016/j.ebiom.2023.104706] [Medline: 37478528]
19. Bhattacharya I, Seetharaman A, Kunder C, et al. Selective identification and localization of indolent and aggressive prostate cancers via CorrSigNIA: an MRI-pathology correlation and deep learning framework. Med Image Anal 2022 Jan;75:102288. [doi: 10.1016/j.media.2021.102288] [Medline: 34784540]
20. Morris E, Comstock C, Lee C, et al. ACR BI-RADS magnetic resonance imaging ACR BI-RADS atlas, breast imaging reporting and data system. 2013 URL: https://www.acr.org/Clinical-Resources/Clinical-Tools-and-Reference/Reporting-and-Data-Systems/BI-RADS [accessed 2026-01-08]
21. QuPath. URL: https://qupath.github.io/ [accessed 2026-01-21]
22. Dung CV, Anh LD. Autonomous concrete crack detection using deep fully convolutional neural network. Automation in Construction 2019 Mar;99:52-58. [doi: 10.1016/j.autcon.2018.11.028]
23. Chen LC, Papandreou G, Schroff F, et al. Rethinking atrous convolution for semantic image segmentation. arXiv. Preprint posted online on Jun 17, 2017. [doi: 10.1007/978-3-030-01234-2_49]
24. Chai ZF. Breast cancer component segmentation. GitHub repository. 2024. URL: https://github.com/ChaiZhifeiF/Breast-Cancer-Component-Segmentation [accessed 2024-07-23]
25. Lee HJ, Kim EK, Kim MJ, et al. Observer variability of Breast Imaging Reporting and Data System (BI-RADS) for breast ultrasound. Eur J Radiol 2008 Feb;65(2):293-298. [doi: 10.1016/j.ejrad.2007.04.008] [Medline: 17531417]
26. Abdullah N, Mesurolle B, El-Khoury M, Kao E. Breast imaging reporting and data system lexicon for US: interobserver agreement for assessment of breast masses. Radiology 2009 Sep;252(3):665-672. [doi: 10.1148/radiol.2523080670] [Medline: 19567644]
27. Ward AD, Crukley C, McKenzie CA, et al. Prostate: registration of digital histopathologic images to in vivo MR images acquired by using endorectal receive coil. Radiology 2012 Jun;263(3):856-864. [doi: 10.1148/radiol.12102294] [Medline: 22474671]
28. Kwak JT, Sankineni S, Xu S, et al. Prostate cancer: a correlative study of multiparametric MR imaging and digital histopathology. Radiology 2017 Oct;285(1):147-156. [doi: 10.1148/radiol.2017160906] [Medline: 28582632]
29. Wildeboer RR, Mannaerts CK, van Sloun RJG, et al. Automated multiparametric localization of prostate cancer based on B-mode, shear-wave elastography, and contrast-enhanced ultrasound radiomics. Eur Radiol 2020 Feb;30(2):806-815. [doi: 10.1007/s00330-019-06436-w] [Medline: 31602512]
30. Zhang Z, Wu HH, Priester A, et al. Prostate microstructure in prostate cancer using 3-T MRI with diffusion-relaxation correlation spectrum imaging: validation with whole-mount digital histopathology. Radiology 2020 Aug;296(2):348-355. [doi: 10.1148/radiol.2020192330] [Medline: 32515678]
31. Schoop RAL, de Roode LM, de Boer LL, Dashtbozorg B. Framework for deep learning based multi-modality image registration of snapshot and pathology images. IEEE J Biomed Health Inform 2024 Nov;28(11):6699-6711. [doi: 10.1109/JBHI.2024.3444908] [Medline: 39150810]
32. Schalk SG, Postema A, Saidov TA, et al. 3D surface-based registration of ultrasound and histology in prostate cancer imaging. Comput Med Imaging Graph 2016 Jan;47:29-39. [doi: 10.1016/j.compmedimag.2015.11.001] [Medline: 26647110]

XSL•FO
RenderX

33. Ma K, Kornecki A, Bax J, Mundt Y, Fenster A. Development and validation of a new guidance device for lateral approach stereotactic breast biopsy. Med Phys 2009 Jun;36(6):2118-2129. [doi: 10.1118/1.3130017] [Medline: 19610301]
34. Nakano S, Imawari Y, Mibu A, Otsuka M, Oinuma T. Differentiating vacuum-assisted breast biopsy from core needle biopsy: is it necessary? Br J Radiol 2018 Dec;91(1092):20180250. [doi: 10.1259/bjr.20180250] [Medline: 29975150]
35. Yashima Y, Fujioka T, Kubota K, et al. Comparison of the clinical and pathological characteristics of ultrasound-guided biopsy for breast masses and non-mass lesions between 16-gauge spring-loaded core needle biopsy and 12-gauge spring-loaded vacuum-assisted biopsy. J Med Ultrasonics 2023 Apr;50(2):205-212. [doi: 10.1007/s10396-022-01279-3]
36. Loving VA, Johnston BS, Reddy DH, et al. Antithrombotic therapy and hematoma risk during image-guided core-needle breast biopsy. Radiology 2023 Jan;306(1):79-86. [doi: 10.1148/radiol.220548] [Medline: 35997610]
37. ChaiZhifeiF/breast-cancer-component-segmentation. GitHub. URL: https://github.com/ChaiZhifeiF/Breast-Cancer-Component-Segmentation [accessed 2026-01-21]

Abbreviations

BI-RADS: Breast Imaging Reporting and Data System
CNB: core needle biopsy
CNN: convolutional neural network
DSC: Dice similarity coefficient
H&E: hematoxylin and eosin
HFUS: high-frequency ultrasound
MRI: magnetic resonance image/imaging
PA: pixel accuracy
ROI: region of interest
WSI: whole slide image

Edited by A Coristine; submitted 23.Jul.2025; peer-reviewed by L Yongping, P Bhatnagar; accepted 17.Dec.2025; published 23.Jan.2026.

Please cite as:
Yao JQ, Zhou WW, Chai ZF, Ren F, Huang TY, Zhen TT, Shi HJ, Xie XY, Zhao Z, Xu M
Identification and Localization of Breast Tumor Components via a Convolutional Neural Network Based on High-Frequency Ultrasound Combined With Histopathologic Registration: Prospective Study
JMIR Med Inform 2026;14:e81181
URL: https://medinform.jmir.org/2026/1/e81181
doi:10.2196/81181

© Jia-Qian Yao, Wen-Wen Zhou, Zhi-Fei Chai, Fei Ren, Tong-Yi Huang, Tian-Tian Zhen, Hui-Juan Shi, Xiao-Yan Xie, Ze Zhao, Ming Xu. Originally published in JMIR Medical Informatics (https://medinform.jmir.org), 23.Jan.2026. This is an open-access article distributed under the terms of the Creative Commons Attribution License (https://creativecommons.org/licenses/by/4.0/), which permits unrestricted use, distribution, and reproduction in any medium, provided the original work, first published in JMIR Medical Informatics, is properly cited. The complete bibliographic information, a link to the original publication on https://medinform.jmir.org/, as well as this copyright and license information must be included.

XSL•FO
RenderX

Original Paper

Prompting and Fine-Tuning Large Language Models for Parkinson Disease Diagnosis: Comparative Evaluation Study Using the PPMI Structured Dataset

Hyun-Ji Shin[1,2], MSc; Young Jin Jeong[1,4,3], MD, PhD; Sungmin Jun[2,4,3], MD, PhD; Do-Young Kang[1,4,3], MD, PhD

[1]Department of Data Sciences Convergence, Graduate School, Dong-A University, Busan, Republic of Korea

[2]Institute of Convergence Bio-Health, Dong-A University, Busan, Republic of Korea

[3]Department of Nuclear Medicine, College of Medicine, Dong-A University, Busan, Republic of Korea

[4]Department of Nuclear Medicine, Dong-A University Hospital, Busan, Republic of Korea

Corresponding Author:
Do-Young Kang, MD, PhD
Department of Nuclear Medicine
College of Medicine
Dong-A University
26, Daesingongwon-ro, Seo-gu
Busan, 49201
Republic of Korea
Phone: 82 51 240 5630
Email: dykang@dau.ac.kr

Abstract

Background: Parkinson disease (PD) presents diagnostic challenges due to its heterogeneous motor and nonmotor manifestations. Traditional machine learning (ML) approaches have been evaluated on structured clinical variables. However, the diagnostic utility of large language models (LLMs) using natural language representations of structured clinical data remains underexplored.

Objective: This study aimed to evaluate the diagnostic classification performance of multiple LLMs using natural language prompts derived from structured clinical data and to compare their performance with traditional ML baselines.

Methods: We reformatted structured clinical variables from the Parkinson's Progression Markers Initiative (PPMI) dataset into natural language prompts and used them as inputs for several LLMs. Variables with high multicollinearity were removed, and the top 10 features were selected using Shapley additive explanations (SHAP)–based feature ranking. LLM performance was examined across few-shot prompting, dual-output prompting that additionally generated post hoc explanatory text as an exploratory component, and supervised fine-tuning. Logistic regression (LR) and support vector machine (SVM) classifiers served as ML baselines. Model performance was evaluated using F_1-scores on both the test set and a temporally independent validation set (temporal validation set) of limited size, and repeated output generation was carried out to assess stability.

Results: On the test set of 122 participants, LR and SVM trained on the 10 SHAP-selected clinical variables each achieved a macro-averaged F_1-score of 0.960 (accuracy 0.975). LLMs receiving natural language prompts derived from the same variables reached comparable performance, with the best few-shot configurations achieving macro-averaged F_1-scores of 0.987 (accuracy 0.992). In the temporal validation set of 31 participants, LR maintained a macro-averaged F_1-score of 0.903, whereas SVM showed substantial performance degradation. In contrast, multiple LLMs sustained high diagnostic performance, reaching macro-averaged F_1-scores up to 0.968 and high recall for PD. Repeated output generation across LLM conditions produced generally stable predictions, with rare variability observed across runs. Under dual-output prompting, diagnostic performance showed a reduction relative to few-shot prompting while remaining generally stable. Supervised fine-tuning of lightweight models improved stability and enabled GPT-4o-mini to achieve a macro-averaged F_1-score of 0.987 on the test set, with uniformly correct predictions observed in the small temporal validation set, which should be interpreted cautiously given the limited sample size and exploratory nature of the evaluation.

Conclusions: This study provides an exploratory benchmark of how modern LLMs process structured clinical variables in natural language form. While several models achieved diagnostic performance comparable to LR across both the test and temporal validation datasets, their outputs were sensitive to prompting formats, model choice, and class distributions. Occasional variability

XSL•FO
RenderX

across repeated output generations reflected the stochastic nature of LLMs, and lightweight models required supervised fine-tuning for stable generalization. These findings highlight the capabilities and limitations of current LLMs in handling tabular clinical information and underscore the need for cautious application and further investigation.

(JMIR Med Inform 2026;14:e77561) doi:10.2196/77561

KEYWORDS

Claude; diagnostic classification; fine-tuning; Gemini; GPT; large language models; LLaMA; Parkinson disease; Parkinson's Progression Markers Initiative; PPMI; prompt engineering

Introduction

Parkinson disease (PD) is the second most common neurodegenerative disorder and presents substantial diagnostic challenges due to the heterogeneity of its motor and nonmotor symptoms [1-3]. Despite sustained research efforts, early diagnostic accuracy remains limited, and the variability of clinical presentations continues to complicate reliable classification [4,5]. Large-scale initiatives such as the Parkinson's Progression Markers Initiative (PPMI) [6] have facilitated systematic evaluation of clinical, imaging, and biomarker variables, providing a foundation for quantitative approaches to PD diagnosis.

Machine learning (ML) models, including logistic regression (LR) [7], support vector machines (SVM) [8], and tree-based classifiers, have demonstrated strong performance when applied to structured clinical variables [9-11]. However, these models operate on fixed feature representations and do not naturally support flexible natural language inputs or generative reasoning, limiting their applicability when structured clinical data must be reformatted into descriptive text.

Recent large language models (LLMs) exhibit strong capabilities in processing natural language information and have shown promise in clinical applications involving unstructured text such as clinical notes and reports [12,13]. LLM-generated rationales typically represent post hoc explanatory text rather than true interpretability [14], and prior studies have reported challenges such as prompt sensitivity, stochastic variability, and susceptibility to distributional shifts when LLMs are applied to medical tasks [15]. However, their ability to perform diagnostic classification when structured clinical variables are reformatted into natural language prompts remains insufficiently explored, and recent work evaluating the performance of LLMs on structured or tabular data has reported limited and inconsistent results [16]. These characteristics highlight the need for careful and systematic evaluation when applying LLMs to structured clinical information.

In this context, the goal of this study was to conduct an exploratory benchmark of modern LLMs for PD classification using natural language prompts derived from structured clinical variables in the PPMI dataset. We compared multiple LLM families with traditional ML baselines and evaluated their behavior across few-shot prompting, dual-output prompting, and supervised fine-tuning. The study aimed to characterize both the capabilities and the limitations of LLMs in handling tabular clinical information, rather than demonstrating superiority over conventional ML approaches.

Methods

Overview

Figure 1 illustrates the overall methodological workflow of the study, detailing the progression from dataset selection and feature preprocessing to prompt construction, model training, and evaluation. It provides a concise visual summary of the experimental pipeline described in the Methods section.

XSL•FO
RenderX

Figure 1. Study design overview illustrating the overall experimental pipeline, including dataset selection, prompting strategies, fine-tuning, and evaluation procedures. HC: healthy controls; LLM: large language model; MD: markdown; MD+ST: markdown with special token; ML: machine learning; PD: Parkinson disease; PPMI: Parkinson's Progression Markers Initiative; PT: plain text; SHAP: Shapley additive explanations; ST: special token; VIF: variance inflation factor.

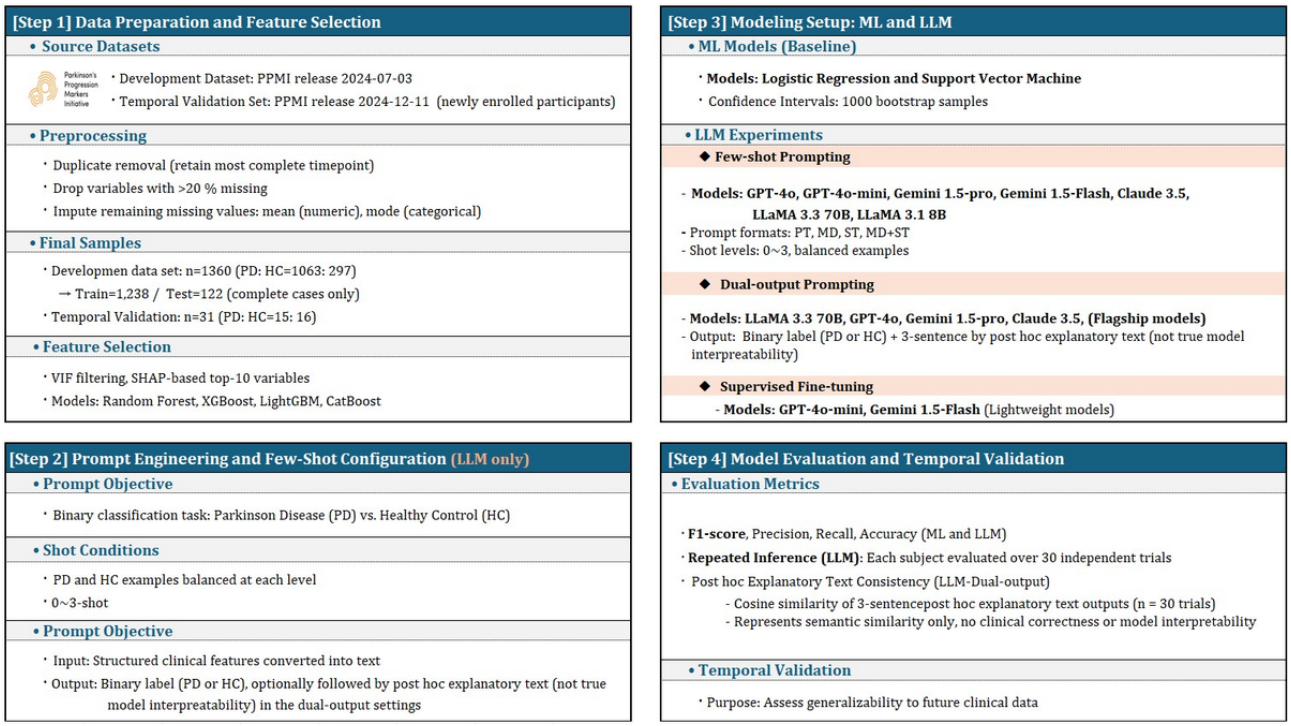

Dataset and Preprocessing

This study used a curated dataset provided by the PPMI, downloaded on July 29, 2024 (data release: July 3, 2024). The initial dataset consisted of 4 participant cohorts: individuals with PD, healthy controls (HC), participants with scans without evidence of dopaminergic deficit, and prodromal participants. For this study, only PD and HC participants were included.

Duplicate observations were removed by retaining the most comprehensive examination timepoint for each participant. Variables with more than 20% of missingness were excluded. Missing values in the remaining viables were imputed using mean imputation for numerical variables and mode imputation for categorical variables [17]. Participants included in the held-out test set and in the temporally independent validation set (temporal validation set) did not contain missing values and therefore required no imputation. Missing-value imputation was performed only for the training portion of the development dataset, which consisted of the train and validation subsets. Imputation statistics (mean and mode) were computed exclusively from the training split and subsequently applied to validation split. This procedure ensured that no information from the test or temporal validation sets influenced the preprocessing of the training data. After preprocessing, the final development dataset consisted of 1360 participants (PD, n=1063; HC, n=297).

A temporal validation set was constructed using the most recent curated PPMI dataset released on December 11, 2024. To ensure temporal separation, all data contained in the July 3, 2024, release were excluded, and only data from participants newly recruited after this release were included. This temporally separated dataset was used to assess the generalizability of model performance to data collected at a later timepoint. In clinical research, obtaining an external dataset with identical conditions is often challenging, and temporally separated datasets serve as a practical and widely accepted alternative for external validation [18,19].

Demographic characteristics of both the development and temporal validation datasets, including age, sex, education, and race, are summarized in Table 1.

XSL•FO
RenderX

Table 1. Demographic information of participants by dataset group.

Characteristic	Development set		Temporal validation set[a]	
	PD[b] (n=1063)	HC[c] (n=297)	PD (n=15)	HC (n=16)
Age (years), mean (SD; range)	63.3 (9.7; 30.7-85.3)	62.4 (10.6; 30.4-83.7)	62.7 (10.9; 31.3-73.0)	63.9 (11.3; 30.4-79.4)
Sex, n (%)				
Male	686 (64.5)	195 (65.7)	8 (53.3)	3 (18.8)
Female	377 (35.5)	102 (34.3)	7 (46.7)	13 (81.3)
Education (years), mean (SD; range)	16.0 (2.8; 6-20)	16.0 (2.7; 8-20)	16.8 (2.0; 11-20)	16.7 (2.0; 12-20)
Race, n (%)				
White	973 (91.5)	272 (91.6)	13 (86.7)	16 (100)
Black	30 (2.8)	10 (3.4)	0 (0)	0 (0)
Asian	21 (2)	2 (0.7)	1 (6.7)	0 (0)
Other	39 (3.7)	13 (4.4)	1 (6.7)	0 (0)

[a]Temporal validation set includes participants newly enrolled after the July 3, 2024, data release (excluded from the development set) and serves as a temporally separated dataset for external validation.

[b]PD: Parkinson disease.

[c]HC: healthy controls.

The development dataset was randomly divided into training, validation, and test subsets following an approximately 7:2:1 ratio. Only complete cases were included in the test set to ensure reliable evaluation. Feature selection and fine-tuning were performed exclusively using the training set. The test set was used solely for final model evaluation and was not involved in any feature selection or model fitting procedures. Class distributions for each subset are summarized in Table 2.

Table 2. Dataset splits and class distribution for diagnostic modeling.

Datasets and subsets	Total, n	PD[a], n (%)	HC[b], n (%)
Development set			
Training set	990	771 (77.9)	219 (22.1)
Validation set	248	193 (77.8)	55 (22.2)
Test set	122	99 (81.1)	23 (18.9)
Temporal validation set	31	15 (48.4)	16 (51.6)

[a]PD: Parkinson disease.

[b]HC: healthy controls.

Feature Selection

Multicollinearity Evaluation

To address multicollinearity, we generated a correlation matrix and computed the variance inflation factor for all candidate variables [20]. Variables with variance inflation factor values exceeding 10, a commonly accepted threshold for severe multicollinearity, were removed to prevent unstable coefficients and improve model reliability [21,22]. A total of 70 variables remained after this screening step and were used for Shapley additive explanations (SHAP)–based feature selection.

SHAP-Based Feature Importance

Feature importance was evaluated using a weighted average of SHAP values obtained from 4 tree-based models, including random forest [23], XGBoost [24], LightGBM [25], and CatBoost [26]. These models were selected because they are widely used for their tabular data and are known to mitigate issues related to multicollinearity while accommodating mixtures of numerical and categorical features effectively [27].

For each model, SHAP values were computed for all remaining variables, normalized, and then combined using a weighted averaging approach based on the diagnostic performance of each model. The performance metrics and assigned weights are summarized in Multimedia Appendix 1.

The weighted average SHAP value for each feature was calculated as [28]:

where:

- φ_{ij} represents the SHAP value of feature j computed by model i
- w_i represents the performance-based weight assigned to model i

XSL•FO
RenderX

- the denominator ensures that weights are normalized so they sum to 1.

The top 10 variables were selected based on these weighted average SHAP values, as shown in Multimedia Appendix 2. The final features set consisted of clinically meaningful motor, olfactory, and imaging features. Specifically, the selected variables were updrs3_score, con_putamen, updrs_totscore, updrs2_score, lowput_expected, upsit_pctl, DATSCAN_PUTAMEN_L, con_striatum, mean_putamen, and DATSCAN_PUTAMEN_R. These features were used consistently across all subsequent ML and LLM experiments.

Prompt Construction

To evaluate the performance of LLMs, we developed 4 prompting formats that express input variables in plain text (PT), markdown (MD), special token (ST) annotations, and a combined markdown with special token (MD+ST) structure [29]. The PT format presents the input features as natural language sentences, whereas the MD format uses a structured table to delineate characteristics and enhance feature recognition, and the combined MD+ST format integrates both structured layout and explicit ST annotation.

Each prompting format was applied under 0-shot conditions to 3-shot conditions. All few-shot settings incorporated balanced PD and HC examples, with 1 pair for 1-shot, 2 pairs for 2-shot, and 3 pairs for 3-shot prompting. For dual-output prompting, the diagnostic label was followed by 3 sentences of post hoc explanatory text, which served as an exploratory output and did not represent true model interpretability [30].

For dual-output prompting, each LLM was instructed to generate a diagnostic label (PD or HC) followed by 3 sentences of post hoc explanatory text with a maximum length of 180 tokens to ensure comparability across models. Examples of all prompting formats, few-shot configurations, and sample outputs are provided in Multimedia Appendix 3.

Modeling Approaches

This study compared traditional ML classifiers with multiple LLMs in order to evaluate diagnostic performance under consistent experimental conditions. As deterministic baselines, we trained LR with L2 regularization and a SVM with a radial basis function (RBF) kernel, using the top 10 SHAP-selected features. Both models were implemented using standard scikit-learn procedures without extensive hyperparameter tuning, since the goal was to establish transparent and reproducible baselines rather than to maximize predictive performance. The complete hyperparameter configurations for the ML classifiers are summarized in Multimedia Appendix 4. These models were evaluated following the procedures described in the "Training and Evaluation Settings" section.

For LLM-based classification, we selected model families that collectively capture diversity in architecture, accessibility, and usage constraints. The included families were LLaMA, GPT, Gemini, and Claude. Each family provided one or more model variants with different parameter sizes or intended applications. The LLaMA models consisted of LLaMA 3.1 8B Instruct and LLaMA 3.3 70B Instruct, both of which were run locally using open-access model weights. The GPT models consisted of GPT-4o-mini and GPT-4o, accessed through the OpenAI application programming interface (API). The Gemini models included Gemini 1.5 Flash and Gemini 1.5 Pro, accessed through the Google Gemini API. For the Claude family, the Claude 3.5 Sonnet model was used. Although lightweight variants such as Claude Instant were available, the Sonnet model was selected due to budget considerations and its expected performance.

All LLMs were accessed through their officially supported APIs or locally hosted implementations using Python-based programmatic interfaces. The same prompting formats, shot settings, and evaluation procedures were applied across all models, except where input-format restrictions required specific handling. Additional implementation details, including software environments and API configurations, are provided in Multimedia Appendix 5.

Training and Evaluation Settings

Overview

The evaluation schedule and prompting phases for each model are summarized in Multimedia Appendix 6, and the hardware and software environments used in all experiments are described in Multimedia Appendix 7. To address the class imbalance between PD and HC, model performance was primarily assessed using the F_1-score, with precision and recall reported as supporting metrics. Accuracy was treated as a secondary measure, given that F_1-score provides a more balanced assessment under imbalanced classification tasks [31].

For all binary classification tasks, PD was assigned as the positive class (label=1) and HC as the negative class (label=0) across all ML and LLM experiments. Numerical features were standardized using *z* score scaling, where each variable was transformed by subtracting the mean and dividing by the SD computed from the training split. This ensured a consistent feature scale for both LR and SVM while preventing data leakage. Standardization using *z* score was applied exclusively to the ML baselines. For LLM-based experiments, models were provided with the original clinical values embedded in natural language prompts, rather than normalized numerical vectors. For ML models, performance uncertainty was quantified using 95% bootstrap CIs based on 1000 resampling iterations [32].

For LLMs, diagnostic classification was evaluated under 0-shot settings to 3-shot settings using 4 prompting formats including PT, MD, ST, and MD+ST. All few-shot experiments incorporated balanced PD and HC examples at each shot level. Across all LLM conditions, each participant was evaluated through 30 repeated model executions under identical prompting conditions to account for the inherent nondeterminism of LLM outputs [33]. Any change in diagnostic labels across these executions was recorded as a label inconsistency event. For dual-output prompting experiments, semantic consistency of the generated post hoc explanatory texts was also evaluated.

For each LLM and prompting configuration, macro-averaged performance metrics (F_1-score, precision, recall, and accuracy) were computed for each of the 30 model executions. Nonparametric 95% CIs for LLM performance were estimated

XSL•FO
RenderX

only for the temporal validation set using a hierarchical bootstrap procedure. In each iteration, participants were sampled with replacement and, for each selected participant, one prediction was randomly drawn from the 30 repeated trials. The 2.5th and 97.5th percentiles of the resulting performance distributions were reported in the temporal validation tables.

All combinations of prompting format and shot number were evaluated for each LLM on the development test set. The prompting configuration reported as the best for each model corresponds to the combination that achieved the highest macro-averaged F_1-score on this test set. During temporal validation, each LLM was evaluated using only under its best-performing configuration. This ensured that temporal validation assessed the generalizability of each model's optimal setting rather than retesting all prompt-shot combinations on temporally independent data.

ML Baseline Training Protocols

Two conventional ML classifiers were trained as deterministic baselines for comparison with LLM-based diagnostic approaches. The models were LR with L2 regularization and a SVM with an RBF kernel, both of which were trained using the same feature subset identified in the SHAP-based feature selection step. Class weights were applied to address the imbalance between PD and HC samples in the development set.

Both models were implemented using standard scikit-learn procedures without extensive hyperparameters optimization, as the primary goal was to establish transparent and reproducible baselines rather than to maximize predictive performance. LR was trained using the liblinear solver with balanced class weights, while SVM used an RBF kernel with probability estimation enabled. Performance for both models was evaluated for direct comparability with all LLM-based experiments.

Few-Shot Prompting Evaluation of LLMs

The LLMs were evaluated using the 4 prompting formats described earlier, applied across 0-, 1-, 2-, and 3-shot settings. Examples of PD and HC were balanced in all few-shot conditions to ensure consistent contextual exposure. All 4 prompting formats were applied to the LLaMA models. In contrast, only the PT and MD formats were applied to the GPT, Gemini, and Claude models because these API-based models do not support ST annotations in their input structure. Importantly, the inclusion of STs substantially influenced both diagnostic performance and output stability. Accordingly, ST-based prompting (including MD+ST) was applied exclusively to the LLaMA models as a model-specific input design choice, and the resulting differences in prompt structuring capability were explicitly considered as a limitation in cross-model comparisons.

Dual-Output Prompting of LLMs for Diagnosis and Post Hoc Explanatory Text

This experiment examined whether requiring LLMs to generate post hoc explanatory text could influence their diagnostic classification performance. Recent studies have shown that step-by-step prompting can improve LLM accuracy in complex decision tasks [34], yet fully stepwise reasoning is often impractical in clinical contexts due to token limitations. Rather than instructing the models to articulate their reasoning step by step, the models were prompted to produce concise post hoc explanatory text. This approach enabled assessment of whether a reduced explanatory demand could affect the diagnostic output.

Each model generated a binary diagnosis of PD or HC followed by exactly 3 sentences of post hoc explanatory text. To ensure consistency across models and to manage token usage, the length of these explanatory outputs was fixed. This dual-output prompting was applied to 4 models, including GPT-4o, Claude 3.5 Sonnet, Gemini 1.5 Pro, and LLaMA 3.3 70B. Among these, the LLaMA model was prompted using the ST format, whereas the other models were prompted using the PT format because these models do not support ST inputs.

Although the generated explanations were not reviewed by clinical experts, their semantic consistency was evaluated to assess the stability of the post hoc explanatory text under repeated prompting. High semantic consistency reflects only the reproducibility of the generated text across repeated runs and does not imply that the explanations are clinically accurate or factually grounded. For each participant, their explanatory outputs per model were collected, and pairwise cosine similarity between sentence embeddings was computed using the all-mpnet-base-v2 model from the Sentence-Transformers library [35,36]. This semantic consistency analysis was performed only on the development set, while the temporal validation set was used exclusively for the primary diagnostic evaluation.

LLM Supervised Fine-Tuning

Supervised fine-tuning was conducted to evaluate whether labeled training data could improve the diagnostic performance and output stability of lightweight LLMs. Unlike prompt-based learning, which is constrained by the number of examples that can be included within a single prompt, supervised fine-tuning allows the model to learn diagnostic patterns directly from the full training dataset.

Among the models tested in this study, GPT-4o-mini and Gemini 1.5 Flash were selected as compact and computationally efficient alternatives to assess how smaller LLMs perform relative to larger models. Both models were fine-tuned using the same dataset that was used in the prompting experiments, and all evaluations were performed under 0-shot conditions on the identical test set. The generation temperature was fixed at 0.1 to ensure consistent and deterministic behavior. Further details regarding fine-tuning platforms, sampling strategies, and training parameters are provided in Multimedia Appendix 8.

The GPT-4o-mini model was fine-tuned through the OpenAI API. Training jobs were submitted from a local workstation after converting the dataset into JSONL format. A total of 1052 samples were used for training and 186 samples for validation. The fine-tuning process followed OpenAI's job-based workflow, in which each training job is versioned and automatically made accessible through the OpenAI API upon completion.

The Gemini 1.5 Flash model was fine-tuned using the Google AI Studio platform. Because the platform restricts training to a maximum of 500 samples, stratified sampling was applied to

XSL•FO
RenderX

preserve the original class ratio, resulting in 383 PD samples and 117 HC samples. The model was trained for 1 epoch with a batch size of 1 and a learning rate of 1, after which the fine-tuned model was deployed via the Gemini API using the assigned model identifier.

All fine-tuned models were trained and evaluated using the PT prompt format to maintain consistency between training and testing conditions.

Ethical Considerations

This study used publicly available, deidentified data provided by PPMI. According to institutional policies and the PPMI Data Use Agreement, additional institutional review board approval was not required for secondary analyses of this publicly accessible dataset. The original PPMI study was conducted under institutional review board approval at all participating institutions, and all participants provided written informed consent permitting data sharing and secondary analyses. All analyses in this study were conducted on anonymized records with no personally identifiable information, and no participant compensation was applicable.

Results

ML Baseline Performance

To establish a deterministic baseline for comparison with LLM-based diagnostic approaches, we evaluated 2 conventional ML classifiers trained on the top 10 SHAP-selected features. LR and a SVM with an RBF kernel were implemented using standard scikit-learn procedures.

As summarized in Table 3, both models achieved identical performance on the test subset of the development set, yielding a macro-averaged F_1-score of 0.960 and an accuracy of 0.975. Precision and recall were balanced across PD and HC, and the 95% CIs ranged from approximately 0.94 to 1.00, reflecting the modest sample size of the test subset (n=122).

Table 3. Performance of machine learning models on the test subset of the development set (n=122; CIs were estimated via 1000 bootstrap iterations).

Model	F_1-score[a] (95% CI)	Precision (macro avg[b]/PD[c]/HC[d])	Recall (macro avg/PD/HC)	Accuracy
LR_L2[e]	0.960 (0.943-1.000)	0.953/0.990/0.917	0.968/0.980/0.957	0.975
SVM_RBF[f]	0.960 (0.944-1.000)	0.953/0.990/0.917	0.968/0.980/0.957	0.975

[a]F_1-scores represent macro avg values across PD and HC classes.

[b]macro avg: macro-averaged.

[c]PD: Parkinson disease.

[d]HC: healthy controls.

[e]LR_L2: logistic regression (L2 regularization).

[f]SVM_RBF: support vector machine (RBF kernel).

Table 4 presents the results from the temporal validation set (n=31). LR demonstrated moderately high generalizability, achieving a macro-averaged F_1-score of 0.903 and an accuracy of 0.903. In contrast, SVM showed a substantial decline in generalizability, producing a macro-averaged F_1-score of 0.484 with markedly reduced recall for PD. The wide CIs observed for both models reflect the limited size of the temporal validation set and the inherent uncertainty associated with evaluating performance on small external samples.

Table 4. Performance of machine learning models on the temporal validation set (n=31; CIs were estimated via 1000 bootstrap iterations).

Model	$F1$-score[a] (95% CI)	Precision (macro avg[b]/PD[c]/HC[d])	Recall (macro avg/PD/HC)	Accuracy
LR_L2[e]	0.903 (0.791-1.000)	0.917/0.833/1.0	0.906/1.0/0.813	0.903
SVM_RBF[f]	0.484 (0.157-0.506)	0.241/0.483/0	0.5/0/1.0	0.484

[a]F_1-scores represent macro avg values across PD and HC classes.

[b]macro avg: macro-averaged.

[c]PD: Parkinson disease.

[d]HC: healthy controls.

[e]LR_L2: logistic regression (L2 regularization).

[f]SVM_RBF: support vector machine (RBF kernel).

Given the small size of the temporal validation set (n=31), results obtained on this dataset should be interpreted with caution, as performance estimates may be sensitive to individual misclassifications.

Figure 2 illustrates the prediction patterns for the 2 classifiers across both datasets. On the development test subset (Figure 2A), both models produced identical predictions, misclassifying 1 HC participant as PD and misclassifying 2 PD participants as HC. In the temporal validation set, LR misclassified only 3 HC cases as PD (Figure 2B), whereas SVM misclassified nearly all HC cases (Figure 2C). Although the two models performed similarly on the development test subset, their stability diverged

XSL•FO
RenderX

substantially when evaluated on data collected at a later timepoint.

Figure 2. Confusion matrix for machine learning classifiers. (A) Test subset of the development set. (B) Logistic regression of temporal validation set. (C) Support vector machine of temporal validation set. HC: healthy controls; PD: Parkinson disease.

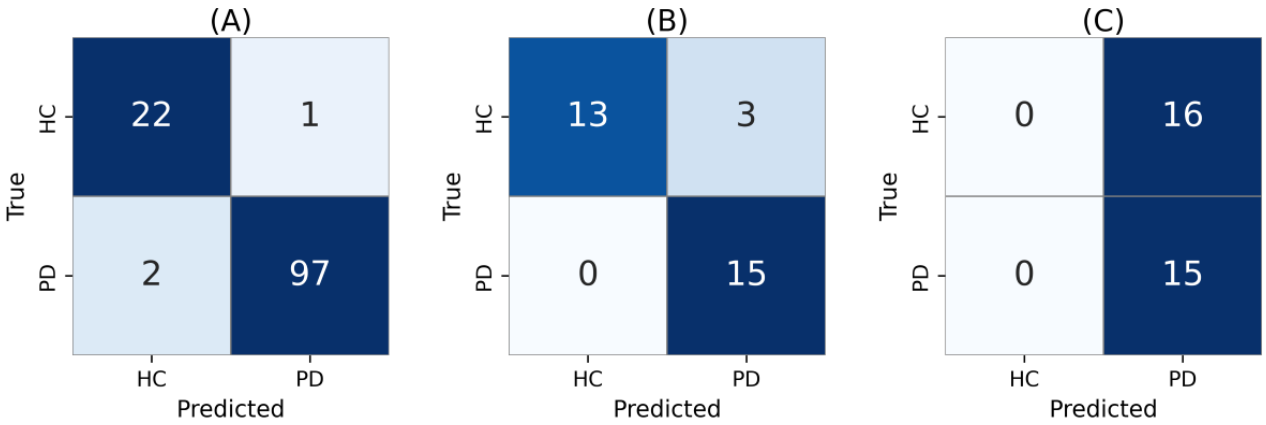

Few-Shot Prompting Performance of LLMs

A total of 4 prompting formats, including PT, MD, ST, and MD+ST, were evaluated under 0-shot conditions to 3-shot conditions to assess the diagnostic performance of LLMs. ST-based prompts were applied exclusively to the LLaMA models because the inclusion of STs substantially affected both classification accuracy and output stability. Non-LLaMA models such as GPT, Gemini, and Claude did not support ST formatting and were therefore evaluated using PT and MD formats.

Table 5 presents the best-performing results for each model on the test dataset (n=122). The best-performing configuration for each model corresponds to the prompt type and shot number that achieved the highest macro-averaged F_1-score on the development test set.

LLaMA 3.3 70B and Gemini 1.5 Pro achieved the highest macro-averaged F_1-score of 0.987 with an accuracy of 0.992 and stable predictions across 30 repeated trials. LLaMA 3.1 8B reached the same F_1-score using the MD+ST prompt at the 3-shot setting but showed one instance of prediction inconsistency. Claude 3.5 Sonnet demonstrated strong performance with an F_1-score of 0.972 and an accuracy of 0.984 under 1-shot MD setting, maintaining complete consistency across repeated runs. GPT-4o and GPT-4o-mini achieved slightly lower but stable performance, with macro-averaged F_1-scores of 0.961 and 0.910, respectively. Gemini 1.5 Flash produced the lowest F_1-score (0.894) despite consistent predictions, reflecting reduced sensitivity for HC cases. Detailed per-participant consistency analyses across 30 trials are provided in Multimedia Appendix 9.

Figure 3 displays the confusion matrices for the best-performing configuration of each model. Most classification errors occurred in HC samples, indicating high sensitivity for PD across the LLMs.

XSL•FO
RenderX

Table 5. Best performance of large language models on the test dataset (n=122).

Model	Prompt	Shot	F_1-score[a]	Precision (macro avg[b]/PD[c]/HC[d])	Recall (macro avg/PD/HC)	Accuracy	Inconsistency[e], n	Inconsistent cases[f]
LLaMA 3.1 8B	MD+ST[g]	3	0.987	0.995/0.990/1	0.978/1/0.957	0.992	1	PD #73 (13:17)
LLaMA 3.3 70B	ST[h]	2	0.987	0.995/0.990/1	0.978/1/0.957	0.992	0	—[i]
GPT-4o-mini	MD[j]	2	0.910	0.972/0.943/1	0.869/1/0.739	0.951	1	HC #103 (19:11)
GPT-4o	PT[k]	0	0.961	0.954/0.990/0.917	0.969/0.980/0.957	0.975	2	HC #26 (28:2); HC #68 (17:13)
Gemini 1.5 Flash	PT, MD	2	0.894	0.967/0.934/1	0.848/1/0.696	0.938	0	—
Gemini 1.5 Pro	PT, MD	2	0.987	0.995/0.990/1	0.978/1/0.957	0.992	0	—
Claude 3.5 Sonnet	MD	1	0.972	0.990/0.980/1	0.957/1/0.913	0.984	0	—

[a]F_1-scores represent macro avg values across PD and HC classes.

[b]macro avg: macro-averaged.

[c]PD: Parkinson disease.

[d]HC: healthy controls.

[e]Number of participants (out of 122) whose predictions were inconsistent at least once across 30 repeated trials.

[f]Example of inconsistent participants showing the final label (eg, PD #73) and the number of predicted labels across 30 runs (eg, 13:17 indicates 13 HC and 17 PD predictions).

[g]MD+ST: markdown with special token.

[h]ST: special token.

[i]Not applicable.

[j]MD: markdown.

[k]PT: plain text.

Figure 3. Confusion matrices of large language models under the best-performing configurations on the test dataset (n=122). HC: healthy controls; PD: Parkinson disease.

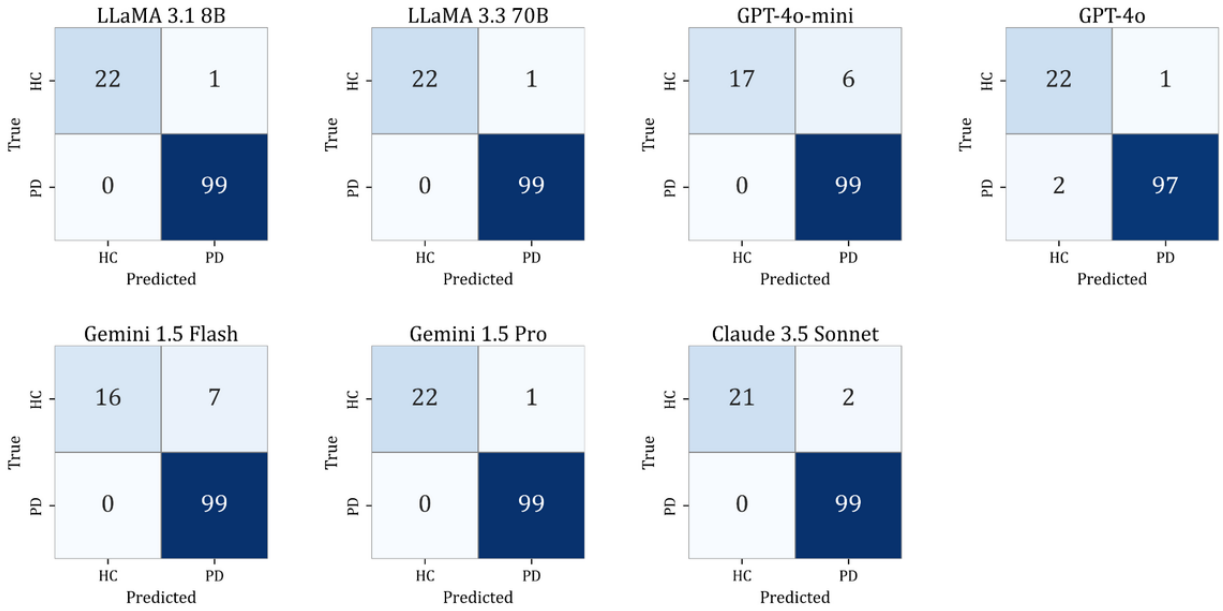

Table 6 and Figure 4 summarize the best-performing configuration of each LLM on the temporal validation set (n=31). LLaMA 3.3 70B achieved the highest macro-averaged F_1-score of 0.968 using the ST format at the 2-shot setting, with recall of 1.00 and consistent predictions across all participants. LLaMA 3.1 8B, Gemini 1.5 Pro, and Claude 3.5 Sonnet showed

XSL•FO
RenderX

comparable performance, each achieving a macro-averaged F_1-score of 0.936 with stable predictions. GPT-4o and Gemini 1.5 Flash achieved moderately high performance (F_1-score=0.903), with consistent predictions across all participants. In contrast, GPT-4o-mini achieved the lowest F_1-score (0.836), driven primarily by reduced recall for HC cases. Across all models, recall for PD remained consistently high (recall≥0.938), demonstrating strong sensitivity even when evaluated on data collected at a later timepoint. Figure 4 shows the confusion matrices for each model under the prompt and shot condition listed in Table 6.

These findings indicate that LLMs generally maintained high diagnostic accuracy and prediction stability under temporally separated data, supporting their potential generalizability beyond the development dataset.

Table 6. Best performance of large language models on the temporal validation set (n=31).

Model	Prompt	Shot	F_1-score[a] (95% CI)	Precision (macro avg[b]/PD[c]/HC[d])	Recall (macro avg/PD/HC)	Accuracy	Inconsistency[e], n	Inconsistent cases[f]
LLaMA 3.1 8B	MD+ST[g]	3	0.936 (0.854-1.000)	0.941/0.882/1	0.938/1/0.875	0.935	2	HC #13 (9:21); HC #23 (7:23)
LLaMA 3.3 70B	ST[h]	2	0.968 (0.899-1.000)	0.969/0.938/1	0.969/1/0.938	0.968	0	—[i]
GPT-4o-mini	MD[j]	2	0.836 (0.708-0.966)	0.875/0.750/1	0.844/1/0.688	0.839	2	HC #10 (4:26); HC #28 (8:22)
GPT-4o	PT[k]	0	0.903 (0.773-1.000)	0.917/0.833/1	0.906/1/0.813	0.903	2	PD #1 (1:29); HC #10 (28:2)
Gemini 1.5 Flash	PT	2	0.903 (0.773-1.000)	0.917/0.833/1	0.906/1/0.813	0.903	0	—
Gemini 1.5 Pro	PT	2	0.936 (0.832-1.000)	0.941/0.882/1	0.938/1/0.875	0.935	0	—
Claude 3.5 Sonnet	MD	1	0.936 (0.832-1.000)	0.941/0.882/1	0.938/1/0.875	0.935	31	—

[a]F_1-scores represent macro avg values across PD and HC classes.

[b]macro avg: macro-averaged.

[c]PD: Parkinson disease.

[d]HC: healthy controls.

[e]Number of participants (out of 31) whose predictions were inconsistent at least once across 30 repeated trials.

[f]Example of inconsistent participants showing the final label (eg, HC #13) and the number of predicted labels across 30 runs (eg, 9:21 indicates 9 HC and 21 PD predictions).

[g]MD+ST: markdown with special token.

[h]ST: special token.

[i]Not applicable.

[j]MD: markdown.

[k]PT: plain text.

XSL•FO
RenderX

Figure 4. Confusion matrices of large language models under their best-performing configurations on the temporal validation set (n=31). HC: healthy controls; PD: Parkinson disease.

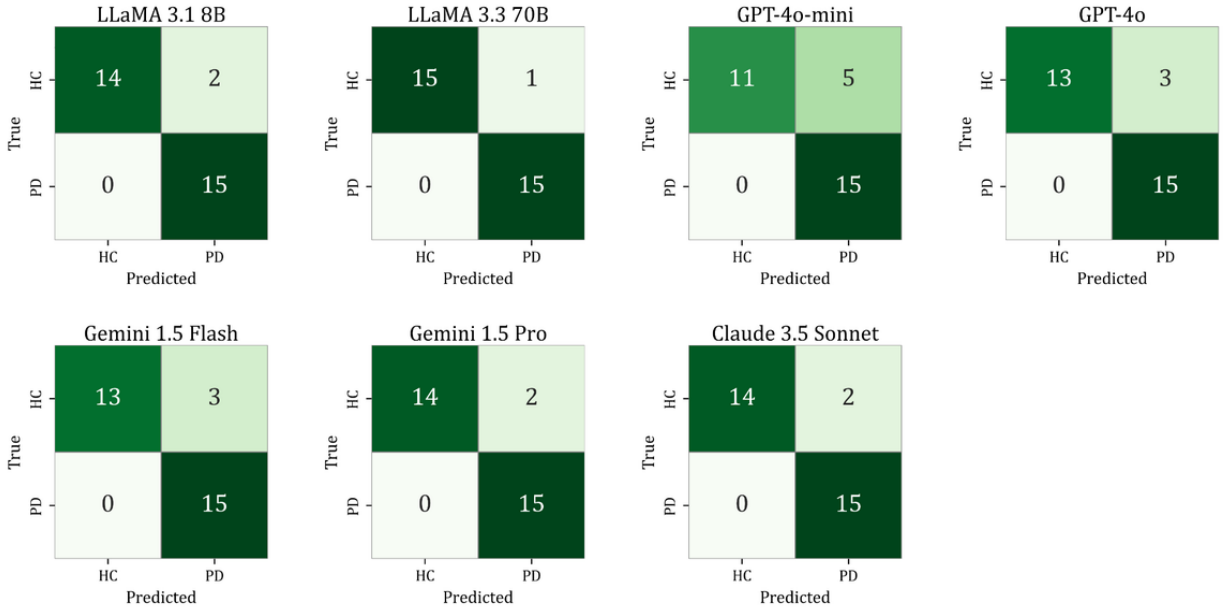

Diagnostic Performance Under Dual-Output Prompting

Dual-output prompting was used to evaluate whether requiring LLMs to generate post hoc explanatory text influenced their diagnostic reliability. This experimental setting included 4 representative models, namely LLaMA 3.3 70B, GPT-4o, Gemini 1.5 Pro, and Claude 3.5 Sonnet. Unlike diagnostic-only prompting, this setup instructed each model to output a binary diagnostic label followed by 3 sentences of post hoc explanatory text. Because the LLaMA models are highly sensitive to input formatting, dual-output prompts for LLaMA 3.3 70B were constructed using the ST format. GPT-4o, Gemini 1.5 Pro, and Claude 3.5 Sonnet do not support ST inputs, and therefore PT prompts were used for these models to maintain compatibility.

As summarized in Table 7, all models achieved high diagnostic performance under dual-output prompting, although overall F_1-scores were slightly lower than those obtained under few-shot prompting. LLaMA 3.3 70B and Claude 3.5 Sonnet each achieved a macro-averaged F_1-score of 0.972 and correctly identified all PD cases. GPT-4o and Gemini 1.5 Pro showed similar results and achieved F_1-scores of 0.958 with an accuracy of 0.975. Most prediction errors occurred in HC cases, whereas all PD samples were correctly classified. Instances of inconsistency across 30 repeated trials were rare, typically affecting no more than 2 participants for each model. The full repeated-trial results are presented in Multimedia Appendix 10.

Figure 5 displays the confusion matrices corresponding to each model's best-performing dual-output configuration.

XSL•FO
RenderX

Table 7. Best performance of large language models on the test dataset under dual-output prompting (n=122).

Model	Prompt	Shot	F_1-score[a]	Precision (macro avg[b]/PD[c]/HC[d])	Recall (macro avg/PD/HC)	Accuracy	Inconsistency[e], n	Inconsistent cases[f]
LLaMA 3.3 70B	ST[g]	3	0.972	0.990/0.980/1	0.957/1/0.913	0.984	122	HC #23 (29:1); HC #68 (28:2)
GPT-4o	PT[h]	1	0.958	0.985/0.970/1	0.935/1/0.870	0.975	122	HC #26 (26:4); HC #77 (6:24)
Gemini 1.5 Pro	PT	3	0.958	0.985/0.970/1	0.935/1/0.870	0.975	122	HC #97 (28:2)
Claude 3.5 Sonnet	PT	0	0.972	0.990/0.980/1	0.957/1/0.913	0.984	122	PD #23 (1:29)

[a]F_1-scores represent macro avg values across PD and HC classes.

[b]macro avg: macro-averaged.

[c]PD: Parkinson disease.

[d]HC: healthy controls.

[e]Number of participants (out of 122) whose predictions were inconsistent at least once across 30 repeated trials.

[f]Example of inconsistent participants showing the final label (eg, HC #23) and the number of predicted labels across 30 runs (eg, 29:1 indicates 29 HC and 1 PD predictions).

[g]ST: special token.

[h]PT: plain text.

Figure 5. Confusion matrices of large language models under best-performing dual-output prompting conditions on the test subset of the development set (n=122). HC: healthy controls; PD: Parkinson disease.

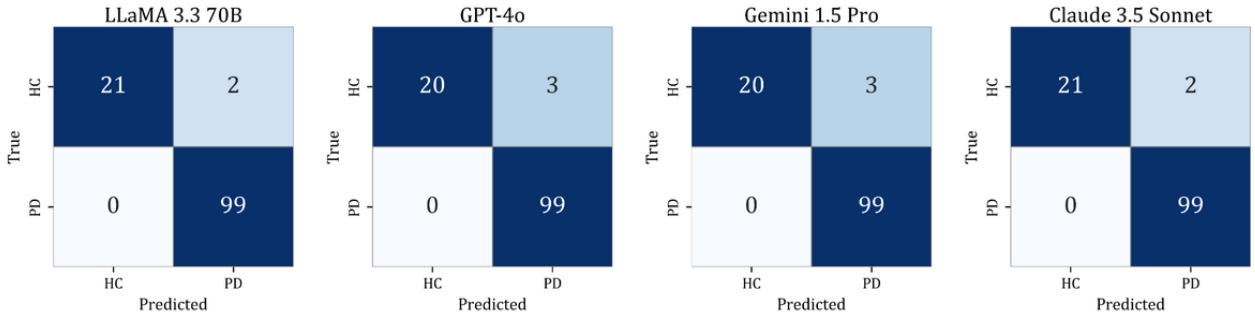

Generalizability was further assessed using the temporal validation set (n=31). As shown in Table 8, all models maintained strong diagnostic sensitivity, and recall for PD remained equal to 1 across all participants. GPT-4o achieved the highest macro-averaged F_1-score of 0.968 with an accuracy of 0.968. LLaMA 3.3 70B followed with a macro-averaged F_1-score of 0.935. Gemini 1.5 Pro and Claude 3.5 Sonnet showed modest decreases in performance with F_1-scores of 0.903 and 0.869, respectively, primarily due to HC misclassifications.

Figure 6 presents the confusion matrices for the temporal validation set under the best-performing configuration for each model.

XSL•FO
RenderX

Table 8. Best performance of large language models under dual-output prompting on the temporal validation set (n=31).

Model	Prompt	Shot	F_1-score[a] (95% CI)	Precision (macro avg[b]/PD[c]/HC[d])	Recall (macro avg/PD/HC)	Accuracy	Inconsistency[e]	Inconsistent cases[f]
LLaMA 3.3 70B	ST[g]	3	0.935 (0.832-1.000)	0.941/0.882/1	0.938/1/0.875	0.935	2	HC #11 (23:7); HC #21 (8:22)
GPT-4o	PT[h]	1	0.968 (0.896-1.000)	0.969/0.938/1	0.969/1/0.938	0.968	1	HC #21 (29:1)
Gemini 1.5 Pro	PT	3	0.903 (0.774-1.000)	0.917/0.833/1	0.906/1/0.813	0.903	0	—[i]
Claude 3.5 Sonnet	PT	0	0.869 (0.735-0.968)	0.895/0.789/1	0.875/1/0.750	0.871	1	HC #10 (1:29)

[a]F_1-scores represent macro avg values across PD and HC classes.

[b]macro avg: macro-averaged.

[c]PD: Parkinson disease.

[d]HC: healthy controls.

[e]Number of participants (out of 31) whose predictions were inconsistent at least once across 30 runs.

[f]Example of inconsistent participants showing the final label (eg, HC #11) and the number of predicted labels across 30 runs (eg, 23:7 indicates 23 HC and 7 PD predictions).

[g]ST: special token.

[h]PT: plain text.

[i]Not applicable.

Figure 6. Confusion matrices of large language models under best-performing dual-output prompting conditions on the temporal validation set (n=31). HC: healthy controls; PD: Parkinson disease.

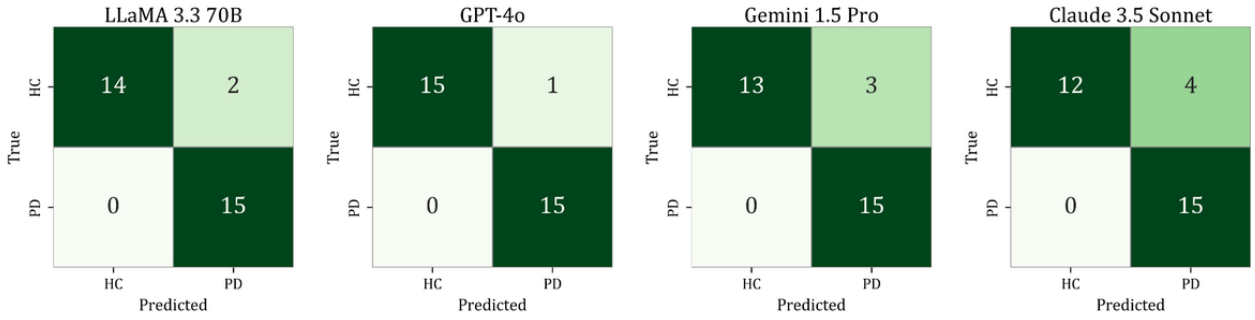

Following the diagnostic classification results presented in Table 7, the semantic consistency of the post hoc explanatory texts was evaluated to assess the stability of generated explanations under dual-output prompting. Pairwise cosine similarity was computed among 30 post hoc explanatory texts generated for each participant, and the resulting mean and SD were averaged across all 122 test participants. As shown in Table 9, all models maintained high semantic consistency, with mean cosine similarity values exceeding 0.95. LLaMA 3.3 70B achieved the highest value under 0-shot prompting (0.997 ± 0.005), and the variation across models and shot settings was small (≤ 0.03). This evaluation was limited to the development set, and additional exploratory metrics for the temporal validation set are provided in Multimedia Appendix 11.

XSL•FO
RenderX

Table 9. Semantic consistency of reasoning outputs on the test dataset (n=122). Semantic consistency was assessed based on pairwise cosine similarity among 30 post hoc explanatory texts generated per participant.

Model	Cosine similarity, mean (SD)
LLaMA 3.3 70B	
0-shot	0.997 (0.005)
1-shot	0.995 (0.009)
2-shot	0.966 (0.016)
3-shot	0.980 (0.011)
GPT-4o	
0-shot	0.973 (0.016)
1-shot	0.980 (0.011)
2-shot	0.981 (0.011)
3-shot	0.975 (0.016)
Gemini 1.5 Pro	
0-shot	0.969 (0.019)
1-shot	0.968 (0.025)
2-shot	0.956 (0.029)
3-shot	0.951 (0.026)
Claude 3.5 Sonnet	
0-shot	0.985 (0.017)
1-shot	0.986 (0.016)
2-shot	0.987 (0.016)
3-shot	0.979 (0.015)

Fine-Tuned Prompting Performance of LLMs

Supervised fine-tuning substantially improved the diagnostic performance of lightweight LLMs and resulted in more consistent classification across the evaluated datasets. Table 10 summarizes the results of GPT-4o-mini and Gemini 1.5 Flash on the development test set (n=122).

Table 10. Fine-tuning performance of lightweight large language models on the development test set (n=122).

Model	Prompt	F_1-score[a]	Precision (macro avg[b]/PD[c]/HC[d])	Recall (macro avg/PD/HC)	Accuracy	Inconsistency[e]	Inconsistent cases[f]
GPT-4o-mini	PT[g]	0.987	0.995 / 0.990 / 1	0.978 / 1 / 0.957	0.992	0	—[h]
Gemini 1.5 Flash	PT	0.973	0.990 / 0.980 / 1	0.957 / 1 / 0.913	0.984	1	HC #23 (9:21)

[a]F_1-scores represent macro avg values across PD and HC classes.

[b]macro avg: macro-averaged.

[c]PD: Parkinson disease.

[d]HC: healthy controls.

[e]Number of participants (out of 122) whose predictions were inconsistent at least once across 30 repeated trials.

[f]Example of inconsistent participants showing the final label (eg, HC #23) and the number of predicted labels across 30 runs (eg, 9:21 indicates 9 HC and 21 PD predictions).

[g]PT: plain text.

[h]Not applicable.

The fine-tuned GPT-4o-mini achieved the highest macro-averaged F_1-score of 0.987, with recall of 1.00 and stable predictions across 30 repeated trials. Gemini 1.5 Flash followed closely with an F_1-score of 0.973, maintaining an accuracy of 0.984 and showing only 1 inconsistent prediction (participant HC #23). Both models were trained and evaluated using PT prompts. The corresponding confusion matrices are shown in Figure 7. Figure 7 displays the confusion matrices of the fine-tuned LLMs on the development test set, showing that nearly all misclassifications occurred among HC participants, whereas both models correctly identified all PD cases in the sample.

XSL•FO
RenderX

Figure 7. Confusion matrices of lightweight large language models after fine-tuning on the development test set (n=122). HC: healthy controls; PD: Parkinson disease.

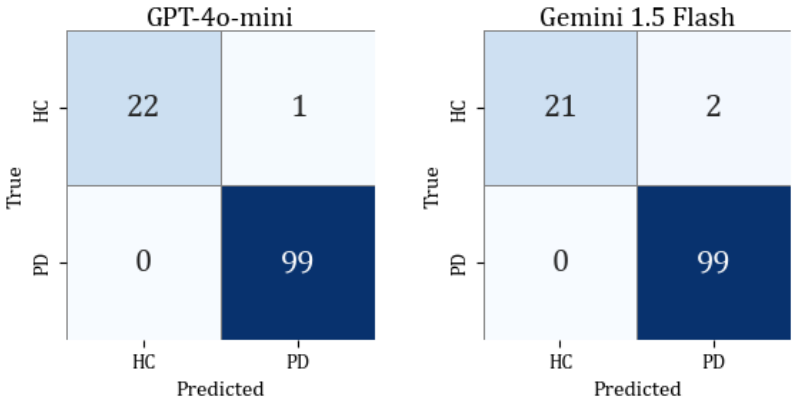

To further assess model generalizability, both fine-tuned LLMs were evaluated on the temporal validation set (n=31). As summarized in Table 11, GPT-4o-mini achieved F_1-score, precision, recall, and accuracy of 1.000 on the temporal validation set, correctly classifying all participants in this sample. In contrast, Gemini 1.5 Flash demonstrated slightly lower but still strong performance with an F_1-score of 0.903 and an accuracy of 0.903. All PD participants were correctly identified, and the few errors were limited to HC participants. Figure 8 presents the confusion matrices under the same fine-tuned PT prompting configuration. These findings confirm that fine-tuning notably improved classification stability while preserving sensitivity to PD in temporally independent data.

Table 11. Fine-tuning performance of lightweight large language models on the temporal validation set (n=31).

Model	Prompt	F_1-score[a] (95% CI)	Precision (macro avg[b]/PD[c]/HC[d])	Recall (macro avg/PD/HC)	Accuracy	Inconsistency[e]	Inconsistent cases[f]
GPT-4o-mini	PT[g]	1 (1.000-1.000)	1/1/1	1/1/1	1	0	—[h]
Gemini 1.5 Flash	PT	0.903 (0.770-1.000)	0.917/0.833/1	0.906/1/0.813	0.903	1	HC #21 (25:5)

[a]F_1-scores represent macro avg values across PD and HC classes.

[b]macro avg: macro-averaged.

[c]PD: Parkinson disease.

[d]HC: healthy controls.

[e]Number of participants (out of 31) whose predictions were inconsistent at least once across 30 runs.

[f]Example of inconsistent participants showing the final label (eg, HC #21) and the number of predicted labels across 30 runs (eg, 25:5 indicates 25 HC and 5 PD predictions).

[g]PT: plain text.

[h]Not applicable.

Figure 8. Confusion matrices of lightweight large language models after fine-tuning on the temporal validation set (n=31). HC: healthy controls; PD: Parkinson disease.

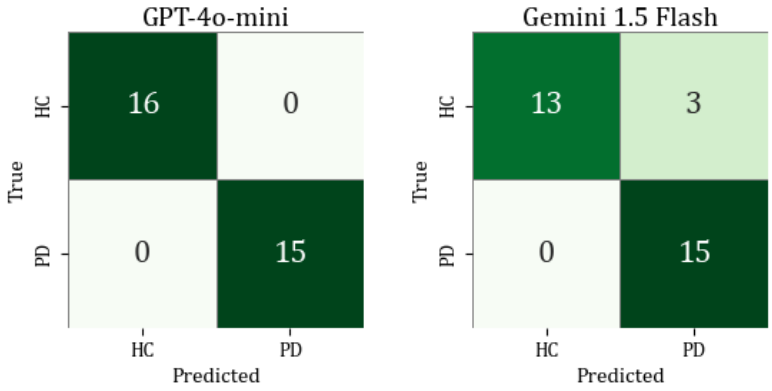

These results confirm that with sufficient training data and consistent prompting formats, even small-scale LLMs can achieve classification accuracy comparable to larger models while maintaining stable performance.

XSL•FO
RenderX

Figure 9 provides an integrated comparison of the best-performing models across all experimental settings, including traditional ML baselines, few-shot prompting with LLM (LLM_F), dual-output prompting with LLM (LLM-D), and fine-tuned prompting with LLM (LLM_FT). Across the development dataset, multiple LLM configurations achieved macro-averaged F_1-scores comparable to LR, and fine-tuned lightweight models reached the highest overall performance.

Figure 9. Comparison of the best macro-averaged F1-scores from the top-performing models in machine learning (ML) and large language model experiments across few-shot, dual-output, and fine-tuned prompting on the development and temporal validation sets.

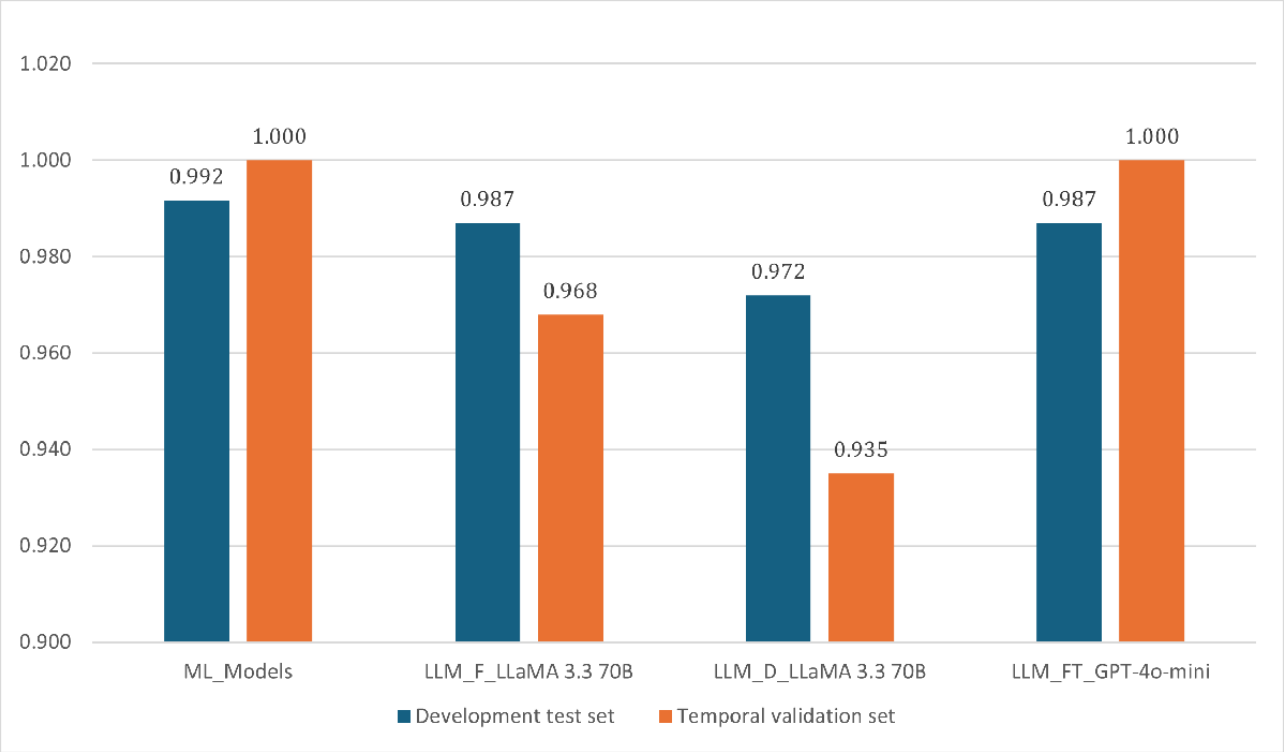

On the temporal validation dataset, LR maintained moderate generalizability, whereas SVM showed substantial degradation when applied to temporally separated data. In contrast, several LLM configurations preserved high recall for PD and sustained overall performance, particularly under fine-tuned and few-shot prompting conditions. These results demonstrate that while ML baselines provide deterministic reference points, LLMs exhibit greater flexibility across prompting strategies and maintain stable sensitivity to PD in both datasets.

Discussion

Overview

This study examined how modern LLMs process structured clinical variables when these variables are reformatted into natural language prompts for the diagnostic classification of PD. Using SHAP-selected features derived from the PPMI dataset, we compared multiple LLM families and prompting strategies with conventional ML baselines. Three main findings emerged. First, several LLMs achieved diagnostic performance comparable to LR while maintaining high sensitivity for PD across both the development test set and the temporal validation set. Second, the diagnostic behavior of LLMs varied depending on prompt format, model family, and shot configuration, whereas the ML baselines produced deterministic and highly stable predictions. Third, supervised fine-tuning markedly improved both accuracy and output stability in lightweight LLMs, allowing a compact model such as GPT-4o-mini to correctly classify all participants in the temporal validation set. In addition, because the ML baselines in this study were minimally tuned, part of any performance gap between ML models and LLMs may reflect limited optimization of the ML baselines rather than true methodological differences. Accordingly, the present comparisons should be interpreted as exploratory rather than definitive.

The performance of the LLaMA family was strongly influenced by input formatting. In particular, the inclusion or removal of STs resulted in notable differences in accuracy and sensitivity, although their classification results varied more widely across different shot settings [29]. Dual-output prompting, which required models to generate diagnostic labels along with post hoc explanatory text, resulted in slightly lower F_1-scores compared with diagnostic-only prompting but did not substantially destabilize predictions. The generated text exhibited high semantic consistency across repeated trials. These explanations should be regarded as post hoc natural language outputs rather than indicators of true model interpretability, since they are produced after the model's primary diagnostic prediction step [14].

To evaluate whether inconsistent predictions reflected clinically ambiguous participants rather than model-level variability, we conducted a qualitative review of cases that exhibited the highest numbers of label inconsistencies. A total of 2 HC participants and 2 PD participants were selected for detailed examination. All 10 SHAP-selected variables, including Unified Parkinson

XSL•FO
RenderX

Disease Rating Scale (UPDRS) motor scores, University of Pennsylvania Smell Identification Test (UPSIT) percentiles, and dopamine transporter single-photon emission computed tomography putaminal uptake metrics, were compared with the overall distributions of the PD and HC groups. None of the reviewed cases demonstrated borderline or contradictory clinical profiles. The HC cases showed preserved dopaminergic uptake and normal motor assessments, with only mild olfactory reductions typical of healthy older adults. The PD cases exhibited reduced dopaminergic activity, clear asymmetry, and motor impairment consistent with established PD patterns. These observations suggest that label inconsistencies are unlikely to arise from underlying clinical ambiguity. Instead, they appear to reflect model stochasticity and prompt-dependent variability [33].

Supervised fine-tuning clarified the role of training data in stabilizing LLM predictions. When provided with labeled examples, both GPT-4o-mini and Gemini 1.5 Flash demonstrated substantial improvements in diagnostic accuracy and showed consistently high sensitivity to PD on the temporal validation set. GPT-4o-mini classified all 31 participants correctly after fine-tuning. This result suggests that compact models can approximate or exceed the performance of larger models when trained on appropriately structured datasets. It also indicates that fine-tuning can reduce susceptibility to prompt-level variability and may support more reliable behavior in clinical decision-support environments. However, this comparison should be interpreted with caution. Although architectural differences may also contribute to the observed performance gap, GPT-4o-mini was fine-tuned on more than twice as many labeled samples as Gemini 1.5 Flash (1052 vs 500) due to platform constraints. Part of GPT-4o-mini's superior performance may therefore reflect the larger amount of training data rather than inherent model advantages, which limits how directly the two models can be compared.

Overall, this study illustrates both the potential and the limitations of modern LLMs for processing structured clinical variables that are presented in natural language form. While several models achieved strong diagnostic performance and generalized well to temporally separated data, their outputs remained sensitive to prompt structures, model architectures, and few-shot configurations. Occasional inconsistencies across repeated runs further highlight the stochastic nature of LLM output generation [33]. These characteristics reinforce the importance of careful interpretation and the need for rigorous evaluation frameworks before LLMs can be integrated safely into real-world diagnostic workflows.

Limitations

Several limitations should be considered when interpreting these findings. First, although temporal validation provided an important assessment of model generalizability, the temporal validation set was relatively small (n=31), which resulted in wide CIs for the reported performance metrics. In addition, models were trained on datasets that included imputed values, whereas evaluation was conducted on datasets restricted to complete cases without missing data, including both the development test set and the temporal validation set. This mismatch may introduce a distributional shift and result in performance estimates that reflect a best-case evaluation scenario rather than real-world clinical conditions where missing data are common.

Second, the 10 features used for model input were selected using SHAP values from tree-based models. Feature sets obtained using alternative selection strategies may differ, so the current feature subset may not fully represent model-agnostic feature selection. Furthermore, the explanatory text generated by LLMs under the dual-output prompting framework was not reviewed by clinical experts. Accordingly, the semantic consistency metric reflects internal textual stability rather than clinically accurate or factually grounded post hoc explanatory text, and the clinical validity of the generated explanations remains unverified.

Finally, several methodological constraints limit direct model-to-model comparisons. Prompt format and shot configuration were selected based on performance observed on the development test dataset, rather than using a separate validation set for configuration selection. This design choice reflects the study's aim to broadly compare model behaviors rather than to establish definitive optimal configurations. In addition, platform-specific constraints limited the extent of fine-tuning that could be performed across LLMs. While GPT-4o-mini was fine-tuned using 1052 training samples with an additional held-out validation set of 186 samples, the Gemini 1.5 Flash fine-tuning interface restricts supervised training to a maximum of 500 samples, and the machine learning baselines were trained on 990 samples. As a result, the observed performance differences across models may reflect differences in training data availability rather than inherent architectural superiority and should be interpreted as exploratory.

Prompt structuring flexibility also differed across platforms, as the ST format was applied only to the LLaMA models due to platform-specific input constraints, further limiting the degree to which direct model-to-model comparisons can be made in this study.

Future Work

Future research should expand these results in several directions. Larger temporal or external datasets, including real-world clinical settings, are needed to strengthen generalizability assessments. Additional work is warranted to examine optimization strategies for prompt design, temperature settings, and calibration methods that may reduce stochastic variability. Expert-based evaluation of generated post hoc explanatory text may clarify how these outputs can be used to support clinical decision-making. Further exploration of supervised fine-tuning for additional lightweight LLMs could help identify resource-efficient models suitable for deployment in constrained clinical environments. Finally, integrating imaging, sensor-derived digital biomarkers, and longitudinal clinical trajectories may clarify how LLMs can combine multimodal biomedical data for diagnostic tasks.

Conclusions

This study provides an exploratory benchmark of how LLMs process structured clinical variables when presented in natural language form. Multiple LLMs achieved diagnostic performance

XSL•FO
RenderX

comparable to conventional ML baselines and maintained high sensitivity for PD under temporal validation. However, their predictions were influenced by prompt format, shot configuration, and model architecture, and occasional inconsistencies reflected inherent stochasticity rather than clinical ambiguity. Supervised fine-tuning substantially improved reliability in lightweight models, demonstrating that compact architectures can achieve stable and high-performing classification when trained on sufficient labeled examples. These findings highlight both the opportunities and the challenges associated with applying LLMs to structured clinical data and emphasize the need for rigorous evaluation before clinical implementation.

Acknowledgments

The authors would like to thank Editage for English language editing. We also acknowledge the use of generative artificial intelligence (AI) tools (ChatGPT by OpenAI and Grok by xAI) under author supervision for language editing and phrasing refinement during manuscript preparation. All analyses, experimental designs, and interpretations related to LLM diagnostics were fully conceived, conducted, and verified solely by the authors.

Funding

This work was supported by 2 funding sources. First, the Regional Innovation System & Education (RISE) program through the Institute of Regional Innovation System & Education in Busan Metropolitan City, funded by the Ministry of Education (MOE) and the Busan Metropolitan City, Republic of Korea (2025-RISE-02-003). Second, the Global-Learning & Academic research institution for Master's·PhD students, and Postdocs (G-LAMP) Program of the National Research Foundation of Korea (NRF), grant funded by the Ministry of Education (RS-2025-2540216). The funders had no role in the study design, data collection, analysis, interpretation of results, manuscript writing, or the decision to submit the work for publication.

Data Availability

The datasets analyzed during this study are available from the Parkinson's Progression Markers Initiative (PPMI) repository, subject to PPMI data access policies. Selected code and processed data supporting the findings of this study are included in Multimedia Appendix 12. Additional materials can be shared upon reasonable request.

Authors' Contributions

HJS was responsible for the conceptualization, methodology, data curation, formal analysis, investigation, visualization, and writing–original draft. DYK, as the corresponding author, provided overall supervision, project administration, funding acquisition, and contributed to conceptualization and writing–review and editing. YJJ and SMJ contributed to validation and provided clinical insights and feedback during manuscript reviews. All authors read and approved the final version of the manuscript.

Conflicts of Interest

None declared.

Multimedia Appendix 1
Performance and weights of tree-based models.
[DOC File , 59 KB - medinform_v14i1e77561_app1.doc]

Multimedia Appendix 2
Weighted mean SHAP values for the top 10 selected variables.
[DOC File , 59 KB - medinform_v14i1e77561_app2.doc]

Multimedia Appendix 3
Prompt formats by structure type and output design.
[DOC File , 51 KB - medinform_v14i1e77561_app3.doc]

Multimedia Appendix 4
Hyperparameter configurations for logistic regression and support vector machine classifiers.
[DOC File , 58 KB - medinform_v14i1e77561_app4.doc]

Multimedia Appendix 5
Description of model families and API.

XSL•FO
RenderX

[DOC File , 63 KB - medinform_v14i1e77561_app5.doc]

Multimedia Appendix 6
Experimental timeline of model evaluations.
[DOC File , 60 KB - medinform_v14i1e77561_app6.doc]

Multimedia Appendix 7
Hardware and software configuration.
[DOC File , 57 KB - medinform_v14i1e77561_app7.doc]

Multimedia Appendix 8
Summary of fine-tuning configurations for lightweight language models.
[DOC File , 60 KB - medinform_v14i1e77561_app8.doc]

Multimedia Appendix 9
Diagnostic performance of large language models in Parkinson disease classification using prompt engineering and few-shot learning.
[DOC File , 169 KB - medinform_v14i1e77561_app9.doc]

Multimedia Appendix 10
Diagnostic generalization of large language models under dual-output prompting on the test dataset.
[DOC File , 85 KB - medinform_v14i1e77561_app10.doc]

Multimedia Appendix 11
Semantic consistency of reasoning outputs on the temporal validation set under dual-output prompting.
[DOC File , 33 KB - medinform_v14i1e77561_app11.doc]

Multimedia Appendix 12
Complete code and dataset package used for all experiments, including preprocessing, few-shot prompting, reasoning consistency analysis, and supervised fine-tuning.
[ZIP File (Zip Archive), 306 KB - medinform_v14i1e77561_app12.zip]

References

1. Shakya S, Prevett J, Hu X, Xiao R. Characterization of Parkinson's disease subtypes and related attributes. Front Neurol 2022;13:810038 [FREE Full text] [doi: 10.3389/fneur.2022.810038] [Medline: 35677337]
2. Tolosa E, Garrido A, Scholz SW, Poewe W. Challenges in the diagnosis of Parkinson's disease. Lancet Neurol 2021;20(5):385-397 [FREE Full text] [doi: 10.1016/S1474-4422(21)00030-2] [Medline: 33894193]
3. Virameteekul S, Revesz T, Jaunmuktane Z, Warner TT, De Pablo-Fernández. Clinical diagnostic accuracy of Parkinson's Disease: Where do we stand? Mov Disord 2023;38(4):558-566. [doi: 10.1002/mds.29317] [Medline: 36602274]
4. Jankovic J. Parkinson's disease: Clinical features and diagnosis. J Neurol Neurosurg Psychiatry 2008;79(4):368-376. [doi: 10.1136/jnnp.2007.131045] [Medline: 18344392]
5. Statistics. Parkinson’s Foundation. URL: https://www.parkinson.org/understanding-parkinsons/statistics [accessed 2025-02-02]
6. Parkinson Progression Marker Initiative. The Parkinson Progression Marker Initiative (PPMI). Prog Neurobiol 2011;95(4):629-635 [FREE Full text] [doi: 10.1016/j.pneurobio.2011.09.005] [Medline: 21930184]
7. Hosmer DJ, Lemeshow S, Sturdivant RX. Applied Logistic Regression. 3rd Edition. Hoboken: John Wiley & Sons; 2013.
8. Cortes C, Vapnik V. Support-vector networks. Mach Learn 1995;20(3):273-297. [doi: 10.1007/bf00994018]
9. Gerraty RT, Provost A, Li L, Wagner E, Haas M, Lancashire L. Machine learning within the Parkinson's progression markers initiative: review of the current state of affairs. Front Aging Neurosci 2023;15:1076657 [FREE Full text] [doi: 10.3389/fnagi.2023.1076657] [Medline: 36861121]
10. Alex JSR. Early detection of Parkinson’s disease using motor symptoms and machine learning. ArXiv Preprint posted online on April 18, 2023 [FREE Full text]
11. Pradeep P, Kamalakannan J. Comprehensive review of literature on Parkinson's disease diagnosis. Comput Biol Chem 2024;113:108228. [doi: 10.1016/j.compbiolchem.2024.108228] [Medline: 39413446]
12. Thirunavukarasu AJ, Ting DSJ, Elangovan K, Gutierrez L, Tan TF, Ting DSW. Large language models in medicine. Nat Med 2023;29(8):1930-1940. [doi: 10.1038/s41591-023-02448-8] [Medline: 37460753]
13. Nazi ZA, Peng W. Large language models in healthcare and medical domain: a review. Informatics 2024;11(3):57. [doi: 10.3390/informatics11030057]

XSL•FO
RenderX

14. Wiegreffe S, Marasović A. Teach me to explain: a review of datasets for explainable natural language processing. ArXiv Preprint posted online on February 24, 2021 [FREE Full text]
15. Wang Z, Zhang G, Yang K, Shi N, Zhou W, Hao S, et al. Interactive natural language processing. ArXiv Preprint posted online on May 22, 2023 [FREE Full text]
16. Sui Y, Zhou M, Zhou M, Han S, Zhang D. Table meets LLM: can large language models understand structured table data? Proceedings of the 17th ACM International Conference on Web Search and Data Mining (WSDM '24) 2024:645-654. [doi: 10.1145/3616855.3635752]
17. Afkanpour M, Hosseinzadeh E, Tabesh H. Identify the most appropriate imputation method for handling missing values in clinical structured datasets: a systematic review. BMC Med Res Methodol 2024;24(1):188 [FREE Full text] [doi: 10.1186/s12874-024-02310-6] [Medline: 39198744]
18. de Hond AAH, Shah VB, Kant IMJ, Van Calster B, Steyerberg EW, Hernandez-Boussard T. Perspectives on validation of clinical predictive algorithms. NPJ Digit Med 2023;6(1):86 [FREE Full text] [doi: 10.1038/s41746-023-00832-9] [Medline: 37149704]
19. Steyerberg EW, Harrell FE. Prediction models need appropriate internal, internal-external, and external validation. J Clin Epidemiol 2016;69:245-247 [FREE Full text] [doi: 10.1016/j.jclinepi.2015.04.005] [Medline: 25981519]
20. Thompson CG, Kim RS, Aloe AM, Becker BJ. Extracting the variance inflation factor and other multicollinearity diagnostics from typical regression results. Basic and Applied Social Psychology 2017;39(2):81-90. [doi: 10.1080/01973533.2016.1277529]
21. Neter J, Nachtsheim CJ, Kutner MH. Applied Linear Regression Models. 4th Edition. New York: McGraw-Hill/Irwin; 2004.
22. O'brien RM. A caution regarding rules of thumb for variance inflation factors. Qual Quant 2007;41(5):673-690. [doi: 10.1007/s11135-006-9018-6]
23. Breiman L. Random forests. Mach Learn 2011;45(1):5-32 [FREE Full text] [doi: 10.1186/1478-7954-9-29]
24. Chen T, Guestrin C. Xgboost: a scalable tree boosting system. In: 22nd ACM SIGKDD International Conference. 2016 Presented at: Proceedings of the 22nd ACM SIGKDD International Conference on Knowledge Discovery and Data Mining (KDD '16); August 13-17, 2016; San Francisco p. 785-794.
25. Ke G, Meng Q, Finley T. LightGBM: a highly efficient gradient boosting decision tree. In: Guyon I, Luxburg UV, Bengio S, Wallach H, Fergus R, Vishwanathan S, et al, editors. Advances in Neural Information Processing Systems 30 (NeurIPS 2017). New York: Curran Associates, Inc; 2017:3146-3154.
26. Prokhorenkova L, Gusev G, Vorobev A, Dorogush A, Gulin A. CatBoost: unbiased boosting with categorical features. In: Advances in Neural Information Processing Systems 31 (NeurIPS 2018). New York: Curran Associates, Inc; 2018:6638-6648.
27. Shwartz-Ziv R, Armon A. Tabular data: deep learning is not all you need. Inf Fusion 2022;81:84-90. [doi: 10.1016/j.inffus.2021.11.011]
28. Lundberg SM, Lee SI. A unified approach to interpreting model predictions. Advances in Neural Information Processing Systems. 2017. URL: https://papers.nips.cc/paper_files/paper/2017/file/8a20a8621978632d76c43dfd28b67767-Paper.pdf [accessed 2025-06-21]
29. He J, Rungta M, Koleczek D, Sekhon A, Wang F, Hasan S. Does prompt formatting have any impact on LLM performance? ArXiv Preprint posted online on November 15, 2024. [doi: 10.48550/arXiv.2411.10541]
30. Creswell A, Shanahan M, Higgins I. Selection-inference: exploiting large language models for interpretable logical reasoning. ArXiv Preprint posted online on May 19, 2022 [FREE Full text]
31. Saito T, Rehmsmeier M. The precision-recall plot is more informative than the ROC plot when evaluating binary classifiers on imbalanced datasets. PLoS One 2015;10(3):e0118432 [FREE Full text] [doi: 10.1371/journal.pone.0118432] [Medline: 25738806]
32. Carpenter J, Bithell J. Bootstrap confidence intervals: when, which, what? A practical guide for medical statisticians. Statist. Med 2000;19(9):1141-1164. [doi: 10.1002/(sici)1097-0258(20000515)19:9<1141::aid-sim479>3.0.co;2-f]
33. Song Y, Gao Q, Bai Y. The good, the bad, and the greedyvaluation of LLMs should not ignore non-determinism. ArXiv Preprint posted online on July 15, 2024 [FREE Full text] [doi: 10.18653/v1/2025.naacl-long.211]
34. Kojima T, Gu SS, Reid M. Large language models are zero-shot reasoners. ArXiv Preprint posted online on May 24, 2022. [doi: 10.48550/arXiv.2205.11916]
35. Reimers N, Gurevych I. Sentence-BERTntence embeddings using Siamese BERT-networks. ArXiv Preprint posted online on August 27, 2019 [FREE Full text]
36. Song K, Tan X, Qin T, Lu J, Liu TY. MPNet: masked and permuted pre-training for language understanding. ArXiv. Preprint posted online on April 20, 2020 [FREE Full text]

Abbreviations

API: application programming interface
HC: healthy controls
LLM: large language model

XSL•FO
RenderX

LLM_D: dual-output prompting with LLM
LLM_F: few-shot prompting with LLM
LLM_FT: fine-tuned prompting with LLM
LR: logistic regression
MD: markdown
MD+ST: markdown with special token
ML: machine learning
PD: Parkinson disease
PPMI: Parkinson's Progression Markers Initiative
PT: plain text
RBF: radial basis function
SHAP: Shapley additive explanations
ST: special token
SVM: support vector machine
UPDRS: Unified Parkinson Disease Rating Scale
UPSIT: University of Pennsylvania Smell Identification Test

Edited by A Coristine; submitted 15.May.2025; peer-reviewed by A Hungbo, N Acharya; comments to author 22.May.2025; revised version received 24.Dec.2025; accepted 24.Dec.2025; published 15.Jan.2026.

Please cite as:
Shin HJ, Jeong YJ, Jun S, Kang DY
Prompting and Fine-Tuning Large Language Models for Parkinson Disease Diagnosis: Comparative Evaluation Study Using the PPMI Structured Dataset
JMIR Med Inform 2026;14:e77561
URL: https://medinform.jmir.org/2026/1/e77561
doi:10.2196/77561
PMID:

©Hyun-Ji Shin, Young Jin Jeong, Sungmin Jun, Do-Young Kang. Originally published in JMIR Medical Informatics (https://medinform.jmir.org), 15.Jan.2026. This is an open-access article distributed under the terms of the Creative Commons Attribution License (https://creativecommons.org/licenses/by/4.0/), which permits unrestricted use, distribution, and reproduction in any medium, provided the original work, first published in JMIR Medical Informatics, is properly cited. The complete bibliographic information, a link to the original publication on https://medinform.jmir.org/, as well as this copyright and license information must be included.

XSL•FO
RenderX

Applicability of Existing Gender Scores for German Clinical Research Data: Scoping Review and Data Mapping

Lea Schindler[1]; Hilke Beelich[1]; Elpiniki Katsari[2], Dr med; Daniele Liprandi[3], Dr ing; Sylvia Stracke[4], Dr med; Dagmar Waltemath[1,5], Dr ing

[1]Medical Informatics Laboratory, University Medicine Greifswald, Walther-Rathenau-Straße 48, Greifswald, Germany

[2]Heart Surgery, University Medicine Greifswald, Greifswald, Germany

[3]Laboratory of Evolutionary Biomechanics, Zoological Institute and Museum, University Greifswald, Greifswald, Germany

[4]Internal Medicine A, Nephrology, University Medicine Greifswald, Greifswald, Germany

[5]Core Unit Data Integration Center, University Medicine Greifswald, Greifswald, Germany

Corresponding Author:
Dagmar Waltemath, Dr ing
Medical Informatics Laboratory, University Medicine Greifswald, Walther-Rathenau-Straße 48, Greifswald, Germany

Abstract

Background: Considering sex and gender improves research quality, innovation, and social equity, while ignoring them leads to inaccuracies and inefficiency in study results. Despite increasing attention on sex- and gender-sensitive medicine, challenges remain with accurately representing gender due to its dynamic and context-specific nature.

Objective: This work aims to contribute to the implementation of a standard for collecting and assessing gender-specific data in German university hospitals and associated research facilities.

Methods: We carried out a review to identify and categorize state-of-the-art gender scores. We systematically assessed 22 publications regarding the applicability and practicability of their proposed gender scores. Specifically, we evaluated the use of these gender scores on German research data from routine clinical practice, using the Medical Informatics Initiative core dataset (MII CDS).

Results: Different methods for assessing gender have been proposed, but no standardized and validated gender score is available for health research. Most gender scores target epidemiological or public health research where questions about social aspects and life habits are already part of the questionnaires. However, it is challenging to apply concepts for gender scoring on clinical data. The MII CDS, for example, lacks all variables currently being recorded in gender scores. Although some of the required variables are indeed present in routine clinical data, they need to become part of the MII CDS.

Conclusions: To enable gender-specific retrospective analysis of routine clinical data, we recommend updating and expanding the MII CDS by including more gender-relevant information. For this purpose, we provide concrete action steps on how gender-related variables can be captured in routine clinical practice and represented in a machine-readable way.

International Registered Report Identifier (IRRID): RR2-10.2196/57669

(JMIR Med Inform 2026;14:e74162) doi:10.2196/74162

KEYWORDS

gender score; gender research; review; clinical routine; clinical research data; German Medical Informatics Initiative

Introduction

Background

Taking sex and gender (see Textbox 1 and Textbox 2) into account improves the quality of research and care, and it supports social equity [1]. Considering sex and gender from the outset can lead to new discovery and foster innovation. Ignoring sex and gender, however, leads to inaccuracies, inefficiencies, and difficulties generalizing results. This is, for example, highlighted by a recent study showing that men with low femininity reported a significant decrease in anxiety during the COVID-19 pandemic, meanwhile women with low femininity reported a significant increase [2].

XSL•FO
RenderX

Textbox 1. Definition of biological sex [3,4].

Biological sex is defined through biological attributes, such as:

- Genetics (ie, chromosomes, gene expression)
- Hormone levels
- Anatomy (ie, internal and external sex organs/reproductive organs)

Deviations regarding the hormonal or chromosomal attributes are possible, where the external appearance can be intersex and it is not possible to decide.

Textbox 2. Definition of (social) gender [3,4].

Gender refers to socially constructed roles, behaviors, expectations, and norms associated with being a woman, man, girl, or boy. It is formed through biological and psychosexual factors and an individual's social biography, and it is shaped by one's role in society. Gender influences how people perceive themselves and others and how they act and interact.

Many health care decisions are influenced by the patients' sex and gender, through social norms and experiences. Sex- and gender-sensitive medicine is receiving increasing attention in international research [5]. However, several publications have shown that women are still not considered equally to men and are poorly represented due to biased study designs [6-8]. It is well known today that this practice leads to an increase in inequality in medical treatment due to inappropriate therapies. Moreover, sex- and gender-specific reporting is often deficient, which leads to a lack of reproducibility and reduced effectiveness of research studies [1].

Even though the situation has improved, it can still be challenging to represent psychosocial gender aspects, as gender is a context-specific construct that is dynamic and multidimensional and can differ across time, geographical regions, and societies [9].

Gender scores are developed and used to assess gender roles and gender identity. They can be created and applied retrospectively to extract frequently missing gender information from already existing data. For this purpose, gender-sensitive variables in the existing data are determined by expert knowledge or statistical algorithms. Gender scores can then be calculated to predict social gender roles. For example, Lacasse et al [10] and Nauman et al [11] each developed a retrospective gender score and applied it to specific datasets from population studies. Examples for the corresponding gender-sensitive variables are specific *professions*, like in health care or construction, and typical *personality trait*s, like agreeableness or neuroticism; *loneliness* or *stress* was considered. In general, retrospective scores cannot capture participants' current gender identity (see Textbox 3).

Textbox 3. Definition of gender identity [3,4].

Gender identity is determined through individual self-perception and the sexual identity of a person, which may differ from someone's physical appearance or biological sex.

Prospective assessments can enhance the collection of gender-specific data from the outset of a study by incorporating further social data or information regarding the identity. Fraser et al [12] and Lagos and Compton [13], for example, evaluated a prospective 2-step gender identity measure on data from huge studies. The 2-step measure differentiates between a person's current gender identity and birth-assigned sex (see Textbox 3 and Textbox 4). The given examples show that gender scores are mostly used in surveys and studies and hardly used on routine clinical data.

Textbox 4. Definition of birth-assigned sex (BAS) [3,4].

BAS refers to the information that can be found on official documents, like a birth certificate, and is assigned based on the child's external anatomy or sex organs. BAS is often measured by a binary choice of response (ie, male or female). Biological sex is not a dichotomy, nor is BAS, where diversity is given.

All 38 university hospitals in Germany are part of the Medical Informatics Initiative [14] (MII), which serves to close the gap between research and routine care. A core dataset (CDS) is being developed by the MII consortia and the participating university hospitals to foster interoperability and allow a shared use of routine clinical data across Germany. Data Integration Centers collect and process routine clinical data and make them accessible to researchers for secondary use. If and how this established dataset considers gender and gender score applications are open questions.

It is important to note that the discussion about the applicability and state of gender scores does not only affect Germany. Critical assessments of sex and gender scores reveal that the problem affects different western cultures [15-18]. Ignoring gender differences in clinical research is a widespread global issue that undermines the validity and applicability of scientific findings across diverse populations [16]. A study conducted in Australia using the Bem Sex Role Inventory (BSRI) [19] found that the majority of participants received different gender scores in at least 1 of the 3 consecutive years, highlighting the complexity and fluid nature of gender identity [18]. This is particularly

XSL•FO
RenderX

concerning because the BSRI yielded inconsistent results even among a relatively stable population of patients older than 75 years — where minimal shifts in habits or identity would be expected over time. Despite being based on outdated social stereotypes, the BSRI is one of the most used gender scores, and other scores are partly based on it, as we later describe.

In this context, where classic gender scores are struggling, new tools are being considered to annotate medical data according to the gender of patients, thanks to the rise of machine learning methods [20]. The results of such methods can then be systematically used to mitigate biases in research, as done by Neufang et al [21], who developed an artificial intelligence model to improve the fairness of attention deficit hyperactivity disorder diagnosis with respect to gender. It is important to understand whether these algorithms are also applicable to general clinical data datasets, such as the MII CDS, to allow large-scale integration of gender debiasing in future research.

The issues outlined in the previous paragraphs indicate that more work needs to be done to update gender scores, taking into account the changes in commonly defined social rules that have occurred in the last century. In practice, outdated scores, such as the BSRI, are often used without considering proper validation and potential biases [22]. Moreover, a gold standard is still missing for how sex and gender should be considered in research with clinical research data. A practicable score should be balanced, comprehensive, and easily applicable. Interestingly, no gender score has so far been established as an international standard.

We therefore conducted a systematic evaluation of gender scores regarding their applicability in health research using German efforts on Data Integration in Medicine as a benchmark. As the world's third-largest economy and one of the World Health Organization's top two donors, we expected the German MII CDS to be a good candidate for our evaluation. In this article, the term gender score refers to the assessment of gender in general (social gender and gender identity), and the term gender identity measure refers exclusively to gender identity.

Related Work

The focus of our scoping review protocol published in JMIR Review Protocols [23] was the applicability and practicability of gender scores in health research. Related to the work described in this paper, Horstmann et al [24] published a review on recently used instruments for the operationalization of sex and gender in health research, and the work by Miani et al [25] summarizes epidemiological aspects in gender scores. The reviews included publications until 2020 and 2021, respectively. For this work, we identified the latest scores and therefore deliberately limited our search to publications between 2019 and 2024. Of the 18 articles from our primary result set, 13 were published after 2020.

In parallel to our work on the systematic review of recent gender scores, another systematic review about the operationalization of gender via composite gender scores in epidemiological studies was published in 2024 by Ballering et al [26]. The authors searched 3 databases (PubMed, Web of Science, and CINAHL) and identified 24 articles with a total of 26 gender scores developed in Europe or North America. They aggregated information on gender scores regarding author, year of publication, methodology, cohort information, and the included variables of the respective gender score and found that many variables overlapped across multiple studies.

Ballering et al [26] criticized theory-driven approaches — developed solely based on expert knowledge — as experts are not free from bias, potentially enhancing sexism or other biases. The authors further claim that data-driven approaches — using statistical models to develop gender scores — only predict female or male sex through identified psychosocial variables and do not consider gender itself. Psychosocial variables that do not associate with sex are excluded, and the quality of the gender scores is strongly dependent on the quality of the dataset. Overall, Ballering et al [26] concluded that data-driven approaches might be good to personalize health care, as gendered variables point out differences between women and men that could lead to improved treatment decisions and patient care.

The work by Ballering et al [26] is a great foundation for our work, and we are able to contribute further insights on the applicability of gender scores on routine clinical data. We had an overlap of 13 articles on both sides, with 13 of 22 articles in our review and 13 of 24 articles in the review by Ballering et al [26] (ie, there was an overlap of more than 50%: 59% ours and 54% theirs). We found further articles regarding gender identity that can be applied from the outset of a study or data collection, which could be of great use to implement gender information in routine clinical practice.

Aim of This Work

In the scope of this work, we identified and categorized state-of-the-art gender scores, systematically assessed their applicability and practicability, and evaluated their applicability on German research data from routine clinical practice (see the Applicability of Gender Scores on the MII CDS section).

The process of our work is illustrated in Figure 1. This work aimed to contribute to the necessary implementation of a standard for collecting and assessing gender-specific data in German university hospitals and the respective research facilities; therefore, we formulated 4 action steps for an extension in health research to enable gender-specific analyses (see Figure 1), which are shown at the bottom of the figure and will be described in detail in the Discussion section.

XSL•FO
RenderX

Figure 1. Overview of the implemented methods. MII CDS: Medical Informatics Initiative core dataset.

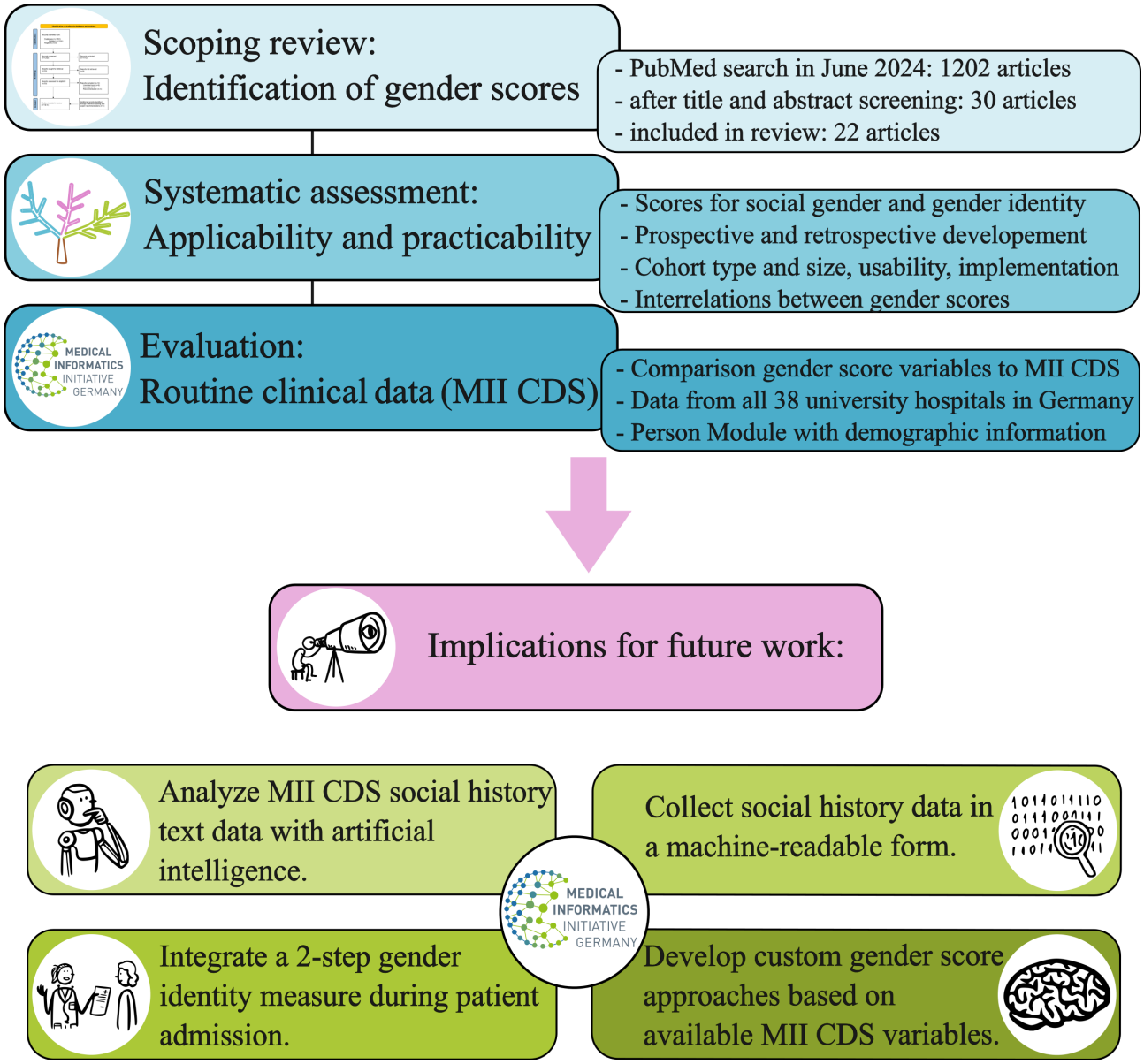

Methods

Scoping Review

We conducted a scoping review to identify articles that reported on the development and implementation of gender scores in health-related studies (see Figure 1). It resulted in 22 articles, which were identified through a title and abstract screening followed by a full-text evaluation. Moreover, we developed a data charting form to extract information on article type and applicability of the gender score in health research. The review protocol was published in JMIR Research Protocols [23].

Assessment of Applicability and Practicability

To assess the applicability and practicability of gender scores, we followed a systematic approach (see Figure 1). In the scope of this work, we extended the data charting process to fully assess the applicability of gender scores on routine clinical data.

Social Gender and Gender Identity

First, we distinguished between scores for gender identity (see Table 1) versus social gender (see Tables 2 and 3). Gender identity (see Textbox 3) is usually measured in a prospective way because it is a purely subjective perception and it is not possible to extract this information when it was not collected. However, social gender includes norms that are expected in society, stereotypes, and certain behaviors (see Textbox 2), and it can be measured prospectively and retrospectively. Typical behavior (eg, specific hobbies, occupational segregation, doing housework or odd jobs) can be analyzed and interpreted after data collection. A typical female or male lifestyle or behavior will lead to different exposure to risk factors for accidents or disease. Social expectations will also influence the process of recovery.

XSL•FO
RenderX

Table . Prospective gender identity measures [12,13,27,28].

Author(s) (year)	Description	Questions and answer option
Lagos and Compton (2021) [13]	2-step gender identity measure	1. What sex were you assigned at birth? (male, female, intersex) 2. What is your current gender? (woman, man, transgender, a gender not listed here [space for answer])
Fraser et al (2020) [12]	Open-ended gender measure	What is your gender? (open-ended item)
McGuire et al (2019) [27]	Genderqueer Identity Scale	1. I am non binary, genderqueer, or an identity other than male or female. 2. I don't want to be seen in the gender binary (as either male or female) 3. I try to deliberately confuse people about whether I am male or female. 4. I try to do things that are masculine and feminine at the same time. 5. I enjoy it when people are not sure if I am male or female 6. The way I think about my gender has always been the same. 7. My gender comes naturally from within me. 8. My gender is something I have spent a lot of time figuring out. 9. The way I show my gender changes depending on who I am with. 10. The way I think about my gender has been influenced by experiences in my life. 11. The way I think about my gender will probably continue to change further as I age 12. I have done research about gender theory and gender roles. 13. I try to convince others that society should not insist on a gender binary. 14. I try to convince others that society expects people to be too gender conforming. 15. Around me, I make sure people are free to express whatever gender roles they want. 16. The way I show my gender is important because I push society to question traditional gender roles. 17. I encourage others to be more open minded about gender and gender roles. 18. In the future, my gender expression will be traditional. 19. In the future, it will upset me if people misgender me. 20. The way I show my gender will probably be mostly the same from day to day. 21. In the future, I expect that people will rarely question my gender. 22. In the future, I think my gender will be fluid or change over time. 23. I will have a non-traditional gender role (be gender non-conforming).
Lombardi and Banik (2016) [28]	2-step gender identity measure	1. What is your sex or gender? (Check ALL that apply; male, female, other: please specify [space for answer]) 2. What sex were you assigned at birth? (Check one; male, female, unknown or question not asked, decline to state)

XSL•FO
RenderX

Table . Prospective gender scores regarding social gender [17,19,20,29-32].

Author(s) (year)	Gender score variables
Pohrt et al (2022)[a] [29]	1. Level of education[b] 2. Civil status[b] 3. Personal net income 4. Households primary earner status 5. Responsibility for caring for other people[b] 6. Responsibility educating and upbringing people[b] 7. Responsibility for picking up people when they become ill 8. Hours per week spent on housework 9. Being mainly responsible for housework, 10. Social support[b] 11. PAQ[c] 12. BSRI[d]: masculinity score 13. BSRI: femininity score 14. Perceived social standing
Tibubos et al (2022) [30]	
PAQ-8	1. Not at all emotional - very emotional 2. Not at all aware of feelings of others -very aware of feelings of others 3. Never gives up easily - gives up very easily 4. Not at all self-confident - very self-confident 5. Feels superior - feels very inferior 6. Not at all understanding of others - very understanding of others 7. Very warm in relations with others - very cold in relations with others 8. Goes to pieces under pressure - stands up well under pressure
Demuth et al (2021) [31]	The questionnaire is not available.
Nielsen et al (2021) [17]	1. Caregiver strain[b] 2. Work strain[b] 3. Independence 4. Risk-taking 5. Emotional intelligence 6. Social support[b] 7. Discrimination
Pelletier et al (2015) [20]	1. Primary earner status 2. Personal income 3. Number of hours per week doing housework 4. Primary responsibility for doing housework 5. Level of stress at home[b] 6. BSRI: masculinity score 7. BSRI: femininity score
Spence et al (1975) [32]	

XSL•FO
RenderX

Author(s) (year)	Gender score variables
PAQ: male score	1. Independent 2. Not easily influenced 3. Good at sports 4. Not excitable, minor crisis 5. Active 6. Competitive 7. Skilled in business 8. Knows ways of world 9. Adventurous 10. Outspoken 11. Interested in sex 12. Makes decisions easily 13. Not give up easily 14. Outgoing 15. Acts as leader 16. Intellectual 17. Self confident 18. Feels superior 19. Takes a stand 20. Ambitious 21. Stands up under pressure 22. Forward 23. Not timid
PAQ: female score	1. Emotional 2. Not hide emotions 3. Considerate 4. Grateful 5. Devotes self to others 6. Tactful 7. Strong conscience 8. Gentle 9. Helpful to others 10. Kind 11. Aware, other feelings 12. Neat 13. Creative 14. Understanding 15. Warm to others 16. Likes children 17. Enjoys art and music 18. Expresses tender feelings
PAQ: sex-specific score	1. Aggressive (M) 2. Dominant (M) 3. Likes math and science (M) 4. Excitable, major crisis (F) 5. Home-oriented (F) 6. Mechanical aptitude (M) 7. Needs approval (F) 8. Feelings hurt (F) 9. Cries easily (F) 10. Loud (M) 11. Religious (F) 12. Sees self running show (M) 13. Needs for security (F)
Bem (1974) [19]	

XSL•FO
RenderX

Author(s) (year)	Gender score variables
BSRI: masculinity score	1. Acts as a leader 2. Aggressive 3. Ambitious 4. Analytical 5. Assertive 6. Athletic 7. Competitive 8. Defends own beliefs 9. Dominant 10. Forceful 11. Has leadership abilities 12. Independent 13. Individualistic 14. Makes decisions easily 15. Masculine 16. Self-reliant 17. Self-sufficient 18. Strong personality 19. Willing to take a stand 20. Willing to take risks
BRSI: femininity score	1. Affectionate 2. Cheerful 3. Childlike 4. Compassionate 5. Does not use harsh language 6. Eager to soothe hurt feelings 7. Feminine 8. Flatterable 9. Gentle 10. Gullible 11. Loves children 12. Loyal 13. Sensitive to the needs of others 14. Shy 15. Soft spoken 16. Sympathetic 17. Tender 18. Understanding 19. Warm 20. Yielding
BRSI: social desirability score (neutral)	1. Adaptable 2. Conceited 3. Conscientious 4. Conventional 5. Friendly 6. Happy 7. Helpful 8. Inefficient 9. Jealous 10. Likable 11. Moody 12. Reliable 13. Secretive 14. Sincere 15. Solemn 16. Tactful 17. Theatrical 18. Truthful 19. Unpredictable 20. Unsystematic

[a]Overlaps with the already published review by Ballering et al [26].

[b]Variables that are potentially covered in routine clinical care in Germany.

[c]PAQ: Personal Attributes Questionnaire.

XSL•FO
RenderX

[d]BSRI: Bem Sex Role Inventory.

XSL•FO
RenderX

Table . Retrospective gender scores regarding social gender [9-11,33-40].

Author(s) (year)	Gender score variables
Cipriani et al (2024)[a] [36]	1. Hostile behavior during childhood 2. Hostile behavior during adulthood 3. Having at least a secondary school diploma[b] 4. Having at least a bachelor's degree[b] 5. Sleep satisfaction[b] 6. Sleep efficacy[b] 7. Having private housing 8. Sexual violence during childhood
Gisinger et al (2023)[a] [35]	1. Level of education[b] 2. Household income 3. Household size[b] 4. Civil status[b] 5. Perceived life stress 6. Sense of belonging to community
Teterina et al (2023)[a] [37]	
ICD-10-CA[c] diagnostic codes with highest effects for predicting male/female gender: male score	1. Fall on and from scaffolding[b] 2. Occupant of heavy transport vehicle injured in noncollision transport accident, driver, traffic accident[b] 3. Driver of other all-terrain or other off road motor vehicle injured in traffic accident[b] 4. Motorcycle rider injured in collision with fixed or stationary object, driver, traffic accident[b] 5. Asymptomatic human immunodeficiency virus (HIV) infection status[b] 6. Motorcycle rider injured in collision with car, pick-up truck or van, driver, traffic accident[b] 7. Motorcycle rider injured in noncollision transport accident, driver, nontraffic accident[b] 8. Motorcycle rider injured in unspecified nontraffic accident[b] 9. Fracture of malar and maxillary bones, LeFort 2, closed[b] 10. Contact with nonpowered hand tool[b]
ICD-10-CA diagnostic codes with highest effects for predicting male/female gender: female score	1. Assault by spouse or partner 2. Esthetic sports[b] 3. Physical abuse[b] 4. Horse riding sports[b] 5. Animal-rider or occupant of animal-drawn vehicle injured by fall from or being thrown from animal or animal-drawn vehicle in noncollision accident[b] 6. Fall while being carried or supported by other persons[b] 7. Other specified gymnastic and esthetic sports and recreational activity[b] 8. Bitten or struck by dog[b] 9. Animal-rider or occupant of animal-drawn vehicle injured in other and unspecified transport accidents[b] 10. Problems in relationship with spouse or partner

XSL•FO
RenderX

Author(s) (year)	Gender score variables
Vader et al (2023)[a] [38]	

XSL•FO
RenderX

Author(s) (year)	Gender score variables
Masculine gender score	1. Work and education (compared with partner)[b] 2. Informal care: household chores, odd jobs, taking care of sick people[b] 3. Lifestyle: physical intensity, type of sport, smoking, alcohol[b] 4. Emotions: emotional problems, nervousness, energetic and vibrant, exhausted and tired
de Breij et al (2022)[a] [33]	1. Working hours[b] 2. Income 3. Occupation segregation[b] 4. Education[b] 5. Informal caregiving[b] 6. Time spent on household chores
Wandschneider et al (2022)[a] [9]	1. A person who is living with their partner for the long term should get married. 2. Children below the age of 6 suffer if their mother works. 3. A same-sex couple can raise a child just as well as a man and woman. 4. It would be good for society if transgender people were recognized as normal. 5. Working experience part-time employment 6. Hours/weekday housework 7. Hours/weekday repairs 8. Hours/weekday leisure, hobbies 9. Worried about global terrorism 10. Worried about crime in Germany 11. Satisfaction with housework 12. Willingness to take risks 13. Worried about own retirement pension
Nauman et al (2021)[a] [11]	1. Chronic stress 2. Civil status[b] 3. Risk-taking behavior 4. Agreeableness 5. Neuroticism 6. Extraversion 7. Conscientiousness 8. Loneliness 9. Level of education
Yuan et al (2021)[a] [39]	1. Risk willingness 2. Loneliness[b] 3. Less participation in household tasks 4. Regular drinking[b] 5. Depression[b]
Ballering et al (2020)[a] [40]	1. Leisure activities (eg, type of sport)[b] 2. Occupation-related components (eg, profession, housewife/-husband)[b] 3. Time spend on household tasks 4. Time spend on odd jobs 5. Lifestyle (eg, dieting, preparing dinner, alcohol, smoking) 6. Experiencing long-term difficulties or negative life events 7. Personality traits and emotions (eg, discipline, impulsiveness, self-consciousness, vulnerability, competence

XSL•FO
RenderX

Author(s) (year)	Gender score variables
Lacasse et al (2020)[a] [10]	1. Civil status[b] 2. Racial/ cultural group 3. Level of education[b] 4. Household income, size, and composition[b] 5. Household food insecurity 6. Ownership of the household 7. Sense of belonging to the local community 8. Occupation: type, working hours, self-employment[b] 9. Amount of stress
Smith and Koehoorn (2016)[a] [34]	1. Responsibility for caring for children[b] 2. Occupational segregation[b] 3. Hours of work relative to partner/spouse 4. Education relative to partner/spouse[b]

[a]Overlaps with the already published review by Ballering et al [26].

[b]Variables that are potentially covered in routine clinical care in Germany.

[c]ICD-10-CA: International Statistical Classification of Diseases and Related Health Problems, Tenth Revision, Canada.

Prospective and Retrospective Scores

Second, we distinguished between prospective (see Tables 1 and 2) and retrospective (see Table 3) scores. It is advisable to include gender variables from the outset of a study; this results in a prospective gender score and is easy to apply to the study dataset. However, the huge amount of existing data drives the development of retrospective gender scores, where gender-specific information can be extracted in hindsight.

Cohort Type and Size

Third, it needs to be considered whether the gender scores themselves are representative. In practice, some gender scores are developed on restricted datasets, for instance, for specific patient groups or other samples that are not representative (eg, older age groups, workers, or specific diagnoses). This is underlined by the finding of Wandschneider et al [9] who showed that gendered practices vary between eastern and western Germany, reflecting a different social development due to the historical political context. As gender norms, stereotypes, or behaviors vary between societies, the relevant gender variables can differ across social groups, countries, and regions or even between different societies within a country.

Furthermore, since retrospective scores depend on statistical modeling, we also considered the sample size on which the models were based. Another analysis we performed was to further classify the background under which the score was developed. We took into account whether the research group used patient or population data to categorize which gender score might be more appropriate for the MII CDS. We also considered the continent where the data collection took place, which is important for consistency due to varying gender-sensitive variables depending on the society or geographical location.

Usability

Fourth, we examined the validity, usability, and practicability of the gender scores. Validity is the main issue because it is of high importance that the score is representative regarding gender. Usability refers to how well the score is established. If a new standard is to be introduced, it is of high importance to use an accepted model to ensure that the scores are usable, comparable, and applicable to large-scale studies and assessments. Practicability refers to how difficult a score would be to integrate into health research.

Implementation

The fifth point we included in our assessment was the level of implementation of scores. To apply scores systematically on existing data, a theoretical model was not sufficient. Instead, it was necessary to have the executable code of a model to integrate it directly. Therefore, we further investigated the applicability of gender scores from the technical viewpoint to evaluate whether models can, realistically, be implemented in a clinical setting. We used the following categories to describe this aspect: code published — refers to a gender score for which an executable model was published; data published — refers to a gender score for which the underlying data are available and a score could be reproduced; statistical parameters published — refers to a model for which all statistical parameters were published and the model could be constructed from them; not published — a model for which not all relevant parameters are available. We considered “code published” the gold standard regarding applicability. “Data published” and “parameters published,” on the other hand, might contain sufficient information to construct an executable model. In the scope of this study, we considered code or data available “on request” as unavailable. However, in practice, there might still be limitations if the description of the article is not concise enough to reproduce all steps.

Interrelations

Based on the extracted data, we performed further analysis to better understand the currently available gender scores. We noticed early on that direct dependencies exist between gender scores. Therefore, we extracted and modeled different types of dependencies between gender scores (see Figure 2). This

XSL•FO
RenderX

analysis allowed us to investigate how scores were developed and whether improvements were made to existing gender scores.

Figure 2. Interrelations between gender scores, where the first 1 or 2 author names identify the work and the developed gender score (see Tables 2 and 3) [9-11,17,19,20,29-41]: (A) gender scores developed with completely new approaches and methods are shown in green; (B) the included or adapted gender scores are in parentheses in the blue branch; (C) gender scores developed based on previous methods and statistical approaches, which are shown in parentheses, are shown in pink. BSRI: Bem Sex Role Inventory; PAQ: Personal Attributes Questionnaire.

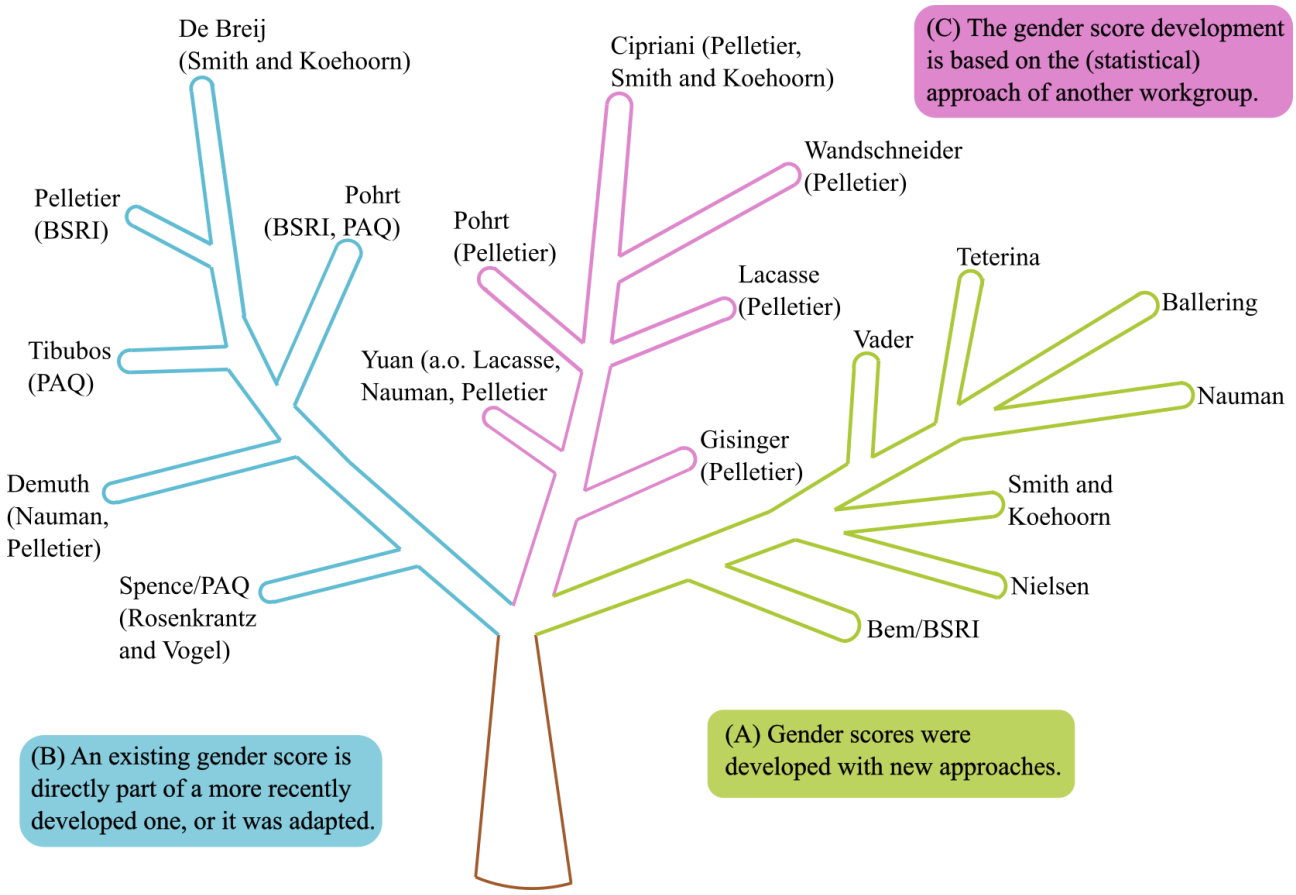

One relation between gender scores captures cases in which an existing gender score was used directly or adapted in another score (see Figure 2B). For instance, the gender score from Pelletier et al [20] includes the BSRI [19]. de Breij et al [33] adapted the score from Smith and Koehoorn [34] but changed "caring for children" to "informal caregiving" as the data were available in their dataset (see Figure 2B).

Moreover, development relationships (see Figure 2C) reflect when one gender score was developed based on the approach, for instance the statistical model, of another research group. For example, Gisinger et al [35], with their statistical model of principal component analysis and logistic regression analysis, were inspired by the approach of Pelletier et al [20].

Applicability on Clinical Routine Data

To assess whether gender scores are applicable on existing data and whether they can be integrated in clinical routine data, we used the technical specification of the MII Core Data Set - Module "Person" as a representative sample against which to evaluate the gender scores (see Figure 1). The MII CDS [14] (see the Background section) is being collected across all 38 university hospitals in Germany. It contains interoperable, consolidated data items with a high degree of standardization in line with international standards to make collaborative data analysis practicable and efficient.

The CDS [42] consists of basic and extension modules that are subject to iterative refinement. The basic modules are generic, and the extension modules are relevant for specific medical fields and disciplines such as oncology or intensive care. We used the *Person Module*, one of the early basic modules, which contains demographic information such as name, date of birth, address, and administrative gender as stated in official documents. The CDS has a comprehensive description of how the data are structured and how the data can be accessed, which allows us to directly compare it against gender scores. The information is available and can be compared based on a sample dataset [43]. Overall, this makes the CDS a suitable choice for studying how gender scores can be applied in realistic clinical data collection.

Retrospective scores required that we compared the variables contained in the gender scores against the variables available in routine clinical data. To perform this comparison, we systematically analyzed all variables contained in the sample dataset of the MII CDS against the variables included in the statistical models of the gender scores.

Ethical Considerations

We did not collect any personal data, so ethical approval was not needed.

XSL•FO
RenderX

Results

The full results of the review are presented in Multimedia Appendix 1 to maintain brevity in the main text.

Scoping Review

Our review results are categorized into prospective development (Tables 1–2) and retrospective development (Table 3) and between gender scores (Tables 2–3) and gender identity measures (Table 1). Articles that overlapped with the already published review by Ballering et al [26] are marked in the tables.

Assessment of Applicability and Practicability

Social Gender, Gender Identity, and Prospective and Retrospective Scores

We distinguished between articles targeting gender identity and articles targeting social gender. We further classified them into prospective and retrospective development and application.

The 4 identified gender identity measures (see Table 1) are prospectively applicable and could be included in future studies for further data collection regarding gender identity. Participants need to be asked explicitly which gender they belong to; this information cannot be analyzed from existing data.

Moreover, we found 18 gender scores to measure social gender in different ways. Of these, 7 are prospective gender scores (see Table 2) that could provide guidance on how to apply (social) gender to a study from the outset. Of the 18 scores, 11 are retrospective (see Table 3) and could be applied on already existing data.

Cohort Type and Size

The background of the cohorts is of importance for the practicability. A score contains different variables, depending on whether it was developed on data from population studies or on patient data. The majority of datasets are based on population studies and thus on specific information that is typically collected in these studies. For a complete comparison of cohorts, see our results in Multimedia Appendix 1.

Only 2 gender scores were developed exclusively based on patient data. Teterina et al [37] focused on patients who entered the emergency department with traumatic brain injuries and published an innovative approach to distinguishing gender by diagnostic codes. These diagnostic codes also describe the background of the accident or incident, enabling conclusions to be drawn about gender. Cipriani et al [36] focused on the effects of gender on emergency patients with psychological crisis. Therefore, they used variables assessing childhood trauma, education, sleep quality, and living situation.

Moreover, the article by McGuire et al [27] assessed gender identity during transition through the collection of patient and population data.

However, all of these studies were restricted by the specific patient cohort group and focused on specific conditions. This hampers their applicability on the general public and their usefulness as broadly applied gender scores for routine clinical data.

In addition, the used population cohorts were neither comprehensive nor inclusive. Many studies used a cohort with a specific age group [11,20,29,31,38,39] or with a specific background like being retired [29] or being a worker [10,33]. This is a major weakness for generalizing results, as a gender score based on a limited cohort is not representative of society as a whole and therefore lacks comprehensiveness.

Furthermore, the majority of cohorts used for developing gender scores are based in the same geographic region, primarily Europe and North America. Only one gender identity measure was used on a cohort in Oceania [12]. We could not find a single gender score publication with a cohort from Asia, South America, or Africa. As a result, the developed scores are not representative for every cohort group and are not universally applicable.

With respect to the size of the cohorts, which forms the basis for the statistical development of retrospective gender scores and influences the reliability of statistical models, we noted that some works used huge cohorts or datasets with n>100,000 [35,37,40] and the outstanding cohort size of approximately 700,000 individuals in the study by Smith and Koehoorn [34]. Other gender scores worked with smaller cohort sizes of n<1000 [19,32,33].

Usability

We examined the validity of scores, meaning how representative the work is regarding gender. Gender can be different in each society, so it is a major task to implement a gold standard. Some research groups used sex as the dependent variable and, therefore, gender as a predictor for sex (eg, [9-11,20]). This approach can be problematic since gender should be considered beyond biological sex.

Statistical regression approaches can be systematically validated by using a control set to test the generalization of the regression model (eg, by systematic evaluation on a dedicated validation set [20,36,37,40]). Researchers who developed a number of scores using the approach by Pelletier et al [20] did not specify whether they performed a systematic validation of their developed scores [9,29,35]. Nauman et al [11] did not use a validation, and Yuan et al [39] reported a performance value without describing the validation setting they used.

3120,2922

Exclusively theory-driven gender scores, where variable scaling is determined by human experts, were not evaluated since there is no gold standard for gender [33,34,38]. Looking at usability, referring to how well established a score already is, some authors did not mention any practical application of their scores [31], whereas other scores were often cited, adapted, and reapplied [19,20,32,34]. Although highly cited scores seem to be widely accepted and used, they might still not be well suited to represent gender. The most cited score was the BSRI, which is also part of other gender scores (eg, [20,29]; see Figure 2), and was often criticized and considered outdated [22].

Regarding practicability, we considered the scope and complexity of questionnaires and how universally applicable variables are on existing data. Some variables were very specific

XSL•FO
RenderX

for the used cohort, whereas others frequently appeared in similar studies. Most gender identity measures are well-suited for clinical data collection, being concise and easy to understand, except for the score from McGuire et al [27], which involves 23 questions and focuses on gender transition, making it less suitable. BSRI [19] and PAQ [32] are lengthy prospective gender scores, same as other gender scores containing them. Tibubos et al [30] developed a shorter form of the PAQ with only 8 variables. We also listed different forms of data collection, from self-reporting questionnaires (eg, [20,34]) to interviews (eg, [13,33,42]). The length of forms could be especially relevant if participants complete a self-reporting questionnaire. Interviews tend to be more time-consuming for the staff conducting them.

Regarding retrospective scores, the length does not have such a big impact, but some scores are much shorter than the majority [34,39]. A minimalistic score can be a trade-off between prediction quality and the number of necessary variables. This was, for instance, investigated by Ballering et al [40], who compared the performance between gender scores including 9 and 85 predictive variables.

Implementation

Only 3 research groups made their analysis code publicly available (*code published*) and provided reproducible gender scores [9,17,40].

Two studies published their data [17] or used publicly available data [39] (*data published*), which are necessary to evaluate their conclusion. All other works did not publish data, which might be justified by data protection regulations. However, anonymized data could still be helpful for recreating a study.

Statistical parameters were published in most retrieved papers (*statistical parameters published*), some more complete than others. However, in the majority of cases, our assessment showed that reconstructing a gender score from the provided parameters would be challenging.

We identified one paper that did not publish the gender score (*not published*) [31]. They adapted the scores from Nauman et al [11] and Pelletier et al [20] to form a new gender score, but they did not provide any specific information regarding their methodology.

Overall, repeatability was made difficult by many of the research groups, and the use of existing scores was made complicated. A systematic overview of the reproducibility of each study is given by our results in Multimedia Appendix 1.

Interrelations

We registered different dependencies and relationships between gender scores and visualized them (see Figure 2). Of the retrieved articles, 7 were developed with totally new approaches or methods (see Figure 2A).

Other scores adapted or included content-related parts of already existing scores (see Figure 2B). For example, Pelletier et al [20] included the BSRI masculinity and femininity scores [19]. Spence et al [32] were inspired by Rosenkrantz et al [41] for the development of the PAQ in 1975, and thereupon, Tibubos et al [30] developed a short form of the PAQ in 2022. It is notable that the BSRI [19] and PAQ [32] each form the basis of 2 other scores.

Sometimes research groups implemented the statistical or methodological approach of another team (see Figure 2C). For instance, the statistical approach of Pelletier et al [20] was frequently used as the basis for current gender scores, for example, by Wandschneider et al [9], Lacasse et al [10], Gisinger et al [35], Pohrt et al [29], Cipriani et al [36], and Yuan et al [39].

Applicability on Clinical Routine Data

Evaluation Overview

We tested all retrieved scores and their published variables for whether they are available in the MII CDS. Initially, we planned to only test retrospective scores developed on clinical data. However, we found that this would limit the number of possible scores too much.

The evaluation of the applicability on clinical routine data required a careful and considerate approach, as variable names are often ambiguous and it is usually not possible to match them directly. This can, for instance, be seen in variables related to care work, which include “responsibility for caring for other people in the household” [29], “dinner is always prepared by someone else” [40], “caregiver strain” [17], “taking care of sick people” [38], “informal caregiving” [33], and “responsibility for caring for children” [34]. Even though some gender scores might be well described and could be used for other datasets, transferring the variables appropriately to a different dataset proved to be complex.

Applicability of Gender Scores on the MII CDS

In the comparison between the variables contained in gender scores and within the MII CDS, we used a two-step approach: We first tried to match the exact gender score variables against the MII CDS, and in case this remained unsuccessful, we extended the search to similar or generic terms.

We found that no variables of any gender score are covered in the MII CDS. This finding is surprising since a high number of variables covered in gender scores, such as occupation, level of education, civil status, children, household composition and size, and social support, are part of social history, which is routine clinical information.

Our principle finding regarding this question was that no gender score can be applied upon the MII CDS. One exception is the score from Teterina et al [37], which includes diagnostic codes and disease-specific data, which could be matched against the MII CDS. This score, however, is highly specific and not usable as a generalized approach. Currently, the MII CDS only encodes the administrative gender as male, female, undifferentiated, or diverse [43]. Administrative gender refers to the gender that is recorded or recognized in official documents (eg, the ID card). It may differ from the birth-assigned sex.

Overall, most scores were applied on population studies or included in studies from the outset. These gender scores frequently include personality traits and psychological

XSL•FO
RenderX

assessments (eg, stress, loneliness scales), which are not part of routine clinical practice and, therefore, also not part of the MII CDS.

To summarize, there are no fitting variables for the MII CDS, and it is impossible to apply an existing gender score to the dataset in order to include gender-specific analysis on clinical routine data.

Discussion

Principal Findings

This work identified and reviewed state-of-the-art gender scores and gender identity measures. These were systematically assessed regarding their applicability and practicability in health research. Last, we tested their applicability on routine clinical data using the MII CDS as a reference dataset.

We found that no gender score is applicable on the MII CDS, because the variables required for the gender scores are not part of the CDS. However, many variables that are commonly included in gender scores are also assessed during a patient's clinical stay. For instance, variables regarding personal background (eg, living with your partner or children, professional field, or self-employment) are often asked during a clinic stay to verify if specific therapies or treatments are feasible. Physicians need to know if patients have responsibilities at home, if they have support, and if they have a stable social environment. A person's background is gender-dependent and influences not only clinical routine but also research data and therapy guidelines (eg, risk factors dependant on lifestyle). This is underlined by the information in Multimedia Appendix 2, which presents examples of current social history documentation practices in a German hospital compared against typical variables used in gender scores. Several variables related to gender scores can be directly inferred from these documentations; however, they are currently not included in the MII CDS. We therefore argue that the current lack of applicability of gender scores on clinical routine data results from missing structured data collection in or extraction methods from clinical information systems. Since the MII CDS is an ongoing effort to standardize research data from routine clinical practice, we recommend that the Person Module of the MII CDS should be updated and expanded to create a sufficient knowledge base for gender health research. Specifically, we formulated 4 action steps that will enable gender-specific analyses (see Figure 1): analyze social history data, collect social history data in a machine-readable form, integrate a 2-step gender identity measure during patient admission, and develop custom gender score approaches for clinical data.

Recommended Action Steps

Analyze Social History Data

Social history is part of routine clinical data collected for many patients. However, the captured information is oftentimes not structured. It can be found in the doctor's notes or additional study data if patients are included in clinical trials. As a first step toward evaluating what information is currently available, we suggest analyzing the full-text information in the patient records using natural language processing and large language models for data extraction. It will be interesting to learn what conclusions and predictions one could draw from the available information and how this information corresponds to the described gender scores. Typical social anamnesis texts are given in Multimedia Appendix 2, showcasing the low information content. A structured analysis of social history data is still ongoing, but the preliminary check of the information content already indicates that the practice of documentation must be significantly improved.

Collect Social History Data in a Machine-Readable Form

We recommend that key components of patients' social histories — such as occupation, education, civil status, number of children, household composition and size, social support — be collected in a structured, machine-readable format. Instead of recording social history solely as narrative text in physician reports, clinical information systems should provide individual fields for each variable, allowing clinicians to select or enter information directly. This approach would reduce the effort required for data processing and aggregation, enable semantic annotation, and facilitate automated export and comparison across datasets.

Several national-level initiatives already exemplify such practices. Scandinavian countries, for instance, collect structured social and demographic data that can be integrated with health care data [44,45]. Similarly, the Canadian Institute for Health Information promotes the standardized collection of social and behavioral data across health care settings, including variables such as family composition, living arrangements, social support, and socioeconomic status. Existing research has also demonstrated how such information can be effectively captured using discrete, machine-readable fields rather than free-text formats [46].

A widely recognized standard that could be further adapted for this purpose is HL7 FHIR [47], which provides a structured framework for encoding social history elements in clinical IT systems. Future work should build on these existing resources — as well as our overview for gender scores — to develop a system that supports the structured capture of variables necessary for calculating gender scores. Although it is important to build future work upon existing standards, ideally, the analysis of clinical data items determining gender should be conducted before designing structured data capture forms for patient social history.

Integrate a 2-Step Gender Identity Measure During Patient Admission

Moreover, to include as many gender dimensions as possible, it would be beneficial to collect more gender-specific data. A promising approach would be to implement the 2-step gender identity measure [13] with open-ended answers during patient admission. Implementing a prospective approach, with minimal effort, would provide valuable insights into gender identity in everyday clinical practice. Although the DIVERGesTOOL [48] was originally developed as an extension of the 2-step approach for the German research context, it may also be well suited for use in patient admission settings. It adds a third question

XSL•FO
RenderX

regarding whether differences in sex development have ever been medically diagnosed.

However, collecting such data must be approached with care, because asking gender-related questions at patient admission can involve sensitive issues and carries potential risks. For transgender, nonbinary, or gender-nonconforming individuals, disclosing gender identity may raise concerns about discrimination or biased treatment. Patients frequently withhold this information due to previous negative experiences and a lack of trust in health care providers [49,50]. Inadequate staff training and poorly designed forms can lead to misgendering or exclusion. To ensure respectful and safe care, it is essential to provide staff with proper training, use inclusive language, and implement supportive documentation systems.

Develop Custom Gender Score Approaches for Clinical Data

Researchers should think beyond the common gender score approaches and develop a gender score that is suitable to clinical data and not only population studies.

An innovative approach was carried out by Teterina et al [37], who used diagnostic codes of patients with traumatic brain injuries in Canadian emergency departments. Researchers should try similar approaches on general — nondisease-specific — clinical data with diagnostic or medication variables. Furthermore, developing a minimalistic retrospective score could prove advantageous in balancing prediction quality with the number of required variables, making the scores applicable even when limited information is available (eg, [40]).

Even though gender is gaining importance in health research, it is still far from being implemented. Our investigation shows that a gold standard is missing that accounts for variations across social groups (eg, including geographical regions, age, time). Due to the lack of a gold standard, some research groups use gender as a predictor for sex when developing gender scores, which contradicts the purpose of introducing gender in research — to move beyond biological sex and gather more detailed information. Solely theory-driven approaches, where experts determine the used variables and their scaling, cannot be validated.

Last, repeatability is a major challenge when aiming at implementing existing gender scores. Due to inconsistent research group practices, existing gender scores are often described only theoretically without providing detailed variables, questions, or complete information on variable weighting. We therefore urge authors to provide complete documentation and executable models when developing gender scores.

To achieve the necessary progress, every inclusion of gender into health research is beneficial, even if it might not be comprehensive or sufficient to cover all aspects.

Limitations

Our collection of gender scores is based on a scoping review conducted to provide a broad overview of the topic. One limitation of this approach is that only one reviewer conducted the full-text screening and the categorization of the retrieved articles. However, during data extraction, more than 30% (7/22, 32%) of the publications were initially double-checked by a second domain expert [23]. The reviewers were in full agreement on all reviewed articles; thus, a single reviewer continued the data extraction. Moreover, our review does not claim to provide a complete list of all existing gender scores but does provide general statements on the current state of gender scores and their applicability in health research.

Moreover, the MII CDS might not be fully representative to test against population-based gender scores. Most gender scores were developed on population or specific patient data, while the MII CDS contains routine clinical data. However, it is important to include gender not only in population research but also in clinical research. This is why we selected the MII CDS as a target dataset for routine clinical data to test the practicability in this setting. As a result, we were able to show that gender scores are not yet a feasible instrument for routine clinical data and are able to make recommendations on how to update and extend the MII CDS in the future.

Comparison With Prior Work

Ballering et al [26] highlighted that gender scores should be the minimum effort in epidemiological studies, but the community should go further than that because the retrospective application of a gender score implies a lack of gender consideration from the outset of the study (eg, the study design). Our findings found several shortcomings with currently available retrospective gender scores. Therefore, our results suggest that self-reported gender assessments are more precise and better suited to assess gender, confirming the theory of Ballering et al [26].

Moreover, we can confirm the findings of Ballering et al [26], specifically that the most common variables in gender scores are related to occupation, income, education, civil status, caregiving and household responsibilities, and ways of spending (leisure) time. Furthermore, our results showed that, even though several of these variables are collected in everyday clinic work, they are not processed and stored in a machine-readable way.

Conclusions

Considering sex and gender enhances equity and research quality. Despite the high importance of the topic, it remains challenging to include gender into health research for several reasons. Ethical implications such as properly defining the concept of “gender” as opposed to “sex,” identifying appropriate ways of asking about a patient’s gender, and raising awareness of the importance with nurses and doctors are nontechnical reasons why the health gender gap remains. Technical implementation is hampered by the absence of a generally applicable clinical gender score. Structured, computer-processable data and metadata about gender-specific aspects in a patient’s social history is also lacking.

In this work, we identified, categorized, and systematically assessed state-of-the-art gender scores from epidemiology and clinical studies. We evaluated their applicability and practicability on a German national research dataset for routine clinical practice, the MII CDS. We found that gender cannot be predicted based on the MII CDS, even though several of the frequently used variables are part of routine clinical practice in Germany.

XSL•FO
RenderX

However, we see an urgent need to include gender-relevant information to the MII CDS in order to narrow the gap between routinely collected clinical data and available research data (see Multimedia Appendix 2). Therefore, further work is necessary to enable gender-specific analysis and to routinely collect more gender-specific data in clinics, for example, during patient admission.

Despite different approaches for assessing gender, no standardized and validated gender score that could be used retrospectively in clinical research exists.

Our study is limited to the German clinical landscape, and our evaluation of possible scores is based on a scoping review. Future investigations into the literature and common practices at clinics inside and outside Germany might give further insights and add to the action items suggested in this work.

Funding

This work was funded by the German Federal Ministry of Education andResearch as part of the project “Inclusive Excellence in Medicine” (01FP23G10A,01FP23G10B) and the “Network University Medicine” (01KXX2121).

Data Availability

Further data underlying our publication are available in Multimedia Appendix 1.

Authors' Contributions

Conceptualization: LS, SS, EK, DW
Data curation: LS
Formal analysis: LS
Funding acquisition: SS, EK, DW
Investigation: LS
Methodology: LS, SS, EK, DW
Supervision: SS, EK, DW
Validation: HB, SS, EK, DW
Visualization: LS
Writing – original draft: LS, DW
Writing – review & editing: HB, DL, SS, EK, DW

Conflicts of Interest

None declared.

Multimedia Appendix 1
Detailed information from the assessment of the retrieved gender scores.
[XLSX File, 18 KB - medinform_v14i1e74162_app1.xlsx]

Multimedia Appendix 2
Three patients showcasing the current social history documentation in clinical practice in a German hospital. Footnotes and color coding indicate the comparison with typical variables used in gender scores. The text examples have been constructed for illustration.
[PNG File, 303 KB - medinform_v14i1e74162_app2.png]

References

1. Tannenbaum C, Ellis RP, Eyssel F, Zou J, Schiebinger L. Sex and gender analysis improves science and engineering. Nature New Biol 2019 Nov;575(7781):137-146. [doi: 10.1038/s41586-019-1657-6] [Medline: 31695204]
2. Arcand M, Bilodeau-Houle A, Juster RP, Marin MF. Sex and gender role differences on stress, depression, and anxiety symptoms in response to the COVID-19 pandemic over time. Front Psychol 2023;14:1166154. [doi: 10.3389/fpsyg.2023.1166154] [Medline: 37207028]
3. Opinion: intersexuality. German Ethics Council. 2012. URL: https://www.ethikrat.org/fileadmin/Publikationen/Stellungnahmen/englisch/opinion-intersexuality.pdf [accessed 2025-11-22]
4. Gender and health. WHO. 2024. URL: https://www.who.int/health-topics/gender [accessed 2024-09-13]
5. Oertelt-Prigione S. Chapter 32 - the operationalization of gender in medicine. In: Legato MJ, editor. Principles of Gender-Specific Medicine 2023:503-512. [doi: 10.1016/B978-0-323-88534-8.00017-1]
6. Geller SE, Koch AR, Roesch P, Filut A, Hallgren E, Carnes M. The more things change, the more they stay the same: a study to evaluate compliance with inclusion and assessment of women and minorities in randomized controlled trials. Acad Med 2018 Apr;93(4):630-635. [doi: 10.1097/ACM.0000000000002027] [Medline: 29053489]

XSL•FO
RenderX

7. Potluri T, Engle K, Fink AL, Vom Steeg LG, Klein SL. Sex reporting in preclinical microbiological and immunological research. MBio 2017 Nov 14;8(6):e01868-17. [doi: 10.1128/mBio.01868-17] [Medline: 29138308]
8. Shah K, McCormack CE, Bradbury NA. Do you know the sex of your cells? Am J Physiol Cell Physiol 2014 Jan 1;306(1):C3-18. [doi: 10.1152/ajpcell.00281.2013] [Medline: 24196532]
9. Wandschneider L, Sauzet O, Razum O, Miani C. Development of a gender score in a representative German population sample and its association with diverse social positions. Front Epidemiol 2022;2:914819. [doi: 10.3389/fepid.2022.914819] [Medline: 38455329]
10. Lacasse A, Pagé MG, Choinière M, et al. Conducting gender-based analysis of existing databases when self-reported gender data are unavailable: the GENDER Index in a working population. Can J Public Health 2020 Apr;111(2):155-168. [doi: 10.17269/s41997-019-00277-2] [Medline: 31933236]
11. Nauman AT, Behlouli H, Alexander N, et al. Gender score development in the Berlin Aging Study II: a retrospective approach. Biol Sex Differ 2021 Jan 18;12(1):15. [doi: 10.1186/s13293-020-00351-2] [Medline: 33461607]
12. Fraser G, Bulbulia J, Greaves LM, Wilson MS, Sibley CG. Coding responses to an open-ended gender measure in a New Zealand national sample. J Sex Res 2020 Oct;57(8):979-986. [doi: 10.1080/00224499.2019.1687640] [Medline: 31729890]
13. Lagos D, Compton D. Evaluating the use of a two-step gender identity measure in the 2018 General Social Survey. Demography 2021 Apr 1;58(2):763-772. [doi: 10.1215/00703370-8976151] [Medline: 33834217]
14. Ammon D, Kurscheidt M, Buckow K, et al. Arbeitsgruppe Interoperabilität: Kerndatensatz und Informationssysteme für Integration und Austausch von Daten in der Medizininformatik-Initiative. Bundesgesundheitsbl 2024 Jun;67(6):656-667. [doi: 10.1007/s00103-024-03888-4]
15. Clayton JA, Tannenbaum C. Reporting sex, gender, or both in clinical research? JAMA 2016 Nov 8;316(18):1863-1864. [doi: 10.1001/jama.2016.16405] [Medline: 27802482]
16. Thibaut F. Gender does matter in clinical research. Eur Arch Psychiatry Clin Neurosci 2017 Jun;267(4):283-284. [doi: 10.1007/s00406-017-0797-7] [Medline: 28389888]
17. Nielsen MW, Stefanick ML, Peragine D, et al. Gender-related variables for health research. Biol Sex Differ 2021 Feb 22;12(1):23. [doi: 10.1186/s13293-021-00366-3] [Medline: 33618769]
18. Morgan R, Yin A, Kalbarczyk A, et al. Reconsidering tools for measuring gender dimensions in biomedical research. Biol Sex Differ 2024 Nov 25;15(1):96. [doi: 10.1186/s13293-024-00663-7] [Medline: 39587652]
19. Bem SL. The measurement of psychological androgyny. J Consult Clin Psychol 1974 Apr;42(2):155-162. [doi: 10.1037/h0036215] [Medline: 4823550]
20. Pelletier R, Ditto B, Pilote L. A composite measure of gender and its association with risk factors in patients with premature acute coronary syndrome. Psychosom Med 2015 Jun;77(5):517-526. [doi: 10.1097/PSY.0000000000000186] [Medline: 25984818]
21. Neufang S, Li F, Akhrif A, Beyan OD. Toward a fair, gender-debiased classifier for the diagnosis of attention deficit/hyperactivity disorder- a machine-learning based classification study. BMC Med Inform Decis Mak 2025 Aug 5;25(1):290. [doi: 10.1186/s12911-025-03126-0] [Medline: 40764552]
22. Donnelly K, Twenge JM. Masculine and feminine traits on the Bem Sex-Role Inventory, 1993–2012: a cross-temporal meta-analysis. Sex Roles 2017 May;76(9-10):556-565. [doi: 10.1007/s11199-016-0625-y]
23. Schindler L, Beelich H, Röll S, Katsari E, Stracke S, Waltemath D. Applicability of retrospective and prospective gender scores for clinical and health data: protocol for a scoping review. JMIR Res Protoc 2025 Jan 20;14(1):e57669. [doi: 10.2196/57669] [Medline: 39832171]
24. Horstmann S, Schmechel C, Palm K, Oertelt-Prigione S, Bolte G. The operationalisation of sex and gender in quantitative health-related research: a scoping review. Int J Environ Res Public Health 2022 Jun 18;19(12):7493. [doi: 10.3390/ijerph19127493] [Medline: 35742742]
25. Miani C, Wandschneider L, Niemann J, Batram-Zantvoort S, Razum O. Measurement of gender as a social determinant of health in epidemiology-a scoping review. PLoS ONE 2021;16(11):e0259223. [doi: 10.1371/journal.pone.0259223] [Medline: 34731177]
26. Ballering AV, Olde Hartman TC, Rosmalen JGM. Gender scores in epidemiological research: methods, advantages and implications. Lancet Reg Health Eur 2024 Aug;43:100962. [doi: 10.1016/j.lanepe.2024.100962] [Medline: 38989448]
27. McGuire JK, Beek TF, Catalpa JM, Steensma TD. The Genderqueer Identity (GQI) scale: measurement and validation of four distinct subscales with trans and LGBQ clinical and community samples in two countries. Int J Transgend 2019;20(2-3):289-304. [doi: 10.1080/15532739.2018.1460735] [Medline: 32999614]
28. Lombardi E, Banik S. The utility of the two-step gender measure within trans and cis populations. Sex Res Social Policy 2016 Sep;13(3):288-296. [doi: 10.1007/s13178-016-0220-6] [Medline: 34956416]
29. Pohrt A, Kendel F, Demuth I, et al. Differentiating sex and gender among older men and women. Psychosom Med 2022 Apr 1;84(3):339-346. [doi: 10.1097/PSY.0000000000001056] [Medline: 35149636]
30. Tibubos AN, Otten D, Beutel ME, Brähler E. Validation of the Personal Attributes Questionnaire-8: gender expression and mental distress in the German population in 2006 and 2018. Int J Public Health 2022;67:1604510. [doi: 10.3389/ijph.2022.1604510] [Medline: 35370535]

XSL•FO
RenderX

31. Demuth I, Banszerus V, Drewelies J, et al. Cohort profile: follow-up of a Berlin Aging Study II (BASE-II) subsample as part of the GendAge study. BMJ Open 2021 Jun 23;11(6):e045576. [doi: 10.1136/bmjopen-2020-045576] [Medline: 34162642]
32. Spence JT, Helmreich R, Stapp J. Ratings of self and peers on sex role attributes and their relation to self-esteem and conceptions of masculinity and femininity. J Pers Soc Psychol 1975 Jul;32(1):29-39. [doi: 10.1037/h0076857] [Medline: 1206468]
33. de Breij S, Huisman M, Boot CRL, Deeg DJH. Sex and gender differences in depressive symptoms in older workers: the role of working conditions. BMC Public Health 2022 May 21;22(1):1023. [doi: 10.1186/s12889-022-13416-1] [Medline: 35597949]
34. Smith PM, Koehoorn M. Measuring gender when you don't have a gender measure: constructing a gender index using survey data. Int J Equity Health 2016 May 28;15(1):82. [doi: 10.1186/s12939-016-0370-4] [Medline: 27233478]
35. Gisinger T, Azizi Z, Alipour P, et al. Sex and gender aspects in diabetes mellitus: focus on access to health care and cardiovascular outcomes. Front Public Health 2023;11:1090541. [doi: 10.3389/fpubh.2023.1090541] [Medline: 36817907]
36. Cipriani E, Samson-Daoust E, Giguère CE, et al. A step-by-step and data-driven guide to index gender in psychiatry. PLoS ONE 2024;19(1):e0296880. [doi: 10.1371/journal.pone.0296880] [Medline: 38271402]
37. Teterina A, Zulbayar S, Mollayeva T, Chan V, Colantonio A, Escobar M. Gender versus sex in predicting outcomes of traumatic brain injury: a cohort study utilizing large administrative databases. Sci Rep 2023 Oct 27;13(1):18453. [doi: 10.1038/s41598-023-45683-2] [Medline: 37891419]
38. Vader SS, Lewis SM, Verdonk P, Verschuren WMM, Picavet HSJ. Masculine gender affects sex differences in the prevalence of chronic health problems - The Doetinchem Cohort Study. Prev Med Rep 2023 Jun;33:102202. [doi: 10.1016/j.pmedr.2023.102202] [Medline: 37223572]
39. Yuan J, Sang S, Pham J, Kong WJ. Gender modifies the association of cognition with age-related hearing impairment in the Health and Retirement Study. Front Public Health 2021;9:751828. [doi: 10.3389/fpubh.2021.751828] [Medline: 34976918]
40. Ballering AV, Bonvanie IJ, Olde Hartman TC, Monden R, Rosmalen JGM. Gender and sex independently associate with common somatic symptoms and lifetime prevalence of chronic disease. Soc Sci Med 2020 May;253:112968. [doi: 10.1016/j.socscimed.2020.112968]
41. Rosenkrantz P, Bee H, Vogel S, Broverman I. Sex-role stereotypes and self-concepts in college students. J Consult Clin Psychol 1968 Jun;32(3):287-295. [doi: 10.1037/h0025909] [Medline: 5666128]
42. The Medical Informatics Initiative's core data set. Medical Informatics Initiative Germany. URL: https://www.medizininformatik-initiative.de/en/medical-informatics-initiatives-core-data-set [accessed 2025-03-03]
43. MII core data set - datasets. Art Decor. URL: https://art-decor.org/art-decor/decor-datasets--mide [accessed 2025-03-03]
44. Ludvigsson JF, Almqvist C, Bonamy AKE, et al. Registers of the Swedish total population and their use in medical research. Eur J Epidemiol 2016 Feb;31(2):125-136. [doi: 10.1007/s10654-016-0117-y] [Medline: 26769609]
45. Pedersen CB. The Danish civil registration system. Scand J Public Health 2011 Jul;39(7 Suppl):22-25. [doi: 10.1177/1403494810387965] [Medline: 21775345]
46. Health inequalities data tool. Government of Canada. URL: https://health-infobase.canada.ca/health-inequalities/Indicat [accessed 2025-08-08]
47. HL7/fhir-sdoh-clinicalcare. GitHub. URL: https://github.com/HL7/fhir-sdoh-clinicalcare [accessed 2025-08-08]
48. Horstmann S, Schmechel C, Becher E, Oertelt-Prigione S, Palm K, Bolte G. DIVERGesTOOL – Entwicklung einer Toolbox zur Erfassung geschlechtlicher Vielfalt in der quantitativen Gesundheitsforschung. Bundesgesundheitsbl 2024 Sep;67(9):1054-1061. [doi: 10.1007/s00103-024-03915-4]
49. Banerjee SC, Staley JM, Alexander K, Walters CB, Parker PA. Encouraging patients to disclose their lesbian, gay, bisexual, or transgender (LGBT) status: oncology health care providers' perspectives. Transl Behav Med 2020 Oct 8;10(4):918-927. [doi: 10.1093/tbm/iby105] [Medline: 30476333]
50. Koch A, Rabins M, Messina J, Brennan-Cook J. Exploring the challenges of sexual orientation disclosure among lesbian, gay, bisexual, transgender, queer individuals. J Nurse Pract 2023 Nov;19(10):104765. [doi: 10.1016/j.nurpra.2023.104765]

Abbreviations

BSRI: Bem Sex Role Inventory
CDS: core dataset
MII: Medical Informatics Initiative
PAQ: Personal Attributes Questionnaire

XSL•FO
RenderX

Edited by A Castonguay; submitted 19.Mar.2025; peer-reviewed by B Hoyt, H Anandan; revised version received 24.Aug.2025; accepted 02.Sep.2025; published 08.Jan.2026.

Please cite as:
Schindler L, Beelich H, Katsari E, Liprandi D, Stracke S, Waltemath D
Applicability of Existing Gender Scores for German Clinical Research Data: Scoping Review and Data Mapping
JMIR Med Inform 2026;14:e74162
URL: https://medinform.jmir.org/2026/1/e74162
doi:10.2196/74162

© Lea Schindler, Hilke Beelich, Elpiniki Katsari, Daniele Liprandi, Sylvia Stracke, Dagmar Waltemath. Originally published in JMIR Medical Informatics (https://medinform.jmir.org), 8.Jan.2026. This is an open-access article distributed under the terms of the Creative Commons Attribution License (https://creativecommons.org/licenses/by/4.0/), which permits unrestricted use, distribution, and reproduction in any medium, provided the original work, first published in JMIR Medical Informatics, is properly cited. The complete bibliographic information, a link to the original publication on https://medinform.jmir.org/, as well as this copyright and license information must be included.

XSL•FO
RenderX

Research Letter

AI-Enabled Customer Relationship Management Platforms for Patient Services in Health Care, Early Lessons From Governance, and Program-Level Outcomes

Anup Kant Gupta[1], MBA

Strategic Management & Leadership, Kelley School of Business, Indiana University Bloomington, Bloomington, IN, United States

Corresponding Author:
Anup Kant Gupta, MBA
Strategic Management & Leadership
Kelley School of Business
Indiana University Bloomington
107 S Indiana Ave
Bloomington, IN, 47405
United States
Phone: 1 (812) 855 4848
Email: anupgupta8@gmail.com

Abstract

This research letter summarizes early lessons from 4 enterprise implementations of artificial intelligence–enabled customer relationship management platforms in health care and describes governance practices associated with improvements in affordability, adherence, and access at program level.

(JMIR Med Inform 2026;14:e83564) doi:10.2196/83564

KEYWORDS

artificial intelligence; health care customer relationship management; salesforce; patient affordability; patient adherence; patient access; digital transformation; governance

Introduction

Health systems continue to face pressure to improve patient outcomes while safeguarding affordability and equitable access [1-4]. Electronic health records support clinical workflows but are not designed for proactive patient outreach or service coordination [5]. Artificial intelligence (AI)-enabled customer relationship management (CRM) platforms support automated eligibility checks, outreach, and risk alerts [6-8]. This research letter summarizes early descriptive insights from enterprise implementations of AI-enabled CRM platforms.

Methods

Program Selection and Sampling Frame

A case-informed thematic analysis was conducted across 4 large health care programs. These were the largest CRM-based patient service deployments accessible to the author during this period. Programs were included if they had live AI-enabled CRM workflows for affordability, adherence, or access for at least 12 months. Each program operated independently with different teams, geographies, and product lines. Data reflect operations recorded between January 2019 and March 2024 across the 4 programs. All outcomes reflect a descriptive analysis of the operational dashboards and do not infer causal relationships.

Data Sources and Definitions

The following three data sources were used, each aggregated at program level.

1. Governance documents summarizing decision logs, compliance checkpoints, and escalation patterns.
2. Stakeholder feedback was gathered through routine program review meetings and documented in standard internal templates.
3. Internal dashboards tracking key operational indicators. These dashboards were deidentified, contained no patient level data, and were part of routine program monitoring.

Program level outcome metrics were defined as follows.

1. Adoption: proportion of active CRM users among provisioned patient service staff within a measurement window.
2. Affordability efficiency: average time for co-pay or financial assistance verification.

XSL•FO
RenderX

3. Therapy initiation time: average days between benefit verification and therapy start.
4. Discontinuation rate: proportion of enrolled patients who stopped therapy during a defined period.

Baseline values came from preimplementation operations, and follow-up reflected the first stable post launch period. Findings are observational.

Ethical Considerations

This work used only aggregated, deidentified operational dashboards and program documents. No patient-level identifiable data or human subject interaction occurred. Institutional review board approval was not required.

Results

Theme 1: Patient Outcome Alignment and Sponsorship

Programs that centered goals on patient experience and outcomes such as therapy initiation time or affordability enrollment sustained stronger executive sponsorship. Programs framed as IT upgrades struggled to maintain alignment.

Theme 2: Continuous Engagement and Adoption

High adoption correlated with structured engagement of patient service teams and compliance officers. Regular feedback cycles supported adoption above 85% vs below 60% in minimally engaged programs [2].

Theme 3: Hybrid Governance Improved Delivery Efficiency

All 4 programs used a hybrid model that combined Agile sprints with scheduled compliance reviews. This approach reduced backlog resolution time by about 30%. Figure 1 summarizes the governance structure.

Figure 1. Hybrid governance framework for artificial intelligence–enabled customer relationship management. The framework illustrates three concentric layers: (1) patient outcomes (affordability, adherence, access) at the core, (2) agile delivery and stakeholder engagement in the middle layer, and (3) governance and compliance checkpoints in the outer layer. Arrows depict how governance structures enable engagement, which in turn drives improved patient outcomes.

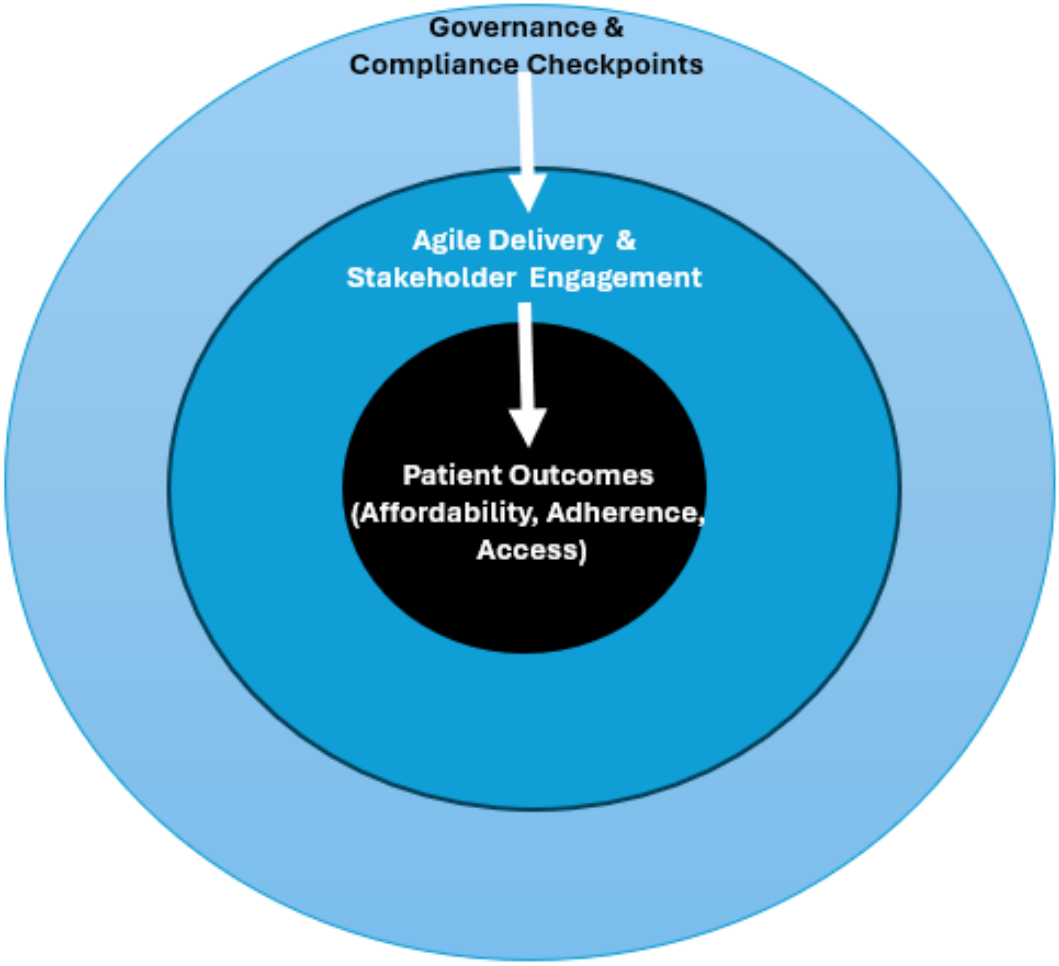

XSL•FO
RenderX

Theme 4: Program-Level Improvements in Affordability, Adherence, and Access

Changes reflect aggregated dashboards and are not causal. Examples include a reduction in co-pay verification time from 4 days to 3 days (25% faster), a 12% reduction in therapy discontinuation rates, and a shortening of therapy initiation time from 20 days to 17 days (15% faster) (Table 1).

Table 1. Program level customer relationship management–enabled improvements.

Patient service	Artificial intelligence functionality	Outcome	Example (anonymized)
Affordability	Automated co-pay verification	Reduced processing time (4 days to 3 days, a 25% improvement)	Fortune 10 rollout (USA)
Adherence	Predictive risk alerts	12% reduction in therapy discontinuation	Consulting-led program
Access	Automated prior authorization	Therapy initiation shortened (20 days to 17 days, a 15% improvement)	Enterprise-wide program

Discussion

Summary of Findings

Across 4 large-scale implementations, AI-enabled CRM platforms supported improvements in affordability, adherence, and access through workflow automation, risk identification, and coordinated service tasks. The most consistent predictors of success were early alignment with patient-centered outcomes, continuous stakeholder engagement, and hybrid governance structures.

Interpretation and Limitations

Results reflect aggregated, unaudited operational dashboards and cannot establish causality [9,10]. Findings describe program-level improvements observed post implementation and may not generalize to organizations with different scales, regulatory environments, or infrastructure maturity.

Future Directions

Future studies should incorporate multi-site comparative designs, validated outcomes, and integration with digital therapeutics and device streams to strengthen evidence for CRM-enabled patient service transformation.

Conflicts of Interest

None declared.

References

1. Digital Health and Innovation. Global Strategy on Digital Health 2020–2025. Geneva, Switzerland: World Health Organization; 2025.
2. Greenhalgh T, Wherton J, Papoutsi C, Lynch J, Hughes G, A'Court C, et al. Beyond adoption, a new framework for theorizing and evaluating nonadoption, abandonment, and challenges to the scale up, spread, and sustainability of health and care technologies. J Med Internet Res 2017 Nov 01;19(11):e367 [FREE Full text] [doi: 10.2196/jmir.8775] [Medline: 29092808]
3. Blease C, Kaptchuk TJ, Bernstein MH, Mandl KD, Halamka JD, DesRoches CM. Artificial intelligence and the future of primary care: exploratory qualitative study of UK general practitioners' views. J Med Internet Res 2019 Mar 20;21(3):e12802 [FREE Full text] [doi: 10.2196/12802] [Medline: 30892270]
4. Topol EJ. High-performance medicine: the convergence of human and artificial intelligence. Nat Med 2019 Jan;25(1):44-56. [doi: 10.1038/s41591-018-0300-7] [Medline: 30617339]
5. Adler-Milstein J, Holmgren A, Kralovec P, Worzala C, Searcy T, Patel V. Electronic health record adoption in US hospitals: the emergence of a digital "advanced use" divide. J Am Med Inform Assoc 2017 Nov 01;24(6):1142-1148 [FREE Full text] [doi: 10.1093/jamia/ocx080] [Medline: 29016973]
6. Davenport T, Kalakota R. The potential for artificial intelligence in healthcare. Future Healthc J 2019 Jun;6(2):94-98 [FREE Full text] [doi: 10.7861/futurehosp.6-2-94] [Medline: 31363513]
7. Obermeyer Z, Emanuel EJ. Predicting the future, big data, machine learning, and clinical medicine. N Engl J Med 2016 Sep 29;375(13):1216-1219. [doi: 10.1056/nejmp1606181]
8. Jiang F, Jiang Y, Zhi H, Dong Y, Li H, Ma S, et al. Artificial intelligence in healthcare: past, present and future. Stroke Vasc Neurol 2017 Dec;2(4):230-243 [FREE Full text] [doi: 10.1136/svn-2017-000101] [Medline: 29507784]
9. Wang Y, Kung L, Wang W, Cegielski C. An integrated big data analytics-enabled transformation model: Application to health care. Information & Management 2018 Jan;55(1):64-79. [doi: 10.1016/j.im.2017.04.001]
10. Rumsfeld JS, Joynt KE, Maddox TM. Big data analytics to improve cardiovascular care: promise and challenges. Nat Rev Cardiol 2016 Jun;13(6):350-359. [doi: 10.1038/nrcardio.2016.42] [Medline: 27009423]

Abbreviations

AI: artificial intelligence

XSL•FO
RenderX

CRM: customer relationship management

Edited by A Benis; submitted 05.Sep.2025; peer-reviewed by E Oluwagbade, A Okoye; comments to author 22.Oct.2025; revised version received 18.Nov.2025; accepted 01.Jan.2026; published 02.Feb.2026.

Please cite as:
Gupta AK
AI-Enabled Customer Relationship Management Platforms for Patient Services in Health Care, Early Lessons From Governance, and Program-Level Outcomes
JMIR Med Inform 2026;14:e83564
URL: https://medinform.jmir.org/2026/1/e83564
doi:10.2196/83564
PMID:41481793

©Anup Kant Gupta. Originally published in JMIR Medical Informatics (https://medinform.jmir.org), 02.Feb.2026. This is an open-access article distributed under the terms of the Creative Commons Attribution License (https://creativecommons.org/licenses/by/4.0/), which permits unrestricted use, distribution, and reproduction in any medium, provided the original work, first published in JMIR Medical Informatics, is properly cited. The complete bibliographic information, a link to the original publication on https://medinform.jmir.org/, as well as this copyright and license information must be included.

XSL•FO
RenderX

Approval of AI-Based Medical Devices in China From 2020 to 2025: Retrospective Analysis

Lingli Zhang[1], PhD; Jianzhou Yan[1,2], PhD

[1]School of International Pharmaceutical Business, China Pharmaceutical University, 639 Longmian Avenue, Jiangning District, Nanjing, China
[2]Research Center of National Drug Policy and Ecosystem, China Pharmaceutical University, Nanjing, China

Corresponding Author:
Jianzhou Yan, PhD
School of International Pharmaceutical Business, China Pharmaceutical University, 639 Longmian Avenue, Jiangning District, Nanjing, China

Abstract

Background: Artificial intelligence–based medical devices (AIMDs) have emerged as transformative technologies in modern health care. However, comprehensive analysis of recent approval trends and characteristics of AIMDs in China remains limited.

Objective: This study aimed to provide an up-to-date overview of AIMDs approved in China up to June 2025.

Methods: We conducted a search of the Drugdataexpy database to identify AIMDs approved up to June 30, 2025, using artificial intelligence–related keywords in the "structural composition" and "intended use" fields. After manual verification and exclusion of non-AIMDs, we collected key characteristics, including name, manufacturer, approval date, risk class, clinical evaluation pathway, medical specialty, data source, review pathway, and algorithm type. Statistical analysis encompassed descriptive statistics and trend analysis. We used the Fisher exact test and Pearson chi-square test to assess the associations between risk class and categorical variables.

Results: A total of 154 AIMDs were identified since the first approval in 2020, with annual approvals increasing from 9 in 2020 to 45 in 2024 (a 49.53% compound annual growth rate), although the 20 approvals in the first half of 2025 suggest a potential moderation in pace. Most AIMDs (123/154, 79.9%) were categorized as class III, and the risk class was significantly associated with approval year (P=.03), manufacturer location (P=.03), and medical specialty (P=.004). Of the 123 class III devices, 19 (15.4%) were approved through innovation review, and 2 (1.6%) each were approved through priority and emergency approval. Deep learning was the dominant algorithm (143/154, 92.9%). Radiology dominated the field (106/154, 68.8%), with computed tomography serving as the primary data source (96/154, 62.3%), particularly for applications in pulmonary nodule detection and cardiovascular assessment. Clinical trials were the primary evaluation pathway for 76.6% (118/154) of all AIMDs. This approach was predominant for class III devices (116/123, 94.3%), whereas most class II devices (21/31, 67.7%) used a clinical exemption pathway. Market concentration was evident, with the top 4 manufacturers accounting for 38.3% (59/154) of all approvals and geographically clustered in major innovation hubs such as Beijing, Shanghai, Shenzhen, and Hangzhou.

Conclusions: China's AIMD ecosystem is experiencing growth, heavily focused on radiology and computed tomography–based solutions within a risk-proportionate regulatory framework. The market is characterized by significant manufacturer and geographic concentration.

(JMIR Med Inform 2026;14:e85538) doi:10.2196/85538

KEYWORDS

medical device; artificial intelligence; AI; artificial intelligence–based medical device; AI-based medical device; medical device approval; regulatory science; China; deep learning; radiology

Introduction

Artificial intelligence (AI) has emerged as a transformative force in modern health care, offering unprecedented capabilities in data analysis, pattern recognition, and clinical decision support [1,2]. Among its many applications, AI-based medical devices (AIMDs) have gained substantial traction, particularly in medical imaging, diagnostics, and predictive analytics [3]. These technologies promise to enhance diagnostic accuracy; reduce physician workload; and, ultimately, improve patient outcomes [4].

Worldwide, regulatory authorities have responded to the rapid development of AIMDs by establishing frameworks to ensure their safety, efficacy, and clinical utility [5-8]. In the United States, the Food and Drug Administration approved 691 AI- and machine learning (ML)–based medical devices by October 2023, with most cleared through the 510(k) pathway and concentrated in radiology and cardiology [9,10]. Similarly,

XSL•FO
RenderX

Europe has witnessed a substantial increase in CE-marked AIMDs, with approval numbers growing significantly since 2015 [11].

China, as a major player in both AI innovation and health care digitalization, has also made significant strides in this domain [12,13]. The National Medical Products Administration (NMPA) approved its first AIMD in 2020. Since then, the number of approvals has grown steadily, reaching 59 by mid-2023, all categorized as class III [14]. In China, medical devices are categorized into 3 classes based on increasing risk: class I (low risk), class II (medium risk), and class III (high risk). This classification dictates the regulatory pathway for market approval. Class III devices, deemed to pose the highest risk, require centralized registration approval from the NMPA itself and are subject to the most stringent review of clinical evidence. Class II devices may receive approval from provincial-level medical product administrations. AIMDs in China are typically categorized as class II or class III. The classification is determined by the algorithm's maturity and its role in clinical decision-making. Specifically, AIMDs with lower algorithm maturity are managed as class III devices if they are intended for auxiliary decision-making. Conversely, if they are intended for non–decision support tasks, they are managed as class II devices. In China, the clinical evaluation pathway for medical devices consists of 3 types: clinical trials, clinical comparison with similar products, and exemption from clinical evaluation. The clinical exemption pathway relies on the *Catalogue of Medical Devices Exempt From Clinical Evaluation* issued by the NMPA [15].

In recent years, the NMPA has actively refined and optimized its review processes for AIMDs. Key efforts include issuing evaluation guidelines, clarifying regulatory classifications, developing clinical evaluation guidance for specific product types, and introducing comprehensive support measures spanning the entire product life cycle [16-19]. These advancements have spurred a new wave of submissions and approvals, fostering a more structured and efficient ecosystem for AIMD market entry. Despite this progress, the literature to date primarily documents AIMD approvals in China up to 2023. There remains a lack of comprehensive analyses covering the most recent developments, particularly those in 2024 and 2025—a period likely marked by regulatory maturation and increased approvals. This study adopted innovation diffusion theory [20] as its primary analytical lens. This theory posits that the adoption rate and pattern of an innovation are influenced by its perceived attributes, including relative advantage, compatibility, complexity, trialability, and observability, within a specific social system.

Therefore, this study aimed to provide an up-to-date analysis of AIMDs approved in China as of June 2025. By examining trends in approval numbers, device characteristics, and regulatory pathways, it may offer insights into the evolving AIMD landscape in China and its implications for future health care innovation.

Methods

Data Source and Search Strategy

To identify AIMDs approved up to June 30, 2025, we searched the Drugdataexpy database [21]. As this is a Chinese-language database, the keyword search was performed using the Chinese equivalents of the following English-language terms in the database fields for "structural composition" and "indications" or "intended use": "deep learning," "machine learning," "neural network," "artificial intelligence," or "algorithm." The NMPA's official website, while providing free access to regulatory announcements, lacks keyword-based filtering capabilities in its search function, thereby limiting efficient retrieval of AIMDs.

This study included AIMDs regulated under the Guidelines for Registration Review of Artificial Intelligence Medical Devices [16], encompassing stand-alone software as a medical device and software in a medical device (SiMD) where AI is a core component. After manual review of full-text descriptions, we excluded records that did not meet the AIMD definition. We also removed entries corresponding solely to routine administrative renewals without changes to the device's core AI software or intended use. Substantive approvals for major changes or modifications to existing devices (eg, the addition of new AI functionality) were retained. Details of the search strategy and process are provided in Multimedia Appendix 1. To minimize omissions, we reran the search for each retained product name to capture devices manufactured by other companies. Our results were cross-validated against the AIMDs approved before July 2023 as listed in the study by Liu et al [14]. Ambiguous entries were checked against the corresponding NMPA evaluation reports or the manufacturers' websites.

Data Extraction

For each eligible AIMD, we extracted the approval number, device name, manufacturer, approval date, structural composition, intended use, risk class, clinical evaluation pathway (clinical trials, clinical comparison with similar products, or exemption from clinical evaluation), and review pathway (innovative, priority, or emergency special review vs standard). From these fields, we derived the city of the manufacturer, medical specialty, body area, and data source of the AIMD. The medical specialty for each AIMD was assigned based on the device's registered intended use and its core function. For devices with applications relevant to multiple specialties, the specialty was determined by the primary clinical context and decision support role stated in the indications for use. The body area for each device was functionally classified into nonoverlapping categories based on the primary anatomical structure and type of clinical analysis specified in the device's intended use: "heart" referred to devices targeting cardiac muscle, chambers, or electrophysiology (eg, electrocardiogram analysis); "cardiovascular" referred to devices focused on the vascular system (eg, computed tomography [CT] or magnetic resonance angiography); "lung" referred to devices analyzing lung parenchyma (eg, nodule detection); and "thorax" referred to devices assessing nonparenchymal structures within the thoracic cavity (eg, rib fracture detection). Algorithm type was determined through a tiered review: it was first identified from

XSL•FO
RenderX

the "structural composition" and "intended use" fields. If not specified there, the full registration dossier was consulted for explicit technical descriptions.

To facilitate downstream data processing, minor lexical variants in device names referring to the same product—such as "medical image" vs "imaging"—were standardized to a single, consistent terminology. For the analysis of market concentration, "manufacturer" referred to the ultimate parent corporate entity. AIMDs approved under the legal names of subsidiaries belonging to the same corporate group were aggregated under the parent company's name. A customized extraction form was piloted on 10 AIMDs and then applied independently by 2 reviewers (LZ and JY). Any disagreements were resolved through discussion until consensus was reached.

Statistical Analysis

Descriptive statistics were used to summarize the extracted variables and assess temporal trends. We calculated the compound annual growth rate for annual approvals from 2020 to 2024 and applied the Mann-Kendall trend test to assess the significance of the growth trend. For AIMDs that used multiple data sources, each modality was counted separately in the subsequent analysis of data source distribution. Associations between categorical variables (approval year, medical specialty, and manufacturer's city) and AIMD risk class were evaluated. The Fisher exact test was used for analyses involving variables with low expected cell counts (approval year and medical specialty), whereas the Pearson chi-square test was used for other comparisons. All tests were 2 sided, with $P<.05$ indicating statistical significance. Analyses were conducted using SPSS Statistics for Windows (version 27.0; IBM Corp).

Ethical Considerations

This study was a secondary analysis of publicly available regulatory records retrieved from a database. No data from human participants or identifiable personal information were used, and no primary data collection was conducted. The data are anonymized and publicly accessible. In accordance with the institutional policy of China Pharmaceutical University, ethics board approval was not required for this study. This study complies with China's Data Security Law [22] and Personal Information Protection Law [23].

Results

Overview of AIMD Approvals in China

As of June 30, 2025, a total of 154 AIMDs had been approved in China since the initial authorization in 2020. Figure 1 shows the inclusion flowchart for AIMDs approved in China. All devices were intended for use by health care professionals, with none designed for direct patient use. The annual approval numbers exhibited a clear upward trend from 2020 to 2024: 9 in 2020, a total of 16 in 2021, a total of 26 in 2022, a total of 38 in 2023, and 45 in 2024. From 2020 to 2024, the compound annual growth rate was 49.53%, and the trend test confirmed a statistically significant increasing trend in annual approvals ($P<.001$). Data for the first half of 2025 show 20 approvals, indicating that the trend may be entering a phase of moderation or plateau (Figure 2). Detailed information on these AIMDs sorted by approval date is provided in Multimedia Appendix 2.

Among the 154 AIMD approvals, 15 device types had at least 3 approvals (Table 1). Pulmonary nodule CT image auxiliary detection software ranked first with 14 (9.1%) approvals. It was followed by coronary artery CT angiography image vessel stenosis auxiliary assessment software with 8 (5.2%) approvals. Coronary artery CT fractional flow reserve calculation software and intracranial hemorrhage CT image auxiliary triage software tied for third, each with 7 (4.5%) approvals. Diabetic retinopathy fundus image auxiliary diagnosis software and pneumonia CT image auxiliary triage and assessment software each had 6 (3.9%) approvals. Pediatric hand x-ray image auxiliary bone age assessment software had 4 (2.6%) approvals. A total of 8 additional products each obtained 3 (1.9%) approvals, spanning various applications from CT image processing and electrocardiogram analysis to specialized endoscopic, angiographic, and x-ray–based diagnostic tools.

XSL•FO
RenderX

Figure 1. Inclusion flowchart for approved artificial intelligence (AI)–based medical devices (AIMDs) in China (2020 - 2025).

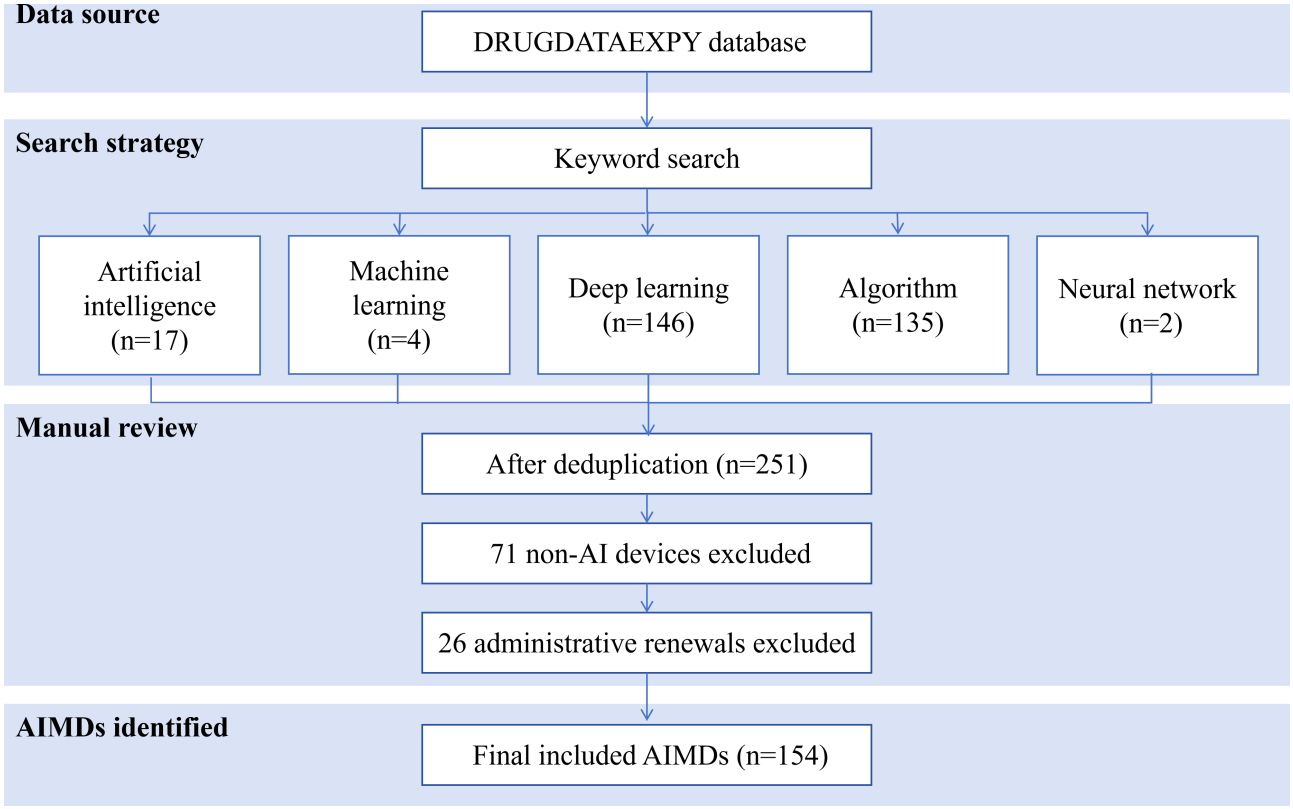

Figure 2. Trends in annual approvals of artificial intelligence–based medical devices in China (2020-2025; n=154). H1: first half of the year.

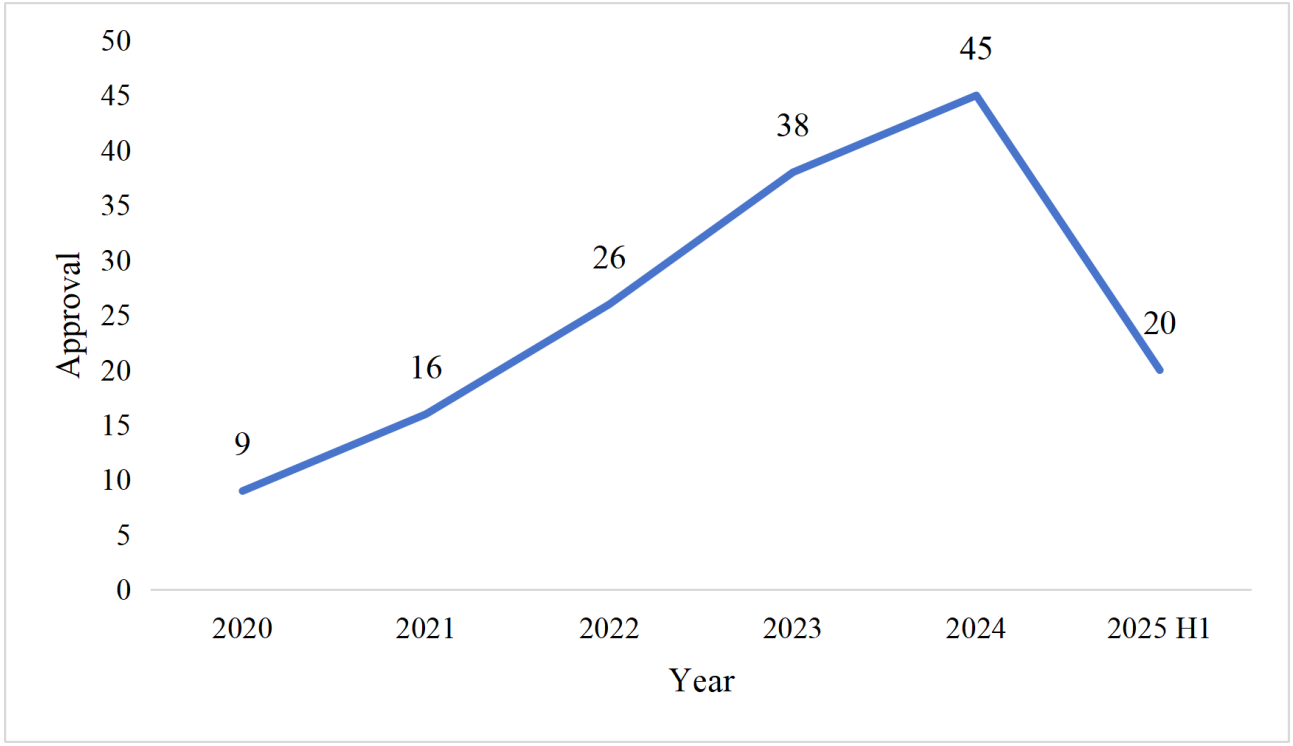

XSL•FO
RenderX

Table . Artificial intelligence–based medical devices with ≥3 approvals in China (2020 - 2025; n=154).

Device description	Approvals, n (%)
Pulmonary nodule CT[a] image auxiliary detection software	14 (9.1)
Coronary artery CT angiography image vessel stenosis auxiliary assessment software	8 (5.2)
Coronary artery CT fractional flow reserve calculation software	7 (4.5)
Intracranial hemorrhage CT image auxiliary triage software	7 (4.5)
Diabetic retinopathy fundus image auxiliary diagnosis software	6 (3.9)
Pneumonia CT image auxiliary triage and assessment software	6 (3.9)
Pediatric hand x-ray image auxiliary bone age assessment software	4 (2.6)
CT image processing software	3 (1.9)
Dynamic electrocardiogram analysis software	3 (1.9)
Electrocardiogram analysis software	3 (1.9)
Electronic lower gastrointestinal endoscopy image auxiliary detection software for intestinal polyps	3 (1.9)
Head and neck CT angiography image auxiliary assessment software	3 (1.9)
Breast x-ray image auxiliary detection software	3 (1.9)
Medical image processing software	3 (1.9)
Rib fracture CT image auxiliary detection software	3 (1.9)

[a]CT: computed tomography.

Data Source of AIMDs

As shown in Table 2, CT was the predominant data source for these AIMDs, identified in 62.3% (96/154) of approvals. This markedly exceeded other data sources, including x-ray (18/154, 11.7%), magnetic resonance imaging (12/154, 7.8%), endoscopy (9/154, 5.8%), electrocardiography (9/154, 5.8%), and fundus photography (9/154, 5.8%).

Table . Data sources used in approved artificial intelligence–based medical devices in China (2020 - 2025). Devices using multiple data sources were counted under each relevant modality. Therefore, the sum of counts exceeds the total number of devices (n=154).

Data source	Devices, n (%)
CT[a]	96 (62.3)
X-ray	18 (11.7)
MRI[b]	12 (7.8)
Electrocardiogram	9 (5.8)
Endoscopy	9 (5.8)
Fundus photography	9 (5.8)
Microscopic images	6 (3.9)
Ultrasound	3 (1.9)
Polysomnography	1 (0.6)

[a]CT: computed tomography.

[b]MRI: magnetic resonance imaging.

Risk Class and Correlation Analysis

The vast majority of AIMDs (123/154, 79.9%) were categorized as class III, with 20.1% (31/154) categorized as class II (Figure 3). Significant associations were found between risk class and 3 key variables: the year of approval (P=.03), the manufacturer's city (P=.03), and the medical specialty (P=.004). In 2020 and 2021, only class III AIMDs were approved. After 2022, the share of class II AIMDs rose each year, from 11.5% (3/26) in 2022 to 35% (7/20) in 2025. The proportion of class III AIMDs was markedly higher in Hangzhou (16/16, 100%) and Beijing (47/54, 87%) than in other cities. The distribution of risk classes varied substantially across medical specialties. Ophthalmology and cardiology exhibited a 100% (16/16) class III rate, whereas 21.7% (23/106) of AIMDs in radiology were class II.

XSL•FO
RenderX

Figure 3. Sankey diagram of approved artificial intelligence–based medical devices in China (2020-2025).

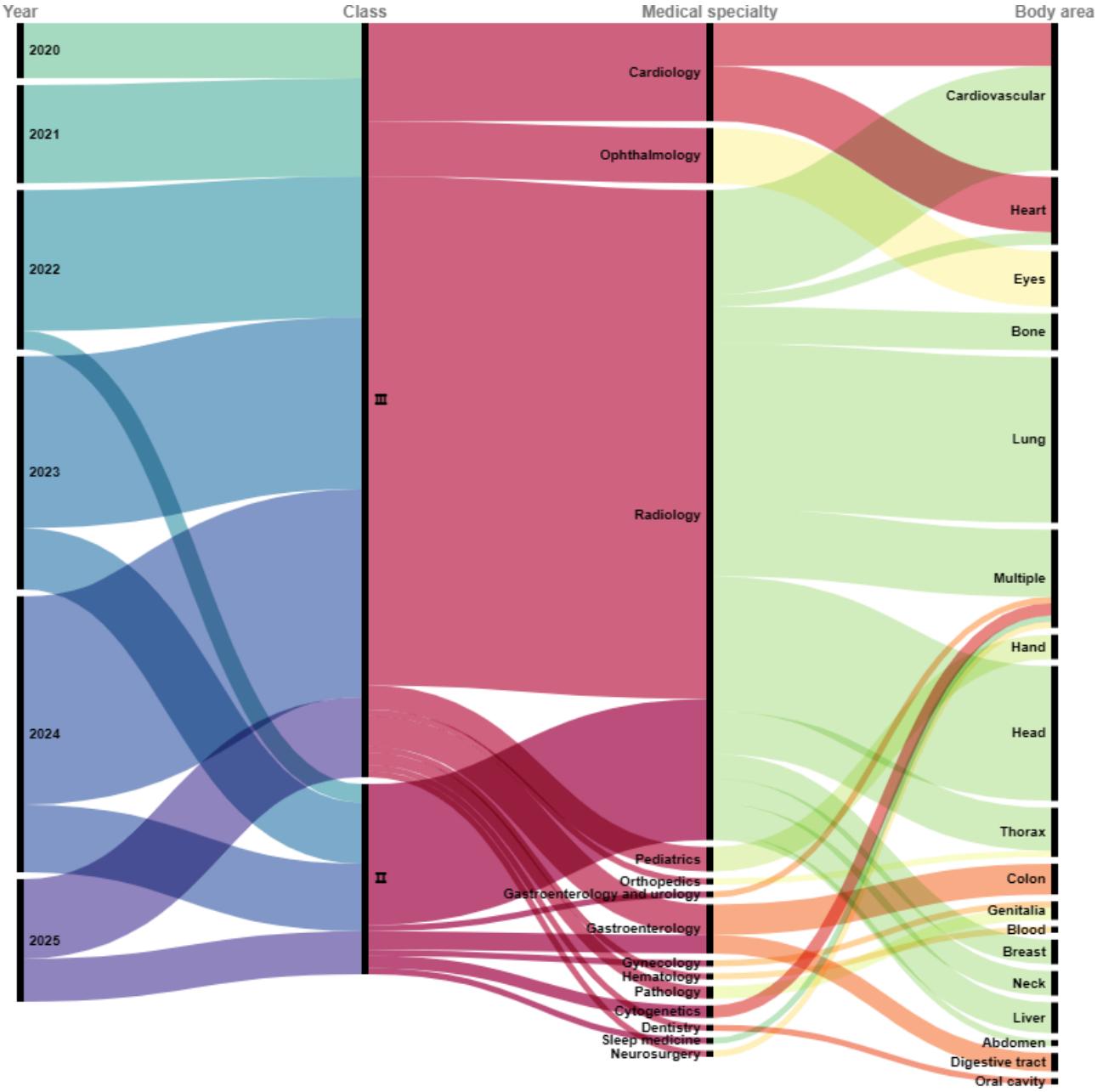

Review Pathway and Algorithm

Of the 154 AIMDs, 23 (14.9%) gained market access through national-level special review pathways, which were exclusively for class III devices. Specifically, of the 123 class III devices, 19 (15.4%) were approved via innovation review, 2 (1.6%) were approved via priority review, and 2 (1.6%) were approved via emergency approval, constituting a combined 18.7% (23/123) of all class III approvals. The remaining 85.1% (131/154) of the devices followed the standard review process. Of the 154 AIMDs, 143 (92.9%) used deep learning architectures; 3 (1.9%) used classic ML methods; and for the remaining 8 (5.2%) devices, the algorithmic approach was not disclosed in the available registration materials.

Clinical Evaluation Pathways

Analysis of the clinical evaluation pathways for the 154 AIMDs (Table 3) showed that most (n=118, 76.6%) submitted clinical trial reports as their primary evidence. The remaining devices were approved either through an exemption from clinical evaluation (n=23, 14.9%) or via a clinical comparison with similar products already available on the market (n=13, 8.4%).

Of the 123 class III devices, 116 (94.3%) used clinical trials, whereas clinical comparison with similar products and clinical exemption were less common (n=5, 4.1% and n=2, 1.6% of devices, respectively). In contrast, among the 31 class II devices, clinical exemption was the most frequent pathway (n=21, 67.7%), followed by clinical comparison with similar products (n=8, 25.8%) and clinical trials (n=2, 6.5%).

XSL•FO
RenderX

Table . Clinical evaluation pathways for approved artificial intelligence–based medical devices in China (2020 - 2025; n=154).

	Total, n (%)	Class III devices (n=123), n (%)	Class II devices (n=31), n (%)
Clinical trial	118 (76.6)	116 (94.3)	2 (6.5)
Exemption from clinical evaluation	23 (14.9)	2 (1.6)	21 (67.7)
Clinical comparison with similar products	13 (8.4)	5 (4.1)	8 (25.8)

Medical Specialty and Body Area

The 154 AIMDs spanned 14 medical specialties. Radiology dominated with 68.8% (n=106) of approvals, followed by cardiology (n=16, 10.4%), ophthalmology (n=9, 5.8%), and gastroenterology (n=9, 5.8%). The remaining AIMDs covered pediatrics, pathology, cytogenetics, sleep medicine, orthopedics, neurosurgery, hematology, gynecology, urology, and dentistry (Table 4).

The most common body areas for these AIMDs were the lung (27/154, 17.5%), the cardiovascular system (24/154, 15.6%), and the head (22/154, 14.3%), with the heart accounting for 7.1% (11/154). Additionally, 10.4% (16/154) of the AIMDs were used across multiple body areas (Table 5).

Table . Distribution of artificial intelligence–based medical devices by medical specialty in China (2020 - 2025; n=154).

Medical specialty	Devices, n (%)
Radiology	106 (68.8)
Cardiology	16 (10.4)
Ophthalmology	9 (5.8)
Gastroenterology	9 (5.8)
Pediatrics	4 (2.6)
Others	10 (6.5)

Table . Distribution of artificial intelligence–based medical devices by target body area in China (2020 - 2025; n=154).

Body area	Devices, n (%)
Lung	27 (17.5)
Cardiovascular system	24 (15.6)
Head	22 (14.3)
Multiple	16 (10.4)
Heart	11 (7.1)
Eyes	9 (5.8)
Thorax	8 (5.2)
Bone	6 (3.9)
Liver	5 (3.2)
Colon	5 (3.2)
Neck	4 (2.6)
Hand	4 (2.6)
Breast	4 (2.6)
Others	9 (5.8)

Manufacturer and Geographic Distribution

We identified 67 manufacturers in total, with a high degree of market concentration. The top 4 companies alone produced 38.3% (59/154) of the AIMDs: Yukun and United Imaging led with 11% (17/154) of the devices each, followed by Infervision with 9.1% (14/154) and Deepwise with 7.1% (11/154). In contrast, 48 manufacturers had only 1 or 2 products each. Manufacturers with more than 2 approved AIMDs are shown in Table 6.

Geographically, of the 154 approved AIMDs, 54 (35.1%) were from manufacturers headquartered in Beijing, 32 (20.8%) were from Shanghai, 18 (11.7%) were from Shenzhen, and 16 (10.4%) were from Hangzhou (Table 7). Thus, these 4 cities accounted for 77.9% (n=120) of all the approved AIMDs. Beijing was home to Yukun and Infervision, Shanghai was home to United

XSL•FO
RenderX

Imaging, and Hangzhou was home to Deepwise, which were precisely the top 4 companies listed above. Shenzhen hosted a broader ecosystem, including Carewell, Tencent Smart Healthcare, RuiXin, and Edan Instruments, but none brought more than 10 AIMDs to market.

Table . Manufacturers with ≥2 approved artificial intelligence–based medical devices in China (2020‐2025; n=154).

Manufacturer	Devices, n (%)
Yukun	17 (11.0)
United Imaging	17 (11.0)
Infervision	14 (9.1)
Deepwise	11 (7.1)
Yizhun	5 (3.2)
SenseTime	4 (2.6)
Carewell	4 (2.6)
Tongxin	3 (1.9)
Tencent Smart Healthcare	3 (1.9)
Siemens	3 (1.9)
RuiXin	3 (1.9)
Neusoft	3 (1.9)
Longwood Valley Medical	3 (1.9)
InnoVision	3 (1.9)
Huiyi Huiying	3 (1.9)
Edan Instruments	3 (1.9)
YiTu	2 (1.3)
Visionary Intelligence	2 (1.3)
Suzhou Volexcloud	2 (1.3)
Shukun	2 (1.3)
Keya Medical	2 (1.3)
Shenzhen Dr. Brain Technologies	2 (1.3)
BioMind	2 (1.3)

XSL•FO
RenderX

Table . Cities of manufacturers of approved artificial intelligence–based medical devices in China (2020 - 2025; n=154).

Cities	Devices, n (%)
Beijing	54 (35.1)
Shanghai	32 (20.8)
Shenzhen	18 (11.7)
Hangzhou	16 (10.4)
Suzhou	4 (2.6)
Xiamen	4 (2.6)
Lishui	4 (2.6)
Shenyang	3 (1.9)
Kunming	3 (1.9)
Changsha	2 (1.3)
Wuhan	2 (1.3)
Guangzhou	2 (1.3)
Chengdu	2 (1.3)
Zhengzhou	1 (0.6)
Wuxi	1 (0.6)
Nanning	1 (0.6)
Nanjing	1 (0.6)
Nanchang	1 (0.6)
Longyan	1 (0.6)
Hefei	1 (0.6)
Guiyang	1 (0.6)

Discussion

Principal Findings

This study provided an overview of AIMDs in China up to June 2025. A total of 154 AIMDs were approved, and annual approvals showed an upward trend. Most of these AIMDs (123/154, 79.9%) were class III and relied on deep learning. They were concentrated in radiology, particularly CT-based; produced by a small number of manufacturers; and located in a few cities.

China did not approve its first AIMD until 2020, later than both the United States and Europe, where approvals for AIMDs occurred as early as 2015 [10] despite variations in the definitions of AIMDs. The number of AIMD approvals in China remains lower than that in the United States and Europe. However, we have observed a rapid increase in AIMD approvals in China, reflecting technological advancements and a supportive regulatory environment.

Our analysis, extending the timeline to mid-2025, built on and updated the foundational work of Liu et al [14]. While confirming the continued dominance of radiology and class III devices previously reported, our data revealed new dynamics. Specifically, we observed a marked increase in the absolute number of approvals and a significant shift with the emergence of class II AIMDs after 2022—a trend that was not fully evident in the earlier data. Furthermore, the sustained market concentration among top manufacturers and in key geographic hubs suggests that these early structural characteristics consolidated rather than dispersed as the market grew. These comparisons highlight the rapid evolution of this field and underscore the value of longitudinal tracking to inform regulatory and market strategies. It should be noted that our counts for 2021 to 2022 were slightly higher than those reported by Liu et al [14]. We identified additional AIMDs, including image processing software and CT fractional flow reserve calculation software. A primary reason for this discrepancy is a fundamental difference in data scope. Our dataset encompassed both centrally approved class III devices and provincially approved class II devices, whereas Liu et al [14] primarily focused on class III approvals granted by the NMPA. Additionally, differences can be attributed to distinct search strategies: our approach incorporated AI-related keywords—such as “deep learning” and “algorithm”—within the “structural composition” and “intended use” fields, whereas their search relied on device-naming conventions, using terms such as “computer-assisted detection” and “computer-assisted triage.”

A prime example of an AIMD category with significant clinical penetration in China is pulmonary nodule CT image auxiliary detection software. This category had 14 approved variants from multiple manufacturers, making it the most widespread AIMD type. According to manufacturer data, United Imaging has deployed its solution in over 2000 hospitals nationwide. Their

XSL•FO
RenderX

clinical evaluations indicate that the software can increase the detection rate of pulmonary nodules by approximately 32% and improve radiologists' reading efficiency by approximately 26% compared with conventional methods [24].

Regarding risk classification, most Chinese AIMDs are designated as class III, whereas all US AIMDs are cleared as class II [25] and Europe has only approximately 1% of AIMDs in class III [11]. The large share of class III in China suggests that many AIMDs were treated as high risk and required the strictest review. From 2020 to 2021, only class III AIMDs were observed; from 2022 onward, this pattern shifted, with a steady influx of class II products. The observed change can be attributed to the *Principles for the Classification Defining of AI-Based Medical Software Products* issued by the NMPA in 2021 [26], which applies to both software as a medical device and SiMD. For SiMD, the assigned risk class applies to the product as a whole, reflecting a holistic regulatory assessment of the AI functionality's clinical role within the device. This guideline allowed AIMDs with mature algorithms that provided only non–real-time assistance—such as measurement, marking, or workflow optimization—to be placed in class II. Previously, any software bearing AI technology had been categorized as class III. The significant association between risk classification and the manufacturer's city likely reflects regional policy support and the clustering of expertise in cities such as Beijing and Hangzhou, where high-risk AIMD development appears concentrated.

Our analysis further revealed that the vast majority of approved AIMDs were supported by premarket clinical evidence through clinical trials or clinical comparison with similar products. Exemption from clinical evaluation was granted for only 23 AIMDs, 21 (91.3%) of which were class II and predominantly consisted of image processing software. This pattern reflects the practical implementation of a risk-based regulatory framework: higher-risk AIMDs generally necessitate more robust premarket clinical validation, while pathways such as exemption or comparison are more frequently applied to lower-risk AIMDs to facilitate efficient market access. Nevertheless, reliance on exemptions and comparative assessments for lower-risk approvals raises concerns about the sufficiency and transparency of premarket evidence. To strengthen the regulatory framework, we recommend clarifying exemption eligibility criteria and tightening the evidentiary standards for demonstrating equivalence.

We did not identify any safety-related recalls among the 154 AIMDs approved as of June 2025. A recent study of Food and Drug Administration–authorized AI and ML devices found that 5.2% were linked to adverse events and 5.8% were recalled, primarily due to software issues [27]. The lack of similar public reports in China may stem from its later market start and differences in data transparency. Accordingly, establishing a robust postmarket surveillance system is essential to detect risks arising from algorithm or workflow changes, and it requires commitments from regulators and manufacturers to ensure the ongoing safety of AIMDs.

Radiology dominated China's AIMD landscape, with an emphasis on CT-based applications, reflecting alignment with the nation's health care needs and its existing technological infrastructure. This focus is evident in the concentration of devices targeting pulmonary nodules and cardiovascular conditions, both representing substantial disease burden. Pulmonary nodules are clinically significant as early indicators of lung cancer, which remains the most common cancer type and the leading cause of cancer death in China [28]. Similarly, cardiovascular diseases rank as the leading cause of overall mortality, accounting for approximately 2 out of every 5 deaths [29].

The high proportion of radiology-related AIMDs approved in China aligns with the trend observed in the United States [25]. Medical imaging modalities such as CT, magnetic resonance imaging, and x-ray generate structured, digital data well suited for AI applications. Among these modalities, CT images have formed the basis for most AIMDs developed in China. The widespread availability of CT scanners in Chinese health care facilities, together with relatively uniform imaging protocols, has accelerated the growth of AI diagnostic software based on CT.

Market concentration emerged as another notable finding, with a limited number of manufacturers accounting for a large share of approved AIMDs. Notably, these dominant manufacturers were primarily headquartered in major cities such as Beijing, Shanghai, and Hangzhou. This market dominance appears to stem from the convergence of several reinforcing factors. These include the concentration of technical and regulatory expertise, preferential access to high-quality medical data through partnerships with leading hospitals, and the availability of substantial venture capital in these regions [30,31].

The observed characteristics of China's AIMD market, specifically its pronounced concentration in clinical specialties and geographic regions, were interpreted through the lens of innovation diffusion theory. First, radiology dominated the field, especially CT-based applications, illustrating innovations with high compatibility through seamless integration into digital imaging workflows and a clear relative advantage in improving efficiency during high-volume screenings, which promotes rapid early adoption. Second, the geographic concentration of approvals in Beijing, Shanghai, Shenzhen, and Hangzhou reflects the social system effect. These megacities concentrate critical resources for diffusion, such as policy incentives, venture capital, and technical talent, forming powerful hubs that accelerate local development and initial market penetration of AIMDs.

The observed approval trends could not be fully understood without considering China's evolving regulatory framework. Our data showed sustained growth consistent with the aims of recent NMPA reforms. Notably, the 2025 measures to optimize full life cycle supervision and support the innovative development of advanced medical devices explicitly aimed to accelerate reviews of advanced devices, optimize premarket processes, and strengthen postmarket surveillance. This policy shift provided essential context for interpreting market dynamics and indicated a regulatory environment oriented toward facilitating efficient innovation while ensuring safety throughout a product's life cycle. Furthermore, the emphasis on fostering

XSL•FO
RenderX

high-level industrial clusters offered a lens to interpret the pronounced geographic concentration of approvals observed in this study. The synergy between concentrated innovation resources in hubs such as Beijing and Shanghai and proactive regulatory support appears to be a defining feature of China's AIMD ecosystem.

Limitations

This study has several limitations. First, the identification of an AIMD depended on the explicit mention of AI techniques in its functional components or intended use. Devices that did not explicitly state the use of AI might have been missed despite cross-checking ambiguous cases with review reports and websites. Second, classifying medical specialties was challenging because many devices spanned multiple clinical domains. We assigned a single primary specialty, which may underrepresent secondary applications. Third, although we standardized device names by merging minor variations that referred to the same product, some inconsistencies may persist, underscoring the need for unified naming conventions.

Conclusions

This analysis indicated that AIMDs in China are experiencing rapid growth. The regulatory landscape is dominated by radiology applications, with CT-based solutions for pulmonary nodules and cardiovascular conditions especially prominent. There is also a high degree of market concentration among leading manufacturers.

Acknowledgments

The authors thank the Drugdataexpy database for providing complimentary access to data on medical devices approved in China.

Funding

This work was funded by the Fundamental Research Funds for the Central Universities (grant 2632025RWPY04) and the National Natural Science Foundation of China (grant 72304150).

Data Availability

The original data supporting this study are publicly available from the Drugdataexpy database. The processed dataset generated and analyzed during this study is provided in Multimedia Appendix 2.

Authors' Contributions

Conceptualization: LZ, JY
Data curation: LZ
Formal analysis: LZ
Funding acquisition: LZ
Methodology: LZ, JY
Project administration: JY
Resources: JY
Software: JY
Supervision: JY
Validation: JY
Visualization: LZ
Writing—original draft: LZ
Writing—review and editing: JY
Both authors have read and agreed to the published version of the manuscript.

Conflicts of Interest

None declared.

Multimedia Appendix 1
Search strategy and process for identifying artificial intelligence–based medical devices.
[DOCX File, 13 KB - medinform_v14i1e85538_app1.docx]

Multimedia Appendix 2
Detailed information of approved artificial intelligence–based medical devices in China.
[DOCX File, 67 KB - medinform_v14i1e85538_app2.docx]

References

1. Yu KH, Beam AL, Kohane IS. Artificial intelligence in healthcare. Nat Biomed Eng 2018 Oct;2(10):719-731. [doi: 10.1038/s41551-018-0305-z] [Medline: 31015651]

XSL•FO
RenderX

2. Moulaei K, Yadegari A, Baharestani M, Farzanbakhsh S, Sabet B, Reza Afrash M. Generative artificial intelligence in healthcare: a scoping review on benefits, challenges and applications. Int J Med Inform 2024 Aug;188:105474. [doi: 10.1016/j.ijmedinf.2024.105474] [Medline: 38733640]
3. Meder B, Asselbergs FW, Ashley E. Artificial intelligence to improve cardiovascular population health. Eur Heart J 2025 May 21;46(20):1907-1916. [doi: 10.1093/eurheartj/ehaf125] [Medline: 40106837]
4. Faiyazuddin M, Rahman SJQ, Anand G, et al. The impact of artificial intelligence on healthcare: a comprehensive review of advancements in diagnostics, treatment, and operational efficiency. Health Sci Rep 2025 Jan;8(1):e70312. [doi: 10.1002/hsr2.70312] [Medline: 39763580]
5. Niemiec E. Will the EU Medical Device Regulation help to improve the safety and performance of medical AI devices? Digit Health 2022 Mar 30;8:20552076221089079. [doi: 10.1177/20552076221089079] [Medline: 35386955]
6. Tang D, Xi X, Li Y, Hu M. Regulatory approaches towards AI medical devices: a comparative study of the United States, the European Union and China. Health Policy 2025 Mar;153:105260. [doi: 10.1016/j.healthpol.2025.105260] [Medline: 39951854]
7. Chen WP, Teng WG, Kuo CB, et al. Regulatory insights from 27 years of artificial intelligence/machine learning-enabled medical device recalls in the United States: implications for future governance. JMIR Med Inform 2025 Jul 11;13:e67552. [doi: 10.2196/67552] [Medline: 40644609]
8. Reddy S. Global harmonization of artificial intelligence-enabled software as a medical device regulation: addressing challenges and unifying. Mayo Clin Proc Digit Health 2024 Dec 24;3(1):100191. [doi: 10.1016/j.mcpdig.2024.100191] [Medline: 40207007]
9. Benjamens S, Dhunnoo P, Meskó B. The state of artificial intelligence-based FDA-approved medical devices and algorithms: an online database. NPJ Digit Med 2020 Sep 11;3:118. [doi: 10.1038/s41746-020-00324-0] [Medline: 32984550]
10. Joshi G, Jain A, Araveeti SR, Adhikari S, Garg H, Bhandari M. FDA-approved artificial intelligence and machine learning (AI/ML)-enabled medical devices: an updated landscape. Electronics (Basel) 2024 Jan 24;13(3):498. [doi: 10.3390/electronics13030498]
11. Muehlematter UJ, Daniore P, Vokinger KN. Approval of artificial intelligence and machine learning-based medical devices in the USA and Europe (2015-20): a comparative analysis. Lancet Digit Health 2021 Mar;3(3):e195-e203. [doi: 10.1016/S2589-7500(20)30292-2] [Medline: 33478929]
12. Han Y, Ceross A, Bergmann J. Regulatory frameworks for AI-enabled medical device software in China: comparative analysis and review of implications for global manufacturer. JMIR AI 2024 Jul 29;3:e46871. [doi: 10.2196/46871] [Medline: 39073860]
13. Zhang S, Li Y, Liu W, et al. A decade of review in global regulation and research of artificial intelligence medical devices (2015–2025). Front Med (Lausanne) 2015 Jul 17;12:1630408. [doi: 10.3389/fmed.2025.1630408] [Medline: 40747091]
14. Liu Y, Yu W, Dillon T. Regulatory responses and approval status of artificial intelligence medical devices with a focus on China. NPJ Digit Med 2024 Sep 18;7(1):255. [doi: 10.1038/s41746-024-01254-x] [Medline: 39294318]
15. Announcement no. 19 of 2025 from the National Medical Products Administration on issuing the list of medical devices exempt from clinical evaluation. National Medical Products Administration. 2025. URL: https://www.nmpa.gov.cn/xxgk/ggtg/ylqxggtg/ylqxqtggtg/20250513095643145.html [accessed 2026-01-21]
16. Guidelines for registration review of artificial intelligence medical devices (no. 8, 2022). Center for Medical Device Evaluation. 2022. URL: https://www.cmde.org.cn//flfg/zdyz/zdyzwbk/20220309091014461.html [accessed 2025-09-11]
17. Guiding principles for clinical evaluation and registration review of artificial intelligence-assisted detection medical devices (software) (no. 38, 2023). Center for Medical Device Evaluation. 2023. URL: https://www.cmde.org.cn//flfg/zdyz/zdyzwbk/20231116154535183.html [accessed 2025-09-11]
18. Announcement no. 101 of 2023 by the National Medical Products Administration on adjusting certain contents of the “medical device classification catalog”. National Medical Products Administration. 2023. URL: https://www.nmpa.gov.cn/directory/web/nmpa/ylqx/ylqxggtg/20230817153633135.html [accessed 2025-09-17]
19. Announcement no. 63 of 2025 issued by the National Medical Products Administration on measures to optimize the whole life cycle supervision and support the innovative development of high-end medical devices. National Medical Products Administration. 2025. URL: https://www.nmpa.gov.cn/xxgk/ggtg/ylqxggtg/ylqxqtggtg/20250703163951182.html [accessed 2025-09-11]
20. Rogers EM. Diffusion of Innovations, 5th edition: Free Press; 2003.
21. DRUGDATAEXPY database. URL: https://db.yaozh.com/ [accessed 2026-02-20]
22. Data security law of the People’s Republic of China. The National People’s Congress of the People’s Republic of China. 2021. URL: http://www.npc.gov.cn/englishnpc/c2759/c23934/202112/t20211209_385109.html [accessed 2026-02-18]
23. Personal information protection law of the People’s Republic of China. The National People’s Congress of the People’s Republic of China. 2021. URL: http://en.npc.gov.cn.cdurl.cn/2021-12/29/c_694559.htm [accessed 2026-02-18]
24. CT lung nodule intelligent screening system: assisting in lung cancer screening. United Imaging Intelligence. URL: https://www.uii-ai.com/product/1.html [accessed 2026-02-17]

XSL•FO
RenderX

25. Zhu S, Gilbert M, Chetty I, Siddiqui F. The 2021 landscape of FDA-approved artificial intelligence/machine learning-enabled medical devices: an analysis of the characteristics and intended use. Int J Med Inform 2022 Sep;165:104828. [doi: 10.1016/j.ijmedinf.2022.104828] [Medline: 35780651]
26. Announcement no. 47 of 2021 issued by the National Medical Products Administration on the guiding principles for the classification and definition of artificial intelligence medical software products. National Medical Products Administration. 2021. URL: https://www.nmpa.gov.cn/ylqx/ylqxggtg/20210708111147171.html [accessed 2025-09-29]
27. Lin JC, Jain B, Iyer JM, et al. Benefit-risk reporting for FDA-cleared artificial intelligence-enabled medical devices. JAMA Health Forum 2025 Sep 5;6(9):e253351. [doi: 10.1001/jamahealthforum.2025.3351] [Medline: 41004181]
28. Cao W, Chen HD, Yu YW, Li N, Chen WQ. Changing profiles of cancer burden worldwide and in China: a secondary analysis of the global cancer statistics 2020. Chin Med J (Engl) 2021 Mar 17;134(7):783-791. [doi: 10.1097/CM9.0000000000001474] [Medline: 33734139]
29. Writing Committee of the Report on Cardiovascular Health and Diseases in China. Report on cardiovascular health and diseases in China 2022: an updated summary. Biomed Environ Sci 2023 Aug 20;36(8):669-701. [doi: 10.3967/bes2023.106] [Medline: 37711081]
30. Beckers R, Kwade Z, Zanca F. The EU medical device regulation: implications for artificial intelligence-based medical device software in medical physics. Phys Med 2021 Mar;83:1-8. [doi: 10.1016/j.ejmp.2021.02.011] [Medline: 33657513]
31. Pinsky MR, Bedoya A, Bihorac A, et al. Use of artificial intelligence in critical care: opportunities and obstacles. Crit Care 2024 Apr 8;28(1):113. [doi: 10.1186/s13054-024-04860-z] [Medline: 38589940]

Abbreviations

AI: artificial intelligence
AIMD: artificial intelligence–based medical device
CT: computed tomography
ML: machine learning
NMPA: National Medical Products Administration
SiMD: software in a medical device

Edited by A Coristine; submitted 09.Oct.2025; peer-reviewed by PT Chen, VK Rathi, WG Teng; revised version received 29.Jan.2026; accepted 30.Jan.2026; published 18.Mar.2026.

Please cite as:
Zhang L, Yan J
Approval of AI-Based Medical Devices in China From 2020 to 2025: Retrospective Analysis
JMIR Med Inform 2026;14:e85538
URL: https://medinform.jmir.org/2026/1/e85538
doi:10.2196/85538

© Lingli Zhang, Jianzhou Yan. Originally published in JMIR Medical Informatics (https://medinform.jmir.org), 18.Mar.2026. This is an open-access article distributed under the terms of the Creative Commons Attribution License (https://creativecommons.org/licenses/by/4.0/), which permits unrestricted use, distribution, and reproduction in any medium, provided the original work, first published in JMIR Medical Informatics, is properly cited. The complete bibliographic information, a link to the original publication on https://medinform.jmir.org/, as well as this copyright and license information must be included.

XSL•FO
RenderX

Tailoring Discharge Summaries to Health Care Providers' Needs (Part 1 of the Framework and Implementation of AI Tools Project): User-Centered Design Approach

Mieke Deschepper[1], MSci, PhD; Helga Rogge[1], MD; Mathias Syx[1], MSCE; Kirsten Colpaert[1,2,3], MD, PhD

[1]Data Science Institute, Ghent University Hospital, Corneel Heymanslaan 10, Ghent, Belgium

[2]Department of Intensive Care, Data Science Institute, Ghent University Hospital, Ghent, Belgium

[3]Department of Internal Medicine and Pediatrics, Ghent University, Ghent, Belgium

Corresponding Author:
Mieke Deschepper, MSci, PhD
Data Science Institute, Ghent University Hospital, Corneel Heymanslaan 10, Ghent, Belgium

Abstract

Background: Medical discharge letters are critical for continuity of care but often lack clarity and personalization, making it difficult for health care providers to retrieve essential information. While large language models (LLMs) offer potential for automating summary generation, their effectiveness depends heavily on the quality and contextual relevance of the prompts used.

Objective: The objective of this study was to develop and describe a human-centered, replicable framework for creating individualized prompts that guide LLMs in generating summaries tailored to the specific needs of health care providers.

Methods: A multidisciplinary workshop was conducted at Ghent University Hospital with 26 health care providers from 5 institutions, including hospitals and general practitioner networks. Participants brainstormed ideal summary formats, generating 170 ideas categorized into themes such as "structure," "medical history," "medication," and "follow-up." These insights informed the development of a 110-item structured questionnaire distributed to 33 participants. Responses were used to generate personalized and generic prompts, refined using the context, objective, style, tone, audience, and response (CO-STAR) framework.

Results: "Structure and layout" (40/170, 23.5%) and "follow-up" (27/170, 15.9%) were the most emphasized categories in the workshop. The questionnaire confirmed the importance of the "follow-up" and "medical history" sections. Prompts were generated per participant and by health care type, incorporating frequently selected responses. The CO-STAR framework was applied to improve prompt clarity and alignment with clinical expectations. Communication emerged as a new category during the workshop and was universally valued in the questionnaire.

Conclusions: This study presents a novel, systematic approach to prompt engineering in clinical artificial intelligence applications. By translating qualitative input into structured, individualized prompts, the framework is designed to improve the usability and relevance of artificial intelligence–generated summaries. It proposes a scalable approach for integrating human-centered design into LLM deployment in health care, with the aim of supporting more accurate, context-aware clinical documentation. However, these outcomes remain to be empirically validated; this study is limited to the design and implementation of a human-centered prompt construction pipeline in a specific multicenter setting.

(JMIR Med Inform 2026;14:e80613) doi:10.2196/80613

KEYWORDS

large language models; clinical artificial intelligence integration; clinical AI integration; prompt engineering; discharge summaries; human-centered design; artificial intelligence; AI

Introduction

Background

Medical discharge letters are essential communication tools, yet their length, complexity, and variability often hinder efficient information retrieval by health care professionals, who frequently encounter difficulties in identifying key elements such as medication changes, follow-up recommendations, and significant diagnostic findings. Moreover, the informational needs of a general practitioner, a surgeon, an intensivist, and other health care providers could differ substantially.

This complexity not only hinders continuity of care but also introduces risk. In recent years, large language models (LLMs) have shown promise in helping extract, summarize, or restructure clinical documents such as medical discharge letters [1]. However, evaluating the quality and safety of such applications remains a human-centered task requiring careful planning and expert validation.

XSL•FO
RenderX

Numerous studies have evaluated the use of LLMs for generating medical discharge letters [2-4]. Despite the growing sophistication of these models, human evaluation remains indispensable for assessing the clinical accuracy, completeness, and safety of the generated outputs. Physicians, in particular, play a critical role in validating whether artificial intelligence (AI)–generated summaries address the nuanced informational needs of health care providers [2,3]. As Tam et al [5] emphasize, a structured planning phase is essential before initiating human evaluation. This phase begins with clearly defining the evaluation objectives and the specific tasks to be assessed. However, while the final evaluation is typically conducted by clinicians, the development of the prompts that guide LLMs is often carried out by engineers or a single physician. This disconnect may result in prompts that do not fully reflect the diverse and context-specific requirements of end users [2-4,6,7].

Effective medical prompt engineering is emerging as a critical skill for health care professionals navigating the integration of AI into clinical practice. As Meskó [8] emphasizes, the rise of LLMs such as ChatGPT represents a paradigm shift in health care, offering unprecedented opportunities for enhancing clinical workflows, patient communication, and decision-making. However, realizing these benefits depends heavily on the clinician's ability to craft precise, context-aware prompts that guide AI systems toward generating accurate and relevant outputs. Patil et al [9] further highlight that well-designed prompts—grounded in medical knowledge and aligned with evidence-based guidelines—are essential for eliciting clinically meaningful responses from AI tools. They argue that prompt engineering should be recognized as a core competency in medical education, enabling physicians to harness AI effectively while maintaining ethical standards and minimizing bias. These perspectives underscore that prompt engineering is not solely a technical task. However, at present, it is neither a skill that all health care professionals possess nor one that they have time to develop in depth. Moreover, as generative AI continues to evolve, its evaluation should be approached as an ongoing process, recognizing that performance, reliability, and clinical relevance may shift over time and require continuous monitoring and adaptation. Furthermore, due to the variability in ChatGPT's responses, evaluating its performance in health care requires repeated testing to ensure reliability. Without incorporating repetition, research findings may be biased and lack credibility [10].

In our project, Framework & Implementation of AI Tools (FRAIT), we aim to develop AI-driven solutions that are tailored to the specific needs of health care providers. The first phase of the project adopts a design thinking approach to design a prompt that accurately reflects the unique requirements and expectations of individual health care professionals. This involves close collaboration to understand their workflows and information needs and the specific clinical contexts in which they operate. Once this tailored prompt is established, the second phase will involve evaluating its effectiveness by applying it to Dutch medical discharge letters, assessing how well it extracts or summarizes relevant information. In this paper, we concentrate on the initial phase: constructing a prompt that is both meaningful and practical for the health care provider, ensuring that it aligns with their clinical and administrative objectives.

Objectives

The aim of this study was to develop a comprehensive process that starts by identifying the needs of health care providers regarding the ideal format for medical discharge letter summaries and results in creating an individualized prompt to generate such summaries effectively.

Methods

Part 1: Workshop

Overview

Health care providers, primarily physicians, were recruited from 5 different institutions: 3 hospitals (Ghent University Hospital, AZ Oudenaarde, and AZ Sint-Lucas Ghent) and 2 general practitioner circles (Huisartsenvereniging Ghent and Huisartsenkring Schelde Leie). The target recruitment range was 20 to 30 health care providers.

The workshop took place on Wednesday, October 16, 2024, at Ghent University Hospital. The workshop followed a 3-part structure consistent with design thinking principles: an energizer to foster engagement, a brainstorming session to elicit ideas, and a feedback round to collaboratively refine and prioritize outputs.

A set of 7 questions, each with 3 possible responses (blue, yellow, and green; Table S1 in Multimedia Appendix 1) was provided to assess the level of LLM use. Results were presented as numbers and percentages. Data were collected through 2 different persons manually counting the groups and a validation based on pictures (Figure S1 in Multimedia Appendix 1).

Following an introduction to the project, the participants were organized into 6 groups, each encompassing a diverse array of institutions and specializations. We used the digital platform Padlet [11] to conduct this brainstorming session, which allowed us to document all steps in the process. The participants had the option to enter their ideas on an available laptop or through their smartphones, which did not require any log-in credentials or other personal information.

The main question for the brainstorming session was the following:

> *What does my ideal generated summary from a medical discharge letter look like? Eg: use of bullet points, Eg: include history. Take us through your thinking: what should be included? All ideas are welcome – personal preference counts. No consensus required, the groups are for cross-pollination / inspiration.*

The emphasis was placed on both layout and content (eg, "I would like to see the accurate medical history, and I would like it to be highlighted").

All ideas were free text, although they required a label or category. The available labels at the start of the brainstorming session were "history," "current problems," "medication,"

XSL•FO
RenderX

"decision," "follow-up," "structure and layout," and "other" or "I don't know." New categories could be added during the brainstorming session.

A preliminary feedback session was held after 15 minutes to discuss the label "other" in more detail for refinement. Subsequently, an additional 15-minute brainstorming session was scheduled.

Statistics

A word cloud was used to visualize and cluster tokens and words based on their frequency within various ideas. The number of ideas by group and category was reported as frequencies and percentages, means and SDs, and medians and IQRs.

During the workshop, results were presented by category as well as the most common words within each category. The full text of the ideas for these specific words was provided to facilitate further discussion within the group if any clarification was required.

Part 2: Questionnaire

The ideas generated from the brainstorming session were systematically categorized. Two independent researchers (MD and HR) conducted data cleaning to eliminate duplicates and segment the ideas into smaller, manageable components. A structured table was developed (Table S2 in Multimedia Appendix 1) where each row represented a primary idea and subsequent columns contained subquestions. Each idea was assigned to a predefined category. For multiple-choice questions, the possible answers were maintained in a separate table (Table S3 in Multimedia Appendix 1). Using this structured table, a complete list of questions was generated. Additionally, we developed a prompt for each potential response in this questionnaire in Dutch, as well as an automated English translation. The questionnaire was designed using Microsoft Forms, with the embedded Microsoft Copilot used to streamline the automation process.

Initially, some general questions were added regarding the type of health care provider and the number of years in practice. An open-ended question for suggestions was included at the end. This questionnaire was distributed to all participants of the workshop and an additional group of general practitioners who will be involved in the ongoing process of the FRAIT project.

The results of the questionnaire were combined with the predetermined prompt for each answer, resulting in a unique prompt for each participant. Additionally, a generic prompt was created overall and by type of health care provider. This generic prompt selected the most frequently chosen answer for each question. For multiple-choice questions, an option must be present in at least one-third of the answers.

To transform the workshop ideas into a structured questionnaire and prompt templates, we applied a systematic multistep process. Each free-text idea was carefully reviewed and split into the smallest meaningful units, with each segment representing a single, actionable suggestion. For example, a statement such as "I want the summary to highlight medication changes and provide a clear follow-up plan" was divided into 2 distinct ideas: highlighting medication changes and providing a clear follow-up plan. Segmentation was guided by the principle that each unit should be assignable to a single category and actionable in prompt design.

Segments were then assigned to predefined categories, such as "medical history," "medication," "follow-up," and "structure and layout." If a segment fit multiple categories, it was assigned to all relevant categories (multilabel coding). New categories were created when multiple participants raised themes not covered by existing categories.

The coding process was iterative and collaborative. Two researchers independently segmented and categorized all ideas. Rather than aiming for consensus or exclusion of divergent ideas, we used a structured framework (Tables S2 and S3 and Figure S2 in Multimedia Appendix 1) to ensure that all contributions from the workshop were systematically included. MD constructed the initial framework by segmenting and categorizing all ideas, whereas HR independently reviewed the results for completeness and accuracy. Any ambiguities or uncertainties were discussed, but the primary objective was the comprehensive inclusion of all perspectives, not convergence on a single interpretation. This approach maximizes methodological transparency and reproducibility, as every idea generated during the workshop is traceable through the coding and questionnaire development pipeline.

Two Python scripts (Python Software Foundation) were created to automate data processing and prompt generation. The first script constructs a dynamic questionnaire by normalizing text, analyzing response frequencies, and reshaping data for optimal mapping between questions and answers. The second script translates completed responses into individualized and generic AI prompts using index-based mapping and neural machine translation for Dutch-to-English conversion. Both scripts aggregate and profile responses to ensure that generated prompts reflect the most common preferences among health care providers, supporting transparent and reproducible prompt engineering.

Finally, we enhanced all prompts by incorporating segments before and after the original prompts, adhering to the context, objective, style, tone, audience, and response (CO-STAR) framework [12-14]. To operationalize the CO-STAR framework, we incorporated both participant input and established clinical communication standards during the prompt enrichment phase. Workshop and questionnaire participants were asked to articulate their preferences regarding the presentation of discharge summaries, including aspects such as clarity, formality, and professional perspective. These responses informed the initial drafting of prompts. Figure 1 illustrates the complete process.

We compared responses in the questionnaire for each category of health care provider, ensuring that there were at least 5 responses per type. Our primary emphasis was on content questions, not layout questions. Because our sample size was limited, we restricted our analysis to descriptive statistics only.

XSL•FO
RenderX

Figure 1. Overview of the full process flow: from multidisciplinary idea generation and categorization, through questionnaire development and automation, to the final context, objective, style, tone, audience, and response framework–optimized prompt for clinical discharge summaries.

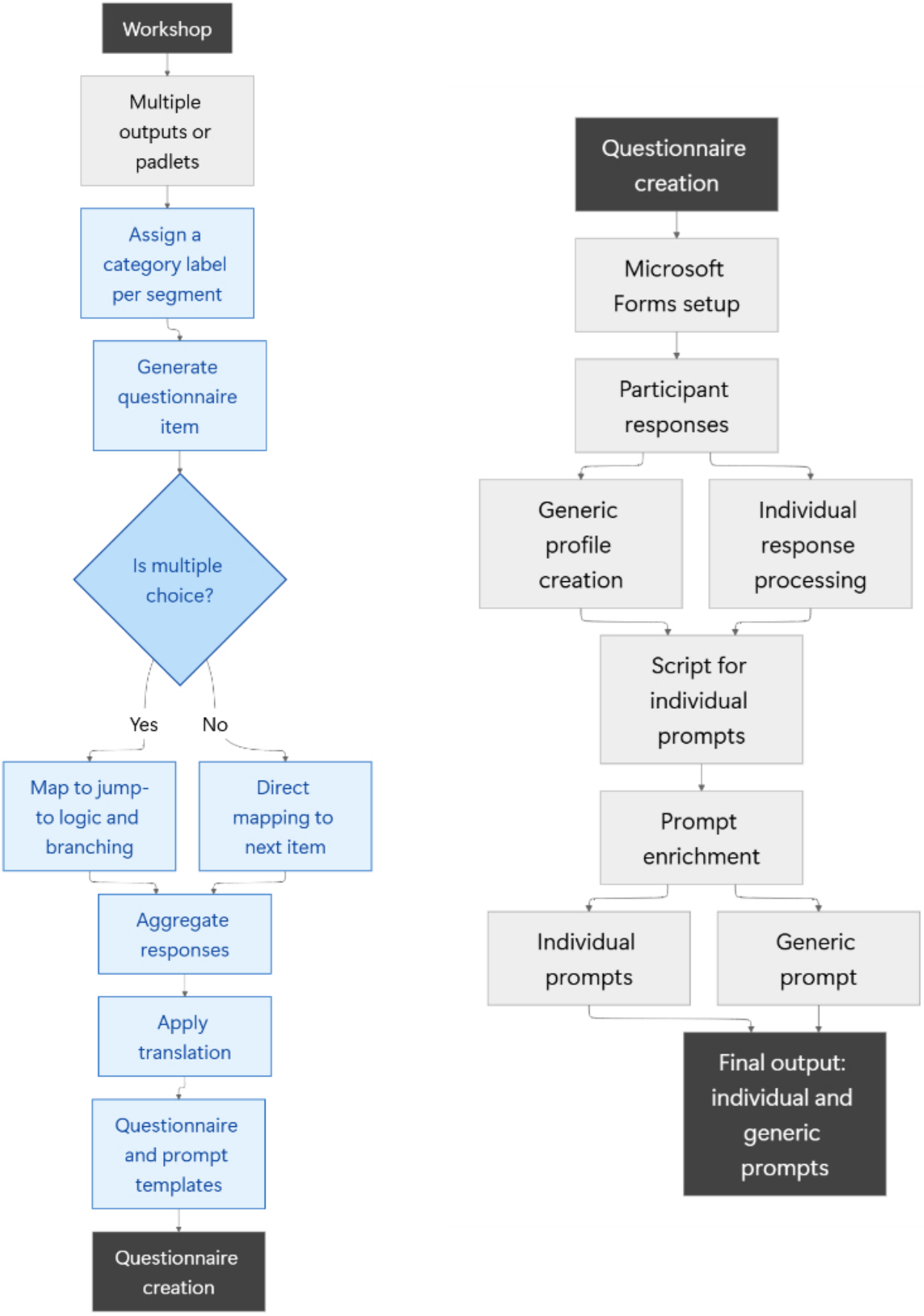

XSL•FO
RenderX

Ethical Considerations

All approvals were granted by the ethical committee of Ghent University Hospital (ONZ-2024 - 0304). The ethical committees of AZ Sint-Lucas Ghent and AZ Oudenaarde were informed of the study. Each participating organization, both hospitals and general practitioner circles, handled recruitment themselves, using their own internal communication channels and procedures to invite participants. The recruitment letter was included with our submission to the ethical committee. Informed consent was obtained from all participants before the start of the workshop (Figure S3 in Multimedia Appendix 1).

To ensure participant anonymity and data privacy, all responses collected during the workshop and questionnaire phases were anonymized before analysis. No personally identifiable information was linked to the responses, and participants were given the option to contribute via digital platforms without requiring log-in or personal credentials. Data were stored securely and accessed only by authorized research team members. These measures were implemented in accordance with institutional guidelines and approved by the relevant ethical committees.

Participants received compensation for the time they spent contributing to the project. This compensation acknowledged the substantial effort required to evaluate the summaries and attendance to the workshop, to ensure that clinicians were remunerated for their professional expertise and time commitment. No additional financial or material incentives were provided beyond this time-based compensation.

Results

Part 1: Workshop

A total of 26 health care providers were recruited for this workshop (Tables S4 and S5 in Multimedia Appendix 1). However, 7.7% (2/26) of the individuals were not present during the first half hour and did not respond to the initial questions. Overall, 5 groups were formed: 4 groups consisting of 5 participants each and 1 group consisting of 6 participants.

Table S1 in Multimedia Appendix 1 lists the questions at the start of the workshop and outlines the profiles of the participants. Figure S4 in Multimedia Appendix 1 presents the outcomes of tokenizing all ideas, which are visualized using a word cloud. Figure S5 in Multimedia Appendix 1 also contains an example of the initial concepts as presented to the participants from one of the groups.

Following a 15-minute feedback session and a plenary discussion on topics categorized as “other,” a new “communication” category was established based on requests from 2 separate groups, demonstrating responsiveness to participant input. Through an iterative process of coding and review, all ideas, including those applicable to multiple categories, were systematically preserved.

At the conclusion of the workshop, a comprehensive compilation of 170 ideas generated by all groups was assembled. The complete list, along with corresponding group names, can be found in Table S6 in Multimedia Appendix 1. The “structure and layout” category contained the greatest number of ideas (40/170, 23.5%), whereas only 6.5% (11/170) of the ideas were left unlabeled by participants. “Communication,” introduced during the second round, constituted the smallest category (Table 1).

The finalized coded table served as the foundation for developing a 110-item questionnaire using branching logic for multiple-choice questions. This systematic approach facilitated the creation of both individualized and generic prompt templates.

Table . Distribution of workshop-generated ideas by category, illustrating the thematic focus and relative emphasis placed by health care providers on different aspects of discharge summary design.

Category	Participant group	Ideas (N=170), n (%)	Ideas (n), mean (SD)	Ideas (n), median (IQR)
Communication	4	8 (4.7)	2 (1.2)	2 (1-3)
Current problems	5	20 (11.8)	4 (2)	5 (3-5)
Decision	5	19 (11.1)	3.8 (1.9)	3 (3-4)
Follow-up	5	27 (15.9)	5.4 (1.1)	5 (5-6)
Medical history	5	24 (14.1)	4.8 (3.8)	4 (3-5)
Medication	5	21 (12.4)	4.2 (3.3)	3 (2-6)
Other or “I don’t know”	4	11 (6.5)	2.8 (1.5)	2 (2-3)
Structure and layout	5	40 (23.5)	8 (2.5)	8 (7-8)

Part 2: Questionnaire

After refining the ideas, a structured table was created as the foundation for the questionnaire. These 2 files, along with their interpretations (available only in Dutch), are included in Tables S2 and S3 and Figure S2 in Multimedia Appendix 1. We provide a Python script that can be used to generate a list of questions and the appropriate “jump-to” points where necessary starting from these files. The resulting 110 questions were uploaded to Microsoft Forms, ready to be answered by the participants. The complete list of questions is available in Table S7 in Multimedia Appendix 1, and a (translated) snippet of these questions can be found in Figure 2. In the same script, when creating questions with multiple possible answers, the corresponding prompt for each answer was also added.

XSL•FO
RenderX

Figure 2. Snippet from the resulting questionnaire list translated into English demonstrating the mapping of provider needs to specific questions and corresponding artificial intelligence prompt template.

Number	Label	Section	Answer	Jump to question	Prompt	Question type
27	Do you want to see Coagulation risk in the History section?	Medical History	['Yes', 'No']	[28, 29]	['Show the coagulation risk in section History Section', '']	item
28	What formatting should be used for this?	Medical History	['None', 'Underlined', 'Italic', 'Bold', 'Strikethrough', 'Fluorescent marking']	[29, 29, 29, 29, 29, 29]	['Coagulation risk: No specific formatting', 'Coagulation risk: Underline the text', 'Coagulation risk: Place the text in italic', 'Coagulation risk: Place the text in bold', 'Coagulation risk: Strike out the text', 'Coagulation risk: Use fluorescent marking']	layout
29	Do you want to see Deep Vein Thrombosis in the History section?	Medical History	['Yes', 'No']	[30, 31]	['Show in section History De Diep Venous Thrombosis', '']	item
30	What formatting should be used for this?	Medical History	['None', 'Underlined', 'Italic', 'Bold', 'Strikethrough', 'Fluorescent marking']	[31, 31, 31, 31, 31, 31]	['Deep Vein Trombosis: No specific formatting', 'Deep Vein Trombosis: Underline the text', 'Deep Vein Trombosis: Place the text in italic', 'Deep Vein Trombosis: Place the text in bold', 'Deep Vein Trombosis: Strike out the text', 'Deep Vein Trombosis: Use fluorescent marking']	layout
31	Do you want to see New diagnoses in the History section?	Medical History	['Yes', 'No']	[32, 33]	['Show the new diagnoses in section History', '']	item
32	What formatting should be used for this?	Medical History	['None', 'Underlined', 'Italic', 'Bold', 'Strikethrough', 'Fluorescent marking']	[33, 33, 33, 33, 33, 33]	['New diagnosis: No specific formatting', 'Nieuwe diagnosen: Underline the text', 'New diagnosis: Place the text in italic', 'New diagnosis: Place the text in bold', 'New diagnosis: Strike out the text', 'New diagnosis: Use fluorescent marking']	layout
33	Do you want to see Allergies in the History section?	Medical History	['Yes', 'No']	[34, 38]	['Show the allergies in section History', '']	item
34	Want to see the type of reaction?	Medical History	['Yes', 'No']	[35, 35]	['Show the reaction on the allergy.', 'Do not show the reaction on the allergy.']	item
35	What allergies do you want to see?	Medical History	['All Allergies', 'Latex', 'Penicillin', 'New', 'Life-Threatening']	[36, 36, 36, 36, 36]	['Show all allergies', 'Show latex allergy', 'Show penicillin allergy', 'Show new allergies', 'Show life-threatening allergies']	item
36	Which list do you want to see?	Medical History	['Table', 'Bullet points - all', 'Bullet points - < 10', 'Prose - short keywords', 'Prose - Full sentences']	[37, 37, 37, 37, 37]	['Allergies: Place this in table form', 'Allergies: Use bullet points', 'Allergies: Use a maximum of 10 bullet points', 'Allergies: Use short keywords', 'Allergies: Use full sentences']	layout
37	What formatting should be used for this?	Medical History	['None', 'Underlined', 'Italic', 'Bold', 'Strikethrough', 'Fluorescent marking']	[38, 38, 38, 38, 38, 38]	['Allergieën: No specific formatting', 'Allergieën: Underline the text', 'Allergieën: Place the text in italic', 'Allergieën: Place the text in bold', 'Allergieën: Strike out the text', 'Allergieën: Use fluorescent marking']	layout
38	Do you want to see section Medication in your summary?	Medication	['Yes', 'No']	[39, 53]	['Show the Medication section in the summary', 'Do not show the medication section in the summary']	section
39	What medication do you want to see?	Medication	['None', 'All Medication', 'Medication on Admission', 'Medication on	[40, 40, 40, 40, 40, 40, 40]	['Show the none', 'Show the all medication', 'Show the medication upon admission', 'Show the medication upon dismissal', 'Show the changed	item

Table S8 in Multimedia Appendix 1 shows the number of questions for each section. “Medical history” and “admission history” constituted the largest parts of the questionnaire.

Most health care providers (30/33, 90.9%) were physicians, with over 81.8% (27/33) having more than 5 years of experience (Figure S6 in Multimedia Appendix 1). The “follow-up” section was highly valued by all participants, whereas the “examination” section received the least interest (Figure S7 in Multimedia Appendix 1).

An example of the resulting individualized and final generic prompt can be found in Figure S8 in Multimedia Appendix 1.

The implementation of the CO-STAR framework produced prompts that effectively reflected both health care provider preferences and established professional standards. The “style” component was defined as “written from the perspective of a medical professional,” and the “tone” element specified the use of formal language. These parameters were selected based on aggregated participant feedback, which underscored the importance of professionalism and clarity in clinical communication. Consequently, the final prompts incorporated user-driven insights alongside best practices, ensuring that AI-generated summaries were both contextually relevant and professionally suitable. A comprehensive overview of the adjustments made to the CO-STAR framework is provided in Figure 3. The prompt structure was enhanced with an introductory segment and a concluding section, whereas the central portion, labeled “<Individual preference>,” reflects findings from the questionnaire.

Table 2 shows the differences in the 10 most common preferences regarding discharge summaries between general practitioners and specialists. General practitioners tend to seek additional details regarding medication and follow-up, whereas specialists more frequently request information pertaining to admission history and examinations.

XSL•FO
RenderX

Figure 3. Illustration of the context, objective, style, tone, audience, and response framework application in prompt engineering: integrating health care provider preferences and clinical standards to optimize artificial intelligence–generated discharge summary prompts.

Color code: C=context - O=objective - S=style - T=tone - A=audience - R=response

"This text is a medical discharge letter (the report of a hospital admission). I would like a summary in Dutch. The intention is that I, as a healthcare provider, can use this letter to properly follow up the patient. The summary must be a maximum of one page long and clearly structured. Use formal language based on the expertise of a physician. Start with the patient's name, date of birth and the name of the hospital. All dates must be in the format day/month/year. If a requested part is not in the letter, bundle the missing parts at the bottom per section in one sentence and use 'Not mentioned' as an indication. “

<Individual preferences>

“We would like to provide some additional explanation: The name of the sections should be translated like: General = Algemeen, Medical History = Voorgeschiedenis, Medication = Medicatie, Examinations = Onderzoeken, Admission history = Opnameverloop, Follow-up = Follow-up, Decision = Besluit. If new diagnoses are requested in the history, this means that you add the new diagnoses that were made during admission to the history. By interventions we mean operations. The admission process describes the path that the patient takes during the admission, the evolution of the condition and the steps that are taken during the admission in chronological order. Here we also expect to report the administration of blood transfusions, radiotherapy or chemotherapy, the performance of diagnostic examinations such as biopsies, endoscopies, the placement of feeding tubes, etc. In Medical imaging / Technical examinations we mean by the protocol all actions that are performed during this examination and all findings that are made in this. If changes in medication are requested, we mean changes in dose, frequency and form and whether medication has been stopped completely or new medication has been started. To do this, make a comparison between the medication on admission on the one hand and the medication on discharge and the medication at the therapy proposal on the other. Medication that has remained the same is not mentioned in the case of changed medication. If the question is about the risk of clotting, mention blood clots/thrombosis and embolisms and the use of blood-thinning medication. Also mention here if you find anything about cerebral infarction/CVA or heart attack/AMIAMI. Clotting disorders should also be mentioned here. Communication is about discussing the condition and the further policy with the patient and his family. If a section should not be mentioned, leave it out of the summary completely. The information in the summary should come from the original letter. An exception to this is if ICD codes or ICPC codes are mentioned. When asking for ICD codes, the ICD-10 code should be mentioned next to the diagnosis, as can be found at https://icd10be.health.belgium.be/. When asking for ICPC codes, you can find them at https://browser.icpc-3.info/. If a patient has come from another hospital, mention this under general.”

XSL•FO
RenderX

Table . Comparison of discharge summary preferences between general practitioners (GPs) and specialists, highlighting the top 20 content areas with the greatest differences in selection rates. Options with negative percentages were favored by specialists, whereas those with positive percentages were preferred by GPs.

Section	Preference	Difference between GPs and specialists (%)
Admission history	Showing acquisition of the interventions performed	−25.3
Admission history	Showing consultations	−14.0
Examinations	Showing the protocol	−13.3
Medical history	Showing life-threatening allergies	−13.3
Examinations	Showing laboratory test results	−12.6
Admission history	Showing main diagnosis	−11.6
Medical history	Showing reaction to allergy	−11.6
Admission history	Showing new diagnoses	−9.8
Examinations	Showing clinical investigation	−8.6
Examinations	Showing medical imaging or technical investigations	−8.6
Follow-up	Showing inclusion in specific care processes	26.8
Follow-up	Showing message for GP	18.7
General	Showing whether the patient is palliative	16.6
Follow-up	Showing the institutions involved	16.6
Medication	Showing changed medication (dose, frequency, and shape)	15.1
Medication	Showing new medication	14.4
Follow-up	Showing in section “follow-up” the communication	13.2
Follow-up	Showing multidisciplinary follow-up (social and home help)	13.2
Medication	Showing stopped medication	12.5
Medication	Showing duration of medication use	12.3

Discussion

Principal Findings

From a single workshop with motivated health care providers, it was possible to generate an automated, individualized prompt tailored to their respective needs, enabling the creation of an ideal medical discharge summary. The process began with the identification of key areas that required attention, such as medical history, medication details, and follow-up procedures. Participants provided input on what specific information should be included in each section, ensuring that the final generated summary would be comprehensive and tailored to the needs of health care professionals. To the best of our knowledge, this is the first study to begin with a multidisciplinary workshop involving physicians from diverse specialties and translate their input into tailored AI prompts.

The collaboration between specialists and general practitioners resulted in an exchange of ideas, leading to a broader perspective from both groups. This synergy allowed for a more holistic approach to the creation of the summary, taking into account both the specialized and general aspects of patient information. At the same time, it became clear that reflecting on one’s ideal summary is not always easy—despite it being a personal matter. Sparring with others did not necessarily lead to adopting their viewpoints but proved valuable in helping participants critically reassess and refine their own preferences.

Dividing the scope into layout and content made the resulting ideas more concrete. By separating these 2 elements, participants were able to focus more effectively on each aspect, leading to clearer and more actionable suggestions. This also leads to a clearer prompt for further evaluation possibilities (in future work), providing a solid foundation for future improvements and refinements based on feedback from health care professionals.

Within the workshop, numerous ideas were generated. The open question at the end—“Do you have any additional comments or suggestions regarding this questionnaire? Are there aspects that you think are missing or not sufficiently addressed? Please note them below.”—received responses primarily on practical issues from only a few participants.

During the workshop, it was observed that all groups contributed an equal number of ideas. Most ideas were related to the

XSL•FO
RenderX

structure of the generated summary, primarily due to the existence of a single category for the broader theme. The "follow-up" category encompassed the highest number of ideas, although there was significant overlap with other categories. The "communication" category, introduced during the workshop, predominantly contained ideas that pertained to the "follow-up" category. This trend was also evident in the questionnaire, where the "communication" section was the only one indicated as desirable by all participants.

The "medical history" and "admission history" sections often included diverse content, resulting in numerous questions from participants. The "medication" and "follow-up" sections also encompassed a wide range of topics, which necessitated their inclusion as multiple-choice questions. This strategy allowed for a targeted approach, meaning that only 1 detailed question on content was asked for each selected topic (eg, "What information do you want to see for the medication? 'Start date,' 'Duration,' 'Dose,' 'Time of intake,' 'Frequency,' 'Form e.g. oral,' 'Show drug substance name,' 'Clinical effect,' 'Criteria for stopping/changing specific medication,' 'Reason for starting, stopping, changing'").

Such a detailed and structured approach ensures that all relevant aspects are thoroughly explored and addressed, providing a comprehensive framework for summarizing medical discharge letters efficiently and effectively.

Comparison With Prior Work

The most significant refinement aligned with the CO-STAR prompt engineering framework was introduced in the "response" section, with a particular emphasis on clarifying the definitions of key terminology embedded within the prompt. This adjustment is crucial for enhancing the model's interpretability and ensuring consistent semantic alignment between the prompt and the generated summary. As demonstrated in the work on SARA [13], a generative AI for legal summarization, precise control over terminology and density within prompts directly influences the coherence and legal validity of the summaries produced. Similarly, the Institute of Electrical and Electronics Engineers Computer Society's International Conference on Computers, Software, and Applications 2024 study [12] on automatic smart contract generation underscores the importance of terminological precision in the response phase to mitigate ambiguity and improve automation reliability. Furthermore, the insights from Teo [14] from the GPT-4 prompt engineering competition highlight how nuanced refinements in prompt structure—especially in the response section—can significantly elevate performance in competitive and real-world applications.

Our findings align with broader trends in health informatics that emphasize the centrality of user needs and adaptive information delivery. For instance, psychoeducational mobile health interventions for parents of small-for-gestational-age fetuses have shown how adaptive, user-centered systems can enhance engagement and outcomes [15]. The ADEPT framework further illustrates how optimizing data flow in dynamic, real-world environments supports effective, personalized care [16]. By translating qualitative input from health care providers into structured, individualized prompts, our framework extends these principles to the domain of clinical AI, ensuring that LLM-generated discharge summaries are not only technically robust but also contextually relevant and responsive to end user needs.

Limitations

An important aspect of this framework's broader impact is its adaptability beyond its original Dutch-speaking setting. Future efforts should focus on translation and cultural adjustment of all materials, questionnaires, and prompts used in workshops. This will require close collaboration with language specialists and domain specialists to ensure accurate terminology, workflows, and compliance. Owing to its modular design, the framework allows for easy alignment of categories and prompts with various health care systems' specific summarization needs. This methodology is applicable across medical specialties by engaging domain experts during assessment and prompt development, ensuring that specialty-specific information needs are addressed. By taking these steps, the framework will become more valuable and help develop AI tools that are effective, equitable, and well-suited to diverse clinical contexts.

Despite aiming for comprehensiveness, the balance between breadth and depth sometimes required trade-offs, prioritizing clarity and efficiency over detailed customization. For instance, preferences were gauged using a multiple-choice question such as "What do you want to see..." followed by only a single question about layout preferences for each item.

This initial prompt is a first step in the improvement in the quality and relevance of AI-generated summaries. It is evident that further refinement is necessary. This ongoing fine-tuning will involve a meticulous evaluation of the generated summaries, taking into account detailed feedback from health care professionals. Such iterative adjustments aim to enhance the precision and contextual accuracy of the summaries, ensuring that they meet the nuanced needs of diverse medical specializations.

Future Steps

The subsequent phase will involve evaluating the generic and individual prompts, with the assessment being developed collaboratively with the health care providers. The prompt will be broken down into smaller components, generating binary questions regarding layout and more specific inquiries related to content accuracy (eg, if an outcome is incorrect, does it constitute a hallucination?). A collection of representative medical discharge letters will be made available for this purpose. Upon completion of the evaluation, it will likely be necessary to review the prompt to identify opportunities for further optimization and integrate additional content informed by the evaluation findings.

Conclusions

This study presents a novel, systematic framework for developing individualized prompts to summarize medical discharge letters grounded in the real-world needs of health care providers. A key strength of this approach lies in the deliberate separation between layout and content preferences, which proved highly effective in capturing both structural and informational expectations.

XSL•FO
RenderX

By translating qualitative input into structured, personalized prompts, this framework aims to improve the relevance and usability of AI-generated summaries and serve as a replicable model for diverse clinical and research settings, although empirical validation remains necessary. The framework supports applications in data collection, data analysis, and personalized feedback generation. This study is limited to the design and implementation of a human-centered prompt construction pipeline in a specific multicenter setting; direct evaluation of AI-generated outputs and broader scalability will be addressed in future work.

Acknowledgments

The authors would like to express their sincere gratitude to the entire team at the Data Science Institute of Ghent University Hospital, as well as to the management, program participants, and coordinators representing the participating organizations. Artificial intelligence was used within the project to enhance efficiency: Figure 1 was created with assistance from Claude (Anthropic). The questionnaire was created in Microsoft Forms using Microsoft Copilot under the Microsoft Office license of Ghent University Hospital.

Funding

The Framework & Implementation of AI Tools project was funded by the Belgian government through the Data Innovation project.

Data Availability

All data generated or analyzed during this study are included in this published article and its supplementary information files (Multimedia Appendix 1). The supporting Python scripts are available in a public GitHub repository [17]. The script frait_part1_questions.py generates a dynamic questionnaire for the Framework & Implementation of AI Tools system. Its primary output is an organized set of questions designed to assist health care providers in selecting relevant sections and details for inclusion in a medical summary. The script frait_part1_prompt.py translates completed questionnaire responses into artificial intelligence prompts, which are used for medical document summarization.

Authors' Contributions

Conceptualization: MD, MS, KC
Data curation: MD
Formal analysis: MD
Funding acquisition: MD, MS, KC
Investigation: MD, HR
Methodology: MD, MS
Project administration: MD, MS, HR
Resources: MD, MS, KC
Software: MD
Supervision: MS, KC
Validation: KC
Visualization: MD, HR
Writing—original draft: MD
Writing—review and editing: MD, HR, MS, KC

Conflicts of Interest

None declared.

Multimedia Appendix 1
Overview of all supplementary materials, including workshop energizer results, input questionnaire structure, informed consent template, participant characteristics, word-cloud analysis, padlet examples, workshop output (in Dutch), full questionnaire, and questionnaire results.
[PDF File, 1061 KB - medinform_v14i1e80613_app1.pdf]

Checklist 1
STROBE checklist.
[PDF File, 137 KB - medinform_v14i1e80613_app2.pdf]

References

XSL•FO
RenderX

1. Patel SB, Lam K. ChatGPT: the future of discharge summaries? Lancet Digit Health 2023 Mar;5(3):e107-e108. [doi: 10.1016/S2589-7500(23)00021-3] [Medline: 36754724]
2. Williams CYK, Subramanian CR, Ali SS, et al. Physician- and large language model-generated hospital discharge summaries. JAMA Intern Med 2025 Jul 1;185(7):818-825. [doi: 10.1001/jamainternmed.2025.0821] [Medline: 40323616]
3. Koh MCY, Ngiam JN, Oon JEL, Lum LHW, Smitasin N, Archuleta S. Using ChatGPT for writing hospital inpatient discharge summaries - perspectives from an inpatient infectious diseases service. BMC Health Serv Res 2025 Feb 10;25(1):221. [doi: 10.1186/s12913-025-12373-w] [Medline: 39924512]
4. Wals Zurita AJ, Miras Del Rio H, Ugarte Ruiz de Aguirre N, et al. The transformative potential of large language models in mining electronic health records data: content analysis. JMIR Med Inform 2025 Jan 2;13:e58457. [doi: 10.2196/58457] [Medline: 39746191]
5. Tam TYC, Sivarajkumar S, Kapoor S, et al. A framework for human evaluation of large language models in healthcare derived from literature review. NPJ Digit Med 2024 Sep 28;7(1):258. [doi: 10.1038/s41746-024-01258-7] [Medline: 39333376]
6. Ntinopoulos V, Rodriguez Cetina Biefer H, Tudorache I, et al. Large language models for data extraction from unstructured and semi-structured electronic health records: a multiple model performance evaluation. BMJ Health Care Inform 2025 Jan 19;32(1):e101139. [doi: 10.1136/bmjhci-2024-101139] [Medline: 39832824]
7. Croxford E, Gao Y, Pellegrino N, et al. Development and validation of the provider documentation summarization quality instrument for large language models. J Am Med Inform Assoc 2025 Jun 1;32(6):1050-1060. [doi: 10.1093/jamia/ocaf068] [Medline: 40323321]
8. Meskó B. Prompt engineering as an important emerging skill for medical professionals: tutorial. J Med Internet Res 2023 Oct 4;25:e50638. [doi: 10.2196/50638] [Medline: 37792434]
9. Patil R, Heston TF, Bhuse V. Prompt engineering in healthcare. Electronics (Basel) 2024;13(15):2961. [doi: 10.3390/electronics13152961]
10. Zhu L, Mou W, Hong C, et al. The evaluation of generative AI should include repetition to assess stability. JMIR Mhealth Uhealth 2024 May 6;12:e57978. [doi: 10.2196/57978] [Medline: 38688841]
11. Visual collaborationfor creative workand education. URL: https://padlet.com/ [accessed 2026-02-18]
12. Napoli EA, Barbàra F, Gatteschi V, Schifanella C. Leveraging large language models for automatic smart contract generation. In: 2024 IEEE 48th Annual Computers, Software, and Applications Conference (COMPSAC): IEEE; 2024. [doi: 10.1109/COMPSAC61105.2024.00100]
13. Bomfim FD, Neto JA, Bezerra Filho G, et al, editors. SARA - a generative AI for legal process summarization based on chain of density prompt engineering. In: Intelligent Systems: Springer; 2025. [doi: 10.1007/978-3-031-79032-4_26]
14. Teo S. How I won Singapore's GPT-4 prompt engineering competition. Medium. 2023 Dec 29. URL: https://medium.com/data-science/how-i-won-singapores-gpt-4-prompt-engineering-competition-34c195a93d41 [accessed 2026-02-14]
15. Balderas-Díaz S, Rodríguez-Fórtiz MJ, Garrido JL, Bellido-González M, Guerrero-Contreras G. A psycho-educational intervention programme for parents with SGA foetuses supported by an adaptive mHealth system: design, proof of concept and usability assessment. BMC Med Inform Decis Mak 2022 Nov 11;22(Suppl 4):291. [doi: 10.1186/s12911-022-02036-9] [Medline: 36357878]
16. Balderas-Díaz S, Guerrero-Contreras G, editors. ADEPT framework: optimizing data flow in dynamic environments for ambient assisted living. In: Ambient Intelligence: Springer; 2025. [doi: 10.1007/978-3-031-83117-1_12]
17. FRAIT (framework & implementation of AI tools). GitHub. URL: https://github.com/miekedeschepperUZG/FRAIT [accessed 2026-02-18]

Abbreviations

AI: artificial intelligence
CO-STAR: context, objective, style, tone, audience, and response
FRAIT: Framework & Implementation of AI Tools
LLM: large language model
STROBE: Strengthening the Reporting of Observational Studies in Epidemiology

XSL•FO
RenderX

Edited by A Benis; submitted 14.Jul.2025; peer-reviewed by G Guerrero-Contreras, J Declerck, S Patel; revised version received 12.Dec.2025; accepted 01.Jan.2026; published 04.Mar.2026.

Please cite as:
Deschepper M, Rogge H, Syx M, Colpaert K
Tailoring Discharge Summaries to Health Care Providers' Needs (Part 1 of the Framework and Implementation of AI Tools Project): User-Centered Design Approach
JMIR Med Inform 2026;14:e80613
URL: https://medinform.jmir.org/2026/1/e80613
doi:10.2196/80613

© Mieke Deschepper, Helga Rogge, Mathias Syx, Kirsten Colpaert. Originally published in JMIR Medical Informatics (https://medinform.jmir.org), 4.Mar.2026. This is an open-access article distributed under the terms of the Creative Commons Attribution License (https://creativecommons.org/licenses/by/4.0/), which permits unrestricted use, distribution, and reproduction in any medium, provided the original work, first published in JMIR Medical Informatics, is properly cited. The complete bibliographic information, a link to the original publication on https://medinform.jmir.org/, as well as this copyright and license information must be included.

XSL•FO
RenderX

Evaluating GPT-4 Responses on Scars or Keloids for Patient Education: Large Language Model Evaluation Study

Mingjun Rao, MD; Tang Xiujun, MSc; Wang Haoyu, BA

Department of Plastic Surgery, Guizhou Provincial People's Hospital, 83 Zhongshan East Road, Nanming District, Guiyang, China

Corresponding Author:
Tang Xiujun, MSc
Department of Plastic Surgery, Guizhou Provincial People's Hospital, 83 Zhongshan East Road, Nanming District, Guiyang, China

Abstract

Background: Scars and keloids impose significant physical and psychological burdens on patients, often leading to functional limitations, cosmetic concerns, and mental health issues such as anxiety or depression. Patients increasingly turn to online platforms for information; however, existing web-based resources on scars and keloids are frequently unreliable, fragmented, or difficult to understand. Large language models such as GPT-4 show promise for delivering medical information, but their accuracy, readability, and potential to generate hallucinated content require validation for patient education applications.

Objective: This study aimed to systematically evaluate GPT-4's performance in providing patient education on scars and keloids, focusing on its accuracy, reliability, readability, and reference quality.

Methods: This study involved collecting 354 questions from Reddit communities (r/Keloids, r/SCAR, and r/PlasticSurgery), covering topics including treatment options, pre- and postoperative care, and psychological impacts. Each question was input into GPT-4 in independent sessions to mimic real-world patient interactions. Responses were evaluated using multiple tools: the Patient Education Materials Assessment Tool-Artificial Intelligence for understandability and actionability, DISCERN-AI for treatment information quality, the Global Quality Scale for overall information quality, and standard readability metrics (Flesch Reading Ease score, and Gunning Fog Index). Three plastic surgeons used the Natural Language Assessment Tool for Artificial Intelligence to rate the accuracy, safety, and clinical appropriateness, while the Reference Evaluation for Artificial Intelligence tool validated references for reference hallucination, relevance, and source quality. We conducted the same analysis to assess the quality of GPT-4–generated content in response to questions from 3 medical websites.

Results: GPT-4 demonstrated high accuracy and reliability. The Patient Education Materials Assessment Tool-Artificial Intelligence showed 75.5% understandability, DISCERN-AI rated responses as "good" (26.3/35), and the Global Quality Scale score was 4.28 of 5. Surgeons' evaluations averaged 3.94 to 4.43 out of 5 across dimensions (accuracy 3.9, SD 0.7; safety 4.3, SD 0.8; clinical appropriateness 4.4, SD 0.5; actionability 4.1, SD 0.8; and effectiveness 4.1, SD 0.8). Readability analyses indicated moderate complexity (Flesch Reading Ease Score: 50.13; Gunning Fog Index: 12.68), corresponding to a 12th-grade reading level. Reference Evaluation for Artificial Intelligence identified 11.8% (383/3250) hallucinated references, while 88.2% (2867/3250) of references were real, with 95.1% (2724/2867) from authoritative sources (eg, government guidelines and the literature). The overall results about questions from medical websites were consistent with the answers to Reddit questions.

Conclusions: GPT-4 has serious potential as a patient education tool for scars and keloids, offering reliable and accurate information. However, improvements in readability (to align with sixth to eighth grade standards) and reduction of reference hallucinations are essential to enhance accessibility and trustworthiness. Future large language model optimizations should prioritize simplifying medical language and strengthening reference validation mechanisms to maximize clinical utility.

(JMIR Med Inform 2026;14:e78838) doi:10.2196/78838

KEYWORDS

scar; keloid; GPT-4; patient education; generative AI; generative artificial intelligence; readability; large language model

Introduction

Scars and keloids are common skin healing outcomes [1], often causing discomfort during the proliferative phase [2]. When located on visible areas such as the face, they can severely impact a patient's appearance, leading to psychological distress such as low self-esteem, anxiety, and depression, which may further hinder social interactions and career development [3]. Scars near joints may cause functional limitations, while perineal scars can result in long-term complications such as dyspareunia and dysmenorrhea [4,5]. Many patients urgently seek to improve both the aesthetic and functional aspects of scars or keloids. However, treatments often require multimodal approaches over weeks to months, making high patient adherence crucial.

XSL•FO
RenderX

Consequently, access to accurate, timely, and comprehensive management information is critical for patients to better understand treatment expectations, options, prognosis, and potential complications [6-9].

Currently, patients increasingly rely on internet-based health information [10]. This trend faces multifaceted challenges, including information overload, variability in source credibility and content accuracy, and the health literacy required to understand the contents [11,12]. Notably, many online resources on scars or keloids are often unreliable, fragmented, or difficult to understand, failing to tackle the fundamental needs of patients with scars or keloids [13].

In recent years, artificial intelligence (AI) tools powered by large language models (LLMs), such as GPT-4 (used by ChatGPT), have demonstrated significant potential in delivering medical information [14]. GPT-4's capacity to generate natural language responses through interactive conversions could aid users in understanding intricate medical concepts, treatment, and management strategies, positioning it as a potentially valuable alternative to traditional search engines for accessing knowledge associated with scars or keloids [15-17].

It is reported that 52% of US adults have used LLMs, and GPT-4, as a leading LLM, receives over 5 billion monthly visits. In total, 39% of LLM users have used LLMs for health care queries [18]. Despite the increasing use of LLMs in health care [19-21], there remains a research gap, and it is currently unclear whether GPT-4 can generate high-quality patient education content related to scars and keloids. Thus, we conducted this study to comprehensively assess the use of GPT-4 in keloid and scar patient education by performing a multidimensional evaluation (encompassing accuracy, reliability, readability, and reference quality) of GPT-4 responses.

Methods

Study Objective

This study aimed to investigate the potential of GPT-4 to provide reliable, accurate, readable, and actual medical information for patients with scars or keloids. To achieve this, we used GPT-4 (OpenAI) to evaluate its accuracy, reliability, readability, and hallucinations in answering questions related to treatments of scars or keloids.

Question Collection

The research questions were manually collected by the authors from Reddit. First, the authors analyzed all posts on the "Hot" page (the most popular and recently active posts) of the r/Keloids subreddit, all posts on the r/SCAR subreddit, and all posts on the r/PlasticSurgery subreddit as of April 6, 2025. We extracted the main text of each post that included the keywords "Scar" or "Keloid" and organized the data using Microsoft Excel. Second, one author (MR) excluded the posts that contained no questions, were duplicates, or had repeated questions. In addition, the same author (MR) performed the initial classification of the questions. To ensure reliability and minimize bias, another author (WH) independently reviewed the process. Consistency between the two authors' classifications was confirmed through discussion. This data collection approach has been adopted in previous Reddit-based research [22]. Furthermore, we adopted 49 questions about keloids or scars from 3 medical websites.

Ethical Considerations

The institutional review board of the People's Hospital of Guizhou Province, affiliated with Guizhou University, deemed this study exempt from ethics approval.

Quality Assessment

Overview

Each question was input individually into GPT-4. Following previous research protocols, a new chat session was initiated for each question to avoid context contamination and to simulate real-world patient interactions [23]. Consistent with real-world activities using GPT-4, no specialized prompt instructions were appended to the question inputs. The contents generated by ChatGPT-4 were evaluated using a modified version of existing health information quality assessment tools.

Patient Education Materials Assessment Tool-AI Tool

The Patient Education Materials Assessment Tool (PEMAT) was used to assess the understandability and actionability of ChatGPT-generated content. The original PEMAT includes 17 items for understandability and 7 for actionability. Since all contents generated by ChatGPT are pure text, the PEMAT was simplified to 8 items for understandability and 3 items for actionability (Multimedia Appendix 1). Each item received 1 point if it met the standard, and scores were reported as percentages. A score of 70% or greater was recorded as a "pass" per PEMAT guidelines [24].

DISCERN-AI Tool

The DISCERN standard, a previously validated tool to help health care consumers and professionals evaluate the quality of treatment information, was adapted for ChatGPT-generated content. Since all contents generated by ChatGPT are pure text, 7 items (questions 3 - 9 from the 15-item DISCERN tool) were selected and scored on a 1 to 5 scale (Multimedia Appendix 2). Each output was rated as follows: very poor (7 - 12 points), poor (13 - 17 points), fair (18 - 23 points), good (24 - 28 points), and excellent (29 - 35 points) [24,25].

Global Quality Scale

The Global Quality Scale (GQS) is a 5-point Likert scale used to evaluate information quality and the flow and ease of use of information. The scores range from 1 (low quality) to 5 (high quality), while scores of 4 or 5 indicated high-quality outputs, a score of 3 was considered moderate quality and scores of 1 or 2 were categorized as low quality.

Readability Assessment

The readability of the ChatGPT-generated content was evaluated using several established readability formulas, including Flesch Reading Ease score, Gunning Fog Index, Flesch-Kincaid Grade Level, Coleman-Liau Index, and Simple Measure of Gobbledygook (SMOG). Each output was copied into Microsoft Word and analyzed via the Readable website [26]. The Flesch Reading Ease score ranges from 0 to 100, and higher scores

XSL•FO
RenderX

indicate greater readability. A score between 60 and 70 corresponds to reading levels of grades 8 and 9 and is generally understandable by the average adult. The Gunning Fog Index and Flesch-Kincaid Grade Level are used to estimate sentence complexity; the scores represent the years of formal education required to understand the contents. For example, a score of 12 implies the output is suitable for readers at the 12th-grade level. The Coleman-Liau Index is similar to the Gunning Fog Index and Flesch-Kincaid Grade Level but uses character counts instead of syllables, making it more suitable for languages where syllable counts may not accurately reflect complexity. The SMOG Index measures syllable density, often used to assess health information materials. A score of 12 indicates that the material is suitable for readers at the 12th-grade level or higher.

Natural Language Assessment Tool for Artificial Intelligence

Three experienced plastic surgeons independently reviewed each GPT-4–generated content using a specially developed Natural Language Assessment Tool for Artificial Intelligence (NLAT-AI) [24]. Using this tool, we assessed accuracy, safety, appropriateness, actionability, and effectiveness. Each output was rated using a 5-point Likert scale (1=strongly disagree, 5=strongly agree; Multimedia Appendix 3). All results were summarized using descriptive statistics.

Reference Evaluation for AI

Given known issues of LLM hallucination (ie, generating plausible but nonexistent references), a brief evaluation tool, Reference Evaluation for AI, was developed to analyze references provided in ChatGPT-generated content [27]. Each reference was verified through direct links or a Google search. The tool assessed (1) reference hallucination (whether references were real or fabricated), (2) relevance and consistency between references and AI output, and (3) source quality (based on the authority of the issuing institution or organization, such as government guidelines, health care organizations, or scientific research; Multimedia Appendix 4).

Results

Question Collection and Classification

A total of 507 posts were identified and analyzed (posts from the r/Keloids subreddit: n=193, 38.1%; posts from the r/Keloids subreddit: n=211, 41.6%; and posts from the r/Scar subreddit: n=103, 20.3%). After removing posts that merely shared information or were duplicates, 354 unique questions were obtained. The questions were categorized into 16 groups based on their contents (Table 1). Furthermore, we obtained 49 questions from 3 medical websites that included 38 unique questions (Table S1 in Multimedia Appendix 5).

Table . Questions on scars or keloids from Reddit (N=354).

Question group	Questions, n (%)
Questions on other respects	28 (7.9)
Questions on other treatments for scars or keloids	4 (1.1)
Questions on common treatments for scars or keloids	46 (13)
Questions on trauma-related scars or keloids	16 (4.5)
Questions on psychological issues caused by scars or keloids	9 (2.5)
Questions on at-home scar or keloid care	3 (0.8)
Questions on preoperative scar or keloid consultation	37 (10.5)
Questions on postoperative scar or keloid consultation	55 (15.5)
Questions on selection of treatments for scars or keloids	80 (22.6)
Questions on impact of scars or keloids on daily life	2 (0.6)
Questions on scar or keloid symptoms	7 (2)
Questions on scar camouflage	6 (1.7)
Questions on the impact of nutrition on scars or keloids	3 (0.8)
Questions on choosing physicians for scar or keloid treatment or related costs	32 (9)
Questions on old scars	14 (4)
Questions on scar or keloid prevention	12 (3.4)

Evaluation of GPT-4–Generated Content

GPT-4 generated content that provided a wide range of medically accurate information. Using the PEMAT-AI, DISCERN-AI, and GQS patient education material evaluation tools, the output of GPT-4 was assessed, with all tools indicating high scores. The overall understandability score using PEMAT-AI easily surpassed the 70% threshold for acceptability (mean 75.5%, SD 12.2%). The DISCERN-AI tool resulted in an overall rating of “good” quality (mean 26.3, SD 3.4), with all 16 groups of questions rated as “good.” The GQS score averaged 4.3 out of 5 (SD 0.8), categorizing the outputs as high quality. More details are shown in Table S1 in Multimedia Appendix 6. Intraclass correlation coefficient (ICC) for

XSL•FO
RenderX

PEMAT-AI, DISCERN-AI, and GQS were 0.73, 0.69, and 0.78, respectively (Table S2 in Multimedia Appendix 5). The results of the ICC demonstrated high reliability of the evaluation tools.

Plastic Surgeons' Evaluation via the NLAT-AI Tool

Using the NLAT-AI tool, 3 independent plastic surgeons evaluated the GPT-4–generated content. All dimensions of the contents received scores above the neutral midpoint of 3 on a 5-point Likert scale. The overall average scores for each dimension were as follows: accuracy 3.9 (SD 0.7), safety 4.3 (SD 0.8), appropriateness 4.4 (SD 0.5), actionability 4.1 (SD 0.8), and effectiveness 4.1 (SD 0.8). More detailed descriptive statistics for each question are presented in Table S2 in Multimedia Appendix 6. Internal validity tests showed an ICC of 0.76 (Table S2 in Multimedia Appendix 5), indicating high reliability.

Readability Assessment

The results of the readability assessments indicated that the GPT-4–generated content was "difficult to read." The average Flesch Reading Ease score was 50.1 (SD 8.1), which is considered moderately difficult. The Gunning Fog Index averaged 12.7 (SD 3.3), and the Flesch-Kincaid Grade Level was 12.4 (SD 2.5), indicating that the text was at a high school level (approximately suitable for individuals aged 16 - 17 years). The Coleman-Liau Index averaged 12.8 (SD 2.6), and the SMOG Index averaged 11.3 (SD 3.16). More detailed evaluation results are shown in Table S3 in Multimedia Appendix 6.

Reference Evaluation for AI Assessment

Most of the references provided in GPT-4's output effectively supported the content. A total of 88.2% (2867/3250) of the references were from actual sources (actual websites or academic papers), while 383 hallucinated references were identified. Among these 2867 real references, 2746 (95.8%) references effectively supported the content. In addition, a total of 95.1% (2724/2867) of the real references were from authoritative sources (government guidelines, health care organizations, or scientific research). More detailed evaluation results are shown in Table S4 in Multimedia Appendix 6.

The Assessment of Questions From Websites

The evaluation results of GPT-4 responses to website-sourced questions were broadly consistent with those from Reddit-derived questions across all assessments (Tables S3-S6 in Multimedia Appendix 1).

Discussion

Principal Findings

This is the first study to assess the overall quality of ChatGPT responses to real-world questions from Reddit about keloids or scars. The results revealed that the content generated by GPT-4 was generally comprehensive and aligned with current medical guidelines and the literature. Using several assessment tools, as well as plastic surgeons' evaluations, the scores were robust, and the plastic surgeons' evaluations were largely positive. The overall results indicate that GPT-4–generated content is reliable, accurate, safe, and actionable, despite there being room for improvement in terms of readability and hallucination.

Over 80% of dermatology outpatients obtain medical information through social media or the internet, with 47% considering it an important source of information [28]. Although patients have access to a wealth of information, studies evaluating the quality of online health information have identified significant deficiencies [29]. As for scars and keloids, the information available to patients contains a lot of low-quality content. A previous study assessing 88 websites related to "burn scars" showed that most of the commercial websites provided information of moderate to poor quality [13]. In contrast, LLMs provide a broad range of fundamentally accurate information and real-time dynamic interactions compared to traditional webpages [30,31]. As a leading LLM, GPT-4 exhibits certain advantages over other LLMs and has demonstrated top-tier performance across diverse evaluations in health care. In answering questions from the American Board of Surgery In-Training Examination, GPT-4 achieved an accuracy rate comparable to that of Copilot, while significantly outperforming Gemini [32]. In other fields of clinical medicine, GPT-4 also attained superior performance relative to other LLMs [33,34]. However, in a substantial number of evaluative scenarios, the performance of GPT-4 did not yield statistically significant differences when compared with Copilot or Gemini. Collectively, the performance of GPT-4 currently represents the best capability of LLMs.

In our study, experienced plastic surgeons evaluated the outputs of GPT-4, confirming that the contents were reliable and accurate. The accuracy of GPT-4 in patient education has also been studied in other clinical contexts (eg, rhinoplasty, sleep apnea, and prostate cancer) where it demonstrated high accuracy and strong reliability [24,35,36]. Such high accuracy and reliability suggest that LLMs such as GPT-4 can effectively address clinical questions from patients with scars or keloids, serving as a valuable auxiliary tool in clinical medicine.

Despite GPT-4's significant potential in responding to keloid or scar patient queries, its outputs commonly had high reading difficulty. Our study revealed that the average reading level of GPT-4–generated content was at a high school level. The results suggest that ChatGPT does not always meet the comprehension needs of all patients. The relatively low readability of GPT-4 can hinder accessibility for certain socioeconomic populations with limited health literacy [37]. Among the latest generation of young adults in the United States, up to 13% have not graduated from high school. This rate reaches 20% among people of color (including African Americans and Native Americans) [38], who are also identified as high-risk groups for developing malignant scars [39]. Due to poor readability, GPT-4 has apparent barriers in its application among these populations [40,41]. To enhance the utility of LLMs for populations with lower educational attainment, it is recommended that developers consider training specialized LLMs based on datasets with good readability [42]. Biomedical text can be simplified through hyperparameter substitution techniques, improving patient understanding [43]. In addition, structured prompting can also contribute to enhancing readability [44].

XSL•FO
RenderX

Moreover, our study also revealed the existence of hallucination, where GPT-4 cited nonexistent references or websites. Fabricated references not only mislead readers and distort their understanding of keloid or scar but also—given the presence of numerous seemingly authoritative yet false information sources—may lead patients to overtrust the content generated by GPT-4 [45,46]. Given the presence of hallucinations, specific clinical diagnosis and treatment must rely on clinicians; LLMs can only serve as auxiliary tools. To address the hallucination issue in LLMs, it is recommended that developers effectively apply retrieval-augmented generation to retrieve documents from an external corpus (such as academic library systems), as this can significantly reduce the hallucinations [47-49]. Integrating external, structured knowledge sources (such as knowledge graphs, databases, or other domain-specific resources) into LLMs can also help ensure that LLMs produce responses with fewer hallucinations [50]. Furthermore, prompt engineering can mitigate hallucination by improving the reasoning capabilities [51].

GPT-4 can provide comprehensive and generally accurate information, which can further assist patients with keloids or scars in accessing timely and precise information. However, current LLMs exhibit limitations, such as hallucinations and relatively low readability; therefore, they are not recommended as the sole source of information for patients. Limited by the lack of clinical background in current LLMs; the insufficient ability to process audio, image, and video information; limited ability to access academic libraries; and the noninterpretability of black box algorithms, current LLMs still require further development to be adapted for applications in health care [52]. The AI agent, as a promising approach, can extend the capabilities of LLMs by enabling them to use external tools, plan and execute multistep tasks, as well as interact dynamically [53]. Multimodal LLM is promising to process text (eg, clinical notes and user-input questions), medical images (eg, photos and computed tomography scans), and videos (eg, treatment procedures) provided by patients, which will more effectively assist patients and health care providers in clinical practice about keloid and scar management [54].

Limitations

Most of the questions collected from Reddit were posts from patients who had not yet sought medical care. Consequently, the questions posed may be biased toward pretreatment information needs, as fewer questions were reported during the treatment phase. This may compromise the generalizability of GPT-4's evaluation across different patient care stages. In addition, Reddit users are concentrated in the age group of 18 to 49 years, with an average age of 23 years, and the majority are aged under 30 years. Thus, the data collected from Reddit clearly fails to represent the middle-aged and older population [55]. Relying solely on Reddit posts for data collection introduces demographic selection bias.

In terms of assessment tools, the qualitative assessment conducted by experienced plastic surgeons was inherently at risk of bias, given the surgeons' attitudes toward the use of GPT-4. Nevertheless, they provided valuable insights owing to their in-depth understanding of scar and keloid education materials. Furthermore, exploratory assessment tools (DISCERN-AI, PEMAT-AI, and NLAT-AI) were used in this study, while their validity requires further testing. LLMs differ from traditional printed educational materials in that their responses to repeated queries of the same question are generated instantaneously and may vary. Currently, existing assessment tools lack the ability to detect such variability in LLM outputs when the same question is posed multiple times [56]. Furthermore, content generated by LLMs is often conveyed with excessive certainty, as these models lack the ability to accurately express information involving uncertainties. Providing definitive answers to such uncertain content may mislead patients, yet current assessment scales fail to evaluate this critical limitation [57,58]. Further research is needed to develop specific tools to enable more robust evaluation of LLM output quality.

Conclusions

Our analysis found that GPT-4 provided high-quality responses to real-world questions related to scars and keloids, suggesting its potential as a useful patient education tool in scar and keloid treatment. The GPT-4 outputs were generally reliable and accurate but need improvement, primarily in readability and hallucinations.

Funding

This study is funded by the Talent Fund of Guizhou Provincial People's Hospital (awarded to MR; [2023]-30).

Data Availability

The datasets generated or analyzed during this study are available from the corresponding author on reasonable request.

Conflicts of Interest

None declared.

Multimedia Appendix 1
Patient Education Materials Assessment Tool for Artificial Intelligence for evaluating the understandability (8 items) and actionability (3 items) of artificial intelligence–generated patient education text.
[DOCX File, 18 KB - medinform_v14i1e78838_app1.docx]

XSL•FO
RenderX

Multimedia Appendix 2
DISCERN-AI tool (7 core items) for assessing artificial intelligence–generated treatment information quality, with 1-3 scoring for each item (relevance, source clarity, date transparency, balance, additional support, uncertainty acknowledgment, and overall quality).
[DOCX File, 21 KB - medinform_v14i1e78838_app2.docx]

Multimedia Appendix 3
Natural Language Assessment Tool for Artificial Intelligence assessment framework: 5 domains (accuracy, safety, appropriateness, actionability, and effectiveness).
[DOCX File, 24 KB - medinform_v14i1e78838_app3.docx]

Multimedia Appendix 4
Reference Evaluation for AI assessment criteria: 3-item tool for validating artificial intelligence–generated references (real or fabricated, content support, and authoritative source status) on large language model reference hallucinations.
[DOCX File, 20 KB - medinform_v14i1e78838_app4.docx]

Multimedia Appendix 5
Supplementary tables for health care website–derived scar or keloid questions: includes 38 unique questions from 3 medical websites (Table S1), intraclass correlation coefficient values for assessment tools (Table S2), and artificial intelligence output evaluation scores (Patient Education Materials Assessment Tool for Artificial Intelligence, DISCERN-AI, Global Quality Scale, Natural Language Assessment Tool for Artificial Intelligence, readability, and reference quality) for website questions (Tables S3-S6).
[DOCX File, 23 KB - medinform_v14i1e78838_app5.docx]

Multimedia Appendix 6
Supplementary tables for Reddit-derived scar or keloid questions: includes subcategory-specific artificial intelligence output evaluation scores for all 16 question groups (Patient Education Materials Assessment Tool for Artificial Intelligence, DISCERN-AI, or Global Quality Scale: Table S1; Natural Language Assessment Tool for Artificial Intelligence: Table S2; and readability metrics: Table S3) and subcategory-specific reference evaluation results (Reference Evaluation for AI) for 3250 total cited references (Table S4), plus overall aggregate scores for all assessments.
[DOCX File, 25 KB - medinform_v14i1e78838_app6.docx]

References

1. Stoica AE, Grumezescu AM, Hermenean AO, Andronescu E, Vasile BS. Scar-free healing: current concepts and future perspectives. Nanomaterials (Basel) 2020 Oct 31;10(11):2179. [doi: 10.3390/nano10112179] [Medline: 33142891]
2. Xiao Y, Sun Y, Zhu B, et al. Risk factors for hypertrophic burn scar pain, pruritus, and paresthesia development. Wound Repair Regen 2018 Mar;26(2):172-181. [doi: 10.1111/wrr.12637] [Medline: 29719102]
3. Hsieh JC, Maisel-Campbell AL, Joshi CJ, Zielinski E, Galiano RD. Daily quality-of-life impact of scars: an interview-based foundational study of patient-reported themes. Plast Reconstr Surg Glob Open 2021 Apr;9(4):e3522. [doi: 10.1097/GOX.0000000000003522] [Medline: 33868874]
4. Schouten H, Nieuwenhuis M, van der Schans C, Niemeijer A, van Zuijlen P. Considerations in determining the severity of burn scar contractures with focus on the knee joint. J Burn Care Res 2023 Jul 5;44(4):810-816. [doi: 10.1093/jbcr/irad016] [Medline: 36752774]
5. Woodward AP, Matthews CA. Outcomes of revision perineoplasty for persistent postpartum dyspareunia. Female Pelvic Med Reconstr Surg 2010 Mar;16(2):135-139. [doi: 10.1097/SPV.0b013e3181cc8702] [Medline: 22453161]
6. Waibel JS, Waibel H, Sedaghat E. Scar therapy of skin. Facial Plast Surg Clin North Am 2023 Nov;31(4):453-462. [doi: 10.1016/j.fsc.2023.06.005] [Medline: 37806679]
7. Gomolin T, Cline A, Ginsberg D, Safai B. Scar tissue I wish you saw: patient expectations regarding scar treatment. J Cosmet Dermatol 2021 Sep;20(9):2739-2742. [doi: 10.1111/jocd.13945] [Medline: 33434326]
8. Cho SB, Ryu DJ, Lee SJ, et al. Scar characteristics and treatment expectations: a survey of 589 patients. J Cosmet Laser Ther 2009 Dec;11(4):224-228. [doi: 10.3109/14764170903341723] [Medline: 19951193]
9. Andrews N, Jones LL, Moiemen N, et al. Below the surface: parents' views on the factors that influence treatment adherence in paediatric burn scar management - a qualitative study. Burns 2018 May;44(3):626-635. [doi: 10.1016/j.burns.2017.09.003] [Medline: 29031888]
10. Jiang S, Beaudoin CE. Health literacy and the internet: an exploratory study on the 2013 HINTS survey. Comput Human Behav 2016 May;58:240-248. [doi: 10.1016/j.chb.2016.01.007]
11. Battineni G, Baldoni S, Chintalapudi N, et al. Factors affecting the quality and reliability of online health information. Digit Health 2020;6:2055207620948996. [doi: 10.1177/2055207620948996] [Medline: 32944269]

XSL•FO
RenderX

12. Khaleel I, Wimmer BC, Peterson GM, et al. Health information overload among health consumers: a scoping review. Patient Educ Couns 2020 Jan;103(1):15-32. [doi: 10.1016/j.pec.2019.08.008] [Medline: 31451363]
13. Bohacek L, Gomez M, Fish JS. An evaluation of internet sites for burn scar management. J Burn Care Rehabil 2003;24(4):246-251. [doi: 10.1097/01.BCR.0000075844.04297.D9] [Medline: 14501424]
14. Li J, Dada A, Puladi B, Kleesiek J, Egger J. ChatGPT in healthcare: a taxonomy and systematic review. Comput Methods Programs Biomed 2024 Mar;245:108013. [doi: 10.1016/j.cmpb.2024.108013] [Medline: 38262126]
15. Neha F, Bhati D, Shukla DK, Amiruzzaman M. ChatGPT: transforming healthcare with AI. AI 2024;5(4):2618-2650. [doi: 10.3390/ai5040126]
16. Jowsey T, Stokes-Parish J, Singleton R, Todorovic M. Medical education empowered by generative artificial intelligence large language models. Trends Mol Med 2023 Dec;29(12):971-973. [doi: 10.1016/j.molmed.2023.08.012] [Medline: 37718142]
17. Iqbal U, Lee LTJ, Rahmanti AR, Celi LA, Li YCJ. Can large language models provide secondary reliable opinion on treatment options for dermatological diseases? J Am Med Inform Assoc 2024 May 20;31(6):1341-1347. [doi: 10.1093/jamia/ocae067] [Medline: 38578616]
18. Lee R. Close encounters of the AI kind: the increasingly human-like way people are engaging with language models.: Elon University URL: https://imaginingthedigitalfuture.org/reports-and-publications/close-encounters-of-the-ai-kind/close-encounters-of-the-ai-kind-main-report [accessed 2025-11-26]
19. Gencer G, Gencer K. Large language models in healthcare: a bibliometric analysis and examination of research trends. J Multidiscip Healthc 2025;18:223-238. [doi: 10.2147/JMDH.S502351] [Medline: 39844924]
20. Kumar D, Sood SK, Rawat KS. Empowering elderly care with intelligent IoT-driven smart toilets for home-based infectious health monitoring. Artif Intell Med 2023 Oct;144:102666. [doi: 10.1016/j.artmed.2023.102666] [Medline: 37783534]
21. Kumar D, Rawat KS, Sood SK. Revolution of artificial intelligence and IOT in healthcare: a keyword co-occurrence network analysis using CiteSpace. In: Shukla AK, Thakur DG, Arabkoohsar A, editors. Recent Advances in Mechanical Engineering 2023:231-237. [doi: 10.1007/978-981-99-2349-6_20]
22. Wang J, Patel P, Jagdeo J. An analysis of keloid patient questions on Reddit. Wound Repair Regen 2024;32(2):164-170. [doi: 10.1111/wrr.13160] [Medline: 38372454]
23. Campbell DJ, Estephan LE, Sina EM, et al. Evaluating ChatGPT responses on thyroid nodules for patient education. Thyroid 2024 Mar;34(3):371-377. [doi: 10.1089/thy.2023.0491] [Medline: 38010917]
24. Gibson D, Jackson S, Shanmugasundaram R, et al. Evaluating the efficacy of ChatGPT as a patient education tool in prostate cancer: multimetric assessment. J Med Internet Res 2024 Aug 14;26:e55939. [doi: 10.2196/55939] [Medline: 39141904]
25. Cassidy JT, Baker JF. Orthopaedic patient information on the world wide web: an essential review. J Bone Joint Surg Am 2016 Feb 17;98(4):325-338. [doi: 10.2106/JBJS.N.01189] [Medline: 26888683]
26. Readable. Our Readability Checker helps you to communicate clearly. URL: https://readable.com [accessed 2026-02-24]
27. Alkaissi H, McFarlane SI. Artificial hallucinations in ChatGPT: implications in scientific writing. Cureus 2023 Feb;15(2):e35179. [doi: 10.7759/cureus.35179] [Medline: 36811129]
28. AlGhamdi KM, Almohideb MA. Internet use by dermatology outpatients to search for health information. Int J Dermatol 2011 Mar;50(3):292-299. [doi: 10.1111/j.1365-4632.2010.04705.x] [Medline: 21342162]
29. Zhang Y, Kim Y. Consumers' evaluation of web-based health information quality: meta-analysis. J Med Internet Res 2022 Apr 28;24(4):e36463. [doi: 10.2196/36463] [Medline: 35482390]
30. Monib WK, Qazi A, Mahmud MM. Exploring learners' experiences and perceptions of ChatGPT as a learning tool in higher education. Educ Inf Technol 2025 Jan;30(1):917-939. [doi: 10.1007/s10639-024-13065-4]
31. Jin Y, Liu H, Zhao B, Pan W. ChatGPT and mycosis- a new weapon in the knowledge battlefield. BMC Infect Dis 2023 Oct 27;23(1):731. [doi: 10.1186/s12879-023-08724-9] [Medline: 37891532]
32. Sanli AN, Tekcan Sanli DE, Karabulut A. Can American Board of Surgery in Training Examinations be passed by large language models? Comparative assessment of Gemini, Copilot, and ChatGPT. Am Surg 2025 Nov;91(11):1923-1929. [doi: 10.1177/00031348251341956] [Medline: 40353502]
33. Gill GS, Tsai J, Moxam J, Sanghvi HA, Gupta S. Comparison of Gemini Advanced and ChatGPT 4.0's performances on the Ophthalmology Resident Ophthalmic Knowledge Assessment Program (OKAP) examination review question banks. Cureus 2024 Sep;16(9):e69612. [doi: 10.7759/cureus.69612] [Medline: 39421095]
34. Tan YZ, Nah SA, Saw SN, Rajandram R, Ong TA. Evaluating the performance of artificial intelligence chatbots in answering urology questions derived from guidelines or board examinations: a systematic review. Urol Sci 2025:10. [doi: 10.1097/us9.0000000000000089]
35. Lim B, Seth I, Kah S, et al. Using generative artificial intelligence tools in cosmetic surgery: a study on rhinoplasty, facelifts, and blepharoplasty procedures. J Clin Med 2023 Oct 14;12(20):6524. [doi: 10.3390/jcm12206524] [Medline: 37892665]
36. Incerti Parenti S, Bartolucci ML, Biondi E, et al. Online patient education in obstructive sleep apnea: ChatGPT versus Google search. Healthcare (Basel) 2024 Sep 5;12(17):1781. [doi: 10.3390/healthcare12171781] [Medline: 39273804]
37. Toiv A, Saleh Z, Ishak A, et al. Digesting digital health: a study of appropriateness and readability of ChatGPT-generated gastroenterological information. Clin Transl Gastroenterol 2024 Nov 1;15(11):e00765. [doi: 10.14309/ctg.0000000000000765] [Medline: 39212302]

XSL•FO
RenderX

38. Veronique I. Report on the condition of education 2024. : Institute of Education Sciences; 2024 URL: https://nces.ed.gov/pubs2024/2024144.pdf
39. Oei F, Putra IB, Jusuf NK. The relationship between skin color and keloid. Bali Med J 2021;10(2):835-838. [doi: 10.15562/bmj.v10i2.2619]
40. DeTemple DE, Meine TC. Comparison of the readability of ChatGPT and Bard in medical communication: a meta-analysis. BMC Med Inform Decis Mak 2025 Sep 1;25(1):325. [doi: 10.1186/s12911-025-03035-2] [Medline: 40890707]
41. Whittaker P, Sun M. Quality and readability of chatbot responses to patient questions: a systematic cross-sectional meta-synthesis. Health Informatics J 2025;31(4):14604582251388879. [doi: 10.1177/14604582251388879] [Medline: 41106853]
42. Li M, Zhang Y, Li Z, et al. From quantity to quality: boosting LLM performance with self-guided data selection for instruction tuning. Presented at: Proceedings of the 2024 Conference of the North American Chapter of the Association for Computational Linguistics; Jun 16-21, 2024; Mexico City, Mexico p. 7602-7635. [doi: 10.18653/v1/2024.naacl-long.421]
43. Swanson K, He S, Calvano J, et al. Biomedical text readability after hypernym substitution with fine-tuned large language models. PLOS Digit Health 2024 Apr;3(4):e0000489. [doi: 10.1371/journal.pdig.0000489] [Medline: 38625843]
44. Daulat SR, Dholaria N, Burnet G, et al. Prompt engineering and follow-up questioning improves the readability of spine surgery questions in large language models. World Neurosurg 2025 Nov;203:124423. [doi: 10.1016/j.wneu.2025.124423] [Medline: 40889596]
45. Aljohani M, Hou J, Kommu S, Wang X. A comprehensive survey on the trustworthiness of large language models in healthcare. Presented at: Proceedings of the 2025 Findings of the Association for Computational Linguistics EMNLP'25; Nov 4-9, 2025; Suzhou, China p. 6720-6748. [doi: 10.18653/v1/2025.findings-emnlp.356]
46. Kim Y, Jeong H, Chen S, et al. Medical hallucination in foundation models and their impact on healthcare. Health Systems and Quality Improvement. Preprint posted online on 2025. [doi: 10.1101/2025.02.28.25323115]
47. Zhang W, Zhang J. Hallucination mitigation for retrieval-augmented large language models: a review. Mathematics 2025;13(5):856. [doi: 10.3390/math13050856]
48. Bhattacharya R. Strategies to mitigate hallucinations in large language models. AMA 2024;10(1):62. [doi: 10.69554/NXXB8234]
49. Wołk K. Evaluating retrieval-augmented generation variants for clinical decision support: hallucination mitigation and secure on-premises deployment. Electronics (Basel) 2025;14(21):4227. [doi: 10.3390/electronics14214227]
50. Agrawal G, Kumarage T, Alghamdi Z, Liu H. Can knowledge graphs reduce hallucinations in LLMs?: a survey. Presented at: Proceedings of the 2024 Conference of the North American Chapter of the Association for Computational Linguistics; Jun 16-21, 2024; Mexico City, Mexico p. 3947-3960. [doi: 10.18653/v1/2024.naacl-long.219]
51. Zhang H, Deng H, Ou J, Feng C. Mitigating spatial hallucination in large language models for path planning via prompt engineering. Sci Rep 2025;15(1):8881. [doi: 10.1038/s41598-025-93601-5]
52. Busch F, Hoffmann L, Rueger C, et al. Current applications and challenges in large language models for patient care: a systematic review. Commun Med (Lond) 2025 Jan 21;5(1):26. [doi: 10.1038/s43856-024-00717-2] [Medline: 39838160]
53. Ferrag MA, Tihanyi N, Debbah M. From LLM reasoning to autonomous ai agents: a comprehensive review. arXiv. Preprint posted online on Apr 28, 2025. [doi: 10.48550/arXiv.2504.19678]
54. AlSaad R, Abd-Alrazaq A, Boughorbel S, et al. Multimodal large language models in health care: applications, challenges, and future outlook. J Med Internet Res 2024 Sep 25;26:e59505. [doi: 10.2196/59505] [Medline: 39321458]
55. Reddit user age, gender, & demographics. Exploding Topics. 2025. URL: https://explodingtopics.com/blog/reddit-users [accessed 2025-11-26]
56. Calloway C. Why do different LLMs give different answers to the same question? Model uncertainty and variability in LLM-based intrusion detection systems ranking: Norfolk State University; 2025. URL: https://digitalcommons.odu.edu/cgi/viewcontent.cgi?article=1123&context=covacci-undergraduateresearch [accessed 2024-05-20]
57. Yona G, Aharoni R, Geva M. Can large language models faithfully express their intrinsic uncertainty in words? Presented at: Proceedings of the 2024 Conference on Empirical Methods in Natural Language Processing; Nov 12-16, 2024; Miami, FL p. 632-702. [doi: 10.18653/v1/2024.emnlp-main.443]
58. Fu T, Conde J, Martínez G, Grandury M, Reviriego P. Multiple choice questions: reasoning makes large language models (LLMS) more self-confident even when they are wrong. arXiv. Preprint posted online on Jan 16, 2025. [doi: 10.48550/arXiv.2501.09775]

Abbreviations

AI: artificial intelligence
GQS: Global Quality Scale
ICC: intraclass correlation coefficient
LLM: large language model
NLAT-AI: Natural Language Assessment Tool for Artificial Intelligence
PEMAT: Patient Education Materials Assessment Tool

XSL•FO
RenderX

SMOG: Simple Measure of Gobbledygook

Edited by A Benis; submitted 10.Jun.2025; peer-reviewed by BAF Assunção, F Fukuzawa, J Klewer, KS Rawat; accepted 29.Dec.2025; published 27.Feb.2026.

Please cite as:
Rao M, Xiujun T, Haoyu W
Evaluating GPT-4 Responses on Scars or Keloids for Patient Education: Large Language Model Evaluation Study
JMIR Med Inform 2026;14:e78838
URL: https://medinform.jmir.org/2026/1/e78838
doi:10.2196/78838

© Mingjun Rao, Tang Xiujun, Wang Haoyu. Originally published in JMIR Medical Informatics (https://medinform.jmir.org), 27.Feb.2026. This is an open-access article distributed under the terms of the Creative Commons Attribution License (https://creativecommons.org/licenses/by/4.0/), which permits unrestricted use, distribution, and reproduction in any medium, provided the original work, first published in JMIR Medical Informatics, is properly cited. The complete bibliographic information, a link to the original publication on https://medinform.jmir.org/, as well as this copyright and license information must be included.

XSL•FO
RenderX

Original Paper

Large Language Models in Patient Health Communication for Atherosclerotic Cardiovascular Disease: Pilot Cross-Sectional Comparative Analysis

Pengfei Li[1*], MD; Yinfei Xu[1*], MD; Xiang Liu[2*], MD; Zhean Shen[1*], MD; Yi Wang[1], MD; Xinyi Lv[1], MD; Ziyi Lu[1], MD; Hui Wu[1], MD; Jiaqi Zhuang[1], MD; Yan Chen[1,3,4], MD

[1]Department of Emergency and Critical Care Medicine, The Affiliated Suzhou Hospital of Nanjing Medical University, Suzhou Municipal Hospital, Gusu School, Nanjing Medical University, Suzhou, Jiangsu, China

[2]Department of Rehabilitation, Shandong Provincial Hospital Affiliated to Shandong First Medical University, Jinan, Shandong, China

[3]Department of Emergency Management, School of Health Policy & Management, Nanjing Medical University, Nanjing, Jiangsu, China

[4]Department of Emergency and Critical Care Medicine, The First Affiliated Hospital of Nanjing Medical University, Nanjing, Jiangsu, China

[*]these authors contributed equally

Corresponding Author:
Yan Chen, MD
Department of Emergency and Critical Care Medicine
The Affiliated Suzhou Hospital of Nanjing Medical University
Suzhou Municipal Hospital, Gusu School, Nanjing Medical University
140 Hanzhong Rd
Suzhou, Jiangsu, 210029
China
Phone: 86 512 6515 53
Email: chenyandoc@njmu.edu.cn

Abstract

Background: Large language models (LLMs) have emerged as promising tools for enhancing public access to medical information, particularly for chronic diseases such as atherosclerotic cardiovascular disease (ASCVD). However, their effectiveness in patient-centered health communication remains underexplored, especially in multilingual contexts.

Objective: Our study aimed to conduct a comparative evaluation of 3 advanced LLMs—DeepSeek R1, ChatGPT-4o, and Gemini—in generating responses to ASCVD-related patient queries in both English and Chinese, assessing their performance across the domains of accuracy, completeness, and comprehensibility.

Methods: We conducted a cross-sectional evaluation based on 25 clinically validated ASCVD questions spanning 5 domains—definitions, diagnosis, treatment, prevention, and lifestyle. Each question was submitted 5 times to each of the 3 LLMs in both English and Chinese, yielding 750 responses in total, all generated under default settings to approximate real-world conditions. Three board-certified cardiologists blinded to model identity independently scored the responses using standardized Likert scales with predefined anchors. The assessment followed a rigorous multistage process that incorporated randomization, washout periods, and final consensus scoring.

Results: DeepSeek R1 achieved the highest "good response" rates (24/25, 96% in both English and Chinese), substantially outperforming ChatGPT-4o (21/25, 84%) and Gemini (12/25, 48% in English and 17/25, 68% in Chinese). DeepSeek R1 demonstrated superior median accuracy scores (6, IQR 6-6 in both languages) and completeness scores (3, IQR 2-3 in both languages) compared to the other models (P<.001). All models had a median comprehensibility score of 3; however, in English, DeepSeek R1 and ChatGPT-4o were rated significantly clearer than Gemini (P=.006 and P=.03, respectively), whereas no significant between-model differences were observed in Chinese (P=.08). Interrater reliability was moderate (Kendall W: accuracy=0.578; completeness=0.565; comprehensibility=0.486). Performance was consistently stronger for definitional and diagnostic questions than for treatment and prevention topics across all models. Specifically, none of the models consistently provided responses aligned with the latest clinical guidelines for the following key guideline-facing question "What is the standard treatment regimen for ASCVD?"

Conclusions: DeepSeek R1 exhibited promising and consistent performance in generating high-quality, patient-facing ASCVD information across both English and Chinese, highlighting the potential of open-source LLMs in promoting digital health literacy

XSL•FO
RenderX

and equitable access to chronic disease information. However, a clinically critical weakness was observed in guideline-sensitive treatment: the models did not reliably provide guideline-concordant standard treatment regimens, suggesting that LLM use should be limited to lower-risk informational subqueries (eg, definitions, diagnosis, and lifestyle education) unless augmented by expert oversight and safety controls.

(JMIR Med Inform 2026;14:e81422) doi:10.2196/81422

KEYWORDS

atherosclerotic cardiovascular disease; large language models; DeepSeek R1; ChatGPT-4o; Gemini; artificial intelligence; AI

Introduction

Atherosclerotic cardiovascular disease (ASCVD) is a major public health concern worldwide, significantly affecting morbidity and mortality rates and contributing to the global burden of disease [1]. Effective management and prevention strategies are paramount in reducing its impact on human health and longevity. In recent years, the development of advanced natural language processing technologies, particularly large language models (LLMs), has introduced a novel paradigm in health care communication [2]. LLMs are deep learning models trained on massive corpora of text data, enabling them to generate humanlike responses, summarize complex information, and interact with users in natural language. Models such as ChatGPT exemplify this technological advancement, offering scalable tools for disseminating medical information and supporting patient education, with the potential to enhance chronic disease prevention and self-management [3,4].

Despite their promise, the application of LLMs in health care—especially in clinical decision-making—remains constrained by several limitations [5,6]. First, LLMs do not inherently possess medical reasoning capabilities; their outputs are generated based on learned language patterns rather than grounded clinical judgment [7]. This introduces risks of producing plausible-sounding but clinically inappropriate advice. Second, the variability in training data sources and lack of domain-specific fine-tuning may result in inconsistent or outdated information [8]. Finally, while individual models may excel in certain tasks, performance can vary widely across different LLMs, especially in medical settings where accuracy and contextual appropriateness are vital [9]. Therefore, rigorous comparative evaluations are needed to identify the models that are most reliable, transparent, and suitable for patient-centered communication within health care and public health contexts.

To our knowledge, there have been no studies specifically focused on the performance of LLMs in providing information about ASCVD. Therefore, this study aimed to assess the performance of various advanced LLMs (ChatGPT-4o [OpenAI], Gemini [Google], and DeepSeek R1) in delivering accurate, comprehensive, and comprehensible information related to ASCVD. Using open-ended questions and simulated patient scenarios, we evaluated the quality and reliability of responses from a patient-centered perspective.

Methods

Question Design and Acquisition of Responses

Our study was conducted from May 15 to 30, 2025. Three qualified physicians (PL, YX, and YW) devised 25 comprehensive questions based on common concerns of patients regarding ASCVD, focusing on patient-centered care and disease management. These queries covered definitions, diagnosis, treatment, prevention, and lifestyle. To mitigate language bias and evaluate multilingual performance, each question was posed in both English and Chinese. To reduce randomness and assess response consistency, each question was submitted 5 separate times to 3 state-of-the-art LLMs—DeepSeek R1, ChatGPT-4o, and Gemini—in both languages, generating a total of 750 responses (25 questions × 3 models × 2 languages × 5 repetitions). To simulate real-world use scenarios, all models were assessed using their default, publicly available versions without any parameter adjustments (eg, temperature, maximum tokens, or top-p nucleus sampling). Crucially, the web-browsing or retrieval-augmented generation capabilities enabled by default in these public interfaces were allowed to function. This ensured that our findings reflected the typical performance accessible to end users who rely on these tools for real-time information retrieval. Each chat was conducted using the “new chat” function to avoid bias from correlation interference and ensure that each session was unaffected by previous prompts. All generated responses were exported as plain text. For DeepSeek R1, the reasoning content and blocks were programmatically removed before human review. Subsequently, all responses were stripped of identifying disclaimers (Figure 1). The complete set of 750 generated responses has been made publicly available in Multimedia Appendix 1 to ensure full transparency and facilitate further research.

XSL•FO
RenderX

Figure 1. Deidentification and preprocessing of model outputs before blinded scoring: raw large language model responses were exported as plain text and stripped of disclaimers and model-identifying metadata, yielding anonymized text for review by 3 cardiologists.

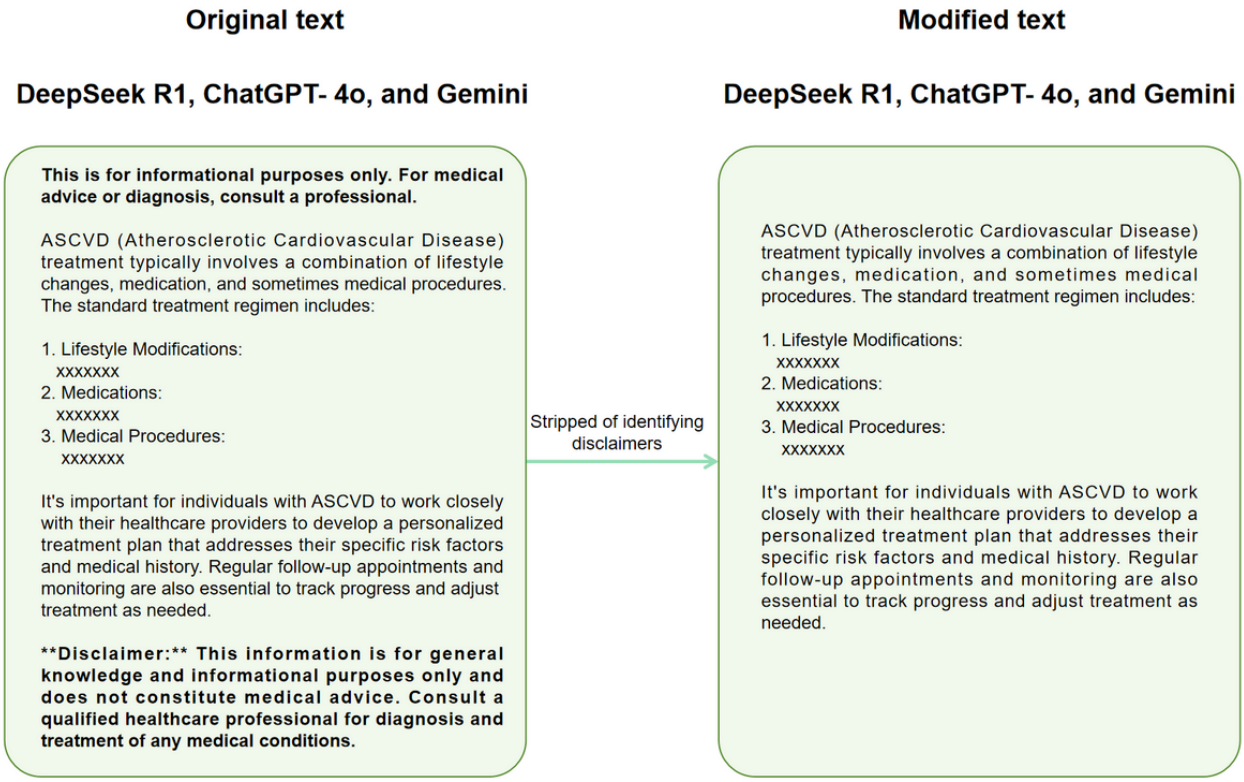

Assessment Methodology

An evaluation panel of 3 board-certified cardiologists assessed the model outputs through a rigorous multistage process. For each of the 25 questions in both languages, 5 independent responses were generated per model. To avoid model selection bias, responses were randomly shuffled within their respective question sets, ensuring that the reviewers remained unaware of the specific language model that generated each response.

To minimize memory bias, 3 cardiologists independently assessed the responses in 3 separate rounds, each conducted on a distinct day with an overnight washout period. Assessments were benchmarked primarily to the 2021 European Society of Cardiology guidelines for cardiovascular disease prevention and the 2024 guidelines for managing chronic coronary syndromes, with cross-checks against the 2025 ACC/AHA/ACEP/NAEMSP/SCAI Guideline for the Management of Patients With Acute Coronary Syndromes [10-12]. We verified that no major guideline updates relevant to our end points were released during the evaluation window (May 15-30, 2025). Using predefined anchors detailed in Table S1 in Multimedia Appendix 2, each reviewer rated every response on 3 dimensions: accuracy (6-point Likert scale: 1="completely incorrect"; 6="completely correct"), completeness (3-point Likert scale: 1="incomplete"; 3="complete"), and comprehensibility (3-point Likert scale: 1="difficult to understand"; 3="easy to understand") [13]. The scoring protocol comprised 3 steps. First, for each question, each model generated 5 responses; the 3 reviewers independently rated every response on the 3 dimensions. Second, the reviewers convened to finalize one consensus score per response per dimension: identical ratings were carried forward, whereas discrepancies were resolved through discussion until unanimity was reached—or, if needed, with brief input from a senior cardiologist. Third, for each question, the arithmetic mean of the 5 consensus scores served as the final per-question score; because per-question scores were nonnormally distributed, between-platform comparisons used the median of the 25 per-question scores. Detailed scoring procedures for the blinded assessment are provided in Tables S2 to S4 in Multimedia Appendix 2.

The overall study design and process are illustrated in Figure 2. We established the following quality thresholds based on the arithmetic mean of the 5 repeated responses per question: an accuracy score of at least 4 was considered acceptable, whereas a score of at least 2 was required for both comprehensibility and completeness. Within the acceptable performance levels, we introduced a new concept called "good response" to facilitate the comparison of the LLMs' excellent responses. A "good response" was defined as having a mean accuracy score of ≥4, mean comprehensibility and completeness scores of ≥2, and a mean total score (sum of accuracy, completeness, and comprehensibility) score of ≥10. The total score threshold (10) was intentionally set higher than the sum of the minimum component scores (8) to ensure that a "good response" exceeded the baseline requirements in at least one dimension (eg, higher accuracy or completeness) rather than merely meeting the minimum acceptable standard in all categories.

XSL•FO
RenderX

Figure 2. Study design and data flow for the blinded comparison of large language models on atherosclerotic cardiovascular disease (ASCVD) questions. Outputs were generated under default settings; all model-identifying markers and disclaimers were removed; and responses were randomized and presented model blind to cardiologists for independent rating, consensus finalization, per-question aggregation, and cross-model comparison.

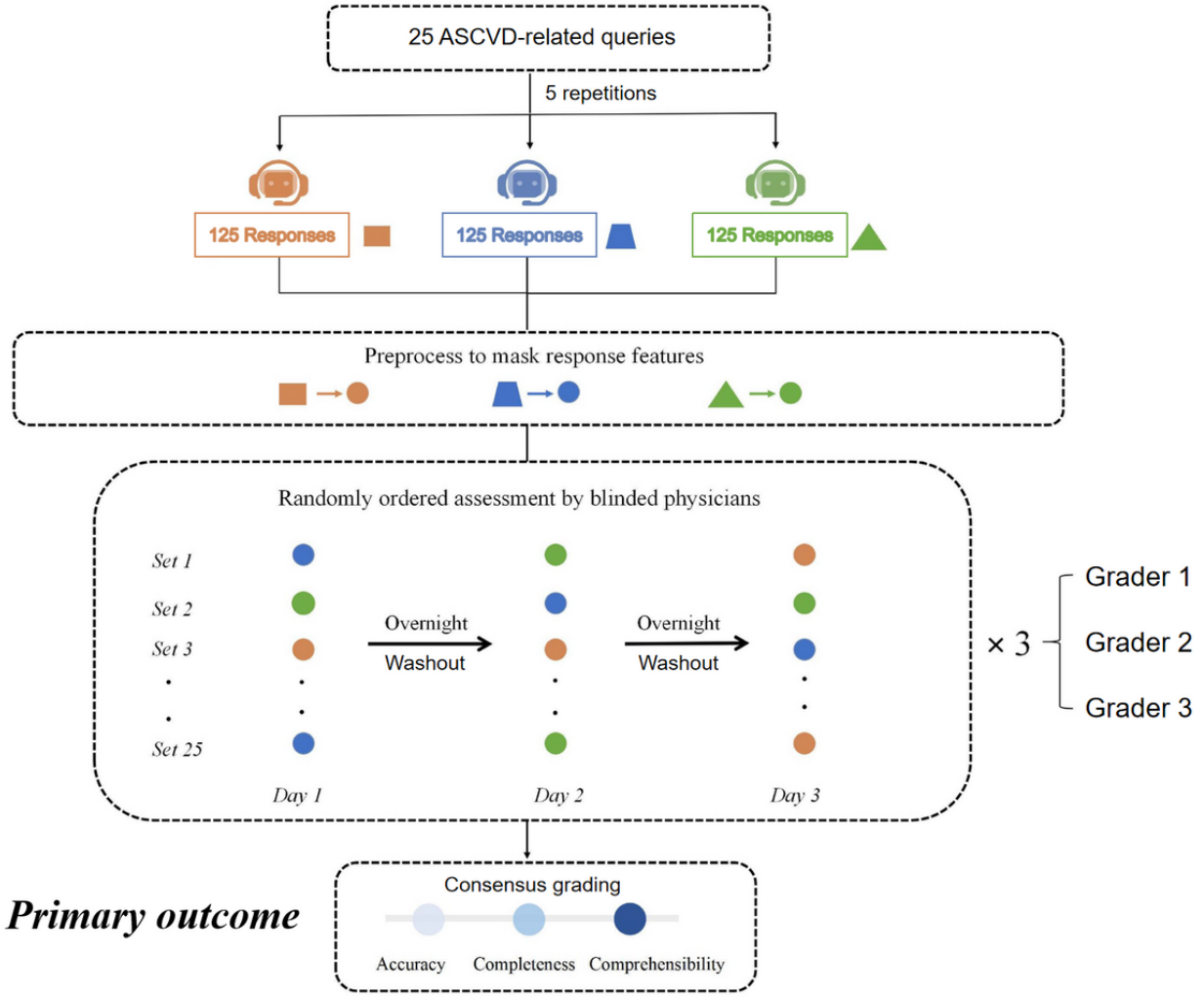

Data Analysis

All data analyses were performed using Prism (version 9.5.1; GraphPad Software) and SPSS (version 26.0; IBM Corp). Continuous variables were described using measures of central tendency and dispersion expressed as median and range. Graphical representations were used to enhance the clarity and interpretability of the data. When the data deviated from a normal distribution, differences between 2 groups were assessed using the Mann-Whitney *U* test, whereas differences among the 3 LLMs were evaluated using the Kruskal-Wallis rank sum test followed by the Dunn multiple-comparison test. The Fisher exact test was used for categorical variables. Interrater reliability was assessed using the Kendall *W* coefficient of concordance, with levels of agreement interpreted as follows: poor (0-0.2), fair (0.21-0.4), moderate (0.41-0.6), good (0.61-0.8), and excellent (0.81-1) [14]. A 2-sided *P* value of <.05 was considered statistically significant.

Ethical Considerations

The data analyzed in our study consisted of deidentified, synthetic outputs generated by LLMs in response to 25 guideline-informed ASCVD questions curated from publicly accessible sources; no patients or personal data were involved. Accordingly, participant recruitment and written informed consent were not applicable, and—per institutional policy—this work did not constitute human participant research and did not require ethics committee review.

Results

Performance

Overview

The “good response” rates for the 3 LLMs were as follows (Table 1): DeepSeek R1 achieved a “good response” rate of 96% (24/25) in both English and Chinese, outperforming ChatGPT-4o (21/25, 84%) and Gemini (12/25, 48% in English and 17/25, 68% in Chinese). Figure 3 illustrates the comparative distribution of scores across the 3 dimensions. In terms of accuracy, DeepSeek R1 maintained a dominant profile with high consistency, whereas Gemini exhibited the widest score variance. Regarding completeness, DeepSeek R1 frequently achieved maximum scores, whereas ChatGPT-4o often provided partially complete responses. Comprehensibility remained high for all models, with DeepSeek R1 and ChatGPT-4o showing slightly more stability than Gemini. Performance analysis revealed a critical pattern: model performance was consistently

XSL•FO
RenderX

and substantially weaker in the treatment domain than in all others, with "good response" rates of 80% (8/10) for DeepSeek R1, a total of 60% (6/10) for ChatGPT-4o, and 30% (3/10) for Gemini (Multimedia Appendix 3). For instance, none of the models consistently provided answers that aligned with the latest clinical guidelines in response to the question "What is the standard treatment regimen for ASCVD?" Similarly, the responses varied significantly in accuracy and detail for the question "How common is coronary artery bypass grafting (CABG) in ASCVD patients?" The following sections provide a detailed analysis of each model's performance across the domains of accuracy, completeness, and comprehensibility.

XSL•FO
RenderX

Table 1. Performance of the 3 large language models on atherosclerotic cardiovascular disease (ASCVD) questions in a blinded, bilingual evaluation. Questions spanned 5 domains (definitions, diagnosis, treatment, prevention, and lifestyle) and were scored by 3 board-certified cardiologists using predefined anchors. A "good response" was defined as an arithmetic mean score across the 5 repetitions of ≥4 for accuracy, ≥2 for completeness, and ≥2 for comprehensibility, with a mean total score (sum of accuracy, completeness, and comprehensibility) of ≥10 after consensus.

	DeepSeek English	DeepSeek Chinese	GPT-4o English	GPT-4o Chinese	Gemini English	Gemini Chinese
Good response (N=25), n (%)	24 (96)	24 (96)	21 (84)	21 (84)	12 (48)	17 (68)
Definitions						
"What is ASCVD?"	✓	✓	✓	✓		✓
"How does ASCVD develop?"	✓	✓	✓	✓		✓
"What diseases does ASCVD specifically include?"	✓	✓	✓	✓	✓	✓
"How does ASCVD affect the heart and blood vessels?"	✓	✓				
"What is the connection between ASCVD and heart disease and stroke?"	✓	✓	✓	✓		
Diagnosis						
"How can I determine my risk for ASCVD?"	✓	✓	✓	✓		
"What are the early symptoms of ASCVD?"	✓	✓	✓		✓	✓
"Which diagnostic tests are used to confirm ASCVD?"	✓	✓	✓	✓		
"Does a family history of cardiac diseases increase my risk of ASCVD?"	✓	✓	✓	✓	✓	✓
"Does my hypertension, diabetes, or hyperlipidemia increase my risk of ASCVD?"	✓	✓		✓		✓
Treatment						
"What is the standard treatment regimen for ASCVD?"						
"Is long-term use of lipid-lowering agents safe for individuals with ASCVD?"	✓	✓	✓	✓		
"Should individuals diagnosed with ASCVD undergo regular coronary angiography?"	✓	✓	✓	✓	✓	
"What are the nonpharmacological treatments for ASCVD?"	✓	✓	✓	✓	✓	✓
"How common is CABG[a] in ASCVD patients?"	✓	✓				
Prevention						
"Can I prevent ASCVD through diet?"	✓	✓	✓	✓		✓

XSL•FO
RenderX

	DeepSeek English	DeepSeek Chinese	GPT-4o English	GPT-4o Chinese	Gemini English	Gemini Chinese
"How important is physical activity in preventing ASCVD?"	✓	✓	✓	✓		✓
"Can antihypertensive and lipid-lowering medications prevent ASCVD?"	✓	✓	✓	✓		✓
"How effective is smoking cessation in preventing ASCVD?"	✓	✓	✓	✓	✓	✓
"How should I monitor my cardiovascular health?"	✓	✓	✓	✓	✓	✓
Lifestyle						
"With ASCVD, how should I adjust my dietary habits?"	✓	✓	✓	✓	✓	✓
"What types of physical activities are safe for someone with ASCVD? Are there any recommended forms of exercise?"	✓	✓	✓	✓	✓	✓
"What is the relationship between ASCVD and body weight?"	✓	✓	✓	✓	✓	✓
"How important is quitting smoking and reducing alcohol intake in managing ASCVD?"	✓	✓	✓	✓	✓	✓
"Can long-term psychological stress affect ASCVD?"	✓	✓	✓	✓	✓	✓

[a]CABG: coronary artery bypass grafting.

Figure 3. Distribution of accuracy, completeness, and comprehensibility ratings for large language model (LLM) responses to atherosclerotic cardiovascular disease–related questions. (A) Shows the distribution of accuracy scores across LLMs. (B) Shows the distribution of completeness scores across LLMs. (C) Shows the distribution of comprehensibility scores across LLMs.

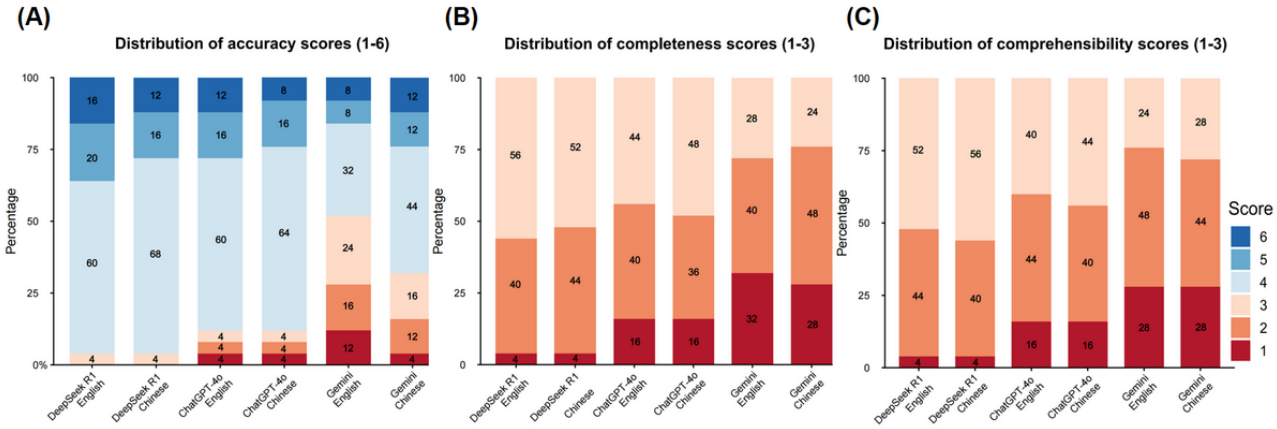

Accuracy

Regarding accuracy, 97% (146/150) of the questions met the acceptable standard, with English-language responses reaching 99% (74/75) accuracy and Chinese-language responses reaching 96% (72/75) accuracy. For both English- and Chinese-language questions, the median accuracy score for DeepSeek R1 was consistently 6 (IQR 6-6 for both languages), whereas for ChatGPT-4o and Gemini, it was 5 (ChatGPT: IQR 5-6 for both languages; Gemini: IQR 4-5 for English and 5-6 for Chinese; Table 2). As detailed in Table 3, for all English-language queries, the mean accuracy score of DeepSeek R1 responses was 5.88 (SD 0.33), whereas the mean scores for ChatGPT-4o and Gemini were 5.40 (SD 0.64) and 4.84 (SD 0.68), respectively. For all Chinese-language queries, the mean

XSL•FO
RenderX

accuracy score for DeepSeek R1 responses was 5.80 (SD 0.40), whereas the mean ChatGPT-4o and Gemini scores were 5.20 (SD 0.76) and 5.00 (SD 0.86), respectively.

Table 2. Median scores for responses from the 3 large language models.

Assessment metric	DeepSeek R1, median (IQR)		ChatGPT-4o, median (IQR)		Gemini, median (IQR)	
	English	Chinese	English	Chinese	English	Chinese
Accuracy (1-6)	6 (6-6)	6 (6-6)	5 (5-6)	5 (5-6)	5 (4-5)	5 (5-6)
Completeness (1-3)	3 (2-3)	3 (2-3)	2 (2-2)	2 (2-2)	2 (2-2)	2 (2-3)
Comprehensibility (1-3)	3 (3-3)	3 (3-3)	3 (3-3)	3 (3-3)	3 (2-3)	3 (3-3)

Table 3. Mean scores for responses from the 3 large language models.

Assessment metric	DeepSeek R1, mean (SD)		ChatGPT-4o, mean (SD)		Gemini, mean (SD)	
	English	Chinese	English	Chinese	English	Chinese
Accuracy (1-6)	5.88 (0.33)	5.80 (0.40)	5.40 (0.64)	5.20 (0.76)	4.84 (0.68)	5.00 (0.86)
Completeness (1-3)	2.72 (0.45)	2.76 (0.43)	2.24 (0.43)	2.12 (0.43)	2.00 (0.57)	2.36 (0.63)
Comprehensibility (1-3)	2.96 (0.20)	2.92 (0.27)	2.88 (0.33)	2.84 (0.37)	2.64 (0.48)	2.92 (0.27)

Completeness

In terms of completeness, 95% (142/150) of responses were acceptable, including 95% (71/75) in both English and Chinese. Regardless of the language of the questions, the median completeness score for DeepSeek R1 was consistently 3 (IQR 2-3 for both languages), with ChatGPT-4o and Gemini both achieving median scores of 2 (ChatGPT: IQR 2-2 for both languages; Gemini: IQR 2-2 for English and 2-3 for Chinese; Table 2). For all English-language questions, the mean completeness score for DeepSeek R1's responses was 2.72 (SD 0.45), with ChatGPT-4o and Gemini achieving mean scores of 2.24 (SD 0.43) and 2.00 (SD 0.57), respectively. For all Chinese-language questions, the mean completeness score for responses from DeepSeek R1 was 2.76 (SD 0.43), with ChatGPT-4o and Gemini scoring a mean of 2.12 (SD 0.43) and 2.36 (SD 0.63; Table 3), respectively.

Comprehensibility

Regarding comprehensibility, all responses were at an acceptable level. Regardless of the language of the questions or the model used, the median comprehensibility score for all questions was consistently 3 (DeepSeek R1 and ChatGPT: IQR 3-3 for both languages; Gemini: IQR 2-3 for English and 3-3 for Chinese; Table 2). As shown in Table 3, for all English-language questions, the mean comprehensibility score for DeepSeek R1's responses was 2.96 (SD 0.20), whereas ChatGPT-4o and Gemini scored a mean of 2.88 (SD 0.33) and 2.64 (SD 0.48), respectively. For all Chinese-language questions, the mean comprehensibility score for DeepSeek R1 responses was 2.92 (SD 0.27), with ChatGPT-4o and Gemini scoring a mean of 2.84 (SD 0.37) and 2.92 (SD 0.27), respectively.

Interrater Reliability

For accuracy scores, the Kendall *W* coefficient of concordance ranged from 0.434 to 0.732, with a mean of 0.578 (SD 0.15). In terms of completeness scores, the coefficient varied from 0.360 to 0.782, averaging 0.565 (SD 0.21). For comprehensibility scores, the range was between 0.386 and 0.581, with a mean value of 0.486 (SD 0.10). This indicates that the scores for accuracy, completeness, and comprehensibility were at a moderate level of agreement.

Model Comparison

In the overall comparison of English- and Chinese-language questions, DeepSeek R1 consistently outperformed the other models in terms of accuracy and completeness. For English-language questions, DeepSeek R1 achieved the highest median accuracy score of 6, significantly surpassing both ChatGPT-4o and Gemini (P<.001 for each pairwise comparison), whereas ChatGPT-4o also outperformed Gemini (P=.008). All 3 models received a median comprehensibility score of 3; the difference between DeepSeek R1 and ChatGPT-4o was not significant (P=.07), although DeepSeek R1 was significantly clearer than Gemini (P=.006), and ChatGPT-4o was moderately clearer than Gemini (P=.03; reflecting significant differences in mean ranks per the Mann-Whitney *U* test despite identical medians). Regarding completeness, DeepSeek R1 again led the models, scoring significantly higher than both ChatGPT-4o and Gemini (P=.009), with ChatGPT-4o also providing more complete responses than Gemini (P=.007). For Chinese-language questions, DeepSeek R1 maintained a significant lead in accuracy over ChatGPT-4o and Gemini (P<.001 in both cases), whereas the difference between ChatGPT-4o and Gemini was not statistically significant (P=.07). All 3 models achieved the same median comprehensibility score of 3, with no significant differences (P=.08). In terms of completeness, DeepSeek R1 again outperformed both ChatGPT-4o and Gemini (P<.001), whereas no significant difference was observed between ChatGPT-4o and Gemini (P=.06). Overall, DeepSeek R1 demonstrated consistently superior performance in both accuracy and completeness across languages. Differences in comprehensibility were minor, with Gemini showing slightly lower clarity in English. These findings affirm DeepSeek R1's leading capabilities and highlight subtle language-specific variations in the outputs of the other models (Figure 4). Specific

XSL•FO
RenderX

examples of LLM failures contrasted with superior responses are detailed in Table S5 in Multimedia Appendix 2.

Figure 4. Comparison of large language model performance on atherosclerotic cardiovascular disease–related questions within languages. Scores are shown for accuracy, completeness, and comprehensibility. *P<.05; **P<.01; NS: not significant.

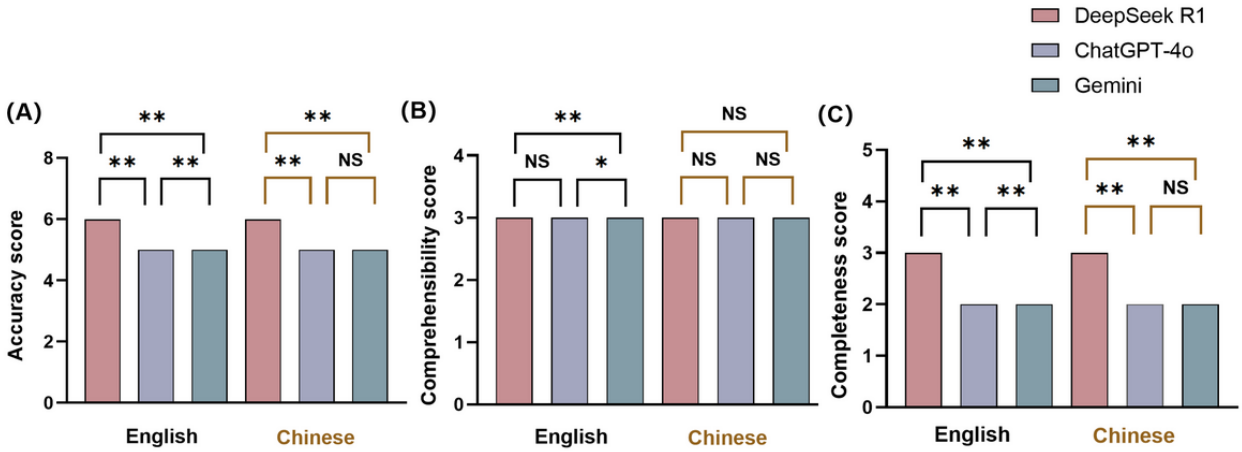

Language-Based Response Comparison

For DeepSeek R1, there were no significant differences between English and Chinese in terms of accuracy, completeness, and comprehensibility scores. Similarly, for ChatGPT-4o, there were no significant differences between English and Chinese across the same metrics, indicating a comparable performance in both languages. For Gemini, the accuracy and completeness scores showed no significant differences between English and Chinese. However, there was a significant difference in comprehensibility scores (P<.001) as the median comprehensibility score for English was 3 (IQR 2-3), whereas for Chinese, it was 3 (IQR 3-3). This indicated that the comprehensibility scores were more consistent in Chinese compared to having more variability in English (Figure 5).

Figure 5. Comparison of large language model performance on atherosclerotic cardiovascular disease–related questions across languages within models. For each model, scores for accuracy, completeness, and comprehensibility are shown for English and Chinese. **P<.01; NS: not significant.

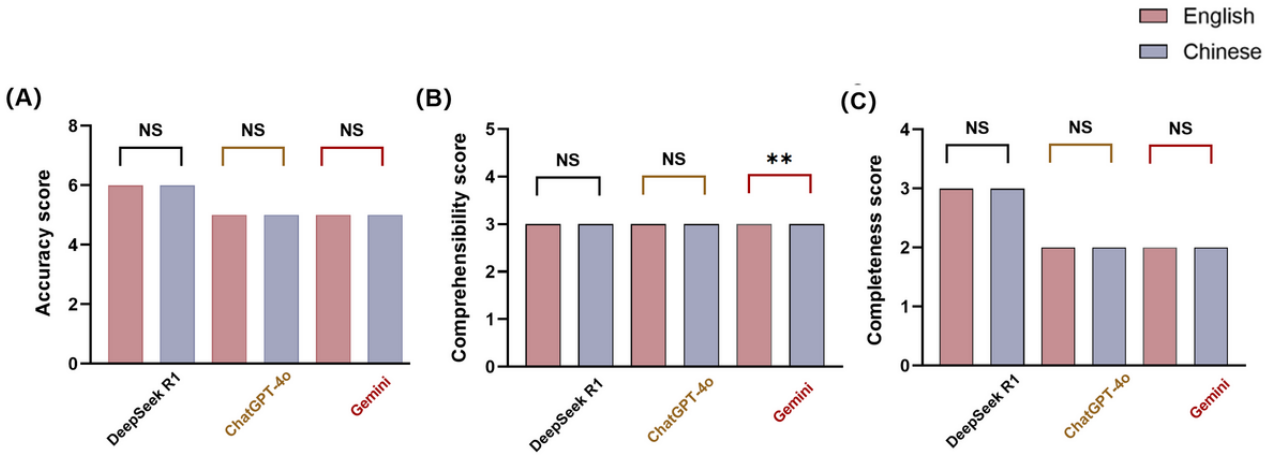

Discussion

Principal Findings

Our study evaluated the performance of 3 advanced LLMs—DeepSeek R1, ChatGPT-4o, and Gemini—in providing accurate, comprehensive, and comprehensible information on ASCVD in both English and Chinese. This evaluation was conducted using a rigorous, blinded study design that incorporated randomization, washout periods, and consensus-based physician assessments. While the widespread emergence of LLMs has significantly expanded public access to medical information—particularly for underserved or non–English-speaking populations [15,16]—concerns about their reliability persist [17,18]. By systematically evaluating multiple LLMs across languages and using patient-centered ASCVD scenarios, our study offers a more holistic perspective on their capabilities and limitations. From a public health standpoint, this approach not only highlights the potential of LLMs to enhance digital health literacy and self-management of chronic diseases but also underscores the need for ongoing oversight and model validation to prevent the spread of misinformation [19,20].

The results demonstrated that DeepSeek R1 generally outperformed the other models in terms of accuracy and completeness and also achieved a slightly higher average score for understandability. Several factors may contribute to this superior performance. DeepSeek R1 is reported to rely heavily on reinforcement learning, which may contribute to improved

XSL•FO
RenderX

logical coherence and multistep reasoning. Additionally, the model is open source under the Massachusetts Institute of Technology license and may offer lower operating costs compared to proprietary models. This open-source nature confers several advantages—including reduced dependency on commercial application programming interfaces (APIs), lower implementation costs, and the potential for institution-specific fine-tuning—making it particularly attractive for health care systems with limited technical resources [21]. Critically, this open-source architecture offers a decisive advantage for clinical implementation: data sovereignty. Unlike proprietary cloud-based models (eg, ChatGPT-4o and Gemini) that necessitate the transmission of sensitive patient data to external commercial servers—raising significant compliance challenges with regulations such as HIPAA (Health Insurance Portability and Accountability Act; United States) and the General Data Protection Regulation (Europe)—DeepSeek R1 allows for local, on-premise deployment [22,23]. Health care systems can host the model within their secure firewalls, ensuring that patient data never leave the institution's control. This capability not only resolves privacy concerns but also creates a secure environment for the aforementioned fine-tuning on proprietary medical records. Furthermore, it is important to clarify that the high comprehensibility scores in this study were achieved without the reasoning chains being visible to the raters. This indicates that DeepSeek R1's internal chain-of-thought process effectively structures the final response for clarity independent of the visible reasoning trace [24]. Taken together, these characteristics suggest that DeepSeek R1 may be a promising candidate for disseminating reliable, cost-effective, and customizable medical information in both clinical and public health contexts.

Language-based comparisons revealed no significant performance differences between English and Chinese for both DeepSeek R1 and ChatGPT-4o. Although Gemini exhibited slightly higher scores in Chinese—particularly in comprehensibility—this difference was not statistically significant, indicating that the variation likely reflects incidental model behavior rather than a systematic language-based advantage. Achieving consistent performance across languages is essential for the global applicability of LLMs in health care communication. Our evaluation indicates a consistent and clinically relevant pattern: across all 3 LLMs, recommendations in the treatment and prevention domain were less reliable than responses to definitional and diagnostic queries. This observation is consistent with external reports that therapeutic, guideline-facing tasks show variable concordance and that performance can be highly sensitive to task framing and evaluation metrics beyond headline accuracy [25-27]. Recent benchmarks likewise describe mixed adherence across clinical scenarios, underscoring the difficulty of encoding and operationalizing rapidly evolving therapeutic knowledge within free-text generation [26-28]. Taken together, these findings suggest that, without explicit retrieval and provenance controls, current general-purpose architectures may not consistently reflect the most up-to-date evidence at inference time, which in turn can pose risks in high-stakes areas such as medication dosing and care timing [25-27]. They also help explain why standard offline evaluations may overestimate real-world reliability ("evaluation illusion") and why even low omission or error rates can have high clinical salience in treatment contexts [9,29].

In practical terms, our findings offer concrete guidance for implementing LLMs in clinical ASCVD care. The encouraging performance of models such as DeepSeek R1 supports adjunctive, nonautonomous use in patient-facing education platforms and, with clinician oversight, selective clinical decision support. For instance, models excelling in comprehensibility are best suited for generating patient education materials, whereas those with superior accuracy on guideline-specific content may better support the drafting of clinical summaries for specialist review. Successful integration will require attention to electronic health record interoperability; comprehensive staff training programs that cover the capabilities, limitations, and appropriate use of these artificial intelligence (AI) tools; and governance (privacy, auditability, and provenance). From a real-world clinical relevance standpoint, cost and deployment considerations (eg, licensing, API use, computing capacity and infrastructure, and local IT constraints) should inform model selection and scaling within existing health care workflows. In particular, open-source options (eg, DeepSeek R1) can lower licensing costs, enable local or hybrid deployment under strict data governance controls, and permit institution-specific tuning with auditable provenance—benefits that may improve feasibility in resource-constrained settings [30]. Given the observed fragility in guideline-sensitive domains, we recommend a clinician-in-the-loop workflow with tiered risk classification, automated guideline-concordance audits, and retrieval-augmented generation to anchor outputs in current evidence, with explicit human sign-off before the information enters care pathways [31,32]. Furthermore, transparent processes for obtaining patient consent for the use of AI-generated content in their care are essential. In addition, institutions should address regulatory and ethical implications (data protection, provenance, and accountability) and establish postdeployment monitoring and incident reporting processes to detect and mitigate potentially harmful responses [33].

Comparison to Prior Work

Unlike prior studies that have primarily examined single models within narrow clinical contexts [34,35], our investigation extends earlier designs by conducting a head-to-head, bilingual comparison of 3 advanced LLMs—DeepSeek R1, ChatGPT-4o, and Gemini—under a rigorous, blinded methodology incorporating randomization, washout, and consensus-based physician scoring. This design enabled more systematic cross-model comparisons than evaluations focused on 1 system or 1 language. The need for such rigor is underscored by reports from multidisciplinary areas such as cardio-oncology, where ChatGPT has answered only 68% of guideline-based queries correctly [36], highlighting the challenges that general-purpose models face when integrating complex clinical knowledge.

Focusing on ASCVD-related patient education and chronic disease self-management, we found that DeepSeek R1 achieved higher scores for accuracy and completeness and acceptable comprehensibility in both English and Chinese in our dataset,

XSL•FO
RenderX

suggesting suitability for patient-facing communication when used nonautonomously. These findings are concordant with recent *Nature Medicine* benchmarks showing that open-source systems can approach the performance of proprietary models in selected tasks [25,37]. Moreover, the open-source nature of DeepSeek R1 may enable privacy regulation–compliant local deployment and institution-specific fine-tuning—features that can support data-governed health systems—whereas its stable bilingual performance in our study aligns with goals of equitable information access [38]. At the same time, our domain-level analysis echoes and extends prior observations by showing that guideline-sensitive content remains comparatively fragile, reinforcing the need for clinician oversight and regular guideline concordance checks [39].

Limitations

Our study has several methodological limitations that should be considered when interpreting the findings. First, composite constraints in study design, item construction, and the evaluation perspective were present. The question set was clinician led, which may introduce selection bias; it used a fixed, evenly distributed, 5-domain preset (ie, definitions, diagnosis, treatment, prevention, and lifestyle) without direct patient involvement for external validation; model comparison was limited to 3 mainstream LLMs; and assessment relied entirely on expert review without patient-side measures such as comprehension or patient-reported outcomes. Collectively, these factors may affect clinical representativeness, diversity, and ecological validity [40].

Second, we acknowledge a moderate level of interrater agreement among the expert cardiologists as measured using the Kendall *W* (accuracy=0.578; completeness=0.565; comprehensibility=0.486). While such moderate reliability is not uncommon when evaluating nuanced, open-ended medical text where a degree of clinical subjectivity is inherent, it must be noted as a key limitation. To mitigate the impact of this disagreement, we used standardized anchors and a consensus adjudication step, and our statistical analysis (using medians and IQRs with nonparametric tests) was specifically chosen to limit the influence of rater heterogeneity. Nevertheless, this variability introduces uncertainty into the statistical significance of the differences found between models and suggests that expert opinions on AI-generated text quality can vary nontrivially. This is particularly relevant for clinical applications, where the use of such AI-generated content, especially for medical pathways or decision support, demands an even higher degree of caution. Consequently, the findings warrant a cautious interpretation. To enhance reliability in future work, we recommend developing more detailed scoring criteria with concrete examples and implementing a formal rater training and calibration process, including a pilot evaluation to establish baseline agreement.

Third, sample size and statistical power were not determined a priori. As an exploratory benchmarking study in a nascent area lacking established effect sizes, we did not perform an a priori power analysis. We used a coverage and stability-oriented design (25 items across 5 domains and 5 independent generations per model per language; 750 responses in total) to balance breadth and response stability. Although primary between-model contrasts reached statistical significance ($P<.001$)—suggesting adequate sensitivity post hoc—the absence of prespecified power planning limits generalizability; future confirmatory studies should use effect sizes and variance estimates from this work for formal power and sample size planning.

In addition, language and cultural generalizability are limited. Performance was evaluated only in English and Chinese. Differences in health beliefs, communication norms, and linguistic nuance across other languages and cultures may affect acceptability and applicability; broader multilingual, multicultural validation is needed.

Finally, geographic variation and reliance on the chosen reference guidelines (“benchmark binding”) may influence concordance judgments across health systems. While we benchmarked against specific international guidelines, ASCVD management varies by region and health system (eg, drug availability, targets, pathways, and reimbursement). Consequently, judgments of being concordant or nonconcordant are bound to the chosen reference standards, and local calibration is advisable for cross-region application.

Future Directions

First, longitudinal performance tracking should be prioritized. Standardized benchmarking with regular retesting across model updates, languages, and domains should be established to quantify performance drift, with early warning triggers for degradation; preregistered, multicenter confirmatory studies should be favored.

In addition, direct head-to-head comparisons with human materials should be conducted. LLM outputs should be benchmarked against human-authored patient education materials, assessing quantitative metrics (eg, accuracy and readability) and qualitative outcomes (eg, patient preference and trust) within a composite evaluation framework.

Moreover, pragmatic integration with clinical systems should be pursued. Low-coupling approaches to clinical systems under data minimization and privacy constraints (eg, standardized APIs, compliance and audit trails, and provenance and version management) should be explored to improve deployability.

Furthermore, communication should be tailored to patient literacy, language, culture, and context. Adaptive presentation methods based on health literacy, cultural background, preferred language, and clinical context should be developed and validated, maintaining clinical correctness while improving accessibility and understanding [41]. To ensure that these tailored communication strategies are effective, future work must include patient-centered validation, assessing the correlation between expert ratings and actual patient understanding and incorporating patient-reported outcome measures.

Finally, safety governance should be strengthened with structured risk management and monitoring. Future work should refine scoring anchors and operational definitions, broaden and diversify rater panels with structured calibration, conduct sensitivity and robustness analyses, implement routine guideline

XSL•FO
RenderX

concordance audits and a risk stratification framework (eg, dosing errors, contraindications, and care delay advice) [27], and establish continuous monitoring and incident reporting mechanisms to detect and mitigate potentially harmful or misleading outputs [26].

Conclusions

Our study evaluated the performance of several advanced LLMs in delivering information related to ASCVD, a major chronic disease burden in public health. In a blinded, bilingual comparison of DeepSeek R1, ChatGPT-4o, and Gemini, DeepSeek R1 demonstrated the highest accuracy and completeness, whereas all models showed comparable comprehensibility. Performance was consistently stronger for definitional and diagnostic queries than for treatment and prevention queries, indicating lower alignment with current therapeutic guidance in those domains. Notably, for the core question regarding the standard treatment regimen for ASCVD, none of the models consistently provided answers aligned with the latest clinical guidelines, representing a safety-relevant limitation of current general-purpose LLMs. These results delineate the present capability profile of LLMs for patient information on ASCVD and establish an empirical baseline for subsequent validation.

Acknowledgments

This work was supported by the National Science and Technology Major Project (2023ZD0503900 and 2023ZD0503902). The authors also wish to acknowledge the developers of the large language models evaluated in this study, whose groundbreaking work made this research possible. While drafting this manuscript, the authors used DeepSeek with the sole purpose of checking the grammar of the text.

Data Availability

All data generated or analyzed during this study are included in this published paper and its supplementary information files.

Authors' Contributions

Conceptualization: PL, YX, X Liu
Data curation: ZS, YW, X Lv
Formal analysis: ZL, HW
Funding acquisition: YC
Methodology: PL, YX
Visualization: PL, X Liu, JZ
Writing—original draft: PL, YX
Writing—review and editing: YC

Conflicts of Interest

None declared.

Multimedia Appendix 1
Full set of large language model responses (N=750; English and Chinese).
[XLSX File (Microsoft Excel File), 732 KB - medinform_v14i1e81422_app1.xlsx]

Multimedia Appendix 2
Detailed scoring rubric with anchors and examples.
[DOCX File , 30 KB - medinform_v14i1e81422_app2.docx]

Multimedia Appendix 3
Domain-specific “Good response” rates by model and language.
[DOCX File , 16 KB - medinform_v14i1e81422_app3.docx]

References

1. Roeters van Lennep JE, Tokgözoğlu LS, Badimon L, Dumanski SM, Gulati M, Hess CN, et al. Women, lipids, and atherosclerotic cardiovascular disease: a call to action from the European Atherosclerosis Society. Eur Heart J 2023 Oct 14;44(39):4157-4173 [FREE Full text] [doi: 10.1093/eurheartj/ehad472] [Medline: 37611089]
2. Li H, Fu JF, Python A. Implementing large language models in health care: clinician-focused review with interactive guideline. J Med Internet Res 2025 Jul 11;27:e71916 [FREE Full text] [doi: 10.2196/71916] [Medline: 40644686]
3. Thirunavukarasu AJ, Ting DS, Elangovan K, Gutierrez L, Tan TF, Ting DS. Large language models in medicine. Nat Med 2023 Aug;29(8):1930-1940. [doi: 10.1038/s41591-023-02448-8] [Medline: 37460753]

XSL•FO
RenderX

4. Ferber D, El Nahhas OS, Wölflein G, Wiest IC, Clusmann J, Leßmann ME, et al. Development and validation of an autonomous artificial intelligence agent for clinical decision-making in oncology. Nat Cancer 2025 Aug;6(8):1337-1349. [doi: 10.1038/s43018-025-00991-6] [Medline: 40481323]
5. AlSaad R, Abd-Alrazaq A, Boughorbel S, Ahmed A, Renault MA, Damseh R, et al. Multimodal large language models in health care: applications, challenges, and future outlook. J Med Internet Res 2024 Sep 25;26:e59505 [FREE Full text] [doi: 10.2196/59505] [Medline: 39321458]
6. Zhang K, Meng X, Yan X, Ji J, Liu J, Xu H, et al. Revolutionizing health care: the transformative impact of large language models in medicine. J Med Internet Res 2025 Jan 07;27:e59069 [FREE Full text] [doi: 10.2196/59069] [Medline: 39773666]
7. Harrer S. Attention is not all you need: the complicated case of ethically using large language models in healthcare and medicine. EBioMedicine 2023 Apr;90:104512 [FREE Full text] [doi: 10.1016/j.ebiom.2023.104512] [Medline: 36924620]
8. Ong JC, Chang SY, William W, Butte AJ, Shah NH, Chew LS, et al. Ethical and regulatory challenges of large language models in medicine. Lancet Digit Health 2024 Jun;6(6):e428-e432 [FREE Full text] [doi: 10.1016/S2589-7500(24)00061-X] [Medline: 38658283]
9. Bedi S, Liu Y, Orr-Ewing L, Dash D, Koyejo S, Callahan A, et al. Testing and evaluation of health care applications of large language models: a systematic review. JAMA 2025 Jan 28;333(4):319-328. [doi: 10.1001/jama.2024.21700] [Medline: 39405325]
10. Visseren FL, Mach F, Smulders YM, Carballo D, Koskinas KC, Bäck M, ESC Scientific Document Group. 2021 ESC Guidelines on cardiovascular disease prevention in clinical practice. Eur J Prev Cardiol 2022 Feb 19;29(1):5-115. [doi: 10.1093/eurjpc/zwab154] [Medline: 34558602]
11. Rao SV, O'Donoghue ML, Ruel M, Rab T, Tamis-Holland JE, Alexander JH, Peer Review Committee Members. 2025 ACC/AHA/ACEP/NAEMSP/SCAI Guideline for the management of patients with acute coronary syndromes: a report of the American College of Cardiology/American Heart Association Joint Committee on Clinical Practice Guidelines. J Am Coll Cardiol 2025 Jun 10;85(22):2135-2237 [FREE Full text] [doi: 10.1016/j.jacc.2024.11.009] [Medline: 40013746]
12. Vrints C, Andreotti F, Koskinas KC, Rossello X, Adamo M, Ainslie J, ESC Scientific Document Group. 2024 ESC Guidelines for the management of chronic coronary syndromes. Eur Heart J 2024 Sep 29;45(36):3415-3537. [doi: 10.1093/eurheartj/ehae177] [Medline: 39210710]
13. Pugliese N, Wai-Sun Wong V, Schattenberg JM, Romero-Gomez M, Sebastiani G, NAFLD Expert Chatbot Working Group, et al. Accuracy, reliability, and comprehensibility of ChatGPT-generated medical responses for patients with nonalcoholic fatty liver disease. Clin Gastroenterol Hepatol 2024 Apr;22(4):886-9.e5 [FREE Full text] [doi: 10.1016/j.cgh.2023.08.033] [Medline: 37716618]
14. Pan A, Musheyev D, Bockelman D, Loeb S, Kabarriti AE. Assessment of artificial intelligence chatbot responses to top searched queries about cancer. JAMA Oncol 2023 Oct 01;9(10):1437-1440. [doi: 10.1001/jamaoncol.2023.2947] [Medline: 37615960]
15. Campbell DJ, Estephan LE, Sina EM, Mastrolonardo EV, Alapati R, Amin DR, et al. Evaluating ChatGPT responses on thyroid nodules for patient education. Thyroid 2024 Mar;34(3):371-377. [doi: 10.1089/thy.2023.0491] [Medline: 38010917]
16. Nielsen JP, von Buchwald C, Grønhøj C. Validity of the large language model ChatGPT (GPT4) as a patient information source in otolaryngology by a variety of doctors in a tertiary otorhinolaryngology department. Acta Otolaryngol 2023 Sep;143(9):779-782. [doi: 10.1080/00016489.2023.2254809] [Medline: 37694729]
17. Iannantuono GM, Bracken-Clarke D, Floudas CS, Roselli M, Gulley JL, Karzai F. Applications of large language models in cancer care: current evidence and future perspectives. Front Oncol 2023 Sep 04;13:1268915 [FREE Full text] [doi: 10.3389/fonc.2023.1268915] [Medline: 37731643]
18. Southwell BG, Otero Machuca J, Cherry ST, Burnside M, Barrett NJ. Health misinformation exposure and health disparities: observations and opportunities. Annu Rev Public Health 2023 Apr 03;44:113-130 [FREE Full text] [doi: 10.1146/annurev-publhealth-071321-031118] [Medline: 36207008]
19. Meskó B, Topol EJ. The imperative for regulatory oversight of large language models (or generative AI) in healthcare. NPJ Digit Med 2023 Jul 06;6(1):120 [FREE Full text] [doi: 10.1038/s41746-023-00873-0] [Medline: 37414860]
20. Ayers JW, Poliak A, Dredze M, Leas EC, Zhu Z, Kelley JB, et al. Comparing physician and artificial intelligence chatbot responses to patient questions posted to a public social media forum. JAMA Intern Med 2023 Jun 01;183(6):589-596 [FREE Full text] [doi: 10.1001/jamainternmed.2023.1838] [Medline: 37115527]
21. Le Guellec B, Lefèvre A, Geay C, Shorten L, Bruge C, Hacein-Bey L, et al. Performance of an open-source large language model in extracting information from free-text radiology reports. Radiol Artif Intell 2024 Jul;6(4):e230364 [FREE Full text] [doi: 10.1148/ryai.230364] [Medline: 38717292]
22. Moor M, Banerjee O, Abad ZS, Krumholz HM, Leskovec J, Topol EJ, et al. Foundation models for generalist medical artificial intelligence. Nature 2023 Apr;616(7956):259-265. [doi: 10.1038/s41586-023-05881-4] [Medline: 37045921]
23. Haltaufderheide J, Ranisch R. The ethics of ChatGPT in medicine and healthcare: a systematic review on Large Language Models (LLMs). NPJ Digit Med 2024 Jul 08;7(1):183 [FREE Full text] [doi: 10.1038/s41746-024-01157-x] [Medline: 38977771]
24. OpenAI. GPT-4 technical report. ArXiv Preprint posted online on March 15, 2023 [FREE Full text] [doi: 10.48550/arXiv.2303.08774]

XSL•FO
RenderX

25. Tordjman M, Liu Z, Yuce M, Fauveau V, Mei Y, Hadjadj J, et al. Comparative benchmarking of the DeepSeek large language model on medical tasks and clinical reasoning. Nat Med 2025 Aug;31(8):2550-2555. [doi: 10.1038/s41591-025-03726-3] [Medline: 40267969]
26. Huo B, Cacciamani GE, Collins GS, McKechnie T, Lee Y, Guyatt G. Reporting standards for the use of large language model-linked chatbots for health advice. Nat Med 2023 Dec;29(12):2988. [doi: 10.1038/s41591-023-02656-2] [Medline: 37957381]
27. Sallam M. ChatGPT utility in healthcare education, research, and practice: systematic review on the promising perspectives and valid concerns. Healthcare (Basel) 2023 Mar 19;11(6):887 [FREE Full text] [doi: 10.3390/healthcare11060887] [Medline: 36981544]
28. Pham C, Govender R, Tehami S, Chavez S, Adepoju OE, Liaw W. ChatGPT's performance in cardiac arrest and bradycardia simulations using the American Heart Association's advanced cardiovascular life support guidelines: exploratory study. J Med Internet Res 2024 Apr 22;26:e55037 [FREE Full text] [doi: 10.2196/55037] [Medline: 38648098]
29. Bhayana R. Chatbots and large language models in radiology: a practical primer for clinical and research applications. Radiology 2024 Jan;310(1):e232756. [doi: 10.1148/radiol.232756] [Medline: 38226883]
30. Dorfner FJ, Jürgensen L, Donle L, Al Mohamad F, Bodenmann TR, Cleveland MC, et al. Comparing commercial and open-source large language models for labeling chest radiograph reports. Radiology 2024 Oct;313(1):e241139. [doi: 10.1148/radiol.241139] [Medline: 39470431]
31. Beltramin D, Bousquet C, Tiffet T. Large language models could revolutionize health care, but technical hurdles may limit their applications. J Med Internet Res 2025 Jun 25;27:e71618 [FREE Full text] [doi: 10.2196/71618] [Medline: 40561496]
32. Forero DA, Abreu SE, Tovar BE, Oermann MH. Automated analyses of risk of bias and critical appraisal of systematic reviews (ROBIS and AMSTAR 2): a comparison of the performance of 4 large language models. J Am Med Inform Assoc 2025 Sep 01;32(9):1471-1476. [doi: 10.1093/jamia/ocaf117] [Medline: 40680299]
33. Lai H, Ge L, Sun M, Pan B, Huang J, Hou L, et al. Assessing the risk of bias in randomized clinical trials with large language models. JAMA Netw Open 2024 May 01;7(5):e2412687. [doi: 10.1001/jamanetworkopen.2024.12687] [Medline: 38776081]
34. Law S, Oldfield B, Yang W, Global Obesity Collaborative. ChatGPT/GPT-4 (large language models): opportunities and challenges of perspective in bariatric healthcare professionals. Obes Rev 2024 Jul;25(7):e13746. [doi: 10.1111/obr.13746] [Medline: 38613164]
35. Wang L, Mao Y, Wang L, Sun Y, Song J, Zhang Y. Suitability of GPT-4o as an evaluator of cardiopulmonary resuscitation skills examinations. Resuscitation 2024 Nov;204:110404 [FREE Full text] [doi: 10.1016/j.resuscitation.2024.110404] [Medline: 39343124]
36. Li P, Zhang X, Zhu E, Yu S, Sheng B, Tham YC, et al. Potential multidisciplinary use of large language models for addressing queries in cardio-oncology. J Am Heart Assoc 2024 Mar 19;13(6):e033584 [FREE Full text] [doi: 10.1161/JAHA.123.033584] [Medline: 38497458]
37. Sandmann S, Hegselmann S, Fujarski M, Bickmann L, Wild B, Eils R, et al. Benchmark evaluation of DeepSeek large language models in clinical decision-making. Nat Med 2025 Aug;31(8):2546-2549. [doi: 10.1038/s41591-025-03727-2] [Medline: 40267970]
38. Normile D. Chinese firm's large language model makes a splash. Science 2025 Jan 17;387(6731):238. [doi: 10.1126/science.adv9836] [Medline: 39818899]
39. Omar M, Agbareia R, Glicksberg BS, Nadkarni GN, Klang E. Benchmarking the confidence of large language models in answering clinical questions: cross-sectional evaluation study. JMIR Med Inform 2025 May 16;13:e66917 [FREE Full text] [doi: 10.2196/66917] [Medline: 40378406]
40. Sumner J, Wang Y, Tan SY, Chew EH, Wenjun Yip A. Perspectives and experiences with large language models in health care: survey study. J Med Internet Res 2025 May 01;27:e67383 [FREE Full text] [doi: 10.2196/67383] [Medline: 40310666]
41. Ji H, Wang X, Sia CH, Yap J, Lim ST, Djohan AH, et al. Large language model comparisons between English and Chinese query performance for cardiovascular prevention. Commun Med (Lond) 2025 May 16;5(1):177 [FREE Full text] [doi: 10.1038/s43856-025-00802-0] [Medline: 40379850]

Abbreviations

AI: artificial intelligence
API: application programming interface
ASCVD: atherosclerotic cardiovascular disease
HIPAA: Health Insurance Portability and Accountability Act
LLM: large language model

XSL•FO
RenderX

Edited by A Coristine; submitted 28.Jul.2025; peer-reviewed by R Kocaaslan, H Pilabré, AA Arafat; comments to author 16.Oct.2025; accepted 17.Dec.2025; published 07.Jan.2026.

Please cite as:
Li P, Xu Y, Liu X, Shen Z, Wang Y, Lv X, Lu Z, Wu H, Zhuang J, Chen Y
Large Language Models in Patient Health Communication for Atherosclerotic Cardiovascular Disease: Pilot Cross-Sectional Comparative Analysis
JMIR Med Inform 2026;14:e81422
URL: https://medinform.jmir.org/2026/1/e81422
doi:10.2196/81422
PMID:

©Pengfei Li, Yinfei Xu, Xiang Liu, Zhean Shen, Yi Wang, Xinyi Lv, Ziyi Lu, Hui Wu, Jiaqi Zhuang, Yan Chen. Originally published in JMIR Medical Informatics (https://medinform.jmir.org), 07.Jan.2026. This is an open-access article distributed under the terms of the Creative Commons Attribution License (https://creativecommons.org/licenses/by/4.0/), which permits unrestricted use, distribution, and reproduction in any medium, provided the original work, first published in JMIR Medical Informatics, is properly cited. The complete bibliographic information, a link to the original publication on https://medinform.jmir.org/, as well as this copyright and license information must be included.

XSL•FO
RenderX

Original Paper

Multi-Evidence Clinical Reasoning With Retrieval-Augmented Generation for Emergency Triage: Retrospective Evaluation Study

Hang Sheung Wong[1], MBBS; Tsz Kwan Wong[2], MBChB, MSc

[1]Department of Accident & Emergency, Princess Margaret Hospital, Hong Kong (SAR), China (Hong Kong)

[2]Department of Accident & Emergency, North Lantau Hospital, Hong Kong (SAR), China (Hong Kong)

Corresponding Author:
Hang Sheung Wong, MBBS
Department of Accident & Emergency
Princess Margaret Hospital
2-10, Princess Margaret Hospital Road, Lai Chi Kok, Kowloon
Hong Kong (SAR)
China (Hong Kong)
Phone: 852 68716917
Email: hs.wong3@ha.org.hk

Abstract

Background: Emergency triage accuracy is critical but varies with clinician experience, cognitive load, and case complexity. Mis-triage can delay care for high-risk patients and exacerbate crowding through unnecessary prioritization. Large language models (LLMs) show promise as triage decision-support tools but are vulnerable to hallucinations. Retrieval-augmented generation (RAG) may improve reliability by grounding LLM reasoning in authoritative guidelines and real clinical cases.

Objective: This study aimed to evaluate whether a dual-source RAG system that integrates guideline- and case-based evidence improves emergency triage performance versus a baseline LLM and to assess how closely its urgency assignments align with expert consensus and outcome-defined clinical severity.

Methods: We developed a dual-source RAG system—Multi-Evidence Clinical Reasoning RAG (MECR-RAG)—that retrieves sections from the Hong Kong Accident and Emergency Triage Guidelines (HKAETG) and cases from a database of 3000 emergency department triage encounters. In a retrospective single-center evaluation, MECR-RAG and a prompt-only baseline LLM (both DeepSeek-V3) were tested on 236 routine triage encounters to predict 5-level triage categories. Expert consensus reference labels were assigned by blinded senior triage nurses. Primary outcomes were quadratic weighted kappa (QWK) and accuracy versus consensus labels. Secondary analyses examined performance within 3 operationally and clinically relevant triage bands—immediate (categories 1 and 2), urgent (category 3), and nonurgent (categories 4 and 5). In 226 encounters with follow-up, we also assigned outcome-based severity tiers (R1-R3) using a published 3-level urgency reference standard and defined a disposition-safety composite.

Results: MECR-RAG achieved a mean QWK of 0.902 (SD 0.0021; 95% CI 0.901-0.904) and accuracy of 0.802 (SD 0.0082; 95% CI 0.795-0.808), outperforming the baseline LLM (QWK 0.801, SD 0.004; accuracy 0.542, SD 0.0073; both $P<.001$) and demonstrating expert-comparable agreement with triage nurses (interrater QWK 0.887). In 3-group analysis, MECR-RAG reduced overtriage from 68/236 (28.8%) with the baseline LLM to 30/236 (12.7%) and maintained low undertriage from 4/236 (1.7%) to 3/236 (1.3%), with the largest gains in the diagnostically ambiguous yet operationally important categories 3 and 4. In a secondary outcome-based analysis defining high-severity courses as R1+R2, MECR-RAG detected high-risk patients more sensitively than initial nurse triage (124/130, 95.4% vs 117/130, 90.0%; $P=.02$) while maintaining nurse-level specificity. MECR-RAG yielded the lowest weighted harm index (13.7, 19.5, and 20.3 per 100 patients for MECR-RAG, nurses, and the baseline LLM, respectively).

Conclusions: A dual-source RAG triage system that combines guideline-based rules with case-based reasoning achieved expert-comparable agreement, reduced overtriage, and better aligned urgency assignments than a prompt-only baseline LLM. Secondary outcome–based analyses in this cohort suggested more favorable triage patterns than initial nurse triage, supporting MECR-RAG as a concurrent decision-support layer that flags discordant or high-risk assignments; prospective multicenter implementation studies are needed to determine effects on emergency department crowding, delays, and patient outcomes.

(JMIR Med Inform 2026;14:e82026) doi:10.2196/82026

XSL•FO
RenderX

KEYWORDS

artificial intelligence; clinical decision support; clinical informatics; DeepSeek; digital health; emergency medicine; large language models; nurses; retrieval-augmented generation; triage

Introduction

Emergency triage is a critical step in emergency department (ED) operations, determining which patients are seen first when demand exceeds capacity. However, triage accuracy varies with clinicians' experience, cognitive load, and the complexity of presenting symptoms, and even trained nurses may misclassify a substantial minority of encounters [1,2]. Undertriage risks delayed recognition of life-threatening illness and preventable morbidity or mortality, whereas overtriage diverts scarce resources toward lower-acuity patients and can exacerbate ED crowding and boarding, both of which are associated with worse outcomes [2]. These challenges are particularly pronounced in mid-acuity categories, which represent most ED visits and where small changes in urgency assignment can translate into large differences in waiting time, crowding pressure, and exposure to harm.

Large language models (LLMs) have emerged as potential tools for clinical decision support because they can interpret free-text notes, integrate medical knowledge, and generate structured recommendations. In emergency care, LLMs have been tested for triage on simulated vignettes and curated cases, but reported performance has been highly variable, with agreement with human raters (Cohen κ) ranging from 0.125 to 0.899 across models, datasets, and evaluation frameworks [3-8]. A fundamental limitation of current "prompt-only" LLMs is their tendency to hallucinate, generating outputs that appear plausible but are factually incorrect or unsupported [9]. In emergency triage, such hallucinations may lead to urgency levels being assigned based on fabricated reasoning, outdated rules, or misinterpretation of presenting complaints, posing potential risks to patient safety and consistency.

Retrieval-augmented generation (RAG) has been proposed as a way to mitigate hallucinations by grounding LLM outputs in external, task-specific knowledge sources such as clinical guidelines, textbooks, electronic health records, and biomedical literature [10-12]. By retrieving relevant evidence at inference time and conditioning generation on that material, RAG can improve access to current, domain-specific knowledge and make model reasoning more transparent. Early work in emergency care has shown that adding retrieval can improve triage or referral accuracy compared with nonretrieval models. Yazaki et al [13] integrated RAG with a triage guideline database and tested GPT-3.5 on 100 structured, simulated scenarios derived from the Japanese National Examination for Emergency Medical Technicians, finding that the RAG-enhanced model achieved 70/100 (70%) accuracy and outperformed both emergency medical technicians and physicians. Gaber et al [14] used a curated dataset of 2000 real-world ED cases from the MIMIC-IV (Medical Information Mart for Intensive Care IV) database and retrieved evidence from a corpus of 30,000 PubMed abstracts, demonstrating superior triage-level prediction and exact-match accuracy compared with nonretrieval workflows.

Despite these advances, existing applications of RAG to emergency triage and referral have important gaps. One study relied largely on textbook-style, simulated examination cases [13], whereas another used routine labels from structured research datasets without clinician-adjudicated ground truth [14]. In both studies, RAG was applied to a single knowledge source—either structured triage guidelines or biomedical literature—rather than explicitly combining protocol-based rules with experiential knowledge from prior cases.

To our knowledge, no prior work has evaluated a dual-source RAG system that jointly retrieves local triage guidelines and real-world past triage cases, or directly compared such a system with a prompt-only LLM using raw, unstructured triage documentation paired with a blinded expert consensus reference standard and outcome-based validity checks. This design better captures the complexity and variability of real-world practice and strengthens the translational relevance of performance estimates.

There is also growing recognition that agreement with human labels alone is an incomplete measure of triage quality. Large cohort studies of systems such as the Emergency Severity Index (ESI) and the Manchester Triage System (MTS) have shown that nurse-assigned categories can underestimate or overestimate "true" acuity when judged against downstream outcomes such as hospitalization, intensive care unit (ICU) transfer, revisits, and short-term mortality [15-17]. In parallel, a *Journal of the American Medical Association* (*JAMA*) editorial on artificial intelligence (AI) in medicine has argued that evaluations of AI tools should prioritize clinically meaningful outcomes, patient-centered care, quality, and equity rather than focusing solely on narrow technical accuracy metrics [18]. Accordingly, evaluations of LLM-enabled triage should explicitly examine how assigned urgency levels align with downstream clinical severity and sentinel safety events, rather than treating concordance with nurse labels as sufficient.

In this context, we developed a dual-source RAG system—Multi-Evidence Clinical Reasoning RAG (MECR-RAG)—that retrieves both structured local triage guidelines (Hong Kong Accident and Emergency Triage Guidelines [HKAETG]) and analogous past triage cases and applies a structured Multi-Evidence Clinical Reasoning (MECR) framework to assign 5-level urgency categories. We retrospectively evaluated MECR-RAG on real ED triage notes, benchmarking it against a prompt-only baseline LLM and against expert nurse consensus labels. Our primary aim was to determine whether a dual-source RAG triage system (MECR-RAG) improves 5-level triage accuracy and agreement (quadratic weighted κ and accuracy) with expert nurse consensus compared with a prompt-only baseline LLM and to benchmark its performance against expert triage nurses. We hypothesized that MECR-RAG would achieve higher agreement than the baseline LLM and noninferior agreement relative to expert nurses. As a secondary aim, in a subset with follow-up data, we

XSL•FO
RenderX

assessed outcome-informed validity by examining how MECR-RAG, the baseline LLM, and initial nurse triage aligned with downstream clinical severity tiers and a composite of sentinel safety outcomes. This early-phase, single-center evaluation, reported in accordance with TRIPOD-LLM (Transparent Reporting of a multivariable prediction model for Individual Prognosis Or Diagnosis - Large Language Models) [19], is intended to provide a methodologically rigorous foundation for future prospective and implementation studies of RAG-enhanced triage decision-support systems designed to augment, rather than replace, nurse-led triage.

Methods

Study Design and Setting

This study was a retrospective, proof-of-concept evaluation of a RAG-enhanced LLM for ED triage classification. The primary objective was to compare the performance of an RAG-based LLM that referenced both historical case data and the HKAETG against a prompt-only baseline LLM in assigning triage urgency levels.

The HKAETG is a 5-level triage system implemented across all 18 government-funded public EDs in Hong Kong. Its structure is conceptually aligned with other internationally recognized systems such as the MTS and ESI. Under the HKAETG, patients are assigned to 1 of 5 categories based on clinical urgency and time-to-treatment targets: category 1 (critical, 0 minutes), category 2 (emergency, 10 minutes), category 3 (urgent, 30 minutes), category 4 (semiurgent, 120 minutes), and category 5 (nonurgent, 180 minutes).

All study data were sourced from a single center, Princess Margaret Hospital (PMH), a major acute public hospital in Hong Kong and one of the city's largest tertiary care facilities. PMH operates a 24-hour ED and manages a high volume of complex and time-sensitive cases. In 2023 and 2024, the ED recorded 113,974 and 110,812 visits, respectively, highlighting its central role in emergency care delivery.

Pilot Study, Sample Size Calculation, and Model Selection

Before the main evaluation, we conducted a pilot study to inform model selection, prompting strategy, and sample size estimation. We randomly sampled 1000 ED triage cases from December 2024; 200 cases were used for pilot testing, and the remaining 800 cases were reserved to simulate a retrieval database. All pilot cases were excluded from the final study.

Three commercially available LLMs (DeepSeek-V3, GPT-4o, and Claude 3.7 Sonnet) were compared in both prompt-only and RAG configurations, with performance assessed against clinician-assigned triage labels using quadratic weighted kappa (QWK) and accuracy. Across models, performance was statistically similar in this pilot. DeepSeek-V3 was therefore selected as the backbone model for the main study primarily on the basis of its inference cost, application programming interface (API) accessibility, and comparable pilot performance.

In the pilot setting, the MECR-RAG configuration achieved an approximate QWK of 0.75 compared with 0.50 for the prompt-only baseline. Using the formula for comparing 2 kappa coefficients described by Fleiss, with α=.05 and power=.80 [20], the minimum required sample size to detect this difference was 48 cases. We nevertheless included 236 consensus-labeled triage cases in the final study to improve the precision of performance estimates and enhance generalizability.

Data Sources and Participants

The test set comprised ED triage cases collected at PMH between January 1 and December 31, 2023. All ED visits during this period were eligible regardless of age, sex, or presenting problem. To ensure temporal representativeness and reflect real-world variation in case mix, we used a stratified sampling strategy in which 1 calendar day was randomly selected from each month and 20 cases were sampled from that day. Within each sampled day, triage categories were sampled to approximate overall category distributions while modestly oversampling rare categories to improve precision for high-acuity strata. Four cases were excluded because case-number identification errors prevented data retrieval, yielding a final test set of 236 triage cases.

Reference labels were assigned using a blinded, multirater consensus process. Two advanced practice nurses with more than 10 years of emergency experience independently reviewed each case. Raters were blinded to the original nurse-assigned triage category and saw only information available at the time of triage: presenting complaint, condition on arrival, vital signs, and relevant past medical history when documented. Downstream data, including investigations, diagnoses, treatments, and ward progress, were withheld so that labels reflected only the initial triage decision context and matched the information provided to the LLMs. Disagreements were adjudicated by a third senior triage nurse to obtain a final consensus category for each encounter.

For retrieval, we constructed a separate database of 3000 anonymized ED visits to PMH between January 1 and December 31, 2024. All encounters in 2024 were eligible, with no clinical exclusion criteria, to preserve the natural diversity of documentation and presentations. Days were randomly sampled from each month, and cases were then drawn from those days to achieve broad temporal coverage; modest oversampling of rare triage categories (categories 1, 2, and 5) ensured sufficient representation while maintaining the real-world skew toward categories 3 and 4. The final database contained 94/3000 (3.1%) category 1, 120/3000 (4.0%) category 2, 1705/3000 (57.0%) category 3, 1035/3000 (34.5%) category 4, and 46/3000 (1.5%) category 5 encounters, with detailed monthly and category-specific sampling shown in Table S1 in Multimedia Appendix 1. To stress-test temporal robustness and reduce bias from contemporaneous documentation habits, 2023 test cases were evaluated against a 2024 retrieval database using the same triage guideline version; the full rationale is provided in Textbox S1 in Multimedia Appendix 1.

Preprocessing

Raw, unstructured triage documentation for both test cases and retrieval-database cases was exported from the electronic medical record, deidentified, and converted into a structured,

XSL•FO
RenderX

machine-readable text format. We retained only nurse-entered information available at the time of triage (eg, demographics, presenting complaint, condition on arrival, vital signs, and relevant past medical history) and excluded any downstream assessments, investigations, treatments, and outcomes. The latest version of the HKAETG (version 6, revised 2022) was similarly digitized and segmented into retrievable guideline sections. Both triage notes and guideline sections were then processed for semantic retrieval; further preprocessing and summarization details are provided in Textbox S2 in Multimedia Appendix 1.

LLM and RAG System Description

For all primary analyses, we used DeepSeek-V3 as the base LLM, accessed via a commercial API without any additional fine-tuning or architectural modification. In what follows, we refer to the DeepSeek-V3 model without retrieval as the "baseline LLM" and the dual-source retrieval-augmented configuration as MECR-RAG. Within each experimental configuration, the same LLM instance handled all stages of the pipeline (preprocessing, retrieval, and generation) with deterministic generation (temperature=0) to minimize stochastic variability. A separate embedding model was used to generate vector representations for semantic retrieval, and the same embedding configuration was applied during database construction and at query time to ensure consistency.

The pipeline was implemented in Python and executed on a standard desktop workstation without graphics processing unit acceleration. End-to-end processing time for the full MECR-RAG configuration was approximately 1 minute per case, including preprocessing, retrieval, and triage prediction, suggesting that near-real-time decision support would be technically feasible. Detailed model versions, libraries, and runtime benchmarks are provided in Section A1 in Multimedia Appendix 1.

MECR-RAG System Architecture

The MECR-RAG system follows a 5-stage pipeline designed to mirror how expert triage nurses combine protocol knowledge with experiential reasoning. First, the raw triage note is summarized into a concise, structured representation optimized for retrieval. Second, the model selects the most relevant sections of the HKAETG using an agentic reasoning step that prioritizes life-threatening conditions and documented physiologic abnormalities. Third, the system predicts the most likely attending specialty (eg, medicine, surgery, and orthopedics) to constrain subsequent case retrieval. Fourth, a hybrid retrieval module identifies similar past triage cases by combining metadata filters (age group and predicted specialty) with vector similarity search. Finally, the model applies a structured, MECR prompt that integrates guideline excerpts, retrieved cases, and the index presentation to assign a 5-level urgency category and provide a textual rationale.

The overall architecture is orchestrated using a modular, node-based workflow that preserves intermediate states, supports full audit trails, and enables systematic component ablation. A schematic overview of the MECR-RAG pipeline is shown in Figure 1, and additional implementation details are provided in Section A2 in Multimedia Appendix 1.

Figure 1. Overview of the Multi-Evidence Clinical Reasoning retrieval-augmented generation system architecture. MECR-RAG: Multi-Evidence Clinical Reasoning retrieval-augmented generation.

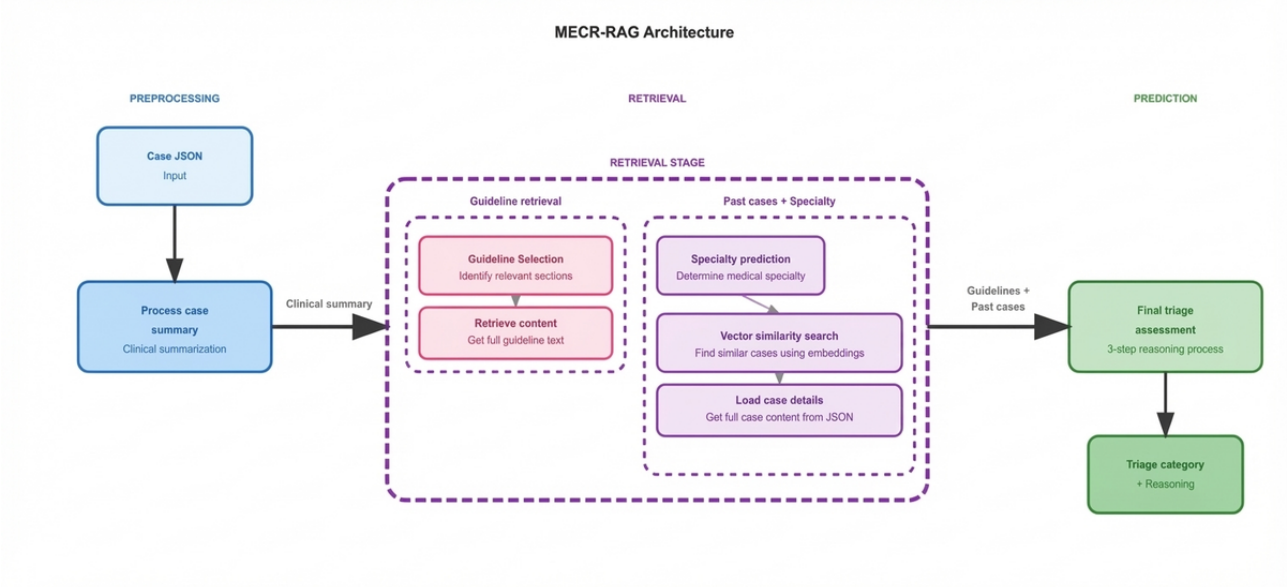

The MECR-RAG pipeline consists of 5 sequential processing stages: clinical case summarization, agentic guideline section selection, specialty prediction for metadata filtering, hybrid past-case retrieval combining metadata and vector similarity search, and multievidence reasoning for the final triage assessment. LangGraph nodes manage state transitions and data flow throughout the pipeline.

Indexing and Database Construction

To support efficient retrieval, both historical triage cases and guideline content were converted into structured, machine-readable representations and indexed in a vector database. Historical cases were transformed into standardized triage-time summaries that captured presenting complaints, key vital signs, and brief clinical context, while preserving links to

XSL•FO
RenderX

metadata such as age group, triage category, and attending specialty. The same summarization template was applied to both database cases and incoming test cases to ensure that queries and indexed documents occupied a comparable embedding space.

The HKAETG document was similarly segmented into discrete sections and summarized to highlight the spectrum of presentations covered by each rule set. Each guideline section was stored with a short synopsis and structural metadata (eg, system, chief complaint, and red-flag criteria) to facilitate targeted retrieval during triage. The combined indexing strategy was designed to balance retrieval quality, computational efficiency, and scalability to larger case repositories. Details of prompt templates, sectioning rules, and indexing parameters are described in Section A3 in Multimedia Appendix 1.

Retrieval System Design

The retrieval layer implements a dual-source strategy that distinguishes authoritative protocol knowledge from experiential case patterns. Guideline retrieval is performed via an agentic selection step: given the summarized index case and a list of guideline section titles and synopses, the LLM selects up to 2 sections it deems most relevant, explicitly favoring conditions associated with high short-term risk or abnormal vital signs. This approach avoids purely lexical matching and aligns guideline selection more closely with clinical reasoning.

Past-case retrieval uses a multistage, hybrid approach. The model first predicts 1 or 2 likely specialties using triage-available information only, then filters the case database by age group and specialty to construct a clinically plausible candidate pool. Within this subset, vector similarity search identifies the closest matches based on the summarized clinical text. A small number of top-ranked cases are returned, along with similarity scores and metadata, for use in the final reasoning step. Similarity thresholds, top-k values, and fallback strategies were chosen empirically and are reported in Section A4 in Multimedia Appendix 1.

Generation and Prompting Strategy

The generation stage uses an MECR prompt that extends conventional chain-of-thought reasoning for the specific demands of triage. Rather than a single undifferentiated reasoning path, the prompt enforces a 3-tier structure: (1) a clinical risk assessment aligned with formal triage category definitions, (2) integration of condition-specific recommendations from the retrieved HKAETG sections, and (3) comparison with retrieved past cases to identify contextual factors that may support escalation or de-escalation (eg, frailty, social circumstances, and borderline physiology). Each evidence source produces an independent provisional triage recommendation.

The model is then instructed to reconcile these recommendations into a single final category, explicitly justifying the choice and indicating which sources carried the most weight. Outputs include the predicted triage category, a structured explanation, and a coarse confidence label (high, medium, or low), enabling clinicians to audit the reasoning process and gauge when additional scrutiny is warranted. The complete MECR prompt details are provided in Section A5 in Multimedia Appendix 1.

Ablation Configurations

To isolate the contribution of individual retrieval components, we implemented 3 reduced configurations alongside the full MECR-RAG system. The baseline configuration used the same triage definition table and reasoning structure but removed all retrieval, relying only on the index case description. The guideline-only configuration added agentic guideline selection but did not use past-case retrieval, whereas the case-only configuration retrieved similar past cases without guideline sections. In all ablation variants, preprocessing steps, LLM model, and evaluation procedures were held constant to ensure that performance differences could be attributed to the presence or absence of specific retrieval sources rather than to implementation artifacts. The details are provided in Section A6 in Multimedia Appendix 1.

Outcome Definition and Label-Based Evaluation

The primary outcome was the 5-level triage category (categories 1-5) predicted by each LLM configuration, compared with consensus labels assigned by expert triage nurses. Two configurations were evaluated: the MECR-RAG system, which incorporated both the HKAETG and retrieval of past triage cases, and a prompt-only baseline model with no retrieval component. Model outputs were assessed against the final adjudicated triage category for each case.

The primary performance metric was QWK, chosen because it accounts for the ordinal nature of triage categories and penalizes larger discrepancies more heavily, in line with their greater clinical consequence. Overall accuracy was reported as a complementary measure summarizing the proportion of exact matches between model predictions and consensus labels.

To provide a more clinically grounded view of performance, we also calculated precision, recall, and F_1-score for each triage category and for a post hoc grouping of triage levels into 3 urgency bands: immediate (categories 1 and 2), urgent (category 3), and nonurgent (categories 4 and 5). This mapping reflects local operational workflows, in which small changes in urgency assignment can translate into large differences in waiting time and risk exposure. These group-level metrics were used to characterize overtriage and undertriage patterns beyond aggregate QWK and accuracy estimates.

Because LLM outputs are probabilistic, all primary comparisons between MECR-RAG and the baseline LLM were repeated across 5 independent runs using identical test cases, prompts, retrieval databases, and API settings. For these analyses, we summarized performance as mean values with 95% CIs calculated across runs. For analyses based on a single representative run—for example, evaluations using the median-performing prediction set or post hoc subgroup comparisons—95% CIs were obtained via nonparametric case-level bootstrapping (1000 resamples). The specific CI method used is reported alongside each result, and full resampling details are provided in Textbox S3 in Multimedia Appendix 1.

XSL•FO
RenderX

Secondary Outcome-Based Validity Analysis

Because there is no universally accepted gold standard for "true" acuity at ED presentation, triage tools are typically judged against surrogate outcomes such as hospitalization, ICU admission, revisits, and short-term mortality [15,16]. Large observational studies have shown that nurse-assigned categories can substantially underestimate or overestimate severity, with mis-triage affecting up to one-third of patients in some cohorts [17,21]. To complement our consensus label-based evaluation, we therefore derived outcome-based severity tiers and a disposition-safety composite (DSC) and re-examined how MECR-RAG, the baseline LLM, and initial nurse triage aligned with downstream clinical courses.

For all encounters with sufficient follow-up, we assigned an ordinal outcome-based severity tier (R1-R3) adapted from the multilevel reference standard used in MTS validation work, in which a multidisciplinary expert panel defined 3 urgency levels [15]. R1 represented high-acuity courses analogous to the "immediate or very urgent" reference category and was defined by the presence of any marker of life-threatening illness, such as markedly abnormal vital signs with modified early warning score ≥5 or depressed consciousness, emergency surgery or other high-intensity interventions shortly after ED arrival, or death in the ED, ICU, or during the index admission. R2 corresponded to an "urgent" course and included patients who did not meet R1 criteria but required substantial acute treatment (eg, intravenous medication, fluids, and nebulizers) or hospitalization. R3 comprised lower-acuity courses in which none of the R1 or R2 markers were present. Patients who left without being seen (LWBS) were coded separately and excluded from outcome-based binary analyses. Full operational definitions and mapping of specific outcome elements to R1-R3 are provided in Table S2 in Multimedia Appendix 1.

To capture sentinel deterioration events that may reflect underrecognition of severity at triage, we additionally defined a DSC based on components commonly used as ED quality and safety indicators. DSC was coded as positive if any of the following occurred after the index ED visit: (1) unplanned ICU transfer within 72 hours of ward admission, (2) ED revisit within 72 hours resulting in unplanned hospital admission (including ICU admission when present), or (3) all-cause death within 7 days [22-24]. A binary variable, DSC_any, was set to 1 if at least one component was present. Outcome adjudication for R1-R3 and DSC_any was performed using routinely collected outcome data and was fully blinded to the index triage category and all model outputs.

Using these constructs, we prespecified 4 binary analytic "lenses" for sensitivity analyses. A classic lens defined outcome+ as R1 only and outcome– as R2 or R3, with test+ as triage categories 1-2 versus 3-5, mirroring conventional MTS validation [15]. An operational lens defined outcome+ as R1 or R2 versus R3 and test+ as categories 1-3 versus 4-5, reflecting the separation between patients who should not wait in the lowest-priority stream and those who can safely do so. Two augmented lenses incorporated DSC_any: an augmented classic lens (outcome+=R1 or DSC_any; test+=categories 1 and 2) and an augmented operational lens (outcome+=R1 or R2 or DSC_any; test+=categories 1-3). These lenses were intended to test robustness across different, clinically motivated definitions of high severity and to align with prior recommendations on composite triage outcomes. Full definitions are provided in Textbox S4 in Multimedia Appendix 1.

For each lens and each triage method (nurse triage, baseline LLM, and MECR-RAG), we constructed 2×2 tables of test+ versus outcome+ and calculated sensitivity, specificity, and 95% CIs, along with positive and negative likelihood ratios (LR+ and LR–) and diagnostic odds ratios (DORs). To compare models on the same patients, we used paired McNemar tests to assess differences in sensitivity (within outcome+ cases) and specificity (within outcome– cases). As additional clinically interpretable summaries, we examined (1) the proportion of R1 cases assigned to immediate (categories 1 and 2), (2) the proportion of R2 cases assigned to nonurgent (categories 4 and 5), and (3) a weighted harm index per 100 patients that assigns higher penalties to more dangerous errors (R1 or R2 assigned to nonurgent) than to overtriage of R3 cases. Case-level harm scores were compared between models using paired signed tests. Detailed formulas for likelihood ratios, DORs, CIs, and harm index computation are provided in Textbox S5 in Multimedia Appendix 1.

Statistical Analysis

All analyses were conducted using R (version 4.5.0; R Core Team). Interrater agreement and kappa statistics were calculated using standard packages for reliability analysis. Classification metrics were obtained using established machine learning libraries, and nonparametric CIs were estimated using bootstrap resampling. Between-model comparisons used tests appropriate to the data structure, including Friedman tests with Nemenyi post hoc procedures for repeated-run summary metrics and Cochran Q and McNemar tests for paired binary outcomes. Exploratory subgroup, scaling, and cross-model generalizability analyses were treated as descriptive and were not formally powered for hypothesis testing. Full details of the statistical workflow, including package names, resampling schemes, handling of multiple runs, and exploratory analyses, are provided in Textbox S6 in Multimedia Appendix 1.

Ethical Considerations

This study was approved by the Hospital Authority Central Institutional Review Board (reference number CIRB-2024-561-4). Because this was a retrospective analysis of anonymized patient records with no impact on clinical care, the Central Institutional Review Board granted a waiver of informed consent. All data used in this study were fully anonymized prior to analysis, and no identifiable patient information was retained or accessible to the study team. No compensation was provided, as no participants were recruited or contacted for this study.

Results

Participants

The final test set comprised 236 ED triage encounters from 2023. After expert consensus adjudication, the distribution of triage categories was 23/236 (9.7%) category 1, 23/236 (9.7%)

XSL•FO
RenderX

category 2, 82/236 (34.7%) category 3, 98/236 (41.5%) category 4, and 10/236 (4.2%) category 5. The mean patient age was 55.1 (SD 26.2; range 0.3-98.0) years. Overall, 131/236 (55.5%) patients were male and 105/236 (44.5%) were female. The most common clinical specialties were medicine (115/236, 48.7%), orthopedics (36/236, 15.3%), surgery (33/236, 14.0%), and pediatrics (13/236, 5.5%), with the remaining 39/236 (16.5%) classified as other specialties.

The retrieval database used by the MECR-RAG system consisted of 3000 anonymized ED encounters from 2024. The triage category distribution was constructed to reflect real-world attendance patterns, which are typically skewed toward lower-acuity presentations, with modest upsampling of categories 1, 2, and 5 to ensure adequate representation of rare but clinically important groups. The mean age in the retrieval database was 56.7 (SD 25.6; range 0.2-104.0) years, with an equal sex distribution (1500/3000, 50.0% male and 1500/3000, 50.0% female). The specialty mix was similar to the test set, with medicine accounting for 1395/3000 (46.5%) encounters, followed by orthopedics (441/3000, 14.7%), surgery (435/3000, 14.5%), pediatrics (210/3000, 7.0%), and other specialties (519/3000, 17.3%). Baseline characteristics of both datasets are summarized in Table 1, and characteristics of the 1000- and 2000-case retrieval subsets used in the scaling analysis are provided in Table S3 in Multimedia Appendix 1.

Table 1. The demographic and triage category distribution of the test set and 3000-case retrieval-augmented generation database.

Characteristic	Test set (N=236)	3000-case database (N=3000)
Age (years), mean (SD; range)	55.1 (26.2; 0.3-98.0)	56.7 (25.6; 0.2-104.0)
Sex, n (%)		
Male	131 (55.5)	1500 (50.0)
Female	105 (44.5)	1500 (50.0)
Triage categories, n (%)		
Category 1	23 (9.7)	94 (3.1)
Category 2	23 (9.7)	120 (4.0)
Category 3	82 (34.7)	1705 (57.0)
Category 4	98 (41.5)	1035 (34.5)
Category 5	10 (4.2)	46 (1.5)
Specialty, n (%)		
Medicine	115 (48.7)	1395 (46.5)
Orthopedics	36 (15.3)	441 (14.7)
Surgery	33 (14.0)	435 (14.5)
Pediatrics	13 (5.5)	210 (7.0)
Others	39 (16.5)	519 (17.3)

Age is presented as mean (SD). Triage category and specialty values are reported as percentages of total cases within each dataset. Other specialties include dentistry; dermatology; ear, nose, and throat; neurosurgery; obstetrics and gynecology; oncology; ophthalmology; and psychiatry. Both datasets were constructed to reflect real-world triage distributions, with modest oversampling of rare categories (eg, categories 1, 2, and 5) to ensure sufficient representation for model evaluation. Full sampling rationale is provided in the “Methods” section. The test set and retrieval database exhibited broadly comparable distributions in age, sex, and specialty.

Comparative Performance of MECR-RAG and the Baseline LLM, Benchmarked Against Expert Rater Agreement

The MECR-RAG system showed substantially higher agreement with consensus triage labels than the baseline LLM. Across 5 independent runs, MECR-RAG achieved a mean QWK of 0.902 (SD 0.0021; 95% CI 0.901-0.904), compared with 0.801 (SD 0.004; 95% CI 0.798-0.804) for the baseline model (mean paired difference 0.101, SD 0.0058; 95% CI 0.097-0.106; P<.001). Classification accuracy followed the same pattern, with a mean accuracy of 0.802 (SD 0.0082; 95% CI 0.795-0.808) for MECR-RAG versus 0.542 (SD 0.0073; 95% CI 0.536-0.548) for the baseline LLM (mean paired difference 0.264, SD 0.0150; 95% CI 0.251-0.278; P<.001). Similar effect sizes were observed when analyses were repeated using single median-run prediction sets, indicating that MECR-RAG’s advantage was robust to run-to-run variability.

To benchmark model performance against human experts, we evaluated interrater reliability between the 2 professional triage nurses who generated the reference labels; their QWK was 0.887. By comparison, MECR-RAG achieved a mean QWK of 0.902 (SD 0.0021; 95% CI 0.901-0.904). Using a prespecified noninferiority margin of −0.05, MECR-RAG met criteria for noninferiority to expert agreement, and this conclusion was unchanged in sensitivity analyses restricted to single median-performing runs. Taken together, these findings suggest that MECR-RAG attains expert-comparable consistency in 5-level triage classification while clearly outperforming a

XSL•FO
RenderX

prompt-only LLM. Confusion matrices comparing triage classification performance between the baseline LLM and MECR-RAG are shown in Figure 2. Results are shown for the median-performing run across 5 stochastic trials in this figure.

Figure 2. Confusion matrices comparing 5-level triage classification performance between the baseline prompt-only large language model (panel A) and the Multi-Evidence Clinical Reasoning retrieval-augmented generation system (panel B) on 236 emergency department triage encounters in the test set. LLM: large language model; MERC-RAG: Multi-Evidence Clinical Reasoning retrieval-augmented generation.

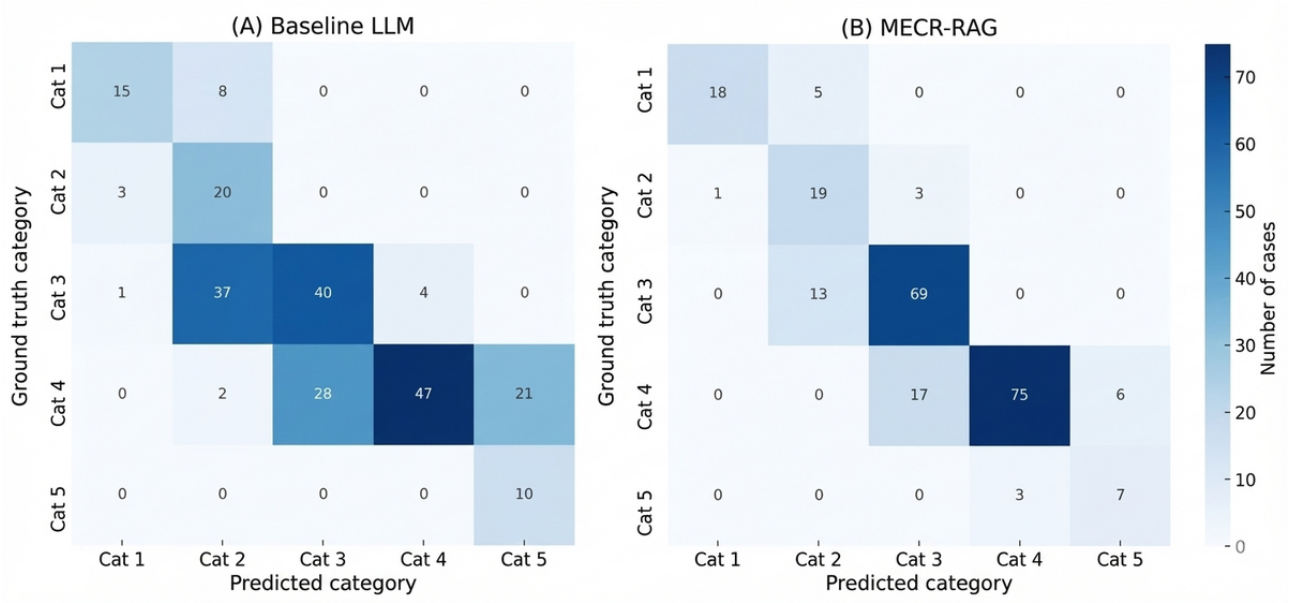

Performance Using Clinically Grouped Triage Categories

To reflect operational priorities in the ED, we conducted a post hoc analysis collapsing the 5 triage categories into 3 clinically meaningful groups: immediate (categories 1 and 2), urgent (category 3), and nonurgent (categories 4 and 5). This schema mirrors local workflows, in which immediate cases are seen without delay, urgent cases typically wait approximately 32 minutes, whereas nonurgent cases typically wait approximately 240 minutes based on 2024 institutional data. All metrics in this analysis were derived from the median-performing model run to approximate single-run deployment. Confusion matrices for grouped predictions are shown in Figure 3. Results reflect the median-performing run across 5 stochastic trials in this figure.

Figure 3. Confusion matrices comparing triage group classification performance between the baseline prompt-only large language model (panel A) and the Multi-Evidence Clinical Reasoning retrieval-augmented generation system (panel B) under a 3-group schema. LLM: large language model; MERC-RAG: Multi-Evidence Clinical Reasoning retrieval-augmented generation.

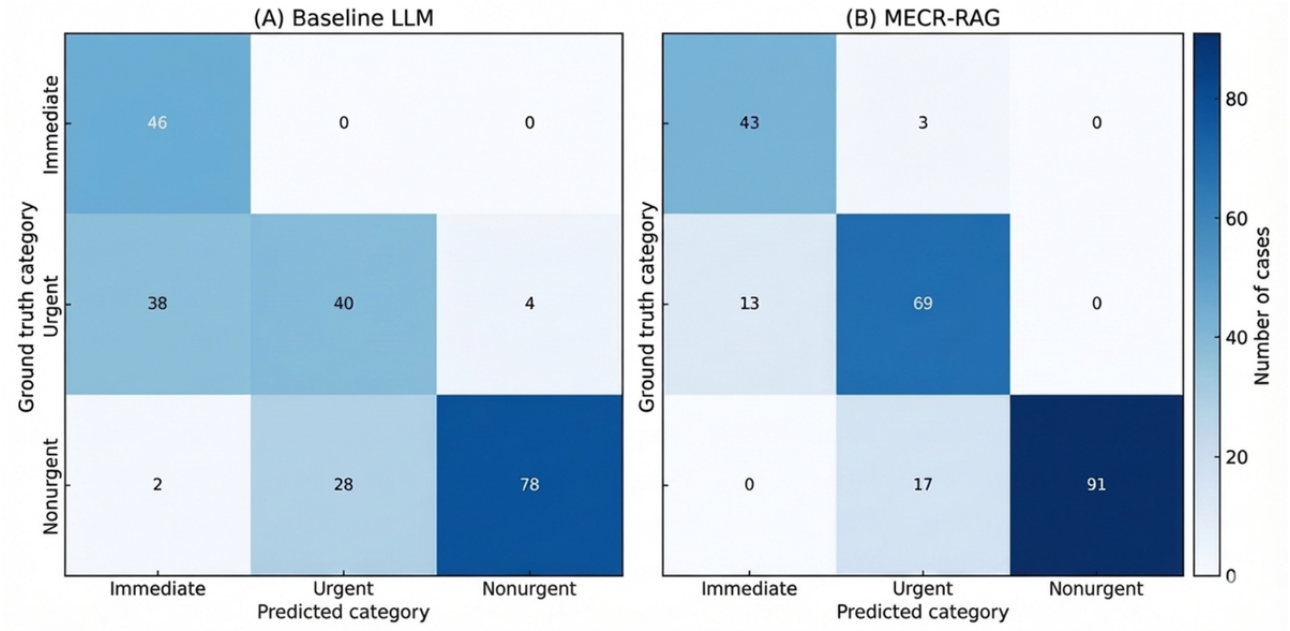

Under this 3-group schema, MECR-RAG maintained high overall performance, achieving a QWK of 0.882 (95% CI 0.840-0.920) compared with 0.759 (95% CI 0.700-0.813) for the baseline LLM (paired difference 0.125, 95% CI 0.077-0.174; P<.001). Accuracy similarly favored MECR-RAG (0.859 vs 0.695; paired difference 0.164, 95% CI 0.110-0.225; P<.001).

XSL•FO
RenderX

Macrolevel precision, recall, and F_1-score were also higher for MECR-RAG (precision 0.848 vs 0.691; recall 0.873 vs 0.737; F_1-score 0.860 vs 0.713).

Error-pattern analysis showed that MECR-RAG slightly reduced undertriage compared with the baseline LLM (3/236, 1.3% vs 4/236, 1.7%; McNemar P=.69), while substantially reducing overtriage. Overtriage decreased from 68/236 (28.8%) with the baseline LLM to 30/236 (12.7%) with MECR-RAG (McNemar P<.001). Thus, the model reduced unnecessary escalation without compromising detection of higher-acuity cases.

Performance advantages for MECR-RAG were consistent across triage groups. For immediate cases, MECR-RAG had slightly lower recall than the baseline LLM (0.935 vs 1.000) but substantially higher precision (0.768 vs 0.535), yielding a higher F_1-score (0.842 vs 0.697). Overall correctness did not differ significantly (McNemar P=.25), suggesting comparable sensitivity with fewer false positives. In the urgent group, MECR-RAG markedly outperformed the baseline model (recall 0.841 vs 0.488; precision 0.775 vs 0.588; F_1-score 0.807 vs 0.532; McNemar P<.001), indicating improved discrimination in this diagnostically challenging and operationally dominant band. For nonurgent cases, MECR-RAG again showed higher recall (0.843 vs 0.722) and F_1-score (0.915 vs 0.823), with perfect precision (1.000 vs 0.951; McNemar P=.01). These patterns, summarized in Figure 4, suggest that MECR-RAG delivers a more favorable balance between safety and operational efficiency, particularly in the mid- and low-acuity groups that account for most ED visits and drive waiting-time differentials.

Figure 4. Comparative model performance across overall and triage group-specific metrics. LLM: large language model; MERC-RAG: Multi-Evidence Clinical Reasoning retrieval-augmented generation. QWK: quadratic weighted kappa.

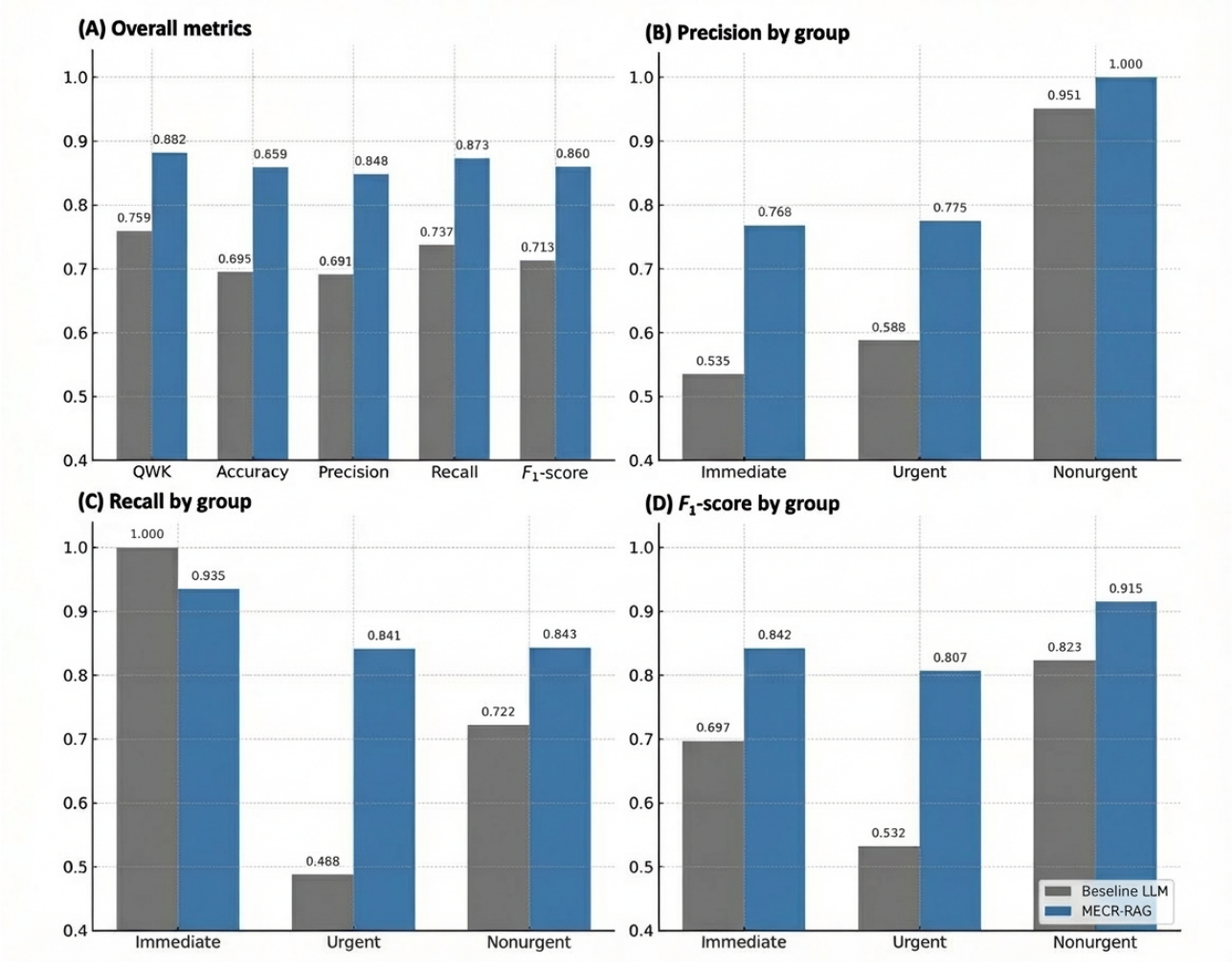

Comparative model performance across overall and triage group-specific metrics. Performance is evaluated using a clinically relevant 3-level grouping: immediate (categories 1 and 2), urgent (category 3), and nonurgent (categories 4 and 5), corresponding to local time-to-physician targets and resource prioritization. Panel A summarizes overall performance across QWK, accuracy, precision, recall, and F_1-score for the baseline prompt-only LLM and the MECR-RAG system; MECR-RAG achieved higher QWK (0.882) and accuracy (0.859) than the baseline LLM (QWK 0.759; accuracy 0.695; both P<.001). Panels B-D show precision, recall, and F_1-score, respectively, by triage group, with MECR-RAG consistently outperforming the baseline LLM across all groups and particularly in the urgent group (F_1-score 0.807 vs 0.532). All results are based on the median-performing model run.

XSL•FO
RenderX

Outcome-Informed Validity Relative to Clinical Severity

Among the 236 triage encounters, 226 (95.8%) had sufficient follow-up information to assign an outcome-based severity tier (R1-R3); the remaining 10 (4.2%) patients were LWBS and were excluded from all outcome-based analyses but retained in label-based performance summaries. Within the 226 encounters with outcome labels, 13/226 (5.8%) met R1 criteria, 117/226 (51.8%) met R2 criteria, and 96/226 (42.5%) were classified as R3. When high-severity outcomes were defined as R1+R2 (n=130) and triage "positive" as categories 1-3 versus 4-5, MECR-RAG achieved the highest sensitivity for high-risk courses at 124/130 (95.4%), compared with 117/130 (90.0%) for initial nurse triage and 122/130 (93.8%) for the baseline LLM. The gain versus nurses was statistically significant (McNemar χ^2_1 =5.14; *P*=.02), whereas sensitivity did not differ from the baseline LLM (χ^2_1 =0.17; *P*=.68). Specificity for low-risk (R3) cases was 77/96 (80%) for MECR-RAG, 78/96 (81%) for nurses, and 66/96 (69%) for the baseline LLM. Thus, MECR-RAG maintained nurse-level specificity (χ^2_1 =0.00; *P*=1.00) while significantly improving specificity over the baseline LLM (χ^2_1 =5.26; *P*=.02). All 3 systems correctly avoided assigning nonurgent (categories 4 and 5) to any R1 cases (0/13 each). The DOR for distinguishing R1+R2 from R3 was 83.8 (95% CI 32.0-218.9) for MECR-RAG, 39.0 (95% CI 18.1-84.1) for nurses, and 33.6 (95% CI 14.6-77.4) for the baseline LLM, consistent with a more favorable overall trade-off between undertriage and overtriage for MECR-RAG, although CIs overlapped because of limited event counts.

To examine clinically important undertriage, we focused on R2 patients assigned to nonurgent triage (categories 4 and 5). Among 117 R2 encounters, 13/117 (11.1%) were initially labeled nonurgent by nurses, compared with 8/117 (6.8%) by the baseline LLM and 6/117 (5.1%) by MECR-RAG. In paired analysis, MECR-RAG approximately halved R2 nonurgent misclassification relative to nurses (13 to 6 cases; McNemar χ^2_1 =5.14; *P*=.02), with a smaller, nonsignificant reduction compared with the baseline LLM (8 to 6 cases; χ^2_1 =0.17; *P*=.68). Considering the entire triage distribution, MECR-RAG also produced the safest nonurgent queue in terms of hidden high-risk patients: among patients predicted as nonurgent, the proportion with R1+R2 outcomes was 6/83 (7%) for MECR-RAG, compared with 13/91 (14%) for nurses and 8/74 (11%) for the baseline LLM. immediate groups were correspondingly enriched for high-severity outcomes, with 47/47 (100%) R1+R2 for nurses, 56/56 (100%) for MECR-RAG, and 82/86 (95%) for the baseline LLM. These patterns suggest that MECR-RAG reduces undertriage of R2 patients into the lowest-priority stream while preserving a clear outcome-based risk gradient across immediate, urgent, and nonurgent groups.

As a complementary summary of mis-triage burden, we constructed a weighted harm index that assigns higher cost to more dangerous errors: R1 assigned to nonurgent (categories 4 and 5) was weighted as 5, R2 assigned to nonurgent as 2, and R3 assigned to immediate or urgent (categories 1-3) as 1. Across the 226 cases with outcome labels, initial nurse triage accumulated a weighted error sum of 44 (harm index 19.47 per 100 patients), the baseline LLM 46 (20.35 per 100 patients), and MECR-RAG 31 (13.72 per 100 patients). At the individual case level, the baseline LLM incurred higher harm scores than MECR-RAG in 19 discordant cases and lower scores in 6, with 201 ties (2-sided sign test *P*=.02), indicating a statistically significant net reduction in weighted harm with MECR-RAG. Compared with nurses, harm scores were lower for MECR-RAG in 14 cases and higher in 8 (204 ties; *P*=.29), suggesting a numerically favorable but underpowered difference. Overall, these outcome-based analyses indicate that MECR-RAG not only improves high-severity sensitivity and reduces R2 undertriage but also yields the lowest aggregate mis-triage burden when accounting for both the direction and severity of errors.

To test robustness to alternative definitions of clinical severity, we repeated binary analyses under classic and augmented outcome "lenses" that defined outcome+ using R1 alone, R1 combined with the DSC, and R1 or R2 combined with the composite (see Methods). Across all lenses, MECR-RAG consistently showed the most favorable trade-off between sensitivity and specificity, with the highest DORs and positive likelihood ratios compared with nurses and the baseline LLM. In a classic Manchester-style lens (outcome+=R1 only; test+=categories 1-2 vs 3-5), all 3 systems achieved perfect sensitivity for R1 cases, but MECR-RAG improved specificity relative to the baseline LLM and approached nurse performance. When the DSC (unplanned ICU transfer within 72 hours, 72-hour revisit with admission, or death within 7 days) was incorporated into augmented lenses, MECR-RAG again maintained the highest discrimination despite wide and overlapping confidence intervals reflecting the small number of sentinel events. Full 2×2 tables, effect estimates, CIs and details for each lens are provided in Tables S4-S7 and Section B in Multimedia Appendix 1. Complementary exploratory analyses, including subgroup performance stratified by age and sex and model behavior on adjudicated disagreement cases, are reported in Sections C and D in Multimedia Appendix 1.

Component-Wise Ablation of Retrieval Mechanisms

To assess the contribution of individual retrieval components, we conducted a component-wise ablation across four configurations: (1) a prompt-only baseline LLM without retrieval, (2) a guideline-only RAG model retrieving sections from the HKAETG, (3) a case-only RAG model retrieving similar past triage cases, and (4) the full MECR-RAG system combining both guideline and case retrieval. Each configuration used an identical preprocessing and generation pipeline and was evaluated over 5 independent runs. QWK was the primary outcome, with overall accuracy, macrolevel precision, and macrolevel recall as secondary metrics.

Across configurations, MECR-RAG achieved the highest agreement with expert consensus (mean QWK 0.902, SD 0.0021; 95% CI 0.901-0.904; accuracy 0.802, SD 0.0082), followed by the case-only model, then the guideline-only model, and finally the baseline LLM. Both guideline-based and case-based retrieval improved performance relative to the baseline, but their combined use in MECR-RAG produced the largest and most consistent gains. Friedman tests on QWK and accuracy across the 4 models were statistically significant, and

XSL•FO
RenderX

post hoc Nemenyi comparisons identified MECR-RAG as the only configuration with a statistically superior rank to the baseline LLM under conservative multiple-comparison control. Full numerical results are shown in Figure 5 (QWK) and Figure 6 (accuracy) and are detailed in Table S8 in Multimedia Appendix 1.

Figure 5. Quadratic weighted kappa performance of model variants and professional raters. LLM: large language model; MERC-RAG: Multi-Evidence Clinical Reasoning retrieval-augmented generation; RAG: retrieval-augmented generation.

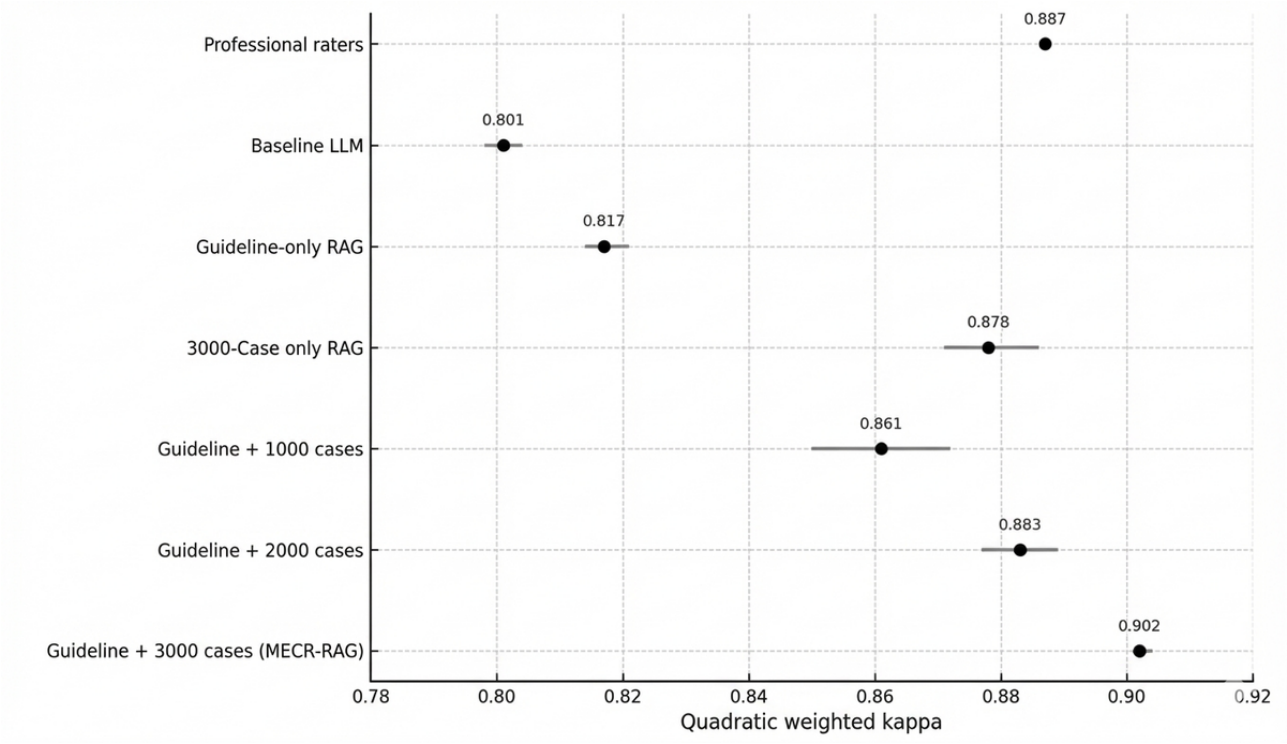

Figure 6. Accuracy performance across model variants. LLM: large language model; MERC-RAG: Multi-Evidence Clinical Reasoning retrieval-augmented generation; RAG: retrieval-augmented generation.

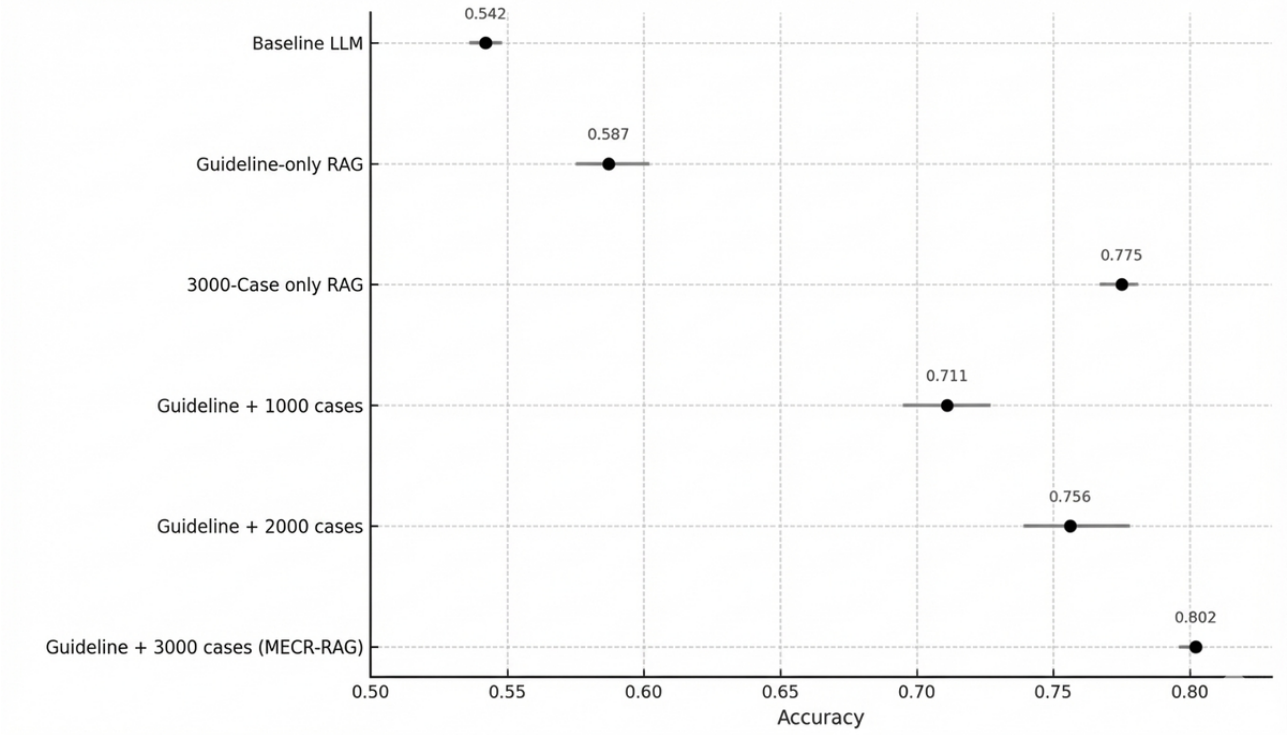

To understand how retrieval affected different acuity levels, we examined per-category accuracy and F_1-scores for triage categories 1-5. Guideline retrieval contributed most strongly to category 1 (critical) performance, where the guideline-only model achieved the highest accuracy and F_1-score, consistent with the value of structured, rule-based protocols for recognizing

XSL•FO
RenderX

life-threatening presentations. In contrast, case retrieval had the largest impact on categories 3 and 4, where the case-only and MECR-RAG models substantially outperformed both the baseline and guideline-only configurations, reflecting the importance of experiential pattern recognition in diagnostically ambiguous, midacuity presentations. For categories 2 and 5, model differences were smaller and not statistically robust, although MECR-RAG generally retained the highest F_1-scores. Overall, MECR-RAG delivered the best balance of precision and recall across all categories, supporting the complementary value of combining guideline-based and case-based retrieval (Figure 7; detailed estimates in Table S9 in Multimedia Appendix 1).

Figure 7. Component-wise ablation analysis of model performance across triage categories. LLM: large language model; MERC-RAG: Multi-Evidence Clinical Reasoning retrieval-augmented generation.

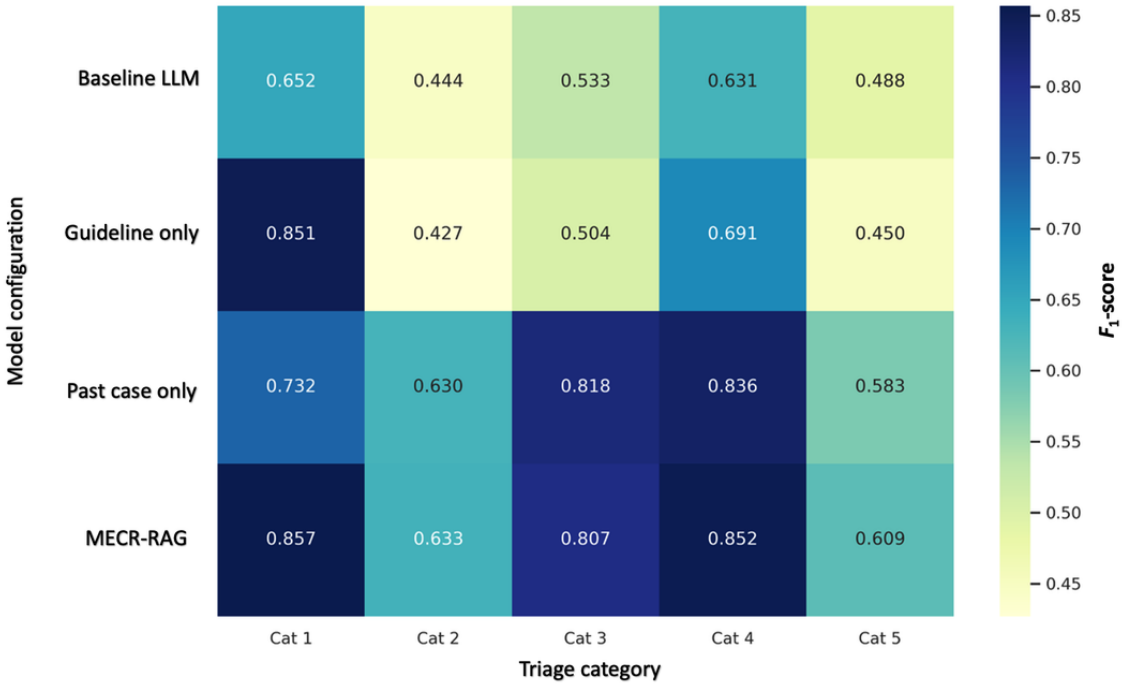

As an exploratory scaling analysis, we also varied the size of the past-case retrieval database from 1000 to 3000 cases and observed monotonic gains in QWK and accuracy with reduced between-run variability at larger retrieval pools (Tables S3 and S10 in Multimedia Appendix 1).

In Figure 5, the mean QWK values with 95% CIs are shown for the baseline and retrieval-augmented model variants. Points represent mean QWK across 5 stochastic runs, and horizontal error bars indicate 95% CIs across these runs. The professional benchmark (QWK 0.887) reflects interrater agreement between 2 expert triage nurses. The figure includes both ablation variants—a guideline-only RAG model and a 3000-case-only RAG model—and scaling variants that combine guideline and past case retrieval with databases containing 1000, 2000, and 3000 past triage cases. The MECR-RAG model (guideline plus 3000 past cases) achieved the highest mean QWK and was statistically superior to the baseline prompt-only large language model (LLM; mean paired difference 0.101, SD 0.0058; 95% CI 0.097-0.106; P<.001), while demonstrating noninferior agreement compared with professional raters.

In Figure 6, the mean accuracy values with 95% CIs are shown for the baseline prompt-only LLM, RAG variants, and combined retrieval configurations. The x-axis shows accuracy, with points representing mean values across 5 stochastic runs and horizontal error bars indicating 95% CIs. The figure includes ablation variants (guideline-only and 3000-case-only RAG) and scaling variants that combine guideline retrieval with 1000, 2000, or 3000 past cases. The MECR-RAG configuration (guideline plus 3000 past cases) achieved the highest accuracy and demonstrated a statistically significant improvement compared with the baseline LLM.

F_1-scores for each triage category (categories 1-5) across 4 model configurations. Rows represent the baseline prompt-only LLM, a guideline-only RAG model, a 3000-case-only RAG model, and the MECR-RAG system, and columns represent triage categories. Values reflect outputs from the median-performing evaluation run. Guideline retrieval contributed most prominently to performance in category 1, while case retrieval improved performance in categories 3 and 4, where patient presentations are more heterogeneous and require contextual interpretation. The MECR-RAG system generally achieved the highest or near-highest F_1-scores across triage categories, illustrating the additive value of combining structured guideline knowledge with experiential case-based retrieval.

XSL•FO
RenderX

Generalizability Across LLM Architectures

The primary model used for all prior evaluations was DeepSeek-V3. To evaluate whether the MECR-RAG framework generalizes beyond this development model, we conducted exploratory assessments using 2 additional foundation models: Claude 3.7 and GPT-4o. Each model was tested on the same 236-case triage dataset with the same 3000-case retrieval database under 2 configurations: the MECR-RAG system and a baseline, prompt-only LLM without retrieval augmentation.

In these single-run evaluations, MECR-RAG consistently outperformed the corresponding baseline configuration. For Claude 3.7, QWK improved from 0.840 under the baseline to 0.890 with MECR-RAG. Similarly, GPT-4o achieved a QWK of 0.890 with MECR-RAG, compared with 0.778 without retrieval. Although these results are based on single inference runs and are not statistically powered for formal comparison, they provide preliminary evidence that the dual-source retrieval framework may confer similar relative gains across distinct LLM back ends. A detailed breakdown of model predictions versus consensus triage labels for Claude 3.7 and GPT-4o, under both MECR-RAG and baseline conditions, is provided in Figures S1 and S2 in Multimedia Appendix 1, respectively.

Taken together, these preliminary findings suggest that the benefits of dual-source retrieval generalize beyond DeepSeek-V3 and may confer cross-model robustness of MECR-RAG across LLMs from different developers, supporting its broader applicability in diverse clinical settings. Further benchmarking across a wider range of model families, input formats, and deployment environments is warranted to validate robustness and assess trade-offs in latency, interpretability, and resource efficiency for real-world clinical deployment.

Discussion

Principal Findings

This retrospective evaluation suggests that a dual-source, retrieval-augmented LLM can achieve expert-comparable agreement with consensus nurse triage labels while substantially outperforming a prompt-only baseline model. MECR-RAG improved QWK and accuracy over the baseline LLM under both the 5-level and 3-group schemas and met prespecified noninferiority criteria compared with professional triage nurses. The largest gains occurred in Categories 3 and 4 and in the urgent versus nonurgent grouping, which together accounted for most ED visits and are operationally dominant, with large differences in waiting times. Ablation analyses indicated that both guideline retrieval and case retrieval contributed to performance, with the full dual-source MECR-RAG configuration consistently outperforming guideline-only and case-only variants. Performance also improved as the retrieval database increased from 1000 to 3000 cases, suggesting that retrieval quality benefits from a richer case pool. Exploratory cross-model experiments with Claude 3.7 Sonnet and GPT-4o further suggested that these benefits generalize across different LLM back ends.

Ground Truth Validity and Construct Interpretation

In this study, the primary reference standard was expert nurse consensus at the time of presentation, which reflects routine clinical decision-making but is an imperfect proxy for underlying acuity. Large US data on ESI version 4 report mis-triage in 32.2% of encounters (3.3% undertriage and 28.9% overtriage), underscoring that nurse-level labels are imperfect proxies for “true” acuity [17]. Even with trained emergency staff, approximately 17% of triage assignments may be inaccurate [21]. To address these limitations, we complemented consensus labels with outcome-informed constructs, ordinal severity tiers (R1-R3) and a DSC, adapted from MTS validation work and recommendations on triage outcome selection [15,22,24].

Within these outcome-based frameworks, MECR-RAG showed higher sensitivity for R1+R2 courses than initial nurse triage at comparable specificity, reduced misclassification of R2 patients into the nonurgent stream, and yielded the lowest weighted harm index, suggesting closer alignment between assigned urgency and downstream clinical course. At the same time, event counts for the most severe outcomes were modest, and both nurse consensus and the composite outcomes remain pragmatic proxies rather than definitive measures of “true” severity. We therefore interpret these findings as supportive evidence that MECR-RAG performs well against clinically grounded, outcome-informed constructs of acuity, rather than as proof that it fully captures an underlying severity state.

Comparison With Prior Work

To our knowledge, this is the first study to evaluate a dual-source, RAG-enhanced LLM for emergency triage using raw triage documentation paired with expert-consensus reference labels and complementary outcome-informed severity constructs. Prior RAG studies in emergency care have shown that retrieval can improve triage or referral performance on simulated exam-style cases or curated ED datasets but have relied on structured scenarios or routine triage labels without independent adjudication [13,14]. Our design addresses the broader evidence gap noted in a recent systematic review, in which only 5% of 519 published evaluations of health care LLMs used real patient care data for testing [25]. This provides a more realistic and stringent test of RAG-enhanced triage than has been reported previously.

Masanneck et al [4] established an early benchmark by evaluating LLM triage performance against expert assessments, but their dataset consisted of physician-curated vignettes from a single day, with selected patient attributes adjusted according to predefined standard operating procedures. In contrast, our study applies dual-source RAG to a year-long sample of anonymized triage notes without manual editing or reinterpretation, preserving the fidelity of frontline documentation and temporal variation. Zaboli et al [3] and Paslı et al [7] have likewise emphasized the importance of handling unstructured narratives and integrating local triage frameworks; our dual-retrieval design directly addresses these needs by combining structured guideline content with real-world case patterns.

XSL•FO
RenderX

Our findings also align with broader work on nurse triage systems, showing that midacuity presentations are both the most common and the most difficult to classify. In a large cohort of over 5.3 million adult ED encounters using ESI version 4, Sax et al [17] found that approximately 29% of visits were overtriaged and that the sensitivity of ESI version 4 for identifying low-acuity, low-resource patients (correctly assigning ESI 4-5 among patients using <2 resources and with no critical interventions) was only 50%. A majority of encounters were assigned to the midlevel category ESI 3, highlighting poor differentiation between lower- and higher-acuity patients. Validation of the HKAETG has similarly shown the lowest interrater agreement for categories 3 and 4, reflecting the intrinsic difficulty of distinguishing "urgent" from "semiurgent" presentations [26]. In our cohort, categories 3 and 4 comprised about three-quarters of all cases, and the prompt-only LLM reproduced the overtriage patterns documented in both human and LLM triage studies. In contrast, MECR-RAG substantially reduced overtriage and improved precision and recall specifically in these mid- and low-acuity strata, suggesting that dual-source retrieval may help address a long-standing bottleneck in emergency triage performance.

Clinical and Operational Implications

Although we did not directly measure ED length of stay (LOS), boarding, or mortality, several findings suggest how MECR-RAG could plausibly influence safety and flow if implemented as decision support. Under a 3-group schema (immediate, urgent, and nonurgent), MECR-RAG achieved higher agreement and accuracy than the prompt-only LLM, with markedly less overtriage and similarly low undertriage. Gains were concentrated in the urgent and nonurgent tiers, which dominate the case mix and are associated with substantially longer waits for lower-priority patients at our center. In outcome-based analyses, MECR-RAG showed higher sensitivity for R1+R2 courses than initial nurse triage at nurse-level specificity, reduced misclassification of R2 patients into the nonurgent stream, and yielded the lowest severity-weighted harm index. Together, these patterns indicate fewer high-risk patients "hidden" in the longest-wait queue and fewer low-risk patients unnecessarily occupying high-acuity resources, aligning urgency assignments more closely with downstream clinical course.

These redistributions of risk are clinically relevant because prolonged ED LOS, crowding, and boarding have been repeatedly linked to delayed treatment, longer inpatient stays, and higher short-term mortality. More efficient separation between urgent and nonurgent queues could, in principle, help decompress monitored areas, reduce avoidable time in high-acuity spaces for low-risk patients, and support more timely care for those with high-severity courses. However, our evaluation was retrospective and did not include LOS, crowding, or mortality as prespecified end points. Any potential contribution of MECR-RAG therefore remains hypothesis-generating and must be tested in prospective, outcome-focused studies.

As illustrated in the proposed human-in-the-loop workflow (Figure 8), MECR-RAG is intended to function as a background triage decision-support layer: triage nurses retain primary responsibility for assigning categories, while a secure, deidentified copy of the triage note is analyzed in parallel, with the system remaining silent for most encounters and surfacing alerts only for predefined safety-relevant discordances (eg, potential undertriage of urgent or immediate cases). Alerts and explanations can then be reviewed by a senior nurse, who may confirm or upgrade the triage category, while all alerts, decisions, and associated operational metrics are logged to support ongoing quality assurance and research on ED LOS, crowding, and downstream outcomes. A staged implementation strategy, beginning with shadow-mode deployment and progressing to focused pilots of discordance alerts with monitoring for automation bias, alert fatigue, throughput, and equity, will be essential before wider rollout.

XSL•FO
RenderX

Figure 8. Conceptual human-in-the-loop workflow for Multi-Evidence Clinical Reasoning retrieval-augmented generation as a background triage decision-support layer in the emergency department. ED: emergency department; LLM: large language model; LOS: length of stay; MECR-RAG: Multi-Evidence Clinical Reasoning retrieval-augmented generation; RAG: retrieval-augmented generation.

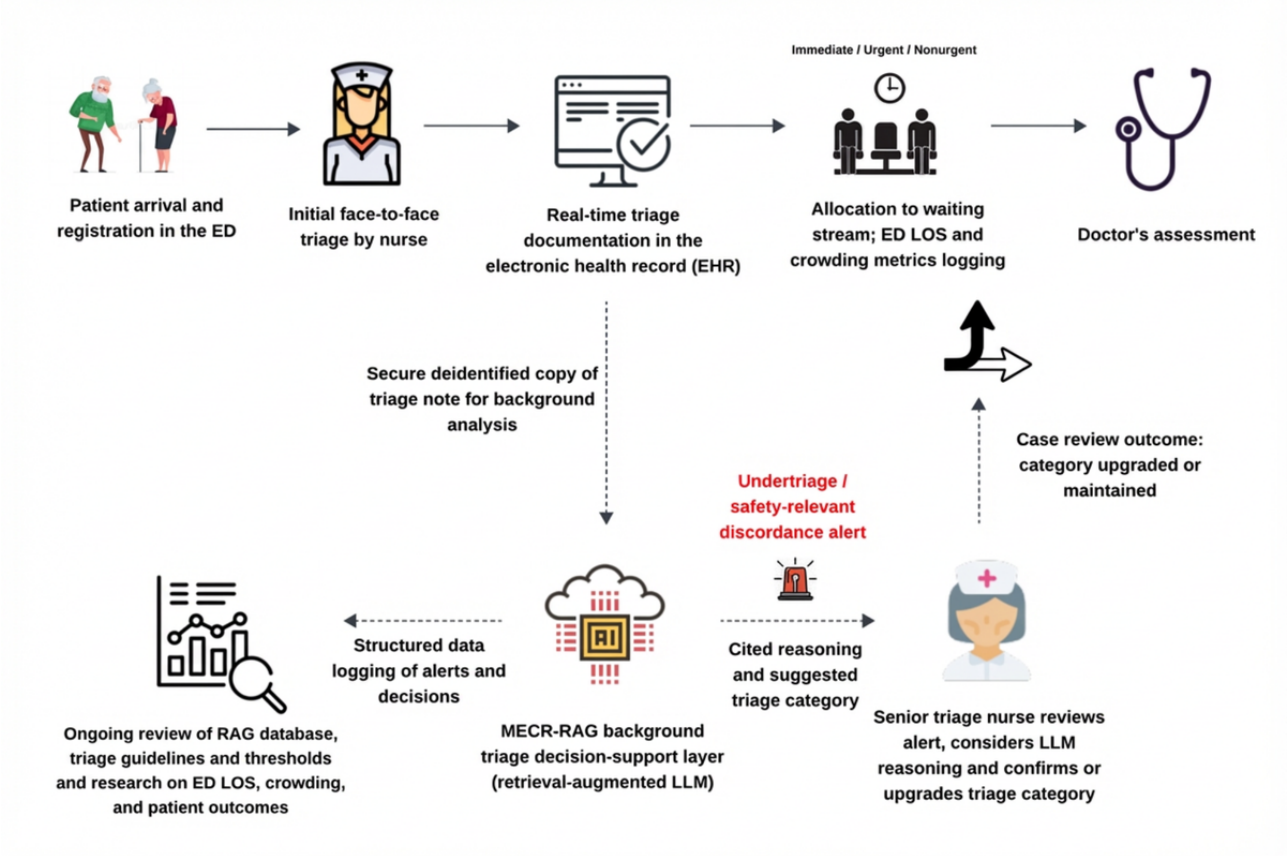

Patients follow the routine care pathway shown in the top row: arrival and registration in the ED, initial face-to-face triage by a nurse, real-time triage documentation in the electronic health record, allocation to an urgency-based waiting stream (immediate, urgent, or nonurgent) with logging of ED LOS and crowding metrics, and subsequent doctor's assessment. In parallel, a secure deidentified copy of the triage note is sent to the MECR-RAG system, which operates as a background triage decision-support layer. MECR-RAG generates its own triage recommendation with cited reasoning and remains silent for most encounters, but triggers an undertriage or other safety-relevant discordance alert when its recommendation conflicts with the nurse-assigned category. Alerts and explanations are routed to a senior triage nurse, who may confirm or upgrade the triage category; all alerts, decisions, and outcomes are logged to support ongoing quality assurance and research on ED LOS, crowding, and patient-centered outcomes.

Limitations and Future Directions

This study has several important limitations. First, within the staged evaluation pathway outlined by DECIDE-AI (Developmental and Exploratory Clinical Investigations of Decision support systems driven by Artificial Intelligence), this retrospective, offline prediction study represents preclinical (in silico) validation and should not be interpreted as evidence of real-world clinical effectiveness or safety [27]. Moreover, strong offline discrimination does not reliably translate into clinical benefit after implementation; prior early warning and sepsis tools (including the Rothman Index and the Epic Sepsis Model) have shown materially weaker performance and limited impact in independent, postdeployment evaluations, partly due to differences in data quality, missingness, case mix, alert logic, and workflow across sites [28-32]. Retrospective deep learning models are also vulnerable to dataset shift, class imbalance, and missing data, further limiting transportability across settings and time [33]. Randomized evaluations of AI-enabled interventions similarly suggest that even high-performing models may fail to improve primary clinical end points without careful workflow integration and attention to system constraints [34,35]. Accordingly, our retrospective, single-center results for MECR-RAG should be viewed as predeployment evidence and require prospective, multicenter evaluation before inferring equivalent real-time performance or improved patient outcomes.

Second**,** the evaluation was conducted in a single ED using the HKAETG; performance may differ under other triage frameworks (eg, MTS and ESI), languages, documentation practices, workflows, and patient case mix. Although the retrieval-augmented design is modular and could, in principle, be adapted by reindexing local guidelines and locally representative triage notes without retraining the underlying LLM, portability remains an empirical question and requires external validation and prospective multicenter evaluation.

Third, the retrieval database and text summaries were constructed automatically from routine triage notes without manual adjudication, and prompts were generated without clinician editing. This reflects realistic deployment conditions and improves scalability, but some retrieved exemplars may be

XSL•FO
RenderX

mislabeled or incomplete, and clinically relevant nuances may be lost during summarization. In addition, we did not directly evaluate usability, interpretability, automation bias, or workflow impact, which are increasingly recognized as critical determinants of the safety and effectiveness of AI-enabled clinical decision-support systems [32,36].

These limitations point to clear priorities for future work. Prospective, multicenter studies across institutions using different triage frameworks (HKAETG, MTS, and ESI) are needed to assess generalizability and to determine how MECR-RAG performs in real-time workflows. Consistent with DECIDE-AI and recent guidance from major journals and professional societies, future evaluations should move beyond agreement metrics to prespecify patient-centered and operational end points, including ED and hospital LOS, crowding and boarding times, unexpected ICU transfer, time-critical treatment delays, and short-term mortality [18,37-39]. Implementation-focused studies should also examine how MECR-RAG is integrated into practice (eg, as a second reader or discordance alert), its effects on clinician behavior, workload, and equity, and unintended consequences such as alert fatigue or overreliance on model outputs, ideally using pragmatic randomized or quasi-experimental designs where feasible [34,35]. Framing this work as an early-phase evaluation and explicitly outlining the need for prospective, outcome-focused trials in line with current AI evaluation guidance positions MECR-RAG as a promising candidate for further study rather than a tool ready for immediate widespread deployment.

Conclusions

In summary, this retrospective, single-center study provides one of the first evaluations of a dual-source, retrieval-augmented LLM for emergency triage on real triage notes with expert consensus labels, extending prior work beyond simulated scenarios and routine labels. MECR-RAG achieved agreement comparable to expert nurses and clearly outperformed a prompt-only LLM, particularly in the high-volume category 3-4 bands, while approximately halving overtriage and keeping undertriage very low. In exploratory outcome-based analyses within this cohort, MECR-RAG also showed higher sensitivity for high-severity courses, a safer nonurgent queue, and the lowest severity-weighted harm index compared with initial nurse triage. These findings support the potential of retrieval-augmented LLMs as clinically coherent decision-support tools that function as background second readers—surfacing guidelines and analogous cases, flagging discordant or high-risk assignments for senior review—and thereby potentially improving allocation of high-acuity resources in ways that could, if replicated prospectively, help reduce ED crowding, LOS, and related adverse outcomes. However, this remains an early-phase, retrospective, single-center evaluation based on proxy outcomes, and rigorous prospective multicenter studies across different triage frameworks, with prespecified patient-centered and operational end points and careful attention to workflow, usability, and equity, are essential before such systems can be recommended for routine clinical deployment.

Acknowledgments

We would like to thank KH Leung for organizing and facilitating the consensus triage labeling process. We are also grateful to the emergency department nursing staff at Princess Margaret Hospital for their triage assessments, which formed the basis of the clinical documentation used in this study.

Funding

No external financial support or grants were received from any public, commercial, or not-for-profit entities for the research, authorship, or publication of this article.

Data Availability

The datasets generated or analyzed during this study are not publicly available due to institutional and regulatory restrictions imposed by the Hospital Authority of Hong Kong, but are available from the corresponding author on reasonable request. The underlying code supporting the findings of this study is available at MECR-RAG-Clinical-Research [40].

Authors' Contributions

HS conceptualized the study design, developed the methodology, collected and curated the data, performed the analysis, created the figures, and drafted the initial manuscript. TK developed the computational architecture, configured the model framework, implemented and executed the MECR-RAG system.

Conflicts of Interest

None declared.

Multimedia Appendix 1
Detailed Multi-Evidence Clinical Reasoning retrieval-augmented generation implementation, prompts, and additional analyses.
[DOCX File , 1124 KB - medinform_v14i1e82026_app1.docx]

XSL•FO
RenderX

References

1. Suamchaiyaphum K, Jones AR, Markaki A. Triage accuracy of emergency nurses: an evidence-based review. J Emerg Nurs 2024;50(1):44-54. [doi: 10.1016/j.jen.2023.10.001] [Medline: 37930287]
2. Hinson JS, Martinez DA, Cabral S, George K, Whalen M, Hansoti B, et al. Triage performance in emergency medicine: a systematic review. Ann Emerg Med 2019;74(1):140-152. [doi: 10.1016/j.annemergmed.2018.09.022] [Medline: 30470513]
3. Zaboli A, Brigo F, Brigiari G, Massar M, Parodi M, Pfeifer N, et al. Chat-GPT in triage: still far from surpassing human expertise - an observational study. Am J Emerg Med 2025;92:165-171. [doi: 10.1016/j.ajem.2025.03.028] [Medline: 40120387]
4. Masanneck L, Schmidt L, Seifert A, Kölsche T, Huntemann N, Jansen R, et al. Triage performance across large language models, chatgpt, and untrained doctors in emergency medicine: comparative study. J Med Internet Res 2024;26:e53297 [FREE Full text] [doi: 10.2196/53297] [Medline: 38875696]
5. Arslan B, Nuhoglu C, Satici M, Altinbilek E. Evaluating LLM-based generative AI tools in emergency triage: a comparative study of ChatGPT Plus, Copilot Pro, and triage nurses. Am J Emerg Med 2025;89:174-181. [doi: 10.1016/j.ajem.2024.12.024] [Medline: 39731895]
6. Pasli S, Yadigaroğlu M, Kirimli EN, Beşer MF, Unutmaz İ, Ayhan A, et al. ChatGPT-supported patient triage with voice commands in the emergency department: a prospective multicenter study. Am J Emerg Med 2025;94:63-70. [doi: 10.1016/j.ajem.2025.04.040] [Medline: 40273640]
7. Paslı S, Şahin AS, Beşer MF, Topçuoğlu H, Yadigaroğlu M, İmamoğlu M. Assessing the precision of artificial intelligence in ED triage decisions: insights from a study with ChatGPT. Am J Emerg Med 2024;78:170-175. [doi: 10.1016/j.ajem.2024.01.037] [Medline: 38295466]
8. Kaboudi N, Firouzbakht S, Shahir Eftekhar M, Fayazbakhsh F, Joharivarnoosfaderani N, Ghaderi S, et al. Diagnostic accuracy of chatgpt for patients' triage; a systematic review and meta-analysis. Arch Acad Emerg Med 2024;12(1):e60. [doi: 10.22037/aaem.v12i1.2384] [Medline: 39290765]
9. Vrdoljak J, Boban Z, Vilović M, Kumrić M, Božić J. A review of large language models in medical education, clinical decision support, and healthcare administration. Healthcare (Basel) 2025;13(6):603 [FREE Full text] [doi: 10.3390/healthcare13060603] [Medline: 40150453]
10. Liu S, Wright AP, McCoy AB, Huang SS, Steitz B, Wright A. Detecting emergencies in patient portal messages using large language models and knowledge graph-based retrieval-augmented generation. J Am Med Inform Assoc 2025;32(6):1032-1039. [doi: 10.1093/jamia/ocaf059] [Medline: 40220286]
11. Xiong G, Jin Q, Lu Z, Zhang A. Benchmarking retrieval-augmented generation for medicine. In: Ku LW, Srikumar V, Martins A, editors. Findings of the Association for Computational Linguistics ACL. Bangkok, Thailand: Association for Computational Linguistics; 2024:6233-6251.
12. Zhang G, Xu Z, Jin Q, Chen F, Fang Y, Liu Y, et al. Leveraging long context in retrieval augmented language models for medical question answering. NPJ Digit Med 2025;8(1):239 [FREE Full text] [doi: 10.1038/s41746-025-01651-w] [Medline: 40316710]
13. Yazaki M, Maki S, Furuya T, Inoue K, Nagai K, Nagashima Y, et al. Emergency patient triage improvement through a retrieval-augmented generation enhanced large-scale language model. Prehosp Emerg Care 2025;29(3):203-209. [doi: 10.1080/10903127.2024.2374400] [Medline: 38950135]
14. Gaber F, Shaik M, Allega F, Bilecz AJ, Busch F, Goon K, et al. Evaluating large language model workflows in clinical decision support for triage and referral and diagnosis. NPJ Digit Med 2025;8(1):263 [FREE Full text] [doi: 10.1038/s41746-025-01684-1] [Medline: 40346344]
15. Zachariasse JM, Seiger N, Rood PPM, Alves CF, Freitas P, Smit FJ, et al. Validity of the Manchester Triage System in emergency care: a prospective observational study. PLoS One 2017;12(2):e0170811 [FREE Full text] [doi: 10.1371/journal.pone.0170811] [Medline: 28151987]
16. Zachariasse JM, van der Hagen V, Seiger N, Mackway-Jones K, van Veen M, Moll HA. Performance of triage systems in emergency care: a systematic review and meta-analysis. BMJ Open 2019;9(5):e026471 [FREE Full text] [doi: 10.1136/bmjopen-2018-026471] [Medline: 31142524]
17. Sax DR, Warton EM, Mark DG, Vinson DR, Kene MV, Ballard DW, et al. Evaluation of the emergency severity index in us emergency departments for the rate of mistriage. JAMA Netw Open 2023;6(3):e233404 [FREE Full text] [doi: 10.1001/jamanetworkopen.2023.3404] [Medline: 36930151]
18. Khera R, Butte AJ, Berkwits M, Hswen Y, Flanagin A, Park H, et al. AI in medicine-JAMA's focus on clinical outcomes, patient-centered care, quality, and equity. JAMA 2023;330(9):818-820. [doi: 10.1001/jama.2023.15481] [Medline: 37566406]
19. Gallifant J, Afshar M, Ameen S, Aphinyanaphongs Y, Chen S, Cacciamani G, et al. The TRIPOD-LLM reporting guideline for studies using large language models. Nat Med 2025;31(1):60-69. [doi: 10.1038/s41591-024-03425-5] [Medline: 39779929]
20. Fleiss JL, Tytun A, Ury HK. A simple approximation for calculating sample sizes for comparing independent proportions. Biometrics 1980;36(2):343-346. [Medline: 26625475]

XSL•FO
RenderX

21. Hinson JS, Martinez DA, Schmitz PSK, Toerper M, Radu D, Scheulen J, et al. Accuracy of emergency department triage using the Emergency Severity Index and independent predictors of under-triage and over-triage in Brazil: a retrospective cohort analysis. Int J Emerg Med 2018;11(1):3 [FREE Full text] [doi: 10.1186/s12245-017-0161-8] [Medline: 29335793]
22. Delgado MK, Liu V, Pines JM, Kipnis P, Gardner MN, Escobar GJ. Risk factors for unplanned transfer to intensive care within 24 hours of admission from the emergency department in an integrated healthcare system. J Hosp Med 2013;8(1):13-19. [doi: 10.1002/jhm.1979] [Medline: 23024040]
23. Gabayan GZ, Derose SF, Asch SM, Yiu S, Lancaster EM, Poon KT, et al. Patterns and predictors of short-term death after emergency department discharge. Ann Emerg Med 2011;58(6):551-558.e2 [FREE Full text] [doi: 10.1016/j.annemergmed.2011.07.001] [Medline: 21802775]
24. Ling D, Sung C, Fang C, Ko C, Chou EH, Herrala J, et al. High-risk return visits to United States emergency departments, 2010-2018. West J Emerg Med 2022;23(6):832-840 [FREE Full text] [doi: 10.5811/westjem.2022.7.57028] [Medline: 36409935]
25. Bedi S, Liu Y, Orr-Ewing L, Dash D, Koyejo S, Callahan A, et al. Testing and evaluation of health care applications of large language models: a systematic review. JAMA 2025;333(4):319-328. [doi: 10.1001/jama.2024.21700] [Medline: 39405325]
26. Fan M, Leung L. Validation of the Hong Kong accident and emergency triage guidelines. The HKU Scholars Hub. 2013. URL: https://hub.hku.hk/handle/10722/210102 [accessed 2026-01-02]
27. Vasey B, Nagendran M, Campbell B, Clifton DA, Collins GS, Denaxas S, DECIDE-AI expert group. Reporting guideline for the early-stage clinical evaluation of decision support systems driven by artificial intelligence: DECIDE-AI. Nat Med 2022;28(5):924-933. [doi: 10.1038/s41591-022-01772-9] [Medline: 35585198]
28. Rothman MJ, Rothman SI, Beals J. Development and validation of a continuous measure of patient condition using the Electronic Medical Record. J Biomed Inform 2013;46(5):837-848 [FREE Full text] [doi: 10.1016/j.jbi.2013.06.011] [Medline: 23831554]
29. Arnold J, Davis A, Fischhoff B, Yecies E, Grace J, Klobuka A, et al. Comparing the predictive ability of a commercial artificial intelligence early warning system with physician judgement for clinical deterioration in hospitalised general internal medicine patients: a prospective observational study. BMJ Open 2019;9(10):e032187 [FREE Full text] [doi: 10.1136/bmjopen-2019-032187] [Medline: 31601602]
30. Wong A, Otles E, Donnelly JP, Krumm A, McCullough J, DeTroyer-Cooley O, et al. External validation of a widely implemented proprietary sepsis prediction model in hospitalized patients. JAMA Intern Med 2021;181(8):1065-1070 [FREE Full text] [doi: 10.1001/jamainternmed.2021.2626] [Medline: 34152373]
31. Habib AR, Lin AL, Grant RW. The epic sepsis model falls short-the importance of external validation. JAMA Intern Med 2021;181(8):1040-1041. [doi: 10.1001/jamainternmed.2021.3333] [Medline: 34152360]
32. Downing N, Rolnick J, Poole S, Hall E, Wessels A, Heidenreich P, et al. Electronic health record-based clinical decision support alert for severe sepsis: a randomised evaluation. BMJ Qual Saf 2019;28(9):762-768 [FREE Full text] [doi: 10.1136/bmjqs-2018-008765] [Medline: 30872387]
33. Mann KD, Good NM, Fatehi F, Khanna S, Campbell V, Conway R, et al. Predicting patient deterioration: a review of tools in the digital hospital setting. J Med Internet Res 2021;23(9):e28209 [FREE Full text] [doi: 10.2196/28209] [Medline: 34591017]
34. Mazor T, Farhat KS, Trukhanov P, Lindsay J, Galvin M, Mallaber E, et al. Clinical trial notifications triggered by artificial intelligence-detected cancer progression: a randomized trial. JAMA Netw Open 2025;8(4):e252013 [FREE Full text] [doi: 10.1001/jamanetworkopen.2025.2013] [Medline: 40257799]
35. Mandair D, Elia MV, Hong JC. Considerations in translating AI to improve care. JAMA Netw Open 2025;8(4):e252023 [FREE Full text] [doi: 10.1001/jamanetworkopen.2025.2023] [Medline: 40257804]
36. Schinkel M, van der Poll T, Wiersinga WJ. Artificial intelligence for early sepsis detection: a word of caution. Am J Respir Crit Care Med 2023;207(7):853-854 [FREE Full text] [doi: 10.1164/rccm.202212-2284VP] [Medline: 36724366]
37. Chiu I, Lin Y, Syue Y, Kung C, Wu K, Li C. The influence of crowding on clinical practice in the emergency department. Am J Emerg Med 2018;36(1):56-60. [doi: 10.1016/j.ajem.2017.07.011] [Medline: 28705743]
38. Sartini M, Carbone A, Demartini A, Giribone L, Oliva M, Spagnolo AM, et al. Overcrowding in emergency department: causes, consequences, and solutions-a narrative review. Healthcare (Basel) 2022;10(9):1625 [FREE Full text] [doi: 10.3390/healthcare10091625] [Medline: 36141237]
39. Armoundas AA, Narayan SM, Arnett DK, Spector-Bagdady K, Bennett DA, Celi LA, American Heart Association Institute for Precision Cardiovascular Medicine; Council on CardiovascularStroke Nursing; Council on Lifelong Congenital Heart DiseaseHeart Health in the Young; Council on Cardiovascular RadiologyIntervention; Council on Hypertension; Council on the Kidney in Cardiovascular Disease;Stroke Council. Use of artificial intelligence in improving outcomes in heart disease: a scientific statement from the american heart association. Circulation 2024;149(14):e1028-e1050 [FREE Full text] [doi: 10.1161/CIR.0000000000001201] [Medline: 38415358]
40. Multi-Evidence Clinical Reasoning RAG for Emergency Medicine Triage - Journal Submission Supporting Code. GitHub. URL: https://github.com/tkwr565/MECR-RAG-Clinical-Research [accessed 2026-01-05]

XSL•FO
RenderX

Abbreviations

AI: artificial intelligence
API: application programming interface
DECIDE-AI: Developmental and Exploratory Clinical Investigations of Decision support systems driven by Artificial Intelligence
DOR: diagnostic odds ratio
DSC: disposition-safety composite
ED: emergency department
ESI: Emergency Severity Index
HKAETG: Hong Kong Accident and Emergency Triage Guidelines
ICU: intensive care unit
JAMA: Journal of the American Medical Association
LLM: large language model
LOS: length of stay
LWBS: left without being seen
MECR: Multi-Evidence Clinical Reasoning
MECR-RAG: Multi-Evidence Clinical Reasoning retrieval-augmented generation
MIMIC-IV: Medical Information Mart for Intensive Care IV
MTS: Manchester Triage System
PMH: Princess Margaret Hospital
QWK: quadratic weighted kappa
RAG: retrieval-augmented generation
TRIPOD-LLM: Transparent Reporting of a multivariable prediction model for Individual Prognosis Or Diagnosis - Large Language Models

Edited by A Benis; submitted 07.Aug.2025; peer-reviewed by S Mohanadas, D Yoo; comments to author 05.Sep.2025; revised version received 05.Dec.2025; accepted 29.Dec.2025; published 26.Jan.2026.

Please cite as:
Wong HS, Wong TK
Multi-Evidence Clinical Reasoning With Retrieval-Augmented Generation for Emergency Triage: Retrospective Evaluation Study
JMIR Med Inform 2026;14:e82026
URL: https://medinform.jmir.org/2026/1/e82026
doi:10.2196/82026
PMID:

©Hang Sheung Wong, Tsz Kwan Wong. Originally published in JMIR Medical Informatics (https://medinform.jmir.org), 26.Jan.2026. This is an open-access article distributed under the terms of the Creative Commons Attribution License (https://creativecommons.org/licenses/by/4.0/), which permits unrestricted use, distribution, and reproduction in any medium, provided the original work, first published in JMIR Medical Informatics, is properly cited. The complete bibliographic information, a link to the original publication on https://medinform.jmir.org/, as well as this copyright and license information must be included.

XSL•FO
RenderX

Original Paper

Machine Learning Algorithms to Predict Venous Thromboembolism in Patients With Sepsis in the Intensive Care Unit: Multicenter Retrospective Study

Yan Zhang[1*], MD; Xia Ren[2*], MS; Luojie Liu[2], MD; Junjie Zha[1], MS; Yijie Gu[1], BS; Hongwei Ye[1], MD

[1]Department of Emergency and Critical Care Medicine, Changshu No.1 People's Hospital, Changshu, Jiangsu, China

[2]Department of Gastroenterology, Changshu No.1 People's Hospital, Changshu, Jiangsu, China

[*]these authors contributed equally

Corresponding Author:
Hongwei Ye, MD
Department of Emergency and Critical Care Medicine
Changshu No.1 People's Hospital
No. 1 Shuyuan Street
Changshu, Jiangsu, 215500
China
Phone: 86 13915657982
Email: zy_rocky@163.com

Abstract

Background: Venous thromboembolism (VTE) is a common and severe complication in intensive care unit (ICU) patients with sepsis. Conventional risk stratification tools lack sepsis-specific features and may inadequately capture complex, nonlinear interactions among clinical variables.

Objective: This study aimed to develop and validate an interpretable machine learning (ML) model for the early prediction of VTE in ICU patients with sepsis.

Methods: This multicenter retrospective study used data from the Medical Information Mart for Intensive Care IV database for model development and internal validation, and an independent cohort from Changshu Hospital for external validation. Candidate predictors were selected through univariate analysis, followed by least absolute shrinkage and selection operator regression. Retained variables were used in multivariable logistic regression to identify independent predictors, which were then used to develop 9 ML models, including categorical boosting, decision tree, k-nearest neighbor, light gradient boosting machine, logistic regression, multilayer perceptron, naive Bayes, random forest, and support vector machine. Performance was evaluated by discrimination (area under the curve [AUC]), calibration, and clinical use (decision curve analysis). A subgroup analysis stratified by the Sequential Organ Failure Assessment score was conducted in the external cohort to assess model stability across sepsis severity levels. Model interpretability was assessed using Shapley Additive Explanations (SHAP) to quantify the contribution of features to the predicted risk.

Results: A total of 25,197 patients from the Medical Information Mart for Intensive Care IV cohort and 328 patients from the external cohort were included, with VTE incidences of 844 out of 25,197 (3.4%) and 30 out of 328 (9.2%), respectively. The light gradient boosting machine model performed best, achieving an AUC of 0.956 in internal validation. Despite the higher VTE incidence and clinical severity in the external validation, the model maintained robust generalization with an AUC of 0.786. Notably, the model achieved enhanced discriminative ability in the severe sepsis subgroup (Sequential Organ Failure Assessment score >6) with an AUC of 0.816, compared with 0.769 in the mild to moderate sepsis subgroup. Calibration curves indicated strong agreement between predicted and observed outcomes, and decision curve analysis showed superior net benefit across clinically relevant thresholds. SHAP analysis identified central venous catheterization, serum chloride and bicarbonate levels, arterial catheterization, and prolonged partial thromboplastin time as the most influential predictors. Partial dependence plots revealed both linear and nonlinear associations between these variables and VTE risk. Individual-level force plots further enhanced interpretability by visualizing personalized risk profiles.

Conclusions: We developed a high-performing and interpretable ML model for predicting VTE in ICU patients with sepsis. The model demonstrated robustness across cohorts and enhanced performance in the severe sepsis population. By integrating

XSL•FO
RenderX

diverse clinical data and leveraging SHAP for transparent explanations, this tool may support personalized prophylaxis and early diagnostic strategies.

(JMIR Med Inform 2026;14:e80969) doi:10.2196/80969

KEYWORDS

venous thromboembolism; sepsis; machine learning; SHAP; MIMIC-IV

Introduction

Sepsis is a life-threatening condition characterized by acute organ dysfunction resulting from a dysregulated host response to infection and remains a leading cause of mortality in the intensive care unit (ICU) [1]. According to the Global Burden of Disease Study, approximately 48.9 million cases of sepsis occur annually worldwide, resulting in an estimated 11.0 million deaths, which accounts for 19.7% of all global deaths [2]. Venous thromboembolism (VTE), comprising deep vein thrombosis and pulmonary embolism (PE), is a common and severe complication of sepsis that significantly worsens patient outcomes. Despite adherence to guideline-recommended thromboprophylaxis, the incidence of VTE in patients with sepsis remains high at 37.2%, up to 10-fold greater than in ICU populations with no sepsis [3]. Previous studies have shown that the presence of VTE is associated with a 28-day mortality rate of 28.6% among patients with sepsis, and the occurrence of PE nearly doubles the risk of in-hospital death (odds ratio [OR] 1.94) [4,5]. These findings underscore the urgent need for early and accurate VTE risk stratification in sepsis to guide timely clinical interventions and reduce morbidity and mortality in this high-risk population.

Current clinical methods for predicting VTE in patients with sepsis have notable limitations. Traditional biomarkers such as D-dimer, although widely used, lack specificity in the context of sepsis, as the condition itself activates coagulation pathways and elevates fibrin degradation products [6,7]. Furthermore, commonly used scoring systems such as the Wells and Autar scores were primarily developed and validated in trauma or postoperative populations. These tools do not account for sepsis-specific indicators, such as the Sequential Organ Failure Assessment (SOFA) score or lactate levels, thereby limiting their predictive use in patients with sepsis [8-10]. Although multivariable logistic regression (LR) models that incorporate clinical and laboratory variables have shown promise, with reported area under the curve (AUC) values reaching up to 0.87, these models are inherently linear and may fail to capture the complex and nonlinear interactions among sepsis-related risk factors [11,12].

Machine learning (ML) techniques have emerged as powerful tools for handling high-dimensional data, uncovering nonlinear associations, and automating feature selection. In recent years, ML models have demonstrated superior performance in predicting complications such as septic shock and acute kidney injury (AKI) in ICU patients, with reported AUC values reaching up to 0.90 [13-15]. However, earlier generations of ML models often functioned as “black boxes,” which limited their adoption in clinical settings due to the lack of interpretability. Explainable ML approaches, such as Shapley Additive Explanations (SHAP), have been developed to address this challenge. By quantifying the contribution of each feature, SHAP enhances model transparency and facilitates clinical understanding [16]. For instance, Liu et al [17] developed an interpretable ML model for septic shock prediction, whose explanatory outputs aligned closely with hemodynamic mechanisms described in the Sepsis-3 guidelines, thereby reinforcing its clinical relevance [18].

Therefore, this study aimed to develop an interpretable ML model that integrates clinical features and laboratory indicators to predict the risk of VTE in ICU patients with sepsis. By applying SHAP to interpret model outputs and identify key predictors, we sought to create a decision support tool that combines high predictive accuracy with strong clinical interpretability, ultimately facilitating personalized prevention strategies.

Methods

Data Sources

The training and internal validation datasets were extracted from the Medical Information Mart for Intensive Care IV version 3.0 (MIMIC-IV v3.0) database, which contains comprehensive and high-quality data from 65,366 patients admitted to the ICU at Beth Israel Deaconess Medical Center between 2008 and 2022. One of the authors (YZ) completed the Collaborative Institutional Training Initiative examination (record ID: 60227322) and was granted access to the database for research purposes.

Ethical Considerations

Ethical approval for the use of MIMIC-IV data was granted by the institutional review boards of Beth Israel Deaconess Medical Center and the Massachusetts Institute of Technology, with a waiver of informed consent due to the use of deidentified data. The data were handled in accordance with the Health Insurance Portability and Accountability Act standards to ensure patient privacy and confidentiality. In addition, ICU patients admitted to Changshu Hospital affiliated to Soochow University between January 2019 and August 2024 were included as an external validation cohort. Ethical approval for this component of the study was obtained from the ethics review committee of Changshu Hospital (number L2024055). As the study was observational in nature and used routinely collected clinical data, the requirement for written informed consent was waived. All electronic data were anonymized before analysis, and access to the dataset was restricted to the primary research team to maintain strict confidentiality. All procedures conformed to the ethical standards set forth in the Declaration of Helsinki. No compensation was provided to any participants involved in this study.

XSL•FO
RenderX

Study Population

This study included adult ICU patients (aged 18 years and older) with sepsis. For patients with multiple ICU admissions, only the first admission was analyzed. Sepsis was defined according to the Third International Consensus Definitions for Sepsis and Septic Shock (Sepsis-3), which require a suspected or confirmed infection accompanied by an increase in the SOFA score of 2 points or more [18]. VTE was defined as an acute episode of deep vein thrombosis (either upper or lower extremities), superficial vein thrombosis (either upper or lower extremities), or PE. VTE diagnoses were identified based on either the *ICD-9* (*International Classification of Diseases, Ninth Revision*; codes 45119, 4512, 45181, 45182, 45183, 45184, 45189, 4519, 4532, 4538, 45381, 45382, 45383, 45384, 45385, 45386, 45387, 45389, 4539, 4150, 41511, 41512, 41513, 41519, 45340, 45341, 45342, 4510, 452, 4530, 4531, and 4533) or the *ICD-10* (*International Statistical Classification of Diseases, Tenth Revision*; codes I808, I809, I8290, I82890, I2699, I2692, I2690, I2602, I2609, I8000, I8001, I8002, I81, I820, and I821) in the MIMIC-IV database, or through diagnostic imaging reports from Changshu Hospital, including duplex venous ultrasonography and contrast-enhanced computed tomography. In the Changshu Hospital cohort, the ICU implemented a routine lower limb venous ultrasound screening protocol for all patients with sepsis meeting high-risk criteria. Patients were excluded meeting any of the following criteria: (1) ICU stay of less than 24 hours, (2) a documented VTE diagnosis prior to sepsis onset, and (3) VTE events occurring within 24 hours following the sepsis diagnosis.

Patients from the MIMIC-IV cohort were randomly split into a training set and an internal validation set in a 7:3 ratio. The training set was used for variable selection and model development, while the internal and external validation sets were used to assess model performance. The overall study workflow is illustrated in Figure 1.

Figure 1. Flowchart of patient enrollment and cohort selection. CatBoost: categorical boosting; DT: decision tree; ICU: intensive care unit; KNN: k-nearest neighbor; LGBM: light gradient boosting machine; LR: logistic regression; MIMIC: Medical Information Mart for Intensive Care Unit; MLP: multilayer perceptron; NB: naive Bayes; RF: random forest; SHAP: SHapley Additive exPlanations; SVM: support vector machine; VTE: venous thromboembolism.

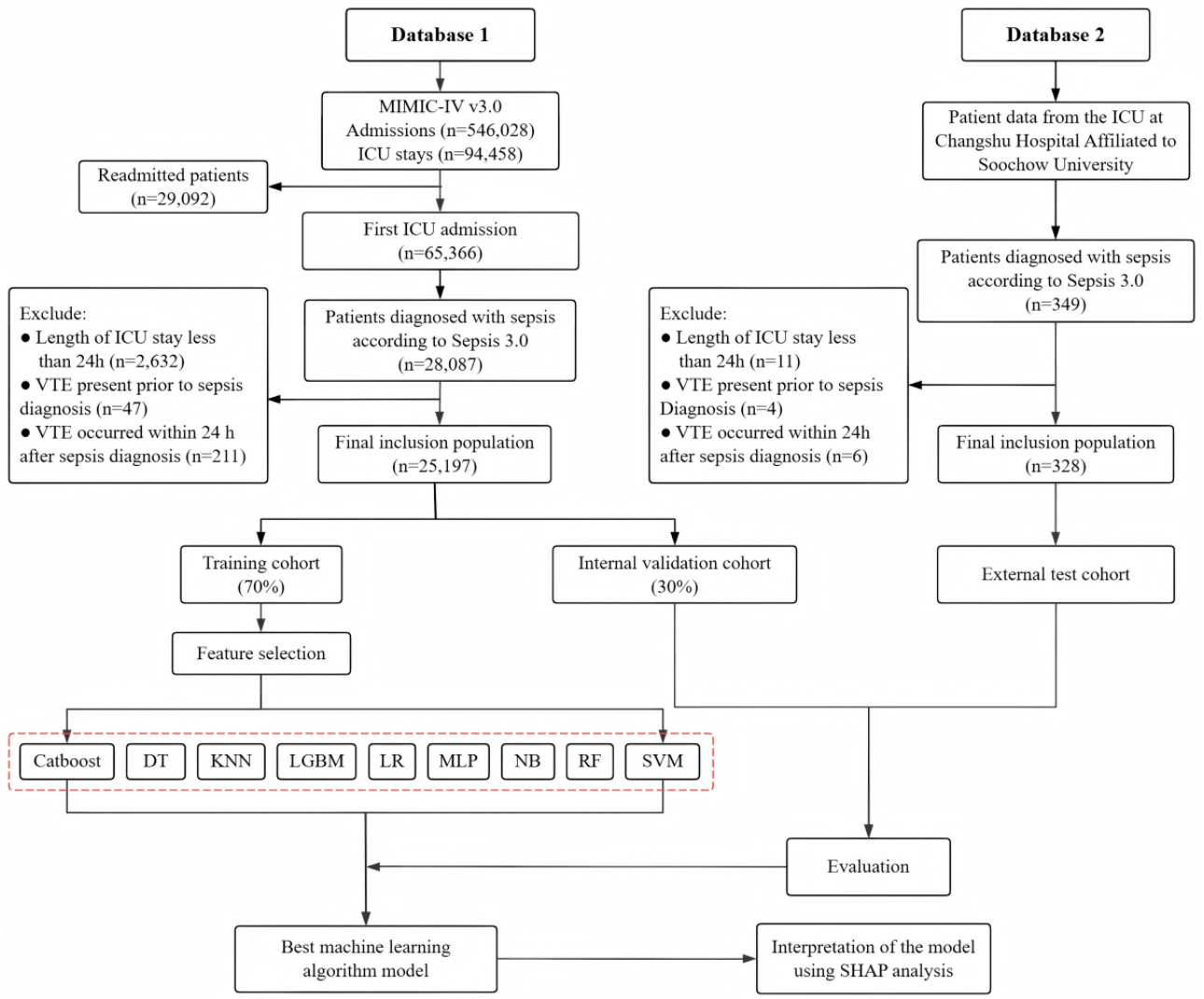

XSL•FO
RenderX

Data Extraction and Processing

Data from the MIMIC-IV database were extracted using Structured Query Language via pgAdmin 4 (version 6.21; pgAdmin Development Team). All clinical and laboratory variables were collected within the first 24 hours of ICU admission, with only the initial measurement included for variables with multiple readings. A set of variables was extracted for each patient, encompassing (1) demographics: age (years), sex, race (Asian, Black, White, Hispanic, and other), height (cm), weight (kg), BMI (kg/m^2), and insurance (Medicare or other); (2) vital signs: heart rate (HR, times per minute), respiratory rate (RR, times per minute), systolic blood pressure (mm Hg), diastolic blood pressure (mm Hg), temperature (°C), and oxygen saturation (SpO_2, %); (3) severity scores: Glasgow Coma Scale, SOFA score, and simplified acute physiology score II (SAPS II); (4) laboratory data: white blood cell count (K/μL), hemoglobin (g/dL), platelet (PLT, K/μL), C-reactive protein (mg/dL), alanine aminotransferase (U/L), aspartate aminotransferase (U/L), albumin (g/dL), creatinine (mg/dL), sodium (mEq/L), potassium (mEq/L), chloride (mEq/L), calcium (mg/dL), blood urea nitrogen (mg/dL), hematocrit (%), glucose (mg/dL), international normalized ratio, prothrombin time (PT, seconds), partial thromboplastin time (PTT, seconds), pH, partial pressure of oxygen (PaO_2, mm Hg), partial pressure of carbon dioxide ($PaCO_2$, mm Hg), base excess (mEq/L), lactic acid (mEq/L), and bicarbonate (HCO_3^-, mEq/L); (5) ventilation parameters: positive end-expiratory pressure (PEEP, cmH_2O), fraction of inspired oxygen (FiO_2, %), and PEEP/FiO_2 ratio; (6) comorbidities: hypertension, diabetes, myocardial infarction (MI), chronic obstructive pulmonary disease (COPD), asthma, pancreatitis, acute respiratory failure (ARF), AKI, acute respiratory distress syndrome (ARDS), and malignant cancer; and (7) therapeutic interventions: arterial catheterization, central venous catheterization, cardiopulmonary bypass, continuous renal replacement therapy (CRRT), ventilation, heparin, aspirin, and vasopressors use. The same set of variables was extracted from the external validation cohort at Changshu Hospital affiliated with Soochow University, ensuring consistency between the datasets.

For missing data, variables with less than 5% missingness were imputed using mean substitution. For those with 5%-30% missing values, multiple imputation methods were used. Variables with more than 30% missing data were excluded from analysis to minimize bias and preserve model robustness. Outliers were identified and treated as missing values and subsequently handled using the same imputation strategies.

Statistical Analysis

All statistical analyses were performed using Stata software (version 16.0; StataCorp LLC), R software (version 4.1.2; R Foundation for Statistical Computing), DecisionLinnc (version 1.0; DecisionLinnc Corp), and Python (version 3.9.12; Python Software Foundation). The Kolmogorov-Smirnov test was used to assess the normality of continuous variables. Variables with a normal distribution were expressed as means and SDs, and group comparisons were conducted using the 2-tailed independent samples *t* test. Non–normally distributed variables were presented as median and IQR and analyzed using the Mann-Whitney *U* test. Categorical variables were summarized as counts (percentages) and compared using the chi-square test. Two-sided *P* values of <.05 were considered statistically significant.

Variable Selection and Model Development

Variables that showed statistically significant differences in the univariate analysis were considered candidate predictors. These variables were further refined using the least absolute shrinkage and selection operator regression to minimize overfitting and reduce multicollinearity. Predictors with nonzero coefficients were subsequently entered into a multivariate LR model. Independent predictors identified through this process were incorporated into the ML models.

Following variable selection, the Synthetic Minority Oversampling Technique (SMOTE) preprocessing algorithm was applied to address class imbalance between VTE and non-VTE cases in the training cohort. In the training cohort, VTE cases (576/17,637, 3.27%) were highly unbalanced compared with non-VTE cases (17,061/17,637, 96.73%). After SMOTE application, the VTE class was balanced to match the non-VTE class, resulting in a 50:50 distribution with a total of 34,122 samples used for model training. This oversampling method helped ensure that the models were trained on a balanced dataset, thereby improving their ability to detect minority class events. A total of 9 ML algorithms were trained on the development cohort, including categorical boosting (CatBoost), decision tree, k-nearest neighbor, light gradient boosting machine (LGBM), LR, multilayer perceptron, naive Bayes, random forest (RF), and support vector machine. For all ML models, we used a 5-fold cross-validation strategy, combined with Grid Search, for hyperparameter optimization and model selection. Notably, SMOTE was applied exclusively to the training folds of the cross-validation process to prevent data leakage into the validation folds or the internal validation set.

Model Evaluation and Interpretation

Model performance was assessed using the internal and external validation datasets. Discrimination was evaluated by plotting receiver operating characteristic curves and calculating the AUC. Calibration curves were used to compare predicted probabilities with observed outcomes. Clinical use was assessed using decision curve analysis, which estimated the net benefit across a range of probability thresholds. In addition, several evaluation metrics were computed, including accuracy, sensitivity, specificity, and the Youden index, to offer a comprehensive assessment of model performance.

The best performing model was selected based on comprehensive evaluation of these metrics. To assess the model's stability and performance in different risk populations, a stratified analysis was conducted on the external validation cohort based on the SOFA score. Patients were divided into 2 subgroups: mild to moderate sepsis (SOFA score ≤6) and severe sepsis (SOFA score >6). To enhance model interpretability, SHAP analysis was conducted. SHAP values were computed to quantify the contribution of individual features to the model's predictions and to explore feature interactions. Visualization

XSL•FO
RenderX

tools from the SHAP package in Python, including feature importance plots, bee swarm plots, force plots, and partial dependence plots (PDPs), were used to provide an intuitive understanding of the model's decision-making process.

Results

Baseline Characteristics

A total of 25,197 patients from the MIMIC-IV cohort and 328 patients from the external validation cohort were included in the study. Among them, 844 out of 25,197 (3.4%) patients in the MIMIC-IV cohort and 30 out of 328 (9.2%) patients in the external cohort developed VTE. The baseline characteristics of all patients are summarized in Table 1. In the MIMIC-IV cohort, patients who developed VTE were younger and exhibited significantly higher HRs and RRs than those with no VTE (all $P<.001$). Laboratory parameters revealed higher PLT counts, serum chloride levels, and PTT in the VTE group (all $P<.05$). In addition, patients with VTE had higher illness severity scores, as indicated by elevated SOFA and SAPS II scores (both $P<.05$). Comorbidities such as ARF, AKI, and ARDS were significantly more common in the VTE group (all $P<.001$). Furthermore, these patients were more likely to have undergone invasive procedures, including arterial and central venous catheterization (both $P<.001$). In the external validation cohort, similar patterns were observed. Patients with VTE demonstrated higher rates of ARDS and more frequent use of mechanical ventilation than patients with no VTE (both $P<.001$). These findings highlight significant differences in demographics, clinical severity, comorbidities, and therapeutic interventions between patients with and with no VTE across both cohorts, emphasizing the relevance of these factors in VTE risk stratification.

XSL•FO
RenderX

Table 1. Baseline characteristics of the MIMIC-IV[a] and external validation cohorts.

Variables	MIMIC-IV cohort (N=25,197)			External Validation cohort (N=328)		
	Non-VTE[b] (n=24,353)	VTE (n=844)	*P* value	Non-VTE (n=298)	VTE (n=30)	*P* value
Demographic data						
Age (years), mean (SD)	66.61 (16.28)	63.83 (16.75)	<.001	73.33 (12.60)	75.90 (9.88)	.19
Sex (male), n (%)	14173 (58.2)	502 (59.5)	.46	210 (70.5)	22 (73)	.74
BMI, mean (SD)	27.71 (6.20)	28.06 (6.15)	.11	22.78 (2.59)	21.93 (3.45)	.20
Race, n (%)	N/A[c]	N/A	.14	N/A	N/A	N/A
Asian	1994 (8.2)	80 (9.5)	N/A	N/A	N/A	N/A
Black	15812 (64.9)	568 (67.3)	N/A	N/A	N/A	N/A
White	806 (3.3)	27 (3.2)	N/A	N/A	N/A	N/A
Hispanic	5038 (20.7)	147 (17.4)	N/A	N/A	N/A	N/A
Other	703 (2.9)	22 (2.6)	N/A	N/A	N/A	N/A
Insurance, n (%)	N/A	N/A	.02	N/A	N/A	.09
Other	4,027 (16.5)	166 (19.7)	N/A	83 (27.9)	4 (13)	N/A
Medicare	20326 (83.5)	678 (80.3)	N/A	215 (72.2)	26 (87)	N/A
Vital signs						
HR[d], mean (SD)	90.00 (20.58)	94.38 (21.12)	<.001	102.86 (24.64)	104.73 (23.56)	.68
RR[e], mean (SD)	19.53 (6.44)	20.38 (6.42)	<.001	22.81 (5.97)	23.97 (6.39)	.35
SBP[f], mean (SD)	121.21 (24.40)	122.17 (25.61)	.29	119.34 (28.29)	119.00 (29.08)	.95
DBP[g], mean (SD)	67.30 (18.12)	68.01 (19.08)	.29	66.14 (14.18)	66.00 (14.80)	.96
Temperature, mean (SD)	36.81 (0.77)	36.81 (0.84)	.88	37.45 (1.71)	37.40 (2.31)	.91
SpO_2[h], median (Q1-Q3)	98 (95-100)	98 (95-100)	.005	92 (88-97)	91 (87-98)	.18
Severity scoring system						
GCS[i], median (Q1-Q3)	15 (13-15)	15 (13-15)	.38	15 (12-15)	14 (11-15)	.32
SOFA[j], median (Q1-Q3)	5 (3-8)	5 (3-8)	.04	6 (5-8)	6 (4-8)	.87
SAPS[k] II, mean (SD)	40.31 (14.22)	41.70 (15.31)	.01	39.69 (14.19)	42.43 (15.58)	.36
Laboratory data						
WBC[l], mean (SD)	12.62 (6.81)	13.05 (7.38)	.10	14.13 (6.88)	13.26 (5.50)	.43
Hemoglobin, mean (SD)	10.51 (2.24)	10.62 (2.13)	.13	10.87 (2.65)	9.71 (2.64)	.03
PLT[m], mean (SD)	195.42 (100.25)	206.41 (111.67)	.005	189.43 (128.43)	191.00 (103.37)	.94
ALT[n], median (Q1-Q3)	26 (16-52)	29 (17-63)	.03	51 (25-81)	27 (19-53)	.11
Creatinine, mean (SD)	1.48 (1.46)	1.41 (1.33)	.12	2.23 (1.82)	2.30 (2.43)	.87
Sodium, mean (SD)	137.89 (5.59)	138.43 (5.64)	.007	137.45 (5.17)	138.38 (5.86)	.41
Potassium, mean (SD)	4.24 (0.77)	4.14 (0.76)	<.001	4.17 (0.72)	4.28 (0.84)	.49
Chloride, mean (SD)	104.04 (6.69)	105.40 (6.80)	<.001	104.44 (7.00)	105.38 (6.74)	.47
BUN[o], median (Q1-Q3)	20 (14-34)	21 (14-35)	.85	14 (9-21)	13 (6-21)	.90
Hematocrit, mean (SD)	31.99 (6.67)	32.03 (6.41)	.85	32.29 (9.06)	29.36 (7.93)	.07
Glucose, median (Q1-Q3)	130 (106-165)	127 (105-162)	.14	8 (6-11)	8 (6-10)	.90
INR[p], median (Q1-Q3)	1.3 (1.2-1.6)	1.3 (1.2-1.5)	.81	1.3 (1.2-1.5)	1.2 (1.1-1.6)	.42
PT[q], median (Q1-Q3)	14.6 (12.8-17.0)	14.6 (13.0-17.1)	.95	15.7 (14.4-17.6)	14.9 (14.2-16.8)	1.00

XSL•FO
RenderX

Variables	MIMIC-IV cohort (N=25,197)			External Validation cohort (N=328)		
	Non-VTE[b] (n=24,353)	VTE (n=844)	*P* value	Non-VTE (n=298)	VTE (n=30)	*P* value
PTT[r], median (Q1-Q3)	31.1 (27.3-37.6)	32.2 (27.7-41.6)	<.001	31.9 (27.7-38.2)	39.9 (35.1-46.8)	.17
pH[s], mean (SD)	7.36 (0.10)	7.37 (0.10)	.15	7.40 (0.10)	7.37 (0.11)	.33
PaO_2[t], median (Q1-Q3)	140.0 (87.0-273.0)	129.0 (84.0-239.5)	.006	93.5 (74.3-121.0)	85.5 (67.0-112.0)	.17
$PaCO_2$[u], mean (SD)	42.35 (12.06)	41.04 (12.52)	.003	38.51 (13.15)	39.59 (17.02)	.74
BE[v], mean (SD)	–1.43 (5.24)	–1.47 (5.44)	.82	–2.05 (5.50)	–2.76 (5.31)	.49
Lac[w], median (Q1-Q3)	1.8 (1.2-2.7)	1.8 (1.2-2.6)	.55	2.3 (1.5-3.5)	2.0 (1.5-3.0)	.82
HCO_3^-[x], mean (SD)	22.62 (4.76)	23.12 (4.81)	.003	22.76 (5.11)	22.27 (5.11)	.62
Ventilation Variables, median (Q1-Q3)						
PEEP[y]	5 (5-5)	5 (5-5)	.14	3 (2-5)	5 (5-5)	.001
FiO_2[z]	60 (50-100)	60 (50-100)	.09	40 (33-500)	40 (33-50)	.82
PEEP[y]/FiO_2[z]	247 (153-352)	245 (146-345)	.52	230 (168-307)	203 (152-295)	.24
Comorbidities, n (%)						
Hypertension	10083 (41.4)	374 (44.3)	.09	214 (71.8)	21 (70)	.83
Diabetes	3521 (14.5)	0 (0.0)	<.001	85 (28.5)	5 (17)	.17
Myocardial infarction	1085 (4.5)	11 (1.3)	<.001	43 (14.4)	4 (13)	.87
COPD[aa]	1647 (6.8)	0 (0.0)	<.001	40 (13.4)	3 (10)	.60
Asthma	1912 (7.9)	78 (9.2)	.14	19 (6.4)	0 (0)	.15
Pancreatitis	600 (2.5)	38 (4.5)	<.001	10 (3.4)	4 (13)	.01
ARF[bb]	8202 (33.7)	339 (40.2)	<.001	180 (60.4)	24 (80)	.04
AKI[cc]	16710 (68.6)	652 (77.3)	<.001	187 (62.8)	16 (53)	.31
ARDS[dd]	5604 (23.0)	260 (30.8)	<.001	54 (18.1)	16 (53)	<.001
Malignant cancer	3829 (15.7)	152 (18.0)	.07	64 (21.5)	8 (27)	.51
Therapeutic interventions, n (%)						
Arterial catheterization	1595 (6.6)	166 (19.7)	<.001	55 (18.5)	30 (100)	<.001
Central venous catheterization	2028 (8.3)	218 (25.8)	<.001	45 (15.1)	27 (90)	<.001
CPB[ee]	2888 (11.9)	77 (9.1)	.02	30 (10.1)	1 (3)	.23
CRRT[ff]	2175 (8.9)	96 (11.4)	.02	30 (10.1)	10 (33)	<.001
Ventilation	12004 (49.3)	416 (49.3)	1.00	148 (49.7)	25 (83)	<.001
Heparin	21304 (87.5)	786 (93.1)	<.001	254 (85.2)	29 (97)	.08
Aspirin	12522 (51.4)	384 (45.5)	<.001	135 (45.3)	7 (23)	.02

XSL•FO
RenderX

Variables	MIMIC-IV cohort (N=25,197)			External Validation cohort (N=328)		
	Non-VTE[b] (n=24,353)	VTE (n=844)	*P* value	Non-VTE (n=298)	VTE (n=30)	*P* value
Vasopressors	7538 (31.0)	290 (34.4)	.04	107 (35.9)	25 (83)	<.001

[a]MIMIC: Medical Information Mart for Intensive Care Unit.
[b]VTE: venous thromboembolism.
[c]N/A: not applicable.
[d]HR: heart rate.
[e]RR: respiratory rate.
[f]SBP: systolic blood pressure.
[g]DBP: diastolic blood pressure.
[h]SpO_2: oxygen saturation.
[i]GCS: Glasgow Coma Scale.
[j]SOFA: Sequential Organ Failure Assessment.
[k]SAPS II: simplified acute physiology score II.
[l]WBC: white blood cell count.
[m]PLT: platelet.
[n]ALT: alanine aminotransferase.
[o]BUN: blood urea nitrogen.
[p]INR: international normalized ratio.
[q]PT: prothrombin time.
[r]PTT: partial thromboplastin time.
[s]pH: potential of hydrogen.
[t]PaO_2: partial pressure of oxygen.
[u]$PaCO_2$: partial pressure of carbon dioxide.
[v]BE: base excess.
[w]Lac: lactic acid.
[x]HCO_3^-: bicarbonate.
[y]PEEP: positive end-expiratory pressure.
[z]FiO_2: fraction of inspired oxygen.
[aa]COPD: chronic obstructive pulmonary disease.
[bb]ARF: acute respiratory failure.
[cc]AKI: acute kidney injury.
[dd]ARDS: acute respiratory distress syndrome.
[ee]CPB: cardiopulmonary bypass.
[ff]CRRT: continuous renal replacement therapy.

Selection of Predictors

Patients in the training set were divided into VTE and non-VTE groups. Univariate analysis identified several variables significantly associated with VTE, including admission age, insurance, HR, RR, SAPS II, alanine aminotransferase, potassium, chloride, glucose, PTT, PaO_2, $PaCO_2$, PEEP, and comorbidities such as diabetes, MI, COPD, pancreatitis, ARF, AKI, and ARDS (all *P*<.05). In addition, therapeutic interventions including arterial catheterization, central venous catheterization, cardiopulmonary bypass, CRRT, heparin use, and aspirin use were significantly associated with VTE (all *P*<.05; Table 2). Least absolute shrinkage and selection operator regression identified 18 variables with nonzero coefficients at the optimal lambda value of 0.0029. These included age, insurance, HR, potassium, chloride, PTT, diabetes, MI, COPD, pancreatitis, ARF, AKI, ARDS, arterial catheterization, central venous catheterization, CRRT, heparin use, and aspirin use (Figures 2A and 2B). These variables were subsequently entered into a multivariate LR model, which revealed that potassium (OR 0.8711, 95% CI 0.7541-0.9756; *P*=.02), chloride (OR 1.0206, 95% CI 1.0081-1.0326; *P*=.001), PTT (OR 1.0086, 95% CI 1.0054-1.0115; *P*<.001), MI (OR 0.2851, 95% CI 0.1101-0.5999; *P*=.003), AKI (OR 1.5274, 95% CI 1.2166-1.9369; *P*<.001), arterial catheterization (OR 1.8985, 95% CI 1.4102-2.5648; *P*<.001), central venous catheterization (OR 2.0805, 95% CI 1.5213-2.8382; *P*<.001), and heparin use (OR 1.5509, 95% CI 1.1203-2.0851; *P*=.01) were independently associated with VTE risk (Table 3). We noted instances of complete separation in the training set for comorbidities such as diabetes and COPD, where the VTE subgroup contained zero cases, leading to extreme ORs in the multivariable LR.

XSL•FO
RenderX

Table 2. Univariate analysis of the clinical features in the training set.

Variables	Total (N=17,637)	Non-VTE[a] (n=17,061)	VTE (n=576)	*P* value
Demographic data				
Age (years), mean (SD)	66.49 (16.30)	66.57 (16.27)	64.10 (16.93)	<.001
Sex (male), n (%)	10268 (58.2)	9934 (58.2)	334 (58.0)	.91
BMI, mean (SD)	27.75 (6.20)	27.74 (6.20)	27.90 (6.04)	.53
Race, n (%)				.42
Asian	1415 (8.0)	1360 (8.0)	55 (9.6)	
Black	11463 (65.0)	11,085 (65.0)	378 (65.6)	
White	604 (3.4)	583 (3.4)	21 (3.7)	
Hispanic	3642 (20.7)	3538 (20.7)	104 (18.1)	
Other	513 (2.9)	495 (2.9)	18 (3.1)	
Insurance, n (%)				.004
Other	2937 (16.7)	2816 (16.5)	121 (21.0)	
Medicare	14700 (83.4)	14245 (83.5)	455 (79.0)	
Vital signs				
HR[b], mean (SD)	90.17 (20.61)	90.06 (20.57)	93.50 (21.61)	<.001
RR[c], mean (SD)	19.52 (6.47)	19.50 (6.46)	20.18 (6.59)	.02
SBP[d], mean (SD)	121.14 (24.40)	121.13 (24.38)	121.45 (25.14)	.77
DBP[e], mean (SD)	67.35 (18.17)	67.34 (18.14)	67.48 (19.10)	.86
Temperature, mean (SD)	36.81 (0.77)	36.81 (0.77)	36.74 (0.84)	.06
SpO_2[f], median (Q1-Q3)	98 (95-100)	98 (95-100)	98 (95-100)	.07
Severity scoring system				
GCS[g], median (Q1-Q3)	15 (13-15)	15 (13-15)	15 (13-15)	.67
SOFA[h], median (Q1-Q3)	5 (3-8)	5 (3-8)	5 (4-8)	.12
SAPS[i] II, mean (SD)	40 (14)	40 (14)	42 (16)	.01
Laboratory data				
WBC[j], mean (SD)	12.65 (6.84)	12.64 (6.82)	13.04 (7.35)	.19
Hemoglobin, mean (SD)	10.51 (2.25)	10.50 (2.25)	10.58 (2.11)	.42
PLT[k], mean (SD)	195.34 (100.17)	195.06 (99.70)	203.51 (113.05)	.08
ALT[l], median (Q1-Q3)	26 (16-53)	26 (16-53)	30 (17-62)	<.001
Creatinine, mean (SD)	1.48 (1.45)	1.48 (1.46)	1.43 (1.28)	.39
Sodium, mean (SD)	137.90 (5.62)	137.89 (5.62)	138.25 (5.65)	.13
Potassium, mean (SD)	4.24 (0.77)	4.24 (0.77)	4.12 (0.73)	<.001
Chloride, mean (SD)	104.10 (6.68)	104.06 (6.68)	105.29 (6.73)	<.001
BUN[m], median (Q1-Q3)	20 (14-34)	20 (14-34)	22 (14-35)	.20
Hematocrit, mean (SD)	31.98 (6.71)	31.98 (6.72)	31.87 (6.37)	.67
Glucose, median (Q1-Q3)	130 (106-165)	130 (106-165)	125 (103-159)	.03
INR[n], median (Q1-Q3)	1.3 (1.2-1.6)	1.3 (1.2-1.6)	1.3 (1.2-1.5)	.54
PT[o], median (Q1-Q3)	14.6 (12.8-17.0)	14.6 (12.8-16.9)	14.6 (13.1-17.1)	.35
PTT[p], median (Q1-Q3)	31.2 (27.3-37.6)	31.2 (27.3-37.6)	32.6 (27.9-42.2)	<.001

XSL•FO
RenderX

Variables	Total (N=17,637)	Non-VTE[a] (n=17,061)	VTE (n=576)	*P* value
pH[q], mean (SD)	7.36 (0.10)	7.36 (0.10)	7.36 (0.10)	.37
PaO_2[r], median (Q1-Q3)	140 (87-273)	141 (87-275)	129 (86-243)	.04
$PaCO_2$[s], mean (SD)	42.32 (12.07)	42.36 (12.04)	41.14 (13.06)	.03
BE[t], mean (SD)	–1.47 (5.26)	–1.47 (5.25)	–1.51 (5.58)	.87
Lac[u], median (Q1-Q3)	1.8 (1.2-2.7)	1.8 (1.2-2.7)	1.8 (1.2-2.7)	.63
HCO_3^-[v], mean (SD)	22.58 (4.76)	22.57 (4.75)	22.87 (4.82)	.14
Ventilation Variables, median (Q1-Q3)				
PEEP[w]	5 (5-5)	5 (5-5)	5 (5-5)	.045
FiO_2[x]	60 (50-100)	60 (50-100)	60 (50-100)	.13
PEEP[w]/FiO_2[x]	246 (152-353)	246 (152-353)	254 (149-357)	.84
Comorbidities, n (%)				
Hypertension	7333 (41.6)	7075 (41.5)	258 (44.8)	.11
Diabetes	2463 (14.0)	2463 (14.4)	0 (0.0)	<.001
Myocardial infarction	793 (4.5)	787 (4.6)	6 (1.0)	<.001
COPD[y]	1142 (6.5)	1142 (6.7)	0 (0.0)	<.001
Asthma	1381 (7.8)	1327 (7.8)	54 (9.4)	.16
Pancreatitis	449 (2.6)	421 (2.5)	28 (4.9)	<.001
ARF[z]	5965 (33.8)	5727 (33.6)	238 (41.3)	<.001
AKI[aa]	12163 (69.0)	11,712 (68.7)	451 (78.3)	<.001
ARDS[bb]	4117 (23.3)	3943 (23.1)	174 (30.2)	<.001
Malignant cancer	2790 (15.8)	2685 (15.7)	105 (18.2)	.11
Therapeutic interventions, n (%)				
Arterial catheterization	1265 (7.2)	1150 (6.7)	115 (20.0)	<.001
Central venous catheterization	1580 (9.0)	1443 (8.5)	137 (23.8)	<.001
CPB[cc]	2090 (11.9)	2038 (12.0)	52 (9.0)	.03
CRRT[dd]	1605 (9.1)	1533 (9.0)	72 (12.5)	.004
Ventilation	8718 (49.4)	8442 (49.5)	276 (47.9)	.46
Heparin	15479 (87.8)	14943 (87.6)	536 (93.1)	<.001
Aspirin	9026 (51.2)	8771 (51.4)	255 (44.3)	<.001

XSL•FO
RenderX

Variables	Total (N=17,637)	Non-VTE[a] (n=17,061)	VTE (n=576)	*P* value
Vasopressors	5492 (31.1)	5294 (31.0)	198 (34.4)	.09

[a]VTE: venous thromboembolism.
[b]HR: heart rate.
[c]RR: respiratory rate.
[d]SBP: systolic blood pressure.
[e]DBP: diastolic blood pressure.
[f]SpO_2: oxygen saturation.
[g]GCS: Glasgow Coma Scale.
[h]SOFA: Sequential Organ Failure Assessment.
[i]SAPS II: simplified acute physiology score II.
[j]WBC: white blood cell count.
[k]PLT: platelet.
[l]ALT: alanine aminotransferase.
[m]BUN: blood urea nitrogen.
[n]INR: international normalized ratio.
[o]PT: prothrombin time.
[p]PTT: partial thromboplastin time.
[q]pH: potential of hydrogen.
[r]PaO_2: partial pressure of oxygen.
[s]$PaCO_2$: partial pressure of carbon dioxide.
[t]BE: base excess.
[u]Lac: lactic acid.
[v]HCO_3^-: bicarbonate.
[w]PEEP: positive end-expiratory pressure.
[x]FiO_2: fraction of inspired oxygen.
[y]COPD: chronic obstructive pulmonary disease.
[z]ARF: acute respiratory failure.
[aa]AKI: acute kidney injury.
[bb]ARDS: acute respiratory distress syndrome.
[cc]CPB: cardiopulmonary bypass.
[dd]CRRT: continuous renal replacement therapy.

Figure 2. Screening predictors of venous thromboembolism using least absolute shrinkage and selection operator regression. (A) Coefficient profile plotted against the logarithm of the lambda sequence. Each colored line represents the coefficient path of an individual candidate predictor. (B) Cross-validation plot for determining the optimal penalty term. The green dots represent the mean binomial deviance with error bars. The left red vertical dashed line indicates the log lambda value that minimizes the deviance (log lambda minimum = –10.683), and the right blue vertical dashed line indicates the log lambda value within 1 standard error of the minimum (log lambda 1se = –5.845).

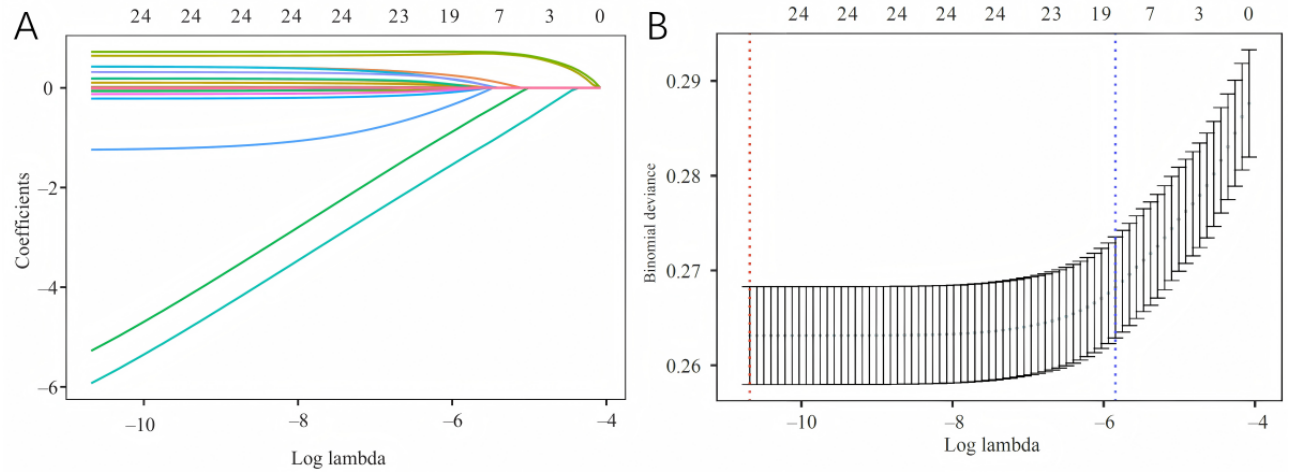

XSL•FO
RenderX

Table 3. Multivariate logistic regression analysis of the selected clinical features in the training set.

Variables	β	*Z* value	Odds ratio	95% CI	*P* value
Admission age (years)	–.0018	–0.6384	0.9982	–0.0072 to 0.0037	.52
Insurance	–.2206	–1.9143	0.8020	–0.4436 to 0.0084	.06
HR[a]	.0035	1.6880	1.0035	–0.0006 to 0.0076	.09
Potassium	–.1380	–2.3558	0.8711	–0.2541 to –0.0244	.02
Chloride	.0204	3.2561	1.0206	0.0081 to 0.0326	.001
PTT[b]	.0085	5.5201	1.0086	0.0054 to 0.0115	<.001
Diabetes	–15.8672	–0.0766	0.0000	–162.9076 to –157.5869	.94
Myocardial infarction	–1.2549	–2.9781	0.2851	–2.1976 to –0.5169	.003
COPD[c]	–15.5638	–0.0530	0.0000	–222.8419 to –215.7841	.96
Pancreatitis	.3493	1.6805	1.4181	–0.0786 to 0.7391	.09
ARF[d]	.1127	1.2010	1.1192	–0.0721 to 0.2957	.23
AKI[e]	.4236	3.9539	1.5274	0.2166 to 0.6369	<.001
ARDS[f]	.1806	1.8616	1.1979	–0.0116 to 0.3689	.06
Arterial catheterization	.6411	5.5322	1.8985	0.4102 to 0.8648	<.001
Central venous catheterization	.7326	6.8935	2.0805	0.5213 to 0.9382	<.001
CRRT[g]	.2571	1.8355	1.2931	–0.0240 to 0.5257	.07
Heparin	.4388	2.5944	1.5509	0.1203 to 0.7851	.01
Aspirin	–.0882	–0.9590	0.9156	–0.2687 to 0.0917	.34

[a]HR: heart rate.

[b]PTT: partial thromboplastin time.

[c]COPD: chronic obstructive pulmonary disease.

[d]ARF: acute respiratory failure.

[e]AKI: acute kidney injury.

[f]ARDS: acute respiratory distress syndrome.

[g]CRRT: continuous renal replacement therapy.

Development and Validation of Models

All selected variables were incorporated into the development of 9 ML models to predict the risk of VTE in ICU patients with sepsis. The 9 ML models exhibited varying degrees of predictive performance in the training set (Figure 3A). Internal validation based on receiver operating characteristic curve analysis demonstrated that the LGBM model achieved the highest predictive performance (AUC=0.956), followed by CatBoost (AUC=0.924), RF (AUC=0.794), decision tree (AUC=0.704), k-nearest neighbors (AUC=0.673), multilayer perceptron (AUC=0.660), support vector machine (AUC=0.621), LR (AUC=0.621), and naïve Bayes (AUC=0.588; Figure 3B). Detailed performance metrics, including sensitivity, specificity, accuracy, precision, F_1-score, and AUC for each model, are shown in Table 4. Notably, the LGBM model exhibited the highest specificity (0.942), accuracy (0.910), precision (0.956), and F_1-score (0.921), consistently outperforming the other algorithms across these key evaluation indicators.

XSL•FO
RenderX

Figure 3. Receiver operating characteristic (ROC) curves of the test and validation sets of 9 machine learning models. (A) ROC curves of the training set. (B) ROC curves of the internal validation set. (C) ROC curves of the external validation set. AUC: area under the curve; CatBoost: categorical boosting; DT: decision tree; KNN: k-nearest neighbor; LGBM: light gradient boosting machine; LR: logistic regression; MLP: multilayer perceptron; NB: naive Bayes; RF: random forest; SVM: support vector machine.

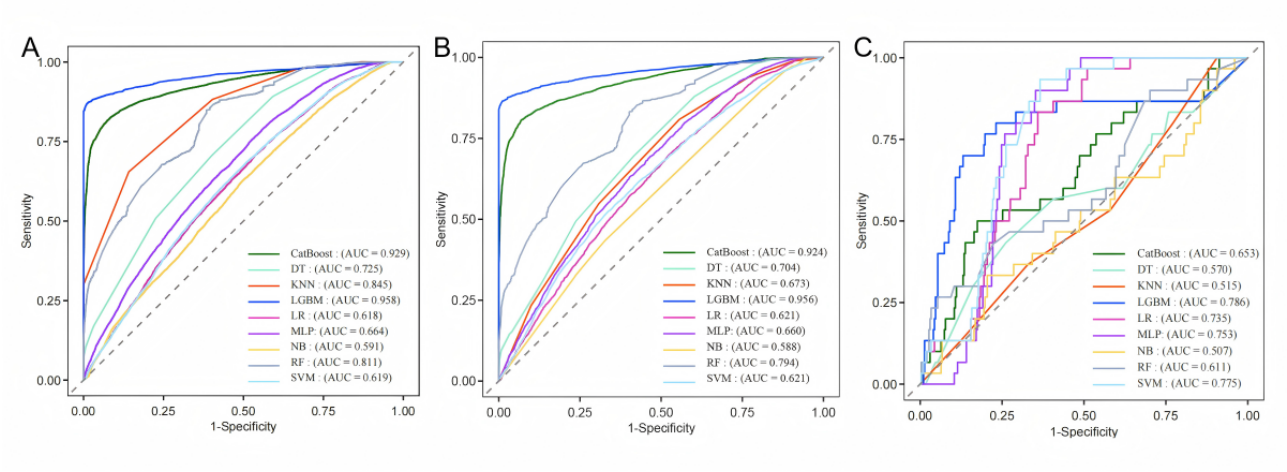

Table 4. Comprehensive evaluation of machine learning model performance.

Methods	Sensitivity	Specificity	Accuracy	Precision	F_1	AUC[a]
CatBoost[b]	0.926	0.598	0.791	0.766	0.839	0.924
DT[c]	0.881	0.394	0.680	0.675	0.764	0.704
KNN[d]	0.809	0.444	0.658	0.674	0.735	0.673
LGBM[e]	0.888	0.942	0.910	0.956	0.921	0.956
LR[f]	0.938	0.199	0.633	0.625	0.750	0.621
MLP[g]	0.803	0.504	0.680	0.698	0.747	0.660
NB[h]	0.308	0.769	0.498	0.655	0.419	0.588
RF[i]	0.893	0.438	0.705	0.694	0.781	0.794
SVM[j]	0.991	0.027	0.594	0.592	0.741	0.621

[a]AUC: area under the curve.
[b]CatBoost: categorical boosting.
[c]DT: decision tree.
[d]KNN: k-nearest neighbor.
[e]LGBM: light gradient boosting machine.
[f]LR: logistic regression.
[g]MLP: multilayer perceptron.
[h]NB: naive Bayes.
[i]RF: random forest.
[j]SVM: support vector machine.

Calibration analysis revealed that the LGBM model demonstrated strong alignment between predicted probabilities and observed outcomes, reflecting robust reliability (Figure 4A). In the decision curve analysis, the LGBM model consistently provided the highest net benefit across a broad range of clinically relevant threshold probabilities, further supporting its clinical applicability in decision-making scenarios (Figure 4B).

XSL•FO
RenderX

Figure 4. Calibration curve of the LGBM model in the internal validation set (A). Decision curve analysis of the LGBM model in the internal validation set (B). CatBoost: categorical boosting; DT: decision tree; KNN: k-nearest neighbor; LGBM: light gradient boosting machine; LR: logistic regression; MLP: multilayer perceptron; NB: naive Bayes; RF: random forest; SVM: support vector machine.

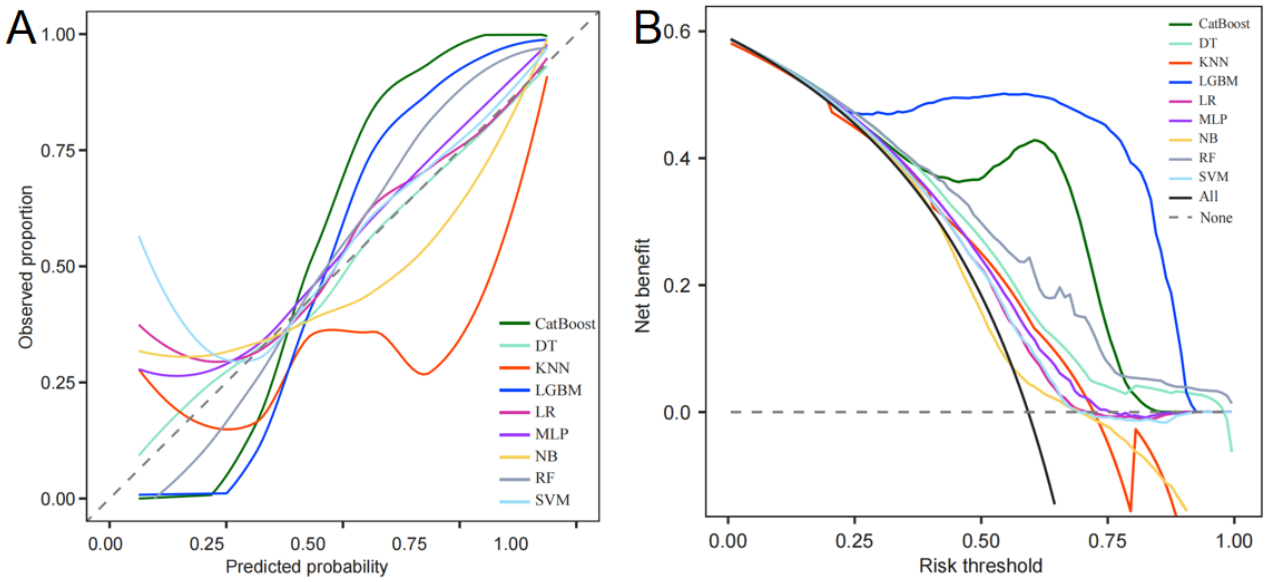

External validation using an independent test cohort further confirmed the robustness and generalizability of the LGBM model, which achieved an AUC of 0.786, outperforming all other ML models in this cohort (Figure 3C). The consistent performance observed across both internal and external validation cohorts underscores the strong generalizability and clinical potential of the LGBM model for predicting VTE in ICU patients with sepsis.

Following stratification based on SOFA score, the LGBM model demonstrated enhanced discriminative ability in the high-risk group. The AUC for the severe sepsis group was 0.816, which was higher than the AUC of 0.769 observed in the mild to moderate sepsis group. The detailed performance metrics are shown in Table 5.

Table 5. Subgroup analysis of LGBM[a] model performance stratified by SOFA[b] score.

Subgroup	SOFA Criteria	Sensitivity	Specificity	AUC[c]
Mild to moderate sepsis	2 ≤ SOFA ≤ 6	0.722	0.839	0.769
Severe sepsis	SOFA > 6	0.667	0.856	0.816

[a]LGBM: light gradient boosting machine.

[b]SOFA: Sequential Organ Failure Assessment.

[c]AUC: area under the curve.

Explanation of the Model

Figure 5 displays the top 15 predictive features for VTE incidence as identified by the LGBM model using SHAP analysis. The feature importance plot, ranked by the mean absolute SHAP values, highlights the variables with the greatest overall impact on model predictions (Figure 5A). The 5 most influential features were central venous catheterization, chloride, bicarbonate, arterial catheterization, and PTT. The corresponding SHAP beeswarm plot (Figure 5B) illustrates each feature's influence on individual predictions, where SHAP values to the right of zero reflect increased predicted risk. It revealed that the presence of central venous or arterial catheters, elevated chloride and bicarbonate levels, and prolonged PTT consistently contributed to a higher VTE risk.

XSL•FO
RenderX

Figure 5. SHAP summary plot for clinical variables contributing to the light gradient boosting machine (LGBM) model. (A) Feature importance ranking plot based on the LGBM model. (B) Scatter plot of variables for SHAP analysis based on the LGBM model. AKI: acute kidney injury; HCO3-: bicarbonate; HR: heart rate; pH: potential of hydrogen; PLT: platelet; PTT: partial thromboplastin time; SHAP: SHapley Additive exPlanations.

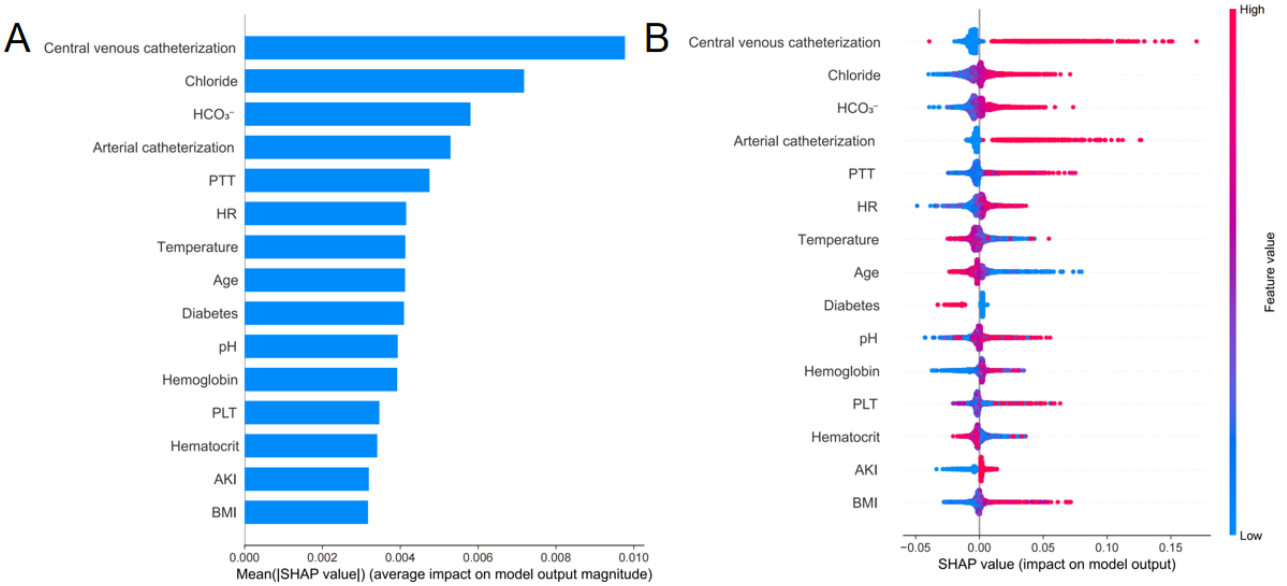

To further examine the marginal effects of key predictors on model output, PDPs were generated for the top-ranked features (Figures 6A-6F). These plots depict how the predicted risk of VTE changes on average with varying values of a single feature, while holding others constant. For dichotomous variables such as central venous (Figure 6A) and arterial (Figure 6D) catheterization, the plots showed a marked increase in the average predicted risk when catheters were present compared with their absence. Continuous variables including serum chloride (Figure 6B), bicarbonate (Figure 6C), and HR (Figure 6F) exhibited monotonic relationships, with risk increasing steadily as the values rose. In contrast, PTT (Figure 6E) exhibited a distinct threshold effect. The predicted risk remained low and stable within the normal range and then increased sharply for values beyond approximately 45 seconds before plateauing at highly prolonged levels, confirming its nonlinear risk association identified by SHAP.

Figure 6. SHapley Additive exPlanations feature PDP of the light gradient boosting machine model. (A) Partial dependence plot of central venous catheter. (B) Partial dependence plot of chloride. (C) Partial dependence plot of bicarbonate. (D) Partial dependence plot of arterial catheter. (E) Partial dependence plot of partial thromboplastin time. (F) Partial dependence plot of heart rate. HCO3-: bicarbonate; HR: heart rate; PDP: partial dependence plot; PTT: partial thromboplastin time.

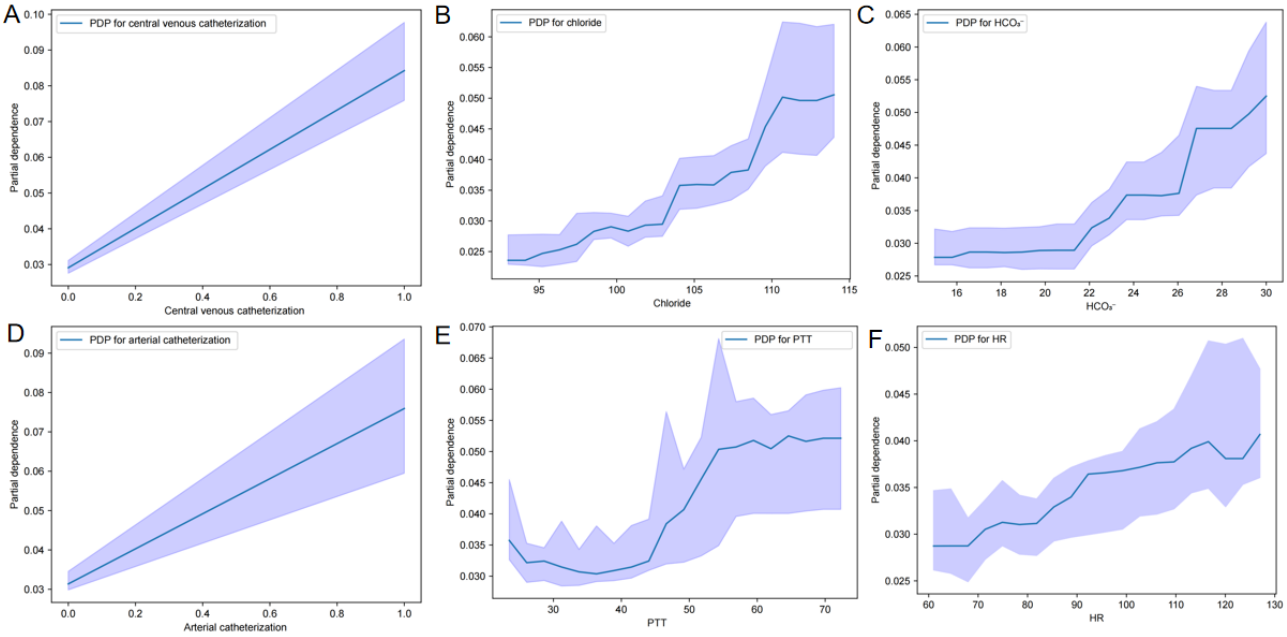

XSL•FO
RenderX

Interpretation of Individual Prediction

To enhance case-level interpretability, SHAP force plots were used to visualize the contribution of individual features to specific predictions (Figure 7). In these plots, each feature was represented as a colored bar that moves the predicted value away from a baseline, which corresponds to the average prediction across the dataset. Features that increase the predicted risk are shown in red, while those that reduce the risk are shown in blue. The length of each bar reflects the extent of the feature's influence. A longer bar indicates a stronger impact on the final predicted probability.

Figure 7. SHapley Additive exPlanations (SHAP) force plots for explaining of individual's prediction results according to the light gradient boosting machine model. (A) SHAP force plot of a high-risk example. (B) SHAP force plot of a low-risk example. AKI: acute kidney injury; HCO3-: bicarbonate; HR: heart rate; PT: prothrombin time; PTT: partial thromboplastin time; SAPS: simplified acute physiology score II; SBP: systolic blood pressure.

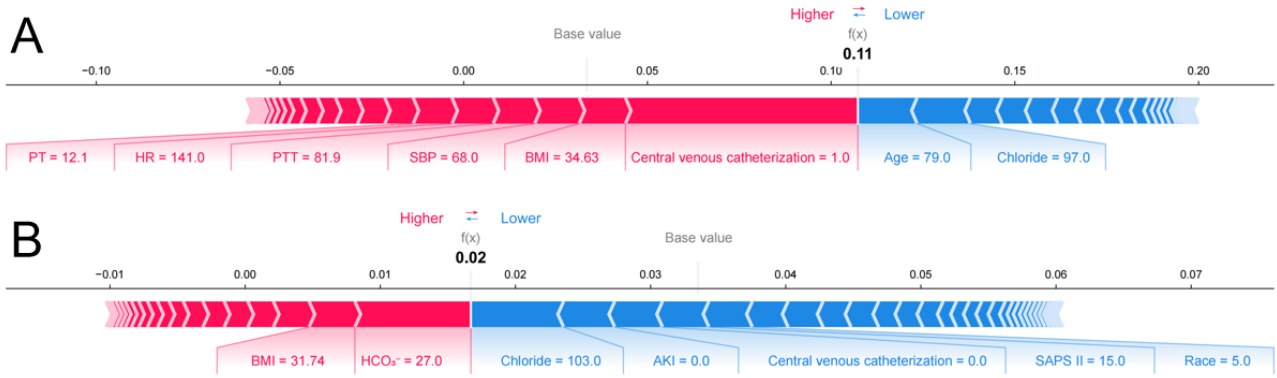

For example, in Figure 7A, the predicted VTE probability for a specific patient was 0.11, which was higher than the baseline value. This elevated risk was primarily attributed to the presence of a central venous catheter, a markedly prolonged PTT of 81.9 seconds, and a high HR of 141 min^{-1}. In contrast, Figure 7B showed a patient with a predicted probability of 0.02, which was lower than the baseline. In this case, protective features including the absence of a central venous catheter, absence of AKI, and a low SAPS II score collectively outweighed the influence of risk factors such as elevated BMI and bicarbonate level. These examples demonstrated that the model was capable of producing clear and clinically relevant explanations for individual predictions.

Discussion

Principal Findings

In this multicenter retrospective study, we developed and validated several ML models to predict the risk of VTE in critically ill patients with sepsis. Among the models tested, the LGBM algorithm demonstrated the highest predictive accuracy with an AUC of 0.956 in the internal validation set and maintained strong generalizability with an AUC of 0.786 in an external cohort. The observed VTE incidence in our external validation cohort (30/328, 9.15%) was substantially higher than the 3.35% (844/25,197) incidence recorded in the MIMIC-IV development cohort. While this difference contributed to the drop in the AUC during external validation, this discrepancy is likely a consequence of multiple factors, including divergent diagnostic practices, disparities in clinical risk profiles, and racial composition differences between the 2 cohorts.

First, variations in VTE surveillance and diagnostic criteria likely served as a primary driver. The MIMIC-IV cohort relied on retrospective identification via *ICD* (*International Classification of Diseases*) codes, a method known to carry a risk of misclassification bias and potential underascertainment, particularly of asymptomatic events. Conversely, the external validation cohort used explicit diagnostic imaging reports and implemented a routine lower limb venous ultrasound screening program for high-risk patients with sepsis. This systematic, active surveillance methodology inherently tends to yield a higher VTE capture rate compared with passive, coding-based case ascertainment. Second, the external validation group exhibited a substantially higher baseline severity and utilization of aggressive life support interventions. Patients with VTE in this cohort showed markedly higher rates of established risk factors such as mechanical ventilation (83.33% vs 49.29% in MIMIC-IV VTE group), ARDS (53.33% vs 30.81%), and CRRT (33.33% vs 11.37%) [19-21]. This heightened clinical severity and iatrogenic risk profile provide a sound clinical explanation for the elevated VTE incidence. Third, the inherent demographic differences between the cohorts represent a major challenge to model generalizability. The MIMIC-IV cohort is composed of a racially diverse population, while the external validation cohort is predominantly Asian, representing a geographically and ethnically distinct cohort. Given that VTE risk is known to vary significantly across different racial groups, this change in demographic distribution may be a contributing factor to the observed performance decrease [22].

Despite these significant differences in cohort characteristics and VTE incidence, the LGBM model maintained the highest predictive performance in both internal and external validation, underscoring its inherent robustness and generalization capacity. These performance advantages align with recent findings that gradient boosting methods often outperform logistic models in predictive accuracy when applied to large clinical datasets [23,24]. Crucially, we applied SHAP to interpret the model's predictions. This analysis identified a set of key risk factors driving VTE predictions, including the presence of central and arterial catheters, serum chloride and bicarbonate levels, and the PTT. By quantifying each feature's contribution to individual risk scores, SHAP facilitated insight into why certain patients

XSL•FO
RenderX

were classified as high-risk. This combination of robust performance and interpretability suggests that our model may assist clinicians in identifying ICU patients with sepsis at an increased risk of VTE, thereby supporting timely prophylaxis or diagnostic evaluation. Conventional instruments such as the Caprini, Padua, or Wells scores were primarily developed for general medical or surgical populations and relied on a linear, additive combination of risk factors [10,25]. These tools lack the specificity required to capture the distinct pathophysiology of sepsis which involves a complex interplay among inflammation, endothelial dysfunction, and coagulopathy collectively referred to as sepsis-induced coagulopathy [26,27]. The pathophysiology of sepsis-induced VTE is inherently nonlinear. Complex interactions among organ failure, systemic inflammation, and iatrogenic factors such as the use of catheters and vasopressors jointly modulate VTE risk in a manner that traditional linear models cannot fully capture [28,29]. In contrast, our LGBM model is consistent with previous ML applications in critical care and automatically captures complex relationships and interactions among predictors while integrating heterogeneous ICU data to generate a more accurate and nuanced risk estimate [30]. Our study found that the LGBM model significantly outperformed the LR model, achieving an AUC value of 0.956 compared with 0.621, which underscores the advantage of advanced ML algorithms in modeling the complex relationships among multiple risk factors. We recognize that prior studies have used advanced ML models for VTE prediction in critically ill patients. For instance, Jin et al [31] developed an RF model for VTE prediction in ICU patients that achieved an AUC of 0.788 in their validation dataset. Our model demonstrates equivalent predictive power in a challenging, sepsis-specific cohort. This robust performance likely stems from 2 key strengths of our approach: first, the inherent efficiency and predictive power of the LGBM algorithm compared with other boosting techniques; second, and more critically, our model's unique inclusion of metabolic and acid-base markers, such as serum chloride and bicarbonate, may offer a more nuanced reflection of the prothrombotic state induced by sepsis-associated organ dysfunction, thereby enhancing predictive accuracy.

The comparative analysis between the LR findings and the SHAP feature ranking reveals the core limitation of traditional statistical approaches in septic VTE prediction. The discrepancy observed for bicarbonate is illustrative. While bicarbonate was not retained in the final LR model, suggesting that its linear signal lacked statistical significance for VTE risk, the LGBM model ranked it as the third most influential predictor overall. This strongly suggests that bicarbonate's predictive power does not stem from a simple linear effect but from its complex nonlinear relationship or crucial interaction with other factors, reflecting the severity of systemic acid-base disturbances. Similarly, MI appeared as a protective factor in the final multivariable regression (OR 0.2851), but its marginal contribution was deemed less vital by SHAP than core metabolic and iatrogenic factors. This protective association in the linear model was likely influenced by confounding or collinearity among chronic conditions, potentially because patients with a history of MI often receive stricter chronic anticoagulation management, which may suppress their VTE risk and mask the true underlying risk in the linear model. The issue of complete separation for variables such as diabetes and COPD further highlights the inherent defect of LR when processing sparse data, as it led to unreliable, extreme coefficients. These findings collectively validate the choice of the nonlinear LGBM model and underscore the necessity of relying on its transparent SHAP feature analysis to evaluate the true, complex VTE risk drivers that are often obscured by the restrictive linearity of traditional statistical methods. Furthermore, the finding that the LGBM model achieved a higher AUC (0.816 vs 0.769) in the severe sepsis subgroup is significant. This enhanced discriminative power in the highest risk population confirms the model's clinical use, suggesting that it is particularly effective for targeted VTE prophylaxis and early intervention in patients with multiorgan dysfunction.

The interpretability enabled by SHAP analysis is essential for clinical translation and offers valuable pathophysiological insights. The top predictors identified by our SHAP analysis are closely related to the pathophysiology of sepsis-associated VTE and reinforce the model's clinical plausibility. The paramount importance of central venous catheterization aligns with Virchow's triad as the catheter can directly cause endothelial injury and lead to local blood flow stasis, both of which are potent triggers for thrombosis [32]. This finding is consistent with numerous studies highlighting indwelling catheters as a major iatrogenic risk factor for VTE in ICU patients [33,34]. The contribution of arterial catheterization, although less pronounced, further underscores the role of endothelial disruption from invasive devices.

Beyond these established risk factors, the model identified the predictive value of metabolic parameters such as serum chloride and bicarbonate. Elevated serum chloride is frequently associated with metabolic acidosis, which commonly develops in severe sepsis and shock [35]. Acidosis has been shown to enhance PLT aggregation and impair fibrinolysis, thereby promoting a prothrombotic state [36]. The association with bicarbonate likely reflects the severity of systemic acid-base disturbances commonly observed in septic shock. These findings suggest that fluid resuscitation strategies and acid-base management may represent modifiable components of VTE risk. The role of PTT is particularly noteworthy. Although a prolonged PTT is traditionally associated with bleeding risk, in sepsis it may paradoxically indicate consumptive coagulopathy in which widespread microthrombosis rapidly consumes clotting factors and leads to their depletion, a hallmark of disseminated intravascular coagulation [37]. The PDP revealed a nonlinear risk profile, where VTE risk increased markedly once PTT exceeded approximately 45 seconds. This nonlinear relationship would likely be overlooked in traditional linear analyses and highlights the model's capacity to identify clinically meaningful physiological thresholds. The contribution of HR appears more direct as its PDP showed a monotonic increase in predicted VTE risk with rising HR. Tachycardia is a cardinal manifestation of the systemic inflammatory response and catecholamine surge in sepsis, reflecting physiological stress and a hyperdynamic state that may promote endothelial dysfunction and a prothrombotic environment [38,39].

XSL•FO
RenderX

Strengths and Limitations

A major strength of our study lies in the integration of rigorous model development with interpretability, which enhances its potential clinical applicability. The model was developed using the large, high-quality public MIMIC-IV database and externally validated it in a geographically and ethnically distinct cohort from our own center. This 2-tiered validation strategy is essential for evaluating model generalizability, which remains a common limitation in single-center ML studies [40]. The decline in AUC from 0.956 to 0.786 during external validation, while still maintaining the best performance among all models, underscores the model's robust generalizability. This performance gap likely reflects intrinsic differences between the 2 cohorts, such as patient genetics, local clinical practices, VTE screening protocols, and data-recording standards. These findings underscore the critical need for local calibration or model retraining before deploying any predictive model in a new clinical setting. In addition, our use of SHAP enhances model transparency and interpretability rather than producing a purely opaque prediction tool. By generating individualized explanations through force plots, our model provides clinicians with transparent and actionable insights that support clinical decision-making and facilitate integration into routine workflows. Such interpretability is essential for translating ML tools from research settings to real-world clinical practice.

Despite these strengths, our study has several limitations. First, its retrospective design allows for the identification of associations but not the establishment of causality. The reliance on *ICD* codes for VTE diagnosis in the MIMIC-IV database may lead to some misclassification, as coding practices can vary and may not capture all clinically recognized events [41]. Second, we included data from only the first 24 hours of ICU admission. While this time frame is critical for early risk stratification, VTE is a dynamic process, and models incorporating time series data may provide greater predictive accuracy [42]. Third, despite comprehensive data extraction, some potential confounders, such as the specific type and dosage of thromboprophylaxis, patient mobility status, or the specific subtypes of malignancy, were not available. This includes the lack of detailed or consistently documented data on heparin dosage, such as prophylactic versus therapeutic, or duration, which forced us to treat heparin use as a binary variable. Finally, although the use of imputation for missing data is standard practice, it may still introduce a small degree of bias.

Future research should aim to prospectively validate our LGBM model in multicenter interventional trials to confirm its clinical use and impact on patient outcomes. Further refinement of the model may involve incorporating dynamic variables throughout the ICU stay and integrating emerging biomarkers related to coagulopathy and endothelial dysfunction. In addition, exploring federated learning approaches could enable the development of more robust and generalizable models across institutions while preserving patient data privacy [43].

Conclusions

This study presents a high-performing and interpretable LGBM model for predicting VTE in ICU patients with sepsis by effectively integrating a broad spectrum of clinical and laboratory data. By leveraging SHAP to enhance transparency, the model extends beyond a simple predictive tool to function as a decision support system capable of elucidating complex risk profiles and enabling clinicians to implement more personalized and effective VTE prevention strategies. This work lays the foundation for the adoption of sophisticated yet interpretable artificial intelligence–driven tools aimed at reducing the burden of VTE in this high-risk patient population.

Acknowledgments

This work was supported by the Suzhou Special Project for Clinical Key Disease Diagnosis and Treatment Technologies (LCZX202334), Key Projects of the Changshu Science and Technology Development Program (CSWS202209), and the Special Research Fund Projects of the China International Medical Foundation (Z-2014-08-2309-1).

Data Availability

The datasets and code used in this study are available from the corresponding author on reasonable request.

Authors' Contributions

YZ and XR designed the study and wrote the manuscript. YZ, XR, and LL collected, analyzed, and interpreted the data. JZ and YG contributed to literature search. XR, and HY critically reviewed and improved the drafts of the manuscript. All authors read and approved the final manuscript.

Conflicts of Interest

None declared.

References

1. Pandey S. Nanotheranostics 2024;8(3):270-284 [FREE Full text] [doi: 10.7150/ntno.94071] [Medline: 38577320]
2. Rudd KE, Johnson SC, Agesa KM, Shackelford KA, Tsoi D, Kievlan DR, et al. Global, regional, and national sepsis incidence and mortality, 1990-2017: analysis for the global burden of disease study. Lancet 2020;395(10219):200-211 [FREE Full text] [doi: 10.1016/S0140-6736(19)32989-7] [Medline: 31954465]

XSL•FO
RenderX

3. Kaplan D, Casper TC, Elliott CG, Men S, Pendleton RC, Kraiss LW, et al. VTE incidence and risk factors in patients with severe sepsis and septic shock. Chest 2015;148(5):1224-1230 [FREE Full text] [doi: 10.1378/chest.15-0287] [Medline: 26111103]
4. Hasegawa D, Sato R, Lee YI, Wang HY, Nishida K, Steiger D. The prevalence, risk factors, and outcomes of acute pulmonary embolism complicating sepsis and septic shock: a national inpatient sample analysis. Sci Rep 2024;14(1):16049 [FREE Full text] [doi: 10.1038/s41598-024-67105-7] [Medline: 38992133]
5. Angus DC, Linde-Zwirble WT, Lidicker J, Clermont G, Carcillo J, Pinsky MR. Epidemiology of severe sepsis in the United States: analysis of incidence, outcome, and associated costs of care. Crit Care Med 2001;29(7):1303-1310. [doi: 10.1097/00003246-200107000-00002] [Medline: 11445675]
6. Innocenti F, Lazzari C, Ricci F, Paolucci E, Agishev I, Pini R. D-dimer tests in the emergency department: current insights. Open Access Emerg Med 2021;13:465-479 [FREE Full text] [doi: 10.2147/OAEM.S238696] [Medline: 34795538]
7. Franchini M, Focosi D, Pezzo MP, Mannucci PM. How we manage a high D-dimer. Haematologica 2024;109(4):1035-1045 [FREE Full text] [doi: 10.3324/haematol.2023.283966] [Medline: 37881856]
8. Shen R, Gao M, Tao Y, Chen Q, Wu G, Guo X, et al. Prognostic nomogram for 30-day mortality of deep vein thrombosis patients in intensive care unit. BMC Cardiovasc Disord 2021;21(1):11 [FREE Full text] [doi: 10.1186/s12872-020-01823-4] [Medline: 33407152]
9. Chopard R, Albertsen IE, Piazza G. Diagnosis and treatment of lower extremity venous thromboembolism: a review. JAMA 2020;324(17):1765-1776. [doi: 10.1001/jama.2020.17272] [Medline: 33141212]
10. Ashrafi Z, Ameri M, Khosravi A, Mirzaei M, Shaker M, Ebrahimi H. Comparison of Autar scale and Wells criteria in DVT risk assessment by nurses in patients with lower extremity trauma. J Vasc Nurs 2022;40(3):148-152. [doi: 10.1016/j.jvn.2022.05.001] [Medline: 36414370]
11. Benfield M, He J, Arnall J, Kaizen W, Jandrisevits E, Eboli-Lopes K, et al. Venous thromboembolism incidence and risk factors in patients undergoing hematopoietic stem cell transplantation. Transplant Cell Ther 2025;31(2):111.e1-111.e10. [doi: 10.1016/j.jtct.2024.10.016] [Medline: 39505211]
12. Viarasilpa T, Panyavachiraporn N, Marashi SM, Van Harn M, Kowalski RG, Mayer SA. Prediction of symptomatic venous thromboembolism in critically ill patients: the ICU-venous thromboembolism score. Crit Care Med 2020;48(6):e470-e479. [doi: 10.1097/CCM.0000000000004306] [Medline: 32187076]
13. Yue S, Li S, Huang X, Liu J, Hou X, Zhao Y, et al. Machine learning for the prediction of acute kidney injury in patients with sepsis. J Transl Med 2022;20(1):215 [FREE Full text] [doi: 10.1186/s12967-022-03364-0] [Medline: 35562803]
14. Fan Z, Jiang J, Xiao C, Chen Y, Xia Q, Wang J, et al. Construction and validation of prognostic models in critically ill patients with sepsis-associated acute kidney injury: interpretable machine learning approach. J Transl Med 2023;21(1):406 [FREE Full text] [doi: 10.1186/s12967-023-04205-4] [Medline: 37349774]
15. Chen Y, Jiang H, Wei Y, Qiu Y, Su L, Chen J, China National Critical Care Quality Control Center Group (China-NCCQC group). Blood pressure response index and clinical outcomes in patients with septic shock: a multicenter cohort study. EBioMedicine 2024;106:105257 [FREE Full text] [doi: 10.1016/j.ebiom.2024.105257] [Medline: 39059317]
16. Qi X, Wang S, Fang C, Jia J, Lin L, Yuan T. Machine learning and SHAP value interpretation for predicting comorbidity of cardiovascular disease and cancer with dietary antioxidants. Redox Biol 2025;79:103470 [FREE Full text] [doi: 10.1016/j.redox.2024.103470] [Medline: 39700695]
17. Liu G, Zheng S, He J, Zhang Z, Wu R, Yu Y, et al. An easy and quick risk-stratified early forewarning model for septic shock in the intensive care unit: development, validation, and interpretation study. J Med Internet Res 2025;27:e58779 [FREE Full text] [doi: 10.2196/58779] [Medline: 39913913]
18. Singer M, Deutschman CS, Seymour CW, Shankar-Hari M, Annane D, Bauer M, et al. The Third International Consensus Definitions for Sepsis and Septic Shock (Sepsis-3). JAMA 2016;315(8):801-810 [FREE Full text] [doi: 10.1001/jama.2016.0287] [Medline: 26903338]
19. Havlicek EE, Palumbo J, Soto-Campos G, Goldenberg NA, Sochet AA. Invasive mechanical ventilation and risk of hospital-acquired venous thromboembolism. Respir Care 2024;69(11):1392-1399. [doi: 10.4187/respcare.11698] [Medline: 38889926]
20. Theochari CA, Theochari NA, Mylonas KS, Papaconstantinou D, Giannakodimos I, Spartalis E, et al. Venous thromboembolism following major abdominal surgery for cancer: a guide for the surgical intern. Curr Pharm Des 2022;28(10):787-797. [doi: 10.2174/1381612828666220217140639] [Medline: 35176975]
21. Chen X, Huang J, Liu J, Deng H, Pan L. Venous thromboembolism risk factors and prophylaxis of elderly intensive care unit patients in a Chinese general hospital. Ann Palliat Med 2021;10(4):4453-4462 [FREE Full text] [doi: 10.21037/apm-21-464] [Medline: 33894730]
22. Chen YW, Fong ZV, Qadan M, Kunitake H, Mullen JT, Chang DC. Should all patients receive the same prophylaxis? Racial variation in the risk of venous thromboembolism after major abdominal operations. Am J Surg 2021;222(5):884-889. [doi: 10.1016/j.amjsurg.2021.05.020] [Medline: 34144805]
23. Chen R, Petrazzini BO, Malick WA, Rosenson RS, Do R. Prediction of venous thromboembolism in diverse populations using machine learning and structured electronic health records. Arterioscler Thromb Vasc Biol 2024;44(2):491-504 [FREE Full text] [doi: 10.1161/ATVBAHA.123.320331] [Medline: 38095106]

XSL•FO
RenderX

24. Seto H, Oyama A, Kitora S, Toki H, Yamamoto R, Kotoku J, et al. Gradient boosting decision tree becomes more reliable than logistic regression in predicting probability for diabetes with big data. Sci Rep 2022;12(1):15889 [FREE Full text] [doi: 10.1038/s41598-022-20149-z] [Medline: 36220875]
25. Hayssen H, Sahoo S, Nguyen P, Mayorga-Carlin M, Siddiqui T, Englum B, et al. Ability of Caprini and Padua risk-assessment models to predict venous thromboembolism in a nationwide study. medRxiv 2023 [FREE Full text] [doi: 10.1101/2023.03.20.23287506] [Medline: 36993603]
26. Maneta E, Aivalioti E, Tual-Chalot S, Emini Veseli B, Gatsiou A, Stamatelopoulos K, et al. Endothelial dysfunction and immunothrombosis in sepsis. Front Immunol 2023;14:1144229 [FREE Full text] [doi: 10.3389/fimmu.2023.1144229] [Medline: 37081895]
27. Iba T, Levy JH, Warkentin TE, Thachil J, van der Poll T, Levi M, Scientific Standardization Committee on DIC ,the Scientific Standardization Committee on Perioperative Critical Care of the International Society on Thrombosis Haemostasis. Diagnosis and management of sepsis-induced coagulopathy and disseminated intravascular coagulation. J Thromb Haemost 2019;17(11):1989-1994 [FREE Full text] [doi: 10.1111/jth.14578] [Medline: 31410983]
28. Su J, Tie X, Zhou R, Zou T, Hong M, Yang L, et al. Risk factors and a nomogram model for deep vein thrombosis in critically ill patients with sepsis: a retrospective analysis. Sci Rep 2025;15(1):16641 [FREE Full text] [doi: 10.1038/s41598-025-01660-5] [Medline: 40360645]
29. van der Poll T, van de Veerdonk FL, Scicluna BP, Netea MG. The immunopathology of sepsis and potential therapeutic targets. Nat Rev Immunol 2017;17(7):407-420. [doi: 10.1038/nri.2017.36] [Medline: 28436424]
30. Li M, Han S, Liang F, Hu C, Zhang B, Hou Q, et al. Machine learning for predicting risk and prognosis of acute kidney disease in critically ill elderly patients during hospitalization: internet-based and interpretable model study. J Med Internet Res 2024;26:e51354 [FREE Full text] [doi: 10.2196/51354] [Medline: 38691403]
31. Jin J, Lu J, Su X, Xiong Y, Ma S, Kong Y, et al. Development and validation of an ICU-venous thromboembolism prediction model using machine learning approaches: a multicenter study. Int J Gen Med 2024;17:3279-3292 [FREE Full text] [doi: 10.2147/IJGM.S467374] [Medline: 39070227]
32. Parienti J, Mongardon N, Mégarbane B, Mira J, Kalfon P, Gros A, 3SITES Study Group. Intravascular complications of central venous catheterization by insertion site. N Engl J Med 2015;373(13):1220-1229. [doi: 10.1056/NEJMoa1500964] [Medline: 26398070]
33. Faustino EVS. Central venous catheter-associated deep venous thrombosis in critically ill children. Semin Thromb Hemost 2018;44(1):52-56. [doi: 10.1055/s-0037-1603938] [Medline: 28778103]
34. Krishnamoorthy A, Hansdak SG, Peter JV, Pichamuthu K, Rajan SJ, Sudarsan TI, et al. Incidence and risk factors for deep venous thrombosis and its impact on outcome in patients admitted to medical critical care. Indian J Crit Care Med 2024;28(6):607-613. [doi: 10.5005/jp-journals-10071-24723] [Medline: 39130389]
35. Filis C, Vasileiadis I, Koutsoukou A. Hyperchloraemia in sepsis. Ann Intensive Care 2018;8(1):43 [FREE Full text] [doi: 10.1186/s13613-018-0388-4] [Medline: 29589205]
36. de Souza JR, Yokoyama AP, Magnus MM, Boin I, de Ataide EC, Munhoz DC, et al. Association of acidosis with coagulopathy and transfusion requirements in liver transplantation. J Thromb Thrombolysis 2022;53(4):887-897. [doi: 10.1007/s11239-021-02609-x] [Medline: 34800258]
37. Levi M, van der Poll T. Inflammation and coagulation. Crit Care Med 2010;38(2 Suppl):S26-S34. [doi: 10.1097/CCM.0b013e3181c98d21] [Medline: 20083910]
38. Vallejos A, Olivares P, Gatica S, Villegas V, Echeverria C, Cabello-Verrugio C, et al. Endotoxemia-induced endothelial fibrosis inhibition improves hypotension, tachycardia, multiple organ dysfunction syndrome, cytokine response, oxidative stress, and survival. Lab Invest 2019;99(8):1173-1192 [FREE Full text] [doi: 10.1038/s41374-019-0237-6] [Medline: 30911151]
39. Sethi P, Peiris CD. A review of catecholamine associated cardiomyopathies and channelopathies. Cureus 2020;12(2):e6957 [FREE Full text] [doi: 10.7759/cureus.6957] [Medline: 32195067]
40. Dung-Hung C, Cong T, Zeyu J, Yu-Shan O, Yung-Yan L. External validation of a machine learning model to predict hemodynamic instability in intensive care unit. Crit Care 2022;26(1):215 [FREE Full text] [doi: 10.1186/s13054-022-04088-9] [Medline: 35836294]
41. Walraven CV. A comparison of methods to correct for misclassification bias from administrative database diagnostic codes. Int J Epidemiol 2018;47(2):605-616. [doi: 10.1093/ije/dyx253] [Medline: 29253160]
42. Cong Y, Wang B, Fei C, Zhang H, Li Z, Zhu Y, et al. Dynamic observation and risk factors analysis of deep vein thrombosis after hip fracture. PLoS One 2024;19(6):e0304629 [FREE Full text] [doi: 10.1371/journal.pone.0304629] [Medline: 38829867]
43. Pati S, Kumar S, Varma A, Edwards B, Lu C, Qu L, et al. Privacy preservation for federated learning in health care. Patterns (N Y) 2024;5(7):100974 [FREE Full text] [doi: 10.1016/j.patter.2024.100974] [Medline: 39081567]

Abbreviations

AKI: acute kidney injury

XSL•FO
RenderX

ARDS: acute respiratory distress syndrome
ARF: acute respiratory failure
AUC: area under the curve
CatBoost: categorical boosting
COPD: chronic obstructive pulmonary disease
CRRT: continuous renal replacement therapy
FiO_2: fraction of inspired oxygen
HR: heart rate
ICD: International Classification of Diseases
ICD-9: International Classification of Diseases, Ninth Revision
ICD-10: International Statistical Classification of Diseases, Tenth Revision
ICU: intensive care unit
LGBM: light gradient boosting machine
LR: logistic regression
MI: myocardial infarction
MIMIC-IV: Medical Information Mart for Intensive Care IV
ML: machine learning
OR: odds ratio
$PaCO_2$: partial pressure of carbon dioxide
PaO_2: partial pressure of oxygen
PDP: partial dependence plot
PE: pulmonary embolism
PEEP: positive end-expiratory pressure
PLT: platelet
PT: prothrombin time
PTT: partial thromboplastin time
RF: random forest
RR: respiratory rate
SAPS II: simplified acute physiology score II
SHAP: Shapley Additive Explanations
SMOTE: Synthetic Minority Oversampling Technique
SOFA: Sequential Organ Failure Assessment
SpO_2: oxygen saturation
VTE: venous thromboembolism

Edited by A Benis; submitted 20.Jul.2025; peer-reviewed by G Wang, S Wan; comments to author 07.Oct.2025; accepted 29.Dec.2025; published 30.Jan.2026.

Please cite as:
Zhang Y, Ren X, Liu L, Zha J, Gu Y, Ye H
Machine Learning Algorithms to Predict Venous Thromboembolism in Patients With Sepsis in the Intensive Care Unit: Multicenter Retrospective Study
JMIR Med Inform 2026;14:e80969
URL: https://medinform.jmir.org/2026/1/e80969
doi:10.2196/80969
PMID:

©Yan Zhang, Xia Ren, Luojie Liu, Junjie Zha, Yijie Gu, Hongwei Ye. Originally published in JMIR Medical Informatics (https://medinform.jmir.org), 30.Jan.2026. This is an open-access article distributed under the terms of the Creative Commons Attribution License (https://creativecommons.org/licenses/by/4.0/), which permits unrestricted use, distribution, and reproduction in any medium, provided the original work, first published in JMIR Medical Informatics, is properly cited. The complete bibliographic information, a link to the original publication on https://medinform.jmir.org/, as well as this copyright and license information must be included.

XSL•FO
RenderX

Original Paper

Evaluation of Large Language Models for Radiologists' Support in Multidisciplinary Breast Cancer Teams: Comparative Study

Hong Jiang[1,2*], MD, PhD; Chun Yang[3*], BM; Wenbin Zhou[4], MD, PhD; Cheng-liang Yin[5], MD, PhD; Shan Zhou[6,7], PhD; Rui He[8], PhD; Guanghui Ran[9], BM; Wujie Wang[9], BM; Meixian Wu[2], MS; Juan Yu[9], MD, PhD

[1]Faculty of Medicine, Macau University of Science and Technology, Macao, China

[2]Department of Statistics, Zhuhai Clinical Medical College of Jinan University, Zhuhai, China

[3]Qiandongnan Prefecture Hospital of Traditional Chinese Medicine, Kai Li, China

[4]Guangdong Provincial Key Laboratory of Tumor Interventional Diagnosis and Treatment, Zhuhai, China

[5]Department of Medical Innovation Research, Chinese PLA General Hospital, Beijing, China

[6]Cancer Virology Program, UPMC Hillman Cancer Center, University of Pittsburgh School of Medicine, Pittsburgh, PA, United States

[7]Department of Microbiology and Molecular Genetics, University of Pittsburgh School of Medicine, Pittsburgh, PA, United States

[8]Grammar and Cognition Lab (GraC), Department of Translation & Language Sciences, Universitat Pompeu Fabra, Barcelona, Spain

[9]Department of Radiology, The First Affiliated Hospital of Shenzhen University, Shenzhen, China

[*]these authors contributed equally

Corresponding Author:
Juan Yu, MD, PhD
Department of Radiology
The First Affiliated Hospital of Shenzhen University
Department of Radiology, Shenzhen Second People's Hospital, The First Affiliated of Shenzhen University, Sungang Road 3002
Shenzhen, 518003
China
Phone: 86 18576685849
Email: yujuan0072@qq.com

Abstract

Background: Artificial intelligence tools, particularly large language models (LLMs), have shown considerable potential across various domains. However, their performance in the diagnosis and treatment of breast cancer remains unknown.

Objective: This study aimed to evaluate the performance of LLMs in supporting radiologists within multidisciplinary breast cancer teams, with a focus on their roles in facilitating informed clinical decisions and enhancing patient care.

Methods: A set of 50 questions covering radiological and breast cancer guidelines was developed to assess breast cancer. These questions were posed to 9 popular LLMs and clinical physicians, with the expectation of receiving direct "Yes" or "No" answers along with supporting analysis. The performances of the 9 models, including ChatGPT-4.0, ChatGPT-4o, ChatGPT-4o mini, Claude 3 Opus, Claude 3.5 Sonnet, Gemini 1.5 Pro, Tongyi Qianwen 2.5, ChatGLM, and Ernie Bot 3.5, were evaluated against that of radiologists with varying experience levels (resident physicians, fellow physicians, and attending physicians). Responses were assessed for accuracy, confidence, and consistency based on alignment with the 2024 National Comprehensive Cancer Network Breast Cancer Guidelines and the 2013 American College of Radiology Breast Imaging-Reporting and Data System recommendations.

Results: Claude 3 Opus and ChatGPT-4 achieved the highest confidence scores of 2.78 and 2.74, respectively, while ChatGPT-4o led in accuracy with a score of 2.92. In terms of response consistency, Claude 3 Opus and Claude 3.5 Sonnet led the pack with scores of 3.0, closely followed by ChatGPT-4o, Gemini 1.5 Pro, and ChatGPT-4o mini, all recording impressive scores exceeding 2.9. ChatGPT-4o mini excelled in clinical diagnostics with a top score of 3.0 among all LLMs, and this score was also higher than all physician groups; however, no statistically significant differences were observed between it and any physician group (all $P>.05$). ChatGPT-4 also had a higher score than the physician groups but showed comparable statistical performance to them ($P>.05$). Across radiological diagnostics, clinical diagnosis, and overall performance, ChatGPT-4o mini and the Claude models achieved higher mean scores than all physician groups. However, these differences were statistically significant only when compared to fellow physicians ($P<.05$). However, ChatGLM and Ernie Bot 3.5 underperformed across diagnostic areas, with lower scores than all physician groups but no statistically significant differences (all $P>.05$). Among physician groups, attending

XSL•FO
RenderX

physicians and resident physicians exhibited comparable high scores in radiological diagnostic performance, whereas fellow physicians scored somewhat lower, though the difference was not statistically significant (P>.05).

Conclusions: LLMs such as ChatGPT-4o and Claude 3 Opus showed potential in supporting multidisciplinary teams for breast cancer diagnostics and therapy. However, they cannot fully replicate the intricate decision-making processes honed through clinical experience, particularly in complex cases. This highlights the need for ongoing artificial intelligence refinement to ensure robust clinical applicability.

(JMIR Med Inform 2026;14:e68182) doi:10.2196/68182

KEYWORDS

breast cancer; large language models; LLMs; radiology assistance; clinical decision-making; ACR BI-RADS; NCCN guidelines; radiologist; National Comprehensive Cancer Network; American College of Radiology Breast Imaging-Reporting and Data System

Introduction

Breast cancer is one of the most common malignancies in women worldwide, with over 2 million diagnoses each year, and it remains the leading cause of cancer-related deaths in women [1,2]. According to a World Health Organization departmental news report in 2021, breast cancer mortality and incidence rates are higher in low- and middle-income countries than in high-income nations, largely due to disparities in early detection and treatment. However, the biological characteristics of breast cancer vary significantly, including imaging features, pathological traits, and lymph node assessment, making early screening and personalized treatment challenging yet crucial.

A mature early screening system relies on well-established professional teams and standardized, specialized guidelines. Although there have been recent advancements, developing countries still face significant challenges in breast cancer care in terms of multidisciplinary coordination among specialist teams (surgeons, oncologists, pathologists, and radiologists), well-balanced medical resources, and adequately trained physicians [3,4]. Furthermore, many physicians rely on empiricism and practice medicine rather than evidence-based guidelines [5,6]. Therefore, there is an urgent need for effective artificial intelligence (AI) tools to support health care professionals in resource-limited settings, improve diagnostic accuracy, and enhance patient outcomes [7,8].

In recent years, several prominent large language models (LLMs) have emerged, including ChatGPT (OpenAI), Gemini Advanced (Google LLC), Claude (Anthropic), Tongyi Qianwen (Alibaba Corporation), ChatGLM (Zhipu AI), and Ernie Bot (Baidu). These models, trained on extensive datasets, offer significant potential in health care by generating complex text through deep learning. ChatGPT, for instance, gained rapid popularity, attracting over 1 million users within days of its release. (knowledge base updated as of October 2023). Studies have shown its potential in medicine, performing well on the United States Medical Licensing Examination and the Board of Radiology-style examination [9,10]. ChatGPT can help radiologists simplify cumbersome diagnostic imaging descriptions [11,12]. Notably, the recommendations provided by ChatGPT for the clinical management of early-diagnosed breast cancer closely align with decisions made by multidisciplinary teams (MDTs) [13]. ChatGPT has indicated a level of congruence with the National Comprehensive Cancer Network (NCCN) guidelines in identifying a wide range of therapeutic agents for the treatment of advanced metastases or advanced primary tumors [14]. However, recent studies highlighted significant limitations in ChatGPT-4.0, revealing a "curse reversal," where a model trained on "A is B" may struggle to infer "B is A" [15].

The rapid advancement of AI has ushered in a new era of innovation, with the emergence and continuous refinement of various LLMs profoundly transforming the health care sector. This study evaluates the performance of various LLMs in addressing breast cancer guideline-related questions, comparing them with radiologists of varying expertise levels to assess their potential in enhancing radiologists' diagnostic capabilities.

Methods

Study Design

The study aimed to evaluate the performance of 9 LLMs in breast cancer imaging diagnosis and to compare their performance with that of breast imaging specialists. We developed a set of 50 questions focused on breast cancer diagnosis and treatment based on the 2013 version of the American College of Radiology Breast Imaging-Reporting and Data System (ACR BI-RADS) classification and the 2024 NCCN Breast Cancer Guidelines. The first 24 questions focused on radiological diagnostics, while the remaining 26 questions pertained to clinical diagnosis and treatment. Questions were then presented to breast radiologists and the 9 LLMs for diagnostic responses. The accuracy, confidence, and consistency of each model in responding to the diagnostic queries were assessed. Furthermore, we conducted a comparative analysis of each model's performance against radiologists possessing varying levels of clinical experience. The study design is provided in Figure 1.

XSL•FO
RenderX

Figure 1. Graph in the full-text abstract: the study design, including question categorization, experiment, and evaluation workflow. ACR BI-RADS: American College of Radiology Breast Imaging-Reporting and Data System; LLM: Large Language Model; NCCN: National Comprehensive Cancer Network.

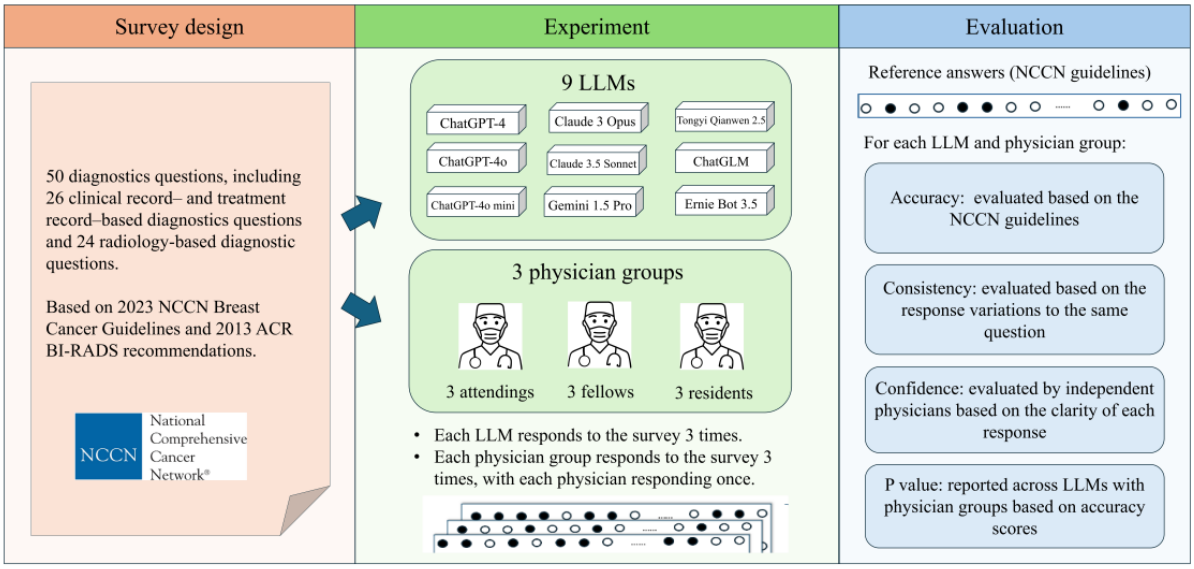

Participants and Models

The 9 LLMs included ChatGPT-4.0, ChatGPT-4o, ChatGPT-4o mini, Claude 3 Opus, Claude 3.5 Sonnet, Gemini 1.5 Pro, Tongyi Qianwen 2.5, ChatGLM, and Ernie Bot 3.5. In addition, the study recruited a total of nine board-certified radiologists, stratified into three distinct experience levels: (1) resident physicians (n=3; 1-5 years of postlicensure experience), undergoing subspecialty training to develop foundational clinical expertise; (2) fellow physicians (n=3; 5-10 years of experience), having completed residency and pursuing advanced fellowship training (1-3 years) to specialize in breast imaging diagnostics; and (3) attending physicians (n=3; >10 years of experience), senior specialists with independent diagnostic authority, responsible for clinical decision-making and trainee supervision. This hierarchical cohort enabled comparative benchmarking of LLM performance against progressive stages of radiologist expertise. Each physician received the same set of 50 questions.

Questions Design

The set of 50 questions was developed based on guidelines extracted from the 2024 NCCN Breast Cancer Guidelines and the 2013 ACR BI-RADS diagnostic criteria, which are widely regarded as the gold standards in clinical breast cancer diagnosis. These criteria are commonly adhered to by physicians in clinical breast cancer diagnosis. In this study, we used these same standards to evaluate the responses provided by the LLMs and physicians to ensure validity and fair comparison. The questions covered a range of common clinical diagnostic decision-making scenarios, providing radiological evidence, such as mammography, ultrasound, and magnetic resonance imaging, as well as clinical information indicators such as medical history, physical examination findings, and laboratory test results, across preoperative, intraoperative, and postoperative stages.

Procedure

Nine physicians were divided into 3 groups based on their experience levels, with each physician answering all 50 questions once. They were prohibited from consulting guidelines or reference materials and were required to complete the questions within 30 minutes. Each physician independently completed the assessment to minimize recall bias. The study aimed to simulate real-world conditions by controlling time and eliminating external aids.

All LLMs were queried via the Google application programming interface on a single date (August 21, 2024) without any additional context (such as task background or medical knowledge priming) and generated responses accordingly. Each LLM independently answered every question 3 times. Standard responses were defined as “yes” or “no.” A response was classified as “yes” if it demonstrated a strong affirmative inclination, supported by compelling theoretical evidence and logical reasoning. Conversely, a response was classified as “no” if it showed a clear negative inclination, backed by equally robust theoretical evidence and sound logic. If an LLM produced an ambiguous response, lacked sufficient evidence, or contained flawed reasoning, it was prompted to reanswer. If the reanswered response remained unsatisfactory, 2 senior physicians with over 10 years of experience were recruited to classify the response based on their professional judgment, thereby evaluating the AI model’s accuracy. In cases of disagreement, the evaluators reevaluated the response based on the 2024 NCCN Guidelines and the 2013 ACR BI-RADS criteria to reach a consensus through discussion.

All LLM-generated responses were anonymized, randomized, and then assessed by evaluators who were blinded to the source (LLM identity) of each response. The accuracy of each response was assessed against the diagnostic NCCN guidelines.

XSL•FO
RenderX

Responses consistent with the guidelines were assigned a score of 1, while inconsistent responses received a score of 0. The accuracy score for each question was calculated by summing the scores of the 3 responses. The overall accuracy performance of both the LLMs and physician groups was determined by averaging the accuracy scores across the 50 questions, resulting in a score ranging from 0 to 3. Subsequently, the accuracy performance of the LLMs was compared to that of the physician groups through rigorous statistical analysis.

Confidence and Consistency

Confidence refers to the clarity of responses, categorized as either "confident" or "nonconfident." A confident answer provides an explicit "yes" or "no" to questions, while a nonconfident answer lacks a direct "yes or no" statement, despite potentially containing detailed explanations, requiring additional prompting to elicit a definitive response. Confident answers received are scored 1, while nonconfident answers are scored 0. The confidence score for each question is calculated by summing the scores from 3 independent response attempts. Each LLM's overall confidence performance is assessed by averaging these scores across 50 questions, resulting in a score ranging from 0 to 3. The confidence ratio represents each LLM's average confidence score divided by the maximum possible score (ie, 3).

Consistency evaluates whether an LLM provides uniform responses across 3 independent attempts to answer the same question. If all 3 answers are identical, the responses are considered consistent, regardless of their alignment with guideline criteria. For consistency assessment, an LLM receives 3 points if all 3 answers to a question are identical, and 2 points if one answer differs from the others. Each LLM's consistency performance is evaluated by averaging these scores across 50 questions, with possible scores ranging from 2 to 3. The consistency ratio is defined as each LLM's average consistency score divided by the maximum possible score (ie, 3).

Statistical Analysis

R software (version 4.4.2; R Foundation for Statistical Computing) was used for data management and statistical analysis. Continuous variables were described using means, and specific group instances were expressed as absolute values. The Wilcoxon rank-sum test was used for score comparisons between 2 different groups. We opted not to perform a Kruskal-Wallis test (for overall multigroup comparison) before pairwise analyses because our research focus was on hypothesis-driven, targeted comparisons between 2 specific groups: each LLM vs each physician subgroup (attendings, fellows, and residents). This design directly aligned with our aim—to evaluate whether single LLMs differ in performance from radiologists at distinct experience levels—rather than testing for overall differences across all groups. Differences between groups were considered significant at $P<.05$. P value correction for multiple comparisons was applied using the Benjamini-Hochberg method. Adjusted P values are provided in Multimedia Appendix 1, Tables 2-4, and corresponding Figures 2-4 to present direct pairwise comparison results; raw P values for multiple comparisons are provided exclusively in Multimedia Appendix 2.

Figure 2. Accuracy scores of large language models (LLMs) compared to physicians in clinical diagnosis and treatment questions of breast cancer. 3-star or dot symbols on each violin from top to bottom represent P values compared to each LLM to attending, fellow, and resident physicians, using the Wilcoxon rank-sum test. Symbols are as follows: "***" represents $P<.001$, "**" represents $.001\leq P<.01$, "*" represents $.01\leq P<.05$, and "black dots" represents $P\geq.05$.

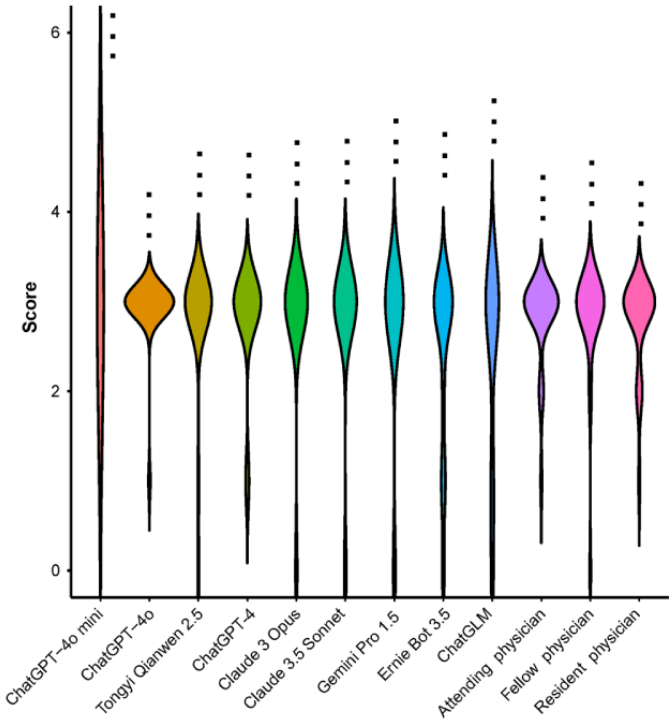

XSL•FO
RenderX

Figure 3. Accuracy scores of large language models (LLMs) compared to those of physicians in radiological diagnosis questions of breast cancer.3-star or dot symbols on each violin from top to bottom represent *P* values compared to each LLM to attending, fellow, and resident physicians, using the Wilcoxon rank-sum test. Symbols are as follows: "***" represents *P*<.001, "**" represents .001≤*P*<.01, "*" represents .01≤*P*<.05, and "black dots" represents P≥.05.

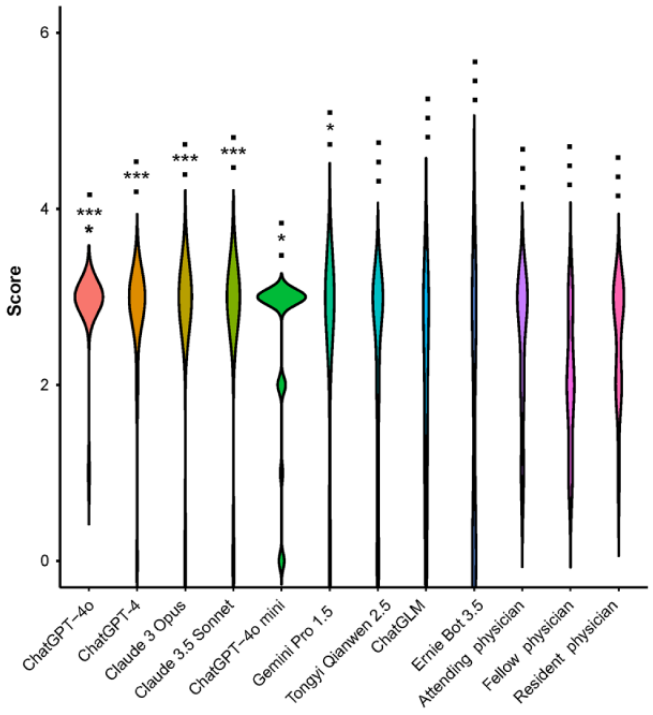

Figure 4. Accuracy scores of large language models (LLMs) compared to those of physicians in totalfor all 50 questions of breast cancer questions.3-star or dot symbols on each violin from top to bottom represent *P* values compared to each LLM to attending, fellow, and resident physicians, using the Wilcoxon rank-sum test. Symbols are as follows: "***" represents *P*<.001, "**" represents .001≤*P*<.01, "*" represents .01≤*P*<.05, and "black dots" represents P≥.05.

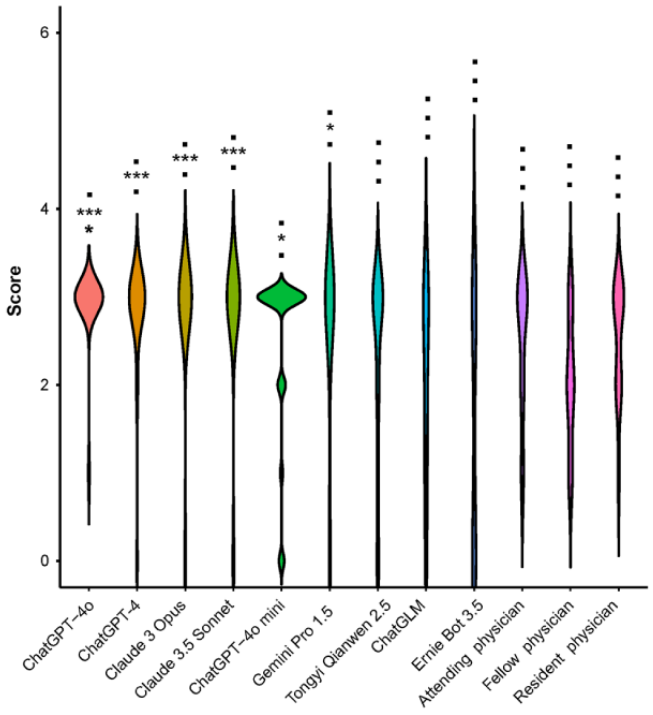

Ethical Considerations

Upon review by the Ethics Committee of Zhuhai People's Hospital, the information and content provided by the researcher did not involve the collection, storage, or use of human samples, and, therefore, met the requirements for exemption from ethical review.

XSL•FO
RenderX

Results

Representative Examples

Textbox 1 provides a representative selection of question-answer examples from the 9 LLMs, while a more comprehensive collection of cases is provided in the Multimedia Appendix 3.

Textbox 1. Representative examples of questions and answers from the 9 large language models (LLMs).

Sample question:

- Can an oval, hypoechoic lesion, growing nonparallel or vertically, with a heterogeneous echo pattern and obscured margins on breast ultrasound, be classified as Breast Imaging Reporting and Data System (BI-RADS 4b)?

ChatGPT-4 response:

- Yes, an oval, hypoechoic lesion growing nonparallel (vertically) with a heterogeneous echo pattern and obscured margins observed on breast ultrasound could be classified as BI-RADS 4b. This classification indicates a moderate suspicion of malignancy, meaning the lesion exhibits characteristics that are more suspicious than those typically found in BI-RADS 4a but not as definitively malignant as those in BI-RADS 4c.
- The characteristics you described—nonparallel orientation (often termed “taller than wide”), heterogeneous echo pattern, and obscured margins—suggest a higher level of concern. These features are often associated with a greater likelihood of malignancy:
  - Nonparallel or vertical orientation: this orientation is more typical of malignant lesions, as benign masses often grow in parallel with the skin.
  - Heterogeneous echo pattern: this can indicate variability within the lesion, which is more common in malignant tumors than in benign growths.
  - Obscured margins: this suggests that the lesion’s borders are not clearly defined, which can be an indication of invasive growth, a characteristic more typical of malignant processes.
- Conclusion: a lesion under 5 mm without a lipid core showing a washout pattern on magnetic resonance imaging should be approached with a high degree of suspicion for malignancy. This situation requires proactive management, including possible biopsy and close imaging follow-up, to ensure timely diagnosis and treatment.

ChatGPT-4o response:

- Yes, an oval, hypoechoic lesion that is growing nonparallel (vertically oriented), with a heterogeneous echo pattern and obscured margins on breast ultrasound can be classified as BI-RADS 4b. BI-RADS 4b is used to describe lesions with a moderate suspicion of malignancy.
- Key features of BI-RADS 4b:
  - Oval shape: while an oval shape can suggest a benign lesion, other features, such as orientation, margin appearance, and internal echo pattern, significantly influence the level of suspicion.
  - Nonparallel growth (vertically oriented): a lesion that grows nonparallel, or “taller than wide,” raises concern for malignancy. This orientation is often associated with invasive tumors because malignant lesions tend to invade tissue in a vertical direction.
  - Heterogeneous echo pattern: a heterogeneous echo pattern, where the lesion appears uneven or varied in echogenicity, is suspicious because it can indicate the presence of both solid and cystic components, or areas of differing cellular density, which is common in malignant tumors.
  - Obscured margins: obscured or indistinct margins are another red flag for malignancy. Clear, well-defined margins are typically seen in benign lesions, while indistinct margins suggest invasion into surrounding tissues.
- In conclusion, the combination of nonparallel growth, heterogeneous echo pattern, and obscured margins justifies a BI-RADS 4b classification, meaning the lesion has a moderate risk of malignancy and requires biopsy for a definitive diagnosis.

ChatGPT-4o mini response:

- Yes, an oval, hypoechoic lesion with a nonparallel (vertically oriented) growth pattern, heterogeneous echo pattern, and obscured margins on breast ultrasound can be classified as BI-RADS 4b.
- Here’s why this classification might be appropriate:
  - Oval shape: while typically less suspicious than irregular shapes, an oval shape alone does not rule out malignancy.
  - Hypoechoic: a darker appearance on ultrasound is often associated with both benign and malignant lesions.
  - Nonparallel growth pattern: a vertical or irregular growth pattern can be more concerning, as it may suggest infiltration into surrounding tissues.
  - Heterogeneous echo pattern: variability in echo patterns within a lesion can be indicative of more complex internal structures, which may be suggestive of malignancy.
  - Obscured margins: margins that are not well-defined or are irregularly shaped can be a sign of malignancy.
- BI-RADS 4b indicates a moderate suspicion of malignancy, with a likelihood of 10%-50%. This classification suggests that while there is a notable suspicion of cancer, the probability is not as high as in BI-RADS 4c. A biopsy is recommended to obtain a definitive diagnosis.

XSL•FO
RenderX

Confidence Level

Claude 3 Opus achieved the highest average score of 2.78, followed by ChatGPT-4 with a score of 2.74. The remaining models scored as follows: ChatGPT-4o 2.52, ChatGPT-4o mini 2.58, Claude 3.5, Sonnet 2.34, Gemini 1.5 Pro 2.28, Tongyi Qianwen 2.5 1.62, ChatGLM 1.98, and Ernie Bot 3.5 1.50. Claude 3 Opus and ChatGPT-4 demonstrated significantly higher confidence compared to the other models (Table 1 and Figure 5).

Table 1. Confidence and consistency levels of the large language models (LLMs).

Methods	Confidence level	Consistency level
ChatGPT-4	2.74	2.90
ChatGPT-4o	2.52	2.96
ChatGPT-4o mini	2.58	2.92
Claude 3 Opus	2.78	3.00
Claude 3.5 Sonnet	2.34	3.00
Gemini 1.5 Pro	2.28	2.96
Tongyi Qianwen 2.5	1.62	2.86
ChatGLM	1.98	2.72
Ernie Bot 3.5	1.50	2.82

Figure 5. Percentage of accuracy, confidence, and consistency levels of large language models (LLMs) across all 50 questions.

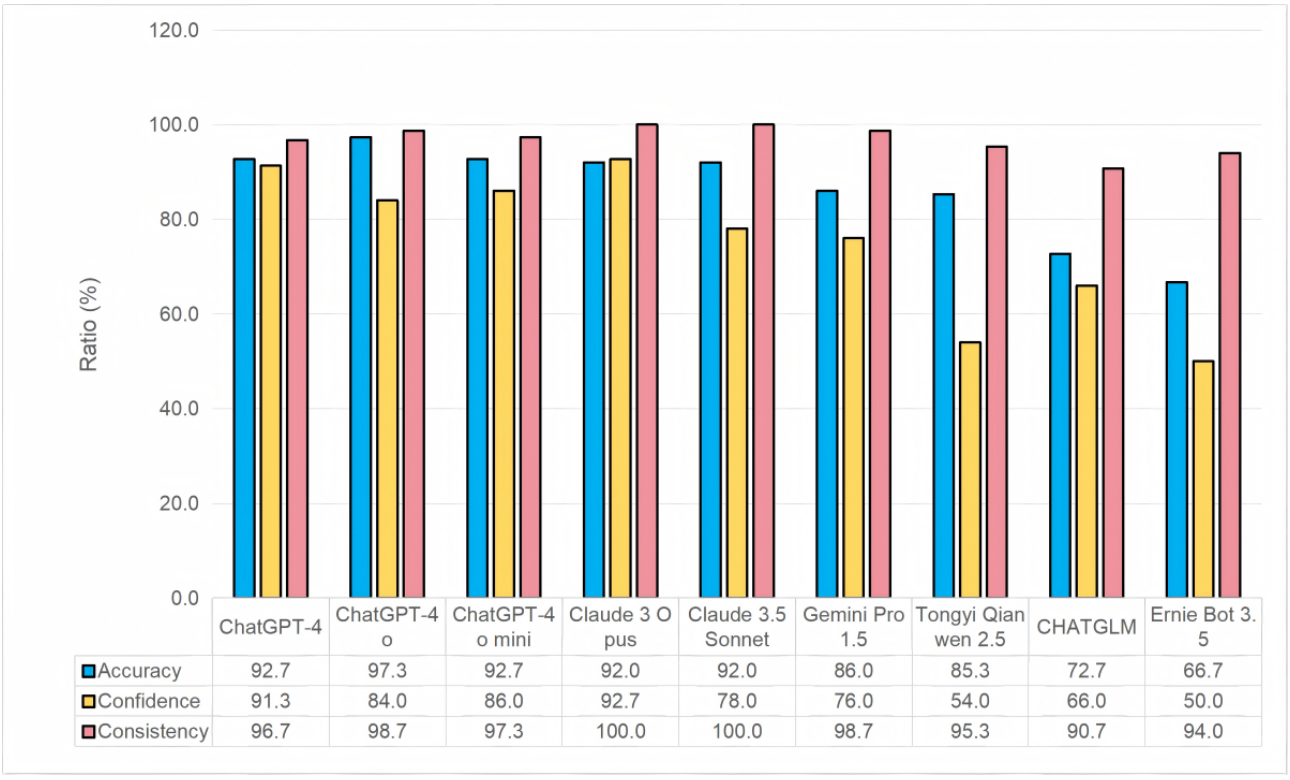

Consistency

Claude 3 Opus and Claude 3.5 Sonnet achieved the highest score of 3.0, demonstrating their superiority. The remaining models achieved the following consistency scores: ChatGPT-4o: 2.96, Gemini 1.5 Pro: 2.96, ChatGPT-4o mini: 2.92, ChatGPT4: 2.90, Tongyi Qianwen 2.5: 2.86, Ernie Bot 3.5: 2.82, and ChatGLM: 2.71 (Table 1 and Figure 5).

Performances on Clinical Diagnostics and Treatment Questions

In the comparison of clinical diagnostic problems, the mean accuracy scores are 3 (SD 0), 2.92 (SD 0.39), 2.81 (SD 0.69), 2.81 (0.49), 2.81 (SD 0.63), 2.77 (SD 0.65), 2.77 (SD 0.82), 2.77 (SD 0.82), 2.65 (SD 0.98), 2.38 (SD 1.02), and 2.35 (SD 1.13) for ChatGPT-4o mini, ChatGPT-4o, Tongyi Qianwen 2.5, attending physicians, fellow physicians, ChatGPT-4, Claude 3 Opus, Claude 3.5 Sonnet, Gemini 1.5 Pro, Ernie Bot 3.5, and ChatGLM, respectively. No significant differences were observed between any language modeling group and the various

XSL•FO
RenderX

physician groups. Regarding comparisons among physician groups, no significant differences were detected between different physician subgroups (Table 2, Figure 2, and Multimedia Appendices 1 and 4).

Table 2. Accuracy score comparisons of large language models (LLMs) with physician groups for clinical diagnostic and treatment questions.

Methods	Value, mean (SD)	FDR[a]-adjusted *P* value		
		Attending physician	Fellow physician	Resident physician
ChatGPT-4	2.77 (0.65)	.84	.97	.66
ChatGPT-4o	2.92 (0.39)	.44	.81	.49
ChatGPT-4o mini	3 (0)	.37	.42	.23
Claude 3 Opus	2.77 (0.82)	.62	.90	.49
Claude 3.5 Sonnet	2.77 (0.82)	.62	.90	.49
Gemini 1.5 Pro	2.65 (0.98)	.84	.97	.66
Tongyi Qianwen 2.5	2.81 (0.69)	.62	.90	.49
ChatGLM	2.35 (1.13)	.44	.44	.49
Ernie Bot 3.5	2.38 (1.02)	.44	.42	.49
Attending physician	2.81 (0.49)	—[b]	.90	.74
Fellow physician	2.81 (0.63)	—	—	.66
Resident physician	2.77 (0.51)	—	—	—

[a]FDR: false discovery rate.

[b]Not applicable.

In Figure 2, 3-star or dot symbols on each violin from top to bottom represent *P* values compared to each LLM to attending, fellow, and resident physicians, using the Wilcoxon rank-sum test. Symbols are as follows: "***" represents $P<.001$, "**" represents $.001\leq P<.01$, "*" represents $.01\leq P<.05$, and "." represents $P\geq.05$.

Performances on Radiological Diagnostics Problems

In the comparison of radiological diagnostic problems, the scores were as follows: ChatGPT-4 2.79, ChatGPT-4o 2.92, ChatGPT-4o mini 2.54, Claude 3 Opus 2.75, Claude 3.5 Sonnet 2.75, Gemini 1.5 Pro 2.5, Tongyi Qianwen 2.29, ChatGLM 2.0, and Ernie Bot 3.5 1.58. The attending physicians scored 2.46, the fellow physicians scored 2.04, and the resident physicians scored 2.5. The differences between ChatGPT-4, ChatGPT-4o, ChatGPT-4o mini, Claude 3 Opus, Claude 3.5 Sonnet, and Gemini 1.5 Pro and the fellow physicians were statistically significant ($P<.05$). There were statistically significant differences between ChatGPT-4o and the resident physicians ($P=.04$). In contrast, the differences between Tongyi Qianwen 2.5, ChatGLM, and the physician groups were not statistically significant ($P>.05$). In comparisons among physician groups, the differences were not statistically significant ($P>.05$; Table 3, Multimedia Appendices 1 and 4, and Figure 5).

XSL•FO
RenderX

Table 3. Accuracy score comparisons of large language models (LLMs) with physician groups for radiological diagnostic questions.

Methods	Value, mean (SD)	FDR[a]-adjusted *P* value		
		Attending physician	Fellow physician	Resident physician
ChatGPT-4	2.79 (0.66)	.10	<.001	.07
ChatGPT-4o	2.92 (0.41)	.06	<.001	.04
ChatGPT-4o mini	2.54 (0.93)	.51	.01	.45
Claude 3 Opus	2.75 (0.85)	.09	<.001	.07
Claude 3.5 Sonnet	2.75 (0.85)	.09	<.001	.07
Gemini 1.5 Pro	2.5 (1.06)	.50	.01	.41
Tongyi Qianwen 2.5	2.29 (1.08)	.81	.15	.97
ChatGLM	2 (1.1)	.22	.84	.22
Ernie Bot 3.5	1.58 (1.44)	.09	.49	.09
Attending physician	2.46 (0.78)	—[b]	.07	.99
Fellow physician	2.04 (0.75)	—	—	.07
Resident physician	2.5 (0.66)	—	—	—

[a]FDR: false discovery rate.

[b]Not applicable.

In Figure 3, 3-star or dot symbols on each violin from top to bottom represent *P* values compared to each LLM to attending, fellow, and resident physicians, using the Wilcoxon rank-sum test. Symbols are as follows: "***" represents *P*<.001, "**" represents .001≤*P*<.01, "*" represents .01≤*P*<.05, and "." represents *P*≥.05.

Performances on Full Set Questions

In the comparison of overall performance, the scores were as follows: ChatGPT-4o 2.92, ChatGPT-4 2.78, ChatGPT-4o mini 2.78, Claude 3 Opus 2.76, Claude 3.5 Sonnet 2.76, Gemini 1.5 Pro 2.58, Tongyi Qianwen 2.56, ChatGLM 2.18, and Ernie Bot 3.5 2.0. The attending physicians scored 2.64, the fellow physicians scored 2.44, and the resident physicians scored 2.64. The differences between ChatGPT-4, ChatGPT-4o, ChatGPT-4o mini, Claude 3 Opus, Claude 3.5 Sonnet, and the fellow physicians were statistically significant (*P*<.05). Significant differences were observed between ChatGPT-4o and resident physicians (*P*=.01) and between ChatGPT-4o and attending physicians (*P*=.03). In the comparisons among physician groups, none of the differences were statistically significant (*P*>.05; Table 4, Multimedia Appendices 1 and 4, and Figure 4).

XSL•FO
RenderX

Table 4. Accuracy score comparisons of large language model (LLM) models with physician groups for all 50 questions.

Methods	Value, mean (SD)	FDR[a]-adjusted *P* value		
		Attending physician	Fellow physician	Resident physician
ChatGPT-4	2.78 (0.65)	.13	.006	.09
ChatGPT-4o	2.92 (0.4)	.03	<.001	.01
ChatGPT-4o mini	2.78 (0.68)	.13	.006	.09
Claude 3 Opus	2.76 (0.82)	.08	.003	.05
Claude 3.5 Sonnet	2.76 (0.82)	.08	.003	.05
Gemini 1.5 Pro	2.58 (1.01)	.47	.06	.30
Tongyi Qianwen 2.5	2.56 (0.93)	.84	.18	.67
ChatGLM	2.18 (1.12)	.09	.47	.12
Ernie Bot 3.5	2 (1.29)	.08	.26	.09
Attending physician	2.64 (0.66)	—[b]	.19	.78
Fellow physician	2.44 (0.79)	—	—	.30
Resident physician	2.64 (0.6)	—	—	—

[a]FDR: false discovery rate.

[b]Not applicable.

In Figure 4, 3-star or dot symbols on each violin from top to bottom represented *P* values compared to each LLM model to attending, fellow, and resident physicians, with the Wilcoxon rank-sum test. Symbols are as follows: "***" represents *P*<.001, "**" represents .001≤*P*<.01, "*" represents .01≤*P*<.05, and "." represents *P*≥.05.

Discussion

Principal Findings

With the global population aging, the rising incidence of cancer, and the increasing complexity of treatment options, there is a growing demand for MDT discussions. However, implementing high-level MDTs in underdeveloped countries remains a significant challenge [16], largely because of the knowledge barriers between specialist doctors. An important question is how specialist doctors in less developed regions can achieve the same medical standards as those in developed regions, easily access authoritative and professional medical knowledge, and overcome barriers between specialties. The recently developed chatbot can theoretically provide instant, evidence-based responses, demonstrating significant potential as an ideal tool for enhancing high-quality health care in underserved regions. In our comparison of 9 LLMs, Claude 3 Opus demonstrated the highest confidence score at 2.78, followed by ChatGPT-4 (2.74) and ChatGPT-4o mini (2.58). These scores suggest that these models exhibit a higher degree of certainty when managing complex medical issues. In contrast, Ernie Bot 3.5's confidence score of 1.50 was significantly lower, indicating a reduced ability to comprehend and process medical problems. These findings underscore the varying levels of proficiency among language models in accurately addressing the same problem. Interestingly, unlike human practitioners, not all chatbots confidently respond to closed-ended questions with a definitive "yes" or "no," suggesting that training data diversity and model architecture significantly impact diagnostic accuracy. This uncertainty may lead to reduced consistency and accuracy of their outputs, thus limiting their independent use in practical clinical applications, making them inseparable from close collaboration with physicians during decision-making.

In addition, in the consistency assessment, Claude 3 Opus and Claude 3.5 Sonnet achieved the highest scores of 3, followed by ChatGPT-4o and Gemini 1.5 Pro, both scoring 2.96, with ChatGPT-4o mini at 2.92. In contrast, ChatGLM and Ernie Bot 3.5 exhibited lower consistency scores of 2.72 and 2.82, respectively. These results highlight the differences in response stability across the LLMs, a factor that is especially critical for clinical decision support. In clinical applications, particularly in dynamic and complex environments, models lacking sufficient consistency may undermine confidence in their outputs. Although Claude 3 Opus and Claude 3.5 Sonnet surpassed the ChatGPT models in response consistency (scoring 3), the ChatGPT models demonstrated superior performance in diagnostic accuracy. However, none of the models provided correct answers to all question sets. Therefore, while AI introduces new possibilities in fields such as medicine, it also presents challenges that require careful expert scrutiny to avoid imposing additional burdens on patients and health care professionals [17,18].

By comparing the nine LLMs with the responses of nine radiologists on the overall 50 guideline questions, ChatGPT-4o achieved the highest score of 2.92, significantly outperforming all physician groups. The difference between ChatGPT-4o and all physician groups (*P*<.05) was statistically significant. ChatGPT-4, ChatGPT-4o mini, Claude 3 Opus, and Claude 3.5 Sonnet all scored higher on average than the physician groups. However, the difference was statistically significant only for the comparison with fellow physicians (*P*<.05). In contrast, Gemini 1.5 Pro and Tongyi Qianwen 2.5 had lower scores, with no statistically significant differences compared to each group

XSL•FO
RenderX

of doctors (P>.05). ChatGLM and Ernie Bot 3.5 showed lower scores than all physician groups, but the differences were not statistically significant. No statistically significant differences (P>.05) were found in the comparisons between each group of doctors, suggesting that attending physicians, fellow physicians, and resident physicians performed comparably in answering the entire question set. Attending physicians and resident physicians both scored 2.64, which may reflect a more consistent ability to answer certain routine questions across all years of experience. Fellow physicians, on the other hand, scored slightly lower, but the difference was not significant, suggesting that their performance in overall diagnostic and therapeutic tasks remains competitive.

In the evaluation of radiological diagnostic performance, ChatGPT-4o scored 2.92. A significant difference was observed between ChatGPT-4o and resident physicians (P=.04), and a significant difference was also detected between ChatGPT-4o and fellow physicians (P<.05). ChatGPT-4 achieved a score of 2.79, surpassing all physician groups on average. However, this difference reached statistical significance solely in the comparison with fellow physicians (P<.05). The difference between ChatGPT-4o mini and the fellow physicians was statistically significant (P=.01). Claude 3 Opus and Claude 3.5 Sonnet both scored 2.75, higher than all physician groups; in particular, the difference between these LLMs and fellow physicians was statistically significant (P<.05), suggesting superior performance in radiological diagnostics. Gemini 1.5 Pro scored 2.50, showing small differences compared with attending physicians and resident physicians but significantly higher than fellow physicians (P=.01). Tongyi Qianwen 2.5 and ChatGLM scored lower, with no statistically significant differences compared to physician groups (P>.05). Ernie Bot 3.5 had the lowest score (1.58) among all LLMs, with no statistical significance compared to any physician group, indicating relatively poorer performance. We conclude that the ChatGPT and Claude series outperform junior medical doctors in addressing complex medical issues, highlighting their potential clinical utility. However, ChatGLM and Ernie Bot 3.5 may require further optimization to improve their performance in medical diagnostics. In the diagnostic radiology domain, the average performance of attending physicians and resident physicians was comparable, whereas the small group of fellow physicians scored lower on average. It is noteworthy that resident physicians, who have recently completed standardized residency training, may be more familiar with the specific guidelines on which the questions were based. Attending physicians, benefiting from extensive clinical experience, would be expected to exhibit an advantage in diagnosing complex imaging findings. The performance variation across the small physician subgroups underscores the preliminary nature of these comparisons.

In the assessment of clinical diagnosis and treatment performance, ChatGPT-4o mini achieved the highest score of 3 among all LLMs, although no statistically significant differences were found when compared with any physician group. ChatGPT-4o scored 2.92 and showed no significant difference compared with physician groups (P>.05); however, it outperformed all physician groups on average. Other LLMs, including ChatGPT-4, Claude 3 Opus, and Claude 3.5 Sonnet, exhibited similar performance to physician groups. ChatGLM and Ernie Bot 3.5 showed weaker performance. Overall, the ChatGPT and Claude series of LLMs outperformed some physician groups with lower seniority in complex health care challenges, indicating potential for clinical applications. Further optimization may be necessary for ChatGLM and Ernie Bot 3.5 to enhance their diagnostic performance. Scores between attending physicians and fellow physicians were identical, while resident physicians scored slightly lower; however, these differences did not reach statistical significance. Radiologists of varying experience levels may possess adequate knowledge of clinical guidelines in diagnosis and treatment, particularly when dealing with standardized procedures or common diseases, resulting in minimal differences. Despite differences in experience, attending physicians and fellow physicians demonstrated similar proficiency in applying clinical guidelines.

It is noteworthy that Tongyi Qianwen 2.5 was the only model unable to generate a response to a specific question, instead providing the feedback, “I’m very sorry, but I don’t think I fully understand what you mean. Let’s change the subject first, shall we?” This issue may be attributable to the complexity and specialized nature of the question, or potential biases and gaps in the model’s training data, leading to insufficient knowledge in specific domains. Our data indicate that when Tongyi Qianwen 2.5 fails to respond, the model’s accuracy may be overstated, and its actual performance is significantly below expectations.

Comparison With Previous Work

In our analysis of the 9 language models, Ernie Bot 3.5, Tongyi Qianwen 2.5, and ChatGLM were more likely to recommend referring the questions to medical experts when faced with specialized imaging terminology and clinical scenarios, rather than providing a definitive answer. In contrast, Claude 3 Opus and the ChatGPT series provided more detailed diagnostic imaging feedback, including recommendations for additional biopsies to support diagnosis and an emphasis on multidisciplinary collaboration. Regarding clinical considerations for surgery, the ChatGPT series excelled by offering surgical recommendations for breast cancer patients, while also demonstrating conventional surgical approaches and discussing recent therapeutic advancements. Furthermore, the ChatGPT family outperformed other language models in breast cancer diagnosis and treatment, with each model excelling in its respective area of expertise. This finding highlights the critical need to select the most appropriate language model based on task-specific performance, thereby enhancing problem-solving across various scenarios. These interactive language models provided feedback significantly faster than breast cancer radiologists, reducing time costs and increasing productivity. With continued iteration and improvement, ChatGPT has demonstrated considerable potential in radiology, including concise report generation, support for medical education, clinical decision aids, patient communication optimization, and data analysis [19,20]. Analyzing the reasons for comparable performance between leading language models reveals several key advantages: (1) large-scale, high-quality training data: both the developers of Claude 3 Opus and Chat

XSL•FO
RenderX

GPT have invested substantial resources in acquiring and curating authoritative medical literature, textbooks, and specialized professional databases; (2) comparable model scale and architecture: as state-of-the-art LLMs, both likely use similar parameter scales and analogous underlying architectural designs; (3) equivalent alignment methodologies: both organizations have likely implemented similar reinforcement learning from human feedback techniques, using extensive human evaluator input to enhance the accuracy of model outputs; (4) competition-driven enhancement: market competition has compelled both companies to continuously improve model performance, particularly in high-value vertical domains such as health care. This competitive environment has resulted in both products demonstrating enhanced logical reasoning capabilities; (5) domain-specific knowledge processing: both models have likely incorporated specialized training methodologies for processing technical terminology and complex semantic relationships within specialized conceptual frameworks; (6) parallel safety control mechanisms: in high-risk domains such as medicine, both models have presumably implemented stringent output controls and prudence measures to ensure responsible performance. Given the continuous evolution of LLMs, their capabilities in complex domains, particularly medicine, are rapidly advancing. Future research should further investigate the potential of these models to maximize their value in clinical diagnosis and treatment [21].

However, LLMs were not specifically trained for the medical field and rely on large datasets collected from public sources, such as web pages, books, and websites. Chinese LLMs have reported average accuracy in general medical question-answering of around 82%; yet, performance drops significantly in complex clinical reasoning tasks, such as breast cancer diagnosis (below 50%) [22]. Advanced models, such as ChatGPT-3.5, ChatGPT-4.0, and Claude-2, achieve slightly higher performance (approximately 60%) in breast cancer clinical assessments, though this still highlights critical limitations in high-stakes medical applications [23]. Despite the vast amount of training data, these models lack comprehensive common sense, which limits their reasoning ability. The literature suggests that LLM performance can be significantly enhanced by guiding reasoning steps incrementally, particularly in tasks involving longer reasoning chains [24,25]. In our study, however, the 9 LLMs were unable to accurately diagnose all rigorous and logical medical problems, and a "curse of reversal" phenomenon was observed. Furthermore, unlike real-time search engines such as Google and Bing, LLMs can only generate responses based on their training data and do not have real-time access to current information [26,27]. In addition, LLMs cannot reliably differentiate between factual and fictional statements, posing a potential risk as sources of misinformation in certain cases [28-30]. Moreover, the training data for these models are not publicly available, and the sources of their information are not disclosed, making it difficult to verify the accuracy of their outputs [31]. Therefore, radiologists must continue to rely on traditional evidence-based education and approach LLMs critically, cross-referencing their outputs with credible medical sources [32].

Limitations

This study has several limitations. First, our findings are subject to the inherent limitations of the author-crafted, closed-ended question format. Although designed for objective assessment, this format may not fully capture the reasoning capabilities of LLMs and could potentially underestimate their performance in real-world, open-ended clinical scenarios. Second, the binary definition of a "confident" response as a direct "yes" or "no" may not adequately reflect clinical decision-making, where acknowledging uncertainty is a sign of expertise. This could have introduced bias by favoring LLMs that generate definitive answers over physicians who appropriately consider diagnostic nuances. Third, the physician sample size, while sufficient for initial comparisons, remains relatively small and may not be fully representative of the broader population of radiologists, which could affect the generalizability of our pairwise comparisons. Fourth, the study's generalizability is constrained by its specific design: the assessment is limited to 50 selected questions that do not encompass all aspects of the guidelines, and the performance of the LLMs was evaluated on a single, specific task (answering structured concordance questions). Consequently, the results may not be directly extrapolated to other clinical datasets or different natural language processing tasks. Fifth, the study conditions, including a strict 30-minute time limit and a "no-consultation" rule for the participating physicians, may not reflect real-world clinical practice, where complex cases often benefit from more time and collaborative discussion. These methodological choices, while necessary for standardization, may have disadvantaged the physicians and thus the conclusions of this study must be heavily qualified by this context. In addition, it has been reported that LLMs may generate different responses to identical prompts at different times, due to model updates [31,33]. Future studies should use larger and more diverse physician cohorts, incorporate more nuanced assessments of confidence, explore the impact of different time constraints and collaborative settings, and use a broader range of question types and clinical tasks to validate and extend our findings.

Future Directions

In medical AI applications, LLMs participating in clinical decision-making face critical responsibility challenges, including decision output liability, misinformation risks, and privacy breach accountability [30]. Typically, LLMs do not independently generate decision outputs but function as tools for physicians. Clinicians must integrate guidelines, relevant literature, and their clinical expertise to formulate final clinical decisions. When using LLMs, it is essential to conceal patients' identifying information to safeguard privacy.

This necessitates establishing explicit legal frameworks that delineate responsibility boundaries among developers, health care institutions, and physicians, while constructing comprehensive accountability mechanisms [34,35]. Concurrently, LLMs present a risk of generating inaccurate medical information that could potentially mislead diagnostic and therapeutic decisions. To address this concern, model developers must implement rigorous content review protocols

XSL•FO
RenderX

and ensure professional, authoritative verification of training corpora.

Conclusions

In conclusion, within the context of our study, Claude 3 Opus and the ChatGPT series, particularly ChatGPT-4o, excelled in addressing breast cancer–related guideline questions and demonstrated significant potential for clinical application. In contrast, the less consistent performance of other LLMs, especially Ernie Bot 3.5 and ChatGLM, suggests that both confidence and consistency should be carefully considered when selecting and applying LLMs to ensure efficacy and stability in clinical practice. This preliminary evaluation indicates that LLMs can provide radiologists with extensive cross-disciplinary knowledge, potentially enhancing contributions within MDTs. However, they cannot fully replace human expertise, particularly in complex diagnostic scenarios that require nuanced decision-making honed by clinical experience.

Acknowledgments

We also sincerely thank Dr Siping Luo, Dr Xiao Luo, Huimei Lü, Zhichunmei Yuan, and Qiuxinmei Chen for their invaluable suggestions in designing the 50 breast cancer questions.

Data Availability

The datasets generated or analyzed during this study are available from the corresponding author upon reasonable request.

Funding

This research was funded by the Department of Science and Technology of Guangdong Province (grant no 112175605105) and the research project “Preoperative Localization and Navigation of Non-Mass Breast Cancer with DCE-MRI and Ultrasound Fusion Imaging” (grant no 2023yjlcyj019), and the Shenzhen Basic Research Project (Natural Science Foundation; grant no JCYJ20220530150416036). The funding period was 3 years, starting in June 2023, with a total budget of CNY $35,615 (US $5000).

Authors' Contributions

CY was responsible for conceptualization, developing the conceptual framework, and formulating the ideas for this study. HJ and CY prepared the original draft, including substantive translation, and contributed to manuscript creation. HJ, CY, JY, and CY participated in the review and editing of the manuscript, covering both prepublication and postpublication stages. Supervision of the study was provided by HJ, CY, and JY, who oversaw and took leadership responsibility for the planning and execution of research activities. Resource support, including the provision of breast cancer–related guideline materials, was provided by JY, HJ, and CY. Formal analysis was conducted by WZ, who applied statistical techniques to analyze the research data, while data curation, including management of LLM models and essential software code, was performed by WZ and SZ. Investigation, including data collection during the study, was carried out by GR, WW, and MW. Project administration was coordinated by JY, who ensured the smooth planning and execution of research activities. Funding acquisition was secured by HJ and JY.

Conflicts of Interest

None declared.

Multimedia Appendix 1
Scores of large language models (LLMs) and physician groups on 50 questions, with comparison analysis.
[XLSX File (Microsoft Excel File), 14 KB - medinform_v14i1e68182_app1.xlsx]

Multimedia Appendix 2
Comparison of accuracy scores between large language models (LLMs) and physicians across 2 domains.
[DOCX File , 23 KB - medinform_v14i1e68182_app2.docx]

Multimedia Appendix 3
Scores of large language models (LLMs) and physician groups on 50 questions, including raw *P* values for comparison.
[DOCX File , 20 KB - medinform_v14i1e68182_app3.docx]

Multimedia Appendix 4
Specific responses from 9 large language models (LLMs) to the 50 questions (each question asked 3 times) and the corresponding physicians’ responses.
[XLSX File (Microsoft Excel File), 854 KB - medinform_v14i1e68182_app4.xlsx]

XSL•FO
RenderX

References

1. Bray F, Laversanne M, Sung H, Ferlay J, Siegel RL, Soerjomataram I, et al. Global cancer statistics 2022: GLOBOCAN estimates of incidence and mortality worldwide for 36 cancers in 185 countries. CA Cancer J Clin 2024;74(3):229-263 [FREE Full text] [doi: 10.3322/caac.21834] [Medline: 38572751]
2. New global breast cancer initiative highlights renewed commitment to improve survival. World Health Organization (WHO). 2021 Mar 8. URL: https://www.who.int/news/item/08-03-2021-new-global-breast-cancer-initiative-highlights-renewed-commitment-to-improve-survival [accessed 2025-01-01]
3. Trapani D, Ginsburg O, Fadelu T, Lin NU, Hassett M, Ilbawi AM, et al. Global challenges and policy solutions in breast cancer control. Cancer Treat Rev 2022;104:102339. [doi: 10.1016/j.ctrv.2022.102339] [Medline: 35074727]
4. Azadnajafabad S, Saeedi Moghaddam S, Mohammadi E, Delazar S, Rashedi S, Baradaran HR, et al. Patterns of better breast cancer care in countries with higher human development index and healthcare expenditure: insights from GLOBOCAN 2020. Front Public Health 2023;11:1137286 [FREE Full text] [doi: 10.3389/fpubh.2023.1137286] [Medline: 37124828]
5. Hisham R, Ng CJ, Liew SM, Hamzah N, Ho GJ. Why is there variation in the practice of evidence-based medicine in primary care? A qualitative study. BMJ Open 2016;6(3):e010565 [FREE Full text] [doi: 10.1136/bmjopen-2015-010565] [Medline: 26962037]
6. Yuan L, Cao J, Wang D, Yu D, Liu G, Qian Z. Regional disparities and influencing factors of high quality medical resources distribution in China. Int J Equity Health 2023;22(1):8 [FREE Full text] [doi: 10.1186/s12939-023-01825-6] [Medline: 36627636]
7. Zuhair V, Babar A, Ali R, Oduoye MO, Noor Z, Chris K, et al. Exploring the impact of artificial intelligence on global health and enhancing healthcare in developing nations. J Prim Care Community Health 2024;15:21501319241245847 [FREE Full text] [doi: 10.1177/21501319241245847] [Medline: 38605668]
8. Geras KJ, Mann RM, Moy L. Artificial intelligence for mammography and digital breast tomosynthesis: current concepts and future perspectives. Radiology 2019;293(2):246-259 [FREE Full text] [doi: 10.1148/radiol.2019182627] [Medline: 31549948]
9. Kung TH, Cheatham M, Medenilla A, Sillos C, De Leon L, Elepaño C, et al. Performance of ChatGPT on USMLE: potential for AI-assisted medical education using large language models. PLOS Digit Health 2023;2(2):e0000198 [FREE Full text] [doi: 10.1371/journal.pdig.0000198] [Medline: 36812645]
10. Bhayana R, Krishna S, Bleakney RR. Performance of ChatGPT on a radiology board-style examination: insights into current strengths and limitations. Radiology 2023;307(5):e230582. [doi: 10.1148/radiol.230582] [Medline: 37191485]
11. Maroncelli R, Rizzo V, Pasculli M, Cicciarelli F, Macera M, Galati F, et al. Probing clarity: AI-generated simplified breast imaging reports for enhanced patient comprehension powered by ChatGPT-4o. Eur Radiol Exp 2024;8(1):124. [doi: 10.1186/s41747-024-00526-1] [Medline: 39477904]
12. Jeblick K, Schachtner B, Dexl J, Mittermeier A, Stüber AT, Topalis J, et al. ChatGPT makes medicine easy to swallow: an exploratory case study on simplified radiology reports. Eur Radiol 2024;34(5):2817-2825 [FREE Full text] [doi: 10.1007/s00330-023-10213-1] [Medline: 37794249]
13. Lukac S, Dayan D, Fink V, Leinert E, Hartkopf A, Veselinovic K, et al. Evaluating ChatGPT as an adjunct for the multidisciplinary tumor board decision-making in primary breast cancer cases. Arch Gynecol Obstet 2023;308(6):1831-1844 [FREE Full text] [doi: 10.1007/s00404-023-07130-5] [Medline: 37458761]
14. Schulte B. Capacity of ChatGPT to identify guideline-based treatments for advanced solid tumors. Cureus 2023;15(4):e37938 [FREE Full text] [doi: 10.7759/cureus.37938] [Medline: 37220429]
15. Berglund L, Tong M, Kaufmann M, Balesni M, Stickland A, Korbak T. The reversal curse: LLMs trained on "A is B" fail to learn "B is A". arXiv. Preprint posted online on Sep 21, 2023 2023. [doi: 10.48550/arXiv.2309.12288]
16. Eaton V, Zambrano A, Sanabria V, Lopez R, Kyei I, Mra R, et al. Innovative methodology for strengthening a multidisciplinary team approach in cities in low- and middle-income countries. JCO Glob Oncol 2022;8:e2200149 [FREE Full text] [doi: 10.1200/GO.22.00149] [Medline: 36252159]
17. Bi WL, Hosny A, Schabath MB, Giger ML, Birkbak NJ, Mehrtash A, et al. Artificial intelligence in cancer imaging: clinical challenges and applications. CA Cancer J Clin 2019;69(2):127-157 [FREE Full text] [doi: 10.3322/caac.21552] [Medline: 30720861]
18. Thirunavukarasu AJ, Mahmood S, Malem A, Foster WP, Sanghera R, Hassan R, et al. Large language models approach expert-level clinical knowledge and reasoning in ophthalmology: a head-to-head cross-sectional study. PLOS Digit Health 2024;3(4):e0000341 [FREE Full text] [doi: 10.1371/journal.pdig.0000341] [Medline: 38630683]
19. Shen Y, Heacock L, Elias J, Hentel KD, Reig B, Shih G, et al. ChatGPT and other large language models are double-edged swords. Radiology 2023;307(2):e230163. [doi: 10.1148/radiol.230163] [Medline: 36700838]
20. Lecler A, Duron L, Soyer P. Revolutionizing radiology with GPT-based models: current applications, future possibilities and limitations of ChatGPT. Diagn Interv Imaging 2023;104(6):269-274 [FREE Full text] [doi: 10.1016/j.diii.2023.02.003] [Medline: 36858933]
21. Hadi M, Qureshi R, Shah A, Irfan M, Zafar A, Shaikh M. A survey on large language models: applications, challenges, limitations, and practical usage. arXiv. Preprint posted online on Jul 19, 2023 2023 Unreviewed arXiv preprint (arXiv:2307.10169); not formally peer-reviewed or published [FREE Full text] [doi: 10.36227/techrxiv.23589741.v1]

XSL•FO
RenderX

22. Shanghai Artificial Intelligence Laboratory, China Software Testing Center (CSTC). Analysis Report on the Development of Large Models in the Healthcare Field (2024). WeChat Official Account (Shanghai Artificial Intelligence Laboratory).: Shanghai Artificial Intelligence Laboratory; 2024. URL: https://mp.weixin.qq.com/s/XCd5FiW2DacnfYXn1XdkSQ
23. Deng L, Wang T, Yangzhang, Zhai Z, Tao W, Li J, et al. Evaluation of large language models in breast cancer clinical scenarios: a comparative analysis based on ChatGPT-3.5, ChatGPT-4.0, and Claude2. Int J Surg 2024;110(4):1941-1950 [FREE Full text] [doi: 10.1097/JS9.0000000000001066] [Medline: 38668655]
24. Jin M, Yu Q, Zhao H, Hua W, Meng Y, Zhang Y. The impact of reasoning step length on large language models. arXiv. Preprit posted online on Jan 10, 2024 2024. [doi: 10.48550/arXiv.2401.04925]
25. Gou Z, Shao Z, Gong Y, Shen Y, Yang Y, Duan N, et al. CRITIC: large language models can self-correct with tool-interactive critiquing. In: Proceedings of the International Conference on Learning Representations (ICLR). 2024 Presented at: 12th International Conference on Learning Representations (ICLR) 2024; May 7–11, 2024; Vienna, Austria URL: https://openreview.net/forum?id=Sx038qxjek
26. Rao A, Pang M, Kim J, Kamineni M, Lie W, Prasad AK, et al. Assessing the utility of ChatGPT throughout the entire clinical workflow: development and usability study. J Med Internet Res 2023;25:e48659 [FREE Full text] [doi: 10.2196/48659] [Medline: 37606976]
27. Liu S, Wright AP, Patterson BL, Wanderer JP, Turer RW, Nelson SD, et al. Using AI-generated suggestions from ChatGPT to optimize clinical decision support. J Am Med Inform Assoc 2023;30(7):1237-1245 [FREE Full text] [doi: 10.1093/jamia/ocad072] [Medline: 37087108]
28. Simon FM, Altay S, Mercier H. Misinformation reloaded? Fears about the impact of generative AI on misinformation are overblown. HKS Misinfo Review 2023 5;4(5):N/A-N/A. [doi: 10.37016/mr-2023-054]
29. Augenstein I, Baldwin T, Cha M, Chakraborty T, Ciampaglia GL, Corney D, et al. Factuality challenges in the era of large language models and opportunities for fact-checking. Nat Mach Intell 2024;6(8):852-863 [FREE Full text] [doi: 10.1038/s42256-024-00872-2]
30. Haltaufderheide J, Ranisch R. The ethics of ChatGPT in medicine and healthcare: a systematic review on large language models (LLMs). NPJ Digit Med 2024;7(1):183 [FREE Full text] [doi: 10.1038/s41746-024-01157-x] [Medline: 38977771]
31. Bernal J, Mazo C. Transparency of artificial intelligence in healthcare: insights from professionals in computing and healthcare worldwide. Appl Sci 2022 Oct 11;12(20):10228. [doi: 10.3390/app122010228]
32. Mello MM, Guha N. ChatGPT and physicians' malpractice risk. JAMA Health Forum 2023;4(5):e231938 [FREE Full text] [doi: 10.1001/jamahealthforum.2023.1938] [Medline: 37200013]
33. Kahng M, Tenney I, Pushkarna M, Liu M, Wexler J, Reif E, et al. LLM comparator: visual analytics for side-by-side evaluation of large language models. In: Extended Abstracts of the CHI Conference on Human Factors in Computing Systems (CHI EA '24). 2024 Presented at: Extended Abstracts of the CHI Conference on Human Factors in Computing Systems (CHI EA '24); May 11-16, 2024; Honolulu, HI p. 1-7. [doi: 10.1145/3613905.3650755]
34. Ferdaus MM, Abdelguerfi M, Loup E, N. Niles K, Pathak K, Sloan S. Towards trustworthy AI: a review of ethical and robust large language models. arXiv. Preprint posted online on Jun 1, 2024 2024 [FREE Full text]
35. Bouhouita-Guermech S, Haidar H. Scoping review shows the dynamics and complexities inherent to the notion of "Responsibility" in artificial intelligence within the healthcare context. Asian Bioeth Rev 2024;16(3):315-344. [doi: 10.1007/s41649-024-00292-7] [Medline: 39022380]

Abbreviations

AI: artificial intelligence
ACR BI-RADS: American College of Radiology Breast Imaging-Reporting and Data System
LLM: large language model
MDT: multidisciplinary team
NCCN: National Comprehensive Cancer Network

Edited by A Coristine; submitted 16.Nov.2024; peer-reviewed by S Matsuda, L Wreyford; comments to author 11.Feb.2025; revised version received 02.Dec.2025; accepted 02.Dec.2025; published 02.Feb.2026.

Please cite as:
Jiang H, Yang C, Zhou W, Yin CL, Zhou S, He R, Ran G, Wang W, Wu M, Yu J
Evaluation of Large Language Models for Radiologists' Support in Multidisciplinary Breast Cancer Teams: Comparative Study
JMIR Med Inform 2026;14:e68182
URL: https://medinform.jmir.org/2026/1/e68182
doi:10.2196/68182
PMID:

XSL•FO
RenderX

©Hong Jiang, Chun Yang, Wenbin Zhou, Cheng-liang Yin, Shan Zhou, Rui He, Guanghui Ran, Wujie Wang, Meixian Wu, Juan Yu. Originally published in JMIR Medical Informatics (https://medinform.jmir.org), 02.Feb.2026. This is an open-access article distributed under the terms of the Creative Commons Attribution License (https://creativecommons.org/licenses/by/4.0/), which permits unrestricted use, distribution, and reproduction in any medium, provided the original work, first published in JMIR Medical Informatics, is properly cited. The complete bibliographic information, a link to the original publication on https://medinform.jmir.org/, as well as this copyright and license information must be included.

XSL•FO
RenderX

Original Paper

Artificial Intelligence Models for Predicting Triage in Emergency Departments: Seven-Month Retrospective Comparative Study of Natural Language Processing, Large Language Model, and Joint Embedding Predictive Architectures

Edouard Lansiaux[1], MD, MSc; Ramy Azzouz[2,3], MD; Emmanuel Chazard[3,4], MD, PhD; Amélie Vromant[5], MD, MSc; Eric Wiel[1,3], MD, PhD

[1]Emergency Department, Lille University Hospital, Lille, France

[2]Centre Antipoison, Lille University Hospital, Lille, France

[3]ULR 2694-METRICS, Lille University, Lille, France

[4]Department of Public Health, EA 2694, Lille University, Lille, France

[5]Emergency Department, Hôpital Pitié-Salpêtrière, Assistance Publique des Hôpitaux de Paris, Paris, France

Corresponding Author:
Edouard Lansiaux, MD, MSc
Emergency Department
Lille University Hospital
2 Avenue Oscar Lambret
Lille, 59800
France
Phone: 33 789222432
Email: edouard.lansiaux@orange.fr

Abstract

Background: Triage errors in emergency departments (EDs), including undertriage and overtriage, pose significant risks to patient safety and resource allocation. With increasing patient volumes and staffing challenges, artificial intelligence (AI) integration into triage protocols has gained attention as a potential solution.

Objective: This study aims to develop and compare 3 AI models—natural language processing (NLP), large language model (LLM), and Joint Embedding Predictive Architecture (JEPA)—for predicting triage outcomes according to the French Emergency Nurses Classification in Hospital (FRENCH) scale and to assess their performance relative to nurse triage and clinical expert consensus.

Methods: We conducted a retrospective analysis of prospectively collected data from adult patients triaged at Roger Salengro Hospital ED (Lille, France) over 7 months (June-December 2024). Three AI models were developed: TRIAGEMASTER (NLP with Doc2Vec + MLP), URGENTIAPARSE (LLM with FlauBERT + Extreme Gradient Boosting [XGBoost]), and EMERGINET (JEPA with variance-invariance-covariance regularization). Of 73,236 ED visits, 657 (0.90%) had complete audio recordings and structured data. Data were split 80:20 into training and validation sets with stratification. Gold-standard labels were established by senior clinician consensus (minimum 5 years of ED experience). The primary outcome was concordance with the gold-standard FRENCH triage level, assessed using weighted κ, Spearman correlation, F1-score, area under the receiver operating characteristic (AUC-ROC) curve, mean absolute error (MAE), and root mean square error (RMSE). Secondary analyses evaluated Groupes d'Etude Multicentrique des Services d'Accueil (GEMSA) prediction and performance by input data type.

Results: URGENTIAPARSE demonstrated superior performance, with a composite z score of 2.514 compared with EMERGINET (0.438), TRIAGEMASTER (–3.511), and nurse triage (–4.343). URGENTIAPARSE achieved an F1-score of 0.900 (95% CI 0.876-0.924), an AUC-ROC of 0.879 (95% CI 0.851-0.907), a weighted κ of 0.800 (P<.001), a Spearman correlation of 0.802 (P<.001), an MAE of 0.228, and an RMSE of 0.790. Exact agreement was 90.0%, with near-agreement (+1 or –1 level) of 92.8%. However, training showed perfect accuracy (1.0) with poor validation performance (~0.5), indicating overfitting. EMERGINET achieved moderate performance (F1-score=0.731, AUC 0.686), while TRIAGEMASTER and nurse triage performed poorly (F1-score=0.618 and 0.303, respectively). For GEMSA prediction, URGENTIAPARSE maintained superiority (κ=0.863, Spearman=0.864, P<.001). Class 1 (highest acuity) was underrepresented (4/657, 0.61%), limiting undertriage risk assessment.

XSL•FO
RenderX

Conclusions: The LLM-based architecture (URGENTIAPARSE) demonstrated the highest accuracy for ED triage prediction among the tested models, outperforming traditional NLP, JEPA, and current nurse triage practices. However, severe overfitting, extreme selection bias (657/73,236, 0.90%, inclusion), a monocentric design, and sparse high-acuity representation limit clinical applicability. Before deployment, the model requires regularization, external validation across diverse EDs, prospective testing, and comprehensive safety evaluation, particularly for undertriage detection. Integration of AI triage support systems shows promise but demands rigorous validation, bias mitigation, and transparent uncertainty quantification to ensure patient safety.

(JMIR Med Inform 2026;14:e83318) doi:10.2196/83318

KEYWORDS

triage; emergency department; artificial intelligence; natural language processing; large language model; Joint Embedding Predictive Architecture; clinical decision support; FRENCH scale

Introduction

Triage in emergency departments (EDs) is vital for prioritizing patients by severity, directly affecting outcomes, efficiency, and resource use. In busy or understaffed settings, accurate triage is essential to ensure safe and equitable care.

In France, the French Emergency Nurses Classification in Hospital (FRENCH) triage scale has become a standardized reference tool for emergency medical services [1]. This 6-level urgency stratification system (1=immediate life-threatening to 6=nonurgent) was designed to promote consistency and reproducibility. However, in practice, its application often varies [2], shaped by disparities in nurse experience, time pressure, interpretive inconsistencies, and fatigue. These factors lead to 2 key errors: undertriage, in which serious cases are underestimated, risking delays in care and potentially preventable mortality; and overtriage, in which minor cases are overprioritized, leading to crowding and inefficient use of resources [3].

Against this backdrop, artificial intelligence (AI) has emerged as a promising complement to traditional triage [4]. AI systems in emergency medicine can process diverse data, operate continuously, and provide consistent and transparent decisions; however, their success over the past decade has been mixed.

Early AI triage systems relied on natural language processing (NLP) to extract clinical meaning from text, using hand-crafted rules or statistical models [5]. Although these early systems were effective, they lacked the ability to understand context, nuance, or rare cases. Advances emerged with large language models (LLMs) such as Bidirectional Encoder Representations from Transformers (BERT) and its French version, FlauBERT [6]. These transformer-based models provided deep contextual understanding. When combined with boosting algorithms such as Extreme Gradient Boosting (XGBoost), LLMs formed hybrid architectures that balanced high performance with interpretability [7], 2 pillars of clinical deployment. More recently, Joint Embedding Predictive Architectures (JEPA) have introduced a third paradigm. JEPA models do not predict outcomes directly; instead, they embed both inputs and targets (eg, triage categories) into a shared latent space. Using techniques such as energy minimization and variance-invariance-covariance regularization (VICReg) [8,9], these models can uncover subtle cross-modal patterns. However, their complexity poses ongoing challenges for interpretability, an essential requirement in medical contexts.

Few studies have compared AI models under consistent conditions [10,11]. Most focus on narrow tasks, rely on limited or noisy data, and are often developed outside the French health care system, reducing their relevance for users of the FRENCH scale. Furthermore, recent work has highlighted concerns regarding judgment biases in triage [11,12], hallucinations in LLMs [13], and the need for robust calibration and uncertainty quantification in clinical AI systems [14].

This study aims to address this gap. We conducted a retrospective analysis of triage encounters at the Centre Hospitalier Universitaire (CHU) Lille ED, one of France's major academic hospitals [15]. Using rich clinical data and nurse-patient dialogues, 3 AI models—TRIAGEMASTER, URGENTIAPARSE, and EMERGINET—were developed to predict FRENCH triage levels. These models were evaluated against expert consensus to identify the best-performing system and to assess their clinical suitability and limitations.

Methods

Study Design

This study was designed as a retrospective, observational, monocentric analysis conducted in the Adult Emergency Department of the CHU Lille, France. The ED is a high-volume academic tertiary care facility serving a diverse patient population, with approximately 73,000 adult visits annually. The investigation covered a continuous 7-month period from June 1, 2024, to December 31, 2024. This time frame was selected to capture seasonal variations in ED activity and to ensure a sufficiently large and heterogeneous dataset.

Ethical Compliance

The study adhered to strict French and European ethical standards, with approval and registration from the Comité d'Éthique de la Recherche en Santé, Health Data Hub filing (project number 18605502), and Commission Nationale de l'Informatique et des Libertés (CNIL) Méthodologie de Référence-004 compliance [16]. Audio recordings were collected with patient information at triage. Personal data were present before anonymization and underwent rigorous deidentification, including removal of names, dates, identifiers, and geographic information smaller than the department level, with transcript verification performed by 2 independent

XSL•FO
RenderX

reviewers. As this was a retrospective analysis of deidentified data, individual informed consent was waived in accordance with French regulations. The study followed the Transparent Reporting of a multivariable prediction model for Individual Prognosis Or Diagnosis (TRIPOD)-AI guidelines (see Multimedia Appendix 1). Owing to patient confidentiality, the full dataset and code are not publicly available; only the code used to define the gold standard is shared (see Multimedia Appendix 2).

Population and Inclusion Criteria

The study included adult patients (≥18 years) evaluated in the Lille CHU ED with complete structured clinical data and recorded nurse-patient audio interviews. Exclusion criteria were minors (<18 years), legally protected adults, patients who declined data use (n=2), and cases with incomplete recordings, corrupted files, missing structured data, or failed transcription quality checks (n=22).

Data Acquisition and Preprocessing

The study relied on 2 primary data sources. First, structured clinical data were extracted from the ResUrgences ED management software (version 2024.1.148; Berger-Levrault). Variables collected included age, sex, vital signs (systolic and diastolic blood pressure, heart rate, temperature, oxygen saturation, and supplemental oxygen requirement), pain score (visual analog scale 0-10), time of presentation, comorbidities, chief complaint category, the initial FRENCH triage decision, and the Groupes d'Etude Multicentrique des Services d'Accueil (GEMSA) scale (corresponding to patient outcome after diagnostic evaluation and treatment in the ED) [17].

Unstructured data from nurse-patient triage interviews were audio-recorded using standardized digital recorders and manually transcribed by trained personnel, with accuracy verified by 2 independent reviewers. Transcripts were linked using unique patient identifiers and time stamps, anonymized in accordance with CNIL guidelines, and securely stored on Health Data Hub–approved servers for modeling. Recording participation was limited to volunteer nurses (n<10) during their regular shifts, introducing potential selection bias in conversation style and patient characteristics.

Comparison of Included Versus Excluded Cohorts

To assess selection bias, we compared demographic and clinical characteristics between included patients (n=657) and the broader ED population (n=72,579) during the study period. The included cohort had a similar mean age (42.6 vs 43.2 years, *P*=.68), sex distribution (330/657, 50.2%, male, *P*=.67), and vital sign distributions. However, included patients had slightly lower acuity (mean nurse FRENCH 3.4 vs 3.1, *P*=.02) and higher admission rates (15.5% vs 12.3%, *P*=.03), likely reflecting volunteer nurse participation patterns and recording feasibility during less chaotic triage encounters (Table 1).

XSL•FO
RenderX

Table 1. Patient demographics, admission characteristics, vital parameters, and triage distributions.

Characteristic	Overall	Training	Validation
Age (years), mean (SD)	42.6 (19.7)	42.5 (19.8)	43 (19.5)
Sex, n (%)			
Male	330 (50.2)	264 (50.2)	66 (50.4)
Female	327 (49.8)	262 (49.8)	65 (49.6)
Admission time, n (%)			
Night (9 PM-6 AM)	211 (32.1)	169 (32.1)	42 (32.1)
Morning (6 AM-2 PM)	241 (36.7)	193 (36.7)	48 (36.6)
Afternoon (2 PM-9 PM)	205 (31.2)	164 (31.2)	41 (31.3)
Chief complaint, n (%)			
Trauma, n (%)	127 (19.3)	101 (19.2)	26 (19.8)
Abdominal, n (%)	102 (15.5)	81 (15.4)	21 (16.0)
Cardiovascular	86 (13.1)	68 (12.9)	18 (13.7)
Neurological	69 (10.5)	55 (10.5)	14 (10.7)
ENT (ear-nose-throat)/stomatology	62 (9.4)	49 (9.3)	13 (9.9)
Other[a]	211 (32.1)	172 (32.7)	39 (29.8)
Comorbidities, n (%)			
None	496 (75.5)	398 (75.7)	98 (74.8)
≥1 comorbidity	161 (24.5)	128 (24.3)	33 (25.2)
Vital signs, mean (SD)			
Systolic blood pressure (mmHg)	143 (24)	143 (24)	143 (23)
Diastolic blood pressure (mmHg)	83 (16)	83 (16)	83 (17)
Heart rate (bpm)	89 (18)	89 (18)	89 (17)
Temperature (°C)	37.5 (0.6)	37.5 (0.6)	37.5 (0.6)
Pain score (0-10)	4 (3.6)	4 (3.6)	4.1 (3.7)
Peripheral capillary oxygen saturation (SpO_2, %)	97 (2)	97 (2)	97 (2)
Supplemental O2 (L/min), mean (SD)	0.04 (0.4)	0.04 (0.4)	0.03 (0.3)
Nurse triage (FRENCH[b]), n (%)			
1 (immediate), n (%)	4 (0.6)	3 (0.6)	1 (0.8)
2 (very urgent), n (%)	86 (13.1)	68 (12.9)	18 (13.7)
3A (urgent, invasive)	0 (0)	0 (0)	0 (0)
3B (urgent, noninvasive)	354 (53.9)	283 (53.8)	71 (54.2)
4 (less urgent)	118 (18.0)	94 (17.9)	24 (18.3)
5 (nonurgent)	95 (14.5)	78 (14.8)	17 (13.0)
Disposition (GEMSA[c]), n (%)			
1	0 (0)	0 (0)	0 (0)
2 (discharged)	509 (77.5)	407 (77.4)	102 (77.9)
3 (short stay)	18 (2.7)	14 (2.7)	4 (3.1)
4 (ward admission)	102 (15.5)	82 (15.6)	20 (15.3)
5 (intensive care unit admission)	10 (1.5)	9 (1.7)	1 (0.8)
Not specified	18 (2.7)	14 (2.7)	4 (3.1)

XSL•FO
RenderX

[a]Other complaints are genitourinary, gynecology/obstetrics, infectious, toxicology, ophthalmology, dermatology, psychiatry, pulmonary, and rheumatology presentations.

[b]FRENCH: French Emergency Nurses Classification in Hospital.

[c]GEMSA: Groupes d'Etude Multicentrique des Services d'Accueil.

Gold-Standard Construction

A gold-standard triage label was established through independent review by 3 senior emergency physicians (minimum 5 years of postresidency ED experience, board-certified in emergency medicine) who were strictly blinded to the original nurse triage assignment, all AI model outputs, and patient outcomes (laboratory results, imaging, disposition, and diagnoses established after the index triage encounter). Each adjudicator independently reviewed the complete triage transcript, vital signs, and demographic data, and then assigned a FRENCH level based solely on information available at the time of triage.

Initial interrater agreement was substantial (Fleiss κ=0.72, 95% CI 0.68-0.76). For the cases with disagreement (155/657, 23.6%), adjudicators met for a structured consensus discussion without knowledge of which assignments were discordant. Final consensus was reached in all cases through majority voting after discussion. This gold standard served as the reference for model training and evaluation. To assess potential incorporation bias, we conducted a sensitivity analysis excluding cases in which the gold standard differed from nurse triage by more than 1 level (n=47), and found similar model performance rankings.

Model Architectures and Training Pipelines

Three distinct AI models were developed, each representing a major class of current machine learning techniques. All models were implemented in Python 3.9 (Python Foundation) with PyTorch 1.12 and scikit-learn 1.1, and trained on NVIDIA A100 graphics processing units (40 GB VRAM), with training times of 2-4 hours per model.

Leakage Safeguards and Hyperparameter Tuning

Overview

Critical measures were implemented to prevent data leakage. All preprocessing steps (Doc2Vec fitting, FlauBERT fine-tuning, and feature scaling) were confined strictly to the training folds, with transformations subsequently applied to validation data. Hyperparameter tuning was performed using 5-fold stratified cross-validation nested within the training set only, without accessing validation data. Random seeds were fixed (seed=42) to ensure reproducibility. Early stopping monitored validation loss with a patience of 10 epochs to prevent overfitting.

TRIAGEMASTER (NLP)

This model used paragraph vector embeddings (Doc2Vec, distributed memory model; vector dimension=100, window=5, min_count=2, epochs=40) to represent free-text input [18], concatenated with *z* score–normalized numerical features derived from structured data (age, sex encoded as binary, and all vital signs). The architecture consisted of a 3-layer feedforward neural network (input→128→64→6 output classes) with Rectified Linear Unit activations [19], dropout regularization (P=.32, applied after each hidden layer), batch normalization, and an L2 weight penalty ($\lambda=1\times10^{-5}$). Optimization used the Adam optimizer with an initial learning rate of 0.001, batch size of 32, and learning rate decay (factor=0.5, patience=5 epochs). The maximum sequence length was 512 tokens. Missing data (<2% of vital signs) were imputed using median values from the training set.

Classification probabilities were derived via softmax activation. CIs for the area under the curve (AUC) were calculated using the DeLong method [20]. Model performance was evaluated across the full range of predicted probabilities. Optimal probability thresholds were defined as the predicted probability that maximized the F_1-score [21]. Inference latency averaged 47 ms per patient on production CPU hardware (Intel Xeon Gold 6248R).

URGENTIAPARSE (LLM)

Built on the FlauBERT language model (flaubert-base-cased, 137 million parameters) [6], this architecture fine-tuned contextual embeddings from patient complaints over 5 epochs with a learning rate of 2×10^{-5}, and then extracted the [CLS (classification)] token embedding (768 dimensions). These embeddings were concatenated with normalized structured variables and fed into an XGBoost classifier (n_estimators=200, max_depth=6, learning_rate=0.1, min_child_weight=3, subsample=0.8, colsample_bytree=0.8, reg_alpha=0.1, reg_lambda=1.0, scale_pos_weight adjusted for class imbalance). This hybrid design enabled both interpretability and high-dimensional pattern recognition [22]. Feature importance was derived using Shapley Additive Explanations (SHAP) values [23], providing transparent model behavior traceable to individual tokens and vital signs. The maximum sequence length was 512 tokens with truncation. Class weights were inversely proportional to class frequencies to address imbalance. Inference latency averaged 312 ms per patient.

EMERGINET (JEPA)

This JEPA encoded textual and structured inputs into a shared latent space (dimension=256) through dual encoders (text encoder: FlauBERT base + 2-layer bidirectional Long Short-Term Memory with hidden size 128 [24]; structured encoder: 3-layer MLP with hidden sizes (64, 128, 256)). The loss function minimized contrastive energy between predicted and target class embeddings using cosine similarity, regularized with VICReg (variance weight=1.0, invariance weight=1.0, covariance weight=0.04) to enforce variance >1.0, invariance via mean squared error, and a near-identity covariance matrix [8]. Training used the Adam optimizer (learning rate=1×10^{-4}, batch size=16, 100 epochs). Final classification was performed using nearest-neighbor matching in embedding space with temperature-scaled softmax (temperature=0.07). Inference latency averaged 189 ms per patient.

XSL•FO
RenderX

Training and Validation Procedures

Each model was trained on 80% of the dataset (n=526) and validated on the remaining 20% (n=131), stratified by gold-standard triage level to maintain class balance (class proportions: 1=4/657, 0.61%; 2=86/657, 13.1%; 3B=354/657, 53.9%; 4=118/657, 18.0%; and 5=95/657, 14.5%; classes 3A and 6 had 0 cases). Hyperparameter grids were searched using 5-fold cross-validation on the training data only. All models were trained 3 times with different random initializations to assess stability; reported metrics are means across runs, with SDs <0.03 for all primary metrics. Training and validation loss curves were monitored to detect overfitting.

Evaluation Metrics

Performance Metrics for Ordinal Outcomes

Model performance was assessed using both absolute error measures and classification agreement metrics. Unless otherwise specified, all *P* values were 2-tailed, with a significance threshold of α=.05. Given the ordered nature of the FRENCH scale, metrics that account for ordinality (weighted κ, Spearman correlation, and mean absolute error [MAE]) were prioritized.

MAE

This measures the average deviation between predicted and actual triage levels.

where is the predicted value, y_i is the true value, and n is the total number of cases.

Root Mean Square Error

This emphasizes larger misclassification errors:

Weighted Cohen κ

This accounts for agreement beyond chance and penalizes larger discrepancies using quadratic weights:

where $fo_{i,j}$ are observed frequencies, $fe_{i,j}$ are expected frequencies under independence, and $w_{i,j}=(i-j)^2/(k-1)^2$ with k classes. Significance was tested via bootstrap (10,000 iterations).

Spearman Correlation Coefficient

This measures the monotonic association between predicted and true ordinal ranks:

$r_s=[\text{cov}(rg_X,rg_Y)]/[\sigma rg_X \sigma rg_Y]$ **(4)**

F1-scores

Macro F_1-score reflects the unweighted average across all triage classes (treating each class equally), whereas micro F_1-score is weighted by class frequency:

F_1-score = (TP)/[TP+1/2(FP+FN)] **(5)**

where TP denotes true positive, FP false positive, and FN false negative. Class-specific F_1-scores were calculated to assess performance in rare high-acuity classes.

Exact Agreement Percentage

This represents the proportion of predictions that exactly match the gold standard.

Near-Agreement Percentage

This represents the proportion of predictions within the +1 or –1 triage level of the gold standard.

Area Under the Receiver Operating Characteristic Curve

This summarizes discrimination across all classification thresholds, calculated using a one-versus-rest strategy for multiclass classification, with 95% CIs estimated via the DeLong method [20].

Composite z Score

This is an integrated performance indicator combining multiple metrics for ranking.

Score = $Z(-\text{MAE}) + Z(-\text{RMSE}) + Z(\kappa_w) + Z(r_s)$ **(6)**

where $Z(X) = (X - \mu_X)/\sigma_X$ standardizes each metric to mean 0 and SD 1 across all models. Negative MAE and RMSE were used, so higher z scores indicate better performance for all components.

Multiclass Brier Score

This is the mean squared difference between predicted probabilities and one-hot encoded outcomes, providing global probabilistic accurac

where is the predicted probability for class j of case i, y_{ij} is a binary indicator (1 if true class, 0 otherwise), and k is the number of classes.

Asymmetric Error Analysis

Given the clinical importance of undertriage (predicting lower acuity than the true acuity, potentially delaying critical care), we analyzed error asymmetry by calculating the undertriage rate (proportion of predictions <true class) and the overtriage rate (proportion of predictions >true class). For classes 1-2 (highest acuity), we report sensitivity, specificity, positive predictive value, and negative predictive value separately, as undertriage in these categories poses the greatest patient safety risk.

Calibration Analysis

Model calibration was assessed by grouping predicted probabilities into quantile-based bins (10 bins per class) and comparing mean predicted probabilities with observed frequencies. Reliability diagrams plotted mean predicted probability versus observed frequency for each bin, with perfect calibration represented by the diagonal. Expected calibration error and maximum calibration error were computed as measures of calibration quality. Additionally, risk distributions were

XSL•FO
RenderX

visualized using density ridge plots stratified by true triage class and faceted by predicted class.

Secondary Analyses

A secondary analysis compared actual versus AI-predicted GEMSA scores (patient disposition: 2=discharged home, 3=short stay unit, 4=admitted to ward, and 5=intensive care unit [ICU]) using models trained separately on nurse-recorded structured histories and full interview transcripts. Another analysis assessed model performance according to input data type (structured data only vs unstructured transcripts only). Both analyses used evaluation methods consistent with the primary analysis. All statistical analyses were performed in R version 4.2 (R Foundation) and Python 3.9.

Results

Population Characteristics

During the inclusion period, 73,236 patients visited the ED of Roger Salengro Hospital. Two patients declined data use. Triage nurse interviews were recorded and transcribed for 681 (0.93%) patients. After excluding 24 cases (6 with missing data and 18 with transcription quality issues), 657 (0.90%) patients met the inclusion criteria (Figure 1).

Included patients had a mean age of 42.6 (SD 19.7) years and a median age of 38 years. The sample was gender-balanced (330/657, 50.2%, male). Most admissions occurred during morning hours (241/657, 36.7%, 6 AM-2 PM). The primary chief complaints were trauma (127/657, 19.3%), abdominal (102/657, 15.5%), and cardiovascular (81/657, 13.1%). One-quarter of patients (161/657, 24.5%) had 1 or more comorbidities, predominantly cardiovascular. Most patients were triaged as FRENCH 3B (354/657, 53.9%), with sparse representation in the highest acuity categories (class 1: 4/657, 0.61%).

Figure 1. Patient flow diagram showing inclusion, exclusion, and dataset splitting. ED: emergency department.

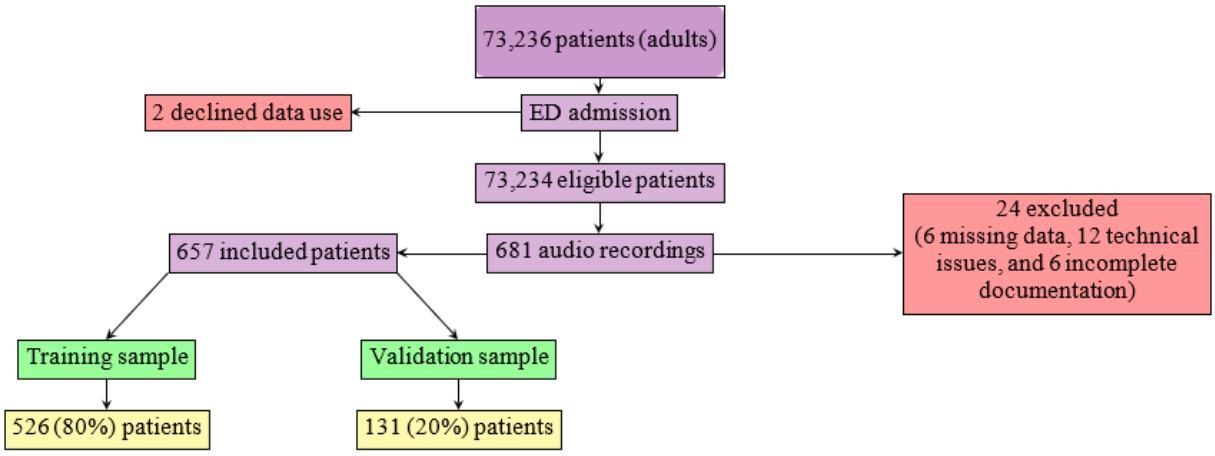

Training Performance and Overfitting Assessment

Over 100 training epochs, TRIAGEMASTER achieved a training accuracy plateau of approximately 75%, with validation accuracy similarly stable at 72%, while log loss decreased and stabilized for both sets, indicating reasonable generalization (Figure 2A).

URGENTIAPARSE exhibited severe overfitting, achieving perfect training accuracy (1.0) by epoch 20 but persistently poor validation accuracy (~0.5 throughout training), indicating memorization rather than learning generalizable patterns (Figure 2B.2). Training log loss approached 0, whereas validation loss remained high and flat at approximately 1.5, with an AUC plateau of 0.69 (Figure 2B.1). This discrepancy indicates that, despite strong performance on the training data, the model fails to generalize to unseen cases—a critical limitation for clinical deployment.

EMERGINET reached a training accuracy of 0.85, but validation accuracy remained at 0.60, indicating moderate overfitting (Figure 2C). Training loss declined steadily, whereas validation loss remained higher and stable, reflecting the performance gap.

XSL•FO
RenderX

Figure 2. Learning curves for 3 artificial intelligence models. (A) TRIAGEMASTER shows stable learning with consistent training and validation performance. (B1) URGENTIAPARSE log-loss evolution demonstrates severe overfitting, with training loss approaching 0 while validation loss remains high. (B2) URGENTIAPARSE accuracy evolution confirms perfect training accuracy (1.0) but poor validation accuracy (0.5). (C) EMERGINET VICReg JEPA learning curves show moderate overfitting, with a gap between training and validation performance. JEPA: Joint Embedding Predictive Architecture; NLP: natural language processing; VICReg: variance-invariance-covariance regularization.

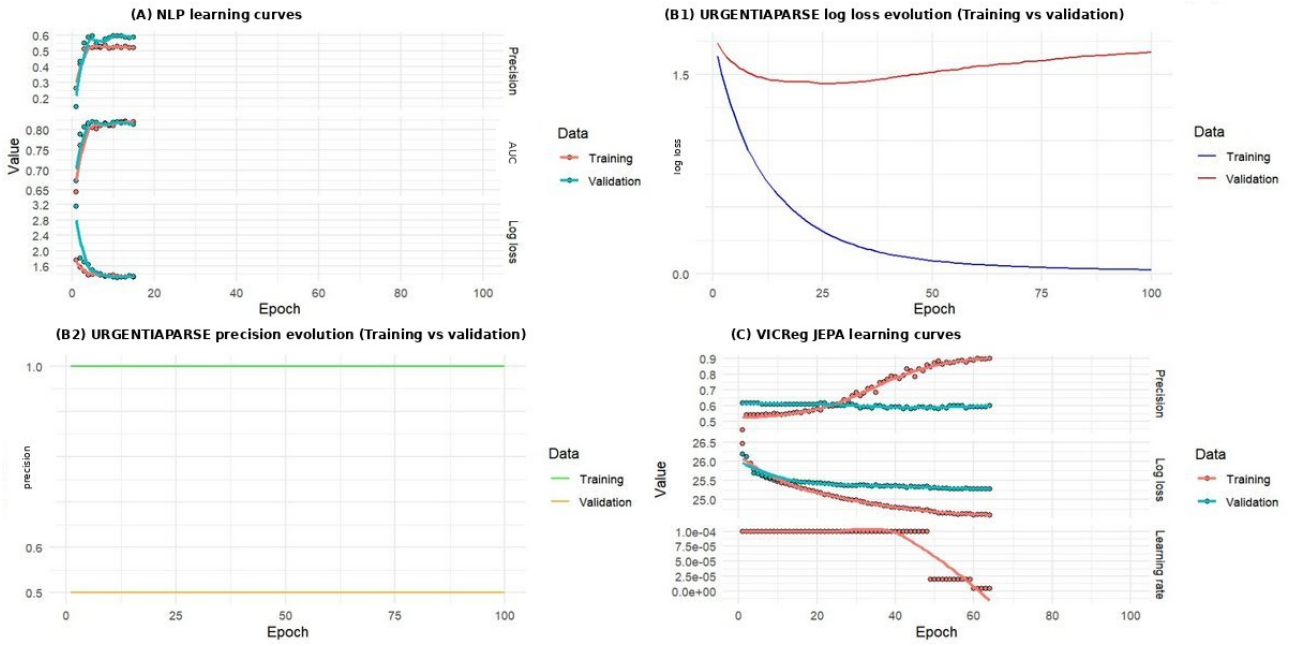

Overall Model Performance

URGENTIAPARSE (LLM) achieved the highest composite score (2.514), outperforming EMERGINET (JEPA, 0.438), TRIAGEMASTER (NLP, –3.511), and nurse triage (–4.343; Table 2). URGENTIAPARSE demonstrated strong discrimination, with a micro F_1-score of 0.900 (95% CI 0.876-0.924), macro F_1-score of 0.894 (95% CI 0.869-0.919), and AUC of 0.879 (95% CI 0.851-0.907). Agreement metrics were substantial: weighted κ of 0.800 (P<.001, 95% CI 0.761-0.839) and Spearman correlation of 0.802 (P<.001, 95% CI 0.768-0.832). Error metrics showed an MAE of 0.228 classes (approximately 1 triage level error every 4-5 patients) and an RMSE of 0.790. Exact agreement was 90.0%, with near agreement (+1 or –1 level) of 92.8%.

EMERGINET achieved moderate performance (micro F_1-score=0.731, macro F_1-score=0.747, AUC 0.686, κ=0.560, P<.001), whereas TRIAGEMASTER performed poorly (micro F_1-score=0.618, AUC 0.642, κ=0.370, P<.001; Spearman=0.005, P=.95). Current nurse triage showed the lowest performance (micro F_1-score=0.303, AUC 0.776, κ=0.080, P=.08; exact agreement=30.3%), likely reflecting the difference between real-time clinical judgment under time pressure and the gold standard established by senior physicians following comprehensive information review.

Receiver operating characteristic (ROC) curve analysis (Figure 3) confirmed the superiority of URGENTIAPARSE across most triage classes, with particularly strong performance for classes 2, 4, and 5 (AUC >0.85). However, class 1 performance was perfect (AUC 1.0) because of extreme sparsity (n=4), limiting the reliability of this estimate. Performance for class 3 was lower (AUC 0.748), likely reflecting the combined representation of 3A (invasive procedures) and 3B (noninvasive), with no 3A cases in the dataset.

Table 2. Primary analysis comparing triage prediction performance across artificial intelligence models and nurse triage.

Model	Mean absolute error	Root mean square error	κ[a]	Spearman[b]	Micro F_1-score	Macro F_1-score	Exact	Near[c]	z score[d]	Area under the curve
URGENTIAPARSE	0.228	0.790	0.800	0.802	0.900	0.894	0.900	0.928	2.514	0.879
EMERGINET	0.401	0.979	0.560	0.602	0.731	0.747	0.820	0.860	0.438	0.686
TRIAGEMASTER	0.637	1.180	0.370	0.005	0.618	0.613	0.554	0.696	-3.511	0.642
Nurse triage	1.393	1.834	0.080	0.024	0.303	0.275	0.303	0.498	-4.343	0.776

[a]Weighted Cohen κ; for all κ values, P<.001 except nurse triage (P=.08).

[b]Spearman rank correlation; all P<.001 except TRIAGEMASTER (P=.95) and nurse triage (P=.76).

[c]Near agreement: proportion within the +1 or –1 triage level.

[d]Composite z score combining standardized mean absolute error, root mean square error, κ, and Spearman metrics (higher is better).

XSL•FO
RenderX

Figure 3. Receiver operating characteristic (ROC) curves for each triage class and the mean curve across all models. URGENTIA-PARSE (large language model) demonstrates superior discrimination for most classes. The results for class 1 (area under the curve [AUC] 1.0 for multiple models) should be interpreted cautiously due to extreme sparsity (n=4). (A) FRENCH inf vs triage — This panel shows ROC curves for a rule-based French triage reference system, where Class 1 achieves near-perfect discrimination (AUC 0.998) but most other classes perform poorly (AUC 0.27–0.63), yielding a modest multiclass AUC of 0.776. (B) TRIAGEMASTER — This panel displays the per-class ROC performance of TRIAGEMASTER, a structured NLP triage model, with moderate overall discrimination (mean AUC 0.641) and relatively homogeneous class-level AUCs ranging from 0.509 to 0.854, suggesting balanced but limited performance across triage levels. (C) URGENTIAPARSE — This panel presents URGENTIAPARSE's ROC curves, the best-performing model overall (multiclass AUC 0.879), with Class 1 achieving perfect separation (AUC 1.0) and strong performance across most classes, reflecting its superior ability to discriminate triage severity levels from free-text clinical notes. (D) EMERGINET — This panel illustrates EMERGINET's ROC curves, showing strong Class 1 discrimination (AUC 0.985) but more heterogeneous performance across the remaining classes (AUC 0.556–0.72), resulting in an intermediate mean AUC of 0.686.

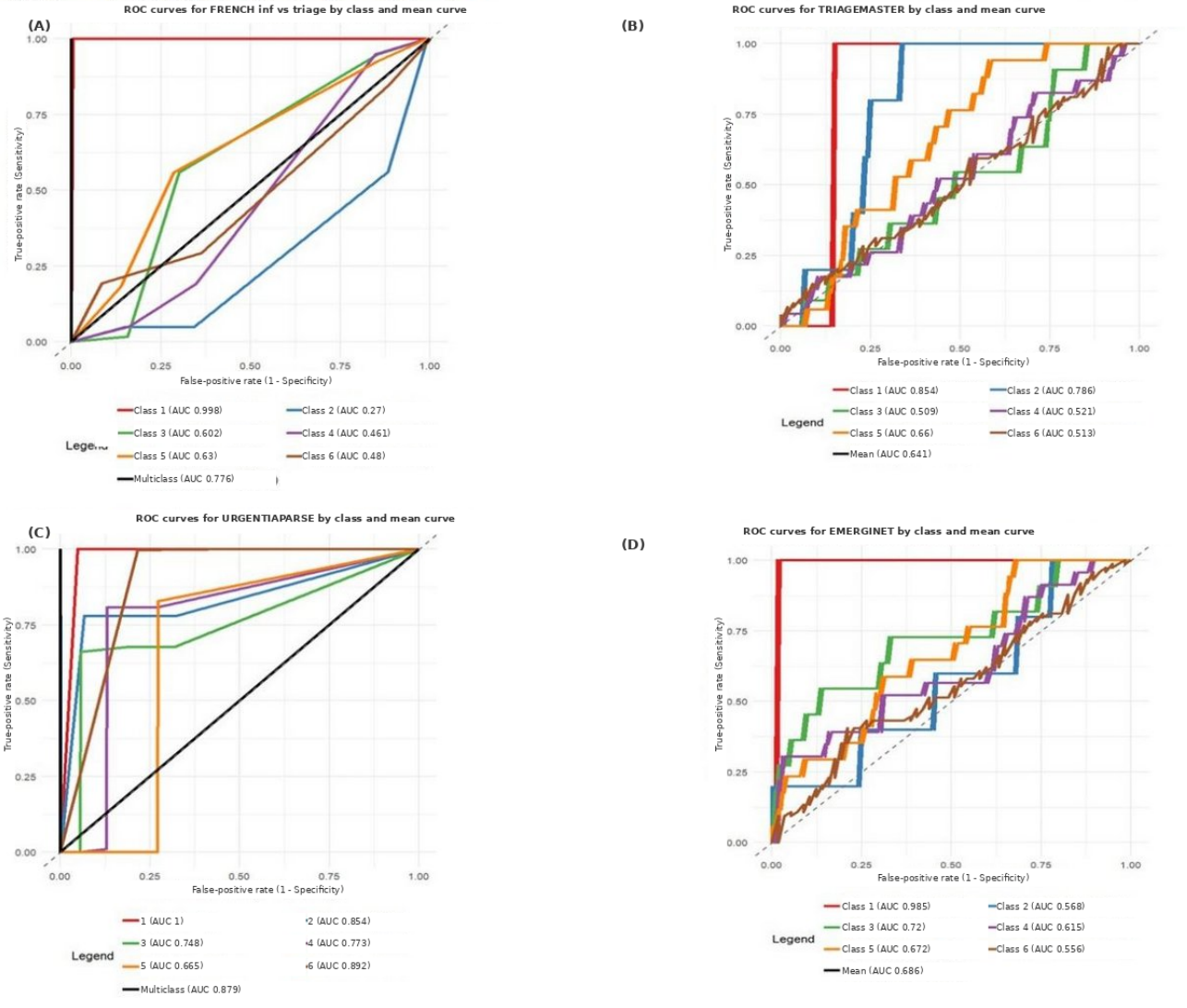

Error Pattern Analysis

Confusion matrices revealed distinct error patterns (Figure 4, top row). URGENTIAPARSE and EMERGINET slightly overestimated acuity for lower triage levels (predicting higher urgency than true), indicating a clinically conservative bias. TRIAGEMASTER systematically underestimated acuity across most classes. Nurse triage showed scattered and inconsistent patterns, with frequent misclassification across nonadjacent categories.

Bland-Altman analysis (Figure 4, middle row) confirmed low, well-centered errors for URGENTIAPARSE (mean difference –0.02, 95% limits of agreement –1.58 to 1.54) and EMERGINET (mean difference 0.08, limits –2.05 to 2.21). TRIAGEMASTER showed larger deviations (limits –3.02 to 2.98), and nurse triage demonstrated extreme disagreement (limits –4.21 to 3.87).

Error distribution analysis (Figure 4, bottom left) showed that URGENTIAPARSE and EMERGINET had narrow, well-centered error distributions (SD <1.0), whereas TRIAGEMASTER and nurse triage exhibited broad, dispersed distributions, indicating less reliable predictions.

Class-specific F_1-scores (Figure 4, bottom right) demonstrated that URGENTIAPARSE maintained consistently high performance across all represented classes (F_1-score >0.75 for classes 2-5), whereas the other approaches showed variable and often poor class-specific performance, particularly for minority classes.

XSL•FO
RenderX

Figure 4. Comprehensive evaluation of four AI-based triage models against the FRENCH gold standard. (A) Confusion matrices comparing predicted versus gold standard triage levels (1–6) for FRENCH inf, NLP, LLM, and JEPA models. (B) Bland-Altman plots assessing systematic bias and limits of agreement between each model and the FRENCH gold standard. (C) Kernel density distributions of prediction errors illustrating the bias and precision of each model. (D) Per-class F1-scores quantifying the discriminative performance of each model across the six triage severity levels.

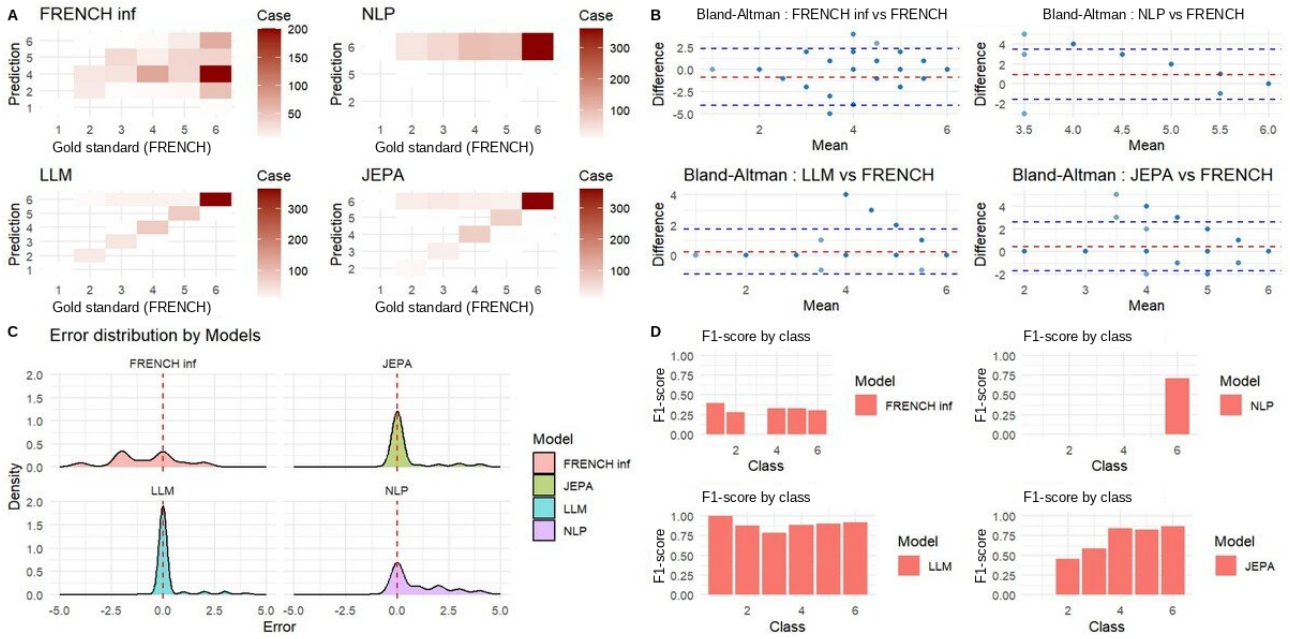

Asymmetric Error and Undertriage Risk

Given the clinical importance of undertriage, we analyzed error directionality. URGENTIAPARSE had an undertriage rate of 4.6% (predicting lower acuity than true) and an overtriage rate of 5.4% (predicting higher acuity), reflecting a slight conservative bias favoring patient safety. For high-acuity classes (1-2, n=90), URGENTIAPARSE achieved a sensitivity of 87.8% (95% CI 79.2%-93.7%) and a specificity of 95.1% (95% CI 91.3%-97.6%), with a positive predictive value of 86.8% and a negative predictive value of 95.6%. However, the limited representation of class 1 (n=4) constrains the assessment of undertriage risk among the most critical patients. Future deployment would require prospective monitoring, with particular attention to undertriage events and associated patient outcomes.

Calibration and Reliability

Multiclass Brier scores indicated superior probabilistic calibration for URGENTIAPARSE (0.142), compared with EMERGINET (0.385), TRIAGEMASTER (0.524), and nurse triage (0.693). However, detailed calibration analysis revealed heterogeneous reliability across classes (Figure 5).

Class-specific calibration analysis showed the following patterns:

- Class 1: Predictions were overconfident, with limited probability range coverage because of extreme sparsity.
- Class 2: Predictions were dominated by high-probability values (>0.8), indicating limited use of intermediate confidence levels.
- Class 3: Displayed a partially calibrated diagonal trend, but with inconsistencies across probability bins.
- Class 4: Demonstrated the most balanced calibration, with broader probability coverage and closer agreement between predicted and observed frequencies.

These findings highlight substantial class-specific differences and underscore the need for post hoc calibration methods (eg, temperature scaling or isotonic regression) before clinical deployment to ensure reliable probability estimates for risk stratification.

XSL•FO
RenderX

Figure 5. Mean predicted probability heatmaps for the four triage models. Each panel displays, for each true triage class (y-axis, 1–6), the mean predicted probability assigned to each predicted class (x-axis, 1–6), with blue intensity encoding probability magnitude (0–1): (A) FRENCH inf, (B) NLP, (C) LLM, and (D) JEPA — blue blocks concentrated along or near the diagonal indicate well-calibrated class-specific predictions. Perfect calibration would be indicated by high intensity only along the diagonal.

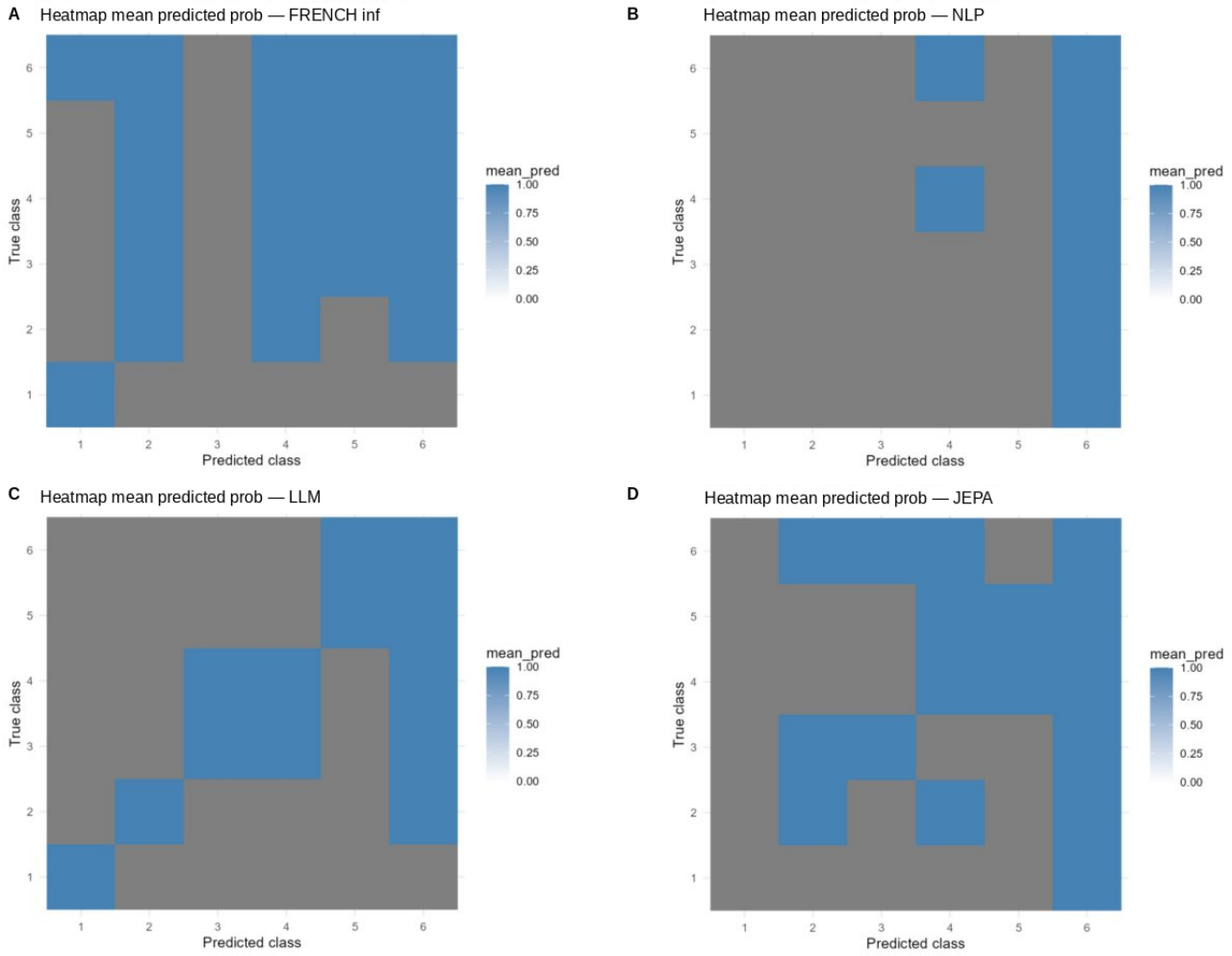

Risk Distribution Analysis

Ridge plot analysis (Figure 6) revealed distinct behavioral patterns across approaches. Nurse triage demonstrated relatively consistent distributional patterns, with moderate overlap between adjacent classes and clear modal peaks, suggesting reasonable discrimination but substantial uncertainty.

TRIAGEMASTER exhibited variable performance, with notable gaps in certain class predictions (particularly panels 1 and 3), indicating an inability to consistently predict across all triage categories. Distributions were concentrated around specific probability values, suggesting either high confidence in limited scenarios or potential overfitting.

URGENTIAPARSE displayed markedly selective characteristics, with substantial gaps in class representation across prediction scenarios. Several triage classes appeared absent in certain combinations, suggesting that the LLM produced more selective predictions. When predictions were generated, distributions were tightly concentrated with distinct modal peaks, indicating high confidence. This sparse prediction pattern may reflect superior discrimination in clear-cut cases but raises concerns regarding coverage across diverse patient presentations. It may also suggest that the model effectively refrains from uncertain predictions—a behavior that requires explicit characterization and validation.

EMERGINET showed heterogeneous patterns, with some classes displaying broad, diffuse distributions and others exhibiting sharp, concentrated peaks, indicating variable predictive confidence across triage categories.

The distinct sparse pattern observed with URGENTIAPARSE warrants careful consideration for clinical implementation. Although it may indicate superior precision in unambiguous cases, the absence of predictions for certain class combinations presents challenges for comprehensive triage coverage. This pattern requires further validation to ensure adequate performance across all patient presentations, including edge cases and ambiguous scenarios.

XSL•FO
RenderX

Figure 6. Risk score distributions by predicted triage class across models (ridge plots). For each model, predicted probability distributions are shown separately per predicted class (facets 1–6, columns) and colored by true triage class (2–6, see legend). (A) FRENCH_inf model (French clinical rule-based inference). (B) NLP model (natural language processing). (C) LLM model (large language model). (D) JEPA model (Joint Embedding Predictive Architecture). The x-axis represents the predicted probability; the y-axis represents the true triage class. Substantial overlap between distributions within a facet indicates high inter-class confusion for that predicted class.

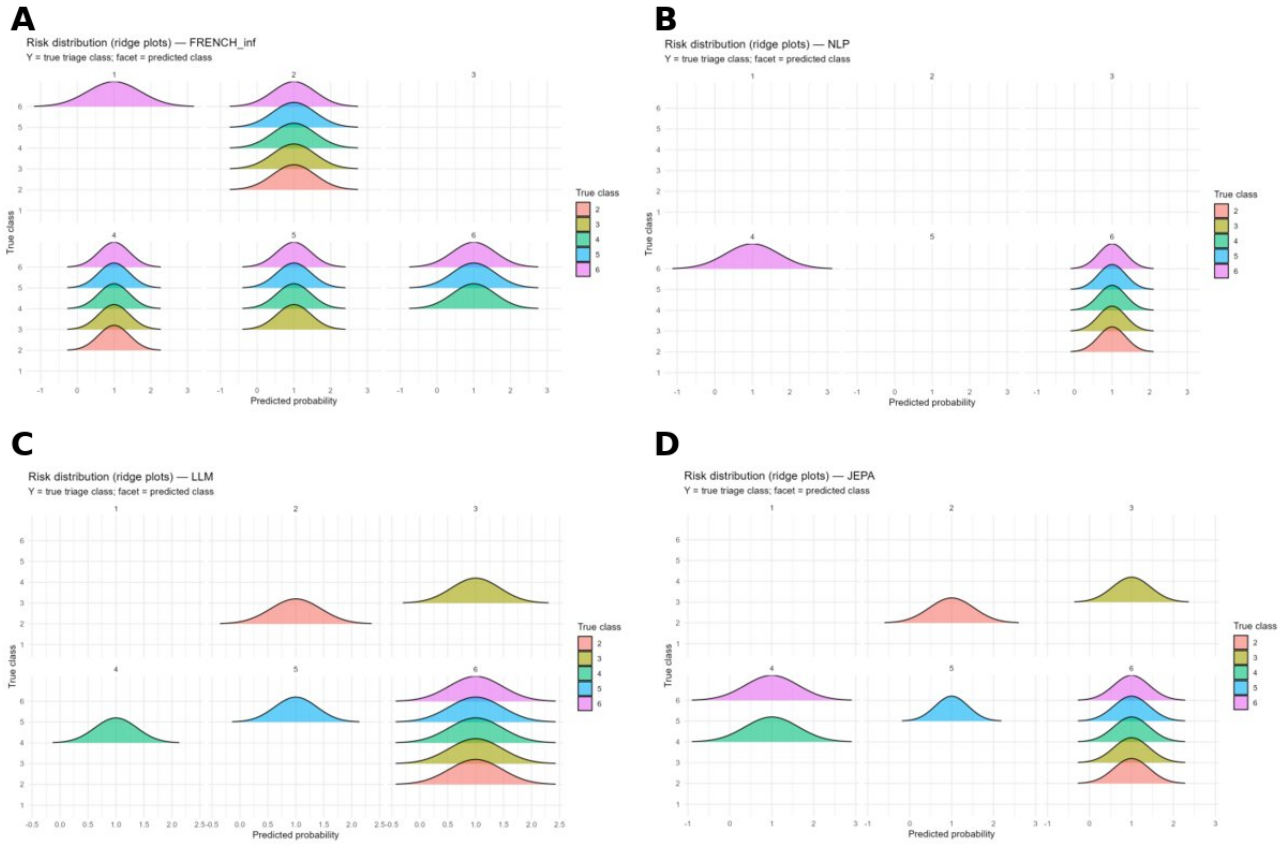

Secondary Analysis: GEMSA Prediction

URGENTIAPARSE substantially outperformed the other models in predicting patient disposition (GEMSA), achieving a composite *z* score of 2.473 versus –2.056 for TRIAGEMASTER and –4.399 for EMERGINET (Table 3). Performance metrics included an MAE of 0.082, RMSE of 0.402, weighted κ of 0.863 (P<.001), Spearman correlation of 0.864 (P<.001), micro F_1-score of 0.957, and macro F_1-score of 0.628. High exact agreement (95.7%) and near agreement (96.0%) further confirmed its accuracy and reliability.

Confusion matrices (Figure 7, top) showed that URGENTIAPARSE produced highly concentrated predictions along the diagonal (accurate), EMERGINET demonstrated moderate accuracy, and TRIAGEMASTER displayed scattered predictions. Bland-Altman analysis (Figure 7, middle) confirmed strong agreement for URGENTIAPARSE (mean difference 0.04, limits –0.83 to 0.91), moderate agreement for EMERGINET (limits –2.12 to 1.96), and large deviations for TRIAGEMASTER (limits –2.51 to 2.25).

Error distributions (Figure 7, bottom left) showed that EMERGINET had small, tightly clustered errors; URGENTIAPARSE exhibited slightly broader but well-centered errors; and TRIAGEMASTER demonstrated wide, poorly centered distributions. Class-specific F_1-scores (Figure 7, bottom right) revealed that URGENTIAPARSE achieved consistently high scores across the represented GEMSA categories, whereas EMERGINET and TRIAGEMASTER showed poorer and more uneven performance.

XSL•FO
RenderX

Table 3. Secondary analysis comparing artificial intelligence models for GEMSA[a] (disposition) prediction.

Model	Mean absolute error	Root mean square error	κ[b]	Spearman[c]	Micro F_1-score	Macro F_1-score	Exact	Near[d]	z score[e]
URGENTIAPARSE	0.082	0.402	0.863	0.864	0.957	0.628	0.957	0.960	2.473
TRIAGEMASTER	0.364	0.863	0.185	0.240	0.811	0.198	0.811	0.840	–2.056
EMERGINET	0.988	1.009	0	0	0.027	0.009	0.027	0.985	–4.399

[a]GEMSA: Groupes d'Etude Multicentrique des Services d'Accueil.

[b]Weighted Cohen κ; URGENTIAPARSE and TRIAGEMASTER, *P*<.001; EMERGINET, *P*=.99.

[c]Spearman rank correlation; URGENTIAPARSE, *P*<.001; TRIAGEMASTER, *P*=.006; EMERGINET, *P*=.99.

[d]Near agreement: proportion within the +1 or –1 GEMSA level.

[e]Composite *z* score (higher is better).

Figure 7. Evaluation of three AI triage models against the GEMSA gold standard. (A) Confusion matrices comparing predicted versus gold standard triage levels for NLP, LLM, and JEPA. (B) Bland-Altman plots showing bias and limits of agreement between each model and GEMSA. (C) Kernel density distributions of prediction errors illustrating model precision and systematic bias. (D) Per-class F1-scores quantifying discriminative performance across triage severity levels.

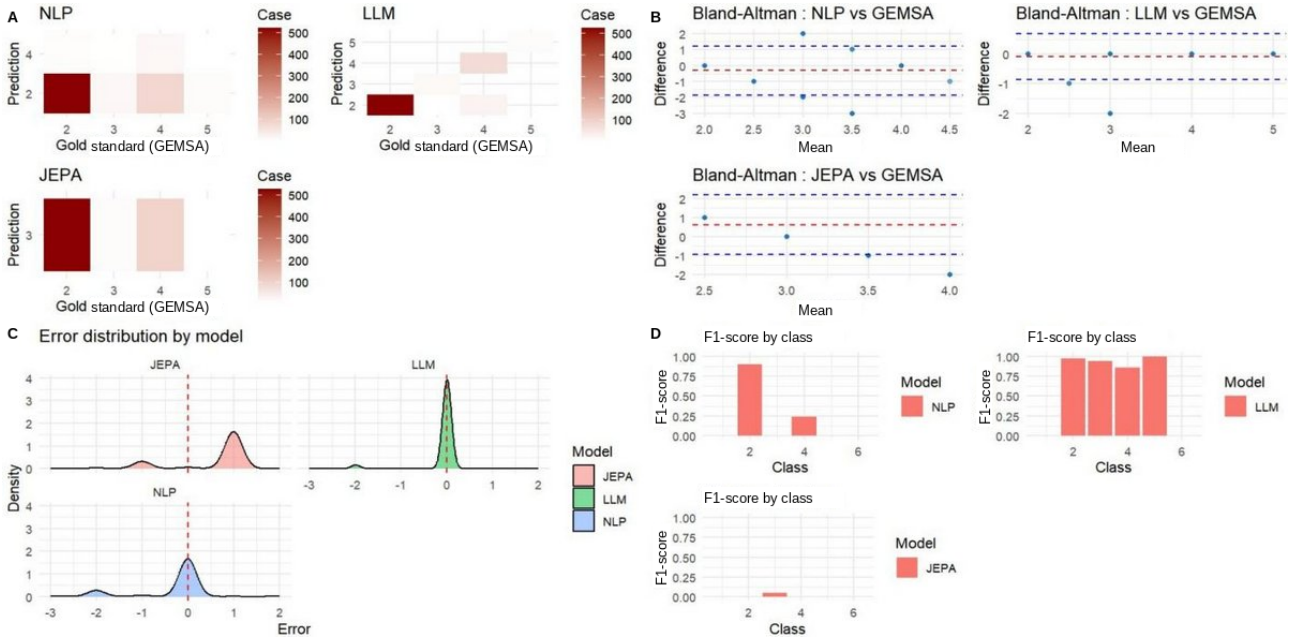

Impact of Data Modality: Structured Versus Unstructured Inputs

Analysis of input data type impact (Table 4) revealed that structured data (vital signs, demographics, and chief complaint codes) yielded slightly better performance than unstructured transcripts for URGENTIAPARSE (*z* score 1.806 vs 1.628) and TRIAGEMASTER (–4.790 vs –4.949), whereas EMERGINET showed minimal difference (–1.357 vs –0.993). These findings suggest that (1) vital signs and demographic data contain substantial triage-predictive information; (2) LLMs can extract meaningful patterns from both modalities; and (3) optimal performance likely requires multimodal integration. The relatively small performance gap between modalities for URGENTIAPARSE indicates that the transcript-based LLM captures much of the clinically relevant information, supporting the feasibility of voice-based triage assistance systems.

XSL•FO
RenderX

Table 4. Performance comparison across data modalities (structured vs unstructured inputs).

Model	Data type	Mean absolute error	Root mean square error	κ[a]	Spearman[b]	Micro F_1-score	Macro F_1-score	Exact	Near[c]	*z* score[d]
URGENTIAPARSE	Structured	0.213	0.748	0.821	0.826	0.903	0.898	0.903	0.928	1.806
URGENTIAPARSE	Unstructured	0.240	0.807	0.790	0.790	0.893	0.891	0.893	0.924	1.628
EMERGINET	Structured	0.510	1.247	0.420	0.559	0.807	0.551	0.807	0.836	–1.357
EMERGINET	Unstructured	0.516	1.240	0.430	0.560	0.791	0.539	0.791	0.843	–0.993
TRIAGEMASTER	Structured	0.916	1.557	0.057	0.160	0.572	0.190	0.572	0.712	–4.790
TRIAGEMASTER	Unstructured	0.991	1.629	-0.003	0.001	0.545	0.118	0.545	0.691	–4.949

[a]Weighted Cohen κ; $P<.001$ for all except TRIAGEMASTER unstructured ($P=.97$).

[b]Spearman rank correlation; $P<.001$ for all except TRIAGEMASTER ($P>.20$).

[c]Near agreement: proportion within the +1 or –1 triage level.

[d]Composite *z* score (higher is better).

Discussion

Principal Findings

This retrospective proof-of-concept study developed and compared 3 AI architectures for ED triage prediction using real nurse-patient interaction data and national triage standards. Of 73,236 ED visits over a 7-month period, 657 (0.90%) patients with complete audio recordings and structured data were included in the analysis. The LLM-based model (URGENTIAPARSE) demonstrated superior performance across multiple metrics (composite *z* score=2.514, F_1-score=0.900, AUC 0.879, weighted κ=0.800, $P<.001$) compared with the JEPA-based EMERGINET (*z* score=0.438), the NLP-based TRIAGEMASTER (*z* score=–3.511), and current nurse triage practices (*z* score=–4.343). Secondary analyses confirmed the superiority of URGENTIAPARSE for disposition prediction (GEMSA) and its robustness across structured and unstructured data modalities. However, severe methodological limitations—particularly extreme selection bias, overfitting, sparse representation of high-acuity cases, and the monocentric design—preclude immediate clinical deployment and underscore the need for substantial additional validation.

Comparison With Prior Work

Our findings align with and extend previous research on AI-assisted triage. The URGENTIAPARSE F_1-score (0.900) substantially exceeds that of prior French ED triage models: Clinical BELGPT-2 achieved an F_1-score of 0.62 [12], while external models such as Mistral 7B and Llama 3 8B demonstrated moderate performance, with larger models (Mixtral 8x7B) underperforming [11]. Our results also surpass those reported in the original FRENCH scale validation studies (AUC 0.83-0.86 for hospitalization prediction [1,25]) when applied by nurses, suggesting that AI has the potential to enhance triage accuracy.

However, unlike previous studies, we observed severe overfitting despite the use of regularization techniques. This likely reflects the extremely small effective sample size relative to model complexity (657 cases for the 137-million-parameter FlauBERT base), the high-dimensional input space (768-dimensional embeddings plus structured features), and substantial class imbalance with sparse representation of high-acuity cases. Recent studies on LLM hallucinations [13] and time-series forecasting [26] suggest potential mitigation strategies, including semantic entropy–based uncertainty quantification, prompt engineering, and backbone reprogramming—approaches that warrant investigation in future iterations.

Our calibration analysis revealed class-specific heterogeneity, consistent with recent findings on proper scoring rules for multiclass classification [14]. The observation that URGENTIAPARSE generates sparse, high-confidence predictions rather than well-distributed probability estimates suggests that the model may benefit from postprocessing approaches such as temperature scaling or Platt scaling to improve probability calibration before clinical implementation.

Prior studies have identified biases in triage decisions related to patient sex, nurse experience, and pain reporting [11,12]. Although our study did not explicitly assess these biases, the gold-standard consensus process and AI model evaluation framework established here could facilitate future bias detection studies. For example, systematic perturbation analyses, such as modifying patient sex references in transcripts while holding all other factors constant, could be conducted to evaluate potential model sensitivity to demographic attributes.

Clinical Implications and Deployment Considerations

If validated prospectively across diverse settings, LLM-based triage support could enhance patient safety and operational efficiency through real-time decision support that highlights high-risk cases for immediate review; quality assurance by flagging discrepancies between nurse and AI triage for senior clinician verification; training tools that provide immediate feedback to novice nurses; and workload redistribution during surge periods by prescreening low-acuity cases. However, multiple critical barriers must be addressed before deployment.

The perfect training accuracy (1.0) with poor validation performance (~0.5) observed for URGENTIAPARSE indicates

XSL•FO
RenderX

severe memorization rather than learning generalizable patterns. Potential solutions include substantial data augmentation, such as paraphrasing, synonym replacement, and back-translation for transcripts, combined with controlled perturbations of vital signs. More aggressive regularization strategies, including higher dropout rates, stronger L2 penalties, and techniques such as mixup or cutmix, may also help. Model simplification through adapter layers or low-rank adaptation (LoRA) fine-tuning of FlauBERT, rather than full model fine-tuning, could further reduce overfitting. In addition, ensemble methods that average predictions from multiple diverse architectures, transfer learning from related domains (eg, ambulance call triage or primary care urgency assessment), and active learning to selectively acquire cases with the highest model uncertainty all warrant investigation.

With only 4 (N=657) class 1 cases (0.61%) and 86 (13.1%) class 2 cases, we cannot reliably evaluate model performance for the most critical patients—those for whom undertriage could be fatal. Prospective deployment would therefore require conservative threshold selection that prioritizes overtriage over undertriage; mandatory senior clinician override for any AI-suggested downgrade relative to nurse triage; and real-time monitoring dashboards tracking undertriage events and associated patient outcomes, including ED length of stay, ICU admission, in-hospital mortality, and 72-hour return visits. In addition, automatic model deactivation should be triggered if the undertriage rate exceeds predefined safety thresholds.

Current probability estimates also require post hoc calibration—using methods such as temperature scaling, Platt scaling, or isotonic regression—to ensure reliable confidence estimates. Furthermore, implementing abstention mechanisms, whereby the model declines to issue a prediction when uncertainty exceeds a predefined threshold, may improve safety by deferring ambiguous cases to human judgment. Techniques from conformal prediction could additionally provide statistically rigorous uncertainty quantification with formal coverage guarantees.

Although SHAP values provide token- and feature-level explanations for URGENTIAPARSE predictions, clinicians require intuitive, actionable insights that align with real-world decision-making. Future work should therefore focus on generating natural language explanations—for example: “Triage level 2 suggested due to elevated heart rate (124 bpm), chest pain complaint, and description of respiratory distress.” Contrastive explanations could further enhance interpretability and trust, such as “If the heart rate were within the normal range, the predicted triage level would be 3.” Such counterfactual framing helps clinicians understand which features are most influential and how changes in patient presentation might alter the recommendation.

Real-time deployment requires inference latency under 5 seconds, a requirement met by the current 312-ms latency. However, seamless electronic health record integration without disrupting nurse workflow remains essential. An intuitive user interface that displays AI recommendations with confidence levels and key supporting features, combined with easy override mechanisms requiring mandatory documentation of the rationale, would facilitate adoption. Establishing feedback loops in which clinician corrections are logged for continuous model improvement completes the integration requirements.

AI triage support raises profound liability questions, with unclear responsibility among nurses, AI developers, and hospitals when undertriage occurs. Algorithmic bias is another concern, as model performance may vary by patient demographics, insurance status, or language. Privacy considerations regarding the secure handling of audio recordings and transcripts must be addressed, and equity requires ensuring that all patient subgroups receive accurate predictions. Comprehensive fairness audits, bias mitigation strategies, and clear governance frameworks must precede any deployment.

Limitations

This study has multiple substantial limitations that constrain interpretation and generalizability across several domains.

The severe selection bias represents perhaps the most concerning methodological limitation. Only 657 of 73,236 (0.90%) ED visits had usable recordings, representing <1% of eligible encounters. Recordings were limited to volunteer nurses (fewer than 10) during feasible moments, likely excluding the highest-acuity cases requiring immediate intervention without time for a structured interview; chaotic shifts with multiple simultaneous arrivals; patients with altered mental status, language barriers, or communication difficulties; nurses uncomfortable with recording technology; and specific periods, such as overnight and weekends. The included cohort had slightly lower acuity than the broader ED population (P=.02), introducing systematic bias that limits generalizability to the real-world case mix. Future studies must implement systematic recording protocols that capture consecutive cases across all shifts, nurses, and patient types to obtain representative samples.

The sparse representation of the highest-acuity classes constitutes the most critical limitation for clinical deployment. Out of 657 cases, class 1 included only 4 (0.61%), class 2 included 86 (13.1%), and no class 3A or class 6 cases were observed. This extreme imbalance severely limits model training on high-risk cases, where undertriage has the greatest consequences. Reliable performance estimation for rare but critical categories becomes impossible, as CIs for class 1 metrics are extremely wide. The ability to detect undertriage patterns that could lead to preventable morbidity or mortality therefore remains fundamentally constrained. Generalization to settings with different acuity distributions also cannot be assessed. Class-specific performance metrics, particularly sensitivity for classes 1-2, have limited reliability and require validation in datasets with adequate representation across the full triage spectrum. Techniques such as the synthetic minority oversampling technique or focal loss to address extreme class imbalance should be explored in future work.

The severe overfitting observed for URGENTIAPARSE fundamentally limits real-world applicability. The model achieved perfect training accuracy (1.0), whereas validation accuracy remained approximately 0.5, clearly indicating that the model memorized training examples rather than learning generalizable triage patterns. This overfitting persisted despite

XSL•FO
RenderX

dropout (P=0.3), L2 regularization ($\lambda=1\times10^{-5}$), and early stopping, suggesting that the effective sample size (n=657) is insufficient for the model complexity (137 million parameters in FlauBERT base). Although we report validation set performance rather than training set performance, the marked training-validation discrepancy signals a high risk of catastrophic failure on truly external data with different patient populations, nurse communication styles, or institutional protocols. Prospective external validation across multiple, diverse EDs is therefore essential before any consideration of clinical use. Potential solutions include more aggressive regularization, model simplification through adapter layers or LoRA fine-tuning, ensemble methods, or the collection of substantially larger training datasets, with a target of over 10,000 cases for stable LLM fine-tuning.

The monocentric design severely constrains external validity. Conducted at a single French academic tertiary care hospital, the results may not generalize to community hospitals with different patient demographics, resource levels, and triage processes. Rural or low-volume EDs, with different case mix and staffing patterns, represent an entirely different operational context. Non-French health care systems using alternative triage scales, such as the Emergency Severity Index, Canadian Triage and Acuity Scale, Manchester Triage System, or Australasian Triage Scale, would require complete model retraining and revalidation. Non-French language contexts would likewise necessitate retraining language models on appropriate corpora. EDs serving culturally, linguistically, or socioeconomically distinct patient populations may exhibit fundamentally different triage patterns. Multicenter validation across diverse settings—including academic and community hospitals, urban and rural locations, and multiple countries—is therefore required to assess transportability and identify factors that affect model performance.

The exclusion of repeat ED visits creates an important gap in our understanding of model performance. By including only index visits, we cannot assess model behavior in patients with frequent ED utilization, complex chronic conditions requiring a longitudinal perspective, or evolving clinical presentations across multiple encounters. Repeat visitors often present atypically and may benefit most from AI-assisted triage, yet they were systematically excluded from model development. This exclusion may bias performance estimates upward if repeat visitors are more difficult to triage accurately.

Several concerns regarding gold-standard construction could introduce incorporation bias. Adjudicators reviewed complete transcripts and vital signs with unlimited time for deliberation, in sharp contrast to real-time nurse triage conducted under time pressure and with incomplete information. This fundamental difference in decision-making context may overestimate AI-human agreement, as both the AI and gold-standard adjudicators had access to complete information unavailable to real-time nurses. Although blinded to outcomes, adjudicators were aware that they were establishing a research gold standard rather than making operational decisions with immediate consequences, which may have influenced risk tolerance and the willingness to assign higher acuity levels. The initial interrater agreement (κ=0.72) indicates substantial but not perfect consensus, with a 23.5% disagreement rate suggesting meaningful variability in expert interpretation even with complete information. The gold standard therefore reflects retrospective expert judgment, which may differ from optimal real-time triage, particularly when information available only after initial presentation is considered. A sensitivity analysis excluding cases with nurse-gold-standard discrepancies over 1 level yielded similar results, partially mitigating this concern but not eliminating it.

Limited independent validation of the FRENCH scale itself represents an often overlooked limitation. Although the FRENCH scale serves as the French national standard, independent validation studies remain limited beyond the original 2009 and 2019 publications [1,25]. The original validation reported an AUC of 0.858 for hospitalization prediction and moderate correlations with resource utilization. A 2019 validation study including 29,423 patients reported similar findings, with an AUC of 0.83 and moderate but significant correlations between triage level and resource utilization or testing [25]. Thus, even compared with FRENCH validation studies, the URGENTIAPARSE model demonstrates superior AUC performance relative to nurses who conducted triage in those studies. However, our gold-standard consensus process effectively establishes an “ideal FRENCH application” and does not validate whether FRENCH itself optimally predicts patient outcomes. Future research should therefore evaluate AI predictions against objective clinical end points, such as ICU admission, in-hospital mortality, 72-hour return visits, and length of stay, independent of triage scale assignment, to assess true clinical utility rather than agreement with an imperfect reference standard.

The lack of prospective validation and real-world testing fundamentally limits our ability to make clinical recommendations. This retrospective analysis cannot assess real-time inference performance or the integration challenges that inevitably arise during deployment. The impact on actual triage decisions and nurse acceptance remains unknown and could substantially affect real-world utility. Effects on patient outcomes, ED workflow, and resource utilization also cannot be determined from retrospective data. Model degradation over time, as patient populations, disease patterns, or institutional practices evolve through concept drift, represents a realistic threat that requires prospective monitoring. Rare failure modes and edge cases typically become apparent only during large-scale deployment involving thousands or tens of thousands of predictions. Unintended consequences, such as deskilling of nurses who become overly reliant on AI recommendations, or gaming of the system if performance metrics become targets, could further undermine potential benefits. Prospective stepped-wedge cluster randomized trials comparing AI-assisted versus standard triage across multiple sites, therefore, represent essential next steps before any clinical implementation can be responsibly considered.

The absence of cost-effectiveness and implementation analyses limits informed adoption decisions. We did not evaluate the computational infrastructure costs required for deployment, including graphics processing unit servers, maintenance, and

XSL•FO
RenderX

updates, which may be substantial for resource-constrained hospitals. Training costs for nurses to use the system effectively also remain unknown and could be prohibitive if extensive instruction is required. The impact on triage time and ED throughput could be positive or negative, depending on implementation details. Cost per quality-adjusted life year gained represents the gold standard for health care economic evaluation, but requires long-term outcome data that are currently unavailable. Scalability challenges related to broad dissemination across diverse health care settings also remain unaddressed. Economic evaluation from a health system perspective is therefore essential for adoption decisions in the context of finite health care resources.

The absence of fairness and bias assessment represents a significant ethical limitation. We did not systematically evaluate whether model performance varies by patient demographics—including age, sex, race or ethnicity, insurance status, language, or socioeconomic status—potentially exacerbating health disparities. Prior work has identified sex-based and other biases in human triage decisions [11,12]; AI systems may perpetuate or amplify these biases if they are not explicitly addressed during development. If the model performs worse for already disadvantaged populations, deployment could worsen existing health inequities. Comprehensive fairness audits stratified by protected characteristics are therefore required before deployment, along with bias mitigation strategies if disparities are identified. Partnerships with ethicists, patients, and advocacy groups to define fairness metrics aligned with societal values should precede any clinical implementation.

Technological and data quality constraints affected the study throughout. Audio recording quality varied substantially, leading to transcription errors that may have affected model input quality in unpredictable ways. Equipment loss and technical failures resulted in 24 exclusions (3.5% of recorded cases), suggesting that real-world deployment would encounter similar challenges. Missing data for certain vital signs (<2%) required imputation using training set medians, which may have introduced bias. Real-world deployment would face these and additional challenges, necessitating robust handling of noisy, incomplete, or corrupted inputs with graceful degradation rather than catastrophic failure. The model's behavior when confronted with poor-quality audio, incomplete vital signs, or technical failures remains unknown.

The lack of uncertainty quantification and explicit abstention mechanisms precludes safe clinical deployment. The model currently provides point predictions without well-calibrated CIs or explicit abstention when uncertainty is high. Clinical deployment requires principled uncertainty quantification—using methods such as conformal prediction, Bayesian approaches, or ensemble disagreement—to determine when deferral to human judgment is warranted. Without such mechanisms, the model may generate highly confident yet incorrect predictions in novel situations outside its training distribution. The sparse prediction patterns observed for URGENTIAPARSE may reflect implicit abstention behavior that should be explicitly characterized; however, we have not systematically examined when or why the model declines to issue predictions.

Limited interpretability persists despite SHAP analysis. Although SHAP values provide mathematical attributions indicating which input features most influenced each prediction, they may not align with clinical reasoning patterns or offer actionable insights for clinicians. A nurse or physician may not find numerical feature importance scores intuitive or helpful in understanding why the AI generated a specific recommendation. Natural language explanation generation that translates SHAP values into clinically meaningful statements remains underdeveloped. User studies assessing interpretability from the clinician perspective are therefore needed to determine whether these explanations facilitate, rather than hinder, clinical decision-making.

Regulatory and legal uncertainties cloud the path to clinical implementation. This research prototype has not undergone regulatory review, such as Conformité Européenne (CE) marking in Europe or Food and Drug Administration (FDA) clearance in the United States, which would likely be required for medical device classification of clinical decision support software. The regulatory pathway for AI-based triage support systems remains unclear and continues to evolve. Legal liability frameworks for AI-assisted triage are also poorly defined. When undertriage occurs with AI assistance, responsibility among nurses, AI developers, and hospitals remains ambiguous. These legal and regulatory uncertainties must be resolved before widespread deployment can proceed.

Finally, the absence of a continual learning framework limits long-term sustainability. Static models trained on historical data inevitably degrade as patient populations, diseases, and clinical practices evolve. Deployment would therefore require active monitoring of model performance in production; detection of performance degradation or concept drift; triggered retraining protocols when performance declines; and potentially online learning mechanisms to adapt to changing patterns while maintaining safety. We have not developed or validated any such infrastructure. Without continual learning capabilities, the model would become progressively obsolete, even if initially successful.

Despite these numerous and substantial limitations, this study provides important proof-of-concept evidence that LLM architectures can achieve high accuracy for ED triage prediction when evaluated using carefully collected retrospective data. The study also establishes a rigorous evaluation methodology that incorporates multiple complementary metrics and comprehensive error analysis, upon which future research can build. The limitations outlined above provide a detailed road map for the substantial additional work required before clinical translation can be responsibly considered, including the specific methodological improvements, additional studies, and infrastructure development necessary to support safe and effective deployment.

Future Research Directions

Building on these findings and addressing the identified limitations, future research should prioritize several key areas.

XSL•FO
RenderX

Trials across more than 10 diverse EDs—including academic and community hospitals, urban and rural settings, and varied patient demographics—with systematic consecutive case enrollment targeting more than 10,000 patients would enable assessment of external validity, detection of site-specific effects, and adequately powered subgroup analyses. A stepped-wedge cluster randomized design would allow causal inference regarding the impact on patient outcomes, including mortality, length of stay, ICU admission rate, and 72-hour return visits, while controlling for temporal trends.

Oversampling the highest-acuity encounters in classes 1-2 through deliberate recording protocols during trauma activations, stroke alerts, cardiac arrests, and other critical presentations would enable reliable detection of undertriage and robust safety evaluation. This targeted data collection would address one of the most important current limitations.

Systematic comparison of advanced overfitting mitigation strategies is also warranted. Such evaluation should include parameter-efficient fine-tuning approaches (eg, LoRA, adapters, and prompt tuning); aggressive data augmentation (eg, back-translation, paraphrasing, synonym replacement, and controlled vital sign perturbations); semisupervised learning leveraging unlabeled transcripts; multitask learning jointly predicting triage, disposition, resource utilization, and outcomes; transfer learning from related domains such as ambulance call triage or primary care urgency assessment; and ensemble methods combining diverse architectures with different inductive biases.

Systematic assessment of model behavior under a range of perturbations would strengthen confidence in its robustness. These should include adversarial attacks representing intentional gaming; distribution shifts due to seasonal variation, pandemics, or novel diseases; missing data resulting from incomplete vital signs, silent patients, or technical failures; transcription errors arising from speech recognition failures; and edge cases, such as rare presentations, complex comorbidities, or psychiatric crises. Developing certified robustness guarantees represents an important objective.

Stratified performance evaluation by protected characteristics—including age, sex, race or ethnicity, insurance status, language, and socioeconomic status—combined with detection of disparate impact, root cause analysis of identified biases, and rigorous testing of mitigation strategies (eg, reweighting, fairness constraints, or adversarial debiasing) would address equity concerns. Partnerships with ethicists, patients, and advocacy groups to define fairness metrics aligned with societal values are essential.

Development of natural language explanation generation, contrastive explanations that articulate how predictions would change if specific features differed, visualization tools highlighting salient features, and user interface optimization informed by clinician feedback would enhance interpretability. Human factors studies evaluating how AI recommendations influence decision-making—including risks of automation bias (overreliance) or dismissiveness (underreliance)—would further inform safe implementation.

Rigorous cost-effectiveness analysis from a health system perspective; budget impact modeling; implementation barrier assessment; stakeholder engagement with nurses, physicians, administrators, and patients; workflow redesign; training program development; and sustainment planning would support adoption. Qualitative studies exploring nurse and physician attitudes, concerns, and acceptance would help identify potential obstacles early.

Infrastructure for continual model performance monitoring, concept drift detection, triggered retraining protocols, online learning mechanisms, and transparent reporting to end users and regulators would maintain performance over time. Development of living systematic reviews tracking field performance as deployment expands would build the evidence base.

Exploration of synergies with AI-assisted diagnosis supporting downstream care decisions, predictive models for ED crowding and resource planning, automated documentation reducing nurse burden, and early warning systems for deterioration after initial triage could create an integrated ecosystem. Emerging work on AI transforming health care from acute care to early prevention [27,28] suggests potential for broader impact across the care continuum.

Collaboration with regulatory agencies, including the European Medicines Agency and FDA, to establish appropriate oversight frameworks balancing innovation with patient safety, defining clinical validation requirements, and clarifying liability and postmarket surveillance obligations for AI medical devices would facilitate responsible translation.

Conclusions

This study demonstrates that LLM-based AI (URGENTIAPARSE) can achieve high accuracy for ED triage prediction, outperforming traditional NLP (TRIAGEMASTER), JEPA (EMERGINET), and current nurse triage practices when validated against a senior clinician consensus gold standard. With an F_1-score of 0.900, AUC of 0.879, weighted κ of 0.800, and 90% exact agreement, the LLM model shows promise for enhancing triage consistency and potentially supporting clinical decision-making.

However, severe methodological limitations mandate extreme caution. Critical barriers to clinical deployment include severe overfitting, with perfect training accuracy but poor validation performance indicating an inability to generalize beyond the training data; extreme selection bias, with only a 0.9% (657/73,236) inclusion rate limiting representativeness; sparse high-acuity case representation, with only 4 class 1 cases precluding reliable undertriage risk assessment where stakes are highest; a monocentric design constraining external validity; retrospective analysis without prospective real-world validation; and absent economic, workflow, fairness, and regulatory analyses.

Before any consideration of clinical deployment, this AI triage support system requires large-scale prospective multicenter validation targeting more than 10,000 cases across diverse settings; comprehensive overfitting mitigation and model robustness enhancement; targeted high-acuity case collection

XSL•FO
RenderX

enabling undertriage safety evaluation; fairness audits and bias mitigation strategies; post hoc calibration and uncertainty quantification with abstention mechanisms; interpretability enhancement with natural language explanations; human factors studies and workflow integration testing; economic evaluation and implementation planning; regulatory review and approval; and continuous performance monitoring infrastructure with concept drift detection.

While this proof-of-concept establishes technical feasibility and identifies the most promising architecture among the tested alternatives, the substantial gap between current evidence and safe clinical deployment must be acknowledged transparently. AI-assisted triage holds potential to improve patient safety, enhance consistency, reduce cognitive burden on nurses during surge periods, and support quality assurance—but realizing these benefits responsibly requires rigorous validation, thoughtful implementation, continuous monitoring, and humility about current limitations. This study provides a foundation and road map for that essential future work.

Funding

The authors declared no financial support was received for this work.

Conflicts of Interest

None declared.

Multimedia Appendix 1
TRIPOD-AI fullfilled checklist.
[PDF File (Adobe PDF File), 302 KB - medinform_v14i1e83318_app1.pdf]

Multimedia Appendix 2
Code for gold-standard.
[ZIP File (Zip Archive), 32 KB - medinform_v14i1e83318_app2.zip]

References

1. Taboulet P, Moreira V, Haas L, Porcher R, Braganca A, Fontaine J, et al. Triage with the French Emergency Nurses Classification in Hospital scale: reliability and validity. European Journal of Emergency Medicine 2009;16(2):61-67. [doi: 10.1097/mej.0b013e328304ae57]
2. Husted JA, Cook RJ, Farewell VT, Gladman DD. Methods for assessing responsiveness: a critical review and recommendations. J Clin Epidemiol 2000 May;53(5):459-468. [doi: 10.1016/s0895-4356(99)00206-1] [Medline: 10812317]
3. Moll HA. Challenges in the validation of triage systems at emergency departments. J Clin Epidemiol 2010 Apr;63(4):384-388. [doi: 10.1016/j.jclinepi.2009.07.009] [Medline: 19875271]
4. Levin S, Toerper M, Hamrock E, Hinson JS, Barnes S, Gardner H, et al. Machine-learning-based electronic triage more accurately differentiates patients with respect to clinical outcomes compared with the emergency severity index. Ann Emerg Med 2018 May;71(5):565-574.e2. [doi: 10.1016/j.annemergmed.2017.08.005] [Medline: 28888332]
5. Ilicki J. Challenges in evaluating the accuracy of AI-containing digital triage systems: a systematic review. PLoS One 2022 Dec 27;17(12):e0279636 [FREE Full text] [doi: 10.1371/journal.pone.0279636] [Medline: 36574438]
6. Hang L, Loïc V, Jibril F, Vincent S, Maximin C, Benjamin L, et al. FlauBERT: unsupervised language model pre-training for French. Paris, France: European Language Resources Association; 2020 Presented at: The Twelfth Language Resources and Evaluation Conference; May 11-16, 2020; Marseille, France.
7. Brossard C, Goetz C, Catoire P, Cipolat L, Guyeux C, Gil Jardine C, et al. Predicting emergency department admissions using a machine-learning algorithm: a proof of concept with retrospective study. BMC Emerg Med 2025 Jan 06;25(1):3-11 [FREE Full text] [doi: 10.1186/s12873-024-01141-4] [Medline: 39762754]
8. Bardes A, Ponce J, LeCun Y. Vicreg: variance-invariance-covariance regularization for self-supervised learning. arXiv. Published online May 11, 2021. 2022. URL: https://arxiv.org/abs/2105.04906 [accessed 2026-02-25]
9. Lansiaux E, Baron M, Vromant A. Navigating the landscape of medical triage: unveiling the potential and challenges of large language models and beyond. Am J Emerg Med 2024 Apr;78:224. [doi: 10.1016/j.ajem.2024.02.013] [Medline: 38395695]
10. Lansiaux E, Ibrahim ES, Minaz A, Itani R, Kukkadi R, Obina OG, et al. Medical triage review: from battlegrounds darkness to the machine light. SSRN. Published online February 13, 2024. 2024. URL: https://papers.ssrn.com/sol3/papers.cfm?abstract_id=4713040 [accessed 2026-02-25]
11. Guerra-Adames A, Avalos-Fernandez M, Doremus O, Gil-Jardiné C, Lagarde E. Uncovering judgment biases in emergency triage: a public health approach based on large language models. 2025 Dec Presented at: The 4th Machine Learning for Health Symposium; December 15-16, 2025; Vancouver, BC, Canada p. 402-439.

XSL•FO
RenderX

12. Avalos M, Cohen D, Russon D, Davids M, Doremus O, Chenais G, et al. Detecting human bias in emergency triage using LLMs. 2024 May 13 Presented at: The International FLAIRS Conference Proceedings; May 18-21, 2024; Sandestin Beach, FL. [doi: 10.32473/flairs.37.1.135586]
13. Farquhar S, Kossen J, Kuhn L, Gal Y. Detecting hallucinations in large language models using semantic entropy. Nature 2024 Jun 19;630(8017):625-630 [FREE Full text] [doi: 10.1038/s41586-024-07421-0] [Medline: 38898292]
14. Ahmadian R, Ghatee M, Wahlström J. Superior scoring rules for probabilistic evaluation of single-label multi-class classification tasks. International Journal of Approximate Reasoning 2025 Jul;182:109421. [doi: 10.1016/j.ijar.2025.109421]
15. Statistique annuelle des etablissements de Santé. DRESS. URL: https://drees.solidarites-sante.gouv.fr/sources-outils-et-enquetes/00-la-statistique-annuelle-des-etablissements-sae [accessed 2026-02-25]
16. Lansiaux E. TIAEU: Triage Intelligent A l'Entrée des Urgences. Health Data Hub. 2023. URL: https://health-data-hub.fr/projets/tiaeu-triage-intelligent-lentree-des-urgences-0 [accessed 2026-02-25]
17. Circulaire DHOS/E 3/PMSI n°-433 du 10 septembre relative au projet de mise en oeuvre progressive d?un financement propre aux urgences dans les établissements de santé. Ministère de la Santé. 2001 Jul. URL: https://sante.gouv.fr/fichiers/bo/2001/01-42/a0422740.htm [accessed 2026-02-25]
18. Milokov T, Chen K, Corrado GS, Dean J. Efficient estimation of word representations in vector space. 2013 Presented at: International Conference on Learning Representations; May 2-4, 2013; Scottsdale, AZ.
19. Ramachandran P, Zoph B, Le QV. Searching for activation functions. 2018 Presented at: International Conference on Learning Representations; April 30 to May 3, 2018; Vancouver, BC, Canada.
20. DeLong ER, DeLong DM, Clarke-Pearson DL. Comparing the areas under two or more correlated receiver operating characteristic curves: a nonparametric approach. Biometrics 1988 Sep;44(3):837. [doi: 10.2307/2531595]
21. Derczynski L. Complementarity, F-score, and NLP evaluation. 2005 Feb Presented at: The Tenth International Conference on Language Resources and Evaluation (LREC 16); May 23-28, 2016; Portorož, Slovenia p. 261-266. [doi: 10.1007/s10579-005-2692-5]
22. Chrusciel J, Girardon F, Roquette L, Laplanche D, Duclos A, Sanchez S. The prediction of hospital length of stay using unstructured data. BMC Med Inform Decis Mak 2021 Dec 18;21(1):351-359 [FREE Full text] [doi: 10.1186/s12911-021-01722-4] [Medline: 34922532]
23. Lundberg SM, Lee SI. A unified approach to interpreting model predictions. 2017 Presented at: NIPS'17: The 31st International Conference on Neural Information Processing Systems; December 4-9, 2017; Long Beach, CA p. 4768-4777.
24. Yu Y, Si X, Hu C, Zhang J. A review of recurrent neural networks: LSTM cells and network architectures. Neural Comput 2019 Jul;31(7):1235-1270. [doi: 10.1162/neco_a_01199] [Medline: 31113301]
25. Taboulet P, Vincent-Cassy C, Squara P, Resche-Rigon M. Validité de la FRENCH, l'échelle de tri des urgences hospitalières élaborée par la Société française de médecine d'urgence. Ann Fr Med Urgence 2019 Jan 15;9(1):10-16. [doi: 10.3166/afmu-2018-0099]
26. Jing M, Wang S, Ma L, Chu Z, Zhang JY, Shi XL, et al. Time-llm: time series forecasting by reprogramming large language models. 2023 Presented at: International Conference on Learning Representations; May 1-5, 2023; Kigali, Rwanda.
27. Ogut E. Graph-theoretical mapping of cortical and subcortical network alterations in preclinical neurodegeneration. Discov Neurosci 2025 Sep 15;20(1):e1. [doi: 10.1186/s13064-025-00214-9]
28. Ogut E. Artificial intelligence in clinical medicine: challenges across diagnostic imaging, clinical decision support, surgery, pathology, and drug discovery. Clin Pract 2025 Sep 16;15(9):169 [FREE Full text] [doi: 10.3390/clinpract15090169] [Medline: 41002784]

Abbreviations

AI: artificial intelligence
AUC: area under the curve
BERT: Bidirectional Encoder Representations from Transformers
CE: Conformité Européenne
CHU: Centre Hospitalier Universitaire
CLS: classification
CNIL: Commission Nationale de l'Informatique et des Libertés
ED: emergency department
FDA: Food and Drug Administration
FN: false negative
FP: false positive
FRENCH: French Emergency Nurses Classification in Hospital
GEMSA: Groupes d'Etude Multicentrique des Services d'Accueil
ICU: intensive care unit
JEPA: Joint Embedding Predictive Architecture
LLM: large language model

XSL•FO
RenderX

LoRA: low-rank adaptation
MAE: mean absolute error
NLP: natural language processing
RMSE: root mean square error
ROC: receiver operating characteristic
SHAP: Shapley Additive Explanations
TP: true positive
TRIPOD: Transparent Reporting of a multivariable prediction model for Individual Prognosis Or Diagnosis
VICReg: variance-invariance-covariance regularization
XGBoost: Extreme Gradient Boosting

Edited by A Benis; submitted 11.Sep.2025; peer-reviewed by AS Mutluer, E Ogut, J Kim; comments to author 11.Nov.2025; revised version received 14.Nov.2025; accepted 22.Dec.2025; published 10.Mar.2026.

Please cite as:
Lansiaux E, Azzouz R, Chazard E, Vromant A, Wiel E
Artificial Intelligence Models for Predicting Triage in Emergency Departments: Seven-Month Retrospective Comparative Study of Natural Language Processing, Large Language Model, and Joint Embedding Predictive Architectures
JMIR Med Inform 2026;14:e83318
URL: https://medinform.jmir.org/2026/1/e83318
doi:10.2196/83318
PMID:

©Edouard Lansiaux, Ramy Azzouz, Emmanuel Chazard, Amélie Vromant, Eric Wiel. Originally published in JMIR Medical Informatics (https://medinform.jmir.org), 10.Mar.2026. This is an open-access article distributed under the terms of the Creative Commons Attribution License (https://creativecommons.org/licenses/by/4.0/), which permits unrestricted use, distribution, and reproduction in any medium, provided the original work, first published in JMIR Medical Informatics, is properly cited. The complete bibliographic information, a link to the original publication on https://medinform.jmir.org/, as well as this copyright and license information must be included.

XSL•FO
RenderX

Original Paper

Application of a Large Visual Language Model on Tongue Image Description Generation and Physical Constitution Reasoning in Traditional Chinese Medicine (TongueVLM): Model Development and Validation Study

Chengdong Peng[1,2], MSc, PhD; Jun Gao[1], Prof Dr, PhD; Nuo Yang[2,3], BE; Yong Wang[2,3], BE; Renming Chen[2], MSc; Changwu Dong[4], Prof Dr Med

[1]School of Computer Science and Information Engineering, Hefei University of Technology, Hefei, Anhui, China
[2]Artificial Intelligence Laboratory, Hefei Yunzhen Information Technology Co, Ltd, Hefei, Anhui, China
[3]School of Information and Artificial Intelligence, Anhui Agricultural University, Hefei, Anhui, China
[4]The Second Clinical Medical School, Anhui University of Traditional Chinese Medicine, Hefei, Anhui, China

Corresponding Author:
Chengdong Peng, MSc, PhD
School of Computer Science and Information Engineering
Hefei University of Technology
Number 193 Tunxi Road
Hefei, Anhui, 230009
China
Phone: 86 055165337378 ext 86
Email: 2020020018@mail.hfut.edu.cn

Abstract

Background: In the field of traditional Chinese medicine (TCM), diagnostic work based on tongue images to recognize the physical constitution is a process of collecting clinical information, reasoning, and combining the patient's tongue image features with questioning. It is necessary to simulate the recognition of pathological information of tongue images by TCM practitioners and professional dialogue based on tongue image features, which helps to develop an intelligent interactive system for TCM diagnosis.

Objective: This study aimed to develop and validate a vertical model of the TCM domain with TCM's understanding and reasoning capability for tongue images.

Methods: A TongueVLM multimodal large model is designed, which includes a visual encoder module, a modal fusion module, and a language decoder module. First, the visual encoder based on the CLIP-ViT (Contrastive Language-Image Pre-Training With Vision Transformer) pretrained model is used for image patch, dimensionality reduction, and migration learning, which maps the high-dimensional tongue features into low-dimensional language encoding vectors. Further, a modal fusion module with a residual architecture is applied to map visual features to a natural language word embedding space, realizing the conceptual alignment between visual encoding and TCM terminology. Finally, fine-tuning of visual instructions is performed based on the LLaMA (large language model meta artificial intelligence), and a TCM-domain large language model with 7B parameters is trained.

Results: The constructed multimodal dataset has 3 test datasets, and experiments are conducted using 3000 samples from each test dataset, respectively. Experimental results indicate that the TongueVLM model outperforms general-purpose large models on all 3 tasks. On the multimodal test dataset, the TongueVLM model achieved accuracy rates of 79.8%, 78.6%, and 60.7% in evaluation tasks respectively, it achieves 9.1%, 8.4%, and 1.1% in greater accuracy than LLaVA-OneVision, and is 7.5%, 7%, and 5.9% more accurate than Qwen2.5-VL-7B, with the text generation time being around 24 tokens per second.

Conclusions: The TongueVLM model, which achieves tongue image description generation and physical constitution reasoning in TCM, is suitable for the application of a Chinese medicine intelligent diagnosis system.

(JMIR Med Inform 2026;14:e87237) doi:10.2196/87237

XSL•FO
RenderX

KEYWORDS

vision-language model; tongue image description generation; visual constitution reasoning; visual dialogue; intelligent diagnosis of traditional Chinese medicine (TCM)

Introduction

In recent years, the research focus on computer vision has gradually shifted toward innovative transformers and their variant architectures. These studies have made significant progress in the 3 basic tasks of image classification, object detection, and image segmentation, along with in-depth experiments on visual-textual multimodal data validity. The visual transformer model, represented by the vision transformer, approaches or even surpasses the convolutional neural network approach in several benchmark tests [1-14]. The key technique of the vision transformer is to construct image-to-vector transformations and effectively maintain the features of the image, bridging the gap between language and vision. Lava family [15-17], GPT-4v [18], and Gemini 1.5 [19] visual-language multimodal modeling have even ushered artificial intelligence-generated content into a new era of visual applications, and the field of medicine has received increasing attention from researchers [20-26].

In the field of traditional Chinese medicine (TCM), diagnostic work based on tongue images to recognize the physical constitution is a process of collecting clinical information, reasoning, and combining the patient's tongue image features with questioning. It is necessary to simulate the recognition of pathological information of tongue images by TCM practitioners and professional dialogue based on tongue image features, which helps to develop an intelligent interactive system for TCM diagnosis. However, the following limitations still exist in the current investigation: (1) high cost of acquisition equipment and collection of clinical data, mostly relying on publicly available datasets, and prominent data sample noise problems; (2) lack of qualitative or quantitative specialized labeling data; (3) lack of validation and analysis of the visual encoding results at the modal fusion stage; and (4) the evaluation metrics of the trained models focus on technical performance and ignore professional human judgments.

Previous studies have shown that, based on the image recognition model in the field of TCM applications, they fused the traditional image features of the tongue with deep tongue features and combined them with a machine learning model to construct a physical constitution identification, which compensated for the lack of information in a single modality and improved the accuracy of constitution classification [27-29]. In terms of training a vertical model of TCM based on a large language model (LLM), we constructed a pretraining dataset and an instruction fine-tuning dataset oriented to TCM and adopted a 2-phase training method of continuous pretraining and supervised fine-tuning to develop an LLM of TCM [30-35]. This model outperforms the existing models in several evaluation metrics and can play a role in TCM consultation.

Medical applications based on multimodal large models are also favored by researchers. A dataset containing 5.3 million+ image-text pairs was used to train the UniMed-CLIP model, which outperforms the existing health care visual language models (VLM) with 0-shot performance [36]. Multimodal health care models, which introduce evaluation metrics and frameworks and perform well in multimodal Q&A (question and answer) and text-based Q&A tasks [33,37]. BiomedCLIP with LLaMA-3 (large language model meta artificial intelligence) to realize a lightweight and efficient medical visual Q&A model [38]. Med-VQA interpretability by localizing image preference regions [39] enhanced the performance of biomedical VLMs by using instruction fine-tuning and multi-image training, respectively [40,41]. Aligned visual features with medical concepts and Med-VQA, enhanced the generation of large models, and achieved excellent performance on public datasets [42-44].

The primary aim of this study is to develop and validate TongueVLM, a specialized VLM for TCM tongue diagnosis. Specifically, our objectives were to (1) design a novel multimodal architecture that effectively aligns visual features of tongue images with domain-specific TCM textual knowledge; (2) construct a high-quality, multimodal dataset for supervised study, and end-to-end training on the TCM dataset; and (3) evaluate the performance of TongueVLM against established baseline models, and validation multimodal capabilities across 3 tasks of tongue feature description generation, physical constitution reasoning, and multiround dialogue.

Methods

Overall Architecture of TongueVLM

Our TongueVLM model uses a hybrid architecture combining the visual encoder module, modal fusion module, and language decoder module. First, the visual encoder based on the CLIP-ViT (Contrastive Language-Image Pre-Training With Vision Transformer) pretrained model is used for image patch, dimensionality reduction, and migration learning. Further, a multimodal fusion module with a residual architecture is applied to map visual features to the natural language word embedding space, realizing the conceptual alignment between visual encoding and TCM terminology. Finally, a visual-textual instruction dataset is constructed to perform multimodal instruction fine-tuning based on the LLaMA general-purpose LLM. As a result, a vertical model of the TCM domain with TCM understanding and reasoning capability for tongue images is obtained. The realization procedure is shown in Figure 1.

XSL•FO
RenderX

Figure 1. Network structure and computation of a large visual-language model. Includes a visual encoder module, a modal fusion module, and a language decoder module. First, the visual encoder based on the CLIP-ViT pretrained model is used for image patch, dimensionality reduction, and migration learning. Further, a modal fusion module with a residual architecture is applied to map visual features to a natural language word embedding space. Finally, fine-tuning of visual instructions is performed based on the LLaMA. AI: artificial intelligence; API: application programming interface; CLIP ViT: Contrastive Language Image Pre Training With Vision Transformer; LLaMa: large language model meta artificial intelligence; SFT: supervised fine-tuning; TCM: traditional Chinese medicine.

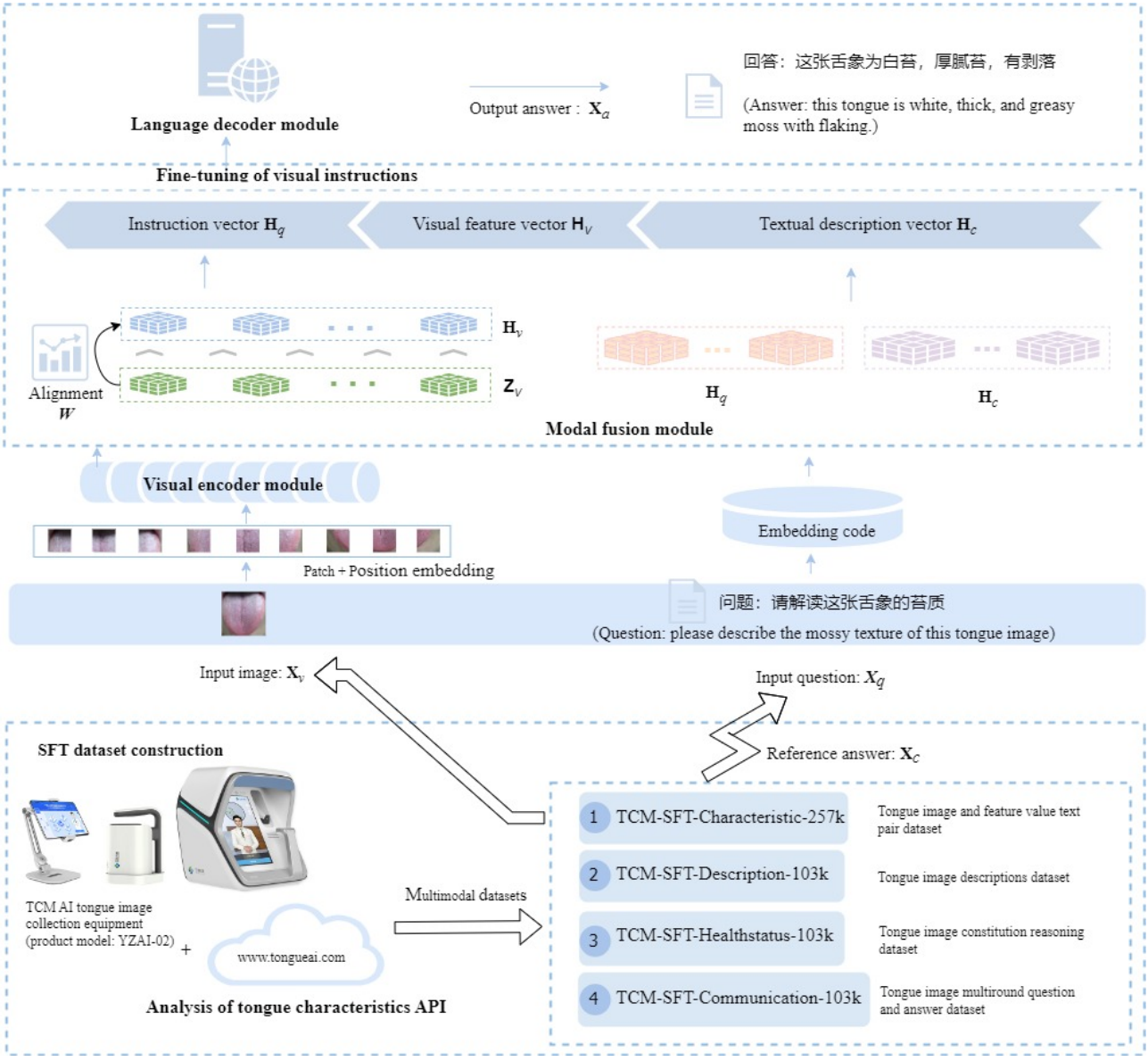

Model Design

Phase 1: Visual Encoder Module

In the first phase, the visual encoder module of the network was designed. Applying tongue images with TCM feature description text pair data in CLIP-ViT pretrained model migration learning. Semantically rich text is used as training labels to project the image feature representations into a kind of encoding that is like the text encoding space, as shown in Figure S1 in Multimedia Appendix 1.

First, we speak of image patch dimensionality reduction preprocessing. Scale the input image $\mathbf{x}_v \in (H,W,C)$ to $\mathbf{x} \in (h,w,C)$ (h is the height, w is the width, and C is the number of channels). Sequence of blocks that transform x into $\mathbf{x}_p \in (N^2,p^2C)$ for image patch operations. The number of blocks is $N^2=(h\times w)/p^2$, and the block dimension is (p^2C); where p is the image patch size. A sequence of blocks is converted into a patch embedding vector $\mathbf{E}_{patch}' \in (N^2,dim)$ by a linear transformation, where dim=1024, p=14, and N= 24. $\boldsymbol{x}_0$ is the zeroth encoding vector taken at the output layer of the transformer encoder, which serves as the visual feature encoding. By adding a learnable embedding vector before the image patch embedding vector E_{patch}, the image block embedding vector becomes $\mathbf{E}_{patch} \in (N^2+1,dim)$. The absolute position encoding algorithm is used to create a learnable position embedding vector $\mathbf{E}_{pos} \in (N^2+1,dim)$ for the block position. The elementwise summation operation on $\mathbf{E}_{patch}$ and $\mathbf{E}_{pos}$ yields an embedding vector $\mathbf{z} \in (N^2+1,\text{dim})$ that incorporates spatial positional encoding and visual representations.

XSL•FO
RenderX

Second, transformer encoder processing. The encoder consists of a stack of **L**=24 encoding layers, and the encoder inputs are image feature embedding vectors $z \in (N^2+1, dim)$. Each encoding layer consists of 2 unitary structures connected: the first unitary structure consists of a multihead self-attention layer and a layer normalization, as well as a residual connectivity module, and the second unitary structure consists of a feedforward fully connected layer multilayer perceptron and a layer normalization, as well as a residual connectivity module.

Phase 2: Modal Fusion Module

The modal fusion module is designed with a multilayer linearly transformed residual architecture, which is a bridging module between the visual model and the language generation model. The tongue visual encoding features are projected into the natural language word embedding vector feature space to solve the conceptual alignment problem of visual encoding with TCM terminology.

The modal fusion module design uses a combination of multiple linear layers and GELU (Gaussian Error Linear Unit) activation functions, as shown in the middle region of Figure S2 in Multimedia Appendix 1. This design allows the modal fusion layers to transform visual features while maintaining essential nonlinear characteristics. In addition, the introduction of the residual structure enables the model to realize efficient feature transformation and projection while fully preserving the integrity of the original visual features.

Splice visual encoding with textual word-embedded encoding to form a sequence of visual-textual instructions. First, the visual encoding feature $\mathbf{Z}_v$ is converted into a visual feature vector $\mathbf{H}_v$, and the textual instruction and textual description are converted into an instruction vector $\mathbf{H}_q$ and a textual description vector $\mathbf{H}_c$ by word embedding encoding, respectively. Thereafter, the vectors are spliced in the order of instruction, visual, and textual description to form the visual-textual fusion instruction sequence data.

Phase 3: Language Decoder Module

The modal fusion module connects the visual encoder and language decoder for end-to-end fine-tuned training on the constructed visual-textual data for a variety of downstream generative output tasks, such as visual quizzing, image description generation, and visual dialogue. The language decoder module chooses LLaMA, a pretrained model with good support for Chinese, which consists of a 32-layer transformer decoder layer, and each decoder layer contains an RMSNorm normalization layer, a grouping attention mechanism, and a multilayer perceptron projection layer. The network architecture is shown on the right side of Figure S2 in Multimedia Appendix 1.

During training, each input image $\mathbf{X}_v$ is associated with a few rounds of dialogue data, where each round of question description can be defined as follows.

The visual encoder module extracts the visual feature V_x (the feature representation obtained by encoding the input image using a visual encoder) and caches it into the context, and the subsequent t-th round (t>1) of training data only needs to input the new instruction and answer . The model automatically fuses the historical dialogue information with the initial visual feature $\mathbf{V}_x$ and builds a spliced sequence of instructions to realize multiple rounds of dialogue training through cross-round dependency.

The instruction sequence of multiple rounds and the corresponding output reply text are temporally spliced into a uniform sequence , the autoregressive training objective is used for instruction tuning, and the maximum likelihood function optimization model is formulated as follows:

where θ is a trainable parameter (the training process is to adjust to maximize the likelihood function) and $\mathbf{X}_{instruct,<i}$,$\mathbf{X}_{a,<i}$ is the instruction sequence and answer sequence of all rounds before the current prediction x_i, respectively. $p(\mathbf{X}_a|\mathbf{X}_v,\mathbf{X}_{instruct})$ is the probability of predicting $\mathbf{X}_a$ under the current $\mathbf{X}_v$ and $\mathbf{X}_{instruct}$ is based on the premise of guaranteeing the accuracy of the result of $\mathbf{X}_a$under the premise that the prediction results of all rounds before the current round takes the maximum probability value.

In other words, the model uses the information accumulated in the history of the previous *t*-1 rounds of the conversation (especially the context of the textual instructions) to accurately estimate the probability distribution of the generated results in the t-th round. In this way, the model can maintain its understanding of the context over consecutive rounds of interactions and accordingly generate accurate responses associated with the content of the previous rounds.

Datasets and Preprocessing

The 90,000 tongue images collected by the TCM artificial intelligence tongue image collection equipment (product model: YZAI-02) jointly developed by Hefei Cloud Diagnostics Information Technology Co and Anhui University of TCM were used, which consists of a standard LED ring light source, a portable collection device, an ultrahigh-definition camera, and a host computer, as well as supporting software. The tongue feature recognition API (application programming interface) was applied to preprocess the collected tongue images with color correction, tongue region segmentation, and tongue moss and tongue texture separation, after which tongue feature analysis was performed on the tongue images to obtain more than 40 types of qualitative or quantitative text containing tongue color, tongue texture, moss color, moss texture, and sublingual collateral data and 10 types of TCM constitution [45].

The TongueVLM training datasets are constructed, including TCM feature description data (traditional Chinese medicine–supervised fine-tuning, TCM-SFT (TCM–supervised fine-tuning)-Characteristic-257k, and TCM-SFT-Description-103k), multiround Q&A data

XSL•FO
RenderX

(TCM-SFT-Healthstatus-103k), and physical constitution reasoning data (TCM-SFT-Communication-103k). The methodology for constructing the dataset is described in Multimedia Appendix 1. The distribution of the tongue image features in the dataset is shown in Figures S3 and S4 in Multimedia Appendix 1.

Model Training Strategy

Stage 1: Pretraining of the Visual Encoder

TCM tongue characterization datasets (TCM-SFT-Characteristic-257k) of 257,000 tongue images and characterization texts are constructed, and the zeroth encoding vector used for learning by comparing the similarity between the tongue images and their corresponding tongue manifestation characterization is used for training the fine-tuning of the tongue visual encoder.

The process to obtain the visual encoder model is as follows: first, the training parameters openai/clip-vit-large-patch14-336 (OpenAI Inc, pretrained weights for the clip model on 400 million text-image pairs) were used as the initial weights for the visual encoder and the text transformer encoder. The Adam optimizer was used in the model training, with the smoothing constant betas set to (0.9, 0.999) and the weight decay parameter weight_decay set to 1e-3, the training batch size was set to 8, the learning rate was 5e-5, the number of training epochs was 3, and the maximum sequence length was 77. Second, the loss function uses the cosine similarity $Cos(I_m,T_n),m\in[1\ldots N^2],n\in[1\ldots N^2]$, where I_m is the embedding vector encoded by visual features and T_n is the embedding vector encoded by textual semantics. The optimization objective is to maximize the cosine similarity $Cos(I_j,T_j)$ between correct image-text pair embeddings while minimizing the cosine similarity $Cos(I^j,T^k),j\neq k$ of incorrect image-text pair embeddings. The results show that the loss value stabilizes after 3 epochs of training, and the loss curves are shown in Figure 2.

Figure 2. Visual encoder training loss and dynamic learning rate curves. The loss curve shows that after 3 rounds of training, the training loss of modal fusion has gradually stabilized, indicating that the model is beginning to converge.

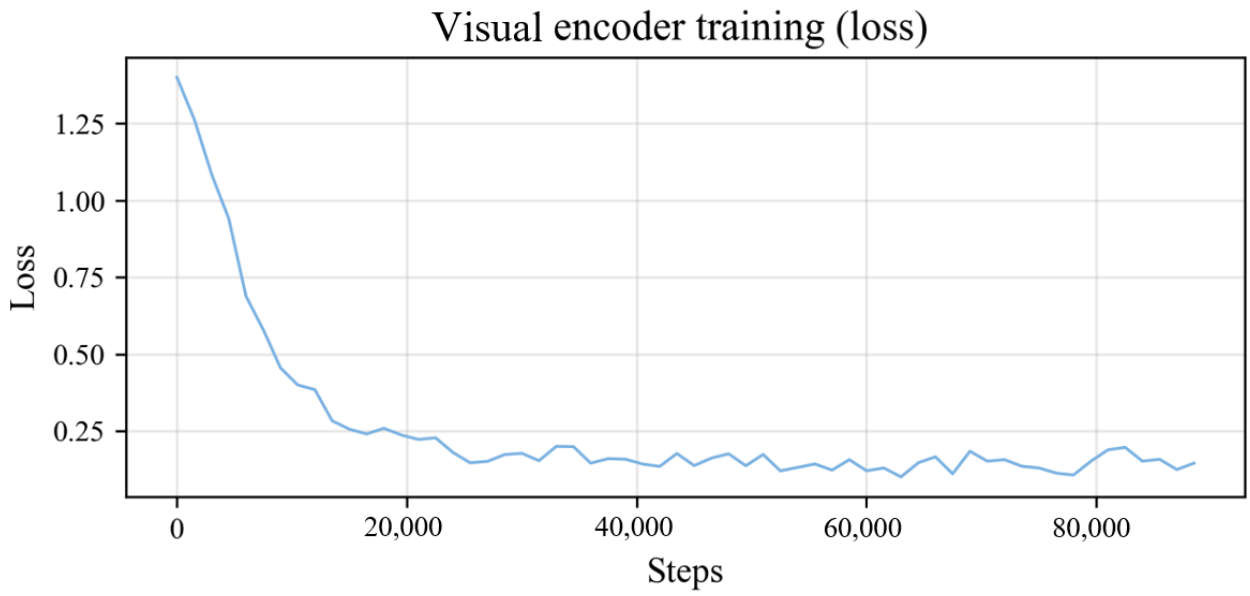

Stage 2: Training of the Fusion Modal

TCM tongue description datasets (TCM-SFT-Description-103k) of 103,000 tongue images and description text are constructed, the visual encoder of TongueVLM and the network weights of the LLM are frozen, the visual-textual multimodal instruction data are fed into the LLM, and the modal fusion module is fine-tuned for training.

The process to obtain the modal fusion model is, first, the training method and parameters are as follows: the pretrained visual encoder weight parameters are loaded, the modal fusion layer weight parameters are randomly initialized, and only the modal fusion layer weights are allowed to participate in the gradient update. The Adam optimizer was used in the model training, with the smoothing constant betas set to (0.9, 0.999) and the weight decay parameter weight_decay set to 1e-4, the training batch size on each GPU is 8, the gradient accumulation step is 8, the learning rate is 2e-5, and the total number of iteration rounds is 3. Spend 30 hours to complete all the training on the Ubuntu (version 20.04.6, Canonical Ltd) platform using 2×RTX4090. Second, the loss function adopts the cross-entropy loss , where C is the total number of word lists, L is the length of the prediction sequence, $S_{n,i}$ denotes the probability that the word in the ith position is the nth word in the lexicon based on the previously known sequence, and $y_{n,i}$ denotes the ground-truth labels in the ith position in the prediction sequence (expressed as 1-hot encoding; ie, if the corresponding word in the position is the nth vocabulary word in the lexicon, only the first element of the 1-hot vector is 1 and the rest are 0), the goal is to minimize the loss; when the probability of each word in the prediction sequence is infinitesimally close to the actual vocabulary 1-hot encoding, that is, for any position i in the prediction sequence, $S_{n,i}\approx y_{n,i}$, the loss will be minimized, and

XSL•FO
RenderX

at this time, the model is considered to be in the optimal state. The results show that the loss value stabilizes after 3 epochs of training, and the loss curves are shown in Figure 3.

Figure 3. Loss curve of the modal fusion model. It shows that after 3 training epochs, the model enters a stable convergence state, and the loss curve for its modal fusion training stabilizes.

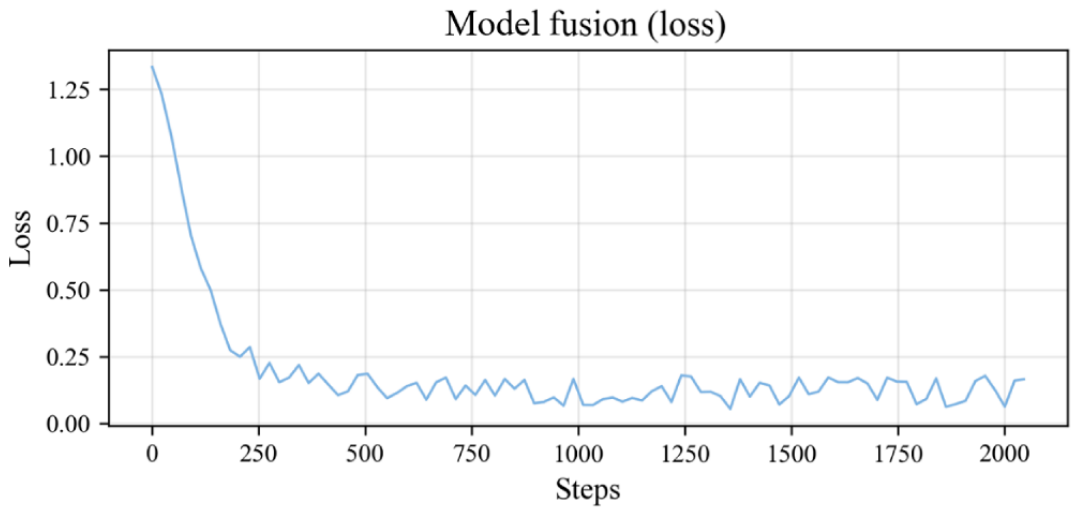

Stage 3: End-to-End Fine-Tuning of TongueVLM

The training data are the TCM multimodal dataset (training set 510,000; validation set 25,000). First, of the training method and parameters, load the pretrained visual encoder weight parameters and modal fusion layer weight parameters, freeze the weight parameters of the visual encoder, and allow only the modal fusion layer and the language decoder weights to participate in the gradient update. The Adam optimizer was used in the model training, with the smoothing constant betas set to (0.9, 0.999) and the weight decay parameter weight_decay set to 1e-4, the training batch size is set to 8 on each GPU, the number of gradient accumulation steps is 8, the learning rate is 2e-5, and the total number of iteration rounds is 3. It takes 135 hours to complete all the training on the Ubuntu (version 20.04.6, Canonical Ltd.) platform using 2×RTX4090. Second, of loss function, the cross-entropy loss function is adopted, and the loss curve is shown in Figure 4. After 4000 iterations, the loss tends to stabilize, and the loss fluctuation is very small when the number of iterations is 8000; currently, the model has converged.

Figure 4. Fine-tuned training loss curve of TongueVLM. It shows that with the increase of training epochs, the fine-tuning training loss of TongueVLM gradually tends to stabilize, indicating the effectiveness of the optimization algorithm and the basic convergence of the model after about 8000 iterations.

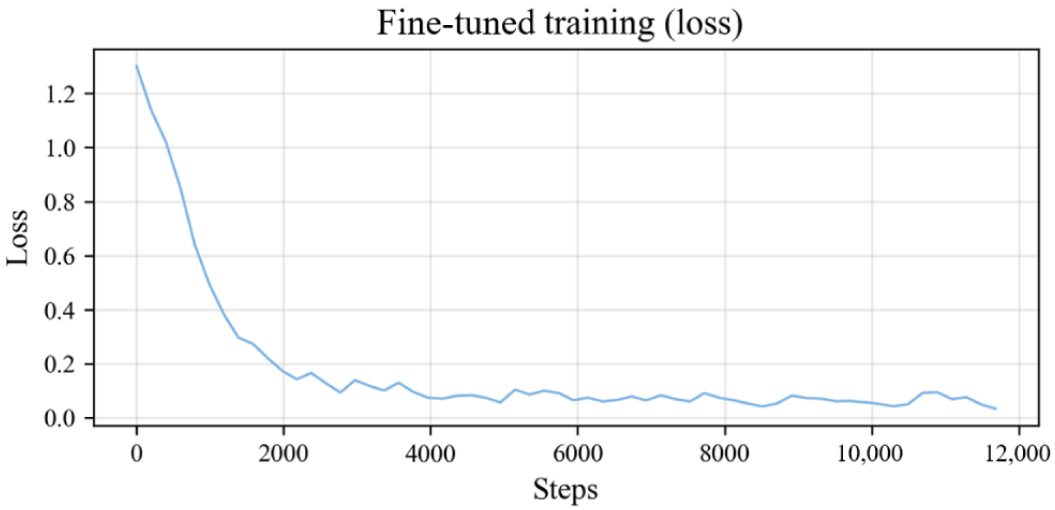

Ethical Considerations

This study was conducted in accordance with the ethical standards of the Declaration of Helsinki and was approved by the ethics committee of the Second Clinical Medical School of Anhui University of Chinese Medicine (Anhui Acupuncture and Hospital). The data used in this research were sourced from 2 distinct origins. First, for data from the Yunzhen 365 app, the data consisted of deidentified user-uploaded tongue images and associated text. All users of the app provided informed consent upon registration, agreeing to the use of their anonymized data for research purposes in accordance with the app's terms of

XSL•FO
RenderX

service and privacy policy. Second, for data from hospital records, the clinical data were obtained with approval from the relevant hospital's institutional review board (2022-zjks-25). Patient confidentiality was strictly maintained, and all personal identifiers were removed before analysis.

All procedures involving human data were reviewed and approved by the appropriate ethics committees. No additional identifiable personal information was accessed or used in this study. Participants received no compensation for their involvement in this study.

Results

Overall Performance of TongueVLM on Benchmark Tasks

The performance evaluation of the TongueVLM on the TCM multimodal test dataset is as follows.

To determine whether the answer texts generated by professional TCM practitioners are close in meaning to the standard answer texts in the corresponding test set, the evaluation is divided into 3 results; according to the degree of similarity in meaning, we define a score value Score for it, in descending order: consistent (Score=100), similar (Score=50), and irrelevant (Score=0); the accuracy of TongueVLM on the test set can be expressed as follows: , where N is the number of test datasets and $Score_i$ is the score of the i-th test dataset.

To directly verify the effectiveness of the improved methods proposed in this study for the field of TCM, we selected visual multimodal models with similar architectures for comparison: LLaVA-1.5 (released in October 2023; Meta Platforms, Inc), LLaVA-1.6 (released in January 2024; Meta Platforms, Inc), and LLaVA-OneVision (released in August 2024; Meta Platforms, Inc). To demonstrate that good results can be achieved in the field of TCM through targeted model design without relying on massive general data, we also compared it with the current open-source multimodal large model benchmark Qwen2.5-VL-7B (released in August 2024; Alibaba Cloud). The accuracy and performance are shown in Table 1. The experimental results show that the TongueVLM model outperforms the general-purpose large model on all 3 tasks; it is 9.1%, 8.4%, and 1.1% more accurate than LLaVA-OneVision and 7.5%, 7%, and 5.9% more accurate than Qwen2.5-VL-7B. The generation time efficiency of each large model is similar, with the generation time of text being 24 tokens per second (approximately 40 words per second, given the word-to-token ratio in our dataset). Due to the optimization of the lexicon in the field of TCM, TongueVLM inference speed is slightly faster than the baseline model.

Table 1. Evaluation indicators for the output of the model. Shows the evaluation metrics of the model output. Experiments are conducted using the test dataset of 3 multimodal datasets, with each test dataset containing 3000 samples with detailed data represented as: number of scores 0, number of scores 50, number of scores 100/total number of test datasets.

Model	TCM-SFT[a]-Description-103k			TCM-SFT-Healthstatus-103k			TCM-SFT-Communication-103k		
	Test result details	Accuracy (%)	Mean time (SD, s)	Test result details	Accuracy (%)	Mean time (SD,s)	Test result details	Accuracy (%)	Mean time (SD,s)
CNN[b] parallel computing	167,58,2775/3000	79	1.48 (>6)	—[c]	—	—	—	—	—
LLaVA-1.5	1730,973,297/3000	26.1	0.27 (1.25)	1828,920,252/3000	23.7	0.24 (1.5)	1174,1653,173/3000	33.3	0.64 (3)
LLaVA-1.6	568,1285,1147/3000	59.7	0.21 (1.55)	545,1241,1214/3000	61.2	0.21 (1.5)	690,1094,1216/3000	58.8	0.62 (3)
LLaVA-OneVision	393,974,1633/3000	70.7	0.17 (1.54)	423,941,1636/3000	70.2	0.25 (1.5)	635,1156,1209/3000	59.6	0.86 (3)
Qwen2.5-VL-7B	412,836,1752/3000	72.3	0.18 (1.48)	420,866,1714/3000	71.6	0.15 (1.4)	519,1672,809/3000	54.8	0.69 (3)
TongueVLM	305,599,2096/3000	79.8	0.11 (1.25)	353,577,2070/3000	78.6	0.20 (1.5)	428,1502,1070/3000	60.7	0.54 (3)

[a]TCM-SFT: traditional Chinese medicine–supervised fine-tuning.

[b]CNN: convolutional neural network.

[c]Not available.

Ablation Studies on the 3-Stage Training Strategy

Visual Encoding Feature Layer Comparison Experiment

The visual encoder extracts image features and outputs a total of 24 hidden layers (disregarding the hidden layer feature values before being input into the visual encoder), and it is necessary to select the appropriate layer as the visual feature information input. Therefore, comparison experiments were conducted on 3 datasets, and the last 5 hidden layers (20th to 24th) features were selected as the visual feature information to train the TongueVLM model; the accuracies on the test datasets are shown in Table 2 below. The experimental results show that the model performs best in all tasks when the penultimate layer of features output from the visual encoder, that is, the 23rd layer of features, is selected as the final visual feature information. These findings reveal that the visual features extracted at that depth level have significant advantages for multimodal intelligent analysis related to TCM tongue diagnosis.

XSL•FO
RenderX

Table 2. Accuracy of different hidden layers as a visual encoder in the test dataset. A total of 500 samples were randomly selected from each of the 3 multimodal test datasets for experimentation. It shows the accuracy of different hidden layers as visual encoders in the test dataset, with detailed data represented as: number of scores 0, number of scores 50, number of scores 100/total number of test datasets).

Hidden layers	TCM-SFT[a]-Description-103k		TCM-SFT-Healthstatus-103k		TCM-SFT-Communication-103k	
	Test result details	Accuracy (%)	Test result details	Accuracy (%)	Test result details	Accuracy (%)
Layer-24	54,102,344/500	79	44,29,427/500	88.3	60,29,411/500	85.1
Layer-23	51,100,349/500	79.8	44,26,430/500	88.6	60,23,417/500	85.7
Layer-22	52,105,343/500	79.1	45,37,418/500	87.3	63,25,412/500	84.9
Layer-21	52,114,334/500	78.2	45,49,406/500	86.1	63,32,405/500	84.2
Layer-20	55,117,328/500	77.3	48,48,404/500	85.6	65,47,388/500	82.3

[a]TCM-SFT: traditional Chinese medicine–supervised fine-tuning.

Modal Fusion Module Structure Experiment

To verify the reasonableness of the structure of the modal fusion module, 3 different neural network structures, namely, numbers 1 (Linear + GELU), 2 (Linear + GELU + Linear + GELU + Linear), and 3 (Linear + GELU + Linear + GELU + Linear + Linear + Res), are designed, and initial weights are randomized with the same datasets; the accuracy on the test datasets is shown in Table 3. The results show that the difference in the effect of the 3 structures on the final performance is not significant. However, the use of the fusion structure of group number 3, containing multilayer linear transformation, together with a multilayer nonlinear activation function and the introduction of residual connections, slightly outperforms the performance of the other schemes. Therefore, group number 3 is chosen as the neural network structure for modal fusion learning.

Table 3. Comparative analysis of the modal fusion neural network structure in terms of accuracy on the test datasets. A total of 500 samples were randomly selected from each of the 3 multimodal test datasets for experimentation with detailed data represented as: number of scores 0, number of scores 50, number of scores 100/total number of test datasets.

Number	TCM-SFT[a]-Description-103k		TCM-SFT-Healthstatus-103k		TCM-SFT-Communication-103k	
	Test result details	Accuracy (%)	Test result details	Accuracy (%)	Test result details	Accuracy (%)
1	55,99,346/500	79.1	46,26,428/500	88.2	62,27,411/500	84.9
2	54,98,348/500	79.4	45,29,426/500	88.1	60,27,413/500	85.3
3	51,100,349/500	79.8	44,26,430/500	88.6	60,23,417/500	85.7

[a]TCM-SFT: traditional Chinese medicine–supervised fine-tuning.

Modal Fusion Module Pretraining Experiment

The weight parameters of the modal fusion are also fine-tuned for training during the overall training of the TongueVLM model; thus, the pretraining of the modal fusion is compared to that of number 1, the pretraining is fine-tuned individually, and number 2 is randomly initialized in TongueVLM without pretraining. The accuracy of the 3 test datasets is shown in Table 4 below. The results show that the accuracy improvement using the individually fine-tuned pretraining approach is significant, with 2.3%, 5%, and 3.5% improvement for the 3 datasets, respectively. Fine-tuning the modal fusion layer using the Chinese interpretation feature description data allows the model to focus more on constructing and optimizing higher-order correspondences between visual-language features.

Table 4. Evaluation of pretraining methods for modal fusion modules. A total of 500 samples were randomly selected from each of the 3 multimodal test datasets for experimentation with detailed data represented as: number of scores 0, number of scores 50, number of scores 100/total number of test datasets.

Numbers	TCM-SFT[a]-Description-103k		TCM-SFT-Healthstatus-103k		TCM-SFT-Communication-103k	
	Test result details	Accuracy (%)	Test result details	Accuracy (%)	Test result details	Accuracy (%)
1	51,100,349/500	79.8	44,26,430/500	88.6	60,23,417/500	85.7
2	53,119,328/500	77.5	46,73,381/500	83.5	63,52,385/500	82.2

[a]TCM-SFT: traditional Chinese medicine–supervised fine-tuning.

Analysis of Module Effectiveness and Interpretability

In this experiment, the visualization of the projection of the attention weight values of the multihead self-attention layer during the forward computation of the visual encoder to the image is investigated, and pseudo-color maps of the regional thermal response during the visual encoding process for typical texture feature locations on the surface of the tongue image are generated.

XSL•FO
RenderX

The multihead attention weights during the forward propagation of the cached visual encoder are Atten_weights$\in R^{(num_heads,dim,dim)}$, where num_heads$\in$(1,2,…,16) is the number of heads of multihead attention, and *dim*=577 is the length of the encoding sequence. The 0th position of the encoding sequence is the classification head, and the $E_i \in R^{(dim-1,dim-1)}$ vector represents the correlation between the 24 × 24 patches of the image in the ith attention header.

As shown in Figure 5, feature locations were selected in the tongue image; Figure 5A for fissured and teeth-marked tongues, and Figure 5B for peeled fur and yellow moss. The attention weights for the specified location are projected into the pseudo-color map of the original image. The text labels of the top 5 tongue features are obtained as output, with red indicating incorrect prediction and green indicating correct prediction, and the length of the color indicates the magnitude of its probability.

Through the feature attention visualization map, it can be seen that the visual encoder for tongue texture features focuses on localized regional positional responses, while the tongue color feature focuses on the overall area response of the image, so that the visual encoder can learn the effective feature information on the tongue, which provides good support for the subsequent feature fusion.

Figure 5. Visualization of the thermal response of the visual encoder's multihead attention. Presents the top 5 categories and their confidence levels of tongue image features predicted by the model in text form. Green represents correctly predicted labels, red represents incorrectly predicted labels, and the length of the color bars intuitively indicates the probability of the prediction.

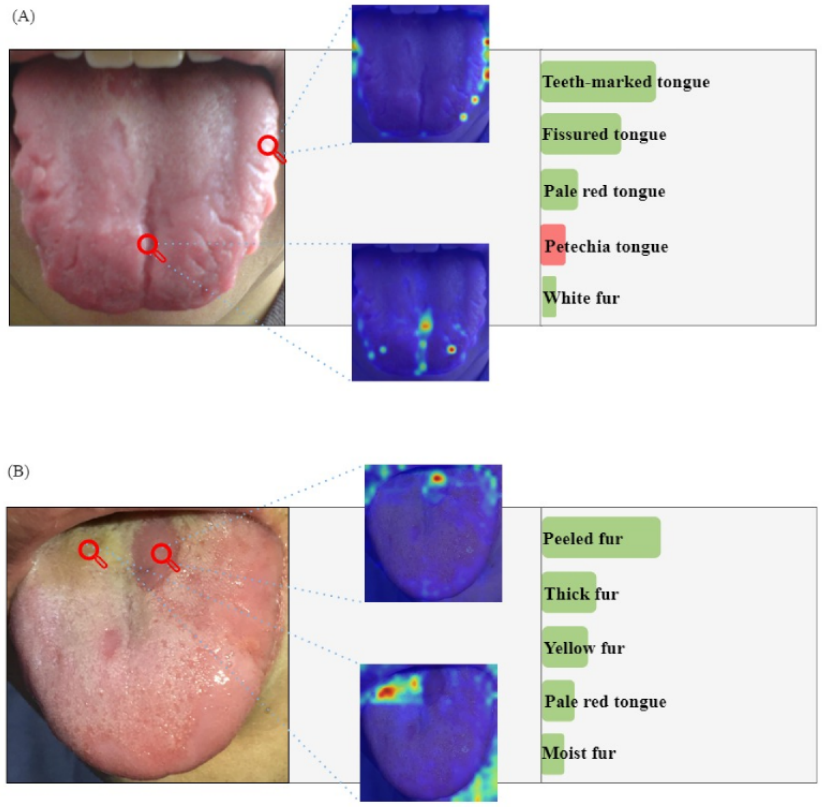

Validation of Multimodal Capabilities Across Tasks

Tongue Image Description Generation Capability

In the task of describing the tongue images, we observe that LLaVA-1.6, LLaVA-OneVision, and Qwen2.5-VL-7B all generate output answers according to structured texts. Moreover, the text of LLaVA-1.6's response to the tongue surface image was intermingled with the description of the tongue sublingual veins. This type of response may be a language hallucination of the LLM. The output text of the TongueVLM is relatively short, but in terms of content, it focuses mainly on image color, texture, and morphological information. Representative examples of model outputs are shown in Table S1 in Multimedia Appendix 1. The tongue feature interpretation of the TongueVLM model is closer to the results of visual model recognition, which fully demonstrates that the TongueVLM model, which has been fine-tuned with the tongue multimodal datasets, solves the conceptual alignment between the visual encoding of the images and the TCM terminology.

Physical Constitution Reasoning and Analysis Capability

In the task of physical constitution reasoning about the tongue image, we observe that the output of the LLaVA-1.5 model completely deviates from the TCM context and seems to lack an understanding of the concept of TCM physique, and the LLaVA-1.6 model outputs the reasoning thinking about TCM physique through the tongue image. The LLaVA-OneVision model misjudges the tongue feature as a red tongue, but can reason about the physical constitution in combination with the tongue feature. Of course, the output is also wrong.

XSL•FO
RenderX

QWen2.5-VL-7B still follows some kind of templated output content, which is accurate in understanding the tongue color and color of the tongue fur features, but misclassifies the tongue shape as fat and large and dentate to the extent that the analysis of the physical constitution is not accurate enough.

In contrast, the TongueVLM model shows professional advantages in the TCM field in terms of effectively recognizing the tongue features and then briefly outputs the results through the tongue features, but its language expression level is slightly rough and needs to be further improved. Representative examples of model outputs are shown in Table S2 in Multimedia Appendix 1.

Tongue Image Dialogue Capability

In the multiround dialogue task of TCM with tongue images, we observe that all the models can accurately recognize the teeth-marked tongue feature in the tongue image in the first round of dialogue, and LLaVA-1.6 not only interprets the tongue feature dimension but also associates more scientific knowledge with the physical condition. However, in the second round of dialogue, LLaVA-1.5 and LLaVA-1.6 gave vague answers of "possibly related." Moreover, LLaVA-OneVision and Qwen2.5-VL-7B were able to provide definite answers, but they were not related to the teeth-marked tongue feature in the previous round of dialogue. The TongueVLM model combines the content of the teeth-marked tongue feature and provides the exact answer; thus, the TongueVLM model still outperforms the other models. Representative examples of model outputs are shown in Table S3 in Multimedia Appendix 1.

The experimental results show that the TongueVLM model outperforms the general-purpose large model on all 3 tasks. First, in terms of tongue feature descriptions, the TongueVLM model is closest to the recognition results of the visual model and includes color and morphological features and local positional features, and the parallel computation time of multiple visual models is greater than that of the large model, which fully reflects the image feature retention ability and computational performance of the TongueVLM visual encoder. Second, in terms of physical constitution reasoning, it is obvious that LLaVA-1.5 does not have expertise in TCM. LLaVA-1.6, LLaVA-OneVision, and Qwen2.5-VL-7B are generated by interpreting the text according to the unified paradigm; it cannot distinguish between tongue photos and sublingual photos, and identifying the positive and negative features is difficult. The TongueVLM model, on the other hand, quantitatively analyzes and localizes the positive features of the tongue image and can reason about the physical constitution based on the tongue image features, with an accuracy of 78.6%. The traditional method requires multiple visual models to extract the tongue features and then input the feature data into decision trees, support vector machines, and other classifiers for supervised learning of somatic qualities, which is less efficient to execute. Third, in terms of multiround Q&As, the TongueVLM model's interactive answers are brief, the contextual correlation is stronger, and the language discourse is not as strong as that of LLaVA-1.6, but its overall answers are more precise and concise, and language generation is not an advantage of the visual model.

Discussion

Principal Findings

This study proposes a TongueVLM network architecture design and a 3-stage training framework, achieving state-of-the-art performance on multimodal tongue image diagnosis tasks. Crucially, ablation experiments confirm that the staged training strategy is essential for stable optimization, while visual analysis demonstrates that the model spontaneously focuses on tongue regions relevant to clinical diagnosis.

The TongueVLM multimodal model proposed in this study is characterized by the following key features. First, the visual encoder characterizes the image features with the language encoding of low-dimensional vectors and approximates the feature extraction capability of the visual model by migration learning of TCM images from the CLIP-ViT pretrained model, which is a key step in the visual-to-large language model. Second, the modal fusion module splices visual and textual instruction data, realizes a seamless connection between natural language and image feature information, and unifies the multimodal data format input to the large model. Third, the TongueVLM model is fine-tuned and trained end-to-end on the TCM dataset. The model exhibits high accuracy in all 3 tasks of tongue feature description generation, physical constitution reasoning, and multiround dialogue.

Limitations and Future Work

This study has several limitations. First, the current data modality only includes tongue image and text-based question-answering data, failing to encompass the complete information system of TCM's "observation, auscultation, inquiry, and palpation." Second, the dataset's diversity requires enhancement, with shortcomings in ethnic distribution and standardization of image acquisition environments, which may compromise the model's generalizability. Third, evaluation of generated texts (eg, tongue pattern descriptions) still relies on expert judgments with inherent subjectivity, lacking objective, fine-grained automated assessment criteria. Finally, the model's generalization capability for clinically rare tongue patterns remains to be validated.

Future research may explore the following directions: first, in terms of model architecture, a gating mechanism is introduced to achieve adaptive attention regulation. Meanwhile, it is considered to incorporate modules such as depth-wise separable convolution to compensate for the shortcomings of self-attention mechanisms in capturing local detail features. Second, expand multimodal data sources by systematically integrating comprehensive information from facial diagnosis, pulse diagnosis, olfactory diagnosis, and physical constitution identification to construct a full-disease-course diagnostic model more aligned with TCM's holistic perspective. Third, fuse multidimensional data acquisition technologies such as 400-1000 nm spectral data and thermal infrared imaging data, and 3D tongue morphology to establish a more refined quantitative tongue pattern characterization system. Fourth, explore automated evaluation frameworks based on LLMs to achieve fine-grained quantitative assessments of the professionalism, consistency, and logical coherence of generated content. Fifth,

XSL•FO
RenderX

advance prospective trials in collaboration with clinical institutions to validate the model's auxiliary diagnostic efficacy and clinical applicability in real-world diagnostic settings. Sixth, currently, TongueVLM is built upon a 7B-parameter model, and its deployment still imposes certain computational requirements. We will explore parameter-efficient fine-tuning techniques (eg, low-rank adaptation) and model quantization. Finally, the model will incorporate continuous learning mechanisms to iteratively improve its tongue image recognition accuracy and diagnostic reasoning ability, thereby advancing research on artificial intelligence–assisted TCM tongue diagnosis.

Conclusions

Intelligent diagnosis and treatment technology in the field of TCM is often based on knowledge graphs, deep learning visual models, and machine learning approaches. Traditional supervised learning is limited by the quality and size of the training data, as well as the difficulty of fusion with natural language and its limited generalizability. The findings demonstrate that the TongueVLM model achieves ideal results in terms of understanding tongue images, constitutive reasoning, and dialogue abilities, and provides a foundational framework suitable for future integration into a Chinese medicine intelligent diagnosis system.

Funding

We are thankful for funding support from the Project of Plans for Major Provincial Science & Technology (202303a07020008) and Xin'an Institute of Medicine and Modernization of TCM Research and Development Project: "Leading the Charge with Open Competition" (2024CXMMTCM002).

Data Availability

The datasets generated and/or analyzed during this study are available from the corresponding author upon reasonable request.

Authors' Contributions

All authors contributed to this study's conception and design. Material preparation, data collection, and analysis were performed by CP, JG, NY, YW, RC, and CD. The first draft of this paper was written by CP, and all authors commented on previous versions of this paper. All authors read and approved this final paper.

Conflicts of Interest

None declared.

Multimedia Appendix 1
Tables (S1-S3) and figures (S1-S4), formulas, and example data.
[DOCX File , 33112 KB - medinform_v14i1e87237_app1.docx]

References

1. Pak S, Son HJ, Kim D, Woo JY, Yang IK, Hwang HS, et al. Comparison of CNNs and transformer models in diagnosing bone metastases in bone scans using Grad-CAM. Clin Nucl Med 2025;50(7):596-604. [doi: 10.1097/RLU.0000000000005898] [Medline: 40237349]
2. Zhang Y, Wang J, Górriz JM, Wang S. Deep learning and vision transformer for medical image analysis. J Imaging 2023;9(7):147 [FREE Full text] [doi: 10.3390/jimaging9070147] [Medline: 37504824]
3. Nurgazin M, Tu NA. A comparative study of vision transformer encoders and few-shot learning for medical image classification. 2023 Presented at: IEEE/CVF International Conference on Computer Vision Workshops (ICCVW); 2025 Oct 19; Honolulu, Hawaii p. 2505-2513. [doi: 10.1109/iccvw60793.2023.00265]
4. Dayan B. Lung disease detection with vision transformers: a comparative study of machine learning methods. arXiv Preprint posted online on Nov 18, 2024. [doi: 10.48550/arXiv.2411.11376]
5. Falqueto P, Sanfeliu A, Palopoli L, Fontanelli D. Learning priors of human motion with vision transformers. In: IEEE. 2025 Presented at: 2024 IEEE 48th Annual Computers, Software, and Applications Conference (COMPSAC); July 02-04, 2024; Osaka, Japan p. 1-9. [doi: 10.1109/COMPSAC61105.2024.00060]
6. Zhang H, Ramachandra R, Raja K, Busch C. Generalized single-image-based morphing attack detection using deep representations from vision transformer. 2024 Presented at: IEEE/CVF Conference on Computer Vision and Pattern Recognition Workshops (CVPRW); June 17, 2024; Seattle, WA p. 1510-1518. [doi: 10.1109/cvprw63382.2024.00158]
7. Sheffield B, Ellen J, Whitmore B. On vision transformers for classification tasks in side-scan sonar imagery. arXiv Preprint posted online on Sep 18, 2024. [doi: 10.48550/arXiv.2409.12026]
8. Gao W, Han B, Sun Z, Yan Y, Ye Y, Feng J, et al. A novel system for precise identification and explainability analysis based on multimodal learning combining laser-induced breakdown spectroscopy and laser-induced plasma acoustic signals. Talanta 2025;293:128182. [doi: 10.1016/j.talanta.2025.128182] [Medline: 40252502]

XSL•FO
RenderX

9. Singh G. Comparative analysis of vision transformers and traditional deep learning approaches for automated pneumonia detection in chest X-Rays. arXiv Preprint posted online on Jul 11, 2025. [doi: 10.48550/arXiv.2507.10589]
10. Alqutayfi A, Almattar W, Al-Azani S, Khan FA, Qahtani AA, Alageel S, et al. Explainable disease classification: exploring Grad-CAM analysis of CNNs and ViTs. JAIT 2025;16(2):264-273. [doi: 10.12720/jait.16.2.264-273]
11. Zhang W, Belcheva V, Ermakova T. Interpretable deep learning for diabetic retinopathy: a comparative study of CNN, ViT, and hybrid architectures. Computers 2025;14(5):187. [doi: 10.3390/computers14050187]
12. Amangeldi A, Taigonyrov A, Jawad MH, Mbonu CE. CNN and ViT efficiency study on tiny ImageNet and DermaMNIST datasets. arXiv Preprint posted online on Feb 13, 2026. [doi: 10.48550/arXiv.2505.08259]
13. Mehdipour S, Mirroshandel SA, Tabatabaei SA. Vision transformers in precision agriculture: a comprehensive survey. Intell Syst Appl 2026;29:200617. [doi: 10.1016/j.iswa.2025.200617]
14. Agarwal A, Gearon J, Rank R, Chenevert E. Fighting fires from space: leveraging vision transformers for enhanced wildfire detection and characterization. arXiv Preprint posted online on Apr 18, 2025. [doi: 10.48550/arXiv.2504.13776]
15. Haotian L, Chunyuan L, Qingyang W, Lee YL. Visual instruction tuning. 2023 Presented at: Proceedings of the 37th International Conference on Neural Information Processing Systems; December 10-16, 2023; New Orleans, LA p. 1516. [doi: 10.5860/choice.189890]
16. Liu H, Li C, Li Y, Lee YJ. Improved baselines with visual instruction tuning. 2024 Presented at: 2024 IEEE/CVF Conference on Computer Vision and Pattern Recognition (CVPR); June 16-22, 2024; Seattle, WA p. 26286-26296. [doi: 10.1109/cvpr52733.2024.02484]
17. Li B, Zhang Y, Guo D. LLaVA-OneVision: easy visual task transfer. arXiv Preprint posted online on Oct 26, 2024. [doi: 10.48550/arXiv.2408.03326]
18. Yang Z, Li L, Lin K. The dawn of LMMs: preliminary explorations with GPT-4V(ision). arXiv Preprint posted online on Oct 11, 2023. [doi: 10.48550/arXiv.2309.17421]
19. Gemini T, Georgiev P, Lei V. Gemini 1.5: unlocking multimodal understanding across millions of tokens of context. arXiv Preprint posted online on Dec 16, 2024. [doi: 10.48550/arXiv.2403.05530]
20. Dehghani M, Djolonga J, Mustafa B. Scaling vision transformers to 22 billion parameters. arXiv Preprint posted online on Feb 10, 2023. [doi: 10.48550/arXiv.2302.05442]
21. Xuyan H, Meng S, Chengxing S, Haoxuan L, Jianlin Z. Visual-language reasoning large language models for primary care: advancing clinical decision support through multimodal AI. Vis Comput 2025;41(13):11327-11348. [doi: 10.1007/s00371-025-04109-y]
22. Thapa S, Naseem U, Zhou L. Vision-language models for biomedical applications. 2024 Presented at: Proceedings of the First International Workshop on Vision-Language Models for Biomedical Applications; Oct 28-Nov 1, 2024; Melbourne, Victoria, Australia p. 1-2. [doi: 10.1145/3689096.3690770]
23. Raminedi S, Shridevi S, Won D. Multi-modal transformer architecture for medical image analysis and automated report generation. Sci Rep 2024;14(1):19281 [FREE Full text] [doi: 10.1038/s41598-024-69981-5] [Medline: 39164302]
24. AlShibli A, Bazi Y, Rahhal MMA, Zuair M. Vision-BioLLM: large vision language model for visual dialogue in biomedical imagery. Biomed Signal Proc Control 2025;103:107437. [doi: 10.1016/j.bspc.2024.107437]
25. Kalpelbe BC, Adaambiik AG, Peng W. Vision language models in medicine. arXiv Preprint posted online on Feb 24, 2025. [doi: 10.48550/arXiv.2503.01863]
26. Peng C, Zhang K, Lyu M, Liu H, Sun L, Wu Y. Scaling up biomedical vision-language models: fine-tuning, instruction tuning, and multi-modal learning. J Biomed Inform 2025;171:104946. [doi: 10.1016/j.jbi.2025.104946] [Medline: 41138953]
27. Liu Y, Fan L, Zhao M, Wei D, Zhao M, Dong Y, et al. Study on a traditional chinese medicine constitution recognition model using tongue image characteristics and deep learning: a prospective dual-center investigation. Chin Med 2025;20(1):84 [FREE Full text] [doi: 10.1186/s13020-025-01126-w] [Medline: 40506765]
28. Jiatuo XU, Tao J, Shi L. Research status and prospect of tongue image diagnosis analysis based on machine learning. Digital Chin Med 2024;7(1):3-12. [doi: 10.1016/j.dcmed.2024.04.002]
29. Tian-Yu GU, Zhuang-Zhi Y, Jie-Hui J. Classifying Chinese medicine constitution using multimodal deep-learning model. Chin J Integr Med 2024;30(2):163-170. [doi: 10.1007/s11655-022-3541-8]
30. Ye Q, Liu J, Chong D. Qilin-Med: Multi-stage knowledge injection advanced medical large language model. arXiv Preprint posted online on Apr 17, 2024. [doi: 10.48550/arXiv.2310.09089]
31. Jia Y, Ji X, Wang X, Zhang H, Meng Z, Zhang J, et al. Qibo: a large language model for traditional chinese medicine. Expert Syst Appl 2025;284:127672. [doi: 10.1016/j.eswa.2025.127672]
32. Yu S, Xu X, Xu F. Enhancing the traditional chinese medicine capabilities of large language model through reinforcement learning from AI Feedback. arXiv Preprint posted online on Nov 1, 2024. [doi: 10.48550/arXiv.2411.00897]
33. Xie J, Yu Y, Zhang Z. TCM-Ladder: a benchmark for multimodal question answering on traditional chinese medicine. arXiv Preprint posted online on Oct 24, 2025. [doi: 10.48550/arXiv.2505.24063]
34. Sun Z, Huang R, Feng J. DoPI: doctor-like proactive interrogation LLM for traditional chinese medicine. arXiv Preprint posted online on Jul 7, 2025. [doi: 10.48550/arXiv.2507.04877]
35. Wei S, Peng X, Wang Y, Shen T, Si J, Zhang W, et al. BianCang: a traditional chinese medicine large language model. IEEE J Biomed Health Inf 2025:1-12. [doi: 10.1109/jbhi.2025.3612415]

XSL•FO
RenderX

36. Khattak MU, Kunhimon S, Naseer M. UniMed-CLIP: towards a unified image-text pretraining paradigm for diverse medical imaging modalities. arXiv Preprint posted online on Dec 13, 2024. [doi: 10.48550/arXiv.2412.10372]
37. LASA Team, Xu W, Chan HP, Li L. Lingshu: a generalist foundation model for unified multimodal medical understanding and reasoning. arXiv Preprint posted online on Jun 13, 2025. [doi: 10.48550/arXiv.2506.07044]
38. Alsinglawi B, Mccarthy C, Webb S, Fluke C, Saidy NT. A lightweight large vision-language model for multimodal medical images. arXiv Preprint posted online on Apr 8, 2025. [doi: 10.48550/arXiv.2504.05575]
39. Wang Y, Liu J, Gao S, Feng B, Tang Z. V2T-CoT: from vision to text chain-of-thought for medical reasoning and diagnosis. Med Image Comput Comput Assisted Intervention – MICCAI 2025 2026;15964:658-668. [doi: 10.1007/978-3-032-04971-1_62]
40. Li C, Wong C, Zhang S. LLaVA-Med: training a large language-and-vision assistant for biomedicine in one day. arXiv Preprint posted online on Jun 1, 2023. [doi: 10.48550/arXiv.2306.00890]
41. Yang X, Miao J, Yuan Y, Jiaze W, Qi D. Medical large vision language models with multi-image visual ability. Med Image Comput Comput Assisted Intervention – MICCAI 2025 2026;15964:402-412. [doi: 10.1007/978-3-032-04971-1_38]
42. Xing Q, Song Z, Zhang Y. MCA-RG: enhancing LLMs with medical concept alignment for radiology report generation. Med Image Comput Comput Assisted Intervention – MICCAI 2025 2026;15964:380-390. [doi: 10.1007/978-3-032-04971-1_36]
43. Yang Y, Ma T, Li R, Zheng X, Shan G. JingFang: an expert-level large language model for traditional chinese medicine clinical consultation and syndrome differentiation-based treatment. arXiv Preprint posted online on Jan 20, 2026. [doi: 10.48550/arXiv.2502.04345]
44. Xu Z, Li Q, Nie W, Wang W, Liu A. Structure causal models and LLMs integration in medical visual question answering. IEEE Trans Med Imaging 2025;44(8):3476-3489. [doi: 10.1109/tmi.2025.3564320] [Medline: 40299735]
45. Traditional Chinese Medicine Identification v2 API. AI Open Platform for TCM Tongue Diagnosis. Beijing: Hefei Cloud Diagnostics Information Technology Co; 2025. URL: https://www.ai-tongue.com/doc_n4t9r9w8/apiapp/composite/home.html [accessed 2026-02-24]

Abbreviations

API: application programming interface
CLIP-ViT: Contrastive Language-Image Pre-Training With Vision Transformer
GELU: Gaussian Error Linear Unit
LLaMA: large language model meta artificial intelligence
LLM: large language model
Q&A: question and answer
TCM: traditional Chinese medicine
TCM-SFT: traditional Chinese medicine–supervised fine-tuning
VLM: visual language model

Edited by A Benis; submitted 06.Nov.2025; peer-reviewed by Y Liu, M Fang; comments to author 05.Dec.2025; revised version received 17.Dec.2025; accepted 17.Feb.2026; published 12.Mar.2026.

Please cite as:
Peng C, Gao J, Yang N, Wang Y, Chen R, Dong C
Application of a Large Visual Language Model on Tongue Image Description Generation and Physical Constitution Reasoning in Traditional Chinese Medicine (TongueVLM): Model Development and Validation Study
JMIR Med Inform 2026;14:e87237
URL: https://medinform.jmir.org/2026/1/e87237
doi:10.2196/87237
PMID:

©Chengdong Peng, Jun Gao, Nuo Yang, Yong Wang, Renming Chen, Changwu Dong. Originally published in JMIR Medical Informatics (https://medinform.jmir.org), 12.Mar.2026. This is an open-access article distributed under the terms of the Creative Commons Attribution License (https://creativecommons.org/licenses/by/4.0/), which permits unrestricted use, distribution, and reproduction in any medium, provided the original work, first published in JMIR Medical Informatics, is properly cited. The complete bibliographic information, a link to the original publication on https://medinform.jmir.org/, as well as this copyright and license information must be included.

XSL•FO
RenderX

Large Language Model–Enabled Editing of Patient Audio Interviews From “This Is My Story” Conversations: Comparative Study

Bikram Bains[1*]; Sampath Rapuri[1*]; Edgar Robitaille[1*]; Jonathan Wang[2], BS; Arnav Khera[2], BS; Catalina Gomez[3], BS; Eduardo Reyes[4], MS; Cole Perry[4], BS; Jason Wilson[5], MS; Elizabeth Tracey[5], MS

[1]Department of Biomedical Engineering, Johns Hopkins University, Baltimore, MD, United States

[2]School of Medicine, Johns Hopkins University, Baltimore, MD, United States

[3]Department of Computer Science, Johns Hopkins University, Baltimore, MD, United States

[4]Technology Innovation Center, Johns Hopkins Medicine, Baltimore, MD, United States

[5]Division of Spiritual Care and Chaplaincy, Johns Hopkins Medicine, 1800 Orleans St, Baltimore, MD, United States

[*]these authors contributed equally

Corresponding Author:
Elizabeth Tracey, MS
Division of Spiritual Care and Chaplaincy, Johns Hopkins Medicine, 1800 Orleans St, Baltimore, MD, United States

Abstract

Background: This Is My Story (TIMS) was started by Chaplain Elizabeth Tracey to promote a humanistic approach to medicine. Patients in the TIMS program are the subject of a guided conversation in which a chaplain interviews either the patient or their loved one. They are asked four questions to elicit clinically actionable information that has been shown to improve communication between patients and medical providers, strengthening medical providers’ empathy. The original recorded conversation is edited into a condensed audio file approximately 1 minute and 15 seconds in length and placed in the electronic health record where it is easily accessible by all providers caring for the patient.

Objective: TIMS is active at the Johns Hopkins Hospital and has shown value in assisting with provider empathy and communication. It is unique in using audio recordings to accomplish this purpose. As the program expands, there exists a barrier to adoption due to limited time and resources needed to manually edit audio conversations. To address this, we propose an automated solution using a large language model to create meaningful and concise audio summaries.

Methods: We analyzed 24 TIMS audio interviews and created three edited versions of each: (1) expert-edited, (2) artificial intelligence (AI)–edited using a fully automated large language model pipeline, and (3) novice-edited by two medical students trained by the expert. A second expert, blinded to the editor, rated the audio interviews in a randomized order. This expert scored both the audio quality and content quality of each interview on 5-point Likert scales. We quantified transcript similarity to the expert-edited reference using lexical and semantic similarity metrics and identified omitted content relative to that same expert interview.

Results: Audio quality (flow, pacing, clarity) and content quality (coherence, relevance, nuance) were each rated on 5-point Likert scales. Expert-edited interviews received the highest mean ratings for both audio quality (4.84) and content quality (4.83). Novice-edited scored moderately (3.84 audio, 3.63 content), while AI-edited scored slightly lower (3.49 audio, 3.20 content). Novice and AI edits were rated significantly lower than the expert edits (P<.001), but not significantly different from each other. AI and novice-edited interview transcripts had comparable overlap with the expert reference transcript, while qualitative review found frequent omissions of patient identity, actionable insights, and overall context in both the AI and novice-edited interviews. AI editing was fully automated and significantly reduced the editing time compared to both human editors.

Conclusions: An AI-based editing pipeline can generate TIMS audio summaries with comparable content and audio quality to novice human editors with one hour of training. AI significantly reduces editing time and removes the need for manual training; with further validation, it could offer a solution to scale TIMS to a large range of health care settings.

(JMIR Med Inform 2026;14:e80205) doi:10.2196/80205

KEYWORDS

audio recording; communication; This Is My Story; TIMS; distress reduction; empathy; patient interview; provider/patient communication; large language model

XSL•FO
RenderX

Introduction

Recent statistics show that health worker burnout is a widespread issue [1]. A 2022 Centers for Disease Control and Prevention report found that 46% of health workers "often" or "very often" felt burned out, increasing from 32% in 2018. Physicians in the United States also report similarly high burnout rates (56% in 2021, 53% in 2022, and 48% in 2023), with an all-time high physician burnout rate of 63% during the pandemic [2,3]. Some reasons for this burnout include excessive work hours, administrative burdens (such as electronic health record documentation), insufficient support staff, and limited organizational and leadership support [4-8]. These chronic stresses impact both patients and clinicians. For example, Andhavarapu et al [9] mentioned that symptoms of depression, anxiety, and posttraumatic stress disorder were reported in 34% of the health care workers surveyed (while 14% reported severe posttraumatic stress disorder), with the highest prevalence among nursing staff (42.8%) and physicians (25.2%). Similarly, the National Academies' 2019 report found that between 35% and 54% of US nurses and physicians and 45% to 60% of medical students and residents experience substantial burnout symptoms throughout their careers [10].

Empathy can serve as a solution, reducing widespread symptoms of burnout while promoting professional fulfillment and strengthening connection with patients [11-14]. Already, health care organizations have recognized the value of empathy and designed personal and patient-centered interventions within their clinical workflows [15]. For example, the This Is My Story (TIMS) program was developed by Chaplain Elizabeth Tracey at the Johns Hopkins Hospital to bring a more patient-centered and empathetic approach to medicine [16]. Patients who participate in the TIMS program take part in a conversation with a chaplain; if the patient is noncommunicative, a chaplain has a conversation with the patient's loved ones. These conversations are guided by four questions: How do you prefer to be addressed? What brings you joy? What does your medical team need to know to care for you best? What brings you peace?

In the words of Dr Charles Cumming, Director Emeritus of Otolaryngology at Johns Hopkins, *"TIMS is about helping us get back to the proper essence of medicine...it's essential to get to know the patient if we're going to be able to help that patient as best we can"* [17]. TIMS conversations have demonstrated clear benefits for clinical communication and empathy, providing an opportunity for meaningful connection with patients to directly target the emotional aspects of burnout [16,18-20]. Past studies by Tracey et al [21] support the positive outcomes the program has had on patients, their families, and the care team. For example, one previous study reported a 74% increase in staff empathy for patients and a 99% improvement in interactions by patients' loved ones with the medical team. Although it has also been shown to be useful in improving staff empathy and reducing distress by 69%, the process of recording and editing conversations can be labor-intensive [21]. By automating the conversation summarization process, these benefits can be made accessible to a wider range of patients and medical institutions.

In this study, we propose an automated editing pipeline for TIMS interviews using a large language model (LLM) and evaluate whether artificial intelligence (AI)–edited interviews are a viable alternative to manual editing. Because medical students were frequently trained to edit TIMS interviews during the pandemic, they are a reasonable baseline for comparing performance. We designed our analysis around two key hypotheses: (1) that AI-edited interviews maintain similar quality to expert-edited interviews in both audio and content metrics, and (2) that AI-edited interviews can be produced more quickly than interviews produced by expert or novice editors.

Methods

Study Design

We used a within - subjects, single - group design in which our reviewer evaluated interviews across three independent editing conditions (expert, AI, novice). Editors were eligible if they had professional experience interpreting patient–clinician audio interviews. Two chaplains from the Johns Hopkins Hospital took part in the study. The novice editors were two medical students who joined the study team from the Johns Hopkins School of Medicine, each having completed an hour-long training session on audio - editing with an expert editor (Chaplain Elizabeth Tracey). The two novice editors edited 12 randomly assigned audio interviews, mirroring the normal workflow for the TIMS initiative without the AI tool.

Patient Audio Dataset

We used a retrospective dataset of audio recordings from 24 patients admitted to the Johns Hopkins Neurosciences Critical Care Unit, a tertiary intensive care unit for patients with diseases of the central or peripheral nervous systems, admitted from departments such as neurosurgery, neurology, and others.

AI Editing Pipeline

Audio recordings were first transcribed using Nvidia's Parakeet-TDT 0.6B v2 automatic speech recognition (ASR) model (Figure 1) [22-24]. ChatGPT-4o [25] processed the transcript using a custom prompt. This prompt asked the model to extract only patient statements that provided essential information about their condition, experiences, feelings, or personal identity. It was also directed to exclude any filler or repetitive content and keep humorous or insightful remarks to preserve patient identity and humanity.

XSL•FO
RenderX

Figure 1. Overview of artificial intelligence–automated workflow for summarizing This Is My Story audio interviews. LLM: large language model.

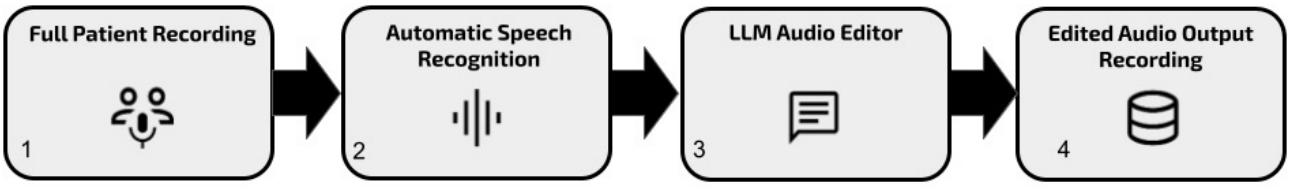

The model was instructed to include the interviewer's four core questions for the TIMS program while excluding interjections or examples provided by the interviewer. Instructions were given to return a processed transcript that the model estimated would take 1.5 minutes during a TIMS interview. The full model prompt is available in Multimedia Appendix 1. The relevant timestamps identified were then used to splice together the final audio file. Examples of cases in which ASR output might have impacted the LLM output are presented in Table S2 in Multimedia Appendix 2. This process was entirely automated and was run on an NVIDIA GeForce RTX 4090 with 24 GB of RAM.

Survey Design

To evaluate both audio quality and content quality for each edited TIMS interview, we created an online questionnaire for our reviewer to complete using a 5-point Likert scale (1=poor, 5=excellent) for each question. The survey included questions grouped into audio (natural flow, pausing/spacing, transitions, pacing, overall listenability of the interview) and content (conversation flow, speaker/topic tracking, patient representation, understanding of patient characteristics, preparation for interaction for patient providers/care team, nuance of the patient's life, relevance of details) quality domains with all details shown in Textbox 1 below. This same survey was used independently for each edited interview for consistent comparison.

Textbox 1. Summary of domain and survey questions following survey administration and data collection.

Audio quality

1. How natural is the conversation flow?
2. How effective are the pauses and spaces between answers?
3. How smooth are the transitions between questions and answers?
4. How does the pacing of the audio feel overall?
5. Overall, how easy is the interview to listen to?
6. Can you understand the flow of the conversation?

Content quality

7. Can you keep track of the speaker and the topic?
8. Is the patient well represented in this conversation?
9. Do you understand the patient's likes/dislikes (proclivities, idiosyncrasies, etc)?
10. Do you feel prepared to interact with the patient in a meaningful way?
11. How well does the conversation capture the depth and nuance of the patient's experience?
12. Does the conversation convey the patient's emotions effectively?
13. How relevant are the details shared during the conversation for understanding the patient's story?
14. How engaging is the conversation in terms of sustaining your interest in the patient's story?

The survey was created and administered using Google Forms. Content experts (ET, JW, CG) provided qualitative feedback on an initial draft of the questions. This feedback focused on improving the clarity and relevance of each item. The questions were then refined based on this input to better capture the intended domains of audio and content quality. It is important to note that because the survey instrument is novel, its reliability and validity have not yet been formally established. The survey asked questions 1, 5, 10, and 11 to gauge general sentiment for the conversation being rated, and more pointed questions to understand where the audios may differ in terms of score (Textbox 1). Since assessing the flow of conversation relies on both audio and content quality, a question about it was used for both parts of the survey. The individual survey responses are available in Figure S1 in Multimedia Appendix 3.

Before rating each edited version, the reviewer listened to the corresponding raw interview as a baseline reference to better understand the context of the interview. Before rating each interview, the reviewer was asked to first listen to two calibration audios—one edited poorly that should score low across all questions, and an expert-edited interview that would score highly. This allowed us to set audio quality expectations for each extreme on the survey. The survey was completed independently for each condition, with the order of the audio

XSL•FO
RenderX

files randomized by condition for each patient to reduce potential order effects.

Editing durations were recorded automatically for the AI pipeline and self‐reported by each novice editor. Expert editing times were not collected due to the limitations of the retrospective dataset.

Content Analysis

For each edited interview, we generated text transcriptions to study the differences in content among the three types of edited interviews. Text transcriptions were created using the Parakeet transcription model. The novice- and AI-edited interviews were compared to the expert edits, and three members of the study team analyzed differences. Types of errors were identified for both AI- and novice-edited conditions across all samples. The most common types of errors were then formalized and described in the results (Table 1). Content similarity between each condition and expert edits was quantitatively measured using ROUGE-L, ROUGE-1, ROUGE-2, bidirectional encoder representations from transformers (BERT), and METEOR on interview transcripts following studies of medical document summarization [26,27]. All metrics measure the similarity of words between summaries and assign a score from 0 to 1, with the ROUGE scores measuring lexical overlap and other scores [28]. METEOR and the BERT scores were used to assess the semantic overlap. Both factor in semantic similarity between words rather than the exact word choice. METEOR also assigns a penalty for differences in phrasing.

Table . Common omissions and inaccurate portrayals by artificial intelligence and novice editors.

Type of error	Artificial intelligence errors	Novice errors
Omission of actionable patient insights	Failure to include specific interests or hobbies of the patient [talking about favorite musical artists bringing her joy]: “She likes Anita Baker, Regina Belle, and Gladys Knight.”	Failure to include information about the patient’s comfort [informing about her medical condition to better care for the patient]: “She has had eczema since she was about three or four, so her skin has to stay moisturized.”
Omission of patient identity and empathy	Failure to include details relevant to understanding the patient’s background [explaining his occupation and hobbies] : “On the church side, he loves to teach. He is a pastor.”	Failure to mention important characteristics about the patient [claiming that her time at Hopkins has made her more independent and resilient]: “She [patient] worked at Johns Hopkins for over 30 years.”
Omission of emotional background	Failure to include framing details relevant for a patient’s background [talking about what brings the patient joy]: “Me [patient’s husband] … We’ve been married 20 years.”	Failure to include details relevant for a patient’s emotional state and anxiety [explaining how he mainly only trusts his partner for everything]: “[He has] a little bit of a trust issue with the medical field.”
Poor narrative fluency	Prompting questions fail to be edited out of the interview: “Introduce yourself and tell me how you’re related to the patient.”	Filler words before prompting questions fail to be edited out of the interview: “That’s great! So, what brings the patient peace?”

Relationships between audio length and content quality were also explored through simple linear regression of each ROUGE metric on the duration of the original interview (in minutes).

Statistical Analysis

We conducted a Friedman test to compare audio‐quality and content‐quality ratings across conditions, with Bonferroni‐corrected Wilcoxon signed-rank post hoc tests to adjust for multiple comparisons. Editing times were analyzed with an independent‐samples *t* test to test significant differences between the two novice editors. We also examined the relationship between the raw interview length and lexical and semantic score overlap for each editor type using Pearson correlation, testing if each slope differed from zero. We then performed an analysis of covariance with transcript length, editor type, and their interaction term to determine if the slope of the length-overlap relationship differed between AI and novice editors.

Ethical Considerations

Ethical approval was not required for this study as it involved a secondary analysis of anonymized data. The original data collection was conducted under Johns Hopkins institutional review board review and approval of the studies with informed consent obtained from all subjects; the consent allowed for future data use and any participants who declined this future use were not included in this secondary analysis. This study was conducted in accordance with all local, institutional, national, and international regulations on human subject research.

Results

Quantitative Comparison of Editing Quality

Across the three types of editors, the mean audio quality ratings were 3.49 (AI-edited), 3.84 (novice-edited), and 4.84 (expert-edited). Similarly, the mean content quality ratings were 3.20 (AI-edited), 3.63 (novice-edited), and 4.83 (expert-edited). The AI-edited interviews demonstrated a higher variability in the rated content quality compared to the novice-edited interviews (SD 0.73 and SD 0.68, respectively). Both interview types were similarly varied in their audio quality ratings (SD 0.77 and 0.78, respectively). Figure 2 highlights the distributions of content and audio quality ratings across each type of edited interview.

XSL•FO
RenderX

Figure 2. (**A**) A comparison of mean audio quality ratings across the three types of editors aggregated across all 24 audio interviews. (**B**) All editors follow similar trends for the content quality ratings. AI: artificial intelligence.

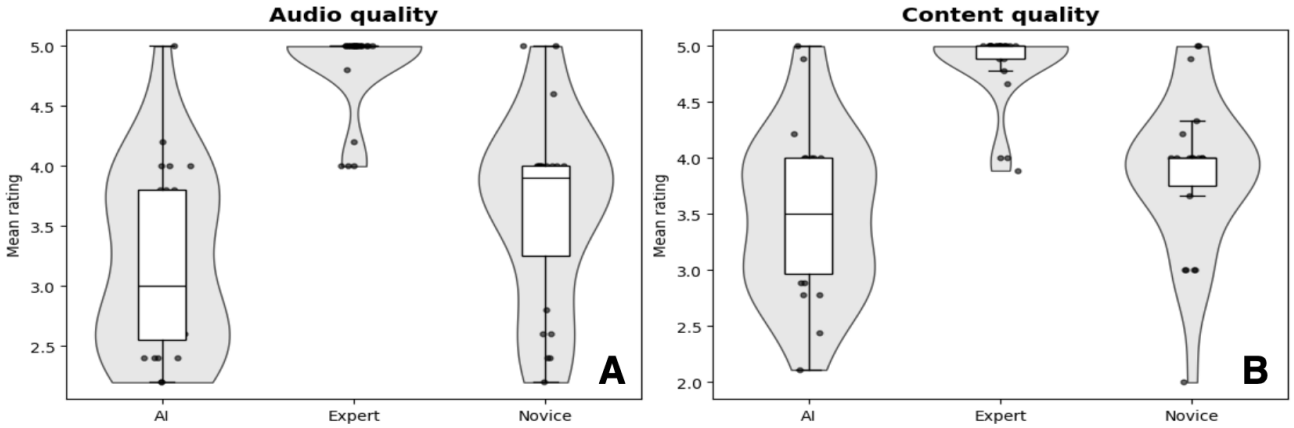

We observed significant differences in audio and content quality between the novice- and expert-edited interviews (P<.001) as well as between the AI- and expert-edited interviews (P<.001). No significant differences were noted between the AI- and novice-edited interviews for either content quality (P=.31) or audio quality (P=.33). A detailed breakdown of the ratings for each individual survey question across all patient interviews can be found in Figure S1 in Multimedia Appendix 3.

To understand the variability between the novice editors, we broke down the differences in rated audio and content quality in Figure 3. Between the two novice editors, we found that novice editor 1 demonstrated a mean content quality score of 3.81 (SD 0.83) and a mean audio quality score of 3.52 (SD 0.76). The second editor's mean content quality score was measured to be 3.88 (SD 0.52), with a mean audio quality score of 3.75 (SD 0.81). However, neither intragroup difference was significant for both content quality (P>.99) and audio quality (P=.51). Figure 4 shows the mean statistical scores across all audio interviews for both the AI and novice editors.

Figure 3. (**A**) A comparison of mean audio quality ratings between the two novice editors, each of whom edited 12 randomly assigned audio interviews. (**B**) Both editors achieved comparable content quality ratings, but the second novice editor exhibited significantly lower variability. All statistical scores of content similarity highlighted the similarities between the artificial intelligence and novice editors, and we report no statistically significant differences between any metric across both types of editors (P>.05). Detailed scores across each metric are contained in Table S1 in Multimedia Appendix 2.

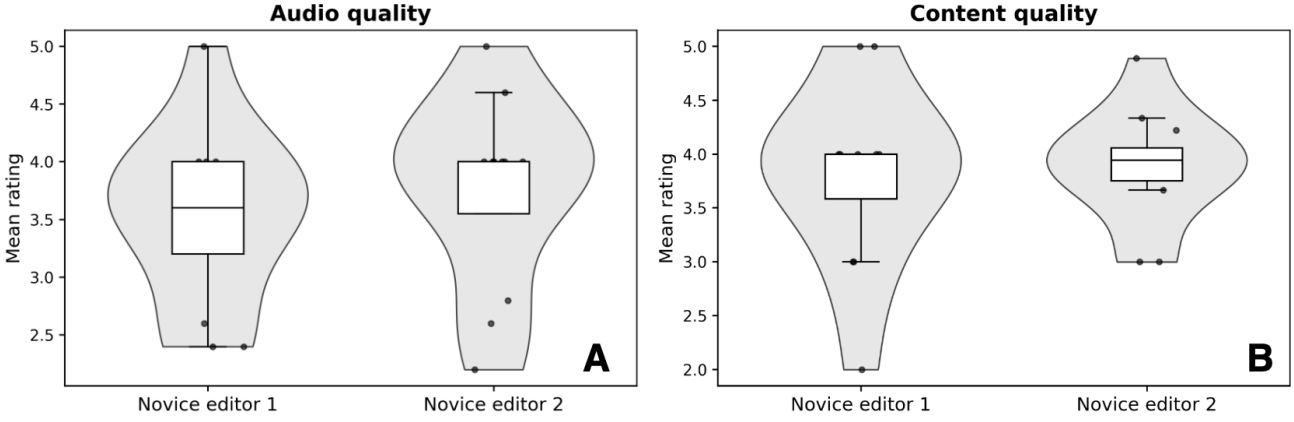

XSL•FO
RenderX

Figure 4. Mean statistical scores across all 24 audio interviews for both the artificial intelligence and novice editors. AI: artificial intelligence. BERT: bidirectional encoder representations from transformers.

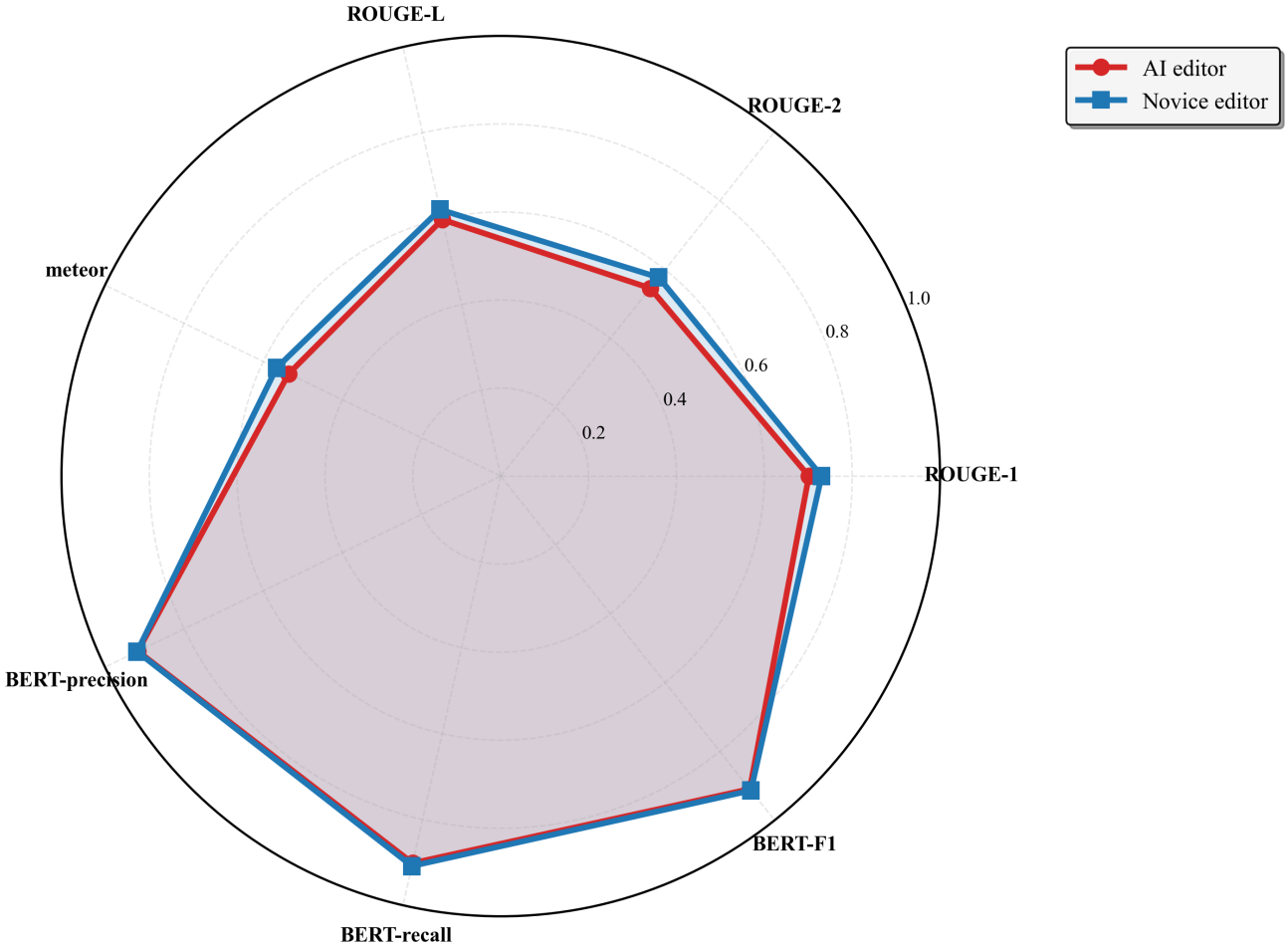

Qualitative Error Analysis

We qualitatively compared the AI- and novice-edited interviews to the expert-edited interviews and found five types of errors repeated across many of the interviews, which are described in Table 1. Many of the errors were similar across the AI- and novice-edited interviews.

Editing Efficiency

On average, each novice editor took 29.54 minutes to edit each interview (SD 12.69 min). However, we report a difference (P=.06) in the time each novice editor takes, with the first editor taking 24.50 minutes (SD 11.18 min) and the second taking 34.58 minutes (SD 13.08 min) to edit each interview. Figure 5 highlights the variability in the time to edit interviews between novice editors. Mean editing times for the expert editor are unavailable as they were not recorded. Based on anecdotal evidence from the expert editor, each audio interview required around 5 to 10 minutes to edit. In contrast to both the expert and novice editors, our automated AI-editing pipeline took less than 10 seconds from ingestion of the raw audio interview to the saving of the edited interview.

XSL•FO
RenderX

Figure 5. Time to edit each interview between each novice editor.

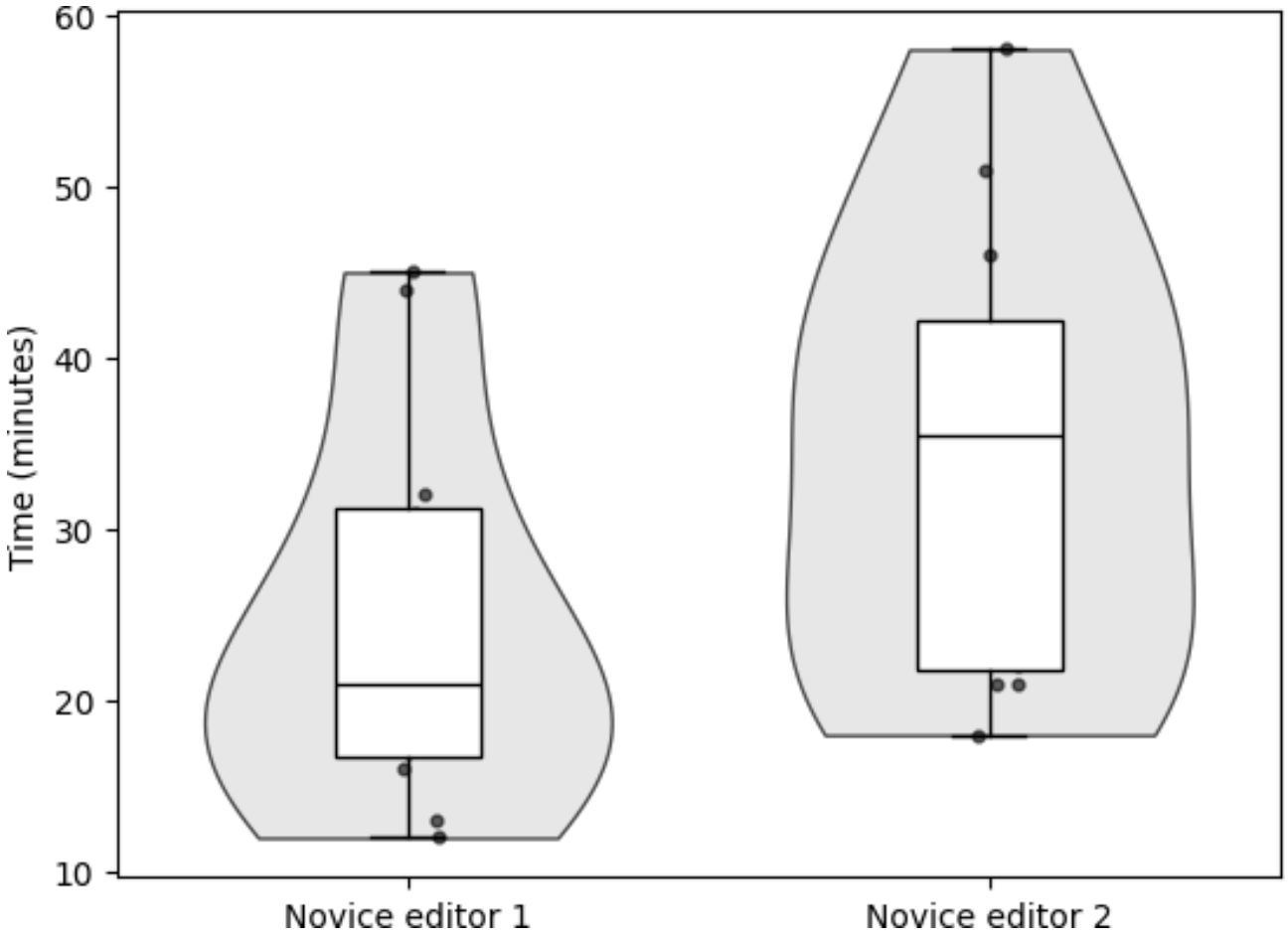

Impact of Interview Length on Editing Quality

We investigated if longer raw audio interviews were associated with changes in the lexical and semantic overlap with the expert reference, as measured by ROUGE-L. For AI-edited interviews, there was a significant negative correlation between transcript length and ROUGE-L scores (r=−0.58, R^2=0.34; Figure 6). This same trend was seen for novice-edited interviews, with a negative correlation (r=−0.52, R^2=0.27). Both slopes were significantly different from zero (P<.05), suggesting longer interviews were associated with lower transcript overlap to expert editor reference for both conditions. Regression plots for ROUGE-1, ROUGE-2, METEOR, and BERT scores showed comparable patterns and are provided in Figure S2 in Multimedia Appendix 3.

XSL•FO
RenderX

Figure 6. Linear regression of the raw transcript length versus ROUGE-L, reflecting the change in lexical similarity to the expert reference with longer interview times.

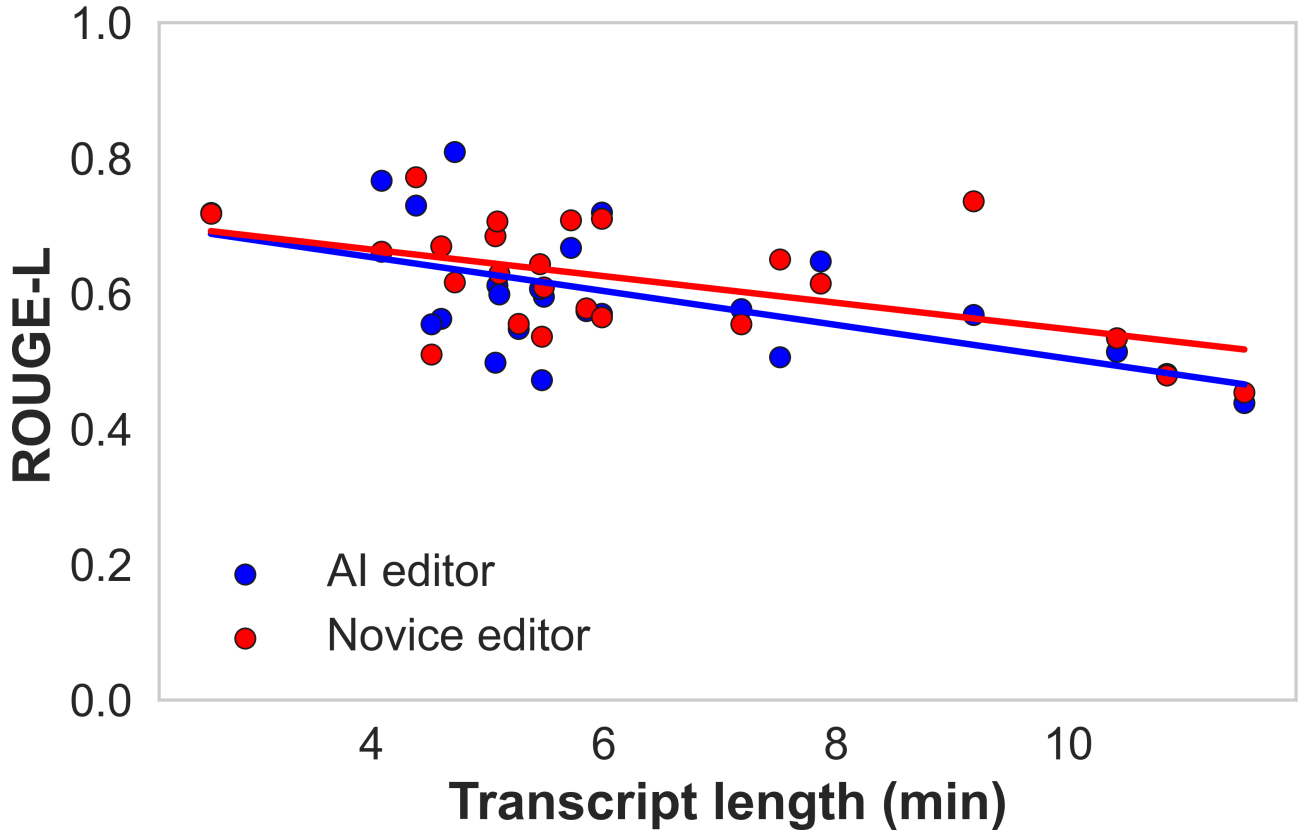

Discussion

Principal Results

Our study compares the listening experience of patient conversations summarized by an expert editor, a novice editor, and ChatGPT-4o. There was no significant difference in content and audio quality between the AI and novice editors, and both showed varying performance across the samples. Further analysis of the edited transcripts revealed that both of these groups omitted key details. The expert editor had a significantly higher audio and content quality rating than both experimental groups and less variability across samples. Exclusion of natural pauses between phrases and auditory cues to break up conversation led to lower audio quality scores.

Comparison to Prior Work

As burnout remains high among health care workers, TIMS provides an opportunity for meaningful connections with patients to target the emotional aspect of burnout. However, the manpower needed to edit audio is a limiting factor for this program's widespread adoption. Although the audio-editing pipeline introduced was originally developed to expand the TIMS program, these results are also broadly relevant to the use of AI in clinical practice and examine a previously unexplored application of LLMs, specifically editing audio content for a medical context. Previous studies have investigated ChatGPT as a clinical decision-making tool, for taking notes, and analyzing literature [26,28-35]. There have also been studies that demonstrate ChatGPT's capability to elicit empathetic feelings in an emergency setting can even exceed that of clinicians [36-38]. However, the combination of a summarization task to build empathy in a third-party listener has not been investigated. In this study, we aim to evaluate whether an LLM is able to extract emotionally relevant details from a conversation. Additionally, we provide a replicable framework for integrating LLMs in the analysis of patient audio for a broad variety of applications within health care settings. We found that our pipeline faced similar issues raised in previous studies examining ChatGPT's ability to summarize in a medical context. Kernberg et al [39] reported that 58% of structured medical notes from patient-physician interactions omitted important information. A manual analysis of the transcripts revealed that details considered important to a patient's story were also often omitted, highlighting a key disadvantage of LLMs in the literature. ChatGPT also tends to vary widely in the quality of responses across the samples. Although this was a shortcoming observed in the novice editors' performance on audio and content quality (SD 0.68 and SD 0.78), the expert editor's performance was consistent.

In addition to the survey, ROUGE scores (ROUGE-1, ROUGE-2, ROUGE-L) for the novice and AI editors indicated a high level of word overlap with the expert-edited transcript, with no significant differences between the two groups. High (~0.9) BERT scores (BERT-recall, BERT-precision, BERT-F_1) were also reported, indicating a high degree of semantic overlap that was not necessarily reflected in the ROUGE score. As the length of the audios increased, there was a statistically significant negative correlation between interview length and the ROUGE-L score for both AI and novice editors (P<.05), indicating longer interviews tended to have less lexical overlap

XSL•FO
RenderX

with the expert reference. This implies that there might be a length of audio that may not be as suitable for AI editing that will become more apparent as longer audios are recorded. These results from an established tool align with the insights from the survey, suggesting some level of construct validity for the survey questions.

Limitations

There are key limitations beyond the strengths of this study. First, there is no standardized or validated survey instrument available, so the introduction of a novel survey to assess the impact of each audio on a listener was necessary. However, abstract questions concerning "patient representation" or "nuance" are susceptible to subjective interpretation, a weakness that is amplified by our use of a single blinded reviewer. We attempted to standardize these ratings with calibration audios that were developed, but we cannot exclude the possibility that these subjective quality scores were influenced by rater bias. Despite this concern, the consistently high scores awarded to the expert-edited interviews provide some evidence of the survey's validity, as the rater reliably scored the gold-standard interviews. This survey could be adopted in the future by studies to measure the efficacy of interventions to increase empathy in medicine.

Second, the sample size of the study was also relatively limited, with only 24 samples and 1 recruited rater who was surveyed, which makes the results prone to bias. To build on this work, a larger sample size of patient audio interviews and experienced interview raters should be recruited. Previous volunteers of the program were able to receive iterative feedback on their work over long periods, but the novice editors had approximately 1 hour of training in comparison, so their skills were not as developed. Lastly, we were unable to obtain granular editing time measurements from the expert editor as these were retrospectively edited. However, the AI pipeline's completion time of under 10 seconds represents a multiple-orders-of-magnitude improvement in efficiency against any manual editing process.

Future Directions

We have presented the groundwork for an audio transcription and editing pipeline for humanistic patient conversations. Future work should test newer models as they improve, and others that are currently available besides ChatGPT-4o, with the same pipeline. Other strategies to improve performance include fine-tuning the LLM model, using AI agents to summarize the transcript, testing other ASR models, introducing patient-specific contextual metadata, and further prompt engineering to optimize the output. Error propagation was not formally tracked through the entire editing pipeline, but we have hypothesized an association between ASR errors and the final output quality. Future work should investigate these errors.

Conclusions

We conclude that ChatGPT-4o can create summarized audio files with similar audio and content quality to a novice editor in just a fraction of the time. However, the expert editor outperforms the AI editing pipeline and the novice editors on all metrics. After further validation, this tool could be implemented in the TIMS program to reduce workload and overcome adoption barriers.

Acknowledgments

This research has been generously supported with grants from the John Conley Foundation for Ethics and Philosophy in Medicine. We additionally acknowledge support from the Catalyst Award and the Diversity Innovation Grant from Johns Hopkins University. Lastly, we thank the Johns Hopkins Technology Innovation Center for providing access to a protected health information–compliant version of ChatGPT-4o.

Data Availability

The original interview recordings are not publicly available for privacy protection considerations but are available from the corresponding author on reasonable request. The relevant code is provided here [40]. This code corresponds to the automated audio-editing pipeline that processes raw audio, uses ChatGPT-4o to extract key segments, and stitches those selected segments into an AI-edited audio.

Authors' Contributions

All authors contributed to the conceptualization and study design. SR, BB, and ER curated the data and conducted the analysis. ET and JW managed and supervised the project. All authors reviewed and edited the manuscript.

Conflicts of Interest

None declared.

Multimedia Appendix 1
GPT-4o summarization prompt.
[DOCX File, 16 KB - medinform_v14i1e80205_app1.docx]

Multimedia Appendix 2

XSL•FO
RenderX

Supplementary tables.
[DOC File, 17 KB - medinform_v14i1e80205_app2.doc]

Multimedia Appendix 3
Supplementary figure.
[DOC File, 231 KB - medinform_v14i1e80205_app3.doc]

References

1. Health worker mental health crisis. Centers for Disease Control and Prevention. 2023 Oct 24. URL: https://www.cdc.gov/vitalsigns/health-worker-mental-health/index.html [accessed 2025-07-06]
2. Shanafelt TD, West CP, Dyrbye LN, et al. Changes in burnout and satisfaction with work-life integration in physicians during the first 2 years of the COVID-19 pandemic. Mayo Clin Proc 2022 Dec;97(12):2248-2258. [doi: 10.1016/j.mayocp.2022.09.002] [Medline: 36229269]
3. Physician burnout statistics 2024: the latest changes and trends in physician burnout by specialty. American Medical Association. 2024 Aug 19. URL: https://www.ama-assn.org/practice-management/physician-health/physician-burnout-statistics-2024-latest-changes-and-trends [accessed 2025-07-06]
4. West CP, Dyrbye LN, Shanafelt TD. Physician burnout: contributors, consequences and solutions. J Intern Med 2018 Jun;283(6):516-529. [doi: 10.1111/joim.12752] [Medline: 29505159]
5. Singh R, Volner K, Marlowe D. Provider burnout. In: StatPearls: StatPearls Publishing. [Medline: 30855914]
6. Belkić K. Toward better prevention of physician burnout: insights from individual participant data using the MD-specific Occupational Stressor Index and organizational interventions. Front Public Health 2025;13:1514706. [doi: 10.3389/fpubh.2025.1514706] [Medline: 40177083]
7. Health worker burnout. Office of the Surgeon General, US Department of Health and Human Services. 2024 May 28. URL: https://www.hhs.gov/surgeongeneral/reports-and-publications/health-worker-burnout/index.html [accessed 2025-07-06]
8. Sipos D, Goyal R, Zapata T. Addressing burnout in the healthcare workforce: current realities and mitigation strategies. Lancet Reg Health Eur 2024 Jul;42:100961. [doi: 10.1016/j.lanepe.2024.100961] [Medline: 39070752]
9. Andhavarapu S, Yardi I, Bzhilyanskaya V, et al. Post-traumatic stress in healthcare workers during the COVID-19 pandemic: a systematic review and meta-analysis. Psychiatry Res 2022 Nov;317:114890. [doi: 10.1016/j.psychres.2022.114890] [Medline: 36260970]
10. National Academies of Sciences, Engineering, and Medicine. Taking Action Against Clinician Burnout: A Systems Approach to Professional Well-Being: National Academies Press; 2019. [doi: 10.17226/25521]
11. Empathy: a critical ally in battling physician burnout. American Medical Association. 2019 Feb 5. URL: https://www.ama-assn.org/practice-management/physician-health/empathy-critical-ally-battling-physician-burnout [accessed 2025-07-06]
12. Cairns P, Isham AE, Zachariae R. The association between empathy and burnout in medical students: a systematic review and meta-analysis. BMC Med Educ 2024 Jun 7;24(1):640. [doi: 10.1186/s12909-024-05625-6] [Medline: 38849794]
13. Delgado N, Delgado J, Betancort M, Bonache H, Harris LT. What is the link between different components of empathy and burnout in healthcare professionals? A systematic review and meta-analysis. Psychol Res Behav Manag 2023;16:447-463. [doi: 10.2147/PRBM.S384247] [Medline: 36814637]
14. Wilkinson H, Whittington R, Perry L, Eames C. Examining the relationship between burnout and empathy in healthcare professionals: a systematic review. Burn Res 2017 Sep;6:18-29. [doi: 10.1016/j.burn.2017.06.003] [Medline: 28868237]
15. Nembhard IM, David G, Ezzeddine I, Betts D, Radin J. A systematic review of research on empathy in health care. Health Serv Res 2023 Apr;58(2):250-263. [doi: 10.1111/1475-6773.14016] [Medline: 35765156]
16. Tracey E, Crowe T, Wilson J, Ponnala J, Rodriguez-Hobbs J, Teague P. An introduction to a novel intervention, “This is My Story”, to support interdisciplinary medical teams delivering care to non-communicative patients. J Relig Health 2021 Oct;60(5):3282-3290. [doi: 10.1007/s10943-021-01379-3] [Medline: 34386889]
17. This Is My Story. Johns Hopkins Medicine. 2022 Jun. URL: https://www.hopkinsmedicine.org/news/articles/2022/06/this-is-my-story [accessed 2025-07-06]
18. Tracey E, Wilson J, Im C, Abshire-Saylor M. A brief patient-recorded audio file called TIMS (This Is My Story) improves communication and empathy for healthcare teams in the hospital. J Patient Exp 2024;11:23743735241274015. [doi: 10.1177/23743735241274015] [Medline: 39161418]
19. Wilson J, Tracey E, Ponnala J, Rodriguez-Hobbs J, Crowe T. An ICU expansion of a novel chaplain intervention, “This is My Story,” to support interdisciplinary medical teams delivering care to non-communicative patients in an academic medical center. J Relig Health 2023 Feb;62(1):83-97. [doi: 10.1007/s10943-022-01567-9] [Medline: 35482270]
20. Tracey E, Wilson J, Mathur R, Hager D. Impressions of recording a brief audio file known as a TIMS (This is My Story) file. J Patient Exp 2025;12:23743735251346585. [doi: 10.1177/23743735251346585] [Medline: 40470310]
21. Tracey E, Wilson J, Abshire Saylor M, et al. TIMS: a mixed methods evaluation of the impact of a novel chaplain facilitated recorded interview placed in the medical chart for the medical staff in an ICU during the COVID-19 Pandemic. J Relig Health 2023 Jun;62(3):1532-1545. [doi: 10.1007/s10943-023-01800-z] [Medline: 37014488]

XSL•FO
RenderX

22. Rekesh D, Koluguri NR, Kriman S, et al. Fast conformer with linearly scalable attention for efficient speech recognition. arXiv. Preprint posted online on May 9, 2023. [doi: 10.48550/ARXIV.2305.05084]
23. Xu H, Jia F, Majumdar S, Huang H, Watanabe S, Ginsburg B. Efficient sequence transduction by jointly predicting tokens and durations. arXiv. Preprint posted online on Apr 13, 2023. [doi: 10.48550/ARXIV.2304.06795]
24. NVIDIA/Parakeet TDT 0.6B V2 (En). Hugging Face. 2024. URL: https://huggingface.co/nvidia/parakeet-tdt-0.6b-v2 [accessed 2025-07-06]
25. OpenAI, Hurst A, Lerer A, et al. GPT-4o system card. arXiv. Preprint posted online on Oct 22, 2024. [doi: 10.48550/ARXIV.2410.21276]
26. Tang L, Sun Z, Idnay B, et al. Evaluating large language models on medical evidence summarization. NPJ Digit Med 2023 Aug 24;6(1):158. [doi: 10.1038/s41746-023-00896-7] [Medline: 37620423]
27. Liu Y, Ju S, Wang J. Exploring the potential of ChatGPT in medical dialogue summarization: a study on consistency with human preferences. BMC Med Inform Decis Mak 2024 Mar 14;24(1):75. [doi: 10.1186/s12911-024-02481-8] [Medline: 38486198]
28. Gan RK, Uddin H, Gan AZ, Yew YY, González PA. ChatGPT's performance before and after teaching in mass casualty incident triage. Sci Rep 2023 Nov 21;13(1):20350. [doi: 10.1038/s41598-023-46986-0] [Medline: 37989755]
29. Rao A, Pang M, Kim J, et al. Assessing the utility of ChatGPT throughout the entire clinical workflow: development and usability study. J Med Internet Res 2023 Aug 22;25(1):e48659. [doi: 10.2196/48659] [Medline: 37606976]
30. Liu J, Wang C, Liu S. Utility of ChatGPT in clinical practice. J Med Internet Res 2023 Jun 28;25(1):e48568. [doi: 10.2196/48568] [Medline: 37379067]
31. Clusmann J, Kolbinger FR, Muti HS, et al. The future landscape of large language models in medicine. Commun Med (Lond) 2023 Oct 10;3(1):141. [doi: 10.1038/s43856-023-00370-1] [Medline: 37816837]
32. Sandmann S, Riepenhausen S, Plagwitz L, Varghese J. Systematic analysis of ChatGPT, Google search and Llama 2 for clinical decision support tasks. Nat Commun 2024 Mar 6;15(1):2050. [doi: 10.1038/s41467-024-46411-8] [Medline: 38448475]
33. Van Veen D, Van Uden C, Blankemeier L, et al. Adapted large language models can outperform medical experts in clinical text summarization. Nat Med 2024 Apr;30(4):1134-1142. [doi: 10.1038/s41591-024-02855-5] [Medline: 38413730]
34. Fraile Navarro D, Coiera E, Hambly TW, et al. Expert evaluation of large language models for clinical dialogue summarization. Sci Rep 2025 Jan 7;15(1):1195. [doi: 10.1038/s41598-024-84850-x] [Medline: 39774141]
35. Goh E, Gallo R, Hom J, et al. Large language model influence on diagnostic reasoning: a randomized clinical trial. JAMA Netw Open 2024 Oct 1;7(10):e2440969. [doi: 10.1001/jamanetworkopen.2024.40969] [Medline: 39466245]
36. Ovsyannikova D, de Mello VO, Inzlicht M. Third-party evaluators perceive AI as more compassionate than expert humans. Commun Psychol 2025 Jan 10;3(1):4. [doi: 10.1038/s44271-024-00182-6] [Medline: 39794410]
37. Ayers JW, Poliak A, Dredze M, et al. Comparing physician and artificial intelligence chatbot responses to patient questions posted to a public social media forum. JAMA Intern Med 2023 Jun 1;183(6):589-596. [doi: 10.1001/jamainternmed.2023.1838] [Medline: 37115527]
38. Elyoseph Z, Hadar-Shoval D, Asraf K, Lvovsky M. ChatGPT outperforms humans in emotional awareness evaluations. Front Psychol 2023;14:1199058. [doi: 10.3389/fpsyg.2023.1199058] [Medline: 37303897]
39. Kernberg A, Gold JA, Mohan V. Using ChatGPT-4 to create structured medical notes from audio recordings of physician-patient encounters: comparative study. J Med Internet Res 2024 Apr 22;26:e54419. [doi: 10.2196/54419] [Medline: 38648636]
40. Rapuris/TIMS_AI_Editing_Pipeline. GitHub. URL: https://github.com/Rapuris/TIMS_AI_Editing_Pipeline [accessed 2025-12-29]

Abbreviations

AI: artificial intelligence
ASR: automatic speech recognition
BERT: bidirectional encoder representations from transformers
LLM: large language model
TIMS: This Is My Story

XSL•FO
RenderX

Edited by A Coristine; submitted 07.Jul.2025; peer-reviewed by A Kernberg, KH Lin, N Thawinwisan, S Biswas; revised version received 04.Nov.2025; accepted 04.Nov.2025; published 09.Jan.2026.

Please cite as:
Bains B, Rapuri S, Robitaille E, Wang J, Khera A, Gomez C, Reyes E, Perry C, Wilson J, Tracey E
Large Language Model–Enabled Editing of Patient Audio Interviews From "This Is My Story" Conversations: Comparative Study
JMIR Med Inform 2026;14:e80205
URL: https://medinform.jmir.org/2026/1/e80205
doi:10.2196/80205

© Bikram Bains, Sampath Rapuri, Edgar Robitaille, Jonathan Wang, Arnav Khera, Catalina Gomez, Eduardo Reyes, Cole Perry, Jason Wilson, Elizabeth Tracey. Originally published in JMIR Medical Informatics (https://medinform.jmir.org), 9.Jan.2026. This is an open-access article distributed under the terms of the Creative Commons Attribution License (https://creativecommons.org/licenses/by/4.0/), which permits unrestricted use, distribution, and reproduction in any medium, provided the original work, first published in JMIR Medical Informatics, is properly cited. The complete bibliographic information, a link to the original publication on https://medinform.jmir.org/, as well as this copyright and license information must be included.

XSL•FO
RenderX

Publisher:
JMIR Publications
130 Queens Quay East.
Toronto, ON, M5A 3Y5
Phone: (+1) 416-583-2040
Email: support@jmir.org

XSL•FO
RenderX